KNOWLEDGEMICHELSON-MORELYEXPERIMENT1887THEORYOFRELATIVITYCARDIACCARECPR

International Society of Biomechanics
XX th meeting

American Society of Biomechanics
29 th meeting

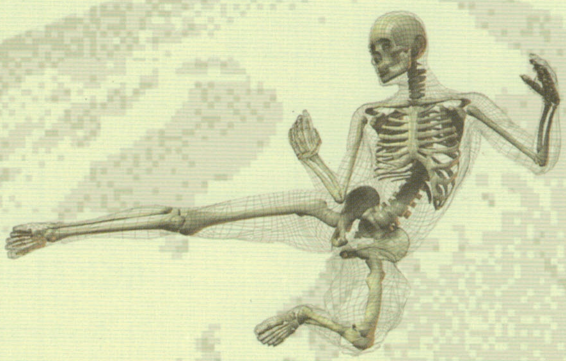

July 31st - August 5th
Cleveland State University

WHEELCHAIRSMEDICALIMAGINGINVENTIONTELEGRAPHCENTRALSTATIONARCLIGHTINGLICKTELESCOPE1STPATENTEDTRAFFICSIGNAL

FUNCTIONALELECTRICALSTIMULATIONMATERIALSOILSTEELPAINTPOLYMERSDISCOVERYLUCYTHEWRIGHTBROTHERSJETPROPULSIONNASA

ENTREPRENEURSHIPROCKEFELLERSTANDARDOILELECTRICITYNELAPARKSPACETRAVEL

Cleveland State University
Main Campus

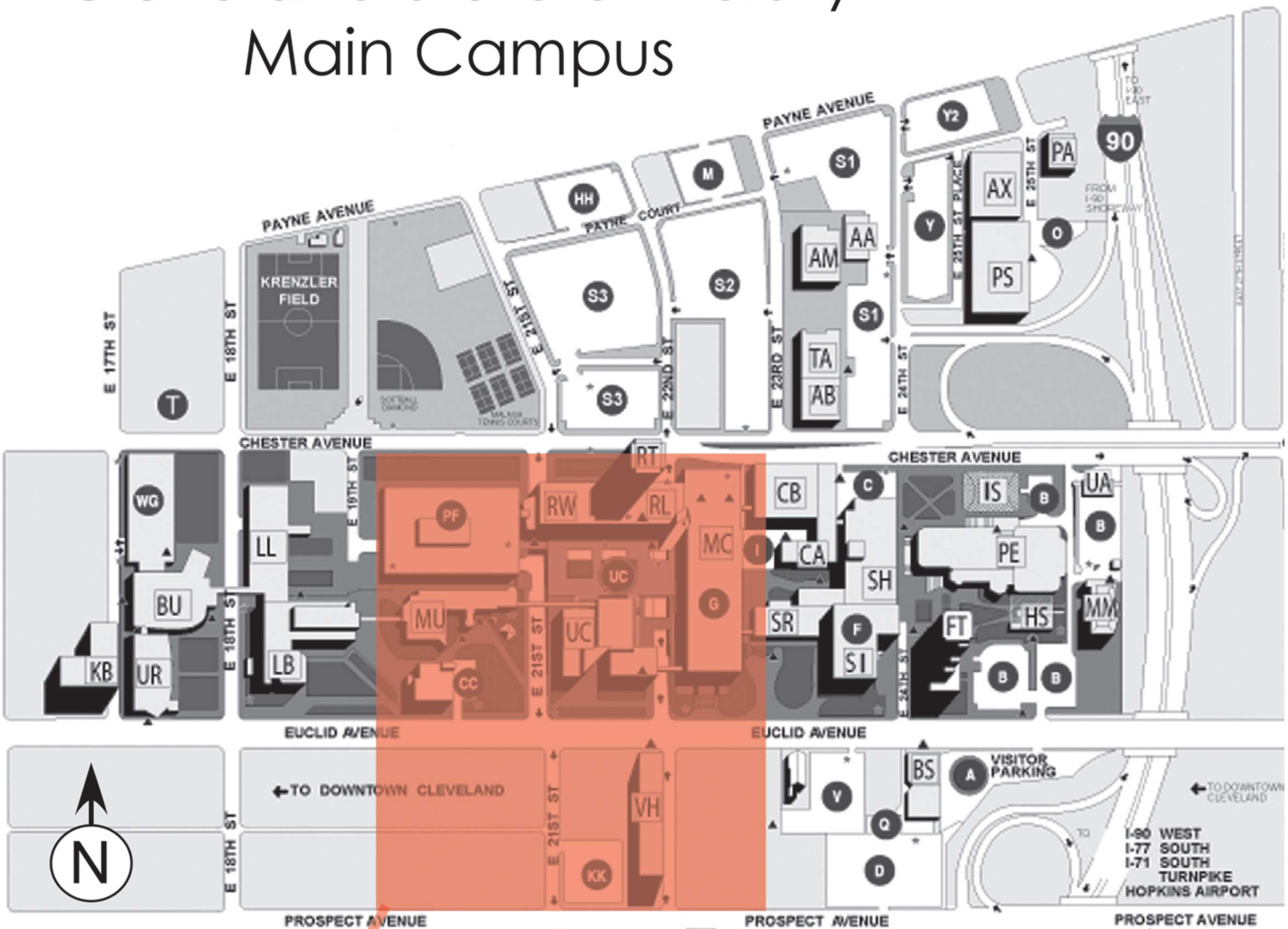

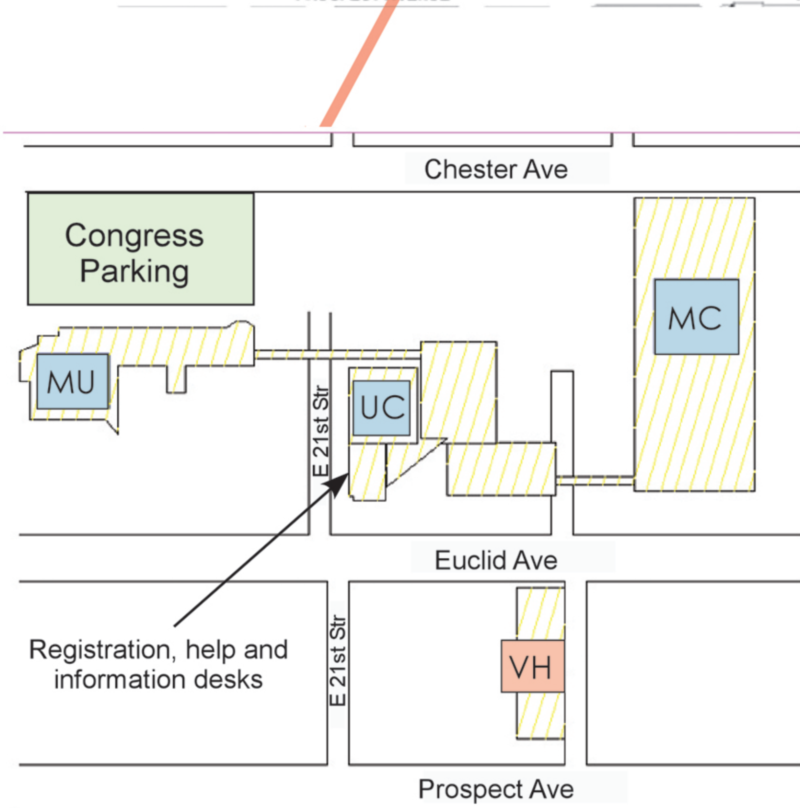

MU: Music and Communication Building
Waetjen Auditorium

UC: University Center

MC: Main Classroom

VH: Viking Hall (campus accommodation)

Welcome

XXth Congress of the International Society of Biomechanics
and
29th Annual Meeting of the American Society of Biomechanics

We are delighted to welcome you to Cleveland, Ohio, for a combined meeting of the International and American Societies of Biomechanics. The last time the ISB held its congress in the USA was in 1989, in Los Angeles, California. In the intervening 15 years, researchers in biomechanics have continued to make significant breakthroughs in a variety of fields including the understanding and treatment of musculoskeletal disorders, preventing workplace injuries and optimizing athletic performance at the elite levels. New medical imaging technologies, microsensors, and computer algorithms add to these breakthroughs on a daily basis. The work of our two societies is in the forefront of advancement of the discipline of biomechanics, in both its academic and applied arenas. Such advancement is especially significant as we progress through what the World Health Organization has designated "The Bone and Joint Decade."
From July 31st through August 5th, 2005, we look forward to meeting colleagues many of whom last gathered in Dunedin in 2003 and to making new acquaintances that will spur collaborations. The underlying emphasis of the Congress this year is to create a program that encourages student participation, with a great variety of educational offerings in all aspects of biomechanics. We have two main objectives for the 2005 meeting: (i) to present an academic program of the highest quality, and (ii) to have a rich social program that will complement the scientific meetings and allow new and old friends to experience all that Cleveland has to offer.

We are confident you will find the meeting to be an outstanding congress that does credit to both ISB and ASB.

Pat

Peter R. Cavanagh, Ph.D., D.Sc.
Virginia Lois Kennedy Chairman of Biomedical Engineering
The Cleveland Clinic Foundation

Patrick E. Crago, Ph.D.
Allen H. and Constance T. Ford Professor and Chairman of Biomedical Engineering
Case Western Reserve University

Organization

Organizing Committee

Brian Davis (Co-Chair)
Ton van den Bogert (Co-Chair)

Peter Cavanagh	William Jirousek
Patrick Crago	Robert Kirsch
George Chatzimavroudis	Melissa Knothe Tate
Susan D'Andrea	Scott McLean
Todd Doehring	Katie Root
A. Seth Greenwald	Paul Sung
Elizabeth Hardin	Ronald Triolo
John Jeziorowski	Guang Yue

Host Institutions

The Cleveland Clinic Foundation
Department of Biomedical Engineering
Orthopaedic Research Center

Case Western Reserve University
Department of Biomedical Engineering
Department of Mechanical Engineering

Louis Stokes Cleveland VA Medical Center
Motion Studies Laboratory

Cleveland State University
Department of Health Sciences
Department of Chemical and Biomedical Engineering

Lutheran Hospital
Orthopaedic Biomechanics Laboratories

ISB and ASB Information

ISB Council Members	ASB Council Members
Mary Rodgers	J.J. Trey Crisco
Sandra Onley	Walter Herzog
Brian Davis	Ted Gross
Julie Steele	Don Anderson
Maarten Bobbert	Art Kuo
Ewald Hennig	Irene Davis
Senshi Fukashiro	Julianne Abendroth-Smith
Mark Grabiner	Steve McCaw
Robert Gregor	Kathy Simpson
Walter Herzog	Andrew Karduna
Jill McNitt-Gray	Melissa Scott-Pandorf
Joseph Hamill	
Alex Stacoff	
Karen Søgaard	
Graeme Wood	
Motoshi Kaya	

ISB General Assembly

The International Society of Biomechanics will hold its General Assembly on Wednesday, August 3rd at 12.00 p.m. in Waetjen Auditorium.

ASB General Assembly

The American Society of Biomechanics will also hold its General Assembly during the Congress. Details will be announced.

ISB Desk

The ISB desk is located in the University Center Atrium (see Map, inside cover). ISB membership questions can be answered throughout the Congress.

General Information

Congress Venue

The Welcome Reception and Scientific program will be held at Cleveland State University Main Campus, from Sunday July 31st through Friday August 5th. Lunches and refreshments will also be provided, Monday through Friday at the congress site. Detailed maps of the congress venue and more information on the scientific and social programs can be found within this booklet. Volunteers will be available on-site throughout through the entire congress to assist you with any queries or concerns. Keep an eye out for the people in the green polo shirts with the congress logo.

Registration Desk

The conference registration desk is located in the University Center Atrium and will be open on Sunday between 8.30 AM and 6.00 PM, and during the remainder of the congress. Please check in at this desk to pick up congress materials or if you have any registration related queries.

Exhibitors

A number of national and international companies will be on hand to exhibit their latest products. All exhibitors will be located in the University Center (Atrium, basement and 2nd Floor), from Sunday 8:30 AM to Wednesday 1:00 PM. See the map on page 9 for details. Please stop by during the conference to see what is the latest and greatest in biomechanics.

Information and Message Service

A congress message board will be provided next to the registration desk. All congress participants are invited to use this board at their convenience.

Banks and ATM's

There three Automatic Teller Machines located on Cleveland State University Main Campus. Each of these is open 24 hours and will take major bank and credit cards. There is also a major bank (Huntington National Bank, 917 Euclid Ave) Bank within walking distance (0.66 miles) from the Congress Center, which is open Monday to Friday between 9.00 a.m. and 4.00 p.m. if you should require additional assistance. Both Bank and ATM locations are included on the Accommodations map for your convenience (page 8).

Internet Cafe

A free internet café will be available throughout the conference, located in the University Center, adjacent to the Atrium. The Cleveland State University is also a wireless network hub for those bringing their own laptops. Please use the following login information to access the CSU computing network (Login: isbasb, Password: csuguest).

Congress Badges

Delegates and accompanying persons are required to wear their official congress identification badges for entrance to all congress activities including the social events and functions.

Fitness Facilities

Access will be provided to Cleveland State University Weight Room and Running Track facilities between 4:00 – 8:00 PM, on Monday, Tuesday and Wednesday. If you are interested in using these facilities, please contact the registration desk for more details.

Safety

As with most large cities, Cleveland has its share of do's and don'ts in terms of keeping safe. We also realize that part of the Congress experience is about exploring what the host city has to offer. To assist you in this process, free transportation will be provided to various destinations on Wednesday afternoon. We strongly encourage you to take advantage of this offer during your stay, both for ease of access and safety reasons. Additional shuttles may be added at other times throughout the conference. Please ask for an update at the information desk. If at any time you require immediate assistance, please contact Cleveland State University Conference Services (216-523-7203) or if it is an emergency, Campus Security (216-687-2020).

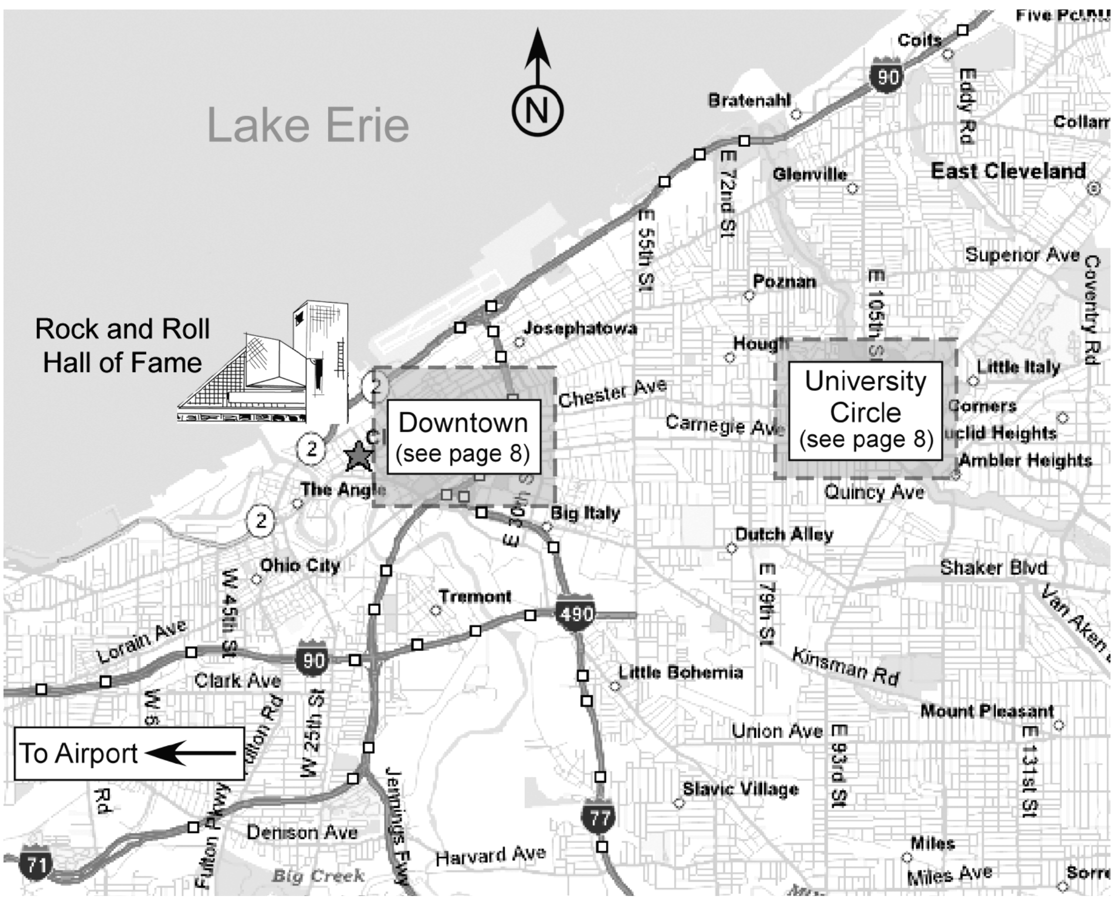

Social Program

Sunday, July 31st	Welcome reception on CSU Campus
Tuesday, August 2st	Open House at Cleveland Museum of Natural History
Wednesday, August 3nd	Tours and excursions
Thursday, August 4th	Baseball: Cleveland Indians and New York Yankees
Friday, Agust 5th	Banquet at Rock and Roll Hall of Fame

Opening Ceremony

The Organizing Committee welcomes you to Cleveland and the XXth ISB Congress and 29th Annual Meeting of the ASB for what promises to be a fantastic scientific and social event. Festivities being with the Opening Ceremony at 3:00 PM on Sunday July 31st, held in the Waetjen Auditorium (MU Building), followed by the Wartenweiler Memorial Lecture at 4:00 PM. The order of events is listed below.

Music: Students from the Cleveland Institute of Music

Welcomes

Mary Rodgers – ISB President
Trey Crisco – ASB President
Ton van den Bogert – Cleveland Organizing Committee
This is Cleveland (Video)
Mark Tumeo – Vice Provost for Research and Dean, College of Graduate Studies
Patrick Crago – Chairman of Biomedical Engineering, CASE

Opening Address: From Marey to Mars – through Ohio
Peter Cavanagh, Chairman of Biomedical Engineering, The Cleveland Clinic

Music: Students from the Cleveland Institute of Music

Introduction to the Wartenweiler Lecture
Benno Nigg, University of Calgary

Wartenweiler Lecture: Bruce Latimer, Director, The Cleveland Museum of Natural History. *Biomechanics and Evolution*

Music: Students from the Cleveland Institute of Music

Welcome Reception

The welcome reception and barbecue will follow the opening ceremony and Wartenweiler Memorial lecture, beginning at 5:00 PM in the area outside the UC building, and will provide an excellent opportunity to meet and socialize with friends and colleagues.

Open House Reception

After the poster session on Tuesday, hop on a trolley at CSU and join your colleagues for an evening at The Cleveland Museum of Natural History in University Circle (6:30 – 10_30 PM). Highlights include planetarium shows, a Late Jurassic sauropod skeleton with a 6-foot, 4-inch femur, a cast of “Lucy’s” originally discovered skeletal materials and her reconstruction; her genuine remains were returned. Also, see live animals native to North America and a Foucault pendulum. Since this is an “Open House”, you can come and go throughout the evening as you please. Trolley shuttles will leave approximately every 20 minutes from CSU for the museum and return you to CSU. This event is free for all registrants and includes food, drinks, exhibits and planetarium shows. If you are still hungry after the reception, you can venture over to Little Italy for a continental dinner. The last trolley back to CSU will depart from the museum at 10:30 p.m.

Wednesday Afternoon Activities

A number of organized (paying) tours are set for the free afternoon on Wednesday. In addition, there will be free transport for the “Cleveland Exploration Excursion”, which incorporates tours of local landmarks and museums, as well as the Orthopaedic Biomechanics Laboratories at Lutheran Hospital, VA Motion Studies Laboratory, Case Western Reserve University Campus, and the Cleveland Clinic Foundation Department of Biomedical Engineering.

Baseball

Join us on Thursday evening at Jacob’s Field to watch our beloved Cleveland Indians take on the New York Yankees. See Newton’s laws of physics in action at this truly amazing sporting extravaganza. Of course, if you would prefer, Shakespeare is also playing at Playhouse Square.

Banquet

The Congress will conclude with a gala banquet on Friday August 5 from 7.00 p.m. until 10.00 p.m. at the Rock & Roll Hall of Fame on Lake Erie. Trolley shuttles will again take you too and from the Banquet.

Accommodations and Places of Interest

Downtown

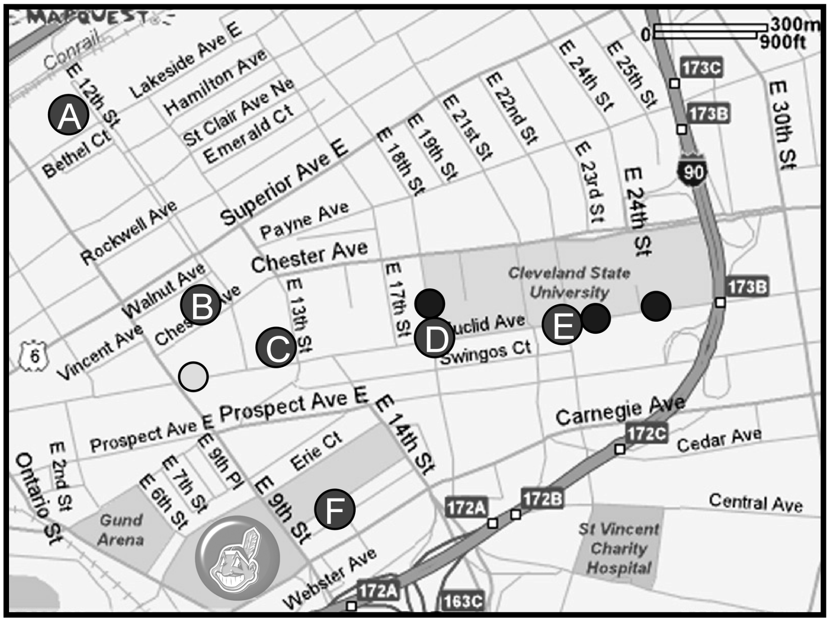

A. Holiday Inn Select

B. Embassy Suites Hotel

C. Wyndham Playhouse Square

D. Comfort Inn Downtown

E. Viking Hall (CSU)

F. Hilton Garden Inn

○ Huntington National Bank

● Automatic Teller Machines

Baseball

University Circle

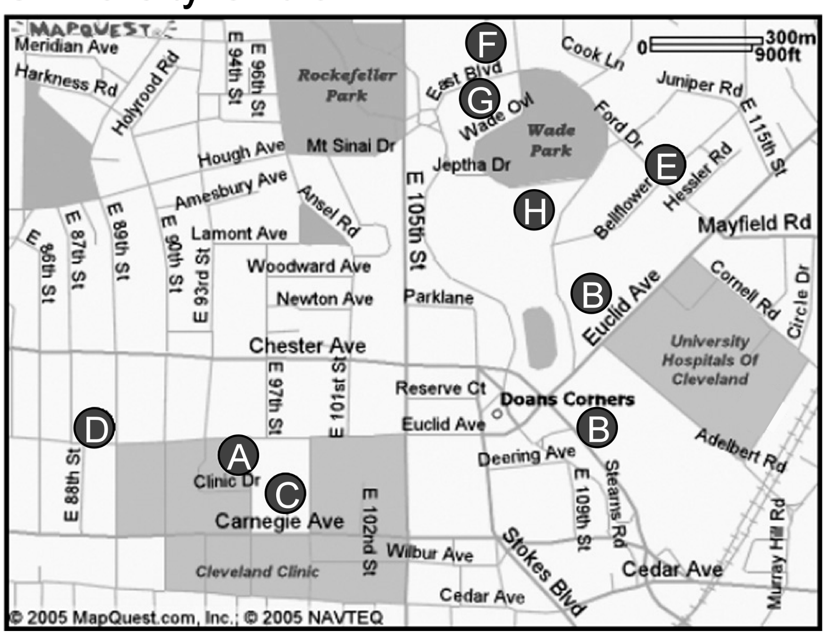

A. Cleveland Clinic Foundation

B. Case Western Reserve Univ.

C. Intercontinental Hotel

D. Intercontinental Suites

E. Glidden House

F. VA Medical Center

G. Cleveland Museum of Natural History

H. Cleveland Museum of Art

1. AMTI
2. Anybody Technology
3. Bertec
4. Bose
5. Cambridge Electronic Design
6. Center for Ergonomics at Univ of Michigan
7. Charnwood Technologies
8. Delsys
9. Human Kinetics Publishers
10. Innovative Sports Training
11. Innovision Systems
12. Instron
13. Inter Institute for Advancement of Medicine
14. Kistler
15. Motion Analysis Corp.
16. Motion Lab Systems
17. Noraxon
18. Northern Digital
19. Novel
20. Parallel Robotics Systems
21. Phoenix Technologies
22. RSscan International
23. Simpleware
24. Tekscan
25. Vicon Peak

R.D. - Registration Desk
I.C. - Internet Cafe

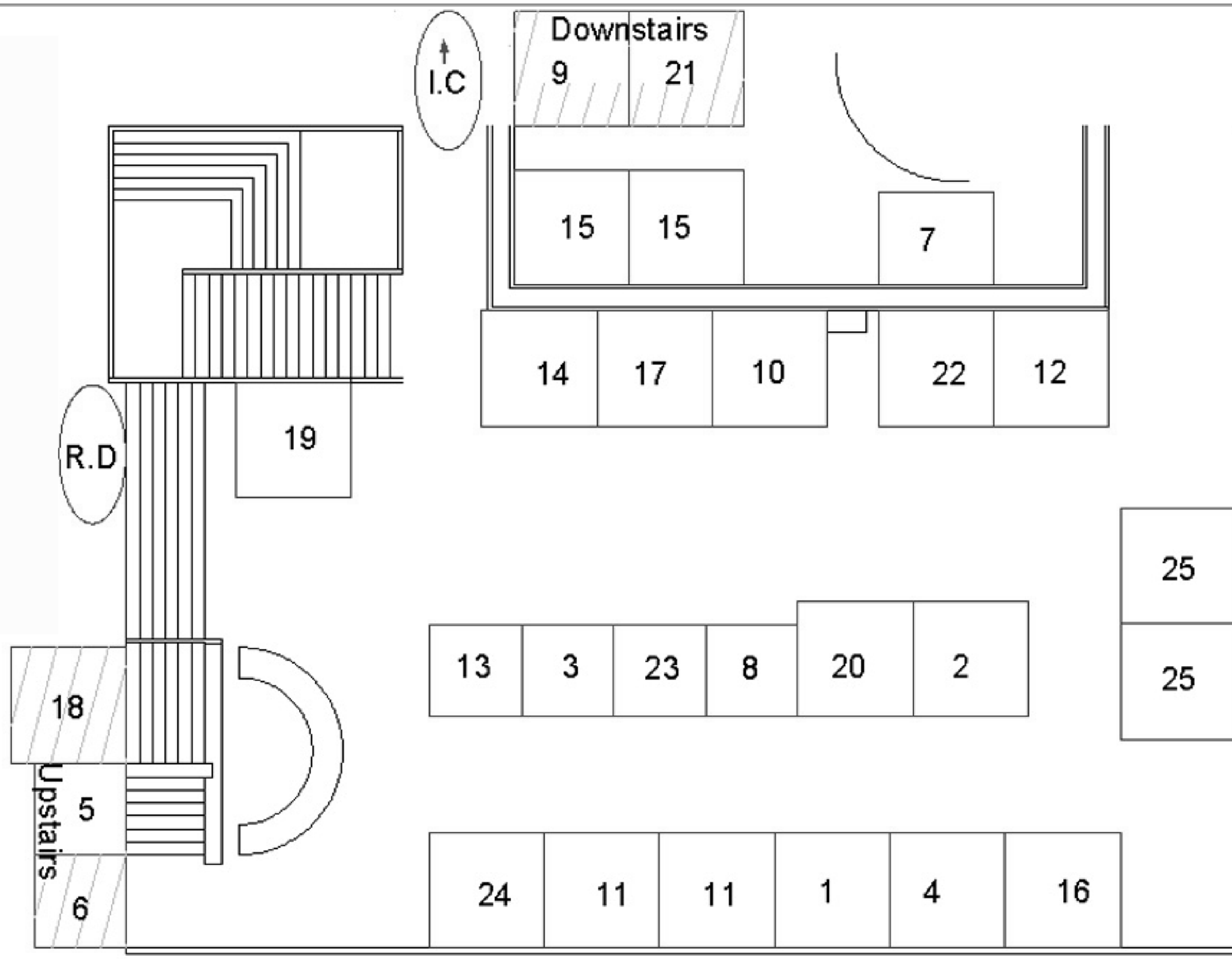

Exhibitor Booths

Presentations

Podium Presentations

Each podium presentation will be limited to ten minutes, allowing five minutes for questions and discussion. Presenters have the option of using their own laptop, or using the computer provided in each room throughout the congress. Those using the latter must have their presentation in PowerPoint format, and saved either on CD, Compact Flash Card, or Memory (USB) Stick. You must go to the speaker ready room (UC - Kiva, near UC1 and UC6) at least 24 hours prior to your presentation. Our Audio-visual (AV) staff will make a copy of your presentation, make sure it works, and install it on the computer in your presentation room. At this time, you should make sure that all fonts appear as expected and that all sound/video clips are working correctly. AV staff will assist you and answer any questions that you may have. If you plan on using your own computer, you must still visit the speaker ready room at least 24 hours prior to your session to test the connection and to inform AV staff that you have arrived. If during your presentation any video files remain black, try switching the laptop from "screen + projector" to "projector only". There will be speaker timers in each of the presentation rooms. Speakers will be shown a green warning light at nine minutes and a red light at ten minutes.

Chairpersons of Podium Presentations

Please arrive in the presentation room 15 minutes before the session in order to introduce yourself to the presenters and AV staff. At the beginning of each presentation please introduce the presenter, their affiliation and title of the presentation. Please ensure that each presentation begins and ends on time so that participants wishing to hear preceding and following talks in other rooms can do so. There will be speaker timers in each presentation room, which will be controlled by the chairpersons. If you have any problems, please contact the AV staff member in your room immediately. In rare cases where the presenter does not show, please take a break for that 15 minute time period rather than move on to the next speaker. This will again ensure no-one misses talks of personal interest.

Poster Presentations

The Tuesday and Thursday poster sessions will be held in rooms UC201 and UC201 and UC Atrium respectively. People with odd numbered posters will be required to stand at their poster from 3:45 PM – 4:45 PM. Those with even numbered posters will need to be at their board for the next hour (4:45 PM – 5:45 PM). For the Tuesday session, presenters should have their posters up by no later than Monday 2 p.m., and should be taken down by 9.00 a.m. Wednesday. For the Thursday session, posters should be up no later than Thursday 9.00 a.m., and should be removed by Friday 6:00 PM. Any posters that are not removed by the required time will be disposed of.

Awards

During the Cleveland-ISB/ASB-2005 Congress, a number of scientific awards will be presented to recognize outstanding scientific contribution in the field of biomechanics. These awards and the respective winners/finalists are listed below.

ISB Awards

Muybridge Award

Winner: Rik Huiskes, Eindhoven University of Technology, The Netherlands
Presentation: Wednesday, August 3, 11:00 AM, Waetjen Auditorium
Sponsor: ViconPeak

Clinical Biomechanics Award

Winner: Magnus Kjartan Gislason, University of Strathclyde, UK
Presentation: Wednesday, August 3, 9:00 AM, Waetjen Auditorium
Sponsor: *Clinical Biomechanics*, Elsevier Science Ltd.

Young Investigator Award (Podium Presentation)

Finalists: Ann Barkowitz, Jill Higginson, Emma Johnson, Craig McGowan, and Thomas Withrow
Presentation: Wednesday, August 3, 9:30 AM, Waetjen Auditorium
Sponsor: Elsevier Science Ltd.

Young Investigator Award (Poster Presentation)

Finalists: Jingzhi Liu, Alena Grabowski, David Suprak, Sicco Bus, Yasushi Enomoto, Elizabeth Chumanov, Steven Blackburn, Sarah Kruger, Veronica Santos, Smita Rao
Presentation: Poster sessions on Tuesday and Thursday

Promising Young Scientist Award

2003 Winner: Constantinos Maganaris, Manchester Metropolitan Univ, UK
Presentation: Wednesday, August 3, 8:30 AM, Waetjen Auditorium
2005 Winner: Kermit Davis, University of Cincinnati, USA
Sponsor: ViconPeak

ASB Awards

Borelli Award
Winner: Kai-Nan An, Mayo Clinic, Rochester, Minnesota
Presentation: Thursday, August 4, 1:15 PM, Waetjen Auditorium

Jim Hay Award for Sports Biomechanics
Winner: Mont Hubbard, University of California, Davis
Presentation Time: Thursday, August 4, 8:30 AM, Waetjen Auditorium

Predoctoral Young Scientist Award
Winner: Katherine Holzbaur, Stanford University, California
Presentation: Thursday, August 4, 9:30 AM, Waetjen Auditorium

Postdoctoral Young Scientist Award
Winner: Stefan Duma, Virginia Polytechnic and State University
Presentation: Thursday, August 4, 9:45 AM, Waetjen Auditorium

Microstrain Award
Winner: Azita Tajaddini, Cleveland Clinic Foundation, Ohio
Presentation: Thursday, August 4, 2:15 PM, Waetjen Auditorium
Sponsor: Microstrain

Clinical Biomechanics Award
Finalists: Wendy Murray and Robert Siston
Presentation: Thursday, August 4, 2:30 PM, Waetjen Auditorium
Sponsor: *Clinical Biomechanics*, Elsevier Science Ltd.

Journal of Biomechanics Award
Finalists: Joseph Crisco and Eun-Jeong Lee
Presentation: Thursday, August 4, 3:00 PM, Waetjen Auditorium
Sponsor: *Journal of Biomechanics*, Elsevier Science Ltd.

Other Awards

NAC-Miyashita Award for best paper from east Asia:
Sponsor: NAC Inc.
To be announced at congress

Delsys Recognition for EMG Innovation
Sponsor: Delsys, Inc.
To be announced at congress

Tutorials

ISB tutorial lectures will be held on Sunday July 31st in the MC building and are limited to registered participants only. Each tutorial requires a separate registration fee of $30. Lunch will be provided for all registered participants between the morning and afternoon tutorial sessions. A list of tutorial sessions is provided below.

Time	Presenter	Title	Room
9:30 AM – 11:30 AM	Mark Latash	Motor Control: The Equilibrium-Point Hypothesis and Internal Models	MC201
9:30 AM – 11:30 AM	Rik Huiskes	Bone and Osteoporosis: Computational Diagnostics	MC202
12:30 PM – 2:30 PM	Richard Baker	3-D Analysis of Movement	MC201
12:30 PM – 2:30 PM	Jeff Weiss	Soft Tissue Mechanics	MC202

Workshops

Two technical workshops will also be held during the congress, which you are welcome to attend. You are required to register for each workshop prior to commencement, but registration is free in each case. For the Novel workshop, you can register online via the congress home page (http://www.isb2005.org). You can register for the Tekscan workshop via their web site (http://www.tekscan.com/medical/meetings.html). Each workshop will present state-of-the-art technologies in pressure distribution measurement and analysis. Workshop sessions will be held at the following times.

Date	Start Time	Session	Room
Monday August 1st	5:30 PM	Novel Workshop	MC201
Monday August 1st	2:00 PM	Tekscan Workshop	UC364

Scientific Program

Sunday, July 31 — 4:00 PM

Wartenweiler Memorial Lecture — Waetjen Auditorium

Chair: Benno M. Nigg

4:00	Bruce Latimer	Biomechanics and Evolution

Monday, August 1 — 8:30 AM

Keynote Lecture — Waetjen Auditorium

Chair: Karen Søgaard

8:30	Don Chaffin	Biomechanical Analysis of Occupational High Exertion Tasks

Monday, August 1 — 9:30 AM

Ergonomics 1 — Waetjen Auditorium

Chair: Don Chaffin, Krystyna Gielo-Perczak

9:30	Kermit Davis	Are There Inherent Differences in How Males and Females Respond to Lifting?
9:45	Allan Wrigley	Principal Component Analysis Of Lifting Waveforms
10:00	Mohammad Abdoli-Eramaki	Impact Of Lift Assistive Device On Lumbar Compressive Force
10:15	Jaap van Dieen	No Single Lifting Technique Minimizes Low Back Load

Locomotion 1 — UC 6

Chair: Art Kuo, Rick Neptune

9:30	Max Kurz	Does Gravity Influence The Structure Of Chaotic Gait Patterns?
9:45	At Hof	Lateral Balance In A/K Amputees And Healthy Controls
10:00	Veerle Segers	Differential Effect Of M. Tibialis Anterior Fatigue On Walk-To-Run And Run-To-Walk Transition Speed In Unsteady State Locomotion Conditions
10:15	Jonathan Dingwell	Tracking Slow-Time-Scale Changes In Movement Coordination

Soft Tissue 1 MC 201

Chair: Kathe Derwin, Ahmet Erdemir

9:30	Kozaburo Hayashi	Effects Of Stress Deprivation On Biomechanical Properties Of Regenerated And Residual Tissues In The Patellar Tendon After Removel Of The Central One-Third
9:45	Naveen Chandrashekar	Effects Of Sex And Mass Density On The Mechanical Properties Of The Human Patellar Tendon
10:00	Kirsten Legerlotz	The Influence Of Different Mechanical Stimuli And Growth On The Mechanical Properties Of The Achilles Tendon In The Female Rat
10:15	Sarah Calve	The Influence Of Aging On The Material Properties Of Tendon

Space Biomechanics MC 202

Chair: Azita Tajaddini, Brian Davis

9:30	Samantha M. Lane	A Dual Track Actuated Treadmill In A Virtual Reality Environment As A Countermeasure For Neurovestibular Adaptations In Microgravity
9:45	Marcus Just	Modeling And Simulation Of Reaction Forces In A Reduced Gravity Exercise System
10:00	John DeWitt	The Effect Of Speed On Ground Reaction Forces During Locomotion In Weightlessness
10:15	Peter Cavanagh	Treadmill Exercise On The International Space Station: The Effects Of External Loading

Bone 1 UC 1

Chair: Serkan Inceoglu, Robert Mensforth

9:30	Dean Lang	Quantitative Trait Loci Influencing Bone Quality In Young And Old Mice
9:45	Michael Bottlang	Strain Field Acquisition On Ovine Fracture Callus With Electronic Speckle Pattern Interferometry
10:00	Luisa Moreno	The Rule Of Creep In The Sex Differences Of Long Bone Resistance To Fatigue Failure
10:15	Jessica Goetz	Three Dimensional Multiscale Reconstruction Of Emu Femoral Head Osteonecrosis: From Cell To Organ Level

Monday, August 1 11:00 AM

Ergonomics 2 Waetjen Auditorium
Chair: Karen Søgaard, Cecile Smeesters

11:00	Scott MacKinnon	Effects Of Reach Distance Upon Electromyographical Activities Of Selected Upper Body Musculature
11:15	Karen Søgaard	Single Motor Unit Activity In The Trapezius Muscles Of Elderly Female Computer Users With And Without Neck-Shoulder Pain During Computer Work
11:30	Nadine Dunk	Gender-Based Postural Responses To Seated Exposures
11:45	Peter Keir	Prediction Of Forearm Muscle Activity During Gripping
12:00	Kathleen Shyhalla	Effects Of Repetitive Work On Discomfort And Performance During Composite Tasks
12:15	Anne Moore	The Effect Of Forearm Support On EMG Activity Of The Upper Extremities During Computer Work: A Chair Intervention Study

Locomotion 2 UC 6
Chair: At Hof, Frank Buczek

11:00	Andrea Lay	Backward Upslope Walking: Implications For The Knee Joint
11:15	Gordon Robertson	Kinetic Analysis Of Gait Initiation
11:30	Frank Buczek	Telescoping Action Improves The Fidelity Of An Inverted Pendulum Model In Normal Human Gait
11:45	Vassilios G. Vardaxis	3D Upper Body Acceleration Magnitude For Self-Selected And Fast Walking Speeds In Young And Older Able-Bodied Adults
12:00	Hartmut Geyer	The Spring-Mass Model For Walking
12:15	Shawn O'Connor	Optimization Of Feedforward And Feedback Control During Walking

Soft Tissue 2 MC 201
Chair: Ivan Vesely, Todd Doehring

11:00	Raffaella De Vita	A Stochastic Model For Ligament Mechanical Failure
11:15	Feng Shen	Rheological Behaviour And Modeling Of Brain Tissue
11:30	Brent Mitchell	Non-Linear Elastic Behavior Of Small Intestinal Submucosa
11:45	Murat Surucu	Micromechanical Modeling Of Nonlinear Viscoelastic Behavior Of Mitral Valve Chordae
12:00	Costin Untaroiu	Identification Of Viscoelastic Properties Of Human Medial Collateral Ligament Using Finite Element Optimization
12:15	John Wu	Estimation Of Viscous Properties Of Skin And Subcutaneous Tissues Via Uniaxial Stress Relaxation Tests

Foot 1 MC 202

Chair: Gert-Peter Brüggemann, Dieter Rosenbaum

11:00	Ricardo Actis	Plantar Pressure Distribution In The Diabetic Foot During Push-Off: Numerical Simulation Using The P-Version Of The Finite Element Method
11:15	Jason Cheung	Biomechanical Effects Of Plantar Fascia Release And Posterior Tibial Tendon Dysfunction - A Finite Element And Cadaveric Foot Simulation
11:30	Carl Imhauser	The Development And Evaluation Of A 3-Dimensional, Image-Based, Patient-Specific, Dynamic Model Of The Hindfoot
11:45	Paul Lundgren	Rotations In Rearfoot Joints At End Of Range Weight Bearing
12:00	William Ledoux	Forefoot Plantar Pressure Is Related To 3-D CT Derived Measures
12:15	Sachin Budhabhatti	Influence Of Foot Orientation And Bone Structure On Plantar Pressure Distribution

Bone 2 UC 1

Chair: Melissa Knothe-Tate, Luisa Moreno

11:00	Todd Ritzman	Mechanobiological Influences On Bone Tissue Engineering Strategies
11:15	Daisuke Tawara	Mechanical Evaluation Of Therapeutic Effect For Osteoporosis Vertebra By Using Patient-Specific Finite Element Analysis
11:30	Anja Niehoff	Voluntary Strength Training And Running Exercise Induce Site-Specific Bone Adaptation In Adult Female Rats
11:45	Grant Goulet	Fluid Flow In Bone Is Correlated To Sites Of Smallest Cross-Sectional Area Perpendicular To Load-Induced Stress Gradients
12:00	Russell Main	How Does Bone Tissue Microstructure Relate To In Vivo Bone Strains In The Goat Radius Through Ontogeny?
12:15	Ted Gross	Muscle Function Locally Mediates Bone Homeostasis

Monday, August 1 — 1:15 PM

Keynote Lecture — Waetjen Auditorium
Chair: Art Kuo

1:15	Andre Seyfarth	Emergence of Gait in Legged Systems

Monday, August 1 — 2:15 PM

Legged Robotics — Waetjen Auditorium
Chair: Jon Dingwell, Andre Seyfarth

2:15	Christopher Vaughan	Comparing The Gait Of Bipedal Robots With That Of Infants
2:30	Juergen Rummel	Stable Locomotion Of Feedforward Controlled One-Legged Robot
2:45	Keith Gordon	Mechanical Performance Of Artificial Pneumatic Muscles To Power An Ankle-Foot Orthosis
3:00	Jesse Dean	Powering The Kneed Passive Walker With Biarticular Springs
3:15	Jimmy Li-Shin Su	Local Dynamic Stability Of Passive Dynamic Walking On An Irregular Surface

Gait Analysis — UC 6
Chair: Tung-Wu Lu, Sicco Bus

2:15	Michael Schwartz	A Comparison Of Two Foot Models Used In Clinical Gait Analysis
2:30	David Stephensen	Gait Deviations In Children With Severe Haemophilia Following Bleeding Into The Ankle Joint
2:45	Sam Augsburger	Assimilating Full Body Gait Graphs Into Single Area Plots
3:00	Matthew Cowley	Effect Of Marker Placement Methods On Calcaneal Rotations
3:15	Adam Fullenkamp	Clinical Usefulness Of Four Functional Knee Axis Algorithms

Shoulder MC 201

Chair: Richard Debski, Mark Pierre

2:15	Toshimasa Yanai	In-Vivo Measurement Of The Compressive Force Under The Coraco-Acromial Arch
2:30	Clark Dickerson	Development Of A Biomechanical Shoulder Model For Ergonomic Analyses
2:45	Joseph Langenderfer	Variability In Isometric Force And Torque Generating Capacity Of Glenohumeral External Rotator Muscles
3:00	Mark Timmons	Arm Abduction Angle And Contraction Intensity Effects On Deltoid And Scapular Rotator Muscle Recruitment During Scapular Plane Isometric Contractions
3:15	Samuel R. Ward	Rotator Cuff Muscle Architecture: Implications For Glenohumeral Joint Stability

Foot 2 MC 202

Chair: Howard Hillstrom, William Ledoux

2:15	Dieter Rosenbaum	Pedographic Assessment Of Clinical And Functional Outcome After Hallux Valgus Surgery - Comparison Of 32 Patients Before And After Scarf Osteotomy
2:30	Gert-Peter Brüggemann	Effect Of Increased Mechanical Stimuli On Foot Muscles Functional Capacity
2:45	Michael El-Shammaa	The Effect Of Muscle Imbalance On Foot Pressure In Pediatric Patients
3:00	Michael Voigt	Foot Pronation In Vivo - Combined Midfoot And Hindfoot Kinematics
3:15	Michael Orendurff	Regional Foot Pressure During Running, Cutting, Jumping And Landing

Simulation UC 1

Chair: Musa Audu, Ton van den Bogert

2:15	Pui Wah Kong	Computer Simulation Of The Takeoff In Springboard Diving
2:30	Sibylle Thies	Stepping On An Obstacle With The Medial Forefoot: Use Of A 3D Dynamic Control Model To Simulate Age And Neuropathy
2:45	Jia-Hsuan Lo	Simulation Of Forward Falls: Effects Of Fall Strategy And Available Muscle Strength On Injury Risk
3:00	Jos Vanrenterghem	Is Efficiency A Viable Criterion For Sub-Maximal Vertical Jumping?
3:15	Leonard Rozendaal	Joint Stiffness Requirements In A Multi-Segment Stance Model

Monday, August 1 4:00 PM

Pelvic Organ and Muscle Biomechanics Waetjen Auditorium
Chair: Margot Damaser, Adonis Hijaz

4:00	Linda McLean	The Relationship Between Pelvic Floor And Abdominal Muscle Activation And The Generation Of Intravaginal Pressures In Healthy Continent Women
4:15	Jiro Nagatomi	A New Approach For Modeling And Analyzing The Viscoelastic Behavior Of Bladder Wall Tissue
4:30	Rebecca Long	MMP-I Up-Regulation As A Potential Mechanism For Increased Compliance In Muscle-Derived Stem Cell-Seeded Sis For Urologic Tissue Engineering
4:45	Chris Constantinou	Direction Sensitive Sensor Probe For The Evaluation Of Voluntary And Reflex Pelvic Floor Contractions
5:00	Kevin Toosi	Time Course Changes In The Mechanical Properties Of The Rat Urinary Bladder Following Spinal Cord Injury
5:15	Chantale Dumoulin	Dynamometry For Measuring Pelvic Floor Function

ISB Technical Group: 3D Analysis of Human Movement UC 6
Chair: Serge Van Sint Jan, Allison Arnold

4:00	Serge Van Sint Jan	Towards An Advanced Clinical Expert System For Patient-Specific Modelling And Musculo-Skeletal (MS) Analysis?
4:15	Bruce MacWilliams	Current Challenges In Clinical Gait Analysis
4:30	Lasse Roren	Gait Data Collection Technology: Where Are We, Where Are We Going?
4.35	Jeff Thingvold	Model-Based Analysis in Biomechanics and New Media Applications
4:45	John Rasmussen	Challlenges In Musculoskeletal Modeling For Clinical Use
5:00	Allison Arnold	Simulation-Based Treatment Planning For Gait Abnormalities: Vision And Challenges
5:15	Marco Viceconti	Fusion Of Biomechanics Data For Patient Monitoring In Pediatric Skeletal Oncology

ISB Technical Group: Shoulder Biomechanics MC 201
Chair: DirkJan Veeger, Ed Chadwick

4:00	Paula Ludewig	Alterations In Scapular Kinematics In Patients With Shoulder Impingement
4:15	Alexis Wickwire	Position Of The Humeral Head Shifts In The Glenoid Due To The Presence Of Osteoarticular Lesions
4:30	Jurriaan de Groot	Arm Mobility Versus Glenohumeral Stability
4:45	Andrew Karduna	Suprascapular Nerve Block Disrupts The Normal Pattern Of Scapular Kinematics
5:00	Jules Dewald	The Effect Of Generating Anti-Gravity Shoulder Torques On Upper Limb Discoordination Following Hemiparetic Stroke
5:15	Thomas Bandholm	Force Steadiness, Neuromuscular Activation And Maximal Muscle Strength In Subjects Suffering From Subacromial Impingement Syndrome

ISB Technical Group: Footwear Biomechanics MC 202
Chair: Joe Hamill, Elizabeth Hardin

4:00	Keith Williams	The Development Of The Footwear Technical Group
4:15	Mario Lafortune	The Footwear Technical Group and Industry
4:30	*Award winners are not known yet*	Nike Award presentation
4:45		Adidas Award presentation
5:00		New Balance Award presentation
5:15		Rsscan Award presentation

ISB Technical Group: Computer Simulation UC 1
Chair: Rick Neptune, Federico Casolo

4:00	Mont Hubbard	History Of the ISB Technical Group Computer Simulation
4:10	Federico Casolo	TGCS Chairman's Report
4:15	Knoek van Soest	Prescribing Skeletal Motion Can Substantially Enhance Mechanical Power Output; A Simulation Study
4:30	Fred Yeadon	The Effect Of Anatomical And Robustness Constraints On Optimum Jumping Performance
4:45	Francisco Valero-Cuevas	Shifting To Population-Based Models And Inferring Model Structure From Data Are Two Directions That Will Enhance The Clinical Usefulness Of Modeling
5:00	B.J. Fregly	Predicted Gait Modifications To Reduce The Peak Knee Adduction Torque
5:15	Alison Sheets	Approximation Of Balanced Landings In Gymnastic Dismounts

Tuesday, August 2 — 8:30 AM

Keynote Lecture — Waetjen Auditorium
Chair: Tim Hewett

8:30	Julie Steele	Developing Textile Biofeedback Technology: From Brassieres to Noisy Knees

Tuesday, August 2 — 9:30 AM

Knee Injuries 1 — Waetjen Auditorium
Chair: Li-Qun Zhang, Julie Steele

9:30	Steven Blackburn	Knee Joint Moments During Sports Activities On Artificial Turf
9:45	Kevin Ford	Effect Of Gender On Knee Abduction And Flexion During Medial And Lateral Landings
10:00	Kelly McKean	Kinematic & Kinetic Differences Between Male & Female Soccer Players
10:15	Mette Kreutzfeldt Zebis	The Effect Of Acute Fatigue On Neuromuscular Activation Pattern During Side-Cutting In Female Team Handball Players

EMG — UC 6
Chair: Carlo De Luca, Graeme Wood

9:30	Michael Hahn	Neural Network Estimation Of Isokinetic Knee Torque
9:45	Paul Sung	Comparison Of Power Spectrum Measures To Entropic Measures Of Electromyography Time Series: Diagnostic Tools For Low Back Pain
10:00	Janessa Drake	Elimination Of ECG Contamination From EMG Signals: An Evaluation Of Currently Used Removal Techniques.
10:15	Didier Staudenmann	Improving EMG Based Muscle Force Estimation Using Principal Component Analysis On A High-Density EMG Array

Muscle Mechanics MC 201
Chair: Maarten Bobbert, Constantinos Maganaris

9:30	Dilson Rassier	Phase Transition Of Force During Ramp Stretch Of Muscle Fibers Treated With BDM
9:45	Hanneke Meijer	Myofascial Force Transmission Is More Important At Low-Frequency Stimulation
10:00	Mir Ali Eteraf Oskouei	Force Enhancement In Sub-Maximal Voluntary Contractions
10:15	Thomas Sandercock	Cat Hindlimb Muscle Response To Slow Movement Shows Poor Relationship To Length-Tension Properties

Sport 1 MC 202
Chair: Peter Milburn, Tzyy-Yuang Shiang

9:30	Federico Casolo	Biomechanics Related To Racket Design And Customization
9:45	Lin-Hwa Wang	Momentum Transfer Of Trunk And Upper Extremity In Tennis Backhand Stroke
10:00	Young-Kwan Kim	Does Warming Up With A Weighted Bat Help Or Hurt Bat Speed In Baseball?
10:15	Hwai-Ting Lin	The Role Of Muscle In Glenohumeral Joint Stability During Baseball Pitching

Bone Modeling UC 1
Chair: Ted Gross, Anja Niehoff

9:30	Daisuke Tawara	Patient-Specific Dynamic Stress Analysis Of Osteoporosis Vertebrae
9:45	Linping Zhao	Three Dimensional Finite Element Analysis Of Maxillary Palate With A Unilateral Cleft
10:00	Carmen Muller-Karger	Finite Element Bone Model Incorporating Heterogeneity And Anisotropy From CT
10:15	Andrea Tami	Finite Element Analysis Of Shockwave Propagation In Cortical Bone

Tuesday, August 2 — 11:00 AM

Knee Injuries 2 — Waetjen Auditorium

Chair: Scott McLean, Tim Hewett

11:00	Tim Hewett	Coupled Biomechanical-Epidemiological studies for the Assessment Of ACL injury Risk.
11:15	Robert Shapiro	Biomechanical Differences Between Genders When Executing A Land And Cut Maneuver
11:30	Gregory Myer	The Effects Of Plyometric Versus Dynamic Stabilization And Balance Training On Lower Extremity Biomechanics
11:45	Ajit Chaudhari	Knee Loading Patterns That Endanger The ACL: Insights From Experimental and Simulation Studies
12:00	Bing Yu	Hamstring Co-Contraction Does Not Necessarily Reduce ACL Loading
12:15	Scott McLean	Sagittal Plane Biomechanics During Sports Movement Does Not Explain Higher Incidence Of ACL Injuries in Females

Gait and Osteoarthritis — UC 6

Chair: Fong-Chin Su, David Sanderson

11:00	Marius Henriksen	Effect Of Intra-Articular Lidocain Injections On Knee Joint Kinetics During Walking In Knee Joint Osteoarthritis Patients
11:15	Michael Anthony Hunt	Dynamic Lower Limb Alignment And Knee Joint Load During Gait In Patients With Knee Osteoarthritis
11:30	Laura Diamond	Adduction Moment During Gait In Patients With Moderate Or End-Stage Knee Osteoarthritis
11:45	Tom Jenkyn	Toe Out Gait And Reduction Of Knee Osteoarthritis Pain
12:00	Jennifer Erhart	Predicting Changes In Knee Adduction Moment Due To Load-Altering Interventions For Medial Compartment Knee OA From Pressure Distribution
12:15	Anne Muendermann	Hip Abductor Strength May Be Critical For Successful Gait Compensation In Patients With Medial Compartment Knee Osteoarthritis

Muscle In Vivo MC 201

Chair: Richard Lieber, Walter Herzog

11:00	Glen Lichtwark	Gastrocnemius Muscle Tendon Unit Interaction Under Variable Gait Conditions
11:15	Sami Kuitunen	Behavior Of The Triceps Surae Muscle In Hopping
11:30	Stacie Ringleb	Bilateral Symmetry Of The Gastrocnemius Stiffness Measured With Magnetic Resonance Elastography In Healthy And Pathologic Muscle
11:45	Wendy Murray	Muscle Operating Range Includes Optimal Length At Extended Joint Postures Following Brachioradialis Tendon Transfer
12:00	Boris Prilutsky	In Vivo Fascicle Velocity Of Cat Gastrocnemius And Soleus Muscles During The Paw-Shake
12:15	Amanda Felder	Sarcomere Length Measurement Permits High Resolution Normalization Of Muscle Fiber Length In Architectural Studies

Sport 2 MC 202

Chair: Fred Yeadon, Richard Nelson

11:00	Mark King	Optimised Tumbling Performances That Are Robust To Perturbations
11:15	Maarten F. Bobbert	Explanation Of The Bilateral Deficit In Human Vertical Jumping
11:30	Alison Sheets	Effects Of Low Bar Avoidance And Gymnast Size On High Bar Dismount Performance
11:45	AJ "Knoek" van Soest	Does Strapping The Rower To The Seat Enhance Rowing Performance?
12:00	Blake Ashby	Optimal Control Simulations Demonstrate How Halteres (Hand-Held Weights) Increase Standing Long Jump Performance
12:15	Rene Ferdinands	Forward Solution Simulation Of The Mixed Action In Cricket Fast Bowling

Hip Replacement UC 1

Chair: Tom Brown, Seth Greenwald

11:00	A Heijink	Generic Design Of The Hip Resurfacing Prosthesis
11:15	Jui-Ting Hsu	The Stability Of Acetabular Cup Under Screw Fixation
11:30	Liam Glennon	Direction-Dependence Of UHMWPE Wear For Metal Counterface Scratch Traverse
11:45	J P Little	A Multiple Material Parameter Finite Element Model Of Hip Resurfacing Arthroplasty
12:00	Marco Viceconti	Subject-Specific FE Model For The Prediction Of The Relative Micromotion In A Total Hip Implant: Verification And Validation
12:15	Jihui Li	Locating Fatigue Microcracks Occurring In Cemented Total Hip Arthroplasty

Tuesday, August 2 — 1:15 PM

Keynote Lecture — Waetjen Auditorium
Chair: Seth Greenwald

1:15	Masahiro Kurosaka	History and Future of Anterior Cruciate Ligament Reconstruction

Tuesday, August 2 — 2:15 PM

Knee Mechanics 1 — Waetjen Auditorium
Chair: Leendert Blankevoort, Masahiro Kurosaka

2:15	Rochelle Nicholls	Implantation Of A Total Knee Arthroplasty Prosthesis Imposes Abnormal Strain On Local Soft Tissues
2:30	David Fung	Changes To The Rat ACL Resulting From Subfailure Impingement Loading
2:45	Choongsoo Shin	Combined Valgus And Internal Rotation Moments Strain The ACL More Than Either Alone: Implications For Non-Contact ACL Injuries
3:00	Kiyonori Mizuno	Gender Dimorphism In Knee Joint Mechanics Affects ACL Loading
3:15	Naveen Chandrashekar	Sex Based Differences In Tensile Properties Of Human Anterior Cruciate Ligament

Methods 1 — UC 6
Chair: Tim Derrick, Peter Quesada

2:15	Daniel Benoit	Skin Movement Artifact During Gait And Cutting Movements Measured In Vivo
2:30	Anthony Schache	Influence Of Thigh Marker Cluster Design On The Estimation Of Hip Axial Rotation
2:45	Tung-Wu Lu	A Kinematic Model Of The Upper Extremity With Globally Minimized Skin Movement Artefacts
3:00	Lars Muendermann	Validation Of A Markerless Motion Capture System For The Calculation Of Lower Extremity Kinematics
3:15	Stefano Corazza	Lower Limb Kinematics Through Model-Free Markerless Motion Capture

Spine 1 MC 201

Chair: Trey Crisco, Takahiro Ishii

2:15	Ryutaro Fujii	In Vivo Three-Dimensional Motion Analysis Of The Lumbar Spine :Coupling Motion Of The Lumbar Spine During Rotation
2:30	Ruth Ochia	In Vivo Segmental Motion Measurement In Asymptomatic And Chronic Low Back Pain Subjects Using Volume Merge Method
2:45	Heydar Sadeghi	Perturbation In Trunk Motion Of Low Back Patients
3:00	Ralph Gay	The Neutral Zone In Human Lumbar Spine Sagittal Plane Motion: A Comparison Of In Vitro Quasistatic And Dynamic Force Displacement Curves
3:15	William Anderst	Three-Dimensional In Vivo Rotation Of Fused And Adjacent Lumbar Vertebrae

Ankle MC 202

Chair: Don Anderson, Tom Buchanan

2:15	Shing-Jye Chen	Effects Of Impeded Foot Arch Height On Calcaneal Eversion And Ankle Joint Forces During Gait
2:30	Yuki Tochigi	The Contribution Of Articular Surface Geometry On Ankle Stabilization
2:45	Leendert Blankevoort	Three-Dimensional Bone Kinematics In An Anterior Drawer Test Of The Ankle Joint
3:00	Kristin Zhao	Mechanical Efficacy Of Tendon Transfer Operations For Foot Drop
3:15	Jane Goldsworthy	Chronic Stress Exposure Following Intra-Articular Ankle Fractures

Head Injury UC 1

Chair: Lars Janshen, David Dean

2:15	Trey Crisco	An Approach To Calculating Linear Head Accelerations Is Not Affected By Rotational Head Accelerations
2:30	Sarah Manoogian	Head Acceleration Is Less Than 10 Percent Of Helmet Acceleration During A Football Impact
2:45	Matthew Craig	Human Mandible Response To Impact Loading Of Chin
3:00	David Pearsall	Durability Of Ice Hockey Helmets To Repeated Impacts
3:15	S. W. Gong	A Novel Approach For A Solid Object Impact On Human Head

Tuesday, August 2 3:45 PM

Poster Session: Ergonomics 3 UC 201

1	Carol Murphy	Children's Postural Changes At Adult Computer Workstations
2	Taylor Murphy	A Comparison Of Task And Muscle Specific Isometric Submaximal EMG Data Normalization Techniques For The Analysis Of Muscle Loads During Hydraulic-Actuation Joystick Controller Use
3	Joshua S. Danker	Investigation Of Shoulder Range Of Motion Limits For Application To Ergonomic Analysis
4	HyunWook Lee	Trunk Stiffness Improvement By Physical Therapy/Exercise During Unstable Sitting
5	Reuben Escorpizo	Work Time And Rest Percentage During Pick-And-Place Task
6	Luke Wooldridge	Kinetic Evaluation Of Right Shoulder And Elbow During Spiccato Technique Violin Bowing
7	Timothy N. Judkins	Electromyographic Correlates Of Robotic Laparoscopic Training
8	Sivaram Shanmugam	Hand Movement Analysis Of The Elderly When Using A Remote Control
9	Kristine Krajnak	The Biodynamic And Physiological Responses Of The Rat Tail To A Single Bout Of Vibration Exposure
10	Kenji Narazaki	Training And Performance Of Robotic Laparoscopy: Electromyographic Analysis To Quantify The Extent Of Proficiency
11	Michael Holmes	Motion Induced Interruptions During Simulated Ship Motions
12	Julie Matthews	Thoracolumbar Kinematics During Lifting Exertions In Moving Environments
13	Hitoshi Yanagi	Upper Limb Motion During Snow Shoveling With Regular And Modified Shovel
14	Joan Stevenson	Theoretical Basis Of A Load Carriage Limit Equation
15	Alvin Au	The Effects Of Submaximal Shoulder Moment, Task Precision And Mental Demand On Muscle Activity During Grip Exertions
16	D. Christian Grieshaber	Forearm Muscle Activity During Three Hose Insertion Tasks As Measured By Surface Electromyography Of The Flexor Digitorum Superficialis Muscle
17	David Andrews	Acceptable Peak Forces And Impulses During Manual Hose Insertions
18	Krystyna Gielo-Perczak	An Investigation Of The Congruity In Geometry Of The Glenohumeral Joint On The Maximum Acceptable Load During Pushing
19	Bente R. Jensen	Reduced Force Control And Increased Contralateral Trapezius Co-Activation Among Subjects With Work Related Musculoskeletal Symptoms
20	Alison Godwin	Virtual Jack Manikin Used To Assess Postural Variables And Visibility Measures
21	Joel A. Cort	An Electromyographic And Psychophysical Examination Of Fastener Initiations In Automotive Assembly
22	Stuart Fraser	Target Acquisition By Pilots Wearing Various Head-Supported Masses During Simulated Flight

Tuesday, August 2 — 3:45 PM

Poster Session: Sport 5 — UC 201

23	Ching-Cheng Chiang	The Effects Of The Tennis Slice Backhand With Different Ball Speeds On The Bounce Angle
24	Yi-Ming Huang	Intermuscular Coordination Analysis Of Skilled Double-Handed Backhand And Single-Forehand Players
25	Yuh-Yih Lin	Vibration Analysis Of Tennis Racket Caused By Impact Between Different Configuration And Additional Weight
26	Jinn-Yen Chiang	Properties Of Tennis Racket Made By Differential Carbon Fibre
27	Tsai, Chien-Lu	Biomechanical Analysis Of EMG Activity Between Badminton Smash And Drop Shot
28	Ti-Yu Chen	The Vibration And Coefficient Of Restitution Analysis In Tennis Racketsvaried With Material Composition And Fiber Arrangement
29	Katie B. O'Keefe	Joint Velocity Sequence Of The Upper Extremity During Fly-Casting
30	Joshua R. Allen	Upper Extremity Kinematics During Fly-Casting
31	Hsiente Peng	Electromyographic Analyses Of Standing Shot Put Throw
32	Michele LeBlanc	Factors Affecting The Javelin's Attitude Angle In American Javelin Throwers
33	Tsung-Ying Hung	Investigatation Of Appropriate Weighted Bat By Muscle Activity
34	Tomoyuki Matsuo	Does Course Of A Preceding Pitch Influence Baseball Batting As They Say?
35	Takahito Tago	The Trunk Twist Angle During Baseball Batting At The Different Hitting Points
36	Brady Tripp	Functional Fatigue Decreases Three-Dimensional Multijoint Position Reproduction In Overhead Athletes
37	Tomohisa Miyanishi	Transfer Of Angular Momentum In The Baseball Batting
38	Tsutomu Jinji	Aerodynamic Characteristics Of Baseballs Delivered From A Pitching Machine
39	Rene Ferdinands	Elbow Angle Excursion Slope As A Determinant Of Bowling Legality
40	Daisaku Hirayama	The Kinematic Changes Of Pitching During A Simulated Baseball Game
41	Yi-Ling Chiang	Rotation Characteristics Of The Shoulder, Torso, And Pelvis During Pitching For Taiwan Elite And Subelite Collegiate Baseball Pitchers
42	Alexander Willmott	A Model For Assessing The Contributions Of Hand Forces And Torques To The Speed Of A Swinging Implement: Application To The Field Hockey Hit
43	David Pearsall	Ice Hockey Stick Recoil Mechanics
44	Chien-Nan Liao	Characteristics Of Muscle Activity In Distal And Proximal Upper Extremities In Different Phases For Taiwan Olympic Female Archery Players
45	Cheng-Ming Hu	Muscle Activation By Olympic Female Archers At Different Releasing Rhythms

Tuesday, August 2 3:45 PM

Poster Session: Biomechanics of Aging UC 201

46	Victoria Hood	Developing A Computer Aided Design Tool For Inclusive Design
47	Susan K M Wilson	Load Distribution During Sit-Stand-Sit Using An Instrumented Chair
48	Victoria Hood	Biomechanics Of Stair Descent In Older Adults
49	Kenneth Meijer	Running Does Not Protect Against Age-Related Gait Adaptations
50	Masaya Anan	The Relation Of The Trunk-Pelvic Movement And Lower Extremity Joint Moment On Elderly People During The Sit-To-Stand Motion
51	Bih-Jen Hsue	Balance And Gait Of Elderly Women During Stairs Locomotion In High-Heeled Shoes
52	Jansen Atier Estrázulas	Kinetic Characteristics Of Gait In Children, Adults And Elderly
53	Hao-Ling Chen	Comparisons Of The Lower Limb Mechanics Between Young And Older Adults When Crossing Obstacles Without Visual Guide
54	Carolina Mitre Chaves	Sit-To-Stand Performance With Young And Elderly Subjects
55	Munetsugu Kouta	Biomechanical Analysis Of Sit-To-Walk Frequently Observed In Daily Living: Effect Of Speed On Healthy Elderly Persons
56	Chia-Huei Shen	Electromyography And Leg Stiffness Comparison Between Old An Young Adults In Descent Stair Walking
57	Hidetaka Okada	Kinetic Characteristics Of Middle-Aged And Older Adults During Walking
58	Robert Shapiro	Biodynamic Changes Accompying Age And Inactivity In Females
59	Misono Sakai	Postural Control Against Perturbation During Walking

Poster Session: Osteoarthritis and Cartilage UC 201

60	Monica Maly	Are The Gait Kinetics Of Women And Men With Knee Osteoarthritis Different?
61	Kurt Manal	Foot Progression Angle And The Knee Adduction Moment In Individuals With Medial Knee Osteoarthritis
62	Le Zhang	Modeling Of Solute Transport In Cartilage Under Static And Dynamic Loading
63	Marius Henriksen	Effect Of Intra-Articular Lidocain Injections On Impact Attenuation During Walking In Knee Joint Osteoarthritis Patients
64	Anneliese D. Heiner	High Shear Stress Induces P53 Expression And Apoptosis In Cartilage Explants
65	Nicole A. Kallemeyn	A Finite Element Analysis Of Cartilage In Cyclic Triaxial Compression
66	Qing Wang	Evaluation Of Osmosis-Induced Deformation Of Articular Cartilage Using Ultrasound Biomicroscopy Imaging
67	Danielle Biton	Heelstrike Dynamics During 6 Minute Walk Test Among End Stage Knee OA Patients
68	Douglas R. Pedersen	Cinematic Measurement Of Cartilage Plugs In Unconfined Compression
69	Sang-Kuy Han	Influence Of The Pericellular Microenvironment On Chondrocyte Modelling

Tuesday, August 2 3:45 PM

Poster Session: Methods in Movement Analysis UC 201

70	Rochelle Nicholls	In Vitro Ligament Strain Measurement: Can Implantable And Non-Invasive Methods Yield Comparable Results?
71	Zhiqing Cheng	Use Of Wavelets In The Analyses Of Biodynamic Responses
72	Sujani N. Agraharasamakulam	Comparison Of Two Ankle Electrogoniometers And Motion Analysis
73	David Miller	An Improved Surrogate Method For Detecting The Presence Of Chaos In Gait
74	Lei Ren	Generalized Approach To Three-Dimensional Marker-Based Motion Analysis Of Biomechanical Multi-Segment System
75	Xiaofeng Wang	Lasr: A New Analytical Tool To Increase Information Retrieval From Complex Images
76	Jill Brimacombe	Validation Of Calibration Techniques For Tekscan Pressure Sensors
77	Maria Lebiedowska	Experimentally Derived Model Of Human Body Growth
78	Stacie Ringleb	Mechanical Properties Of Relaxed And Contracted Thigh Muscles Using Magnetic Resonance Elastography
79	Samuel Bertrand	Estimation Of Human Internal And External Geometry From Selected Body Measurements
80	Frank L. Buczek	Comparing Normal Gait Analyses Using Conventional And Least-Squares Optimized Tracking Methods
81	Andre Plamondon	Validation Of A Dosimeter For The Three-Dimensional Measurement Of Trunk Motion
82	Raviraj Nataraj	Artificial Neural Network Prediction Of Center Of Pressure Using Trunk Acceleration Inputs During Perturbed Human Bipedal Stance
83	David W. Wagner	Dynamic Calibration Of An Extended-Range Electromagnetic Flock Of Birds Motion Tracking System
84	Richard Jones	Prediction Of Lower Limb Segment Kinematics From Foot Accelerations
85	Stephane Armand	Extraction Of Knowledge For Movement Analysis Data - Example In Clinical Gait Analysis.
86	Na Jin Seo	Methods To Measure Static Coefficient Of Friction Between Hand And Other Materials
87	Wangdo Kim	Estimating The Axis Of A Screw Motion From Noisy Data - New Method Based On Plücker Lines
88	Ming Wu	Evaluate The Potential Contributions Of Swing Leg To The Stability Of Body During Single Foot Support Phase Of Walking
89	Timothy R. Derrick	Extraction Of The Impact From Vertical Ground Reaction Forces
90	Lise Worthen	Design Of A Gait Laboratory To Enable Biomechanical Analysis Of Individuals With Post-Stroke Walking Deficits: Force Platform Positioning
91	Sujatha Srinivasan	An Analytically Tractable Model For A Complete Gait Cycle
92	Michelle Sabick	Differences In Joint Kinetics In Girls Due To Choice Of Body Segment Parameters
93	Robert J. Jack	Validation Of The Vicon 460 Motion Capture System For Whole-Body Vibration Acceleration Determination

(session continued on next page)

Tuesday, August 2 3:45 PM

Poster Session: Methods in Movement Analysis (continued) UC 201

94	Young-Hoo Kwon	A 3-Dimensional Camera Calibration Algorithm For Underwater Motion Analysis With Refraction Correction Capability
95	Kurt Manal	A Numerical Method For Determining Ideal Camera Placement
96	Laura Held	Parameterization Of Joint Kinematics Using Quaternions
97	Laura Bray	Development Of A Novel Barefoot Torsional Flexibility Device: A Pilot Study
98	Richard J. Beck	Simulation Of Longitudinal Arterial Stretch In The Lower Limbs During Gait
99	Walter Rapp	Calculating Anatomical Leg Structures From Surface Contours

Poster Session: Tissue and Biomaterials UC 201

100	John Wu	Measurement Of Nonlinear-Elastic Properties Of Skin And Subcutaneous Tissues Via Unconfined Compression Tests
101	Kristen Bethke	Creating A Skin Strain Field Map With Application To Advanced Locomotion Spacesuit Design
102	Donald Sherman	Evaluation And Quantification Of Bruising
103	Pablo-Jesus Rodríguez-Cervantes	Effect Of The Prefabricated Metallic Post Length On Restored Teeth: Fracture Strength And Stress Distribution
104	J. Lawrence Katz	Micromechanical Analysis Of Dentin Elastic Anisotropy
105	Aaditya C. Devkota	Analysis Of Collagenase, Collagen, And Glycosaminoglycan Content Of Cyclically Loaded Tendon Explants In Culture
106	Tim Wrigley	Biomechanical Features Of Normal Patellar Tendons And Those With Patellar Tendinopathy
107	Mikhail Perelmuter	A Micromechanical Model Of The Periodontal Ligament
108	Emika Kato	Repetitive Muscle Contractions Induce Mechanical Changes Of Achilles Tendon
109	Scott Lucas	Failure Properties Of Cervical Spinal Ligaments Under High-Rate Loading
110	Megumi Ohta	Isometric Training Alters Mechanical Properties Of Tendon Structures
111	Brian P. Beaubien	An Experimental Method For Mechanical Analysis Of The Interspinous And Supraspinous Ligaments
112	Yeung Chi Keung	Denervation Impairs Achilles Tendon Healing In Rat Model
113	Robin Adams	Density Changes in Bovine Tendon Resulting from Buffered and Unbuffered Solutions
114	Abhijit Bhatia	The Effect Of Glycosaminoglycans And Hydration On Viscoelastic Properties Of Aortic Valve
115	Judit E. Puskas	Evaluation Of The Fatigue Properties Of Rubbery Biomaterials Using The Hysteresis Method
116	L.Y. Li	Nonlinear Analysis Of The Behaviour Of The Human Cornea
117	Nai-Shang Liou	Investigating Full Field Deformation Of Soft Tissue Under Simple Shear Tests By The Fourier Transter Moiré Method
118	Takatsugu Furukawa	Effect Of Viscosity On Local Impedance Of Biological Gel:

Poster Session: Foot and Ankle UC 201

119	Mehrdad Anbarian	Effect Of Different Wedge Conditions On Joint Angle Changes During Single-Limb Stance
120	Gong Shi Wei	Energy Flow In High Heel Shoes In Walking
121	Karen Julie Mickle	Do Overweight And Obesity Affect Dynamic Plantar Pressure Distributions In Pre-School Children?
122	Weng-Pin Chen	Dynamic Simulation And Experimental Validation Of The Plantar Foot Pressure During Heel Strike
123	Anneleen De Cock	A Foottype Classification With Cluster Analysis On Plantar Pressure Distribution During Barefoot Jogging
124	Yi-Ling Chiu	Effect Of Walking Speed In Change Of The Peak Plantar Pressure Distribution
125	Richard Jones	In Vitro Study Of Foot Kinematics Using A Walking Simulator
126	Jeremy Crenshaw	The Effect Of Laterally Wedged Orthoses On Talus Angle
127	Richard Jones	Effects Of Different Profiles Of Lateral Wedging On Knee Adduction Moments During The Loading Period Of The Gait Cycle
128	David Wallace	Ground Reaction Forces During Level Walking With And Without Lateral Heel Wedge Orthotics
129	Nachiappan Chockalingam	Ankle Joint Dorsiflexion: Assessment Of The True Values
130	XueCheng Liu	Dynamic 6-Segment-Foot Motion Using Electromagnetic Tracking System
131	Christopher G. Neville	The Effect Of Hindfoot And Forefoot Positions On Posterior Tibialis Muscle Length
132	Michael Voigt	Electrogoniometric Evaluation Of Foot Kinematics During Walking At Different Velocities
133	Sicco Bus *Young Investigator Award finalist*	Offloading The Diabetic Foot Using Forefoot Offloading Shoes
134	Matthew Cowley	Differences In Midfoot Rotations Between Foot Types
135	William R. Ledoux	Quasi-Linear Viscoelastic Properties Of The Plantar Soft Tissue In Compression
136	John H. Challis	Mechanical Properties Of The Human Heel Pad: A Comparison Between Populations
137	Philippe Young	An Innovative Tool For Generating Numerical Models Of The Human Foot
138	Kiersten Anas	Medial Longitudinal Arch Motion And The Windlass Effect During Gait
139	Jaebum Son	A New Frontal Plane Foot Model Shows The Effect Of Narrowed Base Of Support On Unipedal Balance
140	Howard J Hillstrom	How Does Shoe Upper Design Influence Plantar Pressure Distribution?
141	Jinsup Song	Can A Sandal Arch Support Reduce Plantar Hallucial Microcirculation?
142	Ahmet Erdemir	Therapeutic Footwear Design: A Finite Element Modeling Approach
143	Zaid M. Hasasneh	Relationship Between Pressure And Shear Under The Foot
144	Michael J. Mueller	Finite Element Analysis On The Effect Of Soft Tissue Thickness On Plantar Pressures In Subjects With Diabetes And Peripheral Neuropathy
145	Donovan J. Lott	Relationship Between Soft Tissue Deformation And Applied Pressure Along The Second Ray Of The Plantar Neuropathic Foot

(session continued on next page)

Tuesday, August 2 3:45 PM

Poster Session: Foot and Ankle (continued) UC 201

146	Dequan Zou	Pressure Gradient As A Potential Indicator Of Plantar Skin Injury On The Neuropathic Foot
147	W.U. Lijun	Computer Simulation For Internal Stability Of Foot Longitudinal Arch
148	Robin Queen	The Reliability And Reproducibility Of Foot Measurements Using A Mirrored Foot Photo Box Compared To Caliper Measurements
149	Jongpeel Joo	Prediction Of Cycle Shoe Performance In Relation To Outsole Materials Based On Biomechanical Testing And Finite Element Analysis
150	Mehrdad Anbarian	Foot Type Classification Using Fuzzy Logic
151	Gautham Gopalakrishna	Biomechanically Designed Scientifically Appropriate Diabetic Footwear
152	Smita Rao *Young Investigator Award finalist*	Changes In Mechanical Characterestics Of The Plantar Flexor Muscles In Individuals With Diabetes Mellitus
153	Annaliese Dowling	How Does Obesity And Gender Affect Foot Shape And Structure In Children?
154	Jason Wilken	The First Metatarsal As A Fixed Strut: New Insights Into Dynamic Arch Function

Poster Session: Rehabilitation UC 201

155	Archana Sangole	Patterns Of Hand Motor Dysfunction In Brain Injury
156	Wen-Lin Tung	Effect Of Bilateral Reaching On Affected Arm Motor Control In Stroke - With And Without Loading On Unaffected Arm
157	Jyh-Jong Chang	Effects Of Bilateral Resistance-Induced Arm Movement Training On Arm Motor Function In Chronic Stroke
158	Tung-Wu Lu	Kinematic And Kinetic Analysis Of Sit-To-Stand With And Without A Cane In Hemiplegic Subjects
159	Shashank Raina	The Effect Of Foot Placement On Sit-To-Stand With And Without Walker Assistance
160	Zhen-Wei Wu	Muscle Coordination In Stroke Patients' Upper Limbs
161	Wen-Shen Liao	Postural Adjustment Of Spinal Cord Injured Subjects With Knee-Ankle-Foot Orthosis
162	Stephanie J. Nogan	Effects Of Trunk And Hip Stimulation During Bimanual Reaching After Spinal Cord Injury
163	Luci Fuscaldi Teixeira-Salmela	Speed Related Changes In Lower Limb Joint Contributions To Mechanical Energy During Gait Of Stroke Subjects
164	Kisik Tae	Repetitive Symmetric Arm Training And Motor Cortex Activation In Chronic Hemiparetic Patients
165	H.A.M. Seelen	Effects Of AFO-Assisted Ankle Angle Position On Dynamic Knee Stability In Brain Injured And Spinal Cord Injured Patients
166	Rong-Ju Cherng	Effect Of Gait Training With Treadmill And Suspension In Children With Spastic Cerebral Palsy
167	Michael D. Ellis	Shoulder-Position Dependant Elbow Torque Coupling During Adduction After Stroke
168	Jose Luis Lujan	Unique Solution For Feed-Forward Control Of Neuroprosthetic Systems Characterized By Redundant Muscles Acting On Multiple Degrees Of Freedom

169	Daniel Theoret	Three Dimensional Knee Joint Kinematics And Lower Limb Muscle Activity Of Anterior Cruciate Ligament Deficient Knee Joint Participants Wearing A Functional Knee Brace During Running
170	Mark E. Dohring	Characterization Of Intralimb Coordination Deficits In Chronic Patients
171	Henry Wang	Biomechanical Analysis Of Sit-To-Stand After Bilateral Total Knee Replacement
172	Mohammad Reza Fotoohabadi	Hip-Spine Interaction During Sit-To-Stand In Healthy Young Subjects
173	Chris Mizelle	Center Of Pressure Measures Predict Hemiparetic Gait Velocity
174	Antoinette Domingo	Muscle Activation During Manually Assisted Treadmill Training After Incomplete Spinal Cord Injury
175	John W. Chow	Bilateral Comparisons Of Isokinetic Knee Strength In Unilateral Total Knee Replacement Individuals
176	Jen-Suh Chern	Center Of Pressure Trajectory During Whole Body Reaching In Hemiplegic Patients

Poster Session: Finite Element Modeling and Imaging UC 201

177	Hsiang-Ho Chen	Biomechanical Study Of Kümmell's Disease By Finite Element Analysis
178	Jill Schmidt	What Is The Accuracy Of Surface Models Created From Visible Human Male Computed Tomography Data?
179	Nicholas John Byrne	Finite Element Analysis Of A Total Ankle Arthroplasty Over One Stance Phase
180	Naira Campbell-Kyureghyan	Prediction Of Intervertebral Disc Creep During Flexion Using A Combined Experimental And Finite Element Approach
181	D. C. Barton	New Method For Coupled Fluid-Structure Interaction Problems In Biomechanics
182	Cheolwoong Ko	Development Of Human Pelvic Bone FE Model By Considering Pelvic Anthropometry
183	Shuo Yang	A Better Image Degradation Method For Converting High Resolution CT Scans Into Finite Element Models
184	Christine Draper	Is Patellar Cartilage Thickness Reduced In Individuals With Patellofemoral Pain?
185	Shuo Yang	A New Voxel Grayscale Based 3D Image Registration Validation Method
186	Wangdo Kim	Objective Ulcer Quantification By Rim Curvature Map
187	Qunli Sun	FE Modeling And Analysis Of Compressed Human Buttock-Thigh Tissue
188	Yang Dai	Quantitative Prediction Of Progression Of Articular Cartilage Degeneration Following Incongruous Intra-Articular Fracture Reduction
189	Viet Bui Xuan	From Reality To Model In Minutes Or On The Aerodynamics Of A Thanksgiving Turkey
190	Heidi-Lynn Ploeg	What Factors Effect The Accuracy Of Solid Models Made From CT Data?
191	Mehran Armand	Parametric Finite Element Model Of Femur From CT Data
192	Sylvana Garcia	A Validation Study: Using CT Scans To Calculate Volume, Weight And Density
193	Todd C. Doehring	New Open-Source Tools For 3D Reconstruction From Medical Images
194	Marc Petre	Using Data From Multiple Tests To Determine Foam Parameters: Modeling Implications

Tuesday, August 2 3:45 PM

Poster Session: Gait and Locomotion UC 201

195	Max Kurz	An Artificial Neural Network That Explores The Role Of Sensory Information For Learning The Neural Connections For Locomotion
196	Tonya Parker	Longitudinal Study Of Gait Stability After Concussion
197	Susanne Lipfert	Leg Stiffness In Walking And Running
198	Chris Hurt	Is There A Gait Transition Between Run And Sprint?
199	Robyn M. Wharf	Kinetic Analysis Of Gait On Inclined Surfaces
200	Wang Xishi	The Stress Level Analysis For Dynamic Cases At Human Hip Joint
201	Dieter Rosenbaum	Leg Length And Leg Torsion Measurement With Ultrasound In Children During One Year - First Results
202	Songning Zhang	Ground Reaction Forces And 3D Kinematics Of Short-Leg Walking Boots In Gait
203	Marina Gouvali	The Variability Of Dynamic And Spatio-Temporal Parameters Of The Running Stride
204	Nobuhiro Kito	Phase Plane Analysis Of Stability In Turning Movement In Subjects With Functional Ankle Instability
205	Alan Hreljac	Kinetic Factors Influencing The Gait Transition Speed During Human Locomotion
206	Lei Ren	Prediction Of Human Walking Based On Simple Gait Descriptor
207	Wolfgang I. Schoellhorn	The Influence Of Music On Kinematic And Dynamic Gait Patterns
208	Christina Danielli C. M. Faria	Relationships Between Iliotibial Band Length And Frontal Plane Pelvic Tilt
209	Jesús Cámara	The Influence Of The Firemen Boots On The Heel Strike Transient During Walking
210	Matthew Seeley	The Effect Of Mild Limb Length Inequality On Able-Bodied Gait Asymmetry: A Preliminary Analysis.
211	Andrea Lay	Control Strategy Transitions During Slope Walking
212	Patricia V. de Souza	Biomechanic Analysis Of The Force Applied In Aquatic Gait Of Humans Immersed At The Sternum Level
213	Shih-Chiao Tseng	Evidence Of Movement Control Adaptation In A Lower Extremity Motor Task
214	Patricia V. de Souza	Dynamometric Analysis Of The Anteroposterior Force Applied In Aquatic Human Gait
215	Kotaro Sasaki	Differences In Muscle Function Between Walking And Running At The Preferred Walk-Run Transition Speed
216	Rong-Ju Cherng	Effect Of A Dual Task On Walking Performance In Preschool Children
217	Chris Rhea	Gait Adaptation: Lead Toe Clearance Continually Decreased Over Multiple Exposures With And Without On-Line Visual Information
218	Philippe Malcolm	Treadmill Versus Overground Run To Walk And Walk To Run Transition Speed In Unsteady State Locomotion Conditions
219	Sam Walcott	Pseudo-Elasticity And Kinetic Energy Storage: Definitions And Applications To Human Movement
220	Prism S. Schneider	Effect Of Dynamic Ankle Joint Stiffness On Joint Mechanics And Muscle Activation Patterns During Locomotion

221	Jeremy Noble	Adaptive Changes In Lower Limb Coordination In Response To Unilateral Loading During Treadmill Locomotion
222	Paul DeVita	Lower Extremity Joint Work Is Larger In Ascending vs. Descending Gaits
223	Cara L. Lewis	Walking In Greater Hip Extension Increases Predicted Anterior Hip Joint Reaction Forces
224	Andre Seyfarth	Hip Control In Locomotion
225	Katrina Simpson	Do Lower Limb Muscle Activity Patterns Change With Prolonged Load Carriage?
226	Ava Segal	The Method Of Using Phase Plane Portraits And First Return Maps To Examine Turning
227	Rebecca Whissell	Is Child Weight To Bag Weight The Best Way To Assess Risk Of Low Back Pain In Children Due To Backpack Use?
228	Robert B. Eckhardt	Short Stature Or Tall Story? Hypothesis And Imagination In Body Size Reconstruction Of LB1 From Flores, Indonesia
229	Shigehito Matsubara	Symmetry And Asymmetry In The Lower Limbs Of Athletes During Gait
230	Robert B. Eckhardt	Was The Early Hominid Brain Musclebound?
231	Michael Bohne	The Effects Of Hiking Downhill Using Two Trekking Poles While Carrying Different External Loads in A Backpack

Wednesday, August 3 — 8:30 AM

ISB Promising Young Investigator Award — Waetjen Auditorium
Chair: Walter Herzog

8:30	Constantinos Maganaris	Adaptive Response Of Tendon To Paralysis

ISB Clinical Biomechanics Award — Waetjen Auditorium
Chair: Kim Burton, Sandra Olney

9:00	Magnus Kjartan Gislason	The Three Dimensional Load Transfer Characteristics Of The Wrist During Maximal Gripping.

Wednesday, August 3 — 9:30 AM

ISB Young Investigator Award finalists — Waetjen Auditorium
Chair: Maarten Bobbert

9:30	Emma A. C. Johnson	The Analysis Of Pressure Response In Head Injury: A Validation Study
9:45	Craig P. McGowan	The Mechanics Of Jumping Vs. Steady Hopping In Yellow-Footed Rock Wallabies.
10:00	Thomas J. Withrow	Valgus Loading Causes Increased In Vitro ACL Strain In Simulated Jump Landing
10:15	Ann M. Barkowitz	A Novel Robotic Device With Haptic Feedback For Lower Limb Rehabilitation
10:30	Jill Higginson	Reduced Plantarflexor Contributions To Support In Post-Stroke Hemiparetic Gait

Posture and Balance 1 — UC 6
Chair: Alan Walmsley, Tammy Owings

9:30	Ian Loram	Paradoxical Muscle Movements In Human Standing
9:45	Erin Wilson	Lumbar Extensor Fatigue Changes Postural Recovery Strategy
10:00	Sukyung Park	The Effect Of Initial Lean On Human Postural Scaling
10:15	Peter M. Quesada	Effects Of Smooth vs "Prickly" Surface Conditions On Tiltboard Performance

Spine 2 MC 201

Chair: Jim Potvin, James Dickey

9:30	Robert Parkinson	Does Load Magnitude Alter Cumulative Load Tolerance? "Weighting" For An Answer
9:45	Erik Cattrysse	3D Arthrokinematic Analysis Of Coupled Motion In The Human Upper-Cervical Spine: In Vitro Analysis Of High Velocity Thrust Techniques
10:00	Dave Glos	Intra-Annular Bilateral Spinal Compression: Novel MEMS Sensors
10:15	David Nuckley	Compressive Mechanics Of The Maturing Human Spine

Lower Extremity Injury MC 202

Chair: Paul DeVita, Kathy Simpson

9:30	Rebecca Zifchock	Kinetic Asymmetry In Left And Right Dominant Female Runners: Implications For Injury
9:45	Tine Willems	Relationship Between Foot Progression Angle And Exercise-Related Lower Leg Pain
10:00	Joseph Seay	Dynamic Symmetry In Female Runners With A History Of Tibial Stress Fractures
10:15	Sara Novotny	The Effects Of Quantitative Feedback On The Reduction Of Landing Force

Prosthetics and Orthotics UC 1

Chair: Sandra Olney, Bob Gregor

9:30	Jack R. Engsberg	Comparison Of Rectified And Unrectified Sockets For Transtibial Amputees
9:45	Martin Twiste	The Effect Of Prosthesis Compliance On Residual Limb-Socket Interface Forces
10:00	Alexander Razzook	Can Passive Dynamic Ankle Foot Orthoses Replicate Natural Ankle Stiffness
10:15	Steven H. Collins	Controlled Energy Storage And Return Prosthesis Reduces Metabolic Cost Of Walking

Wednesday, August 3 11:00 AM

Muybridge Award Lecture Waetjen Auditorium

Chair: Mary Rodgers

11:00	Rik Huiskes	Bone: The Engineer's Ultimate Dream Material

Thursday, August 4 — 8:30 AM

ASB Jim Hay Award Lecture — Waetjen Auditorium
Chair: Walter Herzog

8:30	Mont Hubbard	Spinning Sports Balls

Thursday, August 4 — 9:30 AM

ASB Young Scientist Awards — Waetjen Auditorium
Chair: Walter Herzog

9:30	Katherine Holzbaur *Winner of ASB Predoctoral Young Scientist Award*	Scaling Of Muscle Volumes In The Upper Extremity
9:45	Stefan Duma *Winner of ASB Postdoctoral Young Scientist Award*	A Computational Model Of The Pregnant Occupant: Local Uterine Compression Effects The Risk Of Fetal Injury

Gait Simulation — UC 6
Chair: John Chow, Andre Seyfarth

9:30	Taku Komura	Simulating Pathological Gait Using The Angular Momentum Inducing Inverted Pendulum Model
9:45	Saryn Goldberg	The Influence Of Gastrocnemius Geometry On Its Action At The Knee During Stance
10:00	Ajay Seth	A Neuromuscular Tracking Method For Computing Individual Muscle Forces During Human Movement
10:15	Richard R. Neptune	Ankle Plantar Flexor Force Capacity During Toe Walking

Functional Electrical Stimulation — MC 201
Chair: RonTriolo, Bob Kirsch

9:30	Alicia Koontz	Effects Of Functional Electrical Stimulation On Manual Wheelchair Propulsion
9:45	Anirban Dutta	EMG Based Triggering And Modulation Of Stimulation Patterns For FES-Assisted Ambulation - A Conceptual Study
10:00	Jason Gillette	Lower Back FNS For Stabilization During One- And Two-Handed Reaching Tasks
10:15	Dimitra Blana	Feedback Control For A High Level Upper Extremity Neuroprosthesis

Sport 3 MC 202

Chair: Graham Caldwell, Mike Madigan

9:30	Dieter Rosenbaum	Plantar Pressure Distribution Patterns Used As Biofeedback Information Improve Technical Training And Performance In In-Line Speed-Skating
9:45	Gerald Smith	Ski Skating Force Characteristics: Comparisons Across Speed
10:00	Matthew Major	Aggressive Inline Skating: Biomechanics Of Landing And Balancing On A Grind Rail
10:15	Federico Formenti	Biomechanical And Physiological Determinants Of Skiing Locomotion Development

Injury Biomechanics UC 1

Chair: Jeff Wheeler, Uwe Kersting

9:30	Amber Rath	A Fiber Optic Based Sensor For Measuring Chest And Abdominal Deflection Under Impact Loading
9:45	Robert Catena	Maintenance Of Gait Stability In Concussed College Patients During Dual Tasks
10:00	Sriram Rajagopal	Development And Validation Of The Finite Element Human Body Model For Less - Lethal Ballistic Impacts
10:15	Eric Kennedy	Rupture Pressures For Human And Porcine Eyes Under Static And Dynamic Loading

Thursday, August 4 — 11:00 AM

Hand and Wrist 1 — Waetjen Auditorium
Chair: Trey Crisco, Zong-Ming Li

11:00	William L. Buford	Moment Arms And Moment Potential Balance At The Index MCP Joint
11:15	Jie Tang	Kinematics Of Thumb Opposition
11:30	Sang-Wook Lee	Dynamic Modeling And System Identification Of Finger Movement
11:45	Jaewon Choi	3-Dimensional Kinematic Model For Predicting Hand Posture During Certain Gripping Tasks
12:00	Saurabh Mahapatra	A Mathematical Definition Of Feasible Finger Postures And Movements
12:15	Patrick Salvia	In Vivo Kinematics Of Human Wrist Joints: Combination Of Medical Imaging And Three-Dimensional Electrogoniometry

Diabetic Foot — UC 6
Chair: Peter Cavanagh, Gautham Gopalakrishna

11:00	Robert van Deursen	Functional Outcome In People With Diabetic Neuropathy At Different Stages Of Complications
11:15	Claudia Giacomozzi	Altered Foot Loading In Diabetics. The Role Of Achilles Tendon And Plantar Fascia
11:30	Matthew Cowley	A Prospective Look At Foot Shape And Foot Ulcer Development
11:45	Steve Goske	Reduction Of Plantar Heel Pressures: Insole Design Using Finite Element Analysis
12:00	Sicco Bus	Sub-Calcaneal Fat-Pad Infiltration And Its Effect On Plantar Heel Pressures In The Diabetic Neuropathic Foot
12:15	Brian L. Davis	Metatarsal And Toe Loading Patterns In Diabetic Patients: Possible Role In The Etiology Of Charcot Foot Complications

Gait and Aging — MC 201
Chair: Mike Pavol, Phil Martin

11:00	Chris McGibbon	Neuromuscular Adaptations In Gait With Age And Musculoskeletal Pathology
11:15	Masato Takanokura	Biomechanical Analysis Of Four-Wheeled Walker For An Elderly Person
11:30	Justus Ortega	Elderly Adults Perform Less Limb Work During Walking
11:45	Samantha Winter	The Force-Length Curve Of The Human Gastrocnemius In Vivo.
12:00	Zachary Domire	The Influence Of Seat Height On Sit To Stand In The Elderly: A Simulation Study
12:15	Sukhoon Yoon	Effects Of Short-Term Walking Exercise In Elderly

Running MC 202

Chair: Julianne Abendroth-Smith, Mark Lake

11:00	Anton Arndt	Transmission Of Controlled External Plantar Impacts Along The Tibia In Relation To Muscular Activity
11:15	Katherine Boyer	Soft Tissue Compartment Response To An Unexpected Surface Change
11:30	Caroline Digby	A Preliminary Assessment Of The Effects Of Foot Type On The Movement Coupling Of The Foot And Shank During The Stance Phase Of Barefoot Running
11:45	Stephen C. Swanson	Kinetic Limitations Of Maximal Sprinting Speed Revisited
12:00	Christopher L. MacLean	Short And Long-Term Influence Of A Custom Foot Orthotic Intervention On Lower Extremity Dynamics In Injured Runners
12:15	Uwe G. Kersting	Impact Forces, Rearfoot Motion And The Rest Of The Body In Heel-Toe Running

Wheelchair Biomechanics UC 1

Chair: Mary Rodgers, Joe Sommer

11:00	Shun-Hwa Wei	Joint Workspace Of Shoulder and Elbow Associated with Various Axis Positions During Manual Wheelchair Propulsion
11:15	Jennifer L. Mercer	Kinetic Analysis Of Manual Wheelchair Propulsion Over Three Surfaces
11:30	S. van Drongelen	Shoulder Load During Weight Relief Lifting: A Simulation Study
11:45	Sharon Eve Sonenblum	Kinematics Of Lateral Transfers: A Pilot Study
12:00	Philip S. Requejo	Upper Extremity Kinetics During Wheelchair Lever Propulsion
12:15	W. Mark Richter	Biomechanics Of The Flexrim Low Impact Wheelchair Handrim

Thursday, August 4 — 1:15 PM

ASB Borelli Award Lecture — Waetjen Auditorium
Chair: Kenton Kaufman

1:15	Kai-Nan An	The Evolving Journey of Tendon and Joint Mechanics: Clinical Impacts from Humble Concepts

Thursday, August 4 — 2:15 PM

ASB Awards — Waetjen Auditorium
Chair: James Ashton-Miller

2:15	Azita Tajaddini *Microstrain award winner*	Laser Induced Auto-Fluorescence (LIAF) As A Method For Assessing Skin Stiffness Preceding A Diabetic Ulcer Formation
2:30	Robert A. Siston *ASB Clinical Biomechanics Award finalist*	In-Vivo Passive Kinematics Of Osteoarthritic Knees
2:45	Wendy Murray *ASB Clinical Biomechanics Award finalist*	Significance Of Surgical Attachment Length For Hand Function Following Brachioradialis Tendon Transfer
3:00	Eun-Jeong Lee *ASB Journal of Biomechanics Award finalist*	Modulation Of Passive Force In Skeletal Muscle Fibers
3:15	Trey Crisco *ASB Journal of Biomechanics Award finalist*	Scaphoid And Lunate Rotations Are Minimized With Wrist Motion Along

Posture and Balance 2 — UC 6
Chair: Ge Wu, Robert van Deursen

2:15	Kimberly Ryland	Nonlinear Analysis Of Postural Control In Different Positions And Vision Conditions
2:30	Shirley Rietdyk	Stationary Visual Cues Reduced Centre Of Pressure Displacement In A Dynamic Environment For Experienced Roofers
2:45	Sukyung Park	Optimal Control Model Of Human Postural Scaling With Biomechanical Constraints
3:00	H.J. Sommer III	Postural Control Related To Flexibility Of The Hindfoot When Bearing Heavy Loads
3:15	Kodjo E. Moglo	The Threshold Of Balance Recovery Is Not Affected By The Type Of Postural Perturbation

Rehabilitation Robotics MC 201

Chair: Jay Alberts, Susan D'Andrea

2:15	Margaret Finley	Upper Extremity Robotic Therapy In Stroke Patients With Severe Upper Extremity Motor Impairment
2:30	H.A.M. Seelen	Evaluation Of Upper Extremity Muscle Activity During Manipulation In Robot-Simulated Task Environments
2:45	Theresa Sukal	Discoordination In Stroke Measured Dynamically Using The ACT-3D Robot
3:00	Gregory Sawicki	Therapist Controlled Powered Lower Limb Orthoses To Assist Locomotor Training
3:15	Gail F. Forrest	The Effects Of Locomotor Training On Neural And Muscle Activation.

Cartilage MC 202

Chair: Tammy Haut Donahue, Jaw-Lin Wang

2:15	Salvatore Federico	A Non-Linear, Anisotropic, Inhomogeneous Model Of Articular Cartilage
2:30	Doug Bourne	Cartilage Cell Viability After In Vivo Impact Loading
2:45	Tammy L. Haut Donahue	Biochemical Response Of Meniscal Tissue To Altered Loading
3:00	Matthew Koff	T2 Values Of Patellar Cartilage In Patients With Osteoarthritis
3:15	Seungbum Koo	3D Laser Scan Based Accuracy Test Of In-Vivo Cartilage Thickness Measurement From MRI

Instrumentation UC 1

Chair: Mark Grabiner, Stefan Duma

2:15	Thomas Baer	Calibration And Monitoring Of Piezoresistive Contact Stress Sensor Arrays Using A Travelling Pressure Wave Protocol
2:30	Jennifer Megesi	Validation Of Intramuscular Pressure Sensor In Rat Gastrocnemius
2:45	Philippe Pourcelot	Achilles And Patellar Tendon Loading During Gait Measured Using A Non-Invasive Ultrasonic Technique
3:00	Stephen F. Levinson	Doppler Myography: Ultrasonic Localization Of Acoustic Myographic Signals
3:15	Stephen F. Levinson	Anisotropic Elasticity And Viscosity Deduced From Supersonic Shear Imaging In Muscle

Thursday, August 4 3:45 PM

Poster Session: Musculoskeletal Modeling UC 201

1	Thomas Pressel	Functions Of Hip Joint Muscles
2	Samuel J. Howarth	Using The Eigenvector To Locate Spinal Instability
3	Martijn Klein Horsman	Morphological Muscle And Joint Parameters For Musculoskeletal Modelling Of The Lower Extremity
4	Akinori Nagano	Development Of A Three-Dimensional Simulation Model Of The Human Whole Body
5	Bing Yu	An EMG Driven Optimization Model For Estimating Dynamic Knee Muscle Forces Without Maximum Muscle Voluntary Contraction Test
6	Elizabeth Chumanov *Young Investigator Award finalist*	Lateral Hamstrings Are Stretched More Than The Medial Hamstrings During Sprinting
7	Matthew Pain	Determining Subject Specific Torque-Velocity Relationships
8	Chris Mills	Modeling The Gymnast-Mat Interaction During Vault Landings
9	Costis Maganaris	Muscle Fibre Length-To-Moment Arm Ratios In The Human Lower Limb
10	Dimitrios Baltzopoulos	Can The Patellar Tendon Moment Arm Length Be Predicted From Anthropometric Characteristics?
11	Costis Maganaris	Effects Of Isometric And Isokinetic Contractions On The Patellar Tendon Moment Arm
12	Jim Potvin	Hip Stability: Mechanical Contributions Of Individual Muscles
13	Weidong Luo	Can A Single Scale Factor Be Used To Scale Femur Bone Models?
14	Veronica J. Santos *Young Investigator Award finalist*	Implementing Data-Driven Models Of The Human Thumb Into A Robotic Grasp Simulator To Predict Grasp Stability
15	Daniel Bassett	Predicting Ankle Joint Moments In Subjects With Normal And Abnormal Gait
16	Madhusudhan Venkadesan	The Continuum Of Mixtures Of Feedback And Feedforward Control Strategies Used In Dynamical Dexterous Manipulation Can Be Explored At The Boundary Of Instability
17	Przemyslaw Prokopow	Effects Of Timing Of Muscle Activation On Performance In Vertical Jump

Poster Session: Upper Extremity & Wheelchair UC 201

18	Jean-Sebastien Roy	The Impact Of Using Different Calculation Methods And Local Coordinate Systems When Measuring 3D Scapular Attitudes.
19	Alicia Koontz	Electromyography Of Trunk Muscles During Wheelchair Propulsion
20	Tomoko Aoki	Prehension Synergies: Effects Of Friction
21	Anne Katrine Blangsted	Changes In Mechano- And Electromyogram During Low-Force Static Contraction In Subjects With Unilateral Epicondylitis Lateralis
22	Sungwoo Koh	Mechanical Properties Of The Shoulder Ligaments
23	Paul Pei-Hsi Chou	Relationship Between Elbow Flexion Angle And Joint Loading Of The Upper Extremity During A Close-Chain Exercise
24	Lin, Hui-Ting	Determining The Resting Position Of The Glenohumeral Joint In Normal Subjects
25	Pernille Kofoed Nielsen	Muscle Tissue Composition, Muscular Tenderness, And Force Production In Subjects With Unilateral Epicondylitis Lateralis
26	Duane Morrow	Assessing Shoulder Kinematics In A Subject With A Spinal Accessory Neuropathy
27	Philippe Favre	An Algorithm For Estimation Of Shoulder Muscle Forces For Clinical Use
28	C.G.M. Meskers	Comparison Between Tripod And Skin Fixed Recording Of Scapular Motion
29	David Suprak *Young Investigator Award finalist*	Three-Dimensional Shoulder Joint Position Sense
30	Joseph Langenderfer	Variability Of Glenohumeral External Rotator Muscle Moment Arms
31	Geraldo F. S. Moraes	Scapular Muscle Recruitment And Isokinetic Force Production In Individuals With Impingement Syndrome
32	Paula Ludewig	Volumetric Measurement Of The Subacromial Space At The Shoulder
33	Edward Chadwick	Stiffness Measurement Of The Glenohumeral Joint
34	Hisaichi Ohnabe	Evaluation Of Newly Designed Cushion For Electric Power Wheelchair Driving
35	Laurel Kuxhaus	Reproducing Physiologic Moment Arms With An Elbow Simulator
36	Catarina Tainha	Shoulder Kinematics During Clinical Glenohumeral Tests. Differences Between No-Players And Water Polo Players
37	Philip S. Requejo	Wrist Electromyography And Kinematics When Propelling Standard, Compliant, And Power-Assisted Pushrim Wheelchairs: A Pilot Study
38	Kevin A. Rider	Superposition Of Optimal Submovements In Feedback-Controlled Reaching
39	Yasushi Koyama	The Dodge Movement During The Lat Pull-Down Exercise Increased Scapula Rom
40	Po-Chou Lin	Influence Of Seat Height On Pitch Angle And Pushrim Kinetics During A Wheelie Activity
41	Koh Inoue	Estimation For Dynamic Measurement Of Scapula Kinematics
42	Anamaria Acosta	The Effect Of Shoulder Girdle Coordination On Upper Extremity Workspace In Stroke

Thursday, August 4 3:45 PM

Poster Session: Sport 6 UC 201

43	Ernst Albin Hansen	Performance After Prolonged Cycling At Freely Chosen And Optimal Pedal Rate
44	Felipe Pivetta Carpes	Development Of A Computer Application To Calculate Cyclists Front Area In Studies About Aerodynamics
45	Juliana K. Ribeiro	In-Shoe Pressure Analysis During Aero Jump In Different Cadences
46	Xin-Hai Shan	A Method To Diagnosis The Kinetic Characteristic Of The Straight Kick Performance
47	Mathijs Hofmijster	Effect Of Stroke Rate On Mechanical Power Flow In Rowing
48	Aaron Benson	Force Profile Comparison Of Rowing On A Stationary And Dynamic Ergometer
49	Mutsuko Nozawa	Relationship Between Rotational Movement And Translational Movement During The Golf Swing
50	Toyoaki Aoki	Effect Of Sun Light On Surface Temperature Of Artificial Sport Surfaces
51	Shinichiro Ito	Optimal Arm Stroke For Competitive Free Style Swimming
52	Linda McLean	Differences Between Operated And Non-Operated Shoulder Muscle Activation Patterns Recorded During The Dragon Boat "Long And Hard" Stroke
53	Takeshi Asai	Ball Impact Analysis In Football Using FEM Foot Model
54	Wang Hsiang-Hsin	Effects Of Passive Repeated Plyometric Training On Specific Kicking Performance Of Elite Olympic Taekwondo Player
55	Heather Gulgin	Comparison Of Golfers And Non-Golfers Weight-Bearing Hip Rotation Joint Range Of Motion
56	Chiang Liu	Reflex Modulation After Long Term Passive Repeated Plyometric Training
57	Syn Schmitt	Computer Simulation Of A Human Ski Jumper - A Complete Trial
58	Lee Shuei-Pi	A Comparison Of Isokinetic Leg Flexion And Extension Strength In Elite Adolescent Male Track And Field Athletes
59	Long-Ren Chuang	Biomechanical Analysis Of Punching Different Targets In Chinese Martial Arts
60	Fong-Wei Wang	Dynamical Analysis Of Indoor Eight People Make Tug Of War Attack Movements - European Back-Step And Japanese Back-Step
61	Andrew Chapman	Do Kinematics Of The Pelvis And Lower Limb Vary Between Novice And Highly Trained Cyclists?
62	Min-Chung Shen	Kinematic Analysis Of Kolman Acrobatics In The High Bar Exercise
63	Sekiya Koike	Kinetic Analysis Of Each Hand During Golf Swing With Use Of An Instrumeted Golf Club
64	Walter Quispe Marquez	A Biomechanical Analysis Of Spike Motion For Different Skill Levels Of Male Volleyball Players
65	Luciano L. Menegaldo	Study Of The Inverse Dynamics Optimal Control Technique In Cycling
66	Tetsunari Nishiyama	The Modification Of Pedaling Skill With Real-Time Representation Of Pedaling Force In Non-Cyclists
67	Laurelyn E. Keener	Comparison Of Dressage Rider Posture When Mounted On Different Horses

68	Jiro Doke	A Simple Mathematical Model Of Karate Front Kick
69	Ines Benkhemis	Influence Of Loads To The Joint Moments And Mucle Force Repartition In Sprint Cycling Test
70	Kjartan Halvorsen	The Influence Of Inclined Support Surface On The Biomechanics Of Eccentric Overload In Squats
71	Bryan K. Lindsay	Predictors Of Success In The 3000M Steeplechase Water Jump
72	Tetsu Yamada	Comparison Of The Knee Joint Between The Skilled And Unskilled Subjects During The Kip Maneuver On The Horizontal Bar
73	Alan Lai	Validation Of A Theoretical Rowing Model Using Experimental Data
74	Chih-Hang Lien	Dynamic Stability Strategy For Elite Judoists In Balance Control For Anterior And Posterior Perturbations
75	Chia-Nen Chan	Elelectromyographic Linear Envelope Analysis Of Golf Swing For Trunk Motion In Asian Players: A Case Study
76	Shu-ting Chen	The Comparsion Of Effectiveness Between Grab Start And Track Start In Competitive Swimming
77	Takayuki Sato	The Difference Of Fitness Level Evaluated From The Mechanical And External Work During Bicycle Exercise
78	Bryan Morrison	The Effect Of Aging On Stroke Parameters In Swimming

Thursday, August 4 3:45 PM

Poster Session: Running UC 201

79	Andrew Chapman	The Influence Of Cycling On Lower Limb Movement And Muscle Activation During Running In Triathletes
80	Alena Grabowski *Young Investigator Award finalist*	Modeling The Benefits Of Towing During Adventure Racing, Running With Applied Horizontal Force
81	Laura Hild	Can A Runner's Economy And Arm Motion Be Affected By Feedback Training?
82	Jonas R. Mureika	The Effects Of Temperature, Pressure, And Humidity Variations On 100 Meter Sprint Performances
83	Chien-Hua , Chien-Hua	Mechanomyography And Force Relationship During Concentric And Eccentric Contractions Of The Vastus Lateralis In Sprinters
84	Caroline Digby	High-Speed Coupling Characteristics Of The Foot And Shank During The Stance Phase Of Running
85	Daniel Gales	Ground Reaction Force Asymmetries During Sustained Running
86	Abbey Green	Ankle Plantar Flexor Moments Scale To Planning Time During Unexpected Side Step Cut Tasks
87	Ceri Diss	Quantifying Leg Elasticity In Male Veteran Runners
88	William J. McDermott	Mechanical Constraints Do Not Change The Strength Of Locomotor-Respiratory Coordination During Running
89	Samuel Brethauer	The Effects Of An Over-The-Counter Orthotic On Lower Extremity Kinematics In Male And Female Recreational Runners
90	Andre Seyfarth	Walking And Running On Place
91	Joseph Hamill	Intralimb Coordination In Female Runners With Tibial Stress Fractures
92	Carla Sonsino Pereira	Vertical Ground Reaction Force Differences In Runners With Leg Length Discrepancy - Preliminary Results
93	Yasushi Enomoto *Young Investigator Award finalist*	A Biomechanical Comparison Of Kenyan And Japanese Elite Long Distance Runner's Techniques
94	Lan-Yuen Guo	Lower Extremity Kinematics During Jogging: Influence Of Treadmill Settings

Poster Session: Orthopaedics UC 201

95	Hsiang-Ho Chen	Biomechanical Comparison Of Fixation Techniques For Double Pars Fractures
96	Sang Min Joo	Computer Aided Pre-Operative Planning Of Fracture Reduction And Deformity Correction In Tibia With Hexapod External Fixator
97	Alexandre Terrier	Evaluation Of An Optimal Cement Thickness Around The Glenoid Component
98	Soojung Moon	Biomechanical Analysis On Design Variables In Relation To The Strength Of Compression Hip Screws
99	Suneel Battula	A Biomechanical Study Of The Pullout Strength Of The Self-Tapping Bone Screws In Osteoportic Bone Material Inserted To Different Depths
100	Ching-Lung Tai	Biomechanical Study In The Optimization Of Different Fixation Modes For A Proximal Femur L-Osteotomy- A Three Dimensional Finite Element Simulation
101	Miranda Shaw	A Pedicle Screw Based Design For An Artificial Facet Joint

102	Anthony Au	Internal Bone Stress Analysis Of Tibial Implant With Incorporation Of Soft Tissues
103	Fred Wentorf	Mechanical Evaluation Of Tension Band Orientation
104	Korboi Evans	Adjacent Load Transfer Following Vertebral Compression Fractures Treated By Cement Augmentation
105	Mike Ehlert	Axial Cyclic And Failure Loading Of Pedicle Screws
106	Larry Ehmke	Stability Of Plate Fixation Constructs With Locked And Non-Locked Screws
107	Thaddeus Thomas	Relating Fracture Energy To Clinical Outcome In Tibial Pilon Fracture Cases
108	Paul Weinhold	Three Versus Four Pegged Glenoid Components: A Biomechanical Evaluation Of Fixation Stability With Cyclical Loading

Poster Session: Sport Injuries UC 201

109	Natalie Ann Saunders	Differences In Lower-Limb Neuromuscular Control Between Sports Movements Executed In Laboratory And Game Settings
110	Lester Mayers	Landing Forces Produced In Tap Dance
111	Peter Milburn	Bilateral Symmetry In Single Leg Landings
112	Steven Blackburn *Young Investigator Award finalist*	Development Of A Biomechanically Validated Turf Testing Rig
113	Hsiao-Yun Chang	Muscle Activation Pattern Of Lower Extremity Muscles In Selected Basketball Tasks
114	Thomas W. Kernozek	Changes In Lower Extremity Joint Stiffness With Landing After Fatigue
115	Kurt Clowers	Effects Of Power Generation On Evaluating Impact Attenuation In Landing
116	Thomas W. Kernozek	Rotational Spring And Damper Model Prediction During Landing
117	Eamonn Delahunt	Altered Ankle Joint Positioning During Jump Landing In Subjects With Functional Ankle Instability (FAI)
118	Paula H. Lobo da Costa	Biomechanical Approach To Ballet Movements: A Study Of The Effects Of Ballet Shoe And Musical Beat On The Vertical Reaction Forces
119	Yasuyuki Yoshida	Joint Kinetics And Posture Control During Drop Landings
120	Dieter Rosenbaum	Comparison Of The Effectiveness Of Orthoses Versus Proprioceptive Exercises For The Prevention Of Ankle Injuries In Basketball Players
121	Cheng-Feng Lin	Effects Of Hip And Knee Joint Motions During The Landing Of A Stop-Jump Task
122	John D. Willson	Utility Of The Frontal Plane Projection Angle Of The Knee During Single Leg Squats
123	Michelle Sabick	Differences In Center Of Pressure Movement Between Boys And Girls During One-Footed Landings
124	Scott C. Landry	Neuromuscular Gender Differences Exist During Unanticipated Running And Cutting Maneuvers Within An Elite Adolescent Soccer Population
125	Carla Murgia	Effects Of Proprioception And Strength Training On Injury Prevention In Adolescent And Young Adult Female Dancers
126	Bradley Black	Effects Of Jump Type On Ground Reaction Forces During Landing In Children
127	Radivoj Vasiljev	The Different Influence Of Leg Extensors In Development Peak Of Force In Drop Jump
128	Yang Hua Lin	Effects Of Taping Materials On Isokinetic Performance At The Ankle Muscles

(session continued on next page)

Thursday, August 4 3:45 PM

Poster Session: Sport Injuries (continued) UC 201

129	Wei-Hua Ho	The Difference Of Net Muscle Torque Of Lower Extremity By Using Different Body Segment Parameter In Gymnast
130	Deborah King	Impact Mechanics During Stop And Go Tasks Under Fatigued And Non Fatigued Conditions
131	Brian M. Campbell	The Influence Of Knee And Ankle Bracing On Lower Extremity Kinetics And Kinematics During Jogging
132	Steve McCaw	Joint Torsional Stiffness Contributions To Leg Stiffness
133	Jennifer Jeansonne	Biomechanical Analysis Of Jumping Comparing Low- And High-ACL Injury Risk Groups: Identifying Possible Mechanical Risk Factors
134	Carla Sonsino Pereira	Ankle Muscular Activity During Landing In Volleyball Players With Functional Instability
135	Kristian O'Connor	The Effect Of Lower Extremity Fatigue On Shock Attenuation During Landing
136	Jennifer Earl	Effects Of Exaggerated Pronation And Supination On Lower Extremity Mechanics During A Cutting Maneuver
137	Rhonda Boros	Kinetics And Kinematics Of Males And Females During Two Styles Of Drop Landing
138	Bridget Munro	Quadriceps-Hamstring Muscle Synchrony During Landing Movements: Is It Affected By Movement Direction?
139	Koji Zushi	Changes Of Spring-Like Leg Behavior According To Different Touch Down Velocities In Drop Long Jump

Poster Session: Motor Control UC 201

140	Kazuyoshi Sakamoto	Evaluation Of Function Of Knee Joint By Physiological Tremor In Lower Leg
141	Maya Kawabata	Influence Of Hardness Of Bed On Hip Joint With Use Of Trunk Tremor
142	Maneesha Arashanapalli	Vibration Alters Proprioception And Dynamic Low Back Stability
143	Pete Shull	Bimanual Motor Control: Biological And Robotic System Learning Via Simultaneous Movement Requirements
144	David Sanderson	Recruitment Of Soleus And Gastrocnemius With Restricted And Unrestricted Ankle Motion
145	Akifumi Kijima	Coordination Change Between Gaze, Head And Hip Due To Early Eye Rotation During Open Cut Maneuver
146	Luc Selen	Impedance Modulation With Precision Demands In Discrete Movements
147	Oliver Wirth	Assessing Regularity In Voluntary Motor Activity With Approximate Entropy
148	Huang Yi Ming	The Effect Of Fatigue On The Control Of Targeted Isometric Dorsiflexion In Humans
149	Germano T. Gomes	Quantifying Upper Limb Motor Control: The Peg In Hole Test
150	Christopher Hasson	A Musculoskeletal Model Of Postural Control At The Ankle
151	Jingzhi Liu *Young Investigator Award finalist*	Motor Control Strategy To Manage Central Fatigue
152	Sun Wook Kim	Preparation To A Predictable Perturbation During Multi-Finger Force Production
153	Hiroaki Hobara	Central And Peripheral Control Of Muscle Stiffness In Hopping

154	Ming-feng Kao	The Validity Of Active Squat Keen Joint Propriception
155	Kathy Jagodnik	Proportional Derivative Control for Planar Arm Movement
156	Radhika Kotina	Modeling and Control Of Human Postural Sway

Poster Session: Clinical and Functional Movement Analysis UC 201

157	Wendy Gilleard	The Effect Of A Reference Posture On The Relationship Between Relaxed Calcaneal Standing Measurement And Frontal Plane Rearfoot Motion During Walking In Patellofemoral Pain Syndrome Subjects
158	Steven Jones	The Gait Initiation Process In Unilateral Lower-Limb Amputees Stepping To A New Level
159	Wendy Gilleard	Effect Of Arm Use On Head And Trunk Segment Motion When Rising From A Chair
160	Mirko Brandes	Activity Assessment And Clinical Gait Analysis After Malignant Bone Tumors Treatment With Reconstruction Of Femoral And Tibial Defects
161	Mark Creaby	Are Structural And Gait Biomechanics Indicative Of Tibial Stress Fracture Risk?
162	Mirko Brandes	Basic Gait Parameters Of Healthy And CP Children Assessed By Accelerometry
163	Max Kurz	An Inverted Pendulum Model Indicates That Parkinson's Disease Results In Altered Neuromuscular Stiffness For Controlling Gait
164	Melissa Scott-Pandorf	The Effect Of Peripheral Arterial Disease On Gait
165	Ryo Kanda	Development Of A Web-Based Decision Support System For Acupuncture Treatment
166	James Wakeling	Muscle Dysfunction During Walking In Children With Cerebral Palsy
167	Shyi-Kuen Wu	The Kinetic Changes Of Gait Across Calf Myofascial Intervention
168	Yu-Hsiang Nien	The Ground Reaction Force And Electromyographic Patterns Of Tai Chi Gait
169	Andrej Olenšek	Toe-Walking In Intact Individuals Arising From Emulated Contractures Of Soleus, Gastrocnemius And Hamstring Muscles
170	Urs Wyss	High Range Of Motion Activities Of Daily Living: Differences In The Kinematics Between Hong Kong And Chennai, India Subjects
171	Marietta van der Linden	The Influence Of Subject Characteristics And Joint Kinematics On Function And Quality Of Life In Patients With Osteoarthritis Prior To Total Kee Replacement
172	Ge Wu	Control Of Center Of Pressure During Tai Chi Movement
173	Stephanie J. Nogan	Gait Biomechanics In An Obese Gastric Bypass Surgery Population: Preliminary Results
174	Kevin M. Cooney	Convergent Validity Of Goniometric And Motion Capture Techniques Used To Measure Tibial Torsion
175	Bih-Jen Hsue	Optimal Strategy Of Cane Use During Stair Ascent
176	L.W. Sun	Movement Coordination Between The Lumbar Spine And Hip When Putting On A Sock
177	Hsiu-Chen Lin	Biomechanics Of The Lower Limb During Stair Locomotion In Subjects With Anterior Cruciate Ligament Reconstruction
178	Houng-Chaung Hsu	Influence Of Functional Knee Braces On Lower Limb Mechanics During Stair Locomotion In Patients With Anterior Cruciate Ligament Deficiency

(session continued on next page)

Thursday, August 4 3:45 PM

Poster Session: Clinical and Functional Movement Analysis (continued) UC 201

179	Chen-Yu Lo	Hip And Knee Joint Moment Analysis During Obstacle Crossing In Patients With Unilateral Total Knee Replacement
180	Samuel R. Ward	Patella Alta Is Associated With Patellofemoral Malalignment
181	S. Lee Hong	Dynamical Differences Between Normal And Stereotypic Body Rocking
182	Ruxandra Marinescu	Pediatric Gait Analysis: A Call For Standardization
183	Catherine Stevermer	Investigation Of Sit-To-Stand Performance For Individuals After Total Knee Arthroplasty
184	Victoria Chester	Gait Patterns Of Children With Hypotonia
185	Nicole A. Wilson	Bracing Alters Patellofemoral Contact Mechanics During The Gait Cycle: A Dynamic Biomechanical Study
186	Bee-Oh Lim	Stepping-Over Gait Characteristics In Children With Down Syndrome
187	Nathalie Crevier-Denoix	Effects Of Corrective Shoeings On The Equine Superficial Digital Flexor Tendon Load, Evaluated By A Non-Invasive Ultrasonic Technique

Poster Session: Falling and Fall Prevention UC 201

188	Hyun Gu Kang	Postural Local Dynamic Stability Is Not Predictive Of That During Locomotion
189	Bing-Shiang Yang	Adaptive Changes In Stepping Up And Onto Laterally-Compliant Structures: Age Difference In Healthy Males
190	Chou You-Li	The Correlation Between Energy Absorption Ratio And Pain Score Of The Upper Extremity Under Different Fall Heights
191	Heng-Ju Lee	Dynamic Stability And Energy Efficiency During Different Self-Selected Walking Speeds
192	Karrie L. Hamstra-Wright	Skill Acquisition Occurs During Fall-Preventive Motor Response Training
193	Karen L. Reed-Troy	Wrist Kinetics During Impact Are Affected By Hand Symmetry
194	Lloyd R. Wade	Gait Kinematics On An Elevated Inclined Surafce
195	Youngho Kim	Contributions Of Lower Limb Joints To Support The Body In Unexpected Step-Down Walking
196	April Chambers	Anticipation Of Slippery Floors: Muscle Onsets And Co-Contraction Of The Stance Leg
197	Chien-Ju Lin	Control Of Stability During Slope Lateral Walking
198	Kurt DeGoede	Reaction To A Loss Of Balance In Healthy Menopausal-Aged And Young Women
199	Alaa A. Ahmed	An Analysis Of Losses Of Balance During Tandem Stance On A Narrow Beam
200	Peter Davidson	Arm Fracture In Children's Falls
201	Noriyuki Yamamoto	The Characteristics Of Gait Pattern On The Slippery Surface

Thursday, August 4 3:45 PM

Poster Session: Biomechanics of Jumping UC 201

202	Ikko Omura	Analysis Of The Approach Run And The Takeoff In The Japanese Junior Long Jumpers
203	Chenfu Huang	Optimal Extra Weight On Hands Enhance Standing Jump Performance
204	Yu Liu	Application Of Artificial Neural Network To Predict The Joint Torque Of Lower Limbs Using The Parameters Of Ground Reaction Force During Vertical Jump
205	Sarah E. Kruger *Young Investigator Award finalist*	The Effect Of Load Scaling On The Coordination And Performance Of Countermovement Jumps.
206	Hiroyuki Koyama	Immediate Effects Of An Inclined Board As A Training Tool For The Takeoff Motion Of The Long Jump
207	Shinsuke Yoshioka	Effect Of Bilateral Asymmetry Of Lower Muscle Forces On Vertical Jumping Height: A Simulation Study
208	Yuya Muraki	Kinematic Analysis Of The Preparatory And Takeoff Motion In The Long Jump
209	Kenji Ohisshi	The Relationship Between Leg Length And Velocity Of Center Of Gravity During Contact Phase In The Long Jump
210	Saori Hanaki	Quantification Of Energy Absorbed By The Lower Extremity Depends On Endpoint Of The Impact Phase
211	Kathy J. Simpson	Approach Velocity Profiles Of Elite Male And Female Lower-Limb Amputee Long Jumpers
212	Witaya Mathiyakom	Generation Of Forward Angular Impulse In Tasks With Backward Translation
213	Jill McNitt-Gray	Regulation Of Reaction Force Direction And Angular Impulse During Jumping Tasks Via Redistribution Of Knee And Hip Net Joint Moments

Thursday, August 4 — 3:45 PM

Poster Session: Prosthetics and Orthotics — UC 201

214	Curtis S. To	A Hydraulic Approach To The Development Of A Variable Reciprocating Hip Mechanism For The Reciprocating Gait Orthosis
215	Margrit R. Meier	Obstacle Course Performance: Comparison Of The C-Leg To Two Conventional Knees
216	Glenn K. Klute	Lower Limb Amputee Activity Uneffected By Shock-Absorbing Pylon Or C-Leg Knee
217	Bae Tae Soo	How Much Do The Hip Abductors Contribute To The Gait Stability For Amputee With A Prosthesis?
218	Kang Sung Jae	Kinetic Gait Analysis Of Powered Gait Orthosis Using Fuzzy Logic Controller
219	Michael S. Orendurff	C-Leg Knees Do Not Improve Stance Phase Knee Flexion Or Walking Efficiency In Older Transfemoral Amputees
220	Jeremy D. Smith	Intersegmental Dynamics Of The Swing Phase Of Walking In Trans-Tibial Amputees
221	Zaineb Bohra	Neuromuscular Adjustments To Hopping With An Elastic Ankle-Foot Orthosis
222	Stephen Cain	Motor Adaptation To A Powered Ankle-Foot Orthosis Under Foot Switch Control
223	Dewen Jin	Investigation On Slip Danger To Trans-Femoral Prosthesis User
224	Jiankun Yang	Lower Extremity Muscle Activities Of Trans-Femoral Amputees When A Slip Occurs In Gait
225	Slavyana Milusheva	Virtual Models And Prototype Of Individual Ankle Foot Orthosis
226	Siobhan Strike	One-Foot Vertical Jump With Approach In Unilateral Transtibial Amputees
227	Wei-Ching Hung	The Finite Element Analysis Of Interface Stresses Between The Foot And Ankle-Foot Orthoses

Poster Session: Vascular Mechanics and Fluid Flow — UC Atrium

228	Fariborz Alipour	Measurement Of Turbulence In Glottal Flow
229	Zhi-Yong Li	Identifying Vulnerable Plaques Using MRI-Based Finite Element Analysis
230	Po-Kae Fung	Cardiac Catheter With Variable Head Curvature Actuated By Ipmc (Ionic Polymer-Metal Composite)
231	Jeong Chul Kim	The Paraquat Adsorption Pattern And Hemodynamic Properties Of Charcoal Column In Hemoperfusion
232	Yihkuen Jan	A Time-Frequency Approach Using Wavelets To Study Week-To-Week Variability In Blood Flow Oscillations
233	Zaher Kharboutly	Blood Flow Simulation In An Arterio-Venous Fistula
234	Alejandro Roldan	Simulation Of Blood Flow And Deformations Of Mechanical Heart Valves Using Boundary Integral Techniques
235	James Furmato	Repeatability Of DRT4 Lase Dopler Microvascular Measurements
236	Henry Yu Chen	3-D Finite Element Models Of Arterial Clamping With Fluid-Structure Interactions - A Step Toward Simulating Cardiovascular Surgery
237	Rachamadian Wulandana	Modeling Cerebral Aneurysm Formation And Associated Structural Changes

Thursday, August 4 3:45 PM

Poster Session: Instrumentation UC Atrium

238	Joong Yull Park	Numerical Analysis On Bipolar Hepatic Radio-Frequency Ablation
239	Anita Chan	A New Portable 3-D Gyroscope System For The Evaluation Of Upper Limb Function
240	Elizabeth Ann Hassan	Comparison Of Upperlimb Kinematics Collected By Electromagnetic Tracking Versus Digital Camera Systems In A Gait Analysis Lab
241	Véronique Feipel	Use Of Strain Gauge In The Evaluation Of The Constraint Of Tibio-Femoral Joint In Dynamic Movement: Development, Feasibility And First Results
242	Higa Masaru	Measurements And Modeling Of The Descending Colon
243	Peter Dabnichki	Emotionally-Responsive Clothing For Leisure And Exercise Activities
244	Gail Perusek	Exercise Countermeasures Laboratory At NASA Glenn Research Center - A New Ground-Based Capability For Advancing Human Health And Performance In Space
245	Peter R. Cavanagh	Lower Extremity Loading During Entire Days Of Space Flight
246	Cody Bliss	An Instrumented Scaffold To Monitor Loading Of Cartilage In The Knee Joint
247	Metin Yavuz	A Comparison Of Various Digital Filtering Techniques Applied On Plantar Surface Pressure and Shear Data

Poster Session: Cellular Biomechanics UC Atrium

248	Shigehiro Hashimoto	Measurement Of Red Blood Cell Deformability With Counter Rotating Rheoscope
249	Diane R. Wagner	Cytoskeletal Tension Enhances Osteogenic Differentiation Of Adipose-Derived Mesenchymal Cells
250	T.S. Keller	Influence Of Pericellular Matrix On Cell Strains In The Intervertebral Disc
251	Brandon J. Ausk	Exploring Mechanical Loading Induced Ca2+ Oscillations In Osteocytes
252	Rachna Sah	Cell Deformation In Response To Local Matrix Strain
253	Sylvie Wendling-Mansuy	Cytoskeleton Dynamical Behavior Approched By A Granular Tensegrity Model

Thursday, August 4 3:45 PM

Poster Session: Impact Biomechanics UC Atrium

254	Erica Doczy	Neck Muscle Activity During Short Duration Impacts
255	Jui-Yi Tsou	The Applied Force Patterns Of Chest Compression During Cardiopulmonary Resuscitation
256	Zhifeng Kou	A Comprehensive Approach To Studying Mild Traumatic Brain Injuries In Motor Vehicle Crashes
257	David E McNeely	Cumulative Head Accelerations In College Football Players Differ By Position
258	Lars Janshen	Muscular Stabilisation Of The Head In Car Collisions
259	Sylvie Wendling-Mansuy	Evidence For The Involment Of Muscular Pre-Activation In Impact Loading And In Shock Wave Transmission
260	Elizabeth Drewniak	Do Mechanical Properties Of Chest Protectors Correlate With The Incidence Of Ventricular Fibrillation In A Sudden Death (Commotio Cordis) Swine Model?
261	Cheng-Yu Wu	Computer Simulation Of Motorcycle-Car Accident
262	Wunching Chang	Injury Incidence And Footwear Satisfaction Of Male Competitive Ballroom Dancers
263	David Raymond	A Parametric MADYMO Analysis For The Determination Of Seat Belt Usage In A Frontal Collision
264	Mark B. Sommers	An Organotypic Model Of Traumatic Brain Injury Caused By Acceleration-Induced Shear Strain
265	David Raymond	Occupant Kinematic Analysis Of An Unbelted Minivan Passenger: A Free Body Approach
266	Darrin Richards	Repetitive Head Loading: Accelerations During Cyclic, Everyday Activities
267	Abir Chakraborty	Impact Response Analysis Of Thorax By The Thin-Layer Method
268	Mariusz Ziejewski	Modified Methodology To Determine Head Acceleration

Poster Session: Spine 3 UC Atrium

269	Munier Hossain	A Biomechanical Model Of Sacro-Iliac Joint Dysfunction As A Cause Of Low Back Pain
270	Takahiro Ishii	In Vivo 3D Intervertebral Motion Analysis Of The Cervical Spine In Lateral Bending Using 3D-MRI
271	Veronique Feipel	Head Repositioning Accuracy In Patients With Whiplash-Associated Disorders
272	Christine Herrmann	Increase In Amplitude Of Paraspinal Muscle Reflexes Following Lumbar Extensor Fatigue
273	Michael W. Olson	Activation Patterns Of Trunk Muscles During Cyclic Flexion-Extension
274	Kyungsoo Kim	Increase Of Lumbar Spinal Staiblity Under Follower Load In Sagittal Plane
275	Erik Cattrysse	In Vitro 3D Arthrokinematic Analysis Of Coupled Motions In The Atlanto-Axial Joint During Axial Rotation And Lateral Bending
276	Melanie Bussey	Motion Characteristics Of The Innominate-Hip Complex
277	Naira Campbell-Kyureghyan	Variation In Average And Peak Lumbar Disc Stresses By Level During Flexion Using A Combined Experimental And Finite Element Approach

278	Hongmei Jin	Measurement Of Difference Between Left And Right Rib Lengths On Scoliosis
279	Scott MacKinnon	Motion Induced Interruptions Increase Thoracolumbar Kinematics
280	Angela Viegas Andrade	Functional And Structural Cervical Spine Dysfunctions With Temporomandibular Disorders
281	Sam Augsburger	Analysis Of Inter-Segment Spine Kinematics During Trunk Motion
282	Paul J. Moga	Prevalence Of Back Pain In Seven Sports Based On Self-Reporting By A Sample Of 2268, 8-To-18 Year Old Adolescent Athletes
283	Jamie R. Williams	Comparison Of The Biomechanical Response Of A Lumbar Motion Segment To Loading And Unloading When Loads Are Applied Suddenly And At Normal Lifting Speeds
284	Bonnie Y.S. Tsung	Influence Of Posterio-Anterior Mobilization On Different Level Of The Spine
285	Steve Brown	Muscle Force-Stiffness Characteristics Influence Joint Stability: A Spine Example
286	Véronique Feipel	Upper Cervical Spine Modelling: In Vitro 3D Kinematics
287	Wafa Skalli	Inter Individual Variation In Trunk Muscles Geometry Of Asymptomatic Subjects In Standing Position.
288	Christian Larivière	Back Muscle Fatigue During Submaximal Intermittent Isometric Contractions: The Influence Of Neuromuscular Activation Patterns
289	Jim Dickey	Novel Approach For Studying Human Response To Whiplash-Like Perturbations
290	Chad A. Sutherland	The Accuracy Of Using Postural Assessment To Determine Cumulative Exposure
291	Ryan Milks	Biomechanical Comparison Of Adjacent Level Segmental Motion In The Cervical Spine With Varying Degrees Of Lordotic Alignment
292	L.W. Sun	The Accuracy Of Surface Measurement For Osteoporotic Spine Motion Analysis
293	Jaap van Dieen	Modeling Of Pelvis And Thorax Rotations In Healthy And Pathological Gait
294	L.W. Sun	Automatic Measurement Of Lumbar Spinal Kinematics From Lateral Radiographs
295	Jaap van Dieen	Can Repetitive Shear Loading Of Spinal Motion Segments Cause Disc Injury?

Thursday, August 4 3:45 PM

Poster Session: Muscle UC Atrium

296	Can A. Yucesoy	Acute Effects Of Intramuscular Aponeurotomy Assessed By Finite Element Modeling
297	Sharon Bullimore	Effect Of Stretch Or Shortening Amplitude On Subsequent Isometric Muscle Force
298	Kazuyuki Mito	Influence Of Skin Temperature On Mechanomyogram Of M. Biceps Brachii
299	Huub Maas	In Vivo Fascicle Length Of Cat Medial Gastrocnemius And Soleus Muscles During Slope Walking
300	Ian Loram	Measuring Continuous Changes In Human Muscle Length, In Vivo, Using Ultrasound
301	Laura Frey Law	Accuracy Of Three Mathematical Models vs. Human Trained Paralyzed Muscle
302	Huub Maas	The Origin Of Mechanical Interactions Between Adjacent Synergists In Rat
303	Phu Hoang	Non-Invasive Measurment Of Passive Length-Tension Properties Of Human Gastrocnemius Muscle Fascicles, Tendons, And Whole Muscle-Tendon Units In Vivo
304	Tyler Brown	The EMG-Torque Relationship Of The Knee Extensors During Acute Fatigue
305	Hiroshi Arakawa	Relationship Between Moment-Joint Angle Characteristics Of Knee Flexion And Architecture Of Hamstrings Muscles In Human
306	Toshiaki Oda	In Vivo Muscle Fiber Kinetics During Tetanic Contraction
307	Gregory Sutton	Neuromodulation Changes The Biomechanics And Capabilities Of The Aplysia Feeding Muscle I2
308	Kazushige Sasaki	Shortening Velocity Of Human Plantar Flexors In Vivo And Its Relation To Contraction Intensity And Knee Angle
309	Li Le	In Vivo Determination Of Muscle Architecture Parameters By Ultrasonography: Applications To The Brachialis Muscle Of Normal Subjects And Persons After Stroke
310	Norihide Sugisaki	Behavior Of Aponeurosis And External Tendon Of Medial Gastrocnemius Muscle During Dynamic Plantar Flexion Exercise
311	Nadja Schilling	3D-Fiber Type Distribution In Back Muscles In Small Mammals
312	Toshiyuki Kurihara	Three-Dimensional Architecture Of Human Gastrocnemius And Tibialis Anterior Muscles During Isometric Actions
313	Sampath Gollapudi	Temperature-Dependent Mechanical Properties Of Human Soleus Muscle Fibers
314	Timothy J. Brindle	Sonographic Measures Of Gastrocnemius Length With Two-Joint Passive Movements
315	Lei Cui	Recruitment Order Has Little Effect On The Short-Range Stiffness
316	Yoshiho Muraoka	Heterogeneity Of Change In Muscle Circulation Among Synergists During Dynamic Muscle Action
317	Taku Wakahara	Effects Of Knee Joint Angle On The Force-Length And Velocity Characteristics Of Gastrocnemius Muscle

Thursday, August 4 3:45 PM

Poster Session: Posture and Balance UC Atrium

318	Yun Wang	Stepping From A Narrow Support
319	Kevin Pline	Effects Of Lumbar Extensor Fatigue And Circumferential Ankle Pressure On Ankle Joint
320	Alan Walmsley	Measures Of Postural Stability During Quiet Stance
321	Cristina Sa	Comparative Balance Analysis Between Indoor Climbing Individuals And Control Using Posturography Test
322	Chris Hass	The Relationship Between Knee Extensor Strength And Balance In Parkinson's Disease
323	Attila A. Priplata	Noise-Enhanced Balance Control: The Worse You Are The Better You Get
324	Ellen Rogers	Paraspinal Reflex Behavior As A Function Of Trunk Posture
325	Wen-Chieh Yang	Development Of The Portable Posture Training Device
326	Ge Wu	Postural Control Strategies In People With And Without Peripheral Neuropathy - A Neural Network Approach
327	Clarice Tanaka	Postural Control Under Visual And Proprioceptive Perturbations During Double And Single Limb Stance
328	Haruhiko Sato	Postural Sway On A Sliding Platform: Assessing Spatial And Temporal Stability
329	Clarice Tanaka	Postural Control In Skilled Athletes In Response To Unexpected Perturbation
330	Jeffrey Schiffman	Soldiers' Loads Affect Random Walk Of Center Of Pressure
331	Alessandro Telonio	Effect Of Perturbation Direction On The Threshold Of Balance Recovery
332	Chiung Ling Chen	The Body Center Of Mass Displacement During Various Types Of Support Surface Perturbation
333	Liliam F. de Oliveira	Anticipation Mechanism And Influence Of Fatigue In Mediolateral Stabilogram
334	Kei Masani	Smaller Sway During Quiet Stance Attributes To Effective Use Of Body Velocity
335	Koichi Shinkoda	Characteristics Of Standing And Anterior Tilting Postures In Relation To The Time Of Day
336	Michelle Heller	The Effects Of External Weight Carriage On Postural Stability
337	Jianhua Wu	Fractal Dynamics Of Human Stabilogram In Quiet Stance
338	Marc-Andre Cyr	Effect Of Recovery Restrictions On The Threshold Of Balance Recovery - Prelimnary Results
339	Isabelle Patenaude	A Paradigm To Assess Electromyographic And Kinematic Responses During Anteroposterior Surface Translations In Sitting Following Whiplash Injuries
340	Mark Musolino	Postural Sway Adaptation During Initial Exposure To Periodic And Non-Periodic Optic Flow
341	Esther Kim	Effects Of Arch Height And Accomodation On Postural Stability
342	Hugo Centomo	Postural Control And Postural Mechanisms In Obese And Control Children.

Thursday, August 4 3:45 PM

Poster Session: Bone UC Atrium

343	Thomas Pressel	Mechanical Properties Of Canine Trabecular Bone
344	Andrew Briggs	Distribution Of Bone Mineral Density In Thoracic And Lumbar Vertebrae: An Ex Vivo Study Using Dual Energy X-Ray Absorptiometry (DXA)
345	Sylvie Wendling-Mansuy	Regeneration Of Skeletal Tissues On Joint
346	Sylvie Wendling-Mansuy	Bone Remodeling Model Of A Basic Multicellular Unit
347	Amy Johnson	A Synthetic Model For Mechanical Evaluation Of Vertebral Bone
348	Mary Lou Bareither	Bone Mineral Density Of The Proximal Femur Is Not Related To Dynamic Joing Loading During Locomotion
349	GuoXin Ni	Nanoindentation Study Of Interfaces Between Strontium-Containing Hydroxyapatite Bone Cement And Bone In A Rabbit Hip Replacement Model
350	Won Joo	Cross-Modal Effect Of Damage On Cortical Bone Strength
351	Arzu Gul Tasci	Biomechanical And Histological Evaluation Of Estrogen, Raloxifen, Vitamin K2 And Their Combinations In The Treatment Of Osteoporotic Bone
352	J.E. Brouwers	Resonant Frequency Shifts In Osteotomised Goat Tibiae
353	Hans A. Gray	Validated Finite Element Model Of A Composite Tibia
354	Annie Ming-Tzu Tsai	Effect Of Single Pulsed Electromagnetic Fields Stimulation On The Proliferation Of Mesenchymal Stem Cells
355	Brandi Row	Load-Specific Relationships Between Muscular Power And Bone Mineral Density
356	Cheryl Dunham	Mechanical Properties Of Cancellous Bone Of The Distal Humerus
357	Ger Reilly	Sequential Labelling And Acoustic Emission Analysis Of Damage Occurring In Cortical Bone During Indentation Cutting
358	Jaw-Lin Wang	Regional Variation Of Bone Strain Creep Of Vertebral Body During Repetitive Loading - An In Vitro Porcine Biomechanical Model
359	Renfeng Su	Bone Mechanics From Finite Element Modeling And Micro-Computed Tomography: Validation Of An Orthotropic Material Model With Fused Deposition Modeling
360	Boon Horng Kam	In Vivo Micro CT Scanning Of A Rabbit Distal Femur
361	Jessica Goetz	In Vitro Validation Of Thermal Finite Element Analysis Of Cryoinsult Delivery For Emu Femoral Head Necrosis
362	Stacey A. Meardon	The Effects Of Mechanosensitivity On The Prediction Of Bone Formation Rate
363	Roland Steck	Bridging Organ- And Tissue Level Computational Models Of Bone To Improve Load-Induced Fluid Flow Predictions
364	Nils Goetzen	The Mouse As A Model Organism For Human Skeletal Diseases - A Biomechanical Study
365	Wafa Tawackoli	Vibrational Analysis Of Normal And Osteopenic Trabecular Bone Using Rapid Prototype Duplicates
366	Junghwa Hong	Measurement Sysytem With Nano-Resolution Of Microscopic Bone Propery

367	Eric Anderson	Novel In Silico Virtual & Scaled Up Physical Model Platform To Bridge Gaps In Understanding In Situ Flow Regimes at Multiple Length Scales In Bone
368	David Hudson	Lower Limb Structure And Function Predict Bone Density Of The Proximal Tibia

Thursday, August 4 3:45 PM

Poster Session: Muscle and Exercise UC Atrium

369	Kristina Calder	Practice Distribution And The Aquisition Of Maximal Isometric Elbow Flexion Strength
370	Hiroshi Akima	Neuromuscular Adaptation In Human Calf After Disuse Evaluated By Muscle FMRI And EMG
371	Francisco J. Vera-Garcia	Trunk And Shoulder Muscle Response Comparing One Repetition Maximum Bench And Standing Cable Press
372	Ken B. Geronilla	Age Affects Eccentric Muscle Performance In Vivo During A Chronic Exposure Of Stretch-Shortening Cycles
373	Marco Aurelio Vaz	Long Term Model Of Botulinum Toxin-Induced Muscle Weakness In The Rabbit
374	Sean P. Flanagan	The Effect Of Movement Speed And External Load On Joint Contributions During Lower Extremity Extensions
375	Wen-Lan Wu	The Effects Of Periodized Complex Training Programme On Military Physical Fitness And Fighting Ability
376	Phu Hoang	Passive Length-Tension Properties Of Human Gastrocnemius Change After Eccentric Exercise
377	Kenneth Meijer	A Cross Sectional MRI Study Of The M. Rectus Femoris Morphology In Cyclists, Runners And Sprinters
378	Ben Meyer	A Comparison Of Hip Extension Torques In Conventional And Split Squat Exercises
379	William Bertucci	Validity Of The New Powertap Powermeter And Axiom Cycle Ergometer When Compared With An SRM Device
380	Gustavo Nunes Tasca Ferreira	Impact Of Flexibility On Muscular Performance Of The Knee
381	Jean L. McCrory	Acute Muscle Adaptations To A Resistance Exercise
382	Tetsuro Muraoka	Effect Of 20 Days Of Bed Rest On Passive Mechanical Properties Of Human Gastrocnemius Muscle Belly
383	Dean Hay	Human Bilateral Deficit During Dynamic, Multi-Joint Leg Press Movement
384	Mingfeng Kao	The Validity Of Active Squat Keen Joint Propriception Test
385	Michael Duffey	Fatigue Effects On Bar Kinematics During The Bench Press
386	Raghavan Gopalakrishnan	Effects Of Long-Term Space Flight On Muscle Volume

Thursday, August 4 — 3:45 PM

Poster Session: Hand and Wrist UC Atrium

387	Fan Gao	Does Human Hand Perform Like A Robotic Gripper? -- An Examination Of Internal Forces During Object Manipulation
388	Xun Niu	Effects Of The Grasping Force Magnitude On The Individual Digit Forces During Prehension With Five Digits
389	Fong-Chin Su	Thumb Muscle Forces In Jar Opening
390	Pablo-Jesús Rodríguez-Cervantes	A Virtual Tool For The Clinical Planning Of The Ulnar Palsy Treatment
391	Chris Ugbolue	Kinematics Of Mouse Scrolling
392	Ajay Gupta	Factors Affecting Lunate's Sagittal Alignment
393	Jennifer Di Domizio	The Effects Of Wrist Splinting On Muscle Activity During A Hand Grip Task
394	Asimakis Kanellopoulos	An Investigation Of External Loading Patterns Applied During Maximal Grip
395	Wei Zhang	Accurate Production Of Patterns Of The Total Moment By A Set Of Fingers
396	Warren G. Darling	Perception Of Hand Motion Direction Uses A Gravitational Reference
397	Jeremy Mogk	Modeling Extrinsic Finger Flexor Tendon Kinematics
398	Jae Kun Shim	Enslaving Effects Of Finger Movement On Pressing Forces Of Other Fingers
399	Jessica Woodworth	Impact Of Restricted Pip Joints On MCP Joint Motion In The Human Hand

Thursday, August 4 — 3:45 PM

Poster Session: Joint Mechanics UC Atrium

400	James Cubillo	Numerical Analysis Of A Femur Resurfacing Cup
401	Natasha Lee Shee	In-Vitro Testing Of Knee Joints Using Robotics: Computer Programming Theory
402	Ralph Howald	Factors Affecting The Cement Penetration Of A Hip Resurfacing Implant: An In-Vitro Study
403	Raed Itayem	The Role Of The Femoral Stem In The Stability Of A Metal On Metal Hip Resurfacing Implant. An RSSA Study
404	Lijkele Beimers	Subtalar Joint Kinematics In Healthy Individuals Using Computed Tomography
405	Thomas J. Withrow	Lack Of Hamstring Tension Causes Increased ACL Strain In A Simulated Jump Landing
406	Shahram Amiri	A Simplified Topology For The Tibial Plateau And Meniscal Surfaces And The Role Each Of Its Geometric Features Play In Guiding The Passive Motion
407	Mariana Kersh	Deformation Patterns From A Pre-Clinical Patellar Component Test
408	Andrew R. Fauth	3D Geometrical Optimization Of The Talar Dome
409	Hannah J. Lundberg	Quantifying Fluid Ingress To The Joint Space During Total Hip Implant Subluxation
410	Andrew R Hopkins	Development Of An FE Model Of Uni-Compartmental Knee Replacement
411	Matthew Moran	Computational Assessment Of Anteroposterior Laxity Following Partial PCL Release In Cruciate-Retaining TKR
412	Jihui Li	Initiation And Propagation Of Fatigue Microcracks From A Defect In A Cemented Total Hip Arthroplasty
413	Elena Varini	Primary Hip Stem Micromotion Assessment: Correlation Between Rasp And Stem Stability
414	Frances T. Sheehan	The Talocrural And Subtalar Helical Axes Are Not Fixed During Plantarflexion
415	Robert H. Deusinger	Comparison Of Arthrometer (Passive) And Functional Activity (Active) Anterior Tibial Displacements
416	Ajit Chaudhari	Patellar Ligament Insertion Angle Influences Quadriceps Use During Stair Climbing: Effect Of An Anterior Cruciate Ligament Deficit
417	Jacob Scott	The Effect Of Tibiofemoral Loading On Proximal Tibiofibular Joint Motion

Friday, August 5 — 8:30 AM

Keynote Lecture — Waetjen Auditorium

Chair: Ton van den Bogert

8:30	Martyn Shorten	Cushioning: Mechanics and Biomechanics of Attenuating Loads on the Human Body

Friday, August 5 — 9:30 AM

Rehabilitation — Waetjen Auditorium

Chair: John Jeziorowski, Glenn Klute

9:30	Li Li	Body Weight Support System Influence On The Patterns Of Vertical Forces Applied To The Body
9:45	Janessa Drake	Do Exercise Balls Provide A Training Advantage For Trunk Extensor Exercises? A Biomechanical Evaluation.
10:00	Tine Alkjaer	Biomechanical Analysis Of The Walking Pattern In Healthy Subjects With And Without Rollator
10:15	Janice Flynn	Trunk Muscle Activation Patterns Comparing Cable Press And Body-Blade Exercises

Motor Control – Upper Extremity — UC 6

Chair: Pat Crago, Andy Karduna

9:30	Jae Kun Shim	Prehension Synergies: Trial-To-Trial Variability And Principle Of Superposition During Static Prehension In Three Dimensions
9:45	Yin Fang	Different Motor Planning During Eccentric And Concentric Elbow Muscle Contractions
10:00	D.A. Kistemaker	An Intermittent EP-Model For Fast Point-To-Point Movements
10:15	Eric Perreault	Influence Of Voluntary Posture Selection On Endpoint Stiffness

Muscle Adaptation MC 201

Chair: Véronique Feipel, Paul Sung

9:30	Robert G. Cutlip	Characterization Of Changes In Eccentric Work In Vivo During A Chronic Exposure Of Stretch-Shortening Cycles: Age Effects
9:45	Timothy A Butterfield	The Interaction Between Surface Grade And Exercise Duration For Serial Sarcomere Number Adaptations Following Treadmill Running In Rats
10:00	Sherry Di Jorio	Mitochondrial Adaptation During Rehabilitation And Its Importance In Musculoskeletal Modeling
10:15	Victor Valderrabano	Fiber Selective Muscle Atrophy In Ankle Arthritis

Knee Replacement MC 202

Chair: Dwight Davy, Kiyonori Mizuno

9:30	Christopher J Barr	Knee Kinematics Of Total Knee Replacement Patients: Pre And Postoperative Analysis Using Computer Generated Images
9:45	Monika Zihlmann	3D Kinematic And Kinetic Data Of Total Knee Arthroplasty During The Stance Phase Of Level Walking Using A Moving Video-Fluoroscope
10:00	Elise Laende	Migration Of Medial-Pivot And Posterior Stabilized Implants
10:15	Brendan Joss	Gait Affects Tibial Component Migration In Unicondylar Knee Arthroplasty

Sport 4 UC 1

Chair: Brian Davis, Stefan Duma

9:30	Karine J. Sarro	Rib Cage Motion Patterns In Swimmers During Respiratory Maneuvers
9:45	Hiroyuki Nunome	Segmental Dynamics Of Soccer Instep Kicking
10:00	Ricardo M. L. Barros	Representation And Analysis Of Soccer Players' Trajectories
10:15	Sumiyo Toki	Quantitative Match Analysis Of Soccer Games With Two Dimensional DLT Procedures

Friday, August 5 11:00 AM

Musculoskeletal Modeling Waetjen Auditorium
Chair: Richard Neptune, Douglas Pedersen

11:00	Kotaro Sasaki	Muscle Contributions To The Flight Phase In Running
11:15	Robert F. Kirsch	Musculoskeletal Modeling Of An EMG-Based Neuroprosthesis For Arm Function
11:30	Samuel R. Ward	Scaling Of Human Lower Extremity Muscle Architecture To Skeletal Dimensions
11:45	Clayton Adam	Gravity-Induced Torsion And Vertebral Rotation In Idiopathic Scoliosis
12:00	Serge Van Sint Jan	3D Muscle Moment Arms Using Musculoskeletal Modeling
12:15	Veronica J. Santos	Implementing Data-Driven Models Of The Human Thumb Into A Robotic Grasp Simulator To Predict Grasp Stability

Methods in Gait Analysis UC 6
Chair: Gordon Robertson, Kit Vaughan

11:00	At Hof	Handling Of Impact Forces In Inverse Dynamics In Landing After A Jump
11:15	Lei Ren	A Three-Dimensional Whole-Body Walking Model Based Only On Gait Kinematics
11:30	Raziel Riemer	An Analysis Of Uncertainties In Inverse Dynamics Solutions For Gait
11:45	George Chen	Induced Acceleration Contributions To Locomotion Dynamics Are Not Physically Well-Defined
12:00	Zachary Domire	Comparison Of Methods Used To Determine Induced Vertical Ground Reaction Force
12:15	Ben Stansfield	Optimisation Or Antagonism? Muscle Force Solutions In The Lower Limb

Hand and Wrist 2 MC 201
Chair: Kai-Nan An, Zong-Ming Li

11:00	Zong-Ming Li	Gender Difference In Carpal Tunnel Compliance
11:15	Haoyu Wang	Evaluation Of Five Ligamentous Stabilizers Of The Scaphoid And Lunate
11:30	Fong-Chin Su	Joint Load Of The Thumb In Jar Opening
11:45	Asimakis Kanellopoulos	An Investigation Of Wrist Joint Function Under Load
12:00	Haoyu Wang	Variations In Scapholunate Gap With Various Types Of Ligamentous Sectioning
12:15	Joseph D. Towles	Use Of The Long Flexor And Intrinsic Thumb Muscles To Restore Lateral Pinch In The Tetraplegic Thumb: A Cadaver Study

Knee Mechanics 2 MC 202

Chair: Scott McLean, Jack Engsberg

11:00	Sietske Aalbersberg	Co-Contraction In ACL Deficient Subjects
11:15	Janie Astephen	Postural Gait Changes Are Seen With Severe, Not Moderate, Knee Osteoarthritis
11:30	Hyung-Soon Park	Passive Knee Joint Properties In Tibial Rotation In Men And Women
11:45	Aaron Derouin	Knee Stability: Mechanical Contributions Of Individual Muscles
12:00	Frances T. Sheehan	In Vivo Patellar Tendon Moment Arm And Tibial-Femoral Helical Axis
12:15	Anneliese D. Heiner	A Device To Measure In Vivo Translational And Rotational Laxity Of Rabbit Knees

Running Injuries UC 1

Chair: Irene McClay Davis, Elizabeth Hardin

11:00	Mark Creaby	Comparison Of Static And Dynamic Biomechanical Measures In Military Recruits With And Without A History Of Third Metatarsal Stress Fracture
11:15	Siriporn Sasimontonkul	Estimation Of Stresses And Cycles To Failure Of The Tibia During Rested And Fatigued Running
11:30	Tracy Dierks	Kinematics Of Runners With And Without Patellofemoral Pain During Prolonged Treadmill Running
11:45	Clare Milner	Does Free Moment Predict The Incidence Of Tibial Stress Fracture?
12:00	Wolfgang Potthast	Influence Of Muscle Pre-Activation And Knee Joint Angle On Axial Tibio-Femoral Shock Transmission
12:15	Robert J. Butler	Does Footwear Affect Lower Extremity Variability In High And Low Arched Runners?

Friday, August 5 1:15 PM

Keynote Lecture Waetjen Auditorium
Chair: Mark Grabiner

1:15	J.J. Collins	Noise-Enhanced Sensorimotor Function

Friday, August 5 2:15 PM

Motor Control Waetjen Auditorium
Chair: Jim Collins, Guang Yue

2:15	Scott K. Lynn	Is Lower Limb Joint Proprioception Systemic?
2:30	Daniel M. Krainak	FMRI Brain Imaging During Six DOF Mechanical Measurements Of Upper Limb Isometric Contractions
2:45	Joseph S. Soltys	Velocity Sense In The Lumbar Spine Is Modulated By The Vestibular And Proprioceptive Systems
3:00	J. Maxwell Donelan	Sensory Regulation Of Muscle Activity During Walking In Conscious Cats
3:15	Dirk Jan Veeger	Proprioceptive Disturbances In RSI: A Comparison With CRPS

Locomotion Energetics UC 6
Chair: Art Kuo, Steve McCaw

2:15	Rodger Kram	Metabolic Costs Of Forward Propulsion And Leg Swing At Different Running Speeds
2:30	Brian Umberger	Mechanical Efficiency During Walking At Different Stride Rates
2:45	Jiro Doke	Metabolic Cost Of Generating Force During Human Leg Swinging
3:00	Peter Gabriel Adamczyk	Metabolic Cost Of Walking Varies With Foot Roll-Over Radius
3:15	Manoj Srinivasan	Energetics Of Legged Locomotion: Why Is Total Metabolic Cost Proportional To The Cost Of Stance Work?

Falling and Fall Prevention MC 201
Chair: Jill McNitt-Gray, Mark Grabiner

2:15	Michael Madigan	Age-Related Joint Torque Analysis During Support Phase Of Single Step Recovery
2:30	Karen L. Reed-Troy	Recovery Responses To Surrogate Slips Are Different Than Actual Slips
2:45	Vivi M. Thorup	Ground Reaction Forces In Pigs During Gait On Dry And Greasy Floor
3:00	Lisa Case	Arrest Of Forward Falls Onto Outstretched Hands In Healthy Young Women
3:15	Charles Cejka	Control Of Reach-To-Grasp Reactions During Perturbed Locomotion In Familiar And Unfamiliar Environments: When Does Visual Fixation Of The Handrail Occur?

Knee Mechanics 3 MC 202

Chair: Stephen Piazza, Thor Besier

2:15	Yu Jen Chen	Validation Of A Three Dimensional Model To Quantify Patellofemoral Joint Forces
2:30	William Anderst	Assessment Of Functional Joint Space Repeatability During In Vivo Dynamic Loading
2:45	Josh MacNeil	Preservation Of Periarticular Cancellous Morphology And Mechanical Strength In Post-Traumatic Experimental Osteoarthritis By Antiresorptive Therapy
3:00	Kim McLaughlin	In Vivo Assessment Of Congruence In The Patellofemoral Joint Of Healthy Subjects
3:15	Elvis Chen	Ligament Estimation From In Vivo Knee Motion: An Inverse-Kinematics Model

Animal Biomechanics UC 1

Chair: Boris Prilutsky, Gail Perusek

2:15	Melanie Scholz	Scaling And Jumping: Gravity Loses Grip On Small Jumpers
2:30	Anne Su	Variability In The Direction Of Substrate Reaction Forces In The Locomotor Repertoire Of The Primate Lemur Catta
2:45	Monica A. Daley	Dynamic Stability In A Rough Environment: The Influence Of Initial Limb Posture On Body Dynamics During An Unexpected Perturbation
3:00	David Lee	Proximo-Distal Distribution Of Mechanical Work And Capacity For Elastic Energy Storage In The Limb Joints Of Running Goats
3:15	Peter Zani	The Energetics And Biomechanics Of Turtle Locomotion

Friday, August 4 4:00 PM

ISB President's Lecture Waetjen Auditorium

Chair: Brian Davis

4:00	Mary Rodgers	Rehabilitation & Biomechanics (Do The Locomotion)
5:00	CLOSING CEREMONY	

Presenters and Session Chairs

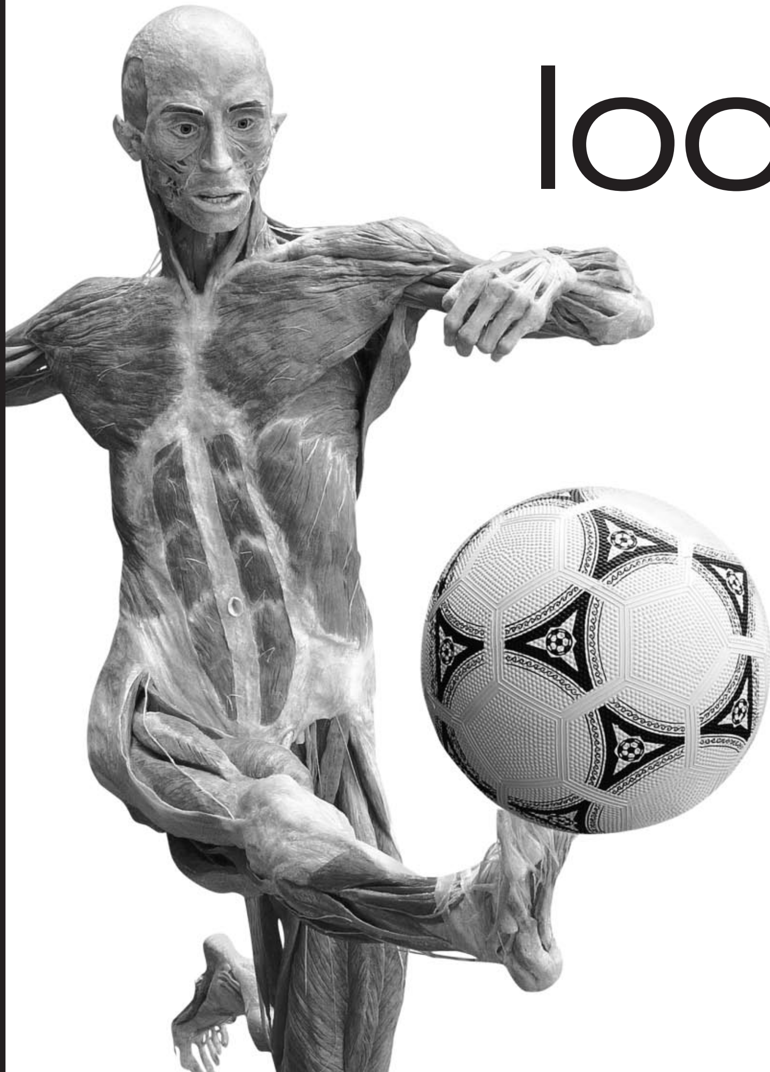

ISB

AMERICAN SOCIETY OF BIOMECHANICS
founded 1977

Sponsors

novel

KISTLER
measure. analyze. innovate.

NIKE

VICONPEAK

MotionAnalysis

Tekscan

DELSYS

Innovision Systems
INCORPORATED

NATIONAL INSTITUTES OF HEALTH

NON SOLUS
ELSEVIER

DEPARTMENT OF HEALTH & HUMAN SERVICES · USA

AMERICAN SOCIETY OF BIOMECHANICS
founded 1977

ISB

ISB/ASB 2005 Congress Overview

	Room A Waetjen Auditorium	Room B UC 6	Room C MC 201	Room D MC 202	Room D UC 1

Sunday July 31, 2005

3:00 PM	Opening Ceremony
4:00 PM	Wartenweiler Memorial Lecture: Bruce Latimer - Biomechanics and Evolution
5:00 PM	Welcome reception and barbecue - University Center

Monday August 1, 2005

	Room A	Room B	Room C	Room D	Room D
8:30 AM	Keynote Lecture: Don Chaffin				
9:30 AM	Ergonomics 1	Locomotion 1	Soft Tissue 1	Space Biomechanics	Bone 1
10:30 AM	Break - University Center				
11:00 AM	Ergonomics 2	Locomotion 2	Soft Tissue 2	Foot 1	Bone 2
12:30 PM	Lunch - University Center				
1:15 PM	Keynote Lecture: Andre Seyfarth				
2:15 PM	Legged Robots	Gait Analysis	Shoulder	Foot 2	Simulation
3:30 PM	Break - University Center				
4:00 PM	Pelvic Organ and Muscle Biomechanics	ISB Technical Group: 3D Analysis	ISB Technical Group: Shoulder	ISB Technical Group: Footwear	ISB Technical Group: Simulation
5:30 PM	NOVEL workshop on pressure distribution measurement - MC 201 (registration required)				

Tuesday August 2, 2005

	Room A	Room B	Room C	Room D	Room D
8:30 AM	Keynote Lecture: Julie Steele				
9:30 AM	Knee Injuries 1	EMG	Muscle Mechanics	Sport 1	Bone - Modeling
10:30 AM	Break - University Center				
11:00 AM	Knee Injuries 2	Gait and OA	Muscle In Vivo	Sport 2	Hip Replacement
12:30 PM	Lunch - University Center				
1:15 PM	Keynote Lecture: Masahiro Kurosaka				
2:15 PM	Knee Mechanics 1	Methods 1	Spine 1	Ankle	Head Injury
3:30 PM	Break and Poster Sessions - UC 201				
7:00 PM	Reception at Cleveland Museum of Natural History				

Wednesday August 3, 2005

	Room A	Room B	Room C	Room D	Room D
8:30 AM	ISB Promising Young Scientist Award: Constantinos Maganaris				
9:00 AM	ISB Clinical Biomechanics Award: Magnus Kjartan Gislason				
9:30 AM	ISB Young Investigator Awards	Posture and Balance 1	Spine 2	Lower Extremity Injury	Prosthetics and Orthotics
10:30 AM	Break - University Center				
11:00 AM	ISB Muybridge Award Lecture: Rik Huiskes				
12:00 PM	ISB General Assembly (until 12:45)				
12:00 PM	Lunch - University Center				
afternoon	Lab tours and excursions				
2-7 PM	Tekscan workshop on pressure distribution measurement - UC 364 (registration required)				

Thursday August 4, 2005

	Room A	Room B	Room C	Room D	Room D
8:30 AM	ASB Jim Hay Memorial Award Lecture: Mont Hubbard				
9:30 AM	ASB Young Scientist Awards	Gait Simulation	Functional Electrical Stimulation	Sport 3	Injury Biomechanics
10:30 AM	Break - University Center				
11:00 AM	Hand and Wrist 1	Diabetic Foot	Gait and Aging	Running	Wheelchair
12:30 PM	Lunch - University Center				
1:15 PM	ASB Borelli Award Lecture: Kai-Nan An				
2:15 PM	ASB Awards	Posture and Balance 2	Rehabilitation Robotics	Cartilage	Instrumentation
3:30 PM	Break and Poster Sessions - University Center				
7:00 PM	Baseball: Cleveland Indians vs. New York Yankees at Jacobs Field				

Friday August 5, 2005

	Room A	Room B	Room C	Room D	Room D
8:30 AM	Keynote Lecture: Martyn Shorten				
9:30 AM	Rehabilitation	Motor Control - Upper Extremity	Muscle Adaptation	Knee Replacement	Sport 4
10:30 AM	Break - University Center				
11:00 AM	Musculoskeletal Modeling	Methods in Gait Analysis	Hand and Wrist 2	Knee Mechanics 2	Running Injuries
12:30 PM	Lunch - University Center				
1:15 PM	Keynote Lecture: James J. Collins				
2:15 PM	Motor Control	Locomotion Energetics	Falling and Fall Prevention	Knee Mechanics 3	Animal Biomechanics
3:30 PM	Break - University Center				
4:00 PM	ISB President's Lecture: Mary Rodgers				
5:00 PM	Closing Ceremony (until 6:00)				
7:00 PM	Conference Banquet at Rock & Roll Hall of Fame				

NUMERICAL ANALYSIS OF A FEMUR RESURFACING CUP

[1]James Cubillo, [1, 2]Chang Jiang Wang
[1]School of Engineering, University of Wolverhampton, UK, TF2 8SD; email: J.P.Cubillo@wlv.ac.uk, Web: www.wlv.ac.uk
[2]Riatec, University of Wolverhampton, UK, WV1 1SB; email: C.J.Wang@wlv.ac.uk, web: www.riatec.org

INTRODUCTION

Wagner [1] developed a method of hip joint arthroplasty by surface replacement. The first clinical trial was in 1976; since then research in this area has continued, and operative techniques and implantation systems have been refined. Hip joint resurfacing offers several advantages over other techniques, most importantly the fact that the femoral neck is left intact.

However, the effects of various designs of femoral resurfacing cup have not yet been fully understood. In this paper, the femoral resurfacing cup was modelled and investigated. Different bone cement materials and various designs of resurfacing femur cup were numerically simulated.

METHODS

A 3D finite element model consisting of a resurfacing cup, bone cement and proximal femur was created using the ANSYS finite element package. The coronal section of the model is shown in Figure 1.

Two types of cancellous bone were considered within the proximal femur. The cancellous bone within the femur head has a Young's modulus of 1300 MPa, and the cancellous bone within the femur trochanteric region has a Young's modulus of 320 MPa [2]; the cortical bone around the trochanter has a Young's modulus of 17000 MPa. The cup is made of Cobalt Chromium, the Young's modulus of which is 210000 MPa and Poisson's ratio 0.3. Two types of bone cement were analysed in this paper with a Young's modulus of 2200 MPa [3] and 2800 MPa respectively.

In this research, we were interested in the region of femoral head and femoral resurfacing cup; only the hip reaction force was applied. In a one-leg stance, a 3 kN load was applied to the femoral head [2]. Ascending and descending stairs and rising from a chair are all activities that increase the posterior component of the joint reaction force and generate large torque, and the anterior-posterior component of force in the joint reaction is up to 45% of the resultant force [4]. The applied forces were distributed over the assumed load-bearing area on the femur head.

For comparative analysis, the following parameters were considered and compared; stress in the cement layer, stress in the bone around the metal stem, and load sharing between the stem and the bone of the femoral neck.

The factors related to the cup design were investigated and discussed. Firstly, the effect of femoral stem bonded or contacted with surrounding bone was investigated. Secondly,

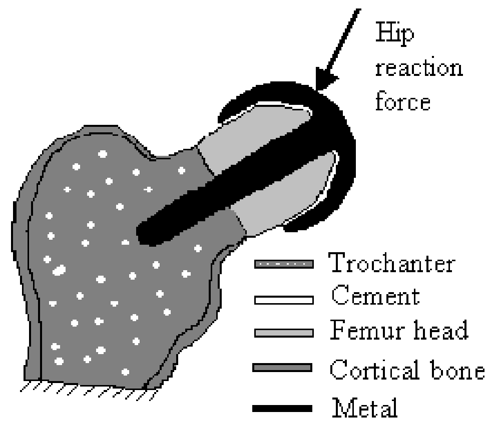

Figure 1: Coronal section of the model and material

the role of the stem in the femoral cup was studied. Finally, the effects of cement thickness, cement material properties, femoral cup depth, stem diameter, and osteoporosis were all investigated.

RESULTS AND DISCUSSION

A femoral cup with a stem reduced the stress in the cement greatly in comparison to a cup without a stem. If a stem was used, the shorter the stem the higher the stress in the cement and femur head bone. When the diameter of stem was decreased, the stress in the cement and femur head bone increased. When the resurfacing cup's depth was reduced, the stress in the cement and femur head bone decreased slightly. Changes in the thickness of the cement layer from 0.5 to 1 and 2 mm did not make much difference to the stresses in the cement and bone. Different material properties of the cement did not change the load sharing between the stem and bone. The more osteoporosis developed in the bone, (i.e. the lower the Young's modulus of the bone), the higher the stress resulted in the cement. All the results showed that the femoral bone carries most of the forces and the stem bears only one quarter to one third of the applied forces in the direction of the stem axis. If the stem were simulated bonded with the bone rather than just in contact with the bone, the stress in the cement was reduced. However, this case may result in stress shielding around the femoral neck with subsequent bone thinning problems.

REFERENCES

1. Wagner H. *ClinicalOrthopaedic and Related Research*, **134,** 102-130, 1978.
2. Fagan MJ and Lee AJC. *J Biomed Eng* **8**, 295-304, 1986.
3. Mann KA et al. *J Orthopaedic Research*, **15**, 62-68, 1997.
4. Harrigan TP and Harris WH. *J. Biomechanics*, **24**, 1047-1058, 1998.

A BIOMECHANICAL MODEL OF SACRO-ILIAC JOINT DYSFUNCTION AS A CAUSE OF LOW BACK PAIN

Munier Hossain, Leonard DM Nokes
Cardiff School of Engineering, Cardiff, UK

email: munierh@doctors.org.uk, web: www.orthobiomech.info

INTRODUCTION

A biomechanical model of sacro-iliac (SI) joint dysfunction is proposed. It was hypothesized that sacro-iliac joint dysfunction in the form of abnormal activation of gluteus maximus and biceps femoris gives rise to lumbopelvic pain by failing to stabilize the sacro-iliac joint during weight bearing. The model was tested on a pilot study of two volunteers.

METHODS

Two male volunteers participated in the study. One subject had no complaint of sacro-iliac joint pain. The other subject had sacral sulcus tenderness, pain over the sacroiliac joint on right side and standing asymmetry of the posterior superior iliac spine.

Electromyogram (EMG) was recorded using pairs of disposable bipolar surface Ag/AgCl electrodes on the symptomatic side for the lumbar multifidus, gluteus maximus and biceps femoris muscles in walking. The surface electrodes were positioned as advised by Snijders et al[1].Baseline activity was recorded at rest. Subjects were asked to walk in a straight line. Each test was taken three times for two full gait cycles. EMG data was taken on the patient before and after a session of physiotherapy. Two dimensional high speed video was used to capture data of walking motion. Surface EMG data were sampled at 1000 Hz and pre amplified at the source. The raw EMG data of the three muscles were full-wave rectified and base line corrected. Then the rectified data were smoothened by passing it through a second order low pass filter with a Butterworth response at 2- 27 Hertz .

RESULTS AND DISCUSSION

Table 1 compares the EMG values from the volunteers. Multifidus was activated throughout the gait sequence but increased activity in swing phases. There was little difference in activity.

Biceps femoris muscle activated in mid swing phase to peak and subsequently relax before initial contact to allow gluteus peak at loading response in the normal volunteer. Gluteus activation remained low in mid stance and terminal stance, but showed another peak activity in pre-swing event .In the patient biceps was activated at terminal swing and at the time of initial contact, it was still relatively active. Gluteus activation was generally poor in the symptomatic individual and failed to reach a peak in loading response. There was consistent activation of biceps on terminal swing event with another peak activation in ipsilateral pre-swing event. Unlike the normal volunteer, gluteus failed to show increased activity in terminal stance to pre swing events. After physiotherapy, there was general decrease in biceps femoris activity and increase in gluteus activity.

SI joint is the key linkage in transmission of weight from the upper limbs to the lower. The joint is vertically oriented and subject to a large shear force and forward momentum on weight bearing. Gluteus is strongly active during initial contact and loading response events when we experience an abrupt limb loading and as such need for SI joint stability is at a premium. Sub-optimal activity of gluteus could disrupt weight transference. Body would attempt to compensate by recruiting biceps femoris, which could exert its influence through its proximal attachment to sacrotuberous ligament [2]. This compensatory strategy might in itself also give rise to pain due to prolong biceps contraction or stretching of long dorsal ligament .

The study showed a difference in gluteus maximus and biceps femoris activity in key events of gait between the two volunteers. A larger study is planned to validate the model.

REFERENCES

1. Snijders CJ, Ribbers MTLM, de Bakker HV, Stoeckart R, Stam HJ. EMG recordings of abdominal and back muscles in various standing postures:validation of a biomechanical model on sacroiliac joint stability. *J Electromyogr Kinesiol* 1998;**8**:205-14
2. Vleeming A. Snijders CJ, Stoeckart R, Mens JMA. The role of the sacroiliac joints in coupling between spine, pelvis, legs and arms. In : Vleeming ADT, Snijders CJ, Stoeckart R, eds. *Movement, stability and low back pain*. New York:ChurchillLivingstone,1997:53-71.

Table 1: Mean electromyogram value compared between normal volunteer (a), patient pre (b)and post-physiotherapy (c) in different events of gait cycle (in mV)

Event of gait cycle	Multifidus			Biceps femoris			Gluteus maximus		
	a	b	c	a	b	c	a	b	c
Initial contact	0.08	0.04	0.08	0.07	0.28	0.04	0.54	0.10	0.07
Loading response	0.04	0.04	0.06	0.05	0.06	0.04	0.92	0.03	0.09
Mid stance	0.04	0.05	0.05	0.06	0.08	0.05	0.10	0.03	0.05
Terminal stance	0.09	0.09	0.06	0.06	0.88	0.12	0.10	0.03	0.05
Pre swing	0.06	0.06	0.08	0.06	1.10	0.19	0.86	0.04	0.09
Mid swing	0.07	0.05	0.06	0.14	0.08	0.03	0.15	0.05	0.06
Terminal swing	0.25	0.22	0.05	0.46	0.44	0.06	0.60	0.14	0.09
Baseline value	0.04	0.04	0.07	0.05	0.06	0.04	0.10	0.03	0.05

A NON-LINEAR, ANISOTROPIC, INHOMOGENEOUS MODEL OF ARTICULAR CARTILAGE

[1] Salvatore Federico, [2] Alfio Grillo, [2] Gaetano Giaquinta, [1] Walter Herzog
[1] Human Performance Laboratory, The University of Calgary, Calgary, Alberta, Canada
[2] Department of Physical and Chemical Methodologies for Engineering, University of Catania, Catania, Italy
Corresponding Author: Salvatore Federico, email: salvatore@kin.ucalgary.ca

INTRODUCTION

Articular cartilage is a biological composite material made of a proteoglycan matrix, and of chondrocyte and collagen fibre inclusions. We have modelled articular cartilage by means of a linearly elastic Transversely Isotropic, Transversely Homogeneous (TITH) model [1]. Here, we extend the TITH model to non-linear elasticity by using a class of transversely isotropic potentials [2,3]. The use of a non homogeneous potential (i.e., explicitly dependent on the point) enables us to identify non-uniformities in the simulation of compression tests.

METHODS

The stress strain relationship for a hyperelastic material is:

$$\sigma_{ij} = \frac{2}{J} F_{ir} \frac{\partial U}{\partial C_{rs}}(C)\; F_{js} \tag{1}$$

where σ is the Cauchy stress, and U is the strain energy potential which is a function of the right Cauchy stretch, C. For a transversely isotropic material, with transverse plane orthogonal to the unit vector $w = e_1$, U is a function of the three principal invariants of C, and the two additional invariants for transverse isotropy [4]. By expressing the invariants explicitly in terms of the components of C, we have:

$$\begin{aligned} U(C) &= a\; \exp(f(C)) \\ f(C) &= -b\; \ln(\det(C)) + \alpha_1(C_{rr}-3) + \\ &\quad + \tfrac{1}{2}\alpha_2((C_{rr})^2 - C_{rs}C_{sr} - 6) + \\ &\quad + \alpha_3(C_{rr}-3)(w_r C_{rs} w_s - 1) + \alpha_4(w_r C_{rs} w_s - 1) + \\ &\quad + \alpha_5(w_r C_{rh} C_{hs} w_s - 1) + \alpha_6(w_r C_{rs} w_s - 1)^2 + \alpha_7(C_{rr}-3)^2 \end{aligned} \tag{2}$$

The coefficients a, b, $\alpha_1,\ldots,\ \alpha_7$ are determined by imposing that, for small strains, Eq. (1) must reduce to the linear theory. If we use Cohen's potential [3], then $b = 1$ and $\alpha_7 = 0$. For a confined compression test, the stress strain relationship is:

$$\sigma_{11} = 2a\;(2P\lambda + Q\lambda^{-1} - \lambda^{-3})\; \exp(P\lambda^4 + Q\lambda^2 - R) \tag{3}$$

where λ is the axial Cauchy stretch, and P, Q and R are linear combinations of $\alpha_1,\ldots,\ \alpha_6$. In the non-linear TITH model, these coefficients explicitly depend on the tissue depth via the non dimensional coordinate, ξ, running from the tidemark (ξ = 0) to the articular surface (ξ = 1). We plotted the stress-strain curve for several values of ξ (Fig. 1). We assumed that, for a transversely homogeneous material in confined compression, the axial stress must be uniform, and imposed a 0.5 MPa stress (Fig. 1). We then plotted the corresponding values of the strain at each depth ξ (Fig. 2) and obtained the spatial distribution of the Green strain, $\varepsilon = (\lambda^2 - 1)/2$, for the non-linear TITH model, and Cohen's non-linear homogeneous model.

RESULTS AND DISCUSSION

The results of this study show that, while the homogeneous model can only give rise to an intrinsic uniform solution (Fig. 2), the non-linear TITH model is able to predict non uniformities in axial strain, due to the variation of the tangent stiffness with depth: the superficial layers deform more than the deep layers because they are softer, a result that is consistent with experimental evidence [5].

Implementation of this model into a Finite Element code might help in studying the mechanical behaviour of chondrocytes during cartilage deformation, which might proof to be an essential piece towards understanding biological responses of articular cartilage as a function of mechanical loading.

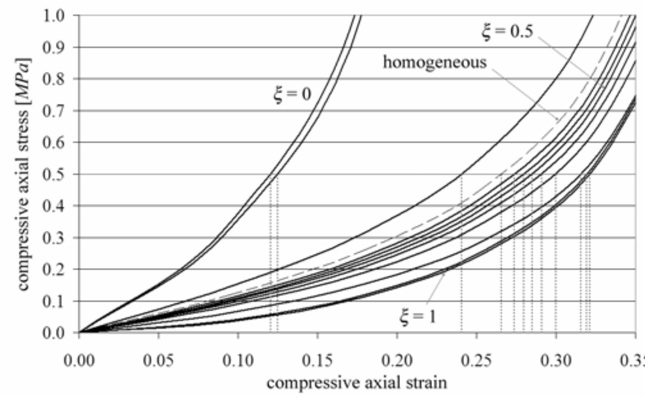

Figure 1: stress-strain curves at various ξ for the non-linear TITH model (solid lines) and Cohen's homogeneous model (dashed line); the dotted lines indicate the strain at each ξ, for a -0.5 MPa stress.

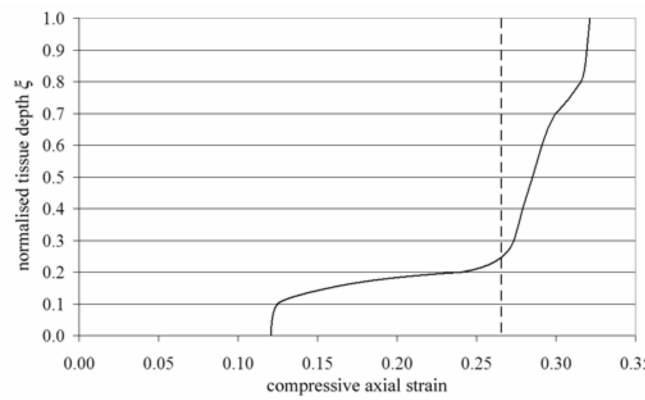

Figure 2: spatial distribution of the strain for the non-linear TITH model (solid line) and Cohen's homogeneous model (dashed line).

REFERENCES

1. Federico, S., Grillo, A., La Rosa, G., Giaquinta, G., Herzog, W., 2004. *J. Biomech.*, in press.
2. Cohen, B., 1992. PhD thesis, Columbia University, 1992.
3. Almeida, E.S., Spilker, R.L., Holmes, M.H., 1995, *BED*-29, *Bioengineering Conference*, *ASME* 1995.
4. Ericksen, J.L., Rivlin, R.S., 1954. *J. Rat. Mech.*, **3**, 281-301.
5. Schinagl, R.M, Gurskis, D., Chen, A.C., Sah, R.L., 1997. *J. Orthop. Res.*, **15**, 499-506.

ACKNOWLEGEMENTS

The Canadian Institutes for Health Research, The Arthritis Society of Canada, and The Canada Research Chair Programme.

COMPUTER SIMULATION OF THE TAKEOFF IN SPRINGBOARD DIVING

Pui W. Kong, Maurice R. Yeadon and Mark A. King
Loughborough University; email: m.r.yeadon@lboro.ac.uk, web: www.lboro.ac.uk

INTRODUCTION

In springboard diving the diver aims to generate sufficient time in the air and angular momentum for somersault and twist, and travel safely away from the board. Since the linear and angular momentum that the diver possesses in the air are determined by the end of the takeoff phase, it is crucial to understand the mechanics of the takeoff in terms of gaining dive height, generating angular momentum and keeping a safe distance. The aim of this study was to develop a computer simulation model in order to investigate springboard diving takeoff techniques in the forward and reverse groups.

METHODS

A planar simulation model of a springboard and a diver was developed using the Autolev 3.4^{TM} software package based on Kane's method of formulating equations of motion [1]. The diver was represented by an eight-segment linked system comprising the head, upper arm, lower arm, trunk, thigh, shank and a two-segment foot. There were extensor and flexor torque generators acting at the metatarsal-phalangeal, ankle, knee, hip and shoulder joint. The torque produced was the product of an activation level and the maximum torque calculated from a torque / angle / angular velocity function. Each activation level was specified using two quintic functions with six parameters.

Input to the model included initial conditions at touchdown obtained using high speed video and activation time histories throughout the simulation. Output of the model comprised time histories of the springboard displacement, the diver's joint angle and angular velocity at each joint, body orientation, CM velocity and whole-body angular momentum. The model was customised to an elite female diver so that simulation output could be compared with the diver's own performance. Model parameters including springboard, strength, inertia and visco-elastic parameters were determined either directly from experiments or indirectly using an angle-driven model. A score was calculated as the average percentage difference in joint angles, orientation, linear momentum, angular momentum, and springboard characteristics. Sixty muscle activation parameters were varied until the best match between simulation and performance was found by minimizing this score using the Simulated Annealing optimisation algorithm [2]. Four dives which required different angular momenta in the forward and reverse groups were selected for this matching process. After satisfactory evaluation, the model was used to optimise takeoff techniques in terms of gaining maximum dive height.

RESULTS AND DISCUSSION

All four simulations matched the performance well with an average score of 6.3%. Graphics comparison of the performance and matching simulation of the forward two and one-half somersault pike (105B) is shown in Figure 1. In the optimisation for height for 105B, there is a 12.7 cm increase in dive height. The good agreement between simulation and performance for all four dives suggests that the model can successfully reproduce springboard diving takeoff movements. The optimised simulation shows that by changing the activation alone the diver can gain more dive height. This model will be further applied to investigate other optimal takeoff techniques.

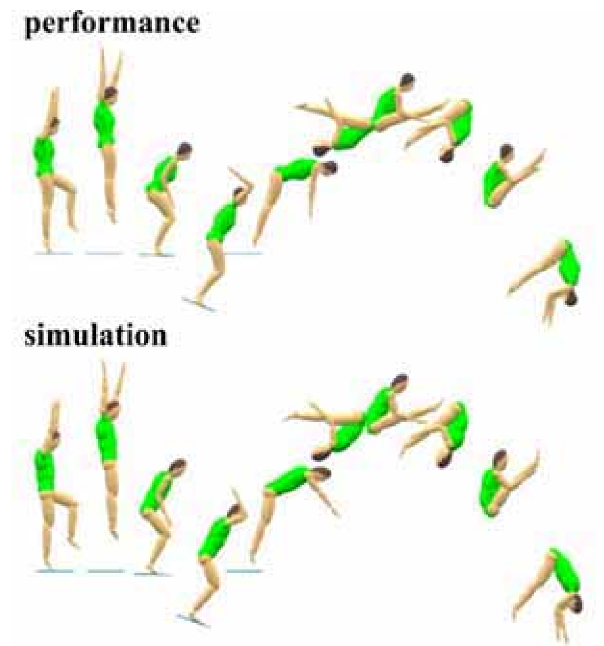

Figure 1: Comparison of the performance and matching simulation of the forward two and one-half somersault pike.

CONCLUSIONS

This study presents a torque-driven simulation model of a springboard and a diver which successfully reproduces realistic springboard diving takeoffs. This model will be used to investigate optimal takeoff techniques in the forward and reverse dive groups.

REFERENCES

1. Kane TR, Levinson DA. *Dynamics: Theory and implementations*, McGraw-Hill, New York, 1985.
2. Corana A, et al. *ACM Transactions on Mathematical Software* **13**, 262-280, 1987

ACKNOWLEDGEMENTS

This study was supported by the International Society of Biomechanics under the Matching Dissertation Grant Program.

PERFORMANCE AFTER PROLONGED CYCLING AT FREELY CHOSEN AND OPTIMAL PEDAL RATE

[1]Ernst Albin Hansen, [2]Kurt Jensen and [3]Preben K Pedersen
[1]National Institute of Occupational Health, Copenhagen, Denmark; email: eah@ami.dk
[2]Team Danmarks Testcenter, University of Southern Denmark, Odense.
[3]Institute of Sports Science and Clinical Biomechanics, University of Southern Denmark, Odense.

INTRODUCTION

The major part of a long cycling road race (>3 h) consists of sub-maximal cycling [1] where cyclists exercise using high pedal rates. In fact, the freely chosen pedal rate (FCPR) is much higher than the one resulting in minimum energy turnover, i.e., the optimal pedal rate (OPR) [2]. Supposing that the choice of a high pedal rate, despite its higher energetic cost, might serve a practical purpose, we examined whether performance was higher after prolonged cycling with FCPR compared to OPR.

METHODS

Nine trained cyclists or triathletes (average±SD: 27±2 years, 73.2±6.7 kg, 179±6 cm) were tested on three different days. On day 1 the subjects performed at random order (without pauses) six 180 W, 6-min, cycle ergometer bouts with 35, 50, 65, 80, 95 rpm, and FCPR. Oxygen uptake (VO_2) was measured continuously, and subsequently plotted against pedal rate for determination of OPR. Afterwards the subjects performed a 5 min time trial test with FCPR for determination of average power output (W_{5min}), peak VO_2 and blood lactate concentration. On days 2 and 3 they cycled 2.5 h at 180 W with either their FCPR or OPR (randomised order) followed by the 5 min time trial test. VO_2 and perceived exertion (RPE) were recorded at 30 min intervals during the prolonged cycling.

RESULTS AND DISCUSSION

U-shaped relationships between pedal rate and VO_2 were observed for 8 out of 9 subjects (for one subject the minimum VO_2 occurred at the highest preset pedal rate). The mean OPR was 73±11 (range: 65-95) rpm while FCPR averaged 95±7 (range: 89-106) rpm ($p<0.05$). Initial peak values averaged for VO_2: 4.65±0.5 l min^{-1}, blood lactate concentration: 13.6±2.3 mM, and W_{5min}: 399±33 W. A workload of 180 W, accordingly, corresponded to 45±4% of the initial W_{5min}. VO_2 during the prolonged cycling was consistently ~7% higher at FCPR than at OPR ($p<0.05$) (Fig 1). RPE increased during prolonged cycling ($p<0.05$) and more so with FCPR than with OPR ($p<0.05$) (Fig 1). The final W_{5min} (359±47W after FCPR and 368±31 W after OPR) was ~10% lower than the initial value ($p<0.05$), which indicated fatigue. The tendency for a greater performance reduction following FCPR, however, did not reach statistical significance.

A high VO_2 reflects a high energy turnover, which at least theoretically, depletes the energy stores sooner. However, performance reduction may also be caused by other mechanisms e.g. linked to neuromuscular function, which could be affected by the relatively high pedal force and muscle stress that follows with the quite low OPR.

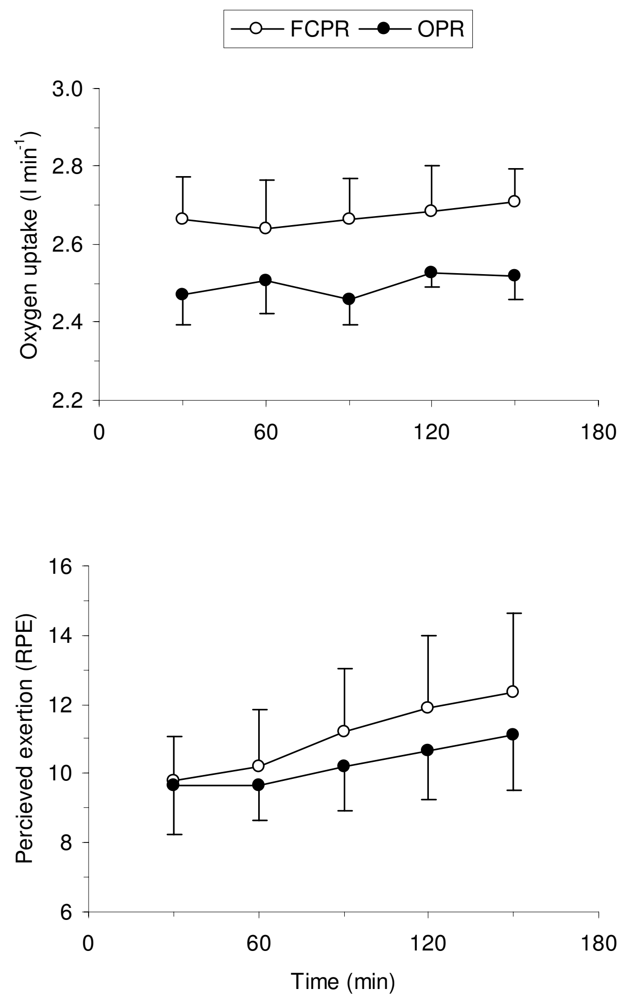

Figure 1: Oxygen uptake and perceived exertion as a function of time during 2.5 h of prolonged cycling.

CONCLUSIONS

Time trial performance was reduced after 2.5 h cycling at 180 W with FCPR and OPR. The reduction of performance did not differ between the two pedal rates, despite VO_2 and RPE being higher with FCPR.

REFERENCES

1. Lucia et al. *Int J Sports Med* **20**, 167-172, 1999.
2. Nielsen JS, et al. *Eur J Appl Physiol* **92**, 114-120, 2004.

ACKNOWLEDGEMENTS

Supported by The Ministry of Culture Committee on Sports Research

MECHANICAL PROPERTIES OF CANINE TRABECULAR BONE

[1]Thomas Pressel, [2]Anas Bouguecha, [2]Matthias Kammler, [2]Bernd-Arno Behrens, [3]Ute Vogt, [3]Andrea Meyer-Lindenberg, [1]Henning Windhagen

[1]Department of Orthopaedic Surgery, Hannover Medical School, Hannover, Germany; E-Mail: pressel@annastift.de,
[2]Institute of Metal Forming and Metal Forming Machines, University of Hannover, Hannover, Germany
[3]Clinic for Small Domestic Animals, School of Veterinary Medicine, Hannover, Germany

INTRODUCTION

Mechanical properties of canine bone are important for a better understanding of skeletal pathologies and are a prerequisite for numerical simulations of the bone. As hip diseases are of particular importance in dogs, we investigated the mechanical properties of trabecular bone in canine femoral heads.

METHODS

Both femora were obtained from eight euthanized dogs and 10x10x10 mm cubic specimens which were oriented along the main pressure trajectories were cut from the centre of the femoral heads (Figure 1). Specimen weights were recorded and sample edge lengths measured. From these results, specimen densities were calculated (Equation 1). Using a custom 100 MHz ultrasound testing device, the runtime through each specimen was recorded ten times in each direction (X, Y and Z) and average runtimes were calculated. From these results the velocity of the ultrasound waves (Equation 2) and the elastic moduli in the three orthogonal directions (Equation 3) could be calculated. Degrees of anisotropy (ratio of elastic modulus to moduli in the other orthogonal directions) were also determined. Statistical analysis using one-way ANOVA (software package SPSS 12.0, Chicago IL, USA) tested the directional moduli for significant differences.

Figure 1: Photograph of a cubic bone specimen which was cut from a canine femoral head

$\rho \quad \frac{m}{V}$ **Equation 1:** density ρ calculated from specimen mass *m* and volume *V*

$c_{long} \quad \frac{s}{t_1 - t_0}$ **Equation 2:** transmission velocity *c* calculated from edge length of the specimen *s* and runtime through the specimen t_1-t_0

$E_{x,y,z} \quad \rho \cdot c_{long}^2$ **Equation 3:** directional Young's modulus *E* along x, y and z axes is calculated from density ρ and transmission velocity *c*

RESULTS AND DISCUSSION

The edge lengths of the specimens varied by ±0.1 mm (±1%). Elastic moduli were found ranging from 6.3 to 14.3 GPa. A mean specimen density of 1.40±0.09 g/cm^3 was calculated. Standard deviations between specimens were much smaller for E_x (the elastic modulus along main pressure trajectories of the femoral head) than for the other orthogonal directions (E_y and E_z). As could be expected from *equation 3*, significant correlations between specimen densities and elastic moduli were calculated ($p<0.005$). No significant differences between directional elastic moduli could be found indicating approximately isotropic specimens ($p=0.34$).
Several authors also have examined trabecular bone in canine and human bone. Works investigating bone of the femoral head [1] or the distal radius [2] found lower elastic moduli, while other authors using ultrasound testing or nanoindentation calculated similar or higher values [3-5]. The differences could be caused by specimens from different sites (e. g. radius or distal femur) and by different properties of human bone. One aspect could also be that several works did not load specimens along the main pressure trajectories which might result in lower elastic moduli.

CONCLUSIONS

The study indicated isotropy of the specimens obtained from canine femoral heads; the results are comparable to similar studies and might provide data for further biomechanical analysis of canine bone.

REFERENCES

1. Ulrich D, Hildebrand T, Van RB, Muller R, Ruegsegger P: The quality of trabecular bone evaluated with micro-computed tomography, FEA and mechanical testing. *Stud Health Technol Inform* 1997, **40:** 97-112.
2. Newitt DC, Majumdar S, van RB, von IG, Harris ST, Genant HK *et al*.: In vivo assessment of architecture and micro-finite element analysis derived indices of mechanical properties of trabecular bone in the radius. *Osteoporos Int* 2002, **13:** 6-17.
3. Jorgensen CS, Kundu T: Measurement of material elastic constants of trabecular bone: a micromechanical analytic study using a 1 GHz acoustic microscope. *J Orthop Res* 2002, **20:** 151-158.
4. Ashman RB, Rho JY: Elastic modulus of trabecular bone material. *J Biomech* 1988, **21:** 177-181.
5. Zysset PK, Guo XE, Hoffler CE, Moore KE, Goldstein SA: Elastic modulus and hardness of cortical and trabecular bone lamellae measured by nanoindentation in the human femur. *J Biomech* 1999, **32:** 1005-1012.

FUNCTIONS OF HIP JOINT MUSCLES

[1]Thomas Pressel and [2]Markus Lengsfeld
[1]Department of Orthopaedic Surgery, Hannover Medical School, Hannover, Germany; E-mail: pressel@annastift.de
[2]Department of Orthopaedic and Trauma Surgery, Hessisch Lichtenau, Germany

INTRODUCTION

Functions of hip joint muscles are important for physical therapy and rehabilitation, but are also useful for reconstructive surgery involving e. g. tendon transfer after plexus or peripheral nerve injuries. Main muscle functions in the neutral position of the joint are well known, but secondary functions or function changes in different joint positions remain under debate. Hence we used a multibody computer model of the hip and knee for further investigation of hip joint muscle functions.

METHODS

A 50th percentile rank male adult model regarding body height was chosen. The mass characteristics and joint positions were determined using the ADAMS/Android software package for the multibody simulation system ADAMS 7.0 (MSC Software, Santa Ana CA, USA). The attachment areas of 27 muscles crossing the hip joint were measured and centre points of the areas were calculated in a previous work[1]. The muscles were represented by straight lines connecting the muscle origin and insertion point; when the course of a muscle differed noticeable from a straight line, one additional wrapping point was used. Hip joint movements were investigated in steps of 20° using a physiological range of motion found in the literature. In each joint position, muscle lengths were determined and muscle lever arms were calculated. Additionally, the new concept of relative torques (torque acting around a single joint axis divided by the total torque which is generated by a standard muscle force) was introduced and relative torques around the three joint axes were calculated. With these parameters the functions of each muscle could be assessed in all investigated joint positions.

RESULTS AND DISCUSSION

Lengths, lever arms and relative torques for 27 muscles of the hip joint were calculated. Due to the large amount of data, two muscles whose functions are under debate in the literature are presented here. There is agreement in the literature that M. adductor longus is an adductor of the hip. In our data, the muscle additionally is a flexor of the hip up to 90° of flexion. At flexion angles greater than 90°, the muscle becomes an extensor (Figure 1). The muscle also was found to be an external rotator of the hip in flexion positions up to 80° or internal rotation of the hip. The rotational function change is not described by most of the authors and internal or external rotation is reported instead.

M. iliopsoas is a flexor of the hip in all anatomical works. In this study, when exceeding 110° of flexion the muscle became an extensor of the hip. We also found an internally rotating moment of the muscle in positions up to 80° flexion and 30° external rotation. In externally rotated positions of the hip the muscle also generated an abducting moment.

In interpretation of our data, the effects of the simplified representation of muscles which were modelled as straight lines have to be accounted for. However, as manifestly curved muscles were modelled by additional wrapping points, the errors due to this simplification were reduced.

The primary functions of hip muscles were the same as in similar studies and in the anatomical literature. Function changes during different hip joint motions were also found in other studies, but there is some debate about the exact joint position of the function change. The data presented here is in most of the cases supported by several authors.

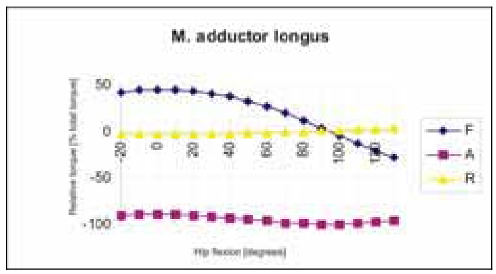

Figure 1: Relative torques of M. adductor longus. *F* designates flexion torque, *A* abduction torque, *R* external rotation torque. Negative values characterise the opposite motion (i. e. negative abduction torque designates an adduction moment)

CONCLUSIONS

The study presented here provides a comprehensive data set of hip joint muscle functions which might be of interest for physical therapy, rehabilitation and further research.

REFERENCES

1. Lengsfeld M, Stammberger U, Reeh S: **Spatial measurement and transformation of muscular attachments at the lower extremity.** *Med Eng Phys* 1994, **16:** 518-525.

THE GAIT INITIATION PROCESS IN UNILATERAL LOWER-LIMB AMPUTEES STEPPING TO A NEW LEVEL

[1]Steven F. Jones, [1]Peter C. Twigg, [2]Andrew J. Scally and [3]John G. Buckley
[1]School of Engineering, Design and Technology, [2]School of Health Studies and [3]School of Life Sciences,
University of Bradford, Richmond Road, Bradford, West Yorkshire, UK; email: s.f.jones1@bradford.ac.uk

INTRODUCTION

Because feedback originating from cutaneous receptors within the foot and leg is only present unilaterally [1], or at best is available via re-mapped receptors within the stump [2], unilateral lower-limb amputees will need to adopt alternative balance and postural control strategies when initiating gait. Also, because amputees are taught to lead with their intact limb when stepping up and with their prosthetic limb when stepping down, they may employ a different gait initiation strategy for each stepping direction. The aim of the present study was to determine the balance and postural control adaptations used by unilateral lower-limb amputees when stepping up and when stepping down to a new level.

METHODS

Ten unilateral amputees (5 transfemoral and 5 transtibial) and 8 able-bodied controls performed single steps up and single steps down to a new level (73 and 219 mm). Amputee subjects stepped up leading with their intact limb and stepped down leading with their prosthesis.

Phase duration, a-p and m-l centre of mass (CoM) and centre of pressure (CoP) peak displacements and CoM peak velocity of the anticipatory postural adjustment (APA) and step execution (SE) phase were evaluated for each stepping direction by analysing data collected using a Vicon 3D motion analysis system. Data were analysed using a random effects population averaged model. Also, to highlight differences in CoM/CoP interactions between each group, data were compared qualitatively (exemplar, Figure 1).

RESULTS AND DISCUSSION

There were significant differences (in the phase duration, peak a-p and m-l CoP displacement, and peak a-p and m-l CoM velocity at heel-off and at foot-contact) between both amputee sub-groups and controls ($P < 0.05$), but not between amputee sub-groups. These group differences were mainly a result of amputees adopting a different gait initiation strategy for each stepping direction (Table 1). In transfemorals this may have been a way, when stepping up, of ensuring the GRF vector was anterior of the knee joint centre; this would have helped to keep the knee of the prosthetic limb fully extended (locked). In transtibials it may have been a way to reduce the knee extensor moment, thereby reducing the force of the prosthesis against the distal end of the tibia. When stepping down (landing on the prosthesis) both amputee sub-groups adopted a 'cautionary' approach.

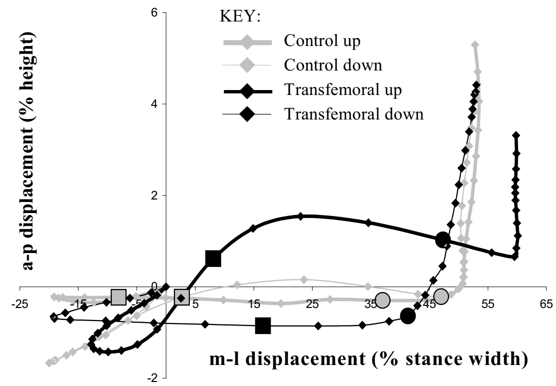

Figure 1. 'Ensembled average' CoP trajectories for transfemoral amputees vs. controls when stepping up to and down from the low step height. Distance between points represents movement speed. Data are shown from movement initiation up to swing limb foot-contact. □ and ○ indicates the instant of heel- and toe-off of the swing limb respectively.

CONCLUSIONS

Findings indicate the gait initiation process utilised by lower-limb amputees was dependent on the direction of stepping and, more particularly, by which limb the amputee led with. This suggests that the balance and postural control of gait initiation is not governed by a fixed motor program, and thus that an amputee will require time and training to develop alternative neuromuscular control and coordination strategies. These findings should be considered when developing training and/or rehabilitation programs.

REFERENCES

1. Geurts ACH, et al. Postural reorganisation following lower limb amputation. *Scand J Rehabil Med* **24**, 83-90, 1992.
2. Schwenkreis P, et al. Reorganization in the ipsilateral motor cortex of patients with lower limb amputation. *Neurosci Lett* **349**, 187-190, 2003.

ACKNOWLEDGEMENTS

Steve Jones is supported by a studentship from the Engineering and Physical Sciences Research Council, UK.
Steve Jones gained a matching 'Doctoral Dissertation Grant' award from the International Society of Biomechanics.
Chas. A. Blatchford & Sons Ltd, Basingstoke, UK, provided prosthetic and clinical support.

Table 1: Mean (SD) temporal and kinematic parameters averaged across step height when stepping up and stepping down.

		Controls		**Transfemorals**		**Transtibials**	
		Up	**Down**	**Up**	**Down**	**Up**	**Down**
APA phase	APA duration (% movement)	30.7 (7.8)	39.1 (7.1)**	47.5 (4.3)**	37.0 (5.4)	42.2 (7.5)**	31.9 (8.2)
	Peak a-p CoP (% height)	-0.81 (-0.5)	-1.8 (-0.7)**	-1.5 (-0.8)**	-1.0 (-0.5)	-1.1 (-0.5)**	-0.8 (-0.4)
	Peak m-l CoP (% stance)	22.81 (7.9)	20.8 (8.5)	13.9 (4.4)**	20.1 (6.7)	16.3 (4.3)	17.9 (4.8)
	m-l CoM vel. HO ($mm.s^{-1}$)	190.1 (56.8)**	178.1 (44.2)	159.9 (32.7)**	150.1 (44.6)	212.8 (34.3)**	175.2 (38.4)
	a-p CoM vel. HO ($mm.s^{-1}$)	91.1 (31.7)	129.6 (37.4)**	112.0 (49.8)*	64.7 (14.3)	86.3 (37.7)*	54.5 (18.9)
SE phase	Peak m-l CoM (% stance)	26.9 (3.4)*	23.6 (4.8)	23.2 (4.8)	24.0 (7.6)	31.0 (5.9)*	27.0 (4.5)
	m-l CoM vel. FC ($mm.s^{-1}$)	334.9 (73.9)**	301.4 (74.0)	303.9 (47.8)**	240.0 (46.2)	360.2 (45.5)**	318.8 (54.6)
	a-p CoM vel. FC ($mm.s^{-1}$)	511.0 (29.1)	622.1 (106.0)**	462.4 (75.7)	457.3 (90.8)	485.7 (64.4)	511.9 (69.7)
	Movement time (s)	1.29 (0.14)*	1.19 (0.16)	1.18 (0.23)	1.31 (0.21)*	1.38 (0.23)	1.47 (0.20)*

Differences between stepping direction are indicated as $^{**}P < 0.001$, $^{*}P < 0.05$. NB, m-l CoP displacements during the APA phase were directed towards the intended swing limb, whereas during the SE phase they were directed towards the stance limb. HO = heel-off, FC = foot-contact.

THE EFFECT OF A REFERENCE POSTURE ON THE RELATIONSHIP BETWEEN RELAXED CALCANEAL STANDING MEASUREMENT AND FRONTAL PLANE REARFOOT MOTION DURING WALKING IN PATELLOFEMORAL PAIN SYNDROME SUBJECTS

Pazit Levinger and Wendy Gilleard
Southern Cross University, NSW Australia.
email: wgillear@scu.edu.au

INTRODUCTION

The choice of a reference posture used in angular motion calculations may play an important role in finding a relationship between the static posture and rearfoot frontal plane of motion in a clinical population such as patellofemoral pain syndrome (PFPS). By using the relaxed standing as a reference posture [1], a frontal plane deviation in the reference posture may mask any appearance of abnormal frontal plane rearfoot motion during walking. This study examined the relationship between rearfoot inversion/eversion during the stance phase of walking and the static relaxed standing measurement in females with PFPS and healthy controls and examined the influence of reference postures used when calculating these measures. Two reference postures were investigated: (1) Vertical Alignment between the rearfoot and the lower leg and (2) Relaxed Calcaneal Standing.

METHODS

Fourteen healthy and 13 females with PFPS were videoed barefoot during five walking trials using a four-camera (50Hz) motion analysis system. External markers attached to a tibia shell and the calcaneus measured peak inversion/eversion motion of the rearfoot relative to the tibia. Two reference postures were assessed: 1. Relaxed Calcaneal Standing posture and 2. Vertical Alignment i.e with the posterior calcaneus and lower leg vertically aligned. For Relaxed Calcaneal Standing reference posture, subjects stood relaxed in a self selected comfortable position. Vertical Alignment posture was achieved when the subjects elevated or lowered their medial longitudinal arch. While this posture was maintained the frontal plane alignment of the rearfoot relative to the tibia was recorded. For Vertical Alignment posture, to enable normalization of the study population to the same zero reference posture for inter-group comparison of the rearfoot relative to the tibia in the frontal plane, the vertical axis was rotated [2] through the individual's angle in the frontal plane previously recorded. All walking trial angles were calculated relative to both the Relaxed Calcaneal Standing and Vertical Alignment postures. Pearson's Correlation was used to investigate the relationship between the Relaxed Calcaneal Standing and stance phase peak inversion and eversion when using the two reference postures.

RESULTS AND DISCUSSION

When using the Relaxed Calcaneal Standing reference posture a significant correlation was found between static relaxed standing measurement and maximum eversion in the control group only (Table 1). When using the Vertical Alignment reference posture, significant correlation was found in PFPS only for both maximum eversion/inversion (Table 1). Thus, indicating that with a more everted posture during relaxed standing there is more eversion and less inversion during walking. As subjects in the control group did not demonstrate an increased calcaneal eversion during static relaxed standing measurement, it is unlikely that these subjects would demonstrate abnormal foot function during walking. A mathematical relationship is therefore unlikely to be found. The relationship between the rearfoot static clinical measurement and dynamic function of the rearfoot during walking therefore may be present in a clinical population rather than healthy control subjects.

CONCLUSIONS

As the Relaxed Calcaneal Standing reference posture may eliminate the inherent compensated foot during dynamic foot function, the use of neutral posture may be necessary. The positive relationship found in the PFPS group between dynamic angular measure and static relaxed standing based on a neutral reference posture indicated that PFPS subjects the clinical rearfoot measurement relaxed standing can be used to explain the pattern of rearfoot motion during walking.

REFERENCES

1. McPoil & Cornwall. JOSPT. **23**: 370-375, 1996.
2. Hunt & Smith. Clinical Biomechanics, **19**, 391-397, 2004

Table 1: The correlation between rearfoot static relaxed standing and rearfoot peak inversion/eversion (Mean±SD) when calculated using the two reference postures (Relaxed Calcaneal Standing and Vertical Alignment) for PFPS and control groups.

Reference posture	**Relaxed Calcaneal Standing**			**Vertical Alignment**		
	Mean±SD	R value	P value	Mean±SD	R value	P value
Control						
Inversion	12.8°±5.46°	-0.04	0.789	10.25°±6.11°	0.457	0.101
Eversion	2.8°±4.63°	-0.770	0.001*	5.41°±2.99°	-0.153	0.602
PFPS						
Inversion	13.14°±4.86°	0.135	0.661	5.57°±6.29°	0.643	0.018*
Eversion	4.21°±2.57°	0.119	0.698	11.64°±4.85°	0.768	0.002*

** Significant at $p \leq 0.05$*

Body Weight Support System Influence on the Patterns of Vertical Forces Applied to the Body

Li Li and Robin Cropper
Louisiana State University, email: lli3@lsu.edu

INTRODUCTION

More and more physical rehabilitation related clinics are using some types of body weight support system (BWSS) in their practices. The use of the BWSS together with the repetition and consistent nature of walking on the treadmill makes the patient repeatedly practice the movement under controlled conditions. In addition to providing postural support, the body weight support system promotes coordination of the lower extremities, which traditional pre-gait training was unable to provide. Furthermore, the BWSS also helps to evaluate patients' gait without requiring the therapist to be at the patient's side to provide physical support. There is little information regarding how BWSS influence the actual gait pattern during treadmill walking. The purpose of this study was to examine how the BWSS influence the external forces at the vertical direction, and how the external forces were influenced by walking speed and the targeted body weight support.

METHODS

Sixteen college students have volunteered for the study. Their mean age (mean ± SD) and body mass were 22 ± 2 years old and 63 ± 11 kg, respectively. The subjects were instructed to walking on a force platform embedded treadmill (Gaitway, Kistler, Amherst, NY, USA) with a body weight support system (Vigor, Stevensville, MI, USA). They were walking at four different speed (.45, .67, .89, and 1.12 m/s) combined with four different levels of targeted body weight support (BWS) at 0, 15, 30, 45 %BWS. The testing order was balanced to prevent any possible order effects. Vertical ground reaction forces were measured by the force pates embedded within the Gaitway treadmill. The actual body weight being supported was measured by a force sensor installed between the harness and the supporting structure of the BWSS.

Maximum vertical ground reaction forces (RMVGRF), maximum and minimum (RMAXSF and RMINSF) suspension forces were calculated relative to participants' body weight and expressed as percentage body weight (%BW). Two factor (speed X %BW) ANOVA with repeated measures were used to analyze the data.

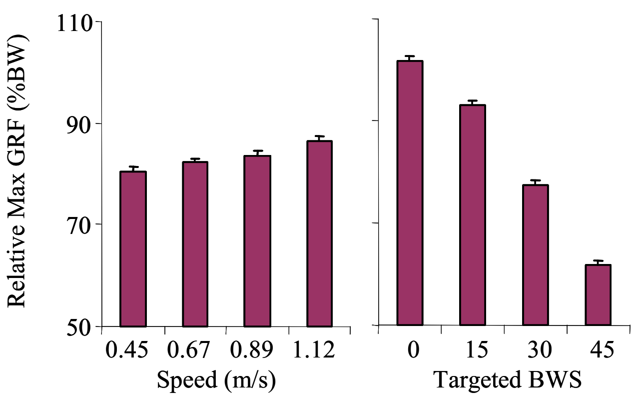

Figure 1: Maximum vertical ground reaction forces increases with walking speed and decreases with the amount of body weight being supported.

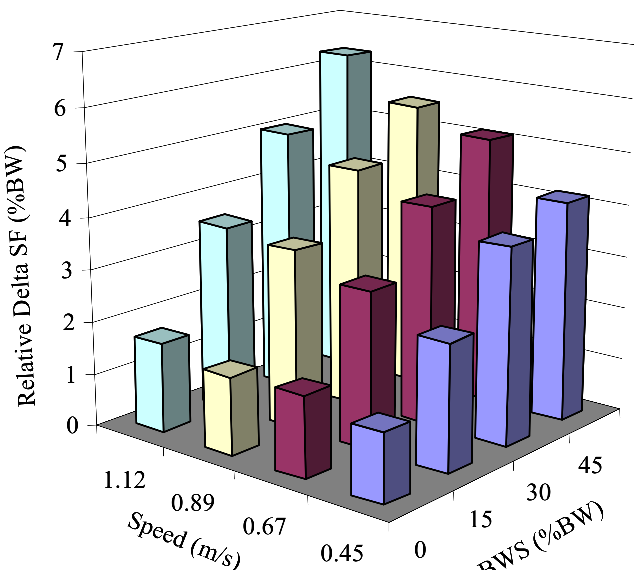

Figure 2: Body weight support amplifies the fluctuation of suspension forces larger then the proportion of body weight support. This influence was enhanced by greater walking speed.

RESULTS AND DISCUSSION

The mean and standard error of mean (SEM) of RMVGRF are reported in **Figure 1**. RMVGRF increased with walking speeds ($F_{3,45}$ = 512, P < 0.001) linearly ($F_{1,45}$ = 50.3, P < 0.001). It decreased with the increase of the targeted BWS ($F_{3,45}$ = 17, P < 0.0001) with both significant linear ($F_{1,45}$ = 1518, P < 0.001) and quadratic ($F_{2,45}$ = 16.3, P = 0.0002) trends. RMVGRF reduced from 101 to 92 %BW when %BWS increased from 0 to 15%, a reduction of approximately 9% BW. RMVGRF further reduced to 77 and 62 %BW (reductions of 15 %BW) when targeted BWS increased to 30 and 45%BW, respectively. RMAXSF ranged from 1.4 to 13.7 %BW and was influenced by both speed and %BWS (interaction, $F_{9,135}$ = 2.01, P < 0.05). The greatest RMAXSF was observed with 45% BWS and walking at 1.12 m/s. The fluctuation (RMAXSF-RMIMSF) of the suspension force is reported in **Figure 2**. The magnitude of this fluctuation changed from 1.3 %BWS, wit the lowest speed and targeted BWS, to 6.3, with the highest level of speed and targeted BWS. The fluctuation was influenced by both speed and targeted BWS (interaction, $F_{9,135}$ = 6.41, P < 0.0001).

CONCLUSIONS

Body weight support system does not provide consistent lift to the body being supported. The fluctuation of suspension force was amplified with greater proportion of body weight support and greater walking speed.

COMPARISON OF RECTIFIED AND UNRECTIFIED SOCKETS FOR TRANSTIBIAL AMPUTEES

[1] Jack R. Engsberg, [2] S. Wayne Sprouse [1] Mary L. Uhrich, [2] Barbara R. Ziegler and [2] F. Daniel Luitjohan
[1]Human Performance Laboratory, Department of Neurosurgery, Washington University in St. Louis,
[2]Precision Prosthetics and Orthotics; email: engsbergj@nsurg.wustl.edu, web: hpl.wustl.edu

INTRODUCTION

The traditional strategy for fabricating a transtibial amputee (TTA) socket is based upon the assumption that the residual limb is not uniform in its ability to tolerate load.[1] Thus, the contours of the residual limb mold are modified by the prosthetist (i.e., rectified socket). We have investigated a new method of shaping the socket using alginate gel.[2] Except for a distal end pad, the mold is shaped to the contours of the patient's residual limb (i.e., unrectified socket). The purpose of this investigation was to objectively compare rectified and unrectified sockets in adults with a TTA.

METHODS

Forty-three adults with a TTA participated (mean age 47±10 years, 36 males 7 females, height 176±8 cm, mass 84±17 kg). Subjects had mature residual limbs. Except for the socket shape, the prostheses were the same.

The prosthetist fabricated the rectified socket using the traditional method. The positive mold was made from a plaster cast and modified by filing down and building up different regions to account for the residual limb's inability to uniformly tolerate load. No more than three check sockets were permitted. In the unrectified socket fabrication process, the positive plaster mold was made using an alginate casting method. The subject placed his/her residual limb into alginate liquid and stood for approximately 5 minutes while the alginate gelled to a semi-solid state. The subject removed the residual limb from the gel leaving a negative mold. Plaster was immediately poured into the mold. This positive plaster mold was removed and very slightly smoothed with sanding screen. A distal end pad was included during socket fabrication, but no other modifications were made.

Subjects were tested after wearing the first randomly assigned socket for at least 4 weeks. They then wore the second socket and were tested after another 4 weeks. Data were collected: 1) from a gait analysis, 2) during a sub-maximal treadmill test (energy expenditure), and 3) from a Prosthetic Evaluation quality of life Questionnaire [PEQ].[3] After participation, the subject chose the socket he/she wished to have on the final prosthesis. Repeated measures ANOVA and a Chi square test were used to determine if significant differences existed ($p<0.05$).

RESULTS AND DISCUSSION

There were no significant differences for any of the variables (Table 1). The present study adds to the body of knowledge in at least two areas. First, there appears to be more than one paradigm for fitting a TTA socket. Despite the two different socket fabrication strategies, the results of the tests for gait, energy expenditure, the quality of life questionnaire (PEQ), and final socket selection were not different.

The second area is related to the simplicity of the alginate method. No shaping is done to the negative mold as it is applied to the residual limb, no modifications are made to the positive mold, and multiple check sockets are not needed. The omission of these steps saves time. The process may not require a prosthetist. The simplicity of the method could be valuable in third world countries where prosthetists and fabrication facilities are scarce or nonexistent. The simplicity of the method might also be beneficial to new amputees, since the effort associated with making a new socket is substantially reduced. Sockets could be fitted more frequently to better account for residual limb volume changes. The simplicity of the method could also save time in a typical prosthetic clinic.

CONCLUSIONS

It is concluded that more than one paradigm exists for shaping prosthetic sockets, and the alginate method is simpler than the traditional method. The alginate method may be helpful in third world countries, permit more frequent socket changes for new amputees, and save time in the typical prosthetic clinic.

REFERENCES

1. Radcliffe CW & Foorte J, *U of Calif, Biomech Lab*, Berkeley, CA. 1961.
2. Engsberg JR, et al. *J Prosthetics and Orthotics* **15**, 119-124, 2003.
3. Legro MW, et al. *Arch.Phys.Med.Rehabil.* **79,** 931-938, 1998.

ACKNOWLEDGEMENT

NICHD of NIH (#R01 HD38919).

Table 1. Means and standard deviations ( ) for key variables.

	Gait Speed	P/NP VGRF ratio	Minimum stance knee flexion (deg)		VO_2	PEQ Total	Final Socket Selection [c]
Socket	**cm/s**	**%**	**P**	**NP**	**ml/(kg*min)**	**%**	
Rectified	125 (22)	95 (7)	11 (6)	11(5)	13.4 (2.3)	82 (11)	16
Unrectified	125 (22)	96 (6)	10 (5)	11 (6)	13.5(2.6)	81 (13)	25
Able-bodied	133 (17) [a]	100	4 [b]	4 [b]			

[a] Waters et al., 1988; [b] Murray et al., 1964; [c] Two subjects decided to use both sockets; P = Prosthetic leg; NP = Nonprosthetic leg; Maximum Vertical Ground Reaction Force [VGRF] ratio

In Vivo Three-Dimensional Motion Analysis of the Lumbar Spine —Coupling Motion of the Lumbar Spine during Rotation—

[1] Fujii R, [1] Mukai Y, [1] Hosono N, [1] Sakaura H, [2] Ishii T, [1] Iwasaki M, [1] Sugamoto K, [1] Yoshikawa H
[1] Department of Orthopaedic Surgery, Osaka University Graduate School of Medicine
[2] Department of Orthopaedic Surgery, Hoshigaoka Koseinenkin Hospital
email: fujii-teddy@rio.odn.ne.jp

INTRODUCTION

In *vivo* 3D kinematics of the lumbar spine during rotation has not been well evaluated by the conventional methods because of inaccuracy. Only *in vitro* studies reported quantitative data in 3D intervertebral motions. However, the lack of physiologic muscle activity makes the results of *in vitro* study impractical [1]. Peacy et al [2] attempted to document *in vivo* coupled motion with axial rotation using biplanar radiography but failed to accurately demonstrate complex coupled motion, because their methods depended greatly on subjective assessments by examiner in tracking bony landmarks on plain radiographs. Considering those facts, in order to evaluate accurately, we developed a 3D imaging system for the relative motion of individual vertebra *in vivo* and reported the kinematics of the cervical spine using this original method [3,4]. The purpose of this study was to evaluate *in vivo* 3D intervertebral motions of the lumbar spine during rotation.

METHODS

Ten healthy volunteers underwent 3D-MRI of the lumbar spine in 9 positions with 15° increments during trunk rotation using a 1.0-T imager. Relative motions of the lumbar spine were calculated by automatically superimposing a segmented 3D-MRI of the vertebra in the neutral position over images of each position using voxel-based registration. 3D motions of adjacent vertebrae were represented with six degrees of freedom by Euler angles and translations on the coordinate system defined by Panjabi, and visualized in animations using surface bone models.

RESULTS AND DISCUSSION

The mean axial rotation of T12/L1, L1/2, L2/3, L3/4, L4/5 and L5/S1 in maximum trunk rotation (56.1°) to each side was 1.3°, 1.6°, 1.5°, 2.0°, 2.1° and 1.7°, respectively. Coupled lateral bending of L1/2, L2/3, L3/4, and L4/5 according to axial rotation was 2.0°, 3.6°, 3.8°, and 1.9°, respectively in the opposite direction and that of T12/L1 and L5/S1 was 0.9° and 0.8° in the same direction (Figure 1). Coupled flexion with axial rotation was observed (L1/2;1.0°, L2/3;1.5°, L3/4;1.5°, L4/5;1.2°, L5/S1;2.5°), while in thoracolumbar junction, extension was coupled with axial rotation (T12/L1;0.1°). These results are consistent with a previous *in vivo* study by Peacy et al (Table 1).

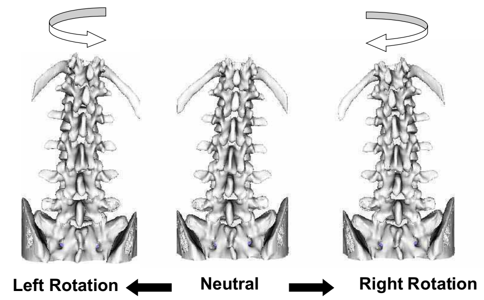

Figure 1: Coupled lateral bending with axial rotation was observed in the opposite direction as axial rotation from L1/2 to L4/5 level, in the same direction T12/L1 and L5/S1 level.

CONCLUSIONS

We investigated the 3D intervertebral motions of the lumbar spine during trunk rotation using a novel *in vivo* 3D motion analysis system, and this is a first report for the *in vivo* coupled motions with accuracy. This result will be helpful for the analysis of other lumber kinematic abnormalities.

REFERENCES

1. Panjabi M, et al. *Spine* **14,** 1002-1011, 1989
2. Pearcy MJ, et al. *Spine* **9,** 582-587, 1984
3. Ishii T, et al. *Spine* **29**, 2826-2831**,** 2004
4. Ishii T, et al *Spine* **29**, E139-E144**,** 2004

Table 1: Comparison of the Mean Range (°±SD) of Coupled Rotational Motion on one side

		T12-L1			L1-L2			L2-L3		
***In vivo* study**	**modality**	**Main AR**	**Coupled LB**	**Coupled F-E**	**Main AR**	**Coupled LB**	**Coupled F-E**	**Main AR**	**Coupled LB**	**Coupled F-E**
Peacy et al (1984)	**Bi-plane X-ray**	-	-	-	1	3	0	1	4	0
Present study	**3D-MRI**	1.3(0.5)	`-0.9(0.6)	`-0.1(0.4)	1.6(0.8)	2.0(0.8)	1.0(1.1)	1.5(0.6)	3.6(1.0)	1.5(0.9)

		L3-L4			L4-L5			L5-S1		
***In vivo* study**	**modality**	**Main AR**	**Coupled LB**	**Coupled F-E**	**Main AR**	**Coupled LB**	**Coupled F-E**	**Main AR**	**Coupled LB**	**Coupled F-E**
Peacy et al (1984)	**Bi-plane X-ray**	2	3	0	2	2	0	1	-2	0
Present study	**3D-MRI**	2.0(0.6)	3.8(1.1)	1.5(0.7)	2.1(0.7)	1.9(0.8)	1.2(0.7)	1.7(0.6)	`-0.8(0.7)	2.5(1.9)

Coupled lateral bending (+) represent the opposite direction of axial rotation   Coupled flexion-extension (+) represent flexion.
AR = axial rotation; LB = lateral bending; F-E = flexion-extension

PLANTAR PRESSURE DISTRIBUTION IN THE DIABETIC FOOT DURING PUSH-OFF: NUMERICAL SIMULATION USING THE P-VERSION OF THE FINITE ELEMENT METHOD

[1] Ricardo L. Actis, [1]Liliana B. Ventura, [2]Barna A. Szabo
[3]Paul K. Commean, [3]Kirk E. Smith, [3]Donovan J. Lott and [3]Michael J. Mueller
[1]Engineering Software Research & Development, Inc.; email: Ricardo.Actis@esrd.com
[2]Center for Computational Mechanics, Washington University
[3]Washington University School of Medicine

INTRODUCTION
The most common cause for diabetic plantar ulcers is excessive plantar pressures in the presence of sensory neuropathy and foot deformity. Proper footwear fitted with a total contact insert (TCI) or TCI with a metatarsal pad are the standard of care for reducing forefoot plantar pressures, although research has not clearly indicated optimal size, location and material properties of orthotic components. One key aspect for achieving this goal is to develop three-dimensional computational models of the foot for enhancing and evaluating a broad range of orthotic device components.

METHODS
In modeling a complex system like the human foot, it is necessary to make simplifying assumptions regarding topological details, constitutive laws, material properties and boundary conditions. Such simplifications are acceptable only if they do not significantly affect the data of interest, in this case the pressure distribution in the regions of the metatarsal heads at push-off. In our investigation, the complexity of the model was increased hierarchically, until the computed pressure distribution was no longer affected by the restrictive assumptions incorporated in the simpler models. The three-dimensional internal structure of the foot was determined using data from SXCT [1], while the reference pressure distribution was measured using the F-scan system [2] with the pressure sensor taped to the subject's foot.

We considered the structure of the foot to be characterized by bone, cartilage, flexor tendon, fascia and tissue. The material properties for the bones were assumed to be linear. Cartilage with linear elastic material properties was included between bones to simulate the flexibility of the connection between bony structures. Muscles and fat were lumped into a single material type (tissue) with nonlinear elastic properties obtained for each individual using an indentor testing device [3]. Fascia and flexor tendon were also incorporated into the model and the properties were assumed to be linear elastic.

RESULTS AND DISCUSSION
Figure 1 shows the section taken through the second metatarsal of the foot in the push-off position of a 63 year-old, male, diabetic subject, with a history of a plantar ulcer. Simpler models were constructed by removing the cartilage between phalanges, or by not including the fascia or the flexor tendon in the model in various combinations.

The p-version FEA program StressCheck was used for the numerical simulation. The influence of the different modeling considerations in the pressure distribution in a region 15 mm proximal and 20 mm distal from the center of the metatarsal head was compared with the one obtained with the F-scan system.

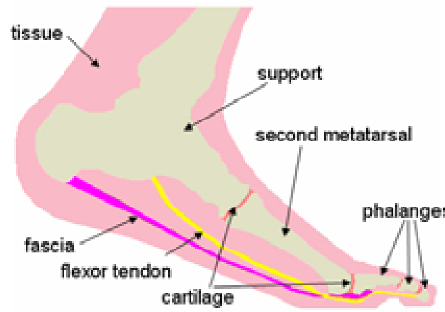

Figure 1: Segmentation for the most complex model considered for analysis.

Predicted and measured pressure distributions were compared in four patients with diabetes and a history of neuropathic ulcer and the agreement was found to be generally good (typically within 12% error in L2 norm) as shown in Figure 2.

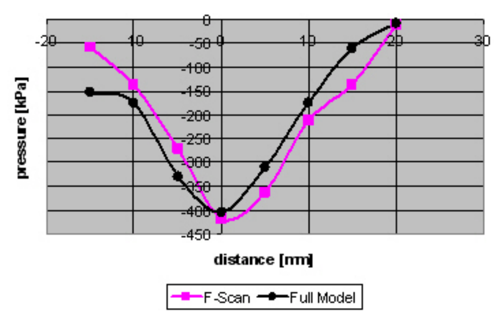

Figure 2: Measured (F-Scan) and computed (Full Model) pressure distributions under the 2nd metatarsal head.

CONCLUSIONS
Initial validation of our computational model is reasonable and future work will seek to determine optimal characteristics of orthotic devices and footwear to distribute plantar pressures evenly.

ACKNOWLEDGMENTS
We acknowledge funding from NCMRR, NIH, RO1 HD 36895.

REFERENCES
1. P. K. Commean, et al., *Arch. Phys. Med. Rehabilitation* 183 (2002): 497-505.
2. M. J. Mueller and M. J. Strube, *Clinical Biomechanics* 11 (1996): 159-164.
3. J. W. Klaesner, et al., *IEEE Trans Neural Systems and Rehabil Eng,* 9 (2001): 232-240.

EFFECT OF ARM USE ON HEAD AND TRUNK SEGMENT MOTION WHEN RISING FROM A CHAIR

[1] Wendy Gilleard, [2]Jack Crosbie and [2]Richard Smith
[1]Southern Cross University, Lismore Australia
[2]University of Sydney; email: wgillear@scu.edu.au

INTRODUCTION

Dynamic analyses during rising to stand from a chair, of the head, and trunk segments have been rarely investigated. Much of the research to date has examined a constrained motion in that the subjects rise with arms folded and kept as close to the body as possible. The use of the upper limbs, however, have been found to significantly affect movement strategies for the body's centre of mass (COM) [1]. When the arms were restricted the COM had a reduced forward displacement, and lowered horizontal and vertical linear momentum [2]. Although a significant difference was found in the ankle joint displacement [1], the effect of restricted arm motion on the motion of the head and trunk segments is unknown. The purpose of the study was to investigate the peak displacement of the head, thoracic and pelvic segments for a rise to stand from a chair when using the arms in a natural manner in comparison to crossed across the chest.

METHODS

Twelve female subjects rose to stand for three trials of each condition: in a natural manner and with the arms crossed across the chest. Data were collected using an 8 camera motion analysis system and a height adjustable chair set to 110% of fibular head to floor distance while standing. Retro-reflective markers were used to define the pelvis, thoracic and head segments with three markers per segment. Sagittal plane displacement of the head, thoracic and pelvic segments. and the thoracolumbar and cervicothoracic spines were calculated throughout the motion. Relative motion of the head and thoracic, and thoracic and pelvic segments were taken as the cervicothoracic and thoracolumbar spines respectively. A single marker each on the right humeral lateral epicondyle and greater tubercle allowed sagittal plane range of motion (ROM) of the right shoulder to be investigated. Paired Students t-tests were used to compare peak displacements.

RESULTS AND DISCUSSION

The head, thoracic and pelvic segments first flexed forward and then extended as the rise continued. During the pre-extension phase the thoracic segment flexed more than the pelvis causing relative thoracolumbar flexion. The thoracic segment flexion then slowed relative to the pelvic segment causing thoracolumbar extension for the remainder of the movement. For the cervicothoracic spine, the head and thoracic segment initially flexed forward, however the head segment forward flexion was less than that for the thoracic segment causing relative cervicothoracic spine extension prior to seat off. Extension of the thoracic segment then resulted in flexion of the cervicothoracic spine as the rise continued.

There was no significant difference between a natural and constrained rise to stand for the peak flexion of the thoracic and pelvic segments and the thoracolumbar spine (Table 1). The head segment was significantly more flexed during a constrained rise and the cervicothoracic spine was consequently less extended (Table 1). It is possible that greater head forward rotation was utilized to compensate for the reduced input to upper body momentum from the restricted arm motion of a constrained movement.

During a natural rise all subjects first flexed the shoulder prior to seat-off, then extended. During a constrained rise some subjects followed a similar movement pattern while others first extended the shoulder joint then flexed ie the upper limbs were bought closer into the trunk. The former strategy was similar to the motion used when the upper limbs were free to move and therefore may be considered a curtailed normal motion in an attempt to minimize the shoulder flexion motion. The latter strategy, however, is opposite in direction to the overall movement. Bringing the upper limbs closer to the chest may, however, increased the thoracic segment forward flexion and therefore the upper body centre of mass was brought forward and assisted in compensating for the loss of normal upper limb contribution to the overall movement. No differences were noted between the thoracic segment peak flexion for a free or constrained rise, however the differences may have been masked by the use of the two shoulder motion strategies within the group.

As would be expected there was a significant increase in shoulder joint ROM with a natural arm movement (Table 1). During the constrained motion, despite requesting the arms be held against the chest, motion still occurred at the shoulder joint as previously reported [1]. Forward upper limb motion was therefore thought to be concomitant to lower limb motion during rising to stand [1].

Table 1: Peak displacement (°).

	Natural	Constrained	p
Head	3.35 ± 4.75	8.39 ± 6.46	0.005*
Thorax	36.76 ± 4.91	37.08 ± 9.13	0.861
Pelvis	36.10 ± 6.73	36.71 ± 9.55	0.668
Cervicothoracic	-38.69 ± 8.27	-30.43 ± 8.66	0.019*
Thoracolumbar	32.48 ± 8.83	32.89 ± 8.07	0.707
Shoulder ROM	13.67 ± 4.45	8.16 ± 3.65	0.001*

Positive values are flexion and negatives values are extension
* significantly different at $p<0.05$

REFERENCES

1. Carr J & Gentile AM. Hum Move Sci **13**, 175-193, 1994.
2. Carr J. Physiotherapy Theory & Practice **8**, 159-164, 1992.

UPPER EXTREMITY ROBOTIC THERAPY IN STROKE PATIENTS WITH SEVERE UPPER EXTREMITY MOTOR IMPAIRMENT

Margaret A. Finley[1, 2], Christopher T. Bever[1, 3] Hermano I. Krebs[4]
[1]VA Maryland Healthcare System, Rehabilitation Research & Development, Baltimore, MD, [2] University of Maryland School of Medicine, Dept of Physical Therapy and Rehabilitation Science, Baltimore, MD., [3]University of Maryland School of Medicine, Dept of Neurology, Baltimore, MD. [4]Massachusetts Institute of Technology, Mechanical Engineering Dept, Cambridge, MA.
Email: mfinley@som.umaryland.edu

INTRODUCTION

Chronic motor deficits in the upper limb are a major contributor to disability following stroke. Although it has been shown that improvements in motor function are most likely in the initial three months following stroke, recent research has demonstrated that gains in motor function can occur with intensive motor learning-based rehabilitation in people even many years post-stroke (1,2). The purpose of this study was to investigate the effect of robotic therapy on motor function and robot derived performance measures in patients with chronic, severe upper extremity (UE) impairments after stroke.

METHODS

As part of a larger study, 15 individuals with chronic, severe UE paresis (Fugl-Meyer <15) after stroke (> six months post onset) performed 18 sessions of robot-assisted UE rehabilitation consisting of goal-directed, planar reaching tasks over a period of three weeks. The robot testing involved the subject reaching for each target, clockwise around the circle pattern without movement assistance from the robot. A movement began when the speed first became greater than 2% of the peak speed and ended after the speed dropped and remained below the 2% threshold again. Kinematic variables derived from the robot evaluation data were aiming error (mean absolute angle between actual direction and a straight line between start and target), mean speed (total distance traveled over total movement duration), peak speed, mean-to-peak speed ratio (mean speed divided by the peak speed which has previously been used as a metric of movement smoothness) (3) and movement duration. Outcome measures included the Fugl-Meyer Assessment, the Motor Power Assessment, the Wolf Motor Function Test, and five robot derived measures (aiming error, mean speed, peak speed, mean: peak speed ratio and movement duration). Student t-tests evaluated differences between baseline and post-treatment outcomes ($p \leq 0.05$). Cohen's *d* was calculated to determine the effect size of treatment on the clinical and robot-derived measures.

RESULTS AND DISCUSSION

Training produced statistically significant improvements from baseline to discharge in the Fugl-Meyer and Motor Power Assessment scores, and in the quality of motion (quantified by a reduction in aiming error and movement duration with an increase in mean speed and speed ratio variables-Table 1). These findings provide evidence that persons with severe UE paresis long after stroke onset can demonstrate reduced motor impairment with a brief, intense robot-assisted intervention. Previous research showed that early in recovery post-stroke, a patient's movements are composed of short, sporadic sub-movements with a series of peaks and valleys. As subjects improved with training, reaching movements became smoother with fewer stops, suggesting improved inter-joint coordination and neural recovery processes (3). In the present study, large treatment effects for the robot-derived measures indicate that movement accuracy and smoothness did improve with practice in these individuals with severe, chronic paresis.

CONCLUSIONS

Our findings indicate that robot-assisted UE rehabilitation can reduce UE impairment and improve the quality of motion in patients with severe UE impairments from chronic stroke.

REFERENCES

Hendricks HT, et al Arch Phys Med Rehabil 2002;83(11):1629-37.
Fasoli SE, et al. Arch Phys Med Rehabil 2003;84(4):477-82.
Rohrer B, et al J Neurosci 2002;22(18):297-3

Table 1: Means (standard error of mean) for robotic outcome variable scores at baseline, post treatment

N=15	Aiming error (radians)	Mean Speed (m/sec)	Peak Speed (m/sec)	Mean-to-Peak Speed Ratio	Movement Duration (sec)
Baseline	1.144 (0.040)	0.038 (0.004)	0.138 (0.012)	0.284 (0.013)	4.850 (0.366)
Post-Treatment	1.009 (0.055)	0.046 (0.004)	0.131 (0.011)	0.360 (0.016)	3.357 (0.334)
Change	-0.136 (0.038)	0.007 (0.002)	-0.006 (0.005)	0.076 (0.012)	-1.492 (0.310)
Effect size (Cohen's *d*)	0.73	0.37	0.14	1.38	1.10
p-values	<0.01*	<0.01*	0.27	<0.01*	<0.01*

* = Significant change baseline to discharge

GAIT DEVIATIONS IN CHILDREN WITH SEVERE HAEMOPHILIA FOLLOWING BLEEDING INTO THE ANKLE JOINT

[1, 2] David Stephensen, [1]Wendy Drechsler, [2]Mark Winter, [2]Gillian Evans, [1]Oona Scott
[1]School of Health and Biosciences, University of East London, London, United Kingdom
[2]Kent Haemophilia Centre, Kent and Canterbury Hospital, Canterbury, United Kingdom
email: W.Drechsler@uel.ac.uk

INTRODUCTION

Haemophilia is an inherited bleeding disorder in which the blood does not clot normally and is characterised by spontaneous and traumatic musculoskeletal bleeding into joints and muscles [1,2]. This paper provides for the first time a description of the gait pattern of children with severe haemophilia who have experienced at least 3 episodes of bleeding into the ankle joint and how this gait pattern deviates from normal gait.

METHODS

Five children, (mean ± SD, age 10.02 ± 2.82 years) with severe haemophilia and 4 age-matched normal controls, (10.05 ± 2.53 years) volunteered to take part in this pilot study. Kinematic and kinetic data for the pelvis and lower limb was collected using a 10 camera Vicon 612 Motion Analysis System (Oxford Metrics Ltd, UK) and 2 Bertec Force Platforms (Model MIE Ltd, Leeds, UK). The force platforms were positioned in the middle of a 7.5 metre walkway and subjects walked barefoot at a self-selected comfortable walking speed. Mean and peak angles and moments in the gait cycle, initial contact and toe off were analysed for differences between the haemophilia subjects and healthy matched controls using the Mann-Whitney U independent t-test for non parametric data. Spearman rank correlations were also used to investigate the relationship between an established clinical haemophilia assessment score [3] and gait changes.

RESULTS AND DISCUSSION

Children with a history of bleeding into the ankle joint adopted a gait pattern which differed from that of normal children. Table 1 shows the differences seen in the ankle and knee angles, while Figure 1 shows the significantly greater ankle plantarflexion ($p=0.01$) and smaller ankle dorsiflexion moments ($p=0.05$). Significantly greater knee flexion moments ($p=0.01$), greater knee flexion angles ($p=0.01$), smaller ankle adduction angles ($p=0.02$), smaller ankle external rotation angles ($p=0.04$) were also found in children with haemophilia.

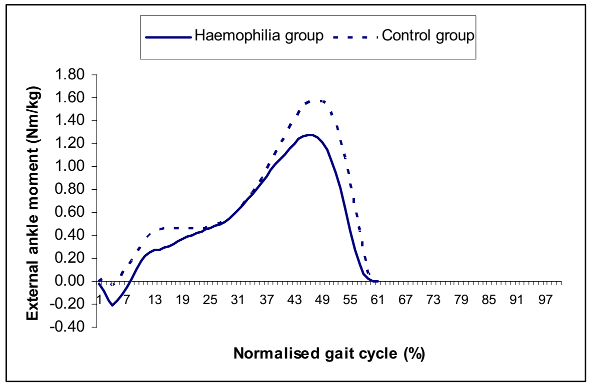

Figure 1. Graph showing sagittal plane ankle moments

Gait velocity was significantly reduced ($p=0.02$) in the children with haemophilia with no apparent relationship was shown between velocity and the clinical haemophilia score [3].

Increased flexion and loading at the knee joint may lead to greater susceptibility to haemarthrosis and disability at the knee joint for these children that may affect lower limb muscle function.

CONCLUSIONS

The results of this pilot study demonstrate that children with haemophilia alter their walking possibly to protect and decrease the load and forces at the ankle joint and increase the load and forces at the knee joint that may affect lower limb muscle function. The subtle gait abnormalities in these children were undetected in either clinical examination or the clinical assessment score.

REFERENCES

1. Wallny T, et al. *Haemophilia*, **8**: 802-808, 2002.
2. Rodriguez-Merchan E.C. *Clinical Orthopaedics & Related Research* **79**: 1421-1427, 1996.
3. Manco-Johnson M, et al. *Haemophilia*, **6**: 649-657, 2000.

Table 1: Means (± SD) sagittal plane joint angles and maximum joint moments during level walking.

		Haemophilia Group	Normal Group
Mean Joint Angles (degrees)	Ankle	2.63 (± 4.08)	1.44 (± 3.28)
	Knee **	24.85 (± 5.84)	15.98 (± 5.03)
	Hip	12.61 (± 6.57)	15.25 (± 4.66)
Max Joint Moments (Nm/kg)	Ankle *	1.30 (± 0.27)	1.59 (± 0.26)
	Knee *	0.79 (±6.57)	0.36 (± 0.27)
	Hip	1.68 (± 0.51)	2.11 (± 0.70)

* $p \leq 0.05$ ** $p \leq 0.01$

DOES GRAVITY INFLUENCE THE STRUCTURE OF CHAOTIC GAIT PATTERNS?

[1]Max J. Kurz, [1]Nicholas Stergiou, [2]Jacob Bloomberg and [1]David Miller
[1]HPER Biomechanics Laboratory, University of Nebraska at Omaha, Omaha, NE
[2] Neuroscience Laboratory, NASA-Johnson Space Center, Houston, TX
E-mail: mkurz@mail.unomaha.edu Web: http://www.unocoe.unomaha.edu/hper/bio/home.htm

INTRODUCTION

Historically, fluctuations in human gait patterns were considered to be random noise or error in the output of the nervous system. However, recent investigations have suggested the contrary and have indicated that such fluctuations have a chaotic structure. A chaotic structure means that the lower extremity kinematics fluctuate from one step to the next with a deterministic pattern. Changes in the chaotic structure appear to be related to the health and stability of the neuromuscular system [1].

The Lyapunov exponent (LyE) is used to quantify the chaotic structure present in a gait pattern [1]. The LyE for a periodic signal (e.g. sine wave) is zero, which indicates no separation in the attractor's trajectory. Alternatively, the LyE for Gaussian noise is positive (+0.469) and indicates divergence in the attractor's trajectory. Hence, a time series that has LyE value close to +0.469 indicates instability, while a time series with LyE close to zero indicates stability or possibly rigidity. The chaotic structure of human locomotion lies somewhere between these two extremes [1]. The degree of stability of a gait pattern can be explored from a chaotic perspective by investigating whether the LyE value shifts towards one of the two extremes, as the independent variable is scaled.

The influence of Newtonian forces on gait stability is not yet completely understood. Here we explore the influence of gravity on chaotic gait stability with a passive dynamic bipedal walking model and experiments where humans walk at simulated micro-gravities.

METHODS

The passive dynamic bipedal model consisted of two rigid legs connected by a frictionless hinge at the hip (Figure 1; [2, 3]). Slight increases in the ramp angle of the walking surface promote a cascade of bifurcations that lead to a chaotic gait pattern [2, 3]. Different micro-gravities were simulated by decreasing gravity in the model's governing equations at the respective ramp angles. A custom built body weight suspension (BWS) system was used to experimentally explore the influence of various micro-gravities on human chaotic locomotion. The BWS supplied a constant upward force on the subject's center of gravity via a cable-spring-winch system that was monitored with a force transducer [4]. Five subjects walked on a treadmill for two minutes under the following micro-gravities: 1.0, 0.9, 0.8, and 0.7 Gs. LyE values were calculated for the sagittal plane joint angle time series of the hip, knee and ankle with an embedding dimension of five.

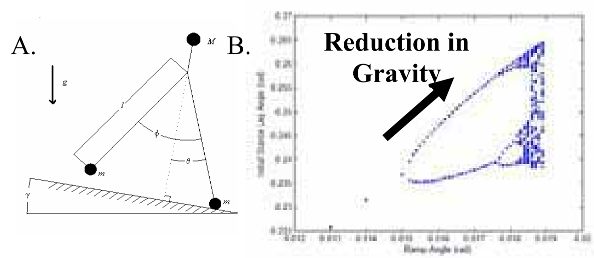

Figure 1. The passive dynamic walking model (A). Bifurcation map of the model's locomotive patterns for the respective ramp angles. Chaotic gait exists when ramp angle is greater than 0.1839 radians [3] (B).

RESULTS AND DISCUSSION

Our simulations provided initial evidence that gravity influences the structure of chaotic gait patterns. As gravity was reduced the model's gait bifurcated towards a chaotic gait pattern that was closer to instability (Figure 1B). The human experiments complemented our model's simulations (Table 1). In general, as gravity was reduced the human chaotic gait patterns shifted towards instability. A significantly increasing linear trend was found for the ankle joint ($p = 0.03$) where lower micro-gravities were associated with less stability. Hence, changes in gravitational forces influenced the performance of the ankle for maintaining stable gait patterns. Although a reduction in gravity is associated with a more economical gait [4], our results indicate that it is not associated with a more stable gait. Alternative counter measures for maintaining a stable gait in micro-gravity environments (i.e. the Moon or Mars) may be necessary. Our future investigations will reveal how changes in other Newtonian forces influence chaotic gait patterns.

REFERENCES

1. Stergiou N *et al.* (2004). *Innovative Analysis of Human Movement*. Human Kinetics:Champaign, IL.
2. Garcia M, *et al. J. Biomech. Eng.* **120(2)**, 281-288, 1998.
3. Kurz MJ, *et al. Chaos, Solitons Fractals* **23**, 485-493, 2005.
4. Farley CT & McMahon TA. *J Appl Physiol* **73(6)**, 2709-2712, 1992.

Table 1. LyE means and standard deviations for the respective lower extremity joints and micro-gravities.

Joint	1G	0.9G	0.8G	0.7G
Ankle	0.176 (.03)	0.189 (.02)	0.196 (.02)	0.213 (.02)
Knee	0.104 (.05)	0.120 (.04)	0.120 (.04)	0.124 (.03)
Hip	0.109 (.03)	0.107 (.02)	0.117 (.02)	0.119 (.01)

AN ARTIFICIAL NEURAL NETWORK THAT EXPLORES THE ROLE OF SENSORY INFORMATION FOR LEARNING THE NEURAL CONNECTIONS FOR LOCOMOTION

Max J. Kurz and Nicholas Stergiou
HPER Biomechanics Laboratory, University of Nebraska at Omaha, Omaha, NE
E-mail: mkurz@mail.unomaha.edu Web: http://www.unocoe.unomaha.edu/hper/bio/home.htm

INTRODUCTION

Human and animal research has indicated that the spinal locomotive neural network wiring is depended on appropriate sensory information. Previous studies have indicated that the loading of the stance limb and the stretch of the hip musculature during the terminal portion of the stance phase are important sensory variables for establishing the spine's neural network connections [1]. However, it is currently not clear which sensory information has a greater influence on the neural wiring. Such difficulties may lie in the fact that it is difficult to completely separate the sensory variables in humans and animals [1].

Artificial neural networks (ANN) are composed of biologically inspired neuron like elements that can be use to model the behaviors of spinal neural networks [2]. ANN are unique because they can be used to simulate the influence of isolated sensory inputs on the wiring of the network's neural connections. Here we use ANN models to further elucidate the effect of limb loading and hip joint sensory information on the development of the neural connections for locomotion.

METHODS

Two feed-forward ANN models that each had six input neurons, three hidden neurons and one output neuron were developed. Neurons between each layer were connected via a series of weighted edges (w_{ij}). Each *i*th neuron had an input value x_i and an output value $y_i = g(x)$. A sigmoid function $g(x) = (1+ e^{x})^{-1}$ was used to determine the excitation of the neuron where the value of x was given by $x_i = \sum w_{ij}y_j$. Through training, the two ANNs learned the proper neural connections to supply a toe-off impulse that actively powered a passive dynamic bipedal model [3] (Figure 1). The simple bipedal model consisted of two rigid legs connected by a torsional spring at the hip. The potential energy of the spring (PE) at the terminal portion of each step was used to model the hip joint sensory information (Eq 1).

$$PE = \tfrac{1}{2}\, k\, (\phi-\theta)^{2=} \qquad \text{Equation 1.}$$

Where k was the stiffness of the hip spring, θ was the stance leg angle, and ϕ was the swing leg angle. k was constant in the bipedal model and was set at 0.01 s^{-2}. The loading force (LF) of the new stance leg was modeled by geometrically calculating the force that occurred at heel-contact (Eq 2).

$$LF = \cos(90-2\theta) * \ddot{\theta} \qquad \text{Equation 2.}$$

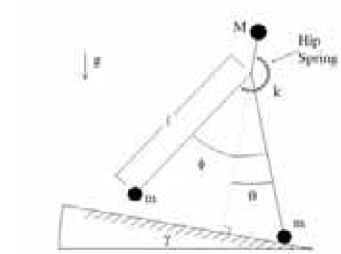

Figure 1. The passive dynamic bipedal walking model [3] that the ANN learned to actively power with a toe-off impulse.

The six sensory inputs for each ANN model were as follows: θ, $\dot{\theta}$, ϕ, $\dot{\phi}$, PE and LF. The first ANN model was not provided with LF, but was provided with PE. The second ANN model was not provided PE, but was provide LF. The initial edge weights for the neurons that were common between the two ANN models were the same. Sensory nodes that were not used in the respective ANN models were set to null. A total of 120,000 training epochs were used in this investigation. The ANN model with the largest mean square error at the respective epochs had a worse learning curve.

RESULTS AND DISCUSSION

Our simulations indicate that the PE and LF played different roles for learning the locomotive neural connections. The ANN trained with LF had a faster initial learning rate. However, as the training exceeded 3000 epochs, the amount of learning that occurred with the LF did not substantially change. Sensory information provided by the PE resulted in a more gradual learning curve and did not influence the neural connections as drastically during the early learning stages. However, as the number of epochs increased, the learning curve from the ANN trained with EPE eventually surpassed the performance of the ANN model trained with LF. These simulations suggest that during the early portions of locomotor training, sensory information from the loading forces may be vital to accelerate the learning process. However, as training progresses, hip joint sensory information may provide more meaningful information for the establishment the neural connections for stable locomotion. These simulations provide insight on the interactive role of these two sensory variables for learning the locomotive neural connections.

REFERENCES

1. Ferris DP, et al. *Spinal Cord* **42**, 14-23, 2004.
2. Russell SR & Norvig P. *Artificial Intelligence a Modern Approach*. Prentice Hall: NJ, 2003.
3. Kuo AD. *J Biomech Eng* **124**, 113-120, 2002.

DISTRIBUTION OF BONE MINERAL DENSITY IN THORACIC AND LUMBAR VERTEBRAE: AN *EX VIVO* STUDY USING DUAL ENERGY X-RAY ABSORPTIOMETRY (DXA).

[1,2] Andrew Briggs, [2]John Wark, [2]Susan Kantor, Nicola Fazzalari, [1,2]Alison Greig, [1]Tim Wrigley and [1]Kim Bennell
[1]Centre for Health, Exercise and Sports Medicine, School of Physiotherapy, University of Melbourne, Australia.
[2]Department of Medicine, Royal Melbourne Hospital, University of Melbourne, Australia.
[3]Institute of Medical and Veterinary Science, South Australia
email: a.briggs3@pgrad.unimelb.edu.au , web: www.physioth.unimelb.edu.au/chesm/

INTRODUCTION

Vertebral fractures are considered to be one of the hallmarks of osteoporosis. The aetiology of these fractures remains unclear, since individuals with comparable bone mineral density (BMD) measured with DXA demonstrate different prevalence rates for fracture. Previous research has demonstrated heterogeneity of bone properties within the vertebral centrum [1]. The distribution of BMD within the centrum may help to explain the aetiology of these fractures. The majority of vertebral fractures occur in the mid thoracic spine. However, DXA cannot be used to measure BMD in this area *in vivo*. The aims of the current study were to determine if regional differences exist in BMD in thoracic and lumbar vertebrae and to determine if the patterns of BMD distribution were similar between these levels.

METHODS

Six embalmed cadaver spines were used for this study (mean 81yrs). Antero-posterior and lateral DXA scans were performed on each specimen with an Hologic QDR4500 densitometer. The lateral scan was used to calculate areal BMD for the whole vertebral body and in 3 subregions orientated longitudinally (posterior, middle, anterior) and 3 subregions orientated transversely (superior, central, inferior) for T7, T8, L2 and L3. Vertebral areas were defined manually by the raters and were of equal size in each plane for each vertebral body. Differences in subregional BMD were examined using a one way repeated measures ANOVA with 4 levels set *a priori* (whole vertebral body with 3 subregions) to prevent *post hoc* comparisons of overlapping subregions.

RESULTS AND DISCUSSION

A significant difference in subregional BMD was found for T7, T8, L2 and L3 (p<0.05). Post hoc tests revealed significantly lower BMD in the central zone of T7, T8, L2 and L3 (p<0.05) (see Figure 1), and in the anterior zone of L2 and L3 (p<0.05) (see Figure 2). Volumetric BMD, rather than areal BMD may be a better variable for longitudinal subregion comparisons due to differences in their 3D geometry.

These results confirm the ability of a commonly used clinical tool, DXA, to detect differences in BMD within vertebral bodies. The results also demonstrate that interpretation of whole vertebral BMD in isolation can obscure potentially important regional density characteristics. The lower BMD observed in the central subregion of thoracic and lumbar vertebrae may help to explain the mechanisms underlying vertebral crush fracture. Compared to the other subregions, the central subregion contains minimal cortical bone and maximal trabecular bone. Therefore, this area may be of significant clinical importance given that trabecular bone is known to be

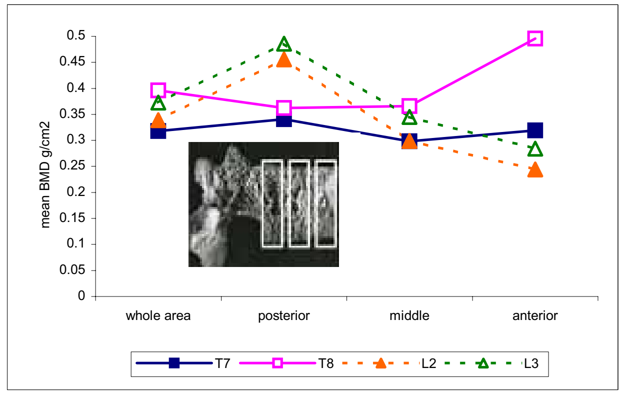

Figure 1: Mean BMD for whole vertebral area and posterior, middle and anterior (transverse) subregions at T7, T8, L2, L3

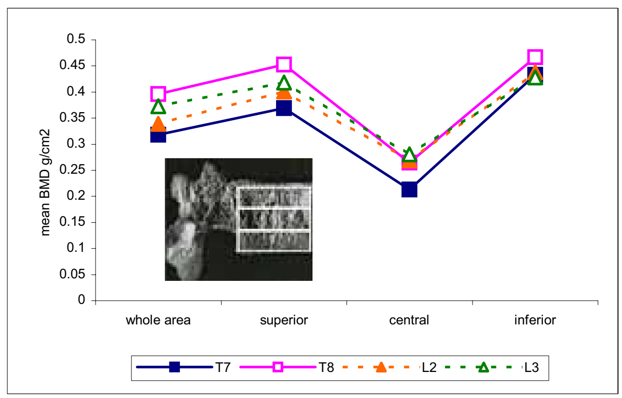

Figure 2: Mean BMD for whole vertebral area and superior, central and inferior (longitudinal) subregions at T7, T8, L2, L3

the dominant structural component in resisting compressive load [2]. Significantly lower BMD in the anterior zone of lumbar vertebrae may help to explain a mechanism for vertebral wedge deformity. Figure 2 illustrates a similar density distribution profile between thoracic and lumbar vertebrae. Given that thoracic BMD cannot be measured *in vivo* with DXA, it may be plausible to assume that measurement of lumbar subregional BMD could be used to predict thoracic BMD distributions.

CONCLUSIONS

DXA can be used to detect differences in BMD within vertebral bodies. These differences may explain, in part, mechanisms underlying vertebral fracture. Intra-vertebral density profiles show some similarities between thoracic and lumbar vertebrae.

REFERENCES

1. Simpson EK, et al. *J Bone Min Res*. **16**, 681-687, 2001.
2. Silva MJ, et al. *Spine* **22**, 140-150, 1997.

In Vivo 3D Intervertebral Motion Analysis of the Cervical Spine in Lateral Bending using 3D-MRI

[1] Takahiro Ishii, [1]Yoshihiro Mukai, [1]Noboru Hosono, [1]Hironobu Sakaura, [1]Ryutaro Fujii,
[2]Eiji Wada, [2]Masayoshi Ishii, [2]Hideo Kawai, [1]Motoki Iwasaki, [1]Kazuomi Sugamoto and [1]Hideki Yoshikawa
[1] Osaka University Graduate School of Medicine, [2] Hoshigaoka Koseinenkin Hospital
Email: ishii-takahiro88@umin.ac.jp

INTRODUCTION

In vivo 3D motion of the cervical spine has not been documented until now, since they are too complicated to follow with conventional radiographs or CT. Although *in vitro* studies using cadaver specimens reported data on the cervical 3D motion, it might not actually reflect physiological motion due to the lack of tonus of musculature. Moreover, understanding 3D motions with only a numerical combination of rotations and translations was difficult. To overcome these problems, we developed a quite unique *in vivo* 3D motion analysis system using 3D-MRI, which can make the 3D animation of the motion, and reported the kinematics of the cervical spine in rotation using this system [1,2]. The purpose of this study is to demonstrate for the first time *in vivo* 3D intervertebral motions of the cervical spine in lateral bending.

METHODS

Twelve healthy volunteers underwent 3D-MRI of the cervical spine in 7 positions with 10° increments during lateral bending using a 1.0-T imager. Relative motions of the cervical spine were calculated by automatically superimposing a segmented 3D-MRI of the vertebra in the neutral position over images of each position using volume registration, which is a method to determine relative position between two volume images by means of superimposing two 3D images to make each voxel value coincide each other maximally, and correlation coefficient was used as similarity measure. Three-dimensional motions of adjacent vertebrae were represented with six degrees of freedoms by Euler angles and translations on the coordinate system defined by Panjabi, and visualized in animations using surface bone models reconstructed with marching cubes algorithm in the Visualization Toolkit (VTK). As we have already declared, the accuracy of this system was 0.24° for flexion-extension, 0.31° for lateral bending, and 0.43° for axial rotation. Mean absolute translational error was 0.52 mm for superoinferior translation, 0.51 mm for anteroposterior translation, and 0.41 mm for lateral translation. [1].

RESULTS AND DISCUSSION

Mean maximum lateral bending of the cervical spine to one side in maximum head lateral bending (30.3°) was 1.9° at Oc/C1, 1.6° at C1/2, 3.7° at C2/3, 3.5° at C3/4, 3.3° at C4/5, 4.3° at C5/6, 5.7° at C6/7, and 4.1° at C7/T1. C6/7 showed the larger lateral bending than other levels (P < 0.05). Coupled axial rotation in the opposite direction to that of lateral

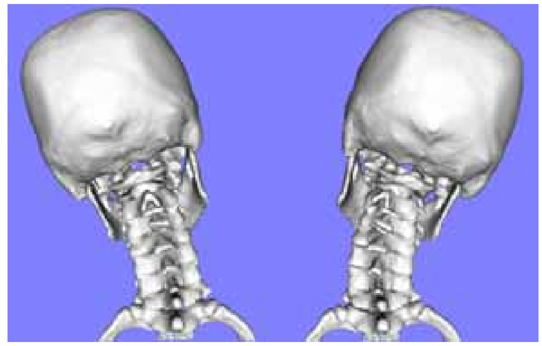

Figure 1: Cervical motion in left and right lateral bending

bending was observed in the upper cervical levels (Oc/C1, 0.2°; C1/2, 17.1°), while in the subaxial cervical levels, it was observed in the same direction as lateral bending except for C7/T1 (C2/3, -0.9°; C3/4, -1.8°, C4/5, -1.1°, C5/6, -1.2°; C6/7, -0.8°; C7/T1, 0.4°). Coupled flexion-extension was small at all vertebral levels (< 1.1°).

In our previous study, we documented that axial rotation of subaxial cervical spine accompanied lateral bending in the same direction as axial rotation. Thus, coupling patterns of subaxial cervical spine were similar between lateral bending and axial rotation. We speculated that the upper cervical spine compensates for subaxial ipsi-axial rotation during head lateral bending by contra-axial rotation.

We could investigate *in vivo* 3D motions of the cervical spine accurately, quantitatively and non-invasively with the use of 3D-MRI to eliminate radioactive exposure. Our system facilitates not only mathematical descriptions of 3D motions, but also 3D visualization of this information, and enabled us to easily understand complicated coupled motion of the cervical spine.

CONCLUSIONS

1. We developed a novel *in vivo* 3D motion analysis system and succeeded in disclosing the *in vivo* coupled motions of the cervical spine in lateral bending for the first time.
2. Lateral bending increases as the cervical level goes downwards, and coupled axial rotation of subaxial cervical spine is in opposite direction to that of the upper cervical spine.

REFERENCES

1. Ishii T, et al. *Spine* **29**, E139-144 2004.
2. Ishii T, et al. *Spine* **29**, 2826-2831 2004.

Table 1: Mean Range (°±SD) of 3-D Intervertebral Motions on one side

Motion	Cervical Level							
	Oc-C1	**C1-C2**	**C2-C3**	**C3-C4**	**C4-C5**	**C5-C6**	**C6-C7**	**C7-T1**
Main Lateral bending	1.9(0.9)	1.6(1.3)	3.7(2.0)	3.5(1.4)	3.3(1.0)	4.3(1.4)	5.7(1.9)	4.1(2.7)
Coupled Axial Rotation	0.2(1.0)	17.1(4.7)	-0.9(0.9)	-1.8(0.7)	-1.1(0.9)	-1.2(1.0)	-0.8(0.9)	0.4(1.0)
Coupled Flexion-Extension	-1.1(1.4)	0.2(2.0)	0(0.9)	0.5(0.9)	0.8(1.0)	0.7(1.2)	0.4(1.8)	0.5(1.5)

IN VITRO LIGAMENT STRAIN MEASUREMENT: CAN IMPLANTABLE AND NON-INVASIVE METHODS YIELD COMPARABLE RESULTS?

[1]Rochelle L. Nicholls, [2]Brenton P. Jenke and [1,3]Markus S. Kuster
[1] School of Surgery & Pathology, University of Western Australia (Australia): rochelle@cyllene.uwa.edu.au
[2] School of Mechanical & Materials Engineering, University of Western Australia (Australia)
[3] Department of Orthopaedic Surgery, Kantonsspital, St. Gallen (Switzerland)

INTRODUCTION

Experimental measurement of ligament strain behaviour is made challenging by the complex geometry of the tissue and the often-invasive nature of measurement devices. There is no gold standard for measurement method, and no direct comparison of the results obtained by implantable and non-invasive measurement methods has ever been made. In this study, two methods for measuring ligament strain *in vitro* were compared: non-invasive optical measurement (OPT) and the implantation of a differential variable reluctance transducer (DVRT).

METHODS

The equivalence of DVRT and OPT was first tested in an isolated tensile test. The anterior fibres of the medial collateral ligament (MCL) were resected from 8 bovine stifle (knee) joints and mounted in a Zwick Z010 materials testing machine. A sub-miniature DVRT (Microstrain, VA.) was implanted parallel to the primary ligament fibre direction. Two optical markers were painted at the extremities of the device (10 mm apart), and also at each end of the ligament (35 mm). A uniaxial tensile load was applied to the ligament at 30 $N.s^{-1}$ until 150 N of force was reached. The ligament was allowed to relax to 30 N of internal force and the process repeated for 3 cycles. Each ligament was tested 4 times at 10 min intervals. DVRT data was sampled at 50 Hz using a National Instruments BNC connector block and 12-bit DAQ card. The optical markers were tracked using a 50 Hz digital camcorder and SIMI Motion Analysis software. Tensile strain (ε) was computed using reference MCL length at 0 deg (l_0) and instantaneous length (l): $\varepsilon = (l-l_0)/l_0$. Strain change ($\Delta\varepsilon$) was defined as the difference between peak and minimum strain.

Quasi-static tests were conducted using intact bovine stifle joints (n=3). Ten cycles of passive flexion and extension were applied via a customised rig at 30 deg s^{-1} between 0-120 deg. DVRTs were implanted in mid-anterior and proximal-anterior MCL fibres. Corresponding optical markers were tracked with two calibrated 50 Hz cameras and SIMI software was used to reconstruct the 3D coordinates using DLT methodology.

RESULTS AND DISCUSSION

There was no significant difference in $\Delta\varepsilon$ detected using OPT or DVRT during cyclic uniaxial tension testing (p=0.184) (Fig.1). The DVRT did report significantly mean higher absolute strain (p=0.001).

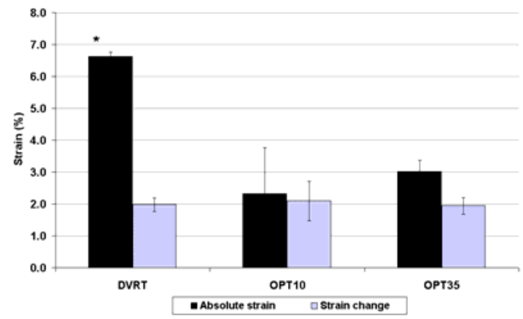

Figure 1: Isolated test results

The DVRT results for quasi-static tests may have been influenced by the motion of deep MCL fibres around the device. OPT can measure only surface strains (Fig2), which may account for the difference in results.

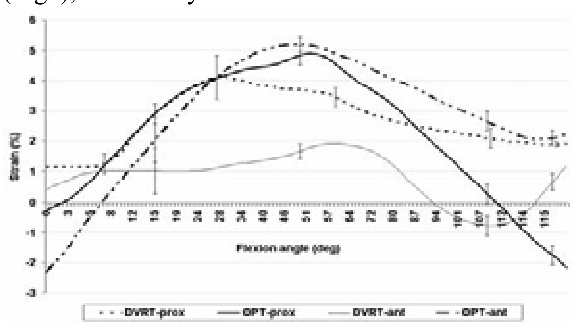

Figure 2: *In vitro* test results

CONCLUSIONS

While no significant difference for measurements of $\Delta\varepsilon$= using DVRT or OPT was shown, practical issues with each method were identified. Ideally for strain measurement in soft tissues, a non-invasive method will be utilized to preserve the ligament structure. However this is unsuitable for intra-articular or multi-layered ligaments. The sensitivity of OPT is dependent on the chosen gage length. Implantable devices should be small and compliant enough to avoid abnormal tissue deformation, and caution used in interpretation of results from multi-layered ligaments.

ACUTE EFFECTS OF INTRAMUSCULAR APONEUROTOMY ASSESSED BY FINITE ELEMENT MODELING

[1, 3] Can A. Yucesoy, [2] Bart H.F.J.M. Koopman, [2] Henk J. Grootenboer and [2, 3] Peter A. Huijing
[1]Biomedical Engineering Institute, Bogazici University, Istanbul, Turkey,
[2]Department of Biomechanical Engineering, Universiteit Twente, Enschede, The Netherlands,
[3]Faculteit Bewegingswetenschappen, Vrije Universiteit, Amsterdam, The Netherlands; email: can.yucesoy@boun.edu.tr,

INTRODUCTION

Aponeurotomy is a surgical technique executed to correct functional problems due to contractures occurring secondary to spastic paresis. Despite its clinical potential importance, the mechanical mechanism of this intervention is not clearly understood. The goal of this study was to investigate this mechanism using finite element modeling. The specific point addressed is modeling changes in lengths of sarcomeres within aponeurotomized muscle due to intramuscular myofascial force transmission [e.g., 1].

METHODS

Finite element modeling of extensor digitorium longus muscle of the rat [see 2 for a description of the model] was performed for two conditions (1) intact and (2) aponeurotomized.

In surgery, aponeurotomy is performed by cutting the intramuscular aponeurosis transversely to its line of pull. In the present study, proximal aponeurotomy was modeled by disconnecting the common nodes of two neighboring aponeurosis elements located in the middle of the proximal aponeurosis of the modeled muscle. Earlier experiments on dissected aponeurotomized rat muscle showed after isometric lengthening that below the location of the intervention a progressive tear occurred in the intramuscular connective tissue in the direction of muscle fibers [3]. As a consequence, a gap opened between the cut ends of the aponeurosis. Present modeling of aponeurotomized muscle allows such a gap and a limited tear.

RESULTS AND DISCUSSION

Major changes in muscle length-active force characteristics were found (Figure 1) after aponeurotomy (1) both active slack length (by approximately 1.2 mm) and optimum length (by 2.0 mm) shifted to higher muscle lengths and the length range of force exertion increased. (2) Muscle active force decreased (e.g., optimum force decreased by 21%).

On lengthening after aponeurotomy, two cut ends of the proximal aponeurosis were separated by a gap and tearing of intramuscular connective tissue along the fiber interface caused the muscle to be divided into a proximal and a distal population of muscle fibers.

Unlike the fairly homogeneous strains in the fiber direction of the intact muscle (Figure 2a), for the aponeurotomized muscle myofascial force transmission was shown to lead to a major strain distribution and thus sarcomere length distributions. Note the contrasting effects for the two fiber populations (Figure 2b): (1) In the distal population (fibers with no myotendinous connection to the muscles' origin), sarcomeres were much shorter than the ones of the proximal population (fibers with intact myotendinous junction at both ends) (2) From proximal ends of muscle fibers to distal ends, the serial distribution of sarcomere lengths varied from the lowest length

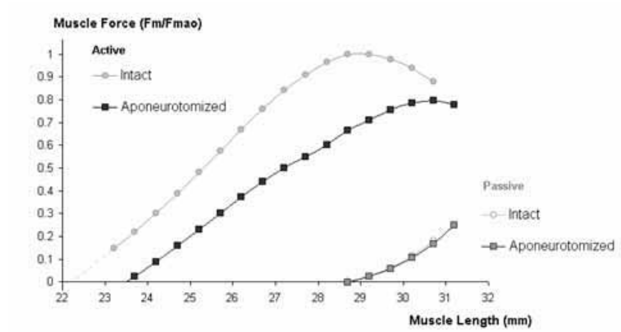

Figure 1: The isometric muscle length-force characteristics of modeled intact and aponeurotomized EDL muscles.

to higher lengths in the distal population and in a reversed manner in the proximal population. Such distributions of sarcomere lengths explain the shifts in muscle active slack and optimum lengths. Muscle force reduction was explained primarily by the short sarcomeres in the distal population. However, fiber stress distributions showed that majority of the sarcomeres (even in the distal fiber population) still contribute to muscle force: myofascial force transmission prevents them from shortening to their active slack lengths.

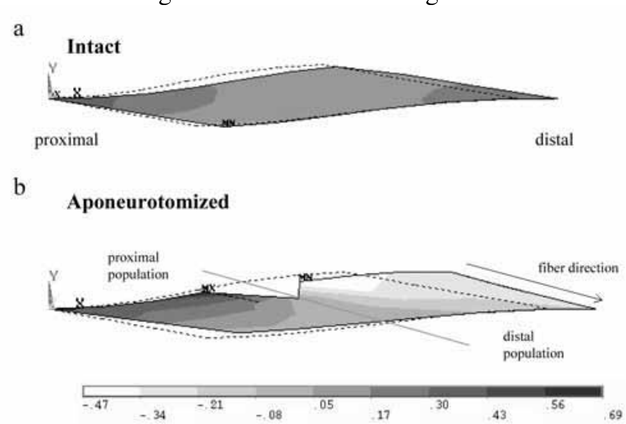

Figure 2: Distributions of fiber direction strain within modeled (a) dissected intact and (b) dissected aponeurotomized EDL muscles at high muscle length.

CONCLUSIONS

We conclude that the mechanism mechanically determining the effects of aponeurotomy is dominated by myofascial force transmission. Accounting for the general characteristics of sarcomere length changes shown in the proximal and distal populations of muscle fibers may help the surgeon make a more controlled decision on the location of the intervention.

REFERENCES

1. Huijing PA, et al. *J Biomech* **32**, 329-345, 1999
2. Yucesoy CA, et al. *J Biomech* **35**, 1253-1262, 2002
3. Jaspers RT et al. *J Biomech* **32**, 71-79, 1999

STEPPING FROM A NARROW SUPPORT

[1]Yun Wang, [2]Elena Yu. Shapkova, [1]Siripan Siwasakunrat,
[1]Vladimir M. Zatsiorsky, and [1]Mark L. Latash
[1]Department of Kinesiology, The Pennsylvania State University, University Park, PA 16802
[2]Children's Surgery Clinic, Institute of Phthisiopulmonology, St. Petersburg, Russia
email: mll11@psu.edu

INTRODUCTION

When a standing person initiates a step, the center of pressure (COP) shifts in the medio-lateral (ML) direction towards the supporting foot and in the anterior-posterior (AP) direction backwards [1,2]. Apparently, COP cannot be shifted beyond the available dimensions of the support area. However, humans can initiate a step forward after balancing for a short time on a support that is very narrow in the AP direction. One possibility is that people use horizontal forces to move the body forward; this would violate the balance and initiate a fall of the body in the required step direction.

We investigated mechanical and electromyographic (EMG) events prior to making a step and their changes associated with changes in the AP dimension of the support area. We hypothesized that a constraint on possible COP shifts will be associated with increased changes in the horizontal force and with changed neural strategies reflected in changes in EMG signals from the leg muscles.

METHODS

Eight healthy subjects participated in the experiment. A force platform recorded the reactive forces and moments. Disposable electrodes were used to record the surface EMG of the following muscles from both sides of the body: tibialis anterior (TA), soleus (SOL), rectus femoris (RF), and biceps femoris (BF), and of the rectus abdominis (RA) and erector spinae (ES) on the left side of the body.

The subjects stood barefoot on the force plate or on one of two specially constructed wooden boards with the same horizontal dimensions as the force plate. One of the boards was fitted with a narrow beam on the undersurface (3.3 cm wide, 5.3 cm high). This board was placed over the force plate such that its narrow dimension was in the AP direction. In other trials, a similar wooden board was placed on the top ridge of a triangular metal wedge (4.9 cm in height, 91.4 cm in length). The wedge was placed on the force plate such that its upper ridge ran horizontally in the ML direction. The subjects performed self-paced steps from quiet stance while standing on either the force plate, or the board fitted with the narrow beam ("narrow support"), or the board resting on the upper ridge of the wedge ("ridge support").

All trials were aligned by the first visible shift of the moment about the vertical axis (time zero, t_0). After alignment, sets of trials performed by the same subject, with the same leg, in the same condition were averaged. Changes in the background EMG were quantified using rectified signals integrated over 100 ms intervals starting 300 ms prior to t_0 and ending 300 ms after t_0. COP shifts and changes in the force in the AP direction (F_X) were quantified within the interval {-300 ms; +300 ms} with respect to t_0.

RESULTS

Stepping from the force plate was associated with COP shifts towards the support foot and backwards and an increase in F_X acting forward on the subject. Stepping from the "narrow support" led to smaller AP COP shifts. Stepping from the "ridge support" was associated with very small COP shift in AP direction, smaller COP shifts in ML direction, and larger F_X changes (Fig. 1). There was a general increase in the level of activation of leg and trunk muscles during stepping from the "narrow support" and "ridge support". Such differences in the activity of ankle extensors were seen in the stepping leg only at the beginning of the preparation period and in the supporting leg over the whole time interval of analysis.

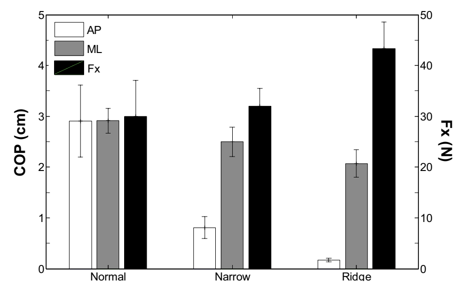

Fig. 1 Shifts of the COP (AP-white bars; ML-grey bars) and Fx (black bars) averaged across the subjects.

DISCUSSION AND CONCLUSIONS

Our observations demonstrate the existence of alternative mechanical strategies that can be used in a task-specific manner to initiate a step. We suggest a hypothesis that a subjectively perceived postural instability may prevent the subjects from using the most common method of step initiation, namely a COP shift backwards. Then, an alternative strategy of an increased F_X change is discovered. If this is correct, training of persons who show an impaired ability to initiate a step may benefit from providing feedback on the horizontal force and practicing on a surface with high friction.

REFERENCES

1. Halliday S, et al. The initiation of gait in young, elderly, and Parkinson's disease subjects. Gait Posture **8**, 8–14, 1998.
2. Couillandre A, et al. Is human gait initiation program affected by a reduction of the postural basis? Neurosci Lett **285**,150–154, 2000.

ACKNOWLEDGEMENTS

This research was supported in part by NIH grants AG-018751, NS-35032, and AR-048563.

EFFECT OF STRETCH OR SHORTENING AMPLITUDE ON SUBSEQUENT ISOMETRIC MUSCLE FORCE

Sharon Bullimore, Tim Leonard, Dilson Rassier and Walter Herzog
Human Performance Lab, Faculty of Kinesiology, University of Calgary, Canada.
email: sbullimore@kin.ucalgary.ca

INTRODUCTION

It is well-known that the force that a muscle can develop during an isometric contraction is influenced by its contractile history [1]. Active stretch increases the force developed during a subsequent isometric contraction (‘force enhancement’, FE), while active shortening decreases subsequent isometric force (‘force depression’, FD). The mechanisms underlying these two phenomena are not well understood, although a number of possibilities have been suggested and the causes of FE and FD are thought to be different [2]. In order to be able to choose between proposed mechanisms, it is necessary to have a detailed knowledge of the characteristics of FE and FD. Here we determine the relationship between the amount of FE or FD and the amplitude of stretch or shortening, respectively. We hypothesised that the nature of this relationship would be different for FE and FD.

METHODS

The experiments were performed using seven cat soleus muscles, as described previously [3]. The muscles were isolated *in situ* and were activated through electrical stimulation of the tibial nerve. An isometric force-length relationship was obtained and optimal length was defined as the length at which active muscle force was highest.

The isometric force developed at a muscle length 9mm longer than optimal length was measured following active stretches of between 3 and 24mm. Total FE was defined as the difference between the isometric force developed after stretch and the force during a purely isometric contraction at the same length. Passive FE [4] was defined as the difference between passive force following a stretch trial and passive force following a purely isometric trial at the same length.

The isometric force developed at a muscle length 9mm shorter than optimal length was measured following shortening contractions of between 3 and 18mm. FD was defined as the difference between the isometric force developed after shortening and the force during a purely isometric contraction at the same length.

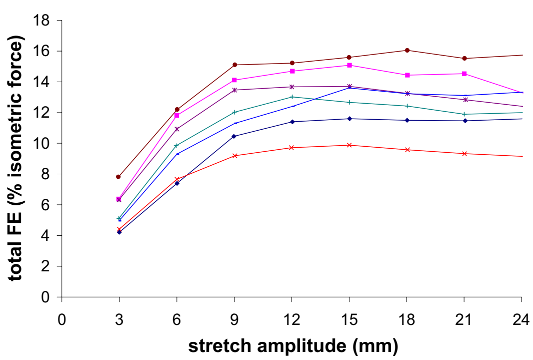

Figure 1: Relationship between total force enhancement (FE) and stretch amplitude in seven cat soleus muscles.

RESULTS AND DISCUSSION

As hypothesised, FE and FD showed different relationships to stretch/shortening amplitude. Total FE increased with stretch amplitude up to approximately 9mm stretch and then levelled off (Figure 1). Passive force enhancement increased with stretch amplitude up to approximately 9mm, then decreased. The relationships of total and passive FE to stretch amplitude were well-fitted by third order polynomials ($R^2 > 0.96$). FD increased with shortening amplitude without levelling off (Figure 2). The relationships of FD to shortening amplitude were well-fitted by second order polynomials ($R^2 > 0.94$). These differences in the behaviour of FE and FD support the hypothesis that they arise from different causes. Any mechanism that is proposed to explain FE must be able to account for the fact that FE increases with stretch only over a limited range of amplitudes before the effect appears to become saturated. Further investigation of the passive component of FE is important for understanding this behaviour.

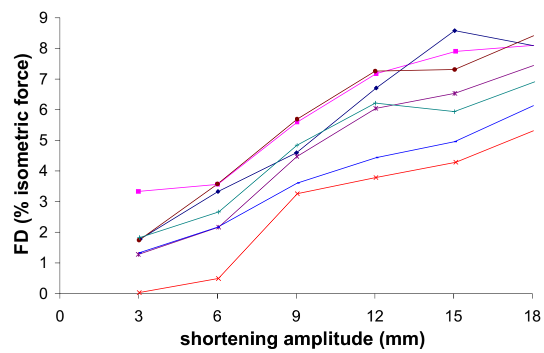

Figure 2: Relationship between force depression (FD) and shortening amplitude in seven cat soleus muscles.

REFERENCES

1. Abbott BC, Aubert XM. *J Physiol* **117**, 77-86, 1952.
2. Rassier DE, Herzog W. *J Appl Physiol* **96**, 419-427, 2004.
3. Herzog W, Leonard TR. *J Biomech* **30**, 865-872, 1997.
4. Herzog W, Leonard TR. *J Exp Biol* **205**, 1275-1283, 2002.

ACKNOWLEDGEMENTS

We thank the Natural Sciences and Engineering Research Council of Canada, the Canada Research Chairs Program and the Alberta Heritage Foundation for Medical Research for financial support.

IMPLANTATION OF A TOTAL KNEE ARTHROPLASTY PROSTHESIS IMPOSES ABNORMAL STRAIN ON LOCAL SOFT TISSUES

[1]Rochelle L. Nicholls, [2]Ben Jeffcote and [1,2,3]Markus S. Kuster
[1] School of Surgery & Pathology, University of Western Australia (Australia)
[2] Dept. of Orthopaedic Surgery, Fremantle Hospital, Western Australia (Australia)
[3] Dept. of Orthopaedic Surgery, Kantonsspital, St. Gallen (Switzerland): Markus.Kuster@kssg.ch

INTRODUCTION

Tension in the medial and lateral collateral ligaments is used to regulate joint tightness during total knee arthroplasty (TKA). Despite accurate ligamentous balancing during surgery, many patients experience restricted range of motion after TKA compared to a healthy knee joint [1]. The reason is not well understood. Preoperative range of motion and altered kinematics such as lack of femoral rollback has been suggested [2]. Our hypothesis was that the medial and lateral ligamentous structures and the extensor envelope are tensioned beyond physiological limits after TKA and prevent further flexion. However, the demands placed on these passive tissues are unknown. The purpose of the present study was to investigate the effect on the soft tissue envelope of TKA implantation.

METHODS

Six fresh cadaver knee joints were tested. A novel method was developed for assessment of soft tissue tension in the intact and TKA knee (Fig.1). A stainless steel rod was inserted in the intra-medullary canal of the tibia and secured using 3 screws through the tibial shaft. At the proximal end, the tibial slope was adjustable via a series of inclined plates connected to the inner rod. A 40 N spring was enclosed in the distal aspect of the device below the inner rod to maintain tibio-femoral contact. To insert the device in the knee, 8 mm of bone was resected beneath the tibial plateau (10 mm below the proximal surface). The plateau was then screwed to the bearing surface of the device. Vertical displacement of the device during motion represented the variation in tibio-femoral forces generated by the collateral ligaments and soft-tissue envelope.

Figure 1: Custom device to assess soft tissue tension.

Each knee was mounted in a customized passive motion rig with the femur secured horizontally. A 40 N spring sutured to the quadriceps tendon mimicked the effects of passive muscle tension. Motion was applied in 15 deg increments from 0 to 150 deg flexion. The procedure was repeated after implantation of an LCS rotating platform TKA prosthesis (De Puy), in which the tibial trial was screwed to the bearing surface of the device. Measurements were obtained using the (standard) 7.5 deg tibial slope, and with 0, 5, and 10 deg slopes.

RESULTS AND DISCUSSION

The device position at 45 deg flexion was selected as the zero reference point as minimal tissue tension was expected in mid-flexion. Fig.2 illustrates the displacement of the tibial plateau by soft tissue tension in the natural and TKA knee relative to this point. In both cases, the joint becomes looser (displacement approaches zero) between 0-45 deg. This is markedly more so after TKA. In the intact knee, the joint remains within 1 mm of the zero position until 135 deg and within 2 mm throughout the full range of motion. After TKA, greater soft tissue tension in flexion was indicated by a mean 6 mm displacement at 150 deg. Changing the slope of the tibial plateau did not approach the behaviour of the intact knee.

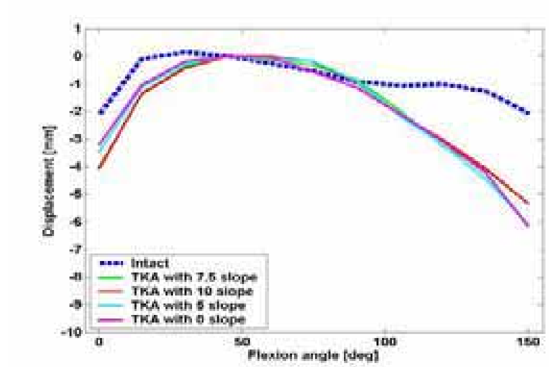

Figure 2: Example of tibial plateau displacement.

CONCLUSIONS

TKA prosthesis implantation imposes additional demands on passive soft tissues beyond 110 degrees and particularly at the extremes of range of motion. This explains the extension deficits and lack of flexion in many knee joints after TKA, and has implications for prosthesis design and implantation technique.

REFERENCES

1. Miner, A. L. *et al. J.Arthroplasty* **18**: 286-294, 2003.
2. Laskin, R. S., Beksac, B. *J.Arthroplasty* 41-46, 2004.

ARE STRUCTURAL AND GAIT BIOMECHANICS INDICATIVE OF TIBIAL STRESS FRACTURE RISK?

[1] Mark W. Creaby, [1]Sharon J. Dixon, [2]Kate McNally, [3]Jonathon Palmer.
[1]School of Sport and Health Sciences, University of Exeter, Exeter, EX1 2LU.
[2]MacLellan Clinic, University of Exeter [3]Northenhay Clinic, Exeter.
email: m.w.creaby@ex.ac.uk

INTRODUCTION

The Royal Marine (RM) Commando training course is believed to be the longest basic infantry training course in the world. Tibial stress fracture is one of the most common injuries in this population [1]. Lower limb structure, joint range-of-movement, gait kinematics and kinetics have all been associated with this injury in different populations, however conclusions are ambiguous. The intensity, frequency and duration of the physical stress experienced during RM training may exacerbate potential risk factors not identified in other populations. The aim of this study was to identify biomechanical differences between RM Commando recruits with, and without tibial stress fracture history.

METHODS

Twenty RM recruits; ten with tibial stress fracture history and ten controls participated in the study. All recruits had failed to complete the full 30-week commando training course due to injury or illness. Recruits were passed fit to return to training at the time of assessment. Measures of lower limb structure and range-of-movement were taken by a state registered podiatrist. Barefoot and shod running gait kinematics (120Hz; Peak Performance Technologies Inc., CO), and ground reaction forces (960Hz; AMTI, MA) were collected. Coordinate data were reconstructed using the procedures of Cole et al [2]. Movement data were referenced to a standing neutral trial.

All data were analyzed using the Wilcoxon signed rank test for matched pairs ($P \leq 0.05$). Twelve tibia with stress fracture history were identified in the injury group, each of these limbs were paired with a limb from the control group. Recruits were matched for the number of weeks of the full training course they completed prior to injury or illness.

Table 1: Selected measures of lower limb structure, barefoot (BG) and shod (SG) running gait (mean ± SD; * $p<0.05$).

		Tibial stress fracture	Controls
Medial hip rotation (deg)		26.6 ± 5.5	32.1 ± 10.1*
GRF impact peak time (sec)	BG	0.012 ± 0.004	0.017 ± 0.007*
	SG	0.028 ± 0.005	0.026 ± 0.005
Peak subtalar eversion (deg)	BG	5.5 ± 3.3	4.6 ± 4.7
	SG	6.0 ± 3.5	7.3 ± 3.5

RESULTS AND DISCUSSION

The reduced passive medial rotation of the hip ($p<0.05$; Table 1) observed in the stress fracture group is suggestive of greater hip retroversion, this is consistent with previous findings [3]. Hip retroversion is believed to result in limited subtalar pronation during gait [4], however this is not supported by the running gait data. During standing hip retroversion results in a supinated foot [4]. This may have masked differences in gait kinematics between the experimental groups because of the defined neutral position employed.

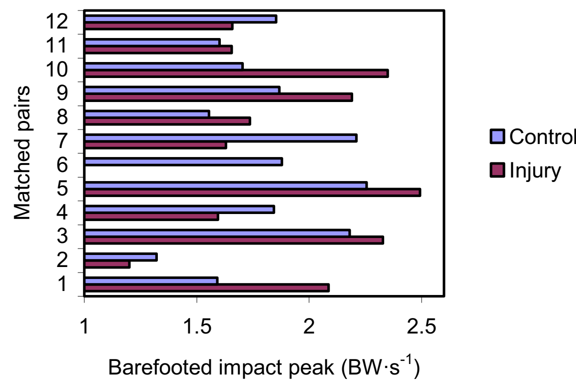

Figure 1: Individual (subject paired) GRF impact peaks.

The vertical ground reaction force (GRF) impact peak occurred significantly earlier in the tibial stress fracture group during barefoot running ($p<0.05$; Table 1), but not during shod running ($p>0.05$). Large variation in measured variables within the study groups contributed to no other significant differences between the groups. Figure 1 illustrates the variation observed in barefoot impact peak values, this is typical of many of the other variables measured. Evidently no cut-off point can be identified between individuals at high and low risk of tibial stress fracture.

CONCLUSIONS

Limited medial rotation of the hip is associated with tibial stress fracture injury. This may be related to increased retroversion of the hip and subsequent implications upon gait. The vertical GRF impact peak time may also be important in tibial stress fracture development, however findings were not consistent between barefoot and shod conditions.

REFERENCES

1. Ross RA, & Allsopp A. *Mil. Med.* **167**, 560 - 565, 2002.
2. Cole G, et al. *J. Biomech. Eng.* **115**, 344 - 349, 1993.
3. Giladi M, et al. *Clin. Orthop.* **216**, 131 - 134, 1987.
4. Root ML, et al. *Biomechanical Examination of the Foot*. Los Angeles, CA: Clinical Biomechanics Corp. 1971.

ACKNOWLEDGEMENTS

© British Crown Copyright 2005/M.D. Published with the permission of the controller of Her Britannic Majesty's Stationary Office.

COMPARISON OF STATIC AND DYNAMIC BIOMECHANICAL MEASURES IN MILITARY RECRUITS WITH AND WITHOUT A HISTORY OF THIRD METATARSAL STRESS FRACTURE

[1]Sharon Dixon, [1]Mark Creaby, [2]Kate McNally and [3]Jonathon Palmer
[1]School of Sport and Health Sciences, University of Exeter, Exeter, EX1 2LU, UK.
[2] Maclellan Clinic, University of Exeter, [3]Northenhay Clinic, Exeter.
email: s.j.dixon@exeter.ac.uk, web: http://www.exbirt.co.uk

INTRODUCTION
For Royal Marines in training, the third metatarsal is the most common site for stress fracture occurrence [1]. Previous evidence regarding factors contributing to stress fracture development is conflicting [2,3], possibly due to the lack of differentiation between stress fracture sites. It has recently been demonstrated that the third metatarsal is less able to withstand horizontal than vertical loads [4], suggesting horizontal loading may be important in development of this injury. The present study compares static anatomical and dynamic biomechanical variables for Royal Marine recruits with and without a history of third metatarsal stress fracture.

METHODS
Ten Royal Marine recruits with a history of third metatarsal stress fracture were matched with control subjects with no previous stress fracture. Selected static variables, including subtalar neutral position, ankle dorsi-flexion and forefoot varus, were measured to describe the anatomy of the lower limb. Each subject also performed running trials in the laboratory wearing military boots. Synchronized ground reaction force and kinematic were collected for 10 trials for both sides of the body. Force plate data were collected at 960 Hz using an AMTI force plate (AMTI, Massachusetts, USA), and three-dimensional kinematic data at 120 Hz using a Peak realtime system (Peak Technologies, USA). For each running trial, peak ankle dorsi-flexion, rearfoot eversion and knee flexion were identified. Horizontal ground reaction force (GRF) was characterized using the peak resultant horizontal force magnitude (contributed to by the anterior/posterior and medial/lateral force components) and the angle of application of this force during braking and propulsion. Application angle was defined as the angle of the resultant horizontal force relative to the sagittal plane, with a negative angle indicating a medially applied force. A matched-pairs Wilcoxon test was used to detect significant differences between the study groups, using data for the stress fracture side for the injury subjects and the same side for each matched control ($p<0.05$).

RESULTS AND DISCUSSION
No significant differences in static anatomical variables were identified between study groups ($p>0.05$). Both static and dynamic ankle dorsi-flexion were lower for the stress fracture group (Table 1), but differences were not significant. During running, rearfoot eversion was found to occur significantly earlier for the stress fracture group than for the matched controls ($p<0.05$, Table 1), suggesting an increased time spent loading the forefoot. No significant differences were identified in peak magnitude of horizontal braking or propulsive force, but the peak horizontal braking force was directed significantly more medially for the stress fracture group ($p<0.05$, Table 1). This suggests a difference in horizontal loading of the foot at this time. Since the third metatarsal is more vulnerable under horizontal than vertical loading [4], this may have implications regarding the mechanism of this injury.

CONCLUSIONS
The measurement of dynamic biomechanical data has highlighted variables associated with third metatarsal stress fracture, indicating the importance of dynamic measurements when investigating risk factors for this injury. The earlier peak eversion, together with the difference in horizontal loading direction during the braking phase, suggest a difference in loading of foot structures that may contribute to this stress fracture development and thus warrants more detailed investigation.

REFERENCES
1. Ross RA, & Allsopp A. *Mil. Med.* **167**, 560 - 565, 2002.
2. Simkin, et al. *Foot and Ankle.* **10**, 25 - 29, 1989.
3. Giladi M et al. *Clin. Orthop.* **216**, 131 - 134, 1987.
4. Arangio, GA et al. *Foot and Ankle Surgery* **4**, 123 - 128, 1998.

ACKNOWLEDGEMENTS
© British Crown Copyright 2005/M.D. Published with the permission of the controller of Her Britannic Majesty's Stationary Office.

Table 1: Static variables, dynamic kinematics and GRF data for stress fracture and control subjects (mean SD, *p<0.05).

	Static variables			Dynamic kinematic variables			Dynamic GRF variables	
	Subtalar neutral (°)	**Forefoot varus (°)**	**Ankle dorsi-flexion (°)**	**Peak eversion (°)**	**Peak eversion time (%)**	**Peak ankle dorsi-flexion (°)**	**Angle of braking force (°)**	**Angle of propulsive force (°)**
Stress fracture	4.9 ± 2.7	5.5 ± 6.1	6.4 ± 2.9	7.7 ± 4.1	39.7* ± 6.5	14.8 ± 3.2	-13.1* ± 6.3	-4.4 ± 7.0
Controls	4.2 ± 4.1	3.1 ± 7.1	7.6 ± 3.0	7.7 ± 2.5	45.6 ± 7.1	16.4 ± 3.2	-6.4 ± 6.7	-7.4 ± 8.2

DEVELOPMENT OF A COMPUTER APPLICATION TO CALCULATE CYCLISTS FRONT AREA IN STUDIES ABOUT AERODYNAMICS

[1,2] Felipe Pivetta Carpes, [1]Mateus Rossato, [2]Alexandre Dias da Silva and [1]Carlos Bolli Mota
[1]Biomechanics Laboratory, [2]Industrial Engineering Post-Graduate Program – Federal University of Santa Maria
felipecarpes@gmail.com   http://www.ufsm.br/gepec

INTRODUCTION

Aerodynamic studies are usually accomplished in the wind tunnels. In the cycling, variables as aerodynamics drag coefficient, surface of the object, front area, were found in the literature [2,3,4,5] and are necessary for the calculations about aerodynamic of the cyclist and/or equipments. Limitations related to this calculation are found. For example, the front area has been considered as constant, and relative at 18% of the total corporal surface obtained by prediction equations [1]. The aim of this study was to propose a method to calculate the cyclist front area through tools of images processing, with the development of a computer application, searching to provide results that can be used in the analysis of aerodynamics in cycling.

METHODS

The first step in the development of the computer application is to determine how to obtain the necessary information. For the development of the computer application the IDL 6.0 (Research Systems Inc.) was used, allowing the work with different forms of data, through computational mathematics. One of the causes of the choice of the IDL was his characteristic multi-platform, facilitating its use in many operating systems. To compile the computer application is only necessary the installation of an IDL Virtual Machine (Virtual IDL Machine – freeware - www.rsinc.com), don't depending of the installation or acquisition of software. Inside of the possibilities of images processing, the second step went verify which would bring a better result. Thus, the computer application was developed based in the image segmentation, with the Roberts operators, the oldest and simple algorithm of detection of borders, using a matrix 2x2 to find the changes in the directions x and y through the Roberts mask (Figure 1).

$$\underset{G_x}{\begin{bmatrix} 0 & 1 \\ -1 & 0 \end{bmatrix}} \underset{G_y}{\begin{bmatrix} 1 & 0 \\ 0 & -1 \end{bmatrix}}$$

Figure 1: Roberts mask

With the mask, if the calculated magnitude is larger than the smallest entrance value (defined in agreement with the nature and quality of the image processed), the pixel is considered, or not, be part of a border. The small size of the mask for the operator of Roberts is easy to implement, and also fast to calculate. The analyses are very sensitive to the image noise. After image segmentation, a method for the calculation of the area is necessary, because the image didn't possess defined dimensions. The third step involved the use of an object of well-known dimensions, photographed with the cyclist, and that supplied parameters for the space calibration in meters.

RESULTS AND DISCUSSION

The tests were accomplished with digital pictures obtained with photographic camera Nikon Coolpix 885 and the computer application presents the necessary characteristics to the front area analysis, with easy use. Using the commands options in the graphic interface of the computer application, the user follows the necessary steps for the analysis. After, the results with image information could be record in a text file for posterior analysis.

CONCLUSIONS

In summary, the computer application has success in the front area calculation and showed an applicable methodology to the cycling, many influenced and dependent of the aerodynamics, as the cyclist body position and equipments or accessories.

REFERENCES

1 - Du Bois, D. & Du Bois, E. F. Clinical calorimeter : a formula to estimate the approximate surface area if height and weight be known. *Archives of Internal Medicine*. 17, p:863-871. 1916.
2 - Di Prampero, P. E., Cortilli, G., Mognoni, P., Saibene, F. Equation a motion of a cyclist. *Journal of Applied Physiology*, 47 (1), p:201-206, 1979.
3 - García-Lopez, J., Peleteiro, J., Rodríguez, J. A., Córdova, A., González, M. A., Villa, J.G. Biomechanical assessment of aerodynamic resistence in proffessional cyclists: methodological aspects. *Proceedings of International Symposium on Biomechanics in Sports*. p: 286-289, 2002.
4 - Padilla, S., Mujika, I., Angulo, F., Goiriena, J. J. Scientific approach to the 1-h cycling World record: a case study. *Journal of Applied Physiology*. 89, p:1522-1527. 2000.
5 - Tew, G. S., Sayers, A. T. Aerodynamics of yawed racing cycle whells. *Journal of Wind Engineering*. 82, p: 209-222. 1999

IN-SHOE PRESSURE ANALYSIS DURING *AERO JUMP* IN DIFFERENT CADENCES

Juliana Koehler Ribeiro, Gabriela Fischer, Felipe Pivetta Carpes & Carlos Bolli Mota
Biomechanics Laboratory, Federal University of Santa Maria, Brazil
julianakr@uol.com.br

INTRODUCTION

The *Aero Jump* is a gym modality with aerobics characteristics, realized with movements and jumps above a little trampoline (figure 1).

Figure 1: Little trampoline of *Aero Jump*

The quantitative description of biomechanical aspects of the human movement is related to the forces that cause the observed movement, as the repercussions in the analyzed phenomenon [2]. The ground reaction forces investigation and the distribution of dynamic pressure in the foot surface, provide important knowledge about the characteristics of the mechanical overload on the human body, in static and sporting situations [1]. The popularizing of the physical activity, besides the benefits for the promotion and maintenance of the health can cause a consequence: injuries [3]. The purpose of this study was to describe the distribution of dynamic pressure during five movements of Aero Jump accomplished in different cadences: 132 bpm (beats per minute) and 145 bpm.

METHODS

The sample was composed by three female (age between 18 and 23 years old, average height of 1.69 m and average weight of 602.66 N), with experience in the *Aero Jump*. The acquisition data was realized by F-Scan version 3.821 (Tekscan, Inc.) and little trampoline *Physicus*® (Physicus, BRA), with dimensions of 20 cm (height) and 96 cm (diameter), supporting until 1500 N. The acquisition frequency selected was 120 Hz, during five seconds to each trial. The selected movement was: basic, double punchinello, simple punchinello, double twist and simple twist. Each subject repeats three times the movements, in each cadence investigated. The all intervals of support were included in the descriptive statistical analysis.

RESULTS AND DISCUSSION

According to table 1, the pressures in the right foot were larger than in the left foot in all movements and in both cadences, varying from 12.7% for the movement simple twist until 43.9% for the movement double punchinello, both in the cadence of 145 bpm. In the movements basic, double punchinello and simple punchinello, the larger pressures was observed in the cadence of 145 bpm. For the double twist and simple twist the larger pressure was observed in the cadence of 132 bpm.

CONCLUSIONS

The results suggest that when cadence increases an increase in the pressure was observed for movements basic, double punchinello and simple punchinello. For movements double twist and simple twist was observed a decrease in pressure according to cadence increased. In summary, the movements of *Aero Jump* realized in elevated cadences don't have a linear relationship with the increase in the pressure.

REFERENCES

1 Amadio, A. C. Características metodológicas da biomecânica aplicadas à análise do movimento humano. In: *Esporte e atividade física, interação entre rendimento e qualidade de vida.* Barueri: Manole, 2002, p.259-279.
2 Nigg, B.; Herzog, W. *Biomechanics of the musculoskeletal system*. Human Kinetics. 1996.
3 Serrão, J. C. Biomecânica: compromisso com o rendimento e com a saúde. In: *Esporte e atividade física, interação entre rendimento e qualidade de vida*. Barueri: Manole, 2002, p.259-279.

Table 1: Peak pressure (g/cm^2) in different cadences.

	Cadence 132 bpm		Cadence 145 bpm	
Movement	Right foot	Left foot	Right foot	Left foot
Basic	2583.4	2221.31	2984.48	1864.26
Double punchinello	2590.08	1961.9	2930.22	1642.88
Simple punchinello	2311.27	1712.61	2962.57	1708.6
Double twist	2373.95	1756.58	2082.67	1728.47
Simple twist	2594.67	1911.07	2157.9	1884.65

ACTIVITY ASSESSMENT AND CLINICAL GAIT ANALYSIS AFTER MALIGNANT BONE TUMORS TREATMENT WITH RECONSTRUCTION OF FEMORAL AND TIBIAL DEFECTS

[1] Mirko Brandes, [1] Dieter Rosenbaum, [2] Winfried Winkelmann, [2]Robert Rödl
[1] University Hospital of Muenster, Orthopedic Department, Motion Analysis Lab, Germany,
[2] University Hospital of Muenster, Orthopedic Department, Germany;
email: mib@uni-muenster.de, web: www.motionlab-muenster.de

INTRODUCTION

Tumors that affect the distal femur and/or the proximal tibia require a resection of the knee joint, which may be reconstructed with modular prostheses. It is reported that current treatment achieves long-term, disease-free survival rates around 60% [1, 2]. Until now, patient activity after tumor prostheses was assessed with questionnaires which do not provide objective and quantitative information about patients' activity in daily living. Thus, the present study assessed the activity patterns of patients with portable measurement devices. Furthermore, the relationship between clinical gait parameters and activities of daily living is unclear.

METHODS

From a larger sample of patients with successful prosthetic treatment, a subgroup of 22 subjects (14 male, 8 female) volunteered. Their mean age was 35±18 years, the follow-up ranged from 2 to 17 years (mean 6±4 yrs.). The tumor was located in the distal femur (n=18) or the proximal tibia (n=4). Clinical outcome was assessed with MSTS and TESS score.
Two measurement devices were applied: The Dynaport® ADL monitor (McRoberts, Den Haag, NL) uses three uniaxial accelerometric sensors and is able to distinguish between different modes of activity, i.e. lying, sitting, standing, walking and cycling. The system is worn around the waist, the third sensor in a strap around the left thigh. The second system is the SAM® Step Activity Monitor (Cyma Inc., Seattle, OR), a 2-dimensional accelerometer that counts and stores steps for several weeks in daily profiles.
The patients were instructed how to handle the devices before taking them home, older patients were visited at home. On the first measurement day, both devices were worn simultaneously from getting up until going to bed. The following six days, the SAM was worn alone.
Data of a clinical gait analysis was available for 14 subjects. In these cases, relations between the number of steps (SAM), activity categories (ADL-Monitor) and main gait parameters (e.g. gait speed, maximum knee flexion) were analyzed.

RESULTS AND DISCUSSION

Three ADL-Monitor measurements had to be excluded due to a handling error. The predominant activity "sitting" accounted for 53.7 ± 15.4% of the total time, followed by standing (27.4 ± 15.6%), locomotion (9.7 ± 5.4%) and lying (8.2 ± 6.3). Only 0.2% of the data could not be classified.
The SAM counted an average of 4786 ± 1770 (Min: 2045, Max: 8135) gait cycles per day which extrapolates to 1.75 million gait cycles per year. These numbers of gait cycles were similar to hip and knee patients assessed in a different study using identical methods, but were slightly lower compared to a group of patients with well functioning hip arthroplasty [3].
Regarding the distribution of daily activities, the activity level of the selected patients was similar to patients with limb salvage surgery and superior to an amputation group reported from the Netherlands [4].
No correlation was found between the number of gait cycles and the clinical scores, age or follow-up of the subjects, whereas the clinical scores (MSTS: 24.7 ± 3.8 out of 30, TESS: 83.6 ± 15.3 out of 100) were nearly identical to tumor patients assessed by Brown in 2002 [2].
If the right knee was affected, the number of steps correlated inversely to the right step length (r=-0.78, p=0.7). This trend was not seen if the left knee was affected and related to the step length of the left leg.

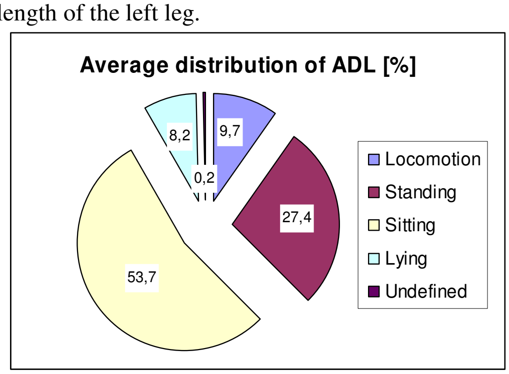

Fig. 1: Average distribution of activities of daily living (ADL-Monitor, n=19)

CONCLUSIONS

Overall, the patients showed a fairly good activity level, whereas strong inter-individual differences were detected, given that the most active subject performed the fourfold number of gait cycles compared to the least active subject. The weak correlations between the clinical gait parameters and the activity level suggest that an estimation of patients´ activity from clinical gait parameters is not solid. Instead, objective devices should be used for a reliable assessment of patients´ activities of daily living.

REFERENCES

1. Kotz et al., *Int Orthop* **26**, 197-202, 2002.
2. Brown et al., *Arch Phys Med Rehabil* **84**, 62-68, 2003.
3. Silva et al., *J Arthroplasty* **17**, 693-697, 2002.
4. Van Dam et al., *JBJS Br* **83**, 1015-19, 2001

ACKNOWLEDGEMENTS

Financial support was kindly provided by the German Cancer Society (Grant # 70-2941 Rö-I)

BASIC GAIT PARAMETERS OF HEALTHY AND CP CHILDREN ASSESSED BY ACCELEROMETRY

[1] Mirko Brandes, [2]Sander Heikens, [3]Wiebren Zijlstra, [2]Rob van Lummel, [1]Dieter Rosenbaum
[1]University Hospital of Muenster, Orthopedic Department, Motion Analysis Lab, Germany,
[2]McRoberts BV, The Hague, The Netherlands,
[3]Institute of Human Movement Sciences, University of Groningen, The Netherlands
email: mib@uni-muenster.de, web: www.motionlab-muenster.de

INTRODUCTION

With modern technology, it is possible to assess and analyze human activities precisely in laboratory settings. However, there is an increasing demand to acquire information about physical activities of subjects under free-living conditions. Spatio-temporal gait parameters can be assessed based on a three-dimensional accelerometer attached to the lower trunk [1]. Until quite recently the measurement systems that are needed for obtaining these acceleration signals were rather bulky and heavy. Recently, the DynaPort MiniMod (McRoberts B.V., The Netherlands) was developed. This miniature device includes three orthogonally mounted accelerometers and it can be used for monitoring human posture and gait parameters. In order to become a useful tool for the assessment of daily activities and gait parameters of children, the system ought to be able to discriminate single steps and to determine the walking distance from the acceleration signals.

METHODS

Group 1: 20 healthy children (aged 3 to 16 years) walked four times 40 meters for the detection of steps in an indoor environment, with no obstacles nearby, at the University Hospital of Muenster. An additional distance, blinded for the analyzer of the data, was walked for detection of walking distance.
Group 2: 20 CP children (aged 5 to 17 years) from the out-patient clinic of the Orthopedic Department walked twice a distance of 20 meters for the detection of steps on a floor in the hospital. Like in group 1, an additional distance was walked for detection of walking distance. The degree of limitations caused by CP was assessed using a self-made classification scale.
Both groups were videotaped for counting steps and distance. Accelerometer signals of the lower back were measured by the MiniMod, a small and lightweight device (5.6 x 6.1 x 1.5 cm, 54g, 100 Hz) and stored on a SD card. The device was firmly fixed to the lower lumbar spine at the level of the second sacral vertebrae with double-sided adhesive tape to avoid movement artifacts. The data sets were send to McRoberts for analysis [2] and compared to the results taken from the video.

RESULTS AND DISCUSSION

Group 1: On average, the healthy children needed 273.7 steps (MIN: 207, MAX: 377) on the 160m tracks for step detection, as counted from the video. The software detected 273.5 steps on average (99.97%, range: 98.5 – 101.5%) regarding the total number of steps. If each misclassified step is counted as an error, regardless if under- or overestimated, the accuracy is 99.6%. The automatically computed walking distance revealed 100.6% of the actually walked distance. The correlation between the medio-lateral displacement of the COM and the age of the subjects was significant ($r = -0.63$, $p < 0.01$).

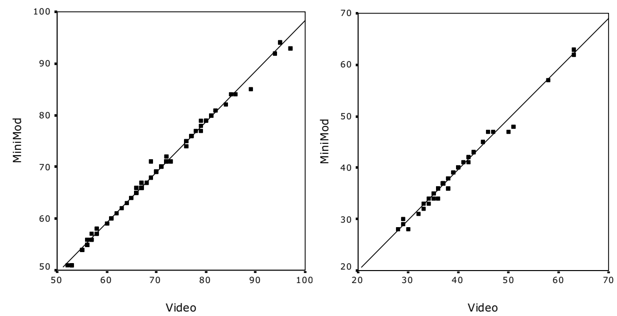

Figure. 1: Steps calculated from the MiniMod compared to the counting from the video for healthy (left) and CP (right) children.

Group 2: One track of one child had to be excluded because of a handling error. On average, the CP children needed 79.8 steps (MIN: 57, MAX: 126) on the 40m tracks for step detection, as counted from the video. The software detected 78.9 steps on average (98.9%, range: 94.1 – 101.8%) regarding the total number of steps. If each misclassified step is counted as an error, the accuracy is 98.7%. The computed distance revealed 101% of the actually walked distance.
The DynaPort MiniMod allows for an accurate assessment of important spatio-temporal walking parameters. Due to its small size and the placement on the back, it does not interfere with most activities and it is comfortable to wear. The opportunity to estimate the medio-lateral displacement of the COM with the MiniMod offers a new tool to analyze the variation of gait within non-laboratory environments.
In healthy children, the displacement decreases with age, whereas this trend does not exist in CP children. Provided that our scale truly reflects the degree of CP, there is no association between the degree of CP and the variation of gait represented by the SDCOM. In both groups, the error of the calculated walking distance was negligible.
Further research will be performed to validate the DynaPort MiniMod for other groups (e.g. children with walking impairments, various adult patient populations) and to enhance the outcome of the device in order to monitor daily activities (e.g. the percentage of standing, sitting, walking).

REFERENCES

1. Zijlstra, Eur J Appl Physiol., **92,** 39-44, 2004.
2. Zijlstra et al., Gait & Posture, **18,** 1-10, 2003.

LONGITUDINAL STUDY OF GAIT STABILITY AFTER CONCUSSION

Tonya M. Parker, Robert Catena, Louis Osternig, Paul van Donkelaar, and Li-Shan Chou
Motion Analysis Laboratory, Department of Human Physiology, University of Oregon
email: chou@uoregon.edu, web: http://biomechanics.uoregon.edu/chou

INTRODUCTION

The need to identify functional impairment following a brain injury is critical to prevent re-injury during the period of recovery. Research to date has focused on neuropsychological tests and static postural control during quiet standing. Little is known about the effect of concussion on dynamic motor function [1,2,3]. A recent study suggested that the ability to control and maintain stability in the frontal plane during walking is diminished in young individuals following a concussion while walking under a divided attention [4]. However, this study did not resolve the issue of how long this pattern continues. Therefore, the purpose of this study was to perform a longitudinal quantification of deficits in maintenance of dynamic stability during gait of individuals following concussion.

METHODS

Fifteen college-age subjects with Grade 2 concussions (CONC) and 15 uninjured controls (NORM) were observed while walking under two conditions: 1) undivided attention (single-task) and 2) while simultaneously completing simple mental tasks (dual-task). Testing began within 48 hours of injury (day 2) and repeated at 5, 14, and 28 days post injury. NORMs were evaluated at the same intervals.

Whole-body motion data were collected using a six-camera motion analysis system and two force plates. A 13-link biomechanical model was utilized to compute whole body center of mass (COM). Center of pressure (COP) was computed with ground reaction forces. In addition to temporal distance gait parameters, anterior and medial-lateral COM motion (APROM, MLROM), peak anterior velocity of the COM (ANTVEL), and the maximum separation between the COM and COP (APMAX) were used to examine dynamic stability. Three-way repeated-measures mixed design ANOVA and Tukey *post hoc* tests were completed to determine differences between group, task, and testing day.

RESULTS AND DISCUSSION

Group by day as well as task by day interactions were found for gait velocity and stride length. Gait velocity was significantly decreased for the CONCs on the dual-task compared to single-task for all days while NORMs were only significantly decreased on the dual-task for days 2 and 5. The CONCs' stride length was significantly decreased compared to the NORMs on both tasks on days 2 and 14. In addition, the stride length on the dual-task was significantly smaller than the single-task for the CONCs on days 2 and 5. Significant group by day interactions were found for MLROM and APMAX. A significant task by day interaction was found for APROM and ANTVEL. Follow-up analyses revealed medial-lateral COM sway was significantly increased for days 2, 5, and 28 for CONCs compared to NORMs on the dual-task

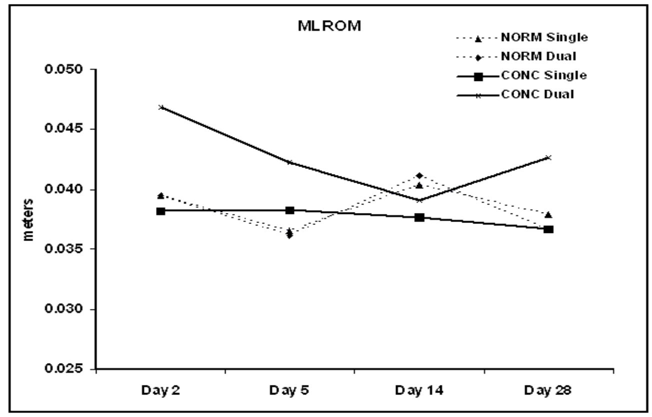

Figure 1: Medial-lateral range of motion of the COM

(Figure 1). One possible explanation may be that when required to divert their attention to a concurrent task, the CONCs could not adequately adjust to the challenge and therefore sway more, compromising their stability. By the last testing the CONCs have returned to play and this increase in activity is likely the cause of the decrease in performance seen on day 28. The CONCs displayed decreased APMAX at days 2, 14, and 28 compared to the NORMs. For CONCs under the dual-task condition, APROM was significantly decreased on days 2 and 5 and ANTVEL was significantly decreased on all 4 days.

CONCLUSIONS

Concussed individuals continue to display significant differences in anterior velocity and COM movement when compared to uninjured controls up to four weeks after injury. The demands of performing a dynamic motor task combined with a mental activity that divides attention may effectively approximate the demands of an athlete in competition. However, if the concussed individuals have difficulty maintaining stability in a controlled environment they may well have difficulty adjusting to the multiple input environment of the athletic arena. The findings of this study demonstrate that concussion has an observable and measurable effect on the body's ability to maintain and control dynamic stability for up to four weeks after injury.

REFERENCES

1. Basford, JR, et al. *Arch Phys Med Rehab*, **84**, 343-9, 2003.
2. Chou, L-S, et al. *Gait and Posture,* **20,** 245-54, 2004.
3. McFayden , et al. *J Head Trauma Rehab*, **18**, 512-25, 2003.
4. Parker, TM, et al. *Clinical Biomech* (in press).

ACKNOWLEDGEMENTS

This study was supported by the Centers for Disease Control and Prevention (R49/CCR021735 and CCR023203).

EFFECTS OF IMPEDED FOOT ARCH HEIGHT ON CALCANEAL EVERSION AND ANKLE JOINT FORCES DURING GAIT

Shing-Jye Chen and Li-Shan Chou
Motion Analysis laboratory, Department of Human Physiology, University of Oregon, Eugene, Oregon, USA
E-Mail: chou@uoregon.edu, web: http://biomechanics.uoregon.edu/chou/

INTRODUCTION

Therapeutic footwear is prescribed to not only control excessive rearfoot motion by aligning tibia and calcaneus, but also retain the medial longitudinal arch (MLA) functions to appropriately attenuate shock and accommodate uneven surface while walking. Changes in the MLA height during midstance have been found to be positively correlated with calcaneal eversion [1]. Excessive calcaneal eversion could be successfully limited by therapeutic footwear [2]. However, small and unsystematic changes of the rearfoot motion [3] and inconsistent peak calcaneal eversion control [4] were found during running with inserted orthoses in shoes. These inconclusive findings may suggest constrained MLA height changes due to the inserted orthoses could affect the calcaneal motion during walking. Therefore, the purpose of this study was to determine effects of impeded MLA height on the calcaneal motion and on 3D ankle joint force (AJRF) in healthy young adults during walking.

METHODS

Fourteen adults (mean age: 25.3±4.7 years, body mass: 71.3±9.8 kg) were tested after being examined by a podiatrist who ruled out any foot-related pathologies. A six-camera motion analysis system (Motion Analysis Corp., Santa Rosa, CA) was used to collect eleven skin based reflective markers placed on left shank/foot during quiet stance and while walking with self selected pace in barefoot (BF) then two types customized arch supports: one deformable (AS1) and one rigid (AS2). Arch supports were directly attached to the plantar surface of the feet using double sided adhesive tapes. Heel cup of the arch support was removed to eliminate any effects on rearfoot motion. KinTrak 6.2 software (Motion Analysis Corp., Santa Rosa, CA) was used to analyze the motion data and 3D AJRF. The MLA height was defined as the perpendicular distance from the navicular marker to the line connected between distal calcaneal and 1st metatarsal head markers. The dynamic change of the MLA height was calculated as differences in heights between walking and standing for each testing condition (BF, AS1 & AS2, respectively). Subject means of MLA height changes were calculated over the stance period. The peak calcaneal eversion (CE) and peak AJRF across subjects were also calculated. Planned contrasts with one way within-subjects ANOVA (SPSS 10.1) was performed to detect arch constrained effect (AS1 and AS2) on changes of the MLA height, peak CEV and peak AJRF, $p < .05$.

RESULTS AND DISCUSSION

Average walking speeds (M =1.31± 0.02 m/s) were found to be consistent across all subjects and among three testing conditions. Mean MLA height changes across stance periods in AS conditions (AS1 M = 0.93±0.33 mm; AS2 M = 0.36±0.47 mm) were found to be significantly less than that in BF condition (M = 1.91±0.18 mm). Significant differences in the peak CE were found between BF (M = 1.51±1.93°) and AS2 condition (AS2 M = 2.59±1.85°, p = .03). Significant arch support effects were found in vertical AJRF (*) at the 1st peak (p1↑) and trough (t1↓) as well as in the AP AJRF at trough 1 (t1↑). Impeded changes of arch height resulted in an increased peak calcaneal eversion and a corresponding increased vertical AJRF during early midstance (Figure 1a and 1b).

SUMMARY

When the MLA vertical motion was impeded, the increased calcaneal eversion might be a compromise for the lack of arch height changes, meanwhile, limiting the arch function in shock absorbing. When therapeutic footwear is designed to control rearfoot motion, its possible effects on the midfoot MLA motion should be considered.

REFERENCES

1. Boozer, et al., (2002). *Biomed Sci Instrum* 38, 203-7.
2. Nester, et al., (2003). *Gait and Posture*, 17, 180-7.
3. Stacoff, et al., (2000). *Clin Biomech,* 15(1): 54-64.
4. William III, et al., (2003). *Med Sci Sports Exerc*, 35, 12, 2060-68.

ACKNOWLEDGEMENTS

This work was supported by the University of Oregon and ISB Dissertation matching grant (to SJC).

a)
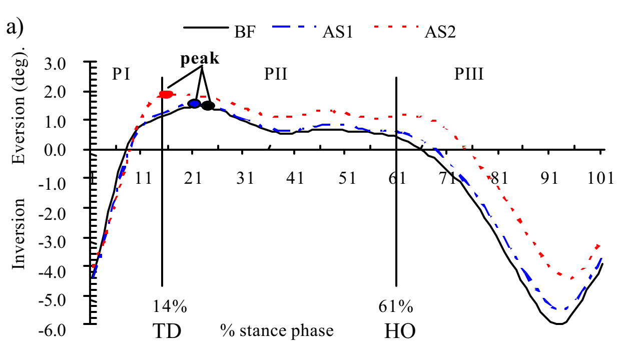

b)
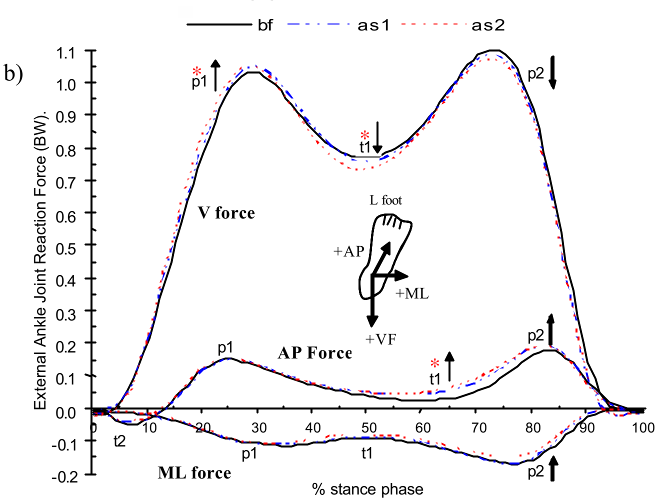

Figure 1. Subject means of a) Eversion/ Inversion change, b) 3D AJRF (Vertical/AP/ML w.r.t. left foot local coordinate system) in each testing condition (BF/AS1/AS2). TD (1st toe down), HO (heel off). * $p < .05$;↑: AJRF increased with rigidity of the arch supports.

STABLE LOCOMOTION OF FEEDFORWARD CONTROLLED ONE-LEGGED ROBOT

[1] Juergen Rummel, [1] Andre Seyfarth and [1,2] Fumiya Iida
[1]Locomotion Lab, Institute of Sport Science, Friedrich-Schiller University Jena, Dornburger Str. 23, D-07743 Jena, Germany,
[2]Artificial Intelligence Laboratory, Department of Information Technology, University of Zurich, Andreasstrasse 15,
CH-8050, Zurich, Switzerland; email: juergen.rummel@uni-jena.de, web: www.lauflabor.de

INTRODUCTION

An accepted model for understanding the dynamics of legged locomotion is the simple spring-mass model introduced by Blickhan [1] and further researched by Seyfarth, et. al. [3]. In reality, however, humans and animals use segmented legs for locomtion instead of simple springs. The combination of both in a motor-driven mechanical application should therefore be more biologically inspired. The aim of this study was to investigate, wether an actuated mechanical system allows stable locomotion without sensory feedback.

METHODS

The mechanical application used in this investigation is a one-legged robot with two segments. The robot body is 150 mm in length, 50 mm in width and 155 mm in height. One motor at the hip actuates a connected thigh segment, that is elastically joined with a shank segment. Two elements of rubber serve as dampers when hitting the ground.

According to Raibert [2], a retaining mechanism constrains motion leaving just two degrees of freedom (vertical and horizontal direction). Rotation about the pitch axis is disabled. Therefore, other stabilizing the robot body is not required.

The hip actuator is realized by a position controlled motor. Here, we used a simple sine oscillation as position signal as follows:

$$P(t) = \alpha \cdot \sin(2\pi \cdot f \cdot t) + \alpha_0 \qquad (1)$$

Frequency f and bias angle α_0 are independent parameters and were varied in experiments (f = 1.5…8 Hz and α_0 = -25…+25 deg) . The amplitude α depends on frequency. This control strategy did not need global sensory feedback.

During experiments, the robot moved in a circle on a wooden plate for 30 seconds for every parameter set and were repeated 3 times. For kinematic analysis of robot movement we attached reflective markers. A high-speed (240 Hz) motion capture system measured and tracked 3D-trajectories of the markers. The Trajectories were split into cycles defined by motor oscillation. For every parameter set, 120 movement cycles were randomly selected for analysis.

The stability of resultant locomotion will be described as equal patterns in horizontal direction whereas standard deviation is used as an opposing reference number in this study.

RESULTS AND DISCUSSION

As shown in figure 1, there are two significant regions with a mean speed of 0.3 m/s in positive horizontal direction. For frequencies between 4 and 6 Hz and bias angles with a range of 0 to 20 deg the robot has a local maximum in speed by using mostly one support point. More important is, that this gait describes a local minimum in variability of speed as shown in figure 2. In the range of the second maximum ($f = 2…5$ Hz, $\alpha_0 < 0$ deg), the robot uses two point contacts. There, horizontal velocity increases and causes low variance in locomotion for a wide area (Fig. 2)

CONCLUSIONS

In this study we observed that feed-forward controlled one-legged locomotion is possible. In two cases we found stable ranges with a remarkable speed.

REFERENCES

1. Blickhan R *The spring-mass model for running and hopping. J Biomechanics* **22**, 1217-1227, 1989.
2. Raibert HM, *Legged Robots That Balance. The MIT Press*, 1986
3. Seyfarth A, et. al. *A movement criterion for running. J Biomechanics* **35**, 649-655, 2002

ACKNOWLEDGEMENTS

This research was supported by an Emmy-Noether grant of the German Science Foundation (DFG) to A.S.: (SE1042/1).

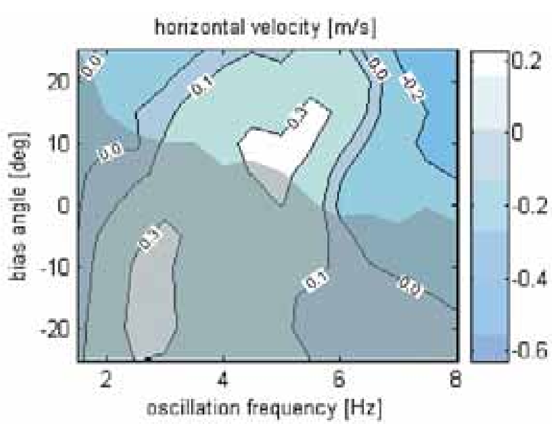

Figure 1: Horizontal speed of robot. Gray layered area shows, where two points touches the ground.

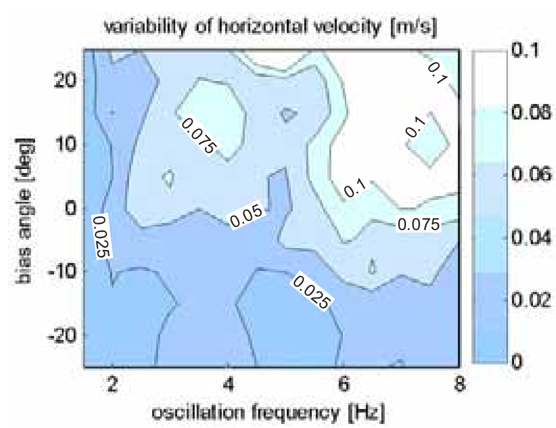

Figure 2: Variation of speed as opposite parameter for stability of motion cycles.

LEG STIFFNESS IN WALKING AND RUNNING

[1, 2] Susanne Lipfert, [1]Andre Seyfarth and [2]Reinhard Blickhan
[1] Locomotion Laboratory, Friedrich Schiller University, Jena, Germany
[2]Biomechanics Laboratory, Friedrich Schiller University, Jena, Germany

INTRODUCTION

There is a good deal of published research available on the mechanics of running regarding leg stiffness and stability [2, 4]. A simple spring-mass model for running had been proposed [1, 5], which provides a basis for further investigations. The work of Seyfarth et al. (2002) exposes spring-like leg operation, minimum running speed, and adjusted leg stiffness and angle of attack as prominent requirements of mechanically self-stabilized running. For walking, however, it seems to be a much greater challenge when attempting to propose respective simple templates. This study targets the leg stiffness, to determine whether running and walking patterns are stable. Aims of this study therefore were a) calculating the correlation coefficients of leg stiffness in running and walking, and b) comparing leg stiffness of both gaits. We hypothesized that vertical ground reaction forces (GRFs) and displacement of the center of mass (CoM) would correlate significantly in a positive linear way for running as well as for walking. We also hypothesized no significant intra- or inter-individual differences for leg stiffness.

METHODS

9 healthy subjects (4 women and 5 men) were randomly selected from an athletic population. Subjects had a number of reflective markers placed over anatomical landmarks to calculate positions of body segments. Ground reaction forces (GRFs) during running and walking were measured on a special split-belt treadmill, where each belt covered a Kistler force plate (2000Hz). 3D coordinates of the reflective markers were recorded simultaneously via six high-speed (150Hz) video cameras (Qualisys). Subjects were required to perform 13 gait transitions (6 x walking, 6x running) at their individual transition speeds, determined in a pretest. Time of transition was signalized by an acoustical signal occurring every 10 seconds. Raw force plate data was processed using custom software (Matlab, Mathworks Inc.). For each stance phase (heel-strike to toe-off), the vertical CoM displacement was calculated by numerically integrating the vertical force. Total vertical GRF (right GRF + left GRF) was then plotted over CoM displacement for each stance phase in running and walking to represent leg stiffness. Correlation coefficients between vertical GRF and CoM displacement and regression lines were calculated on individual stance phase data. A simple analysis of variance (ANOVA) was conducted to determine for significant differences within and between subjects. Both, walking and running were analyzed.

RESULTS AND DISCUSSION

High correlation coefficients of over 0.95 were observed for all data. The results also showed that neither intra-individual nor inter-individual stance phase data did differ statistically with p values being near zero (Figure 1).
Given the fact that stance phase data of both, running and walking, was collected at the same forward speed, it is well justified to compare leg stiffness across both gaits. Two main observations emerged from our comparisons: the vertical stiffness of the leg can be considered as a linear spring not only for running but also for walking. While not exactly the same regressions, there is still a close proximity of the spring-like leg behaviors apparent. The observed smaller vertical excursions of the CoM in walking correspond to the absence of flight phases, where instead single support occurs as opposed to double support.

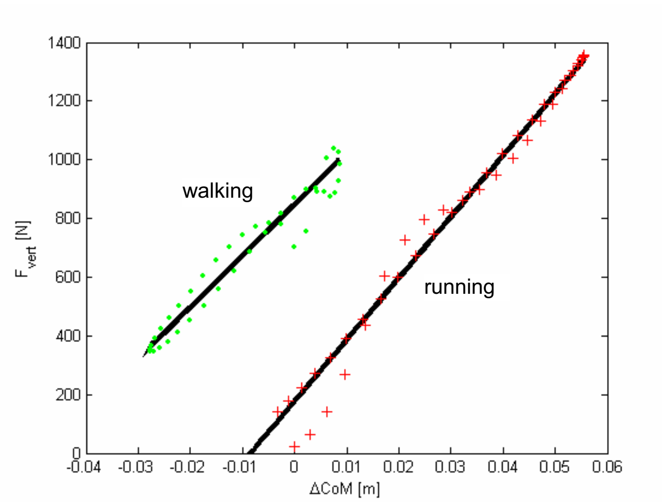

Figure 1 Mean vertical GRFs and CoM displacement data shown as scatter plot and regression line representing leg stiffness in walking (left) and running (right).

CONCLUSION

Mathematical models have already been successfully applied to describe experimentally observed GRFs for running [3, 6]. Further research is currently done to extend these models by a second spring-like leg.

REFERENCES

1. Blickhan, R: The spring-mass model for running and hopping. J. Biomech. 22: 1217-27. 1989.
2. Farely CT et al.: Leg stiffness and stride frequency in human running. J. Biomech. 29: 181-6. 1996.
3. Geyer H, et al.: Spring-mass running: simple approximate solution and application to gait stability. J. Theor. Biol. 232: 315-328. 2005.
4. He JP, et al.: Mechanics of running under simulated low gravity. J. Appl. Physiol. 71: 863-70. 1991.
5. McMahon TA, et al.: The mechanics of running: how does stiffness couple with speed? J. Biomech. 23: 65-78. 1990.
6. Seyfarth A, et al.: A movement criterion for running. J. Biomech. 35: 649-55. 2002.

ACKNOWLEDGEMENTS

This research was supported by an Emmy-Noether grant of the German Science Foundation (DFG).

AN INVERTED PENDULUM MODEL INDICATES THAT PARKINSON'S DISEASE RESULTS IN ALTERED NEUROMUSCULAR STIFFNESS FOR CONTROLLING GAIT

[1]Max J. Kurz, [1]Nicholas Stergiou, [2]Ekaterini Markopoulou and [1]Ugo Buzzi
[1]HPER Biomechanics Laboratory, University of Nebraska at Omaha, Omaha, NE
[2]Neurological Sciences, University of Nebraska Medical Center, Omaha, NE
E-mail: mkurz@mail.unomaha.edu Web: http://www.unocoe.unomaha.edu/hper/bio/home.htm

INTRODUCTION

Inverted pendulums have been used to model locomotion [1,2]. Furthermore, the organization of the dynamic resources available in the neuromuscular system determines the behavior of the inverted pendulum system. These resources can be categorized as the ability of the muscles to produce functional joint torques, passive and active characteristics of the muscles and tendons, and the exchange of potential and kinetic energy [1,2]. An escapement-driven inverted pendulum model has been used successfully to explain how pathological populations (i.e. Cerebral Palsy) utilize these dynamic resources (Figure 1) [1,2].

Parkinson's disease (PD) is a disorder of the basal ganglia that results in a loss of normal motor function [3]. PD patients have irregular stepping patterns and altered lower limb coordination [3]. These movement deficiencies may be related to the inability of PD patients to effectively utilize the available dynamic resources for functional gait. Here we use an escapement-driven inverted pendulum model to reveal how PD patients use the stiffness and dampening resources to control gait.

METHODS

Three-dimensional kinematics of the lower extremity were collected as five subjects with idiopathic PD (Age = 64 $\pm$ 7.0 yrs) and five healthy controls (66 $\pm$ 7.7 yrs) walked on a treadmill at the self-selected pace. All PD subjects were off dopamine treatment and had a Unified PD Rating Scale in the 53rd percentile. Equation 1 represents the dynamics of the escapement-driven inverted pendulum model used in this investigation (Figure 1).

$$ML^2\ddot{\theta} = FL + MLg\theta - kb^2\theta - cb\dot{\theta} \qquad \text{Equation 1.}$$

where M is the mass of the body, θ is leg angle, L is the distance from the axis of rotation to the center of mass of the physical pendulum, F is the active muscle force from the opposite leg, k is the stiffness, b is the distance of the spring from the axis of rotation, g is gravity, c is the dampening, and $\dot{\theta}$ and $\ddot{\theta}$ represent the angular derivatives of the inverted pendulum. Anthropometric measurements were utilized to fit subject's physical characteristics to the model [1,2]. The period of the leg pendulum was computed under the assumption that the time from the start of the stance phase to maxium angular displacement of the leg pendulum represented half of the natural period (τ). The stiffness and dampening of the model was calculated from Equation 2 and 3 respectively [1,2].

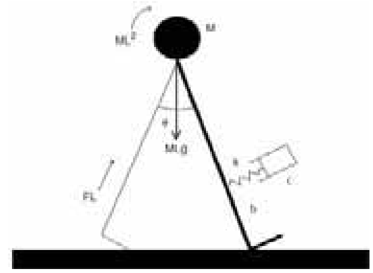

Figure 1. The escapement-driven inverted pendulum model.

$$kb^2 = \frac{ML^2}{(\tau \;\; / 2\pi)^2} + MLg \qquad \text{Equation 2.}$$

$$cb^2 = 2 * \sqrt{ML^2\,(kb^2 - MLg)} \qquad \text{Equation 3.}$$

The stiffness and dampening values were normalized by the subject's walking speed and MLg in order to control for differences in walking speeds and anthropometrics between the two groups [1,2].

RESULTS AND DISCUSSION

PD subjects had significantly less stiffness during locomotion (Table 1). Stiffness in the model is a result of the elastic tissues and active muscular tension [1,2]. The altered stiffness may be related to the impaired reflexes and muscular activation found in PD patients [3]. Stiffness deficiencies may be related to the irregular stepping patterns and higher incidence of falls found in PD patients [3]. Future investigations will investigate if dopamine therapy restores the use of effective dynamic resource strategies in PD patients.

REFERENCES

1. Holt KG, et al. *Human Mov Sci* **19**, 375-405, 2000.
2. Ulrich BD, et al. *Human Mov Sci* **23**, 133-156, 2004.
3. Mitoma H, et al. *J Neurol Sci* ***174**, 22-39*, 2000.

Table 1. Means and standard deviations of stiffness and dampening values. * significant differences between groups at $p < 0.05$.

Group	Stiffness	Dampening
PD	7.78 (3.7)*	1.95 (.84)
Control	12.08 (1.6)	2.09 (.56)

IS THERE A GAIT TRANSITION BETWEEN RUN AND SPRINT?

[1, 3]Chris P. Hurt, [2]Alan Hreljac, [1]Max J. Kurz, and [1]Nicholas Stergiou
[1]HPER Biomechanics Lab, University of Nebraska at Omaha, Omaha, NE,
[2]Kinesiology and Health Science Dept, California State University, Sacramento, CA
[3]Department of Integrative Physiology, University of Colorado, Boulder, CO
email: nstergiou@mail.unomaha.edu, web: www.unocoe.unomaha.edu/hper/bio/home.htm

INTRODUCTION

The walk-to-run behavioral transition has been widely examined in the literature. It has been found that the preferred transition speed from walk to run is approximately 2.0 ms^{-1} [2]. However, the corresponding speed for the behavioral transition from run-to-sprint is unknown. Differences have been reported between run and sprint [3, 5], but it is not clear if run and sprint are two different modes of locomotion or if sprint is actually a fast run [1]. Hreljac et al. [1] found that joint kinetics increased from run-to-sprint over a continuum; without any significant change at some discrete speed. However, they suggested that an analysis of intralimb coordination, based on the principles of Dynamical Systems Theory (DST), might be more sensitive in distinguishing a specific behavioral transition point. In DST, the interacting components are examined while scaling up a control parameter that elicits a new pattern of coordination [4]. The purpose of this study was to examine the intralimb coordination strategies used during running at different speeds that range from a jog to a sprint. By using DST, we investigated the interacting segments, while scaling up the speed as a control parameter.

METHODS

Seven male subjects, all of whom exhibited a heel strike pattern at their preferred running speed, ran at their preferred speed (0%) and at 15%, 30%, 45%, 60%, 75%, and 90% greater than this speed, while sagittal plane kinematics were collected (240 Hz) from the right lower extremity. To examine segmental interactions, the phase portraits from segmental angular position and velocities were used to calculate phase angles [4]. Relative phase curves were calculated for two segmental relationships (foot-shank [F-S] and shank-thigh [S-T]) by subtracting the phase angle of the proximal segment from the distal. Mean relative phase (MRP) was calculated from the relative phase curves of each subject and for each condition. This was done by averaging the absolute values of all points of the curve for the braking and the propulsive periods of stance. A single factor repeated ANOVA was performed on the MRP group means for each segmental relationship and for each stance period. A Tukey test was performed in comparisons that resulted in a significant F-ratio ($p<0.05$).

RESULTS AND DISCUSSION

Statistical significance for both segmental relationships was found only during the braking period of the gait cycle but not for the propulsion period (Table 1). Both MRP F-S and S-T significantly decreased, indicating a more-in-phase relationship between the interacting segments as speed increased. Based on the post-hoc analysis, the 30% speed condition had the greatest effect. It is possible that this is the speed that the landing strategy changed from a heel-strike to a forefoot strike, and may indicate that there is a specific speed where the runner transitions from run to sprint.

Our results indicated that increasing the running speed from a run to a sprint elicited behavioral changes. These changes occurred during the braking period. The 30% above the running self-selected speed condition seems to be a critical speed for the observed changes.

REFERENCES

1. Hreljac A, et al. *Proceedings of ASB*, Toledo, OH, 2003.
2. Hreljac A. *J Biomech* **28**, 669-677, 1995.
3. Mann RA, et al. *Am J Sports Med* 8, 345-350, 1980.
4. Stergiou N, et al. *Gait Posture* **13**, 210-220, 2001.
5. Stefanyshyn DJ, et al. *J Biomech* 30, 1081-1086, 1997.

Table 1: Group means and SDs for the parameters evaluated. Condition numbers underneath the means indicate post-hoc significance.

Variables (deg)	Running Speed						
	0%	15%	30%	45%	60%	75%	90%
MRP F-S Braking	80.7 ± 14.4 30% - 90%	64.1 ± 19.9 60% - 90%	53.8 ± 24.1 90%	44.7 ± 15.7	38.8 ± 24.9	37.3 ± 13.2	26.0 ± 9.4
MRP S-T Braking	68.0 ± 15.5 30% - 90%	53.2 ± 12.2 60% - 90%	45.3 ± 16.6 90%	42.2 ± 11.2	32.8 ± 19.7	35.3 ± 9.4	25.4 ± 7.4
MRP F-S Propuls.	53.8 ± 10.0	51.0 ± 4.1	53.0 ± 4.4	51.1 ± 10.6	50.7 ± 10.6	49.6 ± 4.2	46.4 ± 4.7
MRP S-T Propuls.	46.6 ± 7.2	44.4 ± 5.8	45.2 ± 5.8	43.9 ± 6.2	43.3 ± 8.4	43.3 ± 4.9	41.5 ± 4.2

DOES HUMAN HAND PERFORM LIKE A ROBOTIC GRIPPER? —AN EXAMINATION OF INTERNAL FORCES DURING OBJECT MANIPULATION

[1] Fan Gao, [2]Mark L. Latash, [1]Vladimir M. Zatsiorsky
[1]Biomechanics Laboratory, Department of Kinesiology, The Pennsylvania State University
[2]Motor Control Laboratory, Department of Kinesiology, The Pennsylvania State University
email: fug101@psu.edu, mll1@psu.edu, vxz1@psu.edu,

INTRODUCTION

In multi-digit grasping, a vector of contact forces and moments f can be broken into two orthogonal vectors: the resultant force vector fr (manipulation force) and the vector of the internal force fi ($f = fr + fi$) [1]. Internal force is a set of contact forces which can be applied to an object without disturbing its equilibrium [2,3]. The elements of the internal force vector fi cancel each other and, hence, do not contribute to the manipulation force. The mathematical independence of the internal and manipulation forces allows for their independent (decoupled) control. Such a decoupled control is realized in robotic manipulators [4]. The purposes of this study are to examine whether in human internal force is coupled with the manipulation force and what grasping strategy the performers utilize.

METHODS

The subjects (n=6) were instructed to make cyclic arm movements with a customized handle. Six combinations of handle orientation and movement direction were tested. These involved *parallel manipulations*: (1) VV task - vertical orientation & vertical movement and (2) HH task - horizontal orientation & horizontal movement, *orthogonal manipulations*: (3) VH task - vertical orientation & horizontal movement and (4) HV task - horizontal orientation & vertical movement, and *diagonal manipulations*: (5) DV task - diagonal orientation & vertical movement and (6) DH task - diagonal orientation & horizontal movement. Handle weight (from 3.8 to 13.8 N), and movement frequency (from 1 Hz to 3 Hz) were systematically changed. The analysis was performed at the thumb-virtual finger level (VF, an imaginary finger that produces a wrench equal to the sum of wrenches produced by all the fingers). At this level, the forces of interest could be reduced to the *internal force* (the grip force) and *internal moment*.

RESULTS AND DISCUSSION

During the parallel manipulations, the internal force was coupled with the manipulation force and the thumb-VF forces increased or decreased in phase. During the orthogonal manipulations, the thumb-VF forces changed out of phase; the plots of the internal force vs. object acceleration resembled an inverted V letter (Figure 1). The HV task was the only task where the relative phase (coupling) between the normal forces of the thumb and VF depended on oscillation frequency. During the diagonal manipulations, the coupling was different in the DV and DH tasks. A novel observation of substantial internal moments is described: the moments produced by the normal finger forces were counterbalanced by the moments produced by the tangential forces such that the resultant moments were close to zero.

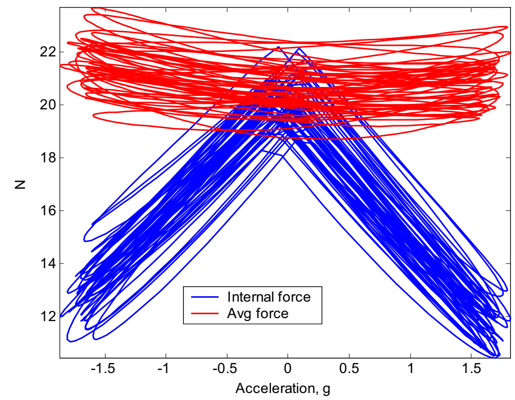

Figure 1: Internal force and average normal force versus the handle acceleration (load, 11.3 N; frequency, 3 Hz).

Internal forces do not affect equations of motion [3] and hence control of manipulation can be broken up into two sub-tasks—'holding' and 'tracking'—which can be controlled independently. Such a control strategy (which is commonly used in robotic grippers – [4]) simplifies the control. This strategy requires, however, exerting unnecessarily large forces and is in this sense uneconomical. This study, however, suggests that the CNS prefers to face larger computational costs rather than produce excessive forces. The CNS uses different patterns of the thumb-VF coordination when the manipulation force is in a tangential direction as compared with the manipulation in the normal direction. When the manipulation force is in a tangential direction, the symmetric pattern of the thumb-VF coordination is used: The thumb and VF work in synchrony to grasp the object stronger or weaker. In contrast, when the manipulation force is in the normal direction the anti-symmetric force changes are recorded: When the normal force of either thumb or VF increases, the force exerted by the opposing digits decreases. It is not clear to which degree such coordination is a consequence of task mechanics as compared with the neural control.

REFERENCES

1. Kerr J, et al. The International Journal of Robotics Research 4, 3-17, 1986.
2. Mason MT, et al. Robot Hands and the Mechanics of Manipulation. MIT Press, Cambridge, Massachusetts, 1985.
3. Murray RM, et al. A mathematical introduction to robotic manipulation. CRC Press, Boca Raton, 1994.
4. Zuo B-R, et al. IEEE Transactions on Systems, Man and Cybernetics 30, 185-192, 2000.

ACKNOWLEDGEMENTS

NIH grants AR-048563, AG-018751, and NS-35032

POSTURAL LOCAL DYNAMIC STABILITY IS NOT PREDICTIVE OF THAT DURING LOCOMOTION

Hyun Gu Kang and Jonathan B. Dingwell
Nonlinear Biodynamics Lab, Department of Kinesiology, University of Texas at Austin
email: jdingwell@mail.utexas.edu web: www.edb.utexas.edu/faculty/dingwell/

INTRODUCTION

Clinical measures of postural stability have been used to predict falls in the elderly with variable success. In particular, several do not predict falls that occur during walking well [1] and these constitute the majority of falls [2]. This could be because inherently different control mechanisms are used to maintain stability during standing and walking [3].

Prior studies comparing postural to locomotor stability [4,5] used different metrics for the different tasks and used metrics that were not *direct* measures of stability *itself*. We resolved these problems by using appropriately defined metrics to define *local dynamic stability* [6] in the same way for standing and walking. We hypothesized that standing stability would be different from walking stability and would not predict walking stability. We also validated our metrics for standing stability against traditional center of pressure (COP) measures.

METHODS

20 healthy subjects (age 18-73) performed three 5-min. trials walking on a motorized treadmill at their preferred speed, and three 5-min. trials standing eyes open on a force plate. Trunk motions were recorded using VICON and used to construct a 12-dimensional state space comprised of the 3D linear and angular trunk positions and velocities. Local dynamic stability was quantified using these trunk trajectories in the 12-D state spaces. The mean divergence over time $\langle d_j(i) \rangle$ of locally perturbed trajectories was calculated to quantify local dynamic stability [6,7]. Mean divergence curves were parameterized using a double exponential function (Equation 1):

$$\langle d_j(i) \rangle = A - B_S e^{-i/\tau_S} - B_L e^{-i/\tau_L} \qquad (1)$$

The parameters (A, B_S, τ_S, B_L, and τ_L) were averaged over the 3 trials of each task. A repeated measures ANOVA was used to determine if standing and walking exhibited different stability properties. Pearson correlations were used to determine if standing stability predicted walking stability. Correlations were also computed between standing stability metrics and traditional COP measures of standing balance: COP excursion, mean speed and mean power frequency (MPF).

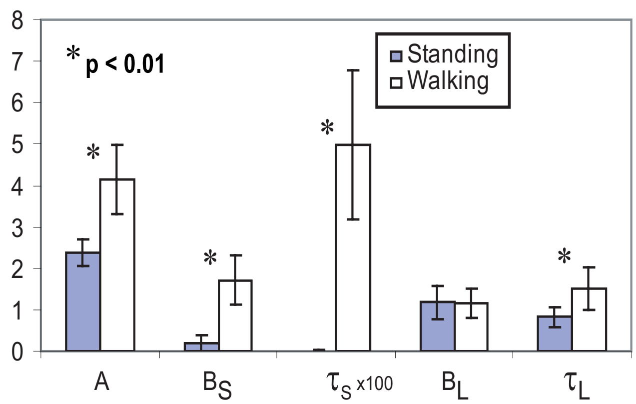

Figure 1: Magnitudes of all mean local divergence curve parameters except for B_L were significantly larger ($p < 0.01$) during walking than during standing.

RESULTS AND DISCUSSION

Local dynamic perturbation responses during standing and walking exhibited different magnitudes and different time scales (Figure 1). Furthermore, local stability metrics for standing were not correlated with those for walking (Figure 2). These results support the idea that postural and locomotor stability are indeed governed by different mechanisms.

COP mean speed and MPF were significantly correlated to A and B_L for standing ($r^2 > 47\%$; $p < 0.001$). Thus, our local dynamic stability metrics are consistent with traditional COP measures for standing balance. None of the COP measures were correlated to any of the local stability metrics for walking ($r^2 < 14\%$; $p > 0.12$). These findings support the notion that traditional postural stability measures based on COP measurements are not predictive of locomotor stability.

REFERENCES

1. Brauer SG, et al. *J. Gerontol A Biol Sci Med Sci*, **55**, M469-M476, 2000.
2. Niino N, et al. *J Epidemiol* **10**, S90-S94, 2000.
3. Winter DA. *Gait Posture* **3**, 193-214, 1995.
4. Shimada H, et al. *Am J Phys Med Rehab* **82,** 511-516, 2003.
5. Cromwell RL, et al. *J Aging Phys Act* **12,** 90-100, 2004.
6. Rosenstein MT, et al. *Physica D* **65,** 117-134, 1993.
7. Dingwell JB, et al. *Chaos* **10**, 848-863, 2000.

ACKNOWLEDGEMENTS

This study was supported by a Biomedical Engineering Research Grant from the Whitaker Foundation.

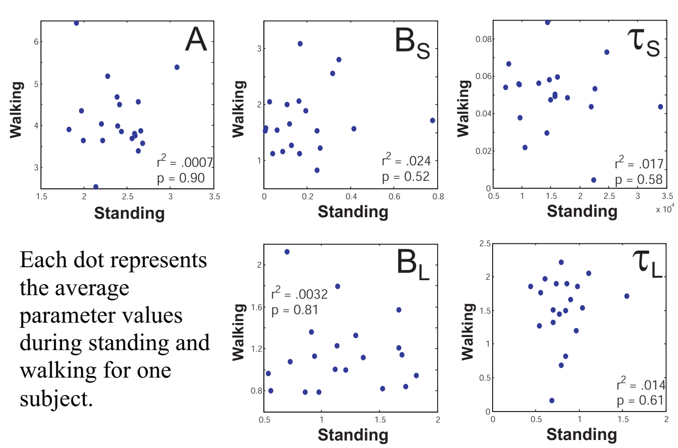

Figure 2: Local dynamic stability of standing did not predict local dynamic stability of walking ($r^2 < 2.5\%$; $p > 0.50$).

EFFECT OF DIFFERENT WEDGE CONDITIONS ON JOINT ANGLE CHANGES DURING SINGLE-LIMB STANCE

[1]Mansour Eslami, [1] Mehrdad Anbarian, [1] Paul Allard, [2]Clarice Tanaka, [1]Sébastien Hinse, [3]Nader Farahpour

[1]Department of Kinesiology, University of Montreal, Montreal, Canada. [2]Department of Physical Therapy, Speech Therapy and Occupational Therapy, University of São Paulo, São Paulo, Brazil. [3]Department of Physical Education, Bouali University, Hamedan, Iran; email: mansour.eslami@umontreal.ca

INTRODUCTION

Wedged foot orthotics are widely prescribed to promote the mechanical alignment of foot joints. However, wedged orthoses can also affect lower limb proximal joints and axial segment as an effect of the weight-bearing closed chain. Therefore, the wedged orthoses prescription should consider the functional relationship between the foot and proximal segments [1]. Conversely, the effect of wedged orthoses on the lower limb proximal joints and axial segment alignment is still unclear. The purpose of this study was to assess the effect of different wedge conditions on angle changes in the subtalar joint, ankle, knee, hip, pelvis, and upper trunk.

METHODS

Fourteen able-bodied young male participated in this study. Participants were tested in single-limb stance under five wedge placements: no wedge (NW); anterior (AW); posterior (PW); lateral heel (LW); medial heel (MW). A Motion Analysis System using five cameras with EVaRT software was used to capture (3 trials of 60s each) joint angle in the trunk and pelvis in horizontal plane, ankle, knee, hip in sagittal plane, and subtalar and hip joint in the frontal plane.

RESULTS AND DISCUSSION

Two repeated-factor (wedge by joint) ANOVA revealed main effect of wedge condition ($F_{4,52}=5.76$, $p=0.002$). Protected t test comparison was conducted on the main effect of wedge condition to detect the significant difference between no wedge condition and the wedge conditions.

In horizontal plane, angle changes in the upper trunk were revealed for all conditions (AW>PW>LW>MW>NW), whereas in pelvis rotation (Fig. 1) were shown in AW and PW conditions (AW>PW>NW).

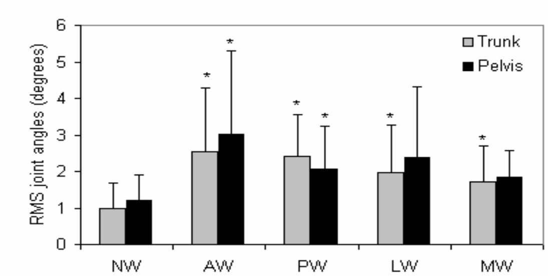

Figure 1: RMS value and standard deviation of upper trunk and pelvis in the horizontal plane across wedge conditions. *statistical difference compared to NW.
NW (no wedge), AW (Anterior wedge), PW (posterior wedge), LW (lateral wedge), MW (medial wedge).

In the sagittal plane (Fig. 2), ankle joint was affected by all wedge conditions (AW>PW>LW>MW>NW). Angle changes in the hip joint was shown in MW, LW and PW conditions (PW>MW>LW>NW) while knee joint revealed in LW (LW>NW) only.

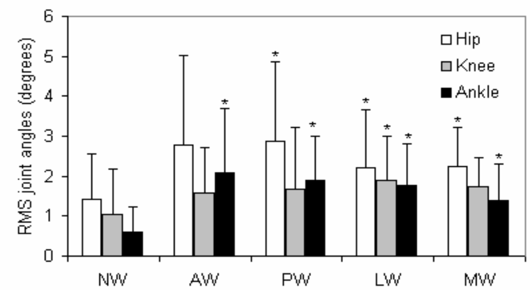

Figure 2: RMS value and standard deviation of hip, knee and ankle joints in the sagittal plane across conditions. *statistical difference compared to NW.

In the frontal plane (Fig. 3), the subtalar joint consistently exhibited angle changes for all wedge conditions (MW>PW>AW>LW>NW), while the hip joint in AW and MW conditions (MW>AW>NW) only.

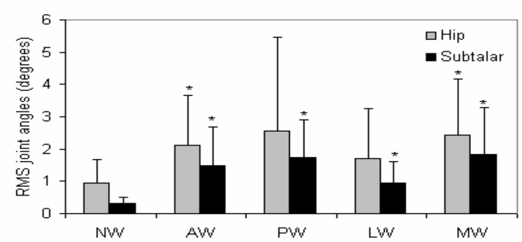

Figure 3: RMS value and standard deviation of hip and subtalar joints in the frontal plane across conditions. *statistical difference compared to NW.

CONCLUSION

Upper trunk, ankle and subtalar joint showed statistically significant changes regardless the wedge conditions. This shows the participation of different planes of movement to compensate a wedge placement. Furthermore, a particular wedge condition changes differently the especial proximal joints in a weight-bearing chain. Thus, it is essential to notice the effect of different posted orthotic on proximal joints and three planes of movement.

REFERENCE

1.Nicolopoulos C.S, et al. Biomechanical basis of foot orthotic prescription: Foot and ankle 2000; 14: 464-469.

Functional outcome in people with diabetic neuropathy at different stages of complications

[1]Robert van Deursen, [1]Rajani Kanade, [2]Patricia Price and [2]Keith Harding
[1]Research Centre for Clinical Kinaesiology, School of Healthcare Studies & [2]Wound Healing Research Unit, School of Medicine, Cardiff University, Cardiff, UK; email: vandeursenr@cardiff.ac.uk

INTRODUCTION

Diabetic neuropathy (DN) frequently leads to ulceration and these patients have an increased risk of lower limb amputation [1,2]. Limited knowledge exists on the functional outcome at various stages of this process. The aim of this study is to investigate multiple aspects of functional outcome/mobility of patients with DN at different stages of complications with trans-tibial amputations (TTA) as the last stage.

METHODS

To date in this ongoing study, 24 subjects with DN and no history of ulceration (control group), 13 with DN and a current plantar ulcer, 9 with DN and partial foot amputation and 21 with DN and unilateral trans-tibial amputation were studied. Informed consent was obtained and functional status was assessed based on the fundamental activities of mobility, largely focused on walking. Physical activity was recorded using Stepwatch Activity Monitors. Patient's perception of mobility was assessed with a self-administered Rivermead Mobility Index (RMI). Plantar pressure was measured with the Pedar in-shoe system while participants walked at their self-selected pace. Gait parameters were measured using digital video. Total Heart Beat Index (THBI), as an indicator of functional capacity/energy expenditure, was measured with a Polar Heart Rate Monitor. Statistical differences between the TTA group and the control group, matched on marginal distributions (age, gender, height, weight), were tested by means of independent t-tests ($\alpha = 0.05$). The other two groups were not sufficient in number and not sufficiently matched to be included in the inferential statistical analysis.

RESULTS AND DISCUSSION

Average daily strides were significantly reduced in the TTA group compared to controls (Table 1). The other two groups showed intermediate activity levels in comparison (Figure 1). Subject's own perception of level of mobility (RMI), gait velocity and functional capacity (THBI) were all significantly different between the TTA group and the controls. Daily plantar cumulative stress [3] was significantly reduced for the TTA group. However, peak pressure over the MT1-2 region was not significantly different between these two groups (Table 1). This also applied to other foot regions but these results are not reported here.

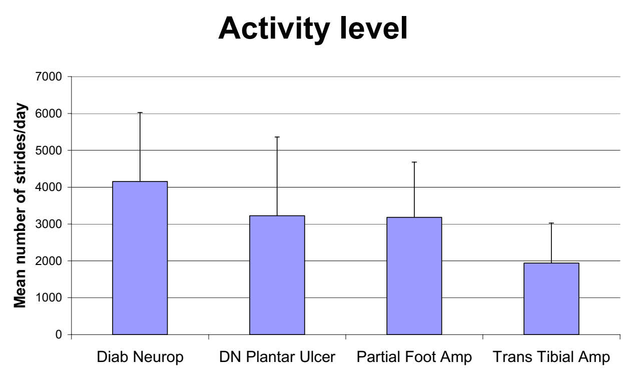

Figure 1: Activity levels measured as a one week average of number of strides per day. Mean and standard deviations are shown for four groups of subjects with DN.

CONCLUSIONS

All groups in this study demonstrated relatively low to very low levels of activity compared to normative values from healthy subjects [3]. Reduced physical activity levels and reduced walking speed seem to limit plantar loading in the TTA group. However, the surviving foot may be at risk of plantar ulceration if functional performance is improved during rehabilitation. This may also apply to the groups at other stages of complications. Therefore, efforts to increase fitness and activity levels should not occur at the expense of foot injury prevention.

REFERENCES

1. Holewski J et al. *J Rehabil Res Dev*; **26**: 35-44, 1989.
2. Apelqvist J, et al. *J Diab Comp*; **6**: 167-74, 1992.
3. Maluf KS & Mueller MJ. *Clin Biomech*; **18**:567-575, 2003.

ACKNOWLEDGEMENTS

Thanks to Michelle Evans, Tim Rebeiro, Jo Burton, Vanessa Davies, Jane Lewis and Scott Cawley for their assistance.

Table 1: Summary of results comparing the control group with DN and no complications and the trans-tibial amputation group.

	Control group Mean (SD)	**TTA group** Mean (SD)	**p**
Activity level (Average strides/day)	4155 (1869)	1941 (1084)	0.001*
RMI (score out of 15) - median	15 (9-15)	11.5 (8-14)	0.001*
Gait velocity (m/s)	1.11 (0.22)	0.76 (0.14)	0.001*
Peak pressure 1-2 MT (kPa)	301.6 (72.3)	316.3 (91.8)	0.574
Daily Plantar Cumulative Stress (MPa /day)	505.7 (235.7)	355.6 (211.1)	0.038*
THBI (beats/m)	1.27 (0.48)	1.71 (0.49)	0.005*

* Significant ($p \leq 0.05$)

THE INFLUENCE OF CYCLING ON LOWER LIMB MOVEMENT AND MUSCLE ACTIVATION DURING RUNNING IN TRIATHLETES

[1,2]Andrew R Chapman, [1]Bill Vicenzino, [2]Peter Blanch, [3]Steve Dowlan and [1]Paul W Hodges
[1]Division of Physiotherapy The University of Queensland, [2]Department of Physical Therapies Australian Institute of Sport,
[3]Department of Biomechanics Australian Institute of Sport
Email: andrew.chapman@ausport.gov.au

INTRODUCTION

Triathletes report a perception of reduced lower limb coordination when running after cycling. This perceived reduction in lower limb coordination may result from interference with control of movement and muscle recruitment. Studies of upper limb coordination have demonstrated interference with control of movement when two previously learnt tasks are performed in sequence or with only short interim periods [1]. These findings can be extrapolated to suggest that control of movement and muscle recruitment in triathletes during running after cycling may be less skilled when compared to running without prior cycling because of interference with movement control. However, interference with control of movement and muscle recruitment in triathletes during running following cycling has not been studied in the absence of fatigue, which is another potential cause of altered control of movement. Therefore, this study investigated the influence of the triathlon transition on movement and muscle recruitment in highly trained triathletes using a protocol designed to provide the triathletes with exposure to cycling without causing fatigue.

METHODS

Participants were nine highly trained Australian national or international level triathletes. Pelvic and lower limb movement (three dimensional kinematics), activation of tibialis anterior (TA, surface electromyography recordings) and stride and stance durations were compared between a control run, which occurred without any prior exercise, and a transition run that was preceded by 20 min of cycling. TA activity during running and cycling was compared using coefficients of multiple correlation (CMC) to test the hypothesis that changes to muscle activity between control and transition runs resulted in activation that more closely resembled that used for cycling. Myoelectric indicators of fatigue (initial values and rate of change of the mean spectral frequency (MNF), average rectified value (ARV), and neuromuscular efficiency (NME)) were measured using a protocol previously described [2] and were used to test the hypothesis that altered TA recruitment was not due to fatigue. Furthermore, repeatability of transition effects was examined and ratings of perceived control of movement were used to investigate if athletes' perceptions of coordination were correlated with transition effects.

RESULTS AND DISCUSSION

Group data of pelvic and lower limb movement, TA EMG, and stride and stance durations did not vary between control and transition runs. Analysis of individual triathlete movement patterns also showed that motion of the pelvis and lower limb, including individual variance of movement patterns and inter-joint coordination, did not vary in any triathlete between control and transition runs. Stride and stance durations also did not vary between control and transition runs in any triathlete. However, analysis of individual triathlete data revealed a decrease in the amplitude of TA EMG during the stance phase of running, which occurred immediately following the cycle leg and continued for the duration of the 30 min control run, in two of the nine triathletes. In these two triathletes, the pattern of activation of TA was more similar to that used for cycling (triathlete three control run-cycling CMC = 0.536 vs. transition run-cycling CMC = 0.746, and triathlete six control run-cycling CMC = 0.444 vs. transition run-cycling CMC = 0.610). Altered recruitment of TA during the transition run was not associated with myoelctric indications of fatigue as initial values and rate of change of MNF, ARV and NME did not vary between pre- and post exercise measures. Interestingly, these two triathletes were not different to the remaining seven triathletes in their ratings of perceived control of movement. Furthermore, the amplitude of TA EMG during the swing phase of running, times of EMG onset, offset and peak amplitude, EMG modulation and individual variance of EMG did not vary between control and transition runs in any triathletes. With the exception of the amplitude of TA EMG during the stance phase of running, absolute magnitudes of all kinematic and EMG variables during running did not vary between triathletes. Data of TA EMG and pelvic and limb kinematics was repeatable (CMC TA EMG = 0.846 ± 0.019, CMC kinematics 0.911 ± 0.029).

CONCLUSIONS

This study suggests that kinematics of the pelvis and lower limb are not influenced by the transition from cycling to running in highly trained triathletes. While activation of TA was not influenced by the cycle-run transition in a majority of highly trained triathletes, the data suggest that leg muscle activity during running may be influenced by cycling in some highly trained triathletes despite years of training and practice of the sequence. Altered recruitment of TA was not associated with myoelctric indications of fatigue but was more similar to that used for cycling, suggesting that it was the cycling task that directly affected running muscle activity. This transition effect was consistent between sessions.

REFERENCES

1. Karniel A, Mussa-Ivaldi FA. Does the motor control system use multiple models and context switching to cope with a variable environment? *Exp Brain Res* **143,** 520-524, 2002.
2. Merletti R, Roy S. Myoelectric and mechanical manifestations of muscle fatigue in voluntary contractions. *J Orthop Sports Phys Ther* **24,** 342-353, 1996

A METHOD TO DIAGNOSIS THE KINETIC CHARACTERISTIC OF THE STRAIGHT KICK PERFORMANCES

Xin-Hai Shan Yun-Xiang Li

Biomech. Lab, College of Phys. Edu., Shandong Normal University, Jinan 250014, China, Xhshan_jn@yahoo.com.cn

INTRODUCTION

Just like the Round Kick[1], the Straight Kick (SK) is another attack method to get score in Chinese Wushu competition. In order to get high effect, the key factor in SK performance is to reach the kick force as large as possible in a short period of time.

However, up to now few have been published related to the kinetic characteristic of this performance. Maybe it was related to the difficulty to test the horizontal kinetic variables of SK by using the force platform directly. Then T-Y Shiang, et al.[2] gave an idea. In order to get the impact data of the baseball, they mounted the force plat vertically on the wall, which makes it possible to test the kinetic characteristic. Therefore, the purpose of this paper is to try to develop a method used to diagnosis the kinetic characteristic of SK performances of China elate Wushu athletes and to present some references for the further research in this area.

METHODS

Participate: 8 Chinese elate Wushu athletes with (age, height, weight) 22.32±0.45year, 1.76±0.03m、72.65±6.62kg.

Apparatus: just as Fig. 1, the metal frame was fixed on the wall. Then the Kistler force platform (9287B) was fixed on the frame. In order to minimize the sore of the foot, a sponge was fixed on the platform with an adhesive tape.

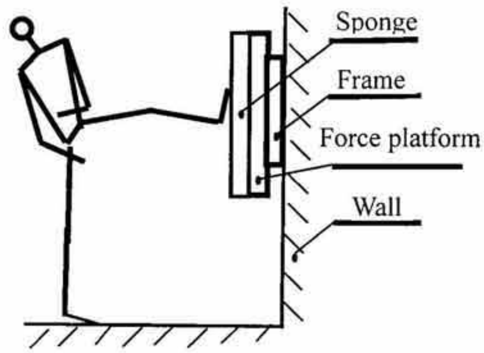

Fig. 1 The experimental apparatus setup

Procedures: in order to avoid injury, every subject was required to warm up more than 5 minutes including running and stretching the tendons. At hearing the start instruction, the athlete moved one step forward to the force platform with One leg standing on the ground, and the other straight kicking horizontally onto the platform with the maximum force.

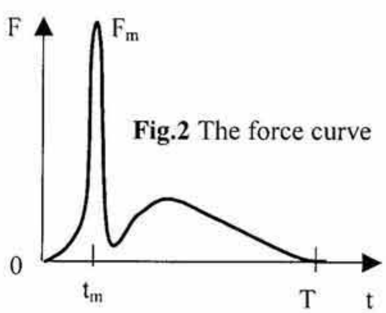

Fig.2 The force curve

Fig.2 is the typical force curve. At beginning, the force is zero. After a short time t_m, the force reaches the top F_m. At time T, the force gets down to zero. $\Delta F/\Delta t$ was calculated by the function F_m/t_m, which was the average force gradient within the time from the contact to the maximum force. Because of the explosive style of the performance, the force data were sampled at 2000Hz for 5s duration.

In the experiment, every athlete was required to complete three trials with the right foot and then with the left foot respectively. The Preferred Leg (PL) was defined in this paper to be the leg with the larger maximum kick force, and the non-Preferred Leg (non-PL) was to be with the less force. The best one of three trials in PL and non-PL respectively was selected as the statistics sample.

Statistics: T-test was used to determine the differences between kinetic variables of PL and non-PL with significant level at 0.05, and 0.01.

RESULTS AND DISCUSSION

From the contact to the maximum force, the time was about 20ms. The total time from contact to separate is about 170ms. In the aspect of time t_m and T, there was no significant difference ($p>0.05$) between the PL and non-PL.

In the maximum force, however, the force of PL was significant larger ($p<0.01$) than that of non-PL. The PL had maximum force 925.51±122.48kgf, while the non-PL was 35.6% lower. The maximum force was about 12 times of Body Weight, which is much larger than the maximum force of vertical jump[3].

Table 1 the kinetic variables of the athletes (n=8)

Variables	PL(M±SD)	Non-PL(M±SD)
t_m(ms)	20±3	21±2
T(ms)	170±21	170±35
F_m(kgf)	925.51±122.48**	595.66±104.44
$\Delta F/\Delta t$ (kgf/s)$\times 10^3$	46.17±9.12**	29.61±6.39
Impact (kgfs)	19.24±5.49*	13.40±5.1

Note. * Significant different ($p<.05$); **highly significant different($p<.01$)

In aspect of force gradient, the difference between LP and non-LP was highly significant ($p<0.01$). The $\Delta F/\Delta t$ of LP is (46.17±9.12)*1000kgf/s, while that of non-LP was 35.7% lower. In the impact, there is still significant difference between the LP and non-LP ($p<0.05$). The Impact of LP is about 19.24kgs, while the non-LP was only about 13.40kgs with 30.4% lower.

REFERENCES

1.X-H Shan, Jie Wang, Proceedings of ISB XIX, Dunedin, New Zealand, Abstract 357, 2003.

2. T-Y. Shiang, et al., The Eng. of Sport **4**, 121-27, 2002.

3.X-H Shan, Proceedings of ISBS XVIII **1**, Hongkong, 76-9, 2000.

Comparison of power spectrum measures to entropic measures of electromyography time series: Diagnostic tools for low back pain

[1]Paul Sung, [2]Ulrich Zurcher and [2]Miron Kaufman

[1]Department of Health Sciences, [2]Department of Physics
Cleveland State University, Cleveland, Ohio

Introduction

The use of surface electromyography (EMG) as a diagnostic tool for low back pain (LBP) is based on the possibility that changes in the fatiguing process can be monitored before the point of mechanical failure has been reached. However, back muscle fatigue studies do not consistently report endurance levels for patients with or without low back pain (LBP). This study is to evaluate a reliable diagnostic tool for low back pain based on power spectrum and novel technique based on nonlinear time series analysis, including entropy and mean square displacement.

Methods

Ten subjects with chronic LBP and ten gender-matched volunteers were recruited as a control group. The endurance of the erector spinae muscle was determined using a modified version of the isometric Sorensen fatigue test. Using standard fast Fourier transform (FFT) of the surface EMG data, the median frequency, the slope of the median frequency, and the coefficient of determination (R^2) were obtained. The signal was interpreted as a random displacement for each discrete time step, and the entropy and mean square displacement as functions of time were computed.

Results and Discussion

The power spectrum measures do not provide a clear differentiation between LBP and healthy individuals. The median frequency was not statistically different between groups ($T_{1,18} = 0.91$, $p > .05$). However, the entropy and the mean-square displacement versus time exhibit a plateau for 10msec < t < 1sec and both of these results were statistically different in the two groups (Figure 1).

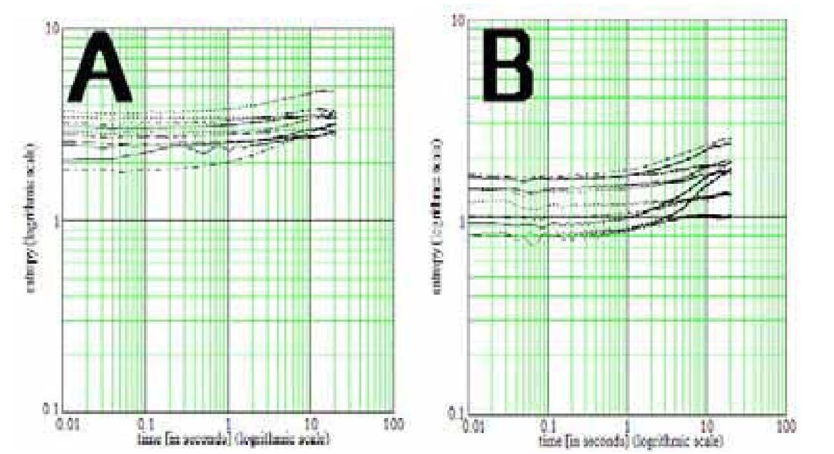

Figure 1. Entropy versus time for healthy group A and LBP group B.

Conclusions

The mean-square displacement and entropy analysis are good diagnostic tools to diagnose LBP. The mean-square displacement versus time has a flat part, which reflects the presence of correlation in the EMG signal. In addition, the entropy values are larger for subjects without LBP than for those with LBP. Further study is required to understand the mechanism of action. The power spectrum seems to indicate a decrease in variability.

References:

Sung P. The efficacy of median frequency on multifidi muscles during one-minute back extension. *Arch Phys Med Rehabil* 2003; 84:1313-8.

Allen PA, Murphy MD, Kaufman M, Groth KE, Begovic A. Age differences in central (semantic) and peripheral processing: the importance of considering both response times and errors. *J Gerontol B Psychol Sci Soc Sci* 2004; 59:P210-9.

Liu JZ, Dai TH, Sahgal V, Brown RW, Yue GH. Nonlinear cortical modulation of muscle fatigue: a functional MRI study. *Brain Res* 2002; 957:320-9.

DOES LOAD MAGNITUDE ALTER CUMULATIVE LOAD TOLERANCE? “WEIGHTING” FOR AN ANSWER

[1] Robert J. Parkinson, and [1]Jack P. Callaghan
[1]University of Waterloo, Waterloo, Ontario, Canada, N2L 3G1
[1]email:callagha@healthy.uwaterloo.ca, web: www.ahs.uwaterloo.ca/kin/people/faculty/callaghan.htm

INTRODUCTION

Previous research examining cumulative compression exposure in the low back has employed a linear summation of force-time magnitudes to obtain estimates of total exposure. More recently, force magnitudes have been weighted (square or tetra power) based on the idea that higher load magnitudes have a greater impact on the development of injury than do lower magnitudes [1,2]. Although researchers have indicated a need to adjust higher loading magnitudes for their role in cumulative injury development, the relationship between load magnitude and cumulative load tolerance has not been quantified. This study was performed to quantify this relationship and provide useable weighting factors to be employed when quantifying cumulative load exposure.

METHODS

40 porcine cervical spinal units were each randomly assigned to one of four loading groups, corresponding to 40, 50, 70, or 90% of the estimated compressive strength of the unit. The compressive tolerance of each spinal unit was estimated using a previously developed equation based on average endplate area [3]. Each spinal unit was mounted inside aluminum cups using non-exothermic dental plaster, mounted in a materials testing machine (8872, Instron Canada, Toronto, ON, Canada) and preloaded with 300N for 15 minutes. The inferior vertebral mounting of the spinal unit was placed on a bearing table to allow unconstrained translations in two directions and rotation about one axis. After preloading, specimens were cyclically compressed with a physiological loading profile at 0.5 Hz until failure occurred or a maximum of 21,600 cycles was reached. Failure was characterized by a distinct drop in stiffness and increase in displacement (figure 1). The relationship between load magnitude and cumulative load tolerance was mathematically characterized and used to generate weighting factors to adjust all loading magnitudes (1-100%) for their contribution to injury development.

RESULTS AND DISCUSSION

The average cumulative load tolerated in each group is provided in table 1. It was found that load magnitudes below 70% did not always induce failure prior to the cycle limit, as indicated in table 1. The measured relationship indicated that load magnitudes below 37.5% resulted in a minimal risk of injury and were therefore assigned a weighting factor of 1. Above this threshold value, equation 1 can be used to determine the necessary weighting factor. The square and tetra power approaches previously employed [1,2] are not supported by the current findings.

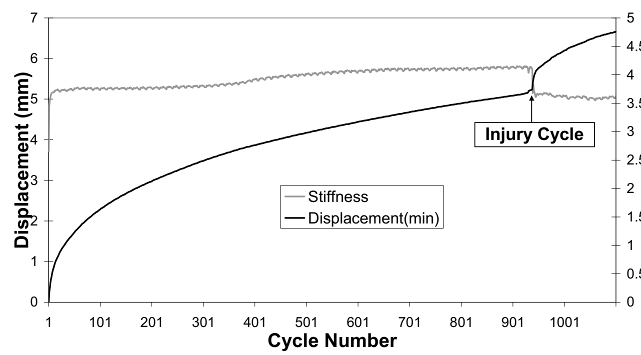

Figure 1: Displacement (mm) and stiffness (kN/mm) versus cycle number obtained from a specimen cycled to a peak load of 50% of the estimated compressive tolerance. Only the peak cycle displacement is plotted for clarity. Plots are overlaid to highlight the simultaneous decrease in stiffness and increase in displacement occurring at failure. The failure cycle is indicated.

REFERENCES

1. Seidler A, et al. *Occup Environ Med* **58**, 735-746, 2001.
2. Jager, M, et al. *Int J Ind Ergon* **25**, 553-571, 2000.
3. Parkinson, RJ et al. *Spine*, Submitted.

Table 1: Average cumulative load tolerance (standard deviation) and number of surviving specimens for each loading group.

Loading Group	Number of Surviving Specimens	Cumulative Load (MN*s)
40%	8	83.2(1.3)
50%	4	3.5(2.1)
70%	0	0.9(1.9)
90%	0	0.1(0.2)

Equation 1:

$$\begin{aligned} \textit{Weighting Factor} &= 5.4617470 \times 10^{-8} \times (\textit{loading magnitude})^5 - 1.3802063803 \times 10^{-5} \times (\textit{loading magnitude})^4 \\ &+ 1.4601005081\;73 \times 10^{-3} \times (\textit{loading magnitude})^3 - 7.8813626392\;557 \times 10^{-2} \times (\textit{loading magnitude})^2 \\ &+ 2.1412519178\;06310 \times (\textit{loading magnitude}) - 22.2341862486\;371 \end{aligned}$$

DIFFERENCES IN LOWER-LIMB NEUROMUSCULAR CONTROL BETWEEN SPORTS MOVEMENTS EXECUTED IN LABORATORY AND GAME SETTINGS

[1] Natalie Saunders, [1]Leonie Otago and [2]Scott McLean
[1] School of Human Movement & Sport Sciences, University of Ballarat, AUS: n.saunders@ballarat.edu.au
[2]The Cleveland Clinic, Cleveland, USA

INTRODUCTION

Anterior cruciate ligament (ACL) injury is a common and traumatic sports injury. While the underlying mechanisms remain unclear, neuromuscular control elicited during high-risk sports movements has become increasingly viewed as a primary risk factor [2]. To date, neuromuscular predictors of ACL injury have typically arisen from lab-based assessments of these movements, as a means to counter the inherently random and unpredictable nature of the true game setting. It is possible however, that this approach excludes important components of actual game-play that contribute directly to the chosen movement response and resultant injury risk [4]. A game-based assessment of high-risk sports movements may thus afford more reliable neuromuscular injury predictors, and hence, more effective injury screening and prevention strategies. With this in mind, the purpose of the current investigation was to compare lab and game-based measures of lower limb neuromuscular control during high-risk sports movements.

METHODS

Ten female subjects (age 24.3, ± 9.5 years) had lower limb EMG data recorded continuously during a fixtured netball game. At a subsequent session, occurring in the lab, EMG data was also recorded for 3 chosen conditions (as below). The movement chosen for investigation was a "leap" land, which is commonly employed in netball and involves taking off on a single leg and landing on the opposite leg. For each subject, bilateral EMG (Mespec 4000, MegaWin) data, sampled at 1000Hz, was first recorded telemetrically for rectus femoris (RF), biceps femoris (BF) and medial hamstring (MH) muscles throughout an entire game (4 x 10 min ¼'s). The game was also videotaped via a 50Hz Panasonic CCD camera, which enabled accurate detection of leap lands, surrounding factors eg. proximity of opposing players, and the moment of foot contact to be analysed in detail. During lab testing, video and bilateral EMG data were again recorded while subjects performed 5 leap land trials for each leg, for 3 specific movement conditions of increasing complexity, namely:

1.Run and leap land.
2.Run, leap land whilst catching a ball, pivot and pass to a team-mate in the same movement.
3.Break from a defender, run, leap land whilst catching a ball, pivot and pass to a team-mate in the same movement

Muscle EMG data obtained from the game movements were then matched to lab-based measures for the ensuing analyses.
The point of initial contact (IC) of the land leg, for both the game and lab trials was first determined via the video camera recordings. EMG data were then analysed for each trial to determine the moment at which each muscle turned 'on' relative to IC (onset to IC), and the resultant duration of the muscle activation burst that occurred concurrent with IC. Specifically, the onset level was defined as the point where muscle activation exceeded baseline levels by at least 1 SD for a minimum of 10 ms [3]. In addition to the landing leg, the same measures were also recorded 2 and 1 step prior to the land, being defined as the contralateral leg land (CL) and ipsilateral leg land (IL) respectively. All dependent measures were subsequently submitted to a 2-way ANOVA to determine for the main effects of test condition and leg.

RESULTS AND DISCUSSION

Onset to IC for the RF and BF muscles was observed to be similar between the game and lab conditions for the landing, CL or IL leg ($p>0.6$). A significant difference ($p= 0.008$) was observed however, for the MH of the land leg, with the onset of activation occurring much closer to IC during the game (73 ± 19ms) compared to the lab (111 ± 14ms) condition. Differences in MH activation were not observed for the IL or CL leg lands. Comparisons of muscle burst duration data also failed to yield significant results for all statistical comparisons.
Previous lab-based investigations for the same sports movement have reported hamstring activation onset times relative to IC, and proposed that onset further from IC, as was found in females when compared to males, increased the likelihood of ACL injury due to an inability to effectively counter tibiofemoral anterior shear forces [1]. Current game observations however, suggest female onset times occur much closer to IC. Thus, the potential for female hamstring activation strategies to contribute to their increased ACL injury risk compared to males may be largely overstated. If this is the case, lab based screening and intervention strategies that focus on this predictor, may have limited success in reducing female ACL injury rates.

CONCLUSIONS

Differences exist in female lower limb neuromuscular control between lab and game-based assessment of high-risk sports movements that may have a significant impact on the ultimate success of current screening and intervention strategies. Further work into this potentially important research disparity is warranted.

REFERENCES

1. Cowling and Steele, 2001, J Electromygr Kinesiol 11:263-268.
2. Griffin et al., 2000, J Am Acad Orthop Surg 8:41-50.
3. Hodges and Bui, 1996, Electroenceph. clin Neurophysiol 101:511-519
4. McLean et al., 2004, Med Sci Sport Ex 36:1008-1016.

EFFECTS OF STRESS DEPRIVATION ON BIOMECHANICAL PROPERTIES OF REGENERATED AND RESIDUAL TISSUES IN THE PATELLAR TENDON AFTER REMOVEL OF THE CENTRAL ONE-THIRD

[1] Kozaburo Hayashi, [2]Hiroyuki Asanuma, [3]Eijiro Maeda, [4]Harukazu Tohyama and [4]Kazunori Yasuda
[1]Osaka University and Okayama University of Science; email: yokohayasi23@yahoo.co.jp
[2]Osaka University; [3]Queen Mary, University of London; [4]Hokkaido University

INTRODUCTION

The central one-third of the patellar tendon (PT) is commonly used as a substitute for reconstruction of the anterior cruciate ligament. The defect made by the resection of the central portion is filled with regenerated fibrous tissue. We have observed in a rabbit model that the strength and elastic modulus of the residual tissue significantly decreased at an initial stage and then increased thereafter, and that those of the regenerated tissue progressively increased during healing [1]. Mechanical stress is considered to affect the remodeling phenomena in both tissues, because the strength and modulus of the normal PT are very rapidly and markedly decreased by the removal of the stress applied to it (stress shielding) [2].
Therefore, we hypothesized that stress shielding significantly affect the properties of both regenerated and residual tissues after the resection of the central one-third of the PT. The purpose of the present study was to test this hypothesis.

MATERIALS AND METHOD

Skeletally mature female Japanese white rabbits were used. After surgical exposure of the PT in each right knee, the PT was relaxed at all knee angles with a stainless steel wire hooked between the patella and the tibial tubercle, for the complete removal of stress [2]. Then, a full-thick, full-long (about 20 mm), rectangular defect, which had the width (about 3 mm) of one-third of the whole width of the PT, was made in the central portion of the PT. Postoperatively, all animals were applied no immobilization procedure, and were allowed unrestricted activities in cages.
At 3 or 6 wks after the operation, patella-tendon-tibia complexes were excised, and each complex was divided into the medial (residual PT tissue), central (regenerated tissue), and lateral (residual PT tissue) portions. Tensile testing was performed for each specimen in ? ? C saline solution at the rate of 20 mm/min; strain was determined at midsubstance with a video dimension analyzer.
The results from these completely stress-shielded tissues (CSS group) were compared with our previous results obtained from the animals which were made same defects in the PT but were applied no sreess shielding treatment (NSS group) [3], and also .with the results obtained from non-treated normal PTs (Control) [4].

RESULTS AND DISCUSSION

Fibrous tissues were regenerated in the PT defects already at 3 wks in both CSS and NSS groups, but their tensile strengths were very much lower compared to the control PT (Figure 1). The strength increased between 3 and 6 wks, although that at 6 wks was still significantly lower than control value. CSS group had significantly lower strength than NSS group at each period. The tensile strength of the residual PT tissue (average for the medial and lateral tissues) was greatly decreased by the removal of the central portion in both groups, possibly due to overstress applied to the residual tissue [1], and the decrease was significantly larger in CSS than in NSS groups. The elastic modulus showed essentially similar results to the tensile strength in both groups. The strain to failure was significantly larger in CSS and NSS groups than in Control group regardless of experimental period, although there were no significant differences between CSS and NSS groups.

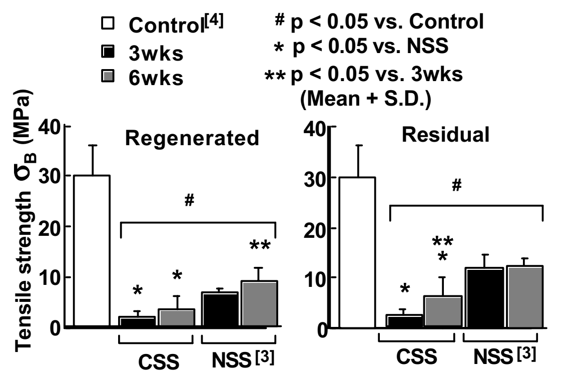

Figure 1 Tensile strength of regenerated and residual tissues after removal of the central one-third of the patellar tendon.

CONCLUSION

These results indicate that stress shielding induces adverse effects on the mechanical properties of the regenerated tissue and the unresected, residual tendon tissue after the removal of the central one-third portion of the PT as a substitute for ligament reconstruction. This fact implies that adequate stress is prerequisite for the healthy remodeling of not only residual tendon tissue but also newly regenerated fibrous tissue.

REFERENCES

1. Tohyama, H, et al., *Clin Biomech* **18**, 765-772, 2003.
2. Yamamoto, N, et al., *Tran ASME, J Biomech Eng* **115**, 23-28, 1993.
3. Noguchi, H, et al. *Proc 13 JSME Bioeng Conf*, Otaru, Japan, 23-24, 2002.
4. Hiro, T, et al. *Proc 13 JSME Bioeng Conf*, Otaru, Japan, 21-22, 2002.

ACKNOWLEDGEMENTS

This work was financially supported in part by the Japan Space Forum for the Ground-Based Research for Space Utilization (no. 181) and by the Grant-in-Aid for Scientific Research (A) (2) (15200036) from the Ministry of Education, Culture, Sports, Science and Technology, Japan.

ESTIMATION OF STRESSES AND CYCLES TO FAILURE OF THE TIBIA DURING RESTED AND FATIGUED RUNNING

[1]Siriporn Sasimontonkul, [2]Brian K. Bay, and [1]Michael J. Pavol
[1]Department of Exercise & Sport Science; [2]Department of Mechanical Engineering
Oregon State University, Corvallis, OR, U.S.A.
Email: fedusrs@ku.ac.th

INTRODUCTION

Many runners suffer from tibial stress fractures. This may be a result of the repetitive loading applied to the tibia during running, as there is evidence of micro-damage in bone tissue after repetitive loading. Therefore, this study investigated 1) whether running-related loads are large enough to cause tibial stress fractures upon repeated application, and 2) whether muscle fatigue alters the potential for tibial stress fractures during running. The potential for tibial stress fractures was predicted, using an integrated experimental and mathematical modeling approach, by estimating the minimum number of loading cycles that would result in the failure of bone (Nfail).

METHODS

Ten male recreational runners with reflective markers attached to their left lower limb ran across a force plate for a total of 6 successful trials within the range of 3.5 – 4 m/s. Subjects then ran on a treadmill until muscle fatigue occurred, as indicated by a decrease of >25% in measured plantarflexion strength. Finally, the fatigued subjects performed 6 more running trials across the force plate within the same range of 3.5 – 4 m/s.

Inverse dynamics analysis was applied to the marker position and force data to estimate the joint reaction forces (JRF) and joint moments at the left ankle, knee, and hip. The forces acting in 21 muscles of the lower limb at each sample time were estimated from the joint moments through optimization, minimizing the sum of the cubed muscle stresses. From the JRF and the muscle forces, the 2-D bone contact forces at the distal end of tibia were computed. Stresses on the anterior and posterior faces of the tibia at 13.7 cm. from the distal end were then estimated from the bone contact forces, based on a beam model [1]. Finally, the tibial stresses were used to predict Nfail [2]. Nfail was log transformed for statistical analysis and a doubly multivariate was used to compare Ln(Nfail) before and after the onset of muscle fatigue.

RESULTS AND DISCUSSION

Compressive stresses were found at the posterior face of the tibia throughout stance, whereas both tensile and compressive stresses acted at the anterior face (Figure 1). This is consistent with strains that have been measured *in vivo* and *in vitro* [3,4]. The maximum compressive stress of -43.4 ± 10.3 MPa occurred at the posterior face of the tibia during mid stance

Table 1: The group mean $\pm$ SD of Ln(Nfail) and the mean of Nfail at the posterior and anterior faces of the tibia.

	Before fatigue	After fatigue	P-value
Ln(Nfail)			
Posterior face	15.48 $\pm$ 2.56	16.07 $\pm$ 2.44	0.004
Anterior face	27.00 $\pm$ 4.95	27.94 $\pm$ 4.01	0.095
Nfail (cycles)			
Posterior face	$5.28*10^6$	$9.53*10^6$	–
Anterior face	$5.32*10^{11}$	$1.36*10^{12}$	–

and resulted in the minimum Nfail. Hence, the posterior face of the tibia was more prone to stress fractures, consistent with the results of a previous epidemiological study [5]. Although Nfail before fatigue averaged $5.28*10^6$ cycles, Nfail varied greatly between runners. The mean Nfails of two runners were only $2.7*10^4$ and $2.7*10^5$ cycles, suggesting that these two runners were at risk of a tibial stress fracture from running.

After muscle fatigue, tibial stresses tended to decrease (Figure 1), which led to a significant increase in Nfail (Table 1). This increase in Nfail implies that fatigue of the plantarflexors from prolonged running did not accelerate the onset of tibial stress fractures. Instead, changes in running technique with fatigue may have served to protect against tibial stress fracture. The results thus indicate that tibial stress fractures in runners result primarily from the repeated application of running-related loads in selected, at-risk individuals, and not from an increase in bone loading due to muscle fatigue.

REFERENCES

1. Sasimontonkul S. *Dissertation*, 2004.
2. Caler WE, et al. *J. Biomech*, **22**, 625-35, 1989.
3. Ekenman I, et al. *Foot Ankle Int.*, **19**, 479-484, 1998.
4. Peterman MM, et al. *J. Biomech*, **34**, 693-8, 2001.
5. Brukner P, et al. *Phys Sportsmed*, **26**, 39-47, 1998.

(a)
(b)

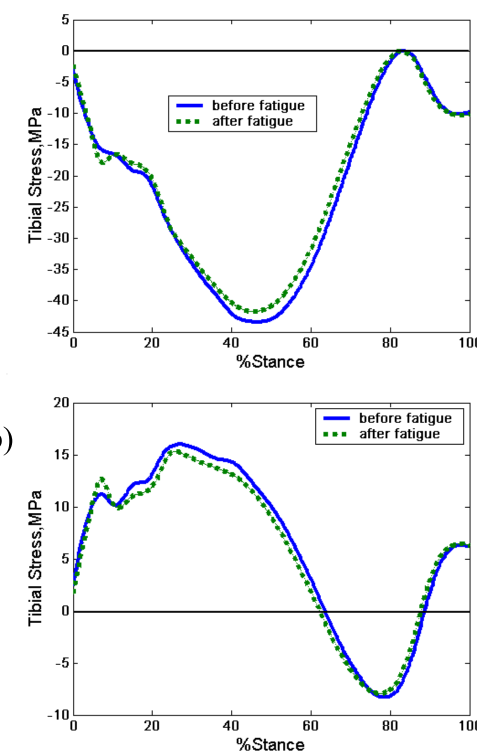

Figure 1: Mean stresses before and after muscle fatigue at the (a) posterior and (b) anterior faces of the tibia during the stance phase of running. Positive stresses are tensile and negative stresses are compressive.

ARE THERE INHERENT DIFFERENCES IN HOW MALES AND FEMALES RESPOND TO LIFTING?

[1] Kermit Davis and [2] William Marras
[1]Low Back Biomechanics and Workplace Stress Laboratory, University of Cincinnati
[2]Biodynamics Laboratory, The Ohio State University

INTRODUCTION

While the evidence is far from conclusive, males appear to be more susceptible to low cost low back injuries (mild low back pain) while females have higher rates of more costly injuries (severe low back pain) [1,2]. Although job requirements do not discriminate between genders, there is reason to expect that the biomechanical effect on the individual may differ as a function of gender. Males are significantly stronger than females [3,4]. Differences in strength and anthropometry between males and females may influence the trunk motions, muscle activities, and subsequent spine loads. Previous work evaluating how males and females respond biomechanically to similar lifting demands provides the evidence that females are not simply proportionally scaled down versions of males [5]. In other words, the differences in spine loading are not just a function of size. Overall, males have significantly greater three-dimensional spine forces than females when lifting. In addition to the differences in spine loading, males and females approached the lifting tasks differently with respect to trunk and hip kinematics as well as muscle recruitment. However, this previous study investigated gender differences but did not control for anthropometic differences. The ***objective*** of the current study was to evaluate males and females performing lifting tasks that were matched on height and body mass.

METHODS

Nine females and nine males were selected from a larger study [6] based on matching anthropometry (within 5 kg and 5 cm). The average weight and height for males was 67.9 kg and 170.5 cm, respectively and for females was 67.5 kg and 168.9 cm, respectively. The experimental tasks consisted of asymmetric lifting of boxes to either a 90^o clockwise or a 90^o counter-clockwise shelf at two different lift rates—2 and 8 lifts/minute. Boxes weighing 6.8 and 11.4 kg were lifted from conveyor and placed on asymmetric shelf. The three-dimensional trunk kinematics as measured by the lumbar motion monitor, trunk kinetics measured by force platform system, and activity of the ten major trunk muscles were inputted into an EMG-assisted spine load model that predicted the three-dimensional spine loads-compression, lateral shear, and anterior-posterior shear forces. A repeated-measures split-plot analysis of variance was performed for all of the dependent variables with all significant effects being further analyzed using Tukey multiple pairwise comparisons.

RESULTS AND DISCUSSION

Although males and females were virtually identical in body size, significant differences in spine loads still existed between the genders. Males were found to produce significantly greater compression forces—about 650 N than females. The direction of the task asymmetry also plays a role in the spine load responses. A small gender-asymmetry interaction effect was found to be significant for compression (Figure 1). In addition, males were found to have significantly greater lateral shear loads (130 N more) when lifting from the counter-clockwise shelf but significantly lower shear loads (about 70 N) when lifting from clockwise shelf. It is interesting to note that females had greater muscle activity in the right and left latissimus dorsi (about 22% MVC), right and left rectus abdominus (about 5% MVC), and left external oblique (about 11% MVC) muscles. Although this increase in muscle activity appears to be counter-intuitive, females lifted in a different way kinematically than the males, counteracting the muscle activity response. Many trunk kinematic differences were not significant but appear to be biomechanically important. Females were found to utilize their hips more (8^o more and 10.5 ^{o}/sec faster) during lifting while males relied on more trunk motion (5^o more and 6 ^{o}/sec faster). Together, the muscle responses and kinematic difference result in different spine load patterns between the genders.

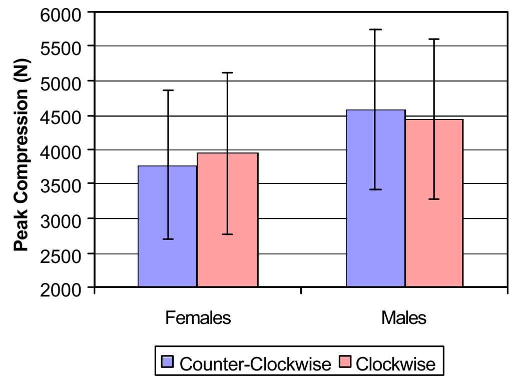

Figure 1: Peak compression for males and females when lifting to counter-clockwise and clockwise shelves.

CONCLUSIONS

As with previous less controlled studies [5], the current study revealed that females are not scaled down versions of males. When exposed to the same lifting conditions, females respond with greater muscle coactivity but in a more neutral trunk posture by utilizing more hip motion. As a result, females minimize the loads on the spine during lifting. Thus, an inherent difference exists between males and females that cause the load pattern to be different.

REFERENCES

1. Alcouffe J, et al. *Occup. Environ. Med.* **56**, 696-701, 1999.
2. Adams MA, et al., *Spine* **24**, 2497-2505, 1999.
3. McNeill TW, et al., *Spine* **5**, 529-538, 1980
4. Kumar S, et al., *Spine* **20**, 160-168, 1995.
5. Marras WS, et al., *The Spine Journal* **3**, 93-99, 2003.
6. Davis KG, et al, *Spine* **27**, 2645-2653, 2002.

ACKNOWLEDGEMENTS

Partial funding was provided by International Society of Biomechanics Dissertation Grant.

THE EFFECT OF PERIPHERAL ARTERIAL DISEASE ON GAIT

[1]Melissa M. Scott-Pandorf, [2,3]Iraklis I. Pipinos,, [2]Leon Robinson, [1]Timothy Judkins, [1]Nick Stergiou
[1] University of Nebraska at Omaha [2] University of Nebraska Medical Center [3] Veterans Affairs Medical Center;
email:mmscott@mail.unomaha.edu, web: http://www.unocoe.unomaha.edu/hper/bio

INTRODUCTION

Peripheral Arterial Disease (PAD) is the result of atherosclerotic occlusion of the leg arteries affecting more than 8.4 million people in US[1]. For PAD patients, walking is a difficult task because the increased metabolic demand of the leg muscles is not satisfied due to the decreased blood flow. The result is claudication, which is defined as pain in the leg muscles during ambulation. When ambulation stops, the muscle is reperfused and the pain subsides. Recent research has examined PAD and the associated claudication as a primary gait disability[2]. However, this work has performed evaluations using only temporal and spatial gait parameters, such as stride length and step time. As a result, these evaluations have been limited in their ability to describe in detail the true gait handicap of PAD patients[1]. For further advancement of the understanding of PAD, kinetics (i.e. ground reaction forces) and kinematics (i.e. joint angles) are warranted[3]. The purpose of this investigation is to examine the ambulatory dysfunction of the PAD claudicating, PAD healthy contralateral, and the healthy control legs using selected kinematic and kinetic parameters

METHODS

Fifteen PAD patients and 5 age-matched (age 45-60 yrs) healthy controls walked through a 10m walkway while kinematic (60Hz) and kinetic (600Hz) data were collected both before and after the onset of claudication symptoms. The patients performed 5 trials at a self-selected pace with each leg while pain free (pre-pain), or with no claudication symptoms. Then patients were asked to walk on a treadmill at 1.5 mph (10% grade) until the onset of pain. After pain was induced, patients completed 5 more trials at a self-selected pace for each leg. The legs of the study participants were divided into 3 groups: PAD claudicating (CL, n=20), PAD healthy contralateral (CO, n=4), and control (HC, n=10). Statistics of selected measures were performed using 2x2 Mixed ANOVA (CL/CO vs HC, pre-pain vs post-pain) and 2x2 repeated measures ANOVA (CL vs CO, pre-pain vs post-pain).

RESULTS AND DISCUSSION

The configuration of the vertical ground reaction force (VGRF) curve depicts a “flatter” configuration (Figure 1) for the CL and CO than the HC. Statistical analysis showed that the minimum values of VGRF (Fmin) for the CL ($p=.02$) and CO ($p=.03$) were significantly larger than the HC. The differences of the VGRF maximums to Fmin (F1-Fmin, F2-Fmin) for CL ($p=.04$,$p=.04$) and CO ($p=.01$,$p=.01$) legs were significantly smaller than the HC. CO revealed larger braking impulse than the HC ($p=.02$). For all legs, braking impulse significantly increased when comparisons included the CO legs from the pre-pain to the post-pain condition (HC:$p=0.01$,CL:$p=0.02$). The stance time for CL ($p=.01$) and

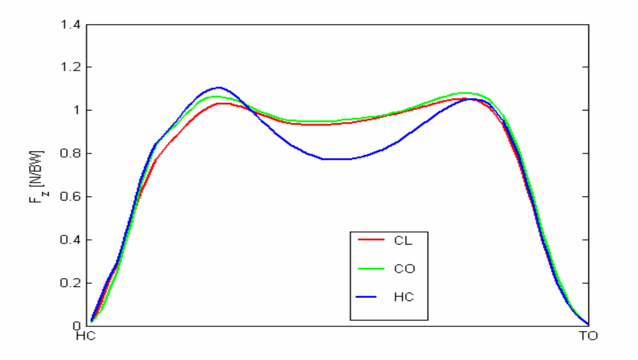

Figure 1. Mean VGRF for CL, CO, and HC legs.

CO ($p=.04$) was found to be larger than the HC. Kinematic results indicated that CL had greater maximum plantar flexion at toe off ($p=.033$) and ankle range of motion during stance than HC. At the knee, maximum flexion during stance decreased for CL from the pre-pain to the post-pain conditions while it increased for the HC ($p=.02$). At the hip, CL had increased maximum hip extension during stance between the pain conditions while in CO decreased ($p=.01$).

CONCLUSIONS

The flatter configuration found in the VGRF curve may represent an attempt by the PAD patients to diminish any vertical fluctuations of the center of gravity and/or inability to accomplish proper knee extension during stance. This may offer a more stable gait to the PAD patient. The decreased knee flexion by CL and the slower walking pace (i.e. higher stance time) of the CL and CO may also indicate an effort toward a more stable gait pattern. In the majority of the patients, the most affected muscles reported were the foot plantarflexors. This may be the reason for the differences noted at the ankle. In addition, the decreased knee flexion observed may have resulted in the compensations found at the ankle. The increased braking impulse of the CO may be an adaptive pattern to slow the system early in stance phase in compensation for the CL. This is also evident by the changes in hip extension between conditions for the CL and CO legs. This again supports the idea of finding a more stable pattern as the gait of the patient slows down. In summary, PAD patients have altered their gait to (1) create a more stable gait and (2) to compensate for the pain induced during walking. Future directions for this investigation include examining stability directly via nonlinear tools.

REFERENCES

1. Gardner A et al. (2001). *Vasc Med* **6**, 223-227.
2. Newman A et al. (1999). *JAGS* **39**, 142-148.
3. Whittle M (1991). *Gait Analysis: An Introduction*.

USE OF WAVELETS IN THE ANALYSES OF BIODYNAMIC RESPONSES

[1] Zhiqing Cheng, [2]Joseph A. Pellettiere
[1]Advanced Information Engineering Services, A General Dynamics Company
5200 Springfield Pike Suite 200, Dayton, OH 45431
[2]Human Effectiveness Directorate, Air Force Research Laboratory
2800 Q Street, Wright-Patterson AFB, OH 45433

INTRODUCTION

Biodynamic responses are usually transient, strongly localized in the time domain, and contaminated with noise, so that conventional statistical analysis, correlation analysis, or spectral analysis used for stationary signals may be neither appropriate nor efficient for the analyses of them. Wavelets, localized in both frequency and time domain, match the major characteristics of biodynamic responses. The use of wavelets in the analyses of biodynamic responses for various applications was investigated by the authors and is briefly described below.

WAVELET/WAVELET PACKET DECOMPOSITIONS

A biodynamic response or signal $S(t)$ can be decomposed on a wavelet basis [1]:

$$S = A_J + \sum_{j \le J} D_j \,, \tag{1}$$

where the approximation A_J retains the lower frequency components of the original signal, and the details D_j contain high frequency components and often display vibrations and noises. In a wavelet packet basis, the decomposition of $S(t)$ at level J can be expressed as [2]

$$S(t) = \sum_{n=0}^{2^J-1} \sum_k q_{Jnk} w_{Jn}(t-k) \,, \tag{2}$$

where $w_{Jn}(t)$ are wavelet packet atoms; q_{Jnk} are wavelet packet coefficients; n is the frequency index, and k is the position index. The wavelet transform allows for a view of biodynamic response in a time-frequency plane, and thus provides the information regarding when events take place.

CORRELATION ANALYSIS

Decompose two signals $x(t)$ and $y(t)$ at a certain level using wavelets. The approximations $x_a^l(t)$ and $y_a^l(t)$ can be treated as deterministic signals, and the linear relationship or resemblance between them can be described by a classic correlation coefficient $\rho_a^l(\tau)$ [3]. The time shift τ is allowed to account for the phase shift between them. A quantity

$$\rho_{am}^l = \rho_a^l(\tau_m) = \max_\tau \{\rho_a^l(\tau)\} \,, \tag{3}$$

can be used to evaluate the agreement in the pulse shape, whereas τ_m can be used to measure the time shift. As dyadic wavelet decomposition provides a multi-resolution analysis, the correlation analysis between the approximations at different levels describes the correlative relationship between the two original signals with different resolutions.

SIGNAL ENERGY DISTRIBUTION ANALYSIS

If a signal is decomposed on an orthogonal wavelet packet basis using Eq. (2), in terms of the signal energy [3],

$$\|S\|^2 = \sum_{n=0}^{2^j-1} \sum_k q_{jnk}^2 \,. \tag{4}$$

The signal energy distribution can be defined in two ways:

- With respect to the frequency index n:

$$E_n = \sum_k q_{Jnk}^2 \,; \tag{5}$$

- With respect to the time position k and the frequency index n:

$$E_{n,k} = q_{Jnk}^2 \,. \tag{6}$$

MODEL VALIDATION

The comparison of the energy distributions of a pair of biodynamic responses from a test and from the simulation shows the agreement or discrepancy in amplitudes between them; thus it can be used for the validation of bio-computational modeling. In order to compare the pulse shape and the peak timing between the two responses, the correlative relationship between the approximations can be used. Based on energy distributions and correlation analysis, several metrics were developed that can be used for quantitative validation. The comparison can be made at different levels so that details at different scales can be taken into account.

PREDICTING HUMAN RESPONSE FROM ATD TESTS

The ATD (Anthropomorphic Test Device) response and human response are considered as the output of a black box system. Based on the decompositions of both responses on a wavelet packet basis, a mapping matrix is built after executing a procedure including de-noising, energy distribution analysis, correlation and regression analysis, and spectral coherence analysis and transfer function identification [4]. With the mapping matrix, an ATD response can be modified or reconstructed into the corresponding human response.

CONCLUSIONS

Wavelet analysis is a useful and effective tool for the analyses of biodynamic responses in various applications.

REFERENCES

1. Strang G, et al. Wellesley-Cambridge Press, Massachusetts, 1997.
2. Misiti M, et al. The MathWorks, Inc., Massachusetts, 1997.
3. Cheng Z, et al. *Proc. of XXII International Modal Analysis Conference*, Michigan, 2004.
4. Cheng Z, et al. *STAPP Car Crash Journal* **48**, 207-225, 2004.

IN VIVO SEGMENTAL MOTION MEASUREMENT IN ASYMPTOMATIC AND CHRONIC LOW BACK PAIN SUBJECTS USING VOLUME MERGE METHOD

[1] Ruth S. Ochia, [1] Nozomu Inoue, [1] Eric Lorenz, [1] Susan Renner, [1] Deepa Gavini, [2] Tae-Hong Lim, [1] Gunnar Andersson, [1]Howard An
[1]Rush University Medical Center, Chicago, IL,
[2]University of Iowa, Iowa City, IA; email: Ruth_S_Ochia@rush.edu

INTRODUCTION

Spinal instability has been suggested as a potential cause of low back pain and axial rotational instability, in particular, has been implicated in its pathogenesis due to the presence of disc degeneration (DD) [1]. The use of radiographs has been under scrutiny in that it has been shown to be difficult to accurately measure vertebral translations and impractical to measure out of plane rotations with the 2D radiographic images [2, 3]. More precise techniques are generally invasive. The current study has expanded on a 3D non-invasive imaging technique to compare *in vivo* vertebral motions in human lumbar spines for healthy and chronic low back pain (LBP) subjects [3].

METHODS

Using serial CT scans, a 3D computer model was developed to analyze lumbar segmental motion under axial torsion *in vivo* (Figure 1A). Male volunteers in their thirties (9 healthy (mean age: 33.8 ± 2.8 years) and 5 LBP (mean age: 33.0 ± 3.5 years)) were recruited to participate in this imaging study (IRB approved). The subjects were placed on a custom jig positioned in the CT scanner. The subjects were scanned in three positions: neutral (supine) and right and left rotated to 50° [4]. Reconstructed lumbar CT images were analyzed using the volume merge method, which virtually merged two 3D vertebrae models to calculate segmental motions in increments of 0.1mm and 0.1° (resolution: 0.2° and 0.1mm) (Figure 1B). Segmental rotations and translations between adjacent vertebral bodies were calculated in three major planes. All subjects were scanned using MRI for determination of disc degeneration using Thompson's grading system. Statistical analysis was conducted using unpaired t-tests with α=0.05.

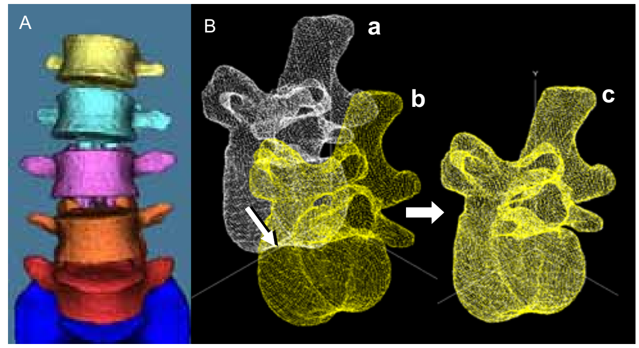

Figure 1: (A) 3D reconstruction of subject's lumbar spine from CT scans. **(B)**Vertebral body in the neutral position (a) was virtually rotated and translated toward the real rotated position (b) with 0.1° and 0.1mm increments, respectively, until the highest value of volume merge was calculated (c).

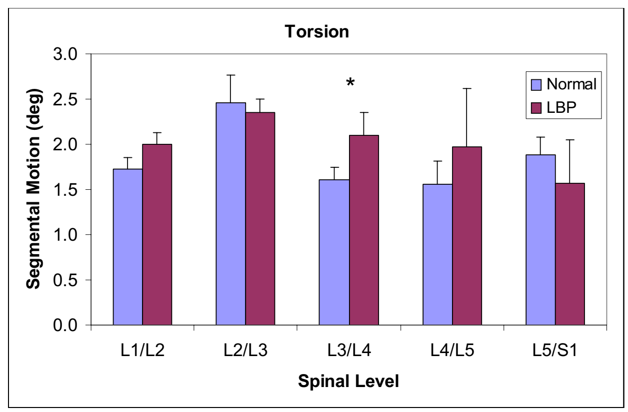

Figure 2: Comparison of torsional segmental motion between healthy and LBP subjects (mean ± standard error of the mean). * p<0.08

RESULTS AND DISCUSSION

Segmental rotations were greatest in torsion with a trend for larger motion at L3/4 in LBP group (2.1° vs 1.6°, p<0.08) (Figure 2). Lateral bending occurred in the direction opposite external rotation for upper vertebrae and with external rotation for the lower vertebrae, but these motions were not significantly different between groups. Segmental translations were neglible, except for the frontal plane with the greatest magnitudes in the upper vertebrae (range -6.0° at L1/2 to 1.4° at L5/S1). In addition, the frontal plane translations showed significant differences between levels (p<0.01) but not between groups (p>0.4). There was a trend for greater degeneration in the LBP versus healthy group at L3/4 and L4/5 (p<0.1 and p<0.09, respectively).

CONCLUSIONS

Eventhough there was a relatively small sample size, some trends were determined. As expected there was greater level of degeneration in the LBP group, which also showed greater motion in torsion in the middle vertebrae. In addition, pure *in vivo* torsion resulted in complex coupled motions with large lateral bending and frontal plane movements, especially in the upper lumbar vertebrae. Additional studies into segmental motion will be conducted in order to determine potential correlations with lumbar DD and LBP subjects' pain mapping.

REFERENCES

1. Fujiwara, A., et al., *Spine*, 2000. **25**(23): p. 3036-44.
2. Haughton, V.M., et al., *AJNR Am J Neuroradiol,* 2002. **23**(7): p. 1110-6.
3. Lim, T.H., et al.,. *Spine*, 1997. **22**(17): p. 1996-2000.
4. Renner, S., et al. *50th Annual Meeting of the Orthopaedic Research Society*. 2004. San Francisco, CA. Poster #1117,

ACKNOWLEDGEMENTS

This study was supported by NIH Program Project AR148152.

PRACTICE DISTRIBUTION AND THE ACQUISITION OF MAXIMAL ISOMETRIC ELBOW FLEXION STRENGTH

Kristina M. Calder and David A. Gabriel
Raymond Nelson Reid Biomechanics Laboratory, Brock University
Email: dgabriel@brocku.ca

INTRODUCTION

Kroll [1] administered five maximal isometric wrist flexion strength trials, on each of three consecutive test days, and observed a significant increase across trials from the first to the last test session. There were then two retest sessions, two weeks and three months later. An 8-15% increase was observed between the first test and retest condition, and it was retained over the 3-month period until the second retest.

Kroll [2] later studied the effects of all contractions given on a single test day. There were three groups corresponding to 5, 10, and 15 maximal effort contractions. None of the three groups exhibited any increase in strength upon retest two weeks later. Thus, fifteen contractions distributed over 3 consecutive days enhanced muscular strength whereas fifteen contractions distributed on the same day did not. Kroll [2] theorized that the results of the two studies could be explained by the observed superiority of distributed versus massed practice in motor skill development. The present study tested Kroll's [2] hypothesis for the elbow flexors.

METHODS

Twenty-six college-aged females were matched and randomly assigned to one of two groups. The massed group (n=13) completed 15 maximal isometric elbow flexion strength trials in one session, while the distributed group (n=13) performed five such contractions on three successive days. After a 2-week and 3 month rest interval, both groups returned to perform another five maximal isometric elbow flexion strength trials to assess retention of any potential strength gains.

Surface electromyographic (SEMG) activity of the biceps and triceps brachii were monitored with bipolar electrodes (DE-2.1, Delsys Inc., Boston, MA). The signals were amplified (1000×), band-passed (20-450 Hz) filtered, before A/D conversion (BNC-2110, National Instruments) at 2048 Hz (DASYLab, DASYTEC National Instruments, Amherst, NH) on a Pentium III PC (Seanix Technology Inc., Blaine, WA). Force was monitored with a load cell (JR3 Inc., Woodland, CA). The force signal was low-passed (100 Hz) before being sampled in the same manner as the SEMG. Figure 1 depicts representative SEMG and force signals.

RESULTS AND DISCUSSION

There was a significant ($p<0.05$) increase in strength in both groups from Block 1 (first 5 contractions) to Block 2 (first retest) and from Block 1 to Block 3 (second retest). Both groups exhibited an increase ($p<0.05$) in biceps root-mean-square (RMS) SEMG amplitude. A significant ($p<0.05$) decrease in triceps RMS SEMG amplitude was found between Block 1 and 2 for both groups. However, a significant ($p<0.05$) increase was found between Blocks 2 and 3.

Both the massed and distributed groups exhibited a learning-related increase in maximal isometric elbow flexion torque that was retained over a three month period. The increase in neural drive to the agonist was also retained [3]. The reduction in antagonist coactivation was a short-term (2 weeks) training effect [4], dissipated over the longer rest interval (3-months). The subsequent increase in antagonist coactivation was necessary to increase joint stability in response to further increases in agonist muscle force output, observed during the last re-test session. The results of this study suggest that there is flexibility in how muscle contractions may be distributed. However, other aspects of motor learning theory should be explored further, such as the role of feedback. To subtract-out learning effects upon strength training studies, only one session in needed, as multiple sessions may be unnecessary.

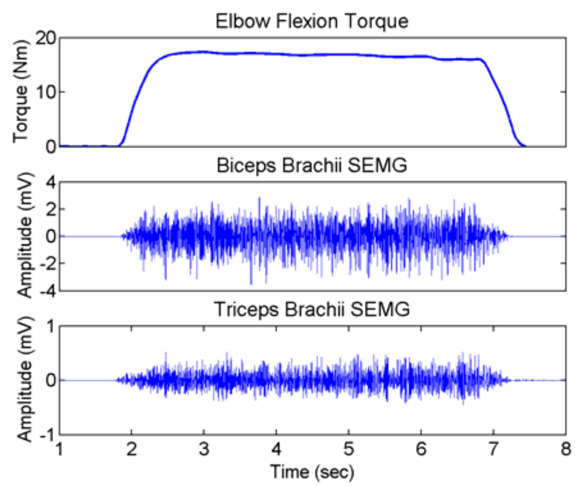

Figure 1. Representative torque (top panel), biceps brachii agonist SEMG (middle panel), and triceps brachii antagonist SEMG (bottom panel) for one subject.

REFERENCES

1. Kroll WP. *RQES* **34**, 50-55, 1963.
2. Kroll WP. *RQES* **34**, 350-355, 1963.
3. Gabriel DA., et al. *MSSE* **33**, 1354-1360, 2001.
4. Carolan B., Cafarelli, E. *JAP*, **73**, 911-917, 1992.
5. Solomonow M., et al. *Am J Sports Med* **65**, 223-244, 1986.

ACKNOWLEDGEMENTS

This study was supported by NSERC of Canada

GASTROCNEMIUS MUSCLE TENDON UNIT INTERACTION UNDER VARIABLE GAIT CONDITIONS

[1] Glen Lichtwark, [1]Kostas Bougoulias and [1,2]Alan Wilson
[1]Stucture and Motion Laboratory, Institute of Orthopaedics, University College London. Email: g.lichtwark@ucl.ac.uk
[2]Structure and Motion Laboratory, Veterinary Basic Sciences, Royal Veterinary College. Website: www.rvc.ac.uk/sml

INTRODUCTION

The interaction of a muscle and its attached tendon during dynamic activities such as locomotion is critical for both force production and economical movement. Sonomicrometry studies have revealed that compliant tendons can store and return elastic energy to change the timing and magnitude of muscular work and allow the contractile components to act nearly isometrically, despite substantial length changes in the muscle-tendon unit [1]. This produces higher forces and reduces the energetic requirements of the muscle fibres. Similar results have been reported for human muscle fibres using ultrasonography during slow walking [2].

Using a novel ultrasound probe and setup, we tested the hypotheses that –

1. the *medialis gastrocnemius* (GM) muscle undergoes a homogenous length and structure change across three sites along the length of the muscle (distal, middle and proximal) during walking and running;
2. the GM muscle fibres shorten more during running than during walking .
3. the elasticity of the Achilles tendon enhances GM muscle fibres efficiency under different locomotion conditions

METHODS

6 volunteers (3 male and 3 female) participated in the study. Participants walked and ran on a treadmill at speeds of 4.5km/h and 7.5 km/h respectively. A flat ultrasound probe was attached to the *gastrocnemius medialis* (GM) muscle such that it imaged a transverse section to the leg in the same plane as line of action of the muscle fibres at a rate of 25Hz. Measurements were made at three levels of the muscle; the midbelly and distally and proximally to this position. Muscle fibre length and pennation angle was measured throughout 3 complete gait cycles for each gait condition for each subject. Sagittal plane kinematics were recorded with an active LED motion analysis system (CODA, Charnwood Dynamics, England) and synchronised with the ultrasound data using a sonomicrometry crystal mounted on the ultrasound probe. Length changes of the *gastrocnemius medialis* (GM) muscle-tendon unit length were derived from joint angle data using the equations derived from Grieve *et al* (1978) [3]. Muscle fibre lengths and the pennation angle from the ultrasound images were used along with the whole muscle-tendon length to estimate the tendon elongation [2].

Identical measures were made with 6 male participants during walking (5km/h) at grades of –5,0 and 10% and also during running (10km/h) at grades of 0 and 10%.

RESULTS AND DISCUSSION

The results of the study show that muscle fibres perform similar functions along the length of the human MG muscle during locomotion, regardless of speed or gait. However, they do not act totally homogenously along the muscle lengths

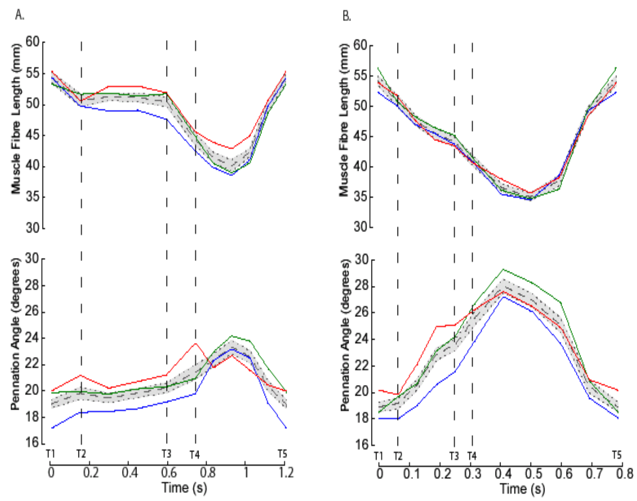

Figure 1: Average length and pennation angle of muscle fibres across one complete stride (heel on to next heel on) during walking (A) and running (B) for each of three three ultrasound sites (distal = blue; midbelly = green; proximal = red). The dashed line represents the average muscle fibre length and pennation angle across all three sites (shaded area is 95% confidence interval). The stride is divided up into the following specific events averaged from the kinematics: T1-Heel strike; T2 – Foot flat; T3 – Heel off; T4 - Toe off; T5 – Heel strike.

(Figure 1). The distal fibres tend to shorten more and act at greater pennation angles than the more proximal fibres. The fibres also shorten more during running compared to walking so that they can produce the forces required to support the body and propel it upwards and forwards. A tendon stretch of approximately 18mm and 25mm during walking and running respectively was estimated. The maximum shortening speed of the muscle tendon complex (6 muscle fibre lengths/s) occurs during the take-off phase of stance. However the muscle fibres never exceed a shortening velocity of above 1.5 lengths per second, even during running. This is a more optimal shortening speed for both power output and efficiency. With variations in grade, the stretch of the Achilles tendon and hence storage of elastic energy is modulated by a change in muscle fibre length. The muscle fibres respond to increases in work demands by activating in an efficient manner to produce the required power output.

REFERENCES

1. Roberts TJ, et al., *Science*, **275**, 1113-1115, 1997.
2. Fukunaga T, et al., *Proc R Soc Lond B Biol Sci,* **268**, 229-233, 2001.
3. Grieve DW, et al., *Biomechanics VI,* **2A**, 405-412, 1978

ACKNOWLEDGEMENTS

The authors would like to thank the British Council, the Royal National Orthopaedic Hospital Trust and the BBSRC for funding.

IN-VITRO TESTING OF KNEE JOINTS USING ROBOTICS: COMPUTER PROGRAMMING THEORY

Natasha K. Lee Shee (B.A.Sc.), James P. Dickey (Ph.D.)
Department of Human Biology and Nutritional Sciences, University of Guelph, Guelph, Ontario, Canada
Email N.K. Lee Shee: nleeshee@uoguelph.ca

INTRODUCTION

The knee is the most used joint in the human body, and thus often succumbs to injury due to trauma and/or aging. Such trauma from accidents, and diseases commonly associated with aging, such as arthritis, can cause pain, inflammation and irregular function of the joint. Studying the knee allows for improved understanding of its injury mechanics as well as knowledge that can be used in improving chemical/surgical treatment of the injured joint and the design of knee prosthetics.

Using robots for *in-vitro* testing of the knee is less invasive than *in-vivo* research while still being able to apply physiologic conditions. The aim of this research is to develop the control theory for controlling a robot to apply physiologic load/motion to the cadaveric knee in order to determine the role and function of each of its structures.

METHODS

An industrial parallel robot (Parallel Robotic Systems Corp., NH, USA) is used, while the knee is described using the floating axis system as described in [1,2,3]. The knee is manipulated by manipulating the tibia (secured to the robot) about the femur (secured to ground) (Figure 1). Local co-ordinate systems are defined through digitizing of the proximal tibia, distal femur, end-effector and load cell. Position and load control programs were then written in Matlab 7.0 to track the mathematical transformations between the systems in order to control the robot kinematics with respect to the knee kinematics and load cell kinetics [2,4]. These programs allow the user to specify either knee kinematic targets or knee kinetic targets respectively.

Both programs were verified using linkage systems that modeled the knee. The position control and load control programs were tested using artificial constructs.

RESULTS AND DISCUSSION

The position control program can reach the target knee kinematics within 0.1^{o} and 0.01mm. To incorporate the floating axis description of the knee, the program recalculates the position/orientation of the floating co-ordinate system after every 0.2^{o} and 0.1mm increment of knee motion. This allows for a step-wise generated position path for the end-effector that can be saved and replayed in a more fluid fashion.

Currently, the load control program can reach the target knee kinetics within 3N and 0.5Nm. Kinetics read at the load cell (secured to the femur) are mathematically transformed to the knee co-ordinate system to represent the knee kinetics [4]. Target knee kinematics are then calculated using its kinetics

Figure 1: Testing set-up. Tibia is secured to the parallel robot (top) and the femur is grounded (bottom).

and a compliance matrix. When the knee reaches the desired kinematics, its kinetics are checked, the compliance matrix is updated; if necessary, new target knee kinematics are set and the process reiterates until the target kinetics are reached.

The position and load control programs are stepping stones for a hybrid control program that simultaneously controls both knee kinematics and kinetics to enable physiological joint loading. This program will allow the user to specify which degrees of freedom are controlled in load and which in position, and is currently being developed.

CONCLUSIONS

Preliminary tests confirm that knee kinematics and kinetics can be controlled independently using the commercial robotic system. When hybrid control programming is complete, physical testing using cadaveric knees will begin.

REFERENCES

1. Dunning, C. et al., *J Biomech* **36**, 1219-1223, 2003.
2. Fujie, H. et al., *J Biomech* 29, no.12, 1577-1585, 1996.
3. Grood, E.S. et al., *J Biomech Eng* **105**, 136-144, 1983.
4. Walker, M., *Master of Science Thesis*, Department of Human Biology and Nutritional Sciences, University of Guelph, 2002.

ACKNOWLEDGEMENTS

Many thanks to Mathew Walker for his continuing guidance with program algorithms, and to Dr. Cynthia Dunning for her help with the initial math regarding the floating axis system. Funding provided by NSERC and CIHR.

THE IMPACT OF USING DIFFERENT CALCULATION METHODS AND LOCAL COORDINATE SYSTEMS WHEN MEASURING 3D SCAPULAR ATTITUDES

[1]Jean-Sébastien Roy, [1,2]Hélène Moffet, [3,4]Luc J. Hébert, [1]Guy St-Vincent and [1,2]Brad J. McFadyen
[1]Center for Interdisciplinary Research in Rehabilitation and Social Integration
[2]Department of Rehabilitation and [3]Department of Radiology, Faculty of Medicine, Laval University
[4]National Defense of Canada; e-mail: jsroy@irdpq.qc.ca

INTRODUCTION

The normal range of scapular rotations during arm elevation of healthy subjects significantly varies from one study to another. Some factors suggested to explain this variation include differences between studies in the kinematic definition of scapular movements. For example, Karduna et al. have shown that, when calculating motion of the scapula, altering the sequence of rotations has a major impact on the magnitude of the estimated scapular motion in each plane [1].

The International Shoulder Group (ISG) has proposed standard definitions of the joint coordinate system for the reporting of shoulder motion to allow a better comparison of results between studies [2]. However, the impact of using different local coordinate reference systems and different methods of calculation when characterising scapular movements remains to be investigated. The objective of this study is to compare the 3D scapular attitudes (3DSA) obtained when using two different local coordinate systems and two different methods of calculation of relative movement.

METHODS

In a seated position, the 3DSA of both shoulders of 15 healthy subjects (mean age 37.8 ± 13.2 years) were measured in two shoulder positions: 70° of flexion and 90° of abduction. The 3DSA was calculated using the Optotrak Probing System (Northern Digital Inc., Waterloo, Ontario, Canada). For each trial, three non-collinear bony landmarks on the scapula (trigonum spinea, angulus inferior and angulus acromialis) and on the trunk (C7 spinous process and the right and left postero-superior iliac spines) were digitized.

Two methods of calculation of relative movement were used to determine the 3DSA. First, the 3DSA with the arm in elevation was calculated with respect to the position of the scapula with the arm at rest; and secondly, the 3DSA was calculated with respect to the trunk. 3DSA were also calculated using the local coordinate reference system proposed by the ISG [2] and by Hébert et al. [3] (Figure 1). The mean of the 3DSA of the 30 shoulders was used to compare the methods of calculation and reference systems. A *t-test* was performed to evaluate the differences.

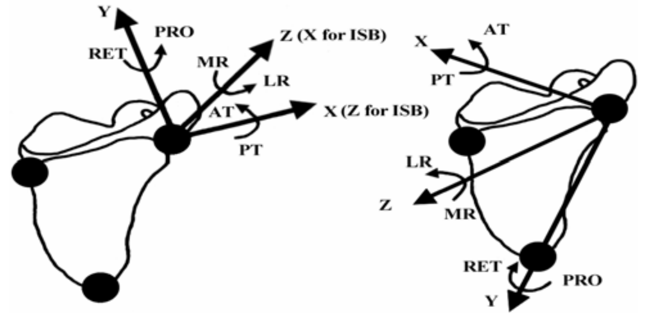

Figure 1: Local coordinate reference system proposed by ISG (left) and Hébert et al. (right)

RESULTS AND DISCUSSION

Altering the method of calculation has the most significant impact on the magnitude of the scapular rotations calculated (Table 1A). This finding is not surprising since the two methods are so different. One method calculates the displacement of the scapula from its position at rest, while the other calculates the changes in the orientation of the scapula with respect to the trunk. When interpreting findings from different studies in which different methods of calculation were used, one must be careful to make comparisons.

Using different local reference systems has less impact on the 3DSA, except in medial-lateral rotation for the method with respect to the trunk (more than 45°) (Table 1B). In this latter plane of movement, the differences in the orientation of the y-axis seem to have brought important changes of attitudes.

These results support the ISG recommendations to adopt standards for joint coordinate systems and method of calculation to allow a better comparison and benchmarking between studies. However, as there is so much variability between methods and systems, the choice of standard parameters must be based on their capacity to best characterise normal and abnormal patterns of movement.

REFERENCES

1. Karduna AR, et al. *J Biomech* **33**, 1063-1068, 2004.
2. van der Helm FCT, et al. (in press) *J Biomech*
3. Hébert LJ, et al. *Clin Biomech* **15**, 1-8, 2000.

Table 1: Differences of 3DSA between **A.** methods of calculation of relative movement and **B.** local coordinate reference systems

		A. Methods of calculation: Scapula at rest vs. Trunk				**B. Local reference system: Hébert et al. vs. ISG**			
		LCRS of Hébert et al.		LCRS of ISG		MC w.r.t. Scapula at rest		MC w.r.t. Trunk	
		Difference (°)	p	Difference (°)	p	Difference (°)	p	Difference (°)	p
Flexion	A-PT	15.0	<.0001	12.7	<.0001	1.2	0.004	1.1	0.0004
70°	L-MR	41.8	<.0001	5.6	<.0001	1.6	0.01	45.8	<.0001
	Pro-Ret	27.5	<.0001	31.0	<.0001	0.0	0.59	3.5	0.0001
Abd	A-PT	23.0	<.0001	22.6	<.0001	0.4	0.44	0.0	0.84
90°	L-MR	38.8	<.0001	9.2	<.0001	0.5	0.54	47.5	<.0001
	Pro-Ret	34.1	<.0001	35.3	<.0001	0.0	0.71	1.2	0.15

Abbreviations: A-PT, anterior-posterior tilting; L-MR, lateral-medial rotation; Pro-Ret, protraction-retraction; w.r.t., with respect to; LCRS, local coordinate reference systems; MC, method of calculation of relative movement; Abd, abduction.

NONLINEAR ANALYSIS OF POSTURAL CONTROL IN DIFFERENT POSITIONS AND VISION CONDITIONS

Kimberly Ryland, Clinton Wutzke, Nicholas Stergiou,
University of Nebraska-Omaha, HPER Biomechanics Laboratory
email: kryland@mail.unomaha.edu, web: www.unocoe.unomaha.edu/hper/bio/home.htm

INTRODUCTION

Despite postural control being a multi-degree-of-freedom mechanical system with highly redundant actuators [1], recent research has demonstrated that postural sway fluctuations like fluctuations present in many other biological systems are not random but rather have order [2]. Unlike traditional linear measures which can mask patterns present during postural sway, nonlinear analysis measures can characterize this order. Quantifying these patterns could enable the pinpointing of the precise contributions of sensory input and the improvement of rehabilitation methods [3]. Our aim was to compare the ability of traditional linear measures to nonlinear measures in differentiating between sitting and standing in the presence or absence of visual information.

METHODS

Eleven healthy young adults were asked to 1) stand quietly on a force platform (10 Hz) looking forward (STAND), 2) sit in a yoga style position directly on the force platform with their hands in their laps (SIT), and 3) sit upright on a stool (base 32x34 cm, height 75 cm) placed in the middle of the force platform with their arms to their sides and their feet not supported by the ground or the stool (SITSTOOL). Each position was maintained for five minutes and repeated three times with eyes open and three times with eyes closed. The coordinates of the center of pressure (COP) in the medial-lateral (ML) and anterior-posterior (AP) were calculated for each trial. Then, the unfiltered COP coordinates were analyzed using Chaos Data Analyzer Professional software to calculate four nonlinear measures (Correlation Dimension CoD, Lyapunov Exponent LyE, Hurst Exponent H, and the Lyapunov Exponent after the time series were surrogated SLyE) [2]. To calculate H, all data were first integrated. To calculate our nonlinear measures, we first reconstructed the state space by estimating the embedding dimensions (ED). ED is a measure of the number of dimensions needed to unfold a given attractor. This parameter was calculated with the Tools for Dynamics software [2]. We also calculated five linear measures (Root Mean Square RMS, Mean Distance MD, Total Excursion TE, Mean Velocity MV, and mean Total Excursion per second TEt) [5]. Statistical analysis was performed by either paired t-tests or ANOVA with further post hoc analysis when necessary.

RESULTS AND DISCUSSION

No significant differences were found for ED (mean=4.83). Thus ED equal with 5 was used for all subsequent nonlinear calculations. Our results showed that postural sway fluctuations for all postures examined had deterministic nature (paired t-tests; mean LyE=0.245, SLyE=0.268, p<.0005). A system is shown to have deterministic nature (orderly fluctuations), if the LyE is positive and is significantly different than SLyE [2]. We also found a mean H=1.005331 with no significant differences between conditions or directions (paired t-tests). H is a measure of persistence (memory) of a given fluctuation in a time series. This H value suggests that the deterministic patterns in posture have long range memory similar to the 1/f noise found in heart rhythms [4]. We also found that nonlinear measures were able to better differentiate between sitting and standing. LyE (a measure of local stability, higher stability equals smaller LyE) in the ML and CoD (a measure of degrees of freedom) in ML and AP demonstrated significant differences between STAND and SIT (p=.002, p=.002, p=.003) and STAND and SITSTOOL (p=.007, p<.0005, p=.003). Significant differences were also found between STAND and SIT in the linear measures of TE, MV, and TEt in the AP (p=.034, p=.034, p=.034) and TE, MV, TEt, and MD in the ML (p=.004, p=.004, p=.004, p=.004, p=.020). In addition significant differences were exhibited between SIT and SITSTOOL for the linear measures TE, MV, and TEt in the AP (p=.001, p=.001, p=.001) and ML (p=.002, p=.002, p=.002). Curiously, no differences were found in the linear measures between STAND and SITSTOOL which suggests that it was the distance from the center of gravity to the force platform that influenced the linear measures, rather than characteristics of the COP time series itself. Also, while the linear measure values were different, they measured the same relationships (identical p values). However when differentiating between vision conditions the nonlinear measures performed poorly while the linear measures demonstrated some differences. Only RMS and TEt in the ML showed significant differences between eyes open and closed (p=.036, p=.018). However significant interactions were found in TE, MV, and TEt in both AP (p=.04, p=.038, p=.038) and ML (p=.018, p=.018, p<.0005) and LyE in ML (p=.027). With the exception of TE and TEt in the AP, these interactions were the result of the eyes open values being larger than the eyes closed values during STAND, while the eyes open and eyes closed values were the same in both sitting conditions. This may be due to differing use of sensory information, while maintaining upright standing vs. sitting. There was also a discrepancy in the general trends found in the data. MD and RMS in AP, CoD and H in ML increased from eyes open to eyes closed, while TE, MV, LyE, CoD, and H in AP and RMS, MD, TE, MV, and LyE in ML decreased from eyes open to closed. This is not altogether surprising as Chiari et al. [5] found that while most subjects' sway increases with their eyes closed, there exists a second class of individuals who sway less with their eyes open. In conclusion, the results demonstrated that posture is deterministic and persistent and that nonlinear tools are able to pierce into the structure of posture. However, more work needs to be done to determine whether these tools can contribute to sensory understanding.

ACKNOWLEDGEMENTS

This work is supported by the Nebraska Research Initiative and NIDRR H133G040118.

REFERENCES

1. Duarte M, et al. *Neurosc Lett*, **283**, 173-176, 2000.
2. Stergiou N. *Innovative Analysis for Human Movement*.
3. Palmieri RM, et al. *J Sport Rehab*, **11**, 51-66, 2002.
4. Ward L. *Dynamical Cognitive Science*.
5. Chiari L, et al. *Gait Posture*, **12**, 225-234, 2000.

ELECTROMYOGRAPHIC CORRELATES OF ROBOTIC LAPAROSCOPIC TRAINING

[1]Timothy Judkins, [1]Kenji Narazaki, [2]Dmitry Oleynikov, [1]Nick Stergiou
[1]HPER Biomechanics Laboratory, University of Nebraska at Omaha
[2]Dept of Surgery, University of Nebraska Medical Center
email: tjudkins@mail.unomaha.edu, web: www.unocoe.unomaha.edu/hper/bio/home.htm

INTRODUCTION

Laparoscopy, a form of minimally invasive surgery (MIS), has revolutionized the treatment of abdominal pathologies. The advent of robotic surgical systems, such as the da Vinci™ Surgical System (dVSS), have further improved MIS by adding three-dimensional viewing [1] and increasing dexterity [2]. However, it is necessary to train and evaluate surgeons on the usage of the robotic system. The current means of evaluating surgical performance, while using a robotic surgical system, are limited to task completion time and number of errors [2, 3] or subjective evaluations. To our knowledge, no studies have examined physiological measures of the surgeons during performance of robotic surgical techniques. Especially, how training affects such physiological measures is unknown. This study seeks to determine how physiological measures, in the form of electromyography, change during training with dVSS.

METHODS

Fifteen right-handed novice dVSS users performed and/or practiced three tasks: bimanual carrying (BC), needle passing (NP), and suture tying (ST). BC required simultaneously picking up two rubber pieces and placing them 50 mm away. NP required passing a 26 mm surgical needle through 6 holes in a latex tube. ST required tying three intracorporeal knots with a surgical suture. All tasks mimicked actual laparoscopic tasks that require significant bimanual coordination. Subjects were randomly assigned to either a training (T) or a control (C) group. The experiment was performed over a period of four weeks and consisted of one pre-training test (PRE), 6 training sessions, and one post-training test (POST). Surface electromyography (EMG) was recorded (1000Hz) from 4 muscles: flexor carpi radialis (FCR), extensor digitorum (ED), biceps brachii (BB), and triceps brachii (TB). Frequency power spectrums for each muscle were calculated using Fast Fourier Transforms. Median frequency and bandwidth were compared using a mixed two-factor (group by testing session) ANOVA for each muscle and for each task.

RESULTS AND DISCUSSION

Median frequency was larger for POST for three muscles (FCR, BB, and TB) during the BC task and for one muscle (FCR) during the ST task (Figure 1). This increase was independent of group. This is not surprising considering that our previous work has found that significant decreases in task completion time are possible even after one training session. Furthermore, the increase in median frequency may be due to a reduction in muscle fatigue, since it has been shown that decreases in EMG frequency are associated with muscle fatigue [4]. It was also found that when a significant difference in median frequency or bandwidth was found, it occurred in muscles that would predominately be used for the given task.

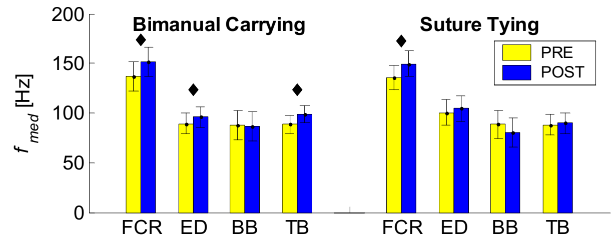

Figure 1: EMG Median Frequency grouped by PRE/POST training for Bimanual Carrying and Suture Tying tasks. A diamond indicates significance ($p<0.05$) between PRE and POST training.

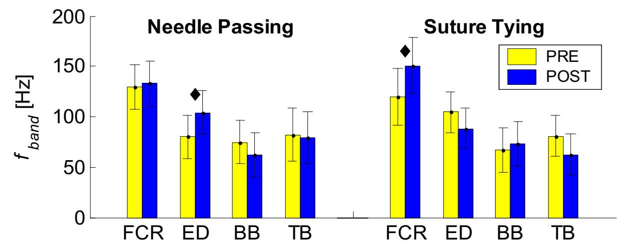

Figure 2: EMG Bandwidth grouped by PRE/POST training for Needle Passing and Suture Tying tasks. A diamond indicates significance ($p<0.05$) between PRE and POST training.

During the BC task, median frequency increased for the muscles used for grasping (FCR) and arm movements (BB and TB). Likewise, the median frequency for the FCR increased POST-training during the ST task, a grasping intensive task. The EMG frequency content is also directly related to the conduction velocities of recruited motor units [5], i.e., the types of motor fibers that are recruited. Therefore, frequency bandwidth may be a representation of the range of motor units that are recruited. For the more complex tasks (NP and ST), we found that POST bandwidth increased for the muscles that are required to perform the respective tasks (ED for NP, FCR and BB for ST; Figure 2). It is likely that different motor units are recruited during different phases of the task depending on the complexity of each phase. In conclusion, an evaluation of the physiological demands of robotic laparoscopic surgery can provide us with a meaningful way to quantify performance and skill acquisition.

REFERENCES

1. D'Annibale AMD, et al. *Surg Laparosc Endosc Percutan Tech*. **14**(1), 38-41, 2004
2. Moorthy K, et al. *Surg Endosc*. **18**(5), 790-795, 2004
3. Hubens G, et al. *Surg Endosc*. **17**(10), 1595-9, 2003
4. Basmajian JV and De Luca CJ, *Muscles Alive*. Williams & Wilkins, Baltimore, MD: 1985.
5. Farina D, et al. *J Appl Physiol*. 96, 1486-1495, 2004

Neuromuscular adaptation in human calf after disuse evaluated by muscle fMRI and EMG

[1] Hiroshi Akima, [2] Ryuta Kinugasa, [3] Toshio Yanagiya, [4] Hiroaki Kanehisa, [4] Hideoki Fukuoka and [5] Tetsuo Fukunaga
[1] Nagoya University, [2] Nippon Sport Science University, [3] Juntendo University, [4] University of Tokyo, [5] Waseda University;
email: akima@nagoya-u.jp

INTRODUCTION

The triceps surae (TS) muscle group plays a key role during postural control and physical activities in humans. It is well known that disuse (e.g. spaceflight and bed rest) induces deconditioning of the TS muscle group. We demonstrated that the neuromuscular adaptation took place in the TS muscle group during fatigable exercise after 20-d bed rest [1]. However, it is not well known whether this adaptation may occur during moderate fatigable exercise in this muscle group. The purpose of this study, therefore, is to elucidate change of function in the TS muscle group during both moderate fatigable and fatigable exercises after disuse using muscle functional magnetic resonance imaging (mfMRI) and surface electromyography (EMG) techniques.

METHODS

Five subjects participated in this study. The subjects were remained a 6 degree head-down tilted bed during 20 days, they were not permitted to be in any weight-bearing posture and all physical activities were kept to a minimum during this period. mfMRI (spin echo, TR 1500 ms, TE 25/70 ms) of the medial and lateral gastrocnemius (MG and LG, respectively), soleus (Sol) muscles was measured at rest and immediately after 25 repetitions (moderate fatigable, 25-rep Ex) and 50 repetitions (fatigable, 50-rep Ex) of unilateral calf-raising exercises [1]. Transverse relaxation time (T2) of the TS muscle group was measured as an index of neuromuscular properties. EMG activity (sampling rate: 1 kHz, band-pass filter: 20 to 450 Hz) was recorded from the MG, LG, Sol, and tibialis anterior (TA) muscles during 25-rep Ex and 50-rep Ex. Raw EMG signals was rectified and root mean squares was calculated. EMG activity was presented as the ratio of the last three repetitions to the first three repetitions. All data are presented as means and standard deviation. A one-way ANOVA and the Newman-Keuls was used for comparison.

RESULTS AND DISCUSSION

There was no significant change in resting T2 due to 20-d bed rest (Fig. 1). Overall, the T2 of the TS muscle group significantly increased with increase of the number of repetitions (Fig. 1). In the MG, Sol muscles, and TS muscle group, the T2 change was significantly higher after bed rest than before bed rest at 25-rep Ex and 50-rep Ex (both $P < 0.05$), suggesting a greater number of muscle fibers were involved in performing during 25-rep Ex and 50-rep Ex under the same absolute load [1, 2].

EMG activity of the Sol muscle and TS muscle group during 50-rep Ex was significantly higher after bed rest than that of before (Fig. 2, $P < 0.05$). No any significant changes of EMG activity were found in the MG, LG, and TA muscles.

We conclude that a short period of disuse affects on muscle function during moderate fatigable exercise as well as fatigable exercise, and that the functional adaptation is muscle-specific in human calf.

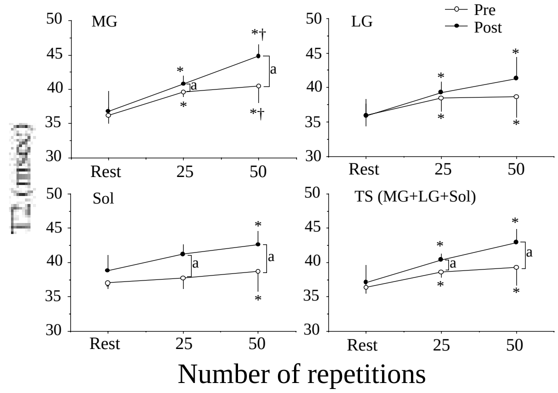

Figure 1: T2 changes of the TS muscle group during unilateral calf-raising exercises before and after 20-d bed rest. *: $P < 0.05$ vs rest, †: $P < 0.05$ vs 25-rep Ex, a: $P < 0.05$ pre vs post.

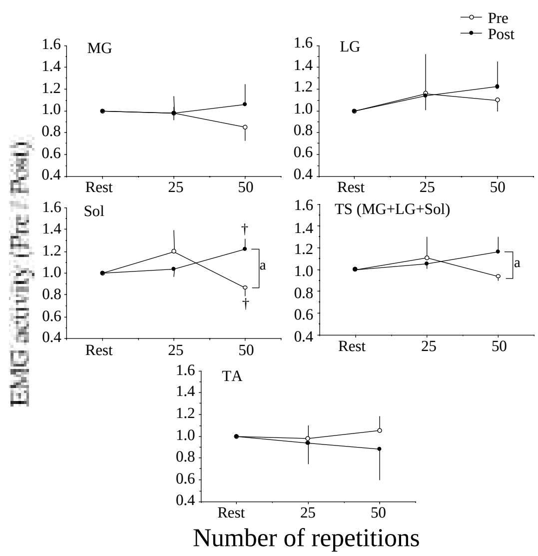

Figure 2: EMG activity of the TS muscle group during unilateral calf-raising exercises before and after 20-d bed rest. †: $P < 0.05$ vs 25-rep Ex, a: $P < 0.05$ pre vs post.

REFERENCES

1. Akima, H., et al. *Med. Sci. Sports Exerc.*, **35**, 655-662, 2003.
2. Ploutz-Snyder, L.L. et al. *J. Appl. Physiol*. **79**, 168-175, 1995.

ACKNOWLEDGEMENTS

This study is funded by a part of "Ground Research for Space Utilization" promoted by Japan Space Forum.

Biomechanical Study of Kümmell's Disease by Finite Element Analysis

[1] Hsiang-Ho Chen, [1] Che-An Pai and [2] Kung-Chia Li
[1] Dept. of Biomedical Engineering, I-Shou University, Kaohsiung, Taiwan; email: hchen@isu.edu.tw,
[2] Dept. of Orthopedics Surgery, Chia-Yi Yang-Ming Hospital, Chia-Yi, Taiwan

INTRODUCTION

Delayed posttraumatic vertebral collapse (Kümmell's disease) is a rarely reported, poorly documented, and poorly understood phenomenon. Schmorl and Junghanns [1] and Resnick and Niwayama [2] supported and defined the delayed vertebral collapse as a form of vertebral osteonecrosis. Based on the Symptoms, radiographies, and MRI findings from 129 patients, classification of the Kümmell's disease has been studied by Li et al in 2004 [3]. Three stages of the disease were found. The object of this study is to understand the stress distribution of vertebral body with various levels of vertebral collapse. The comparison of stress distributed on the vertebral body can be a good reference to the development of three-stage classification system.

METHODS

A three-dimensional finite element model of the intact vertebra was developed. There were 5334 nodes and 25720 elements in this intact model. Four zones of materials, including cortex, cancellous bone, posterior elements and cleft element, were assigned. Various percentages of cancellous bone in other models were excavated to simulate different levels of vertebral collapse (Fig.1). Totally, twenty-two models with various sizes of intravertebral clefts, including 0% (intact), 1%, 2.5%, 5%, 10%, 15%, 20%, 25%, 30%, 35%, 40%, 45%, 50%, 55%, 60%, 65%, 70%, 75%, 80%, 85%, 90% and 95% clefts in vertebral height. Nodes under the inferior end plate of vertebral body were fixed as the boundary condition under loadings. A 1000 N compression was evenly loaded on the superior end plate. In addition to compression, flexion and extension condition were also simulated by loading a 5 N-m torque. The von Mises stress distribution on vertebra was compared among vertebral models with various collapses.

RESULTS AND DISCUSSION

In compression, the maximal von Mises stress in vertebra was much higher than intact and distributed at the bilateral corners of the intravertebral cleft inside the superior endplate (Fig. 2). Comparison among models with various sizes of clefts showed that there were three zones on the curve of maximal von Mises stress along increasing sizes of clefts (Fig. 3). Vertebral collapses with 10 % and 80 % clefts were two transitional points on this curve. In flexion and extension, curves with a similar trend were also found. On the other hand, high stress also concentrated at the posterior cortex behind the cleft.

Three-stage classification has been established by Li et al. The stage I was defined as when the plain x-rays or MRI revealed osteonecrosis signs in vertebral body. The stage II was that body collapsed with intact posterior cortex of body. The stage III was that posterior body cortex collapsed with cord compression. Treatment for each stage was different.

This finite element simulation has shown that the level of stress distributing on vertebral body depended on the size of the intravertebral cleft. Especially, there were three stages in the relation curve between the maximal stress and cleft's size. This becomes a biomechanical evidence to support the clinical finding of three-stage classification for the Kümmell's disease.

Intact (0%) 20% 40% 60% 80%

Figure 1: Models with various sizes of intravertebral clefts.

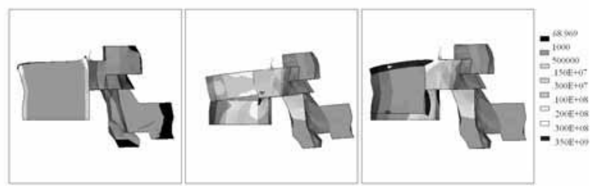

Intact (0%) 10% 80%

Figure 2: The von Mises stress distribution under flexion

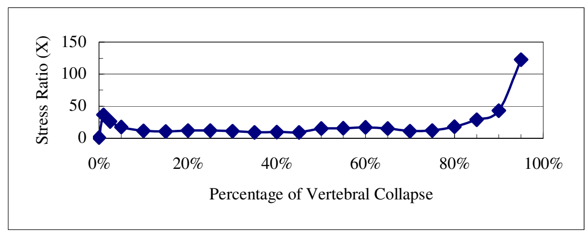

Figure 3: The ratio of maximal von Mises stress in vertebral body with various collapses to the intact under compression. The 0 % of vertebral collapse represents the intact.

CONCLUSIONS

From view points of pathological and biomechanical progress, three-stage classification system is probably appropriate to the diagnosis of Kümmell's disease.

REFERENCES

1. Schmorl G, Junghanns H. *The human spine in health and disease*, 2nd ed., New York, Grune & Stratton, 141-51, 1971.
2. Resnick D, Niwayama G. *Diagnosis of Bone and Joint Disorders*, 2nd ed., Philadelphia, WB Saunders, 3238-53, 1988.
3. Li KC, et al. *Journal of Musculoskeletal Research* **8**, 43-55, 2004.

LATERAL BALANCE IN A/K AMPUTEES AND HEALTHY CONTROLS

[1,2] At Hof, [2]Renske van Bockel and [2]Klaas Postema
[1]Center for Human Movement Sciences and, [2]Dept. of Rehabilitation, University Medical Center Groningen, Groningen, The Netherlands
email: a.l.hof@med.rug.nl, web: www.ihms.nl

INTRODUCTION

In walking the human body is never in balance. Most of the time the trunk is supported by one leg and the center of mass (CoM) is never above some base of support. According to the inverted pendulum model, when support is on the left leg we should fall to the right, and vice versa [4].
Recently it has been shown [2] that in dynamical situations the velocity of the CoM should be acknowledged. The center of pressure (CoP) should be outside the 'extrapolated COM' (XcoM), where XcoM = CoM + velocity of CoM / ω_0. Parameter is ω_0, the pendulum frequency, $\omega_0 = \sqrt{g/l}$. If this condition is not met, the CoM will traverse the CoP position and 'fall' to the wrong side, e.g. to the left of the left foot.

METHODS

CoP position and temporal data were recorded by a treadmill with built-in force transducers [3]. Left-right CoM and XcoM position were computed by filtering the CoP data [1].

Subjects were six above-knee amputees, ages 32-50 yr, with prosthesis for 6-40 years, and six matched healthy controls. They walked at 1 m/s for 2 min.

RESULTS AND DISCUSSION

Amputees showed asymmetric gait with shorter stance (60%) at the prosthetic side vs. 68% at the non-prosthetic side and a wider stride (13 ± 4 cm, mean ±s.d.) compared to controls (8 ± 3cm). At foot placement CoP was just outside of the XcoM, see Figure 1. The margin between average CoP and XcoM at foot contact was only 1.6 ± 0.7 cm in controls. In amputees this margin was clearly different between the prosthetic side (2.7 ± 0.5cm) and at the non-prosthetic side (1.9 ± 0.6cm).

Next to this 'stepping strategy', CoP position was corrected after initial contact by modulating the lateral foot roll-off ('lateral ankle strategy') in non-prosthetic legs up to about 2 cm. Finally there are indications that in prosthetic walkers trunk movements also contribute to balance ('hip strategy').

The inverted pendulum model can explain that 1) a less precise foot placement (greater CoP-XcoM margin) results in a wider stride, and 2) a greater margin at one side, as with a leg prosthesis, should be compensated by a shorter stance duration to achieve a straight path.

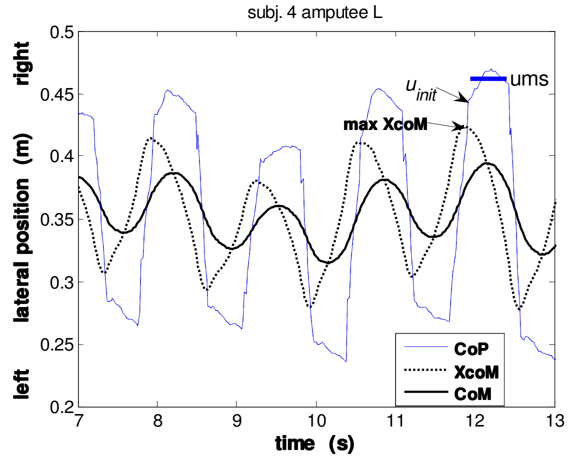

Figure 1 Detail of a recording of CoP, CoM and XcoP in walking at 1 m/s in a subject with a left A/K prosthesis. XcoM shows a maximum 'max. XcoM' when the right foot is initially positioned at $u_{init.}$ After placement the normal right foot corrects itself to achieve an average CoP position *ums*, sufficiently far from the XcoM. Note stereotypical CoP patterns for left (prosthetic) foot, compared to right.

CONCLUSIONS

Foot placement in walking should be remarkably precise to achieve a reasonably narrow and straight path, although some additional correction by ankle- and hip strategy is possible. In patients with a one-sided disability leading to less precise foot placement, as in prosthetic walkers but possibly also in stroke patients, this must be compensated by a shorter stance. Maybe in these patients symmetric gait should not be an aim of rehabilitation.

REFERENCES

1. Caron O, et al. *J Biomechanics* **30**: 1169-1171, 1997.
2. Hof AL, et al. *J Biomechanics* **38**: 1-8, 2005.
3. Verkerke G J, et al. *J Biomechanics*, in press.
4. Winter, D. A. *Gait and Posture* **3**: 193-214, 1995.

PERTURBATION IN TRUNK MOTION OF LOW BACK PATIENTS

[1,2] Heydar Sadeghi, [2] Paul Allard, [2] Somayeh Sadeghi
[1]Department of Kinesiology, Tarbiat Moallem University, Ministry of Sciences, Research and Technology, Tehran, IRAN,
[2]Research Center, Sainte-Justine Hospital, Montreal, PQ, Canada; email: sadeghih@yahoo.com

INTRODUCTION

Analysis of trunk motion consists of a complementary test, which includes the diagnosis and follow-up of patients with low back pain [1,2]. The information provided by the analysis usually shows significant reduction in trunk mobility or functional compensatory behavior. Measuring three-dimensional spine motion in able-bodied subjects and patients with LBP, this study was undertaken to determine: a) if trunk motion and particularly coupling motions were perturbed in LBP patients, which trunk segments are mostly affected, and b) whether or not trunk rigidity was reduced after eight weeks of physiotherapy.

METHODS

The fourteen subjects with low back pain who participated in this study had an age of 33±7.3 years, height of 172±9 cm and weight of 70.9±15.6 kg. The thirteen able-bodied subjects who participated in this study had an age of 35.1±9 years, height of 175±10 cm and weight of 68.5±9.7 kg. Data were collected using a four-camera high-resolution motion analysis video-based system while subjects were performing five principal movements, namely, right and left lateral bending and rotations as well as forward trunk flexion. The amplitude differences of the principal movements and the coupling motions of trunk and thoracic and lumbar segments of the able-bodied subjects and LBP patients were determined using ANOVA with a threshold of $p < 0.05$.

RESULTS AND DISCUSSION

The absence of a difference in the principal motions leads us to believe that there is no limitation of movement because no significant difference was observed between the able-bodied subjects and the patients before and after treatment. Significant differences, however, were observed in the coupling motions between the control subjects and the group of the LBP subjects before treatment (Figure 1).

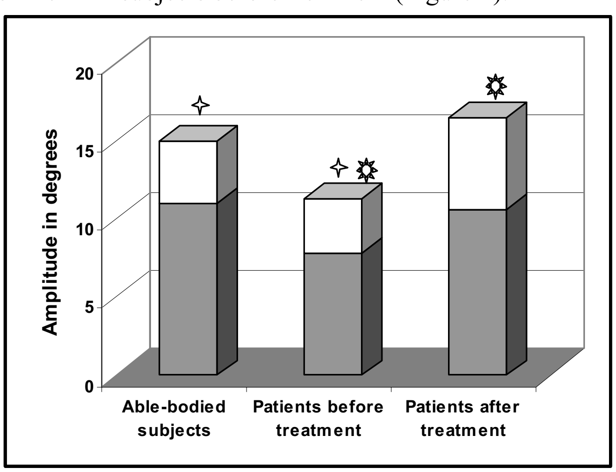

Figure 1: Maximum coupling in rotation for the lumbar segment during lateral bending of the trunk.

The difference for the coupling motions in rotation at the lumbar level during the principal movements of extension was 29% between the able-bodied subjects and LBP patients.

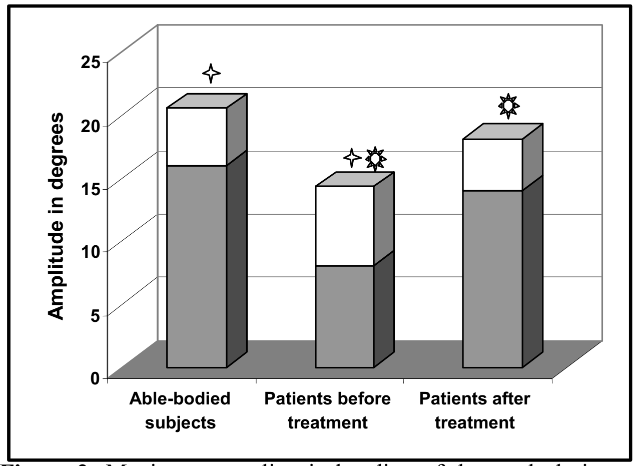

Figure 2: Maximum coupling in bending of the trunk during trunk rotation.

The significant differences in the coupling in lateral extension were recorded at the thoracic level for the principal rotation motion, as indicated in Figure 3. During lateral bending, the coupling rotation at the lumbar level was reduced by 27% in the patient group before treatment while the same group had a 50% reduction in the thoracic coupling bending motion.

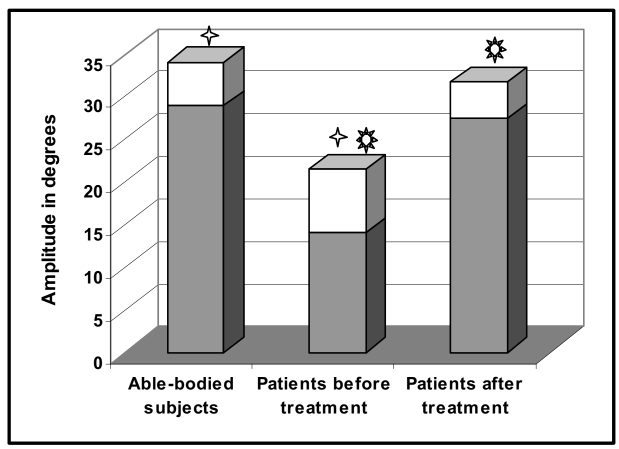

Figure 3: Maximum coupling in bending of the thoracic segment during trunk rotation.

CONCLUSIONS

No indication appeared to locate trunk rigidity in patients with LBP. Reduction in the coupling motion can be expected for LBP patients before treatment. The rigidity might also be manifested for the coupling motions for the segments having the most mobility during the principal motions being executed.

REFERENCES

1. Allard P, et al. Appleton and Lange publishers 357-67, 1999.
2. Beggs JS. Hemisphere Publishing Co, 223, 1966.

WHAT IS THE ACCURACY OF SURFACE MODELS CREATED FROM VISIBLE HUMAN MALE COMPUTED TOMOGRAPHY DATA?

[1]Schmidt J, [1]Engh J, [2]Viceconti M and [1]Ploeg H
[1]University of Wisconsin – Madison, WI, USA
[2]Rizzoli Orthopedic Institute, Bologna, Italy
e-mail: jschmidt1@wisc.edu, web: http://www.engr.wisc.edu/groups/BM/

INTRODUCTION

Three-dimensional (3D) finite element (FE) analysis is used to determine stress and strain distributions in bone in order to predict fracture risk and design orthopaedic implants. Many studies have used computed tomography (CT) data to supply data about geometry and material properties to FE models [1–5]. Both custom-built and commercial segmentation programs have been used to determine the complex bone shape. Yet, few studies have reported the geometric accuracy of the segmentation methods [6-7]. Therefore, the goal of the current study was to determine the accuracy of surfaces created from the visible human (VH) CT data using custom-made and commercial segmentation software programs.

METHODS

The National Library of Medicine's Visible Human (VH) male computed tomography (CT) and cryogenic standardized data sets were used in this study [8]. Two different methods were used to segment both the right (R) and left (L) femurs of the VH CT data. One method uses the custom-made border tracing algorithm, which was developed as part of the HIPCOM project [7], to segment the bones. This method extracts a closed contour as an object, which is an ordered sequence of adjacent pixels. Specifically, once a starting point and direction is located by the user the algorithm searches the eight neighboring points to determine the pixel with intensity greater than or equal to the current pixel. Polygonal surfaces are interpolated from the resulting stack of contour curves. This method is also used to segment the cryogenic VH data.

The second method uses the commercial software Mimics (Materialise, Ann Arbor, MI) to segment the bones. Within this software the primary segmentation command was 'Thresholding'. The 'Thresholding' feature allows the user to specify an upper and lower bound from a range of Hounsfield values, which is known to be related to density. Further processing is uses the 'Edit Masks' commands of 'Draw' and 'Erase'. These commands were only used when needed to fill holes or detach one mask from another.

Polyworks Inspector 8.0.8 software (InnovMetric, Sainte Foye, QC) was used to compare models. The perpendicular distance between points of the CT models and the surface of the cryogenic model was determined. These distances were then used to determine the mean, standard deviation, minimum, and maximum separation distances.

RESULTS

Initial comparisons found no difference between the cryogenic STL and IGS models (L: 0.02 ± 0.11 mm), therefore only the cryogenic STL models were used for the subsequent comparisons. For confidentiality, labels A and B are used to identify the segmentation methods. Method A created models smaller than the cryogenic models (R:-0.29 ± 0.99 mm; L: -0.37 ± 0.62 mm) (Figure1). Method B created models larger than the cryogenic models (R: 0.46 ± 0.61 mm; L: 0.42 ± 0.60 mm) (Figure 1).

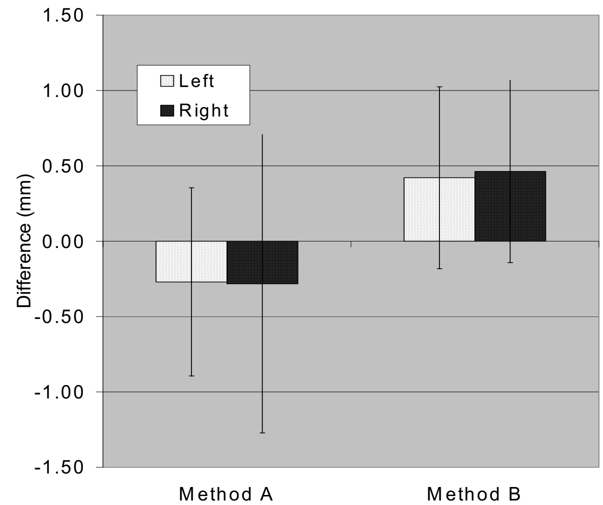

Figure 1: Mean distance and standard deviations between VH cryogenic and CT models created using custom-made and commercial segmentation software.

CONCLUSIONS

The current study reported a smaller mean error (-0.3–0.5mm) compared to a previous study (0.6-0.9 mm) [6]. In addition, this study reported a higher range in standard deviation (0.6 – 1.0 mm) than a previous study (±0.3 mm), which also reported a peak error of 1.5 mm [7].

The current study reported the accuracy of two segmentation methods, while developing a protocol for validation of models created from CT data. This protocol determines the accuracy of a segmentation method using the internationally accessible VH CT data set. This study assumed that the segmented cryogenic VH data set was the gold standard for comparison. A similar method of validation can be used for solid geometry, mesh geometry, and FE deformations and stress. This protocol provides researchers with a method to accurately compare modeling methods created to predict fracture failure or to design orthopeadic implants.

REFERENCES

1. Cattaneo PM, et al. *Proc Instn Mech Engrs* **215,** 203-213, 2001.
2. Donahue TL, et al. *J Biomech Eng* **124,** 273-280, 2002.
3. Keyak JH et al. *J Biomed Eng* **12**, 389-397, 1990.
4. Merz B, et al. *J Biomech Eng* **118**, 387-390, 1996.
5. Prendergast PJ. *Clin Biomech* **12,** 343-366, 1997.
6. Testi D, et al. *Comput Methods Programs Biomed* **65**, 175-82, 2001.
7. Viceconti M. *J Med Eng & Tech* **23**, 77-81, 1999.
8. Spitzer V, et al. *JAMIA* **3,** 118-130, 1996.

ACKNOWLEDGEMENTS

Cryogenic segmentation was performed at Rizzoli Orthopaedic Institute by Debora Testi. Comparisons using Polyworks software was performed at Queen's University, Kingston, ON by Leone Ploeg.

ASSIMILATING FULL BODY GAIT GRAPHS INTO SINGLE AREA PLOTS

Sam Augsburger, MSME, Hank White, MSPT, Chester Tylkowski, MD
Shriners Hospitals For Children Lexington
Email: saugsburger@shrinenet.org

INTRODUCTION

Gait analysis offers detailed kinematic and kinetic assessments of multiple segments and joints. A single condition gait analysis report often includes over 60 graphs of individual segments and joints in multiple planes. The method presented assimilates all kinematic or kinetic gait data from one plane into a single area graph. Deviations from normal are assigned unique colors, creating multi-joint patterns. This visual integration of color patterns uniquely highlights pathologic data in a reproducible manner and facilitates accurate and relevant interpretations of gait analyses.

METHODS

A retrospective review of subjects with a primary diagnosis of Cerebral Palsy resulted in 7 patients for whom bilateral hamstring lengthening only was recommended, and 4 patients for whom bilateral gastrocsoleus lengthening only was recommended. The deviations from normal of these two groups were calculated for each frame of data and each joint/segment in a fashion similar to Manal, et al [1]. The deviation (d) was calculated from the pathological average (x_p), the normal average (x_n), and the normal standard deviation (sd_n), using the equation $d = (x_p - x_n)/ sd_n$.

The trunk and ankle data were plotted horizontally at the top and bottom of the area graphs. The pelvis, hip, and knee data were plotted horizontally with 20 vertical data points between them and adjacent joint data. A continuous gradient of deviations was calculated for the areas between joints. The deviation gradient (d_g) was calculated for each frame using the inferior joint deviation (d_i) and the superior joint deviation (d_s) with the equation $d_g = d_i + g*(d_s - d_i)/20$, where g is the gradient position above the inferior joint (1 to 20).

Each deviation was assigned a color based on a gradient of 56 colors from red (+3 deviations) to violet (-3 deviations). Green was normal (0 deviations). Red was indicative of excessive anterior trunk/pelvic tilt, hip/knee flexion, and ankle dorsiflexion. Violet was indicative of excessive posterior trunk/pelvic tilt, hip/knee extension, and ankle plantar flexion. A total of 8500 data points were assigned colors (85 points high by 100 points wide).

RESULTS AND DISCUSSION

In the hamstring-lengthening-only group (Figure 1a) the predominant patterns were excessive knee flexion at initial contact, excessive ankle dorsiflexion at weight acceptance, and excessive knee flexion during mid-stance. There was mild ankle plantar flexion during mid-stance and hyperextension of the knee during mid-swing.

In the gastrocsoleus-lengthening-only group (Figure 1b) the predominant patterns were excessive knee flexion at initial contact, excessive ankle plantar flexion during mid-stance, excessive knee extension during mid-swing, and excessive hip flexion during late swing. There was a mild increase in ankle dorsiflexion during weight acceptance, and an increase in pelvic anterior tilt during mid-stance and early swing.

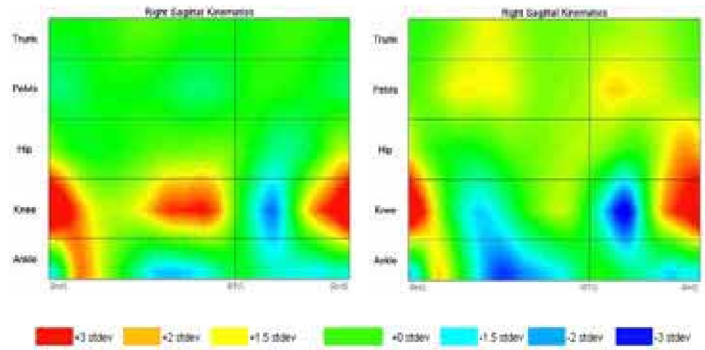

Figure 1: a) Hamstring Lengthening, b) Gastroc Lengthening

CONCLUSIONS

This method of displaying gait analysis data has the advantage of displaying area patterns, which result from multi-joint as well as single joint deviations. The resulting shapes, as well as colors, are indicative of particular pathologies and corresponding interventions. The excessive knee flexion pattern during mid-stance in the hamstring lengthening group (Figure 1a) as well as the knee flexion at initial contact "pouring" into the ankle are characteristic patterns of this population. Likewise, the "chair-like" shape of the ankle plantar flexion/knee extension pattern during mid-stance in the gastrocsoleus lengthening population (Figure 1b) is both indicative and unique.

This method treats gait data as though they are "connected" from one joint to another, rather than disconnected line graphs. Interpretation and integration of the data is still required. However, the patterns assessed are not isolated to single joints and are typical of multi-joint pathologies.

Each clinician has his/her own preferred method of integrating and interpreting gait data. For those who find it difficult to integrate 5 graphs, let alone 60, this method offers an alternative presentation style of data for analysis. Having both color and shape in "zones" from the ankle to the trunk is a potentially useful alternative. The process of applying this method to individual subjects with combinations of pathologies has been enlightening. In doing so we have discovered combinations of the patterns discussed herein as well as new patterns that were not appreciated through more traditional presentation styles of gait data.

REFERENCES

1. Manal, K, et al: A novel method for displaying gait and clinical movement analysis data. Gait & Posture, Volume 20, Issue 2, 222-226, 2004

NEUROMUSCULAR ADAPTATIONS IN GAIT WITH AGE AND MUSCULOSKELETAL PATHOLOGY

[1] Chris A. McGibbon, and [2] David E. Krebs
[1]Institute of Biomedical Engineering, University of New Brunswick, Fredericton NB, Canada,
[2]Massachusetts General Hospital, Biomotion Laboratory, Boston MA, USA; email: cmcgibb@unb.ca

INTRODUCTION

Arthritis and other chronic joint conditions are the leading cause of disability in older adults. Changes in locomotor patterns with age [1-3] and disability [4] may be caused by neuromuscular adaptations, which alter segmental kinematics and kinetics through reorganization of muscle firing patterns to compensate for primary mobility impairments. However, the underlying neuromuscular adaptations that arise from idiopathic, age-related impairment and musculoskeletal pathology are not well understood. The purpose of this study was to explore the underlying mechanisms of gait disorder among older adults, and determine which kinematic and kinetic variables best discriminate between young and old healthy adults, and between healthy and disabled elders.

METHODS

Ankle, knee and hip peak angles, moments and powers in the sagittal plane were acquired during gait in 120 subjects: 45 healthy young (HY), 37 healthy elders (HE), and 38 disabled elders (DE) with functional limitations due to lower-extremity musculoskeletal pathology (primarily arthritis). MANCOVA with discriminate analysis, statistically controlled for gait speed, identified the variables that discriminate between young and old healthy adults, and between healthy and disabled elders. Correlation analysis was used to explore interrelationships among these variables within each group to identify possible mechanisms underlying gait dysfunction among older adults.

RESULTS AND DISCUSSION

Eight variables strongly discriminated among groups (Figure 1). HE subjects were discriminated (sensitivity 76%, specificity 82%) from HY subjects via decreased late-stance ankle plantar flexion angle (AR2), and increased late-stance knee power absorption (KP4) and early-stance hip extensor power generation (HP1). DE subjects were discriminated (sensitivity 74%, specificity 73%) from HE subjects via decreased late-stance ankle plantar-flexor moment (AM2) and ankle plantar-flexor power generation (AP2), and increased early-stance ankle dorsi-flexor moment (AM1), late-stance hip flexor moment (HM2), and late-stance hip flexor power absorption (HP2). Among the eight variables, the number of significant ($p<.005$) correlations increased with age and disability: there were 5 for HY, 7 for HE, and 13 for DE groups. For the DE group, late-stance hip flexor power absorption and hip flexor moment were more tightly coupled to other kinematic and kinetic variables than for healthy groups.

The data suggest that gait changes caused by lower extremity impairment, manifest differently than do gait changes from aging alone. Beyond age-related changes, elders with lower-

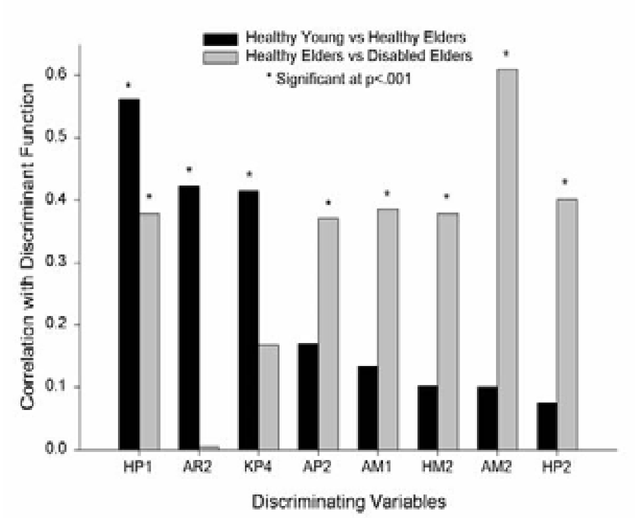

Figure 1. Strength of discriminate functions.

extremity dysfunction rely excessively on passive hip flexion torque to provide propulsion in late-stance, probably to assist with advancement of the swing leg, and ankle dorsi-flexors of the contralateral limb, probably to enhance trunk stability. This compensatory strategy probably increases hip joint stresses, leading to increase OA incidence [5] and promoting hip/trunk muscle overuse and thus fatigue. Furthermore, weak or fatigued ankle muscles could jeopardize control of the body center of mass, and increase risk of falling. Relationships among the biomechanical variables showed a higher degree of coupling for the DE subjects compared to the HY and HE subjects, suggesting reduced flexibility to alter motor strategies.

CONCLUSIONS

This work supports a growing body of evidence that pathological gait changes from age and disability have a neuromuscular basis, which may be informative in a motor control framework for physical therapy interventions. Study of physical therapies, such as optimal functional training, ie, practicing more healthy and younger gait strategies, aimed at reducing the dynamic coupling among neuromuscular control parameters is warranted.

REFERENCES

1. DeVita P, Hortobagyi T. *J Appl Physiol.* **88**, 1804-1811, 2000.
2. Kerrigan DC, et al. *Arch Phys Med Rehabil.* **79**, 317-322, 1998.
3. Judge JO, et al. *J Gerontol Med Sci.* **51**, 303-312, 1996.
4. McGibbon CA, Krebs DE. *J Appl Physiol.* **96**, 149-160, 2004.
5. Amin S, et al. *Arthritis Care Res.* **51**, 371-376, 2004.

MEASUREMENT OF NONLINEAR-ELASTIC PROPERTIES OF SKIN AND SUBCUTANEOUS TISSUES VIA UNCONFINED COMPRESSION TESTS

John Z. Wu, Robert G. Cutlip, and Ren G. Dong
National Institute for Occupational Safety and Health,
Morgantown, WV 26505, USA. email: jwu@cdc.gov

INTRODUCTION

Knowledge of the nonlinear-elastic properties of soft tissues is essential for the development of reliable finite element models for biological systems. The compressive nonlinear-elastic properties of soft tissues are usually determined using unconfined compression tests. To determine the nonlinear-elastic behavior of skin and subcutaneous tissues using a conventional approach, the skin and subcutaneous tissues have to be separated before testing [1,2,3]. Using such an approach, measurement errors may be increased as a consequence of the reduced specimen dimensions and cumulative experimental errors. In the present study, we propose a novel method to determine the nonlinear-elastic behaviors of the skin and the subcutaneous tissues simultaneously using specimens of skin/subcutaneous composites.

METHODS

If two unconfined compression tests (labeled A and B) are performed with specimens of different skin/subcutaneous tissue height ratios (γ_s and γ_f), two different stress-strain relationships will be obtained (Fig. 1a). At the same stress level, the total tissue strains can be obtained from these two distinct stress/strain relationships. Assuming that the tissue samples A and B are taken from two adjacent locations, the mechanical characteristics of the skin and subcutaneous tissues in specimen A should be similar to those in specimen B. Consequently, for a given stress, the strains in the skin (ε_s) and in the subcutaneous tissues (ε_f) for specimen A should be identical to those for specimen B. Therefore, the strains in the skin and subcutaneous tissues for a given stress can be solved from:

$$\varepsilon^A = \gamma_s^A \varepsilon_s + \gamma_f^A \varepsilon_f, \qquad \varepsilon^B = \gamma_s^B \varepsilon_s + \gamma_f^B \varepsilon_f \qquad (1)$$

Because of scattering of test data of soft tissues, multiple unconfined compression tests are to be performed using tissue samples with different skin/subcutaneous height ratios (as sketched in Fig. 1b). The stress/strain curves of skin and subcutaneous tissues are derived from stress/strain curves of the skin/subcutaneous composite soft tissue specimens using a least square method. In the present study, a total of eight samples of skin/subcutaneous composite were used. Tissue samples were collected from the palmar surface of the front feet of a pig (Landrace-Yorkshire-Duroc hybrid).

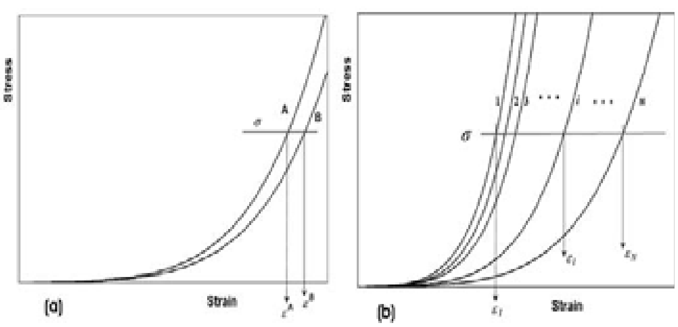

Figure 1: Schematics of the stress/strain relationships of soft tissue samples with different height ratios of skin and subcutaneous tissues. (a) Two samples; (b) Multiple samples

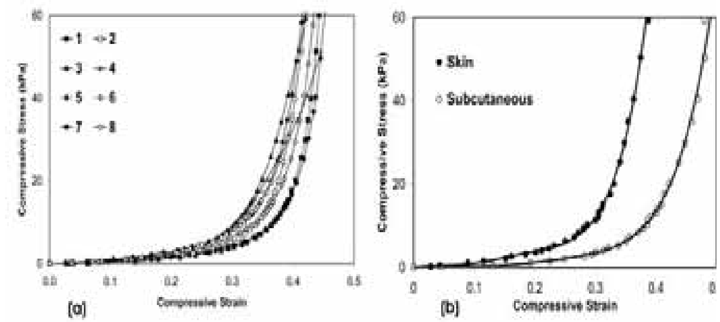

Figure 2: (a) The stress/strain curves of the eight unconfined compression tests using skin/subcutaneous composite specimens. (b) The stress/strain curves of the skin and subcutaneous tissues obtained using the proposed method.

RESULTS AND DISCUSSION

The stress/strain relationships for the eight unconfined compression tests were found to depend on the height ratio of skin/subcutaneous tissue – the specimens with a higher ratio of skin/subcutaneous tissue tend to produce a stiffer stress/strain curve (Fig. 2a). Using the proposed approach, the stress/strain relationships of skin and subcutaneous tissues were derived (Fig. 2b).

CONCLUSIONS

Compared to conventional test procedures, our method offers the advantages that the skin and subcutaneous tissues do not need to be separated prior to testing, and that the soft tissue composite specimens reflect physiological loading conditions much more accurately than testing of isolated skin and subcutaneous tissues. Using the proposed approach, material properties of soft tissues can be obtained in a cost- and time-efficient manner, which simultaneously improves the physiological relevance.

REFERENCES

1. Vogel, HG. *Acta Derm Venereol Suppl (Stockh)* **185**, 39-43, 1994.
2. Wu JZ et al. *Biomed Mater En* **13**, 373-385, 2003.
3. Miller-Young J et al. *J Biomech* **35**, 1523-1532, 2002.

ESTIMATION OF VISCOUS PROPERTIES OF SKIN AND SUBCUTANEOUS TISSUES VIA UNIAXIAL STRESS RELAXATION TESTS

John Z. Wu, Robert G. Cutlip, and Ren G. Dong
National Institute for Occupational Safety and Health,
Morgantown, WV 26505, USA. email: jwu@cdc.gov

INTRODUCTION

Using traditional experimental methodologies [1,2,3], the skin has to be separated from the subcutaneous tissues in order to determine the tissues' viscoelastic properties. Thus, the complex collagen fiber network in soft tissue could be damaged when the skin is separated from the subcutaneous tissue. Therefore, the viscoelastic properties of the skin and subcutaneous tissues measured using isolated samples may be different from those in physiological conditions. The purpose of the present study is to estimate the viscous behaviors of the skin and the subcutaneous tissues using composite tissue specimens.

METHODS

In a creep test using a specimen of skin/subcutaneous tissue composite, dependence of the total tissue strain [$\varepsilon(t)$] on the strain contributions from skin and subcutaneous tissues is derived as:

$$\varepsilon(t) = \gamma_s \varepsilon_s(t) + \gamma_f \varepsilon_f(t) \tag{1}$$

where γ_s and γ_f are the skin and subcutaneous tissue thickness ratios, respectively. The corresponding normalized creep function of the tissue composite [$j(t)$] is related to those of skin and subcutaneous tissues [$j_s(t)$ and $j_f(t)$] by:

$$j(t) = \alpha\, j_s(t) + \beta\, j_f(t) \tag{2}$$

where α and β are parameters depending on the thickness ratios and elastic stiffness of the skin and subcutaneous tissues. If two creep tests (A and B) are performed using specimens of different thickness ratios of the skin and subcutaneous tissues, they will result in two distinct creep curves. Assuming that these two tissue samples are taken from two locations close to each other from the same animal, the mechanical characteristics of the skin and subcutaneous tissues in specimen A should be similar to those in specimen B. Therefore, the normalized creep functions of the skin and subcutaneous tissues [$j_s(t)$ and $j_f(t)$] can be solved from:

$$j(t)^A = \alpha_A j_s(t) + \beta_A j_f(t), \tag{3}$$
$$j(t)^B = \alpha_B j_s(t) + \beta_B j_f(t)$$

Because of scattering of test data of soft tissues, multiple tests are to be performed using tissue samples with different skin/subcutaneous thickness ratios and the equations are to be solved using a least square method. Viscoelastic properties of soft tissues in compression are usually obtained via stress relaxation tests, because the stress relaxation tests are, technically, much easier to perform than the creep tests. The proposed procedure is composed of four steps: (1) perform stress relaxation tests using skin/subcutaneous composite specimens, (2) convert the stress relaxation functions to the corresponding creep functions using Laplace transformations, (3) determine the creep functions of skin and subcutaneous tissue using the proposed method, and, finally, (4) convert the creep functions of the skin and subcutaneous tissues to their corresponding stress relaxation functions using inverse Laplace transformations. The proposed procedure has been applied to determine the viscous properties of the skin and subcutaneous tissues of pig. The tissue samples were collected from the palmar surface of the front feet of a pig (Landrace-Yorkshire-Duroc hybrid).

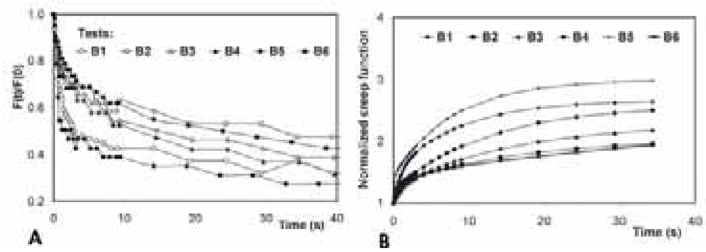

Figure 1: A: The stress relaxations of skin/subcutaneous composite specimens. B: The corresponding normalized creep functions.

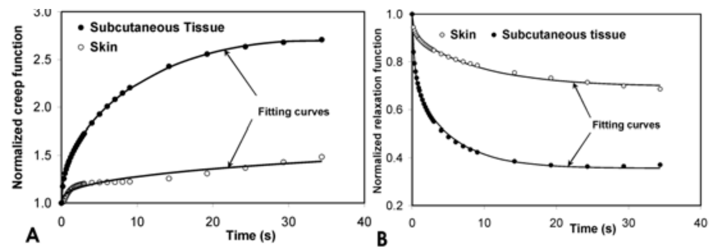

Figure 2: A: The normalized creep functions of the skin and subcutaneous tissues. B: The corresponding stress relaxations.

RESULTS AND DISCUSSION

The six stress relaxation tests were conducted under unconfined compressions using tissue specimens of different skin/subcutaneous thickness ratios (Fig 1A). The stress-relaxation curves have been converted into their corresponding normalized creep functions (Fig. 1B). Using the proposed procedure, the creep and stress-relaxation curves of the skin and subcutaneous tissues were derived, as shown in Figs. 2A and B.

CONCLUSIONS

Using the proposed test procedure, we can simultaneously estimate the viscous properties of the skin and subcutaneous tissues without separating them prior to testing, such that the soft tissue composite specimens reflect physiological loading conditions more reasonably than the specimens of isolated skin and subcutaneous tissues.

REFERENCES

1. Pan, L et al. *Ultrasound Med Biol* **24**, 995-1007, 1998.
2. Miller-Young J et al. *J Biomech* **35**, 1523-1532, 2002.
3. Gennisson JL et al. *Ultrason Ferroelectr Freq Control* **51**, 980-989, 2004.

CARTILAGE CELL VIABILITY AFTER IN VIVO IMPACT LOADING

Doug Bourne[1], Ken Muldrew[2] and Walter Herzog[1]
[1]Faculty of Kinesiology, [2]Faculty of Medicine
University of Calgary; email: dbourne@kin.ucalgary.ca

INTRODUCTION

Injury to articular cartilage is thought to be one of the initiators of osteoarthritis. One possible mechanism of cartilage degeneration is that cells are killed due to impact. The resulting metabolic load on the remaining cells prevents them from properly maintaining the extracellular matrix, leading to matrix degeneration that further impairs the ability of the cartilage to support normal loads leading to further degeneration. Most impact models have used cartilage explants. The validity of taking cartilage out of its natural environment and testing isolated sections is suspect. The only other in vivo impact model in an intact joint has looked at mechanical properties of the cartilage after impact and not biological markers such as cell viability (Haut et al. 1995). The purpose of this study was to look at cartilage viability at different impaction energies in an in vivo rabbit model.

METHODS

14 New Zealand white rabbits were used for this study. Rabbits were injected with acepromazine and then anaesthetized with isoflurane. They were mounted in a custom stereotaxic frame where their hips were pinned and experimental knee supported at approximately 90°. In 13 rabbits, the patella was subjected to either 0J, 2.5J, 5J or 7.5J impacts by dropping a weight from a specific distance. One rabbit knee was subjected to 10 >5J impacts. Cartilage from the patella and the loaded portion of the femoral groove was harvested 24 hours later and 50 μm full thickness sections were prepared with a vibratome. Slices were stained with Syto 13 and Ethidium Bromide and were then viewed under a fluorescent microscope and photographed with a digital camera. Live (green) and dead (red) cells were counted with a custom cell counting program.

Figure 1: Impact set-up showing impactor in approximation to the rabbit's patella.

RESULTS AND DISCUSSION

Cell viability in the first 13 rabbits ranged from 72 -86%. Ten Impacts of the patella caused cell viability to drop to 57%. There was a trend that cell death was occurring more at the intermediate and middle layers than the superficial layer.

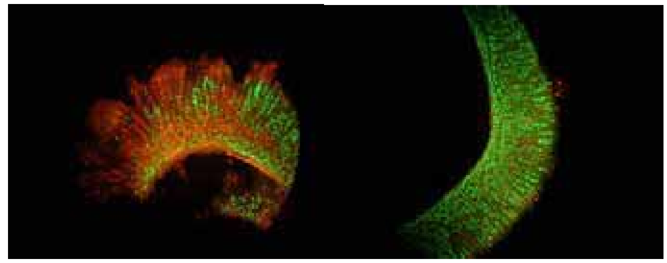

Figure 2: Two sample patella sections. The left section was subject to 10 impacts while the right section was a control (0J).

The cell viability protocol used was not sensitive enough to detect differences between the single impact conditions. This was due to high baseline cell death and variability in cell death in all samples including controls. Impact of the cartilage of one knee 10 times resulted in a much more consistent level of cell death throughout the samples.

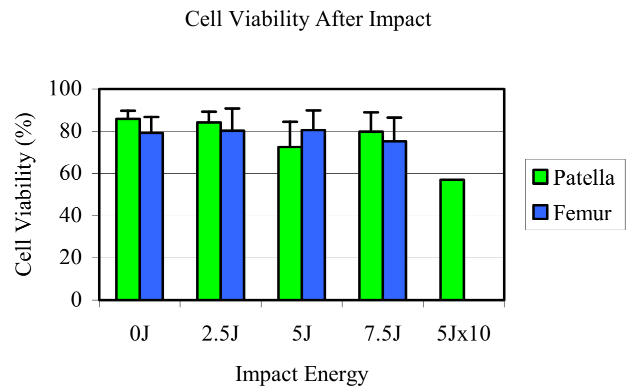

Figure 3: Cell viability for each impact energy.

CONCLUSIONS

Cell viability testing needs to be refined to reduce variability. Future studies will look at cell viability using a confocal microscope to minimize artefacts from cutting the tissue. Despite problems with variability, it appears that cartilage is much more robust in vivo than in vitro explants tests have suggested.

REFERENCES

Haut, R.C., Ide, T.M. and De Camp, C.E. (1995) *J Biomech Eng* **117**, 402-8.

ACKNOWLEDGEMENTS

Supported by the Alberta Provincial CIHR Training Program in Bone and Joint Health, CIHR and the Canada Research Chair Programme.

EFFECT OF THE PREFABRICATED METALLIC POST LENGTH ON RESTORED TEETH: FRACTURE STRENGTH AND STRESS DISTRIBUTION

[1]P.J. Rodríguez-Cervantes, [1] J. L. Sancho-Bru, [2]A. Barjau-Escribano and [2]L. Forner-Navarro
[1]Departament de Tecnologia. Universitat Jaume I, Castelló (Spain)
[2]Departament d'Estomatologia. Universitat de València (Spain); correspondence email: cervante@tec.uji.es

INTRODUCTION

In order to restore devitalized teeth, modern restoring techniques in Dentistry use an external element, the intraradicular post, as a retention system for the material used in the tooth restoration to be carried out later.

Although non-metallic posts are being increasingly used, metallic posts continue to be the standard for most situations because they have stood the test of time [1]. Different aspects of the post design have been studied [2,3,4], but the influence of the post length on the mechanical strength of the restored tooth is lacking. The aim of this work was to study how the prefabricated metallic post length affects the biomechanical performance of restored teeth.

METHODS

A combined theoretical and experimental method was used to analyze the influence of post length (from 3 to 14 mm) for the ParaPost Stainless Steel (Coltène/Whaledent Inc, Ohio, USA).

First, an experimental fracture strength test was performed over thirty extracted human teeth. The purpose of this test was to analyze the differences in strength between the post systems with different post lengths. The teeth were decoronated, treated endodontically and restored with stainless steel posts. The specimens were placed in a retention device and mounted on the universal testing machine. This device allowed the teeth to be loaded on the palatal side at an angle of 30º to the radicular axis, in the vestibular direction. A controlled loading force was applied to the teeth at a rate of 5 N/s, until failure. Three group lengths were considered based on the post length to root length ratio: 'short' (<0.5), 'normal' (0.5 to 0.8) and 'long' (>0.8). The loading force (N) required to cause failure was recorded and the results for the groups were compared by using an ANOVA test.

Secondly, the finite element technique was used to develop a 3D model of the restored tooth. The model allowed us to study the stress distribution pattern on the restored tooth under external loads, for the different post lengths considered. The stress distribution pattern provided information about the fracture mechanism of the restored tooth. To generate the geometry, measurements were taken on 40 extracted human maxillary central incisors: cervico-apical height and mesio-distal and vestibulo-palatal diameters at both cervical and medial root heights were recorded. Mean values from these measurements defined the geometry of the tooth used for the study. Finally, the results from the fracture strength test were used to check the validity of the finite element model and the results from the simulations.

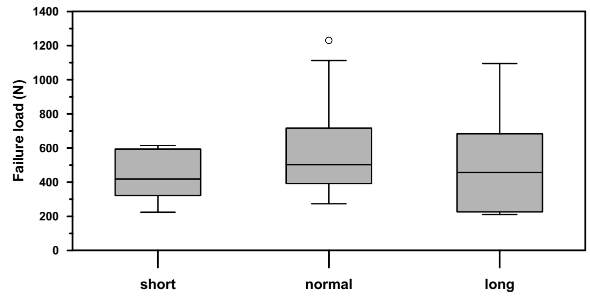

Figure 1: Box-whisker graphs showing spreads of failure load values for the groups of studied specimens.

RESULTS AND DISCUSSION

From the experimental fracture strength test, no significant differences ($p=0.3>0.05$) were observed between the failure loads of the different groups (short, normal and long) of teeth restored using stainless steel posts. Box-whisker graphs showing spreads of values in the data sets can be observed in Fig. 1. Restored teeth showed a fracture of the core along the juncture with the post, on the vestibular side.

The model of the restored tooth predicted similar stress distribution and peak stresses for the different post lengths considered, which agrees with the ANOVA test results. And a stress concentration was predicted along the interface of the post with the composite core, according to the failure mode experimentally observed.

CONCLUSIONS

It has been experimentally proved that the biomechanical performance of teeth restored with stainless steel posts present a low dependency on post length. This is an important finding because the length of the post has a significant effect on its retention. The more apically the post is placed in the root canal, the more retentive it becomes [2,3]. However, it may not always be possible to use a long post, especially when the remaining root is short or curve.

The experimental results corroborated the estimations from the developed model, thus validating the model. The proposed model could be a useful tool for studying the influence that different post design variables have on the biomechanical performance of restored teeth, by means of simulations.

REFERENCES

1. AS Fernandes, et al. *J Prosthet Dent* **90**, 556-562, 2003.
2. I Nergiz et al. *J Oral Rehabil* **29**, 28-34, 2002.
3. JP Standlee et al. *J Prosthet Dent* **39**,400-405, 1978.
4. N Hochman et al. *J Oral Rehabil* **30**,702-707, 2003.

HEAD REPOSITIONING ACCURACY IN PATIENTS WITH WHIPLASH-ASSOCIATED DISORDERS

[1,2]Veronique Feipel, [1,2]Patrick Salvia, [1]Helene Klein, [1,2]Marcel Rooze
[1] Department of Anatomy, Université Libre de Bruxelles, email: vfeipel@ulb.ac.be web: homepages.ulb.ac.be/~anatemb
2 Centre for Functional Evaluation, Université Libre de Bruxelles,

INTRODUCTION

Head repositioning accuracy is commonly evaluated in patients with Whiplash-associated disorders (WAD). Most frequently, only neutral repositioning is assessed [1-4]. Only sparse data on repositioning in remote postures in available [5,8]. Similarly, only a few studies considered the components of HRE in all planes of space. Some bi-dimensional studies are available [1,3], but only one reported three-dimensional information [4] without comparing planes of motion.

In this study head repositioning accuracy in patients with WAD was compared to that obtained in healthy controls. A comparison between different repositioning tasks is proposed.

METHODS

29 patients suffering from WAD (age: 37, SD 14, years, 18 females) and 26 healthy subjects (control, age: 35, SD 11, years, 14 females) were recruited. Of the WAD patients, 71% had a grade III injury and 29% a moderate (grade I or II) injury [6].

Active head kinematics was sampled using a 3D-electrogoniometer (CA 6000 SMA, O.S.I., Union City, CA, USA) mounted using a harness at the level of Th1 and a helmet on top of the head [7]. The tasks consisted of neutral position repositioning tasks after maximal flexion-extension (FE) and of repositioning tasks in pure axial rotation (right and left of 50°) and complex postures (50° right or left axial rotation combined to a 20° ipsi-lateral bending). The former was carried out with eyes open (EO) and blindfolded (BF), the two latter only in blindfolded conditions. Four repetitions were requested for each condition. No feedback was given to the subject before the end of the entire test session.

For neutral repositioning tasks, head repositioning error (HRE) in each plane was computed as the absolute difference between initial head position and the final head position after stabilization (Figure 1a), and the maximal overshoot in each plane, not discussed here. For rotation and complex posture repositioning tasks, HRE in each plane was computed as the absolute difference between the end posture reached during the guided trial and that reached during repositioning trials (Figure 1b). A multiple-way repeated-measures ANOVA was used to compare tasks, motion components and groups.

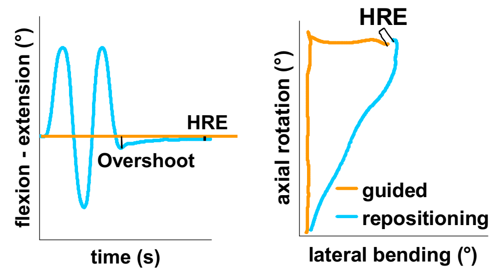

Figure 1: Repositioning parameters for (a) neutral and (b) complex remote repositioning tasks

RESULTS AND DISCUSSION

The HRE values found in the present study are comparable to those reported previously [4,6,7], although some authors found larger values [2,3,8]. These differences could be attributed to methodological differences. HRE was significantly increased ($p=0.009$) in the WAD group as compared to controls (Table 1), confirming several previous studies [3-7], but not all [3,8].

The primary plane HRE was significantly larger than out-of-plane HRE both for neutral ($p=7.1\times10^{-23}$) and remote ($p=3.0\times10^{-23}$) repositioning tasks, confirming previous work [7,8]. Neutral repositioning tasks displayed better head repositioning accuracy than remote repositioning tasks ($p=6.3\times10^{-18}$). The primary component HRE during neutral repositioning was of the same order of magnitude as the out-of-plane component HRE during remote repositioning in rotation. For neutral repositioning tasks, HRE was larger in blindfolded conditions ($p=0.03$). A significant interaction between task complexity and component was obtained for remote repositioning tasks ($p=1.1\times10^{-05}$). Specifically, lateral bending HRE was increased when task complexity was larger, probably due to task difficulty and to the fact that lateral bending is not an out-of-plane component in this task.

REFERENCES

1. Heikkila H, et al. *Arch Phys Med Rehab* **79**, 1089-94, 1998.
2. Revel M, et al. *Arch Phys Med Rehabil* **72**, 288-2-91, 1991.
3. Rix GD, et al. *Arch Phys Med Rehabil* **82**, 911-9, 2001.
4. Treleaven J, et al. *J Rehabil Med* **35**, 36-43, 2003.
5. Loudon JK, et al. *Spine* **22**, 865-8, 1997.
6. Spitzer WO, et al. *Spine* **20,** 2S–73S, 1995.
7. Feipel V, et al. *Clin Biomech* **14**, 462-70, 1999.
8. Kristjansson E, et al. *Clin Rehabil* **17**, 768-74, 2003.

Table 1: Head repositioning errors for neutral and remote repositioning tasks.

	Neutral repositioning tasks				Remote repositioning tasks			
	BF		EO		Pure		Complex	
HRE component (°)	**WAD**	**Control**	**WAD**	**Control**	**WAD**	**Control**	**WAD**	**Control**
Flexion-extension	3.5 (2.4)	2.1 (2.0)	2.3 (1.8)	1.8 (1.6)	2.2 (1.1)	2.0 (1.3)	2.8 (1.4)	2.5 (1.0)
Lateral bending	0.8 (0.6)	0.4 (0.3)	0.5 (0.6)	0.5 (0.5)	1.9 (1.0)	1.7 (0.5)	3.7 (1.8)	3.1 (1.8)
Axial rotation	1.1 (1.1)	0.6 (0.5)	0.6 (0.6)	0.7 (0.6)	7.8 (3.7)	5.6 (3.8)	5.5 (3.6)	4.9 (2.1)

MEASUREMENT OF RED BLOOD CELL DEFORMABILITY WITH COUNTER ROTATING RHEOSCOPE TO DETECT SUBLETHAL DAMAGE

[1]Shigehiro Hashimoto, [1]Masayoshi Omori, [1]Teruyuki Yamanari, [1]Yusuke Morita, [1]Naoki Ogawa, [1]Koichi Imoto, [2]Hajime Otani and [2]Hiroji Imamura
[1]Biomedical Engineering, Osaka Institute of Technology, Osaka, Japan; email: hasimoto@elc.oit.ac.jp
[2]Dept. of Thoracic and Cardiovascular Surgery, Kansai Medical University, Japan

INTRODUCTION

Deformability of red blood cells is an important parameter to maintain blood circulation, because cells have to deform to pass through capillary. Sublethal damage on red blood cells might occur through artificial blood pumps, before hemolysis [1].

METHODS

A parallel-disk type of counter-rotating rheoscope system has been designed and manufactured. In the system, Couette-type shear field is induced in the fluid between two counter-rotating disks, which are made of transparent silica glass. The rotating speed was regulated with a stepping motor, which is controlled by a computer. The shear rate, which is calculated from the velocity deference between two disks, is constant regardless of the distance from the disk. A red blood cell can be observed under shear without translational movement, when it is suspended at the stationary plane in the middle part of the shear field.

A red blood cell deforms from biconcave to ellipsoid in Couette-type of shear field. Deformation of the red blood cell was quantified with an elongation index (E), which was calculated from dimensions of the major (L) and minor (W) axes by E=(L-W)/(L+W). E becomes zero in a sphere (L=W), and approaches to unity as the deformation advances (L>>W). The elongation index (E) was plotted as a function of shear stress (S), and the fitting exponential curve was calculated by E=C(1-exp(-S/R)), where C is the critical elongation and R is the shear stress responsiveness. Both large C and small R indicate large deformability.

A concavo-convex Couette flow system has been designed to damage red blood cells under shear [2]. In the space between a stationary convex cone and a rotating concave cone, the sample blood was sheared in a uniform shear field, where the shear rate is constant regardless of the distance from the axes of rotation. Variation was made on shear rate with the rotational speed of the convex cone.

Human blood was drawn from volunteers with anticoagulant of ethylene-diaminetetraacetic acid and sheared for one hour at the shear rate of 640 per second at twenty degrees Celsius.

Before measurement of deformation, the cells were classified according to the density by a centrifugation method [3]. The

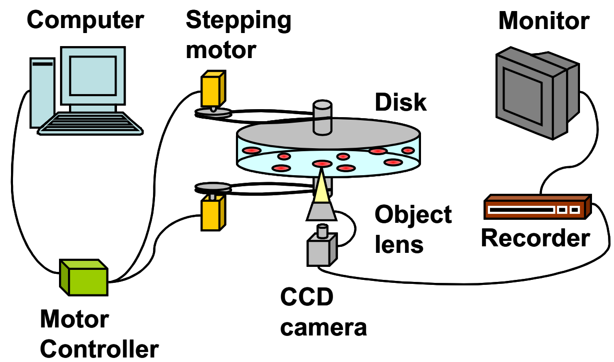

Figure 1: Pattern diagrams of system.

phthalate ester solution with controlled density was used as a separator. After separation, the red blood cells were suspended in a dextran aqueous solution to separate each other and exposed to the high shear stress (<6 Pa) field at low shear rate.

RESULTS AND DISCUSSION

The experimental results shows, that the lighter cells are more compliant than heavier cells and that density of cells increased after exposure to shear fields, although cells of each density level keep their deformability.

One of the advantage of a parallel-disk type of counter-rotating rheoscope system is that a red blood cell deforms in the shear field without contact to the surface of wall, which gives effects to the deformation of the red blood cell.

CONCLUSIONS

The designed system has enough sensitivity to detect sublehtal damage of red blood cells with deformability.

REFERENCES

1. Kameneva MV, et al.. *ASAIO Journal* **41**, M457-460, 1995.
2. Hashimoto S, et al.. *Artificial Organs* **13**, 458-463, 1989.
3. Danon D, Marikovsky Y, *J Lab Clin Med* **64**, 668-674, 1964.

ACKNOWLEDGEMENTS

This work was supported in part by a Grant-in-Aid for Scientific Research from the Japanese Ministry of Education, Culture, Sports, Science and Technology.

MYOFASCIAL FORCE TRANSISSION IS MORE IMPORTANT AT LOW-FREQUENCY STIMULATION

H.J.M Meijer[1], G. C. Baan[1] and P.A. Huijing[1, 2]
[1] Instituut voor Fundamentele en Klinische Bewegingswetenschappen, Vrije Universiteit, Amsterdam, NL
[2] Integrated Biomechanical Engineering for Restoration of Human Function, Faculteit Construerende Technische Wetenschappen, Technische Universiteit Twente, NL
Email: h.meijer@fbw.vu.nl

INTRODUCTION

In addition to myotendinous force transmission, force exerted by the sarcomeres can be transmitted between the muscle and surrounding inter- and extramuscular connective tissue, *i.e.* myofascial force transmission [1]. Proof of such epimuscular force transmission is a difference in force exerted at the origin and insertion of a muscle [2]. For fully activated muscle, myofascial force transmission has been shown to be important for muscle properties. However during *in vivo* motion, firing frequency may vary (in rat EDL muscle between 10 and 60 Hz [3]). Therefore, effects of submaximal stimulation frequencies on myofascial force transmission were investigated for fully recruited rat extensor digitorum muscle (EDL).

METHODS

Male Wistar rats were anaesthetized and the anterior crural compartment was exposed. Proximal and distal tendons of the extensor digitorum muscle (EDL) and the tied distal tendons of the complex of tibialis anterior and extensor hallucis longus (TAEHL) were severed and connected to force transducers. Fully recruited EDL and TAEHL muscles were stimulated at 10, 20, 30 and 100 Hz. The TAEHL complex was kept at constant length, and length-force characteristics after distal lengthening of EDL were determined at the distal and proximal tendons.

RESULTS AND DISCUSSION

At lower firing frequencies, significant proximo-distal EDL force differences exist, indicating epimuscular force transmission (e.g. Fig. 1). Maximal absolute EDL proximo-distal active force differences were highest at 100 Hz ($F_{dist\text{-}prox}$ =0.4 N). However, the percentual difference (Fig. 2) was highest at 10 Hz (F = 30 $\%F_{dist}$). Firing frequency dependent shifts of EDL optimum muscle length were found, although proximally and distally assessed effects of firing frequency differed quantitatively. After distal EDL lengthening, TAEHL distal isometric active force decreased progressively with a peak decrease at 100Hz ($F_{from\ initial}$ = - 0.25 N). However, the highest percentual decrease was found for 10 Hz stimulation ($F_{from\ initial}$ = - 40%).

CONCLUSIONS

Myofascial force transmission becomes more important at lower submaximal firing frequencies: with a decreasing firing frequency, relatively more force is transmitted myofascially relative to the myotendinous path. Evidently, at progressively lower firing frequencies, the stiffness of epimuscular myofascial paths of force transmission decreases less than the stiffness of serial sarcomeres and myotendinous pathways. It is therefore concluded that low firing frequencies as encountered *in vivo,* enhance the relative importance of epimuscular myofascial force transmission with respect to the myotendinous force transmission.

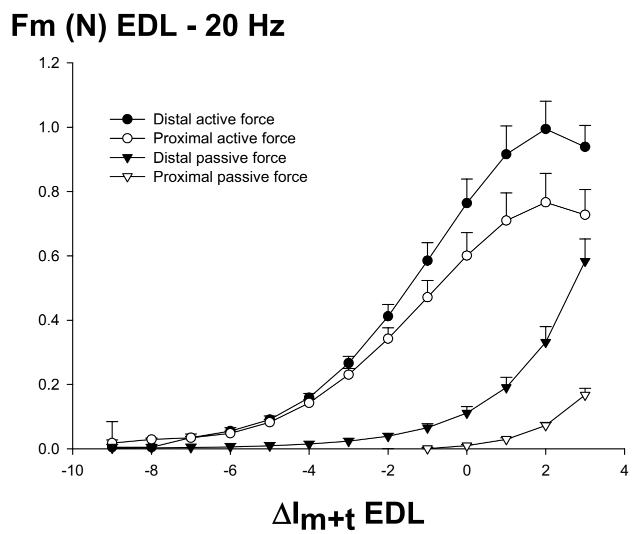

Figure 1: EDL proximal and distal length force characteristics at 20 Hz, as a function of EDL muscle-tendon complex length, increased by distal EDL lengthening (l_{m+t} EDL dist), expressed as deviation from 100 Hz distal optimum length. Error bars represent standard errors.

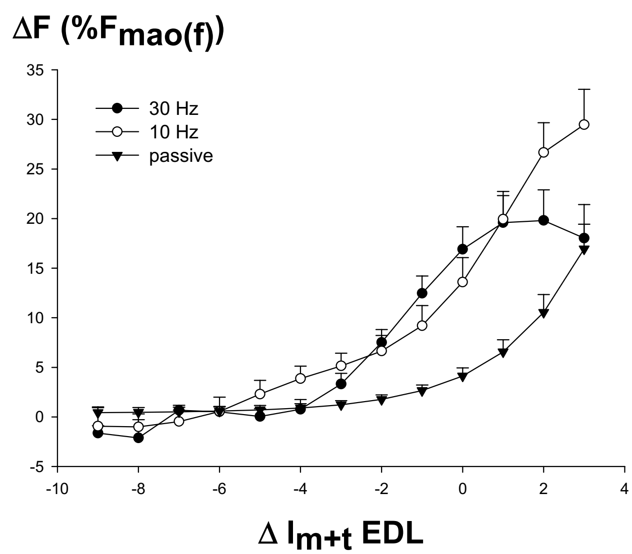

Figure 2: Effects of firing frequency and EDL muscle-tendon complex length on the proximo-distal difference in active force, normalized for distal optimum active force ($F_{mao\ (f)}$), and passive force (normalized for distal 100 Hz optimum force). Error bars represent standard errors.

REFERENCES

1. Huijing, PA, et al.. *J. Exp. Biol.* **201,** 682 – 691, 1998.
2. Huijing, PA, et al.. *Acta Physiol. Scand.* **173,** 297 – 311, 2001.
3. Hennig, R. et al.. *Nature* **314,** 164 – 166, 1985.

BIOMECHANICAL COMPARISON OF FIXATION TECHNIQUES FOR DOUBLE PARS FRACTURES

[1] Hsiang-Ho Chen, [2] Shih-Ting Huang and [3] Kung-Chia Li
[1] Dept. of Biomedical Engineering, I-Shou University, Kaohsiung, Taiwan; email: hchen@isu.edu.tw,
[2] Institute of Biomedical Engineering, National Yang Ming University, Taipei, Taiwan
[3] Dept. of Orthopedics Surgery, Chia-Yi Yang-Ming Hospital, Chia-Yi, Taiwan

INTRODUCTION

Complete pars fracture is one of clinical conditions of spondylolysis and it can lead to spondylolisthesis or degenerative disc disease (DDD) [1]. Double pars fractures (DPF) commonly occur at L4-L5 due to traumatic in juvenile years, whilst occurring at L3-L4 in the elderly from degenerative change. Double pars fracture may decrease spinal stability and more so if complicated with DDD. Posterior instrumentation with cages may restore the biomechanical strength of the spine. Some studies biomechanically compared the spondylolysis fixation techniques [2, 3], but rare comprehensive biomechanical studies on DPF have been reported. The purpose of this study is to compare biomechanically the performance of fixation techniques for the repair of double spondylolytic defect in the pars interarticularis.

METHODS

Eighteen fresh-frozen and thawed porcine lumbar L2-L6 spines were used for mechanical testing. In addition to the control group, DPF group was created by making 2-mm wide defects in the pars interarticularis bilaterally at L3 and L4 using a power saw. Disectomy in combination with the DPF procedure resulted in a DPF&DDD group. The TPS group used transpedicular screw system (TPS) to stabilize DPF defects. The D2TPS group used TPS system to stabilize the spine of DPF&DDD. The D2TPSC group used TPS and interbody cages to stabilize the spine of DPF&DDD. The biomechanical properties were estimated and compared amongst six groups (Fig. 1). Motion segments were mounted and tested on a MTS machine. A series of loadings, including flexion, extension, lateral bending, torsion, and compression, were applied, respectively. The axial stiffness test for this study was 0-250 N compression at the displacement rate of 25 mm/min. In other rotational testing, the torque was 2.5 N-m and the load rate was 25 mm/min [4].

RESULTS AND DISCUSSION

In flexion, DPF had a significantly smaller stiffness (0.55 ± 0.02 N-m/deg) than the intact control group (0.68 ± 0.03 N-m/deg). With TPS fixation, the stiffness was increased significantly (Fig. 2). In extension, DPF had a significantly smaller stiffness than the intact group. With any kind of stabilization, stiffness was increased significantly. In lateral bending, DPF&DDD group had a less stiffness than controls. In compression, DPF and DPF&DDD gradually decreased the stiffness compared to controls. In torsion, DPF and DPF&DDD significantly reduced the intact stiffness. With fixation of TPS or cages, the stiffness was significantly greater than DPF group. In almost all testing, D2TPSC group had the higher stiffness than other groups.

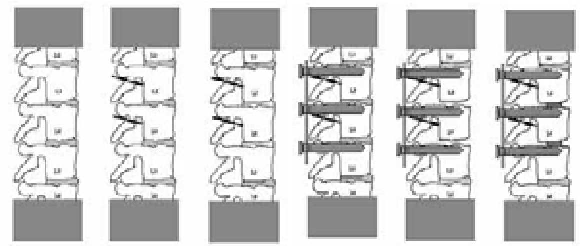

Figure 1: Diagram of 6 groups of device-spine constructs.

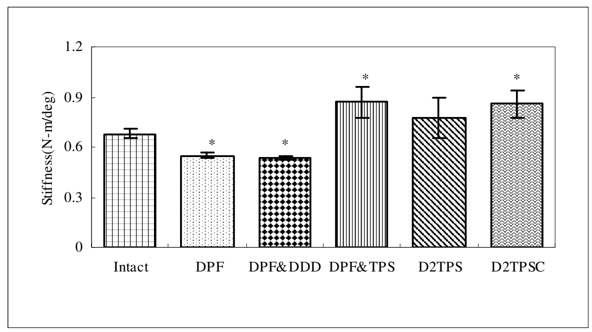

Figure 2: Comparison of flexion stiffness (N-m/deg).
* significantly different from data of Intact group ($p < 0.05$)

Double pars fracture is occasionally found in clinical practice. The treatment depends on the symptoms if DDD and stenosis is severe, decompression and posterior instrumentation is indicated. This study focused on the degenerative situation. Therefore, the facet screw or hook-screw system is not included.

CONCLUSIONS

Double pars fracture significantly reduced spinal stiffness. For spine with double pars fracture only, TPS could retain the intact stiffness. However, TPS seems not to stabilize spine with DPF and DDD. The cage possibly restored the stiffness decreased by the disc degenerative disease in all spinal motion.

REFERENCES

1. Szypryt EP, et al. *Spine* **14**, 977-981, 1989.
2. Mihara H, et al. *Spine* **28**, 235-38, 2003.
3. Deguchi M, et al. *Spine* **24**, 328-33, 1999.
4. Chen HH, et al., *Spine* **29**, E382-7, 2004.

REGENERATION OF SKELETAL TISSUES ON JOINT

[1]Martine Pithioux, [2]Didier Moukoko, [1,3]Mohamed Tellache, [1]Patrick Chabrand, [3]Christian Hochard[1], Sylvie Wendling,
[1]Laboratory of Aerodynamic and Biomechanics Motion, CNRS-University of Méditerranée, Marseilles, France.
[2]Laboratory of experimental surgery, Faculté de médecine, University of Montpellier I, France
[3]Laboratory of Mechanics and Acoustics, CNRS-University of Méditerranée, Marseilles, France.
pithioux@morille.univ-mrs.fr

INTRODUCTION

The study concerns the regeneration of skeletal tissues (bone, cartilage, tendon, and ligament). It is possible to initiate, in vivo as well as in vitro, mesenchymal tissue regeneration, involving progenitor cells. This process recapitulates some cellular event of embryonic skeletal formation. If progenitor proliferation and differentiation pathways can be controlled, it is conceivable that a functional joint may be regenerated. The goal of this study is to analyse the mechanical factors regulating locally mesenchymal cell proliferation and differentiation pathways towards functional skeletal tissues production. This work is a first step to analyse undifferentiated cells as far as bone regenerated.

Experimental studies in vivo and in vitro are developed. This combined approach associating mechanical and biological analyse of the cellular events provides a powerful tool in understanding the regulation mechanisms of functional tissue engineering in vivo and in vitro.

METHODS

Our in vivo experimental studies were coupled together with in vitro experimental studies to be used in numerical modelling. Very few authors have studied the mesenchymal tissue [1, 2] because it is very difficult to analyse this soft tissue before its maturity. A process of skeletal tissue regeneration was initiated by a vascularized periosteal flap transfer in New Zealand white rabbit. Time between the initiation of the regeneration process and the first explants are 7, 14 and 21 days (Figure 1). Fresh samples were preserved in the formaldehyde.

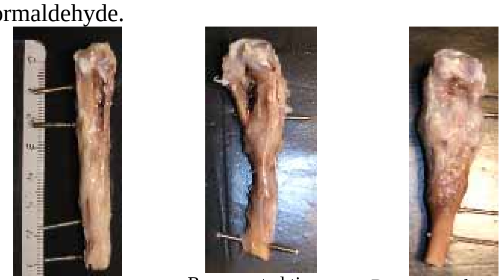

Regenerated tissue at 7 days | Regenerated tissue at 14 days | Regenerated tissue at 21 days

Figure 1: Regenerated tissue

We developed an experimental INSTRON device which was used to analyse the mechanical properties of bones and ligaments [3 and 4]. This device is adapted to analyse the behaviour of the regenerated tissues. Samples were attached by a cable. They were tested with tensile tests as far as failure in order to characterize their mechanical properties and include them in a numerical finite element model. The displacement of the lower traverse beam was measured using an LVDT sensor (Linear Variable Differential Transformer), attached to the machine frame. The tensile load was measured by a strain gauge sensor with an uncertainty of measurement of 1% on the upper traverse beam.

RESULTS AND DISCUSSION

From these results, the mechanical properties of compact bone were deduced where failure occurred. Force-displacement curve obtained for a 14 days sample (Figure 1) was divided into four parts.

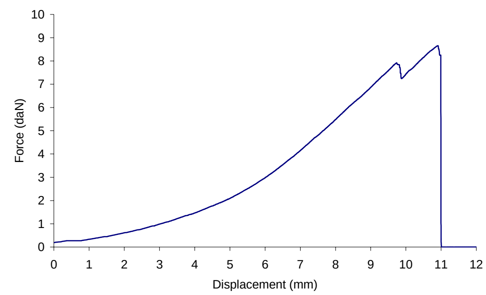

Figure 1

The first part of the curve corresponds to the setting in tension of the cables. On the second part of the curve the behaviour is linear elastic. On the third part, one could observe that the behaviour became non-linear, showing that the material was damaged ductile. In the final stage failure occurred. The damaging part of the bone behaviour is divided in two picks. The first one represents the failure of a first fibre networks constituted by a soft material comparable to a cartilage. The second one represents the failure of second fibre networks which is more mineralised.

CONCLUSIONS

This study is a first step to analyze precisely the tissue regenerated by immature cells. The second step is to regenerate joint cartilaginous tissue because of the weak potential of spontaneous repairing of these tissues. The perspectives of this work concern the development of engineer processes tissue allowing the production of cartilage implants, and of biomaterials of joint resurfacing.

REFERENCES

1. Chakkalakal, D. A et al. Bone, **25**, No. 3: 321-332, 1999.
2. Loboa E.G., et al. Biomech Model Mechanobiol, **2**, 83-96 2003
3. Pithioux M., Subit D., Chabrand P., Medical Engineering & Physics, **26**, 647-653, 2004
4. Subit D. “Modélisation de la liaison os-ligament dans l’articulation du genou, Univ. Méditerranée, 12/2004

NEURAL NETWORK ESTIMATION OF ISOKINETIC KNEE TORQUE

Michael E. Hahn
Movement Science Laboratory, Montana State University, Bozeman, MT, USA
email: mhahn@montana.edu

INTRODUCTION

Rectified, low-pass filtered electromyography (EMG) has been used with Hill-based musculoskeletal models to estimate muscle force and joint moments (Hof & Van Der Berg, 1981). However, it is rather difficult to find a set of neuromuscular activation signals that, when input into such models, produce coordinated movement simulation (Zajac, 1993). This may be due in part to a non-linear response of muscle tissue to activation. Recently, artificial neural network (ANN) models have been used effectively to estimate joint torque in the elbow (Luh et al., 1999; Wang & Buchanan, 2002), but no studies have utilized ANN theory in prediction of lower extremity torque. The purpose of this study was to develop an initial model to estimate isokinetic joint torque produced at the knee during concentric and eccentric contractions. It was hypothesized that ANN mapping would accurately estimate knee joint torque. Linear regression was performed for comparison.

METHODS

Ten young adults (6 female / 4 male; 22.9yrs, 173.7cm, 72.3kg) were recruited for this study within the guidelines of the University I.R.B. All participants were determined to be free of neuromuscular or orthopedic pathologies.

Maximal strength data were collected using a KinCom dynamometer (Rehab World, Hixson, TN, USA). Isometric flexor/extensor maxima were measured at 45°. Isokinetic measures were taken through the knee's functional range of motion in a seated position at 30 and 60°/s. At each isokinetic speed, concentric and eccentric contractions were recorded (two each). Each subject was allowed two sub-maximal practice trials for each joint function. Four total cycles were collected for each direction and speed condition. Subjects were verbally encouraged during each trial to promote maximal motivation.

Joint position and velocity were recorded simultaneously with torque data, at 100Hz. Additionally, EMG signals were sampled at 1000Hz from the vastus lateralis and biceps femoris with passive bi-polar surface electrodes using the Myopac Jr. (Run Technologies, Inc., Mission Viejo, CA, USA). EMG signals were bandwidth filtered (10-1,000Hz), full wave rectified and smoothed with a 4th order Butterworth filter (low pass cutoff = 5Hz). Processed EMG signals were then normalized to the maximal isometric activation.

With all acceptable trials compiled, there were 308 total cases entered for analysis. Linear regression was conducted with age, gender, height, weight, EMG (agonist, antagonist), joint position and velocity as independent variables, and joint torque as the dependent variable. The same inputs were entered into a three-layer back-propagation ANN, with the following settings: training proportion = 0.7, training error goal (E) = 0.1, and hidden units (H) = 5,10,15,20. A bootstrap re-sampling method (50 attempts) assessed each setting of hidden units. Model accuracies were compared using the R-values of each technique.

RESULTS AND DISCUSSION

Linear regression resulted in an R-value of 0.75. Prediction accuracy for the ANN settings reached a maximum of 0.94 (ANN settings: E=0.1; H=10,15,20). Average R-values for those settings were 0.93 (SD, 0.01). The number of epochs needed for solution convergence at those settings averaged from 447.8 (H=20) to 620.2 (H=10). Prediction accuracy was not affected by the number of hidden units, however more hidden units required fewer epochs for convergence (Table 1).

Results indicate that ANN mapping provides a more accurate estimate of knee torque during maximal isokinetic (con/ecc) testing. Performance of the ANN with minimal training (E=0.1) indicates that prediction accuracy is likely without the risk of 'over-training'. Thus, the generality of this system would be more likely to provide accurate estimation for a separate sample of young adults.

CONCLUSIONS

Findings from this initial development of a knee torque prediction model indicate that a more robust estimation of joint torque from muscle activation may be possible using ANN or similar techniques borrowed from the field of computational intelligence. Future efforts will focus on broadening the model to include sub-maximal torque production in more joints and developing adaptive algorithms for estimation of joint moments during locomotion.

REFERENCES

1. Hof, A.L. & Van Der Berg, J.W. *J Biomech* **14**, 771-785, 1981.
2. Luh et al. *J Electromyogr Kinesiol* **9**, 173-183, 1999.
3. Wang, L. & Buchanan, T.S. *IEEE Trans Neural Syst Rehabil Eng* **10**, 30-37, 2002.
4. Zajac, F.E. *J Biomech* **26**(S1), 109-124, 1993.

ACKNOWLEDGEMENTS

This study was funded by the NIH BRIN program of the NCRR (P20 RR-16455-01), and Montana State University. Thanks to Andrea Drew and Briana Fields for assistance in data collection.

Table 1: Effect of hidden units on accuracy, and time to convergence; Mean ± SD

	H = 5	**H = 10**	**H = 15**	**H = 20**
Prediction Accuracy (R)	0.92 ± 0.01	0.93 ± 0.01	0.93 ± 0.01	0.93 ± 0.01
Time to convergence (Epochs)	978.9 ± 94.2	620.2 ± 262.8	523.8 ± 208.6	447.8 ± 216.7

PARADOXICAL MUSCLE MOVEMENTS IN HUMAN STANDING

[1] Ian Loram, [2]Constantinos Maganaris and [1]Martin Lakie
[1]The University of Birmingham, UK, email: i.d.loram@bham.ac.uk
[2]Manchester Metropolitan University, UK; email: c.n.maganaris@mmu.ac.uk

Figure 1: Dynamic bias model**.** CE, contractile element. K, s.e.c., θ COM angle, θ_0 bias exerted on s.e.c. spring.

INTRODUCTION

In human standing the calf muscles soleus and gastrocnemius actively prevent forward toppling about the ankles. It has been generally assumed that these postural muscles behave like springs with dynamic stiffness reflecting their mechanical properties, reflex gain including higher derivatives, and central control. We have used an ultrasound scanner and automated image analysis to record the tiny muscular movements occurring in normal standing and during large voluntary sways. This new, non-invasive technique resolves changes in muscle length as small as 10 microns without disturbing the standing process. This technical achievement has allowed us to test the long established mechano-reflex, muscle-spring hypothesis that contractile element length changes in a spring-like way during sway of the body.

METHODS

Ten subjects stood freely on a footplate that measured ankle torque. Ankle angle was recorded using a laser range finder reflected off the shin. Surface EMG were recorded from left soleus and gastrocnemius. An ultrasound scanner (Esaote Biomedica AU5) recorded 40 s (1000 frames) of sonographs focused on the distal aponeurosis of left soleus and gastrocnemius. Image markers were placed on the proximal and distal aponeurosis of the two muscles. Spatial cross correlation was used to track the changes in position of these markers throughout the 1200 frames. From the differential movement of these markers continuous changes in the length of the contractile element were calculated [1, 2].

Cross correlation was used to assess the relationship between changes in muscle length and changes in CoM angle. A simple model was constructed (Figure 1), incorporating a spring for the s.e.c. of the calf muscles, a contractile element for the muscles and a single mass for the body during standing sagital sway. Using the model and measured values of ankle torque and CoM angle, we computed the predicted cross correlation between muscle length and CoM angle for a variety of values of s.e.c. stiffness. By comparing the actual cross correlation with the predicted, we estimated the stiffness of the s.e.c.

RESULTS AND DISCUSSION

The contractile elements are longest when the subject is closest to the vertical and shorten as the subject sways forwards (paradoxical movements). In quiet standing, muscle length fluctuates at approximately three times the frequency of body sway: on average, shortening during forward sway and lengthening during backwards sway (Figure 2). This counter-intuitive result is consistent with the fact that calf muscles generate tension through a series elastic component (s.e.c., Achilles tendon and foot, Figure 1) which limits maximal ankle stiffness to 92% ± 20% (± S.D) of that required to balance the body (Figure2). The higher frequency of muscle fluctuation is consistent with a central, impulsive controller [3].

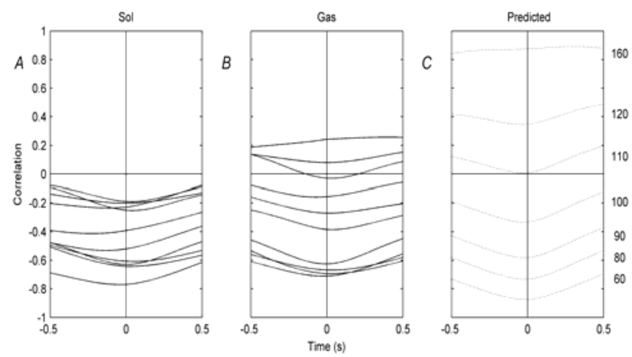

Figure 2 Cross correlation between **A** soleus, **B** gastrocnemius muscle length and centre of mass angle. Each line represents the mean of 6 trials for one subject. **C** shows the predicted correlation for a variety of values of s.e.c. stiffness expressed relative to the load stiffness.. The time lag is shown horizontally.

CONCLUSIONS

The intrinsic length-tension relationship of the calf muscles partially stabilizes the human body in quiet standing while leaving the body mechanically unstable. Stability and balance is achieved by a higher level impulsive process that is poorly correlated with CoM angle.

REFERENCES

1. Loram ID, et al. *J Physiol*, **in press**, 2005a.
2. Loram ID, et al. *J Physiol* **556**, 683-689, 2004.
3. Loram ID, et al. *J Physiol*, **in press**, 2005b.

ELECTROMYOGRAPHY OF TRUNK MUSCLES DURING WHEELCHAIR PROPULSION

[1]Alicia M. Koontz, [1]Yusheng Yang, [2]Ronald J. Triolo, [1]Michael L. Boninger, and [1]Jennifer Mercer
[1]Human Engineering Research Laboratories, VA Medical Center, Pittsburgh, PA, USA
[2] Cleveland FES Center, Louis Stokes Cleveland VA Medical Center, Cleveland OH, USA.
email: akoontz@pitt.edu, web: www.herlpitt.org

INTRODUCTION

Paralysis of the primary trunk musculature likely contributes to ineffective force application during wheelchair propulsion [1]. Functional electrical stimulation (FES) as a modality to improve trunk posture, balance and propulsion efficiency in persons with spinal cord injury is currently under investigation. In order to implement an effective stimulation pattern during propulsion, an understanding of the muscle activation patterns of core trunk musculature is necessary. Therefore, the purpose of this study was to establish and describe muscle activation profiles of selected back and abdominal musculature during wheelchair propulsion using surface electromyography (EMG).

METHODS

Subjects: Fourteen unimpaired subjects (12 male and 2 female) provided informed consent prior to participation in the study. The average age, weight and height were 24.7$\pm$3.6 years, 69.3$\pm$14.3 kilograms and 1.73$\pm$0.07 meters respectively.

Experimental protocol: Bipolar, surface electrodes (Noraxon Inc., Scottsdale, AZ) were placed over three abdominal muscles (rectus abdominis: RA, external oblique: EO and internal oblique: IO), and three back muscles (longissimus thoracis: LT, iliocostalis lumborum: IL, and multifidus: MU). Prior to the propulsion trials, ten seconds of maximum voluntary contraction (MVC) EMG data were recorded during maximal effort exercises for normalization purposes. Subjects were asked to propel at a steady-state speed of 1.8 m/s for 20 seconds using a test wheelchair which was fitted bilaterally with a SMART^{Wheel} (Three Rivers Holdings, LLC., Mesa, AZ), and secured to a computer-controlled dynamometer with a four-point tie down system. Real-time propulsion speed was displayed on a computer screen in front of the subjects. A three-dimensional motion analysis system (Northern Digital Inc., Ontario, Canada) was synchronized with the SMART^{Wheel} and EMG system to record kinematics of the upper limbs, propulsion forces and EMG activity during propulsion.

Data analysis: EMG data were sampled at 1000 Hz, full wave rectified and smoothed with a 10-Hz low pass filter. EMG voltages during propulsion were normalized as %MVC for each muscle. Significant EMG activity was defined as activity with an intensity of at least 5% MVC and for longer than 5% of the propulsion cycle (PC). In order to compare muscle activity across subjects, the time of the PC was normalized to 100% and the push phase to 45% of the cycle for each subject (mean push percentage for the groups). The push phase was further divided into early push (0%–2% of PC) and late push (2%–45% of PC), and recovery was separated into 3 subphases [2] of follow-through (45%–53% of PC), hand return (53%–97% of PC), and pre-push (97%–100% of PC) according to hand motion during an entire PC.

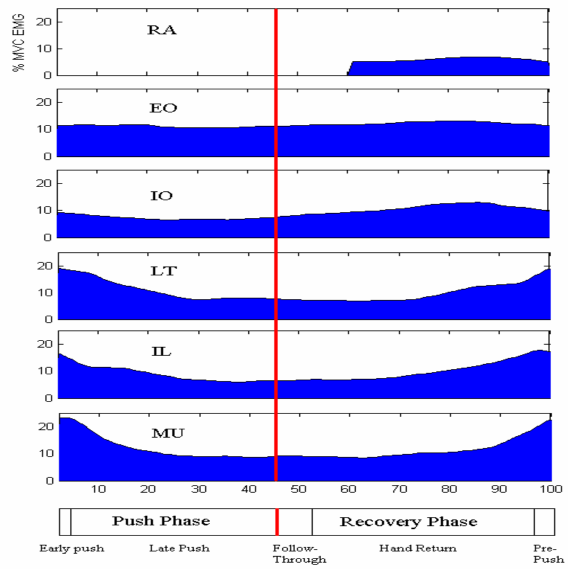

Figure 1: The mean EMG profile of trunk muscles during a propulsion cycle at speed of 1.8 m/sec

RESULTS AND DISCUSSION

During pre-push and early push phases, abdominal muscles (RA, EO and IO), and back muscles (LT, IL, and MU) were active and contracted to provide stability for the trunk while delivering forces to the pushrim (Figure 1). While delivering forces to the rim during late push phase, back muscle activity declines allowing the trunk to lean forward in pushing. During recovery phase (follow-through/hand return), back muscle activity gradually increased to move the trunk upright and abdominal muscles activated to prepare for the next stroke in the late phase of hand return and pre-push.

CONCLUSIONS

Our findings indicate that back and abdominal muscles both showed high activity levels during the pre-push and early push phase. This synchronized activation may provide trunk stability and prevent the trunk from moving in opposition to the arms when applying forces to the pushrim [3]. Researchers can use this profile of trunk muscle activation to develop a muscle stimulation pattern that will increase trunk stability and improve propulsion efficiency of manual wheelchair users with spinal cord injury.

REFERENCES

1. Koontz et al. *Proceedings of ASB'2004*, Portland, OR, 2004
2. CJ Newsam, et al. *Gait Posture*, 223-232, 1999.
3. Rice et al. *Proceedings of RESNA'2004*, Orlando, FL,2004

ACKNOWLEDGEMENTS

VA Rehab R&D (B3043-C) and ASB'2004 Graduate Student-In-Aid Award

EFFECTS OF THE GRASPING FORCE MAGNITUDE ON THE INDIVIDUAL DIGIT FORCES DURING PREHENSION WITH FIVE DIGITS

Xun Niu, Mark L. Latash and Vladimir M. Zatsiorsky
Department of Kinesiology, The Pennsylvania State University, email: vxz1@psu.edu

INTRODUCTION

To control dextrous manipulation of mechanical 5-digit hands, the engineers should know the interrelations existing between the individual digit forces and moments during the performance [1]. The information obtained on humans can be useful in this case. When manipulating hand-held objects, people can grasp them with different forces. In this study, we address the following question: does the pattern of individual digit forces depend on the grip force magnitude? Subjects were asked to keep an instrumented handle with minimal effort and then double the grip force. The following questions are addressed: (a) Does doubling the total grip force double the individual digit forces? (b) Does the sharing percentage of normal forces among the fingers depend on the total force magnitude? (c) Does the percentage contribution of the normal and tangential forces into the total moment exerted on object depend on the grasping force magnitude?

METHODS

Seven right-hand-dominant subjects were required to stabilize in the air an instrumented handle (575 g) using prismatic grip (the tips of the fingers and thumb oppose each other). Four clockwise (negative) and four counterclockwise (positive) torques and one zero torque were applied to the handle. Five six-axis force-torque transducers (Nano-17, ATI Industrial Automation, Garner, N.C.) were mounted on the handle to measure the digit forces. The experiment had two phases. First, the subjects were instructed to hold the handle vertically with minimal normal (grip) force for 3 s. The computer recorded the force and then set a target force level at the double value. Visual feedback on the grip force and on the target force was provided on the computer screen. The subjects were instructed to squeeze the handle until the grip force matched the target. The second phase lasted 17 s.

RESULTS AND DISCUSSION

The doubling of the grip force induced complex changes of the both normal and tangential digit forces (Figure 1). After grip force doubled, the percentages of the individual finger's contribution to the grip force at all torque values changed (Figure 2) although the changes were minimal at the zero torque. The contribution of antagonist fingers (fingers producing moments in the direction of the external torque) increased (e.g. during supination efforts of 460.6 Nmm, the contribution of the little finger changed from 6% to 13%, see Figure 2). The doubling of the grip force also affected the percentage contribution of the normal and tangential forces into the total moment production: the contribution of the moment of the tangential forces increased (e.g. during supination efforts of 460.6 Nmm, the contribution of the little finger changed from 38% to 55%).

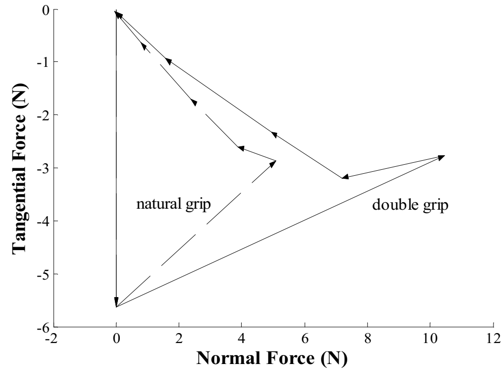

Figure 1: Force polygons. The polygons are obtained by adding tail-to-head the individual forces. Starting from the upper left corner the following forces are shown: gravity, the thumb, index, middle, ring and little finger force. Ideally, in static conditions the polygon should close. Representative example: external torque is zero.

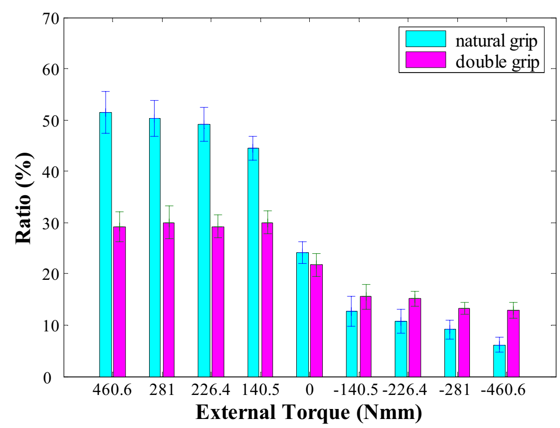

Figure 2: Exemplary little finger's contribution to grip force at different external torques before and after doubling the grip force. Error bars show standard errors.

CONCLUSIONS

The increase of the grip force magnitude during prehension results in increased percentage contribution of (a) the normal forces of antagonist fingers into the total grip force and (b) the moment of the tangential forces into the total moment exerted on the object.

REFERENCES

1. Zatsiorsky VM, Gregory RW, Latash ML (2002) Force and torque production in static multifinger prehension: biomechanics and control. I. Biomechanics. Biol Cybern 87: 50-57.

ACKNOWLEDGEMENTS

NIH grants AR-048563, AG-018751, and NS-35032

THE BIODYNAMIC AND PHYSIOLOGICAL RESPONSES OF THE RAT TAIL TO A SINGLE BOUT OF VIBRATION EXPOSURE

Kristine Krajnak, Daniel Welcome, William G. Lindsley, and Ren G. Dong
National Institute of Occupational Safety and Health, Morgantown, WV
email: Kristine.Krajnak@cdc.gov

INTRODUCTION

In humans, occupational use of vibrating hand tools leads to the development of neural and vascular damage. The goal of this study was to use the rat tail model to characterize the biodynamic response of the tail tissue to different vibration frequencies, and to determine what physiological changes occur in the vascular and neural systems of the tail after a single exposure to vibration.

METHODS

Male Sprague Dawley rats (6 weeks of age) were used for all experiments. Vibration exposures were performed by restraining rats in a Broome-style restrainer. Elastic straps (12 mm wide), located every 3 cm down the length of the tail, were used to hold the tail to a platform without compressing the tissue. The platform was attached to a shaker that produced a controlled, vertical vibration stimulus. The amplitudes of the tail and platform vibrations were measured down the length of the tail using a scanning laser vibrometer. The normalized magnitude (i.e., transmissibility) of the tail vibration was calculated by dividing the measured amplitude of the tissue vibration by the measured amplitude of the platform vibration. Measurements were made a number of frequencies (Figure 1).

The vascular and neural response of the tail to a single 4 h exposure to vibration (125 Hz, 49 m/sec^2 r.m.s.) was also measured to determine if the acute responses of the tail to vibration were similar to those of the human finger. The vascular responses assessed included tail temperature and luminal perimeter. The current perception threshold (CPT) procedure was used to assess the sensitivity of different nerve fiber types by measuring the response of the animals to electrical stimuli of different frequencies.

RESULTS AND DISCUSSION

The magnitude of the tail vibration was greater than the magnitude of the platform vibration at 125-250 Hz (Figure 1). However, the amplified response of the tissue to vibration at these frequencies only occurred in the unrestrained portions of the tail. At 63 Hz, the amplitude of the tail vibration was approximately equivalent to the platform vibration at all locations.

The vascular response of the rat tail to acute vibration was similar to the effects that have been reported in humans. Immediately following the exposure, the tail temperature of both control and vibration exposed rats was reduced (mean ± SEM, control pre 26.4 ± 0.52 and post 22.4 ± 0.33; vibrated pre 26.3 ± 0.51 and post 22.3 ± 0.02), suggesting that restraint caused a vasoconstriction in all rats. Tail temperatures in both groups of rats returned to pre-exposure levels 15 min

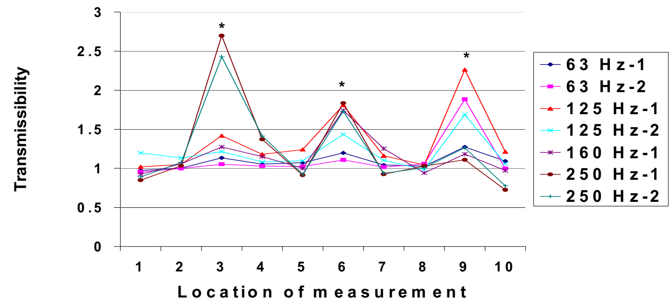

Figure 1: Normalized amplitude of the tail vibration vs. input frequency. The most proximal point on the tail is #1 on the x-axis and * represent un-restrained regions of the tail (N = 2).

following the end of the exposure. However, the internal perimeter of the ventral tail artery was significantly smaller in rats exposed to vibration than in control rats (546.93 ± 51.5 and 747.33 ± 55.7 μM). Therefore, even though skin temperatures recovered, there was a maintained constriction in the tail artery of rats exposed to vibration.

CPT measurements demonstrated that the sensitivity of the Aβ fibers to 2000 Hz stimulation was significantly reduced (i.e. increased stimulus needed to induce a response) in rats exposed to vibration, but increased in the controls (Figure 2). The Aβ fibers carry vibrotactile information from sensory organs to the nervous system. All rats demonstrated slight increases in sensitivity to stimulations of 250 Hz (Aβ fibers) and 5 Hz (C fibers).

CONCLUSIONS

The acute biodynamic and physiological responses of the rat tail to vibration are similar to the responses seen in human fingers (1-3). Future studies will use this model to understand the effects of repeated vibration on soft tissue damage.

REFERENCES

1. Bovenzi M, et al., *OEM* **57,** 422-30, 2002.
2. Dong RG, et al., *J Biomech Eng* **126,**446-456, 2004.
3. Thonnard JL, et al., *Scand J Work, Environ Health* ;**23**, 193-198, 1997.

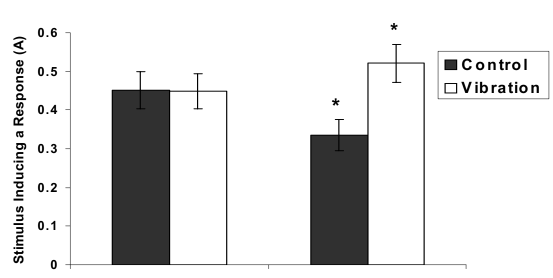

Figure 2. Responses of rats to 2000 Hz stimulation along the tail (data are mean ± SEM, * designates significantly different from pre-exposure test, N = 8/group).

LANDING FORCES PRODUCED IN TAP DANCE

[1]Lester Mayers , [2]Sujani Agraharasamakulam, [2]Sheyi Ojofeitimi, and [2]Shaw Bronner
[1]Division of Sports Medicine, Pace University, Pleasantville, NY;
[2]Analysis of Dance and Movement (ADAM) Center, Long Island University, Brooklyn, NY;
email: lmayers@services.pace.edu

INTRODUCTION

We performed a retrospective survey among experienced tap dancers that suggested a relatively low injury prevalence and occurrence rate (0.31/1000 exposures) among the surveyed cohort.[1] A literature search revealed no information concerning biomechanical aspects of tap dance. To explain the findings of our injury survey, we hypothesized that tap dance might produce less musculoskeletal stress (forces and/or moments) than other dance and sporting activities and initiated a biomechanical analysis by measuring landing forces in a group of experienced tap performers.

METHODS

Six experienced professional tap dancers (3 male and 3 female, mean age 24.5 ± 10.6 years) were recruited. All subjects were injury-free, actively performing when tested, and signed an informed consent.

Four tap dance sequences (flaps, cramprolls, pullbacks, and a subject-selected virtuoso sequence) were repeated 4-8 times within each condition with both feet on the force platform. Three-D kinematic and kinetic data were acquired with a 5-camera motion analysis system (Vicon, Oxford Metrics Ltd, Oxford UK) at 120 Hz and force platform (AMTI, Advanced Mechanical Medical Technology, Inc., Watertown, MA) at 1080 Hz. A full body marker set, comprised of 39 reflective spherical markers 25 mm in diameter, was used to create an 11-segment model.

Peak amplitude Fx (sagittal plane), Fy (frontal plane) and Fz (vertical plane) forces (N) were calculated for each of the four conditions, and normalized to body weight (BW). Means for each kinetic variable were calculated for each subject to minimize intra-subject variability. Descriptive statistics were then calculated for each condition. Separate between-group (gender) t-tests were calculated for each condition ($p < 0.05$).

RESULTS AND DISCUSSION

Between-group t-tests were not significantly different for any condition, so results for all subjects were merged for analysis. Mean peak Fx and Fy for the six subjects were insignificant (< 1.0 BW) for all conditions. For flaps, Fz ranged from 1.16 to 1.96 BW, (mean 1.46 ± 0.32). For cramprolls, Fz ranged from 1.62 to 3.02 BW, (mean 2.35 ± 0.45). For pullbacks, Fz ranged from 1.55 to 2.88 BW, (mean 2.23 ± 0.47). For the optional or virtuoso steps chosen by each performer (n=5), Fz ranged from 1.70 to 4.19, (mean 2.52 ± 0.99). Mean Fz for all conditions and all subjects was 2.14.

Landing forces have been measured in numerous studies involving walking (1-1.4 BW), running (1.6-3.6), jumping (3.5-6.0 BW), gymnastics (9-14.5 BW), various sports activities (4.0-12.6 BW), aerobic dance (1.5-2.6 BW), and dance jump landings (1.4-2.8 BW). It is apparent that Fz forces occurring during tap dance are in the lower range of those reported for these various activities. Although this finding might appear to confirm our initial hypothesis and explain the apparent decreased injury risk for this dance form, there are additional factors to be considered.

CONCLUSIONS

We conclude that the relatively small Fz forces measured during tap dance among experienced professional performers supports our hypothesis that the apparent lower injury occurrence rate among this group may reflect this finding. Nevertheless, the analysis is highly complex and involves many other factors remaining to be studied.

REFERENCES:

1. Mayers LB et al. *J Dance Med Sci* **7**:121-125, 2003.

INFLUENCE OF SKIN TEMPERATURE ON MECHANOMYOGRAM OF M. BICEPS BRACHII

[1] Kazuyuki Mito, [2]Takahiro Tamura, [3]Kenichi Kaneko, [4]Hitoshi Makabe, [5]Masto Takanokura and [1]Kazuyoshi Sakamoto
[1]The University of Electro-Communications, Japan, [2]Sony Corporation Ltd., Japan, [3]Fuji University, Japan,
[4]Yamagata Prefectural University of Health and Sciences, Japan, [5]Kanagawa University, Japan; [1]email: mito@se.uec.ac.jp

INTRODUCTION

Mechanomyogram (MMG) is mechanical counterpart of myoelectric activity and it has gained considerable attention as a new noninvasive tool to investigate the muscular functions. The main mechanisms of MMG signal generation has been considered to be pressure waves generated by lateral expansion of the active muscle fiber [1].

It is well known that the changing of muscle temperature concerns the electrical and mechanical function (i.e., electromyogram: EMG and contraction torque, respectively) of the muscle [2,3]. The present study was therefore performed to examine the relation between the MMG properties and the muscle temperature.

METHODS

Nine healthy male volunteers, aged from 21 to 26 years, participated in this study. The reference condition of skin temperature was attained in room air of 23-25 ºC that resulted in the skin temperature of about 34 ºC which was called "control" condition. The muscles of upper arm were cooled with over 20 minutes down to a skin temperature of 20 ºC (i.e., "cold" condition). At some other day, the muscles were heated up to a 40 ºC (i.e., "heat" condition). In each skin temperature, the EMG and MMG signals were measured on m. biceps brachii during isometric contraction. The maximum voluntary contraction (MVC) was measured in the "control" condition. The subjects maintained contraction level of 20%, 40%, and 60% MVC. The surface EMG signal was picked up by the bipolar Ag/AgCl electrodes (5mm pick-up diameter, 20 mm inter-electrode), placed over the muscle belly along the underlying muscle fiber. The MMG signal was detected by the piezo-electric accelerometer with weight of 2g (9G111BW, NEC Sanei Instruments Ltd.). The accelerometer was placed with double-sided adhesive tape at mid point between the EMG electrodes. The contraction torque, EMG and MMG signals were simultaneously and continuously stored into a personal computer through an A/D converter with 12-bits resolution and with sampling frequency 1-kHz. The root mean square amplitude (RMS) was computed from both signals of EMG and MMG. ANOVA was used to determine the EMG and MMG characteristics at three different temperatures (control, cold, and heat). Significances of individual differences were evaluated by using the Scheffé test if ANOVA was significant.

RESULTS AND DISCUSSION

The mean ± SD of MVC of nine subjects was 22.9 ± 3.6 kg. The effect of skin temperature on the relation between the RMS of EMG and MMG and the contraction level was shown in Fig. 1. The RMS values of EMG and MMG were increased with increasing of the contraction level in all skin temperature. The RMS of EMG was not significantly influenced by the skin temperature. This was in good agreement with the previous studies [2,3]. The RMS of MMG significantly increased with increasing the skin temperature at each contraction level. The present results might be related to the contraction time of muscle fibers and the viscosity of muscular tissue. These data can be extended to the notion that the MMG is a reliable method to investigate muscular function under a wide range of physiological conditions.

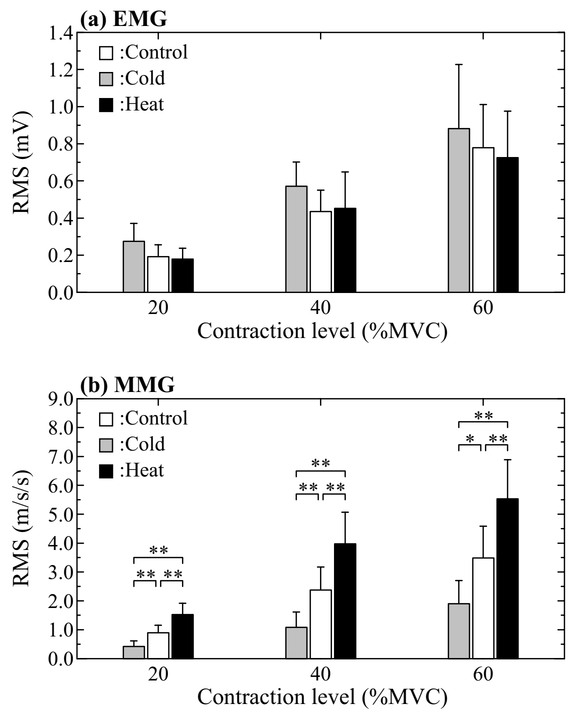

Fig.1: The effect of skin temperature on the relation between (a) RMS of EMG and the contraction level and (b) RMS of MMG and the contraction level. The marks of * and ** are $p<0.05$ and $p<0.01$, respectively.

CONCLUSIONS

The main purpose of this study is to examine whether or not the RMS of EMG and MMG could reflect the contraction properties of muscle during cooling and heating of the skin surface. The results were obtained as the following. (1) RMS of EMG was not almost influenced by the skin temperature. (2) RMS of MMG significantly increased with the increasing of skin temperature.

REFERENCES

1. Orizio C. *Crit Rev Biomed Eng* 21, 201-243, 1993.
2. Holewijn M, and Heus R. *Eur J Appl Physiol* 65, 541-545, 1992.
3. Krause KH, et al. *Electromyogr Clin Neurophysiol* 41, 67-70, 2001.

INVESTIGATION ON SLIP DANGER TO TRANS-FEMORAL PROSTHESIS USER DURING LEVEL WALKING

[1]Jin Dewen, [1]Yang Jiankun, [1]Wang Rencheng, [1]Zhang Jichuan, [1]Ji Linhong,[2]Fang Xin, [2]Zhou Dawei
[1]Division of Intelligent and Biomechanical System, State Key Laboratory of Tribology, Tsinghua University, Beijing (100084), PR China email: jdw-om@tsinghua.edu.cn
[2]China Center of Orthopedic Technology (CHICOT), Beijing (101601), PR China

INTRODUCTION

Slip-related falls have become a major cause of serious injuries, so that more and more researchers dedicate to this field. Grönqvist et al. [1] have indicated that the moment of heel contact is most dangerous for slip occurrence in a gait cycle. Cham et al. [2] have quantified the changes in gait biomechanics when people anticipate slippery environments. Buczek et al. [3] have suggested that the peak required coefficient of friction ($RCOF_{peak}$) can be used to predict slip potentials in gait activities. However, little work has been carried out on the slip events of trans-femoral amputees. The aim of this study is to investigate the slips happening to trans-femoral amputees during level walking on normal and slippery path via the gait analysis.

METHODS

Six male unilateral trans-femoral amputees and ten non-amputees participated in the current study. All of the amputated subjects were active and able to walk independently in daily life. In the experiment, the subjects were required to walk at a self-selected comfortable pace on the dry surface along a 5 m plastic walkway. Then five amputees and five non-amputees were required to walk on the oily surface. Two force plates (OR6-7, AMTI, MA), which were placed in the walkway, were employed to record the ground reaction forces (GRF). At the same time, the Qualysis Motion Capture System (Qualisys Medical AB, Sweden) were employed to record the kinematics data of each trail at 200 Hz synchronously.

The $RCOF_{peak}$ and the contribution ratio of Fx to the RCOF (R_{Fx}) were calculated using the following equations:

$$RCOF_{peak} = \left| \frac{\sqrt{F_x^2 + F_y^2}}{F_z} \right| \qquad R_{Fx} = \frac{F_x^2}{F_x^2 + F_y^2}$$

Where *Fz* represents the force in vertical direction; *Fy* represents the force in forward direction; *Fx* represents the force in lateral direction. A one way analysis of variance (ANOVA) was performed on $RCOF_{peak}$ and R_{Fx}, respectively. Only values of $P < 0.05$ were considered significant.

RESULTS AND DISCUSSION

The values of $RCOF_{peak}$ and R_{Fx} are listed in Table 1 and Table 2. It is indicated from the comparison between the trans-femoral amputees and non-amputees that the $RCOF_{peak}$ and R_{Fx} of amputees were significantly greater than that of non-amputees. And the comparison between sound side and prosthetic side shows that the value of R_{Fx} of prosthetic side is much higher than that of sound side while the R_{Fx} of sound side is close to that of non-amputees.

Table 1: The comparison between the trans-femoral amputees and non-amputees

	$RCOF_{peak}$	R_{Fx}
Amputees	0.220 ± 0.071	0.183 ± 0.150
Non-amputees	0.165 ± 0.025	0.052 ± 0.059
P-value	0.007	0.008

Table 2: The comparison between the sound and prosthetic sides of trans-femoral amputees

	$RCOF_{peak}$	R_{Fx}
Sound Side	0.231 ± 0.094	0.071 ± 0.016
Prosthetic Side	0.209 ± 0.054	0.295 ± 0.137
P-value	0.707	0.017

The results come from the differences of ground reaction forces. The forces in lateral direction of prosthetic side Fx are much greater than that of sound side and both Fx and Fy of sound side are greater than that of non-amputees.

The kinematic data also show the rationality of the results. When the subjects walking on the dry surface, there were obvious lateral swings in amputees' gait pattern. In the slip events the slip direction was completely different between prosthetic side and non-amputees including sound side. When the sound side of amputees or the non-amputees encountered slips, the foot slid mainly in the forward direction while that when slips occurred to the prosthetic side the foot slid mainly sideways.

CONCLUSIONS

1) The large value of peak required coefficient of friction indicates that the trans-femoral amputees face a greater slip danger than normal people during level walking. 2) Swing in the lateral direction of amputees' gait pattern is the main cause of the increase of peak required coefficient of friction. 3) Sideway slip is the peculiar character of the prosthetic side of trans-femoral prosthesis user.

REFERENCES

1. Grönqvist R, et al. An apparatus and a method for determining the slip resistance of shoes and floors by simulation of human foot motions, *Ergonomics* **32** 979-995, 1989.
2. Cham R, et al. Changes in gait when anticipating slippery floors, *Gait and Posture* **15** 159-171, 2002.
3. Buczek FL, et al. High-resolution force plate analysis of utilized slip resistance in human walking. *Journal of Testing and Evaluation* **24** 353-358, 1996.

ACKNOWLEDGEMENTS

Supports: NSFC (No. 30170242) and NHTRD (863) (No. 2001AA320601)

HANDLING OF IMPACT FORCES IN INVERSE DYNAMICS IN LANDING AFTER A JUMP

[1] Rob Bisseling, [1]At Hof
[1]Center for Human Movement Sciences, University Medical Center Groningen, Groningen, The Netherlands
email: r.w.bisseling@ppsw.rug.nl, web: www.ihms.nl

INTRODUCTION

The relation between impact dynamics of a landing after a jump and the cause of chronic injuries, like patellar tendinopathy (jumper's knee), has been the focus for research for many years. During impacts, impact force produces a shock wave, which travels through the subject's extensor mechanism. Net joint moments are a measure of load of the extensor mechanism (patellar tendon).

The purpose of this study was to detect the real contribution of the ground reaction force (GRF) and segmental acceleration in the sagittal net knee moment during the first part of impact of a landing after a jump by comparing a standard inverse dynamic method (SM) with an accelerometer based inverse dynamic method (AM).

METHODS

Seven healthy well trained male volleyball players participated in this study. The subjects were asked to perform a maximal counter movement jump, which was performed according the subject's own preferred style.

Two different inverse dynamic based methods were compared to study the impact dynamics of landing: the SM, using accelerations from filtered (20 Hz) position data and GRF, and the AM, using accelerations from accelerometers and GRF. Measurements of both methods were applied to a three segment rigid body model of the right leg.

RESULTS AND DISCUSSION

The net knee moment, calculated by the SM, showed major differences compared to the AM. These differences mainly took place during the first part of impact, from the time of touch down till approximately 35 ms later. SM showed an extension moment peak during impact, where the AM showed an oscillating effect: flexion moment peak, directly followed by an extension moment peak (figure 1). It turned out that this flexion peak was the result of an 'overestimation' of the moment caused by the horizontal accelerations.

Comparison of the segmental acceleration from position data used in the SM and from the AM showed good correspondence, indicating correctness of method and measurement data. The overshoot in horizontal accelerations can be explained by an underestimated correction factor [1] used to determine the linear acceleration of the centre of mass, using angular velocity and acceleration, which are calculated from position data. Furthermore, our rigid body model assumes that the foot is one rigid segment. Finally, we use a rigid body model without damping [2].

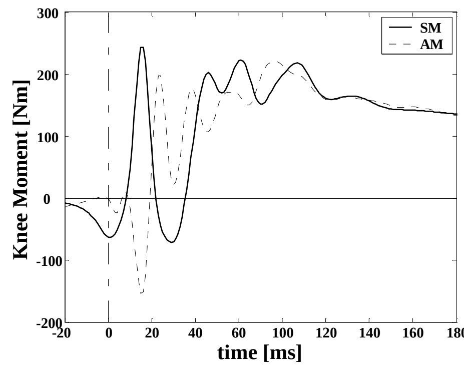

Figure 1. Net sagittal knee moment of a landing. Black line is the moment determined by the SM, and the dotted line is the moment determined by the AM

So, we can state that during impact the real contribution of GRF is for a great part neutralized by segmental acceleration of foot and shank, suggesting that the high impact peak moment shown by the widely used SM moment is be an artifact.

CONCLUSION

Our results showed major differences during impact in sagittal knee moment between the SM and AM. The SM, used in this study, is a widely used method to determine biomechanical parameters. When estimating net joint moments during impact in activities like running and jumping one should take into consideration the inaccuracy of the net joint moment during impact when using rigid body models. To our opinion, adjustments to the widely used filter techniques can overcome artifacts in net impact joint moments, by using the same cutoff frequency for both kinematic and force data. Complementary, we recommend not to consider impact peaks as the source of chronic overuse injuries, like jumper's knee.

ACKNOWLEDGEMENTS

We thank Koen Vaartjes for his technical assistance. Furthermore we thank Dr. Jaap Harlaar and Dr. Caroline Doorenbosch of the VU University Medical Center Amsterdam for their development of the analysis software BodyMech.

REFERENCES

1. Ladin Z., Wu G. *J Biomechanics* 24, 1173-1187, 1991
2. Gruber, K. et al. *J Biomechanics* 31, 439-444, 1998

FACTORS AFFECTING THE CEMENT PENETRATION OF A HIP RESURFACING IMPLANT: AN IN-VITRO STUDY

[1] Ralph Howald, [2] Uldis Kesteris, MD [1] Ralf Klabunde
[1] Zimmer GmbH, Winterthur, Switzerland, email: ralph.howald@zimmer.com
[2] University Hospital Lund, Schweden

INTRODUCTION

Hip resurfacing is increasingly used in orthopedic arthroplasty. In order to plan and conduct the implantation properly, the operating surgeon needs to know how the cementing technique will influence the cement penetration. Breusch et al. [1] quantified the cement penetration in a conventional hip stem and Morberg et al. [2] investigated the cement-bone-interface histologically. However, no information could be found about cement penetration in hip resurfacing prostheses.

OBJECTIVES

Determine the influence of the following parameters on cement penetration: use of jet lavage, type of cement, and the standing period of the cement.

MATERIALS AND METHODS

The Durom™ Hip Resurfacing implant (Zimmer GmbH, Switzerland) and nine fresh frozen paired whole cadaver femora (mean 47 years, range 26 to 66 years) were used in this study. The standard case was the use of jet lavage for cleaning the prepared bone and Simplex® cement (Stryker Orthopaedics, USA) with a three minute standing time. The femora were divided into three paired groups: (A) compared the use of jet lavage to no jet lavage, (B) compared the two low viscosity cements SULCEM™-3 (Zimmer GmbH, Switzerland) and Simplex®, and (C) a 1.5 minute standing time was compared to a 3 minute standing time. All 18 implantations were conducted within a two day period by an experienced surgeon using the standard OR procedures.

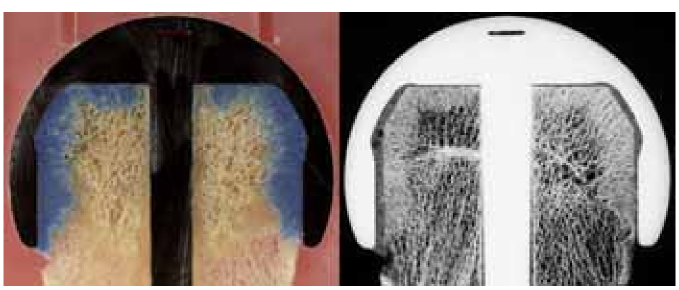

Fig. 1. Section cut of a femoral head (left) and contact x-ray image (right)

A single 2.6 mm thick slice was taken out of the center of each head using a precision diamond blade band saw. Contact x-ray images were then generated using a cabinet x-ray system (Fig. 1). After digitizing the images, computer based measurements were made using Matlab routines. The following measurements were taken: cement penetration *ratio* (penetration area divided by the bone area enclosed by the implant) and mean cement penetration *depth*. The results within each group were compared using a paired t-test. However, since the sample size was only three, the results only indicate tendencies.

RESULTS AND DISCUSSION

Leaving out jet lavage decreased the mean cement penetration *ratio* by 62% ($p = 0.018$), whereas the mean penetration *depth* decreased by 65% ($p = 0.024$). No significant differences were seen between SULCEM-3 and Surgical Simplex when comparing the cement penetration *ratio* ($p = 0.71$) and *depth* ($p = 0.57$). Applying the cement after a standing time of 1.5 minutes instead of 3 minutes resulted in a lower penetration ratio and depth in all cases. However, the results were not significant ($p = 0.15$, $p = 0.16$) (Fig. 2).

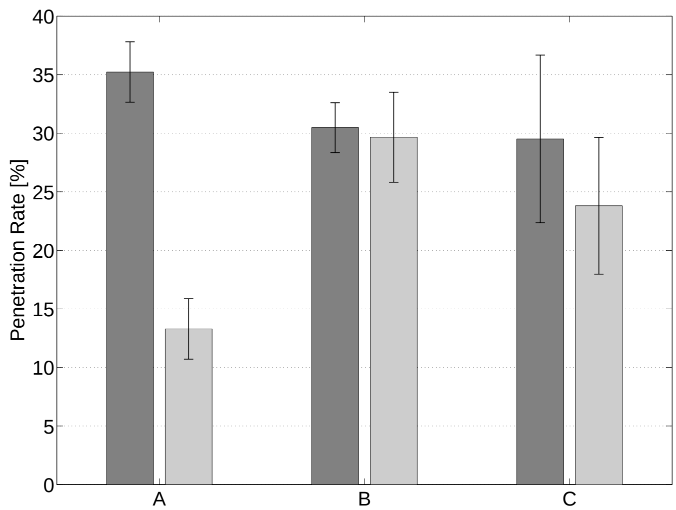

Fig. 2: Comparison of the penetration ratio: (A) Jet Lavage yes vs. no, (B) Simplex® vs. SULCEM™-3, (C) 3 min. vs. 1.5 min. standing period

CONCLUSION

Using jet lavage or increasing the standing time of the cement to 3 min. has the tendency to increase the cement penetration, whereas no difference in cement penetration was found when different cement brands of comparable viscosity are used.

LITERATURE

1. Breusch SJ, et al. *Journal of Arthroplasty* **15**, no. 7, pp. 921-927, 2000
2. Morberg P, et al. *Journal of Arthroplasty* **16**, no. 8, pp. 1004-1009, 2001

ACKNOWLEDGEMENT:

The authors acknowledge the great support of the Biomechanics Group at the Technical University of Munich, Germany.

PATTERNS OF HAND MOTOR DYSFUNCTION IN BRAIN INJURY

[1]Archana P. Sangole, [2]Beatriz C. Abreu, [2]Neil Huddleston, [1]Rita M. Patterson, [1]William Buford Jr. and [1]Kenneth J. Ottenbacher
[1]The University of Texas Medical Branch, Galveston, TX 77555
[2]Transitional Learning Center, Galveston, TX 77550; email: archana.sangole@utmb.edu

INTRODUCTION

Activities of daily living (ADLs) involve smooth voluntary movements between joints that require a synchronized recruitment of relevant muscles. Motion is thus realized by a balance in directional preference of muscular activity. Upper motorneuron syndrome (UMNS) due to lesions in cortico-spinal pathways is common following a stroke or traumatic brain injury. UMNS manifests itself in the form of muscle under- or over-activity which consequently affects motor behavior [1]. An undesirable directional preference is imposed due to involuntary muscle activity thereby inducing spasticity and consequently impeding ADL performance. Muscle under-activity is apparent as weakness, loss of finger dexterity and selective control of muscles. Muscle over-activity is characterized by exaggerated tonic stretch reflexes and tendon jerks. This research is an attempt to identify and study patterns of hand motor dysfunction in ADL performance as a result of brain injury (BI).

METHODS

The research is an on-going study that uses a video-based motion analysis system to record hand activity during grasping. The activity involves grasping a spherical object. Subjects were instructed to reach for and wrap their fingers around the object, without lifting the object, and then gradually release the object. The protocol was set based on [2,3] in order to assess the degree of voluntary finger extension. Data were collected and analyzed to observe patterns of hand coordination during grasping in patients after brain injury.

Prior to data collection, the 3D SIMI motion analysis system was calibrated for spatial alignment and orientation. Reflective markers (5 mm in diameter) were placed on the metacarpal (MCP) and interphalangeal (IP) joints of the fingers and thumb, the base of the 3rd metacarpal and the stylus of the ulna and radius (18 markers). Digital motion data was recorded at 60Hz for at least 8 secs. by three cameras. Spatial coordinate data were extracted from the motion clips of the grasping activity. These were used to calculate MCP and PIP joint angles. Passive range-of-motion for each finger joint and the wrist were also recorded. The abstract discusses a specific case and general observations.

RESULTS AND DISCUSSION

Figure 1 shows the MCP angle plot for the ring finger in the hand of a patient with bilateral hand motor dysfunction. The motion clips indicated that the patient initiated the dynamic phase of grasping by placing the fingers on the object, followed by lowering the wrist to stabilize the object in the palm. This is observed in the MCP angle plot wherein region-1 (R1) shows increased MCP extension followed by R2 with increased flexion due to lowering of the wrist for object stabilization. The same regions are identified in the other hand of the same patient which exhibits relatively better hand motor function.

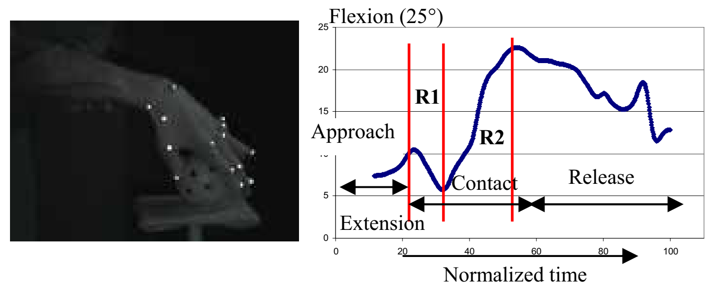

Figure 1: MCP angle plot of the patient's ring finger.

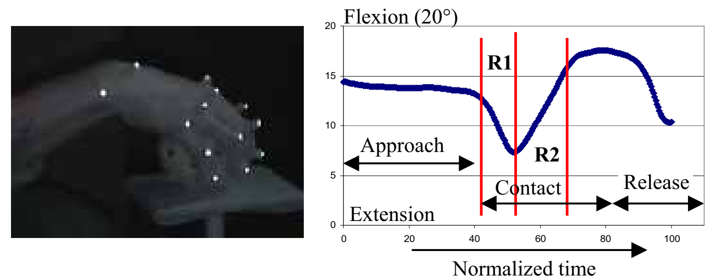

Figure 2: MCP angle plot of the ring finger in the other hand of the same patient.

The MCP and PIP angle plots were almost in phase in the controls, while the same was not the case in the brain injured patients. Table 1 lists the correlation values between the MCP and PIP angle plots of the fingers for the brain injured patients and age- and gender- matched controls.

CONCLUSIONS

In this pilot, it was observed that hand motor dysfunction after BI severely affects the release mechanism of the fingers. Patients tend to use different strategies for stabilizing the object in their hand. Relatively low correlation was observed between the MCP and PIP angles in the brain-injured patients. Further research is required to get a more generalized stratification of hand motor dysfunction in BI.

REFERENCES

1. Mayer NH. *J Head Trauma Rehab* **19**(2), 119-142, 2004.
2. Somia N, et al. *J Hand Surgery* **23B**, 792-795, 1998.
3. Nakamura M, et al. *J Electro Kines* **8**, 295-303, 1998.

Table 1: Correlation between MCP and PIP joint angles.

Subject	Fore		Middle		Ring		Little		Thumb	
	L	R	L	R	L	R	L	R	L	R
Patient-1	0.52	-0.69	0.67	-0.55	0.71	0.47	-0.06	-0.63	0.89	0.49
Patient-2	-0.26	0.97	0.74	0.97	0.64	0.93	0.59	0.75	0.66	0.28
Control-1	0.93	0.74	0.78	0.83	0.83	0.65	0.24	0.77	-0.80	0.23
Control-2	0.97	0.56	-0.05	0.92	0.83	0.95	0.92	0.57	-0.75	-0.75

BEHAVIOR OF THE TRICEPS SURAE MUSCLE IN HOPPING

Sami Kuitunen, Masaki Ishikawa and Paavo V Komi
Neuromuscular Research Center, Department of Biology of Physical Activity,
University of Jyväskylä, Jyväskylä, Finland; email: sami.kuitunen@sport.jyu.fi

INTRODUCTION

Studies with ultrasonography (US) have revealed that muscle fascicle and tendon length changes may not follow the length changes of the whole muscle-tendon complex (MTC) in natural human movements [1]. In jumping, the gastrocnemius (Ga) muscle fascicles have been shown to shorten [2,3] during the ground contact, despite the lengthening-shortening action of the MTC. Fascicle behavior of the soleus (Sol) muscle in natural human movements has not yet been reported. However, modeling the triceps surae function in counter-movement jump indicates similar behavior of Ga and Sol muscle fibers [4]. The present study focused to explore fascicle behavior of the Ga and Sol muscles directly with US in natural stretch-shortening cycle (SSC) muscle action.

METHODS

Eight male subjects performed bilateral hopping at low (LOW), medium (MED) and maximum (MAX) intensity. Ground reaction forces (GRFs) were collected simultaneously with high-speed video (200 Hz) recordings and real-time US (96 Hz) of Sol and medial Ga (GaM). Achilles tendon force (ATF) and MTC lengths of Sol and GaM were calculated.

Ten jumps were selected and data was averaged from each subject for each hopping intensity excluding the US data, where two most representative jumps were chosen.

RESULTS AND DISCUSSION

Fig. 1 represents a typical example of ATF and length changes of MTC and fascicles of Sol and GaM, respectively. Lengthening of MTC increased both in Sol and GaM with increasing loading (ATF). Despite the lengthening of MTC, fascicles of GaM shortened at the beginning of the ground contact. This shortening is similar to the earlier findings regarding counter-movement jumps [2] and drop jumps [3]. It may contribute to the storage of elastic energy by stretching the AT [1,2] and improving energy transfer of the proximal muscles to the ankle joint due to increased muscle stiffness [5]. On the other hand, SOL fascicles showed a lengthening-shortening behavior similarly to the MTC. Similar fascicle behavior has also been observed in the vastus lateralis muscle in drop jumps [3]. It may also be worth noting that the initial shortening of GaM fascicles was followed by a rapid lengthening at MED and MAX, which may imply cross-bridge detachment due to high loading. Similar yielding of GaM fascicles was also observed in the drop jumps [3].

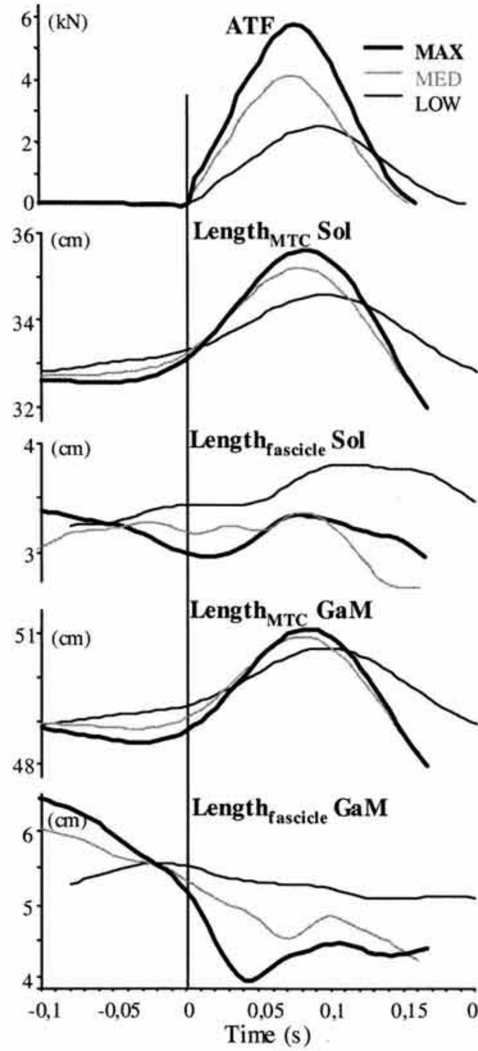

Figure 1: ATF and length-time curves of Sol and GaM MTCs and fascicles of one subject in hopping at different intensities. Vertical line denotes the onset of ground contact.

CONCLUSIONS

The novel finding of the present study was that Sol and GaM fascicles may behave differently in natural SSC muscle action. The Sol fascicles represented a lengthening-shortening behavior similarly to the MTC, whereas GaM mainly shortened during the contact phase in hopping. It is likely that these differences in fascicle behavior between Sol and GaM are related to the suggested different roles of one- and two-joint muscles in human movements [5].

REFERENCES

1. Fukunaga T, et al. *Exerc Sport Sci Rev* **30**, 106-110, 2002.
2. Kurokawa S, et al. *J Appl Physiol* **95**, 2306-2314, 2003.
3. Ishikawa M, et al. *unpublished observations*
4. Bobbert M, et al. *J Biomech* **19**(11), 887-898, 1986.
5. Grégoire L, et al. *Int J Sports Med* **5**(6), 301-305, 1984.

MECHANICAL EFFICIENCY DURING WALKING AT DIFFERENT STRIDE RATES

[1]Brian R. Umberger and [2]Philip E. Martin
[1]Biodynamics Laboratory, University of Kentucky, Lexington, KY, USA
[2]Biomechanics Laboratory, The Pennsylvania State University, University Park, PA, USA
email: umberger@uky.edu web: www.coe.uky.edu/~brian

INTRODUCTION

At any particular walking speed, the rate of metabolic energy expenditure in humans is minimized at the preferred, or self-selected, stride rate [6]. However, our understanding of the underlying factors that determine the global energy rate response, and that ultimately influence the preferred walking pattern, remains incomplete. Mechanical efficiency is a factor that is believed to be important in human locomotion [e.g., 5], but has not received much direct attention in regards to walking stride rate selection. The purpose of this study was to test the hypothesis that maximization of the mechanical efficiency of walking occurs at the preferred stride rate.

METHODS

Six male and four female subjects (M_{age} = 26.7 ± 3.6 yr; M_{ht} = 173.9 ± 9.6 cm; M_{mass} = 67.9 ± 11.9 kg) walked at 1.3 m/s using five different stride rates (preferred, ± 10% of preferred, and ± 20% of preferred). Preferred stride rate was determined as subjects walked on a motorized treadmill, after which the subjects practiced walking at the experimental stride rates for at least 10 min. Following familiarization with the protocol, and after resting for at least 20 min, measurements were made of pulmonary gas exchange while subjects walked on the treadmill at the different stride rates. In a separate trial, ground reaction forces and body segment positions were monitored as subjects walked along a 12 m walkway across a force platform. Subjects matched their stride rates to a metronome for treadmill trials, and to marks placed on the floor for overground trials. For both trials subjects walked with arms folded across their chest, to minimize any influences from outside the lower limbs.

The net (walking minus resting) rate of metabolic energy expenditure (E_{DOT}) was estimated from pulmonary gas exchange [3], and sagittal plane hip, knee, and ankle joint moments were calculated using inverse dynamics [4]. Joint powers were calculated from the net moments and joint angular velocities. Average positive (P_{POS}) and negative (P_{NEG}) power, summed over all three joints, was determined by integrating the instantaneous positive and negative powers over the gait cycle, and dividing by the cycle period. P_{POS} and P_{NEG} were doubled to approximate the power output of both legs. The mechanical efficiency of walking (ε_W) was estimated from P_{POS}, P_{NEG}, and E_{DOT} as $\varepsilon_W = P_{POS} / (E_{DOT} + P_{NEG})$ [1].

Metabolic energy rate and mechanical efficiency data were fit with quadratic polynomials, and the stride rates corresponding to the respective minima and maxima were determined from the resulting equations. Differences between preferred stride rate and the stride rates optimizing energy expenditure and mechanical efficiency were detected using paired t-tests.

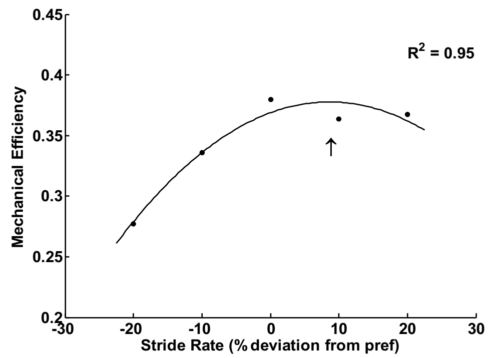

Figure 1: Mechanical efficiency of walking was predicted to be maximized at a stride rate 8.3% above the preferred.

RESULTS AND DISCUSSION

Preferred stride rate (54.3 str/min) and the stride rate minimizing gross metabolic energy expenditure (55.6 str/min) were both similar to previous reports [6], and did not differ significantly ($p > .05$). Mechanical efficiency (Figure 1) was maximized at a stride rate 8.3% higher than preferred (58.8 str/min; $p < .01$). While this difference was statistically significant, the absolute deviation from preferred was modest (4.5 str/min). The present results, combined with earlier work [2] showing that mechanical demand (estimated from net joint moments) was minimized approximately 8.5% below the preferred rate, suggests that these two factor may combine to constrain normal walking stride rates to a narrow range centered around a stride rate of approximately 55 str/min.

CONCLUSIONS

At a single speed, walking with stride rates lower than preferred results in decreased mechanical efficiency, while using stride rates higher than preferred leads to increased loading on the lower limb muscles. The self-selected stride rate in walking appears to represent the best compromise between these two competing factors.

REFERENCES

1. Prilutsky, BI. *J Appl Biomech* **13**, 466-471, 1997.
2. Umberger, BR, Martin, PE. *Proceedings of ASB*, Toledo, OH, Abstract 118, 2003.
3. Weir, J. *J Physiol*, **109**, 1-9, 1949.
4. Winter, D. *Biomechanics and Motor Control of Human Movement*, Wiley, New York. 1990.
5. Zarrugh, MY. *J Biomech*, **14**, 157-165, 1981.
6. Zarrugh, MY, et al. *Eur J Appl Physiol*, **33**, 215-223, 1974.

ACKNOWLEDGEMENTS

Support was provided by NSF IGERT grant DGE9987619 and the Arizona State Univ. Exercise & Sport Research Institute.

KINETIC ANALYSIS OF GAIT ON INCLINED SURFACES

[1]Robyn M. Wharf and [1,2]D. Gordon E. Robertson
[1]School of Human Kinetics, University of Ottawa, Ottawa, Ontario, Canada [2]dger@uottawa.ca

INTRODUCTION

Walking on a level surface usually takes minimal effort and is a daily occurrence. Access to areas on different levels, however, may become a barrier to the injured, elderly or disabled persons. Adding ramps or inclined surfaces is one means of permitting access to different levels of a building. Little data are available concerning the efforts required to negotiate different inclines. Prentice *et al.* [1] analyzed various inclines but only examined the swing phase while Post & Robertson [2], looked at ramp descent at one gradient. The purpose of this investigation was to quantify the moments of force and powers produced in the lower extremity during ascent of inclines of various gradients compared to those of level gait.

METHODS

Twelve subjects (6 female, 6 male) between the ages of 20 and 30 volunteered. Sagittal plane kinematics from a 60 Hz video camera and ground reaction forces from a force platform placed on the ramp were collected. The participant's ascended four different ramp inclinations, five times each (level, 3-deg, 6-deg and 9-deg). The motion data were digitized using the APAS. Kinematic, inverse dynamic and power analyses were done with the Biomech Motion Analysis System [3].

RESULTS AND DISCUSSION

Ankle moments and powers were similar for the level and 3-deg inclined conditions. There were no significant differences in the peak moments of force for any of the four conditions but there was a steady increase in peak power between 3, 6, and 9 degrees of incline. There was a 21% increase in peak power between the 9-degree incline and then level and 3-degree incline (2.99 vs. 2.45 W/kg).

Figure 1 illustrates the average knee moments of force and moment powers for all four conditions. The power burst at K0 was equal for all the inclines excepting for 9-deg, which was significantly less. Other major differences with the 9-deg incline occurred after foot-strike (FS) at K1 where the knee extensors produced almost no negative work compared to the other grades and at K2 where substantially more work and power were required.

There were sequential reductions in the peak eccentric power bursts of the knee extensors at K3 prior to toe-off (TO) and by the knee flexors prior to FS (K4). Thus, the energy demands of ascending inclines are met by reducing the amounts of energy dissipated by knee eccentric muscle contractions.

The peak moments of force at the hip were not significantly different across the four gradients. The peak powers were also similar but there were differences in the extensor work done immediately after FS (H1). Here there was a gradual increase of 138% from level to 9-deg incline (0.29-0.69 W/kg).

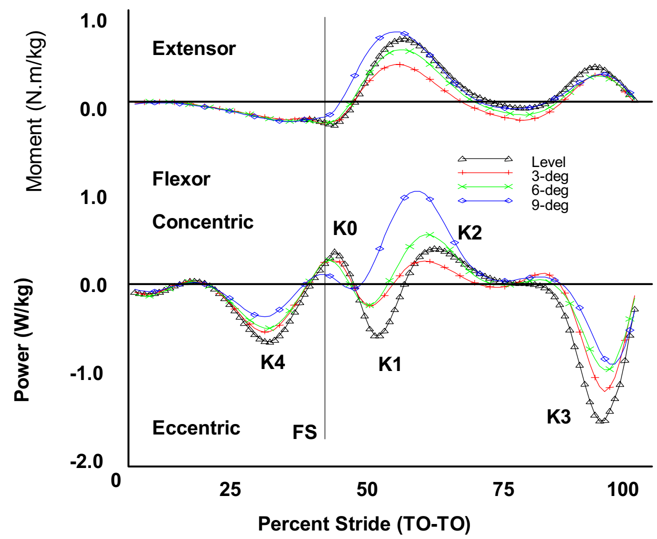

Figure 1: Grand ensemble averages (n=12x5) of the knee moments of force (top) and their powers (bottom) for level, 3, 6 and 9-degree inclines normalized to body mass. Abscissa is percent of stride from toe-off to toe-off.

CONCLUSIONS

There were few differences in the peak moment and power demands between level and 3-deg incline. The demands for 9-deg inclined ascent were significantly greater especially at the knee as compared to level and 3-deg of incline with the 6-deg incline being of intermediate demand.

REFERENCES

1. Prentice SD, et al. *Gait Posture* **20**, 255-65, 2004.
2. Post A & Robertson DGE *Proceedings of CSB XIII,* Halifax, Canada, 2004.
3. Biomech Motion Analysis System, http://www.health.-uottawa.ca/ biomech/software/biomech.

SKIN MOVEMENT ARTIFACT DURING GAIT AND CUTTING MOVEMENTS MEASURED IN VIVO

Daniel L Benoit [1,2,*], Dan K. Ramsey [3,4], Mario Lamontagne [5,6], Lanyi Xu [6], Per Wretenberg [2,4], Per Renström [1,2]
[1]Institution for Surgical Sciences, Section of Sports Medicine, Karolinska Institute, Stockholm, Sweden; [2]Department of Orthopaedics, Karolinska Hospital, Stockholm, Sweden; [3]Department of Physical Therapy, University of Delaware; [4]Institution for Surgical Sciences, Section of Orthopaedics, Karolinska Institute, Stockholm, Sweden; [5]School of Human Kinetics, University of Ottawa, Ottawa, Canada; [6]Department of Mechanical Engineering, University of Ottawa, Ottawa, Canada; dbenoit@magma.ca

INTRODUCTION

Skin movement artifact limits the ability to accurately 3D tibio-femoral kinematics using non-invasive techniques. Previous investigations into the error associated with skin movement artifact have had few subjects and/or been measured under conditions that may not represent healthy populations. The purpose of this study is to measure the effect of skin movement artifact on the reporting of knee joint kinematics in a healthy population during gait and cutting, a movement believed to illicit non-sagittal plane rotations and translations.

METHODS

Eight healthy male subjects participated in this study. Intra-cortical bone pins were transcutaneously implanted under local anaesthetic into the proximal tibia and distal femur. Three reflective markers were attached to each bone pin and four reflective markers were mounted on the skin of the tibia and thigh respectively. Roentgen-stereophotogrammetric analysis was used to determine the anatomical reference frame of the tibia and femur. Knee joint motion was recorded during walking and cutting using infra-red cameras at 120 Hz.

RESULTS AND DISCUSSION

The kinematics derived from the bone-pin markers was compared with that of the skin markers. Rotational errors of up to 4.4 and 13.1 degrees and translation errors of up to 13.0 and 16.1 mm were noted for the walk and cut respectively (table 1).
Although the data was repeatable within subject the direction and magnitude of the error was not repeatable across subjects (figure 1). This suggests that repeatability of motion analysis data can not be used as an indication of accurate data.

CONCLUSION

It was noted that although the skin marker derived kinematics could provide repeatable results this was not representative of the motion of the underlying bones. A standard error of measurement is proposed for the reporting of 3D knee joint kinematics.

Table 1: Absolute error values of skin-marker derived kinematics at three time points during walking and cutting of knee rotations and translations: flexion extension (Flex/ext), adduction-abduction (Add/abd), internal-external rotation (Int/ext); medio-lateral (Med/lat), anterior-posterior (Ant/post) and distraction-compression (Dist/comp). Note: † denotes significant difference between skin and pin-marker data (2 tailed paired Students T-test, $p<0.05$)

		Rotations (degrees +/- StDev)			Translations (mm +/- StDev)		
		Flex/ext	Add/abd	Int/ext	Med/lat	Ant/post	Dist/comp
Walk	Foot-strike	2.8 (2.6)†	2.5 (2.7)	2.8 (2.0)†	5.0 (2.6)	7.7 (4.4)†	5.0 (2.9)†
	Mid-stance	2.4 (2.0)†	3.1 (3.3)	2.4 (1.1)	5.5 (3.1)†	6.2 (5.4)	3.3 (2.4)†
	Toe-off	2.7 (2.4)	4.4 (3.2)†	2.2 (2.1)	8.0 (5.7)	13.0 (5.0)†	5.0 (2.5)†
Cut	Foot-strike	3.9 (2.9)	6.7 (5.4)†	5.4 (4.2)†	7.3 (4.4)	5.6 (5.1)†	6.3 (4.0)†
	Mid-stance	4.0 (2.5)	5.9 (3.1)†	5.4 (4.0)†	5.9 (4.5)†	6.7 (4.4)†	5.6 (3.8)†
	Toe-off	4.2 (2.7)	13.1 (9.8)	3.3 (1.8)†	13.9 (10.1)	16.1 (8.9)	8.3 (6.2)†

Figure2: Progression of error due to skin movement during cutting for all subjects. Figure shows average difference between skin-marker and pin-marker data as it progressive during stance. A positive value describes an over-estimation; zero describes perfect agreement and negative values describe an under-estimation of the skin marker derived knee joint rotations and translations.

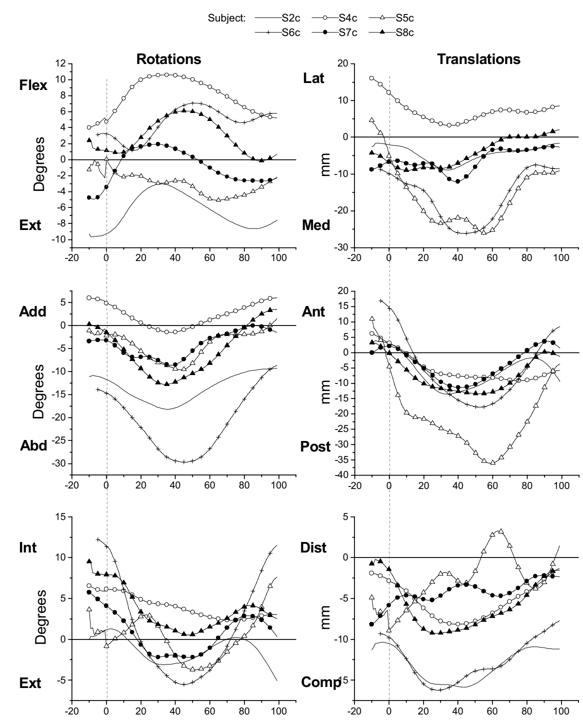

ACKNOWLEDGEMENTS

The authors would like to thank Birgitta Runtz for her expertise with the RSA evaluations.

IN VIVO FASCICLE LENGTH OF CAT MEDIAL GASTROCNEMIUS AND SOLEUS MUSCLES DURING SLOPE WALKING

Huub Maas, Boris I. Prilutsky and Robert J. Gregor
Center for Human Movement Studies, School of Applied Physiology, Georgia Institute of Technology, Atlanta, GA, USA
Email: huub.endemaas@ap.gatech.edu

INTRODUCTION

By changing the slope of a walking surface, mechanical variables (e.g. muscle fascicle length, tendon force) related to proprioceptive feedback can be manipulated. It has been suggested that length-dependent feedback from muscle spindles is more important for limb control during downslope walking compared to level or upslope walking [1]. Such a conclusion is based on length changes of the whole muscle-tendon complex (MTC). However, muscle spindle strain is directly related to changes of muscle fascicle length (L_{fas}).

Fascicle length changes of medial gastrocnemius muscle (MG) have been reported for level walking as well as for modestly sloped surfaces only, i.e. 10% [2]. Therefore, the **aim** of this study was to quantify fascicle length changes of MG as well as soleus (SO) muscles during walking on a level surface as well as on substantially sloped surfaces (i.e. + and −50%, 26.6°).

METHODS

Joint kinematics and kinetics of the hindlimbs, muscle activity patterns, MTC length and L_{fas} were assessed for three walking conditions in the cat: downslope, level and upslope. Four out of six cats were surgically implanted with EMG electrodes in SO and MG [3]. Selected muscles were also instrumented with sonomicrometry crystals to measure L_{fas}. The distance between the sonomicrometry electrodes (fractional L_{fas}) was ≈65% and ≈80% of the total fascicle length of SO and MG, respectively. Resting fascicle [4] and MTC length, as calculated based on a geometrical model, at ankle and knee angles of 90° were used as reference lengths (L_{ref}). For sonomicrometry, 6 step cycles were analyzed for level walking, 10 for the downslope and 13 for the upslope condition.

RESULTS AND DISCUSSION

For all cats, biomechanical gait parameters as well as muscle activity patterns were similar. Significant ($p < 0.05$) differences between changes of MTC length and total L_{fas} were found in early stance of all slope conditions (Figure 1, Table 1). During upslope walking, MTC lengthening of MG occurred in the presence of substantial L_{fas} shortening. For both muscles, fascicle lengthening in early stance during downslope walking was significantly ($p < 0.05$) higher than during level and upslope walking. This suggests a potentially higher contribution of length-dependent feedback for regulation of muscle activation, assuming contant activation of intrafusal fibers. Different muscle-tendon interactions (ΔL_{fas} / ΔL_{MTC}) between muscles and slope conditions can be explained partially by the magnitude of muscle activity [3]:

SO: EMG level < EMG downslope < EMG upslope
MG: EMG downslope < EMG level < EMG upslope.

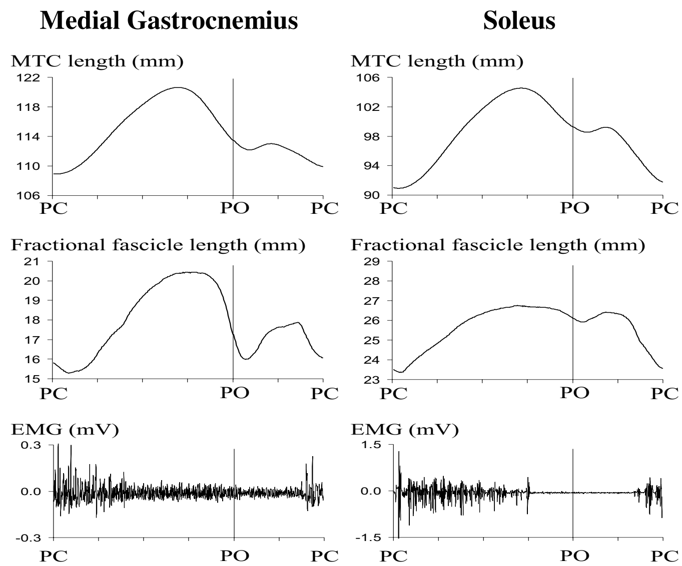

Figure 1: Typical example of MTC and fractional fascicle length as well as EMG recordings during downslope walking.

REFERENCES

1. Abelew TA, et al. *J Neurophysiol*, **84**, 2709-14, 2000.
2. Hoffer JA, et al. *Prog Brain Res*, **80**, 75-85, 1989.
3. Gregor RJ, et al. *Proceedings of the 34th IUPS Congress*, San Diego (CA), 2005.
4. Sacks RD, Roy RR. *J Morphol*, **173**, 185-95, 1982.

ACKNOWLEDGEMENTS

Supported by NIH HD032571 and the CHMS at Georgia Tech

Table 1: Mean (SD) MTC and total fascicle lengthening (+ mm) in early stance for MG and SO muscles. Note that in upslope walking the fascicles of MG are shortening (– mm). * Significantly different from ΔL MTC, † significantly different from ΔL level walking.

Muscle		Downslope		Level		Upslope	
		ΔL (mm)	$\Delta L/L_{ref}$ (%)	ΔL (mm)	$\Delta L/L_{ref}$ (%)	ΔL (mm)	$\Delta L/L_{ref}$ (%)
Soleus	*Fascicle*	4.8 (0.43) *†	11.5 (1.0)	1.4 (0.3) *	3.3 (0.7)	0.27 (0.12) *†	0.6 (0.3)
	MTC	13.6 (0.02) †	12.9 (0.02)	3.2 (0.9)	3.0 (0.8)	2.8 (1.1)	2.6 (1.1)
MG	*Fascicle*	6.2 (0.43) *†	29.5 (2.1)	1.1 (0.2) *	5.0 (1.0)	−3.6 (0.6) *†	−17.2 (2.8)
	MTC	11.6 (0.11) †	9.7 (0.1)	2.4 (0.8)	2.0 (0.7)	2.3 (0.8)	1.9 (0.7)

ADAPTIVE CHANGES IN STEPPING UP ONTO LATERALLY-COMPLIANT STRUCTURES: AGE DIFFERENCE IN HEALTHY MALES

Bing-Shiang Yang and James A. Ashton-Miller
Department of Mechanical Engineering, University of Michigan, email: bsyang@umich.edu

INTRODUCTION

Falls from laterally-compliant structures, such as stepladders, cause injuries in industry and at home across the age spectrum; however, fall-related injuries become more frequent and more serious in older populations [1,2]. Healthy adults, especially the elderly, have been shown to take significantly more time to complete a single step-up movement onto a raised structure with unexpected structural compliance [3]. The purpose of this study was to investigate whether subjects demonstrate practice or learning effects in this behavior. We therefore tested the null hypotheses that there are (a) no significant practice effects in stepping up onto a laterally-compliant structure in repeated trials and (b) no age effects on this behavior between healthy young and older men.

METHODS

Twenty healthy male subjects, 10 young males (YM) aged 26±3 years and 10 older males aged 72±3 years, were asked to stand bare-foot on firm ground, and then step forward and up onto a 7" (0.178 m) -high structure at a self-selected comfortable speed. The mediolateral compliance of the structure could be covertly adjusted to one of three different values (measured at the structural top surface): rigid ($C_0 < 10^{-5}$ m/N), smaller compliance ($C_1 = 1\times10^{-4}$ m/N), and larger compliance ($C_2 = 2\times10^{-4}$ m/N). Six stepping trials were performed with each compliance. Trial order was C_0, C_1, and C_2, interspersed by different numbers of blocks of six C_0 trials to prevent subjects knowing when a compliance change occurred. Adaptive changes in the stepping movements were examined by comparing data from the first to sixth trials in each compliance condition.

The primary parameter investigated was the total time each subject used to complete the step-up movement normalized by the time used from initiating weight transfer till the lead foot contacting the raised structure (Ts). Kinematic and kinetic data were recorded and analyzed, but for brevity are not reported in this abstract. Repeated measure analyses of variance (rm-ANOVA) were performed to examine the effects of practice, structural compliance, and age on Ts. Post-hoc rm-ANOVA were used to examine the effects of structural compliance and age on stepping movements after practice (in the sixth trial). Additional post-hoc rm-ANOVA were performed to compare movement parameters of the first trial of YM with those of the sixth trial of OM. *P*<0.05 (with Bonferroni correction) was considered statistically significant unless otherwise noted.

RESULTS AND DISCUSSION

Practice significantly ($p<0.001$) reduced the stepping duration (Ts) needed for completing a single step-up movement, especially for older males stepping onto the laterally-compliant structures (C_1 and C_2) (Figure 1). The largest practice effect appeared within the first three trials. Ts for OM decreased 21% from the first to second trials on C_1 and 23% from the first to the third trials on C_2, while YM showed relatively smaller amounts of decrease (15%) in Ts from the first to sixth trials on C_2, but no significant changes on C_1. In contrast to results from the first trial only [3], after five repeated trials, the structural compliance did not affecte the total duration of the stepping movements. Although the difference in stepping duration between the two age groups decreased over six consecutive trials, it remained significant, especially on the most compliant structure (Ts for OM was 18% longer than for YM on C_2). By their sixth stepping trial, OM no longer differed significantly from YM in their first trial in either stepping duration or peak lateral structural displacement (p=0.23).

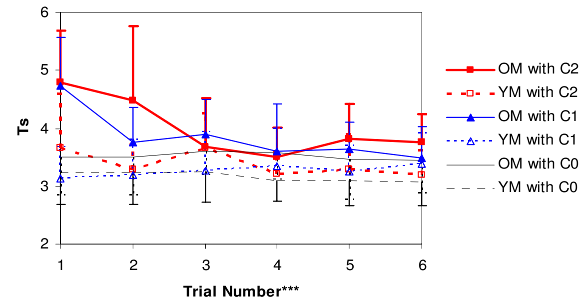

Figure 1: Mean values (error bars: 1SD) of total duration (Ts) of one stepping movement onto the raised structure with three values of structural compliance (C_0, C_1 and C_2) in six consecutive trials each (***: $p<0.001$). For six trials: age effect: $p<0.01$; interaction effect between age and practice: $p<0.01$. In the sixth trial: compliance effect: p=0.15; age effect: $p<0.018$.

Within a small number of practice trials, healthy male adults (both young and older) were able to significantly adjust their stepping movements to adapt to the lateral structural compliance. Older males were able to compensate for the age difference after two or three practice trials.

CONCLUSIONS

Elderly men require more time to adapt to the presence of unexpected lateral ladder compliance than do younger men.

REFERENCES

1. Bjornstig, U., et al. *J. Safety Research*, **23**, 9-18, 1992.
2. Faergemann, C., et al. *Accident Analysis and Prevention*, **32**, 745-750, 2000.
3. Yang, B.-S., et al. *Human Factors*, (in review)

ACKNOWLEDGEMENTS

Supported by US NIH grants P01 10542 and P50 08808.

FORCE ENHANCEMENT IN SUB-MAXIMAL VOLUNTARY CONTRACTIONS

Mir Ali Eteraf Oskouei and Walter Herzog
Human Performance Laboratory, University of Calgary; email: oskouei@kin.ucalgary.ca

INTRODUCTION

Force enhancement (FE) can be defined as an increase in steady-state isometric force after active muscle stretching [1,3,4]. Force enhancement has been observed in single fibers [3], isolated muscles [1], and intact muscles [2,4], and has been reported for maximal and sub-maximal electrical stimulation of muscles [1], as well as for maximal voluntary contraction (MVC) in humans [2,4]. However, it has not been studied for sub-maximal voluntary contractions. Therefore, it is not known if force enhancement occurs during normal everyday movements. The purpose of this study was to test whether force enhancement after stretching exists for sub-maximal voluntary muscle contraction

METHODS

All procedures were identical to those described by Lee and Herzog [4] with two exceptions:
i) All contractions were performed at sub-maximal levels; that is, at either 30% of the maximal isometric voluntary force, or at an activation level (full wave rectified and smoothed EMG, AEMG) corresponding to the value obtained at 30% of MVC, and ii) Visual feedback was provided to the subjects so they could match either 30% of MVC, or the activation level corresponding to 30% of MVC.

In this study, force enhancement was determined in two ways. Force enhancement in the force control protocol was defined as a decrease in steady-state isometric AEMG (activation deficit) in the stretch test contraction compared to the corresponding AEMG of the isometric reference contraction. Force enhancement in the activation control protocol was defined as an increase in steady-state isometric force in the stretch test contraction compared to the corresponding force obtained in the isometric reference contraction. The force enhancement experiment was performed with 17 volunteers.

RESULTS AND DISCUSSION

Subjects fell into two groups showing distinctly different results. Eight of the 17 subjects had statistically significant force enhancement (9 ± 5%) and activation deficit (15 ± 7%) following adductor pollicis stretching (Fig 1, session 1). The remaining nine subjects showed no changes in force or activation after muscle stretching when compared to the corresponding reference contractions

In order to ensure the reliability of the force enhancement results, all force enhancement tests were repeated several weeks after the first testing session. Those subjects who had consistent force enhancement and EMG deficit in the first session also had force enhancement and EMG deficit in the second session (Fig 1, session 2), and subjects who showed no force enhancement in the first session also did not have force enhancement in the second session.

The primary results of this study were that there is force enhancement for voluntary, sub-maximal contractions in the adductor pollicis, and that this force enhancement is clearly and unequivocally apparent in about one half of the tested subjects, while there is not a hint of force enhancement in the remaining subjects. In order to explain these results, we performed a follow up study in which we showed that those subjects who exhibited force enhancement had greater post-activation potentiation and a smaller resistance to fatigue, suggesting that the group showing force enhancement might have had a greater percentage of fast twitch fibers than the group who showed no force enhancement. Therefore, the results suggest that force enhancement might occur exclusively (or to a greater extent) in fast twitch fibers than slow twitch fibers.

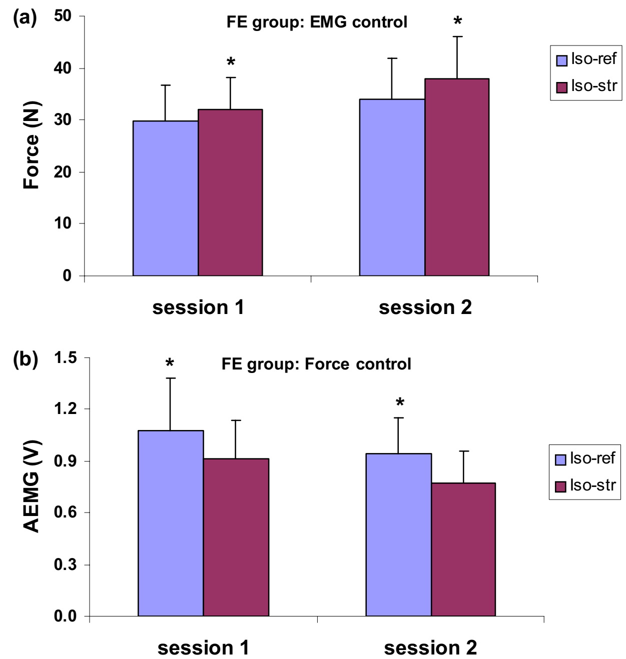

Figure 1: Mean (+1SD) isometric force and EMG during isometric reference contractions (Iso-ref) and following the stretching test (Iso-str) for activation control and the force enhancement group (a), force control and force enhancement group (b). Results for the initial session (session 1) and the repeat session (session 2) are shown. (* p< 0.05)

CONCLUSIONS

Here we demonstrate for the first time that force enhancement exists for sub-maximal voluntary contractions, and we hypothesize that force enhancement might be associated primarily with fast twitch muscle fibers.

REFERENCES

1. Abbott BC and Aubert XM. *J Physiol* **117**, 77-86, 1952.
2. De Ruiter CJ, et al. *J Physiol* **526.3,** 671-681, 2000.
3. Edman KAP, et al. *J Gen Physiol* **80**, 769-784, 1982.
4. Lee HD and Herzog W. *J Physiol* **545**, 321-330, 2002.

LUMBAR EXTENSOR FATIGUE CHANGES POSTURAL RECOVERY STRATEGY

Erin Wilson, Michael Madigan, Bradley Davidson, and Maury Nussbaum
Virginia Tech, Musculoskeletal Biomechanics Lab; email: mlm@vt.edu, web: www.biomechanics.esm.vt.edu

INTRODUCTION

Movements used to maintain standing balance in the sagittal plane following a postural perturbation have previously been described as a hip strategy, ankle strategy, or a combination of the two [1]. Numerous extrinsic and intrinsic factors affect which of these postural strategies are typically employed. To our knowledge, no studies have investigated fatigue in this regard. Therefore, the purpose of this study was to investigate the effect of lumbar extensor fatigue on postural recovery strategy in response to a balance perturbation.

METHODS

Twelve physically active males (20-22 years of age) participated in three experimental sessions, each consisting of four stages: warm-up, three unfatigued balance perturbations, fatiguing protocol, and a fatigued balance perturbation. The perturbation consisted of an anteriorly-directed impulse applied in the mid-sagittal plane at the level of the inferior margin of the scapulae. Typical perturbation characteristics were 170 N and 150 ms for the peak force and duration, respectively. Perturbations were designed to challenge the balance system while not eliciting a stepping response.

The fatiguing protocol consisted of multiple sets of back extensions and intermittent isometric maximum voluntary contractions (MVCs) to assess the level of fatigue [2]. The lumbar extensor muscles were fatigued over 14 minutes to 86%, 73%, and 60% of their unfatigued isometric MVC.

Triaxial ground reaction forces and body segment positions were collected from a force platform and a motion analysis system. Postural strategy was quantified using the trajectory of the center of pressure (COP) along with joint angles and joint torques for the ankle, knee, hip, and "low back" joints derived from inverse kinematics. A repeated-measures ANOVA was used to determine the effect of fatigue on recovery strategy.

RESULTS AND DISCUSSION

Results showed both pre-perturbation and post-perturbation changes in postural strategy with fatigue. Pre-perturbation changes involved a slight anterior lean prior to the perturbation, as evidenced by a 1.1 cm shift in COP position. Post-perturbation changes of the joint angles and torques were consistent with a shift toward more of a hip strategy. Specifically, there was a 3.2 Nm decrease in plantar flexor torque, a 10.2 Nm increase in hip extensor torque, a 2.5° increase in ankle plantar flexion, and a 6.3° increase in low back flexion (Figure 1). Correlations between pre-perturbation COP position and post-perturbation joint angles/torques were low, indicating that the changes in post-perturbation recovery strategy were primarily due to fatigue and not the difference in pre-perturbation COP position.

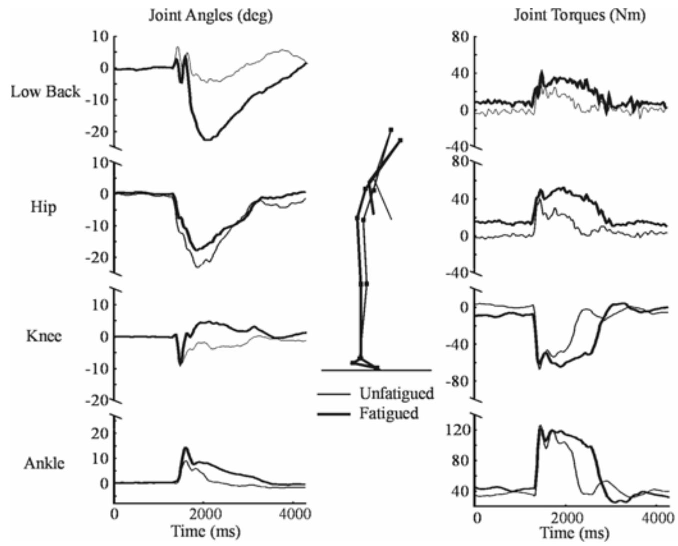

Figure 1: Representative joint angle and joint torque data during unfatigued and fatigued postural recoveries. Positive values indicate extension movement and extensor torque.

Results also suggested that certain subjects, classified prior to fatigue as employing a hip strategy in response to the perturbation, were more affected by fatigue compared to subjects classified as using a combination of hip and ankle strategies prior to fatigue. Increasing fatigue level exaggerated some, but not all, of the changes in postural strategy following fatigue.

CONCLUSIONS

Lumbar extensor fatigue elicited a change in postural strategy in response to a perturbation. Both pre- and post-perturbation postural compensations were identified and demonstrate a general shift toward increasing use of a hip strategy following lumbar extensor fatigue. These findings illustrate that neuromuscular fatigue can influence postural strategy similar to previously reported intrinsic factors.

REFERENCES

1. Horak, FB, Nashner, LM. *J.Neurophysiol*. **55**(6),1369-81, 1986.
2. Davidson, BS, Madigan, ML, Nussbaum, MA. *Eur.J Appl.Physiol Occup.Physiol.* in press, 2004.

ACKNOWLEDGEMENTS

This study was supported in part by grants from the Jeffress Memorial Trust, Richmond, VA (to MLM), and the National Institute for Occupational Safety and Health (to MAN).

EFFECTS OF LUMBAR EXTENSOR FATIGUE AND CIRCUMFERENTIAL ANKLE PRESSURE ON ANKLE JOINT MOTION SENSE

Kevin Pline, Michael Madigan
Musculoskeletal Biomechanics Lab, Virginia Polytechnic Institute and State University; Blacksburg, VA
email: kmpline@vt.edu, web: www.biomechanics.esm.vt.edu

INTRODUCTION

Falls from heights are one of the three leading causes of occupational deaths in the United States, accounting for approximately 700 deaths annually [1]. Increases in postural sway, which suggests a degradation of balance, have been shown following lumbar extensor fatigue [2]. This could conceivably contribute to fall accidents because it is common in many occupational tasks. However it is unclear how lumbar extensor fatigue affects balance. Proprioception at the ankle is critical in maintaining balance and any loss of proprioception could cause increases in sway and contribute to falls. Therefore, the first objective of this study was to evaluate the effect of lumbar extensor fatigue on ankle proprioceptive acuity.

Circumferential Ankle Pressure (CAP) has been shown to improve ankle proprioceptive acuity in individuals with below average proprioceptive acuity [3]. If lumbar extensor fatigue degrades proprioceptive acuity at the ankle, it is possible that the application of circumferential ankle pressure could mitigate the deleterious effects of fatigue on ankle proprioceptive acuity. Therefore, the second objective of this study was to investigate the effect of CAP on ankle proprioceptive acuity both with and without lumbar extensor fatigue.

Proprioceptive acuity in this study was quantified as ankle joint motion sense (JMS) which is the angular displacement at a joint necessary to detect joint motion.

METHODS

Fourteen healthy male subjects participated in the experiment with a mean (SD) age of 23.6 (2.9) years. To measure JMS, subjects were seated on a Biodex System 3 Pro, and the ankle was passively moved at 0.25 deg/sec in either plantar flexion or dorsiflexion until motion was detected by the subject and a hand held stop button pushed. During testing, subjects had their eyes closed and listened to music to prevent ancillary sensory cues of ankle motion. All subjects were tested with and without CAP both before and after a lumbar fatiguing protocol.

JMS was quantified as the angular displacement of the Biodex arm (in degrees) between the initial position and the final position after the subject stopped movement. Both directions were averaged together to give one JMS score for each condition. A square root transformation was used to obtain a normal distribution in the data. A two-way repeated measures ANOVA was used to test for the effect of fatigue on CAP on ankle JMS.

CAP was applied using a pediatric blood pressure cuff placed just above the talocrural joint and inflated to a pressure of 60 mmHg. Subjects were fatigued to 75% of their unfatigued maximum voluntary exertion (MVE) of the lumbar extensors by performing multiple sets of back extensions on a Roman Chair over 14 minutes [2].

RESULTS AND DISCUSSION

Subjects were fatigued to 68.3 (7.2)% of their unfatigued lumbar extensor MVE. Both fatigue and CAP impaired JMS scores (Figure 1). Fatigue induced a 6 (10) % increase in the JMS scores

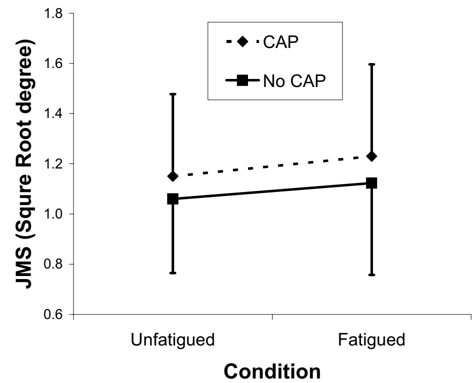

Figure 1: Mean (SD) averaged JMS scores (deg) after square root transformation for unfatigued and fatigued condition with and without CAP

(p=0.031). CAP induced a 7.7 (10) % increase in the JMS scores (p=0.016). The ANOVA performed on the JMS scores revealed no significant interaction between fatigue and CAP (p=0.868).

The explanation for lumbar extensor fatigue impairing proprioception at the ankle joint is not intuitive. One possible explanation is that the general body fatigue, induced by the lumbar extensor fatiguing protocol, hindered joint proprioception at the ankle due to the deficiency of central processing of proprioceptive signals. A number of central changes occur during fatigue and affect, among other things, proprioception [5]. Contrary to previous reports, CAP had a negative effect on ankle proprioception, which may be explained by difference in experimental methods.

CONCLUSIONS

Muscle fatigue of the lumbar extensors decreased ankle JMS. Our results also indicated that the application of CAP decreased ankle JMS. Although this provides a convenient explanation for the previously reported increase in postural sway with lumbar extensor fatigue, this is likely only one contributing factor. Future studies are needed to further understand the relationship between muscle fatigue, JMS, and balance.

REFERENCES

1. BLS, National census of fatal occupational injuries in 2003 US Department of Labor, *Bureau of Labor Statistics* (2004)
2. Davidson BS, et al.. *Eur J Appl Physiol.* **93,** 183-9, 2004.
3. You SH, et al. *J Orthop Sports Phys Ther*. **34,** 449-60, 2004.
4. Matre D et al., *Eur J Pain*. **6,** 245-60, 2002.
5. Gandevia, *Physiol. Rev*. **81,** 1725-1789, 2001.

ACKNOWLEDGEMENTS

This work was supported by grant # J-689 from the Jeffress Memorial Trust, Richmond, VA (to MLM) and grant # R01 OH007882 from the Centers for Disease Control and Prevention (to MAN). Its contents are solely the responsibility of the authors and do not necessarily represent the official views of the sponsor.

BACKWARD UPSLOPE WALKING: IMPLICATIONS FOR THE KNEE JOINT

[1]Andrea N. Lay, [2]Chris J. Hass, and [3]Robert J. Gregor
[1]School of Mechanical Engineering, Bioengineering Program, Georgia Institute of Technology
[2] Dept of Biobehavioral Sciences, Teachers College, Columbia University
[3]Center for Human Movement Studies, School of Applied Physiology, Georgia Institute of Technology
E-mail: gtg449j@mail.gatech.edu (A. Lay)

INTRODUCTION

It has been shown that backwards walking is metabolically more demanding than forward walking at the same speed, in part due to the change in quadriceps activity [1]. During forward walking the quadriceps contract eccentrically in early stance, while during backward walking the eccentric activity is replaced by concentric activity, which has a higher energy cost. This increased demand may contribute to improvements in cardiovascular fitness when backward walking is included in a training program [2]. Reduced joint stresses, in addition to the increased demand also make backward walking beneficial as a rehabilitation strategy for those suffering from knee injuries. Changing the grade of the walking surface may further increase the demands on the muscles and therefore increase the benefits of backward walking for rehabilitation [3]. The purpose of this study was to investigate the knee joint kinetics of backward upslope walking, compared to forward upslope walking, as a means of assessing its functionality as a rehabilitation exercise. [4].

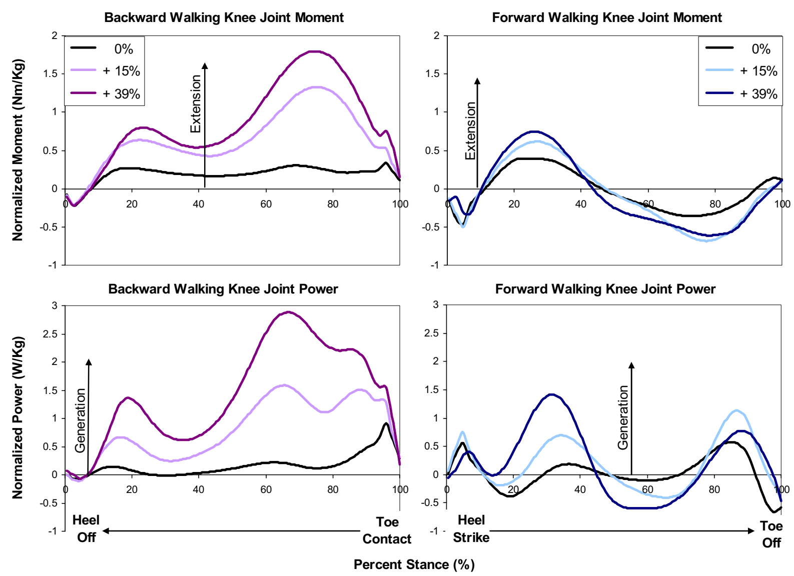

Figure 1: Backward (time-reversed such that the tasks are kinematically similar in time) and forward upslope walking joint moments and powers, ensemble averaged across subjects.

METHODS

Nine healthy adult volunteers (5M, 4F, mean age = 24 yrs) each read and signed an informed consent statement approved by the IRB at Georgia Tech. Participants were then fitted with fifteen retroreflective markers (Helen Hayes system) and performed sixteen walking trials (8 forward, 8 backward) at each of three different grades (0%, +15%, +39%) on a custom ramped walkway [5]. Starting positions were adjusted so each subject struck the force plate with their self-selected limb (8R, 1L). Each participant started at 0% and walked at a self-selected pace; for all subsequent forward trials the stance time was constrained to ±5% of his/her 0% average stance time.

Ground reaction forces (GRF) were sampled at 1200 Hz from a Bertec force platform concealed flush with the walkway surface. Kinematic data were captured at 60 Hz using a six camera Peak 3D Optical Capture system. GRF and kinematic data were exported to in-house software for inverse dynamics calculations. Joint moment and power data were normalized to 300 points over the stride (200 stance, 100 swing) and then ensemble averaged across all subjects for each grade.

RESULTS AND DISCUSSION

The joint moments and powers at the knee joint during backward and forward upslope walking are presented in Figure 1. The knee joint moment during the second half of stance in backward walking is dominated by a large extension moment that is not present in forward walking. The joint power data indicates that the knee extensors act concentrically during the entire stance phase of backward walking. During forward upslope walking the eccentric knee extensor activity also decreases from that at level forward walking, but the demands are much lower than during backward upslope walking. In both activities, the decrease in (or lack of) eccentric quadriceps activity may reduce the patellofemoral joint stresses that are often associated with anterior knee pain [3]. In addition, the large increases in the activity of the knee extensors during backward upslope walking may be useful for strengthening these muscles, a frequent goal in knee rehabilitation. Backward upslope walking also utilizes a greater range of knee joint motion (another common rehab goal) compared to forward upslope walking. In conclusion, backward upslope walking may be a more effective exercise than forward upslope walking for knee rehabilitation, although it is a more difficult task and may not be appropriate for all patient populations.

REFERENCES

1. Flynn TW, et al. *Med Sci Sports Exerc* **26**, 89-94, 1994.
2. Terblanche E, et al. *Int J Sports Medicine* **25**, 1-6, 2004.
3. Cipriani DJ, et al. *J Orth Sprt Phys Ther* **22**, 95-102, 1995.
4. Lange GW, et al. *J Orth Sprt Phys Ther* **23**, 294-301, 1996.
5. Lay AN, et al. *J Appl Biomech*, In Press.

ACKNOWLEDGEMENTS

This work is supported by a NSF GRF.

MEASUREMENT OF TURBULENCE IN GLOTTAL FLOW

Fariborz Alipour and Ronald C Scherer
University of Iowa, Iowa City, IA 52242
alipour@blue.weeg.uiowa.edu

INTRODUCTION

Glottal flow during phonation exits the glottis as a pulsatile jet that has both a repetitive quasi-periodic portion (called the *deterministic signal*), as well as a more random *turbulence* ripple [1]. Studies have suggested that the glottal jet between the vocal folds typically is laminar before the glottal exit, with transitions to turbulence within a short distance of the glottis [2].

This report discusses three different methods of analyzing the velocity signal of the air exiting the glottis into the deterministic (nearly repetitive) signal and the turbulence residual velocities: smoothing, wavelet de-noising, and ensemble averaging. These will be described following discussion of the excised larynx set-up.

METHODS

Canine larynx was mounted on an air tube with a hot-wire probe placed above the glottis outlet. Airflow was passed through a heater and humidifier to achieve 37?C and 100% humidification. The use of sutures, micrometers, and shims controlled glottal length and adduction. The jet velocity above the glottis was measured with hot-wire or hot film sensors using a constant-temperature anemometer system (Dantec 56C01). Analog signals from the hot-wire probe, EGG, and pressure transducer were monitored on a digital oscilloscope and simultaneously recorded on a DAT recorder. The signals were digitized later at a minimum of 10 kHz per channel for 1 to 5 seconds. **Figure 1** shows typically recorded data, including from top to bottom the following signals: EGG, subglottal pressure (Ps), tracheal velocity (Vs), and glottal exit jet velocity (Vj).

In the interest of flow analysis, it is important to separate the turbulence from the velocity. Thus, by time averaging the instantaneous velocity over time, one can find the mean or time-averaged velocity, and by subtraction, an estimate of the turbulence. This works easily in steady flows where time-averaged velocity becomes time independent. However, in pulsatile glottal flow, simple averaging does not work and other ways of separating turbulence are needed. Once the turbulence is separated, the remaining velocity is still time dependent and is called deterministic velocity.

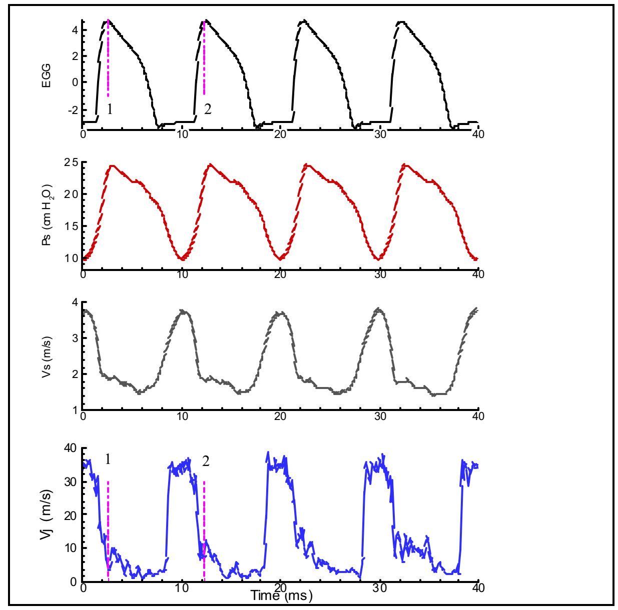

Fig. 1 – Typical waveforms of recorded data

SUMMARY OF RESULTS

The existence of flow turbulence in the glottal jet flow has been shown to be highly likely. The importance of the turbulence has not been well established, although it may appear obvious that it is part of the noise creation for breathy voicing, whisper, and perhaps secondary dipole sound. Thus, it is important to establish methods to measure turbulence associated with phonation. Turbulence intensity is the conventional measure of choice. But what methods should be used to extract the turbulence from velocity signals? This study attempted to examine three different methods, ensemble averaging, smoothing, and wavelet de-noising.

The results suggest that the ensemble averaging is inadequate because it gives the worst representation of the deterministic signal and the lowest cross-correlation between the deterministic signal and the original velocity. It takes away cycle "individuality" by making them all the same (for the chosen group with which to calculate the deterministic signal). The wavelet de-noising scheme would appear to be highly applicable, but the requirement to make a choice of which level of analysis to make lends flexibility for which there is an absence of knowledge. That is, the actual turbulence intensity is unknown, and therefore the level of analysis is not determinable. The smoothing method appears to be a reasonable compromise at this time because of its reasonable calculation of both the deterministic signal and the turbulence intensity, and because of its simplicity.

REFERENCES

1. Alipour F, et al. *J. Fluids Eng.-Trans. ASME*, **117**(4), 577-581, 1995.
2. Hofmans GCJ, et al. *J. Acoust. Soc. Am.* **113**(3), 1658-1675, 2003.

ACKNOWLEDGEMENTS

This work was supported by NIDCD Grant No DC03566.

BILATERAL SYMMETRY IN SINGLE LEG LANDINGS

Barbara Bentley, Peter Milburn, Stephan Milosavljevic and Allan Carman
School of Physiotherapy, University of Otago, Dunedin, New Zealand
email: peter.milburn@otago.ac.nz

INTRODUCTION

Landing on one foot from a jump is a complex task that is required during many sporting activities. An athlete uses muscular energy in an attempt to dissipate these forces with the contractile and articular structures about the knee playing a significant role as a shock absorber [1,2]. It is argued that the high mechanical demand on the knee joint on initial impact and during the landing phase makes it vulnerable to injury [2,3]. Therefore, variations in landing technique and knee movement patterns could contribute to the risk of injury by both increasing the amount of force as well as altering the direction of the load transmitted to the passive structures of the knee [4]. Significant asymmetries have been identified in bipedal landings [5] but there is no information comparing landing strategies of lower limbs in single leg landings. The aim of this project was identify differences in kinematics of the knee joint of the dominant and non-dominant legs during a single leg landing task.

METHODS

Five male and five female healthy university students performed 10 single leg landings on each leg from a fixed height of 37.5 cm. A 12 camera (Eagle™, EGL-500RT) motion analysis system (EVaRT™, Motion Analysis Corporation™, USA) was used to collect 3D kinematic data. Data were captured for three seconds at a sampling rate of 200 Hz and synchronised with the force plate (BP2436, Advanced Medical Technologies Inc™, USA) sampling at 1000 Hz. Calibration markers placed over the medial and lateral malleoli and knee joint lines, and the ASIS and PSIS on each lower extremity established the thigh and shank body fixed coordinate systems and allowed the local coordinates of segment markers to be determined relative to their respective local axes. Seventeen markers per limb allowed a least squared reconstruction of segment trajectory paths for the thigh and shank [6]. These trajectory data were then used to determine the kinematic variables of motion acting at the knee joint prior to foot contact to maximum knee flexion. These data were then filtered with a 6 Hz low pass Butterworth filter and exported into an Excel™ database for further analysis. A one way ANOVA was also used to consider the effect of gender on these kinematic parameters.

RESULTS AND DISCUSSION

While comparisons between the dominant and non-dominant legs demonstrated minimal differences in the sagittal plane knee kinematics, the movement patterns and sampled variables revealed considerable variability both between and within-subjects. However, the presence and formation of these movement pattern asymmetries appeared to occur independently of both limb dominance and gender. In contrast, and consistent with previous research, male to female differences were observed for the discrete variables of both flexion and valgus initial contact and maximum displacement. Importantly when the data were pooled and the leg dominance groups compared, these individual differences were concealed, highlighting the potential error of drawing conclusions regarding individual performance on the basis of group characteristics.

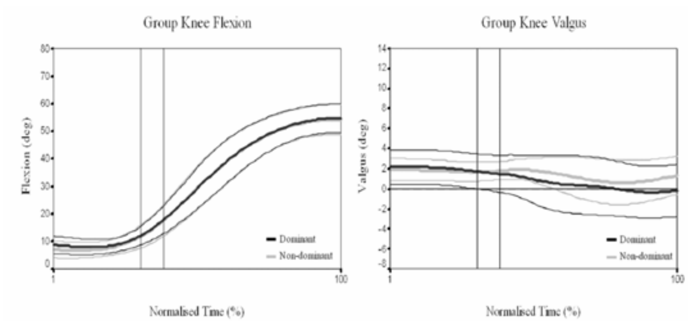

Figure 1: Sagittal and frontal plane knee kinematic patterns of the group means and confidence intervals for the dominant and non-dominant legs. Vertical lines represent the 95% confidence interval for initial contact.

CONCLUSIONS

These findings not only add to our understanding of the kinematics of landing performance and possible risk factors for non-contact ACL injuries, but should also guide methodology and interpretation of results in future research on single leg landings in sports tasks The results question the reliability of pooling data to make conclusions about individual subjects. Further investigations including other biomechanical and neuromuscular parameters are needed to allow a more comprehensive comparison of the dominant and non-dominant legs during landings, which will then provide a clearer illustration of the clinical implications for non-contact ACL injuries.

REFERENCES

1. Decker, MJ, et al *Clin Biomech* **18,** 662-669, 2003.
2. Zhang, S, et al. *Med Sci Sports Ex* **32**, 812-819, 2000.
3. Zhang, S, et al, *Med Sci Sports Ex* **28**(5(suppl)), 122, 1996.
4. Lephart, SM et al, *Clin Orthop Rel Res.* **1**, 162-169, 2002.
5. Ford, KR et al, *Med Sci Sports Ex* **35**, 1745-50, 2003.
6. Veldpaus, FE et al, *J Biomech,* **21,** 45-54, 1988.

MEASURING CONTINUOUS CHANGES IN HUMAN MUSCLE LENGTH, IN VIVO, USING ULTRASOUND

[1] Ian Loram, [2]Constantinos Maganaris and [1]Martin Lakie
[1]The University of Birmingham, UK, email: i.d.loram@bham.ac.uk
[2]Manchester Metropolitan University, UK; email: c.n.maganaris@mmu.ac.uk

INTRODUCTION

Muscle length is a key variable in the understanding and modeling of musculoskeletal dynamics. Direct, continuous measurement of changes in muscle length has traditionally been achieved using animal preparations and invasive methods (e.g. microsonography) in which the muscle and tendon are exposed. There has been no technique for measuring continuous changes in muscle length in humans or animals *in vivo* in a non-invasive manner. Ultrasonography has been used for several years to measure discrete changes in tendon length and aponeurosis length. We have recently developed this technique to continuously track naturally occurring changes in muscle length as small as ten microns [1, 2]. Here we use externally applied perturbations to investigate the spatial and temporal resolution of the technique.

METHODS

Six subjects stood on a footplate that independently measures left and right ankle torque. The subjects were strapped to a vertical back board while they maintained a low, constant level of ankle torque (~ 5 Nm). Every 1.3 s a pneumatic actuator applied a rapid, square pulse, dorsiflexing ankle rotation of defined magnitude and 0.2 s duration to the left ankle joint.

An ultrasound scanner (DIASUS, UK) recorded 40 s (1200 frames, 29 rotations) of sonographs focused on the distal aponeurosis of soleus and gastrocnemius medialis (Figure 1). In subsequent analysis, image markers were placed on the proximal and distal aponeurosis of the two muscles. Spatial cross correlation was used to track the changes in position of these markers throughout the 1200 frames. From the movement of these markers continuous changes in the length of the muscle were calculated from the differential movement between proximal and distal markers along the line of the central, distal aponeuroses [1]. All 29 rotations were averaged and the step changes in footplate angle and muscle length were measured.

RESULTS AND DISCUSSION

The applied ankle rotation and corresponding step increases in muscle length are recorded in Table 1. The ankle rotations are several tenths of a degree which is comparable with the size of rotations that occur naturally during human standing. Changes in gastrocnemius muscle length range from 8 to 300 microns and increase systematically with the size of the ankle rotation. The temporal and magnitude agreement between the measured changes in muscle length and the applied ankle rotations is evidence that the ultrasound tracking technique is recording real changes in contractile element length.

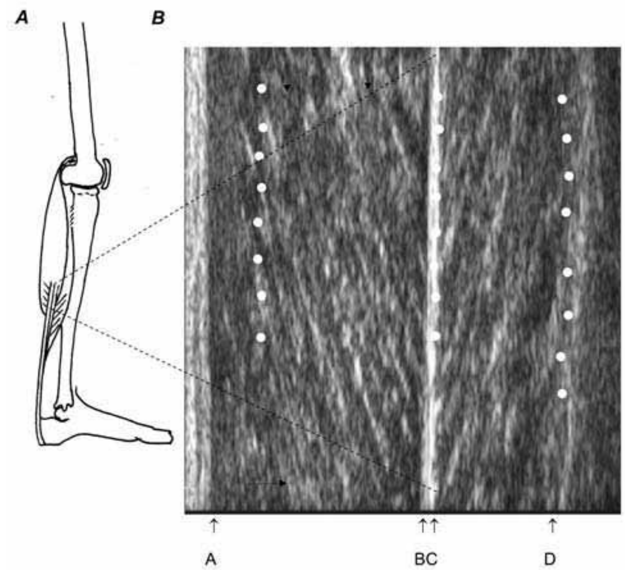

Figure 1: **A** Postural muscles soleus and gastrocnemius, **B** Sonograph showing marker positions (white dots) used for tracking changes in length of the contractile element. A, D proximal aponeuroses of gastrocnemius and soleus. B, C distal aponeuroses which are continuous with the Achilles tendon

CONCLUSIONS

This technique is non invasive and can measure changes in muscle length with high spatial and temporal resolution. It promises new insights into the study of muscle activity that is difficult to assess using surface EMG where muscles are close together or are relatively deep, or where tendon compliance and motion across multiple joints complicates knowledge of the changes in muscle length.

REFERENCES

1. Loram ID, et al. *J Physiol*, **in press**, 2005.
2. Loram ID, et al. *J Physiol* **556**, 683-689, 2004.

Applied ankle rotation (deg)	0.03 ± 0.003	0.16 ± 0.005	0.30 ± 0.01	0.42 ± 0.02	0.5 ± 0.03
Changes in muscle length (μm)	8 ± 3	43 ± 6	92 ± 17	194 ± 28	300 ± 18
Ratio (μm deg^{-1})	354 ± 156	269 ± 31	306 ± 56	458 ± 60	570 ± 32

Table 1: Changes in gastrocnemius contractile element length in response to ankle rotation. Mean ± S.E.M.

THE STRESS LEVEL ANALYSIS FOR DYNAMIC CASES AT HUMAN HIP JOINT

[1]Wang XiShi, [1]Jiang FuChuan and [2]Duan YiXiang
[1]Dept of Mathematics and Physics, QingDao Technological University, No.11, FuShun Rd., QingDao, 266033_P.R.China;
[2]Dept of Orthopaedics, QingDao Hospital, No.1, Jiaozhou Rd., QingDao, 266011_P.R.China; email: wang_xishi@hotmail.com

INTRODUCTION

The estimation of hip joint stress level is very useful for both preoperative planning and postoprerative rehabilitation. Since 1980's, Bergmann and his research group have been pursuing the instrumented hip implants with telemetric data transmission. Their collected gait data were recorded in HIP98, and updated in 2001[1]. So far it is unique gait database of the human hip contact force simultaneously measured in vivo. It is well recognized, however, that intrinsic pathomechanical changes in articulator cartilage depends upon local stress levels rather than upon global joint loading, and the abnormal mechanical stress upon hip joint cartilage is one of the main causes of osteoarthritis. In this paper, based on the Hertzian elasticity contact theory[2] and the hip dynamic measured data in vivo for the human various daily activities[1], such as walking slowly, walking normal, walking fast, going up stairs, going down stairs, standing up, sitting down and knee bending, a realistic stress level analysis for dynamic cases at the human hip joint are presented.

METHODS

1 Coordinate Systems

The three coordinate systems are established for the purpose of describing relationships between the hip motion and resultant load. They are, respectively, X, Y, Z system, X_C, Y_C, Z_C system and a spherical coordinate system ρ, θ, φ, as shown in Figure 1.

2 Stress Distributions on the Hip

The Hertzian theory for the elastic contact of two bodies with nonconforming geometrical shapes, which is suitable to the specific case of a sphere contacting inside a sphere, is employed to calculate the stress distributions on the hip[2]. The formulas are given in the following:

$$\sigma_t(\theta,\varphi) = \frac{3F(t)}{2\pi r^2(t)}\left[1-\frac{d_t^2(\theta,\varphi)}{r^2(t)}\right]^{1/2} \quad (1)$$

where $$r(t) = \left[\frac{3\pi}{8}F(t)\left(\frac{1-\nu_H^2}{\pi E_H}-\frac{1-\nu_C^2}{\pi E_C}\right)\left(\frac{1}{D_H}-\frac{1}{D_C}\right)^{-1}\right]^{1/3} \quad (2)$$

$$d_t(\theta,\varphi) = \frac{D_C}{2}\sin\left\{\cos^{-1}\left[\sin\theta\sin\theta_P(t)\cos(\varphi-\varphi_P(t)) + \cos\theta\cos\theta_P(t)\right]\right\} \quad (3)$$

3 Gait Data in vivo for Routine Activities

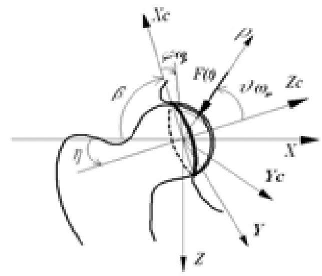

Figure 1: Coordinate System for the peak stress analysis

In 2000 version of HIP 98[1], the gait data in vivo for nine different human routine activities were collected, in which it is assumed to cause high hip joint loads and occur frequently in daily living. In this study, the gait data is taken from the patient H. Sonke[2]. The parameter values for peak stress evaluation are given as following: p=860N, $\eta = 4^0$, $\beta = 56.9^0$, D_c=28.2mm, D_h=28mm, E_c=900MPa, $\nu_c = 0.4$, E_h=206GPa, $\nu_h = 0.3$.

RESULTS AND DISCUSSION

In Figure 1, the comparisons for the peak stress curve in the human eight routine activities are given. The three types of walking cases, the two types of going up/down stairs cases and three types of standing up/sitting down/knee bend cases are, respectively, given in Figure 1(a), 1(b), 1(c). The results show that the higher peak stress level at the human hip joint in the walking fast case is existed. This is probably due to the fact with the higher contact force and with the larger inertia in walking fast case. This may reveals that the hip injury would be more probable when the human walks at the fast speed.

REFERENCES

1.Bergmann G., et al. HIP98 (2001 Version). Biomechanics Lab, Benjamin Franklin School of Medicine, Free University of Berlin, Gemany.
2. Whitehouse, D. J. In Handbook of Surface Metrology, 1994, pp. 749–759 (Institute of Physics Publishing, Bristol).

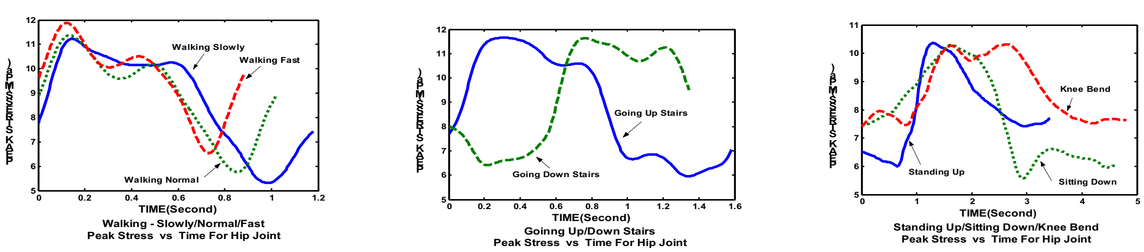

Figure 1 The peak stress comparisons at the hip joint for the human eight routine activities; (a) for walking cases: slowly, normal, and fast; (b) for going up stairs and going down stairs cases; (c) for standing up, sitting down, and knee bend cases.

DOPPLER MYOGRAPHY: ULTRASONIC LOCALIZATION OF ACOUSTIC MYOGRAPHIC SIGNALS

[1]Stephen F Levinson, [2]Hiroshi Kanai and [2]Hideyuki Hasegawa
[1]University of Rochester Department of Orthopaedics, Rochester, NY
[2]Tohoku University Department of Electronic Engineering, Sendai, Japan; email: levinson@ece.rochester.edu

INTRODUCTION

Skeletal muscles generate low-frequency sounds when they contract. These sounds originate from resonant vibrations of muscle fibers and their frequency is related to fiber length and tension. Although more than 2 decades have passed since acoustic myography (AMG) was first described, clinical applications have been limited to neuromuscular junction monitoring during anesthesia [1, 2]. With few exceptions, AMG has provided little more information than surface electromyography (EMG).

Recent improvements in ultrasonic Doppler technology have made it possible to detect sub-micron displacements. Indeed, the measurement of heart sounds propagating in myocardial tissue has been reported [3]. We hypothesize that a similar technique can be used to detect and possibly image skeletal muscle vibrations. This could lead to a biomechanical analog of needle EMG and could provide a noninvasive alternative.

METHODS

As many different terms appear in the literature, we will refer to the *phenomenon* of muscle fiber vibration as AMG, the recording of AMG signals at the skin surface as phonomyography (PMG) and the recording of AMG using Doppler ultrasound as Doppler myography (DMG).

We conducted a single subject exploration of DMG by placing an ultrasound transducer over the flexor forearm group. Doppler signals were obtained during active grasp and the range gate was adjusted to be within the flexor digitorum superficialis (FDS). Surface EMG and PMG signals were simultaneously recorded. Grip strength was measured using a grip dynamometer (Figure 1).

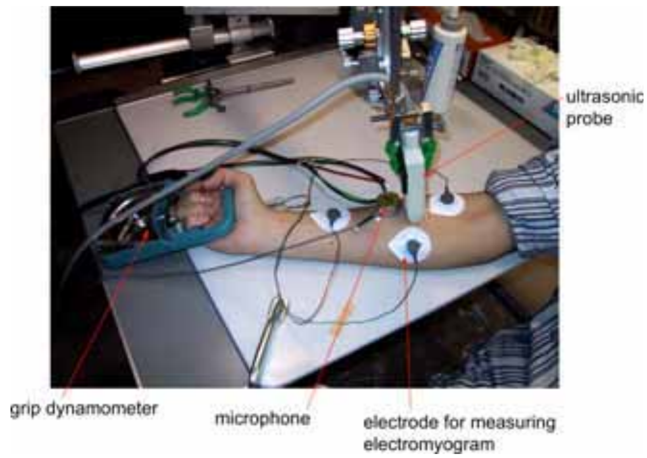

Figure 1: Apparatus for simultaneous measurement of surface electromyogram (EMG), phonomyogram (PMG) and Doppler myogram (DMG) in the forearm during grasp. Grip strength is measured using a grip dynamometer.

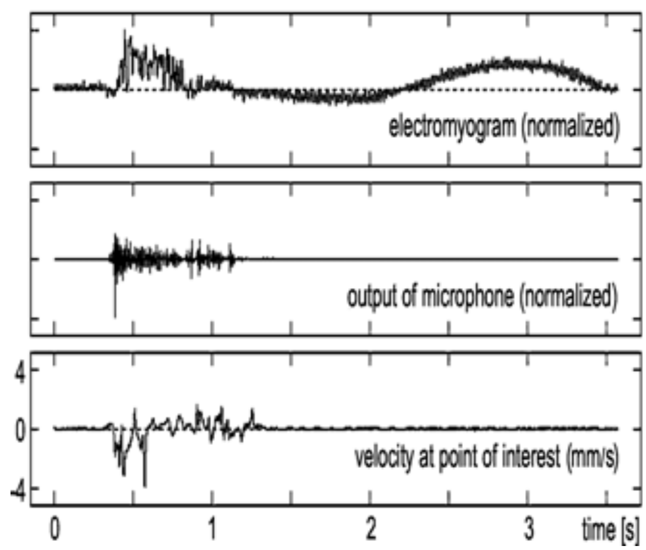

Figure 2: Simultaneous recordings of surface EMG (top), PMG (middle) and DMG (bottom) signals in the flexor digitorum superficialis during 24 kg of grasp.

RESULTS AND DISCUSSION

Simultaneous recordings were obtained for a variety of grip strengths. Vibrations are evident in the DMG recordings, however, translational motion was also observed (Figure 2). As with EMG, it is likely that filters will need to be implemented to remove unwanted components from the DMG signal. Additional experiments will be required to determine the optimum ultrasound parameters and configuration. Still, we believe that this is an important first step and that, with additional research, DMG could become a clinically useful test. The addition of real-time imaging capabilities could lead to a powerful new diagnostic tool.

REFERENCES

1. Barry DT, et al., Acoustic myography: a noninvasive monitor of motor unit fatigue. *Muscle & Nerve* **8:** 189-94, 1985.
2. Hemmerling TM, et al., Phonomyography and mechanomyography can be used interchangeably to measure neuromuscular block at the adductor pollicis muscle. *Anesthesia & Analgesia* **98:** 377-81, 2004.
3. Kanai H, et al., Transcutaneous measurement and spectrum analysis of hart wall vibrations. *IEEE Transactions on Ultrasonics, Ferroelectrics, and Frequency Control* **43:** 791-810, 1996.

ACKNOWLEDGEMENTS

The authors gratefully acknowledge the support of the University of Rochester School of Medicine and Dentistry.

ANISOTROPIC ELASTICITY & VISCOSITY DEDUCED FROM SUPERSONIC SHEAR IMAGING IN MUSCLE

[1]Stephen F. Levinson, [2]Stefan Catheline and [2]Mathias Fink
[1]University of Rochester Department of Orthopaedics, Rochester, NY, [2]Laboratoire Onde et Acoustique, Ecole Supérieure de Physique et de Chimie Industrielles, Paris, France; email: levinson@ece.rochester.edu

INTRODUCTION

Although the role of viscoelasticity in muscle mechanics is well recognized, methods for measurement *in situ* are limited. Recent advances in elastography have made possible the imaging of viscoelastic moduli within individual muscles [1, 2]. We have investigated a new approach, supersonic shear imaging (SSI), which combines high frame-rate (5kHz) ultrasound with acoustic radiation force induction of shear plane waves transients [3]. The elastic moduli can then be deduced from the propagation of these waves, and the viscous moduli from their attenuation.

METHODS

We applied SSI elastography in a single subject. With the subject seated comfortably, ultrasound image sequences were obtained from the right (dominant) biceps during sustained contractions. With the elbow held at 90°, various loads were applied by having the subject hold known weights. In addition, data were collected with the forearm supported (unweighted,) and unloaded (limb weight only). Image sequences were obtained and tissue displacements calculated using frame-to-frame cross-correlation.

RESULTS AND DISCUSSION

Displacement image sequences (e.g. Figure 1) were used to reconstruct speed of sound maps (Figure 2) in both the transverse and axial (longitudinal fiber orientation) directions. Average shear elastic moduli were obtained from these (Table 1) Propagation could not be observed in the transverse direction for loads greater than 0.8 kg. It is evident that the axial elastic moduli are significantly greater than their transverse counterparts, and that both increase with load.

Although we currently lack a direct means of calculating viscosity, it is evident from the observed attenuation of the induced waves that transverse viscosity is significantly greater than axial viscosity and that transverse viscosity increases dramatically with load to the point that propagation is suppressed entirely at greater loads. Whereas the significance of these results is not clear, we anticipate that knowledge of anisotropic and dynamic viscosity could have a significant impact on the field of Biomechanics.

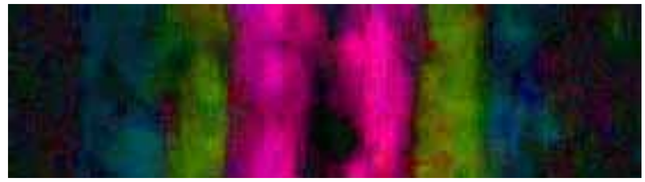

Figure 1: Composite image showing a 3 frame sequence of displacement data. Frame 1 is shown in red, frame 2 in green and frame 3 in blue.

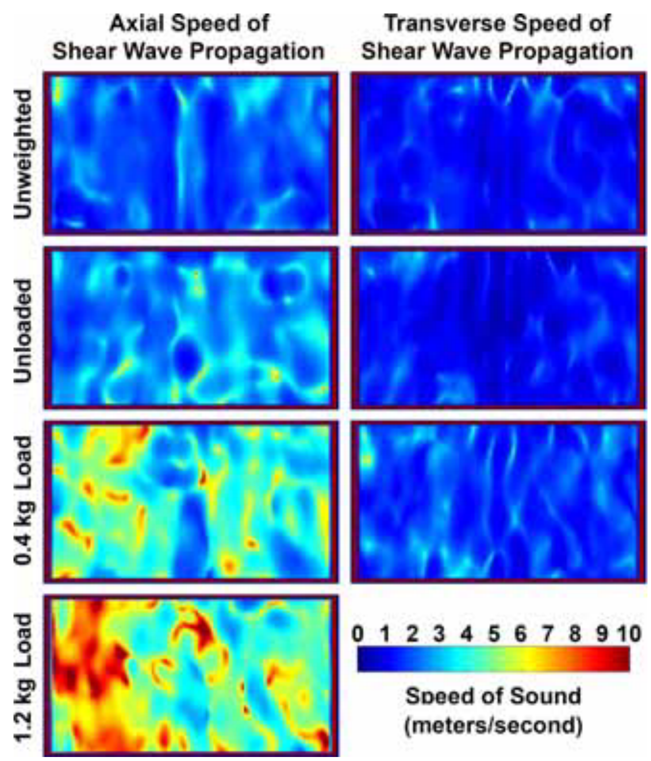

Figure 2: Speed of sound images in a for axial and transverse propagation at 4 applied loads. Propagation in the transverse direction did not occur above the 0.8 kg.

REFERENCES

1. Levinson SF, et al., Sonoelastic determination of human skeletal muscle elasticity. *J Biomech* **28:** 1145-54, 1995.
2. Basford JR, et al., Evaluation of healthy and diseased muscle with magnetic resonance elastography. *Arch Phys Med Rehabil* **83:** 1530-6, 2002.
3. Bercoff J, et al., Supersonic shear imaging: a new technique for soft tissue elasticity mapping. *IEEE Trans Ultrason Ferroelect Freq Control* **51:** 396-409, 2004.

ACKNOWLEDGEMENTS

The authors gratefully acknowledge support from the University of Rochester School of Medicine and Dentistry, and from Ecole Supérieure de Physique et de Chimie Industrielles

Table 1: Axial and transverse shear elastic modulus values (kPa) in the biceps brachii as a function of the applied load

	Unweighted	Unloaded	0.4 kg	0.8 kg	1.2 kg	1.6 kg	2.0 kg
Axial	4.0	7.3	47.2	50.8	59.7	82.5	94.6
Transverse	1.2	1.3	1.8	4.1	—	—	—

KINETIC ANALYSIS OF GAIT INITIATION

[1]D. Gordon E. Robertson, [2]Richard Smith and [2]Nick O'Dwyer
[1]School of Human Kinetics, U. of Ottawa, Canada, [2]School of Exercise and Sport Science, U. of Sydney, Australia

INTRODUCTION

Walking from quiet stance has been analyzed kinematically and kinetically, [2,4] yet little research has been conducted involving inverse dynamics. To understand how gait begins, electromyographic analyses [1,3] have also been carried out to identify the responsible muscles. Although ground reaction forces have often been recorded [1,2,4], net moments and powers were not computed. The purpose of this study was to determine the mechanical causes of gait initiation based on the moments and powers produced in the lower extremities.

METHODS

Subjects were required to stand on two force platforms (9281, Kistler) and then after a signal, begin walking briskly across two additional force platforms (9287, Kistler). Forty-two markers identified thirteen segments in three dimensions. Ten high-speed cameras (Eagle, Motion Analysis) filming at 200 Hz recorded the motion simultaneously with the force signals (EVaRT 4.2). These data were exported to Visual3D for computations of inverse dynamics and moment powers.

RESULTS AND DISCUSSION

Only data for the one-second period immediately before toe-off (TO) of the trailing leg will be presented because the following two steps produced patterns similar to those seen in other walking studies. During these two steps, the subjects accelerated but the moment and power histories had similar shapes to constant-speed gait [5].

Leading leg, stance phase. The moments of force of the leading leg did little work despite the relatively large ground reaction forces. At the hip, flexors initially acted isometrically but before TO and through early swing began hip and consequently knee flexion. Ankle plantar flexors produced small amounts of negative work to control dorsiflexion. Similarly, the knee extensors dominated the stance and early swing phases to control knee flexion. This suggests that initiation of gait began with active hip flexion and a simultaneous controlled collapse of the lead knee and ankle.

Leading leg, swing phase. The ankle moments of force were nearly zero throughout the swing phase doing virtually no work. The knee moments of force were initially extensor until midswing and then became flexor. The knee extensors first worked eccentrically to limit the amount of flexion and then concentrically to extend the knee slightly. Similarly, the knee flexors after midswing acted eccentrically to slow the extending knee (and foot) prior to foot-strike (FS). They then began a concentric phase that continued after FS. During the swing phase, the hip flexors performed positive work to elevate the thigh and thereby enable a longer stride. Like walking, this activity started before TO continuing throughout swing with its peak power occurring early in swing and reducing to zero before FS.

Trailing leg, stance phase (see Figure 1). The hip extensor moment of force was the first lower extremity moment to provide work during the stance phase of the trailing leg. It did the smallest amount of work of the three moments and was essentially inactive before TO. After TO, the hip flexors acted to flex the trail leg and enable swing.

The ankle moment of force did no work until after the leading leg passed midswing, after which it performed largest amount of positive work to provide the body with forward propulsion. At this point, the line of gravity was medial to the trail leg and just past the toes. Similarly, the knee moment was essentially inactive through most of the stance phase doing no work until midswing of the leading leg. At this point, the flexors acted to perform positive work to flex the knee and assist with elevation and forward motion of the foot. The amount of work done by the knee flexors was greater than for the hip extensors but much less than that of the ankle plantar flexors.

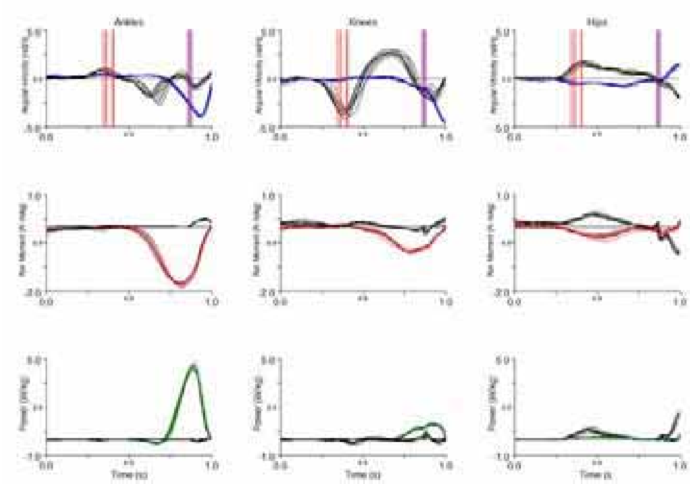

Figure 1: Five trials of one subject showing joint angular velocities (top), moments (middle) and powers (bottom). First column is ankle, second is knee and third is hip. Coloured curves are from the trailing leg--black curves from the leading leg. Data begin one second before toe-off of the trailing leg.

CONCLUSIONS

Initiation of gait begins with the hip flexors of the leading leg and a controlled collapse at the knee and ankle. The trailing leg's moments of force do no work until after the leading leg is midswing. Then the lead leg's hip extensors have a minor role at midswing preceding both the ankle and knee moments performing positive work. The trailing legs' ankle plantar flexors provided the main source of energy during push-off supplemented by work done by the knee flexors.

ACKNOWLEDGEMENTS

Mr. Ray Patton for technical assistance.

REFERENCES

1. Brunt D *et al. Gait Posture* **27**, 297-302, 2005.
2. Halliday SE *et al. Gait Posture* **8**, 8-14, 1998.
3. Mickelborough J *Gait Posture* **19**, 50-7, 2004.
4. Tokuno CD *et al. Gait Posture* **18,** 158-69, 2003.
5. Winter DA *Biomechanics and Motor Control of Human Gait. 2nd Ed.* Waterloo: Waterloo Biomechanics 1991.

EFFECT OF BILATERAL REACHING ON AFFECTED ARM MOTOR CONTROL IN STROKE — WITH AND WITHOUT LOADING ON UNAFFECTED ARM

[1] Wen-Lin Tung, [1] Fong-Chin Su and [1,2] Jyh-Jong Chang
[1] Institute of Biomedical Engineering, National Cheng Kung University, Tainan, Taiwan,
[2] Faculty of Occupational Therapy, College of Health Science, Kaohsiung Medical University, Kaohsiung, Taiwan;
email: minlynn@seed.net.tw, web: http://www.bme.ncku.edu.tw/

INTRODUCTION

Bilateral movements are often used to facilitate symmetrical and smoother movements of the hemiparetic arm in stroke patients. Previous research has shown that bilateral movements with inertial loading on unaffected arm may increase interlimb coupling. The goal of this present study is to investigate the effect of bilateral reaching, with/without inertial loading on the unaffected arm, on hemiparetic arm motor control in stroke.

METHODS

Recruited were twenty unilateral stroke patients (17 males, 3 females), aged between 37 to 75 years (mean ± standard deviation, 56.00 ±10.54 years). All subjects scored at least 30 on the upper extremity subtest of the Fugl-Meyer Motor Function Assessment (total score: 66). Taking the difference of upper extremity function level into consideration, we spilt the subjects into two groups according to the score of FMA. Thirteen subjects in group 1 scored between 50 and 66, indicating a mild motor deficit, and seven subjects in group 2 scored between 30 and 49, indicating a moderate motor deficit. A three-dimensional kinematics analysis equipment (VisualeyezTM Hardware, Canada) was used to collect the movement trajectory data of the hemiparetic arm during performing the experimental tasks. Subjects were asked to perform four movement tasks as quickly as possible: (1) reaching forward with the affected limb only (Uni); (2) reaching forward with both limbs simultaneously (Bil); (3) reaching forward with both limbs while adding a load of 25% upper limb inertia to the unaffected limb (Bil+25%). Kinematic parameters were utilized to quantify the reaching performance of the affected arm.

RESULTS AND DISCUSSION

No matter if loading was applied on the unaffected arm, bilateral reaching task did not significantly facilitate smoother and faster movement. Furthermore, during bilateral reaching with loading on unaffected arm, stroke patients showed slower movement, smaller maximal movement velocity, and less smooth movement in affected arm than bilateral reaching without loading. The greatest proximal active upper extremity range of motion was found during bilateral reaching without unaffected arm loading. More trunk movement was adapted during bilateral reaching either with or without loading on unaffected arm. Patients with moderate upper extremity motor impairment level performed more discontinues and less active elbow range of motion than those with mild upper extremity motor impairment level during performing reaching tasks.

CONCLUSIONS

Bilateral reaching tasks with/without loading on unaffected arm could be considered as adding costs and challenges during motor control. Training with bilateral arm movements may be considered as a treatment strategy and can be incorporated in stroke rehabilitation to facilitate greater active movement and improve motor control performance in affected arm.

REFERENCES

1. Cunningham, C. L., Stoykov, M. E., & Walter, C. B.. *Acta psychologica* **110**(2-3), 321-337, 2002.
2. Mudie, M. H., & Matyas, T. A.. *Disability and Rehabilitation* **22**(1-2), 23-37, 2000.

Table 1: Means and standard deviations for dependent variables calculated from the three movement tasks

	Mild Group (N=13)			Moderate Group (N=7)		
Task / Variables	Uni	Bil	Bil+25%	Uni	Bil	Bil+25%
MV(cm/s)	127.95±48.45	113.27±48.10	114.40±48.26	88.78±25.78	79.51±18.70	80.22±21.60
PRMVO (%)	41.20±5.81	38.40±7.87	39.30±7.60	45.84±15.41	39.14±8.81	34.59±8.91
MT(s)	0.66±0.33	0.77±0.43	0.74±0.39	0.92±0.27	0.97±0.26	0.74±0.39
NMU	1.05±0.18	1.05±0.18	1.03±0.09	1.62±1.11	2.10±0.90	2.00±0.94
NJSM	29.43±34.51	43.50±69.86	39.97±67.85	73.81±43.85	97.64±63.26	95.94±55.67
EFER(deg)	59.67±16.25	65.97±16.32	62.29±13.04	44.81±10.21	47.54±14.76	45.13±12.10
SFER(deg)	52.09±14.83	58.81±16.70	55.16±15.15	46.08±7.82	52.89±10.42	49.98±14.47
TLLV(cm)	2.33±1.55	3.77±2.64	3.58±2.45	4.20±1.70	4.16±1.53	5.29±3.14

MV: maximal velocity, PRMVO: percentage of reach where maximal velocity occurs, MT: movement time, NMU: number of movement units, NJSM: normalized jerk score of movements, EFER: elbow flexion-extension range, SFER: shoulder flexion-extension range, TLLV: trunk linear line value.

Development of a web-based decision support system for acupuncture treatment -The selection of acupuncture points based on a web-based 3-D computer graphic model of the movement used to evaluate motion-induced pain –

Kazuhiko AMANO[1] Ryo KANDA[2] Tatsuya SHIMODA[1] and Yoshito MUKAINO[2]
[1]SEIKO EPSON Corporation Technology Platform Research Center, Japan
[2]The Faculty of Sports and Health Science, Fukuoka University, Japan
e-mail: amano.kazuhiko@exc.epson.co.jp shimoda.tatsuya@exc.epson.co.jp
r-kanda@fukuoka-u.ac.jp mukaino@fukuoka-u.ac.jp

INTRODUCTION

One motion of any part of the human body includes the movement of many joints and axes of the whole body.
When one part of our body moves, our whole body moves simultaneously. It enables us to perform such body movement ranging from the fine motions used in manual labor to the dynamic motions utilized in sport. When a factor exists that disturbs any part of this series of movements in any part of our body, then the whole motion loses its smoothness and thus causes such symptoms as pain. A new diagnostic method for acupuncture treatment which evaluates motion-induced pain[1)] now makes it possible to identify a location that actually causes pain. This method can identify an affected meridian which thus enables us to select an appropriate acupuncture point to reduce pain based on the concept of meridians. The appropriate stimulation of the acupuncture point may help a patient to correct an abnormal motion[2)]. In addition, the effect of a selected acupuncture point is identified by observing that the motion-induced pain decreases after stimulating the acupuncture point. This is a very simple but effective method for identifying the affected meridians and confirming the effect of the selected acupuncture point. To popularize this method, we have developed a web-based decision support system for this method by expressing the loads of movement, which therefore make it possible to precisely identify the exact location that causes a specific pain, using a 3-D computer graphic model for selecting the appropriate acupuncture points.

METHODS

A three-dimensional motion analysis device (Motion Analysis Expert Vision HiRES system) and high-speed camera (FALCON CAMERA) are used to accurately capture an optical motion on film. Next, 32 reflector markers are attached to the parietal region, the cervical vertebra, the lumbar vertebrae and other joints of the subject. Thereafter, the subject is asked to perform the movements similar to those done during orthopedic and neurological tests. Eight high-speed camera takes pictures of these movements which consist of 30 different kinds of movement; the extension of the neck, upper extremities, lower extremities and trunk.
The photographs taken with a high-speed camera are then developed into animation data which are then combined with human body modeling data. Next, such data are run on a human body modeling program using three dimensional computer graphics (hereafter, called 3DCG).
In addition, we also take photographs of all 36 acupuncture points which are each composed of twelve acupuncture points which are suitable for restoring the restriction of extension on either the front, the back or the side of the human body, respectively. We then established a home page in which 30 kinds of movement are connected with the photographs in order to indicate the appropriate acupuncture locations.

RESULTS AND DISCUSSION

The movements consist of the motions which extend from the front, back and side of our body. A total of thirty such movements are considered to exist when performing a physical assessment similar to those performed during orthopedic and neurological tests. Each individual motion influences the 14 meridians of the body. When a specific movement induces pain, then an affected meridian can be found. Next, the optimal acupuncture points to reduce such pain can then be selected based on the concept of meridians. The newly developed home page can show us how to follow such movements based on 3DCG modeling, thus allowing therapists to select the appropriate acupuncture points to reduce pain. When you click on any of the movements shown on screen, then the acupuncture points that need to be stimulated are shown. This tool greatly supports the therapist. Moreover, this system may also be utilized as a self-care tool of pain because it can show the appropriate points to reduce pain which can thus be performed by the patient himself. This system also provides new insight into Oriental Medicine. Further similar research on the motion-induced fluctuation of pulse waves[3)] may therefore eventually lead to the compilation of scientific evidence supporting the theory of a pulse diagnosis in Oriental Medicine.

CONCLUSIONS

A newly developed homepage has been established as a support system for performing effective acupuncture treatment by therapists and also as a tool for self-care, since this homepage is able to clearly demonstrate the movements and thereby can help in selecting the most appropriate acupuncture points.

REFERENCES

1) Mukaino Y, et al. The Meridian Test, IshiIyaku Publishers. Tokyo, 1999.
2) Kondo f, Amano K, Tanaka A, Mukaino Y. Evaluation of acupuncture effect on a motion of meridian test by three dimensional measurement. Technical Report of IEICE MBE 29, 9-12, 2002
3) Amano K. Scientific Grasp of Individual's Vital Information by Checking Pulse Waveform “Seiko Epson Corporation Advances the Basic Research for PULSENSE”, Nature Interface, Vol.2, 60-67, Mar., 2001, http://www.natureinterface.com/e/ni02/

JOINT WORKSPACE OF SHOUDLER AND ELBOW ASSOCIATED WITH VARIOUS AXIS POSITIONS DURING MANUAL WHEELCHAIR PROPULSION

[1] Shun-Hwa Wei, [2] Hsiao-Yun Chang
[1] Chairman of Graduate Institute of Rehabilitation Science and Technology, National Yang Ming University, Taipei, Taiwan, R.O.C.; email: shunhwa@ym.edu.tw
[2] Doctoral student, Graduate Institute of Physical Education, National College of Physical Education and Sports, Taoyuan, Taiwan, R.O.C.

INTRODUCTION

Manual wheelchair propulsion is the primary source of mobility for many persons with disabilities. The user's position relative to the drive wheel has been recognized as an important factor affecting propulsion efficiency [1, 2]. Currently, many wheelchairs provide the ability to adjust the position of the drive-wheel. To justify the effectiveness of this design feature, it is necessary to document the relationship between a user's propulsion performance and the axis position. Therefore, the purpose of this study was to investigate wheelchair users' shoulder and elbow joint workspace associated with various wheel axis positions.

METHODS

Ten persons with disabilities who use manual wheelchairs voluntarily served as subjects for this study. Detailed data for the subjects are presented in Table 1. A wheelchair with adjustable axis positions was used. Six positions including various vertical and horizontal positions were tested (Figure 1). A Zebris ultrasonic motion analysis system was used to measure each subject's upper extremity motion. ANOVA with post-hoc multiple comparisons were used to examine the differences of upper extremity motion among the six positions.

RESULTS AND DISCUSSION

The results showed that different axle position did not significantly affect ($P>0.05$) temporal parameters of push time and recovery time. High and backward axle positions resulted in increasing shoulder initial extension angle. In comparison with low axle positions, high axle positions produced significantly larger shoulder and elbow joint ranges of motion ($p<0.05$). High axle positions also produced larger efficient joint workspace than lower axle positions (Table 2).

Table1. Subject information

Anthropometric data	Mean	SD
Age; years	33.67	8.03
Height; cm	166.92	7.39
Weight; Kg	66.00	7.79
Years of disability; year	15.50	14.63
Years of using wheelchair; year	5.50	5.78
Arm length; cm	53.71	2.73
Trunk length; cm	59.39	2.78
Thigh length; cm	42.71	3.19

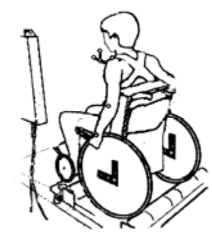

Figure1. Experimental configuration

CONCLUSIONS

The location of the drive-wheel axis determined performance of manual propulsion [3, 4]. This finding provides valuable information for guiding adjustments of the wheel-axis position relative to a user's upper body. An initial shoulder extension angle of 45 degrees and larger shoulder and elbow advantageous joint workspace could be considered adjustment principles. Adjusting the axis upwards and backwards might increase shoulder initial extension angle. Furthermore, adjusting axis height might increase efficient joint workspace.

REFERENCES

1. Van der Woude LVH, et al. *J Rehabil Res Dev* **26**, 31-50, 1989.
2. Wei SH, et al. *Clin J of Biomech* **18**, 46-52, 2003.
3. Boninger ML, et al. *Arch Phys Med Rehabil* **81**, 608-13, 2000.
4. Hughes CJ, et al. *Arch Phys Med Rehabil* **73**, 263-9, 1992.

Table2. kinematics parameters associated with various wheel-axis positions

Parameters		Axel position					
		LB	LM	LF	HB	HM	HF
Temporal	Push; sec (%cycle)	0.43±0.08 (35.3±4.2)	0.46±0.07 (36.9±3.4)	0.46±0.09 (38.4±3.5)	0.42±0.08 (35.3±3.5)	0.43±0.08 (36.6±5.2)	4.09±0.10 (39.1±4.8)
	Recovery; sec(% cycle)	0.79±0.10 (60.9±4.8)	0.80±0.07 (63.4±5.2)	0.76±0.11 (64.7±3.5)	0.79±0.10 (62.0±3.8)	0.76±0.12 (62.2±3.4)	0.79±0.17 (64.7±4.2)
Initial position	Extension; deg	47.4±2.5^{A}	43.7±8.1^{B}	32.8±11.2^{B}	54.7±8.3^{A}	49.5±11.8^{A}	40.0±10.5^{B}
Joint ROM	Sef ROM;deg	41.6±10.1^{A}	42.7±10.5^{A}	38.8±6.2^{A}	56.3±12.1^{B}	51.9±12.4^{B}	52.8±9.1^{B}
	Eef ROM; deg	18.1±4.6^{A}	18.7±7.1^{A}	15.4±8.4^{A}	35.7±8.1^{B}	33.7±6.0^{B}	33.6±6.2^{B}
	Joint workspace; rad^2	0.066±0.017^{A}	0.065±0.013^{A}	0.045±0.017^{A}	0.232±0.026^{B}	0.259±0.037^{B}	0.187±0.022^{A}

LB is wheel axis at low backward position; LM is wheel axis at low middle position; LF is wheel axis at low forward position; HB is wheel axis at high backward position; HM is wheel axis at high middle position and HF is wheel axis at high forward position. All values are mean ± SD. Sef and Eef ROM represents shoulder and elbow range of motion in the direction of extension and flexion, respectively. Mean with the same letter for post-hoc grouping are not significantly different ($p>0.05$). Mean with different letter are significantly different ($p<0.05$).

EFFECT OF STROKE RATE ON MECHANICAL POWER FLOW IN ROWING

[1] Mathijs J. Hofmijster, [1] Erik H.J. Landman, [2] Richard M. Smith and [1] A.J. "Knoek" van Soest
[1] Faculty of Human Movement Sciences and Institute for Fundamental and Clinical Human Movement Sciences, Vrije Universiteit Amsterdam, the Netherlands
[2] School of Exercise and Sport Science, Faculty of Health Sciences, University of Sydney, Australia;
email: m.hofmijster@fbw.vu.nl, web: www.ifkb.nl

INTRODUCTION

In competitive rowing, a large amount of mechanical power is produced. However, only the fraction of power that contributes to average velocity will determine the performance. In this study the previously established power equation of rowing [1] is used to analyze rowing performance. Mechanical power is lost by moving water with the blades. Power is lost to water friction on the hull which is related to velocity cubed. Those power losses are higher when there are larger fluctuations in velocity. Due to the intermittency of propulsion, and due to impulse exchange between the rower and the hull, these fluctuations are substantial. Stroke rate is an important aspect of rowing technique. In this study the effect of stroke rate on the power flow in rowing was investigated.

METHODS

Nine subjects participated in this study. Subjects were instructed to row a minimum of 10 consistant strokes at rates of 20, 24, 28, 32 and 36 strokes per minute with maximal intensity. Subjects rowed 5 trials at each prescribed stroke rate.

Forces on the pin were measured using piezoelectric transducers (Kistler, Switzerland). Oar angle in the horizontal plane was measured using servo-potentiometers (Radiospares). Boat velocity was measured using a trailing turbine with embedded magnets (Nielsen Kellermann). Data was transmitted to the shore using telemetry (ROWSYS, Australia).

Steady state rowing was assumed to be perfectly periodic. In this situation, the average power production during the stroke cycle ($\bar{P}_{rower}$) equals the average power losses to drag ($\bar{P}_{drag}$) and moving water with the blades ($\bar{P}_{blade}$).

Propelling efficiency ($e_{propelling}$) was calculated as the fraction of $\bar{P}_{rower}$ *not* lost to the blades. Velocity efficiency ($e_{velocity}$) was calculated as the fraction of $\bar{P}_{rower}$ *not* lost to velocity fluctuations. From these two terms, the fraction of $\bar{P}_{rower}$ contributing to average velocity ($\bar{v}_{boat}$), defined as total efficiency (e_{total}) was calculated.

A repeated measures ANOVA was used to analyze the data. Pearson's correlation coefficient was also calculated.

RESULTS AND DISCUSSION

A significant main effect of stroke rate was found for $\bar{P}_{rower}$, $e_{propelling}$, $e_{velocity}$, e_{total} and $\bar{v}_{boat}$ (all $p<0.0001$). The correlation of these variables with stroke rate were 0.98, 0.82, -0.72, 0.73 and 0.96 respectively, indicating strong linear relationships (correlation coefficients are averaged over subjects). In table 1 the mean values are presented.

The increase of velocity at higher stroke rates was mainly caused by the increase in $\bar{P}_{rower}$. However, rowers are probably not able to maintain the values found for $\bar{P}_{rower}$ throughout a typical 2000m rowing race.

The decrease of $e_{velocity}$ at increasing stroke rate was expected and is caused by a higher $\bar{v}_{boat}$ and larger accelerations and decelerations by the rower itself. However, e_{total} increases at increasing stroke rate, caused by a substantial increase of $e_{propelling}$. While the mechanical work of the rower remains relatively constant with increasing stroke rate, the energy lost at the blades actually *decreases*. This is most likely related to the finding that at higher stroke rate the blade travels less in the direction opposite the propulsion, thus less water is being moved.

CONCLUSIONS

This study shows the power equation to be an adequate conceptual model to analyze rowing performance. Results indicate that stroke rate not only affects the power output of the rower, but also affects the power loss at the blades and the power loss associated with velocity fluctuations. When similar results become available regarding the effect of other technique-related factors, it may become possible to understand the optimal technique as the optimal compromise between generation of power by the rower and power loss to terms not contributing to average velocity.

REFERENCES

1. Ingen Schenau G.J.v., Cavanagh P.R. *Journal of Biomechanics* **23 (9)**, 865-881 (1990).

Table 1: Average values and standard deviations (between parentheses) for the stroke rates investigated.

Stroke rate	$\bar{v}_{boat}$ (m/s)	$\bar{P}_{rower}$ (W)	$e_{propelling}$	$e_{velocity}$	e_{total}
20	3.84 (0.32)	277 (74.0)	0.785 (0.019)	0.955 (0.0062)	0.740 (0.021)
24	4.07 (0.29)	328 (77.6)	0.797 (0.019)	0.954 (0.0068)	0.751 (0.022)
28	4.33 (0.37)	389 (95.8)	0.812 (0.019)	0.953 (0.0070)	0.765 (0.020)
32	4.52 (0.30)	441 (98.1)	0.821 (0.019)	0.950 (0.0067)	0.770 (0.021)
36	4.76 (0.76)	505 (118)	0.830 (0.017)	0.947 (0.0074)	0.777 (0.019)

BONE REMODELING MODEL OF A BASIC MULTICELLULAR UNIT

Sylvie Wendling-Mansuy, Emmanuel Rixrath, Jean Louis Milan and Patrick Chabrand
Laboratoire d'Aérodynamique et Biomécanique du Mouvement, CNRS USR 2164,
Université de la Méditerranée, Marseille, France. email: wendling@morille.univ-mrs.fr

INTRODUCTION

The bone tissue adapts itself to the mechanical and physiological environment and involves cellular processes of mechanotransduction and remodeling. In fact, bone remodeling results from closely coupled resorption and apposition processes of organized cellular units called Basic Multicellular Units (BMUs) which are controlled by local mechanical signals. Recent studies revealed that osteocytes which are the most abundant cells in bone play a fundamental role as mechanosensors in the early stage of bone remodeling [1]. Moreover it has been shown that osteocyte apoptosis induces bone resorption and appears at very high or very low strains level. However mechanotransduction, biological and biochemical processes involved in the resorption/formation coupling are complex and not yet clearly identified.

The idea of the present study is to develop a model to mechanically simulate the resorption/apposition processes of a BMU taking into account high and low strain energy, microcracks, osteocyte apoptosis, fluid flow effects as well as biochemical factors. The present mechanical model is based on thermodynamic approaches following Silva and Ulm [2] resorption model.

METHODS

The present bone remodeling model is applied to one isolated trabeculae of spongy bone considered as a homogenous isotropic and elastic cylinder containing a network of canaliculae with osteocytes. The biochemical activities of the osteoclasts to dissolve bone matrix and the osteoblasts to synthesize collagenous matrix are translated into energetic quantities which transformations are studied using the two thermodynamical principles. During the resorption phase, the dissolution potential of the cell is balanced by the strain energy of the trabeculae and a chemical energy due to the osteocyte apoptosis. During the apposition phase, the chemical potential of the cell to synthesize collagen is balanced by the trabeculae strain energy through the adherent surface and a chemical energy of the factors released during the resorption phase. Two scenarios of bone remodeling are simulated considering a low strain energy which is defined by *understress* conditions and a high strain energy which is defined by *overstress* conditions.

RESULTS AND DISCUSSION

The numerical results show the variation of the final bone volume (after remodeling) normalized by the initial volume as a function of the strain energy normalized by reference strain energy in two stress conditions (*understress* and *overstress*). Figure 1 shows that the final bone volume obtained after remodeling tends to a non zero minima (i.e. for no stress applied; W*=0). Two parameters have been introduced in the model: the coupling parameter α represents the chemical energy of factors and proteins released in the medium during the resorption phase which might stimulate the recruitment and the differentiation of the osteoblasts.

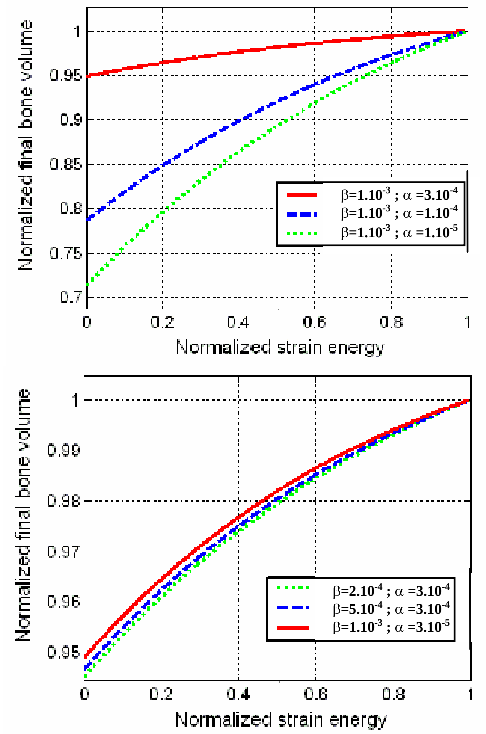

Figure 1: Final bone volume normalized as a function of the applied normalized strain energy in *understress* conditions.

The parameter β represents the mechanical sensibility of the osteoblasts during the apposition phase. It appears that in *understress* conditions, the new bone volume seems to be regulated mainly by chemical factors (the coupling parameter α) because the increase of the mechanical sensibility of the osteoblasts has no effect on the final bone volume (see Figure 1). By contrast, in *overstress* conditions, the numerical results show that increasing β increases the new bone volume more than the coupling parameter α. Since this model could contribute to understanding bone remodeling related to cellular activity and more particularly in pathologic cases (osteoporosis), further studies are needed to validate this model and to identify the parameters introduced in the model.

REFERENCES

1. Knothe Tate M.L., et al., *J. Biomech.* **36**, 1409-1424, 2003
2. Silva E.C., et al. *Proceedings of te 15th ASCE Engineering Mechanics Conf.*, New York, 2002.

TRUNK AND SHOULDER MUSCLE RESPONSE COMPARING ONE REPETITION MAXIMUM BENCH AND STANDING CABLE PRESS

[1]Francisco J. Vera-Garcia, [2]Juan Carlos Santana, [1]John R. Gray and [1]Stuart M. McGill.
[1]Spine Biomechanics Laboratory. Department of Kinesiology. University of Waterloo, Canada.
[2]Institute of Human Performance. Boca Raton, Florida, US.

INTRODUCTION

With the current interest in core and functional training, the use of cables and pulleys in standing positions to train the whole body while emphasizing pressing or pulling motions is becoming more popular [1]. Little is known about the effects of these cable exercises on trunk muscle activity. The purpose of this study was to compare the amplitude of the electromyography (EMG) and the coactivation patterns of the trunk muscles during the single arm staggered stance cable press and the traditional bench press.

METHODS

Fourteen recreationally trained men (age = 28.14 ± 8.33 yr, height = 1.78 ± 0.05 m, mass = 77.78 ± 10.41 kg) were recruited from the university population. All subjects were right-handed and healthy, without current back or shoulder pain. Superficial EMG was recorded bilaterally from rectus abdominis (RA), external oblique (EO), internal oblique (IO), latissimus dorsi (LD) and erector spinae at T9, L3 and L5 (EST9, ESL3, ESL5). EMG was also collected on the right side from pectoralis major (PM) and anterior deltoid (AD).

After warming-up, subjects performed bench and standing press exercises. Resistance was progressively increased until reaching the participant's one repetition maximum (1RM). Rest periods of 2-5 minutes between exercises were utilized in order to avoid muscular fatigue.

The EMG was A/D converted at 12 bit resolution at 1024Hz. Signals were full wave rectified and low pass filtered (single pass Butterworth) at 2.5 Hz, and then normalized to maximal voluntary contraction (MVC) amplitudes. The normalized muscle activity corresponding to the pushing phase of the 1RM was averaged for each press exercise. Differences in average normalized activity for each muscle between exercises and between muscles during each exercise was assessed using a two-way ANOVA (muscle/exercise) with Tukey correction ($\alpha = 0.05$).

RESULTS AND DISCUSSION

1RM bench press performance resulted in an averaged load (74.2 ± 17.6 kg) significantly higher than 1RM single arm standing press (26.0 ± 4.4 kg). Pressing from a standing position imposes greater demands on the motor control system to stabilize and balance the body – this reduces the capacity to push heavy weights.

The significant differences among exercises are shown in Figure 1. EMG amplitudes of the erector muscles (EST9, ESL3, ESL5) and pectoralis major (PM) were larger for the 1RM bench press. However, the pressure of the trunk on the back electrodes when supine on a bench could modify the EMG amplitudes. On the other hand, the activation levels of left abdominal muscles (LRA, LEO, LIO) and left latissimus dorsi (LLD) were higher for the right arm cable press.

Statistically significant differences in normalized EMG amplitudes were found among muscle sites within each exercise. For the 1RM bench press, anterior deltoid (AD) and pectoralis major (PM) were more activated than the most of the trunk muscles, although this exercise produced important mean levels of trunk muscle activation (Figure 1). In contrast, for the 1RM standing cable press, the left internal oblique (LIO) and left latissimus dorsi (LLD) activities were similar to the anterior deltoid activity (AD) and higher than the pectoralis major activation (PM).

CONCLUSIONS

The traditional bench press emphasizes the activation of the shoulder and chest muscles and challenges the ability to develop great shoulder torques. Whereas, a single arm standing press principally activates the contralateral abdominal and latissimus dorsi muscles and challenges the ability to produce smaller forces but in more functional horizontal plane. Coaches and fitness professionals should consider these differences when prescribing exercises to develop pushing or pressing abilities.

REFERENCES

1. McGill SM. *Ultimate back fitness and performance*. Wabuno Publishers, Waterloo, Canada, 2004.

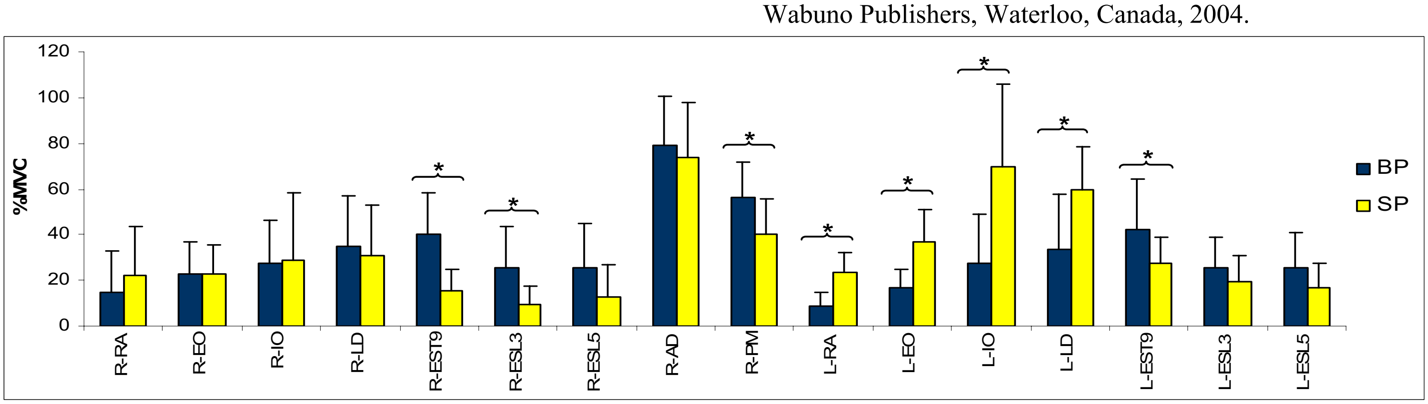

Figure 1. Averages and SD of the mean EMG amplitudes for 1RM Bench (BP) and Standing Press (SP). *Significance ($P < 0.05$).

AGE-RELATED JOINT TORQUE ANALYSIS DURING SUPPORT PHASE OF SINGLE STEP RECOVERY

Kathleen Bieryla, Michael Madigan, and Emily Lloyd
Virginia Tech, Musculoskeletal Biomechanics Laboratory; email: kbieryla@vt.edu

INTRODUCTION

Unintentional falls were the leading cause of non-fatal injury in every age group except for 15 -24 year olds for the year 2002 [1]. In 1995, $64 billion dollars was spent on medical costs stemming from 14 million injurious falls [2]. Falls in the elderly can lead to many health problems including hip fractures or even death. Previous studies have shown that older adults have a reduced ability to recover from a forward fall than younger adults. The purpose of this study was to investigate age-related differences in joint torques during the support phase of recovery from a forward fall.

METHODS

Twenty healthy male subjects, 10 young (20.6 ± 1.3 years) and 10 older (74.0 ± 6.5 years) participated in the study. A forward fall was simulated by releasing subjects from a forward leaning posture. Subjects stood with each foot on a force plate with their weight evenly distributed. Once the cable was released, participants recovered by taking one step with the right leg onto an oversized forceplate. The degree of the lean was measured by the percent body weight on the cable as determined by a load cell. Initial lean was 12% body weight (BW) and increased by 4% BW after successful recoveries. The data collection ended when two unsuccessful attempts at one lean magnitude occurred. Failure to recover was defined as: 1) more than one step was taken by the right leg, 2) greater than 30% BW applied to the harness during the trial, and 3) a step of the left foot greater than 30% of body height. To prevent a fall from occurring, participants wore a full body harness.

A 2-D model of 4 rigid segments (foot, thigh, shank, head-arms-trunk) was used for torque estimation. Peak extensor torques were calculated for the support phase of balance recovery (SPBR). Body segment data was sampled at 200 Hz with an Optotrak optoelectric motion analysis system. Force plate and load cell data were sampled at 1000 Hz.

A repeated measures analysis of covariance was run on the dependent measures of peak extensor torques at the hip, knee and ankle with the independent variables being lean angle and age. Height and weight were used as the covariates. Directional hypotheses based on previous studies of observed age related differences in joint torques were used to improve statistical power [3].

RESULTS AND DISCUSSION

Young subjects were able to recover from a significantly larger lean angle than the older participants (29.9 ± 4.0° vs 20.5 ± 4.0°, $p < .001$). During the SPBR, joint torques of the hip, knee, and ankle were predominately extensor (or plantar flexor) dominant. The order for which the peak torque extensor occurred was the hip followed by the knee and finally the ankle. Peak extensor torque significantly increased with increasing lean angle at the hip, knee, and ankle. Older subjects had a significantly lower peak knee extensor torque during SPBR compared to young subjects. There was no significant age related increase in the hip extensor ($p=0.084$) or decrease ankle plantar flexor torque ($p=.909$) but a trend of larger torques in older adults was seen (fig 1).

Although the general pattern of joint torques is similar for young and older adults, the peak extensor torque values suggest a possible difference in strategy across age groups during the SPBR of single step recoveries. The extensor torques helped decelerate the body rotation about the obstacle and assisted in resisting the buckling of the stepping leg. A post-hoc power analysis was performed and showed a small increase in sample size, 5 for the hip and 6 for the ankle, would have shown significance.

CONCLUSIONS

Age related differences and trends seen in the joint torques is believed to be a combination of age related reduction in muscle strength along with neuromuscular adaptation to lessen the effects of muscle strength loss on physical performance capabilities [3].

REFERENCES

1. Center for Disease Control. WISQARS Leading Causes of Nonfatal Injury Reports. 2002.
2. Englander F, et al.. *J Forensic Sci* **41**, 733-746, 1996.
3. DeVita P, et al.. *J Appl Physiol* **88**, 1804-1811, 2000.

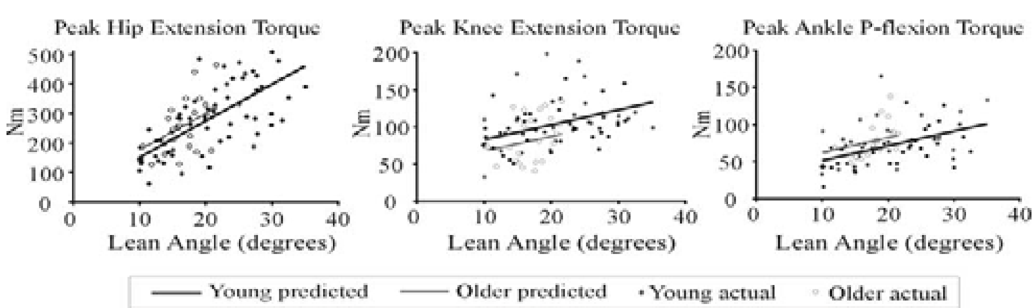

Figure 1: Peak extension and plantar flexion torques for both young (closed circle) and older adults (open circle) at all lean angles. Positive torque corresponds to extensor or plantar flexor dominance.

EFFECTS OF BILATERAL RESISTANCE-INDUCED ARM MOVEMENT TRAINING ON ARM MOTOR FUNCTION IN CHRONIC STROKE

[1,2]Jyh-Jong Chang, [2]Wen-Lin Tung, [3]Wen-Lan Wu, [2]Fong-Chin Su
[1] Faculty of Occupational Therapy, Kaohsiung Medical University.
[2] Institute of Biomedical Engineering, National Chen-Kung University
[3]Faculty of Sports Medicine, Kaohsiung Medical University, Kaohsiung, Taiwan

INTRODUCTION

This study designed an arm movement trainer, called bilateral resistance-induced arm movement trainer, for stroke arm motor rehabilitation. The arm movement trainer integrated robot-aided therapy with bilateral arm movement and arm strength training strategies (Figure 1). The purpose of this study was to analyze the effects of bilateral resistance-induced arm movement training on arm motor recovery in chronic strokes.

METHODS

Twenty unilateral chronic strokes, length of onset over 6 months, were recruited in this study. Each subject received 8 weeks' arm trainer training program and followed up for 8 weeks. The pretest, posttest and follow-up measures of clinical arm motor function and reaching kinematics were compared and analyzed. Data analysis was performed by using repeated ANOVA and post hoc analysis.

RESULTS AND DISCUSSION

After comparing the pretest and posttest of arm motor function and reaching kinematics, We found that arm motor function were significantly improved in total arm strength, grip strength, Fugl-Meyer upper limb scale (Table 1). Reaching kinematics was significantly improved in movement time, normalized jerk score, pick velocity, and percent time to pick velocity (Table 2). There were not significant differences between posttest and follow-up measures in arm motor function and reaching kinematics. Findings from this study might provide evidence that robot-aided therapy combined with bilateral resistance movement training would promote inter-hemispheric disinhibition likely to allow reorganization by sharing of normal movement commands from the undamaged hemisphere. Such "overflow" effect may be more marked under movement with resistance. It is suggested that effect of bilateral resistance-induced arm movement training may also promote a balancing effect on between-hemisphere cortical motor excitability that is associated with brain reorganization and finally contribute to motor recovery.

CONCULUSIONS

Bilateral resistance-induced arm movement trainer might enhance arm motor recovery for chronic strokes. Such simple robot-assisted devices will be more feasible in clinical application for stroke arm rehabilitation.

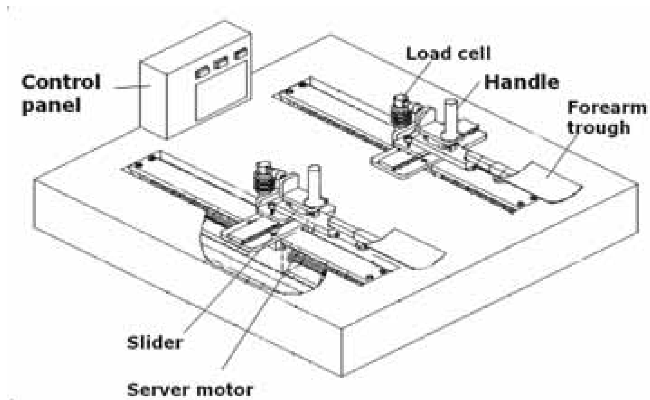

Figure 1. bilateral resistance-induced arm movement trainer

Table1: Measures of arm motor function among pretest, posttest and follow-up (N=20)

Motor	Pre-test	Post-test	Follow-up	F	***P***
FMS	32.70(15.26)	35.55(14.50)	35.35(14.63)	15.09	.000 1
FAT	1.75(2.24)	1.80(2.23)	1.80(2.23)	1.00	.33
GS(kg)	7.54(6.60)	9.75(7.32)	9.27(7.19)	5.65	.009
TAS(kg)	10.85(8.37)	15.71(10.67)	16.59(11.00)	11.41	.0001
MAS	0.95(0.74)	0.77(0.63)	1.00(0.70)	1.18	.31

FMS: Fugl-Meyer Score FAT: Frenchay Arm Test GS: Grip strength
TAS: Total arm strength MAS: Modified Ashworth Scale

Table 2:Measures of reaching kinematics among pretest, posttest and follow-up (N=15)

Kinematics	Pre-test	Post-test	Follow-up	F	*P*
MT(sec)	1.24(0.45)	0.80(0.29)	1.16(1.02)	4.91	0.015
PV(cm/sec)	81.14(34.71)	100.40(33.3)	82.48(36.46)	4.39	0.035
PTPV(%)	30.42(10.33)	37.82(11.66)	31.90(11.66)	6.70	0.004
NJS	173.35(11.41)	76.15(69.44)	136.94(93.95)	5.68	0.008

MT: Movement time PV: Pick velocity PTPV: Percent time to pick velocity NJS: Normalized jerk score

REFERENCES

1. Mudie MH and Matyas TA. *Disabil Rehabil* **22**, 23-37, 2000.

2. Stinear JW, and Byblow WD. *J Clin Neurophysiol* **21**, 124-131, 2004.

3. Whitall J et al. *Stroke* **31**, 2390-2395, 2000.

4. Weiss A, Suzuki T, Bean J, & Fielding R A. *Am J Phys Med Rehabil* **79**, 369-376, 2000.

LEG LENGTH AND LEG TORSION MEASUREMENT WITH ULTRASOUND IN CHILDREN DURING ONE YEAR – FIRST RESULTS

Kerstin Bosch, Dieter Rosenbaum
Movement Analysis Lab - Orthopaedic Department - University Hospital Muenster - Germany
email: boschk@uni-muenster.de , web: www.motionlab-muenster.de

INTRODUCTION

The growth of the lower extremity and the shape changes of leg in infants often lead to uncertainty in parents. The infant's leg can develop from a typical bow leg via a knock-knee to a normal "straight" leg. The reasons for the knock-kneed gait of the infants are the antetorsion of the femur associated with a valgus position of the knee. The reduction of the femoral antetorsion occurs during growth and is pronounced during two phases of detorsion [1]. The aim of the present longitudinal investigation was to quantify the development of leg geometry in children over the course of one year by means of an ultrasound measurement system.

METHODS

33 healthy children (18 male; 15 female) aged 3.5 to 5.2 years were measured during 3 times within one year (every 6 months). To determine leg geometry a sonographic system (Sonoline Prima, Siemens) coupled with a 2.5-dimensional ultrasound measurement system (CMS70P4-K Zebris, Germany) was used. Defined bony landmarks of hip, knee and ankle joint were sonographically displayed. The bony outlines were marked with circles, points and/or vectors. With use of dedicated software (MedMess 2.0, Zebris) the femur, tibia and total leg length as well as femoral and tibial torsion and the mechanical axis were calculated.
For statistical analysis an ANOVA for repeated measurements with $p < 0.05$ and Scheffé test for paired comparison was used.

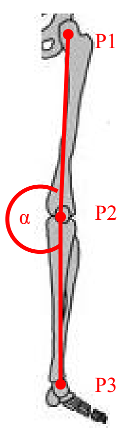

Figure 1: P1- P2 = Femur length; P2-P3 = Tibia length; P1-P3 = Total leg length; α = Mech. axis

RESULTS AND DISCUSSION

In the one-year observation period, a significant increase of the total leg length of 9.4% from 437mm to 477mm could be detected. The femur length increased significantly by 9.4% and the tibia length by 8.7% which confirms the literature [1]. Femoral torsion changed significantly from -31.1° to -28.8° during 1 year but significant changes of tibia torsion were not established. After 6 months a significant decrease of the mechanical axis was detected [Tab. 1].
The significant change of femur torsion can be attributed to the natural decrease of antetorsion during growth. The decrease of 0.7° of mechanical axis can also confirm the development of antetorsion but this low value has no clinical relevance.
Furthermore, it is important to note that the defined bony structures in this age group are not completely ossified. This can lead to complications during the measurement and following calculation.

CONCLUSIONS

Due to the lack exposure to harmful radiation, the ultrasound based measurement system is an adequate medium for determining leg geometry not only in children but also in adults and for follow-up investigations. The degree of ossification of the bony landmarks of children in the demonstrated age group can be problematic and should not be compared with that of adults. Therefore, the results have to be considered and used with caution.

REFERENCES

1. Niethard, F. U.: *Kinderorthopädie.* Stuttgart, 1997.

ACKNOWLEDGEMENTS

This project is supported by the German Research Foundation (DFG grant # RO 2146/3-2).

Table 1: One-year results of all parameters.

	First Examination		+6 Months		+12 Months		p-Level
	Mean	SD	Mean	SD	Mean	SD	
Femur length [mm]	244.08	13.92	256.45	15.0	267.1	15.83	< .0001
Tibia length [mm]	195.59	12.44	205.82	11.92	213.19	12.91	< .0001
Total leg length [mm]	437.12	24.77	459.73	25.29	477.69	26.74	<.0001
Femur torsion [°]	-31.06	9.54	-31.23	8.96	-28.79	9.07	<.0135
Tibia torsion [°]	13.36	6.48	12.12	7.02	11.38	7.98	n.s.
Mechanical axis [°]	181.21	2.06	180.51	1.79	180.60	1.93	<.0095

INCREASE IN AMPLITUDE OF PARASPINAL MUSCLE REFLEXES FOLLOWING LUMBAR EXTENSOR FATIGUE

Christine M. Herrmann[1], Michael L. Madigan Ph.D., Bradley S. Davidson, Kevin P. Granata Ph.D.
Virginia Tech, Musculoskeletal Biomechanics Laboratory
[1] email: herrmacm@vt.edu

INTRODUCTION

Low back disorders (LBDs) are one of the most prevalent and costly musculoskeletal problems in the United States. Abnormal paraspinal reflexes have been linked to low-back pain [1,2] and neuromuscular fatigue has been shown to affect reflexes in multiple muscle groups [3]. Therefore, the purpose of this study was to investigate the effect of lumbar extensor fatigue on paraspinal reflexes.

METHODS

Ten physically active males (20-22 years of age) participated in the experiment. During each experimental session, paraspinal muscle reflexes were measured both before and after a lumbar extensor fatiguing protocol. Reflexes were elicited in response to an anteriorly-directed perturbation applied at the inferior margin of the scapulae while the subjects stood quietly. Perturbation force was recorded using a load cell, and EMG was recorded from the paraspinal muscles (4cm lateral from L4). The fatiguing protocol consisted of multiple sets of back extensions and intermittent isometric MVCs on the Roman chair [4] for a period of 14 minutes to fatigue participants to 60% of their unfatigued lumbar extensor MVC. The reflex measurement began within fifteen seconds of the completion of the fatiguing protocol.

Preparatory muscle activity was computed from 250 msec of data prior to each force impact. Any reflex response after 120 msec was considered voluntary motion and not included in the analysis. Reflex delay was calculated as the time delay from the perturbation onset to the reflex onset, and reflex amplitude was calculated as the peak amplitude of the paraspinal EMG (Figure 1). A paired t-test with a significance level of $p \leq 0.05$ was used for all statistical tests.

RESULTS AND DISCUSSION

Perturbation characteristics differed between fatigue conditions with peak amplitude decreasing an average of 5.8 ± 4.9% with fatigue. Reflexes occurred in 92% of all perturbations. The mean reflex delay was 60 ± 18 msec, and was not affected by fatigue (p=0.278); however, reflex amplitude significantly increased 36 ± 32% with fatigue (p=0.017).

The aim of this study was to examine the effects of lumbar extensor fatigue on paraspinal muscle reflex in response to a sudden perturbation. The results showed fatigue was associated with an increase in reflex amplitude but no significant influence in response delay. Three aspects of the methodology warrant discussion. First, the quantified paraspinal reflexes during a task involved no external constraints on trunk angle and/or response to the perturbation. However, similar conditions have been used in other studies. In addition, analyses of conditions prior to the unfatigued and fatigued perturbation showed that preparatory EMG levels and lumbar flexion angle were not affected by fatigue. Secondly, the perturbation amplitude was not consistent across unfatigued and fatigued conditions which we feel may be due to a decrease in lumbar extensor stiffness with fatigue.

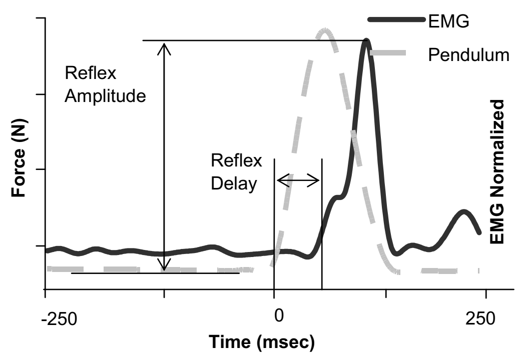

Figure 1: EMG reflex delay and amplitude after pendulum perturbation.

Third, the increase in reflex amplitude may not solely be attributed to fatigue. Dynamic fatiguing can elicit strain in paraspinal tissue in addition to fatigue. Despite this, a dynamic fatigue exercise more closely represents an occupational task.

CONCLUSIONS

Spinal stability is primarily controlled by muscle recruitment, muscle stiffness, and reflex response. Trunk fatigue has been shown to alter trunk muscle recruitment patterns and decrease the force producing capacity of muscle. The increase in reflex amplitude found here may reflect an attempt to compensate for losses in muscle force capacity with fatigue in order to maintain sufficient spinal stability.

REFERENCES

1. Radebold, A., et al. Spine 25(8):947-54,2000.
2. Radebold, A., et al. Spine 26(7):724-30,2001.
3. Hortobagyi, T., et al. Can.J Sport Sci 16(2):142-50, 1991.
4. Davidson, B. S., et al. Eur.J Appl.Physiol 93(1-2):183-9 2004.

USINGTHE EIGENVECTOR APPROACH TO LOCATE SPINAL INSTABILITY

Samuel J. Howarth and Stuart M. McGill
Department of Kinesiology, University of Waterloo, Waterloo, Canada

INTRODUCTION

Models have been developed in the past to evaluate stability of the lumbar spine. One approach to quantify the stability index is to determine the smallest eigenvalue associated with a Hessian matrix comprised of all second partial derivatives from a potential energy function [1]. The system is deemed to be unstable whenever the smallest eigenvalue is less than zero. Clinically the location of potential instability is necessary for developing the buttressing motor patterns to prevent instability. Since eigenvectors associated with particular eigenvalues indicate the buckled configurations, this work proposes a particular form of the eigenvector that would enable investigators to determine the location of spinal instability.

METHODS

The lumbar spine model used here includes six vertebral joints (Pelvis/L5-Ribcage/L1) and three axes (flexion/extension, lateral bend, axial rotation) for a total of eighteen degrees of freedom [2]. Each joint is assigned a passive rotational stiffness component. Instability occurs when the stiffness at a joint is compromised along a particular axis. This study compromised the stiffness at various vertebral levels, and particular axes to investigate the plausibility of the proposed eigenvector format.

As a proof of principle, a theoretical trial of a 25 kg load applied to the upright spine was considered. The rotational stiffness parameters [3] for each joint and axis were made to be identical. This forced the rotational stiffness at each joint to be identical. Lastly, we reduced the rotational stiffness at the L3-L4 joint and lateral bend axis to obtain a compromised joint and axis. Thus, the primary instability will occur at the L3-L4 joint and in the lateral bend axis. Subsequently, the known location of the instability can be checked with the proposed form of the eigenvector described below.

RESULTS & DISCUSSION

The Hessian matrix used for the analysis of spinal stability is a symmetric 18 x 18 matrix whose individual entries are second partial derivatives of a potential energy function taken with respect to generalized coordinates at each lumbar joint and axis. The symmetric nature of the Hessian matrix admits the following relationship between the eigenvalues and eigenvectors of the Hessian matrix:

$$VDV^T = H \quad (1)$$

This is where H is the Hessian matrix, D is a diagonal matrix that contains the eigenvalues along its main diagonal, and V is a matrix whose columns are the eigenvectors associated with a particular eigenvalue. V, D, and H are all 18 x 18 matrices. The individual entries of each eigenvector represent a particular vertebral level and axis (Table 1). Consequently, the joint and axis of buckling is indicated by the largest component of the eigenvector associated with the smallest eigenvalue.

The smallest eigenvalue from the example indicated that an instability had occurred ($?_{min}$ = -18.7231). The largest entry of the eigenvector associated with the smallest eigenvalue occurred along the lateral bend axis of the L3-L4 joint (Table 1). This is precisely the joint and axis with compromised rotational stiffness.

Interestingly, the eigenvector also has large components along the lateral bend axis for all joints above L3-L4. These components are all smaller than the component at L3-L4 along the lateral bend axis, and decrease as the segmental level reaches the top of the spine. This suggests that the entries of the eigenvector demonstrate a deflection of the vertebral joint from some reference orientation.

CONCLUSIONS

The example illustrates the plausibility of the proposed form for an eigenvector in the solution of spinal instability when such instability occurs. This interpretation of the eigenvector allows investigators to develop efficient motor patterns that will buttress instability.

REFERENCES

1. Howarth et. al. *J Biomech* **37**, 1147-1154, 2004.
2. Cholewicki et. al. *Clin Biomech* **11**, 1-15, 1996.
3. McGill et. al. *Spine* **19**, 696-704, 1994.

Table 1: Entries of the eigenvector associated with the smallest eigenvalue. The largest value is noted with an asterisk. RC = Ribcage, PELV = Pelvis, FE = Flexion/Extension, LB = Lateral Bend, A R = Axial Rotation.

Joint		**RC-L1**			**L1-L2**			**L2-L3**	
Axis	**FE**	**LB**	**AR**	**FE**	**LB**	**AR**	**FE**	**LB**	**AR**
Entry	0.0395	0.3350	-0.0093	0.0294	0.4568	0.0099	0.0222	0.5527	0.0272

Joint		**L3-L4**			**L4-L5**			**L5-PELV**	
Axis	**FE**	**LB**	**AR**	**FE**	**LB**	**AR**	**FE**	**LB**	**AR**
Entry	0.0161	0.6049*	0.0477	0.0109	0.0073	0.0295	0.0057	0.0037	0.0127

A FINITE ELEMENT ANALYSIS ON THE EFFECT OF SOFT TISSUE THICKNESS ON PLANTAR PRESSURES IN SUBJECTS WITH DIABETES AND PERIPHERAL NEUROPATHY

[1] Michael J. Mueller, [2]Ricardo L. Actis, [2]Liliana B. Ventura, [2,3]Barna A. Szabo,
[1]Program in Physical Therapy, Washington University School of Medicine; email muellerm@wustl.edu
[2]Engineering Software Research and Development, Inc, [3]Center for Computational Mechanics, Washington University

INTRODUCTION

Excessive localized peak plantar pressures (PPP) are known to contribute to skin breakdown in people with diabetes (DM) and peripheral neuropathy (PN). Previous work has shown a correlation between plantar soft tissue thickness (STT) under the metatarsal heads (where most ulcers occur) and PPP in subjects with DM and PN [1,2]. The purpose of this study was to use a validated finite element analysis (FEA) model to determine the effect of reducing STT on PPP in subjects with DM and PN and a history of plantar ulcers.

METHODS

Data were collected on 4 males with DM & PN. Mean age was 53±26 years, mean BMI was 34±9, and mean duration of DM was 19±9years. All subjects had dense PN (unable to sense 6.10 Semmes Weinstein monofilament) and a history of a plantar neuropathic ulcer.

The 3D internal structure was determined using data from SXCT [3], the reference pressure distribution was measured using the F-Scan system [3], and soft tissue properties were estimated using an indentor testing device and confirmed with values in the literature for each foot.

Individual two-dimensional FEA models in the sagittal plane were developed for metatarsals 2 and 3 using the p-version FEA program StressCheck with the foot in a push-off position for each subject. Bones included a support bone (tibia, talus, calcaneus, navicular, cuneiform), metatarsal and 3 phalanges. Cartilage with linear elastic material properties was included between the bones to simulate the composite stiffness between bones. Fascia and the long flexor tendon were included and the properties were assumed to be linearly elastic. Material properties of bone, fascia, and tendon were obtained form the literature.

The model's ability to predict plantar pressure distribution was tested against measured pressure distribution and found to be good, as reported elsewhere [4]. The effect of reducing STT under the metatarsal head was accomplished by translating the bones, tendon, and fascia vertically downward in 1 mm increments within the soft tissue envelop and keeping the skin outline and boundary conditions unchanged.

RESULTS AND DISCUSSION

Initial STT, PPP, and the % increase in PPP with 1-3 mm reduction in STT for the 2nd and 3rd metatarsal heads are contained in Table 1. Figure 1 shows the change in plantar pressure distribution for a specific subject (D07). There was a strong inverse relationship (r=-0.99) between the reduction in STT and the increase in PPP. According to the model, PPP will increase 14 to 24% under met heads 2 & 3 with a 3 mm reduction in STT depending upon other factors such as the shape and position of the metatarsal head.

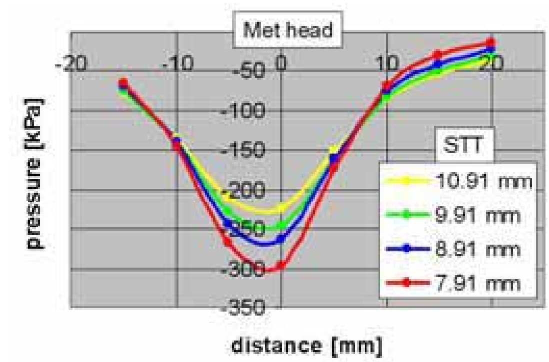

Figure 1: Change in pressure distribution 15 mm proximal to 20 mm distal 3rd met head with changes in STT (3mm).

Although this model is limited by being static and 2D, the results are robust and underlying assumptions for this application seem reasonable, but the effect of reducing STT on PPP may be even greater in reality. Methods currently are underway to establish a 3D model.

CONCLUSIONS

The results have important implications for understanding the factors contributing to skin breakdown in patients with DM and PN. STT has been correlated with PPP [1,2], and these results indicate a reduction in STT is highly correlated to an increase in PPP. Therefore, specific reductions in STT at a localized area, perhaps as a result of previous skin breakdown, could result in higher PPP at that site making it more susceptible to future skin breakdown. We plan to expand the FEA model further to develop strategies to evenly distribute pressures across the plantar foot.

REFERENCES

1. Mueller MJ, et al. *J Biomech* **36**, 1009-1017, 2003.
2. Abouaesha F, et al. *J Am Podiatr Med Assoc 94,39-42, 2004*
3. Commean PK, et al. *Arch Phys Med Rehab*, **183**, 497-505, 2002.
4. Actis RL, et al. *Proceedings of ASME*, IMECE, Anaheim, CA, 59400-2004.

ACKNOWLEDGEMENTS

Funding from NCMRR, NIH, RO1 HD3695

	STT (mm)	PPP (kPa)	%ΔPPP/PPP at –1mm	%ΔPPP/PPP at –2mm	%ΔPPP/PPP at –3mm
2nd met head X ± SD	10.5 ± 3.0	450 ± 147	4.6 ± 1.5	9.0 ± 2.6	15.4 ± 2.1
3rd met head X ± SD	10.0 ± 2.4	264 ± 48	7.8 ± 1.9	13.9 ± 1.9	21.0 ± 3.0

Table 1: Percent increase in PPP for 1-3 mm reduction in STT under the 2nd and 3rd metatarsal heads

THUMB MUSCLE FORCES IN JAR OPENING

[1]Fong-Chin Su, [1]Kun-Yueh Ho, [1,2]Jer-Hao Chang
[1]Institute of Biomedical Engineering, [2]School of Occupational Therapy, National Cheng Kung University
email: fcsu@mail.ncku.edu.tw

INTRODUCTION

Twisting activities such as jar turning and door opening are common functional activities in our daily living. It is a big challenge for the patients with arthritis or after hand injuries. The literature in understanding the muscle contribution of the thumb during jar turning still lacks [1,2]. It is interesting to understand how the muscles of the thumb play their roles in mobility and joint stability. The purpose of this study was to establish a biomechanical model to predict the muscle forces in the thumb and to understand their roles during jar opening.

METHODS

The jar simulator was equipped with one torque sensor (Transducer Techniques, CA, ±22.6*N-m*) and a six-axis force transducer (Nano25, ATI Industrial Automation, NC, Fx, Fy=±111*N*; Fz=±445*N*; Tx, Ty, Tz=±2.8*N-m*). The single-axis torque sensor set inside the jar center was for recording the total torque of the hand and the six-axis force transducer mounted under the tap was for the applied forces and moments of the thumb while jar opening. In addition, three-dimensional kinematical data were captured by a motion analysis system (Motion Analysis Corp., CA). Thirteen 4 mm diameter retro-reflective markers were attached on the dorsal surface of the thumb to define the local coordination system of the thumb and three other markers were on the jar simulator to define its coordination system (Figure 1). The IP joint was represented by a hinge joint with one degree of freedom and three constraint forces (Cx, Cy, Cz) and two constraint moments (Mx, My). The MCP joint was regarded as a universal joint with two degrees of freedom and three constraint forces and one constraint moment. The CMC joint was also regarded as a universal joint. According to the mechanical equilibrium at each joint, the optimization technique was used to solve the redundant system. The objective function minimizing overall muscle stress was selected.

$$\text{Min} \quad \sum (\mathbf{F}_i^M / PCSA)^2$$

$$0 \le \mathbf{F}_i^M \le PCSA * \sigma_{\max} \quad i = 1, \text{m}$$

where PCSAi and F_i^M were cross section area and forces generated in the *i*th muscle or tendon. σ_{max} = 35.3 N/cm^2 was the maximum which a thumb muscle could bear. Eight female and two male volunteers without hand impairment took part in this study. They were all right handed and asked to grip the base of this jar simulator by left hand in a comfortable position. The right hand held the lid of the jar simulator and put the thumb pad on the six-axis force transducer. The subject then turned the jar lid counter-clockwise three times at maximal effort by both power grip and precision handling.

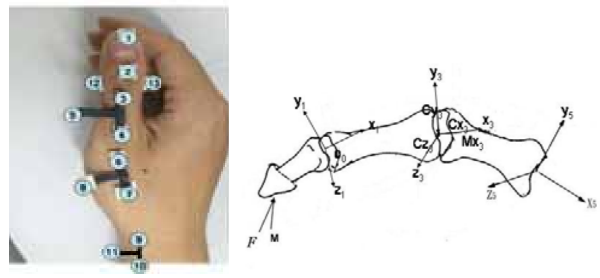

Figure 1: Markers setting and coordination system

RESULTS AND DISCUSSION

Figure 2 shows the muscle forces of the thumb in jar opening. The major active muscles were FPL, FPB, APB, ADP and OPP. The forces of extensor muscles (EPL, EPB, APL) not larger than flexor muscles were average 15N and were about 6 % of total muscle forces. Total muscle forces in precision handling were 5.6 times the applied forces of thumb but that in power grip were 4.7 times. It indicated that power grip was more effective than precision handling. To compare with previous researches, this study adopted measured data instead of assumed value as Cooney et al. and Giurintano et al. did. They measured the moment arms of cadaver muscles by X-ray and CT images. The muscle loads thus varied. This new apparatus here presented a proper method to measure the actual load in jar opening activity and the biomechanical model developed contributed to the prediction of the muscle forces of the thumb during such activity.

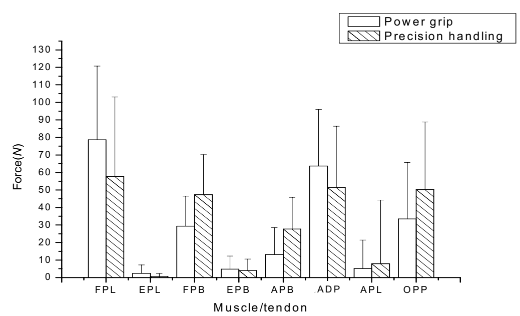

Figure 2: Muscle forces of the thumb in jar opening.

REFERENCES

1. Cooney WP, et al. *J Bone Joint Surg-Am* **59**, 27-36, 1977.
2. Giurintano DJ, et al. *Med Eng Phys* **17**, 297-303, 1995.

ACKNOWLEDGEMENTS

Support from NSC 92-2218-E-006-005.

MUSCLE DYSFUNCTION DURING WALKING IN CHILDREN WITH CEREBRAL PALSY

[1,2] James Wakeling, [2]Roisin Delaney and [2]Israel Dudkiewicz
[1]The Royal Veterinary College, UK ,
[2]The Royal National Orthopaedic Hospital, UK; email: jwakeling@rvc.ac.uk

INTRODUCTION

Cerebral palsy (CP) is a disorder of movement or posture due to a lesion in the immature brain [1]. Release of the gamma system from higher inhibitory control results in the muscles being hyperexcitable [2], and they exhibit elevated muscle tone and excessive co-contraction during walking [3].

CP is typically assessed using gross measures of gait (e.g. walking velocity), or overall motor function and sometimes by the joint kinetics. However, none of these measures are direct measures of the muscle dysfunction.

The purpose of this study was to quantify the differences in the myoelectric activity between children with CP, and healthy controls, in order to determine the extent of the muscle dysfunction during walking.

METHODS

Surface electromyography (EMG) was performed bilaterally on the rectus femoris, semimembranosus, medial gastrocnemius and tibialis anterior from 36 healthy children and young adullts (age range 3.1 – 21.0 years) and 17 children and young adults with CP (4.8 – 21.5 years). Each child walked along a walkway at their preferred velocity. Segmental kinematics were used to determine the time of foot-contact with the ground, and thus to window the walking into stance phase, swing phase, or the entire stride cycles. Data were analyzed from 5-15 strides per individual.

The EMG was resolved into its intensity (a correlate of the power of the signal) in time-frequency space using wavelet techniques [4]. The intensities (at each frequency-band analyzed) were correlated between antagonistic muscles. Correlations were thus calculated across a range of frequencies to make a spectrum. The correlation spectra were used as a measure of the co-contraction. Correlation spectra between the asymptomatic and cerebral-palsied conditions were compared using principal component techniques [5].

RESULTS AND DISCUSSION

Intensity spectra showed that the cerebral-palsied condition had systematically higher mean EMG frequencies than the asymptomatic controls. The extensor muscles (rectus femoris and medial gastrocnemius) showed higher intensities, but the tibialis anterior intensity was less than the asymptomatic condition (Table 1). The results show that the muscle is either activated in a different way, or that the muscle structure is different in the children with CP. This type of analysis can direct future research questions.

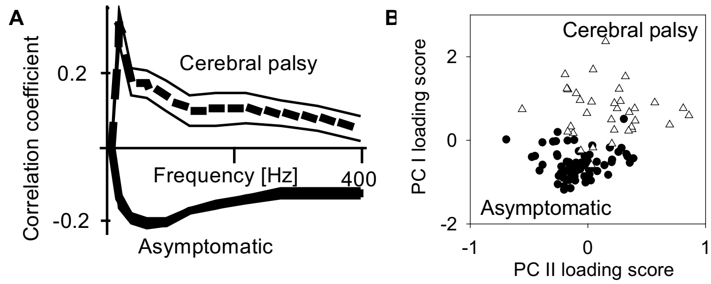

Figure 1: [A] Correlation spectra (mean ± s.e.) and [B] principal component (PC) loading scores for co-contractions for all subjects between the tibialis anterior and medial gastrocnemius during walking

The correlation spectra showed that the cerebral-palsied condition has different (but not always greater) patterns of co-contraction (Fig. 1A). Co-contractions in the cerebral-palsied muscles were always greater in the low-frequency range (<100 Hz) of the myoelectric spectra, and may indicate a greater involvement of the slower motor units for co-contractions [5].

The principal components of the co-contraction could be distinguished between the cerebral-palsied and asymptomatic conditions, and were most different for the more distal muscles (Fig. 1B).

CONCLUSIONS

The EMG signals during walking are markedly different between children with cerebral palsy and asymptomatic controls. Time-frequency analysis of the spectra and the co-contractions provide direct measures of the muscle dysfunction and have an application for quantifying the severity of the condition or the efficacy of treatment.

REFERENCES

1. Bax MCO, *Dev. Med. Child Neurol.* **6**, 295-297, 1964
2. Rushworth G, *J. Neurol. Neurosurg. Psychiatry* **23**, 99-118, 1960
3. Unnithan VB et al. *Med. Sci. Sports Exerc*. **28**, 1498-1504, 1996
4. Von Tscharner V, *J. Electromyogr. Kinesiol.* **10**, 433-445, 2000
5. Wakeling JM et al. *J. Exp. Biol.* **207**, 2519-2528, 2004

Table 1. Changes in the EMG spectra during walking. Arrows indicate if the children with cerebral palsy had significantly (t-test: $p<0.05$), greater or smaller intensity or frequency from their EMG signals compared to the asymptomatic controls.

	Stance phase		Swing phase		Stride	
Muscle	Mean intensity	Mean frequency	Mean intensity	Mean frequency	Mean intensity	Mean frequency
Rectus femoris	↑	↑	↑	↑	↑	↑
Semimembranosus	n.s.d.	↑	n.s.d.	↑	n.s.d.	↑
Tibialis anterior	↓	↑	↓	↑	↓	↑
M. gastrocnemius	↑	↑	n.s.d.	↑	n.s.d.	↑

JOINT LOAD OF THE THUMB IN JAR OPENING

[1,2]Jer-Hao Chang, [1]Kun-Yueh Ho, [1]Fong-Chin Su
[1]Institute of Biomedical Engineering, [2]School of Occupational Therapy, National Cheng Kung University
email: fcsu@mail.ncku.edu.tw

INTRODUCTION

The thumb plays an important role in daily activity because of its opposition characteristics. Jar opening is a common but challenging task for those who could not provide the sufficient twisting torque. Some researchers had developed the biomechanical model of the finger or thumb by means of the hypothetical loads [1,2,3]. This study aimed to develop a novel device to measure the actual three-dimensional loads of the thumb during jar opening and to establish a biomechanical model to reveal the joint loads of the thumb in such activity.

METHODS

The jar simulator was equipped with one torque sensor (Transducer Techniques, CA, ±22.6*N-m*) and a 6-axis force transducer (Nano25, ATI Industrial Automation, NC, Fx, Fy=±111*N*; Fz=±445*N*; Tx, Ty, Tz=±2.8*N-m*). The single-axis torque sensor set inside the jar center was for recording the total torque of the hand and the six-axis force transducer mounted under the tap was for the applied forces and moments of the thumb while jar opening. These data recorded by the jar simulator were used to calculate the normal forces (Fn), tangent forces (Ft), and the torque contribution (C) of the thumb applied to the jar lid. In addition, three-dimensional kinematical data were acquired by a motion analysis system (Motion Analysis Corp., CA). Thirteen 4 mm diameter retro-reflective markers were attached on the dorsal surface of the thumb to define the local coordination system of the thumb and three other markers were on the jar simulator to define its coordination system (Figure 1). The IP joint was represented by a hinge joint with one degree of freedom and three constraint forces (Cx, Cy, Cz) and two constraint moments (Mx, My). The MCP joint was regarded as a universal joint with two degrees of freedom and three constraint forces and one constraint moment. The CMC joint was also regarded as a universal joint. According to the mechanical equilibrium at each joint ($\Sigma F=0$, $\Sigma M=0$), the resultant forces and moments of three thumb joints were computed. Eight female and two male volunteers without hand impairment took part in this study. They were all right handed and asked to grip the base of this jar simulator by left hand and put the right thumb on the 6-axis force transducer of the lid then did jar opening at maximal effort by both power grip and precision handling.

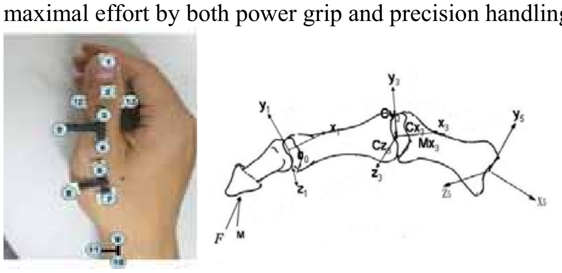

Figure 1: Markers setting and coordination system

RESULTS AND DISCUSSION

The normal force applied by the thumb to the lid was averaged about 45N and the tangent forces were averaged about 15N. The twisting torque contribution of the thumb was averaged about 32.5%. The joint constraint forces and moments of the thumb were calculated and also normalized with respect to applied thumb tip load. The joint contact forces were mainly applied at normal direction (Cx) of each articular surface. The CMC joint bore the largest dorsal and lateral shear forces among three joint. Figure 2 shows the joint resultant forces per unit external applied forces during jar opening. There were 221.5N at the CMC joint, 153N at the MCP joint, and 69N at the IP joint. They were respectively 4.8, 3.3 and 1.5 times the applied forces of the thumb. The external forces and the muscle forces were the major factors to influence the joint constraint forces and moments.

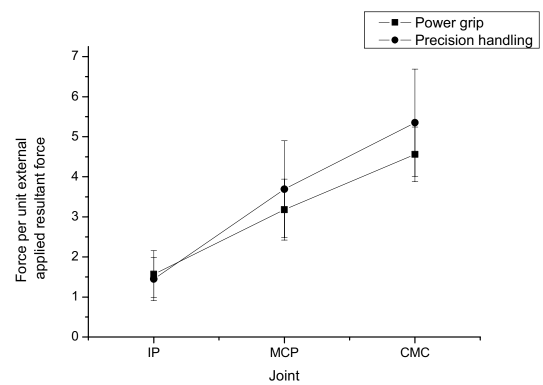

Figure 2: Joint resultant forces per unit external applied force

CONCLUSIONS

This study contributed to the measurement of the biomechanical express and calculation of the joint loads of the thumb in jar opening activity. The new apparatus provides a proper method for measuring the three dimensional load during the activities. The biomechanical analysis model would help to discover more information about the muscle and joint load in other twisting activities by further application.

REFERENCES

1. Cooney WP, et al. *J Bone Joint Surg-Am* **59**, 27-36, 1977.
2. Fowler NK, et al. *Clin Biomech* **14**, 646-652, 1999.
3. Voorbij AI, et al. *Appl Ergon* **33**, 105-109, 2002.

ACKNOWLEDGEMENTS

Support from NSC 92-2218-E-006-005.

PHASE TRANSITION OF FORCE DURING RAMP STRETCH OF MUSCLE FIBERS WITH BDM

Dilson E. Rassier and Walter Herzog
Human Performance Laboratory, Faculty of Kinesiology
University of Calgary (AB), Canada; email:rassier@kin.ucalgary.ca

INTRODUCTION

When muscle fibers are stretched while activated, force increases in two phases: a fast steep increase, and a slow increase. It has been proposed that the breakpoint between phases and the increase in force is due to weakly-bound cross-bridges [1], that do not produce substantial isometric force, but contribute significantly to force when stretched. We tested this hypothesis by stretching muscle fibers while biasing cross-bridges towards a weakly-bound state. If the hypothesis was correct, stretch forces would increase relative to the isometric forces when cross-bridges are biased into a weakly-bound state.

METHODS

Single fibers were dissected from lumbrical muscles of the frog and suspended between a force transducer and a motor arm in an experimental chamber. Fibers were stimulated to produce maximal isometric force, and stretched 5% and 10% of optimal fiber length (L_o) at different velocities, starting at a length 20% above L_o. Experiments were performed at 9ºC in Ringer solution, and with 2, 5 and 10 mM of 2,3 Butanodione-monoxime (BDM). BDM is known to bias cross-bridges into a weakly-bound state [2], preceding phosphate release and the power stroke. Force values were evaluated before and at the end of stretch (peak forces), as well as at the point of transition between the fast and the slow phases of force increase during stretch (critical forces).

RESULTS AND DISCUSSION

When active muscle fibers were stretched while fully activated, force increased significantly. This increase could be divided into a fast rise and a slow rise in force (Fig 1). Increasing concentrations of BDM significantly decreased the isometric force, the absolute forces measured at the end of stretch, and the force at the transition between the fast and the slow phases of force increase. However, BDM significantly increased the peak force and the force at the transition point relative to the isometric force before stretch (Fig. 1). This result was confirmed statistically in 10 fibers, with 5 and 10% fiber length stretches (Fig. 2). Since BDM places a large proportion of cross-bridges in a weakly-bound state [2], we conclude that the force obtained during stretch is caused by weakly- and strongly-bound cross-bridges, while the isometric force is produced only by strongly-bound cross-bridges.

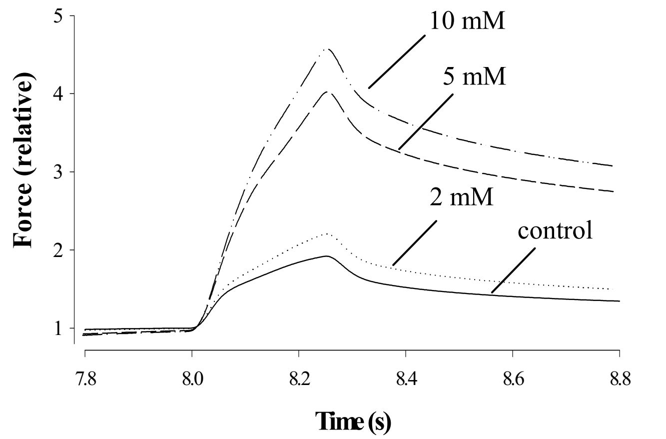

Figure 1: Force during stretch without (control), and with 2, 5 and 10 mM BDM.

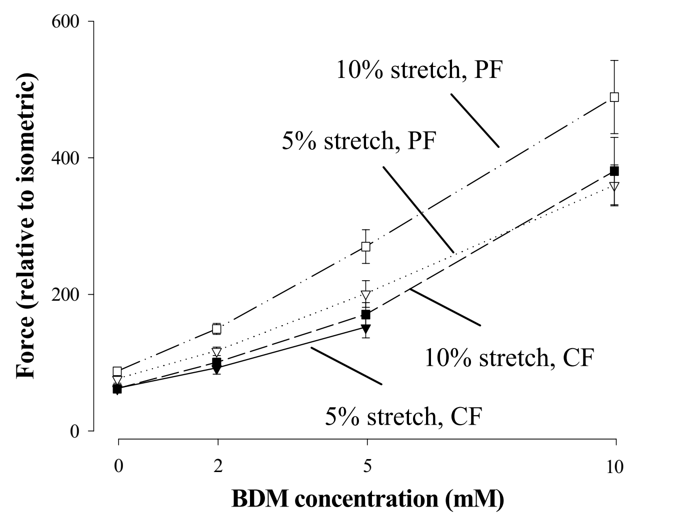

Figure 1: Peak forces (PF) and critical forces obtained at the transition between the fast and the slow phases of force increase during stretch (CF) during stretch, without (control), and with 2, 5 and 10 mM BDM

REFERENCES

1. Getz ,EB et al. *Biophys.J.* **75,** 2971-2983, 1998.
2. Regnier,M et al. *Am.J.Physiol* **269,** C1532-C1539, 1995.

ACKNOWLEDGEMENTS

Canada Research Chair Program and NSERC of Canada.

MODULATION OF PASSIVE FORCE IN SKELETAL MUCLE FIBERS

Eun-Jeong Lee, Dilson E. Rassier and Walter Herzog
Human Performance Laboratory, Faculty of Kinesiology
University of Calgary (AB), Canada; email:walter@kin.ucalgary.ca

INTRODUCTION

When skeletal muscle is stretched while activated, the passive force following deactivation is higher than that produced by passive stretches with the same characteristics (amplitude, initial length), and following isometric contractions at the corresponding lengths [1]. The mechanism behind this phenomenon, referred to as "passive force enhancement", is unknown. Recent evidence shows that increasing Ca^{2+} concentration enhances the force produced by titin [2], suggesting that the passive force enhancement may be caused by modulation of titin upon muscle activation. If that was true, the entire passive force-length relationship would be affected by activation. In this study, we evaluated if the passive force-sarcomere length relationship following active stretches was different from that following isometric contractions and following passive stretches.

METHODS

Single fibers (n = 6) were dissected from lumbrical muscles of the frog (R. Pipiens) and suspended between a motor arm and a force transducer inside an experimental chamber (temperature: 9°C). Sarcomere length was measured using the laser diffraction technique, with a He-Ne laser beam (633nm wavelength) projected perpendicular to the axis of the fiber. Fibers were pre-stretched to different sarcomere lengths along the descending limb of the force-length relationship, activated and stretched ~0.22 µm per sarcomere. Passive stretches were performed with similar characteristics, and isometric contractions were performed at the corresponding final lengths. Experiments were performed in Ringer solution (pH=7.5), and with the addition of 5 and 20 mM of BDM, which inhibits active force production [3].

RESULTS AND DISCUSSION

Passive force measured after stretch of activated fibers was higher than the force measured after passive stretches, and higher than the passive force measured after an isometric contraction at the corresponding length (Figure 1). This result was confirmed statistically in all fibers investigated in this study. The passive force enhancement was length-dependent, as it increased with increasing sarcomere lengths, causing an upwards shift in the passive force-sarcomere length relationship along the Y-axis. Adding BDM to the Ringer solution did not decrease the degree of passive force enhancement after stretches. Therefore, it seems that the increase in passive force observed during an active stretch is not due to cross-bridge kinetics, but due to the engagement of a passive element upon activation and stretch. Based on previous studies [2], we suggest that this passive element is titin, which would be activated by Ca^{2+} when muscle contraction starts.

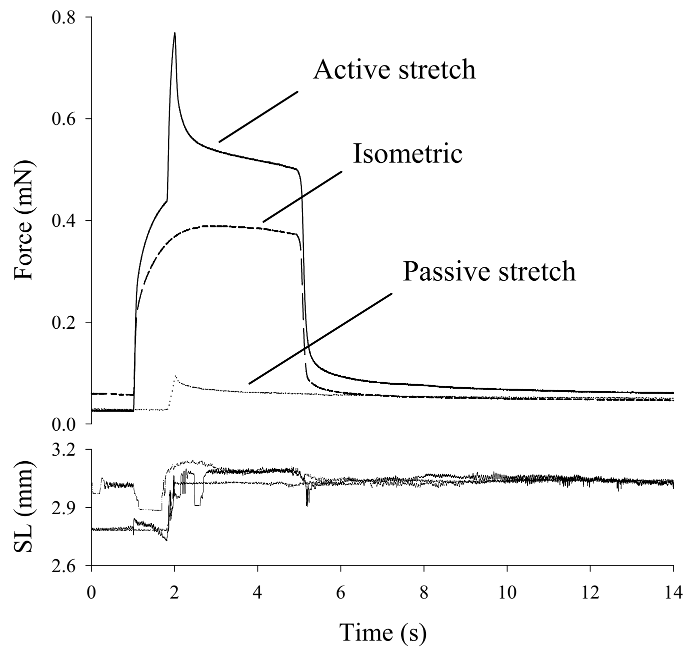

Figure 1: Typical experiment performed with a single fiber in Ringer solution. Force–time traces (top) and sarcomere length -time traces (bottom) are shown for an isometric contraction, an active stretch and a passive stretch. Note that the sarcomere lengths after contractions are similar, but forces following an active stretch are higher than those in the other conditions.

CONCLUSIONS

The passive force-length relationship is shifted upwards along the force axis when fibers are stretched while simultaneously activated. These results might account for the passive force enhancement observed recently in skeletal muscles.

REFERENCES

1. Rassier, et al. *J.Biomech.* **36**, 1309-1316, 2003.
2. Labeit, et al. *Proc.Natl.Acad.Sci.U.S.A* **100,** 13716-13721, 2003.
3. Regnier, et al. *Am.J.Physiol.* **269,** C1532-C`539, 1995.

ACKNOWLEDGEMENTS
Canada Research Chair Program and NSERC of Canada.

DEVELOPMENT OF A BIOMECHANICALLY VALIDATED TURF TESTING RIG

Steven Blackburn[1], Alexander Nicol[1] and Colin Walker[2]
[1]Bioengineering Unit, University of Strathclyde, Glasgow, Scotland. [2]Department of Mechanical Engineering, University of Strathclyde, Glasgow, Scotland. Email: steve_blackburn1@yahoo.com

INTRODUCTION

Many sports are increasing the use of artificial turf, especially with the development of 3rd generation turf. FIFA has decreed that any artificial surface that meets its performance criteria can be used for competitive soccer games [1]. However, it has been suggested that the applied loads in current testing procedures do not reflect the loading actions that occur during actual sporting movements [2,3]. The aim of this study was to develop an artificial turf testing rig that applied biomechanically validated vertical, shear and torque loads to the surface. Results of initial testing on 3rd generation artificial turf and natural grass soccer pitches are presented.

METHODS

The Strathclyde turf testing rig (Fig. 1) was designed to be portable, so that surfaces can be tested *in situ.* The rig was based on a drop-mass/spring/mass system. The basic operation of the test rig involved the use of two weighted pendulum systems to apply loads in a vertical, horizontal and rotational direction. Electromagnets were triggered to release the pendulums at the same time. Loads were applied to a test foot with a pimpled rubber or studded tread design to allow testing on different types of surfaces. A force transducer/ accelerometer complex, positioned just above the test foot provided a measurement of the applied impact loads and accelerations.

Figure 1: Strathclyde turf testing rig

A battery of tests was developed to characterize sports turfs. This included an assessment of linear traction (with a static and dynamic vertical load), rotational traction, vertical impact and a combined vertical, shear and torque impact test. Five trials of each test were conducted on five areas of each pitch.

RESULTS

Table 1 indicates that the traction coefficient and the peak torque measured on the 3G surface were generally lower than the natural grass pitch. The peak vertical forces were similar. The variability in the results reflects the different areas of the pitch tested. The combined impact test (Fig. 2) produced similar loading profiles on both surfaces, although a greater resistance to torque was measured on the natural, dry grass surface.

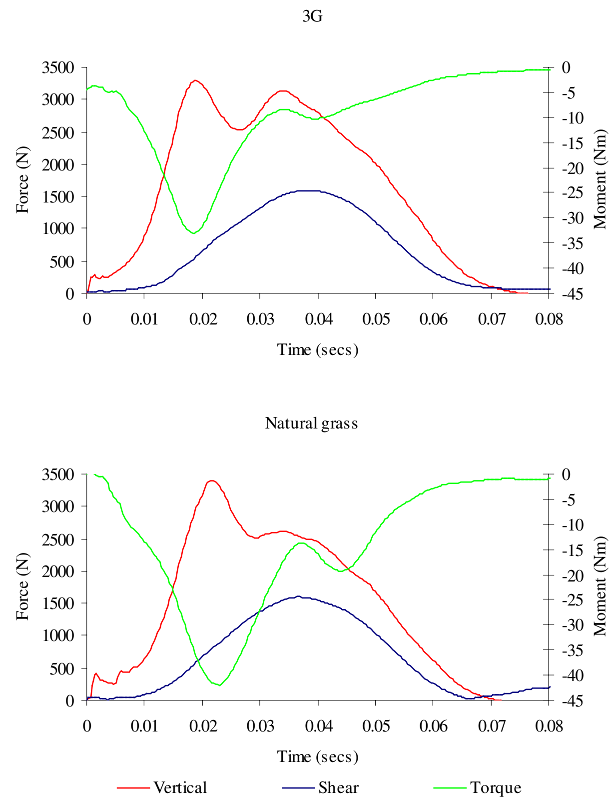

Figure 2: Vertical, shear and torque loads applied during combined impact test on 3G and natural grass surfaces

DISCUSSION

The appropriate loading profiles applied by the test rig were derived from a biomechanical assessment of the player/surface interaction [4].

The operation of the rig is flexible so that different loads can be applied unidirectional or multidirectional in one impact action. This study demonstrated the potential of a new, portable rig to mechanically characterize artificial and natural turfs used in competitive sport.

REFERENCES

1. FIFA. *Laws of the Game*. www.fifa.com, 2004.
2. Nigg, B.M. *Med Sci Sports Exerc*, **22**, 1.131-139, 1990.
3. Dixon, S.J. *Int.J.Sports Med.* **20**, 209-218,1999
4. Blackburn, S.J. *et al. Proceedings of ISB XIX,* Dunedin, New Zealand, 2003.

Surface	Linear traction coeff. (μ)	Peak torque (Nm)	Peak vertical force (N)	Vertical loading rate (kN/s)
3G (*Fieldturf*)	1.9 – 2.9	13.5 – 16.5	3352 - 3405	323.7 – 369.6
Natural Grass	2.1 – 3.2	11-3 – 23.8	3326 - 3478	237.9 – 417.9

Table 1: Ranges of critical surface characteristics derived from test battery.

KNEE JOINT MOMENTS DURING SPORTS ACTIVITIES ON ARTIFICIAL TURF

Steven Blackburn[1], Alexander Nicol[1], Colin Walker[2] and Philippe Brachet[1]
[1]Bioengineering Unit, University of Strathclyde, Glasgow, Scotland. [2]Department of Mechanical Engineering, University of Strathclyde, Glasgow, Scotland. Email: steve_blackburn1@yahoo.com

INTRODUCTION

In team sports, the knee joint is especially susceptible to non-contact injury. With the increased use of artificial turf in sports, there is little evidence regarding the effect of these surfaces on knee joint loading. The aim of this study was to quantify the three-dimensional knee joints moments during different sports movements performed on artificial turf.

METHODS

Ten subjects (ages: 28.2±9.7 years) took part in the study. All subjects played professionally or at a high level of competition and had no history of significant lower extremity injury. Each subject performed three movements on two types of artificial turf. One surface was a short pile, sand-infilled turf and the other was a third generation, long pile, sand/rubber infill turf (3G). The three movements consisted of a straight-line sprint (RUN), a one-stride stopping action during a sprint (STOP) and a 45°-cutting turn to the right (45R). The laboratory was laid out with each turf to provide an area large enough to perform the movements fully. The subjects performed each movement three times on each surface. The players wore their own preferred footwear and were instructed to perform each running movement as fast as possible.

Three dimensional motion analysis was performed using an 8-camer, 120Hz Vicon Motion System. Markers were attached to the body to allow the identification of bony landmarks. Ground reaction forces were measured using a Kistler force plate which was synchronized with the Vicon data. Knee moments were calculated using inverse dynamics and normalized to body weight.

During the stance phase, Peak moments were measured during a weight acceptance (WA) period (0-20% of stance phase) and during a propulsion (PP) period (21-100% of stance phase) for the RUN and 45R. A propulsion period was not defined for the STOP movement, except for moments in the sagittal plane. Moments in this paper are reported as moments that must be generated by the internal musculature.

RESULTS AND DISCUSSION

The magnitudes of the knee joint moments are comparable with published data [1,2]. Internal knee flexor moments of approximately 1-1.5N/kg were applied to the knee during the WA phase of all three movements. These were slightly lower on the 3G turf. Large extensor moments were measured during the propulsion phase, especially in the 45R movements.

Frontal and transverse moments were more variable between subjects, especially during the STOP. During WA, there was an abductor knee moment during the RUN, whereas a larger adductor moment was applied during the 45R. During PP, the RUN produced higher abductor moments than the 45R, with values slightly reduced on the 3G turf. In the WA phase, internal/external moments during the 45R and STOP were much higher than the RUN.

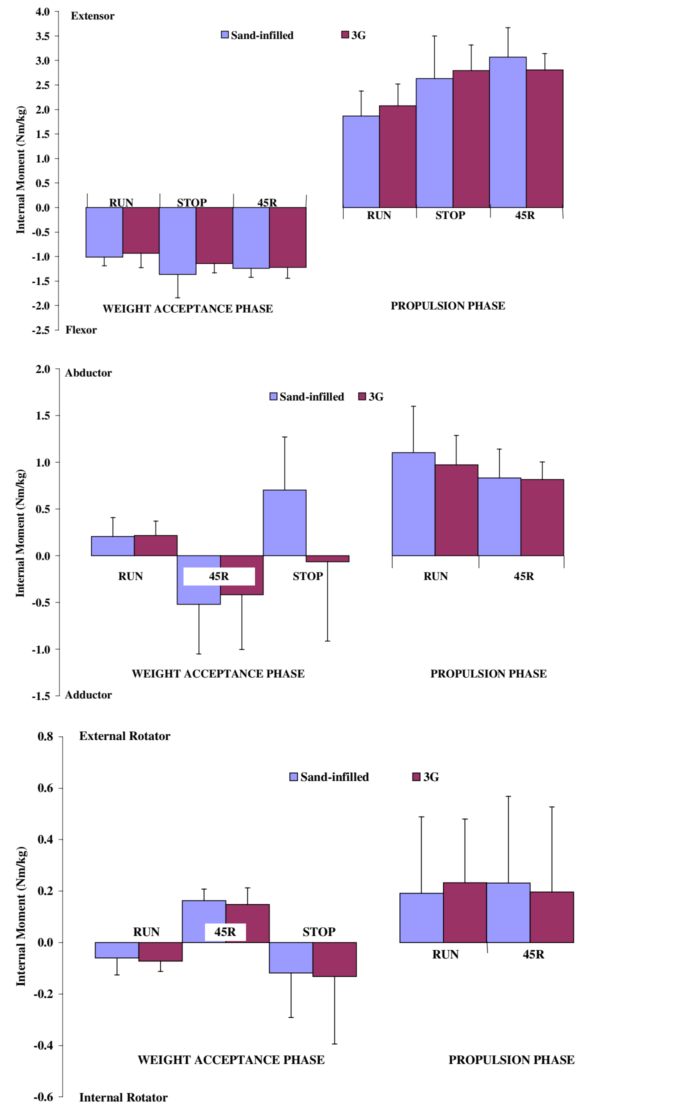

Figure 1 Knee joint moments in transverse, frontal and transverse planes

CONCLUSIONS

Movements that involve rapid deceleration and/or a change in direction produce large knee moments The high moments observed have the potential to significantly load the knee ligaments, increasing the risk of injury.

It is indicated that the sagittal plane loading of the knee during initial impact is generally reduced on third generation turf.

REFERENCES

1. Besier T.F.et al. *Med Sci.Sports Exerc.,* 33. 1168-1175, 2001.
2. Pollard C. *et al*., *Proceedings of ISB XIX*, Dunedin, New Zealand, 2003.

PREHENSION SYNERGIES: EFFECTS OF FRICTION

Tomoko Aoki, Mark L. Latash and Vladimir M. Zatsiorsky
Department of Kinesiology, The Pennsylvania State University
email: vxzl@psu.edu

INTRODUCTION

Friction at the digit-object interface is a critical factor for the central nervous system to adjust digit forces applied to a manipulated object. In two-digit grasps, force normal to the surface becomes greater for an object with a more slippery surface, resulting in a higher normal/tangential force ratio, but the safety margin to prevent slippage is normally kept relatively constant [1]. In multi-digit holding tasks the effects of surface friction have been investigated only for tripod grasps [2]. We therefore investigated these effects in a five-digit object grasping task in relation to changes in the torque acting on the object.

METHODS

Six right-handed healthy young males held an aluminum handle equipped with five six-component force/moment transducers and a level. The level was used to visually guide the subjects to keep the vertical handle orientation. The external torques (-0.5, -0.25, 0, +0.25 and +0.5 Nm) were applied by changing the location of a suspended weight. The total weight of the apparatus was 11.5 N. Sandpaper (S) and rayon (R) materials were used to change friction at the sensor-fingertip interface. There were four surface conditions classified as symmetric — namely SS (all surfaces are S) and RR (all are R) — and asymmetric, SR (S for the thumb and R for the others) and RS (the reverse of SR). Data were collected for each of these conditions while torques were changed (20 trials par subject). Signals were recorded for 3 s after reaching a steady holding condition. In a separate trial for the SS and RR, a hold-to-drop task was performed to measure the minimum normal force to hold the handle, from which we estimated coefficient of static friction (μ), 0.6±0.2 for R and 1.8±0.3 for S. Forces normal (F_n) and tangential (F_t) to the grip surface were analyzed for each digit. Safety margin (SM) was evaluated based on the following equation, SM = $((F_n)_i - |(F_t)_i|/\mu)$.

RESULTS AND DISCUSSION

As expected, both F_n and F_t of all digits were largely influenced by surface condition (Figure). In the symmetric tasks, the F_n was larger in the RR conditions. The effect of friction on F_n was larger than the torque effects: even the smallest value of the F_n for the thumb and virtual finger (VF: an imaginable finger that generates the same mechanical effect of four actual fingers) in the zero torque task was larger than any F_n value in the SS task. There was an equal sharing of the F_t by the thumb and VF for the zero torque condition.

In the asymmetric tasks, force vectors of the thumb and VF differed substantially: the digit force vectors were torque dependent (Figure a). In the zero torque conditions the F_n of the thumb and VF were larger than in the SS and smaller than in RR tasks. At a zero torque, the thumb and VF exerted unequal F_t. Such an unequal sharing of F_t generated a moment of the tangential force that had to be negated by the moment of the normal forces. In the non-zero torque tasks when the torque production required an exertion of a tangential force at the more slippery side, the F_n were as large as in the RR condition (Figure b). The SM values at the zero torque were similar for the thumb and VF for SS and RR, while for the SR and RS tasks they were larger for the S side than the R side.

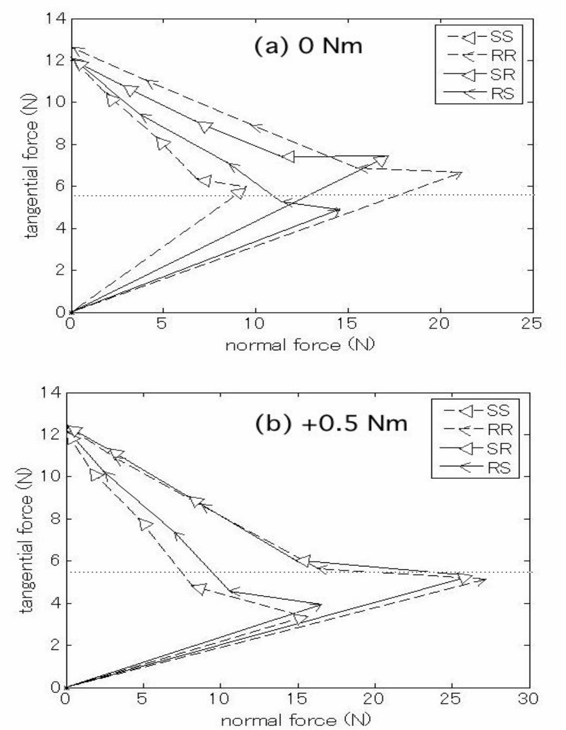

Figure: Mean force vectors for different surface conditions across all subjects. The force polygons have been obtained by adding tail-to-head the individual force vectors. Vectors represent the forces of the thumb, index, middle, ring and little fingers, respectively, in a counterclockwise sequence (starting from the bottom left corner).

SUMMARY

In the asymmetric tasks the subject decrease the F_t production at the places of low friction. Such a strategy results in changes of F_n and the moments produced by the normal and tangential forces (chain effects).

REFERENCES

1. Johansson & Westling. *Exp Brain Res* **56**, 550-564, 1984.
2. Burstedt et al.. *J Neurophysiol* **82**, 2393-2405, 1999.

ACKNOWLEDGEMENTS

Supported in part by NIH grants AR-048563, AG-018751, and NS-35032.

STATIONARY VISUAL CUES REDUCED CENTRE OF PRESSURE DISPLACEMENT IN A DYNAMIC ENVIRONMENT FOR EXPERIENCED ROOFERS

[1]Shirley Rietdyk, [1]Steven R. Torgerud, [2]James D. McGlothlin, [2]Mark J. Knezovich
[1]Health and Kinesiology Department, [2]School of Health Sciences, Purdue University
email: srietdyk@purdue.edu

INTRODUCTION

A worker's postural stability can be compromised by the worksite, work experience and age. Roofers are chronically exposed to a challenging environment: dynamic visual fields, various roof pitch angles and frictional surfaces, gusting winds and handling loads. Recent research has shown that job-specific skills are maintained despite age [1, 2]. These observations might extend to enhanced balance control in roofers due to the challenging environment. Changes to the worksite may improve balance: visual references reduced centre of pressure (COP) displacement in a static lab environment, both at height and on a deformable surface [3].

The purpose of this research was to determine if stationary visual references would reduce COP displacement in a dynamic visual environment, and if the amount of reduction was dependent on work experience and age.

METHODS

Four groups (n = 10 in each group) were examined: younger (26.3 ± 3.1 yrs) and older roofers (50.6 ± 4.2 yrs), younger (26.2 ± 3.7 yrs) and older controls (55.1 ± 4.5 yrs). Roofers had a minimum of two years experience. All subjects were male, healthy and free from any neurologic or otologic disorder. Participants stood on a forceplate (AMTI), either outside (quiet standing) or inside a visual surround (1.2 x 1.2 x 2.3 m), which translated 13 cm in a sinusoidal manner at 0.24 Hz. Six conditions of visual stimuli were examined: (1) 'normal' visual field, (2) static visual field (quiet standing inside stationary surround); the remaining conditions were dynamic visual fields with the following stationary references, (3) no references, (4) two foreground references (inside the moving room), (5) two background references (outside the room) and (6) both foreground and background references. The COP was filtered at 10 Hz with a dual-pass zero-phase-shift fourth-order Butterworth digital filter and quantified by the root mean square (RMS). Statistical analyses were a three factor ANOVA (visual stimuli x age x work experience).

RESULTS AND DISCUSSION

The three way interaction was not significant (p=0.38). The effect of visual stimulus on COP RMS was dependent on work experience (p=0.035). Post hoc analyses revealed that the RMS of the roofers was not different from the controls for four of the six conditions: the quiet standing conditions and the moving room conditions without references or with foreground references (Fig. 1). When background stationary references were present, the COP RMS of the roofers was significantly lower than the controls. When both foreground and background stationary references were present, the COP RMS was reduced compared to the no reference condition, but only for the roofer group. In fact, with both foreground and background references, the response was not different from quiet standing without references. The control group did not reduce the COP RMS with the visual references. Therefore, work experience in a challenging environment did not result in reduced COP RMS either during quiet standing or in a dynamic environment without stationary visual cues in the background. Stationary references in the background did reduce COP displacement, but only for experienced roofers.

The age effect was not dependent on work experience (p=0.17). The roofers had significantly lower COP RMS (p<0.001), and both groups showed similar increases in COP RMS with age (p<0.001). It was interesting to find that the COP RMS of the older roofer was not different from the younger control. Therefore, work experience did not mitigate the age-related changes on COP RMS, but the older roofer had similar postural stability as the younger control.

CONCLUSIONS

Stationary references at the dynamic worksite would only be beneficial for experienced roofers, and need to be in the background. Those at greatest risk of instability due to increased COP displacement, the older, inexperienced roofer, would not benefit from stationary references added to a dynamic worksite.

REFERENCES

1. Guohua L, et al. *Am J Epidemiol,* **157**, 874-880, 2003.
2. Gall B, Parkhouse W. *Ergonomics*, **47**, 671-687, 2004.
3. Simeonov P, Hsiao H. *Inj Prev*, **7**, i50-53, 2001.

ACKNOWLEDGEMENTS

Research supported by the NIOSH Pilot Project Research Training Program of the University of Michigan COHSE.

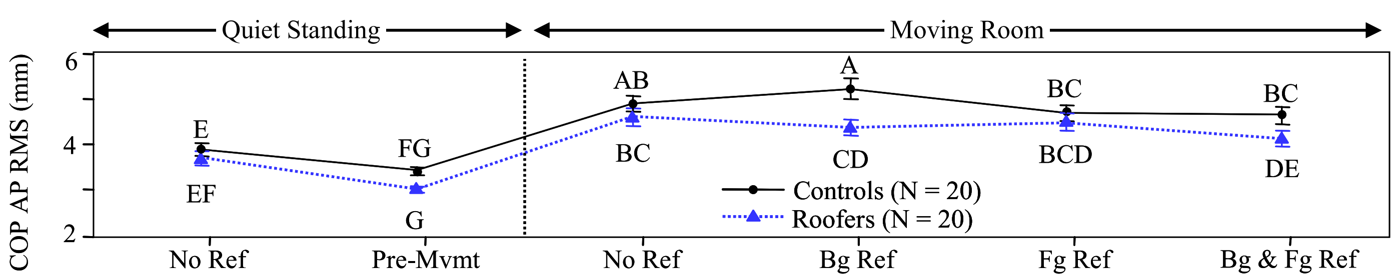

Figure 1: COP RMS compared across work experience and visual background. Bg and Fg = background and foreground references. Letters identify significantly different responses, when more than one letter is present, the response was not different from a response with the same letter (e.g. response with AB was not different from response with A or B).

MICROMECHANICAL ANALYSIS OF DENTIN ELASTIC ANISOTROPY

[1] Anil Misra, [2] Paulette Spencer, [1] Orestes Marangos, [2] Yong Wang, [1, 2] J. Lawrence Katz
[1] Civil Engineering, [2]Oral Biology, University of Missouri-Kansas City
email: misraa@umkc.edu

INTRODUCTION

Stress-strain relationships for materials have been traditionally established through direct phenomenological modeling based upon experimental observations. However, it is widely accepted that the material stress-strain behavior critically depends upon the underlying mechanisms that occur at scales smaller than the material sample scale. Modeling methodologies that account for the underlying mechanisms governing the material behavior and explicitly model material microstructure are expected to provide better insight to the material stress-strain behavior and bridge the scale between continuum and discrete representations. For instance, micromechanical models considering particle interactions have been successfully used for describing stress-strain behavior of granular materials [1]. The objectives of this work are: (1) to develop a micromechanical model that relates the anisotropic elastic properties to the microstructure of dentin using a virtual bond idealization, and (2) to study the average force constants and anisotropy parameters utilizing the developed model in order to understand how the dentin elasticity is affected by the presence of water.

Along this approach, we consider the material-scale to be composed of nano-scale grains (representing molecular bonds) whose centroids represent material points. Similar granular or discrete microstructure models have been considered in the past for developing constitutive relations, such as the virtual internal bond model developed by Gao and Klein [2], the higher order constitutive relationships developed by Chang and co-workers (see among other publications [3]), and the micromechanics models [1,4]. In analogy with atomistic-scale interactions, these nano-scale grains are viewed as interacting with each other through pseudo-bonds.

METHODS

The underlying material microstructure is conceptualized as a collection of interacting grains modeled by virtual bonds. With the view of bridging behavior at nano and micro-scales, the virtual bond force-displacement relationships are formulated taking inspiration from atomic-bond interactions. The force-displacement relationships are formulated for both central and non-central interactions, denoted by the force constants K_n and K_w, respectively. The dentin microstructure is characterized by a virtual bond directional distribution function modeled by first-term of the spherical harmonic expansion denoted by anisotropy parameter a_{20}. Considering the kinematic assumption that the bond displacement is linearly related to the overall strain, the pseudo-bond force-displacement relationships may be combined with its orientation to derive the incremental stress and stiffness tensors. Alternatively, utilizing a static assumption that relates the virtual-bond force to the stress tensor, the pseudo-bond force-displacement relationships may be combined with its orientation to derive the incremental strain and compliance tensors.

RESULTS AND DISCUSSION

Closed form expressions of the transverse isotropic stiffness tensor are obtained for the case of linear inter-granular interactions. These expressions are utilized to compute the stiffness and anisotropy parameters for dry and wet dentin [5] utilizing an optimization method. The stiffness parameters are defined as follows: $A_1 = L_o^2 N_p K_n$ and $C_1 = L_o^2 N_p K_w$, where L_o is the bond length, and N_p is the bond density per unit volume. The stiffness parameters A_1 and C_1, (in GPa) respectively are as follows: 183.2, 0.0 (dry dentin), 199.7, 0.0 (wet dentin) based upon kinematic approach, and 196.5, 45.7 (dry dentin), 243.2, 38.3 (wet dentin) based upon static approach. The anisotropy parameter a_{20} are as follows 0.0 (dry dentin), -0.234 (wet dentin) based upon kinematic approach, and 0.0 (dry dentin), -0.218 (wet dentin) based upon static approach. Measured elastic moduli for dry dentin are isotropic, while those for wet dentin are transversely isotropic with the isotropy plane perpendicular to the tubule direction being stiffer. Consequently, the anisotropy parameter a_{20} vanishes for dry dentin and takes a negative value for wet dentin.

CONCLUSIONS

The force constant for wet dentin is higher than that of dry dentin indicating that the presence of water results in the stiffening of bonds that contribute to the mechanical stiffness at the sample scale. Moreover, the anisotropy parameter of wet dentin indicates that the bond density becomes higher in the isotropy plane in the presence of water.

REFERENCES

1. Misra A, Chang CS *Intl J Sol Strucs*, **30**, 2547-2566, 1993.
2. Gao H, Klein P *J Mech Phys Solids*, **46(2)**, 187-218, 1998.
3. Chang CS, Askes H, Sluys LJ. *Engr Frac Mech*, **69(17)**, 1907-1924, 2002.
4. Thiagarajan G, Misra A *Intl J Sol Strucs*,, **41**, 2919-2938, 2004.
5. Kinney JH *J Biomech*, **37,** 437-441, 2004.

ACKNOWLEDGEMENTS

Supported in part by grant NIH/NIDCR DE014392.

FORCE PROFILE COMPARISON OF ROWING ON A STATIONARY AND DYNAMIC ERGOMETER

[1]Aaron Benson and [2]Julianne Abendroth-Smith
[1]Ithaca College, Ithaca, NY; email: benson_aaron@hotmail.com
[2]Willamette University, Salem, OR; email: jabendro@willamette.edu

INTRODUCTION

Recently developed dynamic rowing ergometers enable part or all of the machine to move back and forth inversely with the rower, akin to the response of a boat. A common dynamic design incorporates a wheeled base beneath a normally stationary machine. Such a setup conserves mechanical energy and enables higher stroke rates, thus better simulating on-water rowing [3]. Comparisons of "fixed" and "floating" conditions using the RowPerfect (a truly dynamic ergometer) have found similar results, as well as decreased work per stroke in the dynamic condition [1,2].

Concept 2 has designed "Slides" to allow dynamic rowing, but research involving this popular equipment is minimal. This study compares the use of a Concept 2 ergometer alone and with Slides, through force profile evaluation.

METHODS

Varsity and novice rowers from the Ithaca College Crew volunteered; 21 women (ht. 1.71 ±0.08 m, mass 67.4 ±7.6 kg) and 16 men (ht. 1.82 ±0.08 m, mass 80 ±11.4 kg) participated. IRB approval and informed consent were obtained.

Subjects completed two 1000-meter trials on a Concept 2 Model C ergometer. The ergometer was alternately stationary or dynamic (counterbalanced). Subjects rowed at their self-selected race pace, maintaining a constant workload within and between trials. All subjects were allowed to warm-up, rest, and familiarize with equipment as needed.

A load cell (Bertec, 2200 N) mounted between the handle and chain provided stroke rate, peak force, mean impulse, and total integrated force (representing work) for the final 30 seconds of each trial. Differences by condition and sex were located with a 2×2 repeated measures ANOVA (α=0.05).

RESULTS AND DISCUSSION

Rowers displayed significantly higher stroke rate and total integrated force, and significantly lower peak force and mean impulse in the dynamic condition than in the stationary (Figure 1). Men exhibited significantly greater peak force, impulse, and integrated force than women. An interaction occurred whereby men decreased impulse on the dynamic ergometer more than women.

The statistical difference in integrated force implies that more work was performed on the dynamic ergometer. Although this is contrary to the literature [1], the small effect size (0.09) indicates minimal practical difference. Measurement over the entire bout could clarify this discrepancy.

These results support the suggestion that dynamic ergometers might reduce injury risk [1], given that the body is subjected

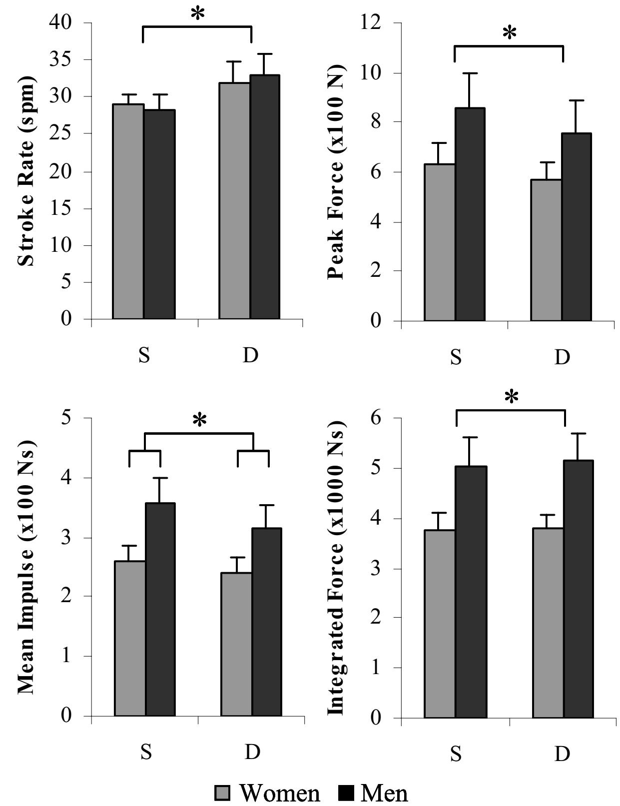

Figure 1: Mean (+SD) stroke rate, peak force, impulse per stroke, and total integrated force on the stationary (S) and dynamic (D) ergometer for women and men. An asterisk indicates a statistically significant difference by condition.

to lower peak forces and load (impulse) during each stroke. It is likely that the reduced musculoskeletal stress is paired with greater cardiovascular stress, in the form of higher stroke rate.

CONCLUSIONS

The dynamic ergometer appears to be more useful for training rowers during the sprinting season, when high stroke rates are desired. Training for strength and endurance might be more effective with the stationary ergometer, providing sufficient overload for muscle and connective tissue development.

REFERENCES

1. Bernstein IA, et al. *Br J Sp Med* **36**, 108-112, 2002.
2. Elliot B, et al. *Sp Biomech* **1**(2), 123-134, 2002.
3. Martindale WO and Robertson DGE. *Can J Appl Sp Sci* **9**(3), 153-163, 1984.

ACKNOWLEDGEMENTS

Thanks to Ken Halpin for his work processing data, as well as to Tom Swensen, Deborah King, and Becky Robinson.

Accuracy of Three Mathematical Models vs. Human Trained Paralyzed Muscle

Laura A. Frey Law and Richard K. Shields
Graduate Program in Physical Therapy & Rehabilitation Science, The University of Iowa
1-252 MEB, Iowa City, IA 52242 USA; email: laura-freylaw@uiowa.edu

INTRODUCTION

Paralysis due to chronic spinal cord injury dramatically decreases physical function, can induce transformation towards fast fatigable muscle fibers [1], and can result in life threatening musculoskeletal deterioration (e.g. pressure ulcers, osteoporosis). Electrical stimulation may be able to improve function of paralyzed muscle and isometric muscle training may attenuate various neuromuscular and skeletal adaptations. Previous work has demonstrated that several mathematical muscle models can represent chronically paralyzed human muscle (untrained) to assist in the development of optimal activation strategies for specific muscle force doses [2]. However, no previous studies have evaluated the ability of mathematical muscle models to represent altered muscle contractile properties resulting from repetitive activation (training) in paralyzed muscle. The purpose of this study was to compare the force predictions of three available muscle models (one linear and two nonlinear) versus human trained (> 1 year) paralyzed muscle.

METHODS

Isometric soleus forces were obtained from 4 individuals with complete spinal cord injury (SCI, 1.5 to 4.2 yrs) who had been continually training their left soleus muscles since the acute injury stage (~6 weeks post injury). Three models of varying complexity, a Hill based nonlinear (Hill NL, [3]), a 2nd order nonlinear (2nd Ord NL, [4]), and a simple 2nd order linear model (Linear), were parameterized using a single force train resulting from a variable ramp of increasing and decreasing stimulation frequencies [4]. The optimal parameter values were then used to predict forces for 9 trains (5, 10, and 20 Hz constant, CT, doublet, DT, and dual doublet, DDT, trains) for each model. Model errors were determined relative to the experimental results for each subject (Matlab 6.0) as an overall error (% error) and specific force property errors: peak force (PF), force time integral (FTI), time to peak tension (TPT), half-relaxation time (HRT), relative fusion index (RFI), and doublet difference (DDiff) to estimate the "catch-like" property of muscle. Model comparisons were made using repeated measures ANOVA, alpha = 0.05, with follow-up tests using Bonferroni correction for multiple comparisons.

The simplest model was the Linear model (3 parameters), followed by the 2nd Ord NL model (6 parameters) and the most complex was the Hill NL model (6 parameters). The Hill NL model was more complex than the 2nd Ord NL model because one of its differential equations had no analytical solution. Numerical analysis techniques (e.g. Runge-Kutta) were required adding to the computational complexity and processing time necessary for optimal convergence.

RESULTS AND DISCUSSION

All three models provided reasonable estimates of force (< 20% mean error), but to varying degrees. Overall, human trained soleus muscle forces were best predicted by the Hill NL, followed by the 2nd Ord NL, and lastly the Linear model (Table 1). However, the 2nd Ord NL model often produced similar errors ($p > 0.05$) as the Hill NL model (e.g. PF, FTI, and DDiff). The 2nd Ord NL model had the greatest difficulty predicting TPT accurately, consistently under predicting contraction times. The simplest Linear model produced the greatest overall error, but had similar errors as the NL models for unfused constant frequencies (5 Hz CT). The relative degree of force fusion (RFI) was best predicted by the nonlinear models, but the Linear model provided reasonable predictions. All three models had difficulty predicting the "catch-like" property of muscle.

CONCLUSIONS

The 2nd Ord NL model produced nearly equivalent force predictions as the Hill NL model, but with less model complexity. Further, the Linear model was the simplest model, producing reasonable force predictions for select force trains. These three models can provide reasonable estimates of human trained paralyzed muscle force, but the 2nd Ord NL model produced the best estimates most simply.

REFERENCES

1. Shields RK. *J Neurophysiol* **73**, 2196-2206, 1995.
2. Frey Law LA, et al. *Proceedings of ACSM*, Nashville, 2005.
3. Ding J, et al. *Muscle & Nerve* **26**, 477-485, 2002.
4. Bobet J, et al. *IEEE Biomed Eng* **45**, 1010-1016, 1998.

ACKNOWLEDGEMENTS

Support was provided by NIH grant RO1 HD39445 (RKS) and The Foundation for Physical Therapy (LAFL).

Table 1: Mean (SEM) errors associated with each mathematical muscle model for predicting human, trained paralyzed muscle forces across stimulation patterns: 5, 10, and 20 Hz: CT and DDT patterns - % error, PF and FTI; CT only – HRT, RFI; 5 Hz CT only – TPT; and mean difference between DDT – DT and DT – CT at 5, 10, and 20 Hz = DDiff.

Model	% error (%)	PF (%)	FTI (%)	TPT (ms)	HRT (ms)	RFI (%)	DDiff (%)
Hill NL	7.8 (0.4)	7.5 (0.7)	9.0 (1.3)	3.0 (2.3)	5.8 (2.0)	3.0 (0.8)	24.9 (2.0)
2nd NL	10.0 (0.8)	7.3 (0.5)	9.3 (2.0)	22.0 (1.8)	11.0 (3.4)	6.6 (1.6)	21.6 (1.6)
Linear	15.8 (1.2)	20.0 (1.1)	17.5 (2.2)	2.8 (1.4)	33.8 (4.8)	12.1 (1.1)	61.6 (8.1)

EVALUATION OF FUNCTION OF KNEE JOINT BY PHYSIOLOGICAL TREMOR IN LOWER LEG

[1] Kazuyoshi Sakamoto, [1]Takuma Igo, [1]Kazuyuki Mito, [1]Hidenori Shimada, [2]Hitoshi Makabe, [3]Masato Takanokura,
[1]The University of Electro-Communications, Japan, [2]Yamagata Prefectural University of Health and Science, Japan,
[3]Kanagawa University, Japan; [1]email:sakamoto@se.uec.ac.jp

INTRODUCTION

Physiological tremor is invisible mechanical vibration of body part. Finger and upper limb have been studied, but the other body parts like lower limb has not reported. The purpose of the study is to elucidate the function no knee joint by physiological tremor under various conditions.

METHODS

Measurement system of physiological tremor of lower leg is shown in Fig.1. The knee angle θ was hold by gazing on the marker connected to ankle with string. The ankle was fixed with use of equipment fastened the ankle (AFO). Tremor was detected by accelerometer (9G111BW, NEC Sanei) glued with both sides adhesive tape on the middle point between knee joint and ankle joint. Tremor was evaluated by total of power spectrum (TP) in frequency range from 0.5 to 50 Hz. The frequency range also divided into two frequency bands, lower band of 0.5 to 5 Hz and higher band of 5 to 50 Hz. The former and the latter showed reflex nervous component and central nervous component, respectively [1, 2]. Three kinds of experiments were performed: **(1)** Experiment of holding posture of lower leg in knee angle from 10 to 90 degrees, **(2)** Experiment of weight load of 5% to 40% MVC (Maximum Voluntary Contraction). **(3)** Experiment of muscular fatigue. The measurement time was 35 seconds for all the experiments. The subjects were ten aged 21 to 24 years old.

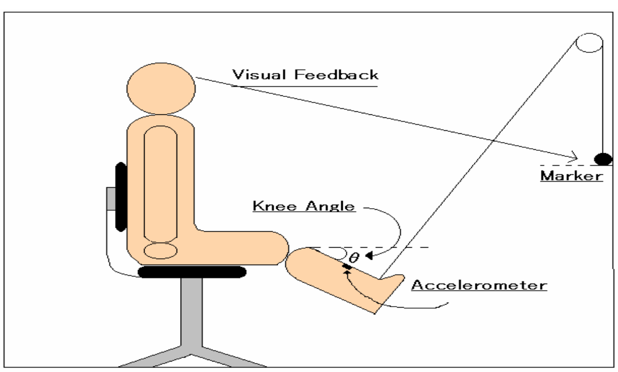

RESULTS AND DISCUSSION

Results of **(1)** experiment of holding posture were presented in Fig. 2. The amplitude of the tremor shown in total power increased linearly as the knee angle θ decreased and the change in lower band was larger than the higher one, but the peak frequencies for various angle remained constant. The function of reflex component was dominant in holing posture. The results of **(2)** experiment under weight load revealed the contribution of higher band when weight load was more than 20 % MVC. The peak frequency decreased significantly at the load more than 20% MVC. The results meant that the central nervous component predominated under higher load. The results of **(3)** are shown in Fig.3. The relative total powers in both frequency bands after all out increased significantly compared with the value before the load. And the value of higher band was significantly larger than that of lower band. Just after the all-out state, the tremor holding posture was controlled by higher band component. The result revealed that the fatigue of central nervous was recognized predominantly.

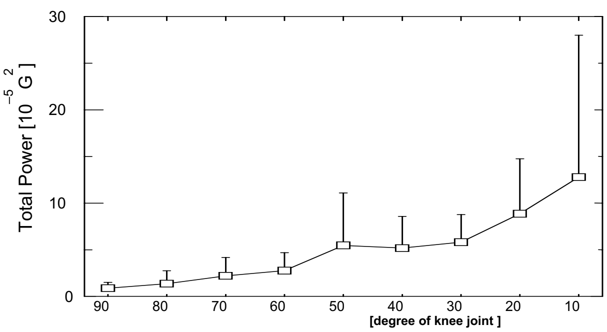

Figure 2: Total power (TP) in full frequency band (0-50Hz) for knee joint angle θ.

CONCLUSIONS

Characteristics of tremor of lower leg under the conditions of knee angle and weight load were obtained. Fatigue of knee joint was evaluated by the total power of the tremor. It was recognized that these results could be applied to the function of knee joint for disease person of knee joint as compared with the fundamental data evaluated in the study.

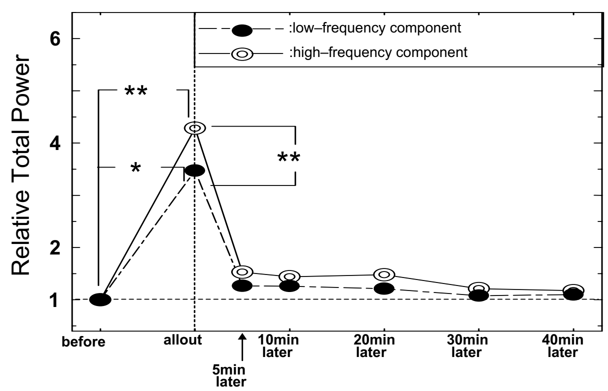

Figure 3: Total power in lower frequency and hither frequency bands before load, at all-out, and after load

REFERENCES

1. Takanokura M and Sakamoto K. *Eur. J. Appl. Physiol.*, **85**, 214-225,2001.
2. Takanokura M, et al. *Electro. Clin. Neurophysiol.* **14**, 297-304, 2001.

THE KINETIC CHANGES OF GAIT ACROSS CALF MYOFASCIAL INTERVENTION

[1,2]Shyi-Kuen Wu, [2]Chang-Zern Hong, [3]Jia-Yuan You, [1]Chiung-Ling Chen, [1]Lin-Hwa Wang, and [1]Fong-Chin Su
[1]Institute of Biomedical Engineering, National Cheng Kung University, Tainan, Taiwan; [2]Department of Physical Therapy, HungKuang University, Taichung County, Taiwan; [3]Department of Physical Therapy, I-Shou University, Taiwan;
email: fcsu@mail.ncku.edu.tw

INTRODUCTION

Myofascial pain syndrome (MPS) is a common clinical problem of muscle pain caused by myofascial trigger points (MTrPs). MTrP has been defined as the hyperirritable spot in a taut band of skeletal muscle fibers [1]. The majority of researches concerning the myofascial pain have been related to pain condition and the areas of head, neck, upper extremities, as well as back, but the lower extremity problems were generally overlooked. The purposes of this study were to investigate the influence of the chronic calf muscle tightness caused by myofascial pain syndrome on gait performance and the treatment effect in order to inform the clinical management of patients with inflexibility of calf muscles.

METHODS

A female subject suffered from chronic knee and ankle pain for five years as a result of calf muscles myofascial pain syndrome. The pain intensity (Visual Analog Pain Scale), ranges of motion on ankle joints, and gait analysis were evaluated before and after myofascial pain therapy. The Expert Vision HiRes motion analysis system (Motion Analysis Corporation, CA, USA) equipped with 6 CCD cameras were synchronized with ground reaction forces measured by two forceplates (Kistler Instrument Corporation, NY, USA) and used to capture the subject's motion at 60 Hz sample rate. The 8-week calf myofascial treatment programs included manual techniques (deep myofascial release, deep friction massage, and proprioceptive neuromuscular facilitation stretching) and home program (self-stretching exercises).

RESULTS AND DISCUSSION

There were significant improvements in the ankle-dorsiflexion ROMs of the affected leg after treatment ($p < 0.01$). A trend of moderate improvement in pain conditions were recorded both in resting and after work. Although the kinematic data of gait analysis were quite similar across treatments except for improved knee flexion angles, the kinetic findings revealed significant effectiveness of myofascial treatments. The significantly decreased peak ground reaction forces ($p < 0.001$), and significantly improved peak joint moments of ankle dorsiflexion ($p = 0.008$), foot supination ($p = 0.002$), and knee extension ($p = 0.009$) were demonstrated during walking. This case study demonstrated the biomechanical abnormality of gait due to chronic myofascial pain in the calf muscles. This greater and prolonged dorsiflexion moment could be due to

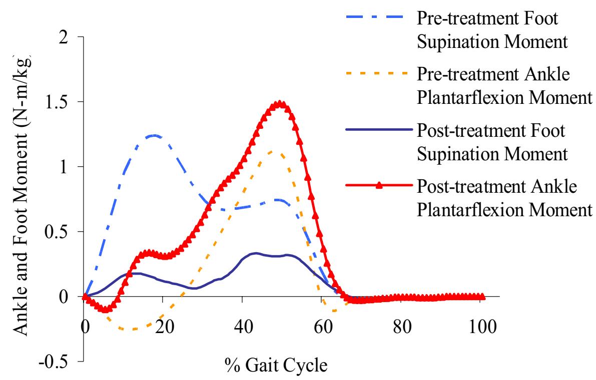

Figure 1: The joint moments of ankle and foot across treatments throughout the gait cycle. (positive values: ankle plantarflexion and foot supination; negative values: ankle dorsiflexion and foot pronation).

greater demands of dorsiflexor muscles to maintain an appropriate heel strike as the result of the tightness of calf muscle. The significantly greater moments of foot supination in the stance phase before treatment may indicate that more supinator efforts to prevent excessive pronated foot that usually compensated for insufficient dorsiflexion flexibility [2]. The significantly greater knee extension moments caused the increase muscle loading of knee extensors and could be the result of excessive knee flexion angles during walking. The excessive knee flexion angles were the obligatory compensation for tight calf muscles in order to have a nearly normal ankle-foot motion. The myofascial treatments improved the clinical symptoms and kinetics of gait.

CONCLUSIONS

The chronic muscle tightness caused by myofascial pain syndrome is a factor influencing the joint motion and easily ignored by clinicians. The quantitative gait analysis is valuable and necessary to clarify the influence of the chronic calf muscles tightness on ankle and knee joints and the effectiveness of myofascial treatments.

REFERENCES

1. Simons DG, et al. *Travell & Simons" Myofascial Pain and Dysfunction: The Trigger Point Manual*, Vol. **1**. Ed. 2. Williams & Wilkins, Baltimore, 1999.
2. Gross M: *J Orthop Sports Phys Ther* **21**, 389-405, 1995.

Table 1: The pain intensity, joint angle, peak ground reaction force, and knee joint moment across myofascial treatments.

		Before treatment	After treatment	P
Pain intensity	ankle resting pain / pain after work	3.1 / 3.8	0.5 / 1.5	
Joint angle (°)	ankle dorsiflexion with knee extended (flexed)	10.3 ± 0.6(20.3 ± 1.5)	18.3 ± 2.1(29.7 ± 0.6)	0.003*(0.001*)
Peak ground reaction force (body weight)		1.75 B.W.	1.13 B.W.	< 0.001*
Knee extension moment (N-m/kg)		0.97 ± 0.07	0.42 ± 0.02	0.009*

BIOMECHANICAL EFFECTS OF PLANTAR FASCIA RELEASE AND POSTERIOR TIBIAL TENDON DYSFUNCTION– A FINITE ELEMENT AND CADAVERIC FOOT SIMULATION

[1]Jason Tak-Man Cheung, [1]Ming Zhang and [2]Kai-Nan An
[1]Rehabilitation Engineering Centre, The Hong Kong Polytechnic University, Hong Kong, China,
[2]Biomechanics Laboratory, Department of Orthopedic Surgery, Mayo Clinic, Rochester, Minnesota, USA;
email: jason.cheung@polyu.edu.hk

INTRODUCTION
The plantar aponeurosis and the posterior tibial tendon are important for maintaining the normal foot arch. Failure or dissection of these structures may lead to arch instability and increase the load bearing of surrounding structures of the foot such as the interlocking tarsal joints, joint capsules and plantar ligaments. In this study, a finite element (FE) and cadaveric foot simulation was done to investigate the biomechanical effects of plantar fascia release (PFR) and posterior tibial tendon dysfunction (PTTD).

METHODS
A geometrical accurate FE model of the human foot and ankle was developed from 3D reconstruction of 2mm coronal MR images from the right foot of a normal male subject in the neutral unloaded position [1]. The FE model (Figures 1) consisted of 28 bony segments embedded in a volume of encapsulated soft tissue. A total number of 72 ligaments and the plantar fascia were included and defined by connecting the corresponding attachment points on the bones.

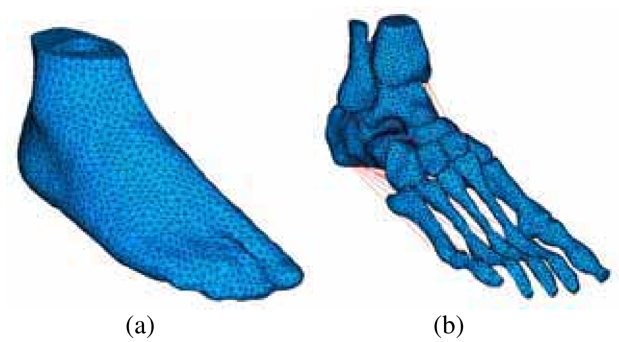

Figure 1: The FE meshes of the (a) encapsulated soft tissue, (b) bony and ligamentous structures.

A hyperelastic material model was adopted to represent the nonlinear and incompressible nature of the encapsulated soft tissue. Other tissues were idealized as homogeneous, isotropic and linearly elastic. The interactions among the bones were defined as contact surfaces to allow relative bone movements. Nonlinear contact stiffness was defined to simulate the contact behavior between the articulating surfaces. A horizontal ground support inclined at 10 degrees relative to the plantar foot was used to establish the frictional contact interaction of the foot-ground interfaces during midstance.

The superior surface of the soft tissue, distal tibia and fibula was fixed throughout the analysis. The ground support was constrained to move in the same direction of ground reaction force vector, which was applied perpendicularly at the inferior ground support. The extrinsic muscles forces during midstance were estimated from muscles cross-sectional area and EMG data with a linear EMG-force assumption [2]. Musculotendon forces were applied at their corresponding points of insertion by defining contraction forces via axial connector elements. Simulation of PFR and PTTD were done by removing the plantar aponeurosis and the tendon forces from the FE model.

The FE predicted results were validated with experimental measurements on six cadaveric foot specimens under similar loading and boundary conditions. Quasi-static foot simulation was done to measure the relative bone rotation, plantar pressure and strain of the plantar fascia (Figure 2).

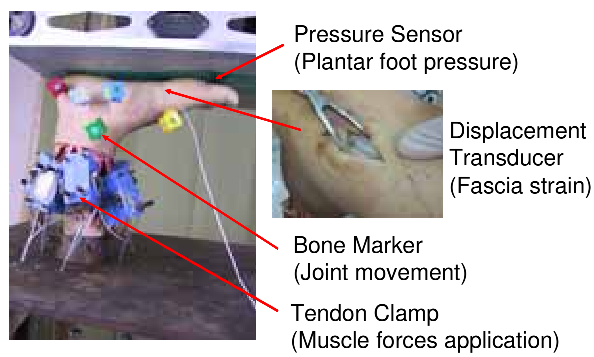

Figure 2: Experimental setup of cadaveric foot simulation.

RESULTS AND DISCUSSION
Both PFR and PTTD decreased the arch height with the former having a greater effect. The reduction of arch height intensified with a combination of PFR and PTTD but did not cause total collapse of foot arch. Both PFR and PTTD increased the strains of the plantar ligaments. The effect of PTTD on the metatarsal stress distribution is minimal while PFR induced medial shift of peak von Mises stress from the third to the second metatarsal. The lack of foot arch support with PFR and PTTD may lead to attenuation of surrounding soft tissue structures and elongation of foot arch, resulting in a progressive acquired flatfoot deformity.

REFERENCES
1. Cheung JT, et al.. *J Biomech* **in press**, 2005.
2. Kim KJ, et al.. *J Musculoskeletal Res* **5**, 113-121, 2001.

ACKNOWLEDGEMENTS
This work was supported by the Hong Kong Jockey Club endowment, the research studentship from The Hong Kong Polytechnic University and a grant from the Research Grant Council of Hong Kong (Project No. PolyU 5249/04E). The support on cadaveric study from the Institute of Clinical Anatomy, Southern Medical University, Guangzhou, China is acknowledged.

ACTIVATION PATTERNS OF TRUNK MUSCLES DURING CYCLIC FLEXION-EXTENSION

Michael W. Olson and Li Li
Department of Kinesiology, Louisiana State University, Baton Rouge, Louisiana, USA
Email: molson2@lsu.edu

INTRODUCTION

A high incidence of low back injuries has been reported in individuals employed in labor intensive work environments [1]. The interactions between the active and passive tissues of the lumbar spine are important factors to consider when identifying the etiology of these injuries [2]. Behavior of the lumbar muscles is affected by the changing mechanical properties of both active and passive tissues.

In healthy individuals the myoelectric activity of the lumbar muscles decreases during deep trunk flexion [3]. This event has been termed the flexion-relaxation phenomenon [4]. Mechanical load-sharing and neural mechanisms have been used to explain this event [4]. However, compensatory mechanisms must be initiated in order to offset the flexion moment applied at the lumbar spine.

The purpose of this study was to explore the behavior of the trunk muscles to identify mechanisms used to compensate for decreased lumbar muscle activity.

METHODS

Data were collected from 13 asymptomatic males [age mean 20 (± SD 1) yrs., height 1.77 (± 0.06) m, body mass 82 (± 11) kg] who performed five separate cycles of trunk flexion-extension. Cycle duration was 10 sec and controlled with the tempo of a metronome. Once collected, the time series of each cycle was normalized to a percentage of the cycle.

EMG signals were collected on the right side by pre-gelled Ag-AgCl electrode pairs. The muscles analyzed were the lumbar paraspinal (LP) at the L3-L4 level, the rectus abdominis (RA), and external oblique (EO). The inter-electrode distance was 2.5 cm from center to center.

Reflexive spheres, 2.5 cm in diameter, were taped onto the skin on the left side at the lateral edge of the twelfth rib, lateral midline of the iliac crest, and greater trochanter. These markers were used to represent trunk inclination and lumbar flexion angles. Kinematic and EMG data were temporally synchronized.

One-way ANOVA with repeated measures was used to evaluate the changes of each variable between trials. The alpha level was set at 0.05.

RESULTS AND DISCUSSION

No trial effects were observed in the data, only means and sd are presented in here as a percentage of the cycle. The LP flexion-relaxation phenomenon occurred in all participants (cessation at 34±7% and re-initiation at 57±7%). The EMG activity of the abdominal muscles, RA (n = 5) and EO (n = 7), were detected (initiation at 42±4% and 39±5%, cessation at 54±5% and 57±%, respectively] at the deepest trunk inclination and lumbar flexion angles in about half of the

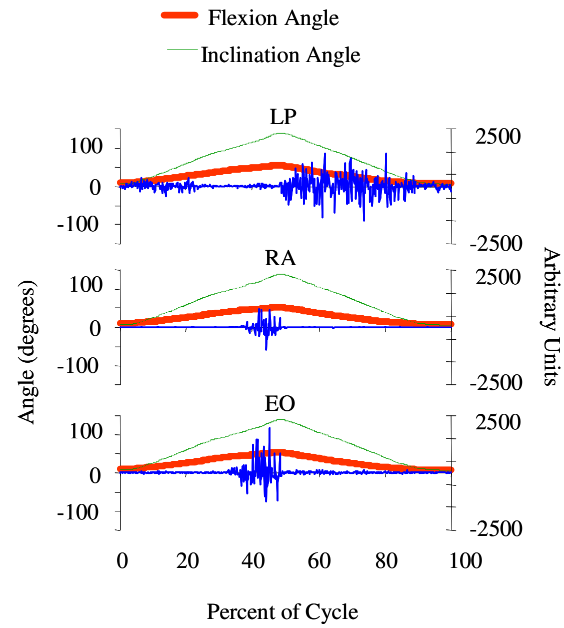

Figure 1: Exemplar EMG pattern of lumbar paraspinal (LP), rectus abdominis (RA), and external oblique (EO) muscles from one participant during a single trial of trunk flexion-extension.

participants (Figure 1). EMG activity of both RA and EO muscles was observed in four individuals. One individual had only RA activity and three had only EO activity detected during this time period.

The activation of the RA and EO muscles may serve to increase the intra-abdominal pressure (IAP). The IAP may also assist with the extension moment at the lumbar region. The involvement of the abdominal muscles leads to increased IAP support for the abdominal cavity. Elevated IAP results in a complementary reinforcement of the integrity of the lumbar vertebrae [5,6].

CONCLUSIONS

Mechanisms responsible for the flexion-relaxation phenomenon need further examination. Likewise, compensatory mechanisms that respond to this myoelectric silent period also require additional attention.

REFERENCES

1. US Dept Labor. http://www.bls.gov/iif/home.htm, 2003
2. Dolan P & Adams MA. *J Biomech* **31**, 713 – 721, 1998
3. Allen CEL. *Brit. J Phys Med* **11**, 66 – 73, 1948
4. Floyd WF & Silver PHS. *J Physiol* **129**, 184 – 203, 1955
5. Cresswell AG & Thorstensson A. *Ergonomics* **31**, 1237 – 1246, 1989
6. Hodges PW, et al. *J Biomech* **34**, 347 – 353, 2001

Measures of Postural Stability During Quiet Stance.

Geoff Walmsley, Alan Walmsley
Massey University, Wellington, New Zealand
email: G.M.G.Walmsley@massey.ac.nz

INTRODUCTION

The control of balance and postural stability has been studied extensively by biomechanists and roboticists, with many interesting results. Postural sway is inherent in all humans during both bipedal and unipedal stance. Time series data of the Center of Pressure (CoP) of a subject on a force plate are most commonly used to analyze postural sway. In this paper we will outline how the time series data may be manipulated to discover what types of process are active, and describe measures that distinguish each series. We follow Zatsiorsky's rambling/trembling concept introduced in [3,4], with particular emphasis given to comparative tests of stability in the elderly. The focus of this paper is to describe the random stochastic movements contained in the tremble component of Zatsiorsky's framework.

METHODS

Force plate data were collected at 50Hz from 12 healthy subjects aged over 60. The data were processed to give (x, y)-coordinates of the CoP. After normalization and mean drift removal, we calculated the distribution of CoP movement in both anterior-posterior (AP) and medial-lateral (ML) directions.

We decided to model the migration of the CoP as a random walk in two dimensions, which is analogous to a particle undergoing diffusion. Inspection of the data revealed that the distribution of particle jump sizes was not Gaussian, and in fact, followed a stable distribution. Denoting the probability of finding the CoP at position x at time t by P(x, t), then the fractional diffusion equation, which has the class of stable distributions as solutions, is given by

$$\frac{\partial P(x,t)}{\partial t} = -D\frac{\partial^{\alpha} P(x,t)}{\partial x^{\alpha}} \quad , \qquad (1)$$

where $0<\alpha\leq 2$. In the case $\alpha=2$, the system is Gaussian, and we observe Brownian motion. This equation can be manipulated into an arbitrary dimensionality, with different α's in different directions [2]. The main feature of equation (1) is that the random walk described by this equation has large but infrequent particle jumps that drive the system.

Finally, a method was developed to calculate an individual measure of postural stability, based on existing theory in fractional calculus. For this, the multiscaling fractional advection-dispersion equation, examined thoroughly in [2] was used. Although heavily mathematical, the theory allows simple computation on data sets to obtain a measure of stability based on the exponent α in both the AP and ML directions.

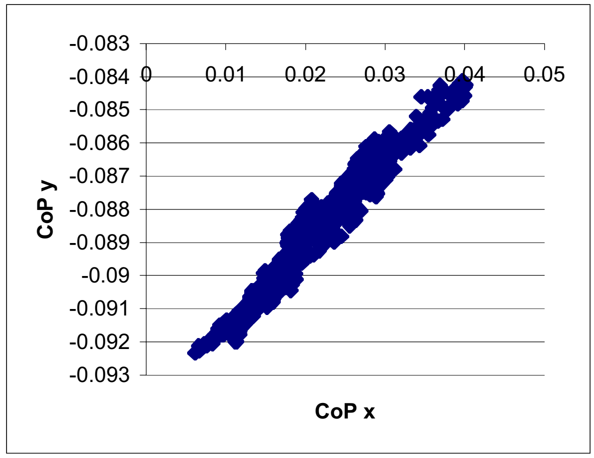

RESULTS AND DISCUSSION

In the data analyzed to date, estimated α values were reduced when subjects moved from bipedal to unipedal stance. There was a further reduction of α when subjects closed their eyes. Figure 1 shows the change in CoP coordinates between consecutive samples for a subject in unipedal stance with eyes closed. Clearly the graph is suggestive of a high correlation between AP and ML movements. Using the multiscaling fractional advection-dispersion equation, we can use this correlation to find the real value of α in each direction.

CONCLUSIONS

From the data collected so far, it is clear that the rambling/trembling framework provides an excellent starting point for describing postural sway. Using the Lambda Model of [1] to describe the main cyclic component of sway combined with the random behavior observed, it is possible to come up with a measure of stability for each subject akin to the concept of Value at Risk (VaR) for a stock portfolio. VaR measures the risk in holding a correlated portfolio of stocks. This would provide a method of indexing subjects according to their relative stability with a minimum amount of a data collection required, which may prove particularly helpful in analyzing changes in stability over time.

REFERENCES

1. Latash M.L. *Control of Human Movement.* Human Kinetics: Urbana, IL. 1993
2. Schumer,R., Benson, D.A., Meerschaert, M.M. and Baeumer, B. *Water Resour. Res.* **39**(1), 1999
3. Zatsiorsky, V.M., Duarte, M. *Motor Control* **3**, 12-27, 1999
4. Zatsiorsky, V.M., Duarte, M. *Motor Control 4*, 185-200, 2000

THE EFFECTS OF THE TENNIS SLICE BACKHAND WITH DIFFERENT BALL SPEEDS ON THE BOUNCE ANGLE

[1] Ching-Cheng Chiang, [2] Jinn-Yen Chiang and [3] Tzyy-Yuang Shiang
[1] National College of P. E. & Sports, Taiwan,
[2] National Changhua University of Education, Taiwan,
[3] Taipei Physical Education College, Taiwan; email: ccchiang@gw.cgit.edu.tw

INTRODUCTION

Nowadays, tennis players are looking to try anything to gain a slight edge over an opponent. Tennis coaches and players are continually searching for ways to improve performance. Past review studies have discussed about the angle at which a ball rebounds from the ground on different types of court surfaces. When a ball bounces on the court, its horizontal speed is usually reduced somewhat by its interaction with the court surface. There are only two characteristics of a court surface that influence what the ball does when it bounces. These are the coefficient of restitution (COR) and the coefficient of friction (COF) between the ball and the surface (Brody, 1987). Brody who derived mathematical relationships between the angles and speeds of a ball before and after the bounce had carried out a theoretical analysis of the bounce process earlier. He distinguished two types of bounce – a low angle high speed bounce (such as the service) when the ball slides along the bounce contact without rolling. At higher angles and lower speeds, such as lobs, volleys etc, the ball rolls during the bounce contact with the surface and the characteristics of the bounce are quite different from the sliding bounce. The purpose of this study was to investigate the effects of the slice backhand with different ball speeds on the bounce angle.

METHODS

Three male tennis players, who rank in the top five domestically, were used as subjects of this study. The court surface was an indoor hard-court with various acrylic types. A ball projector was positioned on the service line. The projector ejected balls without appreciable spin at muzzle speed of 35miles/ hrs. The high-speed video camera was positioned on the ground and about 6m at a distance from the center of the target area. Three male tennis players were asked to stand on the baseline and strike slice backhand for measurements on two different ball speeds – a fast ball (above 50 miles/ hrs) and a slow ball (below 45 miles/ hrs). From these 40 sliced backhand strikes (20 fast balls and 20 slow balls) were subsequently analyzed. The speed gun captured the maximum speed of the ball after being struck by the tennis racquet and direct reading ball speed. The ball trajectory was recorded on a high-speed video camera to determine the bounce angle. Each ball was filmed with 60 frames per second (fps). The frames of each selected slice backhand were stored using a PC and re-digitized and analyzed with a Peak Performance System. The press mouse button was pressed for marking the ball trajectory and court surface when the frame was displayed. We then, printed out the ball trajectory chart from PC. The incident angle and the rebound angle were calculated using a protractor. Mean, standard deviation as well as ball speed, incident angle, rebound angle and the angle difference were determined. Statistically relevant differences were assessed using the dependent T-test.

RESULTS AND DISCUSSION

There is significant difference between the fast ball and slow ball with backspin in incident angle, rebound angle and the angle difference. Both fast ball and slow ball, rebound angle was larger than incident angle. Furthermore, the results showed that there was a significant negative correlation found between the ball speed and incident angle, the ball speed and rebound angle. ($p < 0.01$). It showed that the slice backhand with a faster ball speed had less incident angle, rebound angle. Groppel (1984) showed that, due to frictional factors and the coefficient of restitution between the ball and tennis court, however, the angle of rebound was almost always greater than the approach angle. Bill Murphy and Chet Murphy (1987) indicate that the fast ball with backspin travels in a low trajectory; the ball will skid and remain low as it bounces. As for the slow ball with backspin, High- speed film analyses demonstrate that a soft, lazy ground stroke hit with backspin will cause the shot to sit up and give the opponent a chance for an easy return (Groppel, 1992). Tennis players cannot obtain the ball speed if players hitting the ball without forward motivation. If players chop at the ball, the ball just has spin without forward power (Tony Trabert, 1996). Therefore, a nice slice backhand not only with the fast ball speed but also it has less incident angle and rebound angle.

CONCLUSIONS

Elite tennis players take advantage of a short ball with a slice backhand and hit the ball deep and advance to the net behind the shot. When a under spin shot is hit with a high speed, its incident angle to the court will be low causing it to skid and remain low after the bounce. This forces the opponent to hit upward on the ball so it will clear the net, thus allowing ample time to reach a good volleying position. According to these results, tennis coaches should integrate special training for forearm action as standard practice.

REFERENCES

1. Brody, H. (1987). *Tennis Science for Tennis Players*. (4th ed) University of Pennsylvania Press. Philadelphia, PA.
2. Groppel, Jack L. (1984). *Tennis for Advanced Players*. Champaign, IL: Human Kinetics Publishers, Inc.
3. Groppel, Jack L. (1992). *High Tech Tennis*. (2nd ed) Champaign, IL: Human Kinetics Publishers, Inc.
4. Murphy, B. & Murphy, C. (1987). *Lifetime Treasury of Tested Tennis Tips*. West Nyack, NY：Parker Publishing Company, Inc.
5. Trabert, T. (1996). Graf 's Classic Backhands. *Tennis*. July 1996, 69-71.

The Correlation between Energy Absorption Ratio and Pain Score of the Upper Extremity under Different Fall Heights

You-Li Chou[1], Pei-Hsi Chou[2], Hung-Yu Chen[1], Shen-Kai Chen[2],
[1] Center of General Education, Chang Jung Christian University, Tainan, Taiwan
[2] Department of Orthopedic Surgery, Kaohsiung Medical University, Kaohsiung, Taiwan

INTRODUCTION

A fall onto the outstretched hand is the most common cause of upper extremity injury, including approximately 90% of fractures at the distal radius, humeral neck, and supracondylar region of the elbow. In the study by Chou et al. [1] found if the elbow flexed instead of outstretched after impact would decrease the ground reaction forces. They suggested the elbow-flexed motion represents the effects of damper and spring. In the whole, the total dissipation energy produced by shoulder moment is larger than dissipation energy produced by elbow moment; this means that the shock-absorption effect of shoulder is stronger than that of elbow. Since elbow joint and shoulder joint play important roles to absorb impact energy during falls . The purpose of this study is to find the best joint energy distribution between elbow joint and shoulder joint.

METHODS

The ExpertVison motion system (Motion Analysis Corp., Santa Rosa, CA, USA) with six 120 Hz cameras and two 1000 Hz Kistler force-plates (Type 9281B, Kistler Instrument Corp., Winterthur, Switzerland) was used to measure relative joint positions and ground reaction forces.

The subjects were dropped from a height of 10 cm and 20 cm (i.e. distance between the outstretched hand and the force plate) , and fell onto two hands. The angle between the trunk and the upper arm is maintained at 60° forward flexion of the shoulder.A questionnaire was also designed to record each subject's sensation of pain or uncomfortable index during the impact. The index ranged from 0 to 10, and higher score means more uncomfortable.

RESULTS AND DISCUSSION

Table 1. is the grouping result of all subjects when h=10 cm.

Table 1. energy absorption ratio (h=10 cm)

	comfortable	moderate	uncomfortable
1	1.45	1.50	1.62
2	1.41	1.57	1.60
3	1.69	2.00	2.29
4	1.28	1.38	1.57
5	1.84	1.85	2.08
6	1.53	1.79	2.13
7	1.51	1.55	1.73
8	2.02	2.18	2.45
9	1.66	1.69	1.79
10	1.61	1.69	1.71

Table 2. is the result of the subjects when h=20 cm.

Table 2. energy absorption ratio (h=20 cm)

	comfortable	moderate	uncomfortable
1	1.59	1.67	1.76
2	1.63	1.76	1.89
3	2.00	2.28	2.35
4	1.47	1.57	1.64
5	1.99	2.16	2.17
6	1.71	2.24	2.34
7	1.73	1.73	2.01
8	2.14	2.44	2.63
9	1.78	1.79	2.10
10	1.78	1.85	1.90

Different energy absorption distribution between shoulder joint and elbow joint makes different kind of feeling to the subject. The most comfortable group has the smallest energy absorption ratio since the most uncomfortable group has the highest ratio. In the other words, the most comfortable group has the best energy distribution. In this experiment, all the energy absorption ratios are bigger than 1. So shoulder joint plays the important role during the impact. But smaller ratio makes subjects feel better. If elbow joint can help to share the energy absorption, it is the better way to prevent subjects from injury. Otherwise, when the falling height is higher, the ratio is getting bigger and bigger. That means that we normal people used to use our shoulder to absorb the impact energy. It is not a good way during the impact.

CONCLUSIONS

In this study, different energy absorption ratio really makes subjects feel different. Smaller energy absorption ratio makes subjects feel better. If we can use our elbow joint to help absorbing more energy, it is the better way for us to prevent from injury.

REFERENCES

[1] Chou P.H., Chou Y.L., Lin C.J., Su F.C., Lou S.Z., Lin C.F., Huang G.F., Effect of elbow flexion on impact forces of upper extremity on a fall. Clinical Biomechanics 2001,16:888-894

ACKNOWLEDGEMENT

We acknowledge the financial support of the National Science Council, ROC.
E-mail: ylchou@mail.ncku.edu.tw

PREHENSION SYNERGIES: TRIAL-TO-TRIAL VARIABILITY AND PRINCIPLE OF SUPERPOSITION DURING STATIC PREHENSION IN THREE DIMENSIONS

[1,2]Jae Kun Shim, [1]Mark Latash and [1]Vladimir Zatsiorsky
[1]The Pennsylvania State University and [2]University of Maryland
Email: shimjaekun@hotmail.com

INTRODUCTION

Multi-digit prehension is performed by a redundant system (the hand) which exerts numerous combinations of digit forces and moments to produce a required output of a hand-held object. The human central nervous system (CNS), confronts a choice of selecting a solution of digit forces and moments from an apparently infinite set (Bernstein 1967).

According to the principle of superposition suggested in robotics (Arimoto et al. 2001), some actions can be split in several subtasks that can be controlled by independent control processes. In two dimensions, both simulations of a two-digit robot grasping and experiments with multi-digit human grasping (Shim et al. 2003a; Zatsiorsky et al. 2004) have confirmed the principle of superposition showing the existence of two decoupled subgroups of elemental variables (digit forces and moments): one related to adjustments of the grasping forces, '*grasp control*' and the other associated with control of rotational equilibrium of the hand-held object, '*torque control*'. In the current study, we tested the principle of superposition during multi-digit human prehension in three dimensions (3D).

METHODS

Subjects held a customized handle statically twenty-five times under each of seven external torques (ranged from -0.7 to 0.7 Nm) about a horizontal axis (*X*-axis) in a plane passing through the centers of all five digit force sensors (the grasp plane; Shim et al 2004). *Y*- and *Z*-axes were respectively defined as a vertical axis and an axis perpendicular to *X*- and *Y*-axes. Three force and moment components in 3D were recorded from each sensor.

Regression analysis and principal component analysis (PCA) with varimax rotation and Kaiser criterion were performed on elemental variables (forces and moments) of the thumb and virtual finger (VF: an imagined finger producing a wrench equal to wrenches generated by individual fingers; McKenzie and Iberall 1994; Shim et al. 2004).

RESULTS

PCA performed on all thumb and VF forces and moments under each external torque condition generated three PCs (PC1 to PC3) which accounted for 94.80±0.65 % of the total variance (average ± SD across external torque conditions after the results were averaged across the subjects for each external torque condition). Among the three PCs, one PC had large loadings of thumb and VF grasping forces (F_Z^{vf} and F_Z^{th}), Table 1. The rest two PCs had large loadings on the moments about *X*- and *Y*-axes, respectively. Therefore, the '*grasp control*' variables (F_Z^{vf} and F_Z^{th}) were decoupled from the '*torque control*' variables (all of moment variables). These findings were true for all external torque conditions in each subject.

Table 1. Loadings of principal components (PC1, PC2, and PC3) in all elemental variables under -0.70 Nm external torque condition of a representative subject.

Variable	PC1	PC2	PC3
$M_X^{vf(Y)}$	***0.89***	0.00	-0.27
$M_X^{vf(Z)}$	***-0.92***	0.02	0.26
$M_X^{th(Y)}$	***0.90***	0.03	-0.27
$M_Y^{vf(Z)}$	0.01	***-0.99***	0.07
$M_Y^{vf(X)}$	0.00	***0.97***	-0.04
$M_Y^{th(Z)}$	-0.02	***-0.99***	0.06
F_Z^{vf}	-0.25	-0.10	***0.97***
F_Z^{th}	0.26	0.07	***-0.96***

F_Z^{vf} and F_Z^{th} are VF and thumb forces along Z-axis (grasping forces). $M_X^{vf(Y)}$ is a moment of F_Y^{vf} about X-axis and similar nomenclatures are applied to the other moment variables. The loadings with large magnitudes are shown in ***italics.*** Variables without significant loadings according to the Kaiser criterion are not included in the table.

CONCLUSIONS AND DISCUSSION

The grasping control (the slipping prevention) is realized separately from other subtasks (e.g. maintaining the rotational equilibrium of the object about each axis in 3D) that have to be solved by the CNS during multi-digit prehension. The changes of the grasping forces (F_Z^{vf} and F_Z^{th}) being perfectly matched to each other do not immediately affect the other variables. Therefore, we conclude that the principle of superposition is supported in a 3D static prehension.

REFERENCES

1. Arimoto S. et al. IEICE Transactions E84A, 39-47, 2001
2. Bernstein NA. The Co-ordination and regulation of movements, Pergamon Press, Oxford, 1967
3. MacKenzie CL and Iberal T. The grasping hand, Elsevier Science, Amsterdam, 1994
4. Shim JK et al. Exp Brain Res 152, 173-184, 2003
5. Shim JK et al. J Neurophysiol 10.1152/jn.00764.2004
6. Zatsiorsky et al. Robotica 22, 231-234, 2004

ACKNOWLEDGEMENTS

AG-018751, AR-048563, M01 RR10732, and NS-35032.

MUSCLE ACTIVATION PATTERN OF LOWER EXTREMITY MUSCLES IN SELECTED BASKETBALL TASKS

[1] Hsiao-Yun Chang, [2]Shun-Hwa Wei, [3]Yeu-Jeng Jong, and [4] Chi-Huang Huang
[1] Doctoral student, Graduate Institute of Physical Education, National College of Physical Education and Sports, Taoyuan, Taiwan, R.O.C., email: ncpes920408@yahoo.com.tw; yun1130@seed.net.tw
[2] Chairman of Graduate Institute of Rehabilitation Science and Technology, National Yang Ming University, Taipei, Taiwan, R.O.C.;
[3] Lecturer, Department of Physical Education, National Chia-Yi University, Chia-Yi, Taiwan, R.O.C.
[4] Professor, Graduate Institute of Athletic Training, National College of Physical Education and Sports, Taoyuan, Taiwan, R.O.C.

INTRODUCTION

The anterior cruciate ligament (ACL) injury is a common sports injury in basketball athletes [1]. It needs specific functional task for rehabilitation to assist athletes return to sports [1-4]. Enhance, understanding the safety and adequacy of those specific functional tasks is priority work. Therefore, the purpose of this study was to understand the muscle activation pattern of lower extremity muscles during performing specific functional basketball tasks.

METHODS

Sixteen high school basketball players voluntarily participated this study (mean age: 18.25±2.78; mean height: 184.50±5.35; mean weight: 74.19±6.43). Four specific basketball tasks including sudden stop, jump shot, twist, and cross over movement were investigated in this study. Four channels of electronic signals were measured in this study. Quadriceps and hamstrings were measured by 2 EMG channels. The other channel was used to measure knee joint motion by electrogoniometer. The last channel was used to measure the foot-to-ground contact by self-designed foot switch. All signals were simultaneously collected with sampling 1000Hz. One-way ANOVA was used to examine the differences among four tasks' EMG activities. Scheffe's multiple comparisons were used to examine the difference between each test group.

RESULTS AND DISCUSSION

The results showed that quadriceps and hamstring EMG intensities during sudden stop and jump shot were significantly higher ($p<.05$) than cross over and twist. However, the hamstrings to quadriceps EMG ration showed that sudden stop and jump shot were significantly ($p<.05$) less than cross over and twist.

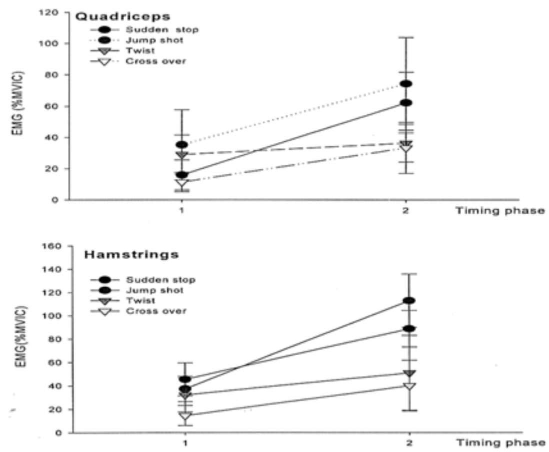

Figure 1: The EMG activation of lower extremities. 1 means pre-airing phase; 2 means landing phase.

CONCLUSIONS

In order to protect a basketball athlete with ACL injury, the clinician and coach have to understand the safety priority among basketball tasks. Based on present study findings, we believed that the sudden stop and stop shot were more dangerous that cross over and twist. These findings can be implicated in knee rehabilitation program, especially in the return-to-sports phase [2-4]. The results suggest that exercise program of sudden stop and jump shot should be described on the last phase of knee rehabilitation program.

REFERENCES

1. Irrgang JJ, et al. *Clin Sports Med* **12,** 797-813,1993.
2. Buz SC, et al. *J Athl Train* **34**, 121-129, 1999.
3. Cicctti MG, et al. *Am J Sports Med* **22**,651-658, 1994.
4. Scott C, et al. *Am J Sports Med* **28**,234-240, 2000.

Table 1 Parameters of four basketball tasks

Parameters		Sudden Stop		Jump Shot		Twist		Cross over	
		Mean	SD	Mean	SD	Mean	SD	Mean	SD
Knee flexion	Pre-airing	59.28 ^{A}	4.19	74.92 ^{A,B}	11.61	70.81 ^{A,C}	5.11	54.80^{B,C}	11.10
angle; deg	Landing	26.99^{A}	9.39	30.72^{B}	7.01	63.06^{A,B}	6.59	56.93^{A,B}	10.25
EMG; mv									
Quadriceps	Pre-airing	15.87 ^{A}	9.58	35.20 ^{A,B}	22.46	29.00^{C}	12.41	11.31^{B,C}	6.26
	Landing	62.27 ^{A}	19.39	74.36 ^{B}	29.79	36.38 ^{A,B}	12.12	33.38 ^{A,B}	16.42
Hamstring	Pre-airing	45.47 ^{A}	14.02	37.25 ^{B}	10.84	32.13 ^{A,C}	14.56	14.57 $^{A, B,C}$	8.59
	Landing	88.80 ^{A}	15.71	112.92 ^{B}	22.91	51.07 ^{A,B}	31.90	40.13 ^{A,B}	21.77
H/Q ratio	Pre-airing	0.36 ^{A}	0.22	1.17 ^{A}	0.78	1.02 ^{A}	0.52	0.89	0.51
	Landing	0.65 ^{A}	0.13	0.86	0.38	1.08 ^{A}	0.39	1.02	1.34

Note: A, B, C, and D mean with the same letter for post-hoc grouping are significantly different ($p<.05$) in the same row.

BIOMECHANICAL ANALYSIS OF FOUR-WHEELED WALKER FOR AN ELDERLY PERSON

[1]Masato Takanokura, [1]Toshihiro Yamauchi
[1]Dept. of Industrial Engineering and Management, Kanagawa University, Japan; email: takanokura@ie.kanagawa-u.ac.jp

INTRODUCTION

Japan goes toward a superannuated society. According to the population projects of National Institute of Population and Social Security Research in Japan, the percentage of the aged population of 65 years and up will reach 25.0% in 2017 [1]. To deal with the superannuated society, the activities of daily living (ADL) have attracted an attention in Japan. Walking is the most important in ADL because a fall of the elderly persons during walking leads to a high possibility of the disuse syndrome. A four-wheeled walker for an elderly person without some disease is a product to assist walking, to carry a baggage, and to take a rest on a street. We analyze the biomechanics of steady walking and step mounting using walkers by an articular angle and torque of a lower limb estimated by a video-based motion-analysis system.

METHODS

The subject was five male students aged 20 to 23 years because we intended developing an analytical method for the biomechanics of elder walking using walkers. Although we used three kinds of walkers as shown in Figure 1 (Mutsumi Medical), we modified the rear wheels to avoid getting them and feet on a force plate by lengthening the wheel axes.

An angle and torque at a hip, a knee, and an ankle joint in a sagittal plane were analyzed by the motion-analysis system (Frame-DIASII, DKH). Reflective markers were attached to ten anatomical landmarks: shoulders, greater trochanters, knees, ankles, and toes. The marker position was estimated by using the DLT method from images filmed by four digital-video cameras of 60 fps (GR-DV5000, Victor). The angle was estimated from the marker positions. Ground reaction force was measured by force plates (9286A, Kistler) and charge amplifiers (9865E1Y28, Kistler). Torque was estimated by the inverse dynamics from the marker positions and ground reaction force.

We formed a floor of 3.6m by a force plate and aluminum floorboards for steady walking. The subject walked at a natural speed with the walker on the floor. We formed a step of 17cm by two force plates, floorboards, and a curb for step mounting. The subject first lifted up front wheels onto the step and then mounted the step along with the walker by lifting up rear wheels. He mounted with a load of 5kg on a basket of the walker and without a load.

(a) Careman (b) You-mate GXN (c) Oscar-mini

Figure 1: Four-wheeled walkers for elderly person.

RESULTS AND DISCUSSION

Figure 2 illustrates flexion torque at hip during steady walking. The ANOVA demonstrated that the main effect of the walker was significant ($F(3,12)=10.67$, $P<0.01$). *Post hoc* analysis showed that the walkers reduced flexion torque at hip ($P<0.01$). Extension torque was not varied. Torque at knee showed similar results. The walkers reduced plantarflexion torque at ankle. The subject supports the body weight not only by the lower limb but by the upper limb through the handgrip of the walker. Articular torque of the lower limb did not depend on the structure of the walker because it went forward at a constant speed during steady walking. Walking using the walkers caused a smaller extension angle at hip, a larger flexion angle at hip, and a larger dorsiflexion angle at ankle.

Figure 3 shows flexion torque at hip during step mounting. The ANOVA demonstrated that the main effects of the walker ($F(2,8)=10.62$, $P<0.01$) and the load ($F(1,8)=12.10$, $P<0.01$) were significant. *Post hoc* analysis showed that the walker "Careman" with a load of 5kg caused larger torque. Torque to hip extension, to knee flexion and extension showed similar results. The handgrip of Careman is positioned just above the rear wheels. The larger moment caused by force to push down the handgrip is necessary to lift up the front wheels because the moment arm is shorter than the other walkers.

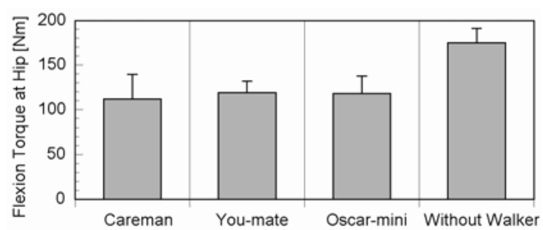

Figure 2: Flexion torque at hip during steady walking.

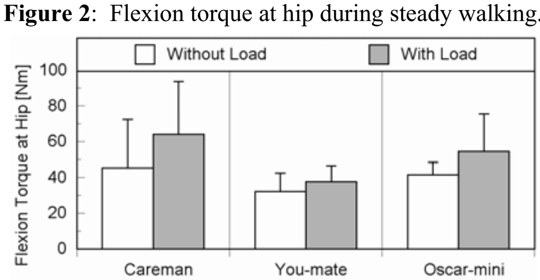

Figure 3: Flexion torque at hip during step mounting.

CONCLUSIONS

During steady walking, the walkers reduce articular torque of the lower limb. During step mounting, torque depends on the structure of the walker and the load on the basket.

REFERENCES

1. National Institute of Population and Social Security Research. *Population Projects for Japan: 2001-2050*, 2002.

A VIRTUAL TOOL FOR THE CLINICAL PLANNING OF THE ULNAR PALSY TREATMENT

[1] J.L. Sancho-Bru, [1] P.J. Rodríguez-Cervantes, [2] D.J. Giurintano, [1] A. Pérez-González and [1] M. Vergara-Monedero
[1]Departament de Tecnologia. Universitat Jaume I, Castelló (Spain); correspondence email: cervante@tec.uji.es
[2]National Hansen's Disease Programs, Baton Rouge (Louisiana)

INTRODUCTION

Mechanical efficiency of the hand can be reduced because of different pathologies. One of these pathologies is ulnar palsy. Ulnar palsy is common in Hansen's disease patients. *Mycobactrium leprae* bacteria attack the ulnar nerve at the elbow level, which reduces the motor capability of the intrinsic muscles of the hand. This paralysis results in the *claw hand* deformity. It occurs because of the loss of the balance between the intrinsic and extrinsic muscles that power the hand [1].

Mathematical models of the finger have been used in the past to study different aspects of hand function. In this work, the use of a 3D model of the index finger for the clinical planning of the ulnar palsy treatment is investigated.

METHODS

A biomechanical model of the finger previously developed by the researchers [2] was used to simulate the ulnar palsy and a tendon transfer for the restoration of the hand function.

The biomechanical model considered the finger as a skeletal open chain of 4 rigid bodies (the bones) connected to the carpus through different joints that characterize the kinematic behavior of the chain. The DIP and PIP joints were modeled as 1 degree of freedom joints capable of flexion-extension movements, while MCP joint is modeled as a 2 degree of freedom joint capable of flexion-extension and abduction-adduction movements with respect to a fixed metacarpal bone. The data for the location and orientation of the rotation axes came from An et al [3] and Brand and Hollister [1]. Muscles, tendons and ligaments control the movement of the chains. A total of 7 muscles (FP, FS, LU, DI, VI, EC and EI) were considered using a Hill's 3 component model that takes into account the muscle activation level and the force-length and force-velocity relationships, as well as the different index of architecture of muscles. Muscles transmit force to the tendons, which finally insert into the bones. To model the effect of tendons crossing the joints, straight lines connecting 2 points were considered, except for the extensors, for which Landsmeer's model I was used. Appropriate force balances were considered in the connecting points of this deformable tendon net, where tendon excursions were calculated by combining the excursions at each joint according to the tendon net configuration. Because tendons were assumed inextensible, tendon excursion defined the change in muscle length. Tendon paths came from the literature [3]. The collateral ligaments of the MCP joint were modeled as non-linear elastic elements.

First, the model was used to simulate the ulnar palsy. The paralysis of the ulnar nerve was modeled by reducing the PCSA of the intrinsic muscles (DI, VI and LU) proportionally to the severity of the palsy. With this model, a search for feasible postures of the finger with ulnar palsy was performed. Moreover, the grasp capabilities of the normal and injured finger were compared for two different grasps (Table 1).

Table 1: Postures defining the grasps that have been analyzed.

Grasps	MCP flex	MCP abd	PIP flex	DIP flex
Wide	60º	0º	60º	45º
Narrow	30º	0º	45º	45º

Second, the model was used to simulate the tendon transfer of the PL muscle to restore hand function. This transfer was modeled by introducing the transferred tendon path in the model, which affected the MCP flexion-extension and abduction-adduction balances. With this model, a new search for feasible postures of the restored finger was performed, as well as the evaluation of grasp capability achieved after the restoration.

RESULTS AND DISCUSSION

From the search for feasible postures performed with the ulnar palsy model, only feasible postures were found for a combination of MCP flexion angles smaller than 20º and PIP flexion angles greater than 90º, i.e. the model predicts that only clawing postures are possible when an ulnar injury occurs. On the other hand, the model predicted a greater reduction of the grasp capability for an 80% injured hand for wide grasp (81%), than for narrow grasp (51%), which agrees with literature [1]. Both results validate the model.

The model for the restored finger predicted feasible non-clawing postures, in contrast with the results of the injured finger model. On the other hand, the restored finger model predicted a 73% improvement of grasp capability for wide grasp and a 38% improvement for narrow grasp.

CONCLUSIONS

Biomechanical models of the hand could be used as virtual tools to investigate the consequences of pathologies such as ulnar palsy and to check the advantages and disadvantages of the different clinical techniques that could be used to restore hand function.

REFERENCES

1. Brand PW & Hollister AM. *Clinical Mechanics of the Hand*, Mosby Inc., St. Louis, 1999.
2. Sancho-Bru JL, et al.. *J Biomech* **34**, 1491-1500, 2001.
3. An KN, et al.. *J Biomech* **12**, 775-788, 1979.

ACKNOWLEDGEMENTS

This research is supported by both the Spanish Government and the EU through the Project "PN I+D+I, PI021662".

COMPUTER AIDED PRE-OPERATIVE PLANNING OF FRACTURE REDUCTION AND DEFORMITY CORRECTION IN TIBIA WITH HEXAPOD EXTERNAL FIXATOR

Sang Min Joo and Yoon Hyuk Kim
School of Advanced Engineering, Kyung Hee University, Korea
email: yoonhkim@khu.ac.kr

INTRODUCTION

When the Ilizarov external fixator is used for fracture reduction and deformity correction, the planning for correction of 3-D multiple deformities is difficult due to the lack of information on required joint rotations and translations in order to correct the deformities [1]. In addition, if the rotational axis is not placed exactly with respect to axis of the deformity, the rotation may generate the unwanted translational shift at the fracture site [1, 2]. Hexapod external fixator, which is also known as the Taylor spatial frame, has an advantage to kinematically calculate the necessary translations of the telescopic struts in order to correct any 3-D deformities at the fracture site. The purpose of this study was to perform computer aided pre-operative planning of fracture reduction and deformity correction in tibia with single or double hexapod fixator system and to compare the results with the clinical ones.

METHODS

Our procedure consisted of four steps (Figure 1). The 3-mm CT data of a tibia in pseudoachondro-plasia was digitized and transformed to the graphic model using the custom made program. Radiographic examination was performed to check the AP and lateral deformities at the proximal and distal bone segments before and after the deformity correction. We used conventional hexapod fixators or modified ones to a double hexapod system, which consists of three rings of 170 mm diameter and twelve telescopic struts of 90 mm length. We developed the CAD model of the fixator system using the CAD software, Solid Works®(Solidworks, USA). The necessary positions of six or twelve telescopic struts to correct given deformities were calculated using the program developed by the authors based on the forward kinematics of parallel manipulators [2-4]. From the calculated values of the telescopic struts, the computer graphic simulation of correction process was performed by simultaneous change of the struts based on simulation software, RecurDyn™ (FunctionBay, Inc, Korea). Finally, the results of planning were compared with clinical outcomes to evaluate the developed analysis and simulation techniques.

RESULTS AND DISCUSSION

A fracture case with 15° of deformity in the AP plane and 15° of deformity in the lateral plane and a deformity correction case with 49° of proximal and 39° of distal deformities in the AP plane and 12° of proximal and 9° of distal deformities in the capital plane were corrected by the pre-operative planning. The graphic simulation could visualize the fracture reduction and deformity correction process by adjusting the telescopic struts simultaneously and showed possible clinical problems such as ring collision and excessive soft tissue distractions (Figure 2).

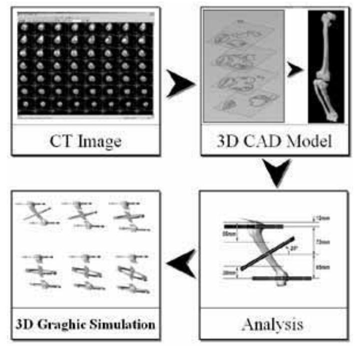

Figure 1: Procedure of computer aided pre-operative planning with double hexapod external fixator system

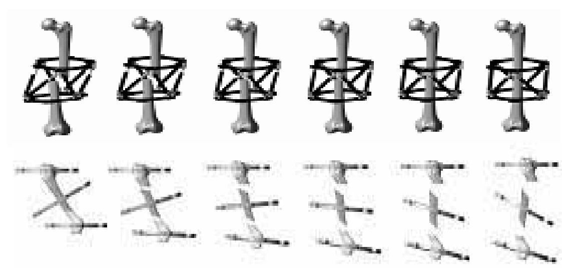

Figure 2: Graphic simulation of sequential adjustment for the fracture reduction (a) and the deformity correction (b)

Pre-op planning for correction of complex multiple deformities is often unavoidable and very difficult. The main reason for this difficulty is the six deformity parameters, which are three translations and three rotations, are coupled. The computer modeling and simulation techniques presented in this study could successfully perform the pre-op planning of tibia with hexapod fixators based on the kinematics analysis.
The results showed that the computer simulation could visualize the fracture reduction and deformity correction procedure and check any surgical problems. This results support the feasibility of the computer-aided planning of fracture reduction and deformity correction.

REFERENCES

1. Seide K, et al. *CORR* **1**, 186-195, 1999.
2. Kim YH, et al. *J Biomech* **35**, 1047-1058, 2002.
3. Ping J, Hongtao W. *IEEE Trans Robot Auto* **17**, 522-526, 2001.
4. Ron BA, et al. *Computer Aided Surgery* **7**, 332-341, 2002.

ACKNOWLEDGEMENTS

This study partly supported by RRC program of MOST and KOSEF

INCREASE OF LUMBAR SPINAL STAIBLITY UNDER FOLLOWER LOAD IN SAGITTAL PLANE

Kyungsoo Kim and Yoon Hyuk Kim
School of Advanced Engineering, Kyung Hee University, Korea
email: yoonhkim@khu.ac.kr

INTRODUCTION

There has been a discrepancy between in vivo and in vitro experiments investigating the load carrying capacity of human lumbar spine. A follower load concept was introduced to explain this discrepancy [1]. A follower load is a compressive load applied along a path that approximates the tangent to the curve of the column. The trunk muscles are supposed to generate the follower load in vivo, but it is still difficult to assess the muscle contraction forces by experimental techniques. Hence a musculoskeletal modeling of the spine and trunk muscles is indispensable. The purpose of this study is to show that there is muscle activations generating the follower load and the lumbar spine is more stable under the follower load using the finite element model of the lumbar spine and trunk muscles in the sagittal plane.

METHODS

A two-dimensional finite element model of a human lumbar spine (T12-S1) and 66 pairs of trunk muscles was developed in the sagittal plane. Each motion segments were assumed to beam elements with elastic stiffness properties in [2], and the muscles were assumed to act statically. A follower load path was defined as having a direction parallel to the bisection of two adjacent segments at each node. At each node, the resultant joint force could be decomposed into two perpendicular force components, follower force in the follower load path direction and shear force.

The forces and moments used in the analysis consist of muscle forces and moments derived by muscle forces, motion segment forces and moments by the stiffness property, and applied external forces and moments. Since the number of unknowns including muscle forces and displacements exceed that of equations describing the equilibrium state of the lumbar spine model, the optimization technique was used. The cost function was the summation of squared muscle stresses and it was minimized in order to decrease the efforts of muscles. The follower load was represented by restricting the shear forces to zero at all vertebral body centers while the non-follower load was unconstrained at all about the shear force. The physiologic limits were assumed as in [2, 3].

In this paper, the deformed shapes of the model and the muscle force combination were examined under the follower load and the non-follower load respectively when 410N of vertical load and 41Nm of moment were applied at T12. The corresponding resultant joint forces (the follower forces and the shear forces) and moments at all nodes were investigated

RESULTS AND DISCUSSION

The patterns of muscle activity on the lumbar spine model generating the follower loads could be estimated under the given external load: 31 pairs of muscles were activated while no muscle acted on the lumbar spine under the non-follower load.

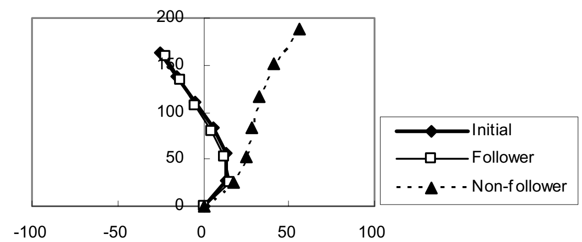

Figure 1: The initial posture of the spine model and the deformed shapes under the follower load and the non-follower load when the external load of 400N and 41Nm applied at T12

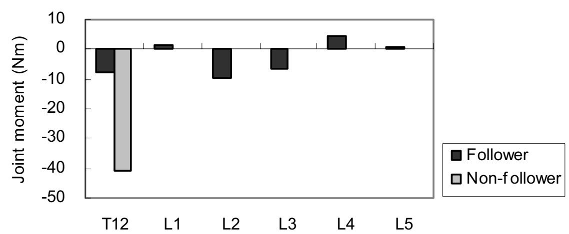

Figure 2: The joint moments at all vertebral body centers under the follower load and the non-follower load when the external load of 400N and 41Nm applied at T12

The deformed shape of the lumbar spine for the follower load was very similar to the initial posture of lumbar spine model in contrast to that for the non-follower load which assumed no muscle activation (Figure 1). The follower forces at all vertebrae under the follower load were around 1000N and there were no shear forces. In contrast, the magnitudes of shear forces were over 100N under the non-follower load though the follower forces were far below those under the follower load. The joint moments under the follower load were smaller that 10Nm while the external moment 41Nm was preserved at T12 under the non-follower load (Figure 2).

It was proved that the follower load could be successfully generated by trunk muscles from the observation that the shear forces were eliminated at all vertebral body centers in contrast with the non-follower load. Also, it was confirmed that the spinal stability under the follower load is much higher since the deformation of posture and the resultant joint moments were much smaller than those under the non-follower load. In addition, the validity of the investigated results is obtained by comparing with the previous studies [1-3].

REFERENCES

1. Patwardhan AG, et al. *Spine* **24**, 1003-1009, 1999
2. Stokes IAF, Gardner-Morse MG. *J Biomech* **28**, 173-186, 1995.
3. Kim YH, Kim K. *JSME Int J C* **47**, 1062-1069, 2004.

THE ROLE OF THE FEMORAL STEM IN THE STABILITY OF A METAL ON METAL HIP RESURFACING IMPLANT. AN RSA STUDY

[1] Itayem Raed, [1,2]Arndt Anton, [3]Derek McMinn, [3]Joesph Daniels and [1]Lundberg Arne
[1]Karolinska University Hospital, Stockholm, Sweden
[2]Stockholm University College of Physical Education and Sports, Sweden
[3]Nuffield Hospital, Birmingham, United Kingdom
email: itayem_r@hotmail.com

INTRODUCTION

The advantage with the minimal resectioning concept is that natural anatomy is more closely replicated than with traditional total hip replacement devices.

Today, the Birmingham Hip Resurfacing (BHR) metal on metal resurfacing implant is the golden standard. It has a narrow, strait femoral stem which requires good bone stock. In many cases, bone stock of the femoral head does not allow resurfacing arthroplasty such as in BHR. A short-stemmed device has been developed with a more robust, curved femoral stem. The load pattern of this type of device is expected to be different than that described in BHR [1] and the different lever arms resulting from the curved design of the stem may result in greater retroversion problems. Will this contribute to a different migration pattern and early loosening as a result?

METHODS

For most joint implants, migration is known to correlate to loosening. Radiostereometric analysis (RSA) was used to measure migration, as this method has been proven to be superior to conventional radiography. This is an ongoing study, which at present includes 9 patients (8 male, 1 female; mean age 51.2, range: 33-62) with data up to 12-months post-operatively. All patients are physically active. Three 0.8 mm tantalum markers were attached on the tip and sides of the short stem implant and 5 – 8 markers were placed in the greater and lesser trochanters at the time of the hip arthroplasty. RSA evaluation was performed post operatively and at 2, 6 and 12 months follow-up. The first patients are expected for the 24-month follow-up this year.

The implant head centre was estimated from the acetabular cup circumference at the post-operative examination and calculated from femoral component markers in subsequent examinations. Standard RSA calculations were used to determine proximal/distal and anterior/posterior translation and implant rotation relative to the femur. The results were compared with the 2 years follow up of the BHR [1].

RESULTS AND DISCUSSION

Migration values for the BHR were very small up to 2 years follow up. The pattern of migration over time indicated limited subsidence. The mean of the BHR migration is presented as a strait line in the figures of the individual results of each migration parameter of the short stem device.

Short stem proximal translation: Values were small. However 2 slightly higher individual distal translation values were seen at 6 and 12 months follow up.

Short stem anterior translation: 2 values were greater in the anterior and 1 value in the posterior direction. No consistent pattern was seen, fig. 1.

Short stem Y rotation: Small values were measured. However individual outliers were seen, fig.2.

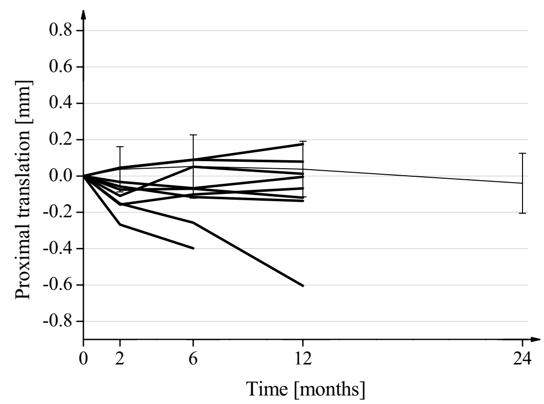

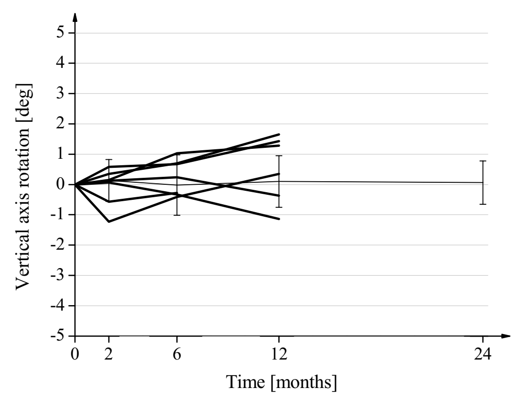

Figure 1. Proximal translation and vertical rotation of individual patients with the short stem hip resurfacing implant. The mean (± SD) of the BHR results is provided as a comparison.

CONCLUSIONS

We found a tendency towards a greater distribution in vertical migration in comparison to the BHR design. A large variation and no clear pattern in anterior migration and individual outliers in rotation could be described. At the 12-month stage no migrations exceeding those expected for conventional hip replacements were found. A follow-up of 20 patients for 2 years will provide final results.

REFERENCES

1. Itayem R, et al. In Press: *J Bone Joint Surg (Br) 87-B.* 2005.

NECK MUSCLE ACTIVITY DURING SHORT DURATION IMPACTS

Joseph Pellettiere, Mary Ann Sanders, and Erica Doczy
AFRL/HEPA
Wright-Patterson AFB, OH

INTRODUCTION

Helmet-mounted systems, such as night vision goggles and helmet-mounted displays, are designed to enhance pilot performance; however, they may also affect pilot safety during ejection due to the change in helmet inertial properties. The effects of variable helmet weight and bracing ability on subject response during impact are unknown. A useful tool for investigating the mechanics of bracing and the relationships to helmet weight and impact acceleration is electromyography (EMG). In addition, EMG can be used to establish the relationship between the potential for neck injury and the force exerted by the neck muscles due to bracing. Two recent studies were conducted at Wright Patterson Air Force Base (WPAFB) to investigate the effect of helmet weight and subject bracing on human response during impact. A better understanding of the relationship between bracing and injury potential can be used to develop detailed instructions for pilots during their training to reduce their injury potential through proper positioning and bracing in the event of an ejection.

METHODS

The methodology for collecting EMG data during short duration acceleration experiments was developed during a -Gx (frontal) impact study on the Horizontal Impulse Accelerator (HIA) at WPAFB. Male and female volunteer subjects, 10 of whom were instrumented with EMG sensors, participated with the approval of an Institutional Review Board (IRB). The MyoMonitor Portable EMG system from DelSys recorded the data separately from the rest of the response measurements, which included head and chest acceleration, belt loads and seat loads. Helmet weights ranged from 0 lb (no helmet) to 4.5 lbs, and acceleration levels were 6, 7, 8 and 10 g. The muscles of interest were those that play a major role in neck position and stability: the upper trapezius and sternocleidomastoid (SCM). Phillips et al. examined the characteristic changes in the EMG data from these muscles that was associated with isometric muscle fatigue [1]. Past research, however, does not quantify timing and level of muscular activation during short-duration impact events. The sensors were placed on the right and left upper trapezius and SCM, over the belly of the muscles.

The collection of EMG data continued during a study that examined neck muscle strength and response during vertical impact with a variable weighted helmet. Male and female volunteer subjects participated in this study on the Vertical Deceleration Tower (VDT), also located at WPAFB. Anatomical landmarks were used for consistency of sensor placement, on the right and left upper trapezius and SCM. An on-board data acquisition system was employed to easily record and synchronize the EMG data with other acceleration and load data. Maximum Voluntary Contractions (MVC) data were collected for each subject before the experiment. Helmet weights were 3.0, 4.0 and 5.0 lbs, with acceleration levels of 6, 8 and 10g.

RESULTS AND DISCUSSION

EMG data were collected for 29 of the HIA tests. Root Mean Squared (RMS) time histories of the EMG voltage were calculated for each successful data collection. RMS amplitude analysis indicated that, in general, the muscular strain increased with increasing –Gx acceleration levels. Activity of both muscle groups was synchronized, by their RMS values, with head and neck motion. It was demonstrated that in fact the neck muscles can respond quickly to the short-duration impacts. Furthermore, the EMG system was able to collect these changes during the impact.

No muscle activity was observed in the SCMs during the -Gx pre-impact bracing period, while measurable muscle activation occurred in the trapezius. This was to be expected since the bracing required of the subjects is that of an isometric extension action and the SCMs primarily act in flexion. The neck muscle activation level generally increased when heavier helmets were worn (Figure 1). This was expected since the bracing levels were similar and the heavier helmet would require higher activation levels to keep the head stable and prevent head rotation during impact.

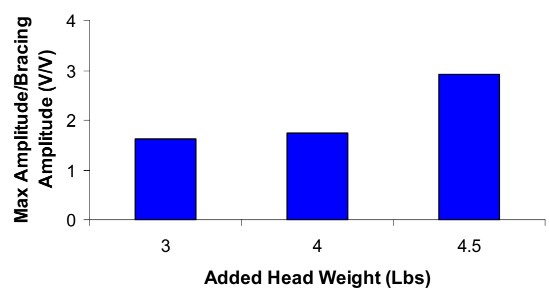

Figure 1. Increase of Trapezium activity with change in helmet weight during 8b impacts

CONCLUSIONS

A method of collecting neck muscle activity data from the trapezius and SCM during short-duration impact experiments was successfully developed. EMG can be used to determine the activation timing of the muscles and to estimate the force produced by the muscles in a dynamic environment. This study showed that the muscles in the neck can and do react during the short time of these impacts. Because of these facts and this unique research, further studies are warranted to establish a relationship between potential for neck injury and muscle force.

REFERENCES

1. Phillips CA, et al. Quantitative Electromyography: Response of the Neck Muscles to Conventional Helmet Loading, *Aviation, Space, and Environmental Medicine*, May 1983.

Age affects Eccentric Muscle Performance *In Vivo* during a Chronic Exposure of Stretch-Shortening Cycles

Ken B. Geronilla[1], Brent A. Baker[1], John Z. Wu[1], Mike L. Kashon[1], Stephen A. Alway[2], and Robert G. Cutlip[1],
(1)National Institute for Occupational Safety and Health, Morgantown, WV, 26506
(2) Laboratory of Muscle Biology and Sarcopenia, Division of Exercise Physiology, West Virginia University School of Medicine, Morgantown, WV, 26506
email: RGC8@cdc.gov

INTRODUCTION

The 55-64 year old demographic comprises the fastest growing sector of the labor force in the United States. However, the effects of age on muscle response and injury resulting from repetitive exposures to mechanical loading have not been studied extensively. It is clear that susceptibility to contraction-induced injury increases with age in both humans [1], and animals [2]. The purpose of this research was to investigate if aging affects the ability of skeletal muscle to adapt to repetitive exposures of stretch-shortening cycles (SSCs). Skeletal muscle adaptation was assessed by characterizing changes in eccentric performance longitudinally during the chronic exposure period. We tested the specific hypothesis that young animals can adapt to repetitive mechanical loading of potentially injurious SSCs while older animals will not be able to adapt. Adaptation was defined by a maintenance or increase in eccentric muscle performance as a result of the repetitive exposures, while mal-adaptation was defined as a decrease in eccentric muscle performance as a result of the exposures.

METHODS

Male F344 x BN F1 rats (N = 11) were obtained from the National Institutes on Aging colony. Young adult (N=6, 330g ± 28 g SD, 12 weeks of age) and old (N= 5, 588g ± 32 g SD, 30 months) rats were housed in an AAALAC accredited animal quarters. The dorsiflexor muscles were tested on a custom-built rodent dynamometer. The dynamometer provides precise control over the muscle length and muscle force output parameters to be studied. Rats were anesthetized with 2% isoflurane gas and placed supine on the heated x-y positioning table of the rodent dynamometer, with an anesthetic mask placed over its nose and mouth. The knee was secured in flexion (at 90 deg) with a knee holder. The young and old age groups were exposed to 80 total SSCs. The SSCs were administered in 8 sets of 10 repetitions each with 2 minute intervals between each set. Within each set, there was a rest of 2 s between each SSC. For each repetition, the muscles were activated for 100 ms and the SSC was initiated with a movement velocity of 60 deg/s over the prescribed range of motion of 90 deg to 140 deg ankle angle. The dorsiflexor muscles were then deactivated 300 ms later. Total stimulation time per repetition was 2.06 s. The exposure protocol and performance tests were administered three times per week for a total of 14 exposures over a 4.5 week period. The eccentric force response was modeled by identifying the peak force from each SSC, and then mathematically characterizing the change in those forces within each set of 10 repetitions and between set using a power law: $T_t = f(t) = P_0 - \alpha \cdot t^{\beta}$

RESULTS AND DISCUSSION The peak eccentric force of the young and old age groups responded differently during the chronic exposure (p = 0.03). The young and old groups were not statistically different at the start of the protocol (p = 0.196), but the young group produced statistically greater eccentric force by the 7th exposure (p = 0.0002), and continued through the 14th exposure (p = 0.0001, Figure 1a). Model parameters (α and β) were quantified (Figs 1b and 1c) and the analytical model fit well to the experimental data for all sets throughout the exposure period (1st, 7th, and 14th exposures shown, Fig 1d).

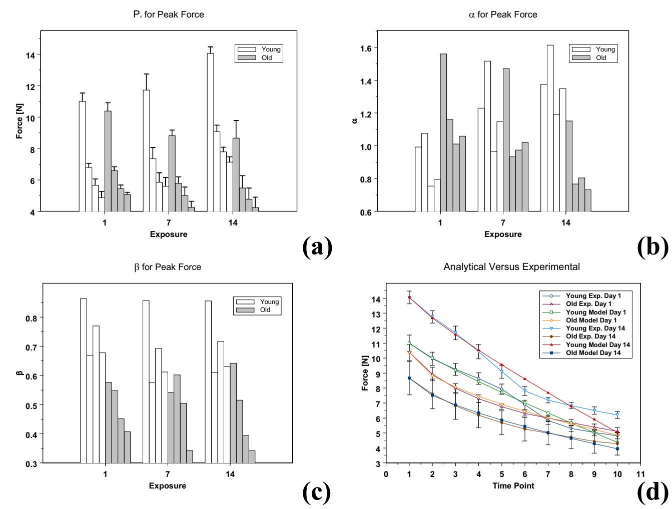

Figure 1: (a) The peak eccentric force of the old and young groups for sets 1-8 of the first, seventh and fourteenth exposures. (b) Parameter (A) of the old and young groups for sets 1-8 of the first, seventh and fourteenth exposures. (c) Parameter (b) of the old and young groups for sets 1-8 of the first, seventh and fourteenth exposures. (d) Analytical versus experimental response for 1st, 7th, and 14th exposures.

CONCLUSIONS

Age negatively affects the ability to adapt to repetitive exposures of SSCs as evidenced by a significant increase in peak eccentric force in the young group as compared with the old group. Also, there was a statistically greater decline in peak eccentric force during each exposure in the old group as compared with the young group. The power law accurately characterizes the changes in eccentric force within each session, and across sequential sessions, and quantifies the difference in dynamic response between age groups during the 4.5 week exposure.

REFERENCES

1. Manfredi TG et al. Med Sci Sports Exerc 1991;23(9):1028-34.
2. Zerba E, et al.. Am J Physiol 1990;258(3 Pt 1):C429-35.

Characterization of Changes in Eccentric Work *In Vivo* during a Chronic Exposure of Stretch-Shortening Cycles: Age Effects

Robert G. Cutlip[1], Ken B. Geronilla[1], John Z. Wu[1], Brent A. Baker[1], Mike L. Kashon[1], and Stephen A. Alway[2],
(1)National Institute for Occupational Safety and Health, Morgantown, WV, 26506
(2) Laboratory of Muscle Biology and Sarcopenia, Division of Exercise Physiology, West Virginia University School of Medicine, Morgantown, WV, 26506
email: RGC8@cdc.gov

INTRODUCTION

Musculo-skeletal injury in aged workers has been identified as an important research focus by The National Occupational Research Agenda [1]. However, the effect of age on skeletal muscle adaptation from repetitive mechanical loading has not been studied extensively. It is clear that susceptibility to contraction-induced injury increases with age [2]. The purpose of this research was to investigate if aging affects the ability of skeletal muscle to adapt to repetitive exposures of stretch-shortening cycles (SSCs). Skeletal muscle adaptation was assessed by characterizing changes in dynamic performance longitudinally during the chronic exposure period. We tested the specific hypothesis that young animals can adapt to repetitive mechanical loading of potentially injurious SSCs while older animals will not be able to adapt. Adaptation was defined by a maintenance or increase in eccentric (negative) work as a result of the repetitive exposures, while mal-adaptation was defined as a decrease in negative work as a result of the exposures.

METHODS

Male F344 x BN F1 rats (N = 11) were obtained from the National Institutes on Aging colony. Young adult (N=6, 330g ± 28 g SD, 12 weeks of age) and old (N= 5, 588g ± 32 g SD, 30 months) rats were housed in an AAALAC accredited animal quarters. The dorsiflexor muscles were tested on a custom-built rodent dynamometer. The dynamometer provides precise control over the muscle length and muscle force output parameters to be studied. Rats were anesthetized with 2% isoflurane gas and placed supine on the heated x-y positioning table of the rodent dynamometer, with an anesthetic mask placed over its nose and mouth. The knee was secured in flexion (at 90 deg) with a knee holder. The young and old age groups were exposed to 80 total SSCs. The SSCs were administered in 8 sets of 10 repetitions each with 2 minute intervals between each set. Within each set, there was a rest of 2 s between each SSC. For each repetition, the muscles were activated for 100 ms and the SSC was initiated with a movement velocity of 60 deg/s over the prescribed range of motion of 90 to 140 deg ankle angle. The dorsiflexor muscles were then deactivated 300 ms later. Total stimulation time per repetition was 2.06 s. The exposure protocol and performance tests were administered three times per week for a total of 14 exposures over a 4.5 week period. The dynamic force response was modeled by calculating the negative work from each SSC, and then mathematically characterizing the change in negative work within each set of 10 repetitions and between set using a power law: $T_t = f(t) = P_0 - \alpha \cdot t^{\beta}$

RESULTS AND DISCUSSION The ability to absorb negative work differed between age groups with subsequent exposures during the chronic exposure period (p = 0.011). Negative work increased in the young group for sets 1-8 during the chronic exposure period, but remained static in the old group (Fig 1a). Negative work was not different with age at the 1st exposure, but was statistically higher in the young group by the 7th exposure (p = 0.001) and the trend continued at the 14th exposure (p < 0.0001, Fig 1a). Model parameters (α and β) were quantified (Figs 1b and 1c) and the analytical model fit well to the experimental data for all sets throughout the exposure period (1st, 7th, and 14th exposures shown, Fig 1d).

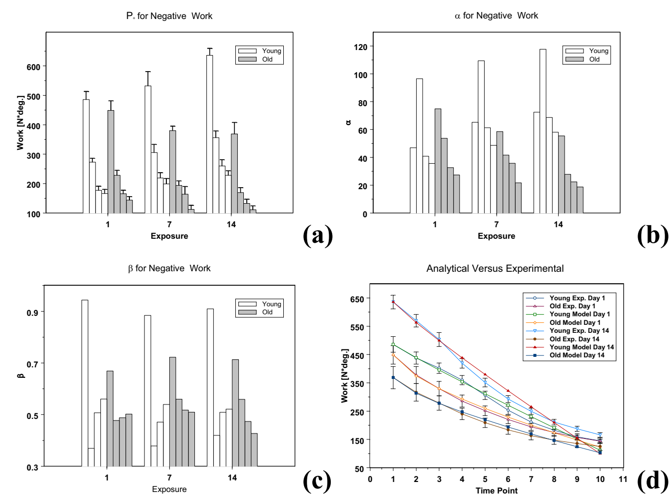

Figure 1: (a) The negative work of the old and young groups for sets 1-8 of the 1st, 7th, and 14th exposures. (b) Parameter (α) of the old and young groups for sets 1-8 of the 1st, 7th and 14th exposures. (c) Parameter (β) of the old and young groups for sets 1-8 of the 1st, 7th, and 14th exposures. (d) Analytical versus experimental response for 1st, 7th, and 14th exposures.

CONCLUSIONS

Age negatively affects the ability to adapt to repetitive exposures of SSCs as evidenced by a significant increase in negative work in the young group as compared with the old group. Also, there was a statistically greater decline in negative work during each exposure in the old group as compared with the young group. The power law accurately characterizes the changes in negative work within each session, and across sequential sessions, and quantifies the difference in dynamic response between age groups during the 4.5 week exposure.

REFERENCES

1. (NRC) NRC, (IM) IfM. Musculoskeletal Disorders and the Workplace. Washington, D.C.: National Academy Press; 2001.
2. Zerba E, et al.. Am J Physiol 1990;258 (3 Pt 1):C429-35.

GROUND REACTION FORCES AND 3D KINEMATICS OF SHORT-LEG WALKING BOOTS IN GAIT

Songning Zhang, Kurt Clowers and Douglas Powell
Biomechanics/Sports Medicine Lab, The University of Tennessee, Knoxville, TN, USA
email: szhang@utk.edu, web: web.utk.edu/%7Esals/resources/biomechanics_laboratory.html

INTRODUCTION

Short-leg walking boots have gained popularity in clinical uses [1, 2] due to several advantages over traditional casts: ease of removal for examination and cleaning, edema treatment, less expensive, and a lesser adverse effect on kinematic and kinetic gait patterns than a synthetic walking cast [1]. They are commonly used in treatment of acute and chronic injuries, and post surgical interventions [3, 4]. Limited information is available on gait biomechanics while walking in these walking boots (walker) [1]. To the knowledge of the authors, no ground reaction force (GRF) profiles of walkers were documented in the literature. Therefore, the objective of this study was to examine the ground reaction force characteristics and lower extremity three-dimensional (3D) kinematics during walking wearing two different short-leg walking boots.

METHODS

Eleven (5 females and 6 males) subjects (Age: 27.4 ± 7.8 years, Body mass: 72.0 ± 13.4 kg, Height: 1.76 ± 0.08 m) participated in the study. The subject performed five level walking trials in each of three randomized conditions: two short-leg walking boots of Gait Walker (DeRoyal Industries, Inc.) and Equalizer (Royce Medical Co.) and one pair of lab shoes. A force platform (1080 Hz, AMTI) and a 6-camera motion analysis system (120 Hz, Vicon) were used to collect GRF and 3D kinematic data simultaneously during the testing session. A pair of photocells was used to determine and monitor the preferred walking speed during testing.

Kinematic and GRF data were smoothed at 6 and 20 Hz respectively, using a fourth-order Butterworth low-pass filter. The 3D kinematic variables were computed using Visual3D software suite (C-Motion, Inc.) in conjunction with a customized computer program. A one-way repeated measures of analysis of variance (ANOVA) was used to evaluate selected GRF and kinematic variables and post hoc comparisons were conducted with an alpha level ($p < 0.05$) adjusted for multiple comparisons through a Bonferroni procedure.

RESULTS AND DISCUSSION

In addition to two normal vertical GRF peaks associated with the loading response (Max 2) and terminal stance (Max 3) in normal walking, one earlier peak (Max 1) occurs before the peak of loading response in the two walker conditions (Table 1). This peak was mostly absent in the shoe walking trials. The statistical comparisons showed no significant differences for the three peaks. Even though the first GRF peaks for the two walkers were below one body weight, it poses loading that may be detrimental to the injured foot/leg structure(s). This risen peak is related to the outsole material and the heel design of the walkers.

The ANOVA comparisons of joint kinematics suggested that the subtalar eversion range of motion (ROM) was greater for the DeRoyal compared to the no walker condition (Table 2). In addition, the hip abduction ROM for the DeRoyal and Royce walkers were significantly smaller than those for the shoes. These data suggest that both walkers restrict motions of the subtalar and hip joints in the frontal plane. Our data basically agreed with the findings of Pollo et al. [1] except for the maximum knee flexion in the earlier stance for the DeRoyal walker, which was greater than walking in the shoes. This may be related to the slight different ground reaction force profile for the condition.

CONCLUSIONS

This study showed both short-leg walking boots, DeRoyal's Intuition Gait Walker and Royce's Equalizer, were effective in minimizing motion of subtalar eversion and hip adduction. Both walkers did not increase the two peak ground reaction forces observed in normal walking in shoes. However, they did impose a small initial peak (less than one BW) in early stance phase.

REFERENCES

1. Pollo FE, et al., *Orthopedics* **22**, 503-507, 1999.
2. Kadel NJ, et al., *Foot Ankle Int* **25**, 406-409, 2004.
3. Kader D, et al., *Br J Sports Med* **36**, 239-249, 2002.
4. King DM, *Aust N Z J Surg* **45**, 54-56, 1975.

ACKNOWLEDGEMENTS

Funded by a grant from DeRoyal Industries, Inc.

Table 1. Average vertical GRF peaks (N/kg).

Condition	Max1	Max2	Max3
Shoe	--	10.77 ± 0.59	10.68 ± 0.41
DeRoyal	8.91 ± 1.49	10.27 ± 0.72	10.47 ± 0.59
Royce	7.37 ± 2.74	10.72 ± 0.61	10.43 ± 0.44

--: No apparent peak observed

Table 2. Average ROM (deg) of lower extremity joint angles.

Condition	Subtalar Eversion ROM	Knee Adduction ROM	Hip Adduction ROM
Shoe	-8.7 ± 3.3	3.3 ± 1.8	8.3 ± 2.4
DeRoyal	-1.8 ± 4.9 [1]	2.4 ± 2.5	6.1 ± 2.00 [1]
Royce	-6.6 ± 4.6	2.1 ± 2.2	6.0 ± 2.3 [1]

[1]: Significantly different from Shoe

STEPPING ON AN OBSTACLE WITH THE MEDIAL FOREFOOT: USE OF A 3D DYNAMIC CONTROL MODEL TO SIMULATE AGE AND NEUROPATHY

[1,2] Sibylle B. Thies, [1,2]James A. Ashton-Miller and [2]Jonathan E. Luntz
[1]Biomechanics Research Laboratory, University of Michigan, Ann Arbor, Michigan, USA, email: sthies@salford.ac.uk
[2]Mechanical Engineering, University of Michigan, Ann Arbor, Michigan, USA

INTRODUCTION

Approximately 24% of falls in the elderly occur while walking on irregular surfaces [1]. Irregular surfaces are known to increase the step width variability in the elderly, particularly those with peripheral neuropathy [2]. Bilateral ankle braces generally decrease this variability [3].

A previous study in healthy young women showed that unexpectedly stepping on a 15 mm-high object with the medial forefoot shifts the center of pressure (COP) medially, thereby decreasing the ankle eversion moment and increasing inversional stance foot acceleration [4]. Increased inversional foot acceleration has been associated with a narrowed recovery step, and sometimes even a crossover step [4].

Our goal was to develop a model to 1) simulate stance leg single support phase dynamics during a sudden medial shift in COP progression during gait, and 2) provide insights in how age, neuropathy, and attachment of an ankle brace might affect maximum inversional stance foot acceleration.

METHODS

A 3D dynamic control model of the stance leg was developed to simulate an unexpected sudden medial shift in COP during the stance phase and to correctly reproduce angular dynamics comparable to those obtained from experimental studies (Figure 1). The equations of motion were implemented in a Matlab Simulink control model with anatomic joint torques under feedback control. The model was then 'aged' through a) reduction of the maximum torque inputs [5], b) adjustment of joint stiffness [6], and c) increased feedback delays [7]. Furthermore, the effect of neuropathic nerve conduction delays on inversional foot acceleration was investigated. Finally, attachment of an ankle brace was simulated by increasing the model's ankle stiffness [8].

RESULTS AND DISCUSSION

Aging the model resulted in increased maximum inversional foot acceleration in presence of a medial shift of the COP (Figure 2). Adjusting feedback delays to those of a neuropathic patient further increased inversional foot acceleration (Figure 2). However, simulating attachment of an ankle brace by increasing ankle stiffness resulted in decreased inversional foot acceleration (Figure 2).

CONCLUSIONS

We conclude that the increased neural latencies and decreased muscle strength associated with old age and neuropathy act to increase maximum inversional stance foot acceleration following an unexpected medial COP shift. Bilateral use of ankle braces help reduce this effect.

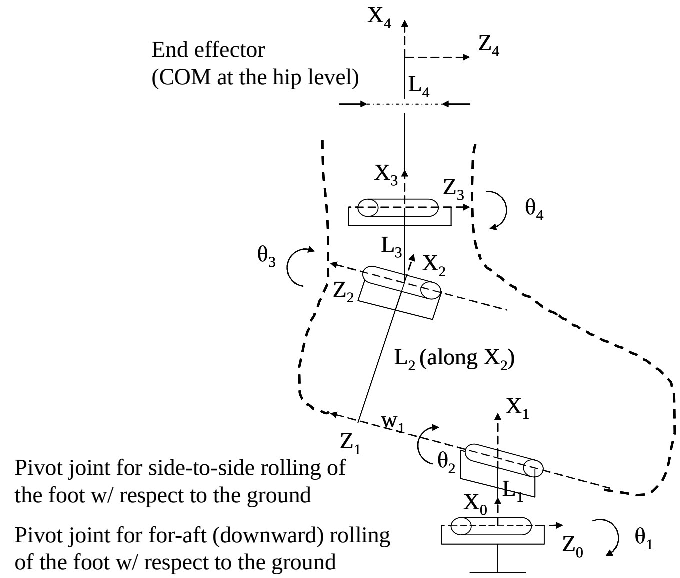

Figure 1: *Model schematic according to Denavit-Hartenberg convention: 2 segments (foot & leg) and 4 rotational joints. The COP (operating point, L1=0) is represented by the 2 lower joints at a given time instant. The two upper (anatomic) joints represent inversion/eversion and plantar/dorsi flexion. Changes in w1 correspond to COP forward progression, while changes in L2 correspond to a medial shift of the COP.*

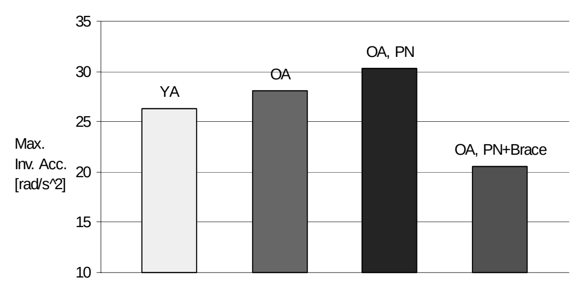

Figure 2: *Effect of age, neuropathy, and ankle brace on maximum inversional foot acceleration (YA: young adult, OA: old adult, PN: peripheral neuropathy).*

REFERENCES

1. Berg WP, et al. *Age Ageing* **26**, 261-8, 1997.
2. Thies SB, et al. *Gait Posture*, in press.
3. Richardson JK, et al. *J Am Geriatr Soc* **52**, 510-5, 2004.
4. Thies SB, et al. *ASB XXVIII*, Portland, Oregon, 2004.
5. Thelen et al. *J Gerontol* **51A**, M226-32, 1996.
6. Lark et al. *Clin Biomech* **18**, 848-55, 2003.
7. Lin et al. *J Mot Behav* **34**, 37-44, 2002.
8. Siegler et al. *JOSPT* **26**, 299-309, 1997.

THE ORIGIN OF MECHANICAL INTERACTIONS BETWEEN ADJACENT SYNERGISTS IN RAT

[1,2] Huub Maas, [2] Hanneke J.M. Meijer and [2,3] Peter A. Huijing
[1] Center for Human Movement Studies, School of Applied Physiology, Georgia Institute of Technology, Atlanta, GA, USA,
[2] Faculty of Human Movement Sciences, Vrije Universiteit Amsterdam, The Netherlands
[3] Institute for Biomedical Technology, Universiteit Twente, Enschede, The Netherlands
Email: huub.endemaas@ap.gatech.edu

INTRODUCTION

It has been shown that adjacent synergistic muscles do not function as independent units with regard to force transmission. Length changes as well as position changes of a single muscle-tendon complex in rat do not only result in force changes of the muscle that is manipulated, but also in force changes measured at the tendons of adjacent synergists [1, 2]. The underlying mechanism for such mechanical interaction between muscles is force transmission to bone via pathways other than the muscular origin and insertion, i.e. epimuscular myofascial force transmission [3]. Two separate pathways for such force transmission exist: (a) connective tissue at the interface between muscle bellies (intermuscular) and (b) extramuscular connective tissues. As both myofascial pathways are possibly involved, the **purpose** of the present study is to investigate the origin of mechanical interactions between synergistic muscles.

METHODS

In male Wistar rats (n = 8), the proximal and distal tendons of extensor digitorum longus (EDL) muscle as well as the tied distal tendons of tibialis anterior and extensor hallucis longus (TA+EHL) muscles were transected and connected to force transducers. Connective tissues at the muscle bellies of the anterior crural compartment were left intact. Supramaximal stimulation (100 Hz) of the common peroneal nerve excited all muscles maximally and simultaneously. Length–isometric force characteristics of distal TA+EHL were assessed. Simultaneously, forces exerted at the proximal and distal tendons of EDL, kept at constant muscle-tendon complex length and relative position, were measured. Intermuscular interaction was tested in two conditions: (a) after full longitudinal compartmental fasciotomy, and (b) after blunt dissection of the intermuscular connective tissue linkages between EDL and TA. Note that in the latter condition, intermuscular myofascial pathways were eliminated.

RESULTS AND DISCUSSION

Distal length changes of TA+EHL altered proximal as well as distal EDL force, despite the fact that EDL muscle-tendon complex length was kept constant (Figure 1). Blunt dissection caused no changes of the TA+EHL length effects on *proximal* EDL force. This indicates that effects of TA+EHL lengthening on proximal EDL force are mediated predominantly by extramuscular myofascial force transmission. In contrast, the amplitude of change in the *distal* EDL force curve decreased significantly (by ≈40%) subsequent to blunt dissection. Therefore, part of the change of *distal* EDL force is mediated by intermuscular myofascial force transmission.

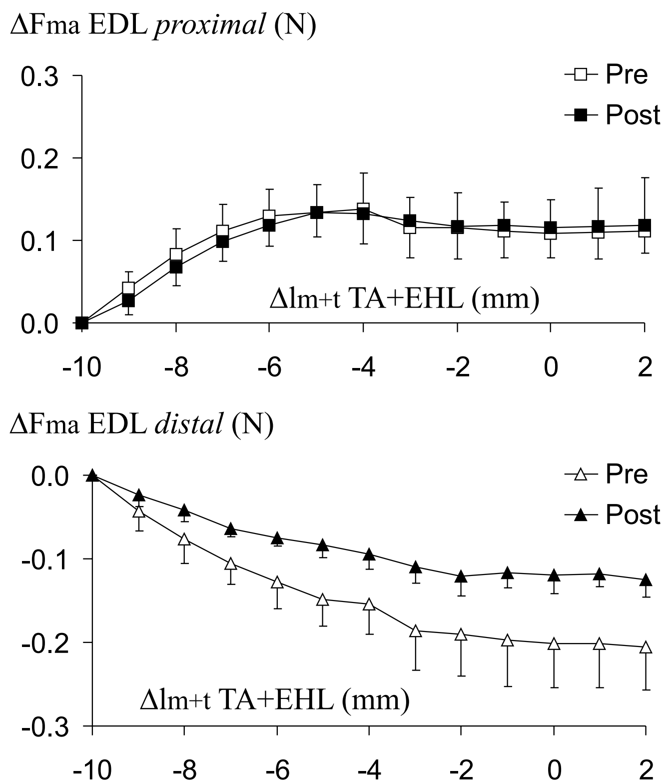

Figure 1: Changes of distal and proximal EDL active forces (F_{ma}) as a function of TA+EHL muscle-tendon complex length. F_{ma} is expressed as the deviation from the initial value (Δl_{m+t} TA+EHL = −10 mm): EDL *distal* $F_{ma,\ pre}$ = 1.74 N (0.10) and $F_{ma,\ post}$ = 1.67 N (0.14); EDL *proximal* $F_{ma,\ pre}$ = 1.45 N (0.14) and $F_{ma,\ post}$ = 1.42 N (0.17). Mean (SD), n = 8.

CONCLUSION

It is concluded that mechanical interaction between synergists originates from both intermuscular as well as extramuscular connective tissues. The highest contribution, however, should be ascribed to the latter pathway.

REFERENCES

1. Maas H, et al. *J Biomech*, **34**, 927-40, 2001.
2. Maas H, et al. *J Biomech*, **37**, 99-110, 2004.
3. Huijing PA, et al. *Acta Physiol Scand*, **173**, 297-311, 2001.

ACKNOWLEDGEMENTS

Congress expenses are funded by the School of Applied Physiology, Georgia Institute of Technology.

EVALUATION OF FIVE LIGAMENTOUS STABILIZERS OF THE SCAPHOID AND LUNATE

[1]Frederick W. Werner, [1]Walter H. Short, [1]Jason K. Green, [2]Haoyu Wang
[1]SUNY Upstate Medical University, email: wernerf@upstate.edu
[2]Bowling Green State University

INTRODUCTION

Ligamentous injuries in the region of the scaphoid and lunate are painful and difficult to treat. This biomechanical study evaluated the function of the scapholunate interosseous ligament (SLIL), radioscaphocapitate ligament (RSC), scaphotrapezium ligament (ST), dorsal radiocarpal ligament (DRC), and the dorsal intercarpal ligament (DIC) and assessed the gap between the scaphoid and lunate. Our hypothesis is that the SLIL is the major stabilizer of the scapholunate joint.

METHODS

Sixteen cadaver forearms were evaluated. Fastrak motion tracking sensors were used to measure the scaphoid and lunate motions. Each wrist was physiologically moved using a wrist joint simulator[1] through repetitive cyclic flexion/extension of the wrist (30° extension to 50° flexion) and wrist radial/ulnar deviation (10° radial deviation to 20° ulnar deviation). Carpal bone motion data were collected in the intact specimens, and in 8 arms after sequentially sectioning the ST, the SLIL, and the RSC. In eight additional arms, data were acquired after sequentially sectioning the DRC, the DIC, and the SLIL. Data were again collected after 1000 cycles of flexion/extension motion. Differences in motion were analyzed using a repeated measures 1 way ANOVA (Duncan's method, $p<.05$). Three dimensional animated models were created of each wrist, based upon serial CT scans. The experimentally collected kinematic scaphoid and lunate data were used to drive the animated motions. To mimic the clinical measurement of carpal instability, the minimum distance between the scaphoid and lunate (excluding the cartilage) was calculated using these models for each arm and for each motion.

RESULTS AND DISCUSSION

Sectioning of the ST alone produced no statistical changes in scaphoid or lunate angular position (fig 1). Additional sectioning of the SLIL resulted in statistically significant increases in scaphoid flexion and lunate extension during wrist flexion/extension and in lunate extension during wrist radial/ulnar deviation. Sectioning of the RSC after sectioning the ST and SLIL did not cause any additional significant angular changes. However, 1000 cycles of motion caused additional significant increases in lunate extension.

Paralleling the angular changes, there was no change in the gap between the scaphoid and lunate with sectioning of the ST ligament. An increase did occur with SLIL sectioning (fig 2).

In the second series of arms, sectioning of the DRC, or the DRC and DIC did not alter the scaphoid motion. Slight increases in lunate radial deviation were observed with sectioning of the DRC, or the DRC and DIC. Subsequent sectioning of the SLIL caused increases in scaphoid flexion, scaphoid ulnar deviation and lunate extension.

In comparing the two groups of arms, there was a greater increase in lunate radial deviation during wrist radial/ulnar deviation after cutting the DRC, DIC, and SLIL and 1000 cycles of motion (Group 2) compared to cutting the ST, SLIL, and RSC and 1000 cycles of motion (Group 1). Group 2 visually demonstrated greater instability compared to group 1 as seen in the 3D animations of carpal motion.

CONCLUSIONS

The SLIL was found to be the major stabilizer of the scaphoid and lunate. The RSC and ST are secondary support structures. The DRC and DIC also are secondary stabilizer structures, but may be more important than either the RSC or ST in stabilizing the scaphoid and lunate. Continued wrist use following ligament injury may result in further changes in carpal kinematics.

REFERENCES

1. Werner et al. J Orthop Res 14:639-646, 1996.

ACKNOWLEGEMENTS

Funded by NIH grant 1R01 AR050099-01.

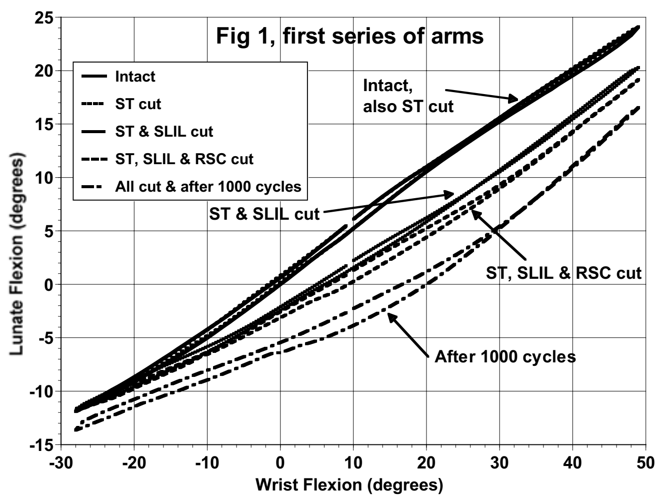

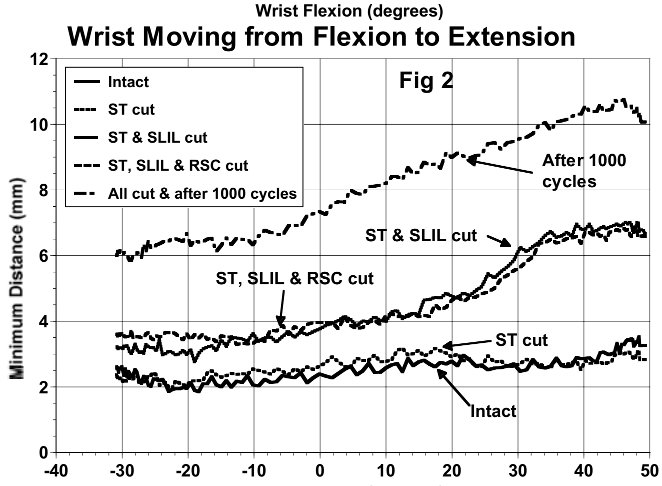

A FIBER OPTIC BASED SENSOR FOR MEASURING CHEST AND ABDOMINAL DEFLECTION UNDER IMPACT LOADING

[1]Amber L. Rath, [1]Sarah J. Manoogian, [1]Stefan M. Duma, [2]Brady J. Bolton, [2]Jeff R. Crandall
[1]Virginia Tech – Wake Forest, Center for Injury Biomechanics, [2]University of Virginia, Center for Applied Biomechanics
email: alrath@vt.edu web: www.cib.vt.edu

INTRODUCTION

Deflection measurements need to be conducted on both crash test dummies and human cadavers in order to evaluate thoracic and abdominal injury risk. Because internal measurement is not always possible on human subjects, an accurate external measurement technique is desired. The objective of this study is to investigate the use of a fiber optic based sensor, ShapeTape, as an alternative method of measuring abdominal and chest deflection in impact biomechanics applications, and to compare its performance to the historically used chestband [1-3].

METHODS

The ShapeTape used in this study was 101.2 cm x 1.6 cm x 1.5 mm with 32 sensors and was covered by a protective ribbed sheath with outside dimensions of 101.2 cm x 2.54 cm x 1.27 cm (Measurand Inc, S1680 Analog-output ShapeTape, New Brunswick, Canada). The chestband used in this study was 140 cm x 3.2 cm x 0.35 cm with 42 sets of 4 gauges along its length (Denton, 42 gauge chestband, Rochester Hills, MI). Drift, pressure, and temperature tests were conducted for ShapeTape alone under static conditions, whereas quasi-static and dynamic loading tests were conducted as comparison tests between the chestband and ShapeTape. For both the quasi-static and dynamic loading tests, a chest form was created to represent the torso of a 50th perctile Hybrid III dummy. The instrumented chest form was secured to a rigid base, which in turn was secured to the base of a material testing machine (Instron, Model 8874, Canton, MA). For both sets of tests, five cylindrical indenters were used measuring 5.08 cm, 7.62 cm, 10.16 cm, 12.70 cm, and 15.24 cm in diameter. For the quasi-static tests, the chest form was compressed by the arm of the impactor with a cylindrical indenter in 1 cm increments until a deflection of 6 cm was reached. For the dynamic tests, a loading rate of 150 cm/s was used to reach the target compression of 7 cm.

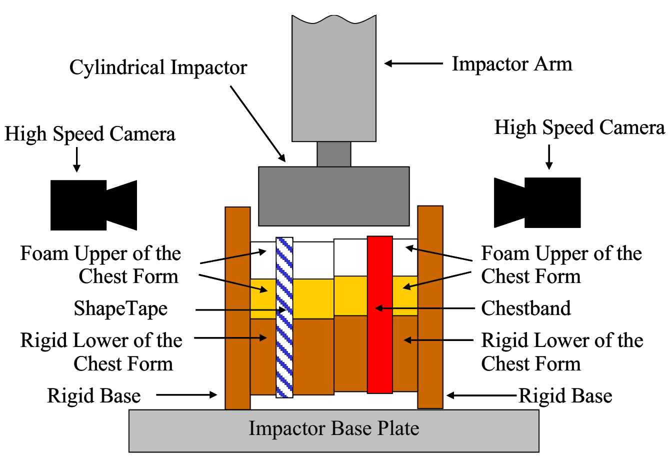

Figure 1: Side view of the set-up for the quasi-static and dynamic loading tests.

RESULTS AND DISCUSSION

Over the period of three hours, there was an average voltage change of 0.26% full scale seen by the 32 ShapeTape sensors, with a maximum of 0.55% full scale drift. This amount of drift is considered negligible. Over the five minute heating of the ShapeTape, the sensors experienced an average voltage change of 1.20% full scale. For the range of forces experienced during distributed airbag loading, 250 N - 750 N, the sensor that was loaded had a 3.24% full scale voltage difference. For the range of forces experienced during focused belt loading, 1000 N - 1600 N, the sensor that was loaded had a 12.32% full scale voltage change. During quasi-static loading, the average error in measuring peak displacement was 3.35% and 1.70% for ShapeTape and the chestband respectively. The average error in measuring peak displacement under dynamic loading was 8.60% and 10.01% for ShapeTape and the chestband respectively. The contour representations of the chest form from the chestband and ShapeTape under both loading conditions were comparable to what was captured from the video analysis (Figure 2).

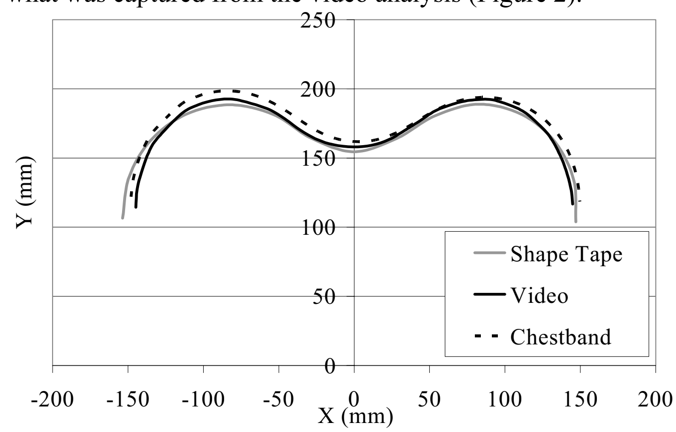

Figure 2: Chestband and ShapeTape contours compared to video data points, taken at 6 cm compression for the quasi-static compression test with a 10.16 cm diameter indenter.

CONCLUSIONS

The contour output for the ShapeTape and chestband were both very similar to the video and overlapped in many cases. From the data collected in this study, ShapeTape appears to demonstrate the same degree of accuracy as the chestband in measuring deflection and visualizing contours during quasi-static and dynamic impact loading.

REFERENCES

1. Danisch L, et al. *Fiber Optic and Laser Sensors and Applications,* SPIE Conference, 3541A, 1998.
2. Butcher JT, et al. *Proceedings of the Twenty Forth Annual Meeting of the American Society of Biomechanics*, 2000.
3. Eppinger RH, et al. *Proceedings of the Thirty Third Stapp Car Crash Conference*, SAE paper no. 892426, 1989.

SUBTALAR JOINT KINEMATICS IN HEALTHY INDIVIDUALS USING COMPUTED TOMOGRAPHY

Lijkele Beimers[1], Gabriëlle JM Tuijthof[2], Leendert Blankevoort[2],
Remmet Jonges[3], Mario Maas[4], C Niek van Dijk[1]
[1]Department of Orthopedics, [2]Orthotrauma Research Center Amsterdam, [3]Department of Medical Physics, [4]Department of Radiology – University Hospital AMC, Amsterdam, the Netherlands
Email: l.beimers@amc.uva.nl

INTRODUCTION

Kinematic profiles of the ankle joint are useful for evaluating pathological joint motion and provide a foundation for the understanding of surgical procedures. No reliable technique exists for accurate in vivo measurements of subtalar joint (SJ) motion. The purpose of this study was to assess normal range of SJ motion in a loaded state using computed tomography (CT).

METHODS

Twenty healthy volunteers (10 m, 10 f) with a mean age of 26,3 yrs (range 22-35 yrs) signed informed consent. CT images of the right foot were acquired in neutral position for bone segmentation of the talus and calcaneus. An external load was applied to force the unconstrained foot in eight different extreme positions; dorsiflexion^{max}, anterolateral^{max}, eversion^{max}, posterolateral^{max}, plantarflexion^{max}, posteromedial^{max}, inversion^{max} and anteromedial^{max}. CT images were acquired in each position using a low-dose technique. After bone contour matching, the positions and orientations of the helical axes were determined for the motions of the calcaneus relatively to the talus between the opposite extreme foot positions. The helical axes were represented in talus-specific anatomic planes as defined by its geometric principle axes.

RESULTS AND DISCUSSION

For inversion^{max}-to-eversion^{max} of the foot, the helical axes of the SJ were found to have a mean inclination from the XY-plane of 49.4±4.3 deg. (Figure 1). The mean deviation of the axes from the XZ-plane was -2.7±7.9 deg. The mean rotation about the helical axes was 37.3±5.9 deg. with a mean translation of 2.3±1.1 mm. Considerable variation of helical axes parameters were found for the motion from dorsiflexion^{max}-to-plantarflexion^{max} (Table 1). In contrast to inversion^{max} and eversion^{max} positions of the foot, dorsiflexion^{max} and plantarflexion^{max} positions were not considered to result in true locking end-positions for the SJ. Helical axes values for the two motions between the intermediate extreme postions were close to the values for inversion^{max}-to-eversion^{max} (Table 1). Despite some apparent differences between subjects, the intersubject variability of the helical axes was smaller than was expected from previous studies.[1,2,3] This finding might be due to studying motions between extreme positions of a loaded foot, resulting in true locking end-positions for the SJ.

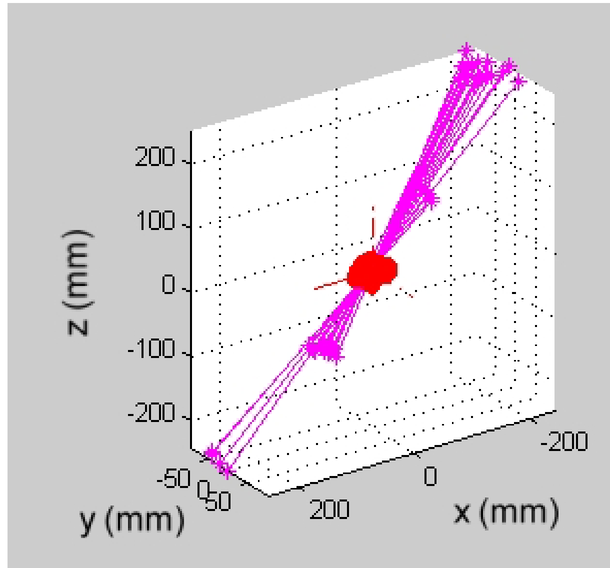

Figure 1. *3D-representation of the helical axes for subtalar motion from inversion^{max}-to-eversion^{max} of 20 normal right feet. The fixed talus (red) and its principle axes are shown in the center. The helical axes are clipped by a bounding box.*

CONCLUSIONS

For motions with a considerable inversion and eversion component, the helical axes were reproducible between the different subjects. The largest mean rotation was found for motion between inversion^{max}-to-eversion^{max}. Dorsiflexion^{max} and plantarflexion^{max} positions of the foot were not considered to result in true locking end-positions for the SJ.

REFERENCES

1. Inman VT. *The Joints of the Ankle,* p.57-66, Waverly Press, Baltimore, USA, 1976.
2. Engsberg JR. *J Biomechanics* **20**, p.429-442, 1987.
3. Arndt A, et al. *Foot&Ankle International* **25**, p.357-364, 2004.

ACKNOWLEDGEMENTS

M. Poulus and M.A. de Graaf for CT assistance

Table 1: *Mean values for the helical axes for the subtalar motions between the opposite extreme foot positions.*

	Inclination (deg)	Deviation (deg)	Rotation (deg)	Translation (mm)
Inversion^{max}-to-eversion^{max}	49.4 (4.3)	-2.7 (7.9)	37.3 (5.9)	2.3 (1.1)
Anteromedial^{max}-to-posterolateral^{max}	49.6 (4.4)	-0.3 (9.2)	35.5 (5.7)	2.8 (1.1)
Anterolateral^{max}-to-posteromedial^{max}	50.7 (4.2)	-9.1 (7.9)	29.7 (5.1)	1.1 (0.6)
Dorsiflexion^{max}-to-plantarflexion^{max}	37.1 (38.6)	-12.3 (38.1)	7.4 (6.0)	1.8 (2.2)

EFFECTS OF FUNCTIONAL ELECTRICAL STIMULATION ON MANUAL WHEELCHAIR PROPULSION

[1,2]Ronald J. Triolo, [3]Yusheng Yang, [3]Alicia M. Koontz , [1]Stephanie Nogan, and [3]Michael L. Boninger
[1]Cleveland FES Center, Louis Stokes Cleveland VA Medical Center, Cleveland OH, USA
[2]Departments of Orthopaedics and Biomedical Engineering, Case Western Reserve University, Cleveland OH, USA
[3]Human Engineering Research Laboratories, VA Medical Center, Pittsburgh, PA, USA
email: ronald.triolo@case.edu, web: http://fescenter.case.edu

INTRODUCTION

Functional electrical stimulation (FES) can facilitate many activities of daily living for individuals paralyzed by spinal cord injuries [1]. Bilateral activation of the paraspinal muscles via implanted electrodes can improve the seated posture of FES users [2], and may also improve manual wheelchair propulsion efficiency. The goal of this preliminary study was to investigate the effect of stimulating the lumbar trunk extensors via an implanted FES system on propulsion biomechanics. The results may provide insight into the benefit of FES during manual wheelchair propulsion.

METHODS

Subjects: Three long-time (>12 months) recipients of the CWRU/VA implanted standing neuroprosthesis [1] with motor complete paraplegia participated in this study. The age, height and years of wheelchair use of the two male and one female volunteers were 40.5 $\pm$ 9.3 years, 1.72 $\pm$ 0.05 meters, and 5.8 $\pm$ 0.7 years respectively.

Experimental protocol: Subjects' own wheelchairs were fitted bilaterally with SMART^{WheelsTM} instrumented pushrims (Three Rivers Holdings, ILL., Mesa, AZ), and secured to a dynamometer with a four-point tie down system. An OPTOTRAK motion analysis system (Northern Digital Inc., Ontario, Canada) was synchronized with the kinetic system to record kinematic data. Subjects were asked to propel their wheelchairs at a steady-state speed of 0.9, and 1.8 m/s for one minute while real time propulsion speed was displayed on a monitor. All propulsion trials were repeated three times: two with electrical stimulation to the erector spinae ON at 50% and 25% maximal recruitment, and one with electrical stimulation OFF. The order of stimulation condition was randomly assigned. To minimize fatigue, at least one-minute of rest was provided between trials.

Data analysis: For each stroke, the start and end of the push phase were determined by the presence/absence of forces detected by SMART^{WheelsTM}. The kinetic data were collected at 240 Hz and linearly interpolated for synchronization with the 60 Hz kinematic data. Since data from both sides were highly correlated ($r = 0.68$; $p < 0.01$), average values of both sides were obtained on all biomechanical variables over ten continuous strokes. Descriptive analyses were reported for each speed condition separately. Since one subject was unable to reach the target speed at 1.8 m/s, only data from two subjects are reported under this speed condition.

RESULTS AND DISCUSSION

Table 1 summarizes the biomechanical variables while propelling with and without FES. Continuous activation of the paraspinal muscles appears to improve propulsion performance. The mechanical effective force (MEF), the percentage of the resultant force leading to forward propulsion, is generally higher with FES for all speed conditions. Higher propulsive forces and longer stroke cadences were generally observed with stimulation ON. Mean trunk angles increased with FES under all conditions. This ability to lean the trunk forward and return facilitated with FES may help the subjects to transfer power from the upper extremities to the pushrim, thereby increasing MEF [3,4]. Although the low level (25%) stimulation showed less advantage than the high level (50%), it may be less fatiguing with prolonged use and allow a greater degree of trunk mobility. The potential benefit of low activation warrants further investigation.

The generalizability of these results is limited by the small sample size due to the limited availability of the CWRU/VA implanted standing neuroprosthesis. Future studies using a non-invasive surface FES system may be needed to further explore the phenomenon and determine benefits of FES on wheelchair propulsion in the larger SCI population.

CONCLUSIONS

Stabilizing the trunk by continuous stimulation of the lumbar erector spinae appears to improve manual wheelchair propulsion. With activation of back muscles, implanted FES users were able to lean forward and thereby increase mechanical effective forces. A future study with a larger sample size is needed to verify these findings.

REFERENCES

1. Davis et al. *J Rehab Res & Dev,* 38, 609-617, 2001.
2. Kukke et al. *IEEE Trans Neural Systems & Rehab Eng*. 12(2): 177-185, 2004.
3. Yang et al. *Proceedings of RESNA 2004*, 374-376, 2002.
4. Yang et al. *Proceedings IFESS 2004,* Bournemouth UK.

ACKNOWLEDGEMENTS

Rehabilitation Research & Development Service, US Department of Veterans Affairs (project B3043-C) and ASB 2004 Graduate Student-In-Aid Award.

Speed Condition	0.9m/s (n=3)					1.8m/s (n=2)				
Stimulation Level	Cadence (stroke/sec)	Max force (N)	Moments (N-M)	MEF (%)	Trunk angle (^{O})	Cadence (stroke/sec)	Max force (N)	Moments (N-M)	MEF (%)	Trunk angle (^{O})
OFF	1.20$\pm$ 0.20	68.0$\pm$ 3.3	6.85$\pm$ 0.63	0.59$\pm$ 0.04	1.9$\pm$ 1.2	1.32$\pm$ 0.01	90.4$\pm$ 3.7	8.24$\pm$ 2.40	0.51$\pm$ 0.06	4.03$\pm$ 10.5
25 %	1.26$\pm$0.19	68.4$\pm$ 3.2	6.33$\pm$ 0.46	0.55$\pm$ 0.02	19.9$\pm$ 14.5	1.40$\pm$ 0.07	89.5$\pm$ 6.1	8.22$\pm$ 2.46	0.55$\pm$ 0.04	18.4$\pm$ 9.7
50 %	1.20$\pm$ 0.20	70.1$\pm$ 3.2	6.98$\pm$ 0.86	0.62$\pm$ 0.05	16.2$\pm$ 9.9	1.39$\pm$ 0.13	97.8$\pm$ 4.7	8.47$\pm$ 2.97	0.55$\pm$ 0.07	18.0$\pm$ 15.7

Table 1: Summary of the effects of trunk stimulation on manual wheelchair propulsion**.**

DEVELOPING A COMPUTER AIDED DESIGN TOOL FOR INCLUSIVE DESIGN

[1]Victoria Hood, [2]David Loudon, [1]Alexander Nicol, [2]Alastair Macdonald, [1]Benard Conway
[1]Bioengineering Unit, University of Strathclyde, Glasgow, UK,
[2]Product Design Engineering, Glasgow School of Art,Glasgow UK; email: victoria.hood@strath.ac.uk

INTRODUCTION

Globally the proportion of older adults in the population is increasing, the fastest growing subgroup being those aged over 80 years. In Europe, it is estimated that 24% of the population will be aged over 65 by 2030 [1]. The majority of these people will remain living in their own home.

The aging process leads to changes in strength, flexibility and balance, which in older adults can combine to limit the use of products or services (transport, buildings etc.)[2]. Inclusive design aims to overcome this by designing products that can be used by all. However, for designers to achieve products that can be used by all it is important to provide them with relevant information on the performance capacity of the older population.

The purpose of this study was to investigate age-related changes in the performance of a range of movement tasks for integration into a computer aided design (CAD) tool for use in inclusive design.

METHODS

Eighty four healthy older adults (age 60 –88 years) underwent full body 3-D biomechanical assessment of five activities of daily living using a VICON 8-camera motion analysis system (120Hz) with 3 Kistler forceplates. Activities consisted of gait, sit-stand-sit, door opening and closing, stair ascent and descent and lifting a small object to different heights (Figure 1). Vicon BodyBuilder was used to analyze the data and export limb segment positions as a series of rotations and translations from the position of the pelvis segment. Maximum isometric joint moments at the hip and knee over a range of angles were also assessed. Maximum upper limb moments for older adults were determined from the literature.

Custom written software was developed in Visual C++ utilizing the OpenGL 3d library. This software imported the processed data and produced an animated model of a subject performing an activity. This model can be manipulated by the designer by changing the position of the limbs. Limits were placed on joint movement to represent loss of motion in the older adult. The resulting change in joint angles and moments were calculated using inverse kinematics. A plug-in was written for the engineering CAD software package SolidWorks using C++. This enabled a potential product developed using CAD to be imported and attached to the hand of the model (Figure 2). The effects on upper limb joint moments as a result of this potential product were determined.

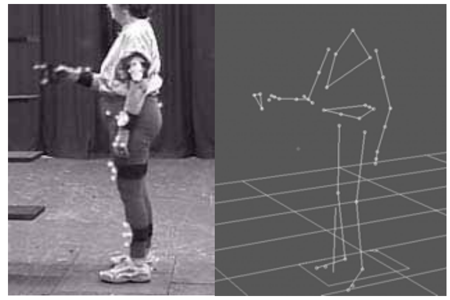

Figure 1: Data collected and processed in VICON.

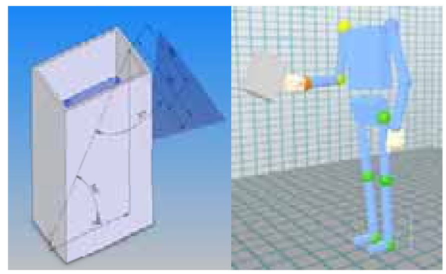

Figure 2: CAD model imported from SolidWorks and attached to model.

RESULTS AND DISCUSSION

Joint moments are presented in both numerical form and graphically on the model. Joint moments are visualized using a colour scale and expressed as the percentage of the expected age related maximum joint moment at that point in time. This allows designers to quickly visualize when a task may prove too difficult for an older adult to accomplish. Changes can then be made to the virtual design in SolidWorks and the usability of the re-engineered product reassessed.

CONCLUSIONS

The study demonstrated that biomechanical data can be interfaced with standard CAD software to aid inclusive design. The prototype CAD tool is currently being tested by designers and work is ongoing to develop it further.

REFERENCES

1. Kinsella, K and Velkoff VA. *An Aging World: 2001 (U.S. Census Bureau Series P95/01-1).* Washington, DC: U.S. Government Printing Office, 2001
2. Fisk AD, et al. *Designing For Older Adults: Principles and Creative Human Factors Approaches,* CRC Press, Boca Raton, Florida, 2004

ACKNOWLEDGEMENTS

Supported by the Engineering and Physical Sciences Research Council Grant GR/R26856/01

EVALUATION OF AN OPTIMAL CEMENT THICKNESS AROUND THE GLENOID COMPONENT FOR UNCONSTRAINED TOTAL SHOULDER ARTHROPLASTY

[1]Alexandre Terrier, [1]Philippe Büchler and [2]Alain Farron
[1]Orthopaedic Research Laboratory, Swiss Federal Institute of Technology Lausanne, Switzerland
[2]Orthopaedic Hospital, University of Lausanne, Switzerland

INTRODUCTION

Although shoulder arthroplasty is an accepted treatment for osteoarthritis, loosening of the glenoid component, which mainly occurs at the bone-cement interface, remains a major concern. At the bone-cement interface, radiolucent lines have been observed in 30-95% of patients at follow-up [1]. Radiolucent lines are associated with fibrous tissue formation and glenoid loosening. In vitro tests have shown that thickness of the cement mantle is important for the primary stability of cemented glenoid components [2]; however there is still a lack of information concerning the optimal cement thickness. The aim of the study was to analyze the effect of this parameter on the glenoid stress transfer by means of a finite element model of the shoulder.

METHODS

The 3D geometry of the scapula was reconstructed from 1 mm CT slices of a cadaver shoulder. The glenoid component was all-polyethylene, keeled with a flat back. Cement thickness was gradually increased from 0.5 to 2.0 mm. Bone, cement and polyethylene were linear elastic. Non homogeneity of bone was derived from CT. At the bone-cement interface two extreme cases were considered: fully bonded and fully debonded. In the latter case, the friction coefficient was 0.6. A 400 N force was applied on the glenoid face, corresponding to the maximal glenohumeral force during abduction [3]. The distribution of this force over the surface was derived from the Hertz theory. Two force distributions were considered: concentric and (posterior) eccentric. Several mechanical quantities were calculated near the bone-cement interface: principal stress within the cement, von Mises stress within the underlying bone, stress and micromotion at the bone-cement interface.

RESULTS AND DISCUSSION

Within cement, the increase of cement thickness induced a continuous decrease of stress (Figure 1). Below 1 mm, the fatigue limit of the cement (~7 MPa) was exceeded, even in the concentric and bonded case. Within bone, and at the bone-cement interface, there was a stress increase from 1.0 to 0.5 and from 1.0 to 2.0, suggesting a minimum between 1.0 and 1.5 mm. Bone stress was below its failure strength, but interfacial stress was close to the failure limit (~3 MPa). The debonding of the interface, as well as the eccentric loading, induced an overall increase of stress. Peak stress was mainly located at the keel tip, but also along the back-keel edges as cement thickness decreased. Micromotion remained moderate (<30µm) and almost constant (vs. cement thickness) in the concentric case, but was excessive (>150µm) and increasing (vs. cement thickness) in the eccentric case. Peak micromotion was located at the keel faces in the concentric case, but under the back in the eccentric case (rocking-horse effect).

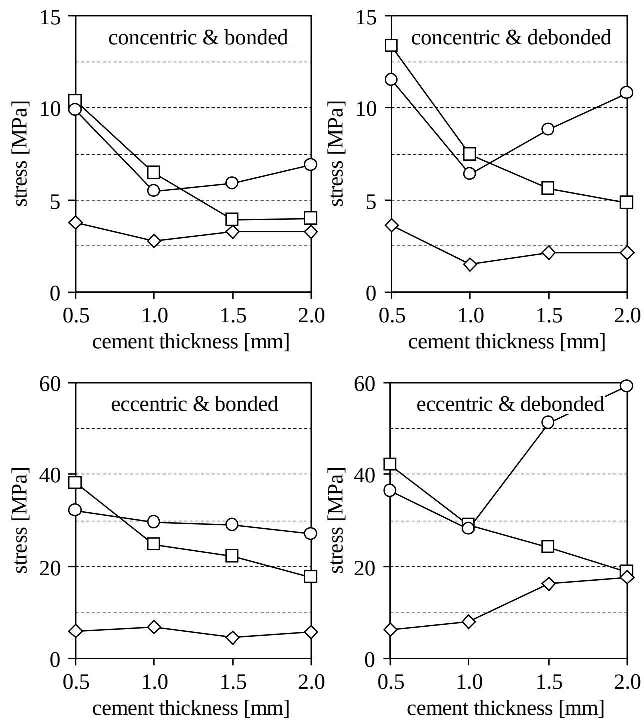

Figure 1: Peak value of cement maximum principal stress (square), bone Misses stress (circle), interfacial shear stress (diamond), for the four cases considered.

CONCLUSIONS

Results showed that cement thinning weakens the cement, but also the bone-cement interface along the back-keel edges. Conversely, cement thickening rigidifies the cemented implant, increasing consequently the overall interfacial stress and micromotion. To avoid both excessive cement fatigue and failure of the bone-cement interface, an optimal cement thickness has been identified between 1.0 and 1.5 mm.

Practically, to avoid the formation of large blocks of cement around the implant, we recommend to correct any bone defect of the glenoid by bone grafting and/or compaction. Moreover, future developments of new glenoid designs should include the ability to ensure a homogeneous cement mantel, with a minimum thickness of 1.0 mm.

REFERENCES

1. Wirth MA et al. *JBJS-A* **78**, 603-16.
2. Nyffeler RW et al. *JBJS-B* **85**, 748-52.
3. Van der Helm FC. *J Biomech* **27**, 527-550.1994.

BIOMECHANICS OF STAIR DESCENT IN OLDER ADULTS

[1]Victoria Hood, [1]Alexander Nicol,
[1]Bioengineering Unit, University of Strathclyde, Glasgow, UK;
email: victoria.hood@strath.ac.uk

INTRODUCTION

Negotiating stairs is one of the most difficult activities of daily living faced by older adults. Falls on stairs are one of the leading causes of accidental death amongst the elderly and the majority of these falls occur during stair descent [1,2].

Many researchers have studied the cardiovascular and musculoskeletal demands of stair ascent but there is little research on the biomechanics of stair descent. The purpose of this study was to investigate the biomechanics of stair descent in older adults.

METHODS

Fifteen healthy men in their 60's (mean age 66.2 years) and thirteen men in their 80's (mean age 82.2 years) underwent full body 3-D biomechanical assessment whilst ascending and descending a flight of four stairs. The second stair of the flight was instrumented using a Kistler forceplate and motion data were captured using an 8 camera Vicon motion analysis system at 120Hz. Subjects attempted 3 trials of stair ascent and descent using a handrail and 3 trials without use of a hand rail. Joint kinetics and kinematics were determined using Vicon BodyBuilder software. Data were normalized to 100 data points from foot contact on one step to foot contact on the step below and then averaged over the subject group.

RESULTS AND DISCUSSION

Men in their 80's descended the stairs significantly more slowly than the men in their 60's. There was no significant change in the amount of time spent in stance phase between the groups (Table 1). Use of a handrail had no significant impact on temporal step cycle parameters. Both groups were slower than younger subjects (mean age = 28.8 years) reported by Reiner et al. [3].

During the weight acceptance phase men in their 80's had a marked reduction in internal plantarflexion moment accompanied by a small increase in knee extensor moment (Figure 1). Throughout stance phase the knee extensor moment remained higher in the older men. This would indicate that the men in their 80's are using the knee extensors of the trailing leg to reduce the moment required by plantarflexors at initial contact. Overall this results in a more smooth moment generation pattern throughout stance. This pattern was observed both with and without use of a handrail.

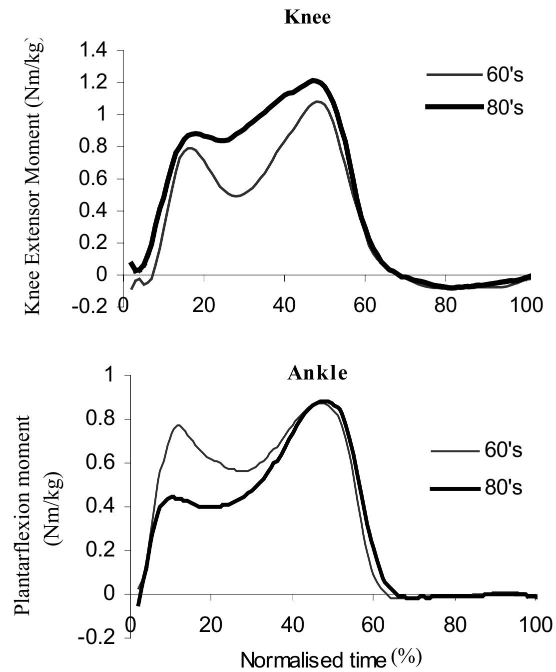

Figure 1: Saggital plane moments at the knee and ankle during stair descent averaged for men in their 60's and 80's

CONCLUSIONS

The strategy older men use to descend the stairs is one which results in a more consistent net moment in the ankle and knee extensors. The increased requirement of the knee extensors with age for stair descent may be a factor that contributes to difficulty performing this task.

REFERENCES

1. Tinetti M et al.. *N Engl J Med* **319**, 1701-1707, 1988
2. Startzell JK et al., *JAGS* **48,** 567-580, 2000
3. Reiner R et al., *Gait and Posture* **15,** 32-44, 2002

ACKNOWLEDGEMENTS

Supported by the Engineering and Physical Sciences Research Council Grant GR/R26856/01

Table 1: Averaged temporal step cycle parameters for stair descent without a rail

Age Group	Cycle duration (s) *	Cadence (steps/min) *	Stance phase (%)
60's	1.28 ± 0.21	48.5 ± 9.2	59.5 ± 3.0
80's	1.65 ± 0.38	38.4 ± 9.4	60.5 ± 2.8

* t-test $p < 0.05$

ELECTROMYOGRAPHIC ANALYSES OF STANDING SHOT PUT THROW

[1]Hsiente Peng, [2]Hsiensen Peng and [1]Chenfu Huang
[1]National Taiwan Normal University, Taipei, Taiwan;
[2]National Taipei Teacher College, Taipei, Taiwan; email: sid125@ms35.hinet.net

INTRODUCTION

The throwing arm plays an important and crucial part in the shot put event. Shot put is a heavy-weighted throwing event compared with others, such as baseball pitching and javelin throw. Standing shot put throw is a basic training movement for the throwing technique in thrust. Electromyography (EMG) of throwing had been studied by many researchers. Nevertheless the applications on studies of upper extremity of throwing events focused mostly on the baseball pitching [1,2,3,4,]. The baseball is a light-weighted throwing event (about 0.145 kg.). There are few studies on the EMG activity of a heavy-weighted throwing event. So, we selected the shot put as our study. The weight of a shot put for adult male is 16 lb. (7.26 kg.). We also asked the subjects to throw lighter shot puts, which are weighted 8 lb. and 12 lb. This study used dynamic EMG analysis to compare the muscle actions in different shot put weight, and to investigate the sequences of the muscular function and the patterns of the muscular activity.

METHODS

Seven shot putters (age of 20±3 years; height of 178±9 cm; weight of 100±24 kg) served as subjects to perform the standing throw with three weights of the shot put (8, 12 and 16 lb.). Each subject at least performed two throws successfully. The best performance was selected to analyze. Two Redlake high-speed cameras (sampling rate: 125Hz; Motion Scope, San Diego, USA.) and one Biovision system (sampling rate: 1250Hz; Biovision, Wehrheim, Germany.) were synchronized to collect the data. The surface EMG of thirteen muscles was recorded. Raw EMG signals were band-pass filtered (20-400Hz), full wave rectified, and passed through a linear envelope at 10Hz for final interpretation. Integrated EMG signals (IEMG) from the onset of thrust to shot put release of the standing throw trials were then normalized by the maximal signal (%max), which was highest EMG value obtained during the standing throw, for each muscle to indicate relative activation levels. The nonparametric statistical test of Friedman two-way analysis of variance by ranks was conducted for the normalized IEMG of each muscle ($p<0.05$).

RESULTS AND DISCUSSION

The distances of 8, 12 and 16 lb. shot put throw were 15.58±1.97, 13.87±2.27 and 11.57±2.42 m, respectively. Figure 1 shows the activation levels of the thirteen muscles. The lower, middle and upper trapezius, anterior deltoid and middle deltoid demonstrated stronger activity than the other muscle groups during the standing shot put throws (23 to 28%max). In addition, forearm extensor and flexor also demonstrated strong activity in 16 lb. shot put throw (23%max). There was a trend in majority of the muscle groups, which showed higher EMG activities when throwing the heavier shot put. Only the forearm flexor demonstrated the statistical significance between the three weights of shot put. Figure 2 shows the time to peak EMG of thirteen muscles of seven subjects. The sequences of the muscular function were a little different in three weights of shot put. Generally, the time to peak EMG sequences corresponded to the proximal-distal segmental sequence. But the serratus anterior was an exception. It's time to peak EMG was emerged just before shot put release.

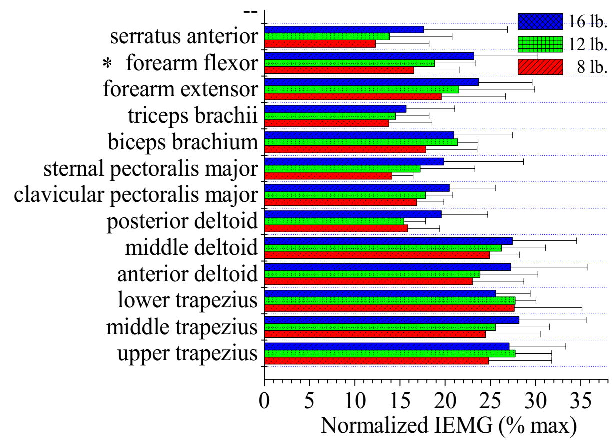

Figure 1: Normalized IEMG of thirteen muscles of seven subjects (mean ± %max) throwing with three weights of shot put (8, 12 and 16 lb.). * The statistical significance was found between the three weights.

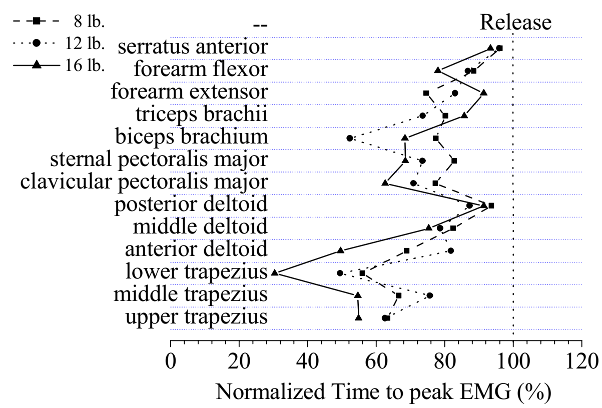

Figure 2: Time to peak EMG of thirteen muscles of seven subjects (mean). Time was normalized to standing throw duration (100%).

REFERENCES

1. Gowan, I. D., et al. *Am. J. Sports Med.* **15**(6), 586-590, 1987.
2. Jobe, F. W., et al. *Am. J. Sports Med.* **11**(1), 3-5, 1983.
3. Jobe, F. W., et al. *Am. J. Sports Med.* **12**(3), 218-220, 1984.
4. Sisto, D. J., et al. *Am. J. Sports Med.* **15**(3), 260-263, 1987.

ANALYSIS OF COLLAGENASE, COLLAGEN, AND GLYCOSAMINOGLYCAN CONTENT OF CYCLICALLY LOADED TENDON EXPLANTS IN CULTURE

[1] Aaditya C Devkota and [1,2]Paul S Weinhold
Departments of [1]Biomedical Engineering and [2]Orthopaedics
University of North Carolina, Chapel Hill; email: aaditya@unc.edu

INTRODUCTION

Overuse injuries comprise a significant portion of tendon injuries. These injuries are a combination of simple material fatigue damage as well as the cells' matrix remodeling response to the load stimulus. To better understand the role of the cellular response in overuse injuries, tendon explants were cyclically loaded across one or twelve days with loading regimens of two magnitudes. The sulfated glycosaminoglycan content, collagen content (by measuring hydroxyproline) and the collagenase content were measured.

METHODS

Avian flexor digitorum profundus tendons were isolated and placed in a custom built load-controlled tissue loading device. Tendons were cyclically loaded to a fixed number of cycles at 3 or 12 MPa (Low, High) across 1 or 12 days (Short, Long). Media was exchanged before and after the full regimen as well as every 3rd day.

Media samples were analyzed for collagenase content by measuring the release of a red dye (Azocoll) impregnated in collagen [1]. Samples were activated with APMA to evaluate total potential collagenase activity. Data was normalized by the day 0 value for each sample. Positive and negative controls were included with collagenase injected and freeze-killed trials, respectively.

Tissue segments were digested with papain, and then analyzed for collagen content [2] and sGAG content [3]. Collagen content was measured by a spectrophotometer from hydrolyzed digests introduced to Chloramine T with an aldehyde dye, DAB and quantified using hydroxyproline standards. sGAG was measured by a spectrophotometer in a DMMB (blue) buffer and quantified using chondroitin sulfate (shark cartilage) standards. All data was normalized by dry weight of the original tendon segment prior to digest.

Table 1: Tissue content of cyclically loaded tendons explants (µg/mg dry weight). Groups without a common letter are significantly different (P<0.05).

	Hydroxyproline	Sulfated GAG
High Long (HL)	91.86 ± 0.661 A	6.725 ± 0.89 A
High Short (HS)	102.0 ± 18.92 A	6.628 ± 1.48 A,C
Low Long (LL)	92.71 ± 16.25 A	4.914 ± 0.94 B,C
Low Short (LS)	82.08 ± 8.882 A	4.203 ± 0.76 B

RESULTS AND DISCUSSION

Sulfated GAG concentrations were found to be in the range of macroscopically normal cadaver tendons [3]. A significant difference in the main effect of magnitude was seen. Both high groups, HL and HS, were statistically larger than the low groups, LL and LS, respectively (Table 1), as measured by a two-way ANOVA. While elevated GAGs were expected in

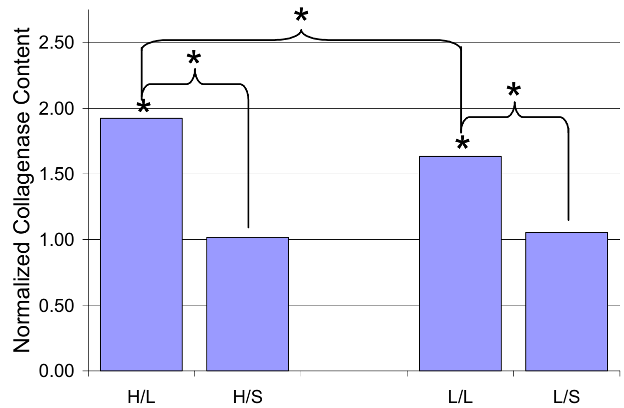

Figure 1: Collagenase content of cyclically loaded tendons, normalized by time 0.

the HL [4], the elevated levels in the HS was not expected because a duration dependence (response time) was expected.

Collagen content, measured by hypro content, was found to be in the range of macroscopically normal, cadaver supraspinatus tendons [2]. However, no differences were seen between any of the groups (Table 1). Though collagen content did not differ, collagenase content did. A significant increase in the collagenase content was seen in the HL and the LL groups relative to time zero. This difference was significant by day 9 for the HL group and day 12 for the LL group. Both long groups were significantly larger than their respective short groups indicating a duration dependence of collagenase release. Magnitude also affected the collagenase content as the HL group was found to be significantly larger than the LL group. This difference was not seen between the short groups however, and could be due to a lack of response time. The high levels of collagenase with a concurrent lack of differences in collagen content potentially suggest a high collagen turnover. However, as active and inactive collagenase was measured with the performed assay, it cannot be concluded with certainty how much collagen turnover occurred.

CONCLUSIONS

Cyclically loaded in vitro tendon explants exhibited significant magnitude dependant GAG increases, as has been observed in overuse tendinopathy lesions. Furthermore, significant differences in collagenase content with a concurrent lack of differences in collagen content was observed, suggesting collagen turnover.

REFERENCES

1. Chavira, et al. *Analytical Biochem* **136**, 446-50, 1984.
2. Riley, et al. *Ann Rheum Dis* **53**, 359-366, 1994.
3. Riley, et al. *Ann Rheum Dis* **53**, 367-376, 1994.
4. Kobayashi, et al *J Comp Path* **120**, 403-414, 1999.

ARE THE GAIT KINETICS OF WOMEN AND MEN WITH KNEE OSTEOARTHRITIS DIFFERENT?

Monica Maly[1]mmaly@yorku.ca, Patrick Costigan[2] and Sandra Olney[3]
[1]School of Kinesiology and Health Science, York University, Toronto Canada
[2]School of Physical and Health Education & [3]School of Rehabilitation Therapy, Queen's University, Kingston Canada

INTRODUCTION

Despite evidence that the mechanical pathology of knee osteoarthritis (OA) might be unique in women, such as different patterns of joint deformity[1] and muscle weakness,[2] no studies have compared loading patterns in knee OA between women and men. We aimed to evaluate the sex-specific knee and hip kinetics in medial compartment knee OA during gait.

METHODS

Female Knee OA (FOA): women over age 50 with medial compartment knee OA. Male Knee OA (MOA): men over age 50 with medial compartment knee OA. Pain, stiffness and function were assessed using the Western Ontario McMaster Universities Osteoarthritis Index.

Gait data were collected using the QUESTOR Gait Analysis in Three Dimensions (QGAIT) system, consisting of an Optotrack optoelectric system (Northern Digital, Canada), a force plate (AMTI, USA) and QUESTOR precision radiographs. QGAIT incorporates joint geometry data from standardized radiographs to more accurately transform the surface marker location into the subject-specific joint centre. The radiographs were obtained with subjects standing barefoot on a calibrated turntable, inside a frame fixed relative to the x-ray source. Surface landmarks to be used for gait trials were marked with a lead bead. Anterior-posterior (knee, hip) and lateral radiographs (knee) were obtained. Radiographs were calibrated. Correction vectors were measured from the surface landmarks into the hip and knee joint centre. In addition, medial joint space narrowing (MJSN, mm) was measured. For gait analysis, 6 infrared emitting diodes (IREDs) were used: greater trochanter, lateral femoral condyle, fibular head, lateral malleolus and 2 IREDs on anteriorly projecting probes attached to thigh and shank. Five walking trials were sampled at 100 Hz. Foot contact was determined using trajectory data from the lateral malleolus. Independent t-tests compared FOA and MOA mean age, MJSN, gait speed and WOMAC subscales. A multivariate analysis of covariance (MANCOVA) was performed to compare FOA & MOA gait characteristics, with gait speed and MJSN as covariates.

RESULTS AND DISCUSSION

The FOA (n=32), aged 66.4 ± 9.4 years were younger than the MOA (n=22), aged 71.0 ± 7.1 years. The MJSN was different between the FOA (2.5 ± 1.6mm) and MOA (1.6 ± 1.5mm, $p<0.05$). Table 1 summarizes participant characteristics.

Table 1: Participant Characteristics

	Gait Speed (m/s)	WOMAC-Pain (%)	WOMAC-Stiffness (%)	WOMAC-Function (%)
FOA	1.1 ± 0.38	29.9 ± 19.2	44.1 ± 26.8	37.4 ± 21.1
MOA	1.3 ± 0.26	30.7 ± 18.2	42.2 ± 22.6	29.9 ± 16.7
p	0.03	0.88	0.78	0.17

Tables 2 and 3 summarize knee and hip kinetics during gait.

Table 2: Peak Knee Forces and Moments

Parameter	FOA	MOA
Anterior Force (N/kg)	3.2 ± 0.67	3.2 ± 0.45
Posterior Force (N/kg)	-0.77 ± 0.29	-0.67 ± 0.23
Medial Force (N/kg)	0.20 ± 0.11	0.17 ± 0.08
Lateral Force (N/kg)	-1.3 ± 0.46	-1.6 ± 0.47
Proximal Force (N/kg)	0.92 ± 0.16	0.82 ± 0.07*
Distal Force (N/kg)	-9.0 ± 0.85	-9.1 ± 0.81
Adduction Moment (Nm/kg•m)	0.42 ± 0.16	0.52 ± 0.17
Abduction Moment (Nm/kg•m)	-0.06 ± 0.03	-0.05 ± 0.03
Flexion Moment (Nm/kg•m)	0.29 ± 0.17	0.24 ± 0.12
Extension Moment (Nm/kg•m)	-0.26 ± 0.10	-0.27 ± 0.10
Int Rot Moment (Nm/kg•m)	0.11 ± 0.04	0.16 ± 0.06**
Ext Rot Moment (Nm/kg•m)	-0.01 ± 0.01	-0.01 ± 0.01

*p value < 0.05, **p value < 0.01

Table 3: Peak Hip Forces and Moments

Parameter	FOA	MOA
Anterior Force (N/kg)	1.6 ± 0.68	1.3 ± 0.36
Posterior Force (N/kg)	-2.0 ± 0.58	-2.3 ± 0.77
Medial Force (N/kg)	0.36 ± 0.23	0.46 ± 0.38
Lateral Force (N/kg)	-0.86 ± 0.51	-0.48 ± 0.32*
Proximal Force (N/kg)	1.4 ± 1.3	1.8 ± 1.0
Distal Force (N/kg)	-9.3 ± 1.8	-8.6 ± 1.2
Adduction Moment (Nm/kg•m)	0.70 ± 0.16	0.61 ± 0.16
Abduction Moment (Nm/kg•m)	-0.13 ± 0.07	-0.21 ± 0.14*
Flexion Moment (Nm/kg•m)	0.63 ± 0.29	0.56 ± 0.21
Extension Moment (Nm/kg•m)	-0.76 ± 0.19	-0.97 ± 0.32**
Int Rot Moment (Nm/kg•m)	0.06 ± 0.03	0.05 ± 0.02
Ext Rot Moment (Nm/kg•m)	-0.08 ± 0.40	-0.12 ± 0.07

*p value < 0.05, **p value < 0.01

CONCLUSIONS

The FOA walked more slowly than the MOA. Though women had the same level of impairment as men, noted by WOMAC scores, women were younger and appeared to have less severe medial OA noted by a larger medial joint space. Despite using gait speed and MJSN as covariates, significantly different knee and hip kinetics were noted between women and men, suggesting that the sex-specific differences in the mechanical pathology of knee OA should be studied further. However, we acknowledge that a larger sample size will be necessary to confirm these sex-related differences in knee OA gait.

REFERENCES

[1]Terauchi, MK. et al (1998). *J Bone Joint Surg* **80B**, 432-436.
[2]Fitzgerald, G. et al (2004). *Arthritis Care Res* **51**, 40-48.

ACKNOWLEDGEMENTS

CIHR Grant# 99034, NSERC, Toronto Rehab Institute.

DYNAMIC STABILITY AND ENERGY EFFICIENCY DURING DIFFERENT SELF-SELECTED WALKING SPEEDS

Heng-Ju Lee and Li-Shan Chou
Motion Analysis Laboratory, Department of Human Physiology, University of Oregon, Eugene, OR
Contact: Chou@uoregon.edu

INTRODUCTION

It is well documented that a high percentage of falls in older adults occur during walking [1]. Numerous studies have shown relations between changes in gait and risk of falling. Walking speed is generally regarded as a control parameter for human gait transitions. Walking with a preferred gait speed is thought to demonstrate a stable phase relationship and minimum energy expenditure [2]. Motion of the whole body center of mass (CoM) has been used to indicate the mechanical energy expenditure [3] and dynamic stability during gait [4]. Out-of-phase oscillation between kinetic (E_k) and potential energy (E_p) of the CoM allows energy to be exchanged from one to another [3]. The timing of exchanges between E_k and E_p at different walking speeds can provide us a better understanding of energy cost in the elderly. It has been found that CoM motion in the medio-lateral (M/L) direction during gait may have particular importance for balance control [4,5]. However, age related differences in the M/L dynamic stability during varied walking speeds are still unknown. Therefore, the purpose of this study was to quantify the relationship between dynamic stability and energy efficiency in three different walking speeds in young and elderly adults.

METHODS

Thirteen healthy elderly adults without neurological or musculoskeletal impairment (6 males and 7 females; 74.7± 5.0 years; 165.4 ± 8.9 cm; 69.4± 11.8 kg) and eighteen healthy young adult subjects (9 male and 9 female; 25.2 ± 4.2 years; 172.6 ± 7.7 cm; 74.4 ± 10.5 kg) were recruited for this study. Subjects were asked to walk with barefoot over level ground along a 10-m walkway. The first condition was their preferred walking speed, and then a distinctly self-selected faster speed followed by a distinctly slower gait.

Whole body motion analysis was performed with a 6-camera ExpertVision™ system (Motion Analysis Corp., Santa Rosa, CA). Three-dimensional marker trajectory data were collected at 60 Hz. Twenty-seven reflective markers were placed on bony landmarks of each subject. Whole body CoM position data was calculated as the weighted sum of 13 segments representing the whole body. Linear velocities of the CoM were calculated with the GCVSPL algorithm. The center of pressure (CoP) position was calculated from the ground reaction forces/moments collected from two force platforms (AMTI, Watertown, MA). Instantaneous sway angles in the sagittal and frontal planes were defined as the angle between the inverted pendulum, defined by the CoP and CoM, and the vertical line (Fig.1). Timing offsets between E_k and E_p were calculated during single stance phase. Effects of subject group and walking speed on CoM sway angles and energy exchange times were assessed using a two-factor ANOVA with repeated measures of walking speeds.

RESULTS AND DISCUSSION

Elderly adults walked significantly slower than young adults for all 3 conditions (preferred, fast, slow: 1.2/ 1.4 m/s, 1.5/ 1.7 m/s, and 0.9/ 1.2 m/s; $p<0.001$). Also, significant group and walking speed effects were found in the max. A/P sway angle and stride length. As the walking speed increased, stride length and max. A/P sway angle increased in both groups. Elderly adults showed a more conservative strategy to control body movement in the A/P direction using a shorter stride length ti maintain a smaller A/P sway angle than young adults. This finding was similar to other studies [6,7]. Neither significant walking speed effects nor significant group differences were found in the max. M/L CoM sway angle and step width. However, timing offsets between E_k and E_p of elderly adults were found to be significantly greater than that of young adults during self selected slower walking speed (81.2 ms vs.56.8 ms; $p=0.038$) (Fig 2).

These findings show that in both groups, decreasing walking speed does not cause greater M/L body movements during gait. The M/L sway angle defined in this study might be a walking speed-independent indicator for dynamic stability. Greater timing offsets between E_k and E_p of elderly adults during slower walking indicate less efficient in the energy transfer. Inefficient energy transfer during gait would require additional energy to be provided from lower extremity muscles [8,9]. Elderly adults walk with a slower speed may require excessive muscle co-contraction or an increase in muscle tone to compensate the inefficient gait. However, this extra energy consumption might be necessary to avoid any dynamic instability.

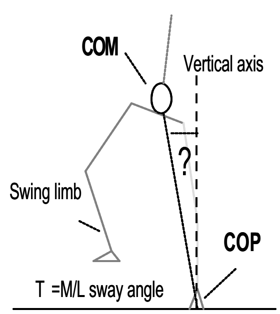

Figure 1: M/L sway angles defined by the CoP and CoM

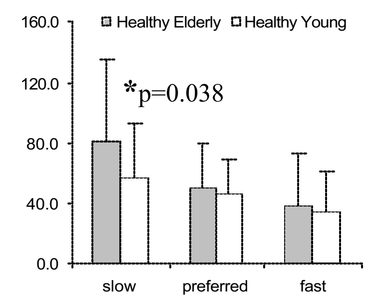

Figure 2: The energy exchange time (msec) in three different walking speeds

REFERENCES

1. Overstall PJ, et al., *Br. Med. J*,1: 261-264, 1977.
2. Diedrich & Warren, *Human perception and performance*, 21:183-202, 1995
3. Cavagna et al., *AM. J. Physiol*, 233:R243-R261, 1977.
4. Chou L-S, et al., *Gait and Posture*, 13:17-26, 2001.
5. Chou L-S, et al., *Gait and Posture*, 18: 125-133, 2003.
6. Tesio L, et al., *Clin Biomech*, 13:77-82.
7. Ostrosky, K.M., et al., *Physical Therapy*, 74: 637-46, 1994.
8. Tucker, et al., *Gait and Posture*, 8: 117-123, 1998.
9. Lamontagne et al., *Arch Phys Med Rehabil*. 81:351-358, 2000.

ACKNOWLEDGEMENT

This study was supported by the NIH (AG 022204-01; HD 042039-01A1).

COMPARISON OF TWO ANKLE ELECTROGONIOMETERS AND MOTION ANALYSIS

Sujani N. Agraharasamakulam, Shaw Bronner and Sheyi Ojofeitimi
ADAM Center, Long Island University, Brooklyn, NY;
Email: an_sujani@yahoo.com, web: www.brooklyn.liu.edu/bbut04/adamcenter/index.html

INTRODUCTION

Flexible electrogoniometers (EG) have been used for gait and sports-specific lower extremity kinematic analysis. The commonly used EG sensor for the ankle is placed parallel to the Achilles tendon (Apara) (SG110, Biometrics, Ltd). Recently, a new ankle EG sensor was developed for placement at the lateral malleolus (Aperp) (SG110/A, Biometrics, Ltd).

In order to test the boundaries of the EG, we selected dancers for our study since they frequently work at extremes of joint motion. The purpose of this study was to examine the concurrent validity of the "new" ankle sensor (Aperp) to Apara EG as well as to a motion analysis (MA) system (the current gold standard), while measuring common dance movements in the sagittal plane.

METHODS

Seventeen dancers (10 female and 7 male), mean age 20.76 ±2.46 years (age range 18 – 27 years), with an average of 10 years of dance training were recruited for this study. The two flexible strain-gauge EGs were placed at the right ankle of each subject, connected to a portable data-logger, and sampled at 100 Hz. Concurrent recordings were made with a Vicon 5-camera motion capture system (MA), sampled at 120 Hz, in order to verify sagittal plane movements recorded by the EGs. Each dancer performed four repetitions of 10 selected dance movements. The EG data were filtered at 5.5 Hz using a 4th order, low pass, zero lag Butterworth filter. The MA data were filtered using an FIR filter and resampled at 100 Hz. Multimodal peak angular displacement data were scored in a custom LabVIEW program.

Concurrent validity intraclass correlation coefficients (ICC) (3, k) comparing: a) the two EGs (Aperp v. Apara), and b) each EG to MA (EG v. MA) were calculated from 2-way ANOVAs ($p < 0.05$), for combined and individual movement conditions (SPSS 13.0).

RESULTS AND DISCUSSION

ICCs comparing the two EG devices were very high for both combined ($r = 0.937$) and individual conditions (range r = 0.842 – 0.971) (Table 1). ICCs comparing each EG device to MA were also high for combined ($r = 0.954$ and 0.958) and individual conditions (range r = 0.829 – 0.992).

Previous analyses of the EGs to a protractor have established a high level of accuracy in measurement, with the mean absolute residual error less than 1.0º [1]. Analysis of relative reliability during repeated measures on the same and following day are currently underway.

When used by the same observer, EGs have demonstrated good reliability for repeated measurement of ankle dorsi-plantarflexion [2]. However, these investigations focused on mid-range movements. Electrogoniometer measurement error increases with extreme positions [3]. Preliminary laboratory MA measurement of common dance movements reported non-weightbearing and weightbearing angular displacements at the ankle ranging from 41.4º(±2.3) dorsiflexion to 55.4º(±2.5) plantar flexion [4]. Because motion greatly exceeds those seen in gait analysis, the selection of EGs to measure dance movement required validation.

Subjects found the new ankle sensor (Aperp) to be more comfortable. Apara sensor breakage was frequent due to the stresses placed upon it by extreme plantar flexion. The Aperp sensor did not break during the course of this study.

CONCLUSIONS

Reliability and validity of EGs to measure basic dance movements in the laboratory is a crucial precursor to workplace exposure-risk analyses. Both ankle EGs were highly correlated to MA and to each other, making them acceptable for use in this population. The greater comfort and durability of the new Aperp sensor makes it appealing for worksite use.

REFERENCES

1. Rowe PJ, et al. *Physiotherapy*, **87**, 479-488, 2001.
2. Rome K, et al. *Foot and Ankle International*, **17**, 28-32, 1996.
3. Hansson GA, et al. *Scandinavian Journal of Work, Environment & Health*, **27**, 30-40, 2001.
4. Ojofeitimi S, et al. *J Orthopaedic and Sports Physical Therapy*, **34**, A-19, 2004.

Table 1: Comparison of ankle sensors and MA: ICC and degrees of freedom (DOF).

Selected Conditions	EGAperp v. EGApara	EGApara v. MA	EGAperp v. MA
Combined (1 – 10)	0.937 (297, 1)	0.954 (309, 1)	0.958 (296, 1)
Grand plié	0.918 (22, 1)	0.960 (25, 1)	0.933 (22, 1)
Passé	0.928 (25, 1)	0.939 (25, 1)	0.992 (25, 1)
Developpé side	0.911 (34, 1)	0.893 (35, 1)	0.878 (34, 1)
Battement arabesque	0.921 (23, 1)	0.937 (23, 1)	0.989 (24, 1)
Jump	0.971 (25, 1)	0.970 (25, 1)	0.978 (25, 1)

HEAD ACCELERATION IS LESS THAN 10 PERCENT OF HELMET ACCELERATION DURING A FOOTBALL IMPACT

Sarah Manoogian, David McNeely, Mike Goforth, Gunnar Brolinson and Stefan Duma
Virginia Tech – Wake Forest, Center for Injury Biomechanics; Email: manoogsj@vt.edu, Web: www.CIB.vt.edu

INTRODUCTION

Sports-related concussions constitute 20 percent of brain injuries each year in the United States.[1] Concussion research has included a variety of instrumentation and techniques to measure head accelerations. These include headbands, helmet attachments, and video reconstructions. Most recently, the Head Impact Telemetry (HIT) System (Simbex, Lebanon, NH), a wireless system that provides real-time data from impacts, is used to measure *in-situ* head accelerations in collegiate football.[2] The purpose of this study is to measure linear head acceleration of a Hybrid III dummy using both accelerometers mounted at the center of gravity of the HIII head and the in-helmet HIT System. By comparing these two measured head accelerations and the helmet acceleration during a pendulum impact, it is shown that the response of the head and the helmet vary greatly and the in-helmet system matches the head and not helmet acceleration.

METHODS

A study of 50 helmet to helmet tests was performed with the impacting helmet mounted on a Hybrid III headform and neck (Figure 1). This assembly was mounted on a pendulum, 20 kg total mass, that impacted at a range of velocities from 3 m/s to 6 m/s. The impacted helmet was mounted to a HIII headform and neck and then to a full HIII body. Instrumentation included an accelerometer mounted directly to the inside of helmet at the location of contact and two measures of head cg acceleration, a triaxial accelerometer cube in the HIII head and the HIT System. Four locations on the struck helmet were tested by rotating the full HIII body while keeping the pendulum configuration the same.

Figure 1: The impacted helmet was mounted to a HIII headform and neck and then to a full HIII body.

RESULTS AND DISCUSSION

These tests illustrated that the helmet acceleration in response to impact varies from the head cg acceleration in amplitude and the time to peak. Overall the peak acceleration for the helmet at the point of contact was 16.6 (+/- 3.2) times greater than the head cg peak linear acceleration for that impact. For example, Figure 2 illustrates that for one impact, the helmet acceleration was approximately 500 g compared the actual head cg of 32 g measured by the dummy. Moreover, the HIT System measured nearly identical to the dummy peak value and curve shape as the HIT System recorded a peak 33 g for the same impact. Additionally, the time from contact to peak head acceleration, 5.82ms (+/-.78ms), is longer than time to peak helmet acceleration, .42ms (+/-.17 ms). The peak magnitude, time to peak, and waveform shape of the HIT System measure match the in head acceleration values and not the helmet shell acceleration values.

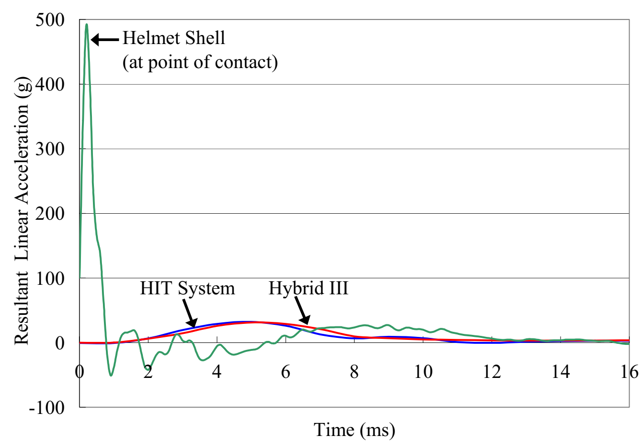

Figure 2: For the same impact, the helmet acceleration was approximately 500 g compared to the Hybrid III cg measure of 32 g and the HIT System measure of 33 g.

CONCLUSIONS

In summary, both the HIT System and the accelerometers in the HIII head measure a similar head acceleration response which varies greatly in magnitude and shape from the helmet response. In 2001 Lewis did a study that proved that wearing a helmet reduced the peak acceleration of the head by approximately a third since the helmet would absorb part of the impact's energy.[3] Therefore this paper presents consistent findings that the impact response of the head cg is much less than that of the helmet.

REFERENCES

1. McCrea, M; et al. JAMA 2003; 290:2556-2563.
2. Duma, SM; et al. Clinical Journal of Sport Medicine 2005; 15(1):3-8.
3. Lewis, LM; et al. Academic Emergency Medicine 2001; 8(6):604-609.

ACKNOWLEDGEMENTS

Simbex, Lebanon, NH

THE VARIABILITY OF DYNAMIC AND SPATIO-TEMPORAL PARAMETERS OF THE RUNNING STRIDE

[1]Marina Gouvali and [2]John H. Challis
[1]Department of Sports Medicine and Exercise Biology, University of Athens, Greece; email: mgouvali@phed.uoa.gr
[2]Biomechanics Laboratory, The Pennsylvania State University, USA; email: jhc10@psu.edu

INTRODUCTION

Variability associated with individual running performance is apparent when an effort has to be repeated, even though conditions remain the same. Variability seems to increase when time between sessions increases [1] suggesting higher biological rather than methodological variability. Previous studies examining day-to-day variability have only measured a limited number of steps, for example 5 or 10 [2], which may not adequately sample the variability which exists in one day. The purpose of this study was to examine the variability of dynamic and spatio-temporal parameters of the running stride between sessions conducted on different days for 90+ steps per day.

METHODS

Seven females and six males voluntarily participated in the study (Age F: 25.8±3.3 yrs, M: 26.9±3.6 yrs, Height F: 167.3±2.3 cm, M: 184.8±5.3 cm, Mass F: 62.9±6.7 kg, M: 83.3±10.7 kg). All subjects provided informed consent for all procedures, which were approved by the Institutional Review Board.

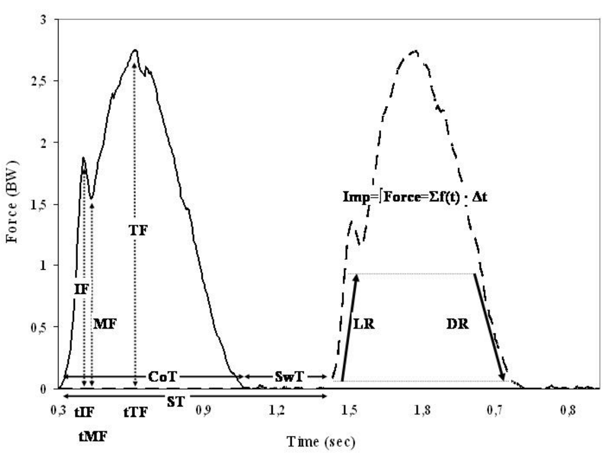

Figure 1: Key variables selected for analysis from a force-time curve.

Vertical ground reaction forces (GRF) and temporal parameters were collected with the aid of a Gaitway Instrumented Treadmill (Kistler Instrument Corporation) with two built-in force plates and were further analyzed with Gaitway Software 1.0 and MATLAB 6.5. Data were sampled at 500 Hz and filtered with a Butterworth filter (2nd order, cutoff frequency 30Hz). They were normalized for force by dividing by body weight. The protocol included 2 sessions separated by a day. Each session consisted of 4 running trials (5 min each) at 4 different speeds (F: 2, 3, 4 m/s, preferred speed, M: 3, 4, 5 m/s, preferred speed). GRF and spatio-temporal parameters for both legs were collected between the 4th and 5th min (~100 strides). The following variables were selected for analysis: *IF*: impact force (BW), *tIF*: time of IF (s), *MF*: minimum force (BW), *tMF*: time of MF (s), *TF*: thrust force (BW), *tTF*: time of TF (s), *Imp*: impulse (BW·s), *LR*: loading rate (BW·s^{-1}), *DR*: decay rate (BW·s^{-1}), *ST*: step time (s), *CoT*: contact time (s), *SwT*: swing time (s), *SL*: step length (m), *SF*: step frequency (steps·s^{-1}) (Figure 1).

Assessment of intra-day variability was evaluated using the coefficient of variation for the whole curve (*CoV*), as well as for each parameter (*CV*). Inter-day effect was tested by multivariate analysis of variance with repeated measures ($p<0.05$).

RESULTS

The coefficient of variability for the whole curve ranged between 4.5-6.0%. Variability between consecutive strides was higher when calculated separately for each parameter (2-20%) and was the least for *ST* and *SF*. Regarding the force variables, the force acting to propel the body (*TF*) was less variable (2.5%) than the force acting to absorb the impact (*IF*) (9.7%).

Table 1: Means and CV of the GRF and temporal parameters. (*$p<0.05$)

Day	1		2	
	Mean	CV	Mean	CV
IF	1.73	10.0	1.73	9.2
tIF	0.036	16.7	0.035	16.1
MF	1.49	11.4	1.46	10.6
tMF	0.047	13.3	0.047	12.7
TF*	2.47	2.6	2.44	2.4
tTF	0.107	7.0	0.106	6.9
Imp*	0.36	1.7	0.35	1.4
LR	63.04	12.1	66.13	12.5
DR	4.58	2.6	4.59	2.2
ST	0.366	3.6	0.363	3.2
CoT	0.237	7.8	0.238	7.7
SwT	0.129	18.4	0.125	16.9
SL	1.249	20.1	1.242	19.8
SF	2.75	2.7	2.77	2.4

The results produced no significant differences for most GRF and temporal means and *CV* between sessions separated by a day; significant, but small, differences existed only for *TF* and *Imp* (Table 1).

CONCLUSIONS

Variability in the force-time pattern between consecutive strides is high and dependent on the nature of the variable, indicating that the number of trials to be analyzed should be determined according to which parameters are of interest. Running performance can be replicated without significant systematic error after one day. In conclusion, one session can be considered as satisfactory for analyzing the dynamic and temporal characteristics of the running stride.

REFERENCES

1. DeVita P, et al. *Hum Mov Sci* **7**, 73-85, 1988.
2. Diss CE, et al. *Gait and Posture* **14**, 98-103, 2001.

RELATIONSHIP BETWEEN SOFT TISSUE DEFORMATION AND APPLIED PRESSURE ALONG THE SECOND RAY OF THE PLANTAR NEUROPATHIC FOOT

[1]Donovan J. Lott, [2]Paul K. Commean, [2]Kirk E. Smith, [1]Michael J. Mueller
[1]Program in Physical Therapy and [2]Mallinckrodt Institute of Radiology, Washington University School of Medicine, St. Louis, MO
E-mail: djlott@artsci.wustl.edu

INTRODUCTION

Neuropathic foot ulcers are one of the most common lower extremity complications for people with diabetes mellitus (DM) and peripheral neuropathy (PN). High plantar pressures commonly seen in people with DM and PN compress and damage soft tissue of the foot contributing to the occurrence of these ulcers. The aim of this study was to determine the relationship between soft tissue deformation and applied pressure along the second ray of feet of individuals with DM, PN, and a history of a plantar ulcer.

METHODS

Ten subjects (6 males/4 females, mean age 58.0 $\pm$ 10.3 years, mean BMI 32.6 $\pm$ 9.5 kg/m^2) with DM (2 Type 1/8 Type 2, mean duration of DM 16.5 $\pm$ 10.0 years), PN, and a history of a plantar ulcer participated.

Plantar pressure data were recorded using the FSCAN system (Tekscan, South Boston, MA, USA) during spiral X-ray computed tomography (SXCT). SXCT scans of the subjects' feet were performed as described in detail elsewhere [1]. The subject applied a load of $\leq$ 45 N (10 lbs.) for the first "preload" scan. For the second "loaded" scan, the subject applied a load of approximately 50% of his/her body weight. The alignment of the anatomical data from the SXCT scans with the pressure data from the FSCAN system was performed as described in detail elsewhere [2]. The second ray was determined in a similar manner by aligning the pressure data with the second metatarsal and second proximal phalanx. All testing was done with the subjects barefoot.

Soft tissue thickness was determined by measuring the distance from the most inferior aspect of the bone to the surface of the skin. Soft tissue deformation (STD) (strain) was defined as: ({[soft tissue thickness from preload scan]–[soft tissue thickness from loaded scan]} / {soft tissue thickness from preload scan})*100. Soft tissue thickness measurements were taken from 11 sensor pixels (5.08 mm spacing) proximal to the metatarsal head to five sensor pixels distal to the metatarsal head (for a total of 17 measurements per condition over 86.36 mm [3.4 inches]).

A Pearson correlation coefficient was performed for statistical analyses to determine the relationship between the STD and the applied pressure along the second ray.

RESULTS AND DISCUSSION

Figure 1 shows the average STD and the pressure difference between the two scans along the second ray. At the location of the second metatarsal head (MTH), the mean STD was 19.5 $\pm$ 6.1%, and the mean pressure difference was 287.3 $\pm$ 145.5 kPa. The mean correlation coefficient for the ten subjects demonstrates a strong relationship between soft tissue deformation and applied pressure along the second ray (r = 0.93 for the 17 points of data).

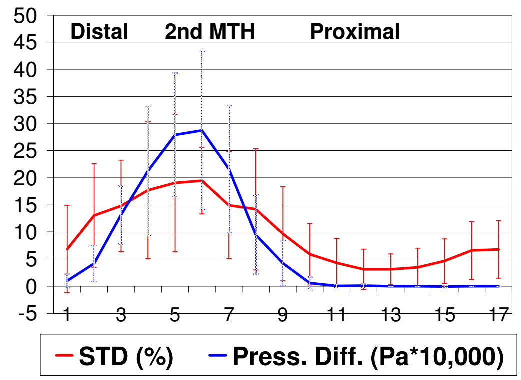

Figure 1: Mean Soft Tissue Deformation (in percentage) and Pressure Difference between loaded and preload conditions (in Pa x 10^4) along the second ray.

SUMMARY

This is the first study that has examined STD at several points along a ray of the plantar foot in patients with DM and PN. Our data suggest that the deformation that occurs along the second ray in patients with DM and PN is strongly correlated with the applied pressure at these same points. Our results at the MTH are generally consistent with those of others. Cavanagh found an average STD of 45.7% at the second MTH with a load of full body weight [3] while we found an average STD of 19.5% with a load of approximately 50% body weight. Future research can build upon these findings by analyzing how the use of footwear and orthotic devices affect the pressure distribution and STD along the second ray of the plantar foot for optimal footwear prescription for people with DM and PN.

REFERENCES

1. Commean P.K. et al. (2002). *Arch. Phys. Med. Rehabil.,* **83,** 497-505.
2. Hastings M.K. et al. (2003). *Clin. Biomech.,* **18,** 877-882.
3. Cavanagh PR. (1999). *J. Biomech.* **32,** 623-628.

ACKNOWEDGEMENTS

Funding from NCMRR, NIH, RO1 HD 36895 and a PODS 1 Award (DJL) from the Foundation for Physical Therapy of the American Physical Therapy Association.

AN IMPROVED SURROGATE METHOD FOR DETECTING THE PRESENCE OF CHAOS IN GAIT

David Miller, Nicholas Stergiou and Max J. Kurz
HPER Biomechanics Laboratory, University of Nebraska at Omaha, Omaha, NE
E-mail: djmiller@mail.unomaha.edu, web: http://www.unocoe.unomaha.edu/hper/bio/home.htm

INTRODUCTION

Surrogate analysis is essential to prevent the misdiagnoses of a purely random signal as deterministic chaos [1]. Several surrogate algorithms have been presented that attempt to destroy the chaotic features of a time series while maintaining the essential linear features. If the original time series is statistically different from the surrogate then, the fluctuations in the time series have a deterministic structure. Alternatively, a failure to find significant differences between the surrogate time series and the original time series indicates that the fluctuations are merely random noise. Recently, the surrogate algorithm of Theiler et al. [3] has been applied to support the notion that fluctuations in human gait have a deterministic pattern [1]. However, inspection of the generated surrogate indicates that much of the essential geometric features of the gait time series are destroyed (Figure 1A and C). In this case, it is questionable if this surrogate can be used to effectively discern the difference between chaotic fluctuations and random noise in a gait time series. Recently, Small and Tse [2] have overcome this difficulty with a pseudoperiodic surrogate (PPS) algorithm that preserves the inherent periodic components of the time series while destroying the subtle nonlinear structure. Although this algorithm appears promising, it has not been tested in human gait patterns. Here we show that the PPS algorithm provides a more robust verification of the presence of chaos in gait by preserving the essential features of the time series.

METHODS

Six subjects walked at a self-selected pace on a treadmill for two minutes while the sagittal knee angles were captured with a 3D optical capture system. Surrogates of the respective time series were generated based on the PPS [2] and Theiler's algorithms [3]. Theiler's algorithm reorganizes the phases of the complex conjugate pairs in the frequency domain such that surrogate contains linearly filtered independent and identically distributed noise. The PPS algorithm generates a surrogate that follows the same vector field as the original time series, but is contaminated with dynamic noise. The PPS algorithm requires that the user define the embedding dimension, the time lag, and the noise radius. The embedding dimension and time lag were calculated with the Tools from Dynamics Software (Applied Chaos, LLC). Noise radius (?) was chosen such that the fine intercycle dynamics were removed, but the intracycle dynamics were preserved. If ? is too small, then the surrogate and the original time series are identical. If ? is too large, then the surrogate is a series of uncorrelated random noise. We selected ? to be the value that maximizes the expected number of short segments (length 2) to be the same between the surrogate and the original time series [2]. The largest Lyapunov exponents of the respective time series were calculated to test the null hypothesis that the surrogate and the original time series had the same dynamics.

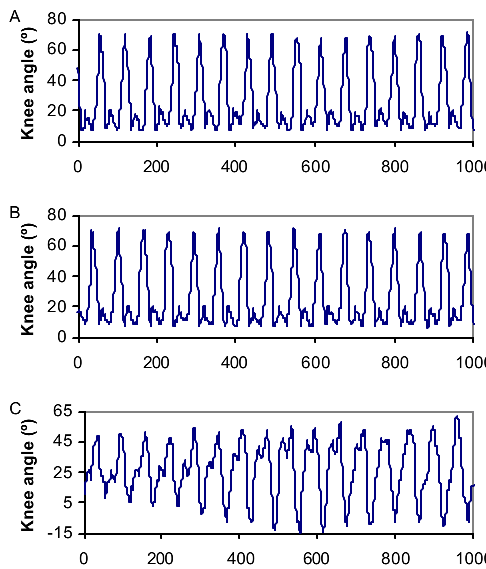

Figure 1: Exemplar original knee angle time series (A), PPS (B), and Theiler's surrogate(C).

RESULTS AND DISCUSSION

Significant differences ($p<0.05$) were found between the original and the respective surrogate time series. Both surrogate tests indicated that fluctuations in the knee time series had a deterministic structure that was significantly different from random noise. However, inspection of Figures 1A and C verifies that Theiler's algorithm alters the original geometric structure of the time series. Hence, it is trivial to find a significant difference between the surrogate generated by Theiler's algorithm and the original time series. It appears that Theiler's algorithm is of limited use for verifying the presence of chaos in gait patterns with an underling periodic structure. Inspection of Figure 1A and B indicates that the PPS algorithm maintains the essential geometric structure of the gait time series. In fact, the surrogate and the original gait time series appear virtually indistinguishable. These results support the notion that the PPS algorithm is more suitable for detecting the presence of subtle chaotic fluctuations that appear in gait. The PPS algorithm should be adopted in future investigations to rigorously verify that fluctuations in gait patterns are in fact chaotic and not random noise superimposed on top of the time series.

ACKNOWLEDGMENTS

This work is supported by the Nebraska Research Initiative.

REFERENCES

1. Stergiou N *et al.* (2004). *Innovative Analysis of Human Movement.* Human Kinetics: Champaign, IL.
2. Small M & Tse CK. *Physica D* **164**, 187-201, 2002.
3. Theiler J *et al. Physica D* **58**, 77-94, 1992.

VALGUS LOADING CAUSES INCREASED *IN VITRO* ACL STRAIN IN SIMULATED JUMP LANDING

[1, 2] Thomas J. Withrow, [1] Laura J. Huston, [1] Edward M .Wojtys, and [2]James A. Ashton-Miller
[1]University of Michigan – Medsport and Department of Orthopedic surgery;
[2]University of Michigan – Department of Biomedical Engineering; email: withrow@umich.edu.

INTRODUCTION

Anterior cruciate ligament (ACL) injury has been associated with abrupt deceleration while running, cutting or landing[3]. Videotape analyses of these injuries has implicated valgus configuration of the lower extremity as a potential injury risk factor.[5] The previous experimental studies that have examined this injury mechanism have done so using sub-physiologic loading magnitudes and rates[2,4]. In this study, we investigated the effect of valgus loading on ACL strain response in a dynamic loading configuration that better simulates landing from a jump with pre-activated knee muscles. We tested the null hypothesis that the addition of a valgus knee impact moment would not significantly increase peak relative strain in the anteromedial ACL bundle compared with a flexion impact moment loading of similar magnitude.

METHODS

Ten fresh cadaveric limbs were studied [mean (SD): 70.3 (15.4) years; 4 males; 6 females; ages 45 to 89]. Specimens were cut 15 cm proximal and distal to the knee joint and potted using polymethyl-methacrylate. A testing apparatus was constructed to simulate the position of a single extremity as it strikes the ground while landing from a jump or during a run/stop maneuver (Figure 1). Pre-impact muscle precontractions of the quadriceps, medial and lateral hamstrings, and medial and lateral gastrocnemius muscle-equivalents were achieved by pretensioning 7 kN/mm springs to maintain the initial angle of 25^o knee flexion prior to impact. The impact force magnitude and its lever arm about the knee joint could be preset. The impact loading direction was standardized to either apply a flexion moment in the sagittal plane ("Flexion only" trial) or by additionally inclining the entire construct into 15 degrees of abduction a "Flexion + Valgus" moment trial.

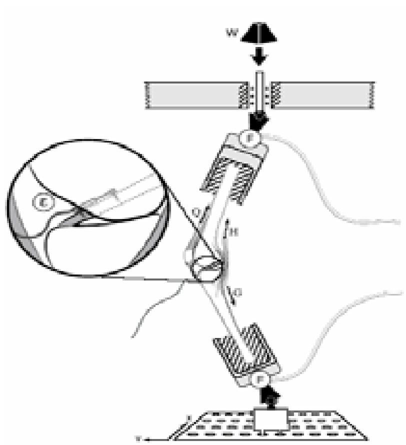

Figure 1. *Schematic of test set-up*

A 150 N weight was released from a fixed height to strike an impact rod in series with the proximal femur. This exerted an impulsive compressive force and flexion moment resulting in an increase in knee flexion angle. Two 3-axis load cells ("F") measured the 3-D forces and moments delivered to the knee construct, as well as the 3-D reaction forces and moments. A 3-mm DVRT (Microstrain, Burlington, VT) mounted on the ACL anteromedial bundle recorded its relative strain[1]. Impact forces, quadriceps muscle force, and ACL strain data were recorded at 2 kHz using a 16-bit A/D board, while tibiofemoral kinematics were tracked at 400 Hz using an Optotrak 3020 system to the nearest mm and degree. A repeated measures ('ABA') experimental design was run consisting of 10 'Flexion only', 10 'Valgus + Flexion', and 10 'Flexion only' trials were run. The last five trials under each condition were analyzed. The peak relative strains for individual specimens were normalized by dividing them by the mean peak relative ACL strain under both 'Flexion only' conditions. A paired Wilcoxon signed rank test was used to test the null hypothesis with a $p<0.05$ significance level.

RESULTS AND DISCUSSION

The mean (SD) peak impact force rose to 1,670 (390) N over a 30 ms time course, thus confirming the physiologic nature of the test. The impact forces did not differ between the 'Valgus + Flexion' and 'Flexion only' tests [1,620 (390) vs. 1,790 (380) N, respectively]. The mean (SD) relative strain during the 'Valgus + Flexion' loading was 4.3 (2.7)%, whereas the corresponding ACL strain measured 3.5 (2.8)% during the 'Flexion only' moment impact. Thus, we rejected the null hypothesis because the peak normalized relative ACL strain in the Valgus + Flexion' configuration was significantly higher than that in both the initial 'Flexion only' configuration (p=0.04) and final 'Flexion only' (p=0.02) conditions. Mean (SD) peak normalized ACL strain when the joint was loaded in 'Valgus + Flexion' was 1.28 (0.38) [non-dimensional units] across all specimens, while the mean (SD) ACL strain when loaded by a 'Flexion only' impact moment was 1.00 (0.32). The pretensioned muscle-equivalent springs gave an immediate rise in tension upon stretch, similar to a lengthening contraction condition *in vivo*. Any test order effect that may have been present was minimal because there was no significant difference in the peak strains measured under the two 'Flexion only' conditions.

CONCLUSIONS

In the slightly flexed knee, preloaded by quadriceps, hamstring and gastrocnemius muscle forces, relative ACL strain was significantly higher under a valgus + flexion impact loading than under a flexion-only impact loading.

REFERENCES

1. Beynnon BD, Fleming BC, J Biomech 31:519-25, 1998
2. Berns GS et al, *JOR* 10: 167-76, 1992.
3. Griffin YL et al, *JAAOS* 8: 141-150, 2000.
4. Markolf KL et al, *JOR* 13: 930-5, 1995.
5. Olsen OE et al, AJSM 32: 1002-12, 2004.

ACKNOWLEDGEMENTS

We gratefully acknowledge the NFL Charities Foundation for funding support.

LACK OF HAMSTRING TENSION CAUSES INCREASED ACL STRAIN IN A SIMULATED JUMP LANDING

[1, 2] Thomas J. Withrow, [1] Laura J. Huston, [1] Edward M .Wojtys, and [2]James A. Ashton-Miller
[1]University of Michigan – Medsport and Department of Orthopedic surgery;
[2]University of Michigan – Department of Biomedical Engineering; email: withrow@umich.edu.

INTRODUCTION

An anterior cruciate ligament (ACL) injury can significantly affect short and long-term physical activity and health in an athlete[4]. ACL injuries have been associated with abrupt deceleration while running, pivoting, awkward landings, and “out of control” play[3]. A factor in these injuries may be the state of lower extremity muscle recruitment at the time of impact. For example, for a given quadriceps activity, a decrease in hamstring muscle activity has long been viewed as hazardous for the ACL. Previous experimental studies have demonstrated the protective effects of hamstring muscle force, but only at low and non-physiologic loading magnitudes and rates[1,2]. In these experiments we investigated ACL strain under more physiological loading levels associated with landing a jump with precontracted quadriceps and gastrocnemius muscles. We tested the (null) hypothesis that, compared with the presence of a hamstring force, lack of hamstring forces would not affect the peak strain measured in the anteromedial bundle of the ACL

METHODS

Ten fresh cadaveric limbs were studied [mean (SD): 74 (17) years; 5 males; 5 females; age 45 to 100 years]. Specimens were divided 15 cm proximal and distal to the knee joint and potted using polymethylmethacrylate. A testing apparatus was constructed to simulate the position of a single extremity as it strikes the ground while landing on one leg from a jump or run/stop maneuver. Pre-impact muscle preloads of the quadriceps, medial and lateral hamstrings, and medial and lateral gastrocnemius muscle-equivalents, the initial angle of knee flexion, and impact force magnitude and its direction about the knee joint could all be preset. The stiffness of each muscle-equivalent was 7 kN/mm. In all trials, an initial knee flexion angle of 25 degrees was used and the impact loading direction was standardized.

A 150 N weight was released from a fixed height to strike an impact rod in series with the proximal femur. This exerted an impulsive compressive force (peak < 30 ms) resulting in an increase in knee flexion angle. Two 3-axis load cells measured the 3-D forces and moments delivered to the construct. A 3 mm DVRT (Microstrain, Burlington, VT) was mounted on the ACL anteromedial bundle to record its relative strain[1]. Impact forces, quadriceps muscle force, and ACL strain data were recorded at 2 kHz using a 16-bit A/D board, while tibiofemoral kinematics were tracked using an Optotrak 3020 system (Northern Digital, Inc, Waterloo, Canada) and recorded at 400 Hz to the nearest mm and degree. Using a repeated measures trial design, three sets of ten trials were run with (“With Hamstring 1”), without (“No Hamstring”) and with hamstring (“With Hamstring 2”) pre-tension, in that order. The last five trials of each condition were then analyzed for each specimen. The peak relative strains for individual specimens are then normalized by dividing them by the mean peak relative ACL strain in the ‘W/ Hamstring’ tests. A non-parametric paired Wilcoxon signed rank test was used to test the null hypothesis with $p<0.05$ being considered significant.

RESULTS AND DISCUSSION

The mean (SD) peak impact force was 1,460 (260) N. The impact forces were not significantly different in the ‘No Hamstring’ and ‘With Hamstring’ tests [1,410 (210) vs. 1,480 (280) N, respectively]. The mean peak (SD) relative strain in the ‘No Hamstring’ conditions was 3.1 (1.3)%, whereas the corresponding data was 2.5 (0.8)% in the ‘With Hamstring’ condition. There was no order effect in that there was no significant difference in peak relative ACL strain between the two ‘With Hamstring’ conditions.

Most importantly, the null hypothesis was rejected in that the peak normalized relative ACL strain in ‘No Hamstring’ condition was significantly higher than the corresponding ACL strain in the ‘With Hamstring 1’ condition ($p=0.004$) or ‘With Hamstring 2’ condition ($p=0.022$). These results were obtained with loading levels exceeding bodyweight and impact loading rates typical of landing from a jump. Our results under these more physiological loadings corroborate earlier results at low loads and quasistatic loading rates[1,2].

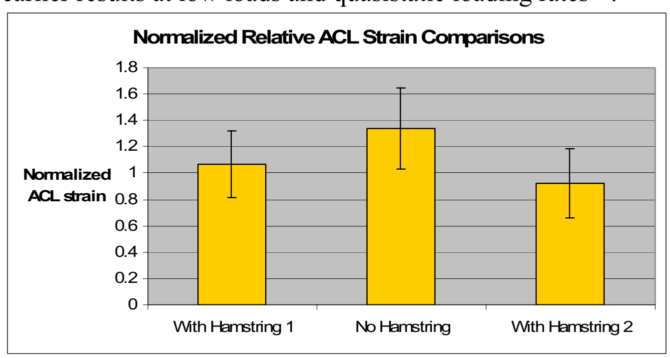

Figure 1: Comparison of the normalized mean (SD, denoted by vertical bars) peak relative ACL strain in the two test conditions.

CONCLUSIONS

At physiological loading levels, decreased hamstring tension (and stiffness) led to increased peak relative ACL strain when simulating landing on a flexed knee with precontracted quadriceps and gastrocnemius muscle-equivalents. Lack of an order effect precludes this result having been due to the sequence of testing or cumulative soft tissue damage.

REFERENCES

1. Beynnon BD, Fleming BC, J Biomech 31:519-25, 1998.
2. Draganich LF, Vahey JW, J Orthop Res. 8:57-63, 1990.
3. Griffin LY et al, *JAAOS* 8: 141-150, 2000.
4. Myklebust G et al, *AJSM* 31: 981-9, 2003.

ACKNOWLEDGEMENTS

We gratefully acknowledge the NFL Charities Foundation for funding support.

FINITE ELEMENT ANALYSIS OF A TOTAL ANKLE ARTHROPLASTY OVER ONE STANCE PHASE

[1] Nick Byrne, [2]Heidi-Lynn Ploeg, and [3]Daren Deffenbaugh
[1] Department Biomedical Engineering, University of Wisconsin, Madison, WI, USA; email: njbyrne@wisc.edu
[2]2Departments of Mechanical and Biomedical Engineering, University of Wisconsin, Madison, WI, USA
[3]DePuy Orthopaedics, Inc. a Johnson & Johnson company, Warsaw, IN, USA

INTRODUCTION

It is known in the biomaterials and orthopedics communities that excessive wear debris in orthopedic implants, in combination with excessive bone-implant interface stress can lead to osteolysis of the supporting bony structures. Osteolysis can cause component loosening, migration, and subsidence [1]. These are the biggest concerns to engineers and surgeons when providing total ankle joint replacements. In total ankle replacement (TAR) specifically, clinical follow-ups have shown the talar component to experience loosening and subsidence more frequently than desired [2].

The purpose of this project is to determine the maximum contact stresses present and maximum polyethylene (PE) deformation resulting between the talar component and polyethylene tibial insert of the size 4 AGILITY Ankle implant (DePuy Orthopaedics, Inc., a J&J co., Warsaw, IN) through one stance phase of the gait cycle under physiological loading. Maximum interface stress between the talar component and the supporting bone will also be investigated to determine the effect of torsion in the transverse plane.

METHODS

Physiological forces and displacements will be applied to the AGILITY components at every five percent of the stance phase of the gait cycle, resulting in 21 total models. A quasi-dynamic analysis of one movement through the stance phase of gait will result from the combination of these 21 models. Component models will be aligned in their respective positions (Figure 1) [3] in Unigraphics, from EDS Corp., Plano, TX.

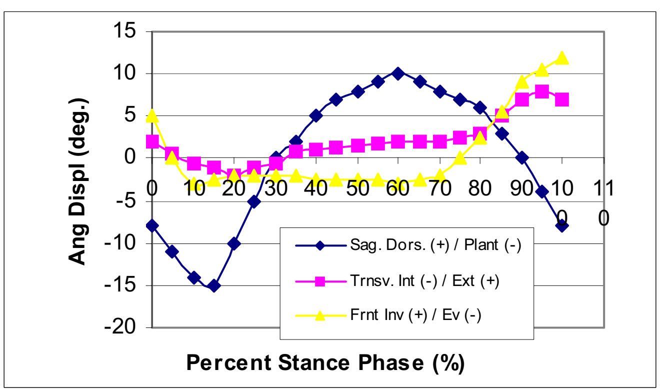

Figure 1: Talus Position in Sagittal, Transverse, and Frontal Planes over Stance Phase of Gait

The solid models will be imported into PATRAN, from MSC.Software Corp., Santa Ana, CA, where the boundary conditions, material properties, and mesh will be defined. Model 15 of 21 is shown below (Figure 3). A physiological varying torsional load will also be applied, although it is not shown.

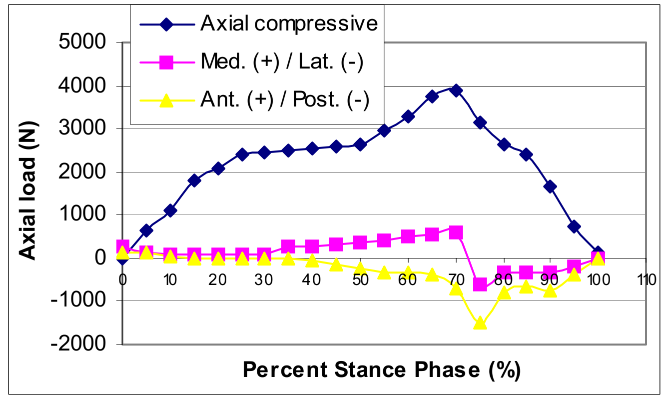

Figure 2: Loads on Ankle Joint in 3 Directions over Stance Phase of Gait Cycle

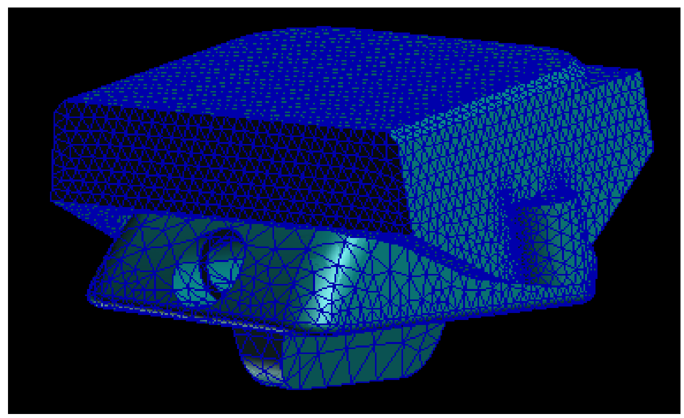

Figure 3: FE mesh of the AGILTY Ankle at 70% of the stance phase of gait: 8° dorsiflexion, 2° external rotation, 2° eversion

RESULTS AND DISCUSSION

Preliminary analysis has shown that maximum contact stresses and polyethylene deformation occur at 70-75% of the stance phase. This was expected, as axial loads (Figure 2) [4] are the greatest and dorsiflexion is also substantial. It is expected that areas of high contact stress and large PE deformation on each of the 21 discreet computational models will combine to closely resemble the wear patterns found on the clinical retrievals of PE tibial inserts. It is also expected that in positions under heavy torsional loading, large medial-lateral contact stresses will be observed in the talus, which may translate into possible large shear forces at the talus-bone interface.

REFERENCES

1. Ratner, B. et al (1996). *Biomaterials Science: An Introduction to Materials in Medicine, Academic Press.*
2. Pyevich, M. et al (1998). JBJS, 80A, 1410-1420.
3. Stauffer, R. et al (1977). *Clin Orthop*, 127, 189-196.
4. Seireg, A., Arvikar (1975). *Biomech*, 8(2), 89-102.

ELIMINATION OF ECG CONTAMINATION FROM EMG SIGNALS: AN EVALUATION OF CURRENTLY USED REMOVAL TECHNIQUES.

[1]Janessa D. M. Drake, [1]Jack P. Callaghan
[1]Faculty of Applied Health Sciences, Department of Kinesiology, University of Waterloo, Canada
Email: jdrake@ahsmail.uwaterloo.ca, web: **www.ahs.uwaterloo.ca/kin/people/faculty/callaghan.htm**

INTRODUCTION

Trunk electromyography (EMG) is often contaminated with heart muscle electrical activity (ECG) due to the proximity of the collection sites to the heart and the volume conduction characteristics of ECG through the torso. Few studies have quantified ECG removal techniques relative to an uncontaminated EMG signal (gold standard or criterion measure), or made direct comparisons between different methods for a given set of data. The purpose of this study was to concomitantly evaluate four current and commonly used methods for ECG contamination removal from EMG signals.

METHODS

ECG recordings at two intensity levels (rest and 50% maximum predicted heart rate) were superimposed on 11 uncontaminated biceps brachii EMG signals (rest, 7 isometric, and 3 isoinertial levels). The removal methods used were high pass digital filtering (HPF: finite impulse response (FIR) using a Hamming window, and 4th order Butterworth (BW) filter) at five cutoff frequencies (20, 30, 40, 50, and 60Hz), a template technique (template subtraction, and a zero-replacement template), combinations of the subtraction template and HPF, and a frequency subtraction/signal reconstruction method. Four performance indicators were calculated from the cleaned signals: root mean square error, mean power frequency, and two coefficients of determination. The indicators were individually ranked from a low of 1 up to 23, averaged, and natural logged for each contraction level. A two-way ANOVA with two repeated measures was used to investigate the effects of the contraction level, heart rate level, and cleaning method. A Least Square Means test was used to decipher interactions.

RESULTS AND DISCUSSION

For muscle activation levels between 10-25% of maximum voluntary contraction (MVC), the template subtraction and BW with a 30Hz cutoff were the two best individual methods for maximal ECG removal with minimal EMG distortion (Figure 1), ranking 3 and 5 out of 23 respectively across all contraction and heart rate levels. Only combinations of the subtraction and filtering outperformed these methods (Table 1). The subtraction method has been shown to be more

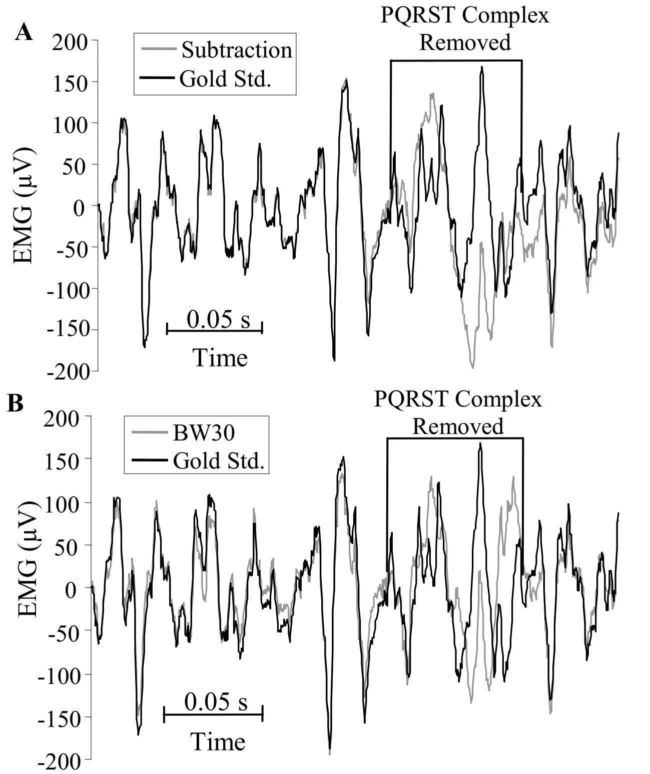

Figure 1: A comparison of the uncontaminated EMG signal (Gold Standard) and the cleaned contaminated signal using the BW30 (A) and subtraction (B) methods.

effective than gating [1], and using a FIR with a 30Hz cutoff to be more effective than with a 60Hz cutoff [2] for ECG removal. This study supports these findings.

CONCLUSIONS

For the EMG levels evaluated in this study, the BW filter with a 30Hz cutoff provided the optimal balance between ease of implementation, time investment, and performance across all contractions and heart rate levels.

REFERENCES

1. Bartolo et al. *J Appl Physiol*, **80**, 1898-1902, 1996.
2. Redfern et al. *Clin Biomech*, **8**, 44-48, 1993.

Table 1: Comparison of the methods (per technique) with the lowest error based on the least mean square probabilities. A lower rank equates to a better performance (in parentheses). The number with the technique represents the cutoff frequency (Hz).

4 Main Techniques	High Pass Filtering		Template (Time Domain)		Combination	Frequency
EMG (% MVC)	FIR	Butterworth	Subtraction	Gating	Sub + HPF	Sub+Inverse FFT
Isometric: Rest	FIR60 (7/23)	BW60 (6/23)	Sub (23/23)	Gate (5/23)	cFIR50 (1/23)	InvFFT (17/23)
Isometric: 10.1%	FIR40 (9/23)	BW30 (4/23)	Sub (6/23)	Gate (13/23)	cBW20 (1/23)	InvFFT (22/23)
Isometric : 13.0%	FIR40 (7/23)	BW30 (5/23)	Sub (4/23)	Gate (15/23)	cBW20 (1/23)	InvFFT (22/23)
Isometric : 15.6%	FIR30 (8/23)	BW30 (4/23)	Sub (2/23)	Gate (12/23)	cBW20 (1/23)	InvFFT (21/23)
Isometric : 24.7%	FIR30 (7/23)	BW20 (4/23)	Sub (2/23)	Gate (13/23)	cBW20 (1/23)	InvFFT (19/23)
Isoinertial: 38.8%	FIR30 (9/23)	BW30 (4/23)	Sub (1/23)	Gate (5/23)	cBW20 (2/23)	InvFFT (20/23)

DO EXERCISE BALLS PROVIDE A TRAINING ADVANTAGE FOR TRUNK EXTENSOR EXERCISES? A BIOMECHANICAL EVALUATION.

[1]Janessa D. M. Drake, [1]Steve L. Fischer, [1]Stephen H. M. Brown, [1]Jack P. Callaghan
[1]Faculty of Applied Health Sciences, Department of Kinesiology, University of Waterloo, Canada
Email: jdrake@ahsmail.uwaterloo.ca, web: **www.ahs.uwaterloo.ca/kin/people/faculty/callaghan.htm**

INTRODUCTION

The use of exercise balls is becoming widespread in the exercise and rehabilitation communities even though the effects of performing trunk extensor exercises on an exercise ball have not been assessed. Only a few abdominal muscle exercises have been quantitatively evaluated in both the traditional (mat) and ball styles [1], but the reported benefits for these exercises on a ball have been equivocally applied to all exercises. To address the effect of an exercise ball on extension exercises, a direct comparison of the same exercises on a mat and on a ball is required. The purpose of this study was to evaluate differences in the biological response of muscle activation, lumbar spine posture, and loading variables for extensor exercises performed on two surfaces.

METHODS

Bilateral muscle activation was recorded from seven sites (rectus abdominis (RA), external and internal obliques (EO/IO), latissimus dorsi, thoracic and lumbar erector spinae (TES/LES), and multifidus (MULT)) on eight subjects. Three-dimensional lumbar spine postures (ISOTRAK, 3Space), and upper body kinematics (video) were recorded while the participants performed the exercises. An EMG-driven model was used to estimate spinal loading. Two-way repeated measures analyses of variance (ANOVA) were used (α=0.05). The surface main effect and surface-exercise interactions were reported since the objective of this work was to assess surface type. A Least Square Means test was used to decipher surface-exercise interactions.

RESULTS AND DISCUSSION

Co-contraction of trunk flexor and extensor muscles was reduced by 30.4% and 9.5% respectively for the contralateral and single leg extension exercises when performed on the ball, but was unchanged for the back extension exercise (Figure 1).

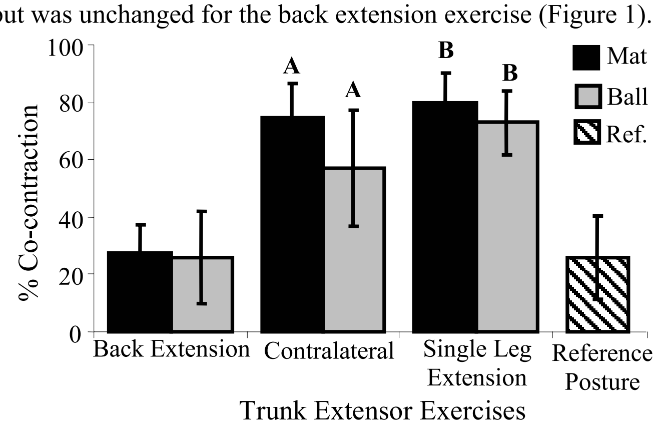

Figure 1: Percent peak co-contraction between left and right trunk flexors (RA, EO, and IO muscles), and trunk extensors (TES, LES, and MULT muscles).

The peak lumbar extension and range of lateral bend and axial twist postures attained during the exercises did not differ between surfaces. Lower spinal loading (compression and anterior-posterior shear) was observed on the ball (Figure 2). Peak muscle activation remained unchanged or decreased when the extension exercises were performed on the exercise ball. The magnitude of muscle activation for the exercises performed on the surfaces were similar to literature values [2,3]. The assumption that the use of an exercise ball will always create a greater challenge for the musculoskeletal system was not supported by the findings of this study.

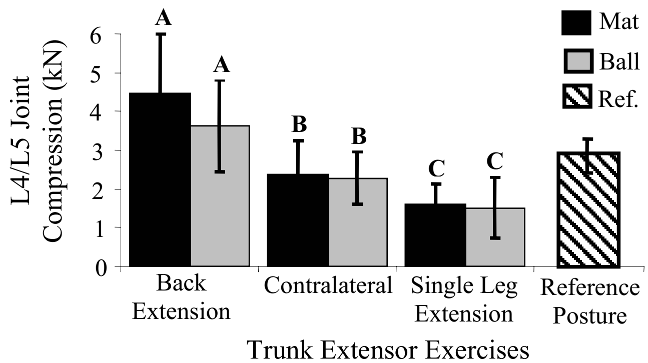

Figure 2: Mean EMG-driven model estimates of maximum L4/L5 joint compression across the participants (N = 8). The significant differences between surfaces for each exercise are indicated with the same letter.

CONCLUSIONS

In a healthy young population there does not appear to be any training advantage to performing extensor exercises on an exercise ball versus a floor surface. However in a rehabilitation scenario, these exercises performed on a ball could reduce low back loading and hence the potential for re-injury would be reduced. Those desiring exercises that elicit high levels of muscle activation and co-contraction can obtain the same or higher levels by performing these trunk extensor exercises on a mat.

REFERENCES

1. Vera-Garcia, et al. *Phys Ther*, **80**, 564-569, 2000.
2. Callaghan, et al. *Phys Ther,* **78**, 8-18, 1998.
3. Mori, A. *Electromyogr Clin Neurophysiol,* **44**, 57-64, 2004.

ACKNOWLEDGEMENTS

We would like to thank the Natural Science and Engineering Research Council of Canada (NSERC) for their financial support. Dr. Jack P. Callaghan is supported by a Canada Research Chair in Spine Biomechanics and Injury Prevention. Janessa Drake is supported by a Canadian Institute for the Relief of Pain and Disability (CIRPD)/Canadian Institutes of Health Research (CIHR) Doctoral Research Award.

MOMENT ARMS AND MOMENT POTENTIAL BALANCE AT THE INDEX MCP JOINT

[1]William L. Buford, Jr., Shukuki Koh, Clark R. Andersen, Steven F. Viegas
Orthopaedic Research Labs, University of Texas Medical Branch,
Galveston, TX, [1]email: wbuford@utmb.edu

INTRODUCTION

This study extends prior investigations of muscle moment arms at the index metacarpo-phalangeal joint (MCPJ) to provide a more detailed description of muscle balance. By combining moment arm data with known tension fractions a renewed understanding of moment potential balance helps to describe clinical conditions as well as provide knowledge relevant to reconstruction and joint arthroplasty.

METHODS

Twelve fresh cadaver arms (6 male, 6 female, average age 71) were acquired through the Texas willed body program. Specimens were dissected through limited incisions but sufficiently to attach nylon cable to the index finger tendons using previously described methods.[2] The muscles studied were the flexor digitorum profundus, flexor digitorum sublimus, extensor digitorum communis, extensor indicis proprius, first palmar interosseous, lumbrical, and two paths of the first dorsal interosseous based on origination on the first metacarpal and the second metacarpal (FDPI, FDSI, EDCI, EIP, 1stPI, Lum, 1DIMc1, and 1DIMc2). Muscle excursions, flexion-extension (FE) and ulnar-radial (UR) MCPJ angles were measured and moment arms determined using methods previously described.[1, 2]

RESULTS AND DISCUSSION

The average UR moment arm values for each muscle with the MCPJ at neutral are combined with the same for FE as described in an earlier study.[2] Results yield the moment arm balance described in Figure 1.

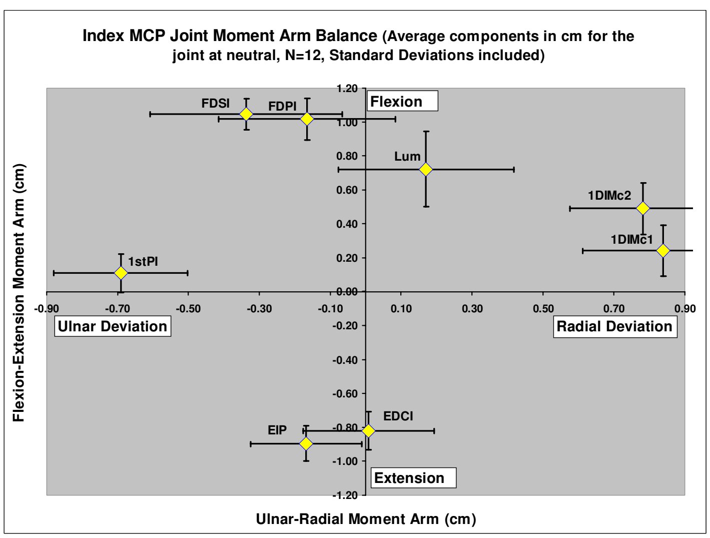

Figure1. Average moment arms for the index MCPJ at neutral, indicating primary FE and UR functions.

To provide an indication of moment potential balance, the moment arms are multiplied by the respective muscle tension fractions[3] and combined to indicate the potential moment in the principal rotation directions (flexion, extension, ulnar and radial deviation). The result for the normal hand appears in Figure 2.

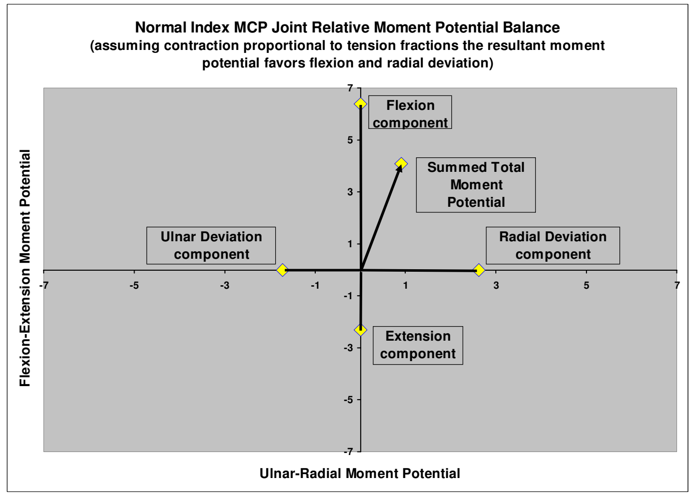

Figure 2. Summary of the moment producing potential of the muscles at the index MCPJ for the normal hand.

When the effects of the intrinsic muscles are removed these results define the moment potential balance for the intrinsic minus hand shown in Figure 3.

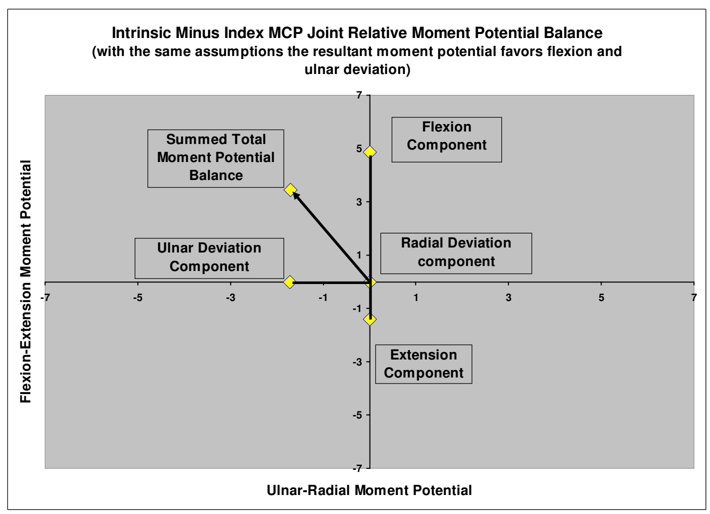

Figure 3. Index MCPJ moment potential balance without the effects of the intrinsic muscles.

CONCLUSIONS

These results combining improved investigations of moment arms for the index in FE and UR motion with previously described tension fractions provide a clear graphical understanding of joint muscle balance. For example, it is readily seen by comparing figures 2 and 3 that the intrinsic minus joint will eventually migrate ulnarly. Also it can be concluded that arthroplasty should seek to reconstruct the balance defined by Figure 2.

REFERENCES

1. An, KN, et al., *J. Biomech* 16:6, 419-425, 1983.
2. Buford, WL et al. **Proceedings**, 59th Annual Meeting, ASSH, NYC, NY, Sep 9-11, 2004.
3. Brand, PW, et al., *J Hand Surg*; 6:209-219; 1981.

KINETIC ANALYSIS OF MANUAL WHEELCHAIR PROPULSION OVER THREE SURFACES

Jennifer Mercer, Michael Boninger, Alicia Koontz, Jon Pearlman, and Rory Cooper
Human Engineering Research Laboratories, VA Medical Center, University of Pittsburgh, Pittsburgh, PA 15206;
email: mercerj@herlpitt.org, web: www.herlpitt.org

INTRODUCTION

Manual wheelchair users (MWUs) encounter a variety of floor surfaces and obstacles during activities of daily living. Some obstacles, such as carpet and ramps, are more difficult to negotiate than a smooth surface [1]. MWUs must increase their propulsion force, stroke frequency, or contact time to propel over these more difficult floor surfaces. Previously, propulsion forces, rate of force application, and stroke cadence have been associated with secondary injuries of the wrist [2] and shoulder [3]. The purpose of this study was to evaluate the biomechanics of wheelchair propulsion over tile, carpet, and up a ramp. We expected to see an increase in propulsion force, torque, rate of force application, pushrim contact time, and cadence, along with decreased velocity, as the MWU propels over carpet and up a ramp as compared to tile.

METHODS

Twenty-three male subjects were consented at The 2004 National Veterans Wheelchair Games (St. Louis, MO). Inclusion criteria included ownership of a manual wheelchair that subjects were capable of propelling and age between 18 and 65 years. Subjects were excluded based on a self-reported history of heart or cardiovascular conditions. Subjects had an average age, height, and weight of 45.8±8.6 years, 1.8±0.14 m, and 99.3±26.4 kg respectively.

The SMART^{Wheel} (Three Rivers Holdings, LLC), a wireless force and torque sensing wheelchair wheel, facilitates biomechanical analysis of wheelchair propulsion over real world obstacles [4]. A SMART^{Wheel} was secured to each subject's manual wheelchair. Subjects were asked to propel at a self-selected comfortable speed over tile, low-pile carpet, and up an ADA compliant ramp while pushrim forces and torques were recorded by the SMART^{Wheel}. All biomechanical variables (Table 1) were calculated based on an average of 5 strokes.

Six separate one-factor ANOVAs with Bonferroni post-hoc analysis were used to compare each of the biomechanical variables (dependent variables) during propulsion over three surfaces (independent factor with three levels).

RESULTS AND DISCUSSION

Table 1 summarizes the comparison of biomechanical variables for wheelchair propulsion over three surfaces. Significant differences were found between the ramp and both tile and carpet for all but one variable (cadence). MWUs used increased resultant force, wheel torque, rate of force application, and contact time. They also propelled slower over the ramp compared to tile and carpet. The same trends were observed for propulsion over carpet compared to the tile, but no significant differences were detected between these two surfaces.

In accordance with our hypothesis, MWUs had to increase their propulsion force, wheel torque, rate of force application, and contact time in order to negotiate the ramp. The MWUs did not increase their stroke cadence but instead went slower up the ramp. Low-pile carpet was used in the study (due to availability) and it may not have provided enough resistance to show significant difference in propulsion over carpet compared to propulsion over tile, as we had expected.

CONCLUSIONS

Unfortunately, using increased force and rate of force application has been previously linked to injury [2,3]. Even with this increased effort, MWUs still propel slower on the more challenging obstacles. It is important that MWUs are able to maintain their independence, without increasing their risk of secondary injuries. Future studies should investigate how changes in wheelchair setup and/or propulsion training protocols can minimize the risk factors for secondary injury that were observed in this study.

REFERENCES

1. Meyers AR, et al. *Soc Sci & Med* **55**, 1435-1446, 2002.
2. Boninger ML, et al. *Arch PM&R* **80(8)**, 910-915, 1999.
3. Boninger ML, et al. *Arch PM&R* **84(11)**, 1615-1620, 2002.
4. Cooper RA, et al. *J Rehab Res Dev* **34(2)**, 162-170, 1997.

ACKNOWLEDGEMENTS

This study was supported by the VA RR+D Center (F2181C).

Table 1: Biomechanical Variables of Wheelchair Propulsion on Three Different Surfaces

	Tile	Carpet	Ramp
Maximum Resultant Force (N)	89.9 (27.1)	95.6 (29.3)	138.3 (22.4)*
Maximum Wheel Torque (N-m)	19.8 (6.8)	22.3 (6.5)	33.9 (5.0)*
Maximum Rate of Resultant Force Application (kN/sec)	1.56 (.87)	1.66 (.75)	2.47 (1.05)*
Contact Time (sec/stroke)	0.51 (.10)	0.54 (.10)	0.74 (.20)*
Cadence (strokes/sec)	0.95 (.17)	1.04 (.20)	1.05 (.23)
Average Velocity (m/s)	1.25 (.27)	1.20 (.31)	0.89 (.33)*

* indicates results significantly different than both Tile and Carpet at $p<.05$ (All Bonferroni corrected p-values were less than .01)
Results listed as mean (standard deviation)

"PRESSURE GRADIENT" AS A POTENTIAL INDICATOR OF PLANTAR SKIN INJURY ON THE NEUROPATHIC FOOT

[1] Dequan Zou, [1]Michael J. Mueller and [1]Donovan J. Lott
[1]Program in Physical Therapy, Washington University, School of Medicine,
4444 Forest Park Blvd., Campus Box 8502, St. Louis, MO 63108, USA
Email: zoud@wustl.edu

INTRODUCTION

Peak plantar pressure (PPP) during walking has been used extensively as an indicator of risk for skin breakdown in the diabetic foot. Although skin breakdown is associated with high PPP, researchers have not been able to identify a critical magnitude of PPP that adequately predicts skin breakdown in the neuropathic population. We speculate that the change in plantar pressure at the PPP location, a "peak pressure gradient, (PPG)", is more important than the PPP because a PPG may identify a concentration of stress (a harmful vertical shearing) to the soft tissues. The purposes of this presentation are to a) describe methods for obtaining the PPG, and b) determine if the PPG at the PPP location is substantially higher in the forefoot than the rearfoot (even compared to PPP) in subjects with diabetes (DM) and a history of plantar ulcer. Skin breakdown typically is in the forefoot rather than the rearfoot despite fairly similar PPPs [1]. A much higher PPG at the PPP location in the forefoot compared to the rearfoot may partially contribute to a differential in skin breakdown location.

METHODS

The PPG at the PPP location can be calculated by

$$\mathrm{PPG} = \max\left(\frac{\partial P}{\partial r}\right)$$

where $\frac{\partial P}{\partial r}$ (space rate of change of pressure on the plantar surface) is the directional derivative of pressure P at the PPP location on the plantar surface in any direction given by vector $\vec{r}$.

Plantar pressure data during walking were collected on 10 subjects (6 Males/4 Females, mean age 58.0±10.3 years, mean BMI 32.6 ±9.5 kg/m^2) with DM (2 Type 1, 8 Type 2, and mean duration of DM 16.5 $\pm$ 10.0 years), PN, and a history of a plantar ulcer.

An F-scan system (Tekscan, South Boston, MA, USA) was used to collect the plantar pressure data during walking at a self-selected pace in standardized shoes with a 1-inch heel [2]. The recorded plantar pressure data were analyzed for the PPP and PPG for the forefoot and rearfoot. The PPG at the location of the PPP was calculated after a bicubic polynomial spline smoothing of the pressure data. The PPP and PPG at the PPP location for each area of interest were averaged over three steps during walking.

Analysis: A one tailed, paired t-test on the ratios of PPP and PPG between the forefoot (FF) and rearfoot (RF) was used to determine differences in PPP and PPG between the FF and RF.

Table 1: Mean PPP and PPG at Forefoot and Rearfoot

PPP FF (kPa)	PPP RF (kPa)	PPG FF (kPa/mm)	PPG RF (kPa/mm)
347.80 ± 75.45	279.17 ± 97.16	32.84 ± 15.52	12.05 ± 5.30

RESULTS AND DISCUSSION

The mean PPG was 171% higher in the FF compared to the RF in subjects with diabetes and a history of plantar ulcer while the mean PPP was only 25% higher in the FF compared to the RF (Table 1). The mean PPG FF/RF ratio (3.09) was significantly greater than the PPP FF/RF ratio (1.41) ($p<0.001$, Table 2). The PPG likely is much lower in the RF than the FF because of differences in soft tissue thickness and shape of the underlying bony structures. A much higher PPG at the PPP location in the FF compared to the RF may be one reason why skin breakdown typically occurs in the FF rather than the RF despite fairly similar PPPs. Because the PPG may identify harmful vertical shearing of soft tissues on the plantar foot, we propose that it is an important variable to characterize the pressure distribution on the plantar surface and to predict potential plantar skin injuries on the neuropathic foot.

Table 2: Mean Ratios of Individual Forefoot to Rearfoot Values for PPP and PPG; and Results of Paired t-test Comparison

(PPP FF)/(PPP RF)	(PPG FF)/(PPG RF)	P value
1.41 ± 0.75	3.09 ± 1.54	0.001

CONCLUSIONS

We describe a new variable, the PPG, which may provide important information about the risk for skin breakdown. PPG is much higher in the FF compared to the RF and this may help to explain why most ulcers occur in the FF despite similar PPPs. Evenly distributed high plantar pressures likely do not cause skin breakdown. We believe that the space rate of change in plantar pressure at PPP location, the PPG, is an important variable to help identify risk for skin breakdown on the neuropathic foot, and that it deserves further investigation.

REFERENCES

1. Pitei DI, et al. Diabetes Care, 22. 1966-1970, 1999.
2. Mueller MJ, et al. *J Biomech,* 36, 1009-1017, 2003.

ACKNOWLEDGEMENTS

Funded by NCMRR, NIH, (RO1 HD36895).

KINEMATICS OF RUNNERS WITH AND WITHOUT PATELLOFEMORAL PAIN DURING PROLONGED TREADMILL RUNNING

[1] Tracy A. Dierks, [1,2]Irene Davis, [1]Kurt T. Manal, and [3]Joseph Hamill
[1]University of Delaware, Newark, DE, USA; [2]Drayer Physical Therapy Institute, Hummelstown, PA, USA; [3]University of Massachusetts, Amherst, MA, USA; email: tdierks@udel.edu, web: http://www.udel.edu/PT/davis/index.htm

INTRODUCTION

It has been suggested that abnormal lower extremity kinematics during running are related to patellofemoral pain (PFP). Specifically, during the first half of stance when the knee is loaded, excessive internal rotation of the femur may result in lateral patellae maltracking [1,2]. Similarly, the patellofemoral joint may also be influenced by excessive knee valgus, which may be partly due to increased femoral adduction [1]. Also, it has been reported that PFP is associated with weak hip abductors and external rotators [3]. Therefore, these abnormal femoral motions may become more exaggerated in an exerted state, such as at the end of a prolonged run. Conversely, PFP has also been associated with decreased knee flexion during functional activities, which is thought to reduce the loads on the patellofemoral joint [1]. Further, the coupling that occurs between the knee and the foot may result in a decrease in rearfoot eversion as well [2].

While abnormal kinematics are believed to be related to PFP, few studies have examined the relationship between kinematics and PFP during running. Furthermore, no studies have investigated kinematics in a PFP group while running with pain and in an exerted state. Therefore, the purpose of this study was to compare the lower extremity kinematics of runners with PFP to uninjured runners over the course of a prolonged run. It was hypothesized that runners with PFP would display larger angular peaks for motions at the hip and that they would increase more than the uninjured group by the end of the run. It was also expected that the PFP group would exhibit smaller peaks at the knee and the rearfoot and that these values would decrease by the end of the run, whereas the uninjured group would display increases.

METHODS

Twenty runners with PFP and 20 healthy, uninjured runners participated in the study. All were between the ages of 18 and 45 and ran a minimum of 10 miles per week. The PFP group consisted of runners who experienced anterior knee pain for a minimum of two months when running. The tested limb in the PFP group was the side with the most painful knee, while the uninjured group was chosen randomly.

Three-dimensional kinematic data (120 Hz) were collected while subjects performed a prolonged run on a treadmill at a self-selected pace. The prolonged run ended when one of three events occur: 1) 85% of the subject's heart rate maximum was reached, 2) a score of 17 was reached on a rating of perceived exertion scale, and 3) for the PFP group, a score of 7 was reached on a visual analog scale for pain. Twenty consecutive footfalls were collected at the beginning and at the end of the run. For each subject, the peak angular values for rearfoot eversion, tibial internal rotation, knee flexion, knee internal rotation, knee adduction, hip adduction, and hip internal rotation were determined for each stance phase and then averaged. A 2-way repeated measures ANOVA (group x time) was used to determine differences for each kinematic variable ($p \leq 0.05$).

RESULTS AND DISCUSSION

The expectation that the PFP runners would display changes different from the uninjured runners in their peak values throughout the run was not supported. No interactions were found for any of the kinematic variables. As expected, the main effect for peak knee flexion was different between the two groups, with the PFP group exhibiting less knee flexion than the uninjured group (Table 1). The observed decreased knee flexion may be a compensatory strategy that was adopted to reduce knee pain because increased knee flexion will increase patellofemoral compressive forces, thus producing greater pain. For the main effect of time (begin to end), peaks for eversion, tibial internal rotation, knee internal rotation, and hip adduction all significantly increased from the beginning of the run to the end (Table 1), which is consistent with the literature [4]. This suggests that, regardless of group, as runners progress from a non-exerted to an exerted state, there is an increase in peak motions. While the majority of these observed increases were only between one to two degrees, both groups changed by approximately the same amount. In the PFP runners, these small increases may have been enough to bring them to their pain threshold, as 13 of 20 runners ended the run due to pain.

CONCLUSIONS

Based on the results of this study, runners with PFP exhibited less knee flexion than uninjured runners, which may be a mechanism to guard against pain. With the exception of knee flexion, both groups displayed similar peak angles at the beginning and end of the prolonged run. By the end of the run, these peak angles typically increased in a similar fashion between the two groups.

REFERENCES

1. Powers CM. *J. Orthop. Sp Phys Ther.* 33, 639-646, 2003.
2. Tiberio D. *J. Orthop. Sp Phys Ther.* 9, 160-165, 19871.
3. Ireland ML, et al. *J. Orthop. Sp Phys Ther.* 33, 671-676, 2003.
4. Derrick TR, et al. *Med Sci Sp Exer.* 34, 998-1002, 2002.

Table 1. Peak angles (deg) for patellofemoral (PFP) and uninjured (UNJ) runners at the beginning and end of the run. Standard deviation in ( ).

	Eversion		Tibial Internal Rotation		Knee Flexion		Knee Adduction		Knee Internal Rotation		Hip Adduction		Hip Internal Rotation	
	Begin	End	Begin	End	Begin	End	Begin	End	Begin	End	Begin	End	Begin	End
PFP	6.4^	7.7^	9.3^	10.9^	42.2*	42.6*	3.1	3.0	2.1^	2.8^	11.6^	12.3^	8.2	8.2
	(3.6)	(4.0)	(3.8)	(4.2)	(6.2)	(6.6)	(4.2)	(4.7)	(4.0)	(4.3)	(2.7)	(2.6)	(4.9)	(5.4)
UNJ	7.6^	9.2^	9.2^	10.7^	46.3*	46.3*	1.5	1.4	3.6^	4.8^	11.9^	12.5^	6.6	7.2
	(3.5)	(3.8)	(3.7)	(4.5)	(5.3)	(5.5)	(3.3)	(3.5)	(5.3)	(5.4)	(3.4)	(3.8)	(4.5)	(4.1)

*Significant group effect. ^Significant time effect.

A SIMPLIFIED TOPOLOGY FOR THE TIBIAL PLATEAU AND MENISCAL SURFACES AND THE ROLE EACH OF ITS GEOMETRIC FEATURES PLAY IN GUIDING THE PASSIVE MOTION

[1] Shahram Amiri, [2]Urs P.Wyss
[1]Ph.D Candidate, Department of Mechanical and Materials Engineering, Queen's University, Canada; amiri@me.queensu.ca
[2]Ph.D, Department of Mechanical and Materials Engineering, Queen's University, Canada; wyss@me.queensu.ca

INTRODUCTION

The goal of this study was to see if the geometry of the tibial plateau and meniscal surfaces in the passive computer knee models can be considered as a combination of simple rigid geometries. It was also desirable to assess the role of each part of the proposed geometry in guiding the passive pattern of motion. The latter was done by eliminating different parts of the geometry from the complete model and comparing the simulation results before and after each elimination. It has been found that the resulting pattern of motion of the proposed geometry matches the experimental data and the constrained-based knee model. The comparisons between the results of different geometrical configurations led to the understanding of the roles of each part of the geometry in guiding the passive motion.

METHODS

The data reported in the literature regarding the profile of the tibial plateau in different planes were used to construct the simplified tibial geometry. The geometry of the tibial plateau surfaces in the sagittal plane has been reported to be flat in the lateral part, and a combination of a flat surface and a 11° slope in the medial portion [1]. The medial side of the tibial eminence in the frontal plane has a radius matching the femoral condyle [2], and it was modeled as a wedge with the profile in the frontal plane and extruded antero-posteriorly [3]. The lateral side of the tibial eminence was simplified as an incomplete cone [3]. The geometry of the medial meniscal surface was considered rigid and located at the extreme end points it can reach in its range of motion [4,5]. The profile of the meniscal geometry was generated considering the fact that the meniscal geometry follows the femoral surface shape. The lateral meniscus was considered as an extension to the flat lateral tibial surface [6].

Ligaments were modeled as non-linear springs and their stiffness, initial strains, and insertions points were extracted as average values reported in the literature [7,8]. A scanned femoral surface was used and all the elements were put together in ADAMS (dynamic simulation software package). A gradual flexion imposed to the model, and the kinematics response of the model was measured. Subsequently, different parts of the tibial geometry were eliminated separately and simulation was performed for each case.

RESULTS AND DISCUSSION

The internal-external rotation of the tibia and its anterior-posterior movement were determined for the complete configuration. Figure 1 compares the internal external rotation of the tibia with the results of the experimental data reported by Wilson et al. [9] and the prediction of the constrained-based model proposed by Feikes et al. [10]. Table 1 shows the internal tibial rotation for different configurations.

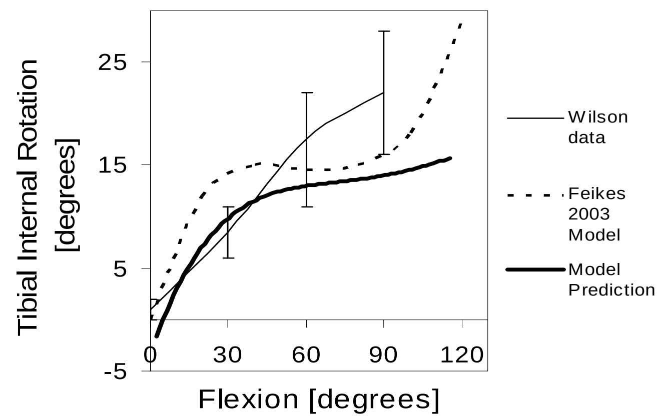

Figure 1: Comparison of the model prediction with the published experimental data and the constrained-based model

Geometric Configuration	Tibial Rotation			
Flexion	**30º**	**60º**	**90º**	**120º**
All Elements present	9.7	13.4	13.8	17.3
Excluding Lateral Meniscal	9.3	15.7	48.1	48.2
Excluding Medial Meniscal	6.2	8.2	10.1	8.7
Excluding Lateral Cone	8.2	13.3	14.1	16.6
Excluding Medial Eminence	8.9	12.9	14.5	28.7

Table 1: Tibial internal rotation for different geometric configurations at different flexion angles.

CONCLUSIONS

Based on the fact that the proposed simplified geometrical configuration replicates the natural passive kinematic patterns, it can be concluded that the recommended geometry includes the important shapes that have influence in guiding the passive motion. The medial meniscus has shown important roles in forcing the joint to undergo higher internal rotation during flexion, while the lateral meniscal extension and medial eminence seem to have a role in preventing the joint from going to excessive internal rotations.

REFERENCES

1. Pinskerova V, et al. Ortopede **29**, S3-S5, 2000
2. Iwaki H, et al. JBJS (Br) **82**, 1189-1195, 2000
3. Martelli S., Pinskerova V. JBJS (Br) **84**, 607-613, 2002
4. Vedi V, et al. JBJS (Br) **81**, 37-41, 1999
5. Thompson W.O, et al. Amercian Journal of Sports Medicine **19**, 210-216, 1991
6. Nakagawa S, et al. JBJS (Br) **82**, 1199-1200, 2000
7. Blankevoort L, et al. J.Biomech **29**, 955-961, 1996
8. Wisman J, et al. J Biomech **13**, 677-685, 1980
9. Wilson D.R, et al. J.Biomech **33**, 465-473, 2000
10. Feikes J.D, et al, J Biomech **36**, 125-129, 2003

ANKLE PLANTAR FLEXOR FORCE CAPACITY DURING TOE WALKING

Richard R. Neptune[1], Judith M. Burnfield[2] and Sara J. Mulroy[3]
[1] Department of Mechanical Engineering, University of Texas, Austin, TX, USA
[2] Institute for Rehabilitation Science and Engineering, Madonna Rehabilitation Hospital, Lincoln, NE USA
[3] Rancho Los Amigos National Rehabilitation Center, Downey, CA USA
Email: rneptune@mail.utexas.edu

INTRODUCTION

Toe walking, a gait deviation associated with a variety of neurological disorders, has been suggested to provide a compensatory advantage due to an observed reduction in net plantar flexor moment in terminal stance compared to heel-toe walking [1, 2]. Perry et al. [3], however, showed that although the net plantar flexor moment decreased during toe walking, muscle activity recorded from the plantar flexors increased, reflecting the need for greater muscle effort (defined by the level of motor unit recruitment). They hypothesized that the dichotomy between increased muscle activity and decreased joint moment was due to a reduction in force generation capacity associated with the increased plantar flexion angle. The goal of the present study was to explicitly test this hypothesis using forward dynamical simulations of toe and heel-toe walking to assess the force generating capacity of the plantar flexors by examining each muscle's contractile state (i.e., fiber activation, length and velocity).

METHODS

Forward dynamical simulations of toe and heel-toe walking were generated using dynamic optimization and a previously described 2D musculoskeletal model developed using SIMM [4], which consisted of a trunk and two legs (femur, tibia, patella and foot for each leg) and fifteen individual muscle actuators per leg [5]. The muscle force generating capacity was governed by normalized force-length and force-velocity relationships (Fig. 1). Muscle excitation patterns were modeled using block patterns and parameter optimization using a simulated annealing algorithm to fine-tune the onset, duration and magnitude of the individual muscle excitation patterns such that the simulations reproduced group averaged experimental kinematic and ground reaction force data previously collected from 10 able-bodied subjects during toe and heel-toe walking [3]. From the walking simulations, individual muscle fiber lengths and velocities during stance were determined from the model and normalized to the optimal fiber length and maximum contraction velocity of each muscle, respectively.

RESULTS AND DISCUSSION

Despite a two-fold increase in soleus (SOL) activation during toe walking, the corresponding SOL muscle force averaged over the stance phase decreased by 13%. Similarly, a 40% increase in gastrocnemius activation during toe walking only produced a 2% increase in muscle force. The lack of increased force production with greater activation was attributed to a poor contractile state during toe walking, primarily muscle fiber lengths (Fig. 2) that were too short on the active force length relationship (Fig. 1A) as a result of the increased plantar flexion angle. The average fiber velocities were similar

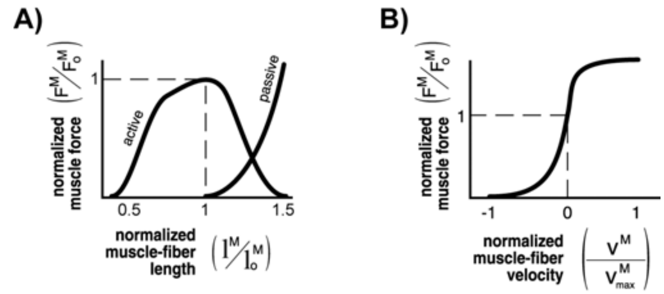

Figure 1: Governing intrinsic muscle properties used in the model: A) normalized force-length and B) force-velocity relationships [4]. With deviations from the muscle fiber's optimal length and increasing rates of shortening, the ability of a muscle to produce force decreases.

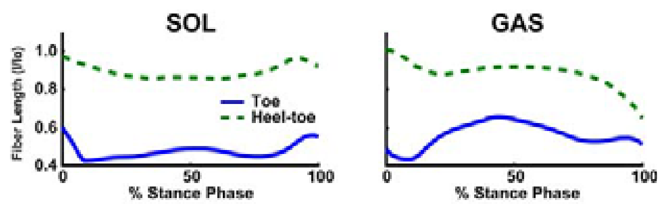

Figure 2: Simulation soleus (SOL) and medial gastrocnemius (GAS) muscle fiber lengths during the stance phase normalized to their optimal lengths.

between the two walking tasks. These results were consistent with Hampton et al. [1] who showed that plantar flexor force decreased during toe walking. Their study used a static decomposition of the ankle joint moment derived from inverse dynamics. However, their analysis did not consider the contractile state of the muscles (i.e., fiber activation, length and velocity) in their assessment of muscle effort. Our simulation-based analysis suggests that toe walking may not be an advantageous compensatory strategy as previously suggested [1, 2] due to the increased muscle activation necessary to overcome the poor contractile state [3]. However, it is possible that spasticity and prolonged equinus foot posture may alter the intrinsic muscle properties such that peak muscle force is generated at shorter fiber lengths [6]. Assessing this possibility remains as future work.

REFERENCES

1. Hampton DA et al.. *J Appl Biomech* **19**: 325-339, 2003.
2. Kerrigan DC et al.. *Arch Phys Med Rehabil* **81**: 38-44, 2000.
3. Perry J et al.. *Arch Phys Med Rehabil* **84**: 7-16, 2003.
4. Delp SL and Loan JP. *Comput Biol Med* **25**: 21-34, 1995.
5. Neptune RR et al. *Gait Posture* **19**: 194-205, 2004.
6. Friden J, Lieber RL. *Muscle Nerve*, **27**: 157-64, 2003.

CHANGES IN LOWER EXTREMITY JOINT STIFFNESS WITH LANDING AFTER FATIGUE

[1] Thomas W. Kernozek, [2]Robert Ragan, [2]David Bushke, [2]John Hart, [1]Mark Iwasaki
[1]Department of Health Professions, [2]Department of Physics, University of Wisconsin-La Crosse, La Crosse, WI; email: kernozek.thom@uwlax.edu; web: http://perth.uwlax.edu/faculty/kernozek/

INTRODUCTION

There may be a specific level of joint stiffness necessary for optimal performance and injury reduction[1]. Too much joint stiffness has been linked to some shock related boney injuries such as stress fractures[2]. Others have suggested that too little joint stiffness may result in soft tissue injury[3]. As a result, there may be an optimal level of joint stiffness to minimize the injury risk. Current focuses of jump-training programs seem to be specific instruction to reduce lower extremity stiffness[4].

Other than paper by Madigan and Pidcoe[5], landing after fatigue has not been investigated. As a result, this study examined the influence of fatigue on the lower extremity stiffness of the knee and ankle in landing.

METHODS

Eight male and eight female recreational athletes volunteered to be in the study. Eight single legged landing trials were performed from a 40-centimeter height. Kinematic data were recorded using a six-camera three-dimensional motion analysis system with 16 retro-reflective markers using the Helen-Hayes marker set. Kinematic data were collected at 240 Hz and raw coordinate data were filtered at 10 Hz. Kinetic data were recorded simultaneously using a Bertec force platform and were synchronized in time with the kinematic data. Kinetic data were sampled at 1200 Hz. Subjects were then asked to perform a protocol consisting of performing a squatting activity on a Smith machine until fatigue ensued. Subjects performed four sets of 60% of their one-repetition maximum squat, each to fatigue failure. Three sets were performed before four single-limb landings were recorded from a 40-centimeter height. The subjects then performed one more squat set to fatigue, to control for muscle recovery, before landing four more times. Inverse dynamics calculations were performed in the Kintrak software package and rotational spring stiffness was calculated with a custom program in Matlab. Joint angles and moments at the knee and ankle were used to calculate rotational stiffness before and after fatigue. Stiffness was calculated by dividing the joint moment by the change in angular displacement respectively for the knee and ankle[6]. Averages of the eight trials per condition were used. A two-way analysis of variance with one between factor (gender) and one within factor (fatigue) were used to compare stiffness at the ankle and knee.

RESULTS AND DISCUSSION

Lower extremity stiffness was different at the ankle and knee joint with fatigue ($p < 0.05$). Figure 1 depicts how these stiffness variables at the knee and ankle change with fatigue. The joint stiffness was not different across gender, nor was there an interaction between gender and fatigue. Stiffness at the ankle increased about 10% with fatigue while knee stiffness decreased about 22% with fatigue.

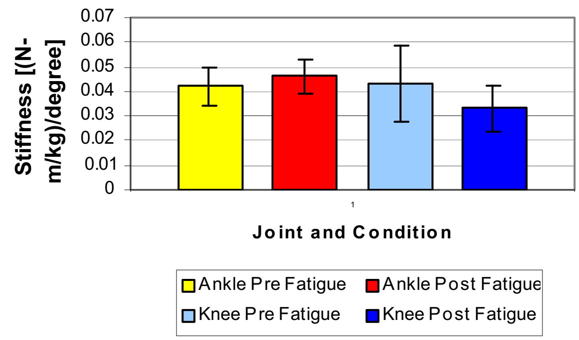

Figure 1. Landing joint stiffness changes pre and post fatigue.

CONCLUSIONS

Not surprisingly, the squat-induced fatigue protocol reduces knee stiffness. The fact that ankle stiffness appears to compensate by increasing is somewhat surprising, and is perhaps in response to the lower knee stiffness. Further research should investigate how this adapted strategy influences injury.

REFERENCES

1. Butler RB, et al. *Clin. Bomech.* **18**, 511-517, 2003.
2. Radin EL, et al. *Clin. Orthop.* **131**, 293-299.
3. Granata, K. et al. *J. Electromyogr. Kinesiol.* **12**, 127-135, 2001.
4. Hewitt, TE et al. *Am. J. Sports Med* 27, 699-705, 1999.
5. Madigan, ML et al. *J. Electromogr. Kinesiol.* **13**, 491-498, 2003.

ACKNOWLEDGEMENTS

Undergraduate research assistants were funded with hi-tech funding from the University of Wisconsin system.

THE APPLIED FORCE PATTERNS OF CHEST COMPRESSION DURING CARDIOPULMONARY RESUSCITATION

[1,2]Jui-Yi Tsou, [3]Chih-Hsien Chi and [1]Fong-Chin Su
[1]Institute of Biomedical Engineering, National Cheng Kung University, Tainan, Taiwan
[2]Department of Physical Therapy, Fooyin University, Kaohsiung, Taiwan
[3]Department of Emergency Medicine, National Cheng Kung University Hospital, Tainan, Taiwan
email: fcsu@mail.ncku.edu.tw

INTRODUCTION

Manual chest compression is essential to maintain adequate blood circulation during cardiopulmonary resuscitation (CPR). It is a skillful movement in demand of proper force control and coordination [1]. Fractures of ribs and sternum due to chest compression during CPR are most commonly reported complications [2]. It not only increases the likelihood of damage to underlying organs but also may impair ventilation and complicate recovery [3].

Therefore, to understand the characteristics of compression force is important for proper force control and decreasing the risk of fractures [4]. The aim of this study was to investigate the three-dimensional (3-D) force patterns of manual chest compression during CPR.

METHODS

Six experienced professional CPR rescuers (3 female, 3 male, age: 36±4.7yrs, height: 165±6.9cm, weight: 65±17kg) participated in this study.

The six-axial force load cell (AMTI MC3A-6-1000, Advanced Mechanical Technology, Inc., Watertown, MA) attached on the standard Resusci® Anne manikin (Laerdal Medical, Wappingers Falls, NY) were used to collect the 3-D compression forces at sampling rate of 1000 Hz. Three markers were attached on the load cell to define the coordination system of the load. The Expert Vision motion system (motion analysis Corp., Santa Rasa, CA) was used to collect the load cell motion at sampling rate of 100 Hz.

The subjects were kneeling beside the manikin and compressed on the load cell to perform CPR with a compression-ventilation ratio of 15/2 and frequency of 100 compressions per min over a session of 5 min. During the 5 min session of CPR, the data was recorded three times at the first, middle and last period. Each period was 20 second. (0:20-0:40, 2:20-2:40 and 4:20-4:40). The applied 3-D forces of chest compression were transformed from the local coordinate system of the load cell to the global coordination system.

RESULTS AND DISCUSSION

The magnitude of up-down direction force was downward 482±29.4N (Figure 1). This force fell on the range between 411 and 548N as expected. There was no significant difference between three periods. It indicates that the experienced rescuers could maintain a constant compression deep during 5 min CPR.

During compression phase, the right direction force rose rapidly to the peak and then decreased (Figure 1). The mean force of right direction was 47±19.2 N. It may account for asymmetry of resultant force of two hands. The rescuers were almost the left hand beneath. While performing CPR with both hands, the shoulders, arms and hands of the rescuer form a triangle, apparently shifting the pressure to the more lateral hypothenar part of the heel of the hand [4] and then result in the right lateral force.

The same observation applies to the force in anterior-posterior direction. While compression, the forward force increased to 31± 9.7 N. It may result from the anterior shifting movement of the trunk.

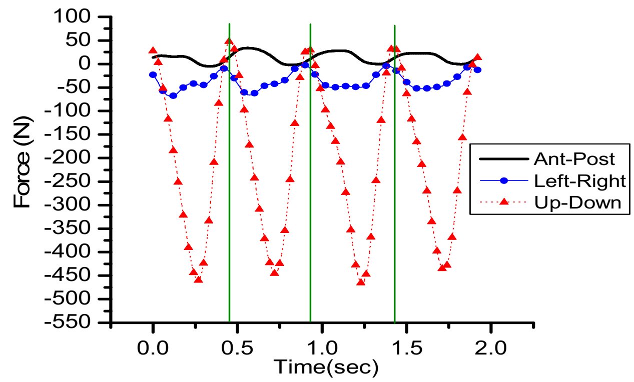

Figure 1: The mean magnitude of 3-D compression force pattern

CONCLUSIONS

From this study, we found that the compression force is not a pure downward force. The other two components of chest compress forces may be affected by body movement. The different resultant force may be also effect the type of fracture. Further researches can use this finding and method to determine the relationship between applied force, body movement, depth of compression, and fracture for developing more efficient and safe CPR.

REFERENCES

1. Larsen PD, et al. *Resuscitation* **53,** 281-7, 2002.
2. Black CJ, et al. *Resuscitation* **63**, 339-43, 2004.
3. Lederer W, et al. *Resuscitation* **60**, 157-62, 2004.
4. Baubin M, et al. *Resuscitation* **35**, 259-63, 1997.

ACKNOWLEDGEMENTS

We acknowledge the financial support of the National Science Council, ROC.

A COMPREHENSIVE APPROACH TO STUDYING MILD TRAUMATIC BRAIN INJURIES IN MOTOR VEHICLE CRASHES

Zhifeng Kou, Mariusz Ziejewski
North Dakota State University
email: zhifeng.kou@ndsu.edu

INTRODUCTION

Mild traumatic brain injury (MTBI) has the incidence rate of 1.2 million people in the United States, and most of whom are caused in motor vehicle crashes (MVC) [1]. However, the biomechanics of MTBI is not well understood. Biomechanical study of the injury mechanisms of MTBI is difficult due to the non-applicability of the various surrogates including animals, volunteers, and cadavers that were traditionally used in impact biomechanical studies. This study was to determine a method used in a comprehensive study of MTBI involved in MVCs.

METHODS

Our biomechanical approach consists of several steps and all of them are well-accepted methods: 1.) Crash investigation of MVCs on scene. In this step, we could determine the Delta V (the maximum change in velocity at the time of collision) by using Crash3 program [2,3], the angle and type of impact. 2.) Computer modeling of vehicle occupant. We used the Articulated Total Body (ATB) computer software to analyze the human body dynamics [4]. The vehicular acceleration time histories employed in the ATB simulations were based on the analyses performed using well-accepted methods in the engineering community that include vehicle-specific bumper rating strength, extent and nature of structural damage to vehicle, etc. The data set of occupant body including the segments' geometric and mass properties are computed using the Generator of Body Data (GEBOD) computer program [5]. 3.) Assessment of the state-of-the-art biomechanical predictors of brain injury. Based on the body kinematics data, we developed a computer program to calculate the results of the following, but not limited to, models published in the literature: a) resultant maximum linear and angular accelerations, the Head Injury Criteria (HIC), the Generalized Model for Brain Injury Threshold (GAMBIT), the Head Impact Power (HIP), and the Power Index (PI). 4.) Correlation of the biomechanical prediction with medical results. All of the patients in our study had complete medical record. If a patient is identified as MTBI by either clinical neurological diagnosis and/or neuropsychological assessment using the definition by American Congress of Rehabilitation Medicine [6], this patient case was called an affirmative MTBI case. We considered the occurrence of MTBI as a dependent variable and the parameters of each biomechanical model as an independent variable. By using logistic regression analysis, we could determine the power and statistical significance of each biomechanical predictor in predicting MTBI and the contribution of each biomechanical predictor in the injury mechanisms of MTBI.

RESULTS AND DISCUSSION

In our ongoing effort of biomechanical reconstruction of motor vehicle accidents, we collected the consent of 20 (n=20) patient cases with complete crash data and medical records. Of these patients, 8 (40%) (n1=8) of them are affirmative MTBI patients and 12 (60%) (n2=12) of them are non-MTBI patients used as control group. Two groups have the similar patterns in their gender and age distributions (Table 1).

Table 1: Patients' demographic data

MTBI		Gender Distribution	Age Distribution			
			Age	#	Age	#
Yes	n1=8	female = 8 male = 4	21-30	3	31-40	3
			41-50	4	>50	2
No	n2=12	Female = 6 Male = 2	21-30	0	31-40	2
			41-50	5	>50	1

The logistical regression results show that all of the biomechanical parameters are statistically significant in predicting MTBI; however, their predicting power are different and categorized from high to low in terms of -2log likelihood ratio shown in Table 2 from left to right.

CONCLUSIONS

Our comprehensive method proved to be effective and practical in studying of MTBI.

REFERENCES

1. Jager T, et al. "Traumatic brain injuries evaluated in US emergency departments, 1992-1994." *Acad Emerg Med.* 2000;**7**:134-140.
2. Ricci L. "NCSS Statistics: Light Trucks and Vans," *NTIS Report DOT-HS-805-531*, 1980a.
3. Ricci L. "NCSS Statistics: Passenger Cars," *NTIS Report DOT-HS-805-531*, 1980b.
4. Cheng H, Rizer AL. *Articulated Total Body Model Version V User's Manual*. United States Air Force Research Laboratory, 1998.
5. Cheng H, et al. "Generator of Body Data (GEBOD) Manual," *Armstrong Laboratory Report, AL-CF-TR-1994-0051*, 1994.
6. American Congress of Rehabilitation Medicine (ACRM). "Definition of Mild Traumatic Brain Injury." *J. of Head Trauma Rehabilitation*, **8**:86-87, 1993.

Table 2: Significance of Biomechanical Predictors (higher is more significant)

Biomechanical Predictor	**Ang Acc (*100r/s*s)**	**Gambit**	**PI**	**HIP**	**Delta V**	**HIC15**	**Linear Peak G**	**HIC36**
-2log likelihood Ratio	47	39	32	29	24	23	22	21

IDENTIFYING VULNERABLE PLAQUES USING MRI-BASED FINITE ELEMENT ANALYSIS

Zhi-Yong Li and Jonathan H Gillard
Department of Radiology, Cambridge, UK; email: ZYL22@cam.ac.uk

INTRODUCTION

Atherosclerotic vascular disease is the most common cause of morbidity and mortality in the world. Plaque rupture has been identified as a critical step in the evolution of arterial plaques[1], whereas the biomechanics of plaque rupture is still not fully understood[2,3]. To explore the role of biomechanics in the assessment of risk of rupture in carotid atheromatous plaque using high-resolution MRI, we used finite element analysis based on the magnetic resource imaging (MRI) method to simulate the mechanism of carotid plaque in asymptomatic and symptomatic subjects.

METHODS

Sixteen subjects, eight symptomatic and eight asymptomatic, underwent high-resolution multi-sequence in vivo MR imaging of the carotid bifurcation. All the imaging studies were conducted on a 1.5 Tesla whole body system using a customized four-channel phased array coil wrapped around the neck. The following axial 2D, ECG-gated, blood-suppressed, fast spin echo pulse sequences were used: intermediate T2 weighted (TR/TE: 2*RR/46) with and without fat saturation, T2 weighted (TR/TE: 2*RR/100), STIR (TR/TE/TI: 2*RR/46/150), and fat-suppressed T1 weighted (TR/TE: 1*RR/ 7.8). The pixel size was 0.4x0.4x3mm in all cases. Segmentation was based primarily on the STIR sequence, which was deemed to be most accurate for fibrous cap and lipid core, when compared with histology. Each patient axial MR slices were segmented manually and all contours were traced to generate the boundaries of lipid core, fibrous cap, vessel lumen and wall based on net intensity characteristics. The mesh was generated for each slice and finite element analysis was conducted in each case to determine the stresses within every plaque. The linear elastic model was used to model the plaque components. The material properties (Young’s modulus and Poisson’s ratio) were chosen based on recent publications[4]. In this study, the Young’s moduli used were: arterial wall 16.8 kPa, fibrous cap 700 kPa and lipid core 6.25 kPa, and a Poisson’s ratio of 0.49999 was used for all components. The internal luminal pressure was assigned at 15kPa. Statistical analysis was carried out for the comparison of symptomatic and asymptomatic patients.

RESULTS AND DISCUSSION

Analysis was carried out for every slice that covers the plaque along the vessel for each patient. The peak stresses are illustrated to be within the disease part of the vessel. The slice with peak stress was chosen for each patient for the comparison between symptomatic and asymptomatic patients. High stress concentration happened at the shoulder region of the symptomatic patient and the maximum stress is 344.2 kPa, while in asymptomatic patient, the stress distribution is much more averaged and the maximum stress is 150 kPa. The mean Principal stresses in the plaques of symptomatic patients are significantly higher than those of asymptomatic patients (533.4±185.3 versus 203.5±121.3 kPa, $p<0.1$). In Figure 1, mean stress with standard deviation is shown for symptomatic and asymptomatic patients and this demonstrates a significant difference between these two groups.

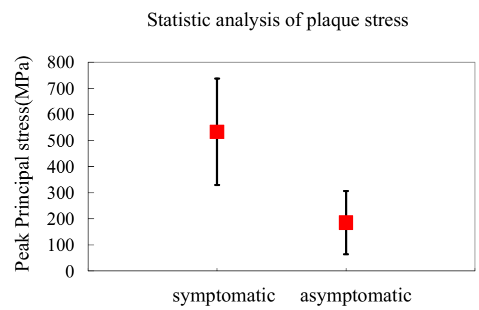

Figure 1: Comparison of plaque mean stress with standard derivation between symptomatic and asymptomatic patients

CONCLUSIONS

This Finite element analysis suggests that the maximum stresses within the plaques of symptomatic patients are higher than those of asymptomatic patients. Mechanical stress in the carotid plaque, therefore, ought to be regarded as a complementary indicator of plaque rupture risk alongside the traditional measure of stenosis. A combination of high resolution MR and finite element analysis could potentially act as a useful tool for assessment of risk in patients with carotid disease.

REFERENCES

1. Richardson, P.D. (2002) Biomechanics of Plaque Rupture: Progress, problems, and new Frontiers. Annals of Biomedical Engineering, 30, pp.524-536.
2. Arroyo, L.H. & Lee, R.T. (1999) Mechanics of plaque rupture: mechanical and biological interactions. Cardiovascular research. 41, pp369-375.
3. Cheng, et. al. (1993) Distribution of circumferential stress in ruptured and stable atherosclerotic lesions: a structural analysis with histopathological correlation. Circulation, 87, pp1179-1187.
4. Radj, et. al. (2004) Finite element modeling and intravascular ultrasound elastography of vulnerable plaques: parameter variation. Ultrasonics, 42, pp723-729.

Vibration Analysis of Tennis Racket caused by Impact between Different Configuration and Additional Weight

Yuh-Yih Lin, Chun-Ling Cho and Chen-Kai Su
Taipei Physical Education College, Taiwan, ROC
email: nigleben@yahoo.com.tw

INTRODUCTION

In the present-day tennis game, it has become the time of power. No matter serve or swing is pointed to the velocity and power. Some tennis players like to add lead to the tennis racket to increase the racket power, but they don`t understand what configuration to reduce vibration of the racket and increase racket power.

The purpose of this research is to analyze the vibration effect of tennis racket caused by impact in different configuration and additional weight to achieve the vibrant minimization. It can also increase the power of ball.

METHODS

In this experiment, we have fixed a tennis racket weight 300$^{\pm}$5 grams to a Kistler Force Plate and kept the face of the tennis racket horizontalized to the ground, and then strung the racket with 50 lb tension on strings. We drop the tennis balls from one meter height to the face of the racket. We add 5,10,15,20,25and 30 grams lead weight to racket in four configurations. These configurations are side of the back , side of the center, side of the forehand and top of the racket. We can analyze relationship of configuration and weight to the vibration of racket. Therefore we drop the ball to the center of percussion (COP) and 4 cm off-COP. We compare the difference with COP and off-COP and analyze the vibration of racket.

At the throat and head of the tennis racket, we have attached two accelerometers to capture the vibration signal of the racket. We then used two different softwares, Bioware and ACQ, to analyze the raw data from different configurations and additional weight.

RESULTS AND DISCUSSION

Data is collected from a total of 250 balls, including four configurations of side of the back , center, forehand and peak of the racket and add 5,10,15,20,25and 30 grams lead weight to racket. The information of the throat accelerometer is in figure 1. We can compare the relationship between impact force and lead weights. The information of the peak accelerometer is in figure 2. We can compare the relationship between impact force and lead weights. For example, we add 30 grams lead weight to the top of the racket. It`s effective to the racket without additional weight. If we add 5,10 and 15 grams lead weight to side of the back and center, it can`t evidently reduce the vibration of racket.

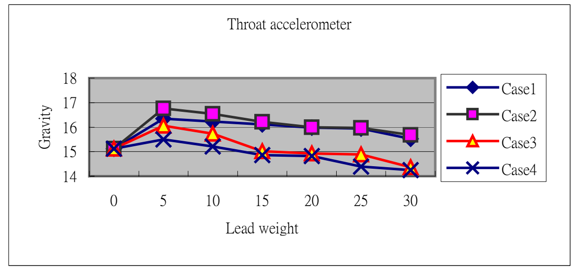

Figure 1: Relationship of the lead weight and impact force in throat accelerometer.

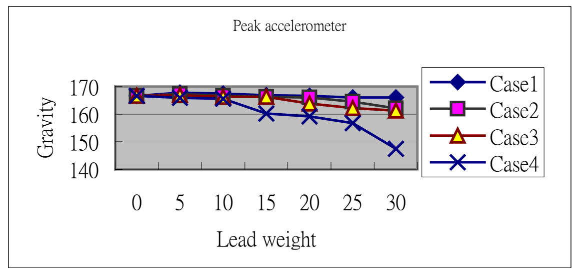

Figure 2: Relationship of the lead weight and impact force in peak accelerometer.

This study demonstrates that the incidence of lead weights and the configuration of adding weights. We find that influence of the weights and configurations. In the side of forehand and peak of the racket, it can reduce the vibration of the racket.

CONCLUSIONS

The study defined the vibration for the different configurations of impact and additional weights. But it is important to understand what configuration we add lead and how many weights we increase.

REFERENCES

1. Duane Knudson (1995), Effect of String Tension and Impact Location on Ball Rebound Accuracy in Static Tennis Impacts, *Journal of Applied Biomechanics.*
2. Howard Brody (2003), Rod Cross and Crawford Lindsey, *The Physics and Technology of Tennis*.

Table 1: The configuration of lead weight locations.

	Case1	**Case2**	**Case3**	**Case4**
Configuration	Side of the back	Side of the center	Side of the forehand	Top of the racket
Lead weight locations		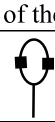		

MOMENTUM TRANSFER OF TRUNK AND UPPER EXTREMITY IN TENNIS BACKHAND STROKE

[1,2]Lin-Hwa Wang, [1,3]Shyi-Kuen Wu, [4]Kuo-Cheng Lo, [1]Hwai-Ting Lin, and [1]Fong-Chin Su
[1]Institute of Biomedical Engineering, National Cheng Kung University, Tainan, Taiwan, [2]Department of Physical Education, National Cheng Kung University, Tainan, Taiwan, [3]Department of Physical Therapy, HungKuang University, Taichung, Taiwan, [4]Department of Physical Education, Kun Shan University of Technology, Tainan, Taiwan;
email: wanglh@mail.ncku.edu.tw

INTRODUCTION

Backhand stroke is a frequently used tennis technique and the improper backhand is believed as a major factor leading to tennis elbow. The effective integration of the whole body segments as a kinetic chain transferring the momentum to the racket via the trunk and upper extremity is essential. The purposes of this study were to develop a kinetic chain model of the upper extremity in one-handed backhand stroke, and to analyze the momentum transfer from the trunk, upper extremity to racket in order to provide valuable information about the mechanisms of tennis backhand stroke.

METHODS

Six right-handed elite male tennis players (age: 26 ± 2.71 yrs, height: 175 ± 7.74 cm, body mass: 73 ± 7.25 kg) with many years tournaments experience were recruited in this study. The skill level of tennis players were rated as 5.5-6.0 according to the United States Tennis Association. The Expert Vision motion system with six cameras (Motion analysis Corp., Santa Rosa, CA, USA) was used to collect the tennis one-handed backhand motion at sampling rate of 60 Hz. Sixteen markers were attached on the selected anatomic landmarks unilaterally, and three attached on the racket to define the coordinate system of the trunk, upper arm, forearm, hand, and racket. Ten trials of backhand stroke were collected with a 3-minute rest between trials. Linear momentum ($\boldsymbol{L}$) is the product of the segment mass ($\boldsymbol{m}$) and velocity ($\boldsymbol{v}$) in the gravitational segment centre of mass position. Angular momentum in the segment coordinate system ($\boldsymbol{H}'$) is defined as the product of the principal moment of inertia ($\boldsymbol{I}$) and angular velocity in segment coordinate system ($\boldsymbol{\omega}'$). The calculation of three components of moment of inertia relative to the segment centre of mass was also adapted from the previous study [1]. The racket's moment of inertia about three orthogonal axes (longitudinal, frontal, and transverse) were computed using the pendulum method [2]. In order to obtain the segmental contribution of the upper extremity to backhand drive performance, we transferred linear and angular momentums from segmental coordinate system into the court coordinate system, in which the opposite of driving (leading) direction is X-axis, right hand side of the court as the Y-axis, and upward direction as Z-axis.

RESULTS AND DISCUSSION

The results showed the time periods of 0.40 seconds (0-24 frames) before impact and 0.27 seconds (25-40 frames) after the impact during the one-handed backhand stroke. Our results showed that the trunk has larger influence on linear momentum than angular one during the backhand stroke. Considering the resultant linear momentums of the backhand stroke, the trunk demonstrated the largest magnitude followed by the racket, forearm, upper arm, and hand. The largest trunk contribution was supported by Field and Altchek [3]. The forward, leftward, and upward trunk movements were essential for generating the racket linear momentum and stabilization of the trunk is also considered to be very effective for the sequential transfer the high force and energy through trunk. However, the insufficient angular momentums of trunk and upper arm external rotation, the potential weak links in the kinetic chain, may predispose the forearm and hand segments to the increased loads (Figure 1). The players relied on the elbow joints to generate the racket velocity and might increase the loads as well as the potential injury to this region [4]. The hand segment had a small resultant angular momentum may suggest that the players keep the hand segment stably throughout the backhand stoke. The possible explanation may be that the skilled players maintained their wrist in a relatively fixed and extended position. The small magnitudes of linear and angular momentums in hand segment may indicate the hand keeps stably in extended position for the momentum transfer rather than power generation throughout the backhand for the prevention of tennis elbow.

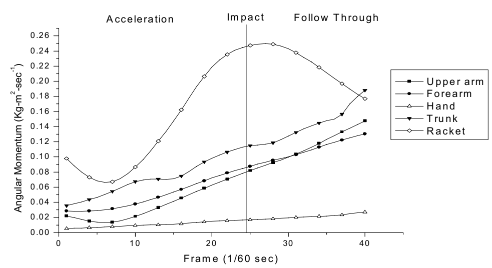

Figure 1: The resultant angular momentums of the segments.

CONCLUSIONS

The efficient kinetic chain of backhand stroke successfully transferred the momentum from proximal trunk to distal hand segments. The segment dropout or kinetic chain breakage decreases the ultimate force and energy available to the racket-ball, and puts abnormally large strains on the surrounding segments. The coaches and clinicians need to advise the tennis players to use the advantage of large trunk muscles and to improve the strength of shoulder rotator cuff muscles to generate the racket momentum for reducing the tennis-related injuries.

REFERENCES

1. McConville JT. *Tech report AFARML-TR-80-119,* 1980.
2. Brody H. *Physics Teacher* **April**, 213-216, 1982.
3. Field LD, et al. *Clin Sports Med* **14**, 59-78, 1995.
4. Kiber WB, et al. *Clin Sports Med* **23**, 545-552, 2004.

ACKNOWLEDGEMENTS

Support from NSC 89-2314-B-006-134-M08, Taiwan.

MECHANICAL EVALUATION OF THERAPEUTIC EFFECT FOR OSTEOPOROSIS VERTEBRA BY USING PATIENT-SPECIFIC FINITE ELEMENT ANALYSIS

[1]Daisuke TAWARA, [1]Jiro Sakamoto, [2]Atsushi Sekimoto, [3]Serina Awamori,
[3]Hideki Murakami, [3]Norio Kawahara, [1]Juhachi Oda and [3]Katsuro Tomita
[1]Graduate School of Natural Science and Technology, Kanazawa University, Ishikawa, Japan,
[2]Department of Human & Mechanical Systems Engineering, Faculty of Engineering, Kanazawa University, Ishikawa, Japan,
[3]Graduate School of Medical Science, Kanazawa University, Ishikawa, Japan,
email: datawara@nihonkai.kanazawa-u.ac.jp, web: http://www.hm.t.kanazawa-u.ac.jp/bionic

INTRODUCTION

To evaluate risk of compression fracture of osteoporosis vertebrae, current diagnosis methods such as measurements of bone mineral density by DXA are not sufficient, because mechanical strength is not evaluated directly. Mechanical strength of vertebra depends on patient-specific factors, which are shape, cortical thickness, density distribution of cancellous, material properties of bone tissue, and so on. So that patient-specific mechanical analysis is required. In previous study, finite-element (FE) analyses based on CT images of osteoporosis patient's vertebrae were carried out and its availability was confirmed. In this study, FE analyses of osteoporosis vertebrae undergoing drug treatment were also performed over time. Effect of drug therapy to mechanical strength recovery of vertebrae was discussed.

METHODS

Analysis target was L1 vertebra because it was located near the inflection point of spine and favorite site of osteoporosis fracture. X ray CT images were taken at 1mm intervals from 4 osteoporosis patients. All of them were Japanese female whose age was 60, 53, 71 and 72 years old respectively. Patient-specific FE models of L1 based on CT images were obtained by using "Mechanical Finder (RCCM Co.)" as shown in figure 1. This is computer software for bone strength analysis considering individual bone shape, cortical thickness and bone density distribution. Shell elements were used for cortical bone. Young's modulus of each element was given one by one calculating from bone density and CT value. Relationship between the mechanical properties and bone density proposed by Keyak [1] was used. Simple compressive loading was considered, that is, bottom surface was fixed and uniform pressure was applied to upper surface of vertebra [2].

RESULTS AND DISCUSSION

Figure 2 shows density and compressive principal strain distribution of model A at the central section before and after therapy. Drug effect in the model A was most significant. High-density area increased after therapy initiation at cortical bone and whole cancellous bone. After a year, local high strain region before therapy was almost disappeared and cancellous bone strain were totally reduced. It would be effective to prevent compression fracture of vertebra. Figure 3 shows average density and compressive principal strain of the 4 models. Drug therapy seemed to work for reinforcing strength of vertebrae in case A and B. Drug effect was also observed in case D, even though average density was not changed. Bone trabecular structure seems to be changed reducing average strain in this case.

CONCLUSIONS

Strength recovery of osteoporosis vertebra due to drug therapy was analyzed quantitatively by patient-specific FE analysis.

REFERENCES

1. Keyak JH, et al., *J Biomech* **31**, 125-133, 1998.
2. Nachemson A, et al., *Spine* **6**, 93-97, 1981.

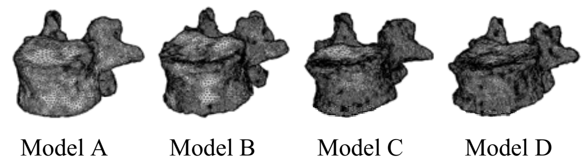

Figure 1: Patient-specific FE models of L1 before therapy

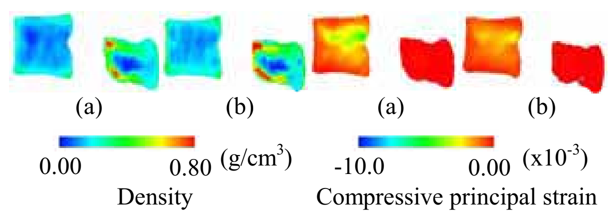

Figure 2: Density and compressive principal strain distribution of model A at central section (a: before therapy, b: after a year)

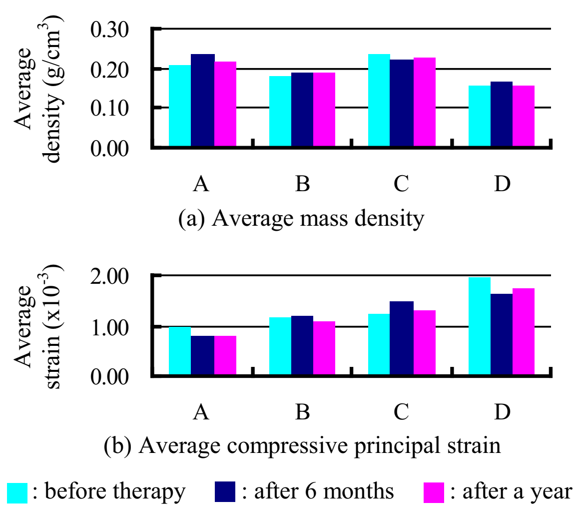

Figure 3: Average density and compressive principal strain of L1 for the patient-specific models

PATIENT-SPECIFIC DYNAMIC STRESS ANALYSIS OF OSTEOPOROSIS VERTEBRAE

[1]Daisuke Tawara, [1]Jiro Sakamoto, [2]Serina Awamori, [2]Hideki Murakami,
[2]Norio Kawahara, [1]Juhachi Oda and [2]Katsuro Tomita
[1]Graduate School of Natural Science and Technology, Kanazawa University, Ishikawa, Japan,
[2]Graduate School of Medical Science, Kanazawa University, Ishikawa, Japan,
email: datawara@nihonkai.kanazawa-u.ac.jp, web: http://www.hm.t.kanazawa-u.ac.jp/bionic

INTRODUCTION

Mechanical strength analysis using finite-element (FE) method is effective to predict a risk of compression fracture of osteoporosis vertebrae. Bone fracture in clinical case of osteoporosis sometimes occurs under the dynamic load condition during transition process from sitting down position to standing position. Patient-specific dynamic FE analysis is necessary to evaluate mechanical strength of osteoporosis for the clinical condition. In this study, dynamic FE analyses of osteoporosis vertebrae were performed considering individual shape and material property based on CT images of patients. Differences of fracture risk depending on patient's case and availability of dynamic analysis was discussed comparing with the results of the static analysis.

METHODS

Finer finite-element meshing is required for patient-specific analysis to reflect individual bone shape and material properties. We used finite-element code "NEXST_Impact (FSIS, Japan)" [1], which can solve large-scale dynamic problem by using parallel processing. Analysis target was L1 vertebra because it was located near the inflection point of spine and favorite site of osteoporosis fracture. X ray CT images were taken at 1mm intervals from 4 Japanese female osteoporosis patients whose age was 60, 53, 71 and 72 years old. Patient-specific FE model of L1 based on CT images were obtained by "Mechanical Finder (RCCM Co.)" that was software to make FE models considering individual bone shape and density distribution. Young's modulus of each element was given one by one calculating from bone density and CT value. Relationship between the mechanical properties and bone density proposed by Keyak [2] was used. An example of FE model and its density distribution of whole model and central section are shown in figure 1. Simple dynamic compressive loading was considered in the analyses, that is, bottom surface was fixed and uniform step pressure was applied to upper surface of vertebra [3]. Dynamic analysis was done in the t=0.0(ms) to t=5.0(ms) range by setting time of loading as t=0.0(ms) and analysis time step was 2.0(μs).

RESULTS AND DISCUSSION

Figure 2 shows Mises stress distribution by time steps in dynamic analysis. Stress wave propagated along high-density region. Peak of stress in dynamic analysis occurred slightly delay after loading. High stress widely occurred at the anterior surface of cortical bone. It is reasonable because load seems to concentrate at cortical bone by low load sharing at cancellous bone in osteoporosis vertebrae. Table 1 shows maximum Mises stress value of dynamic analysis and static analysis of the 4 models. Results of dynamic analysis exceeded that of static analysis in 3 models. It was suggested that static analysis solution give us underestimation of bone fracture risk of vertebrae in comparison with clinical condition that involves dynamic loading.

CONCLUSIONS

Stress wave propagation process of osteoporosis vertebra was shown precisely by patient-specific dynamic FE analysis.

REFERENCES

1. http://www.fsis.iis.u-tokyo.ac.jp/
2. Keyak JH, et al., *J Biomech* **31**, 125-133, 1998.
3. Nachemson A, et al., *Spine* **6**, 93-97, 1981.

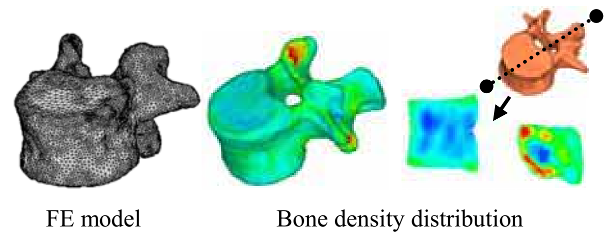

Figure 1: FE model and density distribution of whole model and central section view

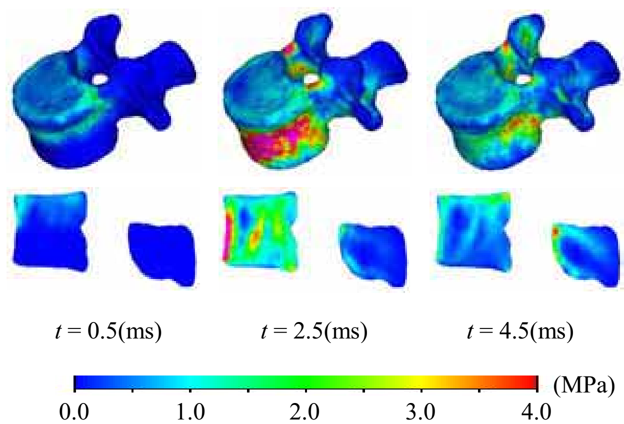

Figure 2: Mises stress distribution of dynamic analysis in model and central section

Table 1: Maximum Mises stress value of dynamic analysis and static analysis of the 4 models

Model	A	B	C	D
Dynamic analysis (MPa)	7.25	12.4	34.3	24.4
Static analysis (MPa)	3.61	13.8	23.5	16.8

INFLUENCE OF HARDNESS OF BED ON HIP JOINT WITH USE OF TRUNK TREMOR

[1]Maya Kawabata, [1]Kazuyuki Mito, [2]Hitoshi Makabe, 3Byung- Chan Min, [4]Kenichi Kaneko, [1]Kazuyoshi Sakamoto
[1]The University of Electro-Communications, Japan, [2]Yamagata Prefectural University of Health and Science, Japan,
[3]Hanbat National University, Korea, [4]Fuji University, Japan; [1]email:sakamoto@se.uec.ac.jp

INTRODUCTION

Researches of tremor, which is invisible mechanical vibration of body parts, have been published for finger and upper limb. The mechanism of tremor was resolved that the generation was caused by both central nervous and reflex nervous systems [1,2]. The study for trunk, however, has not been reported. Therefore, in the study, the function of hip joint was evaluated by trunk tremor after sleep with use of beds with different hardness.

METHODS

In the first place, the characteristics of trunk tremor by the change of bend angle of trunk were measured as fundamental data. In the next place, the influence of sleep on the trunk tremor was researched with different kinds of bed.

Subject slept for eight hours (night sleep) and 90 minutes (day sleep). The former sleep started at 0:00 and latter sleep started from 13:00. The day sleep period was adopted due to one cycle of sleep period. Subject used two kinds of bed, that is, soft and hard beds which rate of the hardness of beds was 1.35. The soft bed made of material with low elasticity, while the hard bed was on the market. Tremor of trunk under the bent posture was measured before and after the sleep.

Measurement system for trunk tremor is shown in Fig.1. Subject gazed a target point P to hold a bent angle θ chosen in the experimental protocol, in which the bent angles were taken to be 0, 20, 40, and 60 degrees. Tremor was detected by accelerometer (9G111BW, NEC Sanei) glued with both sides adhesive tape on upper part of the back around vertebra thoracica I. The resultant raw wave was sampled by 100Hz, transformed by AD converter, and stored to computer. The power spectrum was obtained by FFT (Fast Fourier Transform). The tremor was evaluated by total of power spectra (TP) in frequency range from 2.5 to 40 Hz. The frequency range was also divided into two frequency bands, i.e., lower band of 2.5 to 6 Hz and higher band of 6 to 40 Hz. The former and the latter bands showed the reflex nervous component and the central nervous component, respectively [1,2]. The subjects were ten aged 21 to 64 years old.

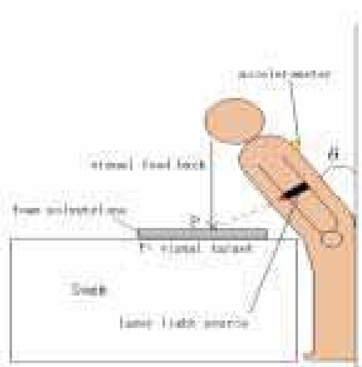

Figure 1: Experimental system for measurement of trunk tremor.

RESULTS AND DISCUSSION

The total power for the change of bent angle was evaluated, since larger angle gave larger load to hip joint for the maintenance of posture. The results showed that larger bent angle was charged, the larger total power was obtained. The tendency was obtained remarkably for the lower frequency band (2.5 to 6 Hz). Namely, the reflex nervous contributed predominantly for the hold of bend posture.

The influence of day sleep for two kinds of beds on the total power of tremor was not recognized significantly, but the influence of the night sleep was recognizeed significantly for the bent angles of 40 and 60 degrees as shown in Fig.2. The sleep with soft bed denoted lower amplitude of tremor as compared the sleep with hard bed. Especially, the bent angle 60 for soft bed showed the value less than unity. The case meant the amplitude of trunk tremor after sleep decreased as compared with the value before sleep. Analyzing the influence of trunk tremor due to sleep, the function of hip joint could be revealed.

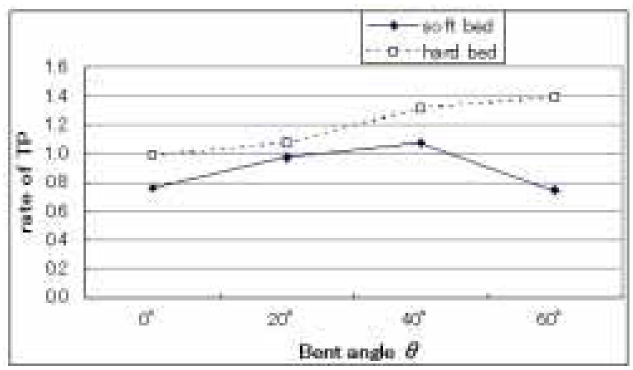

Figure 2: Rate of total power (TP) after night sleep based on TP before the sleep with sue of soft and hard beds for bent angle θ. Unity of the rate value denotes the value before sleep

CONCLUSIONS

Characteristics of tremor in bent posture for normal subjects were elucidated. The results could be applied to evaluate the degree of hip disorder. The influence of night sleep with beds of different materials due to trunk tremor was recognized, so the relax of muscles for hip joint could be evaluated with use of trunk tremor

REFERENCES

1. .Miao T and Sakamoto K *Electromyogr. Clin. Neurophysiol.,* **37**, 343-357, 1997.
2. Sakamoto K et al. *Electromyogr. Clin. Neurophysio.,,***38**, 103-313,1998

CHANGES IN MECHANO- AND ELECTROMYOGRAM DURING LOW-FORCE STATIC CONTRACTION IN SUBJECTS WITH UNILATERAL EPICONDYLITIS LATERALIS

[1]Anne Katrine Blangsted, [1]Pernille Kofoed Nielsen, [2]Michael Kjær and [1]Karen Søgaard
[1]Department of Physiology, National Institute of Occupational Health, Denmark, [2]Sports Medicine Research Unit, Bispebjerg Hospital, Denmark;
email: akb@ami.dk, web: www.ami.dk

INTRODUCTION

In modern information society an increasing number of jobs induce musculoskeletal disorders (MSD) even though the work is characterized by low physical exposure levels. Development of prediagnostic tools may be a step towards efficient strategies aiming to prevent MSD as well as improving the understanding of the basic mechanisms of muscle pain and disorders induced by low-force contractions.

In order to identify possible precursors to muscle pain and disorders, the electromyogram (EMG) has been used to identify muscle fatigue development for prevention purposes. However, during low-force work tasks such as computer work the sensitivity and the ability of the EMG to detect muscle fatigue is limited. Recently, the mechanomyogram (MMG), suggested to reflect the “mechanical counterpart” to the motor unit electrical activity, has been shown to be a promising method for detection of muscle fatigue during such low-force contractions [1]. Since experimentally induced muscle pain seems to be reflected in the MMG rather than the EMG activity [2], it is in this study hypothesized that a low-force contraction of a painful muscle compared to a no pain muscle may evoke a different MMG response. Further, that this pain related difference will be more pronounced in the MMG than in the EMG response.

METHODS

Eight patients (5 females, 3 males) with unilateral epicondylitis lateralis were sitting with the elbows flexed 90 degrees, the forearms pronated and resting on horizontal platforms. In this position they performed static wrist extension at 10% of maximal voluntary contraction (MVC) for 10 min against a force transducer with both the afflicted arm (AA) and the non-afflicted arm (NA) in a random order. During the static contraction, MMG was recorded by an accelerometer placed on m. extensor carpi radialis (ECR) and bipolar surface EMG was recorded from ECR, m. extensor carpi ulnaris (ECU), and a forearm flexor muscle (FLEX). The MMG and EMG were analyzed for root mean square amplitude (MMGrms and EMGrms). Furthermore, subjective perceived exertion was rated by the Borg scale from 0 (no perceived exertion) to 10 (maximum perceived exertion) during the 10% MVC contraction.

RESULTS AND DISCUSSION

The performed force level was on average 9.9 (SD 0.2)% MVC for AA and 10.1 (SD 0.5)% MVC for NA with no significant difference, showing that the task of meeting the target force of 10% MVC was accomplished successfully for both arms. Despite of that, the subjects reported significantly higher level of perceived exertion during the contraction in the AA compare to the NA trial.

EMGrms of ECR increased with time from 45.7 (SD 15.3) to 63.1 (SD 29.5) μV in AA and from 48.6 (SD 18.5) to 58.4 (SD 23.2) μV in NA, with no significant difference between AA and NA. However, the MMGrms of ECR tended to increase more in the AA trial (from 0.05 (SD 0.03) to 0.16 (SD 0.14) $m*s^{-2}$) during the contraction compared to the NA trial (from 0.04 (SD 0.02) to 0.08 (SD 0.06) $m*s^{-2}$). Increase in MMGrms has previously been shown simultaneously with a decreased twitch force [1]. In accordance with this, the pronounced time wise change in the ECR MMGrms of AA during the 10% MVC contraction in the present study may be interpreted as a decreased force output of the activated low-threshold motor units. In order to meet the same force level either an increased activation of the ECR or of some of the synergist muscles is necessary. In line with this, the ECU EMGrms of AA increased significantly from 51.6 (SD 19.5) to 68.8 (SD 18.3) μV while no change was seen with time for NA. For FLEX EMGrms no difference was found between AA and NA. These findings may support the *pain adaptation model* proposing a change in muscle activation due to pain [3]. The increased activation of ECU in AA was not a compensation for a larger antagonist activity. Rather, it may be considered to make up for the corresponding force deficit of the fatigued ECR muscle. A faster fatigue development of the AA was evidenced by the larger increase in perceived exertion.

CONCLUSIONS

The results indicate that the MMG activity in contrast to the EMG is modulated in the afflicted arm of patients with epicondylitis lateralis. MMG could possibly be useful as a non-invasive method to investigate changes in the neuromuscular system and may be developed to serve as a prediagnostic tool for objective identification of MSD.

REFERENCES

1. Blangsted AK, et al. *J Electromyogr Kinesiol* **15**, 138-148, 2005.
2. Madeleine P & Arendt-Nielsen L. *J Electromyogr Kinesiol* **15**, 27-36, 2005.
3. Lund JP, et al. *Can J Physiol Pharmacol* **69**, 683-694, 1991.

ACKNOWLEDGEMENTS

The Danish National Research Foundation supported this work (Grant no. 22-04-0488).

TRUNK STIFFNESS IMPROVEMENT BY PHYSICAL THERAPY/EXERCISE DURING UNSTABLE SITTING

H. Lee, K. P. Granata, M. Piechoski
Musculoskeletal Biomechanics Laboratory, Virginia Tech
Department of Engineering Science & Mechanics.
School of Biomedical Engineering & Science
email: Granta@vt.edu web: http://www.biomechanics.esm.vt.edu/msbiolab/

INTRODUCTION

Many studies have examined the role of physical therapy (PT) and/or exercise on prevention, rehabilitation and recurrence rate of low back pain (LBP). One of the aims of PT exercises is to modify the neuromuscular control of spinal stability. However, effect of PT exercises on neuromuscular control of the trunk is still unclear.

Research demonstrates that seated sway can be used to identify differences in neuromuscular control between patients with LBP and asymptomatic controls [1]. Therefore, the purpose of this present study was to test whether PT exercises influences neuromuscular control of stability by assessment of seated sway.

METHOD

A control group of twenty-seven subjects and a PT-exercise group of twenty-eight subjects with no previous history of low back pain were tested. Subjects in the PT-exercise group participated in a program consisting of 8 PT exercises every day for 12 weeks. Both control and PT-exercise subjects performed a seated sway test at baseline (week 0) and once every 4 weeks for an interval for 12 weeks. To measure trunk sway, each subject maintained an upright seated posture on a flat platform. They sat with thighs resting horizontally on the platform and knee flexed 90^0 hanging over the edge of the platform. Leg and foot supports were provided to prevent any lower-limb movement. Subjects were required to sit quietly for 90 seconds with a barbell of 0% and 30% of body weight on their shoulders. Trunk sway was recorded at 1000 Hz from a force plate underneath the seat/platform and filtered at 10 Hz using a fourth order Butterworth digital filter.

The center of pressure trajectories were calculated from the force and moment data. Analysis included mean sway frequency in anterior/posterior and lateral directions, a total CoP path length traveled per second, and 95% confidence ellipse area of COP.

RESULTS AND DISCUSSION

There was no significant difference in performance between the groups at initial assessment. After 12 weeks of PT the PT-exercise group had smaller ellipse area but longer path length (Table 1). This indicates that the PT-exercise group moved more but constrained the movement within a smaller area. This suggests possible differences in effective trunk stiffness between groups. To verify this, we created a mechanical inverted pendulum held upright by steel springs stretched from the pendulum to its base. When disturbed the pendulum-spring system would oscillate and COP was recorded. Using a stiff spring the ellipse area was smaller but path length was longer than when using a more compliant spring. This was because the system with greater stiffness oscillated at a higher frequency than a system of less stiffness (Figure 1). Similarly, mean sway frequency of the PT-exercise group was greater than in the control group ($p < 0.0001$ anterior/posterior only).

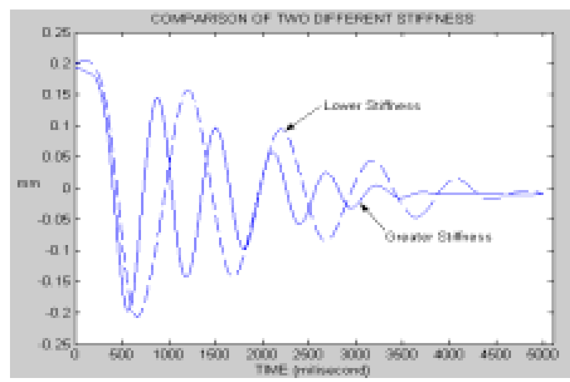

Figure 1: CoP displacements from inverted pendulum with springs of two different stiffness.

CONCLUSION

Following a 12 week program of PT exercise the postural control of the trunk demonstrated characteristics consisted with increased trunk stiffness. Results suggest PT-exercises contribute to improved neuromuscular control of stability. Further research is necessary to identify specific neuromuscular contributions to spinal stability and the factors that influence them.

REFERENCES

1. Radebold, et al.. *Spine* **26**, 724-730, 2001.

Research Support: CDC NIOSH R01 OH07352-01

Table 1, Mean (standard deviation) ellipse area and path length of the seated sway center of pressure (COP) movement while holding a barbell on the shoulders with 0% and 30% of body weight.

VARIABLE	GROUP	LOAD[A]		GENDER[B]		TOTAL[C]
		0 %	30 %	MALE	FEMALE	
Ellipse Area (mm^2)	CONTROL	20.08 (14.68)	48.39 (29.69)	30.05 (23.72)	39.35 (30.57)	34.23 (27.32)
	EXERCISE	13.23 (7.19)	23.02 (11.06)	17.92 (9.89)	18.39 (11.37)	18.12 (10.52)
Path Length (mm/s)	CONTROL	9.58 (2.33)	10.42 (2.56)	9.50 (2.53)	10.55 (2.32)	1.00 (2.48)
	EXERCISE	13.02 (3.57)	13.84 (4.27)	11.95 (3.31)	14.90 (3.99)	13.43 (3.94)

A: Load was significant at $p < 0.0001$ for EA and $p < 0.006$ for PATH.
B: Gender was significant at $p < 0.005$ only for PATH.
C: Total EA and PATH between groups were significant at $p < 0.001$ and $p < 0.001$, respectively.

SIMULATION OF FORWARD FALLS: EFFECTS OF FALL STRATEGY AND AVAILABLE MUSCLE STRENGTH ON INJURY RISK

[1] Jia-Hsuan Lo and [1] James Ashton-Miller
[1] University of Michigan, Ann Arbor
email: joshualo@umich.edu

INTRODUCTION

Skilled use of the upper extremities can significantly reduce the magnitude of the fall-related impact force on the distal forearm during a forward fall [1]. However, simulations have shown that age-related decline in arm muscle strength reduces the ability to arrest a forward fall without a risk of torso and/or head impact [2]. It is not known whether lower extremity movement strategies used during the fall might ameliorate this effect. To investigate this we used direct dynamics simulations to test the hypothesis that the use of knee flexion in a forward fall reduces the impact severity in the presence of an age-related strength decline.

METHODS

A 2-D sagittal-symmetric, 7-segment rigid body model was used to simulate forward falls from a 20º forward inclination. Segments were connected by revolute joints, and the movement of each joint was driven by a pair of agonist and antagonist joint muscle torque actuators. Each actuator employed a Hill-type model with muscle excitation-activation dynamics [3]. A feedback proportional controller was used to drive each joint to a prescribed configuration (given target angle maintained with zero angular velocity) for the first impact. After the first impact, a final prescribed configuration was given to the controller. Gender differences were simulated by appropriate body segment and joint torque data, while age-related strength declines of 30% were assumed for healthy older adults. We simulated two fall strategies with different first impact configurations (Fig. 1): hip flexion with ("H & K") or without knee flexion ("H)", by constraining the prescribed joint angle ranges. The optimal prescribed joint configuration was then found via a global optimization method ("GCLSOLVE" [4]) that minimized the impact injury risk Φ, defined as the maximal ratio of the peak impact forces at wrist, elbow, knee and head to their corresponding fracture tolerances. The objective function was constrained by available joint torques for each age and gender group.

RESULTS AND DISCUSSION

For both young men and women, both fall strategies ('H' and 'H & K') resulted in similar impact injury risks. However, in the presence of age-related strength decline, the 'H' ("Hip

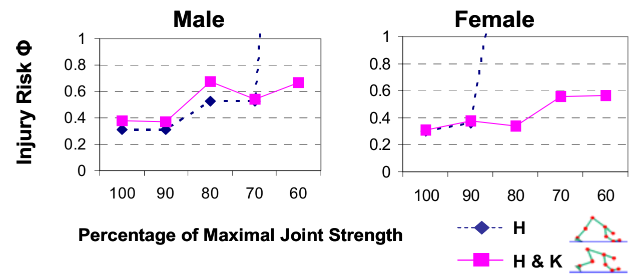

Figure 1: *Injury risk, Φ, versus joint strength relationships.*

Flexion Only") strategy becomes ineffective for avoiding head impact for both genders, as reflected in Φ (Fig 1). The simulations suggest that the better fall strategy for older women is to flex both hips and knees (the 'H & K' strategy) such that they land first on the hands and soon after on the knees. For the older men and young adults the hip flexion strategy ('H') was only slightly better than the 'H & K' strategy, the latter affording the largest head clearance (Fig. 1 & Table 1). The older adult falls resulted in greater injury risks (old: Φ=0.53 & 0.55 vs. young: 0.31 & 0.30 for men and women, respectively; Table 1), while their kinetic energy at impact was similar to those in the young. The optimizer selected straighter elbow angles at impact in order to compensate for strength decline, and this is the main reason for the greater Φ in the old (see θ_{Elbow} in Table 1). These results reflect a forward fall from near-upright stance; further simulations are needed to study arrest behaviors during gait.

CONCLUSIONS

1) Knee flexion reduces the risk of head impact in a forward fall arrest.
2) The hip and knee ('H & K') flexion strategy is the better of the two arrest strategies, particularly in older women.
3) Straighter impact elbow angles are required to avoid head impact in the presence of age-related strength declines.

REFERENCES

1. DeGoede KM, et al. J Biomech **35,** 843-848, 2002
2. DeGoede KM, et al. J Biomech **36,** 413-20, 2003
3. Pandy MG, et al. J Biomech **23,** 1185-1198, 1990
4. Holmstroem K. Adv. Model. Optim. **1,** 47, 1999

Table 1: *The first-impact and final body configurations of the better forward fall arrest strategies for young/old male/female.*

	Body Wt. and Ht.	Strength Factor	Body Configuration: Initial	Body Configuration: First-Impact	Body Configuration: Final	Impact KE (J)	θ_{Elbow} (°)	Injury Risk Φ	Max. Impact Force (N): Wrist	Max. Impact Force (N): Knee
Young Men	75 kg, 1.75m	1		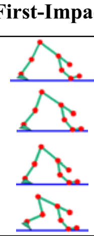	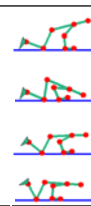	56	36	0.31	616	349
Old Men	75 kg, 1.75m	0.7				57	23	0.53	1054	529
Young Women	60 kg, 1.63m	1				46	32	0.30	607	974
Old Women	60 kg, 1.63m	0.7				44	14	0.55	1115	1722

MECHANICAL PROPERTIES OF THE SHOULDER LIGAMENTS UNDER QUASI-STATIC AND DYNAMIC LOADING

[1] Sung-Woo Koh, [1]John M. Cavanaugh, [1]James P. Leach, and [2]Stephen W. Rouhana
[1]Wayne State University, Detroit, MI and [2]Ford Motor Company, Dearborn, MI, sungwookoh@hotmail.com

INTRODUCTION

The tensile properties of the shoulder ligaments under dynamic loading have not been investigated. A recent finite element model showed the ligaments in the shoulder were subjected to dynamic tensile loading during 8.65 m/s lateral shoulder impact [1]. The mechanical properties of shoulder joints under dynamic loading are needed to better understand shoulder injury mechanisms, to improve shoulder finite element models and to further develop the shoulder of car crash dummies.

METHODS

Thirty-three fresh human shoulders were harvested and bone-ligament-bone specimens of acromioclavicular joint (AC), coracoclavicular ligament (CC) and sternoclavicular joint (SC) were obtained. The age range of test subjects was 47 to 95 years, with 13 shoulders from males and 10 from females. A test fixture and clamps specifically designed for this ligament study and a high-speed Instron machine were used (Fig 1). One quasi-static rate (0.1 %/sec) and two high rates (nominally, 15,000 %/sec and 40,000 %/sec) were used in this study.

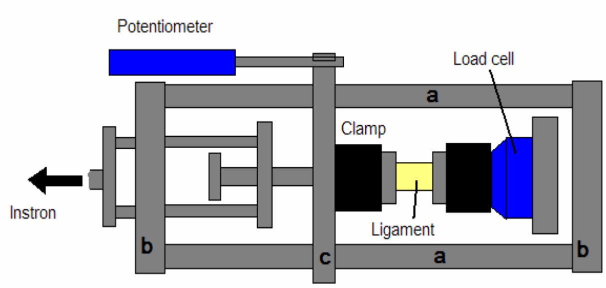

Figure 1. Diagram of the shoulder ligament test setup. Thompson shafts (a) and aluminum plates at the ends (b). The fixture included an additional aluminum plate (c) which was connected and moved with the Instron actuator.

RESULTS AND DISCUSSION

Eighty-three specimens were tested at three different strain rates. In acromioclavicular joint (AC) tests, ligament failure was the most common failure mode. In coracoclavicular (CC) bone-ligament-bone tests, the majority of specimens failed at the ligament. In sternoclavicular joint (SC) tests, the specimen failed at the bone in most cases. In AC and CC tests, 15,000 %/sec tests and quasi-static tests had more bone fracture cases than 40,000/sec tests. The Young's modulus and ultimate load of the three joints were found to be significantly lower in the 0.1 %/sec tests compared to the 15,000 %/sec tests but not significantly different between 15,000 %/sec and 40,000 %/sec tests (Table 1). There was no significant relationship between the ligament cross sectional area and subject age, height and weight. In addition, there was no significant relationship between mechanical properties of the shoulder joints and anthropometric data or age. However, specimens from younger subjects were not available for this study. This appears to be the first published study describing the mechanical and structural properties of the AC and SC. The 40,000 %/sec strain rate is the highest published strain rate ever used and analyzed for ligament studies. Overall, the shoulder ligaments showed larger ultimate strain and smaller ultimate stress and Young's modulus than animal or human knee ligament [2]. The capacity of large ultimate strain in shoulder ligaments may contribute to the large range of motion attainable in the shoulder.

REFERENCES

1. Iwamoto et al. 44th Stapp Car Crash Journal, SAE Paper No. 2000-01-SC19, 2000.
2. Koh et al. 48th Stapp Car Crash Journal, SAE Paper No. 2004-22-0006, 2004.

ACKNOWLEDGEMENTS

This research is supported by a URP grant from Ford Motor Company.

Table 1. Mechanical and structural mean values (+/- standard deviation) of 83 shoulder joints at three different strain rates

	Strain rate (%/sec)	Deflection at failure (mm)	Load at failure (N)	Strain at failure (%)	Young's modulus (MPa)
Acromioclavicular ligament (N=32)	40000 (N=13)	15 (+/- 4.0)	696 (+/- 218.3)	105 (+/- 20)	10.6 (+/- 1.7)
	15000 (N=10)	13 (+/- 7.1)	849 (+/-297.1)	81 (+/- 35)	9.6 (+/- 4.5)
	0.1 (N=9)	11 (+/- 2.1)	464 (+/- 101.1)	80 (+/- 17)	6.3 (+/- 1.2)
Coracoclavicular ligament (N=31)	40000 (N=12)	17 (+/- 7.6)	389 (+/- 194.1)	86 (+/- 34)	10.0 (+/- 3.8)
	15000 (N=10)	14 (+/- 4.3)	345 (+/- 132.1)	58 (+/- 18)	9.0 (+/- 3.8)
	0.1 (N=9)	14 (+/- 4.0)	155 (+/- 80.2)	79 (+/- 39)	3.4 (+/- 1.8)
Sternoclavicular ligament (N=20)	40000 (N=5)	12 (+/- 3.5)	670 (+/- 406.9)	62 (+/- 19)	10.2 (+/- 2.8)
	15000 (N=7)	13 (+/- 3.6)	604 (+/- 255.0)	50 (+/- 13)	12.7 (+/- 2.3)
	0.1 (N=8)	8 (+/- 2.4)	334 (+/- 143.7)	39 (+/- 10)	6.2 (+/- 0.6)

LOWER EXTREMITY MUSCLE ACTIVITIES OF TRANS-FEMORAL AMPUTEES WHEN A SLIP OCCURS IN GAIT

[1]Jiankun Yang, [1]Dewen Jin, [1]Rencheng Wang, [1]Jichuan Zhang, [1]Linhong Ji, [2]Xin Fang, [2]Dawei Zhou, [3]Ming Wu

[1]Division of Intelligent and Biomechanical System, State Key Laboratory of Tribology, Tsinghua University, Beijing (100084), PR China email: jdw-om@tsinghua.edu.cn (Dewen Jin)
[2]China Center of Orthopedic Technology (CHICOT), Beijing (101601), PR China
[3]Northwestern University Medical School, Chicago, IL, 60611, USA

INTRODUCTION

Lower extremity muscle activities always play an important role of human locomotion and balance. In nowadays, surface electromyography (sEMG) is a major method to identify muscle activities. So that, many researchers have used sEMG to investigate the human balance strategies in slips and falls [1, 2]. In comparison with the healthy person, the trans-femoral amputee's ability to recover from slips is weakened obviously due to the absence of one leg. The purpose of this study is to investigate that the sEMG response of trans-femoral amputees when a slip occurs at the heel contact (HC) moment in gait.

METHODS

Six male unilateral trans-femoral amputees and five male healthy non-amputees participated in the current study. Each subject was required to walk at a self-selected comfortable pace along a 5 m plastic walkway, and to perform two walking trials on dry and oily conditions respectively. In oily condition, the motor oil (40#) was evenly applied across 2 m long in the middle of the walkway. A pair of parallel bars was used to protect the subjects against real falls.

The sEMG data were recorded using several bipolar surface electrodes (DE-2.1, Delsys Inc., Boston, MA, USA), which were placed on the skin overlying the muscle bellies of tibialis anterior (TA), gastrocnemius medialis (GM), rectus femoris (RF), biceps femoris (BF), gluteus maximus (GMA), gluteus medius (GME), erector spinae (ES), obliquus externus abdominis (OA) on both sides, unless the muscle was unavailable because of amputation. For analysis, the instantaneous power (IMP) was employed. Each IMP was then low-pass filtered and normalized to its own mean value. At the same time, the Qualysis Motion Capture System (Qualisys Medical AB, Sweden) were employed to record the kinematics data of each trail at 200 Hz synchronously.

RESULTS AND DISCUSSION

When a slip occurred at HC moment for normal people, the power increase of TA, BF, GMA, GME and ES muscles on the anterior leg was observed obviously. All these muscles contracted to lock the ankle, knee, hip and waist joints. And then, if the body fell backward continuously, the power of RF and GMA muscles on the posterior leg increased significantly in order to support the falling body. Thus, it was demonstrated from the muscle activities that there were two steps to recover from a slip-and-fall event, "anti-slip" and "anti-fall", for healthy persons.

However, the muscle responses of trans-femoral amputees differentiated from that of non-amputees for the absence of their legs. When the anterior prosthetic limb encountered a slip at HC moment, which is mostly happened while the subjects walking on slippery surface, the absence of some body parts on the amputated side made the subject unable to sense the slip in time, so that, no timely anti-slip adjustment was implied soon enough. In these cases, slips usually induced complete falls. The function of the GMA muscle on the prosthetic side was mainly to "pull" back the sliding leg when fall had taken place, while the GMA muscle on the intact side contracted to support the falling trunk.

In other cases that the sound limb was anterior and encountered a slip at HC moment, the sliding limb could be locked and stabilized in time but the prosthetic limb was usually not competent for supporting the body. In this situation, the GMA muscle on the sound side cooperated with other muscles together to stabilize the sliding leg. If balance was regained rapidly, the process would continue. Nevertheless, if the adjustments on the sound side could not overcome the perturbation, the GMA muscle on the prosthetic side would act to support the falling trunk. Whether the prosthetic could do so, would depend on the function of the prosthesis. Therefore, the fall danger for amputees is much higher than non-amputees.

CONCLUSIONS

1) For normal persons, the anti-slip and anti-fall response strategies are employed in sequence to regain balance when a slip occurred. But for the absence of some muscles it is difficult for trans-femoral amputees to regain balance. 2) GMA muscles always made enormous contribution to balance control in the slip events, and it was much more obvious for the trans-femoral prosthesis users than for normal people. Moreover, the GMA muscle on the prosthetic limb acted as the compensation of the absent muscles. 3) The sEMG of GMA muscles were very sensitive to slips and could be used for slip detecting. The knowledge could be helpful for detecting the slip event and developing the device preventing the falls.

REFERENCES

1. Ferber R, et al.. Reactive balance adjustments to unexpected perturbations during human walking, *Gait and Posture* **16** (3), 238-248, 2002.
2. Marigold DS, et al.. Role of the unperturbed limb and arms in the reactive recovery response to an unexpected slip during locomotion, *Journal of Neurophysiology* **89**, 1727-1737, 2003.

ACKNOWLEDGEMENTS

Supports: NSFC (No. 30170242) and NHTRD (863) (No. 2001AA320601).

Phase plane analysis of stability in turning movement in subjects with functional ankle instability

[1, 2] Nobuhiro Kito, [3]Koichi Shinkoda and [3] Naohiko Kanemura
[1]Kawashima Orthopaedic Hospital, [2]Programs for Health Sciences, Graduate School of Health Sciences, Hiroshima University, [3]Division of Physical Therapy and Occupational Therapy Sciences, Graduate School of Health Sciences, Hiroshima University, ; e-mail: kito1@muse.ocn.ne.jp

INTRODUCTION

Functional ankle instability (FAI), a tendency for the foot to repeatedly sprain or give way, is a late complication in roughly 10 to 30% of acute ankle sprains. Postural control deficits during quiet standing after acute ankle sprain and in those with FAI have been frequently reported. The task of maintaining posture during quiet standing may not place adequate demands on the postural control system to detect deficits stemming from FAI. In addition, Balance Testing is commonly done using force plates and some measure of the center of pressure movement called, postural sway. Several different parameters are used to quantify postural sway, such as mean sway path, area measures, sway area and velocity measures, mean sway velocity. However, it is now obvious that physical systems are dynamic systems. Their activities are inherently nonlinear, and so nonlinear tools are required in order to understand and manage FAI. The dynamic systems approach suggests a different approach that concentrates not on the number of parameters of stability, but on the consistency of motion as a measure of stability. Our purpose deals with a phase plane analysis of COP (center of pressure) trajectory during the turning movement. This turning movement during in the standing position is one movement complicated by “giving way”. Understanding the normal control mechanisms of the turning movement, based on measuring and analyzing variations in the mechanisms of affected ankles, is a prerequisite to evaluating possible treatment outcome.

METHODS

Three subjects with unilateral FAI (mean age 25.5 years) and one control subject with a healthy ankle (age 24 year) consented to participate in this study. FAI was defined as an individual having sustained an inversion ankle sprain. The same ankle also needed to have had a feeling of “giving way”. Mechanical instability was assessed with the Anterior Drawer and Talar Tilt tests by taking at stress radiography. First, the subject stood with weight evenly distributed on the force plate. Then the subject transferred his/her body weight onto the right leg and turned that produced external pelvic perturbation relative to the weight-bearing femur. After returning to the neutral position, the subject transferred his/her weight onto the left leg and turned again. This was repeated 2 times, with each series of movements being 40 seconds in length.

Phase plane analysis of COP was performed to assess postural stability during the turning movement. Plotting the COP state variables, in this case displacement and velocity, in the medio-lateral (M/L) and anterior-posterior (A/P) direction is an informative tool for quantifying balance control. In addition, plotting the vertical floor reaction force (Fz) variables, in this case the Fz value and 1-time differentiation value, is an informative tool for quantifying the body weight transfer onto the supporting leg.

RESULTS AND DISCUSSION

On the phase plane plot in the M/L direction, difference became clear between subjects with FAI and the subject with a healthy ankle. In the subject with a healthy ankle, the trajectory on the phase plane in the M/L direction was divided into two trajectories: an acceleration trajectory in shifting weight, and a limiting cycle/ convergent trajectory above the x-axis on the phase plane for turning movement (Figure 1). These two trajectories were called Phase 1 and 2, respectively, for convenience. In subjects with FAI, two trajectory patterns on the phase plane in the M/L direction were recognized. One pattern did not show a limiting cycle trajectory for the turning movement, but rather the trajectory rapidly converged above the x-axis on the phase plane (Figure 2). The other pattern did not typically converge at one point above the x-axis on the phase plane during turning posture is maintained (Figure 2).

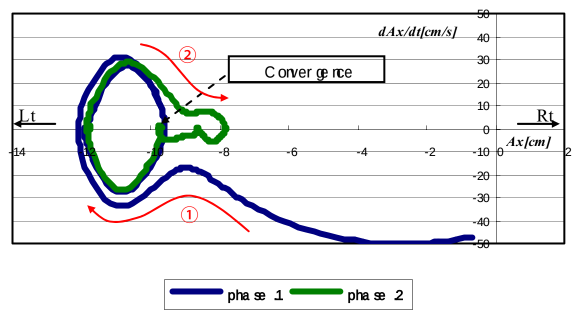

Figure 1: Phase plane in M/L direction of left healthy ankle

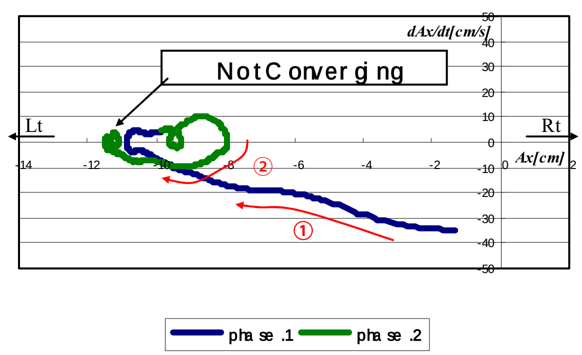

Figure 2: Phase plane in M/L direction of left FIA ankle

CONCLUSIONS

We believe that the quantity and quality of COP during the twisting motion may be connected with a person’s likelihood of “giving way”. Analysis by phase planes in the M/L direction of COP during the twisting motion could potentially be used as a screening tool for people who are at risk for FAI and as an evaluation tool to determine the success of treatments that address the causes of FAI.

RELATIONSHIP BETWEEN ELBOW FLEXION ANGLE AND JOINT LOADING OF THE UPPER EXTREMITY DURING A CLOSE-CHAIN EXERCISE

Paul Pei-Hsi Chou[1], You-Li Chou[2], Shen-Kai Chen[1] , Chia-Ming Kuo[2]

[1]Department of Orthopedic Surgery, Kaohsiung Medical University, Kaohsiung, Taiwan
[2]Institute of Biomedical Engineering, National Cheng-Kung University, Tainan, Taiwan.
e-mail: chou0626@ms3.hinet.net

INTRODUCTION

Push-up is a close-chain exercise that is commonly used to strengthen the upper extremity. Clinically, close-chain exercises are encouraged for the earlier stage of the rehabilitation program because they produce smaller shearing forces across the joints than open-chain exercises. Nonetheless, there is very little research regarding the kinematics of the close-chain exercise of the upper extremity. The purpose of this study is to investigate the relationship between the elbow flexion angle and joint loading during a close-chain exercise of the upper extremity.

METHODS

Fourteen male subjects volunteered in this study. Their average age was 24.5 years, with an average height of 168.9 cm, and average weight of 65.9 Kg. The subjects were asked to perform push-up exercises with their hands in neutral position. The Expert Vison motion system (Motion Analysis Corp., Santa Rosa, CA, USA) with six CCD cameras and two Kistler force-plates (Type 9281B, Kistler Instrument Corp., Winterhur, Switzerland) were used to measure relative joint positions and ground reaction forces. The kinematics and kinetics of the upper extremity were calculated by inverse dynamics and Newton-Eulerian's equation. The correlation between the elbow flexion angle and joint loading during a close-chain exercise of the upper extremity were analyzed.

RESULTS AND DISCUSSION

Results showed that the loading biomechanics of the upper extremity differed with different elbow flexion angles. The maximum loading occurred when the elbow flexion angle was greater than 90° ($p<0.01$). The joint forces in axial, medial/lateral, and anterior/posterior directions increased as the degrees of elbow flexion increased (Figure 1). The maximum valgus moment, flexion moment, and pronation moment were 11.2, 39.9, and 9.8 N-m respectively (Table 1). During the push-up exercise, the greatest loading was calculated with the maximum elbow flexion (the lowest trunk position).

In addition to the effective dampers and springs of wrist and shoulder, the elbow played a very important role of energy dissipation. Taking the effect of elbow motion into consideration, our three-mass-model was more precise in simulating the motion of upper extremity during a close-chain exercise [1].

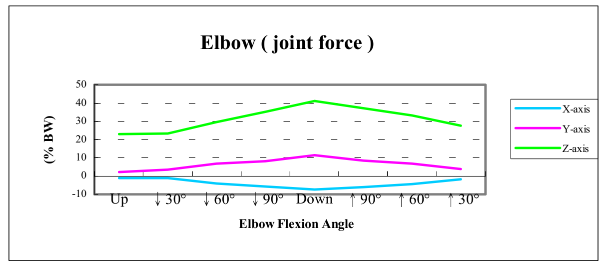

Figure 1: Joint force (% B.W.) vs. degree of elbow flexion angle during a push-up cycle.

Table-1 Joint loading vs. elbow flexion angle

Force	Elbow Flexion Angle					
(% B.W.)	0°	30°	60°	90°	Down	F$^{\#}$ (α)
Med(+) / Lat(-)	-1.3 (1.1)	-1.0 (0.8)	-4.1 (1.7)	-5.9 (2.1)	-7.4 (2.5)	*
Ant(+) / Post(-)	2.2 (1.1)	3.6 (1.9)	6.9 (2.7)	8.2 (3.1)	11.5 (2.9)	*
Axial(+)	23.1 (7.5)	23.4 (9.1)	29.6 (8.7)	35.1 (9.4)	41.0 (11.8)	**
Moment	**Elbow Flexion Angle**					
(N-m.)	0°	30°	60°	90°	Down	F$^{\#}$ (α)
Varus(+) / Valgus(-)	-2.1 (1.5)	3.8 (2.3)	-7.2 (4.1)	-9.9 (3.8)	-11.2 (3.7)	*
Flexion(+) / Extension(-)	12 (3.5)	18.5 (9.6)	22.4 (10.6)	32.6 (12.1)	39.9 (11.5)	**
Supination(+) / Pronation(-)	1.6 (1.1)	3.1 (2.9)	4.6 (3.4)	8.2 (6.3)	9.8 (4.1)	*

F$^{\#}$ value is significance of one-way ANOVA; * ($p<0.05$), ** ($p<0.01$)

CONCLUSION

In this study, the relationship between elbow flexion angle and joint loading during a close-chain exercise were demonstrated. Although the maximum valgus moment during push-up exercise (11.2$\pm$3.7 N-m) was far less than the maximum valgus moment during sports (i.e., 64 N-m in pitching), the peak joint loading occurred between 90 to 120 degrees of elbow flexion. Therefore, keeping elbow flexion less than 90 degrees during a close-chain exercise might be a safer strategy for strengthening of the upper extremity.

REFERENCES

1. Chou, P.H., Lin, C.J., Chou, Y.L., et al. (2002). *Int J Sport Med*, **23(6)**, 457-462

ACKNOWLEDGEMENTS

This study was supported by the National Science Council in Taiwan (NSC 93-2213-E-037-002).

METABOLIC COSTS OF FORWARD PROPULSION AND LEG SWING AT DIFFERENT RUNNING SPEEDS

[1] Bas Moed and [2] Rodger Kram
[1] Faculty of Human Movement Sciences, Vrije Universiteit Amsterdam, The Netherlands
[2] Department of Integrative Physiology, University of Colorado, USA; email: bassiemoed@hotmail.com

INTRODUCTION

We further investigated the cost of forward propulsion and the cost of leg swing across a range of submaximal running speeds by using an applied horizontal force (AHF) at the waist and external swing assist (ESA) forces at the feet. We hypothesized that the absolute costs of forward propulsion and leg swing would be greater at faster speeds.

METHODS

Seven well trained runners volunteered and ran at three different speeds: 2, 3 and 4 m/s. At each speed, they ran normally and completed five trials with 10% body weight (BW) AHF in combination with 0, 1, 2, 3 and 4% BW ESA force, afterwards. The AHF was applied continuously at the waist. ESA was applied at the feet and helped to initiate and propagate leg swing during the first half of the swing phase.

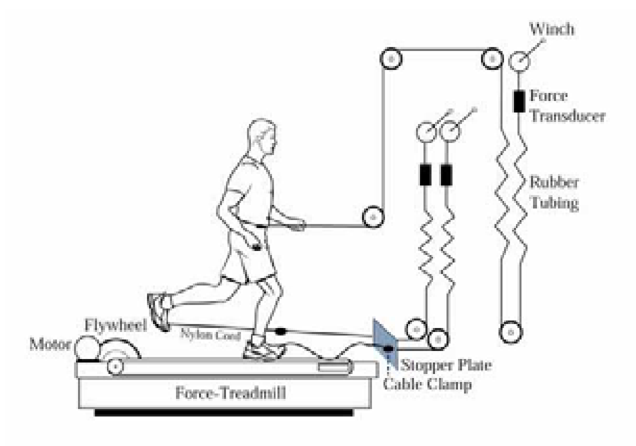

Figure 1: Schematic of the experimental set-up.

Oxygen consumption and carbon dioxide production were measured during a standing trial and were subtracted from gross running values to yield net metabolic rate (W/kg). We estimated the absolute cost of forward propulsion as the difference in metabolic rate between normal running and running with 10% AHF. The difference between running with 10% AHF and the minimum metabolic rate of the 10% AHF combined with ESA, reflected the absolute cost of leg swing.

Kinematic variables (step time, contact time and swing time) and kinetic variables (braking and propulsive impulse of the ground reaction force) were measured for each step, using a force-treadmill.

RESULTS AND DISCUSSION

The absolute costs of forward propulsion and leg swing both increased with speed. The relative costs of propulsion and swing remained at nearly the same percentage of the total.
The increase in the absolute cost of forward propulsion with speed may be explained by shorter contact times and greater braking and propulsive impulses [1]. The increase in the absolute cost of leg swing may be explained by a greater mechanical internal work rate at faster speeds [2].

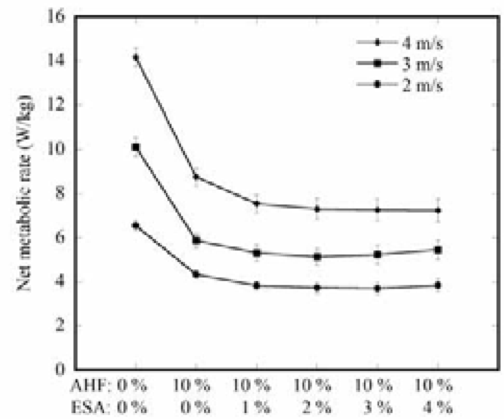

Figure 2: Net metabolic rate versus running condition for each speed. Data points are means ± SEM (error bars).

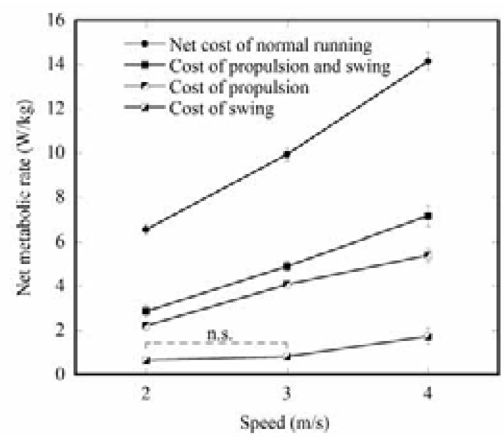

Figure 3: Net metabolic rate versus speed for the cost of normal running, cost of propulsion, cost of leg swing, and the sum of the cost of propulsion and leg swing.

The relative costs of leg swing (~10%), forward propulsion (~40%) and supporting body weight (suggested to be the remaining part; ~50%) are compatible with previous studies [1,3,4].

REFERENCES

1. Roberts TJ et al. *J Exp. Biol.* **201**, 2745-2751, 1998.
2. Willems PA, et al. *J Exp Biol* **198**, 379-393, 1995.
3. Chang YH & Kram R. *J Appl Physiol* **86**, 1657-1662, 1999.
4. Modica JM & Kram R. *J Appl Physiol* (in press)

ACKNOWLEDGEMENTS

This research project was sponsored by VBS-Fund 2004 and the VU-Fund 2004 to B. Moed.

A COMPUTATIONAL MODEL OF THE PREGNANT OCCUPANT: LOCAL UTERINE COMPRESSION EFFECTS THE RISK OF FETAL INJURY

Stefan M. Duma, David M. Moorcroft, Joel D. Stitzel, Greg G. Duma
Virginia Tech – Wake Forest, Center for Injury Biomechanics; Email: Duma@vt.edu; Web: www.CIB.vt.edu

INTRODUCTION

Automobile crashes are the largest single cause of death for pregnant females and the leading cause of traumatic fetal injury mortality in the United States (US) (Weiss, 2002). Unfortunately, fetal injury in motor vehicle crashes is difficult to predict due to the fact that real world crash data is limited and cadaver studies are not feasible. The purpose of this study was to develop a computational model of the pregnant occupant, and to identify the best correlation between uterine compression and risk of fetal injury as predicted by the strain at the uterine-placental interface.

METHODOLOGY

A finite element and multi-body model of the 30 week pregnant small female was created using the MADYMO software package (Figure 1). The finite element abdomen consists of the uterus, placenta, and amniotic fluid that are supported by two pairs of ligaments and surrounded by fat. These structures were imported into a multi-body model of the small female in order to examine overall crash kinematics.

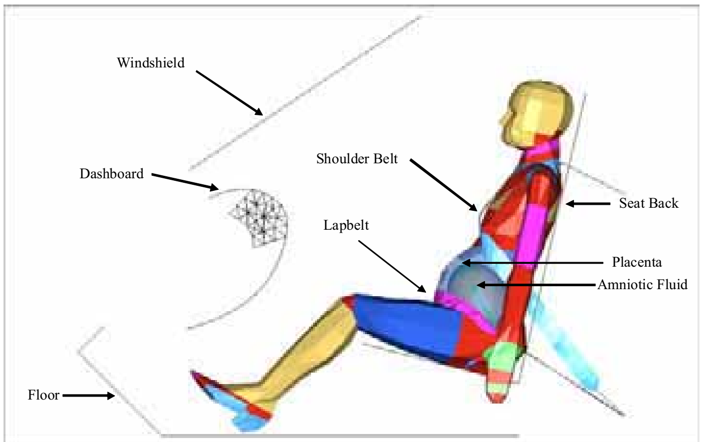

Figure 1: Simulation configuration of pregnant occupant in passenger position with three-point belt.

Four techniques were used to validate the pregnant model. First, a global biofidelity response was evaluated by using a seatbelt to compress dynamically the pregnant abdomen (Moorcroft, 2003). Second, a similar validation procedure was performed with a rigid bar and these results were also consistent with previous data. The third technique involved validating the model against real-world crashes in order to investigate the model's ability to predict injury. The forth method compared the physiological failure strain from placental tissue tests to the model failure strain.

Next, a total of 15 computer simulations were performed on the right-front passenger seat. The test matrix consisted of simulations with five different lap belt locations with each evaluated at three velocities (13 kph, 35 kph, 55 kph). Abdominal measurements were taken at five locations, named AB1, AB2, AB3, AB4 and TH1 ranging from the upper pelvis to the lower thorax. Linear regression analysis was used to correlate the peak uterine compression values to the peak strain at the uterine-placental interface (UPI) and subsequent risk of fetal injury.

RESULTS

Using fatal crashes from pregnant occupants (Klinich et al., 199b), the model showed strong correlation (R2 = 0.85) between peak strain at the uterine-placental interface (UPI) as measured in the model compared to risk of fetal demise as reported in the real-world crashes over a range of impact velocities and restraint conditions. Tissue tests suggest approximately a 60% failure strain for UPI tissues which is in agreement with the model's prediction of 75 % risk of fetal loss at a 60% strain in the UPI. In summary, the global, injury, and tissue level validation techniques all indicate the model is good at predicting injurious events for the pregnant occupant.

The peak uterine strain increased with crash speed and lap belt height except for the top belt location. However, overall compression, which is the peak compression value for all locations, was constant over the range of lap belt locations for a given speed; 20% for 13 kph, 35% - 40% for 35 kph, and 50% for 55 kph. The best correlation was between AB 4 and peak UPI strain for all three impact velocities (Table 1).

Table 1: Correlation coefficient values for each uterine compression measurement versus peak UPI strain.

Measurement Location	13 kph	35 kph	55 kph	All speeds
AB 1	0.48	0.62	0.69	0.53
AB 2	0.50	0.69	0.77	0.65
AB 3	0.24	0.45	0.72	0.05
AB 4	0.92	0.97	0.92	0.93
TH 1	0.20	0.14	0.33	0.26

CONCLUSION

The AB 4 (upper abdomen) measurement location correlated the best because the strain is measured in the uterus at the placental location, which is at approximately the same height as the AB4 measurement location. Therefore, it is suggested as best practice to measure abdominal loading at the uppermost uterine location in an attempt to predict injury to the UPI and risk of fetal demise. It is important to note that all simulations indicate that it is safest for the pregnant occupant to ride in the passenger seat while wearing a three-point belt and utilizing the frontal airbag when possible.

REFERENCES

Klinich KD, et al. UMTRI-99-29. 1999.
Moorcroft DM, et al. **American Journal of Obstetrics and Gynecology**: 189 (2), pp. 540-544, 2003.
Weiss HB, et al. **Injury Prevention**: 8(3), pp. 207-214, 2002.

3D ARTHROKINEMATIC ANALYSIS OF COUPLED MOTION IN THE HUMAN UPPER-CERVICAL SPINE: IN VITRO ANALYSIS OF HIGH VELOCITY THRUST TECHNIQUES

Cattrysse Erik, Baeyens Jean-Pierre, Clarys Jan-Pieter, Van Roy Peter
Dep. Experimental Anatomy, Vrije Universiteit Brussel, Brussels, Belgium
ecattrys@vub.ac.be

INTRODUCTION

Three dimensional analysis of coupled segmental motions in the cervical spine was only studied sparsely and in pure moment analysis. Only preliminary information exists on the kinematics of manual segmental mobilization. The present study focuses on the in vitro registration of upper cervical segmental coupled motions during manually performed therapeutic high velocity thrust techniques (HVT). The aim of the study was to collect qualitative information on the kinematics behavior of the upper-cervical spinal motion segments during planar induced movements and while applying manual therapeutic manipulation techniques. The information can help to understand the effect of manual therapy on spinal motion.

METHODS

Seven cervical spine specimens were taken from embalmed human cadavers at the level of the occiput to the first thoracic spine. Each specimen was clamped on a rigid stand to hold T1 in such a way that the cervical spine was fully free to move. 3D electromagnetic tracking sensors were fixed on the head, C1 and C2. Subsequently, each specimen was first moved in the three main planes of motion. Consecutively in 4 specimens a segmental manipulative high velocity thrust in axial traction direction was performed on the level of C0-C1 followed by a segmental rotational high velocity thrust on the level of C1-C2. The position and orientation of each sensor were collected by an electromagnetic tracking device (Flock of birds-Ascension technologies). At a later stage, the positions of local anatomical landmarks were digitized with a 3D drawing stylus (3DX-Microscribe). The individual sensor data were used to describe coupled movements by means of the parameters of the finite helical axes (Spoor and Veldpaus, 1980; Woltring et al., 1994) for discrete sampling ranges of the movements between the different bones: i.e. orientation, position, shift along and rotation about the estimated helical axis. The anatomical data were used for the definition of local bone embedded co-ordinate systems. To analyze the 3D arthrokinematics of the antlanto-occipital and atlanto-axial joints, the finite helical axes were related to a co-ordinate system based on the centre line through mastoid processes and the transverse processes of C1 and C2. The effect of segmental manual high velocity thrust techniques were analyzed in a six degrees of freedom approach. The results are analyzed by the Euler angle approach and finite helical angles representations.

RESULTS AND DISCUSSION

The results show that all planar induced movements include 3-dimensional coupled motions. During the main flexion-extension motion on the atlanto-occipital segment important associated rotation and lateral bending takes place that can even equal or sometimes exceed the main motion.During HVT traction on the C0-C1 level the thrust results in a 3-dimensional translation. The main direction is lateral, coupled with a smaller axial and sagittal displacement. The rotational HVT on the level C1-C2 results in an additional axial rotation component of approximately 2°, with almost no rotational components in flexion-extension or lateral bending directions (fig 1). This axial rotation component is however again accompanied by translational displacements in all three directions. The largest translation takes place in the lateral direction (fig 1).

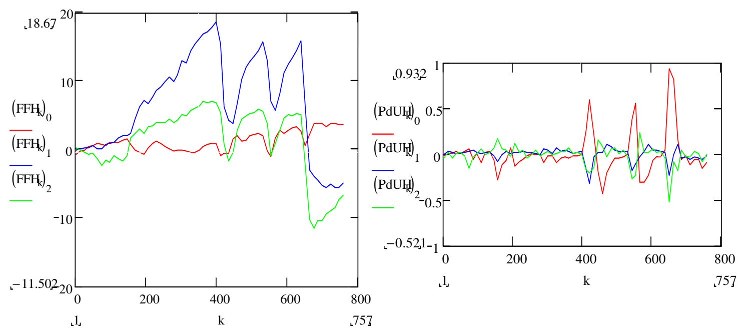

Fig.1 cumulative helical angles (left) and intra-articular translations (right) C1-C2 during rotational HVT (specimen 4)

(FFH1)0≈flexion-extenion	(PdUH1)0≈ lateral translation
(FFH1)1≈axial rotation	(PdUH1)1≈ cranio-caudal translation
(FFH1)2≈lateral bending	(PdUH1)0≈ sagital translation

CONCLUSIONS

These results show that manual induced segmental coupled movements in the upper cervical spine can be analyzed in vitro by means of an electromagnetic tracking device. The largest motion at the atlanto-occipital level is flexion-extension as is described in literature (Panjabi et al., 1993), while at the atlanto-axial level the rotation is the motion whit the largest amplitude. HVT-techniques can induce axial translational displacements andadditional axial rotation in traction and rotation techniques respectively. Therapists have to realize however that coupled rotations and translations take place. In the presented HVT's these coupled motions can not be excluded and may increase stress on vital structures.

REFERENCES

1. Panjabi, M. M., T. Oda, J. J. Crisco, J. Dvorak and D. Grob, 1993. Posture Affects Motion Coupling Patterns of the Upper Cervical- Spine. Journal of Orthopaedic Research 11(4), 525-536.

2. Spoor, C. W. and F. E. Veldpaus, 1980. Rigid Body Motion Calculated from Spatial Coordinates of Markers. Journal of Biomechanics 13(4), 391-393.

3. Woltring, H. J., K. Long, P. J. Osterbauer and A. W. Fuhr, 1994. Instantaneous Helical Axis Estimation from 3-D Video Data in Neck Kinematics for Whiplash Diagnostics. Journal of Biomechanics 27(12), 1415-1432.

3D ARTHROKINEMATIC ANALYSIS OF COUPLED ROTATIONS IN THE ATLANTO-AXIAL JOINT DURING AXIAL ROTATION AND LATERAL BENDING

Cattrysse Erik, Baeyens Jean-Pierre, Clarys Jan-Pieter, Van Roy Peter
Dep. Experimental Anatomy, Vrije Universiteit Brussel, Brussels, Belgium
ecattrys@vub.ac.be

INTRODUCTION

Three dimensional analysis of segmental motion coupling was only studied sparsely and in pure moment analysis. The present study focuses on the in vitro registration of upper cervical segmental coupled motions during manual induced axial rotation and lateral bending. The aim of the study was to create a suitable setup for collecting qualitative information on the kinematics of the atlanto-axial joint during planar induced movements, and to compare patterns of motion coupling.

METHODS

Seven cervical spine specimens were taken from embalmed human cadavers from the occiput to the first thoracic spine. Each specimen was clamped on a rigid stand to hold T1 in such a way that the cervical spine was fully free to move. 3D electromagnetic tracking sensors were fixed on the occiput, C1 and C2. Subsequently, each specimen was moved in the main planes of motion. The position and orientation of each sensor were collected by an electromagnetic tracking device (Flock of birds-Ascension technologies). At a later stage, the positions of local anatomical landmarks were digitized with a 3D drawing stylus (3DX-Microscribe). The individual sensor data were used to describe coupled motions by means of the parameters of the finite helical axes (Spoor and Veldpaus, 1980; Woltring et al., 1994) for discrete sampling ranges of the movements between the different bones. The anatomical data were used for the definition of local bone embedded co-ordinate systems. To analyze the 3D arthrokinematics of the atlanto-axial joint, the finite helical axes were related to a co-ordinate system based on the centre line through the transverse processes of C1 and C2 and the midpoint of the anterior side of the arcus of C1 and corpus of C2. The results are analyzed by the finite helical angles representations

RESULTS AND DISCUSSION

The results show that main planar axial rotation and lateral bending motions include 3-dimensional coupled motions. Tabel 1 shows that the coupling pattern during axial rotation is

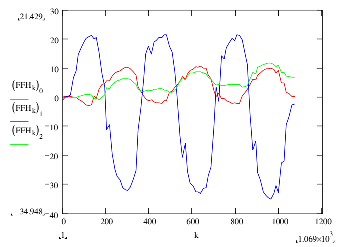

Fig 1. : Cumulative finite helical angles C1-C2 during axial rotation (spec 7) $(FFH_1)_0$≈flexion-extension; $(FFH_1)_1$≈ axial rotation; $(FFH_1)_2$≈ lateral bending

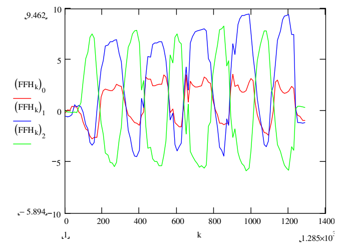

Fig 2. : Cumulative finite helical angles C1-C2 during lateral bending (spec 7) $(FFH_1)_0$≈flexion-extension; $(FFH_1)_1$≈ axial rotation; $(FFH_1)_2$≈ lateral bending

coupled controlateral lateral bending in 5 out of 7 specimens (fig.1). During lateral bending the coupled rotation is ipsilateral in 6 out of 7 specimens.

CONCLUSIONS

These results indicate that the experimental setup is suitable for the analysis of coupled rotations in the upper cervical spine. The results of the arthrokinematic analysis of manual induced planar motions are parallel to the findings of an experimental setup applying controlled forces and moments (Panjabi et al., 1993).

REFERENCES

1. Panjabi, M. M., T. Oda, J. J. Crisco, J. Dvorak and D. Grob, 1993. Posture Affects Motion Coupling Patterns of the Upper Cervical- Spine. Journal of Orthopaedic Research 11(4), 525-536.
2. Spoor, C. W. and F. E. Veldpaus, 1980. Rigid Body Motion Calculated from Spatial Coordinates of Markers. Journal of Biomechanics 13(4), 391-393.
3. Woltring, H. J., K. Long, P. J. Osterbauer and A. W. Fuhr, 1994. Instantaneous Helical Axis Estimation from 3-D Video Data in Neck Kinematics for Whiplash Diagnostics. Journal of Biomechanics 27(12), 1415.

Tabel 1: patterns of motion coupling at the atlanto-axial joint during axial rotation and lateral bending

specimen	*Axial rotation*	Patterns of coupled motions	Direction of coupled motion	Max ROM of main motion	*Lateral bending*	Patterns of coupled motions	Direction of coupled motion	Max ROM of main motion	ROM of major motion component
1		R >> L ≥ F	contro	56°		R ≥ F > L	Ipsi	4°	7°
2		R >> L > F	ipsi	56°		R > F ≥ L	Ipsi	5°	11°
3		R >> L > F	contro	49°		R > F > L	Ipsi	3°	8°
4		R >> L >> F	Ipsi	50°		L ≥ R > F	Ipsi	15°	
5		R >> F > L	Contro	35°		R > F > L	Ipsi	3,5°	10°
6		R >> F > L	Contro	55°		L ≥ R > F	Contro	13,5°	
7		R >> L > F	contro	50°		F > R > L	ipsi	5°	10°

Motion Characteristics of the Innominate-hip complex under increasing passive loads

Melanie Bussey
University of Otago, email mbussey@pooka.otago.ac.nz

INTRODUCTION

The human pelvis provides the bony link between the spinal column and the lower limbs, acting as an intermediary in the load transfer mechanism from the trunk to the legs and *vice versa*. A problem encountered in modelling research is the representation of the pelvis as a solid or rigid body, thus pelvic joint motion is ignored. To increase our understanding of the mechanisms involved in loading injury to the lumbar spine there is a need for research combining lower limb and spine kinematics with pelvic joint kinematics to identify the extent and nature of motion in the lumbar-pelvic-hip complex.
The aim of the present research was to examine the motion characteristics of the innominate-hip complex under normal passive loading conditions and specifically, to determine the contribution of relative innominate bone motion within the complex.

METHODS

Thirty healthy subjects (16 females and 14 males) between the ages of 20 and 40 gave their informed consent to participate in this study. A magnetic tracking device (Fastrack, Polhemus Incorporated, Colchester, VT, USA) was used to track the motion of the pelvis, innominate bones and femurs as the hip was passively loaded in 10° increments. A standardization frame was used to standardize the passive loading of the hip in two separate constraint conditions up to maximum lateral flexion (AB) and external rotation (ER). The frame constrained the hip so that only motions in the frontal and transverse planes were allowed (i.e., the femur was constrained in the directions of flexion and extension). Thus, the hip orientation was described relative to the pelvis as a y x y sequence of Euler angles. In each load position the transverse (I_{NSy}) and sagittal plane ($I_{NSz,}$) angles of the innominate bones were calculated from digitized pelvic landmarks. Finally, the innominate motion was described as absolute angular displacement between the neutral and loaded positions.

To determine whether there was an effect of Hip Condition or Load Position on the ROM of the innominate and hip, means and standard deviations for motion measured in the final positions of each hip condition were calculated. The dependant variables $H_{ABx,}$ $H_{ERy,}$ $I_{NSz,}$ and I_{NSy} were each tested in a GLM univariate analysis, F-ratios and alpha levels derived for each source of variance (Hip Condition, Load Position and Load Position x Hip Condition). Where significant differences between Positions were found a Tukey *post-hoc* test was used to determine which Positions were significantly different.

RESULTS

Firstly, as expected the femur motion increased significantly with each successive Position. So, H_{ERy} increased significantly (p<0.001) with increasing external rotation stress and H_{ABx}, also increased significantly (p<0.001) with increasing lateral flexion stress. Secondly, the only significant Position effect in innominate bone displacement was about the y-axis (I_{NSy}) in the ER condition where there was there a significant change (p=0.001) in innominate motion with increasing stress. The evidence from the Tukey *post-hoc* test showed that the increase in ROM from Position 1 to Positions 3, 4 and 5 was significant, the mean difference between Positions 1 and 3 was -0.84° (95% CI = -1.37 to -0.32°). There was a very low ability to adequately predict I_{NSy} innominate from H_{ERy} of the femur as determined through regression plots (R^2 = 0.10 right, Figure 8 and R^2 = 0.13 left, Figure 7). The combination of small ROM and large individual variability make such across-subject comparisons difficult.

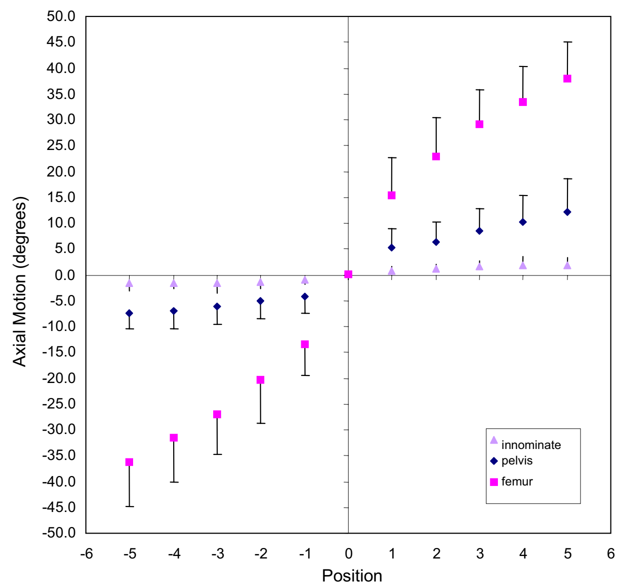

Figure 1: Means and standard deviations for the left (-) and right (+) hip, pelvis and innominate bones in each of the loaded positions of the ER hip condition.

DISCUSSION AND SUMMARY

The present study demonstrated that the greatest change in innominate bone ROM occurs within the first 15-20° of hip motion and that increased load on the innominate from the hip does not significantly increase the displacement of the innominate bones. Although the ranges of innominate bone motion were significantly smaller compared to pelvic or femur motion, the innominate bone motion accounted for 3 to 5% of the total x and y femur rotations. The results of this study support the theory that the main functional role of the pelvic joints (apart from aiding in childbirth) is to reduce the injurious torque from the hip to the lumbar spine.

SCALING OF MUSCLE VOLUMES IN THE UPPER EXTREMITY

[1]Katherine Holzbaur, [4]Wendy Murray, [2]Garry Gold, and [1,3]Scott Delp
Departments of [1]Mechanical Engineering, [2]Radiology, and [3]Bioengineering, Stanford University, Stanford, CA;
[4]Bone and Joint Center, VA Palo Alto HCS, Palo Alto, CA
email: kholzbaur@stanford.edu

INTRODUCTION

Humans vary greatly in size and shape, yet biomechanists often use generic musculoskeletal models with average parameters to examine questions of muscle function and coordination. While this approach allows researchers to investigate general principles underlying human movement, it is unclear how conclusions derived from studies of generic models apply to individuals of different sizes.

Muscle force-generating properties used in musculoskeletal models are often derived from cadaveric studies of muscle architecture. This could complicate scaling of generic models for two reasons. First, cadaveric specimens may not accurately reflect the absolute or relative sizes of muscles in young, healthy subjects. Second, cadaveric studies of muscle architecture often focus on individual muscle groups; this is especially true for the upper limb, where muscle parameters have been quantified separately for the shoulder [1], elbow [4], and forearm [2,3]. This study addresses both issues in the upper extremity by i) measuring volumes for all muscles of the upper limb in young, healthy subjects using magnetic resonance imaging, and ii) comparing these data to the different sources available in the literature.

METHODS

Five subjects (4 females, 1 male, 24-37 years) with no injury or pathology of the upper limb were studied. All subjects provided informed consent. Each subject was imaged supine in a 1.5T MRI scanner (GE Healthcare, Milwaukee, WI). Axial images were acquired from shoulder to wrist using a 3D spoiled gradient echo sequence with 3 mm sections. Shoulder images were obtained with the body coil with TE = 3 ms, TR = 11.6 ms, flip angle (FA) = 30°, matrix = 512x192, and field of view (FOV) = 32 cm. Elbow and forearm images were acquired using a flexed array long bone coil (Medical Advances, Milwaukee, WI) with TE = 5 ms, TR = 23 ms, FA = 45°, matrix = 320x192, and FOV = 16 cm.

To calculate muscle volume, we reconstructed the three-dimensional geometry of the upper limb muscles. Muscle boundaries were segmented in the axial images and a three-dimensional polygonal surface was created for each muscle from the outlines (3D-Doctor, Able Software Corp., Lexington, MA). Muscle volumes were then normalized by the corresponding volume reported in the literature [1-4] to produce a "scaling ratio". For a given muscle, a ratio greater than 1 indicates that its volume is larger than the cadaver data. To determine if muscle volumes obtained from the different literature sources represent the relative proportion of muscle volumes for a single individual, we compared scaling ratios across upper limb segments for each subject.

RESULTS AND DISCUSSION

The ratios between the volumes measured in this study and the volumes from cadaveric data ranged from 0.91 to 3.73. While scaling ratios varied across subjects, all muscles scaled by approximately the same ratio for each subject. For example, the scaling ratios for deltoid, a shoulder muscle, and extensor carpi radialis brevis (ECRB), a forearm muscle, were approximately equal (Fig. 1, red squares). Similarly, the ratios for brachioradialis, an elbow muscle, and pronator quadratus (PQ), a forearm muscle, were comparable (Fig. 1, blue triangles).

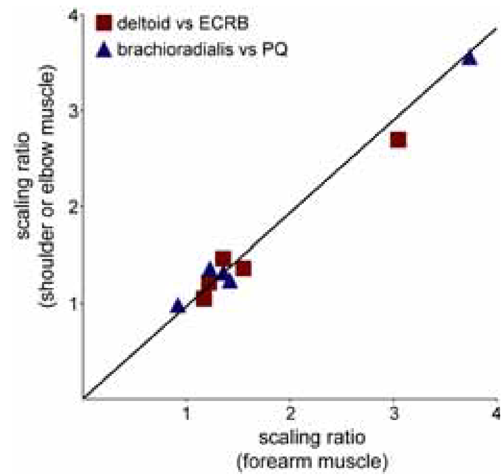

Figure 1: Scaling ratios for example proximal muscles vs. forearm muscles.

Muscle volumes reported in cadaveric studies are equivalent to the volumes measured in the females in this study (height ranged from 157 to 165 cm). The one male subject evaluated here (height = 175 cm) had substantially larger muscle volumes. Data from different architecture studies scaled uniformly to muscle volume for a given subject. That is, when scaling ratios for shoulder or elbow muscles were plotted against ratios for forearm muscles, all points fell close to a line with slope equal to one. This is encouraging for researchers who must combine data sets from multiple studies to estimate force-generating properties for the entire upper limb. It also provides preliminary support for application of modeling results to individuals of varying size. Our ongoing studies will examine muscle scaling in a larger group of subjects.

REFERENCES

1. Langenderfer J, et al. *Clin Biomech* **19**, 664-70, 2004.
2. Lieber RL, et al. *J Hand Surg [Am]* **15**, 244-50, 1990.
3. Lieber RL, et al. *J Hand Surg [Am]* **17**, 787-98, 1992.
4. Murray WM, et al. *J Biomech* **33**, 943-52, 2000.

ACKNOWLEDGEMENTS

Whitaker Foundation, Medtronic Foundation Stanford Graduate Fellowship, NIH R01 HD046774 (Murray), and NIH-EB0002524 (Gold).

EFFECTS OF POWER GENERATION ON EVALUATING IMPACT ATTENUATION IN LANDING

Kurt Clowers and Songning Zhang
Biomechanics/Sports Medicine Laboratory, The University of Tennessee, Knoxville, TN, USA
email: kclowers@utk.edu

INTRODUCTION

A common and acceptable activity used to measure the power output of the lower extremity is the vertical jump [1]. Studies have compared the biomechanical characteristics of landing and jumping with the same level of participation [2, 3] and others have compared the physical activity level or experience in landing and jumping biomechanics [4, 5]. Thus, differences could be observed in the impact attenuation during landing in athletes with different maximum power generation capabilities. Therefore the purpose of this study was to compare the effects of power generation capacity on impact attenuation during a drop landing activity.

METHODS

Twelve male recreational athletes performed five drop landing trials from three heights in two different protocols (PT). Subjects were divided into one of two groups (Grp) based on their maximum vertical jump height: non-elite (Grp 1, N=8) and elite (Grp 2, N=4), which was used as an index for lower extremity power capacity. All subjects performed five landing trials from heights of 40, 60, and 80 cm in the protocol one (PT1) and from 70%, 100%, and 130% of their jump height (H) in the protocol two (PT2).

A force platform (1080 Hz, AMTI) and a 6-camera motion analysis system (120 Hz, Vicon) were used to collect ground reaction force (GRF) and 3D kinematic data simultaneously during the testing session. Kinematic and GRF data were smoothed at 8 and 20 Hz respectively, using a fourth-order Butterworth low-pass filter. The 3D joint kinematic and kinetic variables were computed using Visual3D software (C-Motion, Inc.) in conjunction with a customized computer program. A mixed design three-way repeated measures ANOVA (Grp × PT × H) with Grp as the between-subject factor was used to evaluate selected joint kinematic and kinetic variables ($p < 0.05$).

RESULTS AND DISCUSSION

The mean maximum knee flexion angle was significantly greater in PT2 than PT1 for Grp1. The maximum knee flexion angle increased significantly as height increased for both groups. For Grp1 in PT1 the maximum knee flexion angle increased 11% from H 1 to 2 and 27% from H 1 to 3. However, in PT2 the increases were 11% and 21% from H 1 to 2 and from H 1 to 3 respectively.

The mean peak knee extensor moment was significantly greater in PT1 than PT2 for Grp1 (Table 1). The peak knee extensor moment in PT1 for Grp1 increased 21% and 68% from H 1 to 2 and H 1 to 3 respectively. However, in PT2 the increases were 16% and 31% for Grp1. Conversely, the peak hip extensor moment in PT1 for Grp1 increased 29% and 61% and for PT2 the increases were 31% and 69% from H 1 to 2 and H 1 to 3 respectively. Similarly, the peak ankle plantar flexor moment in PT1 for Grp1 increased 8% and 16% but for PT2 the increases were 16% and 16% from H 1 to 2 and H 1 to 3 respectively.

Table 1: Average peak joint moments (Nm/kg).

Grp	PT	H	Hip Extensor	Knee Extensor	Plantar Flexor
1	1	1	3.4±1.1	2.5±0.4	1.5±0.5
		2	4.4±1.2 [a]	3.0±0.8 [a]	1.6±0.5 [a]
		3	5.5±1.9 [a,b]	4.2±1.0 [a,b]	1.8±0.4 [a,b]
	2	1	2.9±0.9	2.3±0.3 [*]	1.4±0.4
		2	3.8±1.1 [a]	2.7±0.3 [*,a]	1.7±0.5 [a]
		3	4.9±1.3 [a,b]	3.1±0.4 [*,a,b]	1.6±0.3 [a,b]
2	1	1	2.9±0.6	2.3±0.3	1.8±0.3
		2	4.0±0.4	2.8±0.2 [a]	1.9±0.2 [a]
		3	5.0±1.6	3.6±0.8 [a,b]	2.0±0.3 [a,b]
	2	1	4.2±0.9	2.6±0.3	1.8±0.2
		2	4.7±1.0	3.3±0.6 [a]	1.9±0.4 [a]
		3	5.4±1.4	3.8±0.4 [a,b]	2.1±0.3 [a,b]

[*]: Significantly different from protocol 1.
[a]: Significantly different from height 1.
[b]: Significantly different from height 2.

There were greater increases in the hip and ankle moment for PT2 while smaller increases for PT1 in Grp1 but not Grp2. The knee moment demonstrated greater increases for PT1 but smaller increases for PT2 in Grp1 only. The moment data indicates that there is greater effort by the knee musculature for Grp1 to attenuate the impact forces for PT1 but actually less effort by knee and greater effort by the hip and ankle musculature for PT2 to absorb the impact forces.

CONCLUSIONS

Protocol differences were found in individuals who did not participate in jumping sports and who landed from absolute heights. For the PT based on a percentage of maximum vertical jump heights, smaller increases in knee kinematics and knee moments were found in Grp1 only. These results suggest individuals possessing greater power generation capabilities and/or conditioning may be more capable attenuating impact forces in drop landings.

REFERENCES

1. Dowling JJ, et al.. *J App Biomech* **9**, 95-110, 1993.
2. Ford KR, et al.. *Med Sci Sports Exerc* **35**, 1745-50, 2003.
3. Zhang SN, et al.. *Med Sci Sports Exerc* **32,** 812-819, 2000.
4. Hoffman JR, et al.. *Aviat Space Envirn Med* **68**,710-4, 1997.
5. Lephart SM, et al.. *Clin Orthop* 162-9, 2002.

Comparative Balance Analysis Between Indoor Climbing Individuals And Controls Through Posturography Test.

Sá, C.S.C. [1, 2, 3]; Boffino, C.C. [3]; Tsurumaki, A.M. [2]; Durigon, O.F.S. [2]; Tanaka, C. [2]; Ramos, R.T. [3].
(1) Curso de Fisioterapia – IMES; (2) Curso de Fisioterapia – FMUSP; (3) Instituto de Psiquiatria - FMUSP

Introduction

The balance control is needed when an specific skill learning is developed. This is truth when you work with sports techniques learning that needs the refined postural and balance control to optimize the motor performance. So, it could be thought that the sports technique learning would develop a better postural control in the individual that practice those activities. The sportive indoor climbing make the athlete be exposed to certain unusual postural conditions as lower visual inputs defined by the high he is positioned; irregular feet support and the need of an horizontal force avoiding the posterior fall. Those conditions make occur a continuous postural instability during the activity and demand a bigger motor control (reflex, automatic and conscious motor behaviors) developing beside the technique learning, a better balance control. This could be seeing in a posturography test. In the present study, we analyze the equilibrium, the strategy and the sensory analyses score (for somatosensory, visual and vestibular systems) during four stand quietly posturography conditions in indoor climbing individuals and controls.

Methods

Forty normal individuals of both sex and mean age of 23,67 years, divided between two groups according to their sports practice (indoor climbing group – G1 and controls – G2) were called as voluntaries. This two groups were sex and mean age matched. The balance test used was the modified sensory organization test (mSOT) from the Pro Balance Master posturography developed by NeuroCom ® and that presents four defined test conditions: (1) eyes open and fixed platform; (2) eyes closed and fixed platform; (4) eyes open and sway referencing platform; (5) eyes closed and sway referencing platform. The statistics was done as t student-test for independent samples.

Results and Discussion

The results were indicative to a significant difference ($p < 0,05$) in the number 4 mSOT's condition ($p=0,04$) and in the visual system sensorial analyses ($p = 0,01$). Showing the indoor climbing group, G1, to have better performance than controls when the visual system is the biggest responsible for balance control, and the somatosensory and vestibular system are for somewhat being mistaken. This is different to the prevalence of the support surface dependence balance control that is found in controls, when the individual goes better in the test when the support surface is fixed. We can state yet that was found a tendency analyses in the somatosensory system score indicating better balance performance in the G1.
The strategy scores analyses (hip and ankle strategies) didn't show any differences between G1 and G2 in any posturography's condition. As the postural and balance control strategy is specific of standing posture perhaps it's not available during climbing and so it's not learned or developed during this sports practice.

Conclusion

This study has concluded that due to their daily training, climbers presented an increase in the activity in their visual and somatosensory systems. This phenomenon either improved their postural control explaining the large difference in the analysis score of the visual system and a tendency to a significant difference between the groups .in the analysis score of the somatosensory system.

THE EFFECT OF INITIAL LEAN ON HUMAN POSTURAL SCALING

[1,2] Sukyung Park, [3] Fay B. Horak and [1] Arthur D. Kuo
[1]Dept. Mechanical Engineering, University of Michigan, Ann Arbor, MI, USA
[2]Dept. Mechanical Engineering, KAIST, Taejon, South Korea
[3]Neurological Sciences Institute of Oregon Health and Sciences University, Portland, OR, USA
email: sukyungp@kaist.ac.kr, web: me.kaist.ac.kr/~posture

INTRODUCTION

We examined how the central nervous system adjusts postural responses with initial forward lean of the body. Postural feedback responses appear to scale nonlinearly with perturbation magnitude in order to accommodate biomechanical constraints such as allowable ankle joint torque [1]. Initial forward leaning, which is observed among the elderly who are inactive or afraid of falling, brings subjects nearer to the limit of stability [2] and alters the biomechanical constraint. We hypothesized that the central nervous system is aware of body dynamics and further restrains postural responses when subjects initially lean forward prior to a perturbation.

METHODS

We applied fast backwards perturbations of various magnitudes to 12 healthy young subjects (3 male, 9 female) aged 20 to 32 years. Subjects were instructed to quietly stand on a hydraulic servo-controlled force platform with their arms crossed over their chests, and to recover from a perturbation by returning to their upright position. Initially subjects were either standing upright or standing with a half-maximum forward lean. Half-maximum lean is defined as the posture, in which the center of pressure is located at half the maximum magnitude that subjects could achieve without stepping or falling. The force platform translated backward with various ramp displacements ranging 1.2 – 15 cm, all with the duration of 275 msec. Perturbations occurred in blocks of seven displacements, with the perturbation size for each block randomized. For each trial, kinematics and ground reaction force data were recorded and then used to compute net joint torques, employing a least squares inverse dynamics method.

To examine the scaling of multi-joint postural responses, we examined the changes in trajectories of ankle vs. hip joint torques as a function of perturbation magnitude and initial lean. We used optimization methods to identify a set of equivalent feedback control gains for each trial so that the biomechanical model incorporating this feedback control would reproduce the empirical response [1]. There are three components to this identification: a 3-segment inverted pendulum biomechanical model of body dynamics, a linear feedback control to stabilize this model [3], and an optimization procedure to produce model responses with the best fit to the data. We compared the joint torque trajectories with a predicted constraint on allowable ankle torque, and also examined how the identified feedback gains changed with initial learn.

RESULTS AND DISCUSSION

We found that joint torque and feedback gains gradually scaled as a function of perturbation magnitude before they reached the biomechanical constraint, and scaling became more severe with initial forward lean (see Fig. 1). For example, the model suggests that the magnitude of ankle joint angle feedback to ankle torque was smaller in leaning trials than on initially upright trials, as if the subjects experienced a larger postural perturbation in leaning trials. These results imply that the central nervous system restrained postural responses to accommodate a more limiting biomechanical constraint imposed by the forward posture. The gradual scaling of postural feedback gains indicates that the postural control can be interpreted as a feedback scheme with scalable gains.

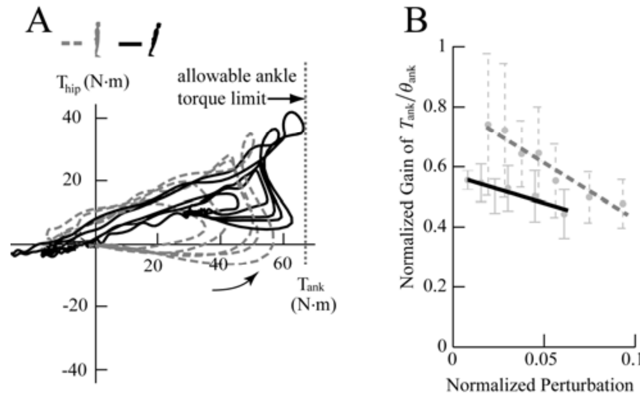

Figure 1: Changes in postural response scaling for two different initial postures. (A) Trajectories of joint torques also scaled with initial lean. Joint torque for leaning trials more conservatively scaled for forward posture. (B) Normalized feedback gains and their linear regressions as a function of perturbation magnitude for upright posture (dashed line) and forward lean posture (solid line).

CONCLUSIONS

Human postural responses scale as a function of perturbation magnitude as well as initial lean to accommodate biomechanical constraints. This scaling implies that the central nervous system is aware of body dynamics and biomechanical effects of initial position so it can restrain postural responses when subjects initially lean forward.

REFERENCES

1. S. Park, et. al.. *Exp. Brain. Res.* **154**, 417-427, 2004.
2. A.P. Woodhull-McNeal. *Aging* **4**, 219-225, 1992.
3. A.D. Kuo, et. al.. *J Biomech* **26**, 137-50, 1993.

ACKNOWLEDGEMENTS

This work support in part by NIH grants DC0231201 and AG06457. C. L. Shupert contributed to data collection.

OPTIMAL CONTROL MODEL OF HUMAN POSTURAL SCALING WITH BIOMECHANICAL CONSTRAINTS

[1,2] Sukyung Park, [3] Fay B. Horak and [1] Arthur D. Kuo
[1]Dept. Mechanical Engineering, University of Michigan, Ann Arbor, MI, USA
[2]Dept. Mechanical Engineering, KAIST, Taejon, South Korea
[3]Neurological Sciences Institute of Oregon Health and Sciences University, Portland, OR, USA
email: sukyungp@kaist.ac.kr, web: me.kaist.ac.kr/~posture

INTRODUCTION

Human postural responses appear to scale as a function of perturbation magnitude to accommodate biomechanical constraints [1]. Scaling occurs in a gradual manner before discrete biomechanical constraints such as limitations on allowable ankle torque become active, implying a continuous neural representation of the constraints. We developed an optimal control model of human postural scaling using a constraint-penalized control objective, and examined whether the model could reproduce this gradually scaling of postural responses as perturbation magnitude increases.

METHODS

Fast backwards perturbations of various magnitudes were applied to 12 healthy young subjects (3 male, 9 female) aged 20 to 32 years [1,2]. Subjects were initially either standing upright or leaning forward on force platform and returned to their upright posture after perturbation stimulus. For each trial, kinematics and ground reaction force data were recorded and then used to compute net joint torques. We previously used system identification to determine subjects' feedback gains for each perturbation [1]. Here, we tested whether a single objective function could reproduce these gains, using a simple parametrization of the constraint dynamics.

We modified a previous linear feedback controller [3] for a 3-linkage biomechanical model of the body. Control gains were obtained by minimizing a control objective including a representation of biomechanical constraints. This representation determines whether the central nervous system (CNS) accommodates the constraints in a gradual manner or by an abrupt change of response. The maximum allowable ankle torque acts as a discrete constraint on postural feedback responses to support surface perturbations. If the CNS were to represent this constraint in a discrete manner, the CNS would uniformly scale postural responses with perturbations until the maximum ankle torque were reached. For larger perturbations, it would abruptly switch feedback gains to a different value to accommodate the discrete constraint. Neural networks are typically better suited to representing constraints in a more continuous manner, similar to a penalty function. If the CNS were to have a continuous representation, it would continuously scale control gains as a function of postural challenges so that the responses would be gradually adjusted to satisfy the constraints. We modeled this concept with an optimal control design. The objective included a penalty against violating the maximum allowable ankle joint torque constraint. We compared the model's feedback scaling behavior against the human experimental data.

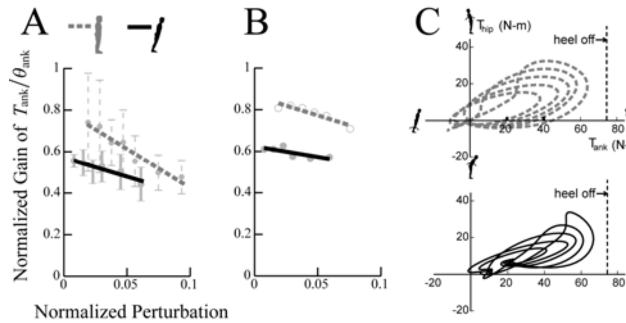

Figure 1: Postural scaling responses. (A) Empirical feedback gains scaled with perturbation magnitude as well as initial lean. (B) Feedback gains computed by optimization model also scaled gradually in a manner similar to data. (C) Joint torque trajectories computed from optimal control model. Gray dotted lines are for upright trials, black solid lines are for leaning trials.

RESULTS AND DISCUSSION

The optimal control model was able to roughly reproduce gradually-scaled postural responses in accordance with biomechanical constraints. The results suggest that the nervous system may represent potentially discrete constraints, such as a threshold torque before heel lift-off, in a continuous manner. It appears unnecessary for the CNS to store postural responses as a large number of muscle activation trajectories. Rather, a family of responses could be encoded by a much smaller number of feedback gains, whose scaling in turn could be encoded by a minimal set of parameters.

CONCLUSIONS

The constraint-penalized objective was able to reproduce the postural scaling with perturbation as well as initial lean. Gradual scaling of postural response by a penalty function implies that the nervous system may represent biomechanical constraints in a more continuous manner. The existence of the global objective based on the biomechanical model also suggests that the CNS is aware of body dynamics and flexibly scales postural response to accommodate biomechanical constraint, rather than discretely selects the preprogrammed responses.

REFERENCES

1. S. Park, et. al.. *Exp. Brain. Res*. **154**, 417-427, 2004.
2. F.B. Horak et. al.. *Gait & Posture.* **1**, 203-10, 1993.
3. A.D. Kuo. *IEEE Trans. Biomed. Eng.* **42**, 87-101, 1995.

ACKNOWLEDGEMENTS

This work support in part by NIH grants DC0231201 and AG06457. C. L. Shupert contributed to data collection.

Relationship between rotational movement and translational movement during the golf swing

[1]Mutsuko Nozawa, [2]Hidetsugu Nishizono and [2]Norihiro Shima
[1]Takeo Maruyama, [1]Syuichiro Yazawa and [1]Kazuhiro Suda
[1]Tokyou Institute of Technology;e-mail:mnozawa@o.cc.titech.ac.jp
[2]National Institute of Fitness and Sports in Kanoya

INTRODUCTION

Several studies of golf swings were investigated the rotation of the trunk and the movement of arms and hands by many researchers. However, a good performance in golf swing is the result of a complex multi-joint movement that is dependent on the forces applied at the feet.

The purpose of this study was to measure and analyze ground reaction forces (GRF) from both feet during the golf swings using a driver. Furthermore, we attempted to clarify the relationship between the rotational movement of the body and the free moment about a vertical axis in the golf swing.

METHODS

Fifteen right-handed male golfers (8 professional golfers in Japan and 7 amateur golfers), with a mean (±S.D) age, height, body mass of 36.2 ± 9.1 years, 170.1 ± 4.0 cm, 72.8 ± 8.0 kg respectively, volunteered to participate in this study. Each golfer carried out 5 shots using a driver. The measurements of kinematics data during the swings were established with the optical motion capture system VICON612 (Vicon Motion Systems Ltd., Oxford, UK) with ten cameras operating at 250 frames per second placed around the subject who performed the golf swing.

At the exact same instant, the GRF's acting at both feet was recorded using one Kistler force platforms. Forces and moments were sampled at 1K Hz using standard coordinate conventions where the positive Fx force was the subject pushing forward, positive Fy was pushing toward the right (away from the direction of the ball flight), and positive Fz was down. We analyzed the golf swing from the start of the downswing to the impact with the ball.3 trials were randomly selected from the 5 shots, and then the data was normalized according to total time

RESULTS AND DISCUSSION

1. Swing time and club head speed

Table 1 show the swing time and club head speed (HS) at impact, hip and shoulder range of the motion (ROM) with the mean (±S.D) respectively.

Table1. Club head speed and hip and shoulder ROM

subject	HSmax (m/s)	Time (s)	ROM Hip (deg)	ROM Shoulder (deg)
Mean± SD	38.8± 2.7	0.3± 0.04	86.0± 10.9	114.2± 13.1

2. The patterns of GRF and free moment forces

The free moment about the vertical axis increased toward middle range between start of downswing and impact with ball, then reached its maximum value (Mzm). Rotations of both the hip and shoulder were going at maximal value in order to build up energy at the top of the backswing. In addition to that, forces acting the both feet also exert a turning effort on trunk rotation. After Mzm appeared, the vertical GRF attained the maximum value (Fzm), which indicates that the free moment decreased toward the impact, resulting in the transfer of force to the target foot (left foot; right-handed). While forces transferred, knee joint and hip joint tended to be flexed. As a result of forces acting on the entire body appeared maximum value in order of increasing the free moment and the vertical GRF during middle downswing. This phenomenon occurred in all subjects for this study.

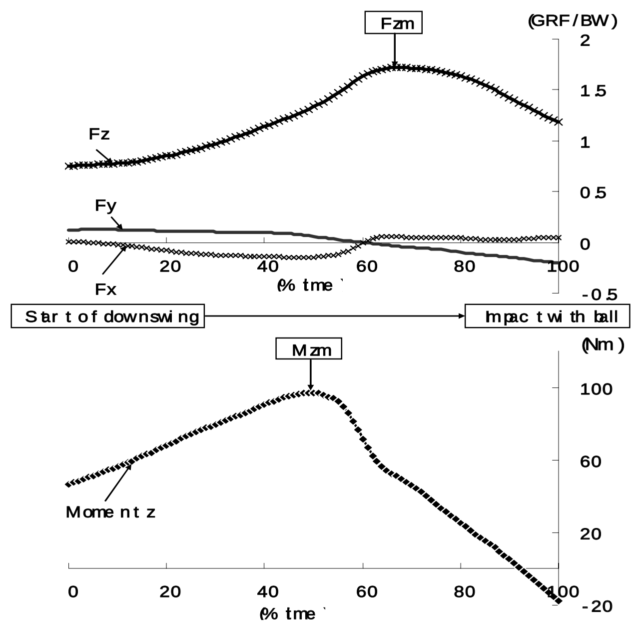

Figure1. The GRF and free moment patterns

CONCLUSIONS

The maximum value of free moment about the vertical axis appeared first during middle downswing in the golf swing, and then the maximum value of vertical GRF appeared in all of the golfers. This suggested that a result of forces acting on the entire body was changed by rotations of hip and shoulder and the flexions of the knee joint and hip joint.

REFERENCES

1. Joseph Hamill, Kathleen M. Knutzen, Biomechanical Basis of Human Movement Second Edition: Lippincott Williams & Wilkins 2003
2. D. Gordon E. Robertson, Graham E Coldwell, Joseph Hamill, Gray Kamen, Saunders N. Whittlesey, Research Methods in Biomechanics: Human Kinetics 2004

LONG TERM MODEL OF BOTULINUM TOXIN-INDUCED MUSCLE WEAKNESS IN THE RABBIT

[1] *M.A. Vaz,* [2] *D. Longino,* [2] *C. Frank,* [3] *T.R. Leonard,* [3] *W. Herzog*
1. School of Physical Education, Federal University of Rio Grande do Sul, RS, Brazil
2. Faculty of Medicine, University of Calgary, AB,Canada
3. Faculty of Kinesiology, University of Calgary, AB, Canada
E-mail: marcovaz@esef.ufrgs.br; walter@kin.ucalgary.ca

Introduction

Muscle weakness is one of the earliest and most common symptoms of patients with osteoarthritis (OA) (1). Although many experimental models of OA include muscular weakness, no model has studied this factor satisfactorily for long periods of time. The purpose of this study was to assess muscle weakness over a period of six months in order to validate an experimental model of muscle weakness for future use in the study of OA.

Methods

Muscle weakness was produced by monthly injections of the neurotoxin clostridium botulinum type A (BTX-A) in the quadriceps muscle of six New Zealand white rabbits. Muscle weakness was assessed by calculating the difference in knee extensor torque between experimental and contralateral hind limb (which was injected with a saline solution). Knee extensor torques were obtained at three different knee angles with a custom-built force sensor bar placed distally on the tibia. Knee extensor torque was produced with supramaximal stimulation (100 Hz, 500 ms) of the quadriceps muscles through the femoral nerve. Maximum isometric knee extensor torque was recorded at multiple knee angles in order to investigate if muscle weakness between hind limbs persists over a physiological range of motion. Muscle mass of the rectus femoris, vastus lateralis, vastus intermedius and vastus medialis muscles was evaluated post mortem using a commercial scale with an accuracy of 0.001g. All outcome measures are reported as relative percent deficits, comparing the BTX-A injected hind limb to the contralateral (sham) hind limb.

Results and Discussion

Muscle weakness across all three tested knee angles was approximately 60%, suggesting that BTX-A had a similar effect across the physiological range of motion and produced weakness over the six months testing protocol (Figure 1).

Atrophy, measured as the deficit in muscle mass between experimental and control limbs, was greatest for the vastus lateralis and smallest for the vastus medialis (Figure 2). This difference in atrophy may represent a difference in fiber type composition between the quadriceps muscles. BTX-A has been reported to have a greater effect on fast-twitch (type II) muscle fibers (2).

Conclusions

Monthly injections of BTX-A, a potent neuromuscular blocking agent, over a six months period, created a chronic functional muscle weakness model in the New Zealand white rabbit. This model may be used to systematically study the possible effects of muscle weakness on joint degeneration, either as an isolated intervention, or in combination with other interventions known to create knee joint degeneration.

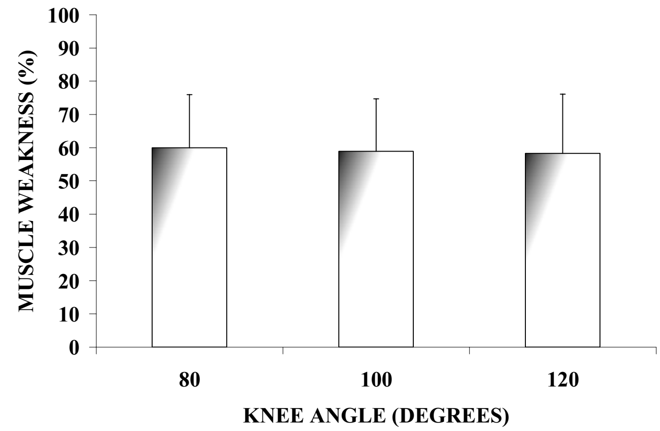

Figure 1. Muscle weakness (mean and standard deviation) of the knee extensor muscles obtained at three different joint angles.

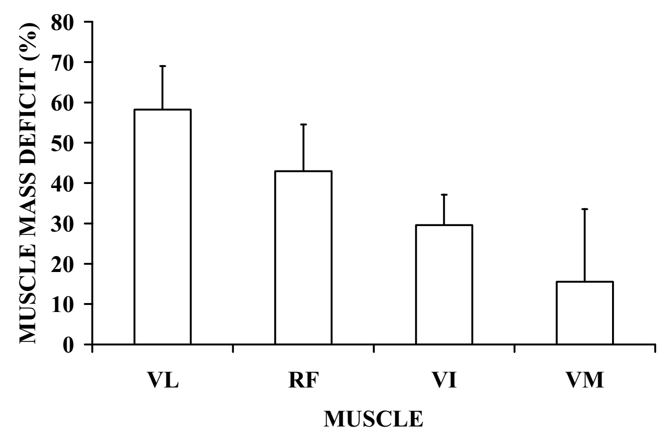

Figure 2. Muscle mass deficit (mean and standard deviation) of the knee extensor muscles (VL = vastus lateralis; RF = rectus femoris; VI = vastus intermedius; VM = vastus medialis).

References

1. Hurley MV, Newham DJ. Br J Rheumatol 32, 127-131, 1993.
2. Duchen LW. J Neurol Neurosurg Psychiatry 33, 40-54, 1970.

Acknowledgements

The Canadian Institutes of Health Research (CIHR), The Canada Research Chair Programme, CAPES-Brazil, UFRGS-Brazil.

Computer simulation for internal-stability of foot longitudinal arch strengthened by plantar soft tissues and plantar static friction

WU Lijun(email: biomech@163.com), KONG Kangmei, QI WeiLi

Laboratory of Surgery, The Second Affiliated Hospital, Shantou University Medical College, Shantou, Guangdong, China, 515041.

【Abstract】 ***Objective*****:** To investigate anatomic structure and biomechanical mechanism for internal-stability of foot longitudinal arch, to offer quantitative academic base for normal arch internal-stability strengthened by plantar soft tissues and plantar static friction, and to calculate the stress distribution in plantar longitudinal arch changed by arch collapse. ***Methods*****:** The method of reconstruction by CT images is adopted, which produces 3D model of foot arch in order to research its anatomic structure of medial and lateral longitudinal arch. The finite element method is also applied to establish biomechanical model of longitudinal arch of second ray of foot, which can analyze its stress distribution in standing phase. ***Results*****:** A 3D computer model of longitudinal arch of normal foot and a finite element model of its second plantar longitudinal arch were created. When simulating naked foot standing with plantar static friction, Von Mises stress of second metatarsal bone and plantar aponeurosis were respectively 1.31MPa and 0.89MPa. When simulating naked foot standing with no plantar static friction, Von Mises stress of second metatarsal bone and plantar aponeurosis increased respectively to 2.35MPa and 1.22MPa. When simulating naked foot standing following surgical plantar aponeurosis release, Von Mises stress of second metatarsal bone and plantar aponeurosis were changed respectively to 3.21MPa and 0.02MPa. When simulating naked foot standing following arch collapse or flat foot standing, Von Mises stress of second metatarsal bone and plantar aponeurosis were changed respectively to 1.66MPa and 1.22MPa. ***Conclusion*****:** Von Mises stress are concentrated mainly on second metatarsal bone and plantar aponeurosis when naked foot standing. Plantar soft tissues and plantar static friction can produce a marked effect to reduce degree of stress concentration in foot longitudinal arch, and can strengthened arch internal-stability. If foot arch collapses or flattens, degree of stress concentration of arch will aggravate over normal arch, and flat arch is disadvantageous to protect internal-stability of foot.

【Keywords】3D model of plantar longitudinal arch, plantar arch collapse, internal-stability, finite element method, biomechanics

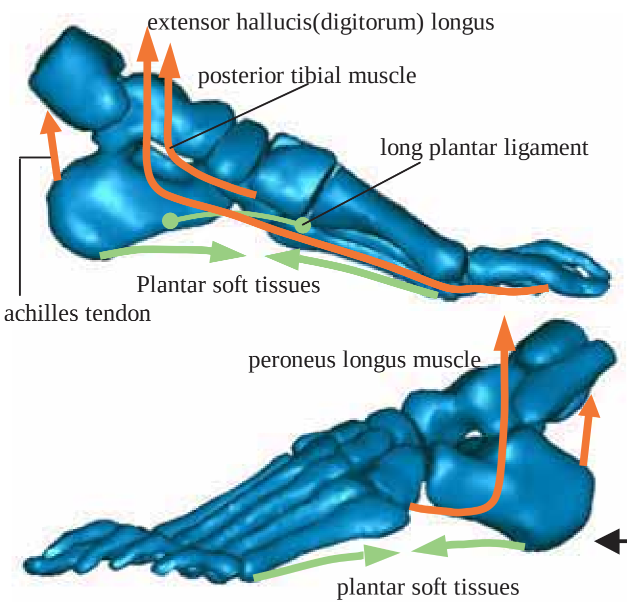

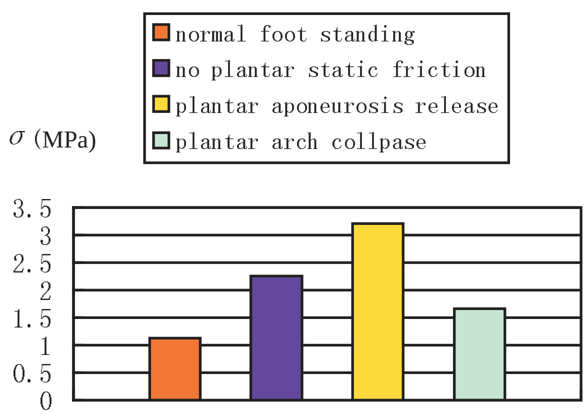

Fig.1 Von Mises stress peak values of 2nd metatarsal bone in several standing conditions

Fig.2 3D-computer model of longitudinal arch of normal foot

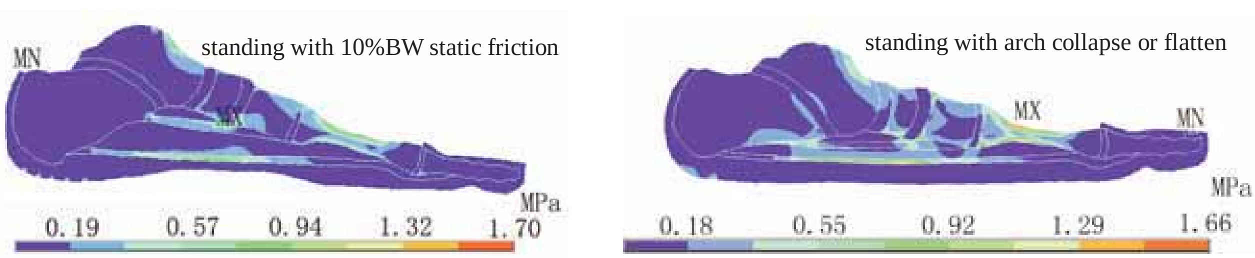

Fig.3 Von Mises Stress distribution in second plantar longitudinal arch under different standing condition

Note: This dissertation is supported by China Postdoctoral science foundation project (No 2004035047)

EFFECT OF SUN LIGHT ON SURFACE TEMPERATURE OF ARTIFICIAL SPORT SURFACES

Toyoaki Aoki
Biwako Seikei Sport College,
Kita-hira, Shiga-cho, Shiga 520-0503 , Japan , e-mail :aoki@bss.ac.jp

INTRODUCTION

Introductions of arttificial sport surfaces such as artificial turf and all-weather track, have been increasing year by year. We have studied the comparisons of surface temperatures of sport surfaces , and reported the results regarding to the seasonal change in the surface temperatures of artificial and natural turfs (1).

In this paper, I would like to report the relationship between the surface temperatures of sport surfaces and illuminance of sun light.

METHODS

The artificial and natural turfs were long-pile type (65mm in depth, sand-rubber infill system) and sand based type (warm season turf), respectively. The all-weather and sand tracks were urethane polymer type(13mm in depth) and soil covered with sand type (100mm in depth), respectively.

The surface temperatures were measured with a infrared thermometer (type UT-02F, Horiba Co., Japan). The illuminances on the surface from the sun were measured with a photo recorder (type PHR-51, T and D Co., Japan).

The measurements of temperatures and illuminances were performed on sunny days fromFebruary 2004 to December 2004 and at 2 hour intervals from 9:00 to 17:00 on each day.

RESULTS AND DISCUSSION

Monthly change in surface temperatures of the artificial turf with time is shown in Fig.1. The surface temperature increased with day from Feb.(winter) to Aug.(summer). The maximum temperature was 67.5'C at 13:00 on Aug.11.

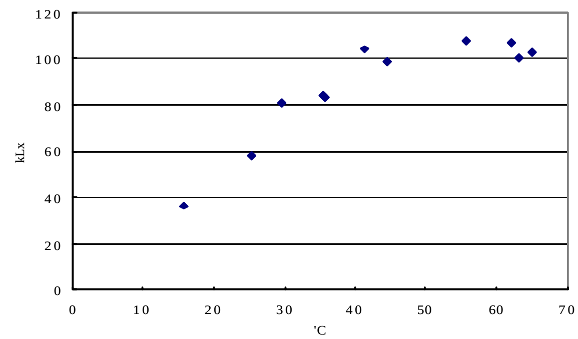

Fig.2 Relationship between surface temp. of artificial turf and illuminance of sun light.

Figure 2 shows relationship between the surface temperature of artificial turf and illuminance of sun light at 11:00 shown in Fig.1. The surface temperature increased with illuminance up to 100 kLx and after that, became a leveling off. In summer, ground temperature had an impact on the surface temperatures.

The other surface temperatures of sport surfaces investigated in this study resulted in the same pattern as shown in Fig.1 and Fig.2.

Details of this study will be presented in the conference.

REFERENCE

1. Aoki T., et al. *Bulletin of Biwako Seikei Sport College,* Vol.2, 2005. in press.

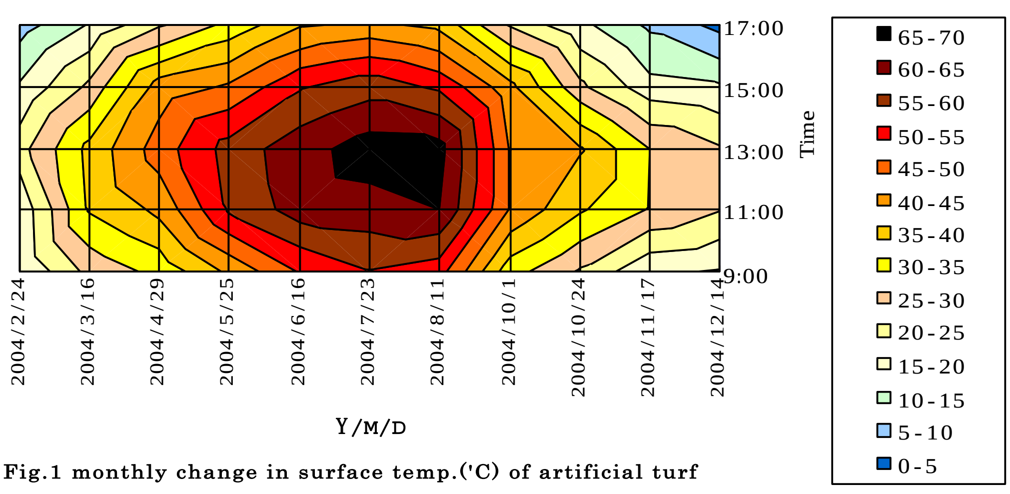

Fig.1 monthly change in surface temp.('C) of artificial turf

VARIATION IN AVERAGE AND PEAK LUMBAR DISC STRESSES BY LEVEL DURING FLEXION USING A COMBINED EXPERIMENTAL AND FINITE ELEMENT APPROACH

Naira Campbell-Kyureghyan and William Marras
Ohio State University Biodynamics Laboratory; email: marras.1@osu.edu

INTRODUCTION

Significant effort has been invested in developing FE models in the field of spinal biomechanics. Various loading conditions have been used for investigation of spinal component behavior. However, nearly all previous studies have applied artificially set loads, which make it difficult to compare to real life situations. Accordingly, the aim of this study was to develop a subject-specific component model of entire lumbar spine capable of determining the response to realistic motion under experimental settings. This paper presents the prediction of the lumbar intervertebral disc stress distribution at different levels during flexion using a human subject-linked FEM.

METHODS

The present study was in-depth, not cross-sectional, and a single subject-specific experiment was performed. A 24-year-old male subject was required to lift a 6.8 kg box from 88 cm above the floor and at a horizontal distance of 74 cm from the subject. The box was lifted from its initial position to approximately waist level at an upright standing posture and then returned to the initial position. Lumbar Motion Monitor (LMM) data was collected throughout the experiment to capture the torso angle change with respect to the initial position.

Stresses in the components of the lumbar spine, vertebral bodies, intervertebral discs, and ligaments, were calculated using a newly developed finite element model [1]. The model is capable of simulating large displacement, dynamic, sagittally-symmetric flexion and the components were validated against experimental results. Subject-specific neutral standing position lumbar spine geometry [2] is predicted as the starting point for the calculation, and the movement of the top of T_{12} is determined using LMM [3] measurements from actual flexion motion. The motion of the remainder of the lumbar spine is calculated from the interaction of the top movement, material properties, and geometry within the finite element model.

The computational model was used to determine the internal motion and forces of the lumbar spine based on the LMM measurements collected during the experiment. Maximum values during the flexion task were extracted for the compressive stress at the disc centroid and the maximum compressive and tensile stresses in the annulus.

RESULTS AND DISCUSSION

Results are presented in Figure 1 for the centroidal axial stress in the disc, maximum annular anterior compressive stress, and maximum annular posterior tensile stress for a lifting task. All

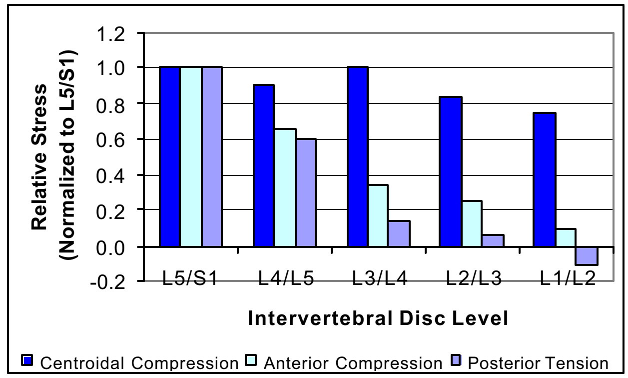

Figure 1: Variation of intervertebral disc stress with level.

stresses are normalized to the L_5/S_1 values. The compressive stress is relatively constant for disc levels from L_5/S_1 to L_3/L_4. In contrast, the maximum anterior and posterior stresses are larger for L_5/S_1 and steadily decrease at higher levels. In fact, at the L_1/L_2 level the stress was almost uniform in compression, even on the posterior annulus.

The relatively constant centroidal stress is due to the somewhat uniform distribution of purely compressive shortening between the discs. However, the rotation due to bending varies greatly between levels, with the largest rotations observed at L_5/S_1. The larger rotations, and hence bending moments, generate larger stresses at the outer layers of the discs.

CONCLUSIONS

The maximum stress in the disc is known to initiate rupture [4]. Although techniques exist for determining the maximum centroidal compression, experimental methods alone are unable to establish the maximum stresses *in-vivo* due to measuring difficulties. Previous finite element models have investigated the distribution of stress within the disc, but have not considered the full lumbar spine under realistic displacement motions. The present model demonstrates the ability to link experimental and analytical methods and calculate the stress distribution for actual motion.

REFERENCES

1. Campbell-Kyureghyan NH. *Computational Analysis of the Time-Dependent Biomechanical Behavior of the Lumbar Spine*, PhD Dissertation, Ohio State University, 2004.
2. Campbell-Kyureghyan NH, et al. *Clin Biomech* (in press).
3. Marras WS. *Int J Ind Ergo* **9**, 75-87, 1992.
4. Shirazi-Adl A. *Spine* **14**, 96-103, 1989.

PREDICTION OF INTERVERTEBRAL DISC CREEP DURING FLEXION USING A COMBINED EXPERIMENTAL AND FINITE ELEMENT APPROACH

Naira Campbell-Kyureghyan and William Marras
Ohio State University Biodynamics Laboratory; email: marras.1@osu.edu

INTRODUCTION

Injuries to the spine can occur through acute trauma, or as the result of the accumulation of damage over time. There is no simple explanation due to the multi-factorial character of low back disorders (LBD), but creep of the intervertebral disc has been identified as a predictor of damage [1]. This study presents the prediction of the intervertebral disc creep during flexion using a combined approach of a human subject experiment and finite element model of the lumbar spine.

METHODS

The present study was in-depth, not cross-sectional, and a single subject-specific experiment was performed. The experiment involved lifting a 6.8 kg box from its initial position, 88 cm above the floor and 74 cm from the subject, to approximately waist level at an upright standing posture and then returning it to the initial position. A 24-year-old male subject was required to repetitively carry out the sagittally symmetric lifting task at 6 lifts/min. for 20 minutes. Lumbar Motion Monitor (LMM) data, capturing the torso angle change with respect to the initial position, was continuously collected for the entire duration of 240 flexion cycles, with rest between the cycles.

A newly developed finite element model [2] was used to calculate the deformations and stresses in the components of the lumbar spine, including the vertebral bodies, intervertebral discs, and ligaments. The model is capable of simulating large displacement, dynamic, sagittally-symmetric flexion and the components were validated against experimental results. The initial model configuration is derived from the subject-specific neutral standing position lumbar spine geometry [3], and the movement of the top of the T_{12} vertebrae is determined using Lumbar Motion Monitor [4] measurements from the actual flexion motion. The finite element model then calculates the motion of the remainder of the lumbar spine from the interaction of the T_{12} movement, material properties, and geometry.

The computational model was used to determine the motion and stress in the lumbar spine based on the LMM measurements collected during the experiment. The axial deformation at each disc level was extracted from the results for further study.

RESULTS AND DISCUSSION

The axial deformation at the L_5/S_1 level over the 20 minutes of repeated flexion is shown in Figure 1. The creep accumulates rapidly at the beginning of the cyclic flexion. The rate of accumulation gradually decreases, with the creep asymptotically approaching a stable value from 15 to 20 minutes into the task. Similar behavior, with slightly different magnitudes, was seen at the other intervertebral disc levels.

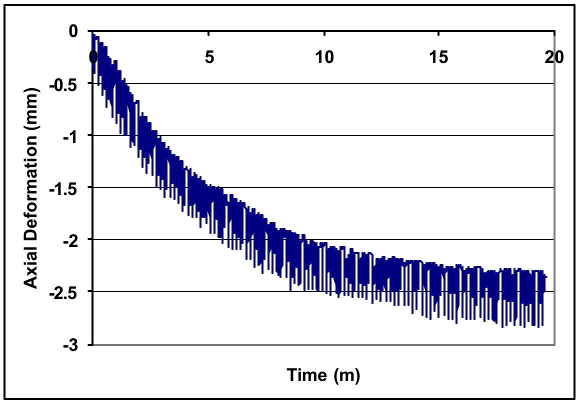

Figure 1: Axial deformation (creep) of L_5/S_1 intervertebral disc.

Limited data is available that considers cyclic loading on the discs over long periods, as opposed to creep or relaxation loading, and presents sufficient information on the testing methods, specimens, and results as to be useful. One set of such data was obtained in a series of experiments performed for 6 hours of pure compressive loading of an intervertebral disc at 1 Hz [5]. The results showed a trend similar to the current study, with creep gradually stabilizing over the course of the experiment at approximately 2.25 mm.

CONCLUSIONS

Creep is an important risk dimension for LBD. Repetitive loading can cause damage to the spine at levels below maximum [6] and creep is an indicator of this cumulative effect. In addition, excessive creep can change the distribution of forces in the spine, increasing loads on the facets and decreasing tension on the ligaments, reducing their effectiveness. The present study demonstrates the ability to link experimental and analytical methods and calculate the disc creep for actual repetitive flexion motion.

REFERENCES

1. Brinkman P, et al. *Clin Biomech* **Suppl. 1**, S1-S23, 1988.
2. Campbell-Kyureghyan NH. *Computational Analysis of the Time-Dependent Biomechanical Behavior of the Lumbar Spine*, PhD Dissertation, The Ohio State University, 2004.
3. Campbell-Kyureghyan NH, et al. *Clin Biomech* (in press).
4. Marras WS. *Int J Ind Ergo* **9**, 75-87, 1992.
5. Koeller W, et al. *Biorheology* **21**, 675-686, 1984.
6. Adams MA, et al. *Spine* **6**, 665-671, 1983.

THE GROUND REACTION FORCE AND ELECTROMYOGRAPHIC PATTERNS OF TAI CHI GAIT

[1] Yu-Hsiang Nien, [2]Shi-Po Chang, [1] Long-Ren Chuang, [1] Wen-Tzu Tang
[1]Institue of Coaching Science, National College of P.E. & Sports, Taiwan
[2]Taipei Physical Education College, Taiwan; email: 930504@mail.ncpes.edu.tw

INTRODUCTION

In the past few years, Tai Chi has become more and more popular in the west. Until now, there are more than one hundred articles about Tai Chi in the MEDLINE database. According to these studies, Tai Chi is beneficial to cardiorespiratory function, balance, postural control, strength, flexibility, and psychological profile [1]. However, most studies focused on Tai Chi training performances, the mechanisms of Tai Chi are still unclear [2,3]. In addition, the subjects in these studies were the beginner (who practiced Tai Chi for only 1 year or less) or amateur. They could not perform the typical characteristics of Tai Chi. In order to understand the mechanisms of Tai Chi, the foundation have to be identified. There are many movements in Tai Chi, like classical Yang style 108 forms, simplified style 24 forms etc. In these different forms, Tai Chi gait is the fundamental movement of Tai Chi. Therefore, the purposes of this study were to understand the ground reaction force and electromyographic patterns in Tai Chi master.

METHODS

A Tai Chi master was selected to be subject in this study (38 years, 166 cm height, 77 kg weight). He has been practicing Tai Chi for at least 2 hours every day for 15 years. The subject was asked to do the Tai Chi gait at a self-determined speed for five trials in the experiment. The gait cycle was determined by the video from digital camera, and divided into four phases: first double support phase (1DS), single limb stance phase (SS), second double support phase (2DS), and swing phase (SW). One digital camera (JVC, 60 Hz) positioned laterally 4m from the subject to check the subject movement, such as foot contact and toe-off. The 3D ground reaction force pattern was collected by a force plate (AMTI, 1000 Hz). The electromyography (EMG) pattern was measured by surface electrodes (Biovision, 1000 Hz) on each of following four muscles of the left leg: gluteus maximus (GM), rectus femoris (RF), biceps femoris (BF), tibialis anterior (TA), and gastrocnemius (GA) to record the muscle activities. The EMG data were processed by full-wave rectification (band-pass filtered at 10-500 Hz). All data was synchronized and calculated by SIMI motion system (SIMI Reality Motion Systems GmbH, Germany).

RESULTS AND DISCUSSION

Tai Chi gait is a slow movement which requires the lower limbs to move with joints in flexion position. The typical GRF and EMG patterns for the Tai Chi master are displayed in Figure 1. The average duration of Tai Chi gait cycle was 3.07± 0.38 second. The percentages of the four phases were: 21% (1DS), 35% (SS), 9% (2DS), and 35% (SW).

By comparing the Tai Chi gait with normal gait [4], the results show that not only the gait cycle duration, but also the

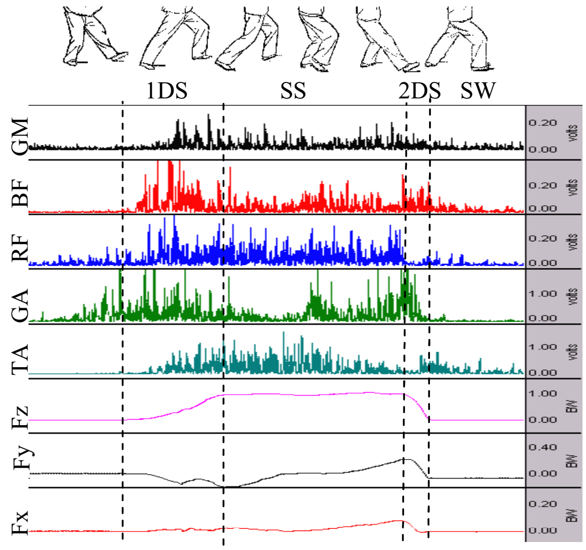

percentage of SS phase of Tai Chi gait was longer than normal gait. According to the GRF, the master demonstrated good control of GRF during the gait. He maintained low level body position while traveling slowly and steadily from one leg to another. A stable GRF was followed during body weight shifting, while the balance of the whole body was maintained. In addition, from EMG patterns, compared to normal gait, the BF and RF muscles had longer proportion of co-contraction. That may also help to maintain the weight shifting during 1DS to SS phase.

Based on these findings, it is not difficult to infer that the improvement of muscle strength after long term Tai Chi training. Therefore, it had also explained some of the effect of Tai Chi training in previous studies.

CONCLUSIONS

Different muscular control strategies involved in Tai Chi gait was determined in this study. The long duration of muscle co-contraction during Tai Chi gait should be one of the important factors of Tai Chi movements. The findings could provide the information for future investigations or Tai Chi training intervention.

REFERENCES

1. Lan Ching, et al. *Sports Med* **32** (**4**), 217-224, 2002.
2. Wayne PM, et al. *Arch Phys Med Rehabil* **85**, 142-152, 2004.
3. Wu Ge. *J Am Geriatr Soc* **50**, 746-754, 2002.
4. Vaughan CL, et al. *Dynamics of Human Gait*, Human Kinetics Publishers.

INVESTIGATING FULL FIELD DEFORAMTION OF SOFT TISSUE UNDER SIMPLE SHEAR TESTS BY THE FOURIER TRANSTER MOIRÉ METHOD

Deng-Lin Guo, Bo-Shao Chen and Nai-Shang Liou
Department of Mechanical Engineering, Southern Taiwan University of Technology
Yuang-Kang City, Tainan Hsien, Taiwan 710 R.O.C; email: nliou@mail.stut.edu.tw

INTRODUCTION

Soft tissues usually exhibit anisotropic and nonlinear material responses. In order to understand the mechanical properties of soft tissues, well controlled mechanical tests are required. Uniaxial tensile tests are the most common mechanical tests for soft tissues since soft tissues mainly sustain tensile load. However the shear deformation of soft tissue could affect the load transfer mechanism of soft tissues when soft tissues are subjected to complex deformations. Finite simple shear is a uniform deformation that can provide information (in addition to what tensile tests provide) about the mechanical properties of planar soft tissues. However test configurations like specimen geometry and the boundary condition can affect the deformation homogeneity during finite simple shear test. In order to ensure that the parameters of constitutive equations obtained from finite simple shear tests are appropriate, the deformation homogeneity of specimens during simple shear tests should be investigated.

The finite element method was used to study finite simple shear deformation of parallel-fibered planar soft tissues [1]. The purpose of this study is to use the Fourier transform moiré method to examine the deformation uniformity of porcine skin during finite simple shear tests. The effects of a different aspect ratio and clamping prestrain of the porcine skin specimen were examined.

METHODS

The Fourier transform moiré (FTM) method was used to investigate the in-plane full-filed deformation of porcine skin specimen under simple shear tests (Figure 1). The FTM method, developed by Morimoto [2,3], is a useful tool for in-plane full-field displacement and strain measurements because the setup is simple, sensitivity and resolution can be varied if necessary and the signal-to-noise ratio is high. The main steps of the FTM method include calculating the Fourier spectrum of the image, obtaining one harmonic of the spectrum, shifting the harmonic toward the origin of the spatial frequency axis and computing the complex moiré fringe pattern. Displacement and strain of the specimen can be obtained from the phase of complex moiré fringe pattern. FTM is an objective method as all computation steps can be done by computer once the image of the deformed specimen is obtained so human error can be minimized.

The procedures for preparing specimen grids on soft tissue specimens and for analyzing deformation in a series of images by using FTM method are detailed in ref [4]. Three aspect ratios (sample dimensions of 5x5, 5x3.75, 5x2.5 cm) were examined. They allowed the effect of different aspect ratios on the strain fields during simple shear tests to be investigated. The deformations of samples due to clamping prestrains were also investigated.

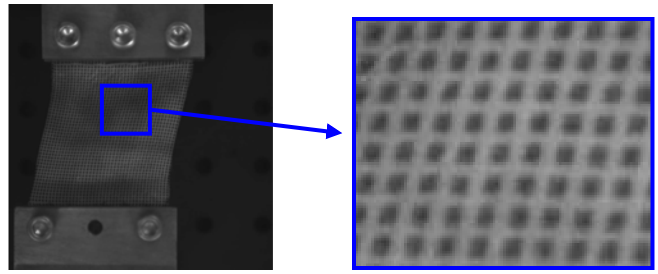

Figure 1: Schematic of in-plane full-filed deformation measurement by the FTM method.

RESULTS AND DISCUSSION

Strain fields, computed from FTM complex moiré fringe patterns (figure 2), were used to examine the in-plane deformation uniformity of samples with different aspect ratios at different shear angles during simple shear tests. The FTM method can be used to validate the soft tissue constitutive model used by the finite element method.

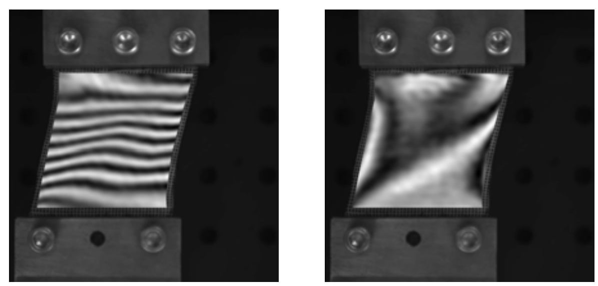

Figure 2: **u** and **v** field complex moiré fringe patterns of a 5x5 cm specimen at 10^{O} shear angle.

If no pre-tension is applied to planar soft tissue sample prior to simple shear test, the out-of-plane deformation of samples under simple shear test can be significant when the shear angle is large. Future work will include out-of-plane deformation measurement and finite element simulations of soft tissues during simple shear tests.

REFERENCES

1. Gardiner JC, et al. *J of Biomech Eng* **123**, 170-175, 2001
2. Morimoto Y, et al. *Opt Eng* **27**, 650-656, 1988.
3. Morimoto Y, et al. *Exp Mech* **29**, 399-404, 1989.
4. Liou N.-S *SEM X Int Congress and Exposition on Exp and App Mech.*, Costa Mesa, USA, article #104 and #106, 2004

ACKNOWLEDGEMENTS

Supported by the National Science Council, Taiwan R.O.C (NSC-93-2213-E-218-010).

DETERMINING THE RESTING POSITION OF THE GLENOHUMERAL JOINT IN NORMAL SUBJECTS

[1]Hui-Ting Lin, [2]Ar-Tyan Hsu, [3]Jia-rea Chang Chien, [4]Ching-Song Yeh and [1]Guan-Liang Chang
[1]Institute of Biomedical Engineering, [2]Department of Physical Therapy,
[3]Department of Electrical Engineering, National Cheng Kung University, Tainan, Taiwan
[4]Mingchi Institute of Technology, Taipei, Taiwan
email: liang@mail.bme.ncku.edu.tw, web: http://www.bme.ncku.edu.tw

INTRODUCTION

The resting position is generally regarded as the position of a joint in which the joint tissues are under least amount of stress and where the joint capsule has its great laxity. It is frequently chosen as the ideal position for evaluation and early treatment of painful and inflammatory joint or joint with hypomobility [1]. For glenohumeral (GH) joint, according to the data in cadaver study reported by Hsu, the resting position was located at an average position of 39 degree of abduction in the scapular plane [1]. However, as far as we know, no research has determined the resting position of GH joint in vivo model. Therefore, the purpose of this study is to define the resting position of the GH joint by investigating the total displacements of humeral head and total rotation range of motion (ROM) of the GH joint at each GH abduction angle in normal subjects.

METHODS

Seventeen normal subjects were recruited. All subjects were seated on the sturdy chair with a designed clamp grapping the spine of the scapula and clavicle. The lateral border of the scapula was also blocked. One adjustable lower arm brace was put on the elbow to immobilize it at 90^{o} flexion. The center of rotation (COR) of GH joint was estimated with the modified methods [2]. The constant relationship between the markers of Fastrack tracking device and COR within local coordinate system were then established.

For measuring the displacements of humeral head, an 80 N force was applied during anterior-posterior (A-P) glide and posterior-anterior (P-A) glide and the markers will be tracked. The displacement of COR could be computed according to the constant relationship. A torque transducer was used during rotation ROM of GH joint to ensure a consistent torque of 4 Nm of internal rotation (IR) moment and external rotation (ER) moment. The markers were tracked during joint play movement and rotation ROM in the plane of scapula form neutral position to end range of GH abduction at 10 degree intervals. Three repeated displacements of COR and rotation ROMs were computed.

All three replicates of displacement measurements and the rotation measurements were used for data analysis. Intra-class correlation coefficient was used to test the Intrasession reliability of the displacements of humeral head and rotation ROMs. To determine the resting position, the method employed by Hsu et al. was followed [2].

RESULTS AND DISCUSSION

Intrarater reliability, ICC(2,1) values, were depicted in Table1. The average values of A-P, P-A displacements, IR and ER ROMs were shown in figure 1 and figure2.

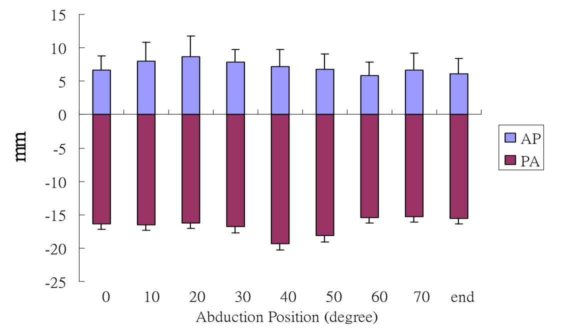

Figure 1: The average values of A-P and P-A displacements at multiple GH joint abduction angles.

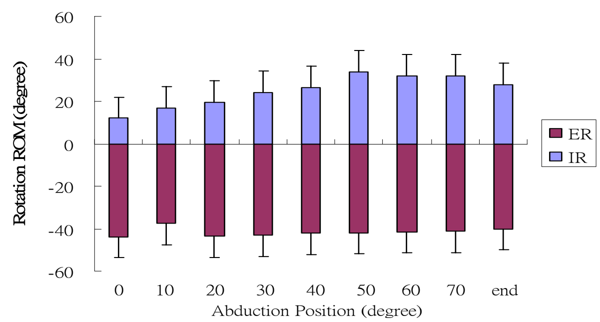

Figure 2: The average values of IR-ER ROMs at multiple GH joint abduction angles.

The resting position is defined as the midpoint of the shared range of 95% confidence intervals of the predicted abduction angles where peaks of maximal displacement and rotation occurred in this study. It provides fundamental information to the practice of orthopedic manual procedures in physical therapy.

ACKNOWLEDGEMENTS

The current research was funded by National Science Council, (grant # NSC 92-2320-B-006-015) and College of Medicine, National Cheng Kung University, Taiwan

REFERENCES

1. Hsu AT, et al..Determining the resting position of the glenohumeral joint: a cadaver study. *J. orthop. sports phys. ther* **32**, 605-612, 2002.
2. Gamage SSHU, Lasenby J. New least squares solutions for estimating the average center of rotation and axis of rotation. *J Biomech* **35**, 87-93,2002.

Table 1: Intraclass Correlation Coefficient among three replicates of A-P, P-A, IR, ER measurement.

	A-P	P-A	IR	ER
ICC(2,1)	0.719-0.936	0.759-0.97	0.807 - 0.979	0.945-0.993

ENERGY FLOW IN HIGH HEEL SHOES IN WALKING

F. Ju, F.S. Cui, Z.S. Liu, *H.P. Lee and C. Lu
Institute of High Performance Computing, 1 Science Park Road,
#01-01 The Capricorn, Singapore 117528; email: hplee@ihpc.a-star.edu.sg

INTRODUCTION

High heel shoes lead the feet weak and prone to injury and serious foot ailments. Hansen et al. [1] investigated the effects of shoe heel height on the rollover characteristics of the biologic ankle-foot system. Stefanyshyn et at. [2] studied the Influence of high heel shoes on mechanical behaviours of normal female gait with four different patterns shoes with high heels. The effect of insoles on the plantar pressure distribution was studied by Lemmon et at. [3] with the finite element method (FEM). More recent research on the foot-shoe system with FEM approaches can be found in [4] and [5]. Studies and observations have found that women walking in high heel shoes experience the excessive side to side motion at the ankle joints and feet, resulting in excessive stresses in the foot ball, calcaneus and joints. These stresses are caused by the contact-impact between the shoe and the ground and, sequentially, propagate into the foot. The whole course can be viewed as a process of energy transformations.

The objective of this study is to investigate the energy flow transmission in high heel shoes under contact-impacts during walking. The effect of the stiffness of shoe soles on the stress distribution in the foot-shoe system will be highlighted.

METHODS

A simplified 2D finite element model including the shoe sole and the foot is established to investigate mechanical and structural characteristics of the foot-shoe system. Only the shoe sole is considered to focus on the interactive effect of the foot and the shoe. The foot is modeled as bones, joints and a layer of soft tissue material at the bottom of the foot. The nominal stiffness, a product of Young's modulus and sole thickness, is used to represent the elasticity of shoe soles.

Structural Intensity (SI) method is employed to characterize the energy flow transmission and stress distribution and propagation in system under various impact-contact conditions. The concept of SI was first introduced to extend the vector acoustics approach to energy flow in structures-born sound fields. SI is the power flow per unit area of cross section elastic medium and offers full information of the paths of energy transmission and positions of sources and sinks [6].

RESULTS AND DISCUSSION

Shoes with the heel height of 3, 6 or 9 cm and various stiffness of shoe soles are used for numerical study. Different stages during walking are considered in the analysis. Figures 1 and 2 show respectively the SI vector and stress contour of the flat and high heel shoes, which clearly indicate the paths of energy transmission and stress distributions in the system. The energy flow patterns show that strain energy distributes and transmits favorably in a flat shoe due to the presence of the soft sole layer, while it reaches the calcaneus with a higher intensity in

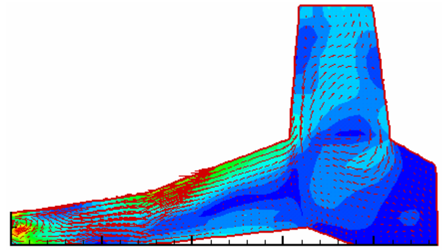

Figure 1: SI vector and stress contour of a flat shoe under contact-impacts

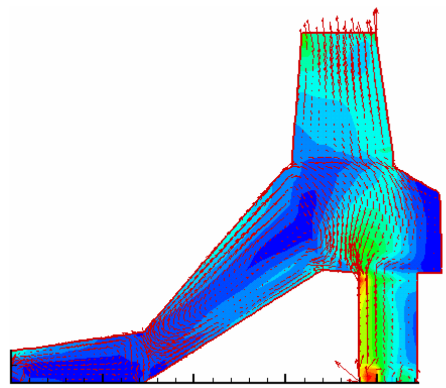

Figure 2: SI vector and stress contour of a high heel shoe under contact-impacts

a high heel shoe regardless of the sole. Soft shoe soles with smaller stiffness can greatly improved the stress concentration at the calcaneus area and ankle joints for flat shoes. However, much greater stress concentrations are found for high heel shoes and soft shoe soles can hardly improve the uneven distribution of stresses in most cases.

CONCLUSIONS

Structural Intensity provides rich information for energy flow transmission in foot-shoe system under the contact-impact during walking. Severe stress concentrations in the calcaneus area are found for high heel shoes, and soft shoe soles do not help much in evening up the stress distribution.

It is relevant to indicate that 2D models are effective to study the mechanical phenomenon of the walking impact of the foot-shoe system but too restrictive for quantitative analyses. 3D models will be developed in our further study.

REFERENCES

1. Hansen AH, et al.. *J of Rehabilitation Research And Development* **41**(4), 547-554, 2004.
2. Stefanyshyn DJ, et al.. *J App. Biomech* **16**,309-331, 2000.
3. Lemmon D, et al.. *J Biomech* **30**, 615-62-, 1997.
4. Chen W, et al.. *Clinical Biomech* **18**, S17-S24, 2003.
5. Lewis G. *Bio-Medical Materials & Engrg* **13**, 75-81, 2003.
6. Liu ZS, et al.. *Int. J .of Impact Engineering*, (Available online 10 August 2004 via ScienceDirect.)

THE EFFECT OF MOVEMENT SPEED AND EXTERNAL LOAD ON JOINT CONTRIBUTIONS DURING LOWER EXTREMITY EXTENSIONS

[1] Sean P. Flanagan and [2]George J. Salem
[1]Department of Kinesiology, California State University, Northridge,
[2]Department of Biokinesiology and Physical Therapy, University of Southern California;
email: sean.flanagan@csun.edu, web: www.csun.edu/~sflanagan

INTRODUCTION

Determining the individual joint contributions during a variety of tasks has been the goal of many biomechanical investigations striving to quantify mechanical demand and provide insight into how multi-joint movement is controlled. Many of these investigations have been conducted with the task performed under a single set of experimental conditions, limiting the generalizability of the results to other movement conditions. They also do not provide information on how the joint contributions are adjusted in order to meet differing task objectives.

The purpose of this investigation was to examine the effect of movement speed on the mechanical demand distribution across the lower extremity joints during the barbell squat activity, and to determine if mechanisms by which this distribution occurred were load-specific.

METHODS

Eighteen healthy, young adults who were familiar with the squat exercise performed 3 sets of 3 repetitions of a squat under two different loading conditions (25% and 50% of a 3 repetition maximum) and two different movement speed conditions (self-selected and as fast as possible). Standard inverse dynamics techniques were used to calculate the instantaneous net joint moment (NJM), angular velocity (ω) and NJM power (P). Average NJM, ω, and P were calculated using numerical integration. The average P at the hip, knee, and ankle were summed to create a lower extremity power score. The percent contribution of each joint was determined as the quotient of the individual P divided by this score. The relative adjustments in the average NJM and ω between the self-selected and fast conditions were calculated by dividing the outcome variables associated with the fast condition by the like outcome variables associated with the self-selected condition (F/SS). For all analyses, alpha was set at 0.05.

RESULTS AND DISCUSSION

The percent contribution for each joint under each condition is presented in Figure 1. The contribution from the hip and ankle significantly increased with load, but significantly decreased with speed. Conversely, the contributions of the knee significantly decreased with load but significantly increased with speed. There were no significant interactions.

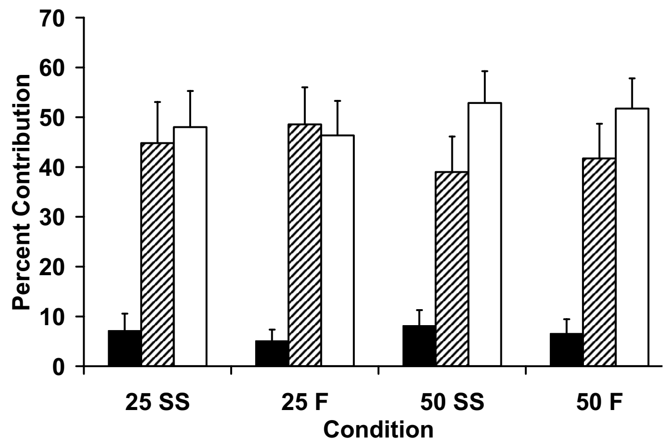

Figure 1. Percent contribution of the ankle (black), knee (striped) and hip (white) for the 25% and 50% self-selected (SS) and fast (F) conditions.

Analyses of the average NJM and angular velocity at each joint (Table 1) indicate that the redistribution of demand as a result of increased movement speed was brought about by specific changes in the average NJM at each joint. While the changes in angular velocities were greater than changes in NJM, they were not significantly different between joints.

CONCLUSIONS

A different, but identifiable movement control strategy appears to be employed in response to increases in movement speed compared to increases in external resistance. However, the magnitude of the speed response strategy is affected by external loading. The results of this investigation indicate that the joint contributions quantified under one set of experimental conditions are not generalizable to other experimental conditions.

ACKNOWLEDGEMENTS

The authors wish to thank James Gordon, Kornelia Kulig, Jill McNitt-Gray, and Christopher Powers for their contributions towards this investigation.

Table 1: Relative adjustment from self-selected to fast movement speed for the average net joint moment (NJM) and average angular velocity (ω).

Condition	Relative Adjustment from Self-Selected to Fast Movement Speeds					
	25%			50%		
	Ankle	Knee	Hip	Ankle	Knee	Hip
Average NJM	0.84 ± 0.37	1.23 ± 0.13	1.09 ± 0.11	0.95 ± 0.25	1.16 ± 0.16	1.08 ± 0.07
Average ω	1.67 ± 0.28	1.70 ± 0.19	1.79 ± 0.26	1.54 ± 0.20	1.56 ± 0.23	1.66 ± 0.33

NUMERICAL ANALYSIS ON BIPOLAR HEPATIC RADIO-FREQUENCY ABLATION

[1,6]Joong Yull Park, [2,3]Jung Min Lee, [4]Chan Young Park and [4,5,6]Byung Goo Min
[1]Interdisciplinary Program in Biomedical Engineering Major, Seoul National University, Seoul, Korea,
[2]Department of Radiology, College of Medicine, Seoul National University, Seoul, Korea,
[3]Department of Diagnostic Radiology, Seoul National University Hospital, Seoul, Korea,
[4]Institute of Medical and Biological Engineering, Medical Research Center, Seoul National University, Seoul, Korea,
[5]Department of Biomedical Engineering, College of Medicine, Seoul National University, Seoul, Korea,
[6]Korea Artificial Organ Center, Seoul, Korea; email: junior74@snu.ac.kr

INTRODUCTION

Hepatic radio-frequency ablation is an important surgical operation that deliver electrical energy of 460~550 kHz into liver tissue by using specified medical device [1]. Ablation probes are inserted percutaneously into tissues where tumors exist. Then electrical energy is delivered through the probes and the electrical energy turn into the thermal energy and heat the tissue to over 45-50 ℃ which cause cell necrosis and get rid of the tumors. It is very important to estimate the effective necrosis range as correctly as possible. Numerical analysis for the bipolar RFA is proposed to do this estimation in this study.

METHODS

The shape of ablation electrode was considered as a straight rod. Ablation electrode consists of the conducting tip and shaft. In this simulation the length of the conducting tip was assumed to be 3 cm, and the diameter to be 2 mm. And the shafts were assumed to be adiabatic. The liver model is a cubic shape having the dimensions of 10 cm × 10 cm × 7 cm.

Heat transfer in the liver tissue is governed by the following heat conduction equation

$$\rho c \frac{\partial T}{\partial t} = \nabla \cdot k \nabla T + \vec{E} \cdot \vec{J} - Q_{ex}$$

where ρ is density, c is heat capacity, k is thermal conductivity, $\vec{J}$ is current density vector, $\vec{E}$ is electric field intensity vector, and Q_{ex} is the metabolic heat source term. We assumed the metabolic heat source term is insignificantly small so that it was ignored.

The surface temperature in the liver model was assumed to be constant at 27℃. For the simplicity, we calculated only the half of the model by using the symmetry condition. AC current of 2000mAh was used for the simulation.

CFD-ACE(U) TM Ver. 2002 (CFD Research Corporation, 215 Wynn Drive, Huntsville, AL 35805) was used for the computation.

RESULTS AND DISCUSSION

The maximum temperature was 101.4℃, and the effective necrosis range, which is in the temperature range of above 60℃, was about 5 cm in length (Figure 1). High temperature regions above 80℃ were near the conducting tips, however, the isothermal surface of 60℃ covers the center part of the liver between the two electrodes.

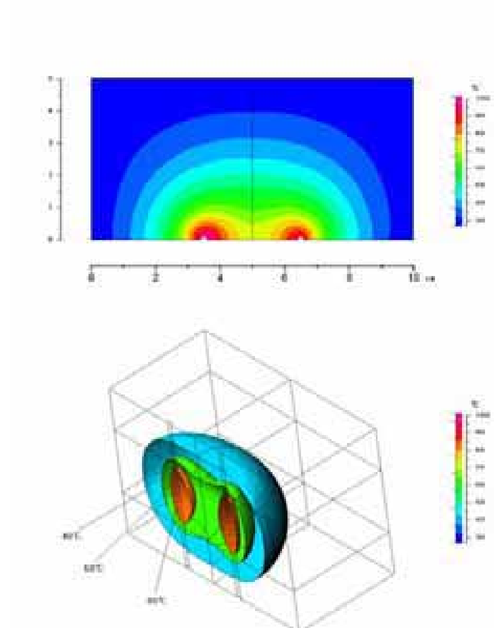

Figure 1: Isothermal surfaces (40℃, 60℃, 80℃).

In Lee et al. the inhomogeneity of liver tissue may cause the complicate electrical, thermal phenomena [2]. In addition, the blood flows in the liver obviously interfere during the RFA treatment. Also the temperature dependent properties of liver such as thermal conductivity, tissue heat capacity, tissue electrical conductivity and so on must be considered in the future work.

CONCLUSIONS

We conducted a three-dimensional numerical analysis on the bipolar hepatic RFA. As a result, we could get a reasonable necrosis range. Though there are significant limitations, this study still shows that the numerical method can be a useful tool for estimation of the effective necrosis range and diagnosis for the RFA treatment in near future.

REFERENCES

1. Alessandro G, et al. *J Hepatol* **33**, 667-672, 2000.
2. Lee TL, et al. *IEEE Trans Biomed Eng* **49(7)**, 836-842, 2004.

ACKNOWLEDGEMENTS

This study is supported by the Brain Korea 21 Project of the Ministry of Education and Human Resources Development, Republic of Korea.

TOE-WALKING IN INTACT INDIVIDUALS ARISING FROM EMULATED CONTRACTURES OF SOLEUS, GASTROCNEMIUS AND HAMSTRING MUSCLES

Andrej Olenšek, Zlatko Matjačić
Institute for Rehabilitation, Republic of Slovenia
email: andrej.olensek@ir-rs.si

INTRODUCTION

Toe-walking is very common gait irregularity in individuals with spastic plantarflexors and hamstrings. Identification of primary cause of toe-walking in particular patient is of utmost importance for deriving appropriate treatment. We therefore need an effective method for proper biomechanical characterization of particular gait irregularity.

Recently two studies investigated compensatory gait deviations where toe walking was imposed in healthy adults by emulating a muscle contracture [1] or using special taping technique to form an equinus constraint [2]. Results lead to conclusion that different gait compensations should be expected when toe-walking is imposed by different constraints.

The purpose of this study is to emulate muscle contractures in individuals free from neuromuscular impairements as described in [1] and investigate which gait compensations arise when toe-walking is elicited by muscle constractures of soleus, gastrocnemius or hamstrings.

METHODS

Figure 1 shows schematic drawing of the system that adds mechanical stiffness in parallel with particular muscle to emulate muscle contractures. Imitating primary gait irregularity by emulating contractures of soleus (SOL), gastrocnemius (GAS) or hamstring (HAM) muscles results in toe-walking but have characteristic compensatory gait deviations.

A volunteer equipped with the system walked along a 7 m walkway with walking speed approximately 1 m/s. We used VICON motion analysis system and two AMTI force plates for recording gait kinematics and kinetics of lower extremities.

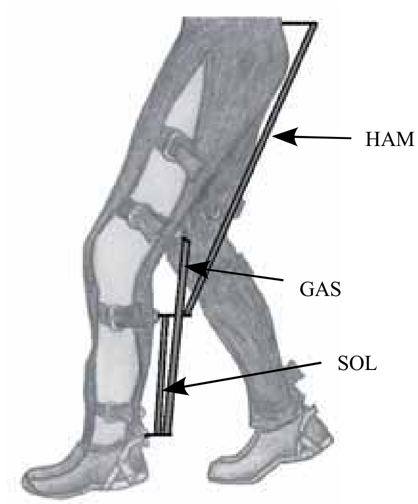

Figure 1: Imposing various mechanical constraints to form muscle contracture emulations forcing the subject to toe-walk

RESULTS AND DISCUSSION

Figure 2 presents ankle and knee angle and moment trajectories for different muscle contracture emulations imposed. All restrictive patterns are characterized with substantial plantar flexion and double-tooth moment trajectory which is consistent with results as recorded in Goodman et al. [1] and Matjačić et al. [2].

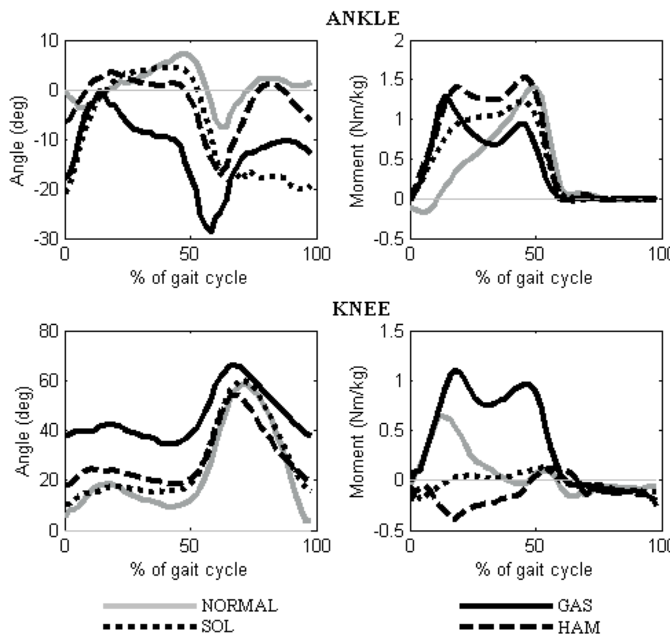

Figure 2: Ankle and knee angle and moment under different experimental conditions

Somewhat more distinctive are knee recordings when observing particular contracture emulation. Prolonged knee flexion and knee extensor moment throughout the stride as recorded in GAS muscle contracture emulations are consistent with results as reported by Matjačić et al. [1] and Goodman et al. [2]. On the other hand knee extensor moment was substantially diminished and excursions in knee angle were less evident when emulating SOL and HAM contractures.

CONCLUSION

Results indicate that particular gait impairment will result in very distinctive secondary biomechanical effects and the proposed methodology for emulating muscle contractures may produce results that are potentially valuable for identifying compensatory gait deviations in clinical practice.

REFERENCES

1. Matjačić Z, et al. *J Biomech*, in press, 2005
2. Goodman MJ, et al. *Gait Posture* **20**, 238-244, 2004

TRANSMISSION OF CONTROLLED EXTERNAL PLANTAR IMPACTS ALONG THE TIBIA IN RELATION TO MUSCULAR ACTIVITY

[1,2]Anton Arndt, [3]Peter Brüggemann, [1]Arne Lundberg, [2]Kjartan Halvorsen and [3] Wolfgang Potthast
[1] Dept. Orthopedic Surgery, Karolinska University Hospital / Huddinge, Sweden, email: toni.arndt@cfss.ki.se
[2] Dept. of Sport and Health Sciences, Stockholm University College of Physical Education and Sports, Sweden
[3] Institute for Biomechanics, German Sport University Cologne, Germany

INTRODUCTION

The shocks transmitted to the musculoskeletal system from external ground reaction impacts have been described as responsible for a number of musculoskeletal pathologies including tibial stress fractures, knee and hip osteoarthrosis and lower back problems [1]. The aim of this study was to ascertain the relationship between lower leg muscle activity and *in vivo* accelerations measured at distal and proximal tibial sites. Previous studies have primarily investigated the relationship between external gorund reaction force and a single proximal tibial site [2] or across joints. These designs exclude the parameter of shock transmission along a single long bone and the possible damping effect of muscle stiffness. In order to avoid the uncertain influence of complicating factors encountered in a previous study [3] in which tibial acceleration transmission was determined during running, this study was restricted to very controlled, static trials.

METHODS

Six voluntary male healthy subjects participated in this study and the data of one subject (36 year, 88 kg) are presented in this abstract. Tibial accelerations were measured using 3D accelerometers (Kistler®, mass <2.5 g) attached to Apex® pins (diameter 3.0mm, length, 60mm) inserted approximately 1.5 cm into the distal and proximal tibia. Pin insertion was conducted under local anaesthetic and the experimental protocol was limited to three hours. Surface electromyography (EMG) electrodes recorded the activity of the gastrocnemius medialis (GM) gastrocnemius lateralis (GL), soleus (SOL), tibialis anterior (TA) and intramuscular EMG wires were used for tibialis posterior (TP). The summed integral of the EMG linear envelopes was referred to as the tibial muscle envelope. A custom made pneumatic impacter initiated impacts under the heel. The ankle joint was maintained in 90º and the knee angle at 180º (full extension). The impact force (F) was measured with a one dimensional force transducer (Kistler®). The sampling rate for all analog data was 1000Hz. Maximal voluntary isometric contractions (MVC) for each muscle were performed and to control muscle pre-activation three activation levels were defined at 0%, 30% and 60% of the MVC EMG amplitudes for GM and vastus medialis (VM). Ten impacts were initiated at each activation level. Accelerometer axes were mathematically aligned with the anatomical tibia axis using a correction algorithm based upon reflective markers recorded by a movement analysis system (ProReflex®, Qualysis, Sweden). F and the tibial accelerations were compared for the three activation levels and the effect of the tibial muscle envelope (sum of EMG integrals 50 ms prior to 50 ms after impact) upon the shock transmission from distal (accTD) to proximal tibia (accTP) was investigated (figure 1). Shock transmission was calculated as accTD – accTP. ANOVA and correlation statistics were calculated in Statistica®.

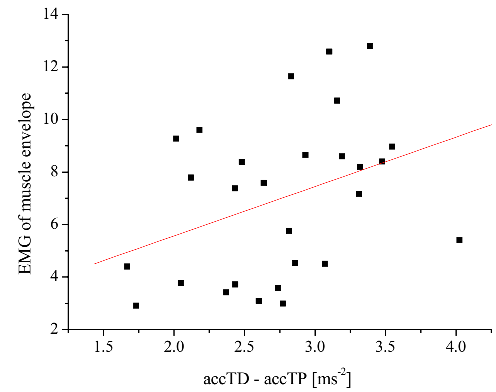

Figure 1: Scatter plot of acceleration damping (accTD-accTP) vs summed EMG integrals of the tibial muscle envelope: r = 0.36, p = 0.06. Two trials were not accepted due to knee angle variation.

RESULTS AND DISCUSSION

Significant differences ($p \leq 0.05$) in F and accTD were found between the 0% and 30% and the 0% and 60% levels, accTP was not significantly influenced. F and accTD correlated significantly with the tibial muscle envelope activity (r = 0.77 and 0.62 respectively, $p \leq 0.05$), accTP did not. Figure 1 shows that the transmission from distal to proximal tibia was not significantly correlated with muscle envelope activity. A trend towards increased damping was, however, shown (r = 0.36, p = 0.06), and it remains to be seen how the inclusion of further subjects in the analysis influences this result.

CONCLUSIONS

The very controlled nature of the external impacts combined with the accuracy in orienting the accelerometer axes provided prerequisites for precise description of shock transmission. The data are an important contribution to the understanding of musculoskeletal control and also raise questions concerning previous studies where accelerations were only measured at one tibial location.

REFERENCES

1. Whittle, et al. *Gait Posture* **10**, 264, 1999.
2. Lafortune et al. *J Biomech* **29**, 1531-1537, 1996.
3. Arndt, et al. *Proceedings of 6th Symposium on Footwear Biomechanics*, Queenstown, New Zealand, 2003.

THE EFFECTS OF PERIODIZED COMPLEX TRAINING PROGRAMME ON MILITARY PHYSICAL FITNESS AND FIGHTING ABILITY

[1] Wen-Lan Wu, [2] Wen-Zen Chen and [2] Jasson Chiang
[1] Faculty of sports medicine, Kaohsiung Medical University, Taiwan, wenlanwu@kmu.edu.tw
[2] Graduate Institute of Sport Coaching Science, Chinese Culture University, Taiwan

INTRODUCTION

Complex training is a way to develop muscle strength, speed and technique, simultaneously [1]. This study is planned to examine the effects of periodized complex training method by comparing the basic physical fitness and fighting ability improvements before and after the training sessions in order to confirm the practical use of periodized complex training in military training promotion.

METHODS

The training program includes one hour of training per day, five days per week, and a total of twelve week. Thirty subjects were randomly assigned to either the control group (n=15) or the experimental (n=15) group. These subjects were currently serving more than six months in the military. A Kistler Quattro Jump force platform system (Kistler 9290AD, Switzerland) and the Biodex System 3 isokinetic dynamometer (Biodex Systems Inc. Shirley, New York) were used in this study to observe the jumping performance and work output from the isokinetic dynamometer, respectively.

RESULTS AND DISCUSSION

In this experiment, the upper extremity muscle strength and muscle endurance tests after twelve weeks of physical trainings that include 60 seconds of pull-up, total work of ten repetitions of isokinetic shoulder flexion/extension at 60º and 180º/sec, both experimental and control groups showed significant improvements after the sessions. However, other than pull-ups, the improvement rates differ significantly between the two groups as experimental group is substantially higher than control group. Although the improvement rates in isokinetic muscle strength at 60º and 180º/sec are greater in experimental group than that of control group, there is no significant difference between the two, reflecting insufficiency of upper extremity training in the routine. In abdomen muscle endurance (60 seconds of sit-up) tests, the improvement rates showed significant differences of 8.17% and 4.93% in experimental and control group, respectively. The experimental group is substantially higher than control group. The lower extremity jumping tests showed 10.92% and 5.59% of significant explosiveness improvement rates in experimental and control group, correspondingly. On the other hand, the muscle endurance improvement rates showed no significant difference between experimental (10.01%) and control (9.43%) group. According to above-mentioned results, we found that the improvement rates for both lower extremity explosiveness and muscle endurance in experimental group are similar. However, the improvement rates in control group are 5.59% and 9.34%, respectively. It revealed that the effects of periodized complex training method are more profound in promoting lower extremity explosive force than in muscle endurance. Furthermore, the influence of twelve-week physical training on cardiopulmonary endurance is shown in the scores of 3000-meter run and bleep-test (indirect VO_2max estimation), where average improvement rates of experimental groups are significantly higher than control group. These results reflected the Fartlek training method used in our physical training program, applying various training velocity in uphill, downhill and stepping exercising modes, could directly elevate the cardiopulmonary performance in exercises. The study also reveals that under fighting ability categories of basic grenade throwing and 500-meter obstacle run the improvement rates are both significantly greater in experimental group than control group. Regression equation demonstrated that shoulder isokinetic muscle strength at 60º/sec and abdomen muscle endurance are factors determining basic grenade throwing scores. Furthermore, shoulder isokinetic muscle strength at 60º /sec, abdomen muscle endurance and the VO_2max are directly related to performances of 500-meter obstacle race.

CONCLUSIONS

In this study we found a close relationship exists between military physical fitness and fighting ability. Simply follow our training program and military people will soon get fitness and wellness results.

REFERENCES

1. Wilson, G.J., et al., *Med. Sci. Sports Exerc* **25**, 1279-1286, 1993.

KINETIC FACTORS INFLUENCING THE GAIT TRANSITION SPEED DURING HUMAN LOCOMOTION

Alan Hreljac, Rodney Imamura, Rafael F. Escamilla, W. Brent Edwards, and Toran Furch
Department of Kinesiology & Health Science, California State University, Sacramento
email: ahreljac@csus.edu

INTRODUCTION

Several researchers [1,2,3,4] have hypothesized that the gait transitions of quadrupeds are triggered by kinetic factors, such as musculoskeletal stresses, particularly at joints. Utilizing invasive techniques, it has been shown [1,2,4] that small horses, dogs, and goats reduced bone and joint strain when changing gait from a trot to a gallop. Non-invasive techniques (ground reaction forces-GRFs), have also been used [3] to make similar conclusions regarding a group of large horses.

Two studies [5,6] which have applied the non-invasive technique [3] to humans, found little evidence to suggest that external kinetic variables (GRFs) were related to the gait transition of humans. No human studies have examined the relationship of joint kinetic variables to the gait transition speed. The primary purpose of this project was to examine whether lower extremity joint kinetic factors are related to the gait transition during human locomotion.

METHODS

Following the determination of the preferred transition speed (PTS) of each of the 16 subjects using methodology described in previous studies [5,6,7], subjects walked down a 25 meter runway, and over a floor mounted force platform at five speeds (70, 80, 90, 100, and 110% of the PTS), and ran over the force platform at three different speeds (80, 100, and 120% of the PTS). Speed was monitored by three sets of infrared photocell timing lights. Reflective markers, placed on the greater trochanter, knee joint center, lateral malleolus, and head of the fifth metatarsal were recorded by a single digital video camera (240 Hz), in the right sagittal plane. A trial was considered successful only if the speed fell within ± 5% of the target speed, the landing foot completely contacted the force platform, and if there was no visible change in stride length.

Two-dimensional (2-D) kinematic data were synchronized with GRF data (960 Hz). The raw 2-D coordinate data were smoothed using a 4th order, zero lag, Butterworth filter. Joint moments were determined by inverse dynamics calculations. Joint powers were calculated as the product of the respective joint moment and angular velocity. Prior to analysis, all variables were normalized by dividing by body mass. Dependent variables (DVs) included maximum ankle dorsi- and plantar flexor moments, maximum knee extensor moment, and maximum power absorption and generation at the ankle and knee. A repeated measures MANOVA compared average values of all DVs between speed conditions. If the hypothesis tested was to be accepted for a DV, the value of the DV would increase as walking speed increased, then decrease when gait changed to a run (at the PTS). For all comparisons, $\alpha = 0.05$.

RESULTS AND DISCUSSION

The maximum dorsiflexor moment was the only DV which increased as walking speed increased, and decreased when gait changed to a run (Table 1). At the low running speeds tested during this study, many subjects exhibited a mid- or forefoot striking pattern, producing an initial dorsiflexion velocity. This movement is controlled eccentrically by the plantar flexors, just as the initial plantar flexion velocity during walking is controlled eccentrically by the dorsiflexors. Changing landing strategy in this way would transfer stress from the dorsiflexors to the plantar flexors at the PTS.

CONCLUSIONS

The dorsiflexor moment which occurs soon after foot contact is the only variable tested which appears to be related to the gait transition during human locomotion. This supports the results of previous studies [7,8] which have concluded that an important factor in changing gaits at the PTS is the prevention of stress in the dorsiflexor muscles.

REFERENCES

1. Biewener AA, et al. *J Biomech* **16**, 565-576, 1983.
2. Biewener AA, et al. *J Exp Biol*, **123**, 383-400, 1986.
3. Farley CT, et al. *Science*, **253**, 306-308, 1991.
4. Rubin CT, et al. *J Exp Biol*, **101**, 187-211, 1982.
5. Hreljac A. *Gait Posture*, **1**, 217-223, 1993.
6. Raynor AJ, et al. *Hum Mov Sci*, **21**, 785-805, 2002.
7. Hreljac A. *J. Biomech* **28**, 669-677, 1995.
8. Hreljac A, et al. *J Appl Biomech*, **17**, 287-296, 2001.

Table 1: Value of DVs at all conditions (M in N·m/kg, P in W/kg, Abs=Absorption, Gen=Generation, *=sig. decrease from W100).

Condition	Ankle-PFM	Ankle-DFM	Knee-ExtM	Ankle-P-Abs	Ankle-P-Gen	Knee-P-Abs	Knee-P-Gen
W70	1.49 ± 0.16	0.25 ± 0.07	1.17 ± 0.44	0.70 ± 0.26	5.02 ± 0.96	3.87 ± 2.01	1.04 ± 0.46
W80	1.52 ± 0.20	0.30 ± 0.13	1.09 ± 0.42	0.74 ± 0.32	5.87 ± 0.97	2.97 ± 2.33	1.59 ± 0.52
W90	1.60 ± 0.17	0.32 ± 0.13	1.24 ± 0.60	0.91 ± 0.38	6.53 ± 1.26	4.74 ± 2.50	1.85 ± 1.02
W100	1.64 ± 0.20	0.37 ± 0.11	1.46 ± 0.46	0.78 ± 0.36	7.49 ± 0.97	4.92 ± 2.89	2.23 ± 0.84
W110	1.67 ± 0.17	0.43 ± 0.19	1.45 ± 0.63	0.45 ± 0.17	7.91 ± 1.13	3.77 ± 2.03	2.49 ± 0.84
R80	1.94 ± 0.28	0.11 ± 0.06*	2.24 ± 0.58	3.51 ± 1.68	6.48 ± 2.30	5.68 ± 1.57	4.49 ± 2.04
R100	2.04 ± 0.29	0.18 ± 0.09*	2.49 ± 0.63	3.58 ± 1.20	7.92 ± 2.49	7.38 ± 2.01	5.43 ± 2.40
R120	2.22 ± 0.37	0.22 ± 0.10*	2.73 ± 0.59	4.12 ± 1.78	9.92 ± 2.45	8.17 ± 2.17	7.21 ± 2.29

PASSIVE LENGTH-TENSION PROPERTIES OF HUMAN GASTROCNEMIUS CHANGE AFTER ECCENTRIC EXERCISE

[1]Phu Hoang, [1]Rob Herbert and [2]Simon Gandevia
[1]School of Physiotherapy, University of Sydney, Australia,
[2]Prince of Wales Medical Research Institute, University of NSW, Australia; email: s.gandevia@unsw.edu.au

INTRODUCTION

It is well documented in animal and human studies that eccentric contractions increase the passive stiffness of muscle. However, the increase in muscle passive stiffness of human muscles after eccentric exercise has only been shown by indirect measurements of the whole muscle group using torque-angle relations or by observing a change in resting joint angles.

This study applied a new method which derives the length-tension relation for human gastrocnemius in vivo [1] to measure changes in the passive behaviors of human gastrocnemius after a bout of eccentric exercise. A second aim of the study was to examine the relations between the changes in muscle passive stiffness and levels of perceived muscle soreness that arises after eccentric muscle damage.

METHODS

Twelve subjects performed one-hour of eccentric exercise with the right leg by walking backwards downhill on a treadmill. Passive ankle torque of the right ankle was measured at 8 different knee angles by rotating the ankle within available range. Measurements were performed in all subjects before and immediately after exercise and 24 hours later. Further measurements were made at 48 hours and one week after exercise in a subset of 6 subjects. Passive length-tension relations of gastrocnemius were computed from passive ankle torque and ankle angle data [1].

Comparisons were made between passive length-tension relations of gastrocnemius before exercise and those at various times after exercise. As soreness after exercise commonly limited passive dorsiflexion by about 10°, especially at 24 hours, we compared muscle passive tension at the longest lengths measured at 24 hours. The tension was normalized as percentage of passive tension at the longest length measured before exercise. Stiffness of gastrocnemius (expressed in N/m) in the sitting (knee and ankle angles at 90°) and standing (knee at 0° and ankle at 90°) postures was also calculated from the measures before and after exercise.

At each time point after exercise, subjects were asked to rate the "level of perceived muscle soreness" during walking based on a visual analogue scale anchored at 0 (no soreness) and 10 (maximal soreness).

RESULTS AND DISCUSSION

An example of passive length-tension curves of gastrocnemius before exercise and at different points of time after exercise for one subject is shown in Figure 1. For this subject, compared with the control value before exercise, passive tension of gastrocnemius at the maximal comfortable length increased 25% immediately after exercise, 77% at 24 hours, 54% at 48 hours and returned within 3% of the control value at one week.

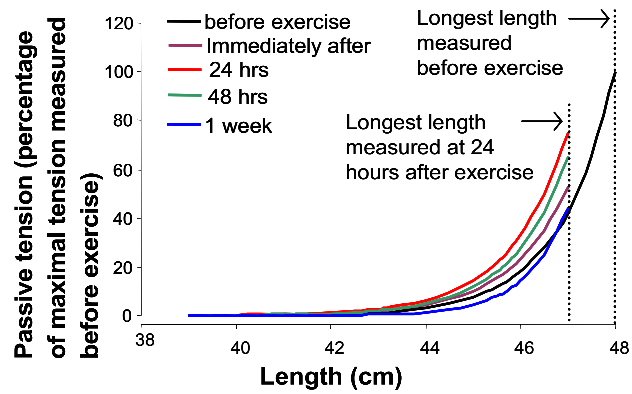

Figure 1: Passive length-tension curves of gastrocnemius of one subject measured before and at various times after exercise

Passive tension was re-scaled as percentage of maximal tension of gastrocnemius measured before exercise. The tension at the longest comfortable length measured at 24 hours was always higher than pre-exercise level during one week after exercise. For this subject there was an increase of 24.7% immediately after exercise, 77.4 % at 24 hours, 54.1% at 48 hours and 3% at one week.

All subjects showed a similar time course. Mean muscle passive tension significantly ($p<0.05$) increased immediately after exercise (34.7±7.3%), peaked at 24 hours (88.4±12.6%), then declined but remained significantly higher than before exercise at 48 hours (45.5±4.4%) and stayed high (but not significant) one week after (14.6±8.7%). These observations support comparable reports in previous studies [2]. Stiffness of gastrocnemius calculated in sitting and standing posture increased immediately after eccentric exercise and stayed increased for at least one week. The relative changes of muscle stiffness were similar in both positions.

All subjects reported some mild soreness immediately after exercise. On subsequent days, the soreness increased and peaked at 48 hours (mean score 3.3 and 3.5 at 24 and 48 hours respectively) and had disappeared at 1 week in all but one subject. There was no correlation between measures of tension or stiffness and the level of pain reported by individual subjects at any time point after the exercise.

CONCLUSIONS

Using a new, more direct measurement method, we report that a single bout of eccentric exercise increases passive stiffness of human gastrocnemius muscles. The increase peaks in 24 hours and is nearly fully resolved within a week. The relative increase in tension was similar across the physiological range of lengths. The levels of pain after exercise did not correlate with the levels of increased muscle stiffness.

REFERENCES

1. Hoang et al. *J Biomech;* **DOI**:10.1016/jbiomech.2004.05.046.
2. Whitehead et al. *J Physiol* **533**, 593-604, 2001.

LOAD DISTRIBUTION DURING SIT-STAND-SIT USING AN INSTRUMENTED CHAIR

Susan K. M. Wilson, Alexander C. Nicol
Bioengineering Unit, University of Strathclyde
Email: s.k.m.wilson@strath.ac.uk , web: www.strath.ac.uk

INTRODUCTION

Older adults have more difficulty in rising from a chair due to physical changes that occur due to ageing, as well as the design of chairs [1]. Ageing causes a decline in muscle strength and a reduction in control noted particularly as the elderly are more prone to falls. There are many aspects of chair design that can influence the ability of the elderly to rise including chair height, type of seating surface, cushions, foot placement, and armrests [2].

METHODS

A portable instrumented chair was designed to measure the forces through the body during standing up and sitting down by means of force plates and transducers. Two Kistler force plates (FPs) are located in the floor for measuring individual foot forces, and a third force plate is located beneath a cushion on the seat. The armrests were instrumented with pylon transducers to measure 3 dimensional forces through the upper limbs. The equipment is integrated with a Vicon 612 motion analysis system (©Oxford Metrics) to enable synchronization of data. The chair can be adjusted in height by means of a hydraulic jack and support rods which are locked in place, and the height of the armrests can also be adjusted (figure 1).

The chair was adjusted to 87.5% of knee height and each subject was asked to stand up and sit down from the chair at their own pace. Two floor mounted force plates were used during testing and the results summed for the graph in figure 2. Each subject was asked to rise without using the armrests. Two different types of seat cushions were used during testing: a polyurethane foam with a vinyl cover (soft cushion) and a high density foam with a cotton cover (hard cushion). Data was recorded in 6 degrees of freedom for both the floor and seat force plates.

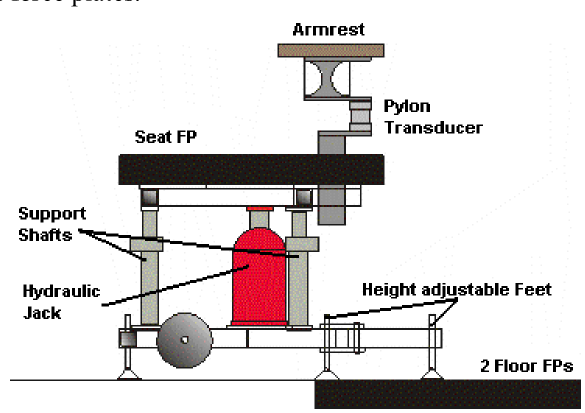

Figure 1: Diagram of components of the instrumented chair.
FP: Force Plate.

RESULTS AND DISCUSSION

Figure 2 illustrates the vertical forces that arose from the seat and floor force plates during testing. At the start of testing the subjects body weight was distributed 80% through the ischial tuberosities to the seat and 20% through both feet to the floor. It can be seen that zero force at the seat FP indicates lift-off from the seat which occurs momentarily before peak vertical foot floor force.

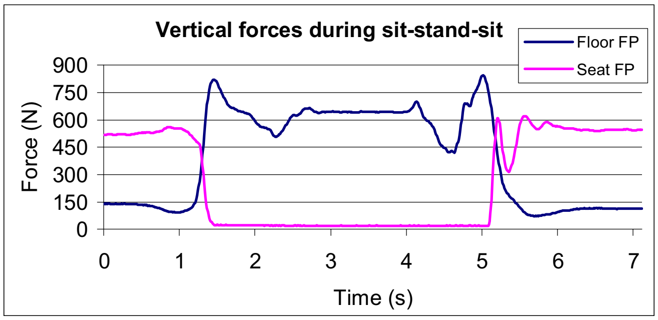

Figure 2: Vertical ground reaction forces at the seat and floor force plates during rising to stand and sitting down.

Figure 3 displays a peak horizontal force measured at the seat of 100N when rising to stand which occurred at the same instant when the vertical forces at both the seat and floor FPs were of equal magnitude (figure 2).

This variation in reaction forces may have been due to the seat height being lower than knee height, requiring more momentum to be generated in the forward direction to assist rising and control in sitting. These results indicate that sit-stand-sit is a complex movement that occurs in more than one plane and requires further detailed analysis in 3dimensions.

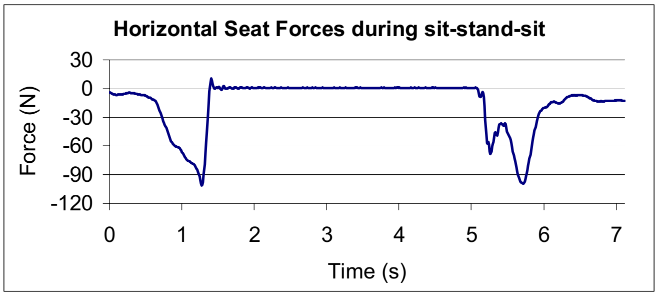

Figure 3: Horizontal forces measured at the seat and floor force plates during rising to stand and sitting down.

REFERENCES

1. Alexander NB, et al. *J Am Geriatr Soc*, **44**, 356-362, 1996.
2. Janssen WMG, et al. *Physical Therapy,* **82(9)**, 866-879, 2002.

NON-INVASIVE MEASURMENT OF PASSIVE LENGTH-TENSION PROPERTIES OF HUMAN GASTROCNEMIUS MUSCLE FASCICLES, TENDONS, AND WHOLE MUSCLE-TENDON UNITS IN VIVO

[1]Phu Hoang, [2]Gabrielle Todd, [2]Robert Gorman , [2]Simon Gandevia and [1]Rob Herbert
[1]School of Physiotherapy, University of Sydney, Australia; email: R.Herbert@fhs.usyd.edu.au
[2]Prince of Wales Medical Research Institute, University of New South Wales, Australia

INTRODUCTION

We present a new method for non-invasive measurement of passive length-tension properties of human gastrocnemius muscle fascicles, tendons, and whole muscle-tendon units *in vivo*. The method relies on the assumption that the gastrocnemius is the only muscle that crosses both the ankle and the knee, so changes in ankle torque-angle properties that accompany changes in knee angle can be attributed to changes in the length of gastrocnemius. The contributions of muscle fascicles and tendons to elongation of the muscle-tendon unit are determined with ultrasonography.

METHODS

Passive ankle torque and ankle angle data were obtained as the ankle was rotated through its full range of motion with the knee in a range of positions. Changes in the length of the whole muscle-tendon unit (MTU) of gastrocnemius were calculated from joint angles and anthropometric data. Passive length-tension curves of the whole gastrocnemius MTU were extracted from torque-angle data based on the assumption that passive ankle torque is the sum of torque due to structures which cross only the ankle joint (this torque was a 6-parameter function of ankle joint angle) and a torque due to the gastrocnemius muscle (a 3-parameter function of knee and ankle angle). Parameter values were estimated with non-linear regression and used to reconstruct passive length-tension curves of the gastrocnemius [1].

We have examined the reliability of the measures of length-tension curves of gastrocnemius MTU by measuring length-tension curves from 11 subjects on three occasions, twice on the same day and on a third occasion at least one week later. The curves were reproducible with average root mean square error was 3% and 6% of maximal passive tension for pairs of measurements within a day and a week apart respectively.

Simultaneously, ultrasonography was used to measure changes in length of muscle fascicles. The methods were similar to those described by Kubo *et al.* [2]. Changes in tendon length were then calculated as change in length of the muscle-tendon unit minus change in length of muscle fascicles. Passive length-tension curves of muscle fascicles and of the tendon were then generated.

Passive length-tension curves provided estimates of muscle-tendon slack length (the length below which there was no tension). The length of muscle fascicles at muscle-tendon slack length provided estimates of muscle fascicle and tendon slack lengths. These were used to calculate strains of muscle-tendon, muscle fascicle and tendon.

RESULTS AND DISCUSSION

An example of a passive length-tension curve of the gastrocnemius MTU from one subject is shown in Figure 1. The mean (± SEM) maximum passive tension from 9 subjects was 280 ± 22 N, the mean slack length of the muscle-tendon unit was 41 ± 1 cm, and the mean maximum in vivo length was 50 ± 1 cm. The muscle-tendon slack length is within the physiological range but close to the shortest in vivo length.

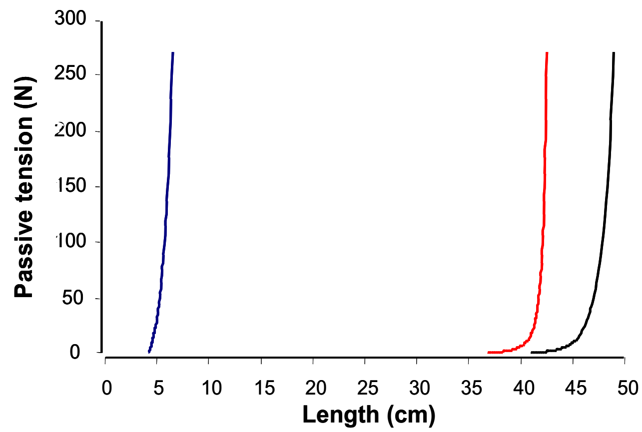

Figure 1: Passive length-tension curves of gastrocnemius muscle-tendon unit (black line, using method in ref [1]), fascicles (blue line, using ultrasonography), and tendon (red line, by subtraction) of one subject. For this subject, the tendon contributed 71% to the total lengthening of the whole muscle tendon unit.

The figure also shows passive length-tension curves of muscle fascicles and tendons. Even at these low passive tensions, tendons undergo functionally important elongation. In the subject shown in the figure, tendon contributed 71% of the total lengthening of the whole MTU. The mean contribution of muscle fascicles and tendons to the changes of the whole MTU from measurements of 9 subjects was 36 ± 4% and 64 ± 4% respectively. These confirm findings of our previous studies in animals [3] and humans [4].

The mean slack length of muscle fascicles (n = 9) was 3.5 ± 0.2 cm. This is similar to the recent findings of Muraoka and colleagues [5]. Average maximum in vivo passive strain of muscle fascicles and tendon was 91 ± 9% and 11 ± 2% respectively.

CONCLUSIONS

The new method enables measurement of passive length-tension properties of human gastrocnemius in vivo. It shows that, even with passive tension, strains in the whole tendon (extramuscular tendon plus aponeurosis) of human gastrocnemius are very large, and tendon elongation accounts for most of the change in muscle-tendon length.

REFERENCES

1. Hoang et al. *J Biomech* **DOI**:10.1016/jbiomech.2004.05.046.
2. Kubo et al. *Acta Physiol Scand* **170**, 127-135, 2000.
3. Herbert R & Crosbie J. *Eur J Appl Physiol & Occ Physiol* **76**, 472-479, 1997.
4. Herbert et al. *J Physiol* **539**, 637-645, 2002.
5. Muraoka et al. *J Biomech* **DOI**:10.1016/jbiomech.2004.06.012.

KNEE KINEMATICS OF TOTAL KNEE REPLACEMENT PATIENTS: PRE AND POSTOPERATIVE ANALYSIS USING COMPUTER GENERATED IMAGES

Christopher J. Barr[1], Alexander.C. Nicol[1], Mark Blyth[2], Martin Sambrook[3]
[1]Bioengineering Unit, University of Strathclyde, [2]Orthopeadic Dept, Glasgow Royal Infirmary, [3]Radiography Dept, Glasgow Royal Infirmary. email: Christopher.Barr.100@strath.ac.uk, web: www.strath.ac.uk/bioeng

INTRODUCTION

Gait analysis has previously been conducted on osteoarthritc patients [1]. Techniques have been developed to study the contact areas of the knee in vivo, but these are in non-weight bearing conditions, and on healthy subjects [2]. The current project aims to show a comparison of knee kinematics in pre- and post– operative knee replacement surgery, using computer animation to represent a patient specific model of the knee joint interactions under every day conditions.

METHODS

Nine patients were recruited from the waiting lists for total knee replacement (TKR) from the orthopeadic department in Glasgow Royal Infirmary hospital. All were selected on the criteria that they suffered from osteoarthritis of the knee joint, and had no secondary conditions that affected their gait.

Each subject underwent preoperative gait analysis using a Vicon 612 Motion Analysis System (©Oxford Metrics). A cluster set of 4 markers was attached to the thigh, shank and pelvis segments. All boney landmarks were then identified, and virtual points were made at each landmark. Each subject was then asked to perform the following every day activities: level walking, ascending and descending stairs, and chair rising and sitting. This was repeated one year postoperatively.

Preoperative magnetic resonance (MR) images were taken for each subject. Postoperatively, Computerized Tomography (CT) scans were taken, as the implant could not be imaged using MR. The scans were rendered into 3D images, which were then combined with gait analysis data and animated in Virtual Reality Modeling Language (VRML).

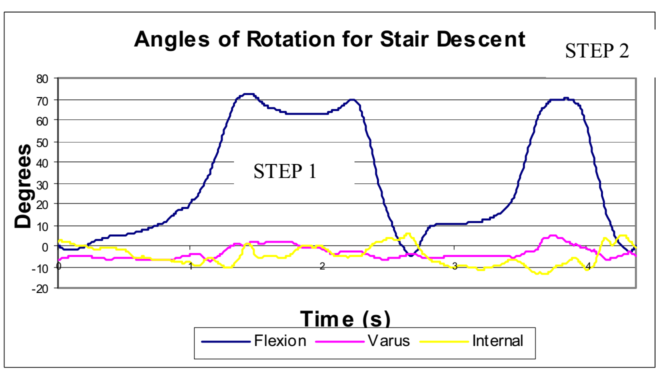

Figure 1: Typical flexion angles stair descent

RESULTS AND DISCUSSION

Figure 1 details angles of rotation during stair descent in the preoperative patient. All subjects reported this to be the most difficult task. The difference in pattern of flexion angle in the two steps demonstrates the difficulties experienced by the subject when descending the stairs. The lack of smooth motion in internal and vulgus rotation illustrates the lack of muscle control during motion.

A 3D surface image of the knee joint was created using MIMICS software from Materialise (figure 2). Preoperatively, 44 axial slices of 3 mm thickness were taken from MRI. Postoperatively 144 slices of 1mm thickness were taken from CT. For each image, each slice was surfaced by outlining the contour of the bone. The dimensions of the scan were input into the software and the slices were then stacked to create a 3 dimensional model.

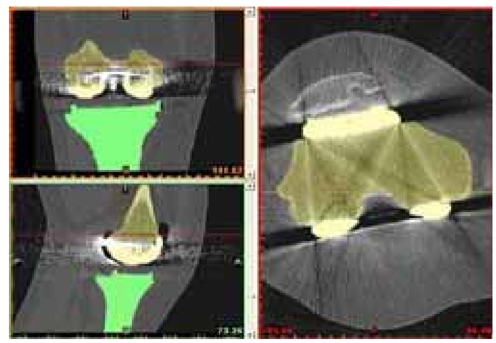

Figure 2: 3D rendering of the knee joint

The 3D model of the knee joint was exported as a VRML file and an animation of the pre- and postoperative knee joint was produced (figure 3). This shows the knee joint at 70° flexion during stair descent, with a slight varus and external rotation, as shown in figure 1. This method allows for the visualization of 3D motion between the tibia and femur during everyday activities. The comparison of pre and postoperative animations will provide data that can be incorporated in preoperative planning of TKR for a wide spectrum of patient groups.

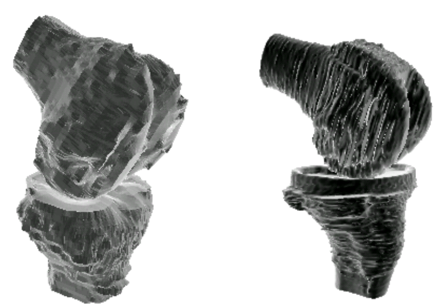

Figure 3: Screenshot of VRML animation (a) preoperation and (b) postoperation

REFRENCES

1. Kaufman KR, et al *J Biomech* **34**, 907-915, 2001.
2. von Eisenhart-Rothe R, et al *J Biomech* **37,** 927-934, 2004.

THE DEVELOPMENT AND EVALUATION OF A 3-DIMENSIONAL, IMAGE-BASED, PATIENT-SPECIFIC, DYNAMIC MODEL OF THE HINDFOOT

[1]Carl Imhauser, [2]Sorin Siegler, [2]Jason Toy, Richard Brand, [3]Jayaram Udupa
[1]Institute of Orthopaedic Research and Biomechanics, Ulm, Germany; email: carl.imhauser@medizin.uni-ulm.de
[2]Drexel University, Philadelphia, Pennsylvania
[3]Medical Image Processing Group, University of Pennsylvania, Philadelphia, Pennsylvania

INTRODUCTION

A confirmed dynamic model of the hindfoot enables parametric analyses to determine how the following injuries or treatments affect hindfoot mechanics (kinematics, flexibility, contact forces and ligament loads): tearing ligaments and repairing them (tenodesis), changing articulating surface geometry (arthroplasty), and constraining a joint (arthrodesis). The model predictions may provide guidelines for altering existing treatments or designing new ones to more closely restore normal hindfoot mechanics. The objective of this study was to develop and evaluate 3D, subject-specific, dynamic hindfoot models (n = 6 *in vitro*) using 3D stress MRI data [1].

METHODS

Existing software (3DVIEWNIX^{TM} [3], Geomagic Studio^{TM}) were used to obtain the subject's bone surface geometry and collateral and subtalar ligament insertion data from MR images. Non-linear load-strain functions described the structural properties of the ligaments [4]. Cartilage's elastic modulus and an exponential term modeled its non-linear compression characteristics [5]. The ADAMS 2003^{TM} software generated and solved the dynamic equations of motion.

Each model (healthy and with ligament injury) was evaluated through subject-specific stress MRI experiments [1] and arthrometer tests [2]. The model used the same forces (inversion, anterior drawer, rotation) and boundary conditions as the experiments. Model output corresponded to the experimental measurements (helical axis parameters, flexibility).

RESULTS AND DISCUSSION

The model with intact ligaments predicted the experimental inversion and anterior drawer kinematic patterns of the ankle joint complex, but under-estimated ankle joint motion and over-estimated subtalar joint motion. Similar to the experimental data, releasing the anterior talofibular ligament and the calcaneofibular ligament caused rotations at the ankle joint complex and at the ankle joint to increase in inversion compared to the intact condition. Unlike the experimental data, the model over-estimated rotations at the subtalar joint.

Similar to experimental data, the modeled ankle joint complex had hysteresis and had high flexibility in the unloaded neutral zone, followed by rapidly decreasing flexibility at the extremes of the range of motion in all directions (Figure 1). The model revealed that hysteresis coincided with low contact forces and with switching contact locations at the articulating

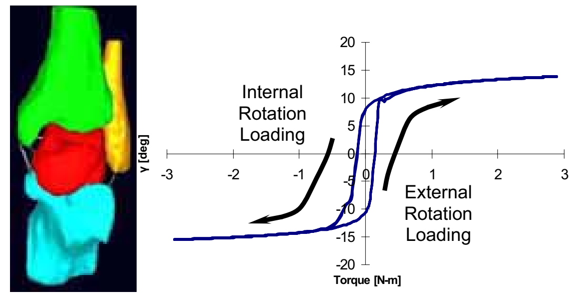

Figure 1: *In vitro* model (left). Predicted load-displacement curve (right).

surfaces. The low flexibility region coincided with increasing contact forces and with no change in contact location.

The ligament strain and loading patterns were sensitive to ligament removal. Sensitivity analyses indicated that rotations caused by altering ligament orientation were smaller than rotations caused by lateral ligament removal; therefore, the model may be sensitive to predicting the changes that occur during ligament rupture. Hindfoot mechanics were sensitive to bone morphology and ligament insertion location.

The results indicate that the structural properties of the subtalar joint's interosseous ligament and cervical ligament must be quantified. The models' assumptions and limitations include differences between the experimental and modeled boundary conditions, exclusion of the cartilage geometry, and estimation of the subtalar ligaments' structural properties.

CONCLUSIONS

Future work will focus on quantifying the structural properties of the subtalar ligaments, developing a larger group of patient-specific models, and performing statistical analysis on output data. Despite the models' assumptions and limitations, they may be a valuable tool to explain fundamental mechanical phenomenon such as joint hysteresis and to do the previously described parametric analyses.

REFERENCES

1. Siegler S, *J Biomech* **38**, 567-578, 2005.
2. Lapointe SJ, *J Orthop Res*, **15**, 331-341, 1997.
3. Udupa JK, *Proceedings of SPIE 2164*, 1994.
4. Funk JR, *J Biomech Eng*, **122**, 15-22, 2000.
5. Gardner TR, *ASME Bioengineering Conference*, 2001.

HAND MOVEMENT ANALYSIS OF THE ELDERLY WHEN USING A REMOTE CONTROL

Sivaram Shanmugam, Victoria Hood, Alexander .C. Nicol, Bernie .A. Conway
Bioengineering Unit, University of Strathclyde, Glasgow
Email: sivaram.s@strath.ac.uk , web: www.strath.ac.uk/bioeng

INTRODUCTION

Hand function decreases with age in both men and women due to age related degenerative changes in the musculoskeletal, vascular and nervous systems [1]. Functional performance in activities of daily living and recreational activity of the elderly are determined to a large degree by in-hand manipulation and dexterity. One of the most predominant activities an elderly person does is to watch television. With the advent of interactive television they are able to watch both digital TV as well as to surf the Internet, and the remote control is the way in which they are able to choose what they want to do. The aim of the current project is to study the ability of older subjects to perform basic remote control manipulations and also to specify the minimal functional requirements to perform this activity of daily living.

METHODS

Three groups of healthy and normal to their age elderly subjects in the age range of 60-69, 70-79, 80+ years were recruited. Three-dimension biomechanical evaluation of the hand was carried out using a Vicon 612 (Oxford Metrics) motion analysis system (Figure 1a). Twenty-three, 6 mm markers were skin mounted at the mid point of each joint (Figure 1b). Subjects were asked to press a number on the remote control for a single button test or a set of three numbers sequentially for a three-button test (Table 1). Subjects preformed 10 single button tests and 10 three-button tests.

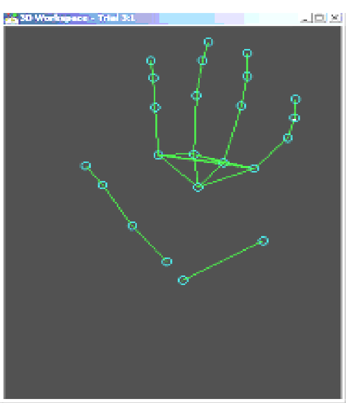

Figure1a Screenshot of image from Vicon software.

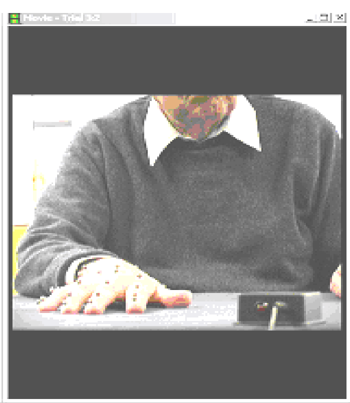

Figure 1b Video image of markers.

The infrared signal from the remote was captured by a video camera, which was in turn connected to the workstation. Digit span of up to nine numbers was assessed to check the short-term memory, and working memory was assessed with the digit span on the remote control. Digit span is the measure of how many sequential digits can be taken in, stored, processed, and recalled in the correct order. Bodybuilder software was used to process and analyze the data.

RESULTS AND DISCUSSION

The measures that were analyzed include velocity and acceleration profiles of the tip of the finger, which is used for the desired activity. Reaction time, time of button contact and time difference between two button contacts were also looked into. The graph (Figure 2) below shows the average velocities of the fingertip between two button contacts, in the three-button test in an 80-year-old subject. Transition 1 is the period from which the fingertip goes from button 1 to button 2 and transition 2 is the period from button 2 to button 3 in the three-button test (Table 1). The graph clearly indicates that the average velocity during transition 1 is more than that of transition 2. Possible explanations include, the emphasis on the pre-planning process, online control and corrective directional measures and other strategic considerations.

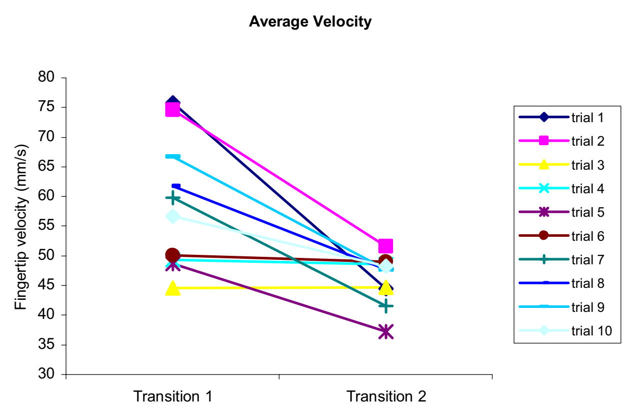

Figure 2 Average velocities during a three-button trial in an 80-year-old subject.

REFERENCES

1. Ranganathan VK, Siemionow V, Sahgal V, and Yue GH. Effects of aging on hand function. *Journal of American Geriatric Society*, **49(11)**: 1478-84, 2001.

	Trial 1	Trial 2	Trial 3	Trial 4	Trial 5	Trial 6	Trial 7	Trial 8	Trial 9	Trial 10
Transition 1	Button 1-2	Button 4-5	Button 7-8	Button 1-2	Button 6-1	Button 3-9	Button 3-4	Button 7-8	Button 5-8	Button 6-9
Transition 2	Button 2-3	Button 5-6	Button 8-9	Button 2-9	Button 1-7	Button 9-1	Button 4-9	Button 8-9	Button 8-2	Button 9-4

Table 1 Details of the three-button test

Kinematic and Kinetic Analysis of Sit-to-Stand with and without a Cane in Hemiplegic Subjects

[1]Po-Ting Hu, [2]Kwan-Hwa Lin,[3]Tung-Wu Lu, [2]Pei-Fang Tang, [2]Ming-Hsia Hu,[4]Jin-Shin Lai
[1] Department of Physical Therapy, Shu-Zen College of Medicine and Management, Taiwan
[2]School and Graduate Institute of Physical Therapy, National Taiwan University, Taiwan
[3] Institute of Biomedical Engineering, National Taiwan University, Taiwan
[4]Department of Rehabilitation Medicine, National Taiwan University Hospital ,Taiwan
email: khlin@ntu.edu.tw

INTRODUCTION

Sit-to-stand (STS) is a requisite activity for most daily activities. The incidence of fall in stroke patients usually occurs during postural transition, and the use of cane is suggested to increase the standing stability [1]. However, the influence of cane on STS has not been well studied yet. The purpose of this study was to determine the effect of cane support on the movement pattern of rising from a chair in hemiparetic patients and the healthy adults.

METHODS

This was a cross-sectional experimental design. The mild-moderate hemiplegic patients with cerevascular accident (CVA) were recruited. Nine hemiplegic patients (mean age: 61.00±13.51 years old; 4 left hemiparesis and 5 right hemiparesis) were chosen as the experimental group, and eleven healthy adults (61.45±12.14years) were the control group. Participants performed rising from a chair in two conditions: (1) arm hanging by sides (no cane; NC), and (2) supported on a regular cane (with cane; WC). The data of 3-dimentional motion analysis (Vicon 250, Oxford, USA) and force (AMTI, USA) were recorded. A symmetry index (SI) was calculated [2] by the differences between the vertical ground reaction forces of the right and left limb (i.e., SI = $(Fz_R\text{-}Fz_L)/\ (Fz_R+Fz_L) \times 2$).

RESULTS AND DISCUSSION

The movement time (MT) in CVA group was longer than normal controls (p<0.01) during STS with and without a cane. Compared with no support, the maximal extension moments of affected knee in CVA patients during STS with a cane were significantly increased (Table 1). In addition, the maximal knee extension moments in the sound side of CVA patients were significantly greater than those of the dominant side of healthy adults (p<0.05) during STS with no support, but no significant difference between 2 groups during STS with a cane. There was a significant improvement in the symmetry of CVA subjects during STS with a cane, because SI decreased significantly from 31 % to 26 % (Figure 1).

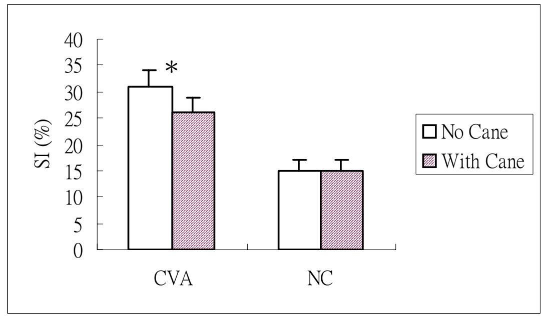

.
Figure 1. Symmetry index (SI) of stroke (CVA) and normal controls (NC) during sit-to-stand with and without a cane.
* $p < 0.05$.

CONCLUSIONS

Hemiplegic patients could exert more force on affected leg during STS with a cane comparing with STS without any support. Using a cane may increase the stability to use the affected side for hemiplegic patients, as well as to reduce the motion time and symmetry during sit-to-stand task [3]. The psychological effect of using a cane to hemiplegic patients needs further studied.

REFERENCES

1. Jeka JJ. *Phys Ther* **77**, 476-487, 1997.
2. Hesse H, et al.. *Scand J Rehab Med* **30**, 81-86, 1998.
3. Chen CL, et al.. *Arch Phys Rehabil Rehabil* **82**, 43-48, 2001.

ACKNOWLEDGEMENTS

The authors thank all the participants for this project.

Table 1: Knee extension moment during sit-to-stand with and without a cane.

	CVA patients (n=9)		Normal Controls (n=11)	
	No Cane	With Cane	No Cane	With Cane
Sound (Dominant) side				
Knee extension moment (NT · M / Kg)	1.00 (0.26) *	0.92 (0.23)	0.86 (0.20)	0.89 (0.24)
Affected (Non-dominant) side				
Knee extension moment (NT · M / Kg)	0.56 (0.19)	0.80 (0.25) †	0.79 (0.27)	0.89 (0.24)

Data were Mean (SD). * Difference between CVA and normal control groups (p<0.05).
† Difference between with and without a cane (p<0.05).

BIOCHEMICAL RESPONSE OF MENISCAL TISSUE TO ALTERED LOADING CAUSED BY PARTIAL MENISCECTOMY

Tammy L. Haut Donahue, Jeff A. McHenry, Barbara Zielinska
Department of Mechanical Engineering
Michigan Technological University; Houghton, Michigan email: thdonahu@mtu.edu

INTRODUCTION: Altered mechanical loading of meniscal tissue occurs following various injuries and surgical treatments such as anterior cruciate ligament (ACL) transection and meniscectomy. The degenerative sequel of the joint following partial meniscectomy is well documented. However, most studies have focused on the degradation of the articular cartilage of the joint. Few studies have focused on how the meniscal tissue responds to the altered loading [1]. Other musculoskeletal tissues, such as cartilage and bone, have been shown to respond to altered loading with a biochemical response that in turn mediates tissue remodeling. The biochemical events resulting from altered loading of meniscal tissue have received little attention.

METHODS: Utilizing a previously validated finite element (FE) model [2], partial medial meniscectomies were simulated by removing various amounts of tissue from varying locations in the white-white or white-red meniscal zones, and documenting the changes in contact mechanics. Either 5%, 10%, 30% or 60% of tissue was removed from the anterior-central (AC), central (C), posterior-central (PC), or posterior (P) region (Figure 1). The change in contact area, maximum and mean contact pressure, and maximum and mean axial strain were documented for both the superior and inferior surface of the meniscus.

This data was then used as input to a custom built bioreactor for unconfined dynamic compression of meniscal explants. Eight porcine knee joints were obtained with 24 hours of death and the menisci aseptically removed and a 6mm biopsy punch used to harvest 6 explants from each meniscus. The explants were maintained in DMEM/F12 media with 10% fetal bovine serum and 1% penicillin/streptomyocin for 48 hours before they were subjected either 0%, 5%, 10% or 20% axial compression at 1 Hz for 2 hours. Following compression, the meniscal explants were bisected into a superficial and deep zone and post-incubated for 24 hours. Regional expression of nitric oxide (NO) released into the media from the explants was quantified using the Griess reaction and was normalized to the wet weight of the explant.

RESULTS AND DISCUSSION: The results indicate that the mean axial compressive strain is approximately 2-3% for the intact, 5% and 10% meniscectomy. The mean strains increase minimally for 30% and 60% meniscectomies (data not shown). The maximum again is fairly consistent at 13% until more than 10% of the tissue is removed, where is increases to over 20%.

When this range of strains was applied to meniscal explants it appears that the deep zone produces more NO, with a significant upregulation following 20% compressive strain which is associated with removing more than 10% of the meniscus. Additionally the unloaded controls appear to produce an elevated amount of NO compared to explants compressed to 5% or 10%, possibly indicating that both overloading and underloading of meniscal tissue is damaging.

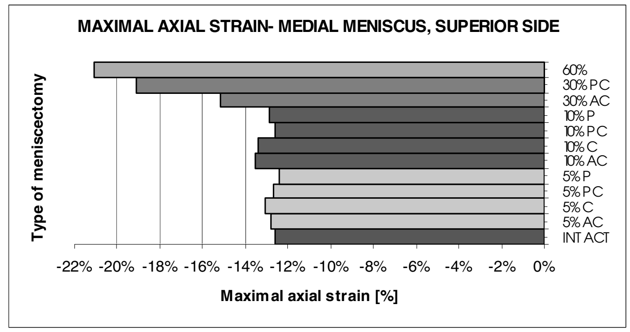

Figure 1. Maximal axial strains in the medial meniscus following various partial meniscectomies.

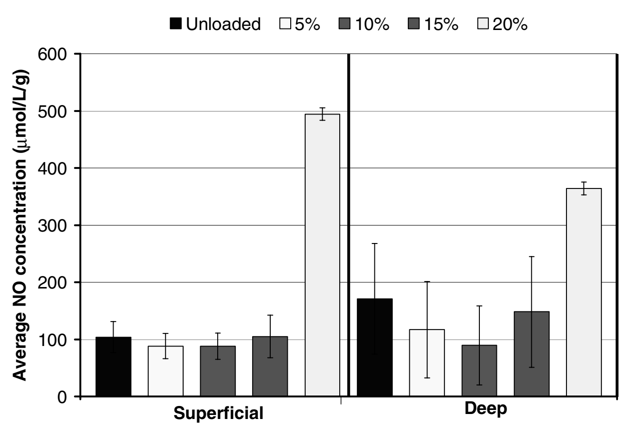

Figure 2. NO production from the superficial and deep zones of medial meniscus explants.

CONCLUSIONS: This work will provide a better understanding of the role of mechanical stimulation in the physiology and pathophysiology of the meniscus. The data gives clear indication to surgeons that removing more than 10% of the meniscus leads to axial strains which produce damaging biochemicals. Joint degeneration is the first step in the etiology of osteoarthritis. Improved treatment following meniscal excision will depend on an understanding of mechanotransduction in meniscal tissue. The findings of this work will have significant implications in the development of pharmaceutical and biophysical interventions for the treatment of the degenerative joint disease osteoarthritis.

REFERENCES: 1) Hellio Le Graverand, M. P.,et.al., Osteoarthritis Cartilage, **9(1)**, 56-64, 2001. **2)** Haut Donahue, T. L., et. al., J. Biomech. Engin. **124**, 273-280, 2002.

ACKNOWLEDGEMENTS: The authors would like to thank the Whitaker Foundation for financial support

MUSCLE TISSUE COMPOSITION, MUSCULAR TENDERNESS, AND FORCE PRODUCTION IN SUBJECTS WITH UNILATERAL EPICONDYLITIS LATERALIS

[1]Pernille Kofoed Nielsen, [1]Anne Katrine Blangsted, [1]Henrik Baare Olsen and [1]Karen Søgaard
[1]Department of Physiology, National Institute of Occupational Health, Denmark;
email: pkn@ami.dk, web: www.ami.dk

INTRODUCTION

Musculoskeletal disorders and pain in the forearm region due to low-force exposure are major problems in the industrialised world. Nevertheless, the pathophysiology is poorly understood.

Prolonged static contractions and ongoing repetitive low-level activity in the forearm muscles is well-known risk factors for development of epicondylitis lateralis. Therefore, it may be speculated that in addition to changes in the tendon also muscular changes may be detectable. Indeed, by the use of biopsy technique, morphological changes in the forearm muscle have been identified in patients diagnosed with epicondylitis lateralis [1]. Such morphological changes could be caused by facilitated formation of non-contractile tissue in the muscle, which may be detectable by non-invasive methods such as ultrasonography [2,3]. Contractile tissue in a healthy muscle will appear dark separated by sharp, bright lines, whereas muscles with different neuromuscular diseases are brighter and more diffuse in the structure [4]. Further, if the contractile tissue is affected it would also be expected to affect the force generating capacity.

The hypothesis of the present study was that in subjects with clinically diagnosed epicondylitis lateralis, the maximal voluntary contraction force (MVC) in wrist extension is lower and the ultrasound image of the muscle is brighter in the afflicted (pain) arm compared to the non-afflicted (no-pain) arm.

METHODS

B-mode ultrasonography was performed bilaterally at the middle part and proximal part of the m. extensor carpi radialis (ECR) on eight patients (5 females, 3 males) with unilateral epicondylitis lateralis. An ultrasound scanner fitted with a 12 MHz linear matrix transducer (LOGIQ 7, M12L, GE-Medical) was used. Gain settings were standardized and kept constant. The transducer was placed perpendicular to the ECR muscle during examination. Each image consisted of pixels with grey-scale values ranging from 0 to 255. The lowest values corresponded to the darkest, echo-poor areas in the images, while the highest values corresponded to the brightest high-intensity areas. A computerized texture analysis calculating the mean grey-scale intensity was used to characterize the images [5].

Next, the muscular tenderness, measured as pressure pain threshold (PPT) was determined with an electronic pressure algometer (Somedic, Hörby, Sweden) [6]. The diameter of the contact area was 10 mm and the pressure was applied perpendicularly to the skin at the middle part of ECR and with a speed of 20 kPa/s. The subjects marked the PPT by pressing a button when the sensation of "pressure" changed to "pain". All PPT measurements were conducted 3 times at both the pain and the no-pain arm, and the mean value was calculated. MVC was measured during a wrist extension. The subjects were sitting with the elbows flexed 90 degrees, the forearm pronated and resting on a horizontal platform. In this position they performed a MVC against a force transducer with both the pain arm and the no-pain arm in random order. Moment arm was measured and the wrist extension torque was calculated. Results are presented as mean (SD).

RESULTS AND DISCUSSION

The mean grey-scale intensity for the middle and proximal measuring sites was 42.86 (10.66) and 46.6 (11.6) for the pain arm compared to 41.50 (8.52) and 37.9 (15.4) for the no-pain arm. The mean PPT was 339 (172) kPa/s for the pain arm compared to 371 (148) kPa/s for the no-pain arm, and the mean MVC torque was 10.3 (4.6) Nm and 11.1 (SD 4.9) Nm, respectively. There were no significant differences.

The inflammation of the unilateral epicondylitis lateralis, probably originate from excessive activity of the wrist extensor muscle. Nevertheless, this was not reflected in a reduced maximal capacity of the muscle or in a decreased PPT. Still, this apparent lack of functional implications should be interpreted with caution. The non-afflicted arm serves as control and the study design does not allow any estimation of the initial condition of the afflicted arm before the symptoms emerged. However, the finding of a well preserved force capacity in the muscle indicating unaffected contractile tissue was corroborated by the results from the ultrasound grey-scale analysis.

CONCLUSIONS

In this study, we found no indications of an influence of epicondylitis lateralis on the function, the PPT, or the tissue composition in ECR. However, a case-control study design may be needed to support this conclusion.

REFERENCES

1. Ljung B-O, et al., *J Hand Surg* **24**, 177-183, 1999.
2. Jensen BR & Bakke M, *Muscle atrophy: Disuse and disease*. Pavia, Italy, 149-161, 1998.
3. Hargens AR, et al., *Bone Joint Surg* **63-A:** 631-636, 1981.
4. Heckmatt JZ, et al., *The Lancet* **June**, 1389-1391, 1980.
5. Nielsen PK, et al., *Clin Biomech* **15 (Suppl 1)**, S13-S16, 2000.
6. Persson AL, et al., *Clin J Pain* **16:** 155-163, 2000.

ACKNOWLEDGEMENTS

The Danish National Research Foundation supported this work (Grant no. 22-04-0488).

3D KINEMATIC AND KINETIC DATA OF TOTAL KNEE ARHTROPLASTY DURING THE STANCE PHASE OF LEVEL WALKING USING A MOVING VIDEO-FLUOROSCOPE

[1] Monika S. Zihlmann, [1] Hans Gerber, [1]Edgar Stüssi
[1]Laboratory for Biomechanics, HCI E411, ETH Zurich, 8092 Zurich, Switzerland
Correspondence to Monika S. Zihlmann: zihlmann@biomech.mat.ethz.ch

INTRODUCTION

Accurate in vivo kinematic and kinetic data of total knee arthroplasties, TKA, are important to understand the complexity of knee joint mechanics after knee joint surgery. This knowledge is crucial to reduce high stresses and strains on the ligamentous structure as well as on the implant parts. A better understanding could lead to better surgical strategies, improved implant designs, and increase patient's satisfactory rate. Video-fluoroscopy is a well established method to get accurate kinematic information of artificial joints by a three-dimensional numeric reconstruction of the single plane projection view of the fluoroscopic images. Until now, this method was limited to kinematic data only. Very accurate in vivo kinematic and kinetic data of TKA can be received by coupling instrumented gait analysis and video-fluoroscopy simultaneously and using a movable fluoroscopic system, proposed by Zihlmann et al. [1]. The goal of the present study was to get kinematic as well as kinetic data of TKA during the stance phase of level walking.

METHODS

One subject with a TKA (balanSys^{TM} fixed bearing, Mathys AG Bettlach, Switzerland) was asked to perform several gait cycles. *Fluoroscopic motion tracking*: The c-arm of the pulsed fluoroscopic unit (Philips Medical Systems, Switzerland) was mounted on a motor driven trolley. The system accelerates and decelerates thereby keeping the knee joint within the field of view of the fluoroscopic image (25frames/s). *Optical tracking*: The subject's condyles and the position of the unit mover were tracked by the optical tracking system VICON (VICON Motion Systems Ltd.) with 100Hz. *Ground reaction forces*: Five force plates (KISTLER AG, Switzerland) were fixed on a basement which was mechanically decoupled from the surrounding ground avoiding an interaction with the unit mover during the level walking tasks. The time of all measurement systems was synchronised. *3D reconstruction of the 2D fluoroscopic images*: Distortion of the fluoroscopic images was corrected by a calibration grid. A full three dimensional analysis of each image was achieved by fitting a synthetic x-ray projection of the tibial and femoral component onto the original in each image [2]. The reconstruction of the implant's position and orientation (6DOFs) was performed relative to the focus of the fluoroscopic image. *Transformation into global coordinate system*: A calibration frame was fixed on one force plate on a defined position. Because the distance of the grid lines were known, the exact position in the global coordinate system of the fluoroscope's focus was calculated.

RESULTS AND DISCUSSION

The fluoroscopic system was able to track the knee joint so that the implant components were in the field of view of the fluoroscope during the stance phase of the gait cycle. During this phase, ground reaction forces were available. Figure 1 shows the finite axis of rotation between femoral and tibial component in the global coordinate system. The force vectors of the third force plate are plotted in the same figure. By reducing the ground reaction force into the axis of rotation the net forces and moments of the TKA can be estimated.

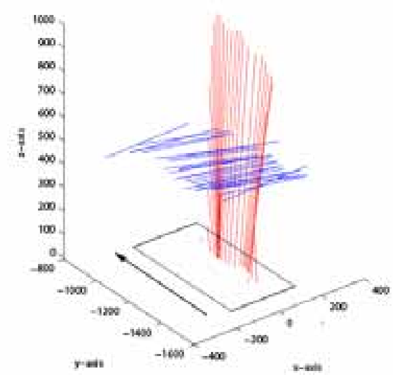

Figure 1: Axis of rotation between tibial and femoral component in the global coordinate system and force vectors of one force plate (4D plot with Δt = 40ms. Y-axis is gait direction)

CONCLUSIONS

This pilot study shows that the presented measuring technique enables the capture of kinematic and kinetic data of the stands phase of level walking simultaneously by coupling instrumented gait analysis and a movable fluoroscopic system.

REFERENCES

1. Zihlmann MS, et al. *Proceedings of CSB 2004*, Halifax, Nova Scotia, Canada, 2004.
2. Burckhardt KV, *PhD thesis Diss ETH No. 14262* ETH Zurich Switzerland, 2002.

ACKNOWLEDGEMENTS

Dr. h.c. Robert Mathys Foundation, Bettlach, Switzerland
Mathys AG Bettlach, Bettlach, Switzerland
Spital Ziegler, Berne, Switzerland
Philips Medical Systems, Switzerland

THE RELATIONSHIP BETWEEN KNEE EXTENSOR STRENGTH AND BALANCE IN PARKINSON'S DISEASE

[1] Chris Hass, [2] Dwight Waddell, [3]Steve Wolf, [3]Jorge Juncos, and [4]Robert Gregor
[1]Teachears College Columbia University, [2]Tulane University, [3]Emory University, [4]Georgia Institute of Technology
email: ch2290@columbia.edu

INTRODUCTION

Balance dysfunction and falls are a major problem in patients with Parkinson's disease (PD). The causes of these falls are multifactorial and may include muscle weakness, sensory defeciencies, postural instability, and extraparamidal dysfunction [1]. The knee extensor muscles are important contributors to postural and locomotor stability. Clinically, loss of strength in these muscles is associated with movement dysfunction [2]. Despite evidence supporting the importance of knee extensor strength in the performance of functional activities, observed associations between measures of knee strength and function in patients with PD have not been made. The purpose of this study was to explore associations between knee extensor peak strength and dynamic balance control in patients with PD.

METHODS

Forty-four patients with idiopathic PD (age: 66±11 yrs; mass: 82.1±17.1 kg; height:174.3± 9.2 cm; Hoehn and Yahr (H&Y) disability score: 2.3± 0.5) volunteered to undergo strength, functional reach, and motion analysis testing.

Isokinetic knee extension strength was measured unilaterally by a KinCom dynamometer (Chattecx, Chattanooga, TN). The participants were positioned against a back support providing a hip flexion angle of approximately 90°. Stabilizing belts were secured over the chest, lap, and distal one-third of the thigh during testing. The resistance pad was positioned approximately 2cm above the lateral malleoli. Knee extension range of motion was 10–90°, and all tests were performed at 60°/s. Participants practiced three submaximal repetitions of extension before the start of testing. During testing, participants performed 3 sets of 3 maximal exertion repetitions with 1~2 minutes rest between sets for both legs. During recording, consistent motivational verbal prompts were given. Peak torque was determined for each repetition and was averaged over the nine repetitions for each leg. The peak torque for each leg was averaged prior to statistical analysis.

The Functional reach test (FRT) was administered as a measure of balance control using a leveled yardstick attached to the wall at the height of the subject's right acromion. To measure the maximal reaching distance, an examiner recorded the subjects initial and end reach positions. Subjects stood comfortably with feet shoulder-width apart, made a loose fist, and, without touching the wall, placed the arm parallel to the yardstick (initial position). Subjects then reached as far forward as they could without raising their heels of the floor (end position). The mean difference between the initial position and the end position for the 3 test trials was calculated as the functional reach.

The peak distance between the center of pressure and whole body center of mass (COP-COM) was calculated as an indicator of dynamic balance control while participants performed gait initiation trials. For each participant, one or two practice trials were followed immediately by three data collection trials for each leg performed at a self selected pace. Kinematic data were collected during the experimental trials using a six camera 3D Optical Capture system (Peak Performance Technologies, Englewood, CO) and ground reaction forces were sampled at 300Hz using a Kistler force platform. Force platform data were subsequently used to calculate the instantaneous COP. Twenty markers placed over boney landmarks were used to construct a simple nine segment model. Estimates of segment mass centers were based on Dempster's anthropometric data and the calculation of the location of the whole body center of mass (COM) was calculated using the Peak performance Software. The distance between the vertical projections of the COM and the COP was calculated using software developed in the Center for Human Movement Studies.

Pearson's correlations were performed to assess relations between PD disability, lower extremity strength, and dynamic balance using SPSS 11.0 for Windows (Chicago, Illinois).

RESULTS AND DISCUSSION

The correlations between dependent variables ranged from poor to moderate in each evaluation (Table 1).

Table 1. Pearson's correlations between PD disability, muscle strength, and balance performance. * p <0.001

	H&Y	*STRENGTH*	*FRT*	*COP-COM*
H&Y score	--------	-0.498*	0.015	-0.554*
STRENGTH	-0.498*	--------	0.006	0.522*
FRT	0.015	0.006	-------	0.054
COP-COM	-0.554*	0.5228	0.054	--------

Greater strength was significantly related to dynamic balance (COP-COM). FRT performance was not related to disease severity, muscular strength, or dynamic balance performance. As expected, the less disabled patients were stronger and displayed greater dynamic balance control.

Strength has been previously associated with both FRT performance and peak COP-COM in older adults [3,4] but appears only to be related to the COP-COM during dynamic tasks in patients with PD. Of interest, FRT performance does not relate to disease severity or dynamic balance control during locomotor activities in this population. These findings highlight the importance of rehabilitative strategies aimed at maintaining strength in patients with PD and suggest that FRT performance is not an appropriate measure of dynamic balance control or a marker of disease severity in this population.

REFERENCES

1. Mallikarjuna N, et al. *Am J Phys Med Rehabil* **83**, 898-908, 2004.
2. Salem GJ, et al. *Med. Sci Sports Exerc* **32**, 1679-184, 2000.
3. Coriveau H, et al. *Arch Gerontol Geriatr* **39,** 163-177, 2004.
4. Davis J, et al. *J Am Geriatr Soc*. **46**,274-279, 1998.

ACKNOWLEDGEMENTS

This project was funded by *NIH #'s* 5 R01 AT000612, 5 P30 AT000609

VIRTUAL MODELS AND PROTOTYPE OF INDIVIDUAL ANKLE FOOT ORTHOSIS

Slavyana Milusheva, Dimitar Tochev, Liliya Stefanova, Yuli Toshev
Institute of Mechanics and Biomechanics, Bulgarian Academy of Sciences, Sofia 1113, Bulgaria
slavyana@imbm.bas.bg; ytoshev@imbm.bas.bg

INTRODUCTION

Ankle-foot orthoses are used mainly in case of disability of neurological origin (cerebral palsy, stroke, spinal cord injury) or musculoskeletal origin (trauma, ageing).
The study is oriented to develop new orthoses to assist the very frequently observed gait abnormalities relating the human ankle-foot complex using CAD modeling.
Computer modeling is a perspective method for optimal design of prosthesis and orthoses. Using CAD geometry different tests could be made without loosing of material and essential design variables could be modified.

METHODS

The main goal is to assist the ankle-foot flexors and extensors during the gait cycle (stance and swing). To realize this aim it is necessary to propose an orthosis model developed based on the 3D biomechanical lower limb model.
Using CAD technology different models of the system AFO (Ankle-Foot-Orthosis) are developed. On the base of the 3D models, the physical AFO models could be elaborated and it is possible to use advanced design and manufacturing technologies: computer aided design (CAD), computer aided manufacturing (CAM) and to combine with computer numerical control (CNC). As result CAD/CAM/CNC could be combine also with rapid prototyping (RP) and rapid tooling (RT). Laser scanning is used to obtain the individual surfaces of patient ankle-foot in order to create a solid model of ankle-foot.

RESULTS AND DISCUSSION

A basic virtual model of the experimental active ankle-foot is developed and shown on (Fig. 1). The model is based on laser scanning and on the contours representing the ankle-foot geometry. Surface and solid models were constructed in Pro/Engineer. The deformation analysis of the 3D model of the new proposed orthoses in Pro/Mechanica is performed. Using Rapid Prototyping technology a physical prototype is manufactured and is under investigation (Fig.2)

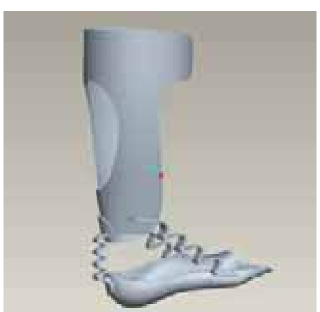

Fig. 1 Virtual ProEngineer Model of Ankle-Foot Orthoses

Fig. 2 Physical Model of Ankle-Foot Orthoses using Rapid Prototyping

CONCLUSIONS

An appropriate AFO design is achieved and manufactured using Rapid Prototyping technology. The difference with the traditional approaches is that the proposed AFO is made using optimal orthoses design on the base of laser scanning by manipulating CAD/CAM methods. The designed AFO is under FEA tests for breaking resistant by frequency and temperature loads.

REFERENCES

1. Milusheva, S. et al. *Acta of Bioengineering and Biomechanics*,Vol.5, Suppl.1,pp.335-339, 2003
2. Stefanova, L et al. *Proceedings of the International Conference on Bionics, Biomechanics and Mechatronics*, Varna, pp. 285-289, 2004

ACKNOWLEDGEMENTS

The study is in the frame of a Royal Society (UK) funded project and a grant NIP-975 by the Bulgarian Research Fund.

OPTIMAL ARM STROKE FOR COMPETITIVE FREE STYLE SWIMMING

[1] Shinichiro Ito
[1]Department of Mechanical Engineering, The National Defense Academy Japan;
email: ito@nda.ac.jp, web: www.nda.ac.jp/~itoh/

INTRODUCTION

Advancing movement of an animal in water can be roughly divided into two categories, locomotion of the maximal efficiency (the minimal energy consumption mode) for an usual motion and that of the maximal speed (the maximal thrust mode) for an urgent evacuation or a predatory action instinctively. For competitive swimming, an operation of the maximal propelling force is desirable. On freestyle swimming, forms of the operation are calculated by using equations of turtles' instinctive locomotion[1].

METHODS

Under a quasi-steady condition, flow induced forces of a hand change by its postures. Thrust force T is generated from a lift force L and a drag force D generated by the flow shown in Figure 1. The thrust force T is balanced with the drag force D_{DP} by the whole body in a constant swimming speed. The formulae of balance of such forces are established, and those formulae are exactly corresponded to the ones of turtles[1]. They are solved concerning the thrust force and the efficiency based on a posture of hand whose lift-drag characteristics are obtained by experiments.

Wind tunnel tests are performed with a plaster replica of a hand including a palm paddle and forearm of an excellent swimmer. As an aspect ratio changes, significant differences in characteristics of lift-drag forces appear with varying sweepback angles ψ whose convention is shown in Figure 2. Sweepback angles of the hand, ψ=135°, 90° and 45° correspond to the catch, the pull and the finish phase on freestyle stroke respectively. With the variation of sweepback angle ψ, the hydrodynamics characteristics against angle of attack α are measured in a wind tunnel with a Reynolds number which is almost equivalent to the relative inflow velocity in water to the hand of actual swimming.

RESULTS AND DISCUSSION

The maximum thrust can be obtained when θ=90°. Namely, the hand plane is perpendicular to the axis of the advancing direction. Each of the maximal points for each ψ has the angle of attack α=90°. That is to say, the hand should be driven along the body axis parallel to the advancing direction for the entire drag forces to be used. The maximal value of the coefficient of thrust at ψ=90° is 0.808, which is 6.2% larger than that at the maximal efficiency. On the other hand, the maximum efficiency η_{max} can be obtained when the motion of the palm paddle corresponds to an S-shaped pull motion. The maximal value of the efficiency at ψ=90° is 0.380, which is 7.1% smaller than that at the maximal thrust.

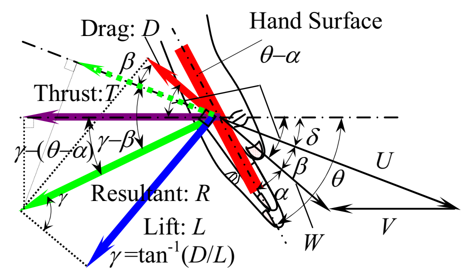

Driving velocity: U Advancing velocity: V
Relative velocity: W Tilt Angle of hand: θ
Angle of attack: α Driving angle: δ

Figure 1: Forces and velocities on a hand paddle

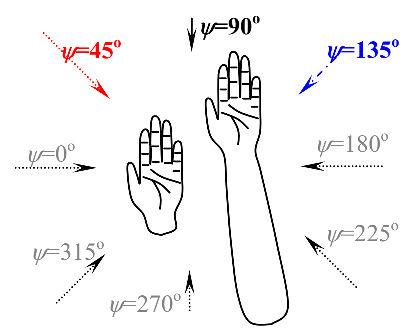

Figure 2: Hand and arm replica used in experiment and Sweepback angle ψ defined by Schleihauf[2].

CONCLUSIONS

The calculations show very interesting and unexpected results which differ from what were said conventionally. An S-shaped pull stroke, a popular form for the conventional front crawl, is resulted as a form of the maximum efficiency mode utilizing lift and drag force by hands. On the other hand, Drag type swimming is the fastest swimming form which generates the maximum thrust. It happened to coincide with the form of Ian Thorpe who has four individual world records.

REFERENCES

1. Ito, S and A. Azuma, Proc. 50th Japan National Congress on Theoretical and Applied Mechanics, Science Council of Japan, 271-280 (2001).
2. Schleihauf, R.E., Swimming III, pp70-109. University Park Press, Baltimore, MD (1979).

NEW METHOD FOR COUPLED FLUID-STRUCTURE INTERACTION PROBLEMS IN BIOMECHANICS

[1]Damian J. J. Farnell, [2]Tim David and [3]David C. Barton
[1]Department of Medicine, University of Liverpool, Liverpool, UK [2]University of Canterbury, Christchurch, New Zealand
[3] School of Mechanical Engineering, University of Leeds, Leeds LS2 9JT; email: d.c.barton@leeds.ac.uk

INTRODUCTION

There are many examples in nature of situations in which a fluid interacts strongly with a flexible structure. Examples range from flapping flags to biological "systems" that are often critical to our survival, e.g. blood flow in the cardiovascular system. The role of numerical simulation of such complex systems is becoming increasingly important as they often yield insight into the fundamental behavior involved. Historically, numerical codes to analyse the dynamic behavior of structures (based on explicit finite element methods e.g. [1]) have evolved separately from those for fluids that are based on computational fluid dynamics (CFD) theory, with the resulting computational complexity and cost reducing the range of applications to which the coupled methodology has been applied. An alternative approach is described here, based on a Lagrangian dynamics approach, embedded in a commercial CFD package (FIDAP). This has the advantage of (relative) computational simplicity and flexibility. The basis of the approach is outlined below followed by a description of its application to two particular problems in biomechanics: blood flow through a heart valve and the swimming action of certain eel-like fish.

METHODS

The flexible structure is treated as an *N*-tuple pendulum with stiffness and damping terms at each "hinge." Each element of the pendulum is assumed to be rigid with uniformly distributed mass. There is only one degree of freedom associated with each element (its rotation), plus an additional freedom for the leading edge of the piecewise-linear structure in the case of the "swimming fish". A Lagrangian is formed from the potential, kinetic and dissipative energy terms of the structure and this is manipulated to form the Euler-Lagrange equations, solution of which yields the motion of the structure. The main external forcing terms in the equations are the pressure differential acting on each element but may also include other terms e.g. due to muscle forces in swimming fish. The structural dynamics solver is written as a subroutine to the commercial CFD package FIDAP that solves the Navier-Stokes equations for the fluid domain in question. The motion of the structure is imposed as a moving boundary condition on the fluid and, in a circular fashion, the pressures generated by the fluid are applied in the Euler-Lagrange equations for the structure. Hence, we solve the two physical problems using a weakly coupled solver, and this approach has been shown to be both highly efficient and accurate [2].

RESULTS AND DISCUSSION

Figure 1 shows a typical result from a 2D coupled analysis of an aortic heart valve. In this case, the two leaflets have been modeled independently, allowing flow asymmetries to develop. Animations of the complete cardiac cycle have been generated which show clearly the full opening and closing of the leaflets and the associated flow vortices.

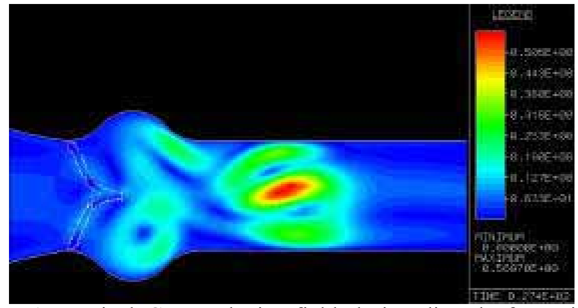
Figure 1: Typical CFD velocity field during diastole for artificial heart valve simulation. The "inlet" from the left ventricle is shown on the left and the two aortic leaflets are shown in outline in white.

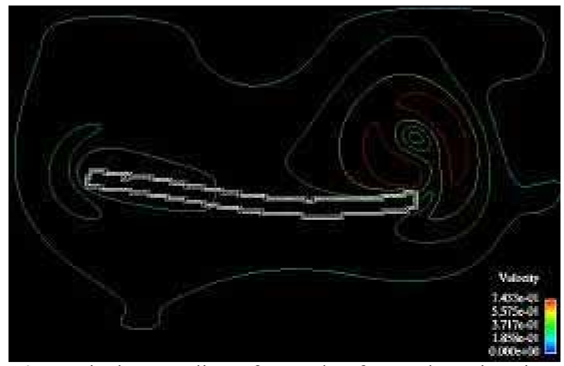

Figure 2: Typical streamlines from the forwards swimming "fish" simulation. The left hand end of the white outline represents the leading end ("head") of the fish.

Figure 2 shows a typical result from the swimming fish simulation. Unlike the heart valve case, the leading edge of the structure is not constrained in space and terms representing the fish's muscle forces are added to the Euler-Lagrange equations. By changing the parameters of the system, it was possible to reproduce both forwards and backwards swimming motions, with quite different vortex structures formed in the two cases. These results are in good agreement with experimental observations [3].

CONCLUSIONS

A novel method has been developed for numerically simulating coupled fluid-structure interaction problems in nature. The method has been applied to several problems, including heart valve dynamics and the swimming action of certain fish, and shown to be robust, efficient and reliable. In principle, it will be possible to extend the method to other problems (e.g. retinal tears in the posterior chamber of the eye) and to fully three-dimensional analysis.

REFERENCES

1. Thornton MA, et al. *Med Eng Phys,* **19**, 588-597, 1997.
2. Farnell DJJ, et al. *J Fluids & Struct,* (in press), 2005.
3. D'Aout K & Aerts P. *J Exp Bio*, **202,** 1511,1999.

A STOCHASTIC MODEL FOR LIGAMENT MECHANICAL FAILURE

[1] Raffaella De Vita and [1]William S. Slaughter
[1]Mechanical Engineering Department, University of Pittsburgh, PA
email: rad15@pitt.edu, web: www.pitt.edu/~rad15

INTRODUCTION

Ligaments are composed of elastin and collagen fibers embedded in a matrix of water, proteoglycans, glycolipids and fibroblasts. Their main function is to guide and to restrain joint motion in order to maintain joint stability. The joint stability is seriously affected when ligament injuries, such as second-degree and third-degree sprains, occur. The treatment and prevention of these injuries require a thorough understanding of the ligament failure mechanisms.

In the present study, a constitutive model will be formulated to describe the failure behavior of ligamentous tissue by taking into account the tissue morphology. The model is able to reproduce the toe region, the linear region and, most importantly, the failure region of the stretch-stress relationship as observed in tensile tests along the fiber direction of the medial collateral ligaments (MCLs) [1].

MODEL FORMULATION

The ligamentous tissue is idealized as composed of N parallel collagen fibers. Elastin and matrix contributions to the tissue mechanical behavior are neglected. The collagen fibers are assumed to contribute to the tissue load only after becoming straight and before breaking. Moreover, they are modeled as a linear elastic material with negligible bending stiffness.

Each fiber is characterized by a straightening stretch, λ^i_s, and a failure stretch, λ^i_f. The fiber straightening stretches and failure stretches for the N fibers are distributed randomly according to Weibull cumulative distributions,

$$G_1(\lambda^i_s) = 1 - e^{\left(\frac{\lambda^i_s - 1}{\beta_s}\right)^{\alpha_s}} \quad \text{and} \quad G_2(\lambda^i_f) = 1 - e^{\left(\frac{\lambda^i_f - 1}{\beta_f}\right)^{\alpha_f}} \quad (i = 1 \ldots N),$$

where α_s, α_f are the shape parameters and β_s, β_f are the scale parameters. The overall tissue stress, σ, and the individual fiber stresses, σ^i, are defined as follows:

$$\sigma = \frac{1}{N}\sum_{i=1}^{N}\sigma^i \quad \text{with} \quad \sigma^i = \begin{cases} K\left(\dfrac{\lambda}{\lambda^i_s} - 1\right) & \text{if } 1 < \dfrac{\lambda}{\lambda^i_s} < \lambda^i_f; \\ 0 & \text{otherwise,} \end{cases}$$

where K is the fiber stiffness, λ is the overall tissue stretch, and λ/λ^i_s is the fiber stretch relative to the taut configuration. Finally, five structural parameters, α_s, α_f, β_s, β_f, K, need to be determined in order to replicate the typical stress-stretch relationship of ligaments.

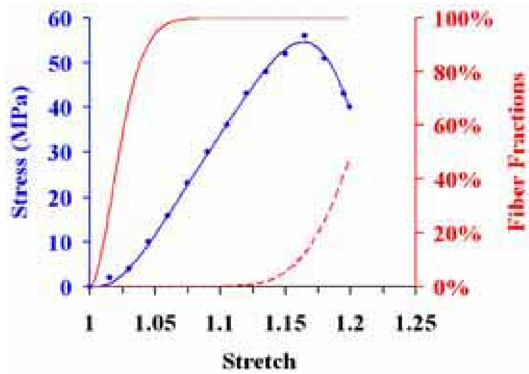

Figure 1: The blue circles are experimental data [1] while the blue line represents the model fit. The red lines represent the straight fiber fraction (—) and the broken fiber fraction (---) predicted by the model.

By following Lanir's approach [2], the presented model is easily generalized to a three-dimensional continuum model to account for the ligament finite deformations and anisotropy.

RESULTS AND DISCUSSION

The model parameter values were determined by curve fitting tensile experimental data on goat MCLs [1]. Their values were found to be K=460 MPa, α_s=1.74, β_s=0.02, α_f=8.10, and β_f=0.18 by implementing the simplex optimization method (R^2=0.99). The experimental data and the model fit at the best fitting parameters are depicted in Figure 1. The fractions of straight fibers and broken fibers, as predicted by the model, are also shown.

The constitutive model is an improvement over the previously presented structural models for connective tissues [3,4] in which the collagen fibers are assumed to have the same failure stretch in the taut configuration.

Three-dimensional constitutive models are necessary to accurately define the ligament mechanical response [5]. However, since quantification of collagen fiber architecture and multiaxial experimental data on ligament failure remain unavailable, the three-dimensional structural model generalization cannot be validated.

REFERENCES

1. Abramowitch SD, et al.. *Knee Surg Sports Traumatol Arthrosc* **11**, 155-162, 2003.
2. Lanir Y. *J Biomech* **12**, 423-436, 1979.
3. Liao H, Belkoff SA. *J Biomech* **32**, 183-436, 1999.
4. Wren TA, Carter DR. *J Biomech Eng* **120**, 55-61, 1998.
5. Weiss J, et al.. *J Biomech* **35**, 943-950, 2002.

A CROSS SECTIONAL MRI STUDY OF THE M. RECTUS FEMORIS MORPHOLOGY IN CYCLISTS, RUNNERS AND SPRINTERS

[1] Kenneth Meijer, [2]Diantha Michels , [1]Henk de Feyter, [1]Gustav Strijkers, and [2]Hans HCM Savelberg
[1] Department of Biomedical Engineering, Technische Universiteit Eindhoven, The Netherlands,
[2] Department of Health Sciences, Maastricht University, The Netherlands; email: Kenneth.Meijer@bw.unimaas.nl

INTRODUCTION

Muscles are highly adaptable. In response to internal and external stimuli they remodel their volume by changing their length and their physiological cross sectional area (PCSA). A recent comparison of knee extension torque in cyclists and runners has indicated that cyclists have a shorter m. rectus femoris (RF) compared to runners, but that the PCSA is similar in both groups [1]. It was argued that this difference was related to a difference in use of the RF in these sports. However, inferring muscle morphology from torque data is prone to error. Therefore, the aim of this study was to study RF morphology more directly. For this purpose we assessed the RF morphology by taking MRI scans for three types of athletes: cyclist (C), distance runners (D) and sprinters (S).

METHODS

Athletes were recruited at sport clubs and assigned to the C, D or S group based on performance criteria. A total of 45 cross sectional MRI scans (weighed T1; 1.5 T Philips S15/ACS scanner) were made of the right upper leg to create muscle images (figure 1). The images were analyzed using Easyvision to quantify the RF muscle belly length, muscle belly width in left-right (L-R) direction and anterior-posterior (A-P) direction as well as muscle volume. This data was fed into a 3-D model of the RF [2] to estimate the muscle fiber length and PCSA. Differences in muscle belly length, L-R and A-P width, volume, fiber length and PCSA between the groups were tested using a one-way ANOVA.

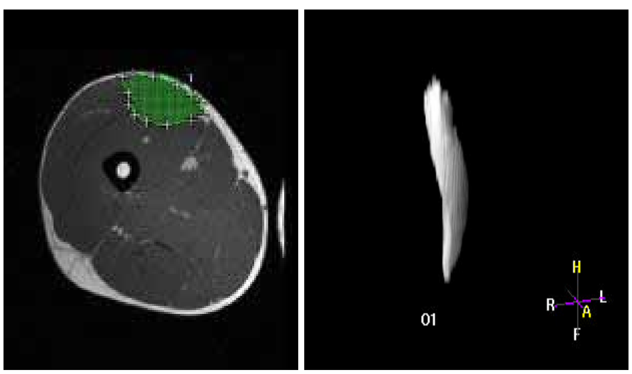

Figure 1: Left panel: region of interest of the m. rectus femoris in cross sectional slice of the upper leg. Right panel: reconstruction of m. rectus femoris volume and the used frame of reference (R=right, L=left, H=head, F=feet and A=anterior)

RESULTS AND DISCUSSION

Each group consisted of nine subjects. There were no significant differences between the subjects in the respective groups in terms of age, height, weight and femur length.

Table 1: Morphological data for m. rectus femoris. Significant differences are indicated by * ($P<0.05$)

Parameter	Cyclists	Distance Runners	Sprinters
volume (cm^3)*	317.3 ± 46.7	338.4 ± 58.5	393.6 ± 74.8
belly length (cm)	33.3 ± 2.5	34.0 ± 2.7	34.4 ± 2.5
L-R width (cm)	7.4 ± 0.6	7.6 ± 0.7	7.9 ± 0.9
A-P width (cm)	5.1 ± 0.6	4.6 ± 0.7	5.6 ± 1.2
fiber length cm	10.4 ± 0.6	10.4 ± 0.8	10.8 ± 0.93
PCSA (cm^2)	30.7 ± 4.3	32.6 ± 5.4	36.5 ± 6.2

Table 1 summarizes the data from the analysis of the MRI images and the model predictions. Statistical analysis revealed that muscle volume was the only parameter that was significantly different between the groups. Post-hoc tests revealed that this was attributed to the difference between the cyclists and the sprinters. It should be noted that the differences in A-P width ($P=0.068$) and PCSA ($P=0.08$) approached significance.

The volumes measured in this study were 106-155% larger than values reported from anatomical studies on cadaver material [3]. Likewise, estimates for fiber lengths were 33-38% larger and PCSAs were 65-82% larger in this study compared to previous studies [3]. These differences probably reflect the high training level of the subjects that participated in this study as well as possible shrinkage of cadaver material.

CONCLUSIONS

The data of this study do not support the hypothesis that a difference in the RF knee extension torque between cyclist and runners results from morphological adaptations [1]. Alternative explanations like length dependent muscle activation and differences in co-contraction levels to explain the results of Savelberg and Meijer (2003) are discussed.

REFERENCES

1. Savelberg and Meijer *J Appl. Physiol.* **94,** 2241-2248, 2003.
2. Savelberg et al. *Proceedings of ICCB Zaragosa*, Spain, Vol. 1, pp185-191, 2003
3. Meijer et al. *J Appl. Biomech.*, **14**, 62-79, 1998

UTILITY OF THE FRONTAL PLANE PROJECTION ANGLE OF THE KNEE DURING SINGLE LEG SQUATS

John D. Willson[1] and Irene Davis[1,2]
[1] Department of Physical Therapy, University of Delaware, Newark, DE, USA
[2] Drayer Physical Therapy Institute, Hummelstown, PA, USA
Email: willson@udel.edu Web: www.udel.edu/PT/davis/index.htm

INTRODUCTION

Abnormal lower extremity mechanics during athletic activities are believed to contribute to the etiology of numerous knee joint injuries [1,2]. The single leg squat test is commonly used by practicing clinicians to identify individuals who display such abnormal mechanics. Presently, due to the restraints of typical clinical settings, analysis of this test is done qualitatively. However, quantification of a patient's performance on this test would facilitate accurate documentation of these mechanics as well as changes due to interventions. Two-dimensional images recorded by a digital camera during this test will reveal the frontal plane projection angle (FPPA) of the knee during this test. However, it is unclear to what extent the frontal plane projection angle determined using such methods is related to actual three-dimensional (3D) kinematics. Specifically, it would be beneficial to know to what degree tibiofemoral (TF) valgus, a widely accepted risk factor for injuries such as ACL rupture and patellofemoral pain, is represented by such images. Additionally, the extent to which performance on the single leg squat test is associated with lower extremity alignment during faster, more demanding tasks has not been determined.

The purpose of this study was to examine the correlation of the FPPA of the knee during single leg squats with hip and knee frontal and transverse plane kinematics. Second, we analyzed to what extent the FPPA of the knee during single leg squats reflects knee and hip kinematics during a single leg landing. We hypothesized that the FPPA during single leg squats would be significantly correlated with TF valgus during single leg squats and landings.

METHODS

As part of an ongoing study, 10 healthy subjects performed five single leg squats and five single leg landings. All trials were collected for the dominant leg of each subject. Retroreflective markers placed on the lower extremity were tracked by a six camera Vicon motion analysis system collecting at 120 Hz. V3D software was used to determine lower extremity kinematics. Markers placed on the leg of each subject bisecting the frontal plane of the proximal thigh, TF joint, and malleoli at the ankle were used to determine the FPPA of the knee in each digital image (CorelDraw). Subjects performed each single leg squat to a cadence and a self-selected depth. Single leg landings were performed from a height of 23 cm. During each squat trial, a digital image was recorded by a camera placed 2m anterior to the subject, perpendicular to the frontal plane, and at the height of the knee joint in single leg stance. Each image was recorded as the subject passed 45º knee flexion as determined by an electrogoniometer on the lateral aspect of the leg. To synchronize the digital camera with the motion analysis, a signal was delivered to the motion analysis workstation as the image was recorded. Pearson correlation coefficients were calculated between the FPPA and selected 3D kinematics during single leg stance and landing conditions.

RESULTS AND DISCUSSION

The FPPA was significantly associated with transverse plane kinematics at the knee (Table 1). 3D TF valgus was weakly associated with the FPPA during single leg squats (Figure 1). During single leg landings, the FPPA was more highly correlated with peak TF internal rotation ($r = .66$, $p = 0.04$) than peak TF abduction ($r = .54$, $p = 0.11$). After ten subjects, it appears that interpretation of the FPPA should not neglect the influence of transverse plane motion on this measure. However, we are collecting additional subjects to sufficiently power the study.

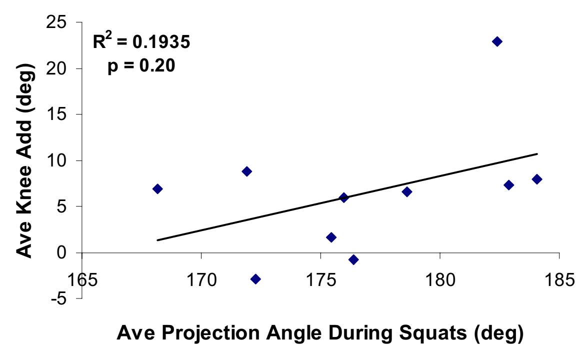

Figure 1: Knee abduction angle determined using rigid body analysis versus the FPPA during single leg squats.

CONCLUSIONS

Based on these preliminary data, the FPPA of the knee during single leg squats appears to indicate the degree of TF valgus to a limited extent. A greater correlation between knee transverse plane kinematics and FPPA has been identified. The FPPA during a single leg squat also appears to lend insight into the degree of knee internal rotation during a single leg landing.

REFERENCES

1. Griffin, L. *J Am Acad Orthop Surg*. **8**:141-150, 2000.
2. McClay Davis, I. *Clin Biomech*. **16**:937-959, 2001.

Table 1. Correlation between the average FPPA and hip and knee frontal and transverse plane kinematics during single leg squats.

	Knee abd/add	Knee IR/ER	Hip abd/add	Hip IR/ER	Femur abd/add (global)	Femur IR/ER (global)
Pearson r *(p)*	0.44 *(0.20)*	0.84 *(0.002)*	-0.29 *(0.42)*	-0.20 *(0.59)*	-0.73 *(0.02)*	-0.27 *(0.46)*

PREDICTION OF HUMAN WALKING BASED ON SIMPLE GAIT DESCRIPTORS

Lei Ren, Richard Jones and David Howard
Centre for Rehabilitation and Human Performance Research, Salford University,
Salford, United Kingdom; email: d.howard@salford.ac.uk

INTRODUCTION

Gait prediction has many potential applications including the investigation of: motor control objectives in gait; the impact of musculoskeletal structure and injury on movement coordination; and the effect of assistive devices on locomotion performance [1]. Dynamic optimisation combined with the forward dynamics method offers a possible solution, however, it leads to very large computational burdens [2]. The inverse dynamics method, with its high computational efficiency, may provide an alternative means of gait prediction [3].

In this study, an inverse dynamics multi-segment model was combined with optimisation techniques to simulate normal human walking in the sagittal plane on level ground. Walking is formulated as an optimal motor task, subject to multiple constraints, with minimisation of mechanical energy consumption being the performance criterion. All segmental motions and ground reactions were predicted from only two simple gait descriptors: walking velocity and cycle period.

METHODS

The human body is modelled as a dynamic coupled multi-segment system containing seven segments: the right and left thighs, shanks, and feet together with a HAT segment (head, arms and trunk). The segments are connected by frictionless hinge joints, and the model accounts only for segmental motions in the sagittal plane. The foot is modelled as a rigid body with a curved surface rolling on the ground without slipping.

A set of kinematic variables (segmental angles) are used to define the motion of the model. During walking, the motion of the stance ankle can be determined by the shape of the plantar surface of the stance foot and its orientation. Thereafter, the motion of each body segment can be derived based on the topology of the model, the segmental angles and the stance ankle motions.

An inverse dynamics method is employed to calculate the joint kinetics and mechanical energy expenditure during walking. As the ground reactions are initially unknown, the inverse dynamics algorithm is based only on segmental motions [4], where a linear transfer assumption is used to solve the indeterminacy problem during the double support phase [4].

In this study, the gait prediction problem is formulated as an optimisation problem, which can be described as: find segment trajectories that achieve the specified gait parameters, whilst minimizing energy cost, and satisfying the constraints associated with a walking gait. Multiple constraints are implemented in the optimisation, which can be broadly categorized as: task constraints, biomechanical constraints and environmental constraints.

RESULTS AND DISCUSSION

The optimisation scheme was implemented in the MATLAB (Mathworks, MA, USA) programming environment using the SQP (Sequential Quadratic Programming) optimisation algorithm. The two input gait descriptors (walking velocity and cycle period) were obtained from the gait measurement data of one subject (age: 38years, weight: 101.7kg, height: 178cm), where the averaged values from four repeated normal walking trials were used.

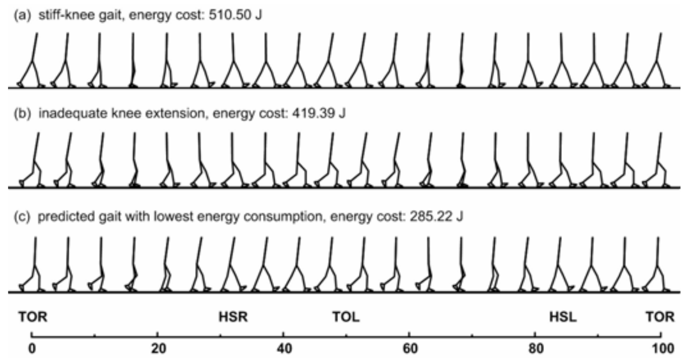

Figure 1: Some typical gait patterns (local minima) found during the random optimisation runs. The model (weight, 101.7 kg) walked at 1.50 m/s, with a cycle period of 1.0 s.

To find optimal solutions (local minima), the minimization was repeated with different random initial values. Due to the high non-linearity of human walking, several local minima were obtained (Figure 1). It was found that the solution with the lowest energy consumption (Figure 1(c)) yields the most realistic gait pattern.

Quantitative comparisons of the predicted ground reactions and segmental motions with gait measurements show that the model reproduced the significant characteristics of normal gait in the sagittal plane. The simulation results suggest that minimising energy expenditure is a primary control objective in normal walking. However, there is also some evidence for the existence of multiple concurrent performance objectives.

REFERENCES

1. Pandy MG. *Annu. Rev. Biomed. Eng.* **3**, 245–273, 2001.
2. Anderson FC et al. *J. Biomech*. Eng. **123**, 381–390, 2001
3. Koopman B. et al. *J. Biomech.* **28**, 1369–1376, 1995.
4. Ren L. et al. *J.Biomech*., In Press

ACKNOWLEDGEMENTS

Funding for this work has been provided by the UK Ministry of Defence.

Noise-Enhanced Balance Control: The Worse You Are the Better You Get

[1] Attila A. Priplata, [2]James B. Niemi, [3]Paolo Bonato, [3]Joel Stein, [4]Aristedes Veves, [5]Lewis A. Lipsitz and [1]James J. Collins
[1]Center for BioDynamics, Boston University, Boston, MA
[2]Afferent Corporation, Providence, RI
[3]Spaulding Rehabilitation Hospital, Boston, MA
[4]Joslin-Beth Israel Deaconess Foot Center, Beth Israel Deaconess Medical Center, Boston, MA
[5]Hebrew Rehabilitation Center for Aged Research and Training Institute, Boston, MA

INTRODUCTION

The human balance control system relies, in part, on somatosensory feedback. In older adults, patients with diabetic neuropathy and patients with stroke, diminished somatosensation is associated with increased postural instability during standing and walking. Recently, it has been demonstrated that subsensory mechanical noise can improve somatosensation in healthy young individuals and older adults[1]. Moreover, it has been shown that subsensory mechanical noise applied to the soles of the feet via vibrating insoles can enhance balance control in healthy young[2], elderly individuals[2], patients with diabetic neuropathy[3], and patients with stroke[4]. The goal of this study was to test the hypothesis that the amount of reduction of postural sway during the application of noise to the soles of the feet is directly correlated with the baseline postural sway of the individual.

METHODS

The postural-sway data of twelve healthy elderly[2] (mean 73 years), 15 subjects with diabetic neuropathy[3] (mean 60 years) and 15 subjects with unilateral stroke[4] (mean 61 years) were pooled from three earlier studies. In each of these studies, subjects stood barefoot with eyes closed on gel-based vibrating insoles that applied subsensory random vibrations to the soles of the feet. With the application of noise, both traditional and random-walk postural sway measures, analyzed from the displacement of a shoulder marker, improved significantly across the groups. These results demonstrated promising improvements in balance control; however, they did not address the contributions that balance impairments have on the level of improvement seen in postural sway during the application of noise. To determine these factors across the three populations, we developed a linear regression model. We compared age, height, sensory threshold, and/or baseline sway of each subject to the difference measure (*difference measure = mean value of control condition - mean value of noise condition*) for each sway parameter of each subject, respectively. We hypothesized that increases in these independent variables would lead to an increase in the difference measure for each sway parameter (indicated by positive coefficient estimates for each sway parameter and $p < 0.05$). With the linear regression model, we also analyzed if interactions were present between stimulation (control vs. noise) and condition (subjects with diabetic neuropathy vs. subjects with stroke vs. elderly) on postural sway.

RESULTS AND DISCUSSION

As indicated in Table 1, all coefficient estimates for the mean value of baseline sway of each sway parameter versus the difference measure of each sway parameter, respectively, are

Parameters	Estimates	*p*-value
Mean Radius	0.2 ± 0.1	< 0.0001
Swept Area	0.2 ± 0.1	0.0038
Max Radius	0.3 ± 0.1	< 0.0001
Range AP	0.3 ± 0.1	< 0.0001
Range ML	0.4 ± 0.1	< 0.0001
$<\Delta r^2>_c$	0.1 ± 0.1	0.0339
D_{rl} (s^{-1})	0.6 ± 0.1	< 0.0001
H_{rl}	0.4 ± 0.1	< 0.0001

Table 1: Coefficient estimates of the traditional and random-walk sway parameters from the model of base-line postural sway versus the difference measure for each sway parameter of each subject, respectively.

statistically significant. Coefficient estimates for age, height and sensory threshold for each sway parameter versus the difference measure for each sway parameter, respectively, were not statistically significant; therefore, these independent variables were removed from the model. No interactions were found between stimulation and age in any of the parameters suggesting that there were no differential effects of mechanical noise in the elderly, patients with diabetic neuropathy and patients with stroke.

This study shows that reduction of postural sway during the application of noise to the feet is greater in individuals with larger baseline postural sway.

CONCLUSIONS

Noise-based devices, such as randomly vibrating shoe insoles, may prove effective in enhancing performance of dynamic balance activities (e.g., walking) in individuals with balance deficits. Moreover, it may be possible to predict the magnitude of the stimulation effect by measuring the baseline performance of the individual.

REFERENCES

1. Priplata AA, et al. *Phys Rev Lett* **89**, 238101, 2002.
2. Priplata AA, et al. *The Lancet* **362**, 1123-1124, 2003.
3. Priplata AA, et al. *Annual Meeting of ACSM*, Indianapolis, IN, Abstract 0078, 2004.
4. Priplata AA, et al. 15th Congress of ISEK, Boston, MA, Abstract 484, 2004.

ACKNOWLEDGEMENTS

We would like to thank Richard Goldstein for guidance with statistical analysis.

GENERALIZED APPROACH TO THREE-DIMENSIONAL MARKER-BASED MOTION ANALYSIS OF BIOMECHANICAL MULTI-SEGMENT SYSTEM

Lei Ren, Richard Jones and David Howard
Centre for Rehabilitation and Human Performance Research, Salford University,
Salford, United Kingdom; email: d.howard@salford.ac.uk

INTRODUCTION

Three-dimensional motion analysis using photogrammetric techniques has been increasingly used in human movement studies recently. Although most 3D applications only focus on specific parts of the body with relatively simple structures (e.g. the lower limbs), real biomechanical systems are more complex as human and animal skeletons are composed of interconnected articulated links with hundreds of degree of freedom (DOF) and complicated topologies; moreover the environmental constraints are various.

This paper presents a methodology for 3D kinematic and kinetic analysis of general multi-body systems using marker-based photogrammetric devices, which can be used for a large range of biomechanical systems, whether human or animal. The proposed methodology is being implemented in a software package, SMAS (Salford Motion Analysis System).

METHODS

The biomechanical system is modelled as a set of rigid segments, connected by generic joints with up to six independent DOF. Three templates are employed to define the biomechanical system: the body template, marker template and force template. All definitions are generic, so that any biomechanical multi-body system can be described.

The body template represents the topology of the multi-body system, which includes the definitions of body segments, their adjacent segments, and interconnecting joints. The marker template defines two marker sets: technical markers and anatomical landmarks. Technical markers are attached to body segments to record their changing positions and orientations, and are associated with technical frames. Anatomical (or bony) landmarks are used to define bone-embedded local frames for each body segment. The force template describes the properties of the external force systems acting on the biomechanical system. These external forces can be set as known (e.g. measured by force plates) or as unknown.

For kinematic analysis, a least square method [2] is used to estimate the position and orientation of body segments from the technical marker coordinates. The CAST protocol [1] is employed, based on a set of calibration procedures, to establish the mapping between the technical and anatomical frames. The calibration procedure allows for the use of different landmark identification techniques (e.g. markers and/or wands). The joint centers can be identified using functional methods or directly from anatomical landmarks. The anatomical landmarks (derived or real) are then used to define anatomical frames and the orientations of body segments. Thereafter the joint kinematics can be described based on the topology defined in the body template.

For kinetic analysis, the inverse dynamics method is employed. However, this differs from the conventional approach where the calculations proceed sequentially, from distal to proximal segments. In SMAS, the calculation sequence depends on the system topology and the environmental constraints defined in the body and force templates. The algorithm starts from all solvable segments, calculates the forces and moments at their adjacent joints, and then runs iteratively until no solvable segment remains. Different approaches are used to derive joint forces and moments according to the determinacy of the system. In the under-determined case, inverse dynamics is used to derive all the solvable joint forces and moments, whereas, in the determinate case, all joint forces and moments can be calculated. If redundancy exists, a least squares method [3] is employed to improve the accuracy of the calculated joint kinetics.

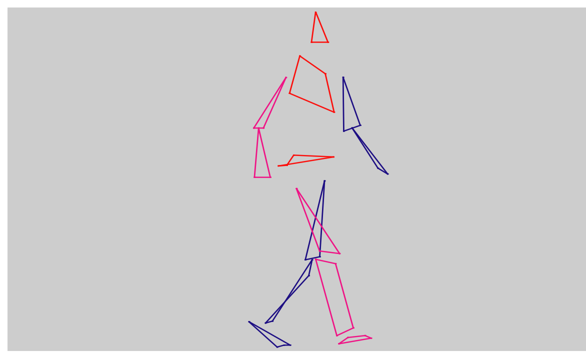

Figure 1: A SMAS 3D model of whole-body walking. The polygons represent the body segments with anatomical landmarks at their vertices.

RESULTS AND DISCUSSION

The methodology is being implemented as a MATLAB based software package, SMAS, which is now almost complete. Figure 1 shows a 3D whole-body SMAS model. The SMAS methodology applies to general biomechanical multi-segment systems, and makes best use of the available kinematic information. Moreover, unknown external forces and moments can be derived, as well as the internal joint forces and moments.

REFERENCES

1. Cappozzo A. et al. *Clin. Biomech.* **10**, 171–178, 1995.
2. Challis JH. *J. Biomech.* **28**, 733–737, 1995.
3. Kuo AD. *J. Biomech. Eng.* **120**, 148–159, 1998.

ACKNOWLEDGEMENTS

Funding has been provided by the UK Ministry of Defence.

HIGH RANGE OF MOTION ACTIVITIES OF DAILY LIVING: DIFFERENCES IN THE KINEMATICS BETWEEN HONG KONG AND CHENNAI, INDIA SUBJECTS

[1]Urs Wyss, [1]Heather Brown, [1]Andrea Hemmerich, [2]Tanya Packer, [1]Stacey Smith
[1]Queen's University, Kingston, Ontario, Canada; e-mail: wyss@me.queensu.ca
[2]Curtin University, Perth, Western Australia

INTRODUCTION

There are regions in the world where for cultural or religious reasons high range of motion (ROM) activities of daily living (ADL), such as squatting, kneeling and cross-legged sitting are common. When patients in these regions suffer from joint disease, it is more difficult for them to be treated with joint replacements, as not many of the current designs allow for a high ROM. Kinematic and kinetic data is limited (3), which is why it is necessary to study high ROM ADL. It was not known if high ROM activities would be following the same kinematic and kinetic patterns in different regions, which is why data was collected from more than one specific group. This study discusses data from subjects from Hong Kong and Chennai in India, and looks at differences between the two populations.

METHODS

In Hong Kong there were 8 female and 3 male subjects assessed. Their mean age was 50.2 years (SD 7.8), the mean mass was 59.3kg (SD 9.9), and the mean height 158.4cm (SD 10.3). In Chennai there were 10 female and 20 male subjects. Their mean age was 48.1 years (SD 7.6), the mean mass was 57.1kg (SD 10.2), and the mean height 158.6cm (SD 7.3). The kinematics were recorded with a Fastrak system (Polhemus), and the ground reaction forces with an non-magnetic force platform (AMTI). The trials were split into a phase going with gravity into the posture, and against gravity out of the posture. Each phase was then normalized to 100%, so that the data can be compared (1).

RESULTS AND DISCUSSION

The mean curves with the standard deviations (+/- 1SD) for the hip and knee angles of the squatting with heels down activity, is shown in Figure 1 for the Hong Kong subjects. It shows the flexion/ extension, abduction/ adduction and external-/ internal-rotation curves. The differences between the Hong Kong and Chennai subjects are mainly in the flexion/ extension movement, which is why only those are summarized in Table 1 for other activities. The kneeling data is not added here, since both groups indicated that it is not an activity that they would do frequently. This, of course would be a very important ADL in Muslim populations. The data in Table 1 shows that the Hong Kong subjects had a higher flexion maximum at the hip as compared to the Chennai subjects. There was, however, a large standard deviation, indicating big differences between subjects. It is interesting to see in Table 1 that the larger hip angles in the Hong Kong subjects are compensated somewhat by smaller maximum knee angles. Furthermore, the standard deviations at the knee of the Chennai subjects are smaller than for the hip angles, indicating much less variation between subjects.

CONCLUSIONS

The kinematics of how the subjects in Hong Kong perform high ROM ADL are different from subjects in Chennai, India. Some of these differences are over 30 degrees. The Hong Kong subjects use less knee flexion, but more hip flexion. Reviewing the position of the sacral marker showed that the compensation of the lower hip angles is mostly taking place in the lower region of the back (2). It is important to be aware of the differences how high ROM ADL are performed in populations with different cultural and religious backgrounds when artificial joints are developed for these persons, so that the technical ROM of the implant is sufficiently large.

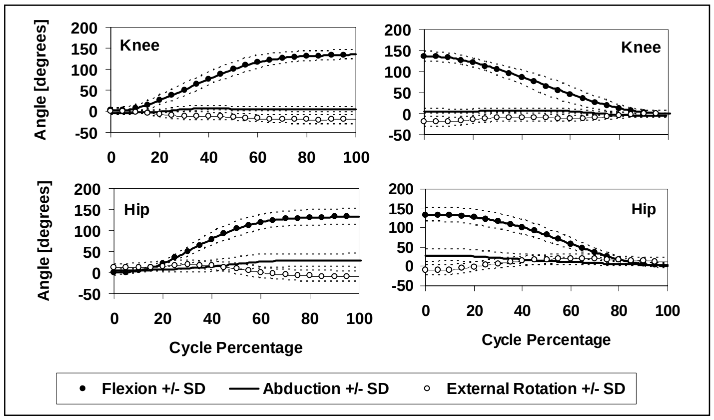

Figure 1: Hip and knee rotations for squatting heels down of Hong Kong subjects.

Table 1: Maximum hip and knee flexion angles for three ADL of the Hong Kong and Chennai subjects.

	Maximum Hip Flexion [degrees]		Maximum Knee Flexion [degrees]	
	Hong Kong	**Chennai**	**Hong Kong**	**Chennai**
Squatting Heels Down	133 (21)	95 (26)	135 (20)	152 (11)
Squatting Heels Up	108 (22)	91 (17)	142 (15)	155 (7)
Sitting Cross-Legged	128 (29)	85 (34)	126 (32)	149 (8)

REFERENCES

1. Brown, H. *M.Sc. Thesis*, Mech. and Mat. Eng., Queen's University, Canada, 2004.
2. Hemmerich, A, et al. *Proceedings of ORS*, 2005.
3. Mulholland, SJ and Wyss, UP. *Int. J. Rehab. Res.*, **24**, 191-198, 2001.
4. Noble, P and Weiss, GM. *Proceedings of ORS*, 2001.

ACKNOWLEDGEMENTS

The study was partially supported by Zimmer, Inc. Switzerland and NSERC.

ONE-FOOT VERTICAL JUMP WITH APPROACH IN UNILATERAL TRANSTIBIAL AMPUTEES

Siobhan Strike and Matthew Taylor
School of Human and Life Sciences, Roehampton University, London, SW15 4JD, UK
Email: s.strike@roehampton.ac.uk

INTRODUCTION

Jumping is a key skill in many team sports and sporting situations, for example a jump shot in basketball, a block in volleyball, an interception in netball or basketball and a jump in football are all common maneuvers in sport and recreation. While many types of jump (countermovement, approach, static etc) have been researched in some way for non-disabled performers [1,2] there is little evidence of research into the mechanisms, compensations and alterations made by disabled performers in similar situations. An understanding of the biomechanics of amputee jumping and the identification of the compensatory mechanisms employed by amputees to achieve controlled flight is justified.

The aim of the study was to assess the biomechanical technique used by transtibial amputees to reach maximum flight height in a 1-footed vertical jump with an approach from the sound and prosthetic sides. Through this assessment, alterations to jump biomechanics could be identified and compensatory mechanisms detailed.

METHODS

Three male transtibial amputees were asked to perform maximal one-legged vertical jump with approach from their right and left limbs. Of the three, only two were comfortable completing the task and achieving height from the prosthetic side. One participant withdrew from the research. Both remaining participants were traumatic left-sided amputees and were healthy and active and free of musculoskeletal injuries. Participant one (P-1) had a mass of 69kg and height of 1.78m. The amputation had taken place 8 years prior to testing. Participant two (P-2) had a mass of 81kg and height of 1.77m. The amputation had taken place 12 years to testing. For the motion capture, a seven camera VICON 512 retro-reflective motion analysis system was used. The cameras were operating at a frequency of 120Hz. Thirty-three retro-reflective markers were placed with tape on the head, trunk, arms and legs. One-foot vertical jumps with an approach were analysed. The participants took a 2-3 step approach followed by a take off from the sound limb or the prosthetic limb. The instruction to the participants was simply to jump as high as possible.

Both participants warmed up for about ten minutes prior to data collection and they were allowed sufficient time to practice the jumps. At least 3 practice attempts were taken. Each participant then performed three jumps of each type and the best jump, defined by maximum height of the Centre of Mass (CoM) was selected for further analysis.

RESULTS AND DISCUSSION

Outcome results for the subjects are presented in Table 1.

Table 1 Outcome results for jump with approach

	Participant 1			Participant 2		
	Sound	Pros	*Diff*	Sound	Pros	*Diff*
Max Height of CoM (m)	1.39	1.26	*0.13*	1.32	1.20	*0.12*
Flight Height of CoM (m)	0.19	0.10	*0.17*	0.17	0.15	*0.02*
Height of CoM @ TO (m)	1.20	1.16	*0.04*	1.15	1.05	*0.1*
Vv of CoM @ TO (m/s)	2.0	1.36	*0.64*	1.80	1.52	*0.28*
Min Height of CoM (m)	0.81	0.98	*0.17*	0.75	0.89	*0.14*
Last step length (cm)	31	14	*17*	61	47	*14*
Vy of CoM at end of approach (m/s)	0.51	0.20	*0.31*	1.13	0.80	*0.33*

For both participants the maximum height achieved was reduced on the prosthetic side compared to the sound side. For P-1 the flight height from the prosthetic limb was substantially lower than that from the sound limb, while for P-2 the flight height was similar from both. This is due to the varied joint angles at take-off.

A key aspect in a jump with an approach is the approach itself. The length of the last step prior to the jump was asymmetrical for both participants and P-2 took a longer step than P-1 on both sides. For both participants the step was longer from the prosthesis onto the sound limb. The horizontal velocity is lower in both cases for P-1 than for P-2. This indicates that P-2 has greater horizontal momentum as he begins the jumping action. However, as P-2 does not jump as high as P-1 it is probable that he cannot make full use of this momentum.

Table 2 Temporal characteristics associated with the approach and take-off phases of the jump

	Participant 1		Participant 2	
	Sound	Pros	Sound	Pros
Final approach (s)	0.57	0.72	0.44	0.40
Countermovement (s)	0.89	0.37	0.89	0.56
Push-off (s)	0.3	0.23	0.48	0.2

The timing of the phases for the jump was asymmetrical for both participants and different between the amputees. For both amputees the jump on the sound side took longer than on the prosthetic side, mainly due to the extended countermovement and push-off phases.

REFERENCES

1. Van Soest AJ et al *Med Sci Sports Exerc,*, **17**, 635-639 1985.
2. Aragon-Vargas LF *Journal of Applied Biomechanics*, **13**, 24-44 1997.

PARASPINAL REFLEX BEHAVIOR AS A FUNCTION OF TRUNK POSTURE

Ellen Rogers, [1] Kevin Granata
Musculoskeletal Biomechanics Laboratory, Virginia Polytechnic Institute, Blacksburg, VA, USA
[1] E-mail: Granata@vt.edu

INTRODUCTION

Prolonged use of flexed postures during manual materials handling is associated with high incidence rates of low back pain (LBP). Spinal instability has recently been considered a potential risk factor for LBP. Previous work indicates that spinal stability is influenced by posture. The ability to accurately assess and reposition the lumbar spine has been shown to decrease with trunk flexion angle[1]. The ability to sense and control spinal curvature is important to spinal stability. Total stability in flexed postures must take into account changes in neuromuscular control, these being important factors in preventing injury during unexpected loading. However, spinal reflex response has not been measured as a function of posture.

Position-dependent reflex behavior has been exhibited in the elbow and the ankle, but not in the trunk. Reflex behavior may depend on anatomical architecture and mechanical advantage of the joint as well as differences in tonic firing rates associated with changes in muscle length. Evidence suggests that a fully flexed spine results in a reduced moment arm for the trunk extensor muscles and load redistribution to passive tissues and deeper spinal muscles. We hypothesize that trunk flexion will reduce paraspinal reflex behavior. The specific aim of this project was to evaluate trunk reflex behavior using data recorded in various trunk flexion angles.

METHODS

Paraspinal reflexes were assessed at four trunk angles (0º, 30º, 60º, and 90º) on twenty-six subjects with no history of low back pain. Subjects were attached to a servomotor via a harness and cable system such that anteriorly directed horizontal loads were applied at the T10 level of the trunk. The servomotor applied a constant isotonic preload. The subject maintained an unsupported upright trunk posture throughout the experiment with their pelvis restrained; trunk angle was achieved via an apparatus that rotated the lower body to the desired angle in order to reduce confounding factors due to changes in spinal load in flexed postures. Each trunk angle was maintained for approximately 3 minutes, to limit exposure to ligament strain. Superimposed on the preload were force perturbations of ±70 N applied in a pseudo-random stochastic fashion with a flat bandwidth from 0-50 Hz. Lumbar paraspinal EMG were measured throughout the trial.

To quantify paraspinal reflex dynamics, the EMG response to a force perturbation was modeled as the closed loop transfer function of the system. Reflex gain was identified as the peak value of the impulse response function relating input force to EMG response using time-domain deconvolution analyses[2].

RESULTS AND DISCUSSION

Reflex gain decreased significantly ($p < 0.0003$) with trunk angle. From upright posture (0º trunk angle) G_R decreased 13.4% at 30º ($p = 0.36$), 24.2% at 60º ($p < 0.02$), and 29.9% at 90º ($p < 0.05$). A significant gender-by-trunk angle interaction indicates possible gender differences in position-dependent reflex behavior. From upright females exhibited a 24.7% reduction in G_R at 60º ($p < 0.02$) and a 31.7% reduction in G_R at 90º ($p < 0.0003$). However in male subjects there was no significant change in G_R due to trunk flexion (Figure 1).

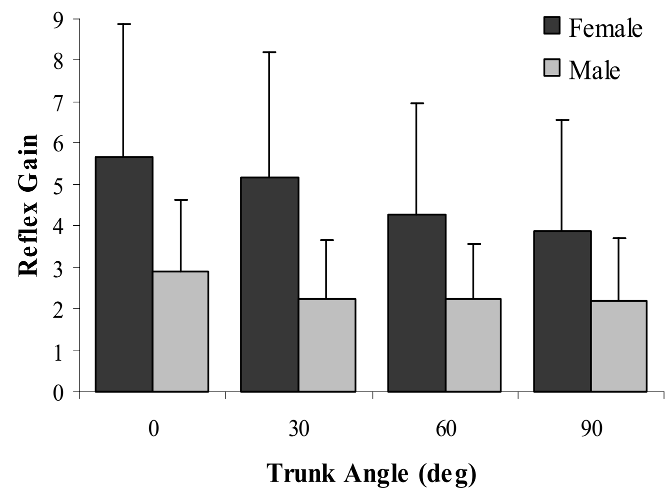

Figure 1. Reflex gain decreased significantly ($p < 0.0003$) with trunk angle.

It has previously been demonstrated that paraspinal reflex gain is altered following prolonged static and cyclic flexion[3]. It is interesting that brief periods of trunk flexion caused an inhibition of reflexes similar to the effects of prolonged flexion. Baseline EMG was also found to decrease with trunk flexion. In response to a perturbation muscles are therefore less excitable and produce a smaller reflex gain.

CONCLUSIONS

Reduced reflex response in flexed postures, even brief periods, can contribute to reduced stability, making unexpected loading events particularly risky. Prolonged flexed posture work is a known risk factor for LBP; possibly even brief flexed postures should be considered a risk factor.

REFERENCES

1. Wilson, S and Granata, KP. Spine 28, 513 – 518, 2003.
2. Hunter IW and Kearney RE. Med.Biol.Eng.Comput. 21, 203-9, 1983.
3. Granata et al., Clin.Biomech. 20, 16-24, 2005.

TRAINING AND PERFORMANCE OF ROBOTIC LAPAROSCOPY: ELECTROMYOGRAPHIC ANALYSIS TO QUANTIFY THE EXTENT OF PROFICIENCY

[1]Kenji Narazaki, [2]Dmitry Oleynikov, [2]Jesse J. Pandorf and [1]Nicholas Stergiou
[1] University of Nebraska at Omaha, Omaha, NE; [2] University of Nebraska Medical Center, Omaha, NE
email: knarazaki@mail.unomaha.edu, web: http://www.unocoe.unomaha.edu/hper/bio/home.htm

INTRODUCTION

In recent years robot-assisted laparoscopy has been developed as a novel surgical procedure [1]. Although this technology promises ease of use and mechanical precision, little has been known about the learning strategies of this new technique [2, 4]. Evaluation of surgical performance and skill acquisition during training are limited in measuring only task completion time and number of errors occurred or a subjective evaluation by an expert [3]. To our knowledge, no studies have examined physiological measures (i.e. electromyography profiles) of the surgeons during performance of robotic surgical techniques. The purpose of this study was to assess changes in robot-based surgical performance through a designed training protocol using electromyography (EMG) in order to identify objective variables for the quantification of learning and dexterity.

METHODS

Seven right-handed medical students, novice users of the da Vinci® robotic surgical system, practiced three inanimate surgical tasks, bimanual carrying (BC), needle passing (NP) and suture tying (ST), with the robotic system for a total of six training sessions during a three weeks period. Before and after the training protocol, performance tests were conducted for all the tasks and muscular activation was monitored from the subject's right arm and forearm using a surface EMG system (DelSys; 1000 Hz). The muscles examined were: flexor carpi radialis (FCR), extensor digitorum (ED), biceps brachii (BB), and triceps brachii (TB). The relative EMG data, percent of raw EMG data relative to maximal EMG output (MVC), for each muscle and for each task were integrated for the entire task completion time (T) to obtain the total volume of muscular activation (EMGV). Moreover, the rate of muscular activation (EMGR) was calculated by dividing the EMGV by T. Mean values of the EMGV and EMGR were compared pre- and post-training using dependent t-tests (α=0.05).

RESULTS AND DISCUSSION

The results revealed significant reductions in EMGV for all muscles in all three tasks; except for the FCR muscle in the BC and ST tasks (Figure 1). However, reductions in EMGV were observed even for the FCR (Figure 1). The relative decreases in EMGV between pre- and post-training testing ranged from 33.2% to 68.6%. These results indicated that less motor units were recruited to perform the same tasks after training which can probably result in decreased fatigue. Significant increases in the EMGR were found for the FCR and TB muscles in all three tasks and for the ED muscle in the ST task (Figure 2). The relative increases in the EMGR in the muscles examined ranged from 30.3% to 84.5%. The EMGR results indicated improvements in the way that motor units are recruited and probably superior efficiency.

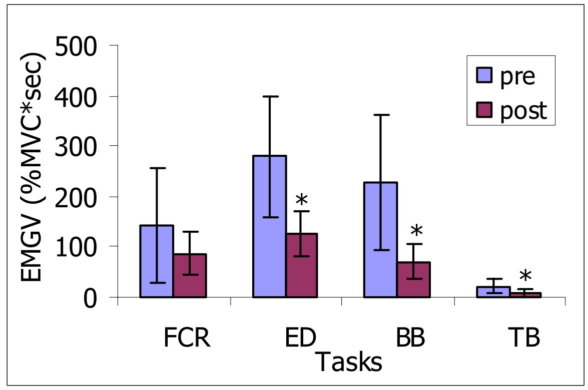

Figure 1: The total volume of muscular activation in the suture tying task (*$p \leq 0.05$).

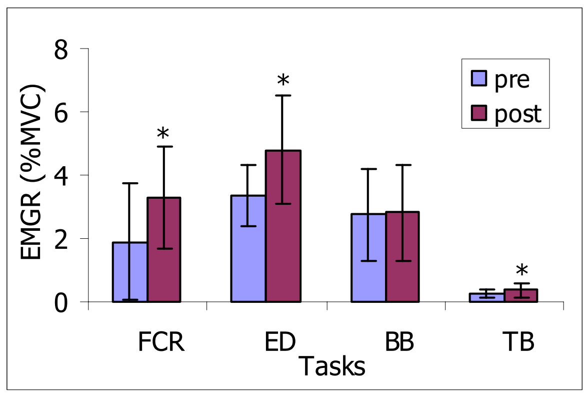

Figure 2: The rate of muscular activation in the suture tying task (*$p \leq 0.05$).

This study objectively demonstrated changes in robotic surgical performance in novice users through a designed training protocol using EMG profiles. The variables examined showed great promise as indicators of learning and dexterity for practical surgical tasks. Future studies will further validate these findings, as well as, incorporate the variables identified to establish valid criteria for the development of integrative surgical systems and virtual training tools.

REFERENCES

1. Dakin GF, Gagner M. *Surg Endosc*, **17**, 574-579, 2003.
2. Hanly EJ, et al. *Am J Surg*, **187**, 309-315, 2004.
3. Prasad SM, et al. *Am J Surg*, **183**, 702-707, 2002.
4. Sarle R, et al. *J Endourol*, **18**, 63-67, 2004.

ACKNOWLEDGEMENTS

This study is supported by the Nebraska Research Initiative.

DEVELOPMENT OF THE PORTABLE POSTURE TRAINING DEVICE

Wen-Chieh Yang, Wei-Hsun Huang, Chih-Han Chang, Kao-Chi Chung
Institute of Biomedical Engineering, National Cheng Kung University, Tainan, Taiwan
E-mail: cchang@mail.bme.ncku.edu.tw

INTRODUCTION

Clinically, an orthosis could be used to support and correct the spine mechanically when moderate abnormal curvature of the spine is detected. The conventional spinal orthoses have been confirmed to be effective in altering the natural history of adolescent idiopathic scoliosis (AIS) [1]. However, employing the orthosis requires the constant corporation from the patient and wearing the orthosis too long might induce muscle atrophy or motion incoordination by this passive correction approach [2].

The aim of this study was to develop a portable posture training system by applying an audio-feedback signal to promote the active correction of the abnormal posture from subject's muscle force [3] and to prevent continue deteriorated. This system could be used to detect a pre-set angle limitation of a joint and remind the patient adjusting to a suitable posture by audio warning when this angle limitation is violated.

METHODS

In order to achieve the portable objective, this posture training system needs to be light weight and low-power consumption. Therefore, the designed system consisted only two components: a flexible bend sensors (FSR, FLX-01 and Images SI Inc, Figure 1) and a self-developed data logger. The bend sensor, stick on the skin by the sport tape, is used to monitor the rotation (bending) on the joint thus detecting the patient posture on his/her activities of daily living. The design chart of the data logger is shown in Figure 2. This data logger used MSP430F169 microprocessor (Texas Instruments) as the MCU which incorporated the A/D function.

In order to prevent constantly calibration and degeneration of the bend sensor, a setting button was built within the data logger. By pressing this setting button, current bend angle of the bend sensor would be recorded into the data logger and used as a pre-set angle limitation of the joint.

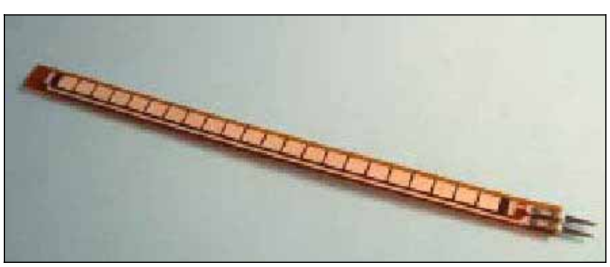

Figure1: Bend sensor

RESULTS AND DISCUSSION

Figure 3 shown the finial layout of the data logger circuit board. The weight of this data logger is less than 120g (including the box) and with two mercury batteries this system

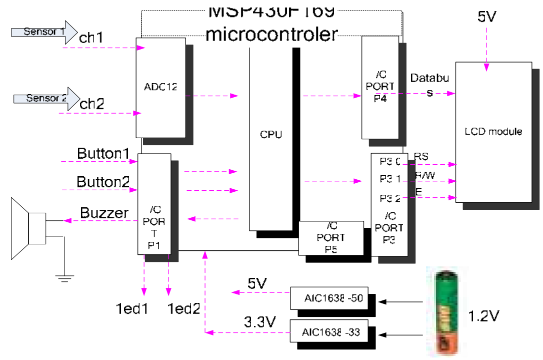

Figure 2: The Data logger design chart

could operate up to 400 hours. To use this system after the bend sensor was stick on the target joint, the user needs to posture the joint at the limitation of the correct angle and press the setting button. If later, the angle of the target joint is larger or smaller (depends on the setting) than this angle limitation, system would provide with am alarm sound. The device provided two modes for alarming: the static mode, if the angle violate the limitation for more than 10 second; the alarm sound will be sent out. The second mode, the dynamic mode, would send out the alarming once the violation of the angle is detected. The current angle sampling setting of this system is set as 10 HZ, and theoretically, with 12 bits of A/D converting, the resolution of this system could up to 2 degree.

Figure 3: The circuit board of the data logger

CONCLUSIONS

A portable posture training system was developed with simple component design and easy to use. Clinical trails of this system are currently being evaluated.

REFERENCES

1. Ashton-Miller J, et al. Basic Orthopaedic Biomechanics, ed. by Mow Van, Lippincott-Raven, 1997.
2. Wych R, et al. Care-Sci. Pract, 7: 100-104, 1996
3. Wong M, et al. Prosthetics and Orthotics International, 25: 60-70, 2001.

Modeling of solute Transport in cartilage under static and dynamic loading

Le Zhang and Andras Z. Szeri
University of Delaware
email: lzhang@me.udel.edu, web: www.me.udel.edu

INTRODUCTION

Articular cartilage consists mostly of chondrocytes and an extracellular matrix, the latter being composed of water, collagen fibers and proteoglycan. Since adult cartilage is avascular, the only way chondrocytes receive nutrient and get rid of waste is by diffusive/convective transport across the articular surface. During its daily routine, cartilage is subjected to a wide range of static and dynamic loading. Osteoarthritis is characterized by a deterioration of cartilage: it is believed that type and intensity of the mechanical loading play a major role in regulating transport activity and, therefore, degeneration. Previous theoretical studies of solute transport in cartilage assumed constant diffusion coefficient; in the present work we relax this assumption.

In this study, a mixture theory based, three dimensional formulation of neutral solute transport in soft tissue is presented [1]. By using Cohen-Turnbull-Yasuda's tortuosity model [2], the diffusion coefficient is made to depend on local deformation. Employing this model, we then study the effects matrix structure, solute size, and the type and intensity of mechanical loading have on the solute transport in soft tissue.

METHODS

We model the tissue as a three phase mixture, consisting of an interstitial fluid, a hyperelastic solid matrix, and a neutral solute. The governing equations for neutral solute transport in cartilage are derived from the conservation of linear momentum, mass of each phase and the mixture. The conservation equations are complemented with the various constitutive equations.

Under appropriate circumstances, the governing equations reduce to the classical convection/diffusion equation and the equations of the biphasic cartilage model. The 3-D formulation is then implemented in the finite element code ABAQUS, following Ferguson[3]. Since convective diffusion is analogous to convection/diffusion of heat, the third equation in the formulation is solved by thermal analogy procedure in ABAQUS.

RESULTS AND DISCUSSION

We validate our model for diffusion of solute in cartilage with Quinn's experimental data[4], as shown in Figure1. Curves represent our model, and symbols represent the experimental data. Quinn's experiments were performed on solute transport in cartilage under unconfined compression.

Confined compression tests are selected to show the application of our theoretical model (Figure2). 400Da and 400kDa dextran transport are investigated. Solute diffuses from the surface into the deep layer of the tissue. Figure2 shows concentration distribution of the solute in the cartilage (through the depth) after 1h diffusion into the tissue under 0%,10% and 20% static compression.

The Y coordinate represents the normalized reduction of concentration when the compression of the tissue varies from 0% to 10% or 20% of its intact thickness. For both solutes, the static loading inhibits their diffusion. 400kDa diffusion shows a higher reduction with increasing loading.

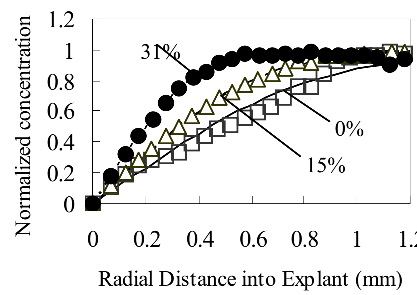

Figure 1. Concentration distribution of 40kDa under static loading (0%, 15%, 30% compressive strain)

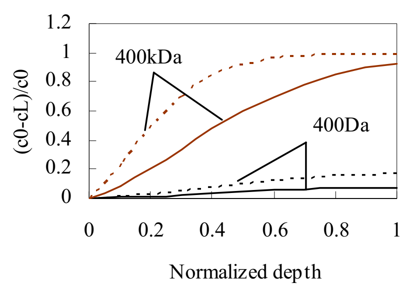

Figure 2: Concentration distribution, static loading : —10%compressive strain---20%compressive strain

CONCLUSIONS

We propose a three phase mixture model on a 3-D finite element platform to predict the diffusive and convective transport of different size solute in cartilage under different mechanical loading.

REFERENCES

1. Rajagopal KR, et al. *Mechanics of Mixtures*, 1995.
2. Yasuda H, et al. *Makromolekular Chemie* **118**, 19-35, 1968.
3. Ferguson SJ, et al. *J Biomech* **37**, 213-221, 2004.
4. Quinn TM, et al. *J Bioche. Biophys Methods* **52**, 83-95, 2002.

RIB CAGE MOTION PATTERNS IN SWIMMERS DURING RESPIRATORY MANEUVERS

Karine Jacon Sarro, Amanda Piaia Silvatti, Angélica Lodovico Pachêco, Carla Maia Aguiar Loula,
Ricardo Machado Leite de Barros
Laboratório de Instrumentação para Biomecânica – Faculdade de Educação Física, Universidade Estadual de Campinas,
Campinas (SP), Brazil; e-mail: ksarro@fef.unicamp.br

INTRODUCTION

Breathing is a dynamic act in which the coordinate motion of the rib cage increases and decreases its volume. Studies show that lung volumes [1] and respiratory motion patterns [2] can be changed by the practice of exercises and respiratory techniques. This work aims to verify if the rib cage motion patterns are altered in swimmers during respiratory maneuvers.

METHODS

The methodology is based on the kinematical analyses of 38 markers attached to the volunteer's trunk representing the rib cage (figure 1) using the DVideo system [3]. A group of 11 male swimmers (SG) was compared to a control group (CG) of 9 non-athletes volunteers during tidal volume (TV) and vital capacity (VC) maneuvers in sitting position. The rotation angles among the coordinate system associated to each pair of ribs and the coordinate system associated to the trunk were calculated in function of time (figure 2). The curves of rotation angle around the quasi-transverse axis were correlated. All combinations of two curves from the 2nd to the 10th ribs were tested. Considering that the correlation coefficient did not present a normal distribution, a transformation was applied according to Fisher (z-transformed correlation coefficient). In order to verify the statistical difference between groups t-tests ($p<0.05$) were performed.

RESULTS AND DISCUSSION

No significant differences were found between the two experimental groups during TV breathings. The figure 3 shows the distribution of the transformed correlation during VC maneuvers using a Box-plot representation. Significant higher values were found in the SG correlating the ribs (2,3,4,6,7,8,9) to the 10th and correlating the 2nd with the 9th rib. It can be seen that the distribution of z-correlation coefficient of the 2nd with the 10th ribs presents significantly higher median values and reduced dispersion in SG. It is also remarkable that the median values of the z-correlation decrease with the increment of the distance between the two ribs considered. The 9th and 10th ribs are important as region of apposition between diaphragm and rib cage. The higher correlation values in SG suggest an optimized pattern and reinforce the idea that practicing swimming can promote positive changes in the respiratory pattern.

CONCLUSIONS

The results obtained suggest that swimming practice lead to the formation of optimized breathing pattern when larger efforts are required from the respiratory system. This study also showed the viability of using the 3-D kinematical analysis to evaluate respiratory motion patterns.

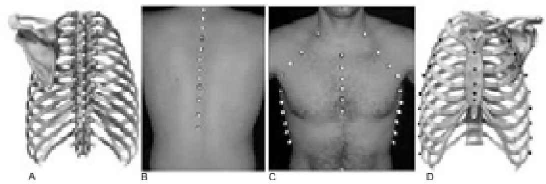

Figure 1: Representation of the rib cage using external markers

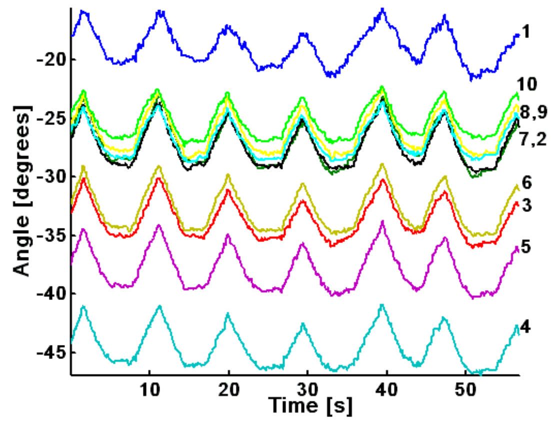

Figure 2: Example of ribs rotation angles around the quasi-transverse axis for one volunteer in VC.

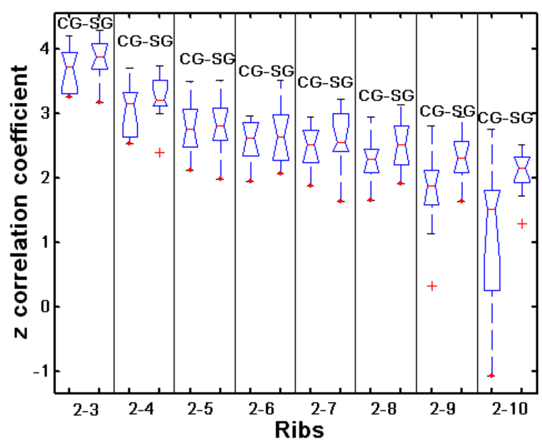

Figure 3: Distribution of the z-transformed correlation coefficient values of the 2nd rib with the other ribs during VC

REFERENCES

1. Courteix, D., et al. *European Journal of Physiology and Occupational Physiology* **76**(3), 264-269, 1997.
2. Barros, R. M. L., et al. J. B.. *Journal of Human Movement Studies* **44**, 387-400, 2003.
3. Figueroa, P. J., et al. *Computer Methods and Programs in Biomedicine* **72**(2), 155-165, 2003.

ACKNOWLEDGEMENTS

Supported by Capes and Fapesp (00/01293-1).

ALTERED ANKLE JOINT POSITIONING DURING JUMP LANDING IN SUBJECTS WITH FUNCTIONAL ANKLE INSTABILITY (FAI)

[1]Eamonn Delahunt, [1]Kenneth Monaghan, [1]Brian Caulfield
[1]University College Dublin School of Physiotherapy, Republic of Ireland
eamonn.delahunt@ucd.ie

INTRODUCTION

FAI, a subjective feeling of ankle instability or, recurrent symptomatic ankle sprains (or both), has been reported to be the most common and serious residual disability following ankle sprains. Single leg landings from a jump are one of the frequent mechanisms of injury to the lateral ligament complex of the ankle joint. To date, there have been no thorough investigations into the kinetic and 3D kinematic patterns of subjects with FAI during jump landing. The purpose of this study was to undertake a comprehensive analysis, of the kinetic and 3D kinematic patterns associated with jumping landing in a group of subjects with FAI, with the aim of determining whether changes in the neural control of movement and dynamic stability of the ankle joint exist in the these subjects.

METHODS

Eleven subjects with unilateral FAI (8male, 3 female) and 13 control subjects (5 male, 8 female) volunteered to participate. Inclusion criteria in the FAI group were based on the criteria used by Caulfield and Garrett [1].

CODA mpx 30 infrared light emitting diodes were attached to the involved lower extremity in the FAI group and the left lower extremity in the control group and were used to provide information pertaining to 3D segment angular displacement and angular velocity. Ground reaction force was measured by a Bertec force-plate. Subjects stood 1m in front of a force-plate with the test leg relaxed and non-weight bearing. The subject then used the contralateral leg to propel him/herself from the start position to land on the test leg on the centre of the force-plate. A jump was deemed unusable if the subject required any form of correction following landing such as touching the floor with the non-test limb or correcting their position on the force-plate. Each subject performed 10 single leg jumps onto the force plate.

Average values for hip, knee and ankle joint 3D angular displacements and velocities were calculated for each subject. Group mean time averaged profiles (500ms pre initial contact (IC) – 500ms post initial contact) were calculated. Differences in FAI and control group time averaged profiles were tested for statistical significance using independent two-sided t-tests. Magnitudes and timing of peak medial/lateral, anterior/posterior and vertical forces were identified for each jump and individual and group mean profiles subsequently calculated. One-way ANOVA was used to test for significant differences in timing and magnitude of peak forces. Furthermore, magnitudes of medial/lateral, anterior/posterior and vertical components of GRF were averaged over time following initial contact for each subject and group mean profiles were calculated. Differences in FAI and control group time averaged profiles were tested for statistical significance using independent two-sided t-tests. The level of significance was set at $p<0.05$ for all analyses.

RESULTS AND DISCUSSION

FAI subjects exhibited a significant increase in ankle joint supination during the period 70ms pre IC to 30ms post IC ($p<0.05$). They also exhibited a significant increase in knee joint flexion from the time period 95ms pre IC to 5ms post IC ($p<0.05$). No statistically significant differences were noted for angular velocities during these times ($P>0.05$). No statistically significant differences in the timing, magnitude or time averaged profiles for any of the components of GRF were noted post IC ($P>0.05$).

Prior to IC with the ground, the process of neuromuscular preparation for the subsequent ground contact is essential to the stability of the ankle joint [2]. Inappropriate positioning of the ankle joint prior to IC could increase the potential for injury. Following IC, the line of action of the GRF is dependent upon the position of the foot in relation to the centre of gravity and inertia [2]. If the ankle joint is held in a more supinated position when IC occurs, an external inversion load is placed upon the ankle joint, thus increasing the potential for a hyperinversion injury.

If the evertor musculature of the ankle joint cannot counteract this external inversion load or if a poorly executed landing occurs, hyperinversion and subsequent injury to the lateral ligament complex of the ankle joint is likely to occur.

CONCLUSION

The disordered positioning of the ankle joint observed in subjects with FAI is likely to result in repeated injury to the chronically unstable ankle, due to the potentially injurious external inversion load created by an excessive supinated position of the ankle joint upon IC.

REFERENCES

1. Caulfield B, et al.. Clin Biomech **19**, 617-621, 2004.
2. Tropp H. J Athl Train **37**, 512-515, 2002.

ACKNOWLEDGEMENTS

This study was supported by the Irish Research Council for Science, Engineering and Technology.

MAINTENANCE OF GAIT STABILITY IN CONCUSSED COLLEGE PATIENTS DURING DUAL TASKS

Robert D. Catena, Paul van Donkelaar, Tonya M. Parker, Louis R. Osternig, Li-Shan Chou
Motion Analysis Laboratory, Department of Human Physiology, University of Oregon
Eugene, OR; contact: chou@uoregon.edu

INTRODUCTION

According to Kahnemn's [2] model of information processing, processing capacity in humans is limited. When two tasks are presented to an individual, the desired outcome(s) will occur so long as the capacity of the system has not been exceeded. Once the capacity has been reached, there will be a decline in performance in one or all tasks. It has been estimated that, between the ages of 15-24 years, 133 people out of 100,000 will receive a traumatic brain injury (TBI) each year [3]. This accounts for 31.7% of all concussions. The maintenance of dynamic stability while perturbed by different secondary tasks is crucial day by day. Motor perturbations have been previously described to have significant detrimental effects on a TBI population [1]. To date, there have been no studies measuring a simple reaction time, a cognitive, and a motor dual-task with level walking, specifically in a concussed population. Our study looked to determine how different secondary tasks affect dynamic stability of patients with concussion and how balance is maintained during each task.

METHODS

Subjects (Conc), n=11, were identified as suffering a grade II concussion within 48 hours of collection. Controls (Norm), n=8, were matched by gender, age, and stature. The whole body motion data were collected with an 8-camera motion analysis system (Motion Analysis Corp., Santa Rosa, CA) during gait. Twenty-nine reflective markers were placed on bony landmarks. A thirteen-link model was created, each with the segmental center of mass (CoM) defined according to Winter [4]. The whole-body CoM was calculated using the weighted sum of each segment [1]. Center of pressure (CoP) location was found with two force plates (AMTI, Watertown, MA). The collection was divided into three parts. The single task session (level) was walking without a concurrent task. The first dual task session (OB) required crossing an obstacle at 10% of body height midway down the walkway. The second dual task session (COG) added in a cognitive task (e.g. backward digit span, spelling backwards) to level walking. Then the 3rd dual task session added a simple reaction time test (RT on) that was imposed with random catch trials (RT off) while walking. During RT trials, the subject responds to an audio perturbation by pressing a button on a wireless remote.

Gait temporal-distance parameters as well as the maximum CoM-CoP separation distances and the time-corresponding CoM linear velocities in the anterior-posterior (A/P) and medio-lateral (M/L) directions were examined [1]. 2x5 ANOVA's with repeated measures were used to assess the differences between tasks and groups. If there was a significant difference ($p<.05$), a post-hoc pairwise comparison was completed to find between which specific tasks there was significance.

RESULTS AND DISCUSSION

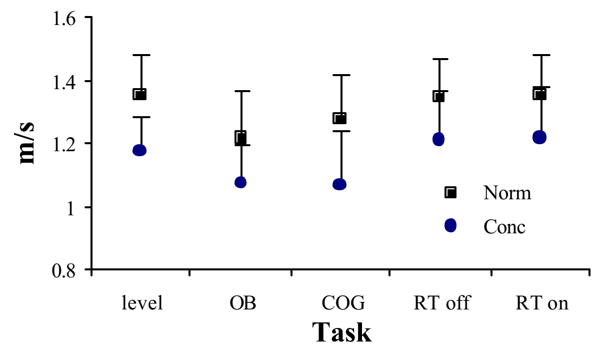

Figure 1. Average Gait Velocity in each task

Significant task effects between OB and level ($p<.001$) and COG and level ($p=.016$) were seen in gait velocity (Figure 1). A significant group effect was also seen ($p=.018$). Norms showed task effects only between OB and level walking for A/P CoM-CoP maximum separation ($p=.029$), and CoM velocity at A/P max separation ($p=.015$). Concs showed significant effects between OB and level walking for A/P range of motion (RoM) ($p=.001$), M/L RoM ($p=.023$), A/P CoM-CoP max separation ($p<001$), and CoM velocity at A/P max separation ($p<.001$). Concs also showed significant effects between COG and level walking for CoM velocity at A/P CoM-CoP max separation ($p=.045$). Even more interesting is that there seem to be differences in Concs between COG and OB for some gait stability parameters. A/P CoM-CoP max separation ($p=.002$) and velocity at M/L CoM-CoP max separation ($p=.025$) are both greater in the OB task.

CONCLUSIONS

Our study shows that a concussion has effects on normal gait regardless of single or dual tasks. Within both groups, only the more difficult tasks have shown to perturb gait stability, leading us to believe there is an attentional deficit in concussed patients. There also seems to be different compensatory actions taken by the individuals with a concussion to overcome these attentional deficits when faced with different types of dual-task situations.

REFERENCES

1. Chou LS, et al. 2004. Gait and Posture. 20:245-54
2. Kahnemn D. 1973. Attention and Effort.
3. Novack T. 1999. TBI facts and stats. Proceedings of the Recovery after TBI Conference.
4. Winter DA. 1990. Biomechanics and Motor Control of Human Movement. Wiley, New York, pp.56-7.

ACKNOWLEDGEMENTS

This study was supported by the Center for Decease Control and Prevention (R49/CCR021735 and CCR023203).

THE INFLUENCE OF SUBJECT CHARACTERISTICS AND JOINT KINEMATICS ON FUNCTION AND QUALITY OF LIFE IN PATIENTS WITH OSTEOARTHRITIS PRIOR TO TOTAL KNEE REPLACEMENT

[1] Marietta van der Linden, [1]Phil Rowe , [2]Paul Gaston [2]Richard Nutton
[1]Queen Margaret University College [2]Royal Infirmary Edinburgh
email: mvanderlinden@qmuc.ac.uk

INTRODUCTION

Osteoarthritis (OA) is associated with increased age, with pain and with functional limitation in joints. The rising proportion of elderly in our society means that optimal management of pain and functional loss in OA is of increasing importance.
In this study the role of pre-operative patient characteristics such as passive knee flexion and muscle strength on knee motion during functional activities and common outcome measures of function were explored. Secondly, relationships between functional knee motion and quality of life measures and daily activity were investigated.

METHODS

Thirty patients with osteoarthritis were assessed an average of 6 weeks before surgery. Fourty age-matched controls were also included in this study. Knee angle was measured using an electrogoniometer during level, stair and slope walking, getting in and out of a chair and getting in and out of a bath. Maximum passive knee flexion was measured in sitting with a manual goniometer. Muscle strength was measured using the MIE Myometer [1] and was normalized for body mass.
Other outcome measures included the American Knee Society Score (AKS), the Western Ontario & McMaster University Osteoarthritis Index (WOMAC) and a quality of life questionnaire, the SF36. The patient's daily physical activity was recorded using an activity monitor (ActivPAL [2]). This monitor records the time spent lying/sitting, standing and stepping. In addition it will display the number of steps made.

RESULTS AND DISCUSSION

Table 1 summarizes the most important patient characteristics. Except age and the SF36 mental score, all characteristics were significantly different between the most affected leg of the patients and the age matched controls ($p<0.01$). Knee flexion during all functional activities was significantly less ($p<0.01$) in the patient group. Further, the affected leg of the patients showed significantly less knee flexion than their contralateral leg in all functional activities except sitting and had significantly weaker knee extensor and flexor strength ($p<0.01$).
Knee flexion strength of the affected leg was relatively less reduced (42%) compared the normal group than knee extensor strength (52%) which corresponds to the findings by Hortobagyi [3].
Passive flexion correlated weakly to moderately ($r=0.41$ to 0.55) with the knee angle during most functional activities except sitting down and getting up from a chair and walking on a flat surface. A total score derived from the knee angle during the functional activities was moderately associated with the functional components of the AKS and the WOMAC ($r=0.56$ and $r= -0.49$ respectively) but less with the SF36 ($r=0.44$ and $r=0.33$ for the Mental and Physical score respectively). Knee extensor and flexor strength were associated with WOMAC function ($r=-0.51$ and $r=-0.54$ respectively) but not or weakly with the AKS function ($r=0.14$ and $r=0.32$ respectively)
The daily amount of steps as measured by the ActivPAL was only associated with age ($r=-0.51$) in the patient group. None of the measured characteristics in the control group showed correlations coefficients higher than 0.34 with any of the outcome measures of the ActivPAL. Interestingly, the mental component of the SF36 was more strongly associated with the function score of the WOMAC ($r=-0.75$) than the physical component of the SF36 ($r=-0.45$).

CONCLUSIONS

This study shows that a score derived from the knee motion during functional tasks as measured by an electrogoniometer is associated with traditional outcome measures of function such as the WOMAC and the AKS. However, this score derived from electrogoniometry is more objective and sensitive than the traditional questionnaire based outcome measures of function and may therefore be more appropriate for the assessment of outcome after knee replacement surgery.

REFERENCES

[1] van der Linden ML et al. *Arch Phys Med Rehabil* **85**, 2058-2064, 2004.
[2] Dahele M et al. *Palliative Medicine* **18**, 409-417, 2004.
[3] Hortobagyi T et al. *Clin Biomechanics* **20**, 97-104, 2004.

ACKNOWLEDGEMENTS

This study was funded by a grant from Zimmer Inc
.

Table 1 Average (std) subject characteristics

Knee	*Age (yrs)*	*BMI*	*Passive flexion°*	*Extensor strength (N/kg)*	*Flexor strength (N/kg)*	*Steps (nr)*	*Walking speed (m/s)*	*SF36 Physical*	*SF36 Mental*
Affected	68.4(10.1)	30.0 (5.6)	102(16)	1.49(0.88)	0.96(0.46)	7569(3961)	0.90(0.88)	36.7(4.35)	54.0(9.9)
Contralateral			110(14)	1.91(0.90)	1.21(0.57)				
Controls	69.6(6.1)	24.9(3.4)*	134(7)*	3.11(1.1)*	1.64(0.47)*	13203(5120)*	1.24(0.10)*	54.5(6.08)*	56.1(4.9)

*significant different $p<0.01$ between the patients (affected leg) and control group
BMI: Body Mass Index

THE FINITE ELEMENT ANALYSIS OF INTERFACE STRESSES BETWEEN THE FOOT AND ANKLE-FOOT ORTHOSES

Wei-Ching Hung, Chih-Han Chang and Chu-Lung Wu
Institute of Biomedical Engineering National Cheng Kung University
e-mail: danaia826@yahoo.com.tw , web: www.bme.ncku.edu.tw

INTRODUCTION

Ankle-foot orthosis (AFO) is often used to correct abnormal gait and maintain ankle and foot in neutral position during ambulation. Unsuitable prescription of AFO would cause the increasing of plantar pressure and even ulceration [1]. Currently, the design of AFO still relies on the orthotist's experience and subjective judgments. This often induced a costly "trail and error" approach to obtain an acceptable AFO. There are some studies to discuss the mechanical behavior in different types of the AFO. But interface stresses between foot and orthoses is seldom discussed especially the shear stresses [2]. The objective of this study was to investigate the interface stress between foot and AFO by establishing a 3D finite element model.

METHODS

A female subject (aged 26) was selected as the modeling target. To setup the material property of the soft tissue, the load-displacement curves of the soft tissues in four regions of the foot were recorded and the Young's modului were calculated from these curves. The contact pressure between the foot and AFO under foot flat condition were measured by the Novel Pedar (NOVEL GmbH Pedar) to valid the finite element results.

The finite element geometry of the foot-AFO structure was established based the CT images. To simplify the computational aspect, the bone structure was modeled as a single entity that is no joint is modeled. The surface-to-surface contact elements were placed between the foot and orthosis with a friction of coefficient 0.5. The proximal anterior surface of the leg was constrained in the anterior and posterior directions to model the strap constraint. The entire bottom area of AFO was fixed to simulate the foot flat condition. Besides, the heel and toe regions of the AFO bottom area were fixed respectively to simulate the heel strike and toe off stages. The loading was applied as a displacement on the superior surface of the leg bone. This displacement increased until the reaction fore reached the body weight for foot flat condition and 125% body weight for heel strike and toe off conditions.

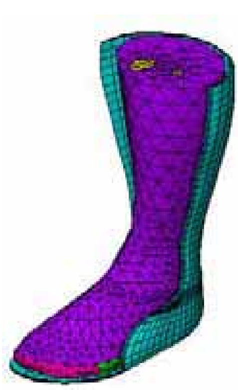

Figure 1: The finite element mesh of the foot-AFO structure.

RESULTS AND DISCUSSION

The finite element mesh of the foot-AFO structure was shown in Figure 1. The differences of averaged contact pressures between the EMED measured results and finite element simulated outcomes were less than 10% which validated the finite element model.

For the foot flat condition the peak contact pressure occurred on the forefoot region which consistent with general biomechanical observation on foot (Figure 2). For the heel strike and toe off conditions, the peak interface stresses happened on the heel and toe regions respectively and this is due to the constrain conditions. Comparing with the foot flat mode, the interface stresses could be increased by more than 200% at toe off or heel strike modes, even though, the loading was increased by only 25%. Moreover, this large increasing of interface stress occurred on both the contact pressure and the shear stress.

CONCLUSIONS

The results of this study indicated that not only the contact pressure but also the interface shear stress plays an important role in the biomechanical evaluation of AFO. Both the loading amount and boundary condition (postural) are vital in determining the interface stresses distributions. The loading and boundary conditions affect the interface stress distribution tremendously; therefore a more realistic loading is necessary for the evaluation of AFO and the modeling of joints might be required for loading conditions other than foot flat.

REFERENCES

1. Chu TM, *et al.*, *Med. Eng. Phys.*, **17** pp. 372-379, 1995
2. Nowak MD, et al., *Journal of Rehabilitation Research and development.*, **37** pp.273-281, 2000

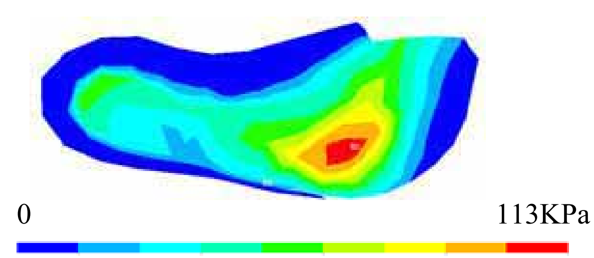

Figure 2: The peak contact pressure occurred on the forefoot region during the foot flat.

Biomechanical analysis on design variables in relation to the strength of compression hip screws

[1]Soo-Jung Moon, [1]Hui-Sung Lee, [1]Sung-Chul Jun, [2]Sae-Young Ahn, [2]Hoon Lee and [1]Sung-Jae Lee
[1]Department of Biomedical Engineering, Inje University, Republic of Korea
[2]Solco Biomedical co. ltd., Republic of Korea
Email: sjl@bme.inje.ac.kr

INTRODUCTION

Compression Hip Screw (CHS) is one of the most widely-used prostheses for the treatment of intertrochanteric fractures because of its strong fixation capability[1]. Fractures at the neck and screw holes are frequently noted as some of its clinical drawbacks, which warrant more in-depth biomechanical analysis on its design variables. In this study, we investigated the effects of the changes in design variables to the strength of the CHS. Particularly, changes in the plate thickness and number of screw holes at the side plate were studied in relation to the strength of the implant.

METHODS

Specimen Preparation

Twenty compression hip screws (Solco Biomedical Co. Ltd., South Korea) with an inclination angle of 135° between the barrel and the long axis of the side plate were used in this study. All side plates were made of Grade 2 titanium and the lag screws of Ti6Al4V. Specimens were classified into four groups (n=5 each):Group I was the control group with the neck thickness of 6-mm and 5 screw holes on the side plate, Group II 6-mm thick and 8 holes, Group III 7.5-mm thick and 5 holes, and Group IV 7.5-mm thick and 8 holes.

Mechanical Test

Each of the specimen(n=3 for each group) and the jig were mounted on the mechanical testing machine (MTS 858, MTS system Corp., MN, USA)[2]. Compressive load was applied at a rate of 0.17mm/sec with the maximum displacement set at 60mm for failure tests. The failure loads were determined by 0.2% offset method which is 0.2% of the lever arm length. Fatigue tests were done (n=2 for each group) to determine the fatigue life. Fatigue loads were applied at 5Hz with data acquisition rate of 20/sec. The 50% and 75% of the failure loads that was obtained earlier from the failure tests were used for each group. Maximum number of loading cycle was set at 1 million cycles according to ASTM[3].

Finite Element Analysis

Finite element models simulating each group were constructed to analyze the change in stress distribution due to changes in thickness and hole numbers.

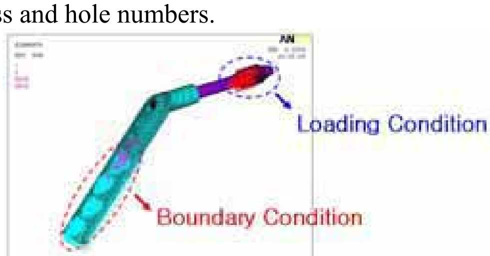

Figure 1: Loading and boundary conditions of finite element models

To reflect the same loading and boundary conditions as in the mechanical test, a compression load of 300N and contact areas between side plate and the jig were restricted in all directions [4](Figure 1).

RESULTS AND DISCUSSION

Experimental Results

Group III was found to be the strongest type with the failure strength of 867N and the bending strength of 49KN-mm, followed by Groups IV. Adding 1-mm of the plate thickness reinforce the CHS by 80% (480N in Group I vs. 867N in Group III) and it was statistically significant ($p<0.05$) (Figure 2). No fatigue failures were found in all specimen groups after 1 million cycles regardless the magnitude of fatigue loads 50% and 75% of the failure loads.

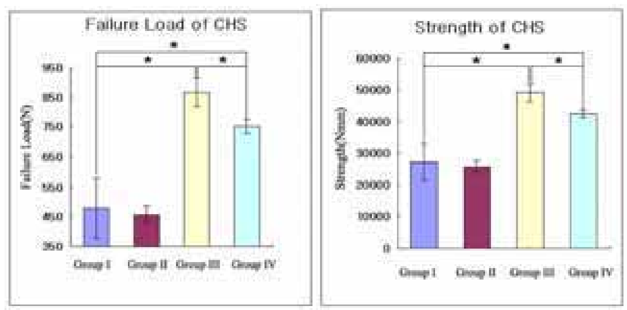

(a) **(b)**

Figure 2: The results of the failure tests of the CHSs: (a) Failure loads, (b) Strengths (*: $p<0.05$)

Finite Element Analysis Results

Peak von-Mises stresses at the neck region are analized. Group Ⅰ(175MPa) showed the highest stress but Group Ⅲ (111MPa) had the lowest. Stresses were appeared to be more concentrated around the perimeters of the lag screw holes than at the junction between the barrel and the side plate.The highest peak von-Mises stresses were found at the most superior screw hole location.

CONCLUSIONS

In this study, both biomechanical tests and finite element analyses showed that the thickness was a far more effective and sensitive design variable for the reinforcement of the CHSs than the screw hole numbers. It was also indicated that more screw holes on the side plate rather decreased the overall strength of CHSs.

REFERENCES

1. B. D. Hartog, et al., *J Bone Joint Surg*. **73A**, 726-733, 1991
2. Moor Douglas C, et al., *J Orthopedic Trauma*, **11(8)**, 577-583, 1997
3. *Annual Book of ASTM standards*, **13. 01**, F384-00
4. K. S. Lee, et al., *J Korean Orthop. Assoc*. **32**, 929-936, 1997

GENERIC DESIGN OF THE HIP RESURFACING PROSTHESIS

[1]Heijink, A.; [1]Zobitz, M.; [1, 2]Morrey, B.F.; [1]An. K N
[1]Biomechanics Laboratory, Division of Orthopedic Research, Mayo Clinic, Rochester, MN.
[2]Department of Orthopedic Surgery, Mayo Clinic Rochester, MN.

INTRODUCTION

Aseptic loosening and femoral neck fractures resulted in unpredictable survival of resurfacing arthroplasty in the past. Introduction of metal-on-metal bearing couples reduced aseptic loosening drastically. Improving prosthesis design in order to optimize load transfer can be an additional means to reduce implant failure. We tested various parametric design changes to explore their influence on the stress pattern in the anatomical and 'resurfaced' proximal femur.

METHODS

Finite element analysis of the proximal femur was performed with a generic, hemispherical deign. Parametric tests were performed for implant stiffness, stem length and shell size. Modeled elastic moduli were 110,000 MPa (titanium), 200,000 MPa (CoCr) and 350,000 MPa (ceramic). Stem length variations were: a) *conventional stem*, as currently is use, b) *half stem*, reaching till the neck, c) *short stem*, reaching till the center of the femoral head and d) *no stem*. Shell sizes, expressed as an angle, included 260°, 220° and 180°.

RESULTS

Cortex. Peak stress concentration at the cortex was at the posterior-medial cortex of the neck, just under the posterior rim of the prosthesis. Surface replacement did not alter the cortical stress pattern of the cortex, independent of design.

Cancellous bone. Resurfacing caused stress concentration at the medial side of the neck. The antero-posterior part of the proximal half of the neck was slightly stress shielded, whereas a slight increase in stress was found at the distal half of the neck. In the femoral head especially the area of the primary trabecular system and the circumference were shielded. This shielding was profound even with the least stiff implants. The stiffer the prosthesis, the more distal the area of stress concentration extended distally. The shielding was independent on prosthesis stiffness. The *short stem* and *no stem* designs did not influence the stress pattern in the femoral neck. The length of the stem has no influence on the stress pattern in the femoral head. With decreasing shell size, the area of stress concentration at the medial neck extended more distally. The antero-posterior shielding slightly decreased, however that change was very small. In the femoral head a smaller prosthesis reduced stress shielding slightly.

DISCUSSION

The shielding of the femoral head in our model showed a pattern similar to the resorption pattern found by Huiskes *et al*. [1]. They suggested prosthetic failure to result from a combination of progressive mechanical effects and interface bone resorption due to micromotion. Possibly, shielding

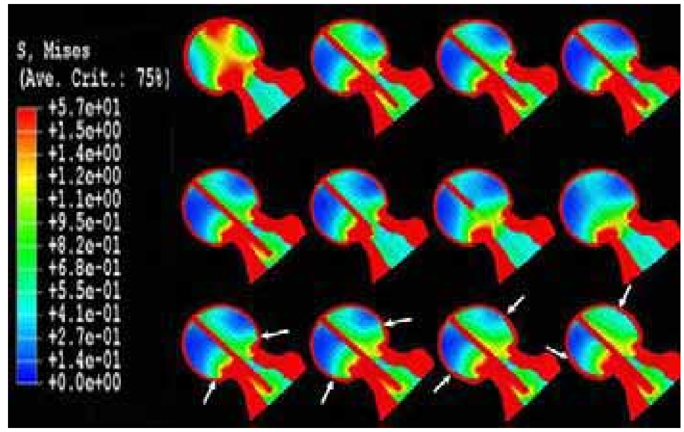

Figure 1: Stress pattern at the proximal femur showing the effect of implants stiffness (top, left to right: anatomical hip, Ti, CoCr, ceramic), stem length (middle, left to right: conventional stem, half stem, short stem, no stem) and shell size (bottom, left to right: 260°, 220°, 180° and 140°). Arrows indicate the edge of the prosthesis. Stresses are Von Mises stresses.

compromises bone quality, to make the femoral head more susceptible to these processes.

Watanabe *et al*. [3] related early fractures to stress shielding of the femoral neck in their finite element analysis. However, using DEXA scans, Kishida *et al*. [2] found bone mineral density in the femoral neck to be preserved after surface replacement. It likely is the stress concentration in the cancellous bone of the medial femoral neck that puts the neck at a greater risk for fractures.

CONCLUSIONS

1. As yet reported, resurfacing arthroplasty leads to stress concentration at the cancellous bone of the femoral neck and stress resorption at the circumference of the femoral head.
2. Less stiff implants reduce stress shielding of the femoral head but lead to higher stress concentration at the neck.
3. Designs with a short stem preserve the stress pattern of the anatomical hip joint at the level of the femoral neck.
4. A smaller shell slightly reduces stress shielding in the femoral head.
5. Thus, designs with a short stem could possibly reduce the risk on stress fractures, while small shells could possible be beneficial in preserving bone quality of the femoral head.

BIBLIOGRAPHY

R. Huiskes: *Acta Orthop Scan*, **56(6)**, 1985
Y. Kishida: *JBJS*, **86-B(2)**, 2004
Y. Watanabe: *J Arthropl*, **15(4)**, 2000

BIOMECHANICAL APPROACH TO BALLET MOVEMENTS: A STUDY OF THE EFFECTS OF BALLET SHOE AND MUSICAL BEAT ON THE VERTICAL REACTION FORCES

Andreja Paley Picon[1], Paula H. Lobo da Costa[2], Isabel de C. N. Sacco[3], Alberto Carlos Amadio[1]
[1]Biomechanics Laboratory, School of Physical Education and Sport - Universidade de São Paulo –Brazil.
[2]Department of Physical Education – Universidade Federal de São Carlos – Brazil. E-mail: paulahlc@power.ufscar.br.
[3]Department of Physical Therapy, Fonoaudiology e Ocupational Therapy – Universidade de São Paulo – Brazil.

INTRODUCTION

Biomechanical studies have tried to explain the loading characteristics of ballet dancing due to the *pointe shoes* and the extreme positions of the foot while standing *en pointe* [1]. Of great importance to the overall ballet performance is also the influence of musical beat, identified by the time signature of the musical tempo, responsible for the speed aspect and thus the correct dynamic of the dance movements and this aspect should also be considered while studying the ground reaction forces. The purpose of this study was to describe the external loads during a ballet movement, sauté - 1st position, while performed with two different footwears (slippers and *pointe shoes*) and two different time signatures (2/4 and 6/8) in order to identify the relative contribution of these two aspects on the loads measured by a force platform. The ¨*saute*¨ is a vertical leap with both feet from the first position and is considered a basic movement performed in an Allegro tempo.

METHODS

Six female ballet dancers (mean age 17 ± 2,1 years-old, mean mass 52 ± 8,4 kg) with at least six years of training volunteered to this study. All dancers practice at least eight hours per week with slippers and *pointe* shoes and had no musculoskeletal injuries at the time of this experiment. All participants signed an informed consent form before testing. While positioned on the force platform, the dancer performed two trials of eight consecutive sautés from the first ballet position with the slippers and the same trial with the *pointe* shoes.

The time signatures 2/4 and 6/8 are binary tempos and the time unit used in this study was the quarter note. Consequently, in the condition 6/8, the movements were performed in the eighth note. This reveals the speed aspect of the dancer performances during this study. Only the vertical components of the resultant ground reaction forces were studied, because it better reflect the external loads applied to the body during landing from a jump. Ground reaction forces (GRF) were measured by a piezoelectrical force platform (Kistler Instruments), sampled at 1000Hz, low pass filtered with a cut off frequency of 200 Hz. Each sauté were divided into three phases: initial position (*demi-plié* or knees flexion), jump and landing (*demi plié* or knees flexion). For each sauté, the selected variables for descriptive purposes were: peak vertical force during landing (Fy), stance time (ST), vertical force rate of increase (Rfy). The time signature was determined by edited extracts from classical pieces, specially prepared for ballet classes, which were played on a CD-player. The data were tested for normality with a Shapiro Wilks test, and differences among the experimental conditions were tested with an analysis of variance one-way and a post-hoc Scheffe test.

RESULTS AND DISCUSSION

The different footwears did not produce significant differences in the profile of the resultant curves. In accordance with typical curves of each condition, the 6/8 time signature produced two vertical peaks and the 2/4 time signature produced only one peak of vertical force. The mean values for Fy1 and Fy2 as well as for the stance time (ST) and the rate of increase of the vertical force (Rfy) for the four conditions studied are presented in TABLE 1.

TABLE 1: Mean values (± sd) for Fy1, Fy2, ST and Rfy for at least 90 sautes-1st position, with pointe shoes (2/4 and 6/8 beats) and slipers (2/4 and 6/8 beats).

	Fy1 (BW) (mean ± sd)	**Fy2 (BW)** (mean ± sd)	**ST (s)** (mean ± sd)	**Rfy** (mean ± sd)
Pointe 2/4	3,89 (± 0,75)	----	$0,37^{\#}$ (± 0,15)	35,14 (± 10,11)
Pointe 6/8	2,89 (± 0,95)	1,67 (± 0,38)	$0,57^{+}$ (± 0,10)	31,74 (± 12,32)
Slipper 2/4	3,60 (± 0,70)	----	$0,35^{*+}$ (± 0,09)	33,11 (± 9,57)
Slipper 6/8	2,80 (± 0,82)	1,83 (± 0,34)	$0,63^{*\#}$ (± 0,09)	26,98 (± 9,78)

With relation to the footwear type, it was observed that the resultant vertical forces measured were not statisticaly different between slipper and *pointe* shoes conditions. In this way, the results pointed out that the musical beat may be a factor of greater influence on the vertical GRF, compared to the footwear type, determining the different curves observed in this study. Significant differences were only found for the stance time for the different conditions. With respect to the vertical force rate of increase no differences were found for footwear and time signature conditions.

CONCLUSIONS

The *pointe* shoes do not produce greater loads than slipper shoes when measured the GRF. The time signature 6/8 produced greater stance times when compared to 2/4 time signature, thus, it is likely that the musical beat influenced more the mechanical aspects evaluated in this study than the footwear types. There is a clear tendency to the fact that the faster the musical beat, the greater the attention should be payed to the landing technique, mainly that of foot positioning on the ground, independently of the ballet shoe used.

REFERENCE

1. Tuckman, A. S., et al. *Foot and Ankle*, 12:.3, 144-148, 1991.

KINETIC ASYMMETRY IN LEFT AND RIGHT DOMINANT FEMALE RUNNERS: IMPLICATIONS FOR INJURY

[1]Rebecca Avrin Zifchock, [1,2]Irene Davis, and [3]Joseph Hamill
[1]Motion Analysis Laboratory, University of Delaware [2]Drayer Physical Therapy Institute
[3]Department of Exercise Science , University of Massachusetts
email: beckyaz@udel.edu

INTRODUCTION

The cause of running injuries continues to elude scientists. While a number of factors have been examined, the role of gait asymmetry and limb dominance has received little attention. Gait asymmetry has been suggested to be both a cause and effect of injury [1]. In addition, previous literature reports that left dominant (LD) people tend to be more symmetrical than right dominant (RD) people [2]. However, the relationship between laterality and gait has not been explored.

Therefore, one purpose of this study was to examine the differences in kinetic asymmetry during gait between LD and RD runners. The difference in injury patterns between LD and RD runners was also examined. The study focused on the symmetry of loading parameters that have previously been linked to chronic running injuries [3]. It was hypothesized that LD runners would be more symmetrical and, as a result, have fewer injuries than RD runners.

METHODS

This is an ongoing study in which, to date, there are 16 LD subjects and 16 age- and mileage-matched RD subjects enrolled. An *a priori* power analysis, based on a 10 point difference in symmetry and variability from previous literature, indicated that 24 subjects were needed per group. All volunteers were female, rearfoot strikers who ran at least 20 miles per week and were free of any lower extremity injuries at the time of data collection. Limb dominance was determined by the foot with which a subject would kick a ball.

Subjects ran along a 25 meter runway at a speed of 3.65 m/s (± 5%), striking a force platform (Bertec Corp., Worthington, OH) at its center. Data were sampled at 960 Hz. Five trials were collected for both the left and right sides. The kinetic variables of interest were peak vertical impact ground reaction force, average and instantaneous vertical loading rates, and peak vertical shock. For each subject, these variables were extracted from the individual trials and averaged across the five trials, within each side.

The symmetry index (SI) [4] was used to evaluate the symmetry of each runner with respect to each of the kinetic parameters: $SI = (X_{dom} - X_{non\text{-}dom})/X_{dom} * 100$

Following the gait assessment, all running-related injuries were monitored for one year. Independent, two-tailed t-tests were performed to compare the kinetic variables and the number of injuries sustained by the LD and RD runners. A value of $p<0.05$ was considered significant for all comparisons.

RESULTS AND DISCUSSION

While the SI values were not significantly different between the LD and RD runners (Table 1), instantaneous loading rate and peak shock were 24.9 and 32.5%, respectively, higher in the RD runners. These individuals also had 38.2% more injuries than LD runners. Based on the *a priori* power analysis, the current number of subjects does not adequately power the study. Therefore, the results may be strengthened as the study continues, and additional subjects are added.

In light of previous literature suggesting that LD people tend to be more symmetrical [5], the kinetic preliminary findings of this study are not surprising. LD people often cite the need to adapt to a “right-handed world.” However, this has much less of an influence on lower extremity tasks. Therefore, the increased symmetry may not necessarily be a learned adaptation, but may be related to neurological control. The fact that the more asymmetrical, RD runners are so much more likely to become injured may lend insight into the role of symmetry in the mechanism of injury.

Future studies will focus upon examining how other gait mechanics (ie. kinematics) differ between LD and RD runners. The link between gait mechanics and the side on which a runner sustains an injury will also be studied.

Table 1: Comparison of SI Values and Number of Injuries between the LD and RD runners

	Impact GRF	Avg. LR	Instant. LR	Peak Shock	# of Injuries
LD	9.0	15.6	9.4	16.6	13
RD	8.0	17.1	12.5	24.6	21
p-value	0.68	0.69	0.30	0.22	0.26
% Diff	12.6	9.2	24.9	32.5	38.1

REFERENCES

1. Subotnick, S.I., *Journal of Orthopaedic and Sports Physical Therapy*, 1981. **3**(1): p. 11-15.
2. Purves, D., L.E. White, and T.J. Andrews, *Proc Natl Acad Sci U S A*, 1994. **91**(11): p. 5030-2.
3. Ferber, R., et al., *Medicine and Science in Sports and Exercise*, 2002. **34**(S5).
4. Robinson, R.O., W. Herzog, and B.M. Nigg, *J Manipulative Physiol Ther*, 1987. **10**(4): p. 172-6.
5. Galaburda, A.M., et al., *Science*, 1978. **199**(4331): p. 852-6.

ACKNOWLEDGEMENTS

This study was supported by Department of Defense grant DAMD17-00-1-0515

LASR: A NEW ANALYTICAL TOOL TO INCREASE INFORMATION RETRIEVAL FROM COMPLEX IMAGES

K Bogie[1,2], X Wang[3], J Sun[3]
[1]Cleveland FES Center, [2]Departments of Orthopaedics & [3] Statistics, Case Western Reserve University. Cleveland, Ohio,
Email: kmb3@case.edu

INTRODUCTION

Interface pressure mapping has been used in research settings for many years, most commonly in the evaluation of seating pressure distributions. Over the past decade, improvements in pressure monitoring technology have led to increasing acceptance in clinical use. However, this brings with it other issues to be considered: evaluation conditions are not as closely controlled as in a research setting and repeated evaluations are often required. Current image analysis is often limited to subjective evaluation of pressure maps, with minimal numerical indices; and gives no objective indication of the significance of any pressure changes observed. Furthermore, intra-assessment comparison of pressure images may be complicated by relative subject movement between assessments. These factors thus limit the clinical utility of the information collected.

We have developed a novel multi-stage image analysis technique that employs data -mining approaches to maximize information retrieval [1]; The LASR (longitudinal analysis and self-registration) tool incorporates fast registration schemes with a customized false-discovery-rate (FDR) controlled statistical procedure.

METHODS

The LASR tool was applied to data obtained from a longitudinal study of the effects on tissue health of using regular gluteal neuromuscular electrical stimulation (NMES) [2]. Repeated assessments of interface pressures were obtained using a Tekscan CliniSeat multi-cell sensor mat (Tekscan Inc., Boston MA). At each assessment, the interface pressure sensor mat was placed over the subject's cushion in the wheelchair prior to transfer. Seating interface pressures were evaluated with the subject sitting still, with no movement or pressure relief procedures, at a scan rate of 2Hz for a 200s period to give a 400 frame 'static data' movie.

The assessment protocol produced large volume data files for a relatively small number of subjects - a statistical challenge known as "huge-p, small-n" problem. In addition, a true reproduction of seating posture on each visit was not always feasible. The LASR algorithm uses a multi- stage procedure to sequentially address these challenges;

Step 1: Spatially register all images using customized self-registration scheme for images with no fixed landmarks.
Step 2: Create pixel-by-pixel (and frame-by-frame) difference images and movies.
Step 3: Filter difference images using local-polynomial smoothing.
Step 4: Create T image/maps and movies by computing test statistic T_x based on neighborhood weighted averages.
Step 5: Compute FDR-controlled P maps and movies with controlled global error rate.

The LASR output map gives a global representation of statistically significant pressure changes. In the clinical application presented, LASR indicates if NMES effectively alters seating interface pressures, with a FDR of <0.05.

RESULTS AND DISCUSSION

Typical LASR analysis output is illustrated in the following case study: Pressure mapping assessment for subject Y showed poor spatial alignment, with both translation and rotation occurring between the baseline and post-treatment images (Figure 1a). Qualitative evaluation of longitudinal changes was difficult. After applying the LASR algorithm it could be seen that pressures were reduced bilaterally over time (Figure 1b). The left and right sacro-ischial regions were equally affected.

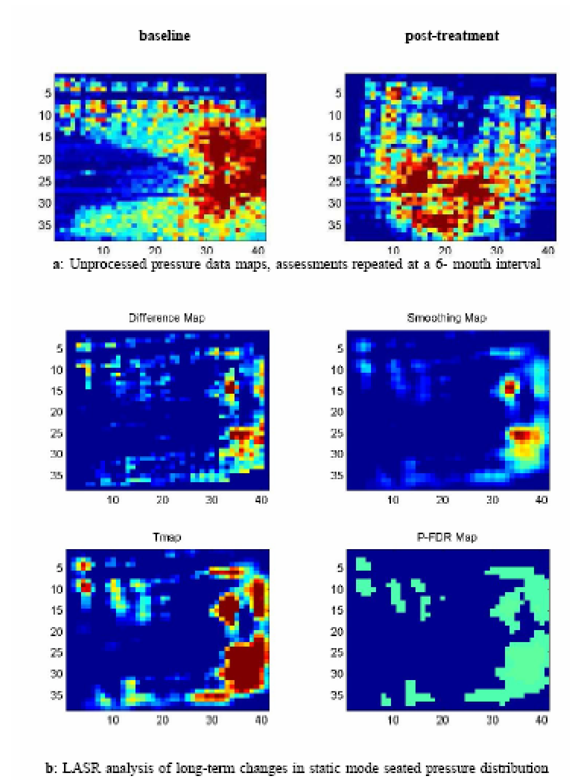

a: Unprocessed pressure data maps, assessments repeated at a 6- month interval

b: LASR analysis of long-term changes in static mode seated pressure distribution

Figure 1: Pressure mapping analysis using LASR

CONCLUSIONS

The LASR tool allows useful quantitative information to be derived from pressure mapping images. In the specific study, LASR analysis showed that statistically significant changes occurred in the ischial region over time. Using LASR we can confirm that NMES improves seating interface pressure distributions thus reducing the risk of developing pressure ulcers.

LASR is an analytical technique to compare 3-D images with no fixed landmarks with many potential applications in the field of image analysis and promises to become a powerful new tool for clinicians and researchers.

REFERENCES:

[1] X Wang, J Sun, KM Bogie. Submitted to *JASA*, 2005.
[2] KM Bogie, RJ Triolo. *J Rehab Res Dev* **40**, 469-475, 2003.

MODELING THE BENEFITS OF TOWING DURING ADVENTURE RACING, RUNNING WITH APPLIED HORIZONTAL FORCE

Alena Grabowski and Rodger Kram
University of Colorado, Boulder; email: alena.grabowski@colorado.edu

INTRODUCTION

Adventure races are typically self-supported, multi-sport, team (3-5 people) races with a wilderness aspect. A team must stay together at all times; therefore, the slowest team member determines overall performance. Adventure racers have used towing as a technique to increase overall team speed during the running portions of a race. Mechanically, towing is accomplished by attaching an elastic cord from the waist of one racer (tow-er) to the waist of a teammate (tow-ee). In theory, the most aerobically fit racer should tow a less fit teammate so that the racers run at the same relative level of exertion (%VO_{2max}), thus achieving a faster speed than the less fit runner could accomplish solo. Our purpose was to predict the optimal towing forces between two runners that would result in the best overall race performance.

METHODS

We used previously established equations [1,2] to model 10, 20, and 42.2 km race distances on a flat course, assuming a constant towing force and negligible aerodynamic drafting. We calculated towing forces and amount of time saved for different combinations of VO_{2max} (ml/kg*min) and body mass. The relationship between $VO_{2submax}$ and running speed established by Daniels and Gilbert [1] is:

$$\mathbf{VO_{2submax}\ (ml/kg{*}min)=0.3744V^2+10.93548V-4.6}$$

(V=velocity in m/sec)

The %VO_{2max} that can be sustained for a defined time [1] is:

$$\mathbf{\%VO_{2max}=80+18.94393{*}e^{(-0.012778T)}+29.89558{*}e^{(-0.1932605T)}}$$

(T=time in min)

We normalized the equation of Chang and Kram [2] to calculate changes in $VO_{2submax}$ due to aiding or impeding towing forces:

$$\mathbf{\%\ Change\ VO_{2submax}=0.155(AHF)^2-4.420(AHF)-0.0000153}$$

(AHF=Applied Horizontal Force in % body weight)

We determined theoretical time saving by combining equations, solving iteratively, and using curve-fitting techniques.

RESULTS AND DISCUSSION

Our model predicts that towing can improve overall running performance by more than 10min in a 10km race (Fig.1, Table1). The effectiveness of towing depends on differences in VO_{2max}; a tow-er must have a higher VO_{2max} than a tow-ee. For a given VO_{2max} difference, performance can be further improved when a tow-er has greater body mass than the tow-ee. However, with optimal towing force, performance may also improve when a tow-ee is heavier than a tow-er. Additionally, towing may improve relative performance more as the race distance increases (Fig.2). Optimal towing force for best overall performance during running depends on runners' VO_{2max}, body mass, and distance. The strongest determinant of running performance due to towing is the VO_{2max} of each runner. Body mass differences and race distance can also influence running performance, but have smaller effects.

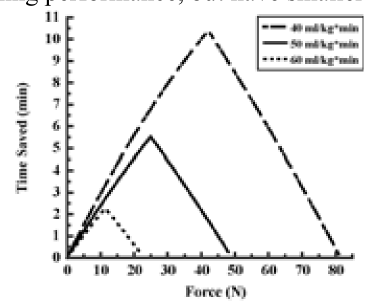

Fig. 1: Time saved in 10km race due to towing force. Tow-er's VO_{2max} = 70ml/kg*min, body mass = 70kg; Tow-ee's VO_{2max} = 40, 50, or 60 ml/kg*min, body mass = 70kg.

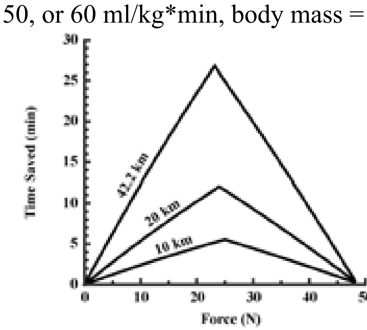

Fig. 2: Time saved in 10, 20, & 42.2km races due to towing force. Tow-er's VO_{2max} = 70ml/kg*min, body mass = 70 kg; Tow-ee's VO_{2max} = 50 ml/kg*min, body mass = 70 kg.

REFERENCES

1. Daniels J & J Gilbert, *Oxygen Power: Performance Tables for Distance Runners*, 1979.
2. Chang Y-H & R Kram, *Journal of Applied Physiology* **86**(5), 1657-1662

Table 1: Solo race times for 10km based on runners' VO_{2max}. Optimal tow force, maximum time saved, & optimal race time based on tow-ees' VO_{2max} & body mass. Tow-er always had VO_{2max} = 70 ml/kg*min, body mass = 70 kg.

VO_{2max} (ml/kg*min)	Body Mass (kg)	Race Dist (km)	Solo Race Time (min)	Optimal Tow Force (N)	Maximum Time Saved (min)	Optimal Race Time (min)
40	70	10.0	50.01	42.1	10.4	39.61
50	70	10.0	41.33	24.9	5.5	35.83
60	70	10.0	35.37	11.4	2.3	33.07
70	**70**	**10.0**	**31.02**	———	———	———

CUMULATIVE HEAD ACCELERATION IN COLLEGE FOOTBALL PLAYERS DIFFERS BY POSITION

[1] David McNeely, Sarah Manoogian, Stefan Duma, [2]Jeffrey Chu, Jonathan Beckwith, Richard Greenwald, [3] P. Gunnar Brolinson, [4]Mike Goforth
[1]Virgina Tech Center for Injury Biomechanics, [2]Simbex, Lebanon, NH, [3]Edward Via Virginia College of Osteopathic Medicine, [4]Virginia Tech Department of Sports Medicine; email: dmcneely@vt.edu, web: www.cib.vt.edu

INTRODUCTION

There are 300,000 incidences of sports-related concussions each year in the United States, with football having the most concussions of any sport [1]. In order to better understand these injuries, the impact event needs to be recorded and analyzed. Head accelerations were recorded during the 2004 Virginia Tech football season. A difference in the average amount of head acceleration per game is seen when comparing different playing positions in football.

METHODS

In-situ linear head accelerations were recorded in real time using the Head Impact Telemetry (HIT) System (Simbex, Lebanon, NH) during practice and games during the 2004 football season. The HIT System measures linear head acceleration of the center of gravity of the head through an array of single-axis linear accelerometers [2,3]. Eighteen players were instrumented as part of a larger study, covering all playing positions. For this study, fifteen players were assessed. Game-only data was compiled from the entire 2004 season, and separated by player. The cumulative accelerations experienced by each player were tabulated and normalized by the number of games recorded for each player. Then, the players were grouped by playing position. Groups were receivers (WR), running backs (RB), offensive linemen (OL), defensive linemen (DL), linebackers (LB), and defensive backs (DB). The average of the cumulative head acceleration experienced by each player position per game played was calculated.

RESULTS AND DISCUSSION

A total of 3,134 impacts were recorded during the 2004 season during games. Average acceleration per impact did not differ by player position. Figure 1 shows the average cumulative head acceleration experienced per game, grouped by position. Distinct difference can be seen throughout the different player positions. Defensive linemen's average cumulative accelerations per game were significantly higher than offensive linemen, wide receivers, and defensive backs ($p<0.05$). Linebackers exhibited significantly higher accelerations than offensive linemen and wide receivers, and running backs saw higher per-game averages than offensive linemen and defensive backs (Table 1).

Figure 1 Average cumulative acceleration per player per game, grouped by position.

CONCLUSIONS

A better understanding of the head accelerations to which football players are subjected will lead to improved protective equipment and more effective treatment. Head accelerations are inevitable in the game of football. Players at all positions experienced similar average accelerations per impact. However, players at the running back, linebacker, and defensive lineman positions appear to experience higher cumulative accelerations each game than do players at the wide receiver, defensive back, or offensive lineman positions. A limitation of this study is the fact that some variability is introduced due to the fact that some of the players were active in a larger portion of the game than others.

REFERENCES

1. McCrea M, et al. *JAMA* **290**, 2556-2563, 2003.
2. Crisco JJ, et al. *J Biomech Engr*, **126**, 2004.
3. Duma SM, et al. *Clin J Sports Med*, **15**, 3-8, 2005.

ACKNOWLEDGEMENTS

Simbex, Lebanon, NH; NIH #R44HD40743

Table 1: Head acceleration data, grouped by player position.

Player Position	Number of Players	Hits Recorded	Player Games Recorded	Average Acceleration per Impact (g)	Average HIC per Impact (g)	Average Cumulative Acceleration per Game (g)
LB	2	590	17	31.3 ± 27.2	29.3 ± 83.7	951 ± 46.7
DL	2	747	17	24.4 ± 20.7	16.7 ± 62.0	847 ± 100.2
RB	2	621	20	27.5 ± 23.4	24.1 ± 53.9	815 ± 67.5
OL	3	297	17	25.1 ± 19.3	23.0 ± 43.2	474 ± 59.2
WR	4	540	33	28.2 ± 17.2	22.8 ± 36.1	469 ± 96.9
DB	2	339	20	23.4 ± 21.6	17.1 ± 64.1	388 ± 71.2

VIBRATION ALTERS PROPRIOCEPTION AND DYNAMIC LOW BACK STABILITY

[1] Maneesha Arashanapalli and [1]Sara E. Wilson
[1]Mechanical Engineering, University of Kansas, email: sewilson@ku.edu

INTRODUCTION

Whole body vibration has long been shown to be a risk factor for low back disorders. Vibration is associated with 1.5-39.5 fold increase in low back injury risk [1]. Vibration has been associated with a higher incidence of low back disorders in occupations such as pilots, tractor drivers and heavy equipment operators [2]. Although a number of investigators have studied the transmissibility of vibration, the mechanism by which vibration results in low back injury is not understood. One potential mechanism by which vibration may lead to low back injury is through changes in the dynamic stabilization of the spine. Muscle and muscle-tendon vibrations of 20 to 120 Hz are known to result in proprioceptive illusions in the extremities due to the stimulation of the muscle spindle organs [3]. After removal of vibration from the muscle, proprioceptive changes have been shown to persist [4]. In this experiment it was hypothesized that vibration-induced proprioceptive changes in the muscle both during and after vibration will correspond to changes in the dynamic stabilization of the low back.

METHODS

Seven healthy subjects were recruited for the study, which was approved by the Human Subjects Committee, University of Kansas. Electromagnetic sensors were placed over the manubrium and the T10, T12, C7 and the S1 spinous processes. Lumbar curvature was defined as the angle between the T10 and S1 markers. Electromyographic sensors were placed on 8 trunk muscles (RA/ES/IO/EO) to measure their activity. The reposition sense protocol consisted of training trials followed by assessment trials. In the training trials, subjects were asked to match their current lumbar curvature with a target lumbar curvature. In the assessment trials, the subjects were asked to reproduce the target lumbar curvature without visual feedback. After two training trials, training and assessment trials were alternated. Reposition Sense Error (RSE) was defined as the absolute difference between the actual curvature assumed and the target lumbar curvature during the assessment trials. Directional error (DE) was defined as the difference between the actual curvature assumed and the target lumbar curvature during the assessment trials. In the sudden loading protocol, the subject wore a harness, which applied a small sudden forward impulse through a dropped weight mechanism. The time from impulse load to peak muscle response was assessed from the EMG data for the erector spinae muscle groups. Both the reposition sense test and sudden loading test were conducted before, during, immediately after, 15 minutes after, and 30 minutes after vibration.

RESULTS AND DISCUSSION

In this experiment, two different effects were observed. First during vibration, kinesthetic illusions were observed resulting in increases in reposition sense error and directional error (Figure 2). Subjects tended to assume more lordotic postures during vibration, which is consistent with previous evidence of muscle lengthening kinesthetic illusions. After vibration, the reposition sense error remained increased while directional error returned to zero suggesting a habituation mechanism for altered position sense. Both during and after vibration, delay in muscle response during dynamic low back stabilization was increased suggesting that proprioceptive changes may indeed be a mechanism for altered low back stability and increased injury risk (Figure 1).

REFERENCES

1. Bernard, B.P., ed. Musculoskeletal disorders and workplace factor. 1997, U.S. D.H.H.S.: Washington, D.C., 94-213.
2. M. L. Magnusson, et al., Spine, **21**, 710-7, 1996.
3. Roll J.P. and J.P.Vedel, Exp Brain Res. **47**(2), 177-90, 1982.
4. Wierzbicka, MM, et al., J Nuerophysiol. **79**, 143-50, 1998.

ACKNOWLEDGEMENTS

This publication was made possible by support from the National Institute for Occupational Safety and Health (1R03 OH007995-01).

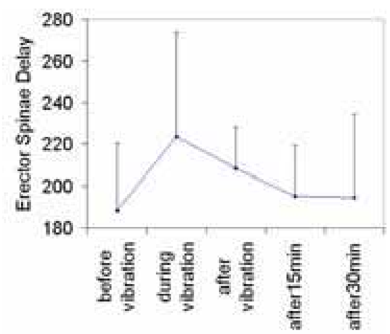

Figure 1: The delay between perturbation and peak initial muscle response was found to increase both during and after vibration returning to baseline after 15 minutes.

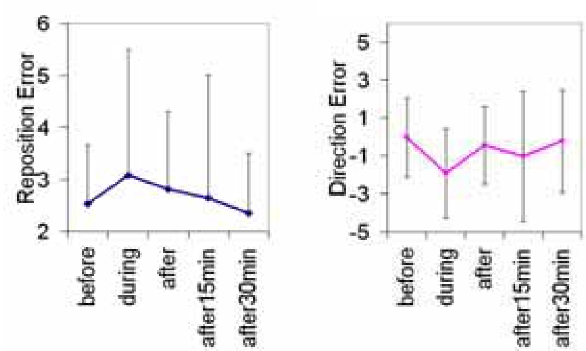

Figure 2: Reposition error was found to increase both during and after vibration, returning to baseline after 30 minutes. Directional error was found to be near zero except during vibration.

VALIDATION OF A THREE DIMENSIONAL MODEL TO QUANTIFY PATELLOFEMORAL JOINT FORCES

Yu-Jen Chen[1], Irving Scher[1,2], Thay Q Lee[3], Christopher M. Powers[1]

[1]Musculoskeletal Biomechanics Research Laboratory, University of Southern Calif., Los Angeles, CA. yujensch@usc.edu
[2]Exponent, Failure Analysis Associates, Los Angeles, CA, USA
[3]Orthopedic Biomechanics Laboratory, Long Beach VA Healthcare System, Long Beach, CA, USA

INTRODUCTION

Although the patellofemoral joint is typically modeled as pulley system where the compressive force acting on the paella is created by the forces in the quadriceps tendon and patellar ligament, this assumption has not been validated. The purpose of this study was to validate a 3D model of the patellofemoral joint. To accomplish this goal, patellofemoral joint reaction forces (PFJRF's) that were directly measured from an in-vitro cadaveric set-up were compared to the PFJRF's, obtained from a computational model.

METHODS

In-vitro measurement of the PFJRF: Seven fresh-frozen cadaveric knees were used in this study. Each was dissected to separate the individual heads of the quadriceps, the central tendon and the patellar ligament. The knee was mounted on a custom jig that was fixed to an Instron machine frame. Quadriceps muscle loads were accomplished using a pulley system and weights, Muscle forces were based on previously reported muscle cross-sectional area data (vastus medialis: 67 N, vastus lateralis: 98 N, rectus femoris and vastus intermedius combined: 111 N). The line of pull of each muscle was based on its 3D muscle fiber orientation. To quantify the magnitude and direction of the PFJRF, a six axis load cell was incorporated into the femoral fixation system so that a rigid body assumption could be made. Care was taken to distract the tibia (5 mm) and cut all soft tissue connection between the tibia and femur so that the only force acting on the femur was from the patella. Using this set-up, PFJRF's (magnitude and direction) were obtained at 0, 20, 40, and 60 degrees of knee flexion. In addition to the PFJRF data, 3D coordinates of the line of pull of each muscle, the orientation of the patellar ligament relative to the tibia, and the patella flexion angle was quantified using a Microscribe digitizer. The force in the patellar ligament was obtained using a buckle transducer. The alignment of the femur relative to the tibia in the frontal plane was measured using a goniometer.

Computer-based estimation of the PFJRF: Following in-vitro testing, computational models based on the three-dimensional coordinates obtained from each of the cadaver knees were created. SIMM modeling software was used to model the four quadriceps muscle force vectors and the patellar ligament force vector. The 3D coordinates of the muscle force vectors relative to the patella and the orientation of the patella and patellar ligament relative to the tibia were identical to that of the in-vitro set-up. In addition, the exact muscle loads and the measured force in the patellar ligament were used. Lower limb alignment also was matched to in-vitro measurements. Based on the unit vectors of each of the quadriceps muscles forces noted above, a resultant quadriceps force vector (relative to the patella) was calculated. The magnitude and direction of the PFJRF was quantified as the resultant of the quadriceps force vector and the patellar ligament force vector. This calculation was repeated at 0, 20, 40 and 60 degrees of knee flexion.

RESULTS AND DISCUSSION

On average, the resultant PFJRF's estimated by the computer model was consistently higher, but similar in magnitude, to the measured in-vitro PFJRF's at all knee flexion angles (9.2% difference at 0˚; 10.0% at 20˚; 13.4% at 40˚; and 15.6% at 60˚, Fig. 1). The PFJRF distribution in all three planes was similar between modeling methods across all knee flexion angles. The Pearson's correlation coefficient revealed a significant association between the resultant PFJRF's estimated from the computer model and the measured PFJRF's from the cadaver specimens (r^2=0.89; $p < 0.001$)(Fig. 2)

SUMMARY

These results suggest that good estimates of the magnitude and direction of the PFJRF can be obtained using a computer-based model. Accurate modeling of PFJRF's is needed to define the biomechanical environment of the patellofemoral joint and to identify the factors contributing to abnormal patellofemoral joint loads during functional activities.

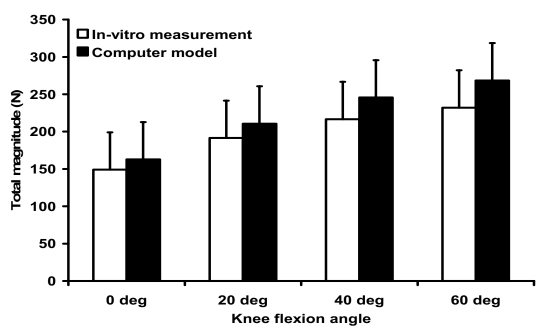

Figure 1. PFJRF output comparison between in-vitro measurements (white) and computer model (black).

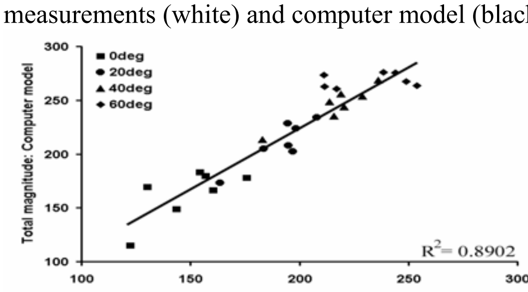

Figure 2. Association between in-vitro measurements and computer model output.

ACKNOWLEDGMENTS: This work was supported by a grant from the Whitaker Foundation

A COMPARISON OF HIP EXTENSION TORQUES IN CONVENTIONAL AND SPLIT SQUAT EXERCISES

Ben Meyer and Jesús Dapena
Biomechanics Laboratory, Indiana University
email: bwmeyer@indiana.edu

INTRODUCTION

Conventional two-leg squats are considered an important part of lower extremity strength training programs, as they serve to exercise the hip and knee extensor musculature. However, the exertion of a large hip extension torque requires a large load and/or a large forward lean of the trunk. In turn, this requires the exertion of large torques by the lumbar extensor musculature, and thus increases the risk of spinal injury. As an alternative to conventional squats, some athletes use split squats as part of their training (Figure 1). The exercise is focused on the forward leg.

The purpose of this study was to examine the relationship between load and hip extension torque in the conventional and split squat exercises, and to draw inferences in regard to the risk of injury for the lumbar spine.

METHODS

Ten male athletes (standing height = 1.76 ± 0.07 m; mass = 88 ± 14 kg) volunteered for the study. The subjects performed conventional squats at 60, 70, and 80% of their raw one-repetition maximum (1-RM), and split squats at 20, 25, and 30% of their raw conventional squat 1-RM. (Raw lifts are those performed without the use of knee wraps or squat suits.) At the low point, the thigh was approximately parallel to the ground.

Each trial was recorded with a Vicon 370 motion analysis system, and the ground reaction forces and torques exerted on the right foot were measured with an AMTI OR6-7-1000 force platform. The sampling rate was 60 Hz for both. Joint torques were computed using the method proposed by Andrews [1,2]. Lifted mass was defined as the sum of the masses of the trunk, arms, head, and barbell. Trunk angles were expressed relative to the vertical. Data were calculated for the low point of the lift, defined as the instant of minimum thigh angle.

RESULTS AND DISCUSSION

Figure 2 shows that the split squat required less lifted mass than the conventional squat to attain any given amount of hip extension torque. In addition, the subjects used a smaller amount of forward lean of the trunk in the split squat (25 ± 12°) than in the conventional squat (35 ± 6°). The combination of a smaller lifted mass and a smaller forward lean of the trunk in the split squat for any given amount of hip extension torque implied smaller lumbar extension torques. In turn, this implied a smaller risk of injury for the lumbar spine when the split squat is used.

CONCLUSIONS

The results of this project indicate that athletes who wish to focus their efforts on the hip extensor musculature should perform the split squat. The use of the split squat reduces the risk of lumbar spine injury by reducing the forward lean of the trunk and the lifted mass in relation to the conventional squat.

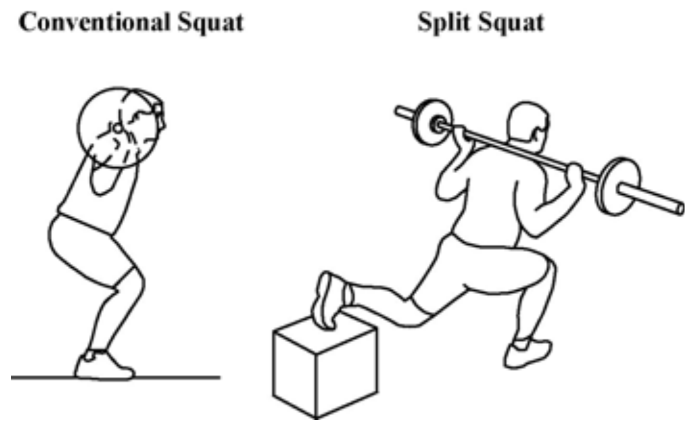

Figure 1: Conventional and split squat exercises.

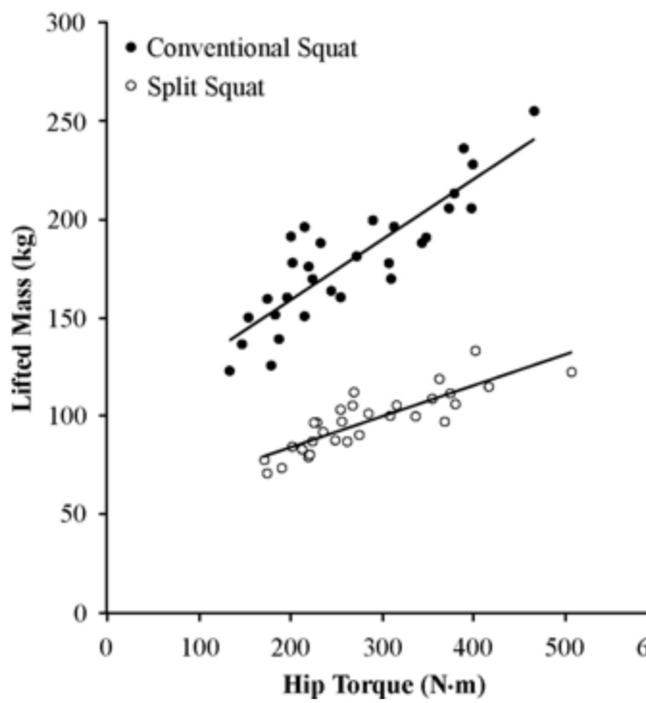

Figure 2: Relationship between lifted mass and hip torque in the conventional and split squat exercises.

REFERENCES

1. Andrews, J.G. *Kinesiology IV*, 32-42, 1974.
2. Andrews, J.G. *Med. Sci. Sports Exerc.* **14**, 361-367, 1982.

ACKNOWLEDGEMENTS

This research was supported in part by a grant-in-aid from the School of HPER, Indiana University.

MUSCULAR STABILISATION OF THE HEAD IN CAR COLLISIONS

Lars Janshen
Humboldt-University Berlin, Institute of Sport Science
email: lars.Janshen@rz.hu-berlin.de web: www.sportbiomechanik.de

INTRODUCTION

Frontal and rear-end collision with low speed are common accident mechanisms in situations with dense city traffic. During a rear-end collision the car occupant of the struck vehicle is pushed forward by the seat-back. Due to its inertia the neck is forced to an extension-flexion movement commonly called 'whiplash'. To improve car safety mainly anthropometric test dummies (ATD) e.g. Hybrid III are used. Although there is an ongoing development of ATD, such as the BioRID P3, and of specific components like the TRID-neck studies in which dummies or cadaver models are used do not reveal neuromuscular control strategies to adjust neck stiffness and to stabilize head position. However: muscular activation is presumably essential for postural control and head stability especially during trunk linear acceleration as they occur in car collisions [1].

The purpose of this study was to investigate differences in muscular coordination patterns of car occupants in frontal and rear-end collisions of small vehicles with low speed.

METHODS

Six male subjects performed five frontal and rear-end collisions with a bumper car (speed = 2.6 m/s) in a randomized order. The instant of car collision and head movement of the occupant were recorded by accelerometers (1000 Hz). Kinematic data was collected using side view high-speed video (1000 Hz). Body motion was related to car motion. In a 2D-model angular amplitude and angular velocity of defined joints located at the cervical spine (C4), between head and neck, neck and shoulder and at the elbow were analyzed in the sagittal plane.

Myoelectric activity of specific neck, upper trunk and arm muscles of either body side was recorded using surface EMG. The signals were pre-amplified and digitized (1000 Hz) to a PDA. After online verification using W-LAN the signals were stored on a PC. EMG-Signals were rectified and filtered using the moving average (MA) method. The analyzed EMG parameters included time, mean amplitude (RMS) and integrals (iEMG) of pre-activation (prior to relative body motion) and main-activation (during relative body motion). RMS and iEMG were described relative to the maximum MA values of the respective muscles and subjects.

In the statistical analysis a MANOVA was performed for the independent factors "subject", "collision type" and "body side". The dependent variables were defined by the measured parameters in the kinematic and EMG analysis.

RESULTS AND DISCUSSION

Within the series of collision types no significant differences between trials were observed. Kinematic data during the frontal and rear-end collisions showed that the complex motion of the head, neck and torso of the car occupant consists of mostly horizontal translational and rotational movements. During

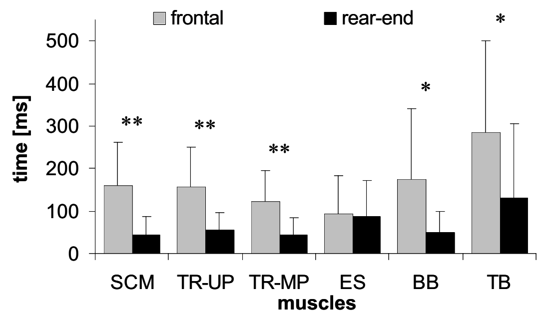

Figure 1 Activation times [ms] of the muscles sternocleidomastoideus (SCM), upper (TR-UP) and middle trapecius (TR-MP), erector spinae (ES), biceps (BB) and triceps brachii (TB) prior to relative head movement (N = 6).

frontal collisions all defined joints except the head-neck joint demonstrated significantly higher flexion compared to the rear-end crashes. During the rear-end collisions a nearly stationary head position observed in the first 70±6 ms of the crash could be attributed to head inertia [2]. This caused significantly higher and earlier maximum flexion in the head-neck joint and higher maximum extension in the other joints compared to frontal crashes.

In frontal collisions all muscles except the erector spinae showed significantly longer activation times prior to relative head movement compared to rear-end crashes (Figure 1). Together with significantly higher mean amplitudes representing the activation intensity this can be attributed to the visual anticipation of the frontal crash. This probably enabled a muscular induced neck stiffness to interlink motion of head and torso. In rear-end collisions EMG showed reflex induced activation time of about 50 ms prior to relative head movement with low intensity for all muscles. This seemed to be insufficient to interlink the head to the forward motion of the trunk.

CONCLUSIONS

In this study a significant difference of the muscular activation during frontal and rear-end collisions was observed. In contrast to currently used passive structures like crash test dummies or human cadavers, the muscular activity seems to play an important role during crashes and therefore should be more considered in future crash-models. Especially the results of the frontal collisions may help to improve occupant safety in the ongoing development of airbag concepts and help to prevent injuries.

REFERENCES

1. Blouin, JS, et al. *Exp. Brain Res.* **150** Attenuation of human neck muscle activity following repeated imposed trunk-forward linear acceleration. 458-464, 2003.
2. Croft, AC, et al. *Accident Analysis & Prevention.* **34**(2). The neck injury criterion: future considerations. 244–255, 2002.

A BIOMECHANICAL STUDY OF THE PULLOUT STRENGTH OF THE SELF-TAPPING BONE SCREWS IN OSTEOPORTIC BONE MATERIAL INSERTED TO DIFFERENT DEPTHS

[1] Suneel Battula, [1]Glen O. Njus and [2]Andrew Schoenfeld
[1]The Department of Biomedical Engineering, The University of Akron,
[2]The Department of Orthopedic Surgery, Akron General Medical Center; email: bsuneel@uakron.edu

INTRODUCTION

Bone screws are commonly used implants for fixation of fractures and are also for stabilizing bone transplants [1,2]. The failure of osteosynthesis is determined by the maximum load that can be transferred between a screw and the bone [3]. This maximum load is referred to as the pullout strength (PS) and can be assessed by axial pullout tests. PS becomes a crucial factor in osteoporotic bone. It is a common practice in orthopaedic surgery to insert the self-tapping bone screws (STS) 2mm past the far cortex to prevent the cutting flutes from remaining in the far cortex.

The purpose of this study was to determine PS of the screws inserted to different depths in the osteoporotic bone material and to evaluate if there is a significant difference in the PS of the STS of different manufacturers.

METHODS

Ninety Stainless Steel (SS) self-tapping cortical bone screws (40mm length, 3.9mm cutting flute length and 3.5mm diameter) from three manufacturers, Zimmer (Warsaw, IN), Synthes (Monument, CO) and Stryker (Mahwah, NJ), were evaluated. These screws were inserted into bone coupons representing osteoporotic bone material. The bone coupons were bicortical with polyurethane foam (density of 0.24 grams/cc and tensile modulus of 143 Mpa) for cancellous bone and E-Glass-filled epoxy sheets (1.7 grams/cc density and tensile modulus of 12.4 GPa) for cortical bone.

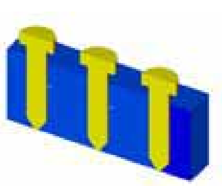

Figure 1: Layout of the bone coupons and the screws.

The screws were subdivided into five groups of six screws per depth per manufacturer. They were inserted -1mm, 0mm, 1mm, 2mm and 3mm relative to the far cortex. Three screws were inserted per coupon (Fig 1) based on the St. Venant's principle.

The axial pullout was performed in agreement with the *ASTM F 543-02* specifications for the metallic medical bone screws. Uniaxial load to failure was applied under displacement control at a rate of 0.1 mm/s using an Instron 8511 materials testing machine.

RESULTS AND DISCUSSION

Fig. 2 shows comparison of the PS of the screws of different manufacturers at different depths of insertion. It may be observed that the PS of the screws inserted 1, 2 and 3mm past the far cortex were significantly higher than the other groups.

Loading energy (LE) was computed as the area under the load displacement curve up to maximum load (PS). Table.1 summarizes the results of the LE at different depths and also for all manufacturers. Two-factor ANOVA and SNK tests were performed to determine the effect of the depth of insertion and manufacturer on the PS.

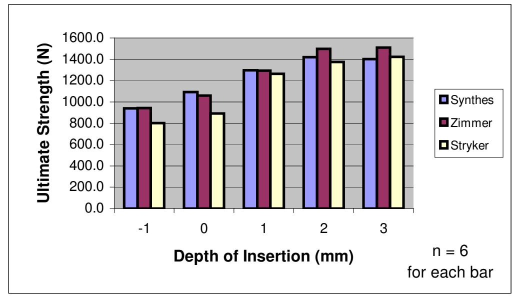

Figure 2: Pullout Strength of Bones screws from different manufacturers inserted to different depths

The statistical results indicate that the PS of the screw when inserted to 2 and 3mm past the far cortex is significantly different ($P<0.05$) from the other depths of insertion. The results failed to indicate any significant difference between the PS of the screws manufactured by different companies.

Table 1: Means ± standard deviation of the Loading energies (N-mm) of the screw pullouts at different depths.

DOI (mm)	Manufacturer		
	Synthes	Zimmer	Stryker
-1	294 ± 60.6	271 ± 83.4	211 ± 31.1
0	344 ± 83.6	337 ± 74.4	251 ± 35.5
1	416 ± 99.9	441 ± 109.3	421 ± 104.4
2	561 ± 87.2	636 ± 83.6	535 ± 51.5
3	560 ± 101.1	616 ± 50.1	628 ± 44.4

CONCLUSIONS

It has been confirmed with the help of biomechanical testing that the optimum depth of insertion for a bone screw in osteoporotic bone material is 2mm past the far cortex. It can also be concluded that the PS of the self-tapping bone screws made by different manufacturers are not statistically different from each other.

REFERENCES

1. Gefen. A, *Medical Engineering and Physics* **24,** 337-347,2002.
2. Glauser C.R, et al. *Orthopaedic and Trauma Surgery* **8**, 388-391, 2003.
3. Seebeck. J, et al. *Journal of Orthopaedic Research* **22**, 1237-1242,2004.

A SYNTHETIC MODEL FOR MECHANICAL EVALUATION OF VERTEBRAL BONE

Amy Johnson and Tony S. Keller
University of Vermont, Burlington VT
email: ajohnson@uvm.edu , web: www.emba.uvm.edu/~keller/mrl

INTRODUCTION

Biomechanical studies of vertebral compression fractures and cement augmentation typically rely on cadaver vertebrae, which exhibit highly variable structural and material characteristics depending on the age and degeneration of the samples. Moreover, cadaveric specimens are increasingly difficult to obtain in sufficient numbers for statistically valid studies. The goal of this project was to create and mechanically test a synthetic vertebral body using commercially available open-cell foam, which is marketed as a structural analog to human cancellous bone. The open-cell structure allows for cement injection making it a desirable testing material for vertebral cement augmentation studies.

METHODS

Blocks of open cell foam (apparent density, ρ_a= 0.12 g/cm^3) were obtained from Pacific Research Laboratories, Inc. (Vashon Island, WA). A 9mm foam cube was digitized using a µCT scanner (36 micron voxels). Volume fraction (BV/TV), three-dimensional (3-D) material anisotropy, and standard morphology (Tb.N, Tb.Th, Tb.Sp) were characterized using a proprietary program based on the parallel plate model method [1]. Ten samples of open cell foam were cut into cylindrical cores (12.8 mm diameter by 19.8 mm height) using a brass-coring tool. Using a servo-hydraulic test machine, the cylindrical foam samples were initially subjected to non-destructive uniaxial compression tests under displacement control. Foam specimens were preloaded to 0.5N, preconditioned for 5 cycles to 0.4% strain using a 1Hz sinusoid, and ramp loaded at 0.016 mm/s to 0.8% strain. 1.5 mm thick fiberglass resin end-plates were molded to the top and bottom surfaces of the foam samples (Fig. 1a). The fiberglass resin end-plate was representative of the cortical bone endplate present in vertebral centrum, and served to reinforce the damaged (cut), load-bearing surface of the foam cylinders. Foam+endplate samples were non-destructively tested as described previously, followed by a failure ramp at a rate of 0.016 mm/s.

Stress-strain data were used to obtain the apparent modulus (E_a), 0.2% offset yield stress (σ_y), 0.2% offset yield strain (ε_y), ultimate stress (σ_{ult}), and ultimate strain (ε_{ult}). The apparent elastic modulus was determined over a 0.5% strain range for the non-destructive tests. A paired-observations t-test (POTT) was used to compare the apparent modulus of foam vs. foam+endplate samples.

Table 1: Apparent modulus (mean ± standard deviation) of foam vs. foam+endplate test specimens.

	Open Cell Foam	Foam + Endplates
Modulus E_a (MPa)	4.97 ± 2.13	6.62 ± 3.04*

*no significant difference (POTT, $p > 0.05$)

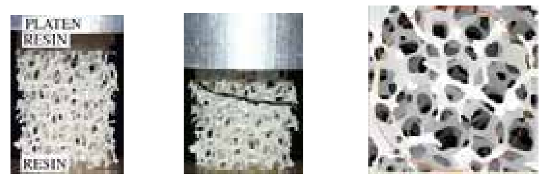

a) b) c)

Figure 1: a) Foam sample with fiberglass endplates prior to compression; b) Post-yield crush zone (highlighted) is visible ($\varepsilon \sim$ 15%); c) µCT 3-D rendering (9 mm x 9 mm).

RESULTS AND DISCUSSION

The foam specimens consisted of an interconnected network of rods similar in morphology to vertebral trabecular bone (Fig. 1c). Foam samples were characterized as transverse isotropic with a BV/TV, Tb.N, Tb.Th, Tb.Sp of 0.106, 0.280mm^{-1}, 0.378 mm, and 3.20 mm, respectively. Human vertebral cancellous bone is transverse isotropic with similar morphology and has an apparent density ranging from 0.05–0.30 g/cm^3 [2]. The latter corresponds to a volume fraction ranging from 0.03 – 0.156 (assuming a bone tissue density ρ_t = 1.9 g/cm^3). The foam+endplate specimens exhibited a crush or fracture consolidation typical of open-celled materials (Fig. 1b). Addition of the endplate increased the stiffness of the foam cores 33%, but this was not statistically significant (Table 1). Mean ± standard deviation for σ_y, ε_y, σ_{ult} and ε_{ult} were 0.231 ± 0.033 MPa, 3.44 ± 0.72 %, 0.241 ± 0.029 MPa and 3.78 ± 0.74 %, respectively. The ultimate apparent strength and stiffness of similar density vertebral cancellous bone is 0.745 MPa and 12.4 MPa, respectively [2]. The lower values obtained for the foam samples (most likely) reflect the 40% lower tissue density of the foam compared to bone tissue (ρ_t= 0.12 g/cm^3 / 0.106 = 1.13 g/cm^3). Strain values, ε_y and ε_{ult} were also lower than lumbar trabecular bone, which are reported as 6.0% and 7.4%, respectively [3].

CONCLUSIONS

Our results indicate that the synthetic open-cell foam exhibits morphology similar to human vertebral cancellous bone, but has a lower density and concomitant lower strength and stiffness in comparison to human bone. Future work will focus on creation of a synthetic foam wedge fracture and cement augmentation model to study vertebral kyphoplasty.

REFERENCES

1. Parfitt AM, et al. *J Clin Invest* **72**, 1396-409, 1983.
2. Keller TS. *J Biomech* **27**, 1159-1168, 1994.
3. Hansson TH. *Spine* **11**, 56-62, 1986.

ACKNOWLEDGEMENTS

Research supported by the Vermont Space Grant Consortium; special thanks to Jeremy Lemoine for µCT scanning.

POSTURAL CONTROL STRATEGIES IN PEOPLE WITH AND WITHOUT PERIPHERAL NEUROPATHY - A NEURAL NETWORK APPROACH

Ge Wu[1], Marc Sarnow[2], Larry Haugh[3], Juvena Hitt[1]
[1.] Department of Physical Therapy, [2.] Department of Orthopaedic Surgery, [3.] Department of mathematics
The University of Vermont, Burlington, VT 05405, USA

INTRODUCTION

Postural control strategies (PCS) during perturbed, upright stance depend on the integration of multiple sensory feedbacks by the central nervous system. People with peripheral neuropathy (PN) have decreased mechanoreception in the foot. This sensory change may lead to modified PCS when their balance is disturbed. The goal of this study was to use an Artificial Neural Network (ANN) model to quantify the motor-sensory relationship during a dynamic, human postural control task in elderly people with PN and without PN (NPN).

METHODS

Five PN (73.6±3.2 yrs) and seven NPN (80.1±8.5 yrs) elderly subjects participated in the postural perturbation experiment – maintaining an upright balance when the supporting base is suddenly rotated toes-up-down around the ankle joints (maximum rotation of 12^o in each direction, maximum speed of 50^o/s). All subjects signed a consent form approved by the IRB at the University of Vermont.

Following measurements were done: the electromyography (EMG) of the tibialis anterior (TA) and gastrocnemius (GAS) muscles of both legs, the distance between the eyes' center to a gaze target in front of the subjects; the head linear and angular accelerations; the ankle rotation; and the normal and shear forces under the feet. All signals were properly low-pass filtered, synchronized, and sampled by a data acquisition system (Bioengineering Technology Systems). Trials 11-25 were collected for each subject, five seconds each trial.

A two layer ANN model was constructed with seven inputs (head angular and linear accelerations (P_1 and P_2), eye-target distance (P_3), ankle rotation (P_4), ankle velocity (P_5), normal and shear forces under the feet (P_6 and P_7)), two outputs (i.e., EMG envelopes of TA (y_1) and GAS (y_2) muscles).

The ANN model was trained based on the Back-Propagation algorithm. For every trial, the ANN model was trained 120 times, 10,000 epochs each, and a goal error of 0.001. For each training, a set of weights was determined and was used to calculate a set of 14 Q values (one for each of the 14 input-output pairs) to estimate the contribution of each sensory stimulus to each leg muscle activity [1]:

$$Q_{ki} = \frac{cp_{ki}^1 \int_T P_i \cdot y_k dt}{4\int_T y_k{}^2 dt} \times 100\% \qquad (k=1,2,\ i=1\text{-}7) \qquad (1)$$

$$cp_{ki}^1 = \sum_j W_{jk}\omega_{ij} \qquad (k=1,2,\ i=1\text{-}7,\ j=1\text{-}50) \qquad (2)$$

where Q_{ki} is the Q value between the i^{th} input variable (P_i) and the k^{th} output variable (y_k), ω_{ij} and W_{jk} the first and second layer weights, respectively, and T the total time duration of the platform movement. The group means of each Q value were compared with a two-sample, unequal variance t-test.

RESULTS

The time trajectories of the input and output variables were consistent, and there were no significant group differences in the peak-to-peak values except for the normal force, shear force and EMG of the GAS muscle (significantly smaller in PN group, $p < 0.009$).

For the Q values, there were marginally significant group differences ($p<0.10$) for each muscle (Table 1). For TA muscle, the PN group had a higher Q value for ankle angle and head linear acceleration than the NPN group ($p<0.06$). For GAS muscle, the PN group had a higher Q value from head angular acceleration than the NPN group ($p=0.075$).

Table 1. Group means and standard deviations of Q values

Outputs	Inputs	NPN	PN	P value
TA	Head ang acc	1.4 ± 1.1	1.4 ± 1.6	0.499
	Head linear acc	0.2 ± 0.1	1.3 ± 1.3	0.061
	Vision	2.4 ± 1.8	1.3 ± 1.1	0.107
	Ankle angle	1.4 ± 0.6	3.3 ± 2.1	0.057
	Ankle velocity	2.8 ± 1.4	2.7 ± 1.2	0.449
	Shear force	3.6 ± 2.9	4.3 ± 2.0	0.267
	Normal force	1.6 ± 1.4	1.0 ± 0.8	0.114
GAS	Head ang acc	0.3 ± 0.2	0.6 ± 0.3	0.075
	Head linear acc	0.6 ± 0.6	0.4 ± 0.3	0.193
	Vision	7.5 ± 11.2	3.5 ± 2.3	0.197
	Ankle angle	1.2 ± 0.6	1.7 ± 1.6	0.294
	Ankle velocity	1.6 ± 1.4	2.5 ± 1.6	0.183
	Shear force	1.7 ± 1.8	2.9 ± 3.4	0.161
	Normal force	2.0 ± 2.4	2.3 ± 1.4	0.310

DISCUSSION AND CONCLUSION

This study examined the quantitative relations between each of the seven mechanical stimuli to the visual, vestibular and somatosensory systems and each of the two leg muscle activities during a sudden toes-up-down rotation of the supporting base among elderly people with and without severe loss of cutaneous mechanoreception in the feet. There were two main findings. First, people with PN have increased dependence on vestibular system or ankle joint receptors. Second, the primary sensory contribution to both muscle activities remains from the somatosensory system in the PN group. It is possible that these subjects still maintain the use of this afferent information from the ankle joint, but with increased assistances from other sensory systems.

These findings are supported by the notion that when portions of the somatosensory receptors are eliminated, there are increased contributions from other sensory systems [2-4]. This study demonstrates the potential of the ANN model in quantitatively studying motor-sensory relationship in human postural control.

ACKNOWLEDGEMENT

This work was supported by the National Institute on Aging. We thank Debra Millon for assistance in data collection.

REFERENCES

1. Shan G et al., Neurocomputing, 61:241-258, 2004.
2. Dieterich M et al., *Brain* 112:1377-1392, 1989.
3. Nashner L. *Trends Neurosci* 5:358-361, 1982.
4. Wu G, Chiang JH. *Exp Brain Res* 114:163-169, 1997.

CONTROL OF CENTER OF PRESSURE DURING TAI CHI MOVEMENT

Ge Wu, Juvena Hitt
Department of Physical Therapy, University of Vermont, Burlington, VT, 05401, email: ge.wu@uvm.edu

INTRODUCTION

Tai Chi Chuan (TCC) is shown to be an effective form of balance exercise for elders [1]. However, its mechanisms in improving balance are not yet clearly understood. The purpose of this study was to examine the control of body center of pressure (COP) during single stance of the TCC movements.

METHODS

A total of ten young subjects (age 27±4 years) participated in this study. All subjects had practiced TCC daily for at least two weeks before testing, and signed an Informed Consent Form approved by the University of Vermont Institutional Review Board.

The kinematics of the trunk and limbs were measured using a marker-based Motion Analysis System (BTS). Surface electromyography (EMG) was recorded from tibialis anterior (TA), soleus (SOL), peronaeus longus (PL), rectus femoris (RF), semitendinosus (ST), and tensor fasciae latae (TFL) muscles. The ground contact characteristics were recorded by two force plates (AMTI) and one pressure plate (Tekscan).

Subjects were asked to perform, five times, with bare feet, one basic Yang-style TCC movement, parting the wild horse mane, over a walkway covered by the force and pressure plates. The distances between these plates were adjusted so that subjects could land with the left foot first on the force plate, followed by the right foot on the pressure plate, and the consecutive left foot on the second force plate. The signals from the force and pressure plates, the Motion Analysis System, and the integrated EMG were collected at 50Hz, 15 seconds each trial.

The single stance time was determined based on the force and pressure plate measurement. Following parameters were computed over the single stance phase: spatial position and angular motion of the ankle, knee, hip and shoulder joints, the RMS value of EMG signals of both stance and swing legs, and the foot COP displacement in the medial-lateral and anterior-posterior directions, normalized by foot width (FW) and foot length (FL), respectively.

The mean and standard deviation of each variable, as well as the temporal features of both SW and TCG were calculated for each subject and compared using two-tailed t-test. They were considered statistically different when the p value was less than 0.05.

RESULTS

The foot COP maintained fairly stationary and centered mainly in the center of the foot (Fig. 1). The maximum range of motion was 14±6%FW and 7±2%FL, as compared to 64±8%FW and 72±7%FL over the complete TCC movement. The stance leg remained fairly stationary, while the swing leg went through a large amount of hip adduction and flexion (Table 1), and the shoulder had a large range of displacement (~25cm) in the transverse plane. All six muscles in the stance leg were activated at or above 20%MVC, and remained active for more than 50% of the single stance time (Table 2).

DISCUSSION AND CONCLUSION

These results suggest that TCC movement involves the precise control of body COP. The fact that the foot COP is centered in the midfoot region with minimal movement during single stance is by no means a coincidence. Earlier studies have shown that during quiet, upright stance, body weight is located more towards the heel region, resulting in more planter pressure in the rearfoot than in the forefoot region [2,3]. Moreover, the large amount of leg and trunk movement during single stance tends to shift the body center of mass. Thus, maintaining foot COP in the midfoot region requires a conscious and precise control of the neuromuscular system. It is perhaps the practice of this precise control of the neuromuscular system that helps improve the stability of upright stance.

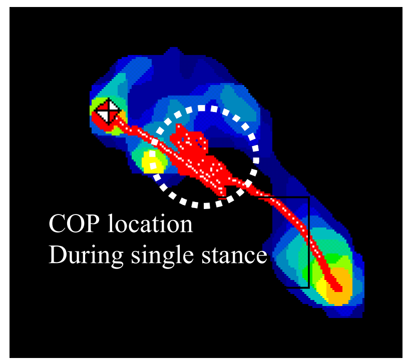

Fig 1. Illustration of foot COP location during single stance.

Table 1. Means and stds of joint ROM (deg)

Joints	Stance leg	Swing leg
Ankle flexion/extension	6±3	14±10
Knee flexion/extension	8±8	74±6
Ankle inversion/eversion	2±5	4±9
Hip flexion/extension	7±3	48±6
Hip abduction/adduction	6±8	20±9

Table 2. Means and stds of stance leg muscle EMG features

Muscles	RMS (%MVC)	On time (% single stance)
TA	38±11	91±19
PL	33±10	80±24
SOL	20±9	57±31
RF	39±15	77±37
TFL	42±16	87±27
ST	21±12	59±38

REFERENCES

1. Wolf S, et al., *J Am Geriatr Soc* 44:489-97, 1996.
2. Cavanagh PR, et al., *Foot & Ankle* 7:262-76, 1987.
3. Chiang JH, Wu G, *Gait & Posture* 5:239-245, 1997.

ACKNOWLEDGEMENT

This work was supported in part by the NSF and the University of Vermont. The authors would like to thank Chris Monberg, Debra Millon and Wei Liu for assistance in data collection.

DIFFERENCES BETWEEN OPERATED AND NON-OPERATED SHOULDER MUSCLE ACTIVATION PATTERNS RECORDED DUIRNG THE DRAGON BOAT "LONG AND HARD" STROKE

[1]Linda McLean, Ellen Keeves, Jen Wolfe, Karen Filion, Anna Smith, Tierney Bowen, Degen Southmayd
[1]Queen's University School of Rehabilitation Therapy,
Email: mcleanl@post.queensu.ca

INTRODUCTION

Surgery for breast cancer often results in muscle weakness, loss of shoulder motion, and pain (Blomqvist et al., 2004). Many women begin to participate in dragon boat training and racing post-operatively as a form of fitness and as a source of social support. Changes in the force couples at the shoulder joint may predispose women who dragon boat to develop shoulder overuse and/or impingement syndromes.

We hypothesized that women who had undergone partial or complete mastectomy with lymph node dissection would demonstrate differences in muscle activation patterns during the performance of the dragon boat stroke on their operated as compared to their non-operated side.

METHODS

Nine experienced female dragon boaters and breast cancer survivors from the Kingston Region participated in this study. Participants were required to have undergone a unilateral partial or complete mastectomy with lymph node dissection.

Delsys™ DE2.1 electrodes were used to record electromyographic (EMG) activity from seven muscles bilaterally, including the anterior deltoid, serratus anterior, pectoralis major, posterior deltoid, teres major, infraspinatus, and supraspinatus based on positioning described by Decker et al.(1999) and Hintermeister et al. (1998). Bipolar fine wire electrodes were used to record the activity of the subscapularis muscle. Each subject performed a series of three repetitions of a maximal voluntary isometric contraction (MVIC) for each muscle. She then performed ten repetitions of the "long and hard" dragon boat paddle stroke on each side, using a water trough and regular dragon boat paddle to simulate the activity.

Maximum voluntary electrical activation (MVE) was determined by using the highest root mean square value (RMS) computed over 200ms moving windows across each data set. The MVE was compared between the operated and non-operated sides for each muscle using a one-way repeated measures ANOVA (alpha = 0.05). The maximum activation amplitudes achieved during paddling were tested using a three-way repeated-measures ANOVA including muscle, recording side (operated vs. non-operated) and paddling side (operated vs. non-operated) as factors, and all two-way interactions (alpha = 0.05).

RESULTS AND DISCUSSION

Four subjects had been operated on their dominant side, while five had been operated on their non-dominant side. Four subjects consented to having fine wires inserted bilaterally.

There were no significant differences between the operated and non-operated sides in terms of the MVE generated during the MVIC at any of the eight muscles studied.

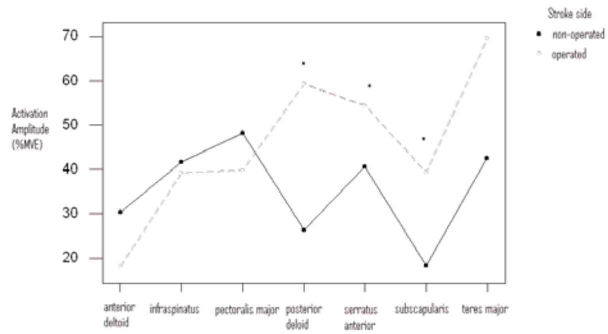

Figure 1: Mean peak muscle activation amplitude on the operated side when paddling on the operated vs. the non-operated side. (* denotes statistically significant differences)

During performance of the dragon boat stroke, there were significant muscle by side (operated and non-operated) and muscle by paddling side interactions ($p<0.0005$). As such the data for each muscle were analyzed separately. Post-hoc analyses revealed that the posterior deltoid, serratus anterior and subscapularis muscles on the operated side worked significantly harder than those same muscles on the non-operated side, particularly when paddling on the operated side.

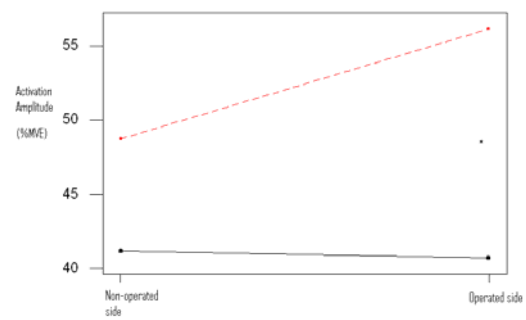

Figure 2: **Ac**tivation amplitude of serratus anterior muscle on the operated and non-operated side during the "long and hard" stroke. (Solid line denotes paddling on the non-operated side; dotted line denotes paddling on the operated side, * denotes statistical significance at alpha = 0.05)

CONCLUSIONS

Due to differences in force couples at the shoulder induced by these muscle activation differences, these results may explain why women who participate in dragon boat training often develop shoulder pain on their operated side.

REFERENCES

Blomqvist L et al., *Acta Oncologica*. Vol. 43(3) pp 280-283, 2004.
Hintermeister RA. Et al. *Am J Sports Med. Vol. 26(2)pp 210-220, 1998.*
Decker MJ et al. *Am J Sports Med. Vol. 27(6)pp 784-791, 1999.*

VALIDATION OF CALIBRATION TECHNIQUES FOR TEKSCAN PRESSURE SENSORS

[1] Jill M. Brimacombe, [1]Carolyn Anglin, [1]Antony J. Hodgson and [2]David R. Wilson
[1]Dept. of Mechanical Engineering, [2]Dept. of Orthopaedics,
University of British Columbia, Vancouver, Canada; email: jillb@mech.ubc.ca

INTRODUCTION

Thin, flexible pressure sensors are often used in orthopaedic biomechanics to measure loads in the knee joint. Prior to using sensors in cadaver and clinical studies, it is important to show that the results they provide are accurate under the proposed testing conditions. Other investigators have previously validated Tekscan I-Scan pressure sensors (Tekscan, Inc., Boston, MA) for accuracy and repeatability of force and force distribution measurements [1]. The current validation study aims to demonstrate that user-defined calibration algorithms provide more accurately calibrated force measurements than the Tekscan built-in calibration routines.

METHODS

Three new, identical I-Scan pressure sensors (model #5051-2500) were loaded using a materials testing machine (Instron 8874, Canton, MA). To simulate the loading in a prosthetic knee joint, each sensor was compressed between a flat disk of UHMWPE (D = 3.82 cm) and a larger aluminum plate. To reduce shear loads at the sensor surfaces, sensors were coated with K-Y lubricant (Johnson & Johnson, Montreal, Canada).

Sensors were conditioned four times at a load of 20.0 kN (120% of the maximum expected pressure). Four different calibration methods were used: a Tekscan linear calibration (performed at two different scales), a Tekscan power calibration, a user-defined 10-point cubic calibration and a user-defined 3-point quadratic calibration. The Tekscan linear calibrations were performed at 20% and 80% of the maximum applied load; the Tekscan power calibration was performed using both of these loads. All Tekscan calibrations pass through (0,0). The user-defined polynomial algorithms used a least squares curve-fitting technique.

Following conditioning and calibration, each sensor was subjected to 3 loading cycles consisting of 10 loads between 0 and 16.7 kN applied in a random order. Throughout conditioning, calibration and loading, forces were ramped up over 10s, held for 5s, and decreased over 10s. Sensors remained unloaded for 120s between load applications. Force data were saved as raw (uncalibrated) values; each calibration algorithm was applied to the same output. Force measurement error was defined as the difference between calibrated Tekscan output and Instron load cell measurements.

RESULTS AND DISCUSSION

Figure 1 shows the typical calibrated output for one sensor using the 5 calibrations. Of the 3 Tekscan calibrations tested, the power calibration was the most accurate (Figure 2); the root mean square (RMS) errors of the measured forces for the 20% linear, 80% linear, and power calibrations were 4.07±0.21 kN, 1.75±0.09 kN, and 0.447±0.16 kN, respectively, corresponding to 24.4%, 10.5% and 2.7% of the tested sensor range. The user-defined polynomial calibrations were markedly more accurate; the quadratic and cubic

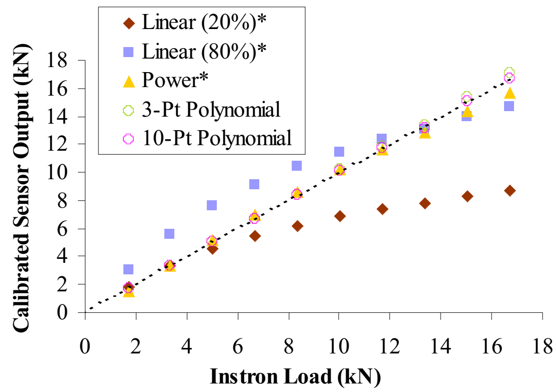

Figure 1: Typical sensor output calibrated using Tekscan (*) and user-defined algorithms.

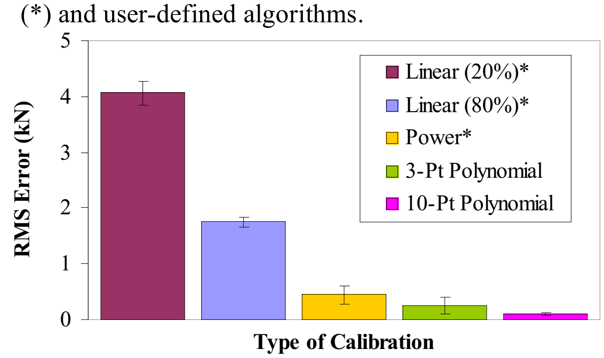

Figure 2: Average RMS errors of Tekscan (*) and user-defined calibration techniques.

calibrations had RMS errors of 0.24±0.15 kN (1.5%) and 0.10±0.03 kN (0.6%), respectively. While most studies do not report their calibration procedure, the previous study which used the Tekscan power calibration found a higher, but comparable, RMS error of 6.5±4.4% [1].

CONCLUSIONS

I-Scan force measurements may be accurate to within 0.6% when calibration algorithms use a least squares minimization technique. Although the 10-point cubic polynomial was the most accurate algorithm, the loading process is considerably more time-consuming. The 3-point quadratic calibration requires only one additional calibration load compared to the Tekscan power calibration and decreases the error in force measurement from 2.7% to 1.5%. Since it is straightforward to export sensor output and calibrate data externally, it is recommended that investigators design their own calibration curves. Since output is dependent on experimental protocol (sensor type, interface materials, sensor range in use, etc.), sensor behaviour must be investigated for each application.

REFERENCES

1. Wilson DR, et al. *J Biomech* **36**, 1909-1915, 2003.

ACKNOWLEDGEMENTS

The authors would like to thank the Michael Smith Foundation for Health Research and CHRP for their generous support.

INTRA-ANNULAR BILATERAL SPINAL COMPRESSION: NOVEL MEMS SENSORS

[1]D.L. Glos , [2]F. E. Sauser, [2,3]I. Papautsky, and [1,3]D. I. Bylski-Austrow
[1]Dept. Orthopaedics, Cincinnati Children's Hospital Medical Center and University of Cincinnati, Cincinnati, OH
[2]Dept. Electrical and Computer Engineering and [3]Biomedical Engineering, University of Cincinnati, Cincinnati, OH
Donita.Bylski-Austrow@cchmc.org; web: cincinnatichildrens.org

INTRODUCTION
Surgical treatment of late stage childhood spinal deformities is successful but invasive. With the goal of creating early, minimally invasive surgical methods, preclinical studies on prototype implants have shown that spine growth may be slowed unilaterally [1]. Spine curvatures were associated with histomorphometric structural gradients of vertebral physes[2]; the mechanism is presumed to be compressive stress gradients across the intervertebral joint, comprised of disc and two growth plates. A clinically successful implant design would require the application of compression levels sufficient to inhibit growth without significantly affecting disc viability.

Many studies have measured spinal pressures in the fluidic disc nucleus. However, to determine side-to-side compression differences in the annulus, thin, flat transducers are required, with sensor faces oriented transversely. The purpose was to design and develop a MEMS transducer capable of measuring compressive stress in the annulus of the intervertebral disc.

METHODS
Piezoresistive sensors were chosen for size, range, and ability to be placed remotely from signal conditioning circuitry. Commercial sensor dies in a full Wheatstone bridge configuration (SM5108: 0.65 mm^3 , Silicon Microstructures Inc., Milpitas, CA) permitted absolute pressure measurements at physiological levels. Carriers of various lengths and pad sizes were tested to define the thinnest functional device. Dies were electrically connected in a clean room complex (Class 10) using photolithography, micro-maching, and wire-bonding techniques [3] The sensors were designed into a small, thin, metallic package (2.5 mm width, 12.5 mm length, 0.8 mm thickness) to withstand dynamic *in vivo* stresses and to allow for firm attachment to vertebrae (Fig. 1).

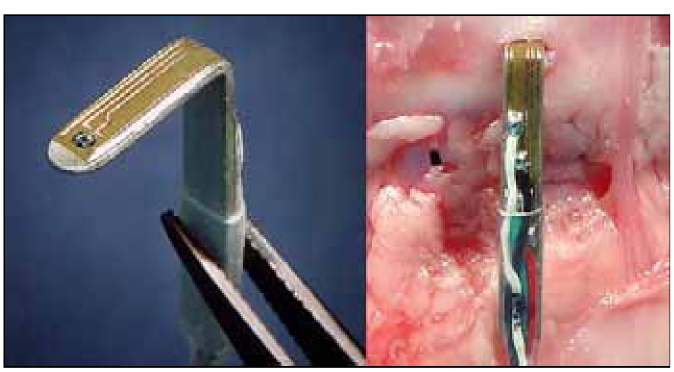

Figure 1: Packaged sensors were small, thin, and rugged.

Packaged sensors were calibrated under both fluid and solid contact conditions by first using a dynamic nitrogen pressure chamber (0-1.6 MPa) with commercial reference pressure sensor, and then using solid contact confined compression tests [3]. Sensors were then placed into the annulus of porcine vertebral motion segments that had been mounted into a materials test system. The segment was tested in cyclic compression (0.05 Hz) with simultaneous acquisition of load and pressure.

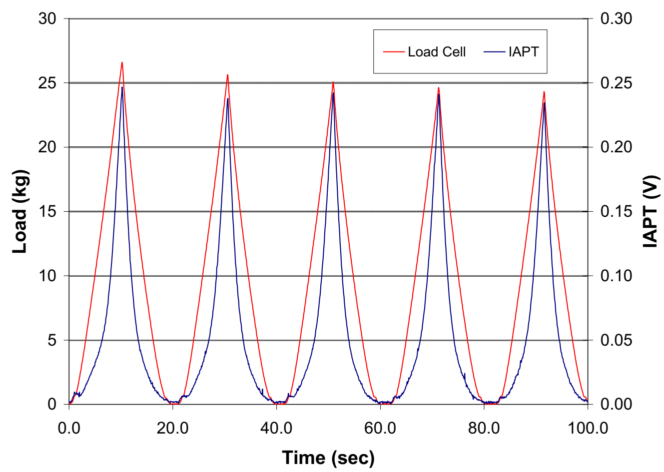

Figure 2: Intra-annular pressure transducer followed load cell.

RESULTS AND DISCUSSION
Intra-annular pressure transducers (IAPT) were successfully connected and packaged to withstand compressive stresses to at least 1.6 MPa. Calibrations performed in fluid versus solid contact tests did not differ significantly; sensors performed consistently with linear output and small offset voltages. Preliminary *in situ* tests indicated that applied loads and sensor response (IAPT) were well-correlated (Fig. 2), and that the sensor is likely to withstand the physiological environment. Testing continues to determine the effects of shear and torsional loading, dynamic range, and long-term reliability prior to their intended application in vivo.

CONCLUSIONS
Novel subminiature (MEMS) compression sensors were successfully fabricated, packaged, and calibrated as isolated transducers as well as *in situ* in the annulus of the intervertebral disc. Further characterization and consideration for *in vivo* and other biomechanical uses are warranted.

REFERENCES
1. Bylski-Austrow DI, et al. *Proc. 50th Orthopaedic Research Society*, #1087, 2004.
2. Bylski-Austrow DI, et al*Proc. 51st Orthopaedic Research Society*, #1331, 2005.
3. Sauser FE, Glos DL, Bylski-Austrow DI, Papautsky I. *Proc. IEEE Engineering in Medicine and Biology*, 2004.

GENDER DIFFERENCE IN CARPAL TUNNEL COMPLIANCE

Zong-Ming Li
Hand Research Laboratory, Department of Orthopaedic Surgery
University of Pittsburgh, Pittsburgh, PA 15213, USA. zmli@pitt.edu; www.pitt.edu/~zmli/handlab/

INTRODUCTION

The carpal tunnel is formed by the carpal bones and the transverse carpal ligament, and is unaccommodating for the expansion of its contents. The detrimental mechanical limitation by the ligament is exemplified by carpal tunnel release, a universal surgical procedure to release the transverse carpal ligament for the treatment of carpal tunnel syndrome. Previous studies have shown that myofascial release manipulation applied to the carpal tunnel caused tunnel enlargement and improvement of carpal tunnel symptoms [1]. The stretchablility of the transverse carpal ligament was also demonstrated in cadaver studies [2]. In addition, hypertrophy of the transverse carpal ligament has been proposed as one of the pathogeneses of carpal tunnel syndrome [3]. To date, little is known about the mechanical properties of the carpal tunnel. The purposes of this study were (i) to characterize the force-displacement relationship resulting from indentation applied to the palmar aspect of the wrist overlying the transverse carpal ligament, and (ii) to study gender difference in carpal tunnel compliance as determined by the indentation test.

METHODS

A hand-held Myotonometer (Neurogenic Technologies, Inc) was used to measure force and displacement during indentation testing. The indentation probe has a flat end with a diameter of 10 mm. To standardize indentation location on the skin overlying the transverse carpal ligament, a line was drawn to connect the palpable pisiform and scaphoid. A point 10 mm distal from the connection line on the bisector was marked as the center of indentation (Figure 1A). During the testing, the hand was placed in an arm holder with the palmar side facing upward (Figure 1B). The probe was manually pressed down perpendicular to the skin surface. The device took measurements from 0.25 to 2.00 kg at an increment of 0.25 kg. Twelve males (age 29.3 ± 6.6 years) and twelve females (age 26.2 ± 4.3 years) who had no neuromusculoskeletal disorders to the upper extremity participated in the study. Effective compliance was defined as the slope of the linear regression line of a set of force-displacement data. Repeated measures 2-way ANOVAs were used to compare the displacement differences. An independent t-test was used to compare the effective compliances between males and females.

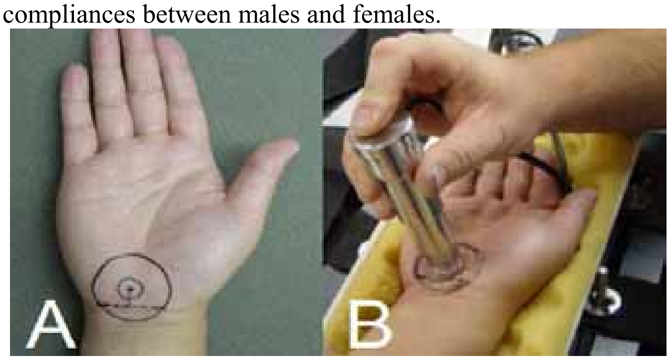

Figure 1. Center of indentation above the transverse carpal ligament (A), and manual indentation testing (B).

RESULTS

In the tested force range, the displacement increased linearly with applied force for either male or female group (Figure 2, R^2 ranges from 0.936 to 0.981). Females showed significantly smaller displacements than males ($F = 30.4$, $P < 0.001$). Force increases from 0.25 to 2.00 kg caused average indentation displacements of 1.82 ± 0.30 mm and 1.38 ± 0.25 mm for males and females, respectively. The effective compliance of females, 0.075 ± 0.012 mm/N, was 24.5% lower than that of males, 0.101 ± 0.018 mm/N ($P < 0.005$, Figure 3).

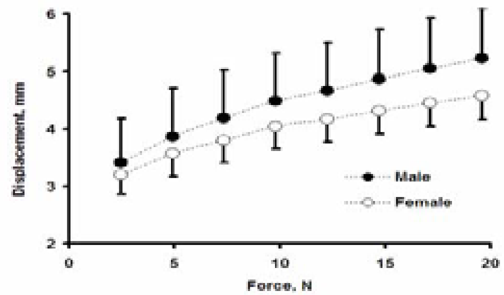

Figure 2. Force and displacement from indentation testing.

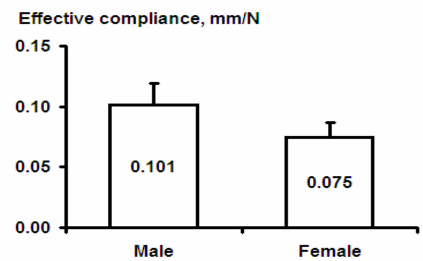

Figure 3. Effective compliance (mm/N).

DISCUSSION

An indentation testing was performed non-invasively to the palmar wrist overlying the transverse carpal ligament. A linear force-displacement relationship was shown in the tested force range. The results confirmed the hypothesis that females have less compliant carpal tunnels than males. This finding may partially explain the higher prevalence of carpal tunnel syndrome in women than in men [4]. Future studies are needed to investigate the material and structural properties of the transverse carpal ligament, the relationship of the ligament to the carpal tunnel pressure, and the biological and biomechanical adaptations of the ligament to repetitive hand use.

REFERENCES

[1] Sucher, B.M., J Am Osteopath Assoc, 1993. 93(12): p. 1273-8. [2] Sucher, B.M. and R.N. Hinrichs, J Am Osteopath Assoc, 1998. 98(12): p. 679-86. [3] Moore, J.S., Am J Ind Med, 2002. 41(5): p. 353-69. [4] Phalen, G.S., J Bone Joint Surg Am, 1966. 48(2): p. 211-28.

ACKNOWLEGEMENT

The author thanks Dr. Leland Albright for providing the Myotonometer device.

SKILL ACQUISITION OCCURS DURING FALL-PREVENTIVE MOTOR REPONSE TRAINING

Karrie L. Hamstra-Wright, Karen L. Reed-Troy, and Mark D. Grabiner
Musculoskeletal Biomechanics Laboratory, University of Illinois at Chicago; email: khamst1@uic.edu

INTRODUCTION

Older adults have a high incidence of trip-related falls that contribute to significant morbidity and mortality. A surrogate treadmill task has been proposed as a potential fall-preventive training tool for older adults. Successful motor response training must elicit stepping strategies as similar as possible to those evoked during actual trips and must demonstrate motor skill acquisition. Differences in the foot trajectories after an actual trip compared to those during the treadmill task have been attributed to the presence of an obstacle [1]. Recent work has shown that the addition of an obstacle to the surrogate treadmill task increases step height and step length to more closely approximate stepping responses elicited during an actual trip [2]. Older adults have demonstrated the ability to modify failed stepping strategies and successfully recover on the subsequent trial during the treadmill task without the obstacle [3], but little is known about the underlying motor control mechanisms regulating the acquisition of this skill.

The purpose of our study was to assess motor skill acquisition while participants successfully stepped over an obstacle during the surrogate treadmill task. We hypothesized that step height, trunk flexion, and trunk angular acceleration would decrease as subjects acquired the skill.

METHODS

Ten healthy young adults (7 females, 3 males) participated in the study (26.9 ± 5.04 yrs, 171.2 ± 6.47 cm). A surrogate trip was induced through sudden treadmill acceleration (maximum speed of 2.5 mph). Subjects were instructed to recover equilibrium and continue walking after the treadmill was unexpectedly activated. Fifty randomized stepping trials, 25 without an obstacle on the treadmill and 25 with a 5 cm obstacle placed 2.5 cm in front of the toes, were conducted. Whole body 3D kinematics were collected with an eight-camera motion capture system (Motion Analysis, Santa Rosa, CA). Maximum step height of the recovery (first leg to step) and trail limb (second leg to step), peak trunk flexion, and peak trunk angular acceleration in flexion and extension were compared between conditions (with, without obstacle) and between trials (trials 1-5 average, trials 20-25 average).

RESULTS AND DISCUSSION

A repeated measures MANOVA revealed a significant reduction in step height, trunk flexion, and trunk angular acceleration in flexion and extension between trials. In the

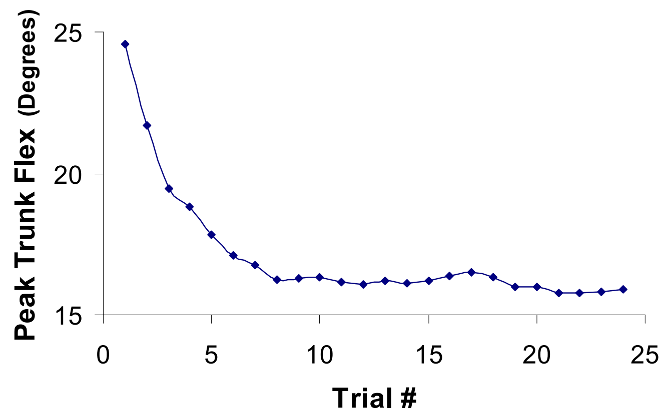

Figure 1: Running mean of peak trunk flexion versus trial number for a typical subject

obstacle condition, recovery and trail step height decreased from trials 1-5 (recover: 30.75 ± 5.85 cm; trail: 34.79 ± 5.77 cm) to trials 20-25 (recover: 27.31 ± 6.88 cm; trail: 30.22 ± 5.13 cm). Regardless of condition, participants demonstrated considerable decreases in trunk flexion and trunk angular acceleration with repetition illustrating skill acquisition of this novel task (Table 1). When subjects stepped over the obstacle, peak trunk flexion reached a steady state whereby further repetition did not result in less trunk flexion (Figure 1). This progressive reduction in peak trunk flexion indicates greater trunk control as trial number increases.

CONCLUSIONS

Twenty-five trials using the surrogate treadmill task with the addition of an obstacle appears to be a more than adequate number of trials to illustrate improvements in foot and trunk control as a measure of skill acquisition. Decreased trunk flexion during tripping events may contribute to successful trip recovery [3] making it a desirable outcome of a fall-preventive training protocol. This work provides further direction in the design and development of a treadmill training protocol as an expedient and effective tool in training older adults how to avoid falling after large postural disturbances.

REFERENCES

1.Troy KL & M Grabiner. *Exp Brain Res* **Oct 23** [Epub], 2004.
2.Hamstra-Wright, KL et al. *J Athl Train*, in press.
3.Owings TM et al. *Clin Biomech* **16**, 813-819, 2001.

Table 1: Values represent means & standard deviations. *Significant ($p \le .05$) decrease from trials 1-5 to trials 20-25.

Trunk Values Trials 1-5 versus Trials 20-25			
	Peak Trunk Flex (deg)	**Trunk Angular Acceleration Flex (deg/s^2)**	**Trunk Angular Acceleration Ext (deg/s^2)**
Trials 1-5	20.38 ± 7.13	1499.78 ± 494.44	-933.88 ± 627.71
Trials 20-25	16.57 ± 4.87	1209.64 ± 413.52	-734.15 ± 424.97
p value (1-5 vs 20-25)	*p = .01	*p = .00	*p = .05

WRIST KINETICS DURING IMPACT ARE AFFECTED BY HAND SYMMETRY

Karen L. Reed-Troy and Mark D. Grabiner
Musculoskeletal Biomechanics Laboratory, University of Illinois at Chicago email: klreed@uic.edu

INTRODUCTION: Falls onto the outstretched hands are the most frequent cause of upper extremity injury, and it has been estimated that older adults experience wrist fractures at a rate of 8 to 10 per 1000 person-years [1]. Previous work has quantified impact forces during symmetrical simulated falls [2,3], and several groups have shown that cadaver wrists fracture when loaded with 1.5 to 3.6 kN [4]. There is evidence that many falls result in temporally and spatially asymmetrical hand impacts [5], however no experimental studies have examined the sensitivity to wrist kinematic and kinetic measures to asymmetry.

The present study was undertaken to quantify wrist kinetics during asymmetrical impacts, and specifically to address three questions. How is spatial asymmetry at impact related to temporal asymmetry? Do asymmetrical impacts result in larger resultant forces than symmetrical impacts? How is loading direction affected by asymmetry?

METHODS: Nine adults participated in this institutionally reviewed and approved experimental protocol. Each subject performed 15 forward falls from a kneeling position onto two force plates. Five asymmetrical combinations of four targets, A_1 through A_5, were selected (Figure 1), based on hand dominance. Each subject performed three consecutive trials at each combination. Force plate data were captured at 2400 Hz. Motion data were captured at 240 Hz (Motion Analysis, Santa Rosa CA).

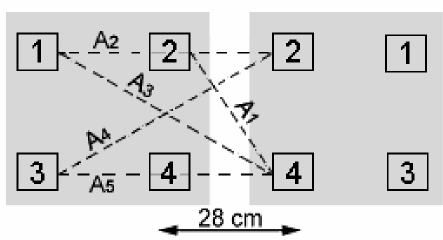

Figure 1 Force plates showing the locations of the four targets. Combinations A_1 through A_5 for a right-handed individual are shown with dotted lines.

The instant of force-plate contact was determined as the time at which each plate measured ≥ 5% body weight (BW). The instant of peak force was measured when the maximum resultant force was reached on each plate. Temporal offset (dtime) between hand-hits was determined for each subject (dtime>0, dominant hand hit first). Force direction for each arm was determined relative to the axis of the forearm (from wrist center to elbow center, Figure 2) and expressed in directional cosines.

RESULTS AND DISCUSSION: Spatial asymmetry caused a temporal offset abs(dtime) between hand-hits of 33±25 ms. On average, 25±9 ms elapsed between the instant of contact and the instant of peak force. In contrast, symmetrical falling data collected with the same set of targets resulted in significantly smaller temporal offsets of 12±11 ms [5].

Asymmetry did not influence peak resultant force magnitude (symmetrical: 92 ± 38 %BW, asymmetrical 94 ± 30 %BW).

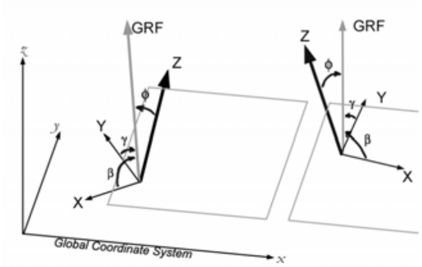

Figure 2 Arm-specific coordinate systems with direction cosines. The z-axis of each system is aligned with the axis of the forearm at the instant of peak force. The axes are mirror-images of each other such that a positive x-value indicates laterally directed force, relative to the forearm (i.e. the left hand coordinate system has left-handed axes). Direction cosine angles are defined such that β is the angle from the x-axis, γ is the angle from the y-axis, and φ is the angle from the z-axis. A force is directed along the axis of the forearm when β=90, γ=90, and ϕ=0. Note that in all cases $\cos^2\beta+\cos^2\gamma+\cos^2\phi = 1$.

However, at the same target location (1 through 4), asymmetry significantly influenced force direction. In targets 1, 2, and 4, asymmetry caused the resultant force to be more axially directed. The 95% C.I. for peak force direction across all asymmetrical positions ranged from 100% axially loaded to β=82.5°, γ=70.4°, ϕ=29.5° (87% axially loaded).

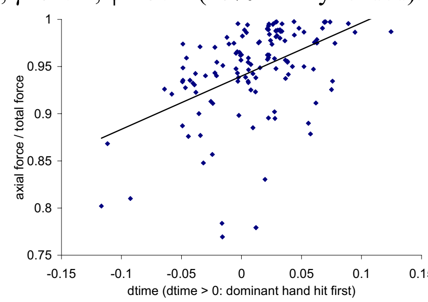

Figure 3 Dominant hand axial force versus temporal offset.

Larger temporal offsets were associated with axially directed resultant ground reaction forces in the first hand to hit (i.e. dominant axial/total force ~ dtime, r = 0.454 $p<0.001$, non-dominant axial/total force ~ dtime, r = -0.335 $p<0.001$, Figure 3). When the ground is contacted asymmetrically, the first hand may be used to reduce the downward and forward velocity of the body, while the second hand may play a more important role in preventing body rotation and in reducing shear.

Although asymmetry doesn't appear to affect peak force magnitude, it does cause more axially directed forces. This appears to be modulated by the magnitude of temporal offset. The extent to which fracture mechanics of the radius are affected by loading direction is still unknown. Furthermore, spatial asymmetry has been shown to cause temporal asymmetry, even for this self-initiated falling task.

REFERENCES: [1]Vogt et al. J Am Geriatr Soc 2002;**50**(1), [2]DeGoede et al. J Biomech 2002;**35**(6), [3]Kim and Ashton-Miller Clin Biomech 2003;**18**(4), [4]Augat et al. J Orthop Res 1998;**16**(5), [5]Troy and Grabiner, ASB Proceedings 2004

ACKNOWLEDGEMENTS: Funding by RO1AG16778 and F32AG025619. Stephanie Donovan helped with data collection.

RECOVERY RESPONSES TO SURROGATE SLIPS ARE DIFFERENT THAN ACTUAL SLIPS

Karen L. Reed-Troy and Mark D. Grabiner
Musculoskeletal Biomechanics Laboratory, University of Illinois at Chicago
email: klreed@uic.edu

INTRODUCTION Slipping and slip-related falls are a common and potentially dangerous problem, especially for older adults. We believe that it is possible to train corrective responses of older adults to reduce the incidence of slip-related falls. However, such an approach requires further understanding of the causal biomechanical distinctions between a successful and an unsuccessful recovery effort. Surrogate tasks are often used to study complex biomechanical events associated with large postural perturbations [1,2]. Although surrogate tasks enhance experimental control over one or more elements of a generally more complex event, such control may change the task of interest by imposing biomechanical constraints that reduce the validity of the surrogate. The purpose of the present study was to quantify the differences in lower extremity and trunk kinematics following a simulated slip versus an actual slip. We hypothesized that the simulated slips would result in significantly different (and less realistic) recovery kinematics, and that individuals who fell on either surface would have larger and faster trunk extensions, and more rapid slipping foot acceleration.

METHODS Twenty-two healthy young adults were each subjected to two types of unexpected slips during a single laboratory visit. Slips were induced in random order using a custom slipping platform and also using artificial ice [3]. The slipping platform consisted of three raised plywood platforms laid end-to-end to create a 7.2 m long walkway. The middle platform had two surfaces (31 x 122 cm), one for each foot, which could be locked in place or move along linear bearings. Each surface could slide a maximum distance of 62 cm in the direction of walking. During trials in which a slip was to be induced the middle platforms were unlocked remotely. The artificial ice consisted of a 1.2 x 1.2 m Plexiglas sheet, the surface of which was coated with a film of mineral oil prior to a slipping trial. Subjects were slipped on the artificial ice after 10 control trials (with no threat of a slip) were collected; they were unaware of the oil. Data from the first slip on the platform were compared to data from the slip on the oil.

From motion capture data (Motion Analysis, Santa Rosa, CA) the onset of the slip and the instant of recovery (the instant the non-slipping foot contacted the surface) were identified. The following variables were quantified for each subject: slip displacement (forward and mediolateral directions), peak slipping foot forward and mediolateral velocities and accelerations, slipping foot internal/external rotation, time to rear foot ground contact, distance the foot was placed behind the body center of gravity, peak trunk extension, and peak trunk extension velocity during the slip. Paired t-tests were used to compare responses during platform slipping and artificial ice slipping.

RESULTS AND DISCUSSION Four subjects (three female) either fell or grabbed the safety harness rope to avoid falling on the artificial ice. Fallers had significantly larger peak lateral flexion angles (30° vs. 13°, p=0.01) and more trunk rotation about the spine (24° vs. 14°, p=0.003). There were no significant differences in trunk extension between fallers and non-fallers. However, the peak slipping heel velocities were larger (214 cm/s vs. 148 cm/s, p=0.04), the slipping displacements were larger (55 cm vs. 30 cm, p=0.02), and the internal/external ankle rotation during the slip was larger (14° vs. 7°, p=0.02) in slips that resulted in a fall.

Four subjects (two male, two female) fell or grabbed the safety harness rope to avoid falling on the slipping platform. Subjects who fell or required rope assistance had significantly larger peak trunk extension angles (38° vs. 17°, p=0.002) but there were no differences in lateral flexion or rotation. Peak heel accelerations were larger (1000 cm/s^2 vs. 602 cm/s^2, p=0.04) and internal/external leg rotation was larger (14° vs. 7°, p=0.008) in those who fell compared to those who recovered.

Recovery from slips on the artificial ice appears to be biomechanically different than recovery from slips on the slipping platform (Table 1). Specifically, on the artificial ice the slipping foot's forward displacement and acceleration were 32% smaller and 85% larger than on the platform, respectively, despite nearly identical pre-perturbation walking velocities (127 cm/s on the platform, 126.7 cm/s on the ice) Slips induced on the slipping platform resulted in smaller slipping foot accelerations than those on the artificial ice. Furthermore, slips on the platform elicited a less conservative recovery response, despite nearly identical pre-perturbation walking speeds in both trials. A conservative response would include rapid placement of the rear foot far behind the center of mass to help prevent excessive trunk extension and reestablish the base of support.

Since several of the variables of interest are influenced by the methodology, providing a realistic perturbation is of great importance. Four of the ten measures that were significantly different between slipping surfaces were the same that distinguished fallers from non-fallers on those surfaces. Simulated slips may be an appropriate vehicle to investigate specific variables associated with sudden postural perturbations, however constraining the direction and displacement of the slip and the additional friction between the slipping foot and the surface, appear to influence the elicited recovery response.

REFERENCES [1] Marigold et al *J Neurophys* **89**(4), [2] Tang et al. *Exp Brain Res* **119**(2), [3] Brady et al. *J Biomech* **33**(7)

ACKNOWLEDGEMENTS Funding from NIH AG10557.

Table 1. Mean (sd) values and paired t-tests results for variables that were significantly different in artificial ice versus slipping platform trials.

	Slipping Foot Variables						*Rear Foot Variables*		*Torso Variables*	
	Forward		M-L						Extension	
	displ. (cm)	accel. (cm/s2)	displ. (cm)	veloc. (cm/s)	accel. (cm/s2)	int/ext rot (deg)	Time to foot placement (ms)	Distance behind CG (cm)	angle (deg)	ang. Veloc (deg/s)
Artificial Ice	33.9 ± 20.1	1279 ± 760	6.7±4.2	56.0 ± 42.7	1040 ± 728	14.7 ± 8.8	303 ± 110	13.2 ± 22.0	12.9 ± 7.6	72.8 ± 46.0
Slipping Platform	50.3 ± 13.3	691 ± 356	**	**	**	8.5 ± 4.8	501 ± 190	-10.4 ± 17.7	21.5 ± 12.8	112.8 ± 52.2
p	0.015	<0.001	<0.001	<0.001	<0.001	0.006	0.003	0.004	0.004	0.002

DOES FREE MOMENT PREDICT THE INCIDENCE OF TIBIAL STRESS FRACTURE?

[1]Clare E Milner, [1,2]Irene S Davis and [3]Joseph Hamill
[1]University of Delaware, Newark, DE, [2]Drayer Physical Therapy Institute, Hummelstown, PA, [3]University of Massachusetts, Amherst, MA; email: milner@udel.edu, web: http://www.udel.edu/PT/davis/Lab.htm

INTRODUCTION

Stress fracture injuries are common in distance runners, and occur most frequently at the tibia. Female runners are twice as susceptible to stress fracture as males. While multiple factors probably lead to the development of stress fractures, biomechanical factors such as loading are considered to play a role. Free moment (FM) is the torsional force about a vertical axis due to friction between the foot and the ground during stance. While FM has been linked to pronation, its potential role in running injuries has not been investigated widely. The relationship of FM to the loads experienced by the lower extremity makes it worthy of further investigation in relation to stress fracture injury. The spiral nature of some stress fractures indicates that torsional stresses on the lower extremity may be involved. If this is the case, the magnitude of the load may be more important than its direction. Furthermore, since FM is calculated directly from a force platform, it may have some value as a simple tool for predicting tibial stress fracture (TSF) in runners.

Preliminary work in our laboratory showed an increase in peak positive FM (resistance to toeing out), and trends towards higher FM at peak braking force and net angular impulse in 13 runners with a history of TSF, compared to runners with no previous lower extremity bony injuries. These trends suggest that there might be significant differences in FM variables between the groups if a larger subject pool were analyzed. Furthermore, the preliminary study did not consider the absolute magnitude of peak FM. An absolute measure (peak regardless of direction) may better represent the size of the torsional force acting on the lower extremity.

The purpose of this study was to investigate the relationships between FM variables and the occurrence of TSF in female distance runners. We hypothesized that maximum positive FM (POSFM), FM at peak braking force (FMBRAK), net angular impulse (IMP) and absolute peak FM (ABSFM) would be greater in runners with a history of TSF compared to uninjured controls. In addition, ABSFM would be predictive of group membership.

METHODS

A group of uninjured female distance runners with a history of tibial stress fracture ($n = 25$, age $= 28 \pm 10$y, weekly mileage $= 116 \pm 39$ miles) and an age- and mileage-matched control group ($n = 25$, age $= 26 \pm 9$y, weekly mileage $= 117 \pm 47$ miles) ran at 3.7m/s on a 25m runway containing a force platform sampling at 960Hz. Data from five trials were scaled to body weight and height and values for each variable averaged for statistical analysis. Differences between the TSF and control groups were examined using independent t-tests ($p \leq 0.05$). All t-tests were one-tailed, as only higher values in the TSF group were of interest. The utility of ABSFM in predicting group membership was investigated using binary logistic regression.

RESULTS AND DISCUSSION

Generally, FM was greater in the TSF group (Table 1). While the magnitude of FM was significantly higher in the TSF group for POSFM and FMBRAK, the highest values in both groups were found in ABSFM. ABSFM also had a larger effect size (0.93, large) than POSFM (0.76, moderate). The higher value of ABSFM, compared to POSFM, indicates that in some runners negative FM (resistance to toeing in) is greater in magnitude than positive FM (resistance to toeing out). This is supported by our observations that some runners have a negative bias in their free moment curve. Therefore, POSFM does not always reflect the highest torsional force experienced by these subjects.

Further support for the importance of ABSFM in TSF was provided by the binary logistic regression. Regression results suggest that increased ABSFM is related to an increased likelihood of being in the TSF group. The model indicated that for every 1.0×10^{-4} increase in ABSFM, the likelihood of having a history of TSF increases by a factor of 1.354 (95% confidence interval 1.086 to 1.688), $p = 0.007$. According to the model chi-square statistic, the model is significant ($p = 0.001$). It also predicted group membership correctly in 66% of the cases. The Nagelkerke R square value was 0.251, suggesting that 25% of the variance between the two groups is explained by ABSFM.

These data suggest a relationship between FM and a history of TSF in distance runners. However, further prospective studies are needed to determine whether ABSFM can be used to predict the occurrence of TSF in female distance runners.

Table 1: Free moment variables in TSF and Control groups.

	POSFM	FMBRAK	IMP (s)	ABSFM
TSF	7.5 ± 4.5	4.0 ± 5.7	6.2 ± 5.7	9.0 ± 4.3
Controls	4.7 ± 2.5	1.6 ± 3.7	1.6 ± 5.5	5.9 ± 2.1
Effect size	0.76	0.49	0.83	0.93
P	0.023	0.043	0.781	0.001

All variables are $\times 10^{-3}$, except IMP which is $\times 10^{-4}$.

CONCLUSIONS

Peak positive FM, FM at peak braking force and absolute peak FM were significantly higher in the TSF group. This suggests an association with history of TSF in female distance runners. The magnitude of absolute peak FM successfully predicted a history of TSF in this group in 66% of cases.

ACKNOWLEDGEMENTS

This study was supported by Department of Defense grant DAMD17-00-1-0515.

THE INFLUENCE OF MUSIC ON KINEMATIC AND DYNAMIC GAIT PATTERNS

Wolfgang I. Schöllhorn, Henrike Kokenge, Karina Fölling, Meike Alichmann, Christiane Bohn
Institute for Sport Science; University of Münster
email: schoell@uni-muenster.de

INTRODUCTION

For the optimization of therapeutic processes different learning strategies have been suggested. From a neurophysiological point of view cognitve processes such as learning and memory are affected by emotions [1]. Beside psychological interventions music can lead to emotional responses [2]. The aim of this study was to investigate the influences of music on everyday movement with extremely individual characteristics [3].

METHODS

Kinematic and dynamic gait patterns were recorded from 16 subjects within three conditions: Stimulating (s), comfort (c), and no (n) music. In all trials headphones were worn. In each condition subjects had to pass in a randomly assigned order three times a 5m zone within which one double step was video recorded (25 Hz). Gait velocity was self determined (0.86-1.49m/s) and measured by means of two pairs of light bars. Subjects were recorded three dimensionally with 2 video cameras (JVC), one in front, and one on the right side of the subject. Angles and angular velocities of the main joints (ankle, knee, hip, shoulder, elbow, trunk) were determined via DLT within SIMI-Motion-Software. Ground reaction forces were measured via Kistler force platform (1000Hz). The time courses of all variables and groups of variables during three right ground contact phases were classified by means of hierarchical cluster analysis. The groups of variables were a) all angles and angular velocities, b) all angles, c) all angular velocities, d) all variables of the lower extremities, e) the ankle angle, and f) ground reaction forces. Assessment rates were determined by $AR = \frac{1}{n}\sum_{i=1}^{n}\frac{m_i}{r_i}100\%$,
with n = number of subjects, m = number of trials clustered in the largest cluster, and r = number of trials per subject. All subjects had to answer a questionnaire about the personal music preferences.

RESULTS AND DISCUSSION

The cluster analysis on the basis of all trial and all variables reveals an AR of 90%, which increases up to 93% when only the angular variables are included. Both ARs with respect to the number of subjects and trials provide strong evidence for the individuality of gait patterns according to [3]. On the background of the ground reaction forces the AR decreases to 70%. Obviously, the angular variables, as the most differentiated type of data, lead to the highest AR. The cluster analyses within single subjects show a strong influence of music in the gait pattern of only two subjects. Most intriguingly some subjects who stated to have no musical or rhythmical sense in the questionnaire displayed fairly good ARs for each type of music. Two subjects achieved a 100% separation by the type of music which they were listening to

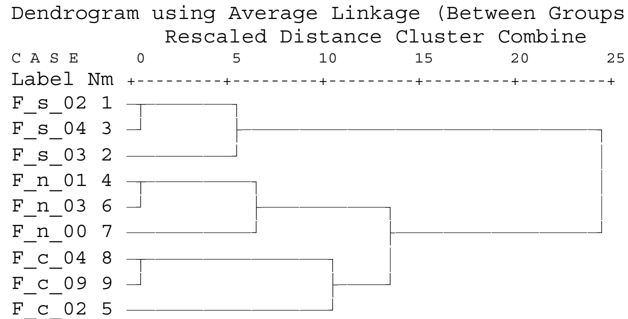

Figure 1: Dendrogram of a single subject (F) based on all kinematic variables with a disjunct separation of gait patterns by type of music (s, n. c).

during gait (figure 1). Very often the single- subject- cluster-analysis leads to a separation of the gait pattern with stimulating or with calming music. When the stimulating music mode was separated the calming and no music mode was merged. When the calming music condition was separated the stimulating and no music condition was clustered together. Whether this provides insight into fundamental personal moods or into situational personal music preferences demands further research.

CONCLUSIONS

Although the applied linear pattern recognition approach is not considered as the most differentiated one[4] , the results verify relevant consequences. This study shows a twofold support for emphasizing research, particularly in clinical applications, on individuals rather than on groups. Firstly, a strong individuality of gait patterns was diagnosed. Secondly, evidence for individual motor reaction when listening to music was shown. However, the presented approach provides a supplementary and sensitive tool for interdisciplinary problems towards more complex or holistic questions.

REFERENCES

1. M. K. Sun and D. L. Alkon, *Neuroscience* 129, 129-139 (2004).
2. J. A. Sloboda, *Psychology of Music* 19, 110-120 (1991).
3. W. I. Schöllhorn, B. M. Nigg, D. Stefanyshyn, W. Liu, *Gait Posture* 15, 180-186 (2002).
4. C. S. Pattichis, C. N. Schizas, L. T. Middleton, *IEEE Trans.Biomed.Eng.* 42, 486-496 (1995).

COMPARING THE GAIT OF BIPEDAL ROBOTS WITH THAT OF INFANTS

Christopher L Vaughan, Victoria Mendel, Nazir Karbanee
MRC/UCT Medical Imaging Research Unit, Department of Human Biology, University of Cape Town,
Observatory 7925, South Africa; email: kvaughan@cormack.uct.ac.za

INTRODUCTION

There has been renewed interest in the capabilities of bipedal robots in the past decade. They may be classified as *active*, (having their own power supply and actuators) or *passive* (driven by the effects of gravity), and *static* (the centre of gravity is always within the base of support) or *dynamic*, where the CG sometimes falls outside the support base [1].

Just as a bipedal robot needs to trade off balance and propulsion, so too does the human infant need to master these two factors when learning to walk [1]. In this paper we compare our recent data for an active and a passive robot with our prior data for young children [2].

METHODS

We based our active robot on the “drunken sailor” design [3], in which two actuators were incorporated, one to drive the legs and the other to tip the robot from side-to-side in order to clear the swinging leg (Figure 1). The robot had adjustable leg lengths (of 122, 137 and 152 mm), a mass of 0.72 kg and a programmable controller, allowing different cadences and step lengths to be implemented. A six camera Vicon system was employed to capture images at 120 Hz from four retro-reflective markers attached to the hip joints and feet of the robot. The 3D data files enabled us to calculate cadence, stride length and velocity, from which dimensionless velocity – the square root of the Froude Number – was derived [4].

Figure 1: Powered bipedal robot driven by two motors.

Our passive robot was based on the design of Garcia *et al.* [5] and implemented in both a physical and computer simulated form. We present here our simulated data. The robot had adjustable leg lengths (520, 770 and 1160 mm), a mass of 3.46 kg and we varied the angle of the inclined slope from 1.0 to 4.5 degrees. The temporal-distance parameters, which enabled us to calculate the dimensionless velocity, were a direct output of the simulation.

RESULTS AND DISCUSSION

Our active robot used a static pattern of movement to maximize stability (Figure 1) and hence sacrificed velocity, having dimensionless velocity values between 0.031 and 0.043 (Figure 2). In contrast, our passive robot used a dynamic gait pattern, achieving dimensionless values up to 0.3 for shorter leg lengths and a slope of 4.5 degrees (Figure 2). With increasing leg lengths, however, stability was critical and the dimensionless velocities dropped off to 0.1. These data are in good agreement with the literature: Collins *et al.* [6] built and tested a 3D passive dynamic walker, while Honda’s ASIMOV robot [7] has an active dynamic pattern (Figure 2). The dimensionless velocities for children [2, 4] increase from 0.25 for an 18 month-old up to a value of 0.45 for teenagers and adults.

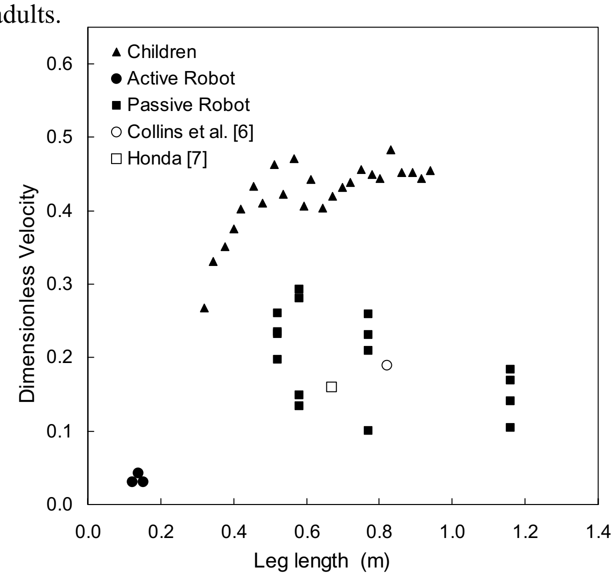

Figure 2: Dimensionless velocity as a function of leg length.

CONCLUSIONS

From a developmental point of view, the gait of sophisticated bipedal robots is just beginning to approach that of infants.

REFERENCES

1. Vaughan CL, *J Biomech* **36**, 513-523, 2003.
2. Vaughan CL, et al. *Exp Brain Res* **153**, 123-127, 2003.
3. Two-legged robots http://www.walkingrobots.com/
4. Vaughan CL, et al. *Gait & Posture* **21**, 2005 (in press).
5. Garcia M, et al. *J Biomech Eng* **120**, 281-288, 1998.
6. Collins SH, et al. *Int J Robot Res* **20**, 607-615, 2001.
7. Honda humanoid robot http://world.honda.com/ASIMO/

KINEMATICS OF MOUSE SCROLLING

U. Chris Ugbolue, Thomas H. Christophel, Nancy A. Baker, Zong-Ming Li
Hand Research Laboratory, Departments of Orthopaedic Surgery, Bioengineering, and Occupational Therapy
University of Pittsburgh, Pittsburgh, PA 15213, USA. zmli@pitt.edu; www.pitt.edu/~zmli/handlab/

INTRODUCTION

One of the most common computer peripherals is a two-button scroll mouse. Studies have shown that the risk of upper extremity musculoskeletal disorders can be increased by intensive mouse use such as clicking and dragging, wheel scrolling, cursor movement, and awkward wrist posture [1-2]. Previous studies on mouse use have focused on finger forces [3-4], wrist positions [5] and hand motion [6] during pointing and dragging. The purpose of this study was to examine the joint kinematics of the index finger during mouse wheel scrolling.

METHODS

Five subjects aged 26 ± 3 years without any musculoskeletal disorders of the upper extremity participated in the study. All subjects were familiar with using a computer mouse. Five reflective markers of 5 mm diameter were placed on the index finger: the center of the nail, distal and proximal interphalangeal (DIP and PIP) joints, metacarpophangeal (MCP) joint, and the midpoint of the 2nd metacarpal bone. A motion capture system (VICON 460, Oxford, UK) was used to collect the marker motion data. Each subject comfortably gripped a two-button scroll mouse (Microsoft® Intellimouse®, Redmond, WA) with their right hand with the index finger over the wheel. They were instructed to maintain a neutral wrist posture. The subjects performed full forward and backward scrolling tasks at 1 cycle/second following a metronome. Ten cycles of scrolling data was collected at 60 Hz. The range of motion and the coefficients of correlation for the DIP, PIP, and MCP joints were calculated. A two-way ANOVA was used to examine the difference in joint range of motion (ROM).

RESULTS

During backward scrolling, the DIP, PIP and MCP joint movements were highly correlated (Figure 1). The DIP and PIP joint moved in phase with correlation coefficient of 0.996 ± 0.025. The MCP joint was correlated in anti-phase with the PIP or DIP joint. For example, the correlation coefficient between the MCP and PIP joint movements was -0.916 ± 0.066. Each backward scroll cycle began with the minimal flexion of the DIP and PIP joints (5.3 ± 2.5° and 14.6 ± 7.4° respectively) and maximum flexion of the MCP joint (21.9 ± 6.9°) and ended with maximum flexion of the DIP and PIP joints (38.1 ± 8.8°and in 57.2 ± 8.5° respectively) and minimal flexion of the MCP joint (8.4 ± 6.1°). A similar, but reverse, pattern was observed during forward scrolling. In backward or forward scrolling the PIP joint ROM was greater than the DIP joint ROM and was more than twice the MCP joint ROM ($P < 0.05$, Figure 2). The scrolling direction did not significantly affect the ROMs of the DIP, PIP or MCP joint.

DISCUSSION

Mouse use requires controlled and stereotypical movements of the DIP, PIP and MCP joints. The negative correlation between the MCP joint and the interphalangeal (IP) joints (i.e. IP joint flexion with MCP joint extension) is advantageous as it prevents excessive muscle shortening or lengthening, preserving optimal muscle lengths for effective force production. On the other hand, our results show that the DIP, PIP and MCP joints move in the ranges of 5-38°, 15-57°, and 8-22°, respectively, during a typical mouse scroll. These motions comprise approximately 40% (DIP), 50% (PIP), and 15% (MCP) of their respective full ROM (see also [7]). In addition, these motion ranges do not surround the functional neutral positions of these joints, which may place these joints under more-than-minimum stress throughout mouse use. Mouse use can account for over 20% of computer use time and more than 78 uses per hour [3]. This repetitive stresses on finger joints could lead to musculoskeletal disorders of hand muscles and finger joints. Further biomechanical studies of mouse usage could help design ergonomic mice to minimize musculoskeletal strain.

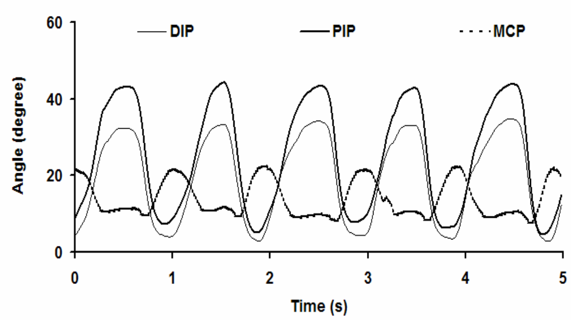

Figure **1**. Representative joint angular motion during 5-cycles of backward scrolling.

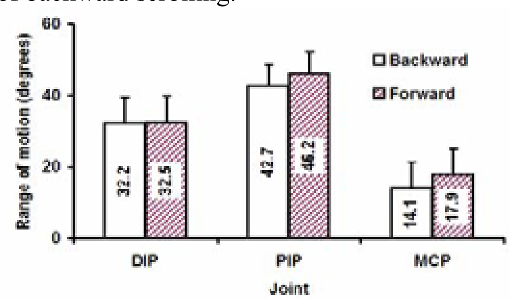

Figure 2. Range of motion of individual finger joints during backward and forward scrolling.

REFERENCES

[1] Karlqvist et al. Ergonomics, 37: 1261-1267, 1994
[2] Fogleman & Brogmus, Ergonomics, 38:2465-2475, 1995
[3] Johnson et al. Scandinavian J Work Environ Health, 26 (5): 398-405, 2000
[4] Rempel et al. Proc Fourth International Scientific Conference: Work with Display Units, Milan, 1994
[5] Damaan et al., Proc Human Factors and Ergonomics Society, p625-629, 1995
[6] Johnson et al., Proceedings of the American Industrial Hygiene Conference and Exposition, Fairfax, VA, p12-13. 1993
[7] Clarkson, Musculoskeletal Assessment, Philadelphia: Lippincott Williams & Wilkins: p200.

KINEMATICS OF THUMB OPPOSITION

Jie Tang, Thomas Christophel, Zong-Ming Li
Hand Research Laboratory, Departments of Orthopaedic Surgery and Bioengineering
University of Pittsburgh, Pittsburgh, PA 15213, USA. zmli@pitt.edu; www.pitt.edu/~zmli/handlab/

INTRODUCTION

One of the most important hand functions is thumb opposition, which results from flexion, abduction and axial rotation at the carpometacarpal, metacarpophalangeal and interphalangeal joints [1]. The thenar muscles, innervated by the median nerve, are critical for coordinated thumb movements. It is commonly observed that thumb opposition is impaired with median neuropathy [2]. The clinical method to assess thumb motion capability is to measure the distance between the thumb tip and the fingertip, or between the thumb tip and distal palmar crease [3]. Goniometric measurement quantifies thumb range of motion in isolated planes, but does not provide information of the dynamic relationship between flexion and rotation. The purpose of this study was to examine the 3D movement of the thumb during opposition.

METHODS

Three young male subjects aged 25.6 ± 3.2 years without any musculoskeletal disorders of the upper extremity participated in the study. Six markers with diameters of 5 mm were attached to the hand (Figure 1). Three markers (1, 2 and 3) affixed to a small triangle plate were attached to the thumb nail. Three markers (4, 5, and 6) were placed on the outstretched fingers to establish a local coordinate frame (*OXYZ*). A motion capture system (VICON 460, Oxford, UK) was used to collect marker motion data. A normal vector (**N**) was defined from the three markers on the plate, pointing in the dorsal direction. The forearm was supinated so that the palm was in parallel to the horizontal plane and faced upward. All fingers were at full extension in parallel with the palm.

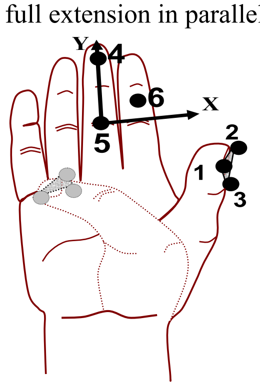

Figure 1: Marker placement on the right hand.

The subjects were instructed to perform thumb opposition, starting with the thumb at full extension in the palm plane, and then moving the thumb tip to the distal palmar crease of the little finger, and then returning to the starting position. Ten cycles of this movement were performed at self-selected paces. The thumb tip was approximated by calculating the middle point between markers 1 and 2. The flexion and pronation angles were determined by computing the projection angles of the vector **N** in the XY and XZ planes, respective.

RESULTS AND DISCUSSION

In the XZ plane, the thumb tip moved in a parabola trajectory during opposition (Figure 2). The thumb tip moved palmarly in the beginning phase and then dorsally as the tip approached the palmar crease. The movement magnitudes in the X and Z directions were 124.8 ± 8.6 mm and 54.2 ± 10.9 mm, respectively. The distal phalanx changed its orientation constantly during opposition, as shown by the non-parallel normal vectors (Figure 2). This change in orientation was produced by concurrent angular movements in flexion and pronation (Figure 3). The angle-angle curves showed piecewise coordination patterns. Thumb pronation was mainly produced in the beginning phase of opposition, perhaps contributing from the movement at the carpometacarpal joint. Flexion motion dominated at the later phase of opposition, likely resulting from movements at the metacarpophalangeal and interphalangeal joints. The ranges of motion in flexion and pronation were 166.7 ± 14.4 degrees and 144.0 ± 16.5 degrees, respectively. These kinematic analyses potentially allow for quantification and discrimination of abnormal motion patterns by hands with neuromuscular disorders such as carpal tunnel syndrome.

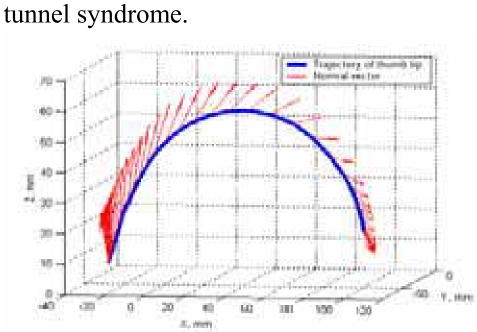

Figure 2: Trajectories of the thumb tip and the normal vector during thumb opposition.

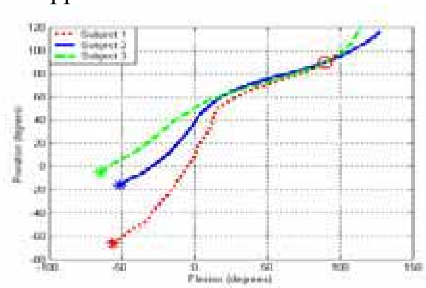

Figure 3: Relationship between flexion and pronation during thumb opposition.

REFERENCES

1. Cooney WP et al.. *J Bone Joint Surg [Am]* **63**, 1371-1381, 1981.
2. Aulicino PL. *The Hand*, Tubiana, Saunders: Philadelphia, 1981
3. Litchman HM & Paslay PR. *J Bone Joint Surg [Am]* **56**, 85-91, 1974.

THE EFFECT OF FOOT PLACEMENT ON SIT-TO-STAND WITH AND WITHOUT WALKER ASSISTANCE

Shashank Raina, Catherine A. Stevermer, and Jason C. Gillette
Department of Health and Human Performance, Iowa State University, Ames, Iowa, USA; email: sraina@iastate.edu

INTRODUCTION

Moving from a sitting to standing position is a transfer that is essential to perform activities of daily living. Individuals having dysfunctional or weak lower extremities may have difficulty performing sit-to-stand movements and may depend on others for assistance. For example, frail elderly and those who have suffered a spinal cord injury may struggle with sit-to-stand movements. If leg strength is insufficient, the upper extremities play an important role in the standing up process. Greater arm assistance reduces maximum hip and knee joint torques by up to 50% [1]. Janssen et al. concluded that repositioning of feet influenced the strategy of the sit-to-stand movement and required lower extension moments at the hip [2]. The present study is aimed at finding how foot placement with or without walker assistance alters the biomechanics of sit to stand in healthy adults.

METHODS

Four subjects (2 male/2 female, age 25 ± 5 yr, height 173 ± 20 cm) participated in this experiment. The subjects did not have any musculoskeletal disorder that would hinder their sit-to-stand performance. An eight-camera video System (Peak Performance, Englewood, CO) was used to track ten reflective markers placed on both sides of the subject's body. The subjects sat on a bench (height 45 cm) with their feet on two separate force platforms (AMTI, Watertown, MA). A Guardian Easy Care adult folding walker was used as an assist device for sit-to-stand. Two triaxial force sensors (Kistler, Amherst, NY) were used for measuring the hand forces applied on the walker.

The subjects sat with their feet shoulder width apart. The protocol involved two independent variables. The first independent variable compared standing with and without the assistance of a walker. The second independent variable that was tested involved three different initial postures: the feet anterior with respect to the knees (foot-forward) at an angle of 80° of knee flexion, the feet even with the knees (foot-even) at an angle of 90° of knee flexion, and the feet posterior with respect to the knees (foot-back) at an angle of 100° degrees of knee flexion. Hand support forces and joint moments were calculated during sit-to-stand movements for these six conditions. Each subject performed three repetitions of the six sit-to-stand conditions for a total of 18 trials.

RESULTS AND DISCUSSION

Maximum hip extension moments increased from foot-back to foot-forward (Fig.1). The hip extension moments without walker assistance were higher than when using a walker for all foot positions. Maximum knee extension moments without walker assistance decreased from foot-back to foot-forward. Knee extension moments with the walker did not show as much of a change with foot positioning. Knee extension moments for foot-forward were higher with walker assistance

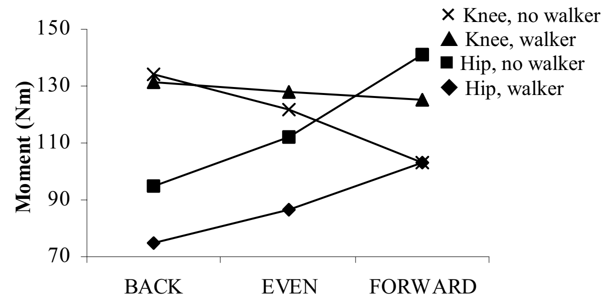

Figure 1: Hip and knee joint moments for alternative foot placements with and without walker assistance.

than without. Maximum ankle plantar flexion moments for foot-back (46Nm) were greater than foot-forward (23Nm) with the walker. The hand forces also showed a consistent trend. The vertical, anterior, and lateral forces increased gradually from foot-back to foot-forward. The average vertical forces were 18% body weight for foot-forward and 11% body weight for foot-back.

The results suggest that if a person has weakness in the hip, a foot-back placement will help reduce the moment requirements on the hip. Walker support in combination with a foot-back placement will facilitate lowering the hip moment requirements even further. This combination will also reduce the hand forces required on the walker, which is important because elderly individuals may have low upper body strength. The knee moments were substantially lower without walker assistance for the foot-forward placement. This may be due to the restricted range of motion of the upper body that reduces the amount of momentum generated. However, there was little difference between knee joint requirements with or without walker assistance when using the foot-back placement.

In addition, the results suggest that the net moment requirements of the body are reduced at the foot-even placement if standing with the help of a walker and the foot-back position if standing without any external support. These results can be used to help optimize stimulation patterns for paraplegics using functional neuromuscular stimulation systems to perform sit-to-stand. They can also be used to choose an appropriate foot placement to help reduce the force requirements for people with weakness in specific joints.

REFERENCES

1. Bahrami F, et al. *Clin Biomech* **15**, 123-133, 2000.
2. Janssen WGM, et al. *Phys Ther* **82**, 866-870, 2002.

ACKNOWLEDGEMENTS

This study was partially funded by a Special Research Initiation Grant from Iowa State University.

IN-VIVO PASSIVE KINEMATICS OF OSTEOARTHRITIC KNEES

[1,2]Robert Siston, [1,2]Nicholas Giori, [1,3]Stuart Goodman, and [1,4]Scott Delp
Departments of [1]Mechanical Engineering, [3]Orthopaedic Surgery, and [4]BioEngineering, Stanford University
[2]Palo Alto Veterans Affairs Health Care System, Palo Alto, California
email: rsiston@stanford.edu, web: http://nmbl.stanford.edu

INTRODUCTION

Osteoarthritis (OA) can lead to pain, disability, and loss of range of motion in the knee. The pre-operative condition of the knee has been shown to influence the functional outcome of treatments for OA [1]. A greater understanding of how motion of the knee is affected by OA may facilitate the assessment of the efficacy of potential treatments. We used a computer-assisted navigation system to study the passive kinematics of osteoarthritic knees intra-operatively and answer two questions: 1) Does the varus or valgus malalignment of the knee measured in full extension persist with flexion of the knee? and 2) Do "femoral rollback" (posterior translation of the femur on the tibia with flexion) and "screw-home" (external rotation of the femur with flexion) motions seen in a normal knee remain in an OA knee?

METHODS

Twelve patients undergoing a primary total knee arthroplasty for treatment of OA gave informed consent to participate in this study. Patients were grouped by limb alignment: mechanical axis varus alignment (six patients), neutral alignment (four patients), and valgus alignment (two patients).

After exposure of the knee joint at the beginning of the operation, the surgeon attached passive optical reference frames from the navigation system onto the medial side of the distal femur and proximal tibia. He circumducted the femur and used a calibrated optical stylus to identify landmarks on the patient's distal femur, proximal tibia, and ankle to establish anatomic reference frames in the femur[2] and tibia[3]. While supporting the leg with an open palm so as to avoid applying external loads to the limb, the surgeon then manipulated the subject's leg through two full cycles of knee flexion and extension. The navigation system recorded the position and orientation of the femur and tibia throughout the motion pattern. We measured the displacement of the origin of the femoral reference frame (OFRF) with respect to the origin of the tibia reference frame to assess translation and determined the flexion, varus/valgus, and internal/external rotations of the knee[4]. Repeated measures analysis of variance (ANOVA) was used to evaluate the differences in kinematics between the three OA groups from 20° to 105° of flexion, the range of motion common to all subjects.

RESULTS AND DISCUSSION

The varus/valgus malalignment measured in full extension did not persist with flexion of the knee, but the neutrally aligned limbs generally maintained their neutral alignment (Figure 1). All groups trended towards a slightly varus alignment in deep flexion, resulting in overall significantly different patterns of varus/valgus rotation between groups ($p < 0.001$).

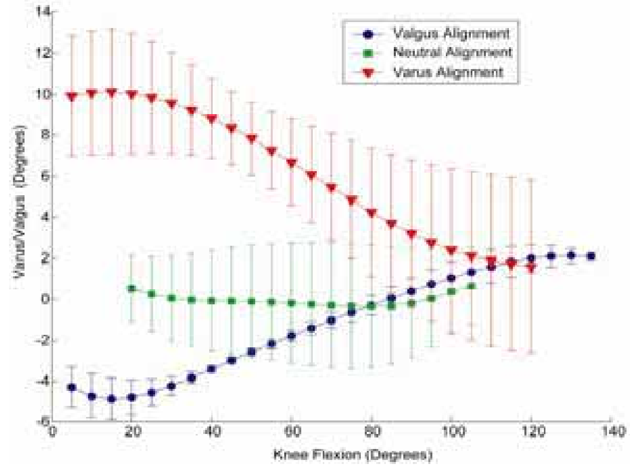

Figure 1: Mean varus (+)/valgus (-) angles for 3 OA groups. Error bars represent 1 standard deviation.

A very limited "screw-home" motion was present in all OA groups. In varus knees, the femur externally rotated by an average of 3.0° ± 4.4° over the common range of knee flexion. In the neutral and valgus groups, we observed an average of 5.0°± 6.9° and 1.0°± 2.6° of external rotation, respectively. No differences existed between the groups ($p > 0.6$). These magnitudes of rotation are all less than what has been observed in normal knees, where as much as 25° of rotation has been reported [5].

The expected "femoral rollback" was present in the varus and valgus groups. In varus knees, the OFRF translated posteriorly an average of 10.7 ± 3.0 mm. Similarly, in valgus knees, the OFRF translated posteriorly and average of 8.0 ± 0.9 mm. However, the motion of the neutral knees was significantly different than the other two groups ($p < 0.001$). In neutral knees, the OFRF translated anteriorly an average of 7.0 ± 5.8 mm before translating posteriorly 7.7 ± 5.0 mm from the most anterior point.

This study represents the first intra-operative characterization of the in-vivo passive kinematics of advanced osteoarthritic knees. Computer-assisted navigation systems, in which reference frames are directly and rigidly attached to bone, are a valuable research tool and represent a safe and reliable means of collecting intra-operative kinematic data.

REFERENCES

1. Harvey, I.A., et. al.. *JBJS Br* 75, 950-955, 1993.
2. Yoshioka, Y. et al.. *JBJS* 69-A, 873-880, 1987.
3. Yoshioka, Y., et al.. *JOR* 7,132-137,1989.
4. Grood, E.S., Suntay, W.J.. *J BioMech Eng* 105, 136-144, 1983.
5. Wilson, D.R., et al.. *J Biomech* **33**, 464-473, 2000.

THE RELIABILITY AND REPRODUCIBILITY OF FOOT MEASUREMENTS USING A MIRRORED FOOT PHOTO BOX COMPARED TO CALIPER MEASUREMENTS

Nathan A. Mall, W. Mack Hardaker, James A. Nunley, MD, and Robin M. Queen, PhD
Michael W. Krzyzewski Human Performance Laboratory, Duke University
Division of Orthopaedic Surgery, Duke University Medical Center

INTRODUCTION

It is widely believed that the height of the medial longitudinal arch (MLA) is a predisposing factor to various types of lower extremity injuries. Discrepancy exists in the literature as to which foot morphologies predispose individuals to certain injury patterns, and whether MLA height plays a role in injury prevention. The controversy surrounding the importance of MLA height and foot morphology could result from inconsistencies in these measurements in the literature. The purpose of this study is to determine the reliability of intertester, intratester, and foot photo box (FPB) versus caliper measurements

METHODS

This study was comprised of 30 subjects (15 male, 15 female) between the ages of 18 and 30 years old. Both feet were tested (n=60) in a 90% weight bearing (WB) stance. First, each foot was palpated and marked for the following bony landmarks in a 90% WB posture: navicular, calcaneus, head of the first metatarsal, and shaft of the first metatarsal. Using a caliper and goniometer, foot length (FL), truncated foot length (TFL), navicular height (NH), height of the dorsum of the foot at 50% of FL (DH), and the angle of the first ray (FRA) were measured. A digital photograph was taken of both feet individually in a 90% weight bearing stance. The mirrored FPB allowed visualization of the posterior, anterior, medial, and plantar aspects of the foot from one picture.

Once the first rater completed measuring and photographing both feet, the marks were erased and the second rater repeated the protocol. The bony landmarks were then digitized and FL, TFL, NH and FRA were measured from the digital photos using the SigmaScan Pro software (Richmond, CA).

The subjects were then asked to return for a second day of testing approximately one week later. Intertester and between measurement condition (FPB versus calipers) reliability were determined using the intraclass correlation coefficient (ICC) (2,k) model and intratester reliability was determined using the ICC (2,1) model.

RESULTS AND DISCUSSION

Preliminary results for the mean, intratester, and intertester reliability for the foot photographs, as well as the FPB to caliper comparisons for the right foot of 15 subjects (7 male, 8 female) are shown in Table 1. While the intratester reliability was slightly higher using caliper measurements, the intertester reliability was higher using the FPB.

Comparing the FPB to the caliper measurements shows good reliability (0.993-0.858), indicating that the FPB could be used in place of caliper measurements with similar reliability. Caliper measurements have already been shown to be valid to radiographic measurements [3], the FPB measurements should also correlate well with radiographic measurements. The FPB values reported are similar to those in the literature from radiographic measurements[1]. The highest between condition reliability was NH/FL and NH/TFL.[3]

	Mean	SD	Intratester	Intertester	Conditions
FL	250.26	21	0.9909	0.9945	0.993
TFL	186.46	14.92	0.9773	0.9774	0.9922
NH	36.8	5.31	0.8644	0.8405	0.9451
DH	60.1	5.76	0.8862	0.9203	0.8897
FRA	24.2	4.39	0.4911	0.5964	0.9197
NH/FL	0.1475	0.0235	0.8885	0.882	0.9282
NH/TFL	0.1984	0.0317	0.8941	0.9011	0.9176
DH/FL	0.2401	0.0172	0.8499	0.8366	0.8601
DH/TFL	0.3232	0.0223	0.7757	0.7448	0.8578

Table 1: Foot Photograph Measurements and ICC values.

The FPB offers several advantages over the caliper measurements; including, speed of measurement, visualization of rearfoot angle, measurement of various footprint indices, and the ability to have the pictures assessed by foot and ankle specialists for a clinical assessment of foot morphology. From the plantar view, various footprint indices[2] were measured, with intratester and intertester ICC values ranging from 0.975 to 0.923 and 0.969 to 0.928, respectively. The average photo took 51.3 ± 19.6 seconds per foot while the caliper measurements took more than 4 times as long with an average of 227.4 ± 68.9 seconds.

CONCLUSIONS

The mirrored FPB is at least as reliable as caliper measurements, and offers better intertester reliability. The speed of testing is faster with the photograph, and also allows calculation of footprint indices. Previously, caliper measurements have been shown to correlate well with radiographic measurements. Our results are similar to results from previous studies which reported caliper and radiographic measurements. [1, 3] Future studies will determine the validity of the FPB to radiographic measurements.

REFERENCES

1. Cavanagh, P, et al. The relationship of static foot structure to dynamic foot function. *J of Biomechanics*. **30**:243-250, 1997
2. Shiang, T, et al. Evaluating different footprint parameters as a predictor of arch height. *IEEE Engineering in Medicine and Biology.* **17**: 62-66, 1998.
3. Williams, D and I McClay. Measurements Used to Characterize the Foot ad the Medial Longitudinal Arch: Reliability and Validity. *Physical Therapy*. **80**:864-871, 2000.

CARDIAC CATHETER WITH VARIABLE HEAD CURVATURE ACTUATED BY IPMC (IONIC POLYMER-METAL COMPOSITE)

M.-S. Ju[1], P.-K. Fung[1], C.-C. K. Lin[2], Y.-Z. Hong[1], C.-K. Chung[1], T.-C. Wu[3]
[1]Department of Mechanical Engineering, National Cheng Kung University
[2]Department of Neurology, National Cheng Kung University
[3]Electronics Research & Service Organization, Industrial Technology Research Institute

INTRODUCTION

The technically difficult part in a catheter surgery is to push a catheter (~ϕ2mm below) through the crotched vessels by using guide wires with different curvatures. The above-mentioned process takes a lot of time and also raises the risk of surgery due to numbers of guide-wire changes.

IPMC (Ionic Polymer-Metal Composite) consists of an electrical active polymer layer sandwiched by metal electrode layers. When a driving voltage is provided, the IPMC membrane bends toward anode direction because the hydrophilic positive ions move toward cathode direction [1-3]. During the design of an IPMC actuator, there are four technical problems to be overcome: (1) how to glue electrode layers on the polymer membrane; (2) how to drive under a wet condition; (3) how to prevent electrolysis when higher driving voltage (>1.23V) is to be applied and (4) how to increase the force output of the actuator (mN order).

The purpose of this study is to develop an active guide-wire by using IPMC membrane and to overcome above technical problems.

METHODS

According to the actuation principle of IPMC, a two segment IPMC actuator is designed. Two pairs of electrodes are joined to the polymer membrane and form a two-segment actuator. While two different phase voltages are applied on the two pairs of electrodes respectively, the actuator can perform a variable S-shape deformation. This design will offer an opportunity to solve the problem that a traditional catheter with a single fixed curvature can not overcome.

The size of the IPMC actuator is decided based on the constraint of the catheter and the length is 20 mm, the width is 1 mm and the thickness is 0.2 mm. The diameter of the whole active guide-wire is constrained to less than 1 mm.

The nafion® is one kind of ion exchange polymers, and a 20% nafion solution is used to make a membrane in this study. In order to attach the electrode layers to the membrane, we mix the nano silver powder with a 5% nafion solution and spread on a glass slide. After drying the solution, a membrane is formed (the electrode layer, ~30μm), and a 20% nafion solution is spread on it and cured to form a film. The film was cut into two halves and glued together by using nafion solution. The electroless silver plating process was applied at the final step and nickel layer was electroplated on two spots as the contacts for electric conduction.

To demonstrate the feasibility of the IPMC actuator, a performance test system was set up and a prototype of IPMC actuator is fabricated and tested. Finally, the IPMC actuator was assembled to form the head of a guide-wire.

RESULTS AND DISCUSSION

The IPMC (length of 20mm, width of 5 mm & thickness of 0.3 mm) driven by 2.8V could perform an approximately 90 degree bending (Fig. 1) and the force was about 0.25gf. The sheet resistances are 0.12 ohm/mm and 0.15 ohm/mm. The elasticity of the IPMC is 3.5GPa (Dry) or 1.16GPa (Wet). According to the test results, the deformation and force output were proportional to the driving voltage, and we found that the oxidations on IPMC surface electrodes made the resistance too high, so its performance was deteriorated under long-term actuation (Fig. 2).

CONCLUSIONS

The active guide wire with the IPMC actuator could change the head curvature according to the magnitude of the applied voltage. Reducing the surface resistance and maintaining the humidity of IPMC can further improve the performance of the active head, and to accurately control the tip position of the IPMC actuator is an on-going work.

REFERENCES

1. Guo S, et al. *IEEE Conference* **3**, 22-28, 1996.
2. Shahinpoor M, et al. *Smart Materials and Structure* **10**, 819-833, 2001.
3. Sia NN, et al. *Journal of Applied Physics* **93** (9), 5255-5267, 2003.

ACKNOWLEDGEMENTS

The study is supported by ITRI and partially supported by National Science Council of R.O.C. under contract number NSC 92-2218-E-006-060.

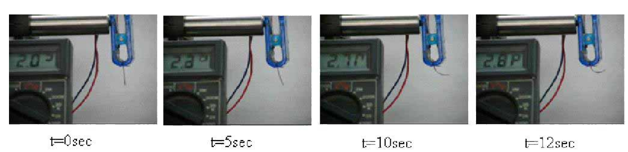

Figure 1: Actuating result of IPMC driven by dc voltage

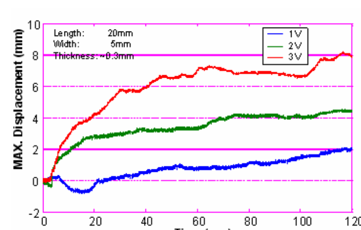

Figure 2: Displacement Response

BALL IMPACT ANALYSIS IN FOOTBALL USING FEM FOOT MODEL

[1]Takeshi Asai, [2]Hiroyuki Nunome, [3]Yasuhisa Kamata and [4]Reiko Sakashita
[1]Yamagata Univ., Yamagata, Japan; email:asai@kescriy.kj.yamagata-u.ac.jp
[2]Nagoya Univ., Nagoya, Japan.
[3]Iwate Univ., Morioka, Japan.
[4]Kumamoto Univ., Kumamoto, Japan.

INTRODUCTION

The motion analysis of kicking in football has been studied by several investigators. However, there are few studies that analyzed the interaction of the kicking foot and ball at impact in football. The purpose of this study is to clarify the relation between the stress distribution, the deformation and the impact point on the foot using a finite element skeletal foot model.

METHODS

The basic shape of the finite element skeletal foot joint model was described using a commercial foot skeletal model for computer graphics and anatomical data, and the solid model was defined after simplifying that model (Fig. 1). The Young's modulus of hard tissue parts was 15GPa and the Poisson's ratio was 0.3 [1], The Young's modulus of soft tissue parts was 1500 MPa and the Poisson's ratio was 0.3 [2]. In the analysis of the ratio of restitution on the foot complex at impact using the instep kick model, the impact point was defined from the axis of the ball –80 to +60 mm at intervals of 20 mm in the vertical direction. The ball velocity and the direction of the ball trajectory after impact were compared by each vertical offset distance. In the curve kick analysis, the generation of spin depends upon the attacking angle and the impact point of the foot on the ball in relation to the axis of the ball. The simulations were carried out with a fixed coefficient of friction of 0.4 with attacking angles from the axis of the ball 5 to 85 degrees at intervals of 10 degrees.

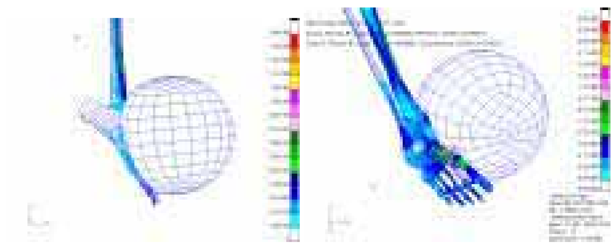

(a) (b)

Figure 1: The instep kick model (a) and the curve kick model (b) using finite element skeletal foot model.

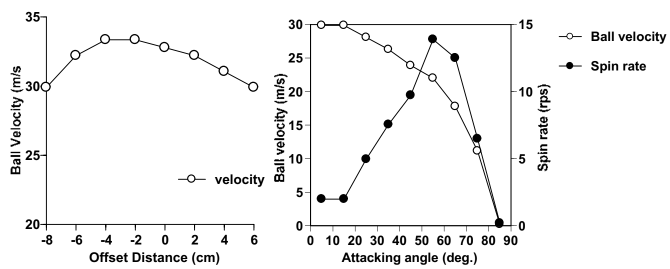

(a) (b)

Figure 2: The relation between offset distance and ball velocity (a) and the relation between attacking angle and ball velocity (b).

RESULTS AND DISCUSSION

In the instep kick analysis using the finite element skeletal foot model, high intensity stress (about 50 MPa) was seen in metatarsal, cuneiform, navicular and tibia at impact. The ball velocity after impact with an offset distance of -20 mm was 33.4 m/s, and that for the offset distance of +20 mm was 32.2 m/s. The maximum ball velocity after impact in this simulation was for the offset distance of -20 mm and –40 mm, while the minimum ball velocity was for the offset distance of +60 mm and -80 mm (Fig. 2(a)). These was a tendency that the deformation of the foot joint in the lower impact case was greater than that of the higher impact case. It is suggested that the energy dispersion of the foot for the lower impact case is greater than that for the higher impact case. The direction of the ball trajectory after impact (shoot angle) in each case indicated a nonlinear trend. The maximum shoot angle was 16 degrees for the offset distance of -20 mm. It seems that the shoot angle was influenced by the location and the deformation of the foot complex and the ball. The relation between attacking angle and ball velocity and the relation between attacking angle and spin rate are shown in Fig. 2(b). It was found that the spin rate of the ball generally increases as attacking angle is increased, but the spin rate falls rapidly in the case of the attacking angle being 75 degrees or greater. The ball velocity simply decreases as the attacking angle is increased. Hence it is considered that, for the infront curve kick, a foot orientation at impact, with the attacking angle between the face vector and the swing vector generates the optimum moment with which to generate ball spin.

REFERENCES

1. Furusu K., Iwamoto M., Miki K. and Kato C., *Proc. of the JSAE spring convention*, Society of automotive engineering of Japan, 5-8, 1999.
2. Jacob S., et al., *Mechanics Research Communications*, Vol. 23, No. 4, 387-393, 1996.

MEASUREMENT OF DIFFERENCE BETWEEN LEFT AND RIGHT RIB LENGTHS ON SCOLIOSIS

[1] Hongmei Jin, [1] Tamotsu Tamaki, [2] Kazuhisa Takahashi, and [2] Tsutomu Akazawa
[1] Department of Mechanical Engineering, Nippon Institute of Technology, Japan,
[2] Department of Orthopaedic Surgery, School of Medicine, Chiba University, Japan;
email: m2021004@mstu.nit.ac.jp

INTRODUCTION

Scoliosis is a disease of spinal deformity accompanied by deformation of costal bones. Some researchers[1] suppose that the difference between left and right costal bones lengths cause the scoliosis in some case of AIS (Adolescent Idiopathic scoliosis). This paper measured the lengths of left and right ribs of 5 scoliosis subjects and 3 healthy subjects. These geometrical data are gotten by 3-D reconstruction of CT images. CAD software executed the measurement of 3-D length of the ribs.

METHODS

CT images including thoracic vertebrae and their costal bones were used. The images were reconstructed by the software, 3D-DOCTOR (Able Software corp. MA, USA). The 3-D data were converted to CAD data. For the measurement of the length of 3-D costal bone, CAD software, Rhinoceros (Robert McNeel &Associates, WA, USA) was used. Figure 1 is an extracted spinal centerline and the illustration of its curvature.
Table 1 shows the Cobb angles and locations of apex vertebrae of curvature of scoliosis on each patient.

RESULTS AND DISCUSSION

The result shows that in scoliosis subjects the difference between the left and the right rib lengths was a little larger than that of healthy subjects. And the average percentage difference to the rib length was 2.2% (SD: 1.5%) in scoliosis subjects (n=5) whereas it was 1.1% (SD: 0.1%) in healthy subjects (n=3). (Figure 2) Each patient's correlation coefficient of CCS (Concave Curvature of Spine) and ΔCV (Difference between the rib length of concave side of spine and that of the conVex side, that is the value subtracted rib length of the convex side of spine from that of the concave side) is shown in Figure 3. The average correlation coefficient of all patients was 0.24 (SD: 0.33) assuming the tendency that the rib of concave side is longer than that of convex side.

CONCLUSIONS

From the measurement of five scoliosis patients, it was suggested that rib of concave side of spinal curvature is longer than that of convex side or that there is no difference between both lengths of the rib.

Table 1: Cobb angle and apex vertebral location of five scoliosis subjects

Case	Cobb angle (deg.)	Location of apex vertebra of the lateral curvature
1	97	T8
2	50	T9
3	57	T7
4	65	T12
5	41	T8

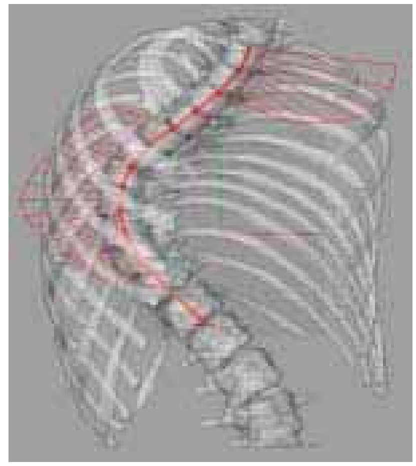

Figure 1: Illustrated magnitude of curvature of the spinal centerline having the direction to the convex side of the line.

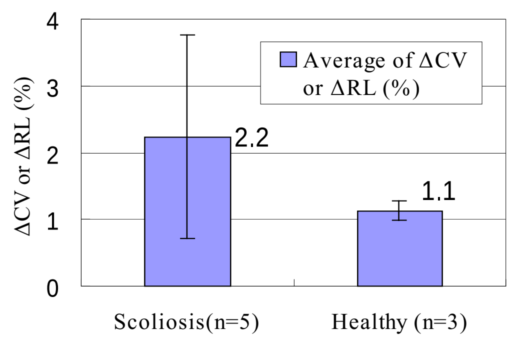

Figure 2: Comparison between Δ CV of scoliosis patients and Δ RL of healthy subjects.

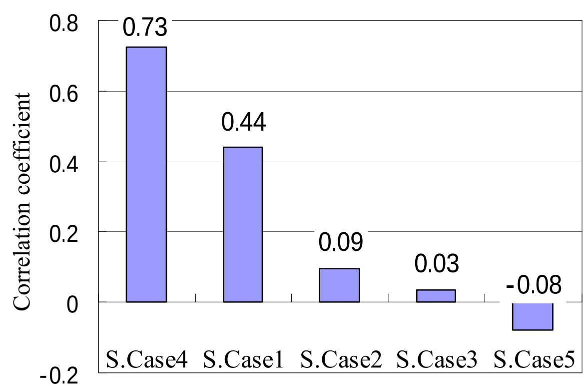

Figure 3: Correlation coefficient between CCS (Concave Curvature of spine) and ΔCV for each patient.

REFERENCES

1. Sevastik JA, New approaches into the etiology, pathomechanism and treatment of idiopathic scoliosis, *International Research Society of Spinal Deformities, Symposium 2004*, Vancouver, Canada, University of British Columbia Press, 31-38, 2004.

THREE DIMENSIONAL FINITE ELEMENT ANALYSIS OF MAXILLARY PALATE WITH A UNILATERAL CLEFT

Linping Zhao[1, 3] P. K. Patel[1, 2, 3]
[1]Shriners Hospitals for Children, 2211 Oak Park Avenue, Chicago, IL 60707 Email: lzhao@shrinenet.org
[2]Northwestern University, Feinberg School of Medicine, Chicago, IL 60611
[3] The Cleft Lip and Palate Institute, Westchester, IL 60154

INTRODUCTION

Cleft lip and palate is the most common congenital craniofacial deformity. Up to 80 % of this population has a skeletal defect. While the surgical procedures for reconstructing the skeletal defects in children with facial clefts is well established [1, 2], it remains unclear how the cleft leads to the alteration in the stress/strain distribution within the maxillary palate, the alveolar arch and the midfacial skeleton. Our preliminary study revealed that unilateral cleft leads to non-uniform, asymmetric stress/strain distribution within the maxillary skeleton during functional tasks [3]. The aim of the current study was to verify such hypothesis that the size (depth and width) of unilateral cleft affects the severity of the non-uniform stress/strain distribution within the mid-facial skeleton.

METHODS

Subject-specific CT scans were obtained following a protocol for clinical examination. Using ANALYZE AVW 4.0 (Biomedical Imaging Resource, Mayo Foundation, Rochester, MN), the maxilla was separated from the mandible and skull, and its surface was modeled with triangular patches. This surface model was imported into ABAQUS/CAE (ABAQUS Inc., Pawtucket, RI). After manually editing, that is, cleaning, repairing, and smoothing, a volumetric mesh was generated using tetrahedral elements. This model acted as a control model (CM). Four models were established to simulate the unilateral cleft with various depths: 1) absent second right incisor (MT), 2) alveolar ridge defect (AR), 3) incomplete unilateral cleft palate (IUCP), and 4) complete unilateral cleft palate (CUCP). Three models were used to simulate complete unilateral cleft with various widths: 1) 1.0 dental unit (CUCP), 2) 1.5 dental units (CUCPm), and 3) 2.0 dental units (CUCPw). For all FE models, the maxilla was modeled as a linear elastic object with elastic modulus of 12.7 GPa and Poisson’s ratio of 0.3. Both the inferior and posterior ends of the maxilla were fixed while forces (100 N in total) perpendicular to the occlusal plane were added to the teeth. The FE analysis was conducted using ABAQUS STANDARD v. 6.4 (ABAQUS Inc., Pawtucket, RI).

RESULTS AND DISCUSSION

The severity of non-uniform stress/strain distribution, indexed using the peak value of Von Mises stress at the paranasal region, increased when the unilateral cleft size (depth and width) increased. The severity was also indexed using the difference in parameters between two sites that were picked up from cleft and non-cleft sides, respectively. Along with the increase of the cleft depth and width, parameters such as Von Mises stress (Fig. 1 middle) and maximum principal strain (Fig. 1 bottom) increased on the non-left side while decreased on the cleft side. This led to an increase in the difference, or in severity of the non-uniform stress/strain distribution.

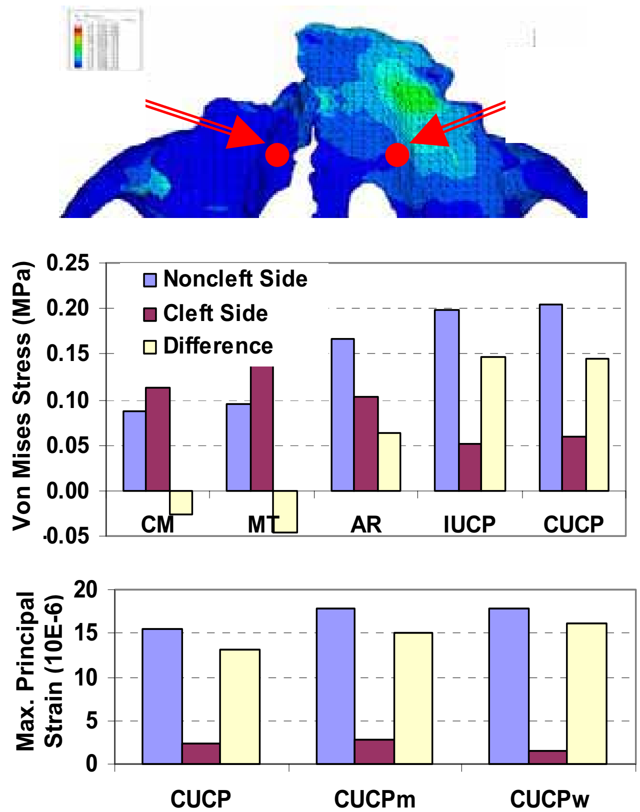

Figure 1: The severity of the non-uniform stress/strain distribution within the maxillary palate indicated in Von Mises stress as a function of unilateral cleft depth (middle), and in maximum principal strain as a function of unilateral cleft width (bottom).

CONCLUSIONS

The existence of unilateral cleft leads to non-uniform stress/strain distribution on the maxillary palate and midfacial skeleton. The size of the unilateral cleft affects the non-uniformity: the larger the depth and width of the unilateral cleft, the more severe the non-uniform stress/strain distribution within the maxillary palate and midfacial skeleton. This has the clinical implication that earlier skeletal reconstruction would restore symmetrical growth and development of the facial skeleton.

REFERENCES

[1]. Boyne PJ, Sands NR. *Oral Surg* **30**, 87-92, 1972.
[2]. Dow JL and Pate PK. *Clin Plastic Surg* **31**, 303-313, 2004.
[3]. Zhao Linping, Patel P, Harris G. *The 26th Annual International Conference of the IEEE EMBS*, San Francisco, CA. 5077-5079, 2004.

Muscle coordination in stroke patients' upper limbs

[1]Zhen-Wei Wu, [1]Ming-Shaung Ju, [2]Chou-Chin K. Lin
[1]Department of Mechanical Engineering, National Cheng Kung University, Tainan, Taiwan; web: http://myweb.ncku.edu.tw/~msju/mml,
[2]Department of Neurology, National Cheng Kung University Hospital, Tainan, Taiwan

INTRODUCTION

Robot-aided rehabilitation is getting popular in the rehabilitation of the strokes. Compared with conventional therapies, a major benefit of rehabilitation robot is that it is able to offer stroke patients repetitive rehabilitation exercise with high intensity and steady quality. Furthermore, sensors deployed on the robot provide abundant information on patient's motor functions. Physiological data such as EMG and biomechanical signals such as joint torque and ROM can be utilized for motor function assessments on stroke patients.
With a laboratory-made rehabilitation robot [1], motion data of patient's upper limb was recorded throughout the treatment [2]. In this work, analyses of load sharing by model simulation were utilized to characterize variation in muscle coordination and improvement of patient's motor function. Model validation was prerequisite for further studies and was the primary topic in this abstract to ensure that the model does reflect faithfully the interaction between patients and the robot to an extent.

METHODS

All the recruited patients were asked to perform horizontal circular tracking motion at shoulder level with visual cues and under resistance applied by the rehabilitation robot. The patients were requested to perform the tracking motion as accurate as possible. A 6-axis load cell and electro-goniometer were fixed to the end-effector of the robot and the patient respectively to measure the force and motion data.
To estimate the muscle force/neural excitation in patient's upper limb during treatment, a neuromuscular model of human upper limb [3] were modified by adding five muscles [4,5]. The kinematic structure of the shoulder was also modified to fit the treatment movement. An optimization was employed to solve the force distribution problem and the neural excitation distribution which could be utilized to characterize the coordination in affected muscles. In the present study, a widely accepted objective function as following [6] was employed for solving the load sharing problem:

$$J = \sum_{j=1}^{9} \left(\frac{F_j}{PCSA_j} \right)^2$$

where F_j is muscle force of the j^{th} muscle. When solve the inverse dynamics problem, only the steady state muscle forces were considered to generate the required muscle activations. When the muscle activations were known, neural excitations could be obtained from the following equation:

$$\dot{A}_j = C_j \left(u_j - A_j \right)$$

where u_j was neural excitation, A_j was muscle activation and C_j was a time constant of the j^{th} muscle.

RESULTS AND DISCUSSION

A simplified human upper limb (Figure 1) was utilized to validate correctness of the optimization procedure. It was assumed that the limb was performing horizontal circular motion with a constant angular velocity ($\omega = 2\pi/5$ (rad/sec)) at shoulder level. For simplicity, only parts of deltoid and pectoralis major muscles were used to generate the required torque at shoulder joint to validate the optimization procedure. In the first 2.3 sec, muscle DS was activated to horizontally extend the shoulder joint and DC and PM were silent. Conversely, during 2.3~4.3 sec, DC and PM were co-activated to horizontally flex the shoulder joint and DS was silent. The resultant torque of these three muscles was equal to the estimated torque. Due to physiological differences, the torque contribution between DC and PM were different. Results of validation showed that the optimization procedure could determine the load sharing condition under the given objective function, the antagonist remained silent while the agonists were both activated.

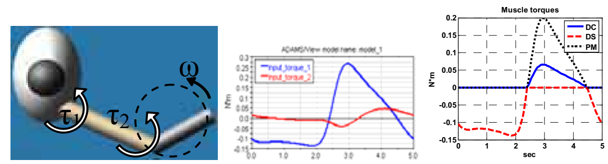

Figure 1: A simplified human upper limb for validation of optimization procedure for the load sharing problem. On the middle, estimated joint torques are depicted. On the right, the torques applied at shoulder joint by DC, DS and PM are depicted.

CONCLUSIONS

The biomechanical model of human upper limb coupled with the optimization procedure was suitable for analyzing load sharing of stroke patient's upper limb. By modeling interaction among muscles, it provided a feasible way for further investigation on various possibilities of a patient's muscle coordination before and after the robot-aided treatment.

REFERENCES

1. Ju MS, et al.. *IEEE Trans Neural Sys. Rehab Eng* (accepted), 2005.
2. Wu SY, et al.. *Proc. 2002 Conference on BME Technology*, 2002.
3. Lemay MA, et al.. *J Biomechanics* 29, 1319-1330, 1996.
4. Langenderfer J, et al.. *J Clinical Biomechanics* 19, 664-670, 2004.
5. Pigeon P, et al.. *J Biomechanics* 29, 1365-1370, 1996.
6. Mohamed KT, et al.. *Computers ind. Engng* 31, 503-506, 1996.

ACKNOWLEDGEMENTS

We are grateful for Dr. Shu-Ming Chen and Prof. Ing-Shiou Hwang's advice on clinical aspects of this study.

BIOMECHANICAL FEATURES OF NORMAL PATELLAR TENDONS AND THOSE WITH PATELLAR TENDINOPATHY

Andrew Simons, Tim Wrigley, Kay Crossley, Ben Metcalf
Centre for Health, Exercise and Sports Medicine (CHESM), University of Melbourne, Australia
email: timw@unimelb.edu.au web: http://www.physioth.unimelb.edu.au/chesm/

INTRODUCTION

The aetiology of patellar tendinopathy commonly suffered by recreational and higher level athletes in jumping sports ('jumper's knee') is uncertain. Currently there is controversy as to whether the most often affected posterior fibres of the patellar tendon (PT) at the patella inferior pole are subjected to greater or lesser stress [1,2]. Particular gross features of PTs that may predispose them to tendinopathy have not been found. Symptomatic PTs are commonly seen to be thickened on MRI [3], however no clear differences in absolute AP width between symptomatic and asymptomatic PTs have been found. Cross-sectional area (CSA) in PTs has not been studied along the entire PT length, with or without tendinopathy. The aim of this study was to characterise this CSA, and determine if tendinopathy resulted in differences in CSA, or PT stress during a maximal contraction, compared to normal PTs.

METHODS

16 symptomatic patients (12M/4F, 27.3±6.6 yr) and 22 asymptomatic controls (15M/7F, 23.0±4.7 yr) were studied. Symptomatic subjects had a PT lesion detected on ultrasound, a stereotypical history of patellar tendinopathy symptoms sufficient to affect exercise activity for 6 months or more, with no previous knee surgery or signs of other knee pathology. Both groups participated in jumping sports at least once a week.

MRI was performed in a 1.5T magnet (GE Sigma Horizon LX) and extremity array coil, on the symptomatic knee in patients and the 'jumping' knee in controls, in full extension. Multiple 3.5 mm PD images (512x384 matrix) were obtained in the sagittal and axial planes. As a proportional indication of the likely moment to which the knee extensor mechanism including the PT might be exposed in jumping sport activities, the maximum isometric knee extension moment was recorded on a Kincom 125-AP dynamometer at 60 degs flexion, with correction for gravitational torque.

The PT was outlined in each axial slice and CSA calculated using Image-J software (NIH). The PT moment arm was measured from the tibiofemoral contact point to the mid-PT in the sagittal plane [4] and adjusted to account for the difference between full extension and 60 degs flexion. Force and stress in the PT were estimated as follows:

$$F_{PT} = M_{KE} / r_{PT} \qquad \sigma_{PT} = F_{PT} / A_{PT}$$

Where: F_{PT} = PT force (N)
M_{KE} = knee extension moment (N.m)
A_{PT} = PT CSA (mm^2)
r_{PT} = PT moment arm (mm)
σ_{PT} = PT stress (MPa)

RESULTS AND DISCUSSION

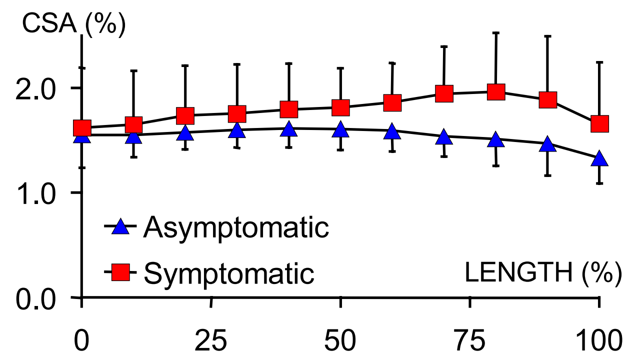

Figure 1: Scaled PT CSA (% tibial width^2) vs PT length (0% = tibial tuberosity; 100% = patella inferior pole).

Table 1: Measured and calculated variables for asymptomatic and symptomatic subjects; mean (SD)

	Asymp.	Symp.	p
Height (cm)	177.9 (7.9)	178.5 (8.2)	.808
Body mass (kg)	70.9 (10.2)	82.9 (15.7)	.007*
Peak isometric moment (N.m)	152.9 (42.9)	163.6 (56.5)	.503
Peak isometric moment (N.m/kg)	2.16 (0.42)	2.00 (0.64)	.356
Max PT CSA (mm^2)	103.1 (24.1)	126.6 (32.8)	.014*
Min PT CSA (mm^2)	72.6 (20.0)	77.3 (29.4)	.557
Mean PT CSA (mm^2)	89.6 (19.0)	103.7 (25.5)	.055
Max scaled PT CSA[1] (%)	1.76 (0.22)	2.18 (0.51)	.007*
Min scaled PT CSA[1] (%)	1.25 (0.25)	1.35 (0.52)	.479
Mean scaled PT CSA[1] (%)	1.54 (0.16)	1.79 (0.41)	.034*
Peak PT force (N)	3588 (991)	3966 (1278)	.305
Stress for max PT CSA (MPa)	35.8 (9.6)	33.3 (12.5)	.481
Stress for min PT CSA (MPa)	54.2 (28.6)	67.5 (65.2)	.392
Stress for mean PT CSA (MPa)	40.9 (10.7)	40.5 (15.7)	.936

[1]scaled to % tibial width squared * $p < 0.05$

PT force and CSA in these young adult PTs (Table 1) were higher than has been reported for elderly PTs, while PT stress (based on mean CSA) was similar [5]. CSA did not increase at the distal insertion (Figure 1) as in the Achilles tendon [6]; in fact PTs tended to *decrease* CSA at the *opposite* end, the patella inferior pole. Maximum PT CSA was greater in the symptomatic group, but PT stress was not significantly different. Greater CSA is consistent with pathological thickening often seen on MRI, although this was highly variable. Future longitudinal studies will be required to identify any differences prior to symptom onset.

REFERENCES

1. Haraldsson BT, et al. *J Appl Physiol* (in press), 2005.
2. Maganaris CN, et al. *Sports Med* **34**, 1005-1017, 2004.
3. Ashford RL, et al. *Phys Ther Sport* **3**, 134-142, 2002.
4. Wretenberg P, et al. *Clin Biomech* 11, 439-446, 1996.
5. Reeves ND, et al. *J Physiol* **548**, 971-981, 2003.
6. Magnusson SP, et al. *Eur J Appl Physiol* **90**, 549-553, 2003.

PREDICTED GAIT MODIFICATIONS TO REDUCE THE PEAK KNEE ADDUCTION TORQUE

[1,2]Benjamin J. Fregly, [2]Kelly L. Rooney, and [1]Jeffrey A. Reinbolt
[1]Department of Mechanical & Aerospace Engineering, University of Florida,
[2]Department of Biomedical Engineering, University of Florida; email: fregly@ufl.edu, web: www.mae.ufl.edu/~fregly

INTRODUCTION

High tibial osteotomy (HTO) is a more conservative surgical procedure than is total knee replacement for treating medial compartment knee joint osteoarthritis (OA). Following HTO surgery, patients with a low peak knee adduction torque during gait tend to have the best long term clinical outcome [1]. As an alternative to HTO surgery, this study uses inverse dynamic optimization of a patient-specific full-body gait model to predict gait modifications that could reduce the peak knee adduction torque.

METHODS

Kinematic and kinetic gait data were collected from a single highly functional knee OA patient with 5º varus alignment and grade 2 medial OA in both knees. The subject walked at a speed of approximately 1 m/sec and also performed isolated joint trials to determine the position and orientation of each lower extremity joint [2]. One complete gait cycle (left heel strike to left heel strike) with clean surface marker and ground reaction data was selected as the nominal data set for the optimization study.

A dynamic, three-dimensional full-body gait model was developed using SIMM. The model possessed 27 degrees of freedom (DOFs) composed of gimbal (3 DOFs), universal (2 DOFs), and pin (1 DOF) joints. External forces and torques acting on the pelvis were calculated from a 6 DOF joint between the ground and pelvis. Since no external loads act on the pelvis in real life, non-zero external force or torque components at any time frame represent error in the model and/or experimental data.

Joint and body segment parameters in the model were tuned via optimization to match the nominal gait data as closely as possible. The cost function simultaneously minimized errors between model and experimental marker locations in the laboratory reference frame, external pelvis forces and torques, and changes in body segment parameters away from their initial values. Design variables were joint positions and orientations in the body segments, body segment parameters, and parameters defining joint translations and rotations (see below). Final root-mean-square (RMS) errors were 1.9 cm in surface marker positions and 3.6 N and 2.8 Nm in external pelvis forces and torques, respectively.

Inverse dynamic optimizations were performed to predict novel gait motions that minimized the left knee adduction torque subject to several reality constraints: follow the prescribed path of each foot, follow the experimental trunk orientation, eliminate external forces and torques on pelvis, and keep the center of pressure under each foot. The 500 design variables were motion and ground reaction torque curves parameterized using a combination of a cubic polynomial and eight Fourier harmonics [3]. Ground reaction forces, shoulder and elbow rotations, and pelvis horizontal translations were prescribed to match the experimental data. The optimizations were performed with and without penalty terms to minimize changes in the leg control torques.

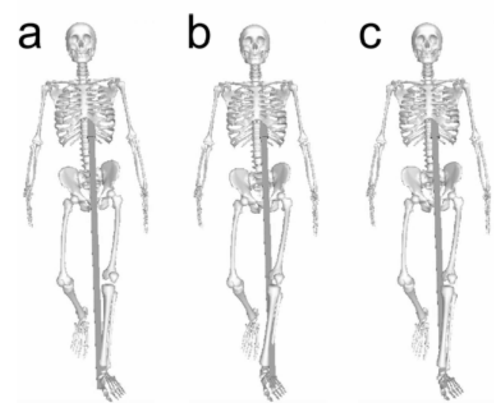

Figure 1: a) Experimental gait motion, b) gait motion predicted without control torque tracking, and c) gait motion predicted with control torque tracking. Arrows indicate line of action of ground reaction force vector.

RESULTS AND DISCUSSION

The optimizations predicted realistic gait motions that reduced the peak knee adduction torque by 72% without control torque tracking and 45% with it (Fig. 1). The optimizations drove the left knee inward in part through increased hip, knee, and ankle flexion, causing the ground reaction force vector to pass more laterally to the knee center than in the experimental situation. These kinematic changes were produced primarily by an increase in knee extension and ankle inversion torque. Predicted changes with control torque tracking were similar but decreased in amplitude compared to those found without control torque tracking.

The optimization results suggest that gait modifications may be able to reduce the peak knee adduction torque by as much as HTO surgery, which has been reported to produce an average 34% reduction [1]. Due to their synergistic effects, even small gait modifications had a large influence on the peak knee adduction torque. If the predicted gait modifications can be achieved in practice, they could help define new rehabilitation strategies for knee OA patients either apart from or in conjunction with HTO surgery.

REFERENCES

1. Prodromos CC., et al. *JBJS* **67A**, 1188-1194, 1985.
2. Reinbolt, JA, et al., *J Biomech*, in press, 2005.
3. Nagurka ML, et al. *J Dyn Sys Meas Cont* **112**, 17-26, 1990.

ACKNOWLEDGEMENTS

This work was funded by the Whitaker Foundation.

Effects of passive repeated plyometric training on specific kicking performance of elite Olympic Taekwondo player

[1]Hsiang-Hsin Wang, [1]Chiang Liu and, [1]Mu-Yen Chu, [2]Wei-Hua Ho, [2]Tzyy-Yuang Shiang
[1]*Institute of Coaching Science, National College of P.E & Sports, Taiwan,*
[2]*Institute of Sports Equipment Technology, Taipei P.E College, Taiwan*; email: mystarmailbox@yahoo.com.tw

INTRODUCTION

Sporting activities involved striking, kicking, jumping, or high frequency rapid acceleration movements require a high power output of the involved muscles (Newton, et.al 1996). Coaches and athletes have modified training method in an attempt to develop explosive power, because velocity of movement is an important factor to reach perfect performance. Therefore, The Passive Repeated Plyometric Training Machine (PRP Training Machine) was designed in order to reach the best power training effect. PRP movement has been shown consisted of many characteristics that set them distinctly apart from other types of movement such as high velocity, high frequency movement and isokinetic contraction during entire range of motion under passive contraction (Wang, et al 2001). Many researches indicated that PRP training could improve neuromuscular system of general players. However, it is not clear how much training effect can beneficial to elite players. Hence, the aim of this study was to determine the effects on specific kicking performance of a 6-wk PRP training program of elite Olympic Taekwondo player.

METHODS

Subject: The subject was an elite athlete who won a gold medal of Taekwondo event in 2004 Athens Olympic games. The subjects' age, height, and weight was 22 years, 173 cm, and 58 kg, respectively.

Specific kick test: Subject chose kicking movements according to his special skills and necessary of competition. The test movements include right leg turning kicking **(RTK)**, left leg turning kicking **(LTK)**, left leg slide step turning kicking **(LSTK)**, right leg axe kicking **(RAK)**, left leg axe kicking **(LAK)**, right leg back kicking **(RBK)**, and left leg 5 continuous kicking **(LCK).** An accelerometer was attached on the back of dummy to catch time and impact acceleration of dummy. When the movement test begins, subject standing in front of dummy and chose a suitable distance. Subject has to kick the target of dummy as rapidly as possible while trigger was flashed red light. The kicking velocity was displacement divided by movement time (m/sec). Besides, total time of 5 kicks (sec) was used to calculate kicking velocity of LCK. The kicking power was the square root of 3 dimensional impact accelerations of the tri-axial accelerometer while the dummy was kicked by subject. The kicking power of LCK was calculated total power of 5 kicks (g).

Training program: PRP machine can control the frequency of pedal and monitor training load during entire movement in passive and repeated form. Training duration was three times a week for six weeks before the pre-competition of Athens Olympic Games. The training load was between 60%MVC to 70%MVC; the frequency of pedal was between 1.5Hz to 3Hz. Exercise duration was set 10 seconds to 15 seconds. The training program was 8 sets a time, and took three minutes rest between each set.

RESULTS AND DISCUSSION

The results indicate that velocity of RTK was significantly increased after PRP training ($p < 0.05$). Beside, the kicking power of LAK and RBK were also significantly increased after PRP training ($p < 0.05$). The velocity and power of most movements were increased after PRP training, but no significant change occurred (Table 1). The subject of this study was elite Taekwondo player who won three times gold medal of international championship during 2002 to 2004. Therefore, breakthrough of physical strength and specific kicking performance was difficult for top athlete. Thus, even very little progress of velocity and power was valuable to an elite player and excited everyone who joined this training project.

Table 1: Training effect of PRP after 6-wk. (n = 3)

Variable	Pre-training M ± SD	Post-training M ± SD	p
Velocity (m/sec)			
RTK	3.496 ±0.167	3.666 ±0.161	.04*
LTK	3.606 ±0.205	3.906 ±0.442	.33
LSTK	2.646 ±0.213	2.630 ±0.160	.81
RAK	3.190 ±0.180	3.436 ±0.211	.11
LAK	3.250 ±0.230	3.080 ±0.235	.57
RBK	2.970 ±0.547	3.196 ±0.083	.52
LCK (sec)	2.406 ±0.041	2.316 ±0.073	.30
Power(g)			
RTK	124.39±6.02	138.51±9.31	.16
LTK	112.65±2.03	122.63±11.44	.24
LSTK	103.91±3.90	109.38±11.44	.38
RAK	32.47±6.96	36.92±9.72	.42
LAK	60.72±3.53	63.24±2.74	.03*
RBK	112.69±5.28	135.06±4.20	.02*
LCK	449.11±47.90	546.47±14.13	.07

* p-value significantly less 0.05

CONCLUSIONS

The results indicate that a PRP training program could improve the velocity and power of kicking of elite Taekwondo player in a sport specific kicking performance. Based on the results of this study, we believe that PRP training is an efficient method of training for elite players to improve strength and power. Therefore, PRP training could be used for those sports activities that involve high muscle speed and power such as Taekwondo, soccer and volleyball etc.

REFERENCES

1. Newton R.U, et al. *J Biomech* **12**, 31-43, 1996.
2. Wang H.H, et al. *Proceedings of ISBS XIX*, San Francisco, U.S.A, Abstract 68-71, 2003

JOINT KINETICS AND POSTURE CONTROL DURING DROP LANDINGS

Yasuyuki Yoshda and Takeo Maruyama
Graduate School of Decision Science and Technology,
Tokyo Institute of Technology, Tokyo, Japan

INTRODUCTION

Landing movement from vertical direction has been investigated in biomechanics since force platforms were developed to measure ground reaction forces. In drop landing studies, control of rotary stability based on the net effect of the three joint moments has not been investigated, previously. Devita & Skelly [1] investigated the relationship between knee joint flexion and kinetic parameters during stiff and soft drop landings. However, this study did not consider rotary stability. Ashby & Heegaard [2] quantified rotary stability in standing long jump study by using the moment about center of mass by ground reaction force (M_{CM}). The purpose of the present study is to investigate the relationship between lower extremity joint kinetics and posture control during drop landings.

METHODS

Ten healthy male subjects (mean±SD: age 22.9±0.99 years; body mass 68.2±7.00 kg; height 174.5±3.57 cm) participated after providing written informed consent. All subjects wore tight fitting shorts and a T-shirts, and were tested in bare feet.
A force platform (Kistler type 9287BA Kistler Instruments, Switzerland) was used to measure the ground reaction force (GRF) at 1kH. The left sagital view was recorded using two high-speed cameras (FASTCAM Photoron, Japan) at 0.25kHz. The motion capture and recording GRF were synchronized using a synchronized pulse generator (PH-1460, DKH, Japan).

Soft and stiff drop landing conditions from a 0.48m height was tested. In soft landing (SOFT), the subjects were instructed to land as soft as possible by using joint flexion. On the other hand, in stiff landing (STIFF) the subjects were instructed to land with minimum joint flexion. Subjects placed their hands on their hips, pushed off from the platform with one leg, closed their legs in midair, and landed on the force platform and dummy platform by each foot simultaneously.

The ankle, knee and hip joint moments were calculated using inverse dynamic analysis combining anthropometric, kinematic, and kinetic data. The segmental masses, the mass center location of the lower extremity, and their moment of inertia were estimated using a four segmental mathematical model [3]. In this study M_{CM} was also calculated

RESULTS AND DISCUSSION

Figure 1 shows a typical example of joint negative work contribution at ankle, knee and hip during STIFF and SOFT. In STIFF, joint negative work contribution was 52.48%, 35.24% and 12.29% in ankle, knee and hip. In SOFT, joint negative work contribution was 30.62%, 48.05% and 21.33% in ankle, knee and hip.

The pattern of power curve was different between STIFF and SOFT. In STIFF after touchdown negative ankle power increased dramatically. On the contrary, in SOFT knee joint negative power decreased slightly after the middle of movement.

In M_{CM} two style landings started with a forward moment, then the moment decreased and became backward. The peak of backward of STIFF was greater than that of SOFT. While M_{CM} is in backward direction, knee flexion moment and hip extensor moment appeared.

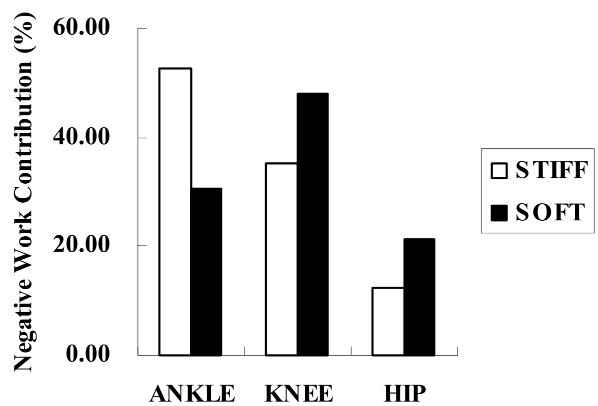

Figure 1: Typical example of ankle, knee and hip joint negative work contribution during STIFF and SOFT.

CONCLUSIONS

In conclusion, these findings indicate that ankle and knee joint contributed shock absorption. Hip joint did not much contributed shock absorption, however, contributed posture control during drop landings.

REFERENCES

1. Devita & Skelly. *Med Sci Sports Exerc* **24**, 108-115, 1992.
2. Ashby & Heegaard. *J Biomech* **35**, 1631-1637, 2002
3. Winter DA *Biomechanics and Motor Control of Human Movement*, 2nd ed, 11-50, John Wiley & Sons, New York, 1990

PROPERTIES OF TENNIS RACKET MADE BY DIFFERENTIAL CARBON FIBRE

[1]Jinn-Yen Chiang, [2]Ching-Cheng Chiang, [1]Ti-Yu Chen and [3]Jong-Her Yang
[1]National Changhua University of Education, Changhua , Taiwan, email:jychiang@cc.ncue.edu.tw
[2] National College of P. E. & Sports, Taoyuan, Taiwan
[3]Taipei Physical Education College, Taipei, Taiwan

INTRODUCTION

Tennis scientist and players dream of finding the excellent racket that will immediately transform them improving high performance and reduce occur sports injury (Brody, 1995). Haake, et al. (2003) advocate several biodynamical properties of tennis racket such as vibratory characteristics. Rackets general are made of new material high strength carbon or graphite composite. Carbon fibre used most often and it is usually combined with high strength carbon fibre. The purpose of this study was to investigate the vibration of various tennis rackets, which were composed by the mixture of high strength carbon fibre and general carbon fibre.

METHODS

There were five different kinds of tennis racket, composed by high strength carbon fibre and general carbon fibre in the ratio of 1 to 0, 3 to1, 1 to 1, 1 to 3 and 0 to 1. All of them had the same string tension, weight, balance point and moments of inertia. The experiments of the study were to collect their vibration amplitudes and to find damping ratio. One tri-axial accelerometer (range 50 g) was fixed on the racket handle and Bio PAC MP100 AcqKnowledge system (2000Hz) were used to acquire the vibratory signals. The ball speed was controlled to be 15 ± 2m/s by a Lobster ball machine. The selected variables in the experiments were tested by one-way ANOVA α= .05 significant level.

RESULTS AND DISCUSSION

The results of this study indicated that the carbon fibre made racket had a lower damping ratio on the center location (0.026) and off-center location (0.038; 0.064) impact (Table 1). The damping ratio was significantly decreased as the content of high strength carbon fibre in the racket was getting increased.

Comparing the results with prior damping ratio showed that the pure carbon fibre racket had a higher damping ratio on the center and off-center impact. And the damping ratio was decreased significantly as the content of high strength carbon fibre in the racket increased. Thereby, based on the vibratory analysis among the various material compose of tennis rackets, it was concluded that by increasing the content of high strength carbon fibre in the racket, it would be decreasing the damping effect of the racket. In other words, it would increase the vibratory wave after impact. Therefore, based on the vibratory analysis among the differential material composition of tennis rackets, it concluded that by increasing the content of glass fibre in the racket, it would be increasing the load in the tennis player's arm.

CONCLUSIONS

These results suggest that the forearm can be easily fatigue in such a high-impact power tennis players. This high-frequency vibration caused much greater stress on the joint of the hand and arm. Then, indirectly, this phenomenon might affect the athlete's performance.

REFERENCES

1. Brody, H. (1995). How would a physicist design a tennis racket. *Physics Today*, **March**, 26-31.
2. Haake, S.J. et al (2003). The dynamic impact characteristics of tennis balls with tennis rackets. *J. Sports. Sci*, **21**, 839-851.

Table 1: Summary of Results (Mean ± SD)

Percentage of high strength carbon fibre Impact Position	**0%**	**25%**	**50%**	**75%**	**100%**
Near Impact*	0.064 ± 0.004	0.064 ± 0.004	0.064 ± 0.004	0.072 ± 0.001	0.083 ± 0.004
2nd amplitude (g)	30.53 ± 2.02	30.52 ± 1.51	30.52 ± 1.56	30.46 ± 1.69	30.44 ± 1.42
6th amplitude (g)	25.51 ± 1.67	23.89 ± 0.94	15.77 ± 1.12	13.44 ± 0.72	10.38 ± 0.64
Center Impact*	0.026 ± 0.003	0.038 ± 0.006	0.048 ± 0.006	0.053 ± 0.005	0.068 ± 0.005
2nd amplitude (g)	35.15 ± 1.60	35.03 ± 1.12	35.05 ± 2.35	35.47 ± 1.48	35.28 ± 1.86
6th amplitude (g)	18.32 ± 2.01	13.54 ± 2.19	10.61 ± 1.97	9.39 ± 1.01	6.42 ± 1.09
Top Impact*	0.038 ± 0.001	0.055 ± 0.002	0.055 ± 0.002	0.069 ± 0.005	0.072 ± 0.004
2nd amplitude (g)	40.49 ± 1.13	41.01 ± 1.15	41.76 ± 1.08	41.02 ± 1.14	40.59 ± 0.95
6th amplitude (g)	15.63 ± 0.67	11.61 ± 0.75	10.47 ± 0.77	7.35 ± 1.14	6.92 ± 0.69

*$p< .05$

THE STABILITY OF ACETABULAR CUP UNDER SCREW FIXATION

[1]Jui-Ting Hsu, [1]Chih-Han Chang, [1]Heng-Li Huang, [1]Guan-Liang Chang, [2]Kuo-An Lai, [3]Weng-Pin Chen
[1]Institute of Biomedical Engineering, National Cheng Kung University, Tainan, Taiwan
[2]Department of Orthopaedics, Medical Center, National Cheng Kung University, Tainan, Taiwan
[3]Department of Biomedical Engineering, Chung Yuan Christian University, Chungli, Taiwan

INTRODUCTION

The total hip replacement is a common surgical procedure in orthopaedics. However, the acetabular cup loosening is one of the major failure modes of cementless acetabular cup. Many researches point out that an unstable cup would induce a large micromotion under dynamic loading. This large micromotion would reduce the bone ongrowth on the cementless cup surface and prohibit the osseous integration [1, 2]. Besides the press fit fixation, the screw-fixation is a widely employed approach. However, how to achieve a better fixation effect with screw is still unclear. The objective of this study was to evaluate the effects of screw numbers and position on the initial stability of acetabular cup.

METHODS

Three dimensional finite element model of pelvis was established from the saw bone.(model and brand names) which included the cancellous bone, cortical shell and subchondral bone. The Osteonic Omnifit (Allendale, New Jersey) acetabular components (including five screw holes, titanium cup, polyethylene liner and ceramic head) were also modeled (Figure 1). The interface of cup and pelvis was simulated with surface–to-surface contact elements with coefficient of friction 0.5 [3]. All the other component interfaces were assumed to be bonded.

To evaluate the fixation, loadings of the five stages of a gait cycle [4] were applied at the center of the femoral head while the cup was fixed on the pelvis with one, two, three, four or five screws respectively. (To simplify the computational aspect, each screw was modeled as a cylinder.) The nodes on sacroiliac joint and pubic symphysis were fixed in all degree of freedom as the boundary condition. The maximum relative micromotion between cup and pelvis was used as the evaluation index for stability. All the finite element analyses were performed using the ANSYS (Swanson Analysis Inc., Huston, PA, USA) software package.

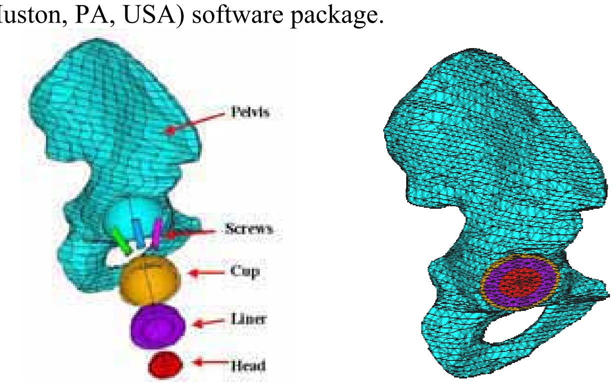

Figure 1: (a) Solid model (3 screws) and (b) Mesh model

RESULTS AND DISCUSSION

In general the maximum relative micromotions between cup and pelvis occurred at the inferior edge of the acetabular cup; that is the opposite side of the screw fixation region (Figure 2). For the same number of fixation screw, different combinations (e.g., five different choices of one-screw fixation) produced various stability effect and the differences could be large. For different number of fixation screw, the five-screw fixation, most stable one, only reduced 16% of peak relative micromotion compared with the best one-screw fixation (Figure 2). What this indicated is that screwing position is more important than screw number and inserting several screws closely together is unnecessary. However, the selection of screw position depends on both absolute location (relative to the loading location) and relative location (area size covered by multiple fixation-screws).

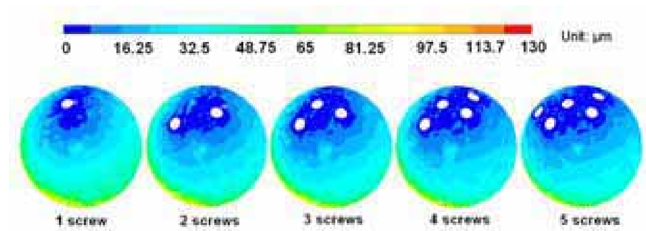

Figure 2: The micromotion distributions of different location screw fixation.

.

CONCLUSIONS

This study suggests that selection of screwing location for acetabular cup is an important factor to achieve better cup stability. The selection of better screw location depends mostly on the loading modes of the cup (the activities of the patient). The general principle is to spread the screw as far as possible so that it can cove most loading cases. However, the bone quality and anatomic consideration were neglected in this research.

REFERENCES

1. Pilliar RM, et al., *Clinical Orthopaedics and Related Research*, 208: 108-113, 1986
2. Litsky AS, et al., *Orthopedics,* 17: 53, 1994
3. Spears, IR, et al., *Journal of Biomechanics*, 34(1): 113-120, 2001
4. Pedersen DR et al., *Journal of Biomechanics,* 30: 959, 1997

ACKNOWLEDGEMENTS

This research was support by the National Science Council (NSC 93-2320-B-006-017) of Taiwan.

A MICROMECHANICAL MODEL OF THE PERIODONTAL LIGAMENT

[1] Mikhail Perelmuter, [2]Francesco Genna, and [2]Angelo Carini
[1]Institute for Problems in Mechanics, pr. Vernadskogo 101-1, 119526, Moscow, Russia (perelm@ipmnet.ru)
[2] Dept. of Civil Engineering, University of Brescia, Via Branze, 38 - 25123 Brescia, Italy (genna@bscivgen.ing.unibs.it)

INTRODUCTION

A micromechanical model of the periodontal ligament (PDL), a thin layer existing between a root of a tooth and the alveolar bone is considered. The PDL is considered as a nanocomposite material comprising corrugated collagen fibrils and viscous gel-like ground substance. The individual cell of the composite material, with the effective properties reflecting the properties of the fibrils and ground substance, is considered.

MECHANICAL MODELLING

It is supposed in the model that the collagen fibrils and the ground substance form a two-layer coaxial cylinder with curvilinear axis. The diameter of the external cylinder is chosen according to the volume fraction of the collagen fibrils. The general equations for the bending/tension strain states of this composite beam are written in the frame of geometrically nonlinear Reissner's beams, supposing that (i) the constituent materials (fibril and matrix) are linearly elastic and isotropic; (ii) there is no mechanical interaction among the fibrils; (iii) each subunit bears the normal and bending loading; (iv) the absence of shear strains; (v) the absence of distributed loads and moments. By assuming a small undulation of the fibrils axis it is possible to get an approximate analytical solution of the governing equations, from which stress-displacement curves can be obtained, showing the dependence of the apparent strain on the external stress, and, thus, the dependence of the PDL elastic modulus on the load level. To model at least the initial locking effect in the PDL under compressive loading we change the Young modulus of the ground substance to its bulk modulus.

RESULTS

Some results are presented for the following values of the mean parameters of the PDL: wavelength of the undulation λ=10, 16, 24 μm, maximal angular deflection of the fibril from the straight axis, $\theta_0 = 15^o$, 20^o, 25^o, average radius of the fibril cross section $r_f = 150\,nm$, Young's modulus of the collagen fibrils E_f = 40 MPa, Young's modulus of the ground substance $E_m = 2\ MPa$, fibrils' volume fraction f = 0.3-0.7.

The dependency of the normal stress in a single fibril on the apparent strain is given in Figure 1. The variation of the maximal undulation angle has a strong influence on the stress-strain distributions. A similar dependency, accounting for the ground substance influence, is given in Figure.2. For strains larger than 6%-7% we can consider the PDL layer as a solid shell with Young's modulus approximately equal to the modulus of the fibrils. The value of the Young modulus at zero strain is the effective modulus of the wavy fibrils.

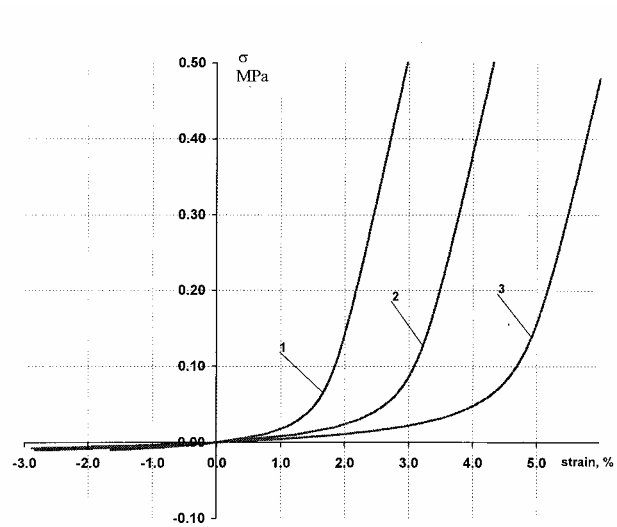

Figure 1: External stress vs. apparent strain in a single fibril: wavelength λ=16 μm, E_f=40 MPa, r_f= 150 nm, lines 1, 2 and 3 correspond to $\theta_0 = 15^0$, 20^0 and 25^0.

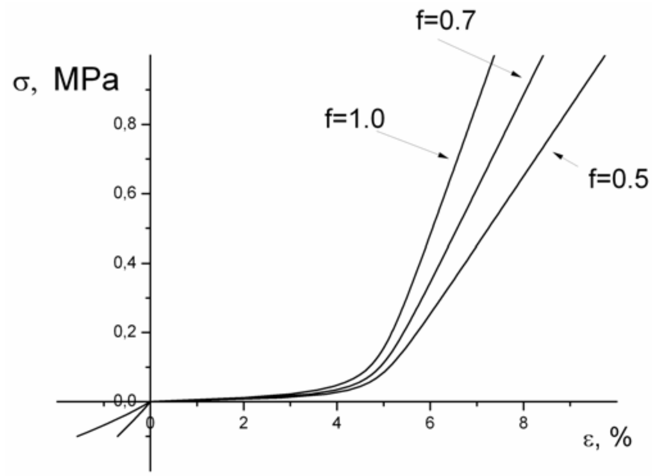

Figure 2: External stress vs. apparent strain, λ=16 μm, $\theta_0 = 25^o$, r_f= 150 nm, f = 0.5 and 0.7 including compression, f = 1.0 without ground substance.

CONCLUSION

The proposed micromechanical model is based on a physical-mechanical ground, and its material parameters are physical quantities that can be experimentally determined; it offers a direct way to determine the influence of the problem parameters on the stress state of the tooth-PDL-bone system.

ACKNOWLEDGEMENTS

Support for this work to M.P. was provided by a fellowship from the Landau Network-Centro Volta and the CARIPLO Foundation (Lombardy, Italy) and is gratefully acknowledged.

COMPARISON OF THE EFFECTIVENESS OF ORTHOSES VERSUS PROPRIOCEPTIVE EXERCISES FOR THE PREVENTION OF ANKLE INJURIES IN BASKETBALL PLAYERS

Dieter Rosenbaum, Ralf Schröter, Eric Eils
Movement Analysis Lab, Orthopaedic Department, University Hospital Münster, Germany
email: diro@uni-muenster.de, web: www.motionlab-muenster.de

INTRODUCTION

Ankle injuries frequently occur in ball games like basketball [1] and may lead to prolonged absences from practice and games. Ankle stabilizing devices such as tape or orthoses are highly recommended as preventive measures against inversion traumata [2]. Alternatively, physiotherapy with exercises addressing a wide variation of strengthening and proprioception has been suggested [3] even though the effectiveness is still under discussion. Furthermore, it has never been shown whether both approaches are equally effective or have a different impact on injury prevention.
The aim of the present study was the prospective randomized investigation of the effect of these two alternative approaches to prevention of ankle injuries in a large sample of active basketball players from various levels of expertise.

METHODS

A total of 337 athletes from 12 women's teams and 23 men's teams of level 1 (Bundesliga) through level 5 (Kreisklasse) leagues participated. All players were actively involved in regular practice sessions and official games in their respective league. 95 athletes were assigned to the orthoses group and were wearing either the AirGo orthosis (Aircast) or their previously used orthosis. Another group of 115 players participated in a proprioceptive training that was carried out in addition to their normal basketball practice session (2 circuits with 6 stations, 15 min duration). The remaining 125 athletes served as a control group and continued their customary practice. All teams were followed for one games season (October 2003 to April 2004) and were asked to report all incidences that involved a basketball related injury that occurred either during practice or in official games and lead to the cessation of active participation. The frequency of injuries was expressed in relation to the amount of participation in basketball activities that were registered in a diary.

RESULTS AND DISCUSSION

A total of 107 reported injuries was located in 54% in the ankle joint, 12% the knee, 10% each the fingers and the head (Fig. 1). There were 28% primary ankle injuries and 68% recurrent injuries. The situations that lead to the injuries were equally distributed between practice sessions and official games and mostly involved direct contact with an opponent. The injuries resulted in a rehabilitation period of 2.5 weeks on average.

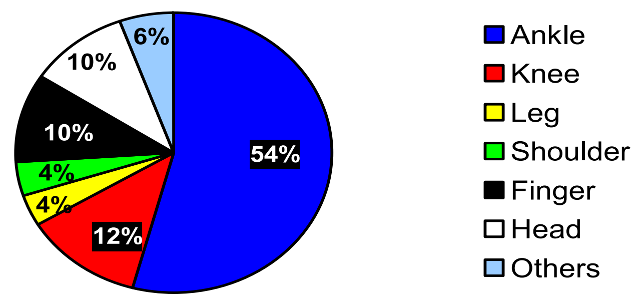

Figure 1: Distribution of the location of injuries (n=107)

Intervention	Control Group (n=125)	Proprio. Group (n=115)	Brace Group (n=95)
Basketball injuries/ 1000 participations	3.37	1.97*	1.00*

Tab. 1: Relative injury frequency for different interventions methods (*=significantly different from control group)

In the control group, the relative injury frequency was determined as 3.37 injuries per 1000 sports participations. In the proprioceptive training group it was significantly reduced to 1.97 injuries per 1000 sports participations. The least injuries occurred in the orthosis group with only 1.00 injury per 1000 sports participations (Tab. 2).
The injury statistics of the control group of active basketball players supports previously reported ankle injury frequencies in basketball [1]. Significant differences between the experimental groups underline the positive effect of both preventive measures with an even more pronounced effect of the ankle stabilizing orthoses.

CONCLUSIONS

Both preventive measures, i.e. multi-station proprioceptive exercises as well as ankle orthoses may be recommended for the prevention of primary and recurrent ankle injuries.

ACKNOWLEDGEMENTS

Supported by the BISP (Bundesinstitut für Sportwissenschaft)

REFERENCES

[1] McKay BJSM 2001
[2] Tropp AJSM 1985
[3] Eils & Rosenbaum MSSE 2001

PEDOGRAPHIC ASSESSMENT OF CLINICAL AND FUNCTIONAL OUTCOME AFTER HALLUX VALGUS SURGERY – COMPARISON OF 32 PATIENTS BEFORE AND AFTER SCARF OSTEOTOMY

[1]Timo J. Lorei, [2]Christian Kinast, MD, [1]Hans Klärner, MD, [1]Dieter Rosenbaum, PhD
[1]Movement Analysis Lab, Orthopaedic Department, University Hospital Münster, Germany
[2] Zentrum für orthopädische Fusschirurgie, München, Germany
email: diro@uni-muenster.de, web: www.motionlab-muenster.de

INTRODUCTION

The Scarf osteotomy has become a standard surgical treatment of pre-arthritic hallux valgus deformities. Several reports evaluated short and long term results but focused on subjective, clinical and radiographic results [5,6]. More recent studies also applied pedographic measurements for a functional evaluation of foot loading characteristics after surgery [1,7]. However, few studies investigated the relationship between subjective, clinical and radiographic outcome with pedographic results and only one study reported also about the behavior of the, contralateral foot in comparison to the operated foot [1].

The aim of this study was to evaluate patient satisfaction, clinical, radiographic and pedographic parameters in order to determine the subjective and functional outcome after surgery.

METHODS

32 unilateral hallux valgus patients that had been treated with a Scarf osteotomy performed by one surgeon (C.K.) were investigated after a mean follow-up of 33 months. Patients reported subjective satisfaction with the surgical outcome, cosmetic appearance, and pain. For the clinical evaluation, the AOFAS score was applied [2]. Hallux valgus and inter-metatarsal angles were determined from weight-bearing x-rays. Pedographic measurements were performed before surgery and repeated at follow-up with a capacitive pressure distribution platform (emed ST-4, novel Munich). Foot prints were subdivided into ten regions and plantar pressure patterns were analyzed with respect to peak pressure, maximum force, and impulse values.

RESULTS AND DISCUSSION

28 of the patients (87.5%) described the result of the operation as excellent or good, one patient (3.1%) as fair and three (9.4%) as poor. The AOFAS Score reached 89 out of 100 points after surgery. The hallux valgus angle improved significantly from 32.5° to 6.6° ($p<0.0001$) and the inter-metatarsal angle from 15.5° to 6.6° ($p<0.0001$). Maximum force and impulse decreased under the lateral forefoot ($p<0.038$) and increased under the medial forefoot ($p<0.001$). Loading also increased significantly under the hallux (maximum force $p<0.0001$, impulse $p<0.001$) indicating that the hallux became more actively involved in the rollover process. Comparison of the operated and contralateral foot revealed a good restoration of loading symmetry. Correlation analyses demonstrated an influence of postoperative pain ($r=0.549$) and hallux valgus angle ($r=0.443$) on patient satisfaction: Patients were more satisfied with lower hallux valgus angles.

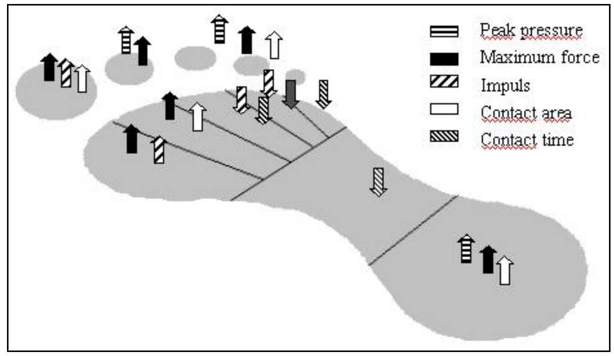

Figure 1: Summary of the significant changes of the operated foot before and after surgery.

The results indicate that the Scarf osteotomy achieved a high rate of subjective patient satisfaction, good restoration of foot function. A good symmetry between affected and contralateral feet was demonstrated. These results are reflected in the patient satisfaction. The correction of the hallux valgus angle is more pronounced than in comparable reports [4,8]. A significant relationship was seen between the postoperative hallux valgus angle and patient satisfaction as well as the extent of medial load shift. This load shift has been described after a follow-up of 20 months [1] and 18 months following Scarf osteotomy [7]. The present results showed a similar load transfer with an off-loading of the first ray before surgery that can be reversed with successful surgery to achieve a more physiologic loading. However, this may take up to one year. The loading changes are not confined to the affected foot but the contralateral foot may also show discrete changes as a consequence of the deformity as well as after surgery. Gait symmetry appeared well restored in the present population after surgery.

CONCLUSIONS

The Scarf osteotomy appears to be a well suited procedure for correction of severe hallux valgus deformities. Pedographic analyses offer an objective evaluation of the complex changes after surgery.

REFERENCES

1. Jones S et al. *J Bone Joint Surg Br*, 86(6): 830-6, 2004.
2. Kitaoka HB et al. *Foot Ankle Int*, 15(7): 349-53, 1994.
3. Kranzl A et al. *Clin Biomech* 18: 19-20, 2003.
4. Kristen KH et al. *Foot Ankle Int*, 23(3): 221-9, 2002.
5. Perugia D et al. *Int Orthop*, 27(2): 103-6, 2003.
6. Petersen W & Seide HW. *Z Orthop* 138(3): 258-64, 2000.
7. Sabo D & Buchner M. *Fuß & Sprunggelenk*, 2: 76-84, 2004.
8. Weil, L. S. *Foot Ankle Clin*, 5(3): 559-80, 2000.

A NEW PORTABLE 3-D GYROSCOPE SYSTEM FOR THE EVALUATION OF UPPER LIMB FUNCTION

A.M.A. Chan and A.C. Nicol
Bioengineering Unit, University of Strathclyde (Glasgow, UK)
Email: anita.chan-@strath.ac.uk

INTRODUCTION

The shoulder joint is extremely important for the positioning of the hand in order to interact with the environment and interest in the restoration of good function to the upper limb is becoming increasingly important. Current clinical methods for functional assessment are limited to subjective pain questionnaires and physical examination which relies largely on the experience of the clinician. While motion analysis techniques have become widely used in research environments, they are not suitable for use in a clinical environment due to their requirement for long and complex testing procedures. The use of kinematic sensors have shown great promise in gait analysis [1, 2] but these systems have tended to be heavy and bulky.

This study aims to develop a lightweight, portable and cost effective system for 3D motion analysis of the upper limb which can be readily applied within a clinical environment.

METHODS

The 3D gyroscope system consists of three identical units (figure 1a) and uses a total of 9 single axis gyroscopes (Murata ENC 03JA). Each gyroscope unit holds three single axis gyroscopes securely at right angles to one another within a rigid plastic housing to allow the recording of angular velocity in three dimensions. The plastic housing (figure 1b) consists of an inner core to which the gyroscopes are mounted, a circular base, and a conical shaped lid.

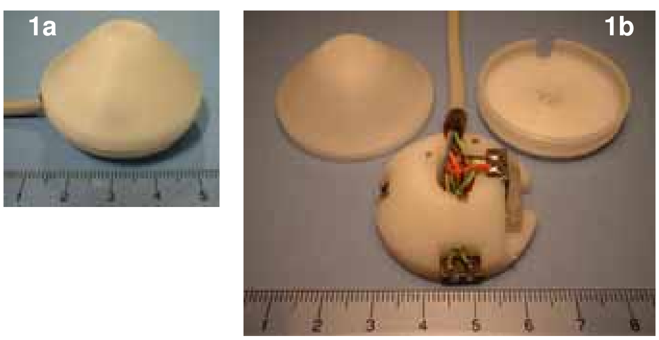

Figure 1: (a) one 3D gyroscope unit, **(b)** components of the plastic housing.

Each 3D gyroscope unit is small (40mm diameter by 25mm high) and lightweight (20g approximately) and is mounted onto the body independently of other system components, thereby minimising size and weight so as not to affect the production of movement when attached to the upper limb of the subject.

Figure 2a and 2b shows the 3D gyroscope system mounted onto the chest, upper arm and forearm. Data from the 3D gyroscope system were sampled simultaneously with an 8 camera Vicon 612 motion analysis system while the subject performed a variety of movements including maximal flexion and extension, and movements to simulate activities of daily living such as brushing hair and dressing.

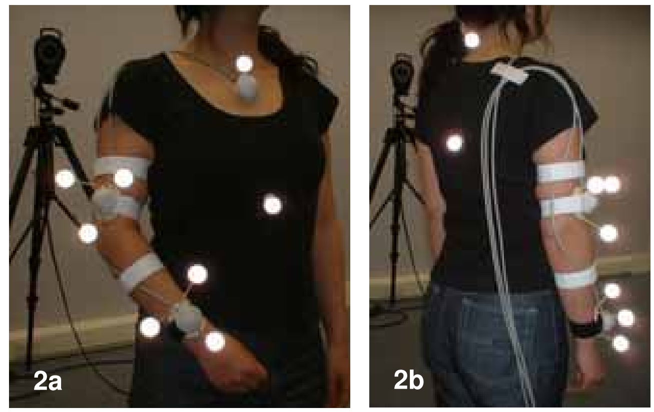

Figure 2a and 2b: Front and rear view of 3D gyroscope system and retroreflective markers mounted onto healthy subject.

RESULTS AND DISCUSSION

Angular velocity data were filtered and integrated to obtain angle data. Figure 3 shows angle data for the upper arm 3D gyroscope unit during a 'reach up back' activity.

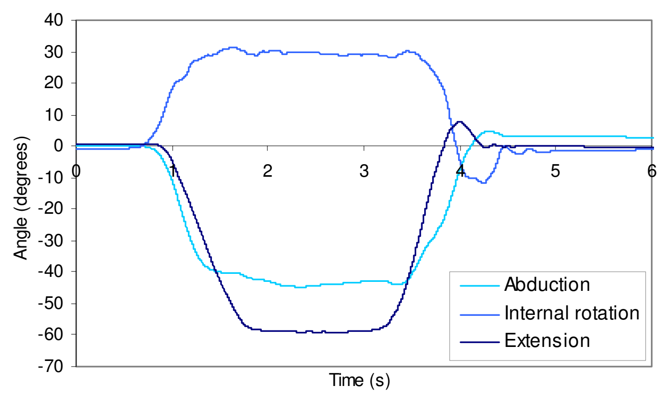

Figure 3: Upper arm 3D gyroscope output for 'reach up back' activity.

The results of this research indicate that the 3D gyroscope system shows potential for use within a clinical setting as a portable motion analysis system for the upper limb.

REFERENCES

1. Mayagoitia, RE, et al. *J Biomech* **35,** 537-542, 2002.
2. Tong, K, and Granat, MH. *Medical Engineering and Physics.* **21,** 87-94, 1999.

ACKNOWLEDGEMENT

Funded by Zimmer USA.

RUNNING DOES NOT PROTECT AGAINST AGE-RELATED GAIT ADAPTATIONS

[1] Hans H.C.M. Savelberg, [1]Lex B. Verdijk, [1]Paul J.B. Willems and [2]Kenneth Meijer
[1] Department of Health Sciences, Maastricht University, The Netherlands; email: hans.savelberg@bw.unimaas.nl
[2] Department of Biomedical Engineering, Technische Universiteit Eindhoven, The Netherlands.

INTRODUCTION

Age effects on human gait have been shown in many studies. DeVita and Hortobagyi [1] argued that a redistribution of joint moments is a most characteristic aspect of age-related gait changes. Elderly were found to increase hip joint extensor torques to compensate for reduced plantar flexion torques. It has been argued that reduced muscle force underlies these age-associated gait adaptations. Physical activity is known to improve muscle function. Combining these observations brings us to the hypothesis that physical active can be applied to prevent gait related retardation of gait function. If anything, running induced adaptations might be most suited to counterbalance the effect of ageing on gait stability.

METHODS

Four groups of subjects were included: young-active, young-inactive, elderly-active and elderly-inactive. All physical active subjects were selected from a group of runners. The inactive participants had not exercised more than once a week for more than one year. Moreover admission to either of the activity groups was based on a physical activity questionnaire.

The subjects were asked to walk over a 12m level walkway, both at a self-selected speed and at a test speed of 1.5m/s. For each trial 2D segmental positions in the sagital plane from video images (50Hz) of reflective markers and vertical and horizontal ground reaction forces (Kistler type 9281A) were obtained. Inertial properties of the lower limb segments were based on a regression model, using subjects' measures. Inverse dynamic analysis was applied to calculate net joint torque moments of the ankle, knee and hip joint. Only when GRF_z exceeded 300N, the point of application of the GRF-vector was determined accurately. Consequently only joint torques between 10 and 90% of the stance phase are presented. Peak values of joint torques and powers were statistically analyzed.

RESULTS AND DISCUSSION

Spatio-temporal characteristics in both the self-selected and the test speed differed between ages not between activity groups. Under both condition elderly walked slower and with shorter step lengths. This resembles previous studies.

Also for joint torques differences between groups occurred as an effect of age not of activity level. In the ankle joint torque elderly displayed a gradual increase from low plantar flexion torques at heel contact to large plantar flexion torques at toe off (Figure1a). Young subjects were characterized by a rapid initial increased, followed by a plateau phase at midstance and a subsequent final rise of plantar flexion moment. Maximal plantar flexion torques were significantly larger in young subjects (152Nm *vs* 132Nm). Elderly had reduced knee extensor torques (Figure 1b) and increased hip extensor torques (Figure 1c) at the initial part of the stance phase. These age-related changes match exactly those presented earlier [1]. No changes in joint torque due to differences in activity were found.

For the same population also function of knee joint extensor and flexor muscle has been reported [2]. An age-associated reduction of knee flexor function was found within the joint angle range used during running and walking. In that study also no effects of activity could be found.

CONCLUSIONS

Based on this study and the previous study evaluating muscle function in the same population [2] it can be concluded that running does not protect against age-associated muscle wasting. Moreover, it is once again suggested that gait changes result from reduced muscle function.

REFERENCES

1. DeVita P, et al. *J Appl Physiol* **88**, 1804-1811, 2000.
2. Savelberg HHCM, et al.. *Isok Exerc Sci* **12**, 34-36, 2004.

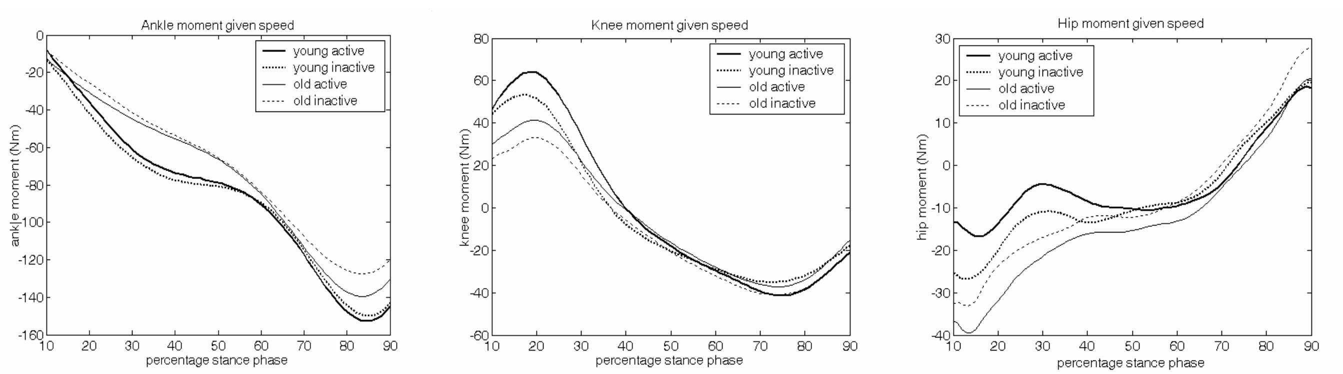

Figure 1a-c: Ankle (left panel), knee (middle) and hip joint torque (right) as function of percentage of the stance phase. Positive torques represent respectively, dorsal flexion, knee joint extension and hip joint anteflexion..

EFFECT OF INTRA-ARTICULAR LIDOCAIN INJECTIONS ON IMPACT ATTENUATION DURING WALKING IN KNEE JOINT OSTEOARTHRITIS PATIENTS

[1] Marius Henriksen [2]Erik B. Simonsen [1]Hans Lund [3]Thomas Graven-Nielsen [1]Henning Bliddal [1]Bente Danneskiold-Samsøe
[1]The Parker Institute, Frederiksberg Hospital, Denmark; email: marius.henriksen@fh.hosp.dk
[2]Insitute of Medical Anatomy, University of Copenhagen. [3]Center for Sensory-Motor Interaction, University of Aalborg.

INTRODUCTION

Impulsive loading of the knee joint caused by heel strike has been suggested to participate in the development and progression of degenerative joint diseases, such as osteoarthritis (OA) [1,2].

Joint pain is one of the cardinal symptoms of OA and is one of the primary aims in conservative treatment of the disease. As pain can be considered a protective mechanism, pain relief may have the potential to increase the impulsive knee joint loads during walking and thus accelerate the degeneration through increased mechanical loads.

Accordingly, the aim of the study was to investigate the effect of local knee joint analgesia on the impulsive knee joint loads during walking in patients suffering from knee joint OA.

METHODS

Ten subjects with painful knee joint OA were included in the study (average age 67.8 (SD 5.0), height 164.2 (SD 4.5), weight 74.0 (SD 12.3)).

Intra-articular lidocain injections (10 cc) were performed using ultrasound guidance to ensure proper placement of the bolus within the joint cavity. The injection was performed in the most affected/painful knee.

Linear accelerations were measured at the tibial tuberosity and sacrum, using a piezoresistent accelerometer, in synchrony with a 3D gait analysis. Acceleration measurements and gait analyses were performed before and immediately after the injections. The subjects were instructed and trained to walk at 4.0 km/h (~1.1 m/s) both pre- and post injection.

Knee joint pain during walking was scored using a 100 mm Visual Analogue Scale after the initial measurements (before injections) and again after the post injection measurements.

Impact attenuation (IA) was quantified using a ratio between the peak accelerations at heel strike measured at the tibia tuberosity (P_{tibia}) and sacrum (P_{sacrum}):

$$IA = P_{tibia} / P_{sacrum}$$

To explain the any changes in acceleration patterns kinematic data were extracted from the 3D gait analysis.

RESULTS

One subject was excluded due to misplacement of the lidocain bolus. All remaining subjects showed a significant decrease in pain during walking (p=0.005, see table).

Impact attenuation significantly decreased after lidocain injections (p=0.01), caused primarily by a decrease in tibial accelerations (p=0.002). Sagittal joint kinematics showed a more extended leg after injections. Both hip and knee joint angles at initial contact turned toward extension after injections (p=0.03 and p=0.0005 resp.). Vertical velocity of the shank prior to impact decreased significantly (p=0.02).

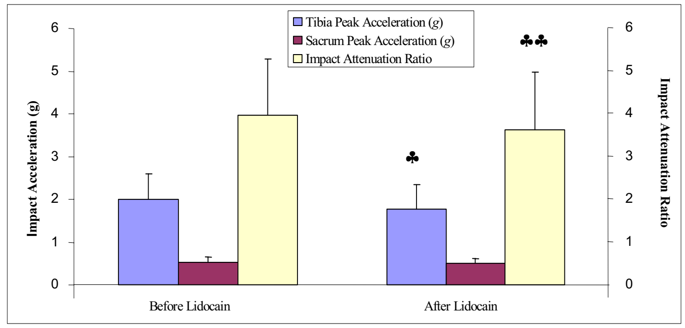

Figure: Peak accelerations (*g*) and impact attenuation ratios before and after lidocain injections. Significant reductions in tibial accelerations ♣ (p=0.002) and impact attenuation ♣♣ (p=0.01) were found.

DISCUSSION

Pain relief affected impact attenuation in a paradoxical way and caused the impact attenuation during walking to decrease, although the impact acceleration at tibia decreased. Extended hips and knees make the leg functionally longer, which could be a possible explanation of the decreased tibial acceleration. Changing knee joint angle at initial contact into more flexion has proved to be highly effective in regulating impact transmissibility [3]. Our results endorsed this, as both knee and hip joint angles changed significantly together with a decreased vertical shank velocity before impact.

CONCLUSION

Local knee joint analgesia may affect the impact attenuation negatively, and this may have clinical implications on the treatment of knee OA in the future.

REFERENCES

1. Radin EL, et al.. *Annals of Rheum Dis* **34**, 132-133, 1975
2. Folman Y, et al.. *Arch Orthop Trauma Surg* **104**, 363-365, 1986
3. Lafortune MA, et al.. *J Biomech* **29**, 1531-1537, 1996

ACKNOWLEDGEMENTS

The Oak Foundation and Copenhagen Hospital Corporation supported the Study.

Table: Average (SD) pain, impact accelerations, impact attenuation ratio (IA) and joint kinematics.

n = 9	Before lidocain	After lidocain	Difference	Paired t-test
Pain VAS (mm)	37.3 (27.8)	1.8 (2.0)	35.6 (27.4)	0.005
Tibial peak acceleration (g)	2.00 (0.59)	1.76 (0.59)	-0.24 (0.18)	0.002
Sacral peak acceleration (g)	0.56 (0.13)	0.50 (0.11)	-0.02 (0.03)	0.07
Impact attenuation ratio (IA)	3.96 (1.32)	3.62 (1.35)	-0.34 (0.33)	0.01
Initial contact knee angle (deg)	8.4 (4.3)	4.0 (5.0)	-4.5 (2.4)	0.0005
Initial contact hip angle (deg)	26.6 (3.9)	24.3 (6.2)	2.2 (2.9)	0.002
Shank vertical velocity (m/s)	0.20 (0.03)	0.18 (0.03)	0.01 (0.02)	0.02

EFFECT OF INTRA-ARTICULAR LIDOCAIN INJECTIONS ON KNEE JOINT KINETICS DURING WALKING IN KNEE JOINT OSTEOARTHRITIS PATIENTS

[1] Marius Henriksen [2]Erik B. Simonsen [1]Hans Lund [3]Thomas Graven-Nielsen [1]Henning Bliddal [1]Bente Danneskiold-Samsøe
[1]The Parker Institute, Frederiksberg Hospital, Denmark; email: marius.henriksen@fh.hosp.dk
[2]Insitute of Medical Anatomy, University of Copenhagen. [3]Center for Sensory-Motor Interaction, University of Aalborg.

INTRODUCTION

Excessive loading of the knee joint during walking in patients suffering from knee joint osteoarthritis (OA) has been hypothesized to participate in development and progression of the disease [1].

Joint pain is one of the cardinal symptoms of OA and is one of the primary aims in conservative treatment of the disease. As pain can be considered a protective mechanism, pain relief may have the potential to affect the knee joint loading pattern during walking and thus accelerate the degeneration through increased mechanical loads.

Accordingly, the aim of the study was to investigate the effect of local knee joint analgesia on knee joint loading patterns during walking in patients suffering from knee joint OA.

METHODS

Ten subjects with painful knee joint OA were included in the study (average age 67.8 (SD 5.0), height 164.2 (SD 4.5), weight 74.0 (SD 12.3)).

Intra-articular lidocain injections (10 cc) were performed using ultrasound guidance to ensure proper placement of the bolus within the joint cavity. The injection was performed in the most affected/painful knee.

Three dimensional gait analyses were performed pre- and post injection. Force plate and movement data was combined to calculate net muscle moments about the joints of the lower extremities. The subjects were instructed and trained to walk at 4.0 km/h (~1.1 m/s) both pre- and post injection.

Knee joint pain during walking was scored using a 100 mm Visual Analogue Scale (VAS) after the initial measurements (before injections) and again after the post injection measurements.

RESULTS

One subject was excluded due to misplacement of the lidocain bolus. All remaining subjects showed a significant decrease in pain during walking (p=0.005, see table).

A significant reduction of the peak extensor moments was found (K2: p=0.04, K4: 0.04) together with a significantly reduced knee flexion angle in early stance (p=0.003). Mid-stance peak flexor moments showed a tendency toward increase (p=0.06). No changes in abduction moments were found.

DISCUSSION

Pain relief caused the peak extensor moments to decrease, which may be interpreted as an unloading of the knee. A

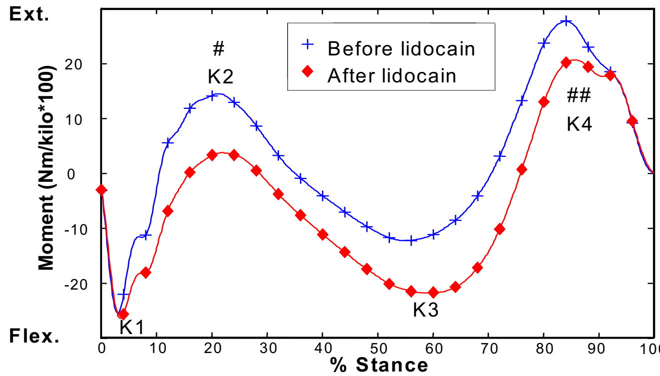

Figure: Knee joint moments during stance before and after intra-articular lidocain injections. Significantly reduced peak extensor moments (K2 and K4) were found (both p = 0.04.). A tendency toward increased flexor moments in mid-stance was observed (p = 0.06).

decreased knee flexion angle makes it to possible to walk with lower extensor moments [2] and thus decrease joint loads in early and late stance. All together this suggests a quadriceps avoidance pattern following lidocain injections.

Decreased extensor moments and knee flexion angles together with unchanged abduction moments have been suggested to results in a dynamically unstable knee joint [3].

We hypothesised that pain relief would remove the protective mechanism of pain and thus increase joint loads, but surprisingly we found the opposite. Increased co-contractions of the hamstring muscles could be a possible explanation, but no EMG data was available in the present study.

CONCLUSION

We surprisingly found that OA patients walked with a quadriceps avoidance-like pattern following pain relief, which represents a paradoxical unloading of the knee joint. The observed changes may suggest an unstable knee following lidocain injections.

REFERENCES

1. Hurwitz DE, et al. *Curr Opin Rheumatol* **11,** 422-426. 1999
2. Baliunas AJ, et al. *Osteoarthritis Cartilag* **10,** 573-79, 2002
3. Schipplein OD, et al. *J Orthop Res* **9,** 113-119, 1991

ACKNOWLEDGEMENTS

The Oak Foundation and Copenhagen Hospital Corporation supported the study.

Table: Average (SD) pain, peak moments (Nm/kilo*100) in sagittal and frontal planes and early stance knee joint angles (degrees).

n = 9	Before lidocain	After lidocain	Difference	Paired t-test
Pain VAS (mm)	37.3 (27.8)	1.8 (2.0)	35.6 (27.4)	0.005
Peak extensor moment (K2)	18.4 (13.7)	7.9 (12.6)	10.5 (12.9)	0.04
Peak extensor moment (K4)	32.2 (12.6)	27.2 (13.9)	5.0 (6.4)	0.04
Peak flexor moment (K3)	-11.4 (12.5)	-22.2 (23.4)	10.8 (15.0)	0.06
Peak abduction moment	58.2 (20.2)	57.7 (22.5)	0.6 (5.2)	0.75
Knee joint angle, early stance	21.3 (5.5)	17.8 (6.2)	3.6 (2.5)	0.003

PRINCIPAL COMPONENT ANALYSIS OF LIFTING WAVEFORMS

[1] Allan T. Wrigley, [1]Wayne J. Albert, [2]Kevin J. Deluzio, and [3]Joan M. Stevenson
[1]Faculty of Kinesiology, University of New Brunswick, Fredericton, NB, Canada [allan.wrigley@unb.ca]
[2]School of Biomedical Engineering, Dalhousie University, Halifax, NS, Canada
[3]School of Physical & Health Education, Queen's University, Kingston, ON, Canada

INTRODUCTION

In a previous investigation [3] we demonstrated the utility of a Principal Component Analysis (PCA) to discriminate between a group of healthy workers; 50 of whom remained healthy (CON) and 56 of whom developed low back pain (LBP) over a two-year assessment period [2]. This discrimination was done on the kinematic and kinetic waveforms associated with individual lifting patterns of a 15kg load performed when all worker were healthy. The purpose of this study is to determine if the PCA approach is robust enough to discriminate the clinical status of the workers when a confounding factor of load is introduced.

METHODS

One kinematic (box velocity) and five kinetic (S1, L1, and T1 extension moments; trunk compression; trunk shear) waveforms describing the 2D motion of the trunk and box of 106 healthy male workers performing sagittal lifts of 5kg, 15kg, and 25kg box loads were analyzed. PCA [1] was applied to matrices consisting of each of the 6-waveform variables from both groups. All waveform data was transformed into principal components (PC)s using an eigenvector analysis of the covariance matrix. By orthonormalizing the covariance matrix (S), the eigenvector matrix (U) is determined. The eigenvalues are extracted by taking the diagonal components of Equation 1.

Equation 1: Calculation of Eigenvalues

$$\underset{p\times p}{L} = \underset{p\times p}{U'} \times \underset{p\times p}{S} \times \underset{p\times p}{U}, \text{ where } \underset{p\times p}{L} = \text{diagonal eigenvalues matrix}$$

The number of PCs retained for comparison (k) was determined using parallel analysis (Jackson, 1991). PC scores were calculated by projecting the original data points (X) into the new coordinate space defined by the k PCs (Equation 2).

Equation 2: Calculation of Principal Component Scores

$$\underset{n\times p}{Z} = \underset{n\times p}{X} \times \underset{p\times p}{U}', \text{ where } \underset{n\times p}{Z} = \text{the matrix of PCscores}$$

The k PC scores for each variable were used as the dependent measures in a two-way MANOVA in order to determine if there were any significant group differences.

RESULTS AND DISCUSSION

The MANOVA results (Table 1) revealed that the PCA was insensitive to confounding load effects as the same clinical status effects that were identified from our previous study [3] were identified again (Figure 1). Furthermore, significant load differences for the first PC of every kinetic variable (Figure 1) indicates that magnitude effects account for the greatest amount of variation in the waveform data sets.

Table 1: MANOVA results for group differences and interaction for the PC scores of each waveform variable.

Effect	*F*	*P*	η_p^2
Clinical Status	3.006	0.001	0.147
Load	54.527	0.001	0.758
Clinical Status * Load	0.519	0.990	0.029

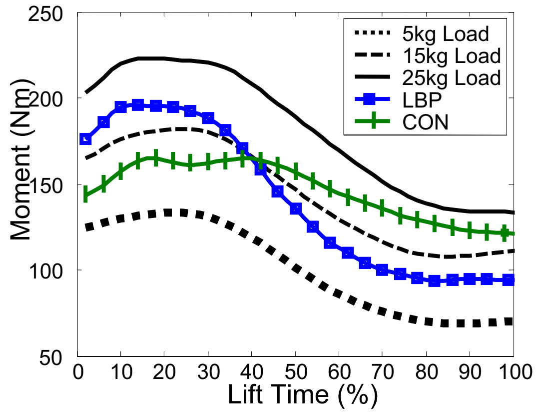

Figure 1: A significant load effect is illustrated with the three lines —, ---, and ··· representing the mean of the trunk extension moment waveforms for each load. Two more lines (+ and □) were plotted to illustrate a clinical status effect based on waveforms that illustrate the PC score and PC coefficient relationship. The differences in load represent a magnitude effect while the differences in extension moment between the CON and LBP group show a change in the trunk loading pattern throughout the lift.

CONCLUSIONS

The PCA technique was able to identify important biomechanical differences between the groups, and was insensitive to confounding load effects. This research has been able to relate differences in lifting technique prior to the development of LBP, and has identified that these differences are not load dependent.

REFERENCES

1. Jackson, JE *A User's Guide to Principal Components* John Wiley & Sons Inc., New York, 1991
2. Stevenson JM, et al. *IOS Press, Inc.*, Burke, 256-260, 1997
3. Wrigley AT, et al.*Clin. Biomech.*(In Press), 2005

BIMANUAL MOTOR CONTROL: BIOLOGICAL AND ROBOTIC SYSTEM LEARNING VIA SIMULTANEOUS MOVEMENT REQUIREMENTS

Pete B. Shull and Roger V. Gonzalez
LeTourneau University; email: RogerGonzalez@letu.edu, web: http://www.letu.edu/people/rogergonzalez/

INTRODUCTION

Bimanual human motor control learning studies have demonstrated that adaptation occurs while using both biological arms to conduct tasks of varying difficulty [1]. Unimanual learning has also been shown to occur when using a robotic system [2]. Though humans can perform tasks of varying complexity, bimanual learning using two contrasting input/output (I/O) systems simultaneously is not well understood. This study tested our hypothesis that humans can adapt spatially and temporally to a bimanual tracing task using both their biological arm and a robotic system simultaneously.

METHODS

Four female and six male subjects (ages 19-29) voluntarily participated in this experiment. All subjects were right-handed by self-report and were tested during the same time each day (±2 hrs) for four consecutive days. Each subject was given the task of tracing 15 cm circle(s) clockwise at 3.2 second intervals using their biological and/or a robotic arm (Figure 1). XY digitizing tablets recorded two-dimensional spatial position every 100ms, and each trial lasted approximately 50 seconds. Subjects traced two circles using both biological arms for the first and last five trials of the experiment to examine normal bimanual performance before and after testing. During stage one of testing, subjects traced one circle with a robotic arm by applying forces and torques to a rigid joystick with their dominant arm. During stage two, subjects used the robotic arm and their non-dominant biological arm to trace both circles simultaneously. The control strategy for the actuation of the robotic arm was intentionally designed to be difficult and non-intuitive so that possible learning could be observed over time.

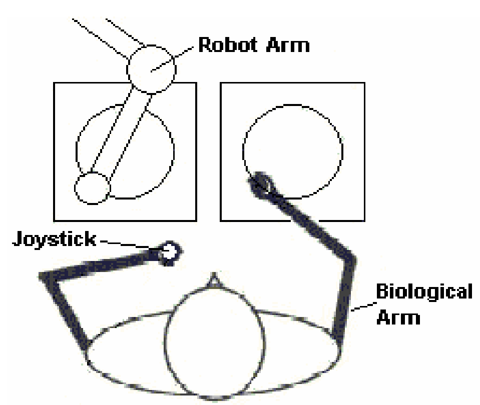

Figure 1: Experimental setup. Subjects traced 15 cm circles on digitizing tablets with the robotic arm by applying forces and torques to the joystick and/or with their biological arm.

RESULTS AND DISCUSSION

Data was analyzed in blocks of five trials. Performance was based on spatial and temporal accuracy in tracing the circle(s).

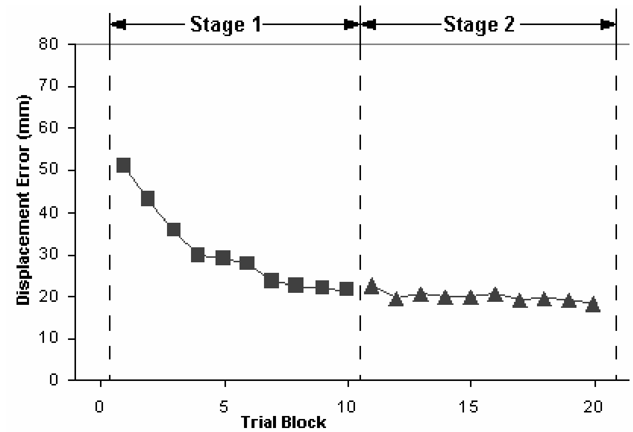

Figure 2: Subject spatial performance using the robotic arm. During stage 1 subjects used only the robotic arm. Stage 2 required using both robotic and biological arms simultaneously.

Spatial accuracy was calculated by averaging the distance from the circle (in millimeters) at each point during the trial. Temporal accuracy was the average of the differences in desired and actual angle (in degrees) at each point of the trial. Compiled results of all subjects show that subjects learned to control the robotic arm by demonstrating spatial learning curves (Figure 2) and temporal exponential learning curves. Biological arm spatial and temporal scores were constant throughout testing and were statistically lower than robotic arm scores since controlling the biological arm was more natural than controlling the robotic arm.

It would seem that moving from stage 1 of testing to stage 2 would be a difficult task because the subject would be controlling two distinct I/O systems simultaneously and that the initial performance of stage 2 would be worse than the final performance of stage 1. However, neither the spatial nor the temporal learning curves were adversely affected when subjects moved from stage 1 to stage 2 of testing.

CONCLUSIONS

Testing indicates that humans can learn to use two distinct parallel I/O systems simultaneously to conduct two-dimensional tracing tasks. It also appears that humans can transition from using one I/O system to using two distinct I/O systems without a decrease in performance in either system.

REFERENCES

1. Walter CB, Swinnen SP, Dounskaia NV. *Journal of Motor Behavior* **34** (2), 183-195, 2002.
2. Shull PB, Gonzalez RV. *J of Applied Biomech*, 2004 (sub.)

ACKNOWLEDGEMENTS

This work was funded in part by NSF-BES Grant (RUI-0201889

UPPER EXTREMITY KINEMATICS DURING FLY-CASTING

[1]Joshua R. Allen, [1]Katie B. O'Keefe, [2]Timothy J. McCue, and [1]Michael E. Hahn
[1]Movement Science Laboratory, Montana State University, Bozeman, MT, USA
[2]Fly Casting Institute, Missoula, MT, USA
email: mhahn@montana.edu

INTRODUCTION

Fly fishing has long been a popular form of recreation among outdoor enthusiasts, and is increasing in popularity internationally. A recent study revealed shoulder and elbow pathologies associated with repetitive, high velocity, overhand movements common to fly-casting [1]. However, no study has formally documented the upper extremity movement patterns during fly-casting. The aim of this study was to determine kinematic patterns of the fly-casting stroke. Documenting the movement patterns common to fly-casting will allow greater understanding of the underlying mechanisms of upper extremity pathologies.

METHODS

Seven subjects (6 male, 1 female; mean age 30.9) participated in the study after signing an informed consent. Subjects ranged from novice to expert, with a number of the subjects being professional fly-fishing guides. Twenty five reflective markers were placed on bony landmarks of the upper body (adapted from Rab et al. [2]). A 6-camera Vicon® 460 system (Vicon Motion Systems Inc., Lake Forest, CA, USA) collected marker position data at a frequency of 200 Hz.

Shoulder motion was calculated with respect to the trunk segment. The order of rotation for the shoulder was sagittal, frontal and transverse. The elbow was modeled as a single-axis pin joint and the wrist as a two-axis pin joint. Range of motion (ROM), peak angular displacement and time to peak displacement were examined for phase patterns, focusing on the following motions: shoulder flex/extension, ab/adduction, ext/internal rotation; elbow flex/extension; wrist flex/extension, radial/ulnar deviation.

Each subject performed multiple casting trials of their preferred casting style. Subjects were instructed to perform a series of "false casts" (usually 2-3), followed by the actual "shooting" cast. Three shooting casts were analyzed from each subject's casting session.

RESULTS AND DISCUSSION

It was determined that the fly-casting motion may be divided into three primary phases. The first phase, the "back cast," is a movement from anterior to posterior, displacing the fly line behind the caster. Primary motions during phase 1 included flexion, abduction, and external rotation about the shoulder. At the end of the back cast, there is a pausing phase (phase 2) in which the caster waits for the line to load the rod prior to the forward cast. Phase 3, the "forward cast," serves to move the rod anteriorly, sending the line to the desired target. Primary motions during phase 3 included shoulder internal rotation and extension, combined with elbow extension.

Average time spent in each phase 1-3 was as follows: 0.72 ± 0.07sec; 0.36 ± 0.09sec; and 0.64 ± 0.12sec, respectively. The greatest ROM for all joints occurred during phase 3, followed by phase 1. Phase 2 showed little motion (<7° per joint) for all joint actions. The greatest ROM during phase 1 and 3 was for external rotation of the shoulder, followed by elbow flexion. Shoulder flexion and abduction also exhibited substantial ROM during the forward cast. Average ROM values are presented in Table 1.

Table 1: ROM during each phase (deg); mean ± SD.

	Motion	Phase 1	Phase 2	Phase 3
Shld	Flex/Ext	26.1 ± 3.1	3.6 ± 2.3	27.9 ± 17.1
	Ab/Ad	19.2 ± 9.6	6.9 ± 5.3	22.1 ± 21.0
	ER/IR	63.4 ± 11.8	6.6 ± 3.7	53.0 ± 17.7
Elbow	Flex/Ext	31.0 ± 6.1	3.4 ± 2.2	41.1 ± 17.0
Wrist	Flex/Ext	21.9 ± 5.8	3.6 ± 1.8	21.9 ± 12.4
	R/U Dev	12.7 ± 1.5	5.1 ± 3.7	11.9 ± 6.5

The time to peak angular displacement within each phase is presented in Table 2. In general, large variation was seen in the timing of peak displacements. However, two distinct patterns showed consistency. Peak shoulder external rotation of 71.6° (± 17.0°) occurred at 4% (± 6%) of phase 3, and peak elbow flexion of 101.7° (± 14.6°) occurred 19% (± 22%) into phase 3. The early external rotation in phase 3 may indicate the effect of anterior trunk motion and inertial delay in the arm and rod segments, similar to the acceleration phase of a baseball pitch.

Table 2: Time to peak displacement (% phase); mean ± SD.

	Motion	Phase 1	Phase 2	Phase 3
Shld	Flex/Ext	22 ± 25	42 ± 30	64 ± 29
	Ab/Ad	59 ± 27	38 ± 33	52 ± 28
	ER/IR	78 ± 25	46 ± 36	4 ± 6
Elbow	Flex/Ext	65 ± 29	38 ± 34	19 ± 22
Wrist	Flex/Ext	54 ± 42	50 ± 38	35 ± 25
	R/U Dev	56 ± 39	53 ± 34	55 ± 24

CONCLUSIONS

Findings from this initial study indicate that there is moderate consistency of basic movement patterns between subjects during fly-casting. Parallel analyses are currently focusing on segmental coordination and joint dynamics, with emphasis on injury prevention. Future work will also quantify the effects of professional instruction on these variables.

REFERENCES

1. McCue, et al. *Wilderness Environ. Med* **15**, 267-273, 2004.
2. Rab, et al. *Gait Posture* **15**, 113-119, 2002.

THE INTERACTION BETWEEN SURFACE GRADE AND EXERCISE DURATION FOR SERIAL SARCOMERE ADAPTATIONS FOLLOWING TREADMILL RUNNING IN RATS

Timothy A. Butterfield, Walter Herzog
Kinesiology Research Centre, University of Calgary, Calgary, Alberta, Canada T2N 1N4
email: walter@kin.ucalgary.ca, web: www.kin.ucalgary.ca

INTRODUCTION

It is well accepted that eccentric exercise results in muscle injury and adaptation. *In-vivo* studies, aimed at quantifying the magnitude of muscle injury, have shown that several extensor muscles of the hindlimb of the rat experience varying degrees of muscle injury following chronic downhill walking [1], illustrating that the damage to these muscles is not uniform. Subsequently, a significant increase in serial sarcomere number (SSN) has been reported in the same knee extensor muscles following long-term downhill walking [2], leading to the hypothesis that eccentric exercise-induced damage results in this cellular adaptation. However, recent studies have shown that one extensor muscle of the hindlimb of the rat undergoes active lengthening during uphill walking [3], which would be expected to result in injury and sarcomere number increase. However, this has not been reported [2]. Recently, we have shown that not only can sarcomere number adaptations differ within a muscle, but can also occur between synergistic muscles, indicating a differential adaptation that may not be damage dependent [4].

METHODS

Protocol I: 24 male Long-Evans rats (age = 150 days) were randomly assigned to one of three groups: uphill (U) group (n=8), downhill (D) group (n=8) and a control (C) group (n=8). All groups were trained in five minute sets, with 1.5 minutes rest between sets for 5 days at 16 meters/min.

Protocol II: 16 male Long-Evans rats (age = 150 days) were randomly assigned to one of two groups: uphill (U) group (n=8), and a downhill (D) group (n=8). All groups were trained in five minute sets, with 1.5 minutes rest between sets for 10 days at 16 meters/min. Total training durations for each group are given in table 1.

Tissue analysis: 72 hours following the last training bout, the rats were killed, and the hindlimbs removed and fixed with the knee maximally flexed. Fascicle and sarcomere lengths of the vastus intermedius were measured using computer software and laser diffraction respectively. A two-way ANOVA was used to assess the differences in SSN with respect to surface grade and time.

RESULTS AND DISCUSSION

There were no significant differences in serial sarcomere number after only five days of exercise in either group, when compared to the control group. However, there was a significant interaction between exercise duration and surface grade with respect to the serial sarcomere number in the vastus intermedius muscle ($p<.001$), illustrating that the adaptation in serial sarcomere number over time was significantly greater in the uphill group compared to the downhill group (Fig. 1).

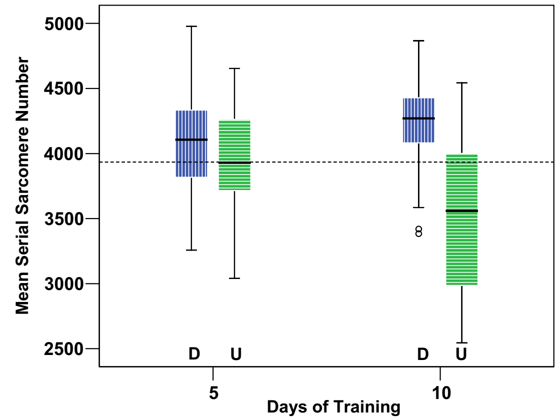

Figure 1. Interaction box plots for the uphill (U) and downhill (D) walking rats of 5 and 10 day duration, for the vastus intermedius muscle. Note the quantitative interaction of grade and duration on serial sarcomere number.

CONCLUSION

Serial sarcomere number changes in the vastus intermedius muscle can be predicted by surface grade only as a function of time. Although a previous study has shown that serial sarcomere numbers may vary depending on surface grade, the lack of a control group in that study does not allow the quantification of a gain or loss of sarcomeres compared to normal [2]. In addition, since knee extensor muscles have been shown to undergo lengthening contractions during uphill walking [3], the loss of sarcomeres in the uphill exercise group questions the role of muscle injury in the process of cellular adaptation.

REFERENCES

1. Armstrong RB et al. *J Appl Phys* **54**, 80-93, 1983.
2. Lynn R et al. *J Appl Phys* **85**, 98-104,1998.
3. Gillis GB, Biewener AA. *J Appl Phys* **93**, 1731-1743, 2002.
4. Butterfield TA, Herzog W. *Proceedings of ASB XXVII*, Toledo Ohio, 2003.

ACKNOWLEDGEMENTS

CIHR Training Program in Bone and Joint Health, NSERC of Canada, The CIHR research Chair program, and Tim Leonard

Table 1. Training duration for each day of each protocol (minutes). 'H' indicates hindlimb tissue was harvested.

Protocol	Day 1	Day 2	Day 3	Day 4	Day 5	Day 6	Day 7	Day 8	Day 9	Day10	Day11	Day12	Day 13
One	15	20	25	30	35			H					
Two	15	20	25	30	35	35	35	35	35	35			H

EFFECTS OF KNEE AND HIP JOINT MOTIONS DURING THE LANDING OF A STOP-JUMP TASK

Cheng-Feng Lin and Bing Yu,
Center for Human Movement Science, University of North Carolina at Chapel Hill
E-mail: feng1368@email.unc.edu

INTRODUCTION

Performance of landing tasks in sports is important for the prevention of lower extremity injuries. Literatures have shown that stiff landing characterized by great impact forces may be a risk factor for knee injuries [1, 2]. Increased hip extensor and knee flexor moments at the initial contact have been found in stiff landing in which the knee flexion angle is less than 90 degree [3]. Female recreational athletes also showed increased knee resultants forces and decreased knee flexion angle during landing compared to the male [1]. However, five degrees increased did not significantly affect the magnitudes of ground reaction forces in stop-jump task [4]. This presentation will show that how the motions of knee and hip affect the ground reaction force.

METHODS

Thirty male and thirty female healthy college students without known history of knee disorder were recruited for this study. Up to five steps approach run followed by stop-jump task was collected. Reflective markers were placed on bilaterally on ASIS, lateral malleolus, upper and lower anterior aspect of tibia. One marker was placed between the lumber vertebrae 4 and 5. The videographic and ground reaction force (Bertec Corporation, Worthington, OH) signals were recorded by the Peak Performance Motus videographic and analog data acquisition system (Peak Performance Technology, Inc., Englewood, CO). The collected 3-D coordinates of the markers during each stop-jump trials were filtered through a Butterworth lower-pass digital filter at estimated optimum cutoff frequencies. All signal processing and data reduction were performed using MotionSoft 3-D motion data reduction program package version 5.5 (MoitonSoft, Inc., Chapel Hill, NC).

Linear regression analysis was performed to determine the relationships of knee and hip kinematics with the ground reaction forces. A type I error rate of 0.05 was chosen to indicate statistical significance in each analysis. A stepwise selection procedure was used to determine the best regression equation for each couple of dependent and independent variables. All statistical analyses were performed using the SYSTAT computer program package, version 5.0 (SYSTAT, Inc., Evanston, IL).

RESULTS AND DISCUSSION

The results are shown in the Table 1. These results indicate that what affect the landing stiffness of the stop-jump task was hip and knee joint motions instead of configurations. A large hip and knee flexion angles at the initial foot contact with the ground do not necessarily make the landing soft, but active hip and knee flexion motions do. Hip joint motion at the initial foot contact with the ground mainly affects the ground reaction force and in the anterior-posterior direction during landing of the stop-jump task. Knee joint motion at the initial foot contact with the ground mainly affects the ground reaction force in vertical direction during landing of the stop-jump task. Hip joint motion at the initial foot contact with the ground appears to be an important technical factor that affects ACL loading during the landing of the stop-jump task.

REFERENCES

1. Chappell JD, et al.. *AJSM* **30**, 261-267, 2002.
2. Malinzak R, et al.. *Clin Biomech* **16**, 438-445, 2001.
3. Devita P and Skelly WA. *Med. Sci. Sports Exss* **24**, 108-115, 1992 .
4. Yu B, et al.. *AJSM* **32**, 1136-43, 2004.

Table 1. Pearson correlation coefficients (p-values) of hip and knee joint kinematics with peak ground reaction forces during the landing of the stop-jump task.

	Peak posterior ground reaction force	**Peak vertical ground reaction force**
Hip flexion angle at initial foot contact with ground	-0.104 (0.429)	-0.150 (0.251)
Hip flexion angular velocity at initial foot contact with ground	-0.630 (0.000)	-0.477 (0.000)
Hip maximum flexion angle during landing	-0.191 (0.144)	-0.123 (0.349)
Knee flexion angle at initial foot contact with ground	-0.102 (0.439)	-0.040 (0.763)
Knee flexion angular velocity in initial contact with ground	-0.490 (0.000)	-0.597 (0.000)
Knee maximum flexion angle during landing	-0.234 (0.072)	-0.381 (0.003)

BONE MINERAL DENSITY OF THE PROXIMAL FEMUR IS NOT RELATED TO DYNAMIC JOINT LOADING DURING LOCOMOTION

Mary Lou Bareither, Karen L. Reed-Troy and Mark D. Grabiner

Department of Movement Sciences, University of Illinois at Chicago, Chicago, IL, USA.
E-mail: mbareith @uic.edu

INTRODUCTION Load bearing provides the most potent influence on bone mass and architecture (1). In 2004 Moisio et al. (2) reported that nearly 40% of the variance of proximal femur bone mineral density (BMD) was associated with peak hip joint moments during walking. This result implies that joint moments acquired using gait analysis during a single session conveys meaningful information regarding daily stress and loading history. We considered the possibility that the result could be an analytical artifact, as the relationships reported were based on joint moment calculations that implicitly included the influence of body mass.

We have previously reported the influences of body size variables on bone mineral density (3, 4). In each of these studies we found a significant relationship between muscle strength variables and bone mineral density of the proximal femur in older adults. However, after accounting for the influence of body size on muscle strength variables, the relationship between muscle strength and bone mineral density was reduced to zero. Based on this work we anticipated that the relationship between joint moments measured during locomotion and bone mineral density would be similarly affected.

The purpose of the present study was to characterize the extent to which body mass influences the relationship between hip joint moments during locomotion and bone mineral density of the proximal femur in a homogeneous sample of healthy young women. We hypothesized that BMD would not be significantly associated with hip joint moments during locomotion independently of body mass.

METHODS Twenty-five women (age and mass: 22.96±2.05 years, 66.8±18.04 kg) participated in this institutionally approved study. The BMD (g/cm^2) of the non-dominant femur was determined by Dual Energy X-ray Absorptiometry (DXA) (Hologic QDR 4500 Elite). Subjects performed 10-15 trials during which they walked at a self-selected velocity along a path of approximately 10 meters. An eight-camera motion capture system (Motion Analysis Corporation, Santa Rosa, CA) and two AMTI force plates operating at 60 Hz recorded gait kinematics and kinetics. Univariate Pearson correlations were calculated to determine the relationships between hip joint moments, body mass, and proximal femur BMD. Significant correlations between hip joint moments and proximal femur BMD were subsequently investigated using an allometric scaling procedure (3,4) to determine the extent to which body mass influenced the relationship between hip joint moments and the BMD of specific regions of interest.

RESULTS AND DISCUSSION A potentially important relationship was discovered between only one of the measures of hip joint moment and one of the regions of interest of proximal femur BMD. Specifically, the peak internal rotation moment and the BMD of the intertrochanteric region were significantly correlated (r= 0.475, p = 0.019). The magnitude of the peak internal rotation moment was 19.77±2.2 Nm. The average BMD of the intertrochanteric region was 1.15±0.03 grams/cm^2. However, the relationship between the allometrically scaled peak internal rotation moment and intertrochanteric BMD was not significant (Figure 1). Prior to scaling, the peak internal rotation hip joint moment (unscaled) was strongly associated with the BMD of the intertrochanteric region; accounting for more than 20 percent of the shared variance. However, scaling of the hip joint moments to account for the influence of body mass reduced the relationship between hip joint moment and bone mineral density to essentially zero. As expected, body mass accounted for a significant proportion of the shared variance of proximal femur BMD

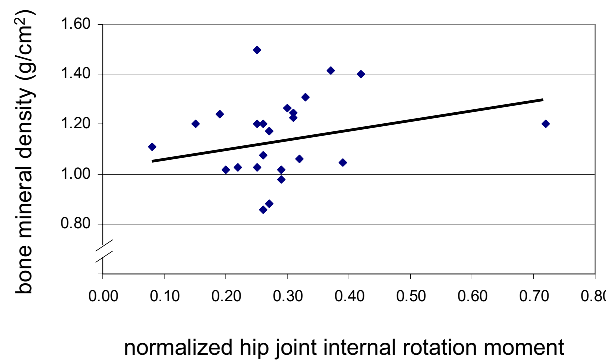

Figure 1: BMD vs. normalized internal rotation hip moment. After removing the influence of body mass on the hip joint moment, the relationship with BMD was not significantly different than zero. The regression equation characterizing the relationship between the peak internal rotation moment normalized to body mass and intertrochanteric BMD: BMD = 1.071 + (.284*normalized internal rotation moment) was not significant (p=0.337). The figure reveals the presence of an apparent outlier on the x-axis. A *post hoc* regression conducted without this data point resulted in an equation that was not significant (p=0.25) and accounted for only 6.3 percent of the shared variance.

In summary, the relationship between bone mineral density of the proximal femur in a sample of young healthy women and peak hip joint moments during locomotion was found to be dependent on the influence of body mass on both variables. After this influence was accounted for, the BMD-hip joint moment relationship disappeared. The results suggest that the dynamic hip joint moments during walking are not independently informative of daily stress stimulus and loading history in young women.

REFERENCES

(1) Lanyon LE. *Bone*, **18**, No. 1 Supplement, 37S-43S, 1996.
(2) Moisio KC, et al. *J of Orthopaedic Research,* **22**:339-345, 2004.
(3) Foley KT, et al. *Calcified Tissue International*, **64**:291-294, 1999.
(4) Owings TM, et al. *Bone*, **30**:515-520, 2002.

ACKNOWLEDGEMENTS Thanks to Stephanie Donovan for assistance with data collection.

HIGH SHEAR STRESS INDUCES P53 EXPRESSION AND APOPTOSIS IN CARTILAGE EXPLANTS

James Martin, Anneliese Heiner, and Joseph Buckwalter
Department of Orthopaedics and Rehabilitation, University of Iowa, Iowa City, IA, 52242
Email: james-martin@uiowa.edu Web: www.uihealthcare.com/depts/med/orthopaedicsurgery/

INTRODUCTION

Joint injuries leading to articular surface incongruities (e.g., step-offs) can cause excessive mechanical shear stress, which promotes cartilage destruction and post-traumatic osteoarthritis (OA). Here we test the hypothesis that excessive shear stress induces chondrocyte stress responses that lead to apoptosis. We cultured human cartilage explants in a mechanically active bioreactor, the Triaxial Compression Vessel (TCV), which is capable of modulating shear stress at physiologically relevant loading levels. This device was used to test the effects of shear stress on chondrocyte viability, apoptosis, and expression of p53, a protein that is involved in the early stages of apoptosis.

METHODS

Cartilage explants harvested from non-osteoarthritic ankle joints from 2 donors were placed in the TCV for mechanical stress treatment. The TCV imposes variable shear stress states at quasi-physiologic levels by applying transverse compression and axial compression simultaneously. The interplay between axial and transverse compression determines shear stress levels. In this study, 2 different treatments (900 cycles, 1 Hz) were applied: 1) 5 MPa axial compression only (high shear stress), 2) 5 MPa axial + 5 MPa transverse compression (minimal shear stress). Treated explants were incubated overnight in calcein AM to stain viable cells (green signal), then were cryoembedded and sectioned. Replicate sections were stained for apoptosis by TUNEL assay using TMR-red-labeled nucleotide (orange signal) or with an anti-p53 antibody using HRP/NBT detection (black signal). Whole sections were scanned using a 10x objective to generate composite images composed of 10-20 frames. Composite images were analyzed by scoring the number of cells stained with calcein AM, TUNEL assay or p53 antibody as a percent of total cells present. At least 3 entire sections from each explant were analyzed for each stain. Student's t-test was used to evaluate statistical significance.

RESULTS AND DISCUSSION

Chondrocyte viability in the superficial and transitional zones of cartilage explants declined from 89% in low shear stress to 62% in high shear stress. Apoptosis increased from 2.4% in low shear stress to 16.7% in high shear stress, while p53 expression increased from 23% to 48% (Figure 1). Differences in viability, apoptosis and p53 expression were significant ($p < 0.05$). No significant changes were seen in the deep zone (data not shown) staining results.

Exposure to high shear stress induced chondrocyte death *via* apoptosis. High shear stress also induced p53 expression, indicating that cell death was imminent. This suggests that high shear stress causes chondrocyte depopulation that could contribute to cartilage degeneration in post-traumatic OA.

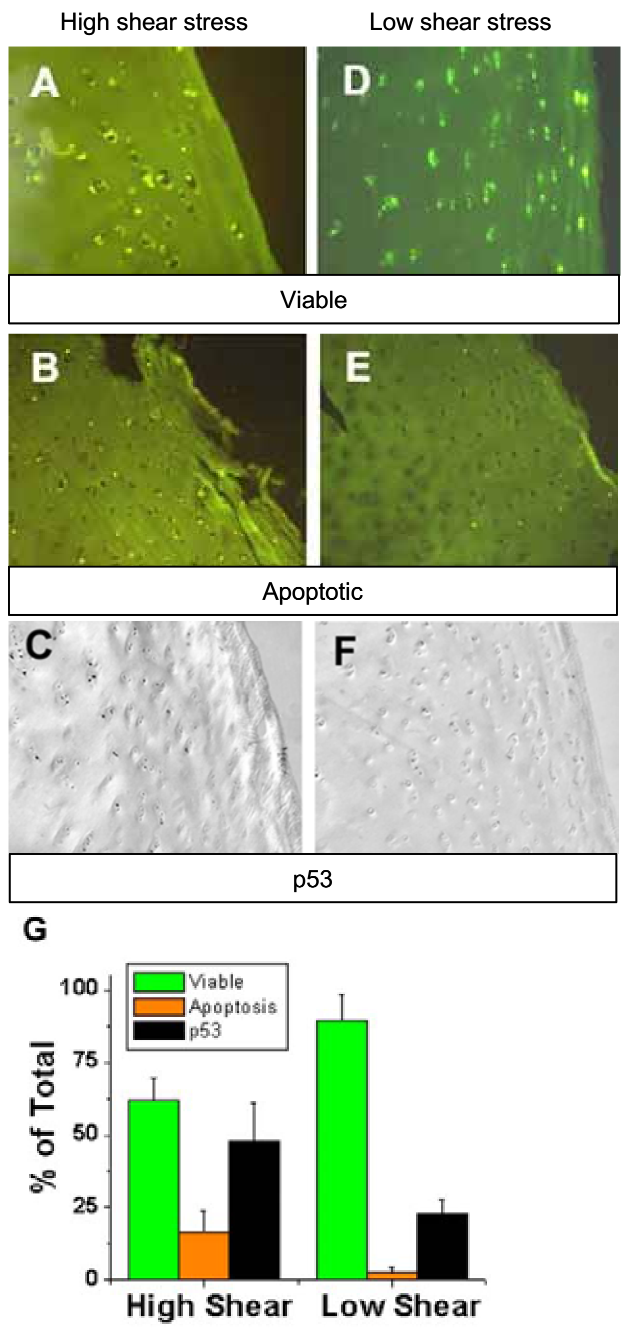

Figure 1: Effects of high and low shear stress on cartilage explants. (A,D) Calcein AM staining for viable cells (green). (B,E) TUNEL reaction for apoptosis (red-orange). (C,F) Immunostaining for p53 (black). (G) High shear stress decreases cell viability, increases apoptosis, and increases p53 expression, as compared to low shear stress.

ACKNOWLEDGEMENT

Supported by award 5 P50 AR048939, NIH Specialized Center of Research for Osteoarthritis.

THE NEUTRAL ZONE IN HUMAN LUMBAR SPINE SAGITTAL PLANE MOTION: A COMPARISON OF IN VITRO QUASISTATIC AND DYNAMIC FORCE DISPLACEMENT CURVES

[1] Ralph E. Gay, [2]Brice Ilharreborde, [2]Lawrence J. Berglund, [2]Kristin Zhao, [2]Kai-Nan An
[1]Department of Physical Medicine and Rehabilitation, and [2]Biomechanics Lab, Mayo Clinic, Rochester, Minnesota
email: rgay@mayo.edu

INTRODUCTION

The neutral zone (NZ) of a spinal motion segment has been defined as "that part of the range of physiological intervertebral motion, measured from the neutral position, within which the spinal motion is produced with a minimal internal resistance." (1) The size of this region of laxity or high flexibility has been considered an indicator of the stability of a motion segment. The NZ has traditionally been measured in degrees of motion using a quasistatic technique that subjects the segment to pure moments that increase incrementally. The ends of the neutral zone are defined by the positions of the motion segment just before beginning the 3rd cycle in each direction (30 seconds after unloading the 2nd cycle). Thus, the NZ is a measure of residual deformation. Thompson et al suggested that the quasistatic NZ may be an artifact of the testing procedure (2). Using dynamic motion, they proposed a definition of NZ which used derivatives of a 4th order polynomial fitted to both the loading and unloading curves. The region most compatible with the NZ concept was confined by a slope of + or -0.05 Nm/degree. They found an area of laxity around the neutral position in a sheep model only during flexion/extension. *The objective of this study was to compare quasistatic and dynamic force-displacement curves from the same motion segments in regard to ROM and characteristics of the NZ region.*

METHODS

Three human cadaveric lumbar motion segments (L1-2, L2-3, L4-5) aged 40-82 were harvested and dissected in the standard fashion leaving bone, ligament and disc tissue. Each segment was wrapped in saline moistened toweling to retard drying and mounted in custom fixtures (upper and lower) using dental plaster and K-wires. Motion segments were then placed in a custom testing device. Dynamic flexion and extension motion was induced using a counter-weighted stepper-motor mounted on a low friction bearing platform in the sagittal plane. The motor was controlled by a LabView program. Pure flexion/extension moments were transferred from the motor to the upper vertebra of the motion segment through low friction sliding bearings to allow lateral flexion to occur. Moments were applied at a rate of 1 degree/second up 5 Nm then the motor reversed and applied a moment in the opposite direction. Force data were measured by a 6DOF load cell. Displacement was measured in degrees by CXTA tilt sensors. Four dynamic preconditioning cycles were completed then a 5th cycle was used for analysis (1 degree/second). Immediately after dynamic testing, the upper specimen mounting was attached to pneumatic cylinders via a cable and pulley system and pure moments were applied in 1 Nm increments from 0 load to 5 Nm. Force-displacement points were taken as the position after 30 seconds was allowed for viscoelastic creep after each new load and after removal of the load. The region between the points taken after load removal (representing residual deformation in both flexion and extension) was defined as the quasistatic NZ.

RESULTS AND DISCUSSION

The ranges of motion attained in both techniques as well as size of neutral zone (degrees) are listed in Table 1. Using 4th order polynomials we found no discrete area with a slope near 0 as did Thompson et al. The region of the dynamic curves prescribed by the quasistatic NZ (centered on 0 load) was isolated and the slopes calculated. Figure 1 shows the two force-displacement curves superimposed for the motion segment with the largest quasistatic NZ (L2-3).

Table 1.

Spec	Q-ROM	D-ROM	Q-NZ	D-slope
L1-2	10.90	11.20	0.78	0.37
L2-3	11.35	10.23	2.11	0.28
L4-5	8.20	9.90	1.43	0.38

Q=quasistatic, D=dynamic, NZ=neutral zone (degrees), D-slope=slope of curve in dynamic NZ region

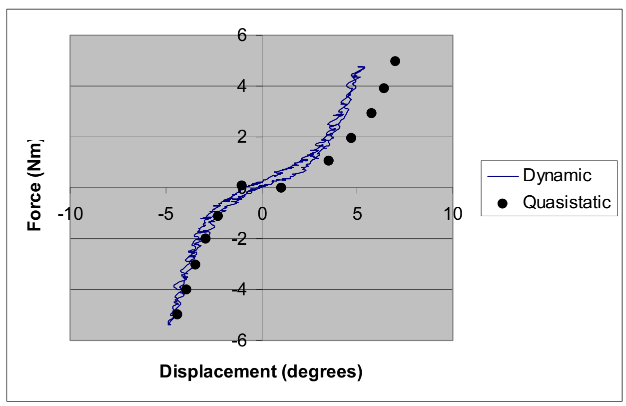

Figure 1: Quasistatic and dynamic force-displacement curves of an L2-3 motion segment superimposed.

CONCLUSIONS

The dynamic force-displacement curves produced by a 1 degree/second moment did not demonstrate an area of laxity about the neutral position as was suggested by the quasistatic curves. This may be due to lack of sufficient relaxation during the dynamic motion despite the low load rate. Alternatively, a true NZ may not exist in these human specimens and the characteristics of motion about the neutral area may be better described by the slope or other functions. Although our results represent only a few specimens, the relevance of the quasistatic NZ, which represents residual deformation after the application of significant load, should be re-examined.

REFERENCES

1. Panjabi MM. Biomechanical evaluation of spinal fixation devices: I. A conceptual framework. Spine 13(10):1129-34, 1988
2. Thompson RE, Barker TM, Pearcy MJ. Defining the neutral zone of sheep intervertebral joints during dynamic motions: an in vitro study. Clin Biomech 18:89-98, 2003

EXPERIMENTALLY DERIVED MODEL OF HUMAN BODY GROWTH

Maria K. Lebiedowska, Steven J. Stanhope,
Physical Disabilities Branch, National Institutes of Health, Bethesda, MD 20892*
email: lebiedowskam@cc.nih.gov

INTRODUCTION

The proportion between body mass and body height serves as a general description of human body shape (HBS).
Different indexes have been used to describe HBS. The most common is Quetelet's body mass index (BMI) that is the ratio between body mass and the second power of body height. The ability of BMI to detect obesity in children is limited by its relatively high level of unexplained variance. Ponderal index (PI) is a geometrically based index (the ratio between body mass and the third power of body height) of HBS. PI is based on a geometrical model, which follows the rules of allometry [1] and scaling of biomechanical parameters [2]. The growth (an age related increase in body height and mass) in children 6-18 years is often considered as geometrically similar, because the body proportions remain almost unchanged. It is unclear how close human growth follows the model of geometrically similar growth.
The aims of this study were to (1) explore the assumption of geometrical growth by developing an experimentally derived model of human body growth; (2) to establish a modified body mass index (MBMI) that is invariant of the effect of growth; and (3) to compare variability of different indexes in a sample population of 6-18 year old children.

METHODS

We used the demographic data collected in able-bodied children age 6-18 years [3] (444 girls and 403 boys). To model growth, the best fit between the body height (H) and body mass (BM) was calculated separately in boys and girls with the function $BM= m_i H^p$. The modified body mass index (MBMI) was calculated as $MBMI= BM/ H^p$ in boys and girls separately. In addition an average body height power across the genders was used to calculate the common modified body mass index (cMBMI) in all children. The BMI ($BMI=BM/H^2$) and PI ($PI=BM/H^3$) were also calculated. The means, standard deviation and variability (standard deviation expressed as a percentage of the mean value) of all indexes were calculated. The correlation coefficients and regression lines were used to assess the relationship between indexes and body height. Statistica, StatSoft Inc. software was used in the analysis at $p<0.05$.

RESULTS AND DISCUSSION

The best mathematical fit between body mass and body height found in girls was $BM_G= 13.6\ H^{2.71}$ ($R^2=0.89$) and in boys $BM_B= 13.9H^{2.65}$ ($R^2=0.91$). The difference between the experimentally obtained powers and the third power of body height reflected the discrepancy between the experimental and geometrically similar model of the human body growth. The different powers obtained in girls and boys may reflect the gender specific differences in body build. There were no statistically significant correlations between indexes and body height, except for BMI, which also exhibited the largest variability (18 % in girls and 17.7 % in boys) (Fig.1). The MBMI, cMBMI and PI exhibited similar variability (12.2%-13.9%) (Table 1). The increase of BMI with the body height in children requires an application of age charts and a z-score or percentile analysis. The fact that the other indexes are independent of body height sanctions a characterization of population with one mean and one standard deviation. Future studies should include the development of models of growth in various populations and in individual subjects.

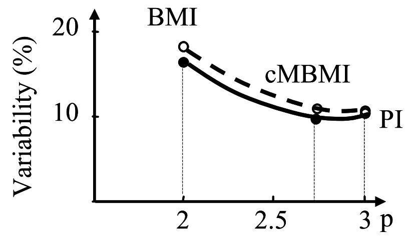

Figure 1 The variability of different body mass indexes in girls (dashed line) and in boys (solid) as a function of p in the equation $BM= m_i H^p$

CONCLUSIONS

Human growth in children 6-18 years old does not follow the geometrically similar growth model.
Using variability as a guide, MBMI and PI appear to be superior to BMI in reflecting the relationship between the body height and geometry.
Based on the differences in the coefficients cMBMI is superior to PI in the context of the differences due to growth in children 6-18 years old.

REFERENCES

[1] Günter B. *Physiological Reviews*, **55**, 659-699, 1975.
[2] Hof A. *Gait and Posture*, **4**, 222-223,1996
[3] Lebiedowska et al. *Disability and Rehabilitation* **18**, 137-142,1996.

* A collaboration between the NICHD and the Warren G. Magnuson Clinical Center, NIH

Table 1 The characteristic of different body mass indexes (mean± std) and their dependency on body height in children 6-18 years old.

Body mass index / Gender	BMI		PI		cMBMI	
	Mean±std (kg/m^2)	Regression equation	Mean±std (kg/m^3)	Regression equation	Mean±std ($kg/m^{2.68}$)	Regression equation
Girls N=444	18±3.2	2.23 + 10.9 H r=0.65	12.47±1.64	15.81-2.28 H r=-0.24	14.02±1.95	12.47+1.07H r=0.1
Boys N=403	17.7±2.9	5.2 + 8.57 H r=0.62	12.21±1.62	17.32-3.46 H r=-0.06	13.76±1.82	14.14+0.5 H r=-0.05

GAIT BIOMECHANICS IN AN OBESE GASTRIC BYPASS SURGERY POPULATION: PRELIMINARY RESULTS

[1] Stephanie J. Nogan, [2] Michele M. Hooper, [3] Thomas A. Stellato, [2] Barbara A. Seitz, [1,4] Ronald J. Triolo, [1] Rudi Kobetic
[1] Motion Study Laboratory, Cleveland FES Center, Louis Stokes Cleveland VA Medical Center, Cleveland, Ohio, USA
[2] Arthritis Translational Research Program, University Hospitals of Cleveland, Cleveland, Ohio, USA
[3] Department of Surgery, University Hospitals of Cleveland, Cleveland, Ohio, USA
[4] Departments of Orthopaedics and Biomedical Engineering, Case Western Reserve University, Cleveland, Ohio, USA
Email: snogan@fes.case.edu, michele.hooper@uhhs.com

INTRODUCTION

Obesity is a major risk factor for knee, but not hip or ankle osteoarthritis (OA). Knee varus malalignment and an increased knee adduction (varus) moment are key variables linked to OA progression. We are studying gastric bypass surgery (GBS) patients with and without knee pain to evaluate gait biomechanics in obese subjects before and after a 100-pound weight loss.

METHODS

Twenty-one subjects were studied, including 18 females and 3 males. The pre-surgery age of the subjects was 49.86 ± 6.81 years and the pre-surgery body mass index (BMI) was 47.15 ± 7.01 kg/m^2. Weight-bearing, semi flexed anterior-posterior radiographs were taken to access radiographic knee OA (rOA). Eighteen (85%) subjects reported knee pain, and of those 18, 14 (78%) had rOA and 4 (22%) had no rOA. Normalized Western Ontario McMaster Arthritis Questionnaire (WOMAC) pain scores were less than 13 for the 3 subjects without pain and ranged from 16 to 73.2 for those with pain. Subjects were able to walk without the use of assistive devices.

Spatial-temporal, kinematic, and kinetic data were collected during natural cadence gait with a 7-camera Vicon 370E system. Peak knee flexion during swing, peak ankle plantarflexion for push-off, peak knee varus moment, and peak ankle plantarflexion power for push-off were determined to be the parameters of interest. Twenty-one subjects completed pre-surgical gait analysis sessions and 6 subjects completed post-surgical sessions. Weight loss for the 6 subjects was 48.41 ± 12.78 kg, for a post-surgical BMI of 29.40 ± 5.78 kg/m^2. Four of the subjects with pre-surgery knee pain reported no knee pain after weight loss. Subjects were compared to published normal control populations, using two-sample t-tests. For pre- and post-surgical assessments, subjects served as their own controls and paired t-tests were used to access significance.

RESULTS AND DISCUSSION

Five sets of comparisons were made for the 4 key parameters: 1) all obese subjects (n=21) versus control, 2) the no pain group (n=3) versus control, 3) the pain group (n=18) versus control, 4) the pain group versus the no pain group, and 5) the 6 post-surgical subjects versus their pre data, as shown in **Table 1**. Control values for peak knee flexion during swing, peak ankle plantarflexion for push-off, and peak ankle plantarflexion power for push-off were taken from Winter [1]. Peak knee varus moment was taken from Gok [2] since Winter only reported on sagittal plane kinematics and kinetics.

	Obese		Control		Significance
	Mean	StDev	Mean	StDev	
Peak Knee Flexion During Swing (deg)	47.01	9.12	64.86	5.41	$p < 0.001$
Peak Ankle Plantarflexion for Push-Off (deg)	-12.07	6.06	-19.77	5.81	$p < 0.001$
Peak Knee Varus Moment (Nm/kg)	0.48	0.21	0.33	0.05	$p < 0.001$
Peak Ankle Plantarflexion Power Before Push-Off (W/kg)	1.74	0.73	3.33	1.02	$p < 0.001$

	No Pain		Control		Significance
	Mean	StDev	Mean	StDev	
Peak Knee Flexion During Swing (deg)	43.81	9.81	64.86	5.41	$p < 0.001$
Peak Ankle Plantarflexion for Push-Off (deg)	-17.45	4.14	-19.77	5.81	None
Peak Knee Varus Moment (Nm/kg)	0.46	0.10	0.33	0.05	$p < 0.05$
Peak Ankle Plantarflexion Power Before Push-Off (W/kg)	2.36	0.52	3.33	1.02	$p < 0.01$

	Pain		Control		Significance
	Mean	StDev	Mean	StDev	
Peak Knee Flexion During Swing (deg)	47.55	9.03	64.86	5.41	$p < 0.001$
Peak Ankle Plantarflexion for Push-Off (deg)	-11.15	5.89	-19.77	5.81	$p < 0.001$
Peak Knee Varus Moment (Nm/kg)	0.49	0.23	0.33	0.05	$p < 0.001$
Peak Ankle Plantarflexion Power Before Push-Off (W/kg)	1.64	0.72	3.33	1.02	$p < 0.001$

	Pain		No Pain		Significance
	Mean	StDev	Mean	StDev	
Peak Knee Flexion During Swing (deg)	47.55	9.03	43.81	9.81	None
Peak Ankle Plantarflexion for Push-Off (deg)	-11.15	5.89	-17.45	4.14	$p < 0.01$
Peak Knee Varus Moment (Nm/kg)	0.49	0.23	0.46	0.10	None
Peak Ankle Plantarflexion Power Before Push-Off (W/kg)	1.64	0.72	2.36	0.52	$p < 0.01$

	Pre		Post		Significance
	Mean	StDev	Mean	StDev	
Peak Knee Flexion During Swing (deg)	43.91	8.49	52.73	3.64	$p < 0.01$
Peak Ankle Plantarflexion for Push-Off (deg)	-9.02	5.42	-10.21	5.86	None
Peak Knee Varus Moment (Nm/kg)	0.45	0.13	0.49	0.19	None
Peak Ankle Plantarflexion Power Before Push-Off (W/kg)	1.83	0.61	1.98	0.70	None

Table 1: Means, standard deviations, and p values for each of the 4 key parameters for the 5 sets of comparisons.

CONCLUSIONS

There were significant differences between the normal controls and the pre-surgical obese group for all 4 of the key parameters. Pain-free subjects demonstrated fewer differences in comparison with normal controls than did subjects with pain. Differences in ankle plantarflexion and ankle power between the pain and pain-free groups were statistically significant. Weight loss is associated with knee pain relief, which can account for improvement in gait biomechanics. The 6 subjects who completed pre- and post-operative evaluations exhibited a significant improvement in peak knee flexion during swing and 4 of these individuals became pain-free post-GBS. We plan to further investigate changes in gait biomechanics due to obesity, OA, or pain by completing post-operative tests after weight loss in all subjects.

REFERENCES

1. Winter DA. *The Biomechanics and Motor Control of Human Gait: Normal, Elderly and Pathological – Second Edition,* Waterloo Biomechanics, Waterloo, Ont., Canada.
2. Gok, et al. *Acta Orthop Scand* **73**, 647-652, 2002.

ACKNOWLEDGEMENTS

The Elizabeth Severance Prentiss Foundation.

ASSESSING SHOULDER KINEMATICS IN A SUBJECT WITH A SPINAL ACCESSORY NEUROPATHY

Duane A. Morrow, Brian R. Kotajarvi, Alexander Y. Shin, Kai-Nan An, and Kenton R. Kaufman
Biomechanics and Motion Analysis Laboratory, Division of Orthopedic Research, Mayo Foundation, Rochester, MN
email: kaufman.kenton@mayo.edu web: mayoresearch.mayo.edu/mayo/research/biomechanics

INTRODUCTION

Kinematic assessment of the upper extremity, particularly the shoulder joint, remains troublesome. Due in part to the technical difficulties in quantifying scapula movement, some investigators choose to report shoulder kinematics as the relative motion between the humerus and trunk [1]. Others, using the method proposed by Karduna [2], report shoulder motion as the angle between the humerus and scapula [3]. A previous report from our laboratory pointed to some of the discrepancies that exist between thoracohumeral pseudo-joint motion and glenohumeral joint motion [4], even in a normal subject. The purpose of this abstract is to report our clinical experience using this technique, examining the results of both methods of UE motion analyses.

Figure 1. Subject with the scapula tracker resting on the scapular spine.

METHODS

UE kinematics were collected on a 17 year old patient with a right spinal accessory nerve palsy which resulted from the biopsy of an enlarged lymph node in the posterior triangle of her right neck. Sixteen retroreflective markers were used to define the head, trunk, scapula, upper arm, forearm, and hand in a six-segment biomechanical model. The three markers used to track the scapula were on a tracker [4] which was attached to the skin using double-sided tape and rested on the scapular spine (Fig. 1). Data was collected at 60-Hz using a 10-camera RealTime Motion Analysis System (Motion Analysis Corp., Santa Rosa, CA). The patient was asked to perform an UE kinematic exam consisting of moving her shoulder throughout her available Flexion/Extension (FE) and Ab/Adduction (AB) ranges of motion as well as reaching across her chest to her opposite shoulder (OS). The patient's elbow and wrist were held in their neutral alignment for the FE and AB trials, but allowed unconstrained motion during the OS trials. Three trials of each motion were collected.

Rotation matrices were calculated between anatomically-defined segment axes constructed using the guidelines established by the International Society of Biomechanics [5]. These rotation matrices were decomposed into clinically relevant coordinates using Woltring's helical-axis method [6].

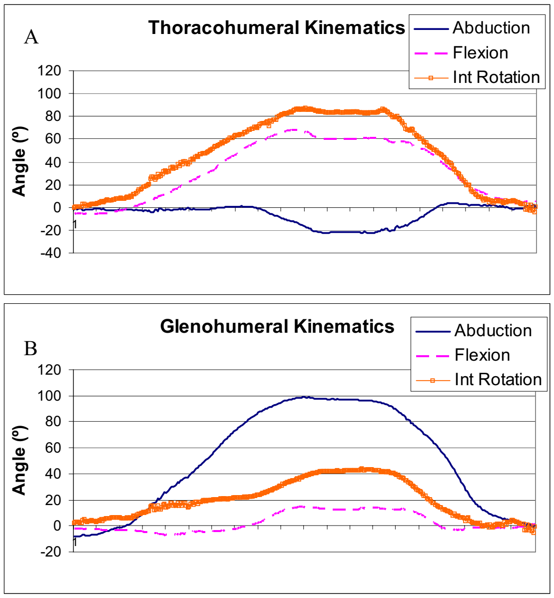

Figure 2. Thoracohumeral (A) and Glenohumeral (B) kinematics of a cross-shoulder reach.

RESULTS AND DISCUSSION

Thoracohumeral and glenohumeral joint kinematics for this subject vary widely using the two techniques. Using only trunk and humerus markers to analyze shoulder motion, it would appear that reaching to the opposite shoulder consists mainly of shoulder flexion and internal rotation (Fig. 2A). However, consideration of the scapula in examination of glenohumeral motion reveals a large contribution of shoulder abduction and substantively less internal rotation (Fig. 2B). The palsy in the spinal accessory nerve lead to weakness in the upper and lower trapezius muscles which are used to keep the scapula retracted. As a result, the patient's scapula was rotated upwards over 52° and protracted by more than 48° (Fig. 1), accounting for the large discrepancy in the kinematics results. Similar results were found for the FE and AB motions.

CONCLUSIONS

Great attention must be paid in the application of UE models used to study patients with clinical pathologies.

REFERENCES

1. Mosqueda T, et al, *J Pediatr Orthop* **24**, 695-699, 2004.
2. Karduna AR, et al, *J Biomech Eng* **123**, 184-190, 2001.
3. Rundquist PJ, and Ludweig PM, *Clin Biomech* **19**, 810-818, 2004.
4. Morrow DA, et al, *ASB Conference*, Portland, OR, 2004.
5. Wu G, et al, *J Biomech*, In Press, 2005.
6. Woltring HJ, et al, *J Biomech*, **18**, 379-389, 1985.

ACKNOWLEDGEMENTS

Funding for this study provided by the Mayo Foundation.

PATELLAR DEFORMATION PATTERNS FROM A PRE-CLINICAL PATELLAR COMPONENT TEST

[1]Mariana Kersh, [1]Heidi-Lynn Ploeg
[1]University of Wisconsin – Madison, Department of Mechanical Engineering
E-mail: mekersh@wisc.edu, web: www.engr.wisc.edu/groups/BM

INTRODUCTION

More attention is being given to the role of patellar components in total knee arthroplasty (TKA) as it is continually cited as a primary cause for TKA revision [1]. Various studies have documented the failure of patellar components [2-4], and as advances in TKA devices are made, it is important to ensure that the history of patellar failure is understood. This information can be used to develop pre-clinical tests to aid the design of clinically successful components. The goal of this study was to compare the polyethylene (PE) deformation of patellar components tested according to a new test protocol [4] against clinical results as one method for test validation.

METHODS

Five metal-backed (Component A) and five all-polyethylene (Component B) patellae were tested using an AMTI knee simulator. All components were fixed with bone cement and tested in bovine serum. A deep knee flexion cycle from 60° to 120° was simulated using a saw tooth waveform developed in a previous study [5]. The femoral component was initially displaced 1.2mm medially with an initial load of 1177N and then translated a total of 6.4mm medially as the load increased to 4258N. Components were tested at 1Hz to 50,000 cycles (20 years of deep knee bending activities), photographed before and after testing, and visually examined.

PE deformation defined as burnishing, creep, and polyethylene transparency, was quantified according to a 4-level scale for each deformation trait: none (0), minimal (1), moderate (2), and extreme (3). This scale was used to evaluate each section of a sixteen-area grid (Figure 1). Each section was assigned a score based on the amount of deformation present. Creep was measured by evaluating circumferential area changes.

RESULTS AND DISCUSSION

The average scores for each area and each component type are found in Table 1. There was no significant difference in the scores for Areas 3 and 4 of Component A or B for any deformation trait and were omitted from overall scores.

Overall, burnishing was more evident in the metal-backed components (score = 2.0) compared to the PE components (1.7). In both components, burnishing scores were higher on the lateral aspect (Area 1) of the patella compared to the medial (Area 2). A more pronounced difference was found in the evaluation of creep: Component A had an average score of 2.0 compared to 0.8 for Component B. PE transparency was only found in Component A.

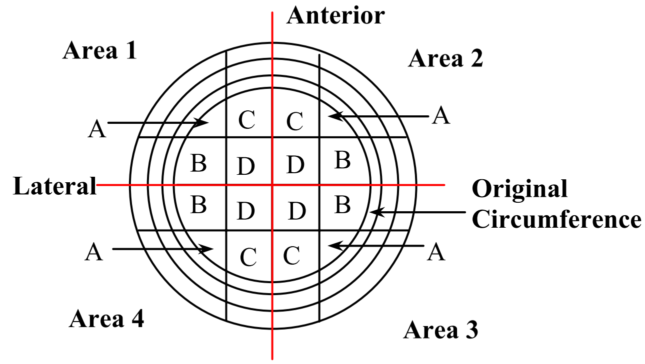

Figure 1. Segmentation of Patella For Evaluation

In a review of TKA revisions, Baech [4] documented asymmetrical wear patterns in metal-backed components. Andersen also found the presence of lateral edge wear [2]. Stulberg noted similar patterns of failure between the metal-backed and all-polyethylene components noting that both groups deformed at the lateral aspect of the component [3].

Regarding test survival, Component A averaged 5200 cycles before excess deformation required the test to be stopped. In contrast, all of the PE components survived 50,000 cycles. Studies have reported an average time to revision range of 11-18 months [2, 4]. The deformation results presented, as well as time to failure results, are similar to those documented in clinical literature indicating potential for the new test protocol to be used as a clinically relevant design tool.

REFERENCES

1. Chew, HT, et al. *Clin Orthop*, **345**, 87-98, 1997.
2. Anderson, HN, et al. *Acta Orthop Scand*, **61**, 1-3, 1991.
3. Stulberg, SD, et al. *Clin Orthop*, **236**, 88-105, 1988.
4. Baech, J et al. *Acta Orthop Scand*, **62**, 166-8, 1991.
5. Kersh, ME et al. *Proc IMECE2004: ASME*, 2004.

ACKNOWLEDGEMENTS

The authors are grateful for the contributions of Dave Blakemore, Les Gilbertson, Brian Kincaid, Lynn Kirkpatrick, Jerry Parcell, The UW Biomechanics Lab, and Zimmer, Inc.

Table 1: Overall Deformation Scores for Metal-Backed Component A and All-Polyethylene Component B

		Burnishing				Creep				PE Transparency			
Area	Component	A	B	C	D	A	B	C	D	A	B	C	D
1	A	3.0	1.6	2.0	1.8	2.4	1.0	3.0	-	2.6	1.0	1.4	0
	B	3.0	2.2	1.4	1.6	1.0	0.6	1.0	-	0	0	0	0
2	A	3.0	2.0	2.0	0.4	2.4	0.8	3.0	-	3.0	1.8	1.0	0.4
	B	2.6	2.4	0.2	0	1.0	1.0	1.0	-	0	0	0	0

THE EMG/TORQUE RELATIONSHIP OF THE KNEE EXTENSORS DURING ACUTE FATIGUE

Tyler Brown and Michael E. Hahn
Movement Science Laboratory, Montana State University, Bozeman, MT USA
email: mhahn@montana.edu

INTRODUCTION

Fatigue has been defined as a transient decrease of performance capacity of muscles during physical activity [1]. Response of knee musculature to acute fatigue may dictate adaptations to knee function during high impact activities, which may result in injury. One technique for assessing muscular adaptation to fatigue is to analyze the ratio of electromyographic magnitude (EMG) to torque production [2]. The purpose of this study was to determine the EMG/torque relationship of the vastus lateralis during acute fatigue.

METHODS

Six male subjects (mean age 24.3) participated in the study. All subjects signed an informed consent before participation. Subjects performed three isometric maximum voluntary (MVC) knee extension (KE) contractions at 45° before performing a fatigue protocol. The fatigue protocol consisted of subjects performing isokinetic KE contractions (concentric and eccentric) at 60°/s through their functional range of motion until acute fatigue was reached. Acute fatigue was defined as when the subject performed two consecutive contractions where the peak concentric torque was below 50% of MVC. All contractions were performed using the subjects' dominant leg.

Knee extensor torque during the isometric and isokinetic contractions was measured using a strain-gauge dynamometer (KIN-COM, Rehab World, Hixson, TN, USA). A passive bi-polar surface EMG recording system (Myopac Jr., Run Technologies, Mission Viejo, CA, USA) was used to collect vastus lateralis (VL) activation magnitudes at a sampling frequency of 1000 Hz. EMG signals were bandwidth filtered (10-10,000Hz), full-wave rectified and smoothed with a 4th order Butterworth filter (low-pass cutoff = 5Hz) before analysis.

For analysis, torque production was normalized to body weight, processed EMG was normalized to maximal isometric activation and the ratio of EMG amplitude to torque production was calculated during each phase of the fatigue protocol. The change of torque produced during each phase was also determined.

RESULTS AND DISCUSSION

It was determined that peak torque production during the fatigue protocol could be broken into three phases. The first phase ("initial") consisted of the first 12 to 15 cycles of the fatigue protocol where subjects maintained roughly 80 to 90% of the torque produced during the isometric MVC. During the second phase ("decline") subjects' torque production dropped from 80% of MVC to below 50% in 12 to 15 repetitions and in the third and final phase ("fatigued"), declines in torque production leveled off and subjects maintained slightly less than 50% of MVC. The change of each subjects' torque production for each phase is shown in Table 1. Torque production during the initial phase increased slightly, in the decline phase there was a dramatic decrease and for the fatigued phase it leveled off with minimal declines.

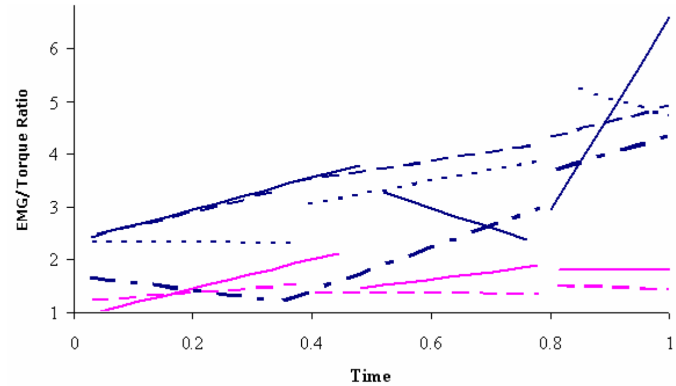

Figure 1: EMG/torque ratio during the fatigue protocol. Time is listed as a proportion of the entire protocol.

Examination of the EMG/torque ratio indicates that responses to the fatigue protocol can be divided into two groups (Fig. 1). One group's EMG/torque ratio essentially doubled as a result of acute muscular fatigue, while a second group responded to fatigue without increasing their EMG/torque ratio. These results indicate that a group of subjects did not need to activate more fibers to sustain torque production of 50% MVC when fatigued. The other subjects needed to increase activation levels in an effort to maintain torque production during acute fatigue. Whether this signal increase resulted from increased recruitment or rate coding is undetermined.

CONCLUSIONS

Further research is needed into the effects of acute muscular fatigue on the knee extensors. Future work will focus on whether the varied responses of the EMG/torque ratio to acute fatigue are due to group-specific training.

REFERENCES

1. Asmussen E. *MSSE* **11**, 313-321, 1979.
2. Eguchi A. *Electro. Clin. Neuro.* **44**, 75-81, 2004.

Table 1. Change in torque production during each phase of the fatigue protocol (Nm/kg)

	Subj. 1	Subj. 2	Subj. 3	Subj. 4	Subj. 5	Subj. 6	Mean (SD)
Initial	-0.010	0.049	0.065	-0.024	0.110	0.030	0.037 (0.049)
Decline	-0.135	-0.181	-0.132	-0.101	-0.203	-0.136	-0.148 (0.037)
Fatigued	0.058	-0.059	0.018	-0.011	-0.012	-0.036	-0.007 (0.041)

DEVELOPMENT OF HUMAN PELVIC BONE FE MODEL BY CONSIDERING PELVIC ANTHROPOMETRY

[1] Cheolwoong KO, [1]Atsuhiro KONOSU, [2]Yukihiro YUKITA and [2]Jiro SAKAMOTO
[1]Japan Automobile Research Institute, [2]Kanazawa University;
email: kcheol@jari.or.jp

INTRODUCTION

In collisions between pedestrians and road vehicles, the incidence of pelvic injuries resulting in serious wounds or death ranks high, following knee and head injuries. In light of this fact, the development of a human pelvis FE model with high bio-fidelity is required for reliable human injury analysis.

Thus far, several human pelvis models have been developed and modified in order to investigate the pelvic injury mechanism due to impact loadings [1,2,3]. However, detailed studies for pelvic anthropometry have been minimal. Therefore, it is necessary to consider pelvic anthropometry in pelvis FE model construction.

METHODS

In this research, a new human pelvic bone FE model (called the JK-model) was constructed on the basis of the CT image data of a Japanese adult. Anthropometry of the JK-model based on anatomical information was investigated by a comparison of measurement data obtained from cadaver pelvic bones.

Figure 1 depicts the reference coordinate of the human pelvis, defined by Reynolds et al., in order to measure anatomical points of cadaver pelves of Americans [4]. In this research, six representative points from A to F (A:Iliocristale, B:Left Iliospinale, C:Symphsion, D:Ischio-Spinale, E:Inferior Turbersity point, F:Inferior Obturator Foramen Point) were selected, as shown in Figure 2. The length from the origin of the reference coordinate to each selected point was defined as a comparison parameter in order to investigate the pelvic anthropometry of the JK-model. In addition, the result was compared to the pelvic anthropometry of commercial pelvis FE models (for example, THUMS and H-model).

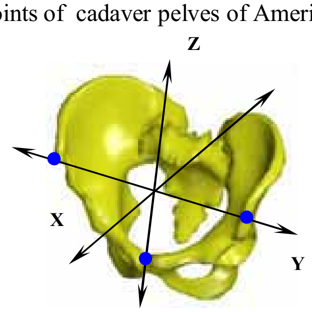

Figure 1: Coordinate System of Pelvis [Reynolds, et al.]

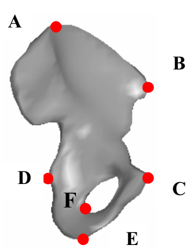

Figure 2: Representative Points

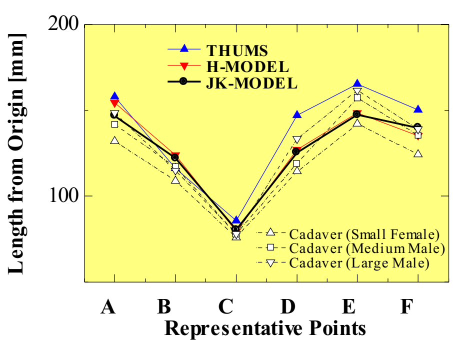

Figure 3: Comparison of Pelvic Anthropometry

RESULTS AND DISCUSSION

The comparison parameters were summarized as presented in Figure 3. It was found that the lengths from the origin to D, E and F points of THUMS are greater than those of the H-model. The overall anthropometrical feature of the JK-model was close to that of the H-model. Also, the comparison parameters of the JK-model lie in the corridor of American measurement data; thus, the JK-model could be used as a standard model for human injury research in the crash safety field.

The appearance of pelvis models is depicted in Figure 4. It was considered that the JK-model has relatively higher bio-fidelity than those of commercial pelvis models with regard to pelvis shape.

CONCLUSIONS

In this research, a new human pelvic bone FE model was constructed on the basis of the CT image data of a Japanese adult. Its pelvic anthropometry was investigated with the use of anatomical information. It is considered that anthropometry study is important and necessary in FE model construction in order to obtain reliable analysis results.

REFERENCES

1. Dalstra, et al. *J of Biomech Engineering* **117**, 272-278,1995.
2. Besnault, et al. **SAE Paper 983147**, 1998
3. Ko, et al. *JSAE 2004 Autumn Conference* **120-04**, 5-8, 2004
4. Reynolds, et al. *FAA Civil Aeromedical Institute* **FAA-AM-82-9**, 1-37, 1982

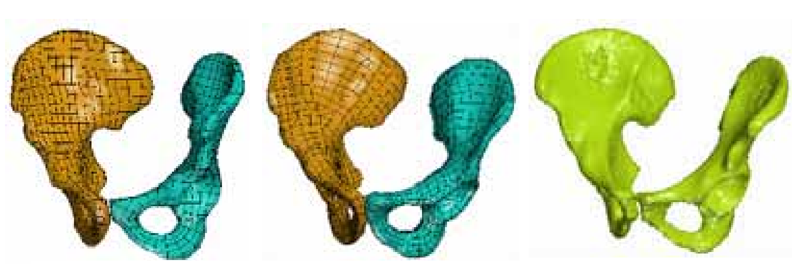

(a) THUMS (b) H-Model (c) JK-Model

Figure 4: Comparison of Human Pelvic Bone FE Model Appearance

In-vivo measurement of the compressive force under the coraco-acromial arch

[1, 2]Toshimasa Yanai and [3]Franz K. Fuss
[1] Chukyo University, Japan; [2] University of Otago, New Zealand; email: tyanai@life.chukyo-u.ac.jp
[3]Nanyang Technological University, Singapore; email: mfkfuss@ntu.edu.sg

INTRODUCTION

Shoulder impingement is a widely recognized mechanism of chronic shoulder pain. With this mechanism, the shoulder pathology is explained as the consequence of repeated impingement, or compression, of the subacromial structures under the coraco-acromial arch. It has not been confirmed, however, if the compressive force that impinges the subacromial structures is sufficiently large to cause micro-trauma that leads to the pathological condition. The purpose of this study was to determine in-vivo the magnitude of the compressive force developed under the coraco-acromial ligament at selected shoulder configurations.

METHODS

Five males with no history of shoulder pain volunteered to participate in this study. After having provided written informed consent, each subject was asked to actively maintain his arm in specified positions: (1) Anatomical (neutral) position, (2) 90° abduction + maximum external rotation, (3) 90° abduction + neutral rotation and (4) 90° abduction + maximum internal rotation. In addition, (5) the subject's shoulder was passively and forcibly configured to form the position for the Hawkins impingement test.

An ultrasound unit (EUB-6500, Hitachi Medico, Japan) was used to visualize and record the shape of the coraco-acromial ligament at each shoulder configuration. The probe was positioned carefully, so that the shape of the ligament's long-axis could be visualized. The contour of the upper, and also lower, surface of the coraco-acromial ligament were identified from the recorded images and digitized manually. The best-fit polynomial equation was determined to express the shape of the ligament mathematically for each shoulder configuration.

The ligament was modeled to have: (a) a uniform elastic property throughout the length between the insertions (Young's modulus = 290 MPa [2]); (b) smooth (no friction) surfaces; (c) a uniform cross-sectional area of 8 mm^2 throughout the length [2]; and (d) the length of a coraco-acromial ligament *in situ* was 5% (pre-strain) longer than the resting length of the ligament [2]. With this model and the measured length, the tensile force acting across the cross-sectional area of the ligament at its attachments and a single resultant of the distributed normal forces that caused the ligament to change its shape were determined. The latter force balances the two tensile forces and compresses the subacromial structures as a reaction (impingement force).

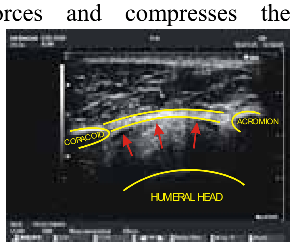

RESULTS

The ultrasound images showed that the coraco-acromial ligament that was flat initially at the anatomical position was pushed, and deflected, upward by the subacromial structures to form a curved shape when the arm was elevated and internally rotated. The extent of the deformation exhibited at the maximum internal rotation was found similar to that provoked at the Hawkins test position. This observation was confirmed with the determined impingement forces (below).

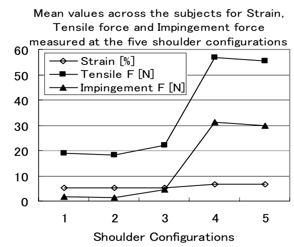

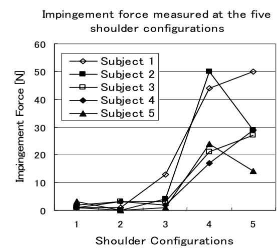

DISCUSSION

The study demonstrated that the impingement force developed under the coraco-acromial ligament increased with the active shoulder internal rotation and that the magnitude of the impingement force recorded during active motion attained similar values to that recorded with the Hawkins test. The first result was consistent with the in-vivo study conducted by Nobuhara [1] in which the impingement force under the coraco-acromial ligament was measured directly from 260 patients during open surgery. The second result indicates that the subacromial structures during active shoulder motions are subject to a compression at the intensity similar to the "impingement sign (localized pain)."

The validity of the present methodology was tested with a cadaveric study in which known amounts of forces applied to ten specimens of coraco-acromial ligament were compared with the corresponding forces determined with the model approach used in the present study. The correlations were found high (0.925-0.986) although the absolute values of the forces were found to involve large error due to the individual variability in the Young's modulus of the ligament. These results suggest that the present methods provide sufficient accuracy in determining the relative magnitude of impingement force and that the ligament Young's modulus needs to be individualized to improve the accuracy in determining the absolute magnitude of the impingement force. It is also important to scan the ligament immediately after the subject has moved his arm into the required shoulder position, in order to keep stress-relaxation and creep to a minimum.

REFERENCES

1. Nobuhara, K. *The Shoulder: Its function and clinical aspects*, World Scientific Publishing, 2003.
2. Soslowsky, L.J. et al. *Clin Orthop Res* **304**, 10-17, 1994.

ACKNOWLEDGEMENTS

This study was partially funded by the Royal Society of New Zealand, ISAT Linkages Fund (99-BRAP-09-YANA).

PREDICTION OF CYCLE SHOE PERFORMANCE IN RELATION TO OUTSOLE MATERIALS BASED ON BIOMECHANICAL TESTING AND FINITE ELEMENT ANALYSIS

[1, 2]Jong-Peel Joo, [1]Soo-Jung Moon, [1]Yoon-Ho Ahn, [3]Seung-Gon Oh, [4]Jin-Bong Kim and [1]Sung-Jae Lee
[1]Department of Biomedical Engineering, Inje University, Republic of Korea
[2]Research Development Team of Korea Footwear Institute, Republic of Korea
[3]Research and development center of Woo Yun Co.,Ltd., Republic of Korea
[4]Korea Institute of Machinery & Materials, Republic of Korea
sjl@bme.inje.ac.kr

INTRODUCTION

Ultra-stiff carbon fiber composites are now being placed in the outsole of both road and mountain cycle racing shoes. They are intended to transfer energy more efficiently from the legs and feet to the pedals. This is based on the belief that higher the stiffness of the outsole, the greater plantar pressure may be produced in the forefoot [1]. In this study, both finite element (FE) analysis and biomechanical experiment were done to assess the performance of the cycle racing shoes in relation to the material properties of the outsole.

METHODS

Three types of outsole FE models outsole were generated for this study (Fig. 1-a). Type I was entirely made of a carbon composite based on the commercially available model (Shimano R-215, Japan); Type II, with a nylon outsole and the carbon composite insert (50 v/o); Type III, of a 100% nylon outsole. Thus, Type I was the stiffest outsole followed by Type II, and then Type III. Also, a foot model was generated from the CT data of a normal person with material properties from literature [2] (Fig. 1-b). The outsole was directly attached to the plantar surface of the foot. The insole part of the shoe was omitted in modeling for the sake of focusing on the outsole only and also to reflect the riding preference of many professional athletes. The material properties of the carbon composite were computed based on the classic lamination theory [3], which allowed us to convert the material properties of carbon composites from anisotropic to isotropic. Bending test of the carbon composite outsole was done to validate with the FE model results. Here, the cleat region of the outsole was held firmly while the heel part was pushed down until bending failure. Displacements under 30kg·f(294N) and 50kg·f(490N) that were within the elastic region were compared with the corresponding FE results.

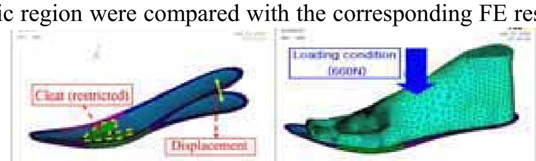

(a) **(b)**

Figure 1: The FE models: (a) outsole, (b) with foot

To obtain the loading conditions for FE analysis, a healthy subject (male, 28 years of age, 735N) rode on a stationary cycle set up (SRM, Germany). In-shoe foot plantar force and pressure were measured with F-scan system (Tekscan Inc., South Boston, USA) while keeping RPM and torque constant during pedaling based on the protocol suggested in the literatures [4]. Maximum force of 660N was recorded and was applied to FE analysis as a loading condition. Performance in relation to different shoe types were assessed by comparing plantar stresses in the forefoot region based on the literature findings on the relationship between the stress-strain and the load transmission and energy absorption at forefoot and heel regions[1, 4]. After applying appropriate loading and boundary conditions based on the experimental data, resulting stresses and displacements were assessed in foot plantar regions of FE models.

RESULTS AND DISCUSSION

The bending test results were in good agreement with the predicted displacements with the FE model, suggesting the validity of our model. The stress at the forefoot was highest with Type I shoes (i.e., the stiffest), followed by Type II and then Type III. It was found that 50 % reduction in carbon composite from Type I resulted in decrease in maximum stress by only 10% in Type II (Fig. 2-a). Corresponding displacement at the heel regions were very small in both Types I and II (Fig. 2-b). However, importance of the carbon composite was clearly shown with significant drop in the maximum stress at the forefoot and leaping increase in the displacement at the heel from Type II to Type III.

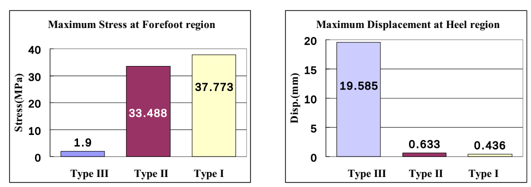

(a) (b)

Figure 2: FEA results: (a) Stresses at forefoot, (b) Displacements at heel

CONCLUSIONS

Our results demonstrated that the inclusion of ultra-stiff material such as carbon composite was very crucial for transferring the energy to the pedal through the outsole. More studies on the optimum amount and locations of the carbon composite material will follow using the FE model constructed from this study.

REFERENCES

1. Gregor R. J, et al., *J injury Sports Med.* **17(2)**, 117-31. 1994.
2. Chen W. P, et al., *J Clinical Biomech.* **16**, 614-620, 2001
3. Ochoa O. O, et al., *Finite element Analysis of Composite Laminates*, 1992.
4. Nathan E. J, et al., *Summer Bioengineering conference*, 2003.

ACKNOWLEDGEMENT

This study was supported by the grant ATC1007805 from Korea Ministry of Commerce, Industry & Energy.

Factors affecting lunate's sagittal alignment

Ajay Gupta
G.T.B.Hospital and University College of Medical Sciences, Shahdara. Delhi. India.
email: drjaygupta@hotmail.com

INTRODUCTION

The lunate classically is described to have tendency to rotate dorsally under the capitate compressive force due to its shape of a wedge with apex towards the dorsum[1]. However no correlation could be demonstrated between the shape of the lunate and the radiolunate angle (RLA)[2]. The sagittal axis of the midcarpal joint lies parallel and dorsal to that of the radiocarpal joint, creating a force couple tending to rotate the lunate dorsally [1,3]. Despite this, lunate is found to maintain an attitude of flexion in most individuals [4].

The dorsal placement of the lunato-triquetral articulation on the lunate provides extension torque to the triquetrum causing lunate to rotate dorsally and balancing the scaphoid's flexion torque. Magnitude of such extension torque should presumably vary among various lunates depending upon inclination and extent of the triquetral's articulation on the lunate and triquetrum's alignment in sagittal and axial plane.

Review of literature failed to provide a study quantifying dorsal orientation of the midcarpal axis. Moreover, there has been no definite description also of how to measure and exactly draw the midcarpal (MCA) and the radiocarpal axes (RCA). It was felt that identifying MCA and RCA accurately on CT, quantifying their displacement with each other and establishing correlation among various parameters might be able to throw some light on the lunate's ambiguous behavior.

METHODS

Database from our earlier studies [5] was utilized to provide material for the present study and included CT wrist of 70 healthy volunteers who never had any symptoms pertaining to their wrist joint. The mean age was 34 years with a range of 19-55 years. There were 49 males and 21 females.

Sagittal section through the middle of the capitate head was used to measure volar tilt of the distal radial articular surface (VT), lunate's sagittal axis (LSA) and the wedge ratio (WR) for the shape of the lunate[2]. Sagittal cuts were also measured for the axis of the triquetrum (TSA) and the midcarpal (MCA) and the radiocarpal axes (RCA). The distance between the two axes was measured and taken as positive value if MCA was found posterior to the RCA while anteriorly placed MCA measured as negative value. The axial sections were reformatted and measured for the lunate axis (LA), triquetro-hamate axis (THA) and luno-triquetral angle (LTA).

RESULTS AND DISCUSSION

The midcarpal axis was found to be dorsal to the radiocarpal axis in 21 patients (30%), volar in 29 patients (41%) while the two axes were nearly collinear in 20 patients (29%). The mean distance between the two axes was 1.6 mm (S.D. 0.87) in the former group and -1.3 mm (S.D. 0.71) in the later. The distance between the two axes showed a strong correlation

Figure 1: Lunate is seen not to rotate towards its thinner side. It is rather rotating in the opposite direction in b, & c.

with the LSA ($p<.001$) and mild correlation with WR measurements ($p<.005$) while it showed no correlation with the VT. The LSA demonstrated significant correlation with TSA and LTA while no correlation was seen with the WR measurements, VT and the LA.

One out of every three persons is reported to have a lunate with shapes not favoring the tendency to dorsiflex. The whole proximal carpal row including the lunate was found to flex, radially deviate and supinate under the axial loading [6]. Elimination of the physiological axial load in anaesthetized patients with complete muscle relaxation reported producing extension of the lunate and the scaphoid and concluded that axial loading due to the normal tone of the forearm muscles tends to flex the scaphoid and the lunate[7]. Despite this, it is rare to find lunate maintaining an attitude of flexion in patients with scapholunate dissociation. The CT measurements of most lunates failed to classify them into the described three shapes since many lunates showed dissimilar typing on the various chosen sagittal sections of the same lunate[5]. It is thus not surprising that lunate's alignment failed to conform to its shapes (Fig.1).

CONCLUSIONS

Relationship between MCA and RCA in terms of the dorso-volar displacement has key role in determining the lunate's sagittal alignment while the lunate's shape may be affecting it secondarily only. The other important factors are scaphoid's flexion torque and extension torque from the triquetrum, with TSA, LTA and THA in turn influencing the latter.

REFERENCES

1. Kaur JM. *Clin Orthop* **202**, 16-26, 1986.
2. Watson HK et al. *J Hand Surg*, **21A**, 759-763, 1996.
3. Kleinman WB:*The Wrist*,.Philadelphia, Lippincott Williams and Wilkins. 2000
4. Sarrafian SK et al. *Clin Orthop* **126**,153-159, 1976
5. Gupta A and Moosawi NA. *J Biomech* **35**,1451-57, 2002
6. Kobayashi M, et al. *J Biomech* **30**,1165-67, 1997
7. Gupta A. *Clin Biomech* **17**,660-65, 2002

ROTATIONS IN REARFOOT JOINTS AT END OF RANGE WEIGHT BEARING

[1]Paul Lundgren, [1]Arne Lundberg, [1,2]Anton Arndt and [3]Adrienne Hunt
[1]Dept. Orthopedic Surgery, Karolinska University Hospital / Huddinge, Sweden
[2]Stockholm University College of Physical Education and Sports, Sweden
[3]School of Physiotherapy, The University of Sydney, Australia
email: paul.lundgren@chello.se

INTRODUCTION

Physiological end of range in the rearfoot joints while under body weight represents a normal functional scenario, as for example in squatting. However, the relative contributions of the relevant joints are unknown. From in-vivo, quasi-dynamic experiments using radiostereometric analysis (RSA) [1], we know: that between 10% and 41% of total foot plantarflexion during ankle joint plantarflexion is due to motion in the joints of the medial longitudinal arch, in particular the talonavicular joint; that during inversion-eversion motion of the foot, frontal plane motion occurs primarily at the talonavicular joint, rather than at the subtalar joint, as is commonly believed. Indeed, from a bone motion study of living subjects, the contribution of talocrural joint to inversion-eversion during the weight bearing phase of walking, has been calculated as 30% [2,3].

Undoubtedly, individual joints will have differing amounts of congruity in different loading circumstances and contribute differently to specific weight bearing functions. In the current study we sought to determine:

- Total rotations required for normal function.
- Joint kinematics during two different approaches to achieving maximal voluntary dorsiflexion.

METHODS

In this descriptive study of joint kinematics of the foot, radiostereometric analysis (RSA) was employed to identify 3D rotation and translation of the joints of the rearfoot (talotibial, talocalcaneal, calcanealcuboid and talonavicular joints) in three normal subjects. Each of the relevant bones had been previously implanted with between 3 and 4 (radio opaque) tantalum markers under local anaesthetic utilising standard surgical procedures. Ethical approval for the study was obtained from the Karolinska University Hospital local ethics committee. Synchronised double X-ray exposures were taken to calculate the relative positions of the segments relative to a calibration coordinate system defined by a cage with tantalum markers.

The subject stood with the examined foot within the calibration cube. X-ray exposures were taken in the following positions: (i) neutral: a neutral (reference) position with the subject standing straight and relaxed with their weight even between both feet, (ii) inversion (foot turned in), (iii) eversion (foot rolled out), (iv) plantarflexion (demi-pointe position), (v) active full dorsiflexion, (vi) lunge (passive dorsiflexion). Individual joint rotations relative to the reference position were calculated using RSA. Rotations about the X-axis (mediolateral axis) were calculated for the two dorsiflexion and the plantarflexion positions, while Y and Z rotations were calculated for the inversion and eversion positions.

RESULTS AND DISCUSSION

The total range of motion at the talus-tib joint between a foot position of maximum plantarflexion and one of maximum dorsiflexion (lunge) was 60º. Whilst plantarflexion was greatest at the talus:tib joint (30º), there were 10º at the nav:talus joint. Not unexpectedly, the lunge position induced more talus-tib dorsiflexion than did active dorsiflexion (30º versus 18º), and therefore more useful in the clinical setting.

Between the positions of maximum eversion and inversion, there were the following total amounts of inversion-eversion: 42º at the nav:talus, and 17º at each of the calc:talus and cub:calc. These figures confirm the nav:talus as the joint that is most important to these end of range foot movements, as indicated previously [1-3]. Interestingly, whilst rotations for both the calc:talus and cub:calc were even between inversion and eversion rotations, eversion motion was only 7º for the nav:talus (Figure 1), compared to 35º for the inversion motion. Associated with this end of range foot inversion, was a notable amount of vertical axis rotation (adduction), especially at the nav:talus joint (28º).

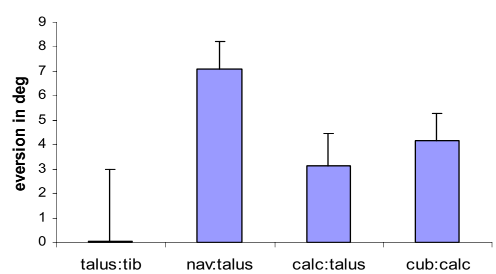

Figure 1. Eversion joint motion (Y axis rotation) for maximum foot eversion.

There was little variability across the 3 current subjects, perhaps indicating that individual joints contribute similarly.

REFERENCES

1. Lundberg, A. Patterns of motion of the ankle/foot complex. PhD Thesis, Karolinska Institute, Sweden, 1988.
2. Westblad P et al.. *Foot & Ankle International,* 23(9):856-63, 2002.
3. Arndt, A et al*., Foot & Ankle International* 25(5), 357-64, 2004.

MORPHOLOGICAL MUSCLE AND JOINT PARAMETERS FOR MUSCULOSKELETAL MODELLING OF THE LOWER EXTREMITY

M.D. Klein Horsman[1], H.F.J.M. Koopman[1], F.C.T. van der Helm[1], L. Poliacu Prose[2] and H.E.J. Veeger[3]
[1]Institute for Biomedical Technology (BMTI), Biomedical Engineering Group, Department of Engineering Technology, University of Twente, P.O. Box 217, 7500 AE Enschede, The Netherlands, e-mail: M.D.KleinHorsman@utwente.nl
[2]Department of Anatomy, Free University, Amsterdam, The Netherlands
[3]Faculty of Human Movement Sciences, Free University, Amsterdam, The Netherlands

INTRODUCTION

To assist in the treatment of gait disorders, an inverse and forward 3D musculoskeletal model of the lower extremity will be useful that allows to evaluate *if-then* scenarios. However, in the current anatomical datasets no sufficiently accurate and complete information is available to construct a sufficiently valid model (e.g. [1]).

The aim of this project was the collection of a complete and consistent anatomical data set. This can be achieved by collection of the three-dimensional location of the rotation centre of the hip and rotation axes of the knee and ankle for joint modelling. For muscle modelling parameters are collected such as optimum length, PCSA, tendon/belly length, and force application parameters such as attachment sites described as point, line, or plane and wrapping surfaces for estimation of curved lines of action.

METHODS & MATERIALS

One lower extremity, taken from a male embalmed specimen (age 77, height 1.74m, weight 105 kg), was studied. Position and geometry were measured with a 3D digitizer. Optotrak was used for measurement of rotation axes of joints. Sarcomere length was measured by laser diffraction [2].

The following steps were taken:

- Collection of anthropometric data of body segments for estimation of mass and moments of inertia.
- Placement of reference screws in 6 body segments (pelvis, femur, tibia, calcaneus/talus, midfoot and phalanges) for the definition of technical coordinate frames.
- Measurement of bony landmarks with respect to screws for definition of anatomical reference frames.
- Dissection of the muscles and ligaments.
- Measurement of attachment sites and underlying geometries.
- Estimation of kinematic axes and centres of rotation for the hip, knee and ankle. Therefore instantaneous helical axes and their optimal pivot point were determined for each joint using the recorded motion data of the associated segments.[3]
- Measurement of macroscopic and microscopic muscle parameters. Pennation angle and the actual length of muscle fibre and tendons were measured with the digitiser.

Optimal fibre length determined by multiplying the actual fibre length with the ratio of optimal and actual sarcomere length.

PCSA at optimal muscle length is calculated as the muscle mass divided by the density (assumed to be 1.056 g/cm^3), resulting in muscle volume and subsequently multiplied by the cosine of the pennation angle divided by optimal fibre length.

RESULTS

A total of 40 muscles were measured. Each muscle was divided in different muscle lines of action based on muscle morphology. For muscles with large attachment areas (such as the gluteus maximus) up to twelve muscle lines of actions were defined. In case of a curvature around an underlying contour, a geometric shape (sphere, cylinder, ellipsoid) was defined, representing the underlying structure. In the model, the shortest distance between origo and insertion over the surface will describe the curved force path of the muscle.

13 Ligaments of the hip, knee and ankle were included and will be modelled as a straight line between point origin and insertion.

Kinematic joint center and axes were constructed from motion data. A reconstruction of the hip joint rotation center by calculation of the optimal pivot point is shown in Figure 1. The mean distance of each helical axis to the pivot point is 9.12 mm.

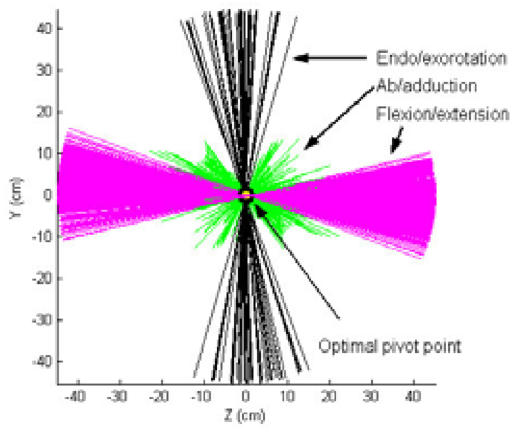

Figure 1: Frontal view of hip rotation centre, defined as the optimal pivot point, calculated with instantaneous helical axes of recorded hip rotations around three anatomical axes.

DISCUSSION

We have now available a unique anatomical dataset comprising all necessary data for modelling. Implementation of these data into an (existing) model of the lower extremity is likely to significantly improve the estimation of muscle forces and will thus make the use of the model as a clinical tool more feasible.

REFERENCES

1. Yamaguchi GT et al.. In: *Multiple Muscle Systems, biomechanics and movement organization*, Winters JM & Woo SL-Y (Eds), Springer Verlag NY, pp. 717 – 774, 1990.
2. Young LL et al.. *Poultry Science* **69**, 1800-1802, 1990.
3 Veeger HEJ et al.. *J.Biomechanics* **30**, 647-652, 1997.

VALIDITY OF THE NEW POWERTAP POWERMETER AND AXIOM CYCLE ERGOMETER WHEN COMPARED WITH AN SRM DEVICE

[1-2] William Bertucci, [2]Sebastien Duc, [2]Frefderic Grappe, [1]Ines Benkhémis and [1]Redha Taiar
[1] Laboratoire d'Analyse des Contraintes Mécaniques, Université de Reims, Moulin de la Housse, 51100-Reims, France,
[2] Laboratoire de Mécanique Appliquée, Université de Franche Comté, 24 rue de l'épitaphe 25030 Besançon cedex, France.
email: william.bertucci@univ-reims.fr

INTRODUCTION

It is common to use laboratory tests in order to evaluate the performance of competitive cyclists. The difference between the winner and the second placed cyclist for track cycling is very small. In this condition it is very important to use a valid and reliable ergometer for tracking small changes in performance.

The aim of this study was to compare two new cycle ergometers, Axiom (Elite, Italy) and PowerTap (CycleOps, USA) with the SRM reference ergometer during maximal intensity exercise (sprint) and during sub maximal intensity exercise (only PowerTap *vs* SRM). The Axiom is an stationary electromagnetically ergometer which permits utilisation of the cyclist personal bicycle. The PowerTap is a mobile cyling powermeter that measures the power output with strain gauges localised in the hub of the rear wheel. The SRM system is a crankset that measures power output from torque and angular velocity continuously. The torque is thereby calculated by strain gauges (depending on the model 4, 8 or 20 strain gauges) that are located between the crank axle and the chain-ring.

METHODS

Ten male competitive cyclists (age 25 ± 3 years, height 180 ± 5 cm, body mass 70.2 ± 4.7 kg) participated in the study. The study comprised two sprint tests in seated position on the Axiom ergometer. Tests were performed on the race bicycle equipped with the PowerTap and SRM ergometers against a 0.6 N/kg resistive loads. The exercise at sub maximal intensity (50 to 400 W) was performed on a treadmill (S 1830, HEF Tecmachine, Andrézieux-Bouthéon, France).

The three ergometers sampled (1 Hz) and stored the power output and the pedalling cadence (rpm). The maximal performance was determined by the maximal power output value. After testing our data for normality and homogeneity of variance, a correlation coefficient, bias, limits of agreement and 95% confidence interval (95% CI) (Bland and Altman, 1986) were calculated to quantify the differences between PowerTap and SRM power output. The analysis of mean differences between the Axiom, PowerTap and SRM power output were assessed with paired Wilcoxon tests, and significant difference was set at $P<0.05$.

RESULTS AND DISCUSSION

During maximal power output test, the results indicate that the Axiom values were significantly lower ($p<0.05$) compared with SRM and PowerTap values. Axiom ergometer underestimates the SRM and PowerTap values by 29 and 30 %, respectively (Figure 1). During exercise at sub maximal intensity, the regression analyses between the PowerTap and SRM power output indicate a high correlation ($r=0.99$, $p<0.001$). The mean differences power output measurement lay between 2.61 and 3.51 W. The mean bias for power output between PowerTap and SRM was 3.1 ± 3.4 W.

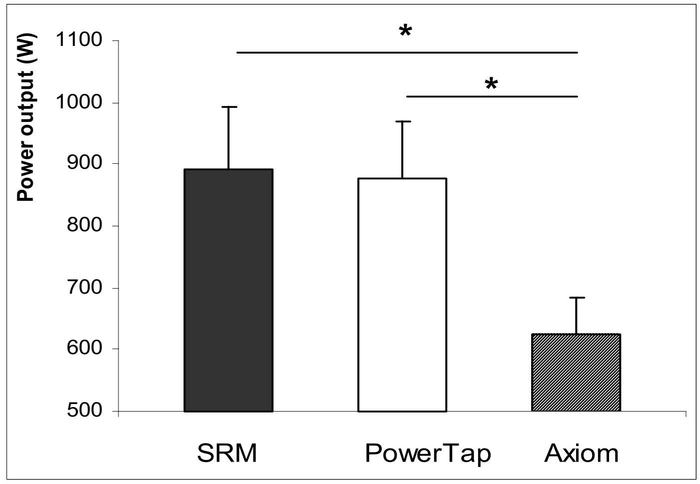

Figure 1 SRM, PowerTap and Axiom maximal power output values during sprint tests.
* : significantly different ($p<0.05$) compared with Axiom

These results indicate that the PowerTap device does provide a valid measure compared with SRM at sub and maximal exercise intensity. The lower bias value indicates that the mean SRM overestimation was only 3 ± 3 W. However, the Axiom was not a valid ergometer when the maximal power output was tested. This result is in accordance with Bertucci et al. [1] who have tested the Axiom validity that shown the Axiom was not valid compared with the SRM during sub maximal intensity exercise. The difference between the SRM and the Axiom device can be explained by the difference between the power output calculation mode. The Axiom power output was calculated from the dubious polynomial equation on the software (taking into account the roller velocity and the braking torque) whereas the SRM and PowerTap ergometer measure the power output from the stain gauges technology.

CONCLUSIONS

This study suggests that the PowerTap mobile cycling powermeter is valid (contrary to Axiom device) for performed scientifics studies in the laboratory or in the actual cycling locomotion.

REFERENCES

1. Bertucci W, et al.. *Int J Sports Med* **26(1)**, 59-65, 2005.

REPETITIVE MUSCLE CONTRACTIONS INDUCE MECHANICAL CHANGES OF ACHILLES TENDON.

Emika Kato[1], Toshiaki Oda[3], Kentaro Chino[3], Toshiyuki Kurihra[3], Toshihiko Ngayoshi[1], Tetsuo Fukunaga[2], and Yasuo Kawakami[2]
[1)] Graduate School of Human Sciences, Waseda University, Saitama, Japan
[2)] Faculty of Sport Sciences, Waseda University, Saitama, Japan
[3)] Department of Life Sciences, University of Tokyo, Tokyo, Japan
E-mail: e-kato@suou.waseda.jp

INTRODUCTION

Muscle contraction induces tendon elongation[1)]. Repetitive muscle contractions are known to induce tendon creep[2)], but the presence of concurrent changes in mechanical properties of the tendon has not been elucidated. The purpose of this study was to investigate changes in the muscle-tendon complex mechanical properties during and after repetitive muscle contractions.

METHODS

Six men (mean±SD for the age, body mass and height was 23.5±1.2 years, 68.3±7.1 kg, 172.7±5.6 cm) performed 15 repetitive isometric ramp contractions. The subject was seated with the knee extended, and the ankle joint was attached to the foot plate at the right angles to the tibial axis. Preceding the experiment, MVC torque was measured, and the target torque was determined based on MVC. Before and after repetitive contractions, the following flexibility test was performed. The subject was seated with the knee extended, and the ankle joint was attached to the foot plate at an angle of 30˚ plantarflexion. The foot plate was connected to a dynamometer (VINE, Japan), by which the ankle joint was passively dorsiflexed with torque gradually increasing from zero to a value at which the passive loading to the ankle joint was just tolerable for each subject. The dorsiflexion angle and passive torque generated by plantar flexor muscles were measured during the test. During the passive loading, real-time ultrasonogram (SSD-6500, Aloka, Japan) was taken to track the movement MTJ (muscle-tendon junction of the gastrocnemius medialis and Achilles tendon). The movement of MTJ with dorsiflexion was assumed to be equal to the elongation of muscle belly (dMus). According to the estimated Achilles tendon moment arm[1)]. The change of MTC (muscle-tendon complex) length (dMTC) during the passive dorsiflexion was estimated from changes in ankle joint angle. Tendon elongation (dTen) was calculated by subtracting dMus from dMTC. Tendon force (TF) was estimated from the torque and moment arm length[3)].

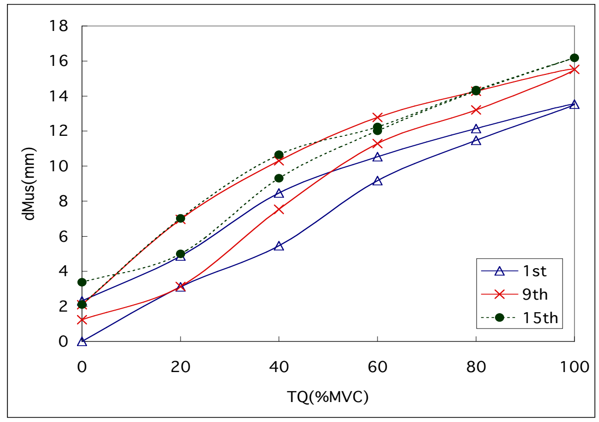

Figure 1: The relation between tendon force and dmus during 15 repetitive contractions, just only the 1st, 9th and 15th contractions are shown.

RESULTS AND DISCUSSION

The changes in dMus during 15 repetitive contractions are shown in Figure 1. The first contraction showed a different pattern compared with other contractions ($p<0.05$), dMus shifted proximally during repetitive contractions. This result indicates that repetitive contractions induced tendon creep. The flexibility test showed dMTC which involved an increase in dTen ($p<0.05$), but dMus did not change significantly. The elongated tendon changed its passive length-force curve, especially at the toe-region. Altered toe-region of the tendon length-force curve suggests structural changes of tendon as a result of repetitive contractions.

REFERENCES

1) Kawakami, Y., et al. *J Appl Physiol* 85, 398-404, 1998
2) Maganaris, C.N., et al. *J Appl Physiol* 93, 2089-2094, 2002
3) Rugg, S.G., et al. *J.Biomech* 23, 495-501, 1990

Table 1: Elongation of MTC, Muscle and tendon during flexibility test.( ):post test, *: p<0.05

Tendon Force (N)	100	200	300	400	500
Elongation (mm)					
MTC	16.0±3.0 (21.9±7.4*)	23.8±7.5 (29.3±5.9*)	28.4±10.3 (32.6±5.2*)	33.1±10.7 (34.9±5.1)	35.0±14.1 (37.0±5.2)
Muscle	11.5±6.0 (13.8±5.4)	18.4±7.4 (20.0±4.8)	20.8±7.1 (22.6±4.6)	23.0±7.3 (23.8±4.4)	24.4±7.1 (25.7±4.5)
Tendon	4.5±3.5 (8.1±2.7*)	5.5±3.1 (9.3±2.3*)	7.6±4.2 (10.0±3.2)	10.1±4.6 (11.1±3.3)	10.7±4.2 (11.4±3.4)

EVIDENCE FOR THE INVOLMENT OF MUSCULAR PRE-ACTIVATION IN IMPACT LOADING AND IN SHOCK WAVE TRANSMISSION

[1]Pascale Chavet, [1]Martine Pithioux, [2]Nancy St-Onge, [1]Sylvie Wendling-Mansuy and [1]Patrick Chabrand
[1]LABM USR 2164 CNRS-University of Méditerranée, Marseilles, France.
[2] McGill University, Montreal, Canada.
chavet@morille.univ-mrs.fr

INTRODUCTION

Biomechanical studies of human beings in a seated position to mimic the driver attitude have increased our knowledge of the effect of the shock on the body structure [1] for accidentology perspective. Potential injuries are generally indirectly estimated from dummies or PMHS paradigms. By consequence, resulting numerical models are limited due to the absence of consideration of potential modifications of functional response of the musculo-skeletal system [3]. This study was conducted to establish the influence of muscular activation of the lower limb prior the impact (pre-activation) on impact loading and on the resulting shock wave.

METHODS

Ten young male adults volunteered in this study. The experimental protocol was approved by the human ethics committee of the University.

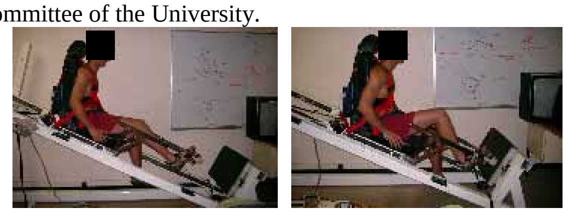

Figure 1. Experimental set : sledge ergometer [2].

The sledge ergometer (Figure 1) was associated to a lower limb guiding device (strain gauge sensor based) which allow the measurement of the overall force exerted by the impacting lower limb before the contact with the force plate. EMG activity of 4 lower limb muscles were monitored and 2 miniature accelerometer measured shank and thigh accelerations of the impacting leg. Three conditions, 25%, 50% and 75% of the maximal force input exerted on the guiding device, were tested in blocks of 3 consecutive trials. Each seated volunteer was dropped from a distance corresponding to 200% of maximal rebound off the force plate he could performed. EMGs, reaction force, displacement of the seat and force before impact were simultaneously recorded at a 2 kHz frequency. ANOVAs tests were run on the averaged measured parameters.

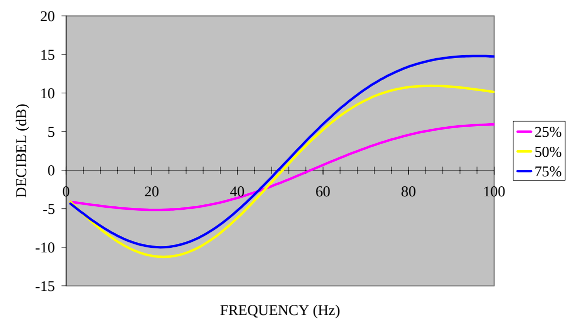

Figure 2. Gain/Attenuation profiles.

RESULTS AND DISCUSSION

On average (Table 1), the lowest pre-activation condition generated highest acceleration peak associated with highest shock transmission ratio and lowest peak force. At the opposite highest condition revealed lowest amplitude peak associated with lowest shock transmission ratio and highest peak force. The computation of gain/ attenuation (Figure 2) showed that attenuation was realized by the human system for the frequency content below 50-60 Hz. The best attenuation was provided for the highest pre-activation conditions.

CONCLUSION

In accordance with recent studies [4] our results showed significant positive relationships between myoelectric input and shock cushioning. Additionally, increasing preactivation would play a role in the damping of the soft tissues.

REFERENCES

1. Klopp GS. et al.. Proceeding of IRCOBI conference, Brunnen, Switzerland 1995.
2. Kyröläinen H. et al.. *Eur J Appl Physiol* **61**, 446-452, 1990.
3. Horita T. et al.. *Eur J Appl Physiol* **88**, 76-84, 2002.
4. Boyer KA.. et al.. *J Biomech* **37**, 1583-1588, 2004.

Table 1: Peak force (PF), peak shank (PS) and peak thigh (PT) accelerations, and calculated acceleration ratio (PS-PT) are reported for the 3 experimental conditions i.e. 25 %, 50% and 75% of maximum force pre-impact.

% maximum force	25%	50%	75%
PF (N/kg)	46 ± 3.7	48 ± 9.3	50 ± 7.3
PS (g)	13 ± 3.45	6.4 ± 4.70	6.4 ± 4.03
PT (g)	8.9 ± 1.10	4.5 ± 1.56	4.8 ± 1.63
PS/PT ratio (a.u)	1.46	1.42	1.33

IMPROVING EMG BASED MUSCLE FORCE ESTIMATION USING PRINCIPAL COMPONENT ANALYSIS ON A HIGH-DENSITY EMG ARRAY

Didier Staudenmann, Idsart Kingma, Andreas Daffertshofer, Dick F. Stegeman and Jaap H. van Dieën
Institute for Fundamental and Clinical Human Movement Sciences, Faculty of Human Movement Sciences, Vrije Universiteit, Amterdam, The Netherlands; d.staudenmann@fbw.vu.nl

INTRODUCTION

The reliability of EMG amplitude measurements when predicting muscle activation is an important issue in EMG based force estimation. Theoretically, two important factors influence the EMG signal. First, the location of the electrode arrangement in relation to the muscle fibre architecture and second, the amount of detected motor units (MUs), contributing to both the EMG and the muscle force. High-density EMG arrays allow the collection of monopolar signal to which also deep MUs are contributing. Principle component analysis (PCA) is a method to classify multidimensional datasets and to detect redundant information [1].

The aim of this experimental study is to analyze whether PCA techniques can improve force estimation from EMG collected with a high-density array.

METHODS

Eleven healthy subjects (age 28.3 ± 4.7 years) performed isometric block-shaped extensions (Figure 1, left panel) with the right-arm at different conditions: Three elbow angles (60°, 90° and 130°) and three levels of maximum voluntary contractions (20%, 50% and 80% MVC). During efforts subjects had online feedback of the contraction level.

Surface EMG of the triceps brachii and force output were measured simultaneously. The EMG was measured with an active monopolar electrode array of 13×10 electrodes (BioSemi, biomedical instrumentation, Amsterdam, NL) [2].

EMG based force estimation from monopolar signals (1), PCA (low eigenvalues) (2) optimally aligned bipolar electrodes (3), Laplacian configuration (5) and conventional bipolar electrodes (5) were compared.

To quantify force estimation quality over the entire contraction pattern (Figure 1) we computed the root mean square difference (RMSD) between normalized EMG and normalized arm extension force.

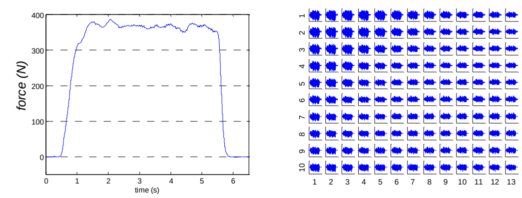

Figure 1: Left panel: Block-shaped contraction pattern with a mean force over the plateau of 370 N. Right panel: raw monopolar 13×10 EMG-signals (at 130° / 80% MVC).

To asses to what extent minor force fluctuations over the plateau were predicted we calculated the correlation coefficient between estimated and measured force.

RESULTS AND DISCUSSION

The EMG processing procedures (Table 1) significantly affected RMSD and correlation (both: $p<0.01$). The two highest RMSD was found for the conventional bipolar electrodes (5) and the monopolar signals (1). PCA reduced RMSD by about 40% compared to conventional bipolar electrodes (5) and by about 12% compared to optimally aligned electrodes (3). In addition, the highest correlations over the plateau were obtained with the PCA procedure.

CONCLUSIONS

High-density EMG is a powerful tool for the prediction of force output of a muscle but its value depends strongly on the EMG signal procedures. PCA can be used as an alternative to spatial filtering with different electrode configurations (3-5). Apparently, any order of spatially filtering electrodes (3-5) suffers from a biased choice of the configuration direction relative to the direction of the underlying muscle fibers. PCA appears to be a valuable tool, extracting the physiologically relevant information independent from the muscle structure and thereby improving the quality of muscle force estimation.

REFERENCES

1. Daffertshofer A, et al. *Clin Biomech* **19**, 415-428, 2004
2. Blok J.H, et al. *Rev Sci Instrum* **73**, 1887-1897, 2002

Table 1: Five EMG procedures (1-5) are shown in the upper row. Small dots represent electrodes, grey surface shows the section of the 13×10 array used and white colors the nature of the electrode configuration (3-5). RMSD over the entire contraction pattern and correlation over the plateau between EMG procedures and the force are shown in the lowest rows.

EMG procedure	1	2	3	4	5
	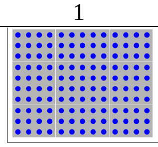	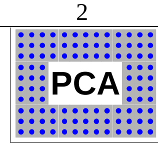	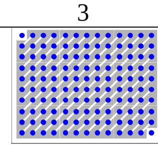	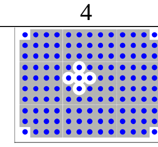	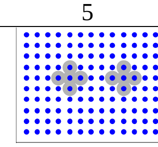
RMSD (%)	16.6 ± 2.7	10.8 ± 2.1	12.2 ± 2.1	15.1 ± 5.1	17.9 ± 2.6
Correlation (r)	0.3 ± 0.2	0.5 ± 0.2	0.4 ± 0.2	0.4 ± 0.2	0.3 ± 0.3

The three dimensional load transfer characteristics of the wrist during maximal gripping.

[1] M.K. Gíslason, [1]N.K Fowler and [2]D.H. Nash.
[1] Bioengineering Unit, University of Strathclyde; email: magnus.gislason@strath.ac.uk
[2] Department of Mechanical Engineering, University of Strathclyde

INTRODUCTION

Wrist instability is a common problem post trauma or through arthritic changes and this can have a profound effect on hand function. With the increasing number of surgical treatments available for the painful wrist, there is a demand for more detailed information on the normal load transfer characteristics of this complex joint. Previous cadaveric studies have measured intra-carpal pressure using pressure sensitive films or conductive rubber [1]. Surface mounted strain gauges have also been used to measure strain levels on a limited number of carpal bones. Both these methods require invasive disruption of the materials under study. A limited number of computational models have been developed but due to the complexity of the wrist joint, many of these have been a two dimensional approach to what is in reality a three dimensional problem. In addition they do not include all 15 bones involved in load transmission or use theoretical/arbitrary loading conditions rather than measured data [2].

The aim of the current study was to develop a fully-representative three-dimensional finite element model of the entire wrist joint in order to study the transmission of force through the carpus during a functional activity. Real biomechanical data were used to define the boundary conditions and the contributions from cartilage and ligaments were incorporated into the model.

METHODS

High resolution 3 Tesla MRI sequences were obtained from a single male subject, with in-plane (axial) resolution of 250x250µm and a slice thickness of 750µm. The MR images were imported into Mimics [3] software where solid models of 15 bones were created (distal sections of radius and ulnar, 8 carpal bones and proximal sections of 5 metacarpals). Physical material properties were assigned according to the pixel grayscale values of the different regions of the MR-image. Regions of cartilage, cortical bone and cancellous bone were defined with transition zones between the different layers. A finite element mesh was created in Abaqus [4] from 10-node tetrahedral brick elements (figure 1). Ligaments were modelled with non-linear spring elements and their origin and insertion points were evaluated manually according to previous anatomical studies.

A series of biomechanical trials were conducted to obtain subject specific loads during a whole hand maximal grip activity. Five six degree-of-freedom force transducers in a grip device were used in conjunction with VICON motion analysis to define the three dimensional load systems applied to each metacarpal according to its coordinate system. These data were applied as loading/boundary conditions in the finite element model to simulate the grip activity.

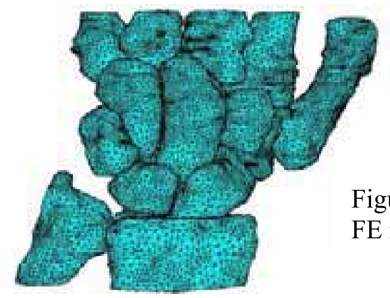

Figure 1: Dorsal view of the FE mesh.

RESULTS AND DISCUSSION

Model results showed that 95% of the load applied to the metacarpals was distributed through the radius and only 5% through the ulna. Previous studies have shown the same ratio to be 90%-radius, 10%-ulna [5]. This discrepancy is consistent with the fact that the current wrist modelled had a negative ulnar variance and the force distribution was determined by the bony anatomy. Approximately 60% of the total load was transmitted from the metacarpals through the trapezoid-trapezium-scaphoid junctions (figure 2). This result is coherent with clinical evidence as the junction between the first metacarpal and the trapezium is a common site for wear.

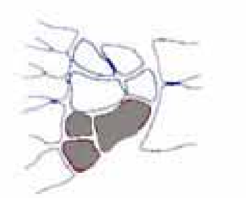

Figure 2: Trapezoid-Trapezium-Scaphoid force transmission.

CONCLUSIONS

This study is an attempt to provide three dimensional finite element modelling of a complete wrist joint using real biomechanical boundary conditions. The results are consistent with previous work but reveal the importance of considering variations in wrist joint anatomy. Future work using this technique will investigate the effects of anatomical variation on wrist joint kinetics.

REFERENCES

1. Tencer AF et al., *J. of Orthop. Research* **6**,509- 517,1988.
2. Carrigan S.D., et al.. *Annals of Biomedical engineering* **31**, 718-725, 2003.
3. Materialise, Leuven, Belgium.
4. ABAQUS Inc., Providence, RI, USA
5. Anderson D.L, et al. *Seminars in arthroplasty* **6**, 1, 30-36, 1995.

ACKNOWLEDGEMENTS

This work was supported by Arthritis Research Campaign grant no. 15468.

AN INVESTIGATION OF WRIST JOINT FUNCTION UNDER LOAD

A.K. Kanellopoulos, M.K. Gíslason, N.K. Fowler
Bioengineering Unit, University of Strathclyde; email: asimakis.kanellopoulos@strath.ac.uk

INTRODUCTION

Previous studies of the wrist joint have considered both individual carpal bone motion and the gross kinematics of the entire wrist complex. A variety of different grip tools have also previously been used to measure loading of the wrist joint during whole hand gripping tasks. Few of these studies however, captured kinematic data in conjunction with kinetic measurements and there is a lack of fully three-dimensional loading data. As a result there is disagreement in the literature, both about the definition of the 'functional neutral' position of the wrist and about the kinematic 'envelope' inside which the hand can provide its maximal gripping force [1].

The aim of the current study was to investigate if the 'functional neutral' position of the wrist joint coincided with the 'anatomical neutral' position in relation to generating the maximal gripping force. The active operating ranges of the wrist during maximal gripping force were also examined.

METHODS

Fifty right-hand dominant adults (25 males, 25 females), with no history of hand trauma participated in the study. The subjects were required to generate maximal gripping force in five different wrist positions: neutral, flexion, extension, radial and ulnar deviation. An eight camera, 120Hz VICON (Oxford Metrics) motion analysis system and a custom-built grip strength tool containing five six-component force transducers were used to obtain concurrent three-dimensional kinetic and kinematic data for each digital segment, the metacarpals, wrist and forearm. Subjects were asked to provide their maximal gripping force in maximal functional positions of wrist flexion, extension, radial and ulnar deviation. For the functional neutral wrist position, subjects adopted a self-defined position of optimal function around the anatomical neutral position.

RESULTS AND DISCUSSION

The functional neutral position of the wrist was experimentally defined as slight extension of the joint, with a mean of 33 degrees extension (SD 17.6) in 94% of the subjects (Table 1). This wrist extension was coupled with a mean of 8 degrees of ulnar deviation (SD 10.1) and it was the position in which the subjects provided their maximal resultant gripping force (Fig.1). In extension, radial deviation and ulnar deviation of the wrist the subjects generated similar

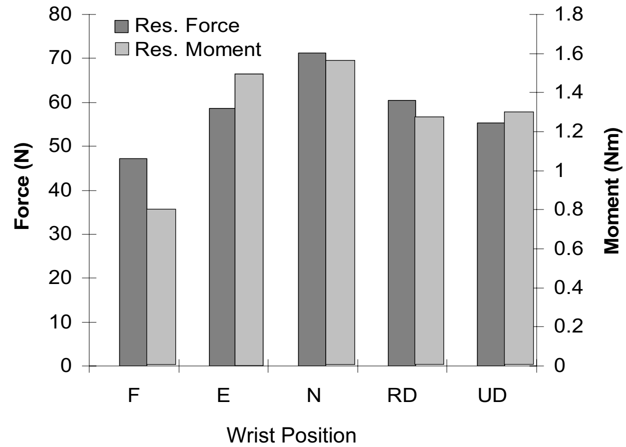

Figure 1: The resultant forces and moments applied to the thumb in flexion (F), extension (E), radial (RD) and ulnar deviation (UD) of the wrist.

maximal resultant forces, whilst in flexion the applied forces were significantly lower. The largest values of the resultant moments were in the neutral and extended positions and the lowest values were obtained for the flexed wrist (Fig.1). For each intended wrist joint position there was a coupling of motion in other planes. Joint flexion was combined with radial deviation, extension with ulnar deviation, radial deviation with extension and ulnar deviation with flexion (Table 1). Previous studies have observed similar coupling patterns during unloaded radial and ulnar deviation but show free wrist flexion coupled with ulnar deviation [2]. This discrepancy may reveal altered kinematic patterns as the wrist is loaded.

CONCLUSIONS

The optimum joint position for production of maximal grip force was a slightly extended and ulnar deviated wrist. This kinematic coupling of flexion-extension with radio-ulnar deviation, together with the definition of the functional neutral wrist position are important characteristics of wrist function under load.

REFERENCES

1. Amis AA, *J Biomed Eng* **8**, 313-320, 1987.
2. Li ZM, *Clin Biomech* **20**, 117-183, 2005.

ACKNOWLEDGEMENTS This work was supported by Arthritis Research Campaign grant no. 15468.

Table 1: Mean wrist angles in each functional position.

Intended Wrist Position	**Mean (SD) (degrees)**		**Mean (SD) (degrees)**
Neutral [flexion (+)-extension(-)]	-33 (17.6)	Combined Ulnar Deviation	8 (10.1)
Flexion	59 (15.5)	Combined Radial Deviation	14 (10.4)
Extension	53 (13.4)	Combined Ulnar Deviation	12 (9.0)
Radial Deviation	13 (8.1)	Combined Extension	12 (15.2)
Ulnar Deviation	25.8 (11.4)	Combined Flexion	8.9 (28.4)

CAN A RUNNER'S ECONOMY AND ARM MOTION BE AFFECTED BY FEEDBACK TRAINING?

[1]Laura Hild, [1]Scott White, [1]Harold Burton, and [2]Louise Gilchrist
[1]State University of New York at Buffalo, Dept. of Exercise and Nutrition Science,
[2]State University of New York at Buffalo, Dept. of Physical Therapy; email: laurah@amtimail.com

INTRODUCTION

It has been shown that among runners with similar VO_{2max} a runner with higher running economy will perform better than one with lower running economy [1]. Several biomechanical variables have been related to running economy [2, 3, 4]. The coaching literature suggests that arm swing is important for "efficient" running. It has been suggested that training with a harness to modify arm swing can improve running economy [5]. The purpose of this research was to determine: 1) if initial reaction (first day of use) to an arm harness affects running economy and arm mechanics; and 2) if a training period with an arm harness improves running economy and arm mechanics.

METHODS

Initial Reaction Study: Eighteen runners (male and female) volunteered to participate. Each subject ran less than 20 miles per week. Running economy, wrist excursion, superior-inferior (S-I) distance from the wrist to the jugular notch, and medio-lateral (M-L) distance from the wrist to the jugular notch were measured while running with and without a harness to modify arm swing [5].

Harness Training Study: Thirteen subjects who exhibited excessive crossover (M-L distance from the wrist to jugular notch ≤ 9.6 cm) or excessively low arm carriage (S-I distance from the wrist to jugular notch ≥ 39.8 cm) trained with the harness. A within subject design was used in which running economy, wrist excursion, S-I distance, and M-L distance were measured prior to training (Test), after 3 weeks of no harness training (Mid Test) and after 3 weeks of harness training (Post Test).

Dependant Variables: Running economy was defined as speed divided by VO2submax (mi*kg/ml). VO2submax was averaged over the last 5 minutes of a 10-minute run. Two video cameras recorded the spatial position of reflective markers at the ulnar stylus and jugular notch. Wrist excursion was defined as the total three-dimensional distance traveled by the wrist in one arm swing. All kinematic variables were averaged over 6 consecutive strides.

Statistical Analysis: One-way repeated measures ANOVA's with a significance level of $p \leq .05$ was used to determine if there was an improvement in running economy, wrist excursion, S-I distance and M-L distance.

RESULTS AND DISCUSSION

Wrist excursion and S-I distance were the only dependant variables that improved for both the initial reaction study (Table 1) and after training with the harness (Table 2). M-L distance did not improve in either study. Also, running economy did not improve despite a change in mechanics. One might suspect that the training period was not long enough; however, Messier et al. reported similar results; 5 weeks of technique training also saw an improvement in running mechanics and not in running economy [6].

Hinrichs reported that arm crossover was necessary to counteract the angular momentum of the legs about the vertical axis while running [7]. Egbuonu et al. reported that restricted arm movement decreased running economy [8]. Since arm crossover was not reduced in our study, angular momentum about the vertical axis was not likely affected and therefore, running economy was unchanged. The arm harness was ineffective for reducing arm crossover and had minimal effect on running economy.

REFERENCES

1. Conley DL, et al. *Med Sci Sports Exerc* **12(5)**, 357-360, 1980.
2. Williams KR, et al. *Proceedings NA Congress Biomechanics*, Montreal, Canada, **2**, 287-288, 1986.
3. Williams KR, et al. *J App Phys* **63(3)**, 1236-1245, 1987.
4. Williams KR, et al. *Int J Sports Med* **8(S)**, 107-118, 1987.
5. Miller TS, *Programmed to Run*, Human Kinetics, 2002.
6. Messier et al. *J Sports Sciences* **7**, 113-126, 1989.
7. Hinrichs RN, *Int J Sport Mechanics* **3**, 242-263, 1987.
8. Egbuonu ME, et al. *Med Sci Sports Exerc* **22(s2),** s17, 1990.

Table 1: Results for the initial reaction study reported as mean ± std. dev. (except Wrist Excursion is reported as the median).

	RE (mi*kg/ml)	**Wrist Exc.** (cm)	**S-I** (cm)	**M-L** (cm)
No Harness	$3.34 \times 10^{-3} \pm 0.32 \times 10^{-3}$	93.7*	$38.3 \pm 7.3^{\#}$	10.7 ± 4.2
Harness	$3.41 \times 10^{-3} \pm 0.40 \times 10^{-3}$	76.7*	$28.4 \pm 4.9^{\#}$	11.6 ± 3.4

Table 2: Results for the harness training study reported as mean ± std. dev.

	RE (mi*kg/ml)	**Wrist Exc.** (cm)	**S-I** (cm)	**M-L** (cm)
Test	$3.37 \times 10^{-3} \pm 0.32 \times 10^{-3}$	$97.0 \pm 16.6^{\#}$	$40.6 \pm 6.8^{+}$	10.7 ± 4.9
Mid Test	$3.50 \times 10^{-3} \pm 0.35 \times 10^{-3}$	$95.6 \pm 17.0^{!}$	39.5 ± 6.6	10.9 ± 4.6
Post Test	$3.48 \times 10^{-3} \pm 0.27 \times 10^{-3}$	$87.7 \pm 14.7^{\#!}$	$37.0 \pm 5.0^{+}$	11.9 ± 4.7

MOTION INDUCED INTERRUPTIONS INCREASE THORACOLUMBAR KINEMATICS

[1]Scott MacKinnon, [1]Michael Holmes, [2]Julie Matthews, [2]Wayne Albert, [1]Steven Mills and [3]Don Bass
[1]School of Human Kinetics and Recreation, Memorial University of Newfoundland,
[2]Faculty of Kinesiology, University of New Brunswick,
[3]Faculty of Engineering and Applied Science, Memorial University of Newfoundland; email: smackinn@mun.ca

INTRODUCTION

Working on a moving platform, such as a seagoing vessel, imposes an increased risk for low back injury [1]. Such a dynamic environment will force a person to make continuous postural adjustments in order to maintain stability while performing a manual materials handling task. In some circumstances, these adjustments may require foot repositioning to maintain the centre of mass location within the confines of the base of support. A motion induced interruption (MII) occurs when the external perturbations are large enough to cause a person to stumble or abandon a task [2]. The purpose of this study was to evaluate the differences in thoracolumbar kinematics between lifts successfully executed and those during which a MII occurred.

METHODS

A ship motion simulator was employed to produce a pitch motion while 19 volunteer participants performed lifting activities. The activities consisted of lifting a 15kg mass under four conditions: a) load starting from floor with a final horizontal displacement of 300mm (Close Floor); b) load starting from floor with a final horizontal displacement of 400mm (Far Floor); c) load starting 250mm above the floor with a final horizontal displacement of 300mm (Close High) and d) load starting 250mm above the floor with a final horizontal displacement of 400mm (Far High). In all conditions the net vertical displacement was 750mm. Lifts were repeated at 10s intervals for a period of approximately two minutes. The 15kg load was connected to a handle which could be easily gripped symmetrically with two hands. The origin and destination of the lift were clearly identified and controlled between subjects. The load was returned to the ground by an investigator in preparation for the next lift. Thoracolumbar motions were collected with a Lumbar Motion Monitor (LMM) and stored on a personal computer for analysis.

A handheld signal was used by one of the investigators to identify the start and finish of each lift as well as the MII incidence. This temporal marker was sampled by an A/D converter and stored on a computer for subsequent analysis. These events were validated during analysis by referring to data collected from a load cell built into the load-handle apparatus. During the analysis procedure each lift was classified into two categories, a successful lift during which no foot adjustments were required or a lift completed but the participant was required to adjust the position of the feet in order to maintain balance (i.e. a stumble).

RESULTS AND DISCUSSION

The maximum LMM velocities in the lateral, sagittal and twisting planes were compared across the four lifting tasks. A repeated measures ANOVA indicated that there were significant increases ($p<0.001$) in thoracolumbar velocities in all three planes of motion for the lifts during which stumbles occurred compared to those lifts executed without MII's (Figure 1). This directional change was consistent across all lifting activities. What was most interesting is that the largest relative increases occurred in the lateral bending and twisting planes. Increases in thoracolumbar velocities in these planes of motion have been related to increased risk for occupationally-related low back disorders [3].

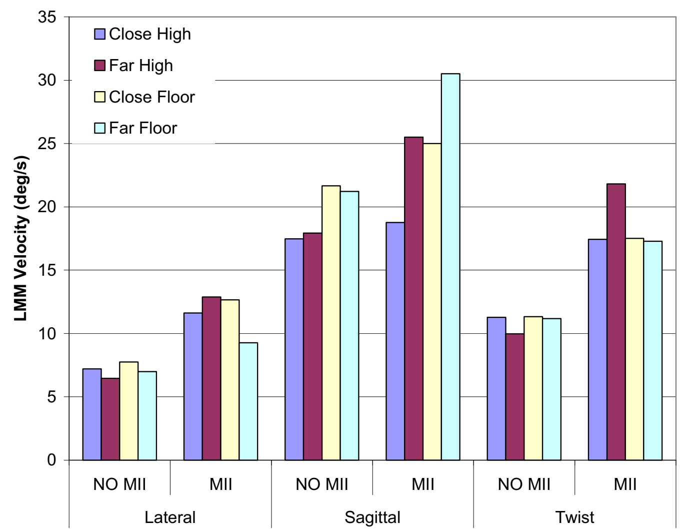

Figure 1: Three-dimensional LMM velocities across lift condition.

CONCLUSIONS

While humans can be quite adept in making dynamic compensatory adjustments to maintain balance, these strategies may not compliment a person's goal of reducing the risk of personal injury.

REFERENCES

1. Kigma I, et al. *In J Ind Erg* **32**, 51-63, 2003.
2. Crossland, P and K Rich *Proceedings of RINA,* London, UK, 2000.
3. Marras W, et al. *Ergonomics* **38**, 377-410, 1995.

ACKNOWLEDGEMENTS

The authors would like to acknowledge Anthony Patterson, Director – Center for Marine Simulation for use of the simulation facilities and NSERC and SafetyNet for financial assistance for this project.

EFFECTS OF REACH DISTANCE UPON ELECTROMYOGRAPHICAL ACTIVITIES OF SELECTED UPPER BODY MUSCULATURE

[1] Scott N. MacKinnon and [2]Christopher L. Vaughan
[1]School of Human Kinetics and Recreation, Memorial University of Newfoundland, St. John's, Canada,
[2]Department of Human Biology, University of Cape Town, Cape Town, South Africa; smackinn@mun.ca

INTRODUCTION

In one-handed, submaximal pulling activities the forces required to move the load are not likely produced from trunk efforts alone, but with contributions from other parts of the body. The upper extremity plays an important role in exerting horizontal pulling forces [1] but more insight into the kinesiological strategies employed by an operator under varying pulling situations is still required.

The purpose of this study was to examine the effects of reach distance on the electromyographical activities (EMG) of eight selected muscles of the trunk and shoulder regions during submaximal horizontal pulling exertions located at elbow height.

METHODS

Eleven healthy male volunteer subjects were asked to execute a right-handed pull on an isoinertial load (12% of lean body mass) located at varying distances (10, 15, 20, 25, 30, 35 and 40% of subject stature) from the frontal plane containing the load handle. Controls were put in place to standardize foot placement, pull direction and tempo. A ME3000P (Mega Electronics Ltd, Kuopio, Finland) unit was employed to collect the EMG activity of the following muscles: left and right erector spinae (at the level of the fourth and fifth lumbar vertebrae), left and right external obliques and the trapezius, latissimus dorsi, deltoid and biceps brachii from the right side of the body. Each channel was sampled at 1000 Hz, band-pass filtered between 20 Hz and 500 Hz, amplified and stored on a personal computer for further analysis. The raw EMG signals were full-wave rectified and low-pass filtered at 4 Hz. The raw signal was then normalized to a maximal voluntary contraction (MVC).

RESULTS AND DISCUSSION

EMG data revealed increasing erector spinae activity as reach distance increased (Figure 1) and this muscle group was found to be co-active with external oblique muscles during the exertion. Shoulder complex muscles were found to be highly active in all conditions, but only the trapezius and deltoid muscles demonstrated significantly decreasing activities as pull reach increased (Figure 1). If any strategy could be identified based on the experimental data, it might be that for closer pull locations (*i.e.* 10-20% stature from frontal plane containing the load) a shoulder strategy is employed, not necessarily because of mechanical efficiency but because the muscles controlling the spine are not in a desirable posture to create an extensor moment and contribute to a pull force. At further pull locations (*i.e.* 30-40% stature from frontal plane containing the load) the subject seems to employ trunk extensor strategies to assist in the pull exertion.

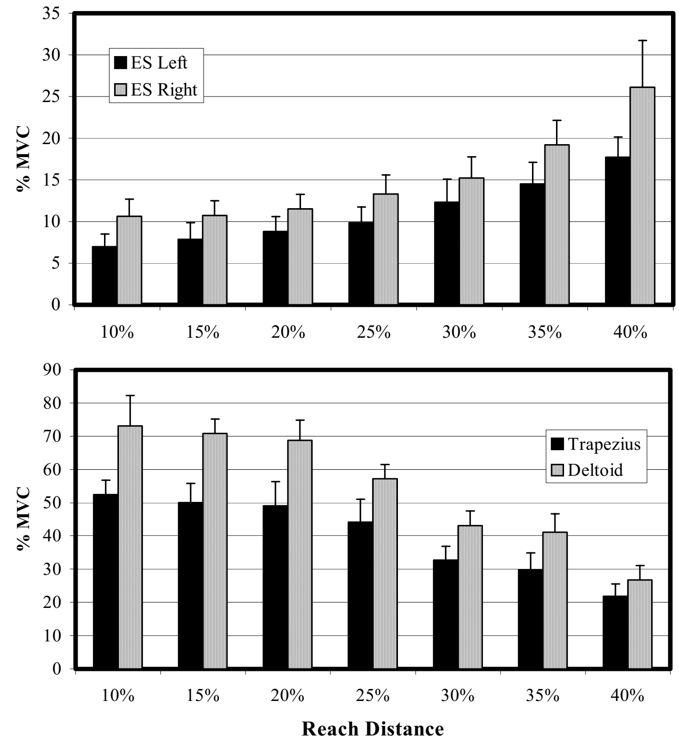

Figure 1: Mean (and standard error of the mean) EMG data. When performing *post hoc* comparisons with $\alpha = 0.05$, the following differences were found for the four muscles: (1) Left ES – 10%/15% different to 40%; (2) Right ES – 10%/15%/20% different to 40%; (3) Trapezius – 10%/15%/ 20% different to 40%; (4) Deltoid – 10%/15%/20% different to 30%/35%/40%; 25% different to 40%.

CONCLUSIONS

Much work must be done to understand better the strategies an operator will attempt to adopt a pull force under various postural conditions. It seems that executing a pull under conditions such as those simulated in this study could be optimized if the subject stood with the front toe at a distance of approximately 25% of stature from the frontal plane containing the load handle. These data provide some direction in positioning the operator within a workstation demanding pull force exertions.

REFERENCES

1. Hoozemans MJM, et al. *Ergonomics* **41**, 757-781, 1998.

ACKNOWLEDGEMENTS

The authors would like to acknowledge the funding provided by the Department of Human Kinetics and Ergonomics, Rhodes University, South Africa to complete this study.

MOTION INDUCED INTERRUPTIONS DURING SIMULATED SHIP MOTIONS

[1]Michael Holmes, [1]Scott MacKinnon, [2]Julie Matthews, [2]Wayne Albert, [1]Steven Mills and [3]Don Bass
[1]School of Human Kinetics and Recreation, Memorial University of Newfoundland,
[2]Faculty of Kinesiology, University of New Brunswick,
[3]Faculty of Engineering and Applied Science, Memorial University of Newfoundland; email: smackinn@mun.ca

INTRODUCTION

Seagoing vessels are designed to minimize the effects of environmental forces in order to reduce the stresses acting on both the structure and those working aboard. However, the external perturbations created by the environment can be considerable in magnitude and unpredictable in occurrence, even in reasonably benign weather conditions. The purpose of this study was to measure the number of motion induced interruptions (MII) a participant will experience while performing manual materials handling tasks typically executed on a seagoing vessel. A MII is defined when a person has to temporarily abandon the task or else execute alterations in the base of support in order to maintain balance [1].

METHODS

A ship motion simulator was employed to produce three different platform motions during which volunteer participants lifted loads. The platform motions where described as pitch, roll and quartering seas. The loads (10 and 15kg) were connected to a handle which could be easily gripped symmetrically with two hands. The connection between the mass and the handle was made by either a solid metal column (i.e. stable load) or a series of chain links (i.e. unstable load). The participants were instructed to ready themselves in a stable position in order to execute a two-handed sagittal plane lift. An audible signal was employed to direct the participants to execute a lift every 10 seconds. The origin and destination of the lift were clearly identified and controlled between subjects. The load began on the floor and was lifted a distance of 750mm in the vertical direction and translated a horizontal distance of 300mm away from the subject at the conclusion of the lift. The load was returned to the ground by an investigator in preparation for the next lift. A handheld signal was used by one of the investigators to identify any MII incidents that may have occurred. This temporal marker was sampled by an A/D converter and stored on a computer for subsequent analysis. Each trial lasted approximately 2 minutes.

RESULTS AND DISCUSSION

A repeated measures ANOVA indicated that there were significant differences in the number of MII per minute for both the motion ($p<0.001$) and load ($p<0.001$) effects (Figure 1). A LSD post hoc analysis revealed that the pitch motion produced significantly more $MII.min^{-1}$ compared to the other motion conditions. There were no significant differences between the three remaining motions. Maintaining balance requires that the vector projection from the system's centre of mass remains within the boundaries of the base of support. In the para-transverse plane located at the foot-floor interface the shortest distance this projection has to travel to leave the boundaries of the base of support is the antero-posterior direction, thus a pitch motion is likely to produce the most MII. Given the significant increases in the $MII.min^{-1}$ for the pitch direction compared to the other motions it would not be unreasonable to recommend that lifting activities be restricted when a vessel is faced with oncoming waves.

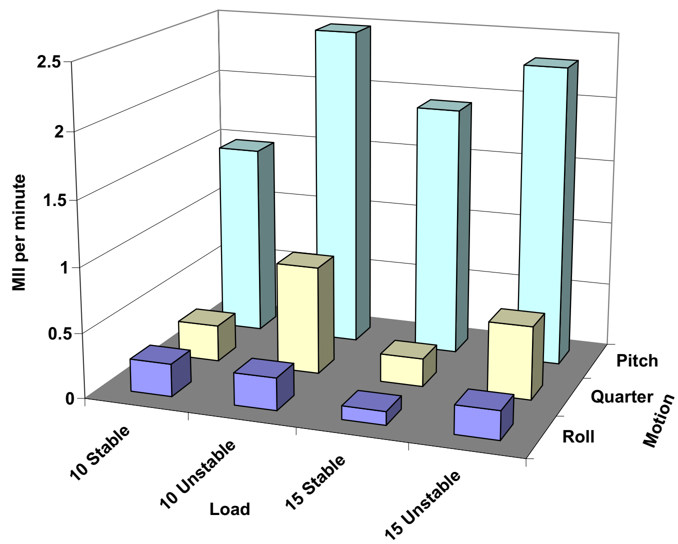

Figure 1: Number of MII per minute as a function of simulated ship motion and load characteristics.

Unstable loads produced significant increases in the rate of MII compared to the stable loads. Interestingly, there were no significant differences in the $MIIs.min^{-1}$ between the 10 and 15kg loads and in some cases the rate of MII was greatest for the lighter load. It is likely that as a person attempts adjustments to regain balance with an unstable load an asynchronicity between the load, segment and floor accelerations occur, making the dynamic corrections to regain stability much more complex and prone to MII.

CONCLUSIONS

Balance control in a complex moving environment is related to the direction of platform motions and the type of load handled. Workers in such environments should be made aware that some situations have a greater risk of accident or injury.

REFERENCES

1. Crossland, P and K Rich *Proceedings of RINA,* London, UK, 2000.

ACKNOWLEDGEMENTS

The authors would like to acknowledge Anthony Patterson, Director – Center for Marine Simulation for use of the simulation facilities and NSERC and SafetyNet for financial assistance for this project.

THORACOLUMBAR KINEMATICS DURING LIFTING EXERTIONS IN MOVING ENVIRONMENTS

[1]Julie Matthews, [2]Scott MacKinnon, [2]Michael Holmes and [1]Wayne Albert
[1]Faculty of Kinesiology, University of New Brunswick,
[2]School of Human Kinetics and Recreation, Memorial University of Newfoundland; email: smackinn@mun.ca

INTRODUCTION

Seafaring occupations have been long recognized as a high risk occupation for injury and accidents and it is hypothesized that the external perturbations associated with vessel motions are responsible for the high incidence of low back exertions common to professional mariners [1]. Studies have shown that large thoracolumbar velocities during lifting activities, as measured by a Lumbar Motion Monitor (LMM), are related to an increased risk of low back overexertion injuries in several industrial occupations [2]. The purpose of this study was to examine the changes in thoracolumbar kinematics of persons performing a lifting activity while exposed to simulated ships motion compared to those collected under stable, laboratory conditions.

METHODS

Nineteen healthy male subjects volunteered to participate in this study. These participants were asked to perform repeated bi-manual symmetrical lifts (6 lifts.min^{-1}) while thoracolumbar kinematics were collected employing a lumbar motion monitor (LMM). 10kg and 15kg loads were considered in this study and lifted through a vertical displacement of 750mm. The articulation between the mass and the handle was made by either a solid metal column (i.e. stable load) or a series of chain links (i.e. unstable load). A ship motion simulator was employed to produce three different platform motions during which the participants lifted loads. The platform motions were described as pitch, roll and quartering seas. Thus a 3 floor motions by 4 loads design was considered in this experiment. The maximum angular velocity in the lateral bending (LB), sagittal (SG) and twisting (TW) planes were calculated from the collected displacement data and were compared across load and motion conditions using a repeated measures ANOVA.

RESULTS AND DISCUSSION

It can be generally stated that the motions of the simulator platform influenced the maximum LB, SG and TW thoracolumbar velocities relative to the baseline laboratory condition. What was most interesting was the direction of these changes. There was a significant increase in the maximum LB ($p<0.001$) and TW ($p<0.001$) velocities for the platform motion conditions relative to the laboratory condition. In both thoracolumbar directions it was the pitch motion that induced the greatest increases in velocity compared to the laboratory values. What was most surprising is that the maximum SG velocities decreased significantly ($p<0.001$) relative to the stable, laboratory condition for all motion conditions, with pitch demonstrating the greatest reduction. SG reduction is characteristic of trunk stabilizing strategies exhibited by low back pain sufferers performing trunk extension activities [3].

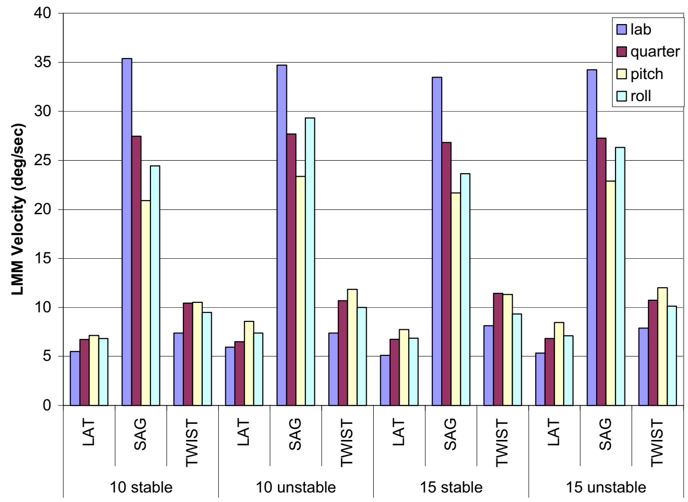

Figure 1: Maximum thoracolumbar velocities across load and motion conditions.

The type of load handled significantly affected the magnitude of the maximum TW velocities ($p=0.026$). In general, there were greater TW velocities when handling the unstable loads compared to the stable loads under the motion conditions.

CONCLUSIONS

Performing lifting tasks in motion environments, particularly with unstable loads will likely increase the risk of overexertion injury to the lower back due to the increases in maximum angular velocities in the lateral bending and twisting planes. Further studies examining if there are changes in lifting strategies while working in a motion environment are warranted given the unexpected decreases in sagittal plane motions occurring at the lower back during the motion conditions.

REFERENCES

1. Kigma I, et al. *In J Ind Erg* **32**, 51-63, 2003.
2. Marras W, et al. *Ergonomics* **38**, 377-410, 1995.
3. Marcal MA, et al. *Advances in Occupational Ergonomics and Safety 3*, 1999.

ACKNOWLEDGEMENTS

The authors would like to acknowledge Anthony Patterson, Director – Center for Marine Simulation for use of the simulation facilities and NSERC and SafetyNet for financial assistance of this project.

POSTURAL CONTROL UNDER VISUAL AND PROPRIOCEPTIVE PERTURBATIONS DURING DOUBLE AND SINGLE LIMB STANCE

Fuad A. Hazime[1], MS, Clarice Tanaka[1,2], PhD, Paul Allard[3], PhD, P.Eng. Martin Simoneau[4], PhD, Normand Teasdale[4], PhD

[1]Division of Rheumatology, School of Medicine, University of São Paulo, Brazil, fuadfisio@hotmail.com
[2]Department of Physical Therapy, Speech Therapy and Occupational Therapy, University of São Paulo, Brazil
[3]Department of Kinesiology, University of Montreal, Montreal, Canada. Laboratoire d'Étude du Mouvement, Research Center, Saint-Justine Hospital, Montreal, Canada
[4]Division of Kinesiology, Laval University, Quebec, Canada

INTRODUCTION

Postural control is known to result from the integration of visual, somesthesic and vestibular information. In the therapeutic settings, proprioception rehabilitation programs often prescribe exercises involving single-leg stance or single-leg hop in order to restore proprioceptive deficits and functional stability of the ankle [1]. We wish to test the hypotheses that, when proprioception is perturbed, the role of vision in postural control increases with the difficulty of the standing task. Additionally, we wish to investigate the effect of vision during postural adaptation after withdrawn of the somesthesic perturbation during double (DLS) and single limb stance (SLS).

METHODS

Eleven healthy and active young male adults (29.6 ± 5.8 years; 181.2 ± 4.6 cm; 81.9 ± 11.5 kg) participated in this study.
To perturb the visual input, the laboratory room was darkened in such a way that participants could not see the environment [2]. Ankle proprioception was perturbed with four vibrators placed transversely to the tendons of triceps surae and tibialis anterior muscles. Four test conditions were collected: normal vision + normal proprioception (20s); reduced vision + normal proprioception (20s); normal vision + perturbed proprioception (10s) to normal vision to proprioception reintegration (10s) and reduced vision + perturbed proprioception (10s) to reduced vision to proprioception reintegration (10s). Five trials of each condition were collected in DLS and SLS using an AMTI force platform. The COP speed of two intervals of proprioception perturbation (V1, V2) and proprioception reintegration (R1, R2) were compared to control conditions using Analysis of Variance (ANOVA) followed by Tukey HSD test ($p<0.01$).

RESULTS AND DISCUSSION

A significant condition by task interaction was revealed. Post hoc comparisons showed that vision has a main effect in SLS ($F(1, 20) = 47.70$, $p<0.001$) while proprioception perturbation showed effect only during DLS ($F(2, 40) = 29.11$ $p<0.001$) (Fig. 1). Postural control in DLS was achieved independently of visual input after 5s of proprioception reintegration (R2). In the present study the difficulty of the task condition seems to be highly related to the visual dependency.
Our results suggest that to perform challenging tasks vision and possibly vestibular system dominates the postural control.

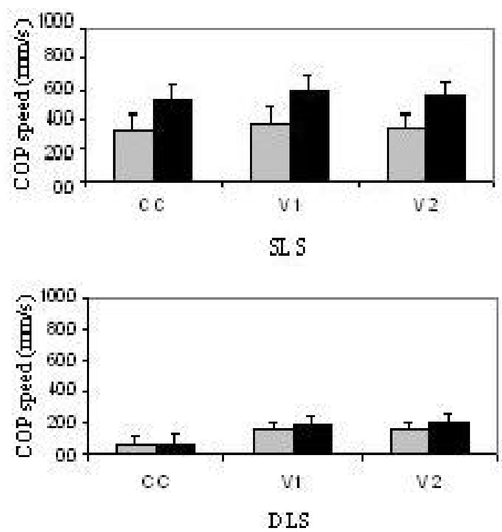

Fig. 1: Mean COP speed during control condition (CC) and two intervals (V1, V2) of proprioception perturbation. Normal vision (■); reduced vision (■); double limb stance (DLS); single limb stance (SLS).

Therefore, exercises involving single-leg stance can improve functional stability probably due to some neuromuscular requirement other than enhance of proprioception system.

CONCLUSIONS

Vision plays a more important role according to the task to be accomplished. The more challenging is the task, more the balance control mechanisms rely on vision. These results can help clinicians and researchers to make decisions about tasks and sensorial availability during assessment and training.

REFERENCES

1. Rozzi SL; Lephart SM; Sterner R; Kuligowski L. Balance training for persons with functionally unstable ankles. *J Orthop Sports Phys Ther* 1999; 29:478-86.
2. Tropp H, Odenrick P, Ekstrand J. Factor affecting stabilometry recordings of single limb stance. *Am J Sports Med* 1984;12:185-188.

INFLUENCE OF MUSCLE PRE-ACTIVATION AND KNEE JOINT ANGLE ON AXIAL TIBIO-FEMORAL SHOCK TRANSMISSION

[1]Wolfgang Potthast, [2]Anton Arndt, [2]Arne Lundberg and [1]Gert-Peter Brüggemann
[1]Instiute for Biomechanics and Orthopedics, German Sport University Cologne, email: potthast@dshs-koeln.de
[2]Dept. Orthopedic Surgery, Karolinska University Hospital / Huddinge, Sweden

INTRODUCTION

A number of cadaver studies has shown a shock attenuating capacity of intra- and periarticular tissues in axial impact loading [1,2]. This shock reduction was mainly explained by deformation. In vivo reductions in shock transmission in walking or running were primarily explained by variations in leg stiffness due to modified joint angles or muscle activity [3,4]. The interdependence of joint angles and muscle activation in locomotor activities makes it difficult to analyze determining factors of shock transmission during locomotion. The purpose of this study was to analyze the role of muscle pre-activation and knee angle on shock transmission in controlled situations.

METHODS

Four male (35-47 years, 70-88kg) healthy subjects volunteered for this study. They were positioned supine with three different goniometric controlled knee angles (0°, 20°, 40°). The forefoot was strapped on the metal plate of an impact device. The hip angle (40°) and ankle angle (90°) were constant. Three muscle activation levels were defined in respect to prior maximal voluntary contractions (0%, 30%, 60% MVC) at each angle condition. Using EMG (Biovision®) the activation was measured at both gastrocnemii (GM, GL), both vasti (VM, VL) and the semitendinosus (ST). In each of the nine different angle-activation conditions ten impacts were initiated under the subjects' heel by means of the pneumatic impacter. The force was measured using a one dimensional transducer (Kistler®). Tibial and femoral shocks were measured using three dimensional accelerometers (Kistler®, m<0.0025kg). This abstract focuses on the longitudinal components only. The sensors were attached to Apex® pins (diameter 3.0mm, length 60mm) inserted under local anesthetic approx. 1.5cm into the right tibia and femur. The insertion locations were medial and approximately 5-7cm below (tibia) and 2–3cm above (femur) the knee joint space. After attaching the sensors their axes were aligned with the anatomical segment axes using a correction algorithm based upon reflective markers recorded by a movement analysis system (ProReflex®). The shock transmission through the knee joint was calculated by the ratio RAT of the acceleration maxima at the tibia (ACCtib) and femur (ACCfem) (RAT=ACCtib/ACCfem·100). The linear displacement of tibia and femur was estimated by double integrating the acceleration time history and the knee compression (KOM) by the difference of tibial and femoral displacement. The sampling rate of all analog data was 1000Hz. An ANOVA ($p<0.05$) was carried out to identify significant differences of the mentioned parameters between knee angle or activation conditions.

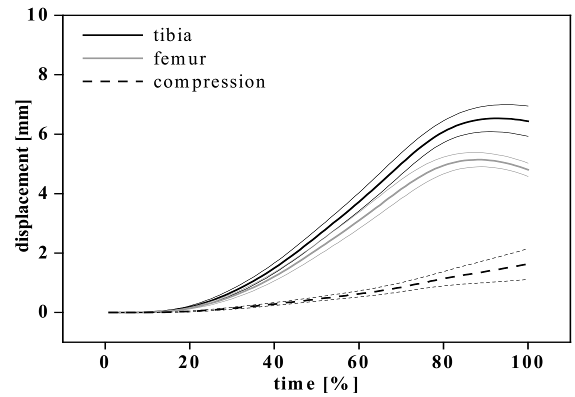

Figure 1: Time normalized time history of mean (±sd) knee compression and femoral and tibial displacement of one subject achieved at 0° knee angle and 0% MVC level (n=10).

RESULTS AND DISCUSSION

In the described study conditions the average peak acceleration at the tibia varied between 2 and 4g and at the femur between 1.5 and 2.5g. With increasing muscle activation levels the tibia acceleration decreased significantly under all knee angles which was also true for the femur at 0° and 20°. ACCtib increased significantly with increasing angles at all MVC levels while ACCfem showed no systematic trend in all subjects. The average shock transmission over all trials was 59.7%. In the 0° and 20° knee angle condition three of the four subjects showed a significant increase in RAT of about 10% with increasing muscle activation levels while one subject showed no substantial change. In the 40° condition increasing muscle activation had a smaller effect on RAT compared to 0° and 20°.

Figure 1 shows the average segmental displacement for one subject at 0° knee angle and 0% MVC. In all knee angle conditions the relative axial movement of tibia and femur (KOM) was significantly decreasing with increasing muscle activation. Apparently the muscle forces pre-load the joint's peri- and intraarticular structures. Considering the facts that RAT was increasing while KOM was decreasing with higher muscle activity and that cadaver studies [1,2] have shown a shock attenuating effect of passive structures it could be assumed that the deformation of peri- and intraarticular tissue also has an effect on shock transmission in vivo. This effect could be substantially influenced by muscle activation.

REFERENCES

1. Radin, EL, Paul, IL. *Arthritis and Rheumatism* **14**: 356 – 362 1971
2. Chu, MA, et al.. *J Biomech* **19**, 979-987, 1986
3. Bobbert MA, et al.. *J Biomech* **24**, 1095-1105, 1991
4. Lafortune MA, et al.. *J Biomech* **24**, 877-886, 1991

A HYDRAULIC APPROACH TO THE DEVELOPMENT OF A VARIABLE RECIPROCATING HIP MECHANISM FOR THE RECIPROCATING GAIT ORTHOSIS

[1]Curtis S. To, [2]Rudi Kobetic, [2,3]Ronald J. Triolo, [1]Musa L. Audu, and [1,2]Robert F. Kirsch
[1]Department of Biomedical Engineering, Case Western Reserve University,
[2]Louis Stokes Cleveland Department of Veterans Affairs Medical Center,
[3]Department of Orthopaedics, Case Western Reserve University
email: cst@po.cwru.edu

INTRODUCTION

The hybrid orthosis system (HOS) is an assistive gait device for individuals with paraplegia that combines the stability provided by an exoskeletal brace with limb mobility controlled via functional neuromuscular stimulation [1]. A type of brace used in the HOS is the reciprocating gait orthosis (RGO) [2]. The RGO facilitates reciprocal gait by mechanically coupling hip extension with contralateral hip flexion. Hip reciprocation is however fixed at a 1:1 flexion/ extension coupling ratio (FECR), limiting hip flexion to the extent of contralateral hip extension [3]. The aim of this research is to develop a hip reciprocating mechanism for the RGO that can couple the hips at variable FECRs. This study focuses of examining the feasibility of utilizing a hydraulic system for variable hip reciprocation.

METHODS

The proposed design of the hydraulic system for variable hip reciprocation consists of a double acting hydraulic cylinder linked to the lever arm of each thigh upright. Corresponding outlets of the opposing cylinders are connected by tubing to produce a closed hydraulic circuit. Thus, hip extension forces the adjoining piston upward, which then pressurizes the contralateral piston to move downward, resulting in contralateral hip flexion. Solenoid valves are employed to control fluid flow through the hydraulic system resulting in the locking/unlocking of a hip joint and/or the disengagement/ reengagement of hip coupling to establish variable FECRs. Pressure relief will be provided by an accumulator.

An initial prototype was developed using off the shelf components to test the efficacy of the design. Pneumatic cylinders with a 5/16 inch bore diameter were used to minimize flow rate and manual shutoff ball valves were used in replace of solenoid valves to simplify operation.

An analysis of determining the operating pressures and flow rates of the hydraulic system during gait was undertaken to resolve optimal cylinder and valve specifications and verify if these components could be supplied off the shelf or necessitated the costs of customization. The goal is to minimize flow rate through the valves while selecting a cylinder with a large enough bore diameter to sustain the pressure ranges experienced during gait. Instantaneous cylinder pressures and flow rates during gait for a series of stock cylinder bore sizes were determined by using dynamic data from a three-dimensional computer model of the HOS that incorporated a RGO with 1:1 hip FECR [4]. A valve coefficient (C_v) was then determined for each cylinder bore diameter.

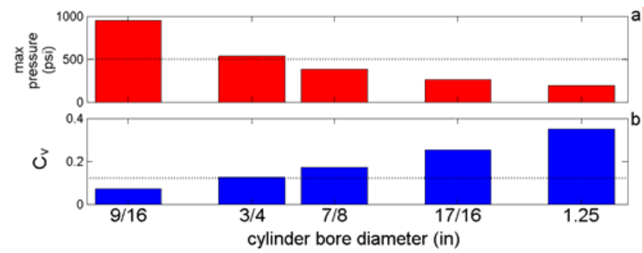

Figure 1: The dotted lines in (a) and (b) indicate the pressure rating for small bore cylinders and maximum C_v for low powered solenoid valves respectively.

RESULTS AND DISCUSSION

The prototype demonstrated the soundness of the proposed hydraulic design by verifying that (1) hip coupling could be readily engaged and disengaged and (2) each hip could be locked and unlocked independently without affecting the kinematics of the opposite hip.

Maximum pressures (Figure 1a) and C_v factors (Figure 1b) during gait indicate that a stock cylinder with a ¾ inch bore diameter and pressure rating of 500 psi and valves with a C_v of 0.12 could be used for the hydraulic variable reciprocating hip mechanism.

Current and future work includes the bench testing of the hydraulic reciprocating hip mechanism with the established optimal components and subsequent able-body testing of the new orthosis.

REFERENCES

1. B. J. Andrews, *et al.* "Hybrid FES orthosis incorporating closed loop control and sensory feedback," *J. Biomed. Eng.*, vol. 10, no. 2, pp. 189-195, April 1988.
2. R. Kobetic, *et al.* "Development of a hybrid gait orthosis: A case report," *J. Spinal Cord Med.*, vol. 26, no. 3, pp. 254-258, 2003.
3. L. Yang, *et al.* "Effects of joint motion constraints on the gait of normal subjects and their implications on the further development of hybrid FES orthosis for paraplegic persons," *J. Biomech.*, vol. 29, no. 2, pp. 217-226, Feb. 1996.
4. C. S. To, *et al.* "The feasibility of a functional neuromuscular stimulation powered mechanical gait orthosis with coordinated joint locking," *Proc. 26th Annu. Int. Conf. IEEE Eng. in Med. and Biol.*, San Francisco, CA, 2004, pp. 4041-4044.

ACKNOWLEDGEMENTS

This work was supported by the VA (Grant #B3463R) and DOD (Grant #PR043074).

CONVERGENT VALIDITY OF GONIOMETRIC AND MOTION CAPTURE TECHNIQUES USED TO MEASURE TIBIAL TORSION

[1] Kevin M. Cooney, [2] Tara Keister, [2] Eugenie Poignard, [2] Elizabeth Rupert, [2] Sarah Zerbe
[2] Thomas Hudson, [1] Michael J. Rainbow, [1,2] Frank L. Buczek
[1] Shriners Hospitals for Children, Erie, PA, [2] Gannon University, Erie, PA; email: kcooney@shrinenet.org

INTRODUCTION

Rotational and torsional abnormalities in the pediatric lower extremity can result in static and dynamic toeing-in or toeing-out, and are two of the most common reasons for parents to seek orthopaedic advice.[1] One common lower extremity torsional abnormality is atypical tibial torsion. Computed tomography (CT) is the gold standard for measurement of tibial torsion,[2] but its practicality is limited due to expense. Several goniometric measurement techniques have been described, but debate remains over which is most valid.[3] One goniometric method as described by King and Staheli was found to be within the accepted variability of CT, and therefore an accurate assessment tool.[4] The purpose of this prospective study was to determine the convergent validity of two other common goniometric methods used to measure tibial torsion, as well as a novel method using motion capture, by comparing them to the validated method described by King and Staheli.

METHOD

Twenty normal subjects (12 female, 8 male) between the ages of 10 and 25 years underwent four different measures of tibial torsion on the right lower extremity, including the CT validated method as described by King and Staheli (MKS), the thigh-foot angle (TFA) [4], a supine trans-malleolar axis measure (TMA) [5], and a novel method using motion capture (MC). One examiner, who was masked from the measurements via modification to a standard goniometer, assessed tibial torsion using the first three methods, while a second examiner recorded the results. After three measurements were obtained for each technique, a third examiner placed 6-mm markers on each subject's right medial and lateral tibial plateau, as well as medial and lateral malleoli.[6] Tibial torsion was then calculated as the rotation between two planes, one containing the tibial plateau markers and mid-point of malleolus markers and the other containing the malleoli and midpoint of the tibial plateau markers, about an axis between the proximal and distal midpoints. Three static motion capture trials were performed on each subject using a 10-camera Vicon 612 system (Oxford Metrics Group, Oxford, England). Biomechanical modeling was performed using Visual3D (C-Motion, Inc., Rockville, MD). Tibial torsion data were compared using a repeated measures analysis of variance with Tukey HSD *post hoc* tests performed in Statistica (Statsoft, Inc., Tulsa OK, USA).

RESULTS AND DISCUSSION

Statistically significant differences ($p < 0.05$) were demonstrated between our goniometric gold standard MKS and the goniometric methods of TFA and TMA (Table 1, Table 2). No significant differences were found between MKS and the novel MC technique, or between TFA and TMA. The results demonstrate discrepancies in the validity of TFA and TMA when compared to MKS, which was found to be a valid measure when compared to CT in previous literature. These findings may be considered when performing goniometric measurement of tibial torsion in the clinical setting. Because motion capture demonstrated convergent validity when compared to MKS, it is concluded that it is also a valid method for measuring tibial torsion. It is recommended that care be taken to ensure accurate placement of the centroid of the markers over the bony landmarks when using the motion capture technique. The absence of comparison to CT, which is the gold standard for measurement of tibial torsion, was a minor limitation of this study. Because the distal reference line for measuring tibial torsion via CT involves the fibular notch of the tibia, but not the medial malleolus,[2] use of the trans-malleolar axis in all four of the techniques described in this study is another area of weakness for determination of true tibial torsion.

Table 1: Descriptive Statistics

Assessment Technique	Range (°)	Mean (°)	Standard Dev. (°)
MKS	20.0	23.3	4.7
TMA	14.0	17.8	3.6
TFA	17.0	17.6	3.8
MC	26.0	19.3	6.7

REFERENCES:

1. Khermosh O., et al. *Clin Orthop* **79,** 25-31, 1971.
2. Jend H.H., et al. *Acta Radiol Diagn,* **22-3A,** 271-276, 1981.
3. Lang L.M., et al. *J Am Podiatr Med Assoc* **88,** 160-165, 1998.
4. Stuberg W., et al. *Clin Orthop* **272**, 208-212, 1991 .
5. Cusick B.D. *Progressive Casting and Splinting for Lower Extremity Deformities in Children with Neuromotor Dysfunction.* Therapy Skill Builders, Tucson, AZ, 1990.
6. Andriacchi T.P., et al. *J Biomechanical Engineering* **120,** 743-749, 1998.

Table 2. Results of Post Hoc Tests (asterisks indicate significant differences at $p < 0.05$)

MKS-TMA	MKS-TFA	MKS-MC	TMA-TFA	TMA-MC	TFA-MC
0.000188*	0.000176*	0.871097	0.991780	0.000640*	0.000460*

ROTATIONAL SPRING AND DAMPER MODEL PREDICTION DURING LANDING

[1] Robert Ragan, [2]Thomas Kernozek, [1]David Buschke and [1]John Hart
[1]Physics Department, 2Department of Health Profession, University of Wisconsin-La Crosse, La Crosse WI 54601
email: ragan.robe@uwlax.edu, web: www.uwlax.edu/faculty/ragan/

INTRODUCTION

Lower extremity stiffness is thought to be an important factor related to performance and injury. There have been three basic approaches to quantifying stiffness during impact related movement activities: vertical stiffness, total leg stiffness and torsional stiffness[1]. The assessment of torsional stiffness allows researchers to quantify changes in stiffness in each joint. This opens the opportunity to assess the relative change in stiffness with experimental perturbations. Some models have also incorporated the use of damping as seen in Derrick et al's study of running[2]. The purpose of this study was to use a spring and damping model to describe landing and describe the relative strength of the fit to drop landing for the joints in the lower extremity.

METHODS

Twelve male recreational athletes performed six single legged drop-landing trials from a 40-centimeter height. Kinematic data were recorded at 240 Hz using a six-camera three-dimensional motion analysis system. Sixteen retro-reflective markers were used with a modified Helen-Hayes marker set. Kinetic data were recorded at 1200 Hz simultaneously with kinematic data using a Bertec force platform. Raw data were smoothed at a 10 Hz cutoff. Inverse dynamics calculations were performed in the Kintrak software package and exported to a custom program in Matlab. Sagittal plane joint angles and moments at the hip, knee and ankle were used to calculate rotational stiffness coefficients[3]. Sagittal plane joint velocities and joint moments were used to calculate damping coefficients for the hip, knee and ankle. Averages of the six trials were used. Descriptive data of the spring and damping coefficients of the hip, knee and ankle were calculated as well as the relative fit using a regression model.

RESULTS AND DISCUSSION

The damped torsion spring model was found to fit the moment data during the impact part of the landing from initial contact until the peak joint moment (approximately 0.1 sec). Spring and damping constants for the knee and ankle maintained high R^2 values with and without the presence of damping (Table 1). Incorporating the effects of damping, however, consistently increased R^2 values in comparison to those without damping. Table 1 also shows that the ankle and knee joint of the lower extremity behave rather spring-like with minimal damping effects. Poor fits of this spring damping model were found for the hip joint where damping coefficients were negative. Also, the model failed to predict joint moments beyond their respective peak moments, where other factors such as central nervous system control need to be considered[4].

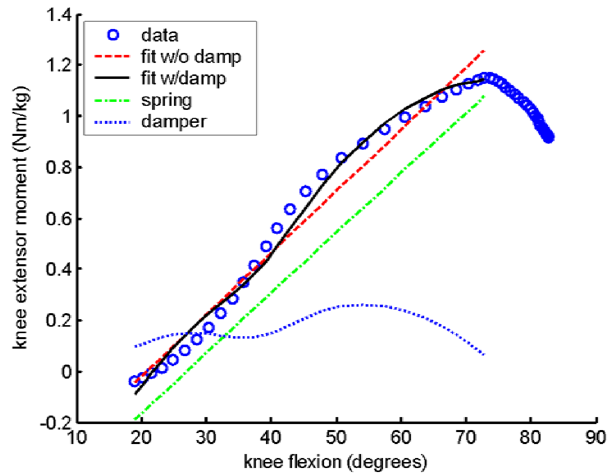

Figure 1 Knee fitting results for a single landing trial from initial foot contact to maximum knee flexion. The spring and damper curves show the contribution from each separately in the fit with and without damping.

CONCLUSIONS

Spring and damping model produces good results for the knee and ankle for the impact portion of landing. The damping effect for drop landing appears to be minimal for the knee and ankle. Much poorer fits were seen at the hip joint. Use of this model should be likely limited to more distal joints like the knee and ankle.

REFERENCES

1. Butler, RJ et al. *Clin. Biomech.* **18**, 511-517, 2003.
2. Derrick TR et al. *J. Appl. Biomech.* **16**, 36-51, 2000.
3. Farley CT et al. *J. Appl. Physiol***. 85**, 1044-1055, 1998.
4. Latash et al. *Movement Science* **12**, 653-692.

ACKNOWLEDGEMENTS

Undergraduate research assistants were funded with hi-tech funding from the University of Wisconsin system, and with a College of Science and Allied Health Dean's Summer Fellowship.

Table 1 Model fitting parameters across subjects (mean ± std. dev.) and R^2 values

	Damping Present			Damping Absent	
Joint	**Damping Constant**	**Spring Constant**	**R^2 Value**	**Spring Constant**	**R^2 Value**
Ankle	.000164 ± .000102	.0398 ± .0078	.9622 ± .0605	.0384 ± .0075	.9865 ± .0057
Knee	.000375 ± .000290	.0495 ± .0150	.9926 ± .0056	.0512 ± .0170	.9536 ± .0615

FOOT TYPE CLASSICATION USING FUZZY LOGIC

Mehrdad Anbarian[1, 2], Paul Allard[1], Nader Farahpour[2], Sébastien Hinse[1], Clarice Tanaka[3]

[1] Kinesiology Department, University of Montreal, Quebec, Canada,
[2]Physical Education Department, Bu-Ali Sina University, Hamadan, Iran,
[3]Department of Physical Therapy, Speech Therapy and Occupational Therapy, University of São Paulo, Brazil,
e-mail: mehrdad.anbarian@umontreal.ca

INTRODUCTION

Foot type classification methods are still controversial in the literature [1]. The difficulty lies in part in the different means of assessing foot disorders such as visual inspection, foot print, radiography, etc. and with the number of parameters to characterize foot morphology. Consequently, foot classification is often based on parameters related to a specifically pathology rather using a single set of angles for all pathologies [2]. The aim of this study was to determine if fuzzy logic (FL) can be applied to classify five foot types using only two geometric parameters and determine its performance.

METHODS

An experienced podiatrist clinically categorized 321 feet into 4 pathological groups, namely, pes planus (n=52), pronation (n=80), pes cavus (n=115) and supination (n=48) and an able-bodied group (n=26).

A digital camera was used to capture two black and white images taken from the postero-anterior and medial views of feet while weight-bearing. Camera-subject distance was fixed at approximately 1.7 meter. The pictures were then processed by a numerical filter where the grey levels were transformed into a color-coded image highlighting muscle and bone prominences. This process facilitated the measurement of two foot parameters. These are the rearfoot and Djian-Annonier angles (Figure 1). In the literature, rearfoot angle is used to describe subtalar joint position while Djian-Annonier is described medial height arch.

The fuzzy logic toolbox in MATLAB was used to develop the classification model. The above two parameters were introduced in the FL model. For estimating the relative accuracy of the classification method, Kappa statistics were applied by comparing the result of the FL classification with that of the clinical sorting.

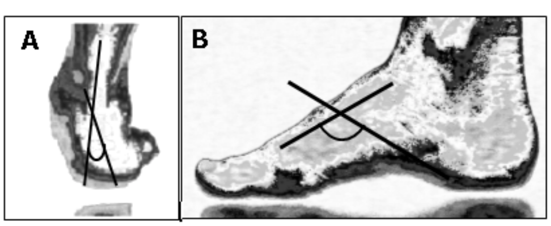

Figure 1: A) Rearfoot and B) Djian-Annonier angles.

RESULTS AND DISCUSSION

The FL technique was successful in classifying 88.8% of all able-bodied and pathological feet. The lowest success rate was found for the able-bodied group (69.2%) as compared to a mean success rate of 93.7% for all pathologies groups (Figure 2). Misclassification of 5 of the 26 feet as pes cavus in the able-bodied group reduced the performance of the FL technique. The misclassification could be related to lower difference value of the rearfoot angle. In the able-bodied group it was 1^{o} greater than in the pes cavus group while it ranged from 7.4^{o} to 10.3^{o} for other pathologies.

A Kappa value of 0.89 was obtained with the FL classification method when compared to the podiatrist's classification. To our knowledge no one has yet reported a classification in which both able-bodied and pathological feet were presented. Furthermore, previous studies were limited to parameters related to a single pathology.

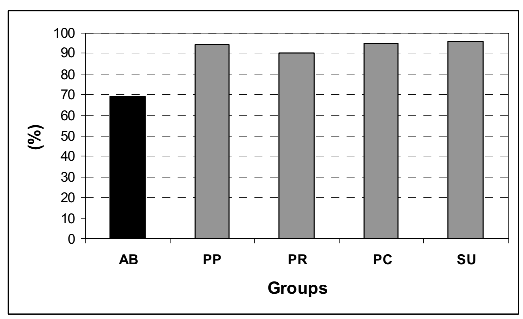

Figure 2: Classification results for able-bodied (AB), pes planus (PP), pronation (PR), pes cavus (PC) and supination (SU) groups.

CONCLUSIONS

The fuzzy logic method was able to classify the five foot types using only two geometrical parameters with high accuracy.

REFERENCES

1. Saltzman CL, et al. *Arch Phys Med Rehabil*, **76**, 45-49, 1995.
2. Razeghi M and Batt ME. *Gait and posture*, **15**, 282- 291, 2002.

CYTOSKELETAL TENSION ENHANCES OSTEOGENIC DIFFERENTIATION OF ADIPOSE-DERIVED MESENCHYMAL CELLS

[1,2]Diane R Wagner, [2]Yue Xu, [1]Dennis R Carter and [2]Michael T Longaker
[1]Department of Surgery and [2]Division of Biomechanics, Stanford University, Stanford CA
email: drwagner@stanford.edu

INTRODUCTION

Cells isolated from adipose tissue possess multilineage potential, but strategies for driving the AMCs to a particular lineage have yet to be elucidated. A recent study has shown that cell density and shape regulate the differentiation of human mesenchymal stem cells (hMSCs) [1]. In hMSCs, RhoA and Rho Kinase (ROCK), which mediate tension in the actin cytoskeleton, are directly involved in density- and shape-dependent differentiation [1]. The RhoA/ROCK pathway is particularly interesting to us because it has also been implicated in the mechanotransduction of signals from the extracellular matrix to a cellular response [2,3].

To explore density-dependent differentiation of AMCs, we varied cell density and examined its effect on adipogenesis and osteogenesis. We inhibited ROCK to determine whether cytoskeletal tension is involved in the differentiation of our cells. Finally, we used microarray analysis to elucidate the mechanisms of density-dependent differentiation in AMCs and to determine whether genes that are regulated by density are also mechanosensitive.

METHODS

AMCs were harvested from inguinal fat pads of three-week-old FVB mice. After expansion, early passage (P1) cells were plated at low (2,500 cells/cm^2) and high (25,000 cells/cm^2) density. Cells were cultured in a bipotent differentiation media containing both osteogenic and adipogenic factors. At 1 week, adipogenic differentiation was determined by staining the cells with Oil Red O. Early osteogenic differentiation was assessed by staining cells for alkaline phosphatase (ALP) and by quantifying ALP activity normalized to total protein. These differentiation assays were performed both with and without the drug Y-27632, which inhibits ROCK.

RNA was harvested from cells at low and high density in bipotent differentiation media 24 hours after plating. Gene expression analysis was performed on cDNA microarrays containing nucleotide sequences for over 20,000 mouse genes.

RESULTS AND DISCUSSION

We observed greater ALP staining in our low density cells. Conversely, Oil Red O staining was more pronounced in the cells plated at high density. Oil Red O staining appeared identical with and without the addition of the ROCK inhibitor Y-27632. However, we saw a decrease in ALP staining at low density with Y-27632 (Fig 1). The quantitative ALP activity assay confirmed the staining results (data not shown). Specifically, ALP activity in cells at low density without Y-27632 was significantly higher than in all other conditions.

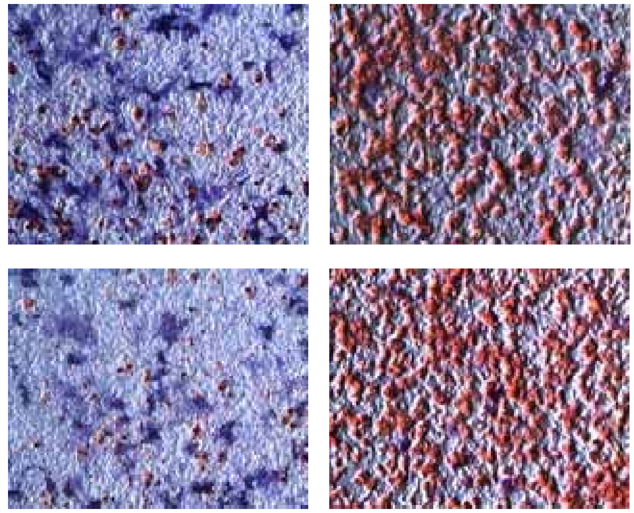

Figure 1: Microscopic (10x) view of ALP staining in blue and Oil Red O staining in red. Left: cells at low density; Right: cells at high density; Top: cells in bipotent media; Bottom: cells in bipotent media with Y-27632.

Some of the genes that are significantly upregulated in low density cells are also mechanosensitive. For example, connective tissue growth factor and thrombospondin 1 were expressed more highly in our low density cells and were upregulated with tensile strain in primary rat calvarial cells [4]. Similarly, calponin was more highly expressed in our low density cells and was upregulated with uniaxial tensile strain in rat bone marrow progenitor cells [5]. A thorough review of our microarray data is ongoing.

CONCLUSIONS

This study demonstrates that cell density influences osteogenesis and adipogenesis in AMCs and strongly suggests that increased cytoskeletal tension in the low density cells enhances osteogenesis. Our microarray data indicate that some similarities exist between genes that are sensitive to density-mediated changes in cytoskeletal tension and mechanosensitive genes. In the future, we plan to explore whether the mechanism of cytoskeletal tension is similar in density-dependent osteogeneisis and in mechanotransduction of AMCs.

REFERENCES

1. McBeath et al *Dev Cell* 2004. 2. Ridley *J Cell Biol* 2000. 3. Chiquet et al *Matrix Biology* 2003. 4. Segev et al *Bone* 2004. 5. Hamilton et al *Tissue Eng* 2004.

ACKNOWLEDGEMENTS

This study was funded by NIH RO1 DE14526.

GAIT KINEMATICS ON AN ELEVATED INCLINED SURAFCE

[1] Lloyd (Chip) Wade and [2]Jerry Davis
[1]Human Movement and Balance Laboratory, Department of Bioengineering, University of Pittsburgh
[2] Department of Industrial and Systems Engineering; Auburn University [1]email: cwade@engr.pitt.edu

INTRODUCTION

Fatal and non-fatal falls from elevation have been documented to be a significant issue in today's workforce. According to the Bureau of Labor Statistics (BLS) in 2003 falls from elevations were reported to be the second-leading cause of fatalities in industry, second only to workplace transportation fatalities, specifically falls from elevation accounted for 13% of all workplace fatalities, with a reported 691 fatalities for the year [1].

In industrial settings, elevated surfaces are typically associated with altered support surfaces (i.e. inclined). While previous research has suggested changes in elevation [2], and exposure to inclined surfaces [3], are risk factors for falls; research is sparse on gait kinematics while exposed to elevation and inclined surfaces simultaneously. Therefore, the purpose of this study was to investigate gait kinematics during exposure to an elevated inclined surface.

METHODS

Twenty subjects, 10 male college students (inexperienced) and 10 male roofers (experienced) between the ages of 19 to 50 years old, participated in this study. The testing protocol was explained prior to providing informed consent consistent with the Auburn University Office of Human Subjects Institutional Review Board (IRB) standards. Exclusionary criteria included a history of neurological, orthopedic, cardiovascular and pulmonary abnormalities as well as any other difficulties hindering normal gait.

Subjects walked (ascending & descending) on an elevated inclined surface (10 to 16 feet from ground level), measuring 16x14 feet at a 6/12 (26^{o}) pitch (Figure 1). A week later, subjects walked on the same inclined surface at ground level. While subjects walked, an 8-camera Peak Performance (Peak 5.0) Motion Analysis System acquired 3D motion data at 120 Hz from markers placed bilaterally on anatomical landmarks to configure the whole body model. Subjects were required to use fall protection that prevented rapid descents if a fall were to occur. Dependent measures included stride length (SL), stride width (SW), step period (SP), and walking velocity (V). A significance level of $\alpha = .05$ was applied.

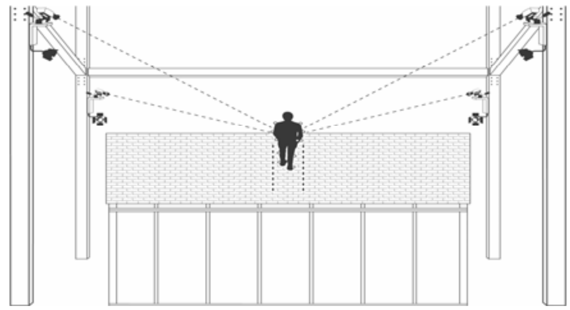

Figure 1. Artist rendering of the elevated inclined surface

RESULTS AND DISCUSSION

Statistical analysis revealed a significant within subject's and between group difference(s) in step length, step width, step period, and walking velocity between the two height conditions and walking directions. Mean values (±SD) for each group, height, and direction are presented in Table 1.

CONCLUSION

An analysis of the kinematics of gait while operating on an elevated inclined surface is important in understanding the effects of elevation on the potential for falls due to slips or loss of balance. While previous research has indicated that step length, width, period, and velocity are correlated to changes in postural stability; it is interesting to note the significant effect of experience at elevation between individuals. This difference may be an underlying factor in fall incidents. Inexperienced individuals demonstrated gait kinematics suggesting a perceived increase in the frictional demands, adjusting their behavior to reduce the risk of a slip or loss of balance. Experienced individuals demonstrated gait characteristics related to postural stability with insensitivity to height. These suggested underestimations of the frictional demands may be a contributing factor related to a loss of balance, resulting in a fall.

REFERENCES

1. Bureau of Labor Statistics: Census of Occupational Injury, 2004.
2. Paulus, W.M., et al. *Brain* **107**, 1143-63, 1984.
3. Redfern, M.S., et al. *Gait & Posture* **6**, 119-25, 1997.

Table 1. Stride length, stride width, step period, and walking velocity, normalized by height, for each direction, height, and group.

	Descending				Ascending			
	Elevation		Ground		Elevation		Ground	
	InEx	Ex	InEx	Ex	InEx	Ex	InEx	Ex
SL(m/ht)	.37±.02	0.46±.01	.41±.02	.49±.01	.44±.01	.53±.01	.47±.02	.55±.01
SW(cm)	11.5±.31	9.6±.25	11.2±.32	8.1±.44	12.4±.27	10.5±.18	12.3±.32	9.1±.44
SP(s)	.39±.01	.57±.02	.47±.01	.63±.02	.47±.01	.64±.01	.53±.01	.69±.01
V(SL/SP)	.71±.02	.83±.02	.8±.02	1.0±.07	.67±.02	.79±.02	.75±.02	1.0±.07

RECRUITMENT OF SOLEUS AND GASTROCNEMIUS WITH RESTRICTED AND UNRESTRICTED ANKLE MOTION

[1] David Sanderson and [2] David Kenyon
[1] School of Human Kinetics, UBC, Canada, [2] Department of Physics, BCIT, Canada
email: david.sanderson@ubc.ca, web: www.hkin.educ.ubc.ca

INTRODUCTION

Marsh and Martin [1] showed that the gastrocnemius and soleus muscles responded differently to cadence manipulations during cycling. Gastrocnemius excitation increased with increasing cadence whereas soleus did not. Subsequently, Sanderson et al. [2] repeated their experiment and presented data on muscle lengthening and EMG activity for gastrocnemius and soleus where cadence was manipulated (50 – 110 rpm in 15-rpm increments). They postulated that the difference in sensitivity to cadence manipulations between these two muscles was associated with their mechanical properties. To assess this postulate individual ankle-foot orthoses that kept the ankle joint at 90° of flexion, or the neutral position were worn as cyclists pedaled a series of cadence conditions at a fixed power output (200 W). In doing so the opportunity for soleus to contribute to pedal force was removed. We postulated that this would result in an increase in gastrocnemius excitation to compensate for the loss of the soleus contribution. Further, with the ankle joint fixed at 90° we would be able to separate the influence of ankle joint ankle changes on gastrocnemius length – i.e. it would solely be determined by knee-joint motion.

METHODS

Participants (n=3) expert cyclists (2M, 1F), with a mean (SD) age of 29 (11) years, mass 68 (2) kg, and height 176 (5) cm.) rode for a minimum of 2.5 minutes at each of five randomly presented cadences (50, 65, 80, 95, and 110 rpm) at a constant nominal power output of 200 W while EMG from soleus and gastrocnemius muscles and lower-limb sagittal-plane video were recorded. Data collection occurred in the final minute of the test protocol and lasted for six revolutions of the crank per collection period. Marker kinematics were used first to compute the angle of the knee and ankle joints and then the muscle lengths of the soleus and gastrocnemius muscles using equations developed by Hawkins and Hull [3] over the complete pedaling cycle. EMG data were normalized to the 50-rpm condition. We used data from Martin et al [4] to provide a baseline condition.

RESULTS AND DISCUSSION

Wearing the ankle-foot orthosis reduced ankle angle motion from a range of 18° to a range of 3° which was consistent with the flexion of the brace. Knee motion range was reduced from 71° to 61°. This was a surprise because with the now limited ankle motion we had anticipated that knee extension would increase. Examination of the motion of the vertical component of hip marker revealed that there was increased hip vertical motion. The cyclists dropped their hip on the down stroke to make up for this shorter leg. Because there was no change in the overall knee-joint range of motion and the limited affect of the ankle joint, the length change of gastrocnemius did not change between conditions. It was concluded that perhaps the strategy was to keep gastrocnemius operating within a specific range. This is consistent with the earlier postulate that the mechanical properties of muscle to some extent dictate their recruitment. Another effect of wearing the ankle-foot orthosis was that both muscle EMG patterns were substantially reduced for all cadence conditions and the sensitivity to cadence shown in gastrocnemius disappeared. Soleus excitation was reduced on average by 48% whereas gastrocnemius excitation was NOT increased by rather decreased by 28%. As we anticipated, the effect of wearing the brace was more marked on soleus. The 28% reduction in gastrocnemius excitation indicated that its activity was primarily affected by knee motion and that this two-joint nature masked any increased loading on the gastrocnemius might have experienced as a result of the reduced contribution by soleus. This project suggests that further work is required to understand fully the interaction of the muscles within the triceps surae complex.

REFERENCES

1. Marsh, A. & Martin, P. *Med. Sci. Sports. Exer.* **27,** 217-225, 1995.
2. Sanderson D. et al. *Med. Sci. Sports Exer.* **31,** S357, 1999.
3. Hawkins, D. & Hull, M. *J Biomech* **23**, 497-494, 1990.
4. Martin, P. et al. *Proceedings of ISB XVIII*, Zurich, Switzerland Abstract 125, 2001.

Figure 1. Mean (SD) normalized EMG for each muscle. Data were normalized to the peak EMG at 50 rpm. Exp.1 refers to data from Martin et al. [4]. Expt. 2 NB refers to data from this study, no brace condition, and Exp. 2 B refers to data from this study, when the cyclists wore the ankle-foot- orthosis.

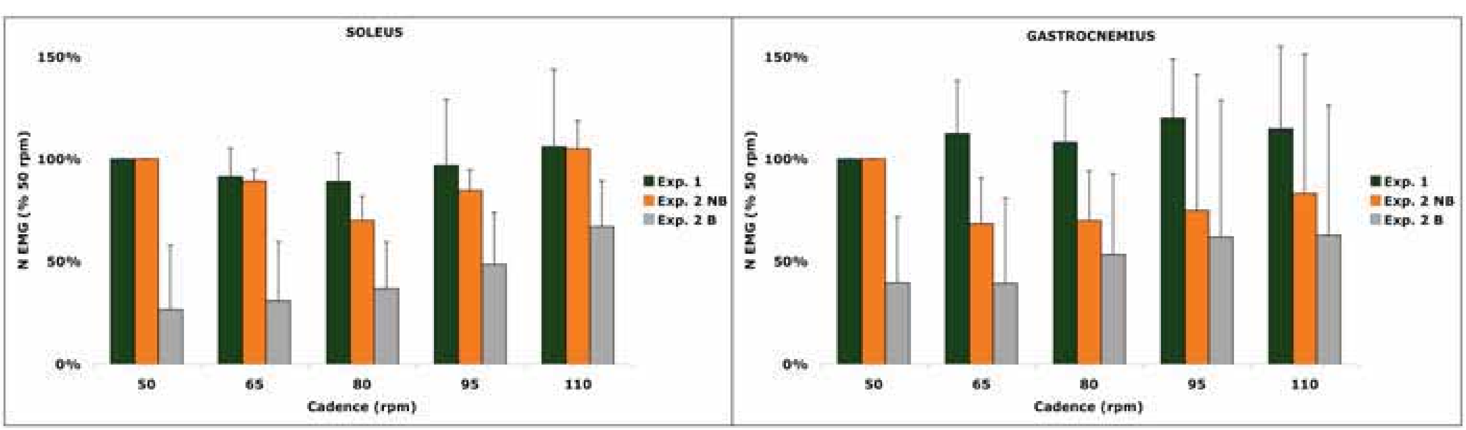

ACCEPTABLE PEAK FORCES AND IMPULSES DURING MANUAL HOSE INSERTIONS

[1]David Andrews, [1]Jim Potvin, [1]Christina Calder, [1]Joel Cort, [1]Heather Loree, [2]Michael Agnew, and [3]Allison Stephens
[1]University of Windsor, Windsor, ON, Canada; [2]Queen's University, Kingston, ON, Canada
[3]Ford Motor Company, Dearborn, Michigan, USA; email: dandrews@uwindsor.ca

INTRODUCTION

Tasks including drilling [1], gripping [2], automobile trim installation [3], and the mating of electrical connectors [4], have been studied recently using psychophysical approaches. However, no study to date has determined the forces that workers find acceptable during manual engine hose installations, even though hose failure in automobiles can in part be attributed to incorrect assembly practices [5].

METHODS

Five women in each of 3 age groups (20 year olds (1.72 (0.07) m; 65.1 (7.9) kg), 30 year olds (1.66 (0.06) m; 72.9 (8.6) kg), and 40+ year olds (1.62 (0.08) m; 82.1 (12.7) kg)), had no previous upper limb injuries or experience with hose insertion tasks, and signed a consent form accepted by the University of Windsor Research Ethics Board.

A tri-axial load cell was mounted to a hose insertion jig supported by an angle iron frame. An ABS plastic hose (length 15.5 cm, diameter 3.8 cm) surrounded a hardwood dowel and base plate that was anchored to the load cell. The jig and load cell could swivel and be adjusted for height. The angle iron frame was mounted to the concrete floor of the lab.

Subjects in each age group were randomly assigned to 9 of 15 total conditions for posture (Lateral Push-Far (LPF), Lateral Push-Near (LPN), Midline Push (MPush), Midline Pull (MPull), and Push Down (PD)), and frequency (1, 3, and 5 insertions/minute. Each subject trained for a total of 24 hours (2.67 hours per posture/frequency condition), and was tested for 3 hours (0.33 hours per condition). Posture conditions were randomly presented. Subjects heard a signal at the set frequencies, via an earphone, after which they applied force to the hose using a power grip until the next signal was presented (750 ms). Subjects applied the maximum force that they found acceptable for 8 hours without feeling fatigued or discomfort. MVCs were executed in each posture.

Force data were A/D converted using a 12-bit card and sampled by computer at 1000 Hz using custom LabVIEW software. Signals were amplified and filtered with a dual pass Butterworth digital filter (f_c = 15 Hz). A total of 1250 samples (1.25 s) of data were collected for each trial: 500 pre-trigger samples, and then 750 samples following the trigger. Data from the last 20 minutes (0.33 hours) of testing in each condition were analyzed.

ANOVAs were performed on mean acceptable peak force (APF), %MVC force, and impulse, with posture and frequency as between subject factors. Tukey/Kramer post hocs were performed for all significant effects ($\alpha = 0.05$).

RESULTS AND DISCUSSION

Significant main effects of posture and frequency were found ($p < 0.0001$ and $p < 0.03$, respectively) for APF. A significant main effect of posture only was found ($p < 0.0001$) for acceptable impulse. The MPull posture condition resulted in the greatest mean APF and impulse, with the lowest seen in the LPF condition. An average decrease of approximately 17% and 13.4% was shown in mean APF and impulse, respectively, as frequency increased from 1 to 5 insertions/min. Average within-subject coefficients of variation (CV) for APF and impulse ranged from 7.2% to 11.2%, and from 5.6% to 9.9%, with means across all conditions being 9.0% and 8.1%, respectively. There were no significant main effects or interactions of posture or frequency for %MVC values. At a frequency of 1/min, subjects selected acceptable forces that were in the range of 63% MVC for each posture, despite the variable physical demands in the different conditions. Fairly comparable levels of APF (as a %MVC) have also been seen in other psychophysical studies in our laboratory involving the hand [4,6].

The results of well-trained novice subjects have been shown in the past not to differ from actual workers using a psychophysical approach [3]. In the current study, each subject executed 4860 trials in training and testing on average. Mean within-subject CVs were low in general and comparable to those reported elsewhere [3,4], suggesting that subjects were consistent and that training was adequate.

Posture conditions used in this study reflected the orientation of the upper limb and not just the wrist or the grip type, as reported in previous work [1]. The LPF posture put increased load on the operators' shoulders, compared to other orientations, as they supported the mass of their extended upper extremity and also applied force to the hose. This likely factored into subjects' decisions to accept less insertion force in this condition. The MVC data support this, with average maximal forces for the LPF condition being the lowest of the postures at 87.0 (±19.2) N.

The decreasing trend in APF and impulse, as frequency increased, is similar to previous work [3]. Declines in maximum APF (and torque) as frequency increases, have been shown in the literature for other tasks that have utilized power grips in a variety of posture conditions [1].

CONCLUSIONS

This is the first study that has quantified APFs and impulses associated with engine hose insertions. Consistent %MVC forces seen across the variety of tested conditions compares favorably with other investigations of hand-intensive mating operations in automobile assembly, and will enable assessments of hose insertion tasks not explicitly tested in this study.

REFERENCES

1. Kim CH, et al. *Int J Ind Erg* **12**, 209-218, 1993.
2. Dahalan JB, et al. *Int J Ind Erg* **12**, 219-230, 1993.
3. Potvin JR, et al. *Int J Ind Erg* **26**, 625-637, 2000.
4. Potvin JR, et al. *Proceedings of CSB*, Halifax, NS, 2004.
5. Mramor R. *Hydraulics & Pneumatics*, Sept., 47-50, 2000.
6. Longo N et al. *Proceedings of ACE*, Banff, Alberta, 2002.

FUNCTIONAL AND STRUCTURAL CERVICAL SPINE DYSFUNCTIONS WITH TEMPOROMANDIBULAR DISORDERS

Ângela Viegas Andrade and Luci Fuscaldi Teixeira-Salmela
Department of Physical Therapy, Federal University of Minas Gerais, Brazil; email: aviegas.bhe@terra.com.br

INTRODUCTION

The incidence of temporomandibular disorder (TMD) has increased and has become a concern for various health professionals [1,2]. The relationship between TMD and cervical spine structural disorders has only been modestly demonstrated [2,3]. The objective of this study was to investigate functional and structural alterations of the head and neck with 17 TMD and 17 age and gender-matched asymptomatic individuals, using a cross-sectional design

METHODS

Functional measures included scores on the temporomandibular index (TMI)[1] and of pain palpation of the superior trapezius, sternocleidomastoideus, and suboccipital muscles assessed by scores on the visual analog scale. Structural assessment of the cervical spine included radiographic measures of lordosis [2], determined by the methods of Cobb and Harrison, as well as the position of the hyoid bone [3]. All radiographic images were digitized using the Autocad software.

Descriptive statistics and tests for normality were carried out for all variables. Student *t*-tests for independent samples with Bonferroni correction were used to investigate differences between groups for all variables, with a significance level of α<0.02. Pearson correlation coefficients were calculated to investigate the relations between cervical alignment measures.

RESULTS AND DISCUSSION

Seventeen subjects (16 female and one male) with a mean age of 23.5 ± 3.6 years comprised the TMD group.

As illustrated in Figure 1, individuals with TMD, when compared with asymptomatic subjects, presented higher scores in total TMI and its indexes (t=11.09; p<0.0001), with the muscular index showing the greatest differences. They also demonstrated higher levels of perception of pain for all cervical muscles (p<0.0001).

Even though no significant differences between groups were found, as shown in Table 1, the TMD subjects presented less cervical lordosis when compared with the reference values of 17° and 26° for the Cobb and Harrison methods [3]. These findings suggest an association between TMD and alterations of alignment of the cervical column, indicating

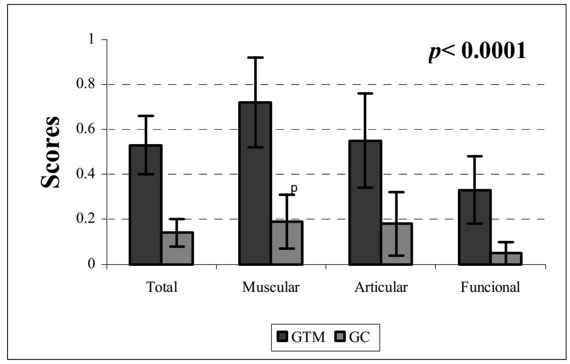

Figure 1: Means (± SD) of the ITM and its indexes

that the cervical column should be evaluated in the presence presence of TMD.

The position of the hyoid in relation to the cervical column was stable, indicating that its position was not influenced by TMD. In that the Cobb and Harrison measures revealed a strong correlation (r=0.82; p<0.0001), it is suggested that either measure can be used to evaluate cervical spine alignment

CONCLUSIONS

The present findings demonstrated that subjects with TMJ demonstrated functional cervical dysfunctions and decreased cervical lordosis, suggesting that cervical assessment should always be performed in the presence of TMJ. Either method, Cobb or Harrison´s, may be used to assess cervical spinal alignment.

REFERENCES

1. Pehling J, et al. Interexaminer reliability and clinical validity of the temporomandibular index : A new outcome measure for temporomandibular disorders. *J Orofacial Pain* **16,** 296-304, 2002.
2. Harrison DE et al. Cobb method or Harrison posterior tangent method : Which to choose for lateral cervical radiographic analysis? *Spine* **25**, 2072-79, 2000.
3. Henriquez J, et al. Anatomia rediológica del hueso hioides. *Rev Chilena Anat* **18**, 149-53, 2000.

Table 1: Means (± SD) of the Structural Measures for both Groups

	Variable	DTM (n=17)	Control (n=17)
Cervical lordosis (deg)	Cobb	9.08 ± 8.05	7.63 ± 10.96
	Harrison	17.40 ± 8.66	16.73 ± 9.73
Hyoid bone position (cm)	Horizontal	3.09 ± 0.28	3.04 ± 0.31
	Vertical	-0.40 ± 0.53	-0.37 ± 0.42

RELATIONSHIPS BETWEEN ILIOTIBIAL BAND LENGTH AND FRONTAL PLANE PELVIC TILT

Christina Danielli Coelho de Morais Faria, Luci Fuscaldi Teixeira-Salmela, Fabiana Fernandes Pereira Lima
Department of Physical Therapy, Federal University of Minas Gerais, Brazil; email: jhsalmela@hotmail.com

INTRODUCTION

The position of the pelvic bone is the key for the postural alignment [1]. Both structural and functional factors may be associated with lateral pelvic tilt [2], one of them being the length of the iliotibial band [1,3]. A lateral pelvic tilt could modify the position of several body structures, overload them, and, thus, causing compensations, dysfunctions and pain [1,3].

Therefore, the aim of this study was to investigate the degree of association between the length of iliotibial band and the frontal plane pelvic tilt.

METHODS

Healthy individuals with no leg-length differences and without pelvic torsion were included in the study. The modified Ober test, performed with a pelvic level and an inclinometer, was used to assess the iliotibial band length. Before data collection, a test-retest pilot study was conducted to determine the reliability of the measurements.

Measures of pelvic alignment were obtained with an anthropometer with the individual positioned on standard support equipment.

Intra-class correlation coefficients were used to investigate intra-rater reliability. The Pearson correlation coefficient was calculated to determine the degree of association between the measure of pelvic alignment in the frontal plane and that of the iliotibial band length. Pelvic alignment was determined by differences in height between the anterior superior iliac spines, whereas the length of the iliotibial band was established by differences between the higher and lower anterior superior iliac spines. The level of significance was set at $\alpha<0.05$.

RESULTS AND DISCUSSION

Thirty-two subjects, 19 women and 13 men (mean age: 22.5 ± 2.6 years) were included in the study. The means, standard deviations, and the intraclass correlation of the measures obtained during the test-retest are presented in Table 1 and demonstrated adequate intra-rater reliability (ICC>0.99).

Descriptive values of the variables obtained to investigate the degree of association between the iliotibial band length and pelvic alignment are presented in the Table 2. No significant correlation was found (r =0.12; p=0.53).

The assumption that pelvic biomechanical disorders lead to pelvic positiining asymmetries is still not completely understood. A possible explanation relies on soft tissue disfunctions [4], mainly of iliotibial band [1,3]. However, the present findings did not provide evidence of significant correlations between pelvic alignment and length of iliotibial band.

These results suggest that alterations in length of the iliotibial band, measured by the modified Ober test, alone does not appear to directly influence pelvic alignment and, thus, might not be a relevant outcome measure for assessment and treatment of pelvic dysfunctions. However, these results should be interpreted cautiously, since only healthy subjects were included.

CONCLUSIONS

Although measures of iliotibial band length showed to be highly reliable, they showed no functional relationship. The present findings indicated that iliotibial band length alone does not appear to influence frontal plane pelvic alignment and that other factors may be involved that still need to be identified.

REFERENCES

1. Kendall FP, McCreary, E K, Provance, P G. *Músculos provas e funções (*4th ed.). São Paulo: Manole, 1995.
2. Badii M, et al. Pelvic bone asymmetry in 323 study participants receiving abdominal CT scans. *Spine* **28,** 1335-1339, 2003.
3. Sahrmann SA, *Diagnosis and treatment impairment syndromes***,** St. Louis : Mosby, 2002.
4. Piva SR, et al. Reliability of measuring iliac crest level in the standing and sitting position using a new measurement device. *J Manipulative Physiol Ther* **26**, 437-441, 2003.

Table 1: Means (± SD) and intraclass correlation (ICC) values of the measures obtained during the test-retest (n=20)

Variable	Measure 1 (cm)	Measure 2 (cm)	ICC
Leg Length	87.23 ± 4.23	87.25 ± 4.27	0.999
Modified Ober test	24.32 ± 4.18	24.3 ± 4.27	0.995
Iliac spine height	96.66 ± 5.27	97.27 ± 5.72	0.994

Table 2: Means (± SD) and range values of the variables used to investigate the correlation (n=32)

Variable	Mean (± SD)	Range
Differences in height between the anterior superior iliac spines	0.54 ± 0.,44	0 – 2.0
Differences between the length of iliotibial band	0.88 ± 4.54	-8.00 – 11.75

Mechanical Properties of Relaxed and Contracted Thigh Muscles using Magnetic Resonance Elastography

[1] Sabine Bensamoun, [1] Stacie Ringleb, [1]Qingshan Chen, [2]Richard Ehman, [1]Kai-Nan An
[1] Biomechanics Laboratory, Division of Orthopedic Research, Mayo Clinic, Rochester, MN 55905
[2] Department of Radiology, Mayo Clinic College of Medicine, Rochester, MN 55905

INTRODUCTION

The determination of the mechanical properties of muscle in passive and active conditions may characterize the physiological changes within the muscle [1]. Thus, the measurement of the *in vivo* mechanical properties of muscles is clinically necessary in order to understand the transformations that occur in muscle with pathologies and treatments. A few techniques (palpation, sonoelastography, elastography) allow measurement of the *in vivo* stiffness of soft tissues but, they are restricted in depth and field of view. Magnetic Resonance Elastography (MRE) is a non-invasive phase contrast MR technique capable of quantifying the *in vivo* mechanical properties and imaging the entire spatial distribution of muscle elasticity [2]. The purpose of this study was to measure the mechanical properties of the vastus lateralis (VL), vastus medialis (VM) and sartorius (Sr) muscles in a relaxed and contracted position.

METHODS

Fourteen volunteers (4 males and 10 females, mean age 25.2 ± 1.78) participated in this MRE study. The volunteers lay supine in a 1.5T General Electric Signa MRI with the right leg resting in a custom MR compatible leg press, capable of measuring the applied load. Shear waves were applied to the thigh muscles with a mechanical (n=7 VL, n=10 VM, n=9 Sr) or pneumatic driver (n=5 VL, n=4 VM, n=4 Sr). Each driver was positioned on the thigh 1/3 of the distance from the patellar tendon to the greater trochanter. The mechanical driver was composed of a coil of copper wire with a hollow aluminum core driven with an alternative current of variable potential, induced shear waves into the thigh muscles at 120Hz. The pneumatic driver was composed of a thin silicone tube connected to a remote pressure driver (i.e., a large active loudspeaker). This system created a time varying pressure wave, which caused the tube around the thigh to expand and contract with the remote driver at 90 Hz. A custom-made Helmholtz surface coil was placed around the thigh. Axial images were obtained and oblique scan planes passing through the VL, VM and Sr were selected from these images. MRE data were collected with a gradient echo technique. The wavelength (λ) was measured in each of the four offsets and the stiffness was calculated ($\mu = \rho * \lambda^2 * f^2$, where ρ=1000 kg/m^3).

RESULTS AND DISCUSSION

Figure 1 showed shear waves propagating in the vastus medialis (VM) and sartorius (Sr) muscles.

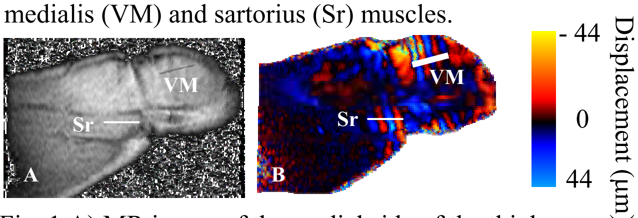

Fig. 1 A) MR image of the medial side of the thigh.
B) Shear waves in the medial side of the thigh

The shear modulus measured at rest (Fig. 2) in the vastus lateralis, vastus medialis and sartorius were 3.73 ± 0.85kPa (VL), 3.91 ± 1.15kPa (VM) and 7.53 ± 1.66kPa (Sr). The stiffness of the sartorius is significantly higher than the vastis stiffness. This may indicate that that the propagation of the waves was influenced by the muscle fiber orientation. The fiber orientation is unipennate in the vasti, while it is longitudinal in the sartorius.

During a thigh contraction of 10% MVC, the stiffnesses of the VL and the VM were 6.11 ± 1.15kPa (P<0.1) and 4.83 ± 1.68kPa, respectively. A faster increase of stiffness was measured for the VL than for the VM. This may be due to a larger percentage of fast fibers in the VL enabling a faster contraction.

With a level of 20% MVC, the stiffnesses of the VL and the VM were 8.49 ± 4.02kPa and 6.40 ± 1.79kPa (P<0.1), respectively. For both levels of contraction, the stiffness of the sartorius muscle did not exhibit any changes. This may be due to the leg press, which solicits the knee extensors while the sartorius flexes the knee.

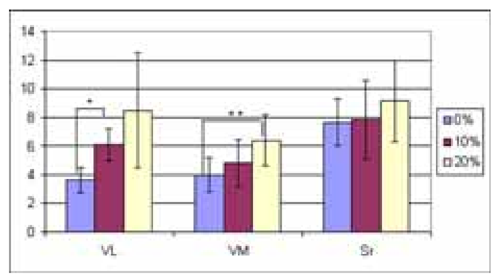

Fig 2. Representation of the muscle stiffness in a relaxed and contracted positions

CONCLUSIONS

We concluded that the MRE technique is able to quantify the stiffness of thigh muscles. Furthermore, the wave length was sensitive to the morphology and fiber composition in each muscle. The MRE technique could be a helpful means to non-invasively improve diagnosises and to understand the effects of pathologies such as Graves Disease which effects proximal muscle strength by changing the composition of the muscle fibers [3].

REFERENCES

1. Masson P, Biophys. *Struct. Mechanism*.4, 15-25, 1978.
2. Jenkyn TR, et al. *J Biomech*. **36**, 1917-1921, 2003.
4. Brennan MD, et al. American Thyroid Association Annual. Washington DC, 2001.

ACKNOWLEDGEMENTS

This study was funded by NIH Grant # and EB00812, EB01981 and CA91959 and Association Française contre les Myopathies (AFM). Special thanks to Thomas Hulshizer and Philip Rossman of the MR Research Laboratory for their technical assistance.

INFLUENCE OF THIGH MARKER CLUSTER DESIGN ON THE ESTIMATION OF HIP AXIAL ROTATION

[1] Anthony Schache, [1] Richard Baker and [2] Larry Lamoreux
[1]Murdoch Childrens Research Institute & Hugh Williamson Gait Laboratory, Royal Children's Hospital, Australia
[2]Gait Dimension, Benicia, California; email: anthony.schache@mcri.edu.au

INTRODUCTION

Measurements of hip axial rotation are prone to considerable error [1]. Given the degree of soft tissue mass surrounding the femur, it is likely that most of this error is a consequence of soft tissue artifacts associated with markers mounted on the thigh. Therefore, the purpose of this study was to evaluate various thigh marker cluster configurations with a view to optimising the estimation of hip axial rotation.

METHODS

Five able-bodied adults (4F; 1M) participated in this study. Mean age, height and body mass were 23.7 years (SD 6.9), 164.9 cm (SD 2.9) and 58.1 kg (SD 7.4) respectively. Ethical approval was obtained prior to commencement. Reflective markers were placed over the pelvis, thigh and shank. A thigh wand fixed to a thermoplastic base plate was firmly mounted on the thigh using circumferential straps. Four different thigh clusters were then configured as defined in Figure 1 (see legend). Three were non-rigid (clusters A, C & D) and one was rigid (cluster B). Cluster A corresponded to the Helen Hayes marker set up. The HJC was estimated from the pelvic markers [2]. Clusters B, C and D were mounted distally on the thigh to optimise rigidity with the underlying femur [1].

A VICON motion analysis system (Oxford Metrics Ltd.) was used to capture 3D kinematic data (120 Hz). A static calibration trial was first captured to define the relationship between all clusters (technical frames) and the relevant anatomical frames. Subjects then performed two tasks: normal gait at a self-selected speed and isolated longitudinal rotation of the lower limb. For the latter task, the test subject stood with the test limb on a ball-bearing turntable and the knee extended. Subjects rotated the test limb about its long axis by internally and externally rotating the hip. As the knee does not permit axial rotation when extended and soft tissue movement in the shank is not expected during this task, markers on the tibia were used to represent true axial rotation of the femur.

Hip axial rotation patterns during gait, as measured from the different thigh clusters, were compared for similarity using the coefficient of multiple determination (CMD or r^2) statistic. Regression analysis was used to describe the relationship between estimated (thigh cluster) and true (tibial markers) hip axial rotation for the isolated longitudinal rotation task. Analyses were performed for the left and right side independently and results were averaged.

RESULTS AND DISCUSSION

Hip axial rotation during gait was highly sensitive to thigh marker cluster design (Figure 1). The mean CMD value was 0.34 (SD 0.29) indicating quite poor similarity between clusters. All clusters underestimated true bone movement during the isolated longitudinal rotation task (Figure 2). Mean regression coefficients were 0.46 (SD 0.06), 0.60 (SD 0.05), 0.56 (SD 0.07) and 0.56 (SD 0.07) for thigh clusters A, B, C and D respectively. This indicates that marker clusters on the distal thigh were only capable of estimating, at best, up to 60% of the true magnitude of movement. When comparing the different clusters, the Helen Hayes convention (cluster A) was associated with the greatest degree of error. Clusters C and D produced near identical results. Thus, the addition of the thigh wand in cluster C had no measurable influence. Clusters C and D tended to produce hip axial rotation patterns during gait that were more systematic across subjects when compared to clusters A and B.

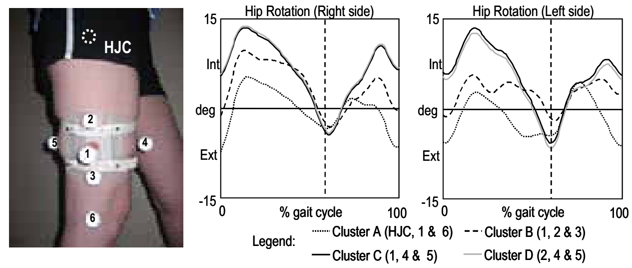

Figure 1 Hip axial rotation during gait as measured using the different thigh marker clusters for a typical subject.

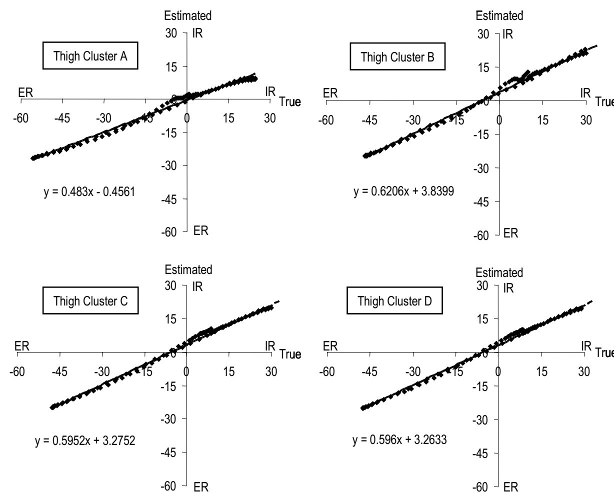

Figure 2 Estimated (thigh cluster) versus true (tibial markers) hip axial rotation during right-sided longitudinal rotation for a typical subject.

CONCLUSIONS

The estimation of hip axial rotation was highly sensitive to thigh marker cluster design. Whilst none of the clusters were capable of satisfactorily estimating true bone movement, clusters C and D appear to be better alternatives than clusters A and B. Until further work provides a definitive solution, one must remain cautious when using estimates of hip axial rotation for purposes of research or clinical interpretation.

REFERENCES

1. Lamoreux LW. *Proceedings of ISB XIII*, Perth, Australia, 1991, pp 372-373.
2. Davis RB et al. *Hum Mov Sci* 10; 1991, pp 575-587.

COORDINATION CHANGE BETWEEN GAZE, HEAD AND HIP DUE TO EARLY EYE ROTATION DURING OPEN CUT MANEUVER

[1]Akifumi Kijima, [2]Koji Kadota, [3]Noriyuki Tabuchi, [4]Tomoyuki Matsuo and [4]Ken Hashizume
[1]Department of Health and Sport Sciences, Fukuyama Heisei University, [2]Osaka University of Health and Sport Sciences,
[3]Graduate School of Human Sciences, Osaka University, [4]School of Health and Sport Sciences, Osaka University
e-mail: kijima@heisei-u.ac.jp

INTRODUCTION

The integration of visuo-vestibular information achieved by eye-head synergy (vestibulo-ocular reflex), is presumed to play an important role in postural control, as it provides a frame of reference for a postural control system [1]. The frame of reference refers to the set of values to which each motor variable refers for planning their own movement. This hypothesis has been supported by previous data demonstrating that the eye-head rotation led to a change in the direction of gravitoinertial acceleration in curvilinear walking [2], or a trunk lateral rotation in a sudden direction change of locomotion (i.e., cutting maneuvers) [3]. However, previous studies have never confirmed that eye-head synergy solely integrates visuo-vestibular information and governs whole body movements.

Subsequently, we tested whether eye-head synergy occurs even when the gaze was experimentally constrained to rotate earlier than in a natural setting. If eye-head synergy exclusively acts to integrate visuo-vestibular information, an early rotation of the head would be emphasized, as it minimizes angular deviation between the eye and the head.

METHODS

Five healthy graduate students were asked to walk a distance of 1.95 m with 2 steps, and cut into one of two directions (60 degrees to the left and right) or step straight ahead. The direction of cut is indicated by a semicircular array with a radius of 0.93 m consisting of 16 LEDs, which was placed at the subjects' eye level.

In the control condition (CNT), the subjects were instructed to start walking straight toward the center of the circular LED array and then step onto the right mat with a cross-over step when the right 8 LEDs placed at 0 to 90 degrees lateral to the approaching direction were turned on. The left 8 LEDs indicated that the subject should step onto the left mat with an open step, and the 8 center LEDs indicated that they should step straight ahead. The timing of the LEDs' onset was controlled by the (left) heel strike of the first approaching step. Eight trials were made for each direction in a randomized order.

To investigate the effects of compulsorily induced lateral gaze rotation, we conducted 24 additional trials for the EHR (eye-head rotation) condition, in which 2 of 8 LEDs located in the cutting direction (i.e., at 54 and 66 degrees) were turned on or off at 0 or 0.5 s after the LEDs' onset. The subjects were required to report when these 2 LEDs turned on or off (e.g., "At first, LEDs turned on (off) and then off (on)"; "remained on (off)"). The lateral rotation of the head, shoulder, and hip as well as that of the left eye during the left open cut maneuver was measured using 4 infrared cameras (ProReflex motion capture unit, Qualysis Medical, Sweden) and a video-based eye-mark recorder (EMR-8, Nac Image Tech., Japan) at a sampling rate of 60 Hz. The lateral angular displacement of the gaze was calculated by summing the lateral rotation of the eye in the orbit and that of the head in space.

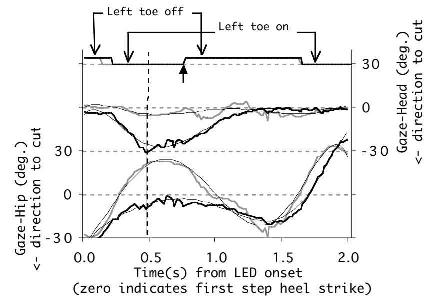

Figure 1: Deviation of angular displacement between Gaze-Head (middle) and Gaze-Hip (bottom) in CNT (gray) and EHR (black)
Thin line on each plot represents a curve fit by a polynominal. Rectangular plot shown on top indicates the timing of left toe contact on the ground. Small upward arrow indicates the timing of the open step onset. Vertical broken line at 0.5 s indicates the timing on which 2 LEDs turned on or off. Mean of 8 trials perfomed by a typical subject.

RESULTS AND DISCUSSION

In the EHR trials, the timing of the saccade onset was concentrated at 0.5 s after the LED onset in order to fixate on the 2 lighting LEDs placed in the cutting direction. The head rotation was not observed in this phase. The saccades in the CNT trials were immediately followed by head rotation, and the timing of those onsets ranged widely from 0.5 to 1.0 s after the LED onset. Thus, the manipulation undertaken in the EHR trials succeeded in guiding the earlier onset of saccade and disturbed eye-head synergy.

An angular deviation of the head relative to the gaze was kept approximately at 0 degree, that is, the eye-head synergy was maintained in every phase in the CNT trials, as reported in a previous study [2]. On the other hand, in the EHR trials, not the head, but the hip was aligned in the gaze direction when the eye fixated on the cutting direction at 0.5 s after the LED onset, following which the head rotated to align in the gaze direction (Figure 1). The results observed in the EHR trials indicate that not only eye-head but also gaze-hip coordination could be employed to integrate visuo-vestibular information.

These results suggest that it is also necessary to achieve the frame of reference for the open cut maneuver. Further, as suggested in a previous study about postural control [1], the strategy for this function is altered or compensated by body segments below the head due to the gaze constraint. We speculated that the earlier rotation of the head relative to the trunk presented in the previous analysis of cutting maneuvers [3] is a part of this dynamic nature of the mechanism to maintain a stable frame of reference.

REFERENCES

1. Berthoz, A and Pozzo, T. *Head and body coordination during locomotion and complex movements.* In S. P. Swinnen et al. (Eds.) *Interlimb Coordination*, 147-165, Academic Press, San Diego, 1994.
2. Imai T, et al. *Exp Brain Res* **136**, 1-18, 2001.
3. Hollands, M. A. et al. *Exp Brain Res* **140**, 223-233, 2001.

ANALYSIS OF THE APPROACH RUN AND THE TAKEOFF IN THE JAPANESE JUNIOR LONG JUMPERS

Ikko Omura[1], Akira Iiboshi[2], Hiroyuki Koyama[3], Yuya Muraki[3], Michiyoshi Ae[4]
[1]Shigakukan Univ., Kagoshima, Japan, [2] Kagoshima Univ., Kagoshima, Japan.
[3]Tsukuba Univ. Grad. School, Ibaraki, Japan. [4]Tsukuba Univ., Ibaraki, Japan email: ioomura@shigakukan.ac.jp

INTORDUCTION

The approach run and the takeoff in the long jump are important factors to determine the distance of the jump. Many studies on the approach or the takeoff in the long jump had been done. Recently, Omura et al. [2, 3] have focused on the characteristics of the step frequency, step length, support time, non-support time and visual control [1] during the approach run to investigate the effective approach run. They reported that Japanese junior long jumpers showed the unsteady step frequency during the approach run, and the longer non-support time during the last three or four steps compared to the Japanese top long jumpers. However, more studies are needed to discuss proper approach run for the junior long jumpers.

The purpose of this study was to investigate the approach run of Japanese junior long jumpers to obtain the fundamental findings on effective approach run and the takeoff.

METHODS

Sixteen boy's long jumpers, with personal best records ranging from 7.17m to 7.87m, were filmed at the final of 2003 and 2004 Japan High School Track & Field Championships by the Biomechanical Project team of the Japan Amateur Athletic Federation. Two digital video cameras were used in this study. One camera was placed at the stands sideway to the runway, and filmed the whole of the steps of the approach (60f/s). All the trials of each jumper were analyzed using FRAME DIAS system (DKH Co., Japan), and calculated step length, step frequency, support time, non-support time. The visual control was calculated from standard deviation of the horizontal distance from the toe of the support foot to the front edge of the takeoff board (i.e. the toe-board distance) [1]. Another camera was placed at a distance of 20m perpendicular to the takeoff board, and filmed the jumpers from the 3rd last steps to takeoff (60f/s). The best performance of each jumper was analyzed, and the several joint angle & angular velocities were calculated. Approach velocities were measured with Laveg Sport (Henley Japan co., Japan)

RESULTS AND DISCUSSION

The approach velocities of the top three jumpers (ranging from 10.3m/s to 10.4m/s) were higher than those of the other junior long jumpers. However, the values were lower than those of the Japanese top jumper (10.8m/s; 8m18) and the World's class jumper (Phillips; 11.0m/s, 8m31). Furthermore, most of the jumpers (including two of top three jumpers) decreased their approach velocities prior to the takeoff. From these results, Japanese junior long jumpers should improve their approach velocity and the preparatory motion for the takeoff.

Hay[1] investigated how the elite long jumper use a visual control strategy, based on the data for the horizontal distance from the toe of the support foot to the front edge of the takeoff board (i.e. the toe-board distance).

As for the visual control in present study, the maximum value of the standard deviation was recorded from the 3rd last stride to the 12th last stride, and the maximum frequency was recorded at the 3rd last stride (five jumpers). Hay [1] revealed that the maximum value of the standard deviation was recorded from the 1st last stride to the 8th last stride, and the maximum frequency was recorded at the 5th last stride for the elite long jumpers. Such a difference between the Japanese junior jumpers and the elite long jumpers reported by Hay might be due to the difference of the physical ability, approach velocity, and the performance level. Hay [1] also established the standard value for assessment of the approach run. According to his study on the elite long jumper, the maximum standard deviation of 0.20m or less was classified as "very good", and that of 0.25m or more was classified as "poor". In this study, more than the half of the jumpers (nine of sixteen jumpers) showed the maximum standard deviation of 0.25m or more (poor), and the maximum value of the junior jumpers was 0.47 m. These results suggested that the approach run of the junior long jumpers were unstable; therefore they have to spend more time to improve and stabilize their approach run.

The peak angular velocities of the free leg during the takeoff for the top three junior jumpers were greater than those of other junior jumpers. And also, the peak angular velocity was observed at the similar phase for the elite long jumpers. These free leg movements for the top three junior jumpers might be effective to obtain the distance of jump. Therefore, it is conceivable that they had mastered the proper technique for the takeoff.

REFERENCES

1. Hay J. G. *Approach Strategies in the Long Jump*, INTERNATIONAL JOURNAL OF SPORT BIOMECHANICS 4, 114-129, 1988.
2. Omura et al. *An analysis of the approach run for the junior long jumpers in the 2001 inter high school game*. XVIIth JSB Congres, Nagoya, Japan, abstract 98-99, 2002.
3. Omura et al. *Analysis of the approach run for the junior boy's long jumpers in the 2003 inter high school game*. XVIIIth JSB Congres, Kanoya, Japan, 2004, abstract(in printing)

DIFFERENCES IN CENTER OF PRESSURE MOVEMENT BETWEEN BOYS AND GIRLS DURING ONE-FOOTED LANDINGS

[1,2]Michelle Sabick, [1]Kristi Unholz, [3]Jeanie Sutter and [1,3]Ron Pfeiffer
[1]Center for Orthopaedic & Biomechanics Research, [2]Department of Mechanical Engineering,
[3]Department of Kinesiology, Boise State University, Boise, ID USA; email: MSabick@boisestate.edu
web: coen.boisestate.edu/cobr

INTRODUCTION

The effects of gender on lower extremity mechanics during landing have been studied extensively in adults, but little is known about landing mechanics in preadolescent populations. By studying landing strategies in preadolescent children, body morphology differences between the genders are essentially eliminated. Hass et al. [1] found that prepubescent females landed with their hips and knees more flexed than post-pubescent females. These results hint that age related morphology changes play a role in landing strategies, at least within female subjects.

Movement of the body's center of pressure (COP) is often used as a measurement of postural stability [2]. The purpose of this study was to determine whether gender in preadolescent soccer players affects postural stability during one-footed landings. To our knowledge, this is the first study to examine the effects of gender in any age group on postural stability during landing.

METHODS

Twelve girls and 11 boys (10 - 12 years of age) were recruited from a local youth soccer league. Subjects dropped from a horizontal bar (net drop 30.5cm) landing barefoot on one leg. The test leg was randomized. The landing surface was a force platform sampling at 1250 Hz. Each subject performed 5 to 10 trials and the first five successful trials were analyzed.

The location of the center of pressure (COP) on the force platform was calculated using the equations provided by the manufacturer (Kistler) for a duration of 100 ms from the time of first contact with the force platform. Displacements and velocities of the COP in the anterior-posterior (D_{A-P}, V_{A-P}) and medial-lateral (D_{M-L}, V_{M-L}) directions, and the mean velocity of COP displacement (V_m) were calculated [3]. Comparisons of kinetic variables between the two groups were made using two tailed Student's t-tests with an α level of 0.05.

RESULTS AND DISCUSSION

While age, height, and weight were not significantly different between groups, the COP displacement and velocity measures tended to be higher in the boys than in the girls (Table 1).

Figure 1: Comparison of COP paths in subjects with low Vm (left) and high Vm (right).

Displacement and velocity in the medial-lateral direction were significantly greater in the boys than in the girls. V_m was also significantly greater in the boys.

Higher values for displacement or velocity of the COP are considered evidence of postural instability [2]. Therefore, it appears that our group of boys were less stable during landing than the girls. Many subjects in both groups appeared to have a difficult time landing and balancing on one foot. Subjects that exhibited low V_m values tended to stabilize within the first 100 ms after contacting the force platform (Figure 1), while many subjects didn't stabilize within that time frame.

CONCLUSIONS

It is not clear whether the boys exhibited greater postural instability during the first 100 ms after landing, or whether they were merely more comfortable using a larger proportion of their base of support. Qualitative evaluation of the COP curves suggested that fewer of the boys reached a stable position within 100 ms than did their female counterparts.

REFERENCES

1. Hass CJ, et al. *J Appl Biomech*, **19**, 139-152, 2003.
2. Murray MP, et al. *J Bone Jt Surg*, **57A**, 510-516, 1975.
3. Raymakers JA, et al. *Gait Posture* **21**, 48-58, 2005.

ACKNOWLEDGEMENTS

Special thanks to Kristof Kipp for his help with data collection and analysis.

	Age (yr)	**Height (m)**	**Weight (N)**	**D_{A-P} (m)**	**D_{M-L} (m)**	**V_{A-P} (m/s)**	**V_{M-L} (m/s)**	**V_m (m/s)**
Girls	11.3 ± 0.7	1.48 ± 0.07	357 ± 75	0.153 ± .038	0.048 ± .018	3.37 ± 1.05	1.45 ± 0.51	4.37 ± 1.38
Boys	11.4 ± 0.8	1.512 ± 0.06	379 ± 35	0.187 ± .054	0.081 ± .035	4.33 ± 1.31	2.21 ± 0.57	6.01 ± 1.95
p-value	0.92	0.31	0.46	0.08	**0.01**	0.06	**0.00**	**0.03**

Table 1: Comparison of demographic and COP data between the male and female groups.

Rheological behaviour and modeling of brain tissue

F. Shen[1], T. E. Tay[1], J. Z. Li[1], S. Nigen[1], P. V. S. Lee[2], H. K. Chan[2]
[1]Division of Bioengineering, National University of Singapore, 9 Engineering Drive 1, Singapore 117576
[2]Defence Medical & Environmental Research Institute, 27 Medical Drive, Singapore 117510
Email: biesf@nus.edu.sg

INTRODUCTION

In order to understand and predict the onset of human head injury due to traumatic impact loads, there is a need to develop realistic constitutive relations so that the biomechanical response of the brain may be modeled more accurately. Although brain tissue is rather complex, possessing both fluid- and solid-like properties, it is common to find simple linear elastic or viscoelastic models in applications such as the simulation of neurosurgery. These models are, however, inadequate in many dynamic impact situations such as automobile accidents, where large strains are often encountered. For example, Bain and Meaney[1] have proposed a threshold strain criterion of nearly 0.21 for axonal injury by comparing morphological injury and electrophysiological impairment to estimated tissue strains. Troseille *et al.* [2] found that a strain above 0.15 would result in irreversible brain injury and a strain above 0.2 could be fatal. These injury criteria are clearly beyond the linear elastic limit, usually taken to be about 1% strain (Brands *et al.*[3]). Therefore nonlinear viscoelastic models must be used for brain injury modeling and prediction.

In this paper, a non-linear model first proposed by Bilston *et al.*[4] is modified and implemented into a commercial finite element (FE) code. To obtain the required model parameters, rheological tests on mechanical properties of brain tissue are performed.

MODELING, TESTING AND IMPLEMENTATION

The proposed 3-dimensional constitutive model consists of three parts: the volumetric, deviatoric and viscoelastic stress components. The long-term elastic stress is modeled by the Mooney-Rivlin rubber model, which is commonly used for hyperelastic materials under large deformation. The upper convected multi-mode Maxwell model is used for the computation of the viscoelastic stresses. The deviatoric stress terms are further modified by a damping function, which is a function of strain invariants.

The parameters in the constitutive model are determined by performing various rheological experiments such as small strain oscillation tests, shear relaxation tests, and compression tests. Porcine brain tissue samples are tested by means of a conventional stress-controlled MCR 300 Paar-Physica rheometer. Furthermore, oscillatory shear tests (both strain and frequency sweeps) and relaxation tests are performed for material property characterization.

We further implemented the 3-dimensional nonlinear constitutive model into the multi-purpose commercial explicit FE code PamCrash. The user-defined material model MAT80

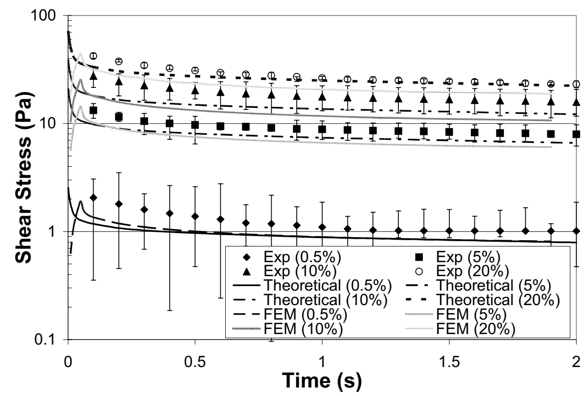

Figure 1: Shear relaxation: comparison between theoretical prediction, FE simulation and experiment

was used in the program. Simulation of the shear relaxation test is performed.

RESULTS AND DISCUSSION

Based on small strain oscillation test, a 12-mode Maxwell model is obtained by curve-fitting procedure. By applying Time-Temperature Superposition principle, the frequency regime is extended to 6 decades ($\omega=10^{-2}\sim10^{4}$rad/s). Shear relaxation tests with different amplitudes of shear strain are performed. A comparison between theoretical and numerical predictions and shear stress relaxation experiment is shown in Figure 1. Good agreement can be observed. Theoretical predictions are within the error bars up to a strain of 20%. Numerical predictions are slightly lower, about 20% lower than the averaged values for large strain case (20%).

CONCLUSION

A 3-dimensional nonlinear viscoelastic constitutive model for brain tissue is proposed and implemented into commercial FE code successfully. The predicted mechanical response of the brain tissue by the FE method show good agreement with shear stress relaxation test data. Combined with a proper head FE model, it is expected that the proposed brain tissue model can be used for head injury analysis.

REFERENCES

1. Bain AC, et al. *J Biomech Eng* **122**, 615-622, 2000.
2. Trosseille X, et al. 36th *Stapp Car Crash Conference Proceedings*, Seattle, WA, 1992.
3. Brands DWA et al. *Stapp Car Crash J* **44**, 249-260, 2000
4. Bilston LE, et al. *Biorheology* **38**, 335-345, 2001

ACKNOWLEDGEMENTS

The support of the Defence Medical & Environmental Research Institute is gratefully acknowledged.

NANOINDENTATION STUDY OF INTERFACES BETWEEN STRONTIUM-CONTAINING HYDROXYAPATITE BONE CEMENT AND BONE IN A RABBIT HIP REPLACEMENT MODEL

Ni GX[1], Lu WW [1], Ngan HW [2]
1 Department of Orthopaedics and Traumatology, The University of Hong Kong, Hong Kong
2 Department of Mechanical Engineering, The University of Hong Kong, Hong Kong, Hong Kong
Corresponding author: Lu WW, wwlu@hkusua.hku.hk

INTRODUCTION

Many bioactive bone cements were developed for total hip replacement, and found to bond with bone directly [1,2]. However, the mechanical properties at the bone/bone cement interface are not fully understood. The aim of the present study was to investigate the interfacial mechanical and morphological properties of newly formed tissue by nanoindentation and microscopic analysis.

METHODS

Unilateral hip replacement was performed with Sr-HA cement in rabbits. Six months later, the femurs were removed and cut into parallel sections. Observations were taken at the interface of Sr-HA cement and cancellous bone for metaphyseal sections and interface of Sr-HA cement and cortical bone at diaphyseal sections.

RESULTS AND DISCUSSION

For the interface between Sr-HA cement and cancellous bone, osseointegration was widespread. Many multinucleus cells covered the surface of the cement, and resorbed the superficial layer of the cement. New bone infiltrated into Sr-HA cement. An interface with a thickness of about 10 µm was found covered on the Sr-HA cement by scanning electron microscopy (SEM). By nanoindentation testing, sharp increase was found at the interface in terms of Young's modulus and hardness (Figure 1).

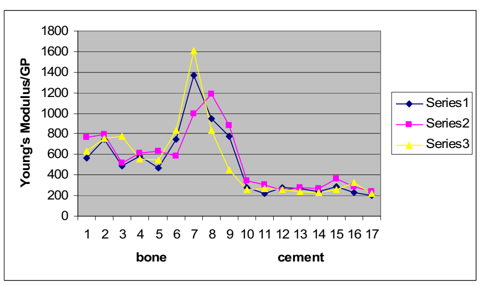

Figure 1: Young's modulus of cancellous bone, interface and Sr-HA cement. The peak was at the interface.

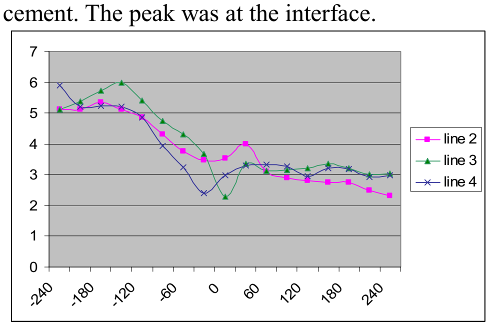

Figure 2: Young's modulus of cortical bone, interface and Sr-HA cement. A smooth transition was found.

As for the interface between Sr-HA cement and cortical bone, intimate contact was observed without fibrous layer intervening by histological and SEM observations. Nanoindentation test showed that, in terms of Young's modulus and hardness, a smooth transition was observed from bone, interface, to Sr-HA cement (Figure 2).

The cement/bone interface is crucial to the stability of the cemented femoral component. However, its mechanical property is far from full understanding because traditional mechanical tests, such as bend testing and compression testing, are not suitable due to specimen size requirements. Fortunately, nanoindentation may offer valuable information about intrinsic mechanical properties, and has been used to evaluate mechanical properties near the implant/bone interface [3].

In the present study, nanoindentation test showed that the Young's modulus and hardness at the interface were higher than those at the Sr-HA cement and cancellous bone. This was further supported by the histological observation. Osseointegration of Sr-HA cement with cancellous was widespread, which is similar to calcium phosphate cement,[4]. Fujita et al found that the bone/cement interface was the weakest point mechanically for the cemented femoral component when a bioactive bone cement consisting of glass powder and Bis-GMA based resin was used in canine total hip arthroplasty [2]. The impregnated ceramic particles which are incompatible with the acrylic cement matrices might be blamed.

Different mechanical properties between cement/cancellous bone interface and cement/cortical bone interface may be explained by the different response of Sr-HA cement to cancellous bone and cortical bone. Further study is needed to explore the way in which the Sr-HA cement bonds with cortical bone.

CONCLUSIONS

Under weight-bearing conditions, intimate contact was found between Sr-HA cement with both cancelllous and cortical bone. The stable interface was further proven by nanoindentation. Sr-HA cement has potential to be an alternative to the conventional bone cement in total hip replacement.

REFERENCES

1 Senaha Y, et al. J Bone Joint Surg 78B, 26-31, 1996
2 Fujita H, et al. J Biomed Mater Res 49, 273-288, 2000.
3 Guo LH, et al. J Biomed Mater Res 54, 554–559, 2001.
4 Ooms EM, et al. J Biomed Mater Res 61, 9-18, 2002

Postural Adjustment of Spinal Cord Injured Subjects with Knee-Ankle-Foot Orthosis

[1]Kwan-Hwa Lin, [2]Tung-Wu Lu, [3]Pei-Pei Hsu, [4]Wen-Shen Liao
[1]School and Graduate Institute of Physical Therapy, National Taiwan University
[2]Institute of Biomedical Engineering, National Taiwan University
[3]Department of Mechanical and Automation Engineering, I-Shou University
[4]Department of Physical Therapy, I-Shou University
email: khlin@ntu.edu.tw

INTRODUCTION

Posture describes body position in space, and the proper control keeps the center of pressure (COP) within the base of support. Most studies investigated the posture control in normal subjects [1]. There is lack of studies concerning the postural control in spinal cord injured subjects (SCI) who may loose balance without support [2]. The purpose of this study was to compare the postural sway, joint angles and postural muscle activities in complete and nearly complete SCI who had to wear knee-ankle-foot orthosis (KAFO) during stance with and without support.

METHODS

The inclusive criteria of this study were SCI who had to wear the KAFO for standing, and would loose balance less than 5 seconds without support. Seven complete and nearly complete mid-low thoracic cord (T6-T12) injured SCI with mean age of 38.6 years old participated in this study. The duration of injury was 94.4 ± 79.2 months. Participants performed standing with each leg on separate force plate (AMTI, USA) for 5 seconds while holding the bars, then released holding until lost balance. Surface electrodes recorded the electromyographic activities (EMG) of trunk muscles and triceps. The joint angles were recorded by 3-D Motion Analysis System (Vicon 250, Oxford, UK). The Wilcoxon signed ranks test was performed to compare the differences in subjects with and without holding. $p < 0.05$ was considered statistically significant.

RESULTS AND DISCUSSION

All the subjects lost the balance within 3 seconds after releasing the hands from the bars. As shown in Table 1, the sway path and sway area are significantly increased in subjects without holding ($p<0.05$). Compared with holding, the hip angle is less hyperextended at the time starting to loose balance, but the pelvis remains to be posterior tilt. The ankle angle between the neutral line and the line from ankle to greater trochanter is reduced at the time starting to loose balance, although it is not statistically significant (Table 1). During standing with holding, the EMG activities of right and left triceps recruit 4.8 ± 1.8%, and 5.1 ± 1.3% of maximal voluntary contractions (Figure 1). The EMG of abdominal and T12 paraspinal muscles seem to recruit more during standing with and without holding. However, the voluntary contractions of abdominal and T12 paraspinal muscles are low, so that the supporting effect of those muscles would be small.

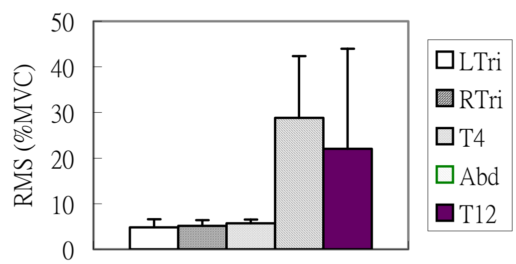

Figure 1. The root mean square (RMS, % maximal voluntary contraction) of triceps and trunk muscle electromyographic activities.

CONCLUSIONS

The postural control in complete SCI depends not only the mechanical alignment of pelvis and other joints, but also on the postural muscle activities [3]. The training of proper alignment of joints and the strength of residual muscles would be important for fall prevention. The anticipatory effect of muscle recruitment needs further study.

REFERENCES

1. Ekdahl C, et al.. *Scand J Rehabil Med* **21**, 187-195, 1989.
2. Matjačič Z,.et al.. *IEEE Trans Rehab Eng* **6**:139-150, 1997.
3. Popvić MR, et al.. *J Biomech* **33**, 1359-1368, 2000.

ACKNOWLEDGEMENTS

The authors thank Chia-Chieh Chang for EMG data analysis.

Table 1: The COP sway and joint angle during stance.

	With Holding	**Without Holding**
Sway path x-axis (mm)	0.8 ± 0.2	2.6 ± 0.7*
Sway path y-axis (mm)	0.8 ± 0.1	2.5 ± 0.5*
Sway area (mm^2)	49.3 ± 6.8	112.0 ± 18.7*
Pelvis angle (-: posterior tilt)	-9.9 ± 4.9	-9.7 ± 5.2
Hip angle (-: extension)	-12.8 ± 5.6	-8.1 ± 4.7*
Ankle to GT (-: extension)	6.7 ± 1.8	4.7 ± 0.9

Data were Mean ± Standard Error. * $p < 0.05$ if compared with and without holding.

The relation of the trunk-pelvic movement and lower extremity joint moment on elderly people during the sit-to-stand motion

[1] Masaya Anan, [1, 2] Nobuhiro Kito and [2] Koichi Shinkoda
[1] Kawashima Orthopedic Hospital, [2] Division of Physical Therapy and Occupational Therapy Sciences, Graduate School of Health Sciences, Hiroshima University; e-mail: an_an0219@ybb.ne.jp

INTRODUCTION

The sit-to-stand motion (STS) is one of the most frequently executed activities although it poses a high risk of falling in elderly. It can be said that an important factor essential to improving movement ability is related to the acquisition of STS during practical activities such as transferring and walking. The purpose of this study was to create a physical therapy strategy related to properly supporting oneself during STS by making a clear relationship between trunk-pelvis movement and lower extremity joint moment.

METHODS

Fourteen elderly subjects (mean age 82.1) with no prior history of CNS-related diseases were recruited for this study. All subjects were able to perform STS without using their arms when the height of the chair equaled the length of their lower leg. Markers were placed on various parts of the body (top of head, tragus, acromion, lowest rib, ASIS, PSIS, great trochanter, lateral knee joint line, lateral malleolus, calcaneal tuberosity, and tip of toe). The movements of the markers on the sagittal plane were taken by a digital video camera (Sanyo, KDR2004) at 30 frames/s, and processed using a picture analysis software (NIH Image). By looking at the data points, the center of gravity (COG) and joint angles were calculated. The center of pressure of the buttocks and foot, and the vertical floor reaction force were measured at a frequency of 30Hz, using 2 force plates. This data was synchronized using an optical stimulus, and the time series behavior of the hip, knee, and ankle joint moments were measured.

RESULTS AND DISCUSSION

Eleven elderly subjects used the predominant hip extension moment during STS, while the other 3 subjects used the predominant knee extension moment from buttocks-off to motion termination. Here, we designated the former subject group as H, and the latter subject group as K. Comparison of the H and K-groups during STS was performed using Mann-Whitney's U Test. In comparison to the H-group, the total STS time of the K-group had a tendency to be longer (p=0.06), while the maximum horizontal velocity and anterior pelvic tilting angle at buttocks-off had a tendency to become smaller (p=0.06, p=0.07). Hip flexion angle and knee extension moment at buttocks-off were significantly larger (p<0.05). Hip extension moment and ankle flexion moment at buttocks-off were also significantly smaller (p<0.05). The data results show that the K-group is unable to use the kinetic energy of the trunk at the hip during STS, but rather uses the motion of the predominant knee extension moment. Specifically, the pelvic movement had an effect on the lower extremity joint moment. It is suggested that during smaller pelvic anteversion STS, the kinetic chain between the pelvic and lower extremity movement is easily broken, and therefore knee extension moment predominates after buttocks-off.

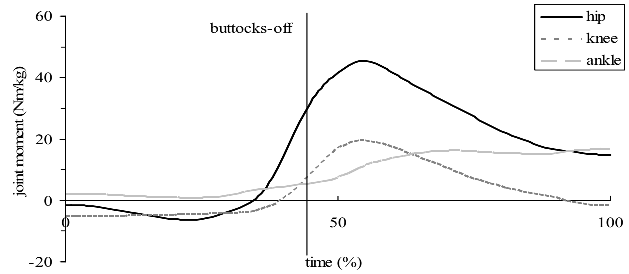

Figure 1: **Lower extremity joint moment in H-group.**

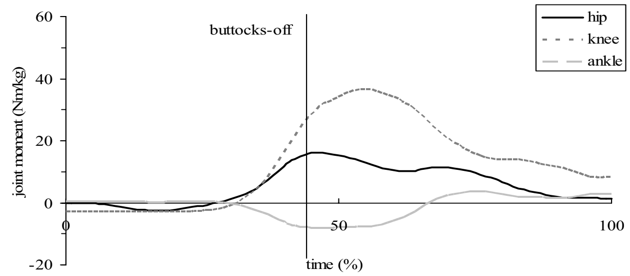

Figure 2: **Lower extremity joint moment in K-group.**

CONCLUSION

In order to make a practical physical therapy strategy for STS, it is necessary to facilitate not only lower extremity extensor muscle strength, but also the kinetics chain which links the pelvic and lower extremity movement.

Table 1: Comparison of H and K-groups

		H-group (n=11)	K-group (n=3)	
Total STS time(s)		2.38 ± 0.53	3.16 ± 0.68	
Maximum velocity (cm/s)	Horizontal	47.9 ± 10.0	33.8 ± 10.7	
Joint angles at the buttocks off (deg)	Pelvis	26.9 ± 8.7	14.9 ± 11.0	
	Hip	112.0 ± 9.4	125.1 ± 9.6	*
	Knee	87.5 ± 5.5	99.0 ± 1.2	*
	Ankle	10.8 ± 5.4	18.7 ± 2.0	*
Joint moment at the buttocks off (Nm/kg) [a)]	Hip	0.91 ± 0.19	0.41 ± 0.05	*
	Knee	0.30 ± 0.14	0.65 ± 0.14	*
	Ankle	0.08 ± 0.14	-0.19 ± 0.10	*

Mean±SD, *: p<0.05

a) each joint moments are normalized by dividing the raw data by the subject's body weight.

OPTIMAL STRATEGY OF CANE USE DURING STAIR ASCENT

Bih-Jen Hsue, Fong-Chin Su
Institute of Biomechanical Engineering, National Cheng Kung University, Tainan, Taiwan
email: fcsu@mail.ncku.edu.tw

INTRODUCTION

Going up and down stairs require strength, range of motion, balance, and coordination, therefore, presents a challenge for the elderly and individuals with disability, and assistive devices may be needed. Therapists and clinicians usually have several approaches for teaching stair locomotion while using an assistive device, i.e. a cane would be for the patient with pain at the lower extremity to start with the stronger leg first followed by the weaker leg and the cane [1]. Some therapist may alter this traditional approach by having the patient progress the cane first, then the stronger leg and weaker leg. However, there is no document in the literature supporting these techniques. The purpose of this study was to compare the effect of placement of a quadricane (four-point cane) during stair ascent on body posture, center of mass (COM), and joint position. The change in the COM and relative orientation of the trunk were examined during five methods: (1) ascending stairs without a cane with right foot stepped up first, then left foot; (2) forward placement of the quadricane at the initiation of stair ascent followed by the ipsilateral foot (ipsilateral to the cane), then contralateral foot (SA1); (3) forward placement of the cane followed by the contralateral, then ipsilateral foot (SA2); (4) lateral placement of the cane with ipsilateral foot stepping up, followed by the contra-lateral foot and the cane (SA3); (5) lateral placement of the cane with contra-lateral foot stepped up, followed by the ipsilateral foot and cane (SA4). All conditions were associated with step-to (non-reciprocal) walking pattern.

METHODS

A five-step wood staircase with a slope of 32.7°, a step height of 18 cm, a tread depth of 28 cm and a width of 90cm was used. Fifteen able-bodied participants in good general health aged from 24 to 30 years old were enrolled. Twenty-five reflective markers were secured to the participant's anatomical landmarks locating on the both sides of the body. An eight-camera Eagle Motion Analysis System (Motion Analysis Corporation, Santa, CA, USA) was used to capture the three-dimensional trajectory data of the markers.

The quadricane was adjusted to ensure that the handgrip was at the height level between the participant's wrist crease and greater trochanter. The participants were asked to ascend stairs with each of the five methods for three times in random orders. One gait cycle was completed as the three weight-bearing points (both legs and cane) were progressed from a tread to another tread one step above. The data were smoothed and normalized to stride period of 100% in one gait cycle. The data was analyzed utilizing repeated measures analysis of variance (ANOVA) at the 0.05 level of significance.

RESULTS AND DISCUSSION

The maximal range of motion of the trunk, hip, knee and ankle from neutral position were list in Table 1. Trunk movements, including flexion, rotation and side-bending are significantly larger in lateral placement of cane, especially in SA4. It agrees with the clinical adaptation to prevent fall from lack of shoulder and trunk extension and the desire to keep the COM anteriorly. The leading leg always demonstrates more hip and knee flexion, and less ankle plantarflexion, no matter what the placement of cane is. As observing the excursions of the joint movement in a stride, some double peaks of the movement at the hip and knee joints of the leading leg in SA3 and SA4.

Table 1: Mean and standard deviation of maximal flexion in degrees of the trunk, hip, knee and ankle in sagittal plane

	No cane	SA1	SA2	SA3	SA4
Trunk	8.0 (2.4)	8.3 (2.3)	7.7 (2.2)	9.1(2.5)	10.9(3.2)
I.Hip*	57.9(4.3)	58.8(5.1)	27.8(7.0)	52.1(13.8)	36.8(7.4)
C.Hip *	27.7(4.7)	27.5(5.2)	58.7(4.6)	30.6(9.2)	56.8(5.1)
I.Knee	79.2(4.2)	80.2(4.1)	56.5(10.4)	73.8(19.5)	69.9(8.4)
C.Knee	55.6(5.6)	54.8(5.4)	77.1(5.3)	62.2(16.7)	79.5(5.0)
I.Ankle**	25.5(5.7)	23.8(4.5)	37.8(6.6)	21.8(6.0)	32.6(5.8)
C.Ankle**	38.6(6.6)	39.2(5.1)	22.54(3.6)	35.3(9.8)	23.4(3.8)

* I: the ipsilateral side; C: the contralateral side
** Degrees of maximal plantarflexion

The excursions of COM displacement in three directions are shown in Figure 1. Significant differences are found in the excursion and maximal medial-lateral COM displacement among five methods.

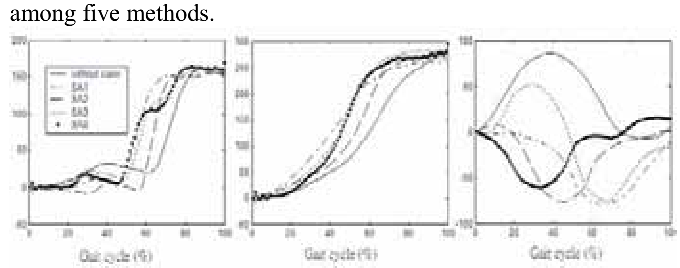

Figure 1: The plot at the left is the COM displacement (in mini-meter) in vertical direction, the plot at the middle is COM displacement in forward-backward direction, and the plot at the right is the COM displacement in medial-lateral direction.

CONCLUSIONS

In order to find an optimal strategy for stair walking while using a cane, not only causes of the disability, i.e. instability or pain at the leg, should be considered, but also the proximal control, such as how to progress with COM within a small base of support and maintain an unavoidable asymmetry posture etc.

REFERENCES

1. Vargo MM, et al. *Am J Phys Med Rehabil* **71**, 170-176, 1992.

ACKNOWLEDGEMENTS

Partial support from grant NSC93-2213-E-006-123, Taiwan.

RELATIONSHIP BETWEEN MOMENT-JOINT ANGLE CHARACTERISTICS OF KNEE FLEXION AND ARCHITECTURE OF HAMSTRINGS MUSCLES IN HUMAN

[1,2] Hiroshi Arakawa, [2]Akinori Nagano and [1]Senshi Fukashiro
[1]Department of Life Sciences (Sports Sciences), The University of Tokyo, Japan
[2]Computational Biomechanics Unit, Riken, Japan

INTRODUCTION

There have been few biomechanical studies that tried to investigate individual variations of human musculoskeletal parameters, e.g., moment of inertia or ratio of fascicle-tendon structure length. Additionally, many synergist muscles that have different moment arm one by one have often been analyzed as a single muscle. However, we need to pay more attention to musculoskeletal differences among individuals, which have a possibility to result in different characteristics of force generation and moment-joint angle relationship. The purpose of this study was to investigate how individual variations of architecture of hamstrings muscle tendon complex, which are agonists of knee flexion, influence moment-joint angle relationship.

METHODS

Ten healthy males (age, 26.4 ± 2.9 yrs; height, 174.5 ± 5.0 cm; mass, 72.0 ± 6.0 kg) participated in this study. A dynamometer (MYORET RZ-450: Kawasaki, Japan) was used to measure isokinetic knee flexion moment. All measurements were performed from the left leg. We measured three maximal-effort voluntary contractions at 30 degree/sec, with different hip joint angles. Subjects were tested at 0 and 90 degrees of hip flexion (Figure 1). We firmly fixed subject's thigh and trunk on the apparatus with straps so that their body did not move while testing. Each testing was performed with sufficient rest. We measured subject's muscle architectural property using ultrasonography. Muscle thickness was measured by B-mode ultrasonography (SSD-2200, Aloka, Japan) at two sites, i.e., posterior thigh at 40% (upper thigh) and 70% (lower thigh) of the thigh length (Figure 2).

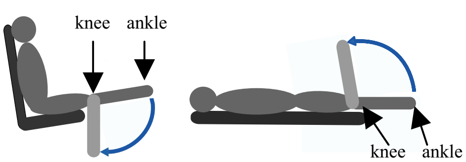

Figure 1: Experimental positions.

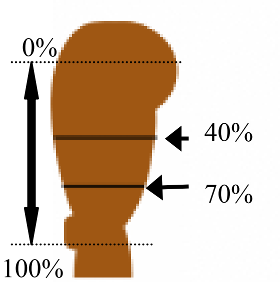

Figure 2: This picture shows the point we measured in muscle thickness measurement.
One is 40% of the thigh length (upper thigh), and the other is 70 % (lower thigh).

RESULT AND DISCUSSION

Figure 3 shows the relationships between the ratio of the upper and lower thigh thickness and the ratio of the knee flexion moment at 0 and 90 degrees of hip flexion. In both cases, the knee flexion angles are at 30 degrees. It was found that subjects whose relative muscle thickness of upper thigh is larger tended to be able to generate larger relative strength when the hip flexion angle is 90 degrees. And there was a significant correlation between the ratio of the upper and lower thigh thickness and the ratio of the knee flexion moment at 0 and 90 degrees of hip flexion ($R=0.828$ $p<0.01$). Several studies have focused on relationship between sprint performance and thigh muscle thickness of upper and lower parts [1,2]. There remains some uncertainty whether the ultrasonography data obtained from skin surface have enough accuracy to address individual differences. Currently we are proceeding with examination using MRI to obtain more reliable architectural data of hamstrings.

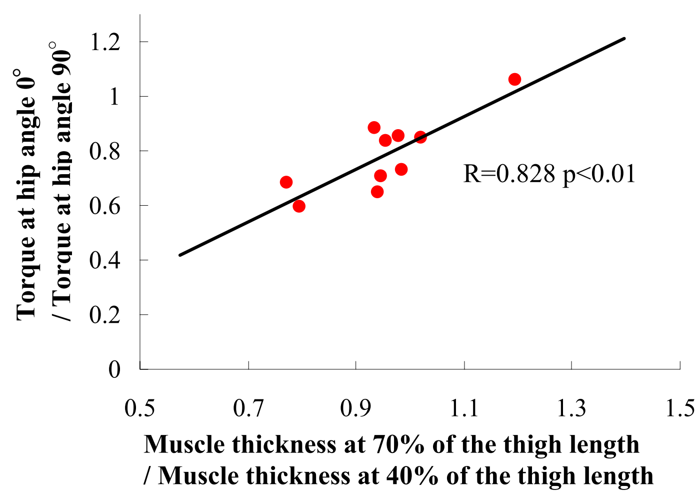

Figure 3: The relationships between the ratio of the upper and lower thigh thickness and the ratio of the knee flexion moment at 0 and 90 degrees of hip flexion. Both of knee flexion angles were at 45 degrees.

CONCLUSIONS

It is likely that differences among individuals in the architecture of hamstrings muscles result in differences of moment-hip angle relationship of their knee flexion.

REFERENCES

1.Kumagai K, et al.. *J Appl Physiol* **33**, 811-816, 2000.
2.Abe T, et al.. *Med Sci Sports Exerc* **31** (10), 1448-1452, 1999.

BIOMECHANICAL STUDY IN THE OPTIMIZATION OF DIFFERENT FIXATION MODES FOR A PROXIMAL FEMUR L-OSTEOTOMY- A THREE DIMENSIONAL FINITE ELEMENT SIMULATION

[1]Ching-Lung Tai, [2]Weng-Pin Chen, [1]Mel S. Lee, [1]Chun-Hsiung Shih and [1]Wen-Jer Chen
[1]Department of Orthopedic Surgery, Chang Gung Memorial Hospital, Taiwan
[2]Department of Biomedical Engineering, Chung Yuan Christian University, Taiwan; email:ortholab@adm.cgmh.org.tw

INTRODUCTION

Numerous surgical techniques have been proposed to manage the femoral neck shortening and the greater trochanter overgrowth secondary to retarded growth of the femoral capital epiphysis but with little success [1]. For the reconstruction of residual deformities of the hip, Papavasiliou et al. performed a new type of proximal femur L-osteotomy with hip spica casts, and achieved good results [2]. Although the results were good with this osteotomy, a thorough understanding and study of the biomechanical characteristics will be helpful to improve the technique and aid in preoperative planning. A three dimensional finite element analysis was thus designed to understand the mechanical characteristics of postoperative femur after L-osteotomy.

METHODS

A patient with left hip dysplasia was recruited as the study model of L-osteotomy. The normal right hip was used as a guide to perform the corrective surgery. The length and the angle of the intersected line between the femoral head center and the most superior point of the greater trochanter in the normal right femur were considered as the final resultant configuration postoperatively (Figure 1). C-T images were used to create the 3-D finite element models. Four FEA models with the same longitudinal length of osteotomy (126mm) but different fixation screw configurations (P2/D2, P2/D3, P3/D2, P3/D3, P: Proximal fixation; D: Distal fixation) together with four FEA models with the same fixation screw number (P3/D2) but different longitudinal length of osteotomy (116, 126, 136 and 146mm) were created. Analysis was performed on a loading condition simulating single legged stance. The von Mises stress distributions of postoperative femora and displacements of the femoral head were analyzed and compared.

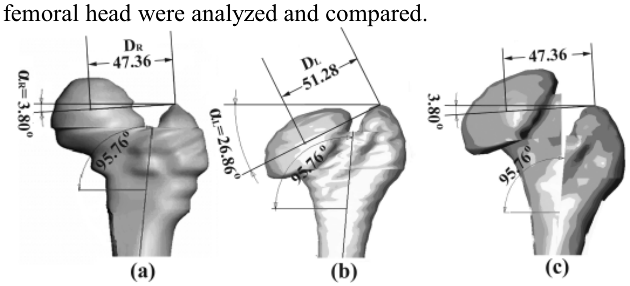

Figure 1: (a) normal right femur, (b) left femur with residual deformity, and (c) resultant configuration after L-osteotomy.

RESULTS AND DISCUSSION

This study achieved the following findings: A). The fixation devices (plate and screws) sustained most of the external loading, the peak value of von Mises stress on the fixation screws decreased with increasing screw number (Figure 2). B). More screws placement on the proximal segment would be more beneficial to improve the postoperative stability as compared to that on the distal segment. C). The extent of osteotomy should be limited because a high local stress concentration might occur around the femoral neck regions with increasing longitudinal length of L-osteotomy (Figure 3).

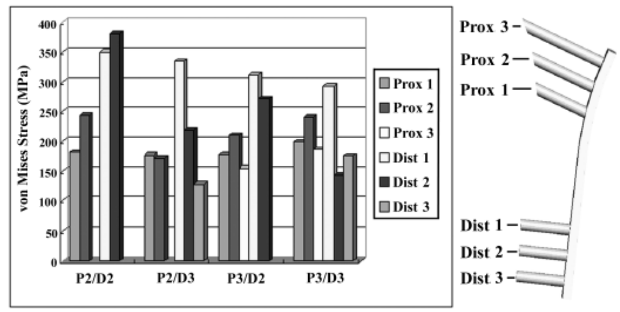

Figure 2: Peak value of Von Mises stress on fixation screws for femora instrumented with four different configurations of screw placement but at the same longitudinal length of osteotomy (126mm). The peak stress of screws increased with decreasing screw number, and the highest value was found on the most distal screw (D2) on condition that the femur was instrumented with four screws (P2/D2).

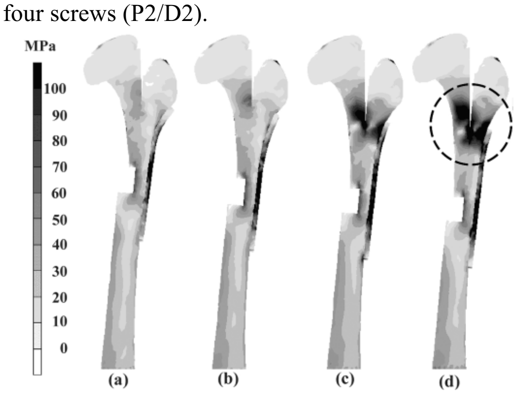

Figure 3: Von Mises stress for femora instrumented with four different longitudinal lengths of osteotomy but the same screw number (P3/D2). (a) 116mm, (b) 126mm, (c) 136mm and (d) 146mm. The von Mises stress around the femoral neck regions progressively increased as the longitudinal length of osteotomy increase from 116 mm to 146 mm.

CONCLUSIONS

The results indicate that the more screws placement on the proximal segment the more the stability improvement in the postoperative femur. Therefore, the cobra type plate with more screw holes on the proximal part might be a good alternative for the L-osteotomy.

REFERENCES

1. Tauber C, et al. *Acta Orthop Scand* **51**, 661-666, 1980.
2. Papavasiliou VA, et al. *Clin Orthop* **341**, 123-127, 1997.

ESTIMATION OF HUMAN INTERNAL AND EXTERNAL GEOMETRY FROM SELECTED BODY MEASUREMENTS

[1]Samuel Bertrand, [2]Ivan Kojadinovic, [1]Wafa Skalli and [1]David Mitton
[1]*Laboratoire de Biomécanique – ENSAM – CNRS UMR 8005, Paris, FRANCE*
[2]*LINA CNRS FRE 2729, Site Ecole Polytechnique de l'Université de Nantes, Nantes, FRANCE*
email: lbm@paris.ensam.fr, web: http://bio-web.paris.ensam.fr/

INTRODUCTION

The development of personalized numerical models of the human being requires a deep knowledge of the human body geometry. Several studies have been performed on the external [1] or on the internal geometry of body parts [2]. As far as the statistical relationships between external and internal geometries are concerned, most studies focused only on the relationships between stature and specific bone dimensions as the length of long bones [3]. The aim of this study is to obtain linear statistical models for estimating internal (trunk bones) and external (full body) human body geometry from a small number of body measurements.

METHODS

The geometrical data used in this work were obtained by combining internal and external measurements performed on 64 healthy adults (20-55 yrs old, 30 yrs on avg.) representative of three morphotypes (16 5th percentile female subjects, 33 50th and 15 95th percentile male subjects) collected by *Bertrand et al.* [4]. The data were analysed using the R statistical environment. The different steps of the statistical analysis are listed hereafter :

1- Agglomerative Hierarchical Clustering of the measured parameters based on the linear correlation coefficient ;
2- Identification of clusters of linearly dependent parameters ;
3- Identification of Isolated Parameters (IP) corresponding to clusters of size 1 ;
4- Selection of a subset of explanatory parameter(s) (Main Parameters, MP) in each cluster ;
5- Estimation of simple linear regression models in order to explain every non-MP parameters in a cluster (Secondary Parameters, SP) by the MP of the cluster.

This procedure was separately applied on external and on subgroups of internal data obtained by regrouping measured parameters belonging to the same anatomical group (i.e. : rib cage, cervical spine, thoracic spine, lumbar spine, pelvis). Thus, external/external and internal/internal anthropometrical models were obtained. Then, the procedure was applied on the whole external parameters associated with internal MP (MP*i*) and internal IP (IP*i*) in order to determine external/internal models, thereby enabling the prediction of MP*i* and IP*i* from external parameters (Figure 1).

RESULTS AND DISCUSSION

The present statistical analysis proposes 189 anthropometrical models (Figure 1, Table 1) enabling to estimate personalized external and internal geometry from 10 external measurements that can be easily measured on any subject : height, acromion-ground height, iliac crest-ground height, sitting height, chest axillary circumference, head (glabella-occiput) circumference, low pelvic circumference, thigh bottom circumference, greatest forearm circumference, weight. The quality of the regressions was evaluated by the Standard Error of Estimate (SEE), with 2·SEE giving the 95% of errors.

Among the 189 models estimated 117 had a 2·SEE≤10% (34 ext/ext, 72 int/int, and 11 ext/int models).

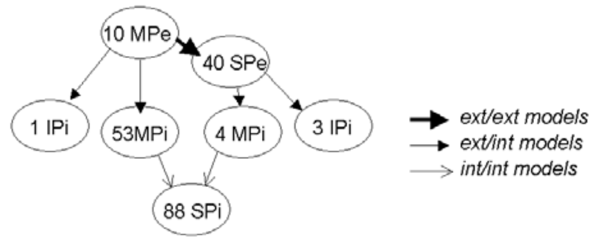

Figure 1: Organigram of MPi, SP*e*, SP*i*, IP*i* estimation from the MP*e* (*e*: external ; *i*: internal).

CONCLUSIONS

Numerous anthropometrical ext/ext (n=40), int/int (n=88), and ext/int (n=61) models were estimated and studied in this work. In particular, 11 external/internal models with 2·SEE≤10% were found, enabling the estimation of internal trunk dimensions from external body measurements. It brings a deeper knowledge on human morphology and opens the way for wide applications (human model personalisation for crash-test simulation, planning of clinical interventions…).

REFERENCES

1. Rebiffe R, et al. Laboratoire de Physiologie et de Biomécanique Peugeot-Renault, 1982.
2. Laporte S et al. *Eur J Orthop Surg Traumatol* **10**, 85-91, 2000.
3. De Mendonça MC *Am J Phys Anthropol* **112**, 39-48, 2000.
4. Bertrand S et al. *Proceedings of SB XXIX,* Paris, France, page 51, 2004.

ACKNOWLEDGEMENTS

This work was funded by the European Community in the framework of the HUMOS 2 project (http://humos2.inrets.fr).

Table 1: Examples of ext/ext, int/int and ext/int models. The table contains for each the intercept, the regression coefficient, and its standard error in mm and in % (explained parameter (*mm*) = *coef* x explanatory parameter (*mm* or *kg*) + *intercept* ± *2·SEE*(*mm*)).

Explained parameters	*Explanatory parameters*	*R²*	*constant*	*coef.*	*2·S.E.E. (mm)*	*2·S.E.E. (%)*
eyes-ground height (standing position) (SP*e*)	height (MP*e*)	0.99	-42.4	0.96	16	1.0
Arm upper circumference (SP*e*)	weight (MP*e*)	0.91	141.2	2.28	26	8.4
height of the right half of the pelvis (MP*i*)	acromion -ground height (standing position) (MP*e*)	0.83	-3.5	0.15	14	6.4
height of the left half of the pelvis (SP*i*)	height of the right half of the pelvis (MP*i*)	0.94	-7.8	1.05	9	4.2
inferior width of the vertebral body of L2 (MP*i*)	height (MP*e*)	0.66	-15.9	0.04	6	12.3
superior width of the vertebral body of L2 (SP*i*)	inferior width of the vertebral body of L2 (MP*i*)	0.87	0.4	0.94	3	8.0

DEVELOPMENT OF A THREE-DIMENSIONAL SIMULATION MODEL OF THE HUMAN WHOLE BODY

[1]Akinori Nagano, [2]Shinsuke Yoshioka, [3]Taku Komura, [1]Ryutaro Himeno and [2]Senshi Fukashiro
[1]Computational Biomechanics Unit, RIKEN; email: a-nagano@riken.jp
[2]Department of Life Sciences (Sports Sciences), University of Tokyo
[3]Department of Computer Engineering and Information Technology, City University of Hong Kong

INTRODUCTION

It is widely recognized that computer modeling and simulation provide valuable contributions to the research of biomechanics. Using forward dynamic computer simulation, it is possible to predict influences of such biomechanical interventions as injury, surgical operations, strength training and so on in quantitative terms.

However, it is also true that the methodology of computer modeling and simulation has not been utilized handily by all researchers / research groups who are interested in using it. One of the reasons is that the procedure of modeling requires very complex technical treatments. Although there are several commercial software packages to help this procedure, even with the aid of these tools, this methodology is not being conveniently utilized by many researchers. This is disadvantageous for the whole society as high-impact contributions can be made by many researchers if this methodology is utilized by more researchers in biomechanics.

We thought that it would be meaningful to present a code (computer program) of a human whole body model to the society of biomechanics for further development of this field. By simply copying the code, interested researchers can easily run a computer simulation. The purpose of this study was to present a three-dimensional linked segment model of the human skeletal system that has large degrees of freedom.

METHODS

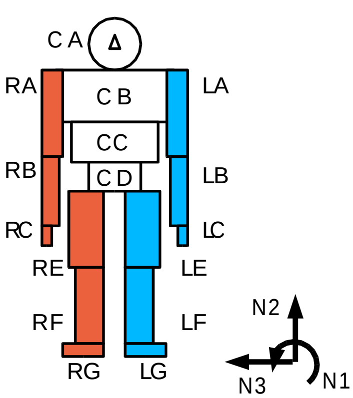

Figure 1: The skeletal model developed in this study.

The model was coded to be processed with a modeling and simulation tool AUTOLEV [1]. The code will be posted on the internet for public access by the time of conference. The model has sixteen rigid body segments in total: head, chest, mid-trunk, lower-trunk, right and left upper arms, right and left lower arms, right and left hands, right and left upper legs, right and left lower legs, right and left feet (Figure 1). The degrees of freedom of the model was thirty-five. Anthropological parameter values were derived from [2-4].

For an example, a hanging motion was simulated using this model. The body was tilted in the forward direction by 45 deg. The upper endpoint of the head segment was fixed in the global coordinate system. Thereafter, a hanging motion was simulated in which the whole body swayed back and forth with an effect of the pull of gravity.

RESULTS AND DISCUSSION

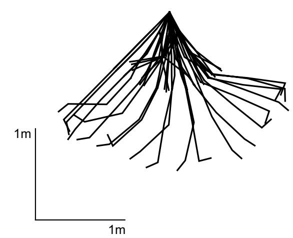

Figure 2: The hanging motion simulated in this study.

It was shown that the code developed in this project can be utilized for simulation of human whole body motions (Figure 2, hanging motion). The following four factors need to be taken into account to simulate a wider range of phenomena that researchers in biomechanics are interested in. Those four major factors are: (1) muscles, (2) ground reaction forces, (3) detailed joint motions and (4) addition or removal of segments. Currently we are trying to address these points utilizing built-in functions of AUTOLEV, and making a steady progress.

REFERENCES

1. Kane TR, Levinson DA. *AUTOLEV 4 User's Manual*. OnLine Dynamics, Inc., Sunnyvale, CA, USA, 2004.
2. De Leva P. *J. Biomech* **29**, 1223-1230, 1996.
3. Delp SL. *Surgery simulation: a computer graphics system to analyze and design musculoskeletal reconstructions of the lower limb.* Dissertation. Stanford University, Stanford, CA, USA, 1990.
4. Winter DA. *Biomechanics and motor control of human movement*. John Wiley & Sons, Inc., New York, NY, USA, 1990.

ACKNOWLEDGEMENTS

This study was partly supported by the special post-doctoral program of RIKEN and by Ministry of Education, Culture, Sports, Science and Technology in Japan (No: 16300205).

DO OVERWEIGHT AND OBESITY AFFECT DYNAMIC PLANTAR PRESSURE DISTRIBUTIONS IN PRE-SCHOOL CHILDREN?

Karen J Mickle, Julie R Steele and Bridget J Munro
Biomechanics Research Laboratory, University of Wollongong, Australia;
Email: kjm06@uow.edu.au

INTRODUCTION

It has been speculated that foot pain caused by high plantar pressures generated during walking may decrease a child's desire to participate in physical activity and, in turn, perpetuate the cycle of obesity. Although obese primary school children have been found to generate higher plantar pressures when walking compared to their leaner counterparts [1], it is not known whether younger overweight and obese children also generate these potentially negative higher pressures. Therefore, the purpose of this study was to determine the effects of overweight and obesity on plantar pressures generated by pre-school children during gait.

METHODS

The height and mass of 86 consenting children (mean age = 4.2 ± 0.6 years) from 10 randomly selected pre-schools in the Illawarra region of New South Wales, Australia, were measured following standard procedures. Each child walked across an emed AT-4 pressure platform (25 Hz; Novel$_{gmbh}$, Munich) using the first-step method, with up to 6 successful trials being collected on each child's left and right foot. A subset of 17 overweight/obese children (BMI = 18.5 ± 1.2 kg.m^{-2}) were then identified from the sample and matched for height, age and gender with 17 non-overweight children (BMI = 15.7± 0.6 kg.m^{-2}).

Peak plantar pressures (N.cm^{-2}), maximum force (N), contact area (cm^{-2}), force-time integrals (N.s) and pressure-time integrals (N.s.cm^{-2}) were then derived for five regions of each child's feet, averaged across all trials. Independent *t*-tests were then applied to the data to determine whether there were any significant differences ($p < 0.05$) in the plantar pressure variables between the two subject groups.

RESULTS AND DISCUSSION

The overweight/obese children had significantly larger contact areas between the total foot (TO), heel (M01), midfoot (M02) and forefoot (M03) and the ground when walking, compared to the non-overweight children. The overweight/obese children also generated significantly larger forces in the total foot, heel, midfoot and forefoot regions of the foot when walking. This was to be expected, as heavier children should generate greater forces than their leaner counterparts. Despite generating the higher forces over larger contact areas, the overweight/obese children displayed significantly higher peak pressures (Figure 1), force-time integrals and pressure-time integrals in the midfoot region of the foot (M02), compared to the non-overweight children.

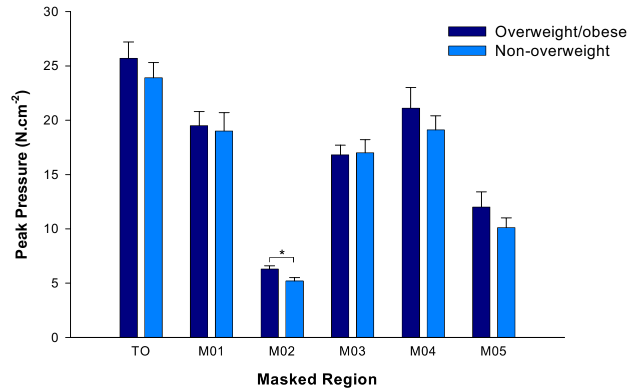

Figure 1: Means (+ SEM) of the peak pressures generated in each masked region of the foot, displayed by the overweight/obese and non-overweight children. * indicates a significant difference between the two subject groups.

CONCLUSIONS

These results imply that the additional contact area displayed by these overweight/obese pre-school children in the midfoot area of the foot was not able to compensate for the high forces generated in that area of the foot during walking, resulting in higher pressures under the midfoot. As force-time and pressure-time integrals provide an indication of the load imparted on particular bony and soft tissue structures in the foot, these results suggest that the midfoot area of these overweight/obese young pre-school children may be exposed to increased stress and, in turn, vulnerable to bony fatigue and soft tissue damage. It is postulated that these changes may be exacerbated if excess weight bearing continues throughout childhood and into adulthood. Therefore, urgent interventions, appropriate to the structural and functional needs of very young overweight and obese children, are required to prevent further weight gain and structural and functional complications to the feet.

REFERENCES

1. Dowling AM, et al. *International Journal of Obesity and Related Metabolic Disorders* 2001; **25**:845-852.

ACKNOWLEDGEMENTS

University of Wollongong small grants.

THE INFLUENCE OF THE FIREMEN BOOTS ON THE HEEL STRIKE TRANSIENT DURING WALKING

[1]Cámara Tobalina Jesús, [2]Begoña Gavilanes
[1]e-mail: txus@libreriacamara.com
[2]Instituto Vasco de Educación Física, web: www.shee-ivef.com

INTRODUCTION

The shape of the first part of the vertical ground reaction force depends on many factors such as the footwear characteristics [1-4, 6], the walking velocity [1, 4], the gait pattern [1], the foot morfology [4, 5] and the sampling rate of the force platforms [1]. These factors have an influence on the presence and magnitude of the heel strike transient (HST). The term "heel strike transient" refers to the impact between the foot and the ground, when a spike of force is superimposed on the upslope of the vertical ground reaction force [5]. We considered the presence of the HST when the spike of force descended 20N. before its final ascending up to the first trust maximum. This force transient is thought to be deleterious [5, 6] The objective of this study was to analyze the influence of different walking conditions on the HST.

METHODS

Fourty five firemen took part in the study. It took place at the Human Motion Analysis Research Laboratory in the Basurto´s Hospital. One force platform was installed flush with the ground in the centre of a 10 meters walkway. The subjects undertook several practice to ensure that they were familiar with the laboratory dimensions and the placement of the force platform. Five trials were conducted under each condition; barefoot (B), with their own runners (R) and with their firemen boots (F). Subjects were asked to walk at self selected speed over the force platform. Trials would be accepted if the speed showed a consistency between conditions, there were no visible alteration of the stride as the subjects walked across the platform and the entire right foot landed on the platform. The vertical ground reaction force was collected at a sampling frequency of 500Hz. Forces were normalized to the subjects´ bodyweight.

RESULTS AND DISCUSSION

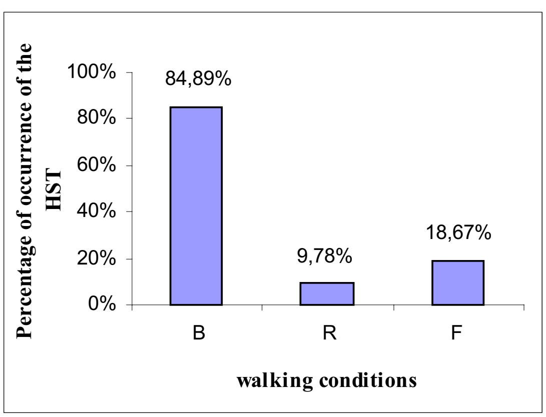

Figure 1: Descriptive statistics of the occurrence of the HST in the three different condicions.

Table 1: Heel strike transient mean magnitudes in each condition.
Numbers in parenthesis are standard deviations.
* indicates a significant difference between groups ($P<0.01$).

	Mean		
Conditions	B	R	F
HST (Bw)	1.00* (0.16)	0.41 (0.32)	0.59 (0.12)

In barefoot walking (B) the HST showed a higher presence (Figure 1) and magnitude (Table 1) than when subjects walked in runners (R) and in firemen boots (F). No significant differences were found between walking in runners and in firemen boots. These results indicate that barefoot walking implies the highest impact of the foot with the ground , whereas walking with runners and with firemen boots reduces significantly the impact of the foot with the ground. This corroborates the statement of Whittle who mentioned that when footwear is used, it provides a line of defense [5] against transient forces. As the walking velocity, the foot morfology and the sampling rate of the force platform did not change among the three walking conditions, the highest presence and magnitude of the heel strike transient during barefoot walking are explained by the differences in the gait pattern and/or by the absence of shoes.

CONCLUSION

Barefoot walking showed a higher presence and magnitude of the heel strike transient than when subjects walked with runners and with firemen boots.

REFERENCES

1. McCaw ST, et al. *Medicine and Science of Sport Exercise* **32**(7), 1258-1264, 2000.
2. Munro CF, et al. *J Biomech* **20**(2), 147-155, 1987.
3. Nigg BM. *Journal of Sports Science* **5**(2), 117-145, 1987.
4. Hamill J. *Proceedings of the XVIV ISBS Symposium,* Madeira, Portugal, 1996.
5. Whittle MW. *Gait and Posture* **10**, 264-275, 1999.
6. Stacoff A, et al. *Gait and Posture* **21**, 24-38, 2005.

ACKNOWLEDGEMENTS

We would like to thank the Bilbao´s Council for its colaboration during the study. We also thank the Basurto´s Hospital and Dr. Anza for the technical support.

AN ALGORITHM FOR ESTIMATION OF SHOULDER MUSCLE FORCES FOR CLINICAL USE

Philippe Favre, Ralph Sheikh, Sandro F. Fucentese, Hilaire A.C. Jacob
Department of Orthopaedic Surgery, Balgrist, University of Zurich, 340 Forchstrasse, Zurich 8008, Switzerland.
Email: pfavre@research.balgrist.ch

INTRODUCTION

The complexity of the shoulder joint, with its extensive range of motion and large number of muscles, calls for close examination of possible muscular strategies involved, to understand some of the disorders of this intricate articulation and to treat these more effectively. Because each muscle can possibly give rise to rotation components about three orthogonal axes simultaneously (for instance, it could abduct, flex, and medially rotate the humerus at the same time), it becomes necessary to describe the muscular effect on the shoulder joint for each of these three actions, separately. Most of the previously developed computational methods have unfortunately been tailored to meet special cases of loading (usually to balance an external moment acting in one principal direction) and therefore do not readily lend themselves for application in a clinical environment where one wishes to test, for instance, the effect of a neurological or muscular deficiency on a model in which an arbitrary combination of external loading conditions would apply. We therefore developed an algorithm to predict muscle forces and test joint stability, for any external load and in 12 discrete positions of the humerus with respect of the scapula.

METHODS

Moment arm length and line of action of each muscle segment was measured off a realistic three-dimensional full-size epoxy model of the thorax, scapula and proximal humerus, based on a fresh cadaver adult specimen, using the tendon travel method [1], in the 12 arm positions of interest. The muscles of the shoulder were segmented to allow for differentiated actions. The algorithm for shoulder force estimation (*ASFE*) involves decision-making iteration loops. In the main loop, muscle segments that can exert a significant moment to oppose the greatest of the three external moment components, while totally disregarding the two lesser ones, and muscle segments that can exert moments which oppose all three external components simultaneously, are first chosen. A small arbitrary force is initially attributed to this set of muscles in proportion to their cross-sectional area and introduced in the system of equilibrium equations. In further, similar, iteration steps, new values of muscular forces are attributed that again equilibrate only a small proportion of the remaining unbalanced external force. Only small increments of muscle force are attributed in each loop to ensure that at no stage, the muscular moment overshoots the external one. The issuing imbalance, also referred to as 'error', converges to an acceptable level. Each thus determined muscle force is stored after every loop and finally summed up to give the final estimate. The resulting joint force is calculated by adding all muscle forces to the external force and is controlled to fall within the glenoid boundaries. If joint stability is not reached at the end of the process, a superimposed force exerted by all the rotator cuff muscles (enforced cavity-compression through co-contraction) is simultaneously raised, and the algorithm restarted until stability is achieved.

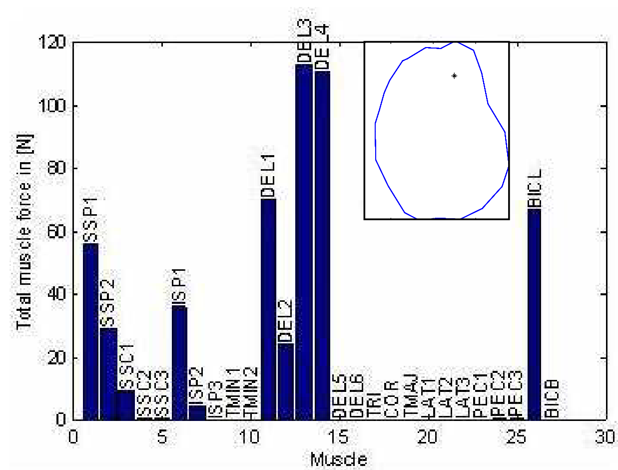

Figure 1: Forces exerted by the 27 muscle segments for abduction with a 9Nm external moment and with the humerus in 30° elevation in the scapula plane and in neutral rotation. The inserted field shows the intersection of the resultant with the glenoid.

RESULTS AND DISCUSSION

The worked-out examples show interesting features of probable muscular activity and give results in good agreement with the literature (simulations, electromyographic studies). Figure 1 is an example. Although stability can be achieved by increasing the overall rotator cuff activity (co-contraction), this is rarely necessary. This also ensures that the magnitude of the resultant is kept as low as possible. Muscle segmentation is of paramount importance for spatial control.

The ASFE offers the advantage of very short calculation time, in generally less than 5 minutes, with a commonly available PC when run with the well-known and widespread Matlab© software.

This algorithm represents a novel force estimation method and a new alternative to the available shoulder simulations.

The strategy of force sharing among muscles opens up the possibility to examine the outcome of muscle deficiencies and to investigate causes of joint instability as encountered in clinical practice.

REFERENCES

1. Fick AE, et al. *Anatomisch-mechanische Studie über die Schultermuskeln, 2. Teil*, Verh Phys-Med Gesell, Würzburg, 1877.

COMPARISON BETWEEN TRIPOD AND SKIN FIXED RECORDING OF SCAPULAR MOTION

Carel G.M. Meskers, Michiel A.J. van der Sande and Jurriaan H. de Groot
Laboratory for Motion Analysis, Departments of Rehabilitation Medicine and Orthopaedic Surgery, Leiden University Medical Center, P.O. box 9600, 2300 RC Leiden, The Netherlands. Email: c.g.m.meskers@lumc.nl

INTRODUCTION

To record 3D scapular rotation, we currently use a scapula-locator: a tripod with an electromagnetic receiver mounted on it, which has to be placed manually and repetitively over the scapula during statical humeral elevations. Measurements of scapular motion by means of an electromagnetic receiver fixed onto the flat part of the acromion (=skin fixed method) potentially enables dynamic and fast motion recording, making it very suitable for clinical measurements. This study was undertaken to: 1) compare tripod to skin fixed recording (concurrent validity); 2) determine the inter-observer variability of skin fixed recording; 3) determine the intra-trial variability; 4) compare statical versus dynamical measurements of scapular rotation at moderate speed.

METHODS

3D shoulder kinematical recordings were performed at eight healthy subjects using both an electromagnetic receiver fixed to an adjustable tripod [1,2] and a receiver fixed to the flat part of the acromion. Measurements were performed according to the standard of the International Shoulder Group [3]. Scapular rotation of the right shoulder was measured during symmetrical elevation in frontal and sagittal plane respectively. Measurements were performed by three observers. Measurements of scapular rotation were performed repetitively to full maximal elevation. Interpolation of data of each of the three scapular rotations (pro-retraction, latero-rotation and spinal tilt) was performed using p-splines [4]. Sampled data at 30, 50, 70, 90, 110 and 130º of humeral elevation were used for statistical testing using a GLM-ANOVA with repeated measurements (SPSS 11.0) to establish the difference between tripod- and skin fixed recordings, intra-trial variability and inter-observer variability of skin fixed measurements and to assess the difference between statical and dynamical (cyclic elevation at about 0.5 Hz) measurements of scapular orientation using the skin fixed method.

RESULTS AND DISCUSSION

The skin fixed method underestimated scapular rotations compared to tripod- based measurements. We found a maximal difference of 6º for orientation (=offset) and 7º for rotation regarding scapula latero rotation during elevation in the frontal plane. These errors exceed the expected error of about 2º evolving from palpation inaccuracies [5] and are attributed to: 1) differences in definitions of local co-ordinate systems (offset error); 2) palpation variability (offset error); 3) skin motion relative to bone (rotational error); 4) influence on acromion receiver position by a stiff receiver cable (rotational error) and 5) interposition of *m. deltoideus* between acromion receiver and scapular bone (rotational error). Inter-observer variability was low compared to tripod measurements (1.91º-4.95º vs. 4.35º-5.15º) and inter trial reliability was high (intra class correlation coefficient > 0.84). The RMSE of statical versus dynamical measurements was below 1º.

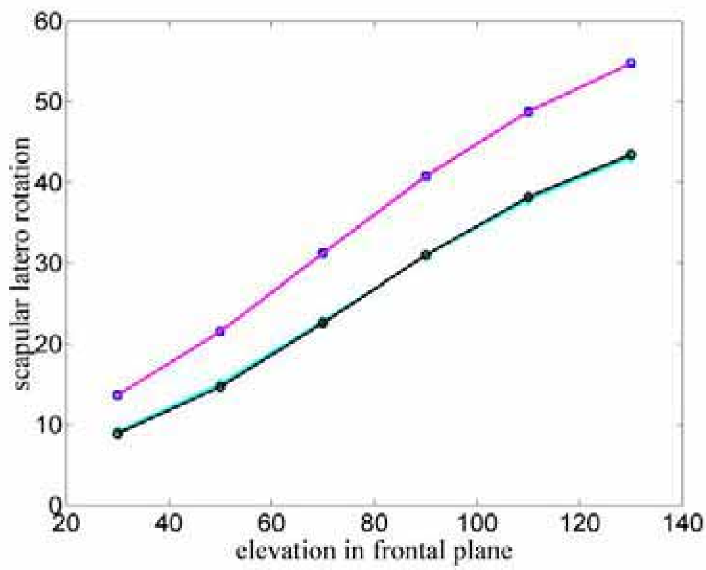

Figure 1: scapular latero rotation as measured by means of a tripod (□) and a skin- fixed method, both statically (Δ) and dynamically (o)

CONCLUSION

A skin fixed method to record scapular rotations is precise but less accurate compared to tripod measurements. Advantages over the latter method are a lower inter-observer variability and the possibility to record scapular motion during low speed continuous arm elevations. Based on the current data, considering a maximal rotational error of 7º, we conclude that shoulder kinematical measurements in a clinical setting can be performed using an electromagnetic receiver attached to the flat part of the acromion.

REFERENCES

1. Johnson GR, et al. *Clin Biomech*. **8**, 269–73, 1993
2. Meskers CGM, et al. *Clin Biomech*. **13**, 280–92, 1998.
3 Van der Helm FCT, www.internationalshouldergroup.org.
4. Eilers PHC, Marx BD, *Statistical Science* **11**, 89-121, 1996
5. De Groot JH*, Clin Biomech* **12**, 461–472, 1997

TELESCOPING ACTION IMPROVES THE FIDELITY OF AN INVERTED PENDULUM MODEL IN NORMAL HUMAN GAIT

Frank L. Buczek, Michael J. Rainbow, Matthew R. Walker, Kevin M. Cooney, James O. Sanders
Shriners Hospitals for Children, Erie, PA, USA
email: fbuczek@shrinenet.org, web: http://www.shrinershq.org/research/erie/

INTRODUCTION

Inverted pendulum models, operationalized in ballistic walking studies [1] and passive dynamic robots [2], have been used to describe normal gait in the absence of active mechanisms, leading some clinicians to minimize the importance of joint powers [3]. We hypothesized that a telescoping action, associated with joint powers, would improve the fidelity of a simple inverted pendulum model applied to normal gait, as measured by its ability to predict horizontal and vertical ground reaction forces (*Fh*, *Fv*, respectively). Unlike previous studies, we made direct comparisons between model predictions and actual gait data for a sample of normal subjects.

METHODS

Kinematic data were collected for 24 normal children at 120 Hz using a ten camera Vicon 612 system, and low-pass filtered (6 Hz cutoff). A thirteen-segment, full-body model was implemented in Visual3D (C-Motion Inc.), and the instantaneous location of the full-body center-of-mass (COM) was calculated. *Fh* and *Fv* were collected at 1560 Hz using three AMTI force plates, and center-of-pressure (COP) coordinates were averaged, consistent with Eqs. (1) and (2) derived for a stationary pendulum pivot. (Here, m is body mass, g is gravitational acceleration, r is pendulum length, and θ, ω, α are the pendulum angular position, velocity, and acceleration, respectively.) Subtracting coordinates of the average COP from those of the instantaneous COM provided a telescoping inverted pendulum. Radial and angular kinematics of this pendulum were calculated using central difference techniques, and input to Eqs. (1) and (2), valid only for single support. Setting radial kinematics ($\dot{r}, \ddot{r}$) to zero removed the telescoping action. Inverse dynamics in Visual3D provided associated lower extremity joint powers. Five separate repeated measures ANOVAs detected differences ($p \leq 0.05$) among measured and predicted kinetic parameters (minima and maxima in *Fh* and *Fv*), with and without telescoping. Root mean square (RMS) errors were also calculated across ensemble averages to quantify differences between actual and predicted *Fh* and *Fv*.

$$Fh = m\left[\left(\ddot{r} - r\omega^2\right)\cos\theta - \left(r\alpha + 2\dot{r}\omega\right)\sin\theta\right] \quad (1)$$

$$Fv = m\left[\left(\ddot{r} - r\omega^2\right)\sin\theta + \left(r\alpha + 2\dot{r}\omega\right)\cos\theta\right] + mg \quad (2)$$

RESULTS AND DISCUSSION

Pendulum compression averaged 1.7 cm over the first 20% of single support, length changes were variable at mid single support, and extension occurred over the last 20% of single support. Ground reaction forces were predicted best when this telescoping action was included (Figure). RMS errors for *Fh* increased from 2.1%BW to 8.0%BW when telescoping was removed, as the predicted force diverged from actual values in early and late single support. RMS errors for *Fv* increased from 6.8%BW to 22%BW, and the double peak pattern was lost, when telescoping was removed. Peaks in *Fh* and *Fv* were significantly different for all comparisons (actual vs. telescoping, actual vs. no telescoping, telescoping vs. no telescoping), but this was not true for a local minimum in *Fv* near 50% single support. In every case, deviations from actual data were worse when telescoping was removed, and these deviations were greatest during lower extremity power bursts calculated for these subjects. We conclude that telescoping contributes to *Fh* and *Fv* during single support, and reflects changes in hip, knee, and ankle angles modulated by joint powers. We expect these findings to be amplified in a companion study of pathological gait, now underway. We also plan to explore correlations between radial powers ($F \cdot \dot{r}$) and joint power bursts.

REFERENCES

1. Mochon S., McMahon T.A. *J Biomech* **13**, 49-57, 1980.
2. McGeer T. *International Journal of Robotics Research* **9**, 62-82, 1990.
3. Perry J. *Gait Analysis*, p. 31, SLACK, Thorofare NJ, 1992.

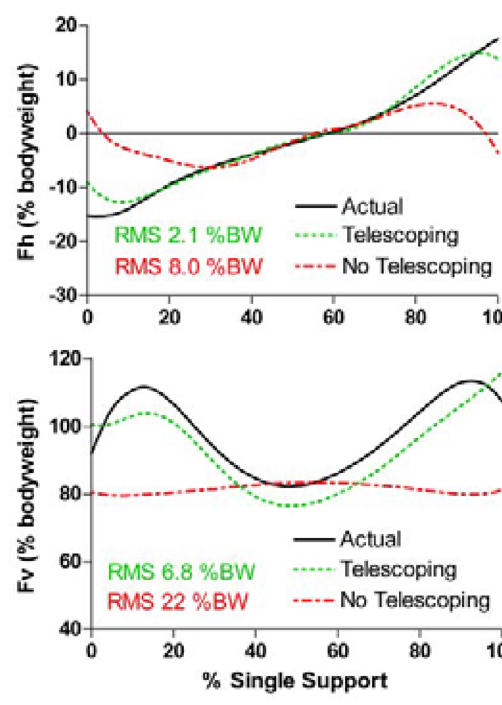

Figure: **Ensemble averages for actual and predicted *Fh* and *Fv*, with and without telescoping action (n = 24).** Note that peaks are attenuated without telescoping. (Standard deviation bands have been omitted for clarity.)

COMPARING NORMAL GAIT ANALYSES USING CONVENTIONAL AND LEAST-SQUARES OPTIMIZED TRACKING METHODS

Frank L. Buczek, Michael J. Rainbow, Kevin M. Cooney, Matthew R. Walker, James O. Sanders
Shriners Hospitals for Children, Erie, PA, USA
email: fbuczek@shrinenet.org, web: http://www.shrinershq.org/research/erie/

INTRODUCTION

The conventional gait model (CN) was pioneered in the late 1960s [1] and has seen widespread clinical use since that time. A desire to minimize the number of motion capture markers in this model was motivated by equipment limitations, including the use of only two or three cameras, and manual digitization of each camera's cine film. This led to the use of markers on one segment to define virtual markers that tracked adjacent segments with no correction for measurement error, and the use of a simple vector to represent the foot. The advent of multi-camera, automated motion capture systems provided opportunities to improve upon these techniques. In particular, an optimized (least-squares), six degree-of-freedom approach (OP) can use an over-determined set of physical markers to track individual segments while adjusting for measurement error [2]. The purpose for this human subjects approved study was to compare gait analysis variables across CN and OP models in normal children. We hypothesized that OP would provide data similar to CN in the sagittal plane, and different from CN in both coronal and transverse planes.

METHODS

Both biomechanical models were created in Visual3D (C-Motion, Inc.). CN was implemented using the Helen Hayes option for the lower extremities and pelvis. OP began with CN joint centers and local reference frames, but tracked all body segments using a minimum of four physical markers. A hybrid marker set allowed a single stride to be analyzed using CN and OP models in 25 normal children. Marker trajectories were collected at 120 Hz using a ten-camera Vicon 612 system, with interpolation and low-pass filtering (6 Hz cutoff) performed in Visual3D. Ground reaction forces were collected at 1560 Hz using three AMTI force plates. Twenty key, functionally-grouped gait analysis variables were calculated in Visual3D (e.g., maxima and minima in hip, knee, and ankle angles, moments, and powers). Dependent t-tests detected differences in these variables across models, using a Bonferroni-adjusted alpha of 0.0025 (i.e., 0.05/20).

RESULTS AND DISCUSSION

Six of nine variables were significantly different in the sagittal plane, yet associated graphical data were unlikely to change clinical interpretations (see sample data, Figure 1a). These differences were attributed to the higher fidelity foot model in OP, and to a more anterior position of the knee center when correctly tracked by four thigh markers in OP, rather than a virtual hip center, a thigh wand, and a lateral knee marker in CN. This latter marker moves posterior to the femoral epi-condyle when the knee is flexed, causing decreased hip and knee flexion angles calculated in CN. No differences were found in five coronal plane variables. Four of six variables were significantly different in the transverse plane, and these were appreciated graphically (see sample data, Figure 1b). In all planes, important, yet untested, features of curves were identified for additional analysis (e.g., maximum knee valgus, etc.). Results for all three anatomical planes require more rigorous accuracy tests. In the meantime, our study shows that for normal children, sagittal and coronal plane biomechanical interpretations, based upon these tested variables, are unlikely to change due to optimized segment tracking alone. The value in these methods seems instead to involve higher fidelity input for forward dynamics [3], and we intend to explore this as one measure of accuracy. These relationships may change when pathological movements exacerbate model differences in a companion study of patients not yet completed.

REFERENCES

1. Sutherland D. *Gait Posture* **16**, 159-79, 2002.
2. Cappozzo A. *Human Movement Science* **10**, 589-602, 1991.
3. Kuo A.D. *J Biomech Engineering* **120**, 148-159, 1998.

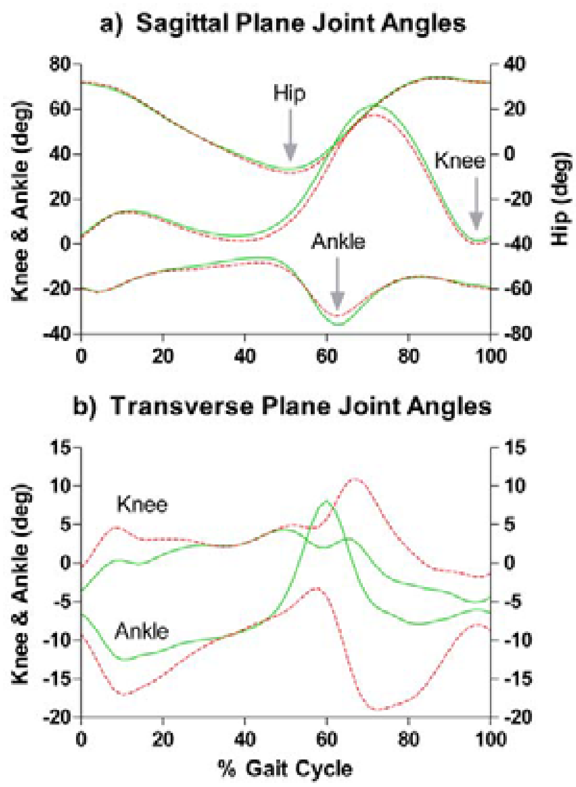

Figure 1: **Sample ensemble average joint angles (n=25). (a)** Significant differences in sagittal hip, knee, and ankle minima (arrows) would be unlikely to change clinical interpretations. **(b)** Transverse plane angles, averaged across the gait cycle, were significantly different between OP and CN models. (OP solid green, CN dashed red.)

IS EFFICIENCY A VIABLE CRITERION FOR SUB-MAXIMAL VERTICAL JUMPING?

[1, 3] Jos Vanrenterghem, [2] Maarten Bobbert, [2] Richard Casius, [1] Dirk De Clercq
[1] Department of Movement and Sport Sciences, Faculty of Medicine and Health Sciences, Ghent University, Belgium
[2] Faculty of Human Movement Sciences, Free University of Amsterdam, The Netherlands
[3] Research Institute for Sport and Exercise Sciences, Faculty of Science, Liverpool John Moores University, UK
e-mail: jos.vanrenterghem@livjm.ac.uk

INTRODUCTION

For the execution of a maximal vertical jump from stance, humans show a unique movement pattern. Over the past decades, researchers have tried to identify the criterion that generates the control signals for this. Through simulation studies it has been shown that a unique movement pattern most likely generates the maximal height achieved by the musculo-skeletal system [1]. In a recent study we found that for jumps towards a sub-maximal target height, humans also have stereotyped movement patterns across individuals [2]. These mainly consisted of decreasing countermovement amplitude for decreasing target heights. According to [2], this indicated that humans could minimize energy-consumption for a sub-maximal jump. Another possibility is that humans simply minimize the total duration of the jump. The purpose of this study was to test the hypothesis that one of these criteria causes the stereotype adaptations for sub-maximal jumping in humans. For this purpose, sub-maximal vertical jumps of a simulation model were generated and the movement patterns were compared with movement patterns observed in humans.

METHODS

An existing 4-segment model with 6 muscle actuators [3] served to simulate countermovement vertical jumps from stance. The initial state of the model was an upright standing position. Switching the muscle actuators “off” and “on” controlled the movement of the model. Two different objective functions were used, one of which generated a given sub-maximal jump height in a minimum amount of time (= minimal time criterion) and the second achieving it with minimal work (= minimal work criterion). The latter criterion involved a rough estimate of energy consumption, counting both eccentric work and concentric muscle work in a ratio of 1:3. Jumps towards heights of 50-60-72-86-93-98-100% of maximal jump height were simulated.

Joint kinematics and kinetics were compared with those of human sub-maximal jumps. The experimental setup was described previously [2], and contained jumps towards heights of 25-50-75-100% of maximal jump height.

RESULTS AND DISCUSSION

Optimizations with both the minimal time and minimal work criterion resulted in unique movement patterns for jumps to heights of 50%-100% of maximal jump height (75% example in figure 1). Both criteria led to similar movement patterns for jumps that were close to maximal jump height (90-100%). For lower jumps (50-90%), solutions of the minimal time criterion were different from those of the minimal work criterion in that they led to incomplete joint extensions and excessive rotational and horizontal energies at toe off. Throughout all jump heights ranging from 50 to 100%, optimizations with the work criterion generated movement patterns that showed a greater resemblance with those of human jumps (representative example in figure 1). Typical adaptations were decreasing hip extension, slightly decreasing knee extension and constant ankle plantar flexion as jump height decreased.

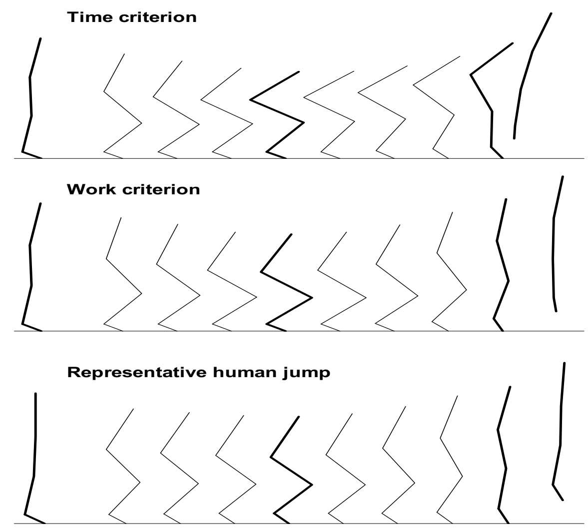

Figure 1: Stick figures showing simulations of minimal time and minimal work optimizations and a human jump for a vertical jump of approximately 75% of maximal jump height.

CONCLUSIONS

Solutions obtained with the minimal time criterion had poor correspondence with humans because of flexed joints, backward velocity and body rotation at take off. Solutions with the minimal work criterion, on the other hand, showed less countermovement in a sub-maximal jump than in a maximal jump and more extended joints and more vertical velocities at take off. This has good correspondence with human jumps and demonstrates that minimized energy-consumption is a viable criterion for sub-maximal jumping.

REFERENCES

1. Pandy MG & Zajac FE, *J Biomech* **24**, 1-10, 1991.
2. Vanrenterghem J et al., *Hum Mov Sc* **22**, 713-727, 2004.
3. Van Soest AJ & Bobbert MF, *Biol Cybern* **69**, 195-204, 1993.

DYNAMIC SIMULATION AND EXPERIMENTAL VALIDATION OF THE PLANTAR FOOT PRESSURE DURING HEEL STRIKE

[1] Weng-Pin Chen, [1,2]Shih-Cherng Lin and [2]Fuk-Tan Tang
[1]Department of Biomedical Engineering, Chung Yuan Christian University, Chungli, Taiwan,
[2]Department of Rehabilitation, Chang Gung Memorial Hospital, Kweishan, Taiwan; email: wpchen@cycu.edu.tw

INTRODUCTION

Computational analysis of the foot biomechanics has its advantage in providing an overall stress distribution of the foot. It is also more economical than in vitro cadaver experiments. In the current study, a general mesh generation software, Gridgen V14, was used to establish a three-dimensional hexahedral foot finite element model with detailed joint characteristics and partial plantar soft tissues. In addition, a dynamic finite element analysis software, LS-DYNA 970, was incorporated with the kinematic data from gait analysis for the dynamic simulation of foot motion during heel strike. The pressure distributions at the heel region during heel strike were investigated. Furthermore, in order to validate the analysis results, the plantar pressures of the same subject who provide the foot geometry was measured during heel strike. Both the analysis and measured results showed similar trends and within the same range.

METHODS

A detailed 3-D finite element foot model was created based on the computed tomography images of the left foot of a 24 yr male subject. A finite element mesh generation program (Gridgen V14, Pointwise, Inc., Fort Worth, Texas, USA) was used to generate 10-node hexahedral elements for the bones (12985 elements), cartilages (536 elements) and portion of the plantar soft tissues (6686 elements).(Fig. 1). The material properties for the bone was assumed to be linear elastic while the cartilage and soft tissue were assumed to be visco-elastic. The Young's modulus, Poisson's ratio, density, bulk modulus (short term and long term) were adopted from literature[1,2]. The kinematic data of the foot of the male subject during heel-strike at normal walking speed (1.2 m/s) was obtained using a Vicon-370 motion analysis system. Also, the plantar pressure of the foot was recorded for ten times using a RS-SCAN foot plate system. The vertical and horizontal velocities of the foot (0.6 m/s; 3.12 m/s) were used as loading condition in the simulation. Initial contact angle of the foot with respect to the ground was assumed to be 23° (Fig. 1). A force varying linearly from 0-420 N was applied on the trochlea of talus to simulate the effect of body weight during heel strike. The analysis was performed using LS-DYNA 970（Livermor, USA） on an HP-SPP2200 supercomputer. The stresses in the bone and plantar soft tissues were computed at each of the 100 increments during the simulation time span of 0.048 s.

RESULTS AND DISCUSSION

Analysis results showed that the plantar pressure increased with respect to the time as the foot starting to be in contact with the ground. The plantar pressures at the heel region obtained from the analysis were compared with the measured results using RS-SCAN plate system. Similar trends were found and the peak value for the analysis results at t=0.48 was

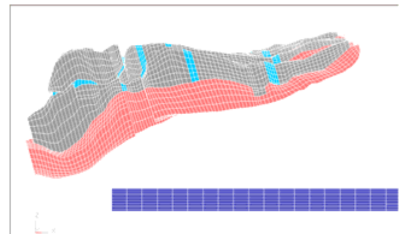

Figure 1: Hexahedral finite element model of the foot bone with plantar soft tissues

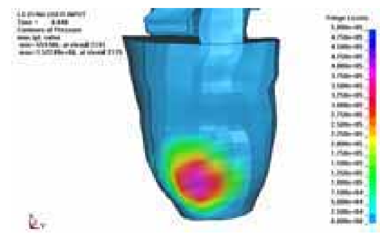

Figure 2: The normal stress of the plantar soft tissue at the heel region at t=0.048s obtained from simulation

found to be 302 KPa. On the other hand, the measured peak plantar pressure was found to be ranging from 248 to 316 KPa (10 measurements). As for the bone stresses, calcaneal stress distribution was transferred gradually from calcaneocuboid joint nearby to posterior calcaneus. Thus, the mean von Mises stress was around 30 ~ 180 KPa. However, anterior and posterior joint surfaces of the subtalar joint sustained compressive stress, and medium joint surface of subtalar joint received tensile stress.

CONCLUSIONS

A 3-D hexahedral finite element model was established and analyzed in this study. The simulation results were validated from plantar pressure measurements. With the application of this model, dynamic finite element analysis for a full gait cycle can be completed in future studies. This model can also provide useful information for footwear and orthosis designs.

.

REFERENCES

1. Chen WP et al. *Clin. Biomech.* **16**, 614-620, 2001.
2. Bandak FA et al. *Int J Solids and Structures* **38**, 1681-1697, 2001.

ACKNOWLEDGEMENTS

This research was supported by the National Science Council, ROC. (grant no.: NSC 91-2614-E-033-001)

SCALING AND JUMPING: GRAVITY LOSES GRIP ON SMALL JUMPERS

Melanie N. Scholz, Maarten F. Bobbert and A.J. “Knoek” van Soest
Institute for Fundamental and Clinical Human Movement Sciences, Vrije Universiteit, Amsterdam, The Netherlands; email: m.scholz@fbw.vu.nl, web: www.ifkb.nl

INTRODUCTION

The current view on the scale effects on jumping is that (1) jumping performance is independent of size in the absence of air friction: all animals would achieve the same jump height (rise of the body center of mass while airborne) if they were geometrically similar and delivered the same amount of work per kg body mass during the push-off (Borelli’s Law), and (2) in the presence of air friction smaller jumpers are at a disadvantage, because they waste relatively more energy on air friction than larger animals due to their larger surface to volume ratio.

It can not be explained from an evolutionary view why jumping locomotion is primarily adopted by small animals, such as insects. Besides, jumping is a battle against gravity and for static situations, i.e. standing with flexed legs, defying gravity becomes easier with decreasing size because the moment of gravity that needs to be counteracted decreases at a higher rate than the muscle moment (L^4 and L^3 respectively, where L is the scaling factor for length). It is evaluated analytically and numerically how this mechanical advantage translates to dynamic situations and affects jumping performance as a function of size.

METHODS

On the basis of energy balances for geometrically similar jumpers consisting of a point mass and massless legs, it is shown analytically that Borelli’s Law is wrong. With the same mass specific work (work per kg body mass), smaller jumpers achieve higher take-off velocities and hence greater jump heights.

$$v_{take-off} = \sqrt{2(W_m - Lg\Delta h)}$$

where $v_{take-off}$ is take-off velocity, W_m is mass specific work, g is the acceleration due to gravity, Δh is the height gained prior to take-off and L is the scaling factor for length.

To assess how the relationship between size and jumping performance contributes to our understanding of real jumping animals, numerical simulations were conducted using a more realistic generic jumper model [1]. One hundred geometrically similar bipedal jumpers ranging from $7{*}10^{-6}$ kg to 70 kg were modeled. Jumpers were actuated by constant knee extensor torques that scaled with mass, so that all jumpers produced the same amount of mass specific work over the same angular knee-extension.

RESULTS AND DISCUSSION

Smaller jumpers achieved greater jump heights than larger jumpers. Absolute jump height increased by 70% when scaling down a jumper from 70 kg to 0.7 g. Figure 1 shows the amount of mass specific work delivered by each jumper during push-off, as well as how it was expended. A division is made in (1) effective kinetic energy (energy due to vertical velocity of the body centre of mass), (2) potential energy and (3) ‘useless’ kinetic energy, energy that does not contribute to jump height (e.g. rotational kinetic energy). Smaller jumpers actually delivered slightly less mass-specific work during the push-off. This is because they took off with more flexed legs, for reasons explained elsewhere [2]. Nevertheless, smaller jumpers jumped higher because they converted a larger fraction of the work into effective kinetic energy. In other words, smaller jumpers achieved higher take-off velocities because of a higher efficacy.

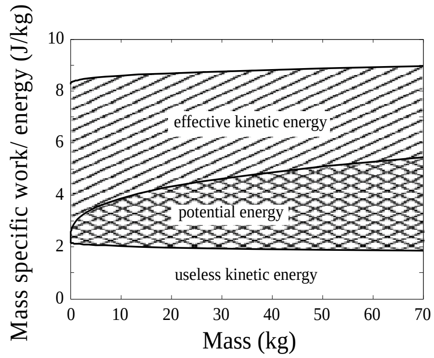

Figure 1: Energy expenditure for different sized jumpers in the absence of air resistance. Total energy expenditure is divided into effective kinetic energy (hatched), potential energy (double hatched) and ‘useless’ kinetic energy (solid white).

CONCLUSIONS

To conclude, size does matter in jumping. If all animals were geometrically similar and delivered the same amount of work per kg body mass, small jumpers would jump higher than larger ones. In nature, small jumpers do not consistently jump higher than larger ones, hence they are not geometrically similar and it can be predicted that small jumpers require relatively less muscle mass. According to the literature, relative jumping muscle mass amounts to 25-40% of the body weight in the galago, 11-15% in various frogs and only 4-6% in locust. A small jumper needs relatively less muscle mass than a large jumper to achieve a certain take-off velocity. Muscle tissue is energetically expensive for an animal because of its high (resting) metabolism. If the benefits of high take-off velocity (i.e. fast escape from predators) are combined with the challenge to sustain as little muscle tissue as possible, being small seems to present the best compromise.

REFERENCES

1. Alexander, R. M. *Philosophical Transactions of the Royal Society of London. Series B: Biological Sciences* **347**, 235-248 (1995).
2. Bobbert, M. F. & Van Soest, A. J. *Exercise and Sport Sciences Reviews* **29**, 95-102 (2001)

FAILURE PROPERTIES OF CERVICAL SPINAL LIGAMENTS UNDER HIGH-RATE LOADING

[1]Scott R. Lucas, [1]Cameron R. Bass, [1]Robert S. Salzar, [1]Chris Planchak, [1]Adam Ziemba
[2]Barry Shender and [2]Glenn Paskoff
[1]Center for Applied Biomechanics, University of Virginia
[2]NAVAIR, Patuxent River, MD
E-mail: slucas@virginia.edu, Web: www.centerforappliedbiomechanics.org

INTRODUCTION

The US Navy is currently developing a finite element model of the human spine to investigate the response of the spine to high-rate loading similar to the input pulse during an aircraft ejection [1]. The University of Virginia Center for Applied Biomechanics is performing experimentation to develop material properties [2] and failure properties of soft-tissues (ligaments and intervertebral discs), which will be implemented into the spine finite element model. This paper presents the failure properties of the anterior longitudinal ligament (ALL), posterior longitudinal ligament (PLL), and ligamentum flavum (LF) in the human cervical spine.

METHODS

Six male and five female human cervical spines were used in this study. The average age of the male and female subjects was 60 yr ± 9 yr and 58 yr ± 6 yr. The average stature and mass were 1749 mm ± 40 mm and 77 kg ± 17 kg for the male subjects and 1626 mm ± 51 mm and 62 kg ± 19 kg for the female subjects. The ALL, PLL, and LF were isolated from each cervical spine at C3-C4, C5-C6, and C7-T1, resulting in a total of 54 male ligaments and 45 female ligaments. Of those, 47 male ligaments and 42 female ligaments were suitable for testing. Ligaments were excluded from testing if they were damaged during specimen preparation. The ligaments were mounted in a universal test machine (Instron, Inc. # 8874 Canton, MA) for uniaxial tests in an orientation that represents physiological conditions. The fixture was enclosed in an environmental chamber to maintain physiological temperature (99 ± 1 ˚F) and humidity (>90%). After the appropriate preconditioning, each ligament was subjected to a battery of material property tests [2], followed by failure tests. The failure tests included step inputs of 75% strain, 100% strain, and 300% strain. A typical strain rate in the failure step tests was 70-150 s^{-1}. Injury risk functions were then generated using a survival analysis on the peak stresses resulting from a 100% step strain input.

RESULTS AND DISCUSSION

The failure analysis was performed using the 100% strain step input tests; therefore, the strain rate (~80 sec^{-1}) did not vary substantially between tests. Otherwise, the viscoelastic nature of the ligaments would result in varying peak stresses depending on the strain rate. A consistent strain rate allows for a direct comparison of peak stress among the ligaments. The engineering stress was calculated using published cross-sectional areas for the ALL, PLL, and LF [3]. The following equations were then used to compute true strain, ε_T, and true stress, σ_T, assuming that the ligaments are incompressible, thus maintaining a constant volume during the tensile loading:

$$\varepsilon_T = \int d\varepsilon = \int_{l_o}^{l_f} \frac{dl}{l} = \ln\frac{(l_o + \Delta l)}{l_o} = \ln(1+\varepsilon_E) \qquad (1a)$$

$$\sigma_T = \frac{F}{A} = \frac{F}{A_0}\cdot\frac{l}{l_0} = \sigma_E(1+\varepsilon_E) \qquad (1b)$$

where F is force, A is cross-sectional area, A_o is initial cross-sectional area, l is length, l_o is initial length, σ_E is engineering stress, and ε_E is engineering strain. Figure 1 and Figure 2 is a representation of the failure strain and corresponding failure stress for each ligament. The similarities of the failure characteristics between genders are consistent with the findings from a statistical analysis of cervical spinal ligament material properties in a previous study by Lucas et al. [2]. From the injury risk functions, the true stress corresponding to a 50% risk of an AIS 3 injury for the ALL, PLL, and LF is 11.6 N/mm^2, 12.6 N/mm^2, and 13.2 N/mm^2.

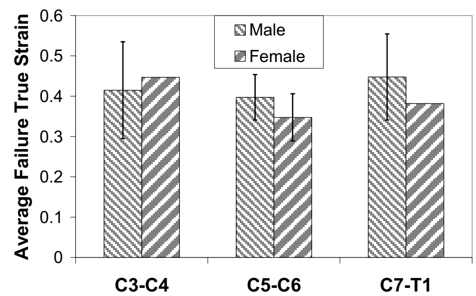

Figure 1: Failure true strain for posterior longitudinal ligament

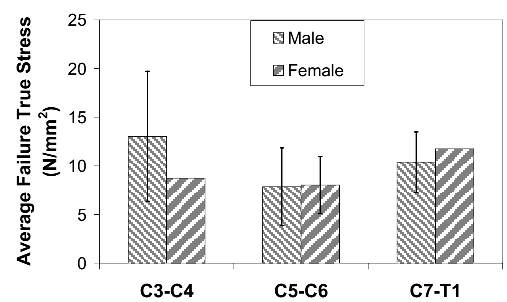

Figure 2: Failure true stress for posterior longitudinal ligament

CONCLUSIONS

The primary objective of this study was to develop failure characteristics of the ALL, PLL, and LF in the human cervical spine under high-rate loading. The injury tolerances are implemented into a finite element model of the cervical spine to assess injury due to aircraft ejection.

REFERENCES

1. Paskoff, G. Influence of Helmet Mass Properties on Head/Neck Forces During High-Speed Ejection. *4th World Congress of Biomechanics*, Calgary, Canada, 2002.
2. Lucas et al. Viscoelastic Characterization of Cervical Spinal Ligaments. *26th ASB Conference*, Portland, OR, 2004.
3. Yoganandan et al. Geometric and Mechanical Properties of Human Cervical Spinal Ligaments. *J Biomech Eng* **122**, 623-629, 2000.

Elderly adults perform less limb work during walking

Justus Ortega and Claire Farley
Locomotion Laboratory, Department of Integrative Physiology
University of Colorado, Boulder, CO, USA
E-mail: Justus.Ortega@colorado.edu

INTRODUCTION

Elderly adults consume more metabolic energy for walking than young adults across a range of speeds (3). It has been hypothesized that the mechanical work performed by the limbs, including the simultaneous positive and negative work by the two limbs during double support, is an important determinant of the metabolic cost of walking (2). This study tests the hypothesis that walking is more metabolically expensive for elderly adults because they perform more mechanical work with their limbs than young adults.

METHODS

Ten young (25 ± 5 yrs, mean ± SD) and ten elderly (75 ± 5 yrs) adults walked at five speeds on a treadmill and on a 40 m walkway with imbedded force platforms. Subjects performed one seven-minute trial at each speed on the treadmill and three trials at each speed on the walkway.

Metabolic cost was determined using indirect calorimetry (1) during the last two minutes of each treadmill trial. We calculated net metabolic cost of transport by subtracting standing metabolic power from gross metabolic power and dividing by body mass and speed.

We measured ground reaction force (GRF) under each limb on the walkway and subsequently calculated individual limb mechanical work (ILW) from the dot product of the GRF and the center of mass (COM) velocity (2). ILW exceeds the traditionally calculated external work because it includes the simultaneous opposing work performed by the two limbs during double support (2).

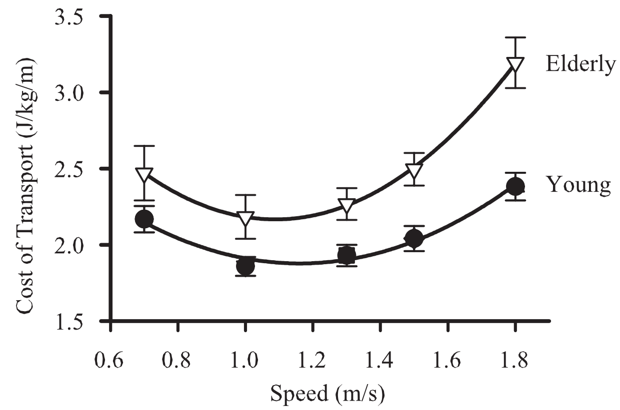

Figure 1: Net metabolic cost of transport (mean ± SEM) versus speed.

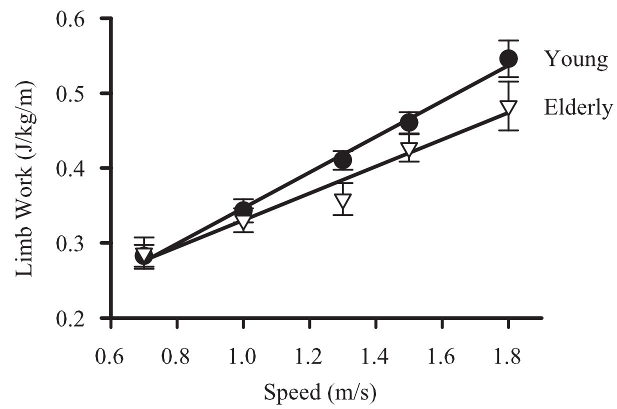

Figure 2: Positive limb work (mean ± SEM) versus speed.

RESULTS AND DISCUSSION

Despite consuming 20% more metabolic energy (p=0.010; Figure 1), elderly adults perform about 7% less limb work to travel a meter than young adults (p=0.028; Figure 2). This difference is mainly due to the elderly subjects performing about 14% less positive limb work during double support than young adults.

The reason why elderly adults perform less individual limb work may be that they take shorter steps at a faster stride frequency. By taking shorter steps, elderly adults exert lower peak propulsive GRF and reduce the vertical excursion of the COM. Both of these factors reduce the mechanical work needed to redirect the COM when it transitions from arcing over one stance limb to arcing over the next stance limb (2).

Elderly adults have a faster stride frequency than young adults primarily because they spend less time in the single limb support phase. It seems likely that the single support phase is the least stable part of a stride, and therefore, shortening this phase may be a response to reduced stability with aging.

CONCLUSIONS

Although elderly adults consume more metabolic energy to travel a meter than young adults, they perform less limb work than young adults. Although the shorter stride length of elderly adults may partly explain the difference in step-to-step transition work, the high metabolic cost of walking in elderly adults is likely due to other factors, such as greater muscle force generation for stabilization.

REFERENCES

1. Brockway, J.M.. *Hum Nutr Clin Nutr* **41**, 463-471, 1987.
2. Donelan, J.M. et al.. *J Exp Biol* **205**, 3717-3727, 2002.
3. Martin, P.E. et al.. *J Appl Physiol* **73**, 200-206, 1992.

ACKNOWLEDGEMENTS

NIH Grants- AG 00279, M01 RR00051

EFFECT OF GENDER ON KNEE ABDUCTION AND FLEXION DURING MEDIAL AND LATERAL LANDINGS

[1]Kevin R. Ford, [1]Gregory D. Myer and [1,2]Timothy E. Hewett
[1]Cincinnati Children's Hospital Medical Center, Sports Medicine Biodynamics Center,
[2]University of Cincinnati, College of Medicine; email: kevin.ford@cchmc.org, web: www.cincinnatichildrens.org/sportsmed

INTRODUCTION

Females who participate in pivoting and jumping sports suffer anterior cruciate ligament (ACL) injuries at a 4 to 6-fold greater rate than males participating in the same sports. ACL injuries often occur during single leg landings or quick changes of direction from either the medial or lateral direction[1]. The purpose of this study was to compare the knee joint kinematics during two types of single leg landings in male and female collegiate athletes. The hypothesis was that females would demonstrate greater knee abduction, but similar levels of knee flexion compared to male athletes.

METHODS

Eleven female and 11 male collegiate athletes were height (female 176±8cm, male 176±8cm) and weight (female 73±7kg, male 74±6kg) matched. Informed written consent was obtained from each subject. Each subject was instructed to balance on one leg on a 13.5 cm block positioned adjacent to the force plate. They were then randomly instructed to drop off the block medially or laterally and land on the same leg and balance for approximately 2 seconds.

An 8 camera motion analysis system (Eagle, Motion Analysis Corp.) with two force platforms (AMTI) were used for data collection. Video and force data were time synchronized and collected at 240 Hz and 1200 Hz, respectively. 37 retroreflective markers were secured to each subject in predetermined anatomical locations. A kinematic model was defined from a standing static trial using Mocap Solver (Motion Analysis Corp.)[2]. Joint rotations in the hip, knee, and ankle were expressed relative to a neutral position where all segment axes are aligned. The data were low-pass filtered with a cubic smoothing spline at a 15 Hz cut-off frequency. A mixed ANOVA was utilized to test for the main effects of gender, task and side with alpha level of 0.05.

RESULTS AND DISCUSSION

Mean and standard deviations for each variable are presented in Table 1. The data are presented as averaged between the two sides as there were no side main effects or interactions. Female subjects had significantly greater knee abduction angles at IC (P<0.001) and maximum (P<0.001) compared to males (Figure 1). In contrast males displayed greater knee adduction maximum during the landings (P=0.005). There were no gender effects on knee flexion angle at either IC or maximum (Figure 2). During the lateral landings both male and female subjects had greater knee flexion and abduction angles at IC (P<0.001)(Table 1). There were no task*gender interactions.

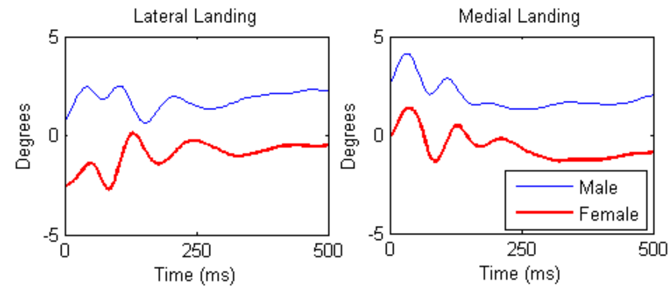

Figure 1. Knee abduction (-) angle in male (thin blue line) and female (bold red line) during the lateral and medial landings.

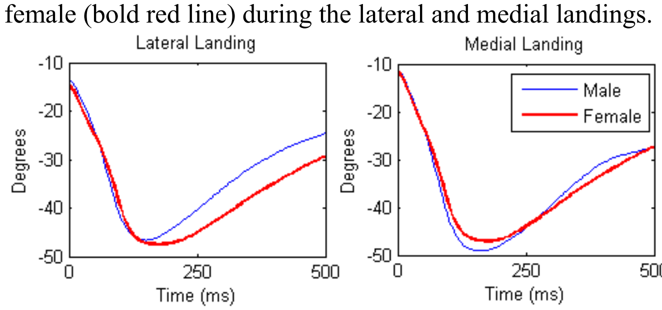

Figure 2. Knee flexion (-) angle in male (thin blue line) and female (bold red line) during the lateral and medial landings.

CONCLUSIONS

Increased knee abduction angles has been previously shown to be predictive of ACL injury risk in female athletes [3]. In the current study females landed with increased knee abduction angles compared to males. Although further research is needed, a higher occurrence of ACL injuries may result from lateral landings as compared to medial landings.

REFERENCES

1. Olsen, OE, et al., *Am J Sports Med* **32**, 1002-12, 2004.
2. McLean, SG, et al., *J Biomech Eng* **125**, p. 864-874, 2003.
3. Hewett, TE, et al., *Am J Sports Med* **33**, 2005.

ACKNOWLEDGEMENTS

This work was supported by NIH Grant R01-AR049735-01A1 (TEH).The authors would also like to acknowledge Scott G. McLean, PhD for his programming expertise.

Table 1. Knee joint flexion and ab/adduction angles during each landing (mean ± SD).

Knee Angles (degrees)	Lateral		Medial		Main Effects	
	Female	Male	Female	Male	Gender	Task
Flexion Initial Contact	-13.6 ± 3.9	-13.5 ± 4.1	-10.8 ± 3.8	-11.2 ± 3.7	F=0.01, P=0.9	**F=43.8, P<0.001†**
Flexion Maximum (-)	-49.2 ± 6.9	-49.0 ± 4.7	-49.0 ± 7.2	-48.9 ± 4.0	F=0.004, P=0.95	F=0.04, P=0.8
Ab/Adduction Initial Contact	-2.4 ± 2.0	1.7 ± 2.3	-0.5 ± 2.2	3.0 ± 2.8	**F=20.0, P<0.001‡**	**F=62.3, P<0.001†**
Adduction Maximum (+)	1.1 ± 3.4	5.0 ± 2.9	2.4 ± 3.2	5.6 ± 3.1	**F=10.0, P=0.005‡**	**F=11.1, P=0.003†**
Abduction Maximum (-)	-4.9 ± 3.1	0.1 ± 3.1	-4.2 ± 3.9	0.5 ± 3.9	**F=14.5, P<0.001‡**	F=4.2, P=0.054

THE EFFECT OF MILD LIMB LENGTH INEQUALITY ON ABLE-BODIED GAIT ASYMMETRY: A PRELIMINARY ANALYSIS

[1]Matthew Kirk Seeley, [1]Jody Clasey, [1]Brian R. Umberger, & [1]Robert Shapiro
[1]University of Kentucky, Lexington, KY, USA
email: mkseel2@uky.edu, web: www.coe.uky.edu/biodynamics/

INTRODUCTION

Gait is one of the most basic of all human movements, but many aspects of gait, such as the causes of bilateral, lower-limb asymmetries, are still not fully understood [1]. Subtle morphological differences have been suggested as one cause of asymmetries [2], but have not been thoroughly investigated. Therefore, the purpose of this study was to investigate the relationship between morphological differences, specifically mild (< 3 cm) limb length inequalities (LLI), and bilateral, lower-limb, mechanical asymmetries during able-bodied gait.

METHODS

Fourteen females and thirteen males participated in this study (Age = 30 ± 6 yrs; Mass = 73.9 ± 16.9 kg; Height = 1.73 ± 0.10 m). Participation included two data collection sessions: 1) limb-length assessment, and 2) gait analysis. All participants signed an informed consent form before participating.

Limb-length was assessed using dual energy x-ray absorbtiometry. Total body scans were performed using a Lunar DPX-IQ bone densitometer. Limb length was calculated by summing femoral and tibial lengths [3]. LLI were quantified by subtracting the left limb length from the right limb length. The absolute value of this calculation served as the measure of LLI.

Gait analysis was performed using a six-camera motion analysis system (60 Hz) and the Cleveland Clinic marker set. Sagittal plane hip, knee, and ankle joint powers, normalized to body mass, were the gait variables of primary interest. Participants walked at a self-selected pace over two embedded force platforms (960 Hz) so that the right and left feet struck separate force platforms during simultaneous gait cycles. Bilateral, lower-limb asymmetry throughout the gait cycle was quantified using the Euclidean distance (ε) formula:

$$\varepsilon = \sqrt{[(X_{R1}-X_{L1})^2 + (X_{R2}-X_{L2})^2 + \ldots + (X_{R100}-X_{L100})^2]} \qquad (1)$$

where X represents the gait variable under consideration; R and L subscripts represent the considered side (left or right); and the numerical subscripts represent the normalized time interval during the gait cycle.

A Pearson's correlation coefficient was used to describe the linearity of the relationships between LLI and gait asymmetries.

RESULTS AND DISCUSSION

Mild LLI were observed (7 ± 7 mm). Using ε as a single measure of joint power asymmetry throughout the entire gait cycle, bilateral asymmetries were observed at the hip (4.84 ± 2.86 W/kg), knee (4.35 ± 2.23 W/kg), and ankle (2.83 ± 1.50 W/kg). However, no significant, linear relationships between LLI and hip power (R^2 = .012), knee power (R^2 = .081), or ankle power (R^2 = .006) were observed (Figure 1). Three other gait variable asymmetries that did result in statistically significant, but weak, linear relationships with LLI were: 1) knee flexion moment (R^2 = .196), 2) ankle abduction moment (R^2 = .158), and 3) ankle flexion angle (R^2 = .183).

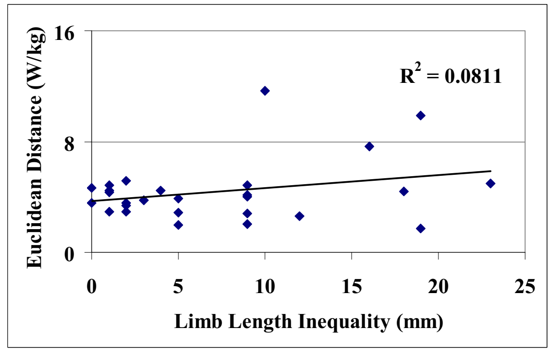

Figure 1: A scatter plot, typical of the plots observed during this study, showing a non-significant, linear relationship between limb length inequality and bilateral, knee joint power asymmetry during able-bodied gait.

Based on the current analysis, there are only weak relationships between mild LLI and bilateral asymmetry during human gait. It is unknown whether a mean LLI closer to our 3 cm threshold might have led to larger gait asymmetries. It is also not clear whether our ε measure is the single best indicator of asymmetry over the gait cycle (as opposed to at a specific point in the cycle). We are currently considering other indicators of asymmetry that might better take into account the whole movement cycle.

CONCLUSIONS

During the present study, only a few weak, linear relationships between LLI and able-bodied gait asymmetry were revealed; no statistically significant, linear relationships were observed between LLI and able-bodied gait asymmetry for the gait variables of primary interest. Further research considering: a) other methods effective in quantifying gait asymmetry; b) variables that resulted in significant correlations during this study; and c) other issues that may contribute to able-bodied gait asymmetry such as footedness, the environment, skill, or neuromuscular factors may also help illuminate this topic.

REFERENCES

1. Sadeghi, H, et al.. *Gait & Posture,* **12,** 34-45, 2000.
2. Subotnick, SI.. *J Orthop Sports Phys Ther* **3,** 11-16, 1981.
3. Durkin, JL, et al.. *J of Biomech* **35,** 1575-1580, 2002.

DEVELOPMENT OF A BIOMECHANICAL SHOULDER MODEL FOR ERGONOMIC ANALYSES

[1]Clark R. Dickerson, [2]Don B. Chaffin and [3]Richard E. Hughes
[1]Department of Kinesiology, University of Waterloo, cdickers@uwaterloo.ca
Departments of [2]Biomedical Engineering and [3]Orthopaedic Surgery, University of Michigan

INTRODUCTION

The study of work-related shoulder disorders has recently elicited an increased amount of attention by scientists [1]. Indeed, load levels in shoulder tissues have been identified as a risk factor for the development of these musculoskeletal disorders [2]. Despite this, few tools are available for the assessment of loading of shoulder structures for dynamic work tasks, especially in prospective job design. Thus, a computerized biomechanical model of the shoulder was developed. There are three major modules in the model: 1) a shoulder geometry module; 2) a dynamic torque module; and 3) a muscle force prediction module. The modules were evaluated empirically with a set of load transfer tasks.

METHODS

The most critical design criterion for the modules was future implementation in prospective job analysis tools, including digital human modeling (DHM) software. Hence, the modules are driven by data types producible in virtual environments: body landmark motion, task and anthropometric properties.

Several aspects of the geometric model were based on prior findings [3,4], including segment and muscle unit definitions, placements of muscle attachment sites, and a mathematical shoulder rhythm. A graphical representation of the internal musculature was developed (Figure 1), allowing visualization of the movements of the shoulder components during motion.

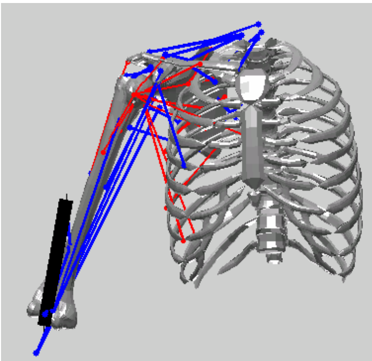

Figure 1: Internal Shoulder geometry. Muscles are shown as having linear and wrapped lines of action.

The external torque module requires 3-D dynamic equilibrium about each of the three joints in the upper arm (wrist, elbow, and glenohumeral), and generates 3-D shoulder joint torques. These torques are inputs to the internal force prediction module. This module distributes these torques amongst 38 muscle units through use of an optimization paradigm. The model includes a novel glenohumeral constraint based on empirical data [5].

Additionally, load transfer tasks were performed by 8 subjects. The tasks were one-handed transfers of loads to locations in the right-handed reach envelope. Hand Loads were varied between 0 and 50% of extended arm flexion/abduction strength. Surface Electromyography (sEMG) data was collected for 11 shoulder muscles to enable model evaluation.

RESULTS AND DISCUSSION

The model showed differential ability across muscles to predict the levels of activation demonstrated by the sEMG recordings as shown by the correlation coefficients in Table 1. Concordance analysis also showed higher concordance ratios for muscles that were primary agonists.

Table 1. Correlation coefficients of predicted and recorded muscle forces levels in the shoulder.

Muscle	*r* value
Infraspinatus	0.63
Biceps	0.61
Deltoid, Total	0.53
Lower Trapezius	0.52
Middle Deltoid	0.42
Latissimus Dorsi	0.32
Posterior Deltoid	0.31
Trapezius, Total	0.27
Anterior Deltoid	0.26
Upper Trapezius	0.01
Pectoralis Major	0
Triceps	-0.20

CONCLUSIONS

The model showed the highest predictive performance for those muscles that were demonstratively most active by sEMG recordings. Muscles that were not mechanical contributors to resisting the calculated external shoulder torques were predicted less accurately. These results are likely due to the combination of the use of a monotonically increasing cost function in the optimization (muscle stress cubed), and the exclusion of potential confounding factors (i.e. segment stiffness, detailed muscle properties). Nonetheless, from an ergonomic analysis point of view, the model is useful for identifying those tissues that are most stressed for a given task.

REFERENCES

1. DHHS (NIOSH) Publication No. 97-141, 1997.
2. Herberts P et al. *Clin Orth*. 191:161-178, 1984.
3. Hogfors C et al. *J Biomech* 20:157-166, 1987.
4. Hogfors C et al. *J Biomech* 24:699-709, 1991.
5. Lippitt et al. *J Shoulder and Elbow Surgery* 2:27-35, 1993

ACKNOWLEDGEMENTS

The authors would like to acknowledge the support of the Automotive Research Center and the HUMOSIM Partners.

3D GEOMETRICAL OPTIMIZATION OF THE TALAR DOME

[1]Andrew R. Fauth, [1,2]Neil A. Sharkey, and [3]James Michelson
[1]Dept. of Kinesiology, The Pennsylvania State University, University Park, PA
[2]Dept. of Orthopaedics and Rehabilitation, The Pennsylvania State University, Hershey, PA
[3]Dept. of Orthopaedic Surgery, The George Washington University, School of Medicine and Health Services
email: nas9@psu.edu url: http://www.biomechanics.psu.edu

INTRODUCTION

The human ankle joint presents a complicated mix of geometry and anatomy that together create an intricate, multi-axis joint capable of complex motions. Past cadaveric and radiographic examinations of the ankle joint have attempted to assess the radii of curvature of the talus by assuming the talar dome to be cylindrical, at least in the 2D sagittal view.[1,4,5,6] Recent studies focused on total ankle arthroplasty applications suggest that the talar dome has a more complicated polyradial and polycentric shape.[2,3] There is little, if any, literature regarding assessments of the surface of the talus with respect to 3D geometry using a numerical optimization approach. The goal of this study was to accurately describe the 3D geometry of the talar dome by combining 3D digitization of cadaveric specimens with numerical optimization.

METHODS

Eight fresh, frozen, non-paired cadaver lower extremities with a mean age of 61.3 years (range 25-80) were used for this experiment. The group was composed of four male and four female specimens equally divided between right and left. Prior to testing, the specimens were thawed, radiographed, and subjected to a number of anthropometric measurements. Each specimen was then dissected and the talus was removed, potted in bone cement (PMMA), and secured in a rigid fixture. A 1mm x 1mm grid was drawn onto the entire articular surface of each talus and a Microscribe 3D digitizing tool (Immersion Corp., CA, USA) was used to collect points along the gridlines.

Following digitization, the data were analyzed in Matlab (V.7.0, Mathworks, MA, USA) using a least-squares optimization approach with the Levenberg-Marquardt algorithm to assess the accuracy of fitting a cylinder to the native shape of the articular surface. First, the superior articular surface of the talar dome was isolated from the medial and lateral walls. Next, a best-guess axis was established by finding the direction vector that connected the most superior point on both the medial and lateral edges of the surface data. This line was then inferiorly offset to provide an initial guess for the cylinder axis. The unit direction vector of this guess axis, a point on the axis, and a radius was provided as an initial estimate to the optimization routine, which then determined the best fit cylinder to all the data points on the superior articular surface of the talus. The resulting output of the optimization was a new axis point, axis direction vector, and a radius that described the best-fit cylinder (Figure 1). The accuracy of the cylinder fit was described by the mean-square error (MSE) of the optimization.

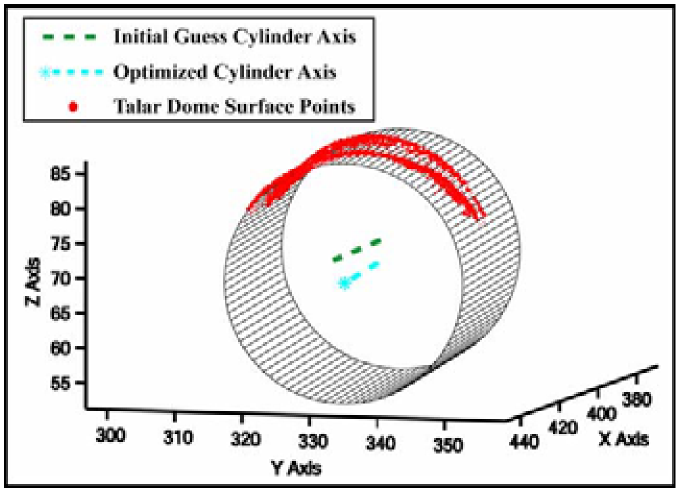

Figure 1. Talar dome surface points for one specimen and the cylinder fit to the points by numerical optimization**.**

RESULTS AND DISCUSSION

According to the results, a cylinder accurately describes the geometry of the superior talar dome (Table 1). MSE for the optimizations ranged from less than 0.1 mm to 0.43 mm. These data confirm that the overall shape of the superior talar dome can be accurately represented by a cylinder in 3D. The optimized cylinder radii were found to be similar for all males (~22mm) and all females (~18mm) respectively, and the difference between the two groups was significant. The calculated radii of curvature are in the range of previous 2D estimates of talar dome radii of curvature.[2,4,6] Examinations of the anthropometric data showed low variance in foot size, however, limiting statistical power. Further examinations are necessary to draw any conclusions regarding predictors of talar dome radii, such as foot size and gender. These data have direct applications to numerical models of the ankle as well as to the design of components for ankle arthroplasty.

REFERENCES

1. Barnett, CH and Napier, JR *J Anatomy* **86**, 1-8, 1952.
2. Buechel, FF, et al., *Foot & Ankle* **6**, 279-290, 1988.
3. Leardini, A, et al., *J Biomech* **32**, 585-591, 1999.
4. Medley JB, et al., *Eng Med* **12**, 35-41, 1983.
5. Pappas, M, et al. *Clin Orthopaedics* **118**, 82-92, 1976.
6. Waugh TR, et al. *Clin Orthopaedics* **114**,180-184, 1975.

ACKNOWLEDGEMENTS

This research was funded by a NIA, grant #2T32 AG00048, Interdisciplinary Training in Gerontology.

Table 1: Output Radii and Mean-Square Error of the Cylinder Optimizations

Specimen #	**1**	**2**	**3**	**4**	**5**	**6**	**7**	**8**	**Mean**	**St.dev.**
Gender	*Male*	*Male*	*Male*	*Male*	*Female*	*Female*	*Female*	*Female*	**--**	**--**
Optimized Radius (mm)	22.54	22.40	21.68	21.30	17.79	18.12	18.72	17.20	20.36	2.073
Cylinder Fit MSE (mm)	0.234	0.424	0.199	0.093	0.184	0.092	0.090	0.189	0.188	0.120

COMPARISON OF GOLFERS AND NON-GOLFERS WEIGHT-BEARING HIP ROTATON JOINT RANGE OF MOTION

[1]Heather Gulgin, [1]Charles Armstrong, [1]Phillip Gribble, and [2]Dan Cipriani
[1]University of Toledo, Toledo, OH
[2]Medical College of Ohio, Toledo, OH
Corresponding author email: hgbuckeye@yahoo.com

INTRODUCTION

Participation in sports places specific demands on the musculoskeletal system that, over time, may cause adaptations in soft-tissue. Athletes who participate in sports requiring repetitive rotational movement on one side and not the other (such as overhead sports) have experienced differences in their side-to-side joint range of motion[1]. Range of motion (ROM) asymmetry such as this has been linked to injury. Although this phenomenon has been documented for the upper extremities, little is known about similar adaptation in the lower extremity structures such as the hip. Athletes who participate in sports experience rotational movement in a functional capacity (weight-bearing status). Although there are established norms for passive and active hip rotation ROM, these measures have typically been made in a non-weight-bearing status. The purpose of the study was to examine anatomical limits of hip rotation ROM (weight-bearing conditions) in elite female golfers and age-matched non-golfing controls to determine if asymmetry between the hips exists.

METHODS

Following a five minute bike warm-up, fifteen healthy, female collegiate golfers (mean age 19.6 ± 1.4 yrs; ht. 163.3 ± 6.5 cm; wt. 59.5 ± 6.6 kg) and twenty age-matched females (mean age 20.5 ± 1.7 yrs.; ht. 166.8 ± 7.7 cm; wt. 61.5 ± 10.2 kg) were evaluated for hip rotation ROM during weight-bearing. All subjects were right-hand dominant, and free from hip or back pain in the past six months. Data were acquired through 3-D videography (Motion Analysis Inc.) and a multi-segment bilateral marker set. Medial and lateral rotation for all subjects was measured on both the right and left side at a stance width equivalent to the distance between each subject's greater trochanters (Cond. A), as well as in a golf stance width (Cond B). For each condition, the mean of each subject's three trials was used for statistical analysis. A two-way ANOVA (group x measure) was run to test for the presence of a significant difference between the two groups (alpha level set at 0.05), as well as separate paired t-tests (golfers and non-golfers) for examining side-to-side differences within groups.

RESULTS AND DISCUSSION

Non-golfers's right lateral ROM was significantly greater than the golfers (48.7° ± 10.3, 40.7±6.5; $p = 0.02$) in Cond A, whereas the remaining hip rotation ROM measurements did not significantly differ between the groups. In condition B, there were no significant differences between the golfer group and non-golfer group hip rotation ROM measurements. In addition, both groups (non-golfers and golfers) demonstrated symmetrical hip rotation ROM, as none of the measured directions were significantly different. Thus, a golfer's right medial rotation did not significantly differ from left medial rotation, and a non-golfers right medial rotation did not significantly differ from left medial rotation.

CONCLUSIONS

Except for a difference in right side lateral rotation during Cond A, the hip ROM of the golfer group was not significantly different from that of the age-matched, non-golfer group. Although the golfer group experiences repetitive unilateral rotations on the left (lead) hip, there does not appear to be an accommodation of joint range of motion, as evidence by the symmetrical range of motion among these subjects. However, previous unpublished data[2] has shown that there is a significant difference when measuring side-to-side hip joint range of motion in a non-weight-bearing status. Thus, there may be a true anatomical adaptation in the soft-tissue, but this does not appear in a dynamic (weight-bearing) measurement.

REFERENCES

1. Ellenbecker T, et al. *Med Sci Sports Exerc*. **34**(12), 2052-2056, 2002.
2. Gulgin H, *ACSM National Meeting*, Nashville, TN, Abstract submission, 2005.

Table 1 WB Hip Rotation Rom Means and Standard Deviations Condition A (gr troch width)

	ROM in degrees			
Group	Rmed	Lmed	Rlat	Llat
Non-golfers	27.8±7.5	28.0±9.4	48.7±10.3*	42.3±11.2
Golfers	29.8±9.2	26.5±9.8	40.7±6.5	39.5±8.4

* $p = 0.02$, significant at $p < 0.05$

Table 2 WB Hip Rotation Rom Means and Standard Deviations Condition B (golf stance width)

	ROM in degrees			
Group	Rmed	Lmed	Rlat	Llat
Non-golfers	27.9±7.7	27.2±7.2	51.9±11.9	47.3±10.9
Golfers	29.9±9.6	27.2±10.2	48.8±6.6	48.2±9.4

ASSESSMENT OF FUNCTIONAL JOINT SPACE REPEATABILITY DURING IN VIVO DYNAMIC LOADING

William Anderst and Scott Tashman
Motion Analysis Lab, Bone and Joint Center, Henry Ford Health System, Detroit, MI 48202; email: anderst@bjc.hfh.edu

INTRODUCTION

More than 20 million Americans have osteoarthritis [1]. The recommended measure for anatomical progression of osteoarthritis is joint space narrowing [2,3], typically measured by radiography or MRI. However, these techniques are not a comprehensive measure of articular cartilage thickness because the joint is imaged in only one orientation and under static loading. Thus, conventional measures do not account for differences in articular cartilage thickness over the entire contact region during active motion or how cartilage responds to dynamic loads common in daily activities.

These shortcomings are addressed by the functional joint space (FJS) score, a measure of subchondral joint space over the entire articular surface during a dynamic loading activity. The purpose of this study was to assess the within-day and between-day repeatability of FJS scores.

METHODS

Subjects were five adult foxhounds that served as controls for a larger study. 3D knee kinematics were determined from pawstrike to .20 s after pawstrike by tracking implanted beads (accuracy $\pm$ 0.10 mm [4]) in x-ray images collected at 250 fps as the dogs ran on a treadmill [5]. Ten tests were performed over two years. Three trials were collected each test session.

Using previously published methods [6], the minimum distances between tibia and femur subchondral bone surfaces were determined for each frame of data. A single parameter, the functional joint space (FJS) score, was created to quantify the minimum joint space over the entire .20 s post-pawstrike.

FJS score was calculated over a 200 mm^2 surface area. This area was big enough to account for large regions of cartilage loss and to reduce the effect of minor irregularities in the calculated close-contact region (e.g. near the spine of the tibia, an unlikely weight bearing region). The FJS score was the average distance between the closest 200 mm^2 subchondral surface areas during the .20 s after pawstrike (Figure 1). A smaller score indicated less joint space.

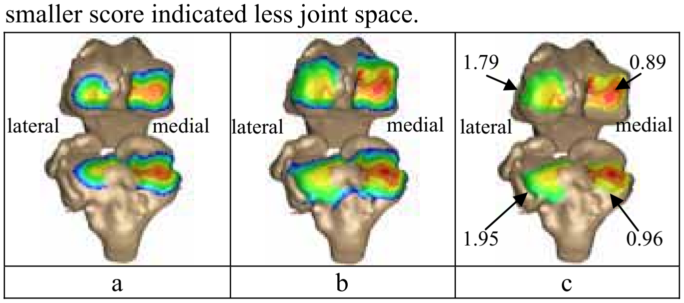

Figure 1: Femur (above) and tibia (below) articulating surfaces colored according to minimum joint space (red=closest, blue=farthest). a) One instant of the analyzed motion. b) The closest distance between surfaces over the entire 0.2 s of motion. c) The closest 200 mm^2 area in each compartment and accompanying FJS score.

The three trials collected each day determined FJS score within-day precision. The average FJS score for the three trials each day was used to calculate the between-day repeatability. The effect of compartment (medial, lateral) and test session (1-10) on FJS score was evaluated with a 2-way repeated measures ANOVA with significance set at $p < 0.05$.

RESULTS AND DISCUSSION

FJS scores were highly correlated between bones within each compartment (medial r=0.95; lateral r=0.95). Thus, for statistical tests, medial femur and tibia scores were averaged to make one medial compartment score, and likewise for lateral scores.

The within-day FJS score precision was 0.09 mm for both the lateral and medial compartments. This result is similar to the most precise static joint space measurements in humans [7,8]. The average between-day FJS score precision was 0.20 mm for both the medial and lateral compartments.

Average FJS scores were greater in the lateral compartment than in the medial compartment (p=.004) (Figure 2). FJS score did not change significantly in either compartment over the 10 test sessions (lateral p=.403; medial p=.637).

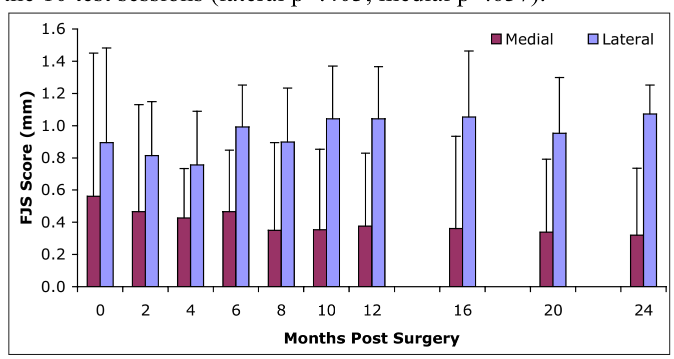

Figure 2:*Medial and lateral FJS score for the 10 test sessions.*

CONCLUSIONS

The FJS method to quantify joint space in vivo produced highly repeatable measurements both within-day and between days, making it a useful tool for serial studies. Unlike conventional joint space measurements, FJS measurements can be performed as the joint is dynamically loaded and moved through a range of motion while variable forces act on the joint. In the future, this tool may be used to serially track in vivo joint space during common activities such as walking in subjects at risk for the development of osteoarthritis.

REFERENCES

1. NIAMS Handout on Health: Osteoarthritis, July 2002.
2. Altman RD, et al. *Arthritis Rheum.* **30**,1214-1225, 1987.
3. Lequesne M, et al. *Journal of Rheum.* **21**, 65-73,1994.
4. Tashman S, et al. *Journ. Biomed. Eng.* **125**, 238-245, 2003.
5. Tashman S, et al. *J. Orthop. Research* **22**, 931-941, 2004.
6. Anderst WJ, et al. *J. Biomech.* **36**, 1291-1299, 2003.
7. Dupuis DE, et al. *Osteo. and Cartilage* **11**, 716-724, 2003.
8. Buckland-Wright JC, et al. *J Rheum.* **31**, 1588-1597, 2004.

The Effects of Temperature, Pressure, and Humidity Variations on 100 Meter Sprint Performances

J. R. Mureika
Department of Physics, Loyola Marymount University, Los Angeles, CA 90045
Email: jmureika@lmu.edu Web: http://myweb.lmu.edu/jmureika/

INTRODUCTION

It is well known that "equivalent" sprint race times run with different accompanying wind speeds or at different altitudes are anything but equivalent races. Adjusting these times for atmospheric drag effects has been the focus of many past studies, including but not limited to [1,2,3,4,5] and references therein. The drag force acting on a sprinter running at speed v in a wind w is a function of air density and the relative wind speed, $F_{\rm drag} \propto \rho_{\rm air}(v-w)^2$, where density has traditionally been calculated using the race venue's elevation above sea level.

However, air density variation is dependent on more than just altitude. This work will quantify how changes in air temperature, barometric pressure, and humidity levels influence 100 m sprint performances. These variables collectively determine an effective altitude known as *density altitude*, which depending on atmospheric conditions can be significantly different than a venue's physical elevation above sea level. The density of hot air is low, yielding a higher density altitude and thus simulating and increase in physical altitude. Increased humidity levels have a similar effect. Conversely, colder temperatures and lower humidity can potentially simulate a decrease in physical altitude.

METHODS

The numerical model of sprinting performances used in Reference [4] is modified using standard hydrodynamic principles to include the effects of air temperature, pressure, and humidity levels on aerodynamic drag. Race times are obtained by numerically-integrating the associated equations for various temperatures in the range 15-35°, relative humidity levels (RH) between 0 and 100%, and atmospheric pressures between 85-105 kPa. These calculations are performed for wind speeds between -3 m/s and +3 m/s. The resulting data are then compared to a defined standard race with no wind, sea level atmospheric pressure and temperature of 25°.

RESULTS AND DISCUSSION

Temperature alone does not have a profound impact on the simulations, giving a performance differential of 0.02 s over the 20°range. Wind and physical altitude corrections under these conditions are thus essentially identical to those discussed in the literature, confirming the earlier result of [3]. The combined effect of relative humidity and temperature plays a slightly more crucial role in adjusting performances, since the air density of hot, saturated air is significantly lower than that of colder dry air.

When the effects of pressure, temperature, and relative humidity changes are considered in combination, the corrections to performances can be very large. Figure 1 shows the range of possible simulation times, bounded by times run in extreme conditions: 85 kPa, 100% RH, and 35° (yielding the least dense atmosphere) and 105 kPa, 0% RH, 15° (most dense). The race times vary by up to or over 0.1 seconds between these extremes even after wind correction is taken into account. The results suggest that a non-negligible difference in race times can be expected for "equivalent" performances run with the same wind speed at the same venue or physical altitude, but under different atmospheric conditions.

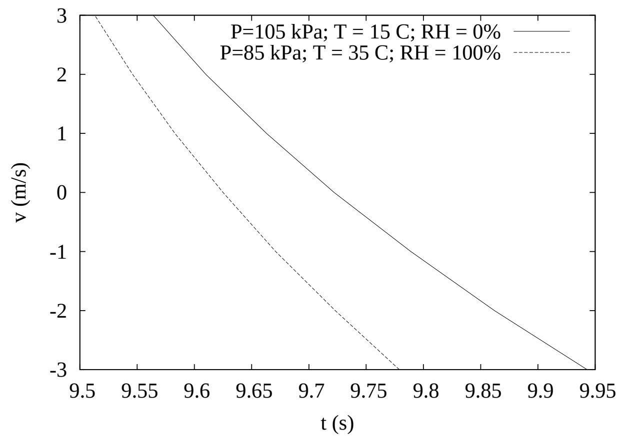

Figure 1: Range of wind-aided and hindered (+3 to -3 m/s) performances equivalent to a "standard" 9.70 second 100 m sprint at sea-level with no wind for extreme high-pressure (top curve) and low pressure (bottom curve) conditions.

REFERENCES

[1] C. T. M. Davies, *J. Appl. Physio.* **48**, 702-709 (1980)
[2] Ward-Smith, A. J; *J. Biomech.* **17**, 339-347 (1984); *J. Biomech.* **18**, 351-357 (1985); *J. Sport. Sci.* **17**, 325-334 (1999)
[3] Dapena, J. and Feltner, M. E., *Int. J. Sport Biomech.* **3**, 6-39 (1987); Dapena, J., in *The Big Green Book*, Track and Field News Press (2000)
[4] Linthorne, N. P., *J. App. Biomech.* **10**, 110-131 (1994)
[5] Mureika, J. R., *Can. J. Phys.* **79**, 697-713 (2001); *New Stud. Athl.* **15 (3/4)**, 53-58 (2000); *Can. J. Phys.* **81**, 895-910 (2003)

ACKNOWLEDGMENTS

This work is made possible through the generous financial support of Loyola Marymount University.

QUANTIFYING FLUID INGRESS TO THE JOINT SPACE DURING TOTAL HIP IMPLANT SUBLUXATION

[2] Hannah J. Lundberg, [1]Douglas R. Pedersen, [3]Marian V. Muste, [1]Thomas E. Baer, [1,2]Thomas D. Brown
University of Iowa [1]Department of Orthopaedics and Rehabilitation, [2]Department of Biomedical Engineering, [3]IIHR-Hydroscience and Engineering; email: hannah-lundberg@uiowa.edu, web: mnypt.obrl.uiowa.edu

INTRODUCTION

Ingress of 3[rd] body debris responsible for femoral head scratching and wear acceleration of total hip implants may be facilitated by convective fluid transport during hip subluxation. To study subluxation-induced particle ingress, a computational fluid dynamics (CFD) model has been developed to quantify the associated fluid motions. Validation of the model was performed using particle image velocimetry (PIV), a method of measuring fluid velocity by tracking marker particles in the flow. Two different femoral head displacement events were evaluated using a fully 3D model.

METHODS

A proof-of-concept 2D CFD model (Figure 1A) was first created for comparison with experimental PIV results. The synovial fluid was assumed to be Newtonian and incompressible (viscosity of 1.0 Pa·s [1]). All external surfaces were designated as "no slip" boundaries. The femoral head was moved (subluxed/separated) out of the cup at a speed of 0.5 mm/s. For PIV validation (Figure 1B) marker particles introduced into the fluid were illuminated and their movement recorded with a digital video camera (Sony DCR-VX2000). EdPIV software was used to track particle movement and calculate fluid velocity.

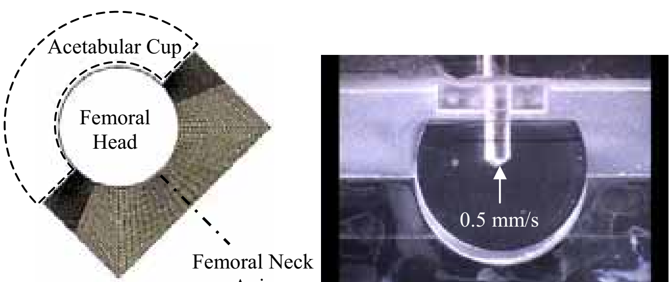

A. B.

Figure 1: A. 2D CFD model mesh and **B.** physical PIV setup.

Two distinct head separation events were then studied using a definitive 3D CFD model (Figure 3A). One implemented the medial separation and femoral head superolateral cup edge pivot reported by Komistek et al. during the swing phase of gait [2]. The other implemented lever-out subluxation due to impingement/lever-out about the inferomedial cup edge [3]. Both regimes resulted in a 0.8 mm separation between the femoral head and acetabular cup after 0.6 s.

RESULTS AND DISCUSSION

The results of the PIV validation are shown in Figure 2. The agreement of PIV versus 2D CFD was 85% or better for velocity vector magnitudes in the clearly visualized areas just away from the entrance to the gap between the femoral head and acetabulum. (The fluid velocity at the gap entrance could not be measured accurately with the physical setup because of high fluid velocity at that point.) Additionally, any incidental fluid motion that might have occurred out of the plane of the image would result in lost/inaccurate vectors.

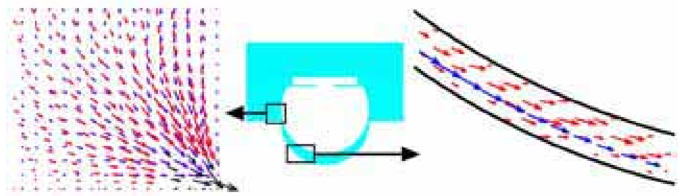

Figure 2: Velocity vectors of the 2D CFD model (red and black) compared to PIV results (blue). CFD velocity vectors shown in red are plotted so that vectors of equal length in the PIV results are equal velocity magnitudes. Black velocity vectors in the left panel, lower right corner, are scaled so that vectors of equal length are 50% greater in the CFD model than PIV.

The 3D CFD results showed markedly different fluid ingress kinematics for swing phase separation versus lever-out subluxation (Figure 3). It was noted that the lever-out femoral head displacement resulted in high velocities at the beginning of the subluxation event at the inferomedial cup edge like that of the gait cycle separation, although at 0.6 s high fluid velocities were located at the superolateral cup edge. The results also suggest that lever-out subluxations may attract debris from multiple locations into the joint space. Dramatic differences in flow patterns suggest that the two subluxation modalities evaluated subject very different regions of the bearing surface to preferential debris embedment, with very different consequences for subsequent head scratching and polyethylene wear acceleration.

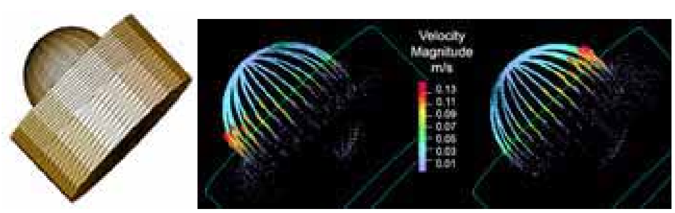

A. B. C.

Figure 3: A. 3D CFD mesh and flow patterns during **B.** swing phase separation and **C.** lever-out, both at 0.6 s.

REFERENCES

1. Mazzucco D, et al. *J Orthop Res* **20**, 1157-1163, 2002.
2. Komistek RD, et al. *JBJS* **84-A**, 1836-1841, 2002.
3. Nadzadi ME, et al. *J Biomech* **36**, 577-591, 2003.

ACKNOWLEDGEMENTS

Supported by grants from the NIH (AR46601, AR47653), DePuy, Inc., and an NSF graduate research fellowship. Thanks to John J. Callaghan and Liam Glennon.

DIRECTION-DEPENDENCE OF UHMWPE WEAR FOR METAL COUNTERFACE SCRATCH TRAVERSE

[1]Liam P Glennon; [1]Matthew C Paul; [2]William D Lack [1]Thomas E Baer; [1]James A Martin; [1]Thomas D Brown
[1]University of Iowa, Iowa City, IA, [2]Harvard University, Cambridge, MA
email: GlennonL@mail.healthcare.uiowa.edu, web: mnypt.obrl.uiowa.edu

INTRODUCTION

Scratches on bearing surfaces of joint prostheses are known to appreciably accelerate wear. The dependence of polyethylene wear rates on counterface motion relative to scratch direction has heretofore not been explored.

METHODS

Arrays of parallel scratches (Fig. 1) were machined at 150 µm intervals on polished stainless steel plates. 25.4mm plugs were machined from conventional and highly-crosslinked UHMWPE.

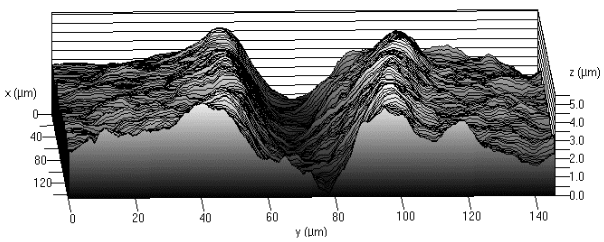

Figure 1. Laser scanning microscopy image of custom profile created on steel. Note axes scales

The scratched counterface plate was immersed in bovine serum and driven reciprocally against the polyethylene plug. The plug was made to traverse the plate at angles ranging from 0° to 90° relative to the scratch orientation, with wear being measured gravimetrically. Based on the scratch geometry of the experiment, a 3-D geometrically and materially nonlinear local finite element (FE) model (Fig. 2) of scratch sliding/ overpassage was developed, to explore continuum-level stress/strain parameters related to orientation-dependent scratch wear. A total of 1,027 candidate surrogate parameters were ranked according to goodness-of-fit to the experimental wear relationship.

RESULTS AND DISCUSSION

Experimentally, steady state wear for all angles was reached by approximately 60,000 cycles. Under this extremely abusive test regimen, in which scratches greatly dominate the surface engagement tribology, the absolute wear rates for both polyethylenes were nominally similar, Fig. 3. Maximum wear rates occurred at 15° for conventional and at 5° for highly-crosslinked UHMWPE. This suggests that at certain low angles, a slicing modality removed large amounts of material as the pin traveled across the scratch lips. The recovered debris was volumetrically dominated by strip/ribbon-like particles often hundreds of µm in length (Fig 4a) unlike the much smaller more bioreactive particles worn by a polished counterface (Fig 4b). In the FEA, computed maximum stress values exceeded polyethylene yield for all scratch orientations. The many FE metrics showed a spectrum of statistical fit with experimental direction-dependence, with (1) cumulative compressive total normal strain in the direction of loading and (2) maximum instantaneous compressive total normal strain transverse to the sliding direction.having best overall performance.

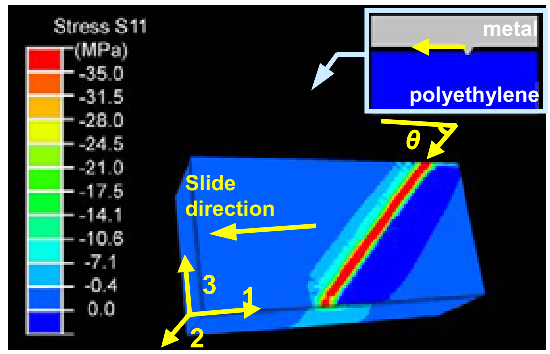

Figure 2. FE model depicting stress contours at θ=45˚.

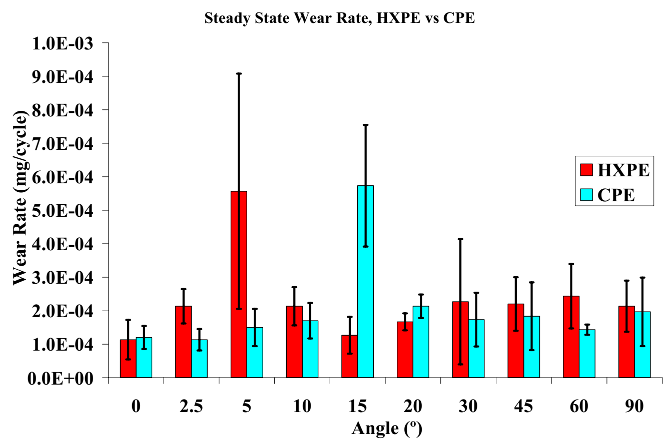

Figure 3. Experimental wear rates vs. scratch orientation.

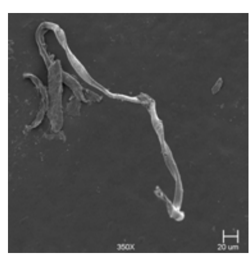

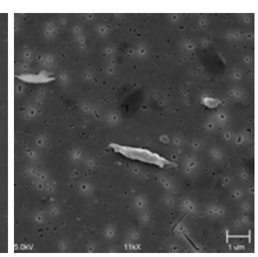

Figure 4a. **Figure 4b.** Polyethylene debris.

CONCLUSIONS

Conventional and highly-crosslinked UHMWPE both showed similar dependence on scratch vs. motion direction, and had comparable volumetric wear rates, in this very abusive regimen. However, the typical particle size was well above the most bioactive range.

ACKNOWLEDGEMENTS

Supported by NIH grants AR46601 and AR47653. Thanks to Katherine Walters for technical assistance.

A PEDICLE SCREW BASED DESIGN FOR AN ARTIFICIAL FACET JOINT

[1] Miranda N. Shaw, [1]Vijay K. Goel, [1]Koichi Sairyo, [1]Srilakshmi Vishnubholta, [1]Ashok Biyani
[1]Spine Research Center, University of Toledo and Medical College of Ohio, Toledo, OH; email: vijay.goel@utoledo.edu

INTRODUCTION

Spinal disorders such as disc degeneration can cause debilitating pain. Currently, several surgical interventions are used to restore spinal stability and normal function in LBP patients. Such surgical techniques include spinal fusion which impairs normal function and the success rate varies. Recently, normal biomechanical motion is restored utilizing artificial discs. Although controversial, if normal function of the spine is to be restored the facet joints may be replaced. Facet replacements may be indicated in cases of facet hypertrophy, spinal stenosis, etc. The following study presents a biomechanical analysis of a pedicle screw based artificial facet design using the finite element technique.

METHODS

A 3-dimensional, non-linear, ligamentous, experimentally validated, finite element model of the L3-S1 segment was used to determine the effectiveness of an artificial facet. The L4 inferior and L5 superior facets were removed and replaced with artificial L4/5 facets constructed of titanium. The artificial facets were attached to L4/5 titanium pedicle screws (Figure 1A). The capsular ligaments and L4/5 facets were removed for simulation of the surgical technique used to replace the facet joint. For comparison purposes, a rigid pedicle screw and rod system was also simulated with a facetectomy at the L4/5 segment. A 400N compression load and 10.6 Nm extension and rotational moment were applied, being the most relevant loading modes for facet function.

RESULTS AND DISCUSSION

Table 1: Angular motion (deg) across L4/5 for 400N compression and a 10.6Nm bending moment.

Relative angular motion across L4/5	Intact Spine	Spine with artificial facet
Extension	3.6	5.1
Rotation	2.9	4.2

Table 2: Facet loads (N) transmitted across the L4/5 facet joint at 400N compression and a 10.6Nm bending moment.

Facet load (N)	Normal facet	Artificial facet
Extension	324	245
Rotation	157	159

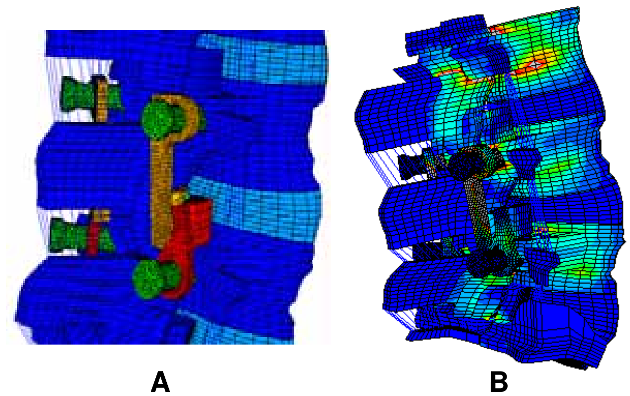

Figure 1: L3-S1 Finite element model. **(A)** Model of facet joint replacement across L4/5. **(B)** Stresses acting on the spine and artificial facet joint in extension.

The relative angular motion across the L4/5 segment increased as compared to intact, in both extension and rotation. Loads through the artificial joint increased in rotation by 1% but decreased in extension by 25% as compared to the intact case. In extension, a peak von Mises stress of 109MPa was located in the L4 artificial facet pedicle screw while in the rigid screw system the peak stress in the pedicle screw was 122MPa. Stresses on the joint and spine are shown in Figure 1B. For the pedicle screw system, a peak stress in the L4 pedicle screw of 107MPa occurred in rotation as compared to 161MPa for the rigid screw system.

CONCLUSIONS

The pedicle screw artificial facet design resulted in increased motion at L4/5 due to capsular ligament removal. Loads transferred through the artificial joint also differed from intact loads. The L4 pedicle screw stresses were less with artificial facets than a rigid screw system suggesting that the artificial facet design will perform similarly to the rigid screw system in the pedicles. Additional investigations are needed for other loading modes and designs to understand the complex biomechanical issues involved with the design of artificial facets.

POSTURAL CONTROL RELATED TO FLEXIBILITY OF THE HINDFOOT WHEN BEARING HEAVY LOADS

[1] H.J. Sommer, [1] Michelle Heller, [2] John Challis and [2] Neil Sharkey
[1] Mechanical and Nuclear Engineering, and [2] Kinesiology, The Pennsylvania State University, University Park, PA, USA
email: hjs1@psu.edu, web: www.biomechanics.psu.edu

INTRODUCTION

Flexibility of the hindfoot is often used to help prescribe in-shoe orthotics for intervention or treatment of overuse injuries to the lower extremity. The high incidence of stress fractures in military recruits during basic training is of particular concern because high frequency of loading is exacerbated by carrying a heavy backpack. Properly designed in-shoe orthotics could potentially reduce the incidence of stress fractures and shorten recovery time, but clinical assessment of hindfoot flexibility is generally qualitative, and prescription of orthoses is often subjective and occasionally contentious. Concomitantly, this study investigated a quantitative measure of hindfoot flexibility versus postural control with a heavy load, as a prelude for future gait studies.

Karlsson et al. [1] suggest a load-unload strategy for medial-lateral (ML) postural control by shifting weight from one foot to the other, and a more active strategy for anterior-posterior (AP) stability using the muscles crossing the ankle joint. ML load-unload is typically actuated by lateral sway of the torso with feet and ankles in a more passive role.

Random walk analysis has been applied to center of pressure (COP) measurements under the feet during quiet standing to investigate control characteristics of postural stability [2]. It employs the mean-square-difference (MSD) in digitized signal x_i over different latency intervals τ as shown in Equation 1. Correlating MSD with τ as shown in Equation 2 permits estimation of scaling exponent H.

$$MSD(\tau) = \Sigma [(x_{i+k} - x_i)^2] / (n\text{-}k) \qquad \text{for } \tau = k\,\Delta t \qquad (1)$$

$$MSD \sim \tau^{2H} \qquad (2)$$

Scaling exponent H equals 0.5 for classical Brownian motion, is above 0.5 for more active control, is below 0.5 for less active control, and equals 0 for a purely random signal. Typical plots of *log(*MSD*)* versus *log(*τ*)* for COP during quiet standing with shoes exhibit characteristic H_1 between 0.4 to 0.7 for τ below a critical time interval (CTI) of approximately 1 second, and H_2 between 0.1 to 0.2 for τ above the CTI.

METHODS

A vernier caliper was used to measure navicular drop [3] for each foot of 22 female volunteers. At least two measurements per foot by different investigators were averaged. The sum of right and left navicular drop was used to quantify hindfoot flexibility. The subjects then donned cross-training shoes and stood on a force platform under two conditions: two feet quiet standing, and wearing a military backpack (18.1 kg). COP data were collected at 1000 Hz over 30 seconds per trial. One trial per condition was used. Correlation coefficients for scaling exponent H_1 in ML and AP directions for each trial were computed as linear functions of navicular drop.

RESULTS AND DISCUSSION

AP scaling exponent H_1 for two feet was effectively constant across all values of navicular drop with mean 0.60 (r^2 = 0.01). AP scaling exponent H_1 while wearing the backpack was effectively constant with mean 0.68 (r^2 = 0.03). These values indicate moderately active control in the AP direction with slightly more active control effort when wearing a backpack.

ML scaling exponent H_1 for two feet was effectively constant across all values of navicular drop with mean 0.38 (r^2 = 0.04) indicating less active control than AP. However ML scaling exponent H_1 while wearing the backpack was moderately correlated to navicular drop (r^2 = 0.32) as shown in Figure 1. More flexible feet exhibited less ML active control while stiffer feet exhibited more active control.

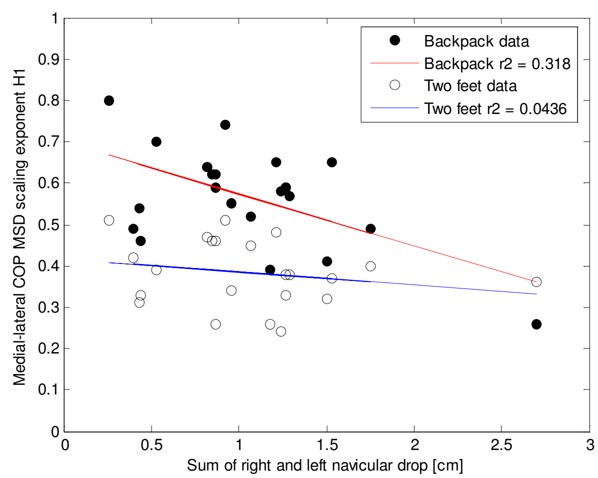

Figure 1: ML postural control versus hindfoot flexibility

CONCLUSIONS

These data support active AP ankle strategy with higher H_1 in the AP direction compared to ML for two feet, and even higher H_1 when a heavy load is carried on the back. In regard to the ML load-unload model, a flexible foot would provide a better damping mechanism and require less ML control than a more rigid foot.

A correlation with r^2 = 0.32 is not definitive. However the relationship between ML postural control when wearing a backpack and hindfoot flexibility quantified by navicular drop warrants further investigation, particularly in regard to prescribing in-shoe orthotics to reduce lateral ankle forces.

REFERENCES

1. Karlsson A, et al. *Clin Biomech* **15**, 365-369, 2000.
2. Collins JJ, et al. *Exp Brain Res* **95**, 308-318, 1993.
3. Brody DM. *Orthop Clin North Amer* **13**, 541-548, 1982.

BILATERAL SYMMETRY OF THE GASTROCNEMIUS STIFFNESS MEASURED WITH MAGNETIC RESONANCE ELASTOGRAPHY IN HEALTHY AND PATHOLOGIC MUSCLE

[1]S.I. Ringleb, [1]K.R. Kaufman, [2]J.R. Basford, [3]R.L. Ehman, [1]K.N. An
[1]Biomechanics Laboratory, Division of Orthopedic Research, Mayo Clinic College of Medicine, Rochester, MN
[2]Department of Physical Medicine and Rehabilitation, Mayo Clinic College of Medicine, Rochester, MN
[3]MRI Research Laboratory, Department of Radiology, Mayo Clinic College of Medicine, Rochester, MN
E-mail: Ringleb.stacie@mayo.edu Web:mayoresearch.mayo.edu/mayo/research/biomechanics

INTRODUCTION

Quantifying the changes in skeletal muscle stiffness that occur with pathologies will improve our understanding of disease and injury and should lead to advances in treatment. Magnetic Resonance Elastography (MRE), a non-invasive phase contrast MRI technique, can visualize small displacements from applied shear waves and quantify the stiffness of soft tissues *in vivo* [1]. This technique has shown significant differences in the medial gastrocnemius muscle stiffness between the healthy volunteers and patients with spastic paraplegia, flaccid paraplegia and poliomyelitis, however, variations in the muscle stiffness in the left and right legs were observed in both populations [2]. Currently, we would like to use MRE to evaluate the effects of hemiplegic stroke and unilateral disuse atrophy on muscle stiffness by comparing the muscle stiffness in the affected limb to the unaffected limb. However, before this study can be conducted, it is necessary to determine a confidence interval to indicate if the differences are due to anatomic variations or if they are caused by pathology.

METHODS

Five healthy volunteers (4 female, 1 male, mean age: 26.4±3.3 years, BMI 21.3±2.0) were placed in a test jig with integrated MR compatible torque cells (Interface, Scottsdale, AZ). This jig fixed the ankle position in a range from 20˚ dorsiflexion (DF) to 40˚ plantarflexion (PF) in 10˚ increments. The loading was monitored with a custom LabView program (National Instruments, Austin, TX) including visual feedback to ensure that a constant load was applied by the subject. The volunteers' ankles were fixed at 10˚ of PF and they were asked to resisted isometric loads of 5-20 Nm in 5 Nm increments. MRE data were also collected with no contraction at 10˚ of DF, 10˚ of PF and 30˚ of PF in healthy volunteers and in one patient with hemiplegic stroke.

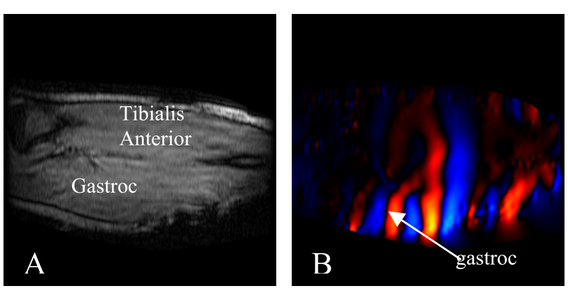

Fig 1. A) 2D MR image B) MRE image of gastroc

To collect MRE data, an electromechanical driver was strapped around the lower leg to induce shear waves into the gastroc at 100 Hz (f_e). A 2D 5 mm thick slice including the lateral gastroc was imaged with a gradient-echo, cyclic motion sensitizing sequence (TR/TE of 100ms/min full, 256x64 acquisition matrix, 24cm FOV) (Fig. 1). Each scan took 64 seconds to complete. The stiffness was calculated using a phase gradient technique after the data were smoothed with a directional filter. A 1D profile was drawn along the direction of the wave propagation in the complex first harmonic. The spatial frequency (f_s) was measured from the 1D profile and stiffness was defined as: $\mu = f_e^2/f_s^2$.

Left to right symmetry was assessed using the Bland-Altman technique [3]. For each volunteer, the side-to-side difference in gastrocnemius stiffness was plotted against the mean stiffness. The confidence interval of anatomic variations was defined as the mean value of the difference in stiffness ± two standard deviations of the difference.

RESULTS AND DISCUSSION

The left to right difference and confidence interval ranged from -9.27 to 7.88 kPa. and -7.89 to 8.11 kPa, respectively in the Bland-Altman plot (Fig. 2). In the stroke patient, the difference between the gastroc stiffness in the affected and unaffected limbs was -3.45, 32.28 and 32.41 kPa when the ankles were fixed at 30˚ of PF, 10˚ of PF and 10˚ of DF, respectively. These differences exceeded the confidence interval in two of the three conditions tested, indicating a change in the muscle properties after a stroke.

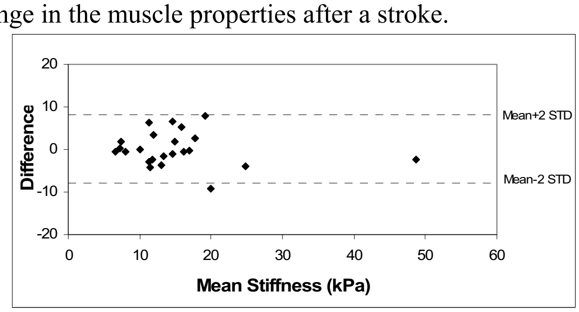

Fig. 2 Bland-Altman Plot of the left to right difference of gastrocnemius stiffness in five healthy volunteers.

CONCLUSIONS

A symmetry threshold was determined for the gastroc in PF loading and with no load at various ankle positions. While more data must be collected to include a more representative population, the preliminary results suggest that comparing the affected to unaffected limb when unilateral pathology is present will enable us to detect changes caused by injury or disease.

REFERENCES

1. Manduca, A, et al. *Med Image Analysis* **5**, 237-254, 2001.
2. Basford, JR, et al. *Arch Phys Med Rehal* **83**,1530-36, 2002.
3. Bland JM and Altman DG *Lancet* **346**, 1085-1087, 1995.

ACKNOWLEDGEMENTS

This study is supported by NIH grants EB00812, EB01981, CA91959 and HD07447 We thank T.C. Hulshizer for his technical assistance.

THREE-DIMENSIONAL SHOULDER JOINT POSITION SENSE

David N. Suprak and Andrew R. Karduna
Department of Human Physiology, University of Oregon, Eugene, OR, USA
email: dsuprak@darkwing.uoregon.edu

INTRODUCTION

Joint position sense (JPS) is an important ability contributing to coordinated joint function, and is especially important for the stability and function at the shoulder [1]. The vast majority of studies in this area focus on movement about one axis of rotation, whereas there exists a scarcity of information concerning how shoulder joint position sense behaves in three dimensions. Therefore, the purpose of this study was to examine the effects of elevation angle on three-dimensional (3D) active repositioning error of a presented joint position. We hypothesized that error magnitude, defined as the angle between the presented and reproduced joint positions, would increase as the humeral elevation angle moved away from 90°, the position in which torque due to gravity about the shoulder joint is maximized.

METHODS

A total of 20 subjects (12 males, 8 females), with a mean age of 23.3 yrs. (± 4.8 yrs.) participated in the study. Following a standardized warm-up procedure, subjects were fitted with a head-mounted display and asked to remove shirts (females wore sports bras) to minimize visual and tactile cues (Figure 1). Kinematic data were collected via the Polhemus Fastrak magnetic tracking system, with one receiver on the thorax and one on the humerus. Testing involved the presentation of five target positions, consisting of various elevation angles in the scapular plane (35° plane). These positions were presented via custom-made Labview software through the head-mounted display. Once the target position was achieved, the display turned black and remained so for the remainder of the trial. Subjects held the position for five seconds, and returned to the side. Subjects then attempted to replicate the target position in three dimensions, in the absence of visual cues. Target positions were presented in a randomized order.

Figure 1: Experimental Set-up.

RESULTS AND DISCUSSION

A one-way repeated measures ANOVA revealed a significant main effect for elevation angle. Pairwise comparisons across elevation angle showed significantly smaller repositioning error at 90° compared to that at 30°, 50°, and 70° of elevation (Figure 2). The trend indicating improved JPS as the presented position is moved toward 90° elevation may be related to the torque generated at the shoulder joint due to gravity. Greater muscle activation is required in order to counteract this increase in torque and maintain the presented shoulder position. This finding may implicate muscle spindles as a primary source of afferent input related to JPS, due to the increased stimulation of these receptors with increasing muscle activation. This role of the muscle spindles has been hypothesized by various authors in the past [2, 3].

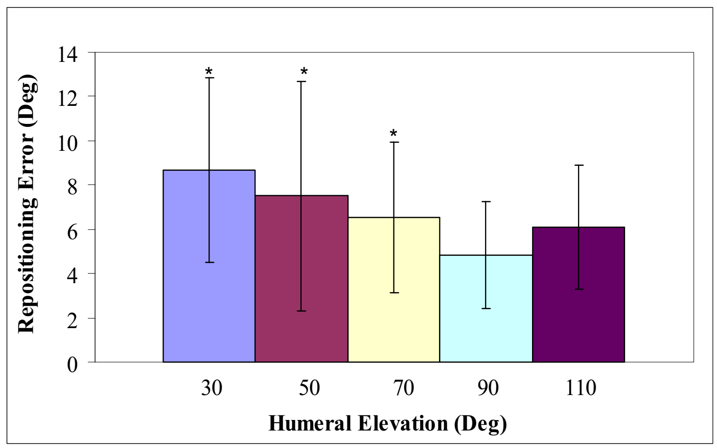

Figure 2: Error Magnitude Across Elevation Angle (Mean ± SD).

CONCLUSIONS

The results of this study indicate that 3D JPS in the shoulder is affected by the humeral elevation angle. More investigation is necessary to elucidate the role of muscle contraction intensity in 3D JPS.

REFERENCES

1. Voight, ML, et al. *JOSPT* **23**, 348-52, 1996.
2. Radovanovic, S, et al. *J Electrom Kines* **8**, 139-45, 1998.
3. Ribot-Ciscar, E, et al. *Exp Brain Res* **149**, 512-19, 2003.

ACKNOWLEDGEMENT

Brian Fedor, for technical assistance.

Influence of Pericellular Matrix on Cell Strains in the Intervertebral Disc

Prabhu, R.D., Iatridis, J.C and Keller, T.S.
Department of Mechanical Engineering, University of Vermont,
Burlington, Vermont 05405, email:rdprabhu@cem.uvm.edu

INTRODUCTION

Mechanical signals on intervertebral disc cells are important determinants of biosynthetic activity and can result in cell death if excessively large. Computational modeling demonstrated that a narrow pericellular matrix (PCM) surrounding the chondrocytes substantially alters the cell's micromechanical environment [1]. In cartilage, alterations to the cell and PCM are implicated in the initiation and progression of arthritis [2,3]. The PCM has been observed around the cells of the annulus and nucleus of the intervertebral disc with the suggestion of increasing PCM thickness with degeneration [4,5]. However, the role of the PCM in determining the micromechanical environment of cells in the disc has not been investigated. The purpose of this study is to investigate the influence of PCM thickness on cell strains in the three different regions of the intervertebral disc.

METHODS

Cells in the outer annulus fibrosus (AF) region of the disc are elongated and embedded in a highly anisotropic extracellular matrix whereas cells in the nucleus pulposus (NP) are spherical and surrounded by isotropic tissue. The cells of the transition zone (TZ), or inner annulus, are ellipsoids and surrounded by matrix with a moderate degree of anisotropy. To model the micromechanical environment in and around the cells a 2-D transversely isotropic axisymmetric model of the cell, PCM and tissue was developed using FEMLAB (Comsol, Natick, MA). The model computed the volume averaged cell strains normalized by the far-field matrix strains as a function of varying PCM thickness. For all disc regions, the PCM thickness was varied from 0 to 3 microns. Uniaxial loading conditions were applied, and effective strain fields were calculated. Material properties and geometries for the cell, PCM and the extracellular matrix in the three disc regions were taken from literature [6] and assumed linearly elastic. To further elucidate the effects of cell aspect ratio and extracellular matrix anisotropy on cell strains, four baseline cases were investigated (spherical-isotropic, spherical-anisotropic, non-spherical-isotropic and non-spherical-anisotropic) and cell averaged radial, azimuthal and axial strains were calculated. Anisotropy was simulated by varying the matrix modulus along the axial (E_z) and radial (E_r) directions and cell aspect ratio (a/b) was varied from 1 to 5.

RESULTS AND DISCUSSION

For uniaxial loading, relative variations in effective strain both within and across the cells in the TZ were larger than that for the cells in the AF region (Figure 1). The presence of the PCM 'amplified' the cell strains in a nearly linear increase in strain with PCM thickness (Figure 2). Anisotropy in the extracellular matrix enhanced the dependence of cell-strains on PCM thickness while cell-elongation reduced the dependence.

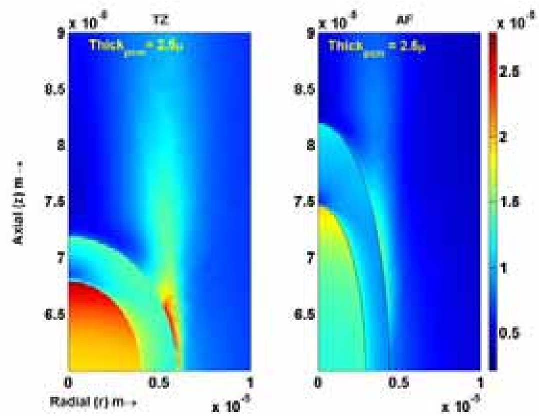

Figure 1: Effective Strain fields for TZ and AF regions

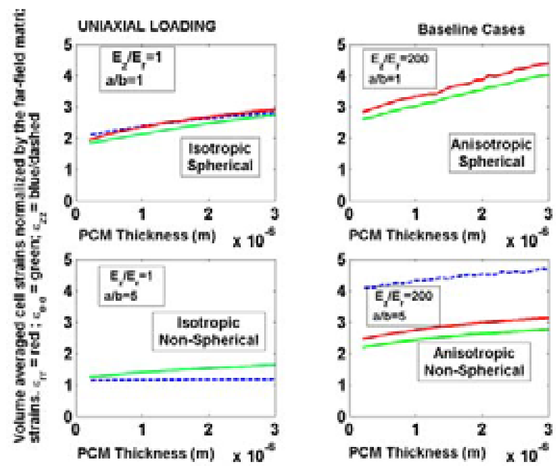

Figure 2. Average cell strains for the baseline cases

Thus cell strains are a function of the competing effects of anisotropy and cell elongation. Large strain amplification in the TZ region is consistent with increased apoptosis in this region found in a mouse tail model of degeneration [7]. This model coupled with detailed information on microstructural geometry, properties and other loading conditions will help in understanding the mechanobiology of health and disease.

REFERENCES

1) Guilak F and Mow VC. *J Biomech*, **33**, 1663-1673, 2000.
2) Poole CA. *J Anat* **191**, 1-13, 1997.
3) Horikawa O et al. *J Orthop Sci* **9**, 29-36, 2004.
4) Gruber HE et al. *Biotech Histochem* **77,** 1, 37-41, 2002.
5) Trout JJ et al. *Anat Rec* **204**, 4, 307-314, 1982.
6) Baer AE & Setton LA. *J Biomech Eng* **122**, 245-251, 2000.
7) Lotz JC et al. *Spine* **23,** 2493-506, 1998.

ACKNOWLEDGEMENTS

Funded by The Whitaker Foundation grant RG-03-0030 and DOE-EPSCoR

DEVELOPMENT AND VALIDATION OF THE FINITE ELEMENT HUMAN BODY MODEL FOR LESS – LETHAL BALLISTIC IMPACTS

Sriram Rajagopal, Cynthia Bir, Jong Lee and King Yang
Wayne State University
Email : rs.sriram@wayne.edu

INTRODUCTION

The need to test less lethal kinetic energy rounds before their deployment in the field is becoming increasingly necessary with the increase in their usage and potential associated injuries. A cost effective and efficient way to test these rounds is by observing their effects on previously validated finite element human body models. This paper deals with development and validation of the Wayne State Human body model and comparison of the model response with the physical tests performed on cadavers for the assessment of blunt ballistic impacts [1].

METHODS

The Wayne State Human Body Model includes a detailed representation of the lung, heart, liver, spleen, spine, ribcage, sternum and major blood vessels [2,3]. Material properties for various tissues of the model were derived from those reported in the literature and the material tests performed at Wayne State University. The model was developed using Hypermesh (Altair Engineering) as the pre/post processor and LS-DYNA (Livermore Software Technology Corporation) as the solver.

The model was tested for three impact conditions listed in Table 1. Displacement of the projectile was calculated using the nodal displacements and the force was calculated based on the contact interaction forces. Displacement-time, force-time and force-displacement graphs were plotted so as to compare the results with the corridors developed from the experimental test results [1].

RESULTS AND DISCUSSION

Results obtained from the FE analysis show good correlations between numerical simulations and experiments. It was observed that the properties and thickness of the skin covering the thorax plays a major role in the response characteristics. Based on the stresses observed in the FE model, sternum and rib fractures can be predicted. Figure 1 shows the force-displacement plot for Condition B. Similar co-relation was observed for the remaining two conditions. The displacements and the forces were computed until 4 ms after which the impactor is not in contact with the body in all the three conditions.

Table 1: Impact conditions from experimental testing.

Impact Conditions	Diameter *(mm)*	Length *(mm)*	Mass *(grams)*	Velocity *(m/s)*
Condition A	37	100	140	20
Condition B	37	100	140	40
Condition C	37	28.5	30	60

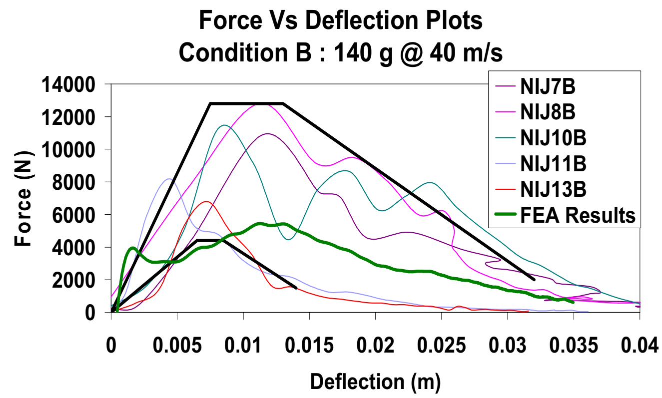

Figure 1: Force-Deflection Plot for Condition B

The energy balance was maintained by reducing the hourglass energies and the skin was given a fully integrated element formulation. In the force-time curves an initial steady rise in force is observed due to the energy absorbed by the skin.

CONCLUSIONS

Results from this study demonstrate that finite element thorax model is powerful tool for assessment of the injury mechanisms to the human thorax against blunt ballistic impacts.

REFERENCES

1.Bir, C. A. (2000). The Evaluation of Blunt Ballistic Impacts of the Thorax. Detroit, MI., Wayne State University.
2.H.C. Wang (1995). Development of a Side Impact Finite Element Human Thoracic Model. PhD Dissertation. Detroit, MI., Wayne State University.
3. Ruan, J., R. El-Jawahri, et al. (2003). "Prediction and Analysis of Human Thoracic Impact Responses and Injuries in Cadaver Impacts Using a Full Human Body Finite Element Model." *Stapp Car Crash Journal* 47: 299-321.

ACKNOWLEDGEMENTS

This project was funded by a grant from the National Institute of Justice.

INVESTIGATATION OF APPROPRIATE WEIGHTED BAT BY MUSCLE ACTIVITY

[1]Tsung-Ying Hung, [2]Ya-Chen Liu, [1]Chiang Liu, and [1]Tzyy-Yuang Shiang
[1]Taipei Physical Education College, Taiwan. [2]Chung-Hua University, Taiwan

INTRODUCTION

Swing velocity is a critical factor for batting performance. There is a certain relationship between swing velocity and bat weight (Fleisig *et al,* 2002). Some studies have demonstrated that baseball player could significantly improve swing velocity through using regular bat, weighted bat, and combine weighted and lighter bat for several weeks training period (Sergo & Boatweight, 1993, DeRenne et al, 1995). During warm-up in the on-deck circle, using lighter bat could produce significantly higher velocity compared to using regular or weighted bat (DeRenne & Branco, 1986). On the other hand, Tu *et al.* (2002) found that swing weighted bat could significantly improve velocity. But only in the first swing after warm-up with weighted bat (Otsuji *et al*, 2002). Each player has specific ideal weight bat (Bahill & Karnavas, 1991). However, there are big gap between ideal weight bat and general use bat for practice or game. Therefore, the purpose of this study was to determine appropriate weighted bat by analyzing muscle activity.

METHODS

Eleven collegiate baseball players were voluntary participated in this study. Each subject randomly swung nine different weighted bat: 1200g (weighted bat), 900g (general using bat), 850g, 800g, 750g, 700g, 650g, 600g, and 490g (fungo bat). After finished warm-up session, participant swung each kind of bat three trials. Each swing has a break period for 30 seconds. In order to discriminate swing phases, the desk bell and sound recorder were use to be a trigger and record sound signal. Surface active electrodes (Biovision system) were used to detect muscle activity of triceps and biceps brachii muscles. Integral EMG and Mean EMG during swing phase were calculated after normalizing by MVC. We also calculated the ratio of biceps and triceps muscle activities for intermuscular coordination between agonist and antagonist muscle. The sound signal was collected including sound of bell (I), bat-ball impact (Ⅱ), and ball flight into protective net (Ш) (shown in Figure 1, channel 1 is sound signal, channel 2 and 3 are EMG of triceps and biceps brachii muscles). Swing phase was defined as I to Ⅱ.

RESULTS AND DISCUSSION

In table 1, muscle activities in triceps and biceps of right arm appeared slightly change with increasing bat weight. Triceps is agonist muscle result from extending elbow during swing. Triceps is the major contributing muscle during swing phase because of higher muscle activity. As Figure 2 shown, 850g-bat and 650g-bat also have better intermuscular coordination between triceps and biceps brachii muscles. According to muscle force-velocity relationship, swing velocity and muscle activity could be used as index to find suitable weight bat (Liu *et al*, 2003). Our other study found that 850g-bat and 650g-bat could induce higher swing velocity. Combining description above, 850g-bat and 650g-bat have some advantage characteristics, such as higher IEMG and MEMG in triceps, lower IEMG and MEMG in biceps, as well as better intermuscular coordination. Therefore, 850g-bat and 650g-bat are appropriate weighted bats for game and practice.

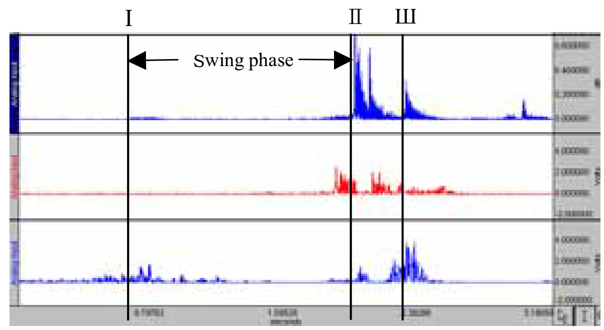

Figure 1: Signals of sound and muscle activity.

Table 1: Muscle activity with different weighted bats

Bat	Triceps		Biceps	
	IEMG	MEMG	IEMG	MEMG
1200g	13.29±1.89	25.04±5.75	3.17±1.23	5.92±2.38
900g	11.18±2.28	21.22±2.99	3.24±1.37	6.20±2.53
850g	11.73±2.68	21.14±4.64	3.06±0.76	5.66±2.11
800g	10.31±1.78	21.13±3.10	3.06±1.28	5.94±2.26
750g	11.00±2.60	19.82±4.38	3.00±0.66	5.67±1.58
700g	11.72±2.59	22.24±4.52	2.74±0.80	5.28±1.66
650g	13.05±5.75	20.16±2.52	2.37±0.52	4.98±1.56
600g	9.81±1.87	19.77±3.49	2.63±0.92	5.20±2.29
490g	11.01±2.36	21.72±4.55	2.72±0.57	5.48±1.84

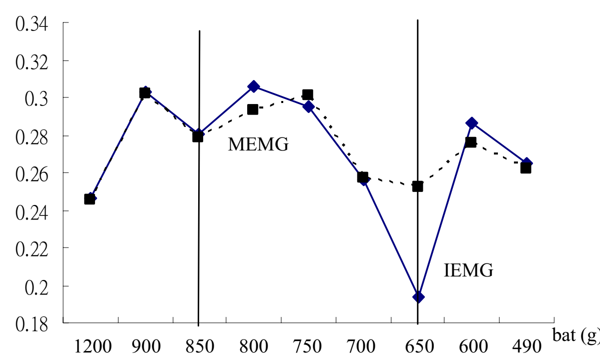

Figure 2: Intermuscular coordination of swing weighted bats

CONCLUSIONS

The results reveal that triceps brachii muscle was a major muscle group during swing. IEMG and MEMG decreased with decreasing bat weight. Consequently, 850g-bat is appropriate bat weight for hitting in competition. 650g-bat is suitable bat weight for improve swing velocity and intermuscular coordination in swing practice.

REFERENCES

1. Liu, et al. *Proceedings of ISB XIX*, New Zealand, 2003.

AN EMG DRIVEN OPTIMIZATION MODEL FOR ESTIMATING DYANAMIC KNEE MUSCLE FORCES WITHOUT MAXIMUM VOLUNTARY CONTRACTION TESTS

Bing Yu and Evan J.X. Tong
Center for Human Movement Science, Division of Physical Therapy, The University of North Carolina at Chapel Hill, Chapel Hill, NC, USA; email: byu@med.unc.edu

INTRODUCTION

Anterior cruciate ligament (ACL) injuries are common in sports. Women are at a greater risk for ACL injuries than men. Previous studies show significant gender differences in lower extremity kinematics and kinetics when performing athletic tasks, but have not establish the relationship between the observed gender differences in motion patterns and the risk for ACL injuries. To investigate the biomechanical risk factors for ACL injuries, a musculoskeletal model is needed to estimate dynamic knee muscle forces in athletic tasks. The purpose of this study was to develop an EMG driven optimization model to estimate dynamic knee model forces in athletic tasks without maximum voluntary contraction tests.

METHODS

The muscle fiber force was expressed as the sum of forces generated by the contractile and parallel elastic elements. The force generated by the contractile element was expressed as a function of dynamic EMG, EMG-to-force gain, muscle specific stress, muscle physiological cross section area, muscle length-tension adjustment, and velocity-tension adjustment. The force generated by the parallel elastic element was expressed as a function of muscle specific stress, muscle physiological cross section area, and parallel elastic length-tension adjustment. The muscle origin and insertion coordinate, physiological cross section area, optimum fiber length, muscle tendon length, muscle maximum contraction velocity, and muscle pinnation angle data, and length-tension and velocity-tension relationships in the relevant literature were used in the model to determine muscle length, PCSA, length-tension adjustments and velocity adjustments. Force fiber force was converted to the muscle tendon force using the muscle pinnation angle. Vastus medialis, lateralis, and intermedius, rectus femoris, semimembranosus, semitendinosus, biceps femoris long and short heads, medial and lateral gastrocnemius were considered as the knee flexion-extension moment generators. EMG-to-force gains and muscle specific stresses were optimized to minimize the sum of squares of the differences between the muscle generated knee flexion-extension moment and knee resultant flexion-extension moment, subject to the constraints to the muscle EMG-to-force gains and muscle specific stresses.

Five male and five female recreational athletes were recruited as the subjects. Three-dimensional (3D) kinematics and kinetics, and EMG were collected for a stop-jump and a running task. The kinematics data were collected at 120 frames/second while the kinetic and EMG data were collected at 1200 sample/channel/second. The raw coordinate data of critical body landmarks were filtered at the estimated optimal cutoff frequencies. Knee joint resultants were estimated using an inverse dynamic procedure. EMG signals were band-pass filtered (10 – 300 Hz) and then low-pass filtered (6 Hz) for linear enveloped EMG. The stop-jump and running tasks were rotated as calibration and validation tasks to validate the estimated EMG-to-force gains and muscle specific stresses. Regression determinant (R^2) and mean error (e) between muscle generated knee flexion-extension moment and knee resultant flexion-extension moments were used to evaluate the quality of predicated knee flexion-extension moment. Paired t-tests were performed to compare the regression determinants and mean errors between calibration and validation tasks.

RESULTS AND DISCUSSION

The proposed EMG driven optimization model predicted knee flexion-extension moment for calibration and validation tasks with a good accuracy (Table 1). Although the accuracy of the predicated knee flexion-extension moment was lightly decreased for validation tasks, there was not statistically significant difference in the regression determinant of the predicted knee flexion-extension moment between calibration and validation tasks (Table 1).

The ability of the proposed EMG driven optimization model to predict knee flexion-extension moment for the calibration task was comparable to the similar models in literature. The decreased ability to predict knee flexion-extension moment for the validation task is likely due to assumed linear EMG-to-force relationship. The lack of consideration of the relationship between muscle activation level and muscle length-tension relationship did not seem to have critical effects on the ability to predict knee flexion-extension moment for the validation task. Further studies may be needed to further validate estimated muscle forces and joint structure loadings.

REFERENCES

Kaufman, K.R. et al. *J. Biomech*, **22**, 943-949, 1989.
Kaufman, K.R. et al. *Am. J. Sports Med.* **40**, 781-992, 1991.
Lloyd, D.G., Besier, T.F. *J. Biomech*, **36**, 765-976, 2003.

Table 1. Regression determinant between predicted knee flexion-extension moment and knee resultant flexion-extension moment.

Calibration Task	**Gender**	**Validation Task**	
		Jump	Run
Jump	M	0.9118	0.8346
	F	0.9282	0.8511
Run	M	0.8539	0.9368
	F	0.8409	0.8986
Jump and Run	M	0.8946	0.8849
	F	0.8807	0.8628

POSTURAL SWAY ON A SLIDING PLATFORM: ASSESSING SPATIAL AND TEMPORAL STABILITY

[1] Haruhiko Sato, [1]Yoshitaka Shiba, [1]Toyokazu Saito and [1]Toshiro Futami
[1]Allied Health Sciences, Kitasato University
email: haru@kitasato-u.ac.jp

INTRODUCTION

If a fall is regarded as a situation in which a person fails to recovery the body center of mass from the edge of the base of support, balance assessment is required to measure the excursion distances of the center of pressure (COP) as well as reaction time [1]. A quick response is preferable to achieve efficient recovery from stability limits. In order to assess spatial and temporal stability [2], we designed a sliding platform anchored at one end of a sliding rail. The platform helps the subject to transfer his or her weight from heel to toe or from toe to heel when performing voluntary anterior-posterior (AP) sway of the COP on the platform. The aim of the present study was to describe the various characteristics of AP sway among young, and elderly subjects, as well as in subjects with Parkinson's Disease (PD).

METHODS

Our subjects consisted of 37 healthy university students (17 female and 20 male; age range = 18-27 years, mean = 20.1 ± 2.3 years), 29 healthy elderly subjects (13 female and 16 male; age range = 65-89 years, mean = 69.9 ± 4.7 years), and 7 subjects with PD (4 female and 3 male; age range = 55-72 years; mean = 63.7 ± 6.6 years). PD subjects were recruited from Kitasato University East Hospital and elderly subjects were recruited from the local community.

Wearing a safety harness, subjects performed voluntary cyclic AP sway standing on the sliding platform or a fixed platform, each of which contained three load cells to measure vertical ground force. Data were recorded at 100 Hz and the associated COP was then computed. An auditory metronome guided subjects to sway the COP at 0.5 Hz. Once the subject swayed rhythmically, force data were recorded for 10 seconds. Time series were analyzed for each trial corresponding to COP sway (Fig. 1). COP amplitude was calculated using the distances between the peaks and the valleys, and duration was defined as the times between the peaks. The calculated values were averaged across three trials per subject.

RESULTS AND DISCUSSION

The mean duration achieved by elderly and PD subjects was found to be longer than that of young subjects under both fixed and sliding conditions (Fig. 1, Table 1). Most young subjects were able to pace their AP sway with the auditory cue, while elderly and PD subjects did not maintain the pace. The ranges of duration on the sliding platform were 1.8 to 3.0 sec for the

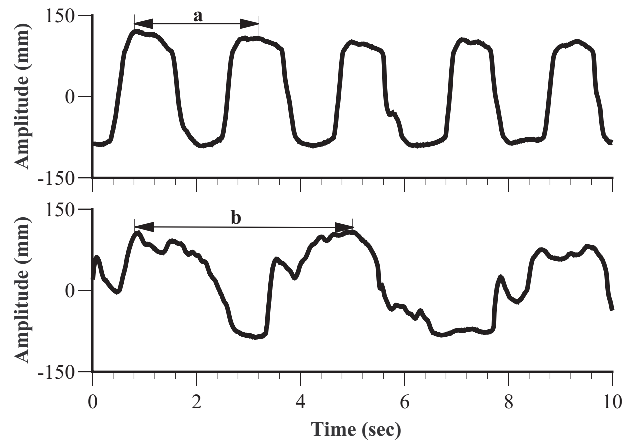

Figure 1: Representative AP displacements of the COP on the sliding platform in a young subject (top) and an elderly subject (bottom). The intervals designated by "a" and "b" indicate duration.

young, 1.0 to 6.4 sec for the elderly, and 1.8 to 6.1 sec for PD subjects. Both elderly and young subjects showed shorter duration under sliding conditions than under fixed conditions ($p < 0.001$ and $p < 0.05$, respectively), and the mean amplitude of elderly and PD subjects was significantly smaller than that of the young under both conditions ($p < 0.01$). Sliding conditions produced smaller amplitude than fixed in the young and the elderly ($p < 0.01$). The sliding mechanism was found to be an effective method of testing the speed of sway, especially in elderly subjects, however, this method was less effective in the case of PD subjects.The duration of voluntary AP sway was found to decrease with decreasing amplitude.

CONCLUSIONS

The sliding platform was found to help subjects perform fast AP sway provided that they were able to easily move their body weight. In subjects with a balance problem, fast AP sway is more difficult to achieve.

REFERENCES

1. Owings TM, et al.. *J Am Geriatr Soc,* **48,** 42-50, 2000.
2. Hof AL, et al.. *J Biomech*, **38**, 1-8, 2005.

ACKNOWLEDGEMENTS

This work was supported by Grant-in-Aid for Young Scientists 15700370 (MEXT).

Table 1: Amplitude and duration of COP time series under fixed and sliding conditions for young, elderly, and PD subjects.

	Young		Elderly		PD	
	Fixed	Sliding	Fixed	Sliding	Fixed	Sliding
Amplitude (%FL)	82.2 ± 4.8	78.1 ± 4.6	74.5 ± 7.3	70.9 ± 9.6	68.4 ± 4.9	63.9 ± 8.5
Duration (sec)	2.2 ± 0.4	2.0 ± 0.2	4.2 ± 2.5	2.6 ± 1.4	3.1 ± 1.2	3.8 ± 2.1

FL denotes foot length.

IN VIVO MUSCEL FIBER KINETICS DURING TETANIC CONTRACTION

[1] Toshiaki Oda, [1] Toshiyuki Kurihara, [1] Kentaro Chino, [1] Hiroaki Kanehisa,
[2] Toshihiko Nagayoshi, [2] Emika Kato, [3] Tetsuo Fukunaga and [3] Yasuo Kawakami
[1] Department of Life Sciences, University of Tokyo, [2] Graduate School of Human Sciences, Waseda University,
[3] Faculty of Sport Sciences, Waseda University;   E-mail: pesu@sannet.ne.jp

INTRODUCTION

The muscle fiber force is a function of muscle fiber length (MFL), muscle fiber shortening velocity (MFV) and active state (AS) [1, 2]. However, little is known how these factors determine the time-course of muscle fiber force in human muscles *in vivo*. The present study aimed to investigate the time-course of muscle fiber kinetics during isometric tetanic contractions. For this aim, we measured MFL and MFV, and estimated the time-course of the force generating capacity (FGC) determined from each of MFL, MFV and AS.

METHODS

Six healthy male volunteers participated in this study as subjects. The subject was seated with the knee joint fully extended. To change the initial length of MFL, three ankle joint angles (30, 10 and -10 deg; 0 deg is an anatomical position) were chosen . Isometric tetanic contractions (2s at 50Hz) were evoked by percutaneous supramaximal electrical stimulations to the common peroneal nerve. The ultrasound apparatus (SSD-6500SV, Aloka, Japan) having a 10 MHz linear-array probe was used to measure the sequence of longitudinal ultrasonic images (96.4Hz) of the tibialis anterior muscle at the level of 40 % of the lower leg length. From the serial images, MFL, MFV and pennation angles were measured using an image analysis software. Muscle fiber force was estimated using measured dorsi-flexion torque, moment arm length and pennation angle. FGC related to MFL and MFV were estimated from force-length and force-velocity relationships. FGC related to AS was calculated using the following equation:

$$F_{exp}=P_0 \cdot FGC_{F-L}(MFL) \cdot FGC_{F-V}(MFV) \cdot FGC_{F-AS}(AS)$$

where F_{exp}=estimated muscle fiber force, P_0=maximal force at optimum length, FGC **a** (**b**)=force generating capacity related to **a** as function of **b**. F-L, F-V and F-AS mean force-length, force-velocity and force-active state relationships, respectively.

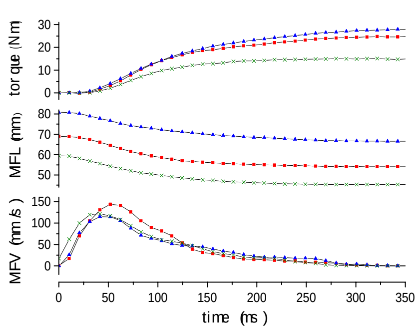

Figure 1: Time-courses of dolsi-flexion torque, muscle fiber length (MFL) and muscle fiber shortening velocity (MFV). (average of six subjects) [30deg, ■10deg, ×-10deg]

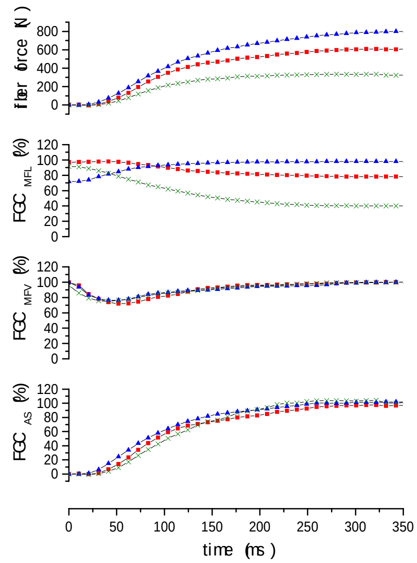

Figure 2: Time-courses of fiber force and force generating capacity of each muscle fiber length (MFL), muscle fiber shortening velocity (MFV) and active state (AS). (average of six subjects) [30deg, ■10deg, × -10deg]

RESULTS AND DISCUSSION

The time courses of the measured dorsi-flexion torque, MFL and MFV are shown in Figure 1, and the estimated time-courses of FGC for each of MFL, MFV and AS in Figure 2. For MFL, the magnitude of FGC changed by as much as 27% at the initial phase of contraction (~100 ms). The shapes of the time-course curves were considerably different between joint angle conditions (maximal difference; 31%). For MFV, the magnitude of FGC decreased rapidly at the initial phase (maximal change; 28%) and then increased gradually in all joint angle conditions. For AS, although the magnitude of FGC increased gradually from 0 to 100% in all joint angle conditions, the shape of the time-course curve differed among joint angle conditions (~17%). These findings suggest that the time-course of muscle fiber force developed during tetanic contraction of the tibialis anterior muscle is determined by summation of various changes of the time-course of FGC as a function of MFL, MFV and AS, and that, when the joint angle is changed, it is influenced mostly by the force-MFL and force-AS relationships rather than the force-MFV relationship.

REFERENCES

1. Bobbert MF and Ingen schenau JV. *J Biomech* **23**, 105-119. 1990.
2. van Zandwijk JP et al. *Biol Cybern* **79**, 121-130, 1998.

REFLEX MODULATION AFTER LONG TERM PASSIVE REPEATED PLYOMETRIC TRAINING

[1]Chiang Liu, [2]Ya-Ju Chang, [3]Chuan-Show Chen, and [1]Tzyy-Yuang Shiang
[1]Taipei Physical Education College, Taiwan. E-mail: chiangliu1974@yahoo.com.tw
[2]Chang Gung University, Taiwan. [3]National Taiwan College of Physical Education, Taiwan.

INTRODUCTION

Resistance training results in improved strength by increasing muscle size and by altering the pattern of nervous drive (Sale, 1988). Resistance training changes the functional properties of spinal cord circuitry in humans, but does not substantially affect the motor cortex (Carroll et al, 2002). Hoffman reflex (H-reflex) was evoked by an electrical stimulus applied on peripheral nerve. It reflects the excitability of motorneuron pool in spinal cord (Schieppati, 1987). Almeida-Silveira et al (1996) monitored the H-reflex and found a decrease in reflex excitability after repeat Stretch-Shortening-Cycle training in rats. Passive Repeated Plyometric training (PRP training), a new training method for strength and power, was developed based on the concepts of Stretch-Shortening-Cycle training (Chen & Shiang, 1996). Several researches have found that PRP training significantly improved strength and power in elite athletes (e.g. Liu *et al*, 2001). However, how neuro-muscular system contributes to the gain of strength and power after PRP training is still not well understand. Therefore, the purpose of this study was to investigate the excitability of the reflex arc and the presynaptic inhibition (PSI) could be modulated by the PRP training.

METHODS

Ten male collegiate (aged 20.30± 0.82 yr; weight 68.87±10.26 kg; height 171.70±3.53 cm) voluntary participated in the study. The subjects participated in a 10-wk PRP training program with three sessions per week (see Figure 1). In each of the training sessions, five sets of PRP training were carried out with a 2min break between sets. Each set lasted for 20 sec and the movement frequency was at 2.5Hz. The assessment of H-reflex and M-wave amplitudes were conducted before 1st, 15th, and 30th training session. The subjects were positioned on a leg extension machine with ankle and knee joints fixed. The surface EMG was recorded from the soleus muscle of non-dominant leg by using bipolar surface electrode with 2k Hz sampling frequency. The maximum H-reflex was elicited by stimulating the posterior tibial nerve with a constant-current stimulator (DS7H, Digitimer, UK) at 0.2 Hz to detect motorneuron excitability and at 2 Hz to detect PSI. The intensity of the stimulation was gradually intensified to elicit the maximal M-wave. Ten peak-to-peak amplitude of the H-reflexes at each frequency and ten M-waves were recorded. The $H_{max}$to-M_{max} ratio (H/M) at 0.2 Hz was calculated for indicating the excitability of alpha neuron pool. The averaged amplitude of 2nd to 10th H-reflex at 2 Hz was divided by first H-reflex (PSI ratio= Σ H2-H10/H1) for indicating PSI changed.

Figure1: *PRP training*

RESULTS AND DISCUSSION

A Repeated Measures of ANOVA revealed that the H/M ratio significantly depressed at 30th training session (p=0.015) (Figure 2), indicating about 23.5% decrease of motorneuron pool excitability after 10-wk PRP training. This result was consistent with the findings of previous studies (Almeida-Silveira et al, 1996; Scaglioni et al, 2002). Almeida-Silveira et al (1996) found that H-reflex decreases were accompanied by relative increases in the number of type II fibres after SSC training, suggesting the decrease of motorneuron pool excitability after long term PRP training might relate to the change of fiber type composition. In Figure 2, there was significantly increased in PSI ratio after 10-wk PRP training (p=0.037). The PSI mechanisms are considered mainly responsible for depression of the H-reflex (Zehr, 2002), which might relate to the function of Ia inhibitory interneurons. The long term PRP training induced PSI ratio increase about 9.7% indicating the PRP training might be able to inhibit effect of Ia inhibitory interneuron and decrease presynaptic inhibition in spinal circuitry.

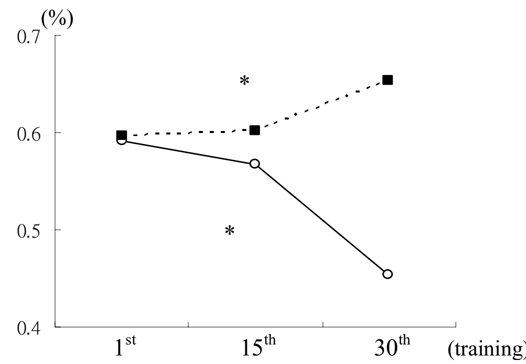

Figure 2: Variety of H/M ratio (○) and PSI ratio (■) via the PRP training for ten weeks. (*means significant difference between 1st and 30th, p<.05).

CONCLUSIONS

The findings revealed that excitability of motorneuron pool significant decreased and PSI significant increased by the long term PRP training. The PRP training affected reflex modulation of spinal cord and induced plasticity change of spinal circuitry.

REFERENCES

1. Almeida-Silveira et al, *E J Appli Physiol* **72**, 261-266, 1996.
2. Chen & Shiang, *PRP Training Machine*, Taiwan, 1996.
3. Carroll et al, *J Physiology* **544. 2**, 641-652, 2002.
4. Liu *et al*, *Proceedings of ISBS XIX*, San Francisco, 2001.

ACKNOWLEDGEMENTS

This research, *NSC 92-2413-H-028-005*, has been financially supported by National Science Council in Taiwan.

BALANCE AND GAIT OF ELDERLY WOMEN DURING STAIRS LOCOMOTION IN HIGH-HEELED SHOES

Bih-Jen Hsue, Fong-Chin Su
Institute of Biomechanical Engineering, National Cheng Kung University, Tainan, Taiwan
email: fcsu@mail.ncku.edu.tw

INTRODUCTION

It is well known that a large number of falls occur on stairs, and females appear to be at higher risk of stair injury based on the high incidence of stair accidents in the elderly women. But, only few studies have been conducted to evaluate the specific factors that contribute to falls on stairs [1,2], or what the strategies are as one's balance is challenging during stair locomotion (SL). The high falling rate and the threatening consequences indicate important needs for the understanding of biomechanics, the identification of the risk factors and the development of preventive strategies. The purposes of this study are (1) to determine the differences in gait pattern between young and elderly females by examining the changes in temporal and kinematics parameters, and (2) to determine the balance strategies in terms of the changes in body posture, center of mass (COM), and joint position while the balance is challenging by wearing high-heeled shoes (HHS).

METHODS

A five-step wood staircase of 18x28x90 cm in dimension was used. The fifth step was created by a 60cm x 90cm platform. Twenty-five reflective markers were secured to the participant's anatomical landmarks locating on the both sides of the body. An eight-camera Eagle Motion Analysis System (Motion Analysis Corporation, Santa, CA, USA) was used to capture the three-dimensional trajectory data of the markers.

Participants were limited to the individuals who were able to ambulate without using any assistive device and ascend and descend stair without handrail. Five medium body-sized elder females (> 65 y/o) and five young women were enrolled. The participants walked from a start point about 3-5 steps away from the stair to the top platform reciprocally and descended stairs to the start point at their preferred walking speeds under two conditions: wearing low-heeled shoes (LHS) with heel height less than 2 cm and HHS with stiletto more than 5.5 cm. One stride for stair ascent (SA) began with heel contact on the second step and ended with subsequent heel contact of same foot on the step four. For stair descent (SD), one stride began with toe contact on step three and terminated with toe contact of same foot on step one. The data was analyzed utilizing repeated measures analysis of variance (ANOVA) with one within, and one between factor at the 0.05 level of significance.

RESULTS AND DISCUSSION

The temporal phases for SA and SD under two shoe conditions are listed in Table 1. The walking speed of elder females is slower to either in SA or SD. The elder females seem to gain stability by increasing the stance phase, and this tendency is more obvious while wearing HHS. In young female, the major changes of joint and segment motion while wearing HHS are the decreases in hip and knee flexion. For elder females, the most significant changes caused by wearing HHS are increases of hip internal rotation both in SA and SD, and foot varus in SD.

Table 1: Stance and swing phases in percentage and the period of one cycle in second (*Y*: 5 young females; *E*: 5 elder females)

		SA			***SD***		
		Cycle*	ST (%)**	SW (%	Cycle*	ST (%)**	SW (%)
LHS	*Y*	1.19	58.17	41.83	1.16	55.01	44.99
	E	1.58	62.12	37.88	1.59	56. 46	43.54
HHS	*Y*	1.24	60.07	39.93	1.19	55.25	44.75
	E	1.65	64.16	35.84	1.68	58.47	41.53

* The unit is in seconds; **ST: stance phase, SW: swing phase

The maximal peak-to-peak COM displacement in medial-lateral (ML), anterior-posterior (AP) and vertical (V) directions are shown in Table2. The findings in COM displacement agree with the trunk motions in Figure 1. The changes in the trunk movement are also more apparent in transverse plane and frontal plane than in sagittal plane.

Table 2: The peak-to-peak COM displacement in centimeter (*Y*: 5 young females; *E*: 5 elder females)

		SA			***SD***		
		ML	AP	V	ML	AP	V
LHS	*Y*	4.56	67.62	34.14	4.04	66.71	33.03
	E	7.41	64.73	34.22	8.36	65.62	34.13
HHS	*Y*	4.37	68.38	35.58	4.05	68.76	34.32
	E	7.00	64.96	34.84	7.31	63.64	34.05

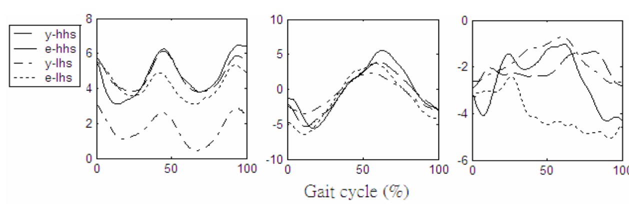

Figure 1: Trunk flexion (+)/extension (-) (right), side-bending (middle), and rotation (left) in degrees

CONCLUSION

The body is like an inverted pendulum during SL, and the elder females accommodate the temporal parameters, and the motion at proximal parts to complete the task. A decrease in maximal excursion of COM displacement in AP direction, and an increase in ML in elder group may suggest that as the elderly restrict the body motion in AP direction to prevent from confronting the risk of falls. Therefore, they need to increase body motion in transverse plane to advance to next step.

REFERENCES

1. Templer, J. et al. J Safety Res 16,183-196, 1985.
2. Simoneau, G. et al. J Gerontol 46, M188-195, 1991.

ACKNOWLEDGEMENTS

Partial support from grant NSC93-2213-E-006-123, Taiwan.

BIOMECHANICAL ANALYSIS OF THE WALKING PATTERN IN HEALTHY SUBJECTS WITH AND WITHOUT ROLLATOR

[1] Tine Alkjær, [1]Peter K. Larsen, [1]Gitte Pedersen, [1]Linda H. Nielsen and [1]Erik B. Simonsen
[1]Institute of Medical Anatomy, The Panum Institute, University of Copenhagen, email: t.alkjaer@mai.ku.dk

INTRODUCTION

The rollator is a commonly used walking-aid in elderly and in disabled subjects. The purpose of using the rollator is to improve the walking performance and minimize the risk of falling. Studies have shown that the walking performance in elderly subjects measured as distance, cadence and velocity is improved when they walk with a rollator [1]. However, knowledge about the specific changes in the joint moment patterns of the ankle, knee and hip joint are limited. Thus, the purpose of the present study was to investigate the biomechanical effects of walking with a rollator on the walking pattern in healthy subjects.

METHODS

Seven healthy women (age: 34.7 (range: 25-57) years, height: 1.70 (range: 1.64-1.78) m, weight: 64.7 (range: 55-75) kg) participated in the study, which was approved by the local ethics committee. The subjects were asked to walk across two force platforms (AMTI, OR6–5-1) both with and without a rollator (Dolmite Maxi 650, Dolomite AB, Anderstorp, Sweden) at a speed of 4.5 km/h. Fifteen small, reflecting spherical markers were placed on the subjects according to the marker set-up described by Vaughan et al. [2]. In addition, 14 markers were placed on the upper extremities and on the rollator.

Five video cameras (Panasonic WV-GL350) operating at 50 Hz were used to record the movements. The video signals and the force plate signals were synchronized electronically with a custom-built device. The device put a visual marker on one video field from all cameras and at the same time triggered the analogue-to-digital converter, which sampled the force plate signals at 1000 Hz. The subjects triggered the data sampling and synchronization when they passed the first pair of photocells. Three-dimensional coordinates were then reconstructed by direct linear transformation using the Ariel Performance Analysis System (APAS). Prior to the calculations, the position data were digitally lowpass filtered by a fourth-order Butterworth filter with a cut-off frequency of 6 Hz, and the 1000 Hz force plate signals were down sampled to 50 Hz to fit the video signals.

An inverse dynamics approach was used to calculate the kinematics and kinetics for flexion and extension. Six gait cycles were normalized and averaged for each subject and situation (with and without rollator, resp.). Normalization was performed by interpolating data points to form 500 samples for each gait cycle. Only the stance phase of the left leg was analyzed. A Students t-test for paired data was used to identify statistically significant differences between walking with and without rollator in selected kinematic and kinetic variables of the walking patterns. The level of significance was set at 5%.

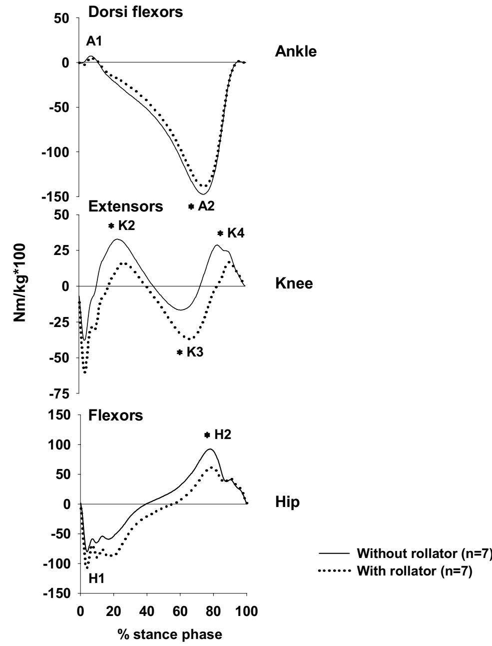

Figure 1: Average joint moments (Nm/kg*100) of the left ankle, knee and hip. 0% indicates heel strike and 100% indicates toe off on the x-axis. * indicates significant difference between walking with and without rollator.

RESULTS AND DISCUSSION

The hip was significantly more flexed during the stance phase when walking with the rollator (p=0.007). The peak ankle plantar flexor moment (A2, p=0.02) and knee extensor moments (K2 + K4, p=0.01) were significantly smaller during walking with rollator, while the peak knee flexor moment (K3, p=0.000) was larger than without rollator (Figure 1). The peak hip flexor moment (H2) was smaller during walking with rollator than without (p= 0.000) (Figure 1).

CONCLUSIONS

The results showed that walking with a rollator unloaded the plantar flexors and knee extensors. The hip was more flexed when walking with rollator because the trunk was leaned forward. This resulted in a smaller hip flexor moment during walking with rollator. However, the more flexed hip position should result in better conditions for the hip extensors to produce moment. Further investigation is needed to answer this question.

REFERENCES

1. Mahoney J, Euhardy R, Carnes M. A comparison of a two-wheeled walker and a three-wheeled walker in a geriatric population. *J Am Geriatr Soc* 1992; **40**(3):208-212.
2. Vaughan CL, Davis BL, O'Connor JC. *Dynamics of human gait*. Champaign, Illinois: Human Kinetics Publishers, 1992.

SEGMENATAL DYNAMICS OF SOCCER INSTEP KICKING

[1] Hiroyuki Nunome, [2]Takeshi Asai and [1]Yasuo Ikegami
[1]Nagoya Univ., Nagoya, Japan; e-mail: nunome@htc.nagoya-u.ac.jp
[2] Yamagata Univ., Yamagata, Japan

INTRODUCTION

An open kinetic chain model generally used for the detailed biomechanical analysis of the kicking leg motion allowed the moment due to muscular force input and other sources to be computed separately. Putman (1991) illustrated the actions of the resultant joint moment and motion-dependent interactive moment simultaneously during punt kicking. The procedure was applied by Dörge et al., (2002) to soccer instep kicking. However, as the integrated parameters was solely reported in their study, the time-series changes of the resultant joint moment and motion-dependent interactive moment during soccer instep kicking were still concealed.

The purpose of this study, therefore, was to reveal the detailed time-series actions of the resultant joint moment and motion-dependent interactive moment during soccer instep kicking

METHODS

The kicking motions of five highly skilled club players (age: = 16.8 ± 0.4 yrs; height: = 176.2 ± 6.1 cm; mass: = 70.6 ± 7.2 kg) were captured using a three-dimensional cinematographic technique at 200 Hz. The resultant joint moment (muscle moment) and the motion-dependent interactive moment (interactive moment) were computed using a two link kinetic chain composed of the thigh and lower leg (including shank and foot).

To avoid a systematic distortion of the data caused by ball impact, the moments were computed from unsmoothed coordinates until three frames before ball impact and then extrapolated for fifteen points by a linear regression line. The regression line was defined for each change. To resemble the final change of the data, the final eight to twelve data points were fitted to the linear regression line. For angular velocities, a quadric regression line was fitted to the unsmoothed data in the same manner. After these extrapolations, all parameters were digitally smoothed by a fourth-order Butterworth filter at 12.5 Hz, and then the extrapolated regions after ball impact were removed.

RESULTS AND DISCUSSION

During the final phase of kicking, though the forward hip muscle moment rapidly decreased, its backward moment was rarely seen toward ball impact. This indicated that the backward hip muscle moment had no substantial influence to decelerate the thigh during kicking. As shown in Figure 1, it is obvious that the deceleration of the thigh was initiated by the reaction knee muscle moment as Nunome et al., (2002) argued, and this motion was later emphasized by the interactive moment due to the distal end force.

For the lower leg motion, as shown, the knee muscle moment dominates the lower leg motion until the final phase of kicking.

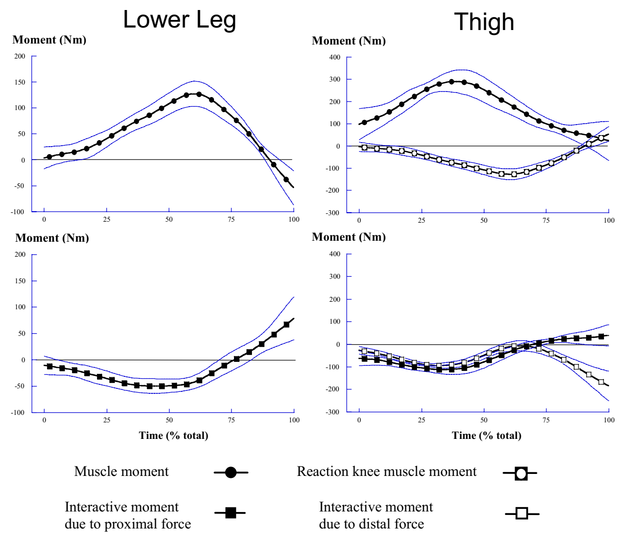

Figure 1: The average (±SD) changes of muscle moment and motion-dependent interactive moment acting on the lower leg and thigh.

After this, the knee muscle moment was rapidly inhibited. It is assumed that as the angular velocity of the lower leg exceeded the inherent force-velocity limitation of muscles immediately before ball impact, the muscular system related to the lower leg motion became incapable of generating any concentric force. Thus, it can be speculated that the backward knee muscle moment was mainly due to the resistance of the muscular system when it was forced to be stretched.

In contrast to the inhibition of the knee muscle moment, the interactive moment began to dominate the accelerative motion of the lower leg immediately before ball impact.

CONCLUSIONS

Detailed time-series data of the muscle moment and interactive moment during soccer instep kicking was clearly illustrated. The deceleration of the thigh was initiated by the reaction knee muscle moment and was later emphasized by the interactive moment due to the distal end force.

The acceleration of the lower leg immediately before ball impact was dominated by the interactive moment due to the proximal end force.

REFERENCES

1. Putnam. *Med Sci Sports Exerc* **23**, 130-144, 1991.
2. Dörge et al., *J Sports Sci* **20**, 293-299, 2002.
3. Nunome et al., *Med Sci Sports Exerc* **34**, 2028-2036, 2002.

RELATIONSHIP BETWEEN FOOT PROGRESSION ANGLE AND EXERCISE-RELATED LOWER LEG PAIN

[1]Tine Willems, [2]Dirk De Clercq, [2]Anneleen De Cock, [3]Philip Roosen and [1]Erik Witvrouw
[1]Department of Rehabilitation Sciences and Physiotherapy, Ghent University, Belgium; E-mail: Tine.Willems@ugent.be
[2]Department of Movement and Sport Sciences, Ghent University, Belgium
[3]Arteveldehogeschool, Ghent, Belgium

INTRODUCTION

Exercise-related lower leg pain (ERLLP) is a common and enigmatic overuse problem in athletes and military populations [1]. Runners, track athletes and athletes participating in jumping sports are frequently diagnosed with ERLLP which is usually induced by repetitive tibial strain imposed by loading during intensive, weight bearing activities. Retrospective and prospective studies have identified a relationship between an increased subtalar eversion and ERLLP [2,3,4]. As highly potential risk factor, also an increased medial pressure distribution during the forefoot contact phase has been identified [4]. In clinical practice, an increased foot progression angle (abducted) is often linked with an increased eversion as it is suggested that the lower leg follows the direction of progression. Therefore, we hypothesize that ERLLP could be related to an increased foot progression angle which could relate to the increased eversion and the increased medial pressure distribution. However, to our knowledge, in the literature, the relationship between foot progression angle and ERLLP or the eversion excursion or the medio-lateral pressure distribution has not been investigated. Therefore, the purpose of this study was 1) to investigate the relationship between the foot progression angle and the amount of eversion and the medio-lateral pressure distribution and 2) subsequently gain insight in a potential underlying mechanism that might be implicated as precursor to ERLLP.

METHODS

Subjects were 400 healthy undergraduate physical education students. 3D-gait kinematics combined with plantar pressure profiles were collected during barefoot running at a speed of 3.33m/s. The experimental set-up consisted of a 2m x 0.4m AMTI-force platform set into a 16.5m indoor running surface. Plantar pressure data were collected with a Footscan pressure plate (RsScan Int, 2m x 0.4m, 2 sensors/cm², 480Hz, dynamic calibration with AMTI), mounted on top of the force platform. The foot progression angle was derived from the plantar pressure data and was defined as the angle between the direction of progression and the mid heel - head of metatarsal II axis. Kinematics were collected at 240Hz using 7 infrared cameras (Proreflex) and Qualisys software. Marker placement and modeling was based on that of McClay and Manal (1999). The eversion was calculated through positioning the rearfoot with respect to the lower leg and the excursion was measured around the sagittal axis trough modeling with Visual3D (C-motion). Three valid right and three valid left stand phases were measured and analysed.
After the evaluation, all sports injuries were registered by the same sports physician during a certain period.
First, intrasubject variability of the foot progression angle of 30 healthy subjects was evaluated by means of Intraclass Correlation Coefficients (ICC) for three consecutive trials. Second, foot progression angle was correlated with the eversion excursion and the medio-lateral pressure distribution during the forefoot contact phase, which were both risk factors for ERLLP.
And third, Cox regression analysis was performed to test the effect of the foot progression angle on the hazard of injury.

RESULTS AND DISCUSSION

Intraclass Correlation Coefficient showed low intrasubject variability (ICC=0.92), which demonstrates that positioning of the foot is very constant in barefoot running.
Pearson correlation showed no significant correlation between foot progression angle and the eversion excursion (R=.121) and between foot progression and the medio-lateral pressure distribution during the forefoot contact phase (R=.116).
During the follow-up period, 46 of the subjects developed ERLLP, of whom 29 subjects had bilateral complaints. So 75 symptomatic lower legs, 35 left and 40 right were classified into the ERLLP group. As control group, bilateral feet of 167 subjects who had no injuries at the lower extremities were selected. Cox regression analysis showed no significant differences between the foot progression angle between the uninjured and ERLLP group (P = .533).
Our hypothesis that ERLLP could be related to an increased foot progression angle which related to the increased eversion and the increased medial pressure distribution can be rejected.

CONCLUSIONS

Results of this study show that the foot progression angle is not a risk factor for ERLLP. In addition, the foot progression angle is not related to the amount of eversion or the medio-lateral pressure distribution during the forefoot contact phase. We therefore hypothesize that during the roll off, the lower leg is not following the direction of progression, but rather the direction of the foot axis. However, this should be investigated further.

REFERENCES

1. Beck BR. *Sports Med* **26**, 265-279, 1998.
2. Messier et al. *Med Sci Sports Exerc* **20**, 501-505, 1988.
3. Viitasalo et al. *Am J Sports Med* **11**, 125-130, 1983.
4. Willems et al. *Gait Posture*, **in press**, 2004.
5. McClay et al. *Med Sci Sports Exerc* **31**, 1629-37, 1999.

ACKNOWLEDGEMENTS

This research was supported by BOF-RUG 01109001

PLANTAR PRESSURE DISTRIBUTION PATTERNS USED AS BIOFEEDBACK INFORMATION IMPROVE TECHNICAL TRAINING AND PERFORMANCE IN IN-LINE SPEED-SKATING

[1] Olaf Hoos, [2]Dieter Rosenbaum, [2]Eric Eils and [3]Kuno Hottenrott
[1]University of Marburg, Institute of Sports Science, Marburg, Germany
[2]University of Münster, Movement Analysis Lab, Münster, Germany,
[3]University of Halle, Institute of Sports Science, Halle, Germany
email: hoos@mailer.uni-marburg.de

INTRODUCTION

In-line speed-skating (ISS) is a rather new competitive discipline with biomechanical characteristics similar to ice speed-skating (3,4). In both disciplines knowledge and feed-back of push-off mechanics appear essential for performance optimization (1,2). Therefore, the goal of the study was to evaluate whether plantar pressure distribution patterns are useful as biofeedback information to develop exercises for technical training that are beneficial for performance optimization in ISS.

METHODS

The study consisted of two parts. **Part 1:** Foot pressure distribution (Novel-Pedar, 50 Hz) was assessed for eight elite in-line speed skaters (age: 28±5 years, weight: 72±4 kg) skating 1000 m at 35 km/h behind a car on a smooth road track. All athletes skated the road track four times with different push-off conditions in randomized order: normal technique (N), focused on normal technique (F), push-off with the forefoot/toes (T) and push-off with the heel (H). For each condition, five consecutive steps were analyzed yielding contact time (CT), peak pressure (PP), maximum force (MF) and force-time-integrals (FTI) for 10 anatomical regions. Furthermore, all subjects completed a questionnaire about their experience and sensation concerning push-off mechanics for the different conditions. Pressure distribution patterns and the results of the questionnaire were used to extract main characteristics of push-off dynamics in elite ISS and a training program with specific push-off exercises was developed accordingly. **Part 2:** The developed program was evaluated in a 6 week trial of technical training with 69 recreational inline-speed-skaters, randomly separated in a training group (TG; n=39; age 37±10 years, weight 70±12 kg) and a control group (CG; n=39; age 38±9 years, weight 67±10 kg). Technical training volume was similar for both groups (once a week, 105 min) with the major focus on basic technical aspects of the ISS technique. While CG focused only on basic technical drills, TG additionally used the specific push-off exercises. The effect on skating performance was evaluated by a 200 m sprint test before (PRE) and after (POST) the 6 week program.

RESULTS AND DISCUSSION

Table 1 shows the PP-values of the elite skaters. The plantar pressure values indicated that the major characteristics during push-off are a well-distributed load between heel and medial forefoot and a push-off with pronounced heel impulse. This specific pressure distribution pattern is only altered by the condition push-off with toes, which is further mentioned in the questionnaire as most ineffective and "unusual". The results had shown that for technical training in Part 2 of the study specific exercises for plantar sensation during skating and for pronounced sideways push-off with high-heel impulse had to be used.

The results of the 200m sprint test yielded a significant improvement for TG (pre: 35.1±4.5 s; post 33.9±4.0 s, p=0.0005) and no changes for CG (pre: 38.9±7.0 s; post: 39.1±6.3 s, n.s.), underlining the positive effect of the developed technical training program on skating performance.

CONCLUSIONS

Plantar pressure distribution patterns yield useful biofeedback information for coaches and athletes and may help to improve technical training programs and performance in ISS.

ACKNOWLEDGEMENT

Supported by the BISP (Bundesinstitut für Sportwissenschaft; VF 0407/06/16/2002-2003).

REFERENCES

1. Publow, B. *Speed on Skates*, Human Kinetics, Champaign/ILL, 1999.
2. Gemser, H. et al. *Handbook of competitive speed-skating*, Eisma Publishers, Leeuwarden (NL), 2000.
3. De Boer, R. W. et al. *Eur J Appl Phys* **56**, 562-69, 1987
4. Hoos, O. *Movement structure, movement technique and speed regulation in in-line speed-skating.* PhD Thesis, Görich & Weiershäuser, Marburg, GER, 2003.

Table 1: Peak Pressure (PP, n=8) of 10 plantar regions of the foot at 4 push-off conditions. „*" marks a significant difference between conditions (ANOVA), „<" and „>" a trend (p<0.10) between conditions normal (N), focused (F), toes (T) and heel (H). Further abbreviations: med.= medial, lat.= lateral, cent.= central, n.s.= non-significant

Peak Pressure [N/cm²]	Push-off conditions				Differences between conditions
	normal (N)	focused(F)	toes (T)	heel (H)	
Med. Heel	21,4±6,8	22,5±6,9	15,4±7,7	23,8±6,5	trend (T<H)
Lat. heel *	21,1±7,3	21,5±6,1	15,2±7,3	23,4±6,3	trend (T<H)
Med. Midfoot	8,0±4,7	8,0±4,4	8,2±5,2	8±4,3	n.s.
Lat. Midfootl	5,9±2,7	6,1±2,2	6,3±1,8	6,1±2,4	n.s.
Med. forefoot	18,0±7,9	17,7±7,9	19,0±9,3	16,8±7,8	n.s.
Cent. Forefoot	7,7±2,9	8,2±3,0	10,9±5,3	7,7±3,4	n.s.
Lat. Forefoot	7,8±2,0	7,1±2,0	10,9±3,2	7,0±3,9	trend (T>F; T>H).
Hallux	19,3±14,9	16,9±12,1	19,4±9,0	13,0±8,5	n.s.
Second toe	7,8±2,0	7,1±2,0	10,9±3,2	7,0±3,9	n.s.
Lat. Toes	8,7±3,5	9±2,7	11,3±4,7	7,4±3,6	n.s.

COMPUTER SIMULATION OF A HUMAN SKI JUMPER - A COMPLETE TRIAL

[1,2] Syn Schmitt, [1]Helmut Mutschler, [2]Albert Gollhofer and [1]Hanns Ruder
[1]Section Biomechanics, Department of Astronomy and Astrophysics, University Tuebingen
[2]Department of Sport and Sport Science, University Freiburg; email: sschmitt@tat.physik.uni-tuebingen.de

INTRODUCTION

Recent computer simulation results make a good contribution to understanding human movements [2,4]. But the control algorithms used there, are very complex and numerically more expensive. The purpose of this contribution is to present a robust method to model and simulate a complex human movement with aerodynamic interaction. In detail the squat position control at start-up and the calculation of lift and drag forces during the complete ski jump are considered.

METHODS

The ski jumper model was created on the bases of a HANAVAN [3] model (height: 1,78m, weight: 60kg) consisting of 17 rigid bodies. Each joint has a 1-dof rotational spring damper representing stiffness and elasticity of the real body joints except for the following joints: ankle, knee, hip, upper body, shoulder and neck. These joints are the actuators of the model. To create and solve the equations of motion we used DySim, a self-coded rigid body simulation package. The animation of the data was made with AniDySim also self-coded using OpenGL.

The actuators are built with 1-dof rotational spring dampers (ARSDA) with adaptable resting length. Therefore we created a control algorithm to switch between different states to adapt the resting length to the desired motion. The torque produced by the spring is directly transmitted to the body mechanics. In this presented simulation we used eight different angular configurations (states/resting lengths) for the complete trial.

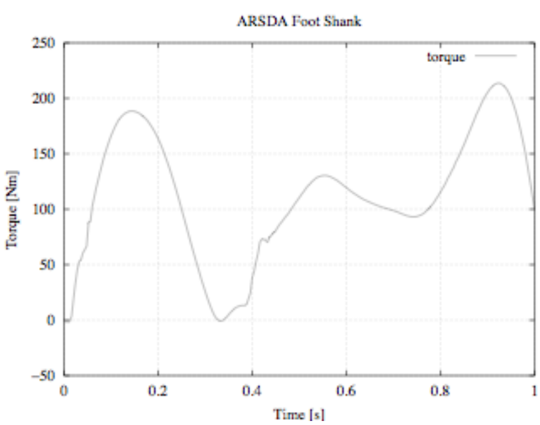

Figure 1: Movement control of the foot-shank joint: The control algorithm switches between two states, one to bring the ski jumper more to the front and the other more to the back (positive and negative torque changes).

During the start-up and the landing phase the ground reaction forces were modeled with contact elements between the skis and the jumping hill. In the flight phase we used a newly written aerodynamic algorithm. Lift and drag forces where calculated separately with drag force $\underline{F}_D = 0.5 \cdot c_R \rho_A A_R \underline{v}^2$ as a

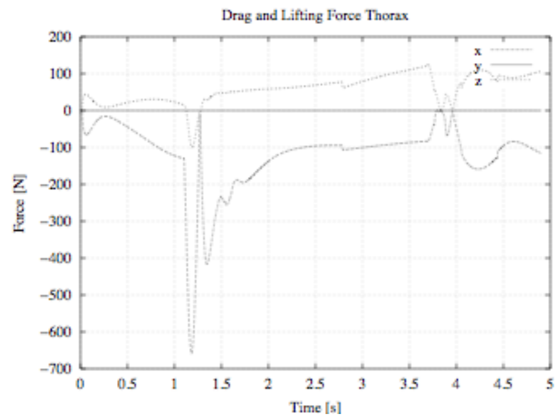

Figure 2: Aerodynamic forces in x-, y-, z-direction. Where -x marks the drag direction and z marks the lift direction.

standard formula. The lift force, largely dependent on the variable aerodynamic conditions like position and surface conditions, was estimated by the modified formula $\underline{F}_L = 0.5 \cdot c_L \rho_A A_W \underline{v}^2$.

RESULTS AND DISCUSSION

The result of this computer simulation is an entire ski jumping trial, encompassing the start-up and the landing including the calculated aerodynamic forces. Figure 1 displays the ankle torque for the movement control during the start-up phase. The swift-like regulation between forward and backward position is clearly observable. Figure 2 shows the lift and drag forces of the thorax body calculated for the entire trial. At t~1,2s the takeoff of the jumping movement takes place, thus high drag forces are considerable.

This example of a entire and complex movement model on the basis of realistic physical constraints demonstrates a powerful tool for better understanding of complex biomechanical structures. However, the validation of the results is still in progress using detailed position and velocity data from real ski jumper collected with a GPS receiver.

CONCLUSIONS

Even with this approach to model human movement we showed that a complex computer simulation could be done according to the λ-model [1]. Furthermore it is obvious that modeling of aerodynamics of a dynamic multibody system enables to identify the most critical flight phases in relation to optimize horizontal velocity.

REFERENCES

1. Feldman A, Journal of Motor Behavior **18**, 17–54, 1986.
2. Guenther M, et al. *Biol Cybernetics* **89**, 2, 89-106, 2003.
3. Hanavan EP, *Techreport*, Wright-Patterson AFB, OH, 1964.
4. Pratt J, *PhD thesis*, MIT, Cambridge, Massachusetts, 1995.
5. Schlichting HJ, *Praxis Naturwiss - Physik* **35**, 5–7, 1986

DOES COURSE OF A PRECEDING PITCH INFLUEBCE BASEBALL BATTING AS THEY SAY?

[1,2] Chizuru Toriki, [1] Tomoyuki Matsuo, [3] Takayuki Shigetani, [3] Ryutaro Himeno, [4] Kazushi Tezuka, [1] Ken Hashizume
[1]Faculty of Health and Sport Science, Osaka University
[2]Asahi Broadcasting Corporation
[3]Advanced Computer Center, The Institute of Physical and Chemical Research
[4]Beta-Endorphin; email: tmatsuo@skill.hss.osaka-u.ac.jp

INTRODUCTION

It is generally believed that a certain combination of pitches influences the performance of baseball batting. However, it is difficult to elucidate it in real game situation, because several factors involve it (not only characteristics of pitches but also game situations). Gray (2002) ascertained, in his virtual batting study, that there were both the expectancy effect concerning the preceding pitch sequence and the pitch count effect [1]. He focused on change of pitch speed. In the current study, we focused on change of the course of pitch, especially whether the course of the preceding pitch individually influence the movement of batting the succeeding low-and-outside ball.

METHODS

Eight experienced college-level baseball players voluntarily participated in this study. Their mean height was 1.75 m (SD = 0.06), mean body mass was 71.9 kg (SD = 25.4), mean age was 20.6 years (SD = 1.2), and mean number of years of playing experience was 12.3 years (SD = 2.5). After detailed explanation of the experiment and filling out an informed consent, they were provided sufficient amount of time for warm-up including bat swings.

Three reflective markers with 19 mm in diameter were put at the distal end of an aluminum bat. Its length was 0.85 m and its mass was 0.87 kg. Reflective markers were also put on the top of participant's head, both of lateral tip of the acromions, and both of anterior superior iliac spines. A four-camera ProReflex system (Qualisys) was used to collect the three-dimensional coordinates of the reflective markers with sampling frequency at 200 Hz during swings.

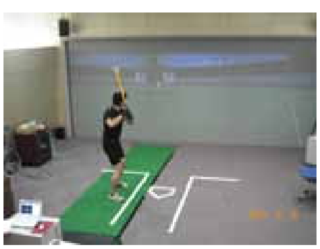

The task was to 'hit' a virtual ball, simulating an approaching baseball. The virtual pitch was displayed on a large display (2.1 m in vertical X 6 m in horizontal) with a pitcher (height was 1.78 m) in a baseball stadium. The trajectories of pitches were computed based on the pitch velocity, the angle of incidence, air resistance, and spin of the ball (Himeno, 2001). The ball velocity at the instant of ball release was always set at 33.3 m/s. Each participant first swung in the control condition in which he was informed where the ball was thrown, then swung in the pseudo-random condition in which the course of pitch was strategically decided so as not to be noticed by the participants. A block consisted of approximately 22 swings with a 20 sec. rest between swings, and eight blocks were performed with 2–10 min. rest between blocks.

Several kinematic variables concerning trunk and bat movements during swing for the pitch into low-and-outside corner of the strike zone were calculated and compared among the conditions of the course of the preceding pitch.

RESULTS AND DISCUSSION

Although angle of trunk forward bending did not differ among conditions, both of maximum angles of the pelvis rotation and the upper trunk during backswing were significantly smaller in the condition where the preceding pitch was the low-and-outside pitch (pre-LO condition), than in the condition where the preceding pitch was high-and-inside (pre-IH condition) (Figure 1).

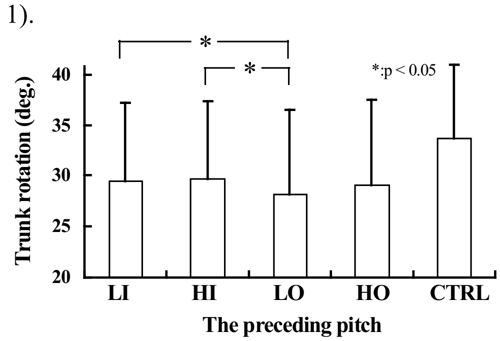

Figure 1: Maximum upper trunk rotation during backswing for the low-and-outside strike. LI, HI, LO, HO, CTRL stand for low-and-inside, high-and-inside, low-and-outside, high-and-outside, and pre-informed conditions, respectively.

Maximum angular velocity of the upper trunk during forward swing had a tendency to be slightly lower in the pre-OL condition than in the pre-IH condition.

From the above results, it is suggested that the participants expected that the probability of successive low-and-outside pitches was low and the probability of the low-and-outside pitch after high-and-inside pitch was high.

CONCLUSIONS

From the results of the swings for the same course of the pitch but different course of the preceding pitch, it was found that even only the course of the preceding pitch influenced the trunk movement during batting for the low-and-outside ball.

REFERENCES

1. Gray R. *J Exp. Psycho. Human Perception & Performance*, **28**, 1131-1148, 2002.
2. Himeno R, et al. *J visualization*, **4**, 198-207, 2001.

A FOOTTYPE CLASSIFICATION WITH CLUSTER ANALYSIS ON PLANTAR PRESSURE DISTRIBUTION DURING BAREFOOT JOGGING

[1] Anneleen De Cock, [2]Tine Willems, [2] Erik Witvrouw and [1] Dirk De Clercq
[1] Ghent University, Department of Movement and Sport Sciences, Belgium
[2]Ghent University, Department of Rehabilitation Sciences and Physiotherapy, Belgium

INTRODUCTION

The foot provides stabilisation, shock absorption, balance and propulsion during stance phase, but how these functions are realised is still not fully understood[1]. Plantar pressure measurements have the potential to unravel the relations between foot structure and foot function. It is a common belief that different functional foot types exist, but a classification into functional foot types is mostly based on morphological characteristics, measured in a static position [2,3]. Dynamical measurements, linked to the functional behaviour of the foot, may provide a better basis for a classification system. The aim of the present study was to develop a foot type classification based upon dynamical plantar pressure measurements.

METHODS

Plantar pressure data were collected from 215 healthy subjects (age: 18.3 ± 1 years; 129 men and 86 women) . A footscan pressure plate (RsScan Int. , 2m x 0.4m x 0.02m, 10sensors/ 4cm², dynamic calibration with AMTI force plate) was mounted in the middle of a 16.5m long running track. The subjects ran at a speed of 3.3m/s (± 0.17m/s). Three stance phases were measured for each side. For each trial, eight important anatomical areas (medial en lateral heel, metatarsal I-V and the hallux) were identified on the footprint. For each area descriptive statistics (mean, SD) were calculated for relative regional impulses (% of summed impulses of all subareas, RI_R). To classify into foot types, a K-means clustering analysis was used, based on the relative regional impulses of the forefoot. A multivariate ANOVA with post-hoc Tukey test was used to study differences between the four clusters.

RESULTS AND DISCUSSION

With the K-means cluster analysis, four clusters of pressure patterns were identified (figure 1): (a) Medial M_2 pattern with large pressure loading underneath M_2 (b) Central-lateral pattern with a more overall scattered pressure loading, (c) Central pattern with larger pressure loading underneath M_3 and M_2 and (d) Medial M_1 pattern with a large pressure loading underneath M1. Significant differences were found between the four clusters for peak pressures, regional impulses, relative regional impulses and some timing factors. In three of the four patterns and certainly in the M_2 pattern, M_2 sustains high impulses, since specific characteristics of this metatarsal make it a cantilever during push off. The forefoot contact phase (when meta's make contact) for the M_1 pattern is significant shorter in duration compared to other foot types,

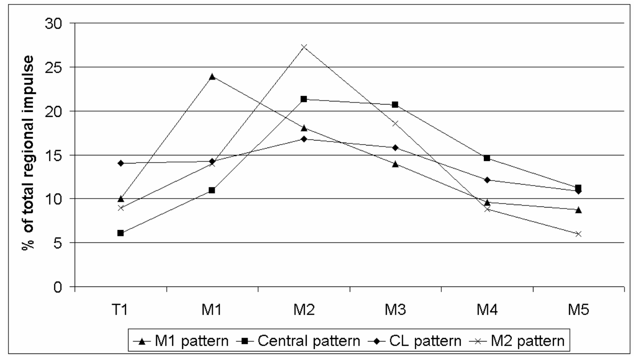

Figure 1: Relative regional impulses for the four loading patterns.

which could indicate a fast initial plantar flexion and initial eversion. [4] The high pressure loading on the first metatarsal might also arise from a rigid first ray, which then sustain allmost all pressure loading during push off.
The pressure load patterns found in the present study are very similar to the pressure patterns found by Hughes et al (1993) [5], which were based on peak plantar pressure underneath the forefoot of 100 adults in a walking condition. Although peak pressures and pressure-time integrals are higher in running, the distribution of the pressure over the foot is comparable to that of walking. This could indicate that in both locomotion forms, similar loading mechanisms exist.

CONCLUSIONS

An interpretation of foot types was suggested by classifying four foot types on differences in dynamical plantar pressure distribution. Further research combining plantar pressure data with morphological measurements and 3D kinematic data is expected to get a better insight in the functional behaviour of the different foot types.

REFERENCES

1. Giacomozzi C et al. Med. Biol. Eng. Comp. 2000; 38: 156-163
2. Razeghi M et al. Gait Posture 2002; 15: 282-291
3. Cavanagh PR et al. J Biomech 1987; 20 (5): 547-51
4. McClay et al. Clin Biomech. 1998; 13: 195-203
5. Hughes J. et al. Foot Ankle 1993; 14 (9): 514-19

ACKNOWLEDGEMENTS

This research was supported by BOF-Ghent University 011/046/04 and BOF-Ghent University 0141/090/04

SHOULDER LOAD DURING WEIGHT RELIEF LIFTING: A SIMULATION STUDY

[1] Stefan van Drongelen, [1] Luc van der Woude, [2] Ed Chadwick, [1] DirkJan Veeger
[1] Institute for Fundamental and Clinical Human Movement Sciences, Vrije Universiteit, Amsterdam, The Netherlands.
[2] Department of Biomedical Engineering, Case Western Reserve University and VA FES Center, Cleveland, Ohio, USA
Email: s.vandrongelen@fbw.vu.nl, web: www.fbw.vu.nl

INTRODUCTION

High and frequent loading during wheelchair ADL is a generally recognized factor contributing to the development of shoulder complaints. A previous study has shown that the external load on the shoulder in subjects with a spinal cord injury (SCI) is high (40 Nm) during weight relief lifting [1]. Simulation of internal load that includes the effect of (partial) muscle paralysis is likely to lead to higher glenohumeral contact forces and forces in the remaining muscles, when compared to a complete musculoskeletal system. The purpose of this study was to evaluate the effect of lesion level on the estimated glenohumeral contact force and muscle load.

METHODS

Four subjects with tetraplegia (TP) and four able-bodied (AB) male subjects participated. Three-dimensional kinematics of the thorax, humerus, clavicula, scapula, forearm and hand were recorded with a 3-camera opto-electronic system (Optotrak, Canada) during 3 trials of weight relief lifting. External forces were recorded with an instrumented wheelchair (AMTI 6df; Quickie Triumph, The Netherlands). The orientation of the scapula was determined in a calibration measurement with a scapula-locator system. From this measurement and the orientation of the humerus during the tasks, the orientation of the scapula and clavicula were calculated using a regression model [2]. Position and force data were used as input for the Delft Shoulder and Elbow Model which calculates muscle forces and joint glenohumeral contact forces (GHCF). To simulate complete lesion levels, we made a classification of muscle force at each lesion level, based on muscle segment innervations as described in Gray [3], based on the assumption that the maximum relative force of each muscle was relative to the number of innervating segments above the lesion. By this method the model was modified to simulate lesions from C5 to T1, whereby a T1 lesion was equal to the complete, fully functional, shoulder-elbow model. All 24 input profiles (3 trials x 8 subjects) were used. This implied that the profiles of the AB subjects were used as input to a model with a SCI and vice-versa.

RESULTS AND DISCUSSION

The peak GHCF (Figure 1) was higher for the TP profiles than for the AB profiles (P=0.037) and for the TP profiles the peak GHRF was significantly higher for the first successful simulation (S1) compared to T1 (P=0.029). For the T1 simulation, higher forces are calculated for the TP profiles in the serratus anterior, pectoralis major, deltoideus and in the rotator cuff compared to the AB profiles. However the muscle forces are not significantly higher for the TP profiles compared to the AB profiles (P=0.36). The calculated forces for the biceps and triceps show much more predicted force in the triceps for the AB profiles compared to the TP profiles.

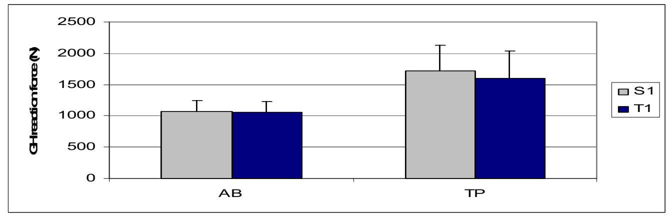

Figure 1: GHCF (mean + SD) for AB and TP profiles for the first successful (S1) and complete model simulation (T1).

Results show that it is possible to have a successful simulation of the performance of a weight relief lift with a complete C6 SCI but not with a C5 lesion, which appears indeed to be the case in real life. At the C6 lesion level, fewer successful AB profiles suggest an adaptation in the kinematics of the subjects with TP. The lesion modifications do have a small effect on the GHCF: T1 is 7.3 % higher than S1 for TP profiles. We expected the effect to be larger, but it is well likely that the adaptations in the TP kinematics already compensate for the loss of muscle force and the loss of muscle function by the use of different muscles.
A critical issue in this study is the question of whether the forces and particularly the forces of the triceps are correct. The predicted maximum triceps force for the TP profiles still 11 % of the maximum triceps force in the model. This percentage is close to the percentage measured by Needham-Shropshire [4]. They reported that subjects with a manual muscle test score of 3/5 for the elbow extension only had 9 % of the maximum voluntary force production of healthy controls. However, especially for TP subjects, the EMG intensity in terms of %MVC is of little value without information about the moment that can be generated at 100 % MVC. Information about muscle force instead of muscle activity is an important reason to use a biomechanical model.

CONCLUSIONS

The higher GHCF found in our simulations was mainly due to a different task performance by the TP subjects. The model modifications had a minor effect on the calculated GHCF.
Due to the higher load on the shoulder joint and shoulder muscles in subjects with tetraplegia, these subjects run a higher risk of muscle overload and damage to the shoulder joint.

REFERENCES

1. Van Drongelen S, et al. *Arch Phys Med Rehabil*, accepted.
2. Pascoal AG. *Ombro e Elevação do Braço*, Universidade tecnica de Lisboa, Lisboa.
3. Gray H. *Gray's Anatomy*, Churchill Livingstone, New York NY.
4. Needham-Shropshire BM, et al. *J Spinal Cord Med* **20,** 324-30, 1997.

IMPEDANCE MODULATION WITH PRECISION DEMANDS IN DISCRETE MOVEMENTS

Luc P.J. Selen, Peter J. Beek and Jaap H. van Dieën
Institute for Fundamental and Clinical Human Movement Sciences, IFKB, Vrije Universiteit, van der Boechorststraat 9, 1081 BT Amsterdam, The Netherlands; email:Luc.Selen@fbw.vu.nl

INTRODUCTION

Human motor performance is intrinsically variable, but this variability is tuneable, as evidenced by the speed-accuracy trade-off. Recently, impedance modulation has been suggested as a means to decrease motor output variability [1,2]. Unlike previous studies, in which impedance was estimated from muscular (co)-activation, we conducted an experiment in which we estimated the impedance from mechanical perturbations.

METHODS

Twelve subjects participated in the experiment. Their right forearm was cast (NobaCast) to a splint, which was attached to a torque controlled motor. Two targets were presented on a ledbow placed 1.5m in front of the subject. A laserpointer attached to the splint indicated the pointing direction of the arm on the ledbow. Three different targets (3, 6 and 9cm in width) were presented in blocks. Subjects were instructed to make discrete, 35^{o}, target-to-target flexion movements, with a movement time between 270 and 330ms. After each trial, the performance was fed back to the subject. Each blok consisted of 165 flexion movements of which 20 were perturbed by a torque pulse of 5Nm and a duration of 70 ms duration.
For the unperturbed trials that matched the time and precision constraints we determined the trajectory variability. The perturbed trials were matched to the best fitting unperturbed trial [3] to find the trajectory deviation after perturbation. These trajectories were normalized to the maximum deviation in all trials of each subject individually. The maximum deviation was used as a first order estimate of the impedance. ANOVAs for repeated measures were performed on both the trajectory variability and the impedance changes.

RESULTS AND DISCUSSION

Figure 1 shows the standard deviation over all correct unperturbed trials for the different targets for all subjects. Trials were aligned to movement onset. Notice the decrease in variability when entering the target region (300-400ms) and the subsequent increase. This monotonic behavior was present in the correct trials of all subjects. Figure 2 shows the normalized maximum trajectory deviation after perturbation. Although overall the deviation increases with target width, the large standard deviations reflect that impedance modulation is not present in all subjects.
So far, only the maximum trajectory deviation was analyzed as an impedance estimate. In future work we will try to explicitly model the elbow joint as a second order system, resulting in quantitative measures of stiffness and damping.

CONCLUSIONS

This study shows that impedance modulation and precision demands go hand in hand. Whether this impedance modulation is a strategy for reducing motor output variability in the face of precision constraints remains unclear. Osu et al. [1] presented a similar result, based on EMG activity. Although group averages indicate that impedance is modulated with precision demands, in single subjects this is not always the case. Apparently, other strategies to meet precision demands are available, even in single degree of freedom, time-constrained movements.

REFERENCES

1. Osu R., et al. J. Neurophysiol 92, 1199-1215, 2004
2. Gribble P.L., et al. J Neurophysiol 89, 2396-2405, 2003.
3. Popescu F., et al. Exp Brain Res 152, 17-28, 2003

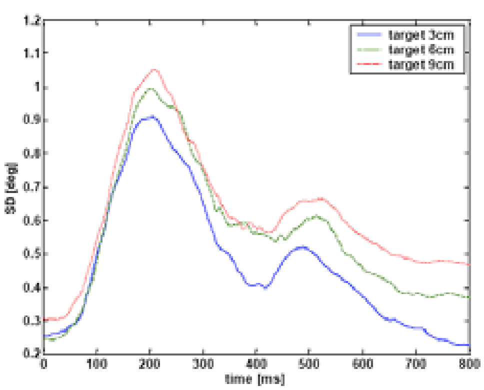

Figure 1: Kinematic variability over all subjects in the correct trials. The variability of the 3 cm target is different from the 6cm and 9cm target after 300ms

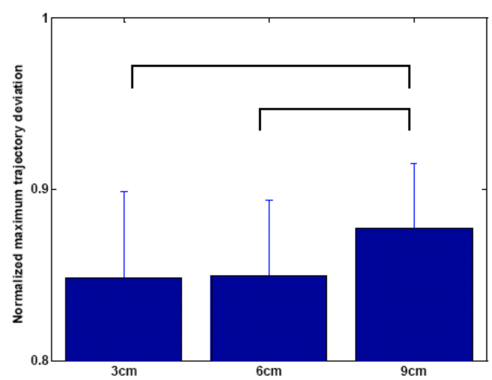

Figure 2: Impedance estimate (expressed as the normalized maximum trajectory deviation) for all subjects . The 9 cm target is significantly different from the 3cm and 6 cm target.

GROUND REACTION FORCES IN PIGS DURING GAIT ON DRY AND GREASY FLOOR

[1, 2]Vivi M. Thorup, [2]Frede A. Tøgersen and [1]Bente R. Jensen
[1]Institute of Exercise and Sport Sciences, University of Copenhagen, Denmark; email: ViviM.Thorup@agrsci.dk,
[2]Dep. of Animal Health, Welfare and Nutrition, Danish Institute of Agricultural Sciences, Denmark

INTRODUCTION

Leg weakness, meaning clinical leg and claw disorders, joint diseases and locomotion disturbances, form a large welfare concern in modern pig production. Inappropriate flooring is a major contributor to these leg problems [1].

The dual purpose was to study the normal walk of slaughter pigs on solid (non-slatted) dry floor and to examine the effect of greasy floor condition on the gait.

METHODS

Kinetic data were collected from 12 healthy Danish crossbred slaughter pigs, with 6 pigs walking on dry and 6 on greasy concrete floor, respectively. Rape oil was used to make the floor greasy. Ground reaction forces were recorded at 1KHz from a force plate in the floor. Three to four trials were obtained for both right limbs. Vertical forces (Fz) were normalized to percentage body weight. For the stance phase vertical peak force (PeakFz), vertical mean force (MeanFz), horizontal craniocaudal peak (PeakFy) and minimum (MinFy) forces and stance phase duration were examined. Video recordings (50 Hz) were used to calculate walking speed.

Average vertical force curves were aligned according to a registering method [2]. Representatives of front and hind limb were chosen as templates. Then average of forces for each point of time was taken.

Results are reported as average (SD). Ratios are front/hind limb. Paired t-tests were used to compare limbs and unpaired t-tests to compare conditions. Level of significance was 5%.

RESULTS AND DISCUSSION

Average weight of the pigs was 75 (6) kg. Average walking speed was 0.86 (0.12) m/s on dry and 0.75 (0.11) m/s on greasy floor, with pigs tending to move faster ($P<0.07$) on dry floor. Figure 1 shows the vertical force exerted by front and hind limbs on dry floor. Kinetic parameters are reported in Table 1. Front limb MeanFz was significantly higher than hind MeanFz for both conditions, with a mean ratio of 1.2, that is the front limb carried more weight. Correspondingly, front limb PeakFz was significantly higher for both floor conditions meaning that the front received higher vertical peak forces

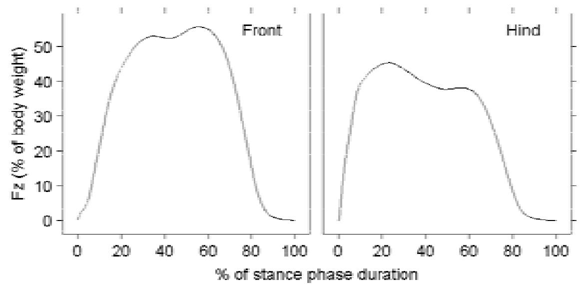

Figure 1: Average vertical ground reaction force of walking pigs during stance phase on dry floor (n=6). Left: front limb (24 trials), right: hind limb (23 trials).

than the hind (mean ratio 1.3). Front PeakFy in dry condition tended ($P<0.06$) to be higher than for the hind limb (ratio 1.1), whereas for greasy condition it tended ($P<0.07$) to be lower than the hind PeakFy (ratio 0.9). Front limb MinFy tended ($P<0.09$) to be lower than hind for dry condition (ratio 0.8). Comparing conditions, front limb PeakFy was significantly higher for dry than greasy condition, whereas hind limb PeakFy for greasy condition tended ($P<0.06$) to be higher than for dry. MinFy for the front limb tended ($P<0.1$) to be larger for greasy condition. Regarding stance phase duration, front limb stance phase lasted significantly longer than hind for both conditions. Stance phase duration of the hind limb was significantly longer than the front for greasy condition.

CONCLUSIONS

Pigs carry more weight on the front limb, and the front limb absorbs higher vertical peak force than the hind limb. Front limb peak horizontal force is higher on dry than on greasy floor. On dry floor horizontal peak force tends to be largest on the front limb and horizontal minimum force tends to be largest on the hind limb, however, on greasy floor the situation is reversed. Front limb stance phase lasts longer than hind for both dry and greasy floor. On greasy floor pigs have longer hind limb stance phases and tend to walk slower.

REFERENCES

1. Jørgensen B. *Anim Sci* **77**, 439-449, 2003.
2. Ramsay JO and Li X. *J Roy Stat Soc, B*, **60**, 351-363, 1998.

Table 1: Average (SD) stance phase parameters from pigs on dry and greasy floor. Percentages are force normalized to body weight. Significant differences ($P<0.05$) between a) front and hind limbs, b) floor conditions.

	MeanFz (%)		PeakFz (%)		PeakFy (N)		MinFy (N)		Stance phase duration (ms)	
Condition	**Front**	**Hind**	**Front**	**Hind**	**Front**	**Hind**	**Front**	**Hind**	**Front**	**Hind**
Dry	37.0 (2.7)[a]	31.7 (1.4)	57.2 (3.2)[a]	45.1 (2.7)	58 (8)[b]	51 (6)	-51 (14)	-63 (15)	665 (118)[a]	556 (41)[b]
Greasy	38.2 (1.5)[a]	32.3 (1.6)	57.7 (2.1)[a]	45.2 (2.7)	48 (9)	57 (5)	-59 (5)	-56 (12)	711 (79)[a]	635 (68)

KINEMATICS OF LATERAL TRANSFERS: A PILOT STUDY

[1] Sharon Eve Sonenblum, [1] Stephen Sprigle, [2] Leslie VanHiel, [2] Chris Maurer and [1]Eric Whittaker
[1] CATEA, Georgia Institute of Technology, [2] Shepherd Center; email: Sharon@catea.org

INTRODUCTION

People with spinal cord injuries (SCI) must transfer many times daily. Despite the importance of proper transfers, researchers have not completely described the kinematics of lateral transfers. Nyland *et al* identified transfer technique as a risk-factor for upper extremity degeneration and cited the need for quantitative measures of transfers and additional transfer research [1]. The purpose of this pilot study was to collect kinematic data on lateral transfers and identify different transfer strategies.

METHODS

A convenience sample of 19 male adults was recruited from Shepherd Center (an acute SCI rehabilitation center) with IRB approval. Subjects had to be able to perform lateral transfers independently or with minimal assistance and could not have pressure sores or upper extremity orthopaedic conditions. Data was collected with a motion capture system from Motion Reality Inc. (Marietta, GA). We used eight 60Hz cameras and 41 markers on the body and 8 on the wheelchair. After providing written consent, subjects performed three lateral transfers to their stronger side between their own wheelchairs and a 20" high therapy mat. They were provided as much assistance as they generally used.

For each subject, two average values (transfer to the mat and transfer to the chair) were calculated for the following descriptors of transfers: **maximum buttock height, minimum head height, wrist spacing and torso angle**. Wrist spacing (the distance between the left and right wrist body segments) and torso angle (the angle between the projections of lines running through the shoulders and through the hips) were measured at the mid-transfer point. Time zero was set at the **mid-transfer point,** which was defined as the point where the buttocks reached a maximum height between the final lift-off from the chair (or mat) and the initial contact with the mat (or chair). Paired t-tests were used to compare maximum buttock height, minimum head height, wrist spacing and torso angle during transfers to and from the wheelchair.

RESULTS AND DISCUSSION

Subjects elevated their buttocks an average of 11 inches above the therapy mat at mid-transfer (Table 1). They lowered their heads to approximately 21 inches above the mat. Subjects did not display a significant difference in buttock and head heights when transferring to the mat versus transferring to the wheelchair. On average mid-transfer (or maximum buttocks height) and minimum head height were separated by 0.3±0.5 seconds for transfers to the mat and 0.1±0.6 seconds for transfers to the wheelchair.

Subjects' wrists were spaced similarly at mid-transfer in transfers from the wheelchair (25.5") and transfers to the wheelchair (26.2"). The amount of torso rotation varied greatly between the subjects. The average angles formed by the shoulders and hips were nearly identical in transfers to and from the wheelchair (24° & 23°).

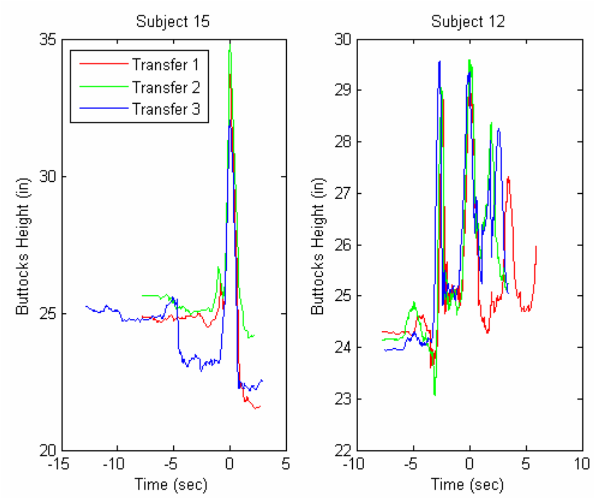

Figure 1: Two subjects' transfers to the mat are shown. Transfers to the wheelchair looked similar. Subject 15 (C6/7, Asia A) performed a smooth transfer with only one peak of buttock elevation while Subject 12 (T8, Asia C) used more buttock elevations to complete the transfer task.

A variety of transfer strategies were used by our subjects to complete the transfer task (Figure 1). The variation in buttock height within each subject's transfers was greater for transfers to the wheelchair than transfers to the mat ($p=0.0335$).

CONCLUSIONS

People with SCI use a variety of strategies to transfer between two surfaces. The different transfer strategies might be correlated to such factors as injury level, time since injury or body weight. Future work will cluster the transfer strategies in order to determine these relationships. Additionally, it is possible that the repeatability of the transfers might be related to upper extremity pain or safety of transfers. Further work with a greater number of subjects is needed to determine these relationships.

REFERENCES

1. Nyland J, et al. *Spinal Cord* 38: 649-657, 2000.

ACKNOWLEDGEMENTS

Funded by NIDRR in the RERC for Wheeled Mobility

	Transfer to Mat		Transfer to Wheelchair	
	Mean ± Stdev	**Range**	**Mean ± Stdev**	**Range**
Max Buttock Height	11.6" ± 1.6"	8.4"-14.8"	11.4"±2.0"	7.7"-17.3"
Min Head Height	21.2"±3.4"	13.9"-28.0"	21.8"±2.7"	35.1"-47.5"
Wrist Spacing at Mid-Transfer	25.5"±3.9"	18.3"±35.5"	26.2"±4.1"	19.0"±36.9"
Shoulder-Hip Twist Angle	23° ± 8°	6° - 38°	24° ± 8°	8° - 47°

Table 1: Summary of transfer measurements shows minimal variation in maximum buttock height and much greater variation in torso rotation. No significant differences were seen between transfers to the mat and the wheelchair.

DIFFERENTIAL EFFECT OF M. TIBIALIS ANTERIOR FATIGUE ON WALK-TO-RUN AND RUN-TO-WALK TRANSITION SPEED IN UNSTEADY STATE LOCOMOTION CONDITIONS

[1]Veerle Segers, [2]P. Aerts, [1]M. Lenoir and [1]D. De Clercq
[1]University Ghent, Department of Movement and Sport Sciences, Belgium
[2]University of Antwerp (UA), Functional Morphology lab,Department of Biology, Belgium
veerle.segers@ugent.be

INTRODUCTION

There are basically two forms of human locomotion, namely walking and running, kinematically distinguished from one to another by presence resp. absence of a double stance phase. When increasing resp. decreasing speed, a gait transition occurs at the point people intuitively feel that it is easier, more naturally to run resp. to walk even though it is possible to walk faster or run slower than the preferred transition speed. [1]. One of the most puzzling aspects of the transition-dilemma is to reveal the reason why gait transitions occur at that specific speed.

The purpose of the present study was to examine the role of the m. tibialis anterior -a possible trigger [2]- in a protocol with gradually changing speed before and after fatigue of the m. tibialis anterior. Our hypotheses are (1) that there is a relationship between the m. tibialis anterior and transition speed also in a protocol with gradually changing speed and (2) that within burst endurance rather than the strength is determinative for transition speed. Muscular fatigue of the dorsiflexors is therefore assumed to affect the transition speed.

METHODS

A group of 20 active female human subjects participated in the study after given informed consent. The WRT (walk-to-run transition) and RWT (run-to-walk transition) speed were determined on a treadmill in a protocol with gradually changing speed. The accelerations used in this research were 0.1 ms^{-2}; 0.07 ms^{-2}; 0.05 ms^{-2} for the WRT and -0.1 ms^{-2}; -0.07 ms^{-2} and -0.05 ms^{-2} for the RWT. WRT and RWT speed were determined using high speed video-images (200 Hz) before and after a fatigue protocol, in which the subjects performed submaximal dorsiflexions (ROM : 30°, ±75% 1RPM) until exhaustion was reached.

EMG of the m. tibialis anterior was obtained using bipolar electrodes and Noraxon-software. The signal was rectified, filtered (bandpass 4-500 Hz) and integrated. EMG-intensity (integral) and duration of the first peak of the m. tibialis anterior (end swing- begin stance), being the most dominant activity in RWT and WRT, were calculated. A 2 (fatigue) x 3 (acceleration) ANOVA and with step number as factor and Post Hoc Tukey tests were used for WRT and RWT to find differences for transition speed, energy-intensity and duration of the burst of the m. tibialis anterior.

Table 1. Transition speed

	Acceleration	Transition Speed (ms^{-1}) Before fatigue	After fatigue
WRT	0.1 ms^{-2}	2.16 ± 0.12	2.06 ± 0.07*
	0.07 ms^{-2}	2.10 ± 0.06	2.00 ± 0.07*
	0.05 ms^{-2}	2.12 ± 0.08	2.04 ± 0.09 *
RWT	-0.1 ms^{-2}	2.19 ± 0.14	2.19 ± 0.14
	-0.07 ms^{-2}	2.12 ± 0.09	2.20 ± 0.14*
	-0.05 ms^{-2}	2.17 ± 0.06	2.18 ± 0.06

Asterisk: significant difference between transition speed before and after fatigue $*p<0.01$ $*p<0.05$

(a) 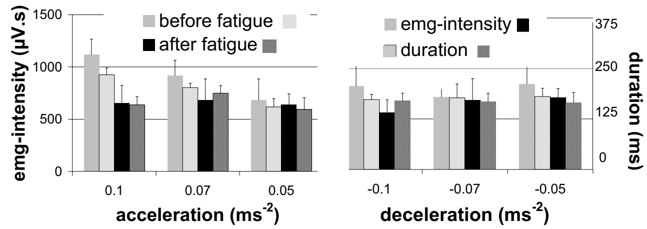 (b)

Figure 1: EMG -intensity and duration of energy burst of the m. tibialis anterior for the (a) WRT and (b) RWT

RESULTS AND DISCUSSION

Transition speed is significantly changed after introducing muscular fatigue. After fatigue, WRT speeds are lower for all accelerations. RWT-speeds do not change, except for the intermediate deceleration (Table 1). The differential effect of fatigue of the m. tibialis anterior is in agreement with the findings of Prilutsky and Gregor [3]. They claim that WRT is triggered by the increased sense of effort due to the augmented activity in the muscles activated during swing (m. tibialis anterior, m. rectus femoris and hamstrings), and, on the other hand, that RWT would be triggered by the activity during stance (m. soleus, m. gastrocnemius and m. vastii). [3]

Post hoc Tukey tests reveal that tibialis anterior EMG–intensity is higher in the steps around transition (step0) in both WRT and RWT. Therefore, EMG– intensity of the burst is averaged over 3 steps in the transition-zone (step-1 → step+1).

In the WRT before fatigue EMG-intensity is higher, except for the lowest acceleration and duration is higher for the highest acceleration. In the RWT there is no significant effect, nor for duration nor for EMG-intensity. This might indicate that in the WRT the m. tibialis anterior is no longer capable of maintaining the desired muscle tension, a combination of both a loss in power and duration, resulting in a higher sense of effort [4] accompanied by a change in locomotion pattern[3].

CONCLUSIONS

Walk-to-run transition speed is clearly affected by fatigue of the m. tibialis anterior. The increased sense of effort, due to the muscular fatigue, might explain this phenomenon. Further research is necessary since evolution of EMG-intensity on a step to step basis can provide meaningful information.

REFERENCES

1. Thorstensson and Roberthson, *Acta Physiol Scan*, **131**:211-214, 1987
2. Hreljac et al, *J Appl Biomech*, **17**: 287-296, 2001
3. Prilutsky and Gregor, *J Exp Biol*, **204**: 2277-2287, 2001
4. McCloskey et al, *Adv Neurol*. **39**:151-67,1983

ACKNOWLEDGDEMENTS

This research is supported by BOF–UGent B/03796/01– IV1.

A MULTIPLE MATERIAL PARAMETER FINITE ELEMENT MODEL OF HIP RESURFACING ARTHROPLASTY

[1] J P Little, [2]F Taddei M, [2]Viceconti and [1]H S Gill
[1]Oxford Orthopaedic Engineering Collaboration, University of Oxford, Oxford, UK,
[2]Instituti Ortopedici Rizzoli, Laboratorio di Tecnologia Medica, Bologna, Italy;
email: paige.little@ndos.ox.ac.uk

INTRODUCTION

Hip resurfacing arthroplasty (HRA) is increasingly carried out as an alternative to total hip arthroplasty (THA) in young, active patients. The primary indication for this surgery is osteoarthritis. It is favoured over THA as it preserves bone stock and it is claimed not to cause stress shielding. However, fractures of the femoral neck result in short term failure of the procedure in approximately 2% of patients [1]. Previous finite element (FE) analyses have employed over-simplified material parameters to define the femoral bone and non-physiological loading conditions [2,3]. Furthermore, it is unclear from the literature whether the surface interaction between the implant and bone cement is a 'sticking/sliding' contact best represented using a Coulomb friction model or whether it is a 'glued' contact. In this study an experimentally validated FE model of a cadaveric femur pre- and post- HRA surgery was analysed to determine the change in mechanics. This model included physiological loading conditions and more accurate multiple material parameters represented nonhomogeneous bone distribution in the femur.

METHODS

Material properties were assigned to the femoral bone using the data from a detailed CT of a cadaveric femur [4]. Intact and implanted FE models were validated using experimentally measured strains compared with model calculated strains. The surface interaction between the retro-surface of the implant and the underlying bone cement was represented using either a Coulomb friction model (μ=0.3) or as rigidly bonded (μ=infinity). A physiological load case representing the muscle and hip contact forces at an instant 10% through the level walking gait cycle was applied to the intact and implanted models. Von Mises stresses were compared in three cross-sections through the neck of the femur (Figure 1a) and in the femoral head. To determine the potential for femoral bone fracture under this physiological loading condition, a risk of fracture (RF) scalar was calculated as the ratio between the Von Mises stress and the ultimate strength of bone. A value greater than one indicated a potential failure.

RESULTS AND DISCUSSION

It was found that the use of 381 separate material parameters to define the femoral bone was optimum. The correlation between the experimental and calculated strain values for the two material model had R^2=0.87, while in the model incorporating 381 materials R^2 was 0.92. Von Mises stress in the femoral head was 0.8 to 3.2% higher when the implant and bone cement were rigidly bonded; however, Von Mises stress in the femoral neck was the same in both the implanted models. Therefore, only results for the Coulomb friction model are considered. For this physiological load case the

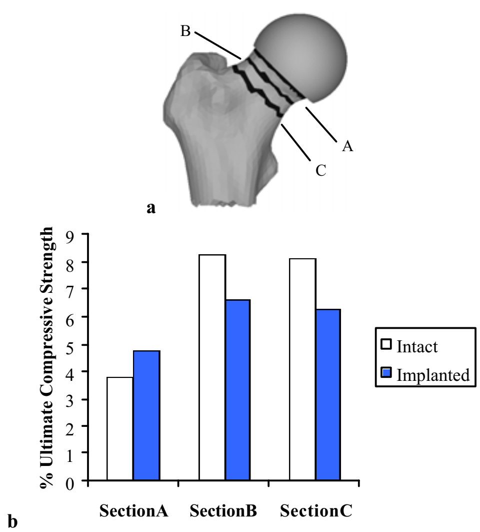

Figure 1: **a.** Cross-sections in the femoral neck; **b.** Peak Von Mises stress in femoral neck as a percentage of ultimate compressive strength

change in maximum Von Mises stress after resurfacing, expressed as a percentage of the reported ultimate compressive strength of cortical bone (193MPa) ranged from -1.8% to 1.0% (Figure 1b). Of the 47,984 elements in the implanted model, 72 had an RF value greater than 1. As these elements were remote from one another and it was unlikely that localized volumes of bone would be sites of fracture, the fracture risk post-HRA surgery was assessed to be low.

CONCLUSIONS

A multiple material property model more closely simulates real bone mechanical properties than a 2 material model. This is the first fully validated FE model of a femur implanted with an HRA. These results indicate that the geometry and direction of loading on the implant result in implant-cement interface stresses that are transmitted to the underlying bone as if these two materials were rigidly bonded. Analysis of the intact and implanted FE models under physiological loading conditions appears to support the claims that HRA does not result in stress shielding in the femoral neck. Furthermore, the calculated bone stress in the femoral neck was not sufficient to be a potential cause of fracture.

REFERENCES

1. Pearson AM, et al. *Proceedings of British Hip Society*, Sheffield, UK, 2004.
2. Huiskes R, et al., *Acta Orthop Scand*, **56**, 474-478, 1985.
3. Watanabe YN, et al.. *J Arthroplasty* **15**, 505-11, 2000.
4. Taddei F., et al., *Med Eng Phys*, **26**, 61-69, 2004.

DYNAMIC LOWER LIMB ALIGNMENT AND KNEE JOINT LOAD DURING GAIT IN PATIENTS WITH KNEE OSTEOARTHRITIS

[1]Michael A. Hunt, [1]Trevor B. Birmingham, [1]Ian C. Jones, [1]J. Robert Giffin and [1] Thomas R. Jenkyn
[1]Wolf Orthopaedic Biomechanics Laboratory, University of Western Ontario, London, Ontario, Canada
email: tjenkyn@eng.uwo.ca

INTRODUCTION

Factors suggested to be associated with the development and progression of osteoarthritis (OA) of the knee include lower limb malalignment and high dynamic knee joint loads. Due to the high, repetitive knee joint loads associated with walking, gait analysis has become an important tool in the evaluation of OA in patients. The peak external knee joint adduction moment (EKAM) has been the most commonly reported variable in the gait literature for patients with OA of the knee due to its hypothesized association with medial compartment knee joint load during walking [1]. The EKAM is calculated as the product of the frontal plane lever arm (FPLA) and the frontal plane ground reaction force (GRF). While numerous studies have reported GRF data, no previous studies have reported data pertaining to the FPLA in patients with OA. Since the FPLA can be thought of as a dynamic measure of alignment, it would be beneficial to understand how lower limb alignment contributes to knee joint load during gait. The purpose of the present study was to examine the inter- and intra-limb relationships between the peak EKAM, peak FPLA, and peak frontal plane GRF during gait in patients with knee OA.

METHODS

Prior to medial opening wedge high tibial osteotomy, gait analyses were performed on 125 patients (98 males, 27 females; mean age = 46.8 +/- 10.5 yrs.) with knee joint OA primarily affecting the medial compartment. Patients walked across the laboratory at a self-selected velocity while three-dimensional kinetic and kinematic data were collected bilaterally. These data were combined to calculate the EKAM and the FPLA – defined as the perpendicular distance from the GRF to the knee joint centre of rotation (Figure 1). Inter-limb comparisons (operative vs. non-operative) were made among the peak values during stance for the following dependent variables: EKAM, FPLA, and frontal plane GRF. Pearson product moment correlations were computed to assess the magnitude of the intra-limb relationships between variables. Lastly, intra-limb comparisons were made regarding the time during stance (% stance) where the peak value of each variable occurred.

RESULTS AND DISCUSSION

Compared to non-operative limbs, the peak EKAM and peak FPLA magnitudes were significantly greater in the operative limbs (Table 1). In contrast, peak frontal plane GRF magnitudes were significantly larger in the non-operative limbs. The peak EKAM was more highly correlated with the peak FPLA (r=0.77) than the peak frontal plane GRF (r=0.18). Within limbs, the positions during the gait cycle where the peak values occurred were significantly different among all variables (Table 1).

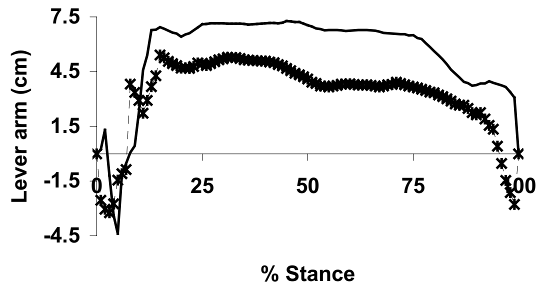

Figure 1: Frontal plane lever arm values for a single patient during stance. Solid line indicates operative limb while dashed line indicates non-operative limb.

These results indicate that although the peak magnitude of the frontal plane GRF was greater in non-operative limbs, the peak magnitude of the EKAM was larger in operative limbs mainly due to an increased lever arm length. The increased dependency of the EKAM on the lever arm magnitude was further highlighted by a higher correlation with the FPLA than with the frontal plane GRF.

CONCLUSIONS

Results from this study support the claim that knees affected with OA experience higher dynamic medial compartment knee joint loads during walking. However, this is the first study to report data pertaining to the FPLA during stance in this patient population. Given the hypothesized association between lower limb alignment and OA development and progression [2] and the finding of a high association between EKAM and FPLA peak magnitudes, the FPLA appears to be an important biomechanical measure of dynamic lower limb alignment in the study of knee joint OA.

REFERENCES

1. Andriacchi TP. *Orthop Clin North Am* **25**, 395-403, 1994.
2. Cooke D, et al. *Osteoarthritis Cartilage* **5**, 39-47, 1997.

Table 1: Mean (SD) peak magnitudes and gait cycle positions where peak values occurred.

	Non-operative Limb		Operative Limb	
	Peak	**Time of Peak (% stance)**	**Peak**	**Time of Peak (% stance)**
Force	1.09 (0.07) BW	59.2 (20.5)	1.06 (0.06) BW	56.2 (19.9)
Lever arm	3.19 (1.08) %ht	33.5 (16.1)	3.70 (1.21) %ht	33.4 (17.0)
Moment	2.52 (0.79) % BW*ht	41.2 (18.3)	2.94 (0.90) % BW*ht	41.7 (17.6)

A THREE-DIMENSIONAL WHOLE-BODY WALKING MODEL BASED ONLY ON GAIT KINEMATICS

Lei Ren, Richard Jones and David Howard
Centre for Rehabilitation and Human Performance Research, Salford University,
Salford, United Kingdom; email: d.howard@salford.ac.uk

INTRODUCTION

Biomechanical investigations of human movement often involve a simplified mechanical model of the human body, consisting of a collection of articulated rigid segments subject to external forces and moments. Many models only focus on a portion of the body, whereas whole body models have been used for activities involving both lower extremities and the upper body, such as balance control [1], weight lifting [2] and load carriage [3].

This paper presents a 3D whole body multi-segment model for gait analysis studies, where inverse dynamics analysis over a whole gait cycle is based only on kinematic data. It differs from the conventional application of inverse dynamics used in gait laboratory studies, where the calculations start from measured ground reactions. This is useful for test conditions where force plates are not suitable (e.g. outdoor gait trials or traversing obstacles). Whole body gait measurements using a multi-camera motion analysis system have been used to validate the model. The predicted ground reaction forces and moments on each foot were compared with force plate data.

METHODS

The human body was modeled as a dynamic coupled multi-segment system, which includes 13 rigid body segments: the head, torso, pelvis, right and left forearms, right and left humerii, and both legs (thighs, shanks and feet). Anthropometric data for each body segment are based on de Leva [4], but modified for the forearm and torso due to the different definitions used. A set of bone-embedded local coordinate systems based on anatomical landmarks are defined for each body segment [5].

An inverse dynamics method is employed to calculate the joint kinetics during walking based only on segmental motions. From the sum of the translational equations of motion of all the body segments, the sum of the ground reaction forces (GRFs) can be derived. In single stance, the GRFs on the supporting foot can be obtained directly. For double support, a “Smooth Transition Assumption” (STA) is used to solve the indeterminacy problem. The ground reaction forces and moments acting on the trailing foot move smoothly towards zero by following simple mathematical functions. Thereby, the GRFs on each supporting foot can be calculated, and then the forces at each joint derived by applying inverse dynamics segment by segment.

Similarly, from the sum of the rotational equations of motion of all the body segments, the sum of the ground reaction moments (GRMs) can be derived from the segmental motions and joint forces. Thereby, the GRMs on the supporting foot in single stance can be obtained directly. In double support, the STA assumption is used to calculate the GRMs on each foot. Thereafter the net muscle moments at each joint can be calculated by applying inverse dynamics segment by segment.

Whole body gait measurements were conducted to validate the model [5], using a set of specially designed plastic plates carrying marker clusters and a set of calibration procedures based on the CAST technique. Four male subjects walked along a walkway at two speeds, normal and fast. The motion data was collected at 100 Hz using a 6-camera Qualisys motion analysis system. Two Kistler force plates were used to record ground reactions. The raw marker data was processed by a MATLAB software package SMAS (Salford Motion Analysis Software), which was developed for 3D kinematic and kinetic analysis of general multi-body systems. The processed segmental motion data were then input into the whole body model, which was validated by comparing the calculated GRFs and GRMs with measured data.

RESULTS AND DISCUSSION

For all subjects, the calculated GRFs and GRMs at each foot were compared with force plate data. The results show that the calculated GRFs are in good agreement with the measured values. Figure 1 shows a typical result for one subject (38 yrs, 101.7 Kg). However, the estimated GRMs are larger than the measured data, and this problem needs further investigations.

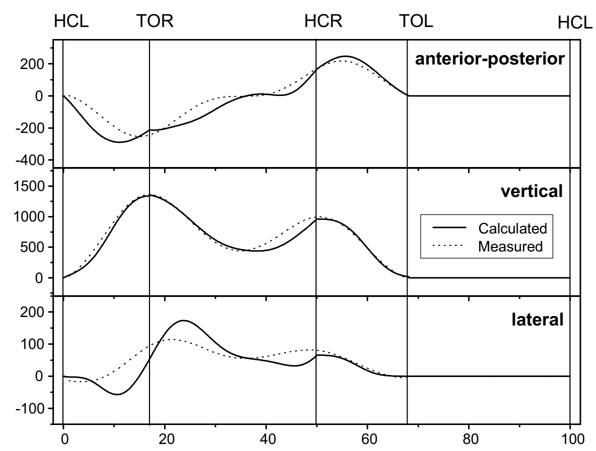

Figure 1: Calculated and measured ground reaction forces on left foot over a whole gait cycle (walking velocity: 2.11 m/s)

REFERENCES

1. MacKinnon CD, et al. *J. Biomech.* **26**, 633–644, 1993.
2. Kingma I, et al. *Hum. Mov. Sci.* **15**, 833–860, 1996.
3. Ren L. et al. *J.Biomech*., In Press
4. de Leva P. *J. Biomech.* **29**, 1223–1230, 1996.
5. Ren L. et al. *ASB 28th Meeting*, Portland, USA, 2004.

ACKNOWLEDGEMENTS

Funding has been provided by the UK Ministry of Defence.

VARIABILITY OF GLENOHUMERAL EXTERNAL ROTATOR MUSCLE MOMENT ARMS

[1]Joseph E. Langenderfer, [1]Cameron Patthanacharoenphon, [2]James E. Carpenter, and [1,2]Richard E. Hughes
[1]Department of Biomedical Engineering, [2]Department of Orthopaedic Surgery,
University of Michigan, Ann Arbor, MI USA
email: rehughes@umich.edu

INTRODUCTION

Glenohumeral rotator muscle moment arms have been determined in previous studies [1,2,3]. These studies did not examine the interaction between portions of the rotator cuff, or between sub-regions of cuff tendons. This study's purpose was to empirically determine rotation moment arms for sub-regions of supraspinatus, infraspinatus, and for teres minor. There were 2 hypotheses: 1) that muscles and their sub-regions possess differences in moment arm due to joint angle, and 2) that sub-regions of the cuff tendons increase their effective moment arms through connections to other sub-regions.

METHODS

Data were collected from 10 normal cadaver specimens for supraspinatus (SSP), infraspinatus (INF), and teres minor (TM). SSP and INF were divided into 3 and 4 sub-regions, respectively. The change in tendon excursion relative to humeral head rotation was measured with a custom instrument. The instrument has demonstrated error less than 0.5 mm. Data were collected for the full range of external rotation at 10^{o} and 60^{o} abduction in the scapular plane. Two conditions were tested: 1) tendon divided just up to musculotendinous junction (intact cuff), and 2) tendon divided all the way to the insertion to bone (divided cuff). Three trials were recorded for each abduction angle - tendon condition combination. Polynomials were fit to the tendon excursion vs. rotation angle data. Moment arm was determined at one degree increments as the derivative of the tendon excursion versus joint angle relationship [4]. Moment arm data were analyzed with an ANOVA model.

RESULTS AND DISCUSSION

Rotation moment arms were dependent upon abduction angle, rotation angle, cuff condition and muscle sub-region, and demonstrated significant inter-specimen variability (Figures 1&2) (Mean±S.D.). Moment arms for INF were significantly greater at 10^{o} abduction ($p<0.001$). Moment arms of SSP ($p<0.05$) and teres minor ($p<0.001$) were significantly greater at 60^{o} abduction. Moment arms of sub-regions of INF ($p<0.001$) and SSP ($p<0.001$) were significantly different. Moment arms of INF ($p<0.001$) and SSP ($p<0.001$) were significantly greater with an intact rotator cuff. TM moment arm was not significantly affected by cuff condition ($p=0.46$).

CONCLUSIONS

Moment arm differences between muscle sub-regions and for different cuff conditions have possible clinical implications. At neutral rotation the SSP has a very small rotation moment arm suggesting it contributes little to external rotation strength. Some loss of strength seen clinically with isolated SSP tears is likely due to muscle inhibition or pain. Additionally, the results of interaction between cuff regions have potential for explaining why some subjects retain strength after small cuff tear. This finding also helps explain why a partial cuff repair may be beneficial when a complete repair is not possible. Such data can help differentiate between cuff tear cases which would benefit from cuff repair and cases for which cuff repair might not be as favorable.

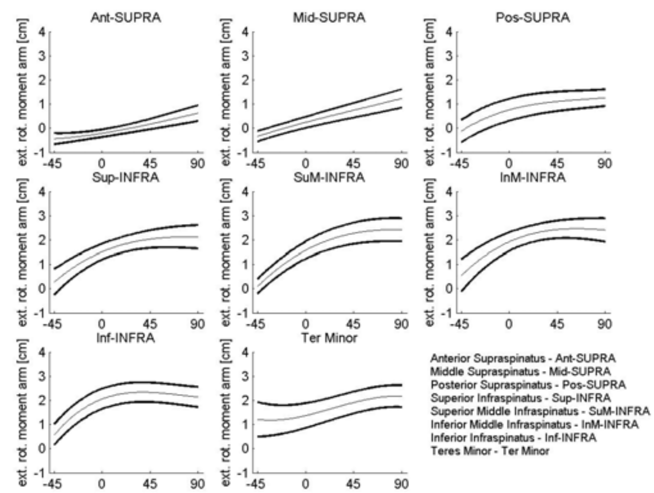

Figure 1: Moment arms, Intact cuff, 10^{o} abduction.

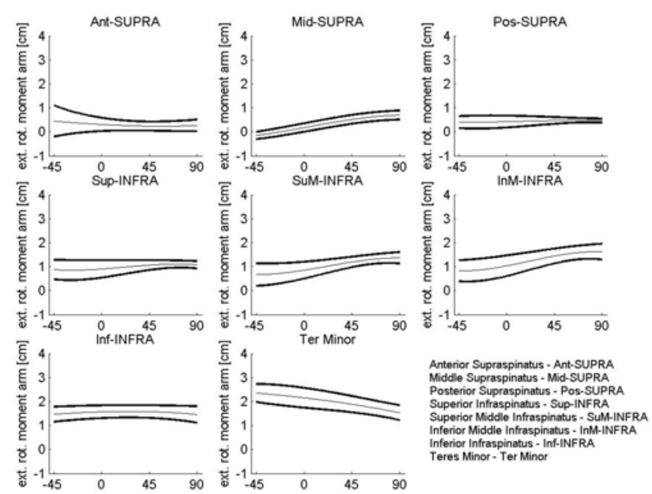

Figure 2: Moment arms, Divided cuff, 60^{o} abduction

REFERENCES

1. Bassett RW et al. *J. Biomech.* **23**, 405-415, 1990.
2. Otis JC et al. *J.B.J.S.* **76-A**, 667-676, 1994.
3. Kuechle DK et al. *Clin. Biomech.* **15**, 322-329, 2000.
4. An KN et al. *J. Biomech. Engin.* **106**, 280-282, 1984.

ACKNOWLEDGEMENTS

Whitaker Foundation
NIH grant AR048540

VARIABILITY IN ISOMETRIC FORCE AND TORQUE GENERATING CAPACITY OF GLENOHUMERAL EXTERNAL ROTATOR MUSCLES

[1]Joseph E. Langenderfer, [1]Cameron Patthanacharoenphon, [2]James E. Carpenter, and [1,2]Richard E. Hughes
[1]Department of Biomedical Engineering, [2]Department of Orthopaedic Surgery,
University of Michigan, Ann Arbor, MI USA
email: rehughes@umich.edu

INTRODUCTION

Glenohumeral external rotator muscles possess varying ability for generating forces and torques due to differences in muscle architecture, moment arm, and the interaction of these two factors. Previous authors have measured muscle architecture [1], and moment arms [2,3] at the shoulder. Due to parameter covariance, it is advantageous to utilize parameters from a unique dataset rather than from disparate sources. This study's purpose was to determine a complete dataset of parameters for predicting the length-tension (L-T) dependence and torque generating capacity of infraspinatus, supraspinatus and teres minor for shoulder external rotation.

METHODS

Data were collected from 10 normal cadaver specimens for supraspinatus (SSP), infraspinatus (INF), and teres minor (TM) muscles. SSP and INF were divided into 3 and 4 sub-regions respectively. Muscle-tendon units were dissected from the specimens. Tendon length, muscle belly length and muscle fascicle length were measured with a digital caliper. Muscle volume was measured via water immersion. Pennation angle was measured with a goniometer. After muscle fixation, fascicles were dissected and sarcomere lengths measured via laser diffraction. Tendon area, PCSA, optimal muscle length and optimal fascicle length were determined from empirical data. Tendon excursion relative to humeral head rotation was measured with a custom instrument from 45° internal to 45° external rotation with the humerus at 10° abduction. Muscle moment arms were determined as the derivative of tendon excursion versus rotation angle [4]. Inelastic tendon was assumed, and fascicle excursion as a function of joint angle was calculated from tendon excursion and pennation angle. Rigor was assumed to develop with the humerus in neutral rotation and abduction. Length-tension relationships were determined by normalizing fascicle excursion to optimal fascicle length [5]. Maximum isometric rotation torque generating capacity was estimated as the product of PCSA, maximum moment arm, and cosine of pennation angle, at 10° and 60° abduction. ANOVA models were used to determine if muscle sub-regions were operating on different portions of the length-tension relationship, and to test the effect of abduction angle, cuff condition and muscle sub-region on maximum torque capacity.

RESULTS AND DISCUSSION

The muscles demonstrated differences in their maximum isometric torque capacities (Figure 1), and length tension relationships (Figure 2). Abduction angle ($p<0.001$) and muscle sub-region ($p<0.01$) had a significant effect on maximum isometric torque capacity. Cuff condition did not have a significant effect on maximum torque capacity. Sub-regions of INF were operating on different portions of the L-T relationship ($p<0.001$), but SSP was operating over the same L-T region ($p=0.49$).

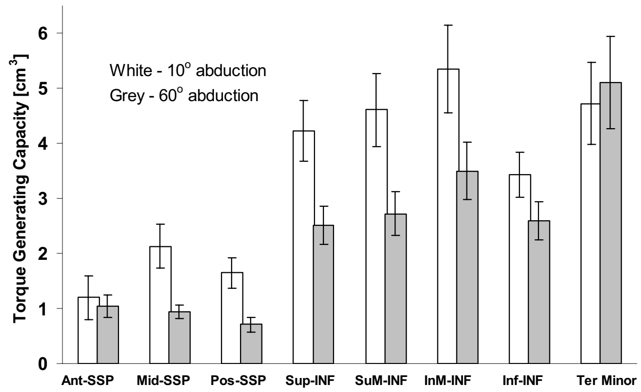

Figure 1: Maximum isometric rotation torque generating capacity (mean±standard error).

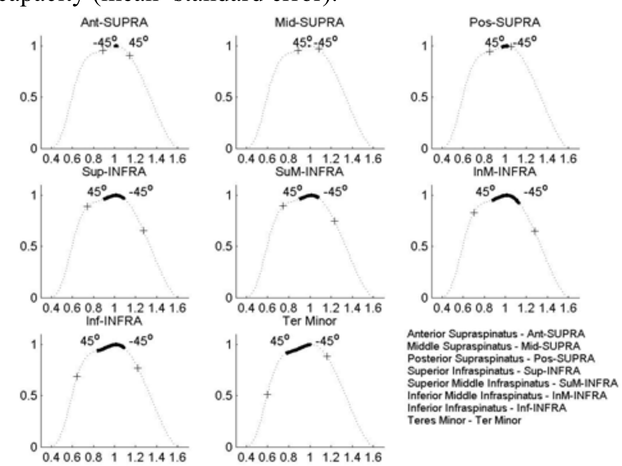

Figure 2: Normalized force versus normalized fascicle length. (Mean (+) S.D.) [5].

CONCLUSIONS

Functional capabilities of these muscles depend on muscle architecture and moment arm and their combined effects. Significant variability was detected between specimens. Parameter covariance can be determined from this unique dataset and is important for probabilistic modeling.

REFERENCES

1. Veeger HEJ, et al. *J. Biomech.* **24**, 615-629, 1991.
2. Otis JC, et al. *J.B.J.S.* **76-A**, 667-676, 1994.
3. Kuechle DK, et al. *Clin. Biomech.* **15**, 322-329, 2000.
4. An K.N. et al. *J. Biomech. Engin.***106**, 280-282, 1984.
5. Murray WM, et al. *J. Biomech.* **33**, 943-952, 2000.

ACKNOWLEDGEMENTS

Whitaker Foundation
NIH grant AR048540

TRUNK MUSCLE ACTIVATION PATTERNS COMPARING CABLE PRESS AND BODY-BLADE® EXERCISES

Janice M. Flynn, Francisco J. Vera-Garcia, Stephen H.M. Brown, Stuart M. McGill
Spine Biomechanics Laboratory, Department of Kinesiology, University of Waterloo, Canada
Email: jflynn@uwaterloo.ca

INTRODUCTION

Rehabilitation professionals often rely on intuition and subjective observation to choose treatment techniques. Our objective is to provide some quantitative information to assist decision-making. The Body-blade®, a 122 cm, .68 kg flexible rod with a resonance frequency of 4.5 Hz. is frequently used for recruiting the stabilizing muscles of the trunk and shoulder girdle, yet no in-depth analysis has been undertaken to justify this treatment choice. The purpose of this study was to compare the electromyographic (EMG) amplitudes and recruitment patterns of the trunk muscles during simple cable pulleys and compare them with various exercises using the Body-blade®.

METHODS

Fourteen recreationally trained men (age = 28.14 ± 8.33 yr, height = 1.78 ± 0.05 m, mass = 77.78 ± 10.41 kg) were recruited from the university population. All subjects were right-handed and healthy, without current back or shoulder pain. Superficial EMG was measured of the right anterior deltoid (AD) and pectoralis major (PM), bilateral rectus abdominis (RA), external oblique (EO), internal oblique (IO), latissimus dorsi (LD), and erector spinae at 3 levels (EST9, ESL3, ESL5), while subjects performed standing cable press and Body-blade® exercises.

The EMG was A/D converted at 12 bit resolution at 1024Hz. Signals were full wave rectified and low pass filtered (single pass Butterworth) at 2.5 Hz, and then normalized to maximal voluntary contraction (MVC) amplitudes. The normalized muscle activity corresponding to a 2-second window of co-ordinated Body-blade® or cable press use was then averaged over the 14 subjects for each exercise.

RESULTS AND DISCUSSION

Cable presses resulted in high levels of EMG activation in the shoulder muscles, followed by the left IO and LD. Large amplitude Body-blade® oscillations, with the blade in a vertical orientation and oscillations in a medial/lateral direction, produced large increases bilaterally in the IO amplitude, as well as moderate bilateral EO activity. When oriented horizontally (vertical oscillations), the highest muscle activity was seen in the back muscles: LD and UES, as well as RAD (Figure 1).

Vertical orientation of the Body-blade® resulted in the greatest activation levels of the IO (avg 48% MVC bilaterally) and EO (avg 26% MVC) muscles, thought to be critical contributors to lumbar spine stability [1]. Previous research has demonstrated that IO surface electrodes adequately represent Transverse Abdominis (TA) activation within 15% RMS difference [2], suggesting that TA is equally trained with this exercise.

Horizontal orientation of the blade resulted in very little EO or IO activity.

CONCLUSIONS

The Body-blade® is a superior exercise modality for recruitment of the IO and EO muscles, when used in a vertical orientation. As such, it could be a valuable asset to exercise programs aimed at optimizing muscle recruitment patterns, which are known to stabilize and support the lumbar spine.

REFERENCES

1. McGill SM. *Ultimate back fitness and performance.* Wabuno Publishers, Waterloo, Canada, 2004.
2. McGill SM, et al. *J Biomech* **29**, 1503-1507, 1996.

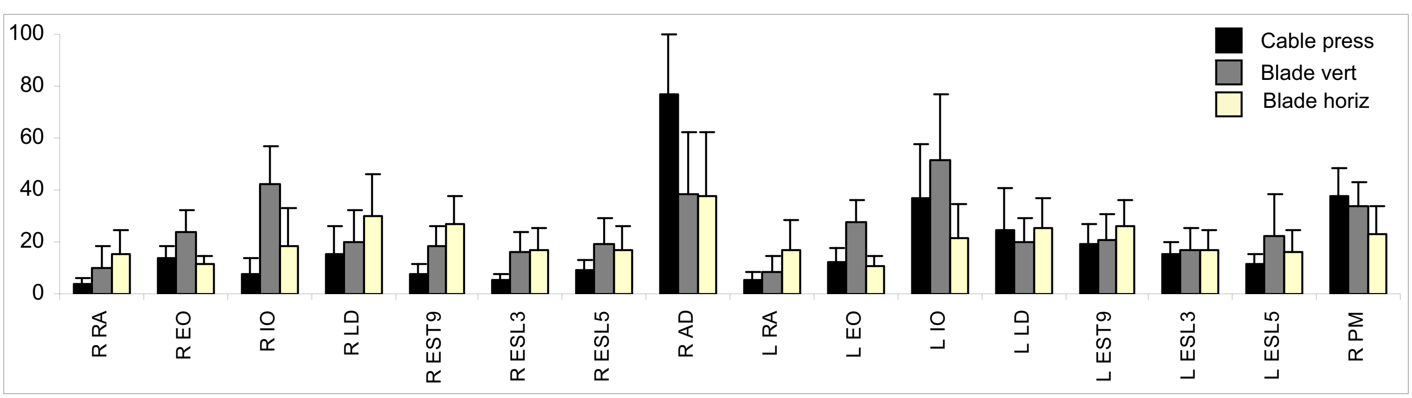

Figure 1. Mean EMG amplitudes (mean, SD) for cable presses, vertical and horizontal orientation Body-blade® oscillations.

EFFECT OF RECOVERY RESTRICTIONS ON THE THRESHOLD OF BALANCE RECOVERY PRELIMINARY RESULTS

Marc-André Cyr, Kodjo E Moglo and Cécile Smeesters
Research Center on Aging, Sherbrooke Geriatric University Institute, Sherbrooke, QC, Canada
Department of Mechanical Engineering, Université de Sherbrooke, Sherbrooke, QC, Canada
email: Cecile.Smeesters@USherbrooke.ca web: www.cdrv.ca

INTRODUCTION

It is only recently that studies have focused on postural perturbations at the threshold of balance recovery, i.e., postural perturbations large enough that balance recovery is not always possible and a fall can occur. The knowledge at the threshold of balance recovery is thus very limited. In particular, the effect of recovery restrictions on the threshold of balance recovery has not been quantified, despite evidence of its importance during small and medium postural perturbations [1-4]. Therefore, the purpose of this study is to quantify the effect of recovery restrictions on the threshold of balance recovery.

METHODS

Balance recovery following sudden release from an initial forward lean was performed by six healthy younger adults, three males and three females (23.3 ± 2.3 yrs, 1.74 ± 0.07 m, 67.1 ± 11.5 kg). The maximum forward lean angle that these younger adults could be released from and still recover balance was determined using i) only a single step, ii) no more than 2 steps and iii) no recovery restriction. The forward lean angle was sequentially increased until the subjects failed to recover balance twice at a given angle and the types of recovery restrictions were randomly ordered. Forward lean angles, reaction times, weight transfer times, first step times, first step lengths and first step velocities were measured using force platforms (AMTI, Newton, MA) and an Optotrak motion measurement system (NDI, Waterloo, ON). One-way analyses of variance with repeated measures were used to determine the effect of the type of recovery restriction.

RESULTS AND DISCUSSION

The type of recovery restriction did not significantly affect maximum forward lean angles that younger adults could be released from and still recover balance (Figure 1 and Table 1). Moreover, at the maximum forward lean angles, the type of recovery restriction did not significantly affect reaction times, weight transfer times, first step times and first step velocities (Table 1). However, at the maximum forward lean angles, the type of recovery restriction significantly affected first step lengths (Table 1). Specifically, first step lengths using only a single step were significantly longer than those using no more than 2 steps ($p = 0.008$).

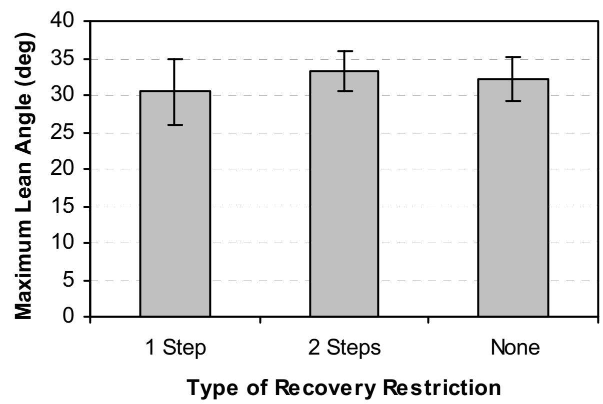

Figure 1: Effect of the type of recovery restriction on the maximum forward lean angle that younger adults could be released from and still recover balance ($p = 0.156$).

CONCLUSIONS

Preliminary results have shown that, despite possibly lengthening the first step, restricting balance recovery to only a single step does not significantly decrease the postural disturbance younger adults could sustain. Therefore, recovery restrictions do not seem to affect the threshold of balance recovery. Further experiments are needed to confirm these preliminary results in a larger sample of younger adults and, more importantly, in a sample of older adults.

REFERENCES

1. Hsiao ET and Robinovitch SN. *J Gerontol* **56**(1), M42-47, 2001.
2. Luchies CW, et al. *JAGS* **42**(5), 506-512, 1994.
3. Maki BE, et al. *J Gerontol* **55A**(5), M270-277, 2000.
4. McIlroy WE and Maki BE. *J Gerontol* **51A**(6), M289-296, 1996.

ACKNOWLEDGEMENTS

We gratefully acknowledge the assistance of Noémie Séguin-Tremblay, José-Carl Harnois and Mathieu Hamel along with the support of grant 298229-04 from the Natural Sciences and Engineering Research Council of Canada.

Table 1: Effect of the type of recovery restriction on the threshold of balance recovery.

Type of restriction	1 Step	2 Steps	None	p
Maximum Lean Angle (deg)	30.4 ± 4.5	33.2 ± 2.7	32.2 ± 3.0	0.156
Reaction Time (ms)	82 ± 5	82 ± 11	80 ± 11	0.754
Weight Transfer Time (ms)	138 ± 10	130 ± 17	138 ± 15	0.321
First Step Time (ms)	192 ± 25	164 ± 16	170 ± 27	0.098
First Step Length (m)	1.029 ± 0.082	0.842 ± 0.050	0.872 ± 0.155	0.034
First Step Velocity (m/s)	5.415 ± 0.717	5.184 ± 0.638	5.147 ± 0.636	0.213

Control Strategy Transitions during Slope Walking

[1]Andrea N. Lay, [2]Daniel K. Lai, [3]Chris J. Hass, and [2]Robert J. Gregor
[1]School of Mechanical Engineering, Bioengineering Program, Georgia Tech (E-mail: gtg449j@mail.gatech.edu)
[2]Center for Human Movement Studies, School of Applied Physiology, Georgia Tech
[3]Department of Biobehavioral Sciences, Teachers College, Columbia University

INTRODUCTION

Investigations of slope walking in quadrupeds have revealed motor programs (control strategies) for up and downslope walking different from that for level walking [1]. Similar results would be expected in humans during slope walking based on the changes in biomechanics and muscle activity [2; 3]. One interesting question that then follows is at what grade does the nervous system switch from the level walking strategy to the slope walking strategy? For the first step of upslope walking, a transition grade has been suggested to exist between 6˚ and 9˚ (11% and 16%) [4]. Although the question of transition grades has not been addressed in detail for slope walking, it has been studied for the similar task of stepping on a wedge [5]. Based on kinematic and EMG patterns, the authors identified two distinct control strategies, with a transition grade at 15˚ (27%) [5]. The goal of this study was to investigate kinematic patterns during upslope walking in order to identify common control strategies, and potentially identify a transition grade between control strategies.

METHODS

Five healthy volunteers (4M, 1F, mean age = 28 yrs) gave their informed consent and then were fitted with fifteen retroreflective markers (Helen Hayes system) and walked at five different grades (0%, +10%, +15%, +25%, +39%) on a modified LifeFitness treadmill. Each participant selected a comfortable pace at +39% and maintained this speed for all trials. After participants adjusted to each condition data were collected for two 10 second trials. Kinematic data were captured at 60 Hz using a six camera Peak 3D Optical Capture system and were exported to in-house software to calculate joint angles. Joint angle data from each leg (L and R) were normalized to 300 points for every stride (200 stance, 100 swing) and then ensemble averaged across all strides for each trial. Ankle-knee angle-angle plots of the stance phase were used to classify the control strategies [5]. Each plot was given a shape score (s-shaped = 0, c-shaped = 1) and a knee angle (KA) score for the value of the knee angle during mid to late stance at the same ankle angle as at heel strike (HS) (larger angle than at HS = 0, smaller angle than at HS = 1). The sum of the two scores was used to classify each plot.

RESULTS AND DISCUSSION

Sample ankle-knee angle-angle plots and their scores are presented in Figure 1. Because of the similarity between the three highest grades, only data from +39% is shown (Fig 1B). All 0% plots (n=18) received a cumulative score of 0 (Fig 1A), and all +15%, +25%, and +39% plots (n=20 for each) received a total score of 2. These findings suggest that a different control strategy is being used for the steeper grades than for level [5]. In contrast, the 10% (n=18) plots received

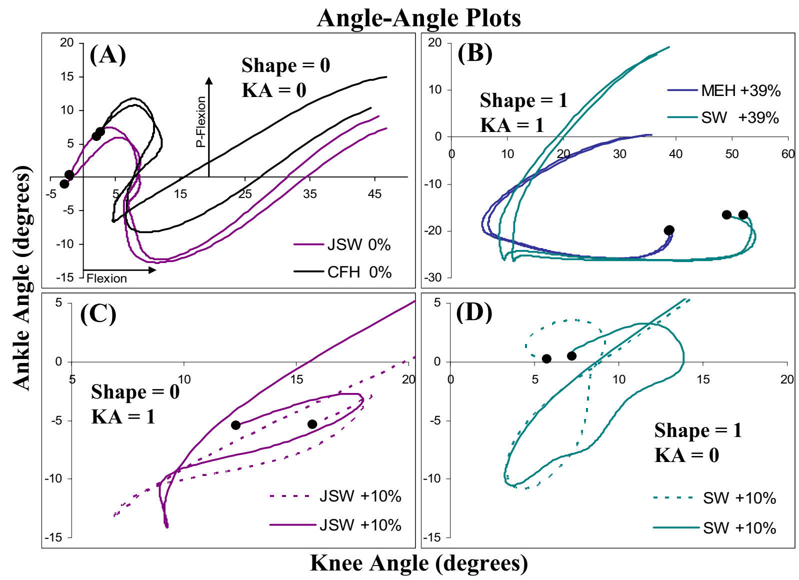

Figure 1: Representative angle-angle plots for stance (● = HS). Knee flexion and ankle p-flexion are indicated in (A). The scales of (C) and (D) are expanded to show the shapes.

mixed scores: 4 received a total score of 0, 9 received a total score of 1 (Fig 1C and 1D), and 5 received a cumulative 2. A cumulative score of 1 indicates a mixed control strategy, and therefore a possible transition grade. The four plots that received a total score of 0 were from one subject (2L and 2R), who used only the level walking form. Another subject used only the mixed strategy shown in Fig 1C, and the remaining three subjects used both pure and mixed strategies. These data suggest the presence of a 10% transition grade for upslope walking. This transition grade is lower than that observed during wedge stepping (27%) [5] and than that predicted for the first step of upslope walking (11-16%) [4]. It is possible that the level walking strategy may be sufficient for a single step on a grade above 10%, but inadequate when sustained walking is required. In light of these findings we expect that for grades of less than 10% the level walking control strategy will prevail. Exploration of this idea, as well as its extension to downslope walking, warrants future research.

REFERENCES

1. Smith JL, et al. *J Neurophysiol* **79**, 1702-16, 1998.
2. Redfern MS, et al. *Gait Posture* **6**, 119-125, 1997.
3. Leroux A, et al. *Exp Brain Res* **126**, 359-68, 1999.
4. Prentice SD, et al. *Gait Posture* **20**, 255-65, 2004.
5. Earhart GM, et al. *J Neurophysiol* **84**, 605-15, 2000.

ACKNOWLEDGEMENTS

This work is supported by an NSF GRF and the Center for Human Movement Studies at Georgia Tech.

ANALYSIS OF INTER-SEGMENT SPINE KINEMATICS DURING TRUNK MOTION

JoAnne Resig, Sam Augsburger, Hank White, Donna Oeffinger, Chester Tylkowski
Shriners Hospitals for Children, Lexington, KY.
Email: saugsburger@shrinenet.org

INTRODUCTION

The purpose of this study is to develop a technique that models the spine as a multi-segment system and determines kinematic patterns in multiple planes. Past studies have used motion analysis systems to examine the lumbar spine with respect to the pelvis [1,2,3] and total spinal segment range of motion in scoliosis [4,5]. However, these studies did not report kinematics of the spine segments while moving in all three planes. The method described here has the potential to document changes in dynamic spine motions following therapeutic interventions for spinal pathologies.

METHODS

Eight reflective skin markers were placed over the following anatomical landmarks: sternum, the spinous processes of 3 thoracic vertebrae (T1, T8, T12), 1 lumbar vertebra (L3), sacrum (Vs), and both anterior superior iliac spines (L.ASIS, R.ASIS). Each participant performed four trunk motion tasks while standing: flexion/extension, lateral bending, axial twist, and a cone (moving trunk through a continuous maximum circular motion, starting with flexion, then lateral bending, extension, opposite lateral bending, and ending with flexion). Using custom software, seven segments were created for analyses of the trunk motions: thorax (T1, T8, Sternum), pelvis (L.ASIS, R.ASIS, Vs), total spine (Vs-T1), and 4 spine segments: (Vs-L3), (L3-T12), (T12-T8), and (T8-T1).

For the first three movement tasks, a transformation matrix was determined from the pelvis coordinate system. Spine segment angles were calculated in the frontal and sagittal planes based on the pelvis coordinate system. Inter-segmental angles were calculated between adjacent spine segments and angular data were normalized based on the position of the T1 marker at four events within each motion: 0% = onset of motion; 25% = change in direction of motion (i.e. end flexion); 75% = change in opposite direction of motion (i.e. end extension); and 100% = end of motion.

For the multi-planar cone motion, segment angles (Z-angles) were found with respect to the vertical axis, which was defined by the pelvis coordinate system. Data were normalized based on the angular location of the T1-Vs segment as a 360° arc was created in space during the motion.

RESULTS AND DISCUSSION

Figure 1 shows sagittal plane flexion/extension angles for one person. Motion of the L3-T12 segment with respect to the Vs-L3 segment contributed to over half of the thorax flexion motion, but this segment had little contribution in extension. For this person, minimal motion occurred in the frontal plane during flexion/extension (data not shown). Figure 2 shows the Z-angle of the pelvis with respect to the room and the lumbar segments with respect to the pelvis. Circular gridlines

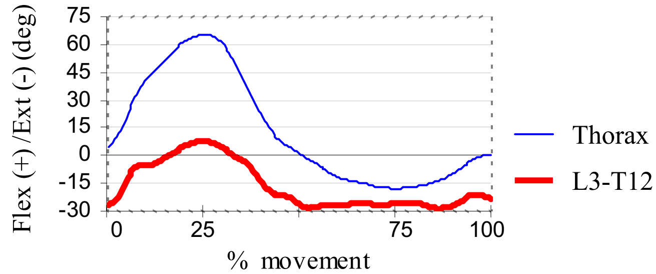

Figure 1: Sagittal plane angles for the Thorax segment with respect to Pelvis and the L3-T12 segment with respect to Vs-L3 during trunk flexion-extension (mean of 3 trials).

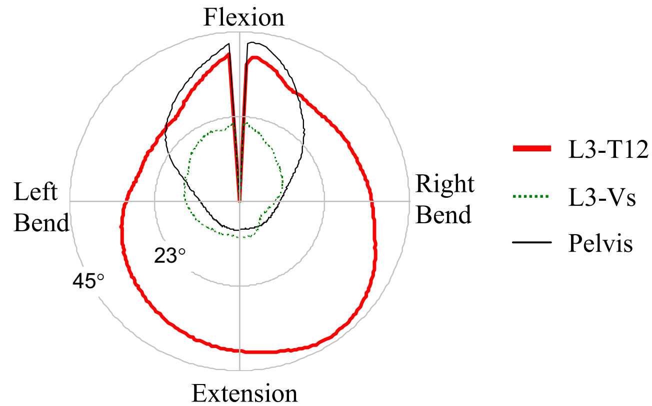

Figure 2: Z-angles during cone movement for the Pelvis with respect to room vertical and L3-Vs and L3-T12 segments with respect to Pelvis vertical (mean of 3 trials).

represent the angular value. For this participant, flexion at the beginning of the cone movement occurred almost equally with tilting of the pelvis and bending of the L3-T12 segment. However, as the person rotated the trunk towards the right and extension, most of the motion of the trunk occurred in the lumbar region with the L3-T12 segment.

CONCLUSIONS

One advantage of this technique is that the contributions of different spine segments to total motion are quantified. Trunk motion can be compared within a subject or between subjects to determine differences in flexibility at certain spinal segments. Limitations of the model include marker obstruction and/or coalescence during extreme motions and skin motion artifact. A database for comparison of normal and pathological spine kinematics is under development.

REFERENCES

1. Lee RYW, et al. *Hum Mov Sci* **21**, 481-494, 2002.
2. McClure PW, et al. *SPINE*, **22(5),** 552-558, 1997.
3. Peach JP, et al. *Arch Phys Med Rehabil,* **79,** 663-669, 1998.
4. Engsberg JR, et al. *SPINE*, **27(12):** 1346-1354, 2002.
5. Feipel V, et al. *Med. Biol. Eng. Comput,* **40**, 497-505, 2002.

CO-CONTRACTION IN ACL DEFICIENT SUBJECTS

[1]Sietske Aalbersberg, [1]Idsart Kingma, [2]Leendert Blankevoort and [1]Jaap H. van Dieën
Institute for Fundamental and Clinical Human Movement Sciences; [1]Vrije Universiteit Amsterdam;
[2]Academic Medical Center, University of Amsterdam, Amsterdam, the Netherlands; email: s.aalbersberg@fbw.vu.nl

INTRODUCTION

Co-contraction of the Hamstrings muscles is proposed in the literature as one of the strategies that anterior cruciate ligament deficient (ACLD) subjects can use to compensate the loss of ACL function. This study examined the response of ACLD and control subjects to shear forces in isometric knee extensions.

METHODS

Twelve chronic ACLD and 10 control subjects performed submaximal isometric knee extensions. The task was a positioning task with knee flexion target angles ranging from 5º to 45º with two external flexion moments both applied at two distances on the lower leg in a custom made chair (Figure 1). The shear force was controlled by changing the moment arm without changing the moment. A more proximal placement of a resistance pad will decrease the tibiofemoral displacement [1] and will thus lead to less force on the ACL [2]. Subjects received real-time position feedback about their knee joint angle (Optotrak). The subject was asked to extend the knee to one of the six target angle and hold it there for 5 seconds. Electromyographic data were collected from three Quadriceps and three Hamstring muscles. All EMG signals were normalized to the average EMG during a reference positioning task (30 Nm extension moment for extensors and 25 Nm flexion moment for flexors).

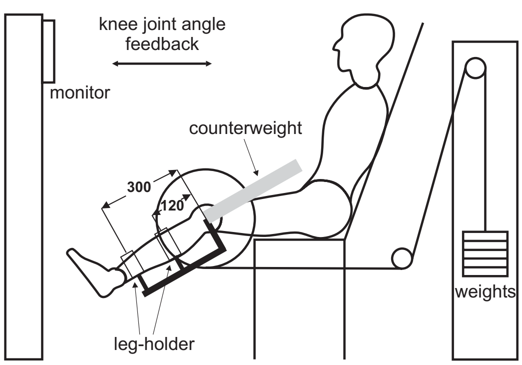

Figure 1: Experimental set-up

RESULTS AND DISCUSSION

The EMG of four muscles during positioning tasks is shown in Figure 2. In the analysis of variance, no significant effect of subject group was found in positioning across all muscles (p-values>0.2). There was a significant interaction between knee angle and subject group for the Biceps Femoris, but this effect was very small and will not have a great impact on the resulting shear forces.

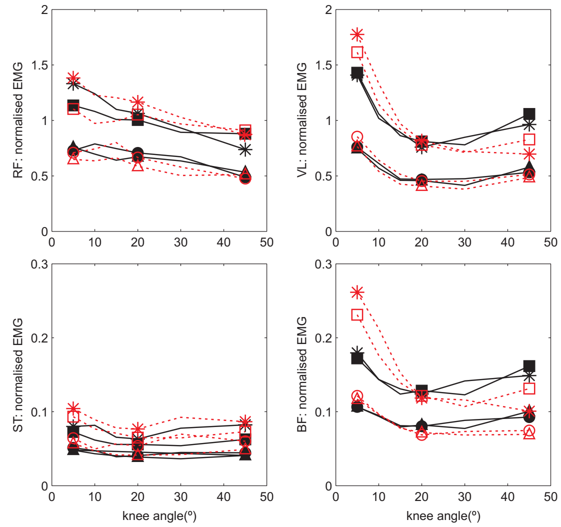

Figure 2: Normalized EMG of four muscles during positioning tasks for control (dashed red line) and ACLD group (solid black line). ✳ = 30 Nm at 120 mm, □/■ = 30 Nm at 300 mm, ○/● = 15 Nm at 120 mm, ▲/Δ = 15 Nm at 300 mm, RF = Rectus Femoris, VL = Vastus Lateralis, ST = Semitendinosus, BF = Biceps Femoris.

Interestingly, neither moment arm nor moment arm x knee angle interacted with subject group, indicating a comparable strategy between the control group and the ACLD group in response to shear force challenges to the knee joint.

CONCLUSIONS

The hypothesis that ACLD subjects increase co-contraction in situations with an increased shear load in sub-maximal isometric knee extensions was rejected.

REFERENCES

1. Jurist KA, et al. *Am J Sports Med* **13** 254-258 1985
2. Zavatsky AB, et al. *Am J Sports Med* **22** 418-423 1994

PREVALENCE OF BACK PAIN IN SEVEN SPORTS BASED ON SELF-REPORTING BY A SAMPLE OF 2268, 8-to-18 YEAR OLD ADOLESCENT ATHLETES

Paul J. Moga
College of Osteopathic Medicine, Michigan State University,
East Lansing, MI U.S.A. email: moga@msu.edu

INTRODUCTION

Pediatric back pain is an important problem for at least two reasons. First, it may restrict activity [e.g. 1]. Second, it has been associated with back pain later in life [e.g. 2]. This study is aimed at identifying back pain prevalence in youngsters, both by gender and by sport. This information may be helpful in the development of preventative measures.

METHODS

Data from the study of Wojtys, et al. [3] were used for this post-hoc analysis. That study was originally designed to investigate the relation between athletic training and thoracic kyphosis angle. Part of the original data were collected using written survey instruments that were completed by each of the nearly 2300 adolescent athlete participants.

The original survey instruments included questions regarding general health and injury history, sport participation, and the presence of back pain. Those subjects who experienced back pain were asked to identify which area of the spine was involved: cervical, cervico-thoracic, thoracic, thoracolumbar, or lumbar, or combinations thereof.

Back pain prevalence was then calculated with subjects divided by gender and by primary sport. The primary sports of volleyball, wrestling, swimming, football, gymnastics, and ice hockey were grouped according to the gender predominance of the participants.

RESULTS AND DISCUSSION

There were 2268 respondents to the backache question--406 females [mean age 13.8 (± 2.3) years] and 1862 males [mean age 14.8 (± 2.0) years]. The overall prevalence of pain in one or more spine areas was about the same for both genders (females: 27.3%; males: 27.9%).

Table 1 lists back pain prevalence by spine region for each of seven sports. Of these sports, only male athletes reported having cervical pain (<1.5%), while more female swimmers reported cervicothoracic pain (1.8%). Male ice hockey players reported having the most thoracic pain (2.7%). Thoracolumbar pain had a prevalence of at least twice that of thoracic pain in female volleyball players (5.8%), male swimmers (5.7%), and male ice hockey players (5.3%). Finally, the prevalence of lumbar pain was the largest for each sport, most notably in female gymnasts (about 37%) and male football players (about 29%).

CONCLUSIONS

Of five spine regions, lumbar pain was the most prevalent, as reported by our sample of 2268 adolescent athletes, ages 8 to 18 years. This finding holds true for participants of female volleyball, swimming, and gymnastics, as well as male wrestling, swimming, football, and ice hockey. These findings should be considered by those involved in designing training programs for adolescent athletes.

REFERENCES

1. Olsen TL, et al. *Am J Public Health* **82(4)**, 606-8, 1992.
2. Papageorgiou AC, et al. *Pain* **66(2-3)**, 181-5, 1996.
3. Wojtys EM, et al. *Am J Sports Med* **28(4)***,* 490-8, Jul-Aug 2000.

ACKNOWLEDGEMENTS

The author wishes to thank J. A. Ashton-Miller, Ph.D., E.W. Wojtys, M.D., and L. J. Huston, M.S.E., all of the University of Michigan, for their support during the original data acquisition, and for the use of the data set in this analysis.

Table 1: Prevalence of Back Pain by Spine Region and Sport (divided by Gender Predominance). *s.d. = standard deviation; C-T = Cervicothoracic; T-L = Thoracolumbar.* Note the prevalence of lumbar pain in gymnasts and football players.

Sport	*n*	Mean Age (yrs.)	*(s.d.)*	*No Pain*	Cervical	C-T	Thoracic	T-L	Lumbar
Female									
Volleyball	*52*	14.4	*1.5*	*69.2*	.	.	1.9	5.8	9.6
Swimming	*217*	13.3	*2.0*	*76.5*	.	1.8	0.5	1.8	15.2
Gymnastics	*35*	12.8	*2.4*	*57.1*	.	.	.	2.9	37.1
Male									
Wrestling	*951*	15.0	*1.5*	*71.1*	1.0	1.1	1.0	3.1	20.6
Swimming	*175*	13.9	*2.2*	*76.6*	0.6	.	1.1	5.7	14.9
Football	*391*	16.1	*1.1*	*62.2*	0.3	1.3	0.5	2.8	28.9
Ice Hockey	*188*	13.3	*2.1*	*77.3*	.	0.5	2.7	5.3	13.3

OPTIMAL EXTRA WEIGHT ON HANDS ENHANCE STANDING JUMP PERFORMANCE

Chenfu Huang, Hung-ying Chen and Hsiente Peng
National Taiwan Normal University, Taipei, Taiwan; email:t08001@cc.ntnu.edu.tw

INTRODUCTION

Standing long jump is one of events in ancient Olympic game and in the eighteenth ancient Olympiad in 708BC; extra weights (halteres) were used either to make the challenge more difficult or to enhance the jumping performance. Minetti et al. [1] used computer simulation to determine the optimal extra weights that would be needed to maximally increase a jumping distance. They suggested that the extra mass 2-9 kg would increase a 3-meter jump by at least 17 cm. However, they only asked subjects to perform the vertical jump with halteres instead of standing long jump. Huang et al [2] suggested optional extra weight for extending distance is 6-12% of body mass. However, their subjects dropped the extra weights in the air which may gain more distance during jumping. The purpose of this study was to investigate the effect of different levels of extra weights on standing long jump performance.

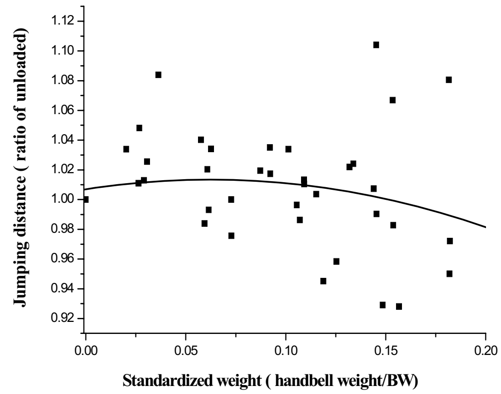

Figure 1: Effect of different weights on jumping performance.

METHODS

Twelve male athletes (age 21.8±1.7yr, height 175±5cm, body mass 67.8±12.0kg) served as subjects for this study. Each subject performed maximal standing long jump while loaded with one pair of handbell that ranged from zero (unloaded) to 10 kg of total extra weights. The extra weights were defined as four loading levels: zero, low (2kg or 4kg), middle (6kg or 8 kg), and high weight (10kg). Each subject was randomly assigned one weight on both low and middle levels. Each subject performed two trials for each level. Four best jumps from each subject (one unloaded and three loaded trials) were selected for analysis. A Redlake camera (125Hz) was synchronized with a Kistler force platform (9287B, 1250Hz) to collect standing jump data. Nine body landmarks (ear, shoulder, elbow, wrist, hip, knee, ankle, toe and heel) were digitized by Kwon 3D software. Dempster's study [3] was used to calculate body segment parameters.

RESULTS AND DISCUSSION

Figure 1 shows the effect of different extra weights on jumping distance. Average values of the best jumps for each loads (handbell weight / BW) are shown as a fraction of the value for an unload jump. Curve is best-fit by using second-degree polynomial regression. For the average mass of subjects in this study, the optimal extra weight for enhancing performance is 4.24 kg or 6.25% of body mass. The results of selected variables were listed in Table 1. The vertical velocity of body CG and body CG angle at takeoff were reduced as extra weights increased during the jumps. The results showed a longer time to peak horizontal force (T max) and a greater horizontal impulse (H Impulse) as extra weights increased. In addition, the peak vertical power (Max V_P) decreased as extra weights increased. Minetti suggested that 5-6 kg of extra weight is optimal for extending jumping distance. This study indicated that 4.24 kg or 6.25% BW of extra weight is optimal for extending jumping distance.

REFERENCES

1. Minetti AE, et al. *Nature*. **420**, Nov 14, 141-142, 2002.
2. Dempster WT. *WADC Technical Report,* 55-159. OH:Wright-Patterson Air Force Base, 1955.
3. Huang C, et al. *Proceedings of ISB XIX*, Dunedin, New Zealand, Abstract 169, 2003.

Table 1：Variables of four levels of extra weight during jumps.

N=12	unloaded	low	middle	high
Distance (m)	2.92±0.16	2.98±0.17	2.95±0.22	2.92±0.23
V velocity (m/s)	2.09±0.2	1.98±0.2	1.72±0.16*	1.62±0.14*
H velocity (m/s)	3.06±0.25	3.16±0.22	3.18±0.25	3.13±0.29
CG angle (deg)	34.4±4.3	32.1±3.3	28.4±3.3*	27.6±3.5*
Tmax (s)	0.76±0.16	0.86±0.2	0.96±0.17*	1.02±0.16*
H Impulse (N*s)	237.6±42.0	253.6±42.5	273.2±41.8*	283±44.5*
Max V_P (Watt)	2479±619	2185±500	1924±405*	1747±406*

* = significance with unloaded jump

COMPARISON OF UPPERLIMB KINEMATICS COLLECTED BY ELECTROMAGNETIC TRACKING VERSUS DIGITAL CAMERA SYSTEMS IN A GAIT ANALYSIS LAB

[1,2] Elizabeth Hassan, [1,2]Thomas Jenkyn, PhD, PEng and [1]Cynthia E. Dunning, PhD, PEng
[1]Department of Mechanical and Materials Engineering, University of Western Ontario, London Ontario, Canada,
[2]Wolf Orthopaedic Biomechanics Lab, Fowler-Kennedy Sports Medicine Clinic, London, Ontario, Canada

INTRODUCTION

The purpose of this study is to dynamically quantify the accuracy of kinematics measured by an electromagnetic tracking device compared to a digital optical motion analysis system for applications in the upper limb. Unlike lower limb motion, there is currently no standardized marker set for collecting upper limb kinematic data. [1] Complicating upper limb kinematic are joint motion pathways with fewer biomechanical constraints, smaller segments, and larger skin movement errors. These factors make collecting accurate and reliable in vivo data of the upper limb difficult. [2] However, innovations in motion analysis technology combined with optimized marker set design and placement could allow investigators to study upper limb kinematics in a gait analysis lab as an alternative to electromagnetic tracking systems.

METHODS

All of experiments were performed in the Wolf Orthopaedic Biomechanics Lab (WOBL) at the University of Western Ontario, which is equipped with an 8 camera Eagle Digital Motion Capture System (Motion Analysis Corp., Santa Monica, CA, USA). Rigid clusters of spherical reflective markers and electromagnetic sensors were attached to a mechanical articulator that mimicked elbow motion (Fig. 1).[3] Kinematic data were collected simultaneously using the camera system and an electromagnetic tracking system (Flock of Birds, Ascension Technologies, Burlington VT, USA) while the mechanical 'elbow' was moved through known ranges of flexion (i.e. 1, 2, 3, 5, 20, 110°), with and without coupled varus-valgus and/or internal-external rotations.

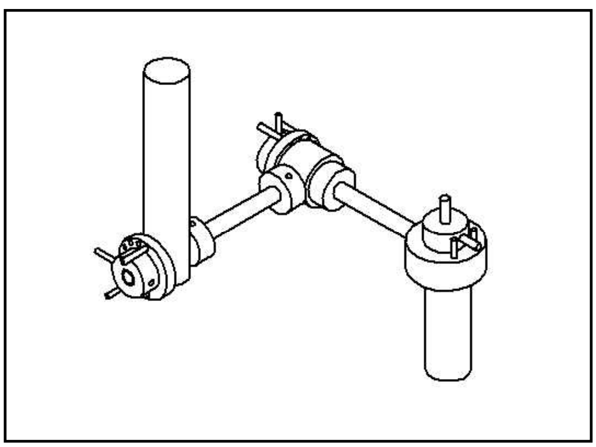

Figure 1 – Mechanical Articulator

RESULTS AND DISCUSSION

Compared to the known magnitudes, both the electromagnetic system and the optical system tended to overestimate the motion with mean differences of 0.96° and 3.28°, respectively (confidence intervals from 0.67°-1.24° and 2.55°- 4.06°, respectively). Two-way ANOVA analysis showed that for large (110°) flexion arcs, there is no effect of adding coupled motions ($p=0.53$) and no significant difference between systems ($p=0.09$). Both systems are able to accurately describe upper limb motion (Fig. 2), although they tended to over-estimate the magnitude of the motion. This appeared to be more pronounced for the optical system, but optimization of the marker cluster design may improve these results.

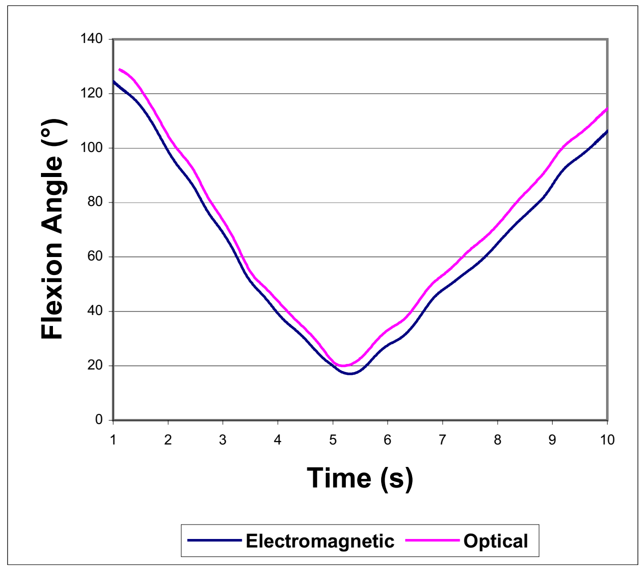

Figure2 – Reported Flexion Angle for Both Systems as a Function of Time.

REFERENCES

[1] Measurement of lower extremity kinematics during level walking. Kadaba MP. J Orthop Res. 1990 May; 8(3):383-92.
[2] Review of arm motion analyses. Anglin C. Proc Inst Mech Eng [H]. 2000; 214(5):541-55. Review.
[3] Quantifying translations in the radiohumeral joint: application of a floating axis analysis. Dunning CE. J Biomech. 2003 Aug;36(8): 1219-23

ACKNOWLEDGEMENTS

The authors acknowledge the funding support of the University of Western Ontario and NSERC (Natural Sciences and Engineering Research Council of Canada).

THE EFFECT OF MUSCLE IMBALANCE ON FOOT PRESSURE IN PEDIATRIC PATIENTS

[1]Michael El-Shammaa, [1]Nicholas Gryfakis, [1]Kelly Lenard, [2]Nathan Lashley, [2]Louis Santangelo, [1]Luciano Dias
[1]Motion Analysis Center, Children's Memorial Hospital, Chicago, IL
email: melshammaa@childrensmemorial.org; web: www.childrensmemorial.org/depts/motionanalysis/
[2]College of Podiatric Medicine, Finch University of Health Sciences, Chicago Medical School

INTRODUCTION

Foot pressure data is frequently collected during gait analysis. Analysis of this data is typically done by dividing the foot pressure into regions with a mask that is not customized to the shape of the individual foot. Previous studies have successfully used these generic foot masks to evaluate varus and valgus foot deformities [1]. The effect of posterior tibialis [2] and anterior tibialis [3] dysfunction on foot pressure data has also been examined in vitro. This study examined average peak foot pressure on patients with a strength imbalance between a major evertor and invertor of the foot.

METHODS

Five able-bodied subjects (ten limbs; mean age = 11.8 yrs) and 15 patients with a mean age of 10.5 yrs (12 cerebral palsy, 1 pdd, 1 lipoma, and 1 clubfoot) were included. The same physical therapist measured all patients' muscle strengths. A minimum difference in muscle strength grade of 1 (on the 0 to 5 scale) between the peroneus brevis (evertor) and the posterior tibialis (invertor) was observed for inclusion. The patients were divided into 2 groups. Group 1 (n=7 limbs) showed greater posterior tibialis strength. Group 2 (n=10 limbs) showed greater peroneus brevis strength.

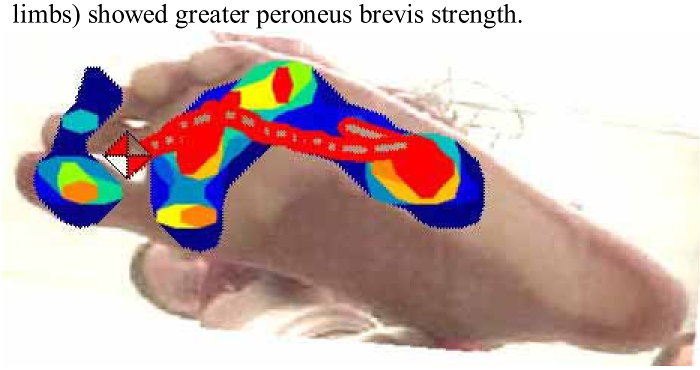

Figure 1: Foot pressure overlay with plantar surface picture

Barefoot pedobarograph data was collected for all subjects using a Tekscan, Inc. FMAT pressure mat. A static photo of the plantar surface of the foot was taken for each subject while in bilateral self selected weight bearing. The peak foot pressure data was overlaid on the static image of each patient's foot as seen in Figure 1. This facilitated a more thorough evaluation by displaying the peak pressure relative to the individual shape, size and anatomical landmarks of the foot. Simultaneous gait analysis data was collected on select subjects (as needed) to verify that the foot progression angle of the image matched the foot progression angle of the foot pressure. The long axis of the foot, from the center of the heel to the 2nd interspace was rotated to vertical and used to create the medial/lateral division. The foot was then divided at 32.9% and 62.3% of the overall foot length from the posterior aspect to give the midfoot and forefoot sections. The four regions evaluated were the medial midfoot, medial forefoot, lateral midfoot, and lateral forefoot. The average (over the area) peak pressure of each region was normalized to the maximum peak pressure of the entire foot. The ratio of

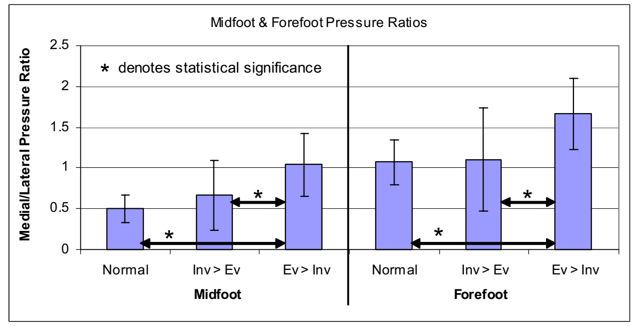

Figure 2: Medial/lateral pressure ratios for the midfoot and forefoot.

medial to lateral average peak pressure was examined for the midfoot and for the forefoot.

RESULTS AND DISCUSSION

Group 1 (Inv. > Ev.) showed an average posterior tibialis strength of 3+/4- and an average peroneus brevis strength of 2+. Group 2 (Ev. > Inv.) showed an average peroneus brevis strength of 3 and an average posterior tibialis strength of 2-.

Figure 2 shows that the medial to lateral ratio was not statistically different between the normal group and the Inv. > Ev. group, for both the midfoot ($p = 0.38$) and the forefoot ($p = 0.91$). The normal ratio is approximately 0.5 for the midfoot (the medial midfoot shows approximately half the mean peak pressure as the lateral midfoot), and approximately 1.0 for the forefoot (same mean peak pressure for both medial forefoot and lateral forefoot). The Ev. > Inv. group showed significantly increased mean peak medial pressure for both the midfoot ($p = 0.001$) and the forefoot ($p = 0.002$).

CONCLUSIONS

The overlaid image of the plantar surface of the foot is a useful tool in orthotic fabrication, foot pressure analysis and research. These results show that a foot evertor/invertor strength imbalance can have a significant effect on foot pressure data. In subjects where the posterior tibialis is significantly stronger than the peroneus brevis, the pressure ratio is not significantly affected; however, when the posterior tibialis is significantly weaker than the peroneus brevis, there is a significant shift of pressure towards the medial aspect of the forefoot and midfoot. This may be an important factor when considering the implications of a surgery that may weaken the posterior tibialis. Future studies will focus on the effects of an imbalance between other muscle groups.

REFERENCES

1. Chang CH, et al. *J Pediatric Orthopedics*,**22**, 813-818, 2002
2. Inhauser CW, et al. *J Clinical Biomech*, **19**, 161-169, 2004
3. Wulker N, et al. *Foot & Ankle Int*, **24**(8), 623-9, 2003

ACKNOWLEDGEMENTS

Children's Memorial Hospital Motion Analysis Center Research and Education Fund, Claudia Kelp-Lenane.

ASSESSING REGULARITY IN VOLUNTARY MOTOR ACTIVITY WITH APPROXIMATE ENTROPY

Oliver Wirth and Israel R. Hall
National Institute for Occupational Safety and Health
email: owirth@cdc.gov

INTRODUCTION

The objectives of the present study were to: 1) extend the use and analysis of the regularity statistic *approximate entropy* (ApEn) [2] to voluntary motor performances of rats, and 2) describe how ApEn changes as a function of other biomechanical measures of motor performance including pull force and power spectral density. Because previous studies have shown that vibration affects muscle activity [1], we also attempted to determine how a mechanical stressor (i.e., vibration) affects motor activity and thus ApEn.

METHODS

Eight rats were trained with operant conditioning techniques to perform a voluntary and repetitive bar-pulling response [3]. After training, a single 5-hr exposure session was conducted in which food rewards were earned for performing pull-bar responses of at least 1-s duration and 0.1 N peak force. For one half of the rats, a vibration stimulus (125 Hz, 49 m/s^2) was applied to the pull bar with every response. Because thousands of bar-pull responses were performed by each rat, 4 to 7 bar pulls of at least 2-s duration were sampled at 1000 Hz in each successive 30-min time bin of the session. To eliminate any signal noise from the vibration stimulus, the vibration was turned off briefly during the recording of those forces.

Among the record responses, several time-domain measures were computed, including peak force, mean force, and standard deviation of the force-time series. In addition, a Matlab routine was developed to calculate ApEn for each response on the basis of an algorithm previously published [2]. The force-time series for each response was truncated, and only the middle 1024 data points were used in the calculation of ApEn. In addition, the power spectral density (PSD) was computed to obtain the total power of the force-time series of each response. The total power of the spectrum was calculated as the integral of the PSD between 5 Hz and 40 Hz – the range often associated with physiological force tremor. The modal frequency also was determined from that range. ApEn and the other time-domain measures were compared and plotted as a function of exposure group and session time.

RESULTS AND DISCUSSION

All rats were trained successfully to perform repetitive bar pulls for food rewards with or without vibration. 3-5 thousand bar-pulling responses were generated in the 300-min session with each rat with and without the vibration stimulus. Global measures of performance, including peak force, mean force, and standard deviation of the force-time series, total power, the modal frequency, and ApEn, when averaged across the recorded pull-bar responses, revealed no significant differences between the vibration and no vibration groups. In both groups, however, there was a significant decrease in pull

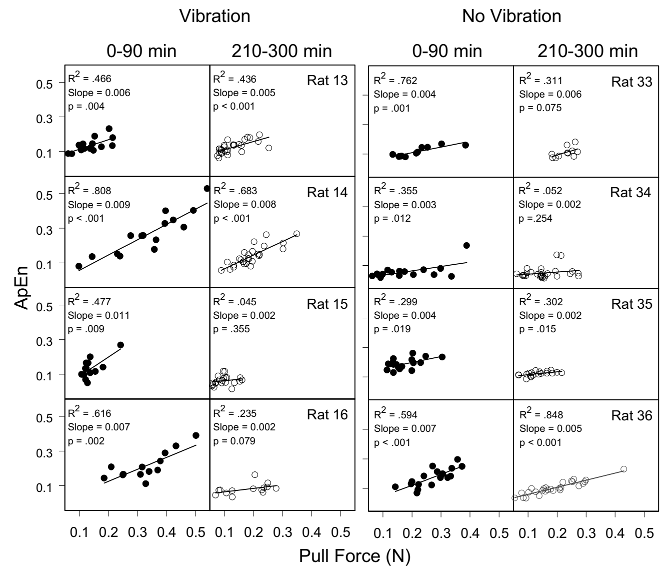

Figure 1. ApEn for the vibration and no vibration groups in the first and last 90-min periods of the session plotted as a function of pull force.

force, total power, and ApEn. Furthermore, orderly relations were found when ApEn was compared with other measures. For example, Figure 1 shows significant positive correlations between ApEn and pull force and, in the vibration group only, the slopes of the functions that describe the relation between ApEn and force significantly decreased across session time. Additional results (not shown) indicated similar relations between total power and force. Increases in ApEn were associated with increases in total power; however, the relation between ApEn and total power did not change across session time. The time-dependent decreases in ApEn and changes in the functions relating ApEn to force and total power in the vibration group indicate that regularity in each force-time record increased with increased exposure to the repetitive task and that vibration may have exacerbated this change. It is tempting to speculate that a physiological response such as tremor or fatigue might have played a role.

CONCLUSIONS

The present study demonstrated that high-gain force records obtained from voluntary bar-pull activity of rats revealed systematic changes in ApEn, total power, and other measures of performance. In addition, vibration may have had direct motor effects contributing to changes in force output, and that the regularity statistic ApEn was sensitive to those changes.

REFERENCES

1. Necking LE, et al. Scand J Plast Reconst Surg Hand Surg 1996;30:99-103.
2. Pincus SM. Proc Natl Acad Sci USA 1991;88(6):2297-301.
3. Wirth.O. Proc. 10th Int Hand-Arm Vibration Conf; 2004; 145.

TRACKING SLOW-TIME-SCALE CHANGES IN MOVEMENT COORDINATION

Jonathan B. Dingwell [1], Domenic F. Napolitano [2], and David Chelidze [2]
[1] Nonlinear Biodynamics Lab, Dept. of Kinesiology, University of Texas, Austin, TX, USA
[2] Dept. of Mechanical Engineering, University of Rhode Island, Kingston, RI, USA
E-mail: jdingwell@mail.utexas.edu Web: http://www.edb.utexas.edu/faculty/dingwell/

INTRODUCTION

Diseases like osteoarthritis and repetitive strain injuries lead to changes in coordination that develop slowly over time. It is important, but often very difficult, to track the progression of these disease processes. By contrast, changes in movement coordination patterns can be easily measured. Our goal is to develop methods to track changes in underlying (i.e. "hidden") disease states from easily obtainable biomechanical data.

METHODS

We borrowed a method for tracking similar hidden damage processes in mechanical systems [1,2]. We assume our system can be modeled as a hierarchical dynamic system of the form:

$$\dot{x} = f(x, \mu(\phi)), \qquad \dot{\phi} = \varepsilon\, g(\phi, x) \qquad \text{(1a, 1b)}$$

where $x \equiv$ the *observable* states of the fast-time-scale system, $\phi \equiv$ the *hidden* slowly-varying dynamics, $0 < \varepsilon << 1$, and $\mu(\phi) \equiv$ the parameters in (1a). If $\varepsilon = 0$, $\mu(\phi)$ would be constant. We form a topologically valid state space from a single measured time series, $x(n)$, using delay embedding (Figure 1*A*):

$$y(n) = [x(n), x(n+\tau), \ldots, x(n+(d-1)\tau)] \qquad (2)$$

where τ is a time delay and d is the embedding dimension [3]. Data from the unperturbed system are used to build a locally linear model of the system behavior (Figure 1*B*). Drift in ϕ leads to "errors" ($\mathbf{E}_k$) between actual and predicted behavior. If our model is good, the model error ($\mathbf{E}_k^M$) will be small and $\mathbf{E}_k \approx \varepsilon_k \equiv$ the true error or drift in the system dynamics. $\mathbf{E}_k$ can then be used to define the following *tracking metric*:

$$\varphi = \left\langle F \left\| \mathbf{E}_k(y(n), \phi) \right\| \right\rangle \approx \left\langle \left\| \varepsilon_k(y(n), \phi) \right\| \right\rangle \qquad (3)$$

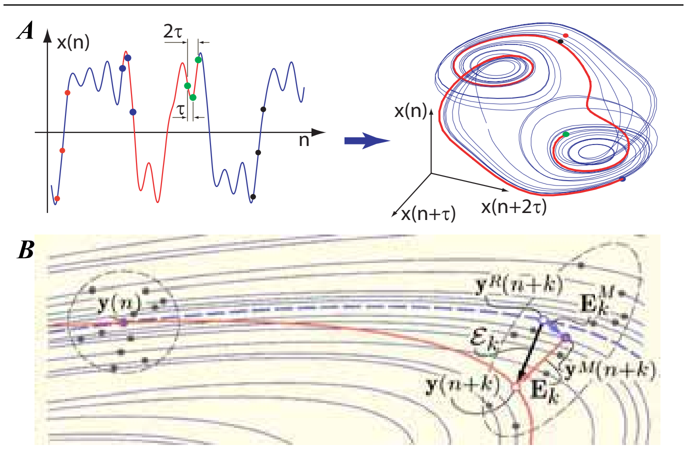

Figure 1. ***A:*** "Embedding" a 1-dimensional time series in a multi-dimensional vector space defining equivalent states of the system. ***B:*** Tracking function estimation: (—) is the current trajectory. (– –) is the corresponding model trajectory. $\mathbf{E}_k$ is the estimated error, $\mathbf{E}_k^M$ is the modeling error, and ε_k is the true error, or drift in the system.

where $\langle\cdot\rangle \equiv$ the RMS over the index n and F is an appropriate filter [2]. Thus, this metric essentially tracks the average error, over time, in the predicted fast-time-scale dynamics that is introduced by the slow-time-scale dynamics.

Five healthy subjects walked on a motorized treadmill at their self-selected pace. The treadmill incline was increased from 0° to +8° slowly over 25 minutes. Kinematic data were recorded (Vicon-612, Oxford Metrics, Oxford, UK) continuously at 60 Hz to obtain sagittal plane hip, knee and ankle angles. These joint kinematics defined $x(n)$, the fast-time-scale dynamics. Tracking metrics (φ) were computed from joint angle data and regression analyses were used to determine how well these metrics tracked the "hidden" treadmill incline angle.

RESULTS AND DISCUSSION

Basic patterns of joint kinematics changed little across trials. Tracking metrics (φ) generally increased with treadmill angle (Fig. 2). Regressions yielded adj-r^2 of 86% to 98%. Although these predictions were not perfect, no attempt was made to adjust or alter the original algorithm of [2]. By accounting for additional features specific to biological systems (e.g. noise, multiple time scales, etc.), better results may be obtained.

By using a state space formulation, the proposed method yields valid measures of slow-time-scale dynamics, without the need for "guessing" or for highly detailed first-principles models of system dynamics [2]. We anticipate this approach can be used to track other "hidden" biological processes like muscle fatigue, repetitive strain injury, or disease progression.

REFERENCES

1. Chatterjee A et al. *J. Sound & Vibr.* **250**: 877-901, 2002.
2. Chelidze D et al. *J. Vibr. & Acoust.* **124**: 250-264. 2002.
3. Sauer T *J. Statistical Physics,* **65** (3-4): 579-616, 1991.

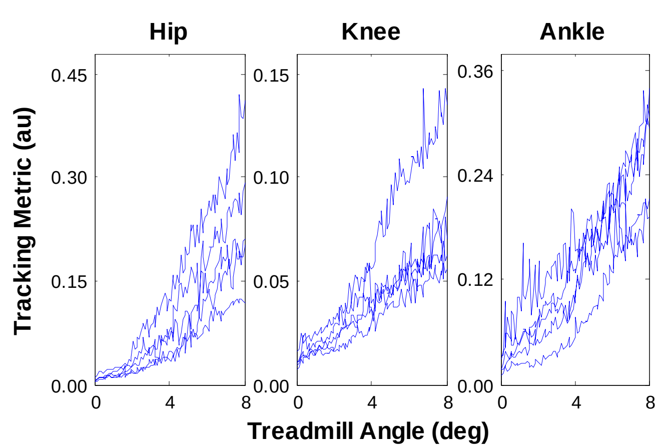

Figure 2: Tracking metrics computed from joint kinematic data as a function of treadmill angle (85.6% $\le r^2 \le$ 98.4%).

KINETIC EVALUATION OF RIGHT SHOULDER AND ELBOW DURING SPICCATO TECHNIQUE VIOLIN BOWING

Luke Wooldridge, Peter Visentin[1], Gongbing Shan[1]
[1]University of Lethbridge
email: Luke.Wooldridge@uleth.ca

INTRODUCTION

Musicians are a group particularly susceptible to overuse syndrome (OS), with up to 65% of professionals afflicted [1]. Violinists are at particularly high levels of risk for developing OS, due to the repetitive nature of the movements they use. Of 227 music students surveyed, string players reported shoulder pain more often than any other group at any other injury site [2]. Previous work has provided biomechanical descriptions of the legato (smooth bowing) technique during violin performance. It was discovered that kinetic considerations for risk of OS include the type and quantity of loading [3]. The current study examines the right shoulder (RS) and right elbow (RE) for the spiccato (bounced bow) technique.

METHODS

3-D motion capture using a nine-camera VICON v8i system (<0.76mm accuracy) was used to collect kinematic data. Inverse dynamic modeling technique was applied to capture data for obtaining joint kinetics. A ten-segment biomechanical model (upper body, violin and bow) designed for the capture was utilized. Subjects consisted of eight professional violinists. The protocol had the performers play G major scale cycles covering all four stings of the violin from the lateral G-string to the medial E-string and back at different tempi (varying bowing speeds) using the spiccato technique.

RESULTS AND DISCUSSION

Violin play can be described by two types of muscle load, the fundamental load from the process of moving the arm during a stroke, and the impact load resulting from overcoming the inertial forces of string crossings and bow direction changes (Fig. 1). In legato bowing it was found that fundamental loads dominated total joint moments at lower tempi, gradually giving way to impact loads at higher tempi [3].

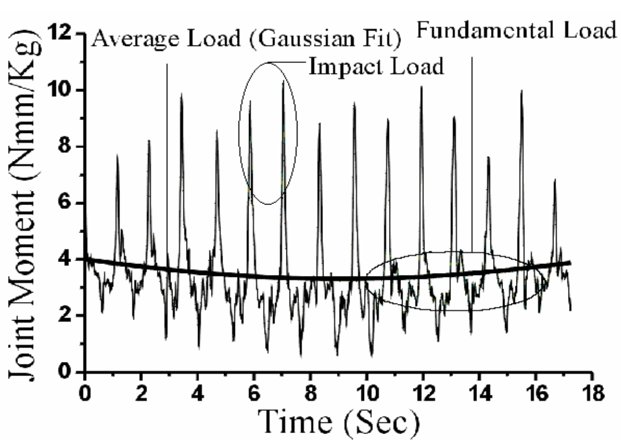

Figure 1: Wrist moment representative of legato bowing during the cycle of the scale at a low tempo.

Figure 2 shows spiccato bowing to produce a moment curve composed solely of impact load. Thus, playing spiccato even at low tempos exposes the muscles to loading patterns similar to those experienced during high tempo legato bowing. Impact loads have been identified as a significant factor in the cause of OS, and results suggest that spiccato bowing carries a higher risk for the development of OS than legato [4].

Kinetic analysis of spiccato bowing revealed that string played had a large effect on RS loads. RS moment is greatest when the G-string is played (88.9 Nmm/kg +/-SD 11.03) and lowest on E (64.2 Nmm/kg +/-SD 10.48). In contrast to the RS, the RE moment is greater for E than G-string bowing, although the difference is much smaller (31.13 Nmm/Kg +/-SD 5.05 vs. 29.97 Nmm/Kg +/- 4.61 respectively)

The height of the oscillations in Figure 2 gives an indication of the effect of string on moment range. Large ranges of moment indicate a more dynamic movement, while small ranges are indicative of quasi-static movement. There are some indications that static loads may increase risk of injury relative to more dynamic loads [3]. Moment ranges are larger when playing the E-string than G for both RS (41.44 Nmm/Kg vs. 34.68 Nmm/Kg) and RE (26.05 Nmm/Kg vs. 19.84 Nmm/Kg respectively).

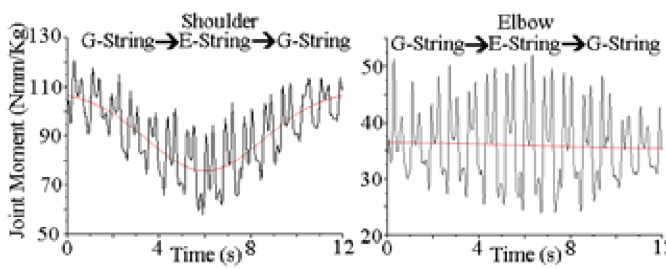

Figure 2: RS and RE joint moments at 144 bows/min during the cycle of a scale.

CONCLUSIONS

The current study reveals that playing on the G-string for extended periods using the spiccato technique increases risk of injury in the right shoulder, due to the higher overall loads and the narrower load range (approaching quasi-static conditions) experienced under these conditions. It follows that apportioning practice time with consideration of the factors identified should reduce the risk of RS injury due to overuse.

REFERENCES

1. Hoppmann R, et al. *Semin Arthritis Rheum* **19**, 117-126, 1989.
2. Zetterberg C, et al. *Med Probl Perform Art* **14(4)**, 160-166, 1998.
3. Visentin P & Shan GB. *Med Probl Perform Art* **18(3)**, 91-97, 2003.
4. *Nat Code Prac Prev Occup OS*, Australian Government Publishing Service, NOHSC, Canberra, p.2013, 1994.

ACKNOWLEDGEMENTS

This research is supported by Westgrid (Canada). The authors thank Brandie Dunn for her technical support.

DEVELOPMENT OF AN FE MODEL OF UNI-COMPARTMENTAL KNEE REPLACEMENT

[1] Andrew R Hopkins, [1] Mark Taylor, [1] Sara Checa Esteban, [1] Andrew New and [2] Lorin P Maletsky
[1] Bioengineering Science Research Group, University of Southampton.
[2] Department of Mechanical Engineering, University of Kansas.
E-Mail: a.r.hopkins@soton.ac.uk,
Web: http://www.ses.soton.ac.uk/projects/Bioengineering_Sciences/bioengineering_sciences.html

INTRODUCTION

Uni-compartmental replacement of the knee is recognized as a suitable treatment for localized damage of the tibiofemoral joint, whilst often allowing for later revision to a total knee replacement [1]. Several clinical studies have followed the progress of this implant device, however to date there have been very few computational studies [2]. The purpose of this project is the development of a Finite Element testing suite for the uni-compartmental knee, and its validation against existing clinical data. This paper will consider the steps involved in the development of such a model.

METHODS AND MATERIALS

Loading of the knee has been applied using data gathered from the Kansas Knee Simulator. This device uses five axes of dynamic control to apply loads to the components of the total knee replacement during activities such as walking and squatting. The loading profile consists of a vertical component applied to the centre of rotation of the hip, a prescribed rotation of the femur during walking (12-37° flexion), an applied quadriceps loading, tibial torque and abduction-adduction of the tibia. An FE model of one of the tested component sets was developed from CAD data (Fig. 1). The femur, tibia and patella were modeled as rigid bodies for this analysis, with the quadriceps modeled as a 2D membrane. Following successful application of the Explicit Finite Element time-stepping scheme to the analysis of total knee kinematics with the Stanmore simulator [3], all analyses were conducted in the Explicit FE solver PAMCRASH (ESI Software). The femur was free to rotate and translate relative to the vertical axis. The tibia was permitted to rotate around the ankle centre, but not to translate in the vertical axis. The resulting unconstrained movement of the knee components was recorded during these different activities and compared to the experimental findings.

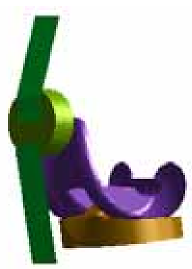

Figure 1 – FE models of TKR used to validate loading configuration.

Using the software package AMIRA (TGS Software) it is possible to extract surface representations of the anatomy of the lower extremity. Surface meshes of the osseous geometry have been developed from this data (Fig. 2), and in the first instance a model of the intact knee has been developed, inclusive of cartilage and ligaments. Following successful modeling of this configuration, a uni-compartmental knee device will be developed from CAD data and introduced to the lateral and medial compartments in separate analyses.

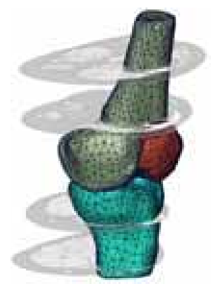

Figure 2 – Surface meshes of femur, tibia and patella developed from CT

RESULTS AND DISCUSSION

Displacements of the patella, tibia and femur were recorded during loading and compared with experimental data. The FE model managed to reproduce predicted kinematics to within 8% for all three components. Time-step size was not found to influence kinematics, however due to the large ranged of movement in the unconstrained knee system mass and inertial forces were found to be of critical relevance. The model was extremely sensitive to misalignment of the components.

The surface meshes of the tibia, femur and patella have been introduced to the finite element model of the total knee replacement. Initial results suggest that precise positioning of these osseous geometries and the inclusion of accurate inertial qualities of the mesh will influence the kinematics of the intact knee.

REFERENCES

1. Marmor L, *Clin Orthop Rel Res* **94**, 242-248, 1973.
2. Iseaka K, et al. *J Biomech* **35**, 969-974, 2002.
3. Godest A-C, et al. *J Biomech* **33**, 435-442, 2000.

ACKNOWLEDGEMENTS

This work has been funded jointly by EPSRC and DePuy International.

KINETIC CHARACTERISTICS Of THE GAIT IN CHILDREN, ADULTS AND ELDERLY

Jansen Atier Estrázulas, Roberta Pires,Diego Murilo dos Santos, Lígia Raquel O. G. Stolt and Sebastião Iberes Lopes Melo.
Santa Catarina Universaty State – UDESC – Brazil – email: jansenef@hotmail.com

INTRODUCTION

The gait is a simple activity of daily life and one of the main abilities of the human,that starts to develop the gait in the first years of life, and in agreement with Delisa (1992), the bipede gait standard is acquired in infancy for around 7 or 8 years old, where the sensory-motor system becomes suitable automatically to generate a repetitive set of motor control commands to allow a person to walk without conscientious effort. In adults, for being a daily movement, the gait pattern is characteristic of each person and well defined. In the elderly, in general way, one of the biggest functional limitations is the fall, or the fear of it, that implies in diminished levels of activities with subsequent loss of the muscular function, joint tissue and information processing.

Studies have been carried through in the search for characterizing the gait in these cited populations above, however, one can find little comparison between them. Thus, the search for a bigger understanding of kinetic characteristics of the gait was objectified in this study comparing children, adults and elders, trying to identify a possible difference between these populations.

METHODS

This disgnostic descriptive study was carried through in the Laboratory of Biomechanics of the Center of Physical Education, Physiotherapy and Sports of UDESC. There were as population children, adults and elders of the city of Florianópolis – SC - Brazil.

The sample was constituted by individuals of the feminine sex, being 34 children(G1) with age between 10 and 12 years old, 24 adults (G2) with age between 18 and 41 years old, and 12 elders (G3), with age between 64 and 74 years old. The sample was intentional type. One selected only subjects that had not presented any type of pathology or disfunction.

As measure instrument one used an ergometric treadmill Kistler-Gaitway 9810SI, with two force platforms of piezoeletric crystals connected to their bases that register the ground reaction force. The data processing was made through the instrument software.

For data collection, it was initially did a period of adaptation to the equipment and wheightning for the data normalization by the corporal weight (CW). Finally, one collected data with sampling frequency of 600 Hz and acquisition with 12s, speed average for the citizens of 4,0km/h. The average value of both sides of the sample was used. One used descriptive statistics in the characterization of the variáveis(média and standard deviation) and to comparison used ANOVA One-Way and the Scheffe Post Hoc test. The level of significance adopted was of 95%.

In this study some kinetic variables related to the vertical component of the ground reaction force had been analyzed: First Force Peak (FFP), Second Force Peak (SFP), Force of Medium Support (FMS), Tax of Wheight Acceptance (TWA).

RESULTS AND DISCUSSION

The results show that the groups that had participated of this study had presented the First Force Peak with a statisticly significant difference between the groups, and when applied the Scheffe Post-hoc test one did not find where this difference occurred, being able to have been influenced by the size of the sample. However, analyzing the results, it can be verified that the average value for the G1 (1,08CW), was greater than the average values of G2 and G3 (1,05 CW).

The variable Second Force Peak occurs in the phase of propulsion of the foot to stimulate it for the following step during the gait. The groups of this study had differed in this variable, having the G3 the lesser value (1,00 CW) and the G1 the greater (1.11 CW).

The Medium Support Force was the only kinetic variable that did not present significant difference statisticly. This can be explained by this variable occur in the phase of transistion of the weight of the citizen on the support foot, not happening many variations from a citizen to the other.

The Tax of Weight Acceptance consists in the form the citizen is cushioning the first impact in the phase of weight reception. In this study, the citizens of G2 had differed from G1 and G3, presenting lesser values for this variable, what demonstrates a less harmful gait for health.

COCLUSIONS

With results and the theoretical referencial this study conclude that: The FFP was bigger for the children, what it demonstrates the lack of maturation for the protection of the locomotive device during walking of this group. The SFP was lesser for the elderly, that it tells to the lesser force used for this population for the translation of the step. The children and the elderly group had presented a bigger TWA compared with the adults. The two groups execute the gait with lesser protection of the locomotive device, for the lack of maturation (children) and degenerative deficiency of the advanced age (elderly). For in such a way, it can even be concluded that these groups possess distinct characteristics of locomotion, although some variables present similarities.

REFERENCES

DAVID, A.C. Aspectos biomecânicos do andar em crianças: cinemática e cinética. Tese de Doutorado. UFSM, 2000.

DELISA, J. A. Medicina de Reabilitação Princípios e Prática .São Paulo, Ed. Manole, 1992. vol. 2.

McCRORY, J. L.; WHITE, S.C. and LIFESO, R. M. Vertical ground reaction forces: objective measures of gait following hip arthroplasty. Gait and Posture, Oxford, Reino Unido. n. 14, pag 104-109, 2001.

SUTHERLAND,D.H.; OLSHEN,R.A.;BIDEN,E.N. & WYATT,M.P. The development of mature walking. London: MacKeith Press, 1988.

WINTER,D.A. The biomechanics and motor control of human gait: normal, elderly and pathological. Canadá: University of waterloo Press, 1991.

AN ANALYSIS OF UNCERTAINTIES IN INVERSE DYNAMICS SOLUTIONS FOR GAIT

Raziel Riemer, Elizabeth T. Hsiao-Wecksler, and Xudong Zhang
Department of Mechanical and Industrial Engineering, University of Illinois at Urbana-Champaign, Urbana, IL 61801, USA
E-mail: xudong@uiuc.edu

INTRODUCTION

Inverse dynamics is a powerful tool for analysis of human movement [1], but is subject to error from various sources; these include estimates of segmental properties [2], skin artifacts [3], inaccuracies in center of pressure (COP) locations [4], and inherent noise in instrumentation. Previous studies have focused on the effect of only one or two error sources [2, 3, 4]. The combined effect of all sources of error on the calculated joint torques has not been investigated. A comprehensive analysis can provide a thorough understanding of uncertainties in inverse dynamics solutions. It can also lead to more effective error controls and improved algorithms for error correction such as the variance-weighted least-squares method [5].

This study seeks to provide a comprehensive analysis of most sources of error in inverse dynamics and their effects on computed lower extremity joint torques during gait.

METHODS

A three-segment linkage (foot, shank and thigh) represented the human leg, and served as the basis for Newton-Euler equations incorporating ground reaction force measurements (bottom up). An inverse dynamics solution was then computed for the joint torques at the ankle, knee and hip.

The magnitudes of the uncertainties in the leg joint torques are determined using an error analysis method [6]

$$E = \sqrt{\left(\frac{d\tau}{dx_1}\Delta x_1\right)^2 + \left(\frac{d\tau}{dx_2}\Delta x_2\right)^2 + \ldots\ldots + \left(\frac{d\tau}{dx_n}\Delta x_n\right)^2} \qquad (1)$$

where τ is the torque at a given joint, and Δx_i are estimated inaccuracies associated with the input variables in the equation of motion of interest. The uncertainty, E, is a statistical representation of the possible 3σ-error in the torque value. The magnitudes of the inaccuracies (Δx_i) were derived from literature data [2, 3, 4] and our own experimental studies. Since the reported values for Δx_i varied across the studies, and because different systems and methods where used to determine input parameters to the equations of motion, two sets of Δx_i where used to represent the range of values: Set 1 (small Δx_i) and Set 2 (large Δx_i).

Five males and five females (weight: 75.98±14.74 kg; height: 1.69±0.06 m) walked at their normal speed, with the right foot landing on a force plate (AMTI) while motion capture system (Vicon) recorded their movements. These measurements, the estimated segment parameters, and Δx_i where then input into Equation 1 to estimate the uncertainties in each joint torque.

RESULTS AND DISCUSSION

The magnitudes of the uncertainties changed over time (Fig. 1) and show temporal resemblance to the vertical ground reaction force profiles during stance, but not at all to the torque profiles. Similar trends where observed for both sets of Δx_i. The values of estimated uncertainties relative to peak joint torque for the ankle, knee and hip are: 4 %, 29 %, 56 %, respectively, when using Set 1, and are 7 %, 70 % and 140 %, respectively, for Set 2. This suggests that the difference between the inverse dynamics results and the true joint torque at knee and hip can be substantial.

The main contributors to the uncertainty in the joint torques are the inaccuracies in the segment angles, the distance from the COP to the ankle center of rotation, and the foot mass (Fig. 2). Other studies have suggested that inaccuracy in the joint torques is closely related to the quality of the acceleration estimation [7]. Our findings, however, indicate such is not the case for the leg joint torques at least during normal gait.

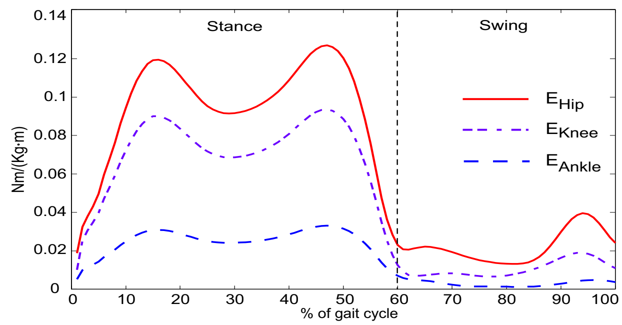

Figure 1: Estimated uncertainties (Set 1) in calculated joints torques during a gait cycle (normalize by weight and height).

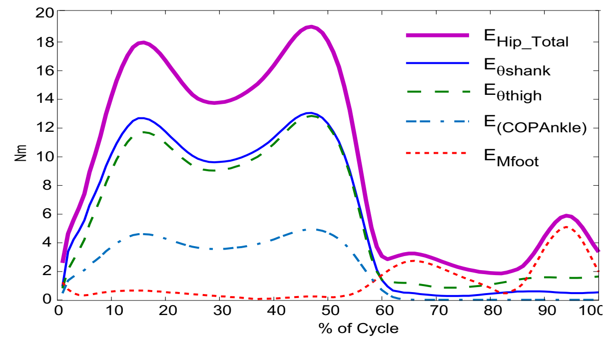

Figure 2: Main contributors for estimated uncertainty in hip joint torque for a 1.8 m and 80 kg subject in one cycle (Set 1).

REFERENCES

1. Winter, A.D., *Biomechanics and motor control of human movement*, 2nd ed. John Wiley & Sons, Inc, 1990.
2. Challis, H., John. *J. Applied Biomech*, **12**, 517-530, 1996.
3. Cappozzo, A., et al. *Clinical Biomech*, **11**(2): 90-100, 1996.
4. McCaw, S.T., P. Devita. *J. Biomech,* **28** (8): 985-988, 1995.
5. Kuo, A.D. *J. Biomech. Eng.*, **120**: 148-159, 1998.
6. Doeblin, O.E. *Measurement Systems: Application and Design*, McGraw Hill, 1966.
7. Cahouët, V. et al. *J. Biomech,* **35**: 1507-1513, 2002.

REPRESENTATION AND ANALYSIS OF SOCCER PLAYERS' TRAJECTORIES

Milton Shoiti Misuta, Rafael Pombo Menezes, Pascual Jovino Figueroa, Sergio Augusto Cunha, Ricardo Machado Leite de Barros
Laboratório de Instrumentação para Biomecânica – Faculdade de Educação Física, Universidade Estadual de Campinas, Campinas (SP), Brazil; e-mail: misuta@fef.unicamp.br

INTRODUCTION

The increasing interest in quantifying variables related to the athlete's performance has been stimulated the development of systems to collect data. In [1], we proposed an automatic method of tracking soccer players from video sequences. This kind of method provides a great amount of data to be summarised and interpreted. In this paper, we propose and evaluate two ways of representation and analysis of players' trajectories.

METHODS

A first division Brazilian championship game was recorded using four stationary digital video cameras. Applying [1], the 90 minutes players' positions were obtained (sampled at 7.5 Hz). To each player's position data set, linear regression of the covered distance in function of time was performed and the slope of the best fit regression line (α) was determined. This parameter was used to characterise the physical performance of each player. Principal components analysis (PCA) was performed to model the regions more visited by the players. In the Figure 1, the ellipses are centred in the player's median position. The ellipse's major axis has his direction driven by the eigenvector associated to the largest eigenvalue. The lengths of the axes are one standard deviation long symmetrically to the origin. The slope of the major axis related to the longitudinal axis of the field was also calculated (θ). To evaluate the stability of the proposed variables, the variations of slopes ($\Delta\alpha$) and ($\Delta\theta$) were analysed increasing the time of sampling from 2 to 90 minutes (2 minutes step). In this evaluation, the trajectories of just 14 players were considered, excluding therefore the goalkeepers and the players replaced during the game.

RESULTS AND DISCUSSION

An individual analysis of the PCA can be used to distinguish the players' characteristics of moving, as shown in the Figure 1. Considering that the PCA is obtained *a posteriori*, the representation can be associated to the tactical organization of the team. The Figure 2 exemplifies the players' covered distances at any time interval for 8 players. Furthermore, it is remarkable that the curves seem to be characteristic to each player. The Figure 3 shows the tendency of stabilization of the mean value and standard deviation of ($\Delta\alpha$) and ($\Delta\theta$) for the 14 players with the increment of the time interval used to determine the variables. This result suggests that it is not necessary to analyse the full time game to determine, at a given error level, the variables proposed. In conclusion, the proposed variables showed to be useful to represent and analyse important aspects of the soccer players' performance.

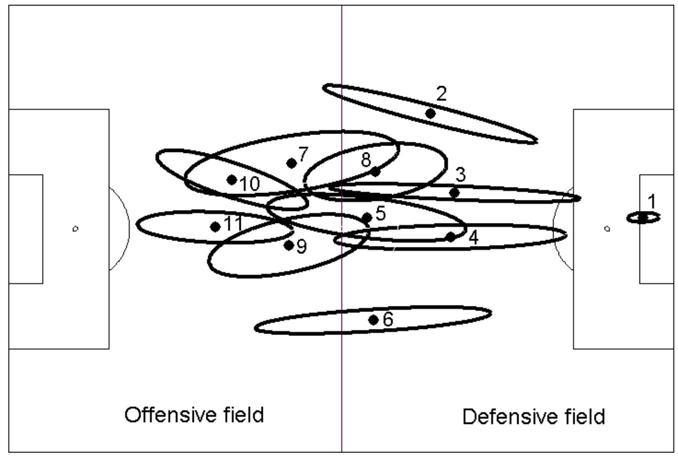

Figure 1: Representation of the players' region of moving using Principal Components Analysis (PCA).

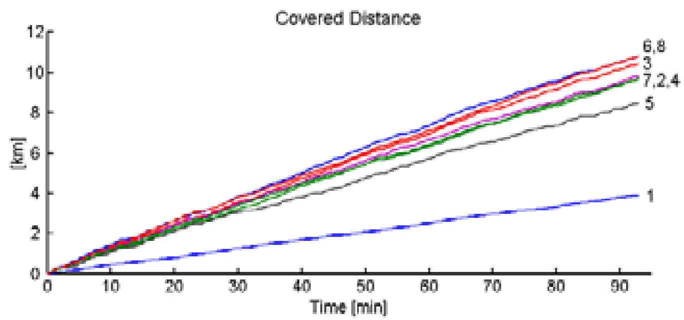

Figure 2: Example of covered distance of 8 players in function of the time

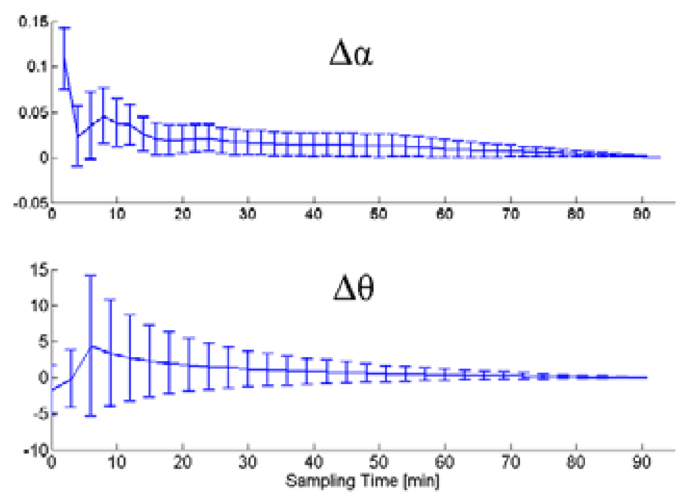

Figure 3: Mean value (n=14) and SD of the variation of slope of ($\Delta\alpha$) and ($\Delta\theta$) with the increment of the time interval used to determine the variable.

REFERENCES

1. Barros, R.M.L., et al. *Proceedings of ISB XVIII*, Zurich, Switzerland, p.236-239, 2001.

ACKNOWLEDGEMENTS

Supported by Capes, CNPq and Fapesp (00/01293-1).

A FINITE ELEMENT ANALYSIS OF CARTILAGE IN CYCLIC TRIAXIAL COMPRESSION

[2]Nicole A Kallemeyn, [1,2]Nicole M Grosland, [1]Douglas R Pedersen, [1]James A Martin, [1]Anneliese D Heiner, and [1,2]Thomas D Brown
[1]Department of Orthopaedics and Rehabilitation, The University of Iowa, Iowa City, IA
[2]Department of Biomedical Engineering; email: vosn@mail.medicine.uiowa.edu web: http://mnypt.obrl.uiowa.edu

INTRODUCTION

When compared to other forms of mechanical testing of articular cartilage, triaxial testing holds the unique advantage of accommodating independent modulation of physiologically relevant shear stress states within the matrix, by varying the axial and radial (transverse) applied loads. However, owing to the proximity of loading/constraint boundaries, stress heterogeneities may confound the interpretation of *in situ* experiments performed in this configuration. A poroelastic finite element (FE) model of a cartilage specimen in cyclic triaxial compression testing was developed in order to investigate the effect of variation in loading conditions, geometry and material properties.

METHODS

A baseline FE model of a cartilage explant (4 mm diameter, 1.5 mm thick) and containment sheath (0.0254 mm thick) was created to mimic triaxial testing conditions [1]. The specimen was modeled using axisymmetric, poroelastic elements. In the radial (*r-z*) plane, the specimen was discretized into 150 8-noded bi-quadratic elements. The sheath was modeled using 100 2-noded axisymmetric shell elements. The experimentally measured modulus of the containment sheath was 5.5 GPa and Poisson's ratio $\upsilon = 0.4$. The cartilage had an initial void ratio (volumetric ratio of fluid to solid) of $e = 4.0$, $\upsilon = 0.1667$, a depth-dependent modulus ranging from 10 MPa in the superficial zone to 20 MPa in the deep zone, and void ratio-dependent permeability [2].

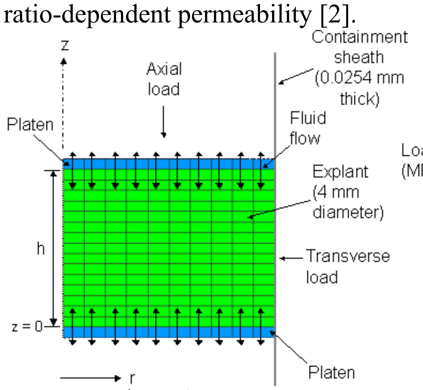

Figure 1a.

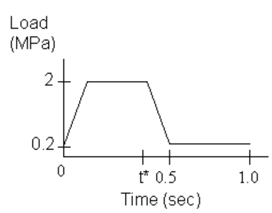

Figure 1b.

The cartilage explant was compressed between two rigid porous platens (diameter = 4 mm). Consequently, the interstitial fluid was free to flow in and out of the surfaces adjacent to the platens (Fig 1a). Transverse fluid flow was assumed to be restricted by the impermeable containment sheath. Six hundred cycles of trapezoidally-modulated loading were applied at a frequency of 1 Hz (Fig 1b); axial and transverse load magnitudes were 0.2 to 2.0 MPa.

Parametric testing was performed by independently modifying model attributes from the baseline model. The series included the cartilage radius, thickness, modulus, Poisson's ratio, and initial void ratio, as well as load magnitude, rate, and frequency. For the purpose of this abstract, only the results from the thickness and void ratio parametric series are shown.

In all cases, data were collected at the centroid of each element. The thickness was decreased from the 1.5 mm baseline case to 0.75 mm and 0.375 mm. In the void ratio series, three models were run in addition to the baseline case ($e = 4.0$) in which the initial void ratio was 2.0, 8.0, and 16.0.

RESULTS AND DISCUSSION

Throughout the 600 cycles, the cartilage peak-to-peak axial strain range decreased and total strain increased for all cases (Fig 2). As the thickness decreased from the baseline, peak-to-peak strain increased, in addition to the maximum strain for each cycle.

The pore pressure is shown (Fig 3) at 0.1 mm off the symmetry axis of the cartilage at time t* (Fig 1b) for the 1st and 600th cycles of loading. At the onset of loading, pore pressures were higher compared to 600 cycles, where the effect of the different void ratios was seen.

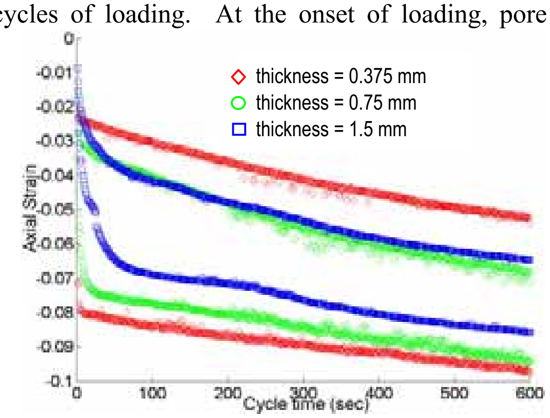

Figure 2. Peak-to-peak axial strain.

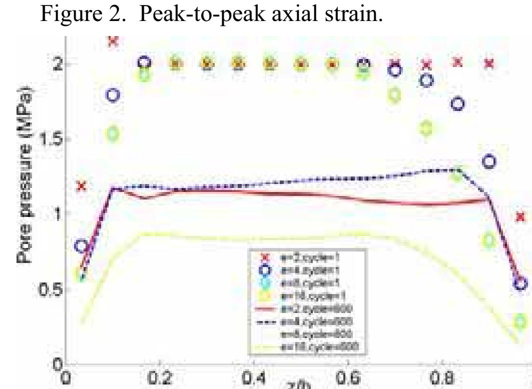

Figure 3. Pore pressure at t* for 1st and 600th cycles.

This FE model is a powerful tool to explore cartilage behavior for a wide range of physiological conditions. Additionally, changes in thickness, water content, permeability, stiffness, etc. are commonly associated with cartilage degradation [3], and can therefore be simulated to better understand these pathological conditions.

REFERENCES

1. Heiner AD, et al. *J Biomech*, **37**, 689-695, 2004.
2. van der Voet, AF. *Proc Instn Mech Engrs Part H,* **211**, 209-211, 1997.
3. Buckwalter, JA et al. *Instr Course Lect.* **49**:481-489, 2000.

ACKNOWLEDGEMENTS

This study was financially supported by the NIH AR 48939.

SOLDIERS' LOADS AFFECT RANDOM WALK OF CENTER OF PRESSURE AND EMG ACTIVATION DURING POSTURAL SWAY

Jeffrey M. Schiffman, Carolyn K. Bensel, Leif Hasselquist, Karen Norton, and Louis Piscitelle
U.S. Army Natick Soldier Center, Natick, MA, 01760, USA
Email: Jeffrey.Schiffman@natick.army.mil

INTRODUCTION

Carrying loads may contribute to poor balance resulting in falls when soldiers perform marches, negotiate obstacles, and maneuver during operations. We investigated the effects of carrying loads on soldiers' center of pressure trajectories during postural sway using a general stochastic model; we also examined EMG activity changes as a function of load carried.

METHODS

Fourteen Army enlisted men (mean: 19.6 yr, 1.75 m, 74.11 kg) participated after giving informed consent. We tested the soldiers under three load weight configurations: 6, 16, and 40 kg. At the heaviest load, soldiers wore/carried: M16A1 rifle, boots, minimal clothing (6 kg), plus a helmet and armor vest with ammo, grenades, and canteen (+10 kg), plus a backpack containing a 20-kg steel block (+24 kg). The 20-kg block was located either high on the back and close to the shoulders (h&c) or low on the back and away from the body (l&a) to create two unique backpack center of mass positions.

We recorded postural sway as the volunteers stood comfortably on a force plate for ten trials of 30-s each. Foot placement on the force plate was controlled. The presentation order of the load configurations was based on a Latin square. Force plate outputs were recorded and converted to physical units (mm). From a stabilogram diffusion analysis (SDA), we determined Hurst scaling exponents for short-term and long-term regions for axial and planar movements [1]. Percent of EMG on-time activation for 8 bilateral muscle pairs (Tibialis Anterior, Vastus Lateralis, Rectus Femoris, Gluteus Medius, Biceps Femoris, Erector Spinae, Upper Trapezius, Paraspinals) was calculated as described elsewhere [2].

For each configuration, each measure was averaged over the ten trials. A one-way repeated measures ANOVA with three levels was run on each averaged measure to determine the effects of weight (6 kg, 16 kg, 40 kg h&c). A significant ANOVA finding was followed up with a trend analysis using a within-subjects polynomial contrast. A paired samples t-test was used to determine the effects of load position (h&c vs. l&a) on the measures. Alpha was set at .05 and we corrected for multiple comparisons.

RESULTS AND DISCUSSION

SDA--For the medio-lateral Hurst exponent over the short-term time intervals, a significant linear trend for weight was found, with the heaviest load being the least random with values ranging from 0.81 to 0.85. The l&a load position was significantly less random than the h&c position, 0.84 vs. 0.85. For both the planar and anterior-posterior Hurst values (both with similar means) over the long-term time intervals, a significant linear trend for weight was found (Figure 1): The lightest load was the most random. Also, the l&a position was significantly more random than the h&c position, about 0.20 vs. about 0.12.

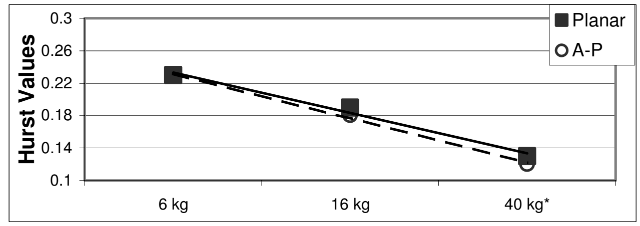

Figure 1: A-P and planar long-term mean Hurst values results. (H < 0.5, correlated anti-persistent motion)

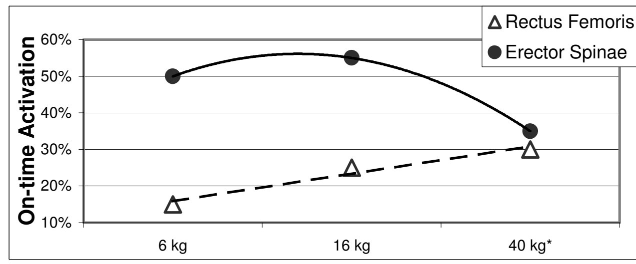

Figure 2: Rectus Femoris and Erectors Spinae mean on-time activation results.
*40 kg load includes pack with block in h&c position.

EMG—For bilateral Rectus Femoris, a significant linear trend was found: On-time percentage increased with an increase in load weight from 15% mean on time at 6 kg to 20% at 16 kg to 30% for 40 kg (Figure 2). For Erector Spinae, a significant quadratic trend was found: on-time percentage increased with an increase in load carried from 50% at 6 kg to 55% at 16 kg, but then decreased to 35% at 40 kg (Figure 2). The Paraspinals increased significantly in on-time percentage as a function of load position, from 65% for h&c to 80% average on-time for the l&a position.

Postural sway became less random as load weight increased. However, as the load position was changed from high and close to low and away from the body at the heaviest load, postural behavior became less structured. Thus, a load placed low and away in the backpack may be quite difficult for a load carrier to control precisely. In contrast, a load placed close and high on the back required more control to balance, but was easier and more predictable to manage.

At the heaviest load, Rectus Femoris activity continued to increase while Erector Spinae activity decreased. These muscular changes at the heaviest load may be attributable to forward lean of the trunk when the backpack was worn. The changes may reduce the efficiency of the muscular control scheme, which aims to maintain posture while minimizing fatigue.

REFERENCES

1. Collins JJ, et al. *Exp. Brain Res* **95**, 308-318, 1993.
2. Laughton CA, et al. *Gait Posture* **18**, 101-108, 2003.

SCAPHOID AND LUNATE ROTATIONS ARE MINIMIZED WITH WRIST MOTION ALONG THE DART THROWER'S PATH: IMPLICATIONS FOR STABILITY IN HIGH-DEMAND TASKS

[1] Joseph J. Crisco, [1]James C. Coburn, [1]Douglas C. Moore and [2]Scott W. Wolfe
[1]Department of Orthopedics, Brown Medical School/Rhode Island Hospital, [2]The Hospital for Special Surgery
email: joseph_crisco@brown.edu, web: brownbiomechanics.org

INTRODUCTION

The radiocarpal joint (radio-scapho-lunate articulation) is responsible for as much as 85% of overall wrist motion, depending on direction the wrist is moved in [3]. However, there appear to be directions of wrist motion where radiocarpal motion is significantly reduced [2,4]. An interesting example is the "dart thrower's" motion, which involves movement of the wrist from a position of combined extension and radial deviation (radial extension) to a position of combined flexion and ulnar deviation (ulnar flexion). The dart thrower's motion is used for activities that require fine control, such as fly casting, as well as high-demand activities that require maximal grip and stability, such as hammering. This study was performed to explore possible motion minima in the 3-D kinematics of the radiocarpal joint *in vivo*, throughout the entire range of wrist motion.

METHODS

The 3-D kinematics of the capitate, scaphoid and lunate were measured *in vivo* in both wrists of 14 male (25.6 years; range 22-34), and 14 female (23.6 years; range 21-28) healthy volunteers using CT volume images of 481 static wrist positions and established segmentation and registration procedures for markerless bone tracking [1]. This study was approved by the IRB and all volunteers were enrolled after informed consent. Carpal kinematics were calculated relative to the radius, with respect to the neutral wrist position, and described using helical axis of motion variables. Multiple linear regression was used to analyze carpal rotation as a function of wrist position.

RESULTS AND DISCUSSION

For all wrist positions, regardless of direction, the scaphoid (Fig. 1) and lunate rotated primarily in flexion or in extension. Scaphoid and lunate rotations and translations were minimized *only* at wrist positions along the path of the dart thrower's motion (Fig. 1, dashed line). This behavior was independent of gender and was consistent across all subjects (RMS errors of scaphoid and lunate rotation as a function of wrist rotation were 6.6° and 6.9°). The scaphoid and lunate translated radially 1.5 ± 0.9 mm and 1.3 ± 0.9 mm when they extended, but only 0.5 ± 0.4 mm and 0.5 ± 0.4 mm when they flexed.

CONCLUSIONS

Using the largest database of subjects and wrist positions to date, we found that the kinematics of the radiocarpal joint is dominated by flexion and extension rotations of the scaphoid and lunate, regardless of the direction of wrist motion. We also found that radiocarpal motion was *uniquely* minimal only along the path of the dart thrower's motion. It is unclear why wrist motion along this path is shifted to the midcarpal joint (esp. scaphocapitate and lunocapitate), but it is consistent with the unique functional importance of this motion which is used for both low and high demand activities that require exquisite control and stability.

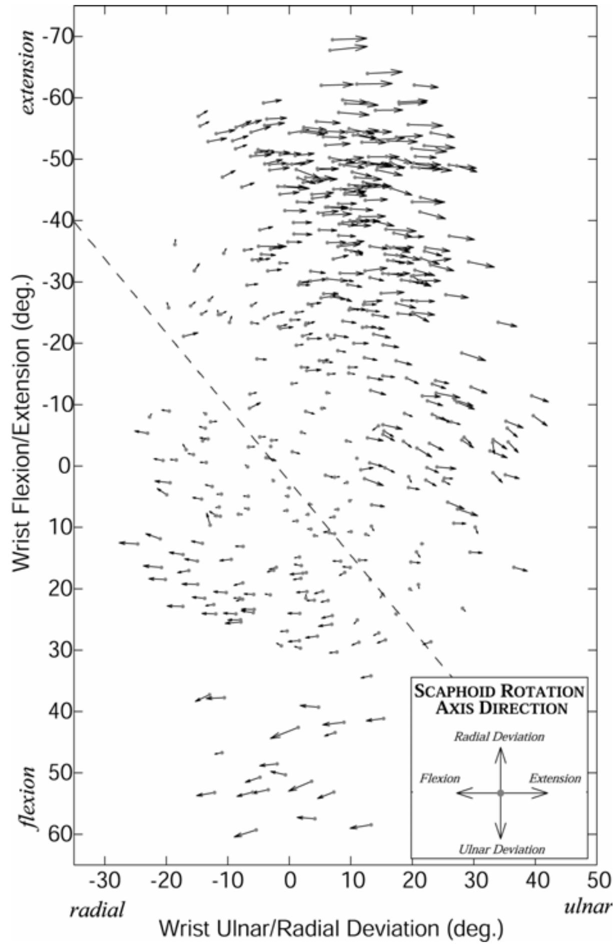

Figure 1: The scaphoid rotation axes (see legend) were almost exclusively in the flexion-extension direction for all wrist positions. The dart thrower's path of motion (dashed line) differentiated wrist positions at which the scaphoid flexed from those at which it extended. Scaphoid rotation values near this path approached zero (the length of each vector is a measure of the magnitude of scaphoid rotation).

REFERENCES

1. Crisco et al. *J Ortho. Res.*, **17(1)**:96-100, 1999.
2. Ishikawa J, et al. *J Hand Surg [Am],* **24(1)**:113-20, 1999.
3. Kobayashi et al. *J Biomechanics*, **30(8)**:787-93, 1997.
4. Werner et al. *J. Hand Surg. [Am],* **29(3)**:418-22, 2004.

ACKNOWLEDGEMENTS: Funded by NIH AR044005

DO MECHANICAL PROPERTIES OF CHEST PROTECTORS CORRELATE WITH THE INCIDENCE OF VENTRICULAR FIBRILLATION IN A SUDDEN DEATH (COMMOTIO CORDIS) SWINE MODEL?

[1] Elizabeth Drewniak, [1]David B. Spenciner and [1]Joseph J. Crisco
[1]Department of Orthopaedics, Brown Medical School/Rhode Island Hospital
email: joseph_crisco@brown.edu, web: brownbiomechanics.org

INTRODUCTION

For young healthy athletes, Commotio cordis is the second leading cause of death is commotio cordis. Commotio cordis (CC) is the sudden death (or aborted sudden death) due to a non-penetrating chest wall impact that, in the absence of injury to the ribs, sternum and heart, occurs in a vulnerable window on the T-wave of the cardiac cycle (10 to 30 ms prior to the T-peak) and results in ventricle fibrillation (VF). The fatal impact mostly occurs to the left chest wall in the region of the cardiac silhouette by a projectile (ball or puck) traveling at speeds consistent with youth play. Despite increases in the use of protective gear, to date, 7 young athletes (3 lacrosse goalies, 2 baseball catchers, and 2 hockey goalies), all wearing chest protectors, have died from commotio cordis [1].

We hypothesized that the efficacy of chest protectors could be predicted from quasi-static compression testing. The purpose of this study was to determine if a correlation existed between the incidence of VF [2] and three quasi-static mechanical properties, displacement, stiffness, and pressure distribution, for various baseball and lacrosse chest protectors.

METHODS

Quasi-static compression testing was performed on eleven models of lacrosse and baseball chest protectors evaluated in a previous animal model of CC [2]. Each model was placed on a rigid plate and a compressive load was applied by a rigid spherical object positioned on each chest protector using a servo hydraulic material tester (Instron Corp., Canton, MA). The spherical object was a hardwood ball with a diameter of 6.35 cm and 7.62 cm for the lacrosse and baseball chest protectors, respectively. A preload of 10 N was applied and then cycled up to 6000 N five times at 1 Hz. Load and actuator position data were collected at 100 Hz.

During the quasi-static compression testing, displacement, stiffness, and pressure distribution were measured. Displacement was defined as the difference from the minimally and maximally compressed positions of each model. Stiffness was calculated from load-displacement measurements, first for the region of low stiffness between 0 and 400 N and second for the region of high stiffness between 2400 and 5000 N. A pressure sensitive film (Ultra Super Low Fuji Film, Fuji Photo, Co., Ltd., Tokyo, Japan) was used to measure the distribution of applied pressure.

Linear regression (SigmaStat3.1, Systat, Point Richmond, CA) was used to examine correlations between these mechanical properties and the incidence of VF, which was determined for the same chest protector models in a previous animal model [2]. We computed the R^2 and P values for the regression equation. A significance value of $P < 0.05$ was set *a priori*.

RESULTS AND DISCUSSION

The displacement of each model ranged from 7.09 to 21.03 mm. There was a trend of increasing displacement with decreasing incidence of VF, but no significant linear correlation was found ($R^2 = 0.14$, $P = 0.06$).

The compression testing revealed a highly nonlinear load-displacement behavior in all chest protector models. There was an initial range of very low stiffness (10.88 to 48.24 N/mm), then a transition region, followed by a region of high stiffness (2425.42 to 7335.44 N/mm) that was assumed to be associated with the bottoming out of the chest protector. Neither the low stiffness region ($R^2 = 0.1$, $P = 0.12$) nor the high stiffness region ($R^2 = 0.05$, $P = 0.25$) demonstrated a linear correlation with the occurrence of VF.

The area of the pressure distribution ranged in shape from circular to rectangular. Grouping all models together, we found that there was a significant ($P = 0.01$) decrease in the incidence of VF as the area of the pressure distribution increased.

This study was performed to determine if quasi-static compression testing could explain the variance in the incidence of VF. While none of the models significantly increased or decreased the risk of VF in the previous study [2], we did find that the incidence of VF significantly decreased as the pressure distribution increased. While this finding seems logical and intuitive, it is still surprising considering the complexity and the dynamic nature of CC.

CONCLUSIONS

The goal of this experiment was to develop an experimental protocol that could be incorporated into performance standard test protocols for chest protectors to ensure that all models meet a minimal standard performance requirement. Surprisingly, we found that increases in quasi-static pressure distribution were associated with a significant decrease in the incidence of VF. It remains to be demonstrated that chest protectors constructed using these findings as design criteria can significantly reduce the incidence of VF.

REFERENCES

1. Maron BJ, et al.. *JAMA* **287** (9), 1142-1146, 2002.
2. Weinstock et al.. *Heart Rhythm* **1**, 692, 2004.

ACKNOWLEDGEMENTS

Funded in part by The RIH Orthopaedic Foundation

BIOMECHANIC ANALYSIS OF THE FORCE APPLIED IN AQUATIC GAIT OF HUMANS IMMERSED AT THE STERNUM LEVEL

SOUZA, Patricia Vieira de[1], HAUPENTHAL, Alessandro[1], SCHUTZ, Gustavo Ricardo[1], & ROESLER, Helio[1].
1- Santa Catarina State University – UDESC – Brazil – email: patricia@posturall.com.br

INTRODUCTION

The human gait is one of the most studied movements in terrestrial environment [1,2,3], but this fact does not occur in the aquatic environment [4]. Despite of the aquatic environment be a lot utilized for training and rehabilitation, there are few works about the aquatic gait.

This study analyzed the Ground Reaction Force (GRF) vertical component during the aquatic gait. For so much, the objectives of this work were: 1) Verify the maximum value of the GRF vertical component; 2) Compare the GRF inside and outside the water.

METHODS

This diagnostic descriptive study was carried through in the Laboratory of Aquatic Biomechanics Research of UDESC. One invited to participate of this study individuals that possessed stature from 1,60 to 1,85m and no gait disorders. With these criteria, 63 subjects (31 female and 32 male) carried out the experiment. The average ages were 23±5 years old. The average height was 1,70±0,15 m. The water depth was 1,30m. Although that depth of immersion corresponds to a level for each subject, they all had the water reaching their sternum.

In the bottom of a thermal swimming pool (30±1oC) one had put a footbridge of 6,15 m of length containing two underwater force platforms [5] (A and B). One acquired the GRF in the vertical components (Fy) in a rate of sample of 600hz. One has used the acquisition system SAD 32 version 3.0 [6].

Each subject carried out four passages in the footbridge at the maximum speed they could obtain. The average speed was 0,55± 0,05 m/s.

To analyse the reduction in the GRF vertical component in the aquatic gait, their values have been compared to the land gait values. The value used to calculate the force reduction was 1,2N/BW [1,2,3]. For data analysis one utilized descriptive statistics through the program Microsoft Excel.

RESULTS AND DISCUSSION

In the vertical component the forces had varied 59% of the subjects' corporal weights., as one can see in Table 1 .

Table 1: Maximum Force in Fy e Fx (N/BW) and reduction compared to land gait values (%).

	FyA	FyB
(N/BW)	**0,59**±0,09	**0,58**±0,08
(%)	**51±8**	**52±7**

For a better understanding of the alteration that occurs in the underwater gait, a force×time curve for GRF vertical component at the sternum level is compared to a GRF curve outside the water. One can visualize that occurs a curve rectification, the peaks are next to deflection and the load absorption happens in a larger time until the first force peak (Figure 1). The "M" look curve common in the outside water gait [2.3] is not characterized inside the water and the curve morphology is similar to a trapezium.

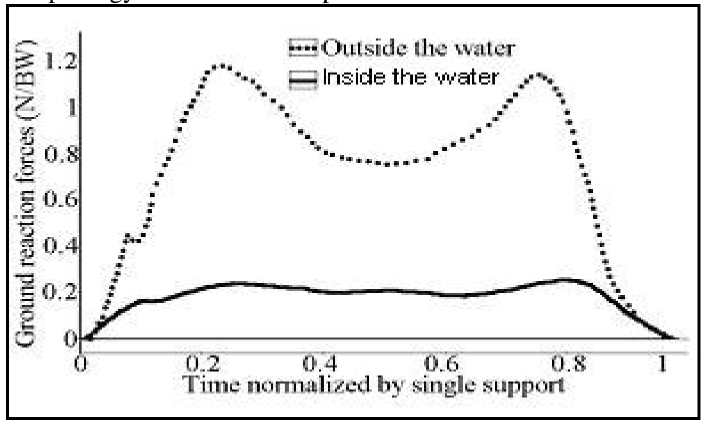

Figure 1: Comparing the force×time curves for GRF vertical component outside the water and aquatic gait.

The found values in this study for maximum force in the GRF vertical component are inferior to the ones previously reported by Harrison et al [7]. The BW reduction values are similar to the ones found by Brito [8], in wich study the immersion level was at the hip and the speed was smaller.

CONCLUSIONS

One can conclude that at the sternum immersion level the GRF vertical component can be altered in significant values. The curve shape is similar to a trapezium, differently from the land curve.

This work values point out that submmiting the individual to an exercise inside the water at this immersion level can bring benefits when it comes to reducing the resultant load. Knowing these values and their relations to other immersion levels is crucial to activities prescription in aquatic environment.

REFERENCES

1. Perry J. *Gait analysis: normal and pathological function*. New York: MacGraw-Hill; 1992.
2. Nigg BM Herzog W *Biomechanics of the musculo-skeletal system*. Chichester: John Wiley & Sons; 1994.
3. Winter DA *The biomechanics and motor control of human gait: normal, elderly and pathological.* Second edition. Canada: Waterloo Cover; 1991.
4. Becker BE, Cole, AJ *Terapia Aquática Moderna*. São Paulo: Manole; 2000.
5. Roesler H. *Tese de Doutorado* - Programa de pós-graduação em Engenharia Mecânica, UFRGS, Porto Alegre; 1997.
6. Silva LM, Zaro MA. *"SAD 2 VERSÃO (3.0) - Sistema de Aquisição de dados – Manual de Operação"*. Caderno Técnico da Engenharia Mecânica CT 07 – DEMEC, Porto Alegre, 1997.
7. Harrison R. Et Al. *Physiotherapy*. .**78**, 164-166, 1992.
8. Brito RN, et al. *Revista Brasileira de Fisioterapia* **8**, 7-12, 2004.

DYNAMOMETRIC ANALYSIS OF THE ANTEROPOSTERIOR FORCE APPLIED IN AQUATIC HUMAN GAIT

SCHUTZ, Gustavo Ricardo[1], SOUZA, Patricia Vieira de[1], HAUPENTHAL, Alessandro[1], & ROESLER, Helio[1].
1- Santa Catarina State University – UDESC – Brazil – e-mail: patricia@posturall.com.br

INTRODUCTION

Walking in water is a major rehabilitation therapy for patients with orthopedic disorders. However, data about kinetic variables while walking in water is still unclear [1]. It is important to the professionals who work with rehabilitation to know informations as the gound reaction force components during gait in water. Acccording to Brito et al[2], few works exist about the subject, and also there aren´t knew studies about the behavior of the anteroposterior component during walking in water. This work had the objective to analyze the anteroposterior component of the ground reaction force (GRF) during the aquatic gait and the influence of the speed and the upper limb position on the GRF anteroposterior component values.

METHODS

This study took place at the swimming pool and Aquatic Biomechanics Research Laboratory of Santa Catarina State University.

The sample was composed by 60 individuals that possessed stature from 1,6 to 1,85m and no gait disorders. The water depth was 1,30m. One opted for dividing the sample in three groups, according to their levels of immersion: (1) manubrium sterni, (2) medial point between the manubrium sterni and xiphoid process sterni distance (3) Xiphoid process sterni.

Two underwater force platforms [3] were set on the bottom of a thermal swimming pool (30±1oC), in a footbridge of 6,15 m of length. One acquired the GRF in the anteroposterior component in a rate of sample of 600hz. One has also used the acquisition system SAD 32 version 3.0 [4]. The subjects were supposed to walk along the footbridge in two speeds (Slow and Quick) and two different upper limb positions (Inside and Outside the water). The four situations imposed for the three groups in this study are described on Table 1.

Table 1: Aquatic Gait Situations

	Gait Situation	Speed
ISG	Slow gait with the upper member inside the water beside the body slow gait with the upper member inside the water beside the body - named inside slow gait	0,42 m/s
OSG	Slow gait with the upper member outside the water - outside slow gait	0,42 m/s
IQG	Gait with the upper member inside the water the fastest speed the subject obtained - inside quick gait	0,55 m/s
OQG	Gait outside the water the fastest speed the subject obtained - outside quick gait	0,66 m/s

RESULTS AND DISCUSSION

The GRF anteroposterior maximum force reduction for aquatic gait compared to the reference values for land gait [5](Table 2).

Table 2: Maximum force reduction of the GRF anteroposterior component for aquatic gait compared to the reference values for land gait (%).

	Group 1	Group 2	Group 3
ISG	55	55	55
OSG	50	50	50
IQG	45	35	15
OQG	30	20	5

Comparing each group separately in different speed situations (slow and quick), one can realize that the values raise as the speed raises, with statistic significance for all the three groups. Comparing the upper limb inside and outside the water gait situation, the values do not raise significantly.

In the slow situations the values had been cut off to half the values outside the water. Indeed, in the quick situations, there wasn't such a significant reduction, specially when it comes to group 3 OQG, where the values are very close to land gait values, despite of a slower speed in the water. The alteration of immersion level does not increase the maximum force in this component.

The Fx curve has a negative peak in land gait, related to the movement breakdown, and a positive peak, due to acceleration [5]. For the positive peak, one can observe that the maximum force increases significantly with the aquatic gait speed upgrade.

CONCLUSIONS

This work values point out that an increase in the gait speed results an increase in the anteroposterior component. This is very important for underwater exercise prescription. For instance, if the treatment goal is to train gait of a subject not so functionally injured, the aquatic gait that most approximates to land gait is in the xiphoid process immersion level, upper limb outside the water and the fastest speed the subject can carry out. An alteration in the curve pattern also can be confirmed: it looks like a triangle.

REFERENCES

1.Miyoshi, et al. *Clinical Biomechanics* **20,** 194-201, 2005.
2 Brito RN, et al. *Revista Brasileira de Fisioterapia* **8**, 7-12, 2004.
3 Roesler H *Tese de Doutorado* - Programa de pós-graduação em Engenharia Mecânica, UFRGS, Porto Alegre; 1997.
4 Silva LM, Zaro MA. *"SAD 2 VERSÃO (3.0) - Sistema de Aquisição de dados – Manual de Operação"*. Caderno Técnico da Engenharia Mecânica CT 07 – DEMEC, Porto Alegre, 1997.
5. Winter DA *The biomechanics and motor control of human gait: normal, elderly and pathological.* Second edition. Canada: Waterloo Cover; 1991.

Validation of a dosimeter for the three-dimensional measurement of trunk motion

[1] A. Plamondon, [1]A.. Delisle, [1]C. Larue, [2]P. Desjardins, [1]D. McFadden, [1]D. Brouillette and [1]C. Larivière
[1]Institut de recherche Robert-Sauvé en Santé et en Sécurité du Travail (IRSST), Montréal, Canada
[2]Centre de recherche interdisciplinaire en réadaptation du Montréal métropolitain
email: plamondon.andre@irsst.qc.ca ; web: http://www.irsst.qc.ca/

INTRODUCTION

Back injuries still affect many workers. There is evidence that bending and twisting of the trunk and lifting at work are risk factors for back pain. Various methods are available for assessing bending and twisting of the trunk within a job. Recently, new types of instrumentation have been developed which combine different sensors. Backmann (2000) developed such a system consisting of a gyroscope, a magnetometer and a linear accelerometer. The data of each sensors are processed into a filter and produces orientation estimates. However, their system has not been validated exhaustively with human subjects. The purpose of this study was to evaluate a dosimeter composed of two sensors each including accelerometers, magnetometers and gyroscopes for the three-dimensional (3D) measurement of trunk motion.

METHODS

The instrument (dosimeter) consisted of two three-dimensional inertial tracking sensors (Micro Strain 3DM-G. Burlington) linked by a flexible rod with a potentiometer (figure 1). The two sensors were used to measure the orientation of the thorax relative to the pelvis. Each sensor comprised of three orthogonal gyroscopes which measured the angular rate of rotation, three orthogonal accelerometers which sensed the gravitational acceleration and three orthogonal magnetometers which are sensitive to earth magnetic field. The signals from the two sensors were transmitted to a computer (Casiopeia Five 230 MZ; Casio). The sample frequency was set to 76 Hz.

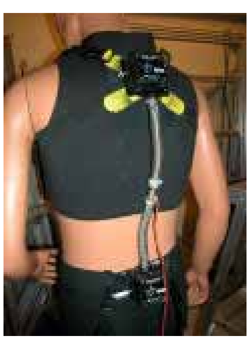

Figure 1. Illustration of the dosimeter

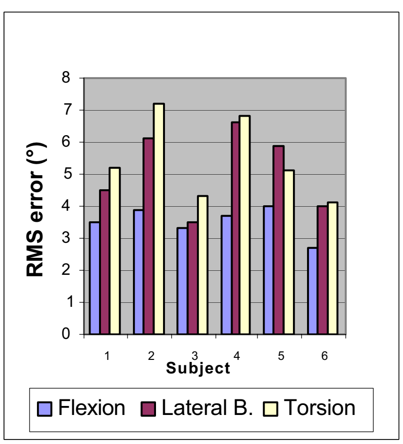

Figure 2. RMS errors during the long trial (30 min)

The data from the gyroscope were adjusted with the accelerometer and magnetometer estimates using a complementary filter [1]. The data of each sensors were processed into the filter which produced orientation estimates in quaternion form. These outputs were transformed into direction cosines where the three orthopaedic angles of Grood & Suntay [2] were computed: flexion-extension (angle α), lateral bending (angle β) and torsion (angle γ).

To validate the dosimeter, six male subjects were asked to perform manual handling tasks with empty boxes. They had to adopt different static postures (20) as well as to perform slow, moderate and fast lifts over a short period of time (30 sec) and, finally, to transfer boxes during 30 minutes. The task forced the subjects to exert large amplitude back motions. The dosimeter was tested by comparing the orientation as calculated by the complementary filter to the orientation that was obtained from a 3D optoelectronic system (Optotrak 3020 with four bars, Northern Digital Inc). The sensor orientation was obtained from six active markers attached securely to each sensor box. The root mean square difference (RMS) between the dosimeter and the Optotrak system was calculated for the three orthopaedic angles (α, β, γ)

RESULTS

Figure 2 illustrates the RMS errors for the three orthopaedic angles between the thorax and the pelvis during the long dynamic trials (30 minutes). RMS errors varied between 3 and 7° and were generally higher for the torsion angle (γ). Coefficient of multiple correlation was found to be higher than 0.90 for most of the long trials. Static and short dynamic trials resulted in smaller errors than the long trials, with the torsion angles having the highest level of errors (5°). Maximal errors were generally below 16° for the short trials. Speed of movement had a significant effect on the level of error but only in the order of 1 to 2°.

DISCUSSION AND CONCLUSION

Errors about the torsion angle (γ) can be explained by small disturbances from local magnetic field which affect the magnetic sensor. Gyroscopes also drift over time and the accelerometers used as inclinometer are influenced by quick motions. The filter worked well to overcome these sources of error, particularly during the long duration task. The results of this study indicates that the dosimeter is a valid system for the three-dimensional measurement of trunk motion. Future work should focus on obtaining more accurate data from long duration tasks .

REFERENCES

1. Backmann (2000). Inertial and magnetic tracking of limb http://movesinstitute.org/bachmann/dissertation.pdf
2. Grood ES, et al. *J. Biomec. Eng* **105**, 136-144, 1983.

ACKOWLEGEMENT

Study supported by a grant from IRSST, Montréal, Canada

NEUROMODULATION CHANGES THE BIOMECHANICS AND CAPABILITIES OF THE *APLYSIA* FEEDING MUSCLE I2

[1] Gregory Sutton, [2]Bryan Higashikubo and [2,3,4] Hillel Chiel
Case Western Reserve University, Departements of [1]Mechanical Engineering,
[2]Biology, [3]Biomedical Engineering, and [3]Neurosciences

INTRODUCTION

Neuromodulation is often used by the nervous system to change a muscle's response to nervous system stimulation. Invertebrate preparations are well suited for study of neuromodulation because of their experimentally tractable nervous systems and biomechanics. The *Aplysia* smooth muscle I2 is a good model for neuromodulation because it is a muscle with known behavioral correlates [1], and it responds to serotonergic neuromodulation [2]. During two feeding behaviors, biting and swallowing, I2 moves the grasping structure toward the jaws [1]. During swallowing behaviors, the I2 muscle is sufficiently strong to move the grasper throughout the grasper's full range of motion, but, during biting, an unmodulated I2 is insufficiently strong to generate the full motion of the grasper [3]. We used *in vitro* studies of I2's response to serotonin to show that serotonergic neuromodulation can sufficiently strengthen I2 to allow the I2 to generate biting behaviors.

METHODS

Aplysia californica were anesthetized by injection of 60% body mass of 333 mM $MgCl_2$ and the feeding apparatus (the buccal mass) was removed. The I2 was dissected out of the buccal mass, and the I2 nerve was suctioned and attached to a stimulus isolation unit (WPI A360). I2's length was controlled by a serovomotor system (Aurora Scientific, 300B-LR).

In order to characterize how I2's mechanical properties would change in response to serotonergic neuromodulation, we measured the descending limb of I2's length-tension curve in response to increasing concentrations of serotonin. I2's maximum contractile force and rate of contraction were both recorded.

The changes in I2's contractile properties were then programmed into a kinetic model of the feeding apparatus [3] to predict whether these changes in biomechanics were sufficient to allow the I2 to produce biting behaviors.

RESULTS AND DISCUSSION

In response to serotonin application, I2's maximal contractile force increased as a function of serotonin concentration and length (3 concentrations are shown in **Figure 1**). At longer lengths, both lower and higher concentrations of serotonin caused a near doubling of I2's maximum contractile strength. In contrast, at shorter lengths, lower concentrations of serotonin had little effect, while higher concentrations of serotonin caused a tripling of I2's maximum contractile force. Serotonin did not cause a significant change in the speed of I2 activation (data not shown).

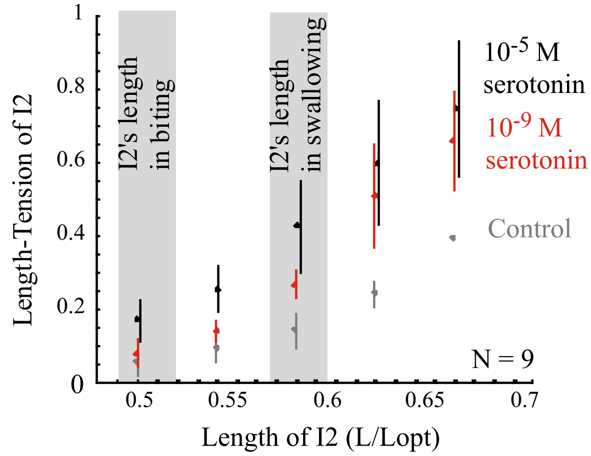

Figure 1: I2's length-tension curve in response to different concentrations of serotonin

It has been previously shown that tripling of I2's maximal contractile force is sufficient to allow I2 to generate biting behaviors [3]. To achieve this increase of I2's contractile force, however, the serotonin concentration had to be quite high (10^{-5} M). In a different *Aplysia* feeding muscle (I5), stimulation of a serotonergic neuron (the metacerebral cell) has been observed to cause the same change in muscle contraction as application 10^{-9} M serotonin [4], suggesting that, while serotonergic neuromodulation can strengthen I2 sufficiently to allow I2 to generate biting behaviors, the amount of serotonin needed to do so is greater than the concentration that is biologically observed.

When this change in contractile strength is programmed into the kinetic model of the feeding apparatus, the model predicts that 10^{-5} M serotonin would be required to strengthen the I2 sufficiently to generate biting behaviors.

CONCLUSIONS

Serotonergic neuromodulation is sufficient to strengthen the I2 enough to allow I2 to generate biting behaviors. This does, however, require the nervous system to apply a very large amount of serotonin to the muscle. Serotonergic strengthening of a muscle represents a concrete example of a neuromodulating neuron (the metacerebral cell) acting to change the biomechanics of a muscle (I2). It is probable that another mechanism assists I2 with moving the grasper. These data are consistent with a complimentary hypothesis that another muscle (I1/I3) assists I2 with moving the grasper [3].

REFERENCES

1. Hurwitz I, et al. *J. Neurophysiology* **75**(4):1309-1326, 1996.
2. Hurwitz I, et al. *J Neurophysiology* **84**(6):2810-2820, 2000.
3. Sutton GP, et al. *Biol. Cybernetics* **91**(5): 333-345, 2004.
4. Weiss KR, et al. *Brain Research* **99**, 381-386, 1975.

NEUROMUSCULAR GENDER DIFFERENCES EXIST DURING UNANTICIPATED RUNNING AND CUTTING MANEUVERS WITHIN AN ELITE ADOLESCENT SOCCER POPULATION

[1] Scott Landry, [1]Kelly McKean, [2]Cheryl Hubley-Kozey, [1]Kevin Deluzio and [3]William Stanish
[1]School of Biomedical Engineering, Dalhousie University,
[2]School of Physiotherapy, Dalhousie University, [3]Department of Surgery (Orthopaedics), Dalhousie University
email: landrys@dal.ca

INTRODUCTION

The anterior cruciate ligament (ACL) is an extremely important ligament for knee joint stability and proper function, particularly during sporting activities that involve running, jumping and cutting. Injury to the ACL can be detrimental to an athlete's career, with approximately 70-80% of these injuries being non-contact in nature [1,2] and females being 2-8 times more likely of sustaining an ACL injury than males [3]. The non-contact mechanism of this injury most often involves landing from a jump or cutting to change directions during activities such as basketball or soccer. The purpose of this study was to identify gender related neuromuscular differences of the lower limb in unanticipated running and cutting maneuvers within an elite soccer population.

METHODS

20 elite male and 20 elite female adolescent soccer players underwent a complete 3D kinematic, kinetic and electromyographic (EMG) analysis of the lower limb, with only the EMG findings being discussed in this abstract. Subjects were required to run at 3.5+/-0.2 m/s down the laboratory runway and just prior to the right foot landing on the force plate, a light system randomly cued the individuals to either 1) cut to the left (side-cut), 2) continue running straight or 3) cut to the right (cross-cut). For the stance portion of the maneuver, muscle activation patterns of the rectus femoris, vastus medialis and lateralis, lateral and medial hamstring and medial and lateral gastrocnemius were normalized to maximum voluntary isometric contractions (MVIC). All cuts were made at 35°-60° from the direction of travel and all waveforms were analyzed for gender differences using principal component analysis (PCA) [4].

RESULTS AND DISCUSSION

While all subjects were free from injury at the time of testing, many reported minor lower limb injuries previously in their soccer careers (Male=62%, Female=86%). The most common injuries included ankle sprains and muscle strains of the hip flexors, quadriceps, adductors and hamstrings. Descriptives comparing the male and female subject groups indicated that the only group differences were that males were taller and heavier than the females (Table 1).

Table 1: Descriptives for male and female subject groups. * indicates stat. sign. ($p<0.05$). Values are mean (STD).

	Males	Females
Age (yrs)	17.2 (0.8)	16.9 (1.0)
Weight (kg) *	69.6 (6.6)	60.8 (5.5)
Height (m) *	1.8 (0.1)	1.6 (0.1)
BMI (kg/m^2)	22.1 (1.7)	22.4 (1.8)
Soccer (yrs)	10.7 (1.7)	9.8 (2.1)

Using PCA to compare the EMG waveforms between males and females, it was determined that females had on average higher lateral gatrocnemius activation magnitudes than their male counterparts during the side-cut, cross-cut and straight run ($p<0.05$) throughout stance. The overall activation magnitude of the rectus femoris in females was also larger than males during the both the cross-cut (Figure 1B) and straight run ($p<0.01$). For the lateral hamstring, however, females generated a smaller overall activation magnitude than the male soccer players (Figure 1A) ($p<0.01$) and this difference was only evident for the cross-cut maneuver.

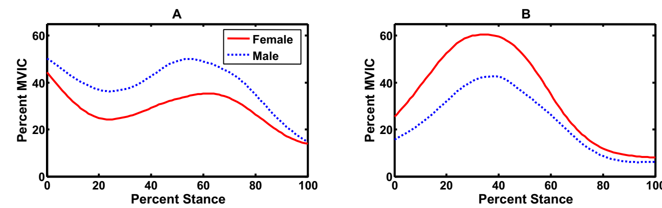

Figure 1: (A) Lateral hamstring and **(B)** rectus femoris activation patterns for males and females during the stance phase of the cross-cut, normalized to % MVIC and % stance.

Comparing only peak stance activation levels between gender, females had an approximate 30% larger activation level for their lateral gastrocnemius for the run and two cutting maneuvers. For the cross-cut only, females had a 40% smaller lateral hamstring peak activation level and an approximate 40% larger peak activation compared to males.

These results confirm that athletic females tend to be more quadriceps dominant and do not use their hamstrings to the same degree as males [5] during cutting and running tasks. Having the higher rectus femoris and lateral gastroc-nemius activity may also potentially expose females to earlier fatigue onset and may thereby result in reduced knee joint stabilization. Proper muscle function is crucial in preventing knee injuries while landing from a jump and/or cutting to change direction during activities like soccer and basketball.

CONCLUSIONS

Neuromuscular differences between genders were most evident in the unanticipated cross-cut maneuver. The higher rectus femoris and lower lateral hamstring activity in females, in combination with specific knee joint loading patterns, appears to play a significant role in predisposing females to higher non-contact ACL injury rates.

REFERENCES

1. Noyes F, et al. *J Bone Joint Surg* **65A**, 154-162, 1983.
2. Boden B, et al. *Orthopaedics* **23**, 573-578, 2000.
3. Arendt E & Dick R. *Am J Sports Med* **23(6)**, 694-701, 1995.
4. Deluzio K, et al. *J Hum Mov Sci* **6**, 201-217, 1997.
5. Huston L & Wojtys E. *Am J Sports Med* **24**, 427-436, 1996.

ACKNOWLEDGEMENTS

Nike Global Research Grant

OBSTACLE COURSE PERFORMANCE: COMPARISON OF THE C-LEG TO TWO CONVENTIONAL KNEES

[1] Margrit-R. Meier, [1]Andrew H. Hansen [1,2]Steven A. Gard, and [1,2]Dudley S. Childress
[1]Northwestern University Prosthetics Research Laboratory and Rehabilitation Engineering Research Program,
[2]Jesse Brown VA Medical Center, Chicago, Illinois; email: m-meier@northwestern.edu

INTRODUCTION

Previous investigations of some microprocessor-controlled (MC) knee joints have produced conflicting results, indicating clear benefits for amputees while others suggested there were no differences compared to conventional knee mechanisms [1-4]. Further quantitative analyses are needed to determine if it is beneficial to prescribe expensive MC knee mechanisms over passive knee units that cost significantly less.

The specific objectives of this study were to: (1) examine participants' walking performances while walking over an obstacle course (OC), and (2) test the influence of mental loading (ML) while walking over the OC using three different knee units.

METHODS

General: In a crossover study design, participants wore each prosthetic knee joint—Otto Bock C-leg, Otto Bock 3R60 and Mauch SNS—for a period of four weeks. Test prostheses were fabricated using a duplication of the participant's current prosthetic socket and each participant was fitted with a Dynamic Plus foot to reduce variability. *Participants:* Persons with unilateral transfemoral amputation, aged between 40 and 60 years, with a body-weight less than 125 kg, were included if they: presented with no serious complications that interfered with their walking ability; had six or more months of experience with a definitive prosthesis; and were able to walk unassisted at a comfortable speed without undue fatigue and without health risk. *Protocol:* The OC was set up in the VA Chicago Motion Analysis Research Laboratory. It consisted of a foam section (3m long, 1m wide (3x1), 20 durometer on a shore A scale), narrow slaloms around three chairs, a vacuumized bean-bag section (3x1) simulating sand, a rock section (3x1), a short downward sloping ramp (1.5x1.4), a 90-degree left turn, and a final stair step (height: 12cm). The ML test consisted of an arithmetic calculation task where the participant had to count aloud backwards in 3-step increments (1st visit), in 7-step increments (2nd visit) and in 3-step increments (3rd visit). Participants completed the OC twice, once without and once with ML. No familiarization run was allowed. Time was measured from a videotape recording of participants navigating the OC. *Statistical Analysis:* Friedman Test assessed the overall performance of the three knee joints. If a variable reached significance level, Wilcoxon Signed Rank Test was used to determine differences between each knee joint. A Bonferroni correction was applied to account for multiple testing, lowering the significance level to 0.016.

RESULTS

Data from 2 women and 9 men were analyzed. Their mean age was 45.8 ±9.5 years, mean height was 175 ± 9 cm, and mean weight was 81.8 ± 14.1 kg. They were all established walkers with their amputation having occurred 20.1 ± 14.2 years ago. The median time taken to complete the OS with the 3R60 knee was 34.9 seconds (s). Adding the ML altered the time minimally: 34.2s. For the C-leg, the total time without ML (32.1s) was slightly lower when compared to the 3R60 knee but increased with ML to 33.9s. The difference between the 3R60 and the C-leg was non-significant for both conditions (without ML: p=0.169; with ML: p=0.045). Participants performed best on the OC when fitted with the SNS unit: total median time without ML was 30.9s, with ML 32s. The difference between the SNS and the 3R60 was significant for both conditions. However, the difference between the C-leg and the SNS knee joint was not significant (without ML: p=0.674; with ML p=0.678) (Figure 1).

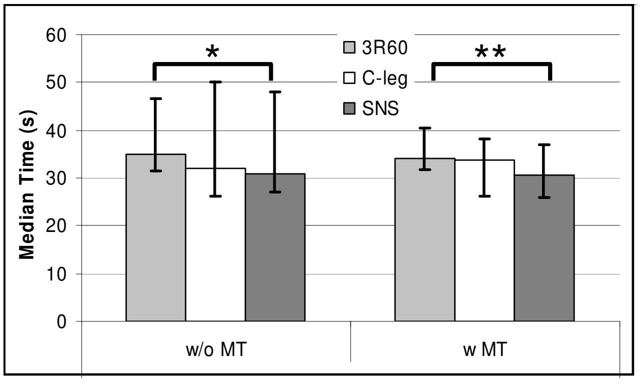

Figure 1: Total time taken (in sec) to complete the obstacle course for each prosthetic knee joint. w/o MT: without Mental Task * SNS-3R60: p=0.011 w MT: with Mental Task ** SNS-3R60: p=0.005

DISCUSSION AND CONCLUSIONS

The participants completed the OC in the shortest time when fitted with the SNS unit, followed by the C-leg, and they were slowest with the 3R60 knee regardless if ML was administered or not. The more mechanically complex (3R60) and the more sophisticated (C-leg) knee joints performed less favorably in this context. These two knees may require more time and training to take full advantage of their characteristics than the given 4-week accommodation period. However, it could also mean that for soft or uneven walking surfaces, a simpler knee (like a SNS unit) simply performs better, as participants may have a quicker and direct impact on its behavior.

REFERENCES

1. Smith DG, et al. *Proceedings of 11th ISPO*, Hong Kong, Abstract FP 3C3.2, 2004.
2. Stinus H. *Z Orthop Ihre Grenzgeb* **138**, 278-282, 2000.
3. Buckley JG et al. *Arch Phys Med Rehabil* **78**, 330-333, 1997
4. Datta et al. *Prosthet Orthot Int* **22**, 129-135 ; 1998

ACKNOWLEDGEMENTS

This work was supported by the Department of Veterans Affairs, Rehabilitation Research and Development Service, and is administered through the Jesse Brown VA Medical Center, Chicago, IL.

CROSS-MODAL EFFECT OF DAMAGE ON CORTICAL BONE STRENGTH

[1] Won Joo, [1]Dwigth T. Davy
[1]Case Western Reserve University, email: dtd@cwru.edu

INTRODUCTION

Bone is a complex biological material which continually undergoes damage accumulation and repair in-vivo [1]. The effects of damage are often studied in terms of the mechanical property degradation in the loading mode (e.g. tension, torsion, etc.) in which damage was accumulated [2]. However, in-vivo loading is more complex, and it is important to understand how damage accumulated in one loading mode affects mechanical properties in other loading mode. Our previous studies demonstrated complex cross-modal effects of damage on viscoelastic properties [3]. The purpose of this study was to determine how monotonic strength in each of three loading modes (tension, compression or torsion) is affected by damage mode and magnitude.

METHODS

Cortical bone samples were machined from the mid-diaphyses of 18 human femurs (7 females and 11 males, 38-55 years old age). The final machined samples had a reduced diameter section (4 mm diameter x 18mm long) with the axis along the nominal bone axis. During all machining and testing, specimens were kept wet and testing was performed at 37°C. Samples were randomly assigned to experimental and control groups. For control groups, 10 undamaged specimens were tested under strain control in each loading mode (Tension (T), Compression (C), Rotation (R)). Loading rates of ±1 %/s or 8 degree/s were used. The results from control group were used as undamaged measures and the yield strain of each loading mode used to prescribe the damage cycle magnitudes shown in Figure 1.

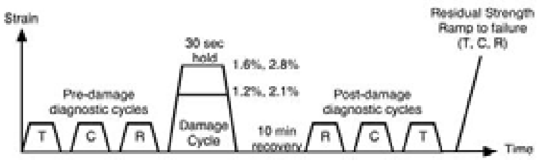

Figure 1. The protocol for strength degradation test.

Before and after the damage cycle, diagnostic cycles in three modes were performed to measure the change of viscoelastic properties by damage (Data shown in [3]). Damage was induced in one of three loading modes (T, C, or R) during damage cycle with two different magnitudes for each mode, which for tension were 1.2% and 1.6% (150% and 200% tension yield), compression were 1.2% and 1.6% (120% and 160% compression yield) and torsion were 2.1% and 2.8% (150% and 200% rotation yield). Following the damage cycle, 10 minutes recovery time was allowed at zero-stress (zero-torque) hold condition. After the recovery period, each specimen was monotonically loaded to failure in one of the three modes. Six specimens were tested for each test group. For the torsional tests, the following equation [4] was used to calculate shear stress.

$$\gamma = \theta \frac{a}{l}, \qquad \tau = \frac{1}{2\pi r^3}\left[\theta \frac{dT}{d\theta} + 3T\right]$$

Changes in properties due to damage were compared using 1-way ANOVA (with Tukey's pairwise comparisons) and paired t-tests ($p<0.05$).

Table 1: Measured parameters from monotonic failure test after damage. All values are normalized to mean values of control group (mean±SD).

Damage mode	failure mode	Damage strain	Yield strain, ε_y	Yield stress, σ_y	Failure stress, σ_f
Tension damage	T	1.2%	0.82±0.03	0.62±0.05	0.91±0.05
		1.6%	0.78±0.03	0.60±0.05	0.80±0.08
	C	1.2%	0.85±0.04	0.66±0.04	0.92±0.05
		1.6%	0.79±0.04	0.62±0.05	0.77±0.05
	R	1.2%	0.97±0.03	0.93±0.06	1.03±0.08
		1.6%	0.90±0.04	0.80±0.03	0.84±0.11
Compression damage	T	-1.2%	0.95±0.02	0.79±0.05	0.81±0.09
		-1.6%	0.69±0.06	0.45±0.07	0.79±0.10
	C	-1.2%	0.87±0.06	0.68±0.07	0.88±0.05
		-1.6%	0.65±0.03	0.44±0.04	0.68±0.14
	R	-1.2%	0.97±0.06	0.89±0.13	0.97±0.14
		-1.6%	0.94±0.05	0.92±0.10	0.98±0.09
Rotation damage	T	2.1%	0.99±0.01	0.87±0.01	0.93±0.07
		2.8%	0.96±0.06	0.82±0.07	0.83±0.04
	C	2.1%	1.05±0.06	0.90±0.03	0.94±0.04
		2.8%	1.00±0.07	0.89±0.07	0.97±0.13
	R	2.1%	0.88±0.03	0.79±0.04	0.97±0.06
		2.8%	0.80±0.04	0.65±0.06	0.87±0.08

RESULTS AND DISCUSSION

There were significant and mode dependent inter-modal damage effects on monotonic strength of human cortical bone. Axial (compressive and tensile) damage reduced tensile and compressive yield strain and stress (Table 1). Higher damage strains tended to produce greater property degradation, although not all differences were significant. Compression damage of -1.6% strain induced more degradation than tensile damage of 1.6% strain on tension and compression strengths. Axial damage modes affected torsion properties far less than axial properties. Conversely, shear (torsion) damage induced small degradations in tension and compression compared to shear strength degradation. The failure stresses showed significant decreases but smaller magnitudes of degradation than yield stress and strain (Table 1).

The un-coupling between axial and rotation damage modes is consistent with our earlier observations on viscoelastic properties [3]. They also are consistent with the qualitative differences in damage morphologies that have been observed [2,5]. Work in histological measurements of damage is ongoing to further explore the relationship between the observed cross-modal mechanical property changes due to damage and the morphological nature of the damage in each mode.

REFERENCES

1. Burr DB, Turner CH, et al. J. Biomech. 31:337, 1998
2. Jepsen KJ, Davy DT, J. Biomech. 30:891, 1997
3. Joo W, Jepsen KJ, Davy DT, Trans. ORS 29, 2004
4. Nadai A. Theory of flow and fracture of solids, pp. 347-352. McGraw-Hill, New York. 1950
5. Carter DR, Hayes WC, Clin. Orthop. Rel. Res., 127, 265-274, 1997

ACKNOWLEDGEMENTS

Supported by NIH Grants AR43785 and AR44927. Tissues provided by Musculoskeletal Transplant Foundation.

COMPARISON OF THE BIOMECHANICAL RESPONSE OF A LUMBAR MOTION SEGMENT TO LOADING AND UNLOADING WHEN LOADS ARE APPLIED SUDDENLY AND AT NORMAL LIFTING SPEEDS

[1]Jamie Williams, [1,2]Raghu Natarajan and [1]Gunnar Andersson
[1]Department of Orthopedic Surgery, Rush University Medical Center, Chicago, Illinois,
[2]Department of Bioengineering, University of Illinois at Chicago, Chicago, Illinois; email: Jamie_Williams@rush.edu

INTRODUCTION

Repetitive lifting and sudden or unexpected loading have been attributed to the development of back injuries. Experimental studies have considered the response of the spinal musculature under both types of loading conditions. While it is important to understand how the muscles surrounding the spine react in these situations, it is equally important to understand how the spine itself reacts, specifically how the intervertebral disc behaves, under such conditions. However, studying the response of the various disc tissues to these types of loading conditions is difficult using standard experimental techniques. Therefore, the purpose of this study was to use a previously validated poroelastic finite element model (PEFEM) to compare the biomechanical response of a lumbar motion segment when subjected to physiological loading conditions when applied suddenly and under normal lifting speeds.

METHODS

A previously validated three-dimensional PEFEM of an L4-L5 motion segment in which biological parameters such as swelling pressure and strain dependent permeability and porosity had been included, was used as the basis for this investigation [1]. The loads, compression, AP shear and lateral shear, were determined for a lifting activity in which a box was lifted from elbow height on the right side and placed at elbow height on the left side. This activity was found to have a significant AP shear component (818N) and lateral shear component (1489N) that occur at approximately the same time as the peak compressive load (5083N). While these loads were measured at normal lifting speed, for the sake of comparison the same load magnitudes were assumed for the suddenly applied load analyses. The peak loads were applied using a triangular waveform with the time taken to reach the peak load equal to 0.01sec, 0.1sec to simulate suddenly applied loads and 1sec to simulate the normal lifting speed. In all three analyses, following the release of the peak load a recovery period of 5 sec was modeled in which a constant 400N compressive load was applied.

RESULTS AND DISCUSSION

Figure 1 shows the maximum effective stress in the endplates and annulus and the maximum pore pressure in the nucleus pulposus both when the peak load was applied and following the recovery period. The magnitude of the maximum effective stresses in the endplates and annulus for the two suddenly applied loading cases were very similar when the peak load was applied. When the loads were applied at a normal lifting speed, over 1sec, the magnitudes of these stresses were reduced. A similar effect was observed with respect to the maximum pore pressure in the nucleus. The loss of disc height was greatest when the loads were applied in 1sec (5.06mm), as

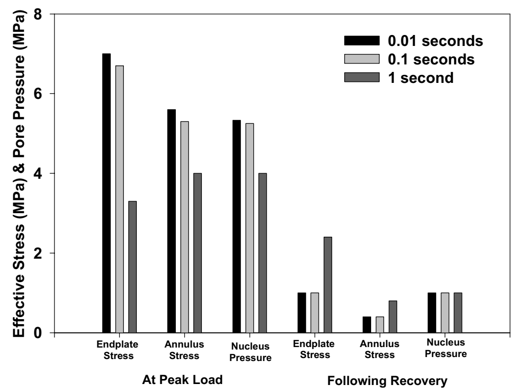

Figure 1: Maximum effective stress in endplates and annulus and maximum nucleus pore pressure at peak load and following the 5 second recovery.

compared to when the loads were applied in 0.01sec (3.61mm) and 0.01sec (3.62mm). Following the recovery period the maximum stresses and maximum pore pressure in the nucleus were greatly reduced as compared to when the loads were applied at a normal lifting speed. Also, the original disc height was restored following the recovery period in the two suddenly applied loading analyses; however, at a normal lifting speed only 90% was recovered.

CONCLUSIONS

The results of the current study support that suddenly applied loads do create circumstances that can result in failure of disc tissues, particularly when the peak load is applied. The PEFEM results also suggest that the disc is able to quickly recover from such loads. When the same loads were applied at a rate representative of normal lifting, the stresses in the disc tissues were significantly less when the peak load was applied however, they remained elevated and the total disc height loss was not completely recovered at the end of the recovery period. If this were a repetitive lifting situation, additional fluid would be lost with each subsequent lift. Therefore, the disc tissues must resist more of the applied load in turn resulting in higher stresses in these tissues. Hence, without appropriate time to recover between bouts of lifting, normal lifting speeds also put the disc at risk of injury.

REFERENCES

1. Williams JR, et al. *Proceedings of the 50th Annual Meeting of the ORS*, San Francisco, CA, Vol. 29, Poster 1147, 2004.

ACKNOWLEDGEMENTS

NIH: AR48152-02. The authors wish to acknowledge Steve Lavender, Ph.D. at the Ohio State University who is responsible for collecting the spine loads used in this study.

SEX BASED DIFFERENCES IN TENSILE PROPERTIES OF HUMAN ANTERIOR CRUCIATE LIGAMENT

[1] Naveen Chandrashekar, [1]Javad Hashemi and [2]James R Slauterbeck
[1]Texas tech University, Lubbock, TX-79415
[2]University of Vermont, Burlington, VT-05405 email: jhashemi@coe.ttu.edu

INTRODUCTION

Females participating in athletic events injure their ACL more frequently than males [1]. The disparity may be due to a smaller ACL size or inferior ACL tensile properties in females among other cited reasons. Any sex differences in the mechanical properties of the ACL might reflect a difference in the internal ACL structure. Therefore it is important to investigate how the tensile properties of ACL vary by sex. We hypothesize that male ACLs have superior structural properties than female ACL even after considering the size of the ACL as a covariant indicating a sex-based difference in the mechanical properties.

METHODS

Seventeen fresh-frozen unpaired knees (8 male and 9 female) were thawed and dissected. The average length of the ACL was measured using a vernier caliper and the minimum cross-sectional area and volume of the ACL were measured using a 3D Scanner[2]. The femur and tibia were tested in tension at 100%/s along the ligamental axis. The structural properties* were calculated and multivariate regression analysis, with age and body mass index (BMI) as covariants, was performed. To test for existence of a sex difference in mechanical properties** of the ACL, the size variables of the ACL were added as covariants and the regression analysis was repeated.

RESULTS AND DISCUSSION

As shown in Table 1, the structural properties of the male ACL are superior to those of the female ACL when age and donor body mass index (BMI) were considered as covariants. The male ACL showed a significantly higher load at failure, stiffness and absorbed energy before failure. This was expected as the female ACL (minimum area =57.32 ± 15.7, volume = 1996 ± 530) was significantly smaller than the male ACL (minimum area =72.9 ± 18.9, volume = 2772 ± 706) [3]. In order to test if any sex based differences in mechanical properties of the ACL existed, the size of the ACL was added as a covariant and the regression analysis was performed again. ACL length, cross-sectional area, area per unit length, and volume of the ACL were added as a covariate for regression analysis with displacement, load, stiffness and energy absorbed, respectively. Still, the male ACL was found to have superior tensile properties. This indicates that the female ACL is not weaker just because it is smaller [3] but also of lower mechanical quality. This might significantly contribute towards greater incidence in ACL tear rate in females. A lower torsional stiffness of female knees has also been cited as a potential reason for this disparity [5]. In our study, we found the female ACL to have lower stiffness and elastic modulus when compared to male ACL. Since ACL is the primary restraint for the internal rotation of the knee, decreased stiffness of the ACL might be a major contributor for lesser rotational knee stiffness in females. Though the reason for inferior mechanical properties of the female ACL is unclear, the influence of sex hormones can be one of the possibilities. For instance, estrogen is known to lower the failure of rabbit ACL [6] but this could be species dependant and tissue specific. Ultrastructural studies are needed to support such theories. This study also emphasizes the need for considering sex as a variable while testing mechanical properties of human ACL. One limitation of this study is that the activity levels of the donors were unknown and therefore its impact on the results could not be assessed.

REFERENCES

1. Arendt E, Dick. R *Am J Sports Med* **23**, 694-701, 1995
2. Hashemi et al. *J Biomech* **38**, 551-555, 2005
3. Chandrashekar et al. *Am J Sports Med*, [In Press], 2005
4. Shelbourne KD, *Am J Sports Med*. **26**,402-408, 1998
5. Hsu WH et al. *Transactions of 50th annual meeting of ORS* San Fransisco, California. Abstract **1305**, 2004.
6. Slauterbeck et al. *J Orthop Res* **17**, 405-408, 1999.

Table 1. Tensile properties of the ACL (Mean ± SD) and *P*-values of difference between the sexes.

Sex (age in years)	Elongation at failure, mm	Load at Failure, N	Stiffness, N/mm	Energy absorbed, N-mm
Male (36.6 ± 10.1)	8.95 ± 1.95	1810 ± 292	308 ± 87	7280 ± 3605
Female (36.8 ± 11.4)	7.48 ± 1.77	1272 ± 234	199 ± 63	4691 ± 1956
P-value (Age & BMI as covariate)	0.09	0.002	0.009	0.033
P-Value (Age, BMI and size as covariates)	0.16	0.008	0.02	0.027

* Structural properties are not normalized to geometrical variables of the tissue and include load at failure, linear stiffness, energy at failure, and elongation at failure.

** Mechanical properties are structural properties normalized based on the corresponding geometrical variables of the tissue and include Failure strength, modulus of elasticity, strain energy density, and strain at failure.

EFFECTS OF SEX AND MASS DENSITY ON THE MECHANICAL PROPERTIES OF THE HUMAN PATELLAR TENDON

[1] Javad Hashemi, [1]Naveen Chandrashekar and [2]James R Slauterbeck
[1]Texas Tech University, Lubbock, TX-79415; [2]University of Vermont, Burlington, VT-05405 email: jhashemi@coe.ttu.edu

INTRODUCTION

A diverse range of values for the mechanical properties of the human patellar tendon has been reported in the literature. These discrepancies persist even though similar test environments and specimen cross-sectional areas are used [1,2,3]. Since patellar tendon is used as an autogenous graft for ACL reconstruction, it is important from a clinical point of view to know the reasons for the variations in the reported properties. Donor age has been excluded as a factor that causes this disparity; at least in the age range below 50 years [2,3]. Since sex and collagen content are known to affect mechanical properties of some connective tissues [4,5], it is reasonable to believe these factors might be causing variability in the properties of patellar tendon. In this study, we hypothesize that 1) female patellar tendons have inherently inferior mechanical properties as compared to male patellar tendons and 2) the mechanical properties of the patellar tendon are correlated to its mass density.

METHODS

Twenty patellar tendons were harvested along with their bony attachments from unpaired knees (10 male and 10 female). The mean age of male donors was 39 years (range 26-50) and that of female donors was 37.7 years (range 17-50). The central portion of patellar tendon (average width of about 5mm) was trimmed. Its length, average width and thickness were measured using a caliper. The patellar tendon was tested to failure at a strain rate of 100%/s in a tensile testing apparatus. After the test, the tendons were carefully removed from their attachment sites and weighed accurately. The mass density of patellar tendon was calculated. The PT was kept moist by 0.1N saline solution throughout the experiment. Statistical tests were performed to compare mechanical properties of male and female patellar tendons. Correlation analysis was performed to test the correlation between the mass density of the tendon and mechanical properties.

RESULTS AND DISCUSSION

As shown in Table 1, no evidence of a sex-based difference in mechanical properties of human patellar tendon was found.
The results revealed a diverse range of mass densities extending from a low of 0.76 g/cm^3 to a high of 2.68 g/cm^3 (250% difference) and the same was true with mechanical properties. The ultimate strength (Figure 1), elastic modulus

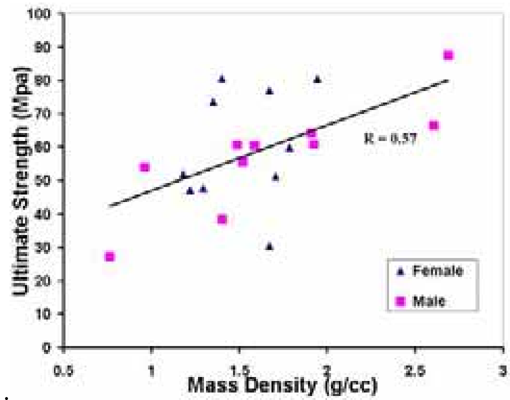

Figure 1. Correlation between mass density and ultimate strength

and toughness of patellar tendons were found to be correlated to the mass density. The tensile strength and elastic modulus were significantly higher for those patellar tendons having a mass density greater than 1.67 g/cm^3. Sex does not seem to affect the mechanical properties of patellar tendon and hence the effect of sex might be tissue specific. The ranges in mass density and mechanical properties highlight the need for considering the quality of autograft before ACL reconstruction. Based on our findings, it is evident that mass density can be used as a predictor of mechanical properties of human patellar tendon. The need for such predictors is highlighted by some researchers [6]. Modern imaging techniques such as CT scans can be used to find the mass density of the patellar tendon to assess its suitability for use as a graft. Higher mass density might reflect higher amount of collagen and hence reflect better tissue quality [5]. Biochemical and histological studies are needed to verify our results.

REFERENCES

1. Butler DL et al. *J Biomech* **19**,425-432, 1986
2. Blevins FT et al. *Am J Sports Med* **22**, 328-333, 1995
3. Flahiff CM et al. *Am J Sports Med* **23**, 354-358, 1995
4. Kubo K et al. *Eur J Appl Physiol* **88**, 520-526, 2002
5. Haut RC et al. *J Biomech* **25**, 163-173, 1992.
6. Beynnon BD et al. *Am J Sports Med* **29**, 161-166, 2001

Table 1:Mechanical properties of male and female patellar tendons and P-values based on t-test.

	Ultimate strength - MPa	***Failure strain***	***Elastic modulus MPa***	***Toughness MPa***
Male	57.5 ± 15.2	0.18 ± 0.03	501.4 ± 143.6	4.37 ± 1.1
Female	59.9 ± 17.2	0.18 ± 0.04	513.4 ± 134.1	4.82 ± 0.8
***P*-value**	0.63	0.61	0.57	0.84

EFFECT OF PERTURBATION DIRECTION ON THE THRESHOLD OF BALANCE RECOVERY PRELIMINARY RESULTS

Alessandro Telonio, Marc-André Cyr, Kodjo E Moglo and Cécile Smeesters
Research Center on Aging, Sherbrooke Geriatric University Institute, Sherbrooke, QC, Canada
Department of Mechanical Engineering, Université de Sherbrooke, Sherbrooke, QC, Canada
email: Cecile.Smeesters@USherbrooke.ca web: www.cdrv.ca

INTRODUCTION

It is only recently that studies have focused on postural perturbations at the threshold of balance recovery, i.e., postural perturbations large enough that balance recovery is not always possible and a fall can occur. The knowledge at the threshold of balance recovery is thus very limited. In particular, the effect of perturbation direction on the threshold of balance recovery has not been quantified, despite evidence of its importance during small and medium postural perturbations [e.g.: 1-2]. Moreover, understanding the effect of perturbation direction is particularly important given that case controlled studies have shown that sideways falls, compared to other fall directions, increases hip fracture risk [e.g.: 3-5]. Therefore, the purpose of this study is to quantify the effect of perturbation direction on the threshold of balance recovery.

METHODS

Balance recovery following sudden release from an initial lean was performed by six healthy younger adults, three males and three females (23.3 ± 2.3 yrs, 1.74 ± 0.07 m, 67.1 ± 11.5 kg). The maximum lean angle that these younger adults could be released from and still recover balance using a single step was determined for i) forward, ii) dominant side, iii) non-dominant side and iv) backward leans. The lean angle was sequentially increased until the subjects failed twice at a given angle and the lean directions were randomly ordered. Lean angles, reaction times, step times, step lengths and step velocities were measured using force platforms (AMTI, Newton, MA) and an Optotrak motion measurement system (NDI, Waterloo, ON). One-way analyses of variance with repeated measures were used to determine the effect of the lean direction.

RESULTS AND DISCUSSION

Since there were no significant differences between dominant and non dominant side results, non dominant side results were not considered in the analyses of variance. The lean direction significantly affected the maximum lean angles that younger adults could be released from and still recover balance using a single step (Figure 1 and Table 1). Moreover, at the maximum lean angles, the lean direction significantly affected reaction times, step times, step lengths and maximum step velocities (Table 1). Specifically, forward results were different from dominant side and backward results ($p < 0.034$) but dominant side and backward results were not different ($p > 0.452$). On the other hand, at the maximum lean angles, the lean direction did not significantly affect mean step velocity (Table 1).

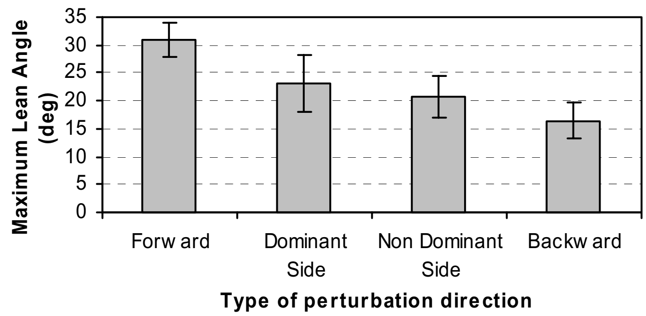

Figure 1: Effect of the lean direction on the maximum lean angle that younger adults could be released from and still recover balance ($p = 0.018$).

CONCLUSIONS

Preliminary results have shown that the perturbation direction significantly affects the postural disturbance younger adults could sustain. It is thus conceivable that different mechanisms could be responsible for balance recovery in different directions. Further experiments are needed to confirm these preliminary results in a larger sample of younger adults and, more importantly, in a sample of older adults.

REFERENCES

1. Hsiao ET and Robinovitch SN. *J Gerontol* **56**(1), M42-47, 2001.
2. Maki BE, et al. *J Biomech* **29**(3), 343-353, 1996.
3. Greenspan SL, et al. *Am J Med* **104**(6), 539-545, 1998.
4. Hayes WC, et al. *Calcif Tissue Int* **52**(3), 192-198, 1993.
5. Nevitt MC and Cummings SR. *J Am Geriatr Soc* **41**(11), 1226-1234, 1993.

ACKNOWLEDGEMENTS

We gratefully acknowledge the assistance of Jean-Sébastien Gosselin, Vincent Deschamps-Sonsino and Mathieu Hamel along with the support of the Junior I Research Fellow Grants 6391 and 5393 from the Fonds de la Recherche en Santé du Québec for Cécile Smeesters.

Table 1: Effect of the perturbation direction on the threshold of balance recovery.

Lean direction	Forward	Dominant Side	Non Dominant Side	Backward	p
Maximum Lean Angle (deg)	30.9 ± 3.1	23.1 ± 5.2	20.8 ± 3.8	16.4 ± 3.1	0.018
Reaction Time (ms)	153 ± 13	215 ± 21	203 ± 13	206 ± 31	0.030
Step Time (ms)	238 ± 7	184 ± 22	167 ± 13	193 ± 28	0.020
Step Length (m)	1.032 ± 0.082	0.694 ± 0.075	0.634 ± 0.090	0.724 ± 0.047	0.018
Maximum Step Velocity (m/s)	6.282 ± 0.559	4.589 ± 0.439	4.558 ± 0.576	4.782 ± 0.332	0.017
Mean Step Velocity (m/s)	4.327 ± 0.334	3.796 ± 0.474	3.806 ± 0.527	3.807 ± 0.656	0.122

DOES FOOTWEAR AFFECT LOWER EXTREMITY VARIABILITY IN HIGH AND LOW ARCHED RUNNERS?

Robert J. Butler[1], Irene McClay Davis[1,2], Joseph Hamill[3], & Chris Knight[4]
[1]Department of Physical Therapy, University of Delaware, Newark, DE, USA 19716 email: rbutler@udel.edu
[2]Drayer Physical Therapy Institute, Hummelstown, PA, USA
[3]Department of Exercise Science, University of Massachusetts, Amherst, MA, USA
[4]Department of Health and Exercise Science, University of Delaware, Newark, DE, USA

INTRODUCTION

High and low arches have been reported to be predisposing factors for an increased injury risk (Kaufman et al., 1999) Running shoes have been designed to decrease this injury risk. Motion control shoes help to reduce excessive motion in low arch (LA) feet and cushioning shoes assist in attenuating impacts in high arched (HA) rigid feet. Recent data suggest that running in the recommended running shoe for a given foot type reduces injury rates (Knapik et al., 2001). However, the biomechanical changes that occur when running in the recommended shoe have not been evaluated.

Coupling variability, as it relates to injury, has received recent attention in the literature (Hamill et al., 1999) although no inferences have been made to joint variability. Two studies have examined how footwear influences joint variability. Kurz et al., (2003, 2004) reported no difference in frontal and sagittal plane variability of the ankle joint when running in motion control and cushioning shoes. However, variability should also be examined amidst the fatigue that is typical of a prolonged run, when most overuse running injuries are thought to occur. It was reported that the variability of foot position placement on the treadmill increased when subjects became fatigued during a prolonged run (Verkerke et al., 1998). These changes in variability may be a function of arch type, and may be influenced by footwear.

Therefore, the purpose of this paper was to examine changes in lower extremity joint variability when low and high arched individuals run in motion control and cushioning shoes over the course of a prolonged run. It is possible that the shoes may have a greater effect on variability at the end of a prolonged run when the runner is in an exerted state. Since the motion control shoe is more rigid than the cushioning shoe, it was hypothesized that it will reduce variability compared to the cushioning shoe in low arched runners. It was expected the more flexible cushioning shoe will increase variability compared to the motion control shoe in high arched runners during the prolonged run.

METHODS

Subjects for the study included twelve LA and twelve HA recreational runners (>10mpw). These subjects were classified as LA or HA by being at least 1.5 sd below or above, respectively, a mean arch height index value of a reference population of 60 healthy individuals. The average arch height index was 0.273 for the LA runners and 0.390 for the HA runners. The motion control shoe used was the New Balance 1021 and the cushioning shoe was the New Balance 1022. Subjects were given a 5 minute warm-up jog before starting a prolonged run at their self-selected average training pace. Data were collected 5 min into the prolonged run and just prior to the termination of the run. The run was terminated when the subject exceeded a "hard physical activity intensity" as defined by the American College of Sports Medicine (>85% age specific HR max or the rate of perceived exertion >16).

The variables of interest were the average variability during stance for sagittal plane motion of the knee and ankle, tibial internal rotation and rearfoot eversion. Average variability was determined by calculating the point by point standard deviation of 5 trials for each subject and averaging across the trial. A two-way repeated measures (shoe, time) ANOVA for each arch type was used to analyze the data. Interactions and main effects were analyzed using a significance level of $p<0.05$.

RESULTS AND DISCUSSION

A significant interaction in the HA runners for tibial rotation variability was found (Fig. 1). A similar trend was observed for tibial rotation in LA runners. No other interactions or main effects were observed

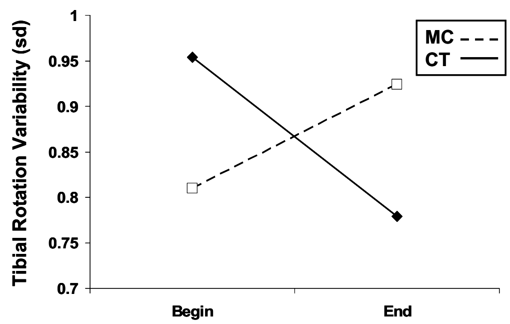

Figure 1. Interaction of footwear and time in High Arched runners (MC=motion control, CT=cushioning shoe)

The hypothesis that the cushioning shoe would increase variability in high arched runners and the motion control shoes would reduce variability in low arched runners over the course of the run was not supported. In fact, the single significant interaction was in the opposite direction of the expectation. Tibial internal rotation variability, while higher at the beginning of the run in the cushioning shoe, increased in the motion control shoe and decreased in the cushioning shoe oier the course of the run. A similar trend was observed in the LA runners although not significant ($p=0.16$). While we observed a shoe-related difference in variability, the benefits of this effect in injury prevention remain theoretical and require further study.

CONCLUSION

High arched runners increased tibial rotation variability in motion control shoes and decreased tibial rotation variability in cushioning shoes over a prolonged run.

REFERENCES

Hamill et al.(1999) *Clin Biomech,* 14, 297-308.
Kaufman et al.(1999) *Amer J Sports Med,* 27(5), 585-593.
Knapik et al.(2001) *US Army Hth Prev Med,* 12-MA-6558-01.
Kurz and Stergiou(2003) *Gait Post,* 17, 132-135.
Kurz and Stergiou(2004) *JAPMA,* 94(1) 53-58.
Verkerke et al.(1998) *Gait Post,* 8, 37-42.

ACKNOWLEDGEMENTS

This study was supported the American College of Sports Medicine Doctoral Research Grant and New Balance Athletic Shoes.

Arm abduction angle and contraction intensity effects on deltoid and scapular rotator muscle recruitment during scapular plane isometric contractions

Mark K. Timmons, Staci M. Stevens, Danny M. Pincivero
Email: mark.timmons@utoledo.edu
Human Performance and Fatigue Laboratory, Department of Kinesiology
The University of Toledo, Toledo, OH

Purpose: To investigate the effects of arm elevation angle and voluntary isometric contraction intensity on deltoid and scapular rotator muscle recruitment.

Methods: Nine healthy, young adults (5 men, 4 women) performed maximal and sub-maximal isometric arm abduction contractions in the scapular plane on a Biodex isokinetic dynamometer. The subject's right arm was secured to the resistance arm of the dynamometer immediately proximal to the wrist. The arm was positioned in the plane of the scapula in an abducted position. Subjects performed five isometric maximal voluntary abduction contractions (MVCs), followed by randomly ordered ten-second sub-maximal contractions at 10-90% MVC (10% increments) (CI), at the following arm abduction angles (AA): 15, 30, 45, 60, 75 and 90 degrees.

During each contraction electromyograms (EMG) were obtained from the deltoid (DEL), upper trapezium (UT), lower trapezium (LT) and serratus anterior (SA) muscles. EMG signals were collected at 2000 Hz, bandpass filtered (20-500 Hz) and fullwave rectified. A 3 second analysis window was chosen during the point of maximal torque for the MVC's and during the point at which the subject was producing the target torque. The integrated EMG (IEMG) value was calculated for each analysis window, and were expressed in absolute (ABS) and normalized to the MVC (NORM) units.

Results and Discussion: The MVC torque (TOR) decreased significantly ($F_{5, 40} = 7.44$, $p<0.001$) as AA increased (Table 1). Absolute IEMG demonstrated significant main effects for AA ($F_{5,160} = 15.82$, $p<0.001$) and CI ($F_{9,288} = 171.79$, $p<0.001$).

Analysis of the NORM IEMG demonstrated significant main effects for both AA ($F_{5,160} = 15.18$, $p<0.001$) and CI ($F_{8,256} = 637.15$, $p<0.001$), and an AA by CI interaction ($F_{40,128} = 5.82$, $p<0.001$). The lower AA levels (15, 30, and 45 deg) were each significantly different from the higher AA levels (60, 75, and 90 deg). No significant muscle main effect or interaction effects were observed to be significant. Figure 1 displays the normalized IEMG as a function of CI for the DEL muscle (only the 15, 45 and 90 deg levels are shown for clarity). A similar pattern of higher NORM IEMG, plotted as a function of CI, was shown for the UT, LT and SA muscles.

The results of this investigation agree with the results from previously reported studies. Lawrence and DeLuca (2) reported a nonlinear increase in EMG intensity with increasing CI. Coury et al (1) reported an increase in deltoid EMG and a decrease in deltoid force with increasing shoulder flexion. Ringelberg (3) reported that normalized IEMG increased during sub-maximal isometric contractions, as a function of increasing AA. EMG from the upper trapezius has been shown to display a linear increase with increasing CI; however the rate of EMG increase was greater during higher force contraction, 50-90% MVC than lower force contractions (4).

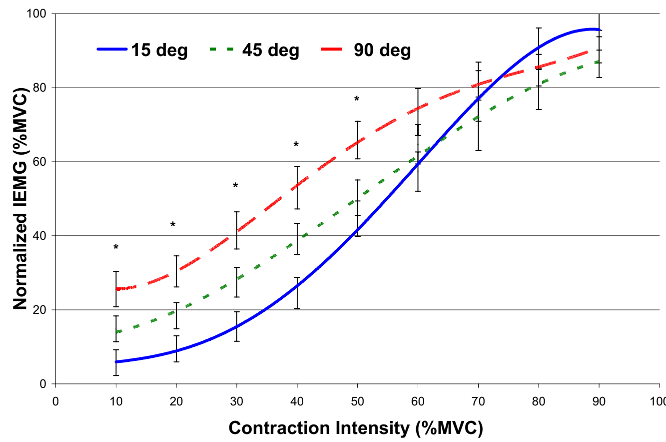

Figure 1. Normalized deltoid muscle IEMG vs. CI, 15°, 45° and 90° AA (*p<0.05).

Conclusions: The results of this investigation demonstrate that the recruitment of the shoulder muscles during isometric abduction contractions is dependant upon the position of the shoulder, as well as the intensity of the contraction. The increased muscular recruitment that is exhibited at higher AA during relatively low CI is possibly explained by changes in muscle length produced by altering orientations of the bony components of the shoulder girdle.

References:

1. Coury HG, et al. *J Electromyogr. Kinesiol,* **8** 157-168, 1998
2. Lawrence JH and DeLuca CJ, *J Appl Physiol* **54** 1653-1659, 1983
3. Ringelberg JA, *J Biomech* **18** 939-947, 1985
4. Hagberg C and Hagberg M, *Eur J Appl Physiol* **58** 641-645, 1989

Table 1. MVC torque and IEMG.

	15 deg	30 deg	45 deg	60 deg	75 deg	90 deg
Torque (N•m)	55.2 (7.7)	54.1 (7.5)	49.9 (6.7)	48.1 (7.0)	45.4 (6.9)	45.7 (8.3)
Deltoid (V•s)	3.468	3.45	3.611	3.884	3.862	3.78
Upper Trapezium (V•s)	1.903	2.775	2.558	2.988	3.199	3.165
Lower Trapezium (V•s)	1.914	1.92	1.719	1.75	1.95	1.867
Serratus Anterior (V•s)	0.84	0.783	0.967	1.102	0.906	1.117

EFFECTS OF PROPRIOCEPTION AND STRENGTH TRAINING ON INJURY PREVENTION IN ADOLESCENT AND YOUNG ADULT FEMALE DANCERS

Carla Murgia
Exercise Science, Kean University
Biomechanics & Kinesiology; email:docmurg@aol.com, web: www.kean.edu

INTRODUCTION

The positive effects of strength and proprioceptive training in the rehabilitative process of the injured athlete are well documented in the literature [1,2,3}. It has been suggested that deficits in neuromuscular pathways associated with injuries have a detrimental effect on joint position sense, protective and defensive mechanisms of the injured joint, balance, and delay of return to activity [4,5]. As a result, progressive strength and proprioception training have been incorporated early into the rehabilitation protocol of injured athletes to restore joint stability and a quicker return to functional performance activity levels [6,7]. The purpose of this study was to examine the effects of strength and proprioception conditioning in the prevention of injuries in female dancers.

METHODS

One hundred subjects were randomly selected from professional dance studio advanced classes. Female subjects, aged 13 to 21 years of age, were cross trained in dance forms. Subjects were randomly assigned to four treatment groups: strength and proprioceptive conditioning (group 1); strength conditioning and relaxed static stretching (group 2); proprioceptive conditioning and relaxed static stretching (group 3); and static stretching (group 4). Progressive strength protocols for the knee and ankle included use of Thera-Band (silver strength) resisted motion and specialized weight training of the inferior extremity. Proprioception protocol consisted of a regimen commonly used in ankle and knee injury rehabilitation regimens. Stretch protocol incorporated the use of relaxed focused static stretch positioning. Positions were held for 30 seconds. All groups trained in front of a mirrored wall 3 times per week for 10 weeks. Pre and post-tests were compared for ankle and knee stability, kinesthesia, and postural sway. Pre and post treatment surveys were used to determine occurrence and severity of knee and ankle joint injury. Ankle stability was assessed using the anterior draw and tilt tests. Knee stability was assessed using varus-valgus, Lachman, and a-p drawer tests. Active and passive joint position sense for the knee and ankle were evaluated using isokinetic instrumentation. Postural sway was measured by identifying center of mass using a 3D automatic digitizing video system and a force platform. Subjects were required to maintain a flat-foot and demi-pointe one-foot stance for 30 seconds on the platform. Postural sway was determined by measuring the amount of center of gravity excursion in the frontal and sagittal planes. Quantity of sway in each plane was summed to determine total center of gravity excursion. A one-way ANOVA with repeated measures was used to analyze the data. Scheffe′ post hoc tests were used to analyze the nature of the differences when significance was found.

RESULTS AND DISCUSSION

Groups that participated in any combination of strength and/proprioceptive conditioning (groups 1, 2 & 3) had significantly ($p<.01$) greater ankle and knee joint stability and less postural sway than the controls (group 4)). When combination protocol (group 1) and the two combination relaxation protocols (groups 2 & 3) were compared for joint stability and postural sway, positive effects were found, although not significant. Joint position sense scores significantly increased ($p<.01$) in the two proprioception training groups (1, 3). In addition, dancers who participated in any combination of strength and proprioceptive training sustained fewer leg injuries of lesser severity ($p<.05$) and when injured, returned to full activity sooner than the controls. Anecdotally, surveys administered at the end of the study revealed that general complaints of discomfort about the knee and ankle joints decreased in number and severity ($p<.01$).

CONCLUSIONS

The results indicate that stronger muscles in proper strength ratios and educated sensory receptors produce stable joints that are more proficient in the identification of joint position and correction of sudden abnormal positions. The lack of significance between "treatment" regimens 1 and 2 or 3 does not necessarily indicate that all three treatment groups are equally effective. It may reflect the restorative effect of relaxed focused stretching. Dancers do not usually take the time to rest. They work through fatigue and minor injuries despite symptoms of pain and paresthesia, which result in poor movement mechanics, as evidenced by "harder" landings from jumps and leaps, "sagging ankles" in releve′ and foot pronation in turn-out. The results of this study clearly demonstrate the positive effects of strength and proprioceptive conditioning when included in training cycle of the dancer. Inclusion of these components is recommended for enhancement of the quality of the performance life of the dancer.

REFERENCES

1. Baltaci G & Kohl H. Phys Ther Rev; 8, 2003.
2. Hassan B et al. Ann of the Rheum Dis; 61(5):422. 2002.
3. Kaminski T et al. J Athl Training; 36(2):S93, 2001.
4. Matsusaka N et al. Am J Sport Med; 29(1):25, 2001.
5. Bouer V & Yvews G. Neurosci Lett; 289:143, 2000.
6. Hiller C, Refshauge K, & Beard D. Am J Sport Med; 32(1):216, 2004.
7 Benton J, et al. J Athl Training; 36(2):: S-87, 2001.
8 Willems T et al., J of Athl Training; 37(4): 487

THREE-DIMENSIONAL IN VIVO ROTATION OF FUSED AND ADJACENT LUMBAR VERTEBRAE

William Anderst and Scott Tashman
Motion Analysis Lab, Bone and Joint Center, Henry Ford Health System, Detroit, MI 48202; email: anderst@bjc.hfh.edu

INTRODUCTION

Over 300,000 spinal fusion operations were performed in the United States in 2001 and the frequency is increasing [1]. Vertebral motion is three-dimensional (3D) and dependent upon bone, ligament and disc constraints in addition to active musculature. To understand normal vertebral motion and the effects of surgical procedures on spine function, in vivo 3D studies must be performed during muscle driven activities.

Previous in vivo 3D lumbar vertebrae motion studies have included only static measurements [2-4], while dynamic motion has been studied only in 2D [5]. The present pilot study investigated the in vivo 3D motion of lumbar vertebrae during movement. The purpose was to measure the relative rotation between fused and unfused vertebral segments.

METHODS

Five lumbar fusion surgery patients served as subjects (44±12 yrs). Informed consent was received prior to surgery. Three to five tantalum beads were implanted into each of the fused vertebrae and the vertebrae adjacent to them. Subjects were tested 2, 3 and 6 months after surgery. Implanted beads were tracked (accuracy ± 0.10 mm [6]) in biplane x-ray images (50 fps, 100 kV, 100 mA) to determine 3D vertebral kinematics. Subjects performed six motions: forward and backward bending, lateral bending to both sides and axial twisting in both directions. Data collection began with the subject seated upright and continued for 1.0 s per movement. Subjects moved until they reached the end of their range of motion. Reflective markers placed on the shoulders, C7, suprasternal notch, ASIS and PSIS tracked trunk rotation.

Vertebrae were CT scanned and reconstructed into 3D surface models [7]. Relative rotations between adjacent vertebrae (e.g. L3/L4 means "L3 relative to L4") were calculated by body-fixed, ordered rotations about vertebral body anatomical axes (defined by CT reconstructions) in the order flexion/extension, axial (twist), and lateral bending.

RESULTS AND DISCUSSION

Data collected 2 and 3-months post surgery showed less than 2° of relative motion between vertebrae for all subjects, likely because their range of motion was still limited. Patient mobility increased six months post surgery. Between subject variation (fusion site, number of vertebrae fused, type of fusion) was wide ranging and grouping results was inappropriate. Thus, results from one patient 6 months post surgery are presented here. This subject had an L4-L5 fusion. Rotation of L5/Pelvis (inferior to fusion), L4/L5 (fused site) and L3/L4 (superior to fusion) were calculated.

In the left lateral bend (Figure 1), there was less than 0.3° of rotation between fused vertebrae. The vertebra inferior to the fusion had a relative rotation opposite the trunk rotation and the vertebra superior to the fusion had a relative rotation in the direction of trunk rotation. The relative rotation between vertebrae did not necessarily change linearly with trunk rotation, as there was little movement in L3/L4 until after the trunk rotated 10° (Figure 1). Conversely, L5/Pelvis varied more linearly with trunk rotation.

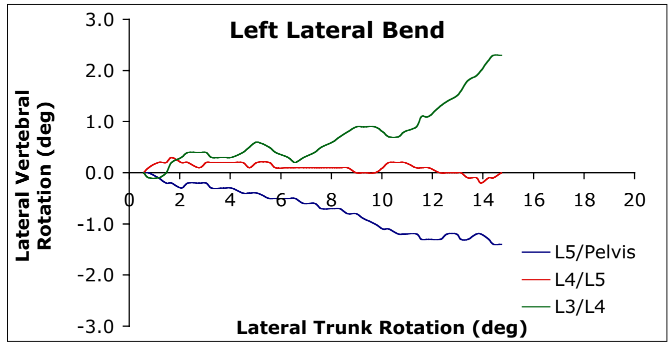

Figure 1: *Relative vertebrae rotation during a left lateral bend. Positive values are in the direction of trunk rotation.*

Forward bending induced relative motion between the fused vertebrae (Figure 2). Also, relative motion between vertebrae occurred near the initiation of trunk rotation. After 7° of trunk rotation, there was little change in relative rotation between adjacent vertebrae in spite of continued trunk flexion.

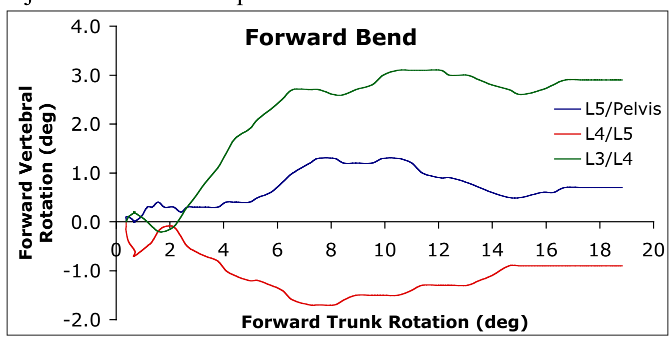

Figure 2: *Relative vertebrae rotation during a forward bend. Note relative motion of fused vertebrae (L4/L5). Note also the non-linear relationship between trunk rotation and relative rotation between vertebrae.*

CONCLUSIONS

The primary findings were: 1) relative rotation between adjacent vertebrae was not always linearly related to trunk motion; 2) motion in different planes should be studied to investigate relative motion between fused vertebrae, and 3) relative rotation of the vertebra superior to the fused site tended to be in the same direction as the trunk, however relative rotation of the vertebra inferior to the fused site was often in the direction opposite of trunk rotation.

REFERENCES

1. Agency for Healthcare Research and Quality, http://www.ahrq.gov/data/hcup/ 2. Pearcy M, et al. *Spine* **9**, 294-294, 1984. 3. Pearcy M, et al. *Spine* **9**, 582-587, 1984. 4. Plamondon A, et al. *Spine* **13**, 1027-1032, 1988. 5. Takayanagi K et al. *Spine* **26**, 1858-1865, 2001. 6. Tashman S, et al. *Journ. Biomed. Eng.* **125**, 238-245, 2003. 7. Treece GM, et al. *Comp. and Graphics* **23**, 583-598, 1999.

THE EFFECTS OF WRIST SPLINTING ON MUSCLE ACTIVITY DURING A HAND GRIP TASK

Jennifer Di Domizio & Peter J. Keir Ph.D.*
School of Kinesiology and Health Science, York University, Toronto, Canada M3J 1P3
*email: pjkeir@yorku.ca

INTRODUCTION

Wrist splints are commonly used in the rehabilitation of carpal tunnel syndrome and other wrist disorders. While they are usually prescribed for night use, they have become common for both day and workplace use. Theoretically, splinting of the wrist should lower muscle activity by stabilizing the wrist and reducing the need for co-contraction. However, the effectiveness of decreasing muscle activity through wrist restraint is inconclusive [1, 2]. The purpose of the study was to examine the relationship between forearm muscle activity and splinting during grip force production.

METHODS

Ten healthy volunteers (5 male, 5 female) participated. Forearm muscle activity was examined during four grip force exertion levels (12.5, 25, 50 and 100% $Grip_{max}$) in three wrist postures, with and without a wrist splint. EMG was recorded from flexors carpi radialis (FCR) and ulnaris (FCU), flexor digitorum superficialis (FDS), extensors carpi radialis (ECR) and ulnaris (ECU) and extensor digitorum communis (EDC). Plexiglass splints were affixed to the dorsal aspect of the right forearm and hand with tape for each posture (0°, 30° flexion, 30° extension). Experimental set up and procedures followed a previous study [3]. A grip dynamometer (MIE Medical Research Ltd., Leeds, UK) was used with a 5 cm grip span and was not supported, while the forearm rested on a platform. An oscilloscope provided visual feedback with the instantaneous grip force overlaid on the target grip force. Differential raw EMG and grip force data were collected at 1000 Hz, with EMG digitally linear enveloped at 3 Hz. Each trial lasted 10 s and was initiated with a "pre-exertion" (zero force) phase lasting a minimum of 1.5 s, followed by an increase to the desired target force, which was maintained for a minimum of three seconds. Average EMG (AEMG) was calculated for "pre-exertion" and target force phases.

RESULTS AND DISCUSSION

No significant differences in activity were observed between splinted and non-splinted conditions for any muscle during low to moderate target forces (12.5, 25, 50%). However, the use of a splint significantly increased muscle activity for ECR, ECU, EDC, FCR and FCU during maximal efforts (100% $Grip_{max}$) at postures specific to each muscle (all $F > 13.6$, all $p < 0.044$). These increases ranged from 7.3% MVE for FDS to 28.2% MVE for FCU. The largest difference was observed for FDS (39.1% MVE), but it was not statistically significant. During pre-exertion (0% $Grip_{max}$), wrist splinting appeared to support the wrist, as evidenced by lower AEMG for ECR and FDS (all $F > 6.1$, $p < 0.036$). ECU, EDC and FCR also exhibited lower activity, but did not attain significance. However, this finding may be explained by lower grip forces required to hold the dynamometer in the pre-exertion phase when splinted (approx. 0.6 N less). Figure 1 illustrates the general result that AEMG was generally lower at zero grip force, similar from low to moderate target forces (12.5, 25, 50%) and higher at maximal (or near maximal) grip exertions. True maximal grip force was not attained by most participants, especially in the flexed wrist posture; however, there was no difference with or without splinting. While the splints created for this study are not representative of most commercially available products, these data indicate that the effectiveness of splinting may be governed by force level and wrist posture. These data also suggest that industrial wrist bracing to reduce operator effort with power hand tool use, such as with power screwdrivers [4], may require further assessment using EMG.

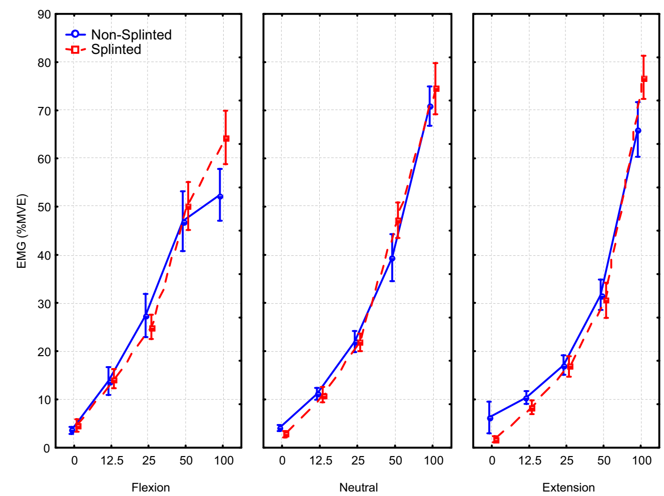

Figure 1. Mean ECU muscle activity (% MVE) versus grip force (% $Grip_{max}$) for the three wrist postures in splinted (dashed line) and non-splinted (solid line) conditions.

CONCLUSIONS

At low to moderate grip effort levels, muscle activity was not altered by using a wrist splint, however, at maximal effort, AEMG increased with the splint. It would appear that a dorsal wrist splint does not reduce muscular effort in what might be considered "active" use. In addition, under the conditions tested, dorsal wrist splints did not reduce co-contraction. Thus, the increasingly common use of wrist splints during daily activities should be reconsidered, if the intent is to reduce wrist loading by decreased muscle activity.

REFERENCES

1. Johansson L, *Appl Ergon*, **35**, 129-136, 2004.
2. van Elk, *J Orthop Sports Phys Ther*, **34**(5), 228-234, 2004.
3. Mogk JPM & Keir, PJ. *Ergonomics*, **46**(9), 956-975, 2003.
4. Johnson, SL. *Human Factors*, **31**(1), 61-69, 1988.

ACKNOWLEDGEMENTS

This study was funded by NSERC (Canada), grant #217382.

THE FORCE-LENGTH CURVE OF THE HUMAN GASTROCNEMIUS IN VIVO.

Samantha Winter and John H. Challis
Biomechanics Laboratory, The Pennsylvania State University, USA
email: slw294@psu.edu, jhc10@psu.edu

INTRODUCTION
The variation in isometric force produced with changing muscle length has been investigated extensively and ascending, plateau and descending limbs of this force-length relationship have been explained in terms of the cross bridge theory [1]. However, in vivo different skeletal muscles may operate over all or only part of the force-length curve, and for a given muscle, different individuals may be adapted to operate on different parts of the curve. The purpose of this study was to determine the force-length relationship for the gastrocnemius, which has not been reported previously in vivo for humans. A modified method based on the algorithm of Herzog & ter Keurs [2] was used to reconstruct the force-length curves of the muscle.

METHODS
Fourteen male and fourteen female subjects aged between 18 to 27 years performed maximal isometric plantar flexions in a Biodex dynamometer (females: mass 60.9 kg ± 10.0, height 1.66 m ± 0.02; males: mass 86.1 kg ± 11.9, height 1.81 m ± 0.07). Plantar flexion moments were recorded at five ankle angles: -15, 0, 15 30 and 40 degrees, with negative angles defined as dorsi-flexion. These measurements were repeated for four different randomly ordered knee angles (0, 50, 90, 115 degrees of flexion) over two testing sessions four to ten days apart.

The change in normalised gastrocnemius muscle length was computed as a change from the reference position, defined as full knee extension and a 0 degree (neutral) ankle angle. The force in the Achilles tendon was computed from the active moment and the ankle moment arm [3]. The ankle moment arm was scaled according to the shank length of the subject. Robust regression techniques [4] were used to fit first and second order polynomials to each set of four forces measured at the same ankle angle, but at different knee angles. The second order equation was selected as long as it produced a monotonic relationship. This step produced five curves corresponding to different sections of the gastrocnemius force-length curve. The curves were separated along the vertical force axis by the monoarticular force contribution, but they overlapped in terms of the length change on the horizontal axis. The entire length change represented the length change produced by all of the various experimental joint configurations. In order to subtract out the mono-articular contribution from each data set, the polynomial equation of the first data set was used to predict the force value of the first data point in the second set, and the force difference was then subtracted from all the data points in this second set. This procedure was repeated for all subsequent sets. Points were then normalised to the maximum force, and second and first order polynomials were fitted to the entire normalised data set.

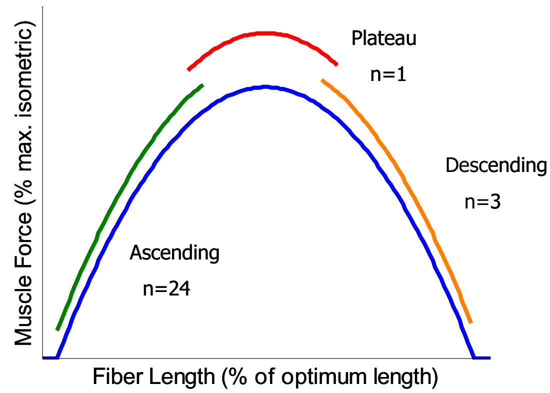

Figure 1: Number of subjects operating over each portion of the force-length curve.

RESULTS AND DISCUSSION
The majority of the 28 subjects operated over the ascending limb; however, three subjects operated over the descending limb, and one subject operated over the plateau region (Figure 1).

Sensitivity analyses indicated that the reconstructions of the force-length curves were robust to changes in the moment arm and maximal tendon stretch parameters used.

Previous work has also determined that there is variation in the portion of the force-length relationship that the rectus femoris operates over [5]. There was, however, a higher degree of consistency in the portion operated over for the gastrocnemius. This might be reflective of more consistent functional demands placed on the gastrocnemius.

CONCLUSIONS
In vivo variation exists, for the gastrocnemius, in the portion of the force-length curve operated over. The source of this variation, that is, whether it arises as a result of genetic expression or as a result of functional adaptation, is unknown, but the variation should be recognised when conducting modelling studies or when performing surgery.

REFERENCES
1. Gordon, A. M. et al. *J Physiol* **184**, *170-192*, 1966.
2. Herzog, W., & ter Keurs, H. E. D. J. *Pflügers Archives* **411**, 637-641, 1988.
3. Visser, J. J. et al. *Eur J Appl Physiol Occup Physiol* **61**, 453-460, 1990.
4. Huber, P. J. *Robust Statistical Procedures* (2nd ed.). Philadelphia: SIAM. 1996.
5. Herzog, W., & ter Keurs, H. E. D. J. *Pflügers Arch*, **411**, 642-647, 1988.

THE CONTRIBUTION OF ARTICULAR SURFACE GEOMETRY TO ANKLE STABILIZATION

Yuki Tochigi, M. James Rudert, Charles L. Saltzman, Annunziato Amendola, and Thomas D. Brown
University of Iowa, Department of Othopaedics and Rehabilitation
Email: yuki-tochigi@uiowa.edu, web: http://poppy.obrl.uiowa.edu/

INTRODUCTION

Passive stability of the ankle under weight-bearing conditions is thought to rely substantially on the role of the articular surfaces[1,2]. Ligament-sectioning paradigms previously utilized to study the relative contribution of ligamentous vs. articular restraints have not allowed direct study of the mechanism by which surface resistance contributes to ankle stabilization. This study hypothesized that ankle stabilization by surface resistance involves specific contact stress changes that plausibly explain the contribution of articular surface geometry to passive ankle stability.

METHODS

Six cadaver ankles with the significant peri-ankle ligaments intact were subjected to an experiment to explore articular contact pressure changes associated with various external loads. The loads were anterior/posterior (A/P) shear forces (40 and 80 N), inversion/eversion torques (150 and 300 N-cm), and internal/external rotation (IR/ER) torques (150 and 300 N-cm); these magnitudes are similar to those occurring during gait. An MTS-based custom fixture held a specimen at a predetermined ankle position (15º dorsiflexion, neutral, 15º plantar flexion, or 30º plantar flexion) under 600N axial force. At each position, one of the three external loads was applied for all load increments, while motion associated with the two remaining loads was unconstrained.

Contact stress on the superior tibial plafond surface was recorded by a purpose-designed transient stress transducer (Tekscan Inc., Boston, MA, USA), which reported local stress at each of the 1472 (32x46) sensing units (sensels). For each load/position, the pressure changes due to the applied external load were calculated from the recorded pressure map by subtracting the corresponding axial-load-only map obtained at that position, on a sensel-by-sensel basis.

Plafond geometry was modeled as two adjacent spherical sectors (Fig.1). The force at each sensel, assumed to act normal to the surface, was resolved into three components: axial, A/P, and medial/lateral (M/L). The sum of the A/P components was assumed to represent the surface resistance to the applied external A/P load. Version and IR/ER torques about the zero-load center of pressure were calculated from the appropriate force components and were assumed to represent the surface resistance to the corresponding external loads. Frictional forces were assumed negligible.

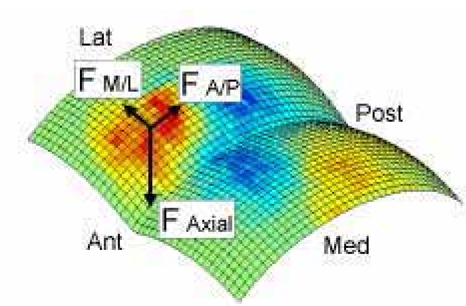

Fig.1 Ankle geometric model with a pressure change map (external load = 300 N-cm IR torque). The plafond geometry consists of two partial spheres (radius = 25mm, separation b/w centers = 20mm). The force is regarded as applied from the tibia to the talus. Pressure change is converted to the corresponding force perpendicular to the sensel surface. The axial, A/P, and M/L components of the force are utilized to estimate the magnitude of the surface resistance associated with the external load.

For each of the three external loading conditions, and at each position, the resisting force/torque was linearly regressed against the magnitude of the externally applied force/torque (Fig.2). The slope was considered to represent the contribution of the measured pressure changes to restraining the ankle. (A slope of 1.0 would indicate that articular surface engagement provided 100% of the resistance). This analysis was individually applied to each specimen.

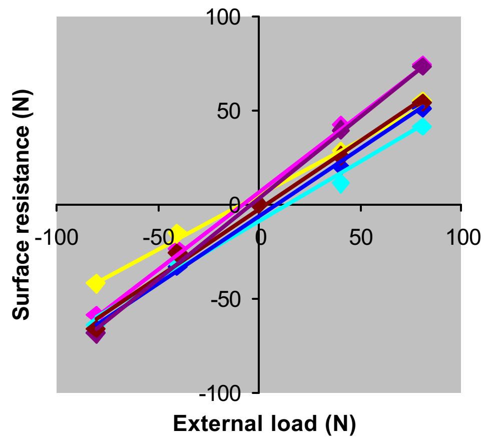

Fig.2 External load vs. surface resistance in the A/P force test at the neutral position (n=6). Each specimen has five data points (plotted for the four external-load magnitudes and the axial-load-only condition) and a trend line based on linear regression. In this case, correlation coefficient (R) is greater than 0.99 in every specimen, and the slopes range from 0.61 to 0.98.

RESULTS AND DISCUSSION

In the neutral position, the pressure changes on the tibial plafond accounted for 73 ± 11% (average ± standard deviation) of the external AP force, 39 ± 14% of the version torque, and 30 ± 14% for the IR-ER torque. Significant effect of ankle position was revealed only in the version test ($p = 0.01$, single factor ANOVA), in which the contribution linearly decreased in the plantar-flexed positions.

The results indicate that the superior-inferior tibial-talar surfaces play the primary role in A/P stabilization under weight-bearing conditions. Contribution of these surfaces in helping to resist version and IR-ER torque was also evident, even without counting the effect of the lateral and medial ankle "gutter" surfaces (a subject inviting future investigation).

CONCLUSION

Ankle stability under weight-bearing conditions appears to be substantially dictated by the ankle surface geometry.

REFERENCES

1. Stormont DM, et al. *Am J Sport Med* **13**, 295-300, 1985.
2. Watanabe K, et al. *49th ORS abstract*, #0119, 2003.

ACKNOWLEDGEMENTS

AOFAS Research Grant and NIH Grant AR48939

AN INVESTIGATION OF THE CONGRUITY IN GEOMETRY OF THE GLENOHUMERAL JOINT ON THE MAXIMUM ACCEPTABLE LOAD DURING PUSHING

Krystyna Gielo-Perczak
Liberty Mutual Research Institute for Safety and Health, Hopkinton, MA U.S.A.
email: Krystyna.Gielo-Perczak@LibertyMutual.com web: www.libertymutual.com/research/

INTRODUCTION

Occupational ergonomics and safety analyses of the human body require a new biomechanical approach that combines the geometric complex nature of the human joints with the requirements of the workplace in order to explain the mechanism of musculoskeletal disorders. Recent analyses of the glenohumeral joint have not focused on the contribution of geometric parameters like the radii of the glenoid fossa of scapula and the humerus, and their functional relationship to strength. However, Saha (1961) pointed out the variance of shoulder anatomy relating to the congruity of the glenoid and humeral head. In the general population we can distinguish the three most common characteristic shoulder joints: 1) Type A, the glenoid with a radius that is larger than that of the humerus, 2) Type B, the glenoid and the humerus with the same radius, 3) Type C, the glenoid with a smaller radius than that of the humerus [1]. The purpose of the current study was to answer to question is the strength used in one-handed pushing related to the congruity of the glenoid and humeral head?

METHODS

The coefficient of congruity(conformity) (R/r) was defined as a ratio of the humerus radius (R) and radius of the glenoid fossa of the scapula (r) curvature. This coefficient for type A was defined as ≤ 0.75, where components were with unequal radii of curvature (glenoid larger) nonconforming articulation; for type B as <0.75; 1.25>, as a conforming articulation where humeral and glenoid components were almost equal and for type C as ≥ 1.25, nonconforming articulation with glenoid radius smaller than the humerus.

Frontal MRI images of the glenohumeral joint of the right arm were obtained from 12 healthy men who had never experienced chronic shoulder pain, stress fracture, or joint injury. Data were recorded by using a 1,5-T Sigma system (GE Medical Systems). The subject lay in an MRI tube in a prone position with his arm in 0° of adduction. The elbow was flexed to 90° with the forearm lying on the chest. The magnetic resonance images were taken at the same arm positions for all subjects.

The same 12 subjects performed a series of simulated pushing tasks in laboratory conditions. A special constrained framework was designed with twelve force sensors. Subjects exerted maximum push force during maximum voluntary contraction (MVC) on a handle in a sidewise direction. The subjects were asked to push on the handle and MVC loads were recorded when the arm was abducted from 5 to 30 degrees in the frontal plane. Over a two-week period, each subject performed two and four repetitions of constraint range upper-limb abduction and abduction at six different randomized angles while standing. For each repetition, participants were instructed to gradually increase their effort to what they felt was an acceptable maximum force. Once the maximum force was reached, subjects sustained MVC on the instrumented handle for three seconds.

Subject	*R/r*	Type
1	1.41	C
2	0.72	A
3	0.70	A
4	0.69	A
5	1.13	B
6	0.77	B
7	0.86	B
8	0.70	A
9	1.39	C
10	0.47	A
11	1.05	B
12	1.38	C
Mean	0.71	

Table 1: The coefficient of congruity (R/r) and type of joint for 12 participants.

RESULTS AND DISCUSSION

The participants' mean age and standard deviation was 40.5 ± 8.7 years, with an average height of 178 ± 7.08 cm and body weight of 81.5 ± 14.9 kg. The coefficient of congruity and related type of joint for the 12 participants are presented in Table 1. The three most common types of shoulder joint congruity among 12 subjects do not correlate with mean forces recorded at the handle during maximum voluntary contraction when arm was abducted from 5 to 30°.

The results from study [2] relating to one-handed pushing showed that the maximum forces exerted were higher than in the current study, but the subjects had free movement and were not constrained. Perhaps the constrained position of participants in the current experiment was a very unique factor which was never before considered during the strength measurements.

CONCLUSIONS

The investigation didn't reveal the influence of the coefficient of congruity on the maximum acceptable load applied to the hand during pushing. However, the study confirmed that the relation of different geometric parameters of glenohumeral joint should be analyzed which have an influence on the strength of the subject.

REFERENCES

1. Gielo-Perczak et al. *Proceedings of HFES 49th*, New Orleans, USA, 233-237, 2004.
2. Mital et al, *A guide to Manual Materials Handling,* 1997.

BIOMECHANICAL ANALYSIS OF EMG ACTIVITY BETWEEN BADMINTON SMASH AND DROP SHOT

Chien-Lu Tsai[1], Huang, Kwei-Shu[1], and Shaw-Shiun Chang[2]
[1]National Taiwan Normal University, [2]National Taiwan Ocean University
email: cltsai@cc.ntnu.edu.tw

INTRODUCTION

The forehand overhead stroke is one of the most typical and powerful badminton techniques. It can be divided into several types of stroke. Previous studies related to badminton skills had been conducted by several researchers, Gowitzke and Waddell, 1979, they used 2D model to describe the smash strokes. Tsai, et al, 1996, they used 3D model to analyze the smash strokes. Tsai, et al, 2001 used the inverse dynamic to investigate the upper extremities of Taiwan elite badminton players, they found the wrist joint exerted the greatest velocity and power value in both kinds of strokes than the elbow and shoulder, the extensor muscles of wrist were performing the eccentric contraction around contact. The purpose of this study was to analyze the kinematics and the surface EMG methods on the upper extremities of the elite badminton players when they were performing smash and drop shots.

METHODS

Four elite badminton players (age 21yrs, high 175cm, weight 68kg) in Taiwan were served as the subjects. The patterns of the shuttle in this study were divided into two different trajectories. While the players were performing the smash, the target of the shuttle was on the ground of opponent's middle court. The drop shot was landing on the opponent's frontal court. The upper extremity of the subject was separated into three segments. The segments were estimated by using the Dempster's parameter. Two Redlake 1000 high-speed digital cameras (Motion Scope, San Diago, USA, 250Hz) were used to record the 3D kinematics data, one Biovision EMG system was used to record the raw EMG signals of upper limb muscles, such as flexor carpi ulnalis, extensor carpi radialis, biceps brachii, triceps brachii, deltoid and pectoralis major. A dependent-pared t-test was used to test the selected variables at .05 significant levels.

RESULTS AND DISCUSSION

Table 1: The Kinematics Variables of the Smash and Drop Strokes

Variables	Smash	Drop	Sig.
Time of Contact (sec)	0.004	0.008	*
Shuttle Velocity(m/s)	75	27	*
Shuttle Angle (deg)	-7	-2	
Shoulder Angle (deg)	169	147	
Elbow Angle (deg)	189	164	*
Wrist Angle (deg)	187	185	
Shoulder Ang Vel..(deg/s)	-709	-302	
Elbow Ang. Vel.(deg/s)	-678	-404	
Wrist Ang. Vel..(deg/s)	-2040	-498	*

* *p< .05*

Table 1 shows the kinematical data of the smash and drop shots at the contact point. There were significant differences between the smash and drop shots in shuttle velocity, the contact duration time, the elbow angle at the contact point and the wrist angular velocity. contact.

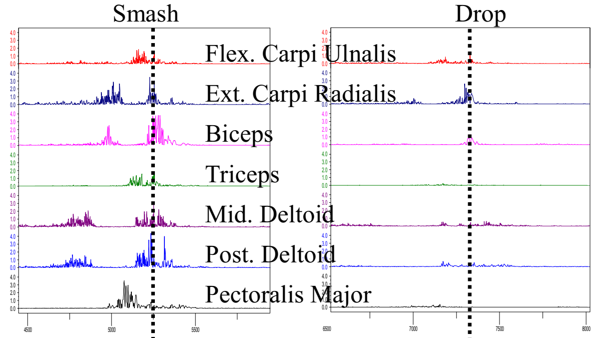

Figure 1: The EMG Signals of the Smash and Drop Shots

Figure 1 shows the raw surface EMG signal patterns of smash and drop strokes around contact. From the EMG patterns, we found the sequence of smash and drop shots were similar. The surface EMG activity of smash stroke was stronger than the drop shot. The Deltoids were acting in the very first period of the movement to raise the upper arm. Then the Ext. Carpi Radialis and Biceps to backward and downward the racket to prepare swing the racket upward. The Pectoralis Major acted to move the upper arm swing the arm upward. Before contact, the Triceps and the Flex. Carpi Ulnalis contracted to swing up the racket. The Biceps, the Ext. Carpi Radialis and the Deltoid acted to stable the upper extremities. Tsai, et al in 2001 had deducted that the Ext. Carpi Radialis and Biceps might be engaged in the eccentric contraction during the contact phase in the smash stroke. In this study, we verified that not only the extensor muscles of wrist but also the biceps were suffering the eccentric contraction around contact.

CONCLUSIONS

The results showed that there were significant differences in initial flight angle, contact duration time and initial shuttle velocity between the smash and the drop shots. The surface EMG activity of smash stroke was stronger than that of drop shot. The sequence of the movement of smash and drop were very similar. The EMG signal of smash was significant greater than that of drop shot. In this study, we verified the biceps and the wrist extensor were performing the eccentric contraction at the contact point.

REFERENCES

1.Gowitzke, B.A., Waddell, D.B. Technique of Badminton Stroke Production: *Science in Badminton. In Racquet Sports*, d. J. Terauds. Del Mar, CA: Academic Publishers , 1979.
2.Tsai,Chien-Lu, et al. Biomechanical Analysis of the Upper Extremity Between Badminton Smash and Drop Shot. *Proceeding of ISB XVIII*th, Zürich, Abstract 249, 2001.

ACKNOWLEDGEMENTS

We like to thank the financial support from the National Science Council in Taiwan.

EVALUATION OF OSMOSIS-INDUCED DEFORMATION OF ARTICULAR CARTILAGE USING ULTRASOUND BIOMICROSCOPY IMAGING

Qing Wang and Yongping Zheng
Rehabilitation Engineering Centre, The Hong Kong Polytechnic University
email: 03900369r@polyu.edu.hk

INTRODUCTION

Articular cartilage, a biological connective tissue, covers the bony ends of articulating joints. It has been found that the unique composition and multilayered structure of articular cartilage contribute to its intrinsic biomechanical properties.

In recent years, ultrasound has been utilized to measure not only the acoustic properties but also the mechanical properties of cartilage combined with compression and indentation methods. This study introduced an ultrasound biomicroscopy imaging method to evaluate the osmosis-induced deformation of artilage cartilage and its mechanical properties.

METHODS

The ultrasound biomicroscopy system consisted of a computer-controlled stepper-motor, 3-D translating device and the signal acquirement system (Figure 1). Ultrasound transducer could be moved vertically and horizontally in the *x*, *y* and *z* directions to obtain the maximum echoes from the tissue. Using the custom-made software, the digitalized A-mode ultrasound signals and B-mode images were stored for the offline analysis.

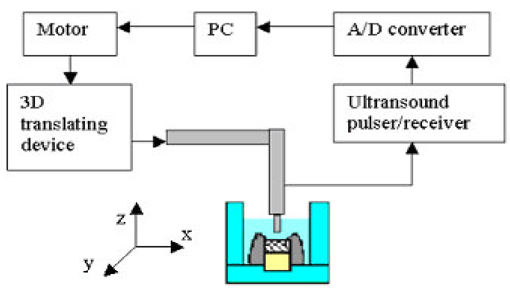

Figure 1: Schematic of the ultrasound system.

Cartilage-bone plugs (n = 5) with a diameter of 6.35 mm and the cartilage thickness ranged from 1.39 mm to 1.70 mm were prepared from the proximal-lateral side of bovine patellae. Specimen was fixed on the bottom of the container and equilibrated for one hour in physiological saline solution (0.15 M NaCl), and then the solution was immediately replaced by the hypertonic saline (2 M NaCl). The deformation of cartilage under the osmotic loading was monitored by the ultrasound biomicroscopy imaging system.

RESULTS AND DISCUSSION

The section (full-thickness of cartilage × 1.5mm) of the central portion of specimen was scanned (Figure 2). From the deformation of cartilage specimens under the osmotic loading due to the increase of the concentration of the external saline bath, the compressive strains were measured from 0.003 to 0.025 for the five samples. The mean ultrasound speeds in 2 M saline and in cartilage immerged in 0.15 M saline were 1646 m/s and 1652 m/s, respectively, measured using a noncontact method reported earlier [1].

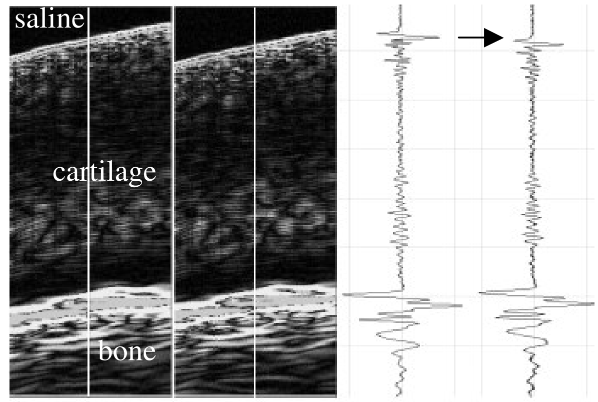

(a) (b) (c) (d)

Figure 2: B-mode ultrasound images of one specimen equilibrated (a) in physiological saline and (b) in hypertonic saline. Ultrasound beam propagated along the thickness direction. The grey levels of the image linearly represent the amplitudes of the RF signals. RF signals in (c) and (d) correspond to the positions indicated by the white solid lines in (a) and (b), respectively. The black arrow indicated that the echoes reflected from cartilage surface shifted slightly due to the alteration of the saline concentration.

Swelling behavior is thought to be important for the overall mechanical properties and functions of cartilage and provides a high resistance to compressive loads. Most of previous studies reported the swelling-induced strains of cartilage, but not along a cross-section *in situ* [2-4]. The present study investigated the transient response of cartilage to the osmotic loading *in situ*. The results showed that the ultrasound biomicroscopy scanning technique could be feasible to assess the fine deformation of cartilage of both large and small animals.

CONCLUSIONS

In comparison with traditional mechanical methods and optical methods, this method is potential to be applied for *in-vivo* applications due to the capacity of recording the transient deformation of the intact tissue nondestructively.

REFERENCES

1. Patil, S.G., et al., Ultrasound Med Biol 30, 953-963, 2004.
2. Mow, V.C., Schoonbeck, J.M., *Transaction of the 30th Annual ORS.* Altanta, Georgia. 9, 262, 1984.
3. Narmoneva, D.A., et al., *J Biomech* 32, 401-408,1999.
4. Zheng, Y.P., et al., *Ultrasound Med Biol* 30, 841-849, 2004.

ACKNOWLEDGEMENTS

This project was partially supported by the Research Grant Council of Hong Kong (PolyU5199/02E, PolyU 5245/03E) and The Hong Kong Polytechnic University.

THE RELATIONSHIP BETWEEN PELVIC FLOOR AND ABDOMINAL MUSCLE ACTIVATION AND THE GENERATION OF INTRAVAGINAL PRESSURE IN HEALTHY CONTINENT WOMEN

Stéphanie J.Madill and Linda McLean
School of Rehabilitation Therapy, Queens University, Kingston, Ontario, Canada

INTRODUCTION

Stress urinary incontinence (SUI) is "the complaint of involuntary leakage [of urine] on effort or exertion, or on sneezing or coughing"[1]. It affects 26% of women aged 30 to 59, peaking in the 40 to 49 year age group[2]. It is caused by the failure of the pelvic floor muscles (PFM) and the urethral sphincters to resist increases in intra-abdominal pressure[3], however, the mechanism by which the PFM and abdominal muscles work together to maintain continence is not well understood.

METHODS

PFM electromyography (EMG) data were acquired using a Femiscan™ probe seated in the vagina[4]. The probe had two pairs of bipolar bar electrodes mounted laterally, and was modified by mounting a pressure transducer in a hole cut through its posterior surface. Surface EMG data were recorded from rectus abdominis (RA), transversus abdominis (TA), internal obliques (IO) and external obliques (EO) using Meditrace™ 133 surface Ag-AgCl adhesive electrodes. All EMG data were amplified using Bortec AMT-8 amplifiers, and both EMG and pressure data were acquired at 1kHz using a 16-bit Analog to Digital Converter and Labview v. 6.1.

Resting data were recorded first, with each subject positioned in supine and asked to relax their PFM and abdominal muscles. After a period of instruction to familiarize subjects with the proper performance of a PFM contraction, volunteers performed three repetitions of a maximum voluntary contraction of their PFM while EMG and pressure data were recorded simultaneously from all sensors.

All pressure and EMG data were smoothed by computing the root mean square (RMS) value using a moving window of 20ms across the contraction time, less the resting RMS value The data were then normalized based on the maximum smoothed pressure or EMG amplitude achieved during each contraction. The normalized pressure vs. EMG curves were ensemble averaged, and the equations of these curves were computed and tested ($p<0.05$). Significant curves were used to model the EMG vs. pressure relationship.

RESULTS AND DISCUSSSION

Thirteen urinary continent women, mean age 36.3 ±9.9 years (10 nulliparous, three parous) participated in the study. Since the EMG amplitudes from the two sides of the PFM were highly correlated in all cases (cross-correlation coefficient 0.90, 95% confidence interval 0.89-0.92), the side with the larger EMG amplitude was used in the analysis for each subject and each contraction.

The ensemble average EMG vs pressure curves for three of the abdominal muscles (RA, TA and IO) were "S" shaped (See Figure 1), whereas that for the PFM showed a steep initial rise followed by a leveling off. (Figure 2) The EO versus pressure curve did not produce any predictable pattern ($p>0.09$). All of the curves, except that for RA, were best defined by second order polynomial equations ($p<0.05$). RA was best defined by a third order polynomial equation.

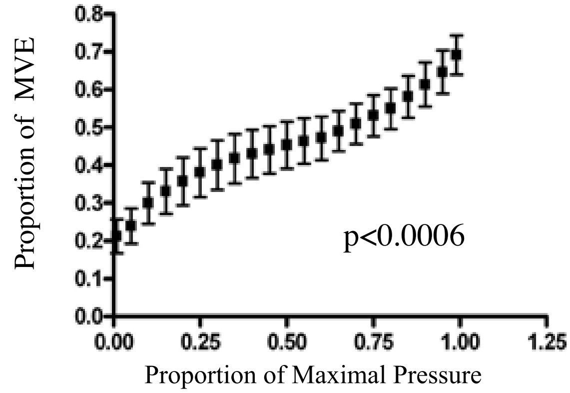

Figure 1. Ensemble average curve (n=13) for normalized IO EMG versus lower vaginal pressure. Squares indicate the mean proportion of MVE for each pressure increment while the whiskers indicate one standard deviation.

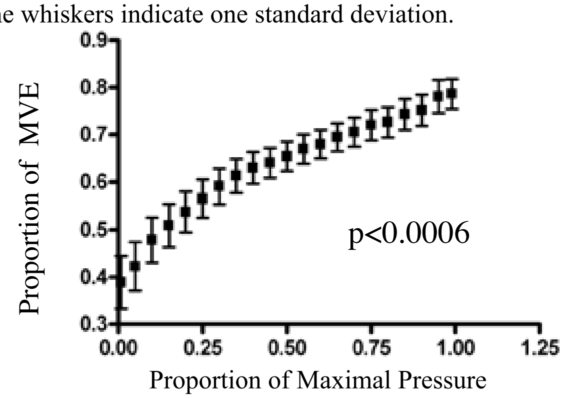

Figure 2. Ensemble average curve (n=13) for normalized PFM EMG versus normalized vaginal pressure. Squares indicate the mean percent MVE for each pressure increment while the whiskers indicate one standard deviation.

In voluntary PFM contractions, lower intravaginal pressure in urinary continent women is not solely the product of PFM activation; it receives significant contributions from TA, RA and IO. The EO muscles did not appear to have a predictable pattern of activation in response to a voluntary PFM contraction and are therefore thought to contribute minimally to the generation of lower intravaginal pressure.

REFERENCES

1. Abrams P, et al. *Neurouro Urodyn* **21**, 167-178, 2002.
2. Cardozo L and Stanton SL. *Br J Obstet Gynæcol* **87**, 187-190, 1980.
3. Abrams P, et al. eds. *Incontinence, 2nd International Consultation on Incontinence.* Paris, Health Publications Ltd. 2002
4. Aukee P, et al. *Accupunct Electrother Res* **27,** 27-44, 2002.

ACKNOWLEDGEMENTS

Funding for this project was provided by the Physiotherapy Foundation of Canada. Roy Young provided technical assistance to modify the probe.

A Comparison of Isokinetic Leg Flexion and Extension Strength in Elite Adolescent Male Track and Field Athletes

Lee Shuei-Pi, Tsai Yeh-Jung, Gu Guo-Hong
National Taiwan Normal University
Email: koftp@:yam.com

INTRODUCTION

The characters of muscle could be specific to different kinds of sports events after long-time training, such as sprinters may perform better in power, poor in endurance, and marathonian may have reversed results. The isokinetic peak torque and torque ratio are important parameters to evaluate the athletic performance or to prevent knee injury (Costill, et al, 1968). So the purpose of this study was to investigate the differences among young male sprinters, jumpers and throwers in the two parameters. We hope the results could be benefit to the information for coaches or athletes in muscular training.

METHODS

Three groups of well trained, adolescent male athletes were subjects in this study. One group consisted of 17 short-distance runners (<400m, age:17.8±1.4 yrs, weight:65.3±4.41 kg). Another group consisted of 10 long or high-jumping jumpers (long and high jumping, age:17.5±1.4 yrs, weight:64.0±6.4 kg). The last one consisted of 12 throwers (javelin, shot-put, discus, age:17.4±1.7 yrs, weight:91.7±16.8kg). They were asked to stop training at least one day, and signed informed consent for the information about basic procedures before experiment.

Quadriceps and hamstring were analyzed in this study. The measurement was mainly divided into three portions. First is the peak torque of quadriceps (QUAD PT) during concentric (QUAD con) and eccentric (QUAD ecc) periods. Second is the peak torque of hamstring (HAM PT) during the concentric (HAM con) and eccentric (HAM ecc) periods. The peak torque was maximum torque within certain period in dominant leg and measured by using a Cybex-6000 isokinetic dynamometer. The concentric data were collected at angular velocity of 180^0/sec for 4 consecutive contractions, and eccentric ones were at angular velocity of 120^0/sec for 4 consecutive contractions. The relative peak values (divided by body weight) were also analyzed. Last is the ratio of H/Q (HAM PT / QUAD PT) during their concentric period. SPSS one-way ANOVA was used to compare the difference in peak torques of the three groups. The significant value was set at .05, and Scheffe method was used for post-hoc comparisons.

RESULTS AND DISCUSSION

Table 1 and 2 showed that the throwers' absolute peak torques were significantly higher than sprinters' and jumpers' during both types of quadriceps' contractions (P< .05). The hamstrings' absolute values were similar to quadriceps', although without significant difference among the three groups. However, reversed results that the sprinters' and jumpers' relative peak torques were higher than throwers', but without significant difference among them, could be seen during both types of contractions in the two muscles. It indicates that runner and jumper may need faster movement than thrower do, so the influence of body weight should be taken into consideration.

The mean H/Q ratios of sprinters, jumpers and throwers were 0.61, 0.58 and 0.56 respectively, and there was not much difference among the three groups. The values were similar to those observed in young basketball players in Gerodimos et al.

CONCLUSIONS

In healthy adult, the H/Q ratios ranges betweens 0.56~0.8. If the athlete value lower than those, the training in hamstring should be increased for maintaining muscular balance.

REFERENCES

1. Costill, D. L. et al. *Research Quarterly for Exercise & Sports,* ***39***, 780 -785, 1968.
2. Gerodimos, N. et al. *J Sports Medicine & Physical Fitness,* ***43(4)***, 444 -452, 2003.

Table 1: The absolute (ABS) and relative (REL) peak torques (PT) of quadriceps in concentric and eccentric contractions.

Type of action	**Concentric period (knee extension)**			**Eccentric period (knee flexion)**		
Sports Event	**Runner**	**Jumper**	**Thrower**	**Runner**	**Jumper**	**Thrower**
Abs PT (Nm)	150.9 ± 21.3*	152.4 ± 32.4+	203.8 ± 36.9*+	176.7 ± 39.8*	197.8 ± 50.5	228.2 ± 43.1*
REL PT (Nm/kg)	2.0 ± 0.2	2.3 ± 0.5	2.2 ± 0.2	2.7 ± 0.7	3.1 ± 0.6	2.6 ± 0.6

Table 2: The absolute (ABS) and relative (REL) peak torques (PT) of hamstring in concentric and eccentric contractions.

Type of action	**Concentric period (knee flexion)**			**Eccentric period (knee extension)**		
Sports Event	**Runner**	**Jumper**	**Thrower**	**Runner**	**Jumper**	**Thrower**
Abs PT (Nm)	91.2 ± 11.4	86.6 ± 14.3	114.1 ± 21.7	98.2 ± 22.1	114.9 ± 30.8	140.6 ± 22.2
REL PT (Nm/kg)	1.4 ± 0.1	1.3 ± 0.1	1.2 ± 0.2	1.5 ± 0.3	1.8 ± 0.4	1.6 ± 0.3

* and + ： P < .05

Biomechanical Analysis of Punching Different Targets in Chinese Martial Arts

[1] Long-Ren Chuang, [2]Wei-Hua Ho, [1]Yu Liu, [2]Tyzz-Yuang Shiang
[1] Department of Chinese Martial Arts, Chinese Culture University, e-mail: allen@faculty.pccu.edu.tw
[2] Institute of Sports Equipment Technology, Taipei Physical Education College

INTRODUCTION

The research of punching motion in martial arts was focus on different gloves type, skill levels and styles of punching (Smith, 1986, Powell, 1989, Whiting, 1988). Only Yoshihuku [1] has compared the punching motion with target and none. So far, no one has done a thorough study to determine the difference among punching different targets. Our hypothesis was the martial arts athletes' punching motion would be affected by different material and mass of targets. The difference will show on kinematics of the upper extremity and muscle moment calculated by inverse dynamics. The results will help us to understand the coordination of upper extremity when punch different targets.

METHODS

Nine healthy Chinese martial arts athletes of Chinese Culture University aged 18-24 years, weight 70.1±14.2 kg and height 168±4.9 cm volunteered to participate in the experiment. They have to punch three different targets that include cardboard (0.2kg), small punching bag (9.2kg) and big punching bag (29.2kg). We used a Sony PD150 digital camera and Peak Motus 6.0 motion analysis system (60Hz) to catch the kinematics data of upper extremity. Then we applied the intersegmental dynamics formula that developed by Zernicke & Smith [2] to calculate the joint moment, muscle moment and interaction between the segments. One-way repeated-measures ANOVA were carried out for each of the dependent variables in the study. The probability level was set at $P < .05$.

RESULTS AND DISCUSSION

The fist peak velocity was significantly different when punching three different targets ($P<.05$). The fastest velocity of fist was punching the cardboard target (6.98±0.72 m/s), then was punching the small bag (6.06±0.68 m/s), and the lowest velocity was punching the big bag (5.43±0.82 m/s) . The contact time was significantly different when punching different targets, too. The shortest contact time was found in punching the cardboard (0.03±0.00 sec), then the small bag (0.10±0.01 sec), and the longest contact time was found in punching the big bag (0.14±0.05 sec). The kinematics results are similar to Yoshihuku's [1] study.

Figure 1 shows similar trend of elbow and shoulder moment curve when subjects punched three different targets. The results of elbow and shoulder moment were similar with penetrating strike in previous study [3]. In all moments, only the maximum shoulder flexion moment in the cardboard (156.51±142.22Nm), small bag (90.29±64.09Nm) and big bag (61.16±40.58Nm) were significantly different (P<.05).

The shoulder muscle flexion moment was larger when subjects punch the cardboard target than small and big targets

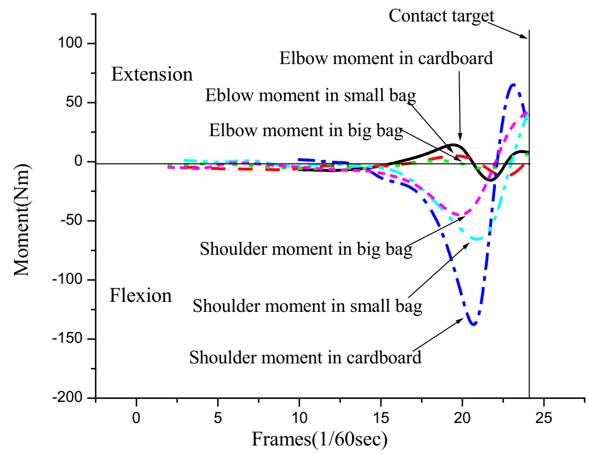

Figure 1. The subject 7 punched the different targets.The curve displayed the muscle moment of elbow and shoulder before contact

which indicated shoulder joint can fully flexion that make the fist velocity faster. On the contrary, the subjects wanted to recruit more muscle fibers and to raise the effective mass to participate when punching the heavy target. This phenomenon causes the shoulder muscle flexion moment and fist velocity decrease when punching the heavy target. The results agree with the principle of muscle loading and contraction velocity.

CONCLUSIONS

Different target mass will affect punching motion of subject's upper extremity. These results showed differences in the fist peak velocity, contact time and the maximum flexion shoulder muscle moment which could provide useful information for the athletes and coaches.

REFERENCES

1. Yasuo Yoshihuku & Yasuo Ikegami (1988), Biomechanical analysis of Tsuki motion. *Japan Journal Sports Science. 7*(12), 818-824.
2. Zernicke, R.F., Smith, J. (1996), Biomechanical insights into neural control of movement. In L. B. Rowell & J. T. Shepherd (eds.). *Handbook of Physiology Sec. 12: Exercise: Regulation and Intergration of Multiple System* 293-330.Oxford, NY: Oxford University Press.
3. Chuang, L.R., Liu Yu, & Yang Norman (1998), Intersegmental Dynamics Analysis of the Penetrating Strike and Surface Strike in the Chinese Martial Arts. *Abstracts of 1998 XVI International Society of Biomechanics in Sports,* 20.

ACKNOWLEDGEMENTS

This study was supported by a grant from National Science Council, Taiwan (NSC91-2413-H-034-001).

BIOMECHANICALLY DESIGNED SCIENTIFICALLY APPROPRIATE DIABETIC FOOTWEAR

Gautham Gopalakrishna, Mohamed Sadiq, Bhabendra Nath Das, Gnanasundaram Saraswathy
Shoe Design and Development Centre, Central Leather Research Institute, Chennai.India
email: gautham@clrim.org

INTRODUCTION

Mechanical factors play an important role in the etiology of a majority of foot ulcers. The stress and strain experienced by the diabetic foot is significantly different from that of the non-diabetic foot. This is because of the biomechanical abnormalities in the foot as a consequence of diabetic neuropathy. This paper looks at the factors responsible for the abnormal stresses and also examines the vital role of the footwear which is designed after the biomechanical analysis of the diabetic foot. Many foot complications due to external sources are prevented only by footwear and it is illustrated in this paper that prescription of footwear is a pre-requisite for the diabetic foot along with medical treatment.

The paper also highlights the use of biomechanical principles in designing the correct footwear and details criteria and materials for satisfying the requirements of a scientifically appropriate footwear for diabetics which is designed to provide for better shock absorption, reduced friction, better comfort and wear properties and most importantly helps in redistributing pressure uniformly on the plantar surface of the foot.

METHODS

a) A careful selection of patients was made and an adjusted sandal was fabricated for them. The footwear were fabricated with specially derived Rocker bottomed soles[1], to relieve biomechanical stresses
b) This was tested for its pressure reduction using an optical pedobarograph [2]
c) Pressure reduction was analysed
d) Wear trials was carried out and Wear pattern assessed

RESULTS AND DISCUSSION

From the pressure contours generated the significant changes in the pressure pattern as compared to the barefoot is evident. The pressure has been well distributed and reduced.

Sl. No	Bare foot Press. (KPa) **BFTP**	Inshoe Press. (KPa) **ISHP**	Sl No	**BFTP (KPa)**	**ISHP (KPa)**	Sl. No	**BFTP (KPa)**	**ISHP (KPa)**
1.	960	52	6.	534	33	11.	665	21
2.	670	45	7.	491	33	12.	676	35
3.	717	38	8.	694	40	13.	546	32
4.	786	45	9.	680	38	14.	684	40
5.	486	26	10	773	33	15.	645	37

Table 1: Plantar pressure readings - Barefoot Vs Specially designed footwear

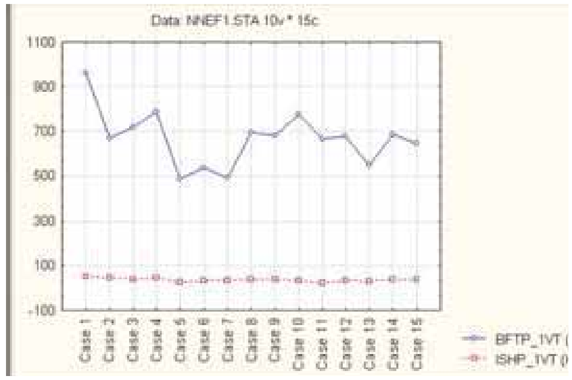

Figure 1 : Graphical representation of plantar pressures : Barefoot Vs Specially designed Footwear (BFTP = Barefoot Pressures; ISHP = Inshoe Pressure after wearing special footwear)

Table 1 and Figure 1 highlight the Barefoot pressures as well as the Inshoe pressures of subjects measured after wearing the specially designed footwear. As is amply demonstrated from the table, the underfoot pressures have reduced drastically on wearing the new footwear. On some of the patients, a follow-up study was done after three months and while there have been no drastic reduction in pressures in the follow up period as compared to the time when the initial pressures were measured on wearing the new footwear, in most of the cases the plantar pressures have either reduced or have remained unchanged.

The tabulated results clearly demonstrate that the design methodology adopted, selection of last and materials for the specially designed footwear have proven to be efficacious in minimizing underfoot pressures resulting in more comfort to the wearer.

The developed footwear targets specific high pressure areas particularly susceptible to neuropathic ulceration [3] and with the right combination of lasts, materials and design markedly reduces the pressures in these areas. The pedorthic therapeutic footwear, through use of specially designed rocker bottomed soles and custom moulded footbeds, relieves underfoot biomechanical pressures to a very large extent.

REFERENCES

1. Frykberg RG, Bailey LF, Matz A, et al. *J Am Podiatr Med Assoc 2002*;92(1):48-53Offloading properties of a rocker insole. A preliminary study.
2. Vijay Viswanathan et al. ***Diabetes Care***, February 1, 2004, Effectiveness of different types of footwear insoles for the diabetic neuropathic foot: a follow-up study.
3. Matthew L. Maciejewski et al. ***Diabetes Care***, December 1, 2004,Effectiveness of diabetic therapeutic footwear in preventing reulceration: response to Chantelau

MOVEMENT COORDINATION BETWEEN THE LUMBAR SPINE AND HIP WHEN PUTTING ON A SOCK

[1, 2]Gary LK Shum, [1]Jack Crosbie, [3]LW Sun and [3]Raymond YW Lee

[1] School of Physiotherapy, the University of Sydney, Sydney, Australia; [2] Physiotherapy Department, United Christian Hospital, Hong Kong; [3] Department of Rehabilitation Science, the Hong Kong Polytechnic University,Hong Kong;

Email: garyshum@student.usyd.edu.au

INTRODUCTION

Low back pain (LBP) is a major health and socioeconomic problem and is frequently associated with a change in the mobility of the lumbar spine and hips [1], resulting in various forms of functional disabilities. Many back pain patients complain of aggravation of their back pain during activities of daily living. However, there is a paucity of information on the coordination of movements between lumbar spine and hips during activities of daily living especially for those pathological spines. This study was to examine differences in the kinematics and joint coordination of the lumbar spine and hips when putting on a sock in asymptomatic subjects and patients with sub-acute low back pain.

METHODS

Subacute (with symptoms between 1 and 12 weeks) back pain subjects with (n=30) or without (n=30) straight leg raise (SLR) signs and normal asymptomatic subjects (n=20) were recruited. A three-dimensional electromagnetic tracking device was used for measuring movements of the lumbar spine and hips. Kinematic data was captured while each subject put on a sock from a sitting position and each subject was asked to put on the sock on legs of both the painful side (PS) and non-painful side (NP). The kinematic patterns of lumbar spine and hips were analyzed. Coordination between the two joints was studied by cross-correlation. This identifies the strength of correlation and phase lag of the two movements.

RESULTS AND DISCUSSION

The results generally showed that LBP has altered the lumbar-hip coordination accordingly (Table 1). It is interesting to note that when putting on a sock on the painful side (PS), there were marked alteration in the strength of cross-correlation between lumbar spine and hip. In groups 2 and 3, there was a significant decrease in the strength of correlation between flexion of the lumbar spine and hip. However, there were significant increases in the strength of the cross-correlation in other planes of motion. It is suggested that subacute back pain patients developed well-coordinated compensatory responses in performing activities of daily living.

It was also found that when back pain subjects putting on a sock with positive SLR sign there was altered lumbar-hip coordination in regard to the phase lag. When putting sock on the painful side, the lumbar spine flexed much earlier than hip in subjects with limited SLR when compared to normal subjects (phase lag = 0s, 0s and 2s for Groups 1, 2 and 3). Moreover, the coordinated activity with different planes of hip movements was affected by the presence of SLR sign. This further suggests that joint coordination is markedly influenced by the presence of SLR sign while putting on a sock with a positive SLR sign.

CONCLUSIONS

Our study showed that low back pain will affect not only the lumbar-hip coordination but also the coordination within the hip joint. Assessment of back pain patients should include kinematic analysis of the spine as well as hips.

REFERENCES

1. Shum GLK, Crosbie J and Lee RYW. *Spine*, **in press**, 2005.

Table 1. Mean (SD) maximum normalised cross-correlation coefficient for different the lumbar spine and hip movements.

Cross-correlation coefficients	Group 1 Normal	Group 2-LBP PS	Group 2-LBP NP	Group 3-SLR PS	Group 3-SLR NP
LxF & Hip F	0.98 ± 0.01	0.96 ± 0.02*	0.97 ± 0.02	0.95 ± 0.05*	0.96 ± 0.04*
LxR & Hip F	0.75 ± 0.23	0.84 ± 0.21*	0.87 ± 0.14*	0.89 ± 0.11*	0.89 ± 0.2*
LxR & Hip R	0.64 ± 0.2	0.76 ± 0.16*	0.69 ± 0.22	0.73 ± 0.17*	0.66 ± 0.17
LxSF & Hip F	0.72 ± 0.22	0.84 ± 0.19*	0.8 ± 0.23	0.89 ± 0.11*	0.81 ± 0.19
LxSF & Hip S	0.62 ± 0.23	0.75 ± 0.18*	0.72 ± 0.23	0.74 ± 0.15*	0.67 ± 0.2
Completion Time	4.8 ± 1.0	8.0 ± 2.5*	8.4 ± 3.0*	9.4 ± 3.2*	9.2 ± 2.8*

Lx = Lumbar; F = Flexion; R = Rotation; S = Lateral Flexion; NP = putting socks on non-painful side; PS = putting socks on painful side.

* $P < 0.05$, significant difference in symptomatic subjects when compared with asymptomatic subjects (Group 1).

CONTRIBUTIONS OF LOWER LIMB JOINTS TO SUPPORT THE BODY IN UNEXPECTED STEP-DOWN WALKING

[1] Sungjae Hwang, [1] Seongsik Myeong, [1,2] Hansung Kim and [1,2] Youngho Kim
[1]Dept of Biomedical Engineering, Yonsei University, Korea,
[2]Institute of Medical Engineering, Yonsei University, Korea;
email: yhkim@dragon.yonsei.ac.kr, web: biomecha.yonsei.ac.kr

INTRODUCTION

The generation of the forward movement and the stable support of the upper body are two important roles of the lower limb in walking [1]. The function of the body support has been recently received much attention. The concept of the support moment, defined as the sum of all joint moments in the lower limb, has been used to determine the relative contribution of the lower limb joint moments to prevent the collapse [2].

Falling is a serious problem among the elderly population, frequently resulting in physical injuries. The unexpected walking is one of the most probable cause of falling in the elderly [3]. However, the postural recovery mechanism based on the support moment in the unexpected walking has not been clearly defined yet.

In this study, dynamic simulations were performed to analyze contributions of the lower limb joints for the support moment in the unexpected step-down walking based on 3-D motion analysis data.

METHODS

A 27 year-old male subject (height: 170cm, weight: 68kg), with no gait problems in gait, participated in the 3D motion analysis. Six infrared cameras (Vicon 612, USA) were used to capture movements of sixteen reflective markers based on the Davis protocol for the gait analysis of the lower extremity [4]. For the unexpected step-down walking, a movable platform was designed to provide vertical perturbations during gait. Computer simulations were performed using Lifemode (Biomechanics Research Group, USA). A 3D virtual skeletal model for the simulation was composed of seven segments. Gait simulations were performed by translational and rotational motion capture data. Motion capture data obtained by the 3D motion analysis system were imported to the generated skeletal model. The model for this study calculated the vertical acceleration of the upper body, which was produced by the support moment estimated at each joint. In order to calculate joint moments for the support in walking, gait phases were divided into right mid-stance, double limb support, and left mid-stance (Figure 1).

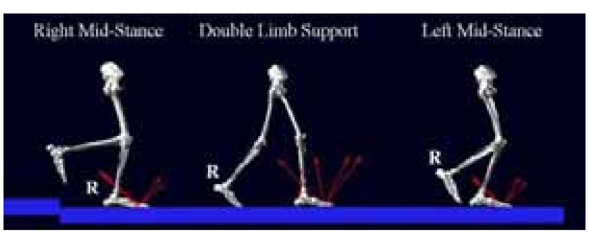

Figure 1: Simulation results from the forward dynamics in unexpected step-down walking.

RESULTS AND DISCUSSION

Figure 2 shows vertical accelerations of the pelvic center in the unexpected step-down walking. In the unexpected step-down walking, the right ankle joint was the most primary contributor for vertical accelerations. In the unexpected step-down walking, the vertical acceleration at right mid-stance, contributed by the right ankle and knee joints, was very large. Since in the unexpected step-down walking, no roll-over mechanism of the foot exists, at first the forefoot contacted to the ground and then progressed to double-limb-support. At left mid-stance phase, the subject kept his balance for repositioning of the over-advanced COG through that the subject stepped left foot forcefully. This caused the left ankle moment large during left mid-stance.

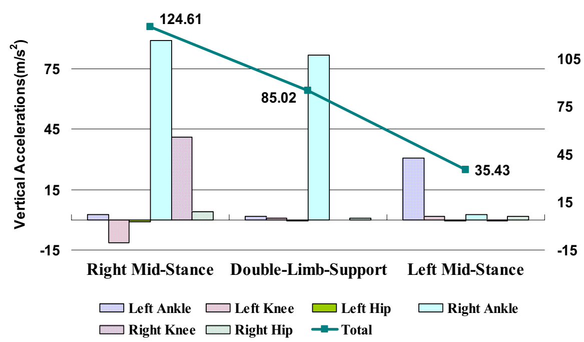

Figure 2: Vertical accelerations of the pelvic center in unexpected step-down walking.

CONCLUSIONS

In the unexpected step-down walking, the important contributors during single-limb-support are not only ankle plantar flexors but also knee extensors.

This study, analyzing the relative contributions of the lower limb joint moments for the body support would be helpful to understand many unexpected walking and compensatory mechanisms for various pathological gaits.

REFERENCES

1. Winter DA. *The Biomehcanics and Motor Control of Human Gait*, University of Waterloo Press, 1991.
2. Winter DA. *J Biomech* **13**, 923-927, 1980.
3. Runge CF. *Gait and Posture* **10**, 161-170, 1999.
4. Davis RB, et al. *Human Movement Science* **4**, 575-578, 1991.

ACKNOWLEDGEMENTS

This research was supported by the Program for the Training of Graduate Students in Regional Innovation which was conducted by the Ministry of Commerce, Industry and Energy of the Korean Government.

Dynamical Analysis of Indoor Eight People Make Tug of War Attack Movements- "European Back-Step" and "Japanese Back-Step"

Fong-Wei Wang and Chien-Lu Tsai
Nation Taiwan Normal University
Email : s08048@yahoo.com.tw

INTRODUCTION

The "European Back-Step" Indoor Tug of War attack movement has been developed for more than one hundred years, and it is the most popular movement style in Europe. The "Japanese Back-Step" Indoor Tug of War attack movement is new technique from Japan. Both of the techniques have their own supporters. The purposes of this study were to investigate the kinetics parameters of Indoor Eight People Make Tug-of-War "European Back-Step" and "Japanese Back-Step" attack movements. We would like to find out which movement style is more powerful and more efficient.

METHODS

The subjects were 8 Taiwan Indoor Tug-of-War national team pullers (174.1±3.6cm, 72.7±2.4kg, 22.1±2.4 year). Two Redlake High-Speed video cameras (60Hz) and a Kistler (9287) Force Plateform (600Hz) were used to collect the 3D kinematical data and the ground reaction force of the subjects. The 3D data were analyzed by Kwon3D motion analysis system and the 6-second duration time of ground reaction force were analyzed by Bioware software. A Paired–samples t-test was used to compare the differences between "European" & "Japanese" back-step attack movements. The level of significance was $\alpha = .05$ in this study, and the statistical software was SPSS 12.0 version.

RESULTS AND DISCUSSION

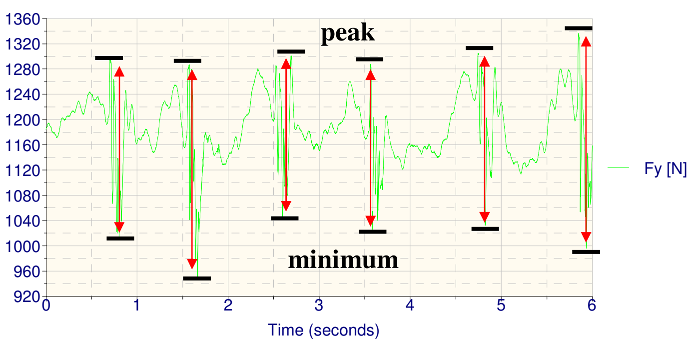

Figure 1: The curve of the peak and minimum backward ground reaction force (GRF)

We found that there were several cycles with peak and minimum backward ground reaction force (GRF) in the duration time in figure 1. The athletes should increase both the peak and minimum GRF in the competition. From the figure 2, we found there was a greater peak backward GRF in "Japanese Back-Step" (1.9bw) than "European Back-Step" (1.85bw). And there was a greater minimum backward GRF value in "Japanese Back-Step"(1.55bw) than the value of "European Back-Step"(1.47b w) (P< .05). That meant the "Japanese Back-Step" was more powerful than the European style both in the peak and the minimum GRF.

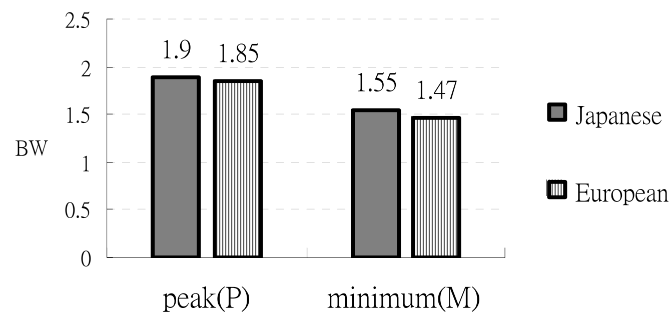

Figure 2: The peak and the minimum backward GRF of "European Back-Step" and "Japanese Back-Step"

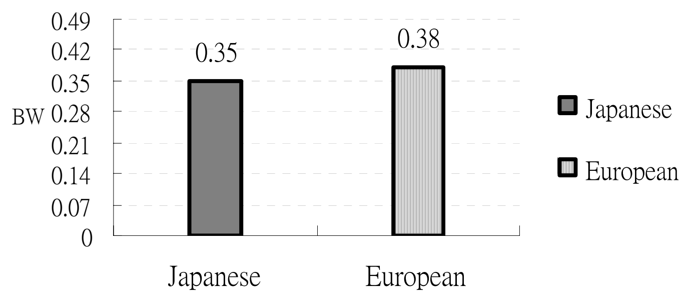

Figure 3: The value between the peak and minimum backward GRF

From the figure 3, the value between the peak and the minimum backward GRF of "Japanese Back-Step" (0.35bw) attack movement was less than that of "European Back-Step" (0.38bw) (p< .05). That meant the "Japanese Back-Step" was more constant than the European style. As the results, there was better performance in the "Japanese Back-Step" than that in the "European Back-Step" in the kinetics parameters.

CONCLUSIONS

As result showed, there were greater the peak, the minimum and the less value between peak and minimum backward ground reaction force of the "Japanese Back-Step" than those value of the "European Back-Step". That meant the "Japanese Back-Step" was more powerful and more efficient than the European Back-Step style. It is recommended that athletes should practice the Japanese Back-Step attack movement in the future.

REFERENCES

1. Dempster, W. T.(1958). Analysis of two-handed pulls using free body diagrams. *Journal of Applied Physiology,* ***13****(3)*, 469-480
2. Da,K.(1995).*Technique indoor tug-of-war.Training Manual: Basic Training*. DC: Tug of War International Federation.

DO KINEMATICS OF THE PELVIS AND LOWER LIMB VARY BETWEEN NOVICE AND HIGHLY TRAINED CYCLISTS?

[1,2]Andrew R Chapman, [1]Bill Vicenzino, [2]Peter Blanch, [3]Steve Dowlan and [1]Paul W Hodges
[1]Division of Physiotherapy The University of Queensland, [2]Department of Physical Therapies Australian Institute of Sport,
[3]Department of Biomechanics Australian Institute of Sport
Email: andrew.chapman@ausport.gov.au

INTRODUCTION

Previous studies have shown that novice and highly trained cyclists use different patterns of leg muscle recruitment when cycling [1, 2]. Novice cyclists are characterized by greater individual variance, greater population variance, longer durations of muscle activity, more extensive and more variable muscle coactivation, and less modulation of muscle activity. The data also show that modulation of muscle activity decreases with increasing cadence in novice cyclists but is not influenced by cadence in highly trained cyclists. However, kinematics were not controlled in these studies of cycling so differences in leg muscle recruitment between novice and highly trained cyclists may relate to kinematic variations. The purpose of this study was to determine if kinematic variations are likely to account for differences in leg muscle recruitment between novice and highly trained cyclists.

METHODS

Participants were ten novice and ten highly trained cyclists. Four experimental conditions of cycling at 55-60, 75-80 and 90-95 rpm and preferred cadence were investigated in random order. Three dimensional kinematics of the pelvis and lower limbs and orientation of the bicycle crank arms were measured. Coordinates of 14 mm reflective markers were sampled at 250 HZ using a VICON 620 eight-camera motion analysis system (Oxford Metrics Ltd, Oxford, England). Marker trajectories were filtered using a GCVSPL algorithm to remove low frequency movement artifact and three dimensional kinematics were calculated using the Plug in Gait® model which has been described and validated previously (Version 1.8, Oxford Metrics Ltd: Oxford, England). Electromyographic (EMG) activity of leg muscles was also measured using methodology previously described [1] in three novice and two highly trained cyclists to confirm comparisons were of novice and highly trained cyclists in whom muscle activity varied as previously reported.

RESULTS AND DISCUSSION

The comparison of EMG data was consistent with previous findings of varied muscle activity between novice and highly trained cyclists. Patterns of movement (i.e. time series kinematic data) did not vary between novice and highly trained cyclists, but the absolute range of sagittal plane motion of the ankle was significantly less in novice cyclists (13.2 ± 7.7^{o}) than in highly trained cyclists (21.5 ± 9.0^{o}). Absolute ranges of motion of the pelvis, hip and knee was not different between groups. Cadence did not influence kinematics of the pelvic, hip, knee or ankle in either group.

Sagittal plane motion of the hip and ankle (i.e. hip flexion-extension and ankle dorsiflexion-plantarflexion) and knee and ankle (i.e. knee flexion-extension and ankle dorsiflexion-plantarflexion) were more coordinated in highly trained cyclists (r = 0.85 ± 0.07 and 0.76 ± 0.08) than novice cyclists (r = 0.65 ± 0.10 and 0.53 ± 0.08). Sagittal plane motion of the hip and ankle, and knee and ankle, were also more consistently coordinated (i.e. the degree of coordination between these movements varied less between pedal stokes) in highly trained cyclists (0.04 ± 0.02 and 0.05 ± 0.02) than in novice cyclists (0.09 ± 0.03 and 0.11 ± 0.02). Coordination and variability of coordination of sagittal plane hip and knee motion did not vary between groups.

Individual variance (i.e. variability of movement patterns between pedal strokes) did not vary between groups. Population variance (i.e. variability of movement patterns between cyclists) of flexion-extension of the hip was greater in novice cyclists (8.0 ± 1.6°) than in highly trained cyclists (4.2 ± 1.8°), but population variance of frontal motion of the knee was greater for highly trained cyclists (7.1 ± 1.1°) than novice cyclists (4.4 ± 1.2°). Population variance of other joint motions was not different between groups.

CONCLUSIONS

This study suggests that kinematics of the pelvis, hip, and knee do not vary between novice and highly trained cyclists. Differences in leg muscle recruitment between novice and trained cyclists may be explained in part by kinematic variations at the ankle. However, kinematic variations between novice and highly trained cyclists revealed in this study are unlikely to explain all aspects of varied leg muscle activity (e.g. longer durations and less modulation of muscle activity in novice cyclists). Greater coordination of motion between the hip and ankle and knee and ankle joints may reflect more skilled control of movement in highly trained cyclists. Furthermore, differences in the response of leg muscle recruitment to altered cadence in novice cyclists and highly trained, in whom decreased modulation of muscle activity with increased cadence was seen, are not likely to be associated with kinematic variations as cadence did not influence kinematics.

REFERENCES

1. Chapman A, Vicenzino B, Blanch P, Hodges P. Do muscle recruitment patterns differ between trained and novice cyclists? Medicine and Science in Sports and Exercise 2004;36:s169
2. McLean B. Neuromuscular and kinematic correlates of performance in cyclists. Masters Thesis. The University of Queensland, Brisbane, Australia: 1987

THE VIBRATION AND COEFFICIENT OF RESTITUTION ANALYSIS IN TENNIS RACKETS VARIED WITH MATERIAL COMPOSITION AND FIBER ARRANGEMENT

[1]Ti-Yu Chen , [1]Jinn-Yen Chiang, [2]Ching-Cheng Chiang , [3]Jong-Her Yang and [4]Der-Chia Lin
[1]National Changhua University of Education, Taiwan; email: chentiyu@yahoo.com.tw
[2]Chang Gung Institute of Technology, Taiwan
[3]Taipei Physical Education College, Taiwan
[4]National Council on Physical Fitness and Sports, Taiwan

INTRODUCTION

The increase in power of modern tennis could be attributed to stronger, better conditioned players, but the major reason was the modern racket of the consistent power making it possible (Groppel, 1992). However, there are strong indications that impact shock and post-impact vibration transfer in tennis racquet may lead to the epicondylitis humeri syndrome. This study was to investigate how the vibration on wrist joint of the player and rebounding velocity of the ball from each racket were affected by the vibration of various tennis rackets which were composed by the mixture of carbon fiber and glass fiber.

METHODS

There were eight different kinds of tennis racket, composed by mixing carbon fiber and glass fiber in the ratio of 1 to 0, 6 to 1, 5 to 2, and 4 to 3. The angles of the fiber were arranged in 22 degrees and 30 degrees with respect to the longitudinal axis.

The experiment 1 was to monitor the vibration on the wrist joint of participant and to find the logarithmic decrement ratio of vibration. Accelerometer was attached to participant's wrist joint to acquire the vibratory signals. The logarithmic decrement ratio, δ, was calculated using,

$$\delta = \ln\left(\frac{X_m}{X_{m+k}}\right)$$

where X_m and X_{m+k} are the amplitudes of vibratory wave between k periods.

For experiment 2, Peak Motus system with one high-speed video camera was used to record the kinematics data and to calculate the coefficient of restitution. The coefficient of restitution, e, was calculated using,

$$e = -\frac{V'}{V}$$

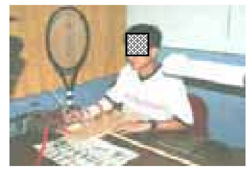

Figure: The accelerometer (attached to the wrist joint of participant) measuring chain.

where V and V' were the pre-impact and post-impact ball velocities.

RESULTS AND DISCUSSION

The results of the vibration logarithmic decrement ratio on wrist indicated that the pure carbon fiber made racket at 22 degrees had a higher value, and the value was significantly increasing as the content of carbon fiber in the racket was increasing. On the other hand, pure carbon fiber made racket had higher stiffness that its coefficient of restitution was higher than glass fiber made racket. This phenomenon indicated that the wrist joint would absorb more vibratory energy from racket made by pure carbon fiber.

CONCLUSIONS

By increasing the content of glass fiber in the racket, it might be decreasing the load in the tennis player's arm on center or off-center impact. But it would affect the performance on ball rebound. On the other hand, the rackets with fiber angle at 22 degrees had lower vibration than that at 30 degrees.

REFERENCES

Groppel, J.L. (1992). *High Tech Tennis* (2nd ed.), 15-27. Champaign, IL: Leisure Press Inc.

Table: The mean and standard deviation of vibration logarithmic decrement ratio (δ) and the coefficient of restitution (e) with various tennis rackets material and fiber angles (mean ± SD)

Fiber Angle	Percentage of Carbon							
	100%		86%		71%		57%	
	δ	e	δ	e	δ	e	δ	e
22 Degrees								
Center Impact	2.14±0.13	0.33±0.02	1.68±0.12	0.31±0.01	1.86±0.37	0.32±0.02	2.16±0.16	0.32±0.02
Top Impact	1.71±0.10	0.16±0.02	1.41±0.10	0.13±0.03	1.58±0.24	0.11±0.02	1.25±0.10	0.11±0.02
Bottom Impact	0.42±0.07	0.37±0.02	0.65±0.07	0.36±0.02	0.57±0.15	0.36±0.04	0.77±0.06	0.32±0.01
30 Degrees								
Center Impact	2.04±0.14	0.32±0.01	1.21±0.16	0.30±0.02	1.71±0.22	0.31±0.03	1.29±0.08	0.31±0.02
Top Impact	1.15±0.07	0.16±0.01	1.40±0.10	0.15±0.01	1.16±0.07	0.12±0.01	1.35±0.12	0.13±0.03
Bottom Impact	0.73±0.14	0.41±0.02	0.61±0.07	0.37±0.02	0.56±0.08	0.35±0.02	0.69±0.14	0.34±0.02

THE BODY CENTER OF MASS DISPLACEMENT DURING VARIOUS TYPES OF SUPPORT SURFACE PERTURBATION

[1,2] Chiung Ling Chen, [1]Fong Chin Su, [3]Hong Wen Wu [2]Kwok Tak Yeung and [4]Chia-Wei Liu
[1]Institute of Biomechanical Engineering, National Cheng Kung University, Tainan, Taiwan,
[2] School of Occupational Therapy, Chung San Medical University, Taichung, Taiwan; email: joelin@csmu.edu.tw
[3] Department of Physical Therapy, and [4]Institute of Medical Science, China Medical University, Taichung, Taiwan

INTRODUCTION

Previous studies have revealed differences of muscle responses between translational and rotational platform perturbation [1,2]. The differences in the organization of postural responses were ascribed to the different mechanical demands of the perturbations. Regulation of the body center of mass (COM) seemed to be the main function of postural control. No kinematic data including COM trajectory were collected to test the effects of all four of the platform displacements (forward/backward translation, F/B and toe-up/toe-down rotation, U/D), perform at same velocity, on the same subjects. Allum et al (2001) used combinations of support surface rotation and backward translation (BU and BD) to induce balance corrections [3]. It seemed to increase task difficulty. Two additional types of combination of support surface rotation and forward translation (FU and FD) were not studied in the literature. Therefore, the purpose of this study was to investigate the differences of COM trajectories under various types of support surface perturbations including uni-axial (F, B, U and D) and bi-axial (BU, BD, FU and FD) perturbations.

METHODS

Six healthy subjects (4 males, 2 females; ages 19-22 years) consented to participate in the study. A tri-axial postural perturbation platform was used to provide both uni-axial and bi-axial support surface perturbation. The velocity and amplitude of platform movement was 50 mm/s for 70mm or 50 degree/s for 7 degrees, respectively. All subjects were tested under eight types of perturbations with 3 trials of each perturbation. These perturbations were delivered in a random sequence and commenced 1 second after the start of the data collection. A six-camera video-tracking motion analysis system (Motion Analysis Corp., CA, USA) was used to collect three-dimensional kinematic data with thirty-nine retro-reflective spherical markers fixed over the whole body of the subjects. The data was collected at 200Hz for 3seconds. The 13-segment model was used to calculate the total body COM. We divided the COM trajectories into two phases: a passive imposed postural sway and an active automatic postural reaction phases. The maximal horizontal (anterior/posterior, A/P), vertical and medial-lateral displacement of the body COM with respect to support surface in two phases was measured respectively.

RESULTS AND DISCUSSION

There were no differences of the maximal medial-lateral COM displacement among various types of perturbation, and the means were range from 10 to 20 mm. Table 1 presents the COM displacement and Figure 1 shows the COM trajectories in A/P horizontal and vertical directions. During uni-axial perturbation, all the four types of perturbation induced quite a large horizontal COM displacement, while the forward translation induced larger displacement than the others. Platform rotation (U and D) induced more vertical COM displacement than translation. All the bi-axial perturbation induced more horizontal displacement than uni-axial perturbation. The BD and FU tests demonstrated the adding effects of the imposed sway. However, the vertical displacement conformed to the expected adding and counterbalanced effects. In automatic postural reaction phase, translational tests recovered more displacement than rotational tests. Because rotational tests changed the end COM position by bringing the COM forward in D test and backward in U test. During bi-axial BU and FD test, the subjects recovered larger displacement in horizontal and vertical directions than BD and FU tests. It was assumed that the “enhanced” ankle input of BU and FD generated agonist stretch reflex that stabilizes the posture. Whereas the “nulled” ankle input of BD and FU tests produced weaker balance-reaction responses regardless of the greater imposed postural disturbance. It was presumed that BD and FU tests are the more challenge tests for balance control.

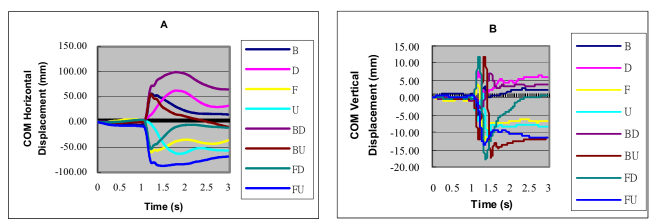

Figure 1: The horizontal trajectory (A) and the vertical trajectory (B) of the body COM of eight types of support surface perturbation.

REFERENCES

1. Keshner EA, et al. *Exp Brain Res* 71, 455-466, 1988.
2. Nardon A, et al. *Brain* 113, 65-84, 1990.
3. Allum JHJ, et al. *Gait and Posture* 14, 217-226, 2001

ACKNOWLEDGEMENTS

Supported by NSC 93-2320-B-040-036, Taiwan.

Table 1: Mean of the maximal horizontal and vertical displacement of the body COM during the passive imposed sway and active postural reaction phases in eight types of support surface perturbation

Displacement (mm)	Horizontal								Vertical							
	B	D	F	U	BD	BU	FD	FU	B	D	F	U	BD	BU	FD	FU
Imposed Sway	63.25	53.06	-66.97	-63.98	91.31	71.89	-69.69	-89.3	-8.25	12.88	4.56	-9.47	4.31	-15.89	18.05	-9.24
Postural Reaction	-65.46	-23.41	55.89	23.66	-55.30	-74.93	68.92	32.38	13.6	8.45	9.57	12.52	14.74	32.34	-21.48	10.26

ARREST OF FORWARD FALLS ONTO OUTSTRETCHED HANDS IN HEALTHY YOUNG WOMEN

[1,2]Lisa Case, [1]Jia-Hsuan Lo, [1,2]James Ashton-Miller
[1]University of Michigan, Department of Mechanical Engineering
[2]University of Michigan, Department of Biomedical Engineering; email: lcase@umich.edu

INTRODUCTION

Fall-related injuries are projected to cost the United States $85 billion per annum by the year 2020 [1]. Some 60% of all falls in older adults are in the forward direction [2]. Past studies have examined the biomechanics of forward fall arrests from different heights, onto different surfaces, and using different strategies. These studies, however, involved men; none address how forward falls are arrested by women. This is surprising since elderly women have 1.2 to 2.2 higher rates of falls [3], and are 1.8 to 2.2 times more likely to sustain an injury in a fall [4], than men. We first quantified how a group of healthy young women use their upper extremities to arrest standardized forward falls from three different heights, one of which was similar to that used in a two-height test protocol developed for men [5]. We tested the null hypothesis in women that fall height would not affect the magnitude of the ground reaction force, pre- and post-impact arm kinematics, or arm muscle EMG patterns. Finally, by comparing these results with the published male data [5] obtained using similar methods, we tested the hypothesis that there is no effect of gender on these parameters.

METHODS

Ten healthy young women [mean (SD): age: 24.5 (2.1) yrs, body weight: 585 (61) N; height: 163.7 (4.3) cm] volunteered for this study. Kinematic markers were affixed to the subjects on both upper arms and forearms, left side of the head, neck and left thigh, as well as the left malleolus to collect kinematic data at 200 Hz with an Optotrak 3020 motion-tracking system. Three AMTI force plates were used to collect force and moment data at 2 kHz using the following protocol. RMS surface EMG was measured at 1 kHz in the left triceps, biceps, deltoid, pectoralis, neck extensor, and serratus anterior and a 50 ms window analyzed just prior to impact. Subjects were leaned 20° forward from vertical and held with a tether. The subject was then asked to bend at the waist with her arms out toward the force plates in front of her. The subject was then released, at the count of three, to arrest the fall, with each hand landing on a force plate. Two falls were performed from a neck marker height of 70 cm, followed by two falls from 80cm and three falls from 90 cm. Subjects were asked to fall naturally using only their arms. Because the fall heights were 75 and 100 cm in the male study and since the women's data appeared linear across fall heights, linearly-interpolated male values at 80 and 90 cm were used in the gender comparisons. Repeated measures analysis of variance (rm-ANOVA) were used to test the hypotheses (using $p<0.05$ for significance).

RESULTS AND DISCUSSION

In the women, the peak ground reaction force, F1, normalized by body weight, increased with fall height (Table 1, rm-ANOVA, $p<0.05$). Their elbow flexion angle at impact, Θ, did not vary significantly across the fall heights ($p>0.10$). The increase in elbow flexion from impact through the first 500 ms of the fall arrest, $\Delta\Theta$, however, did increase with fall height ($p=0.003$), leading us to reject the first hypothesis. Pre-impact triceps activation, EMG_{tri}, shown as a percentage of a maximum triceps contraction, did not vary with fall height ($p>0.05$). Comparing these parameters with published results for men [5], no gender difference was found in F1 after normalization by body weight ($p=0.376$). There was also no difference in the elbow flexion at impact ($p=0.177$) or in pre-impact triceps activation ($p>0.05$). The remarkable finding was the significant, almost 4-fold difference, in the post-impact increase in elbow angle ($p = 0.039$; Figure 1). Therefore, we rejected the null hypothesis of no gender differences in the forward fall arrest strategy under these test conditions. We speculate that these healthy young women may have limited post-impact elbow flexion to reduce the risks of elbow buckling and, thereby, head impact.

Table 1: *Mean (SD) initial elbow angle (**Θ**) at impact, post-impact increase in elbow angle (**$\Delta\Theta$**), maximum impact force (**F1**), and triceps EMG (**EMGtri,** % max) for the women. [Θ = 180° = full arm extension]*

Fall Ht.	Θ (°)	$\Delta\Theta$ (°)	F1 (N)	EMG_{tri} (%)
70 cm	166 (6)	15 (7)	482 (75)	66 (30)
80 cm	169 (7)	22 (12)	584 (79)	67 (34)
90 cm	168 (7)	31 (12)	648 (90)	70 (31)

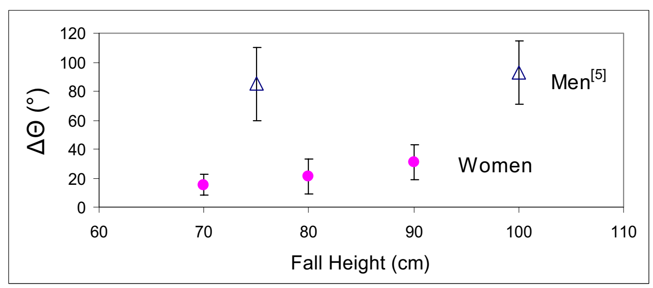

Figure 1: *A 4-fold gender difference in the mean post-impact change in elbow flexion (**$\Delta\Theta$**) was found. Bars denote SD.*

CONCLUSIONS

1) In healthy young women, increasing fall height:
   a. Did not affect elbow flexion angle at impact
   b. Did increase normalized impact forces
   c. Did increase post-impact elbow flexion.
2) Healthy young women permit significantly smaller increases in post-impact elbow flexion than men.

REFERENCES

1. Englander, F., et al., *J Forensic Sci* **41**, 733-764, 1996.
2. O'Neill, T.W., et al., *Annals Rheum Dis* **53**, 773-775, 1994.
3. Luukinen H., et al., *J Clin Epid* **47**, 843-850, 1994.
4. Malmivaara, A., et al., *Am J Epid* **138**, 384-394, 1993.
5. DeGoede, K.M., *J Biomech* **35**, 843-848, 2002.

A KINEMATIC MODEL OF THE UPPER EXTREMITY WITH GLOBALLY MINIMIZED SKIN MOVEMENT ARTEFACTS

[1] Tung-Wu Lu, [1] Yen-Sheng Lin, [1, 2] Mei-Ying Kuo, [2] Horng-Chaung Hsu, [1] Hao-Ling Chen
[1] Institute of Biomedical Engineering National Taiwan University, Taipei, Taiwan
[2] Department of Orthopaedics, China Medical University Hospital, Taichung, Taiwan
Email: twlu@ntu.edu.tw

INTRODUCTION

The human upper extremity plays an important role in activities of daily living. Knowledge of the kinematics of the joints of the upper limb is helpful for the understanding of its normal function. Most published kinematic models of the upper extremity oversimplified the shoulder complex and forearm due to their great complexity and huge skin movements [1,2]. These simplifications may lead to erroneous results that can be further magnified by skin movement artefacts, limiting their clinical applications. No quantitative validation was offered for these models. Measurement of the scapular kinematics presents another problem due to its large relative movement underneath the skin.

In motion analysis, segmental positions and orientations were mostly calculated without joint constraints, leading to errors in calculated joint motion and artifactual joint dislocations[3]. This problem can be resolved by the global optimization method (GOM) [3]. The purpose of the study was to develop an upper extremity model considering all the bones and joints, and to use the GOM to reduce skin movement artefacts. The model was validated with skeletal marker data of the scapula.

METHODS

The human upper extremity was modelled as a series of 25 rigid links connected by 24 single-degree-of-freedom (SDOF) joints. The shoulder complex was modeled as a spatial mechanism with 14 rigid links, including the trunk, clavicle, scapula and humerus. The scapulothoracic (ST) joint was modelled as a 5-DOF joint; sternoclavicular (SC) joint as a 3-DOF joint; acromioclavicular (AC) as a 3-DOF joint; and glenohumeral (GH) joint as a 3-DOF joint. The forearm was modeled as a mechanism with 11 rigid links, including the ulna, radius and hand. The distal and proximal radioulnar joints were each modelled as 3-DOF joints, the elbow joint as 1-DOF and wrist as 2-DOF joints.

These multi-DOF lower-pair joints were modelled as a series of SDOF joints connected by virtual links and described following the Denavit-Hartenberg notation [4]. There were a total of 12 DOFs in this upper limb mechanism, Fig. 1. These 12 independent variables (IV) were obtained using measured data and the other dependent variables (DV) obtained by solving loop equations at the shoulder and forearm. Minimization of the skin movement artefacts was achieved with the GOM.

For the validation of the model, scapular kinematic data from 5 healthy male subjects implanted with bone pins were obtained by a 7-camera motion analysis system (Vicon 370, Oxford Metrics, U.K.) during humeral elevation (HE) in the scapular plane, forward reaching and manual wheelchair propulsion (MWP). The measured skin marker data were input into the model and the predicted scapular kinematics were compared with those measured with the skeletal markers.

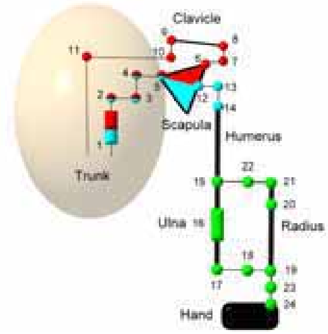

Figure 1: The mechanism of the upper extremity model. Prismatic joints are represented as rectangles and revolute joints circles.

RESULTS AND DISCUSSION

The root mean squared errors (RMSE) of the model-predicted scapular protraction, rotation and tilt during HE were 4.61°, 1.54° and 4.14°, respectively. The corresponding values were 3.21°, 2.90° and 3.07° for reaching and 2.20°, 2.96° and 1.70° for MWP. The RMSEs of translation were all within 8mm.

A three-dimensional kinematic model of the human upper extremity was developed, allowing the prediction of the scapular orientation and position as well as all other joints during dynamic movements using skin markers with GOM to minimize the skin movement artefacts. Comparisons of the model predicted scapular kinematics with those measured with skeletal markers provided a direct and quantitative validation of the model. The model will be useful for the study of the function and biomechanics of the upper extremity and with further development to include the kinetic analysis of the upper extremities.

REFERENCES

1. Davis JL, et al. *J Rehabil Res Dev* **35**, 61-72, 1998.
2. Garner BA and Pandy MG *Computer Methods in Biomedical Engineering* **2**, 107-124, 1997.
3. Lu TW and O'Connor JJ, *J Biomech*, **32**, 129-134, 1999.
4. Denavit BJ and Hartenberg RS, *J App Mech*, 215-221, 1955.

REDUCED PLANTARFLEXOR CONTRIBUTIONS TO SUPPORT IN POST-STROKE HEMIPARETIC GAIT

[1,2,4]JS Higginson, [1,2]FE Zajac, [5]RR Neptune, [6,7]SA Kautz, [1,2,3]SL Delp
[1]VA Palo Alto Rehab. R&D Ctr., [2]Depts. of Mech. Eng. and [3]Bioeng., Stanford University,
[4]Dept. of Mech. Eng., Univ. of Delaware, [5]Dept. of Mech. Eng., Univ. of Texas at Austin,
[6]VA Brain Rehab. Research Ctr., [7]Dept. of Phys. Ther., Univ. of Florida; email: higginson@me.udel.edu

INTRODUCTION

Muscle-actuated forward dynamic simulations of self-selected and slow walking speeds have shown that the ankle plantarflexors are supplemented by the uniarticular knee extensors to provide body weight support in midstance [1,2]. Patients with severe ankle plantarflexor weakness show reduced walking speed and compensatory strategies related to the strength of hip and knee extensors [3]. This case study presents the first muscle-actuated forward dynamic simulation of post-stroke hemiparetic gait over the entire gait cycle and demonstrates one way that post-stroke muscle contributions to support differ from those of neurologically healthy older adults.

METHODS

Two forward dynamic simulations of slow gait (0.3 m/s) were developed based on the walking patterns of healthy older adults [4] and an individual with post-stroke hemiparesis who walked with his paretic knee abnormally flexed during midstance. A 2D musculoskeletal model consisting of a trunk, pelvis and two legs was developed using SIMM [5] and actuated by 15 Hill-type muscle-tendon units per leg, including the soleus (SOL), gastrocnemius (GAS), vasti (VAS), tibialis anterior (TA), gluteus maximus (GMAX) and biceps femoris short head (BFSH). Muscle excitation patterns (i.e., onset, offset, magnitude) were assumed symmetric for healthy slow gait, and asymmetric for post-stroke gait. Dynamic optimization was used to find the appropriate muscle excitation patterns that best emulated the experimental kinematics and kinetics during slow and post-stroke hemiparetic gait. To assess the contribution of each muscle to support of the center of mass (COM), individual muscle forces were reduced to zero during midstance (i.e., middle third of the total stance duration) while all other muscle forces remained unchanged. The effect of each muscle force perturbation on vertical position of the COM was quantified 0.06 seconds later.

RESULTS AND DISCUSSION

Experimental kinematics and vertical ground reaction forces were reproduced by the simulations of slow and post-stroke hemiparetic gait. Muscle excitations agreed reasonably well with EMG [6]. Compared to healthy slow gait, peak excitation of the paretic and non-paretic plantarflexors were unaltered, paretic TA and BFSH excitations prolonged and increased, and paretic and non-paretic VAS excitations shortened.

In midstance, on the non-paretic side, SOL, GAS and VAS contributed less to support than in speed-matched healthy older adults (Figure 1) due to reduced contributions to extension of the ankle, knee and hip by SOL and GAS. The non-paretic TA no longer opposed COM support, thus less effort was required by the plantarflexors.

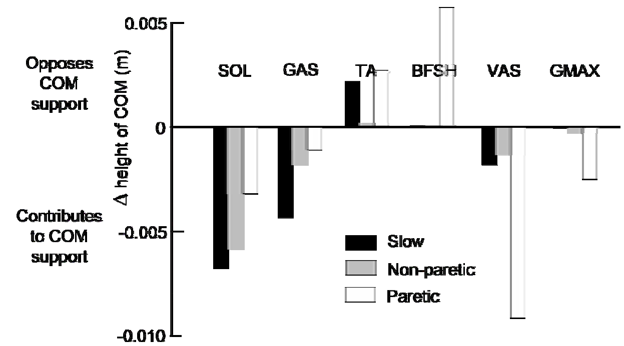

Figure 1: Contributions of key muscles to midstance support of COM in slow and post-stroke hemiparetic gait.

On the paretic side, the plantarflexor contributions were reduced even further (Figure 1), with compensation to COM support provided by VAS, GMAX and other muscles not shown. Although paretic TA and BFSH midstance activity may enhance ankle and knee stability, respectively, these muscle actions opposed COM support. Because the model used in the analysis was 2D, the hip abductor contributions to COM support have been neglected and may be significant [7].

CONCLUSIONS

These simulations represent the first muscle-actuated forward dynamic simulations of healthy slow and post-stroke hemiparetic gait, characterized by a flexed paretic stance knee posture. Despite reorganization of paretic and non-paretic muscle coordination patterns with respect to that of speed-matched healthy older adults, adequate body weight support was provided by altered muscle contributions.

REFERENCES

1. Neptune et al., *J Biomech*, 34(11): 1387-98, 2001.
2. Higginson et al., submitted. *J Biomech*.
3. Mulroy et al., *Gait & Posture,* 18: 114-125, 2003.
4. Chen et al., in press. *Gait & Posture*.
5. Delp and Loan, *Comput Biol Med,* 25: 21-34, 1995.
6. den Otter et al., *Gait & Posture*, 19(3): 270-8, 2004.
7. Anderson and Pandy, *Gait & Posture,* 17: 159-169, 2003.

ACKNOWLEDGEMENTS

We thank G. Chen and D. Kothari for providing the slow gait data [4], L. Worthen and M. Kim for collecting the post-stroke gait data, and the supercomputing resources at Stanford University. Funding was provided by the Rehabilitation R&D Service of the U.S. Department of Veterans Affairs and NIH GM 63495. This work is based on Jill Higginson's Ph.D. thesis (2005).

INTERNAL BONE STRESS ANALYSIS OF TIBIAL IMPLANT WITH INCORPORATION OF SOFT TISSUES

[1]Anthony G. Au, [2]V. James Raso, [2]Adrian B. Liggins and [1]A. Amirfazli
[1]Department of Mechanical Engineering, University of Alberta, Edmonton, Alberta, Canada
[2]Capital Health Authority, Glenrose Rehabilitation Hospital Site; email:a.amirfazli@ualberta.ca, web: www.mece.ualberta.ca

INTRODUCTION

Stress shielding at the proximity of total knee replacement (TKR) implants can cause of aseptic loosening and weakened implant fixation. Reduction of stress shielding is therefore a focus of current TKR design. A finite element (FE) tool was recently developed, improving upon the state of the art for stress analysis of the tibia. It addresses deficiencies of past FE models by giving special consideration to the incorporation of realistic geometry, material properties, and loading to provide improved analysis of bone stress states. A better representation of stress states in the post-TKR tibia will allow for better implant design. This paper presents a parametric analysis of the effects of TKR tibial component design on stress shielding.

METHODS

A 3D tibia, incorporating orthotropic and heterogeneous bone properties mapped directly from experimental data, was used. Loading representative of the stance phase of gait was applied. Tibiofemoral and patellofemoral surfaces were loaded with non-uniform distributed compressive forces while 4 ligament (ACL, PCL, MCL, LCL) and 6 muscle (gracilis, sartorius, semitendinosus, semimembranosus, popliteus, iliotibial tract) forces were distributed over experimentally determined attachment areas. The ACL and PCL were each divided into anterior and posterior bands; the MCL was divided into deep and superficial bands. The lines of action for each ligament and muscle were assigned for various intervals of the gait cycle. This realistic approach to incorporating loading conditions is rarely done in FE models.

The tibial TKR component, modeled after a commercially available implant, consisted of a metal tray, a polyethylene insert, and a post fixed to the tibia by bone cement. Three FE tibia implant models were created featuring a Ti6Al4V tray (E=117 MPa, ν=0.3), a CoCrM tray (E=220 MPa, ν=0.3), and a stainless steel (AISI 316 L) tray (E=200 MPa, ν=0.3). Cement-bone interface forces were examined for the models at 3 locations: beneath the tray, around the periphery of the post, and beneath the post. Stresses were compared with those from a model representing the natural tibia (with identical loading conditions) to examine the stress changes associated with introduction of an implant. Stress shielding was assessed by examining global changes in stress distribution and stress changes in the cancellous bone immediately surrounding the post.

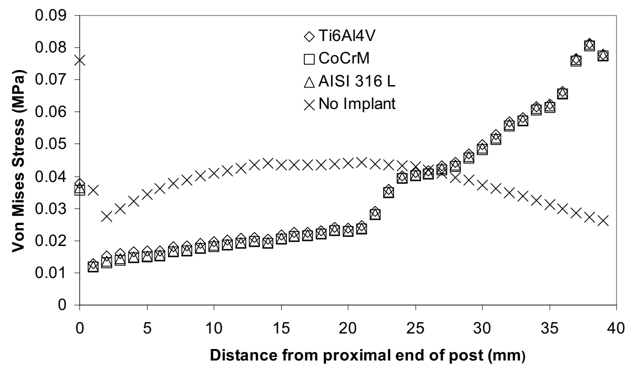

Figure 1: Stress in cancellous bone posterior to implant post from the proximal end to the distal end of the post.

RESULTS AND DISCUSSION

Introduction of a metal post generally reduced stress in the surrounding cancellous bone at the more proximal portion of the post and increased stress in the more distal portion (Fig 1). High stress increases were observed in the bone directly beneath the post. Globally, bone stress was seen to decrease in both cortical and cancellous bone (except in the proximal anterior bone). Inserting an implant into the tibia greatly reduced bone stress; the type of metal composing the tray component slightly affected stress levels in the cancellous bone. In addition, the interface forces between the bone and the cement used to secure the implant were not affected by the material composition of the implant (Table 1). In a previous work, it was found that the shape of the post had a noticeable influence on interface forces [1]. The presentation will discuss the influence of different post shapes and different implant materials on cement-bone interface forces and stresses distribution in the tibia.

CONCLUSIONS

While inserting a metal implant significantly alters the stress fields, the material composition appears to have only a slight effect.

REFERENCES

1. Au AG, et al. *Med Eng Phys* 27, 123-134, 2005.

Table 1: Load distribution of cement-bone interface forces for 3 different implant material types.

Interface	Implant Metal		
Location	Ti6Al4V	CoCrM	AISI 316 L
Beneath Tray	72%	73%	73%
Post Periphery	24%	23%	23%
Post Base	4%	4%	4%

EVIDENCE OF MOVEMENT CONTROL ADAPTATION IN A LOWER EXTREMITY MOTOR TASK

[1] Shih-Chiao Tseng and [2]Steven J. Stanhope
[1]Department of Physical Therapy and Rehabilitation Science, University of Maryland, School of Medicine
[2]Physical Disabilities Branch, National Institutes of Health; email: tsengs@cc.nih.gov, web: pdb.cc.nih.gov

INTRODUCTION

Movement control adaptation (MCA) is designed to optimize dynamical characteristics of movement (such as effort, power, joint torque, or muscle force) in response to a change in the physical demands of movement. [1-3]. Results from previous studies on movement adaptation for upper extremities suggest that a delay in the onset or poor execution of movements in response to environmental change would form the basis of impaired MCA. The purpose of this study was to develop a method for measuring MCA in a more complex, functional lower extremity motor task. We hypothesized that MCA will begin in the motor preparatory phase and continue in the motor execution phase.

METHODS

Data from one healthy young subject are presented. The tests consisted of training an individual to react to a light cue by stepping forward as fast as possible to the light target, a distance equaling to 30% of maximal step length (MSL). Following the training period, an MCA trial (60%) was inserted into a series of trained step trials (30%) by shining the light cue at 60% of MSL.

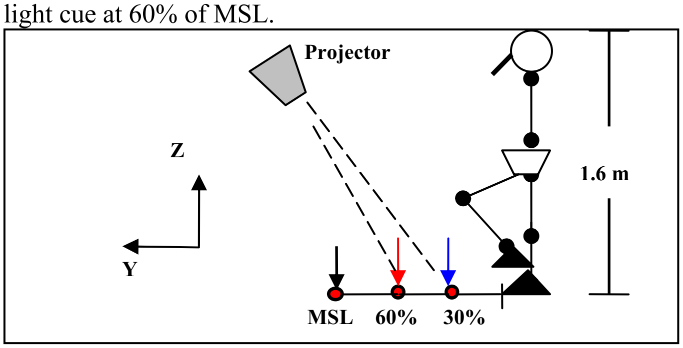

Figure 1: Stepping Test. MSL: maximal step length (1.06 m)

Force plates were used to measure kinetic data during stepping tests (Figure 1). Movement analyses were divided into three phases of forward stepping: Reaction time phase (RTP)- defined as time period from onset of light-cue stimulus to onset of step initiation. Motor preparatory phase (MPP)- defined as time period from onset of step initiation to toe-off of swing foot, and motor execution phase (MEP)- defined as time period from toe-off of swing foot to toe-off of stance leg.

RESULTS AND DISCUSSION

The results from a single subject showed there is no observed delay in reaction time at 60% of MSL (253 and 254ms at 30% and 60% of MSL, respectively). This finding indicated the subject has approached the motor tasks the same way as previously trained tasks via a feedforward control mechanism, which means the motor program has been processed prior stimulus. The evidence of identical motor programming is indicated by generation of similar slope of anterior/posterior (A/P) force in the early stage of MPP, and later modified the ongoing motor program, which has been shown in this study as the timing of departure in slopes at 30 and 60%, defined as onset of MCA (Figure 2). The finding in this study showed the onset of MCA occurred at 40% of a step cycle (500ms after onset of stimulus). The capability of developing MCA is very important for humans to overcome unexpected environmental challenges and achieve an optimal motor control. On the other hand, a delay of MCA would result in poor motor execution in the later phase.

In addition, MCA also was demonstrated by relatively higher peak force (60 vs. 47 N) and impulse in the A/P direction (14523 vs. 8218 N*ms) at 60% compared to 30% of MSL (figure 2) in swing leg. A longer period for weight transfer (Tw) was observed at 60% of MSL (369 vs. 290 ms). During MEP, the stance leg in the late phase of MEP showed relatively higher second peak A/P force at 60% compared to 30% of MSL (53 vs. 39 N). Increasing Tw in MPP indicated further generation of propulsion force for the swing leg. Occurrence of a second Peak A/P force in stance leg at 60% of MSL indicated MCA existed in stance leg. In summary, occurrence of MCA coexisting in swing and stance legs is governed by highly coordinated motor programs.

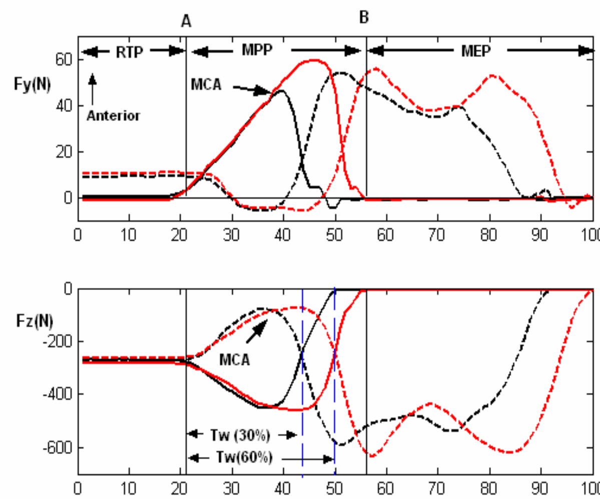

Figure 2: Ground reaction forces in A/P direction (Fy) and in vertical direction (Fz) for 30% (black lines) and 60% (red lines) of MSL (upper and lower figures, respectively). Time is normalized by 100%. Solid lines represent force measures of the swing leg. Dash lines represent force measures of the stance leg. The time point at 0 represents onset of the stimulus (light cue) and time point at 100 represents toe-off of stance leg. A: onset of stepping; B: toe-off of swing leg.

CONCLUSIONS

This study demonstrated the feasibility of measuring the onset and characteristics of MCA in a complex, lower-extremity motor task, and provided insight into understanding underlying control mechanisms of human locomotion.

REFERENCES

1. Gordon J, et al. *Exp Brain Res* **99**, 112-130, 1994.
2. Scheidt RA, et al. *J Neurophysiol* **84**, 853-862, 2000.
3. Ito, et al. *Neurosci Lett* **352**, 285-230, 2003.

Artificial Neural Network Prediction of Center of Pressure Using Trunk Acceleration Inputs During Perturbed Human Bipedal Stance

[1]Raviraj Nataraj, [1,2]Ronald J. Triolo, [1,2]Robert F. Kirsch, [1,2]Musa L. Audu, [2]Rudi Kobetic
[1]Case Western Reserve University,
[2]Louis Stokes Veteran's Administration Medical Center; e-mail: rxn25@po.cwru.edu

INTRODUCTION

This study investigates the feasibility of artificial neural network (ANN) prediction of changes in center of pressure (COP) during perturbed human bipedal stance using current and past COP and trunk acceleration inputs. The COP – COM (center of mass) variable has been shown to be correlated to COM acceleration during quiet standing [1]. We hypothesize that accelerations of a point on the trunk (estimate of COM) can be implemented by an ANN to predict COP. We seek to employ this ANN in a dynamic, feed-forward manner for controlling standing posture using functional neuromuscular stimulation (FNS) following spinal cord injury (SCI). Due to the delay in peak muscle force production after initial stimulation, we will apply a control loop that acts predictively by minimizing the difference between a desired COP and a *future* COP determined by the ANN.

METHODS

Two able-bodied male subjects (25-27 yrs) have participated thus far. Each subject wore two belts, one around the waist and one around the chest (figure 1). Both belts were fastened to four non-elastic cotton-cloth ropes. Each rope was aligned in either the anterior-posterior (A-P) or medial-lateral (M-L) directions relative to the subject. Ropes were used to manually apply perturbations to the subject standing on an instrumented force-plate that actively measured COP. The subject wore a retroreflective sternum marker whose 3-D position was tracked using a VICON© camera system. The position data were double-differentiated off-line using a derivative-filter [2] to obtain trunk accelerations. Trials consisted of perturbing the subject, initially in erect stance, in different combinations of rope-pulls. Perturbations were moderate such that significant COP deviations were incurred yet the subject could make postural corrections to maintain bipedal stance without stepping.

Data from the aforementioned trials were used for training and testing an ANN for COP prediction at several future time increments (100, 150, 200, 250, 300 msec) on the order of neuromuscular delay. A three-layer, time-delayed feed-forward network [3] for back-propagation training was created. The inputs into the network were current and past values of three orthogonal acceleration components (x, y, z) and two horizontal-plane COP components (A-P, M-L). The outputs were changes in the two COP components at the previously specified future time-instants.

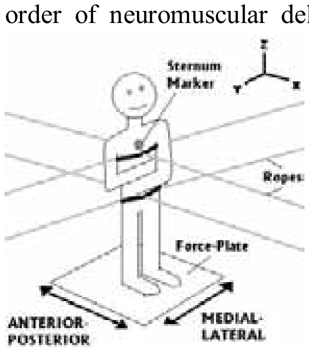

Figure 1. Experimental Set-up (not to scale)

RESULTS AND DISCUSSION

After ANN training, correlation coefficients (R^2) between true COP change and ANN-predicted output for test data were calculated as a measure of their respective fit. Results from a test sample having both A-P and M-L perturbations are shown in figure 2. Substantial correlation (> 0.7) exists for both the A-P and M-L components.

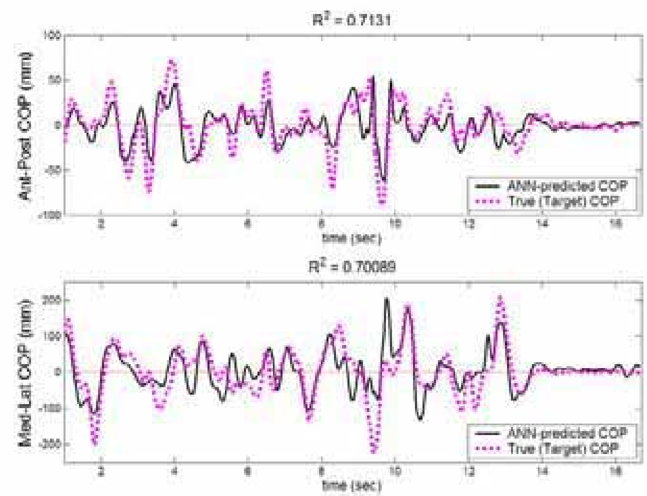

Figure 2. ANN prediction (200 msec in future) of changes in Ant-Post (top) and Med-Lat (bottom) COP for 1000-point (60 Hz sampling rate → 16.7 sec) test sample.

Improved correlation is expected with additional inputs (more markers, additional past values) and a more dynamic neural network structure that includes recurrent connections. Future investigations will implement accelerometer outputs rather than numeric differentiation of VICON position data. Accelerometer readings are likely not as accurate as the numerically-derived values currently used. However, it is expected that the accelerometer will be more sensitive to larger deviations in posture relative to steady-state swaying, making correlations during a perturbation trial higher. While feasibility has been demonstrated, the required accuracy of the ANN predictor can only be assessed when integrated in the full FNS control system. This will be done first in simulation prior to experimental evaluation.

REFERENCES

1. Winter DA, et al. *J Neurophysiol* **80**, 1211-2, 1998.
2. Kaiser JF, Reed WA. *Rev. Sci. Instrum* **48**, 1447-1455, 1977.
3. Lan N, Feng H-Q, Crago PE. *IEEE Trans Rehab Eng* **2**, 213-223, 1994.

ACKNOWLEDGEMENTS

NIH: R01NS040547-03 Research Project Grant
NIH: 9T32EB04314-06 Training Grant

LOWER LIMB AMPUTEE ACTIVITY UNEFFECTED BY SHOCK-ABSORBING PYLON OR C-LEG KNEE

[1-3]Glenn Klute, [1]Jocelyn Berge, [1]Michael Orendurff, and [1,4]Joseph Czerniecki
[1]Dept. of Veterans Affairs, Seattle, Washington USA
Depts. of [2]Mechanical Engr., [3]Electrical Engr., and [4]Rehabilitation Med., Univ. of Washington, Seattle, Washington USA
email: gklute@u.washington.edu, web: www.seattlerehabresearch.org

INTRODUCTION

Prosthetic prescription is widely believed to have a strong influence on lower limb amputee activity levels. Optimum prescription should equate to maximum performance. Field measurements of activity is one method to access performance on a functional level, yet few investigators have used this metric to explore how amputees actually use their prostheses in the community [1] and how prosthetic prescription might influence activity [2]. The purpose of this study is to discover if variation in prosthetic prescription can affect the activity levels of lower limb amputees. The secondary purpose was to discover the characteristics of their activity; specifically, how long are their bouts of activity, how frequently do they occur, and how many steps do they average during each bout.

METHODS

Ten *transtibial* and five *transfemoral* amputees gave informed consent to participate in this Institutional Review Board-approved protocol. Activity levels were measured using a pager-sized instrument (StepWatch2; Cyma) attached to the distal end of the prosthetic pylon. The number of steps taken was collected for 1 week using a 1 minute sample and record interval. The prosthetic components of all subjects were held constant throughout the study except for the intervention of interest. The *transtibial* amputees (5 traumatic, 4 dysvascular, 1 infection; age 52 ± 6 years; Ht. 178 ± 6 cm; Wt. 91 ± 18 kg), all long term prosthetic users, were provided with a SAP (Mercury™ Telescopic Torsion Pylon; Blatchford) and rigid pylon in random order. The activity of each subject was recorded following 3 weeks of acclimation. The *transfemoral* amputees (5 traumatic; age 48 ± 14 years; Ht. 171 ± 4 cm; Wt. 76 ± 10 kg), all previous long term Mauch SNS (Ossur) users, were provided with a C-Leg (Otto Bock) and a Mauch SNS in random order. The activity of each subject was recorded following 3 months of acclimation.

RESULTS AND DISCUSSION

The activity levels of neither *transtibial* nor *transfemoral* amputees were affected by their prosthetic prescription. Among *transtibial* amputees, no difference in activity level was observed across pylons (Rigid: 3191 ± 2230 steps/day, SAP: 3192 ± 2207 steps/day, $p > .99$). Among *transfemoral* amputees, no difference in activity level was observed across knees (Mauch SNS: 2675 ± 976 steps/day, C-Leg: 2657 ± 737 steps/day, $p > .96$). A study of *transtibial* amputees (n=13) did find a difference across liners: subjects were more active while wearing a closed-cell low-density polyethylene liner (4135 steps/day) than a silicone liner (2262 steps/day) [2]. Considering that activity levels can vary widely between individuals [3], a large sample population might be necessary to adequately determine a functional activity level ceiling for lower limb amputees. However, if appropriate controls are placed on age and amputation etiology [1], a small sample

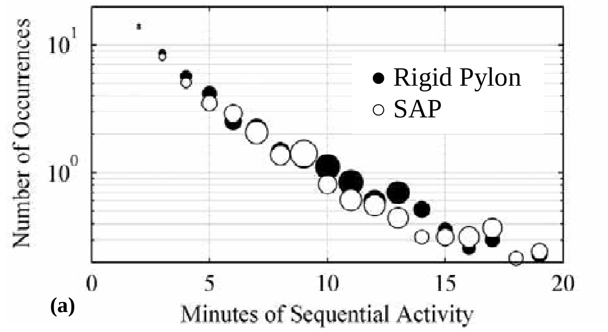

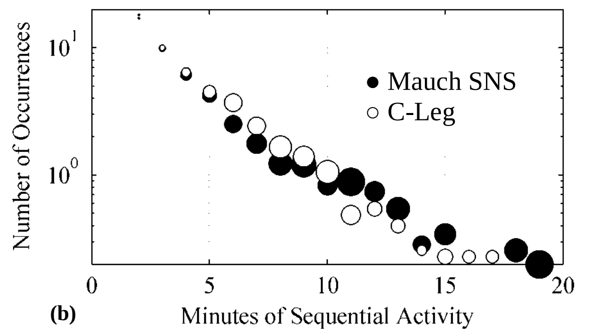

Figure 1: Bouts of daily activity (averaged over 1 week) for **(a)** *transtibial* amputees wearing rigid pylon or SAP and **(b)** *transfemoral* amputees wearing Mauch SNS or C-Leg. Circle diameter is proportional to number of steps per minute (1mm=20 steps/minute).

population might suffice to distinguish differences due to prosthetic prescription in within-subject experiments.

No differences were distinguishable in the characteristics of their daily activities averaged over a 1 week period (see Figure 1). When amputees walked for at least 5 minutes in a row, they averaged ~50 steps/minute. However, rarely were amputees active for more than 10 minutes at a time. Most of their activities (number of occurrences) consisted of short bouts of 3 minutes or less and during these short bouts they averaged ~14 steps/minute. Subjects in this study did not achieve the recommended minimum of 30 minutes moderate-intensity activity on most days of the week to promote health, psychological well-being, and a health body weight [4].

REFERENCES

1. Holden JM et al. *J Orthop Res*, **5**, 562-8, 1987.
2. Coleman KL et al. *Proceedings International Society for Prosthetics & Orthotics*, Glasgow, Scotland, 2001.
3. Marsden JP et al. *Ergonomics*, **15**, 439-51, 1972.
4. Dept. of Health & Human Services, *Dietary Guidelines for Americans 2005*, 2005.

ACKNOWLEDGEMENTS

This research was supported by Dept. of Veterans Affairs Grants A2770I and A2448R.

KINEMATIC & KINETIC DIFFERENCES BETWEEN MALE & FEMALE SOCCER PLAYERS

[1] Kelly McKean, [1]Scott Landry, [2]Cheryl Hubley-Kozey, [1]Kevin Deluzio and [3]William Stanish
[1]School of Biomedical Engineering, [2]School of Physiotherapy, Dalhousie University
[3]Department of Surgery, Division of Orthopaedics, Dalhousie University
email: kmckean@dal.ca

INTRODUCTION

Anterior cruciate ligament injuries occur 2-8x more often in females than males [1,2]. Over 70% of these injuries occur in a non-contact situation including cutting, pivoting and landing from a jump [3]. Several factors have been implicated in this predisposition including biomechanics [4]. The purpose of this study was to detect differences in kinetics and kinematics during cutting maneuvers that may contribute to this gender predisposition.

METHODS

21 elite male and 21 elite female soccer players between the ages of 14-18 years underwent a complete 3D kinematic, kinetic and electomyographic (EMG) analysis of the lower limb during unanticipated running and cutting maneuvers. Hip, knee and ankle angles, forces and moments were collected during the stance phase of each maneuver. Subjects were instructed to run down the walkway of the lab at 3.5 ± 0.2 m/s. Just prior to their right foot landing on the force plate, a light system randomly directed the individuals to either 1) cut to the left (side-cut), 2) continue running straight or 3) cut to the right (cross-cut) until 5 successful trials were obtained for each direction. All cutting maneuvers were made at a 45-60° angle. The kinematic and kinetic waveforms for the entire stance phase of each task were analyzed using principal component analysis [5].

RESULTS AND DISCUSSION

There was no significant difference between males and females in age, body mass index (BMI), years of soccer experience or speed of the cutting manuevers (Table 1). All players were injury free at the time of testing; however, many reported lower limb injuries previously in their soccer careers (M=62%, F=86%).

For the cross-cut and side-cut conditions principal component analysis revealed females exhibit a significantly smaller magnitude of hip flexion than males throughout stance (p=.01) (Figure 1A). In the cross-cut maneuver females also exhibited a significantly larger magnitude knee adduction moment than their male counterparts (p=.03) (Figure 1B).

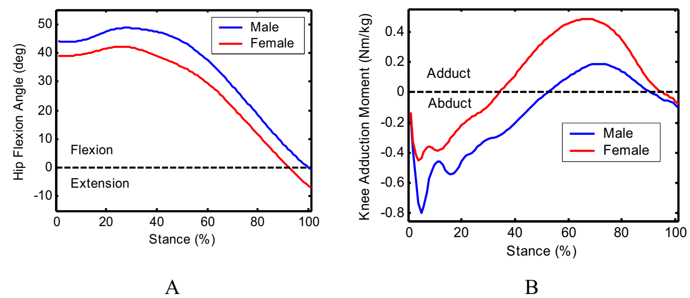

Figure 1: A) Females exhibit less hip flexion than males during cross-cuts & side-cuts (p=.01). B) Females exhibit a greater knee adduction moment than males during cross-cuts (p=.03).

CONCLUSIONS

The cross-cut was the most successful maneuver for identifying gender related differences in this elite soccer population. Females generated less hip flexion and a larger knee adduction moment than their male counterparts. These biomechanical differences may place the female ACL at greater risk for injury. Knowledge of these differences will aid in developing prevention programs to reduce non-contact ACL injuries in females.

REFERENCES

1. Arendt & Dick. *Am J. Sports Med* **23**:694-701, 1995.
2. Elias et al. *Med & Sci Sport Exer* **33**:359-367, 2001.
3. Nyland et al. *J Ortho & Sport Phys Ther* **20**:132-137, 1994.
4. Sigward et al. *Clin Biomech* **16**:952-3, 2001.
5. Deluzio et al. *Hum Mvmt Sci* **18**:701-711, 1999.

ACKNOWLEDGEMENTS

This study was funded by the Nike Sports Research Laboratory, Beaverton, Oregon.

Table 1: Demographics of elite males and female soccer players.

	Age (yrs)	Weight (kg)	Height (m)	BMI (kg/m^2)	Soccer (yrs)	Speed (m/s) side	run	cross
Males	17.2 ± 0.8	69.6 ± 6.6	1.8 ± 0.0	22.1 ± 1.7	10.7 ± 1.7	3.5 ± 0.1	3.5 ± 0.1	3.5 ± 0.1
Females	16.9 ±1.0	60.8 ± 5.5	1.6 ± 0.1	22.4 ± 1.8	9.8 ± 2.1	3.4 ± 0.1	3.5 ± 0.1	3.4 ± 0.1
p-value	.25	<.01	<.01	.63	.15		.22	

DIFFERENCES IN MUSCLE FUNCTION BETWEEN WALKING AND RUNNING AT THE PREFERRED WALK-RUN TRANSITION SPEED

Kotaro Sasaki and Richard R. Neptune
Department of Mechanical Engineering, University of Texas, Austin, TX, USA
Email: rneptune@mail.utexas.edu

INTRODUCTION

Walking and running are the two most common forms of human gait. Understanding differences in muscle function between the two gait modes would further our understanding of the neuromotor control principles that govern human locomotion. Recent modeling and simulation studies have identified individual muscle contributions to the body mechanical energetics during normal walking [1]. However, it is unclear whether these contributions are preserved when the gait mode switches from walking to running. Therefore, the objective of this study was to use forward dynamical simulations of walking and running at the same speed and assess whether individual muscles contribute to the same body segment mechanical energetics during the two gait modes.

METHODS

Forward dynamical simulations of walking and running at the preferred walk-to-run transition speed (~2 m/s) were generated using dynamic optimization such that the simulations reproduced the averaged experimental kinematic and ground reaction force data collected from 10 healthy subjects. A 2D musculoskeletal model with nine degrees-of-freedom (trunk anterior-posterior tilt, horizontal and vertical translation, hip, knee and ankle flexion-extension for both legs) consisting of a trunk and two legs (femur, tibia, patella and foot for each leg) and seventeen individual muscle actuators per leg was developed using SIMM [2]. The muscles included the gluteus maximus, anterior and posterior gluteus medius, adductor magnus, iliacus, psoas, biceps femoris long head, medial hamstrings, biceps femoris short head, vastii, rectus femoris, tibialis anterior, soleus and medial and lateral gastrocnemius. Thirty visco-elastic elements were attached to each foot segment to model the foot-ground contact [e.g. 1]. Individual muscle excitation patterns were derived from EMG data collected from the same subjects. Parameter optimization using a simulated annealing algorithm was used to fine-tune the onset, duration and magnitude of the EMG patterns to produce well-coordinated movements. A state-space segment power analysis was performed to quantify how individual muscles contribute to the body segment energetics [3].

RESULTS AND DISCUSSION

The primary difference in how individual muscles distribute body segment mechanical power between walking and running was observed in the soleus (SOL). In walking, SOL absorbed ipsilateral leg power and transferred much of that power to the trunk from mid to late stance, then in late stance simultaneously generated power directly to the trunk (Fig. 1: SOL, Walking, 25-50% gait cycle). In running, SOL absorbed power from both the leg and trunk in the beginning of stance and then generated power to both the leg and trunk in mid stance (Fig. 1: SOL, Running, 0-30% gait cycle). In addition,

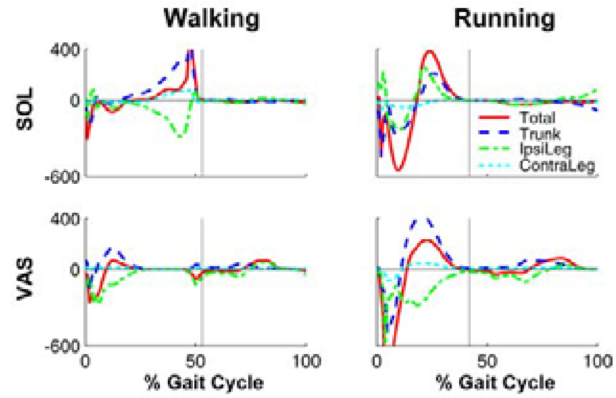

Figure 1: Distribution of total musculotendon power (*Total*) to the trunk (*Trunk*), ipsilateral leg (*IpsiLeg*) and contralateral leg (*ContraLeg*) during walking and running over the gait cycle. The vertical lines indicate toe-off. SOL: soleus; VAS: vasti. Units are in watts.

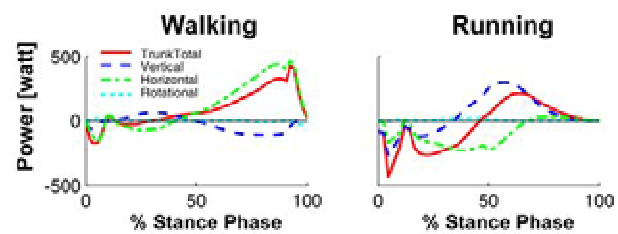

Figure 2: Trunk mechanical power generated by the soleus (SOL) during stance in walking and running. *Total*: total power; *Vertical*: vertical kinetic and potential power; *Horizontal*: horizontal kinetic power; *Rotational*: rotational power.

the power generated to the trunk by SOL exhibited different patterns between gait modes (Fig. 2). In walking, SOL provided positive horizontal and negative vertical power in late stance, which indicated that SOL acted to accelerate the trunk forward and decelerate the downward motion of the trunk. In running, near mid-stance SOL absorbed power from the trunk in the horizontal direction (i.e., decelerated its forward motion) while providing positive power in the vertical direction for body support. All other muscle contributions to body segment power were similar between walking and running, although the magnitudes and durations often differed between the two modes (e.g. Fig. 1: VAS).

REFERENCES

1. Neptune RR, et al. *Gait Posture* **19**, 194-205, 2004.
2. Delp SL and Loan JP. *Comput Biol Med* **25**, 21-34, 1995.
3. Fregly BJ and Zajac FE. *J Biomech* **25**, 81-90, 1996.

ACKNOWLEDGEMENTS

This work was supported by The Whitaker Foundation.

MUSCLE CONTRIBUTIONS TO THE FLIGHT PHASE IN RUNNING

Kotaro Sasaki and Richard R. Neptune
Department of Mechanical Engineering, University of Texas, Austin, TX, USA
Email: rneptune@mail.utexas.edu

INTRODUCTION

One of the most distinctive differences between walking and running is the existence of a flight phase in running rather than the double support phase that occurs in walking. This fundamental difference in gait mechanics indicates the need for muscles to generate greater vertical acceleration of the body's center of mass (COM) in running. Previous modeling studies of normal walking have shown that the uniarticular hip and knee extensors, and the ankle plantar flexors are the primary contributors to vertical acceleration of the COM from early to mid stance, and from mid to late stance, respectively [1, 2]. However, little is known about how individual muscles work in synergy to accelerate the COM upward to produce the flight phase in running. Therefore, the objective of this study was to identify which muscles contribute to the acceleration of the COM vertically and how these contributions differ between walking and running at the same speed.

METHODS

Individual muscle contributions to the vertical acceleration of the COM were obtained by quantifying each muscle's contribution to the vertical ground reaction force (GRF) using forward dynamical simulations of walking and running. A 2D musculoskeletal model with nine degrees-of-freedom (trunk anterior-posterior tilt, trunk horizontal and vertical translation, hip, knee and ankle flexion-extension for both legs) consisting of a trunk and two legs (femur, tibia, patella and foot per leg) and seventeen Hill-type muscle actuators per leg was developed using SIMM [3]. The muscles included in the model were the gluteus maximus, anterior and posterior gluteus medius, adductor magnus, iliacus, psoas, biceps femoris long head, medial hamstrings, biceps femoris short head, vastii, rectus femoris, tibialis anterior, soleus and medial and lateral gastrocnemius. The equations of motion were derived using SD/FAST (PTC, Needham, MA). Visco-elastic elements were attached to each foot segment to model the foot-ground contact [2]. Muscle excitation patterns were derived from measured group-averaged EMG patterns. A simulated annealing optimization algorithm was used to fine-tune the onset, duration and magnitude of the EMG patterns such that the simulations emulated group averaged experimental kinematic and GRF data collected from 10 young healthy subjects during walking and running at the preferred walk-to-run transition speed (~2 m/s). The contributions of each muscle to the vertical GRF were then quantified using a GRF decomposition [1, 2].

RESULTS AND DISCUSSION

The primary contributors to vertical GRF were the soleus (SOL), vasti (VAS) and gluteus maximus (GMAX) in both walking and running (Fig. 1). In walking, VAS and GMAX contributions occurred primarily in early stance phase (~0-30% stance phase), and then SOL contributed from mid to late stance (~30-100% stance phase, see also [1, 2]). In running,

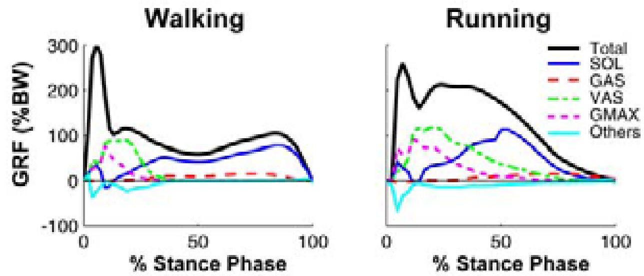

Figure 1: Individual muscle contributions to vertical GRF. Total: the total GRF including muscular and non-muscular components, Others: hamstrings, gluteus medius, tibialis anterior, rectus femoris, biceps femoris short head and iliacus-psoas combined.

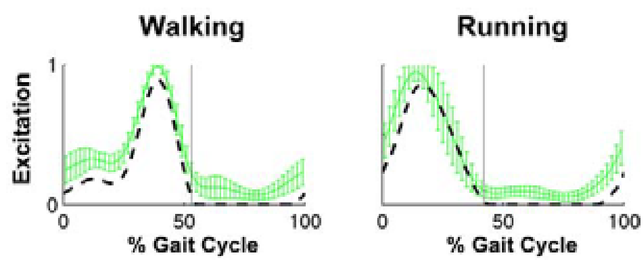

Figure 2: SOL excitation patterns for the walking and running simulations (dashed line) and group average EMG linear envelopes (solid line, average ± S.D.) at the preferred transition speed from heel-strike to heel-strike of the ipsilateral leg. The EMG data were normalized to the maximum value observed over the gait cycle. The vertical lines indicate toe-off.

the magnitude of the VAS and GMAX contribution increased and extended into mid stance (~0-60% stance), while the SOL contribution shifted earlier in the stance phase (~0-70% stance), which corresponded with a shift in SOL muscle activity (Fig. 2, [4]). These results indicate that the flight phase in running is produced by increased and prolonged VAS and GMAX and phase-advanced SOL contributions to the vertical GRF which provides the necessary vertical acceleration of the COM.

REFERENCES

1. Anderson FC and Pandy MG. *Gait Posture* **17**, 159-169, 2003.
2. Neptune RR, et al. *Gait Posture* **19**, 194-205, 2004.
3. Delp SL and Loan JP. *Comput.Biol.Med.* **25**, 21-34, 1995.
4. Mann RA, et al. *Am. J. Sports Med.* **14**, 501-510, 1986.

ACKNOWLEDGEMENTS

This work was supported by The Whitaker Foundation.

IMPACT OF FLEXIBILITY ON MUSCULAR PERFORMANCE OF THE KNEE

Gustavo Nunes Tasca Ferreira, Luci Fuscaldi Teixeira-Salmela, Cristiano Q Guimarães, Geraldo Fabiano de Souza Moraes
Department of Physical Therapy/Universidade Federal de Minas Gerais – Brasil; e-mail: jhsalmela@hotmail.com

INTRODUCTION

Despite the popularity of stretching programs for sport rehabilitation, little it is known about the relationships between gains in flexibility and changes in muscular performance. This aim of this study was to investigate the impact of static stretching on flexibility of the hamstrings and muscular performance of knee flexor and extensor muscles.

METHODS

Thirty subjects (19 women and 11 men; aged:22.8 ± 4.9 years) with shortened hamstrings (60 legs), operationally defined as the loss of knee extension greater than 30°, took part in the study. Measures of flexibility were obtained with a goniometer and the amount of applied force was controlled by a manual dynamometer. Muscular performance measures on the isokinetic dynamometer at 60° and 300°/s were obtained before and immediately after the intervention. The intervention program consisted of 30 sessions of static stretching, performed bilaterally five times a week for six weeks. Measures of flexibility were reassessed six weeks after the cessation of the intervention (follow-up). Descriptive statistics and tests for normality (Shapiro-Wilk) were calculated for all outcome measures. The impact of the intervention was investigated using parametric and non-parametric analyses, depending on data distribution ($\underline{\alpha}<0.05$).

RESULTS AND DISCUSSION

As presented in Table 1, after the intervention, there were significant gains in measures of flexibility (p=0.000) and muscular performance for the following parameters: angle of peak torque for hamstrings at 60°/s and 300°/s (p<0.0001 and 0.018); for work normalized by body weight at 60°/s and 300°/s for knee flexors (p=0.012 and 0.005); for knee extensors (p<0.0001). Of the 10 subjects who comprised the follow-up group, repeated measures ANOVA revealed that gains in flexibility obtained with the intervention, were maintained ($\underline{p}$= 0.183).

The observed gains of flexibility corroborated previous findings [1,2]. Considering evidence of stretching-induced sarcomerogenesis [2,3], it is possible to infer that after the intervention, the number of sarcomers in series in the hamstrings increased, and thus, improved their capacity to vary length, which may explain changes of angle of peak torque in the direction of knee extension.

It is possible to speculate that the hamstrings became more capable of moving the leg over a larger angular distance during the same time interval. Increases in the number of sarcomers in series represent a larger capacity of the muscle-tendon unit to vary its length in a certain time interval [4], which can be translated by increases of angular velocity. Therefore, the slope of the curve is increased until the segment reaches the isokinetic programmed speed, generating a larger area below the curve, and thus increasing the generated work.

The observed increases in work generated by knee extensors after the intervention can be related to smaller passive resistance imposed by the knee flexors [2,3], once the range of motion used during tests was the same.

The retention of gains in flexibility can be explained by the fact that the stretching exercises were performed bilaterally and may have allowed the subjects to incorporate these gains in their daily lives, thus, attenuating the detraining effects.

CONCLUSIONS

These findings indicated that the intervention resulted in gains in measures of flexibility and muscular performance and suggest that these gains had a positive impact on various parameters of muscular performance.

REFERENCES

1. Bandy WD et al. The effect of static stretch and dynamic range of motion training on the flexibility of the hamstrings muscles. *J orthop Sports Phys Ther* **27**, 295-300, 1998.
2. Chan SP et al. Flexibility and passive resistance of the hamstrings of young adults using two different static stretching protocols. *Scand J Med Sci Sports* **11**, 81-86, 2001
3. Gajdosik RL. Passive extensibility of skeletal muscle: Review of the literature with clinical implications. *Clin Biomech* **16**, 87-101, 2001.
4. Lieber RL. Bodine SC. Skeletal muscle mechanics: Implications for rehabilitation. *Phys Ther* **73**, 12, 844-85, 1993.

Table 1: Means (± SD) of Outcome Measures over Time

Variable		Pre	Post
Flexibility (°)		142.6 ± 5.9	157.1 ± 11.2
Angle of peak torque (°)	60°	59.2 ± 8.4	55.3 ± 8.4
	300°	88.6 ± 12.9	85.2 ± 15.6
Work of Knee flexors (J/kg)	60°	121.3 ± 27.4	125.6 ± 28.5
	300°	61.2 ± 16.4	63.5 ± 18.5
Work of knee extensors (J/Kg)	60°	240.7 ± 48.0	248.6 ± 53.0
	300°	116.0 ± 27.7	119.3 ± 28.0

LATERAL HAMSTRINGS ARE STRETCHED MORE THAN THE MEDIAL HAMSTRINGS DURING SPRINTING

Elizabeth S. Chumanov[1], Darryl G. Thelen[1,2,3], Dina M. Hoerth[2], Thomas M. Best[2,3], Bryan C. Heiderscheit[3], Stephen C. Swanson[4]
Depart of Mech Engr[1], Biomed Engr[2], Ortho and Rehab[3] Univ. of Wisconsin–Madison, Orthopedic Specialty Hospital[4] Murray, UT
Email: easchmerr@wisc.edu

INTRODUCTION

Acute hamstring strains are one of the most frequent injuries in sports involving sprinting [1,2]. Radiological analyses have shown that a large majority of hamstring injuries occur in the lateral hamstrings (BF-biceps femoris), while the medial hamstrings (ST-semitendinous, SM-semimembranous) are less frequently involved [3,4]. However, there is currently limited scientific data to understand injury mechanisms during sprinting and differences in injury rates between muscles.

The objective of this study was to characterize medial and lateral hamstring kinematics across sprinting speeds. We hypothesized that the BF would be subjected to greater stretch than the ST or SM. Our secondary hypothesis was that increasing sprinting speed would both increase and delay the occurrence of peak hamstring stretch within the gait cycle.

METHODS

Fourteen athletes (6 female, 8 male, 16-31 yr old) participated in this study. Subjects had no previous hamstring injuries within one year prior to being tested. Whole body kinematics were recorded at 200 Hz while each subject sprinted on a high-speed treadmill at 80, 85, 90, 95, and 100% of his/her maximum sprinting speed. Hamstring kinematics were estimated using a 3-D, 29 degree-of-freedom model that included geometric descriptions of the BF, ST and SM muscles (Fig. 1). Model predictions of hip extension and knee flexion moment arms for the individual hamstring muscles were consistent with published data. [5,6].

Figure 1: Musculoskeletal model shown with markers and in posture of peak hamstring muscle stretch

The model was scaled to individual subjects. An optimization-based inverse kinematics routine was employed to compute joint angles from marker kinematics. At each time step, muscle-tendon lengths were determined by computing the distance from origin to insertion and accounting for wrapping about structures at the knee. Muscle stretch was defined as the lengthening of the muscle-tendon unit relative to the length in an upright posture. Repeated measures ANOVA were used to test for the significance ($p < 0.01$) of the effects of speed and muscle on peak stretch and the time at which peak stretch occurred within the gait cycle (GC).

RESULTS AND DISCUSSION

Average maximum sprinting speed was 9.4 m/s for the males and 8.1 m/s for the females. Peak muscle-tendon stretch occurred at ~90% GC (Fig. 2a). The BF was stretched an average of 9.5% beyond the nominal upright length, which was significantly more than the peak stretch of the SM (7.4%) and ST (8.1%). However, there was no significant variation in peak hamstring stretch with speed (Fig. 2b). There was a slight delay (~2% of the GC) in the occurrence of peak hamstring stretch at the maximum sprinting speed.

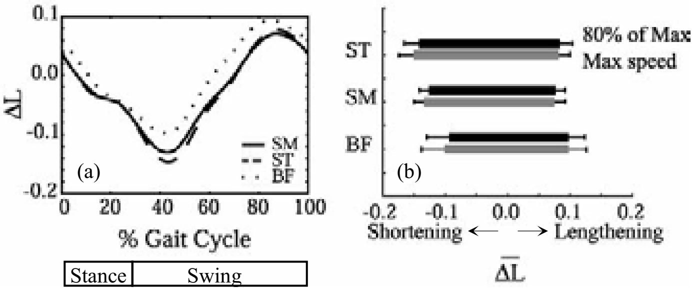

Figure 2: a) Peak hamstring muscle-tendon stretch ($\Delta\overline{L}$) occurs during late swing prior to foot strike. b) Overall excursions of the hamstrings over a sprinting gait cycle ranged from 19 to 23%, but did not vary with sprinting speed over the range (80-100% max) considered.

The differences in peak stretch between the medial and lateral hamstrings found in this study are primarily a result of differences in knee flexion moment arms between muscles. The ST and BF have similar hip extension moment arms [5], and thus each undergo similar stretch due to hip flexion. However, because the BF has a smaller knee flexion moment arm than the ST and SM muscles, knee flexion during late swing (Fig. 1) reduces the BF length less than the medial hamstrings. The net effect is that the BF experiences greater overall stretch, relative to the upright length, than ST or SM

SUMMARY

Animal models of muscle-tendon injuries have shown that mechanical strain is a strong indicator of injury potential [7]. Therefore, the muscle-tendon stretch measures reported in this study provide insights into hamstring injury potential during sprinting. Our data support the idea that the potential for a lengthening strain injury to the hamstrings is greatest during the late swing phase of sprinting, when the muscles are maximally stretched and active [8]. Furthermore, we conclude that the higher injury rates for the BF may in part arise from differences in knee flexion moment arms between the hamstring muscles.

REFERENCES

1. Seward, H., et al. *Med J Aust*, 1993. **159**: 298-301.
2. Kujala, U.M., et al. *Sports Medicine*, 1997. **23**: 397-404.
3. Garrett, W., et al. *Med Sci Sports Exerc*, 1989. **21**: 506-514.
4. De Smet, A.A., et al. *Am J Roent*, 2000. **174**: 393-399.
5. Arnold, A.A., et al. *Comp Aided Surg*, 2000. **5**: 108-119.
6. Buford, W., et al. *IEEE Trans. Rehabil. Eng*, 1997. **5**:367–379.
7. Best, T., et al. *J. Biomech.Eng*, 1995. **117**: 262–265.
8. Kuitunen, S., et al. *Med. Sci. Sports Exerc*, 2002. **34**: 166–173.

ACKNOWLEDGEMENTS

Contributions of Allison, Li Li, and Michael Young. Support of Aircast Foundation Inc. and NFL Charities.

SCAPULAR MUSCLE RECRUITMENT AND ISOKINETIC FORCE PRODUCTION IN INDIVIDUALS WITH IMPINGEMENT SYNDROME

Geraldo F. S. Moraes, Luci F. Teixeira-Salmela, Christina D.C.M. Faria, Gustavo N.T. Ferreira
Department of Physical Therapy/ Universidade Federal de Minas Gerais, Brazil e-mail: geraldmoraes@terra.com.br

INTRODUCTION

Dynamic neuromuscular imbalance of scapulohumeral rhythm has been related to the onset of the impingement syndrome and other related pathologies [1-2].

The aim of this study was to investigate muscular imbalance of the rotator cuff and scapular muscle recruitment in 10 individuals with impingement syndrome graded I and II compared to 10 asymptomatic subjects.

METHODS

Recruitment patterns and latencies were determined by the electromyographic activity of the scapular stabilizer muscles (trapezius and serratus anterior) during shoulder elevation in the scapular plane. Isokinetic measures of muscular performance were determined by the antagonist/agonist work ratios of the medial (MR) and lateral rotators (LR) obtained with the dynamometer Biodex at speeds of 60 and 180°/s in the supine position. Descriptive statistics and tests for normality (Shapiro-Wilk) were performed for all outcome variables. ANOVA (2x2) was used to investigate side and group differences, as well as interactions, with a significance level of $\alpha < 0.05$.

RESULTS AND DISCUSSION

No group or side differences were found for the recruitment patterns. Supporting previous studies, the activation sequence involved first, the superior trapezius, followed by serratus anterior, middle, and inferior trapezius [1-2], However, as illustrated in Figure 1, subjects on the impact group showed significantly higher latencies for all scapular muscles (F= 27.18 – 50.13; $p<0.001$). In addition, a group-by-side interaction was found, indicating that the differences were significant only for the affected side (F= 18.75–37.39; $p<0.001$).

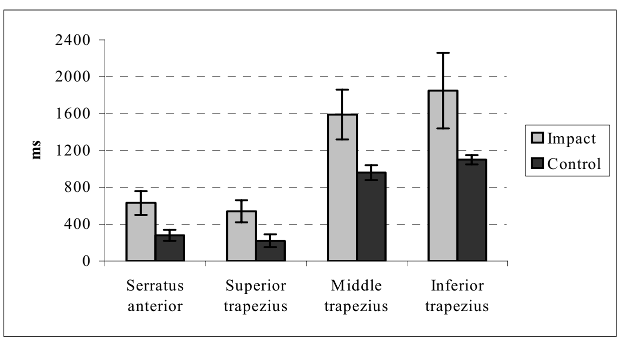

Figure 1: Means (± SD) of latencies (ms) for the impingement (affected side) and control groups

No significant group or side differences were found for the muscular performance measures (Figure 2), which are opposite to the findings reported by Leroux et al. [3], in which the measurements were taken in the seated position. Ng and Lam [4] also reported significant differences for the antagonist/agonist work ratios of athletes obtained in the supine position.

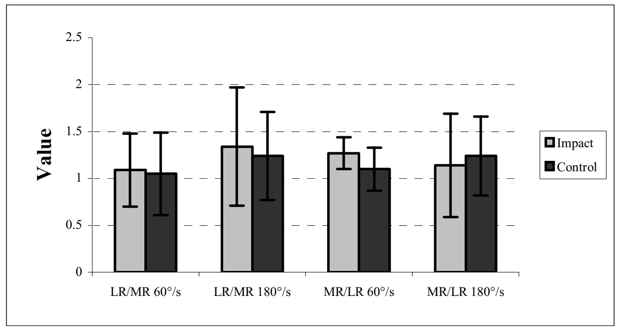

Figure 2: Means (± SD) of isokinetic ratios for both groups

CONCLUSIONS

Individuals with impingement syndrome presented significant delays for the recruitment of scapular muscles, indicating alterations of dynamic neuromuscular balance. Therefore, assessment of performance of the scapular stabilizer muscles appears to be more important for the detection of functional deficits in individuals with impingement syndrome, to better guide therapeutic interventions.

Isokinetic performance of shoulder rotators was not affected by the presence of impingement. Subject positioning during the isokinetic assessment may have provided a mechanical advantage for the rotator muscle actions and explain the lack of significant differences between groups for the muscle performance measures. These findings suggest that when performing shoulder isokinetic assessment, subject positioning should be controlled.

REFERENCES

1. Cools AM et al. Scapular muscle recruitment pattern: Electromyographic response of the trapezius muscle to sudden shoulder movement before and after a fatiguing exercise. *J Orthop Sports Phys Ther* **32**, 221-229, 2002.
2. Cools AM et al. Scapular muscle recruitment patterns: Trapezius muscle latency with and without impingement symptoms. *Am J Sports Med* **31**, 542-549, 2003.
3. Leroux J et al. Isokinetic evaluation of rotational strength in normal shoulders and shoulders with impingement syndrome. *Clin Orthop* **304**, 108-115, 1994.
4. Ng GYF & Lam PCW. A study of in men who play badminton. *J Orthop Sports Phys Ther* **32,** 399-404, 2002.

THE THRESHOLD OF BALANCE RECOVERY IS NOT AFFECTED BY THE TYPE OF POSTURAL PERTURBATION

Kodjo E Moglo and Cécile Smeesters
Research Center on Aging, Sherbrooke Geriatric University Institute, Sherbrooke, QC, Canada
Department of Mechanical Engineering, Université de Sherbrooke, Sherbrooke, QC, Canada
email: Cecile.Smeesters@USherbrooke.ca web: www.cdrv.ca

INTRODUCTION

Only recently have studies focused on postural perturbations at the threshold of balance recovery, i.e., perturbations large enough that balance recovery is not always possible and a fall can occur. The knowledge at the threshold of balance recovery is thus very limited. In particular, the effect of initial velocity on the threshold of balance recovery has not been quantified, despite experimental [1-2] and theoretical [3-5] qualitative evidence of its importance. This study quantified the effect of initial velocity on the threshold of balance recovery and developed a method to compare experiments with different initial velocities, regardless of the postural perturbation.

METHODS

Three male and three female healthy younger adults participated (24.5 ± 4.2 yrs, 1.72 ± 0.05 m, 67 ± 8.1 kg). The maximum forward pull force that they could sustain and still recover balance using a single step was determined for three different walking velocities with no initial lean. The maximum forward lean angle that they could be released from and still recover balance using a single step was also determined for three different forward pull forces with no initial velocity. The forces and angles were sequentially increased and the postural perturbations were randomly ordered. Walking speeds, pull forces, angular positions and velocities, reaction, weight transfer and step times, and step lengths and velocities were measured using load cells and a motion measurement system. One-way ANOVAs with repeated measures were used to determine the effect of the type of postural perturbation.

RESULTS AND DISCUSSION

The experiments showed that (Figure 1 and Table 1):

- The maximum pull force younger adults could sustain decreased as initial walking velocity increased.
- The maximum lean angle younger adults could be released from decreased as initial pull force, which in effect adds initial velocity, increased.
- At the thresholds of balance recovery (maximum pull and leans trials), the type of perturbation did not affect weight transfer times, step times, step lengths and step velocities but did affect reaction times although only by 12 ms.
- The equivalent disturbance angular position and velocity points at the thresholds of balance recovery formed a disturbance threshold line separating falls from recoveries, regardless of the postural perturbation.

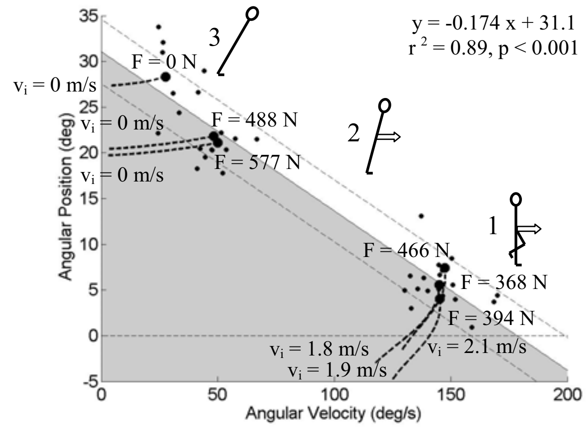

Figure 1: The equivalent disturbance angular positions and velocities, i.e., the angular positions and velocities from the vertical of the line connecting the stance ankle and the center of mass at the time of joint torque activation.

CONCLUSIONS

Initial velocity, produced by walking or added by pulling, has a detrimental effect on the threshold of balance recovery. However, results from experiments with no initial velocity do predict results of experiments with initial velocity. In other words, the threshold of balance recovery is not affected by the type of postural perturbation. Experiments are currently underway to confirm these results in older adults.

REFERENCES

1. Berg WP, et al. *Age Ageing* **26**(4), 261-268, 1997.
2. Pavol MJ, et al. *J Gerontol* **56A**(7), M428-437, 2001.
3. Maki BE and McIlroy WE. *IEEE Trans Rehabil Eng* **7**(1), 80-90, 1999.
4. Pai YC and Patton J. *J Biomech* **30**(4), 347-354, 1997.
5. Van den Bogert AJ et al. *J Biomech* **35**(2), 199-205, 2002.

ACKNOWLEDGEMENTS

We gratefully acknowledge the assistance of Véronic Francoeur-Castilloux, Emmanuel Côté, Philippe Fauteux and Mathieu Hamel along with the support of grant RG-02-0585 from the Whitaker Foundation.

Table 1: Effect of the type of postural perturbation on the threshold of balance recovery.

Type of perturbation	Walking Trials			Leaning Trials			p
Walking Velocity (m/s)	**1.809 ± 0.174**	**1.925 ± 0.130**	**2.108 ± 0.239**	**0.000 ± 0.000**	**0.000 ± 0.000**	**0.000 ± 0.000**	
Maximum Pull Force (N)	466 ± 75	394 ± 59	368 ± 55	**0 ± 0**	**488 ± 44**	**577 ± 39**	0.051
Maximum Lean Angle (deg)	**-2.8 ± 1.9**	**-4.9 ± 2.5**	**-1.7 ± 3.6**	27.3 ± 4.7	20.4 ± 3.6	19.7 ± 3.1	0.029
Reaction Time (ms)				80 ± 1	91 ± 8	92 ± 7	0.034
Weight Transfer Time (ms)				153 ± 25	171 ± 13	169 ± 18	0.189
Step Time (ms)	256 ± 22	241 ± 15	242 ± 30	196 ± 24	206 ± 18	207 ± 17	0.528
Step Length (m)	1.071 ± 0.110	1.039 ± 0.070	1.113 ± 0.050	0.984 ± 0.110	1.066 ± 0.060	1.085 ± 0.140	0.158
Step Velocity (m/s)	4.196 ± 0.408	4.319 ± 0.394	4.695 ± 0.896	5.048 ± 0.576	5.209 ± 0.676	5.235 ± 0.340	0.106

Note: Bolded values are controlled by the very nature of the postural perturbations and are thus not included in the statistical analyses.

Dynamic Calibration of an Extended-Range Electromagnetic Flock of Birds Motion Tracking System

David W. Wagner and Matthew P. Reed
University of Michigan - Ann Arbor,
email: dwwagner@umich.edu, web: www.HUMOSIM.org

INTRODUCTION

Electromagnetic (EM) motion tracking systems are a popular alternative to optical motion tracking systems. EM systems provide both position and orientation data from each sensor and can be used in environments with line-of-sight obstructions that would limit the use of camera-based systems. However, the presence of metal in the environment distorts the electromagnetic field and can cause significant errors [1,4]. Calibration procedures have been developed to improve accuracy by characterizing the distortion [2,3,4]. Previous efforts have used specialized fixtures with carefully controlled geometry to generate the reference data for calibration.

A new calibration technique is proposed that uses an optical motion tracking system as the source of reference data. The electromagnetic sensors are attached to a hand-held calibration wand that is also marked with optical targets. The wand is moved throughout the capture volume while data are gathered from both systems. Translation and rotation offsets are calculated for volume elements (voxels) of the capture space and subsequently applied to data from the electromagnetic system using an interpolating kernel.

METHODS

An Ascension Technology 'Flock of Birds' (FOB) electromagnetic tracking system with an extended range transmitter (ERT) was calibrated. Four sensors reporting both position and orientation were sampled at 50 Hz. Optical data were obtained using a Qualisys ProReflex MCU240 6-camera tracking system at 50 Hz. Five reflective markers, 25 mm in diameter, were placed on the wand, as shown in Figure 1. The configuration of the wand allowed the orientation of the FOB sensors to be calculated from the optical data.

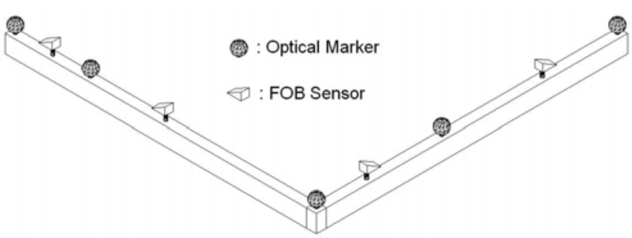

Figure 1. Calibration wand, showing optical markers and electromagnetic sensors.

The FOB system was calibrated throughout a 3.6 x 4.8 x 2.0 m volume adjacent to the FOB transmitter. Data were gathered simultaneously from the two systems as the wand was moved slowly through the capture volume. Data were collected for 3 to 5 minutes for the main calibration dataset. The optical data were examined to verify that the capture volume was adequately spanned. Holes in the calibration dataset were filled with shorter 1-2 minute trials.

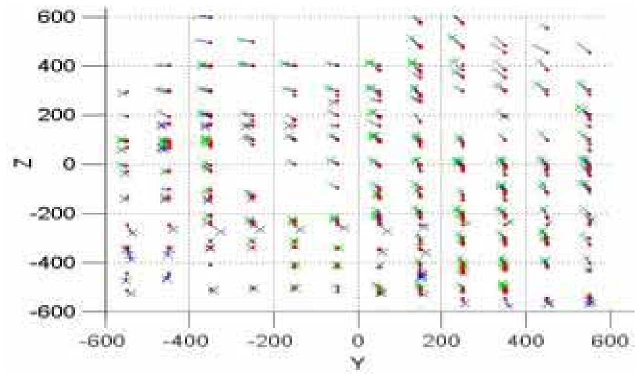

Figure 2: Positional offsets for all voxels in subset of the measurement volume.

Locally weighted linear regression was used to interpolate the scalar positional offsets for the FOB output position using a method similar to that reported by Day et al 2000 [2]. A Gaussian kernel centered at the FOB output position was used to determine weighting factors for the local regression. Orientation offsets were decomposed into Euler angles and handled in a similar fashion.

RESULTS AND DISCUSSION

Three-dimensional translational offsets are shown for a subset of the capture volume (Figure 1). Voxel size is 50mm^3. Circular dots indicate the reported FOB position and the connected cross is the associated global position. In practice, voxel size can be varied depending on the observed local field distortion, or the data can be used directly in the local interpolating functions, rather than aggregated into voxels. The accuracy with which the EM data match the optical data can be controlled in part by adjusting the density of the data gathered. Visual and quantitative tools provide feedback during the calibration process of the accuracy of the fit, allowing additional data to be gathered where needed.

Most previous approaches to EM system calibration have used specially constructed fixtures to move the EM sensors throughout the capture volume. The method reported here is faster and can easily be used around obstacles or with a changing environment. One group has reported using an optical system to obtain reference data [4], but only to improve the accuracy of measurements from a fixed-position calibration grid. Although the current approach is only practical when an optical system is available, it provides a relatively fast and accurate way of ensuring that data gathered from the two systems can be accurately merged for analysis.

REFERENCES

1. Day JS, et al. *J Biomech* **31**, 957-61, 1998.
2. Day JS, et al. *J Biomech* **33**, 1039-45, 2000.
3. Meskers CG, et al. *J Biomech* **32**, 629-33, 1999.
4. Perie D, et al. *J Biomech* **35**, 293-7, 2002.

EFFECTS OF JUMP TYPE ON GROUND REACTION FORCES DURING LANDING IN CHILDREN

Bradley A. Black, Christine M. Snow, and Michael J. Pavol
Dept. of Exercise and Sport Science, Oregon State University, Corvallis, OR, U.S.A.
email: mike.pavol@oregonstate.edu

INTRODUCTION

Bone loss associated with osteoporosis increases the risk of fracture in older adults. However, osteoporosis might be delayed and the incidence of fractures among older adults reduced by increasing peak bone mass during growth. In particular, pre-adolescence appears to be more responsive to interventions for increasing bone mass than adulthood. Known stimuli for increasing bone mass are large forces applied at high loading rates, such as those during landing from a jump. Indeed, a 7-month program of drop landings from a 61cm height enhanced gains in bone mass in children [1]. In this study, we determined whether other types of jumping activities in children produced ground reaction forces similar to those of the previously-reported drop landings.

METHODS

22 healthy children (11 girls; mean ± SD age: 8.2 ± 0.6 years) provided informed consent to participate in this study. After a warm-up, each participant performed 5 trials each of 13 types of jumping activities. One type was a drop from a 61cm-high box. The other 12 types were performed from the ground and comprised all possible combinations of three factors: direction (vertical, forward, lateral), feet used (1-footed hops, 2-footed jumps), and continuity (single, continuous). All hops were on the dominant foot. In continuous trials, participants performed 2 identical hops/jumps (in opposite directions for the lateral trials) without coming to rest in between. Vertical hops/jumps were as high as possible. Forward and lateral hops/jumps were over marked distances of 80 and 55% of body height, respectively. Lateral hops/jumps were toward the dominant foot. The ground reaction forces acting on the dominant foot during the first landing of each trial were measured at 1080Hz using a force plate. The activity order was counterbalanced across participants. Practice was provided for each activity.

The peak force and peak rate of force increase (determined over a moving window of 4.6ms) on the dominant foot during the first landing of each trial were normalized to body weight and pooled across the 5 trials for each activity. Three-factor repeated-measures ANOVA identified loading differences across direction, feet used, and continuity. Paired *t*-tests with a Bonferroni correction compared the loading for each activity to that of the drop landings. An α of 0.05 was used.

RESULTS AND DISCUSSION

The peak forces during landing were greater for hops than for jumps, were greater for single than for continuous hops/jumps (except in the lateral direction), and were greater for forward hops than for vertical or lateral hops (Table 1). Peak forces during the drop landings exceeded those during all other jumping activities except the single, 1-footed, forward hops.

Similarly, the peak loading rates during landing were greater for single than for continuous hops/jumps (except in the lateral direction) and typically greater for forward than for vertical or lateral hops/jumps (Table 1). Peak loading rates for hops were greater than for jumps only in the lateral direction. Peak loading rates during the drop landings exceeded those during all other jumping activities.

The results make sense. Two-footed jumps allow sharing of the impact forces between the limbs at landing, reducing the peak loading. Continuous forward hops/jumps do not require forward momentum to be arrested upon landing, while continuous vertical hops/jumps likely include a large countermovement after landing, reducing the loading. Forward hops/jumps likely involved greater momentum at landing, hence greater forces and/or loading rates, than did vertical or lateral hops/jumps due to the greater horizontal velocity associated with the greater horizontal distance traveled. Yet, in no hop or jump from the ground did the participants generate energy equivalent to the potential energy at take-off of the drop jump, resulting in smaller impact forces and/or loading rates for these other activities.

CONCLUSIONS

Compared to a variety of other jumps from the ground, single, 1-footed, forward hops produced the largest peak impact loadings in our sample of children. These hops were the only jumping activity from ground level that may produce as great an osteogenic stimulus as drop landings from a 61cm height.

REFERENCES

1. Fuchs et al., *J Bone Miner Res* **16**, 148-156, 2001.

ACKNOWLEDGEMENTS

Funded by NIH R01-AR-45655 (to CMS)

	Drop	Vertical		Forward		Lateral	
Peak Force (bw):		**Single**	**Continuous**	**Single**	**Continuous**	**Single**	**Continuous**
1-footed hop	–	3.7 ± 0.7 ^{abcd}	3.2 ± 0.5 ^{ad}	4.6 ± 0.7 ^{ab}	3.8 ± 0.7 ^{ad}	3.6 ± 0.5 ^{acd}	3.3 ± 0.3 ^{ad}
2-footed jump	5.3 ± 1.2	3.1 ± 1.0 ^{bd}	2.5 ± 0.6 ^{d}	3.6 ± 1.1 ^{bd}	2.7 ± 0.8 ^{d}	2.7 ± 0.7 ^{d}	2.8 ± 0.5 ^{d}
Peak Loading Rate (bw/s):							
1-footed hop	–	296 ± 147 ^{bcd}	227 ± 97 ^{cd}	449 ± 110 ^{bd}	364 ± 120 ^{d}	277 ±101 ^{acd}	223 ± 61 ^{acd}
2-footed jump	669 ± 190	322 ± 186 ^{bd}	221 ± 115 ^{d}	406 ± 186 ^{bd}	277 ± 126 ^{d}	204 ±107 ^{cd}	194 ± 78 ^{cd}

Table 1: Peak force and peak loading rate during landing as a function of hops vs. jumps, direction, and continuity
^{a} p<.05 vs. 2-footed hop; ^{b} p<.01 vs. Continuous; ^{c} p<.05 vs. Forward; ^{d} p<.001 vs. Drop; bw = body weight

ANTICIPATION OF SLIPPERY FLOORS: MUSCLE ONSETS AND CO-CONTRACTION OF THE STANCE LEG

April J. Chambers and Rakié Cham
Human Movement and Balance Laboratory, Department of Bioengineering, University of Pittsburgh, Pittsburgh, PA, USA
email: ajcst49@pitt.edu, web: www.engr.pitt.edu/hmbl

INTRODUCTION

Falls are a major cause of injury, death and disability in the elderly [4,6,8]. In relatively healthy older adults, falls are often precipitated by base of support (BOS) perturbations such as slips and trips [1,5,6]. The use of proactive strategies has been revealed in gait studies using testing paradigms involving repeated exposure to a known perturbation [2,3]. The goal of this study, which has not been previously addressed, is to investigate the impact of anticipating real slippery floors on the muscle activity (onset and co-contractions) in the leading/left leg during gait on dry surfaces.

METHODS

Eleven young (20-33 yrs) and 9 older subjects (55-66 yrs), screened for neurological and orthopedic abnormalities, were instructed to walk at a self-selected pace across a vinyl tile walkway, while ground reaction forces and whole body motion were sampled at 1080 and 120 Hz, respectively. Also, EMGs were collected from the vastus lateralis (VL), medial hamstring (MH), tibialis anterior (TA), and medial gastrocnemius (MG) at 1080 Hz. Subjects were informed the first few trials would be dry, 'baseline dry' (BD). Without the subjects' knowledge, a glycerol solution was applied at the left/leading foot-floor interface, generating an 'unexpected slip. Subjects were then alerted that all remaining trials might be slippery, 'alert dry' (AD). Only the EMG data of the first 2 trials in the BD and AD conditions were analyzed here to minimize adaptation effects.

EMGs were rectified, low-pass filtered at 50 Hz using a zero-phase elliptical filter, and time normalized with respect to stance time (left foot) with 0% = Heel contact (HC) and 100% - Toe off (TO). The magnitude of the resulting EMG envelope was normalized within subject to the average peak value collected in the BD trials. Onsets were determined using a threshold of two standard deviations above baseline activity (with visual confirmation). A co-contraction index (CCI) was calculated based on the integrated (from -20% to HC and from HC to 20% into stance) ratio of the EMG activity of antagonist/agonist muscle pairs (TA/MG and VL/MH) using the equation proposed by Rudolph [7]. Within subject repeated measures ANOVAs were conducted on the onset, ankle and knee CCI using age (young/older), condition (BD/AD), and their interaction effect as independent variables. Significance level was set at 0.05

RESULTS

In general (exception is TA), muscle onsets were significantly affected by condition (Table 1). Specifically, the MG and MH were activated earlier in stance in the AD trials compared to the BD condition, finding that was evident in both age groups. Also, a significant age x condition interaction effect was seen in VL, with the older group delaying the activation of this muscle when anticipating slippery surfaces, while young subjects did not. Also, older subjects activated their MH earlier in stance with anticipation compared to young subjects.

Table 1: Mean Onset (standard error)

Onsets in % Stance	CONDITION			
	BD		AD	
	Older	Young	Older	Young
VL	-13.91 (1.02)	-14.27 (1.08)	-10.64 (2.02)	-15.84 (1.47)
MH	-14.26 (5.05)	-24.12 (1.15)	-19.10 (1.56)	-25.38 (.93)
TA	-9.62 (1.29)	-2.39 (3.09)	-9.03 (2.08)	-3.70 (3.14)
MG	20.39 (6.48)	23.18 (4.65)	8.04 (6.50)	3.22 (5.78)

Anticipation resulted in increased stiffness at the ankle and knee in both age groups (Figure 1). Additionally, significant age x condition interaction effects were seen at the knee as younger subjects increased stiffness in the AD trials compared to their BD levels more than older subjects, especially post HC. Interesting age-related differences in knee stiffening strategies exist between the pre- and post- HC phases as well.

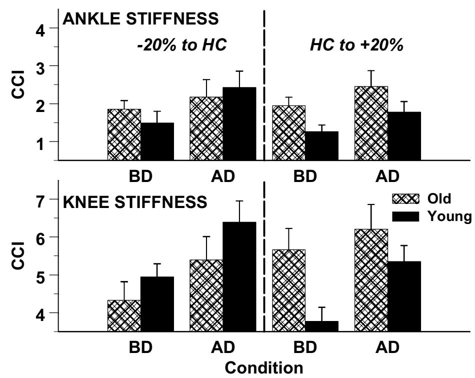

Figure 1: Ankle (top) and knee (bottom) CCI from -20% to HC (left) and from HC to 20% into stance (right) (standard error bars)

DISCUSSION AND CONCLUSIONS

In summary, anticipating slippery surfaces affects lower leg muscle activation onsets and ankle/knee stiffness. While young and older subjects adopted similar strategies at the ankle when anticipating slippery floors, there were age-related differences associated with the upper leg muscles. It is worth noting the most critical recovery responses to slips are generated at the knee and hip, not the ankle [9].

REFERENCES

1. Berg WP et al. *Age and Ageing*, 26:261-8, 1997.
2. Cham R et al. *Gait and Posture*, 15:159-71, 2002.
3. Marigold DS et al. *J Neurophysiol*, 88(1):339-53, 2002.
4. Masud T et al. *Age and Ageing*, 30 (Suppl 4):3-7, 2001.
5. Nyberg L et al. *J Am Geriatrics Scty*, 44:156-60, 1996.
6. Rubenstein LZ et al. *Clin Geriatric Med*, 18:141-58, 2002.
7. Rudolph KS et al. *Knee Surg, Trau, Arth*, 9:62-71, 2001
8. Sterling DA et al. *J Tra-Inj, Inf, Crit Care*, 50:116-9, 2001.
9. Cham R et al. *J biomech,* 34(11): 1439-45, 2001.

ACKNOWLEDGEMENTS

Funding source: NIOSH R03 OH007533
Neurological screening: Dr. Joseph Furman

COMPARISONS OF THE LOWER LIMB MECHANICS BETWEEN YOUNG AND OLDER ADULTS WHEN CROSSING OBSTACLES WITHOUT VISUAL GUIDE

Hao-Ling Chen and Tung-Wu Lu
Institute of Biomedical Engineering, National Taiwan University, Taiwan, twlu@ntu.edu.tw

INTRODUCTION

Since tripping over obstacles during locomotion has been reported as one of the most frequent causes of falls in the elderly [1], research on the kinematics and kinetics of the lower extremities during this functional activity has received much attention [2-4]. The majority of previous studies in young adults during obstacle-crossing have been limited to presenting the kinematics of the leading swing limb and the kinetics of the trailing stance limb. It is noted that one has no visual cue when the trailing limb is crossing the obstacle, increasing the chance of tripping. Thus, a complete knowledge of the mechanics of obstacle crossing should include that of the limbs when the trailing limb is crossing, Fig. 1.

The kinematics of the crossing trailing limb has been reported for young adults [4] but the kinetics of the leading stance limb has not. Moreover, since aging may affect the performance of locomotion and obstacle negotiation, age effects on the mechanics of the leading stance limb and the trailing swing limb require detailed investigation. The purpose of the present study was thus to investigate the kinematics of the trailing swing limb and the kinetics of the leading stance limb when crossing obstacles of different heights in the healthy old people and to compare the results with those of the healthy young people.

METHODS

Fifteen young adults (age: 23±3 years, height: 176.1±6.3 cm, mass: 68±8.6 kg) and fifteen older adults (age: 72±6 years, height: 160±5.7 cm, mass: 58±10.4 kg) participated in the present study with informed consents. They all had normal corrected vision and were free of neuromusculoskeletal pathology. In a gait lab, each subject walked at self-selected pace and crossed obstacles of three different heights (10, 20 and 30% of leg length). Twenty-eight markers were used to track the motion of both limbs. Kinematic and kinetic data were measured with a 7-camera motion analysis system (Vicon512, Oxford Metrics, U.K.) and two force plates (AMTI, Advanced Mechanical Technology, U.S.A.) placed on each side of the obstacle. Height effects on temporal-distance gait parameters and joint angles of the trailing swing limbs as well as peak and crossing moments of the leading stance limbs were tested using RMANOVA for each age group (α=0.05). Independent t-test was used for between-group comparisons.

RESULTS AND DISCUSSION

The trailing clearance distances were not affected by height and age in both groups (p>0.05), in agreement with the literature [5-6]. Smaller leading heel-obstacle distances were found in the older group for all heights (p<0.05), suggesting that the older subjects may have higher risk of stumbling when the leading limb was crossing.

When the trailing toe was above the obstacle, the older group adopted bigger trailing hip flexion angles as well as bigger hip extensor, hip abductor and knee abductor crossing moments of the leading limb for all heights. Similar results were also found in the leading peak moments. Bigger joint crossing moments and more flexed positions of the stance limb may help to maintain a better stability. Bigger peak moments indicate that higher muscular demand was needed in the older group. In order to achieve the same trailing toe clearance as the young group, the older adults adopted bigger trailing hip crossing flexion angles.

The results of the study suggest that different temporal-distance, kinematic and kinetic strategies were used by the two age groups. The older group, with age-related muscle weakness, degradation of balance control and coordination, adopted a more conservative strategy possibly due to safety requirements.

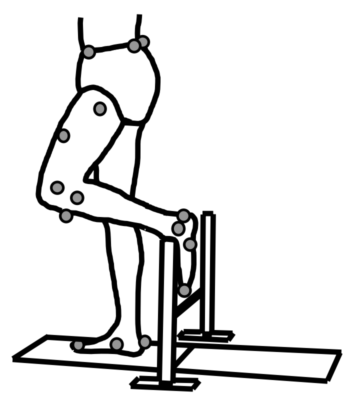

Figure 1: Schematic diagram showing a subject's trailing limb crossing a height-adjustable obstacle while the leading limb is the stance limb.

REFERENCES

1. Tinetti ME, et al. *N Engl J Med* **319**, 1701-1707, 1988.
2. Chen HS, et al. *J Gerontol* **46**, M196-M203, 1991.
3. Patla AE, Rietdyk S. *Gait Posture* **1**, 45-60, 1993.
4. Chou LS, Draganich LF. *J Biomech* **30**, 331-337, 1997.
5. McFadyen BJ, Prince F. *J Gerontol* **57A**, B166-B174, 2002.
6. Draganich LF, Kuo CE. *J Biomech* **37**, 889-896, 2004.

MECHANOMYOGRAPHY AND FORCE RELATIONSHIP DURING CONCENTRIC AND ECCENTRIC CONTRACTIONS OF THE VASTUS LATERALIS IN THE SPRINTERS

[1]Chien-Hua Peng, [1]Yu Liu, [1]Shu-Mei Peng, [1]Jia-Yean, Chen, [1]Yi-Fang Lee
[1]Chinese Culture University, Department of Kinesiology
email: jessiepeng@sparqnet.net

INTRODUCTION

It has been investigated the mechanomyographic (MMG) signal may respond linear [1] or non-linear [3] relationship with force development Different relationship depends on contraction types, force levels, angular velocities and the muscles studied [1, 3]. Studies suggested that the MMG properties may also differentiate muscle fiber types [5]. The purpose of this study was to investigate the MMG and EMG (electromyographic) amplitude responses of vastus lateralis to different force levels during concentric and eccentric contractions in the sprinters.

METHODS

Subjects. Six male sprinters (26.1 ± 1.6 yrs) were recruited for this study.

Experimental procedures. Subjects were in seated position with belt over the hip and chair of leg extension machine, then randomly performed 30%, 50%, 70% and 85% MVC leg extension each 5 tests with starting knee angle 90° and extending to 180° at the speed of 1.5s up and 1.5s down controlled by beat metronome (40bpm, 1beat up, 1 beat down). Each subject practiced the speed control 2 times on nonconsecutive days one week ahead.

Signal processing. The MMG and EMG signals from vastus lateralis of nondominant leg were detected by biaxial accelerometer (acceleration range ± 2g, Biovision), and surface electrodes (Biovision) respectively with both sample rate 1000Hz and bandpass filtering (2nd order Butterworth) 5-100Hz for MMG and 5-500Hz for EMG. The concentric and eccentric phases were separated by goniometer signal, and the middle 0.5s of each 1.5s recording was used to avoid initial burst [6]. The mean root mean square (time constant 100ms) of MMG (rmsMMG) and EMG (rmsEMG) for middle 3 of 5 tests were calculated.

Statistical analysis. The relationship between concentric and eccentric rmsMMG/rmsEMG with force and the difference between two phases of two signals were examined by linear regression model (y = a + bx, x: force, y: rmsMMG or rmsEMG) and two-way ANOVA respectively.

RESULTS AND DISCUSSION

MMG signal. The rmsMMG showed positive linear relationship with increasing force level for both concentric (r^2= 0.45, regression coefficient b=0.67, P<.001) and eccentric (r^2= 0.64, b=0.80, P<.001) contractions. The eccentric rmsMMG was greater than concentric rmsMMG for all levels of force (P<.05).

EMG signal. The rmsEMG also showed linear relation with increasing force for concentric (r^2= 0.71, b=0.84, P<.001) and eccentric (r^2= 0.54, b=0.73, P<.001) contractions. Contrary to MMG, all levels of concentric rmsEMG were significantly greater than eccentric rmsEMG (P<.05).

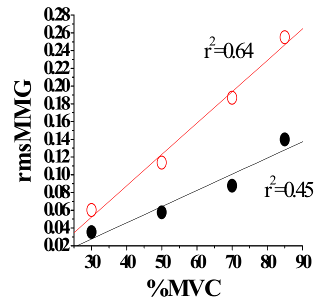

Figure 1

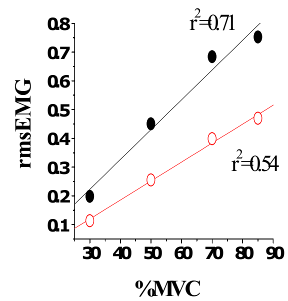

Figure 2

Figure 1:MMG-force relationship during concentric (●) and eccentric (○) contractions.
Figure 2: EMG-force relationship during concentric (●) and eccentric (○) contractions.

Discussion. The results of linear relationship of MMG/EMG amplitude and force during concentric and eccentric contractions conformed to previous study [1]. The lower EMG activity demonstrated decreased active motor units during eccentric phase [4]. The greater MMG activity during eccentric contraction of this study disagreed with the previous investigations of no difference [1] or lower activity [3] may result from faster speed of our experiment and fast-twitch fiber type subjects. Studies reported at higher velocities muscle sounds were from more superficially located fast-twitch fibers [2] and were less damped by surrounding tissues may result in greater MMG amplitude [7], and these may account for our study result.

CONCLUSIONS

The MMG signal may detect the active motor units recruitment during isotonic concentric and eccentric contractions and also response the selectively activated fast-twitch fibers at faster velocity and with fast fiber type muscle during eccentric contraction.

REFERENCES

1. Dalton, PA, et al. & Stokes, M.J. (1991). *European Journal of Applied Physiology,* **63**, 412-416, 1991.
2. Johnson MA, et al. *Journal of the Neurological Sciences,* **18**(1), 111-29, 1973
3. Madeleine P, et al. *Journal of Electromyography & Kinesiology,* **11**(2), 113-121, 2001.
4. Moritani T, et al. *American Journal of Physical Medicine,* **66**(6), 338-350, 1987.
5. Orizio C, et al. . Veicsteinas A. *International Journal of Sports Medicine.* **13**(8), 594-599, 1992.
6. Oster G, et al. *Biophysical Journal,* **30**(1),119-127, 1980.
7. Smith DB, et al. *Journal of Applied Physiology,* **82**(3), 1003-1007, 1997.

APPLICATION OF ARTIFICIAL NEURAL NETWORK TO PREDICT THE JOINT TORQUE OF LOWER LIMBS USING THE PARAMETERS OF GROUND REACTION FORCE DURING VERTICAL JUMP

[1] Yu Liu and [2]Shi-Ming Shih
[1]Chinese Culture University, Taipei, Taiwan; email: yliu@faculty.pccu.edu.tw;
[2]National College of Physical Education, Taoyuan, Taiwan

INTRODUCTION

The measurement of ground reaction force (GRF) during vertical jump was often used to evaluate the athlete's muscular strength and power of lower limbs. However, the GRF could only specify the muscular power ability of lower limbs in whole and it couldn't reflect the muscle joint torque and neuromuscular control ability at each joint of lower limbs. To get the information of the joint torque, inverse dynamics calculation must be conducted by inputting the kinematic data and the data of GRF [1]. The purpose of this study was to develop an artificial neural network (ANN) model for predicting the joint torque at ankle, knee and hip by using the relevant parameters of GRF during vertical jump.

METHODS

10 male sport students (age: 20.10 ±1.91 yrs; height: 179.34 ± 4.25 cm; weight: 69.58 ±3.91 kg) performed counter-movement-jump (CMJ) on a Kistler force platform (1200Hz). Meanwhile, the kinematic data of CMJ were recorded and digitized with a Peak Performance System at 120Hz. The GRF and kinematic data of support phase were than normalized as 100%. To calculate the joint torque at ankle, knee and hip, 2D inverse dynamics model was developed by inputting the GRF, kinematic data and Dempster's body segment parameters [1].
In this study we used a fully-connected, feed-forward network comprised of one input layer, one hidden layer and one output layer trained by back propagation using Gradient Steepest Descent Method [2]. The input parameters of this ANN model were time variables obtained by GRF measurement: time percentage, GRF, vertical displacement of center of mass (c.m.), speed of c.m. and power; the output parameters of the model were time data of joint torque at ankle, knee and hip. The data were scaled before input and rescaled after output. We used the software PCNeuron 4.1 to develop the ANN model and the root mean square (RMS) error of prediction to measure the network fitness..

RESULTS AND DISCUSSION

One subject from the ten was chosen randomly as test sample for evaluating the network fitness. The data of rest nine subjects was used for modeling and training of the ANN. After trial-and-error optimization procedure, a "5-10-3 ANN model" was found, in which there were 5 neurons in the input layer, 10 neurons (nodes) in the hidden layer and 3 neurons in the output layer.

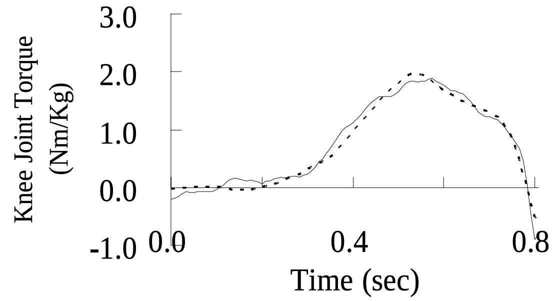

Figure 1: The measured （solid line） and predicted (dotted line) joint torque at knee joint during CMJ.

The results of the test sample (Table 1) showed that, compare to the measured curves, the relative errors of the predicted peak joint torque at three joints were less than 4%. The RMS errors for all three joints were smaller than 0.04 revealing that the prediction errors of this model were well convergent. The predicted and the measured time curve of joint torque were also significantly correlated, the correlation coefficient were 0.967, 0.987 and 0.979 at ankle, knee and hip respectively. The figure 1 demonstrates that the predicted curve of joint torque at knee was fit well to the measured curve. Since the GRF could be simply measured in the sport science, the application of ANN using GRF is meaningful to study of joint torque without inverse dynamics during vertical jump.

CONCLUSIONS

A back propagation ANN was developed by trial-and-error optimization technique to predict the lower limb's joint torque by using GRF during CMJ. We conclude that the ANN using GRF is feasible in the study of joint torque without kinematic measurement and inverse dynamics during vertical jump.

REFERENCES

1. Robertson DGE, et al. *Research Methods in Biomechanics.* Human Kinetics, Champaign, IL, 2004.
2. Schalkaff RJ. *Artificial Neural Network*, New York, McGraw-Hill Companies Inc. 1997.

Table 1: The peak values of measured and predicted joint torque and their relative errors; RMS errors and the correlation coefficient between the measured and the predicted time curve of joint torque at ankle, knee and hip（**: p<.01）.

Joint	Peak Torque Measured [Nm/kg]	Peak Torque Predicted [Nm/kg]	Relative Error [%]	RMS Error (n=100)	r (n=100)
Ankle	-1.908	-1.938	1.56	0.0309	0.967**
Knee	+1.882	+1.972	3.16	0.0327	0.987**
Hip	-2.459	-2.359	3.59	0.0335	0.979**

SKI SKATING FORCE CHARACTERISTICS: COMPARISONS ACROSS SPEED

Gerald Smith, Bent Kvamme and Vidar Jakobsen
Norwegian University for Sport and Physical Education; email: Gerald.Smith@nih.no

INTRODUCTION

Two primary ski skating techniques, V1 and V2, have been typically thought of as uphill and flat terrain techniques, respectively. However it has become common for ski racers to push the V2 skate on steeper uphills. A recent physiological comparison of the techniques across a range of slopes found a cross-over point of relative effectiveness with similar costs on moderate uphills of about 4 to 5 degrees [1]. A 5° uphill slope was used for the measurements of the current experiment, allowing both techniques to be evaluated under similar physiological demands. Kinetic characteristics of ski skating have been measured in only a few situations [2], none involving V2 technique on uphill terrain and across a range of speeds. The objective of this experiment was therefore to determine how V1 and V2 kinetic characteristics change with skiing speed on moderate uphill terrain where racers commonly use both techniques.

METHODS

Instrumented roller skis and poles were used to measure reaction forces during V1 and V2 skating on a large treadmill with a 5° uphill slope. A small electronic device was carried which telemetered the force data to a computer for synchronous recording along with 3-D position data. Markers on skis and poles were tracked using a Qualisys ProReflex system at 240 Hz. Using ski and pole positioning to orient the resultant reaction forces in the lab coordinate system, force components were calculated. From the force data, cycle characteristics, impulse, peak and average force (over a cycle) were determined.

Eight elite-level male skiers participated in two data collection sessions which were randomly assigned to a technique (V1 or V2 skating). After a warmup, ski speed was systematically increased from moderate to faster than race-pace relative to each skier's capability. Three speeds within this range were analyzed. At each speed, 15 seconds of force and position data were recorded from which six cycles were analyzed. Mean values across the six cycles were used to represent a skier's characteristics at that speed.

RESULTS AND DISCUSSION

Cycle characteristics changed systematically for both skating techniques with both cycle length and frequency increasing with speed ($P < 0.001$). Thus, control of skating speed on uphill terrain follows a different pattern than on the flat where frequency dominates [3]. Ski angle with respect to forward direction affects the proportion of reaction force which is propulsive. While ski angles were different for V1 and V2 techniques (about 19° vs. 15°) these changed little with speed. Peak forces (Figure 1) of both skis and poles increased with speed ($P < 0.02$) while average forces over a cycle were nearly constant. Average propulsive force summed across skis and poles did not change with speed (Figure 2). The proportion of propulsive force from poling was about 50-55% for V1 and 70-75% for V2 skating with each decreasing slightly with increased speed ($P < 0.03$).

CONCLUSIONS

Treadmill ski skating forces change systematically in magnitude and timing as speed increases. However propulsive force component remains relatively constant with increasing speed as the resistive forces opposing motion (gravity and ski drag) do not change with speed.

REFERENCES

1. Kvamme B, et al. *Eur J Appl Phys*, in press.
2. Millet GY, et al. *MSSE* **30**, 1645-1653, 1998.
3. Nilsson J, et al. *Sports Biomech* **3**, 85-107, 2004.

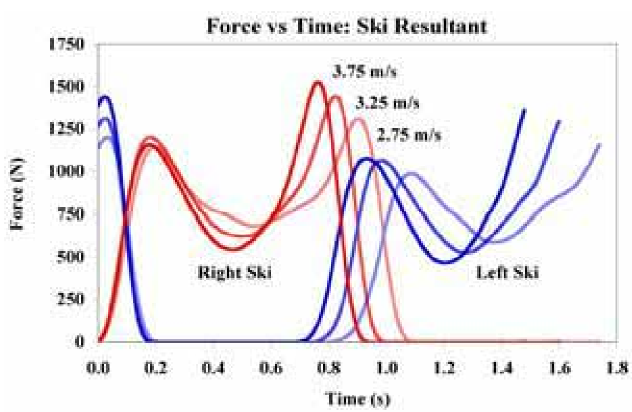

Figure 1: Resultant Ski Force vs. Time. These graphs from one skier illustrate the typical pattern of decreasing phase time and increasing peak forces as speed increases.

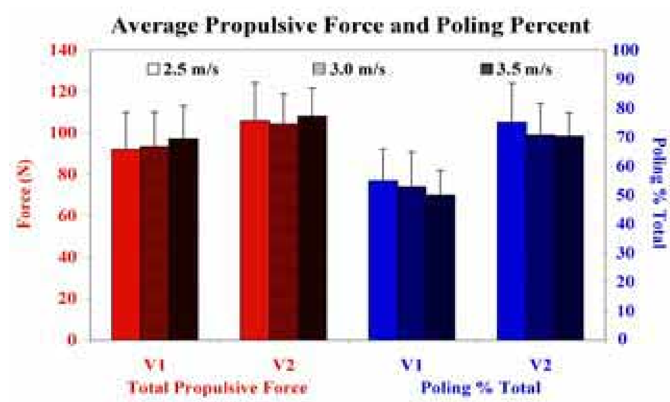

Figure 2: Total propulsive force was nearly constant across speeds however the proportion between ski and pole propulsion was different for the two techniques (V1 and V2 Poling % Total).

THE PARAQUAT ADSORPTION PATTERN AND HEMODYNAMIC PROPERTIES OF CHARCOAL COLUMN IN HEMOPERFUSION

[1,4]Jeong Chul Kim, [1,4]Jung Chan Lee, [1,4]Joong Yull Park, [2]Gil Jun Suh, and [2,3,4]Byoung Goo Min
[1]Interdisciplinary Program in Medical and Biological Engineering Major, Seoul National University, Seoul, Korea,
[2] Department of Biomedical Engineering, College of Medicine, Seoul National University, Seoul, Korea,
[3]Institute of Medical and Biological Engineering, Medical Research Center Seoul National University, Seoul, Korea
[4]Artificial Organ Center, Seoul, Korea; email: jckim80@snu.ac.kr

INTRODUCTION

Hemoperfusion is a therapy for the drug intoxicated patients using the activated charcoal column. Although studies on the charcoal adsorption in the industrial field are active, in medical applications, quantitative prescription is not available. More quantitative standard on the hemoperfusion prescription is required. In this study, hemodynamic analysis on the hemoperfusion was quantitatively performed with a mathematical model of the paraquat adsorption was represented.

METHODS

HEMODYNAMIC MODEL

The paraquat adsorption in the charcoal column was simulated by solving the chemical reaction equation and mass balance equation simultaneously. The chemical reaction of adsorption was defined as the finite-rate reaction and stoichiometric coefficient and rate exponent were obtained from animal experiment. Langmuir model was used to fit the animal experiment data and calculate the parameters required to predict the absorption kinetics

Blood flow rate of 120 m/min was given as an inlet boundary condition and venous pressure of 10mmHg condition was set for the far enough from the column outlet. Darcy's law was used to model the porous media of the activated carbon and experimentally determined the porosity and flow resistance in the porous media.

To estimate the paraquat adsorption, the amount of paraquat absorbed and the time required for the adsorbent to take up half as much parauat as it will at equilibrium. Mass flux distribution was also calculated by dividing the charcoal column into three parts from central region to peripheral region.

A commercial computer-aided design software package, GAMBIT 2.0 (Fluent, Inc.), was used to generate the two dimensional axisymmetric geometry and computational surface mesh of the charcoal column (Figure). A commercial CFD code, FLUENT6 (Flunet, Inc.) was used to discretize and solve the mass and momentum equations governing fluid flow through the porous media

ANIMAL EXPERIMENT

For Six dogs (Body Weight = 30 kg), 50 cc diluted paraquat solution was injected in intravenous injection. The paraquat level an hour after injection was 61.8 mg/L. Hemoperfusions were started one hour after injection for four hours and blood was sampled at 30, 60,120, 180, 240 min from arterial line. Blood flow rate was maintained at 120 mL/min and pumped with peristaltic roller pump (Gambro AK95). The Adsorption Charcoal Column used was ASRORBA 300C (Gambro). The paraquat concentration analysis of the blood samples were entrusted to Inha University Hospital.

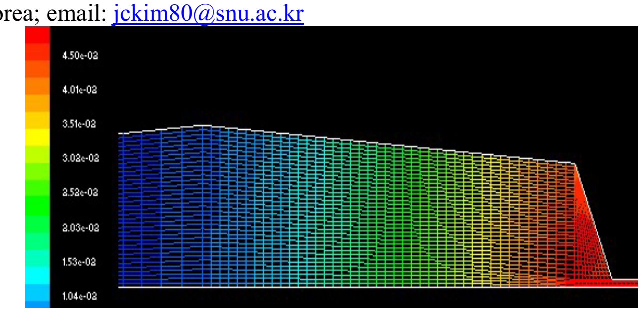

Figure: Praquat concentration distribution in the charcoal column.

RESULTS AND DISCUSSION

The peristaltic roller pump generated sine wave like mass flow with pressure drop about 15 – 20 mmHg. The charcoal column surface mesh was dissected in radial direction into three parts to assess the flow distribution. As shown in Figure, the concentration of the toxin is higher in the central region than that of peripheral region. This phenomenon is due to the mass flux inequality per unit volume. The mass flux ratio calculated per unit charcoal volume in each dissected part was 1: 1.7: 5.3 implying that 65% more influx was passed through the central region of the column and might lead to decrease in adsorption efficiency. At the interface of the porous media and blood inlet, secondary flow was observed, which possibly results in the risk of thrombosis formation in clinical application and this is an important factor in the life of charcoal column. The amount of paraquat absorbed during the hemoperfusion was 2.976g and the time required for the adsorbent to take up half as much parauat as it will at equilibrium was16.5 min implying the strong electrostatic interaction between negatively charged surface and paraquat cation.

CONCLUSIONS

This simulation may be helpful to determine the quantitative prescription of hemoperfusion dose for the drug intoxicated patients. And more optimized flow pattern and geometry of the charcoal column are required to maximize the paraquat adsorption efficiency in the activated carbon.

REFERENCES

1. W.T. Tasi, et al. Chemosphere **55**, 829-837, 2004
2. Hampson EC, et al. *J Pharmacol Exp Ther* **254**, 732-740, 1990.

ACKNOWLEDGEMENTS

This Study is supported by the Brain Korea 21 Project of the Ministry of Education and Human Resources Development, Republic of Korea.

BIOMECHANICS OF THE LOWER LIMB DURING STAIR LOCOMOTION IN SUBJECTS WITH ANTERIOR CRUCIATE LIGAMENT RECONSTRUCTION

[1,2]Hsiu-Chen Lin, [1]Tung-Wu Lu and [2,3]Houng-Chaung Hsu
[1]Institute of Biomedical Engineering, National Taiwan University,
[2]School of Physical Therapy, China Medical University,
[3]Department of Orthopedics, China Medical University Hospital; email: hclin@mail.cmu.edu.tw

INTRODUCTION

The anterior cruciate ligament (ACL) is one of the most commonly injured ligaments in the knee. Its injury would lead to the degradation of stability and/or mobility of the joint. To regain stability and restore function after ACL injury, surgical reconstruction is frequently considered and a proper rehabilitation program is crucial for the recovery of the function. The accelerated rehabilitation program, which emphasizes early full knee extension and weight bearing as well as closed kinetic chain (CKC) exercises, has been proven to have good results after a long-term follow-up [1]. Being one of the most frequently used CKC exercises and a frequent activity of daily living, studies on the three-dimensional dynamics of stair locomotion in ACL-injured patients were limited. Previous studies of stair activities in ACL patients focused on the mechanical changes at the knee joint [2,3]. However, stair locomotion is achieved through a complicated mechanical interaction among the lower limb joints in three dimensions. The present study aimed to provide a more complete account of the possible biomechanical changes among the lower limb joints.

METHODS

Ten ACLR subjects (28.3±8.5 years) and ten normal controls (21.4±1.7 years) were recruited in this study. Each subject performed stair ascent and descent on a three-step stair in a gait laboratory. A seven-camera motion analysis system (VICON 370, Oxford Metrics, U.K.) was used to measure the movement trajectories of each segment of the lower extremity. The ground reaction forces (GRF) were measured with a force platform (AMTI, Mass., U.S.A.), which served as the second step of the three-step stairs. Peak joint angles, peak joint moments and angular impulses of the lower limb joints in three dimensions during the stance phase of the stair activities were calculated and compared between groups using t-test and between affected and unaffected limbs using paired t-test. A significance level of 0.05 was used.

RESULTS AND DISCUSSION

Compared to the normal knees, significantly smaller peak moments and angular impulses of the extensors and internal rotators at the affected knees were found during both stair activities while larger peak moments and angular impulses of the adductors and peak abduction angles were needed at the unaffected knees. Larger hip extensor impulses and smaller hip external rotation angles and smaller peak ankle plantarflexor moments at the affected limb during stair ascent were found (Figure 1). During stair descent, larger hip internal rotation angles, and smaller peak hip abductor moments and ankle plantarflexor moments in the affected limb were found while larger hip flexor impulses in the unaffected limb were required.

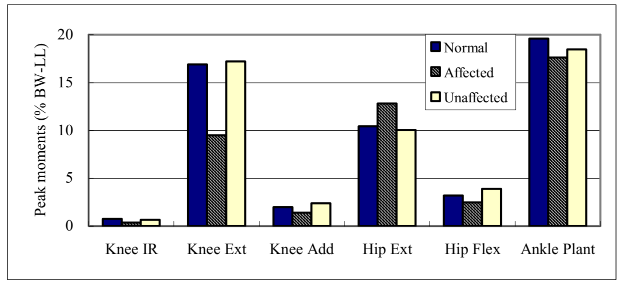

Figure 1: Peak joint moments during stair ascent.

These results suggest that the ACLR knees had significant reduction in the mechanical loadings in the sagittal and transverse planes during both stair activities, possibly due to the need to protect the ACL graft as well as the deficit of the quadriceps strength, which may persist even at 24 months after reconstruction [4]. The compensations to these changes occurred mainly in the coronal components of the unaffected knees and at the hip joints, with different strategies for stair ascent and descent. The increased hip extensor impulses were used to compensate the reduced knee extensor impulses in the affected limb during stair ascent. During stair descent, the increased hip flexor impulses in the unaffected limb helped controlling the movements of the trunk.

CONCLUSIONS

Significant mechanical changes in the sagittal and transverse components at the ACLR knees were found during both stair activities and the compensations occurred mainly in the coronal components of the unaffected knees and also at both hip joints with different strategies for stair ascent and descent.

REFERENCES

1. Shelbourne KD, et al. *Am J Sport Med* **25**, 786-795, 1997.
2. Andriacchi TP. *J. Biomechanics* **23**(Suppl. 1), 99-105, 1990.
3. Kowalk DL, et al. *Med. & Sci. Sports & Exerc* **29**,1406-1413, 1997.
4. Kobayashi A, et al. *International Orthopaedics* **28**, 48-51, 2004.

ACKNOWLEDGEMENTS

The authors gratefully acknowledge the supports from the National Health Research Institute of Taiwan (NHRI-EX93-9126EP) and China Medical University.

INFLUENCE OF FUNCTIONAL KNEE BRACES ON LOWER LIMB MECHANICS DURING STAIR LOCOMOTION IN PATIENTS WITH ANTERIOR CRUCIATE LIGAMENT DEFICIENCY

[1,2]Horng-Chaung Hsu, [3]Tung-Wu Lu, [2,3]Hsiu-Chen Lin
[1]Department of Orthopedics, China Medical University Hospital
[2]School of Physical Therapy, China Medical University
[3]Institute of Biomedical Engineering, National Taiwan University; email: hchsu@mail.cmu.edu.tw

INTRODUCTION

Anterior curciate ligament (ACL) provides passive stability of the knee and involves in the guidance of the joint motion. Injury of the ACL would lead to the degradation of stability and/or mobility of the joint. Functional knee braces have been suggested to provide necessary stability for ACL injured individuals and to be a factor causing the change of the kinetics of the lower limb during gait [1]. But, knee braces only resulted in minor kinematic changes in the ACL deficient (ACLD) knees during single leg hops [2]. The efficacy of knee braces may be different for different activities. The efficacy of braces on ACLD subjects during stair locomotion, one of the most common daily activities, has not been reported. The purpose of this study was to examine the immediate effects of functional knee bracing on the mechanics of the lower limb joints in ACLD individuals during stair locomotion.

METHODS

Ten ACLD subjects (26.1±7.3 years) were asked to perform stair ascent and descent in a gait laboratory first without and then with knee braces (DonJoy Goldpoint, Smith & Nephew DonJoy Inc.). The kinematic data were measured with a seven-camera motion analysis system (VICON 370, Oxford Metrics, U.K.) and the kinetic data with a force platform (AMTI, Mass., U.S.A.) that served as the second step of a three-step stairs. Joint angles, moments and angular impulses were calculated during the stance phase of the stair activities from the measured kinematic and kinetic data with a 3-D lower limb model. Peak joint angles, joint moments and angular impulses at the hip, knee and ankle joints in three dimensions were calculated and compared between bracing conditions and between affected and unaffected knees using paired *t*-test. Data from ten normal controls without bracing were also obtained.

RESULTS AND DISCUSSION

The affected knees adopted quite similar movement patterns to the normal ones (Figure 1) while significant alterations at the affected hip and in the unaffected limb were noticed during stair activities. Bracing did not affect the biomechanics of the lower limb during stair locomotion except for minor changes in the flexion angle and flexor impulse at the affected hip and in the internal rotation angle and external rotator moment at the unaffected knee during stair ascent, Table 1. The adaptations of the locomotor system to ACL deficiency were evident although there had no significant mechanical changes at the affected knees. The bracing did not result in any significant alteration of the mechanics of the affected knees. These results suggest that the mechanical condition at the ACLD knees remained relatively unchanged mainly because of the adaptations at the other joints instead of knee bracing.

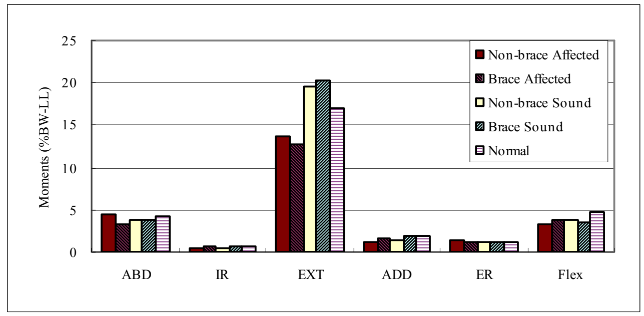

Figure 1: Peak joint moments at the knee during stair ascent.

CONCLUSIONS

The influence of knee bracing on the lower limb mechanics was not significant in ACLD subjects during stair locomotion. Bracing may not be used as a device to improve the performance of stair locomotion in these subjects.

REFERENCES

1. DeVita P, et al. *J Biomech* **29**, 583-588, 1996.
2. Ramsey DK, et al. *Clin Biomech* **16**, 61-70, 2001.

ACKNOWLEDGEMENTS

The authors gratefully acknowledge the support from the National Health Research Institute of Taiwan (NHRI-EX93-9126EP).

Table 1: Variables affected by functional knee bracing for the ACLD subjects during stair ascent.

	Normal		Affected					Unaffected				
	Non-brace		Non-brace			Brace		Non-brace			Brace	
	Mean	SD	Mean	SD		Mean	SD	Mean	SD		Mean	SD
Hip extension (deg)	3.35	5.17	0.05	5.34	*	3.36	5.72	1.64	5.24		0.47	3.99
Hip flexor impulse (%)	0.41	0.39	0.15	0.16	*	0.11	0.15	0.33	0.28		0.32	0.32
Knee IR (deg)	0.42	8.50	2.62	10.45		0.87	4.64	-6.34	4.04	*	-3.37	3.39
Knee ER moment (%)	1.30	0.57	1.52	1.31		1.08	0.42	1.19	0.53	*	1.11	0.52

* $p<0.05$ between brace conditions using paired *t*-test

DETERMINING SUBJECT SPECIFIC TORQUE-VELOCITY RELATIONSHIPS WITH THE INCLUSION OF HIGH VELOCITY TORQUE DATA

Matthew Pain, Chris Mills and David Jessop
School of Sport and Exercise Sciences,
Loughborough University, LE113T, UK email: M.T.G.Pain@lboro.ac.uk

INTRODUCTION

Modelling of the muscle force-velocity relationship normally utilizes a Hill type function in the concentric phase and a rapid increase to a plateau region in the eccentric phase. Muscle experiments in humans show depression in eccentric and low velocity concentric torque production [1], they have also been limited to joint angular velocities of less than $\pm 400\ ^{o}s^{-1}$. The introduction of a 'differential activation' function [2] explains a possible mechanism for the force suppression observations. However without high concentric velocity torque data the bounds chosen for maximal velocity of contraction can have an important influence on the final fit of the curve to the experimental data.

The aim of this paper is to examine the variation of a Hill type 4 parameter function, and a 7 parameter function, including differential activation, when maximal velocity torque data are included.

METHODS

Measurements were taken on an elite martial artist, height 1.78 m, weight 90 kg, the protocols were approved by Loughborough University Ethical Advisory Committee.

Isovelocity torque data in concentric-eccentric cycles were collected in 50 $^{o}s^{-1}$ intervals up to a crank angular velocity of 450 $^{o}s^{-1}$ for flexion and extension of the knee and hip. Corrections for weight and differences between crank and joint angle were calculated. Peak isovelocity torques were determined for 17 angular velocities. High speed video (500 Hz) was used along with subject specific anthropometrics to determine joint torques during unloaded maximal flexion and extension of single joints. Joint torque near maximal velocity was used to provide an 18th torque-velocity value.

The Direct Optimization routine [3] was used to calculate the 4 and 7 parameter values that gave the best fit to the 17 data points. The upper bound for maximal angular velocity was set sufficiently high that it was not reached. The error between the 18th data point and that predicted by the two functions was calculated. The parameters were then re-optimized including 18 data points and its effect examined.

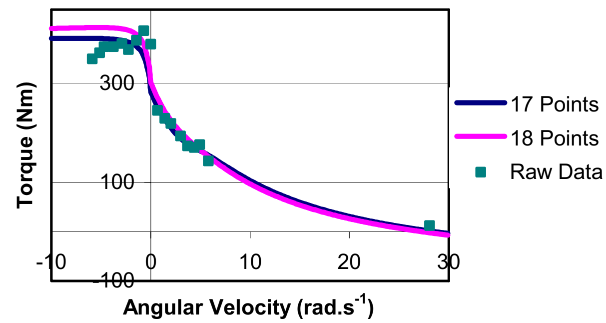

Figure 1: Torque profiles for knee extension using a 7 parameter function

RESULTS AND DISCUSSION

As expected the 7 parameter function produced better fits to the dynamometer data than the 4 parameter function. The average RMS error for the 7 parameter fits was 24 % and for the 4 parameter fits 45 %. The 7 parameter function using 17 data points was better at predicting torque at higher angular velocities, 13 % error, than the 4 parameter function, 38 % error (Table 1). Optimizing for the 18 point dataset improved the 4 parameter error at high velocity to 8.9 % and the 7 parameter to 6.5 %. The 7 parameter function appears more robust at extrapolating to higher velocities when only dynamometer data are available.

CONCLUSIONS

The 7 parameter function gives a better fit to the data than the 4 parameter function. It also extrapolates more accurately to predict high velocity data. The 7 parameter function is less sensitive to the maximum voluntary contraction bounds. The use of a 7 parameter function with dynamometer data should be used rather than a 4 parameter function even if eccentric data are not required.

REFERENCES

1. Westing et al. J. App. Physiology. **58**,100-104 1988.
2. Yeadon et al. *J Biomech* **38**, in press.
3. Finkel. CRSC, N.C. State University, March 2003

Table 1: Difference between the 18th data point and that predicted by the optimized curve.

Movement	RMSD (percentage of maximum torque)			
	Four parameters 17points	Seven Parameters 17points	Four parameters 18points	Seven parameters 18points
Hip Extension	30.15	23.47	5.28	3.02
Hip Flexion	6.12	4.02	2.06	2.22
Knee Extension	79.21	1.00	7.27	1.83
Knee Flexion	37.81	24.21	20.79	19.03
Mean Average	38.32	13.17	8.85	6.53

MODELING THE GYMNAST-MAT INTERACTION DURING VAULT LANDINGS

Chris Mills, Matthew Pain and Fred Yeadon
School of Sport and Exercise Sciences,
Loughborough University, LE113T, UK. email: M.T.G.Pain@lboro.ac.uk

INTRODUCTION

Landings are an essential element in gymnastics and are a time when injuries may occur. Most injuries to gymnasts affect the lower extremity [1]. The landing surface and the landing control strategy adopted by the gymnast contribute to the dissipation of forces at landing.

The aim was to design a model of the landing surface and gymnast's body in order to obtain reasonable estimates of the landing forces experienced by the gymnast. Modeling the gymnast-mat interaction may help to reduce the forces experienced by the gymnast at landing and improve performance.

METHODS

A subject-specific 6 link wobbling mass model of a gymnast was developed using Visual Nastran4D. Torque-angle-angular velocity functions for the model's joint torque generators were derived from isokinetic dynamometer measurements of the gymnast. A landing mat model based on independent mat testing [2] was also developed in Visual Nastran 4D. These two model were used to simulate the gymnast landing.

Landings from four vaults were recorded: a backward somersault, a forward somersault, a handspring vault and a tsukahara vault. Sixteen Vicon cameras (250Hz), a Phantom (v5) high-speed camera (1000Hz), a Kistler force plate (1000Hz) and a Biovision surface EMG system (250Hz) were used to collect data.

Simulation inputs for model evaluation were the body orientation, centre of mass velocity, joint angles and angular velocities of the gymnast during landing. Torque activation histories were optimized using a Simplex algorithm to minimize the difference between simulated and experimental ground reaction forces, joint angle and body orientation time histories.

RESULTS AND DISCUSSION

The landing mat model matched the experimental material tests to within 1.4 % of the peak force and had an RMS difference of 1014.2 N. The majority of the RMS error arose from the latter half of the simulation. In the experiment the mat could lift from the force plate during the rebound phase

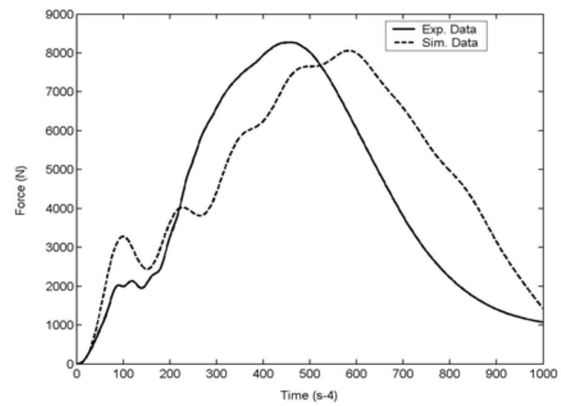

Figure 1: A comparison of the vertical ground reaction forces for the gymnast-mat model and equivalent experimental data during the landing of a front somersault.

which could not occur in the simulation. The simulation of the gymnast only included a small part of the rebound phase.

The model of the gymnast and mat matched the actual performances with overall scores between 12 % and 21 %. The best match was obtained for the forward somersault skill (Table 1). This produced a difference between simulated and actual vertical peak force of 3 % with an RMS of 21 % (Figure 1). The computational run time limited the number of simulations and the complexity of the optimization routine. Manual variations in activation time histories produced better ground reaction force fits but slightly worse scores overall.

CONCLUSIONS

The gymnast-mat model was able to reproduce the key elements of the landing dynamics. Optimization of the mat parameters and / or the torque activation patterns may provide an insight into equipment modifications or landing strategy changes that may reduce injuries in gymnastics.

REFERENCES

1. Meeusen and Borms. *Sports Medicine* **13,** 337-356, 1992.
2. Pain, Mills and Yeadon. Proceedings of the 27^{th} Annual Meeting of the American Society of Biomechanics, Toledo, USA. Abstract 139, 2003.

Table 1: Evaluation of the mat-gymnast model against the actual performance.

Gymnastic Skill	RMS (all joints)	RMS (body orientation)	RMS (Vert GRF)	RMS (Hor GRF)	Peak (VGRF)
Front Somersault	8 %	4 %	21 %	15 %	3 %
Back Somersault	15 %	1 %	15 %	36 %	23 %
Handspring	11 %	1 %	25 %	31 %	33 %
Tsukahara	35 %	8 %	20 %	21 %	2 %

HIP AND KNEE JOINT MOMENT ANALYSIS DURING OBSTACLE CROSSING IN PATIENTS WITH UNILATERAL TOTAL KNEE REPLACEMENT

[1]Chen-Yu Lo, [2]Saiwei Yang and [3]Horng-Chaung Hsu
[1]School of Physical Therapy, China Medical University, Taichung, TAIWAN.
[2]Institute of Biomedical Engineering, National Yang Ming University, Taipei, TAIWAN; email: swyang@bme.ym.edu.tw
[3]Department of Orthopedics, China Medical University Hospital, Taichung, TAIWAN.

INTRODUCTION

Total knee replacement (TKR) may be the best choice for improvement of the quality of life as the severity of knee osteoarthritis is progressing. Many clinical studies have examined the differences in kinematics during locomotion, such as level walking and stair climbing, and their results have been controversial [1,2]. Stepping over obstacles is a non-stereotyped, functional task which the elderly may be encounter on their activities of daily living. For performing the task safely, the person will need good postural control, providing by good lower limb strength and coordination, and proper joint proprioception. Reduced proprioceptive sensory feedback, muscle strength or balance may disturb balance control. Such a mechanism may allow acceleration of degenerative joint conditions, and may account for the increased prevalence of falls seen in elderly subjects. According to Saari et al [1], hip extension tended to decrease, and decreased hip extension moment was noted in TKR patients during stair climbing. The purpose of this study was to investigate the kinetics of lower limb in patients with unilateral TKR during obstacle crossing, the more physical demanded daily activity and the relationship between moment and muscle strength.

METHODS

Ten subjects with average age of 68 years old receiving primary unilateral TKR participated in this study. The posterior cruciate ligament was retained in knees with 5° or less varus/valgus alignment. Motion analysis was done between half and one year after surgery. Eleven healthy, age-matched elderly were recruited to the control group. Each subject was instructed to walk on level and to cross obstacle. Seven digital cameras (Vicon, Oxford Metrics, U.K.) synchronized with 2 force plates (AMTI, U.S.A.) were connected to the motion system to provide 3D kinetic and kinematic data during obstacle crossing. The height of obstacle was 20 cm, chosen for the relevance to daily activities, equal to the height of non-standard curb or doorstop. The average peak values of hip and knee joint moments during stance phase were measured. Moments were normalized by dividing body mass and leg length to reduce intersubject variability. Isokinetic concentric strength of hip flexor and extensor and isometric strength of knee flexor and extensor were collected at the same session.

Nonparametric tests were used as the distribution material was skewed. For kinetic data, Kruskal-Wallis one-way analysis of variance by ranks was used for group difference (operated side, non-operated side and control group). Spearman correlation coefficients were introduced to evaluate association between joint moment and isokinetic concentric muscle strength. Statistical differences were defined as significant at the $\alpha = 0.05$ level.

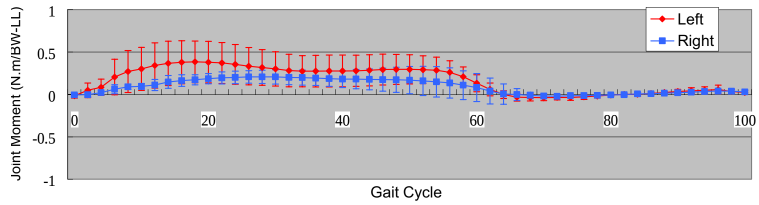

Figure 1: The knee adduction moment of right TKR (subject 8)

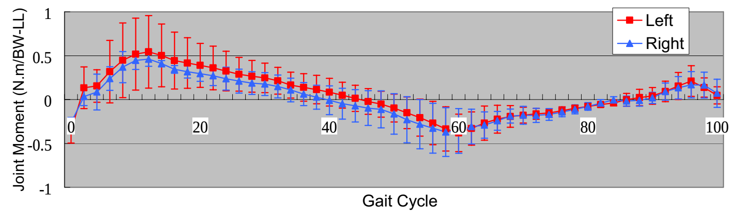

Figure 2: The hip adduction moment of right TKR (subject 8)

RESULTS AND DISCUSSION

The first peak adduction moment of knee joint at the non-operated leg was higher than the contralateral side of the TKR group (Fig. 1). The difference between the non-operated leg and control group was not significant. The peak hip extension moment of non-operated extremities was higher than the operated side (Fig. 2). The hip joint moment was correlated with isokinetic hip extensor strength significantly.

Decreased hip extension moment may reflect a need to stabilize the lower leg in the beginning of stance. Higher knee adduction moment has been suggested as an indicator of static varus knee alignment [2]. Obstacle crossing could be sensitive to frontal plane movement of hip joint.

CONCLUSIONS

Objective gait analysis assists for evaluation of the functional recovery and musculoskeletal deficiency after TKR. Hip adduction moment of the limb may be an indicator of medial knee compartment loading. Decreased hip extensor may influence the stability of knee joint. For patients with TKR, rehabilitation after surgery should focus not only on the gain of range of motion but also on of the strength training of knee joint as well as hip joint.

REFERENCES

1. Bolanos AA, et al. *J Arthtoplasty* **13,** 906-915, 1998.
2. Cloutier JM. *J Bone Joint Surg [Am]* **65,** 906-919, 1983.
3. Saari T, et al. *Int Orthop* **28,** 82-86, 2004.
4. Andrews M. *J Orthop Res* **14,** 89–95, 1996.

ANTICIPATION MECHANISM AND INFLUENCE OF FATIGUE IN MEDIOLATERAL STABILOGRAM

[1] Roger G. T. de Mello, [2]Liliam F. de Oliveira and [1]Jurandir Nadal
[1]UFRJ/Biomedical Engineering Program, COPPE, Rio de Janeiro, Brazil,
[2]UFRJ/Biomechanics Laboratory, EEFD, Rio de Janeiro, Brazil; email: roger@peb.ufrj.br

INTRODUCTION

An important feature of the Central Nervous System (CNS) is its capability to foreseeing future movements of the body [1]. This control does not act by feedback and is named anticipation. Several investigators have focused anticipation by studying the synergism between anti-gravitational muscles and the ones responsible for limbs movements [2]. Others report that anticipation can be affected by fatigue [3]. This study aims to detect the anticipation mechanism and the latency between the gastrocnemius muscle myoelectric signal and the mediolateral (x) stabilogram during static posture and test the fatigue influence.

METHODS

The instrumentation consisted of a vertical force platform and an electromyographic system, synchronized to register the stabilometric and myoelectric signals (EMG), with sampling frequencies of 50 and 1 kHz, respectively. Superficial silver/silver chloride electrodes (Ag/AgCl) were fixed on the lateral head of the gastrocnemius muscle. A group of 23 individuals (15 males and 8 females) were tested after free consent. The age was 23.2 ± 3.6 years (mean ± standard deviation), body mass 70.6 ± 10.9 kg and height 169.9 ± 7.0 cm. The individual stood on the force platform, with the feet together and the arms relaxed, for 120 s. Then he was asked to perform a maximum plantar flexion and maintain this position as much as he can support until muscle failure. During this time the right hand was gently placed on a stem on the platform side to avoid body unbalance. After muscle failure, the individual returned to the initial position for more 120 s data acquisition. The EMG RMS (RMS-EMG) values were calculated after mean removal at windows of 200 ms and stabilometric signals were subsampled to 5 Hz. The normalized cross correlation function (NCCF) was estimated for both pre- and post-fatigue data sets. The maximum correlation value and the corresponding lag were extracted from the NCCF of each individual. This lag was considered as estimation of the latency between signals. To test the presence of latencies as well as the differences between pre- and post-fatigue conditions, Students' t-test was applied ($\alpha = 0.05$). Monte-Carlo simulation was applied to determine the critical value of the cross correlation function ($\alpha = 0.01$).

RESULTS AND DISCUSSION

The mean latency of the body displacement was significantly different from zero, either before ($p < 0.001$) and after fatigue ($p < 0.0015$). The fatigue caused a increase to the ensemble mean latency between RMS-EMG and mediolateral stabilogram, equal to 0.82 ± 0.91 s before and 0.90 ± 1.17 s after fatigue, however this increase was not significant ($p = 0.80$) (Figure 1). Only three individuals presented no significant correlation between RMS-EMG and the body sways. The mean maximum correlation decreased significantly later the fatigue of the 0.39 ± 0.23 for 0.28 ± 0.16 ($p < 0.05$), decreasing ankle strategy for mediolateral control.

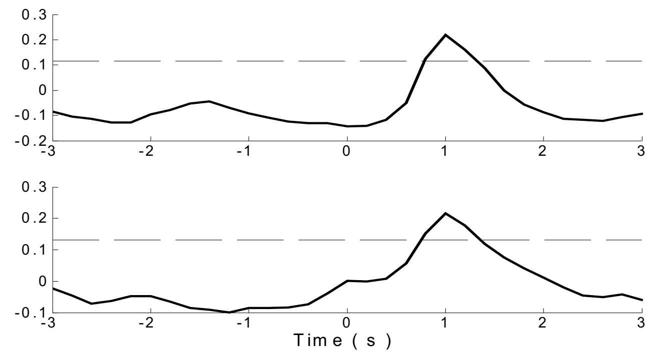

Figure 1: NCCF between RMS-EMG and x stabilogram (subject FA12), before (upper) and after (lower) fatigue (-- critical value by Monte Carlo simulation, $\alpha = 0.01$).

The cross correlation function permits the anticipation mechanism to become evident, in accordance to prior study [4]. These authors found a delay of the CP oscillations in relation to the rectified EMG signal, at magnitudes between 240 and 270 ms. This values differ from the ones in the present study, that are between 400 and 1.400 ms, agreeing with prior result for anterior-posterior stabilogram [3].

The results strengthen the hypothesis that an anticipatory control mechanism plays an important role on the body oscillation regulation. The plantar flexors fatigue decreases the ankle strategy control of the mediolateral sway and do not causes an increase to the time delay between the EMG signals of these muscles and the effective mediolateral sway of the center of pressure.

REFERENCES

1. Shumway-Cook A, Woollacott M. *Motor Control: Theory and Practical Applications*, Baltimore: Lippincott Williams & Wilkins, 1995.
2. Brown JE, Frank JS. *Exp Brain Res* **67**, 645-650, 1987.
3. Mello RGT, Oliveira LF, Nadal J. *Proc 25th Ann Internat Conf IEEE Eng Med Biol Soc*, Cancún, p 2905-2908, 2003.
4. Gatev P, Thomas S, Kepple T, Hallett M. *J Physiol* **514**, 915-928, 1999.

ACKNOWLEDGEMENTS

This study was supported by FUJB and FAPERJ.

MIGRATION OF MEDIAL-PIVOT AND POSTERIOR STABILIZED IMPLANTS

[1] Elise Laende, [1]Kevin Deluzio, [2]Allan Hennigar, [2]Chad Munro, [2]Stephen Arany, [2]Michael Dunbar
[1]School of Biomedical Engineering, Dalhousie University, Halifax, Canada
[2]QEII Health Sciences Centre, Halifax, Canada

INTRODUCTION

The fixation of the tibial component of a total knee replacement is critical to long-term function of the joint and is indicative of the success of the implant design and surgical technique. The pattern of implant migration, as measured by radiostereometric analysis (RSA), in the first two post-operative years has been shown to be predictive of the long-term fixation of the implant [1]. The purpose of this study was to compare the migration of the new ADVANCE® Medial-Pivot knee to the existing ADVANCE® Posterior Stabilized implant (Wright Medical Technology, Inc., Arlington, TN). There is evidence that in normal knees the lateral condyle pivots about the medial condyle in flexion and extension; the Medial-Pivot implant is designed to replicate this function [2].

METHODS

Radiostereometric analysis (RSA) is an accurate radiographic technique for measuring relative motion between an implant and bone [3]. Tantalum beads inserted in the tibia and implant polyethylene component during surgery are highly visible in bi-planar x-rays taken during follow-up exams. Using a calibration box, the 3D co-ordinates of the beads define the positions and orientations of the implant and bone. Comparing the relative positions of the implant and bone in successive exams identifies movement of the implant with respect to the bone. The migration of the implant can be represented as the maximum total point motion (MTPM) of the prosthetic bead that moved the most, indicating the magnitude of migration without direction [1]. Commercial software (RSA-CMS, MEDIS, Leiden, The Netherlands) was used to determine the bead 3D co-ordinates from the stereo x-rays.

Sixty-six patients (48 female) with osteoarthritis were randomized to receive either a Medial-Pivot (MP) or Posterior Stabilized (PS) implant. Surgeries were performed by three surgeons following a standard protocol of PCL resection, patellar resurfacing, and RSA bead placement. Stereo x-rays were taken within 4 days post-operatively and at 6 and 12 months. General health and disease-specific health questionnaires, including WOMAC and KSS, were administered to all patients pre-operatively and at 6, and 12 months post-operatively.

RESULTS AND DISCUSSION

The subject characteristics and did not significantly differ between groups (Table 1).

Table 1. Subject characteristics. Mean ± SD.

Subject Characteristic	MP (n=32)	PS (n=24)	p value
Age (years)	65.4 ± 7.4	65.9 ± 8.2	0.813
Weight (kg)	88.7 ± 17.4	86.4 ± 15.8	0.622
Height (cm)	163.8 ± 10.1	165.3 ± 7.3	0.535
BMI	33.0 ± 5.9	31.9 ± 5.5	0.453

The results of the health outcome questionnaires differed significantly between groups only for the KSS knee scores (Table 2).

Table 2. Health outcome questionnaire results. All scores out of 100, 100 being ideal. Mean ± SD.

Questionnaire	MP (n=28)	PS (n=22)	between group p-value
Womac			
pre-op	43.9 ± 20.4	41.7 ± 13.1	0.105
6 months post-op	76.4 ± 15.9	91.3 ± 6.0	
12 months post-op	78.7 ± 18.1	87.4 ± 9.4	
KSS Knee Score			
pre-op	38.7 ± 21.1	50.9 ± 21.7	0.005
6 months post-op	68.0 ± 25.4	71.9 ± 18.8	
12 months post-op	64.5 ± 21.8	72.4 ± 21.8	
KSS Function Score			
pre-op	43.8 ± 25.0	50.7 ± 15.0	0.293
6 months post-op	65.5 ± 14.8	74.3 ± 14.7	
12 months post-op	69.4 ± 24.2	71.0 ± 22.7	

The migration of the MP and PS groups were not different at the time points measured (Figure 1). The consistent level of migration at 6 and 12 months indicates favourable tibial component fixation and long-term success.

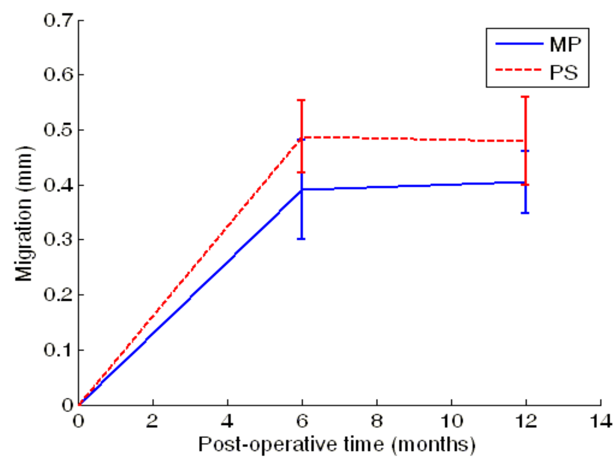

Figure 1. Maximum Total Point Motion (MTPM) of MP and PS implants at 6 and 12 months post-op for analyzed RSA cases to date (nMP=8, nPS=14). Mean and standard error of the mean shown. Between group p-value = 0.482.

CONCLUSIONS

The similar migration pattern for the Medial Pivot implant to the accepted functional Posterior Stabilized implant supports the use of this implant in total knee arthroplasties. Long-term monitoring will continue to confirm the results to date.

REFERENCES

1. Ryd L, et al. *J.Bone Joint Surg.Br*. **77**, 377-383, 1995
2. Nakagawa, et al. *J.Bone Joint Surg.Br* **82**, 1199-1200, 2000
3. Selvik G. *Acta Orthop.Scand.Suppl* **232**, 1-51, 1989

3D UPPER BODY ACCELERATION MAGNITUDE FOR SELF-SELECTED AND FAST WALKING SPEEDS IN YOUNG AND OLDER ABLE-BODIED ADULTS

Vassilios G. Vardaxis, PhD
Division of Physical Therapy, Human Performance Laboratory, Des Moines University
Des Moines, Iowa; email: vassilios.vardaxis@dmu.edu

INTRODUCTION

Changes in the aging neuromuscular system contribute to the decline of the functional capacity of the elderly with serious implications with respect to increased frequency of falls [1]. Quantification of the trunk/head kinematics (passenger of the locomotion system) during gait for different age groups, under various conditions may help identify potential degenerations in the control of the head [2]. A significant body of research exists examining trunk motion during gait, however, most of it includes a small number of subjects and a limited number of it includes head kinematics in 3D [2,3]. The purpose of this study was to assess whether any age or speed-related differences exist in the acceleration magnitude of the head and pelvis during self-selected normal and fast walking speeds.

METHODS

A total of 162 healthy adults/elderly participated in the present study. These subjects were classified in three age groups (G1, N=54, 24.4±5.8 yr; G2, N=60, 49.7±5.4 yr; G3, N=48, 70.4±5.7 yr). Subjects were asked to walk with a steady velocity of progression across a 10 m walkway at self-selected normal and fast walking speed, while 5 gait trials were collected at each speed using a 6-camera VICON system. A full-body marker set was used (31 markers) for gait analysis. The 3D location of the center of the pelvis and center of the head were determined. Velocity of progression, cadence, and stride length were determined. The instantaneous acceleration patterns for the pelvis and head in 3D (laboratory coordinate system) were derived using finite differences. The magnitude of the 3D accelerations: antero-posterior (AP), medio-lateral (ML), and vertical (VER) for pelvis and head were calculated using the root mean square (RMS) of the waveform patterns over the gait cycle. Univariate two-way repeated measures ANOVA was used to test for differences between age-groups (between effect) and between walking speeds (within effect).

RESULTS AND DISCUSSION

The older group walked with slower velocity of progression than the 2 younger groups for both speed conditions (Table 1). The average increase in velocity between speed conditions was 18.3% (normal, 1.32 m/s; fast, 1.56 m/s). There were no group differences in percent velocity of progression increase.

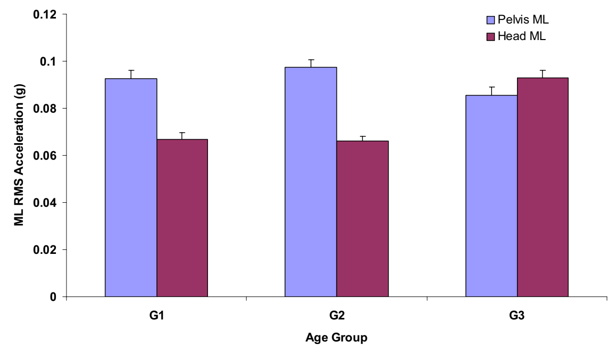

Figure 1: Mean (±SE) of pelvis and head acceleration magnitude (RMS) in the ML direction for all three groups.

The acceleration magnitude in all directions increased with speed, as expected. Between groups differences in acceleration magnitude were found for the pelvis in the AP direction ($p < .001$) and for the head in the ML direction ($p < .001$). There were no group differences in the VER direction. The elderly group walked slower than the younger groups and for both speed conditions exhibited greater head acceleration magnitude in the ML direction. Interestingly, the magnitude of the ML acceleration for the head in the older group was significantly higher than the ML acceleration magnitude of their pelvis ($p < .05$) for both speed conditions (Figure 1). This data suggests that, while accelerometric 3D analysis is a promising tool in accessing dynamic balance for older adults, the dual reference point (pelvis, head) techniques can provide further insights in the control of the head motion for vestibular and visual field stability.

CONCLUSIONS

The musculoskeletal structures of the trunk in the elderly are unable to filter locomotion perturbations in the ML direction. The younger subjects use their trunk effectively to adjust the disturbances introduced by the locomotion to the pelvis.

REFERENCES

1. Winter DA. ABC: Waterloo Biomechanics, 1995
2. Menz HB, et al. *Gait & Posture* **18**, 35-46, 2003
3. Moe-Nilseen R. *Clin Biomech* **13**, 320-7, 1998

Table 1. Descriptive statistics of the spatio-temporal gait parameters for normal and fast self-selected speed for the 3 age groups.

	Normal Speed			Fast Speed		
Age Groups	Velocity (m/s)	Stride Length (m)	Cadence (steps/min)	Velocity (m/s)	Stride Length (m)	Cadence (steps/min)
G1: 20–39 yrs	1.32 (±0.14)	1.33 (±0.13)	119.2 (±5.2)	1.59 (±0.17) †	1.48 (±0.14)	128.5 (±7.7) †
G2: 40–59 yrs	1.35 (±0.12) †	1.39 (±0.12) †	117.0 (±8.3)	1.58 (±0.14) †	1.51 (±0.14) †	126.6 (±8.9)
G3: 60–79 yrs	1.26 (±0.19)	1.31 (±0.14)	115.8 (±9.5)	1.48 (±0.21)	1.44 (±0.17)	123.7 (±9.5)
	p < .019 *	p < .005 *	NS	p < .002 *	p < .041 *	p < .021 *

NS = no significant group effect, * Significant univariate group effect, † Significant different from G3

MUSCULOSKELETAL MODELING OF AN EMG-BASED NEUROPROSTHESIS FOR ARM FUNCTION

Robert F Kirsch (robert.kirsch@case.edu), Juan Gabriel Hincapié, Dimitra Blana, and Edward Chadwick
Department of Biomedical Engineering, Case Western Reserve University (http://bme.case.edu/)
Cleveland VA Functional Electrical Stimulation Center (http://feswww.fes.case.edu/)

INTRODUCTION

Individuals with C5/C6 Spinal Cord Injury (SCI) lose control over a number of upper extremity muscles. Specifically the hand muscles are paralyzed, there is partial loss of wrist and elbow extension, and several shoulder functions are lost, including horizontal flexion and adduction. Functional Electrical Stimulation (FES) can be used to stimulate paralyzed muscles to restore function to these individuals. The goal of this project is to determine an appropriate set of muscles to stimulate and the pattern of muscle stimulation that, when combined with retained voluntary function, would provide improved arm function. The proposed approach will eventually extract movement intention from the EMG activity of muscles that are under voluntary control and uses this information to specify the stimulation levels of needed for the paralyzed muscles.

METHODS

Experiments were performed to measure the kinematics of a set of arm movements that reflect a wide range of daily activities. These kinematics were used as the input to a musculoskeletal model [1] in the performance of inverse dynamic simulations. These simulations generated a set of muscle activations that would produce each of the movements while minimizing the sum of squared muscle stresses. Figure 1 shows a set of arm kinematics [2] in the upper panels and the activations of several key muscles predicted by the inverse simulations (lower panels).

We then trained a time-delayed artificial neural network (TDANN) that took several of the muscle activation patterns as inputs and another set of muscle activation patterns as outputs. Specifically, we used muscles that would be expected to have voluntary function (clavicular trapezius, scapular trapezius, clavicular deltoid, and scapular deltoid) in individuals with C5/C6 SCI as the inputs and muscles that would be expected to be paralyzed (pectoralis major, serratus anterior, medial triceps) as outputs. This TDANN was designed to predict *needed stimulation* of paralyzed muscles based on the *natural activity* of muscles with voluntary control.

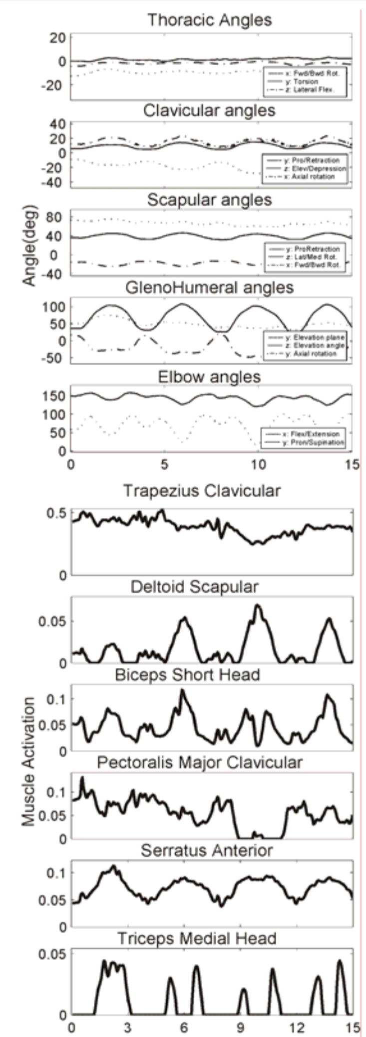

Figure 1: Musculoskeletal model inputs and outputs.

RESULTS AND DISCUSSION

Figure 2 shows an example of the ability of the TDANN to predict appropriate muscle activity. The upper panel shows the relevant arm kinematics. The next lower panel shows the "voluntary" activity of 4 muscles used as TDANN inputs. The lower 3 panels show the desired muscle activations (dotted lines) and those predicted by the TDANN (solid lines). Overall, the TDANN predictions were quite good across a wide range of different movements.

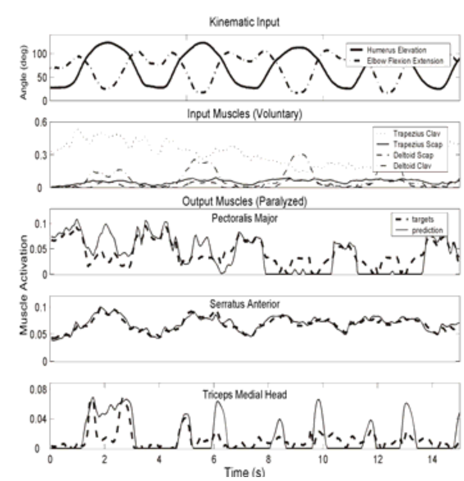

Figure 2: TDANN predictions of "paralyzed" muscle activity based on "voluntary" muscle activity.

CONCLUSIONS

The TDANN approach to predicting needed muscle activation for "paralyzed" muscles from the activation of several "voluntary " muscles has been shown to be accurate for dynamic movement conditions. This result indicates that an arm neuroprosthesis with EMG-based FES of key elbow and shoulder muscles should be feasible.

REFERENCES

1. van der Helm, F.C.T. "A finite element musculoskeletal model of the shoulder mechanism". *Journal of Biomechanics.* **Vol 27**. No 5. pp 551-569. 1994.
2. van der Helm, F.C.T. et al. "ISB recommendation on definitions of joint co-ordinate system of various joints for the reporting of human motion: Pt II. Shoulder and Elbow. *Journal of Biomechanics.* **In press.**

ACKNOWLEDGEMENT

This work was funded by contract N01-NS-1-2333 from the National Institute of Neurological Disorders and Stroke.

CONTROL OF STABILITY DURING SLOPE LATERAL WALKING

[1]Chien-Ju Lin, [1, 2]Lin-Hwa Wang, [3]Yi-Wen Chang and [1]Fong-Chin Su
[1]Institute of Biomedical Engineering and [2]Department of Physical Education, National Cheng Kung University, Tainan, Taiwan, [3]Department of Exercise and Health Science, National Taiwan College of Physical Education, Taichung, Taiwan;
email: fcsu@mail.ncku.edu.tw

INTRODUCTION

Nowadays, the workers' occupational safety is highly emphasized for all the developing countries. Tubular steel scaffolding, which is regulated not to be narrow than 30 centimeters is commonly used in Taiwan as construction false work and finishing structure of high headroom buildings. In this condition, the workers need to walk laterally on a narrow slope while lateral walking is not a usual gait pattern in our daily life. Center of pressure (COP) is the point where the ground reaction force is collectively exerted at the surface [1], and it has been wildly used to analyze the control of stability [2,3].Very little research concerns gait pattern in lateral walking and slope walking. Kawamura, et al. determined step length, width, time factors and deviation in the COP during upslope and down slope walking, and found that walking speed, deviation in COP and the ratio of stance phase to stance phase were different between level and slope walking [2]. Lerous, et al. investigated postural adaptation to walking on inclined surface. They concluded that it was necessary to modify trunk and pelvis alignment during slope walking [4]. The purpose of this study was to investigate the COP trajectory in level and slope lateral walking. Hopefully the results will provide useful information on improving labors' working safety.

METHODS

Five normal subject (three males and two females, ages: 25±4.8 years, height: 166.9±7.2 cm and weight: 62.0±11.6 kg) participated in this study.

Two Kistler force plates (Kistler Instrument Corporation, NY, USA) were used in this experiment to collect the data of ground reaction force for further computation of COP. Foot switches (Motion Lab System, LA, USA) were synchronized with the force plates to identify gait phases during walking. The entire lateral walking cycle can be divided into two double support phases and two single support phases (right and left). The first double support phase started with the leading foot contact, and ended with the trailing foot off. The second started with the contact of trailing foot and ended with the leading foot clearing off from the floor. Slope inclinations were set at 5 degree. The subjects were instructed to walk with right leg leading from the bottom of the slope to the top at self-selected speed.

RESULTS AND DISCUSSION

According to the COP trajectories (Figure 1), we found these subjects performed two kinds of gait patterns. Four subjects performed toe contact with their leading foot while only one subject performed heel contact. Those who walked with toe contact had a U-shaped COP trajectory. The COP moved backwards after contact and then turned left before trailing foot contact. At this moment, COP moved laterally until the leading foot off. After that, COP kept moving to the left and turned

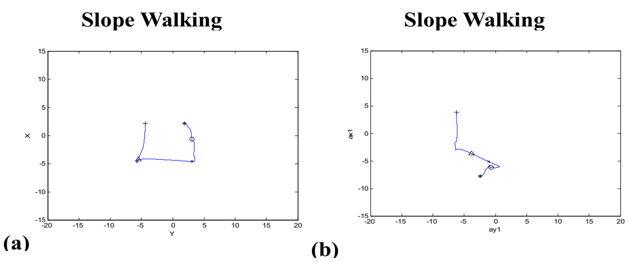

Figure 1: (a) U-shaped COP and (b) S-shaped COP (*: right foot contact; o: left foot off; x: left foot contact; Δ: right foot off; +: 2^{nd} right foot contact)

forwards when the leading foot was performing hip abduction for next stride. However, the S-shaped trajectory indicated that the subject performed heel contact thus the COP moved forwards after contact.

Besides, the mean single-to-double support ratio (single support phase/double support phase) for level lateral walking and slope lateral was 0.31±0.04 and 0.24±0.03, respectively. The single support phase had a trend to be shorter during slope walking because walking on the slope was more unstable. Furthermore, the maximum velocity of the shift of COP during each phase is shown in Table 1. The result showed that during second double support phase the maximal velocity of COP shift during slope lateral walking was significantly larger than that during level lateral walking.

Table 1: Maximal sway velocity during four phases (unit: m/s)

	1^{st} Double Phase	**Right Single Phase**	**2^{nd} Double Phase**	**Left Single Phase**
Level	1.02±0.50	0.65±0.28	0.97±0.18	0.71±0.10
Slope	1.10±0.67	0.74±0.19	0.95±0.18	0.83±0.14 *

* p<0.05

CONCLUSIONS

The most obvious difference in maximal COP shift velocity happened in the second double support phase. It is unstable for human to walk laterally on a slope. Therefore, the muscle activation and joint adaptation of lower extremities will be important to control the movement.

REFERENCES

1. Winter DA. *Gait Posture* **3**, 193-214, 1995.
2. Kawamura K, et al. *Acta Medica Okayama* **45**, 179-184, 1991.
3. Hass J, et al. *Arch Phys Med Rehabil* **85**, 1593-1598, 2004.
4. Leroux A, et al. *Gait posture* **15**, 64-74, 2002.

ACKNOWLEDGEMENTS

Support from grant NSC 91-2316-B-006-002-CC3, Taiwan

BIOMECHANICAL AND HISTOLOGICAL EVALUATION OF ESTROGEN, RALOXIFEN, VITAMIN K2 AND THEIR COMBINATIONS IN THE TREATMENT OF OSTEOPOROTIC BONE

[1] Arzu G. Tasci, [2]Hasan Bilgili, [3]Hikmet Altunay, [4]Kaan Erler, [1] M. Ruşen Gecit, [1]Dilek Sendil Keskin,
[1]Middle East Technical University, Engineering Sciences Department
[2]Ankara University, Department of Veterinary Medicine
[3] Ankara University, Department of Histology
[4] Military Academy of Gulhane, Department of Traumotology
email: dkeskin@metu.edu.tr, atasci@metu.edu.tr

INTRODUCTION

In this study, **Estrogen**, the most common hormone replacement therapy (HRT) agent, was used as single and combined with **Raloxifen**, a SERM type **osteoporosis** drug. Despite their high clinical uses, they have not been tried before, in combination. They act as agonist of each other in uterus and mammary glands. Therefore, it was expected to prevent HRT side effects by using the combinations while enhancing the healing of osteoporotic bone. As a third agent, **Vitamin K2** was chosen to be applied alone or in combination with Raloxifen. Although the recent studies mentioned the effects of Vit K2 on bone, its rebuilding and repair effect was not completely established. Hence, Vit K2-Raloxifen combination was applied and compared with the other groups as a new treatment. To understand the single and combined effects of these three agents, mechanical properties of bone was studied with both **strain gage** and **bending** theory methods on **ovariectomized** rat model**.** Also, histological evaluations of bone and uterine tissues were carried out together with blood analysis.

METHODS

Rats (56) were divided into 7 groups as Estrogen (E), Raloxifen (R), Vit K2 (K), Estrogen and Raloxifen (E+R), Vit K2 and Raloxifen (R+K), Ovariectomized controls (C), and Sham operated group (S). All drug groups were ovariectomized before the treatments. Drug treatments were started three months after the surgery, and continued for 12 weeks. Estrogen and Vit K2 were applied by subcutaneous injection, while Raloxifen was administered orally. Uterus and right tibia were taken for histological analysis. Left tibia and both femora were wrapped in saline soaked gauze sponge and stored at -20^{o}C until DEXA measurements and biomechanical testing.

RESULTS AND DISCUSSION

All the treatments have resulted in numerically higher values for mechanical properties of femora and even significantly better values for tibia when compared to untreated controls (Table 1). The combined therapies performed better than the individual administrations and both of the controls. The modulus of elasticity was calculated from the strain gage data and compared with that obtained from the beam deflection formula. Computed moduli were consistent with literature. [1-3] However, there was a significant difference (about 13 times) between the values obtained from the two approaches. Similar difference was also observed and explained in another study for healthy rat tibia [2].

Table 1: Comparison of mechanical properties for tibia

TIBIA	ULTIMATE STRENGTH (MPA)	MODULUS OF ELASTICITY (GPA)	ENERGY ABSORBED (NMM)
C	**100.11***	3.26	46.08
S	176.71	5.53	51.13
E+R	202.22	5.87	**73.59 ***
E	174.95	4.28	63.63
R	187.96	4.44	65.59
K	170.09	5.12	59.58
R+K	189.94	5.30	57.77

* Statistically different from other groups

Biochemical analysis of blood showed an increase in bone formation (ALP activity) compared to controls. The highest ALP activity among all was observed in R group. Quantitatively, E+R had the maximum BMD values for proximal and distal of femur and tibia. As a general trend, treatment groups had better BMD values than the ovariectomized controls. Histologically, enlargement in uterus, and degeneration in connective tissue were highly observed in E group. However, such changes were less in combined groups and in the groups not involving estrogen. This implied that the adverse effects of estrogen on uterus could be reduced by using R.aloxifen.

CONCLUSIONS

Antiresorptive agents are effective in osteoporosis prevention and treatment, but their combination was found to be much better mechanically, histologically and densitometrically than their separate usage. Strain gage data was thought to be more informative than the deflection data while determining the mechanical properties of rat femur under three point bending. Vit K2 was found to be an important factor in increasing the strength of bone especially at high stresses.

REFERENCES

1. Akhter, et al. *J Biomech* **25**, 1241-1246, 1992
2. Turner C.H., Burr D.B., *Bone* **14**, 595-606,1993
3. Erickson, et al., *The Anatomical Record* **268**, 115-124, 2002

ACKNOWLEDGEMENTS

We would like to thank Eisai Co.Ltd. (Tokyo, Japan) for supplying Vitamin K2 as a generous gift.

EFFECTS OF TRUNK AND HIP STIMULATION DURING BIMANUAL REACHING AFTER SCI

[1] Stephanie J. Nogan, [1, 2] Ronald J. Triolo, [1] Jonathan L. Sakai
[1] Motion Study Laboratory, Cleveland FES Center, Louis Stokes Cleveland VA Medical Center, Cleveland, Ohio, USA
[2] Departments of Orthopaedics and Biomedical Engineering, Case Western Reserve University, Cleveland, Ohio, USA
Email: snogan@fes.case.edu, Website: fescenter.case.edu

INTRODUCTION

Functional electrical stimulation (FES) can be used to restore a variety of functional tasks in individuals paralyzed by spinal cord injuries (SCI). Individuals with low cervical or thoracic level spinal cord injuries (SCI) do not have control of all of the postural muscles of the trunk and hip, and therefore have difficulty during uni- or bimanual reaching tasks and often must rely on using one arm to hold onto the wheelchair for balance. Since mechanical stabilization of the trunk improves reach after SCI [1, 2], activation of the trunk and hip extensor muscles via FES should also positively impact spine and pelvic angles (**Figure 1**) and increase absolute sagittal reach length (**Figure 2**) during bimanual reaching.

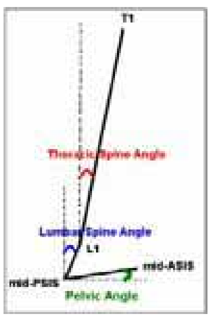

Figure 1: Definitions of thoracic spine, lumbar spine, and pelvic angles.

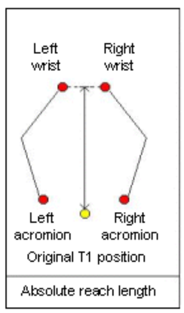

Figure 2: Definition of absolute sagittal reach length.

METHODS

Three recipients of a CWRU/VA implanted neuroprosthesis for exercise, standing, and transfers participated in this study [3]. Subject 1 (S1) had a T6 motor complete (ASIA A) SCI, and Subjects 2 (S2) and 3 (S3) had sensory incomplete (ASIA B) injuries at C7 and T5, respectively. All three had been using their neuroprosthesis for at least 3.5 years.

Stimulation patterns were created to activate the erector spinae, semimembranous, and gluteus maximus for trunk stability during seated reaching. Six Vicon 370E optical markers were placed on the left and right acromion, wrist, and lateral femoral epicondyle, and T1 while seven Polhemus Fastrak radio frequency markers were placed on the left and right ASIS and PSIS, L1, and L3, since the wheelchair would obscure those markers from view.

After calibration and static postural data were collected, bimanual reaching trials were performed with no stimulation, trunk stimulation alone, and simultaneous activation of trunk and hip extensors. For the trials involving stimulation, the subject first turned on the appropriate stimulation pattern and became accustomed to the new posture (**Figure 3**). The subject reached to one of three target heights, held a box of one of three weights at the target for three seconds (**Figure 4**), and then returned the box to his/her lap.

Figure 3: Subject finds a new posture for sitting when the stimulation is on.

Figure 4: Subject reaches towards the high target with stimulation on.

RESULTS AND DISCUSSION

Thoracic spine, lumbar spine, and pelvic angles did not change significantly during the trials without stimulation as maintaining balance during bimanual reaching was very difficult without the use of trunk and hip muscles. The angles and absolute reach length generally improved with FES (**Figure 5**) since balance was achieved by the activation of the hip and back muscles.

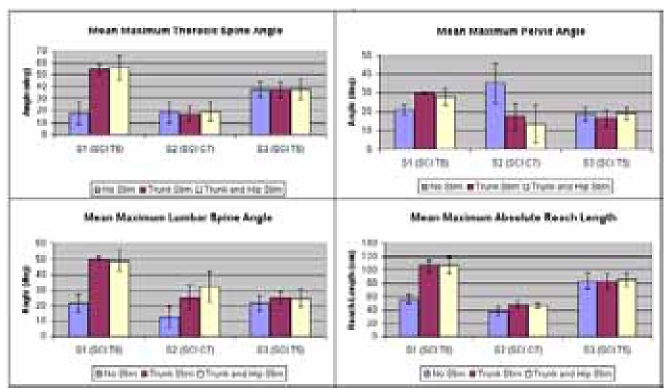

Figure 5: Mean spine and pelvic angles, along with absolute reach length, for each of the 3 subjects for each of the 3 stimulation conditions.

CONCLUSIONS

Trunk stimulation allowed neuroprosthesis users to reach further and carry heavier loads with more stability than without FES. Stimulation positively impacts posture and can augment reaching function after SCI. Inter-subject differences from this small study demonstrate the need for further investigation on how to optimize stimulation of the trunk and hips during bimanual tasks. The interactions between target height and weight carried, as well as the relative magnitudes of trunk and hip activation, remain to be determined.

REFERENCES

1. Curtis KA, et al. *Arch Phys Med Rehabil* **76**, 360-367, 1995.
2. Allison GT, Singer KP. *Spinal Cord* **35**, 217-222, 1997.
3. Davis JA, et al. *J Rehab Res & Dev* **38**(6), 609-617, 2001.

ACKNOWLEDGEMENTS

VA Merit Review #B3043C and NIH R01-NS40547.

Is Lower Limb Joint Proprioception Systemic?

[1] Giselle Cross, [1]Patrick A. Costigan and [1]Scott K. Lynn
[1]School Of Physical and Health Education, Queen's University, Kingston, ON, Canada
Email: 3PAC13@post.queensu.ca

INTRODUCTION

Proprioception, or joint position sense, provides feedback to the central nervous system that assists in appropriate muscle coordination during joint motion. Poorly controlled joint motion may lead to abnormal joint forces which are thought to be a risk factor for osteoarthritis (OA) in certain joints such as the knee. Proprioception decreases with age [1] and is further decreased in persons with knee OA [2] but we do not know if poor proprioception is a cause or effect of the disease [3]. It is also not known if proprioception is systemic across all joints.

If proprioception is systemic, then young and elderly persons will have different proprioceptive scores at all joints but the ratio of one joint to another will be similar regardless of age. If this were the case, we might be able to resolve the cause-effect relationship between proprioception and OA. The purpose of this study was to compare the ratio of ankle to knee proprioception between young and elderly group.

METHODS

Ankle and knee proprioception were tested on 15 young (24 ± 4 years) and 14 elderly subjects (70 ± 4 years). Active to active angle reproduction (AR) was tested twice at each of 30, 45 and 60 degrees of knee flexion. The error between experimenter positioning and subject repositioning was averaged across all trials. Threshold of movement detection (TD) tests were performed at a knee angle of 45 degrees with an angular speed of 0.3 deg/sec. The subject signaled when they detected their leg moving and could correctly indicate the movement direction. The range of motion (ROM) before signaling was averaged across 5 flexion and 5 extension trials. Repeatability of both tests was assessed on 10 subjects over two separate days. The ankle TD score was divided by the knee TD score to determine the ankle:knee ratio. An AR ankle:knee ratio was also calculated. For all tests the subjects were blindfolded and listening to music to reduce information received from other sources. T-tests were used to determine differences between groups on all variables.

RESULTS AND DISCUSSION

Repeatability testing showed that the AR test was not consistent (ICC < 0.6) and consequently there were no differences on the ankle and knee AR scores or the AR ankle:knee ratio between the young and elderly (Table 1). The TD test was repeatable (ICC > 0.8) and the elderly had an increased ROM before movement was detected (Table 1) at both the ankle and the knee. There were no differences between the groups on the TD ankle:knee ratio variable.

The AR tests at the knee and ankle used protocols similar to those in the literature and also used different equipment at each joint, suggesting that the lack of repeatability was not due to equipment or the joint. Agreeing with the literature, the TD scores showed that proprioception acuity decreased at both the ankle and knee with increased age [1]. The TD ankle:knee ratio was not different between the age groups suggesting that the decline in proprioception is similar at both joint. This lends support to the notion that at least some forms of proprioception may be systemic.

This information may shed some light on the spectrum of results collected from persons with knee OA. We expect the proprioceptive test scores from OA knees to be worse than those from aged-matched controls. Since the ankle is seldom affected by OA, if subjects with knee OA also have poor ankle proprioception, we can assume that poor proprioception preceded the disease. If the ankle score is normal, then we can assume that the poor knee score resulted from the disease process.

CONCLUSIONS

Active to active angle reproduction was not reliable at either the ankle or the knee. Both the ankle and knee threshold of movement detection scores were worse for the elderly but the ratio between the ankle and knee was not different between the age groups. These results suggest that some aspects of proprioception may be systemic.

REFERENCES

1. Skinner H, et al. *Clin Orthop* **184**, 208-211, 1982
2. Barrett D, et al. *J Bone Joint Surg* **73B**, 53-56, 1991.
3. Sharma L. *Rheum Dis Clin North Am* **25**, 299-314, 1999.
4. Deshpande, N. *Arch Phys Med Rehabil* **84**, 883-889, 2003.

ACKNOWLEDGEMENTS

Motor Performance Laboratory, School of Rehabilitation Therapy, Queen's University.

Table 1: Proprioception test scores.

	Active to Active Angle Reproduction (AR)			Threshold of Movement Detection (TD)		
	Ankle (deg)	Knee (deg)	Ankle:Knee	Ankle (deg)	Knee (deg)	Ankle:Knee
Young	**2.2 ± 1.2**	**3.3 ± 1.6**	**0.88 ± 0.7**	**0.9 ± 0.4***	**0.62 ± 0.3***	**1.53 ± 0.6**
Elderly	**1.8 ± 1.0**	**3.9 ± 1.7**	**0.59 ± 0.5**	**1.4 ± 0.4***	**0.93 ± 0.3***	**1.60 ± 1.0**

* A significant difference exists between the young and elderly ($p < 0.01$).

T2 VALUES OF PATELLAR CARTILAGE IN PATIENTS WITH OSTEOARTHRITIS

[1]Matthew F. Koff, [2]Kimberly K. Amrami, [1]Kenton R. Kaufman
[1]Biomechanics/Motion Analysis Laboratory, Department of Orthopedic Surgery, Mayo Clinic, Rochester MN
[2]Department of Radiology, Mayo Clinic, Rochester MN; email: kaufman.kenton@mayo.edu

INTRODUCTION

Osteoarthritis (OA) is a debilitating disease which affects articular joints throughout the human body. Recently, the calculation of T_2 values for articular cartilage obtained from MRI has been developed to aid the diagnosis of OA [1]. T_2 values of cartilage are sensitive to the disruption of collagen fibers and changes in water content of cartilage seen during the onset of OA. Limited studies have been performed *in vivo* across varying degrees of OA (e.g. [2]). Relating T_2 values of cartilage to standard clinical staging methods of OA would be beneficial for determining the clinical applicability of this new technique. Therefore, the purpose of this study was to quantify differences of T_2 values of patellar cartilage across different stages of OA as defined by radiological examination.

METHODS

Following IRB approval with obtained consent, 39 subjects (56 ± 11 y.o., 12 M, 27 F) were enrolled in the study. Standing lateral radiographs centered on the patella were obtained for each subject. Radiographs were graded for patello-femoral OA based on the Kellgren and Lawrence (KL) scale from 0 (no OA) to 4 (end-stage OA). Following the radiological exam, MR images of each subject's patellae were obtained. Examinations were performed with a clinical 1.5 T MRI system (Signa Excite 11.0, GE Healthcare, Waukesha, WI). A series of axial T_2-weighted single spin-echo images were acquired along the length of the patella: TR = 1000ms, TE = 8,17,26,34,43,51,60,68,77 ms, 256x256 image matrix, slice thickness = 2mm, slice spacing = 4mm. After image acquisition, patellar cartilage was manually segmented on each image. T_2 values of patellar cartilage were calculated on a pixel-by-pixel basis using a custom written linearized least-squares program. Data from the first echo image was discarded in calculating T_2 values [3]. Pixels with T_2 values greater than 200 ms were considered outliers and were excluded from statistical analysis [4]. An average T_2 value generated from all analyzed pixels of each patella was used for statistical analysis. A one-way ANOVA was performed to determine any differences of patellar cartilage T_2 values across the KL stages of OA. Statistical significance was set at $p<0.05$.

RESULTS AND DISCUSSION

A representative T_2 map of patellar cartilage is shown in Figure 1. Average calculated T_2 values of patellar cartilage across the KL stages of OA is shown in Table 1. The calculated T_2 values are similar to those in previous studies [1]. The T_2 values of patellar cartilage were approximately 63 ms for KL stages 0, 1, 2 and 3 with an increase to 74 ms for KL stage 4 OA. The statistical analysis found no significant differences among T_2 values across the KL stages of OA.
The lack of differences of T_2 values across OA stages may be due to several factors. First, the KL staging of a joint assigns an OA stage based on the overall radiographic appearance of a joint. Therefore, the KL staging is more likely to detect advanced stages of OA rather than the initial onset of the disease. If there is a rapid change of T_2 values during the onset of OA and not at later stages, then we would not expect to find differences using a KL protocol for staging OA. Second, the effects of volume averaging and chemical shift near the cartilage-subchondral bone interface may have artificially increased the calculated T_2 values. Finally, we had a limited number of patellae for KL stage 4 OA (n=2). An increase in the sample number may have resulted in T_2 differences among the OA groupings.

CONCLUSIONS

T_2 mapping of patellar cartilage may provide a non-invasive method for accurate staging of OA within the knee. Additional studies evaluating different methods of grading OA may highlight the benefits and sensitivity of T_2 mapping in a clinical setting.

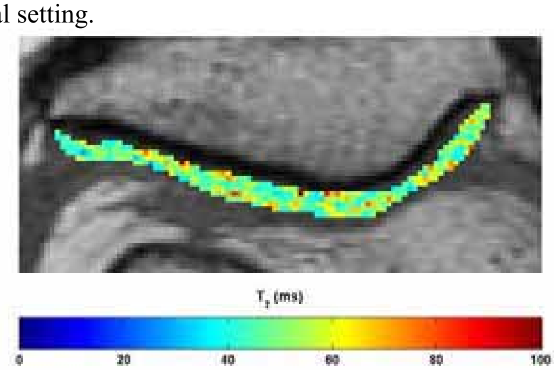

Figure 1. Representative T_2 map of patellar cartilage

Table 1. T_2 values of patellar cartilage at each stage of OA

Kellgren-Lawrence OA Stage	n	T_2 Values (ms) (Average ± Std.Dev.)
0	16	63.02 ± 6.25
1	25	62.15 ± 10.24
2	22	63.72 ± 7.85
3	10	64.18 ± 10.66
4	2	73.97 ± 2.33

REFERENCES

1.Mosher TJ, et al. *Semin Musculoskelet Radiol* **8,** 355-68, 2004.
2.David-Vaudey E, et al. *Magn Reson Imaging* **22,** 673-82, 2004.
3.Maier CF, et al. *JMRI* **17,** 358-64, 2003.
4.Dunn TC, et al. *Radiology* **232,** 592-8, 2004.

ACKNOWLEDGEMENTS

NIH Grant AR048768-03

ACUTE MUSCLE ADAPTATIONS TO A RESISTANCE EXERCISE

[1]Yusheng Yang, [1]Eliana Chaves, [2]Jean L. McCrory
[1] Human Engineering Research Laboratories, University of Pittsburgh
[2] Neuromuscular Research Laboratories, University of Pittsburgh
email: yuy7@pitt.edu, web: www.herlpitt.org

INTRODUCTION

The neural factor (NF) and hypertrophic factor (HF) are the two major mechanisms related to improvements in neuromuscular efficiency [1]. Progressive resistance training results in neural and muscle hypertrophic adaptations that are primarily responsible for improved efficiency. Initial gains are related to the NF, which involves the interaction of facilitatory and inhibitory phenomena at various levels of the nervous system. Subsequent increases are attributed to the HF [2,3]. However, the timing of the neural adaptations is not yet documented. The purpose of this study is to examine neural adaptations resulting from a single-session of resistance exercise training. We hypothesized that the neural adaptations will be observed following a single session of resistance exercise training.

METHODS

Subjects: Twenty-six healthy subjects (14 M, 12F) provided informed consent prior to participation in this study. Their age, height and mass were 28.9 ± 5.8 yrs, 1.8 ± 0.1 m and; 68.3 ± 11.6 kg, respectively.

Experimental protocol: Surface electromyographic (EMG) activity of biceps brachii and triceps brachii on the dominant arm were recorded (2000 Hz, gain 1000, bandpass filter 15-500 Hz, CMRR 130 dB) during an elbow flexion task with resistances of 0 lbs and 3 lbs (pre-training). Subjects were then asked to perform the same task with 10 lbs resistance as a heavy resistance training exercise. Subsequently, EMG data were again obtained during the same task with resistance of 3 lbs and 0 lbs (post-training), respectively. Each lifting task was repeated five times within a 15 second period. The pace of movement was controlled by an audible cue of 60 bpm. The start and end of each repetition was determined with an electrogoniometer placed at the elbow.

Data analysis: Median frequency (MF) and integrated EMG (iEMG) were calculated for the concentric (CON) and eccentric (ECC) phases of each repetition. Data of middle three repetitions of each task were averaged for statistical analysis. A two-factor ANOVA [load (0 lbs, 3 lbs) × training (Pre, Post)] with repeated measures was employed to test for significant changes in iEMG and MF. Separate analyses were performed for the CON and ECC data for each muscle. An alpha level of 0.05 was used for all tests of significance.

RESULTS AND DISCUSSION

Following a single session of resistance exercise, significant reductions of biceps MF ($p<0.05$) and iEMG ($p<0.05$) during the CON action were noted (Table 1). Similar trends were noted in the ECC triceps MF ($p=0.17$) and iEMG ($p=0.08$). No changes were noted during the ECC action of the biceps. This CON neuromuscular efficiency gain of the biceps may be explained by the NF. Neural adaptations involve prime-mover motor unit activation and synchronous coactivation of the antagonist [4]. Given a hierarchical slow-twitch to fast-twitch motor unit recruitment pattern, decreased biceps CON iEMG in the post-training condition may indicate that less fast-twitch motor units were necessary to effectively accomplish the same task. The lower median frequency of stimulation may also be indicative of less fast-twitch motor unit involvement. The fact that no significant decreased changes of the iEMG or MF were found for the biceps during ECC action may reflect that there is less potential for neural adaptations with ECC than CON contraction. In the ECC action of the biceps, gravity could be considered the agonist while the biceps was the antagonist. It is not known how long these neural adaptations will persist or if there will be any carryover in the next training session. Also, a future study with isokinetic dynamometer at both directions may be needed to discriminate the dominance of neural adaptations in either CON or ECC muscle action.

CONCLUSIONS

Our research indicates increased neuromuscular efficiency following a single session of resistance training can be observed in the agonist muscle during CON activation. This improved efficiency is attributed to neural activation rather than to muscle hypertrophy. This information must be considered when interpreting data of subjects who have performed multiple trials in various conditions in the laboratory. Our results may provide alternative training for athletes to improve their performance within a short period of time.

REFERENCES

1. Hakkinen K et al. *Acta Physiol Scand*, **125**, 587-600,1985.
2. Hakkinen K et al. *Electromyogr Clin Neurophysiol* **35**, 137-147, 1995.
3. Keen DG et al. *J. Appl Physiol*, **77**, 2648-2658,1994.
4. Sale, DG. *Med. Sci. Sports Exercise*, **20**, S135-S145, 1988

Table 1: Mean iEMG and MF values during 3 continuous elbow flexion tasks. * significant difference due to main effect of training

		Concentric action of Biceps		Eccentric action of the Triceps	
		Pre-training	**Post-training**	**Pre-training**	**Post-training**
0 lb load	iEMG ($\mu v{*}s$)	41.95 ± 23.92 *	34.67 ± 17.05 *	9.03 ± 7.25	7.18 ± 5.04
	MF (*Hz*)	53.87 ± 12.47 *	51.21 ± 12.79 *	49.21 ± 19.54	42.95 ± 32.59
3 lb load	iEMG ($\mu v{*}s$)	81.81 ± 38.91 *	78.60 ± 32.90 *	12.21 ± 9.39	12.05 ± 8.38
	MF (*Hz*)	55.71 ± 8.63 *	52.92 ± 9.86 *	50.67 ± 11.30	47.31 ± 17.39

THE DIFFERENT INFLUENCE OF LEG EXTENSOR'S IN DEVELOPMENT PEAK OF FORCE IN DROP JUMP

Radivoj Vasiljev[1], Milinko Dabovic[2], Dusko B. Ilic[3]
[1]Department of Biomechanics, Faculty of Physical Culture, University of Novi Sad, Serbia, email: vasiljev@uns.ns.ac.yu
[2]Department of Sport's Gymnastics, Faculty of Sport and Physical Education, University of Belgrade, Serbia
[3]Department of Biomechanics, Faculty of Sport and Physical Education, University of Belgrade, Serbia

INTRODUCTION

Although great number of researches has done to pointing the role of Peak Force (PF) and Rate of Force Development (RFD) in jumping, sprinting and other dynamic sports activity, their role in drop jump performance was not investigated. Young et al [4] investigated relationships between the strength qualities of the leg extensor muscles and performance in vertical jumps performed from a standing position (double leg takeoff) and a run-up (single leg takeoff). They were reported that speed strength tests correlated significantly with both jump types, but maximum strength did not. A few experiments determine the best dropping height and find the best method for drop jump with small angular displacement of the knee from 0.3m [5]. Stone et al [3] investigated relationships between power output in countermovement jump and squat jump at different load conditions, among stronger and weaker subjects. They were reported that stronger subjects have had greater power output at greater load conditions and concluded that maximal strength development is primary factor in jumping ability enhancement [2]. In the presence of different reports, to distinguish the influence of maximal strength and speed-strength in jumping abilities, role of leg extensor's peak force (PF), rate of force development (RFD), rate of force development normalized with peak force (RFD/PF) and time interval from generating 30% to 70% of peak force (T30-70%) in counter drop jump (CDJ) and bounce drop jump (BDJ) performance were tested [1]. RFD/PF and T30-70% represented rate at which force were produced independently of peak force.

METHODS

Forty six male students of physical education, 23±1.9 years of age, 180.8±5.8 cm of height and 77.8±6.7 kg of weight, took part in a study. Isometric PF, (isometric) RFD, RFD/PF and T30-70% for hip and knee extensors, as well as foot plantar flexors, were measured with a strain-gauge dynamometer (Hottinger Baldwin Messtechnik, Germany; 0-5000N; 50Hz). Better of two attempts for every measured muscle groups were analyzed. Subjects also performed two CDJ and BDJ from height of 0.2, 0.3, 0.4, 0.5, 0.6 and 0.7 m. Jumps data: counter -bounce drop jump height and time (CDJH, BDJH, CDJT, and BDJT) presented in (Table 1). Count-bounce drop jump power output (CDJP BDJP), were collected using Ergo-Jump contact mat - Bosco's test system. Better CDJ and BDJ from every height vere analyzed. Dynamometry data were compared with CDJH and BDJP, using Pearson's product – moment correlation.

RESULTS AND DISCUSSION

With dynamometry data, PF for all muscles groups correlated significantly with RFD ($p<0.001$). Correlations between RFD/PF and T30-70% were the strongest ($p<0.001$), we found significantly correlation also, between CDJH and BDJP ($p<0.001$). PF and RFD of measured muscles groups, correlated significantly with CDJH and BDJP, but RFD/PF and T30-70%, did not. Since RFD depend upon amount of produced force (i.e. peak force) and rate at which force were produced, it is not known whether the peak force produced by muscles or rate at which they were generated force, had greater influence on RFD. For the hip extensors, correlations with RFD were stronger in CDJ from lower heights, only. Bounce drop jump power output (BDJP) showed stronger correlations with RFD of knee extensors in jumps from lower heights. Factor analysis showed that peak force factors for all measured leg extensor muscles, have had greater overall influence on drop jump performance, even if their influence on RFD variability were lower. It was concluded that peak force factors have a greater role in CDJ and BDJ performance, regardless of stronger correlations between BDJP and RFD of knee extensors, as well as between CDJH and RFD of knee and hip extensors in some jumps.

CONCLUSIONS

From a practical approach, to improve impact jumping ability, depending upon stretch shortening cycle, these results suggests that improving a maximum strength, rather than speed strength, should be a primary component of training programs.

REFERENCES

1. Abernety P., et al., *J. Sports Med.* **19**, 401-417, 1995.
2. Bobbert M. F., *J. Sports Med.* **9**, 7-22, 1990.
3. Stone M. H., et al., *J. Strength Cond. Res.* **17**, 140-147, 2003.
4. Young W., et al., *J Sports Med Phys Fitness.* **39**, 285-293, 1999.
5. Zushi K., et al., *Japan J. Phys. Educ.*, **38**, 265-278, 1993.

Table 1: Jumps data: Counter drop jump height (CDJH) and time (CDJT) - Bounce drop jump height (BDJH) and time (BDJT).

	Height (m)					
	0.20	**0.30**	**0.40**	**0.50**	**0.60**	**0.70**
CDJH (m)	0.32 ± 0.056	0.34 ± 0.053	0.35 ± 0.061	0.36 ± 0.057	0.35 ± 0.058	0.34 ± 0.064
BDJH (m)	0.28 ± 0.054	0.31 ± 0.057	0.31 ± 0.058	0.32 ± 0.062	0.32 ± 0.062	0.31 ± 0.070
CDJT (ms)	230.0 ± 40.3	217.6 ± 35.9	222.9 ± 41.3	226.8 ± 35.9	220.4 ± 42.7	236.6 ± 43.9
BDJT (ms)	144.1 ± 28.3	141.9 ± 22.4	148.5 ± 26.0	151.1 ± 27.3	149.6 ± 25.7	155.7 ± 26.0

VOLUMETRIC MEASUREMENT OF THE SUBACROMIAL SPACE AT THE SHOULDER

[1]Paula M Ludewig, [2]Edward Gonda, and [3]Fred A Wentorf
[1]Program in Physical Therapy, [2]Biomedical Engineering, and [3]Department of Orthopaedics
University of Minnesota, Minneapolis, MN; email: ludew001@umn.edu

INTRODUCTION

Shoulder pain is a common and debilitating condition. One theorized mechanism for the development of shoulder pain and associated rotator cuff tendonitis is compression of the soft tissues within the subacromial space of the shoulder as the arm is elevated. However, current methods of subacromial space measurement are limited. The purpose of this study was to develop and validate a volumetric description of the subacromial space at the shoulder, and describe changes in this space during passive humeral scapular plane abduction.

METHODS

The subacromial volume was defined as an extension of the supraspinatus outlet area described by Zuckerman et al.[1] Shoulder anatomical landmarks for 3 cadaveric specimens and an anatomical shoulder model were digitized in 3-D from CT scans (1mm contiguous helical slices) of the scapula and humerus with the arm in a neutral position (at side). Sets of 3 specific anatomical landmarks were used to define planes representing superior, medial, lateral, anterior and posterior borders of the subacromial space (Figure 1). Sequential triangular volumes were defined within the space and summed to define the overall volume (Vo). This volume is then further subdivided into anterior (Va), middle (Vm), and posterior (Vp) subvolumes representative of specific anatomic subcomponents of the subacromial space.

A portion of the humeral head crosses the plane defining the lateral border of the Vo, and the volume of this intersecting portion of the humerus is determined (Vi). Finally, Vo-Vi = the remaining space available to accommodate the rotator cuff soft tissues (Vr). Reductions in this remaining volume may increase impingement risk. Motion data is also collected for each specimen using 3-D electromagnetic motion sensors rigidly fixed to the bony segments via intercortical pins. Registration blocks which can be defined in the sensor frames by surface digitizing and are visible in the CT are used to build reference frames linking the motion data to the CT anatomical data.[2] The Vi and Vr can then be calculated in multiple arm positions using matrix transformations from the sensor data to rotate the anatomical data. Motion and CT data from 1 cadaver were used to describe these changing volumes at neutral, 40°, 60°, 90°, and 120° of humeral scapular plane abduction relative to the thorax. For validation, the anatomical model was rigidly fixed in 2 positions, anatomical neutral and with the humerus abducted ~ 90° relative to the scapula. Sensor orientation data and CT scans were collected in both positions. Volume measures calculated from the rotated anatomical data (experimental method) were compared to calculations based on the CT scan in the second position (criterion reference).

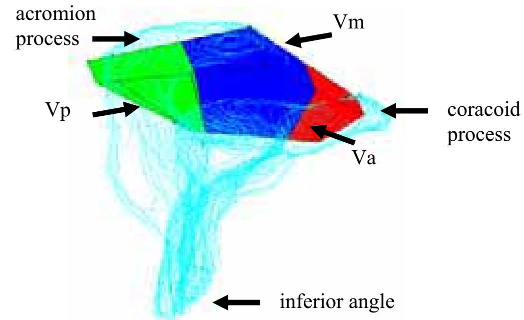

Figure 1. Superior/medial view of the subacromial volume superimposed on the scapula.

RESULTS AND DISCUSSION

The available subacromial volumes prior to considering humeral intersection are represented in Table 1. The Vr progressively decreased as humeral elevation increased with the smallest value at the 90° arm position, consistent with the clinically described position of shoulder impingement. The Vr then increased slightly in the 120° arm position (Table 2). The Vr calculated from the experimental method was 20.43 ml and the criterion reference value 20.45 ml, representing a 0.1% error. These volumetric measures may provide additional insight into mechanisms of development and rehabilitation for shoulder impingement syndrome.

REFERENCES

1. Zuckerman JD, et al. *J Shoulder Elbow Surg* **1**, 4-14, 1992.
2. Fischer KJ, et al. *J Biomech* **34**:377-383, 2001.

ACKNOWLEDGEMENTS

Funded by NIH/NICHD/NCMRR K01-HD42491.

Table 1. Non-intersected subacromial volumes (ml).

	Specimen				
Volume	**Model**	**# 1- Right Shoulder**	**# 2 - Right Shoulder**	**# 3 - Left Shoulder**	**Mean (SD)**
Overall	38.42	21.43	29.98	39.44	32.32 (8.41)
Middle	23.27	16.20	15.37	21.61	19.11 (3.92)
Anterior	4.84	1.56	2.47	4.68	3.39 (1.63)

Table 2. Remaining subacromial volumes (Vr -ml) across humeral elevation angles.

	Neutral	**40°**	**60°**	**90°**	**120°**
Middle	21.61	20.22	19.03	14.37	17.45
Anterior	4.68	3.90	3.29	0.17	2.59

SPEED RELATED CHANGES IN LOWER LIMB JOINT CONTRIBUTIONS TO MECHANICAL ENERGY DURING GAIT OF STROKE SUBJECTS

Luci Fuscaldi Teixeira-Salmela, Marie-Helène Milot, Sylvie Nadeau, Denis Gravel, France Piotte

CRIR, Site IRM, École de Réadaptation, Université de Montréal, Canada, E-mail: jhsalmela@hotmail.com

INTRODUCTION

Estimations of the relative contributions for each joint to the total energy involved in gait at different speeds may be central to precisely understanding the nature, extent, and degree of compensation across joints in subjects with locomotor disorders to provide more efficient rehabilitation.

The purpose of this study was to determine the relative contributions of the ankle, knee, and hip joint muscles to the total energy generated and absorbed during gait at natural and maximal speeds with stroke subjects.

METHODS

Fifteen subjects (five women and 10 men), mean age (58.3 ± 13.8 years), walked with their low-heeled shoes (five wore ankle-foot orthoses) without ambulatory aids. They were asked to walk at their natural speed and then, as fast as possible along a 9-meter walkway. Data were obtained with a 3-D Optotrak system and AMTI force platforms. An inverse dynamic approach was used to yield kinetic variables. Work generated and absorbed during gait by flexors and extensors for all joints were summed and the relative contributions to total positive and negative work for both speeds were calculated for each joint. Three within-factor repeated measures ANOVA, followed by contrasts, were used for laterality, joint, and speed effects.

RESULTS AND DISCUSSION

Mean (±1 SD) values for the natural and maximal speeds of 0.70 (± 0.30) m/s and 1.28 (± 0.37) m/s, were similar to those previously reported [1].

Side effects: For the generation contributions, significant differences between sides for both speeds were found only for the ankle and hip joints For absorption, differences were significant for the ankle and knee (Table 1).

The relative contributions of the affected (AS) /non-affected (NAS) sides to the total energy generated at natural speed were 40/60%. Corresponding values for absorbed work were 41/59%. At maximal speed, the respective values were 38/62% and 36/64%, demonstrating, as opposed to healthy subjects [2], the asymmetric nature of hemiparetic gait [1].

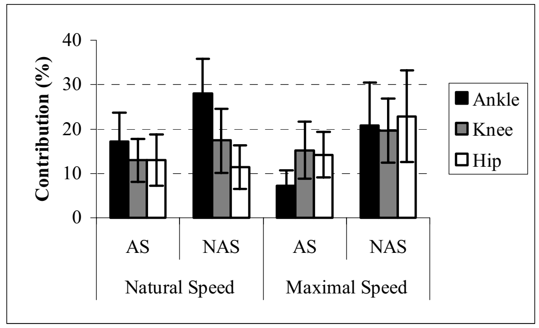

Figure 1: Relative contributions (%) of ankle, knee, and hip to total energy (generation + absorption) across speeds

Joint effects: For AS, contributions at the ankle were different from the other joints at both speeds, whereas for the NAS, all differences across joints were significant only for natural speed.

Speed effects: Supporting previous findings with healthy subjects [2], contributions at the knee and hip increased at maximal speed, while those at the ankle substantially decreased (Figure 1). Increases in generation were higher at the hip, whereas those in absorption were higher at the knee.

CONCLUSIONS

These findings demonstrated the interplay between limbs and joints associated with increases in walking speed. The asymmetry of hemiparetic gait indicates greatest contributions of the NAS side at both speeds. This model easily identifies segments that compensate for others with different task demands. The next step is to apply this model to determine effects of lower limb strengthening programs on these relative contributions for stroke victims.

REFERENCES

[1].Olney SJ et al. Work and power in gait of stroke patients. Arch Phys Med Rehabil 72, 309-314, 1991.

[2].Teixeira-Salmela et al. Lower limb joint contributions to energy generation and absorption during gait: Effects of cadence and laterality. Submitted, 2005.

ACKNOWLEDGEMENTS

Project financed by CHIR. Dr. Teixeira-Salmela is supported by CAPES/Brazil and Dr. Nadeau, and M-H. Milot by FRSQ.

Table 1: Contributions (%) to Generation and Absorption of Energy at Ankle, Knee, and Hip for Natural and Maximal Speeds

Joint	Natural Speed				Maximal Speed			
	Generation		Absorption		Generation		Absorption	
	AS	NAS	AS	NAS	AS	NAS	AS	NAS
Ankle	14	27	18	27	12	22	2	20
Knee	10	9	14	22	9	10	23	31
Hip	16	24	9	10	17	30	11	13
Total	**40**	**60**	**41**	**59**	**38**	**62**	**36**	**64**
	100		100		100		100	

SIT-TO-STAND PERFORMANCE WITH YOUNG AND ELDERLY SUBJECTS

Carolina Mitre Chaves, Fátima Goulart, Marcia Chagas-Vallone, Patricia Brito, Luci F. Teixeira-Salmela
Department of Physical Therapy, Federal University of Minas Gerais, Brazil; E-mail: carolinamchaves@uol.com.br

INTRODUCTION

Sit-to-stand is an often performed functional task in daily life and an important requirement for other functional movements. Among the elderly, the difficulty to stand is common and has been considered as a risk factor for institutionalization and falls [1,2,3].

The aim of this study was to evaluate the sit-to-stand task with gender-matched healthy young and elderly individuals at three distinct seat height conditions.

METHODS

Fourteen young (28.14± 5.91 yrs.) and 14 elderly individuals (68.71± 2.49 yrs.) were included. The sit-to-stand task was investigated using an accelerometer, electromyography (EMG), and force platforms. Investigated variables included: reaction times, movement times, latencies, and EMG activity of the tibialis anterior, erector spinal, hamstrings, and soleus muscles, as well as the body elevation index. Conditions were determined according to subjects` knee height, with the seat adjusted to 80, 100, and 115% of knee height. Three within-factor repeated measure ANOVA (2X2X3) was used to investigate age, gender, and seat height effects

RESULTS AND DISCUSSION

Reaction time did not differ between conditions, however, both reaction and movement times were greater for the elderly (Figure 1) and the latencies were slower for all muscles (p<0.01), except for the tibialis anterior. The elderly increased their movement times when the seat was lowered and decreased it when it was elevated (p<0.01). This demonstrated that regardless of gender, increases in seat height affected functional performance for elderly individuals. Significant interactions between age and gender for the young subjects were found, indicating that men were faster than women.

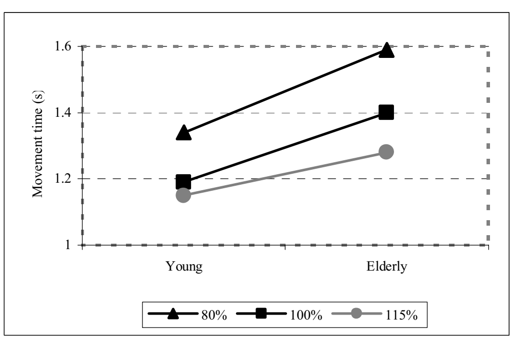

Figure 1: Effect of seat heights on movement time (s)

When the seat was lowered (80% condition), there was observed greater EMG activity for the tibialis anterior and quadriceps muscles (p<0.01), but no differences between the other conditions. In addition, the tibialis anterior was recruited earlier in the 80% condition (p<0.05), demonstrating its function as a preparatory muscle for the sit- to-stand task [3].

When the seat was elevated, decreases in EMG activity were found for all muscles, with the quadriceps being the main generator in the sit-to-stand task. Large variability was observed for the erector spinal muscles, probably indicating different individual strategies [3]. Hamstring activity was not influenced by seat heights

The body elevation index was determined by the amount vertical force generated, when standing from a chair. Differences in the body elevation index were found between groups and were gender-related, indicating that for young subjects, men showed a higher index (Figure 2).

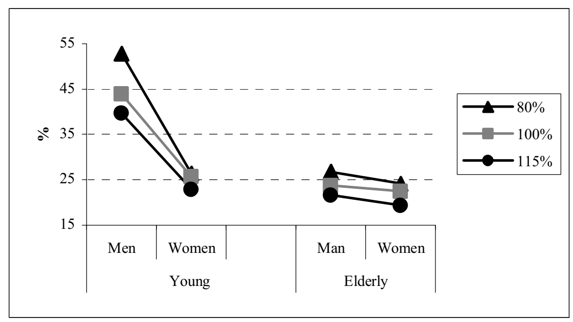

Figure 2: Body elevation index (% body weight) for the young and elderly groups across conditions

CONCLUSIONS

The present findings showed that increases in seat height were associated with decreases in movement time for the elderly and for EMG activation of the tibilais anterior and quadríceps for both young and elderly subjects. When the seat was lowered, movement time and EMG muscle activity increased for both groups. Based upon these findings, these strategies may be adopted by rehabilitation professionals to train the sit-to-stand task, especially with elderly subjects

REFERENCES

1. Luukinen H et al. Risk factors for recurrents falls in the elderly in long-term institucional care. *Public Health* **109**, 57-65, 1995.
2.Tinetti ME et al. Shared risk factors for falls, incontinence, and functional dependence. Unifying the approach to geriatric syndromes. *JAMA* **273**, 148-1353, 1995.
3 Janssen WGM et al. Determinants of the Sit-to-Stand Movement: A Review. *Phys Ther* **82**, 66-878, 2002.

RESONANT FREQUENCY SHIFTS IN OSTEOTOMISED GOAT TIBIAE

JE Brouwers, PAJ de Leeuw, GJ Streekstra, L Blankevoort
Orthotrauma Research Center Amsterdam,
Academic Medical Center, University of Amsterdam, the Netherlands.
guido@brouwersweb.com

INTRODUCTION

Diagnosing a bone fracture without the availability of X-rays is sometimes difficult. Osteophony is the assessment of bone integrity by analyzing its vibrations and is a non-invasive technique that could eventually assist general practitioners in correctly diagnosing fractures [1]. In case of a hip fracture, percussing the patella and auscultating the symphysis pubica results in a different sound, as compared to the healthy contra lateral side [2]. The pitch of the sound represents the resonant frequency. Nevertheless, listening with a stethoscope provides subjective results. By recording and analyzing the signals, the results become objective. Bone can be easily excited on prominences without much soft tissue coverage. The skin covering this prominence could influence the resonant frequency [3].

The goal of this study is to assess the influence of skin covering the point of excitation and to assess the influence of a standardised osteotomy on the resonant frequency of bone.

METHODS

For the experiments, 16 goat tibiae (8 fresh cadavers) are used. The medial malleolus is percussed with a hammer, instrumented with a force transducer. The response is measured with an acceleration sensor screwed into the tuberositas tibiae. After a measurement with skin covering the malleolus, the skin is removed and the experiment is repeated by percussing the bare malleolus. Subsequently, halfway between the malleolus and the tuberositas, a stepwise osteotomy is made (1/3, 2/3 and completely through). An osteophonogram is made by analyzing the transfer function between both signals, using a 2 channel data acquisition and analysis system (Pulse, Bruel & Kjaer, Denmark) coupled to a notebook PC (Figure 1). In the osteophonogram the resonant frequency is detected by the software.

RESULTS

There is no statistically significant difference between the resonant frequency of a goat tibia with or without skin covering the medial malleolus (paired T-test), the Pearson correlation coefficient is 0.992 ($p < 0.05$).
Also, no significant difference is found between intact bone and a 1/3-osteotomy or between intact and a 2/3-osteotomy (Figure 2).

There is a significant decrease in the mean resonant frequency between an intact and a fully osteotomised goat tibia (521 vs. 428 Hz; Anova and Bonferonni post hoc analysis: $p < 0.05$).

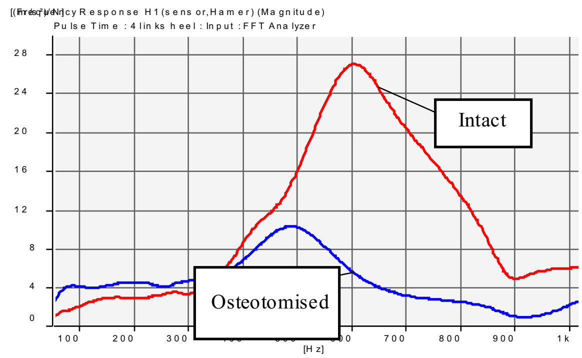

Figure 1: Typical example of an osteophonogram with the resonant frequency shift between an intact (red curve) and a completely osteotomised goat tibia.

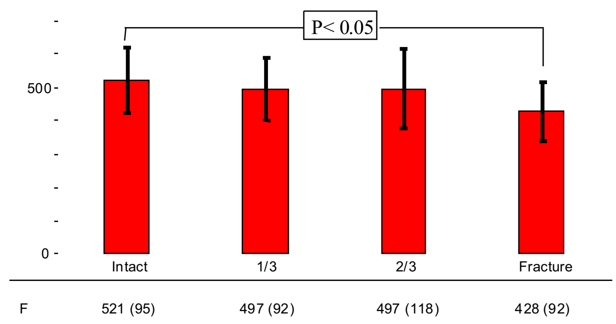

Figure 2: Average resonant frequency in Hz (with standard deviation) of the intact and the osteotomised (1/3, 2/3 and 3/3= fracture) goat tibiae.

CONCLUSIONS

Soft tissue covering bone prominences at the point of excitation does not influence the resonant frequency.

The resonant frequency of a fully osteotomised goat tibia is significantly decreased as compared to the intact tibia.

Osteophony seems to be a promising non-invasive method to detect bone fractures.

REFERENCES

1. Lipmann, RK. *J Bone Joint Surg Am* **14**, 118-126, 1932
2. Tiru M., et al. *Singapore Med J* **43**, 467-469, 2002
3. Nokes L. *Proc Inst Mech Eng [H]* **213**, 271-290, 1999

STIFFNESS MEASUREMENT OF THE GLENOHUMERAL JOINT

Edward Chadwick, Robert Kirsch and John Chae

Case Western Reserve University and The Cleveland FES Center

INTRODUCTION

Stroke is the leading cause of activity limitation among older adults in the United States. More than 700,000 strokes occur each year [1], with a prevalence of approximately 4 million (AHA, 1997). A common complication of stroke is hemiplegic shoulder pain with reported prevalence ranging between 34% and 84% [3][2].

Shoulder pain following stroke has been associated with subluxation in the gleno-humeral (GH) joint, but this is disputed and the aetiology is poorly understood. It is hypothesised that dynamic stability is a better predictor of pain than subluxation, which is a simple measure of joint instability.

The objectives of this research are to identify the mechanical and neuromuscular changes in the hemiplegic shoulder following stroke and their relationship to the development of pain, and to investigate possible mechanisms underlying that pain. Mechanical characteristics of the gleno-humeral joint will be determined using a system identification technique, modelling the shoulder as a second-order system.

METHODS

Displacement perturbations in the range 0-6Hz, 0-2cm, were applied to the arm during a constant force task, using a mechanical manipulator, while measuring end-point forces using a force transducer. The subject was firmly attached to the manipulator by means of a cast from the mid humerus level to the wrist, with the elbow in $90°$.

System Identification techniques were used to quantify dynamic stiffness of the shoulder, with humeral end-point motion as input and end-point force as output for the system.

$$\begin{bmatrix} F_x(f) \\ F_y(f) \end{bmatrix} = \begin{bmatrix} H_{xx}(f) & H_{xy}(f) \\ H_{yx}(f) & H_{yy}(f) \end{bmatrix} \begin{bmatrix} X_x(f) \\ Y_y(f) \end{bmatrix} \tag{1}$$

RESULTS AND DISCUSSION

Figure 1 shows stiffness curves for the three principal directions (leading diagonal) as well as the interaction between directions (off-diagonal). The curves for K_{xx} (top left) and K_{zz} (bottom right) have the typical tick-mark shape of a second-order system, but the curve for K_{yy} (centre) is all over the shop.

Partial and multiple coherence values for the identifications were found to be very good in the principal directions.

CONCLUSIONS

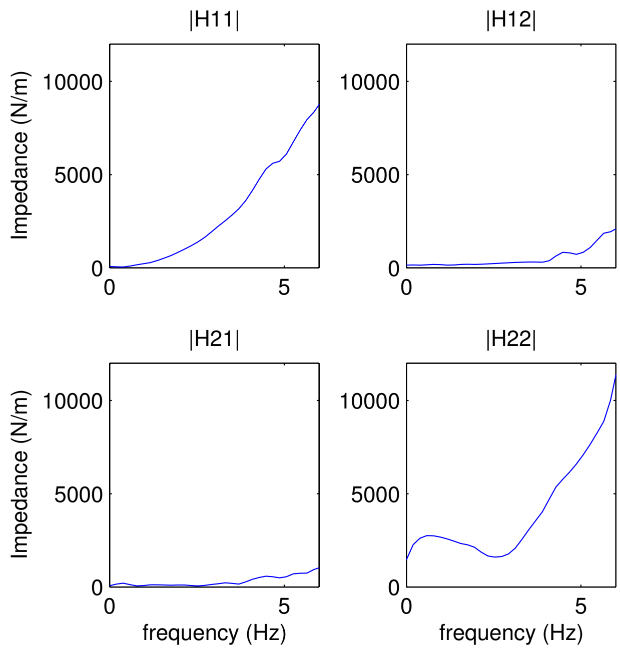

Figure 1: Dynamic stiffness of the shoulder during a 10N vertical (up) push task.

References

[1] J. Broderick, T. Brott, R. Kothari, R. Miller, J. Khoury, A. Pancioli, J. Gebel, D. Mills, L. Minneci, and R. Shukla. The Greater Cincinnati/Northern Kentucky Stroke Study: preliminary first-ever and total incidence rates of stroke among blacks. *Stroke*, 29(2):415–21, 1998.

[2] T. Najenson, E. Yacubovich, and S.S. Pikielni. Rotator cuff injury in shoulder joints of hemiplegic patients. *Scand J Rehabil Med*, 3(3):131–7, 1971.

[3] M. Peszczynski and T.T. Rardin, Jr. The incidence of painful shoulder in hemiplegia. *Pol Med Sci Hist Bull*, 29:21–3, 1965.

SMALLER SWAY DURING QUIET STANCE ATTRIBUTES TO EFFECTIVE USE OF BODY VELOCITY

[1, 3] Kei Masani, [2]Albert H. Vette, [3]Masaki Abe, [3]Kimitaka Nakazawa and [2]Milos R. Popovic
[1]University of Tokyo, [2]University of Toronto,
[3]Research Institute NRCD; email: masani@idaten.c.u-tokyo.ac.jp

INTRODUCTION

The nature of the control mechanism responsible for ensuring stability during quiet standing has attracted the attention of many researchers, since larger sway is supposed to relate to falling, which is a serious problem in elderly. However, the mechanism that determines the sway size remains unclear.

Using cross-correlation analysis, we found that the modulation of calf muscle activity matches body sway during quiet standing, and that the muscle activity precedes body sway with about 200ms [1]. It was also demonstrated that the central nervous system attributes a significant role to the body velocity information in order to generate the preceding motor command [1, 2].

In the present study, we tested the hypothesis that a more effective utilization of the body velocity information leads to an improved stabilization of the body.

METHODS

Experimental study: 24 young (Mean age 27yrs; Male 11, Female 13) and 22 elderly (66yrs; M 11, F 11) healthy subjects were asked to stand quietly for 90 sec and five trials. The body sway and electromyogram (EMG) in the right soleus muscle were measured. Due to the space limitation, we do not compare distinct age group characteristics in this abstract.

Simulation study: We provided an explanation for the experimental results by means of a numerical simulation. Human quiet stance was simulated using an inverted pendulum model regulated by a proportional and derivative (PD) controller. The parameter sets of the simulation, such as proportional gain (Kp), derivative gain (Kd) and closed-loop time delay, were selected with the goal of generating a realistic cross-correlation function (CCF) between the motor command and body sway as demonstrated in [2].

Analysis: The correlation coefficient (CC) and time shift (TS) were determined using the peak of CCF between body sway and EMG (Experimental study) or motor command (Simulation study). Sway size was evaluated as the standard deviation of body sway.

RESULTS AND DISCUSSION

Figure 1 shows the results of the experimental study. The results indicate that for a person, who sways less, CC is smaller (A) and TS longer (B). For both age groups, this tendency is more distinct in male than in female subjects (not shown in this abstract).

The experimental results inspired us to consider the contribution of the velocity information in the central nervous system. We reported in [1] that a larger Kd generates a faster fluctuation of the motor command. Therefore, the CC between body sway and motor command is expected to be smaller when the body is controlled by means of a larger Kd gain. The relation is shown in Figure 2A. Also, a controller with a larger Kd gain is capable of producing a longer TS, since the phase of the derivative time series leads the position time series [2], as shown in Figure 2B. Additionally, since a larger Kd is more capable of compensating the noise torque, the ratio of Kp/Kd correlates with the sway size (r=0.316, p<0.01). As a result, a smaller sway size relates to a smaller CC and longer TS for the simulation as well (Figure 2C, D).

Comparing the results in the experimental and simulation studies, we conclude that the person who shows the smaller body sway utilizes the larger body velocity information.

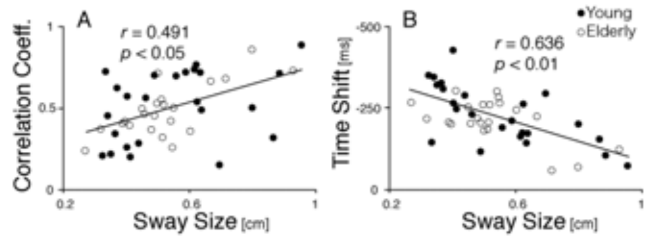

Figure 1: Results of the experimental study. Sway size vs. CC (A) and TS (B) of the CCF between EMG and body sway. Note that the positive CC indicates that the larger EMG correlates with the forward body position, that the negative TS indicates that the EMG precedes the body sway, and that the vertical axis of B is reversed.

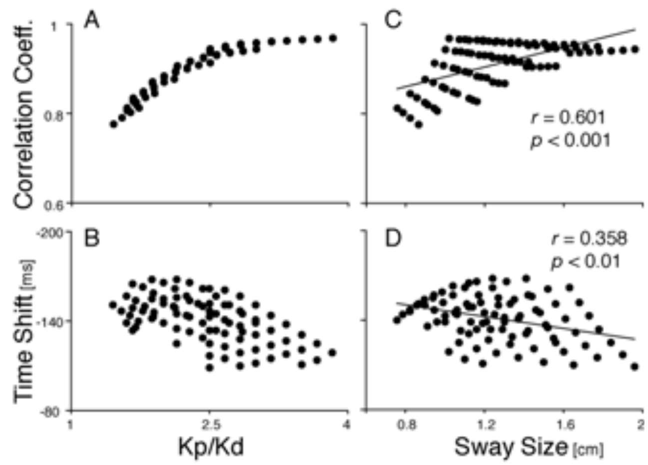

Figure 2: Result of the simulation study. The ratio of Kp/Kd vs. CC (A) and TS (B) of the CCF between motor command and body sway. Sway size vs. CC (C) and vs. TS (D). Plots are from 89 simulations. See notes in Fig. 1.

REFERENCES

1. Masani, et al. *J Neurophysiol* **90**, 3774-3782, 2003.
2. Masani et al. *Gait and Posture*, in press.

CHANGES IN MECHANICAL CHARACTERESTICS OF THE PLANTARFLEXOR MUSCLES IN INDIVDUALS WITH DIABETES MELLITUS

[1] Smita Rao, [1]Jason Wilken, [2]Charles Saltzman and [1]H John Yack
[1]Graduate Program in Physical Therapy and Rehabilitation Science,
[2]Orthopedics and Rehabilitation; email: smita-rao@uiowa.edu

INTRODUCTION

Foot ulcers are estimated to develop in 15% of all individuals with DM[1] and have been linked to repetitive mechanical stress. Loss of ankle range of motion (ROM) and increased stiffness are two factors that have been implicated as potential contributors to plantar loading[2].

Attempts to document changes in passive ankle ROM and stiffness in individuals with DM have uncovered mixed results[3,4]. Differences in criteria for determining passive end ROM and for quantifying stiffness, as well as variations in the extent of pathology in subjects with DM, may account for ostensible differences in ankle ROM and stiffness. During gait: attempts to document plantar loading have not controlled for the confounding effect of walking velocity, which has been shown to influence plantar loading[5]. The biomechanical relationships between passive and dynamic gait measures of ankle ROM and stiffness, and plantar loading are not well understood. The **purpose** of our study was to examine the association between passive ankle ROM and stiffness measured at rest and during gait, in individuals with DM and neuropathy, and to use this information to help understand how ankle ROM and stiffness may influence plantar loading.

METHODS

Twenty-five subjects with DM, neuropathy and no ulcer and 80 age and gender matched non-diabetic controls participated in clinical ankle ROM and stiffness testing. Ten subjects from each group were tested during gait. In subjects with DM, type and duration of DM, most recent HbA1c levels and presence of neuropathy (using Semmes-Weinstein monofilaments) was documented.

Passive Testing: Passive ankle ROM was quantified as angular displacement between the tibial crest and the plantar aspect of the foot, measured with a custom built device, while applying torques of 15, 20 and 25 Nm. Passive ankle stiffness was calculated as the slope of the curves over 15-25 Nm intervals. **During gait:** Plantar pressures were recorded at 60 Hz using in-shoe insoles (Novel Inc, MN), ankle ROM was measured using kinematic data collected using infrared markers (Northern Digital Inc, Waterloo, Canada) placed on the foot, leg and thigh segments, kinetic data was collected using a force-plate embedded in the walkway (Kistler Inc., NY) as subjects walked at 0.89 m/s. Data was processed to yield sagittal plane ankle kinematics and kinetics and ankle stiffness was calculated during second rocker.

RESULTS AND DISCUSSION

Passive: Subjects with DM showed higher ankle stiffness (0.016 vs. 0.005 Nm/kg/º, p<0.001) and less peak dorsiflexion (13.5 vs. 21.5º, p<0.001) than age and gender matched control subjects during clinical testing. **Gait:** The groups did not show differences in stiffness (0.068 vs. 0.076 Nm/kg/º, p=0.97) or peak dorsiflexion (9.8 vs. 11.7º, p= 0.93) utilized during gait.

Passive: Ankle stiffness with the knee extended was significantly associated with ankle stiffness with the knee

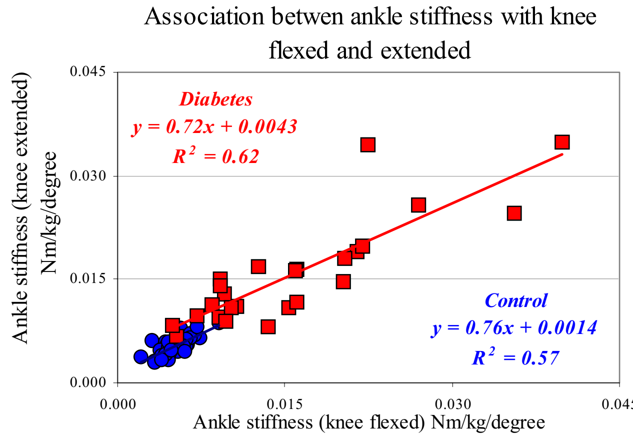

Figure 1: Graph depicting association between passive ankle stiffness with the knee flexed and extended in subjects with diabetes (red squares) and non-diabetic controls (blue circles)

flexed in subjects with DM, as well as in non-diabetic individuals (Figure 1). In subjects with DM, HbA1c levels and duration of DM showed fair association with ankle stiffness in the knee extended position (r^2 = 0.48 and 0.24 respectively, p<0.01). **Gait:** In subjects with DM: peak plantar pressure showed a positive association with ankle stiffness during gait (r^2=0.51, p=0.02) and stride length (r^2=0.49, p=0.03). In control subjects: peak pressure was positively associated with stride length (r^2=0.42, p=0.02) but not with ankle stiffness during gait (r^2=0.06, p=0.68).

CONCLUSIONS

The unique findings of our study revealed that while subjects with DM had restricted passive ankle ROM and increased stiffness compared to control subjects, these measures did not represent ankle motion or stiffness utilized during gait. Peak passive stiffness was about 18 and 23% of ankle stiffness during gait, in control and DM groups respectively, suggesting that individuals with DM may utilize higher contribution from passive stiffness to ankle stiffness during second rocker in gait.

In spite of differences in ankle ROM and passive stiffness, subjects with DM demonstrated ankle stiffness and plantar pressures, similar to control subjects, while walking at identical speed, 0.89 m/s. This may represent an effective strategy adopted by subjects with DM to modulate plantar loading using kinematic pattern.

REFERENCES

1. Gordois, A., et al., Diabetes Care, 2003. 26(6): 1790.
2. Fernando, D.J.et al. Diabetes Care, 1991. 14(1): 8.
3. Salsich, G.B., M.J. Mueller, and S.A. Sahrmann, Phys Ther, 2000. 80(4): 352.
4. Trevino, S.G., et al., Foot Ankle Int, 2004. 25(8): 561.
5. Mueller, M.J., et al., Phys Ther, 1994. 74(4): 299.

ACKNOWLEDGEMENTS This study was supported by NIH RO1 NR 07721-03

EFFECT OF 20 DAYS OF BED REST ON PASSIVE MECHANICAL PROPERTIES OF HUMAN GASTROCNEMIUS MUSCLE BELLY

[1] Tetsuro Muraoka, [2]Masanobu Tachi, [3]Junichi Ushiyama, [3]Tadashi Muramatsu,
[4]Hideoki Fukuoka, [1]Tetsuo Fukunaga and [4]Hiroaki Kanehisa
[1]Waseda University, [2]Japan Institute of Sports Sciences, [3]Keio University,
[4]The University of Tokyo; email: muraoka@aoni.waseda.jp

INTRODUCTION

Immobilisation affects mechanical properties of muscle [1, 2]. Animal experiments showed that passive mechanical properties of muscle belly, which play an important role in movement, changed with immobilisation [1]. However, these results might not be directly applicable to humans in vivo because of the differences in species. Moreover, the influence of immobilisation differs muscle to muscle [2]. Recently, the passive mechanical properties of the human gastrocnemius (GAS) muscle belly in vivo can be measured using ultrasonography [3].

The aim of this study was to investigate the effect of 20 days bed rest (BR) on passive mechanical properties of the human GAS muscle belly in vivo.

METHODS

Subjects were four healthy males (20 ± 0 yr). Each subject provided written informed consent. Subjects remained at a continuous 6° head-down tilt throughout a 20-days BR period. Five days before the start of the BR period and a day after the end of the BR period, passive mechanical properties and muscle thickness of the GAS muscle belly were measured. This study was approved by the ethical review board of NASDA and the Faculty of Medicine, the University of Tokyo.

Each subject lay on his right side with the right hip joint flexed and held constant within the range of 30° to 50°. Transverse ultrasound images of the medial head of the GAS were taken during passive slow knee extension from 65° to 5° with a constant ankle joint angle of 10° dorsiflexion. The change in passive ankle joint moment (Mp), which is produced only by the GAS length change, was also measured.

Baseline of the Mp was defined as the plantarflexion moment in the knee joint angle range of 55° to 60°, in which the moment was almost constant for all subjects. The first point to rise above the 99 % confidence interval of the baseline of the plantarflexion moment for 5° while extending the knee joint was set as the onset of the Mp produced by the GAS, and the knee joint angle at this onset was defined as the slack knee joint angle for the GAS (θs). The slack length of the GAS muscle fascicles (Lfs) was defined as the length of the GAS muscle fascicles (Lf) at θs. The relationship between Lf and Mp in the knee joint angle range from 5° to θs° was fitted with a linear regression equation using a least squares method.

Muscle thickness of the GAS (Tm) was measured from left leg at 70% of the lower leg length proximal to the lateral malleoluls using a B-mode ultrasonography.

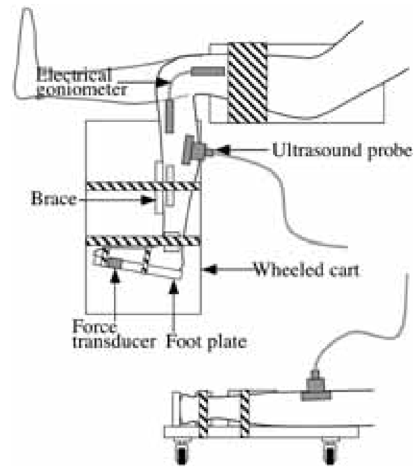

Figure 1: Top and side view of the experimental setup used for the measurement of the passive ankle joint moment during passive slow knee extension.

RESULTS AND DISCUSSION

Tm slightly decreased from 60 ± 2 mm to 59 ± 2 mm with BR. θs decreased from 42° ± 6° to 28° ± 12°, but Lfs was almost constant (the pre-BR Lfs was 42 ± 4 mm and the post-BR Lfs was 44 ± 5 mm). Thus, BR had little effect on Lfs, which was in agreement with the previous result [1]. The slack length of the human GAS tendinous tissues in vivo might be lengthened with BR, although the tendinous tissues of rabbit soleus muscle in vitro were shortened with immobilisation [1]. The slope of the relationship between Lf and Mp in the knee joint angle range from 5° to θo° decreased from 0.085 ± 0.027 Nm/mm to 0.071 ± 0.042 Nm/mm with BR. Thus, BR decreased the passive stiffness of the human GAS muscle belly in vivo, although the stiffness of rabbit soleus muscle fascicles in vitro was unchanged with immobilisation [1].

CONCLUSIONS

Twenty days of bed rest had little effect on the slack length of gastrocnemius muscle belly, but decreased its passive stiffness.

REFERENCES

1. Herbert RD & Crosbie J. *Eur J Appl Physiol* **76**, 472-479, 1997.
2. Kubo K, et al. *Br J Sports Med* **38**:324-330, 2004.
3. Muraoka T, et al. *J Biomech* in press.

ACKNOWLEDGEMENTS

This study was carried out as a part of Grand-based Research for Space Utilization, proposed by the Japan Space Forum.

HOW MUCH DO THE HIP ABDUCTORS CONTRIBUTE TO THE GAIT STABILITY FOR AMPUTEE WITH A PROSTHESIS?

Tae Soo Bae, Jae Youn Lee, Song Hak Im, S.K. Kim, M.S. Mun
Korea Orthopedics and Rehabilitation Engineering Center, email: bmebae@iris.korec.re.kr, web: www.korec.re.kr

INTRODUCTION

The appropriate abduction torque by hip abductor muscle is essential to the balance and stability control of frontal plane stability of pelvis during walking. Without adequate abduction torque on the stance limb, above-knee amputees tend to lean trunk toward the amputated side during single-limb support in the frontal plane. The aim of the present study was to analyze the role of hip abductors which control the gait stability at walking speeds using 3-D musculoskeletal dynamic models for amputees by the inverse dynamic analysis.

METHODS

Ten transfemoral amputees with lower-limb prosthesis and ten healthy subjects were involved and gait analysis was performed by motion analyzer. Subjects were instructed to walk at three speeds at which they felt fast, most comfortable, and slow. Using SIMM, we made the musculoskeletal model for stump using anthropometric data which were obtained from computed tomography and MRI. After consultation with clinicians and references, the insertion points of muscles related to hip motion were redefined. Four primary abductors-the gluteus medius (GMed), the gluteus minimus (GMin), tensor fasciae Latae(TFL) and two secondary abductors-the piriformis (PF) and the satorius (SAT) were considered in this study. Next, we made the 4-bar linkage prosthetic model scaled to the stump model. (Figure 1) The dynamic equation of motion for amputee and normal subject was derived using SD/FAST and an inverse dynamics simulation was produced by Dynamics Pipeline. We adapted the muscle parameters of normal subjects to those of amputees through the sensitivity analysis referred to the comparative results from isokinetic and isometric test using dynamometer (Biodex) and also to the help of clinicians.

RESULTS AND DISCUSSION

During single-limb support period in the frontal plane, the pelvic obliquity of right legs of normal was 3~8 degrees greater than those of amputated leg of amputees which showed the negative sign of obliquity for amputees meaning that they tend to lean trunk toward amputated leg.

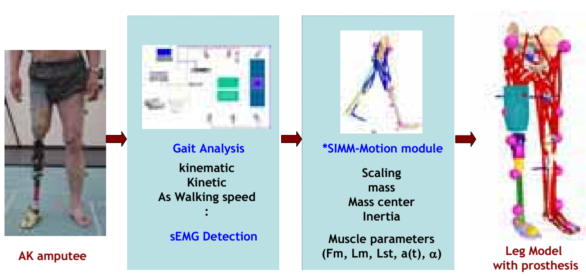

Figure 1 The configuration of experiment and simulation

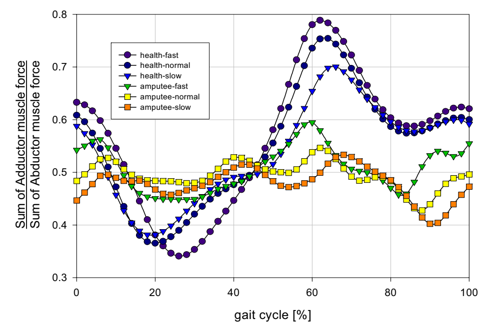

Figure 2: Comparison of the ratio of the sum of adductor muscle force with that of abductor muscle force

The muscle force of GMin is 11% (about 80N) and that of GMed is 20% (about 100N) over bodyweight(BW) less than those of the normal. The force of TFL and SAT is not different in pattern and scale. But that of PF is 39% of BW (about 390N) less than normal. The sum of adductor and abductor muscle force was less than that of normal at swing phase and at stance phase respectively. In view of the ratio of the sum of adductor muscle force to that of abductor muscle force, the weakened abductor during stance phase and the weakened adductor during swing phase were observed in contrast to normal subjects. And as walking speed increases, the force of abductor and adductor is vertically increased and decreased for normal gait. But for amputee gait they are shifted back as walking speed increases. (Figure 2)

CONCLUSIONS

From musculoskeletal model for normal and amputee gait as walking speed increased, weaken abductor results in excessive adduction in the frontal plane and then inadequate valgus torque was generated. The PF, GMin and GMed in order were significantly weak ($p<0.05$). The abductor and adductor forces are vertically increased and decreased for normal gait but shift-back for amputee gait as the walking speed increase. By dynamic modeling of musculoskeletal motion during gait, it was found that the magnitude or pattern of muscle forces and moments was different between amputees and normal subjects in three dimensional planes.

REFERENCES

1. Zajac FE., *CRC Crit. Revs. Biomed. Eng*, Vol. 17(14), 359~411, 1989
2. Delp SL, Loan JP. *Computers in Biology and*, Vol. 25, No.1, 21~34, 1995

ACKNOWLEDGEMENTS

This work was supported by Ministry of Health & Welfare (No. 02-PJ3-PG6-EV03-0004)

BIOMECHANICAL ANALYSIS OF SIT-TO-WALK FREQUENTLY OBSERVED IN DAILY LIVING: EFFECT OF SPEED ON HEALTHY ELDERLY PERSONS

[1] Munetsugu Kouta, [2]Koichi Shinkoda, [2]Naohiko Kanemura, [1]Michele Eisemann Shimizu, [1]Morihiro Tsujishita
[1]Hiroshima Prefectural College of Health Sciences
[2]Hiroshima University
e-mail: kouta@hpc.ac.jp

INTRODUCTION

There has not been enough biomechanical research done about how motions occur in a series and about task-oriented motions. In particular, biomechanical characteristics of the sit-to-walk component of the Timed Up and Go Test have not been accounted for [1], although this series of motions is observed most frequently in daily living. Additionally, there is not enough intervention done to improve the sit-to-walk sequence. We often see people with physical disorders stand up and initiate gait unstably, and we often treat patients who have a history of falls and fractures from attempting to stand up and initiate gait.

The purpose of this study was to clarify the normal characteristics of this series of motions for healthy elderly people.

METHODS

At first, as a pilot study we researched the patterns of the sit-to-walk for healthy elderly people [2]. We asked 18 healthy elderly people to stand up and walk as fast as possible, and we found that there are two patterns for this series of motions. One pattern involved small movements of the lower extremities, which is advantageous for fast motion. The other included large movements of the lower extremities, which are advantageous for stability, in spite of slower motion.

We defined these two motion patterns as the fast motion and the slow motion. In the present study, we analyzed the biomechanical characteristics of these two motions, while constraining the speed of the motions. The characteristics of 8 healthy elderly people (69.8±3.9 years old) were obtained.

Kinematic data was obtained by VICON 512 3D motion capture system (Oxford Metrix Ltd.). Kinetic data was obtained using two Kistler force plates. Ground reaction force (GRF) data was represented as *Fx,* right-left (left is plus), *Fy*, anterior-posterior (anterior is plus), and *Fz*, vertical (upper is plus).

Table 1: Difference between fast and slow motion

		fast	slow
GRF	*Fx* [N]	64.7±12.8	61.6±11.9
	Fy [N]	163.2±27.4	115.7±33.3
	Fz [N]	592.1±70.3	605.2±75.5
COM - CFP inclination			
First toe off [deg]		89.4±4.5	83.2±4.3
First heel contact [deg]		105.5±5.9	93.8±5.7

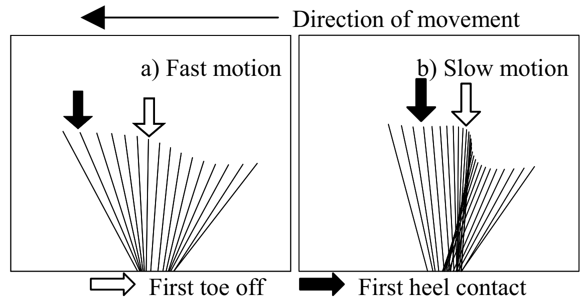

Figure 1: Movement of COM and CFP at y-z plane from starting movement of the head to first heel contact

RESULTS AND DISCUSSION

The maximal value of GRF is indicated in Table 1. Only the component of *Fy* was significantly different between the fast and the slow motions (p<.001). Inclination of the center of the body mass (COM) to the center of the foot pressure (CFP) at the first toe off and the first heel contact was larger in the fast motion than in the slow motion (more than 90 deg; forward inclination, less than 90 deg; backward inclination) (p<.001) (Table 1). During the fast motion, the OFP barely moved at stand up, and then gradually moved forward. During the slow motion, the CFP moved forward at stand up, then moved backward and the first toe off was achieved (Table 1).

In the first swing of the sit-to-walk series, the maximal values of the vertical and lateral GRF of the stance leg were not different for both fast and slow motions. But the forward GRF was significantly larger in the fast motion. GRF means acceleration of COM. So only forward acceleration was larger in the fast motion. In the fast motion, the CFP moved forward gradually and constrained the forward movement of the COM, because the COM moved faster. In the slow motion, the CFP moved forward at stand up in order to constrain the COM movement. COM movement was slower in the slow motion, so the CFP moved backward in order to induce a forward COM movement. We believe that the forward GRF shows a force couple on the sole of foot, and the COM-CFP movement shows a reverse pendular model.

We did not analyze the motions that subjects actually carried out in daily living. This point is a limit of this study. But we think it is important to analyze sit-to-walk as a series of motions.

REFERENCES

1. Janssen WG, et al. *Phys Ther* **82**, 866-79, 2002.
2. Kouta M, et al. Proceedings of the First Asian Pacific Conference on Biomechanics, 109-110, 2004

REPETITIVE SYMMETRIC ARM TRAINING AND MOTOR CORTEX ACTIVATION IN CHRONIC HEMIPARETIC PATIENTS

[1]Kisik Tae, [1]Sayup Kim, [2]Sungjae Song, [3]Soyoung Lee, [3]Giyoung Park, [4]Chulho Sohn and [1]Youngho Kim
[1]Dept of Biomedical Engineering, Institute for Medical Engineering, Yonsei University, Korea,
[2]Dept of Mechanical Engineering, Wonju National College, Korea,
[3]Dept of Physical Medicine and Rehabilitation, [4]Dept of Diagnostic Radiology,
Keimyung University Dongsan Medical Center, Korea;
email: yhkim@dragon.yonsei.ac.kr, web: biomecha.yonsei.ac.kr

INTRODUCTION

With the development of functional neuroimaging in recent years, several studies have been reported upon cortical reorganization induced by intervention in stroke patients [1,2]. The repetitive bilateral exercises improved functional motor performance of the affected upper extremity of hamiparetic patients [3].
The purpose of this study was to demonstrate the effect of repetitive symmetric arm training, which was designed to improve upper limb function, on functional recovery and upon cortical activation changes in chronic hamiparetic patients using functional magnetic resonance image (fMRI).

METHODS

A symmetrical upper limb motion trainer was made of M.C. Nylon suitable for MR environments and designed the affected side can be passively controlled with the same movement according to the active motion of the unaffected side. Totally six subjects participated in this study. As a control group, three of them were right-handed healthy male subjects (age: 34±5 years). In three patients (age: 43.3±6 years), two patients were left hemiparesis and the other was right hemiparesis. All patients received the training at 1hr/day, 5 days/ week during 6 weeks. Fugl-Meyer scores (FMS) were obtained every two weeks during the 6-week training. Before and after the 6-week training program, the blood oxygen level dependent (BOLD) fMRI measurements employing the echo planar imaging (EPI) technique (TR/TE/α=1900/40/90°, FOV=240mm, matrix size= 64×64 and slice thickness=5mm), were performed using a 3T MR scanner (GE Medical System, Milwaukee, USA) with a head coil. A T2-wighted anatomical volumetric images (FSE, TR/TE/α= 4500/104/90°, FOV=240 mm, matrix size=256×256 and slice thickness=5mm) were obtained. During fMRI experiments, two motor tasks were assigned to each subject: Task 1 was an only active wrist extension/flexion on the unaffected and Task 2 was the passive wrist extension/flexion of affected hand by an active wrist movement of unaffected side using the nonferritic device. Significance of the activation between the rest and the task was threshold at $p<0.001$.

RESULTS AND DISCUSSION

In all three patients, FMS of the affected hands improved significantly after the 6-week training program ($p<0.05$). In Task 1, the only dominant wrist movement, in control group, activations in the primary contralateral sensori-motor cortex (SMC) were observed. In Task 2, on the other hand, the passive wrist movement of the non-dominant hand driven by the active wrist movement of the dominant hand, activations in the primary bilateral SMC, supplementary area (SMA) and premotor area (PMA) were observed. In fMRI results in Task 1, a cortical activation in the contralateral (affected) side was observed after the training (Figure 1 (a)). However, Task 2 showed that the contralateral PMA of the unaffected wrist and the bilateral SMA were newly activated and activations in contralateral SMC increased in Patients 1 and 3. However, cortical activations in contralatral SMC of unaffected wrist, bilateral PMA and bilateral SMC were newly activated in Patient 2 (Figure 1 (b)).

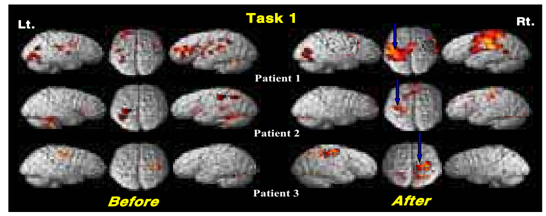

(a)

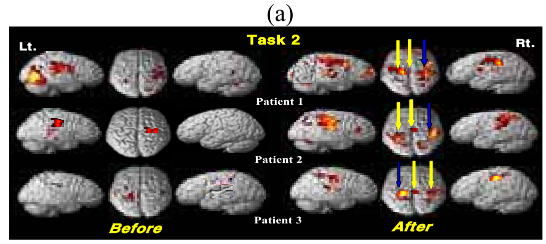

(b)

Figure 1: Cortical activations before and after training during Task 1(a) and Task 2(b) ($p<0.001$), increasingly activated (blue arrow) and newly activated (yellow arrow) areas compared before the training.

CONCLUSIONS

In three patients with chronic hamiparesis after brain injury, specific repetitive symmetric upper limb training appears to improve FMS and induce cortical reorganization. This association supports that developed arm trainer improves arm function by inducing reorganization of motor cortex networks.

REFERENCES

1. Carey JR, et al. *Brain* **125**, 773-788, 2002.
2. Nelles G, et al. *Neuroimage* **13**, 1146-1154, 2001.
3. Whitall J, et al. *Stroke* **31**, 2390-2395, 2000.

ACKNOWLEDGEMENTS

This work was partially supported by RRC program of MOST and KOSEF.

EFFECTS OF TAPING MATERIALS ON ISOKINETIC PERFORMANCE AT THE ANKLE MUSCLES

[1] Yang Hua Lin and [1]Chung Hung Wu
[1]Graduate Institute of Rehabilitation Science, Chang Gung University, Taoyuan, Taiwan; email: linyh@mail.cgu.edu.tw

INTRODUCTION

Athletic taping has been one of the most popular methods to support the weakened joint. Although there have been the positive effectiveness of ankle taping on the range of ankle motion there are few reports about the effect of taping materials on the joint performance such as muscle activity. The purpose of this study was to examine effects of different taping materials on isokinetic performance of the ankle muscles. The null hypotheses was proposed as taping could not affect significantly neiether the isokinetic performance of the underlying muscles nor those in accordance with different taping materials.

METHODS

Forty-five young healthy adults (mean age=24.7 ± 3.4 yr) without any history of ankle sprain within past six months were volunteered to participate in this study and randomized into three groups as a non-elastic taping group (n=15) with athletic white tape, an elastic taping group (n=15) with kinesio tape and a control group (n=15). Tapings was done along the tibial anterior and the peroneal group according to the principles provided by Illustrated Kinesio-Taping [1]

CYBEX NORM™ system was used to measure isokinetic performance of ankle muscles with concentric dorsiflexion-plantarflexion and eversion-inversion movements of the ankle, which were interpreted as ratio of peak torque to body-weight values ratio for reciprocal concentric contraction at angular velocity of 60°/sec and 120°/sec. There were three conditions to be tested as (1) untaped condition, (2) taped condition, and (3) untaped condition for the two groups with using two different tape materials

Each subject did three repetitions of contraction at each condition with assigned slow and fast speeds. The data were examined with ANOVA to determine the statistical significance of the factors of conditions and groups.

RESULTS AND DISCUSSION

Types of taping material did not show the significant difference in isokinetic peak torque of ankle muscles except ankle invertors with non-elastic taping compared with that in the control group without any taping (Table 1.). The isokinetic peak muscle torque significantly affected by the testing speed as previous studies but did not show a combined effect by the taping materials used.

Regardless the taping materials were used, the isokinetic peak torque of ankle evertors at slow speed and fast speed showed significantly better performance under taped condition than those showed under untaped condition (Figure 1.), which occurred in the ankle invertors at fast speed as well.

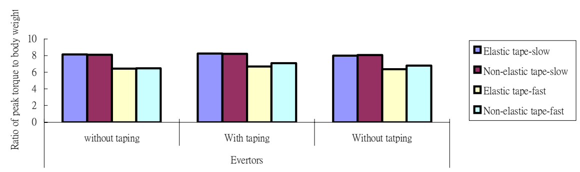

Figure 1. Isokinetic peak torque of ankle evertor under taped vs untaped condition

CONCLUSIONS

In this study, taping materials did not demonstrated significant effects on the isokinetic peak torque of ankle muscles. When the ankle was taped the ankle evertors showed significantly increased isokinetic peak torque, which was compared with those under untapped conditions before and after.

REFERENCES

1. Kase K. *Illustrated KinesioTaping.* KMS LLC.

ACKNOWLEDGEMENTS

The authors would like to thank the National Science Council of the Republic of China for financially supporting this research under Contract No. NSC 92-2314-B-182 -050 -.

Table 1: Isokinetic performance of ankle muscles with different taping materials interpreted as ratio of peak torque to body weight.

Groups	Ankle Muscles			
Slow speed	**Dorsiflexors**	**Plantar flexors**	**Evertors**	**Invertors**
Elastic tape	5.95±1.72	22.71±9.37	8.23±2.63	10.28±3.03
Non-elastic tape	6.34±2.39	17.15±8.27	8.21±3.20	9.15±2.99*
Control	6.58±2.64	24.63±13.85	8.75±2.19	13.87±7.76*
Fast speed				
Elastic tape	5.59±1.33	16.37±8.08	6.70±2.31	8.24±2.76
Non-elastic tape	5.86±1.88	14.00±6.43	7.07±2.71	7.52±2.74
Control	5.94±1.63	20.78±13.96	7.16±2.19	10.70±5.93

PATELLA ALTA IS ASSOCIATED WITH PATELLOFEMORAL MALALIGNMENT AND REDUCED CONTACT AREA

Samuel R. Ward, Michael R. Terk, and Christopher M. Powers
Musculoskeletal Biomechanics Research Laboratory, Department of Biokinesiology and Physical Therapy
University of Southern California, Los Angeles, CA email: srward@ucsd.edu

INTRODUCTION

Patella alta or "high riding patella" is a condition that is thought to predispose individuals to patellofemoral joint dysfunction. The purpose of this study was to compare patellofemoral alignment and contact area in persons with patella alta to subjects with normal patellar position and determined the association between the vertical position of the patella, patellofemoral malalignment, and contact area.

METHODS

Twelve patients with patella alta and thirteen subjects with normal patellar position participated. The presence of patella alta was determined using the Insall-Salvati index as measured on sagittal magnetic resonance images of the knee [1]. Medio-lateral patellar displacement, tilt, and patellofemoral joint contact area were quantified from axial MR images of the patellofemoral joint obtained with the quadriceps contracted and the knee at 0°, 20°, 40°, and 60° of flexion.

Statistical comparisons between groups were made as a function of joint angle using two-way ANOVAs with repeated measures. *Post-hoc* Tukey tests were used to identify between group differences at each knee flexion angle when significant interactions were present. Values are reported as mean ± SE unless otherwise noted.

RESULTS AND DISCUSSION

Lateral patellar displacement was greater in subjects with patella alta compared to subjects with normal patellar position at 0° of knee flexion (85.4% ± 3.6% versus 71.3% ± 3.0 % of patellar width lateral to midline, $p < 0.007$). However, group differences were not observed between 20° and 60° of knee flexion. Lateral patellar tilt was also greater in subjects with patella alta compared to subjects with normal patellar position (21.6° ± 1.9° versus 15.5° ± 1.8°, $p = 0.028$). Again, group differences were not observed between 20° and 60°. Subjects with patella alta had systematically less patellofemoral joint contact area compared to subjects with normal patellar position. On average, these individuals had 19% less contact area in the range of knee flexion angles tested (231.2 ± 9.1 mm^2 vs. 286.7 ± 8.8 mm^2, $p < 0.001$; Figure 1). However, a maximum difference of 26% was observed at 20° of knee flexion (158.5 ± 10.6 mm^2 vs. 214.9 ± 10.2 mm^2).

The vertical position of the patella was positively associated with lateral patellar displacement ($r^2 = 0.365$, $p < 0.020$) and lateral patellar tilt ($r^2 = 0.274$, $p = 0.002$) at 0° of knee flexion. At knee flexion angles between 20° and 60° these associations were no longer significant. The vertical position of the patella was negatively correlated with patellofemoral joint contact area at all knee flexion angles tested (r^2 = 0.404 - 0.196, $p < 0.05$) with greater degrees of patella alta being associated with less contact area.

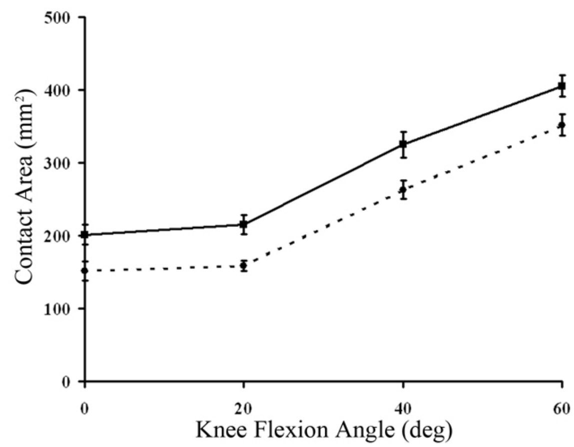

Figure 1. Total patellofemoral joint contact area was measured as a function of knee flexion angle in control subjects (solid line) and patients with patella alta (dotted line). There was a significant reduction in contact area in the patients with patella alta across all knee flexion angles tested.

CONCLUSIONS

Our data confirm the clinical assumption that patients with patella alta have greater degrees of patellofemoral joint malalignment compared to persons with normal patellar position. The reduced contact area observed in this population supports previous investigations that have found persons with patella alta demonstrate elevated patellofemoral joint stress (force per unit area) during functional tasks [2]. The association between patellar position and patellar malalignment was strongest at full knee extension, which suggests that this is a position of instability in this patient population.

REFERENCES

1. Insall J and Salvati E: *Radiology* **101,** 101-104, 1971.
2. Ward SR and Powers CM. *Clin Biomech* **19**, 1040-1047, 2004.

ACKNOWLEDGEMENTS

Financial support provided by a Promotion of Doctoral Studies level II award from the Foundation for Physical Therapy.

SCALING OF HUMAN LOWER EXTREMITY MUSCLE ARCHITECTURE TO SKELETAL DIMENSIONS

Samuel R. Ward, Laura H. Smallwood and Richard L. Lieber
Department of Orthopaedic Surgery, University of California and VA Medical Center, San Diego, CA; email: rlieber@ucsd.edu

INTRODUCTION

Modeling is widely used by investigators to understand neuromusculoskeletal disorders. Architectural properties of the muscles in these models are based on estimates from a relatively small sample of cadaveric specimens [1,2]. Given that the skeletal dimensions of modeled individuals will almost certainly vary from the skeletal dimensions of the cadaveric specimens, architecture must be scaled to match the skeletal dimensions of the modeled subjects. However, these assumptions have never been tested in humans. Therefore, the purpose of this study was to define the scaling functions of human architecture to measured skeletal dimensions.

METHODS

Eight formaldehyde-fixed cadavers were prepared by skinning and isolating the quadriceps and hamstring muscles. The mass of each muscle was measured after dissection and isolation from adjacent muscles. Fiber lengths and pennation angles were measured from three to five predetermined locations within each muscle using digital calipers and a goniometer. Sarcomere lengths for each muscle fiber bundle were determined by laser diffraction using the zeroth to first order diffraction angles as previously described [3]. To account for variations in muscle fiber length that occur during fixation, fiber bundle lengths were normalized by scaling measured sarcomere length to a standard sarcomere length for human muscle of 2.7 μm [4]. Using these normalized muscle fiber lengths, PCSA was calculated using the following equation [5]:

$$\text{PCSA (cm}^2\text{)} = \frac{\text{Mass (g)} \bullet \cos\theta}{\rho\ (\text{g/cm}^3) \bullet L_f\ (\text{cm})}$$

where ρ represents muscle density (1.112 g/cm^3) [6] and θ represents surface pennation angle.

Femur length (cm; distance from the greater trochanter to the lateral epicondyle) and body mass (kg) were measured as potential scaling factors for fiber length and PCSA, respectively. Since body mass was only available for five cadaveric specimens, statistics scaling PCSA based on mass was restricted to these samples. Simple linear regression was used to determine the slope and strength of the association between architectural measurements and skeletal dimensions.

RESULTS AND DISCUSSION

Muscle fiber length scaled poorly with femur length. In fact, only fiber length of the short head of biceps femoris scaled with femur length. In contrast, PCSA scaled well with body mass (Table 1). Although rectus femoris, vastus medialis and semitendinosus did not have statistically significant model fits, the PCSA of these two quadriceps muscles had good model fits and were close to achieving significance (*p-values* 0.05-0.06).

CONCLUSIONS

Although more data are needed to fully elucidate these scaling relationships, these data represent a more robust sample than previous studies estimating architectural values [1,2]. However, based on these data, it appears that PCSA scales well with body mass but muscle fiber length does not scale, in general to femur length.

REFERENCES

1. Friederich JA and Brand RA. *Journal of Biomechanics* **23,** 91-95, 1990.
2. Wickiewicz TL, *et al. Clinical Orthopedics and Related Research* **179**, 275-283, 1983.
3. Lieber RL, Fazeli BM, Botte MJ. *Journal of Hand Surgery (American Volume)* **15A**, 244-250, 1990.
4. Lieber RL, Loren GJ, Fridén J. *Journal of Neurophysiology* **71**,874-881, 1994.
5. Sacks RD and Roy RR. *Journal of Morphology* **173**, 185-195, 1982.
6. Ward SR, and Lieber RL. *Journal of Biomechanics* 2005; (in press).

ACKNOWLEDGEMENTS

Veterans Affairs Medical Center San Diego.

Table 1: Scaling relationships for muscle fiber length versus femur length and PCSA versus body mass.

	Fiber Length		**Physiological Cross-Sectional Area**	
Muscle	**Slope**	**r^2**	**Slope**	**r^2**
Rectus femoris	-0.033	0.012	0.307	0.749
Vastus lateralis	0.124	0.142	1.125*	0.994
Vastus intermedius	0.201	0.173	0.338*	0.793
Vastus medialis	0.046	0.025	0.566	0.764
Biceps femoris LH	0.352	0.260	0.424*	0.881
Biceps femoris SH	0.395*	0.571	-	-
Semitendinosus	-0.0441	0.005	0.035	0.027
Semimembranosus	0.0286	0.004	0.548*	0.925

*indicates significant regression model fit.

ROTATOR CUFF MUSCLE ARCHITECTURE: IMPLICATIONS FOR GLENOHUMERAL JOINT STABILITY

Samuel R. Ward[1], Laura H. Smallwood[1], Jan Fridén[2], and Richard L. Lieber[1]
[1]Department of Orthopaedic Surgery, University of California and VA Medical Center, San Diego, CA; email: rlieber@ucsd.edu
[2]Department of Hand Surgery, University of Göteborg and Sahlgrenska University Hospital, Göteborg, Sweden

INTRODUCTION

Muscle architecture provides insight into the excursion and force generating ability of muscles. Previous studies comparing the architecture of the shoulder rotator cuff muscles failed to normalize muscle fiber lengths to sarcomere length and, consequently, the position of shoulder fixation influenced previous fiber length and physiological cross-sectional area (PCSA) estimates. The purpose of this investigation was to determine the architecture of the four rotator cuff muscles using fiber lengths normalized to sarcomere length.

METHODS

Ten fresh-frozen shoulders were prepared by skinning, Formalin fixing, and rinsing in 1X PBS. The mass of each muscle was measured after sharp dissection from bony attachments. Fiber lengths and pennation angles were measured from three to five predetermined locations within each muscle using digital calipers and a goniometer. Sarcomere lengths for each muscle fiber bundle were determined by laser diffraction using the zeroth to first order diffraction angles as previously described [1]. To account for variations in muscle fiber length that may occur during fixation, fiber bundle lengths were normalized by scaling measured sarcomere length to a standard sarcomere length for human muscle of 2.7 µm [2]. Using these normalized muscle fiber lengths, PCSA was calculated using the following equation [3]:

$$\text{PCSA (cm}^2\text{)} = \frac{\text{Mass (g)} \bullet \cos\theta}{\rho\ \text{(g/cm}^3\text{)} \bullet L_f\ \text{(cm)}}$$

where ρ represents muscle density (1.112 g/cm^3) [4] and θ represents surface pennation angle.

One-way repeated measures ANOVAs and *post-hoc* T-tests with Bonferroni corrections were used for between muscle comparisons. Values are reported as mean ± SE unless otherwise noted.

RESULTS AND DISCUSSION

Masses were significantly different among all muscles. Subscapularis was the heaviest (101.8 g ± 11.5 g), followed by infraspinatus (78.0 g ± 7.5 g), supraspinatus (34.0 g ± 4.3 g) and teres minor (21.2 g ± 2.0 g) muscles.

Fiber lengths were significantly shorter in the supraspinatus muscle (4.50 cm ± 0.32 cm) compared to the infraspinatus (6.57 cm ± 0.33 cm), teres minor (6.10 cm ± 0.35 cm) and subscapularis (6.00 cm ± 0.47 cm) muscles (Figure 1). This is interesting in light of the fact that the supraspinatus and infraspinatus sarcomere lengths (3.23 µm ± 0.05 µm and 3.18 µm ± 0.06 µm) were significantly longer than the teres minor (2.80 µm ± 0.07 µm) or subscapularis (2.52 µm ± 0.09 µm) muscles. This implies that, at approximately neutral shoulder positions, the intrinsic length of the fibers is relatively long in these muscles. Secondly, it demonstrates that architectural studies that do not normalize muscle fiber lengths to sarcomere length significantly overestimate fiber lengths in supraspinatus and infraspinatus muscles.

The PCSA of supraspinatus (6.6 cm^2 ± 0.6 cm^2), infraspinatus (10.7 cm^2 ± 1.0 cm^2), teres minor (3.2 cm^2 ± 0.3 cm^2) and subscapularis (15.5 cm^2 ± 1.4 cm^2) muscles were all significantly different from each other (Figure 1).

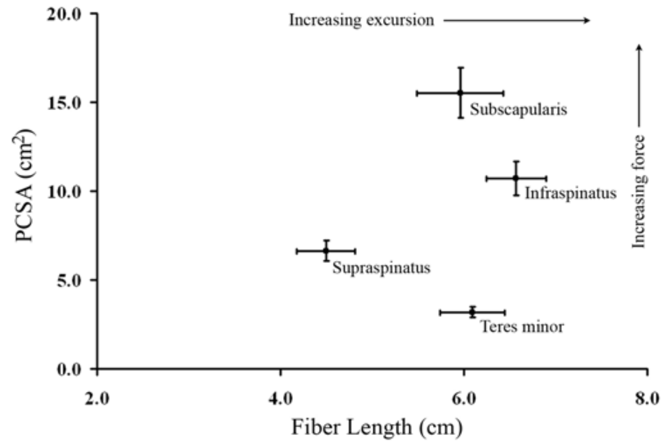

Figure 1. Scatter plot of normalized muscle fiber length versus PCSA. Supraspinatus muscle had significantly shorter muscle fiber lengths than the other three rotator cuff muscles and all muscles had significantly different PCSAs.

CONCLUSIONS

Based on architecture, subscapularis would produce the largest forces, while infraspinatus would operate over the widest range of shoulder positions. Surprisingly, supraspinatus has the shortest muscle fibers, indicating that its function as a glenohumeral stabilizer is limited to a relatively narrow range.

REFERENCES

1. Lieber RL, Fazeli BM, Botte MJ. *Journal of Hand Surgery (American Volume)* **15A**, 244-250, 1990.
2. Lieber RL, Loren GJ, Fridén J. *Journal of Neurophysiology* **71**,874-881, 1994.
3. Sacks RD and Roy RR. *Journal of Morphology* **173**,185-195, 1982.
4. Ward SR, and Lieber RL. *Journal of Biomechanics* 2005; (in press).

ACKNOWLEDGEMENTS

Veterans Affairs Medical Center San Diego.

THE EFFECT OF LOAD SCALING ON THE COORDINATION AND PERFORMANCE OF COUNTERMOVEMENT JUMPS

[1] Sarah E. Kruger, [1] Eric L. Dugan, [1] Philip B. Newell, and [2] Tim L.A. Doyle
[1] School of Physical Education, Sport, and Exercise Science, Ball State University, Muncie, IN 47306, USA
[2] School of Biomedical and Sports Sciences, Edith Cowan University, Perth, WA 6027, Australia
email: sekruger@bsu.edu web: www.bsu.edu/biomechanics/

INTRODUCTION

In recent years, numerous studies have been conducted using dynamic systems theory (DST) as a means to examine kinematics and stability in human movement patterns. While the performance aspects of the countermovement jump have been studied heavily [1,2], the effect of load scaling on the coordination of the jump squat movement is currently unknown. It is likely that the changes in jump squat performance are mirrored by changes in jump squat coordination. Therefore, the purpose of this project was to assess the coordination and performance of the jump squat movement for multiple loading conditions using the principles of DST.

METHODS

This study involved seventeen male participants ranging in age from 18 to 30 years (mean age 21.1 ± 2.6 years). The mean body mass was 94.5 ± 18.2 kg while the mean body height was 1.78 ± 0.06 m. All participants were free of lower body injury at the time of data collection. Each participant was required to undergo an initial familiarization session which was utilized to determine the participants' three repetition maximum (3 RM) for the squat movement. That 3 RM value was then used to predict the one repetition maximum (1 RM) which was necessary to establish the amount of weight required for each loading condition during the jump squat testing session. For that actual testing session, two jump squats were performed for each loading condition, 0-60% of each participants' 1 RM incremented by 10% for each trial. Two-dimensional video capture was used to assess kinematics and a force platform in combination with a linear position transducer was used to determine power.

RESULTS AND DISCUSSION

Regardless of the participants' strength background, the power output values decreased as the applied load was increased from 0-60%. No difference was found in the power values achieved during the lower loading percentages of 0-20%, which is significant because all but two participants reached their peak power by 20% of their 1 RM value. This finding indicates that peak power is produced with little to no applied load. The mean power values for all participants can be observed in Table 1.

However as the power outputs were decreasing, the mean absolute relative phase (MARP) values for the shank-thigh and thigh-trunk relationships were increasing. This increase in MARP signifies that a more out-of-phase relationship was occurring between segments and two segments working in greater opposition indicates that a change in coordination is taking place. The MARP values calculated from 0-30% were found to be statistically similar and can be identified as the more highly coordinated jump squat trials. The values achieved above 30% of 1 RM, confirm that as the applied load was increased that the participants' were shown to deviate from their normal jump squat movement pattern. The mean MARP values can also be found in Table 1.

CONCLUSIONS

More highly coordinated movement patterns and greater power output values were found to occur at lower percentages of load (0-30%). The lack of change observed from 0-30%, indicates that the participants were efficient in carrying out the jump squat movement at those percentages and that the movement pattern observed was the preferred pattern of motion. Since the results established for the unloaded condition were consistent with those found up to and including 30%, it can be concluded that jump squat performance was stable throughout that range of 1 RM percentages. On the whole, these results indicate that optimal jump squat performance is achieved at lower loading percentages and also suggest the existence of a relationship between power output and coordination.

REFERENCES

1. Wilson, G.J., et al. Medicine Science Sports Exercise, **25**(11), 1279-86, 1993.
2. Stone, M.H., et al. Journal of Strength and Conditioning Research, **17**(1), 140-147, 2003.

Table 1: The mean and standard deviation values of the power outputs and MARPs calculated for all participants.

Loading Percentage	Power Output (Watts)	Shank-Thigh MARP	Thigh-Trunk MARP
0	5521.00 ± 1346.83	100.47 ± 14.92	97.70 ± 6.38
10	5631.42 ± 1366.34	98.94 ± 12.61	97.84 ± 6.03
20	5536.93 ± 1250.01	102.91 ± 13.93	97.55 ± 5.06
30	5353.10 ± 1161.52	102.07 ± 11.75	97.56 ± 4.95
40	5232.36 ± 1183.10	105.42 ± 10.41	101.03 ± 5.21
50	4981.22 ± 1177.06	105.82 ± 14.48	101.78 ± 6.08
60	4765.56 ± 979.53	109.79 ± 10.08	102.07 ± 5.47

Kinematic Analysis of Kolman acrobatics in the High Bar Exercise

[1]Min-Chung Shen and Chien-Lu Tsai
National Taiwan Normal University, Taiwan
[1]Corresponding author; email: fast1123@mail.taipeilink.net

INTRODUCTION

The high bar exercise is one of the six events in men's artistic gymnastics. Kolman, which is an element with super E difficulty, is categorized into the flight-acrobatic element group in the high bar exercise (Figure 1) [1]. The well execution of the flight-acrobatics witch is difficult to perform is critical for getting a high score in a competition.

In this study, we used Kwon 3D analysis software to analyze the kinematical parameters of the images of Kolman acrobatics performed by an outstanding Taiwanese gymnast. The present results could provide some critical information to gymnasts to safely and perfectly perform Kolman.

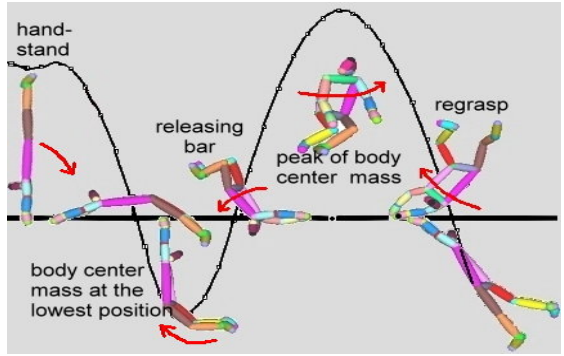

Figure 1: The schematic process of completing Kolman. The change of the position of the gymnast's body center mass was illustrated by the curve.

METHODS

We used two high speed cameras (Redlake) with 125Hz recording frequency and 1/625 sec shutter speed were used to synchronously record the 3D images of the Kolman acrobatics. Digitalization of the recorded images and analysis of the kinematical parameters of the gymnast's body segments were carried out by Kwon3D 3.1 Performance System [2]. The values of the parameters were analyzed with the Mann-Whitney test to reveal the kinematical characteristics of Kolman and the important factors which determine the successful execution of this acrobatics.

RESULTS AND DISCUSSION

In the period of gymnast swinging down from handstand, no parameter had significantly different values in the successful and failed Kolman. When the center-of-mass (COM) of gymnast's body arrived at the lowest position, the projected position of the COM in the failed Kolman was significantly farer away the projected position of the bar on the X-axis in the coordinate (0.24±0.02 m, P=0.034), comparing to that in the successful Kolman (0.17±0.05m). The value of the horizontal acceleration of the COM in the failed Kolman (-2.68±0.77m/s^2) was significantly smaller than that in the successful Kolman (1.19±1.56m/s^2) (P=0.034). The results indicated that the gymnast may plucked the bar too early and then had an excessive component of force along the horizontal direction of body movement while he failed to perform Kolamn (Table 1).

Table 1: Two kinematical parameters of the center-of-mass of gymnast's body when the center-of-mass arrived at the lowest position.

Kolman	Parameters	
	Projected position on the X-axis (m)	Horizontal acceleration (m/s^2)
Successful	0.17±0.05	1.19±1.56
Failed	0.24±0.02	-2.68±0.77
P value	0.034	0.034

The gymnast plucked the bar twice at different time points before released from the bar. The first pluck occurred when the gymnast's COM arrived at the lowest position; the second one occurred after the COM passed the lowest position. After the second pluck, the value of the horizontal acceleration of the COM in the failed Kolman (36.03±2.05m/s^2) was significantly higher than that in the successful one (30.42±2.28m/s^2) (P=0.034). That probably caused an excessive force to overfly the bar and then leaded to a drawback in regrasping the bar.

CONCLUSIONS

The timing to pluck the bar and the horizontal component of the bar-plucking force are likely to be the important tipping points to affect the performance of the gymnast who carries out the Kolman. We suggested that gymnasts and coaches should pay attention to the timing and the skills with which to pluck the bar for getting an adequate force to complete the whole acrobatics successfully.

REFERENCES

1. International Gymnastics Federation Men's Technical Committee. *Code of points for men's artistic gymnastics competitions,* 3-22, 113-132, 2001.
2. Kwon, Y. H. *The effects of body segment parameter estimation on the experimental simulation of a complex airborne movement*, Doctoral dissertation, Pennsylvania State University, 1993.

UPPER EXTREMITY KINETICS DURING WHEELCHAIR LEVER PROPULSION

Philip Requejo, Ernest Bontrager, and Sara Mulroy
Pathokinesiology Laboratory, Rancho Los Amigos National Rehabilitation Center, Downey, CA, USA
email: prequejo@larei.org, web: www.larei.org

INTRODUCTION

Lever-propelled wheelchairs (WC) have been described as more efficient and less physically demanding than pushrim-propelled WC [1]. Propelling with a lever mechanism is thought to provide a more effective transfer of power by placing the arms in a more natural segmental position and orientation [2]. In particular, those with limited energy resources or those with upper extremity pain/weakness may benefit from this alternative mode of manual WC ambulation. While demand on the upper extremities during standard WC propulsion has been documented [3,4], investigation of the upper extremity forces and moments magnitude and direction is required to better understand demands during ambulation with lever-propelled WC. The objective of this work was to determine the joint forces and moments during lever propulsion using a kinematic and kinetic model and an instrumented lever.

METHODS

A set of prototype levers (Wijit®, SuperQuad) were custom fabricated and the right lever was instrumented with foil strain gauges (Micro Measurements) mounted below the handles (Figure 1A). Reflective markers were placed at the lever shaft and on the right upper extremity and trunk to define the three-dimensional motion of the lever, hand, forearm, upper arm, and trunk segments. Subjects propelled a lever-mounted Quickie GPV® WC positioned on a stationary custom WC ergometer [3]. Data were recorded at a self-selected free and fast propulsion speed (level ground simulation) and at a simulated 8% grade. Wheel torque (2500Hz, A/D Data Translation) and three-dimensional motion of the right upper extremity and lever was recorded (50Hz, Vicon®) during each 10-sec propulsion trial. Reaction force normal to the lever was determined from wheel torque and lever length. Upper extremity joint kinematics was determined from the recorded motion data using a Euler/Cardan rotation sequence. A 4-segment 3D upper extremity inverse dynamics model of the right upper extremity was implemented (Visual3D) to calculate the joint forces and moments during lever propulsion. Onset of reaction force was used to determine the push and recovery phase timing of each propulsion cycle (%CYCLE).

RESULTS AND DISCUSSION

Mean hand reaction force (Figure 1B) and glenohumeral net joint forces (Figure 2) are shown for a 41 year old subject with T12 complete paraplegia (ASIA-A) for 17 years while propelling at free, fast, and graded propulsion. Vertical dashed lines represent the mean transition from the push to recovery phase. Peak lever forces occurred in the middle of push phase in free, the end of push phase in fast, and the beginning of push phase in graded propulsion. Peak posterior joint force was seen during the push phase in the free and graded

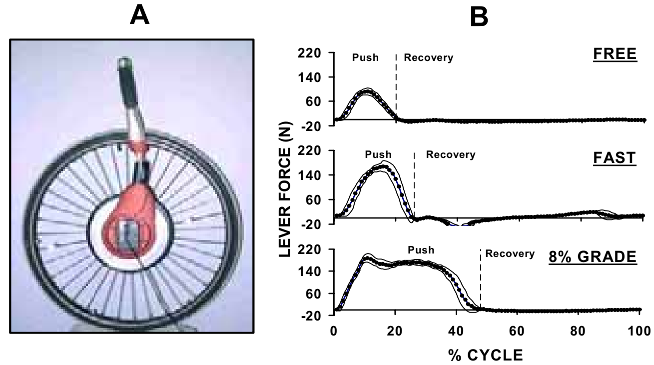

Figure 1: A) Instrumented Wijit® lever design. B) Lever reaction force during propulsion

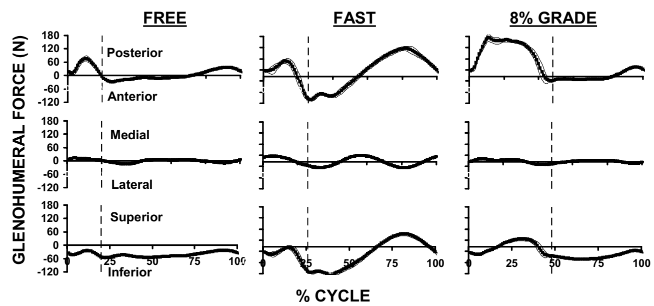

Figure 2: Glenohumeral net joint forces during lever propulsion.

propulsion while peak force was seen during the recovery phase of fast propulsion. Medial/lateral forces were minimal. Inferior joint forces were seen in the push phase of free and fast while superior forces were seen in the push phase of graded and the recovery phase of fast, indicating the increased effects of inertial loads at high velocities and cadence. The relative difference between posterior and upward joint forces reflected a shift in upper extremity demands from vertical to horizontal direction compared to previously reported push phase forces with a standard pushrim WC [3,4]. Within-subject comparison of the upper extremities demands during lever and standard WC propulsion will be studied. The joint kinetic model allows us to investigate these demands during lever WC propulsion.

REFERENCES

1. van der Woude, L. H., et al. *Am J Phys Med Rehabil* **80**(10), 765-777, 2001
2. van der Woude, L. H., et al. *J Rehabil Res Dev* **34**(3), 286-294, 1997
3. Kulig, K., et al. *Clin Orthop Rel Res,* **354**, 132-143, 1998
4. Kootz, A. M., et al. *J Rehabil Res Dev* **39**(6), 635-650, 2002

ACKNOWLEDGEMENTS

NIDRR grant H133E020732, SuperQuad®

EFFECT OF VISCOSITY ON LOCAL IMPEDANCE OF BIOLOGICAL GEL: MEASUREMENT WITH MICRO-VIBRATING ELECTRODE

[1]Takayuki Okamoto, [1]Shigehiro Hashimoto, [1]Takatsugu Furukawa, [1]Yusuke Morita, [1]Tomohiro Sahara, [1]Kenichi Yamasaki, [1]Hideo Kondo, [1]Wataru Ikeda, [2]Hajime Otani and [2]Hiroji Imamura
[1]Biomedical Engineering, Osaka Institute of Technology, Osaka, Japan; email: hasimoto@elc.oit.ac.jp
[2]Dept. of Thoracic and Cardiovascular Surgery, Kansai Medical University, Japan

INTRODUCTION

A biological body includes various electrolytes. Some studies tried to analyze the structure of organs with measurement of local electric impedance [1, 2]. To avoid the change of structure by movement of ions with a direct current, an alternating current is applied to measure electric impedance of electrolyte solutions. High impedance of a micro-electrode disturbs to distinguish signal of local impedance at specimen from that of the other part of the electric circuit. In the present study, a new methodology to measure local mechatronic property has been proposed, and measurement system has been designed with a micro-vibrating electrode. The effect of viscosity on local impedance of the biological gel was evaluated with the proposed system.

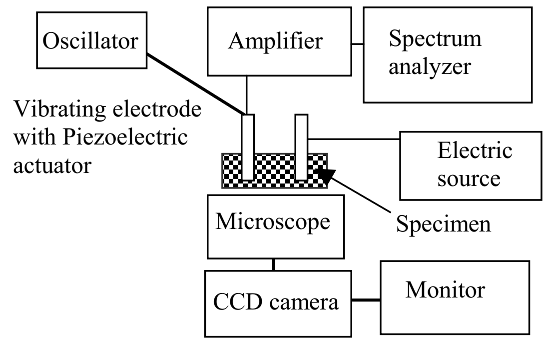

Figure 1: Measurement system.

METHODS

The impedance between two electrodes soaked in an electrolyte solution varies with the distance between them. When the distance oscillates sinusoidally with a mechanically vibrating electrode, the impedance oscillates, too. The oscillation corresponds to the variation of impedance of the local space, where the electrode is vibrating. The variation was analyzed with spectrum and the amplitude at the corresponding frequency was measured. The electrode was made of a glass micro-capillary filled with a potassium chloride aqueous solution (3 mol/L). A platinum wire was inserted in the center of the capillary to decrease impedance of the electrode. The diameter of the tip of the capillary is 0.01 mm. One of the electrodes was vibrated with a piezoelectric actuator. The measurement system consists of an oscillator, an amplifier, a spectrum analyzer, a phase-contrast optical microscope, a charge-coupled device camera, and a monitor (Fig. 1).

The manufactured system was applied to measure electrolytes: the sodium chloride aqueous solution, the potassium chloride aqueous solution, a quail egg, and human blood. Variation was made in the viscosity of the solution with dextran. The viscosity was measured with a cone and plate viscometer. The measurement has been performed at 25 degrees centigrade.

RESULTS AND DISCUSSION

The experimental data show that impedance increases with the decrease in the concentration of sodium chloride in the solution from 9.0 to 0.1 percent, and with the increase in the amplitude of vibration of the electrode to 0.023 mm. The results also show that impedance depends on the variation of electrolytes and that the ratio of impedance between the potassium chloride (0.1 percent) and sodium chloride (0.1 percent) is 1.15, which can be approximated to 1.21 calculated from electric conductivity of chronological scientific tables. The experiment with a quail egg shows that the impedance is independently measured of that of the surroundings, when the electrode stuck into the yolk is vibrating: while the impedance varies with the concentration of electrolyte in the surroundings, when the electrode is not vibrating.

The signal was also picked up as a function of viscosity, when the electrode was vibrated in the sodium chloride aqueous solution including dextran. The impedance increases with viscosity at higher frequency (>100 Hz), and with frequency at higher viscosity (>0.01 Pa s).

The result with human blood shows that impedance of the blood varies with coagulation process.

CONCLUSIONS

The experimental data show that the designed system is effective to detect the effect of viscosity on local impedance of biological gel.

REFERENCES

1. Tsai JZ, Cao H, *IEEE Transactions on Biomedical Engineering*, **47**, 41-47, 2000.
2. Wang Y, Haynor DR, Kim Y, *IEEE Transactions on Biomedical Engineering*, **48**, 1390-1401, 2001.
3. Grosse C, Tirado M, *IEEE Transactions on Instrumentation and Measurement*, **50**, 1329-1333, 2001.

ACKNOWLEDGEMENTS

This work was supported in part by a Grant-in-Aid for Scientific Research from the Japanese Ministry of Education, Culture, Sports, Science and Technology.

EMG BASED TRIGGERING AND MODULATION OF STIMULATION PATTERNS FOR FES-ASSISTED AMBULATION – A CONCEPTUAL STUDY

[1]Anirban Dutta, [2]Rudi Kobetic and [1,2]Ronald Triolo, PhD
[1]Departments of Biomedical Engineering and Orthopaedics, Case Western Reserve University,
[2]Motion Studies Laboratory, Louis Stokes VA Medical Center; email: adutta@case.edu

INTRODUCTION

The surface electromyogram (sEMG) from the rectus-femoris is a good indicator of the gait-speed in able-bodied subjects [1], and may be used to temporally scale functional electrical stimulation (FES) patterns to change the speed of assisted gait [2]. The purpose of this study was to investigate the potential of utilizing the sEMG as both a proportional and discrete control source for FES-assisted ambulation after incomplete spinal cord injury (ISCI). The ability to modulate volitional sEMG was measured in two subjects with ISCI and four able-bodied volunteers to determine its suitability as a proportional command input for FES to paralyzed synergists. The muscle activations during over-ground walking of the able-bodied subjects were further analyzed to determine whether the sEMG can provide a consistent trigger that could replace of the mechanical switches currently employed during FES-assisted ambulation.

METHODS

Two subjects with incomplete spinal cord injury (age 22 and 36 yrs, C7 ASIA C and T4 ASIA D respectively) and four able-bodied volunteers (ages 25 to 54 years) participated in the study. Subjects were positioned on a Biodex System3 dynamometer (Biodex Medical Systems, USA) with the knee fixed isometrically at 30 degrees of flexion while surface recording electrodes were positioned over the rectus-femoris. The sEMG was pre-amplified by a CED 1902 preamplifier (Cambridge Electronic Design, England) and low-pass (1000 Hz) filtered before sampling at 2200 Hz by AT-MIO-64F-5 data-acquisition card (National Instruments, USA). The rectified sEMG was normalized by the average value during maximum voluntary contraction (MVC) before modulating the vertical position of a tracking signal displayed to the subjects on a computer monitor. Subjects were instructed to track a rectified 0.01 Hz sinusoidal target signal of amplitude 0.7. A set of five, 100-second trials were taken for each subject and the results were ensemble averaged. Mean square tracking error (MSE) between the target and sEMG modulated pursuit signals were computed separately for the ascending and descending phases of each trial. Able-bodied subjects then participated in walking trials in which linear envelopes of the sEMGs were derived bilaterally from the tibialis, quadriceps, hamstrings, triceps surae and gluteal groups with the VICON motion analysis system (Oxford Metrics Ltd., Oxford, UK). Principal component analysis was performed to reduce the order of the data [3]. Analysis was then performed in the eigen-space of the sEMGs for pattern identification.

RESULTS AND DISCUSSION

The MSE for the ISCI subjects were 6.72 % MVC during phases of increasing muscle activity, and 9.69 % MVC for the relaxation phases. The MSE for the able-bodied subjects were 6.39 and 5.59% MVC for the increasing and relaxation phases, respectively.

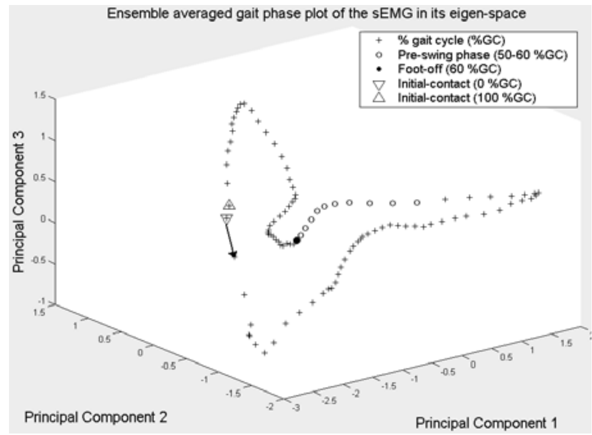

Figure 1: Gait sEMG trajectory in its eigen-space

The first four principal components (PC) of the sEMG during able-bodied gait accounted for about 98% of the variance (%VAF) in the data. **Figure 1** shows the sEMG in its eigen-space defined by the first three PCs (90.67 %VAF). The data-points representing the pre-swing phase of the gait cycle were clustered together in a pattern and may be appropriate for use as a gait event detector. The presence of such a pattern of volitional muscle activations remains to be confirmed in a set of partially paralyzed muscles in individuals with ISCI.

CONCLUSIONS

ISCI subjects performed as well as the able-bodied subjects during increasing muscle activity, while their performance degraded during relaxation of the muscle, implying that the sEMG may potentially be a proportional control source. Furthermore, a consistent pattern of muscle activation exists during the pre-swing phase in the able-bodied subjects. If such a pattern of volitional muscle activation exists during the switch activated FES assisted gait in ISCI subjects, then it might be used to replace the manual mechanical triggers and better integrate and coordinate stimulation with their intact voluntary function. This is the topic of current investigation.

REFERENCES

1. Nene A, et al. *Gait Posture* 9 **(1)**, 1-9, Mar, 1999.
2. Kobetic R, et al. *IEEE Trans Biomed Eng* **2(2)**, 66-79, Jun, 1994.
3. Wootten ME, et al. *J Orthop Res* **8(2)**, 247-258, Mar, 1990.

ACKNOWLEDGEMENTS

The research was supported by the Merit Review project B2933R from the Rehabilitation Research and Development Service of the United States Department of Veterans Affairs.

GRAVITY-INDUCED TORSION AND VERTEBRAL ROTATION IN IDIOPATHIC SCOLIOSIS

[1] Clayton Adam, [1]Mark Pearcy and [2]Geoff Askin
[1]Queensland University of Technology, Brisbane, Australia
[2]Mater Children's Hospital, Brisbane, Australia

INTRODUCTION

Vertebral rotation is an important aspect of spinal deformity in scoliosis, associated with ribcage deformity (rib hump). Although both lateral curvature and axial rotation appear to increase together in progressive scoliosis, the mechanisms driving vertebral rotation are not clearly established and it is not known whether lateral curvature precedes rotation, or vice versa. This study investigates the hypothesis that intravertebral (within the bone) rotation in idiopathic scoliosis is caused by growth in the presence of gravity-induced torsions, the twisting moments generated by gravitational forces acting on the scoliotic spine.

METHODS

The twisting moment T_p acting at an arbitrary point P on a three-dimensional spinal curve is given by

$$T_p = M_p \cdot \hat{a},$$

where $M_p = r \times F$ is the total moment due to gravity force F acting at (vector) distance r, and $\hat{a}$ is the tangent to the spinal curve at P (Figure 1).

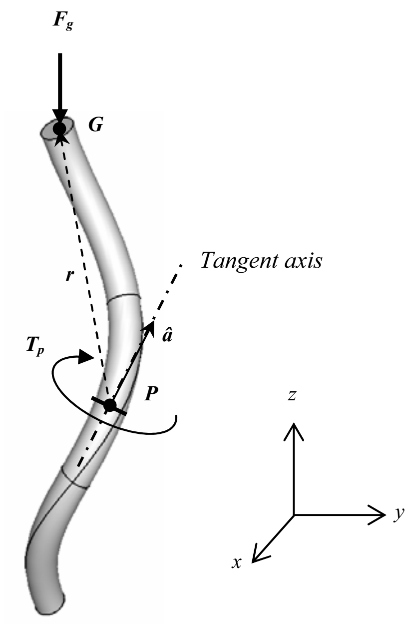

Figure 1: Torque T_p about a 3D curved column due to gravity loading F_g

Standing radiographs for five idiopathic scoliosis patients were used to define three-dimensional curves representing the approximate axes of rotation of each spine, running along the anterior edge of the neural canal from T1 to S1. The equilibrium equations above were then solved to calculate gravity-induced torsions exerted by head and torso weight about the spinal axes for each patient. Intravertebral rotations were measured for the same patients using Aaro & Dahlborn's technique [1] with reformatted computed tomography images in the plane of superior and inferior endplates of each vertebra. The gravity-induced torsion curves were compared with intravertebral rotation measurements to see whether gravity-induced torsion is a likely contributor to intravertebral rotation.

RESULTS AND DISCUSSION

Gravity-induced torques as high as 4 Nm act on the spines of idiopathic scoliosis patients due to static body weight in the standing position. Maximum intravertebral rotations (for a single vertebra) were approximately 7°. There appears to be general agreement between the measured intravertebral rotations and profiles of gravity-induced torsion along the length of the spine (Figure 2). Rotation measurements confirm the finding of previous authors [2] that maximum intravertebral rotations occur at the ends of a scoliotic curve (with little relative rotation at the apex), and this finding is consistent with the gravity-induced torsion profiles calculated.

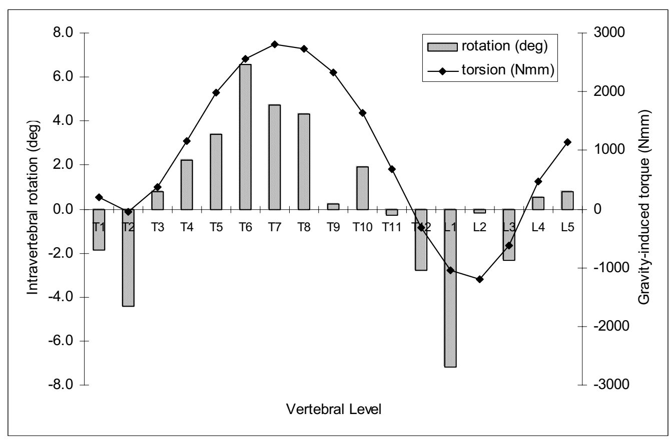

Figure 2: Comparison of gravity-induced torsion and measured intravertebral rotation for a single patient

CONCLUSIONS

Gravity-induced torsion is a potential cause of vertebral rotation in idiopathic scoliosis. Since the spine must be curved in three-dimensions (out of plane) to produce such torques, vertebral rotation would be expected to occur subsequent to an initial lateral deviation, suggesting that coronal curvature precedes axial rotation.

REFERENCES

1. Aaro S & Dahlborn M. *Spine* **6**, 460-7, 1981.
2. Birchall D et al. *Spine* **22**, 2403-7, 1997.

COMPUTER SIMULATION OF MOTORCYCLE-CAR ACCIDENT

Cheng-Yu Wu, Saiwei Yang,
Institute of Biomedical Engineering, National Yang Ming University, Taiwan
email: swyang@ym.edu.tw, web: http://rehab.ym.edu.tw

INTRODUCTION

Motorcycle is a highly mobile transportation vehicle, due to least or no add-on protective device for the motorcyclist the accidence is to result in severe spinal injury or fetal death. Head, knee and leg are reported over 45% of injury rate [1]. The accident reconstruction presentation is necessary to inspect the rationale and mechanism of accident occurring and responsibility due, For the purpose of injury mechanism and protection devices development computer simulation has been used extensively [2, 3, 4, 5].

The purpose of this study was to construct a light weight motorcycle-automobile accident computer simulation to understand the impact locations and forces on the body segments for the accident presentation and protective device development.

METHODS

A motorcycle weighted 100Kgs and a car weighted 1200Kgs were modeled using ADAMS 11.0 (MSC software Co., USA). The motorcyclist was simulated as Hybrid III50% and constructed using LifeMod (Biomechanics Research Inc, USA). In addition, **Standard Pendulum-Hybrid III** impact experiment was used to validate computer construction of the dummy. Four common collision types were studied namely head-on, 90 degrees lateral impact, 45 degrees side-swipe, and bumper-rear-end collision.

.

RESULTS AND DISCUSSION

The pendulum-dummy simulation showed well correspondence in acceleration-time slope. In the head-on collision simulation the motorcycle had speed of 35 Km/hr and car was 55 Km/hr at the time of collision. The head was hit on the windshield first with impact force of 7586N and then the head hit the ground first in prone position with force of 15,874 N (at time of 0.85 second)(Fig. 1). For the 90 degree side collision, the motorcycle speed was 34 Km/hr and car was35 Km/hr, the motorcyclist had the arm and head hit on the front hood with impact force of 6976N and then had the shoulder hit on the ground in supine position first then turned to site wall(Fig. 2). The impact on the scapular was 10,033N (at 0.75 second). For the 45 degree-side collision, the speed of motorcycle and car was 35 and 55 Km/hr, respectively. The head hit on the engine hood first (at 0.93 second) and then fell across the hood with head on the ground (650N, 1.19 second) in prone position. For the bumper to rear collision, the speed of motorcycle and car was 22 and 62 Km/hr, respectively. The buttocks were hit on the hood first with impact force of 9507N, then thrust anteriorly to the ground with butt hit first (Fig. 3). The force on the butt was 11320N and 9391N on the head at the time of impact to the ground.

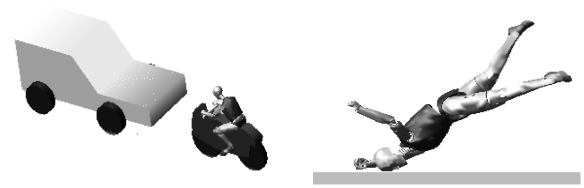

Fig. 1 : Head-on collision

Fig. 2 : 90 degrees side impact

Fig. 3: Bumper to rear end collision

CONCLUSIONS

The simulations showed the head was the most injured part, especial impacted to the ground after crashed by a car in any direction. 90 degree side collision resulted in shoulder severe injury when impacted to the ground. The bumper to rear end collision created a large momentum and resulted in sacrum-back trunk severe injury.

This simulation demonstrates a useful means for the motorcyclist garment development.

REFERENCES

1. Bradbury A, et al. *Scotland. Health Bulletin*. 51(2):86-91, 1993 Mar.
2. Nieboer JJ, et al.*TNO Crash-Safety Research Centre Delft*,Nov. 4-7,1991
3. McGuan S. *SAE 930226*,1993.
4. Wang YO, et al. *SAE* , 1999-01-0719.
5. Giavotto V, et al. *International Journal of Crashworthness,* Vol. 3, No. 5, pp. 328-336.,1998.

ACKNOWLEDGEMENTS

This study was supported by National science Council of R.O.C. (NSC91-2622-E010-006, 93-2213-E010-008).

The difference of net muscle torque of lower extremity by using different body segment parameter in gymnast

[1] Wei-Hua Ho [2]Ching-Wen Hu [1] Tzyy-Yuang Shiang, [3]Chan-Chin Lee
[1]Taipei Physical Education College, Taiwan; email: afa@tpec.edu.tw
[2]Nanshan High School, Taiwan [3]Tzu-Chi medical center, Taiwan

INTRODUCTION

Body segment parameter (BSP) is an important data of biomechanics research, due to the difference of races, age, sex, fitness level, sports event and other factors of subjects, which would lead to disparity between reality and research results. Consequently, the purpose of this study is to compare and discuss the difference caused by using different body segment parameters models and ground reaction force to calculate net muscle torque during gymnasts during vertical jump.

METHODS

Four Taiwanese elite (2 male and 2 Female) participated in this study. Kistler force platforms and Kodak high speed video camera (10K Hz) were used to obtain the ground reaction force and kinematics data during vertical jump, then inverse dynamics formula (Enoka,2000) and three BSP models were applied to calculate the net muscle torque of joint of lower extremity. Three BSP models included cadaver method (Dempster, 1955), gamma-ray method (Zasiorsky 1983), and young Taiwanese male from MRI method（Ho, 2002）, and the subject's individual BSP which also established by MRI method.

$$SEE = \sqrt{\frac{\sum (x' - x)^2}{n}} \quad \text{...........} \ (1)$$

Those subjects individual BSP was used as the standard to calculate Standard Estimate Error (SEE) value and compare the difference of ankle, knee and hip joint kinetic data among the BSP models (equation 1).

RESULTS AND DISCUSSION

Table 1 show that the male and female gymnast SEE value of ankle, knee and hip joint net muscle torque during vertical jump. The joint net muscle torque of lower extremity determined from MRI method and gamma-ray method was similar. But, the joint net muscle torque determined from the cadaver method was obviously larger than other BSP models. Especially, the SEE of hip joint net muscle torque was 7.4902 and 6.4252 for both male subjects. In the past, the most often used approach to establish segment inertial properties was the data obtained from elderly male cadavers (e.g. Dempster, 1955 et al.). But the results of this study show that Dempster's cadaver model has the largest SEE value when determine the joint net muscle torque. Therefore, appropriate BSP model should be chosen when the subjects' individual BSP is not available.

CONCLUSIONS

It is very important to choose the appropriate BSP model when doing human subject study which can reduce the inaccuracy of results. Researches should consider the similarity between the subjects of study and the subjects of BSP model, such as sex, age, race, living style, diet, fitness level, and representative of samples.

REFERENCES

1. Dempster, W.T. (1955). Space Requirements of the seated operator. Wright-Patterson Air Force Base, Ohio, (*WADC-TR-55-159.*)
2. Enoka, R. M. (2002). *Neuromechanics of human movement*. Champaign, IL: Human Kinetics.
3. Wei-Hua Ho, Tzyy-Yuang Shiang, and Chan-Chin Lee (2004). The study of body segmental parameters of Taiwanese young people from MRI, *Journal of Medical and Biological Engineering*, 24: page 1-6.
4. Zatsiorsky, V., & Seluyanov, V. (1983). The mass and inertia characteristics of the main segmental of the human body, *Journal of Biomechanics*, 8B, pp.1152-1159.

Table 1: The comparison of SEE value of ankle, knee and hip joint net muscle torque among different BSP models.

Variables	Researcher	Method	Male 1	Male 2	Female 1	Female 2
Ankle joint net muscle torque	Dempster(1955)	Cadaver	1.0934	0.4616	0.7889	0.2823
	Zatsiorsky(1983)	Gamma ray	0.0713	0.1066	0.0472	0.0566
	Ho(2004)	MRI	0.0911	0.1705	0.0521	0.1194
Knee joint net muscle torque	Dempster(1955)	Cadaver	1.9306	1.6489	1.0374	0.8853
	Zatsiorsky(1983)	Gamma ray	0.0503	0.1535	0.3602	0.1048
	Ho(2004)	MRI	0.0909	0.1775	0.2787	0.0965
Hip joint net muscle torque	Dempster(1955)	Cadaver	7.4902	6.4252	2.9255	4.5742
	Zatsiorsky(1983)	Gamma ray	0.7052	0.3849	0.7386	0.4083
	Ho(2004)	MRI	1.0394	0.5931	0.8005	5.6605

HOW DOES OBESITY AND GENDER AFFECT FOOT SHAPE AND STRUCTURE IN CHILDREN?

[1] Annaliese Dowling, [1] Julie Steele and [2] Louise Baur
[1] Dept of Biomedical Science, University of Wollongong, Wollongong, NSW Australia,
[2] Dept of Paediatrics and Child Health, The Children's Hospital, Westmead, NSW Australia; email amd02@uow.edu.au

INTRODUCTION

Obesity is a prevalent disease of today's society which has many negative consequences which affect an individual's quality of life. One system of the human body which is affected by obesity is the musculoskeletal system as it must endure the added mass and adiposity on a daily basis. It has been suggested that pathologies of the lower extremity may be exacerbated in obese individuals as a consequence of increased mechanical loading of the lower limbs by their additional mass (1-3).

As the feet are the foundation for stance and dynamic tasks, it is postulated that the increased loading associated with obesity would place the feet at risk of pathology. Obese children have been found to display an increased plantar contact area compared to non-obese children (3-5). In addition the foot shape and dimensions of obese children's feet were found to be different from children of normal mass. However, this was found in a small sample of 10 obese children therefore it is unclear whether this relationship exists in a larger sample of obese children. These children displayed significantly larger foot shape dimensions for 17 out of the 26 measurements recorded. These children's feet were broader, taller and thicker in comparison to the non-obese children (7). Therefore the purpose of this study was to determine whether the foot shape and foot structure characteristics of obese children's feet could be replicated in a larger population of children and whether it was moderated by gender.

METHODS

Forty-five obese (30 girls and 15 boys; 9.2 ± 1.4 years; BMI 24.98 ± 2.6 kg/m^2) children in the 7 to 12 year age group were matched to 45 non-obese children (9.2 ± 1.4 years; BMI 16.34 ± 1.2 kg/m^2), for gender, age and height. Height and weight were measured to calculate body-mass index and classified according to international cut-off values. Right and left static footprints were obtained using a pedograph to calculate the Arch Index of each child's feet to characterise foot structure. Twenty-six foot shape variables (lengths, breadths and circumferences) for both the right and left feet were recorded to characterise foot shape (8). Paired *t*-tests revealed 10 significant differences between the right and left limbs of the 90 subjects. Therefore, a random foot was selected for each subject via a random number generation for each subject before further analyses in order to limit any bias in the data.

Means and standard deviations were calculated for the total sample for Arch Index derived from the footprints and the foot shape values. After testing for normality and equal variance, two-way analyses of variances (ANOVA; $p<0.05$) were calculated using the random foot data to determine whether there were any main effects of age and/ or gender on the dependent variables.

RESULTS AND DISCUSSION

The mean Arch Index values obtained for the obese and non-obese children were 0.23 ± 0.05 and 0.17 ± 0.08, respectively. While standing the obese children generated significantly greater plantar contact area indicating flatter feet compared to their non-obese counterparts, plantar contact area however was not affected by gender. Similarly, obese children have significantly greater foot dimensions for 17 of the 26 variables ($p \leq 0.05$). The non-obese children displayed greater mean values for only two ankle dimensions although this was not significant. However, gender did affect the shape of the foot in children regardless of body type. In general the foot shape parameters were greater for the boys compared to the girls.

From these results, it is evident that obese children have significantly broader, higher, and thicker structural features in their feet compared to their non-obese counterparts. The results in this study encompass a larger population of children and similar trends are showing through this data set more clearly than Dowling & Steele's (2001) and have greater mean foot shape values in comparison which may reflect the increasing prevalence of obesity in children. However, no significant interactions between gender and obesity were found for the dependent variables.

CONCLUSIONS

Gender did affect the foot shape and structure in children regardless of their body type. The mechanism behind the obese child's foot shape and structure is currently unknown therefore more research is warranted examining the bone density and bone stresses to determine definitely whether obesity is detrimentally affecting the musculoskeletal architecture of obese children.

REFERENCES

1. Gehlsen GM, et al. *Res Q Ex Sport* **51**:3, 478-85, 1980.
2. Messier SP, et al. *Foot Ankle* **15**:1, 29-34, 1994.
3. Messier SP, et al., *MSSE* **20**:5, 501-5, 1988.
4. Bordin D, et al. *Minerva Paediatrica* **53**:1, 7-13, 2001.
5. Riddiford-Harland DH, et al. *Int J Ob* **24**:5, 541-4, 2000.
6. Dowling AM, et al. *Int J Ob* **25**:6, 845-52, 2001.
7. Dowling AM, et al. Proceedings of 5th Footwear Symposium, Zurich., Switzerland, p30, 2001.
8. Parham K et al., Anthropometry of the foot and lower leg of US Army Soldiers, Fort Jackson S.C.1992.

ACKNOWLEDGEMENTS

I would like to acknowledge funding from Australian Research Council (SPIRT scheme).

EFFECT OF WALKING SPEED IN CHANGE OF THE PEAK PLANTAR PRESSURE DISTRIBUTION

[2]Yi-Ling Chiu, [1]Saiwei Yang, [2]Fen-Ling Kuo, [1]Chia-Chi Lin, and [1]Yen-His Chen
[1]Institute of Biomedical Engineering, National Yang Ming University, Taiwan
[2]Institute of Rehabilitation Science and Technology, National Yang-Ming. University, Taiwan
Email: swyang@ym.edu.tw, Web: http://rehab.ym.edu.tw

INTRODUCTION

The plantar pressure pattern has been used as the evaluation tools for foot disorders, the numerical values of peak pressure in heel and metatarsal areas are usually critical, however, these local maximum values are highly affected by the walking speed, measurement sensing hardware as well as software used. By using an in-shoe pressure measurement system, Kernozek found that the plantar peak force tended to increase with gait speed mainly in the heel region, and almost no changes in the forefoot regions [1]. Hsiang et al [2] used a force plate and found out the path of center of gravity changed in faster walking speed which also resulted in an adverse effect on the variability and the reliability of the gait pattern. White et al [3]also found that increasing the walking speed induced higher peak ground reaction forces in loading response of a gait cycle but the reaction forces decreased linearly in mid stance, and no profound changed in push off phase. Zhu's study showed that as walking cadence increased, pressure-time integrals and foot-to-floor contact durations decreased, and peak plantar pressures increased [4].

The objective of this study was to find out the effect of walking cadences to the plantar pressure by an innovative pressure platform-type system with higher sampling rate.

METHODS

Ten healthy young volunteers without any foot pain or disorders, five for each male and female gender with mean ages of 22 ± 3 years old and body weight of 61 ± 13 kgs were recruited. The subjects were asked to walk along a 10M pathway with barefoot in three speeds normal walking speed, and 30% higher and lower of normal one on the RS-Scan 1M Footscan high frequency platform system (Rsscan Int. Belgium). Ten successful foot-print data of each cadence were collected for further analysis in nine interesting region namely toe mask (T1) five metatarsal head masks (M1,M2,M3,M4,M5), and two heel masks (H1, H2).

RESULTS AND DISCUSSION

The average self-path normal walking speed was 98.23 $\pm$ 4.53 steps/min, 30% lower was 72.46 $\pm$ 4.22 steps/min, and 30% higher was 132.57 $\pm$ 6.37 steps/min. The maximum peak plantar pressure was 17.02 N/cm^2 (±3.39), 21.02 N/cm^2 (±3.65), and 21.79 N/cm^2 (±4.05) for lower, normal, and higher walking speed, respectively. These peak values were at the left medial heel region. The pressures were linearly increased as walking speed increased, except at the left forefoot region which showed highest at the speed of normal walking (Figure1 and 2). The contact time at each marked region was decreased as the walking speed increased. The maximum contact times of all subjects were at the right 3rd metatarsal head. The impulses were also decreased as the speed increased but the maximum values were at left 2nd metatarsal head for all subjects.

These results are similar to that of referred studies except the plantar pressure at the left forefoot regions. Inman reported that the flexion angle at the loading response reduced by 67% when walked at 60m/min and by 38% at 120 m/min in comparison with 90 m/min. This study showed similar result at the left foot during midstance to push off response. This may imply taht, the dominate leg (left foot in this study) is used to control the walking speed path which may result in changing of ground reactions

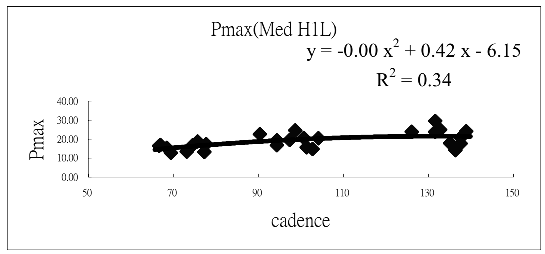

Fig. 1: The relationship of Peak pressure and cadence at left foot medial heel region

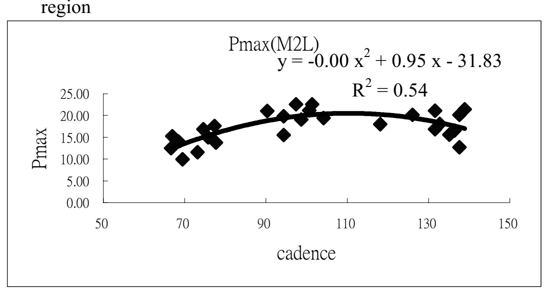

Fig. 2: The relationship of Peak pressure and cadence at left foot second metatarsal head

CONCLUSIONS

The results showed that with second order linear regression the peak plantar pressure was basically increased as the walking speed increased except the left forefoot region which had its highest value at the normal speed. The contact time and impulse were decreased as the speed increased.

REFERENCES

1. Kernozek TW, et al. *Foot & Ankle International*, 0198-0211, 1996
2. Hsiang SM, Chang CC. *Safety Science*, 40:639-657, 2002
3. White SC, et al. C.A. *Gait and Posture*, 4:206, 1996
4. Hongsheng Zhu HS, et al. *Arch Phys Med Rehab*, 76:1000-5, 1995
5. Inman VT, etal. *Human walking*, Baltimore, Willians and Wilkins Co. 1981

ACKNOWLEDGEMENTS

This study was supported by National science Council of R.O.C. (NSC93-2622-B010-003)

IMMEDIATE EFFECTS OF AN INCLINED BOARD AS A TRAINING TOOL FOR THE TAKEOFF MOTION OF THE LONG JUMP

Hiroyuki Koyama, [1] Yuya Muraki, [1] and Michiyoshi Ae [2]
1. Doctoral Program of Health and Sport Sciences, 2. Institute of Health and Sport Sciences
University of Tsukuba, Japan, koyama@lasbim.taiiku.tsukuba.ac.jp

INTRODUCTION

Various methods have been used to learn and improve long jump techniques in training. Since simplifying practice conditions with the use of auxiliary tools is effective in improving techniques, jumpers frequently use auxiliary training methods. An inclined board from which a jumper takes off may be one of the most frequently used technical training tools. Although there have been some investigations on the characteristics of the takeoff motion from an inclined board, changes in the takeoff motion immediately after the use of an inclined board have not been investigated thoroughly. Therefore, the purpose of this study was to investigate immediate effects of the use of an inclined board on the takeoff motion of the long jump.

METHODS

Eight male long jumpers from the varsity athletic club were videotaped with two high-speed VTR cameras (250 Hz) set perpendicular to the runway. Four different kinds of jumps were performed: normal long jump, long jumps on upward inclined boards with different inclinations (2.5 and 5.0 deg), and jumps on a raised flat board (0 deg, but at height of 5 cm). To investigate immediate effects of the boards on the takeoff motion, pre and post trials were performed by subjects, using their normal technique, before and after the jumps from the boards. Two-dimensional coordinates of the body segments were reconstructed by using reference markers set on both sides of the runway. Linear and angular kinematics of joints and segments and the location of the center of gravity (CG) were calculated. To test differences between pre and post trials, dependent t-tests were used with a significance level set at 5%.

RESULTS AND DISCUSSION

Jump distance for the post trial was significantly longer than that for the pre trial (post, 6.59±0.29 m; pre, 6.48±0.38 m; p<0.05). Table 1 shows the CG velocity at touchdown (TD) and toe-off (TO) of the takeoff phase. There was no significant difference in the vertical velocity at the TD and TO between pre and post trials. The horizontal velocity at the TD and TO for the post trial was significantly greater than that for the pre trial, and the rate of decrease in the horizontal velocity during the takeoff phase for the post trial was significantly smaller than that for the pre trial. No significant difference between the pre and post trials was observed in the ratio of the vertical velocity at the TO to the reduction in the horizontal velocity during the takeoff phase. However, six of the eight subjects enhanced the ratio for the post trial (116.1±10.3%) in comparison to that for the pre trial. These results indicate that the jumpers in the post trial were able to convert the horizontal velocity to the vertical velocity more effectively than in the pre trial, regardless of the higher approach velocity for the post trial.

Figure 1 shows the average thigh and shank angular velocities of the takeoff leg during the takeoff phase. Although there were no remarkable differences in patterns of the thigh and shank angular velocities during the takeoff phase, the forward rotation of the thigh just after the TD for the post trial was faster than that for the pre trial. Moreover, in the middle of the takeoff phase for the post trial, the thigh rotated faster than it did for the pre trial. An intersection of the thigh and shank angular velocities indicated the instant at which the takeoff leg knee flexed to its maximum. The intersection for the post trial appeared significantly earlier than that for the pre trial, resulting in less flexion of the takeoff leg knee for the post trial (post, 28.6±4.1 deg; pre, 32.4±2.8 deg; p<0.05) and a larger knee joint angle at the maximum knee flexion for the post trial (post, 134.6±4.9 deg; pre, 130.6±6.5 deg; p<0.05). The reduced knee flexion of the takeoff leg for the post trial was effective in exerting large extension torque because leg extension force abruptly decreased for a knee joint angle less than 130 degrees. These results reveal that inclined boards can induce immediate effective changes in the takeoff motion for the long jump, and that they would be an appropriate training tool for learning and improving the takeoff techniques of the long jump.

Table 1 Mean values of horizontal and vertical velocity (HV, VV) of the CG at the touchdown (TD) and toe-off (TO) of the takeoff, decreasing rate of the horizontal velocity during the takeoff phase, and ratio of the vertical velocity at toe-off to the reduction in the horizontal velocity during the takeoff phase (V-H ratio) for the pre and post trials

		Pre		Post		Difference
		Mean	SD	Mean	SD	(*p < 0.05)
TD	HV_{TD} (m/s)	8.89	(0.35)	9.01	(0.31)	post > pre *
	VV_{TD} (m/s)	-0.50	(0.17)	-0.61	(0.12)	ns
TO	HV_{TO} (m/s)	7.42	(0.47)	7.69	(0.36)	post > pre *
	VV_{TO} (m/s)	3.11	(0.16)	3.03	(0.14)	ns
	ANG_{TO} (deg)	22.8	(1.4)	21.5	(1.2)	pre > post *
Decreasing rate of HV (%)		-16.6	(2.7)	-14.6	(2.0)	pre > post *
V-H ratio		2.17	(0.36)	2.34	(0.20)	ns

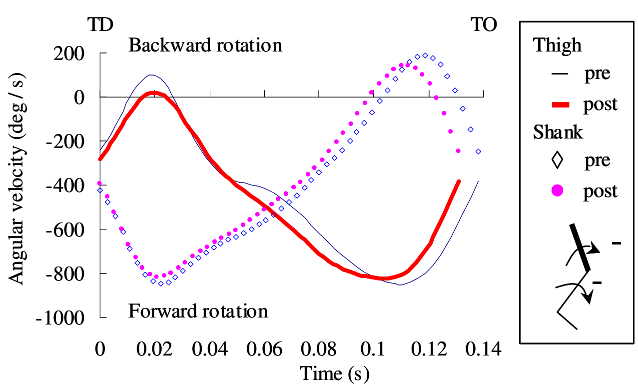

Figure 1 Averaged patterns of angular velocities of the thigh and shank of the takeoff leg during the takeoff phase for the pre and post trials

KINETIC ANALYSIS OF EACH HAND DURING GOLF SWING WITH USE OF AN INSTRUMETED GOLF CLUB

Sekiya Koike, Hitoshi Shiraki, Norihisa Fujii and Michiyoshi Ae
University of Tsukuba, Ibaraki Pref., Japan
Institute of Health and Sport Sciences, koike@taiiku.tsukuba.ac.jp

INTRODUCTION

The roles of the upper extremities during golf swing are transfer of the energy generated by the lower extremities into a golf club and control the club head to place in a hitting point. Since the golf club is manipulated by both hands in swing motion, the upper extremities and the club make a closed multi-segment loop. Therefore it is impossible to determine the forces and moments acting on the club by each hand with only visual information of motion of the club. The purpose of this study was to investigate three dimensional kinetics of each hand using an instrumented golf club to measure forces and moments exerted on the grip handle of the club.

METHODS

Figure 1 shows the structure of the instrumented grip handle. Eleven pairs of strain gages were attached on the outer diameter of an aluminium light weight rod. These strain gages were used to calculate: 1) The torsional moment acting on the grip axis between the hands; 2) The bending moments; and 3) The tensile and compressive axial forces. The output of the sensors was converted into the values of forces and moments by resolving the static equilibrium equations. Two spherical markers with negligible-mass shafts were attached on the club shaft for the purpose of measuring the orientation of the moving club. Two professional golf players volunteered to participate in this study as subjects. They swung three kind of clubs such as driver, number 5 Iron club and sand wedge. The positions of markers of the body segment endpoints and of the clubs were captured with VICON motion analysis system operating at 250Hz. A personal computer was used to store the strain gauge signals that were amplified through dynamic strain amplifiers. The sampling frequency of the force and moment data collection was 500Hz.

RESULTS AND DISCUSSION

Figures 2 (a) and (b) show the forces exerted by each hand with respect to subject B during forward swing motion with the number 5 Iron club. These values are expressed in a swing club coordinate system Σ_{swc}, where the unit vectors of Σ_{swc} were defined as follows: z_{swc} is a normal unit vector of the swing plane, y_{swc} is a unit vector from club head to grip-end and x_{swc} is a unit vector perpendicular to these vectors. The horizontal axes of the figures denote normalized time from the beginning of forward swing motion (0%) to the impact (100%). The x_{swc}-axial force of the head side hand decreased slightly toward 30% time and increased gradually in the period of about 70% time, and then decreased rapidly toward the impact. The x_{swc}-axial forces of the hands showed inversion patterns approximately with respect to sign. The result indicates that the forces acted as couple force and did not accelerate the rotational motion along the swing plane just before impact. The y_{swc}-axial force of the head side hand kept constant value by 70% time and increased dramatically and reached the peak at approximately 90% time, and then it kept the peak value toward the impact. On the other hand, the y_{swc}-axial force of the grip-end side hand showed a different pattern, increased gradually from 80% time to the impact. The resultant force increased gradually toward the impact due to increase in centrifugal force.

CONCLUSIONS

To investigate kinetics of each hand during golf swing motion, an instrumented golf club with strain gauges was used to solve the closed multi-segment loop problem. From the results, the kinetic responses of the two players showed considerably different patterns with use of the clubs. The ability to quantify acting forces and moments of each hand during golf swing has the potential to (1) understand the mechanics of swing motion, (2) provide useful information for prediction of injury due to inappropriate swing.

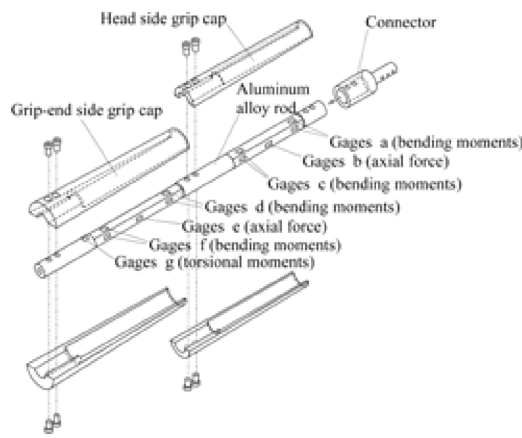

Figure 1: The structure of the instrumented grip handle.

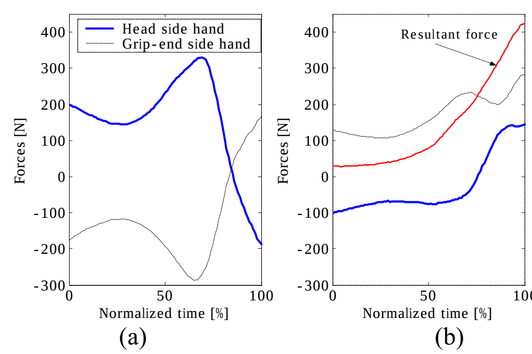

Figure 2: Kinetic responses of each hand during swing motion with the number 5 Iron club. (a): The forces along x_{swc}-axis. (b): The forces along y_{swc}-axis.

REFERENCES

Koike, S. et al. Kinetics of the upper extremities during baseball batting, *Proceedings of ISB XIX*, Dunedin, New Zealand, Abstract 212, 2003.
Koike, S. et al. An instrumented bat for simultaneous measurement of forces and moments exerted by the hands during batting. *The Engineering of Sport* 5, **2**, 194-200, 2004.

EVALUATION OF UPPER EXTREMITY MUSCLE ACTIVITY DURING MANIPULATION IN ROBOT-SIMULATED TASK ENVIRONMENTS

[1,2] H.A.M. Seelen, [1] R.P.J. Geers, [1] Y.J.M. Janssen-Potten
[1] Institute for Rehabilitation Research, Hoensbroek, The Netherlands
[2] Rehabilitation Foundation Limburg, Hoensbroek, The Netherlands
ham.seelen@irv.nl

INTRODUCTION

Arm-hand function (AHF) is essential in activities of daily living. In patients suffering from cervical spinal cord injury (C-SCI) AHF is severely impaired. During rehabilitation they have to learn to use their residual capacities to (partially) compensate for the loss of function [1]. In some cases muscle transpositions are carried out to restore a specific arm or hand function. Many AHF test use a time score as a critical factor. However, such tests do not provide insight in either the quality of movements, nor in the mechanisms that govern compensation of function loss and the associated changes in muscle co-ordination that occur in C-SCI patients [2].

A 3D robotic arm (HapticMaster, FCS Control Systems BV, NL) has been developed with which movement-specific force may be exerted on a subject performing an upper extremity task, thus controlling the movement trajectory/position, velocity and acceleration of the arm (figure 1).

The aim of the present study is to investigate the potency of the HapticMaster (HM) in simulating activities of daily living (ADL) and to investigate the effects of specific changes in the applied force and resistance on muscle activation patterns during upper extremity task performance.

Figure 1: Experimental setup

Figure 2: Cylinder grip

METHODS

15 healthy volunteers, (m/f=6/9; mean age 24.6 yr, range 21-30 yr; mean height 1.76 m, range 1.50-2.00 m) participated. Subjects, while seated, performed 2 standardised ADL tasks, i.e. lifting a full soft drink can vertically over a distance of 30 cm (phase 1) and back (phase 2) using a cylinder grip (task A) (figure 2) and moving a small light weight object horizontally over a distance of 30 cm from left to right and back using a 3-point grip (task B). Task C and D were identical to A and B as to spatial displacement, but objects' masses were simulated by the HM. Each task was performed 8 times (trials).

Activity of 21 (focal and postural) muscles of the arm and trunk was recorded using surface EMG (sample rate: 1000 Hz; Sample time: 7s. Also object displacement was recorded using an IR-camera system (PRIMAS, Delft Motion Analysis, Delft, NL). Data were analysed off-line using MATLAB (The Math Works Inc., Natick, Mass). EMG data were full wave rectified, low-pass filtered (2nd order Butterworth filter) and normalised to the movement cycle (figure 3). Within-subject signal reproducibility and between-subject signal similarity were assessed using intraclass correlation coefficients (ICC) across trials. Similarity between muscle activation patterns between task A/C and B/D was assessed by calculating correlation coefficients (R) for all muscles.

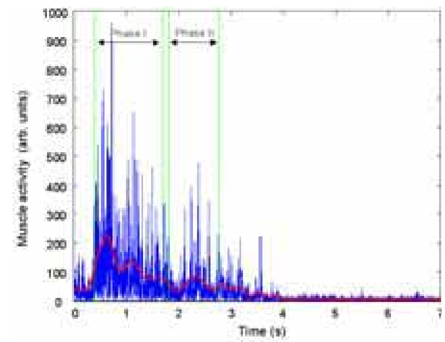

Figure 3: Example of EMG recording

RESULTS AND DISCUSSION

Within-subject reproducibility, expressed as mean ICC, was higher than 0.80 in 77.4% of all cases. ICC values in task A and C were generally higher than in task B and D. ICC values associated with between-subject reproducibility were higher than 0.60 in 79.8% of all cases. Mean R-values were above 0.60 in 81.0% of cases for task A and C and in 95.2% of cases for task B and D.

CONCLUSIONS

During the 'real world' ADL tasks and the HM simulated tasks similar muscle coalitions were activated. This finding corroborates the idea that the HM may be used to develop and adequately simulate upper extremity tasks conditions with which arm muscle function may be evaluated. This is especially important in those persons whose arm function is impaired and who receive rehabilitation treatment to improve their arm-hand function performance. Next to the evaluation aspects the HM may offer the opportunity to train arm performance in patients with sensorimotor deficits caused by impairments of the central nervous system.

REFERENCES

1. Seelen H.A.M. (1997). *Reorganisation of postural control in spinal cord injured persons.* PhD-thesis. University Maastricht
2. Van Tuijl J. et al. (2002). *Spinal Cord* **40**, 51-64.

ACKNOWLEDGEMENTS

The authors wish to thank M. van Kroonenburgh PT, F. Brendel PT and B. von Birgeln PT for their assistance during data collection.

EFFECTS OF AFO-ASSISTED ANKLE ANGLE POSITION ON DYNAMIC KNEE STABILITY IN BRAIN INJURED AND SPINAL CORD INJURED PATIENTS

[1)] D. Beckers , [1)] A. Waelen, [1,2)] H.A.M. Seelen
[1)] Rehabilitation Foundation Limburg, Hoensbroek, The Netherlands
[2)] Institute for Rehabilitation Research, Hoensbroek, The Netherlands
ham.seelen@irv.nl

INTRODUCTION

In stroke patients and patients with an incomplete spinal cord injury (SCI) normal gait is affected. One of the problems is the lack of ankle control due to either paresis of the ankle dorsiflexors and/or spasticity of the calf muscles, causing either primary toe-strike or, in mild paresis, drop foot. Another phenomenon observed is (often extreme) knee hyperextension in the latter part of the stance phase, often aggravated by weakness of the quadriceps muscles. This knee hyperextension can be viewed as an attempt to stabilise the knee to facilitate push-off. However, next to the kinematic inefficiency, this hyperextension will, over time, cause severe damage to the joint at its ligaments. Whereas it has been shown that the use of an ankle foot orthosis (AFO) does not impair lower leg muscle function [1], the effect of AFO use on knee dynamics has not been investigated systematically. Aim of the present study was to assess the effect of AFO-assisted ankle angle position on knee motion and walking symmetry in patients with unilateral dropfoot or pes equinus due to stroke or incomplete SCI.

METHODS

14 subjects (4 incomplete SCI and 10 stroke patients; m/f=8/6; mean age 48.5 (13.6)) participated. All subjects were able to walk unaided for at least 20 m. Gait was evaluated in three AFO conditions: no-AFO (NA), AFO with an ankle angle of 0° dorsiflexion (AA0), and AFO with an ankle angle of 10° dorsiflexion (AA10). Each patient used a custom-built AFO. A hinge at the ankle level facilitated the use of several (fixed) ankle angles (figure 1).

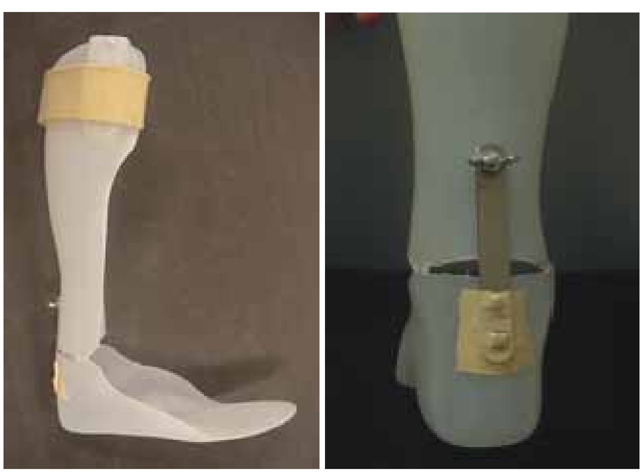

Figure 1: Ankle foot orthosis with variable ankle angle.

Gait timing parameters were recorded using bilateral insole pressure sensors (IDM, RIS GmbH, Berlin, Germany). Sample rate was 50 Hz. Sample time was 1 minute. Bilateral knee joint movement was recorded using 2 biaxial electrogoniometers (Penny & Giles, XM110, Biometrics, Gwent, UK). Data were recorded at 100 Hz on a portable data logger (Porti-24/ASD, TMS Int., Enschede, NL) (see figure 2).

Figure 2: Equipment used.

Maximum knee extension and knee flexion ratio (FR) between affected an unaffected limb were calculated. Data were analysed off-line using Matlab software (The Math Works Inc., Natick, Mass). Statistical analyses included Friedman two-way analysis by ranks. Post-hoc multiple comparison was performed using Wilcoxon signed ranks tests.

RESULTS AND DISCUSSION

Average maximum knee extension at the affected side was 4.8° larger in condition NA relative to condition AA10 ($p<0.01$), whereas differences between NA and AA0 (NA: 3.3° more knee extension) as well as between AA0 and AA10 (AA0: 1.7° more knee extension) failed to attain significance levels. As to walking symmetry, ankle angle manipulation did not lead to significant changes in either the FR between AFO conditions or in the stance phase duration between conditions.

CONCLUSIONS

Changing the ankle angle of an AFO may be used in stroke patients and in incomplete SCI patients suffering from either dropfoot or pes equinus to reduce harmful knee hyperextension during gait. Optimal active knee control is present when the knee remains (slightly) flexed. In contrast, gait symmetry seems not to be influenced by manipulation of the AFO ankle angle in these patients. Although other AFO parameters may also influence knee hyperextension during gait, like stiffness of the AFO and heel height, a stiff AFO or a high heel may reduce or even prevent normal rocking of the foot during the stance phase, thus reducing walking ability. This trade-off between different AFO characteristics should always be kept in mind.

REFERENCES

1. Geboers J. et al. *Arch Phys Med Rehabil* **83**,240-245, 2002.

A BIOMECHANICAL ANALYSIS OF SPIKE MOTION FOR DIFFERENT SKILL LEVELS OF MALE VOLLEYBALL PLAYERS

[1]Walter Quispe Marquez, [1]Masanao Masumura, [2]Michiyoshi Ae
[1]Master Program of Health and Sport Sciences, [2]Institute of Health and Sport Sciences
University of Tsukuba, Japan

PURPOSE

The purpose of this study was to three-dimensionally analyze the spike motion for world elite and Japanese university volleyball players, and identify differences in swing motion to obtain information for coaching spike techniques.

METHODS

Eighteen male volleyball players (1.94±0.07 m, 85.7±8.67 kg) participated in this study as subjects. Nine were national players from Canada, Serbia Montenegro, and Japan, and seven university players of Japan. Spike motions of Serbia Montenegro and Japanese players were recorded during two official games of the World League (2002, Osaka) with two high-speed VTR cameras (250 Hz, 1/1000 sec). Canadian players and Japanese university players' spike motions were captured with Vicon Motion System 612 (eight cameras, 120 Hz) using 39 reflexive markers. 3D data from VTR were reconstructed using a DLT method. Data smoothing was done with a Butterworth digital filter and the Wells and Winter method at optimum cutoff frequency of 5~12Hz. The trial in which the fastest right hand velocity at impact was obtained for each subject was used for further analysis. The subjects were grouped by the right hand velocity as a criterion. The five fastest and the five slowest players were referred to as the top and lower groups, respectively. Upper arm joint angle and joint angular velocity were primary variables for comparison of spike motions. Right hand height and velocity at the impact, trunk kinematics and relative velocity between segment end points were also computed. The data were normalized from the toe-off to the impact as 100% and averaged every 1%. Right hand velocity at the impact was related to the other variables by Pearson's correlation coefficient with $P<0.05$. Differences between the two groups were tested with t-test at $p<0.05$.

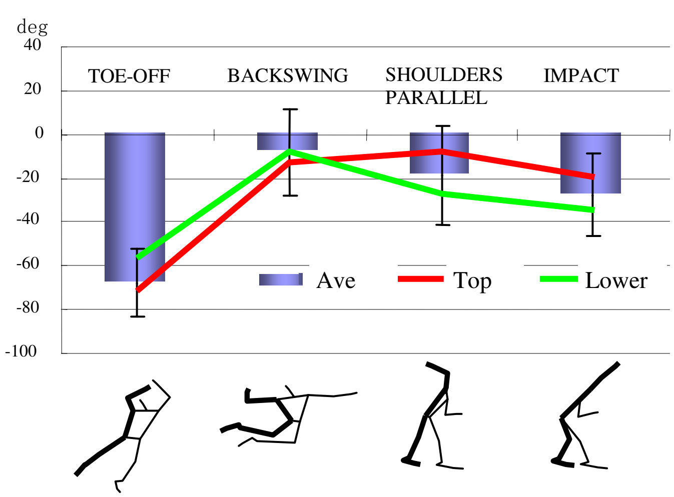

Figure 1: Right shoulder horizontal adduction/abduction angle.

RESULTS AND DISCUSSION

Right hand velocity at the impact was significantly related to the shoulder abduction and horizontal adduction angles at the toe-off.

Figure 1 shows the right shoulder horizontal add/abd angle at the events of spike motion for the average, top and lower groups. During the backswing phase following toe-off, the top group elevated the upper arm. However, the lower group abducted the right shoulder considerably smaller than the top group. Figure 1 indicated that the lower group started the horizontal abduction earlier and greater than the top group. Moreover, the horizontal adduction at the impact was greater in the lower group than that of the top group. The right shoulder was accelerated through the forward rotation of the trunk, and then, the upper arm horizontal adduction was retarded in the top group in the forward swing, whereas the lower group precociously adducted the shoulder mentioned above.

Figure 2 shows the change in angular velocity of the right elbow joint after the toe-off. Although there was no difference in the pattern of the elbow angular velocity before the start of rapid shoulder abduction (indicated by a vertical dotted line in figure 2), after the start, the elbow angular velocity for the top group became negative, and then increased rapidly toward the impact. This indicated that the lower group continued extending the elbow after the start of shoulder abduction while the top group could use stretch-shortening cycle to increase the elbow extension velocity.

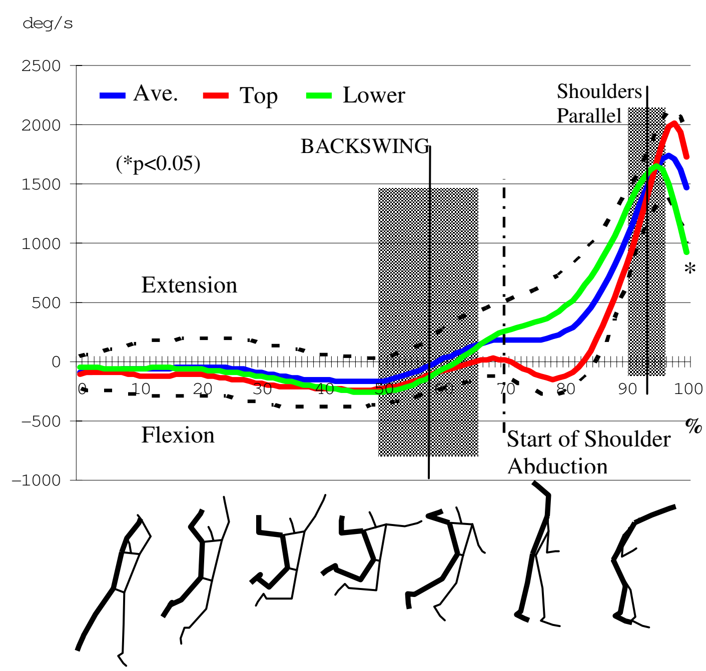

Figure 2: Right elbow angular velocity from toe-off to impact moment. Ave=average

EFFECTS OF GAIT TRAINING WITH TREADMILL AND SUSPENSION IN CHILDREN WITH SPASTIC CERERBRAL PALSY

[1]Rong-Ju Cherng, [1]Chuan-Fei Liu, [2]Tien-Huey Liu, [2]Rong-Bin Hong, [3]Fong-Chin Su
[1]Department of Physical Therapy, College of Medicine, National Cheng Kung University, Tainan, Taiwan,
[2]Department of Rehabilitation Medicine, Chi-Mei Medical Center,
[3]Institute of Biomedical Engineering, College of Engineering, National Cheng Kung University, Tainan, Taiwan
email: rjc47@mail.ncku.edu.tw

INTRODUCTION

Independent ambulation is a big concern for the family of the children with cerebral palsy (CP). How to improve the children's ambulatory ability is considered the primary focus of most therapeutic interventions. The purpose of the study was to examine the effect of a 12-week gait training with treadmill and suspension on the gross motor function measure and gait performance in children with spastic CP.

METHODS

Eight children with spastic CP met the inclusion criteria and participated in the study. Children were pair matched based on their functional category with Gross Motor Function Classification System and then randomly divided between two groups AB and BA. Children in the AB group first received regular therapeutic exercises except gait training for 12 weeks then received treadmill and suspension gait training for another 12 weeks. The sequence of treatment program was reversed for children in the BA group.

A commercial treadmill (Trackmaster TM210AC) capable of slow speeds with a minimum speed of 0.1 m/s and able to increase its speed with an increment of 0.1 m/s was used for gait training in this study. Suspension was achieved with LiteGait (LiteGait, Scottsdale, AZ). A harness was provided to subjects for weight suspension and safety during gait training. One therapist sat behind the child and corrected for foot placement during gait training. The regular therapeutic exercises were based on traditional pediatric exercises. The treatment duration of treadmill gait training or therapeutic exercises was 2-3 times a week and 30 minutes a time.

Gaitrite electronic walkway system (GAITRite, CIR. Systems Inc. Clifton, NJ 07012) was used to measure the gait temporal-spatial characteristics of the subjects in the study. Other than temporal-distance parameters of gait, muscle tone, selective motor control, gross motor function measure were assessed and measured three times: before treatment (baseline), after the first phase of treatment and after the whole session of treatment.

RESULTS AND DISCUSSION

The gait performance of each subject at three measurement times is presented at Figure 1. The results showed that gait velocity, and stride length improved after gait training with treadmill and suspension. No change of cadence was noted. As the gross motor function measure was concerned, the treadmill gait training effect was significant on the sub-scores of standing, walking and the total score. The effect on sitting sub-score was only marginal (p = 0.0587).
Our results are consistent with previous preliminary studies or case reports of nonambulatory patients [1-3], showing that the task-oriented gait training is a promising treatment program.

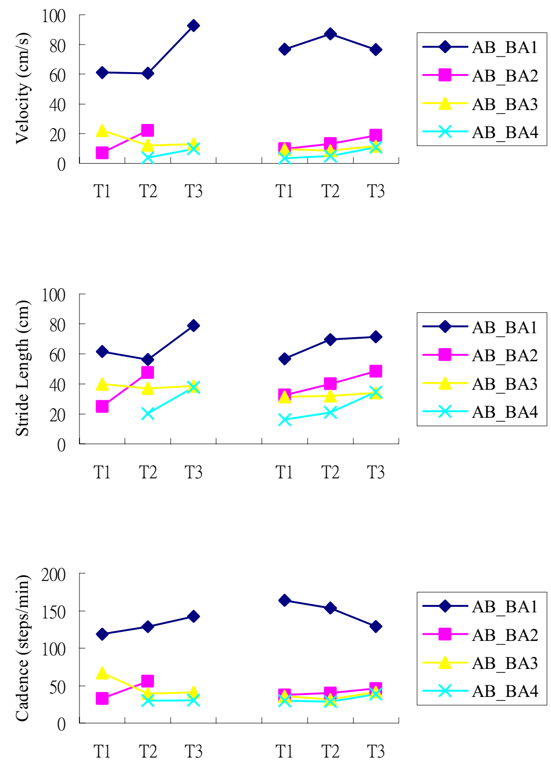

Figure 1: Gait performance of each subject at three measurement times

CONCLUSIONS

Children with spastic CP benefit from gait training with treadmill and suspension with partial weight support in stride length, gait velocity and certain gross motor functions. It is suggested that gait training with treadmill and suspension with partial weight support is a promising treatment for children with spastic CP.

REFERENCES

1. Richards CL, et al.. *Pediatr Phys Ther* **9**, 158-165, 1997.
2. Schindl MR, et al.. *Arch phys Med Rehabil* **81,** 81:301-306, 2000.
3. Day JA, et al.. *Pediatr Phys Ther* **16**, 106-113, 2004.

ACKNOWLEDGEMENTS

This project was partially supported by NSC 92-2218-E006-003.

EFFECT OF A DUAL TASK ON WALKING PERFORMANCE IN PRESCHOOL CHILDREN

Rong-Ju Cherng, Ling-Yin Liang and Yang-Ting Young
Department of Physical Therapy, College of Medicine, National Cheng Kung University, Tainan, Taiwan
email: rjc47@mail.ncku.edu.tw

INTRODUCTION

In many situations, children at preschool need to perform motor or cognitive tasks concurrently while walking. For example, they may be talking, carrying a lunch tray, listening to the teacher's instructions, etc. when they walk. Therefore it is important to understand the potential effect of concurrent tasks on walking. The purpose of the study was to examine the influence of a concurrent motor or cognitive task on walking performance in typically developing preschool children.

METHODS

Fifty-five typically developing 4- to 5- year-old (M = 60.1 months, SD = 6.9) preschool children, 28 boys and 27 girls participated in the study. Each child performed 3 trials for each of the following 5 test conditions: free walking (single task), walking while carrying an empty tray (concurrent motor task – easy), walking while carrying a tray with 7 marbles inside the tray (concurrent motor task – hard), walking while performing a forward digit rehearsal task (concurrent cognitive task – easy), walking while performing a backward digit rehearsal task (concurrent cognitive task – hard). The sequence of the conditions was randomly determined for each child. The digit rehearsal task was adjusted individually according to each child's digit span assessed before the experiment. Several measures of walking performance were collected, three of which were reported here: velocity (cm/s), stride length (cm), and cadence (steps/min). Repeated measures one-way ANOVA was used to analyze the differences of walking performance among single task: free walking, and dual motor task, and dual cognitive tasks. Two-way ANOVA (2 task x 2 level) was used to further analyze the dual-task cost interaction between type and difficulty level of secondary tasks. A level of 0.05 was used for statistical significance.

RESULTS AND DISCUSSION

Table 1 presents the walking performance under single and dual task conditions. There were significant difference of walking performance (velocity, stride length and cadence) between free walking and motor dual or cognitive dual tasks. However, there was no significant difference of walking performance between motor dual or cognitive dual condition. Figure 1 presents the dual-task cost of gait velocity between motor and cognitive dual tasks. The results showed a significant level effect ($p<0.001$) and the interaction effect of the type and level of the secondary tasks ($p<0.001$). However, there was no significant difference of the type effect (n.s.)

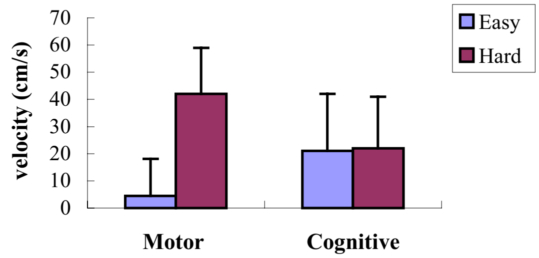

Figure 1: Dual task interference cost of gait velocity

The reaction time of easy and hard cognitive task at single task test condition was significantly different with 1.16 s and 1.43 s respectively ($F=23.929$, $p<0.000$). However, the reaction time of easy or hard cognitive task was not significantly different between at single task and at dual task. (1.16 s vs. 1.23 s; $F=2.666$, $p=0.105$ and 1.43 s vs. 1.69 s; $F=3.121$, $p=0.080$ respectively).

Combining the results of reaction time and the walking performance, we proposed that the reason of no difference of gait velocity between easy and hard cognitive task is that the interference of the cognitive task on gait velocity may be a fixed amount, not affected by its difficult level. Carrying a tray (motor dual task) needs visual monitoring, which may share a common visual motor control of gait. Carrying a tray with marbles in it needs more load of visual motor control than carrying an empty tray. Therefore, the interference effect was bigger with hard level than easy level of the task. Future studies are needed to investigate which phases or events of gait cycle are affected by the dual motor or dual cognitive tasks.

CONCLUSIONS

Children of 4- to 5-year-old have difficulty maintaining walking performance by decreasing their walking efficiency (decreasing speed, stride length and cadence) while concurrently performing other motor or cognitive task.

Table 1: Walking performance under single and dual task conditions

	Single Task Free Walking	Dual Task-Motor Task			Dual Task-Cognitive Task		
		Easy	Hard	Total	Easy	Hard	Total
Velocity (cm/s)	85.86 ± 22.33	82.54 ± 20.30	42.69 ± 17.88	62.62 ± 27.62	64.68 ± 18.79	62.77 ± 19.87	63.73 ±19.28
Stride Length (cm)	81.74 ± 9.30	79.81 ± 6.75	51.38 ± 9.99	65.60 ± 5.93	70.5 ± 8.06	68.44 ± 9.27	69.49 ± 7.87
Cadence (steps/min)	125.62 ± 22.55	125.28 ± 18.95	97.90 ± 21.57	111.59 ± 24.44	110.43 ± 22.73	108.29 ± 23.66	109.36 ± 23.12

SHORTENING VELOCITY OF HUMAN PLANTAR FLEXORS IN VIVO AND ITS RELATION TO CONTRACTION INTENSITY AND KNEE ANGLE

Kazushige Sasaki and Naokata Ishii
Department of Life Sciences, University of Tokyo
email: cc47710@mail.ecc.u-tokyo.ac.jp

INTRODUCTION

To measure the intrinsic shortening velocity of human muscles in vivo, we have recently developed a technique, the principle of which is based on the 'slack test' developed by Edman [1] for single muscle fibers. Using this technique, the unloaded shortening velocity (V_0) of contractile component can be determined without an effect of the recoil of series elastic component (SEC).

The purpose of this study is to measure V_0 of human plantar flexors at varied levels of contraction intensity. In consideration of the biarticular structures of medial and lateral gastrocnemius muscles, we also examined if a change in knee angle affects V_0.

METHODS

Eight male subjects participated in the present study. Each subject performed voluntary contractions on a custom-designed ankle dynamometer, with which high angular velocities (up to 20 rad s^{-1}) can be attained. During the testing session, the subject's right foot was attached firmly to the footplate by using inelastic straps.

Isometric plantar flexion force was measured during maximum voluntary contraction (MVC) at an ankle angle of approximately 10-15º dorsiflexion. Then, while the subject performed an isometric contraction with a given force level (10%, 50%, and 80% of MVC), the footplate was released and rotated at a high speed (quick-release movement). The distance of release (ΔL) ranged between 35º and 50º, which is above the SEC strain of plantar flexors during MVC estimated in the previous studies [2,3].

Since a considerable ankle rotation occurs even during an isometric plantar flexion [4], ΔL was corrected for the ankle rotation during an isometric contraction preceding the release by using an electrical goniometer. In addition, the force signals were corrected for passive force and inertia by using a transfer function. After correction, the time between the onset of release and the beginning of force redevelopment (Δt) was determined (Figure 1). Relations between Δt and ΔL for varied release distances were fitted with a linear regression, the slope of which provided V_0 of plantar flexors.

All the subjects completed two testing sessions with the knee extended or flexed, which were taken on separate days. In the flexed knee position, the knee was flexed 120º, at which the biarticular gastrocnemius muscles can transmit negligible contractile forces to the calcaneus, as suggested previously [5]. Even in the extended knee position, the knee was slightly flexed (within 20º) to prevent pain or discomfort due to immoderate stretch of the gastrocnemius muscles.

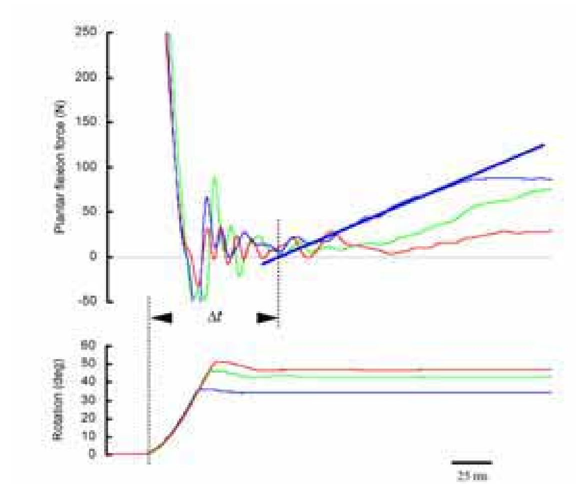

Figure 1: Superimposed force and angle recordings from three quick releases with different release distances.

RESULTS AND DISCUSSION

Representative results from one subject (Figure 2) showed that V_0 increased with contraction intensity in the extended knee position, suggesting progressive recruitment of faster motor units. In the flexed knee position, however, such a tendency was not observed. This may be due to the ineffectiveness of the gastrocnemius, which has a higher percentage of fast-twitch fibers and longer fascicles, to produce and transmit muscle forces.

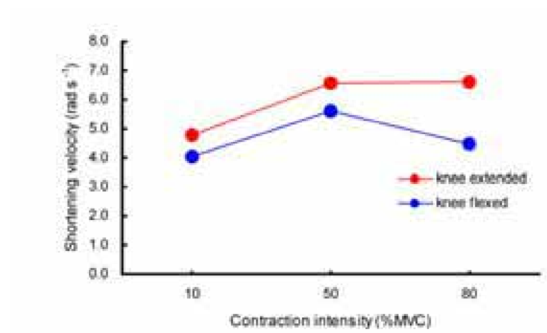

Figure 2: Representative relations between contraction intensity and V_0.

REFERENCES

1. Edman KA. *J Physiol* **291**, 143-159, 1979.
2. Hof AL. *J Biomech* **31**, 793-800, 1998.
3. de Zee M and Voigt M. *J Biomech* **34**, 1399-1406, 2001.
4. Magnusson SP, et al. *J Physiol* **531**, 277-288, 2001.
5. Maganaris CN. *Clin Anat* **16**, 215-223, 2003.

THE INFLUENCE OF DIFFERENT MECHANICAL STIMULI AND GROWTH ON THE MECHANICAL PROPERTIES OF THE ACHILLES TENDON IN THE FEMALE RAT

Kirsten Legerlotz, Gert-Peter Brüggemann and Anja Niehoff
Institute for Biomechanics and Orthopedics, German Sport University of Cologne, Cologne, Germany
e-mail: Legerlotz@dshs-koeln.de

INTRODUCTION

Even though tendon injuries rank among the most frequently occurring sport injuries [1], the adaptation of the tendon to exercise is not well investigated. It is known that different kinds of physical activity create different mechanical stimuli on biological materials leading to different adaptation effects. This has been shown for example for bone tissue [2] but had not yet been investigated for the tendon. Therefore, the aim of this study is to analyze the effect of running exercise, which creates single impacts with short rest periods between the impacts (~2.4 Hz)[3] in contrast to vibration strength training, that creates close following impacts; and growth on the mechanical and morphological properties of the rat Achilles tendon.

METHODS

Forty-two female Sprague Dawley rats of 11 weeks age (233 ± 20g) were divided into four groups: a basis control group (BC, n=10) that was killed at the beginning of the study; a non-active age matched control group (AMC, n=10); a voluntary wheel running group (RT, n=10) that was single housed and had free access to a running wheel; and a vibration strength training group (VST, n=12). The VST group trained voluntarily in a rat squat machine, where the rats had to lift a weight to reach a special food. When the weight was lifted a vibration plate (25 Hz) under the rat's feet was activated. Three rats of the VST group had to be excluded from the study, because they did not use the squat machine frequently enough. After a 12 week training period the rats were killed by decapitation and the Achilles tendon was dissected. The left Achilles tendons were at first cyclically tested with 30 cycles up to 10 N. With the last cycle the hysteresis and creep (in % of the original length) were determined. Afterwards the tendons were tested until failure to determine the ultimate load, ultimate load per body mass, stiffness and deformation. The right Achilles tendons were embedded in paraffin and will be sectioned and stained to determine the cross sectional area.

The significance of difference between the groups was determined by an one-way ANOVA. All statistical tests were evaluated using $\alpha < 0.05$.

RESULTS AND DISCUSSION

The average running distance of the rats in the RT group was 9.6 ± 2.9km/day. The animals of the VST group lifted the weight (250 - 450g at the end of the study) for 161 ± 112s/day. At the end of the study the AMC group (327 ± 31g) was significantly heavier than RT group (283 ± 25g, p = 0.010). There was no significant difference between the VST group (305 ± 36g) and the other two groups concerning the body mass. Regarding the mechanical properties of the Achilles tendon, no significant differences could be found between the groups (Table 1). But if the ultimate load is adjusted according to body mass, the BC group revealed significantly ($p \leq 0.001$) higher values than the AMC and the VST group. Thus, neither vibration strength training nor growth cause an increase in the ultimate load of the tendon but rather the ultimate load per body mass decreases. Running training seems to compensate an age related decrease of the ultimate load per body mass. These results indicate that the kind of mechanical stimulus has an influence on the mechanical properties of the Achilles tendon but that the tendon is predominantly influenced by growth effects in younger adult rats. These results are in line with the hypothesis of Smith et al. [4] who formulated that once an optimised tendon is formed during skeletal maturity no more distinct adaptation will occur.

REFERENCES

1. Majewski M, et al. *Orthopade* **29**, 670-676, 2000
2. Liu L, et al. *J Appl Physiol* **95**, 219-224, 2003
3. Clarke KA and Parker AJ, *Physiol Behav* **38**,345-351, 1986
4. Smith RK, et al. *Comp Biochem Physiol A Mol Integr Physiol* **133**, 1039-1050, 2002

Table 1: Mechanical properties of the Achilles tendon. Values presented are means ± SD. *Values significantly ($p \leq 0.001$) different to the BC group

Group		**Achilles Tendon**					
		F_{max} [N]	**F_{max}/mass [N/kg]**	**Stiffness [MPa]**	**Deformation [mm]**	**Hysteresis [%]**	**Creep [%]**
BC	[n=10]	47.1 ± 5.1	203 ± 25	40.5 ± 8.7	2.10 ± 0.41	20.8 ± 5.4	0.25 ± 0.06
AMC	[n=10]	45.0 ± 9.6	138 ± 27*	49.9 ± 11.4	1.59 ± 0.48	18.4 ± 5.8	0.28 ± 0.09
RT	[n=10]	47.7 ± 9.1	169 ± 35	49.5 ± 11.0	1.67 ± 0.56	17.4 ± 3.4	0.28 ± 0.04
VST	[n=9]	42.0 ± 9.4	137 ± 38*	42.8 ± 14.1	1.65 ± 0.40	16.6 ± 2.6	0.25 ± 0.06

INFLUENCE OF POSTERIO-ANTERIOR MOBILIZATION ON DIFFERENT LEVEL OF THE SPINE

[1]Bonnie YS Tsung, [2]John Evans, [3]Pin Tong, [1]Raymond YW Lee
[1]Department of Rehabilitation Sciences, The Hong Kong Polytechnic University, Hong Kong
[2] Centre for Rehabilitation Science and Engineering, Queensland University of Technology, Australia
[3] Department of Mechanical Engineering, The Hong Kong University of Science and Technology, Hong Kong
Contact: email: bonnie.t@polyu.edu.hk

INTRODUCTION

Postero-anterior mobilization involves the application of vertical forces on the human spine when the subjects lying prone. It is commonly used clinically for changing the spinal stiffness and symptoms of back pain patients. Previous research modeled posteroanterior mobilization as three-point bending of the lumbar spine, which was considered to be a beam supported at the pelvis and the thoracic cage [1]. But geometric effect of the spine on the segmental stiffness of the spine was still not be considered. The aim of this study was to measure the curvature change of the lumbar spine to PA mobilization of different lumbar spinal segments.

METHODS

Seventeen normal subjects (mean age = 30.71 ± 5.82, mean height = 1.71 ± 0.05m, mean weight = 65.53 ± 8.12 kg) agreed to participate in this study. Subject was requested to lie on the unpadded plinth with the face down. Posteroanterior mobilization force was applied to the spinous process of each level of lumbar spine by an experienced physiotherapist.

The spine was modeled as a beam support at thoracic cage and pelvic (Figure 1). Force applied to the spine was continuously monitored and captured by the use of a non-conductive force plate (4060-NC Bertec Corporation, Columbus, OH 43229, USA), which was mounted underneath the unpadded plinth. An electromagnetic tracking system (Fastrak, Polhemus Navigation, Colchester, VT) was used to measure the change in curvature of the spine. Two electromagnetic sensors were used to measure the local curvature change of the spine (e.g. Mobilizing L3, measure angle between L1 and L5 level). The bending stiffness (EI) of the spine was derived from the bending force and the local change in curvature of the spine by moment area method (Equation 1).

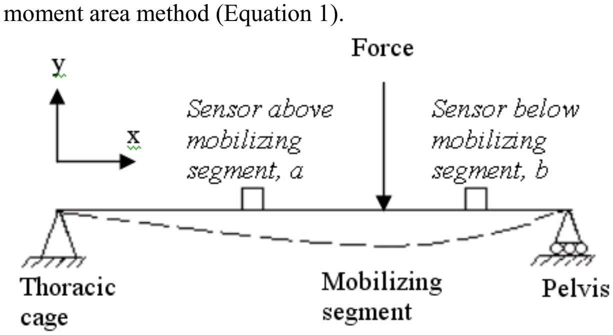

Figure 1: A beam model representing deflection of spine under posteroanterior mobilization.

$$EI = \frac{\int_b^a M dx}{\theta_{ab}} \qquad \textit{(Equation 1)}$$

RESULTS AND DISCUSSION

Figure 2 shows the result of mobilizing different lumbar level. The mean frequency of mobilization for all five lumbar levels was 1.64 ± 0.13 Hz. Higher force was applied to the spine when mobilizing L4 & L5 level, and more resulting spinal curvature change was found on these levels than the remaining levels. However, these levels were found to be stiffer than the remaining levels.

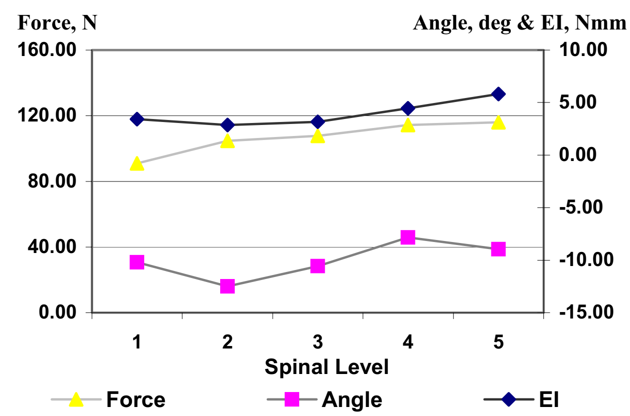

Figure 2: The average center of oscillation of the mobilizing force, change in spinal curvature (angle between L1and S2) and stiffness (EI).

CONCLUSIONS

The influence of spinal level and geometry on bending stiffness should be considered when clinical changes in spinal stiffness were evaluated.

REFERENCES

1. Lee RYW and Evans JH. Physiotherapy **80,** 68-73, 1994

ACKNOWLEDGEMENTS

The authors wish to thank the Hong Kong Research Grant Council in providing funding of this research project (Competitive Research Grant PolyU 5195/01E).

VOLUNTARY STRENGTH TRAINING AND RUNNING EXERCISE INDUCE SITE-SPECIFIC BONE ADAPTATION IN ADULT FEMALE RATS

Anja Niehoff, Kirsten Legerlotz and Gert-Peter Brüggemann
Institute for Biomechanics and Orthopedics, German Sport University of Cologne, Cologne, Germany
email: Niehoff@dshs-koeln.de

INTRODUCTION

Previous studies have confirmed that physical activity has a positive effect on morphological and mechanical properties of bones [1,2]. Nevertheless, one has to consider that different types of exercise affect specific bone adaptation [3,4]. The loading pattern of the mechanical stimulus, including strain rate, loading cycle frequency, strain direction and distribution, peak strain magnitude and number of cycles is of critical importance. Thereby, a high-frequency low-risk mechanical loading pattern turned out to be strongly osteogenic [5]. In addition, it was found that a low-frequency loading regime is osteogenic with a rest period between each loading cycle [6].
The purpose of the study was to analyze the effect of vibration strength training with a high frequency of 25 Hz in compared to running exercise with a low frequency of ca. 2 Hz [7] and rest between the loading cycles on bone mechanical and morphological properties in the adult female rat.

METHODS

Forty-two 11 weeks old (233 ± 20g) female Sprague-Dawley rats were randomly assigned to a basic control group (BC; n=10), a voluntary wheel running group (RUN; n=10), a vibration strength training group (VST; n=12) and a non-active age-matched control group (AMC; n=10). The RUN group had free access to a running wheel. The VST group trained voluntarily in a rat squat machine, where the rats had to lift a weight to reach special food. When the weight was lifted a vibration plate (25 Hz) under the feet was activated. The time of lifting the weight was monitored. After 12 weeks of exercise the rats were killed by decapitation and the right femur and tibia were dissected.
Peripheral quantitative computed tomography (pQCT) was performed by transverse image sets of multiple slices at 7%, 7% + 5mm from the proximal tibial plateau and at 50% the total tibial length. Femora were scanned at 5, 5.5 and 6 mm from the distal plateau and at 50% of the total bone length.
To determine the mechanical properties the bones were loaded until failure by a 3-point bending test using a material testing machine (Z2.5/TN1S, Zwick, Germany). The support distance was 15 mm for tibia and 16 mm for femur. The broadness of support points was 2 mm for tibia and 4 mm for femur. The crosshead speed during testing was 10 mm/min. The cross-sectional moment of inertia was calculated from the pQCT measurements at 50% of the total length of the bone.
The significance of difference between groups was determined by one-way ANOVA ($\alpha < 0.05$).

RESULTS AND DISCUSSION

Three rats of the VST group had to be excluded from the study, because they did not use the squat machine on a regular basis. The average running distance of the RT group was 9.6 ± 2.9km/day. The VST group lifted the weight (mass: 250-450g) for 161 ± 112s/day. At the end of the study animals of the AMC group (327 ± 31g) were significantly heavier than those of the RT group (283 ± 25g, p=0.010). The mechanical properties of tibia and femur in the different groups are summarized in table 1.
Tibia: The cancellous BMD was significantly (p=0.001) higher in the RUN group compared to the BC group. There were no significant effects of vibration strength training on the analyzed pQCT parameters. The BC group had always significantly ($p<0.05$) lower values in contrast to the AMC, RUN and VST group.
Femur: On the diaphyseal site the RUN group had a significantly lower cortical area (p=0.003), cortical (p=0.003) and total (p=0.011) BMC compared to the AMC group.

CONCLUSIONS

Mechanical stimulation by exercise with different frequency regimes affects site-dependent bone adaptation.

REFERENCES

[1] Mosekilde L, et al.. *Bone* **15**, 293-301, 1994. [2] Myburgh KH, et al.. *J Appl Physiol* **66**, 14-19,1989. [3] Bourrin S, et al.. *J Bone Miner Res* **10**, 1745-1752, 1995. [4] Honda A, et al.. *J Bone Miner Res* **16**, 1688-1693, 2001. [5] Rubin C, et al.. *J Bone Miner Res* **17**, 349-357, 2002. [6] Srinivasan S, et al.. *J Bone Miner Res* **17**, 1613-1620, 2002. [7] Mosley JR, et al.. *Bone* **20**, 191-198, 1997.

Table 1: Mechanical properties of tibia and femur. Values presented are means ± SD. *Values significantly ($p<0.05$) different to the BC group. #Values significantly ($p<0.05$) different to the RUN group. BM = bending moment; BS = bending stress

		F_{max} [N]	BM [Nmm]	Energy [mJ]	E-modulus [MPa]	BS [MPa]	Strain [%]
Tibia	**BC**	82 ± 7	315 ± 65	34.7 ± 8.3#	15.7 ± 33.3	218 ± 45	4.2 ± 0.9
	AMC	117 ± 21*	468 ± 83*	36.4 ± 9.9#	10.4 ± 23.8*	218 ± 28	4.2 ± 0.9
	RUN	127 ± 17*	506 ± 68*	46.5 ± 6.7	10.7 ± 22.2*	244 ± 24	4.6 ± 0.5
	VST	115 ± 16*	461 ± 62*	38.4 ± 8.0	11.2 ± 39.1*	221 ± 26	4.1 ± 0.6
Femur	**BC**	96 ± 9	358 ± 33	37.6 ± 15.6	33.4 ± 11.1	135 ± 13	4.5 ± 1.6
	AMC	130 ± 31*	487 ± 116*	42.1 ± 21.2	36.6 ± 14.9	137 ± 31	4.2 ± 1.6
	RUN	120 ± 22	450 ± 83	30.6 ± 16.0	43.5 ± 13.3	141 ± 28	3.6 ± 1.6
	VST	141 ± 25*	528 ± 95*	50.4 ± 17.2	30.9 ± 11.0	142 ± 17	5.1 ± 2.1

Kinetic Gait Analysis of Powered Gait Orthosis using Fuzzy logic Controller

SungJae Kang, Jei Cheong Ryu ,Gyo Suk Kim, Seung Mun
Korea Orthopedic & Rehabilitation Engineering Center(KOREC)
Email: kangsj@iris.korec.re.kr, web: www.korec.re.kr

INTRODUCTION

At KOREC, a prototype of a powered gait orthosis has been developed to reduce the energy consumption and the muscle fatigue. Each hip joint of the PGO is flexed by an air muscle operated by pressurized air enabling the patient to walk. The air muscle behaves like a human muscle and connects one side of the torso section to the upper part of the same side of the brace. The role of artificial muscle is to assist hip flexion during swing phase. Therefore, the patient can walk with less energy expenditure by using a PGO than using an RGO.The PGO a modification of an RGO[1] incorporating two pneumatic muscle actuators(PMA), a compressed air system,pressure and joint angle sensors.
In the present study, PGO which controlled by fuzzy algorithm for hip flexion and analyzed for SCI patients who used the developed PGO with the three-dimensional motion analysis system.
.

METHODS

The concept of the PGO driving system is to couple the right and left sides of the orthosis by specially designed hip joints and pelvic section. The driving system of powered gait orthosis(PGO) consists of the orthosis, sensor, control system. An supply system is composed of an air compressor, 2-way solenoid valve(MAC, USA), accumulator, pressure sensor. Role of this system provide air muscle with the compressed air at hip joint constantly(Fig. 1). PGO which controlled by fuzzy algorithm for hip flexion.

Two subjects(39±2.8 years) who were two adult normal male and one paraplegic male participated in this study. Subjects were recruited from the laboratory staffs and patient of the hospital. Their heights and weights ranged from 170±1.7 ㎝, 60.5±7.5kg, respectively.

Subjects were performed the gait analysis five times per one month after gait training on PGO during about three months.

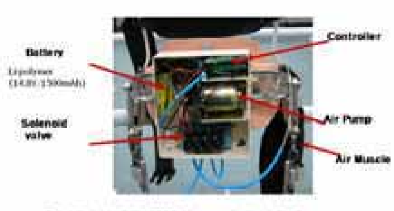

Figure 1: PGO system

RESULTS AND DISCUSSION

This figure 2 shows the sagittal plane internal joint moment during a single gait cycle. As a results, the maximum hip flexion angles PGO's gait was 57^{o} during swing phase and maximum hip flexion moment was 0.86Nm/kg. Maximum knee flexion/extension moments were about 0.89Nm/kg and 0.68Nm/kg. Maximum ankle dorsiflexion moments is 1.08Nm/kg. PGO’s moment curve was similar to normal gait. The ratio of the duration of the swing phase of fuzzy controlled PGO gait shows 40.4% as an approximation to the normal gait.

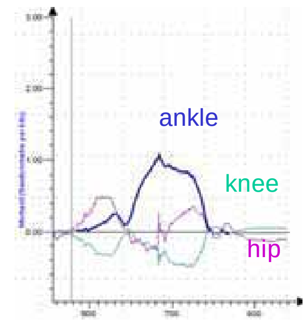

Figure 2:Hip, Knee, Ankle moment

CONCLUSIONS

We are proposed fuzzy controlled PGO's system using air muscle of hip joints for SCI patients. This PGO controlled by fuzzy controller looks like a excellent device comparative of others. Because the ratio of the duration of the swing phase of fuzzy controlled PGO was similar to the characteristic curve of normal gait. it directly became the causes to increase the gait speed of PGO.

REFERENCES

1. Douglas R, Larson PF, DAmbrosia R, McCall RE. ,“The LSU reciprocation gait orthosis”, Orthopedics.,Vol.6,pp 834-839, 1983

ACKNOWLEDGEMENTS

This study was supported by a grant of the Korea Health 21 R&D Project, Ministry of Health & Welfare, Republic of Korea. (02-PJ3-PG6-EV03-0004)

EFFECT OF BILATERAL ASYMMETRY OF LOWER MUSCLE FORCES ON VERTICAL JUMPING HEIGHT: A SIMULATION STUDY

[1,2] Shinsuke Yoshioka, [2]Akinori Nagano and [1]Senshi Fukashiro
[1] Department of Life Sciences (Sports Sciences), University of Tokyo, Japan; email: syoshioka@riken.jp
[2] Computational Biomechanics Unit, RIKEN, Japan

INTRODUCTION

Properties and function of each bilateral component of the human body are basically symmetrical. Thus, when human movements such as jumping and walking are investigated, a bilateral symmetry is assumed. However, in reality, they are not precisely symmetrical. Additionally, little is known about the effects of bilateral asymmetry of musculoskeletal properties on various human movements. It is hard to address this question using experimental protocols because of the difficulty in controlling the asymmetry of the human body.

The purpose of this study was to investigate the effects of bilateral asymmetry of lower muscle forces on the biomechanics of a vertical jumping motion using computer simulation.

METHODS

A model of 3D human body musculoskeletal system was developed using DADS-3D (LMS International). Segment inertial parameter and muscle parameter values were derived from [1] and [2], respectively. A dynamic activation mechanism to represent the transfer lag between the neural input signal and the musculotendon force development [3] was implemented. In addition, Hill-type muscle F-V-L relations, elements to limit the joint range of motion, and ground reaction force [4] were implemented. Fifteen muscles for each leg were implemented. Properties of each muscle were bilaterally symmetrical and derived from [5] and [6].

Two types of models were developed. One model had the same construction and properties as above mentioned (Model-Bal). Another model had basically the same construction and properties as above mentioned, except for the muscle force (Model-Imbal). All muscle forces in the right leg of Model-Imbal were 5% greater than those of Model-Bal, while All muscle forces in the left leg of Model-Imbal were 5% smaller than those of Model-Bal.

Mathematical representations of the skeletal, muscle and activation dynamics were programmed in FORTRAN, then compiled with DADS-3D. Muscle activation profiles were searched using Bremermann's [7] numerical optimization method (Figure 1). The objective function was vertical jumping height.

RESULTS AND DISCUSSION

Jump movements were generated with the models above mentioned (Figure 2, 3). The jump movement of Model-Imbal was similar to that of Model-Bal. The jumping heights of Model-Bal and Model-Imbal were almost the same. However, actions of a few muscles such as m.gluteus medius were different between Model-Bal and Model-Imbal. It was revealed that the actions of those muscles are important for the coordination of jumping in Model-Imbal.

REFERENCES

1. de Leva, *J Biomechanics* **29**: 1223-1230, 1996.
2. Delp SL, Dissertation, Stanford University, 1990.
3. He J, *et al.*, *IEEE Transactions on Automatic Control* **36**: 322-332, 1991.
4. Nagano et al., *Am J Phys Anthropol* **126**: 2-13, 2005.
5. Friederich et al., *J Biomechanics* **23**: 91-95, 1990.
6. Brown et al., *Exp Brain Res* **121**: 76-91, 1998.
7. Bremermann, *Mathematical Biosciences* **9**: 1-15, 1970.

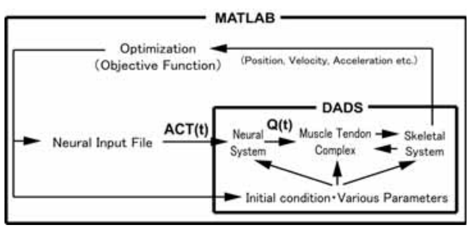

Figure1: Schematic of the simulation

Figure 2: Stick figures of the vertical jumping of Model-Bal generated through the numerical optimization.

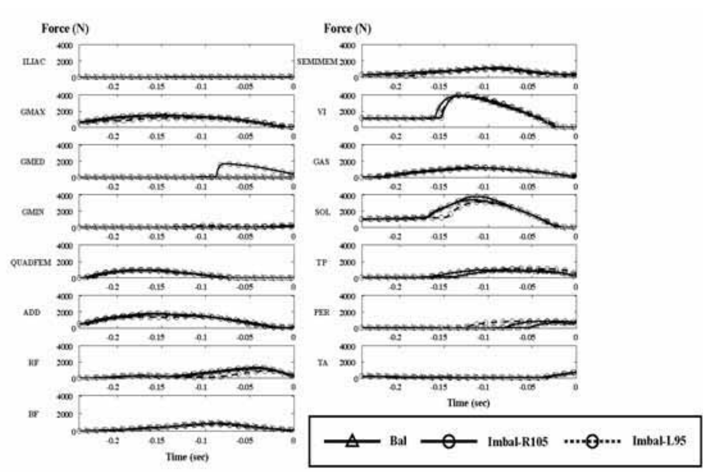

Figure 3: Time-Force relation profiles of the contractile element during jump movement. 0 sec is take-off time.

VALIDATED FINITE ELEMENT MODEL OF A COMPOSITE TIBIA

[1]Hans Gray, [1]Amy Zavatsky, [3]Marco Viceconti, [3,4] Luca Cristofolini and [2]Harinderjit Gill
[1]Dept of Engineering Science and [2]Dept of Orthopaedic Surgery (OOEC), University of Oxford; [3]Laboratorio Di Tecnologia Medica, Istituti Ortopedici Rizzoli and [4]DIEM, Engineering Faculty, University of Bologna; email: hans.gray@st-catherines.ox.ac.uk

INTRODUCTION

Composite bones are synthetic bones made of a hard glass-fibre reinforced epoxy shell (representing cortical bone) with a foam centre (representing trabecular bone). They are useful tools for experimental studies on orthopaedic implants as they have little variability between them, are more convenient to handle and store than cadaveric bones, and are cheaper and easier to source. Finite element (FE) models of composite bone can be used to evaluate new and modified designs of joint prostheses and fixation devices. Although FE models of the composite femur have been created and validated [1,2], no validated FE models of the composite tibia yet exist.

The aim of this study is to create an FE model of the composite tibia (Mod. 3101 Pacific Research Laboratories, WA, USA) and validate it against experimental results. As an initial step, the FE model was validated against the results obtained by Cristofolini and Viceconti [3], who measured deflections in the bone due to simple loading conditions.

METHODS

CT (HiSpeed CT/i, GE Medical Systems, USA) images of a composite tibia taken at 2 mm intervals in the transverse plane were segmented, and 3D models of the outer surface geometry of the bone and the geometry of the surface between the epoxy shell and the foam were created (sliceOmatic, TomoVision, Virtual Magic Inc., Montreal, Canada). These two surface geometries are now available at the BEL Repository, http://www.tecno.ior.it/VRLAB/. The surface geometries were used to create a 10-node tetrahedral solid mesh of the tibia (MSC.Patran, 2004 r2, MSC.Software Corporation, USA). Five different meshes consisting of 64349 to 110363 nodes were created; convergence of the results was checked. The reinforced material and the foam were both assumed to be isotropic with Poison's ratios of 0.3 and with Young's moduli of 14200 MPa and 69 MPa, respectively [3].

In the reported experimental study [3], the bending stiffnesses of eight composite tibiae were estimated by bending them in the latero-medial and antero-posterior planes. A four-point bending jig was used for load application (up to 500 N), while an extensometer was used to measure the mid-diaphysial deflection. The average results of five tests done on each bone, as well as the overall average, were presented. The experiments were simulated on the FE model (MSC.Marc, MSC. Software Corporation, USA) and model deflection and stiffness results compared to experiment.

In the reported experimental study [3], the torsional stiffness of the eight composite tibiae were estimated by applying a 5 Nm moment to the proximal end and measuring the angle of twist. The average torsional stiffness for each specimen, as well as the total average, was presented. To simulate the experiments on the FE model, two forces, parallel to each other and to the transverse plane, were applied to the proximal tibia. The surface nodes in the distal 30 mm of the tibia were fixed. Model displacements were used to calculate the angle of twist and torsional stiffness and compared to experimental results.

RESULTS AND DISCUSSION

For anterior-posterior bending, the FE analysis gave a deflection of 0.266 mm and a bending stiffness of 1880 N/mm. This stiffness is within 1% of the average experimental value and is well within the reported range of values [1]. For latero-medial bending, the FE analysis gave a deflection of 0.553 mm and a bending stiffness of 904 N/mm. This stiffness is within 4% of the average measured value and within the range reported [1].

For torsion, the FE analysis gave an angle of rotation of the proximal tibia with respect to the distal tibia of 0.762° and a torsional stiffness of 6.56 Nm/degree. This stiffness is just over 20% higher than the measured average and outside the maximum measured value as well [1]. While the reasons for this large discrepancy are not clearly understood, it is possible that simplified boundary conditions in the FE model which ignored the two end mounting pots in the experiment may have led to slight, yet unwanted, deflections in the model. The assumption that the material properties of the composite bone were isotropic may also have contributed to the error.

It is of interest to note that only the bending stiffness and torsional stiffness were compared between the experimental results and the FE model, as this was the only information reported on the experimented tibiae. The surface strains generated due to these types of loading were not measured in the reported study. Therefore, while the model can be used reasonably accurately in cases where deformations are concerned, it may not yield accurate results if stresses or strains are analysed. Further experiments using more comprehensive loading conditions have been done on a strain gauged composite tibia. These results are now being compared against FE results. Additional attention is being dedicated to the proximal epiphysis.

CONCLUSIONS

This study has used the only reported experimental data on the second generation composite tibia (Mod. 3101 Pacific Research Laboratories, WA, USA) to validate an FE model of the same. The FE model can be used to evaluate conditions where bending predominates and should generate accurate results. However, for loading situations where torsion is predominant, less accurate results may be generated.

REFERENCES

1. Stolk J, et al. J. Biomech, 35(4):499–510, 2002.
2. Waide V, et al. Clin Biomech, 18(6):523–36, 2003.
3. Cristofolini L, Viceconti M. J Biomech, 33(3):279–88, 2000.

ACKNOWLEDGEMENTS

Hans Gray is funded by a Felix Scholarship at the University of Oxford.

Fusion of biomechanics data for patient monitoring in pediatric skeletal oncology

[1] Fulvia Taddei, [2]Marco Manfrini, [3]Alberto Leardini, [3]Maria Grazia Benedetti and [1]Marco Viceconti
[1]Laboratorio di Tecnologia Medica, [2]Dipartimento di Oncologia Muscolo-scheletrica, [3]Laboratorio di Analisi del Movimento
Istituti Ortopedici Rizzoli, Bologna, Italy; email: tecno@tecno.ior.it; web; www.tecno.ior.it

INTRODUCTION

The term *data fusion* indicates the methods and the technologies that allow the synergistic combination of disparate data into a new dataset, which potentially contains more information than the sum of the original data. We applied data fusion to combine medical imaging, movement analysis, muscolo-skeletal modeling, and finite element analysis data, into a coherent representation of local skeletal loading during certain motor tasks. This approach has been used to estimate the risk of fracture under fully unprotected walking in pediatric patients, which underwent a major skeletal reconstruction due to the presence of a bone sarcoma.

METHODS

At each periodic control the patient is examined with a CT scan of the reconstructed and of the contro-lateral regions. In the first post-operative control, we also perform a complete MRI examination of the lower limbs.

Whenever possible, before the imaging session, the patient is instrumented with a redundant set of radio-opaque and reflective markers, firmly attached to the skin. This includes four markers per segment in addition to those used for a standard gait analysis [1]. The movement analysis session is accurately planned in advance among the surgeon, the physiatrist, and the bioengineers, in order to maximize the collected information, while minimizing the risk of spontaneous fractures. This required the development of a special protocol for children, which considers the need, in the early stages of the follow-up, of protected walking.

CT, MRI and all movement analysis data (kinematics, ground reaction forces, EMG) are imported into a data fusion application (Data Manager, B3C, Italy), which allows the complete spatial and temporal registration of all data, using the skin landmarks as fiducial points. Data are then processed to extract the skeletal geometry, the distribution of mineral density inside each bone, the joint centers, the line of action and the lever arm of all relevant muscles, etc. The software provides also a virtual palpation environment that allows the accurate definition of the joint reference systems following the ISB standardization, and let you compute all biomechanical quantities necessary to predict the muscle and the joint forces with static optimization. At the same time the bone data are processed to create a subject-specific finite element model. Loaded with muscle and joint forces, the model predicts the stresses and strains induced in the bone for each time frame of the recorded task [2]. Robust quality insurance protocols are used to monitor all instrumentations. All uncertainties are factored into a Montecarlo simulation that provides a full sensitivity analysis on the stress predictions [3]. The stress results are then imported back in the Data Manager and fused with the rest of the data. Using the advanced interactive visualization features of the Data Manager, the stress results are reported to the medical professionals fused with the anatomical (imaging) and functional (gait analysis) data of the patient (Fig. 1). This dramatically improves the efficacy of doctor-engineer communication.

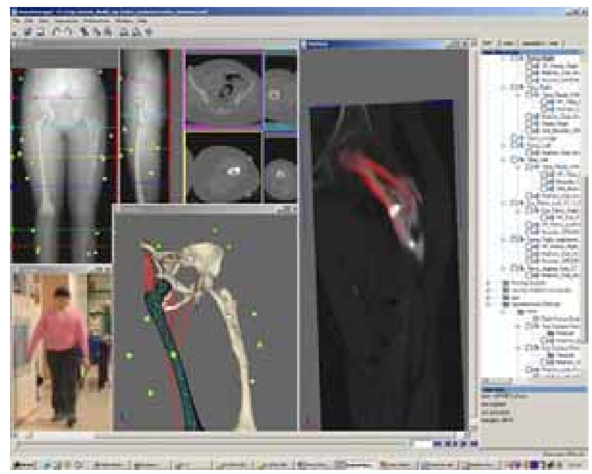

Fig. 1 The DataManager environment. In clockwise order, from top-centre: the CT dataset taken with the markers attached to the patient skin; the FEM results mapped onto the CT volume; the FEM model of the right femur within the muscle-skeletal model used to predict muscle forces; a movie of the walking task. On the right the tree structure used to organize the different data.

RESULTS AND DISCUSSION

So far the method has been used with 4 patients; for 2 of them we already have more than 5 controls. The only warning raised with this procedure so far, was confirmed by sub-capital slippage complication during unprotected walking, occurred a few months later.

The method is becoming in our hospital the *de facto* standard for planning the rehabilitation protocol in these very difficult cases. This poses major problems, as the whole procedure currently requires a large amount of time to collect, process and analyze all these data. However, we are optimistic that improvements in the software algorithms can provide the level of automation that is necessary for large-scale clinical usage. In the meanwhile, preliminary attempts are being made to use this methodology also in the pre-operative planning phase.

REFERENCES

1. Benedetti MG, et al. *Gait Posture*, **18** (Suppl. 1), S11, 2003.
2. Taddei, et al.. *Proc Inst Mech Eng [H],* **217**, 111-119, 2003.
3. Taddei F., et al.. Istituti Ortopedici Rizzoli, Bologna, Italy, 2004, Internal Report.

DOES STRAPPING THE ROWER TO THE SEAT ENHANCE ROWING PERFORMANCE?

A.J. "Knoek" van Soest, J. van Zeil and T. Guhr
Faculty of Human Movement Sciences and IFKB, Free University Amsterdam, the Netherlands
email: k.vansoest@fbw.vu.nl

INTRODUCTION

A well-known coordination problem in rowing is to prevent "shooting the slide"; rowers must prevent lifting themself from the sliding seat, which may occur when pulling too hard on the oar handle. We have three indications that this constraint may limit performance. First, novice rowers are known to shoot the slide quite often. Second, the vertical seat reaction force in expert rowers approaches zero during the pull phase [1]. Third, a simulation study indicated that eliminating the no-slide-shooting constraint on coordination by "strapping the model to the sliding seat" may increase performance during the first stroke [2]. Thus, in this experimental study we address the question if rowing performance can be improved in well-trained rowers by strapping them to their sliding seat. As the mechanics of ergometer rowing have been shown to be comparable to on-water rowing, this question is addressed in the context of ergometer rowing.

METHODS

Six well trained rowers participated in two ergometer rowing tasks, using an instrumented Concept IIC rowing ergometer. The first task, mimicking the start of a race, was to perform a series of two maximal strokes, starting from zero flywheel velocity. The second task, mimicking high-intensity steady state rowing, was to was to row 500 meters, where the first and last 150 meters (approximately 15 strokes each) were performed at maximal intensity. Both tasks were performed three times, both under normal conditions and while strapped to the sliding seat. Apart from a warming up period of 20 minutes, the participants had no training with the strap. The rowing ergometer was instrumented with 6-channel AMTI force transducers under the feet and under the sliding seat; a one-channel force transducer was mounted between the handle and the chain. An Optotrak system was used to measure kinematics. From these data, mechanical work and average mechanical power delivered by the rower to the ergometer during the stroke phase were calculated. Data were analyzed using paired Student's *t*-tests and ANOVA ($p=0.05$).

RESULTS AND DISCUSSION

Results for the first two strokes after the start are summarized in Table 1. The significant difference in min(F_seat_z), the minimum of the vertical force under the seat, indicates that subjects used the strap. This resulted in a higher peak handle force, which in turn resulted in higher stroke work and higher average power output during the stroke. Together, these results indicate that in this task, removing the no-slide-shooting-constraint on coordination by strapping the rower to the sliding seat allows rowers to pull harder at the handle and thus to perform better.

Results for the the high-intensity steady state rowing task investigated were less clear. While min(F_seat_z) was significantly lower when strapped, and rowers thus appear to use the strap, this did not result in a significantly higher average power output in a group analysis (data not shown). However, ANOVA's on the individual subjects indicated that in 3 out of 6 subjects, average power output was significantly higher in the strapped condition, with relative differences between 2.0% and 3.7%.

One possible explanation of the results is that during high-intensity steady state rowing (as opposed to short-duration sprinting), physiological limitations on power output are such that the no-slide-shooting constraint is "inactive". This would imply that during steady state rowing, removing this constraint by strapping the rower to the sliding seat is ineffective. Another possibility, that will be addressed in a future study, is that subjects need to learn to exploit the strap during steady state rowing.

Table 1. Results for strokes 1 and 2; * indicates significance

	Stroke number	Normal	Strapped	Rel. diff. (%)	
Min(F_seat_z) (N)	1	54	-5	-108.9	*
	2	27	-15	-155.5	*
Max(F_handle) (N)	1	1114	1177	5.6	*
	2	1091	1163	6.6	*
Max(v_handle) (m/s)	1	1.69	1.80	6.4	
	2	2.17	2.23	2.7	*
Work (J)	1	977	1020	5.2	
	2	940	990	5.4	*
Average power (W)	1	768	839	9.2	*
	2	1474	1574	6.8	*

.

REFERENCES

1. Smith RM. *Ph.D. thesis*, University of Sydney, Sydney, Australia, 1996.
2. Soest AJ van, et al. *Proc. of VIII TGCS Symposium*, Milan, Italy, 105-108, 2001.

ACKNOWLEDGEMENTS

We acknowledge Concept2 Benelux for providing us with a rowing ergometer.

EFFECT OF SINGLE PULSED ELECTROMAGNETIC FIELDS STIMULATION ON THE PROLIFERATION OF MESENCHYMAL STEM CELLS

Ming-Tzu Tsai, Walter H. Chang, Ru-Jyuan Hou, Dai-Wei Wu
Bone Tissue Engineering Research Center, Chung Yuan Christian University, TAIWAN, E-mail: g9102504@cycu.edu.tw

INTRODUCTION

Mesenchymal stem cells (MSCs), which have the capacity of self-renewal and multipotent potential of differentiation, is the promising tool for bone tissue engineering, such as bone repair and reconstruction [1]. However, the origin and number of MSCs are still the problems in clinics. Based on the few population of MSCs contained from adult bone marrows, the main objective of this research was to enhance the recruitment of MSCs in vitro by using physical stimuli, single pulsed electromagnetic fields (sPEMF) stimulation. The activity of MSCs was estimated by MTT assay as well as the histomorphological stain.

MATERIAL AND METHOD

Bone marrow MSCs primary culture. MSCs were isolated from bone marrows of bilateral femora and tibiae acquired from 4-6-week-old male Wistar rats. Isolated MSCs were resuspended in α-MEM containing 10% FBS [2].

sPEMF system. sPEMF was well-established in our lab for many years. The parameters of sPEMF were: single pulse, 7.5 Hz, 1.3, 2.4, and 3.2 Gauss of magnetic intensities. The stimulation period of sPEMF was two hours a day for 14 days.

Experimental design. Isolated bone marrow MSCs were cultured in 8-well chamber slides for two days, and then cells were exposed to sPEMF stimulation with specific parameters for 2 hr/day for 14 days. Conditioned medium and cells were collected and assayed at day 0, 3, 6, 9, 12, and 14.

Proliferation and differentiation assay. The proliferation and of MSCs was determined by MTT assay. The differentiation of osteoblasts and adipocytes from MSCs were evaluated by von Kossa stain and Oil Red stain.

RESULT AND DISCUSSION

Fig. 1-2 showed von Kossa stain of osteoblasts and oil-red O stain of adipocytes differentiated from bone marrow MSCs. It indicated that bone marrow MSCs still had multipotent ability of differentiation after appropriate PEMF stimulation with specific parameters. Fig. 3-5 showed the proliferation of MSCs with three original MSCs densities with/without PEMF stimulation with different intensities. PEMF-50, PEMF-500, and PEMF-1000 maintained higher proliferation than their controls during 14-day period (Fig. 3). The effect of PEMF stimulation with 2.4 G and 3.2 G inhibited cell viability of MSCs, especially 3.2 G of magnetic intensity. The original cell densities of MSCs also had dose-dependent relationship with their growth rate with or without PEMF exposure.

CONCLUSION

The purpose of this study was to estimate the ability of PEMF stimulation on MSCs proliferation in vitro. It indicated that physical stimuli might be a promising physical stimulus for MSCs expression in the future.

ACKNOWLEDGEMENT

The authors thank National Science Council (NSC 93-2213-E-033-037, NSC 93-2120-M-033-001) for financial support to this research.

REFERENCE

[1] Long MW, "Osteogenesis and Bone-Marrow-Derived Cells," *Blood Cells, Molecules, and Diseases*, **27(3)**: 677-691, 2001
[2] Meirelles LDS and Nardi NB, "Murine Marrow-Derived Mesenchymal Stem Cell: Isolation, in vitro Expansion, and Characterization," *British Journal of Haematology*, **123**: 702-711, 2003


Fig. 1. Von Kossa stain of osteoblasts.

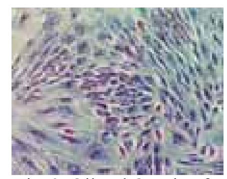
Fig. 2. Oil-red O stain of adipocytes.

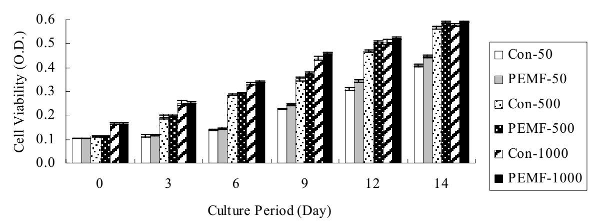

Fig. 3. Proliferation of MSCs by MTT assay (PEMF = 1.3 Gauss).

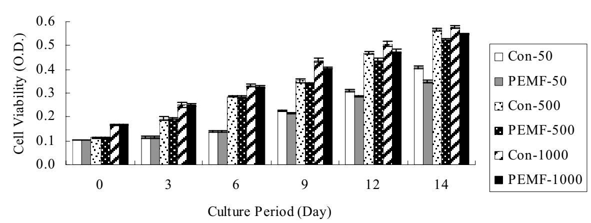

Fig. 4. Proliferation of MSCs by MTT assay (PEMF = 2.4 Gauss).

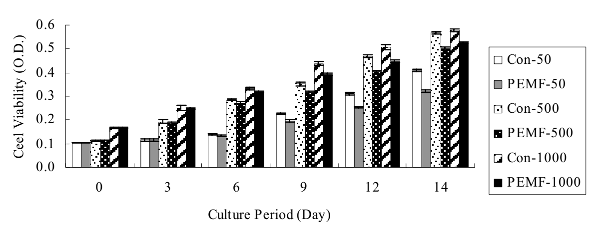

Fig. 5. Proliferation of MSCs by MTT assay (PEMF = 3.2 Gauss).

INDUCED ACCELERATION CONTRIBUTIONS TO LOCOMOTION DYNAMICS ARE NOT PHYSICALLY WELL-DEFINED

George Chen
Honda Fundamental Research Laboratories, Mountain View, CA
Rehabilitation R&D Center, VA Palo Alto Health Care System, Palo Alto, CA
Mechanical Engineering Department, Stanford University, Stanford, CA; email: chen@rrdmail.stanford.edu

INTRODUCTION

Induced segmental acceleration and power analysis has been advocated in the assessment of muscle and joint moment function during locomotion [1-4]. The analysis quantifies the contributions of individual forces and moments to the accelerations, reaction forces, and powers produced during a task [5]. The purpose of this study is to assess whether induced acceleration contributions to locomotion dynamics are physically well-defined or whether contributions depend very much on the formulation of the model. The assessment was made possible by the analyses of simple, theoretical locomotor task using different models.

METHODS

The theoretical locomotor task was based on a planar, rigid-body simulation created using dynamical-equations-of-motion generated by SD/FAST. The body consisted of four rigid segments – the trunk, and thigh, shank, and foot of the supporting leg. The contralateral leg was not included. Joint moments at the hip, knee, and ankle were prescribed to posturally support the configuration of the body as it rolled forward, in a pendular motion, over a pin joint connecting the tip of the foot to the ground.

Induced acceleration analyses [5] were performed, using four models, to determine the contributions of joint moments and centrifugal and gravity forces to the mechanical power of the trunk and leg. Model 1 represented all body degrees of freedom, and Models 2 through 4 represented progressively fewer degrees of freedom by locking the ankle, knee, and hip joints. Since these degrees of freedom were posturally supported and did not accelerate during the task, all four models completely described its simulated dynamics.

RESULTS AND DISCUSSION

The trunk powers contributed by each moment or force differed (both in magnitude and direction) between models, even though the total contributions were identical for all models and equal to the simulated powers (Fig. 1). Since the joint moments did not generate nor absorb energy, the contributed leg powers (not shown) were equal in magnitude to the contributed trunk powers but opposite in sign. In Model 1, the knee moment directed much power away from the trunk (i.e., power contribution was negative), but its effect was mostly cancelled by the positive contributions from the hip and ankle moments. The total power contribution to the trunk was modest and negative. As degrees of freedom were progressively eliminated in Models 2 through 4, the power contributed by each joint moment changed and were reduced in magnitude, overall. However, the total contributions

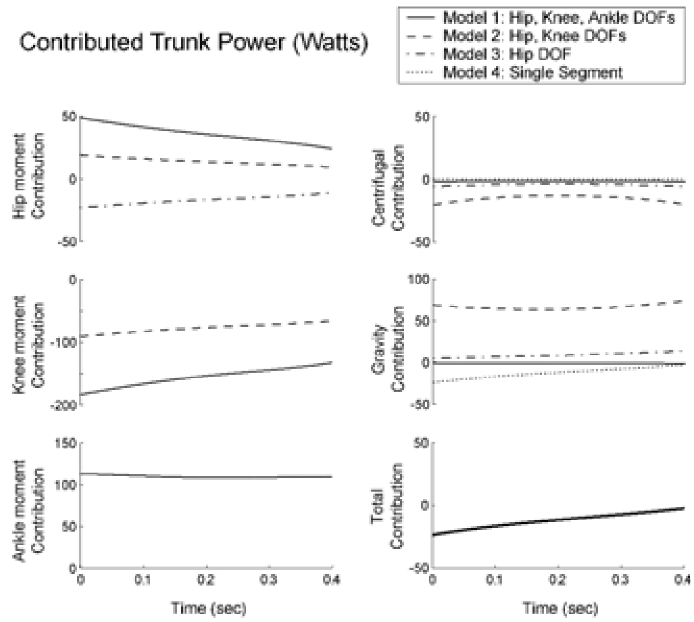

Figure 1: Using models 1 through 4, trunk power contributed by each moment or force and total contribution by all moments and forces. Note: Total contribution was the same for all models.

remained the same. In Model 4, the effect of gravity, by itself, accounted for the total power contribution to the trunk.

CONCLUSIONS

Even though all four models completely described the simulated dynamics of the theoretical locomotor task, the induced acceleration decomposition of mechanical powers differed between models. To conclude, induced acceleration contributions to the dynamics of a task are not physically well-defined. The application of the analysis in the assessment of muscle and joint moment function during locomotion should be critically reevaluated.

REFERENCES

1. Anderson FC, et al.. *Gait & Posture* **17**, 159-69, 2003.
2. Neptune RR, et al.. *Gait & Posture* **19**, 194-205, 2004.
3. Siegel KL, et al.. *Gait & Posture* **19**, 69-75, 2004.
4. Zajac FE, et al.. *Gait & Posture* **17**, 1-17, 2003.
5. Zajac FE, et al.. *Gait & Posture* **16**, 215-32, 2002.

In vivo determination of muscle architecture parameters by ultrasonography: applications to the brachialis muscle of normal subjects and persons after stroke

[1]Le Li, [1] KaiYu Tong
[1]Jockey Club Rehabilitation Engineering Centre, The Hong Kong Polytechnic University, Hong Kong, China
Correspondence author email: rctong@polyu.edu.hk

INTRODUCTION

It is believed that muscle architectural parameters have effects on the muscle's force generating capacity. The pennation angle, fibre length and thickness of the muscle has been described mainly with the data obtained in preserved cadavers or specimen before. However, cadaver data are limited in their usefulness since muscle undergo shrinking during the fixing process.

Ultrasonography can be used to measure the changes of muscle fibre length and pennation angle reliably and non-invasively. It has become possible to describe human muscle architecture in vivo by ultrasound. This study is aim to quantitatively describe the brachialis muscle architecture parameters in rest and muscle contraction condition for normal and subjects after stroke.

METHODS

Brachialis muscle's architecture parameters including pennation angle, muscle fibre length for six unimpaired subjects and six hemiparetic subjects after stroke were measured using ultrasound imaging technology at rest and different levels of muscle contraction. At rest, the measurements for normal subjects were done at elbow positions from 0°–90° flexion with increase of 10° and measurements for pathological subjects were done from 10°-80° since some of them could not extend their arms to full extension. In muscle contraction, the subjects were asked to perform 20%, 40%, 60%, 80% and 100% maximum voluntary contraction(MVC) isometrically at the fixed position of 90° elbow flexion(elbow fully extended called 0° flexion).

RESULTS AND DISCUSSION

Ultrasound measurement of muscle pennation angle and muscle fibre length were comparable with results from cadaver data in literatures. These parameters changed with elbow joint position and muscle contraction activity. The changes in muscle parameters were different between normal and pathological subjects. The finding was that fibre length of pathological subjects change less than normal subjects which may indicate the effects of spasticity.

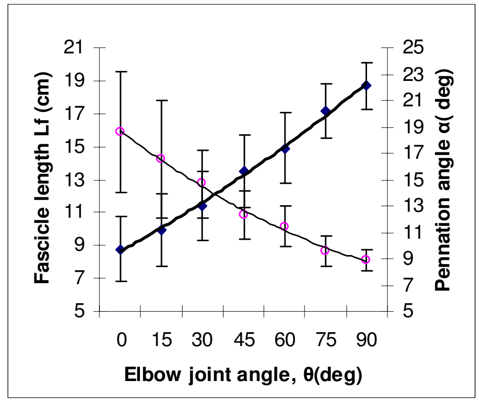

Figure 1: Muscle pennation angle and fibre length change with elbow flexion angle in rest(data from normal subjects)

CONCLUSIONS

This preliminary study finds in vivo ultrasonography could measure muscle architecture parameters and the results are comparable with anatomical data from unimpaired cadavers. Pathological subjects' muscle architecture parameters are different from normal subjects by ultrasonography. The results can be used to study the muscle properties and give useful information for force and tension calculation in the neuromusculoskeletal modelling. Application of in vivo ultrasound study on musculotendon complex is to find the relationship between the force generating of the muscle and muscle's architecture parameters. Other aspect of the applications is to have the musculoskeletal model parameters on specific subject with difference in architecture.

REFERENCES

1. Amis AA, Dowson D, Wright V., 1979. Muscle strengths and musculo-skeletal geometry the upper limb. Eng Med. 8, 41-48.
2. An K.N., Fui F.C., Morrey B.F., Linscheid R.L., Chao E.Y., 1981. Muscles across the elbow joint. J Biomech.14,659-669
3. Winters J.M., Stark L.,1988 Estimated mechanical properties of synergistic muscles involved in movements of a variety of human joints. J Biomech.21,1027-1041
4. Lieber R.L., Jacobson M.D., Fazeli B.M., Abrams R.A., Botte M.J., 1992. Architecture of selected muscles of the arm and forearm: Anatomy and implications for tendon transfer. J.Hand Surgery[AM].17A, 787-798

Table 1: Summary of literature data on brachialis muscle parameters and results of this study

Muscle Parameter	**Literature data and results of this study**					
Mean.(SD)	An et al.,(1981)	Amis et al(1979)	Winters(1988)	Lieber et al.,(1992)	Normal Subjects in this study	Pathological Subjects in this study
Fibre Length(cm)	9.0(2.9)	12.3	9.11	12.1(0.8)	11.75(2.2)	9.1(2.7)
Pennation angle(°)	---	0	15.0	2(0.6)	15.8(3.5)	15(4.2)

THE TRUNK TWIST ANGLE DURING BASEBALL BATTING AT THE DIFFERENT HITTING POINTS

[1] Takahito Tago, [2]Michiyoshi Ae and [2]Sekiya Koike
[1]Doctoral Program in Health and Sport Sciences, University of Tsukuba ; email: tago@lasbim.taiiku.tsukuba.ac.jp
[2] Institute of Health and Sport Sciences, University of Tsukuba

INTRODUCTION

Most of investigations on the baseball batting have focused on the batting motion for hitting a ball at the center of strike zone. However, since a pitcher in real baseball game tries not to throw the ball toward the center of strike zone, it is useful to identify how batters change the batting motion to hit the ball at various points in the strike zone. Although we can easily observe how the arms and legs are changed to carry the bat toward various hitting points, we have no information enough to teach an appropriate trunk motion to batters, which has been advocated to be important.

The purpose of this study was to investigate the change in twist angle between the shoulders and hips during baseball batting at the different hitting points.

METHODS

Subjects were ten right-handed male skilled batters of a varsity baseball club. Informed consent was collected after the explanation of the experiment procedure. Nine hitting points were set in the strike zone according to the baseball rules: three heights (high, middle, low) based on the subject's height and three courses (inside, center, outside) based on the width of a home plate. The subjects were randomly assigned nine hitting points and hit at least five times at each hitting point. The ball was set on a batting-tee stand at the hitting points assigned. The trial in which fastest ball velocity and good feeling of subjects were obtained was chosen at each hitting point for analysis.

Kinematic data were collected by using Vicon 612 system with nine cameras operating at 120Hz. Batting motion was divided into six phases by seven instants of motion event: Take-back start (TBS), Toe-off (TOF), Knee high (KH), Toe-on (TON), Swing start (SS), Left upper arm parallel (LUP), and Impact (IMP).

A trunk twist angle was defined as the angle between a line connecting the hips and a line connecting the shoulders, which were projected on a horizontal plane. A positive angle of the trunk twist means that the shoulder rotation to the hitting direction, i.e. forward rotation, is larger than that of the hips.

A repeated two-way ANOVA was used to test differences in the angular kinematics among hitting points at a significant level of 0.05.

RESULTS AND DISCUSSION

The upper figure of Figure 1 shows changes in trunk twist angle for hitting the ball at three heights (high, middle, low). The shoulder rotation to the opposite hitting direction, i.e. backward rotation, was significantly larger in the low ball hitting from SS to LUP than that of the high ball hitting, and the shoulder forward rotation significantly

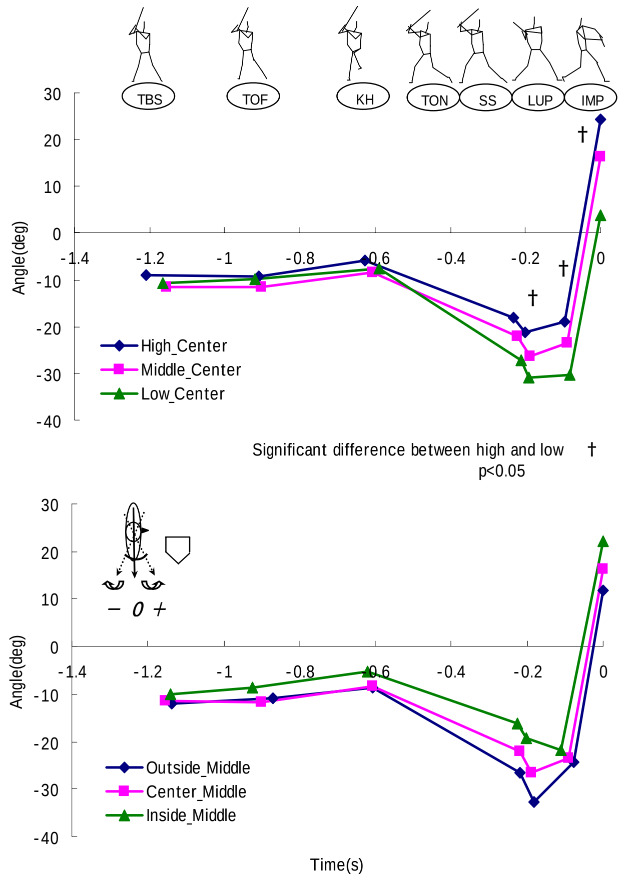

Figure 1. The trunk twist angle in the High－Low and Outside－Inside ball hitting.

smaller in the low ball hitting at IMP than that of the high ball hitting. These differences in the shoulder rotation between the high and low ball hitting indicated that the different trunk motion and timing were used in swinging the bat for high and low ball hitting.

The lower figure shows changes in trunk twist angle for hitting the ball at three courses (outside, center, inside). The shoulder backward rotation was larger in the outside ball hitting from TON to LUP than that of the inside ball hitting, and the shoulder forward rotation tended to be smaller in the outside ball hitting at IMP than that of the inside ball hitting. However these differences were not significant.

These results suggest that when hitting a high ball a batter should rotate the shoulders backward in small range from SS to LUP and use the large forward rotation from LUP to IMP, and that in hitting a low ball a batter should use large backward rotation of the shoulders from TON to LUP and use the small forward rotation from LUP to IMP.

STUDY OF THE INVERSE DYNAMICS OPTIMAL CONTROL TECHNIQUE IN CYCLING

[1] Olavo Luppi Silva, [1]Franco Giuseppe Dedini [2]Luciano Luporini Menegaldo.
[1]Faculty of Mechanical Engineering – State University of Campinas/UNICAMP - Brazil,
[2]Department of Mechanical and Materials Engineering – Military Institute of Engineering/IME – Praça General Tibúrcio, 80; CEP 22290-270, Rio de Janeiro/RJ - Brazil; email: lmeneg@ime.eb.br,

INTRODUCTION

In recent developments, the authors have shown the possibility of considerable decreases of computational time, if a hybrid technique optimal control technique is applied [1,2] to find muscle activation patterns in musculoskeletal systems. The so-called Inverse Dynamics Optimal Control (IDOC) method breaks the classical Forward Dynamics Optimal Control Problem (OCP) in two steps:

a) Finding the joint torque curves through the Inverse Dynamics analysis of a real or simulated system;
b) Formulate an OCP that minimizes a cost function comprising a muscle-activation related expression augmented with an error function part between the moments calculated by inverse dynamics and the actual moment generated by muscles. Only muscle dynamics is considered in the OCP dynamic constraints, removing Multi-Body System (MBS) differential equations of the OCP formulation. These equations greatly increase the numerical cost of the OCP, as discussed in [3] for posture.

In this paper, the IDOC method was applied to cycling. The low numerical cost associated with the IDOC method should contribute to improve clinical applicability of mathematical modeling and optimal control, in the prescription of custom rehabilitation programs.

METHODS

Initially, a MBS of human pedaling was formulated. The crank, ankle, knee and hip torques in both sides were calculated for a subject performing a constant angular velocity cycling movement. The multi-body system is a 2-D, eight bars and three degrees of freedom linkage with two closed loops. Each bar represents crank, stationary bar, thigh, shank and ankle for right and left sides (Figure 1). The model dimensional and inertial parameters, as well as the measured pedal forces, were taken from [4,5].

The IDOC problem was formulated considering ten lower-limb muscles (*gluteus medius,* hamstrings*, biceps femoris* short head, *gluteus maximus*, ilipsoas, *rectus femoris, vasti, gastrocnemius, soleus, tibialis anterior*). A Hill-type muscle contraction dynamics was used. The dependence of the muscle moment arms with joint angles was taken from [6]. The OCP was formulated and solved in the framework of the Consistent Approximations Theory, using the RIOTS toolbox for Matlab [7].

RESULTS AND DISCUSSION

The torque curves obtained by the MBS inverse dynamics analysis has shown a good agreement with data published by other authors [8]. In addition, the joint torque curves formed by the sum of the individual muscle contributions, after the IDOC solution, were very similar to the inverse dynamics outputs. A series of numerical tests was carried out to find the most suited cost function that should lead to a reasonable matching between the calculated and EMG muscle activation patterns. This exploration is still in progress. However, feasible solutions were found for some muscles, compared to EMG and OCP data presented by [9]. Namely, *soleus, gastrocnemius*, hamstrings and *rectus femoris* has shown similar shapes. Other muscles, however, showed a good agreement with [9] in the maximum activation amplitudes, but with some phase distortion. Other classes of constraints, like endpoint equality and inequality constraints are currently being explored. The computational time used to perform the IDOC solution in one cycle of pedaling at 60 rpm was around 3-4 hours using a 450 MHz Pentium III processor. The results suggest that the method may a suitable alternative to low-cost optimal control analysis of cycling.

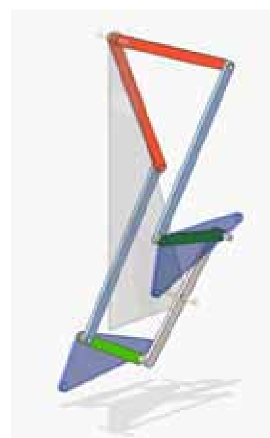

Figure 1: Geometry of the cycling model

REFERENCES

1. Menegaldo, LL., et al. Proceedings of 6th Int. Symp. CMBBE, Madrid, 2004.
2. Menegaldo LL, et al.. *J Biomech* **submitted**, 2005.
3. Menegaldo LL, et al. *J Biomech* **36**, 1701-1712, 2003.
4. Redfiled R, et al. *J Biomech* **19**, 317-319, 1986
5. Gonzalez H et al. *J Biomech* **22**, 1151-1161, 1989
6. Menegaldo LL, et al. *J Biomech* **37** 1447-1453, 2004
7. Schwartz, AL. et al., *SIAMM J. Control Optim.*, **34**, 1235-1296, 1996.
8. Kautz S.A., et al. *J Biomech*, **28**, 1391-1401, 1995.
9. Kaplan ML. et al., *J Biomech* **34**, 1077-1083, 2001.

ACKNOWLEDGEMENTS

This work received a scholarship from the Conselho National de Pesquisa e Desenvolvimento (CNPq).

LOAD-SPECIFIC RELATIONSHIPS BETWEEN MUSCULAR POWER AND BONE MINERAL DENSITY

[1]Brandi Row and [2]Peter Cavanagh
[1]The Centre for Studies in Aging, Sunnybrook and Women's College Health Sciences Centre, Toronto, Canada, [2]Cleveland Clinic Foundation, email: Brandi.Row@sw.ca

INTRODUCTION

Lower extremity muscular strength (STR) influences bone mineral density (BMD) of the proximal femur (PF) and lumbar spine (LS) in older adults [1]. However, when body size is taken into account, STR is not independently associated with BMD of the PF in older adults [2]. In various lower extremity muscle groups, normalized STR and power (PWR) contributed to the best predictive models of BMD in older adults [3]. Further, PWR of lower extremity muscles contributed uniquely to BMD, even when taking sex, age, BMI, and STR into account [3]. The purpose of this study was to determine 1) which factors of PWR (force and velocity) are most predictive of BMD, and 2) at which loads relative to maximal STR is the relationship between PWR and BMD optimized in older adults.

METHODS

Pre-intervention STR, PWR and BMD data were collected for 48 healthy older adults (28 females, 20 males; ages 65-82 yrs) who were accepted into an exercise intervention study previously described [4]. Subjects with osteoporosis, joint replacements and those already participating in resistance-training programs were excluded. Dual X-Ray Absorptiometry (DXA) scans (Hologic, Inc., Bedford, MA) were used to assess whole body lean body mass (LBM) and BMD at the PF and LS. Subjects performed STR tests (one-repetition maximum, 1RM) for Leg Press (LP), Hip Abduction (AB), Hip Adduction (AD) and Hip Flexion (HF) using resistance-training machines. PWR was determined for each exercise: the concentric motion was completed 'as fast as possible' at loads of 30, 50 and 70% of 1RM (except for LP, where 30% 1RM is too light to perform safely). PWR (force*velocity during the PWR test), and STR (in kg and Watts, respectively) were normalized by dividing by the lean body mass of the total leg in kg. Regression analyses were conducted using statistical software (Minitab, State College, PA). The 'best subsets' feature was used in order to determine the combination of variables (lowest bias, highest adjusted R^2) accounting for the most variance in BMD. Systematic variations of the regressions were conducted in order to determine the optimal relationship between the load (% 1RM) used during the PWR tests and BMD, and to determine which component of PWR (force or velocity, VEL) was the most influential for BMD.

RESULTS AND DISCUSSION

While sex was the leading predictor of BMD (women < men), the VEL component of PWR was also an important predictor of PF BMD, while the normalized force component was not. For LS BMD, however, *both* VEL and force parameters were important predictors (Table 1). Regression models for Proximal Femur BMD were optimized with PWR tested at a load of 50% 1RM (Figure 1). Conversely, models for Lumbar Spine BMD were optimized at a load of 70% 1RM.

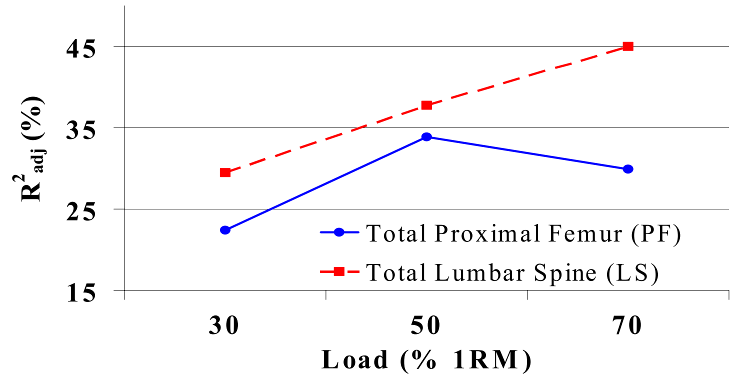

Figure 1: R^2_{adj} for PF and LS BMD for models as in Table 1.

CONCLUSIONS

This study revealed that PWR tests at moderate loads (50% 1RM) produced the best relationship between PWR parameters and PF BMD. A load of at least 70% 1RM was required to optimize this relationship with LS BMD. Given the predominance of VEL as a predictor of BMD, particularly for PF BMD, high velocity resistance training should be evaluated as a method for improving BMD in older adults. Further, investigations should focus on whether such load-specific relationships optimize training outcomes for PF and LS BMD.

REFERENCES

1. Layne, JE, & Nelson, ME, *MSSE* **31(1)**, 25-30, 1999
2. Owings, TM, et al., *Bone* **30(3)**, 515-20, 2002
3. Row, BS & Cavanagh, PR, *Proceedings of GCMAS*, Lexington, KY, 2004.
4. Row, BS & Cavanagh, PR, *Proceedings of ISB XIX*, Dunedin, New Zealand, 2003.

This work was performed at the Pennsylvania State University.

Table 1: P-values and R^2_{adj} for the best model for each BMD parameter at loads of *50% 1RM, and $^+$70% 1RM (Force (F)/ leg LBM). Blank cells indicate that the indicated parameter was not a part of the best model.

BMD	Sex	Age	BMI	AD VEL	AB VEL	HF VEL	LP F	AD F	AB F	HF F	R^2_{adj} (%)
Femoral Neck	0.000		0.039		0.113	0.164					27.7^+
Greater Trochanter	0.000	0.037	0.157	0.012	0.006						43.9*
Inter-Trochanteric Crest	0.000		0.077	0.026	0.090						34.4*
L1	0.000		0.060	0.056	0.027					0.283	48.7^+
L2	0.000		0.183	0.009			0.017		0.181		43.8^+
L3	0.003			0.004	0.312	0.197	0.147	0.127			37.6^+
L4		0.019		0.035			0.101	0.019	0.042		30.8^+

IMPACT MECHANICS DURING STOP AND GO TASKS UNDER FATIGUED AND NON FATIGUED CONDITIONS

[1] Deborah King, [1]John Sigg and [2]Barb Belyea, [1]Chris Hummel, [2]Mike Buck
[1]Department of Exercise and Sport Sciences, Ithaca College
[2]Department of Physical Therapy, Ithaca College; email: dking@ithaca.edu; web: www.ithaca.edu/hshp/ess

INTRODUCTION

Fatigue affects muscle activation and coordination during complex tasks such as walking, jumping, and landing [1,2,3]. Moreover, it is commonly believed, and there is some evidence to support, that injuries occur more often near the end of practices and competitions when athletes are fatigued [1]. However, few studies have examined the effects of fatigue on landing mechanics during stop and go tasks [e.g. 4,5]. The fatiguing protocols used in these exemplar studies targeted the musculature used specifically for jumping, which may not be representative of the cardiovascular and muscular fatigue that develops during a game or practice. The purpose of this study was to examine landing mechanics in male and female athletes performing stop and go landing tasks in fatigued states representative of game conditions.

METHODS

Twenty healthy athletes (10 male, 10 female) participated in this study after giving their written informed consent. The testing session involved warm-up, pre-fatigue testing, a fatiguing protocol, and post-fatigue testing. The pre and post fatigue testing involved 4 different tasks: 1) 90 degree cut, 2) 45 degree cut, 3) forward step, and maximum vertical jump after landing from a 0.5 m high box.

The fatigue protocol consisted of a 10 minute progressive incline treadmill run followed by an “M-drill”. The M-drill was a 3 by 3.5 m pattern of forward, backward, and side ways steps with vertical jumps. The pattern was repeated until 1) lap time slowed to 150% of their fastest time or 2) completion of 10 laps and inability to achieve maximum jump height.

During pre and post testing, GRFs were measured with two AMTI force plates. High speed digital video data were collected using two Photron cameras. The subjects performed 3 vertical jumps between each post trial to maintain their level of fatigue. The GRF data for the 90 degree cut and vertical jump tasks only are presented in this abstract. Data were analyzed with a three way repeated measures ANOVA at $\alpha = 0.05$.

RESULTS AND DISCUSSION

The initial vertical impact GRF peak of the cutting leg was significantly greater in the post fatigue trials as compared to the pre fatigued trails (Figure 1). Additionally the time to the

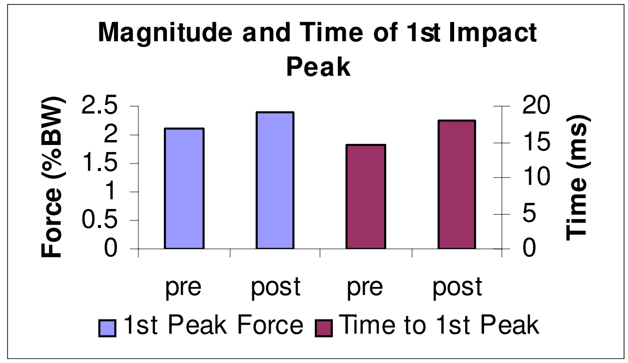

Figure 1: Impact peak & time to peak pre and post fatigue.

first vertical GRF peak was significantly longer in the post fatigue trials (Figure 1). A non significant decrease in impulse was also observed pre to post fatigue (p=0.056; Table 1). There was no significant gender or task interaction.

The increased peak impact forces and times to peak impacts suggest altered landing strategies utilized by the subjects in the fatigued state. This is supportive of previous research using localized fatiguing protocols which suggests subjects respond to fatigue with varying combinations of increased bilateral variability and increased impact forces during the landing phase of stop and go tasks [4].

CONCLUSIONS

Significant increases were found in vertical GRFs during the landing phase of stop and go tasks in pre and post fatigued conditions, along with significant difference in the timing of the GRF peaks. Alterations in landing mechanics observed in fatigued states, such as those that might be encountered in practice and game situations, may pre-dispose athletes to increased risks of injury. Further research in the relationship to fatigue and injury occurrence appears to be warranted.

REFERENCES

1. Johnston, et al. *Med Science Sports Exerc*, 30, 1703-1707, 1997.
2. Pinnerger, et al. *Med Sci Sports Exerc*, 23, 647-653, 1999.
3. Podacki et al. *Med Sci Sports Exerc*, 33, 1157-1167, 2000.
4. McNitt-Gray, et al. *23rd Annual Meeting of American Society of Biomechanics*, Atlanta, GA, 1996.
5. Nyland, et al. *Orthop Sports Phys Ther*, 25, 171-184, 1997.

Table 1: Vertical GRF variables pre and post fatigue across stop & go task. All values are mean ±SD. *p<0.05.

	First Impact Peak* (% BW)	Time to Impact Peak* (ms)	Contact Time (ms)	Impulse (Ns/BW)	Peak Force (%BW)
Pre	2.06 ± 1.8	14.5 ± 3.8	401 ± 86	0.63 ± 0.30	3.67 ± 1.8
Post	2.27 ± 1.9	17.0 ± 7.3	396 ± 71	0.61 ± 0.29	3.81 ± 1.9

THE EFFECT OF FATIGUE ON THE CONTROL OF TARGETED ISOMETRIC DORSIFLEXION IN HUMANS

[1] Yi Ming Huang, [2]Ya Ju Chang, [2]Chung Hsun Hsieh and [2]Mong Chiech Jiang
[1] Graduate Institute of coaching science, National College of Physical Education and Sports, Tao-Yuan, Taiwan
[2] Department of physical therapy & Graduate Institute of Rehabilitation Science, Chang Gang University, Tao-Yuan, Taiwan
E-mail: imin127@ms55.hinet.net

INTRODUCTION

Fast and target orientated movement is common in daily life and in sports. Skeletal muscle fatigue is defined as the failure to maintain required or expected torques or the increasing efforts to maintain the same torque output level (2). Previous study has shown that torque of maximal voluntary contraction (MVC) declined and the contraction and relaxation prolonged after fatigue (1). It is possible that the ability of movement control after fatigue declines by fatigue, especially in fast movement. Co-contraction is one form of the controlling strategies defined as the simultaneous recruitment of two muscles. Since fatigue results in slowing of contractile speed and increase recruitment during submaximal isometric contractions (3), the error of movement, especially fast movement, should increase. It is not clear whether this increased movement error can be corrected by adjusting the control pattern of agonist- antagonist muscle pairs.

METHODS

10 volunteers with averaged age 22.9 ± 1.97 participated. Subjects sat on a rigid chair with one foot fixed firmly on the platform of the torque measurement system (fig.1). The signal from the force transducer as well as a target line was displayed on a screen where subjects can clearly view. The electromyography (EMG) signals were recorded from soleus and tibia anterior muscle (fig.2).

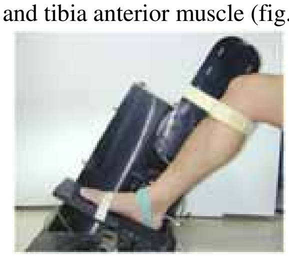

Fig1. Torque measurement system

Fig2. Tibialis anterior and Soleus EMG electrode placement

The test was started with 5 MVC of dorsiflexion. Fatigue was defined as subjects' torque was hard to reach 50% MVC. 40% of the MVC was calculated to set the target line. Following the MVC test, the subject conducted 5 fast and 5 slow isometric dorsiflexions with peak torque just hitting the target line before and after TA fatigue. The systematic errors of torque generation and co-contraction ratio of EMG firing were calculated. Two-way repeated-measures of ANOVA was used to examine the effects of fatigue and speed on systematic error, co-contraction ratio. A significance level of $p < 0.05$ was used.

RESULTS AND DISCUSSION

In this study, we observed the higher systematic errors and co-contraction ratio in the fast contractions (Table 1 & 2). We expected participants used co-contraction for improving the performance of force generation.

Table1. The mean and Std. of Systematic error in pre-test and post-test in the fatigue and control session.

	Systematic error (%)			
	Experimental group		Control group	
	fast	slow	fast	slow
Pre	11.69±4.80	4.55±2.16*	9.10±3.91	3.38±0.99*
Post	24.31±6.53†	10.27±4.10*†	8.16±3.77	4.65±1.92*

Table2. The mean and Std. of co-contraction ratio of the TA and Sol in the pre-test and post-test in the fatigue and the control session.

	Co-contraction ration (%)			
	Experimental group		Control group	
	fast	slow	fast	slow
Pre	0.81±0.14	0.67±0.24*	0.76±0.19	0.67±0.28*
Post	0.82±0.10	0.80±0.20*†	0.80±0.15	0.58±0.34*

If the phasic activation associated with the accuracy control of the force, it is interesting to know if the pattern switched to reduce error after fatigue. According to the result (Table2), the co-contraction ratio was only increased in the slow contractions but was unvaried in the fast contractions. This increase of the co-contraction ratio was parallel to the change of systematic error (Table1). After fatigue, the magnitude of the systematic error increment was higher in the fast contractions than in slow contractions indicating the accuracy was adjusted in the slow contractions. It is possible that the change of co-contraction ratio in the slow contractions was for increasing the accuracy of movement.

CONCLUSIONS

Our results supported that the systematic of force generation increased after fatigue in both the fast and slow isometric contractions. The slow isometric contractions had smaller increment in the systematic error related to the change of the agonist-antagonist activation patterns.

REFERENCES

1. Buttelli O, Seck D, Vandewalle H, Jouanin JC, and Monod H. Effect of fatique on maximal torque during short exhausting cycling. Eur J Appl Physiol 73:175-179, 1996.
2. Edwards RHT, Hill DK, and Jones DA. Fatigue of long duration in human skeletal muscle after exercise. J Physiol(Lond). 272:769-778, 1977.
3. Marsden CD, Obeso JA, and Rothwell JC. The function of antagonist muscle during fast limb movement in man. J Physiol 335:1-13, 1983.

ACKNOWLEDGEMENTS

The work was supported by grants from the National Science Council, Taiwan (NSC92-2314-B-182-0)

REDUCED FORCE CONTROL AND INCREASED CONTRALATERAL TRAPEZIUS CO-ACTIVATION AMONG SUBJECTS WITH WORK RELATED MUSCULOSKALETAL SYMPTOMS

Bente R. Jensen, Theis B. Hansen and Marianne Pilegaard
Institute of Exercise and Sport Sciences, University of Copenhagen, Denmark.
email: brjensen@ifi.ku.dk

INTRODUCTION

Increased values of vibro-tactile sensory threshold indicating entrapment of peripheral nerves have been documented among computer users with severe upper extremity symptoms [1]. However, our knowledge regarding potential functional consequences is limited. The aim was to study fine motor control and upper extremity muscle activation in subjects with and without symptoms.

METHODS

Three groups of female subjects participated. The +sPC group (44 yrs, n=15) had severe upper extremity symptoms and worked at the computer for 75 % of the working day. The -sPC group (43 yrs, n=11) had no symptoms and worked at the computer for 73 % of the working day. The control group (44 yrs, n=9) had no symptoms and worked at the computer for 2 h or less per day. Upper extremity fine motor control was measured in a submaximal handgrip force control task. The task (12 s) was to increase the handgrip force (right hand) as fast as possible to a level above a predetermined upper threshold force level (led feedback) and then decrease the force to below a predetermined lower threshold (led feedback) as fast as possible [2]. The force control task was performed at 3 submaximal absolute force levels, corresponding to 5, 10 and 20 %MVC (maximum voluntary contraction) for a healthy reference group. Each task was repeated 3 times. Task frequency (number of cycles per second), peak force and rate of force increase and decrease for the three groups were calculated. Surface EMG was recorded from mm. trapezius (left and right), right m. extensor carpi radialis, m. extensor digitorum, m. extensor carpi ulnaris and m. flexor carpi radialis during the task and related to maximum values. Average forearm muscle activity expressed as static, mean and peak activity was calculated. Finally, handgrip strength (highest 1-s value out of 3 trials) was measured.

RESULTS AND DISCUSSION

Handgrip strength was 32.0(SE 1.6) kg, 33.1(1.4) kg, and 33.3(1.4) kg for the +sPC, -sPC, and the ctrl group, respectively. Thus, no group differences in muscle strength were found. Task frequency decreased with increasing upper force threshold level for all three groups. However, the frequency of the force control task (across all force levels) was lower for the +sPC group compared to the control group (Figure 1). This could be explained by a slower force increase and a slower force decrease in the +sPC group compared to the control group, whereas no between group differences were found in the peak force during the force control task. Rate of force increase and rate of force decrease was highly correlated ($r = 0.84$, $p < 0.001$).

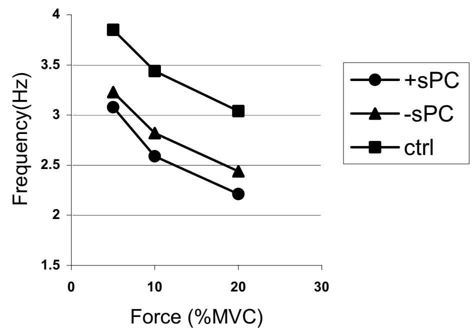

Figure 1: Task frequency during the force control task.

The +sPC group had minor but significantly lower static forearm muscle activity level at all three force levels, a lower mean activity level at the 20 %MVC task and a tendency to a lower mean activity level at the 5 %MVC task than the ctrl group. These differences may be explained by the lower frequency of the force control task in the +sPC group. The increase of the upper force threshold was mainly reflected in the peak activity levels while the static activity remained unchanged. In general, the activity of the mm. trapezius was significantly lower than in the forearm muscles during the force control tasks. The peak activity level of the left m. trapezius was higher in the +sPC and the –sPC groups at the two lowest force levels and higher in the –sPC at the highest force level compared to the ctrl group, while no group differences were found for the right m. trapezius.

CONCLUSION

Impaired fine motor control and increased contralateral shoulder muscle activity were found in the symptomatic group despite of well-maintained muscle strength.

REFERENCES

1. Jensen B.R., Pilegaard M., Momsen A. *Int Arch of Occup and Environ Health* , **75**: 332-340, 2002.
2. Jeng O-J., Radwin R.G., Rodriques A.A. *Ergonomics* **36(7)**: 1055-1069, 1994.

ISB XXth Congress - ASB 29th Annual Meeting
July 31 - August 5, Cleveland, Ohio

UPPER CERVICAL SPINE MODELLING: *IN-VITRO* 3D KINEMATICS

[1,2,3]Dugailly PM, [1]Sobczak S, [1,3]Salvia P, [1]Sholovkha V, [2]Klein P, [1]Van Sint Jan S , [1]Hilal I, [1]Feipel V, [1]Rooze M
[1] Laboratory of Anatomy, [2] Research Unit for Manual Therapies, Université Libre de Bruxelles, Belgium.
[3] Department of Physiotherapy, Erasmus Hospital , ULB, Brussels, Belgium
Corresponding author: pdugaill@ulb.ac.be http://homepages.ulb.ac.be/~anatemb

INTRODUCTION

For the global kinematics of the cervical spine, the upper cervical spine plays a considerable role for maintaining the head in the horizontal plane or for compensating coupling motion occurring at cervical lower segments. Presently, for a better understanding of human biomechanics, procedures using computerized human models have been implemented to analyze the structural mechanics of the human body in attempt to obtain accurate virtual models [1,2,3]. The aims of this study are to develop a standardized protocol for analyzing the *in-vitro* kinematics of the upper cervical spine, and to combine individual kinematics data with anatomical data for 3D bone modelling and simulation.

METHODS

Specimens were sampled from donators and processed according to strict ethical regulations. Medical imaging was acquired by computed tomography (Siemens SOMATOM) in neutral position for nine specimens. Individual morphometric data were extracted for each osseous segment. 3D reconstruction was performed after object segmentation and identification using Amira® (Germany).
For each specimen, the lower cervical segments and related soft tissues were removed as well as the mandible and anterior neck viscera. The upper cervical segments and their ligaments, suboccipital muscles and fascias were kept intact. Fiducial markers (Fidm) (aluminium balls: ∅ 4mm) were placed on the atlas, axis and skull (figure 1). Using a 3-D digitizer (Faro® arm, model 08 Bronze, USA), each Fidm was identified in 5 successive specimen positions of each flexion-extension and axial rotation. For each bone, a local reference system was defined using anatomical landmarks according to the International Society of Biomechanics recommendations [4]. For each vertebral displacement, rotation and translation were computed according to anatomical axis (x,y,z). Helical axis orientation and location were also computed and implemented in kinematics models (figure 2).

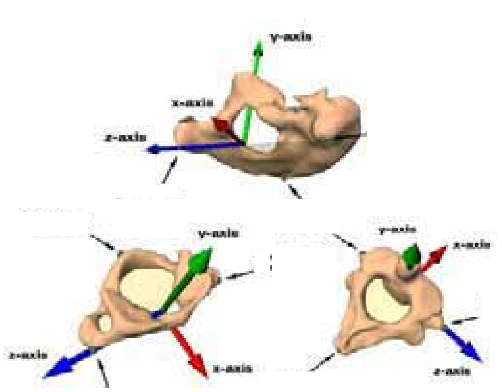

Figure 1: Anatomical landmarks and local reference system of the occipital bone.

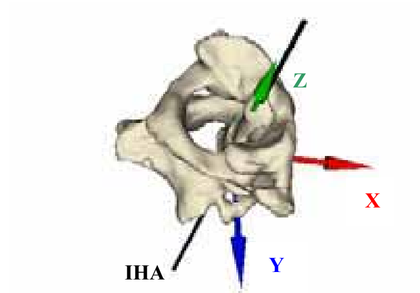

Figure 2: Kinematics model and instantaneous helical axis (IHA) during axial rotation at C1-C2 level

RESULTS

The different steps of this protocol for combining morphological data and interpolation of kinematics data from discrete positions were carried out using a validated registration method[2]. Moreover, a reliability study performed for anatomical and metallic marker digitizing demonstrated good reproducibility of the 3D digitizing. For each specimen, different kinematics patterns were observed, although primary motion was similar (figure 3).

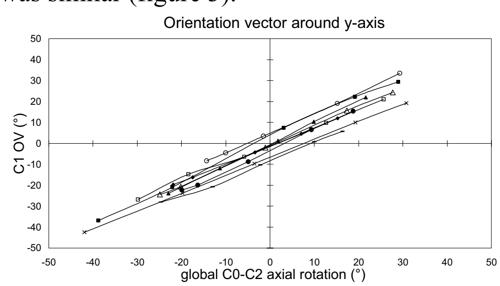

Figure 3: Axial rotation of C1 on C2 (orientation vector, OV) as a function of global C0-C2 movement for each specimen.

DISCUSSION

Considering the presence of surrounding tissues (muscle, fascia) our results are comparable to those found in the literature for the global range of movement as well as for motion patterns. Sampling of human morphological data and modelling represents a significant source of information in the understanding of the biomechanical processes. Such validated models are also needed in the field of advanced care and health knowledge. Moreover, combining *in vitro* and *in vivo* data analysis of the normal mechanical behaviours of the musculoskeletal system would provide the design of specific biomechanical models for understanding of pathogenic functional mechanisms of the upper cervical spine.

REFERENCE

1. Hilal I, PhD Thesis, Université de Rennes I, 2000.
2. Van Sint Jan S et al. J Biomech , 2002, 1475-1484
3. Vasavada AN, Spine 1998, 412-422.
4. Wu G, J Biomech, 2002, 35, 543-548.

DYNAMICAL DIFFERENCES BETWEEN NORMAL AND STEREOTYPICAL BODY ROCKING

[1] Karl Newell, [1] Lee Hong and [2]James Bodfish
[1]The Pennsylvania State University,
[2]J. Iverson Riddle Developmental Center;email: slh343@psu.edu

INTRODUCTION

Stereotypical body rocking has been noted as one of the most common repetitive behaviors exhibited by patients diagnosed with mental developmental disorders [1]. It has been argued that such behaviors should not be classed as being independent of the instrumental activities of daily living [2]. The aim of this experiment was to compare differences and similarities between the dynamics of sitting and body rocking in adults with profound mental retardation and healthy adult controls.

METHODS

7 adults (aged between 31 and 45 years) diagnosed with severe or profound mental retardation (Vineland Adaptive Scales), residents of a state developmental center, were selected due to their regular engagement in body rocking stereotypies (MR group). These participants were not on any regimens of medications. 3 adult males and 3 adult females from the University community served as the controls, matched to be within 10% of the age, weight and height of the disordered patients. The Institutional Review Board of the Pennsylvania State University and the Western Carolina Center provided approval for the informed consent and experimental procedures involved.

A force platform (AMTI Model SG6-4) placed beneath a wooden block (length 46.4 cm x width 50.8 cm x height 48 cm) served as the data collection device, while the participants were seated upon this block, which had no back, thus preventing the participants from leaning against it. The motion of the centre of pressure (CoP) of generated by the participants force outputs served as the dependent variable.

MR group participants were measured while exhibiting stereotypical body rocking behavior and during a protocol in which they were sitting still. Matched control participants were asked to simulate body rocking by oscillating at a preferred frequency and amplitude and were then asked to sit as still as possible. 3 trials lasting 10 s were recorded for each participant in the still and body rocking conditions.

RESULTS AND DISCUSSION

For the controls, similar modal CoP oscillation frequencies were noted during both sitting still and voluntary rocking (Figure 1). However, the complexity of the CoP time series was higher during quiet sitting, marked by increased approximate entropy (values). The MR group however, demonstrated an opposite direction of change. While the modal frequency of CoP oscillations was lower during sitting ill, no differences were noted between the complexity of the CoP time series during quiet sitting and body rocking.

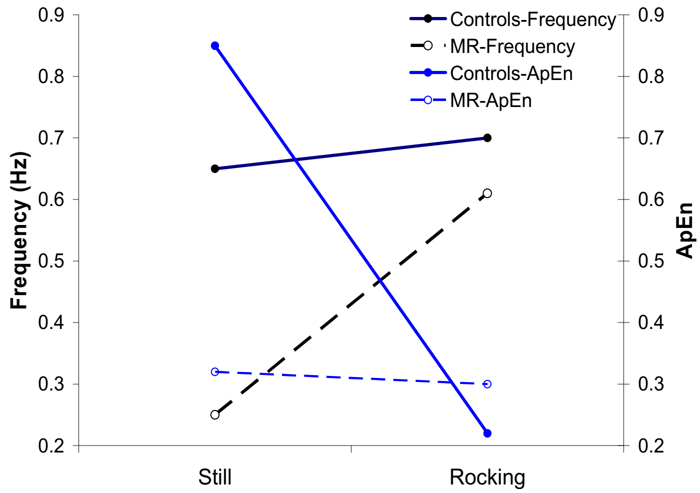

Figure 1. Mean ApEn and modal frequency values during both sitting still and body rocking in both the MR group and matched controls.

CONCLUSIONS

The results are supportive of the idea that sitting and body rocking possess similar dynamics in healthy adults. Similarities in the dynamics of body rocking in controls and MR group suggest that both behaviors possess similar modes of organization, though with different scaling values. Greater dynamical stability afforded by body rocking as opposed to sitting still could be a contributing explanation for the regular occurrence of such stereotypical behaviors in MR patients.

REFERENCES

1. Lewis MH Baumeister AA (1982). Stereotyped mannerisms in mentally retarded persons: Animal models and theoretical analyses. In N. R. Ellis (Ed.), *International review of research in mental retardation* (Vol. 11. pp. 123-161). New York: Academic Press.
2. Sprague RL & Newell KM (Eds.) (1996). *Stereotypies: Brain and behavior relationships.* Washington, D.C: American Psychological Association.

3D MUSCLE MOMENT ARMS USING MUSCULOSKELETAL MODELING

[1,2,3]Dugailly PM, [1]Dermience G, [1]Sobczak S, [1,3]Salvia P, [2]Klein P, [1]Van Sint Jan S, [1]Hilal I, [1]Feipel V, [1]Rooze M
[1]Laboratory of Anatomy, [2]Research Unit for Manual Therapies, Université Libre de Bruxelles, Belgium.
[3]Department of Physiotherapy, Erasmus Hospital , ULB, Brussels, Belgium
Corresponding author: pdugaill@ulb.ac.be http://homepages.ulb.ac.be/~anatemb

INTRODUCTION

Upper cervical muscle biomechanics is poorly reported in the literature. However, these muscles seem to play an important role in head stabilization during cervical spine movement. The objectives of this study were to analyze the *in vitro* 3D moment arms of the suboccipital muscles during upper cervical spine movement and to implement these biomechanical muscle data in a musculoskeletal model.

METHODS

Kinematics data were sampled from digitizing technical markers (aluminum balls: diameter, 4mm) placed on the upper cervical segments (skull, C1 and C2) of 7 fresh specimens. Suboccipital muscles (rectus capitis posterior major (RCPM), rectus capitis posterior minor (RCPm), obliquus capitis superior (OCS), obliquus capitis inferior (OCI)) were kept intact to assure accurate digitizing of their insertions (Mmark) and fiber orientation in a maximal flexion position. Five successive positions for axial rotation (AR) and flexion-extension (FE) were processed. Axial rotation was achieved from maximal right rotation to maximal left rotation. All kinematics and muscle data were obtained using a 3-D digitizer (Faro® arm, model 08 Bronze, USA). Moreover, medical imaging of each specimen supplied morphometric data for 3D reconstruction (Amira®,Germany). According to a validated registration method [2], registration of kinematics and muscle data with morphometric data was processed using the DataManager software (http://www.tecno.ior.it). Muscle orientation was defined by the line of action, a straight line between attachment centroids (figures 1 and 2).
Then, for both movements, muscle lengths were computed for the five positions. Muscle moment arm was computed using a tendon excursion method previously described [4].

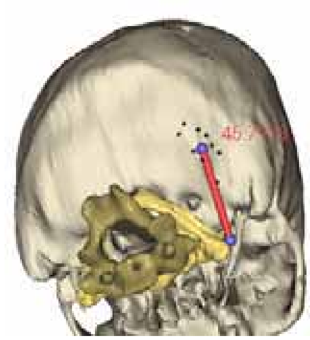

Figure 1: Surface muscle markers (●) after digitizing of the right occipital insertion of the OCS. Centroid of attachment site (●), muscle action line (▬) and length (mm).

RESULTS AND DISCUSSION

Average moment arms (table 1) showed comparable value between right and left muscles for both movements. Absolute moment arms were similar for RCPM, OCS and OCI in AR and for RCPm, RCPM and OCS in FE. Moment arm magnitude was close to zero for RCPm in AR and for OCI in FE. In general, moment arms were larger for AR except for RCPm. For AR, our results confirmed the antagonist role of OCS compared to RCPM and OCI.

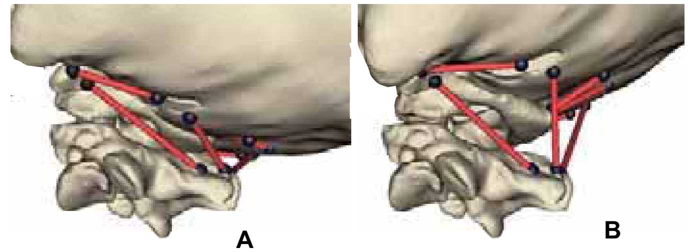

Figure 2: Musculoskeletal model of one specimen in extension (A) and maximal flexion (B) of the C0-C2 complex. Muscles action line (▬) and insertion (●).

	AR		FE	
	left muscle	**right muscle**	**left muscle**	**right muscle**
RCPm	1.9 (12.4)	-0.7	19.3 (7.1)	22.1 (5.3)
RCPM	-23.3 (5.0)	22.3 (5.8)	14.9 (3.6)	18.8 (5.0)
OCS	24.5 (6.5)	-22.8 (11.1)	17.2 (3.4)	17.5 (5.1)
OCI	-24.6 (2.1)	24.8 (3.0)	-2.2 (8)	-2.2 (6.6)

Table 1: Average suboccipital muscle moment arms (mm) and SD during AR and FE. Negative values represent antagonist action regarding the primary movement.

Our data were sampled using an accurate device that is commonly used in the literature. Kinematics data were computed using validated method for registration of different data sets. If some morphometric and biomechanical data are found in the literature, only few are available about suboccipital muscle length variations and moment arms. Our results are partially in agreement with previous studies [3]. Vasavada et al [3] have observed similar data in AR concerning the investigated muscles but differences are observed for flexion extension. These differences are most probably due to different methodological approaches.
In this study kinematic and muscle data were obtained from the same specimens. This integration provides an interesting source for the analysis of musculoskeletal mechanic using an integrated computer graphic environment.

REFERENCE

1. Hilal I, PhD Thesis, Université de Rennes I, 2000.
2. Van Sint Jan S et al. J Biomech , 2002, 1475-1484
3. Vasavada AN et al. Spine 1998, 412-422.
4. Klein P et al. J Biomech, 1996,21-30.
5. Dugailly PM et al. Arch Physiol Bioch vol 106b,80 ,1998

ACKNOWLEDGEMENTS

Research project partially funded by the EC through MULTIMOD project (contract # IST-2000-28377)

CHARACTERISTICS OF STANDING AND ANTERIOR TILTING POSTURES IN RELATION TO THE TIME OF DAY

[1] Koichi Shinkoda, [1]Naohiko Kanemura, [2]Saburo Ohmine and [2]Kenji Hachisuka
[1]Hiroshima University Graduate School of Health Sciences,
[2]University of Occupational and Environmental Health;email: shinkoda@hiroshima-u.ac.jp

INTRODUCTION

Standing balance and mobility has been essential to our daily lives and physical wellbeing, especially to the aged and/or people with physical disabilities [1]. Understanding its functions is important in improving safety in their daily lives, especially in decreasing fall risks and improving their physical wellbeing. The purpose of this study was to investigate the characteristics of anterior tilting movement and the difference in balance and mobility function in respect to the time of day, i.e. AM and PM by analyzing coordinates of the center of foot pressure (CFP) and the minimum jerk theory [2].

METHODS

Fourteen older subjects (older group: OG; female: 8, male: 6; age 63.3±6.04 years) and nine younger female subjects (younger group: YG, age 20.5±0.53 years) were recruited for this study with informed consent. On the Kistler force platforms, the subjects were instructed to stand still barefoot for the first five seconds. When they hear a beep, they were to tilt their body forward as quickly as possible around the ankle joint keeping the heel on the force platforms and holding that position until the second beep. When the third beep is heard, they were instructed to go back to the previous erect position as quickly as possible. The subjects kept the anterior tilt position for about 15 second and the total time was 30 seconds per trial (Figure 1). The OG subjects had two trials in a single day. The YG subjects were evaluated three times in a single day i.e. AM (around 8:30) and PM (around 15:30), and were tested over five non-consecutive days in a span of two weeks. The subjects sat down for about a minute to rest between the tests. The signals from the force platforms were sampled at 30Hz using A/D converter and PC. Analyses were done using variables derived from *x-y* coordinates (*x*: medial-lateral; *y*: anterior-posterior) of CFP. Each CFP data was analyzed statistically, and the level of significance was set at $P<0.05$.

Figure 1: Standing and tilting postures. A: standing still; B: anterior tilting; C: return to the previous position

RESULTS AND DISCUSSION

The mean anterior-posterior CFP coordinate (*Cy*) for 5 seconds when the OG subject returned to the previous erect position was found to be significantly more posterior than for 5 seconds prior to the tilting position (paired t test, $P<0.05$). Similar results were also obtained from YG subjects. The subjects appear to lose their sense of positioning when a relatively stressful posture is applied to their lower extremity muscles. This phenomenon was observed in both groups. Therefore, there is a possible risk of posterior fall, when a person tries to lift a relatively heavy object, which is in front of her/him.

The *Cy* of YG while maintaining the anterior tilting position was found to be significantly more anterior in PM than in AM (Figure 2, Repeated measures ANOVA; $P<0.05$). Conversely, this means that a person does not have better mobility in AM as in PM. The human foot is long and narrow and the distance between the ankle and toe is longer than that of between the ankle joint and the heel. In other words, a more anterior CFP is advantageous in controlling the standing position using the braking function of the triceps surae. Therefore, when treating patients and caring for older people, we need to keep in mind that there is a difference in the standing balance and mobility in respect to the time of day.

There were no significant difference in the jerk costs (JC) [2] of *x-y* coordinates of CFP in respect to the time of day during the standing still and maintaining the anterior tilting positions as well as the phases of the anterior tilting and posterior returning motions in YG. This suggests that the task adopted in this study was linear movement, indicating that a significant difference in JC motion smoothness was not obtained between AM and PM.

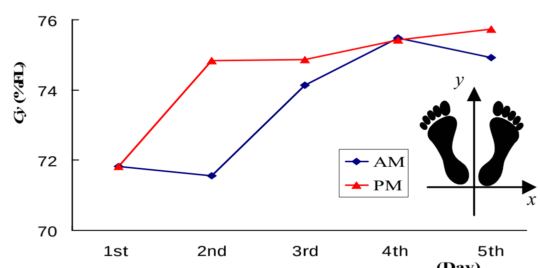

Figure 2: Mean CFP *y*-coordinate *Cy*. Values are expressed in percentages to the foot length (FL) from the heel ($P<0.05$).

CONCLUSIONS

Since there seems to be an illusion of postural control to some extent, we have to keep that in mind when we care for not only older adults but also healthy persons who require physical therapy. For a much better detailed understanding in the differences of postural control and mobility in time of day, additional evaluations, such as electromyography and three dimensional motion analysis, are needed.

REFERENCES

1. Shinkoda K, et al. *Jpn J Traumatol Occup Med* **47**, 30-38, 1999.
2. Hreljac A, *Gait Posture* **11**,199-206, 2002.

THE INFLUENCE OF KNEE AND ANKLE BRACING ON LOWER EXTREMITY KINETICS AND KINEMATICS DURING JOGGING

Brian M. Campbell, PhD[1], Charles W. Armstrong, PhD[2], Daniel Cipriani, PhD, PT[3], and James A. Yaggie, PhD, RKT[4]
[1]Bowling Green State University, Kinesiology Division, Bowling Green, OH
[2]The University of Toledo, Department of Kinesiology, Toledo, OH
[3]Medical College of Ohio, Department of Physical Therapy, Toledo, OH
[4]San Diego State University, Department of Exercise and Nutritional Studies, San Diego, CA
email: campbeb@bgnet.bgsu.edu

INTRODUCTION

There is substantial research on the effects of both ankle and knee braces on lower extremity kinetics and kinematics, when these braces are worn independently [1,2,3]. However, bracing of the knee and ankle simultaneously, for both prophylactic and rehabilitative purposes, is a common practice in athletics. While prophylactic bracing in athletes may be beneficial, some research has demonstrated potentially detrimental effects on lower extremity function. Of particular concern in this regard, are the effects that may be due to the combined use of ankle and knee braces. It has been speculated that that the mobility limitations induced by multiple braces may create aberrant motion and forces at other joints that may result in injury. Therefore, the purpose of this investigation was to determine how ankle bracing alone, knee bracing alone, and ankle and knee bracing together affect lower extremity kinetics and kinematics during straight ahead jogging in healthy subjects.

METHODS

Eighteen subjects with no history of lower limb pathologies within the two years prior to this study participated in the investigation. Each of the subjects performed a series of jogging trials with each of four brace conditions (no brace (NB), ankle brace (AB), knee brace (KB), ankle and knee brace (ABKB)). An Ankle Stabilizing Orthosis (Medical Specialties Inc.) and the functional knee brace (dj Orthopaedics, LLC.) were fitted to each subject according to manufacturers' guidelines. The subject rode a stationary bike, at a comfortable self selected pace for 5 minutes to provide a period of accommodation to the braces prior to the jogging trials. Each subject was then required to complete five to seven trials of straight ahead jogging for each of the randomized bracing conditions. Gait data was collected using a six camera, 3-D HIRES video system, a gait analysis software package and two force platforms. This data was analyzed for each of the subject's trials to determine the affects of the different brace conditions on the individual's gait pattern.

RESULTS AND DISCUSSION

Average knee, ankle and hip joint angles for the NB, AB, KB and the ABKB groups were calculated and statistically compared at the point of peak knee moment (PKM). Figure 1 illustrates a statistically significant reduced knee joint angle at PKM in the KB and ABKB conditions compared to the NB condition. Results also revealed significantly reduced ankle joint plantarflexion ($p = .046$) at PKM in the AB trials and a significantly reduced hip flexion angle ($p = .034$) in the KB and ABKB trials.

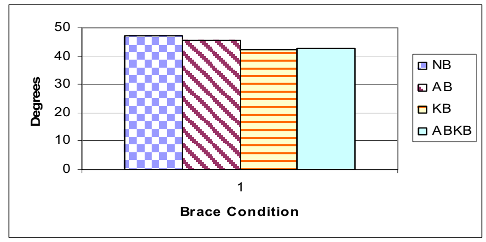

Figure 1: Left Knee Position at PKM. $p = .007$

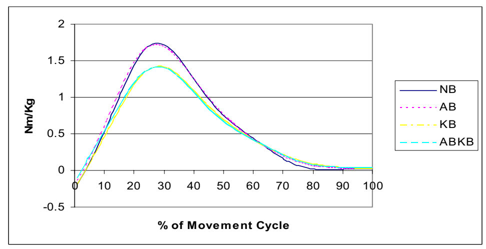

Figure 2: Left Knee Moments

Additionally, although not statistically significant, there were interesting trends in the joint moment data that illustrated a decreased knee extension moment in the KB and ABKB conditions (Figure 2). Additionally, there appeared to be a reduced ankle joint moment in the AB condition when compared to the other conditions. Finally, the ABKB condition appeared to evidence a slightly higher peak hip moment compared to the other conditions.

Previous studies have demonstrated a pattern of knee extensor torque adaptation during jogging, associated with FKB use, indicative of reduced stress on the ACL [1,2]. However no previous research has addressed the influence of simultaneous knee and ankle bracing on lower extremity function. It does appear from the current results that knee and ankle bracing may be protecting their respective joints, through a reduction in the moments. However these bracing conditions may be predisposing other areas of the body, specifically the hip and low back, to potential injury. With the rise in the use of prophylactic combined knee and ankle bracing in athletics, it is important for clinicians to be aware of these possible predisposing factors, even though the braces may be of some benefit in reducing injury.

REFERENCES

1. DeVita P., et al. *J Biomech*, **29**, 583-588, 1996.
2. DeVita P., et al. *Am J of Sports Med*, **26**, 778-784, 1998.
3. Miller E, et al. *P Clin of N America*, **37:5**, 1175, 1990.

FINITE ELEMENT BONE MODEL INCORPORATING HETEROGENEITY AND ANISOTROPY FROM CT

C.M. Müller-Karger, C.A. Larrazabal
Departamento de Mecánica, Universidad Simón Bolívar, Caracas, Venezuela.
email: cmuller@usb.ve, http://www.did.usb.ve/biomecanica

INTRODUCTION

This investigation seeks to achieve a heterogeneous and anisotropic characterization of bone in a simple form and with low computational cost. The ultimate purpose is to create a model and a platform to design and simulate medical devices. CT is used to develop a geometric reconstruction of the bone, and to assign the heterogeneous and symmetric mechanical properties to the elements of the model. The directions of symmetry of the material are determined based on prior knowledge that they are aligned with the principal stresses (Wolf Law). Bone material is considered to be orthotropic.

Several models based on CT consider the bone to be heterogeneous and isotropic. Only a few models take into account anisotropy, using either bone remodeling theories [1,2] or complex trabecular models [3].

METHODS

A femur model was constructed using 197 images, spaced every mm at the epiphisis and every 4mm in the diaphisis. The images were 211x211 pixels, with a resolution of 0.7 mm/pixel, calibrated with a phamton.

Segmentation of the images produced a wire model that was imported to ANSYS. This FE software was programmed for the automatic construction of the solid model. Using 10 nodes tetrahedrons, various meshes were created for a convergence study. Plots of von Mises stresses, equivalent deformation and energy of deformation were evaluated for twenty points of all models. Then, a mesh of 43125 elements was choseen. The load condition used was the same as the one presented by Doblaré and Garcia [2]. Assignment of mechanical heterogeneous properties was computed at every centroid of the elements using a program developed by the authors.

If the bone behaves as an object with ortotropic symmetry, it is necessary to determine nine non-zero elastic constants of the flexibility matrix: three Young modules E_1, E_2, E_3; three shear modules G_{12}, G_{13}, G_{23}; and six Poisson ratios ν_{12}, ν_{21}, ν_{13}, ν_{31}, ν_{23}, ν_{32}, of which only 3 are independent. Young modulus in the axial direccion (E_3) is related to density estimated from the CT using known equations. To obtain the remaining elastic constants, information of previous studies that have determined these properties by mechanical tests [4] was used. Resulting the following relations:

$$\begin{array}{lll} E_3 = 1 & E_2 = 0.67 * E_3 & E_1 = 0.67 * E_3 \\ G_{32} = 0.3 * E_3 & G_{13} = 0.27 * E_3 & G_{12} = 0.22 * E_3 \\ \upsilon_{21} = 0.3 & \upsilon_{31} = 0.95 * \upsilon_{21} & \upsilon_{32} = 0.79 * \upsilon_{21} \end{array} \quad (1)$$

The FEM analysis provides the stress components of the three coordinated planes for each element. These are then used to solve the eigenvalue and eigenvector problem of the Stress Matrix, in order to obtain the principal directions for every element of the model. The principal directions obtained for a heterogeneous and isotropic model are used as seed for an iterative process to find the actual direction of the mechanical properties. Convergence is verified for the three angles of every element.

To define local coordinate system in FEM programs the Euler angles (α, β, χ) are required. These are obtained from the principal stresses vectors with a rotation matrix.

RESULTS AND DISCUSSION

A comparison between isotropic and anisotropic models of the femur is performed. Results indicate that it is necessary to consider anisotropy to model bone tissue. Figure 1 shows results for a heterogeneous and anisotropic model.

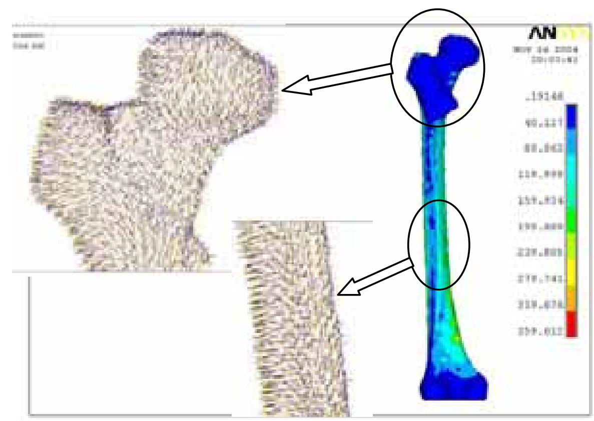

Figure 1: Orientations of the coordinates systems are shown for the epiphisis and diaphisis. Plot of von Misses stress is for the whole model.

CONCLUSIONS

We developed methodology to represent a bone model with a mechanical property and a material symmetry system for every model element. Numerical results indicate that even models with a relatively small number of elements leads to reliable results. The model reflects the highly heterogeneous and anisotropic characteristics of the bone, and operates at very low computacional cost, using normal CT. The model is not intended as a substitute of microscopic bone models [3].

REFERENCES

1. Fernándes et al. *Computer Methods in biomech. and biomedical engineering*. **2**: 125-138.,1999.
2. Doblare and Garcia. *J. Biomech.* 35 (**1**): 1-17, 2002
3. Van Rietbergen B., et. al. *ESB Conference*. Dublin, 2000.
4. Van Buskirk, Ashman, Tulane University, 1980.

BEHAVIOR OF APONEUROSIS AND EXTERNAL TENDON OF MEDIAL GASTROCNEMIUS MUSCLE DURING DYNAMIC PLANTAR FLEXION EXERCISE

[1] Norihide Sugisaki, [2]Hiroaki Kanehisa, [3]Yasuo Kawakami and [3]Tetsuo Fukunaga
[1]Graduate School of Human Sciences, Waseda University, [2]Depertment of Life Sciences, University of Tokyo,
[3]Faculty of Sport Sciences, Waseda University; email: nori-sugisaki@toki.waseda.jp

INTRODUCTION

Pennate muscles have aponeuroses and external tendons, both of which have been regarded as elastic materials. However, limited information is available on the behavior of each of the two tissues of human muscles during contractions. Some attempts have been made to determine mechanical properties of these structures in vivo [1, 2], but the data have been obtained in a 'static action' of the muscle-tendon complex, not in a 'dynamic action' in which most human movements are performed. The purpose of this study was to investigate the differences between the behavior of the aponeurosis and external tendon of the medial gastrocnemius muscle (MG) in dynamic actions. We determined the length changes of the aponeurosis and external tendon of MG during concentric and eccentric actions of the ankle joint using ultrasonography.

METHODS

Nine male subjects (23.5 ± 1.4 yr, 171.5 ± 6.6 cm, 64.1 ± 6.1kg, mean ± SD) performed concentric (CON) and eccentric (ECC) plantar flexion exercises preceded by an isometric action (Pre-iso) on an isokinetic dynamometer (CON-TREX, CMV AG, Switzerland) with pre-set velocity of 5°/s. The range of motion of the ankle was set from 100° to 60° (90° was the neutral anatomic position; positive values for dorsiflexion). Each of concentric and eccentric exercises was performed at three contraction intensities; maximal voluntary contraction (CONmax, ECCmax), and 30 and 60% of MVC (CON30%, CON60%, ECC30%, ECC60%). From Pre-iso to the end of joint motion, the subjects kept the pre-set level of contraction intensity through a visual feedback of the exerted torque. In addition, the subjects performed static ramp actions with the ankle positioned at 100° and 60°.

During the exercises, ankle joint angle and torque were measured, and simultaneously length changes of the aponeurosis and external tendon of MG were determined using two ultrasound apparatuses (SSD-5500, SSD-6500SV, Aloka, Japan) with electronic linear array probes of 10 MHz and 7.5 MHz wave frequency, respectively. The Achilles' tendon force was calculated by dividing the torque by the moment arm of MG, estimated with a procedure described in a prior study [3].

Table 1 Length changes of aponeurosis and tendon (mm)

	Aponeurosis	Tendon
CONmax	-2.5 ± 1.2†	-11.3 ± 3.3†*
CON60%	-0.6 ± 2.0	-9.3 ± 3.7†*
CON30%	-0.8 ± 2.2	-7.4 ± 2.9†*
ECCmax	0.6 ± 1.5	10.3 ± 3.3†*
ECC60%	0.6 ± 2.0	9.9 ± 2.4†*
ECC30%	0.9 ± 1.8	8.2 ± 2.7†*

Values are mean ± SD. †indicates that the length change significantly ($p<0.01$) differs from Pre-iso. * indicates that the length change in tendon significantly ($p<0.01$) differs from that in aponeurosis.

RESULTS AND DISCUSSION

In CON, the length of external tendon significantly shortened from the level of Pre-iso in all test conditions, with decreasing Achilles' tendon force.However, those change of aponeurosis was significant only in CONmax (Table 1). In ECC, the external tendon was elongated in all test conditions with increasing Achilles' tendon force, while aponeurosis was not elongated even in ECCmax (Table1, Fig. 1). In static action at 60°, the lengths of both aponerurosis and external tendon increased across force level. However, the length of aponeurosis did not change in static action at 100°.

The present results indicate that, in concentric and eccentric actions, the behaviors of the tendon tissues of MG differ between aponeurosis and external tendon. From the findings obtained here, it may be assumed that the external tendon of MG plays a role of storing and releasing elastic energy. On the other hand, it is suggested that the aponerurosis of MG releases the pre-stored elastic energy in concentric actions, while it acts just for transmitting the muscle force in eccentric actions.

CONCLUSIONS

The present study provides evidence that there is a difference between the length changes of aponeurosis and external tendon in dynamic actions. In addition, the present results indicated that the elastic behavior of aponeurosis differ depending on the types of exercises (concentric or eccentric).

REFERENCES

1. Muramatsu T, et al. *J Appl Physiol* **90**, 1671-1678, 2001.
2. Magnusson SP, et al. *Acta Physiol Scand* **177**, 185-195, 2003.
3. Grieve DW, et al. *Biomechanics VI-A*, University Park Press, Baltimore, MD.

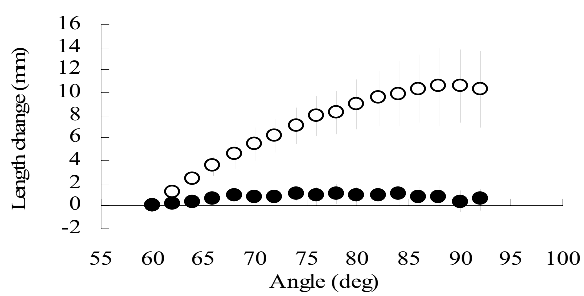

Figure 1 Length changes of the aponeurosis and external tendon from Pre-iso as a function of ankle joint angle during ECCmax. Values are mean ± SD. ● and ○ indicate aponeurosis and tendon respectively.

IN VITRO STUDY OF FOOT KINEMATICS USING A WALKING SIMULATOR

[1] Anmin Liu, [1]Chris Nester, [2]Erin Ward, [1]David Howard, [2]Jay Cocheba, [2]Tim Derrick, [2]Pat Patterson.
[1]Centre for Rehabilitation and Human Performance Research, university of Salford,
[2] Dept. Engineering and Dept Health and Human Performance, Iowa State University.
email: c.j.nester@salford.ac.uk , web: www.healthcare.salford.ac.uk/crhpr

INTRODUCTION

Previous published descriptions of foot and ankle kinematics are incomplete because they are selective in their location of measurement devices on the foot. There is a particular dearth of information on navicular, cuboid, cuneiform and metatarsal kinematics. We aimed to describe the kinematics of the tibia, talus, calcaneus, navicular, cuboid, three cuneiforms, five metatarsals and proximal phalanx of the hallux during a cadaver based simulation of walking.

METHODS

A dynamic cadaver model (walking simulator) was used to apply load to the tibia and leg tendons in a manner to move the specimen in a manner similar to walking. The walking simulator consists of a rigid metal frame supported by four wheels, which is pulled along a track by a motor and cable. Attached to the frame is a pneumatic cylinder which applies vertical load to the below knee cadaver specimen. Artificial muscle forces are applied through attachments to nine individual tendons (tibialis posterior, tibialis anterior, flexor hallucis longus, flexor digitorum longus, Achilles, peroneus brevis, peroneus longus, extensor digitorum longus and extensor hallucis longus) using eight motors (extensor hallucis and digitorum longus are tied together). The tibial loading, forward progression of the tibia and tendon force actuators are open loop controlled and adjusted manually. The duration of stance is approximately 2 seconds and ends prior to toe off, at about 80% of normal stance. Data were collected on 13 specimens (age 32 to 80). Clusters of 4 reflective markers were attached to each bone using 1.6mm K wires.

Eular angles were computed for 22 anatomical joints. To assess the repeatability of the walking simulation, the coefficient of multiple correlation (CMC) was calculated for the kinematic data and ground reaction forces.

RESULTS AND DISCUSSION

The simulator produced repeatable simulations of gait for each foot. CMC for the major rearfoot joints (ankle, sub talar, talonavicular and calcaneo cuboid joints) were all > 0.6. Table 1 shows mean range of motion at each joint during the simulated stance phase (mean of 13 feet). The kinematic pattern at the ankle and sub talar joints was in line with in vivo kinematic data [1]. We found greater frontal and transverse plane motion at the talonavicular joint (mean of 11.6° and 15.5° respectively) than at the calcaneocuboid joint (mean of 5.9°, 6.8° respectively). The concept of the 'mid tarsal' joint, at which the navicular and cuboid move as a single functional unit relative to the calcaneus and talus, is broadly supported by the data. Whilst there was relative motion between the navicular and cuboid, both joints dorsiflexed during the first 60% of the simulated stance phase, and plantarflexed thereafter. Both joints everted and abducted during the first 30% of the simulated stance phase, and inverted and adducted thereafter.

The motion between the cuneiforms and navicular, and the cuboid and cuneiforms was greater than we had anticipated At the medial cuneiform/navicular joint there was on average 9.8°, 6.5° and 3.1° in the sagittal, frontal and transverse planes respectively. The motion between metatarsals 4 and 5 and the cuboid was consistently larger than the motion between the other metatarsals and their cuneiforms. Metatarsals 1-3 moved an average of just 4.7° and 5° in the sagittal and frontal planes relative to the cunieforms, whereas metatarsals 4 and 5 moved 9.8° and 9° respectively in relation to the cuboid.

Our data demonstrate that all mid and forefoot joints have an important role in the overall kinematic function of the foot. For example, based on the mean data sagittal plane motion between the navicular and talus, navicular and medical cuneiform, and medial cuneiform and the first metatarsal, totaled 23.9° during the part of stance simulated. This is comparable to the motion at the ankle and sub talar joints. The motion between the cuneiforms and navicular (9.8°, 8.5° and 10.5° for the medial, central and lateral cuneiforms respectively in the sagittal plane) was comparable to, or in some cases exceeded, the motion between the talus and navicular (9.6°) and between the calcaneus and cuboid (6.9°).

REFERENCES

1. Arndt et al. Foot & Ankle. 2004. 25: 5: 357-364.

ACKNOWLEDGEMENTS

This project was funded by the UK EPSRC

	Calc-Tib	Tal-Tib	Calc-Tal	Nav-Tal	Cub-Calc	Mcun - Nav	Ccun - Nav	Lcun - Nav	Lcun-Ccun	Ccun-Mcun	Cub-Lcun	Cub - Nav
Sag	23.5	21.4	5.5	9.6	6.9	9.8	8.5	10.5	5.2	4.4	8.2	6.0
Front	11.9	12.4	8.4	11.6	5.9	6.5	6.3	5.8	4.7	3.4	5.4	6.3
Trans	7.8	7.9	6.0	15.5	6.8	3.1	3.7	6.8	3.3	3.1	3.7	5.4

	Met1 - Mcun	Met2 - Ccun	Met3 - Lcun	Met4 - Cub	Met5 - Cub	Met2 - Met1	Met3 - Met2	Met4 - Met3	Met5 - Met4	PrxP-Met1
Sag	4.5	4.4	5.2	9.7	9.9	5.1	3.4	4.3	5.0	40.4
Front	5.6	3.6	6.0	7.2	10.8	5.4	4.4	6.2	7.0	14.2
Trans	4.3	3.4	3.9	4.2	4.4	3.6	2.2	2.8	3.4	15.0

Table 1. Mean (of 13 feet) total range of motion at each of the joints

INJURY INCIDENCE AND FOOTWEAR SATISFACTION OF MALE COMPETITIVE BALLROOM DANCERS

[1]Wunching Chang, [2]Chein Kheng Koh, and [2]Chun-Hsien Chen
[1]Department of Vehicle Engineering, MingChi University of Technology, Taiwan
[2]School of Mechanical and Production Engineering, Nanyang Technological University, Singapore
Email: wlylechang@mail.mit.edu.tw

INTRODUCTION

In recent decades, ballroom dancing has become very popular around the world. With an increasing number of people putting on their dance shoes, ballroom dancing has, in fact, became more than just a predominant social activity. Many competitive ballroom dancers had sustained dance-induced injuries. The goal of this study was to investigate the injury incidence and footwear satisfaction in competitive ballroom dancing.

METHODS

Personal interviews were conducted on 29 male competitive ballroom dancers in Singapore. The personal particulars of each subject were acquired in section I of the survey. This was to categorize subjects into different age groups, dancing experience, and level of expertise. Section II of the survey investigated the injury profile of each subject whereby the average number of injuries per year sustained was documented. In addition, each subject was asked to describe during which actions were injuries occurred. In section III, the level of satisfaction of dance footwear in use was recorded. Subjects rated dance shoes in terms of satisfaction on a scale of 1 (least satisfied) to 5 (most satisfied). Factors taken into account were traction, fit, impact absorption, support, height, comfort, and arch.

RESULT AND DICSUSSION

Injury Incidence

The male Latin dancers generally had a higher injury profile as compared to the Standard dancers. The most common injuries in male Latin dancers occurred at the back (14.0 ± 7.5 injury/year), ankle (13.4 ± 7.4 injury/year), hip (11.8 ± 8.2 injury/year), and foot (10.7 ± 5.4 injury/year). The injuries at the back and hips were probably due to the vigorous upper body actions required in the Latin dances. The Samba and Cha Cha Cha especially required a lot of hip rotation and hip thrust. The Samba roll required extreme stretching and bending of the back in anti-clockwise directions. The basic Cha Cha Cha steps, on the other hand, had the dancer thrusting the hips to move forward, backward, or sideways. When acute actions were performed sharply at a fast tempo, the male Latin dancers were easily prone to injuries if no proper care was taken. Male dancers generally had the exaggerated jumping and landing actions in the routine for Paso Doble. When these actions were not executed properly, dancers could injure the foot. Furthermore, male dancers were sometimes required to support their partners, causing extra stress on the body. Footwork was a very important factor in competitive ballroom dancing. Whether it is the sensual Rumba or the lively Jive, tremendous stress was placed on the dancers' feet. Furthermore, dancing in heels (1 ~ 1.5 inch) had aggravated this stress. Thus, proper warm-up must be performed before engaging in vigorous dance training.

The main locations of common injuries sustained by the male Standard dancers were found at the foot (5.1 ± 3.2 injury/year), ankle (4.8 ± 3.1 injury/year), shin (3.8 ± 3.1 injury/year), and wrist (3.5 ± 3.1 injury/year). Although the nature of the Standard dances differed greatly from the Latin dances, amount of stresses placed on the dancers' feet could also be very enormous. Adequate control in the foot and ankle was required to maintain the up-down motion in the Waltz, and the Slow Foxtrot. On the contrary, fast galloping and jumping actions were required in the Viennese Waltz, and the Quickstep. In the Standard dances, the couple covered huge distances on the dance floor with the male dancer taking the lead over his partner. The male dancer prompted the female dancer by means of the upper and lower extremity contact. For example, in the Standard ballroom dance Waltz, the male dancer would take the first step forward. And when his shin touched the partner's, she received the cue and subsequently took a step backwards. The constant rubbing and collision of the shin could have resulted in the occurrence of shin injuries.

Footwear Satisfaction

The subjects were generally satisfied with the dance footwear in use. The more significant variables include the fit (4.0 ± 0.8), impact absorption (3.6 ± 1.0), support (3.6 ± 1.0), and comfort (4.0 ± 1.0). One possible explanation for the high satisfaction rate of the fit may be that the front of the foot was completely covered by the footwear of male dancers. And the fit of footwear could also be adjusted with the tightening or loosening the shoelaces. For impact absorption of dance footwear, subjects had a more uniform pressure distribution on the feet due to the relatively high contact area with the surface of the dance floor. The arch of the dance shoes became steeper as the heel height increased. Since the heel heights of the dance shoes for male dancers were significantly lower than female's at 1 to 1.5 inch, the tendency for developing foot problems with the shoe arch was greatly reduced.

PREDICTION OF LOWER LIMB SEGMENT KINEMATICS FROM FOOT ACCELERATIONS

Yannis Goulermas, David Howard, Lei Ren, Richard Jones, Chris Nester, Jiri Canderle
Centre for Rehabilitation and Human Performance Research, University of Salford, UK
Project: (Real-Prof) : IST 2001/38429, c.j.nester@salford.ac.uk, www.realprof.eu.com

INTRODUCTION

Whilst gait analysis has proved useful for clinical applications its use is still limited by the cost of the facilities, the time and resource required for data collection and analysis, and the fact that the data is only a snapshot of how a patient walks under laboratory conditions. We do not know how representative gait assessment in a laboratory is of gait during daily lives. As a result of these limitations there are efforts to develop "wearable" gait laboratories that provide continuous and daily monitoring of gait. The basis of these systems is that a suitably small number of wearable sensors can be used to measure and represent human motion and activity. Through these systems 1000's rather than 10's of gait cycles from real world situations can be assessed and a truly representative quantification of patient gait (and other activities) acquired. Of the technical challenges in this development, the use of as few and simple motion sensors as possible and the extraction of the maximum amount of motion information as possible is paramount. This would lead to small, inexpensive, light weight and therefore acceptable wearable systems, and yet little or no compromise on data quality for gait researchers. The work described here uses acceleration data of the foot to predict sagittal plane foot, shank and thigh kinematics. For the "wearable gait laboratory" concept this emulates the use of accelerometers to measure foot acceleration, but the extraction from that of full lower limb sagittal plane kinematic data.

METHODS

Kinematic data were collected on 8 subjects using the CAST marker system for the foot, shank, thigh and pelvis and 10 Vicon cameras. From the foot markers the acceleration of the foot in two directions were determined. Also, foot, shank and thigh angles in the sagittal plane are calculated. Several different regression techniques were used (eg: Linear regression, Multi Layer Perception, Polynomial, Functional Link and Radial Basis Neural Networks and k-Nearest Neighbours, Generalised Regression Networks), to predict the foot, shank, and thigh motion patterns from the foot acceleration data. Data from 5 gait cycles for each of the 8 subjects was used with a 4-fold Cross-Validation process. The 8 subjects are split to 4 groups of 2, and each time we use 3 groups for training of the regression tools and 1 for testing of the tools. The final errors are calculated from averaging the errors for the 4 runs of the training-testing stages. The errors measured were the used Cross-Correlation coefficient (CC), the Root Mean Square (RMS), the Maximum Absolute Deviation (MAD) and a Thresholded Absolute Deviation (TAD) that represents the percentage of angle error predictions exceeding a user-defined threshold set to *5°*. Table 1 presents these errors for each of the six redicted signals. Figure1 (top) displays single (1 out of the four) repetitions of Cross-Validation (where subjects 7 & 8 are used to test algorithms and all other 1,..,6 are used for training). Figure 1 (bottom) presents the training (top graphs -6 subjects)Figure 3 displays testing of θ_{rf} prediction (r = right leg, l = left leg, f = foot, s = shank, t = = thigh..

	testing stage				training stage			
	CC	RMS	MAD	TAD	CC	RMS	MAD	TAD
θ_{rf}	0.98	9.19	7.72	62.3	0.99	5.31	3.72	25.3
θ_{rs}	0.99	4.27	3.27	20.5	0.99	2.76	1.78	06.9
θ_{rt}	0.98	4.19	3.38	23.3	0.99	2.71	1.91	07.8
θ_{lf}	0.98	7.95	6.36	53.3	0.99	4.77	3.40	24.4
θ_{ls}	0.99	4.11	3.00	16.7	0.99	2.82	1.85	07.4
θ_{lt}	0.98	4.06	3.23	21.7	0.99	2.36	1.66	04.5
avg	0.98	5.62	4.49	32.9	0.99	3.46	2.39	12.7

Table 1: errors in the prediction of segments kinematics from foot accelerations.

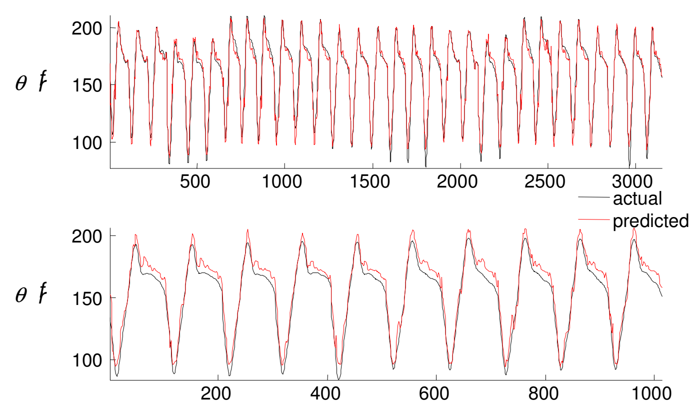

Figure 1: training the algorithms

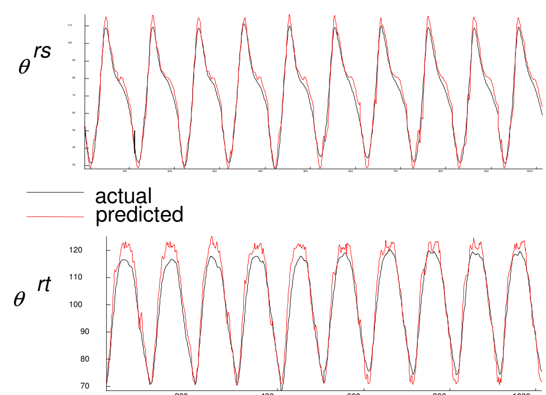

Figure 2: Testing of θ_{rs} and θ_{rt}.

ACKNOWLEDGEMENTS

This project (Real-Prof) was funded by the IST programme of the EU RTD funding (1.2 Million Euros, Jan 2003-Oct 2005).

REACTION TO A LOSS OF BALANCE IN HEALTHY MENOPAUSAL-AGED AND YOUNG WOMEN

[1]Doug Wisner and Kurt DeGoede
Elizabethtown College, Department of Physics and Engineering, Elizabethtown, PA, degoedek@etown.edu
[1]presently enrolled in the Penn State College of Medicine, Hershey Medical Center, Hershey, PA, dmw294@psu.edu

INTRODUCTION

Falls and fractures related to those falls are a significant problem in elderly adults [1]. Epidemiological studies have also shown that there is a greatly increased risk for distal forearm fracture in women that are not elderly, but experiencing menopause [2]. Osteoporosis cannot explain why other fracture sites do not show the same increase in fracture rate [3] or why these women are also falling much more frequently than their younger counterparts [4].

This is a pilot study designed to determine the reaction of menopausal-aged women, MW, to a fall situation (balance disturbance) and compare that reaction to those of younger women, YW. It is hypothesized that the menopausal-aged women will have slower arm reaction time, RT, than the younger women in an actual balance disturbance and that the older women would have slower movements while attempting to regain their balance with their arms. Most previous work has focused on differences between young women and those over the age of 65 and only a few studies have looked at reactions to actual fall conditions or at upper extremity reactions to these conditions [5].

METHODS

Three healthy young women and three healthy menopausal-aged women were recruited from the Elizabethtown College community. The young women had a mean age of 20 ± 1 years and the menopausal-aged women had a mean age of 50 ± 1 years. Subjects were screened by a written health evaluation, signed an informed consent form, and all procedures were approved by the institutional review board.

Subjects were asked to step onto a balance disturbance platform, with hands at their sides, wrists contacting switches placed at their hips. Each was fitted in a safety harness to prevent any fall to the ground and told to try to keep her feet in place at all times, but that she was free to move her hands. Subjects were asked to react as naturally as possible to any loss of balance that may happen during the study. The electronic switches captured timing data and arm movements were recorded by two Sony digital cameras and a SIMI motion capture system (SIMI Reality Motion Systems, Germany).

Twenty trials were conducted with the YW at multiple drop heights (up to 8.25 cm) to determine a minimum effective balance disturbance. With this determined, ten trials were conducted with the MW at this height.

The hypothesis was tested in using a student t-test assuming unequal variance. Two-tailed t-values below .05 were considered significant. RT's that were more than 4 stdev from the mean of the other trials for that subject were discarded as outliers (3 instances).

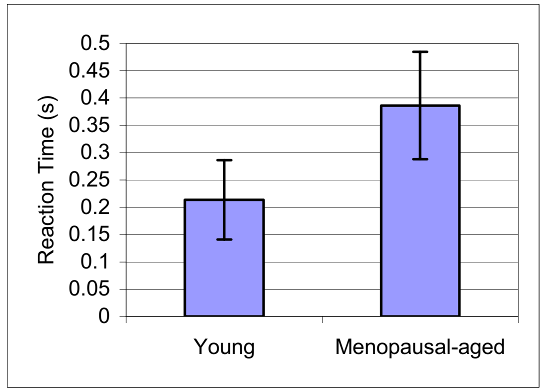

Figure 1: Average reaction time for the two groups.

RESULTS AND DISCUSSION

There was no relationship between trial number and RT in the YW and MW and that there was no relationship between drop height and RT in the YW ($r < 0.5$ for all subjects).

The YW and MW responses at the minimum effective balance disturbance (5.7 cm drop) showed YW reacted with a mean RT of 214 ± 73 ms and MW reacted with a mean RT of 386 ± 98 ms. A trend is noticeable, as shown in figure 1, but there is not a statistically significant difference with the limited number of subjects here ($p = 0.08$). The YW reactions times were just faster than those reported in slips while walking (250 – 300 ms) [5]. The movements themselves were very similar between YW and MW, table 1.

This data, though limited, suggests a potential decline in the ability to respond to a fall disturbance as early as at 50 years of age in women. However, surprisingly, the velocity and magnitude of the responses appears essentially unchanged.

	YW	MW
Movement amplitude (m)	0.12 ± 0.07	0.17 ± 0.12
Maximum velocity (m/s)	1.3 ± 0.5	1.2 ± 0.7

Table 1: Average movement measurements.

REFERENCES

1. Blake AJ, et al. *Age Ageing*, **17**, 365-72, 1988.
2. Owen RA et al. *Am J Pub Health*, **72**, 605-7, 1982.
3. Donaldson LJ, et al., *J Epid Comm Health*, **44**, 241-5, 1990.
4. Winner SJ, et al. *BMJ*, **298**, 1486-8, 1989.
5. Marigold DS, et al. *J Neurophysiol*, **89**, 1727-1737, 2003.

ACKNOWLEDGEMENTS

This project was funded through the Elizabethtown College faculty grants program.

GAIT ADAPTATION: LEAD TOE CLEARANCE CONTINUALLY DECREASED OVER MULTIPLE EXPOSURES WITH AND WITHOUT ON-LINE VISUAL INFORMATION

Chris Rhea and Shirley Rietdyk
Health and Kinesiology Department, Purdue University
email: srietdyk@purdue.edu

INTRODUCTION

Reduced vision of the lower limbs is a common occurrence in activities of daily living. Carrying a laundry basket up stairs reduces vision of both the lower limbs and the obstacle (stair). Patla [1] has shown that absence of vision of the lower limb relative to an obstacle changed the trajectory of the swing limb. Rietdyk et al. [2] found that similar visual interference did not change the trajectory of the swing limb when accomodating an elevated surface, and suggested that the lack of change may have resulted from increased exposure. The purpose of this research was to determine if increased exposure to an obstacle with visual interference and full vision modified toe clearance of the lead limb during gait.

METHODS

The lower limb kinematics of six subjects (23.8 yrs) were examined while stepping over a 10 cm obstacle. Subjects performed 50 blocked trials with full vision and 50 blocked trials with visual interference which were randomized so half of the subjects received full vision first. Goggles blocked the view of the lower limb and the obstacle two steps prior to stepping over it. Lead toe clearance was examined. A 2x2x3 (vision x order x trials (grouped as first, middle, and last five trials)) ANOVA was run.

RESULTS AND DISCUSSION

Subjects tripped on 1% of the obstacle crossing trials, all trips occurred with the trail limb. A significant interaction was observed for lead toe clearance (vision x order x trials, $p < 0.0001$). Post hoc analyses for the full vision trials revealed that toe clearance decreased 12.1% over the first 50 trials (solid line in figure 1). While the initial large margin (17.3 cm) reduced the risk of tripping with the lead limb, the proactive strategy would require an increase in energy consumption and also reduced stability [3]. Therefore, an ideal toe clearance should be high enough to prevent tripping, but low enough to maintain stability and reduce energy costs. With increased exposure, and without specific instructions or external feedback from the experimenters, the subjects reduced their toe clearance. This indicates that subjects were attending to 'internal' feedback to decrease the toe clearance during this dynamic task. Visual feedback, presumably from view of the knee in the periphery [1], would allow the subject to continually reduce the limb elevation.

Toe clearance was 19.9 cm for the first five trials with visual interference, an increase of 2.5 cm (14%) relative to the full vision condition, consistent with Patla [1]. Due to visual interference, feedback would not be received from the view of the knee in the periphery. Generally, spatial estimates with vision are considered to be less variable than other sensory modalities [4]. As only kinesthetic information could provide the feedback, limb elevation increased to compensate for variability. Subjects reduced toe clearance by 23.4% during

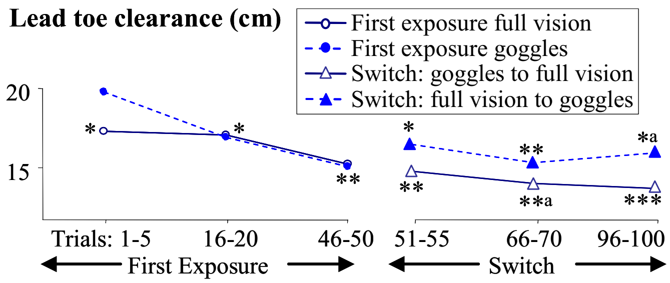

Figure 1: Lead toe clearance across 100 trials for full vision (open circles and triangles) and goggles (closed circles and triangles). Asterisks indicate significantly different responses, *a indicates the response was not different from * or **; ***a was not different from ** or ***.

the first 50 trials, the reduced toe clearance values were not different from the full vision group after 20 and 50 exposures.

Following 50 exposures with full vision, subjects who received visual interference for the first time showed an increase in toe clearance (dotted line in right half of Fig. 1), which did not decrease over 50 trials. However, the subjects who received visual interference first did not demonstrate a decrement in performance when vision was provided. These findings are consistent with the motor control literature where motor learning during aiming tasks has been shown to be specific to the sources of afferent information used to optimize performance during practice [5]. These findings are especially interesting as we did not specifically instruct subjects or provide feedback regarding toe clearance.

It is important to note that the toe clearances observed here were slightly higher than those observed in the literature [e.g. 1]. This between subject difference may affect the overall magnitude of the decrease, but we would still expect to see a decrease with repeated exposures. Further analyses will examine clearance of the trail limb and toe clearance variability during this task.

CONCLUSIONS

During initial exposure, toe clearance decreased for both full vision and visual interference conditions, and after 20 trials the toe clearance was not different across the visual conditions. However, when subjects switched to another visual condition, those with initial visual feedback showed a decrement in performance, which was not observed when the initial trials were without visual feedback.

REFERENCES

[1] Patla. *Ecol Psychol,* **10**:287-302, 1998.
[2] Rietdyk et al. *Exp Brain Res*, in press, 2005.
[3] Patla & Rietdyk. *Gait Posture*, **1**:45-60, 1993.
[4] Ernst & Bülthoff. *Trends Cogn Sci,* **8**:162-69, 2004.
[5] Proteau. In Proteau, Elliot (eds) *Vision and motor control*, North Holland, Amsterdam, pp 67–103, 1992.

HUMAN BILATERAL DEFICIT DURING DYNAMIC, MULTI-JOINT LEG PRESS MOVEMENT

Dean Hay, Vinicius Aguiar de Souza, Senshi Fukashiro
Department of Life Sciences, University of Tokyo, Japan
email: w_dean_c_hay@hotmail.com

INTRODUCTION

Bilateral Deficit (BLD) is used to describe the decrement of the maximum performance elicited by two limbs working simultaneously when compared to the sum of each limb working independently. Both impaired reaction time and decreased force production have been observed in humans during bilateral movements [1, 2]. However, other studies have demonstrated no bilateral deficit [3], or differences dependent upon the motor task and type of athlete [4].

The purpose of this study was to determine whether or not BLD was present during a dynamic movement **(horizontal leg press)** under conditions where the relative load was equal for single and two-legged jumps.

METHODS

Five healthy male subjects (Age: 27.8 ± 3.5 yrs; Weight: 72.2 ± 4.7 kg; Height: 1.76 ± .03 m; mean ± SD) participated in this study with informed consent. Subjects were positioned in the supine position on a horizontal leg press machine and performed a randomized series of left, right, and double leg maximal jumps. Loads were adjusted for single leg (0.5x and 1x body weight - BW) and double leg (1x and 2x BW) jumps. Each condition was repeated 4 times for a total of 24 trials.

Kinematic (200 Hz) and reaction force (1000 Hz) data were recorded along with EMG (1000 Hz) from 6 muscles of the left leg (Sol, MGas, BFem, VMed, RFem, GMax). Joint torque, power, and work were calculated for the ankle, knee, and hip of the left leg (Armo, G-sport, Japan). EMG root mean square (RMS) was also determined. Single and double leg jumps were normalized then statistically analyzed using a repeated measures general linear model (5 subjects x 6 conditions x 4 trials).

The bilateral deficit index was calculated by the formula:

BI = 100 * (single leg – double leg) / single leg)

A positive value denotes a bilateral deficit.

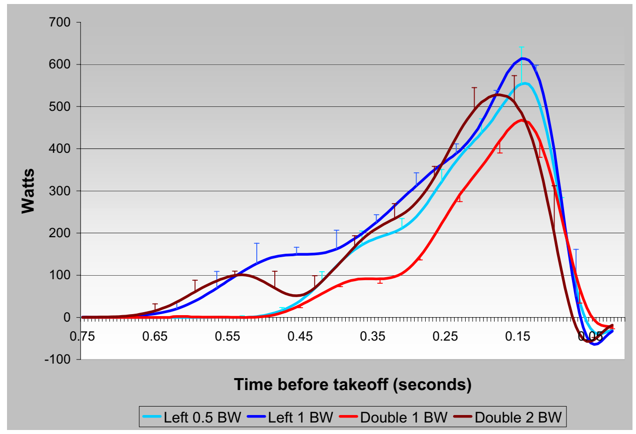

Figure 1: Average knee joint power for 4 conditions with standard deviation bars (one subject).

RESULTS AND DISCUSSION

As there was no significant difference between left and right leg impulse, subsequent analyses were limited to left leg - double leg trials. Left leg jump impulse was significantly greater than double leg impulse (Left 0.5BW vs. Double 1BW; Left 1BW vs. Double 2BW, respectively). Sol, RFem, and VMed showed BLD, while MGas and GMax exhibited bilateral facilitation. Work for each joint exhibited significant BLD (Table 1).

CONCLUSIONS

Bilateral deficit during a multi-joint leg press movement is negatively associated with load. Our data show that BLD is greater during explosive, rapid movement, suggesting general impaired fast-twitch motor unit recruitment. Implications of the results are discussed.

REFERENCES

1. Ohtsuki, T. *Percep. Motor Skills*, 53: 27-30, 1981.
2. Secher NH, et al. *Acta Physiol Scand* 134: 333-339, 1988.
3. Jakobi, JM, et al. *J Appl Physiol* 84: 200-206, 1998.
4. Howard JD, et al. *J Appl Physiol* 70: 306-316, 1991.

Table 1: Bilateral deficit indices for impulse, EMG, and normalized joint work. Statistical significance: * p <0.05; ** p <0.01.

Condition	Impulse	RMS Electromyography						Joint Work		
		Sol	MGas	BFem	VMed	RFem	GMax	Ankle	Knee	Hip
Left 0.5BW vs. Double 1BW	26%**	15.2%**	-2.5%	4.2%	4.8%	14.6%**	-15.1%*	15.1%**	11.1%**	38.35%**
Left 1BW vs. Double 2BW	11.7%**	9.5%**	-7%*	-7.6%	7.1%*	12.1%**	-12.7%*	11.5%**	6.2%**	29.4%**

THE MODIFICATION OF PEDALING SKILL WITH REAL-TIME REPRESENTATION OF PEDALING FORCE IN NON-CYCLISTS

[1] Tetsunari Nishiyama and [1] Takayuki Sato
[1] Human Performance Laboratory, Nippon Sport Science University
; email: nisiyama@nittai.ac.jp, web: www.nittai.ac.jp/

INTRODUCTION

By the real-time representation of the force on the pedal during bicycling, even non-cyclists can quickly modify the pedal force. The effect of such feedback instruction will vary in individuals. We examined the effect of modification on the pedaling mechanics induced by the real-time representation of the force-pattern applied to the pedals during bicycling in non-cyclists. Also the modified force pattern was examined in relation to the energy consumption.

METHODS

Seven males (23-31yrs) participated in a maximal Vo_2 test, baseline test, and feedback test. In the baseline test, the subjects were asked to pedal naturally without any feedback instruction using a racing type ergometer. Both feet were fixed to the pedals. They pedaled the load of 30, 50 and 70% Vo_2max, at a cadence of 70 rpm. The pedaling forces of tangential (F_{tan}) and radial (F_{radial}) directions to the crank arm were measured in the left and right pedals using a strain-gauge method. The resultant force (F_{result}) was determined from F_{tan} and F_{radial}. The crank angle was measured by a potentiometer and defined 0 degree at the top position. Each pedal force was averaged on thirty revolutions of the crank. The Vo_2 was averaged on the last 30 seconds of each 5 minute load. The delta mechanical efficiency was calculated from oxygen consumption and mechanical work in each load. After two to five days of the baseline test, the feedback test was conducted with visual and oral instructions. The visual instructions show the subjects the PC monitor displaying F_{result} and F_{tan} on the clock diagram every 30 degree of crank cycle. The subjects were given an explanation of the mechanisms of F_{tan} and F_{result}. After at least 5 minutes practice periods, the subjects were asked to try the following movement, "F_{result} turn to the direction of F_{tan} in 90-180 and 180-360 degree of crank cycle on the both pedals". The representation of the clock diagram on the both sides continued during the bicycling while oral instruction was sometimes given.

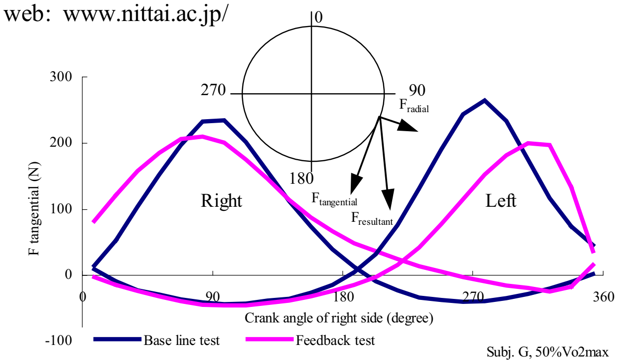

Figure 1: Averaged tangential force in thirty cycles.

RESULTS AND DISCUSSION

In the modification of the pedaling mechanics with the feedback intervene, the F_{tan} decreased in the push phase (0-180 degree of crank angle) and increased in the pull phase (180-360 degree) (Fig. 1, 2). Generally, as shown in Fig. 2, the modified right F_{tan} in the pull phase showed large increase, which was the predominant side in all subjects, in comparison with the left one, and the left F_{tan} of the push phase showed large decrease than the right one.

In the load of 30%Vo_2max, the increase of the right F_{tan} in the pull phase was correlated to the increase of Vo_2 in the modified pedaling. Such the modification of pedaling force was not always reflected effectively for the oxygen consumption. Thus, the excessive modification of the pedaling force made the mechanical efficiency decrease. However, the changes of the pedaling mechanics, such in pull or push phase and the left or right leg, was varied in the subjects. It was confirmed that the feedback effect of the pedaling skill should be evaluated in the relationship between the individual difference of the pedaling modification and energy consumption.

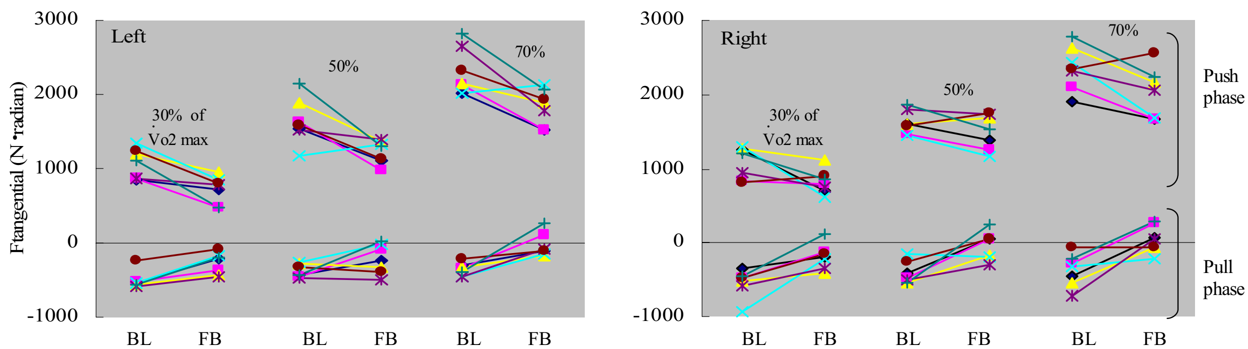

Figure 2: The modification of integrated tangential force by the feedback instruction in seven subjects. BL; base line test, FB; Feedback test.

EFFECT OF INCREASED MECHANICAL STIMULI ON FOOT MUSCLES FUNCTIONAL CAPACITY

Gert-Peter Brüggemann, Wolfgang Potthast, Björn Braunstein and Anja Niehoff
Institute for Biomechanics and Orthopaedics,
German Sport University Cologne; email: brueggemann@dshs-koeln.de

INTRODUCTION

As biological structures receive mechanical stimuli they are getting stronger. If muscles, tendons and bones are not in use they will decrease strength and their functional capacity. The biological structures of the foot can be trained by barefoot walking or workout through the speculated higher loading. No scientific evidence for a causal relationship between increased foot loading and functional improvement of foot structures could be found in the literature. The foot arch and the foot functional capacity is strongly related to the strength of the flexor muscles of the metatarsophalangeal joints (MPJ): M. flexor hallucis longus (FHL) and M. flexor digitorum longus (FDL) [1,2,3]. It was shown that a special designed minimal shoe (Nike FREE) increases the range of motion on the metatarsophalangeal joints (MPJ) and the ankle joint in normal walking and modifies the plantar pressure distribution in a way close to barefoot walking on grass. In a pilot study using wire EMG technique the muscle activity of the FHL was shown to be significantly increased during walking in the minimal footwear in comparison to walking in traditional running shoes. If training with the minimal footwear mimics barefoot training one can assume that using the minimal shoe will increase the loading of the foot structures and make them stronger.

The purpose of the study was to demonstrate the capacity of biological structures to adapt to mechanical stimuli modified through footwear and to quantify effects on strength and morphology of the foot and shank muscles. The research question was to quantify the impact of increased mechanical stimuli on (1) muscle strength and (2) anatomical cross sectional area (ACSA) of intrinsic foot and shank muscles.

METHODS

The research question was solved by a prospective longitudinal designed approach. The prospective study operated with an experimental (n_E =25) and a control group (n_C=25) both consisting of male and female subjects. The experimental intervention over a period of five months was the use of the minimal footwear in athletes preparatory (warm up) training while the control group used traditional training shoes for the same training programme. The measurement of muscle strength was performed by special custom build dynamometers. ACSA of FHL, FDL, M. triceps surae (TS), Mm. tib. post (TP) and ant.(TA), M. peroneus (PER) at the greatest circumference of the shank and ACSA of four of the intrinsic foot muscles (M. abductor hallucis, M. quadratus plantae, M. abductor digiti minimi, M. flexor digitorum brevis) were estimated by MRI (Siemens Symphony, 1.5 Tesla).

RESULTS AND DISCUSSION

The muscle strength changes through the intervention showed a significant ($p<.01$) increase of the MPJ flexors in the experimental group; no significant change in the controls.

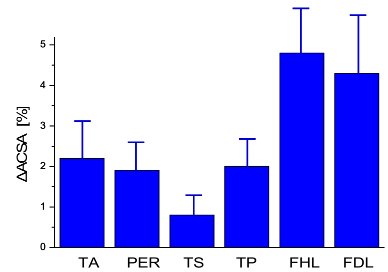

Figure 1: Relative increase of ACSA of six extrinsic foot muscle through the five months intervention (Mean and SEM); experimental group (n_E=25).

Table 1: Changes in MPJ flexor strength [N], subtalar inversion strength [Nm], plantar and dorsi flexors strengths [N]. Means and SEM. *: p<.05, **:p<.01.

	Experimental group		Control group	
	Pre	Post	Pre	Post
MPJ flexor strength	232 (10.9)	279 (11.6) **	228 (11.1)	237 (11.6) ns
Inversion moment	18.0 (1.4)	21.8 (1.6) *	17.5 (1.3)	17.7(1.2) ns
Plantar fl. strength	1065(72.2)	1254(73.2) *	1296(68.0)	1242(63.1) ns
Dorsi fl. strength	432(18.0)	460(18.9) *	415(20.6)	419 (14.8) ns

Plantar flexion strength increased only significantly ($p<.05$) in the experimental group. The maximum supinator muscles torque increased for the experimental group ($p<.05$) and showed no effect on the control group. While for the Mm tibialis anterior, peronei, tibialis posterior and triceps surae no significant changes in the ACSA were found, the ACSA of the Mm flexor hallucis and flexor digitorum increased by approximately 4% and by 5% for the Mm abductor hallucis and quadratus plantae in the experimental group.

CONCLUSIONS

The use of minimal footwear was related to changes in muscle strength and morphology. It was demonstrated that the footwear increased mechanical stimuli on the tendon muscle units. The muscle strength capacity of those muscles which were more intensively used by the minimal shoe increased significantly. Muscles which were similar activated in both conditions did not respond. One can conclude that footwear technology impacts the mechanical loading as well as the biological response of the loaded tissues.

REFERENCES

1. Jacob, HAC. *Clin Biomech* **6**, 783-792, 2001,
2. Kitaoka, HB et al. *Foot Ankle Int* **15**(10), 557-560, 1994.
3. Tochigi,Y. *Foot Ankle Int* **24**(8), 634-639,2003.

ACKNOWLEDGEMENTS

This study has been financially supported by Nike.

AN INVESTIGATION OF EXTERNAL LOADING PATTERNS APPLIED DURING MAXIMAL GRIP

A.K. Kanellopoulos, M.K. Gíslason, N.K. Fowler
Bioengineering Unit, University of Strathclyde; email: asimakis.kanellopoulos@strath.ac.uk

INTRODUCTION

The external loads applied to the fingers have been previously measured using different gripping tools in several wrist orientations [1],[2],[3]. Uniaxial or planar forces applied to a grip tool are typically measured in order to examine the force distribution across the digits. These kinetic studies have not been concurrent with kinematic measurement and there is therefore little information on the external moments generated at the finger joints during whole hand grip.

The aim of the current study was to investigate the three dimensional externally applied forces and moments on each individual finger during whole hand grip. The variation of the external loading patterns and the finger force distribution was also studied in relation to the orientation of the wrist joint.

METHODS

A cohort of fifty healthy right-hand dominant adults (25 males, 25 females) were required to provide their maximal gripping force in five different wrist orientations: maximal flexion, extension, radial (RD) and ulnar deviation (UD) and a position of 'functional neutral' (N). A custom-built gripping tool with five independent six-degree-of-freedom force transducers was used to measure the three dimensional forces and moments applied to individual digits during each grip task. The kinetic data was synchronized with an eight-camera VICON (Oxford Metrics) motion analysis system in order to obtain concurrent kinematic data of each finger/thumb segment, the wrist and forearm. These kinematic data were used to express the transducer loads in terms of individual metacarpal axis systems.

RESULTS AND DISCUSSION

The mean (SD) percentage distribution across the fingers of the applied normal transducer force for the neutral wrist position was found to be: 35% (7.6%) in the index, 30% (6.9%) in the middle, 21% (5.5%) in the ring and 14% (5.9%) in the little finger. These results are comparable with several previous studies [2]. Others suggest however that the middle finger exerts the highest normal force during maximal grip with a neutral wrist [3]. Figure 1 shows the force distribution across the digits in the coronal plane for three wrist positions. It is evident from this figure (and table 1) that during maximal grip trials there is a significant contribution from shear forces which cannot be neglected.

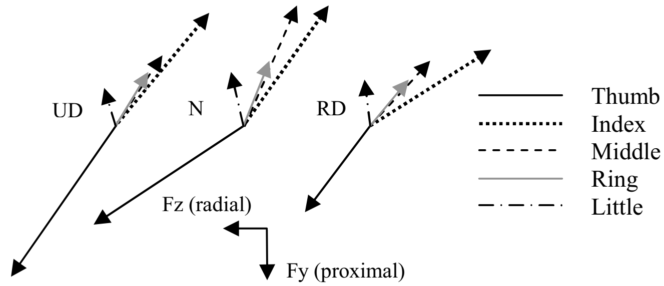

Figure 1: Force vector diagrams showing the force distribution between the digits for three wrist positions in the coronal plane with respect to the metacarpal axis systems.

Table 1 shows how the external loading patterns applied to the index finger (with respect to the metacarpal axis systems) vary with wrist joint orientation in maximal grip. The maximum resultant grip loads are generated in a neutral wrist position. The largest ulnarly directed forces occur during ulnar deviation and this coincides with the largest applied adduction moments. This evidence agrees with current knowledge of hand biomechanics and is clinically important because it explains the contribution of external loading patterns on the development of several deformities in the pathological hand.

CONCLUSIONS

The three dimensional loading patterns generated during whole hand grip are complex and vary with wrist orientation. Significant shear force components are produced during simple grip activities and these can generate large adduction/pronation moments at the finger joints. These results have important implications for both biomechanical modelling and joint implant design.

REFERENCES

1. Amis AA. *J Biomed Eng* **9**, 313-320, 1987.
2. Kinoshita H, et al. *Ergonomics* **38**, 1212-1230, 1995.
3. Ohtsuki T. *Ergonomics* **24**, 21-36, 1981.

ACKNOWLEDGEMENTS This work was supported by Arthritis Research Campaign grant no. 1546

Table 1: Averaged maximum external loads (SD) applied to the index finger with respect to the metacarpal axis system.

Wrist Position	Fx (N) +ve volar	Fy (N) +ve proximal	Fz (N) +ve radial	Mx (Nm) +ve adduction	My (Nm) +ve pronation	Mz (Nm) +ve flexion
Neutral	-3 (4.6)	-19(7.3)	-13 (4.5)	1.0 (0.35)	0.6 (0.23)	-0.1 (0.49)
Flexion	-5 (3.5)	-14 (5.0)	-7 (2.9)	0.7 (0.25)	0.2 (0.17)	-0.8 (0.44)
Extension	-6 (4.5)	-14 (5.4)	-12 (6.4)	0.8 (0.32)	0.4 (0.31)	-0.9 (0.43)
Radial Dev.	1 (4.2)	-18 (6.6)	-15 (7.5)	1.0 (0.42)	0.6 (0.33)	-0.7 (0.45)
Ulnar Dev.	1 (5.2)	-12 (4.4)	-19 (9.3)	1.1 (0.34)	0.7 (0.42)	-0.4 (0.28)

TREADMILL VERSUS OVERGROUND RUN TO WALK AND WALK TO RUN TRANSITION SPEED IN UNSTEADY STATE LOCOMOTION CONDITIONS

[1]P. Malcolm, [1]M. Lenoir, [2]P. Aerts, [1]V. Segers, [1]D. De Clercq
[1]Ghent University, Department of Movement and Sport Sciences,
[2]University of Antwerp, Department of Biology; email: philippe.malcolm@ugent.be

INTRODUCTION

Recently it has been argued that the transition between walking and running is a gradual process instead of a distinct event [2]. If this is true then transitions should preferably be studied in a protocol with gradually changing speed. Furthermore it has been found that the magnitude of acceleration has an effect on the transition speed. The easiest way to impose such a constant acceleration is by the use of a motor driven treadmill. Although the mechanics of treadmill locomotion and overground running do not fundamentally differ, various kinematical [1], physiological and perceptual differences exist. It might be possible that one or more of these differences affect the run to walk transition (RWT) or the walk to run transition (WRT).

The purpose of this preliminary study was to determine whether treadmill versus overground locomotion differ in transition speed in a protocol with gradually changing speed.

METHODS

4 female subjects (height: 170.8 ± 2.3 cm) performed several RWT's and WRT's at 3 constant accelerations (±0.05, ±0.07 and ±0.10ms^{-2}) on a motor driven treadmill and an overground walkway. They were instructed to change from walking to running or vice versa when it felt most natural to them.

In the treadmill protocol transition speed was defined as the average speed of the treadmill belt during the transition step. The transition step was defined as the first step with a double stance phase in a RWT or the first step with a flight phase in a WRT. In the overground protocol the constant acceleration was imposed by means of a row of flashing lights which the subjects had to "follow" as closely as possible. The transition speed was defined as the average forward speed of a marker at C7 during the transition step. This speed was obtained from motion analysis (Qualisys, 240 Hz).

In each condition 3 trials were retained. Statistical analysis was done in MS Excel 2002 and SPSS (11.0)

RESULTS AND DISCUSSION

Visual inspection of the results showed that intra subject variability was acceptable so further analysis could be done with average values of each subject. The average transition speed of each subject is shown in two scatter plots: one for the RWT's (figure 1) and one for the WRT's (figure 2). In figure 1 we see no systematic relation between the average RWT speed in the overground condition and the treadmill condition. From figure 2 however it seems that all subjects started running sooner (i.e. at a lower speed) when they performed a WRT on the treadmill. Non parametric analysis with a Wilcoxon test showed a trend towards significant differences between the overground condition and the treadmill condition in all three WRT accelerations. (p = .068, Z = -1.83)

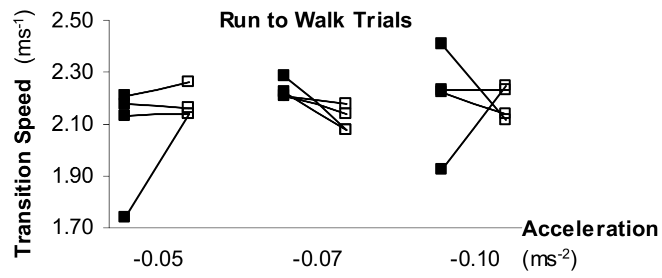

Figure 1: RWT transition speed of four subjects in the overground condition (filled squares) and the treadmill condition (open squares)

Figure 2: WRT transition speed of four subjects in the overground condition (filled squares) and the treadmill condition (open squares)

These results can probably be linked to the fact that many authors found that on a treadmill subjects tend to change their kinematics to "a pattern that provides them with more security" as a means of avoiding falling off the back of the treadmill [1]. It makes sense that the subjects only alter their transition speed in the WRT condition because the WRT is probably more intimidating than the RWT. In the WRT the subjects face the risk of being thrown off the back of the treadmill if they are unable to match the increasing speed whereas in the RWT they probably perceive this as less likely because the treadmill is slowing down.

CONCLUSION

The results of this preliminary study should be interpreted with caution, because of the small population. Nevertheless a clear difference in WRT transition speed has been found between treadmill and overground locomotion. We believe that it is worthwhile to continue this research on a larger scale so that we will be able to use more stringent statistical methods and be able to determine if the use of a treadmill can be justified in transition studies with a gradually changing speed protocol.

REFERENCES

1. Alton F, et al. *Clin Biomech* **13**, 434-440, 1998.
2. Li L, et al. *Res Q Exercise Sport* **73**, 229-237, 2002.

POSTURAL GAIT CHANGES ARE SEEN WITH SEVERE, NOT MODERATE, KNEE OSTEOARTHRITIS

[1] Janie Astephen and [1]Kevin Deluzio
[1]Dalhousie University School of Biomedical Engineering

INTRODUCTION

Knee osteoarthritis (OA) is a very common disease of the musculoskeletal system that is a major cause of morbidity and disability in the world. It is a progressive disorder that involves multiple, interacting biomechanical and biochemical factors, making it very difficult to understand the pathological process of the disease. Although many biomechanical changes with knee OA have been identified (i.e. knee joint loading and orientation), most previous studies have included only patients with severe knee OA. Without data from patients from varying levels of knee OA severity, it is difficult to determine whether these factors are a result of the disease process, or are important to the onset and progression of the disease. Differences in the knee flexion angle during gait with knee OA have been found [2], but simultaneous changes that occur at the other joints in the lower limb have not been explored in previous studies.

Using a multidimensional gait data analysis technique, we compared the postural changes (hip, knee and ankle angles in the sagittal plane) over different levels of knee OA disease severity.

METHODS

Two patient populations, a moderate knee osteoarthritis (OA) population (n=40) and an end-stage knee OA population (n=38), as well as an age-matched control group (n=40) were included in this study. Disease severity of the moderate knee OA group was based on radiographs, physical exams and functional tests. The severe knee OA patients were within six months of total knee replacement surgery.

Three-dimensional kinematic and kinetic data during gait were collected for all patients using two optoelectronic motion analysis position sensors (Optotrak 3020, Northern Digital, Inc.), and a force platform (Advanced Mechanical Technology, Inc.) embedded in the walkway. These data were combined with specific anthropometric measures in an inverse dynamics model.

A multidimensional gait data analysis technique [1] that uses principal component analysis (PCA) and discriminant analysis was applied to the sagittal plane hip, knee and ankle angle waveforms to extract the important features of the data that describe differences in sagittal plane posture between the groups.

RESULTS AND DISCUSSION

A scree plot of the data indicated that the first three principal components (PCs) explained the majority of the variation in the sagittal plane waveforms. A stepwise discrimination procedure indicated that two of these three PCs, PC1 and PC3, contained valuable discriminatory information between the groups. The two discriminatory PCs, combined in linear discriminant functions that represented boundaries between the groups, successfully discriminated between the normal and severe knee OA groups (with a cross-validation error of 9%), but did not discriminate between the normal and moderate knee OA groups. Postural gait differences are therefore characteristic of severe knee OA gait, and not characteristic of moderate knee OA gait.

The third principal component, PC3, was the most discriminatory feature. This feature had equal contributions from all three lower limb angles, and therefore represented an overall range of motion of the lower limb. This difference is most important from late stance to early swing (approximately 40 – 80% of the gait cycle) (Figure 1a). The severe knee OA group had higher PC3 scores than the normal group, and these higher scores were associated with lower overall ranges of motion in all three joints (Figure 1b). These changes are likely in response to the increased levels of pain during gait that are common with end-stage knee OA. The lack of difference between the normal and moderate OA groups suggests that these postural changes are not involved in the pathomechanics of knee OA. PC1 was interpreted as a difference in the magnitude of the knee flexion angle during early stance, which supports the results of previous knee OA studies. The identification of PC3, however, points to the importance of synergism between the joints of the lower limb during gait.

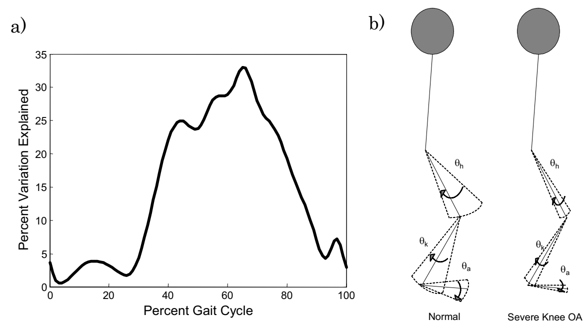

Figure 1: a) A plot of the percentage of the variation explained by PC3 at each percentage of the gait cycle shows that PC3 is most important from approximately 40-80% of the gait cycle. b) Severe knee OA patients exhibited less sagittal plane angular motion in all three lower limb joints during gait than normal subjects.

CONCLUSIONS

Postural gait changes between normal and severe knee OA subject groups were identified, but no significant postural changes were identified between the normal and moderate knee OA groups. This suggests that the kinematic changes are more a response of the disease than a contributing factor to the onset and progression of knee OA. The most discriminatory feature identified an important synchronicity in the joints of the lower limb that is often not accounted for in gait studies. The results of this study indicate the need for more simultaneous considerations of multiple joints in gait analysis.

REFERENCES

1. Astephen, JL, KJ Deluzio. *Proc Inst Mech Eng [H]* **218**(4):271-279, 2004.
2. Kaufman, K.R. et al. *Jbiomech*, **34**, 907-915, 2001.

COMPUTATIONAL ASSESSMENT OF ANTEROPOSTERIOR LAXITY FOLLOWING PARTIAL PCL RELEASE IN CRUCIATE-RETAINING TKR

Matthew F. Moran[1,2], Damon Servidio[5], Charles M. Davis III[4], and Stephen J. Piazza[1,2,3,4]
[1]Biomechanics Laboratory and Departments of [2]Kinesiology, [3]Mechanical Engineering, and [4]Orthopaedics and Rehabilitation,
The Pennsylvania State University, University Park, PA and Hershey, PA
[5]Stryker Orthopedics, Mahwah, NJ; E-mail: steve-piazza@psu.edu

INTRODUCTION

Proper tensioning of the posterior cruciate ligament (PCL) achieved by adequate joint line restoration has been cited as a key determinant of success in PCL retaining total knee replacement (PCR-TKR) [1]. Tensioning of the PCL is thought to be important because it affects anterior-posterior (AP) stability and knee kinematics following PCR. Modifying the joint line following total knee replacement (TKR) could affect PCL tensions and consequently alter knee stability and function. Joint line elevation commonly follows PCR-TKR [2] and has the potential to tighten the PCL and restrict range of motion (ROM). In cases where PCL tightness limits ROM, a partial PCL release has been advocated [1], but few studies have addressed the effect of this procedure on AP laxity. The purpose of the present study was to create a computational model to investigate the effect of partial PCL release on AP laxity characteristics following PCR-TKR as compared to a posterior cruciate-substituting (PS) knee design. Varying degrees of release and three PCR tibial insert designs (condylar, anteriorly-lipped, and ultra-conforming) were tested for AP laxity. It was hypothesized that partial PCL release would increase AP displacements at higher flexion angles, but an ultra-conforming insert would limit these displacements more than the other two designs.

METHODS

A forward-dynamic computer simulation of the American Society for Testing and Materials protocol for testing AP constraint (ASTM F1223-04) was created and its output was found to compare well to experimental results obtained for PS knee components [3]. The model for this study incorporated 8 spring-like elements representing the anterior-lateral (AL) and posterior-medial functional bundles of the PCL respectively. Ligament insertions, stiffness, and slack lengths were assigned based on values reported in literature [4, 5]. The natural knee motions reported by Walker et al. were applied to the model and the resulting ligament length patterns were found to compare favorably to experimental values [6]. Anterior-posterior laxity test simulations were run at 0º, 30º, 75º and 90º for all three PCR tibial inserts and for intact PCL, partial AL-PCL release (half of the bundle was released), and complete AL-PCL release. At each flexion angle an 80 N anterior force and 80 N posterior force were applied to the tibial insert and the total AP displacement was recorded. The inserts were under a constant 200 N compressive axial load, the femoral component was free to move in the frontal plane, and contact friction was not modeled.

RESULTS

With the PCL intact, the design of the tibial insert affected AP laxity measures at smaller flexion angles but did not influence displacements at either 75º or 90º flexion. The standard condylar insert exhibited 70% more and 215% more AP displacement than either the anterior-lipped or ultra-conforming inserts at 0º and 30º flexion, respectively. AL-PCL release, either partial or complete, affected AP laxity measures at larger flexion angles while having minimal influence at smaller flexion angles (Figure 1). With a partial release of the AL bundle over all angles, the standard condylar and anterior-lipped insert displayed an average displacement increase of 1.2 mm, while displacement for the conforming insert increased by only 0.6 mm. With a complete release of the AL bundle, the standard condylar and anterior-lipped insert displayed an average displacement increase of 3.3 mm, while the conforming insert increased only 1.9 mm.

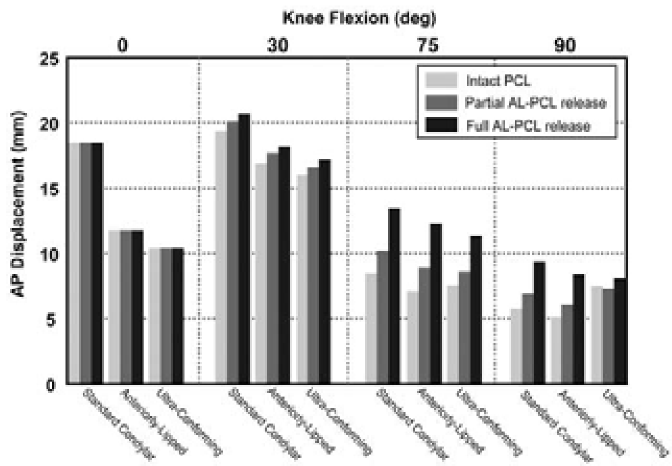

Figure 1: Effect of partial and complete release of the anterolateral (AL) bundle of PCL on AP laxity.

DISCUSSION

Selective release of the PCL to attain a proper flexion arc substantially increased the maximum AP displacement at 75º and 90º flexion regardless of insert design. At higher flexion angles PCL tension contributes more to AP stability than does insert conformity. When the knee is near full extension and PCL tensions are lower, conforming designs provide a more stable joint. The changes in AP displacement determined in this study are likely to be functionally significant; smaller changes in displacement have been used clinically to differentiate between injured and healthy knees [7].

REFERENCES

1. Arima J, et al. *Clin Orthop Rel Res* **353**: 194-202, 1998
2. Figgie HE, et al. *JBJS* **68A**: 1035-1040, 1986
3. Moran MF, et al. Proc. 28th ASB, 2004.
4. Harner CD, et al. *Arthoscopy* **15**: 741-749, 1999.
5. Essinger JR, et al. *J Biomech* **22**: 1229-1241, 1989
6. Walker PS, et al. *J Biomech* **21**: 965-974, 1988.
7. Eakin & Cannon. *Am J Sports Med* **26**:96-102, 1998.

ACKNOWLEDGMENTS

This work was funded by an Academic Computing Fellowship (PSU) and from an ISB Matching Dissertation Grant.

3D-Fiber type distribution in back muscles in small mammals

Nadja Schilling
Institute of Systematic Zoology and Evolutionary Biology, Friedrich-Schiller-University Jena, Germany
email: nadja.schilling@uni-jena.de, web: www.zoo.uni-jena.de

INTRODUCTION

The evolution of the locomotor apparatus in vertebrates is marked by major reorganizations of the trunk's musculature. The plesiomorphic segmental organization was dissolved in the hypaxial but also in the epaxial muscles. In mammals, three epaxial tracts allow for high mobility in all three rotational degrees of freedom as for lateral bending and tilting at symmetrical gaits and for sagittal bending at asymmetrical gaits.

Different roles in stabilizing and mobilizing of the vertebral column were hypothesized for the diverse paravertebral muscles. Large, superficial back muscles are supposed to produce the range of movement, whereas small, deep muscles control the range of movement and especially control segmental motions.

Since metabolic profiles of muscles relate to their function (as shown for limb muscles) it can serve as an indicator of function. Therefore, the aim of the study was to investigate and compare the muscle fiber type distribution in back muscles of different species of small mammals. In order to test current hypothesis on back muscle function the overall, 3D-distribution pattern of fiber types was investigated.

METHODS

Adults of 4 small mammalian species (*Galea musteloides* - the cui, *Ochotona rufescens* - the pika, *Rattus norvegicus* - the rat, *Tupaia belangeri* - the tree-shrew) were used for this study. Serial sections were made from the complete backs including the vertebral column to preserve the topographical relationships between muscles and their intramuscular architecture. Only the posterior thoracic and the lumbar regions were used in this study. Samples were quick frozen in liquid nitrogen cooled isopentan.

Sections were made using a kryostat microtome (SLEE, D-knife, 12 µm) and processed for muscle fiber type characterization using alkaline combination reaction based on Ziegan's protocol [1]. As a result, fiber type I (SO) is stained blue, type IIa (FOG) dark brown, and type IIb (FG) light brown. Drawings were made at different cranio-caudal levels from the serial sections.

RESULTS AND DISCUSSION

Surprisingly, the overall fiber type distribution pattern was highly similar between the species investigated. Most of the muscles showed a heterogeneous distribution of the different fiber types over the muscle's cross section but also along the cranio-caudal axis. Only few of the muscles showed the same fiber type composition from deep to superficial regions or from cranial to caudal direction.

The highest percentage of glycolytic fibers was present in the m. sacrospinalis (longissimus lumborum et iliocostalis) and in the m. psoas major. Only a few oxidative fibers were observed in the posterior thoracic part of the m. sacrospinalis. The m. psoas major was more or less free of oxidative fibers. The fiber type composition of both muscles make them suitable to generate forces and speed for a wide range of movement.

The highest percentage of oxidative fibers were found in the mm. intertransversarii et interspinales as well as in the mm. rotatores et multifidi. In caudal direction, the proportion of oxidative fibers is decreased in the superficial regions of the mm. multifidi. As inferred from their anatomical position and their high percentage of fatigue resistant, oxidative fibers, these muscles are best suited to maintain segmental stability.

A regionalisation of oxidative fibers was found in the m. quadratus lumborum. Around the huge intramuscular tendon oxidative fibers were distinctly arranged. Especially, in the caudal thoracic but also in the cranial lumbar part this oxidative region was extensive. Towards the caudal region the proportion of the oxidative fibers was decreased. Such regionalisation of oxidative fibers in deep parts of a muscle are well known from limb muscles in so called anti-gravity muscles. These muscles enduringly counteract passive limb flexions due to gravitational force. As a muscles involved in ventilation, the oxidative region of the m. quadratus lumborum is supposed to be involved in inspiration movements.

CONCLUSIONS

Diverse back muscles were related to different functions in stabilization and mobilization of the vertebral column. An overall distribution pattern of different muscle fiber types was found in all species under investigation. The major reorganization in the trunk's musculature during the evolution of mammals is suggested to include not only macroscopic changes but also the fiber type distribution pattern.

REFERENCES

1. Ziegan J. *Acta histochem* **65**, 34-40, 1979.

ACKNOWLEDGEMENTS

Technical support by Ingrid Weiß and Leila AlKuweiti is gratefully acknowledged.

KINEMATICAL ANALYSIS OF THE PREPARATORY AND TAKEOFF MOTION IN THE LONG JUMP

[1]Yuya Muraki, [1]Hiroyuki Koyama and [2]Michiyoshi Ae
1Doctoral Program of Health and Sport Sciences, 2Institute of Health and Sport Sciences,
University of Tsukuba, Japan; email: yuya@lasbim.taiiku.tsukuba.ac.jp

INTRODUCTION

Approach velocity is one of the most important factors in the long jump. However, it is difficult for a jumper to prepare for the takeoff with a minimum loss of approach velocity. The purposes of this study were to investigate motion variability of the preparatory and takeoff motions for skilled long jumpers and to compare their motions between different approach velocity groups.

METHODS

The last two steps of the approach and takeoff motions of thirty-three skilled male long jumpers (height, 1.79 ± 0.06 m; body mass, 69.9 ± 6.9 kg; and effective jump distance, 7.78 ± 0.31 m) were videotaped with two high-speed VTR cameras (250 Hz) during official competitions. Two-dimensional coordinates were used to calculate linear and angular kinematics of joints and segments and the location of the center of gravity (CG). The VTR images were collected by the Scientific Committee of Japan Association of Athletics Federations.

The preparatory and takeoff motions were divided into three support and two flight phases. Coordinate data were normalized by the body height and the duration of each phase and averaged [1]. Since the takeoff time was set at 100%, the support and flight time of the last two and last steps were 76, 91, 111 and 62%. Coefficients of variation (CV) of the angles of the shank, thigh and torso were determined by the following equation.

$$CV = \frac{SD}{|Mean + 360|} \times 100$$

Subjects were divided into two groups by the horizontal CG velocity at the touchdown of the takeoff phase, i.e. fast group (FG: n=14; height, 1.82 ± 0.07 m; body mass, 71.7 ± 9.1 kg; effective jump distance, 8.01 ± 0.30 m) and slow group (SG: n=19; height, 1.78 ± 0.05 m; body mass, 68.47 ± 4.7 kg; effective jump distance, 7.61 ± 0.19 m). Student's t-test was used to test significant differences between FG and SG for the angles of the shank, thigh and torso. The significance level was set at $p<0.05$.

RESULTS AND DISCUSSION

The horizontal CG velocity at the touchdown of the FG, 10.38 ± 0.15 m/s, was significantly larger than that of the SG, 9.91 ± 0.12 m/s ($p<0.001$). The FG kept significantly larger horizontal CG velocity than the SG at all instants of all phases ($p<0.01$).

Figure 1 shows changes in coefficients of variation of the shank, thigh and torso angles during the preparatory and takeoff phases. The takeoff leg was identical to the support leg during the second last step. The CV of the segment angles of the leg during the support phase was small. In the flight phase, the CV of segment angles of the swing leg increased during forward swing and decreased during backward swing before the touchdown. These results indicated that all the subjects moved the support leg in a consistent manner during the support phase but they swung the free leg in more various manner.

Figure 2 shows changes in the torso angle of the FG and SG during the preparatory and takeoff phases. The significant differences were found between the FG and SG only in the torso angle around the touchdown of the last support, which indicated that the FG inclined the torso more forward than the SG. Although the horizontal CG velocity of the FG was larger than that of the SG, there was no significant difference in the decrease of the horizontal CG velocity during the support phase of the last step. These results indicated that a jumper with the torso tilted forward slightly before the touchdown of the last step may minimize the loss of the horizontal CG velocity during the preparatory phase.

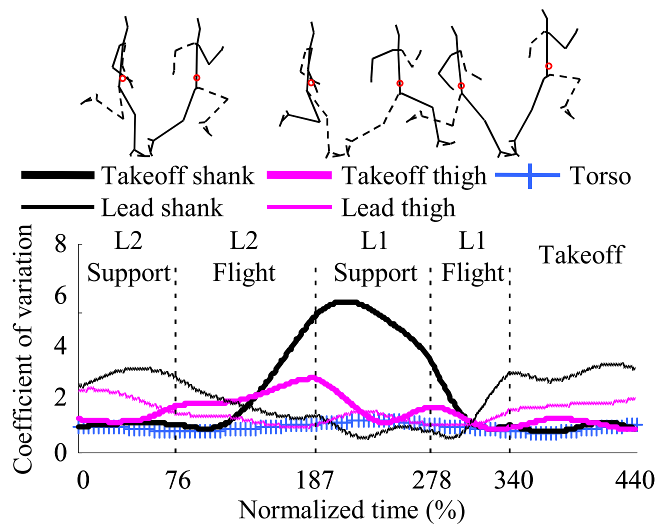

Figure 1 averaged changes in coefficients of variation of the shank, thigh and torso angles from the last two step (L2 and L1) to the toeoff. Stick pictures showed the averaged preparatory and takeoff motions of all the subjects

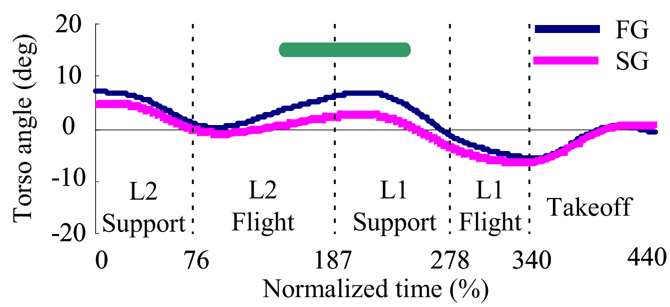

Figure 2 averaged changes in the torso angles of the FG and SG from the last two step (L2 and L1) to the takeoff. Positive value indicated that torso tilted forward. Horizontal bar above the curves showed significant difference between FG and SG ($p<0.05$)

GROUND REACTION FORCE ASYMMETRIES DURING SUSTAINED RUNNING

Daniel J. Gales and John H. Challis
Biomechanics Laboratory, The Pennsylvania State University, USA
email: djg153@psu.edu, jhc10@psu.edu

INTRODUCTION

Gait is a complex activity that has served as a major area of research in the biomechanics community. A common assumption in gait analysis and research is that the lower extremities behave symmetrically during able-bodied gait. This assumption may be inaccurate and have significant impact in clinical gait analysis, rehabilitation of patients, and artificial limb design.

Previous research examining running and ground reaction forces have utilized a limited number of footfalls in their analyses of symmetry, and have reached different conclusions. Hamill et al. [1] used ten-trial mean values to examine ground reaction force symmetry during walking and running and concluded that there appeared to be symmetry in ground reaction force parameters. Munro et al. [2] used six trials from each subject to examine ground reaction forces in running and indicated that right-left asymmetries were clearly present in these subjects. The purpose of this study was to examine ground reaction force symmetry during running using 700 pairs of footfalls per subject.

METHODS

Eight healthy young adult subjects with mean (sd) age 24.6 (3.5) years and body mass 627.0 (61.8) N, with no known musculoskeletal or neurological pathology volunteered for the study. The subjects were all experienced runners.

Vertical ground reaction force (VGRF) data were collected at 250 Hz using a Kistler Gaitway Instrumented Treadmill. Data were collected for two different running trials. Trial one (slow speed) consisted of running at 3, 4 or 5 $m.s^{-1}$ for 600 s for male subjects and 2, 3 or 4 $m.s^{-1}$ for 600 s for female subjects. Trial two (fast speed) consisted of running at a self-selected velocity for 600 s. Data collection began once the subject was running at the required velocity for each trial.

Data were processed with force and center of pressure data filtered with a 2nd order Butterworth filter with a cut-off of 30 Hz. The start and end of footfalls were identified using a 30 N threshold and data below this value were assumed to be noise. To quantify symmetry, a symmetry index was computed [3]. This index computed the difference between right and left limbs of a gait variable divided by the average of this variable.

Statistical differences in the following parameters were assessed using paired t tests: symmetry indices, mean impact peak VGRF, mean active peak VGRF, and mean VGRF impulse.

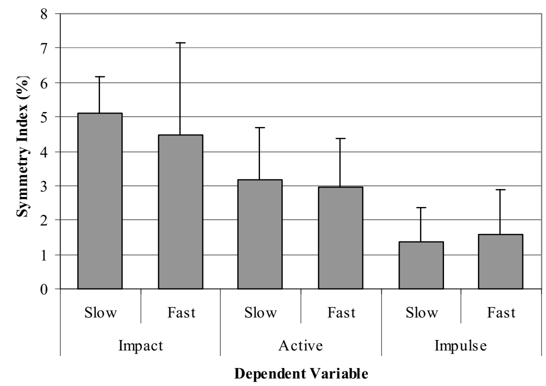

Figure 1: Mean and standard deviation o f symmetry index of mean impact VGRF, mean peak VGRF and VGRF impulse.

RESULTS AND DISCUSSION

Subjects completed an average of 1641.6 (83.2) steps per trial. Paired t-tests indicated significant differences between speeds for mean impact peak VGRF ($p < 0.001$), mean active peak VGRF ($p = 0.001$), and mean VGRF impulse ($p = 0.008$). As the speed of running was increased, there was a significant change in these variables. These results may have significance relative to injury rates in runners.

The symmetry index indicated that all of the subjects demonstrated asymmetrical behavior in mean peak VGRF, mean active VGRF and impulse across all trials. The presence of asymmetry in these variables for this period supports the concept that right and left lower extremities are not symmetrical during sustained running.

Paired t-tests indicated no significant differences ($p > 0.2$) for symmetry indices for impact peak VGRF, active peak VGRF, and VGRF impulse at different speeds (Figure 1).

CONCLUSIONS

This study provides evidence for the asymmetrical behavior of the lower extremities during running, but did not demonstrate any change in symmetry as running speed is increased.

REFERENCES

1. Hamill, J, et al. *Res Q Exerc Sport*, **55,** 289-293, 1984.
2. Munro, C, et al. *J Biomech,* **20**, 147-155, 1987.
3. Sadeghi, H, et al. *Gait Posture,* **12**, 34-45, 2000.

Extraction of knowledge for movement analysis data – example in clinical gait analysis.

[1]Stéphane Armand, [1]Eric Watelain, [2]Emmanuel Roux, [1]François Xavier Lepoutre
[1]LAMIH – UMR CNRS 8530, UHVC, Valenciennes, France, stephane.armand@univ-valenciennes
[2]LTSI - INSERM U642, Université de Rennes 1, Rennes, France.

INTRODUCTION

A major challenge in the field of human movement analysis is the interpretation of data acquired. For example, this interpretation could lead to optimization of performances in sport, to better space organization in ergonomics or to define therapeutic planes in medicine. The large amount of data provided by motion capture devices makes interpretation a difficult task for human reasoning [1]. Techniques of artificial intelligence could decrease the subjectivity and give a helpful tool for interpretation. The aim of this study is to provide a method to link a movement with the elements of interpretation of this movement. For application example, toe-walking - considered as a major gait deviation in many diseases - will be linked with its possible clinical causes provided by physical examination.

METHODS

The first step of the method is to extract (from trials) the different patterns or expressions of a considered movement. In order to reach this aim, a fuzzy space-time windowing of variables permitting to quantify the considered movement can be performed. And then a fuzzy c-means algorithm can be used to extract the different expressions of this movement. Each trial is assigned to these different patterns with membership values. Next, each pattern is characterized by the weighted mean of motion analysis data.

The second step is to link these expressions with their possible causes. Literature and experts could provide the different possible causes. Measurements of cause variables - which are interesting in interpretation process - are coded in fuzzy modalities. Fuzzy decision trees are then induced to create “if-then” rules linking expressions of movement with their possible causes. The accuracy of these rules can be evaluated with a stratified ten-fold cross validation.

For application example, toe-walking was explored with this method. A database of 2511 clinical gait analysis containing 11950 trials is used in input to extract the different expressions of toe-walking. Subsequently, toe-walking patterns are linked with their clinical causes. Possible clinical causes are extracted from clinical examination measurements including range of movement, muscular tone and strength which are coded in membership values according to the three modalities: {low, medium, high}.

RESULTS AND DISCUSSION

In this clinical example of extraction of knowledge; the first step of the method has permitted to extract three different patterns of toe-walking (figure 1). The second step of the method has highlighted clinical possible causes of these three patterns represented by 12 main rules. A rule is a combination of clinical elements leading to one of the three groups. An example of rules, corresponding to the possible causes, is presented on Table 1. The classification accuracy of the rules has been evaluated at 81%. Results were in agreement with literature and clinical gait analysis experts. For a given pattern of a new patient, it is now possible to determine possible causes of this pattern: *abduction approach*. It is also possible to predict the pattern of movement as from clinical measurements: *deduction approach*. Results of this clinical example provide an overview of possibilities of such method. Compared to classical statistical method, this method of extraction of knowledge has the advantage of not considering linear relationship between variables and permits to deal with a large amount of data. Fuzzy coding introduces the notion of vagueness and allows manipulation of language terms as “high” or “medium” rather than numerical values.

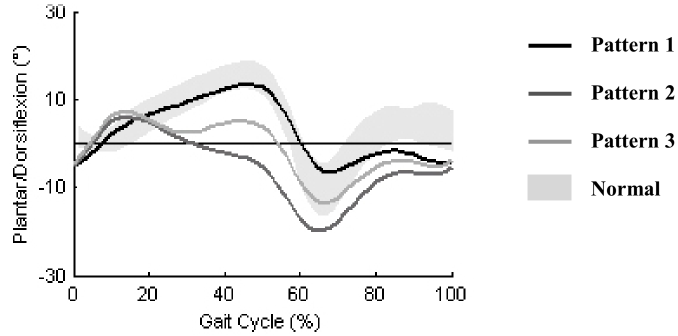

Figure 1: Three ankle gait patterns identified for toe-walkers

CONCLUSIONS

This two steps method using fuzzy c-means and fuzzy decision trees is an original method to extract knowledge from motion analysis data. It provides intelligible rules permitting identification of possible movement causes. This artificial intelligence method can be a helpful tool for all the people who have to deal with a large amount of data in the field of human motion analysis and who want to understand which elements influence movement patterns.

REFERENCES

[1] Chau T. *Gait Posture* **13**, 49-66, 2001.

Table 1: Examples of rules explaining movement patterns of toe-walkers.

Rules	Rules conditions		
	Condition 1	Condition 2	Condition 3
Rule 1 – Pattern 1	Low **tone** triceps surae	Medium **strength** quadriceps	
Rule 2 – Pattern 1	Low **tone** triceps surae	Medium **strength** tibialis anterior	
Rule 3 – Pattern 2	High **tone** triceps surae	Low **range of motion** dorsiflexion	High **tone** quatriceps

ADDUCTION MOMENT DURING GAIT IN PATIENTS WITH MODERATE & END-STAGE KNEE OSTEOARTHRITIS

[1] Laura Diamond, [1]Kevin Deluzio, [2]Cheryl Kozey and [3]William Stanish
[1]School of Biomedical Engineering, Dalhousie University,
[2]School of Physiotherapy, Dalhousie University, [3]Department of Surgery (Orthopaedics), Dalhousie University
email: ldiamond@dal.ca

INTRODUCTION

Osteoarthritis (OA) is a progressive degenerative joint disease that often results in significant disability and loss of function. This chronic joint disorder can be particularly debilitating in the knee because it is stressed in activities of daily living including walking. There is a distinctly higher prevalence of medial compartment OA within the diseased population [1]. The adduction moment of the knee is considered to be the mechanical factor most highly correlated with knee OA. However, not all studies have found higher adduction moments in OA patients [2]. In the latter case, the patient severity level was unknown, and comparisons were made at the peak adduction moment only. The purpose of this study was to characterize the changes in adduction moment that are associated with different severities of knee OA. Principal component analysis was used to detect differences in adduction moment waveform magnitude and shape.

METHODS

Fifty patients affected with moderate OA, 32 end-stage OA patients and 37 asymptomatic controls underwent a complete 3D kinematic, kinetic and electromyographic (EMG) analysis of the lower limb, with only the kinetic findings being discussed in this abstract. Patient severity levels were established through the Kellgren-Lawrence radiographic grading system [3] (Mod=1-3; End-stage=4). A Joint space narrowing grade [4] difference$\geq$ 1 (medial-lateral) was used to establish predominantly medial compartment OA. The subjects were required to walk along a 5-meter walkway in the laboratory a total of five times at a self- selected pace. The lower limb kinetics were calculated using the three dimensional orientation and position of the markers and the force plate data. The joint moment data was normalized with respect to bodyweight to Newton-meter/kilogram. All adduction moment waveforms were analyzed for group differences using principal component analysis (PCA) [5].

RESULTS AND DISCUSSION

Descriptives comparing the subject groups indicated that the control group was slightly younger and lighter than the patient groups, while the end-stage OA group walked significantly slower than the other two groups (Table 1).

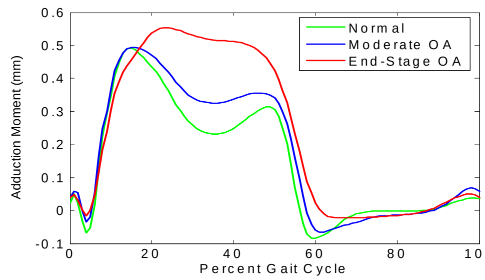

Figure 1: Mean adduction moment gait waveforms for moderate OA, end-stage OA, and control groups.

Using PCA to compare the adduction moment waveforms between the groups revealed that all three groups were significantly different ($p<0.05$) with respect to the overall magnitude of the curve during the stance phase (0-60%)(Figure 1). This magnitude difference (S>M>N) was represented by PC1. PC2 represented the shape of the adduction moment curve during the first 20% of the gait cycle. The end-stage OA group was significantly different than the other two groups with respect to PC2 ($p<0.01$). PC3 represented the variation found in the curve during the latter half of the stance phase (20-60%). The shape of the loading vector revealed that this PC was a difference operator contrasting mid-stance to late stance. The end-stage OA group was significantly different than the other two groups with respect to PC3 ($p<0.05$).

CONCLUSIONS

The overall magnitude of the adduction moment waveform during gait increases with both disease presence and severity level. End-stage OA patients exhibit a modified adduction moment curve shape when compared to moderate OA patients and asymptomatic controls.

REFERENCES

1. Baliunas A, et al. *Osteo Cartilage* **10**, 573-579, 2002.
2. Kaufman K, et al. *J Biomech* **34(7)**, 907-915.
3. Kellgren & Lawrence, *Ann Rheum Dis* **16**, 494-502, 1957.
4. Altman R, el al. *Osteo Cart*, **3 Suppl A**, 3-70, 1995.
5. Deluzio K, et al. *J Hum Mov Sci* **6**, 201-217, 1997.

Table 1: Descriptives for moderate OA, end-stage OA and normal subject groups. Values are mean (STD).

	Normals (N)	Moderate OA (M)	End-Stage OA (S)	Significant Diff ($p<0.05$)
Age (yrs)	50.5 (10.5)	59.7 (8.2)	64.1 (7.7)	N < (M = S)
Weight (kg)	72.9 (14.2)	94.7 (19.1)	94.3 (16.3)	N < (M = S)
Height (m)	1.7 (0.1)	1.7 (0.1)	1.7 (0.1)	NONE
BMI (kg/m2)	24.8 (4.0)	31.1 (5.7)	33.2 (5.0)	N < (M = S)
Speed (m/s)	1.3 (0.1)	1.2 (0.2)	0.9 (0.2)	S < (M = N)

The Effect of Laterally Wedged Orthoses on Talus Angle

[1] Jeremy Crenshaw, [1] Todd Royer, [2] Irene Davis, [1] Stephanie Crenshaw, and [2] Robert Butler
[1] Health, Nutrition and Exercise Sciences, and [2] Physical Therapy, University of Delaware, Newark, Delaware, USA.
email: jcrensha@udel.edu

INTRODUCTION

Laterally wedged insoles are a conservative treatment for medial knee osteoarthritis (OA). These insoles, typically inclined 5-10 degrees, attempt to alter lower extremity alignment and redistribute forces at the knee, potentially reducing knee pain. However, there are conflicting reports of static alignment measured with frontal plane radiographs. A few studies [4,5,6] did not find significant differences in tibio-femoral angle between wedged and non-wedged conditions, whereas another study [7] reported a shift in the mechanical axis, but not in the tibio-femoral angle during one-legged stance.

We previously reported no differences in tibiofemoral angle or mechanical angle with laterally wedged orthoses [3]; however, it is possible that wedged insoles affect ankle alignment as determined by talus position on frontal plane radiographs. The purpose of this study was to determine the effects of laterally wedged insoles on frontal plane talus angle in patients with medial knee OA. It was hypothesized that the talus would rotate medially with the use of a laterally wedged insole.

METHODS

Eleven males and ten females (M_{age}= 61.6±7.0 yrs; M_{height}= 169.9±9.8 cm; M_{mass}= 93.9±18.6 kg), all diagnosed with medial knee OA of grade II or higher on the Kellgren-Lawrence scale, volunteered to be subjects in this study. Full length laterally wedged foot orthoses were fitted for each subject's affected knee side. Wedging amount (9.2 ± 3.5˚) was determined for each subject based on the greatest reduction in knee pain during a lateral step-down task. A two-week period was allowed for accommodation to the orthotic device. Frontal plane radiographs allowed analysis of the affected limb in a bilateral stance with and without the wedged insole in the shoe.

A line was drawn on the radiograph to connect the two most superior articulations of the talus; the angle between this line and horizontal, measured manually with a standard goniometer, defined the talus angle. Positive angles represent a medially rotated (laterally elevated) talus.

A paired samples t-test was used to determine significant differences between wedged and non-wedged conditions for talus angle ($p < .05$).

RESULTS AND DISCUSSION

Talus angle (Figure 1) for the wedged condition (-1.67±3.93 deg) did not rotate medially from the non-wedged condition (-0.95±4.25 deg) as hypothesized ($p = 0.197$). Change in talus angle ranged from -4 to +4 degrees, indicating a highly variable subject response to the wedged orthosis.

Despite wedging of 5-15 degrees, lateral wedging does not seem to affect talus angle during a bilateral static stance. Previously we reported increased subtalar eversion during gait with wedged orthoses, suggesting the calcaneus is altered during the stance phase [1]. Therefore, potential changes in calcaneus alignment do not appear to affect static talus alignment. Additionally, changes in talus angle are not consistent with reductions in frontal plane knee moment [2] or knee pain associated with wedged orthotic use.

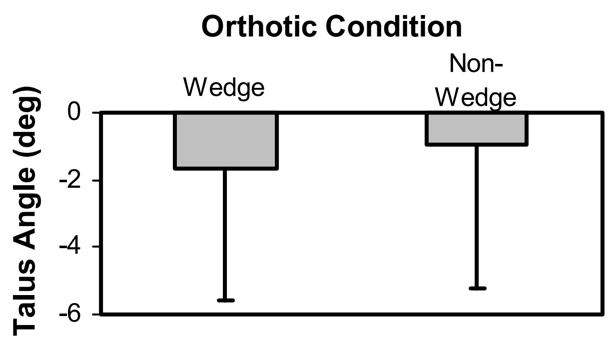

Figure 1: There were no significant differences in talus angle between insole conditions. Positive angles reflect a medially rotated (laterally elevated) talus.

CONCLUSIONS

Laterally wedged orthoses did not alter talus angle in subjects with medial knee OA.

REFERENCES

1. Butler RJ, et al. *National ACSM Conference*, Indianapolis, Indiana, The effect of wedged orthotics on hip and ankle mechanics, 2004.
2. Butler RJ, et al. *Proceedings of ISB XIX*, Dunedin, New Zealand, Acute effects of wedged orthoses on knee mechanics in patients with knee OA, 2003.
3. Crenshaw SJ, et al. *Gait and Clinical Movement Analysis Annual Meeting*, Lexington, Kentucky, Functional test performance and pain in subjects with medial knee osteoarthritis treated with laterally wedged insoles, 2004.
4. Giffin JR. et al.. *JPO* **7**, 23-28, 1995.
5. Maly MR, et al.. *Clin Biomech* **17**, 603-10, 2002.
6. Toda Y, et al.. *J Rheumatol* **28**, 2705-10, 2001.
7. Yasuda K, Sasaki T. *Clin Orthop* **215**, 162-172, 1987.

ACKNOWLEDGEMENTS

Support from NIH-RR16548 (Tom Buchanan, PI) is acknowledged.

MECHANICAL PROPERTIES OF CANCELLOUS BONE OF THE DISTAL HUMERUS

[1] Cheryl E. Dunham, [2]Sarah E. Takaki, [1,2]James A. Johnson, and [1,2,3]Cynthia E. Dunning
[1]Departments of Biomedical Engineering and [2]Mechanical and Materials Engineering
Biomechanical Testing Laboratory, University of Western Ontario, London, Ontario, Canada; email: [3]cdunning@eng.uwo.ca

INTRODUCTION

Mechanical properties of cancellous bone in the distal humerus are of interest for a number of reasons. An understanding of variations in modulus and strength across several transverse sections may determine optimal fixation techniques and locations for prosthetic components. These results may also suggest optimized surgical procedures to allow better fixation in stronger bone [1,2,3]. An understanding of these mechanical properties is of value in developing finite element models, as well as providing comparative data to validate synthetic bones for implant testing. The objective of this study was to quantify the strength and modulus of distal humerus cancellous bone, and identify any regional variations.

METHODS

Three consecutive transverse slices (3 mm thick) were sectioned from the distal cancellous region of seven fresh-frozen cadaveric humeri (ages 70-92, mean age 79.4 years). Each slice was marked with a 3x3 mm^2 grid, and subjected to compressive testing using a flat cylindrical indenter (1.6 mm diameter). A servohydraulic testing machine (Inston Corp., Canton, Mass., USA) collected load-displacement data during testing. Indentation modulus and strength were calculated for each test site, and pooled into nine regions defined by anatomical directions (anterior, posterior, medial, lateral and central) for each slice (Figure 1). Results were analyzed using two-way repeated measures ANOVAs to determine differences in strength and modulus among regions and slice levels. All statistical tests were performed with $\alpha = 0.05$.

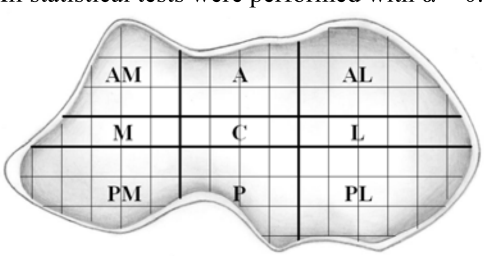

Figure 1: Transverse slice showing 3x3 mm^2 test sites and nine regional divisions [defined by anterior (A), posterior (P), medial (M), lateral (L) and central (C) sections].

RESULTS AND DISCUSSION

Stress-strain curves for the indentation tests were reasonably consistent in shape, with all exhibiting a characteristic yield followed by a slight softening and then a large region of nearly constant load (Figure 2). Mean modulus was found to be 309.8±242.0 MPa (range: 2.9-1041.7 MPa). Yield strength averaged 4.4±2.5 MPa (range: 0.6-16.3 MPa). The highest modulus was found in the distal-most slice ($p<0.05$). The lowest modulus region was the posterior lateral ($p<0.05$) (Figure 3). There were no differences in strength among slices or across the nine regions.

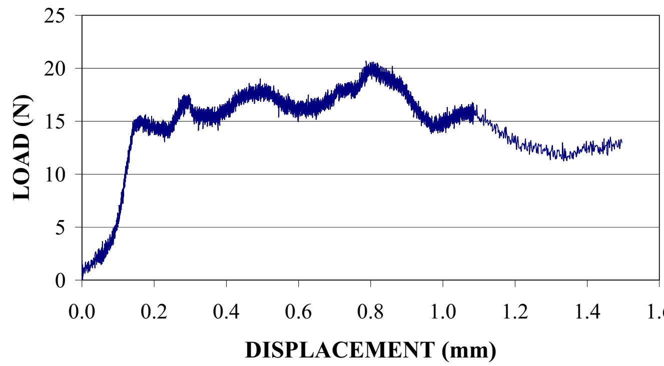

Figure 2: Representative load-displacement curve for one indentation site.

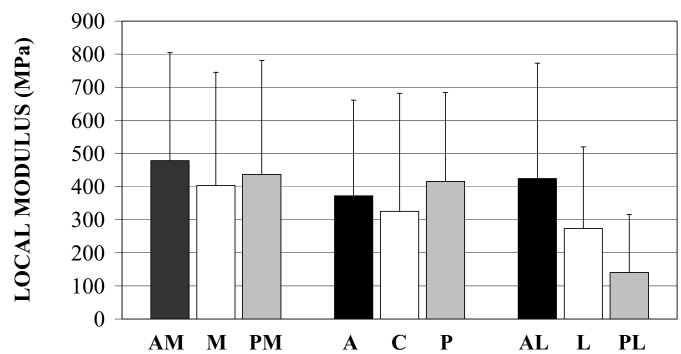

Figure 3: Indentation modulus for the 9 regions of the distal humerus. (See Figure 1 for region definitions.)

CONCLUSIONS

This study determined the indentation strength and modulus of cancellous bone of the distal humerus at three transverse levels and nine anatomically-defined regions within each cross-section. Mean strength was 4.4 MPa and mean modulus was 309.8 MPa, with large variations both within and among humeri. Cancellous bone modulus decreased with movement from distal to proximal. The posterior lateral region had a lower modulus than the other regions of the distal humerus. The influence of slice depth may be important with regard to the amount of bone removed during prosthetic replacement requiring cancellous fixation. Regional variations in modulus suggest that the posterior lateral region may be an inferior site for screw purchase during fracture fixation.

REFERENCES

1. Anglin, C. et al. *J. Biomech* **32,** 1091-1097, 1999.
2. Gordon, K. D. et al. *J.Orthop.Trauma* **17,** 285-289, 2003.
3. Batte, S.W.P. et al. *Proceedings of ORS XLII,* Atlanta, Georgia, USA, 1996.

SEQUENTIAL LABELLING AND ACOUSTIC EMISSION ANALYSIS OF DAMAGE OCCURRING IN CORTICAL BONE DURING INDENTATION CUTTING

[1] Ger Reilly, [1]Ashkan Safari, [2]David Taylor and [1]Brendan McCormack
[1] School of Mechanical and Electronic Engineering, Institute of Technology, Sligo, Ireland, reilly.ger@itsligo.ie
[2] Trinity Centre for Bioengineering, Trinity College, Dublin, Ireland

INTRODUCTION

When a surgeon uses a wedge shaped blade or an osteotome to cut cortical bone during an operative procedure the bone will fail by a process of microcracking and primary crack propagation. It has previously been observed that crack propagation is dependent on the direction of cutting relative to the main axis of the bone [1]. It has also been observed that microcracks occurring during fracture release acoustic signals that facilitate real-time monitoring of a cutting process [2].

In these novel studies, we labelled damage accumulation during cutting of cortical bone using sequential chelating dyes [3] and we correlated recorded AE signals during cutting with load-displacement curves.

METHODS

8mm cubes of cortical bone were located in a chamber and cut using a wedge-shaped blade in longitudinal and transverse directions. Chelating dyes were used at different loading stages. Specimens were sectioned and examined for evidence of damage using UV microscopy post-test.

Similar specimens were also tested using AE monitoring techniques and various AE parameters were recorded and correlated with load curves; number of AE hits, and amplitude of AE signals. A threshold value of 40dB was used to eliminate background noise and low-amplitude signals were amplified by a fixed gain of 40dB with a (0.1-1) MHz band pass filter [4].

RESULTS AND DISCUSSION

The chelating dyes label the progressive damage occurring during different stages of the cutting process and indicate the extent of the damage zone around the cutting area. The zone is different for different cutting directions; extending longitudinally for longitudinal cutting and confined to lateral regions for transverse cutting as shown in Figure 1. For both cutting directions fracture cracks grow along the lamella interfaces.

Figure 2 shows that the number of recorded AE pulses increased prior to main cutting fracture as previously reported for tensile fracture [5]. High amplitude, high duration signals may be associated with the main crack propagation, as they occurred predominantly during this period of loading.

CONCLUSIONS

It is difficult to clearly distinguish different stages in the crack growth from current results however there is clearly labelling of damage (flame effect) by all dyes used, indicating damage occurring at different stages of the loading process, and the labelled zone shows the direction of the damage process occurring relative to cutting. The AE technique is useful for real-time monitoring and prediction of fracture processes, and the increase in AE pulses prior to fracture may be used as an indicator of onset of fracture during bone cutting.

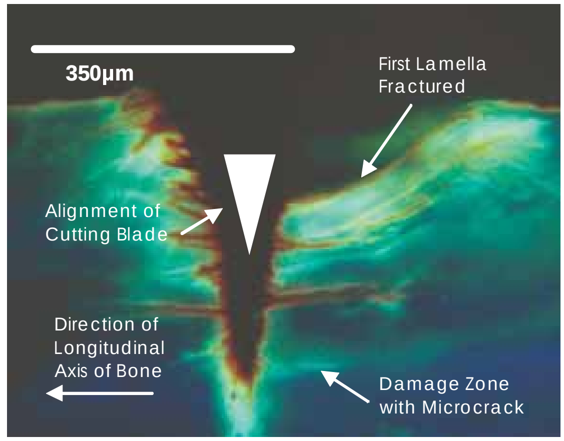

Figure 1: Cutting zone - transverse cutting specimens.

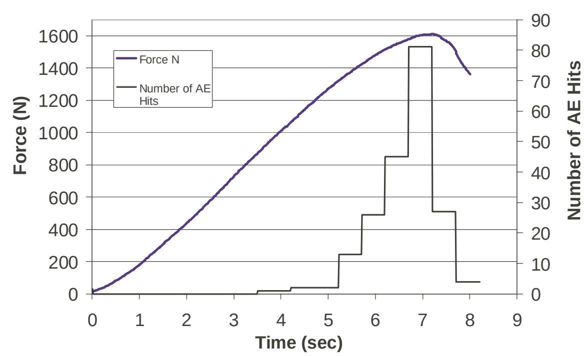

Figure 2: Force and number of AE hits versus time during longitudinal indentation loading.

REFERENCES

1. Reilly G.A. & Taylor D., *Proceedings of ESB14*, Hertogenbosch, Holland, 2004.
2. Safari A., Reilly G.A., McCormack B.A.O., *Proceedings of Bioengineering in Ireland 11*, Dublin, Ireland, 2005.
3. O'Brien F.J., et al., *J Biomech* **35,** 523-526, 2002.
4. Rajachar R.M., et.al., *ASTM STP1353*, Vahaviolos, S.J., Ed., PA, 1999.
5. Zioupos P., et al., *Med Eng Phys* **16,** 203-212, 1994.

ACKNOWLEDGEMENTS

This work was funded by the Council of Directors Strand I and III Research Programs.

VALIDATION OF INTRAMUSCULAR PRESSURE SENSOR IN RAT GASTROCNEMIUS MUSCLE DURING ISOMETRIC CONTRACTION

JL Megesi[1], TR Jenkyn[1,2]
[1]School of Kinesiology, University of Western Ontario, Canada
[2]Dept. of Mechanical and Materials Engineering, University of Western Ontario, Canada

INTRODUCTION

The inability to directly measure the internal loads acting within articular joints has been a limitation in biomechanics. Currently, skeletal muscle loads must be estimated from EMG measurements or calculated computationally. Intramuscular pressure (IMP) has been shown to be well correlated with muscle tension and has recently become a feasible *in vivo* measure [1,2]. The sensor used in this study is based on fiber-optic technology and has been used extensively in rabbit [3]. The purpose of this study was to evaluate the performance of the fiber-optic IMP sensor during galvanic isometric contractions in intact rat skeletal muscle.

METHODS

Sprague-Dawley rats (weight 200-300g) were anaesthetized and secured to a custom-made jig with the knee fixed at 90°. Hind limb muscles were exposed, but left intact. The foot was attached to a lever articulating about the ankle from which force was measured. The biceps femoris was reflected and the sciatic nerve exposed. Platinum wire electrodes were placed around the nerve and isometric contractions of the hind limb muscle group were elicited (Grass Instruments, S-88 stimulator). A 360 µm diameter fiber-optic pressure sensor (Luna Innovations Inc., Blacksburg, VA) was inserted into the belly of the gastrocnemius muscle via a 22-gauge needle, parallel to the direction of the muscle fibres. IMP, force and muscle length were measured simultaneously at stimulation levels of 2.4, 3.0, 3.5, 4.0, 4.5, 5.0 and 5.5 volts with at least 1 minute rest between levels to minimize fatigue.

RESULTS

The results of this experiment indicate that the length-tension curve for isometric contractions was mimicked by the length-pressure curve for active conditions (Figure 1). To confirm this finding, muscle force and IMP were plotted against each other and linear regression was performed (Figure 2). There was a strong linear correlation (R^2=0.76) between IMP and muscle force.

DISCUSSION

This study quantified the relationship between IMP and muscle force during galvanic isometric contractions in intact rat skeletal muscle. These findings confirm previous work done in rabbit skeletal muscle [3]. Further work must now be concentrated on the validity of the sensor under dynamic contraction conditions.

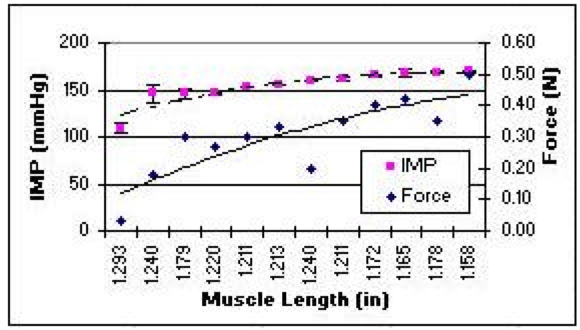

Figure 1. Relationship between IMP and isometric muscle force for rat gastrocnemius muscle at varying lengths.

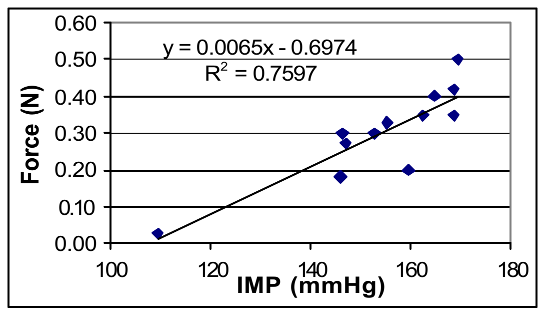

Figrure 2. Relationship between isometric force and intramuscular pressure at various stimulation levels. Force and IMP were well correlated (R^2=0.76).

REFERENCES

[1] Baumann J.U., Sutherland D.H., Hanggi D.H. (1979) *Clin Orthop Rel Res* 145:292-299.
[2] Kaufman K., Wavering T., Morrow D., Davis J., Lieber R. *J* (2002) *Biomech* 36: 283-287.
[3] Davis J., Kaufman K.R., Lieber R.L. (2002) *J Biomech* 36: 505-512.

ACKNOWLEDGEMENTS

Special thanks to Earl Noble and Tom Dzialoszynski for their continued input and help on the project.

DYNAMIC SIX-SEGMENTAL FOOT MOTION USING ELECTROMAGNETIC TRACKING SYSTEM

[1] XueCheng Liu, [2]John Thometz, [2]Roger Lyon, and [3]Chris Boudreau
[1]Motion Analysis Lab, [2]Dept. of Orthopaedics, Children's Hospital of WI, [3]Dept. of Biostatistics, Medical College of Wisconsin. Email: xcliu@mcw.edu, web: www.chw.org

INTRODUCTION

Multi-segmental foot motion during walking has been mostly investigated using passive markers and the Video Motion Analysis System (1,2,3). These foot segments mainly are limited to the hindfoot and forefoot. Since the Electromagnetic Tracking System (ETS) was introduced to our biomechanical and clinical society, one study was conducted to determine the ankle joint kinematics (4). The goal of this study is to develop a newly designed anatomically based six-segmental foot model using the ETS, including the hindfoot, midfoot and forefoot kinematics, and to find out the reliability of intraobserver.

METHODS

The study was performed on six children with 12 normal feet. Their ages ranged from 9 to 15 years with a mean age of 12 years. The ETS consists of: a long range StarTrak transmitter (Polhemus Inc., Colchester, VT) with 12 sensors, electronics unit and the 6D Skill Technologies' Gait motion capture and software (Skill Technologies, Inc., Phoenix, AZ). There is a two-inch cubic transmitter used as the global reference frame within a maximum radius is 12 ft. Each sensor with half-inch cubic coils compute with 6 degrees of freedom in real-time. The motion is sampled at a rate of 120Hz. A fourth order Butterworth digital filter with a cut-off frequency of 6Hz is also used.

Six sensors were placed on each foot with double stick tape at the following locations: the tibia tuberosity, posterior calcaneus, navicular tuberosity, cuboid tuberosity, middle dorsal shaft of the 1st metatarsal bone and dorsal hallux. The children were initially asked to stand in a neutral postion, which is defined as a static standing with weight-bearing and their feet parallelling the y-axis of our global reference. Each sensor is used as a local reference frame for the segment to which it is attached and aligned with the global reference during calibration. After defining the neutral position, the subjects walked with 6 sensors on each foot along a 20 ft walkway at their natural speed. Data was captured over a 4 second period and three separate trials were completed for each subject. Four subjects were randomly selected for repeated tests during the same day and by the same satff. Correlation between two times measurements was calculated by Intraclass coefficient (ICC).

We always calculate angles by the distal sensor with respect to the proximal sensor. Hence the Cardan sequence is the angle around the medial/lateral axis first (dorsiflexion/plantarflexion as pitch angle), followed by the angle around the anterior/posterior axis (inversion/eversion as yaw angle), finally the angle around the vertical axis (internal/external rotation as roll angle).

RESULTS AND DISCUSSION

In the sagittal plane, mean peak dorsiflexion of the hindfoot at the mid stance is 10.4°. The navicular-1st metatarsal segment displays mean peak dorsiflexion of 4.9° before toe-off. The 1st metatarsal-hallux joint gives mean peak dorsiflexion of 43° at toe-off (Figure 1). In the coronal plane, mean peak inversion of the hindfoot is 5.2° and eversion is 2.9°, whereas the navicular-1st metatarsal segment, and 1st metatarsal-hallux joint yield smaller range of motion. In the transverse plane, the hindfoot displays dominated external rotation during 1st and 2nd rocker. The midfoot and forefoot expresses minimal internal rotation during stance phase yet external rotation during swing. In sagittal plane, ICC between two measurements are 0.62 for hindfoot, 0.40 for navicular-1st metatarsal segment, and 0.34 for 1st metatarsal-hallux joint. In the coronal plane, coefficients are 0.86, 0.52, and 0.79, respectively. In the transverse plane, coefficients are 0.94, 0.66, and 0.72, respectively.

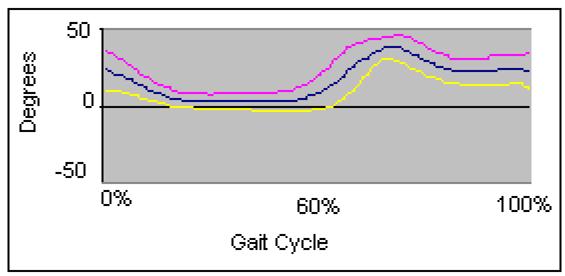

Figure 1. Dorsiflexion and plantarflexion of the 1st metatarsal-hallux joint in mean ± SD as a function of gait cycle.

CONCLUSIONS

Our foot model has a moderate to high reliability to determine hind and forefoot rotation. Movements derived from the navicular-1st metatarsal enhance our understanding of midfoot kinematics during walking. Further studies are needed to evaluate the interobserver variation across days.

REFERENCES

1. Kaufman,et al. *Technique for measurement of foot and ankle kinematics.*GCMAS, 2003.
2. P. Smith,et al. *3D motion analysis of the pediatric foot and ankle*. Editor, G.Harris. IEEE,2000.
3. MacWilliams BA,et al. *Foot kinematics and kinetics during adolescent gait. Gait & Posture* **17**, 214-224, 2003.
4. Woodburn J, et al. *A preliminary study determining the feasibility of electromagnetic tracking for kinematics at the ankle joint complex. Rheumatology*;**38**:1260-8, 1999.

SUBJECT-SPECIFIC FE MODEL FOR THE PREDICTION OF THE RELATIVE MICROMOTION IN A TOTAL HIP IMPLANT: VERIFICATION AND VALIDATION

[1,3] Barbara Reggiani, [1,3] Luca Cristofolini, [2,3] Elena Varini, and [3] Marco Viceconti
[1] DIEM, [2] DEIS, Università degli Studi di Bologna, Italy, [3] Laboratorio di Tecnologia Medica, I.O.R., Bologna, Italy
Corresponding author: barbara.reggiani@mail.ing.unibo.it

INTRODUCTION

The most common reason for the aseptic loosening of cementless hip stem is the lack of primary stability as the presence of an excessive relative micromotion at the bone-implant interface [1]. Despite pre-clinical validation has remarkably improved over the last few years, some important factors affecting implant biomechanics have still to be considered. Most of the previous numerical studies on hip arthroplasty were based on the solid model of a composite femur replica. However, subject-specific factors (skeletal anatomy, mechanical properties, implant position) are needed to produce helpful outcomes for clinical practice. In addition, these models were developed using time consuming structured meshes frequently lacking of careful verification and validation phases.

Aim of the present work is the development of a Finite Element (FE) model of an implanted femur taking into account the specificity of subject as well as the planned surgery technique parameters.

Specific aims are the verification of the numerical accuracy of the FE model and the analysis of the predicted relative micromotions compared to experimental results (validation).

METHODS

The 3D model of an intact cadaveric femur, taken *in-vivo* for clinical purpose, was generated from the CT dataset using a previously validated procedure. A linear convergence test on seven meshes with increasing refinement levels was performed to ensure the numerical accuracy of the model. Afterward, the position of an anatomic cementless hip stem (ANCAfit, Cremascoli-Wright, Italy) inside the femur was defined by a skilled surgeon using a pre-operative CT based software (Hip-Op, B3C, Italy). Surgical parameters and hip stem geometry were then imported within the FE model. An unstructured mesh was generated for both femur and hip stem consisting of tetrahedral elements (Figure 1*a*). The coefficient of friction was set to 0.3. Frictional contact was modeled at the bone-implant interface by means of face-to-face contact elements.

The peak compenetration was recorded since it must be very small to get a good level of numerical accuracy. The validation process ensured that the numerical model accurately predict the physical phenomenon it was designed to replicate. This was assessed by comparing the predicted history of sliding micromotion at the femur calcar level to *in-vitro* experimental measurement of Intra-operative Stability Assessment Console (ISAC) [2] replicating the same boundary conditions (Figure 1*a*). Two indicators were selected to judge the quality of the model: the root mean square error and the peak error of predicted micromotions.

RESULTS AND DISCUSSION

Over the seven generated meshes, the percentage error in energy norm and the differences in terms of stress, strain and displacement were less than 2.2%. The model that guarantee the best compromise among computational time and accuracy was chosen (40460 elements). The peak compenetration was 3.2 microns, less then previously reported best value [3].

The model predicted the sliding micromotions measured experimentally with an average (RMS) error of 12 μm and a peak error of 21 μm (Figure 1*b*). The errors are comparable to those reported in studies with synthetic femurs and clearly acceptable for most applications. The different pattern of predicted versus experimental micromotions is explainable through a small volume of very soft cancellous bone in the femoral endosteum that may exceed the yield strain limit, e.g. 0.78% (Figure 1*b*). This hypothesis is confirmed by other measurements on different cadaveric femurs that have shown a similar pattern of experimental micromotions.

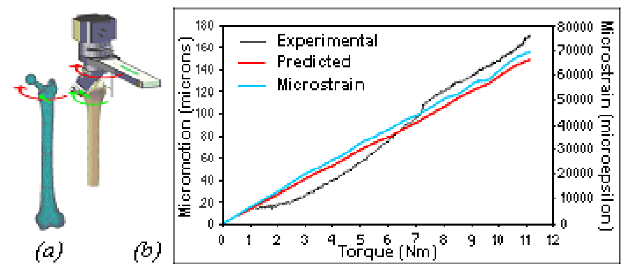

Figure 1: *(a) FE model and the applied boundary conditions compared to experimental set-up used as benchmark problem; (b) Predicted and experimental micromotions over the applied torque. Peak microstrains over the entire FE model are also reported.*

CONCLUSIONS

Verification and validation are necessary preliminary steps to consider any finite element model predictions of scientific value. Using the method proposed it was possible to asses the confidence of predicting the bone-implant relative micromotions account for the patient and surgeon. Furthermore, unstructured mesh was proved to have the same degree of accuracy of the more time-consuming structured meshes.

REFERENCES

1. Total Hip Replacement. NIH Consensus Statement 1994 Sep 12-14, **12**(5): 1-31
2. Varini E. et al. *Proceedings of ESB XIV*, 's Hertogenbosh, the Netherlands, 2004
3. Viceconti M. et al.. *J Biomech* **33**, 1611-1618, 2000

AN ANALYSIS OF LOSSES OF BALANCE DURING TANDEM STANCE ON A NARROW BEAM

[1]Alaa A. Ahmed and [1,2]James A. Ashton-Miller
Biomechanics Research Laboratory
Departments of [1]Biomedical and [2]Mechanical Engineering
University of Michigan, Ann Arbor, MI, USA; email: aaahmed@umich.edu

INTRODUCTION

Most falls are preceded by a loss of balance. Given that there are few mechanistic explanations for 'loss of balance', we have hypothesized it to be a loss of effective control, detectable as a control error anomaly (CEA). We have used a model-reference adaptive controller to represent the central nervous system along with a failure detection algorithm to mimic how it makes decisions based on input and output signals obtained during the task [1,2]. In this paper we examine the ability of this method to detect a loss of balance in a three-dimensional, multi-degree of freedom (dof) balancing task: tandem stance on a narrow beam. We hypothesize that a control error anomaly will predict the occurrence of a compensatory step off the beam at least 100 ms, and no more than 2 s, later.

METHODS

Ten young (18-30 yrs) female subjects were tested. Subjects were asked to stand in tandem (heel-to-toe) stance on a narrow beam (2.5 cm wide) for a maximum of 60 seconds (Fig 1). Each subject performed a minimum of 15 trials.

The human was modeled using eight three-dimensional rigid body segments: trunk, pelvis, right and left feet, calves, and thighs. Twenty-eight optoelectronic markers recorded the segment kinematics; ground reaction forces and torques were also recorded from two force plates to which the beam was bolted. Joint torques were calculated using inverse dynamics.

We considered the joint torques to represent the system inputs, while the segment accelerations represent the 8x3 system outputs in the three orthogonal planes. The corresponding control error signals were defined as the residuals generated when each of the actual system outputs is compared to the corresponding predicted output of a nominal forward internal model using the given torque inputs. CEA was detected once an error signal crossed a threshold level set at three standard deviations (3Σ) beyond the mean value in a 2-second-wide moving window, **b**, which trailed the current time instant, **t**, by 100 ms (**δ**). (Fig 1: The threshold calculation begins at 'Start', initially using baseline data in window **a**.) LOB was confirmed by the occurrence of a step within 2 s of, and no earlier than 100 ms from, CEA detection (window **c**). The occurrence of a step was defined as a compensatory response and evidence of CEA perception.

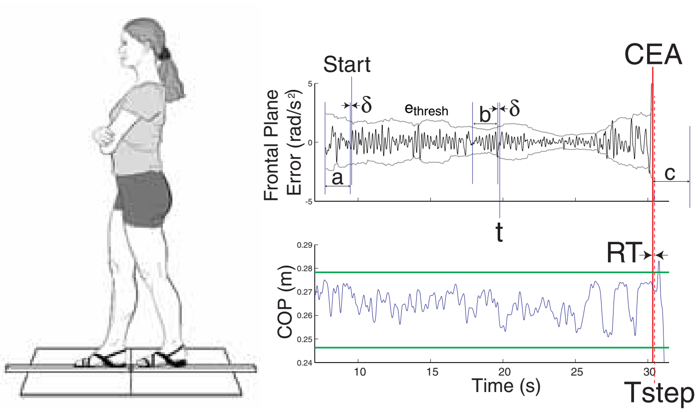

Figure 1 *Left: Subject in tandem stance. Right (top): Algorithm schematic of one of the 22 control error signals analyzed and (bottom) center-of-pressure (COP) in the frontal plane with time of step initiation, Tstep, marked by a vertical dotted line. The horizontal lines (bottom figure) delineate the beam outline.*

RESULTS AND DISCUSSION

This is the first test of the CEA hypothesis in a 3D multi-dof balancing task. The 3Σ algorithm correctly detected a loss of balance in 71.6% of 148 trials by either predicting the step off the beam when one occurred, or by not predicting a step when one did not occur. In this case, the first of the 8 segment control error signals in the frontal plane to reach 3Σ was used to detect CEA. Similar results were obtained when monitoring control error in either the sagittal (64.9%) or transverse plane (64.2%). Control error within a given plane was a better step-predictor than individual segment control error ($p<0.05$, Table 1), and segments performed equally ($p>0.05$). Importantly, kinematic signals such as segment and whole-body center of mass (COM) position, velocity and acceleration were significantly less reliable than CEA ($p<0.01$, Table 1). The optimal threshold level for CEA detection was 3Σ, supporting earlier results in sagittally-symmetric seated [1] and standing reach [2] balance tasks. In contrast to kinematic measures, CEA emphasizes the importance of the control input, and the input/output relationship in the perception of a loss of balance.

CONCLUSIONS

The results support the definition of a loss of balance as a loss of effective control. Control error is a more reliable predictor of a compensatory response than body kinematics in this three-dimensional, multi-input, multi-output balancing task.

REFERENCES

1. Ahmed AA, Ashton-Miller JA, *Gait Posture* **19**, 252-262, 2004.
2. Ahmed AA, Ashton-Miller JA, *Proceedings of ASB XVIII*, Portland, OR, 2004.

Table 1: Success Rate of Various Algorithm Detection Schemes (χ^2 probability relative to Within-Plane Error, * p<0.05, ** p<0.01)

	Within-Plane Error	Segment Error	COM Acceleration	COM Velocity	COM Position
Success Rate (%)	71.6	60.8^*	31.8^{**}	56.1^{**}	38.5^{**}

PEDIATRIC GAIT ANALYSIS: A CALL FOR STANDARDIZATION

[1] Ruxandra Marinescu, [1]Sherry Mitchell, [2]Donald McCartney and [1]Jean Wright
[1]Pediatric Rehabilitation Department, George and Marie Backus Children's Hospital, Savannah, GA, USA
[2]Orthopedic Center, 4600 Waters Ave, Savannah, GA, USA
email: marinru1@memorialhealth.com

INTRODUCTION

The objectives of the study were to identify the gait assessment practices currently used in pediatric motion analysis laboratories and to evaluate the need for a standardized approach [1].

Gait analysis is recognized today as an essential tool in clinical rehabilitation [2,3]. Generally, gait analysis is successfully used to assess and to identify motor disability, to develop treatment plans, to evaluate the effectiveness of a treatment and to study clinical and pathological gait. However, because of differences in the equipment, personnel training and the methods used for gathering data, comparing and sharing gait analysis results between gait analysis laboratories is very difficult, if not impossible [4].

A questionnaire was developed in the Pediatric Rehabilitation Department, at the George and Marie Backus Children's Hospital at Memorial Health University Medical Center. Several important issues emerged from the current study. The results of the study highlight the current inconsistency between gait assessment practices of various motion analysis laboratories and the importance of standardization.

METHODS

A multiple-choice questionnaire assessed the current practices in pediatric motion analysis laboratories, and the perceptions of the staff regarding the standardization of their laboratory's data. The questionnaire had 15 questions regarding motor evaluation tests used for children with motor impairment, methods to determine treatment effectiveness, normative database used, etc.

A consecutive sample of 13 pediatric motion analysis laboratories were recruited out of 15 centers to complete the questionnaire based on availability of pediatric evaluation, testing capabilities and peer recognition. All the participants completed the same questionnaire. Four recruited participants did not answer the questionnaire.

RESULTS AND DISCUSSION

Currently, to evaluate the results of a gait analysis, diverse resources are used. No two laboratories listed the same protocols as part of their evaluation. Most of the participants are using normative data that is collected on-site. The remaining participants are using data developed by other laboratories.

Four of the participants consider "functionality" as the most essential characteristic of gait for children with motor impairment. Symmetry, normality, comfort and patient's goals were also considered. Four of the participants are using Gross Motor Function Measure (GMFM) to evaluate motor impairment in children. The remaining participants are using various other evaluation tests: Gross Motor Function Classification System (GMFCS), Pediatric Outcomes Data Collection Instrument (PODCI), etc.

Determining the necessity of a treatment and the treatment's effectiveness varies among participants. These determinations are usually performed using instrumented and observational examinations, as well as other evaluations such as team review, interview with the family, etc.

Determining the optimal duration of a physical therapy treatment is particular for each participant. Multiple criteria are used: specific goals, post surgery assessment, functional potential, severity of motor impairment, patient's ability to cooperate, insurance reimbursement, etc.

Despite the availability of expensive and sophisticated equipment, there is no standardized protocol or series of tests that laboratories agree to as a basis for evaluation. Most of the participants are interested in using a new normative database as reference.

CONCLUSIONS

Gait assessment practices vary significantly between different laboratories. While developments in technology are rapidly progressing, the tools to standardize the information are lagging. This gap is particularly noticeable in children under the age of eight, where there is little to no normative tools.

Lack of consistency between centers, rapid development of technology, and perceived interest of current laboratories for a common assessment and normalization tools calls for the standardization of data.

REFERENCES

1. Wu G, et al. *J Biomech*. **35**, 543-8, 2002.
2. Cooper RA, et al. *Am J Phys Med Rehabil*. **78**, 278-80, 1999.
3. Craik R, Oatis C. *Gait Analysis: Theory and Application*. Mosby, 1995.
4. Kaufman KR, *Future Directions in Gait Analysis*, <http://www.vard.org/mono/gait/kaufman.htm> (24 May 1999).

ACKNOWLEDGEMENTS

The authors would like to thank the participants in the study.

THE VALIDITY OF ACTIVE SQUAT KEEN JOINT PROPRIOCEPTION TEST

Ming-Feng Kao
National Taiwan College of Physical Education
email: eric3456733@yahoo.com.tw

INTRODUCTION

Proprioception is a sense of position and movement of one's own limbs and body in the absence of vision, termed "limb-position sense" and "kinesthesia," respectively. Proprioception has been shown to diminish with injury, age, and so on. Position sensibility can be measure by many methods. Several different testing techniques have been developed to measure the conscious submodalities of Proprioception. There are 3 submodalities (joint position sense, JPS; Kinaesthesia and sense of tension). The JPS test measures the accuracy of position replication and can be conducted actively or passively in both open and closed kinetic chain position. Variety of equipment and instrument were developed to measure conscious appreciation of Proprioception, such as commercial isokinetic dynamometers, electromagnetic tracking devices, custom-made jigs, and some new device. Recently a functional squat system (FSS) was introduced by MONITORED REHAB SYSTEMS that mimics the movement co-ordination pattern of squat jump, under the control of an external load. This device can be measure Proprioception in actively closed kinetic chain. Compared to some open chain device, it shows more similar to daily activity. Therefore, some test need to investigate the reliability for FSS. The intraclass correlation coefficient (ICC) is used to measure inter-rater reliability. Although Pearson's r may be used to assess test-retest reliability, ICC is preferred when sample size is small (<15) or when there are more than two tests (one test, one retest) to be correlated. Therefore, The purpose of the present study was to compare repeat-measures proprioceptive test in Functional Squat System.

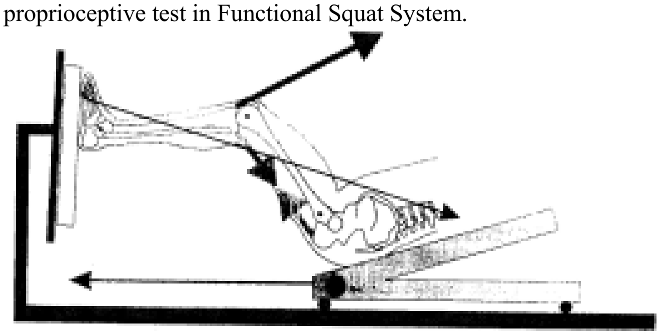

Figure 1: Functional Squat System when performed repetitive squat exercises with one leg in standardized pace.

METHODS

Eighteen college students participated in this study (male=9, female=9; mean age, 22.1±3.5 years). Subject were used FSS in Proprioception test program to measured low extremity in 25, 50 and 75 three different knee joint angel. For intrasession intratester reliability of the figure-of-two measurement, ICC (2,1) and the SEM were used. The ICC (2,1) was based on a subjects ×2-way analysis of variance (Shrout & Fleiss, 1979).

RESULTS AND DISCUSSION

The ICC (2,1) for repeat-measures knee proprioceptive test was 0.94 (P< .05). The means, SDs, and SEMs for these measurements and the repeat-measures proprioceptive test are summarized in table 1. the results of the correlations between two test are summarized in Table 2. In order to get an accurate measurements, the reliability coefficients should exceed 0.90 to ensure valid interpretations (Portney and Watkins, 1993). In this study, results demonstrated excellent intrasession intratester reliability and small measurement error for the repeat-measures proprioceptive test.

Table 1: Means, SDs, and SEMs, for 3 different knee angles repeat measurement test in FSS.

Measurement	Distance (cm)		
	Mean	SD	SEM
25°	16.04	11.05	5.41
50°	15.81	11.81	7.06
75°	9.22	4.29	3.49

*Means based on 3 measurements obtained from 25 subjects.

Table 2: Pearson Product Moment correlation coefficients ( ) of the relationship between repeat-measures proprioceptive test in FSS.

Measurement	r*
25°	0.89
50°	0.84
75°	0.96

*$p < .001$

CONCLUSIONS

This study was conducted to determine the intrasession-intratester reliability and criterion-related validity of the repeat-measures knee proprioceptive test. The result shows that the FSS Proprioception test was reliable and valid indirect method of measuring knee Proprioception in individuals with this test.

REFERENCES

1. Lephart SM, el al. Proprioception and Neuromuscular Control in Joint Stability, Human Kinetics Publishers, 2000.
2. Shrout, P. E., & Fleiss, T. L. (1979). Intraclass correlations: uses in assessing rater reliability. *Psychology Bull, 86*, 420-428.

Investigation of Shoulder Range of Motion Limits for Application to Ergonomic Analysis

Joshua S. Danker and Matthew P. Reed
University of Michigan - Ann Arbor,
email: danker@umich.edu, web: www.HUMOSIM.org

INTRODUCTION

Ergonomic analysis using human figure models requires detailed knowledge of worker postures. Because tendonitis, carpel tunnel syndrome, impingement syndrome, and other musculoskeletal disorders can result from awkward upper extremity postures, accurate simulation of upper-extremity postures is critical for job analysis. Posture-prediction algorithms used in digital human models include joint range of motion (ROM) limits, and these limits affect the ranges of postures that can be applied to the figures. Inaccurate or inappropriate joint ROM may result in inaccurate posture prediction.

Due to its complexity, versatility, and susceptibility to injury, the shoulder is of primary importance in any comprehensive ergonomic analysis of the upper extremities. This abstract describes the first steps of an investigation of the influence of shoulder ROM on work postures, beginning with a comparison of shoulder motions in seated reaching tasks with the ROM data provided by Tumer and Engin [2].

METHODS

Widely cited data on shoulder ROM [2] were compared with shoulder motions in seated upper extremity reaches measured in the laboratory using motion capture equipment. The experimental data contain the locations of the sternoclavicular and glenohumeral joints calculated from the position and orientation information obtained from electromagnetic transducers (Flock of Birds, Ascension Technologies). Data from 12 men and women seated in a truck seat reaching to a wide range of push-button target locations were used for the current investigation. Because the experimental data provide a single claviscapular segment to approximately the linkage of the thorax to the humerus, the data are not directly comparable to Tumer and Engin's three-segment model (clavicle, scapula, humerus) for which ROM data are provided. To facilitate the comparison, a composite ROM cone was created to define the combined motions of Tumer and Engin's sternoclavicular and claviscapular joint segments.

Figure 1 shows the joint sinus cones from Tumer and Engin along with the three-link shoulder system. A MATLAB simulation incremented the two joints independently through their ranges of motion. The endpoint of the claviscapular segment, the glenohumeral (GH) joint center, was stored for each increment. This cloud of roughly 5×10^5 points defined a region of allowable glenohumeral joint center locations relative to the torso for the average joint ROM cones given by Tumer and Engin. The resulting simulated GH locations were compared to the measured GH locations, expressed with respect to an equivalent thorax coordinate system.

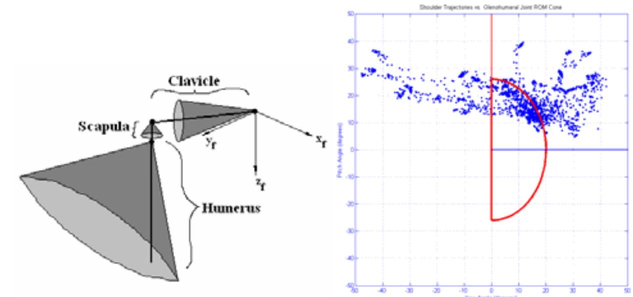

Figure 1: Diagram of the three-link shoulder complex used by Tumer and Engin [2] (left). Comparison of measured glenohumeral joint locations with respect to the thorax with the combined clavicle-scapula ROM (right).

RESULTS AND DISCUSSION

GH locations often deviated from the region defined by the Tumer and Engin clavicle and scapula ROM limits (Figure 1). The patterns of deviation persisted even when the data were normalized within subject to a neutral posture. Most of the deviations were in the upper right quadrant, corresponding to reaches to targets in front of and above the shoulder. The greatest GH excursions occurred in near-maximal reaches, precisely the reaches that are of greatest interest for ergonomic analysis. Perhaps unsurprisingly, given the large amount of inter-individual variability in shoulder ROM [1, 3], most of the population may have shoulder ROM that exceeds the average mobility provided by the Tumer and Engin joint sinus cones. The current investigation also suggests that the shape of the shoulder ROM used by individuals for seated reaches varies considerably.

More investigation will be necessary to determine how best to include the large amount of variability in shoulder ROM in ergonomic analyses. If an average ROM limit is used, the figure model may not be capable of motions that many or most people could perform, posing a model credibility problem. Moreover, because individuals with more limited ROM will not always be the individuals most at risk in a particular task, the utility of DHM figure models as a screening and evaluation tool may be compromised without improved methods for incorporating ROM limits.

REFERENCES

1. Dempster, WT. *Archives of Physical Medicine and Rehabilitation* **46**, 49-69, 1965.
2. Tumer ST and Engin AE. *ASME Journal of Biomechancial Engineering* **111**, 113-121, 1989.
3. Webb Associates, *Anthropometric Source Book* 1, NASA Ref. 1024, Chapters VI & VII, 1978.

THE FIRST METATARSAL AS A FIXED STRUT: NEW INSIGHTS INTO DYNAMIC ARCH FUNCTION

[1,2] Jason Wilken, [2]Charles Saltzman, [1,2] Smita Rao, [1]H. John Yack
[1]Grad Program in PT and Rehab Science, [2]Orthopaedics and Rehabilitation
The University of Iowa, email: jason-wilken@uiowa.edu

INTRODUCTION

The truss and tie rod theory has long provided the framework through which motion of the medial longitudinal arch during loading is viewed [1,2]. Early insights gained from static loading of cadaveric feet resulted in a conventional understanding that describes arch lowering during the stance phase of gait via simultaneous downward motion of the proximal first metatarsal and distal calcaneus. In the process of quantifying the effects of ankle arthroplasty and fusion on dynamic foot function it was observed that arch motion occurred in a manner different than commonly accepted. The purpose of this work is to define the segmental kinematics that expose a new perspective on arch motion during gait in which arch elongation occurs about a stationary first metatarsal.

METHODS

Motion of the first metatarsal in the global (relative to the floor) and of the first metatarsal relative to the calcaneus (arch elongation) was assessed in a total of 23 limbs. Of the limbs tested 7 had undergone ankle fusion, 9 had undergone ankle arthroplasty and 7 had no previous surgical intervention. An Optotrak motion analysis system was used to record the 3-D position of the first metatarsal and calcaneus during gait. Motion of the first metatarsal was tracked with a lightweight marker triad mounted on the first metatarsal, medial to the extensor hallucis longis tendon in a manner similar to Leardini et al. [3]. Hindfoot motion was assess by two markers on the lateral and one on the posterior aspect of the calcaneus. A digitizing process in conjunction with lateral and AP x-rays of the foot in the patient population, and palpation of the foot in control subjects were used to identify the location of underlying bony geometry relative to each segment's marker triad. Visual 3D (C-motion Inc.) was used to calculate 3-D displacements. The mean of five trials at self selected, 0.9, 1.1, 1.3 and 1.6 m/s were used for variables of interest.
To determine arch kinematics during gait motion of the first metatarsal relative to the calcaneus (arch motion) and sagittal plane angular motion of the first metatarsal in the global (lowering of the proximal end of the first metatarsal) were assessed during stance phase.

RESULTS AND DISCUSSION

Kinematic patterns and peak values were highly consistent both within and between walking velocities with standard deviation values of less than 1 degree on average. To our surprise arch and first metatarsal kinematics were not significantly different between groups and therefore, grand mean values were used. Once forefoot contact occurs the first metatarsal was found to maintain a nearly static position from 17.0 ± 3.3 % until 67.0 ± 6.4% stance (Figure 1). During this

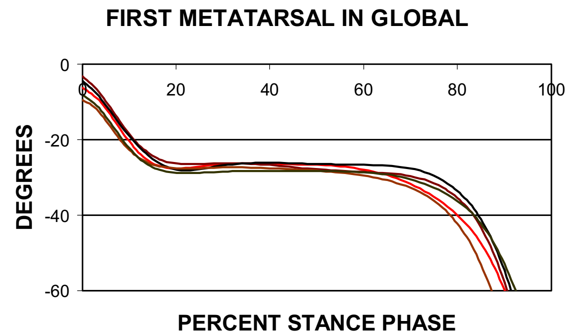

Figure 1: Sagittal plane kinematics of the first metatarsal relative to the floor for five subjects demonstrating nearly static positioning for approximately 50% of stance.

interval the first metatarsal was found to lower only 1.5 ± 1.2 degrees while the arch flattened 10.5 ± 3.0 degrees on average. These data suggest that during the stance phase of gait arch elongation occurs as the calcaneus is pulled up and over the nearly stationary first metatarsal. The elevation and resulting unloading of the calcaneus that produces this motion is substantiated by plantar pressure data in which the calcaneus is unloaded in mid stance

Contrary to the current understanding of normal arch motion, the first metatarsal appears to maintain a nearly static sagittal plane orientation during midstance. These findings are quite robust and exist following surgical interventions and across different walking velocities where the stress on the arch would vary.

CONCLUSIONS

These data suggest a new insight into medial longitudinal arch motion in which the calcaneus is pulled over a nearly stationary first metatarsal causing arch elongation. This calls into question the current understanding of medial longitudinal arch lowering and may in part explain the mixed results observed with current interventions used to control arch motion during gait.

REFERENCES

1. Hicks, JH. *J Anat* **88**, 25-30, 1954.
2. Hicks, JH. *Acta Anat* (Basel) **25**, 34-45. (1955).
3. Leardini, A., et al.. *Clin Biomech (Bristol, Avon)* **14**, 528-36 1999.

ACKNOWLEDGEMENTS

Foundation for Physical Therapy, Inc.
American Orthopaedic Foot and Ankle Society

THE EFFECTS OF EXTERNAL WEIGHT CARRIAGE ON POSTURAL STABILITY

[1]Michelle Heller, [2]John Challis, and [2]Neil Sharkey
[1]Mechanical and Nuclear Engineering, and [2]Kinesiology, The Pennsylvania State University, University Park, PA, USA
email: nas9@psu.edu, web: www.biomechanics.psu.edu

INTRODUCTION

Postural stability has been defined as "the ability to return the body close to the equilibrium point when exposed to a perturbation" [1]. Karlsson and Frykberg suggested that two different mechanisms keep an individual in a stable position: the load-unload strategy and the ankle strategy [1]. Medial-lateral stability is maintained through the load-unload strategy when a person shifts his/her weight from one foot to the other. The ankle strategy is used to maintain anterior-posterior stability by employing the muscles crossing the ankle joint to create a moment to resist loss of balance and is the mechanism of greatest interest when investigating the effect of load distribution on postural stability. Both load carriage and associated muscle fatigue have the potential to decrease a person's postural stability. Compensatory mechanisms such as increased trunk inclination during load carriage serve to keep the center of mass over the feet, and the degree of flexion is dependent on the magnitude of the external load. This observation illustrates that there may be a correlation between load carriage and stability; such information could be valuable in combating common injuries encountered by military personnel.

Kinematic changes of load carriage include a greater degree of knee flexion after heel strike [2], decreased transverse pelvic and thoracic rotation, decreased phase shift between pelvic and thoracic rotation, increased hip excursion [3], and increased musculoskeletal stiffness [4]. The changes in gait kinematics are partially a result of energy-saving mechanisms, but may also function to help increase dynamic postural stability. Static postural control studies may begin to unravel some of these relationships.

METHODS

Twenty-two female subjects (mean: 20.8 years, S.D.: 1.7 years) with no history of musculoskeletal disorders volunteered to participate in the study. Each subject was asked to stand upright on a Kistler force platform under each of three conditions: one foot quiet standing, two feet quiet standing, and while wearing an 18.1 kg military pack. The subjects were asked to concentrate on an "X" located 1.5 meters from the ground. Data were collected at 1000 Hz in conjunction with a Motion Analysis system. One thirty-second trial was collected for each condition, as LeClair et al. [5] determined this was sufficient to see differences between conditions.

The standing trials involved standing quietly on two feet and the one-foot trials involved standing while one first metatarsal head was placed against the opposite medial malleolus. During the external load condition, the subjects were asked to wear a standard issue military pack, which was obtained from the Penn State ROTC program.

RESULTS AND DISCUSSION

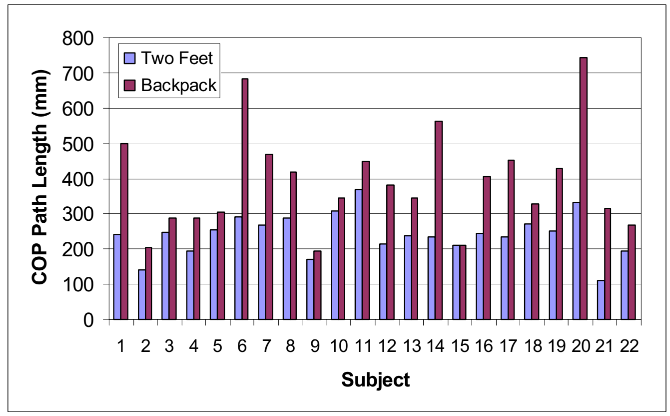

Figure 1: The center of pressure path lengths for each of the subjects indicates more sway under the backpack condition than during quiet standing.

Standard measures of postural stability indicated that the subjects were less stable while carrying the military pack. The data were analyzed using a paired t-test. The center of pressure (COP) path lengths were higher under the load carriage condition than the two foot quiet standing ($P < 0.001$), as shown in Figure 1. The area of the ellipse that included 85% of the data points was calculated for each trial. The COP areas were higher for the load carriage condition ($P < 0.001$). Both of these results indicate more postural sway when carrying an external load. Furthermore, the anteroposterior (AP) and mediolateral (ML) excursions were both greater under the load carriage condition, with $P = 0.019$ and $P < 0.001$ respectively. All standard measures of postural stability indicate a decrease in stability when the subjects donned the military pack.

CONCLUSIONS

Wearing an external load of 18.1 kg, which is less than the minimum load carried by military personnel, reduces postural stability in healthy, young females. This could translate into a higher likelihood of injuries such as ankle sprains in this population.

REFERENCES

1. Karlsson A, et al. *Clin Biomech* **15**, 365-9, 2000.
2. Tilbury-Davis DC, et al. *Hum Mov Sci* **18**, 693-700, 1999.
3. LaFiandra, M, et al. *J Biomech* **36**, 87-95, 2003.
4. Holt, KG, et al. *J Biomech* **36**, 465-71, 2003.
5. Le Clair K, et al. *Clin Biomech* **11**, 176-178, 1996.

VIRTUAL JACK MANIKIN USED TO ASSESS POSTURAL VARIABLES AND VISIBILITY MEASURES FROM THE CAB OF LOAD-HAUL-DUMP MACHINES

[1] Alison Godwin, [2]Tammy Eger and [2]Sylvain Grenier
[1]Queen's Ergonomic Research Group, Queen's University
[2]Biomechanics Ergonomics and Kinesiology Lab, Laurentian University; email:4aag@qlink.queensu.ca

INTRODUCTION

Load-haul-dump (LHD) machines were previously shown to have significant visibility deficits within a computer-aided design environment known as Classic JACK [1]. The virtual human simulation program was then used to assess the postural deviations of the head and trunk that may be associated with obtaining a line-of-sight from the cabin of these machines. Since minor retro-fit modifications were insufficient to create a large increase in visibility measures [2], a concept change was tested in the virtual environment for feasibility.

A rotating operator seat has been successfully used to reduce postural deviations for tractor operators and other, sideways-seated machine operators [3,4]. A rotating seat and console was incorporated into the virtual environment to allow testing of a 20º and 45º seat rotation intervention. Postural load variables and visibility measures were evaluated as dependent variables.

METHODS

Virtual human operators representing a range of anthropometric sizes (1st to 99th percentile) were placed in the cab of a 7yd3 LHD machine. A series of movement strategies (n=15) representing typical neck and trunk movements used by actual operators to view specific hazards around their vehicles were developed. These movement strategies were constrained by known biomechanical tendencies (twist developed by thoracic vertebrae and flexion developed by lumbar vertebrae). The virtual hands and feet were constrained to hand controls and foot pedals. A variety of biomechanical variables were collected while the virtual human used their unique movement strategy to view the left-most target point. Selected dependent variables included muscular activity of five trunk muscles (N), compression (N), shear (N), L4/L5 moment (Nm), trunk rotation (º), neck rotation (º), trunk flexion(º) and trunk lateral bend (º). Data was assessed using t-tests to determine if differences existed between the current cab condition and a seat rotation of 20º and 45º. Using the Bonferroni correction, a $p<0.0167$ was required for significance.

RESULTS AND DISCUSSION

There was a lack of statistical significance to demonstrate that a seat rotation will unequivocally reduce the risk factors that may lead to injury for LHD operators. Compression, shear, L4/L5 moment and muscular activity all showed decreasing trends. It was possible to demonstrate that a virtual environment can show decreases in postural load variables when a proposed beneficial solution is tested. All postural angle values decreased as seat rotation increased with a concomitant increase in visible area available to the operator (Figure 1).

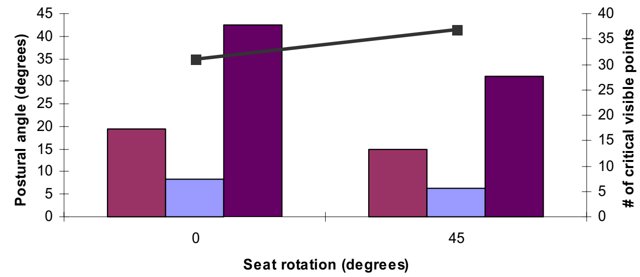

Figure 1: Trunk rotation, trunk lateral bend and neck rotation decreased as seat rotation increased from 0 to 45. An advantageous increase in the number of visible critical points was also achieved.

Even without statistical significance, these results can be used by manufacturers to evaluate and refine potential designs and concepts. Limitations to consider before implementation of these types of modifications include the ability to obtain accurate machine representations and validated operator movements.

CONCLUSIONS

Despite some reservations, this research shows promise for the ability to analyze a virtual human in industrial machinery. Most industrial manufacturers use 3-D programs to design future equipment. It is advantageous to the eventual human user if ergonomic principles and biomechanical considerations can be assessed and refined prior to building prototypes.

REFERENCES

1. Jeffkins AA, et al. *Ergonomics in* Design,**12(2)**,12-17, 2004.
2. Godwin AA, et al. *International Journal of Industrial Ergonommics*, submitted, 2004.
3. Eklund J, et al. *Ergonomics*, **37(4)**, 623-639, 1994.
4. Bottoms DJ and Barber TS. *Applied Ergonomics*, **9**,77-84, 1980.

ACKNOWLEDGEMENTS

The authors would like to thank the Workplace Safety and Insurance Board (WSIB) of Ontario for their continued support of visibility studies.

AN ELECTROMYOGRAPHIC AND PSYCHOPHYSICAL EXAMINATION OF FASTENER INITIATIONS IN AUTOMOTIVE ASSEMBLY

[1] Joel A. Cort, [2]James R. Potvin and [3]Allison Stephens
[1]Department of Human Biology and Nutritional Sciences, University of Guelph, Guelph, ON, Canada, [2]Department of Kinesiology, University of Windsor, Windsor, ON, Canada, [3]Ford Motor Company, Dearborn, MI, U.S.A.
email: jcort@uoguelph.ca

INTRODUCTION

Injuries to the upper extremity region rank second among all reported occupational injuries [1]. Currently, limits are non-existent for low force, repetitive tasks such as Fastener Initiations (FI) performed in the automotive industry. The purpose of the current study was to determine acceptable human tolerance limits values (TLVs) for a fastener initiation task, which is commonly performed in the automotive industry.

METHODS

A psychophysical methodology was utilized to examine 24 non-skilled female subjects while performing fastener initiation tasks on a simulation device. The independent variables were: 1) wrist posture: neutral, flexion and extension, and 2) fastener size: large (10 mm depth, 20 mm diameter) and small (5 mm and 10 mm). For each condition, subjects were instructed to complete their maximal acceptable number of FIs over the course of a 60 minute trial. Subjects trained for 2 hours on each condition and were tested for 1 hour (total of 18 hours). The kinematic dependent variables were: 1) average number of 720 degree FIs per minute, 2) average duration of each FI and 3) average number of individual movements (efforts) per 720º FI.

Surface EMG was also used to monitor the muscle activity of forearm (biceps brachii (BB), brachioradialis (BR), flexor carpi ulnaris (FCU), extensor carpi ulnaris (ECU) and hand muscles (thenar (TR) and first dorsal interosseous (FDI)). A repeated measures ANOVA with Tukey's significance post hoc test were used to determine any significance within the measured variables ($p<0.05$).

RESULTS AND DISCUSSION

Both Posture and Fastener Size variables had significant main effects on all kinematic variables. Results indicated a 10% decrease in FIs per minute when the small fastener size was used, as well as a 10% increase in the average time to complete each FI when performing the task with the small compared to large fastener. In addition to the fastener size, posture was shown to have a significant effect on the kinematic data. Compared to the extended posture, the average number of FIs/min increased 12% and 7% for the neutral and flexed posture, respectively. In addition, the average duration of each FI was affected by posture with the extension being 12% greater than flexion and flexion being 8% greater than neutral.

The kinematic data used to determine the TLV showed interesting results as the large fastener/neutral wrist condition had the highest number of FIs (9.1±2.6), they were performed with the lowest number of efforts per FI and shortest duration

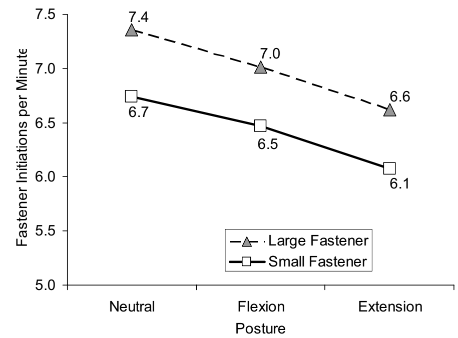

Figure 1: TLV for FI/minute calculated as the values acceptable to 75% of females (n = 24).

per FI. TLVs were calculated as those acceptable to 75% of the female subjects (Figure 1). These ranged from 6.1 to 7.4/min depending on the fastener size and wrist posture.

Electromyography data showed that posture, age and fastener size did, in certain instances, demonstrate significant interactions. In particular, posture had an effect on EMG from the BB, BR and TR muscles. The EMG of the BB was at its lowest (% of Maximal Voluntary Exertion (MVE)) during flexion and BR and TR were at their highest during extension. Interestingly, the ECU had the highest activity for all six conditions (mean of 13.5% MVE). This result parallels that of Mogk and Keir (2003), where the ECU higher activation is believed to be due to it role as a stabilizer to the internal and external moments about the wrist joint.

The kinematic and surface EMG data from this study show that both Posture and Fastener Size are important factors that affect the performance and acceptability of FIs. As the Posture variable deviated from neutral, and as the fastener became smaller, a significant decrease in the FIs per minute resulted. Thus, this study provides data to support the need for the design of more neutral hand-wrist human interfaces along with larger objects for the hand to manipulate. Such designs will potentially decrease the risk of musculoskeletal injury and/or increase productivity. Thus, this study has provided recommendations on acceptable human tolerances for the task of fastener initiations used in the manufacturing industry. Furthermore, EMG data provided valuable information regarding forearm and hand muscle activity during a low force, high frequency task.

REFERENCES

1. Workplace Safety and Insurance Board of Ontario's 2002 Annual Report.
2. Mogk, J. & Keir, P. *Ergonomics* **46**, 956-975, 2003

ACKNOWLEDGEMENTS

This study was funded by The Ford Motor Company.

ACCURATE PRODUCTION OF PATTERNS OF THE TOTAL MOMENT BY A SET OF FINGERS

Wei Zhang, Naoki Yoshida, Mark L. Latash
Department of Kinesiology, The Pennsylvania State University, University Park, PA 16802
email: mll11@psu.edu

INTRODUCTION

During isometric force production by an effector, force variability typically increases with the level of force [1]. When several fingers of the hand press down in parallel to produce a required time profile of the total force, there is little variation in the total force variability over a wide range of the total force [2]. This results from force-stabilizing multi-finger synergies. Tasks of accurate total force production are also accompanied by synergies stabilizing the total moment in pronation/supination, even when the subjects are instructed and get visual feedback on the total force but not on the total moment [2]. These findings have been interpreted as consequences of everyday practice with tasks that typically impose more strict accuracy constraints on total moment production. We investigated the relations between the total moment and its variability during the multi-finger production of accurate time profiles of the total moment. We expected the hypothetical multi-finger synergies to lead to complex relations between the moment magnitude and its variability.

METHODS

Twelve healthy, right-handed volunteers, six males and six females participated in the experiment. The subjects sat comfortably in a chair and positioned the right forearm on the horizontal board directly in front of the subject. The fingertips of the right hand were placed on unidirectional force sensors spaced to fit the subject's individual anatomy. Changes in the forearm and hand position were prevented by a set of Velcro straps and using a custom-fitted wooden piece placed under the palm. The subjects watched a 17" monitor that showed a target moment time profile and the actual total moment in pronation/supination produced by the normal finger forces with respect to the midpoint between the middle and ring fingers (effort into pronation was considered positive).

After a few practice trials, the subjects were required to follow, as closely as possible, a pattern shown on the screen with the cursor. There were two tasks, the Ramp-Task and the Sine-Task illustrated in Figure 1. Each task required accurate production of a moment profile starting from a certain level into pronation (normalized by subject's index finger maximal force), on average about 20 Ncm, to the same level into supination and then back to the original pronation moment. The total time of a trial was 12 s; the time intervals of moment changes were 3 s each. Twenty-five trials were performed at each task. Average force and moment time profiles and their variance profiles were computed over each set of 12 trials.

RESULTS

Both ramp and sine changes in the total moment showed two phases, a decrease in the forces by fingers that produced the moment in one direction followed by an increase in the forces of fingers that produced the moment in the opposite direction.

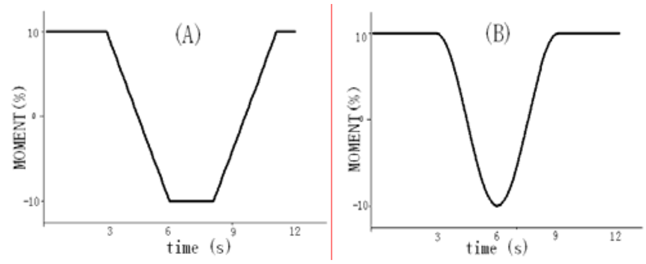

Figure 1: The Ramp-Task (A) and the Sine-Task (B). Moment axes are in percent of the product of index finger MVC by its lever arm.

In both tasks, the total normal force produced by the fingers increased over the trial duration such that it was significantly higher at the end of the task (on average, a two-fold increase from 8 to over 16 N) while the subjects produced the same moment as at the trial initiation. No clear relations were observed between total force and its variability and between total moment and its variability. However, moment variance was significantly higher, on average by 70%, when the total moment was close to zero than at its peak values; this was more pronounced during moment changes from pronation to supination. High moments into supination were accompanied by higher variance, on average by 66%, than high moments into pronation.

DISCUSSION AND CONCLUSIONS

Our observations suggest the existence of complex relations between magnitude of a moment produced by a set of fingers in isometric conditions and moment variability. Apparently there is no simple rule that would predict moment variability based solely on its level. Moment variability depends on the rate of moment change, on the time history of getting to a particular moment value, and it shows differences between the pronation and supination moments. Moment changes from a steady-state to another level and back to the same steady-state are accompanied by an increase in the finger force level, which is not dictated by the task and looks counter-intuitive: It involves unnecessary force production by fingers opposing the required moment. Further studies of multi-finger moment production are needed to resolve these mysteries.

REFERENCES

1. Newell KM, Carlton LG, Hancock PA (1984) Kinetic analysis of response variability. Psychol Bull 96: 133-151
2. Latash ML, Scholz JF, Danion F, Schöner G (2002) Finger coordination during discrete and oscillatory force production tasks. Exp Brain Res 146: 412-432

ACKNOWLEDGEMENTS

This research was supported in part by NIH grants AG-018751, NS-035032, and AR-048563

Use of strain gauge in the evaluation of the constraint of tibio-femoral joint in dynamic movement: Development, feasibility and first results

[1]Stéphane Sobczak, [1]Benjamin Gilbert, [2]Véronique Feipel, [1]Serge Van Sint Jan, [2]Philippe Lefèvre, [1]Patrick Salvia and [1,2]Marcel Rooze
[1] Laboratory of Anatomy and Embryology, University of Brussels, Belgium.
[2] Laboratory of Functional Anatomy, University of Brussels, Belgium.
Corresponding author: ssobczak@ulb.ac.be http://homepages.ulb.ac.be/~anatemb

INTRODUCTION

The mechanism behind medial or lateral tibio-femoral gonarthrosis remains partially unexplained [1]. According to Maquet's theories, the surgical treatment of this pathology seems to give good results [3]. However poor results are observed in more or less 25 % of the cases. It is true that the cartilaginous and osseous lesions of this pathology can explain the long-term pain. The purpose of this work was the development of a new method to record in-vitro tibio-femoral variations of the constraints, during dynamic flexion-extension movement of the knee. Further goals behind this study include analysis of the constraint variations during 3D low femoral osteotomy.

METHODS

Specimens: Five fresh human right lower limbs were used (Age: 84,2 ± 8,7; 4 men, 2 women). Each limb was thawed during 24 hours before preparation: - dissection of thigh muscles; - replacement of muscle tendons by fishing wires for loading (240N on each head of quadriceps and 75N for all flexors). The specimens were placed on a metal bracket allowing their fixing in the hip and femoral bone (Figure 1).

Figure 1: Experimental setup

Strains gauges (SG): Six SGs (FCA-1-17, ø 4.5 mm, 120 Ω, TML) were molded in epoxy resin (LX 112) to obtain sensors that were inserted into the spongy bone of the tibial proximal epiphysis in anterior, posterior and lateral locations of both tibial condyles perpendicular to the cartilaginous surface. The SGs were inserted about 10 mm below the edge of the tibial plateau and below the articular cartilage.

Data logger: Twelve gauges amplifiers were built. These modules consist of low-pass filters and different gains to allow increasing of the sensitivity of the SGs. The amplifiers were connected to a Pc-Data acquisition board Dap2003a (DAP, National Instruments).

Protocol: Cycles of two movements of leg flexion-extension were applied manually. An 6 DOF-electrogoniometer [2] samlped tibio-femoral kinematics, and allowed to normalize results according to the range of motion. Three repetitions were carried out for each specimen. Intra- and inter-observer reproducibility was studied on one specimen. Three observers performed 10 motion cycles at three intervals of time.

RESULTS AND DISCUSSION

Intra- and inter- observer reproducibility: the Root Mean Square (RMS) difference to the mean curve was compared. The results show small differences between observers and repetitions, compared to the maximal peak value of 3 N/cm^2 (Table 1).

Table 1: Intra- and inter- observer RMS differences for SG 1

	Experimenter 1	Experimenter 2	Experimenter 3
Intra (N/cm^2)	0.08 to 0.25	0.06 to 0.15	0.05 to 0.09
Inter (N/cm^2)		0.08 to 0.25	

Inter-individual variations: Figure 2 shows the interindividual variability obtained for SG 1. Results also depend on the quality of the spongy bone [4] and the placement of the sensors.

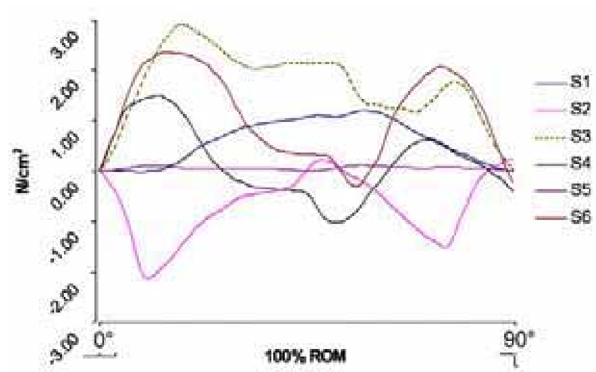

Figure 2: Interindividual variations

CONCLUSIONS

This study shows the feasibility of analyzing articular constraint variations during dynamic movements. Reproducibility of measurements was satisfactory, and a significant inter-individual variability was found. This reinforces the idea to use this technique to study the changes of joint constraints before and after knee surgical procedures (e.g., osteotomy). Such a study is currently being performed by the authors.

REFERENCES

1. Goutallier D, et al.. *Rev Chir Orthop* **83**, 613-621, 1997.
2. Sholukha V, et al.. *Med Eng Phys* **26(3),** 251-260, 2004.
3. Aglietti P, et al.. *Am J Knee Surg* **13(2)**, 89-95, 2000.
4. Khodadadyan-Kostermann C, et al.. *Clin Biomech,* **19**, 370-376, 2004.

ACKNOWLEDGEMENTS

Special thanks to Mr Dupuis for his help in the development of the SG setting, and Mr Sterckx for his help in the experiment.

A COMPARISON OF TASK AND MUSCLE SPECIFIC ISOMETRIC SUBMAXIMAL EMG DATA NORMALIZATION TECHNIQUES FOR THE ANALYSIS OF MUSCLE LOADS DURING HYDRAULIC-ACTUATION JOYSTICK CONTROLLER USE.

Taylor Murphy and Michele Oliver
School of Engineering, University of Guelph ON; email: taylor@uoguelph.ca

INTRODUCTION

Joystick manipulation involves low level, but nearly constant contractions of the shoulder musculature [3]. This combination makes it difficult to choose an appropriate technique for electromyography (EMG) normalization. Results from investigations using maximal voluntary contraction (MVC) normalization techniques are equivocal with some studies observing increases [1] with others finding decreases [4] in reliability. Normalization using MVC methods is also questionable, as it can be difficult for subjects to reliably elicit a maximal contraction. Sub-MVC normalization, on the other hand, has been shown to increase reliability [4]. Further studies [2] have exposed severe compromises (as the result of motion artifacts and contraction type) to the quality of data when a dynamic task is normalized by a single isometric contraction. Moreover, a study of joystick manipulation did not find dynamic normalization procedures to be better than isometric ones [3].

The purpose of this study was to determine an appropriate submaximal isometric electromyography (EMG) normalization technique that will later be used to assess the efficacy of a dynamically moveable armrest for joystick operators.

METHODS

The experimental set-up involved a mock-up of a common excavator cab, including a chair and right-hand hydraulic-actuation joystick. Surface EMG data were collected from 3 muscles (upper trapezius – UT, posterior deltoid – PD, and anterior deltoid – AD) using a Noraxon Telemyo (model 500, Noraxon USA Inc) telemetered EMG system (fixed gain of 2000, bandwidth of 10-500Hz, common mode rejection ratio of >100dB at 60Hz, input impedance 2 mega ohms). Six subjects performed three trials of three contraction types consisting of a muscle-specific reference isometric voluntary contraction (mRVC) (one for each of UT, PD, and AD), six task-specific isometric reference voluntary contractions (tRVC) (start, middle and end range of joystick motion), and two dynamic occupation tasks (forwards and backwards joystick motions). The mRVC's were accomplished by holding a 1kg weight in three standardized non-task related positions. Muscle activation levels during tRVC trials were approximately equivalent to activation levels during mRVC trials where force was monitored by strain gauges oriented in a full-Wheatstone bridge and displayed to subjects on a monitor to allow them to produce a constant level of muscle activation. The average RMS values of the middle 10 seconds of all RVC trials were used as the normalization values. Joystick angles (6 VICON M2 cameras, Oxford, UK) were used to segment the EMG data into 5% intervals of the joystick motion cycle for the forward and backward dynamic trials. After ensemble averaging, and dividing the dynamic trials by the various RMS values, the four normalization procedures were assessed using an inter-subject coefficient of variation (CV) [4].

RESULTS AND DISCUSSION

The un-normalized CV's were generally lower than those of normalized ensembles with CV values being consistently higher for backward than forward motions (Table 1). The lowest CV's varied randomly across muscles and normalization methods but remained relatively low throughout. A potential explanation for the low CV values is that joystick motion involves small displacements (approximately 20° for each of forward and backwards motions) and is relatively constrained.

The purpose of normalization is to reduce the variability between subjects, therefore, the low CV values reported for all normalization techniques indicate that one isometric method is not superior to another when normalizing shoulder EMG during joystick manipulation.

REFERENCES

1. Knutson, L.M., Clarke, W.R., and Sodberg, G. (1994) A study of various normalization procedures for within day electromyographic data. *Journal of Electromyography and Kinesiology* **4**, 47-59.
2. Mirka, G.A. (1991) The quantification of EMG normalization Error. *Ergonomics* **34**, 343-352.
3. Northey, G., Oliver, M., MacLean, A., and Sexsmith, J. (2003) A comparison of four movement specific EMG data normalization techniques for the analysis of muscle loads during hydraulic actuation joystick controller use. Proceedings of the Association of Canadian Ergonomists Annual Conference, London, Ontario.
4. Yang, J. and Winter, D. (1984) Electromyographic amplitude normalization methods: improving their sensitivity as diagnostic tools in gait analysis. *Archives of Physical Medicine and Rehabilitation* **65**, 517-52.

Table 1: Intersubject Coefficients of Variation (%) for Un-normalized and Eight Amplitude Normalized Ensembles. Start, Middle and End refer to the joystick position at which point the normalization trial took place.

	Forward					Backward				
Muscle	Un-Normalized	mRVC	tRVC start	tRVC middle	tRVC end	Un-Normalized	mRVC	tRVC start	tRVC middle	tRVC end
UT	15.39	17.45	10.74	11.37	15.52	15.33	17.36	15.85	22.28	23.35
PD	12.62	18.19	14.12	11.40	13.31	12.61	21.83	23.55	36.40	21.54
AD	10.31	12.74	23.97	14.61	13.90	12.68	13.98	19.29	23.33	25.24

A BETTER IMAGE DEGRADATION METHOD FOR CONVERTING HIGH RESOLUTION CT SCANS INTO FINITE ELEMENT MODELS

[1, 2] Yang, S, [2]Voor, MJ and, [1]Hnat WP
[1]Mechanical Engineering Department of University of Louisville,
[2]Orthopaedic Bioengineering Laboratory of University of Louisville; email: s0yang01@gwise.louisville.edu

INTRODUCTION

When performing finite element analysis of voxel-based images converted directly from CT scans, image degradation is often necessary to decrease the size of the finite element model when the model is too large to be solved due to time or memory constraints. The region average (RA, Figure 1: left) image degradation method is widely used. The degraded voxel is generated by combining a particular number of adjacent voxels of the original model and averaging their grayscale values. A voxel expansion (VE Figure 1: right) degradation method is proposed for which the degraded voxel is generated by directly expanding a single original voxel. A reliable method should render high fidelity for the degraded model in three areas: bone indices, image grayscale distribution, and biomechanics.

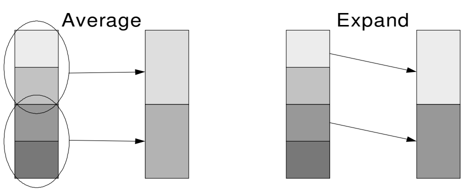

Figure 1: Left: Region average. Right: Voxel expansion

METHODS

Three New Zealand white rabbit distal femurs were scanned in a micro-CT system (ACTIS 150/225 FFi-HR CT, BIR Inc., Chicago, IL) with 14µm nominal resolution. A 3.5mm trabecular cube was generated from each of the three image stacks. Models at this size satisfied the continuum assumption for a porous material [1]. The voxel size of each model was then degraded by both methods to 28µm and 42µm which is smaller than 1/4 of the mean trabecular thickness (Tb.Th) as recommended for solution convergence [2]. The trabecular volume fraction, mean Tb.Th, grayscale distribution and apparent stiffness of the degraded models were compared to that of the original models to evaluate the performance.

RESULTS AND DISCUSSION

For the trabecular indices calculation, the Otsu method [3] was used to threshold the image stacks. The indices percentage errors for the two methods are shown in Figure 2. The volume fractions of the degraded models rendered by the VE method were essentially unchanged whereas the values from the RA method changed. The mean Tb.Th increased for both methods but significantly less for the VE method compared to RA.

The RA method affects the model grayscale distribution significantly. A distribution comparison between the two methods is shown in Figure 3. The grayscale distribution of the VE rendered model is similar to that of the original model whereas the distribution for the RA rendered model changed.

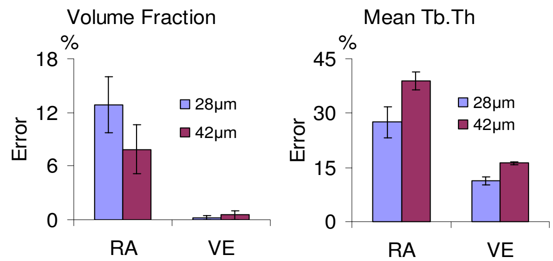

Figure 2: Trabecular indices comparison between two degradation methods

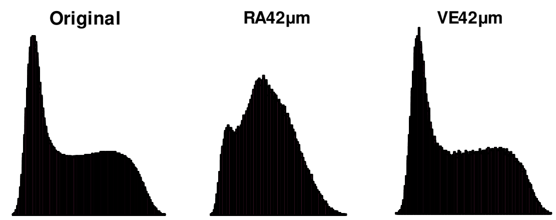

Figure 3: Grayscale distribution comparison between two degradation methods

Six finite element models created by two methods and two degraded levels were evaluated. Homogeneous material properties were assumed and tissue stiffness was set to 10GPa. All models were fixed at one end and a 0.2% axial strain was applied at the other end. Results for the degraded models were compared to the original models (Figure 4).

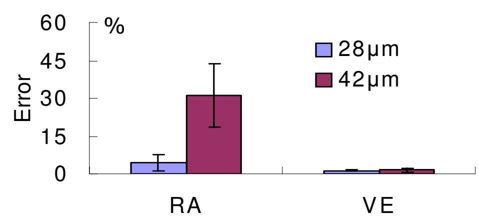

Figure 4: Finite Element Analysis apparent stiffness comparison between two degradation methods

All differences between the VE and RA methods (Vol. Frac., Tb. Th., App Stiff.) were statistically significant except the apparent stiffness for the 28µm voxel size.

CONCLUSION

The widely used RA degradation method produced less desirable results than the VE method. The reliability does not decrease significantly as the degraded voxel size increases for the VE method.

REFERENCE

1. Harrigan et al. J. Biomech. 21, 269-275.
2. Guldberg et al. J Biomech 120, 289-295.
3. Otsu, N., 1979. IEEE Trans. Systems, Man, and Cybernetics, 9(1), 62-66.

Pseudo-Elasticity and Kinetic Energy Storage: Definitions and Applications to Human Movement

[1] Sam Walcott and [2]Andy Ruina
[1,2]Theoretical and Applied Mechanics, Cornell University
[1]Gradutate Student; email: scw11@cornell.edu

INTRODUCTION

Tasks such as throwing and jumping often have a short preliminary phase where movement is away from the target. Traditionally this countermovement is explained by one of four mechanisms: 1) elastic energy storage in soft tissue allows muscular work done in the countermovement to be stored and released, 2) stretch from the countermovement increases the muscle forces in the later movement through force potentiation, 3) because of activation delays, countermovement allows full activation at an earlier time in the forward movement, and 4) stretching muscles in countermovement leads to reflex stimulation and hence higher forces.

We present an alternative explanation for countermovement that depends on the multi-link nature of the body. The idea, that kinetic energy storage in some links can be used in a manner analogous to elastic energy storage, is foreshadowed in a sketch in [1] in the context of jumping, and is discussed in the context of throwing in [2].

Here, to make the point especially clear in the extreme, we show that a collection of links with no springs whatsoever can behave almost identically to a spring. The idea has long been known at the molecular level where rubber elasticity is explained by the entropic contributions of numerous identical links [3]. Here we show that macroscopic multi-link systems, with no a-priori statistical or thermal inputs, naturally behave as a spring, with the end-point motion putting work in and out of the links almost reversibly.

This multi-link example is not meant to be literally applied to macroscopic biomechanics, but rather gives a cartoon that may apply partially and approximately in normal throwing and jumping tasks.

METHODS

We simulated various multi-link systems that illustrate the ideas. One example is a simple multi-link 2D pendulum with the last link more massive than the others (Figure 1). When dropped from a typical static configuration the lower mass turns out to move as if it was connected to an appropriate nonlinear spring instead of collection of links (Figure 2). With more degrees of freedom (more links or 3D rather than 2D) the elasticity emulation becomes more accurate.

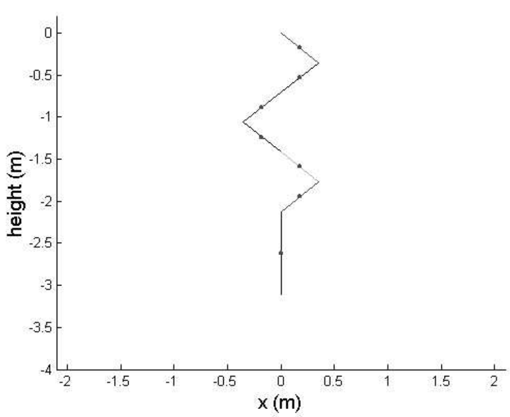

Figure 1: A 2D seven link pendulum with symmetric initial displacement. Gravity points down. The pendulum is anchored to the fixed frame at 0,0.

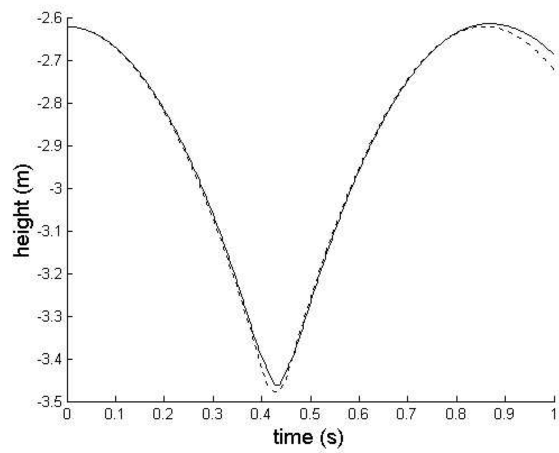

Figure 2: The height of the center of mass of the final link of a 2D seven-link pendulum (solid) and the position of a point mass on a spring in a gravity field (dotted).

RESULTS AND DISCUSSION

The relatively small number of links required to show this pseudo-elasticity, especially in 3D, suggests the relevance to human motions such as throwing and running.

In throwing, for example, it has long been known that kinetic energy transfer is important – the so-called "kinetic chain", but here we suggest that this kinetic energy transfer can act like a spring. From the point of view of the ball, the kinetic energy is stored in the arm and then returned to result in a faster, further, or more efficient throw. And, in detail, our model of throwing also illustrates the effect, although the spring analogy is somewhat disguised by the small number of links.

REFERENCES

1. Tucker. V.A, *Am. Sci.* **63**, 413-419, 1975.
2. Walcott, S. *Proceedings of ISEA 5*, Davis, California, Volume 1, 2004.
3. Noggle, J. *Physical Chemistry,* Harper-Collins, New York, NY.

TENDON ADAPTIVE RESPONSE TO PARALYSIS

Constantinos N. Maganaris[1], Neil D. Reeves[1], Joern Rittweger[1], Anthony J. Sargeant[1,3], David A. Jones[1,2], Karin Gerrits[3] & Arnold de Haan[1,3]
[1]Manchester Metropolitan University, U.K; [2]University of Birmingham, UK; [3]Vrije University, Netherlands
email: c.n.maganaris@mmu.ac.uk

INTRODUCTION

A well-established adaptation to long-term paralysis is an increase in the speed of muscle contraction and/or rate of force development. This characteristic behaviour has been associated exclusively with transformation of type I muscle fibres to type II muscle fibres due to changes in the expression of relevant myosin heavy chain isoforms [e.g. 1-3]. Information is lacking, however, regarding the degree to which potential disuse-induced changes in the mechanical properties of tendons contribute to the above phenomenon.

To address this issue, we examined in vivo the tensile behaviour of the patellar tendon in spinal cord injured (SCI) and able-bodied (AB) humans.

METHODS

Six SCI men (age: 36±5 y, height: 186±9 cm, body mass: 80±15 kg; mean±SD) and six age-matched AB men (age: 37±4 y, height: 183±7, body mass: 78±7 kg) volunteered to participate after the study was approved by the local Ethics Committee. The measurements were taken at 90 deg knee angle. Ultrasonography (ALOKA, SSD 5000SV) was used to obtain the patellar tendon resting dimensions and its elongation during isometric contractions of increasing intensity elicited by tetanic (150 Hz) stimulation of the quadriceps muscle [4]. The maximal current used corresponded to 50% of the current producing maximal knee extension torque during femoral nerve stimulation. The patellar tendon forces during contraction were estimated from the torque values produced and moment arm lengths measured on lateral-view pQCT scans (XCT 2000). From the slope of the force−elongation curves produced, the stiffness and Young's modulus of the tendon were calculated in the force region 0-450 N. Independent samples student *t*-tests were used to test for differences in all relevant measured or calculated parameters between the SCI and AB groups.

RESULTS AND DISCUSSION

The resting length of the patellar tendon was similar in the two groups (P>0.05), but the cross-sectional area (CSA) of the tendon was smaller by ~17% (P<0.05) in the SCI subjects compared with the AB subjects. Tendon stiffness was lower by ~59% (P<0.01) in the SCI subjects compared with the AB subjects. Tendon Young's modulus was lower by ~49% (P<0.05) in the SCI subjects compared with the AB subjects (Table 1).

Table 1. The main parameters examined.

Parameter	SCI	AB	P
Tendon length (mm)	44±7	47±6	P>0.05
Tendon CSA (mm^2)	101±23	122±18	P<0.05
Stiffness (N/mm)	163±101	401±158	P<0.05
Young's modulus (MPa)	77±43	152±76	P<0.01

The present results indicate that long-term paralysis deteriorates the intrinsic and structural properties of tendon. A reduction in tendon stiffness means that the changes in contractile speed of the whole muscle-tendon complex underestimate the extent of fibre type transformation in paralyzed muscles.

REFERENCES

1. Lieber RL et al. *Exp Neuro* **91,** 423-434, 1986.
2. Burnham R et al. *Spinal Cord* **35,** 86-91, 1997.
3. Gerrits HL et al. *Muscle Nerve* **22,** 1249-1256, 1999.
4. Reeves et al. *J Physiol* **548,** 971-981, 2003.

ACKNOWLEDGEMENTS

- Peak Performance Technologies (PYS Award 2003 to CNM)
- Biomedic Nederland BV (provision of ALOKA system)

SHOULDER-POSITION DEPENDANT ELBOW TORQUE COUPLING DURING ADDUCTION AFTER STROKE

[1]Michael D. Ellis, MPT, DPT and [1,2,3]Jules P.A. Dewald, PT, PhD
[1]Northwestern University, Department of Physical Therapy and Human Movement Sciences, [2]Department of Physical Medicine and Rehabilitation, [3]Department of Biomedical Engineering ; email:m-ellis@northwestern.edu

INTRODUCTION

Previous work [1] has identified abnormal elbow torque coupling during isometric shoulder abduction and adduction of the impaired upper extremity after stroke. Changes in heteronymous (proprioceptive) reflex pathways, that link shoulder and elbow joint muscles [2], may underlie the expression of this coupling due a stroke-induced loss in descending corticospinal input to the spinal cord. In an effort to test this hypothesis, elbow/shoulder torque coupling was measured isometrically in two shoulder positions.

METHODS

Eleven individuals ranging from 14 to 289 months after stroke participated in the study. All subjects were able to support the upper limb against gravity and demonstrate the ability to generate some concurrent active elbow extension. In each of the two positions studied, the elbow angle was 90º while the shoulder angle (abduction) was either 75º or 20º.

Single-Task Protocol: Maximum voluntary torques [1] were measured isometrically at the shoulder and elbow for each shoulder position. Joint torque data was collected concurrently for both the shoulder and elbow while the subject attempted to maximize torque in a primary direction.

Dual-Task Protocol: Subjects maintained various percentages of isometric maximum shoulder adduction (25%, 50%, and 75%) while attempting to maximize either elbow flexion or extension.

RESULTS AND DISCUSSION

A significant effect of shoulder position was found on elbow/shoulder torque coupling (fig. 1). Specifically, a profound torque direction reversal occurred in the adducted or

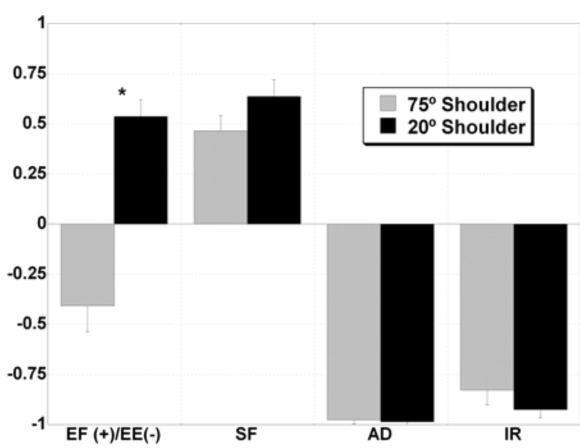

Figure 1: Normalized maximum shoulder adduction (AD) and coupled elbow flexion (EF)/extension (EE), shoulder flexion (SF), and internal rotation (IR) torques during the single-task protocol for the 75º-and 20º-shoulder positions.

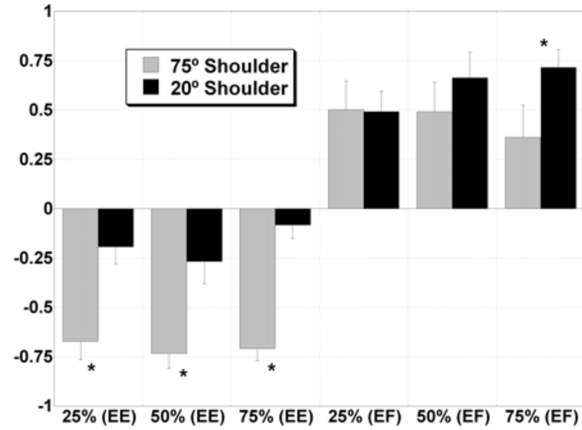

Figure 2: Normalized maximum elbow flexion (EF) (+) or extension (EE) (-) torque during various percentages of maximum adduction torque (25%, 50%, and 75%) for the 75º- and 20º-shoulder positions.

20º-shoulder position. This reversal suggests an alteration in the "stereotypical" extension pattern previously described [1] as coupling of shoulder adduction with elbow extension. This phenomena was further examined during a dual-task protocol. Consistent with previous results, [1] subjects generated considerable elbow extension and progressively less elbow flexion during higher levels of adduction in the 75º-shoulder position (fig. 2). However, in the 20º-shoulder position, subjects generated less elbow extension and greater elbow flexion during higher levels of adduction. The effect of shoulder position on joint torque coupling may be explained by position-dependant differences in proprioceptive feedback from shoulder abductor and adductor muscles and/or reorganization at the level of the spinal cord affecting the integration of ascending proprioceptive input.

CONCLUSIONS

Abnormal torque coupling of shoulder adductors with elbow extensors appears to be dependant upon shoulder position.

REFERENCES

[1] J. P. Dewald and R. F. Beer, *Muscle Nerve* **24**, 273-83, 2001.
[2] V. M. McClelland, S. Miller, and J. A. Eyre, *Brain Res* **899**, 82-93, 2001.

ACKNOWLEDGEMENTS

This work was supported by a National Institutes of Health RO1 Grant (HD39343).

A NEW VOXEL GRAYSCALE BASED 3D IMAGE REGISTRATION VALIDATION METHOD

[1, 2] Yang, S, [1]Hnat, WP and [2]Voor, MJ
[1]Mechanical Engineering Department of University of Louisville,
[2]Orthopaedic Bioengineering Laboratory of University of Louisville; email: s0yang01@gwise.louisville.edu

INTRODUCTION

Registration, or accurately aligning multiple images of the same subject or specimen, is vital to three-dimensional analysis of bone microstructure. Validation is required during development of new registration techniques and for evaluating the performance of existing techniques. Physical landmark methods are usually employed to validate other registration techniques because they have a reputation for accuracy [1]. However, it is difficult to implement a landmark validation method for micro level registrations or to evaluate the registrations with a geometry variance problem caused by bone growth or adaptation.

We developed a new validation technique that can be used without limitations for mono-modality registration validation.

METHODS

This voxel grayscale based technique takes advantage of the similarity of the net bone formation percentage (%NBF) in the adjacent regions within a bone. A small region, A_1 (Figure 1), from the reference image is selected and the bone volume fraction (BV) calculated. A region A_2, which has the same size and same position as A_1, is selected from the registered floating image and the bone volume fraction calculated. The %NBF or volume fraction ratio R_A is given by

$$\% \, NBF = R_A = \frac{BV_{A2} / TV_A}{BV_{A1} / TV_A} = \frac{BV_{A2}}{BV_{A1}} \quad (1)$$

A region B_1 from the reference image, in close proximity to A_1, is selected together with B_2 in the registered floating image and the %NBF calculated by

$$\% \, NBF = R_B = \frac{BV_{B2} / TV_B}{BV_{B1} / TV_B} = \frac{BV_{B2}}{BV_{B1}} \quad (2)$$

For well registered images with geometry variance, the %NBF should be approximately equal for equation (1) and (2). That is $R_A/R_B \approx 1$ which is defined as the ratio of percentage (RP). A good image registration will have a RP mean of approximately 1.0 with a small standard deviation.

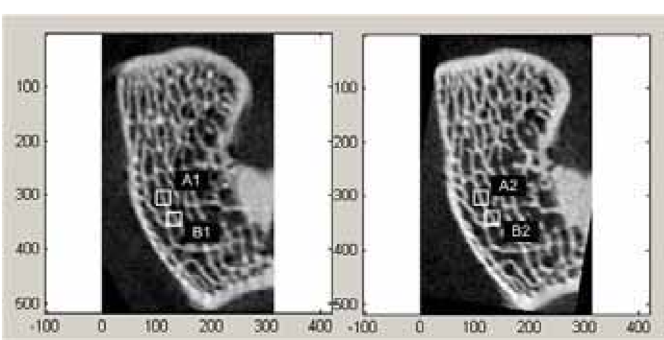

Figure 1: Slices chosen from reference image (left) and corresponding registered image (right).

This method is able to distinguish the registered images from unregistered images for nearly all the selected region sizes (SRS), as shown in Figure 2, where three registered and unregistered image pairs were tested. The SRS was set to 25 voxels in this study. The distance between A_1 and B_1 was set to 10 voxels which was shown to have no significant effect on the validation results. For each validation, twenty selected region groups were used to stabilize RP and the STDV.

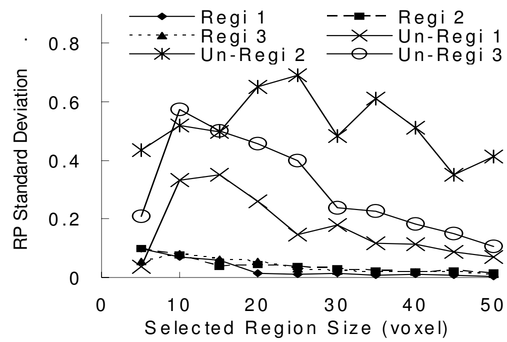

Figure 2: Validations for registered and unregistered images.

RESULTS AND DISCUSSION

Seven rabbit distal femurs were scanned, in vivo, at 28μm nominal resolution in a custom open frame micro-CT system (ACTIS 150/225 FFi-HR CT, BIR Inc., Chicago, IL) with 14 or 28 days time-intervals. The images were registered by a custom designed software package using the maximization of mutual information method which is considered to be accurate [1] and then validated. The RP means were all nearly 1.0 and the standard deviations were approximately 0.1 as shown in Figure 3.

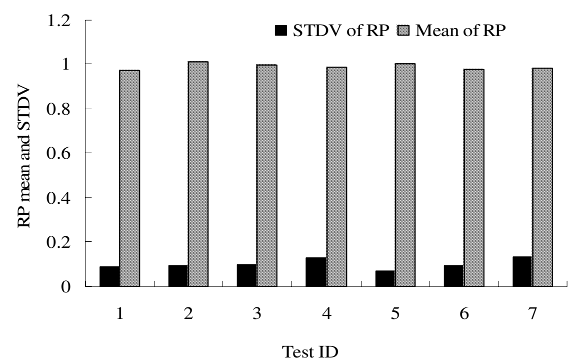

Figure 3: The RP mean and standard deviation for seven registrations.

This new grayscale based method can be used case by case to validate the registrations where existing techniques do not apply. The minimum registration error it can detect has been shown to be one voxel.

REFERENCE

1. West et al. Journal of Computer Assisted Tomography. 21 (4): 554-566.

UNIQUE SOLUTION FOR FEED-FORWARD CONTROL OF NEUROPROSTHETIC SYSTEMS CHARACTERIZED BY REDUNDANT MUSCLES ACTING ON MULTIPLE DEGREES OF FREEDOM

[1,2,3,4] Jose Luis Luján, [1,2,3,4] Patrick E. Crago
[1]Case Western Reserve University, Department of Biomedical Engineering,
[2]MetroHealth Medical Center, [3]Cleveland FES Center, [4]Cleveland VA Medical Center;
email: jll7@case.edu

INTRODUCTION

We previously developed a method for implementing feedforward neuroprosthetic controllers for musculoskeletal systems with multiple degrees of freedom and complex mechanical interactions [1]. These controllers employed inverse models of the musculoskeletal systems under control. Experimental tests showed poorer performance than expected, which we attribute to redundancy of the data used to develop the inverses. The inverse relationship between muscle output and electrical stimulation is not unique (most joints have redundant actuation with non-stationary input-output muscle properties and coupled degrees of freedom) and if left unrestricted, neural networks trained to model the inverse may produce undesirable solutions. To overcome this problem, we automated a method to choose a single optimal inverse prior to network training [2]. Our present work involves obtaining this unique inverse solution and training a controller capable of independently controlling coupled degrees of freedom. We evaluate our solution method by testing the controllers in simulation and experimentally with able-bodied and spinal cord injured human subjects.

METHODS

For simulation studies, we developed a forward model of static isometric force production at the tip of the thumb, controlled by four extrinsic and intrinsic muscles. This model, which parallels our experimental model, allows us to generate time-varying forces in three directions. Muscle activation is modeled as a nonlinear function of the electrical stimulus. The model includes random noise and a linearly-decreasing fatigue factor that scales the maximum muscle force with every muscle contraction.

Our general approach (Figure 1) is to first create a system model of the time-varying input-output data with a time-invariant artificial neural-network. The system model smoothes the output muscle forces at the tip of the thumb, eliminating their time-variance. The system model also allows us to increase the amount of time-invariant input-output data by means of its interpolation capabilities. We choose unique input-output patterns from this time-invariant data that optimize specific performance criteria, such as minimum co-activation, which allows us to eliminate redundancy and thus obtain a unique solution. We train an inverse-model, static, feedforward, artificial neural network controller (Figure 2) with these optimal input-output data.

Figure 1: Process for obtaining a unique solution.

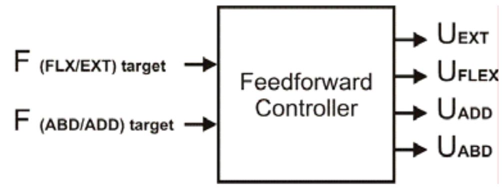

Figure 2: Feedforward controller. The inputs are the target flexion/extension and abduction/adduction forces at the thumb tip. The outputs are the stimulus required for the extensor, flexor, adductor and abductor muscles.

We first study redundancy by stimulating only a pair of antagonists (extensor pollicis longus and abductor pollicis brevis) controlling flexion/extension of the thumb's carpometacarpal joint. We then incorporate coupling to the system by stimulating two additional muscles (flexor pollicis longus and adductor pollicis) allowing us to control abduction/adduction as well.

RESULTS AND DISCUSSION

We demonstrated the feasibility of this approach with a simplified model of a pair of antagonist muscles controlling a single degree of freedom [2]. The system model eliminated redundancy due to noise, and the optimization produced training data that eliminated mechanical redundancy by optimizing co-contraction. We expect similar results with the more realistic simulation model we are implementing currently, which will be followed by experimental tests. The methodology is general enough that it will be suitable for a wide variety of musculoskeletal systems. The use of neural networks for the controller allows us to improve generalization of muscle stimulation. Furthermore, by allowing independent control of redundant systems with coupled degrees of freedom, the function restored by neuroprostheses can be improved.

REFERENCES

1. Lujan JL, Crago PE. "Computer-based test-bed for clinical assessment of hand/wrist feed-forward neuroprosthetic controllers using artificial neural networks", *Med Biol Eng Comput.*, **42**(6), 754-61, Nov 2004.
2. Kirsch RF. et al, "Restoration of Hand and Arm Function by Functional Neuromuscular Stimulation", *Quarterly Progress Report #5, NIH Neuroprosthesis Contract N01-NS-1-2333*, 21-27, June 2002.

ACKNOWLEDGEMENTS

This work is supported by the NIH/NINDS Neuroprosthesis Program under contract N01-NS-1-2333.

MUSCLE FIBRE LENGTH-TO-MOMENT ARM RATIOS IN THE HUMAN LOWER LIMB

Constantinos N. Maganaris, Vasilios Baltzopoulos and Dimitrios Tsaopoulos
IRM, Manchester Metropolitan University, Alsager, U.K.; email: c.n.maganaris@mmu.ac.uk

INTRODUCTION

The fibre length (*L*)-to-moment arm (*d*) ratio (*L/d*) is functionally significant because it determines the active excursion range and the relative contributions of the contractile element and its mechanical advantage to the pattern of the torque-angle relation. Despite their importance, data on *L/d* ratios are rather scarce [e.g., 1,2], but suggest that the *L/d* ratio in a given muscle-joint is constant between individuals. In the present study we have quantified the *L/d* ratio in main human knee extensors and ankle plantarflexors from in vivo measurements of *L* and *d*. A secondary aim was to examine whether the *d* values in the knee extensors and ankle plantarflexors scale with each other.

METHODS

Twenty-one men (age: 25±6 years, body height: 182±8 cm, body mass: 79±8 kg; mean±SD) without any musculoskeletal injuries in the lower limbs volunteered to participate after the study was approved by the local Ethics Committee. Measurements of *L* were taken from the vastus lateralis (VL), vastus intermedius (VI), gastrocnemius medialis (GM), gastrocnemius lateralis (GL), and soleus (SOL) muscles, using ultrasonography [e.g., 3,4]. The sonographs were taken from the central region of each muscle, with the knee fully extended and the ankle at the anatomically neutral position. Measurements of *d* were taken at the above joint configuration in the Achilles tendon (AT) and the patellar tendon (PT) using magnetic resonance imaging [e.g. 5,6]. From the measurements taken, the relations between a) *L* in each ankle plantarflexor muscle and d_{AT}, b) *L* in each knee extensor muscle and d_{PT}, and c) d_{AT} and d_{PT}, were analyzed with Pearson correlation coefficients.

RESULTS AND DISCUSSION

The L/d_{AT} ratios ranged from 0.78 to 1.35 in the GM muscle, from 0.72 to 1.32 in the GL muscle and from 0.61 to 1.1 in the SOL muscle. The L/d_{PT} ratios ranged from 1.5 to 2.24 in the VL muscle and from 1.1 to 2 in the VI muscle. The d_{AT}/d_{PT} ratios ranged from 1.21 to 1.61. None of the relations examined was significant (P>0.05), which therefore also precludes that the quantities involved in each relation scaled with each other. The Pearson correlation coefficients obtained ranged from -0.2 to 0.29 (Table 1).

Table 1. Relations between the parameters examined.

Relations	r	P
L_{GM} vs. d_{AT}	0.059	P>0.05
L_{GL} vs. d_{AT}	0.129	P>0.05
L_{SOL} vs. d_{AT}	0.092	P>0.05
L_{VL} vs. d_{PT}	-0.203	P>0.05
L_{VI} vs. d_{PT}	-0.245	P>0.05
d_{AT} vs. d_{PT}	0.29	P>0.05

The varying *L/d r*atios in the present in vivo study contrast previous findings in other muscle-joint systems [1,2], indicating that *d* differences in a given joint between individuals may not always accounted for by differences in muscle length caused by *L* differences. It may be the case that in some pennate muscle-joint systems the above inter-subject muscle length differences are primarily accommodated by differences in muscle fibre number and/or cross-sectional area. The present findings indicate that *L* may not always scale to *d* and need to be accounted when the *L/d r*atio of a given muscle-joint system needs to be known, e.g., when seeking a donor muscle to surgically substitute functional loss.

The lack of relation between d_{AT} and d_{PT} precludes that these quantities can be predicted from one another when one of these *d* values is already known.

REFERENCES

1. Lieber RL. *Acta Anat* **159**: 84-89, 1997.
2. Lieber RL et al. *J Exp Biol* **200**: 19-25, 1997.
3. Maganaris CN et al. *J Physiol* **512**: 603-614, 1998.
4. Kawakami Y et al. *J Appl Physiol* **85**: 398-404, 1998.
5. Rugg SG et al. *J Biomech* **23**: 495-501, 1990.
6. Maganaris CN et al. *J Physiol* **510**: 977-985, 1998.

EFFECT OF DYNAMIC ANKLE JOINT STIFFNESS ON JOINT MECHANICS AND MUSCLE ACTIVATION PATTERNS DURING LOCOMOTION

[1]Prism S. Schneider, [2]James M. Wakeling and [1]Ron F. Zernicke
[1]Human Performance Laboratory, University of Calgary, Calgary, Canada
[2]Department of Basic Veterinary Sciences, Royal Veterinary Collage, London, United Kingdom
email: prism@kin.ucalgary.ca, web: www.kin.ucalgary.ca

INTRODUCTION

Ankle-foot orthotics (AFOs) are external orthopaedic devices that provide support for foot-drop or ankle instability associated with many neuromuscular disorders. Currently, AFOs are articulated or rigid. Dynamic joint stiffness (JS) can be calculated as the slope of a joint angle vs. moment plot and is an important constraint on the motor control system as it affects the generation of voluntary movements and the displacement resulting from an external perturbation [1]. Understanding JS is essential to orthotic design and the quantitative evaluation of neuromuscular diseases [2]. JS has not been examined experimentally or dynamically with the use of AFOs in human locomotor activities. The effects of dynamically varied AFO stiffness on joint kinematics, kinetics, muscle activation patterns and resultant JS during walking and stepping down from a platform were the focus of this study.

METHODS

Bilateral AFOs were instrumented with electro-hydraulic disc brakes to allow for computer-adjustable AFO stiffness, which permitted varied external resistance of ankle motion. The study design was prospective, randomized, and was comprised of six healthy adult males. 3D kinematics were acquired using unilateral, lower-extremity active marker placement and a high-speed, motion analysis system (CODAmotion MPX30; Charnwood Dynamics Ltd., UK). Force plate (AMTI; 2000 Hz), electromyographic (EMG) (MA-310; Motion Lab Systems, Inc. Los Angeles, CA, USA; 2000 Hz), and video (200 Hz) data were collected during a minimum of 15 successful walking and 10 step down trials per subject for Shod (shoes only) and 3 AFO stiffness conditions: rigid (Rigid), articulated (Art), and intermediate (Inter). Time-frequency analysis, using wavelets, was used for EMG analysis to identify low (20-38 Hz) and high (128-218 Hz) frequency content of the EMG signals. Multivariate analysis of variance with a *post-hoc* test (α=0.05) revealed significant differences.

RESULTS AND DISCUSSION

During both gait and step downs there were no significant differences in mean resultant ankle or knee joint stiffness, independent of AFO use and AFO stiffness for both tasks. During the stance phase of gait, there was a significant decrease in ankle joint energy production at toe-off when AFO conditions were compared to Shod (Fig. 1). There was also a significant decrease in energy absorbed at the knee joint following heel-strike in the AFO conditions. During the step down task, there was a significant increase in energy absorbed across the ankle and knee joints in all AFO conditions compared to Shod (Fig. 1). The tibialis anterior (TA) muscle showed a significant increase in activation for all AFO conditions for walk and step down trials across all frequency bands (Fig. 2). There was significantly greater recruitment of the lateral gastrocnemius (LG) in all AFO conditions for step downs, but a decrease in activation for the AFO walking trials (Fig. 3). There were AFO condition and frequency dependent changes in EMG signals for both tasks.

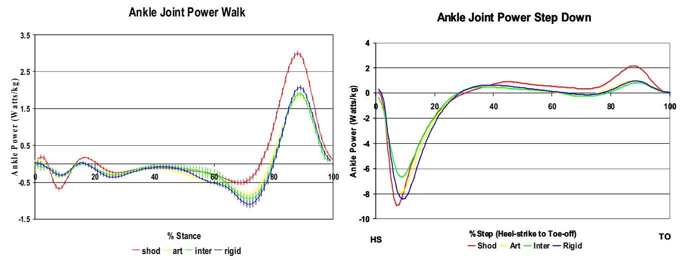

Fig. 1: Mean (±se) ankle joint power for walk (left) and step downs (right) for Shod (red) Art (yellow), Inter (green) and Rigid (blue). N=6

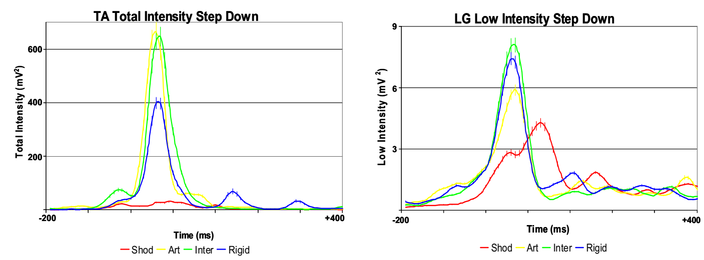

Fig. 2: Mean (±se) TA total intensity (left) and LG low intensity (right) for 200ms pre- and 400ms post-step down for Shod (red) Art (yellow), Inter (green) and Rigid (blue) conditions. N=5

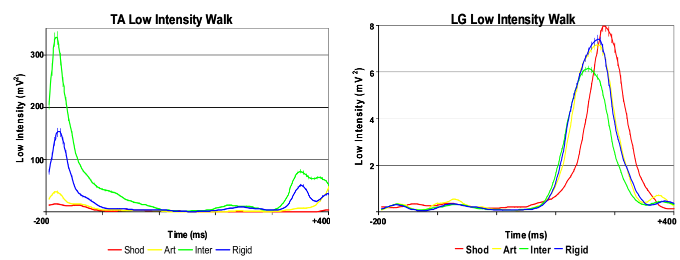

Fig. 3: Mean (±se) TA low intensity (left) and LG low intensity (right) for walking trials for Shod (red) Art (yellow), Inter (green) and Rigid (blue) conditions. N=5

CONCLUSIONS

Despite changes in AFO stiffness, resultant ankle and knee joint stiffnesses remained unchanged for both walking and step down trials; however, there were changes in muscle activation patterns and mechanical joint energetics. That suggested that a neuromotor and joint dynamics response helped maintain a task-specific resultant joint stiffness. These findings are consistent with JS being a function of task [3] and therefore, task-specific AFO stiffness may be more desirable in clinical populations. Results from this study provide data to help in our understanding of how AFO prescription may affect internal joint mechanics and muscle activation patterns.

REFERENCES

1. Hunter I. & Kearney R. *J Biomech* **15**, 747-52, 1982.
2. Davis R. & DeLuca P. *Gait & Posture* **3**, 79-80, 1995.
3. Stefanyshyn DJ. & Nigg BN.*J Biomech* **14**, 292-99, 1998.

ACKNOWLEDGEMENTS

NSERC, AHFMR, CIHR, Wood Professorship in Joint Injury Research, Colman Prosthetics and Orthotics

MUSCLE FORCE-STIFFNESS CHARACTERISTICS INFLUENCE JOINT STABILITY: A SPINE EXAMPLE

Steve Brown and Stuart McGill
Department of Kinesiology, University of Waterloo
email: shmbrown@ahsmail.uwaterloo.ca

INTRODUCTION

The muscle force-stiffness relationship has often been modeled as linear, while in-situ muscle research has clearly demonstrated a non-linearity [1,2]. Estimation of rotational joint stability relies on both a muscle's instantaneous pre-perturbation force and stiffness [3]. Under conditions of static equilibrium, a muscle's stiffness will function in a stabilizing manner, while its force can function in either a stabilizing or destabilizing manner depending on the muscle's orientation about the joint.

In joint stability research, it has generally been assumed that a muscle's direct contribution to stability increases with force and activation and theoretically peaks at maximum force and effort. The purpose of this study was to theoretically test this notion, by comparing the joint stabilizing effects of a muscle with a linear force-stiffness relationship to the same muscle after imparting a slight non-linearity into the relationship.

METHODS

A single muscle (rectus abdominis) was modeled and its individual direct stabilizing potential about lateral bend axis of the L4-L5 spine joint was analyzed. Muscle force profiles were simulated from 0 to 100 percent of maximum Muscle stiffness was calculated using the following equation from Bergmark (1989): $k_m = q\frac{F_m}{L_m}$

where: k_m = muscle stiffness ($\frac{N}{m}$)

q = dimensionless multiplier
F_m = muscle force (N)
L_m = muscle length (m)

Force-stiffness relationships were developed by adjusting q through a range of values generally reported in the literature, and to replicate the general form of the non-linear relationship (Profiles 2 and 3) between muscle force and stiffness seen in the literature. Three profiles were examined: 1) linear; 2) non-linear with moderate stiffness magnitudes; 3) non-linear with higher stiffness magnitudes.

RESULTS AND DISCUSSION

With a linear force-stiffness relationship, stability increased proportional to muscle force; with a non-linear relationship, stability peaked and subsequently decreased at submaximal muscle forces. When considering the lower, as opposed to the higher non-linear stiffness magnitudes, the stabilizing potential of the muscle peaked at a lower muscle force level and actually became negative (destabilizing) at a "critical" stiffness magnitude (Figure 1).

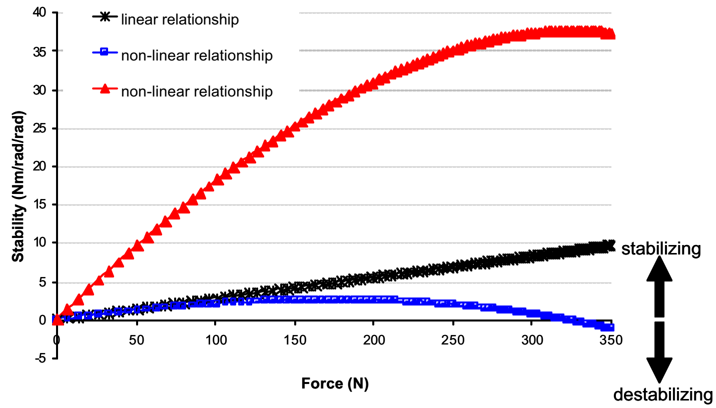

Figure 1: Stabilizing contribution of the RA muscle about the lateral bend axis of the L4L5 spine joint in upright standing. The muscle is simulated to have either a linear or non-linear force-stiffness relationship.

The primary concept demonstrated in this proof of principle study is that a muscle's individual contribution to joint stability may not necessarily peak at its maximum force output. Considering a non-linear relationship between force and stiffness and a muscle whose orientation is such that it's pre-tension is destabilizing, there may exist a critical force level at which any additional force increase becomes dominant over the corresponding stiffness increase, thereby reducing the muscle's stabilizing potential.

This apparent dichotomy in the muscle force-stiffness relationship, and its effect on joint stability, may provide an explanation for the phenomena of joint buckling under high loading situations. As muscles generate force towards maximum, corresponding stiffness increases taper off, thus reducing the stability margin of safety. Based on this, it appears possible that the likelihood of joint buckling may be lowest during moderate loading conditions, and become higher as loading conditions approach the minimum or maximum of the end loading range.

CONCLUSIONS

It was concluded that a non-linear muscle force-stiffness relationship greatly alters the individual stabilizing potential of the muscle throughout its progression of force development.
A muscle's stabilizing contribution may actually peak at and subsequently decrease above a critical submaximal force level. Incorporating this knowledge into stability models may assist in recognizing unstable events that lead to injury at higher levels of muscle activation.

REFERENCES

1. Hoffer JA & Andreassen S. *J Neurophysiology* **45**, 267-285, 1981.
2. Joyce GC & Rack PMH. *J Physiology* **204**, 475-491, 1969.
3. Potvin JR & Brown SHM. *J Biomechanics*, in press.

FRACTAL DYNAMICS OF HUMAN STABILOGRAM IN QUIET STANCE

[1] Jianhua Wu, [2]Ning Pan and [3]Keith R. Williams
[1]Division of Kinesiology, University of Michigan, Ann Arbor, MI 48109;
[2]Biological & Agricultural Engineering, [3]Exercise Biology, University of California, Davis, CA 95616;
Email: wjhwu@umich.edu

INTRODUCTION

To reveal the dynamics of center of pressure (COP) such as the magnitude and direction of displacements between COP points, a stabilogram-diffusion analysis (DFA) was proposed [1]. The DFA assumes a COP profile as a fractional Brownian motion (fBm), and applies the basic relation of a long-memory process, which expresses a typically unbounded process with an unlimited diffusion, to estimate the Hurst coefficient. As COP profiles are usually bounded due to physiological limits, the DFA thus conducted to COP naturally biases the results [2]. We first examined if a COP profile is a fBm signal, and then used a bridge detrended scaled window variance method (bdSWV) to estimate the Hurst coefficient if applicable.

METHODS

Twelve healthy female college students volunteered in this study. The subjects stood barefoot on a Kistler® 9287 force platform as still as possible in 1) eyes open (EO) and 2) virtual dynamic vision (DV). Three trials were collected for each subject at 100 Hz for 60 seconds. COP data in anterior-posterior (AP) direction were analyzed. Raw data were filtered by a second order Butterworth with cutoff frequency 5 Hz.

A power-law $q(f) \sim 1/f^{\beta}$ exists in the Fourier power spectrum of a fBm signal, where $q(f)$ is the power at a frequency f, and β is the scaling exponent with $1<\beta<3$. A power spectral analysis (PSA) was conducted to raw COP data, and β was estimated for the frequencies lower than 1/8 of the sampling rate [3].

A fBm signal obeys the scaling law $Var(\Delta x) \sim \Delta t^{2H}$, where $Var(\Delta x)$ is the variance of the displacement Δx, Δt is the time interval, and H is the Hurst coefficient with $0<H<1$. When $H>0.5$, COP is positively correlated (persistence), i.e., the direction of the past COP movement will be likely continued in the future movement. A higher H in this context denotes a higher level of persistence. Conversely, when $H<0.5$, COP is negatively correlated (anti-persistence). A lower H here represents a higher level of anti-persistence [2]. The bdSWV [4] was conducted to the filtered COP data such that 1) data were partitioned into non-overlapping windows in one time interval, 2) a bridge detrending was performed and standard deviation (SD) was calculated within each window, 3) average SD was calculated for each time interval, 4) H was estimated in the log-log plot of average SD versus time intervals.

RESULTS AND DISCUSSION

Scaling exponent β (Table 1) was within the range of 1 to 3, indicating that a COP profile is a fBm signal regardless of visual condition. Two linear portions were observed through the bdSWV method irrespective of visual condition (Figure 1) such that the short- and long-term regions were separated by a transition point T, which was close to 1 second (Table 1). H_s was higher than 0.5 and H_l was lower than 0.5 in both visual conditions (Table 1), similar to the findings by a DFA analysis [1]. Two control schemes may be expected in quiet stance such that persistence dominates in the short-term region while anti-persistence governs in the long-term region [1]. This implies that the postural control system may not use input from the visual, vestibular and somatosensory systems to regulate muscle activities unless the input reaches a threshold.

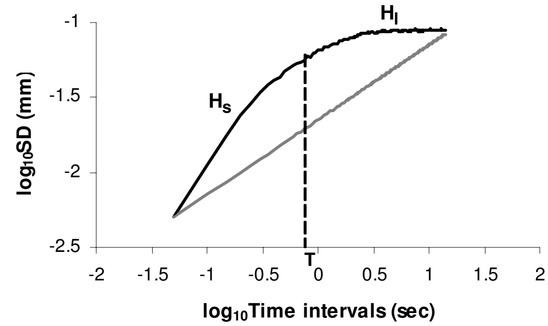

Figure 1: A representative log-log plot of average SD vs time intervals. T is transition point, H_s and H_l is the Hurst coefficient for short- and long-term regions, respectively.

H_s in DV was significantly higher than that in EO, while H_l in DV was significantly lower than that in EO (Table 1). Dynamic visions yielded higher levels of persistence and anti-persistence in the short- and long-term regions, respectively. The higher anti-persistence in DV may be due to the increase of the activity of musculature in quiet stance.

CONCLUSIONS

It was concluded that a COP profile is a fBm signal, and the bdSWV is able to reveal the fractal dynamics of COP profiles.

REFERENCES

1. Collins JJ, et al. *Exp Brain Res* **95**, 308-318, 1993.
2. Delignieres D, et al. *J Mot Behav* **35**, 86-96, 2003.
3. Eke A, et al. *Eur J Physiol* **439**, 403-415, 2000.
4. Cannon MJ, et al. *Physica A* **241**, 606-626, 1997.

ACKNOWLEDGEMENTS

Thank National Textile Center for funding this study.

Table 1: Results of PSA and bdSWV method (* denotes a significant difference between EO and DV at p<0.05 level)

	β	T	H_s	H_l
EO	2.34	0.84	0.89	0.12
DV	2.60*	0.90	0.94*	0.08*

JOINT TORSIONAL STIFFNESS CONTRIBUTIONS TO LEG STIFFNESS VARY DURING DROP LANDINGS ONTO ONE OR TWO LEGS

[1] Steven T. McCaw, [2]Tibor Hortobágyi and [2]Paul DeVita
[1]Illinois State University, Normal,
[2]East Carolina University, Greenville, NC; email: smccaw@ilstu.edu, web: cast.ilstu.edu/mccaw

INTRODUCTION

Vertical ground reaction force (GRFv) descriptors of landing on one leg are less than twice the two leg landing values[1], suggesting neuromuscular control strategy adjustments according to the number of limbs available to absorb energy. Quantifying leg stiffness and individual joint stiffness allows evaluation of neuromuscular control strategies [2]. When hopping in place, leg stiffness adjustments to alter hopping frequency or height occur primarily by adjusting ankle joint stiffness [2]. Landing differs from hopping since landing does not require a subsequent flight period. Landing research identifies the knee as the primary contributor to energy absorption, but the ankle contribution increases if a "stiffer" landing technique is used [3,4]. The purpose of this study was to compare measures of leg and joint stiffness between one and two leg drop landings. It was hypothesized that higher vGRF values in one leg landing reflect increased leg stiffness. We were also interested in how the individual joint stiffnesses contribute to the altered leg stiffness.

METHODS

Eleven physically active females, each accustomed to landing, participated in the study. All landings were performed from a box set at 25% of body height. Ten trial blocks of one leg and two leg landings were collected in random order from each subject. Instructions were to "land comfortably".

To collect ground reaction force data (GRF), subjects landed with the right foot on a force platform (960 Hz). Markers secured on the right side of the body defining the trunk, thigh, shank and foot segments were digitized with a high-speed infra-red tracking system (240 Hz). Custom software was used to calculate joint torques (JMF) using an inverse dynamic analysis combining the synchronized GRF, kinematic, and subject anthropometric data. Leg stiffness (k_{leg} = Peak $GRF_{vertical}$ / Leg compression) and individual joint stiffness ($k_{joint} = \Delta JMF / \Delta$Joint Angle) were subsequently calculated [2]. Paired t-tests were used for statistical comparisons ($\alpha = .05$)

RESULTS AND DISCUSSION

All GRF and kinematic measures were significantly different between one and two legged landings (table 1). Peak GRFv values were not twice as high. A more extended body position was used in a one leg landing and the leg compresses less. Joint positions are more extended at contact and less flexion ROM is utilized at all joints when landing on one leg; peak knee flexion is reached in a shorter period of time. All joint and leg stiffness measures were significantly different between one and two leg landings (figure 1). Leg stiffness was ~2 times higher during a one leg landing compared to a two leg landing. The increase in leg stiffness was attained by increasing joint stiffness slightly more than 50% at the ankle and hip, and tripling joint stiffness at the knee.

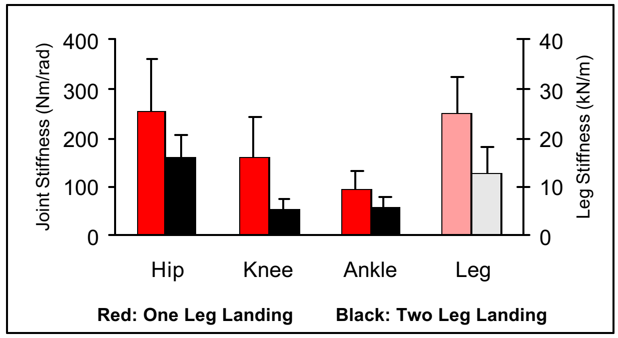

Figure 1: Leg and joint stiffness measures.

CONCLUSIONS

A twofold increase in leg stiffness during landing on one leg results in GRFv values that are 1.5 fold as high as when landing on two legs. While increased joint stiffness is evident at the hip, knee and ankle, the disproportionate increase in knee joint stiffness suggests modulation of knee joint stiffness is the primary mechanism of adapting to a landing on one leg.

REFERENCES

1. McCaw, ST et al. *Proceedings ASB (CD),* 2004.
2. Farley CT & Morgenroth DC. *J Biomech,* **32**,267-273, 1999.
3. Zhang, S et al. *Med Sci Sprt Ex,* **32**, 812-819, 2000.
4. DeVita P & Skelly WA. *Med Sci Sprt Ex,* **24**,108-115, 1992.

ACKNOWLEDGEMENTS

STM received a Travel Grant from the American Society of Biomechanics. Data collection was assisted by ECU students Joe Helseth and Brandon Noyes.

Table 1: Descriptive statistics of selected GRF and kinematic variables.

	GRFv (kN)	Leg Compress (m)	Time to Mx Knee ? (seconds)	TD Angle (radians)			Joint Flexion ROM (radians)		
# Legs				Hip	Knee	Ankle	Hip	Knee	Ankle
One	2.62 ± .59	.11 ± .02	.179 ± .043	2.92 ± .08	2.96 ± .06	2.15 ± .08	.38 ± .17	.79 ± .16	.89 ± .09
Two	1.71 ± .50	.15 ± .03	.199 ± .050	2.86 ± .09	2.86 ± .07	2.09 ± .17	.66 ± .24	1.05 ± .18	.89 ± .13

THREE-DIMENSIONAL ARCHITECTURE OF HUMAN GASTROCNEMIUS AND TIBIALIS ANTERIOR MUSCLES DURING ISOMETRIC ACTIONS

[1] Toshiyuki Kurihara, [1]Toshiaki Oda, [1]Kentaro Chino, [2]Toshihiko Nagayoshi, [2]Emika Kato, [1]Hiroaki Kanehisa, [3]Tetsuo Fukunaga, and [3]Yasuo Kawakami
[1]Department of Life Sciences (Sports Sciences), University of Tokyo, Komaba, Japan, E-mail: t-kuri@mti.biglobe.ne.jp
[2]Graduate School of Human Sciences, Waseda University, Japan, [3]Faculty of Sport Sciences, Waseda University, Japan

INTRODUCTION

The architecture of a muscle, characterized by the length (fascicle length) and the angle (pennation angle) of fascicles of muscle fibers, is a primary determinant of its function. Recent in vivo approaches employing ultrasonography have shown that architecture of human skeletal muscles change during contractions even in isometric actions [1-4].

Most previous sonographic studies measured muscle architecture only at the midbelly of the muscle, based on the notion that there is a marked uniformity in architecture throughout a muscle [5]. As for the medial gastrocnemius muscle (MG), however, Kawakami et al. [1] found that pennation angle measurements significantly varied among positions, while fascicle length was constant. In their results, the differences in pennation angles still remained when the muscle contracted. Moreover, Nagayoshi et al. [4], who examined the architecture of the tibialis anterior muscle (TA), reported significant differences in fascicle length measurements between proximal 30% and 50% positions in a relaxed condition, without differences in pennation angles. On the other hand, some researchers claimed that homogeneous architecture at the various sites of muscle belly of MG [2] and TA [3] were found both at rest and during contraction. Thus, whether architectural parameters, such as the fascicle length and pennation angle, differ within a muscle at rest and/or during contraction still remains a question.

The present study aimed to ascertain the uniformity of the architecture of human medial gastrocnemius and tibialis anterior muscles both in the relaxed and contracted conditions.

METHODS

Four healthy men (27.8 ± 2.2 yrs) volunteered for the measurements. The subject's right foot was firmly attached to an electric dynamometer. The ankle joint was fixed at 0 deg (for MG) or at 30deg dorsiflexion (for TA), and the knee joint was fully extended while the subject was in a prone position and seated position for MG and TA measurements, respectively. During the ultrasound data acquisition, the subject was asked to relax, then to maintain isometric plantar flexion or dorsiflexion at five force levels (20, 40, 60, 80, 100%MVC).

By moving a 7.5MHz, linear, B-mode, ultrasonographic probe (SSD-5500, Aloka, Japan) on the skin along the center of the muscle belly, serial cross-sectional images of muscles were obtained. An electromagnetic position sensor was attached to the ultrasonic transducer to provide position and orientation information for each image acquired. All the serial ultrasonic images (recorded at 30 frames/s) were stored in a computer simultaneously with the positional information, by which, three-dimensional ultrasound (3D-US) images were reconstructed.

The 3D-US images could be cut at any planes with respect to the muscle orientation. Several planes were taken from different regions over the longitudinal axis of the muscle belly so that fascicles of interest were visualized throughout their lengths. In each image, the fascicle length was measured along the fascicle as the distance between its aponeurotic attachments, and the pennation angle was measured as the angle between the deep aponeurosis and fascicles.

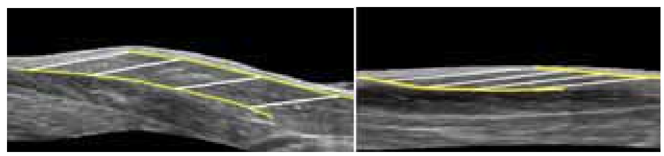

Figure 1: Typical examples of reconstructed ultrasound images of the MG (left) and TA (right) at rest condition.

RESULTS AND DISCUSSION

A preliminary study for 2 subjects showed that the fascicle length of MG was constant throughout the muscle in the relaxed and contracted conditions. On the other hand, fascicle length of TA showed an increasing trend along the center line of the muscle belly towards the distal direction in rest conditions, which remained when the contraction levels increased. The uniformity of fascicle length for MG and the nonuniformity for TA support previous reports [1,2,4].

The pennation angles of MG and TA both differed among various sites. In the relaxed condition, pennation angles were maximal at the middle position and minimal at the extreme ends in both muscles. The site of the maximal values moved proximally with increasing contraction levels. The position-related differences within muscle are similar to a previous finding [1] for MG, while no reports have been made for the nonuniform pattern of TA pennation angles at rest and/or during contraction.

The present results indicate that MG and TA have heterogeneous architecture within muscle that change by contraction, and that they should not be treated by planimetric models.

REFERENCES

1. Kawakami Y, et al., *J Appl. Biomech.* **16**, 88-98,2000.
2. Maganaris CN, et al., *J Physiol.* **512**, 603-614, 1998.
3. Maganaris CN and Baltzopoulos V, *Eur. J Appl. Physiol.* **79**, 294-297, 1999.
4. Nagayoshi T, et al., *Int. J Sport Health Sci.*, **2**, 216-221, 2003.
5. Wickiewicz TL, et al., *Clin. Orthop.* **179**, 275-283, 1983.

ISOMETRIC TRAINING ALTERS MECHANICAL PROPERTIES OF TENDON STRUCTURES.

[1]Megumi Ohta, [1]Yoichi Katsumata, [1]Koichiro Murata, [2]Hiroaki Kanehisa [3]Yasuo Kawakami and [3]Tetsuo Fukunaga
[1]Graduate School of Human Sciences, Waseda University, [2]Department of Life Sciences, University of Tokyo
[3] Faculty of Sport Sciences, Waseda University; e-mail:blessing@akane.waseda.jp

INTRODUCTION

The mechanical properties of tendon structures are related to the functional characteristics of muscle-tendon complex (MTC), such as the rate of torque development (RTD) and electromechanical delay (EMD) [1]. On the other hand, resistance training changes the tendon tissues to be stiffer [1, 2], which could result in faster RTD and shorter EMD.

The present study aimed to examine the effect of isometric resistance training on elastic and functional properties of human elbow flexor muscles.

METHODS

Nine healthy males (age, 24.4±2.3 years; heights, 172.8±6.7cm; weight, 68.1±8.9kg; mean ± SD) voluntarily participated in this study. They were requested to perform maximal isometric elbow flexion torque at 90° of elbow joint for ten seconds, five times a day (interval between trials was one minute each), five days a week, for six weeks. Before and after the training period, the distal myotendinous junction of the biceps brachii (MTJ) was visualized on the real-time ultrasonic image (Aloka SSD6500). Excursion of the MTJ during ramp isometric elbow flexion was considered as the elongation of the tendon structure. Maximal isometric elbow flexion torque (MVC), RTD, EMD and muscle thickness of elbow flexors were measured before and after the training period. RTD was determined as the rate of torque increase from 0 to 50% MVC. EMD was calculated as the time interval between the onset of electromyogram and torque development.

RESULTS AND DISCUSSION

The relationships between the tendon elongation (L) and tendon force (F) before and after the training period are shown in Fig 1. Before the training, the L-F curve consisted of two phases, i.e., phase 1 (Ph1), the region below 40%MVC of force with a large tendon elongation, and phase 2 (Ph2), the region above 40%MVC. The training changed the point dividing Ph1 and Ph2 from 40%MVC to 25%MVC. The decrease of tendon elongation in Ph1 may be related with a decreased slack of tendon or joint laxity. The slope of the regression line for the relationship between L and F in Ph2, representing the tendon stiffness as reported previously [1, 2, 3], increased significantly after the training. There were tendencies for RTD to increase and EMD to decrease by the training, which could be attributed to less tendon elongation at the lower force region. However these changes were not significant (Table 1).

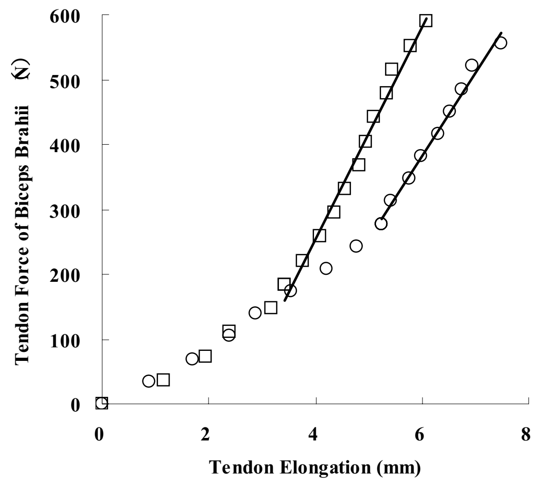

Figure 1: The relationship between tendon elongation and %MVC before (○) and after (□) the training.

REFERENCES

1. Kubo K. et al., J Appl Physiol **91**, 26-32, 2001.
2. Reeves DN.et al., Muscle Nerve **28**, 74-81, 2003.
3. Butler DL et al., Exerc Sport Sci Rev **6**, 125-181, 1978.

Table 1: Measured variables before and after the training.

	Berofe the training		After the training	
MVC (Nm)	62.01±6.09		65.79±7.03	
Muscle thickness (mm)	32.12±2.02		32.47±2.71	
EMD (ms)	35.33±6.30		30.78±3.80	
RTD (Nm/s)	537.75±147.46		578.80±220.30	
	Phase1(0-40%MVC)	Phase2 (40-80%MVC)	Phase1 (0-25%MVC)	Phase2 (25-80%MVC)
Tendon elongation (mm)	5.24±1.64	7.22±1.69	3.42±1.89	6.07±2.43
Slope of regression equation (N/mm)	53.91±16.64	130.95±35.08	41.79±40.66	174.05±113.98 *

MECHANICAL EVALUATION OF TENSION BAND ORIENTATION

[1] Joseph J. Signorelli, [2]Greg Brown, [1]Fred A. Wentorf, [2]Michael Zlowodzki and [2]Peter Cole
[1]University of Minnesota Orthopaedic Biomechanics Laboratory,
[2]Department of Orthopaedic Surgery, Regions Hospital;
email: wento001@umn.edu

INTRODUCTION

The modified AO tension band method is commonly used for the fixation of transverse patellar fractures. Despite its wide spread use, the orientation of tension bands has not been tested directly. Free body diagrams of a tension band suggest that the vertically oriented figure eight *(*Fig. 1A*)* that has traditionally been used does not provide as much compression across the fracture fragments as would a horizontally oriented figure eight (Fig. 1B*)*. Based on the free body diagrams, a simple rotation of 90 degrees of the tension band will more than double the compressive force between fracture fragments. The objective of this study is to experimentally evaluate the mechanical effect of orientation of the patella tension band.

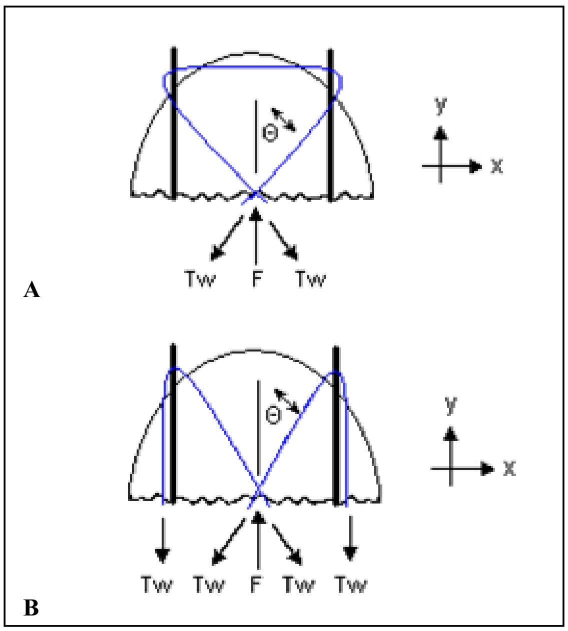

Figure 1: Free body diagrams of a vertically (A) and horizontally (B) oriented patella tension band

METHODS

Tension bands of both orientations were tested on a model constructed to simulate patellar fracture fragments. Two parallel aluminum cylinders were mounted on an Instron 5865 material testing machine (Instron, Canton MA, USA) by perpendicular lag screws. 5.0cm segments of 2.0mm Kirchner wires (K-wires) were inserted perpendicularly into the aluminum cylinders into pre-drilled holes to simulate the free ends of the K-wires in the proximal and distal patellar fragments. The K-wires were located on the anterior slope of the cylinders to simulate the curvature of the anterior surface of the patella. A tension band of 316L 18 G monofilament stainless steel wire was applied to the construct using either in the vertical or horizontal orientation. The ends of the tension

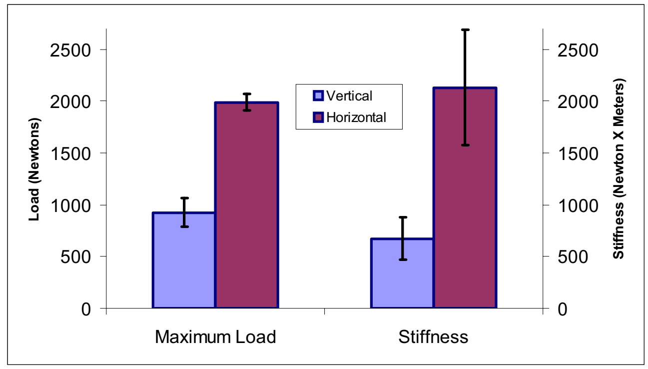

Figure 2: Comparison of the experimental maximum load and stiffness values of a horizontally and vertically aligned patellar tension band construct (Mean values and standard deviations are shown).

bands were twisted until each specimen had a pre-tension of 40N. The cylinders were then distracted on the material testing machine at a rate of 25 N/sec to a preload of 250N and held for ten seconds to allow tension to equalize throughout the tension band. The load was then increased at a rate of 50 N/sec until failure of the wire. Maximum load, stiffness, and mode of failure were recorded for fifteen trials of each wire orientation.

Limited cyclic testing was also performed using this model. The tension bands were subjected to 50 cycles consisting of increasing the load from the preload (250N) to 500N and back to the preload in four seconds. Five samples were tested in each orientation. Statistical comparisons between both models were performed using Student's t-test.

RESULTS AND DISCUSSION

In load to failure testing the horizontal construct was found to have a significantly higher maximum load and stiffness than the vertical construct ($p<0.0001$, Figure 2). Cyclic testing showed significantly less extension for the horizontal figure eight, with a mean value of 1.1 mm, than for the vertical figure eight, with a mean value of 2.7 mm ($p<0.0001$). For both constructs, over 80% of the extension was seen in the first fifteen cycles.

There is much debate over the proper method of patellar fracture fixation including methods with screws, and a combination of screws and wires. This study strengthens the position of tension bands in patellar fracture fixation and may require that this improved method be evaluated against other methods in use.

CONCLUSIONS

Overall, the results from this study confirm the theoretical advantages of the horizontal figure eight tension band compared to the vertical orientation

HEELSTRIKE DYNAMICS DURING 6 MINUTE WALK TEST AMONG END STAGE KNEE OA PATIENTS

[1]Danielle Biton, [1]Peter M. Quesada, [2]John Nyland, [3]Michael Durham, [4]Claudia A. Angeli, [3]Robert V. Topp and [5]Ann Swank
[1]Department of Mechanical Engineering, University of Louisville, Louisville, KY: email: d0bito01@gwise.louisville.edu
[2]Orthopaedic Surgery Dept., UofL; [3]School of Nursing, UofL; [4]Frazier Rehab. Inst.; [5]Ex. Phys. Lab., UofL, Louisville, KY

INTRODUCTION

Osteoarthritis (OA) is one of the most common chronic conditions among older adults with the knee joint being the most commonly affected joint. Symptoms of the disease involve gait alterations and difficulty completing activities of daily living. The involvement of mechanical factors in OA is widely recognized. Heelstrike phenomenon can reflect abnormal loading patterns that standard kinematic variables are unable to detect.

This study investigated the effect of performing a 6 minute walk on gait speed, vertical velocity of the ankle marker just prior to heelstrike, and maximum ankle vertical displacement during swing.

METHODS

Data from thirteen subjects recruited for a larger overall research project were collected and analyzed. All subjects signed a consent form approved by an IRB. Our study population consisted of 6 men, and 7 women, ages 54 to 70 years old (61.38 ±6.25). Patients were diagnosed with unilateral end stage knee OA and scheduled for TKA. Only subjects capable of walking at a velocity greater than 0.75m/s for 6 minutes were included in this study to limit the influence of speed on gait parameters.

Each patient was asked to perform a 6 minute walk along a 35 meter loop and was instructed to cover as much distance as they could in 6 minutes. One side of the walkway was instrumented with an 8-camera motion tracking system (Hawk system; Motion Analysis Corp.) Patients had reflective markers placed on their body in a Helen Hayes marker arrangement. Markers trajectories were recorded while walking and data for the first and last loops (beginning and end of the 6 minute walk) were retained for analysis. Motion data were collected at 100 Hz.

Gait speed (GS) was calculated as an average over one loop, for the first and last loops. Maximum ankle vertical displacement (Z_{max}) during swing prior to heelstrike for the affected leg (i.e. limb not scheduled for surgery) was considered for analysis. Vertical velocity of the ankle marker was derived from marker vertical displacement data, and the the peak, occurring prior to heelstrike ($\dot{Z}_{max}$) for the affected leg, was retained for analysis.

Paired t-tests were used to assess the differences in these parameters, between the beginning and end of the 6 minute walk, for the involved limb.

RESULTS AND DISCUSSION

No significant difference was found in gait speed (p=0.72) between the beginning and end of the 6 minute walk (figure1). Significant differences were found for the vertical velocity of the ankle marker prior to heelstrike (p=0.012), and the maximum vertical displacement of the ankle during swing (p=0.019) between the beginning and end of the 6 minute walk (figure1). Means, standard deviations and t-test values are reported in table 1.

Table 1: Mean, standart deviation and t-test value for GS, Z_{max}, and $\dot{Z}_{max}$ at the beginning and the end of the 6 min walk.

	Mean	Std Dev	t-test
GS_0	1.25 m/s	± 0.30	P = 0.72
$GS_{6\ min}$	1.24 m/s	± 0.27	
$Z_{max\ 0}$	226 mm	± 22	P = 0.019
$Z_{max\ 6\ min}$	220 mm	± 21	
$\dot{Z}_{max\ 0}$	0.219 m/s	± 85	P = 0.012
$\dot{Z}_{max\ 6\ min}$	0.265 m/s	± 75	

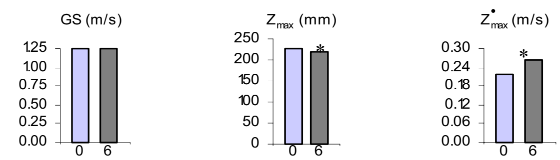

Figure 1: GS, Z_{max}, and $\dot{Z}_{max}$ at the beginning and the end of the 6 min walk. (* P≤0.05).

While gait speed remains unchanged, between the beginning and end of the 6 minute walk test, subtle changes in GS, Z_{max}, and $\dot{Z}_{max}$ are noticeable. At the end of the 6 minute walk, the vertical velocity of the ankle marker prior to heelstrike increases and patients don't lift their ankle as high in preparation for heelstrike. Gill et al. [1] in a study among healthy adults demonstrated that higher heelstrike ankle vertical velocity and lower ankle rise in preparation for heelstrike are associated with higher loading rate at heelstrike. These findings suggest that in order to maintain their gait speed throughout the 6 minutes, patients develop compensatory mechanisms modifying their loading pattern, possibly due to fatigue. These subtle changes are not noticeable with usually reported gait variables but as suggested by Gill et al. [1], can be responsible for large differences in impulse loading experienced at heelstrike and cause one's knee OA condition to worsen.

The results of this study may need to be interpreted with caution, at this time, since the sample size is still somewhat small. Subject recruitment, however, is continuing. Future investigation in this area hopes to establish means for utilizing these biomechanical variables as fatigue indicators, which could help assess end stage knee OA treatment outcomes.

REFERENCES

1. Gill HS, et al. *J Biomech*, **36**, 1625-31, 2003.

LOWER BACK FNS FOR STABILIZATION DURING ONE- AND TWO-HANDED REACHING TASKS

[1] Jason Gillette, [2]JoAnne Resig, [2]John Alton, and [2]Eric Hartman
[1]Department of Health and Human Performance, Iowa State University, Ames, Iowa, USA; email: gillette@iastate.edu
[2]customKYnetics, Inc., 304 Crossfield Drive, Suite A, Versailles, Kentucky, USA

INTRODUCTION

An individual with a complete thoracic-level spinal cord injury (SCI) experiences a loss of voluntary control to the lower extremities, the pelvis, and a portion of the trunk. These limitations may make it difficult or impossible to perform seated tasks such as reaching, lifting, and pulling. A prototype functional neuromuscular stimulation device was developed to activate the trunk muscles for added stiffness during seated tasks. The particular studies described here involved evaluation of one-handed and two-handed reaching tasks using the Stimulation for Improved Trunk Stability (SITS) system prototype. The hypothesis was that using the SITS system would result in increased postural stability when compared to reaching tasks performed without stimulation.

METHODS

Subject #1 was a 34 year-old male with a T3 level complete injury, and Subject #2 was a 38 year-old male with a T6 level complete injury. The SITS system consisted of a control module that interfaced with an Octostim muscle stimulator. Adhesive surface electrodes were placed on the skin over the paraspinal muscle mass just lateral to the vertebral column. During one-handed reaching, three conditions were tested while seated in a wheelchair: unconstrained (U), constrained (C), and constrained with assistance from the stimulation system (SITS). Compensatory movements such as hooking an arm around the wheelchair frame were allowed in the U condition. Use of the non-dominant arm was deterred in the C condition by having the participant hold his arm to the side of his body. The two-handed reaching tasks were tested using the U and SITS conditions. Reflective markers were tracked by a Motion Analysis video system, and the wheelchair wheels were positioned on four load cells. Video data were used to determine object trajectory, targeting accuracy, and trunk displacement.

One-handed reaching tasks involved moving a 1 kg mug between nine targets on a table. Targets were located at 60% (6), 90% (9), and 120% (12) of seated reach (measured with trunk vertical) at the midline (M) and half the shoulder width to the left (L) and right (R). For example, L6R6 indicates moving from the left 60% to the right 60% target. A successful movement was defined as the final object position being within 80% reaching distance from the target. Five repetitions of six reaching combinations for three conditions (U, C, SITS) were performed over two days (180 trials). For the two-handed reaching tasks, the table was removed, and the mug was manipulated through a series of movements. The three tasks were moving and holding the object: 1) above the head, 2) at eye-level with arms extended, and 3) with the arms extended on the dominant side of the body. Five repetitions of the three two-handed tasks for two conditions (U, SITS) were performed over two days (60 trials).

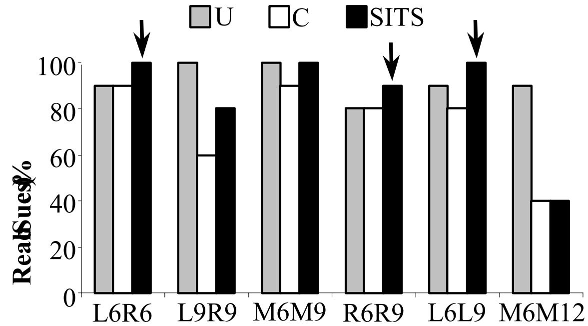

Figure 1: One-handed reaching success. Arrows indicate movements where the SITS system appeared beneficial.

RESULTS AND DISCUSSION

Combining data for one-handed reaching tasks, the percentage of successful movements was highest for the U condition (92%), followed by the SITS (89%) and C (84%) conditions. Similarly, trunk displacement was minimized in the U condition (1.8 cm), followed by the SITS (2.6 cm) and C (3.1 cm) conditions. Figure 1 shows representative data from Subject #1 for the percentage of successful movements as a function of reaching combination. When combining data for the two-handed reaching tasks, trunk displacement did not show differences between the U and SITS conditions. Wheelchair center of pressure displacements were reduced for the SITS condition (7.4 cm) as compared to the U condition (10.8 cm). Maximum wheelchair center of pressure velocities were also reduced for the SITS condition (68.1 cm/s) as compared to the U condition (84.5 cm/s) indicating that the task was more controlled with the stimulation than without.

Compensatory movements such as arm hooking (U condition) may be ergonomically unfavorable. One goal of designing the SITS system was to provide enough trunk stability that compensatory movements would be unnecessary. The SITS system appeared to be helpful for the one-handed combinations that involved reaching to the right or left (Figure 1). In addition, the SITS system may have been most beneficial for two-handed reaching tasks, particularly those that involved lifting an object over the head. Center of pressure data supported observations that the SITS system provided additional postural stability to maintain targeted two-handed reaching postures. Overall, the participants continued to reach most effectively with the U condition, while the SITS system provided additional lower back stiffness that resulted in consistent improvement over the C condition.

ACKNOWLEDGEMENTS

The authors thank Robert Shapiro, Sarah Berizzi, and Larry Goodrich at the University of Kentucky. This study was funded by a SBIR grant from NIH (R43HD41286).

BIOMECHANICAL ANALYSIS OF JUMPING COMPARING LOW- AND HIGH- ACL INJURY RISK GROUPS: IDENTIFYING POSSIBLE MECHANICAL RISK FACTORS

Jennifer J. Jeansonne, Vanessa A. West, and Jennifer R. Hoenig
Southeastern Louisiana University, Hammond, LA, USA; email: jjeansonne@selu.edu

INTRODUCTION

It is well known and documented that anterior cruciate ligament (ACL) knee injuries occur more frequently in women, at a rate of 4-8 times that of men [1]. Of the 30,000-100,000 ACL injuries reported in various years, most injures were a result of a non-contact mechanism and sports such as soccer, basketball, and volleyball, report the highest prevalence of ACL injuries especially when compared to males in the same sports [2, 3]. Research associated with knee injuries in females has observed hormonal, neuromuscular, and anatomical differences in men and women [4]. What has not been reported is why certain groups of athletes have a higher incidence of injury than others, or if it is due to training and teaching techniques. If dancers and cheerleaders also jump, why are they less likely to injure their knees? The purpose of this study was to compare kinematics and kinetic data from low- and high- ACL injury risk groups, and controls, to identify possible mechanical risk factors.

METHODS

Thirty-six female collegiate undergraduates volunteered for this study; however, only 32 (m=20±2.3yrs) completed the study. Subjects were placed in one of three groups: high-risk (volleyball players, n=11), low-risk (dancers & cheerleaders, n=12), and controls (non-athletic, n=9). All participants completed an informed consent and medical questionnaire.

Each participant performed 3 vertical jumps at maximal effort with joint markers on the right and left legs placed at the hip, knee, ankle, heel and toe. Each participant faced the same direction and had only the right foot on the Bertec force platform when jumping. The jumps were videotaped using three cameras, two anteriorly and one posteriorly positioned relative to the subject. The video was digitized and then filtered and processed to calculate flexion/extension at the knee and ankle, knee varus/valgus, jump height, and jump time using Peak Motus® 8. The force data was synchronized with the kinematics data to calculate peak forces during the loading and landing phases of the jump. The force plate collected at 600 Hz, while the cameras collected data at 60 Hz.

RESULTS AND DISCUSSION

A 3 X 9 (group X measure) ANOVA found significant differences ($p<0.05$) between the groups for all but 2 of the dependent measures (Table 1). Post-hoc tests revealed the high-risk group to be significantly different from both the controls and the low-risk group for the kinematic measures (dorsi/plantarflexion at load & land, knee flexion at load & land, & jump time) (Figure 1), while the low-risk group was significantly different from the high-risk and controls for the kinetic measures (GRF at load & land). Measures of knee varus and valgus were not significant.

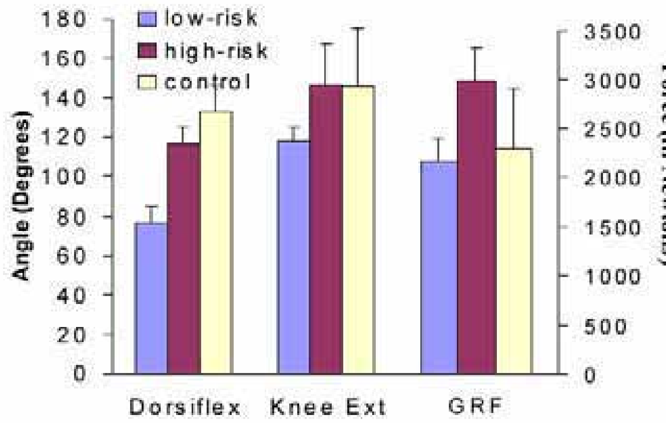

Figure 1: Maximal dorsiflexion, knee extension and ground reaction force during the landing phase of the jump.

This study revealed several differences between the three groups. The high-risk group was observed to load the least out of the three groups (knee angles: loading 120 deg, landing 147 deg), yet had longer jump times (0.48s vs. 0.42s). This is possibly due to training, needing to get to the net and quickly jump high to spike or block the ball. This landing style transmits a high amount of force to the knee and puts excessive stress on the ACL. The high-risk group also had higher GRF (loading: 2128 N, landing: 2979 N) than the low-risk group (loading: 1936 N, landing: 2165 N). These high forces could be attributed to the higher prevalence of ACL tears. The similar GRF for loading and landing in the low-risk group could be due to their training and teaching. Dancers are taught to go through the same flexion/extension path and depth during loading and landing. This could indicate why they have fewer ACL injuries compared to the high-risk group. The low risk groups must make jumps look smooth and symmetrical, while the high-risk athletes have a responsibility to make an athletic play regardless of how it looks.

CONCLUSIONS

Prevention programs have been developed to retrain females' firing patterns, increase hamstring strength, and improve jumping and landing mechanics to reduce the number of incidences and risk of injury. The research presented here supports the need for preventative jumping programs to decrease the ground reaction forces during landing and increase joint flexion, to reduce risk factors.

REFERENCES

1. Karageanes, Blackburn, Vangelos. *Clin J of Sports Med*, **10**, 162-168, 2000
2. Ardent, Bershadsky, Agel. *J of gender-specific med*, **5** (2), 19-26, 2002.
3. Romani et al. *J of Women's Health* **12** (3) 287, 2003.
4. Hewett, T. *Sports Med*, **29** (5) 313-327, 2000.

	Dorsiflexion (degrees)	Knee Flexion (degrees)	GRF (Newtons)	Jump time (seconds)
Load	[L]74±9, [H]88±9, [C]70±13	[L]105±17, [H]120±18, [C]99±8	[L]1936±223, [H]2128±348, [C]1685±610	[L]0.416±.04, [H]0.479±.04, [C]0.443±.07
Land	[L]76±8, [H]116±20, [C]133±29	[L]118±13, [H]147±18, [C]146±14	[L]2165±314, [H]2979±325, [C]2296±728	

Table 1: Means and standard errors for the low-risk (L), high-risk (H), & control (C) groups for the measures with significant findings.

A TIME-FREQUENCY APPROACH USING WAVELETS TO STUDY WEEK-TO-WEEK VARIABILITY IN BLOOD FLOW OSCILLATIONS

[1]Yih-Kuen Jan, PhD, PT; [1]David M. Brienza, PhD and [2]Michael L. Boninger, MD
[1]Department of Rehabilitation Science and Technology,
[2]Department of Physical Medicine and Rehabilitation, University of Pittsburgh; email: yij2@pitt.edu

INTRODUCTION

Laser Doppler flowmetry has been used extensively to quantify skin perfusion response to compressive loading (1). The study of blood flow responses is confounded by temporal variability in blood flow measurements (2). Several methods have been reported to compensate for temporal variability in baseline blood flow measurements. However, the success of these methods in reducing temporal blood flow variability has been mixed. Spectral analysis has been shown to be useful in isolating the effects of distinct control mechanisms to various stimuli in the microcirculatory system (1). However, the sensitivity of spectral analysis to temporal blood flow variability has not been reported. This study investigated the effectiveness of a wavelet analysis technique in reducing week-to-week variability in blood flow measurements.

METHODS

Ten healthy subjects were brought into the laboratory on three occasions separated by 7±2 days for measurements of baseline and thermally induced maximal sacral blood flow for three consecutive weeks. Blood flow over the sacrum was recorded during 10 minutes of rest to establish baseline flow followed by 15 minutes of incremental heating from 35°C to 45°C. Laserflo Blood Perfusion Monitor 2 (BPM^2, Vasamedics, Eden Praire, MN) and Softip pencil probe (P-435, Vasamedics) were used to measure capillary blood perfusion (ml/min per 100g tissue). A temperature control module (TCO, Vasamedics) with heater probe (P-422, Vasamedics) was used to heat the skin to 45°C to obtain a maximal skin blood flow response. Laser Doppler blood flow was sampled at 20 Hz using a 16-bit data acquisition card (PCI-MIO-16XE, National Instruments, Austin, TX).

Wavelet analysis was used to decompose blood flow signals into frequency components determined to be associated with metabolic (0.008-0.02 Hz), neurogenic (0.02-0.05 Hz), myogenic (0.05-0.15 Hz), respiratory (0.15-0.4 Hz) and cardiac (0.4-2.0 Hz) control mechanisms (1). Analysis methods were used to study relative contributions in each characteristic frequency band to total blood flow (1). The rationale for designation of frequency range for each characteristic frequency band's control mechanism is described in Geyer et al. (1).

Maximal blood flow ratio was defined as the ratio of baseline blood flow to thermally induced maximal blood flow at 45°C. The coefficient of variation (CoV), independent of units of measurements, was used to analyze the impact of inherent skin blood flow variability on various normalization methods by comparing its magnitude between total skin blood flow at baseline, power within each characteristic frequency band at baseline and baseline skin blood flow normalized to the maximal blood flow according to the ratio method.

RESULTS AND DISCUSSION

The CoV for the blood flow signal power in each individual frequency band at baseline (CoV range from 0.08 to 0.15) were smaller than that of blood flow at baseline (0.28) or maximal blood flow ratio (0.41) ($p<0.05$) (Figure 1). The maximal blood flow ratio method failed to reduce variability in baseline blood flow.

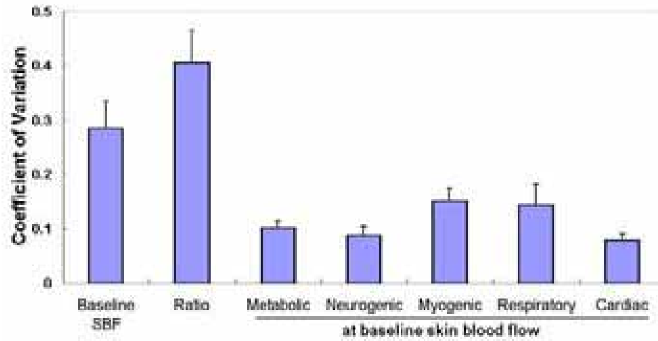

Figure 1. Comparisons of coefficients of variation of skin blood flow at baseline, maximal blood flow ratio method, and five characteristic frequency bands isolated from baseline blood flow in three consecutive weeks (values are mean±S.E.).

CONCLUSIONS

Our study suggests that wavelet analysis is effective in reducing temporal blood flow variability. To best of our knowledge, this is the first study published using wavelet analysis to investigate temporal variability of laser Doppler blood flow measurements. However, time-frequency approaches have been used widely in the study of heart rate variability. We postulated that the study of skin blood flow variability has great potential to advance understanding of blood flow control mechanisms and to provide early detection of pathological changes in the skin (i.e. foot ulcers in diabetes mellitus, survival of free flap and stage I pressure ulcer).

REFERENCES

1. Geyer, M. J., Jan, Y. K., Brienza, D. M., & Boninger, M. L. (2004). Using wavelet analysis to characterize the thermoregulatory mechanisms of sacral skin blood flow. *Journal of Rehabilitation Research & Development, 41*(6), 797-806.
2. Bircher, A., de Boer, E. M., Agner, T., Wahlberg, J. E., & Serup, J. (1994). Guidelines for measurement of cutaneous blood flow by laser Doppler flowmetry. A report from the Standardization Group of the European Society of Contact Dermatitis. *Contact Dermatitis, 30*(2), 65-72.

ACKNOWLEDGEMENTS

This project is partly supported by the National Institute on Disability and Rehabilitation Research (H133G040222) and the Department of Veterans Affairs, Rehabilitation Research and Development Service (F2181C).

The relationship between leg length and velocity of center of gravity during contact phase in the long jump

[1] Kenji Ohishi , [1]Tetsunari Nishiyama and [2]Kazuhisa Anraku
[1] Human Performance Laboratory, Nippon Sport Science University, [2]Physical Training School of Japan Defence Forces
e-mail: kenji@nittai.ac.jp, web: http://www.nittai.ac.jp/

INTRODUCTION

The take-off velocity of the center of gravity (CG) is one of important factors in the performance of the long jump. The horizontal velocity of CG gained by approach run was decelerated during the contact phase. Therefore, it is important to study the mechanisms of velocity changes during the stance phase. We examined the relationship between the changes of the CG velocity and leg length of the take-off leg during foot contact phase.

METHODS

Ten male long jumpers and ten male no-athletes participated in this study. The long jump movement during foot contact phase of take-off was recorded in the sagittal plane at 250f/s using high-speed video camera (nac, inc.). Two –dimensional coordinates of each marker on whole-body of subjects were obtained using MOVIAS software (nac, inc.). The kinematics data were smoothed two-order digital Butterworth low-pass filter with a cutoff frequency of 8Hz.

The horizontal and the vertical velocity of CG and the leg length were calculated from the coordinates. The leg length is defined as the distance from the CG to the point of metatarsophalangeal joint. The leg length was normalized to the length at the take-off. And, horizontal velocity of the CG was normalized to the horizontal velocity of the CG at the touchdown.

RESULTS AND DISCUSSION

The mean long jump distance was 6.99(6.31-7.33) m in the athlete, and 4.97(4.33-6.13) m in the non-athlete.

The %leg length was decreased in the first half of foot contact phase, then it was lengthened during the last of phase. The first half was defined as the period from touchdown to the appearance of shortest %leg length, and the latter half was defined as the period from the appearance of shortest %leg length to take-off.

Figure show the relationship between ⊿%horizontal velocity at the latter half and %horizontal velocity at the take-off. In all the members, there was the significant relation. This result show that the increase of ⊿%horizontal velocity at the latter phase approaches the velocity of approach run. However, there was no correlation in the athlete and no-athlete groups.

The relationship between velocity of CG and ⊿%leg length was show in the table. And, there was the correlation on ⊿%leg length at the latter half and it at the first half. In all the members and athlete group, there was the significant relation in ⊿% horizontal velocity at the latter half and ⊿%leg length at the same phase($p < 0.05$). The significant relation could not be observed between other elements.

From these results, there was no relation on ⊿%leg length and ⊿velocity of CG in many phases. However, the ⊿%leg length affects the ⊿%horizontal velocity of CG at the take-off, which ⊿%leg length will be considered as one element of the performance decision.

REFERENCES

1. Seyfarth A., Friedrichs A. et.al. *J Biomech* **32**, 1259- 1267,1999.

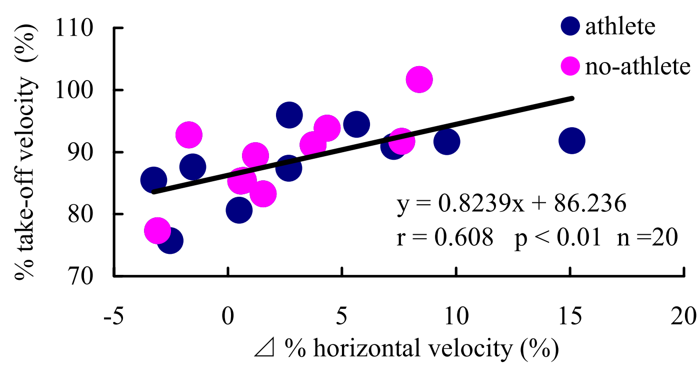

Figure. The relationship between ⊿% horizontal velocity at the latter half and %horizontal velocity at the take-off.

Table. The value of correlation coefficient and level of significance

		⊿%leg length at the first half			⊿%leg length at the latter half		
		all(n=20)	athlete(n=10)	no-athlete(n=10)	all(n=20)	athlete(n=10)	no-athlete(n=10)
⊿vertical velocity	first half	0.177	-0.527	-0.379	0.402	0.454	0.026
		ns	ns	ns	ns	ns	ns
	latter half	-0.120	-0.366	-0.019	0.273	0.610	-0.140
		ns	ns	ns	ns	ns	ns
⊿%horizontal velocity	first half	0.131	-0.028	0.028	0.051	0.294	-0.289
		ns	ns	ns	ns	ns	ns
	latter half	-0.283	0.449	-0.014	-0.453	-0.679	-0.329
		ns	ns	ns	0.05	0.05	ns

INITIATION AND PROPAGATION OF FATIGUE MICROCRACKS FROM A DEFECT IN A CEMENTED TOTAL HIP ARTHROPLASTY

Jihui Li[1]; Gang Qi[1, 2]
[1]Dept. of Biomedical Engineering, [2]Dept. of Mechanical Engineering. The University of Memphis, Memphis, TN 38152
E-mail: jihuili@memphis.edu Web: http://www.me.memphis.edu/mar_lab/mar_lab/home.htm

INTRODUCTION

Voids/defects in cement mantle or at interfaces were reported as a major source of fatigue microcracks (MCs) that occurred in cemented total hip arthroplasty (THA) [1,2]. Presently, it is difficult to monitor the progression of MC activities in real time. In this work, we presented a case study to reveal the initiation and accumulation of MCs from a proximal defect in a cemented THA, using acoustic emission microcrack graphs (AEMG) technique [3].

METHODS

A series of standard hand mixed cemented THA specimens were prepared using Spectron stem, Palacos R cement and Sawbone femurs. In X-ray examination, one specimen with a proximal defect of 6.5 × 2.5 × 14.0 mm (in anterior-posterior, medial-lateral and distal-proximal direction, respectively) was identified (Fig. 1a) and selected to study the influence of the defect on MCs activities. The specimen was subjected to 5 million cycles of fatigue loading (267/2670 N at 2 Hz) on a MTS machine. MC signals were detected by an AE system and their locations were calculated. Six virtual sections (A1 to A6, 5 mm thick each) were selected from the defect area (Fig.1b). MCs that occurred in each section were counted and plotted onto the anterolateral quadrant (Fig.1c) to visualize the initiation and accumulation of MCs (a process called AEMG [3]). After the experiment, the specimen was sectioned at seven locations (A-G in Fig.1a) for SEM inspections.

RESULTS AND DISCUSSION

The AEMG and the number of MCs of virtual sections in the first three hours (Fig.2) indicated that the fatigue damage initiated from the lower lateral end of the defect (section A4) 4 seconds after test started. The damage spread to the surrounding area of the defect (A2-A5) immediately and the number of MCs increased dramatically. Damage propagation (evaluated by number of MCs) decreased as the test proceeded, but with three recover periods which started from the 12th, 18th and 22nd days, respectively (Fig. 3c). Most MCs accumulated around the middle-lower defect (A3-A5). SEM observed a continuous debonding at cement-stem interface next to the defect at physical section A (Fig.3a). A large amount of cement debris could be identified in the debonding (Fig.3b). This indicated the MCs in the middle and final fatigue process was caused mainly by the grinding between damaged interfaces instead of the damage propagation. No MCs located along cement-bone interface and on either side of the defect. Few insignificant MCs were detected in other physical sections.

CONCLUSIONS

AEMG analysis indicated that defect was indeed the key reason of fatigue MCs. These MCs initiated at the lower lateral end of the defect and propagated upward to the surrounding area. Damage propagation was slow down then and interface grinding became the major source of MCs.

REFERENCES

[1] Powers et al., J Arthroplasty, 1998; [2] Topoleski et al., J Biomed Mater Res. 1992; [3] Qi et al., ibid, 2004.

ACKNOWLEDGEMENTS

The project was supported by Whitaker Foundation RG-01-0482.

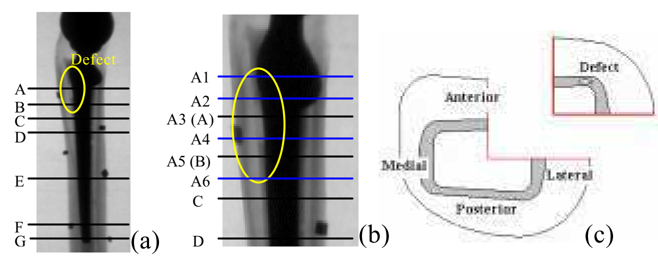

Fig. 1. (a) X-ray of the specimen, sectioned at A to G. (b) Six virtual sections (A1 to A6). (c) Anterolateral quadrant of A3.

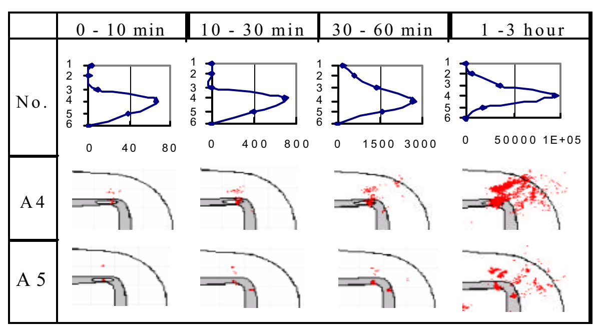

Fig. 2. Number of MC cumulated in A1 to A6, (represented by 1 to 6) and their distribution (A4 to A5) in the first 3 hours.

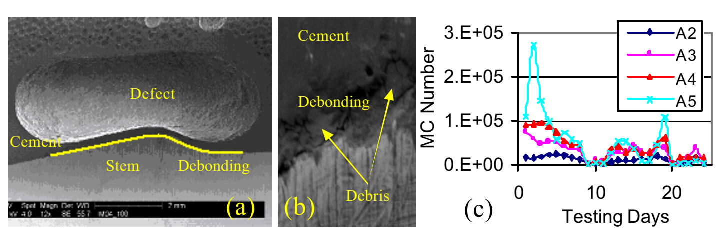

Fig. 3. (a) ESEM image of the defect with debonding marked by yellow curve (12×). (b) Details of the debonding (333×). (c) Number of MCs occurred in A2 to A5.

OPTIMISED TUMBLING PERFORMANCES THAT ARE ROBUST TO PERTURBATIONS

Mark A. King and Maurice R. Yeadon
Loughborough University; email: M.A.King@lboro.ac.uk, web: www.lboro.ac.uk

INTRODUCTION

Determining optimum tumbling performance in artistic gymnastics has previously focused on maximising somersault rotation in simulations, with a double straight somersault being possible [1]. Gymnasts may develop their optimum performance in a different way, however, since their technique must have some robustness to perturbations. Therefore using an optimisation criterion that merely maximises somersault rotation in a simulation is unlikely to give a realistic solution. In particular there is no guarantee that such an optimum simulation will be robust to small perturbations of the touchdown conditions and the technique used. The aim of this paper is to determine the effect of incorporating perturbations of technique into the optimisation of simulated tumbling performance.

METHODS

A planar five-segment model was developed with torque generators at each joint for simulating the foot contact phase in tumbling. The elastic properties of the interface between the feet and tumbling track were represented by horizontal and vertical massless damped linear springs (Figure 1).

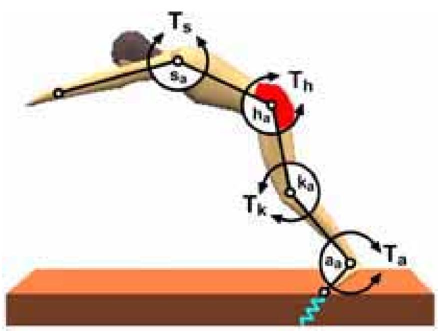

Figure 1: A five segment simulation model of the foot contact phase in tumbling.

The model was customised to an elite gymnast by determining subject-specific segmental inertia and joint torque parameters. Anthropometric measurements of an elite gymnast were taken and segmental inertia parameters were calculated using a mathematical model [2]. Torque measurements were taken during eccentric-concentric movements at the ankle, knee, hip and shoulder joints using an isovelocity dynamometer (KinCom 125E), with crank angular velocities ranging from 20°/s to 250°/s, in order to express torque as a function of joint angle and angular velocity [3].

A performance of a double layout somersault was used to provide initial conditions for simulations. Maximising rotation potential (angular momentum × flight time) subject to a flight time constraint (greater than the actual performance) produced sufficient somersault rotation for a double straight somersault [3]. This original optimised simulation was then perturbed by varying the initial conditions (body orientation ±3°, linear momentum ±3% and angular momentum ±3%), and the onset activation times (±20ms) of the knee and hip torque generators in order to determine its robustness to perturbations. Two modified optimisations were then carried out with the perturbations to the initial conditions and the onset activation times included in the optimisation procedure (lowest rotation potential score chosen for each combination of parameters and simulations with flight times less than that of the actual performance discarded).

RESULTS AND DISCUSSION

The optimisation for robustness to perturbations of initial conditions had 4% less rotation potential than the original optimisation while the onset time optimisation had 3% less rotation. Perturbing the initial conditions for the original optimised simulation and the two robust optimisations resulted in maximum reductions in rotational potential of 5%, 5% and 5% respectively. Perturbing onset times to the torque generators resulted in reductions in rotation potential of 3%, 2% and 1% respectively. The flight times for the perturbed original optimisation were as much as 6% less than in the actual performance while the flight times for the perturbed robust optimisations were all greater than the actual flight time. In summary, including perturbations within the optimisation procedure resulted in simulations that had less rotation potential but were more robust (in terms of rotation potential and flight time) to perturbations than the original double straight optimum simulation.

CONCLUSIONS

When maximising performance it is important that the robustness of the optimum simulation to perturbations is considered and is included in the formulation of the optimisation procedure used. Failure to do this can result in maximal solutions that are unrealistic and not achievable. In the development of such gymnastic skills it is likely that robustness and consistency are an inherent part of optimised performance. Considerations of robust and consistent performance may therefore have parallels in both motor learning and evolution.

REFERENCES

1. King MA, et al. *J Biomech* **37**, 471-479, 2004.
2. Yeadon MR. *J Biomech* **23**, 67-74, 1990.
3. King MA, et al. *J App Biomech* **18**, 207-217, 2002.

Different Motor Planning During Eccentric and Concentric Elbow Muscle Contractions

Yin Fang, Vlodek Siemionow and Guang H. Yue
Biomedical Engineering Dept. The Cleveland Clinic Foundation
Email: fangy@bme.ri.ccf.org

INTRODUCTION

Eccentric contractions are characterized by greater force production but lower muscle activation, depressed monosynaptic reflex excitability, reduced ability to fully activate the working muscle, motor unit recruitment strategy altered from the "size principle", reduced stability of the movement, and greater susceptibility to muscle tissue damage. The results of many studies suggest that the CNS may control concentric and eccentric muscle actions differently though direct evidence is few. The purpose of this study was to measure electroencephalography (EEG)-derived movement-related cortical potential (MRCP) during the two types of muscle actions and determine if the level and timing of cortical activation differ between eccentric and concentric human elbow flexor contractions.

METHODS

Eight right-handed men (29.13 ± 2.36 years old, range 26-31 years) participated in the study performed on Kin-Com isokinetic dynamometer. They performed 40 maximum voluntary concentric contractions (when exerting elbow flexion force against the lever arm and rotating it toward the body) and 40 eccentric contractions (when lever arm rotating away from the body). Surface EMG signals were recorded from the biceps brachii (BB), brachioradialis (BR), triceps brachii (TB), and deltoid (DT) muscles. Scalp EEG signals were simultaneously recorded by a 64-channel NeuroScan EEG system. The force, EMG, and EEG data were trigger-averaged across the 40 trials and movement related cortical potential was derived. Two dimensional MRCP mapping was draw based on the mean value of the entire group.

RESULTS AND DISCUSSION

The force exerted by the subjects during eccentric MVCs (210.63 ± 94.68 N) was significantly higher ($P < 0.05$) than the force during concentric MVCs (184.06 ± 87.07 N). The EMG of the major elbow flexor muscles (BB) during eccentric

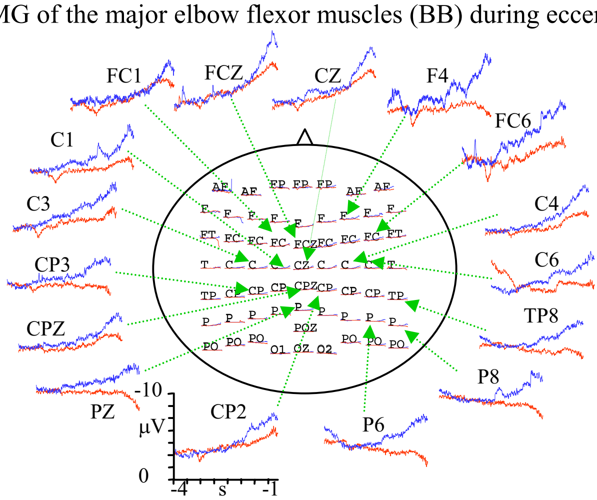

Figure 1: A multi-channel display of MRCP for concentric (red) and eccentric (blue) muscle activities.

contraction (321 ± 175 µV) was significantly lower ($P < 0.01$) than the EMG of the muscle during concentric contraction (447 ± 264 µV). A majority of electrodes showed a greater NP for eccentric than concentric movements in the brain potential maps (Fig 1). Detailed analysis suggested there is a bigger brain activation area for eccentric than concentric movements, and the activation starts earlier (from MRCP start to EMG start) when compared with concentric movements (Fig 2).

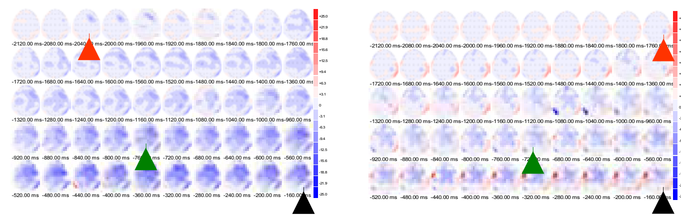

Figure 2: Group average of topographical maps of cortical potential (µV) showing spatial and temporal distributions of electrical activity at the cortical surface for eccentric (left panel) and concentric (right panel) contractions. Red arrow: MRCP onset; Green arrow: EMG onset; Black arrow: Movement onset;

Our data imply that the level of cortical activation was substantially higher and the preparation time was significantly longer for eccentric than concentric tasks during the specific planning and execution phases of the controlling process. Several factors related to distinct eccentric characteristics might contribute to these different cortical activities. It is well known that eccentric muscle contractions induce greater tissue damage than do concentric muscle activities [1]. The adaptive changes following repetitive eccentric training may be an indication of CNS-modulated adaptations to protect muscle from further injury [2]. The unusual brain activities could be the results of such adaptation. Eccentric contraction is also more difficult to control than concentric ones, represented by greater force fluctuation and more EMG spiking [3]. Greater voluntary effort is required when a person performs a motor task that is more difficult to control. Associated with this difficulty is that the motor unit pool cannot be fully activated during maximal voluntary eccentric contraction [4]. This incapability to fully activate motor units could also related to some mechanism protecting muscle tissue from damage, since more force would be generated while the motor unit pool was fully activated.

REFERENCES

1. Fridén J, et al.. *Int J Sports Med* **4**: 170-176, 1983.
2. Westing SH, et al.. *Acta Physiol Scand* **140**: 17-22, 1990.
3. Owings TM, et al.. *Isokinetics in Human Performance.* Champaign: Human Kinetics. 209-228, 2000.
4. Sale DG. *Med Sci Sports Exerc* **20(Suppl)**: S135-S145, 1988.

METHODS TO MEASURE STATIC COEFFICIENT OF FRICTION BETWEEN HAND AND OTHER MATERIALS

Na Jin Seo, Thomas J Armstrong, Philip Drinkaus
University of Michigan; email: najins@umich.edu

INTRODUCTION

The friction between hand and other materials affects our ability to grasp and manipulate objects. Friction data are needed for the design of tool/consumer products, job analysis, and workstation design. This coefficient of friction is difficult to measure consistently, because it is affected by many factors including: contact force, hydration [1], area of contact, contaminates [2], and direction [3]. The purpose of this study is to develop a simple method of measuring the static coefficient of friction between skin and other materials so that this information can be readily calculated in the field.

METHODS

The proposed method is referred to as the "tilt" method. A flat plate is held in the hand. The hand is then tilted at a steady rate until the plate begins to slide. The static coefficient of friction (μ_s) is equal to the ratio of the shear (friction) force (F_f) to the contact (normal) force (F_n) just before the object starts to move.

F_f is equal to $W\sin\theta$ and F_n is equal to $W\cos\theta$, where W is the weight of the plate and θ is the angle of the plate with respect to the horizontal at the time the plate begins to slide. It can be shown that μ_s is approximately equal to $\tan\theta$.

The standard method entails holding the flat plate on the hand as in the tilt method, but the plate is attached to a force transducer. The subject then increases the horizontal force on the plate until it begins to slide. The μ_s is then calculated as the ratio of the F_f (measured by force transducer at the time the plate begins to slide) to its weight.

Independent variables for the tilt method were: contact area (fingertips vs. flat palm), materials (rubber (Rb), aluminum (Al), cardboard (Cb)), and plate weights (10, 20, 30N). The average F_n and shear force buildup rate (dF_f/dt) at which slippage occurs were calculated for each condition (subjects pooled). The F_n values ranged from 4.2–27N. The dF_f/dt values ranged from 0.8–5.4 N/s. Using the results from the tilt method, the appropriate F_n and dF_f/dt were chosen for each material and contact area, and used for the standard method. The dependent variable was μ_s. Subjects were allowed to practice tracking a constant dF_f/dt by following a bar indicator.

5 university students (3 males, 2 females) volunteered to participate. To remove possible contaminants, subjects washed their hands with soap and rinsed with tap water. They dried their hands with paper towels and air dried for 15 minutes. Each condition was tested 3 times, and trials were randomized.

RESULTS AND DISCUSSION

The μ_s measured by the tilt and standard method for each F_n and material is shown in Figure 1.

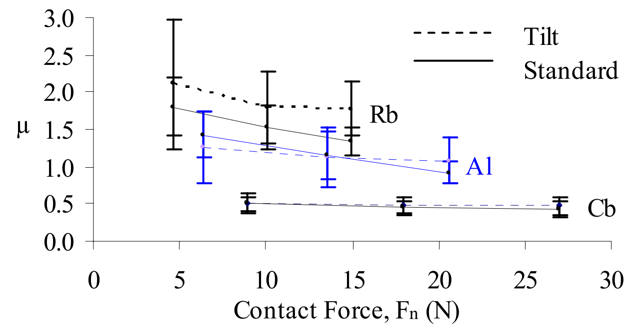

Figure 1: Static coefficient of friction from "tilt" and standard method between palmar skin and three different materials for different F_n's (contact area and subjects pooled, Rb: rubber, Al: aluminum, Cb: cardboard).

Analysis of variance revealed that the μ_s's from the tilt and the standard methods were not statistically different (p>0.05).

The μ_s's decreased with increasing F_n (p<0.05), as observed in the previous studies [1,2,3]. The relatively high μ_s's (2.11±0.88, for the tilt method with Rb) may have resulted from the low F_n's tested.

The μ_s's of fingertips were lower than those of the flat palm. This difference was statistically significant for Rb and Al, while only a trend was observed for Cb. This trend that a narrower skin contact area tended to have a lower μ_s than a wider contact area under clean skin condition was also observed in [2], even though a different material and kinetic coefficient of friction were investigated in [2].

In this study, the μ_s's for Al and Cb were found 1.15±0.37 and 0.48±0.12, respectively (F_n, contact area, method pooled). These values were higher than those calculated from the regression model in [1]: 0.39 and 0.30 for Al and paper, respectively (F_n pooled). This could be due to the difference in skin contact area, since only an index finger and a thumb were used in [1]. Higher values for dF_f/dt and F_n in [1] (15N/s and 22–39N, respectively) could also be the reason for the large difference in μ_s's between the two studies. The dF_f/dt was controlled in this study. However, the effect of different dF_f/dt on μ_s needs to be investigated.

The tilt method is easy to perform, and can be performed in the field. This provides timely, relevant information about μ_s in the workers' environment.

REFERENCES

1. Buchholz B, et al. *Ergonomics* **31**, 317-325, 1988.
2. Bobjer O, et al. *Applied Ergonomics* **24**, 190-202, 1993.
3. Bullinger HJ, et al. *Bundesanstalt für Arbeitsschutz und Unfall-forscung,* Dortmund, Germany, 1979.

TEMPERATURE-DEPENDENT MECHANICAL PROPERTIES OF HUMAN SOLEUS MUSCLE FIBERS

Sampath K. Gollapudi[1] and David C. Lin[1,2,3]

[1]Dept. of Mechanical and Materials Engineering, [2]Programs in Bioengineering and Neuroscience, [3]Dept. of Veterinary and Comparative Anatomy, Pharmacology and Physiology, Washington State Univ., Pullman, WA, USA
Email: sampath@vetmed.wsu.edu

INTRODUCTION

Temperature-dependent mechanical properties of different skeletal muscle fibers (slow and fast) are related to the differences in their crossbridge kinetics [1]. Previous studies have employed complex multi-state crossbridge models for analysis of temperature-dependent mechanical properties, mostly in isometric condition and for shortening contractions. There has been no study of the variations in contractile properties during lengthening contractions at different temperatures. This study will record the lengthening and shortening force-velocity (F-V) data from human type I fibers at different temperatures to examine the variations in these properties within the context of a simplified Huxley's two-state crossbridge model [2]. Also, this study will serve as the experimental basis of how to utilize data obtained at lower temperatures to extend the model to *in vivo* temperatures.

METHODS

Single fibers were chemically skinned and dissected free from biopsies of human Soleus muscles. Institutional Review Board approval was obtained for these procedures. Fibers were attached between the force transducer and motor hooks via aluminum foil T-clips. The initial sarcomere length of all fibers in relaxing solution was set to 2.2 µm, and each fiber is maximally activated in a Ca++ solution at a specific test temperature (10, 15, and 20^0 C). A perturbation was then applied as a linear change in force (force ramp) for both lengthening and shortening contractions to measure the F-V behavior. For this study, a total of 15 type I fibers have been measured. Each fiber was later analyzed by gel electrophoresis for myosin heavy chain type.

RESULTS AND DISCUSSION

Figure 1 shows the averaged F-V curves for human Soleus fibers during lengthening and shortening contractions across all trials at 10^0 C (n=5), 15^0 C (n=5) and 20^0 C (n=5). In all these fibers, a good homogeneity of the sarcomere pattern was maintained after repeated activations. These experimental curves clearly demonstrate that the mechanical properties of both shortening and lengthening contractions are quite sensitive for changes in temperature. A temperature rise from 10^0 C to 15^0 C causes an increase of ~43% in the maximum shortening velocity during shortening and an increase of ~135% during lengthening, thereby affecting the muscle's peak power production. A similar trend can also be observed among these properties at higher temperature steps.

By simulating the Huxley's crossbridge model for these ramp pertubations, it is possible to estimate the model parameters (crossbridge attachment rate, *f* and detachment rate parameter,

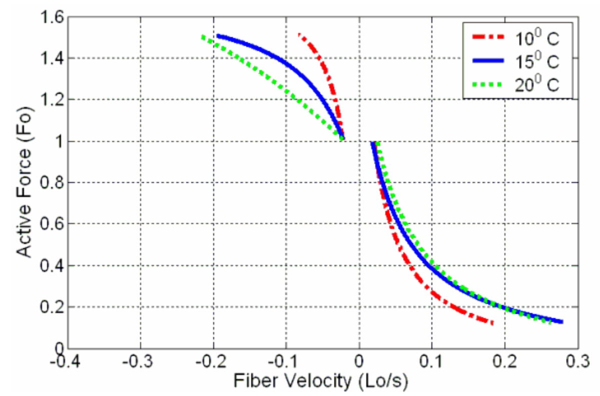

Figure 1: Averaged F-V curves at 10^0 C, 15^0 C and 20^0 C. Positive velocity is shortening.

g) [3]. These analyses provide valuable information about how crossbridge kinetics at the microscopic level influences macroscopic behavior. Also, these data at lower temperatures can be used to extrapolate *in vivo* function at physiological temperature. Furthermore, this study can be extended to investigate the temperature-dependent mechanical behavior of fast (Type II) fibers. These data would be critically important in understanding the differences of distinct muscle fiber types at both the microscopic and macroscopic levels [4].

SUMMARY

Mechanical properties of human Soleus (type I) muscle fibers are found to be highly-temperature sensitive. Specifically, both the lengthening and shortening force-velocity relationships were found to vary with the test temperature. These data will be used with a simplified crossbridge model to tie the temperature controlled biophysical experimental data to macroscopic force predictions. A need to further extend this study to *in vivo* temperatures is also justified in order to better understand the differences in contractile properties among various fiber types.

REFERENCES

1. Gollapudi, S. K., and Lin, D. C., *Proceedings of ASB 28th Meeting*, Portland, OR, USA, 2004.
2. Zahalak, G. I, *Mathematical Biosciences*, Vol. **55**: p. 89-114, 1981
3. Lin. D. C., and Nichols T. R., *Transactions of the ASME*, Vol. **125**: p. 132-140, 2003
4. Bottinelli. R., Canpari. M., Pellegrino. M. A., Reggiani, C., *Journal of Physiology*, **495.2**: p. 573-586, 1996

ACKNOWLEDGEMENTS

Support provided by the Whitaker Foundation.

FUNCTIONAL FATIGUE DECREASES THREE-DIMENSIONAL MULTIJOINT POSITION REPRODUCTION IN OVERHEAD ATHLETES

Brady Tripp, Tim Uhl, Carl Mattacola, Cidambi Srinivasan, Robert Shapiro
University of Kentucky; E-mail: brady_tripp@yahoo.com

INTRODUCTION

The sensorimotor system (SMS) is responsible for providing the awareness, coordination and feedback to maintain stability and function. Therefore, acuity of this system is a major component of injury-free athletic performance. Evidence suggests that muscular fatigue [1,2] and injury [3] compromise SMS function in the upper-extremity. However, investigations of joint position sense often employ methods that hamper our ability to apply results to functional activity. The purpose of this study was to examine the effect of functional fatigue on unconstrained, multijoint position reproduction of the upper-extremity. We measured position reproduction acuity of the upper-extremity as a functional unit and acuity of four individual joints.

METHODS

We used a single-session repeated-measures design. Subjects consisted of 16 healthy male NCAA baseball players (21.0 ± 1.6 years, 175.8 ± 10.2 cm, 82.8 ± 4.3 kg). We recorded position of the throwing-side thorax, scapula, humerus, forearm and hand using an electromagnetic tracking device (Ascension Technology, Burlington, VT, USA) and MotionMonitor software (Innovative Sports Training, Chicago IL). We blindfolded subjects and tested their ability to reproduce two self-selected upper-extremity positions (arm-cock and ball-release) before and after a fatigue protocol. Subjects were in a single-knee stance position for the testing and throwing protocol. Subjects identified a target position followed by three-reposition trials. The functional fatigue protocol was a single bout of throwing a baseball at a target with maximum velocity (1 every 5 seconds). After every 20 throws, subjects rated their local (upper-extremity) exertion level on the Borg Rating of Perceived Exertion scale [4]. We considered subjects fatigued after reaching a level greater than 14. Immediately after the throwing protocol, we retested participants in the same manner as prefatigue measures. Post-testing began within 1 minute after completion of the throwing protocol and both positions were completed within 3 minutes. We calculated 3-dimensional variable error scores (3DVE) to represent overall reposition acuity for each arm position using hand position in relation to the thorax. We calculated additional 3DVE scores for each individual joint (scapulothoracic, glenohumeral, elbow and wrist).

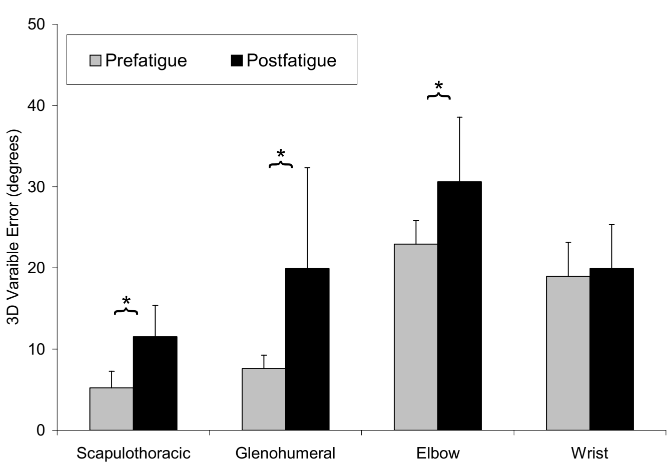

Figure 1: Comparison of prefatigue to postfatigue acuity scores (3DVE) for the arm-cock position.
* Significant difference between conditions ($P < 0.05$)

RESULTS AND DISCUSSION

Subjects were fatigued after 62 ± 28 throws. We used Wilcoxon matched-pairs sign-rank tests to compare prefatigue to postfatigue error scores. Fatigue had a significant effect on position reproduction acuity (increasing 3DVE scores) for the arm-cock (12.4 to 24.1mm) and ball-release positions (20.8 to 41.7mm) ($P < .001$). Comparisons of prefatigue 3DVE scores for scapulothoracic, glenohumeral, elbow and wrist joints with postfatigue reveal decreased acuity for both the arm-cock (Figure 1) and ball-release (Figure 2) positions.

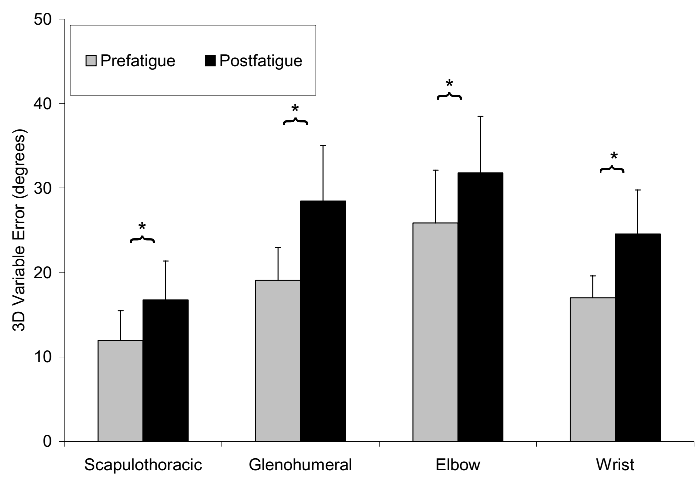

Figure 2: Comparison of prefatigue to postfatigue acuity scores (3DVE) for the ball-release position.
* Significant difference between conditions ($P < 0.05$)

CONCLUSIONS

Using multijoint, 3-dimensional measures and a functional throwing protocol, we demonstrated fatigue reduced 3D position reproduction acuity in both positions tested and at multiple upper-extremity joints. Our results indicate that after prolonged throwing, SMS deficits effect the entire upper-extremity and may put multiple joints at risk for injury.

REFERENCES

1. Carpenter JE, et al. *Am J Sports Med* **26**, 262-265, 1998.
2. Myers JB, et al. *J Athl Train* **34**, 362-367,1999.
3. Lephart SM et al. *J Shoulder Elbow Surg* **3**, 371-380, 1994.
4. Borg G. *Borg's Percieved Exertion and Pain Scales,* Human Kinetics, Champaign, Il. 1998.

THE MECHANICS OF JUMPING VERSUS STEADY HOPPING IN YELLOW-FOOTED ROCK WALLABIES

[1] Craig P. McGowan*, [2]R. V. Baudinette and [1]A. A. Biewener
[1]Concord Field Station, Harvard University, Bedford, Massachusetts, USA
[2]Department of Zoology, University of Adelaide, Adelaide, South Australia, AU
*e-mail: cmcgowan@oeb.harvard.edu

INTRODUCTION

Previous work has suggested that a musculoskeletal design that favors elastic energy recovery, like that found in wallabies and kangaroos, may be constrained in the ability to generate mechanical power [1]. Yet rock wallabies regularly make large jumps while maneuvering through their environment. The goal of our study was to explore the mechanical power requirements associated with jumping in yellow-footed rock wallabies and to determine how these requirements are achieved relative to steady speed hopping mechanics. As jumping can be a high power activity, we hypothesized that yellow-footed rock wallabies would be able generate substantial amounts of mechanical power.

METHODS

Four adult yellow-footed rock wallabies, *Petrogale xanthopus* (one male and three female, ranging from 5.10 to 5.50 kg body mass) were trained to hop through a straight runway with no obstacles and through a runway containing a jump 1.10m high. High-speed video recordings (Photron Fastcam-X 1280 PCI) and ground reaction force measurements from a runway mounted force platform (Kistler type 9286AA) were used to calculate whole body power output and to construct a simple mass-spring type model to determine whole limb mechanics. The combined mass of the hind limb extensor muscles was used to estimate muscle mass-specific power output.

Changes in mechanical energy and whole body power outputs were calculated via integration of the vertical and horizontal ground reaction forces [2]. The legs were modeled as a spring in series with a linear actuator and the body was considered to be a point mass located at the ilium point, which was a proxy for the position of the CoM. The actuator in this model can only produce positive work, and it is assumed that all of the negative energy associated with leg spring compression is recovered elastically. Leg stiffness was determined at the point of maximum leg compression.

RESULTS AND DISCUSSION

Net extensor muscle power outputs averaged 155 W kg^{-1} during steady hopping and 495 W kg^{-1} during jumping (Figure 1). The highest net power measured reaching nearly 640 W kg^{-1}. As these values exceeded the maximum power producing capability of vertebrate skeletal muscle [3], it was determined that back, trunk and tail musculature likely played a substantial role in contributing power during jumping. Inclusion of this musculature produced a maximum power output of 452 Wkg^{-1} muscle.

Similar to human high-jumping, rock wallabies used a moderate approach speed (not significantly different than steady hopping) and a relatively shallow leg angle of attack (45-55º) during jumps [4]. Leg stiffness increased nearly twofold in jumping (steady: 2.98 kN m^{-1} vs. jumping: 5.50 kN m^{-1}), which facilitated the transfer of horizontal kinetic energy into vertical kinetic energy. Time of contact was maintained during jumping despite greater leg stiffness and smaller leg excursions by a substantial extension of the leg, which kept the foot in contact with the ground. Additionally, rock wallabies appeared to minimize potential pitching moments by adjusting their leg angle to match the angle of ground reaction force vector.

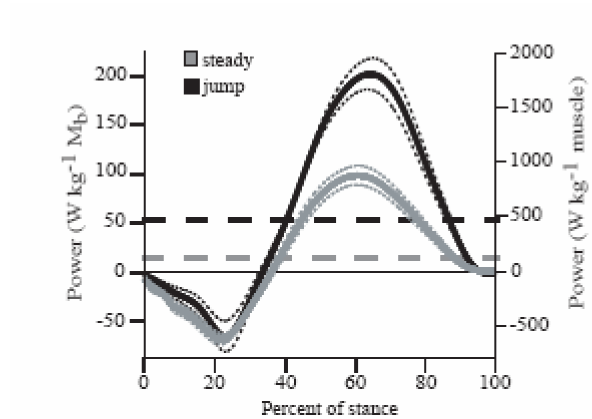

Figure 1. Mean power output during stance normalized to body mass (M_b, left axis) and hind limb extensor muscle mass (right axis). Horizontal dashed lines represent the net power produced during stance.

CONCLUSIONS

Our results clearly show that rock wallabies are capable of producing very high power outputs. For the jumps recorded in this study, estimates of muscle mass-specific power output (450 W kg^{-1} muscle) suggest that all of the musculature of the legs, back and tail were recruited to produce jumps and that power output is near the maximum expected for vertebrate skeletal muscle. However, whether this comes at the expense of tendon and aponeurosis strain energy savings by rock wallabies during steady level hopping requires a more detailed kinetic analysis of their level hopping mechanics.

REFERENCES

1. Biewener, A. A. *Amer. Zool.* **38**, 703-717, 1998.
2. Cavagna, G. A. *J. Applied Physiol.* 39,174 -179, 1975.
3. Weis-Fogh, T. and Alexander, R. McN. *Scale Effects in Animal Locomotion.* ed. Pedley, T. J. Chapter 30. New York: Academic Press, 1977.
4. Alexander, R. McN. *Phil. Trans. R. Soc. Lond.* B **329**, 3-10, 1990.

ARM FRACTURE IN CHILDREN'S FALLS

[1]Peter L. Davidson, [1]David J. Chalmers and [2]Barry D. Wilson
[1]Department of Preventive and Social Medicine, [2]School of Physical Education
University of Otago, Dunedin, New Zealand; email: peter.davidson@ipru.otago.ac.nz, web: www.otago.ac.nz/ipru/

INTRODUCTION

Arm fractures in children are a significant public health problem in New Zealand and other industrialized nations. Computer simulation has been used to model the risk of arm fracture in children as a function of fall height, surface stiffness and damping, child age and fracture history; taking into account physical properties of children such as body weight, arm stiffness, bone density and bone size [1]. This 'biomechanical impact model' generated a 'Factor of Risk' (FR) ratio of the impact force to the fracture force. The model was validated using data gathered for an epidemiological case-control study of falls from playgrounds [2]. The FR values were found to be significantly associated with the actual fracture probability (FP) and an 'injury risk curve' was generated to predict fracture probabilities for given values of FR [3]. The purpose of the current study was to use the biomechanical impact model and the injury risk curve to predict distal radius fracture for a series of playground fall scenarios. This study assessed the risk relationship between child age, equipment heights and surfaces currently used in playgrounds in New Zealand and other countries with the aim of providing information on which to recommend measures for reducing arm fractures in falls from playground equipment.

METHODS

Playground fall scenarios were defined by child age (5, 9 and 13.5 years of age), fall height (0.5 to 3m at 0.5 m intervals), and surface type. The surface types are listed in Table 1. These scenarios were chosen to represent the range of fall situations that are expected to be encountered at typical playgrounds. FR values were generated for each of the fall scenarios using the biomechanical model, with FR being the estimated impact force (based on the child's age and mass; fall height and surface impacted) divided by the estimated fracture force (based on the child's age and fall height dependent strain rate). The biomechanical model is a rheological two-mass model with the wrist and shoulder joints represented as linear spring and damper elements [1, 4]. The impact properties of childrens' joints were derived from a gymnastic study of head-first wrist impacts [5] and surfaces were modeled as linear or exponential springs [3]. Presented here are analyses conducted for the high-frequency force component representing the initial hand impact. FP values as a function of FR were derived from the injury risk curve (Figure 1) [3].

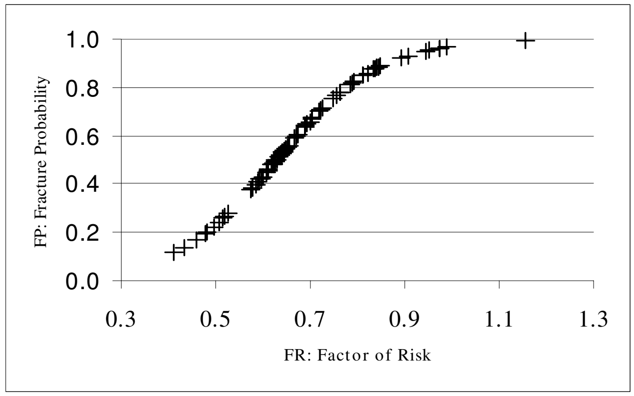

Figure 1: Injury Risk Curve [3].

RESULTS AND DISCUSSION

The fall scenarios for a child aged 9 are listed in Table 1. Surfaces are listed in order of decreasing risk. Earth, grass, rubber mats and dry 15cm deep bark chips produced very similar risks. Wet bark produced a lower risk compared to dry bark, likely due to an increased energy absorbing capacity. The scenarios for ages 5 and 13.5 years of age produced similar pattern of results but with lower and higher values respectively, compared to 9 years of age. Risk increased dramatically with fall height with 3m falls having a high probability of arm fracture. Due the limitations of the case-control study upon which the injury risk curve was based; the model is limited to falls onto a single arm and that are serious enough to require attention (medical or reassurance) by a caregiver.

CONCLUSIONS

This study showed that non-rigid surfaces typically used playgrounds give similar risks of fracture and this risk reached high values for 3m fall heights. This study demonstrates how the biomechanical model is a valuable tool in evaluating interventions aimed at reducing arm fractures in children.

REFERENCES

1. Davidson PL et al. *Comp. Meth. Biomech. Biomed. Eng*. **7**:2, 63-71, 2004.
2. Chalmers DJ et al. *Inj. Prev*. **2**:2, 98-104, 1996.
3. Davidson PL et al. *J. Biomech*. in press, 2004.
4. Chui J et al. *J. Biomech*. **31**, 1169-1176, 1998
5. Davidson PL et al. *J. Appl. Biomech*. in press, 2004.

Table 1: FP values as a function of fall height and surface type for a child 9 years of age (D: dry; W: Wet; 15 & 30: cm depths)

Fall Height (m)	Impact Surface Type							
	Rigid	Earth	Grass	RubberMat	Bark D15	Bark W15	Bark D30	Bark W30
0.5	0.16	0.11	0.11	0.10	0.09	0.08	0.08	0.06
1.0	0.45	0.30	0.29	0.28	0.25	0.23	0.22	0.17
1.5	0.71	0.55	0.54	0.52	0.50	0.44	0.41	0.32
2.0	0.86	0.73	0.74	0.71	0.70	0.64	0.59	0.49
2.5	0.94	0.87	0.87	0.84	0.82	0.78	0.74	0.66
3.0	0.96	0.93	0.93	0.91	0.90	0.87	0.83	0.77

Simulating Pathological Gait using the Angular Momentum Inducing Inverted Pendulum Model

[1]Taku Komura, [2]Akinori Nagano
[1]Department of Computer Engineering and Information Technology,
City University of Hong Kong
Email:taku@ieee.org

[2]Computational Biomechanics Unit, RIKEN
Email: a-nagano@riken.jp

INTRODUCTION

In this study, we propose a new method to simulate human gait motion when muscles are weakened. The method is based on the enhanced version of 3D linear inverted pendulum model that is used for generation of gait in robotics. After the normal gait motion is generated by setting the initial posture and the parameters that decide the trajectories of the center of mass and angular momentum, the muscle to be weakened is specified. By minimizing an objective function based on the force exerted by the specified muscle during the motion, the set of parameters that represent the pathological gait was calculated. By using our method, it is possible to find out the general idea how an impairment of a muscle can affect biped gait. By doing further concise modeling of the musculoskeletal and development of techniques to import parameters from individual humans, it will be possible to use the proposed method for analysis, diagnosis, and rehabilitation training of patients with impairments at the muscles. The effects of weakening the gluteus medialis were analyzed. Important similarities were noted when comparing the predicted pendulum motion with data obtained from an actual patient

METHODS

The 3D Linear Inverted Pendulum Mode [1], a method to plan biped locomotion of robots, was enhanced so that angular momentum can be generated around the center of mass. Since angular momentum is consistently generated around the center of mass when human perform gait motion, this function is essential to generate gait motion similar to humans. This model is called Angular Momentum inducing inverted Pendulum Model (AMPM). Using AMPM, the human gait was modeled. We then introduce a method to combine using the musculoskeletal model with AMPM. A musculoskeletal model based on Delp's data [2] was prepared to estimate the muscle force by using static optimization [3]. The gait motion was first modeled using AMPM, and then the motion was tuned by changing the parameters that define the behavior of AMPM by optimizing a criteria based on the musculoskeletal dynamics.

RESULTS AND DISCUSSION

To examine the validity of the method proposed in this paper, we have generated normal and pathological human gait motion using our method, and compared the kinematical and dynamical data with those by humans. A set of AMPM parameters that produce a gait motion with a step length of 0.6 m and velocity of 1 m/s were used. By minimizing an objective function based on muscle dynamic, the effects of weakening the gluteus medialis, was simulated. As the optimization proceeds, features known as lateral trunk bending appears in the motion. The trunk swings from one side to the other, producing a gait pattern known as waddling. During the double support phase, the trunk is generally upright, but as soon as the single support phase begins, the trunk leans over the support leg, returning to the upright attitude again at the beginning of the next double support phase.

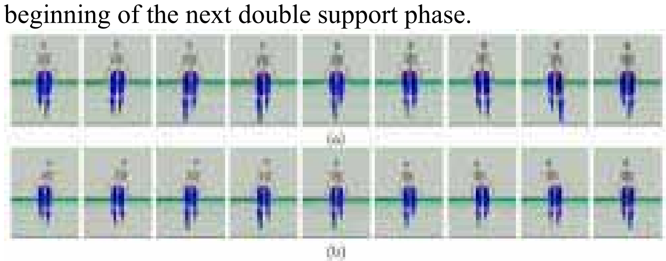

Figure 1 The trajectory of the AMPM-generated motion before (a) and after (b) the optimizing an objective function based on gluteus medialis.

The method proposed in this study has the following advantages compared with previous methods:

- Since the gait motion is described by the AMPM parameters, there is no need to specify all the input parameters of the muscles. As a result, the computational cost for the optimization is much less than previous methods.
- As the balance of the human body model is explicitly kept by using the AMPM model, the optimizer only needs to search for the optimal set of parameters in terms of muscle force, and hence does not need to go through a large number of trials to generate the balanced motion.

REFERENCES

1. Kajita S, Matsumoto O and Saigo M, *Real-time 3D walking pattern generation for a biped robot with telscopic legs* Proceedings of the 2001 IEEE International Conference on Robotics and Automation, pp2299-2306, 2001
2. Delp SL. *Surgery simulation: a computer graphics system to analyze and design musculoskeletal reconstructions of the lower limb.* Dissertation. Stanford University, Stanford, CA, USA, 1990.
3. Crowninshield RD and Brand RA, *A physiologically based criterion of muscle force prediction in locomotion,* Journal of Biomechanics, vol. 14, pp793-800, 1981

ACKNOWLEDGEMENTS

The work described in this paper was partially supported by a grant from City University of Hong Kong (Project No. 7001743).

ADAPTIVE CHANGES IN LOWER LIMB COORDINATION IN RESPONSE TO UNILATERAL LOADING DURING TREADMILL LOCOMOTION

Jeremy W. Noble and Stephen D. Prentice
Gait and Posture Lab, Department of Kinesiology, University of Waterloo, Waterloo, ON, Canada.
email: jwnoble@uwaterloo.ca

INTRODUCTION

In order for the Central Nervous System (CNS) to effectively control the movement of the limbs during locomotion it must have sufficient knowledge of the mechanical properties of the lower limb. With this knowledge the CNS is able to coordinate actions at the three major joints of the lower limb to provide safe and effective locomotion. Previous studies have manipulated limb mechanics by placing an additional mass on the lower limb and reported the changes in limb kinematics and kinetics [1,2]. However none of these studies have examined the resulting disruptions in interjoint coordination in the lower limb when the mechanical properties of the limb were altered. The goal of this study was to determine how interjoint coordination is affected during the adaptation to addition of mass to the limb, and its subsequent removal.

METHODS

Participants (n=8) were instructed to walk on a treadmill moving at 1.56 m/s for three 5 minute trials (PRE, WEIGHT, POST). During the WEIGHT condition a 2 kg mass was placed at the centre of mass of the leg segment of the left lower limb. Bilateral limb and trunk kinematics were obtained from an OPTOTRAK system (Northern Digital Inc., Waterloo ON) and infrared emitting diodes placed on anatomical landmarks defining a seven segment representation of the limbs and trunk.

Segment and joint kinematic time histories were determined using the conventions described by Winter [3] and net joint moments the sagital plane were calculated at the ankle, knee and hip joints during the swing phase using standard inverse dynamics [3]. Time series data from the WEIGHT and POST conditions was then averaged into bins of five consecutive strides so that the time course of the adaptation to the mass could be analyzed. In order to investigate interjoint coordination between the hip and knee joints knee vs. hip angle plots were determined for each stride.

RESULTS AND DISCUSSION

During the PRE condition the Hip vs. Knee angle graphs were similar to those previously reported [4]. With the added mass, there was decrease in knee flexion during the swing phase of the first bin of 5 strides although the range of hip motion was similar to the PRE condition. Once accustomed to the mass the swing phase of the angle-angle plot approached that which was observed in the PRE condition however knee flexion never fully returned to that observed in the PRE condition.

When the mass was removed the peak angles observed at both the hip and knee joints during the swing phase were greater than the PRE condition. There was also a period of additional hip extension during early stance. This extra hip extension during weight acceptance diminished over the first 25 strides of the POST condition.

A

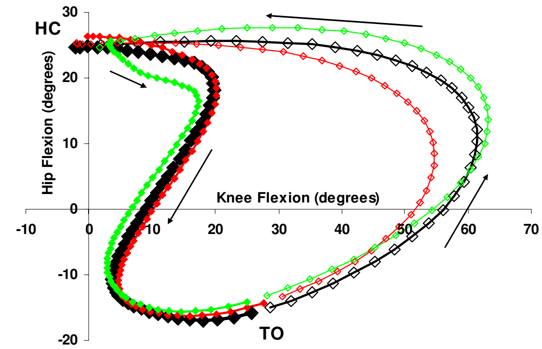

B

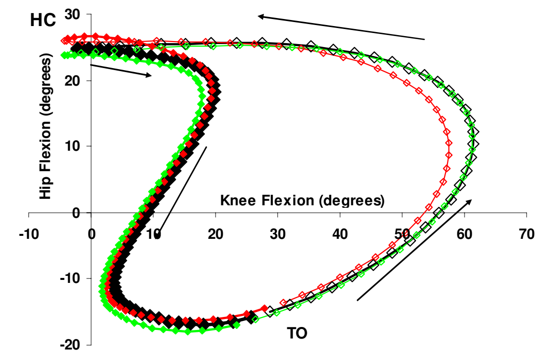

Figure 1: Hip vs. Knee Angle Plots comparing the first (A) and 25th (B) bins of the WEIGHT (Red) and POST (Green) to the mean of the PRE (Black) condition.

CONCLUSIONS

Adaptive changes in knee-hip coordination were observed primarily during the swing phase when the mass would have the greatest effect. Early exposure to the weight (or its removal) brought a disruption to the normal coordination between the knee and hip which returned close to PRE coordination within 25 strides. Additional changes in the coupling between the knee and hip during weight acceptance following the removal of the mass would indicate the influence of swing limb mechanics upon the actions of weight acceptance.

REFERENCES

1. Martin PE et al (2000) IV WCB Calgary AB.
2. Reid MJ & Prentice SD (2001) *Neurosci Res Com* **29:**79-87.
3. Winter DA (1991) The Biomechanics and Control of Human Gait. Waterloo, Waterloo Biomechanics.
4. Hershler C & Milner M (1980) *Am J Phys Med* **59**:109-25.

ACKNOWLEDGEMENTS

Financial support for this project was provided by NSERC

ANKLE MUSCULAR ACTIVITY DURING LANDING IN VOLLEYBALL PLAYERS WITH FUNCTIONAL INSTABILITY

Eneida Yuri Suda[1, 2] , Carla Sonsino Pereira[2] and Isabel de Camargo Neves Sacco[2]
[1] Centro Universitário Capital, Physical Therapy Course
[2] Physical Therapy, Speech and Occupational Therapy Department, School of Medicine, University of São Paulo – São Paulo – Brazil; email: yurisuda@usp.br

INTRODUCTION

The ankle sprain is one of the most common injuries in athletes, particularly in sports in which participants frequently jump and land on one foot like the volleyball. 90% of ankle injuries in volleyball occur during landing after a blocking maneuver. The most common complication following ankle sprains is functional ankle instability (FI) that has been defined as a tendency for the foot to give away after an ankle sprain with no evidence of ligament injuries [1]. The pathogenesis of FI is considered to be multifactorial, with mechanical, muscular, and sensorimotor factors playing a role [2]. The purpose of this study was to compare the muscle activation patterns of selected ankle muscles of volleyball athletes with and without FI performing a landing after the blocking maneuver. We believe that subjects with functional ankle instability present different patterns of muscular activation when compared with normal ones.

METHODS

Nine subjects were studied (age 24.1±3.1 years). Four had complaints of FI with no clinical evidences of mechanical injury and were considered as the functional instability group (FIG). Five subjects had no complaints about instability and had no history of lower limbs injuries and were considered as the control group (CG). All subjects were professional or recreational volleyball players. Surface electromyography were collected from peroneus longus (PL), tibialis anterior (TA) and gastrocnemius lateralis (LG) muscles while subjects performed a jump in the volley blocking. Electrodes were placed on the muscle belly, far away from the innervation zone [3]. The task was performed 8 times and a synchronized electrogoniometer signal placed on the ankle allowed the recognition of the landing phase. The RMS values and temporal variables in linear envelopes, both normalized by each subject's maximal voluntary isometric contraction (MVIC), were obtained for each muscle. The linear envelope's variables obtained were TA maximum peak, TA minimum peak, PL maximum peak and GL maximum peak. Groups were compared using t test for independent samples when normal distribution was present, and Mann-Whitney tests when the data was not normal. We adopted p value lower than 0.05.

RESULTS AND DISCUSSION

Results are displayed in Table 1. The RMS values showed significant differences in TA muscle activation between groups but not in the PL or LG muscles. The PL is a potentially critical muscle in preventing ankle sprains injuries as a protective mechanism to balance inversion [4], but interestingly we observed a significant difference only in the TA muscle: a lower activation in FIG subjects. TA is also an important muscle in preventing ankle sprains by impeding excessive plantar flexion, a primary mechanism in ankle sprain injuries since the inversion movement has a plantar inversion component associated [4]. The linear envelope variables showed that TA has an earlier peak of activation in FIG subjects; therefore this TA activation is statistically lower than the CG. A study showed a decrease in onset latency for the TA muscle after 8 weeks of proprioceptive training [5]. Although our subjects hadn't been specifically trained, they are active athletes and this pattern may be due to a compensatory learning. We can also observe that subjects in FIG had an earlier LG peak of activation than the control ones. This activation can help individuals to diminish impact during landing and it can also be due to a compensatory pattern. If the LG is activated earlier, the TA as an antagonist also has to be active earlier in order to counteract the LG action. This GL earlier activation can also predispose the individuals with FI to an inversion sprain since a more plantar flexion position during landing can predispose the individual to an inversion sprain.

CONCLUSIONS

Our results showed that individuals with FI have a muscle activity pattern that predisposes to an ankle inversion sprain since subjects in FIG showed a lower TA activation during landing when compared to controls. Besides that subjects with FI also showed an activation pattern probably compensatory, with TA and GL muscles activating earlier.

REFERENCES

1. Hertel J. *Sports Med* **29**, 361-371, 2000.
2. Konradsen L. *Knee Surg Sports Traumatol Arthrosc* **8**, 246-251, 2000.
3. Hermens HJ, et al. *J Electromyogr Kinesiol* **10**, 361-374, 2000.
4. Neptune RR, et al. *Med Sci Sports Exerc* **31**, 294-302, 1999.
5. Osborne MO, et al. *Am J Sports Med* **29**, 627-632, 2001

Table 1: RMS values (% of MVIC) and linear envelope variables (% of movement cycle) for TA, PL and LG muscles of CG and FIG.

Muscle	RMS **CG**	RMS **FIG**	p	Envelope variables	CG	FIG	p
TA	**83,51±7,8**	**66,73±3,7**	**0,002***	**TA max peak**	**20,56%±1,429%**	**13,22%±1,85%**	**0,009***
PL	45,12±3,07	49,11±3,45	0,301	**TA min peak**	39,66%±2,256%	44,96%±3,979%	0,56
GL	48,7±3,99	44,2±3,81	0,504	**PL-max peak**	14,47%±1,653%	14,06%±1,912%	0,165
				LG-max peak	**13,90%±1,695%**	**3,125%±1,564%**	**0,000***

SINGLE MOTOR UNIT ACTIVITY IN THE TRAPEZIUS MUSCLES OF ELDERLY FEMALE COMPUTER USERS WITH AND WITHOUT NECK-SHOULDER PAIN DURING COMPUTER WORK

[1] Karen Søgaard, [3]Stefan Thorn, [2]Laura Kallenberg, , [5]Marco Gazzoni, , [3]Leif Sandsjö [4]Peter Schenk, [2]Hermie Hermens, [4]Thomas Laübli , [3]Roland Kadefors, [1] Gisela Sjøgaard, [5]Roberto Merletti
[1]Department of Physiology, National Institute of Occupational Health, Denmark; [2]RRD, Enschede, The Netherlands,
[3]National Institute for working life, Göteborg , Sweden, [4]ETH, Zürich, Switzerland, [5]LISIN, Politecnico di Torino, Italy.
email: ks@ami.dk, web: www.ami.dk

INTRODUCTION

Musculoskeletal disorders in the neck and shoulder regions of female computer users are a major occupational concern in the European countries and the incidence of disorders increases with age and hours of work per week. It has been reported that neck shoulder cases (NS-cases) compared to neck shoulder controls (NS-controls) have a significantly lower muscle strength and a lower muscle activation measured as a lower EMGrms value at the same relative force demand [1]. This finding supports the pain adaptation model supposed to protect the painful muscle from further activity by an inhibitory effect of pain. In contrast, another study has reported an increased trapezius activity during computer tasks in the NS-cases compared to controls evaluated from the total number of motor unit action potentials (MUAP) per second [2]. Such an activity pattern would be in agreement with the vicious circle theory suggesting a pain induced increase in activity in the painful muscle. The aim of the present study was to investigate if the results of a decreased muscle strength and lower activation in a large field study of subjects with and without neck-shoulder pain can be supported by an analysis on single motor unit (MU) level during a typing and editing task in a sub sample of the study population.

METHODS

Two groups of computer users were recruited: 88 NS-cases, who reported trouble in the neck and/or shoulder region for more than 30 days during the last year, and 164 NS-controls who reported trouble in the neck and/or shoulder region for no more than 7 days during the last year. Their mean (SD) values were: age 53 (5) years, height 1.66 (0.06) m, weight 70 (14) kg with no significant difference between NS-cases and NS-controls. An adhesive electrode array composed of eight linearly arranged bar electrodes (size 1x5 mm, 5mm inter electrode distance) was placed on right upper trapezius muscle attempting a position distal to the endplate zone without covering the tendon. Measurements started with a bilateral MVC of the trapezius muscle during shoulder elevation and a 30% MVC test. Further, the subjects performed a 10 min typing and editing task. EMGrms was calculated using an inter electrode distance of 20 mm. On a sub sample of 11 cases and 19 controls MUAP were detected in the typing and editing composite EMG signals with a wavelet based method, separating action potentials from the background noise. MUAP rate is defined as the total number of action potentials divided by the total activity time. A MU was defined when at least 20 action potentials could be allocated to the same MU. Of the total number of action potentials a fraction of 20.8 (19.2) % for cases and 30.8 (18.1) % for controls, could be clustered into single MU.

RESULTS AND DISCUSSION

In the large group of NS-cases and NS-controls a significantly lower MVC was found for the NS-cases (mean 310 (122) N) compared to the NS-control (mean 364 (122) N). In the sub sample the corresponding values were 400 (88) N and 395 (136) N with no significant difference. During the 30% MVC test a significantly lower EMGrms was found both in the large group (NS-cases =194 (105)µV vs. NS-controls 256 (169)µV) and in the sub sample group (NS-cases= 195 (77) µV vs. NS-controls= 248 (93)µV). However, in the more functional typing and editing task similar levels of EMGrms were found in NS-cases and NS-controls. This was supported by the more detailed muscle activity analysis in the sub sample. From the right trapezius muscle a total of 4938 (2836) and 4852 (3480) MUAP per subject was detected in NS-cases and NS-controls, respectively. MUAP rate, the combined measure of MU number and firing rate, was similar, being 10.8 (6.1) MUAP per sec in NS-cases and 11.7 (5.3) MUAP per sec in NS-controls. A total of 22 MU were defined for NS-cases and 44 MU for NS-controls giving a mean of 2 MU per subject in both groups. For each subject mean values of the properties of the detected MU were calculated. Table 1. presents the results as group mean (SD). Only MUAP area was significantly different between the groups.

Table 1.

	NS-Cases	NS-Controls
No. of MUAP per MU	612 (560)	915 (820)
MU Activity duration (s)	312 (173)	258 (163)
MUAP Area (mV*s)	0.774 (0.382)*	1.136 (0.762)
MUAP MPF (Hz)	112 (13)	107 (15)

* indicates significant difference between cases and controls ($p < 0.05$)

CONCLUSIONS.

In the present study lower muscle activation, measured as EMGrms, in NS-cases compared to NS-controls was found both in the large study group and in a sub sample during a 30%MVC. In contrast, for the more functional typing and editing task, neither EMGrms nor MUAP rate, could confirm a lower level of activation in NS-cases. The significantly smaller MUAP area for NS-cases may indicate a selective recruitment of smaller MU or a pain related change in properties such as fibre diameter of the low threshold MU for the NS-cases.

REFERENCES

1.Schulte E et al., *Eur J Appl Physiol,* 2005 (in press).
2. Kallenberg LA et al., *Eur J Appl Physiol,* 2004 (Epub ahead of print).

QUANTIFYING UPPER LIMB MOTOR CONTROL: THE PEG IN HOLE TEST

Germano T. Gomes, Farshid Amirabdollahian, Garth R. Johnson
CREST, University of Newcastle
email: G.T.Gomes@ncl.ac.uk, web: http://www.ncl.ac.uk/CREST

INTRODUCTION

The *I-match* project (www.i-match.org), funded by the European Commission under the Information Society Technologies program, is a three-year project that began in 2002. It focuses on quantifying user's upper limb performance and skills in order to aid in selecting the most suitable interface for use with an assistive device. Within this project a new technique, the 'Peg in Hole Test' was developed making use of virtual reality and haptic robotics in order to access motor control.

The Peg-in-Hole assessment is essentially a 3D movement task presented in a virtual space (Figure 1). It has a simple geometry and objective. It consists of a table with two cylindrical holes and one cylindrical peg that is to be placed in the holes alternately using the hand. It is inspired by the validated, used in clinical assessment, Nine-Hole-Peg-Test [1].

METHODS

The PHANToM haptic interface (SensAble Technologies, USA) was used. It offers 3 active and 3 passive degrees of freedom. The orientation of the virtual peg follows that of the PHANToM stylus in real-time. Shadow cues are used to provide better depth perception and a novel collision detection algorithm was developed, allowing for multiple contacts points between the peg, the table and holes and the walls thus adding realistic touch feeling. The peg insertion and removal is preceded by a guiding arrow and a beep sounds at each successful peg insertion. It is possible to modify, on the fly, the peg diameter, peg height and weight, hole diameter, separation between holes and clearance (peg vs. hole) .

A pilot study involving 12 healthy subjects (6 females, 6 males, age 32 ± 8) was conducted. Subjects were instructed to (starting from mid-position) insert the peg into the left hole, remove it and insert it into the right hole as quickly as possible while trying to minimise the collision with the table and the walls of the holes. This was performed 20 times (10 cycles) before moving to the next experimental setting.

Two virtual tables were selected: one with a separation between holes of 50mm and the other 150mm. The diameter of the holes was set at 20, 30 and 40mm. Two peg weights were used: one with simulated weightless (0 N) and the second with a weight of 0.981N (~100g). The virtual peg diameter was set constant at 10mm. These combined variables made for a total of 12 different testing conditions.

Data was logged at an average sampling frequency of 1000Hz. Forces, positions, orientations and velocities were recorded. In order to exclude learning effects, only 5 full cycles were analysed (cycles 4 to 8) for each of the 12 settings.

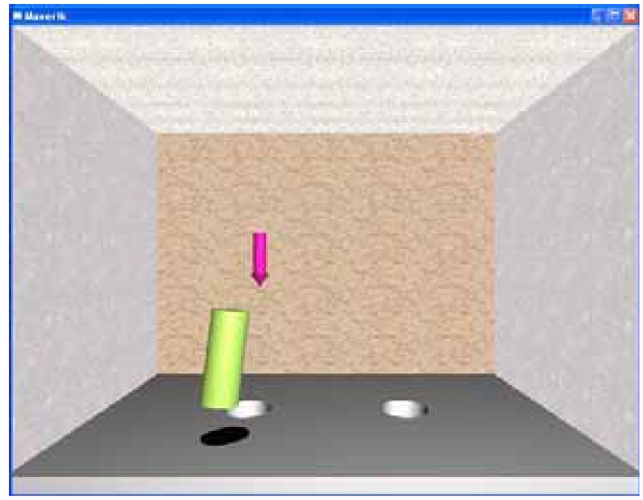

Figure 1: The Peg-in-Hole test

RESULTS AND DISCUSSION

The following results were calculated from the 144 tests: time of each full cycle, time of left-to-right and right-to-left half-cycles, FFT, spread of velocities, collision energies, spread of positions at mid-travel and at insertion for right and left holes, deviation of Y positions from a straight line and deviations from Fitts law [2].
All frequencies were below 0.5Hz and corresponded to the gross movement (no tremor). Adding weight appeared to lower collision energy. The accuracy and repeatability of the movements were analysed using the distribution of positions (error and STD) at bottom of right and left holes ($z = 0$), these varied with the clearance and the side considered.
X-Y plots showed a consistent double arched pattern clearly different from the expected shortest projected path (straight line fits produced RMSE>0.8). Fitts 'law' failed to apply, the movement time did not correlate linearly to index of difficulty.

CONCLUSIONS

It appears that a more compressive measure of "difficulty" of a task must be introduced. Real world human arm movement tasks are in nature 3D, have a goal, might involve obstacle avoidance and eventually face collisions. The Peg-in-Hole test, despite its simplicity, has embedded in its design all of these factors and as such can be a powerful tool in studying and accessing general upper limb movement. A single compounded factor involving collision energy, duration of collisions, repeatability, accuracy and cycle time of the movement may prove to be a more realistic measure of quality or difficulty of these movements.

REFERENCES

1. Wade, D.T., *Measurement in Neurological Rehabilitation*. 1992: Oxford University Press. 408.
2. Fitts, P.M., The information capacity of the human motor system in controlling the amplitude of movement. Journal of Experimental Psychology, 1954.**47**:p.381-391

A MUSCULOSKELETAL MODEL OF POSTURAL CONTROL AT THE ANKLE

Christopher J. Hasson, Jeff L. Gagnon, Richard E.A. van Emmerik, and Graham E. Caldwell
Biomechanics and Motor Control Laboratories, University of Massachusetts, Amherst, USA; E-mail: cjhasson@excsci.umass.edu

INTRODUCTION

Changes in postural stability associated with the aging process may be due to alterations in neural, skeletal and muscular characteristics. The effects of such changes are difficult to study experimentally, as they typically occur over a long time period. Therefore, many have studied postural control using analytical or numerical models, such as the simple inverted pendulum [3]. However, most models do not incorporate specific representation of the individual muscles involved in the balance process. The purpose of this paper is to describe a musculoskeletal model for studying control of sagittal plane postural sway at the ankle [3]. Development of this model will allow the study of how age-related changes in muscular properties will affect postural control.

METHODS

For initial testing of the model, experimental data were collected on a single male subject undergoing voluntarily upright sway in the sagittal plane at a frequency of ~1/3 Hz for 20 s. Center of mass motion (CoM) was measured in 3-D with an eight-camera Qualysis™ system, center of pressure (CoP) was measured with two AMTI™ force platforms, and muscle activity of the right limb soleus (SO), gastrocnemius (GA), and tibialis anterior (TA) muscles was recorded with a Delsys™ electromyography (EMG) system. Segment lengths were measured, and their masses and inertial characteristics were estimated with standard anthropometric scaling.

The musculoskeletal model was comprised of two segments representing the feet and rigid body, linked by a frictionless hinge ankle joint, confined to sagittal plane movement. The model's segment anthropometrics were matched to the subject. The equations of motion for the model were found with Autolev™, and can be expressed in general form as:

$$A(\theta)\alpha = B(\theta,\omega) + gC(\theta) + F_A + F_C$$

where θ, ω and α are vectors of segment angle, angular velocity and angular acceleration respectively; $A(\theta)$ is the inertia matrix; $B(\theta,\omega)$ is the vector describing Coriolis and centrifugal effects; $gC(\theta)$ defines the gravitational effects; and F_A is the net ankle joint torque. F_C represents foot-floor constraint forces, modeled with a series of 21 spring-damper elements along the length of the foot [1]. The ankle torque was generated by three Hill-type models representing the SO, GA, and TA muscles. Each Hill actuator consisted of non-linear series elastic and contractile components, with model parameters drawn from the literature. The experimental EMG signals were rectified, smoothed, and scaled to use as control signal shape templates for the Hill models. Muscle lengths and moment arms were computed using subject-scaled polynomial functions of joint angle modeled from SIMM™.

A variable step-size Runge–Kutta–Merson integrator was used to simulate the model motion, using initial conditions from the experimental data. A differential evolution genetic algorithm [2] was used to find the control signal scaling levels (λ), which maximized the time the model was able to remain upright. The same λ was used for SO and GA. Model performance was assessed by comparison of CoM and CoP time series with experimental data. Model sensitivity was studied by changing maximum isometric force (P_0) values in the Hill muscle models using five different literature sources (Table 1).

RESULTS AND DISCUSSION

The model was able to stay upright for the entire 20 s trial, indicating that the muscle models, control signals, and foot-floor interaction were realistic. The shape of the model's CoM and CoP motion closely matched the experimental data, with the major difference being that the model did not "lean back" as far as the subject (Figure 1).

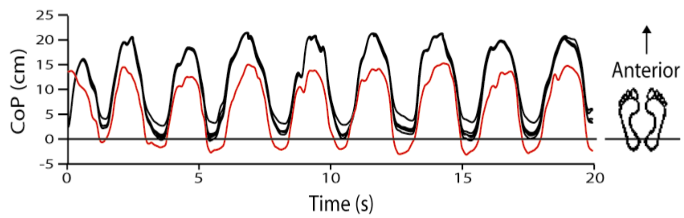

Figure 1. Experimental (thin / red) and model (Mod 1 to Mod 5; black) CoP sagittal displacement referenced to the ankle joint.

Optimized λ values (Table 1) and simulation performance were sensitive to the P_0 values used for the Hill actuators. With increases in the absolute TA P_0, the model leaned back farther as measured by its CoM minimum (r = -.94). Weaker relationships were found between the SO (r = -.57) and GA (r = -.70) P_0 values and the model CoM minimum. Although the TA P_0 values had a large range (1253 to 3114 N), the optimized λ values did not (0.72 to 0.82). The SO / GA λ values varied more (0.48 to 0.75). This suggests that the model results were dictated by the dorsiflexor TA. With a weaker TA, the model kept its CoM farther in front of the ankle joint to prevent unstoppable backward sway that would result in falling. Future work on age-related changes in muscular properties will focus on the inclusion of subject-specific parameters using MRI and ultrasound technology.

Table 1. Optimization parameters and results.

	Actuator	Mod 1	Mod 2	Mod 3	Mod 4	Mod 5
P_0 (N)*	SO	8367	8674	6976	5377	5898
	GA	5039	4854	4850	2869	3116
	TA	3114	2867	2303	2295	1253
λ	SO, GA	0.49	0.48	0.53	0.75	0.70
	TA	0.72	0.74	0.82	0.73	0.80

*Model P_0 sets [Mod 1 to Mod 5] drawn from studies in the literature.

REFERENCES

1. Anderson FC and Pandy MG. *Comput Methods Biomech Biomed Engin* **2**, 201-231, 1999.
2. Storn R and Price K. *Technical Report TR-95-012, International Computer Science Institute*, 1995
3. Winter DA, et al. *J Electromyogr Kines* **13**, 69-56, 2003.

GROUND REACTION FORCES DURING LEVEL WALKING WITH AND WITHOUT LATERAL HEEL WEDGE ORTHOTICS

David A. Wallace, and Rod A. Harter
Sports Medicine Laboratory, Oregon State University, Corvallis OR
email: wallaced@onid.orst.edu,

INTRODUCTION
Osteoarthritis (OA) affects an estimated 21 million Americans and is responsible for more than 7 million physician visits per year. Knee OA is a debilitating condition that frequently transforms physically active individuals into sedentary persons. Heel wedge orthotics are designed to mechanically lower the magnitude of the tibiofemoral joint loads in order to reduce pain and disability in knee OA patients. Heel wedge orthotics have been shown to effectively reduce knee pain[1] but few studies have compared the ground reaction forces of both medial and lateral orthotics. The purpose of this study was to characterize the effects of medial and lateral heel wedge orthotics on peak ground reaction forces during level walking.

METHODS
Ten healthy volunteers (6 females, 4 males; mean age, 24 ± 7 yr) with no history of knee injury participated in the study. Three-dimensional kinematic data (6-camera, Vicon Motion Systems, 120 Hz) and ground reaction forces (2 Kistler force plates, 1080 Hz) were collected as subjects ambulated at a self-selected pace along a 10m walkway. Each subject was tested under 3 conditions (10 trials per condition): lateral wedge (LAT), medial wedge (MED) and no wedge (CONTROL). The order of testing was selected randomly.

Peak ground reactions forces in the medial (GRF_x), anterior (GRF_y) and vertical (GRF_z) directions were analyzed from the initial contact to mid-stance phase of the gait. Force data was filtered using a second order recursive Butterworth filter with a 50Hz low-pass cutoff frequency. For reach direction of force, a repeated measures ANOVA was used to detect differences between three conditions. When appropriate, Bonferroni *post-hoc* tests were employed to determine significant differences between pairs of the three conditions.

RESULTS AND DISCUSSION
Peak GRF_x was significantly higher in the MED condition compared to both the LAT (p=.0005) and CONTROL conditions (p=.0025). Although the LAT condition tended to be lower than the CONTROL, no significant differences were determined (p>0.05). There were no significant differences between conditions found in either peak GRF_z or peak GRF_y (p>0.05).

Table 1: Peak Ground Reaction Forces

Condition	Peak Ground Reaction Force		
	GRFx	GRFy	GRFz
CON	36.3 ± 19.4	36.5 ± 24.4	878.5 ± 207.3
MED	40.2 ± 22.8	36.6 ± 19.4	898.2 ± 206.8
LAT	34.5 ± 21.1	33.3 ± 19.8	894.9 ± 197.1

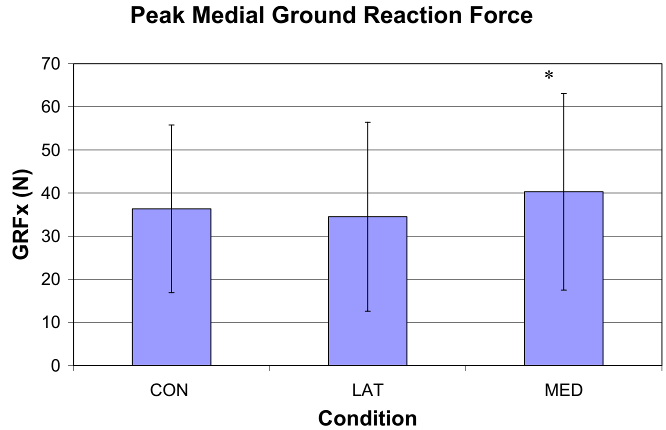

* Significant difference between MED and both CON and LAT

CONCLUSIONS
These data suggest that heel wedge orthotics can effectively alter ground reaction forces during gait. In the current study, the application of a medial heel wedge created a much larger medially directed force during the initial loading phase of gait thus potentially increasing the varus joint torques of the lower extremity. However, in agreement with previous studies, the orthotics did not reduce vertical peak forces.[2] Previous studies have suggested that lateral heel wedge orthotics reduce the varus joint torque at the knee.[3] These findings suggest the mechanism by which this occurs is through a change in the medial/lateral ground reaction force rather than by a reduction in the magnitude of the vertical ground reaction force.

REFERENCES
1. Keating EM, et al. *Orthop Rev* **22**, 921-924, 1993.
2. Maly MR, et al. *Clin Biomech* **17**, 603-610, 2002.
3. Kerrigan DC, et al. *Arch Phys Med Rehabil* **83**, 889-893.

ACKNOWLEDGEMENTS
This study was partially supported by HAPAD, Inc.

EXPLANATION OF THE BILATERAL DEFICIT IN HUMAN VERTICAL JUMPING

Maarten F. Bobbert, Wendy W. de Graaf and Jan N. Jonk
Institute for Fundamental and Clinical Human Movement Sciences, Vrije Universiteit, Amsterdam, The Netherlands;
email: M_F_bobbert@fbw.vu.nl

INTRODUCTION

In the literature, it has been reported that in two-leg jumps, humans achieve less than twice the jump height and work they are able to achieve in a one-leg jump [1, 2]. The seemingly submaximal performance in two-leg jumps has been coined bilateral deficit. It has been speculated that the deficit is primarily caused by a reduction in neural drive to the muscles in the two-leg jump and only secondarily by differences in non-neural factors [1, 2]. The purpose of the present study was to investigate the contribution of differences in active state and shortening velocity to the bilateral deficit in vertical squat jumping. For this purpose, we performed experiments on human subjects and simulations with a forward dynamic model of the musculoskeletal system.

METHODS

Eight male subjects performed maximum height vertical jumps, pushing off with only their right leg or with both legs together. In the one-leg jumps, the left leg was kept as passively as possible. Except for the position of the left leg, the initial body configuration was the same in both types of jumps (Figure 1). Kinematics and ground reaction forces of the individual legs were collected at 200 Hz, and EMG activity was recorded at 1000 Hz from soleus, gastrocnemius, vasti, rectus femoris, glutei and hamstrings of the right leg. Off-line, the EMG signals were high-pass filtered, rectified and low-pass filtered at 5 Hz to produce SREMG (Smoothed Rectified EMG). Inverse dynamics was used to calculate work produced by the right and left leg during the push-off.

One- and two-leg jumps were also simulated with a forward dynamic model of the musculoskeletal system [3]. The model had 7 rigid segments (foot, shank and thigh of each of the two legs and a head-arms-trunk segment), and was actuated by 15 muscle-tendon complexes (MTC): soleus, gastrocnemius, vasti, rectus femoris, glutei and hamstrings of the left and right leg, and tibialis anterior, short head of biceps femoris and iliopsoas of the left leg. Each MTC was represented as a Hill-type unit. The model calculated the segmental motions corresponding to stimulation (STIM) input to the muscles. Initial STIM levels were chosen such that static equilibrium was achieved in the starting position, which was close to that of the subjects. Subsequently STIM of each muscle was allowed to switch between “on” and “off” several times, and switching times were optimized to find maximum jump height using a parallel genetic algorithm. Once the optimal solutions had been found for the one-leg and two-leg jumps, we used them to determine the cause for differences in muscle work performed. We estimated the effect of differences in active state by substituting at each MTC length in the two-leg jump the active state at the same MTC length in the one-leg jump, and subsequently re-calculating muscle force and work (this step will be called: correction for active state). The same procedure was followed to estimate the effect of differences in CE velocity (correction for CE-velocity).

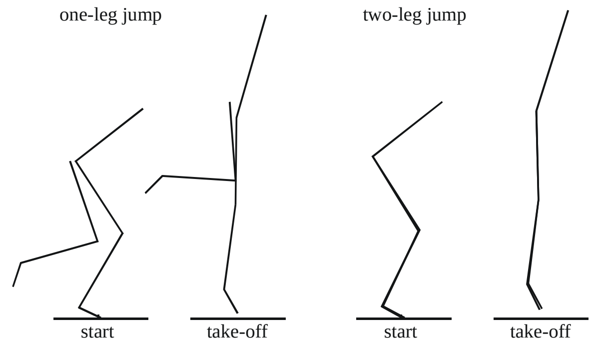

Figure 1: Average initial and take-off body configurations of the subjects in the one-leg and two-leg jumps.

RESULTS AND DISCUSSION

No differences occurred between the two types of jumps in the range over which the subjects extended the joints of their right leg (Figure 1). Obviously, in the two-leg jump, greater velocities were reached and the range of motion was traveled in less time than in the one-leg jump. Mean vertical displacement in the airborne phase was 23.7 cm in the two-leg jump and 12.6 cm in the one-leg jump. Work performed by the right leg was 195 J in the two-leg jump and 248 J in the one-leg jump. Ratio’s of peak SREMG values in the two-leg jump to peak SREMG values in the one-leg jump, averaged over all subjects, ranged from 0.9 to 1.0 for the different muscles, suggesting that any reduction of neural drive in the two-leg jump was at best minimal. In the simulation model, the work performed by the right leg was 160 J in the two-leg jump and 234 J in the one-leg jump. In the model, the difference in work output of the right leg was, of course, completely caused by non-neural factors. Correction for active state caused the work in the two-leg jump to increase by 24 J, while correction for CE-velocity caused it to increase by 58 J. This shows that the differences in active state and shortening velocity between two-leg jumps and one-leg jumps can have a substantial effect on the force and work output of the muscles.

CONCLUSIONS

SREMG-results indicate that at best a minimal reduction in neural drive occurred in two-leg jumps compared to one-leg jumps. However, in a two-leg jump, initial active state is lower than in a one-leg jump and less time is available to increase active state. Moreover, the muscles travel their range of shortening at greater speed. In the model, these two factors combined caused the muscles to produce substantially less work in the two-leg jump than in the one-leg jump. It seems that the bilateral deficit in jumping is primarily caused by non-neural factors rather than by a reduction in neural drive.

REFERENCES

1. Challis JH. *Hum. Mov. Sci.* **17**, 307-325, 1998.
2. van Soest AJ, et al. *Med. Sci. Sports Exerc.* **17**, 635-639, 1985.
3. van Soest AJ, et al. *J. Biomech.* **26**, 1-8, 1993.

POSTURAL CONTROL IN SKILLED ATHLETES IN RESPONSE TO UNEXPECTED PERTURBATION

Sheylla K. Yoshitomi[1], MS, Clarice Tanaka[1,2], PhD, Marcos Duarte[3], PhD, Fuad A. Hazime[1], MS
[1]Division of Rheumatology, School of Medicine, University of São Paulo, Brazil, sheyllaky@uol.com.br
[2]Department of Physical Therapy, Speech Therapy and Occupational Therapy, University of São Paulo, Brazil
[3]School of Physical Education and Sport, University of São Paulo, Brazil

INTRODUCTION

Judo is an Olympic sport modality based on a straight combat between two athletes, whose main objective is to dominate the adversary leading him to knock down. The achievement of a good performance requires the development of athletes' equilibrium and muscular force [1]. The role of balance is enhanced by the end of the fight with the disequilibrium of one of the adversaries, followed by his immobilization or giving up. According to the judo techniques, athletes are constantly subjected to unexpected movements imposed by their adversaries with the objective of creating opportunities to break their equilibrium to define the combat [2]. This modality leads the athlete to develop news sensorial-motors strategies and mental abilities that contribute to improve his postural control [3]. This study aimed to test the hypotheses that athletes of this modality presents better postural control in responses to unexpected perturbation than a healthy and recreationally active young group.

METHODS

Ten skilled male judo athletes and ten healthy and recreationally active young male adults (age and weight matched) participated in this study. Subjects were asked to stand still on an AMTI force plate. Using a resistant non-extendable thread we applied at the subject's upper mid spine (i.e., at the level of the inferior border of the scapulae) an external posterior perturbation (EPP) by means of halters equivalent to 6% of the subject body weight. Three trials of 40s were collected with data acquisition beginning 2s prior to the EPP. After observing that the subject reacquired apparent stability with EPP, the EPP was then unexpectedly released. Postural control was analyzed in 8 intervals of 1s each (T1 to T8) starting at the moment of EPP release. Analysis of variance was used to compare mean of COP speed and COP displacement for T1 to T8 and maximum COP displacement during T1. The α level was preset at p less than 0.05 and post–hoc (Tukey HSD test) were conducted when necessary.

RESULTS AND DISCUSSION

Athletes showed better postural control than control group. In the first second (T1) after EPP release ANOVA showed that athletes presented COP speed 16.4% lower than control group ($p=0.01$) (Fig. 1). Intragroup analysis showed similar COP displacement from T2 to T8 for control group. However, in athletes, COP displacement was higher during T2 than others intervals (Fig. 2). Summarizing (1) both groups presented similar reflexive response to the perturbation with no inter-groups difference in the maximum COP displacement in T1, (2) the athletes presented lower COP speed in T1 and (3) athletes were slower to bring the COP backward ($T1 \neq T2$, $T2=T3=...T8$). These results reveal better postural control of the athletes than the control group after the perturbation

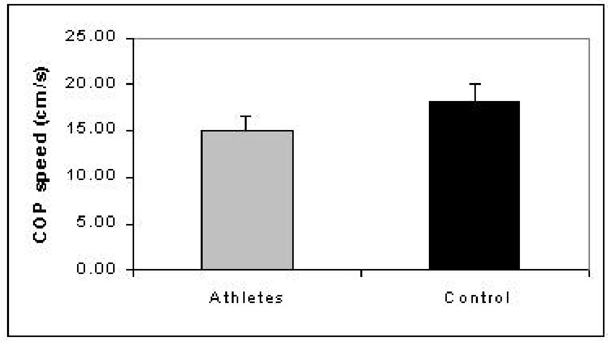

Figure 1: Mean of COP speed for athletes and control group in the T1.

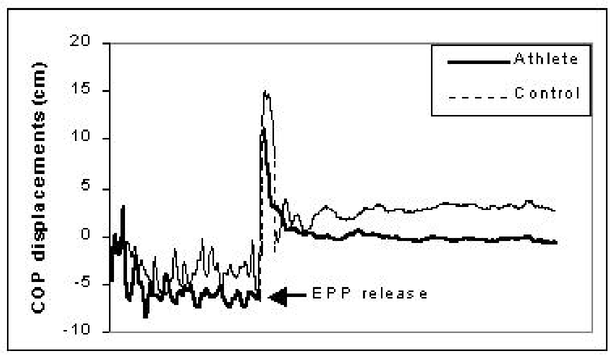

Figure 2 – Example of athlete and control subject postural control. Athlete (dark line) and control subject (light line) cop displecement during trial 2 and 3 respectively.

CONCLUSIONS

Athletes presented better postural control in response to unexpected perturbation compared to healthy and recreationally active young male adults.

REFERENCES

1. Fracarolli JL. *Biomecânica: análise dos movimentos.* 2ª ed. Rio de Janeiro: Cultura médica; 1981.
2. Perrin P, Deviterne D, Hugel F, Perrot C. Judo, better than dance, develops sensorimotor adaptabilities involved in balance control. *Gait and Posture*. 2002;15:187-94.
3. Perrot C, Deviterne D, Perrin PH. Influence of training on postural and motor control in a combative sport. *Journal of Human Movement Study.* 1998; 35:119-36.

IS PATELLAR CARTILAGE THICKNESS REDUCED IN INDIVIDUALS WITH PATELLOFEMORAL PAIN?

[1] Christine Draper, [1]Amy Fiene, [1]Thor Besier, [2] Garry Gold, [3]Gary Beaupre, [1,3,4]Scott Delp
[1]Department of Mechanical Engineering, Stanford University, Stanford, CA, [2]Dept. of Radiology, Stanford University Medical Center, Stanford, CA, [3]VA Rehabilitation Research and Development Center, Palo Alto, CA, [4]Dept. of Bioengineering, Stanford University, Stanford, CA; email:cdraper@stanford.edu

INTRODUCTION

Patellofemoral pain is a common and debilitating knee disorder. Increased stress in the articular cartilage may lead to stimulation of pain receptors in the subchondral bone. Thinning of the articular cartilage is one possible mechanism leading to increased cartilage stress. We tested the hypothesis that subjects diagnosed with patellofemoral pain have thinner patellar cartilage than control subjects.

Magnetic resonance imaging (MRI) has been used to accurately and non-invasively measure cartilage thickness [1,2]. Patellar cartilage thickness has been estimated in pain-free control subjects using MRI [3]. However, comparisons of cartilage thickness between control subjects and individuals with patellofemoral pain have previously not been performed.

METHODS

Sagittal plane MR images were obtained from 10 pain-free control subjects and 10 subjects with patellofemoral pain. All subjects were between the ages of 20 and 35 to minimize the effect of osteoarthritis on cartilage thickness. Equal numbers of male and female subjects were present in each group. Subjects were imaged while lying supine with the knee in full extension, minimizing cartilage load and deformation. Images were acquired with a 1.5T scanner (GE Healthcare, Milwaukee, WI), using a standard knee coil and a 3D fat-suppressed spoiled gradient echo MR sequence, with a scan time of approximately 15 minutes. The following scan parameters were used: TR: 60ms, TE: 5ms, Flip Angle: 40°, Matrix Size: 256x256, FOV: 12cmx12cm, slice thickness: 1.5mm, Sections: 60.

The subchondral bone and articular cartilage boundaries of the patella were manually segmented using custom software to generate 3D point clouds representing the cartilage surface. Triangulated surfaces were created of the subchondral bone boundary (Geomagic, Raindrop Geomagic, NC). Cartilage thickness was determined by computing the minimum distance between the subchondral bone surface and the articulating cartilage surface, along the surface normal vectors of the subchondral bone (Figure 1). The peak and average thicknesses of the cartilage were computed and compared between subject groups. To account for differences in subject size, we normalized the thickness measurements by scaling according to (body mass)$^{\wedge 0.45}$ [4]. The significance of the differences was evaluated using a one-tailed t-test.

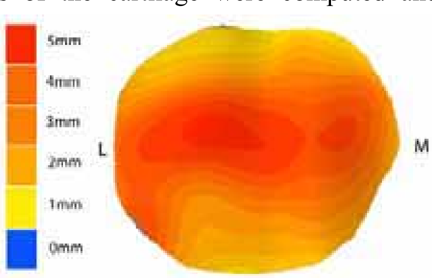

Figure 1: Cartilage thickness distribution on patella of a female volunteer.

RESULTS AND DISCUSSION

We found that the average peak thickness among control subjects was 5.8±1.6 mm while the average mean thickness was 2.9±0.7mm. These results are comparable to previous measurements of patellar cartilage thickness in active, healthy subjects made using MRI ([1], peak = 5.8-5.9mm, mean = 2.8-2.9mm). The average peak thickness among subjects with patellofemoral pain was 5.2±0.7mm while the average mean thickness was 2.9±0.3mm. Compared to the control subjects, the male subjects with patellofemoral pain had significantly lower peak cartilage thickness both before and after normalization ($p<0.05$) and showed a trend towards a lower mean cartilage thickness ($p<0.1$). There were no significant differences in cartilage thickness between the female control and patellofemoral pain subjects both before and after normalization (Figure 2). When both genders were pooled, there was a trend for the patellofemoral pain subjects to have a smaller normalized peak cartilage thickness than the control subjects ($p<0.1$).

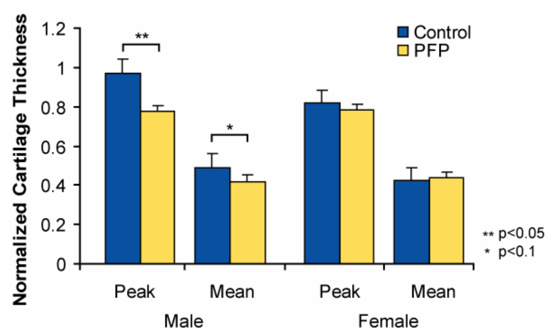

Figure 2: Comparison of Peak and Mean Cartilage Thickness between Subject Groups

These data suggest that thin cartilage may be correlated with patellofemoral pain in male subjects. Future studies that examine patellar and femoral cartilage thickness on a larger group of subjects are required to confirm this finding.

REFERENCES

1. Stammberger T, et al. *Magn Reson in Medicine* **41**, 529–536, 1999.
2. Hardy PA, et al. *JMRI* **13,** 120-126, 2001.
3. Sittek H, et al. *Skeletal Radiol* **25,** 55-62, 1996.
4. Simon WH. *Arthritis Rheum*, **13(3),** 244-256, 1970.

ACKNOWLEDGEMENTS

We would like to acknowledge funding from the VA Rehabilitation R&D Service (VA RR&D grant #A2592R), the National Science Foundation, and a Stanford Graduate Fellowship.

INTER INDIVIDUAL VARIATION IN TRUNK MUSCLES GEOMETRY OF ASYMPTOMATIC SUJETS IN STANDING POSITION.

[1]Renée Saintonge, [1]Vincent Pomero, [1]Olivier Gille, [1]Dominique Bonneau, [2]Jean-Marc Vital, [2]Vincent Dousset and [1]Wafa Skalli
[1]Laboratoire de Biomécanique, ENSAM CNRS, France,
[2]CHR Bordeaux, France

INTRODUCTION

Biomechanics models of the lumbar spine need specific muscular geometry data as maximal physiological area, centroid location of muscular areas in the intervertebral plane and muscular line of action or contraction. Those geometry data are usually acquired for supine subject. However, a significant difference exist when considering muscular centroid locations between the supine and the upright position [1]. The aim of this study was to characterize personalized muscular geometries of asymptomatic subjects in upright position and their related parameters in the L3/L4 intervertebral plane.

METHODS

19 asymptomatic subjects were recruited. Two exams were performed. First, a stereoradiographic exam consisting of two full spine X-Ray (frontal and lateral views) in standing position into a calibrated device was done [2]. With a specific software, the 3D personalized reconstruction of the vertebras (T1-L5), the pelvis and the ribs of the subject in upright position were obtained. Then, ten MRI axial slices were obtained from T9-T10 to L5-S1 levels and the femoral heads. The muscles outlined on the MRI were the Rectus Abdominis (RA), the External Oblique (EO), the Internal Oblique (IO), the Transversus Abdominis (TA), the Psoas (P), the Transverso Spinalis (TS), the Longissimus Dorsi (LoD), the Iliocostalis (IC) and the Latissimus Dorsi (LaD). The outlined muscles were then reconstructed and repositioned into the 3D spine reconstruction coordinates system using a specific technique based on muscles geometry adaptation regarding skin configuration in standing position and muscular bone attachment points [3]. A personalized volume reconstruction in standing position of each studied muscle was obtained between T9-T10 level and the femoral heads. Muscular volumes and intersection areas between the muscular reconstructions and the L3/L4 intervertebral plane were evaluated on left and right muscles. The centroid location of the muscular area was calculated with regard to the intervertebral disc centre. The orientation of the muscular line of action was quantified. The maximal physiologic area was evaluated as the maximal area of the intersected volume by a normal plane to the muscular line of action.

RESULTS AND DISCUSSION

The trunk muscles volumes and maximal physiologic area are shown in Figure 1. The largest muscles volumes were the Psoas (242 mL) and the RA (255 mL). The smallest volume was obtained for the QL (69 mL). The biggest variation between subjects was observed for the left Psoas (77%). The Psoas had the highest maximal physiologic area with 14 cm², followed by the LaD (11 cm²) as well as the IC and the LoD (9 cm²). A maximal physiologic area inter subject variability of 34% was observed for the LoD and the RA. The IO, LaD and RA had a high inter subjects variability for the postero-anterior centroid position (6.5-7.1 cm). The inter subject variability of the lateral centroid position for the IO, the LaD, the EO and the TA was between 4.6 and 6.8 cm. As for orientation of muscle line of action, variability between subjects could reached 46° for the LaD in the sagittal plane and 25° in the coronal plane. Furthermore, the TA had 70° of variation in the coronal plane. The muscles TS, Psoas and LoD had few variations between subjects for the area centroid position and the line of action orientation. Our data were in accordance with the few available data in the literature [4, 5].

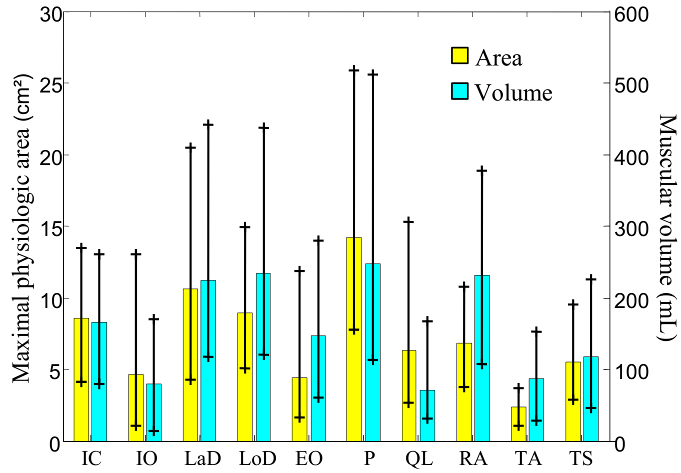

Figure 1 Maximal physiological areas and muscular volumes (mean, min, max).

CONCLUSIONS

The proposed muscular geometry in the L3/L4 plane took into account the muscular geometry shape and the muscular fiber orientation. A wide inter variability among subjects was observed, which underlined the need to personalized the muscular geometry for trunk muscular modelization.

REFERENCES

1. McGill SM, et al. *J Biomech*, **29**, 643-6, 1996
2. Dumas R, et al. *J Biomech*, **36**, 827-34, 2003
3. Pomero V, et al. *Eur Spine J*, **submitted**, 2005
4. Delp SL, et al. *J Biomech*, **34**, 371-5, 2001
5. Tracy MF, et al. *Spine*, **14**, 186-93, 1989

ACKNOWLEDGEMENT

Renée Saintonge was supported by a PhD grant from IRSST, Québec, Canada.

REGIONAL VARIATION OF BONE STRAIN CREEP OF VERTEBRAL BODY DURING REPETITIVE LOADING – AN IN VITRO PORCINE BIOMECHANICAL MODEL

Chun-Kai Chiang, M.S., Yuan-Chuan Tsai, M.S., *Jaw-Lin Wang, Ph.D.
Institute of Biomedical Engineering, National Taiwan University, Taipei, Taiwan, ROC
e-mail: jlwang@ntu.edu.tw , web: biomech.bme.ntu.edu.tw

INTRODUCTION

The compressive fracture of osteoporotic vertebra is the consequence of accumulated micro fracture caused by the mechanical repetitive loading. However, how the micro fracture or strain accumulated during repetitive loading within the vertebra is not well understood yet. The purpose of this study is to explore the distribution and progression of strain and strain field of vertebral body during repetitive loading.

METHODS

Seven fresh-frozen thoracic porcine spinal motion segments (T10/T11/T12) were used in the experiments. All ligamentous, capsular, and intracapsular structures were preserved. The T10 and T12 were mounted in polyester resin casts with the T11 vertebral body aligned. The surface of vertebral body was cleaned with alcohol. Two 3-axial strain gages rosettes (Kyowa KFG-1-120-D17-11N50C2, Kyowa Electronics Instruments Co., Ltd., Tokyo, Japan) were mounted at the anterior and posterior sites of T11 vertebral body.

A "drop-tower type" impact testing apparatus was used for the testing (Figure 1). The vibrator was guided by two rods to give a vertical motion. The energy of the vibration was produced with the two eccentric rotors droved by a motor. The energy was transmitted to the specimen through the impounder. The fixed frame, which is fixed to the guiding rode, is used to align the vertical movement of impounder. The specimen was mounted vertically below the impounder with a uni-axial load cell (Kistler 9021, Kistler Instrumente, Winterthur, Switzerland).

The magnitude of external loading was 200N compression and 100N tension from peak to peak. The loading frequency was 5 Hz, and the loading period was five hours; hence 90,000 cycles in total were applied. We recorded one second data every 5 minutes. Sixty sets of data were collected through the loading period. Signals of two strain gages rosettes and axial forces were recorded at 10 kHz sampling frequency. The signals were then low pass filtered at 250 Hz frequency using Butterworth filtering algorithm. The two principal strains at anterior and posterior sites of vertebral body were calculated from the measurement of two strain gage rosettes.

RESULTS AND DISCUSSION

The tensile strain of anterior site reached equilibrium after 30,000 cycles (1500 $\mu\varepsilon$), while the compressive strain kept progression through out the loading period (820 $\mu\varepsilon$ max) (Figure 2a). The tensile strain of posterior site reached equilibrium after 30,000 cycles (200 $\mu\varepsilon$), while the compressive strain did not reach steady state even after 90,000 cycles loading (850 $\mu\varepsilon$ max) (Figure 2b). We found that the compressive principle strain of both site of vertebral body did not reach the steady state even after 90,000 cycles of loading, while the tensile strain reached steady state at about 30,000 cycles of loading. The magnitude of the tensile principle strain is two times as large as the magnitude of the compressive principle strain at anterior site of vertebral body. It showed that tensile strain induced by the long-time fatigue loading maybe the reason for the wedge compressive fracture of vertebral body (Figure 3).

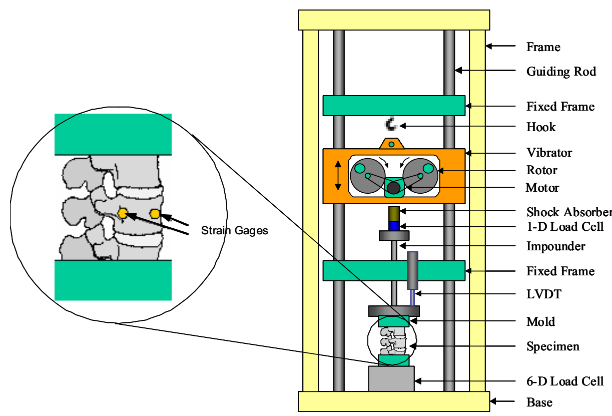

Figure 1: The schematic plot of testing apparatus.

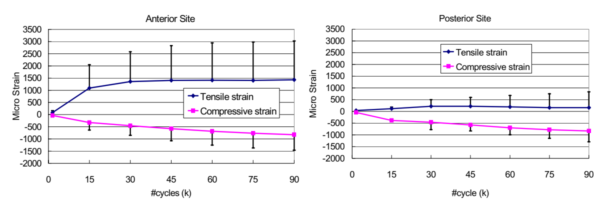

(a) (b)

Figure 2: Principal strain of vertebral body at (a) anterior site, and (b) posterior site.

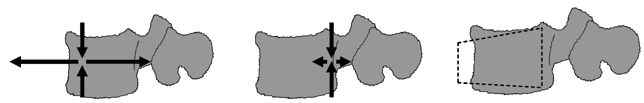

Figure 3: Schematic plot of principal strain of vertebral body.

REFERENCE :

1. MIchio Hongo, et al. *Spine* **24**, 1197-1202, 1999.

ACKNOWLEDGEMENTS

We acknowledge the financial support of the National Science Council, Taiwan, ROC, NSC 93-2320-B-002-030.

ANKLE JOINT DORSIFLEXION: ASSESSMENT OF THE TRUE VALUES

John Weir and Nachiappan Chockalingam
Faculty of Health and Sciences, Staffordshire University, Stoke-on-Trent, ST4 2DF, UK
email: jweir40@eircom.net; n.chockalingam@staffs.ac.uk

INTRODUCTION

The amount of ankle joint dorsiflexion required for human ambulation is claimed to be 10 degrees [1,2,3,4,5]. Motion of a reduced quantity has been referred to in the literature as “equinus” and the widely accepted theory is that when equinus is present abnormal foot function occurs. Clinical experience suggests that the majority of patients evaluated, display an amount of ankle joint dorsiflexion during stance, which falls short of this figure. However, patients presenting within the clinical environment normally complain of some discomfort and therefore may not be a good representation of the normal population. One of the main purposes of this study is to determine how and when this arbitrary figure of 10 degrees became established and accepted as the norm and is it in fact a correct figure.

METHODOLOGY

Fifteen subjects consisting of 8 men and 7 women, aged 19-49 years (mean 27.07), with a body mass ranging between 51.5-126 kg (mean 71.96), height ranging between 161-189 cm (mean 173) and no known gait abnormalities were recruited from a population of university students. All subjects reported to have a passive ankle joint motion of between 12.2 and 25.6 degrees. Ethical approval was sought and received from the university ethics committee. As a result of the prescribed exclusion criteria, one male subject was eliminated from the study (ankle surgery due to fracture). All subjects were supplied with a written explanation of the study and gave a written consent.

A three dimensional opto electronic motion analysis system consisting of five infra-red cameras, sampling at a rate of 60 Hz was employed for data collection and analysis (Motion Analysis Corp, Santa Rosa, CA). Reflective skin markers were placed on predetermined anatomical landmarks. Once the markers were placed on the subject, they were asked to stand on a dynastat weight bearing goniometer (Dynastat, Stafford, UK), with their ankle joint maintained at 90 degrees, whilst their subtalar joint was placed in neutral position [6]. The positioning of the subject in neutral was performed by the same researcher (JW). Two trials of data were taken for each subject whilst they were in this position. The information from this data was later used as a zero reference point to correct the walking data for subtalar neutral position during data analysis. The markers were used to define a segment coordinate system for each limb segment, 3 markers per segment i.e. foot, shank, thigh. This set up allowed for analysis of motion between the foot and leg for each subject. While the data was collected for several trials, three trials were chosen at random for each subject to measure the dorsiflexion values. The 3D co-ordinates were be smoothed using a Butterworth filter (Fc = 7Hz) and all foot angles were expressed relative to the subtalar neutral position. Data were subjected to analysis for similarities using the co-efficient of multiple correlation (CMC) [7].

RESULTS AND DISCUSSION

Results (Table 1) show ankle joint dorsiflexion values of between 12 degrees and 22 degrees dorsiflexion with a wide variation between subjects. Data from a particular subject was discarded due to errors in analysis.

Table 1: Maximum values for ankle joint dorsiflexion/ plantarflexion

	Max Dorsiflexion (degrees)		Max Plantarflexion (degrees)		
Subject No:	**Mean**	**St.Dev**	**Mean**	**St.Dev**	**Typical CMC Values**
1	14.07	*0.25*	-12.33	*1.10*	0.983
2	14.70	*0.11*	-3.79	*1.11*	0.755
3	12.43	*1.18*	-12.24	*2.11*	0.732
4	17.31	*2.07*	-6.03	*3.69*	0.823
5	17.85	*0.34*	-4.02	*2.15*	0.989
6	18.93	*0.52*	-3.68	*1.03*	0.955
7	21.97	*1.36*	-1.48	*1.19*	0.914
8	16.97	*0.34*	-7.61	*2.59*	0.989
9	13.77	*0.15*	-3.77	*0.66*	0.992
10	17.67	*0.38*	0.58	*3.83*	0.917
11	13.37	*0.26*	-6.11	*0.50*	0.757
12	20.39	*0.82*	3.69	*1.76*	0.773
13	22.53	*0.29*	0.44	*1.51*	0.941

The results appear to show ankle joint dorsiflexion in normal subjects is greater than the value traditionally espoused by clinicians for walking. This may have clinical implications. More research is needed to determine the effect of terrain, footwear and muscle length on the measurements.

REFERENCES

1.Subotnik S, Journal of the American Podiatry Association, **61**(11), 423-27, 1971.
2. Root ML, et al., Normal and Abnormal Function, Los Angeles, Clinical Biomechanics Corporation, 1977.
3.Lang L, The Chiropodist, **39,** 4-7, 1984.
4.Waller RM, Podiatry Now, 183-190, 2000.
5. Wright et al, The Journal of Bone and Joint Surgery, **46-A**(2), 361-382, 1964
6.Branthwaite H et al, Clinical Biomechanics, **19(9)**, 972-977, 2004.
7. Kadaba *et al*, Journal of Orthopaedic Research, **7(6)**, 849-860, 1989.

C-LEG KNEES DO NOT IMPROVE STANCE PHASE KNEE FLEXION OR WALKING EFFICIENCY IN OLDER TRANSFEMORAL AMPUTEES

Michael Orendurff, Ava Segal, Martin McDowell, Glenn Klute, Rhonda Williams, Aaron Turner, Jan Pecoraro, Joseph Czerniecki
Motion Analysis Laboratory, Rehabilitation Research and Development, Seattle Veterans Hospital
Seattle, Washington USA email: michael.orendurff@va.med.gov , web: www.seattlerehabresearch.org

INTRODUCTION

Microprocessor-controlled prosthetic knees are hypothesized to improve stance phase knee flexion, sagittal knee moments and walking efficiency for transfemoral amputees. Few rigorous examinations of the kinematic, kinetic and energetic[1] improvements in transfemoral amputee gait have been published in peer-reviewed journals. The goal of this study was to compare the differences between the C-Leg (Otto Bock, Minneapolis, MN) and Mauch knees in stance phase knee flexion, knee extensor moment and gait efficiency across walking speeds in older, experienced transfemoral amputees.

METHODS

Eight traumatic transfemoral amputees (age 48.5 ± 13.2 years; Ht 172.5 ± 4.2 cm; Wt 80.1 ± 10.5 kg) gave informed consent to participate in this IRB approved protocol. Subjects were all previous long term Mauch swing and stance (SNS) users. Each subject was evaluated following a 3-month acclimation period in the C-leg and the Mauch SNS prosthetic knees with identical sockets; order of knee type was randomly assigned. Full body gait kinematics and kinetics were collected at each subject's self-selected walking speed (SSWS) using a 10-camera Vicon 612 system and Plug in Gait (Lake Forest, CA.). Peak knee flexion in single limb stance, peak knee flexion in swing and peak knee extensor moment in early stance was extracted using Event Analyser (Vaquinta Software, Southampton, UK). Later, oxygen consumption (ml/kg/min) was measured at 0.8, 1.0, 1.3 m/s and SSWS overground with a Sensormedics VmaxST mobile metabolic system (Loma Linda, CA) with seated rest between speeds. Oxygen consumption was converted to net oxygen cost (ml/kg/m) by subtracting resting levels and dividing by walking speed to estimate gait efficiency. Overground speed was enforced using a velocity-detecting cart pushed parallel to the subject by an investigator. Oxygen data was monitored in real time and the trial continued until 2 minutes of steady state metabolic data was collected, usually within 8 minutes. Knee flexion in stance and swing, knee extensor moment in early stance, and oxygen cost for the C-Leg versus the Mauch SNS were compared using repeated measures mixed effects ANOVAs.

RESULTS AND DISCUSSION

There was no significant difference observed between stance phase knee flexion with the C-Leg or Mauch SNS knee; both knees remained in full extension through terminal stance phase. The C-Leg had lower (more normal) peak knee flexion during swing phase compared to the Mauch SNS (54.2 ± 4.2 vs. 59.1 ± 8.1; $p < 0.0001$). The peak knee extensor moment in early stance showed no significant difference between the knee types ($p < 0.59$), although the moment was shifted slightly toward extensor (closer to normal) in the C-Leg knee. Oxygen costs at each of the 4 walking speeds were not statistically different with the C-Leg compared to Mauch SNS knee ($p > 0.19$), indicating that the subject's gait was not more efficient with the C-Leg. This is consistent with previous literature[1].

CONCLUSIONS

Older, experienced transfemoral amputees did not demonstrate significant improvements with the C-Leg despite a 3-month acclimation period. Even with the long acclimation period, these subjects were not able to take advantage of the eccentric knee flexion feature during early stance phase. This may be related to the subjects' previous long-term use of a Mauch SNS limb. Many subjects commented that they still found it difficult to break the habit of providing extensor force to the prosthetic limb in stance phase. Subjects described the C-Leg as having better stumble recovery and therefore fall prevention, although this was not explicitly measured in this study. Despite the lack of significant improvements observed in the kinematics, kinetics or energitics, 7 of the 8 subjects chose to keep the C-leg as their primary limb after the study was completed.

REFERENCES

1. Buckley, JG, et al. *Arch Phys Med Rehabil* 78: 330-3, 1997.

ACKNOWLEDGEMENTS

This work was funded by Dept of Veterans Affairs Grant #A2770I.

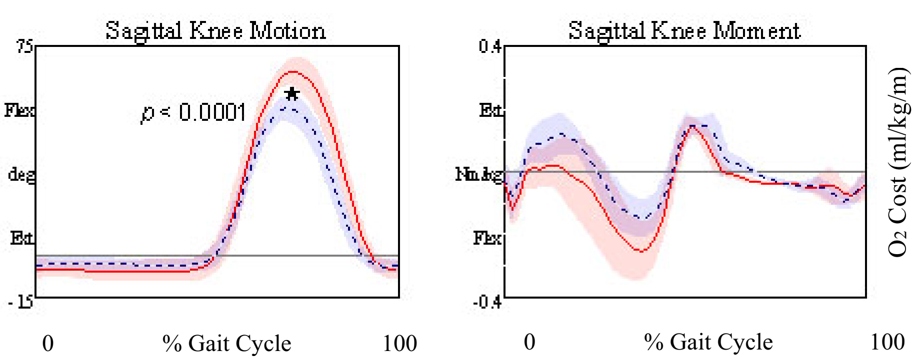

Figure 1: Sagittal prosthetic knee motion, moment across the gait cycle for the C-Leg (dashed blue line) and the Mauch SNS (solid red line). Shaded area is ± 1SD.

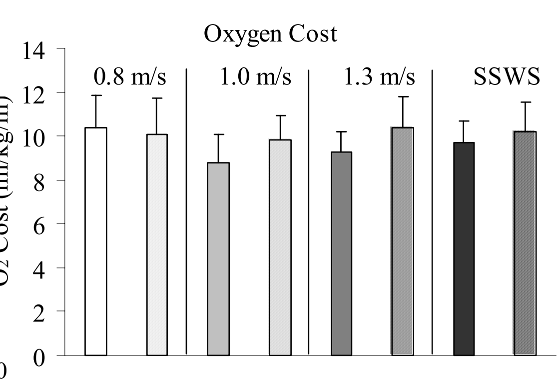

Figure 2: O_2 cost for the C-Leg (solid) and Mauch (hatched bars) across 4 gait speeds. (Mean + 1SD)

Mitochondrial Adaptation During Rehabilitation and Its Importance in Musculoskeletal Modeling

[1] Sherry L. Di Jorio, [2]Michael B. Vergason, [1,3]Gary T. Yamaguchi and [1,4]James T. Ryaby
[1]Harrington Department of Bioengineering, Arizona State University; email: sherry.dijorio@asu.edu
[2]Department of Chemistry and Biochemistry, Arizona State University; [3]Exponent Inc.; [4]OrthoLogic Corporation

INTRODUCTION

Musculoskeletal models are widely used in assessment and predication of rehabilitation or surgical outcome. In many of these models [1,2], muscle parameters such as specific force are considered constant throughout the healing process. We hypothesized that muscle properties change during healing. This change may be significant enough to alter model outputs and therefore render the model invalid if the changes are not taken into consideration.

METHODS

8-10 month old male Sprague-Dawley rats (n=105, 500 grams mean weight) were divided into five groups: Control, Sham, Fracture Only (Fx), Tenotomy only (Ten), or Fracture plus Tenotomy (FxTen). Prior to treatment, all animals underwent two weeks of treadmill training. In the Fx group, mid-diaphyseal fractures in the right femur were made as described by Bonnarens and Einhorn [3]. The Ten group had the patellar tendon completely severed just proximal to the patella, rendering the knee extensors ineffective. Animals in the sham group had a knee incision and exposure of the femoral condyles. Food and water were given ad libitum.

A subset of the animals walked on a forceplate-fitted rodent treadmill wearing reflective markers. Measured ground reaction forces and joint angles were used as inputs to a dynamic 3D musculoskeletal model of the hindlimb.

Animals were euthanized after 2, 4, 6, and 8 weeks. Contralateral knee flexors were harvested (semitendinosis and biceps femoris- caudal head) along with both femurs. Muscles were immediately placed in liquid nitrogen. To determine presence of mitochondrial adaptation, the method of Srere [4] was used to quantify the activity of citrate synthase (CS). CS activity was statistically compared using ANOVA, with α=0.05. All animal procedures were approved by the Arizona State University IACUC committee.

RESULTS AND DISCUSSION

CS activity, and indicator of oxidative capacity, is directly proportional to the amount of mitochondrial activity in the muscle [5], and its activity has been shown to decrease in association with decreased ability of the muscle to produce force [6]. The decrease in CS activity associated with fracture, tenotomy, or both indicates a potential need to adjust muscle properties in musculoskeletal models whose purpose is to assess movement capability during fracture or muscle injury rehabilitation.

Mean CS activity was significantly greater in control and sham animals than in animals receiving fracture, tenotomy, or

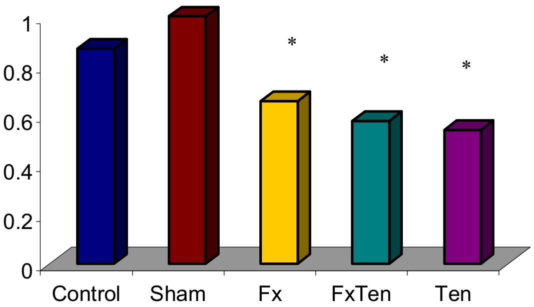

Figure 1: Normalized mean 8-week citrate synthase activity in semitendinosis. *Mean is different from control and sham, $p<0.05$.

both ($p<0.05$) (Figure 1). A common pattern is seen at all time points analyzed.

Kinetic and kinematic gait analysis shows that there is indeed a difference in the gait of animals that have undergone femoral fracture, patellar tenotomy, or both ($p<0.05$). Differences arise in ground reaction forces, knee and ankle joint angles, and stride characteristics. Dynamic musculoskeletal modeling of measured rat gait calculates a significantly different joint reaction force at the knee as the specific force in the knee flexors is changed. To accurately model muscle force during rehabilitation, direct experimental evidence relating mitochondrial content to specific force is needed.

CONCLUSIONS

Femoral fracture, patellar tenotomy, or both significantly reduce CS activity in the knee flexors, indicating a reduction in those muscles' ability to produce force. Because the gait of these animals is significantly different from normal rat gait, there is a need for musculoskeletal models to be individualized and customized. Based on these results, specific force can be treated as an adjustable parameter.

REFERENCES

1. Hurwitz DE, et al. *J of Biomechanics* **36**, 113-119, 2003.
2. Gonzalez RV et al. *J of Biomechanics* **30**, 705-712, 1997.
3. Bonnarens F and Einhorn T, *J Orthop Res* **2**, 97-101, 1984.
4. Srere, PA. *Methods Enzml.* **13**, 3-5, 1969.
5. Schwerzmann K, et al. *Proc Nal Acad Sci* **86**, 1583-7, 1989.
6. Lowe DA, et al. *J Appl Physiol.* **96**, 498-506, 2004.

ACKNOWLEDGEMENTS

Authors would like to acknowledge Wayne Willis for technical advice. This research is funded by OrthoLogic Corporation, Tempe, AZ. Sherry Di Jorio is an IGERT fellow under NSF grant# DGE-9987619.

JOINT STIFFNESS REQUIREMENTS IN A MULTI-SEGMENT STANCE MODEL

Leonard A. Rozendaal, A.J. "Knoek" van Soest
Institute for Fundamental and Clinical Human Movement Sciences, Amsterdam/Nijmegen, The Netherlands
email: l_rozendaal@fbw.vu.nl

INTRODUCTION

Currently, there is a vivid debate on the control mechanisms involved in human stance, in which the required and available ankle joint stiffness play a key role. Ankle stiffness values are typically discussed in the context of a one-segment stance model. Considering other joints as well, in particular the knee and the hip, it is found that the ankle stiffness should be substantially higher than the one-segment model suggests.

METHODS

In an n-segment model of the standing human moving in the sagittal plane, the gravitational potential energy $U_g(\varphi_1,...,\varphi_n)$ can be expressed as a function of the joint angles φ_i. The Hessian (second derivative matrix) of U_g is $\boldsymbol{G}$, the joint stiffness matrix due to gravity, which typically has negative values. The joint stiffness matrix $\boldsymbol{K}$ due to intrinsic muscle-tendon properties and reflexive control, when symmetric, can be considered the Hessian of an elastic energy potential function $U_k(\varphi_1,...,\varphi_n)$. A quasi-static requirement for stability is that the Hessian of the total potential energy, i.e., $\boldsymbol{G}+\boldsymbol{K}$, has all positive eigenvalues. We consider only local control of the joints, where $\boldsymbol{K}$ is a diagonal matrix with local joint stiffness values K_i at the diagonal. At the boundary of the region of stabilizing K_i the eigenvalues of $\boldsymbol{G}+\boldsymbol{K}$ become zero. Hence this boundary can be found by determining the combinations of K_i for which $\det(\boldsymbol{G}+\boldsymbol{K})$ equals zero. Analytical expressions can be obtained for systems up to at least order 3.
Besides these boundaries, as scalar measures we use the minimum required stiffness: 1) when all joint stiffnesses are equal, $K_i = K_0$; 2) when all joint stiffnesses exceed their single-joint requirement by the same amount, $K_i = -G_i+\Delta K_0$. Here G_i is the gravitational stiffness for joint i when all other joints are considered fixed. Model parameters are based on Winter (1979); resulting values of the G_i are indicated in Table 1.

Table 1 (left). *Gravitational stiffness per joint, in Nm/rad.*
Table 2 (right). *Measures for the required joint stiffness in several multi-segment stance models. All values in Nm/rad.*

joint	G_i
ankle	-754
knee	-432
hip	-160
neck	-8
shoulder	25

model	K_0	ΔK_0
ankle	754	0
ankle-hip	794	160
ankle-knee	1054	432
ankle-knee-hip	1106	528
ankle-knee-hip-neck	1106	529
ankle-knee-hip-shoulder	1107	532

RESULTS AND DISCUSSION

In a one-segment model, stability requires that $K_{ankle}+G_{ankle}>0$; i.e., the ankle joint stiffness must be at least 754 Nm/rad. However, in a two-segment ankle-hip model stability is not guaranteed when $K_{ankle}>754$ Nm/rad and $K_{hip}>160$ Nm/rad, the single-joint requirements for each joint separately. The actual stability boundary is an arm of a hyperbola with $K_{ankle}=754$

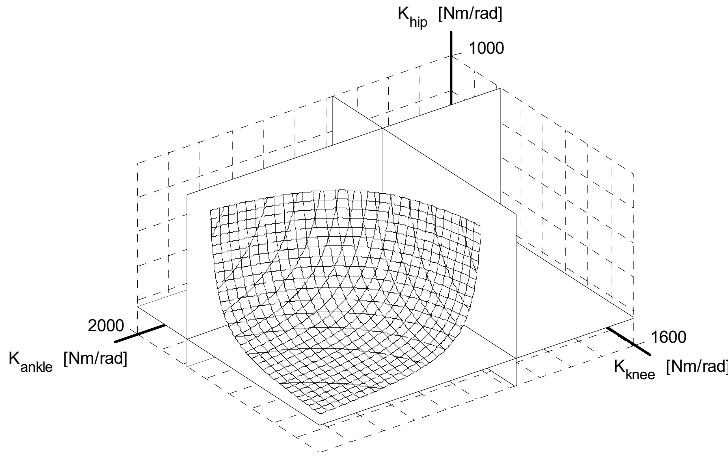

Figure 1. *Joint stiffness requirements for the ankle-knee-hip model. The straight planes represent the single-joint requirements, i.e., $K_{ankle}>-G_{ankle}$, $K_{knee}>-G_{knee}$, $K_{hip}>-G_{hip}$. Joint stiffness combinations at the near side of the curved surface actually result in quasi-statically stable stance.*

Nm/rad and $K_{hip}=160$ Nm/rad as asymptotes. As a result of the interaction between segments, typically both joint stiffnesses must exceed their single-joint requirement considerably to obtain stable stance (see Table 2). Only when one of the joints has a very high stiffness, its influence on the other joint can be ignored. When the knee is included instead of the hip, the interaction effect is stronger, as G_{knee} is larger than G_{hip}. In a three-segment ankle-knee-hip model, the stability boundary becomes a hyperbolic surface in a three-dimensional joint stiffness space (Figure 1). The numerical measures indicate that the stiffness requirements are heightened further in this case (Table 2). Modeling the head or the arms as additional segments separate from the trunk has only a minimal effect.

CONCLUSIONS

Inclusion of additional joints in a stance model substantially increases the local stiffness requirements for the joints already present. Assuming equal stiffness for all joints, in the ankle-knee-hip model the ankle stiffness must be at least 1106 Nm/rad, compared to 754 Nm/rad in the conventional single-segment stance model. Hence, stabilizing the inverted multi-segment pendulum of the standing human appears to be even more challenging than assumed previously.

REFERENCES

1. Winter, D.A., 1979. *Biomechanics of Human Movement*. John Wiley & Sons, New York.

ACKNOWLEDGEMENTS

Grant 575-23-014 of the Netherlands Organization for Scientific Research (NWO) to L.A. Rozendaal.

THE EFFECT OF LOWER EXTREMITY FATIGUE ON SHOCK ATTENUATION DURING LANDING

Kristian M. O'Connor, Evan Coventry, Barbara A. Hart, Sarika K. Monteiro, Jennifer E. Earl and Kyle T. Ebersole
Department of Human Movement Sciences
University of Wisconsin - Milwaukee: krisocon@uwm.edu, web: www.uwm.edu

INTRODUCTION

The forces that are imposed on the body due to landings must be absorbed primarily in the lower extremity. Muscles assist in the absorption of these impact forces [1], and it has been shown that a fatigued muscle decreases the body's ability to attenuate shock from running [2]. The purpose of the study was to determine the effect of lower extremity fatigue on shock attenuation and joint mechanics during a drop landing. It was hypothesized that lower extremity fatigue would cause a decrease in the shock attenuation and alter joint mechanics.

METHODS

Ten active, non-pathologic male participants, 19 to 27 years of age, were recruited for participation. Each participant took part in a fatigue landing protocol (FLP) that was similar to that utilized by Madigan & Pidcoe [3]. The FLP included cycles of a drop landing, a maximal countermovement (CM) jump, and five squats repeated until exhaustion. Accelerometers attached to the skin were used to measure tibia and head accelerations. Shock attenuation was calculated through a transfer function [4]. Sagittal plane lower extremity kinematics were collected using an electromagnetic tracking system and kinetics were collected using a force plate. A repeated-measures ANOVA ($p < 0.05$) was performed on each of the dependent variable across the cycles of the FLP.

RESULTS AND DISCUSSION

The power output for the CM jumps performed in each cycle significantly decreased from 1197 ± 273 W to 805 ± 182 W. This indicated that the FLP elicited fatigue, and the individual joint work values indicated that the knee experienced the greatest decrement in performance (Figure 1a), as was anticipated. However, there were no significant changes in tibia and head acceleration or in the shock attenuation (Table 1). The range of motion at the ankle significantly decreased as the FLP progressed, but the knee and hip ranges of motion were not significantly different (Table 1). Hip joint work significantly increased, and ankle work showed a decreasing trend, consistent with a distal to proximal redistribution of joint work (Figure 1b). The total work done by the lower extremity remained approximately constant throughout the FLP, which was expected since the drop height remained constant. Interestingly, the knee joint work during landing was not significantly different from the beginning to end, even though the corresponding jump performance dramatically worsened at the knee.

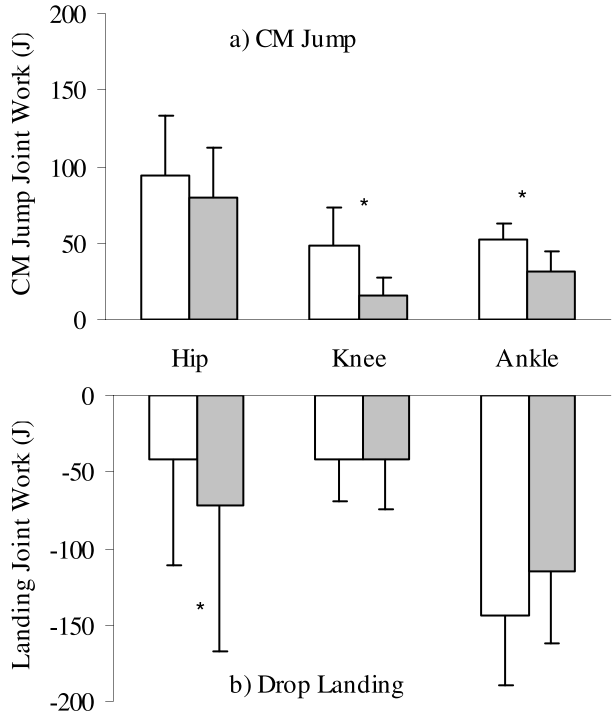

Figure 1. Group mean net joint work for the a) countermovement jump and the b) drop landing for the first (white bars) and last (gray bars) cycles. * indicates significant difference ($p < 0.05$).

CONCLUSIONS

This change in work distribution is thought to be a compensatory response to utilize the larger hip extensors that are better suited to absorb the mechanical energy of the impact. The results suggested that the lower extremity is able to adapt to fatigue though altering kinematics at impact and redistributing work to larger proximal muscles.

REFERENCES

1. Mizrahi J & Susak Z. *Eng Med* **11**, 141-147, 1982.
2. Voloshin O, et al.. *Clin Biomech* **13**, 513-520, 1998.
3. Madigan ML & Pidcoe PE. *J Elect & Kines* **13**, 491-498, 2003.
4. Derrick TR et al.. *MSSE* **30**, 128-135, 1998.

ACKNOWLEDGEMENTS

UWM College of Health Sciences.

Table 1: Group mean (± SD) acceleration and kinematic variables for the first and last cycles of the FLP. * indicates a significant difference between time points ($p < 0.05$).

	Tibia Acceleration (g)	Head Acceleration (g)	Transfer Function (dB)	Ankle ROM (°)	Knee ROM (°)	Hip ROM (°)
First Cycle	13.2 ± 4.2	3.9 ± 1.3	-12.1 ± 3.2	48.1 ± 6.4*	46.7 ± 11.9	37.9 ± 15.4
Last Cycle	12.3 ± 1.9	3.8 ± 1.1	-14.1 ± 3.9	43.6 ± 5.0	44.2 ± 16.5	45.9 ± 27.5

THREE DIMENSIONAL KNEE JOINT KINEMATICS AND LOWER LIMB MUSCLE ACTIVITY OF ANTERIOR CRUCIATE LIGAMENT DEFICIENT KNEE JOINT PARTICIPANTS WEARING A FUNCTIONAL KNEE BRACE DURING RUNNING

Daniel Théoret, M. A., and Mario Lamontagne Ph. D.
University of Ottawa,
email: dtheo087@uottawa..ca, web: www.biomech.uottawa.ca

INTRODUCTION

Knee braces have been found to provide limited stability to the ACL deficient (ACLD) knee in situations where the knee is loaded during sporting movements [1,3]. The increased laxity in the joint requires the patient's body to compensate for the ACLD by also altering muscle recruitment patterns, such as the hamstrings and quadriceps to adequately stabilize the knee during such activities [4,5]. Different adaptation strategies have been found between patients that can cope with the injury and patients that cannot. One of the expected changes can be muscle activation characteristics of the injured knee during strenuous activity with and without a functional knee brace.

METHODS

A group of 11 ACLD male participants (mean: 33.5, ± 7.7 yrs, 89.1, ± 12.5 kg, 185.7, ± 7.8 cm) took part in the experimentation. At the time of the testing session, all participants exhibited full knee range of motion and no pain during walking. Three dimensional (3D) kinematic and electromyography (EMG) data were collected for ten consecutive gait cycles during running on a treadmill under both braced (B) and unbraced (UB) conditions. Video was collected using the SIMI* Motion system (SIMI* Reality Motion Systems GmbH) from four digital video cameras (JVC GR-DVL9800) set at 60 Hz. EMG data was collected at 1000 Hz (Bortec Biomedical Ltd.) for vastus lateralis and medialis, biceps femoris, semitendinosis, lateral and medial gastrocnemius muscles. Statistical analysis of both the EMG and 3D kinematic data using one-way Anova (p=0.05) focused on comparisons between the braced and unbraced conditions.

RESULTS AND DISCUSSION

Fairly similar flexion/extension knee joint patterns were observed between the braced and non-braced conditions. Bracing significantly reduced ($p<0.05$) the peak abduction angle, and the total range of motion during running (Table 1). The internal/external rotation curve for the braced condition showed a significantly ($p<0.05$) lower range of motion than in the unbraced condition (Table 1). Bracing also prevented the ACLD knee from going into internal rotation during the running cycle. Overall analysis demonstrated that bracing reduced the overall range of motion of the knee joint in the frontal and transverse planes but did not affect the motion in the sagittal plane for ACLD participants during running.

Comparisons of muscle activity between the braced and unbraced conditions revealed some changes in timing and amplitude characteristics of the EMG signal. Muscle activity (measured as the area under the LE EMG curve) increased for all the muscles in the braced condition. This increase ILE EMG was not significant most likely because of high variability within participants. Our results showed a tendency that at heel-strike, the EMG amplitude of the quadriceps (vastus medialis and lateralis) decreased while hamstrings (biceps femoris and semitendinosis) increased in the braced condition.

CONCLUSIONS

The findings of this study suggested that bracing significantly affected the kinematic profile of ACLD patients during running. Although no significant differences were observed for the EMG variables, tendencies were noted both in terms of muscle activity and timing, especially for the semitendinosis muscle. The tendencies in EMG activity changes caused by the brace to the semitendinosis muscle were not however in accordance with the added mechanical restrictions expected while wearing a functional knee brace. This led us to believe that the brace had a proprioceptive effect on the injured limb, resulting in added active muscular stability. These findings are therefore in accordance with the phenomenon of a proprioceptive contribution of the functional knee bracing [2]. We must point out that the sample size might have a large influence in the statistical difference in the EMG findings.

REFERENCES

1. Beynnon BD, et al. *Am J Sports Med* **31,** 99-105, 2003.
2. Németh G, et al. *Am J Sports Med* **25**, 635-641, 1997.
3. Ramsey DK. et al. *Clin Biomech* **16**, 61-70, 2001.
4. Rudolph K. et al. *Knee Surg Sports Traumatol Arthros* **9**, 62-71.
5. Smith J. et al. *Arch Phys Med Rehab* **84**, 1680-1686.

Table 1. Kinematics data in the sagittal, frontal, and transverse planes over the duration of the running cycle, n=11.

	Peak angle (deg.)						**Total ROM (deg.)**		
	Flex.	Abd.	Ext. rot.	Ext.	Add.	Int. rot.	Flex./Ext.	Abd./Add.	Int./Ext. rot.
UB	82.4±8.0	15.3±4.2*	-10.8±5.9	13.2±5.5	1.2±2.7	5.1±8.0	69.2±8.9	14.7±4.7*	15.9±5.6*
B	83.4±7.1	10.2±2.9*	-9.7±5.4	14.2±4.6	1.0±2.4	1.2±3.0	68.7±6.4	9.2±2.8*	10.9±4.8*

*Significant difference in the angular value between bracing conditions ($p<0.05$)

COMPARISON OF DRESSAGE RIDER POSTURE WHEN MOUNTED ON DIFFERENT HORSES

Laurelyn E. Keener[1] and Morris Levy[2]

[1]Dept. of Biology
[2]Biomechanics Laboratory, Dept. of Health Physical Education and Recreation
University of Minnesota Duluth
E-mail: keen0070@d.umn.edu

INTRODUCTION

The equine sport of Dressage subjectively judges how well a horse and rider move together. Dressage experts believe that a horse cannot move at its potential without the optimal level of balance and communication with the rider.

Measurable differences can be observed in the kinematics of multiple horses when ridden by a professional vs. amateur rider [2]. The availability of measurable horse-rider interactions would further benefit Dressage training, instruction and judging. Therefore, the purpose of this study was to compare rider posture with two horses, and to assess the resulting effect on the horses.

METHODS

Two well-conditioned Dressage horses, accustomed to the arena in which data collection occurred, were fitted with identical 17.5-inch Dressage saddles and their usual Dressage bridles. Ten adult amateur Dressage riders rode both horses. All riders had at least 4 years of riding experience and 50 hours of formal Dressage education. Two calibrated pan and tilt cameras were positioned 15 meters apart to gather position-time data as the horses trotted along a 12-meter track.

Reflective markers were placed on the following landmarks of each rider: top of the head, jaw, shoulder, hip, knee and ankle. Markers were also placed over palpable skeletal regions along the horses' right hind limbs to aid in later identification of joint angles. Each rider was given a 5-minute warm-up period with the horse. Five consecutive trials of each horse-rider combination were filmed. All pairs were filmed within a five-hour period, and their order was randomized.

Using Peak Motus® Pan and Tilt Software, one stride cycle, beginning with the right hind limb in perpendicular stance phase, from each trial was captured and digitized. The average stifle-, hock-, hip- and knee- angle ranges were calculated to assess horse movement and rider posture. Figure 1 illustrates the angles of interest from which comparisons were made.

RESULTS AND DISCUSSION

Table 1 described the average angular ranges of riders and horses. Separate paired t-tests ($\alpha = 0.05$) were used to compare the rider hip and knee angle ranges while riding two different horses. The hip angle ranges changed significantly ($t_9 = 2.50$, $p = 0.0337$), while the knee angle ranges remained similar between horses ($t_9 = 0.064$, $p = 0.95$). Paired comparisons of horse angular ranges revealed significant differences for both the stifle and hock ($t_9 = 11.10$ and 6.78, respectively; $p < 0.0001$). These results suggest that riders change their movement, adjusting to the movement and potential aptitude of the horse in relationship to the skill involved (trotting action in this case).

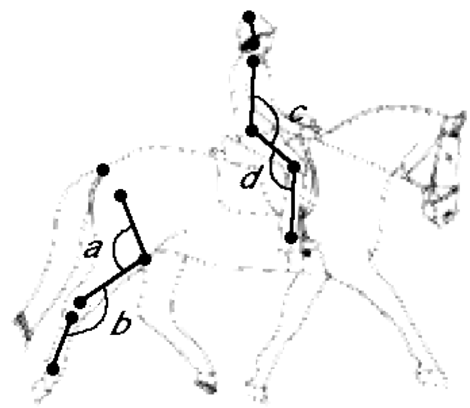

Figure 1: Outline of horse and rider shown for orientation purposes. Horse and rider marker placement and joint angles (*a* = stifle, *b* = hock, *c* = hip and *d* = knee).

CONCLUSIONS

Dressage, a sport based on qualitative observations, would benefit from quantitatively defining desirable interaction characteristics. In analyzing joint angles of ten riders on two horses, we found that a rider's hip kinematics vary when riding horses whose movement patterns are different. Thus, when teaching and judging a pair, the rider position must be flexible depending upon the horse' gaits.

REFERENCES

1. Cano, M. R. et al. (1999). *J. Vet. Med.,* **46**, 91-101.
2. Peham, C. et al. (2001). *Sports Eng.,* **4**, 95-101.

ACKNOWLEDGEMENTS

This project was funded in part by the University of Minnesota's Undergraduate Research Opportunity Program. Expressed appreciation to Nic Matack, Josh Turbes, Krissy Falk and Charles Luoma for help in data processing.

Table 1: Descriptive angular values (Mean ± SD)

Joint Angle Ranges (deg)	Stifle (a)	Hock (b)	Hip (c)	Knee (d)
Horse A	28.7 ± 1.7	46.7 ± 1.4	11.1 ± 2.7	13.8 ± 2.2
Horse B	41.7 ± 2.2	52.9 ± 2.8	14.2 ± 5.3	13.7 ± 6.1

RUPTURE PRESSURES FOR HUMAN AND PORCINE EYES UNDER STATIC AND DYNAMIC LOADING

[1]Eric Kennedy, [1]Katherine Voorhies, [1]Amber Rath, [2]Frederick Brozoski, and [1]Stefan Duma
[1]Virginia Tech – Wake Forest, Center for Injury Biomechanics,
[2]United States Army Aeromedical Research Laboratory; email: eric_kennedy@vt.edu, web: www.CIB.vt.edu

INTRODUCTION

More than 30,000 people lose sight in at least one eye every year in the United States alone [1]. Among the severe injuries that can result in the loss of an eye is globe rupture. Previous studies have attempted to determine the rupture pressure of both human and porcine eyes; however, no studies have been conducted at a dynamic rate. Porcine eyes are frequently used as human eye surrogates in ocular research due to their anatomical similarities. Since biological tissue typically displays viscoelastic behavior, it is hypothesized that the rupture pressure of the eye will be directly affected by the pressurization rate of the eye. Therefore, the purpose of this study is to determine the static and dynamic rupture pressure of human and porcine eyes.

METHODS

A pressure system was developed to internally pressurize the eye with physiological fluid via a needle inserted through the optic nerve. Static testing was accomplished by increasing the internal pressure of the eye by approximately 0.02 MPa/second, using 10 human and 10 porcine eyes until the eyes ruptured at their maximum static pressure. The dynamic testing of 10 human and 10 porcine eyes was accomplished by setting the initial pressure to release at 2.8 MPa, resulting in a loading rate of approximately 2.77 MPa/second, and measuring the pressure at which the eyes ruptured.

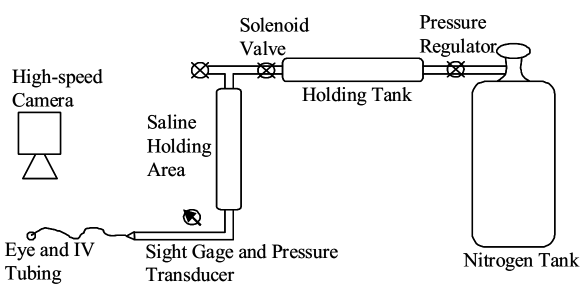

Figure 1: Schematic of eye pressurization system used for both static and dynamic tests.

RESULTS AND DISCUSSION

Globe rupture occurred primarily at the equator for both static and dynamic tests. The average loading rate under static loading was 0.02 ± 0.01 MPa/second while the average loading rate for dynamic tests was 2.77 ± 0.58 MPa/second. Static test results displayed an average rupture pressure for porcine eyes of 1.00 ± 0.18 MPa while the average rupture pressure for human eyes was 0.36 ± 0.20 MPa. Porcine eyes under static loading were found to be significantly stronger than human eyes ($p = 0.01$). For dynamic loading, the average porcine rupture pressure was 1.64 ± 0.32 MPa, and the average rupture pressure for human eyes was 0.91 ± 0.29 MPa. Again, the porcine eyes were found to be significantly stronger than the human eyes ($p = 0.01$). Additionally, the dynamic rupture pressures for both porcine and human eyes were significantly higher ($p = 0.01$) than their respective static rupture pressures.

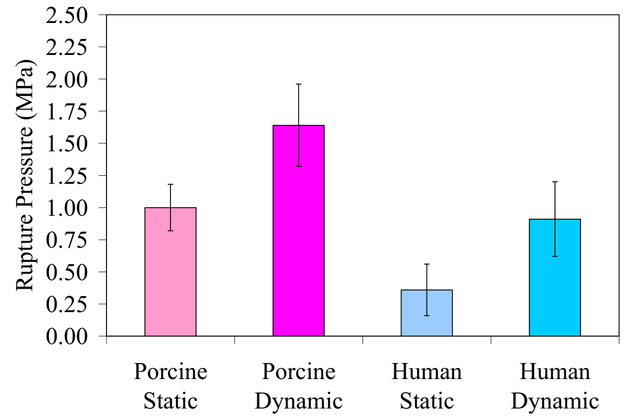

Figure 2: Averages of results of rupture pressure testing with standard deviations. Porcine eyes ruptured at a higher pressure than human eyes ($p = 0.01$). For both human and porcine eyes, dynamic rupture pressures were higher than static rupture pressures ($p = 0.01$).

CONCLUSIONS

Both human and porcine eyes exhibit large viscoelastic effects when loaded dynamically. The viscoelastic behavior of the eye under dynamic loading is consistent with that seen in other biological tissue [2]. Under dynamic loading the human eye can withstand approximately 150% more pressure before rupture than under static loading, while under the same circumstances the porcine eye can withstand approximately 64% more pressure before rupture. This behavior proves that previously determined material characteristics of the eye from static tests will lead to inaccurate predictions of the rupture pressure of the eye, both human and porcine. Finally, due to differences in their response versus human eyes, separate criteria must be utilized to interpret results of porcine eye tests versus human eye tests.

REFERENCES

1. Parver, L.M. Eye Trauma: The Neglected Disorder. *Archives of Ophthalmology* **104**, 1452-1453, 1986.
2. Yamada, H and Evans, F.G. *Strength of Biological Materials.* Williams and Wilkins, Baltimore.

ACKNOWLEDGEMENTS

The authors would like to thank the United States Army Aeromedical Research Laboratory for their support of this research. This paper does not represent the official practice or policy of the United States Army.

BLOOD FLOW SIMULATION IN AN ARTERIO-VENOUS FISTULA

[1] Zaher KHARBOUTLY, [1] Marianne FENECH, [2]Jean-Marc TREUTENAERE, [1] Isabelle CLAUDE, [1] Cécile LEGALLAIS
[1]Université de Technologie de Compiègne (UTC), UMR CNRS 6600, Biomécanique et Génie Biomédical
Centre de Recherche de Royallieu - BP 20529-60205 Compiègne, France
[2]Département de Radiologie, Polyclinique Saint-Côme, Compiègne, France

INTRODUCTION

Patients with ESRD "end stage renal disease" require haemodialysis. Its most desirable form of vascular access is the arterio-venous fistula. We propose an investigation protocol to understand the correlation between hemodynamic changes in this very specific blood vessel and the associated clinical complications. Realistic 3D reconstruction geometry of the fistula is the result of segmenting CT angiography images. Then the geometrical model is treated with industrial computation fluid dynamics software for blood flow simulation.

METHODS

A non pathologic fistula realized in 1987 is the base for this study. CT images are therefore acquired using "Lightspeed Ultra CT, General Electric" & the smartPREP technology. The images are then exported in a DICOM format. Vessel contour segmentation is the output of the region growing algorithm to be finally reconstructed into a three dimensional volume by applying "NURBS". This volume is introduced into Gambit 2.1® (Fluent, Lebanon, NH, USA) to produce the biomechanical model. At the entrance of the fistula (arterial side), a straight tube of sufficient length is added to allow the blood flow profile development. The volume is perpendicularly divided into seven sub-volumes taking into consideration the vascular central axis as a reference. Each face of the sub-volumes has been meshed with a 524 quadrilaterals at the input & at the output. A boundary layer at the wall of four rows has been added to calculate the velocity gradients & wall shear stress. The Cooper algorithm is implemented to propagate into the volume meshing it with hexahedral mesh of total number 150 288[1]. The blood flow in the vessels of the meshed biomechanical model is calculated using Navier-Stokes equation solved using Fluent 6.1® (Fluent, Lebanon, NH, USA). The post treatment and interpretation of the results are affected using Ensith7.6® (CEI, Apex, NC, USA). In such vessels the blood is considered a Newtonian fluid of viscosity 0,004 Pa.s and density of 1050 kg/m3 [2]. In our study, a non stationary flow of a cardiac frequency 76 beats/ minute with a period of (0,8 sec) is applied. The entrance velocity follows the physiological curve presented in the literature [3].

RESULTS AND DISCUSSION

As a result of the numerical simulation, the non stationary flow enables flow pattern visualization during the cardiac cycle in the artery, anastomosis & vein. Figure 1a & 1b shows respectively an axial & a sagittal plane of the arterio-venous fistula at two different cardiac instants.

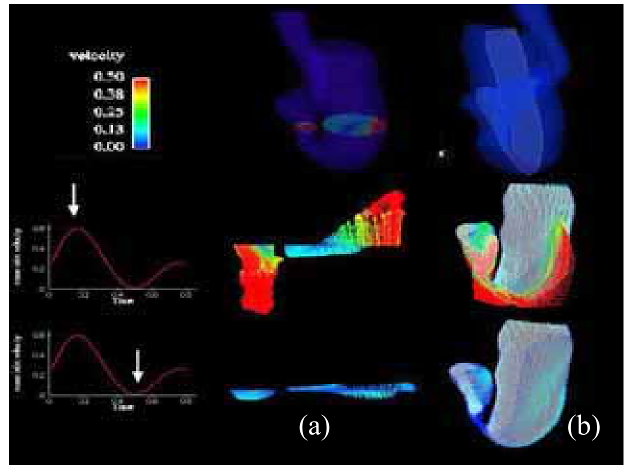

Figure 1: (a) velocity profile axial plane. -(b) velocity profile sagittal plane of the anastomosis

In the axial plane we can notice the parabolic velocity profile in the artery. Whereas in the vein, we see a partial inversion of the velocity profile at the systolic peak. At the beginning of the diastole, there is low velocity. For the sagittal plane we can see a jet towards the external wall of the vein due to the acceleration at the anastomosis, which produces constraints over the wall of the vein and noticeable recirculation phenomena at the low velocity zone at the interior.
We validate our results by comparing it to an Echo-Doppler examination for the same patient. We measure the flow at the artery and visualize approximated velocity profiles at different cross-sections. The obtained flow representation is less accurate than our method. In addition our simulation allows wall shear stress calculation which can not be obtained in the Doppler study.

CONCLUSIONS

The simulation indicates the risk zones, weak shear rates & views of the recirculation zone. The obtained flow representation is more precise than the Doppler velocity measurements. Therefore our method represents for the clinicians an additional tool to prognostic and diagnosis. Indeed low constraints may predict atherosclerosis generation and high constraints may lead to potential changes in the venous shape serious structural changes

REFERENCES

1. S. Prakash and C. R. Ethier, *J. Biomech. Eng*., vol. 123, no. 2, pp. 134–144, 2001.
2. Comolet , R. Biomécanique circulatoire. Masson, Paris 1984.
3. Piljs, N.H.J., de Bruyne, P. *Kluwer Academic Publishers*, The Netherlands 1997.

PRIMARY HIP STEM MICROMOTION ASSESSMENT: CORRELATION BETWEEN RASP AND STEM STABILITY

[1,2] Elena Varini, [3]Marco Vandi, [1,3]Luca Cristofolini, [2]Angelo Cappello and [1]Marco Viceconti
[1]Laboratorio Tecnologia Medica, Istituti Ortopedici Rizzoli, Bologna, Italy, cristofolini@tecno.ior.it
[2]DEIS, University of Bologna, Bologna, Italy, evarini@deis.unibo.it
[3]DIEM, University of Bologna, Bologna, Italy

INTRODUCTION

Primary stability achieved by press-fit is critical for the long-term success of cementless hip stems [1]. It is recognized that micromotions over 30-150 micron prevent osteointegration and lead to implant failure [2]. Conversely, excessive press-fit can cause intra-op fractures [3]. A device able to intra-operatively assess stem stability was developed and validated [4]. It consists of an angular sensor and a torsional load cell, which are embedded in a real-time torque wrench. The device is manually operated by the surgeon, who can use this quantitative information to decide whether more press-fit is needed.

This device could successfully discriminate between stable and unstable stems intra-operatively [4]. The goal of the present work was to find a correlation between rasp and stem stability. This could provide the surgeon with a quantitative information concerning the quality of the femoral canal just prepared before inserting the stem, thus enabling a prediction of the implant stability possibly achievable.

METHODS

The device [4] is meant to measure a stem/femur relative rotation when a torque is applied. It incorporates two high accuracy transducers, an RVDT angular sensor and a torsional load cell. A custom designed connector allows an easy and rigid insertion of the device in the stem neck modularity. As a reference point for the angular probe, a Kirschner nail is driven anteriorly on the greater trochanter prior to the insertion of the device. All the electronics is hosted in a cavity machined inside the handle. Data acquired (sampling frequency 200Hz) are recorded in a separate memory, for post-op evaluations. The surgeon interface, located in the upper side of the handle, is composed by: (i) a display, for the visualization of the stem size; (ii) four buttons to select a function of the device; (iii) two bi-colored series of LEDs, indicating the amount of torque applied and the extent of micromotion achieved.

Three composite and two embalmed re-hydrated cadaveric femurs were tested. An experienced surgeon prepared the femurs to be implanted, in a single session and following the standard surgical protocol. The tests were performed as follows: a first torque-micromotion acquisition was made with the last rasp used by the surgeon to prepare the canal still inserted into the femur. The measurement device was connected to the rasp and the angular and torsional data were acquired when a torque (up to 20Nm) was manually applied. Five to ten repetitions were performed on each femur. The same measurement protocol was repeated with the corresponding stem inserted and press-fitted in the femoral canal. Data were acquired and processed.

RESULTS AND DISCUSSION

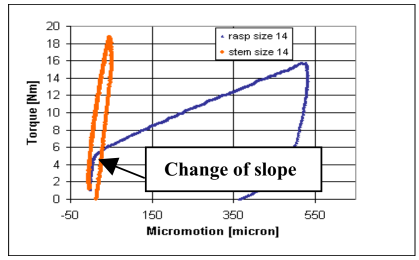

Fig.1 Typical torque-micromotion curves for the rasp and the stem on the same femur

Observing the increasing part of the torque-micromotion curve (Fig.1), the stem micromotions increase linearly, while the rasp shows a highly non-linear trend (with a pronounced "knee" corresponding to a sudden increase of the micromotion rate). Thus it was decided not to directly compare the rasp-stem motion patterns, but to search for a parameter of the rasp curve to correlate with the stem-micromotion.

The best-correlated rasp-parameter was the level of torque corresponding to the slope change in the torque-micromotion curve. This rasp parameter presented a linear trend if plotted against the stem micromotion (Fig.2), thus showing the presence of a good correlation (R^2>0.93) between rasp and stem stability.

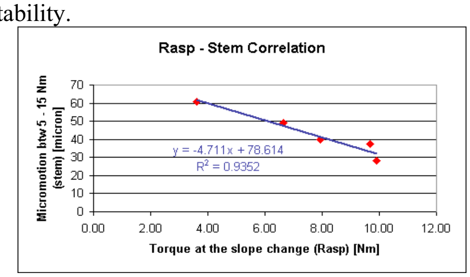

Fig.2 Correlation between rasp and stem stability

CONCLUSIONS

The aim of the present work was to investigate if it was possible to evaluate the quality of the femoral canal and predict the stem stability, by using the torque wrench, prior to the stem implantation.The correlation tests yielded satisfactory results. The rasp and stem stability seems to be strictly related.

REFERENCES

1. Maloney WJ, et al. *Clin Orthop* **249**,129-140, 1989.
2. Søballe K, *Acta Orthop Scand* **255**, 1-58, 1993.
3. Fishkin Z, et al. *J Arthroplasty* **14**, 98-101, 1999.
4. Cristofolini L, et al. Submitted to *Med Eng & Phys*

ACKNOWLEDGEMENTS

Work financed by EC: ISAC Project IST-1999-20226.

CHARACTERIZATION OF INTRALIMB COORDINATION DEFICITS IN CHRONIC STROKE PATIENTS

[1] Mark Dohring, PhD [1] Karen Sng. and [1,2]Janis J Daly, Ph.D.
[1]Louis Stokes Cleveland Department of Veterans Affairs Medical Center,
2 Department of Neurology, Case Western Reserve University School of Medicine

INTRODUCTION

Many stroke survivors experience deficits in coordination that cause gait deficits. Normal gait is dependent on intralimb coordination among hip, knee, and ankle joint movements. Although the presence of intralimb coordination deficits were noted in stroke survivors, a credible quantitative measure has not been reported. The purpose of this study was: 1) quantitatively characterize intralimb coordination in stroke survivors with persistent gait deficits; and 2) determine whether quantification of intralimb coordination discriminated improvement following an innovative treatment with or without functional neuromuscular stimulation (FNS) using intramuscular (IM) electrodes (FNS-IM).

METHODS

Twenty-nine stroke survivors (0.23 to 14.92 yrs post stroke) and three healthy controls were enrolled in the study. The study was conducted under the supervision of the Louis Stokes Cleveland Department of Veterans Affairs Medical Center, Committee for Human Subject Protection (VAMC,IRB). Informed consent was obtained.

Subjects were randomly assigned either to Group 1, FNS-IM or Group 2, No-FNS. Both groups received conventional gait training and body weight supported treadmill training for 1½ hours/day, 4 days/week for 12 weeks. Group 1 (FNS-IM) had implantation of up to 8 electrodes for paretic muscles. An 8-channel research stimulator delivered the FNS patterns that were custom-designed for each individual.

A VICON 370 V3.5 was used to acquire pre-treatment and post-treatment hip and knee joint kinematic data during over-ground walking. No FNS was activated during the testing.

Hip and Knee angle consistency across multiple steps was analyzed using a vector analysis method [1]. Incremental change in hip and knee angle between frames of a step was used to define a vector in hip-knee angle space. The directions of these vectors were used to define the angular component of correspondence (ACC) across multiple steps for each limb. Comparisons were made for stroke vs. control and FNS-IM vs. no FNS-IM.

RESULTS AND DISCUSSION

According to ANOVA model analysis (summarized in Tables 1, 2, and 3, below), there was a significant difference in intra-limb coordination for the following: stroke vs. control (both limbs); involved limb vs. uninvolved limb for the stroke survivors; and involved limb pre-treatment vs. post treatment for the FNS-IM group.

The results indicated that the ACC measure successfully differentiated intralimb coordination between controls and stroke survivors for both limbs and between the involved and uninvolved limbs in stroke survivors, meeting the first goal of this study. The ACC also discriminated an improvement following treatment in the FNS-IM group, meeting the second goal of the study. There was no gain detected for the non-FNS-IM group.

Table 1. Stroke vs. Control

	Stroke mean (std dev)	Control[a] mean (std dev)	Comparison p
Involved limb	0.78 (± 0.11)	0.97 (± 0.01)	0.003*
Uninvolved limb	0.86 (± 0.10)	0.97 (± 0.00)	0.042*

[a] Left leg used for control subjects
* $p < 0.05$ is significant

Table 2. Limb comparison for stroke

	Involved mean (std dev)	Uninvolved mean (std dev)	Comparison p
Pre-treatment	0.78 (± 0.11)	0.86 (± 0.10)	0.005*
Post-treatment	0.82 (± 0.12)	0.88 (± 0.07)	0.028*

* $p < 0.05$ is significant

Table 3. Pre- vs. post- treatment change

	Pre-treatment mean (std dev)	Post-treatment mean (std dev)	Comparison p
Stroke-involved FNS	0.81 (± 0.08)	0.87 (± 0.07)	0.042*
Stroke-involved Non-FNS	0.75 (± 0.13)	0.77 (± 0.14)	0.747

* $p < 0.05$ is significant

REFERENCES

1. Tepavac D, et al. *Journal of Applied Biomechanics* **17,** 259-270, 2003.

ACKNOWLEDGEMENTS

This work was supported by the Department of Veterans Affairs, Office of Rehabilitation Research and Development, Grant 2226R, Principal Investigator: Janis J Daly, Ph.D.

ESTIMATING THE AXIS OF A SCREW MOTION FROM NOISY DATA — NEW METHOD BASED ON PLÜCKER LINES

[1] Koon Kiat Teu, [2]Wangdo Kim
[1]School of Mechanical & Production Engineering, Nanyang Technological University, Singapore
[2]Biomechanics Laboratory, Legacy Clinical Research & Technology Center; email: wkim@biomechresearch.org

INTRODUCTION

Screw axis has been employed to describe joint kinematics mainly in clinical assessments. It is intuitive that the geometry of the screw axis of a spatial displacement can be fully and easily studied using Plücker's coordinates that define the line directly [1]. One of the fundamental problems in calculating screw axis is noisy data. The new algorithm presented in this paper takes advantage of set of line patterns, which are derived from point data using dual number relationship. The method involves mapping a set of lines to the corresponding lines after movement. The mapping of vectors is made possible by the use of dual transformation matrix. The dual transformation matrix (DTM) has been shown to be effective means of three-dimensional *line* transformation in displacement analysis [2].

METHODS

The method in this paper involves obtaining the DTM from coordinated points. This method has been mentioned in [2]. After solving for DTM $[\hat{R}]$, we solve for the dual vector associated with DTM using the eigenvector.

$$[I - \hat{R}]\hat{V} = 0 , \qquad (1)$$

and seek solution other than $\hat{V} = 0$. This is easily done if we separate it into the pair of vector equations compromising the primary and dual component respectively

$$[I - R]\boldsymbol{V} = 0$$

$$[I - R]\boldsymbol{W} = [D]\boldsymbol{V} \qquad (2)$$

Where $[D]$ is the skew-symmetric matrix defined by $[D]\boldsymbol{V} = \boldsymbol{d} \times \boldsymbol{V}$ for any translation and we used the property of $[R]\boldsymbol{V} = \boldsymbol{V}$.

The proposed method was tested on simulated data. The simulations follow closely to that of [4].

RESULTS AND DISCUSSION

The simulation results in [4] ("new" and "FHA" method) were used as references for the proposed algorithm. The results of the "new" methods were superimposed to our simulation results in Figure 1 and 2 as a comparison. The general trend of the error follows that of those reference methods. The errors in direction and position were lower when there's significant noise. For skin movement artefact simulation, the estimation of the position using the proposed method was better. The error in direction is reasonably good and follows closely to that of the "FHA" method. The simulation results showed that the proposed method worked well, especially in estimating the direction of the screw axis when noise is present. The mapping of vectors gives a better estimate of the rotation than mapping of points data. The results are highly significant as they demonstrate an advantage of using line instead of points.

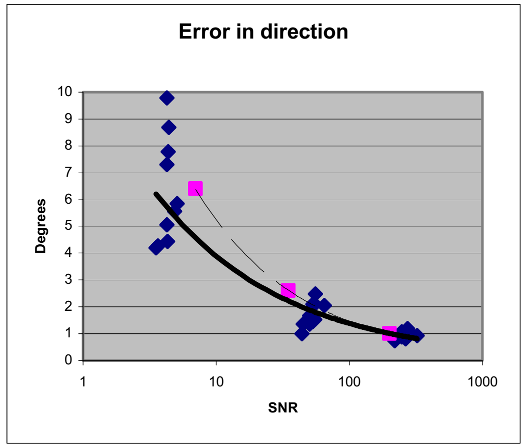

Figure 1: Mean error in the estimated direction of the axis plotted against the SNR (Signal To Noise Ratio). The solid lines correspond to the presented method and the dotted lines to the "new" method.

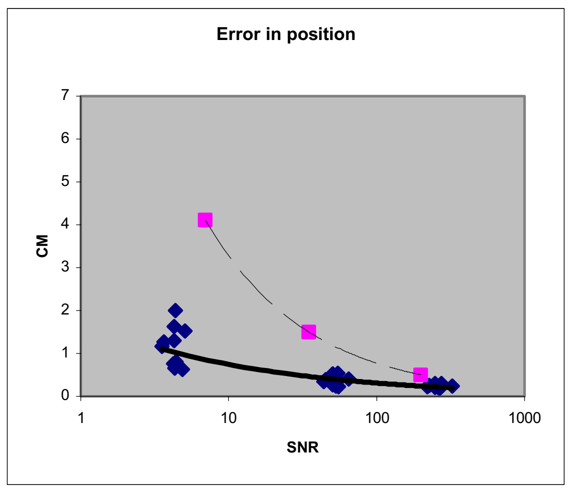

Figure 2: Mean error in the estimated position of the axis plotted against the SNR

CONCLUSIONS

In our study, the estimation of screw axes from a set of Plücker lines clearly outperforms the conventional methods using points data. This opens the range of new practical applications of Plücker lines in bio-kinematics situation. The method provides an alternative analysis tool for estimation of screw axes and can be applied to any actions such as gait analysis in clinical setting to estimate the screw axis.

REFERENCES

1. McCarthy, J. M. *Geometric Design of Linkages,* 2000.
2. Ying, N., et al. *J Biomech* **35,** 1647-1657, 2002.
3. Press, W. H., et al. *Numerical Recipes in C.*, 1992.
4. Halvorsen, K., et al. *J Biomech* **32,** 1221-1227, 1999

MECHANICAL PERFORMANCE OF ARTIFICIAL PNEUMATIC MUSCLES TO POWER AN ANKLE-FOOT ORTHOSIS

[1]Keith E. Gordon, [1,3]Gregory S. Sawicki and [1,2]Daniel P. Ferris
[1]Departments of Movement Science, [2]Biomedical Engineering, [3]Mechanical Engineering
University of Michigan, Ann Arbor, MI; email: kegordon@umich.edu

INTRODUCTION

A powered ankle-foot orthosis could be very useful for investigating neuromechanical control of human locomotion. Plantar flexor muscles are critical to the generation of forward velocity and support of the center of mass during human walking. The purpose of this study was to quantify the mechanical performance of a pneumatically powered ankle-foot orthosis that assists plantar flexion during the stance phase of walking.

METHODS

Three subjects walked at a range of speeds (0.5-2.0 m/s) wearing a unilateral ankle-foot orthosis (~1.5 kg) with either one or two artificial muscles working in parallel (Figure 1). Foot switches on the ball of the foot activated the artificial pneumatic muscles (6.2 bar) using on-off control. We hypothesized that two artificial muscles would provide greater torque and mechanical work than one artificial muscle.

Figure 1: Powered Ankle-Foot Orthosis. Left) Orthosis fit with a single artificial muscle. Right) Orthosis fit with two parallel artificial muscles to provide plantar flexor torque.

RESULTS AND DISCUSSION

Contrary to our hypothesis, the orthosis produced similar total plantar flexor torque and net work independent of the number of artificial muscles (Figure 2). The orthosis generated 57% of the peak ankle plantar flexor torque during stance and performed ~80% of the positive plantar flexor work done during normal walking. The similarity in torque and work between single and double muscle conditions can be explained by the artificial muscle force-length properties. Peak artificial muscle force will decrease linearly as artificial muscle length decreases during contraction. Subjects altered their ankle kinematics between single and double muscle conditions. During the double muscle condition subjects increased plantar flexion resulting in shorter artificial muscles lengths. At shorter artificial muscle lengths, the peak artificial muscle force was less.

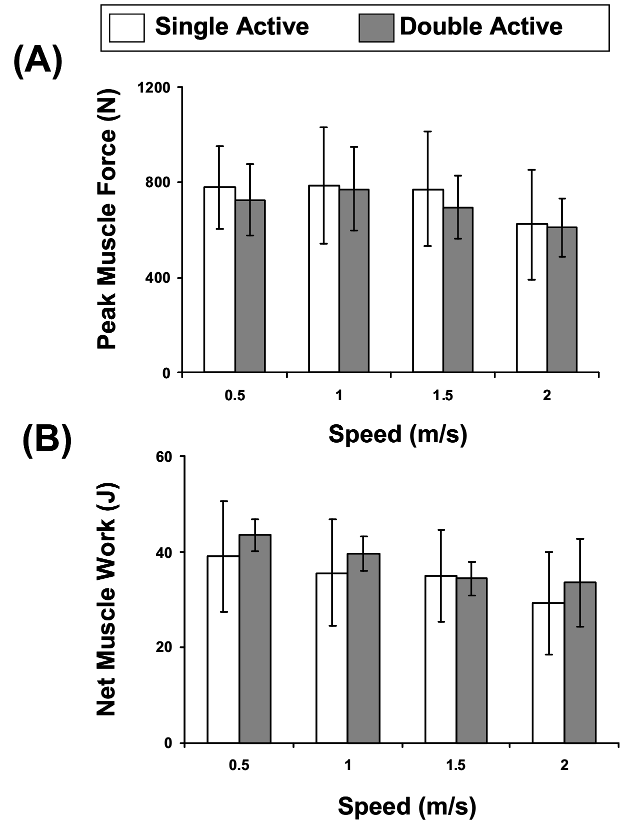

Figure 2: A) Peak artificial muscle force (mean ± s.d.). B) Net artificial muscle work (mean ± s.d.). Double muscle data is the sum of both muscles.

Positive work performed by the orthosis on the ankle joint (torque-angle) was about 29% less than work performed by the artificial muscles (force-length). Compliance in the muscle attachment brackets and orthosis shell resulted in the artificial muscles shortening without concomitant changes in joint angle.

CONCLUSIONS

These findings emphasize the importance of human testing in the design and development of robotic exoskeleton devices for assisting human movement. In this study, subjects modified their joint kinematics when walking with the powered orthosis, resulting in similar joint kinetics between conditions.

ACKNOWLEDGEMENTS

Supported by NIH R01NS045486 and NSF BES-0347479.

OBJECTIVE ULCER QUANTIFICATION BY RIM CURVATURE MAP

[1]Xiang Liu, [2]Wangdo Kim, [3]Reiner Schmidt, [3]Burkhard Drerup and [4]Jinsup Song
[1]School of Mechanical and Production Engineering, Nanyang Technological University, Singapore,
[2]Biomechanics Laboratory, Legacy Clinical Research & Technology Center, Portland, Oregon, USA
[3]Klinik und Poliklinik für Technische Orthopädie und Rehabilitation, Universtätsklinikum, Münster, Germany
[4]Advanced Wound Healing Center, Temple University School of Podiatric Medicine, Philadelphia, USA
email: wkim@biomechresearch.org

INTRODUCTION

A method of 3D optical technique for quantifying wound size is presented. More traditional measures of the wound length and width fail to account for irregular wound shape. A reliable and accurate wound size assessment is needed to objectively evaluate efficacy of various wound care modalities.

METHODS

A special platform was constructed to position the wand of the laser scanner and a digital camera in a common coordinate system when the ulcer surface is scanned. Using a FastSCAN laser scanner (Polhemus, Colchester, Vermont, USA), the ulcer's rim curvature map [1-2] is computed. Utilizing a specified rim curvature value, the wound edge is detected and processed via a cubic spline smoothing. The digital photo is, then, transformed into the same coordinate system as the laser scanner to qualitatively verify the wound boundary. The wound dimensions are reconstructed by interpolating the surface regions outside the ulcer using a second order polynomial fitted to the points outside the ulcer boundary. The averaged difference between the reconstructed surface and the scanned ulcer surface is taken as the mean ulcer depth. The volume is the product of area and the mean depth. Using this technique, a venous status ulcer at the lateral malleolus was scanned ten times during one month period. Three repeated measurements are made for each session.

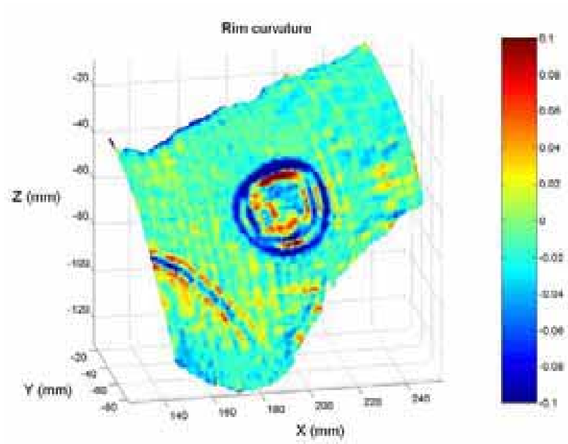

Figure 1: The rim curvature map of the ulcer.

RESULTS AND DISCUSSION

From the map of rim curvature (Fig. 1), the ulcer boundary can be readily delineated. Calculated wound depth, area, and volume are shown in Fig. 2 with the maximum, minimum and mean values of the three independent measurements. While there is slight increase in area, the ulcer depth and the volume have decreased over time, which are in agreement with the clinical observation.

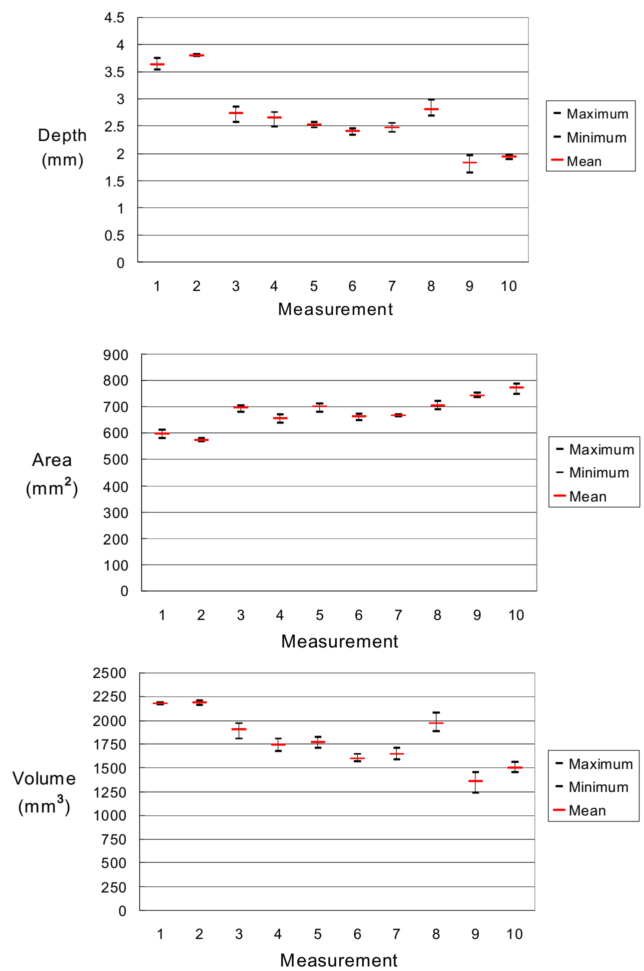

Figure 2: Calculated dimensions of the ulcer over a month.

CONCLUSIONS

The surface scanning aided by rim curvature maps and photograph is shown to be a potentially viable non-contact method of wound measurement. Additional studies are needed to test its reliability, accuracy, and utility of this technique in wound related studies.

REFERENCES

1. Frobin W. and Hierholzer, E. *Moiré Fringe Topography and Spinal Deformity* 71-82, 1983.
2. Liu X, et. al. *Real-Time Imaging* **10,** 217-228, 2004.

TARGET ACQUISITION BY PILOTS WEARING VARIOUS HEAD-SUPPORTED MASSES DURING SIMULATED FLIGHT

[1]Stuart Fraser, [2]Nabih Alem
[1]UES, Inc. at U.S. Army Aeromedical Research Laboratory, Fort Rucker, Alabama, USA, [2]U.S. Army Aeromedical Research Laboratory, Fort Rucker, Alabama, USA; email: stuart.fraser@us.army.mil

INTRODUCTION

The modern U.S. Army helicopter helmet has evolved from a simple crash protection device to a mounting platform for advanced technologies, greatly increasing the effective combat power of the pilot. Current helmet designs are capable of supporting such devices as night vision goggles (NVGs), forward looking infrared (FLIR) display and weapon aiming systems. All of these devices add weight and displace the center of gravity (CG) of the helmet system forward to head and neck CG. This increased helmet load relative to the head and neck CG adds biomechanical stress to the neck and upper body of the pilot, which ultimately could lead to decrements in performance, including such tasks as searching for targets. To date, the relationship between the head-supported loads and the CG of the system and the effects on the pilots in low-G maneuvers has not been explored systematically. This paper investigates the effects of mounting additional mass on the helmet and displacing the CG location on the ability of a pilot to acquire targets placed throughout an NUH-60 helicopter cabin.

METHODS

To simulate various helmet weight moments, an HGU-56/P aviator helmet was modified to include fixtures that consisted of graduated rods extending forward relative to the direction the pilot was facing. This allowed for the addition of various weights at different distances. In addition to these modifications, a head motion tracker was attached to the top of the helmet using Velcro®. Within an NUH-60 flight simulator, five liquid crystal display targets were placed around the subject; and a computer controlled the presentation of targets and integrated information from the motion tracker, requiring the pilot to actually face the target to successfully 'acquire' it. The pilots flew a 2-hour flight pattern, with 5-minute blocks of target acquisition repeated six times. The time and accuracy of the acquisitions were recorded.

RESULTS

Multivariate analysis of variance was performed on the effect of the helmet on the acquisition times (Figure 1). The results showed that for targets lower left, upper left, upper center and upper right of the pilot, helmet mass had a significant effect, but center of gravity location did not. Post-hoc analyses showed that increasing mass increased acquisition time for these targets, except for the lower left target; where increasing mass decreased acquisition time. Comparisons of target-hit ratios were compared across all subjects for all targets, with no significant differences discovered. Also, there were no significant effects observed when testing for the effect of flight time on target hit ratios.

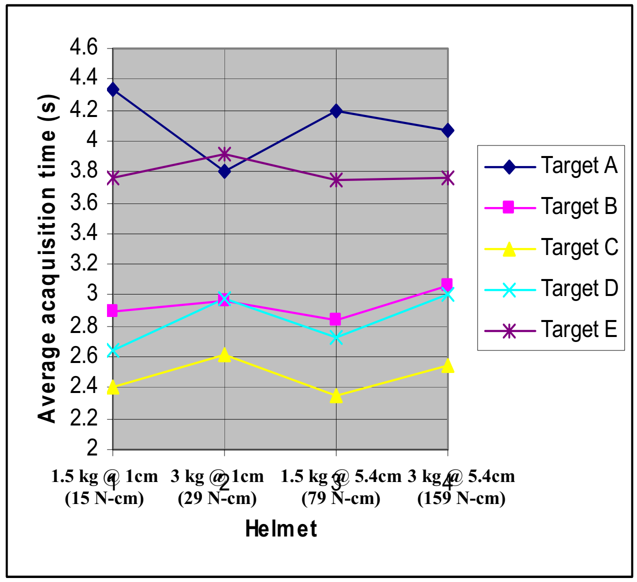

Figure 1: Average acquisition times by helmet and target

DISCUSSION

At six 5-minute intervals throughout a 120-minute flight, pilots were tasked to acquire targets placed throughout the cabin by pointing their helmet at the active target as quickly as possible. These tasks were repeated while the pilot wore four different head supported mass configurations. Overall, changes in helmet configuration did have a significant effect on target acquisition time, and it was the mass component of the system that produced the most significant effects in this aspect of performance. Helmets of greater mass (even if there was a lesser overall weight moment) performed worse on targets above the shoulders of the pilots, whereas a target on the center console of the aircraft performed better with the additional mass. The performance of the pilots in acquiring targets over the course of a 2-hour session did not change significantly. These results would indicate that reducing the mass of the helmet should be a priority in enhancing the effectiveness in pilots' head motion to detect and focus on targets in their environment.

LOWER EXTREMITY JOINT WORK IS LARGER IN ASCENDING VS. DESCENDING GAITS

Paul DeVita, Joseph Helseth, Brandon Noyes and Tibor Hortobagyi
Dept of Exercise and Sport Science, East Carolina University, Greenville, NC, USA
email: DeVitaP@mail.ecu.edu

INTRODUCTION

Metabolic rate (i.e. rate of O_2 consumption) is ~3-fold higher walking up vs down stairs and inclines [1,2]. This difference is attributed to the lower metabolic efficiency of generating muscle force through shortening vs lengthening contractions. Two reports however showed that mechanical work from joint powers is ~1.4 to 2.0-fold larger in stair ascent vs descent [3,4]. We also reported that this joint work was only 6% less than the change in potential energy (PE) in stair ascent but was 24% less than the change in PE in stair descent despite equivalent changes in total body PE in these gaits [5].

These data lead to a generalized hypothesis about mechanical work through joint powers in ascending and descending gaits. We hypothesize that lower extremity muscles will produce more mechanical energy during gait tasks in which humans raise their center of mass compared to the energy they absorb in gait tasks in which humans lower their center of mass. The purpose of this study was to compare joint work in stair and ramp ascent and descent gaits.

METHODS

Ground forces and sagittal plane kinematics were obtained from 34 young, healthy volunteers (mass: 69 kg) as they ascended and descended a 4-step stairway and a 10° ramp. The kinematic and force data were combined through inverse dynamics to calculate lower extremity joint torques during the stance phases. Joint power and joint work were calculated as the product of the torque and angular velocity at each joint and as the area under the power-time curves, respectively. We assume that work from joint powers is produced by muscle force since joint powers are derived from joint torques. Total work was assessed by summing the work performed at each joint. Changes in PE (d PE) were calculated as the change in total body PE per step up or down the ramp and stairs. All descent values were negative but are shown in absolute values for comparison purposes. 2-way ANOVA with specific comparisons was used to compare sample means, $p<.05$.

RESULTS AND DISCUSSION

Total joint work was 28% lower in descent vs ascent in both gaits (figure 1, table 1). The mean vertical displacements per step were 12 and 20 cm on the ramp and stairs yielding d PEs of 82 and 132 J of work. Total joint work in ascent and descent were 17% and 40% lower than d PE on the ramp and 22% and 44% lower than d PE on the stairs (all $p<.05$).

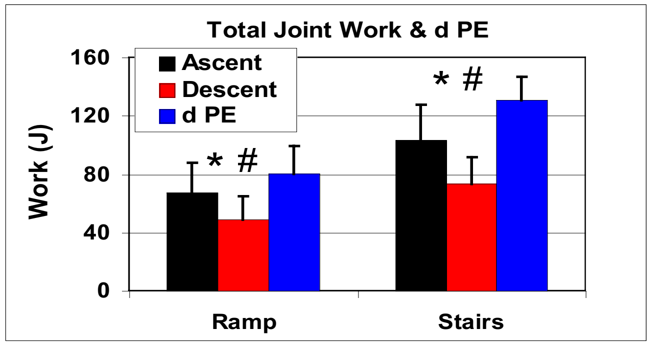

Figure 1: Total joint work and d PE on the ramp and stairs. Descent values in |J|. * Ascent > Descent, $p<.05$, # Ascent & Descent < d PE, $p<.05$.

While both gaits had less joint work in descent, the pattern of responses across the individual joints varied between gaits. Stair descent vs ascent had similar decreases at each joint (~10 J). Ramp descent vs ascent had large decreases in hip and ankle work (~25 J) but a large increase in knee work (35 J).

By ignoring work due to ligament forces we may be slightly overestimating muscle work. We also did not report swing phase energetics. Based on predicted masses of the limbs we estimate that 13 J and 20 J of work were needed to displace the limb on the ramp and stairs which account for ~75% of the difference between joint work and d PE in the ascending gaits but only 36% in descending gaits. We suggest the unidentified work in descending tasks is produced by other tissues including bone, cartilage and spinal discs. Results suggest the higher metabolic cost of ascending gaits is partially due to larger contributions from muscles in these tasks.

CONCLUSIONS

Despite the limitations, the results suggest lower extremity muscles produce more mechanical energy during gait tasks in which humans raise their center of mass compared to the energy they absorb in gait tasks in which humans lower their center of mass despite equivalent changes in total PE.

REFERENCES

1. Basset DR et al. Med Sci Sports Exer, 29, 1250-1254, 1997.
2. Laursen B et al. Appl Ergonomics, 31, 159-166, 2000.
3. Reiner R et al. Gait & Posture, 12, 32-44, 2002.
4. Duncan JA et al. Gait & Posture, 5, 204-210, 1997.
5. Noyes et al. Proceedings SEACSM, 33, 40, 2005.

Table 1: Mean (Sd) for d PE, total work and work at each joint (J, absolute values)

	Ramp					Stairs				
	d PE	Total	Hip	Knee	Ankle	d PE	Total	Hip	Knee	Ankle
Ascent	82 (19)	68 (20)	24 (14)	4 (6)	40 (9)	132 (17)	103 (25)	13 (10)	52 (12)	38 (12)
Descent	82 (19)	49 (16)	5 (5)	39 (13)	6 (7)	132 (17)	74 (18)	4 (4)	45 (12)	25 (8)

BONE MECHANICS FROM FINITE ELEMENT MODELING AND MICRO-COMPUTED TOMOGRAPHY: VALIDATION OF AN ORTHOTROPIC MATERIAL MODEL WITH FUSED DEPOSITION MODELING

[1,2] Renfeng Su and [1,2] Steven Boyd
[1]Department of Mechanical and Manufacturing Engineering, University of Calgary, Alberta, Canada
[2]Calgary Center of Innovative Technology, Alberta, Canada; email:skboy@ucalgary.ca,web:www.enme.ucalgary.ca/~skboyd

INTRODUCTION

Bone diseases such as osteoporosis result in bone loss and weakened bone micro-structure and could lead to spontaneous fractures. Detection of bone micro-structural changes and their impact on bone mechanics is important for the successful treatment of bone diseases and progression of joint injuries.

It is commonly postulated that local mechanics (tissue stress or strain) is related to stimuli for bone remodeling [1]. A micro finite element (μFE) solver was developed in our lab to numerically predict the local stress and strain in bone structure [2,3]. Micro-computed tomography (μCT) can provide high resolution image data suitable to the μFE solver and allows non-destructive, three-dimensional morphological and mechanical analysis of bone. With newly developed in vivo μCT, μFE simulation of bone mechanics can be evaluated over time. However, it is important that μFE models be validated for numerical accuracy. This is problematic because it is difficult to perform experiments on 1:1 scaled bone.

A method has been developed to validate μFE models using rapid prototyping: fused deposition modeling (FDM). FDM prototypes can be built based on μCT image data and scaled up so that local stress values can be measured in an experimental setup using strain gauges for comparison with μFE models to estimate accuracy.

METHODS

Five identical FDM prototypes were manufactured (FDM Titan, Stratasys, Minnesota, U.S.A) based on a $1.7 \times 1.7 \times 1.7 mm^3$ volume of trabecular bone scaled to 30:1. Two rosette strain gauges were mounted on each prototype: one on a flat and one on a curved surface. Uniaxial compression (1%ε) was performed on the five prototypes. Two data acquisition systems were used for recording. Apparent stress (E_{app}) and local 1st principal stresses calculated from rosette readings were obtained experimentally.

The μFE model is based on the same trabecular bone image data used for the prototypes, and boundary and loading conditions mimicked the experiments. The material properties used were the orthotropic properties of FDM material which were previously determined experimentally [4]. Our in-house μFE solver was upgraded to solve this orthotropic model. Results from μFE (stress results in elements in a 3x3 region corresponding to each gauge were averaged) were compared to experimentally measured strains.

RESULTS AND DISCUSSION

The FDM Titan machine was tested for volumetric reproducibility (five models; 0.1% error), and the FDM prototype volumes were matched to the μFE mesh volumes. The μFE model predicted E_{app} measured experimentally within <1% (Fig. 1). The local 1st principal stress calculated by μFE was within 9% of experimental data on the flat surface and 56% on the curved surface (Fig. 1). The accuracy of our in-house μFE model at the apparent level (1%) indicates that global orthotropic material properties can be predicted well based on digital FE models. The error of prediction on the curved surface was largest due to the jagged hexahedron mesh used, as well as due to the problems of attaching strain gauges to curved surfaces. The reduced error in local stress measurements on the flat surface is due to the reduced effect of jagged surfaces in that region of the μFE model.

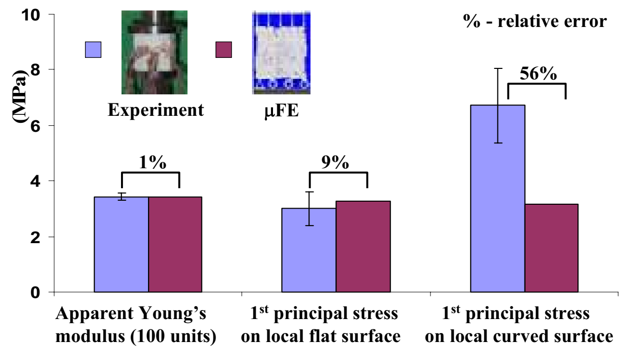

Figure 1: Comparison of experiment and μFE results at both global (left) and local levels (middle/right) on a trabecular bone model.

CONCLUSIONS

The prediction of trabecular bone mechanical properties by our in-house μFE solver is more accurate at the apparent level than local level. This result is expected, and smoothing these μFE models may reduce these local errors (work in progress). The results presented here reinforce that μFE models used to predict bone remodelling based on local stress/strain should account for the large errors that may occur on the model surface.

REFERENCES

1. Huiskes R, et al. *Nature* **405,** 704-706, 2000.
2. Boyd SK, et al. *J Bone Miner Res* **17**, 687-694, 2002.
3. van Rietbergen B, et al. *J Biomech* **28**, 69-81, 1995.
4. Su R, et al. *Trans 5th Combined ORS*, Banff, Canada, Abstract 338, 2004.

ACKNOWLEDGEMENTS

Research funded by NSERC.

VARIATIONS IN SCAPHOLUNATE GAP WITH VARIOUS TYPES OF LIGAMENTOUS SECTIONING

[1]Haoyu Wang , [2]Frederick W. Werner, [2]Walter H. Short, [2]Jason K. Green
[1]Bowling Green State University
[2]SUNY Upstate Medical University, email: wernerf@upstate.edu

INTRODUCTION

Instability of the scapholunate joint is frequently manifested by wrist pain but determining which ligament or ligaments are torn is difficult. Most studies agree that the scapholunate interosseous ligament (SLIL) is the primary stabilizing structure. However, there are secondary stabilizing structures such as the dorsal intercarpal (DIC) and dorsal radiocarpal (DRC) ligaments. Pre-surgical determination of which structures are damaged would be of value to the surgeon when attempting to repair the torn ligaments. The purpose of this study was to determine if various gap patterns between the scaphoid and lunate could be related to which ligaments were ruptured. A secondary purpose was to determine which wrist position might best differentiate these effects.

METHODS

Ten cadaver forearms were evaluated. Fastrak motion tracking sensors were attached to the scaphoid, lunate and third metacarpal to measure angular and translational motion of these bones. Each wrist was physiologically moved using a wrist joint simulator through repetitive cyclic flexion/extension of the wrist (30° extension to 50° flexion) and wrist radial/ulnar deviation (10° radial deviation to 20° ulnar deviation). Carpal bone motion data were collected in the intact specimens, and in 5 arms after sequentially sectioning the DRC, the DIC, and the SLIL. In five additional arms, data were acquired after sequentially sectioning the DIC, the SLIL, and the DRC. Data were again collected after 1000 cycles of flexion/extension motion following complete ligament sectioning to mimic continued use after injury. 3D animated models were created of each wrist, based upon serial CT scans to aid in analyzing the data. The experimental kinematic scaphoid and lunate data were used to drive the animated motions. Two anatomical landmarks were identified on the lunate (dorsal lunate, volar lunate) and two on the scaphoid (dorsal scaphoid and volar scaphoid). Using the models and kinematic data, the distances between the dorsal points and between the volar points were determined during each motion (fig 1) for each level of ligament sectioning using customized CAD software. Additionally, a projected quadrilateral area was computed from these four points.

RESULTS AND DISCUSSION

Sectioning of only the DRC (1st group of arms) or only the DIC (2nd group of arms) caused no increase in the gap between

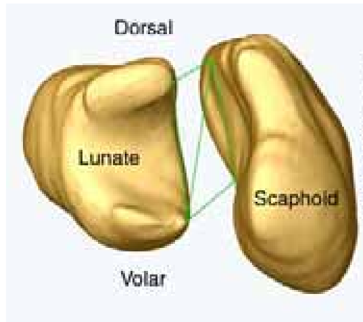

Fig 1: Transverse view as from fingers showing location of dorsal and volar landmarks

the bones (fig 2, table 1). Subsequent sectioning of the SLIL caused an average 35 to 55% increase in the dorsal and volar gaps during flexion/extension and an average 10 to 40%

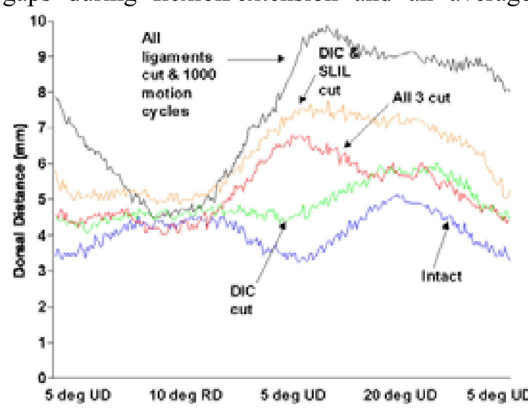

Fig 2: Gap between dorsal points on scaphoid and lunate during wrist radial/ulnar deviation

increase during radial/ulnar deviation. Even though the gaps during wrist flexion/extension were greater than during radial/ulnar deviation, the wrist angle during flexion/extension at which the largest gap occurred varied among arms. Typically the gap increased the least in wrist extension. However, during radial/ulnar deviation, the largest gaps were consistently observed in ulnar deviation. With cyclic motion, the gaps increased, especially during the radial/ulnar deviation motion.

CONCLUSIONS

Following wrist ligament injury, detection of major gap changes, between the scaphoid and lunate, may be best detected in wrist ulnar deviation.

ACKNOWLEDGEMENTS

Funded by NIH grant 1R01 AR050099-01.

Group 1 arms - Table 1	Average % increase from intact flexion/extension motion			
	DRC cut	DRC&DIC cut	DRC, DIC, & SLIL cut	All 3 cut and 1000 cycles
Dorsal Gap	-1.0	1.7	53.1	70.1
Volar Gap	0.4	1.4	37.9	49.6
Areal gap	0.7	3.5	40.9	54.4

IDENTIFICATION OF VISCOELASTIC PROPERTIES OF HUMAN MEDIAL COLATERAL LIGAMENT USING FINITE ELEMENT OPTIMIZATION

[1] Costin Untaroiu, [1]Kurosh Darvish, [1]Jeff Crandall, [2]Bing Deng and [2]J.T. Wang
[1]Center for Applied Biomechanics (CAB), University of Virginia, Charlottesville, VA, email: cdu4q@virginia.edu
[2]General Motors R&D, Warren, MI

INTRODUCTION

Current finite element (FE) models of the human lower extremity lack accurate viscoelastic material properties of the knee ligaments, which are needed for computational evaluation of pedestrian injuries [1]. Medial collateral ligament (MCL) is the most frequently injured ligament in lateral impacts. Therefore, the accuracy of the viscoelastic mechanical properties of the MCL FE model is of crucial importance in modeling pedestrian impacts [2]. The focus of this work is to determine the global viscoelastic material properties of MCL using a representative human MCL tested under dynamic and quasi-static loadings.

METHODS

The bone-MCL-bone specimen was extracted and its ends were potted in the fully extended position. The proximal potting cup was rigidly fixed and the distal cup was pulled along the longitudinal axis of tibia. First, the specimen was subjected to a ramp-and-hold test with constant tensile ramp of 3 mm in 30 ms and approximately 600 seconds hold time. The second test was a quasi-static test to failure on the same specimen. In both tests the time histories of force and displacement were recorded. For identification of the material properties, the components of the UVA-GM FE model [2] were used (Figure 1). The insertion sites were modeled using tied contact between bones and ligament. The material model was assumed as transversely isotropic quasi-linear viscoelastic (QLV). The direction of anisotropy (of collagen fibers) was defined in the material definition as the element normal along the insertion sites. First, the quasi-static test was simulated. The material coefficients were optimized using LS-Opt [4], assuming the quasi-static test data as the target values and defining minimization of the root-mean-square (RMS) error as the objective function. The range of values of hyperelastic coefficients (C_1-C_5) used in the optimization process were defined based on the reported data in [5]. The viscoelastic properties of the ligament were then determined from the dynamic ramp and hold test. A three-term Prony series was considered for the relaxation behavior. The long-term Prony coefficients (S3 and T3) were estimated directly from the relaxation data. The two additional Prony coefficients (S1, T1, S2, and T2) were determined by considering both the ramp and hold periods and the same FE optimization procedure described above was conducted.

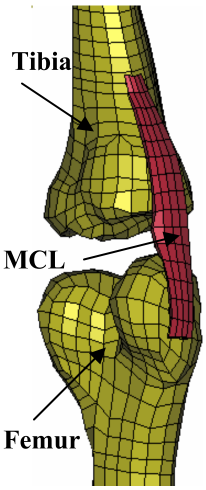

Figure 1: FE Simulation of the MCL Tensile Tests

RESULTS AND DISCUSSION

The material coefficients obtained by FE optimization are provided in Table 1. The results of the simulations of quasi-static failure tests and dynamic ramp-and-hold tensile tests of MCL in comparison with experimental data are shown in Figures 2-a, and 2-b respectively. In the dynamic test with 0.1 mm/ms displacement rate, approximately 15% increase in the peak dynamic force was observed, which suggests that tissue viscoelasticity plays certain role in the response during impact scenarios. The elastic stress-strain relationship in a cubic sample of MCL in tension along the collagen fibers with optimized parameters was compared with the corridor provided in [5]. The current material model was slightly stiffer at strains above 13%. This material model was determined by assuming a homogeneous anisotropic material for the whole MCL and optimizing its global tensile properties. However, MCL is inhomogeneous particularly at the insertion sites, which could explain the difference observed in its local (anterior-central two-third region) and global properties.

Table 1: Optimized MCL material properties

K (GPa)	C_1 (MPa)	C_3 (MPa)	C_4 -	C_5 (MPa)	S_1
3.75	7.85	0.25	60.4	307.5	0.15
S_2	S_3	T_1 (ms)	T_2 (ms)	T_3 (ms)	λ
0.026	0.348	100	11710	162633	1.055

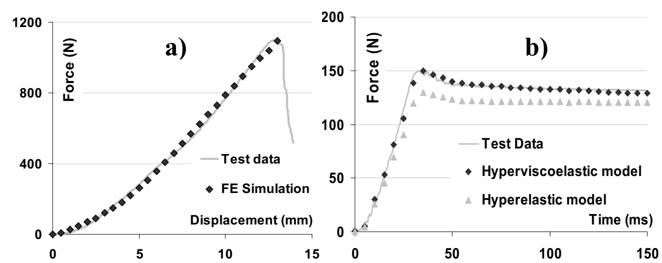

Figure 2: FE Simulation of the MCL Tensile Test

CONCLUSIONS

The global viscoelastic material properties of an MCL specimen were derived by FE optimization. Results showed that tissue viscoelasticity increases the peak dynamic force by 15%. Studies of more specimens are underway and will be reported in the future.

REFERENCES

1. Weiss, J. et al., *Critical Rev. Biom. Eng.* **29**(4): 1-70, 2001
2. Untaroiu, C, et al., *ASME Int. Congress*, Paper 61583, 2004
3. Hallquist, J. O., *LS-Dyna Theoretical Manual*, May 1998
4. Stander, N, et al., “LS-OPT User’s Manual”, LSTC, 2003
5. Quapp, KM, et al., *J. Biomech. Eng.* **120**, 757-763, 1998.

EFFECTS OF EXAGGERATED PRONATION AND SUPINATION ON LOWER EXTREMITY MECHANICS DURING A CUTTING MANEUVER

Jennifer E. Earl, Sarika K. Monteiro, and Kristian M. O'Connor
Department of Human Movement Sciences
University of Wisconsin – Milwaukee; email: jearl@uwm.edu, web: www.uwm.edu

INTRODUCTION

The mechanism of non-contact ACL injury is commonly associated with a position of knee valgus and tibial external rotation which occurs during sudden twisting or cutting. The literature is contradictory about how foot pronation relates to knee motion and ACL injury. While excessive pronation has been identified as a risk factor [1], this motion is typically coupled with tibial *internal rotation*, and it is tibial *external rotation* that is observed at the time of injury. The purpose of this study was to determine how exaggerated pronation or supination influenced lower extremity kinetics and kinematics during a side cutting maneuver.

METHODS

Ten active college-age males, with no current lower extremity impairment, volunteered to participate. Three-dimensional kinematic data were collected at 200 Hz and ground reaction force data were collected at 1000 Hz. Subjects ran 4.5-5.0 m/s, and watched for a visual cue to run straight ahead, cut 45° to the left, or stop quickly. This design was intended to elicit an unanticipated cutting response, which has been shown to differ from anticipated cutting maneuvers [2]. The right leg of all subjects was tested. Only the cutting trials were analyzed.

Subjects wore custom-made running shoes: a pair with a neutrally-posted midsole, a pronated pair with an 8° lateral rearfoot wedge, and a supinated pair with an 8° medial rearfoot wedge [3]. Five trials of each activity (run, cut, stop) were collected in each of the three shoes, for a total of 45 trials.

Three-dimensional hip, knee, and ankle joint kinematics and kinetics were calculated. Peak joint angle and moment data were extracted from the stance phase and analyzed using repeated measures ANOVA ($p<0.05$).

RESULTS AND DISCUSSION

The pronated shoe caused a significant change in ankle mechanics. Peak ankle eversion angle ($f_{2,18}=3.51$, $p=0.05$), and ankle inversion moment ($f_{2,18}=10.96$, $p<0.001$) were significantly increased in the pronated shoe. It was expected that any change that occurred at the ankle would be transferred up the kinetic chain and result in changes at the knee and hip. However, no significant changes in either knee or hip kinematics were seen. Joint angle patterns observed in this study are similar to those previously reported [4,5]. The pronated shoe did cause the knee external rotation moment to be significantly lower ($f_{2,18}=5.03$, $p=0.02$), and there was a trend that the pronated shoe also caused the knee varus moment to be lower ($p=0.10$) (Table 1). This indicates that in the pronated shoe there was less demand on the knee joint to maintain transverse plane stability.

These findings seem to contradict the theory that excessive pronation increases the stress at the knee during a cutting maneuver, and is therefore a risk factor for ACL injury. The pronated shoe with its lateral wedge seemed to provide an inclined push-off surface that re-oriented the ground reaction force vector in such a way that the stability of the knee was enhanced.

These findings may not be directly related to the mechanics of an individual with anatomical excessive pronation. These individuals would not have the benefit of the angled push off surface that existed in the pronated shoe design. The supinated shoe, however, could have approximated the effect of a posted orthotic, which did not lead to significant differences in kinematics or kinetics as compared to the neutral shoe.

CONCLUSIONS

The shoe that exaggerated pronation enhanced the transverse plane stability at the knee, and caused less rotational torque on the knee joint. Additional research is needed to identify if this pattern is consistent in females, and if anatomical pronation causes the same effect.

REFERENCES

1. Loudon JK et al.. *JOSPT* **24**, 91-97, 1996.
2. Besier, TF et al.. *MSSE* **33**, 1176-1181, 2003.
3. O'Connor KM & Hamill J. *Clin Biomech* **19,** 71-77, 2004.
4. McLean SG et al.. *Bull Hosp Joint Diseases* **57**, 30-38, 1998.
5. Neptune RR et al.. *MSSE* **31***,* 294-302, 1999.

ACKNOWLEDGEMENTS

UWM College of Health Sciences SEED Grant

Table 1: Group mean (± SD) differences in ankle (A) and knee (K) mechanics (peak values) between medial (supinated), neutral, and lateral (pronated) posted shoes during a cutting maneuver. * = Significantly different from the neutral and supinated shoes ($p < 0.05$)

	A Eversion Angle (°)	A Inversion Moment (Nm)	K Int. Rot. Angle (°)	K Ext. Rot. Moment (Nm)	K Valgus Angle (°)	K Varus Moment (Nm)
Supinated shoe	-3.3 ± 5.3	21.5 ± 16.3	4.2 ± 4.3	-28.1 ± 17.1	-5.9 ± 5.4	132.2 ± 68.1
Neutral shoe	-3.8 ± 5.6	22.9 ± 17.5	3.2 ± 3.8	-30.6 ± 18.8	-6.3 ± 4.7	124.7 ± 56.6
Pronated shoe	*-5.2 ± 5.7	*25.9 ± 17.7	3.4 ± 3.3	*-20.7 ± 12.7	-6.5 ± 5.3	109.3 ± 56.8

fMRI BRAIN IMAGING DURING SIX DOF MECHANICAL MEASUREMENTS OF UPPER LIMB ISOMETRIC CONTRACTIONS

[1]Daniel M. Krainak, [1, 2]Todd B. Parrish, and [1, 3]Julius P.A. Dewald
Northwestern University [1]Department of Biomedical Engineering, [2]Department of Radiology,
and [3]Department of Physical Therapy & Human Movement Sciences; e-mail: krainak@northwestern.edu

INTRODUCTION

A six degree of freedom (DOF) load cell technology is used to measure joint torques in a functional magnetic resonance imaging (fMRI) environment in an unprecedented manner. This system offers substantial improvement over existing methods that monitor at most one DOF during fMRI motor experiments. Developing a functional brain map depends on adequate characterization of motor output. Collecting multiple joint torques and fMRI simultaneously surpasses all current methods used to assign brain areas to motor functions.

METHODS

A novel system using a non-ferrous six degrees of freedom load cell (JR3, Inc., Woodland, CA) to monitor shoulder and elbow joint torques is developed to conduct functional MRI investigations of the human motor cortices (Figure 1). The subject's arm is surrounded by a fiberglass cast to prevent wrist movement and insure proper joint position [1]. A combination of delrin and garolyte provides an interface

Figure 1: Subject position and load cell mounting setup used during function MRI sessions.

surface to evenly distribute the loads generated by the subject across the entire load cell surface. A wooden frame holds the load cell in position. Load cell signals are filtered using 8^{th} order low-pass Butterworth filters with a cutoff of 15-Hz and 4^{th} order elliptical filters with a sharp 10-Hz cutoff. The filters remove artifacts caused by the gradients and radio frequency signals used in the functional MRI sequence. This system preserves the force and torque information used to calculate joint torques during contractions of the upper limb and provides feedback to the subject. Using a TTL pulse from the MRI system, joint torque samples are synchronized with the MRI recordings.

Functional MR images are collected from a 3.0-Tesla MR scanner (Siemens Trio, 3T) using a 2D gradient echo, echo-planar imaging sequence (TR=2000ms, TE=30ms, FA=80°, voxel=3.4x3.4x3mm^3, 31-slices, 64x64 matrix). Following the functional imaging an anatomical scan of the entire brain is acquired as a reference image for functional data using an MP-RAGE T1 weighted 3D gradient echo sequence (TR=2100ms, TE=4.38ms, FA=8°, voxel=1.0x1.0x1.0mm^3). Visual stimuli for the functional MRI paradigms are observed through an MR compatible mirror mounted on the head coil aimed at a rear-projection screen fitted in the magnet. An event-related protocol using short, low-effort contractions with approximately 30-seconds between tasks is designed to minimize head movement artifacts during analysis [2].

RESULTS AND DISCUSSION

The technique is verified both with a phantom MRI study and an incremental mass study. No artifact is caused by the presence of the load cell on phantom images. Load cell recordings inside the magnet match load cell recordings outside the magnet for the same masses. A study of shoulder and elbow activation in the motor cortices during elbow flexion and shoulder abduction confirms the feasibility of this measurement technique. An isolated joint torque is difficult to produce voluntarily without cocontraction. Substantial secondary torques are observed while monitoring multiple isometric joint torques during tasks such as elbow flexion and shoulder abduction. Thus, functional activity on the motor cortex may be related in large part to these secondary joint torques. For example, shoulder flexion is prominent during elbow flexion tasks and therefore, accounts for some portion of the neural activity.

CONCLUSIONS

This methodology offers a unique and novel approach to investigate cortical control of the upper limb. It permits a greater association of cortical activity with the multi DOF nature of motor output. The system records multiple isometric joint torques generated by a subject and enables detailed study of the relationship between elbow/shoulder torques and associated cortical activation sites. To date, neuroimaging motor studies incorrectly associate most observed neural activity with a single motor output measurement consequently not accounting for unmonitored motor events. Assigning cortical regions based on a single DOF measurement grossly undermines the complexity of human movement. By incorporating multiple elbow/shoulder torques, we can better characterize the cortical activation map in both healthy and neurologically impaired subjects.

REFERENCES

[1] Dewald JP, et al., *Brain*, **118 (Pt 2)**, 495-510, 1995.
[2] Birn RM, et al., *Hum Brain Mapp*, **7**, 106-14, 1999.

ACKNOWLEDGEMENTS

This work was supported by a National Institutes of Health RO1 Grant (HD39343).and by the RIC Women's Board.

DYNAMIC MODELING AND SYSTEM IDENTIFICATION OF FINGER MOVEMENT

Sang-Wook Lee and Xudong Zhang
University of Illinois at Urbana-Champaign
email: xudong@uiuc.edu

INTRODUCTION

Biomechanical models for hand movement can aid in various industrial design and clinical evaluation processes. There exist kinematic models for grip posture prediction [1, 2] and inverse dynamic models for estimating muscle forces in static poses or movements [3, 4]. However, a forward dynamic model of finger movement, particularly one that is empirically based and computationally efficient, has been lacking.

This study aims to develop a dynamic model for predicting human finger movements during manipulative actions. The model incorporates a control scheme modulating dynamic stiffness and damping of the fingers to generate desired movements, and parametric system identification allowing empirical estimation of the parameters characterizing the dynamic properties.

METHODS

The database for model development was from an experiment in which an anthropometrically diverse group of 28 subjects performed grasping motion tasks. Joint angular profiles derived were found to be of sigmoidal shape, which were then represented compactly by parametric hyperbolic tangent functions [4]. A constrained non-linear optimization was formulated to determine the parameter values of hyperbolic tangent functions best fitting the joint angular profiles.

A proportional-derivative (PD) control scheme was proposed to govern the system dynamics. The torque at joint i (i=1, 2, 3) was computed as:

$$T_i = -K_i^p\left(\theta_i - \theta_i^f\right) - K_i^d\left(\dot{\theta}_i - \dot{\theta}_i^f\right), \quad T_i \le M_i^{max} \qquad (1)$$

where θ_i denotes the angle of joint i, θ_i^f the joint angle in terminal posture, K_i^p the proportional feedback gain, K_i^d the derivative feedback gain, and M_i^{max} the upper limit of torque value generated at joint i. K^p and K^d characterize two main movement-specific properties: dynamic joint stiffness and damping. M^{max} corresponds to the torque maximum, i.e., the peak value of torque profile. In forward solutions given the parameter values, the 4th-order Runge Kutta method was employed.

The controller parameters were estimated in an optimization routine that minimized the discrepancy between the model-predicted and measured movement profiles. The discrepancy was represented as the difference between two sets of profile attributes: response time, peak velocity, and peak acceleration. These attributes are in fact the parameters in the aforementioned hyperbolic tangent functions fitting the measured profiles. The optimization routine iteratively estimated the control parameters resulting in model response that best matched the measurement. It should be noted that the movement speed affects the parameter values (e.g., faster movement requires greater feedback gain and torque values). To remove the effect of speed, the obtained control parameters were normalized using a linear regression model. This parameter estimation scheme was applied to the movement database to determine the speed-scaled K^p, K^d and M^{max} values.

RESULTS AND DISCUSSION

The mean and standard deviation values of K^p and M^{max} are shown in Figure 1. K^d values showed a similar pattern across the digits as K^p (means for digit 2 to 5 were 6.9, 6.4, 6.1 and 2.5 × 10^{-3} N s m/rad, respectively). The grand mean RMSE (SD) value for 336 model-reproduced joint angular profiles was 4.88° (3.75°).

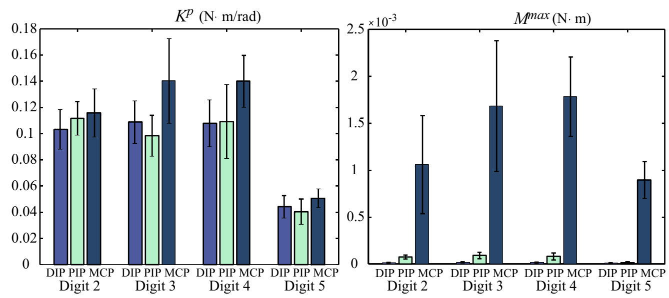

Figure 1: Mean and SD of estimated K^p and M^{max} values.

Estimated active joint stiffness K^p values were in a comparable range for digits 2 to 4, but were considerably smaller for digit 5. This can be considered as a reflection of the difference in anthropometric properties. A similar pattern was exhibited by K^d values. The K^p and K^d values for MCP were slightly greater than those for DIP and PIP, while the M^{max} values of the MCP joints were 10-100 times greater. These results are consistent with the understanding that most physical work in grasping motion is done by MCP flexion. They also are corroborated by an invasive EMG study [5] that discovered significantly higher levels of muscle activation associated with MCP flexion during grasping motions.

The proposed model enables computationally efficient and physically interpretable prediction of finger movement, owing to the simple control and parametric system identification scheme. Potential applications include computer-aided design of hand-operated products, clinical diagnosis of hand-related disorders or impairment.

REFERENCES

1. Buchholz B, et al. *J Biomech* **25**, 149-162, 1992.
2. Lee SW, et al. *J Biomech,* in press.
3. Sancho-Bru JL, et al. *J Biomech Eng* **125**, 78-83, 2003.
4. Buchner HJ, et al. *J Biomech* **21**, 459-468, 1988.
5. Braido PB, et al. *Hum Mov Sci* **22**, 661-678, 2004.
6. Long C, et al. *J Bone Joint Surg* **46A**, 1683-1706, 1964.

ADJACENT LEVEL LOAD TRANSFER FOLLOWING VERTEBRAL COMPRESSION FRACTURES TREATED BY CEMENT AUGMENTATION

[1] Mark Kayanja, [1] Daisuke Togawa, [2]Korboi Evans, [1] Isador Lieberman
[1] Cleveland Clinic Spine Institute, Cleveland Clinic Foundation, 9500 Euclid Avenue Cleveland Ohio 44195
[2] Case Western Reserve University, 10900 Euclid Avenue, Cleveland Ohio 44106
Presenting author Korboi Evans; email: Kravan8@yahoo.com

INTRODUCTION

Osteoporosis is a common clinical problem affecting more than 24 million people in the United States [1] and is a "systemic skeletal disease characterized by low bone mass and micro-architectural deterioration of bone tissue, with a consequent increase in bone fragility and susceptibility to fracture." [2]. Vertebral compression fractures (VCFs), the most common osteoporotic fractures, lead to significant and progressive physiologic and functional limitations [3], that are compounded when subsequent VCF occur with serious long term consequences. There is up to a 30% age-adjusted increase in mortality and a 9% loss in lung function with each vertebral fracture [4,5]. Subsequent VCF may result from the continued osteoporotic process, from altered load transfer to adjacent levels as a result of altered biomechanics or a combination of both. This study was designed to investigate whether bone mineral density significantly alters adjacent level load transfer following polymethylmethacrylate augmentation, a minimally invasive technique used to treat VCF.

METHODS

11 spines were used to obtain 21 five level segments composed of 12 upper thoracic (T3-7) and 9 lower thoracic segments (T8-T12). The segments underwent DEXA scanning to determine their bone mineral density (BMD). The segments were divided into two groups based upon BMD, a normal group (11 segments, mean BMD 1.0 ± 0.1 gm/ cm^2) and an osteopenic/osteoporotic group (10 segments, mean BMD 0.8 ± 0.1 gm/ cm^2). The superior and inferior vertebrae (T3, T7, T8 and T12) were fully embedded in polyester resin, and strain gauges (SGs) were applied to the anterior vertebral shells of T3, T7, T8 and T12, while force sensing resistors (FSRs) were inserted into the centers of the same vertebrae. Both the SGs and the FSRs were connected to signal conditioning equipment for data collection. The multilevel segments were biomechanically tested non-destructively in compression and flexion, a defect in the intermediate vertebrae (T5 and T10) was created using either inflatable bone tamps (osteoporotic segments) or bone drill and curettes (normal segments) to ensure a reproducible location of the initial VCF, the VCF was then reduced and augmented and the non-destructive testing in compression and flexion was repeated. Measurements of stiffness, superior and inferior adjacent level strain, superior and inferior centrum load were taken from all the tests and compared using general linear modeling with two groups of multilevel segments (high and low BMD). The significance level was set at 0.05 with 95 % confidence interval limits with post hoc least significant difference tests.

RESULTS AND DISCUSSION

The osteoporotic segments had significantly lower compressive stiffness than the normal segments, but there were no significant differences between the two groups in adjacent level load transfer (Table 1). In both groups there was higher adjacent level load transfer following fracture augmentation (strain $p = 0.10$, centrum load $p = 0.41$) and flexion created a greater load transfer than compression (strain $p = 0.001$, centrum load $p = 0.54$). Osteoporosis significantly reduced compressive stiffness from the reduced bone mass and deterioration of bone micro-architecture. Osteoporosis affects trabecular bone of the centrum to a more significant degree than the compact woven bone of the vertebral shell resulting in the reduced centrum load but increased strain at the adjacent levels.

CONCLUSION

Augmentation of osteoporotic multilevel segments does not alter segment biomechanics.

REFERENCES

1. Consensus Development Conference on Osteoporosis. Hong Kong, April 1-2, 1993. Am J Med 1993;95:1S-78S.
2. Consensus development conference: diagnosis, prophylaxis, and treatment of osteoporosis. Am J Med 1993;94:646-50.
3. Haczynski J, Jakimiuk A. Vertebral fractures: a hidden problem of osteoporosis. Med Sci Monit 2001;7:1108-17.
4. Kado DM, Browner WS, Palermo L, Nevitt MC, Genant HK, Cummings SR. Vertebral fractures and mortality in older women: a prospective study. Study of Osteoporotic Fractures Research Group. Arch Intern Med 1999;159:1215-20.
5. Leech JA, Dulberg C, Kellie S, Pattee L, Gay J. Relationship of lung function to severity of osteoporosis in women. Am Rev Respir Dis 1990;141:68-71.

Table 1 - Biomechanical comparisons between the normal and osteoporotic segments before and after VCF

Measurement	Normal	Osteoporotic	P value
BMD (gm/cm^2)	1.0 ± 0.1	0.8 ± 0.1	<0.0001
Compressive stiffness (N/mm)	1079 ± 66	749 ± 84	0.01
Bending stiffness (Nm/degree)	6.2 ± 1.2	3.1 ± 1.2	0.78
Adjacent level strain (micro strain)	1172 ± 313	985 ± 343	0.69
Adjacent level centrum load (millivolts)	104 ± 26	87 ± 28	0.66

BACK MUSCLE FATIGUE DURING SUBMAXIMAL INTERMITTENT ISOMETRIC CONTRACTIONS: THE INFLUENCE OF NEUROMUSCULAR ACTIVATION PATTERNS

[1] Christian Larivière, [2]Denis Gravel, [2]Bertrand Arsenault, [3]Denis Gagnon and [4]Phillip Gardiner
[1]Occupational Health and Safety Research Institute Robert-Sauvé, Montreal, Canada, [2]Research Center, Montreal Rehabilitation Institute, Montreal, Canada; [3]Faculty of Physical Education , University of Sherbrooke, Canada, [3]HLHP Research Institute, University of Manitoba, Winnipeg, Canada; email: larchr@irsst.qc.ca

INTRODUCTION

Three groups of factors are known to explain muscle endurance: (1) anatomical factors (muscle mass and composition, capillary-zation), (2) physiological factors (hormones, enzymes, energy stores), and (3) neuromuscular activation patterns (NMAP). However, NMAP (variable activation of motor units within and between muscles, etc.) has rarely been quantified using indices derived from surface electromyography (EMG). This would help to estimate the role of NMAP when muscles fatigue. The aim of this study was thus to quantify the relationship between the NMAP of synergist muscles and fatigue using different EMG indices.

METHODS

Seventy-four subjects (43 males and 31 females; age: 20-55 yrs) performed 3 maximal voluntary contractions (MVC) and a fatigue test while standing in a static dynamometer measuring L5/S1 moments [1]. Surface EMG signals were collected from 4 pairs of back muscles (multifidus at the L5 level, iliocostalis lumborum at L3, and longissimus at L1 and T10). The fatigue test, assessing absolute endurance (90 Nm load), consisted of repeating an 8-s cycle extension task (1.5 s ramp to reach 90 Nm + 5 s plateau at 90 Nm + 1.5 s rest). For all subjects, a familiarization session (MVCs + 10 min. fatigue test) was followed by a test session (MVCs + fatigue test to exhaustion or 60 min). A subsample of 31 subjects (19 males and 11 females) performed a 3rd session, but the fatigue test was performed to exhaustion using a relative load (41% MVC), thus assessing relative endurance.

Strength was defined as the peak MVC while our fatigue criterion was defined as the time to reach exhaustion either during the absolute ($Tend_{abs}$) or relative ($Tend_{rel}$) fatigue test. For each plateau, the time-series of the RMS amplitude (125 ms) of the EMG signals were computed. The EMG RMS time-series (first 5 min) were used to quantify NMAP between back synergists using 2 types of EMG indices (Ind1 and Ind2 adapted from [2]), both accounting for the effect of fatigue on EMG RMS (linear trends in the EMG time-series were removed). Ind1 basically reflects the variation in EMG activity of each muscle while Ind2 quantify the alternating activity between 2 muscles. Ind2 being the proportion of time of alternating activity (P_{ALT}) times the amplitude of this activity, P_{ALT} was also studied separately. For Ind2 and P_{ALT}, various pairs of muscles (homolateral and contralateral) were assessed.

RESULTS AND DISCUSSION

$Tend_{abs}$ values of subjects (27 males and 27 females) who reached exhaustion before 60 min (median = 14.4 min; range: 2.7-56.7 min), $Tend_{rel}$ values (median = 8.7 min; range: 2.0-24.3 min) as well as Ind1 and Ind2 indices (not P_{ALT}) were first log-transformed to obtain normal distributions. From the **absolute endurance protocol (load = 90 Nm;** session 2; n = 54 subjects**)**, the associations (Pearson correlation) between the EMG indices and $Tend_{abs}$ were all significant ($P < 0.05$) and ranged between -0.29 and -0.61 (positive sign for P_{ALT}). Higher Pearson correlations were observed between the EMG indices and *Strength* (range: -0.38 to –0.81; positive sign for P_{ALT}). Stepwise regression analyses revealed that the EMG indices (2 to 4 selected depending on the model) can explain 57% of $Tend_{abs}$ and 68% of *Strength*. From the **relative endurance protocol (load = 41 % MVC**; session 3 ; n = 31**)**, few EMG indices (6/38) were significantly correlated to $Tend_{rel}$ and only three correlated with *Strength*. In the regression models, EMG indices explained only 29% of $Tend_{rel}$ and 22% of *Strength*. To verify whether Ind1, Ind2 and P_{ALT} were sensitive to the progression of fatigue, these indices were computed for each 25% interval of the absolute fatigue test to exhaustion (n = 54 subjects). The one-way ANOVAs for repeated measures (4 time-intervals) showed, but only for Ind1 and Ind2, a significant ($P < 0.05$) increase across intervals (fatigue effect).

It can be speculated that P_{ALT} was more specific to measure alternating activity while Ind1 and Ind2 was more sensitive to EMG amplitude variations due to the recruitment of motor units (due to force or fatigue increase). In fact, the negative association between Ind1 and Ind2 indices and *Strength* during the absolute endurance protocol showed that Ind1 and Ind2 increase proportionally with the relative load. Hence, *Strength* being a predictor of absolute endurance ($R^2 = 0.31$), negative associations between these indices and $Tend_{abs}$ were expected. During the relative endurance protocol, the relative load being equal across subjects, the relations between the EMG indices and $Tend_{rel}$ or *Strength* almost disappeared, except for some P_{ALT} indices. The differential effect of fatigue on Ind1-Ind2 versus P_{ALT} suggest that EMG amplitude variability increased but alternating activity was stable as fatigue progressed.

CONCLUSIONS

The quantification of NMAP using surface EMG is complex but can reveal relations with the strength and endurance of an individual, particularly during an absolute endurance protocol.

REFERENCES

1. Larivière C, et al. *Clin Biomech* **16,** 80-83, 2001.
2. van Dieen JH, et al. *Eur J Appl Physiol* **66,** 70-75, 1993.

ACKNOWLEDGEMENTS

This project was co-funded by the Occupational Health and Safety Research Institute Robert-Sauvé (IRSST) of Quebec and the Canadian Institutes for Health Research (CIHR).

NOVEL APPROACH FOR STUDYING HUMAN RESPONSE TO WHIPLASH-LIKE PERTURBATIONS

James P. Dickey, Loriann M. Hynes, Christopher D. Jackson
Human Biology and Nutritional Sciences,
University of Guelph, Guelph, Ontario, Canada; email: jdickey@uoguelph.ca

INTRODUCTION

Whiplash is a common and disabling condition with a significant associated health and economic burden. Much biomechanical research has attempted to understand the mechanism of this injury, and therefore enable strategies to lessen the severity and prevalence of whiplash injuries. This research has identified several primary sites of injury during whiplash including the facet joints [1] and musculature [2]. While the facet joint contribution can be studied using in vitro experimental approaches[1], in vivo human testing is necessary in order to evaluate the physiologic muscle responses to whiplash-type perturbations. To date the human testing experiments have either used experimental impacts with entire automobiles [3, 4], or have applied accelerations to sleds guided by rails [5-8]. Previous experiments have determined that awareness of the impact timing [7], impact direction [5] and head rotation [6] modulate the muscular response, however previous investigations have not been able eliminate the subjects' awareness of the impact direction; the nature of the automobile setup, or the orientation of the rails, has provided clues about the impact direction. Placebo "collision" experiments show that the physiological and psychological factors strongly influence the observed responses to perturbations [4]. Accordingly, as the majority of rear-end collisions are unexpected, experiments must incorporate unknown timing and direction in order to gain insight into "typical" responses to whiplash impacts. The purpose of this paper is to describe the novel experimental system that we have developed for applying low-velocity whiplash-like perturbations in arbitrary directions.

METHODS

We have assembled a novel experimental system for performing human studies using low-velocity whiplash-like perturbations. This system consists of an automobile seat, leg rest, and seatbelt restraint system mounted on a six degree-of-freedom parallel robotic platform. The six degree-of-freedom capacity make this system ideally suited for applying perturbing motions in any direction. Preliminary efforts have been limited to developing appropriate motion pathways for producing the whiplash-like perturbations, and for developing the necessary associated instrumentation. To date we have concentrated on anterior accelerations/displacements, simulating rear end impacts.

RESULTS AND DISCUSSION

The robotic testing platform, showing the platform, automobile seat, seatbelt and footrest is shown in Figure 1. We have determined, through experimentation, that the system is limited to translations less than 20 cm, velocities less than 0.8 m/s (3 km/hr) and accelerations less than 1 g. Pilot testing has determined that platform motions with 1 g peak accelerations (peak acceleration at 0.05 s) result in head accelerations of less than 4 g (Figure 2). These perturbation parameters are similar to one previous study [8], and less severe than the low-velocity impacts that are frequently reported in the literature (either 4 , 8 or 9.3 km/hr) [2-6]

Figure 1: Automobile seat mounted on robotic platform. The platform motion has been programmed to simulate whiplash-like perturbations.

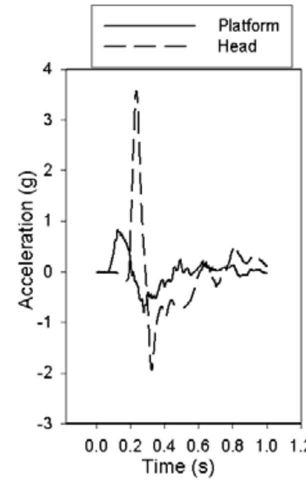

Figure 2: Platform and Head accelerations during whiplash-like perturbation.

CONCLUSIONS

We have assembled a powerful and versatile testing platform for evaluating the biomechanics of whiplash-like perturbations. This system offers unparalleled flexibility due to the ability to translate and/or rotate in any direction. Accordingly, this system is ideally suited to assess the biomechanical effects of low-velocity whiplash-like perturbations due to impacts in different directions, or combinations of directions, more closely simulating real-world (unexpected) impact situations.

REFERENCES

1. Siegmund GP, et al. *Spine* **26**: 2095-2101, 2001.
2. Brault JR, et al. *Clin Biomech* **15**: 426-435, 2000.
3. McConnell WE, et al. *Annu Proc Assoc Adv Automot Med* **47**: 467-492, 2003.
4. Castro WHM, et al. *Int J Legal Med* **114**: 316-322, 2001.
5. Kumar S, et al. *Spine J* **4**: 656-665, 2004.
6. Kumar S, et al. *J Orthop Res* **23**: 224-230, 2005.
7. Siegmund GP, et al. *Spine* **28**: 671-679, 2003.
8. Magnusson ML, et al. *Eur Spine J* **8**: 118-125, 1999.

ACKNOWLEDGEMENTS

Funding provided by the Canadian Foundation for Innovation, NSERC, as well as the Department of Human Biology & Nutritional Sciences and the College of Biological Sciences at the University of Guelph.

IN VIVO MICRO CT SCANNING OF A RABBIT DISTAL FEMUR

[1,2]Boon H. Kam, [2]Shannon B. Antekeier, [1,2]Michael J. Voor, [1,2]Shuo Yang, [2]Seid W. Waddell and [2]Robert L. Burden Jr.
[1]University of Louisville Department of Mechanical Engineering,
[2]University of Louisville Department of Orthopaedic Surgery; email: bhkam002@gwise.louisville.edu

INTRODUCTION

High resolution computed tomography (micro-CT) is a powerful research tool for the study of the detailed structure of cancellous (trabecular) bone [1, 2]. In vivo scanning of only small animals such as rats has been described [3-5]. There are obvious advantages to scanning larger animals using similar techniques so that greater volumes of bone and larger implants can be studied. The objective of this investigation was to demonstrate the successful scanning of a live rabbit distal femur and obtaining accurate high-resolution micro-CT images of 3-D trabecular architecture. A volume fraction comparison was made from in vivo micro-CT images to in vitro micro-CT images on the same femurs after excision to ensure the in vivo scanning produced accurate results.

METHODS

Two six-month-old New Zealand White rabbits (weight: 4-5 kg) were used. All procedures were approved by the university institutional animal care and use committee. The rabbits were anaesthetized with 37.5 mg/ml of Ketamine and 5mg/ml of Xylazine). It took approximately 10 to 20 minutes for the rabbit to be sedated. A rabbit holder was custom made for this scanning procedure. It consists of three sections include the top column of 2.25 inches in length and 40.055 inches in diameter, the second column of 9.22 inches in length and 21.6 inches in diameter and the last column is similar to a tube which has 12.00 inches in length and 2 inches in diameter.

The rabbit was situated in the holder resting its front legs against the top column of the fixture. The right hind leg was resting in flexion and the left hind leg was extended into the transparent column and held in place with a strap. Fabric padding was placed around its head and neck to provide anatomical support in its seating position. The holder was then placed on the specimen manipulator in a custom open acrhitecture micro-CT scanner ((ACTIS 150/225 FFi-HR CT, BIR Inc., Chicago, IL) (Figure 1).

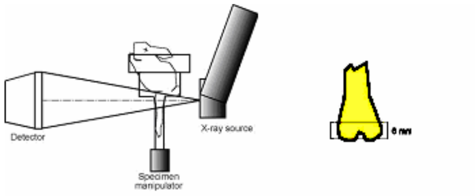

Figure 1: Scanning a live rabbit distal femur 28-micron nominal resolution. Scans were performed in two rotations with a total radiation exposure time of approximately six minutes.

The specimen manipulator is rotated around the z-axis and raised or lowered along the z-axis. The best nominal resolution obtained in scanning a live rabbit distal femur in this arrangement is a voxel size of 28 microns. After in vivo scanning, the femurs were excised and scanned again in vitro in a smaller specimen holder at 14-micron nominal resolution. These two sets of data were registered and compared using VG StudioMAX (Volume Graphics, Heidelberg, Germany) to allow direct comparison.

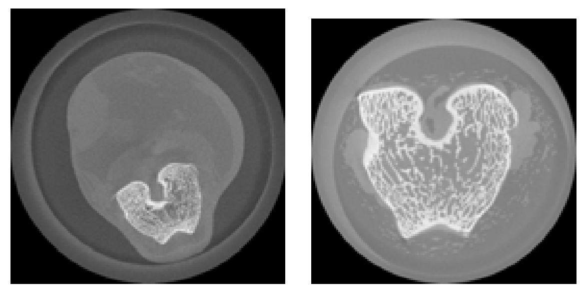

Figure 2: Examples of in vivo (28 micron) and in vitro (14 micon) slice images from the same rabbit femur.

RESULTS

The volume fractions calculated for these two rabbits are 0.25 vs. 0.262 and 0.37 vs. 0.374 (in vivo micro-CT scanning vs. in vitro micro-CT scanning) respectively. The accuracy of in vivo micro-CT scanning is well within 5% of the in vitro method.

DISCUSSION AND CONCLUSIONS

Our studies have demonstrated that the volume fraction from in vivo micro-CT images matches the in vitro micro-CT images. These accurate high-resolution images show the true trabecular architecture can be further utilized in obtaining other trabecular measurements such as trabecular thickness and in analyzing the changing mechanical properties of trabecular structure in micro-FEA on living animals.

REFERENCES

1. Hildebrand T, et al. CMBBE 1,15-23, 1997.
2. Mueller R, et al. Bone 23, 59-66, 1998.
3. Kinney JH, et al. J Bone Miner Res 10, 264-270, 1995.
4. Laib A, et al. Osteoporos Int, 12, 936-941, 2001.
5. Waarsing JH, et al. Bone 34, 163-169, 2004.

ACKNOWLEDGEMENTS

The study was made possible by grants from the NSF and NIH/NIA AG022299-01.

METABOLIC COST OF GENERATING FORCE DURING HUMAN LEG SWINGING

Jiro Doke and Arthur D. Kuo
Department of Mechanical Engineering, University of Michigan, Ann Arbor, MI, U.S.A.
email: jdokeh@umich.edu

INTRODUCTION

When people walk at a particular speed, they choose a step frequency that is the least metabolically demanding [1]. This optimal selection of preferred step frequency can be attributed to determinants such as the cost of stance leg push-off during step to step transitions [2] and the cost of swinging the legs quickly. Sharp increase in metabolic cost during one-legged isolated leg swinging has been seen [3]. We hypothesized two potential causes to the cost of leg swinging: *work hypothesis* and *force/time hypothesis* [3]. According to the work hypothesis, the metabolic cost would increase proportionally to the positive mechanical work performed on the leg, which is assumed to be continuously fueled by the muscles. With the force/time hypothesis, the muscles are generating short bursts of forces, which result in a metabolic cost that is proportional to the force but inversely proportional to the duration of the bursts. Force/time hypothesis has been shown to better predict the preferred speed-step frequency relationship than the work hypothesis [4].

The purpose of this study is to test the force/time hypothesis on the metabolic cost of fast leg swinging. In order to isolate the effect of the work hypothesis, we maintained a constant rate of positive mechanical work over all swing frequencies. If the metabolic rate increases in spite of constant positive work rate, then we can conclude that work hypothesis has little contribution to the increase of metabolic cost at high frequency leg swinging.

METHODS

We measured the mechanics and metabolics of swinging a single human leg, using a frame inside which subjects stood on one leg and swung the other leg at prescribed amplitudes and frequencies (Figure 1). The amplitude was set at 50 degrees at the lowest frequency of 0.75 Hz and decreased with higher frequency, in order to assure a constant rate of positive mechanical work. We measured ground reaction forces, swing leg angle, and oxygen consumption rate, which we used to estimate the metabolic rate.

Six male subjects (aged 29.8 ± 4.9 yrs., mean ± s.d.) consented and participated in this study. They performed single-leg swings at five different frequencies ranging from 0.75 Hz to 1.08 Hz. Each frequency trial lasted six minutes, and the last three minutes were used for analysis in order to ensure steady state metabolic rate.

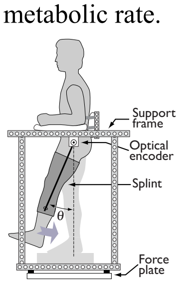

Figure 1: The apparatus consisted of a metal frame with back and arm rests for support, and a raised block for single-leg standing. The subject was securely strapped inside, and the leg angle was measured by an optical encoder at the hip. The whole frame was place on top of a force plate.

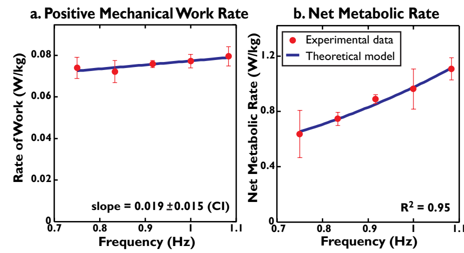

Figure 2: **a.** Positive mechanical work rate remained nearly constant. **b.** Metabolic rate increased with frequency to the 2.5th power, as predicted by the force/time hypothesis.

We created a theoretical model that consisted of a simple pendulum representing the swing leg, with the equations of motion

$$\ddot{\theta} + \omega_n^2 \theta = T,$$

where ω_n is the pendular natural frequency and T is the hip torque. Assuming a sinusoidal motion with amplitude A and frequency $\omega \triangleq 2\pi f$,

$$\theta(t) = A\cos\omega t.$$

In leg swinging, force/time cost is defined as a cost proportional to hip torque amplitude and inversely proportional to swing period [3]. With a constant positive work rate, the force/time hypothesis yields a metabolic rate prediction of

$$\dot{E} \propto f^{2.5}.$$

RESULTS AND DISCUSSION

The metabolic rate increased substantially by 74.3% from 0.75 Hz to 1.08 Hz, despite the nearly constant positive mechanical work rate (Figure 2). Moreover, the metabolic rate increased with frequency to the power of 2.5, as predicted by our force/time model (R^2 = 0.95). The rate of positive work had a slope of 0.019 ± 0.015 (95% confidence interval) W/kg. If the work hypothesis was to hold, the cost would amount to a mechanical to metabolic efficiency of 1.5%. Assuming a typical efficiency of about 21% in isolated muscles [5], the result suggests a weak link between mechanical and metabolic work.

CONCLUSIONS

We isolated the effect of muscular work by keeping the positive work rate constant. There was a substantial increase in metabolic rate. This strongly suggests that the work hypothesis alone does not explain the increase in metabolic cost during high frequency leg swinging. Instead, the increase is better explained by the force/time hypothesis, which credits the cost to muscles generating short bursts of force.

REFERENCES

1. Zarrugh MY. et al. *Eur. J. Appl. Physiol. Occup. Physiol.* **33**, 293-306, 1974.
2. Donelan JM. et al. *J. Exp. Biol.* **205**, 3717-3727, 2002.
3. Doke J. et al. *J. Exp. Biol.* **208**, 439-445, 2005.
4. Kuo AD. *J. Biomech. Eng.* **123**, 264-269, 2001.
5. Hill AV. *Proc. R. Soc. Lond. B* **126**, 136-195, 1938.

SONOGRAPHIC MEASURES OF GASTROCNEMIUS LENGTH WITH TWO-JOINT PASSIVE MOVEMENTS

Timothy J. Brindle, Jeri L. Miller, Maria K. Lebiedowska , and Steven J. Stanhope
**Physical Disabilities Branch, National Institutes of Health, Bethesda, MD 20892
email: Tbrindle@cc.nih.gov, web: http://pdb.cc.nih.gov/

INTRODUCTION

In-vivo ultrasound is a non-invasive method to identify gastrocnemius (GAST) length changes with passive and active movements.[1-3] Predicted ratios of ankle movement, relative to knee movement, can be varied to generate conditions where the GAST will homogeneously elongate, shorten or where the GAST will heterogeneously maintain its length.[4] The purpose of this study is to determine, with 95% confidence, the feasibility of sonographic imaging to derive quantifiable measures of GAST length in order to identify conditions when the GAST homogeneously shortens, elongates, or a condition when there are heterogeneous or minimal changes in GAST muscle length during knee and ankle movements.

METHODS

Ten subjects were seated on a Biodex (*Biodex Inc., Shirley NY*) with their legs positioned in a custom-made foot/ankle apparatus, controlled by a linear actuator (*Ultramotion, Inc, Mattituk, NY*), that passively extended knee and plantar flexed ankle, respectively. A 7.5 MHz linear transducer (*SonoSite, Bothell, WA*) imaged the mid-third of the GAST in the longitudinal plane. The transducer array was set in a jig, attached to the Biodex arm, and held in place with an elastic wrap to maintain image planes of site GAST targets during

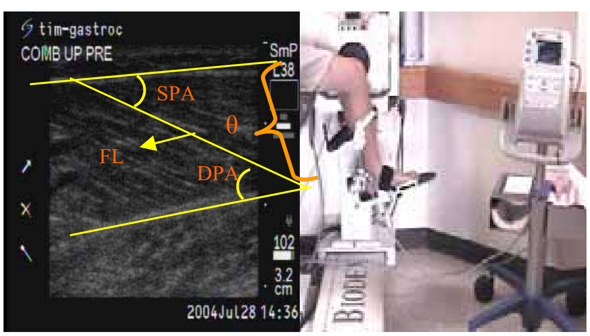

A. **B.**

Figure 1: A) Ultrasound image with angles to calculate: SPA, IPA, and θ. B) Biodex and Linear actuator, with custom foot plate to move the knee and ankle.

data acquisition.[1] As the knee was extended (60^o-20^o at 2 ^{o}/s) the ankle rotated (0^o-6.4^o at 0.32^o/s) for med GAST measurements or rotated (0^o-10.8^o at 0.54 ^{o}/s) for lateral GAST measurements. Off-line ultrasound measures, aquired every 10^o of knee angle (α) included: muscle fiber length (FL); superficial and deep pennation angle (SPA, DPA) and the angle between the superficial and deep aponeuroses (θ).(Fig.1) Commercial software enabled calculation of muscle fiber length (*Carnoy. Schols, P.&E. Smets.2001*) and pennation angle(*Photoshop8,Adobe,Seattle,WA*). Mean values from three trials for each condition were used to calculate a linear regression, with 95% confidence interval, and descriptive data for each movement (*Statistica,StatSoft,Ltd. Tulsa, OK*).

RESULTS AND DISCUSSION

Med GAST FL increased (p<0.05) as the knee extended (FL= 9.1-0.05α: r=-0.32). Lat GAST demonstrated a non-significant trend (p=0.051) to shorten with knee extension (FL=9.2+ .014α: r =0.052). (Figure 2) Greater variability of the lateral GAST FL data warrants reporting pennation angles. (Table 1) During knee extension, increased pennation angles support the trend of GAST shortening during combined knee and ankle movements.

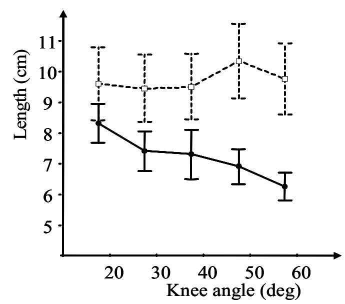

Figure 2: Mean med GAST (—■—) and mean lat GAST (--- □ ----) FL, with 95% confidence interval, relative to α.

Because sonographic techniques are highly user-dependent, future reliability studies are needed to determine accuracy of quantification of muscle length data for estimating forces and muscle function involving two joint movements.

CONCLUSIONS

This is the first study to use sonographic techniques to identify how two joint movements affect GAST muscle fiber length. Homogeneous elongation of the GAST was demonstrated at the predicted ratios of knee and ankle movement. However, heterogeneous changes in the GAST length are apparent with the reported insignificant trend of FL measures. Shortening of lateral GAST would occur with increased plantar flexion velocity, relative to given knee movements.

REFERENCES

1. Chow RS, et al. *Eur J Appl Physiol.* **82**, 236-244, 2000.
2. Muraoka T, et al. *Cells Tissues Organs*. **171**, 260-268,2002
3. Narici MV, et al. J Physiol. **496**, 287-297, 1996.
4. Refshauge KM, et al. J Physiol. **488**, 231-241, 1995.

**A collaboration between the NICHD and the Warren G. Magnuson Clinical Center, NIH.*

Table 1: Lateral GAST Pennation angle: ***Knee Angle (deg)***

	20	30	40	50	60
SPA	6.4+/-3.8	6.5+/-4.1	6.2+/-3.6	5.7+/-3.6	5.4+/-2.9
DPA	10.3+/-3.2	11.1+/-4.1	10.1+/-4.1	9.1+/-4.1	7.7+/-3.2
θ	5.7+/-2.3	5.6+/-2.3	5.1+/-2.1	4.5+/-2.3	3.6+/-1.9

EFFECTS OF DIFFERENT PROFILES OF LATERAL WEDGING ON KNEE ADDUCTION MOMENTS DURING THE LOADING PERIOD OF THE GAIT CYCLE

[1] Richard K Jones, [1] Christopher Nester and [2] Jim Richards
[1] Centre for Rehabilitation and Human Performance Research, University of Salford, UK
[2] Allied Health Professions Unit, Faculty of Health, University of Central Lancashire, UK
email: r.k.jones@salford.ac.uk, web: www.healthcare.salford.ac.uk/crhpr

INTRODUCTION

The aim of lateral wedging is to force the foot into pronation. This will have the effect of altering the centre of pressure and the ground reaction force line of action, which will theoretically modify the loading at the knee joint. This is especially important in conditions such a medial compartment osteoarthritis where off loading of the affected medial compartment is desirable by moving the knee into this position will relieve the pain in this compartment.

The use of lateral wedging has been reported since the first study by Yasuda and Sasaki in 1987[1]. However, there is still a dearth of literature available on biomechanical variables during walking with lateral wedging. A recent study [2] investigated the effects of different elevations of wedging in a group of individuals with no pathologies. They found that laterally wedged insoles significantly reduced the knee joint adduction moment compared with the no wedged insole. However, it is not known if the insoles were inside the shoe or attached to the outside, and also a very simple marker set were used which could bring errors into the calculation of frontal plane motion and moments. It has been clinically shown that wearing a laterally wedged insole provides some perceived pain and function benefit for OA patients, although the guidelines for prescription of the insole such as the degree of incline to use has not been thoroughly studied in respect of controlled shoes and insoles.

The purpose of this study was to assess the effect of wearing two different degrees of lateral wedging on the knee joint adduction moment during loading in healthy adults.

METHODS

Twelve, healthy, male subjects participated in the study. Subjects performed ten walks whilst wearing standard shoes (ECCO Zen) and standard insoles (slimflex). Three conditions were investigated: a) no wedge b) 5 degree wedge, c) 8.5 degree wedge. The insoles were all manufactured by a podiatrist with a full sole up to the metatarsal heads on the lateral border of the insole. Data was collected using eight camera Qualisys Proreflex MCU240 system with bilateral force collected using two Kistler force platforms. Markers were located on the calcaneus, 1st metatarsal, fifth metatarsal, 2nd metatarsal, with clusters of four on the shank, thigh and pelvis. Anatomical reference frames were based on the ISB stardardisation protocol [3]. Hip joint centre was calculated with the functional hip joint method [4].

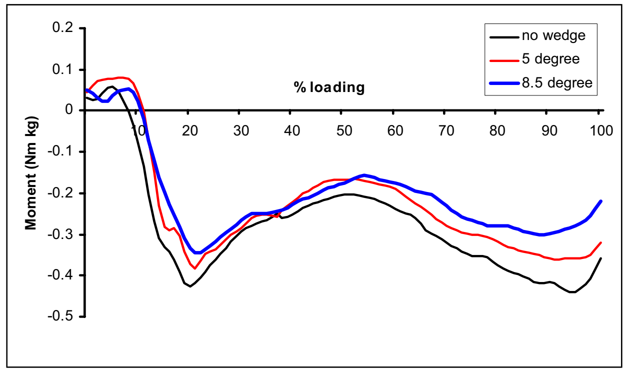

Figure 1: Knee adduction moment in the three wedges N=12)

Data were exported to Visual 3D where 3-dimensional coordinates were interpolated, and low pass filtered using a Butterworth 4th order filter at 6 Hz. Analog data was filtered at 25 Hz. The knee adduction moments were calculated and the peak moments during loading were identified between heel strike and the contralateral heel strike. A one way analysis of variance was performed with an alpha level of 0.05 with a Bonferroni adjustment.

RESULTS AND DISCUSSION

The data for the knee adduction moment was significantly lower for both the 5 degree and 8.5 degree lateral wedging in both limbs during the loading period of both limbs.

CONCLUSIONS

It can be seen from the data presented in this paper that lateral wedging on a standard insole changes the adduction moment of the knee joint during walking. This has implication for the future study on medial compartment osteoarthritis where three conservative treatment options will be evaluated against standard surgical procedures in the aim at reducing pain and increasing functional independence.

REFERENCES

1. Yasuda K et al.. *Clin Orthop*, **215**, 162-172, 1987
2. Kaikana W et al. *Am J Phys Med Rehábil*, **83**, 273-278, 2004.
3. Wu W et al. *J Biomech*, **35**, 543-548
4. Leardini A et al. *J Biomech*, **32**, 99-103, 1999

ACKNOWLEDGEMENTS

The authors would like to thank ECCO and Algeo's for their support in this project

Variable	Degree of Wedge Profile		
	No wedge	5 degree wedge	8.5 degree wedge
Knee Adduction Moment (Nm / kg)	0.425	0.384	0.345

Table 1: Knee adduction moment data for the different wedge

A SIMPLE MATHEMATICAL MODEL OF KARATE FRONT KICK

Jiro Doke and Arthur D. Kuo
Department of Mechanical Engineering, University of Michigan, Ann Arbor, MI, U.S.A.
email: jdokeh@umich.edu

INTRODUCTION

A front kick is one of the most common forms of kick in karate. From observation, the hip and knee joint of the kicking leg go through a sequence of flexion and extension. Experimental studies have shown that, kinematically, the kick starts with hip and knee flexion, then the knee starts to extend, and the hip extends slightly at impact [1]. The front kick is often taught as a maximal effort technique, and we might superficially expect the hip and the knee muscles to be activated with a bang-bang control. However, torque and EMG data has shown the muscles to be not maximally active. We created a simple mathematical model to test whether bang-bang control is the optimal technique and to examine the effects of activation and coordination on kicking performance.

METHODS

We derived a simple, two-segment model with anthropomorphic inertial properties to simulate a closed stance front kick (Figure 1a). The hip and knee joints were actuated by a simple Hill-type muscle model with force-velocity dynamics. We activated the muscle model with an adjustable, constant activation level during flexion and extension phase, with no activation dynamics. Coordination was controlled by two timing parameters (Figure 1b). The first timing was the time from the beginning of the kick to when the knee torque switched from flexion to extension. The second timing was the time from the knee switch timing to when the hip torque switched from flexion to extension. We performed a forward-dynamic simulation, with a terminating condition of 60-degree knee flexion angle. We noted whether the kick terminated with the foot in the target area, which was an area of about 4 mm^2 around the hip height level. As a performance measure, we used horizontal foot velocity at kick completion. For each combination of joint activation levels, we optimized about the switch timings to find the maximum final horizontal foot velocity.

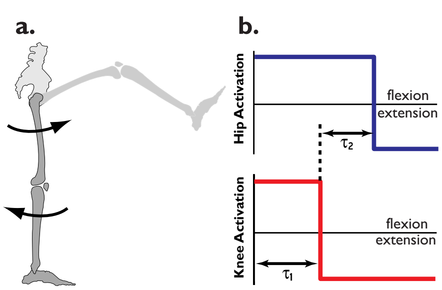

Figure 1: **a.** Simple two-segment karate front kick model. **b.** The torques at the hip and the knee are activated with specified activation levels and switch timings.

RESULTS AND DISCUSSION

We found that the hip needed to be fully activated in both flexion and extension, and the knee had to be maximally extending to achieve maximum performance. However, the knee had an optimal flexion activation level that was not maximal (Figure 2a). Maximum final horizontal foot velocity of 3.874 m/s was achieved at only 15% knee flexion activation and 100% knee extension activation. High activations at the knee caused the knee joint to rotate too fast and kick below the target. At lower knee flexion activations, maximum horizontal foot velocity was achieved at an intermediate activation level (i.e. in the range of 0% ~ 35%, Figure 2a "star"). This optimality arises from the kinematic coupling between the thigh and the shank. At 15% knee flexion activation, the knee is optimally flexed for increasing the horizontal foot velocity during the latter half of the kick. For knee extension, greater activation resulted in increased the foot velocity. These results agree with observations of human kicks, which show relatively low knee joint activity in the flexion phase, but greater activity in the extension phase [2]. Furthermore, a parametric study showed that hip parameters, such as maximum hip torque and velocity, played a greater role in improving kick performance than did knee parameters.

A qualitative analysis of the optimal kick revealed that hip extension torque just prior to kick termination increased the horizontal velocity of the foot (Figure 2b), which can be observed in human data [2]. As the knee straightened, the foot velocity decreased, and this suggested that foot impact should occur before the knee is fully extended, ideally, when the velocity is at its local maximum.

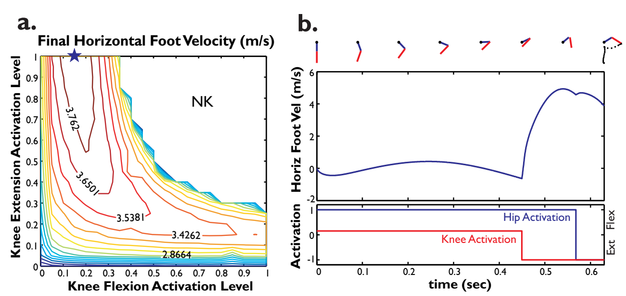

Figure 2: **a.** The optimal kick is indicated by a star, with final horizontal foot velocity of 3.874 m/s. The "NK (no-kick)" region is where no successful switch timing combination was found. **b.** Horizontal velocity profile of the foot during an optimal kick.

CONCLUSIONS

We simulated a karate front kick using a model with simple muscle activation mechanics. We reduced the degree of freedom of the complex kicking motion in order to study the essence of the movement. We found the hip to have a more significant role in kicking performance, and the knee had to be moderately activated during flexion in order to ensure target placement and high horizontal foot velocity. Hip extension just before impact also increased foot velocity. These results resemble what has been observed in experiments, and moreover, give insights to coordination of joints in performing an effective kick.

REFERENCES

1. Robertson DGE. et al. *World Congr. of Biomech.*, 2002.
2. Sorensen H. et al. *J. of Sports Science,* **14**, 483-495, 1996.

Influence of loads to of the joint moments and muscle force repartition in sprint cycling test

Inès Benkhémis, Mathieu Boucher
[1]Laboratoire de mécanique des solides UMR-CNRS6610, Université de Poitiers, 86962 Futuroscope-Chasseneuil Cedex, France.
email: ines@etu.univ-poitiers.fr web : www-lms.univ-poitiers.fr

INTRODUCTION

The pedalling technique requires a complex muscular activation which depends on a few factors like the frequency, the loads [1]. The aim of this preliminary study is to compare the muscular force obtained when using the physiological cross-section area (PCSA) during a sprint test performed by a road and a track cyclists.

METHODS

The cycling tests were realized in laboratory conditions seated on a bicycle (Monark 824) equipped with clipless pedals fixed to a 6-axis sensor (Médicapteur Ex114-45-200). The two subjects (road cyclist: 70kg, 1.75m and track cyclist: 55kg, 1.65m) performed sprints on the ergo-trainer against a 2 and 8kg load. The motion was recorded at 50 Hz by an optoelectronic system (Saga3[rt]). We analyze the first pedalling cycle for each test. The lower limb is considered as a planar 3 degree of freedom. The moment arm and the PCSA values used are taken from [2]. The joint moment at ankle, knee and hip are obtained by the resolution of the inverse Dynamic equations and the muscular force by the minimization method.

RESULTS AND DISCUSSION

The first result indicates that the track cyclist (TC) develops more joint force than the road cyclist (RC). In fact, the figure 1 shows how the joint moments of TC are more important than RC. So, it is logical to obtain the greater muscular force values from the TC. However, the minimum value of the sum of joint moment and the sum of muscular forces are inferior (table 1). In this case we can conclude that the pedalling strategy is different.

The most important muscular force participation is the Long Head Biceps Femoris (BFL: a knee flexor and hip extensor) and the least are the Tibialis Anterior (TA: an ankle flexor) and the Short Head of Femoris (BFS: a knee extensor). At 8kg, the muscular force increases about 19% for TA and BFS and about 10% for BFL of the two cyclists.

Six of the nine low limb muscles fit into the knee.But the knee moments are the least at any load for the two subjects.

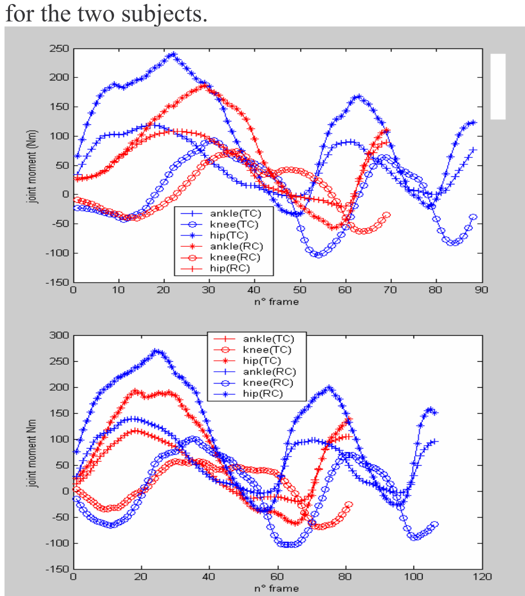

Figure 1: joint moments for the two cyclists at 2kg (top) and 8kg (bottom)

CONCLUSION

Our preliminary study shows the importance of the use of the individual muscle force to compare pedalling motion. It is useful to determinate the energy cost per muscle to define a cycling profile.

The inferiority in the knee moment needs more investigation and probably to relate it to the height of the seat.

REFERENCES

1. Baum B.S., Li Li, *J. electromyo. Kinesio*. **13**, 181-190, 2003.
2. Raikova R.T., Prilutsky B.I. *J Biomech* **34**, 1243-1255, 2001.

Table 1 : Minimum, maximum and mean values of the sum of joint moments and muscular force.

	2 kg				8 kg			
	TC		RC		TC		RC	
	moment	force	moment	force	moment	force	moment	force
min	20.6Nm	1200N	46.02Nm	1715N	34.65Nm	1196N	42.55Nm	1810N
max	406.6Nm	19800N	336.9Nm	15710N	460.8Nm	21790N	360.4Nm	17480N
mean	216.7Nm	9739N	175Nm	7560N	245.9Nm	10990N	186.5Nm	8401N

Ankle Plantar Flexor Moments Scale to Planning Time during Unexpected Side Step Cut Tasks

Jeff Houck[1,2], Abbey Green[2], Allison Baxendale[1], Kenneth Dehaven[3]
[1]Ithaca College – Rochester Campus, Rochester, NY Contact: jhouck@ithaca.edu
[2]University of Rochester, Department of Biomedical Engineering Rochester, NY
[3]University of Rochester Medical Center, Department of Orthopedics Rochester, NY

INTRODUCTION

During sports play quick movements such as cut tasks are believed to place athletes at risk. The ankle joint plantar flexors, responsible for controlling tibial progression during midstance,[1] may play a key role in successfully completing a quick cut task.[2] As planning time is reduced, rapid development of large plantar flexor moments and restraint of tibial progression (dorsiflexion range of motion) during second rocker are expected. Further, we theorized that as planning time decreased the plantar flexor response would show a non-linear increase to control tibial progression. The purpose of this study was to examine the relationship between indicators of ankle plantar flexor function (Table 1) and planning time during second rocker (10-60% of stance) of an unexpected side step cut task.

METHODS

Nineteen healthy subjects (22.6 ± 5.5 years old, 172.8 ± 9.0 cm, and 71.9 ± 14.3 kg) participated in this study. Data were collected using an Optotrak Motion Analysis System (Northern Digital, Inc.) and force plate (Kistler) integrated with Motion Monitor Software (Innsport Training, Inc.) to generate ankle joint angles, moments and power. Position data were sampled at 100 Hz and force and analogue data at 1000 Hz. Each testing session included expected tasks, straight walking (ST) and 45° side step cut (SS), followed by a set of unexpected straight walking (STU) and unexpected side step cut (SSU) tasks in a random order. For all tasks speed was maintained at 2 m/s using infrared timing gates (Bower Timing Systems, Draper UT). Only the SSU tasks are included in this analysis. Planning time is defined as the interval between the visual cue and initial contact (Figure 1). The relationship between the dependent variables (Table 1) and planning time were examined using SPSS 10.0.

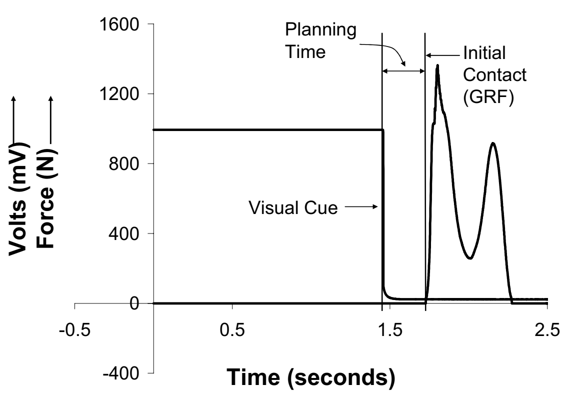

Figure 1. Subjects went straight or cut when given a visual cue to turn. Planning time was the interval between an analogue signal synchronized with the light cue and initial contact determined from the ground reaction force data.

RESULTS AND DISCUSSION

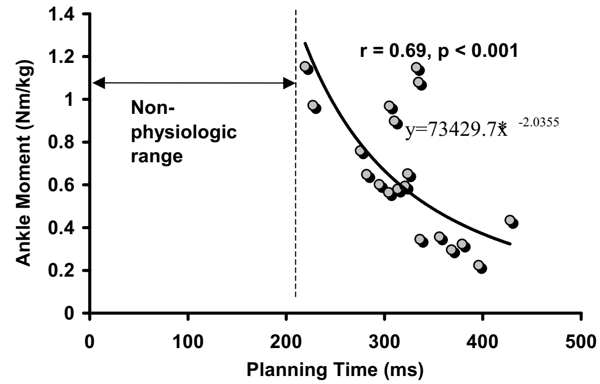

Figure 2. The non-linear relationship between peak ankle plantar flexor moments and planning time showed increased moments with decreasing planning time.

Table 1. Pearson Product Moment Correlations between Planning Time and Ankle Variables During Second Rocker.

Variable	Mean (SD)	r - value
Planning Time (ms)	321±52	
Dorsiflexion Range of Motion (°)	11.7±4.8	-0.31
Plantar Flexion Moment (Nm/kg)	0.66±0.3	**-0.66**
Power Absorption Integral (W/kg * %Stance)	6.6±7.8	-0.09

Bold values indicate significance at $p < 0.05$

The findings of this analysis suggest that the peak ankle plantar flexor moments scale to planning time during an unanticipated cut task (Figure 2). The range of planning times executed during this task varied from ≈200 – 450 ms (Table 1). The shorter planning times (< 350 ms) are associated with large plantar flexor moments (> 0.6 Nm/kg). These large responses, in some cases equal to the plantar flexor moment at push off, may challenge athletes. The longer planning times (> 350 ms) are associated with smaller plantar flexor moments (< 0.4 Nm/kg), suggesting longer planning times have less effect on limb loading. This data supports the view that ankle plantar flexor weakness or poorly timed control of plantar flexor function may impact performance during unexpected cut tasks.

REFERENCES

1.Perry, J., Phys Ther, 1967. **47**(9): p. 778-801.
2.Patla, A.E., et al., J Exp Psychol Hum Percept Perform, 1991. **17**(3): p. 603-34.

ACKNOWLEDGEMENTS
Support from the Whitaker Foundation (RG-02-0645)

BIOMECHANICAL DIFFERENCES BETWEEN GENDERS WHEN EXECUTING A LAND AND CUT MANEUVER

Robert Shapiro and Jeff Buhr
Department of Kinesiology and Health Promotion, University of Kentucky
email: rshap01@uky.edu web: http://www.coe.uky.edu/biodynamics/

INTRODUCTION

It is well documented that the knee is a commonly injured joint in male and female athletes. Many researchers have investigated the significantly higher incidence rate of non-contact ACL injuries in female athletes. [1,2,3]. It has been suggested that females are at risk for an ACL injury because they land with less knee flexion, and greater knee abduction than males while having weaker hip strength. Cutting and landing from a jump are most often identified as the activity at the time of injury. Consequently, investigators have tried to recreate these activities in an effort to define the injury mechanism and deduce factors that cause the injury rate difference between males and females. It has become apparent that a static landing activity, asking a subject to land and hold that position, does not adequately reproduce an authentic sport motion. In an effort to create a more realistic task, investigators have introduced landings followed by a vertical jump, while others have examined the cutting in an unanticipated direction to simulate a sport-related motion. The combination of landing and cutting has yet to be studied in the laboratory setting The purpose of this study was to attempt to recreate a landing condition that more closely resembled that seen in sport competition and evaluate landing kinematics. In this study landing and cutting were combined into a single event, more closely simulating motions seen in basketball, volleyball and soccer.

METHODS

Healthy, male (n = 22, age = 23(1.4)yrs, wt = 745(100)N, ht = 1.76(0.05)m) and female (n = 23, age = 22.4(1.5)yrs, wt = 600 (69.8)N, ht =1.65 (0.06)m) subjects provided informed consent prior to participating in this study. Subjects were marked with 37 reflective markers enabling 3-D reconstruction of a rigid linked model of the body. Six Falcon high-speed cameras (120Hz) imaged subjects while two Kistler force platforms measured ground reaction forces (960 Hz). Video and GRF data were synchronized at collection onset. Motion Analysis Corp. Eva software was utilized to obtain marker object-space coordinates. Subjects were imaged in a static position to enable determination of anatomically relevant coordinate systems [4]. Subjects were then instructed to land from a 60 cm platform and cut right, left or remain stationary after impact. The direction of cut was provided immediately prior to the subject leaving the platform. Table 1 provides a list of dependent variables. Three-dimensional kinematic variables were calculated using both KinTrak® and OrthoTrak® software T-tests, $p<.05$, were used in this preliminary analysis to compare the groups.

RESULTS AND DISCUSSION

Only kinematic data from the right leg (dominant leg in 44 of 45 subjects) for the land and right cut maneuver are reported here (Table 1). Subjects generally landed in slight knee and hip flexion. Males landed in greater knee flexion and reached a greater maximum knee flexion angle but total range of motion was not different between males and females. Both groups landed with slightly abducted hips and slightly adducted knees. Females remained abducted at the hip while the males obtained an adducted position through the remainder of stance. At the knee both groups moved into an abducted position. This knee motion is similar to that reported by Pollard et al. for a cutting maneuver [2]. No between group differences were observed for knee rotation, knee abduction, hip flexion or hip rotation variables.

Variable	Male (±SE)	Female(±SE)	P<.05
Angle at Impact (degrees)			
Knee Flexion	22.35 (1.50)	18.42 (1.02)	*
Knee Adduct	6.17 (1.40)	2.84 (1.60)	
Knee Ext Rot	4.23 (0.84)	2.54 (0.80)	
Hip Flexion	18.50 (1.39)	19.12 (1.03)	
Hip Adduct	-3.24 (0.83)	-5.05 (0.88)	
Hip Ext Rot	7.61 (1.03)	9.65 (0.88)	
Maximum or Minimum Angle after Impact (degrees)			
Knee Flexion	93.3 (1.54)	87.9 (1.52)	*
Knee Adduct	-6.17 (1.83)	-13.68 (3.34)	
Knee Ext Rot	5.17 (1.62)	9.56 (1.61)	
Hip Flexion	63.83 (1.73)	64.08 (1.80)	
Hip Adduct	5.68 (1.31)	-2.5 (1.21)	*
Hip Ext Rot	3.87 (1.22)	7.02 (0.99)	

Table 1: Comparisons (mean (SE)) of right leg hip and knee angles at impact and maximum range.

CONCLUSIONS

While the premise that females tend to land with less knee flexion and reach less maximal knee flexion while landing is supported in this study, no differences in knee abduction or rotation were observed. The greater hip abduction angle in females supports the idea that weakness at the hip may prevent females from establishing a safe landing position. With both the thigh and knee abducted, the knee is placed at risk for an injury upon landing as the weight of the body can, given sufficient hip abduction, potentially place a torque at the knee that cannot be actively controlled. Further evaluation of hip kinetics and associated muscle activity is warranted.

REFERENCES

1. Ford KR, et al. *Med. Sci. Sports Exerc* **35**, 1745-1750, 2003.
2. Pollard CD, et al.. *Clin Biomech* **19**, 1022-1031, 2004.
3. Fagenbaum R, & Darling W. *Amer J Spt Med* **31**, 233-240, 2003.
4. Grood E, & Suntay WJ. *J Biomech Eng* **105,** 136-144, 1983.

FEEDBACK CONTROL FOR A HIGH LEVEL UPPER EXTREMITY NEUROPROSTHESIS

Dimitra Blana (dimitra.blana@case.edu), Juan Gabriel Hincapie, Edward K J. Chadwick and Robert F. Kirsch
Department of Biomedical Engineering, Case Western Reserve University, Cleveland OH

INTRODUCTION

Individuals with C3/C4 spinal cord injury lose voluntary control of almost all muscles of the upper extremity. A neuroprosthetic system that applies electrical stimulation to paralyzed muscles can be used to restore function to these individuals. The controller for this system will generate the appropriate levels of muscle activation, based on the user commands. It also needs to compensate for errors caused by external disturbances and fatigue. This is necessary, because at that level of injury, voluntary correction for errors in the performance of the neuroprosthesis is not possible. In addition, due to the large number of shoulder and elbow muscles that must be controlled in high tetraplegia, purely experimental methods for developing the neuroprosthesis are inefficient and impractical. The goal of this project is to use a model-based approach to develop and test a feedback controller for this system.

METHODS

The musculoskeletal model of the shoulder and elbow used in this project is a finite element model built in SIMM (Software for Interactive Musculoskeletal Modeling, Musculographics, Inc.). It includes 28 muscles, six bones and five joints, with a total of 17 degrees of freedom. The morphological and muscle contraction parameters were obtained from cadaver studies performed by the Van der Helm group in Delft [1].

The open-loop controller that calculates the muscle activations required for a desired movement was designed as a static two-layer artificial neural network (ANN). It has a tangent-sigmoidal activation function for the hidden layer and a linear activation function for the output layer. In order to correct for position and orientation errors that are caused by fatigue or external disturbances, such as masses added to or removed from the hand, a feedback loop needs to be added to the previously designed controller. Its role is to model the relationship between error and the changes in muscle activation that will move the arm toward the desired position. Both the open-loop and the feedback parts of the controller are being developed using the musculoskeletal model, which was customized to simulate a person with C3-C4 level spinal cord injury.

RESULTS AND DISCUSSION

Figure 1 shows the predictions of the open-loop controller, which is an ANN with 20 neurons in the hidden layer, for the activation of two muscles, middle deltoid and upper trapezius, during a humeral abduction movement. The RMS error is 4.47% for the middle deltoid, and 6.05% for the upper trapezius. The performance of the ANN can be improved by optimizing its parameters.

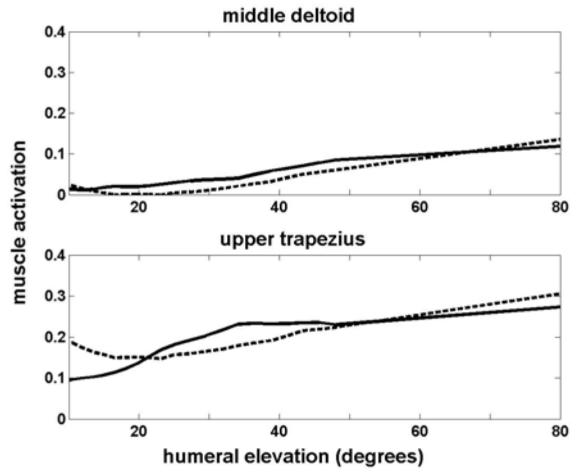

Figure 1: The solid lines are the activations calculated by the model, and the dotted lines are the ANN predictions.

When the feedback loop is added, the performance of the overall controller will be evaluated using the model in series with the system. A set of forward simulations will be performed with the output of the controller as input to the model, and the resulting endpoint position and orientation will be compared with the desired ones.

CONCLUSIONS

The preliminary results show that the ANN can accurately predict the muscle activations needed for a desired posture, and can therefore be used as the open-loop part of the neuroprosthesis controller. It is also demonstrated that the use of a musculoskeletal model can facilitate the development of the feedback controller, by simulating a C3-C4 SCI individual and realistic conditions of fatigue and external disturbances, both for designing and for testing the system.

REFERENCES

1. Klein Breteler M.D, Spoor C.W. and van der Helm F.C.T: *Measuring muscle and joint geometry parameters of a shoulder for modeling purposes*, J Biomech 32: 1191-1197, 1999.

ACKNOWLEDGEMENTS

Peter Loan and Musa Audu, Ph.D. are acknowledged for their help with SIMM and optimisation methods, respectively.

FOREARM MUSCLE ACTIVITY DURING THREE HOSE INSERTION TASKS AS MEASURED BY SURFACE ELCTROMYOGRAPHY OF THE FLEXOR DIGITORUM SUPERFICIALIS MUSCLE

D. Christian Grieshaber, Thomas J. Armstrong and Na Jin Seo
University of Michigan, Ann Arbor, MI
email: gries@umich.edu, web: http://umrerc.engin.umich.edu/

INTRODUCTION

When the physical demands of a task exceed the capacities of the worker performing those tasks can often lead to losses in production, fatigue and sometimes pain or injury to the worker. Hose installation tasks during automotive assembly operations are an example of a physically demanding task. In a recent survey, automotive truck assembly plant workers rated hose insertion tasks as the most physically demanding part of their job [1].

This study examines the effect that insertion method has on subject exertion levels, as measured by surface finger flexor EMGs.

METHODS

This experiment involved the measurement of insertion loads and EMGs in subjects as they inserted a rubber radiator hose onto a horizontal flange. The hose had an inner diameter of 25.4 mm and a wall thickness of 5 mm. The tasks simulated three insertion methods similar to those observed in field studies of hose installation tasks – Straight Push, Rocking Push and Twisting Push. Surface EMG electrodes (AMBU Neuroline 720 Wet Gel Ag/AgCl) were placed over distal muscle belly fibers of the Flexor Digitorum Superficialis muscle. Exertion levels were normalized using maximum static power grip (MVC) prior to testing.

For straight insertions, subjects were instructed to insert the hose directly onto the flange. For rocking insertions, subjects were instructed to push the hose on while rocking the hose back and forth in either the vertical or horizontal direction. For twisting insertions, subjects were instructed to push the hose on while rotating it about the long axis of the flange.

6 male and 6 female university students volunteered to participate in the experiment. All subjects were free of known upper extremity disorders and gave informed consent prior to testing. The experimental design was approved by the University of Michigan Internal Review Board.

RESULTS AND DISCUSSION

Axial loads and exertion levels increased with fit and varied by the insertion method used (Figure 1). Axial insertion forces were 35% higher for the straight method (150.0 N) compared to the twist method (110.6 N), $p<0.0001$. There does not appear to be an advantage to using the twisting method over the straight or rocking method, even though the axial insertion force is reduced by 26%. There was a 64% increase in pooled exertion levels for the twisting method over the straight method. The increase in muscle activity is consistent with decreased power grip strength capabilities due to deviations of the wrist during twisting and rocking insertions [2, 3]. It is also possible that tighter grip is required to twist or rock the hose.

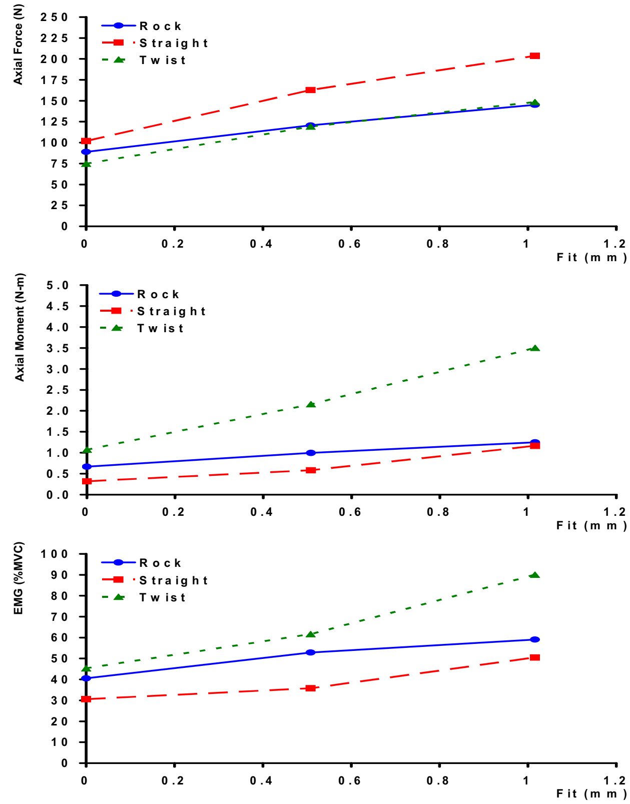

Figure 1: Average force, moment and EMG recordings for 12 subjects and three insertion methods. Fit is a measure of the amount of interference between the flange and the hose as it is inserted.

CONCLUSIONS

The greatest muscle activity was recorded while inserting hoses with the twisting method. The straight push has higher axial loading than the rocking push, but allows the subject to work in preferred static wrist posture. Future studies will investigate whether subjects use a tighter grip during twisting and rocking insertions.

ACKNOWLEDGEMENT

This project was funded in part by joint funds from the UAW-GM National Joint Committee on Health and Safety. The results presented herein represent the conclusions and opinions of the authors. Its publication does not necessarily imply endorsement by the International Union, UAW, or General Motors Corporation.

REFERENCES

1. Ebersole, ML and Armstrong, TJ. *Proceedings of the HFES 48th Annual Meeting*, New Orleans, LA, 2003.
2. O'Driscoll, SW, et al. *J of Hand Surgery* **17A**, 169-177, 1992.
3. Lamoreaux, L and Hoffer, M. *Clinical Orthopedics and Related Research*, **314**, 152-155, 1995.

CHANGES IN THE RAT ACL RESULTING FROM SUBFAILURE IMPINGEMENT LOADING

[1]David T. Fung, [2]J. Scott Quinby, [2]Jason L. Koh, [1]Shu Q. Liu and [1-3]Li-Qun Zhang
[1]Depts. of Biomed. Eng., [2]Ortho. Surg., and [3]Phy. Med. & Rehab., Northwestern University; email: d-fung@northwestern.edu

INTRODUCTION

While many noncontact ACL injuries may have resulted from direct over-stretching of the ligament, the ACL may also be injured due to its impingement against the intercondylar notch. Previous cadaveric studies have shown the ACL to impinge against the lateral wall of the notch during abduction and external tibial rotation at moderate knee flexion [1,2]. How impingement loading may alter the biomechanical properties of the ACL remains unknown. The purpose of this study was to evaluate changes in the force-length relationship of the ACL resulting from impingement, in corroboration with histological examinations on its superficial tissue, in a subfailure impingement injury model in rats

METHODS

Seven female musculoskeletally mature Sprague-Dawley rats with an average weight of 370±60 g (mean±SD) were used in this study. Under anesthesia, both lower limbs were disarticulated at the hip. Soft tissue on the disarticulated limbs was carefully dissected leaving only the ACL intact (Fig. 1a). The lateral tibial condyle of each femur-ACL-tibia complex (FATC) was then removed with a burring tool, allowing the knee to assume excessive abduction.

Each FATC was then mounted on a custom-designed loading apparatus with special clamps to hold the femoral and tibial shafts in a saline bath (Fig. 1b). In the apparatus, a linear motor with a precision of 0.4mm was used to load the ACL. A load cell was connected on one end to the motor shaft with its axis aligned with that of the load cell and, on the other end, to the tibial clamp. The FATC was secured into the apparatus by first fixing the tibia in the tibial clamp with the tibial axis aligned with the motor shaft and load cell axis. The femur was fixed to the femoral clamp, which, in turn, was attached to the multi-degree-of-freedom adjustable arm. Each FATC from each pair was randomly selected to be loaded in one of two knee postures by manipulating the position of the adjustable arm: 1) at ~30º flexion; and 2) at ~30º flexion, ~15º abduction, and ~5º external tibial rotation. Linear movement of the motor directly stretched the ACL longitudinally in the first posture and induced impingement of the ACL in the second.

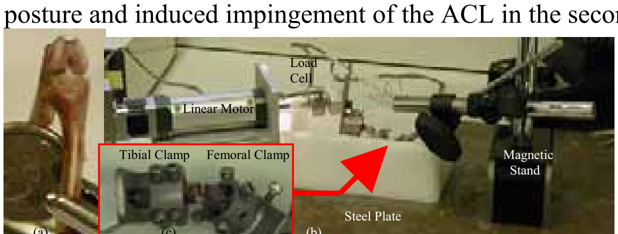

Figure 1. Experimental Setup. An FATC (a) mounted on the loading apparatus (b). Femoral and tibial clamps (c) secure the FATC, allowing the motor shaft the load the ACL cyclically.

Initially, the ACL was loaded cyclically to a minimal load to locate the 'inflection point' on the force-length curve, which established the ACL's normal length. The ACL was then preconditioned by loading the ACL 10× to 0.28 mm of displacement. Following preconditioning, the ACL was loaded repeatedly 10× at the same displacement (Sequence 1). The ligament was given a 15-min rest and loaded cyclically to 0.36 mm of displacement (Sequence 2) for 10 trials of 10 cycles per trial. Subfailure injury, if any, would have occurred during this Sequence, reaching 12% strain in the ligament. Following another 15-minute rest, the ligament was loaded cyclically 10× again at 0.28 mm of displacement (Sequence 3). All loading was applied at 1 mm/sec. Force-displacement data in Sequences 1 and 3 were plotted separately for impinged and nonimpinged ACL for each pair of FATC's. Using linear regression, the stiffnesses for the impinged ligament ($k_{1,imp}$ and $k_{3,imp}$) and for the directly-stretched ligament ($k_{1,ds}$ and $k_{3,ds}$) were determined in Sequences 1 and 3. Differences between the Sequences and between the mode of loading was evaluated statistically (Paired t-test). Significance was established at p=0.05.

Immediately following Sequence 3, the ACL was harvested and stained with a cell viability assay (Live/Dead® L-3224, Molecular Probes) with Hoechst 33258 added to locate the cell nuclei. Under the fluorescent microscope, live cells show green fluorescence and necrotic cells show red. Images were captured at 20× magnification and overlaid at randomly selected regions on impinged aspect, and the non-impinged aspect of the impinged ACL, and on the directly stretched ACL. The images of the three regions were compared to assess the effect of impingement.

RESULTS AND DISCUSSION

Among the seven pairs of ACLs, $k_{1,imp}$ (11.9±5.7 N/mm) (mean±SD) was significantly greater than $k_{3,imp}$ (9.6±6.0 N/mm) (p=.014). Insignificant difference was observed between $k_{1,ds}$ (12.9±7.1 N/mm) and $k_{3,ds}$ (12.1±5.5 N/mm) (p=0.20), and between $k_{1,ds}$ and $k_{1,imp}$ (p=0.67), demonstrating the impingement led to a reduction in the ligament's stiffness. Representative micrographs showed that impingement resulted in the disruption of the tissue organization and cell necrosis on the impinged surface of the ACL (Fig. 2).

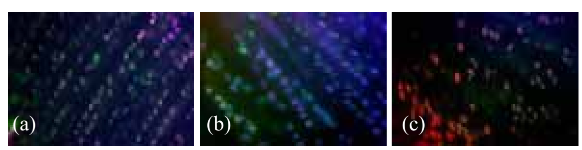

Figure 2. Representative fluorescent micrographs showing the directly stretched ACL (a), and the impinged ACL at its nonimpinged aspect (b) and impinged aspect (c).

CONCLUSIONS

Cyclic impingement loading has shown to decrease the stiffness of the ACL in the ex-vivo rat model, corroborated with reduced cell viability and disrupted tissue organization on the impinged surface of the ACL as observed on fluorescent micrographs. The loads and displacements reached during cyclic loading were within physiological limits. Results from this study contributed to our understanding of ACL injury resulting from impingement at the tissue level.

REFERENCES:

1.Fung, DT, Zhang, L-Q. (2003) *Clin. Biomech.* (18) 933-941.
2.LaPrade, RF, Burnett, QM. (1994) *AJSM*, (22) 198-203.

THE EFFECTS OF SUBMAXIMAL SHOULDER MOMENT, TASK PRECISION AND MENTAL DEMAND ON MUSCLE ACTIVITY DURING GRIP EXERTIONS

Alvin K. Au and Peter J. Keir, PhD
School of Kinesiology and Health Science, York University, Toronto, Canada; email: pjkeir@yorku.ca

INTRODUCTION

Over 100,000 new cases of musculoskeletal disorders (MSDs) reported annually in the U.S. resulted from overexertion or repetitive motion of the upper extremity [1] and cost the health care and insurance systems hundreds of millions of dollars [2]. Despite the prevalence and cost associated with upper extremity MSDs, the underlying mechanisms for these injuries are still not well understood. In the workplace, external forces have been relatively well evaluated, but internal muscular loads are not as easily assessed. Further complicating matters is that, in addition to external forces, laboratory studies have identified several other factors that increase muscle activity in the upper extremity, including the nature of loading, increased task precision and mental demands. Failure to account for these factors by assessing external loads alone in the workplace will likely underestimate muscle load. For example, the addition of a submaximal grip or mental load to maximal shoulder exertions have been shown to interfere with the ability to produce maximal shoulder moment without necessarily reducing muscle activity; this effect was greatest when all tasks were combined [3]. The purpose of this study was to determine the influence of task precision, mental demands and shoulder exertions on forearm and shoulder muscle activity during a grip exertion task.

METHODS

Participants (8 males, 8 females) were recruited from the university community and visited the lab on two occasions. On the first visit, participants were oriented to the protocol and had their maximal grip and shoulder strengths determined. The experimental protocol was conducted during the second visit. In total, there were 4 grip conditions, 3 shoulder loads and 2 mental loading levels. Each of the 24 conditions was repeated 3 times in a randomized block design. Participants were seated with the right arm abducted to 90°. They then exerted grip forces of 0, 30 and 100% MVC while simply maintaining shoulder posture or exerting a 40% MVC shoulder moment. To create the 40% MVC shoulder moment, participants either pushed upwards against a force transducer (*force-controlled*) positioned just proximal to the elbow or supported an equivalent weight (*posture-controlled*) hung from the same location. The 30% MVC grip force was maintain under two levels of precision: high precision required the grip force to be maintained within ±5% and low precision within ±10%. The increased mental loading condition was achieved by the simultaneous use of the Stroop test [3]. All forces and linear envelope EMG (3 Hz analog) were collected at 100 Hz. Surface EMG was recorded from 8 muscles on the right upper extremity: trapezius (TR), anterior deltoid (AD), middle deltoid (MD), posterior deltoid (PD), flexor carpi radialis (FCR), flexor digitorum superficialis (FDS), extensor carpi ulnaris (ECU), and extensor digitorum communis (EDC). Each trial lasted 10 s and participants received a minimum rest of 1 minute between trials and 5 minutes between blocks.

RESULTS AND DISCUSSION

Preliminary analysis (n=3) indicated that maintaining 90° arm abduction while holding the grip dynamometer required shoulder moment of 20-30% MVC. Middle deltoid activity was approximately 30% MVE for these contractions, as previously found [4]. Force- and posture-controlled shoulder exertions at 40% MVC increased trapezius and deltoid activity by 20-25% MVE beyond that required to support the arm alone. Interestingly, for both 40% MVC moments (force- and posture-controlled), forearm extensor muscle activity increased by 2-3% MVE without an increase in grip force (Fig. 1). The need for greater precision in grip force also appeared to increase forearm muscle activity slightly. Based on these preliminary data, there appears to be a slight reduction in deltoid activity between the force- and posture-controlled moments with 0 and 30% MVC grip. The ability to generate a maximal grip exertion was compromised during simultaneous force-controlled shoulder exertions but not in any other condition. This 10-15% MVC reduction in grip force was paralleled by a similar decrease in forearm muscle activity. The findings of this study will improve our knowledge of the interactions of physical and cognitive demands in the workplace and their role in upper extremity MSDs.

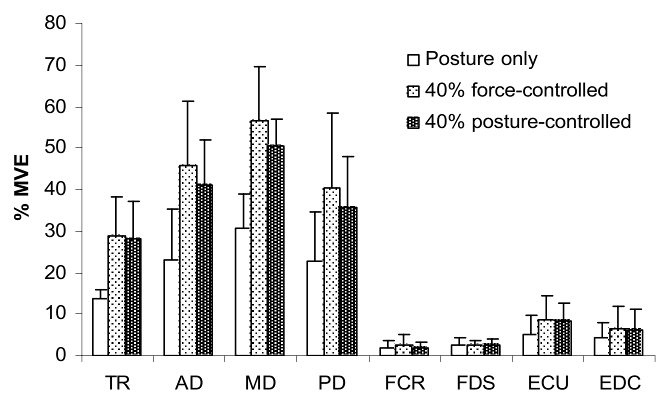

Figure 1: Muscle activity at 90° shoulder abduction with and without a 40% shoulder moment (no grip force).

REFERENCES

1. NIOSH, *Worker Health Chartbook 2004*, Cincinnati, OH.
2. NIOSH, *MSDs and Workplace Factors*, Cincinnati, OH.
3. MacDonell C, M.Sc. thesis, York University, Toronto, ON.
4. Sjogaard G, et al. *J Appl Physiol* **96**, 1522-1529, 2004.

ACKNOWLEDGEMENTS

This study was funded by NSERC (Canada), grant #217382.

WALKING IN GREATER HIP EXTENSION INCREASES PREDICTED ANTERIOR HIP JOINT REACTION FORCES

[1]Cara L. Lewis, [2]Shirley A. Sahrmann and [3]Daniel W. Moran
[1]Movement Science Program, [2]Program in Physical Therapy, School of Medicine, [3]Department of Biomedical Engineering; Washington University in St. Louis; email: lewis@wustl.edu

INTRODUCTION

Acetabular labral tears are a recently recognized source of anterior hip pain. Excessive forces have been implicated as one cause of these tears. A clinical sign of a tear is anterior hip pain during late stance phase of gait. We propose that this pain is due, in part, to excessive force on the anterior structures of the hip, especially when the hip is extended. Our hypothesis is supported by the fact that, in patients with this pain, the pain is reduced when the patient is instructed to walk in less hip extension. This gait modification may help to decrease the anteriorly directed force, thus decreasing the pain.

The purpose of this study is to use a 3D dynamic musculoskeletal model to estimate the hip joint reaction forces while walking. We hypothesize that, within subjects, the gait trials with the greatest maximum hip extension will have a greater maximum anterior hip joint reaction force when compared to trials with the least maximum hip extension.

METHODS

A six degree of freedom, 3D musculoskeletal model of a lower leg was developed to calculate joint reaction forces in the hip, knee, and ankle. Musculoskeletal parameters were adapted from Delp [1]. Kane's Method [2] and AUTOLEV 3.1 (OnLine Dynamics, Inc., Sunnyvale, CA) were used to generate the dynamic equations of motion. The general form of the dynamic equations of motion is:

$$\mathbf{M}(\vec{\mathbf{Q}})\ddot{\vec{\mathbf{Q}}} = \vec{\mathbf{T}} + \vec{\mathbf{P}}\left(\vec{\mathbf{Q}},\dot{\vec{\mathbf{Q}}}\right) + \vec{\mathbf{V}}\left(\vec{\mathbf{Q}},\dot{\vec{\mathbf{Q}}}\right) + \vec{\mathbf{G}}(\vec{\mathbf{Q}}) + \vec{\mathbf{E}}\left(\vec{\mathbf{Q}},\dot{\vec{\mathbf{Q}}}\right)$$

where M is the mass matrix, T is the net joint torques contributed by the force in the muscles spanning all joints, P is the torques developed passively in the joints due to viscoelastic damping and passive joint structures, and V, G, and E are the instantaneous segmental torques caused by the inertial, gravitational, and external forces, respectively. Q is the column vector of joint angles. Using kinematic and kinetic data from gait trials, the required segmental torques due to muscles were obtained for each trial. At each time point, a pseudoinverse optimization routine was used to solve for the optimal set of muscle forces [3] to create the needed joint torques. Once the optimized muscle stresses were solved simultaneously across all joints, the model calculated the resulting 3D reaction forces in the hip due to muscular contraction.

The gait data used in this study was collected from 5 healthy college-aged male subjects who participated in a previous study [4]. Each subject walked at a self-selected speed while 3D kinematic and kinetic data were collected. As we were most interested in anteriorly directed joint reaction forces, we only analyzed the terminal stance phase of gait. Within each subject, the reaction forces at the hip for the 2 trials with the most hip extension (MHE) range of motion and the 2 trials with the least hip extension (LHE) range of motion were each averaged. Paired t-tests were used to detect differences ($p < 0.05$).

RESULTS AND DISCUSSION

The average anterior reaction forces are presented in Table 1. Despite only a 2 degree difference between the MHE and LHE trials on average, ambulating with greater hip extension results in anteriorly directed forces that are significantly higher than ambulating with less hip extension.

Table 1: The average maximum hip angle and average anterior joint reaction force for the two groups.

Variable:	**MHE**	**LHE**	**p**
Max Hip Extension Angle (°)	13.5	11.5	0.01
Anterior Joint Reaction (N)	1791	1428	<0.01

CONCLUSIONS

A 3D musculoskeletal model was modified to estimate joint reaction forces in the hip during ambulation. During gait trials with greater maximum hip extension, anterior joint reaction forces are higher than with less hip extension. Instructing patients with anterior hip pain to ambulate in less hip extension may help to decrease forces on the anterior hip joint and thereby decrease pain.

REFERENCES

1. Delp SL. Surgery simulation: a computer graphics system to analyze and design musculoskeletal reconstructions of the lower limb. [PhD dissertation] Department of Mechanical Engineering. Palo Alto, California: The Stanford University, 1990.
2. Kane TR and Levinson DA. *Dynamics: theory and application,* McGraw-Hill, New York, NY, 1985.
3. Yamaguchi GT, Moran DW, and Si J. Computationally efficient method for solving the redundant problem in biomechanics. *J Biomech* **28**, 999-1005, 1995.
4. Carhart MR. Biomechanical analysis of compensatory stepping: implications for paraplegics standing via functional neuromuscular stimulation. [PhD dissertation] Tempe, Arizona: Arizona State University, 2000.

AN INTERMITTENT EP-MODEL FOR FAST POINT-TO-POINT MOVEMENTS

Dinant Kistemaker, Knoek van Soest and Maarten Bobbert
Institute for Fundamental and Clinical Human Movement Sciences,
Vrije Universiteit, Amsterdam, The Netherlands; e mail: d.kistemaker@fbw.vu.nl.

INTRODUCTION

It has been widely acknowledged that the visco-elastic properties of muscles are beneficial to the control of posture and movement. An important class of control models that exploit these properties are equilibrium point (EP) models. Extensions of EP-models for fast point-to-point movements (e.g., co-contraction and 'virtual' trajectories) have been proposed to overcome limitations in terms of movement speed. Unfortunately, EP-models and their extensions have often been tested with models that lack a realistic description of the (dynamic) behavior of the muscle-tendon complex. The purpose of this study was to investigate whether EP-models can account for experimentally observed fast single-joint point-to-point movements [1], without making use of 'virtual' trajectories. To this end, we used an arm model with muscle models that reproduced the salient dynamical properties of muscles. We also examined intermittent control as a neurophysiologically plausible method to increase maximal movement speed.

METHODS

The 2D model of the arm (Fig. 1) was actuated by four Hill-type muscles consisting of a contractile element (CE), a series elastic element (SE) and a parallel elastic element (PE). Activation dynamics was modeled to describe the relation between muscle stimulation ($STIM$) and active state. Feedback of contractile element length (l_{CE}) and contraction velocity (v_{CE}) was linear, and a 25 ms time delay (denoted by δ) in the feedback loop was adopted using a fifth-order Padé approximation.

Figure 1. Schematic drawing of the arm model. φ_e = elbow angle (extension positive).

The desired trajectories were based on experimental data of Gottlieb (1998) and covered 100^0 in 0.2 s (Fig.2E). In accordance with the experiments, the model was constrained to move in the elbow joint only. The musculoskeletal model was respectively driven by an α-controller:

$STIM = STIM_{open}$

a λ-controller:

$STIM = k_p[\lambda - l_{CE}(t-\delta)] + k_d[-v_{CE}(t-\delta)]$

and a hybrid EP-controller:

$STIM = STIM_{open} + k_p[\lambda - l_{CE}(t-\delta)] + k_d[\dot{\lambda} - v_{CE}(t-\delta)]$

In these controllers, $STIM_{open}$ was the open-loop muscle stimulation that created a stable EP with maximal stiffness. Stiffness was calculated using a linearization of the model in an equilibrium point. k_p and k_d are feedback gains and λ and $\dot{\lambda}$ denote desired l_{CE} and v_{CE}. In the intermittent controllers $STIM_{open}$, λ and $\dot{\lambda}$ were updated with a frequency of 10 Hz.

RESULTS AND DISCUSSION

All implemented EP-models gained maximal movement speed when control signals were sent out intermittently. The implementation of intermittent control was based on experimental studies indicating that humans control their movements with a frequency of 6-10Hz. Maximal movement speed of the α-controller depended on the stiffness in the EP that was set. The stiffness produced by the present model was in accordance with values reported in the literature. Although $STIM_{open}$ was chosen such that it maximized stiffness, the α-controller was not capable of producing fast movements as observed by Gottlieb (1998). The λ-controller was also incapable of generating sufficiently fast movements, because time delays imposed limits on feedback gains to prevent stability problems.

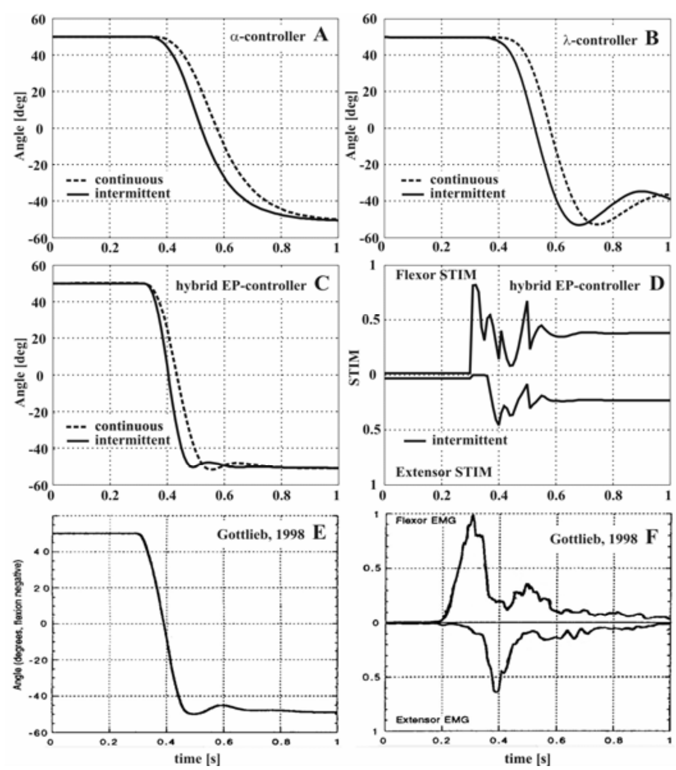

Figure 2. Experimental data of Gottlieb (1998) and model simulations with the three different EP-controllers.

The hybrid EP-model was able to accurately reproduce fast movements as observed experimentally [1], albeit only when control signals were sent out intermittently (Fig. 2C). Furthermore, this model showed a stimulation pattern (Fig. 2D) that resembled the observed tri-phasic EMG pattern, indicating that this pattern does not need to be pre-programmed.

REFERENCES

1. Gottlieb GL. *J Neurophysiol*. 80, 1860-7, 1998.

A COMPARISON OF TWO FOOT MODELS USED IN CLINICAL GAIT ANALYSIS

[1,3]Krista J Evans and [1,2,3]Michael H. Schwartz
[1]Graduate Program in Biomedical Engineering, University of Minnesota, Minneapolis, Minnesota USA,
[2]Department of Orthopaedic Surgery, University of Minnesota, Minneapolis, Minnesota, USA,
[3]Gillette Children's Specialty Healthcare, St. Paul, Minnesota, USA; email: KJEvans@gillettechildrens.com

INTRODUCTION

The location and orientation of talo-crural (TC) and sub-talar (ST) joint axes play an important role in determining foot kinematics and kinetics. The single rigid segment foot model (conventional model) commonly used in clinical gait laboratories contains several significant shortcomings including i) reliance on physical exam based measurements, which are susceptible to significant random and systematic errors [1], and ii) approximating the foot as a single rigid vector [2]. As a result, foot motion data has been widely viewed as a weak link in clinical gait analysis. Other foot models have been proposed, and this study aims to evaluate the clinical usefulness in two proposed foot models: the three-segment foot model, proposed by Kaufman, et al., (Mayo model) and the functional model. The Mayo model defines three rigid segments (tibia, hindfoot, and forefoot), aligns the segments using anatomical landmarks, and computes Euler angles between the segments [3]. The second model considered here, the functional model, uses optimization to estimate functional TC and ST axes [4]. The TC and ST axes are used to create a four-segment foot model (tibia, talus, calcaneous, and forefoot). This study consists of an *in-vivo* assessment of the two proposed models in both typical and pathological feet.

METHODS

Three-dimensional marker trajectories were collected for multiple subjects using a 12 camera Vicon 612 system (Oxford Metrics, Oxford, England). Both physical and virtual markers, as well as functional calibrations were used to define required parameters for all three foot models. Functional calibrations consisted of range-of-motion trials performed to locate the centers and orientations of the subject's TC and ST axes. Each subject then performed five walking trials, which were used to calculate foot kinematics. For both multi-segment foot models (Mayo and functional), marker trajectory data was low-pass filtered using a Savitzky-Golay smoothing filter, and was rigidly-transformed with respect to each model-defined rigid body segment using Procrustes analysis. The location of the TC and ST joint axes can be described by a position vector in a marker-based coordinate system. The orientation of these axes can be described by 2 rotations in the same coordinate system.

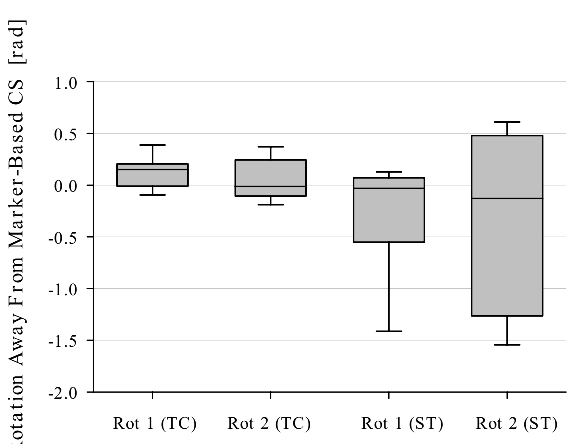

Figure 1: Rotations of the talo-crural and sub-talar joint axes, as calculated by the functional method [4]. The talo-crural axis is expressed relative to the bi-malleolar axis.

RESULTS AND DISCUSSION

Initial comparisons between the marker-based bimalleolar axis (Mayo model) and the estimated TC axis (functional model) show good agreement (Figure 1). The transverse plane orientation of the estimated TC axis (Rot 2 TC) relative to the marker-based bi-malleolar axis was the most accurate estimation of the calculated four rotations when compared to the marker-based bi-malleolar axis. The measure of coronal plane orientation of the estimated TC axis (Rot 1 TC) had the most precise results. The functional method allows objective location of the TC axis without the need for subjectively placed skin-mounted markers to identify the bimalleolar axis. Furthermore, the bimalleolar axis is based on anatomical landmarks, and is different than the TC orientation described by Inman [5]. This difference may be especially important in clinical gait analysis of pathological feet.

Initial results also show that the ST axis is not as precisely located as the TC axis. Since there is no gold-standard to compare the ST axis, the accuracy was not quantified. Current efforts are focused on using anatomical landmarks to assist in consistently describing the ST axes [5]. Using anatomical landmarks as initial estimations of both the ST and TC joint axes is meant to decrease computation time, provide indirect assessment of accuracy, and increase the precision.

CONCLUSIONS

The functional model provides precise and objective location of the TC axis. However, current studies suggest that the location of the ST axis is not as consistent or reliable as has been reported [4]. Current efforts are focused on improving the estimation of the ST and TC axes using the functional method in combination with the Mayo foot model.

REFERENCES

1. Schwartz MH, et al. *Proc. of the ESMAC Meeting*, Warsaw, Poland, 2004.
2. Davis RB, et al. *Human Movement Science* **10**, 575-587, 1991.
3. Kaufman KR, et al. *Proc. of the 8 th Annual GCMAS*, Wilmington, DE, 2003.
4. van den Bogert AJ, et al. *J Biomech* **27**, 1477-1488, 1994.
5. Stiehl, JB (ed.). *Inman's Joints of the Ankle*. Baltimore, Williams & Wilkins, 1991.

THE INFLUENCE OF SEAT HEIGHT ON SIT TO STAND IN THE ELDERLY: A SIMULATION STUDY

[1]Zachary J. Domire, and [2]John H. Challis
[1]Division of Kinesiology and Health, The University of Wyoming, Laramie, WY, USA
[2]Biomechanics Laboratory, The Pennsylvania State University, University Park, PA, USA
email: zdomire@uwyo.edu, jhc10@psu.edu

INTRODUCTION

Lowering seat height has been shown to increase the difficulty of rising from a chair [1]. The impact of this increasing difficulty is particularly important for elderly individuals, because rising from a chair can be a near maximal strength task [5]. Two strategies while in contact with the seat have been proposed for dealing with decreases in seat height: moving the trunk farther forward or increasing the forward momentum of the trunk [9, 7]. The purpose of this study was to examine performance of the sit to stand from progressively lower seat heights, using a validated model of the elderly.

METHODS

The model consisted of three links (shank, thigh, and head arms and trunk). The inertial parameters for the links were the same as those for a typical experimental subject (mean age 71.8 years) from the study of Burgess [2]. The model was actuated by eight muscle models representing the major muscle groups of the lower extremity. Each muscle model had force-length and force-velocity properties as well as activation dynamics [4]. The original parameters values for the muscle model were based on the data in the literature [3, 8], and adjusted to make them reflective of an older subject.

The neural excitations required for the model to perform the sit to stand were determined by solving an optimal control problem. The objective function found the muscle neural excitations required to perform the sit to stand while minimizing the muscle stresses and the rate of change of the muscle forces [6].

The sit to stand was simulated from three different seat heights of 38, 42, and 50 cm. The shank and the trunk were vertical at the start of each of the simulations. Changing seat height was accommodated by rotation of the thigh segment.

RESULTS AND DISCUSSION

The simulation produced a similar kinematics and kinetics as the elderly subjects in Burgess [2]. Trunk movement prior to seat off, as seat height decreased, did not support either of the proposed strategies. The hip angle at seat off increased as seat height decreased. However, because of the higher initial hip angle, the resulting anterior trunk rotation decreased as seat height decreased. Maximum hip flexion velocity also decreased as seat height decreased.

The peak moments required to stand did not necessarily increase as seat height decreased (Table 1). However, if these moments are expressed as a percentage of the moment the muscles are capable of given their current length and velocity then the moments increased as seat height decreased. The maximum knee moment (98 %), and the knee moment at seat off (93 %) for the lowest seat height were close to maximal.

To accommodate the lower seat heights initial hip flexion had to increase. This moved the hip extensors to a less favorable region of the force-length curve. This is complicated by the knee extensors being near maximally stressed at this time, therefore activation of the hamstrings is undesirable. In the simulation from the lowest seat height the gluteal muscles are 90 % activated to reverse the direction of the hip movement, thus not allowing increased forward trunk rotation.

CONCLUSIONS

Two strategies for motion prior to losing contact with seat have been proposed for dealing with decreases in seat height: rotating the trunk farther forward, or increasing the forward momentum of the trunk. Evidence from this study does not support adoption of either of these strategies, because higher initial hip angles during seat contact places great demands on the hip extensors. Clearly decreasing seat height presents a significant challenge to the elderly, with no obvious strategy for meeting this challenge.

REFERENCES

1. Arborelius UP, et al. *Ergonomics* **35,** 1377-91, 1992.
2. Burgess RM. Unpublished M.S. thesis, Penn State. 2003.
3. Friederich JA & Brand RA. *J Biomech*. **23**, 91-95, 1990.
4. Gallucci JG & Challis JH. *J App Biomech* **18**, 15-27, 2002.
5. Hughes MA, et al. *J Biomech* **29,** 1509-13, 1996.
6. Pandy MG, et al. *J Biomech. Eng* **117,** 15-26, 1995.
7. Schenkman M, et al. *J Am Geriatr Soc* **44,** 1441-6, 1996.
8. Van Soest AJ, et al. *J Biomech* **26**, 1-8, 1993.
9. Weiner DK, et al. *J Am Geriatr Soc* **41,** 6-10, 1993.

ACKNOWLEDGEMENTS

Supported in part by a grant from The Whitaker Foundation.

Table 1: The maximum joint moments (as a percentage of maximum moment) during the sit to stand from three seat heights.

	Seat Height		
	38 cm	**42 cm**	**50 cm**
Maximum Hip Extension Moment	70 Nm (67%)	82 Nm (36%)	87 Nm (41%)
Maximum Knee Extension Moment	266 Nm (98%)	271 Nm (96%)	229 Nm (74%)
Knee Extension Moment at Seat Off	245 Nm (93%)	239 Nm (84%)	200 Nm (66%)

Note - Moments presented are for both legs.

EVALUATION OF NEWLY DESIGNED CUSHION FOR ELECTRIC POWER WHEELCHAIR DRIVING

Junichi Kubo[1], Yusheng Yang[2], Hisaichi Ohnabe[2], Rory A Cooper[2],
Rosemarie Cooper[2], Tokuji Okada[1], Diane M. Collins[2]
[1]Niigata University, Japan
[2]University of Pittsburgh, VA Pittsburgh Healthcare System, USA

INTRODUCTION
Whole-body vibration can resulted in low-back pain, disc degeneration and other harmful effects to the body [1]. Researchers are investigating optimal solutions for reducing vibration and seat pressure exposure of electric power wheelchair users [2, 3, 4]. The purpose of this study was to investigate the effectiveness of the newly designed water-filled cushion (NDWF), based on vibration amplitude transmissibility from the wheelchair seat to the head, and pressure mapping while driving an electric-powered wheelchair, as compared to other typical wheelchair cushions (Air-filled (AF), Viscoelastic fluid (VF), Water-filled (WF)).

METHODS
A triaxial accelerometer (ARJ-A-T ±10g) was mounted on a seat frame to measure the vibration on the seat frame. Another accelerometer was mounted on a Bite-Bar that was held between the teeth of subjects in order to measure the whole-body vibration experienced by subjects. Signals from the accelerometers were amplified and sampled at 200Hz via a battery-powered acquisition system, and pressure distribution mapping was recorded simultaneously. The subjects sat on the different cushions placed on a sensor seat (BIG-MAT) in order to measure two values: the peak pressure and the contact area. Subjects drove the electric-powered wheelchair (JW1-22B) over four different surfaces: pavers, asphalt, brick and gravel, while sitting on four different cushions: AF, VF, WF, and NDWF. The electric-powered wheelchair was driven at one meter per second over these four surfaces. Ten subjects participated in this experiment. Their average age, weight and height were 22.2 ± 1.03years old, 62.2 ± 9.39kg, and 171.7 ± 8.32cm tall respectively. Each driving trial was repeated three times, resulting in each subject driving the wheelchair for 36 trials (3 surfaces x 4 cushions x 3 times). From the collected signals, the Vibration Dose Value (VDV) was calculated for each direction (XYZ) respectively, then determined the resultant vibration dose value (VDV_{total}). The Vibration Dose Value Ratio (VDVR) which represented the effective amplitude transmissibility of a cushion was also calculated. From the peak pressure and contact area data, the decreasing rate of the peak pressure (DP) and the increasing rate of the contact area (IC) were calculated based of those normative data when cushions were not used. To evaluated the effect of different cushion designs on a user's whole-body vibration, the variables VDVR, DP and IC were compared for significant differences between cushions using a mixed-model ANOVA, with an alpha of p=0.05.

RESULTS AND DISCUSSION
The average and standard deviation of VDVR on each surface, peak pressure (DP) and increasing rate of the contact area (IC) are shown in Fig. 1, 2 respectively. Results showed that the

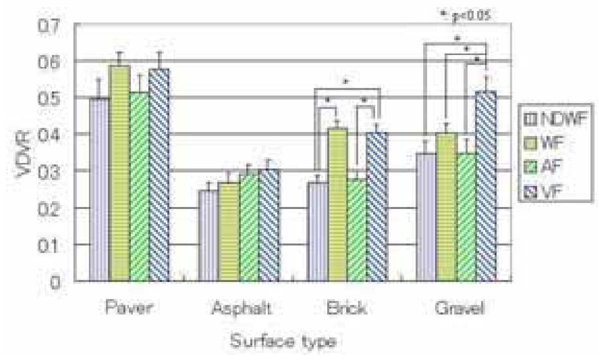

Fig.1 The VDVR on each surface

VDVR on the paver and asphalt surfaces did not have significantly differences between cushions. The VDVR of the NDWF and AF cushion showed significant less than WF, VF cushion on the brick and gravel surfaces (p<0.05). VF cushion showed a significant highest VDVR value compared to other three cushions. (P<0.05)

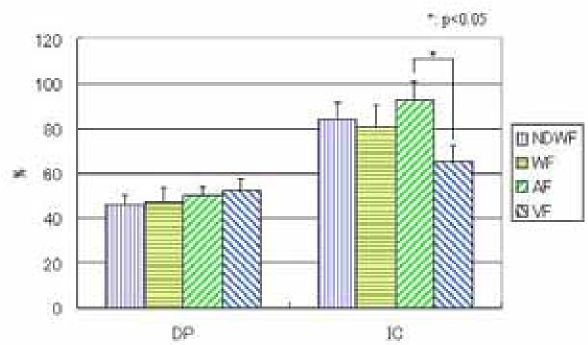

Fig.2 The DP and IC on paver surface

The DP and IC of the NDWF, WF and AF cushion were almost identical while driving wheelchair on the paver surface (Figure 2). From present results, whole-body vibration of NDWF cushion users was significant reduced and did not change the pressure distribution compared to others three cushions. Based on present limited data, the NDWF cushion was comparable to commercial cushions and might be able to provide a comfortable ride and had a comparable effect in the prevention of pressure sores for power wheelchair users.

REFERENCES
1. Seidel et. al., *Int Arch Occup Environ Health* 58, 1-26, 1986
2. Dobson et al, *Proceedings of RESNA'2004* , Atlanta, GA,2003.
3. Cooper RA, et al. *J Spinal Cord Medicine*, 27, 468-475, 2004
4. Kubo J, et al. *Proceedings of 21th ISS,* 117,118.

A MODEL FOR ASSESSING THE CONTRIBUTIONS OF HAND FORCES AND TORQUES TO THE SPEED OF A SWINGING IMPLEMENT: APPLICATION TO THE FIELD HOCKEY HIT

Alexander Willmott and Jesús Dapena
Department of Kinesiology, Indiana University, Bloomington, IN, USA
Email: awillmot@indiana.edu

INTRODUCTION

The motions of any striking implement are determined by the force and torque exerted by the hands on it and by the force of gravity [1]. However, the contributions of these factors to an implement's final speed have never been quantified.

The goal of this study was to develop a theoretical model for the analysis of the roles of hand force, hand torque and weight in the generation of the speed of any selected point on a swinging implement, and to apply it to the field hockey hit.

METHODS

The velocity of any point P on the implement other than its center of mass, G, can be broken down into the absolute velocity of G ($\mathbf{v}_G$), and the velocity of P relative to G ($\mathbf{v}_{P/G}$). The velocity of G is generated by the forces acting on the implement: force **F**, applied by the hands at the mid-grip position, and the weight of the implement, **W**. (See Figure 1.) The relative velocity $\mathbf{v}_{P/G}$ is linked to the angular motion of the implement, and therefore ultimately results from the torques acting about G: the mid-grip couple **T** exerted by the hands, and the torque produced by force **F** about G.

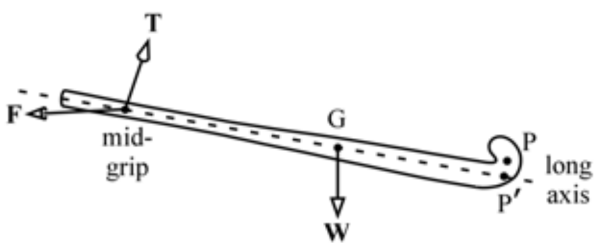

Figure 1: Free-body diagram of a field hockey stick, including the locations of all points used in the model.

In the model, **F** is separated into $\mathbf{F}_N$ and $\mathbf{F}_L$, its components normal and parallel to the longitudinal axis of the implement. **T** is similarly broken down into $\mathbf{T}_N$ and $\mathbf{T}_L$. The roles of these factors and of **W** during any given period are calculated as follows. To assess contributions to the linear acceleration of G, each force is divided at every instant by the mass of the implement, and the resulting acceleration vector is projected onto the current $\mathbf{v}_G$ vector. The acceleration is considered positive or negative, depending on whether the projected vector points in the same direction as $\mathbf{v}_G$ or opposite to it. These projected accelerations are integrated over the period to compute cumulative contributions to the change in the magnitude of $\mathbf{v}_G$. The contribution of each force to the final $\mathbf{v}_P$ is obtained by multiplying its contribution to $\mathbf{v}_G$ by the cosine of the final angle between $\mathbf{v}_G$ and $\mathbf{v}_P$.

To calculate contributions to $\mathbf{v}_{P/G}$, each contributing torque is integrated over the period to calculate an angular impulse. The latter is separated into components normal and parallel to the implement's longitudinal axis at the end of the period. This yields contributions to changes in "somersaulting" and "twisting" angular momentum, respectively. Each is divided by the corresponding moment of inertia to calculate contributions to somersaulting and twisting angular velocity. A linear velocity contribution is calculated for each angular velocity as the cross-product of the angular velocity with the position vector pointing from G to P at the end of the period. The projection of this linear velocity onto the final $\mathbf{v}_P$ gives the contribution of the corresponding torque to $\mathbf{v}_P$.

This model was applied to the downswing of hits by eight female collegiate field hockey players. The DLT method was used to determine the 3D motion of the stick. Inverse dynamics was used to calculate the mid-grip force and torque.

The point selected for analysis in the field hockey application was P′, the point on the stick's longitudinal axis closest to P, the center of the hitting surface. (See Figure 1.) The reason for this decision was that accurate estimates of the moment of inertia of each stick about its longitudinal axis were not available. This made it impossible to measure the effects of the twist rotation of the stick. The latter, however, plays only a minor role in a field hockey hit: the impact speeds of P and P′ differed by 0.7±0.7 m/s.

RESULTS AND DISCUSSION

The speed of point P′ at impact was 28.7±3.4 m/s. The contributions from the forces and torques applied to the stick during the downswing accounted for 27.1±2.9 m/s of this amount. The main positive contributions during this period came from the longitudinal force (54±9%) and from the normal torque (62±18%). Weight made a very small positive contribution (4±1%), and the normal force made a rather small negative contribution (-19±9%). The negative contribution of the normal force was due largely to its effect on the stick's rotation: when this force is in the direction of the hit, the associated torque about G causes a backward linear acceleration of P′ relative to G that more than outweighs the beneficial linear acceleration of G.

CONCLUSIONS

The impact speed of a point near the distal end of the field hockey stick is produced in approximately equal proportions by the pull along the length of the stick and by the couple applied at the mid-grip. The effects of weight and of the force component perpendicular to the stick are much smaller.

REFERENCES

1. Vaughan CL. *Biomechanics VII-B*, University Park Press, Baltimore, 325-331, 1981.

QUANTIFYING LEG ELASTICITY IN MALE VETERAN RUNNERS

[1] Ceri Diss and [2] David Kerwin
[1] University of Roehampton UK,
[2] University of Bath UK; email: c.diss@roehampton.ac.uk

INTRODUCTION

Biological changes during aging that are related to running form six categories. They are cartilage, ligament and tendon, muscle, the nervous system, bone and the cardiovascular system. Within these categories one may see a reduction in elasticity, muscle mass, reaction time to stimuli, bone mass and the efficiency of the cardiovascular system. A reduction in elasticity is a result of muscle lengthening, loss of contractile properties, tendon and ligaments' lengthening and stiffening [1]. To quantify leg elasticity a linear spring model has been applied effectively to symmetrical rebound jumping and hopping [2].

The purpose of this study was to determine whether a linear spring model can be applied to a modified asymmetrical rebound jump for the quantification of leg elasticity in veteran runners.

METHODS

A seven camera infra red system (Vicon 512) operating at 120Hz was synchronised with a force platform (Kistler 9281B11) operating at 1080Hz to obtain kinematic and kinetic data. A static calibration procedure for the identification of the position of the force platform and a dynamic (wand) calibration for 3-D reconstruction of body markers throughout the measurement volume. 36 reflective markers were used to create a full body model for each subject. Davis, R.B. et al (1990) developed the model with normal subjects and based on marker placements and static anthropometric measurements. Quintic spline filtering based on Woltring's method was applied to the real marker trajectory data prior to the modelling of upper and lower body kinematics and kinetics. The kinematic model allowed for point displacement and angles of and between segments to be determined. The kinetic models used mass and moment of inertia of the segments to facilitate the calculation of segmental 'reactions'.

Six veteran (V60) runners (mean mass = 74.66 kg, height = 1.74 m) performed two sets of five modified vertical jumps from which six were selected for analysis for each subject. The approach to the jump was from a step-in, to a two-footed landing on the force platform followed by a maximal vertical rebound, termed a Step in Jump (SIJ). All subjects signed a consent form and were given a familiarisation period prior to data collection.

RESULTS AND DISCUSSION

The linear least square values were greater than 0.9 for all subjects indicating that a linear spring model can be used when evaluating leg elasticity of the veteran runner when performing a modified asymmetrical SIJ. This is because the horizontal displacement during the step-in phase is small. If this were to increase the asymmetry would increase hence making the linear spring model unsuitable for such a movement.

Leg elasticity (Kleg) values are quite high for the veteran runner. This is mainly due to the small amount of leg compression (ie leg flexion) during the ground contact phase of the SIJ, since the force values at minimum leg compression (F peak) are similar to those previously reported. The reduced leg compression in turn influences a veteran athlete's ability to jump. This is shown by the reduced rise in the centre of mass (CM Rise) compared to the literature [3].

CONCLUSIONS

A linear spring model can be used to evaluate leg elasticity of the veteran runner. Their leg stiffness effects their ability to jump mainly because there is in reduction leg flexion during the ground contact phase of the jump.

REFERENCES

1. Taunton JE, et al *British Journal of Sports Medicine* **31**, 5-10, 1997.
2. Farley CT, et al *Journal of Applied Physiology* **71**, 2127-2132, 1991.
3. Bedi JF,et al *Research Quarterly for Exercise and Sport* **58**, 11-15, 1987.

ACKNOWLEDGEMENTS

Oxford Metrics, UK. Kistler, UK.

Table 1: Mean and standard deviation for each subject.

Subjects	1	2	3	4	5	6
Linear least squares value	0.94 ± 0.01	0.98 ± 0.01	0.94 ± 0.02	0.98 ± 0.01	0.94 ± 0.02	0.97 ± 0.02
Kleg (BW/s)	56.1 ± 9.50	33.15 ± 16.86	17.54 ± 5.52	28.36 ± 3.85	11.65 ± 3.43	46.33 ± 23.91
Spring Compression (m)	0.09 ± 0.02	0.12 ± 0.04	0.17 ± 0.05	0.12 ± 0.01	0.21 ± 0.05	0.08 ± 0.03
F peak (BW)	4.66 ± 0.29	3.38 ± 0.28	2.68 ± 0.21	3.44 ± 0.25	2.29 ± 0.22	3.12 ± 0.33
CM rise (m)	0.26 ± 0.05	0.26 ± 0.06	0.34 ± 0.06	0.19 ± 0.02	0.23 ± 0.05	0.15 ± 0.04

PRESERVATION OF PERIARTICULAR CANCELLOUS MORPHOLOGY AND MECHANICAL STRENGTH IN POST-TRAUMATIC EXPERIMENTAL OSTEOARTHRITIS BY ANTIRESORPTIVE THERAPY

[1,2] Josh MacNeil, [1,2,4] Steven Boyd, [3] Michael Doschak and [1,3,4] Ron Zernicke
[1]Department of Mechanical and Manufacturing Engineering, University of Calgary, Alberta, Canada
[2]Calgary Center for Innovative Technology, Alberta, Canada
[3]Department of Surgery, University of Calgary, Alberta, Canada
[4]Faculty of Kinesiology, McCaig Centre for Joint Injury and Arthritis Research, University of Calgary, Alberta, Canada
email: skboyd@ucalgary.ca, web: http://www.enme.ucalgary.ca/~skboyd/

INTRODUCTION

Osteoarthritis (OA) is the most common joint disease in humans and results in a severe degradation of joint structures that ultimately leads to joint degradation and failure [1]. The onset of OA is joint dependent and its probability increases with age or joint injury [2]. An anterior cruciate ligament transection (ACLX) is a well established animal model for post-traumatic OA, and changes in the periarticular bone in experimental OA occur as early as 3 weeks after injury [3].

This project is aimed at investigating whether antiresorptive bisphosphate (BP) drug therapy conserves long term joint function and retards OA progression. The effectiveness of BP therapy was assessed in conserving bone mineral at the MCL enthesis, periarticular cancellous bone architecture and the apparent mechanical properties of the periarticular bone in the distal femur and at the MCL insertion in an ACLX joint.

METHODS

Skeletally mature, female New Zealand White rabbits were used as an experimental OA model and were randomly assigned to three groups (N=10/group). ACLX was performed in two groups; the first group was dosed with BP (risedronate, 0.1 mg/kg s.c. daily for 6 wk), the second group was untreated. The third group was comprised unoperated normal controls. After 6 wk, all animals were sacrificed, and the femur-MCL-tibia complex was dissected free. The medial and lateral femoral condyles were separated with a band saw to reduce the size of the specimen to facilitate scanning of the entire condyle.

Micro computed tomography (μCT) scans of the medial condyle of each cohort group were obtained (Skyscan 1072, Skyscan, Aartselaar, Belgium) at 100 kV through 180° with a rotation step of 0.9°, at an x12 magnification that produced serial cross sectional images of isotropic 19.4 μm^3 voxels. All data were filtered (sigma = 1.2, support = 2) and a global threshold was applied to extract the mineral phase. The μCT data were input for large-scale finite element (FE) models to determine differences between groups in their apparent mechanical properties using a direct mechanics approach [4]. The approach accounted for the variation in bone micro architectural geometry, but not variation in tissue modulus.

A morphological analysis for each group was also completed and provided a quantification of periarticular cancellous bone architecture by determining trabecular thickness (Tb.Th), trabecular number (Tb.N), trabecular separation (Tb.S), bone surface to volume ratio (BS/BV), structural model index (SMI) and anisotropy (by mean intercept length, MIL).

RESULTS AND DISCUSSION

The experimental results revealed that BP therapy conserved medial collateral ligament (MCL) bone complex laxity and bone mineral at the MCL enthesis [5]. It was previously shown by our group (Doschak et al. 2004) that BP therapy conserved periarticular cancellous bone mineral density, elastic modulus, and maximal energy to failure [6]. A qualitative assessment of the μCT scans indicated that periarticular cancellous bone architecture was conserved. Full morphological and finite element results are proceeding.

Conservation of bone mineral density, bone mineral at the MCL enthesis, elastic modulus and energy to failure in the cancellous bone indicated that primary and secondary joint structures were being maintained through BP therapy. A reduction in joint laxity may also have reduced the effect of an ACL injury on joint loading conditions. Those improvements in joint structure and function may have a long term effect on retarding the pathogenesis of OA.

CONCLUSIONS

Based on a qualitative assessment of the data and on the experimental results obtained, BP therapy appeared to have a positive effect on joint structure and function in the post-traumatic ACLX joint that may retard long term OA progression.

ACKNOWLEDGEMENTS

Supported in part by Canadian Institutes for Health Research and the Wood Professorship in Joint Injury Research.

REFERENCES

1. Kelsey JL. *Epidemiology of musculoskeletal disorders*. New York: Oxford University Press, 1982
2. Praemer A, Furner S, Rice DP. *Musculoskeletal conditions in the United States*. American Academy of Othopaedic Surgeons, Park Ridge, IL, 1992.
3.Boyd SK, et al. *J Bone Miner Res*. **17**:687-694, 2002
4.van Rietbergen, et al. *J Biomech*. **12**:1653-1657, 1996
5. Doschak MR, et al. *Osteoarthritis Cartilage.* **11**:S85; P236, 2003
6. Doschak MR, et al. *J Orthop Res*. **22**:942-948, 2004

The Effect of Hindfoot and Forefoot Positions on Posterior Tibialis Muscle Length

[1] Christopher G. Neville, [1] Adolf Flemister, [1] Josh Tome, [1,2] Jeff Houck
[1]University of Rochester, Rochester, NY
[2]Ithaca College – Rochester Campus, Rochester, NY contact: christopher_neville@urmc.rochester.edu

INTRODUCTION

Posterior Tibial Tendon Dysfunction (PTTD) is a primary cause of flat foot deformity. The flat foot deformity seen in PTTD is expected to produce increased strain on the posterior tibial (PT) tendon causing eventual rupture. A recent in-vivo study suggests subjects with PTTD show hindfoot (HF) eversion as well as significant forefoot (FF) abduction compared to controls [1]. However, current management of PTTD focuses on relieving strain with orthotics by supporting the HF and medial longitudinal arch, without directly influencing forefoot position. [2]. The differential effects of HF eversion and FF abduction on PT muscle length remain unclear, making it difficult to judge the relative importance of forefoot abduction. The purpose of this study was to describe differential changes in PT muscle length due to non-weight bearing foot positions of FF abduction and HF eversion at three different angles of ankle motion.

METHODS

Four fresh frozen human cadaver limbs were potted and mounted on a platform. The PT tendon was dissected proximal to the medial malleolus and a 5 kg weight was sutured to the tendon via a string. Bone pins were inserted into the tibia, calcaneous, navicular, and first metatarsal to track motion of each bone. A 6 camera Optotrak Motion Analysis System (Northern Digital Inc, CAN) was used to track 3 infrared emitting diodes (IREDs) mounted to each bone pin. The platform was arranged so vertical displacement of an IRED on the 5 kg weight tracked PT muscle length. Using Motion Monitor Software (Innsport Training Inc, USA) online feedback of 3D angles (Z-X'-Y'' sequence) were used to achieve reproducible 3D FF and HF positions. After neutral foot position was determined, the foot was moved into 9 specified testing positions designed to stretch and shorten the PT muscle (listed in Table 1). These 9 positions were repeated at 30º of ankle plantarflexion, neutral ankle, and 10º of ankle dorsiflexion, resulting in 27 tested positions. PT muscle length was recorded at each foot position. Data were averaged across limbs for each position to describe differences across positions.

RESULTS AND DISCUSSION

Across ankle positions isolated FF abduction and HF eversion produced muscle lengthening while FF adduction and HF inversion produced muscle shortening (Table 1). FF adduction neutralized the effect of HF eversion in the HF EV + FF ADD position (Figure 1). This effect occurred to an even greater extent in the HF INV + FF ABD position where FF motion surpassed the effect of the HF and produced lengthening. These results demonstrate a trend where the FF produces an equal or greater change in muscle length to that of the HF (Figure 1).

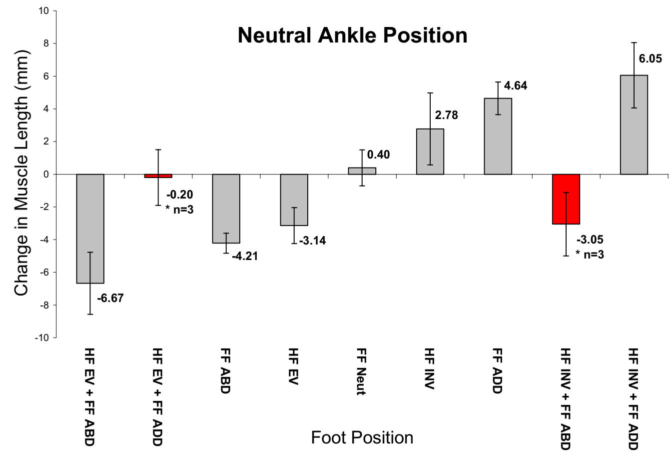

Figure 1: Muscle Length for 9 Neutral Ankle Tests with standard deviation bars.

CONCLUSIONS

The results from this study suggest FF abduction and HF eversion play an integral role in determining length of the PT muscle. If replicated in weight bearing studies, this would suggest that controlling the FF and HF during gait is necessary to decrease strain on the PT muscle. This may require designing braces to control the FF after heel off, when only the FF is in contact with the ground, in addition to controlling the HF during early stance.

REFERENCES

1. Tome, J., et al. *The Effect of Posterior Tibial Tendon Dysfunction on Dynamic Foot Motion*. GCMAS 10th Annual Meeting. Portland, OR, 2005.
2. Myerson, M.S., *Adult acquired flatfoot deformity: treatment of dysfunction of the posterior tibial tendon.* Instructional Course Lectures, 1997. **46**: p.393-405.

ACKNOWLEDGEMENTS

This work supported in part, by the Center for Foot and Ankle Research at Ithaca College.

Table 1: PT muscle length relative to neutral expressed in millimeters ±1 standard deviation for each position tested. Negative values indicate lengthened position, positive values indicate shortened position. Hindfoot (HF), Eversion (EV), Inversion (IV), Forefoot (FF), Abduction (ABD), Adduction (ADD).

	HF EV + FF ABD	HF EV + FF ADD	FF ABD	HF EV	Neutral	HF INV	FF ADD	HF INV + FF ABD	HF INV + FF ADD
Plantarflexion	-2.0±2.2	5.8±1.0	-0.7±1.8	0.4±2.6	2.9±1.9	5.0±2.3	6.8±1.2	-0.4±1.2	10.1±1.9
Neutral	-6.7±1.9	-0.2±1.7	-4.2±0.6	-3.1±1.1	0.4±1.1	2.8±2.2	4.6±1.0	-3.1±1.9	6.1±2.0
Dorsiflexion	-9.3±3.1	-2.6±2.9	-6.7±2.0	-2.0±1.8	-2.6±3.5	1.3±2.7	3.1±3.4	-5.3±1.7	3.6±3.5

3-DIMENSIONAL KINEMATIC MODEL FOR PREDICTING HAND POSTURE DURING CERTAIN GRIPPING TASKS

[1]Jaewon Choi and [2]Thomas J. Armstrong
[1]Mechanical Engineering, University of Michigan; email: jaewonc@umich.edu ,
[2]Industrial and Operations Engineering, University of Michigan

INTRODUCTION

Hand posture has a pronounced effect on hand grip strength in a given work condition. Even though many studies have addressed hand grip strength capacity, relatively few models have quantitatively explained how hand posture affects grip strength. Buchholz predicted the posture by iteratively increasing joint angles until ellipsoidal finger segment contacts an ellipsoid representing object [1]. Lee suggested a hand posture prediction model using optimization [2]. In the model, he minimized objective function which is summation of distances from center of rotation to the object surface. In this paper, a model for simulating hand posture by use of a contact algorithm has been developed. The distances between object surface and finger segments were calculated as increasing joint angles successively. This model has advantages over the previous models, in that it can estimate hand posture during real grasping scenarios and it considers the effect of finger movement patterns on hand postures. It can also be applied to various types of grips.

METHODS

The computational model was developed in a Visual C++ environment and OpenGL graphic functions were used to display the hand and object. The hand was modeled as open chain of rigid body segments, which was described as a truncated cone, the simplest reasonable representation of hand segments. 25 degrees of freedom were used to characterize the joints of the five fingers and wrist. A collision detection algorithm was used to determine when contact occurred between hand and object. Quadratic surface meshes were created for the surfaces of both hand and object. The distance between the meshes on hand and those on object was calculated as the joint angle increased. When the minimum distance between hand and object was smaller than a preset threshold value, it was regarded as a collision occurrence.

Two subjects participated in the experiment. Independent variables considered in this experiment were: 1) object size (cylinder diameter: 26.2mm, 60.0mm, 114.3mm); 2) hand size (hand length/breadth: 192/85.5mm vs. 171/91.0mm). Object location and elbow angles were controlled. Joint angles of each joint were measured for each condition. Each condition was repeated five times for each subject. The markers secured on dorsal side of the hand were tracked by OptoTrak® Certus™ motion tracking system (Northern Digital Inc.).

Table1 Mean(SD) values of the model prediction error of difference between observed and predicted joint angle(Middle finger, 2 subjects, 6 trials per subject)

Diameter	MCP	PIP	DIP
26.2mm	-3.9°(2.4°)	9.1° (1.6°)	-24.3° (12.2°)
60.0mm	1.0° (1.6°)	4.5° (2.0°)	5.2° (4.6°)
114.3mm	-5.1° (1.4°)	7.9° (1.4°)	-5.0° (7.1°)

(a) **(b)**

Figure 1: Predicted prehensile postures for different object and hand sizes. Left (a): a 95% male hand grasping a 20 mm diameter cylindrical object. Right (b): a 25% female grasping a 40 mm diameter cylindrical object.

RESULTS AND DISCUSSION

Table 1 shows the model prediction error between observed and predicted joint angle for varying cylindrical object sizes. The hand model gave reasonable predictions of joint angles for different object sizes (R^2=0.79). The errors between observed and predicted joint angle ranged from -24.3° to 9.1°. The greatest error was found in the small object size. For the larger sized objects, errors ranged from -5.1° to 7.9°. Joint angles appear to be very sensitive to object location for the small object.

Figure 1 shows different views of grasping objects when 1) a 95% male grasps a 25 mm diameter cylinder; 2) a 25% female grasps a 50 mm diameter cylinder, which were simulated by the computational model.

By applying a simple contact algorithm, prehensile hand postures could be predicted for various object attributes and hand size; however, because this model considered only kinematic relationship, the effects caused by force were not included. The rigid body modeling of the hand without assessing deformation also could also result in errors, probably overestimating angles. The effects of the object location on the hand posture will be studied in the future.

REFERENCES

1. Buchholz B. et al., J. of Biomechanics: 25(2), 149-162, 1991
2. Lee, S.W et. al., Proceedings of HFES 48th annual meeting, 1459-1463, 2004

ACKNOWLEDGEMENTS

The project was funded in part by joint funds from the UAW-GM National Joint Committee on Health and Safety. The results presented herein represent the conclusions and opinions of the authors. Its publication does not necessarily imply endorsement by the International Union, UAW, or General Motors Corporation.

PERCEPTION OF HAND MOTION DIRECTION USES A GRAVITATIONAL REFERENCE

[1] W.G. Darling, [1]C.R. Peterson, [1]A. Viaene and [2]J.P. Schmiedeler
[1]Department of Exercise Science, University of Iowa
[2]Department of Mechanical Engineering, Ohio State University
email: warren-darling@uiowa.edu,

INTRODUCTION

Kinesthetic sense, or perception of motion, has primarily been studied at the joint level by considering measures such as the time to detect passive motion or the angle through which a limb segment is slowly moved until motion is detected[1]. Such measures may be important in relation to control of joint stability, but the purpose of most limb movements is to place the endpoint (hand or foot) in a specific location. Thus, understanding the frame of reference used in sensing direction of hand motion would provide important information relevant to mechanisms underlying control of upper limb movements. Thus, the purpose of the present research was to determine whether the frame of reference used for kinesthetic perception of hand motion uses intrinsic (i.e., body-fixed) or extrinsic (earth-fixed or visually specified) axes.

METHODS

Adult human subjects (n = 6) were instructed to set unseen motion of the hand (imposed by a motorized linear slide apparatus operating in the frontal plane) parallel to specific axes while in two different body postures: (1) Fixed - normal upright seated posture and (2) Varied - experimenter-imposed tilt (lateral flexion) of the head and trunk to the right or left to different orientations on each trial. Direction of hand motion was controlled by the subject pressing the right and left buttons on a mouse to rotate the hand motion counter-clockwise (ccw) and clockwise (cw), respectively. Hand motion was aligned to visually specified axes presented on a head-mounted display (that also blocked vision of the external environment), to the trunk-fixed longitudinal axis and to the earth-fixed gravitational axis in different conditions. Subjects completed 42 trials when aligning hand motion to visual axes (six trials each for seven visual axes) and 24 trials when aligning the hand to the trunk-fixed longitudinal axis and the earth-fixed vertical axis. Digital encoders in the motorized slide apparatus recorded motion of the hand in the frontal plane. Orientations of the head and trunk were recorded using a 3D electromagnetic system (Ascension Technologies minibird system).

Errors on individual trials were computed as the signed angular difference between hand motion direction and target axis direction in the frontal plane. Constant errors (CE) were computed as the mean of the signed errors. Variable errors were computed as the standard deviation of the signed single trial errors. In addition, correlation analysis was used to assess whether single trial errors for each axis depended on orientations of the head, neck and visual axis.

RESULTS AND DISCUSSION

CEs clearly differed ($p < 0.05$) for the different visual axes with axis angled ccw (-30°, -20°, -10°) having positive (cw) errors and axis angled cw (10°, 20°, 30°) having negative (ccw) errors (Fig. 1). Constant errors for setting hand motion parallel to the trunk and vertical axes were generally small and cw. VEs were clearly smaller ($p < 0.05$) for setting hand motion parallel to earth-fixed vertical than to visual axes and the trunk-fixed longitudinal axis when head and trunk orientation were varied (Fig. 1). Furthermore, single trial errors depended strongly on neck orientation when setting hand motion to visually specified axes in each subject ($R = 0.6$ to 0.9), but not to trunk or vertical ($R = 0.0$ to 0.8).

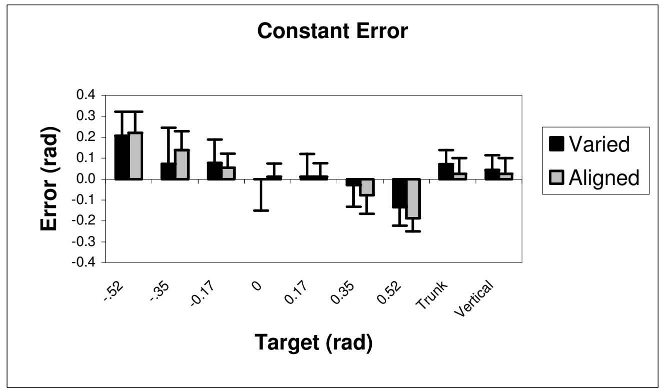

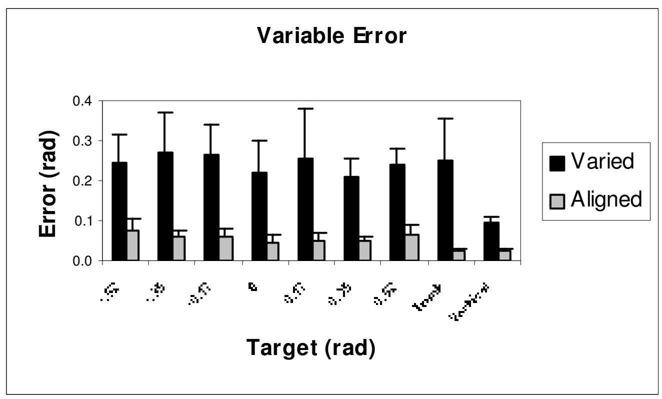

Figure 1: Constant errors (top) and variable errors for aligning hand motion to visual axes (-0.52 to +0.52 rad), trunk-fixed longitudinal axis (Trunk) and earth-fixed vertical (Vertical).

CONCLUSIONS

The low errors, and lack of dependence of errors on neck angle, when setting hand motion to vertical show that perception of hand motion uses an earth-fixed frame of reference. This is consistent with our previous findings on perception of static forearm orientation perception[2] and motion of an external object[3].

REFERENCES

1. Hall LA & McCloskey DI J Physiol 335:519-533
2. Darling WG & Bartelt R Exp Brain Res 149:40-47
3. Darling WG, Pizzimenti MA Exp Brain Res 141:174-183.

PASSIVE KNEE JOINT PROPERTIES IN TIBIAL ROTATION IN MEN AND WOMEN

[1] Hyung-Soon Park, [1]Chulhyun Ahn and [1,2]Li-Qun Zhang
[1]Rehabilitation Institute of Chicago, [2]Northwestern University, Chicago, IL 60611, l-zhang@northwestern.edu

INTRODUCTION

The anterior cruciate ligament (ACL) is an important structure for controlling knee joint movement and maintaining stability. The incident rate of ACL injury is two to eight times higher in women than in men [1]. ACL impingement against intercondylar notch during excessive tibial external rotation and abduction has been considered as a main mechanism of ACL injury, especially in women [2]. On one hand, the intercondylar notch geometry ("narrower", loosely speaking) makes it more likely for female knees to have ACL impingement than male knees [2]. On the other hand, women may have larger laxity in tibial rotation and abduction than men, which also makes it more likely for women to have ACL impingement than men under the same knee loading. The purpose of this study was to evaluate passive knee joint properties in tibial rotation in male and female subjects.

METHODS

The subjects (5 men and 5 women) were seated in a custom designed joint driving device (Fig. 1). The knee and hip flexion angles were 60° and 80°, respectively. The ankle was cast in the neutral position and coupled to one end of an L-shaped aluminum angle located distal and posterior to the foot-ankle cast. The L-shaped attachment was mounted onto the motor shaft through a six-axis force sensor.

To measure tibial rotation, LED markers were attached on the bony and flat anteromedial surface of the tibia, and the 3-D movements of the markers were measured by an Optotrak system at 100 Hz. The femur was fixed by clamping the lateral and medial femoral condyles to the seat (Fig. 1).

The zero tibial rotation was taken with the second toe pointing forward. With the position and torque limits set at the internal and external directions, the motor rotated the tibia at the constant speed of 1.5 deg/sec within the limits.

Joint laxity in tibial rotation is measured in two ways: 1) terminal rotation measured at 7Nm torque, and 2) intermediate rotation measured at the slope of 2 deg/Nm [3]. Joint stiffness and energy loss in tibial rotation were measured at 15 degree rotation (shaded area in Fig. 2).

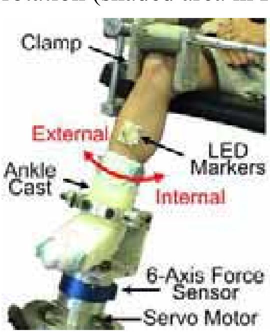

Figure 1: Experimental setup for knee axial rotation. The servo motor rotates the knee about the tibial long axis with the six-axis forces/moments measured by the JR3 force sensor. The ankle was cast for tight coupling. Optotrak markers on the flat tibia surface measure the angle of tibial rotation.

RESULTS AND DISCUSSION

Under the controlled load, women showed significantly higher laxity in tibial external rotation with larger terminal rotation (31.9±4.2° vs 19.5±2.2°, P=0.001) and larger intermediate rotation (28.1±4.2° in women vs 15.5±2.4° in men, P=0.001). Women also showed lower joint stiffness in external rotation (31.9±13.1Nm/rad vs 47.5±6.68Nm/rad in men, P=0.028). In contrast, there was no difference in the passive knee properties in tibial internal rotation between the men and women.

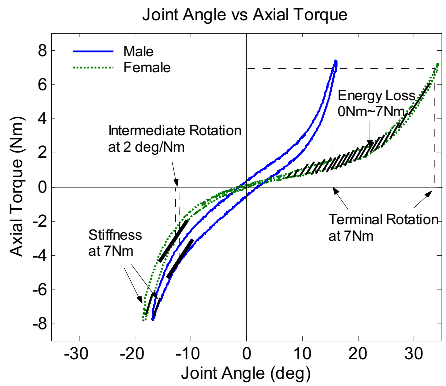

Figure 2. Typical tibial rotation torque-angle relationship in a man (solid blue line) and a woman (dotted green). Intermediate rotation at 2deg/Nm, terminal rotation at 7Nm, stiffness and energy loss at 7Nm are shown.

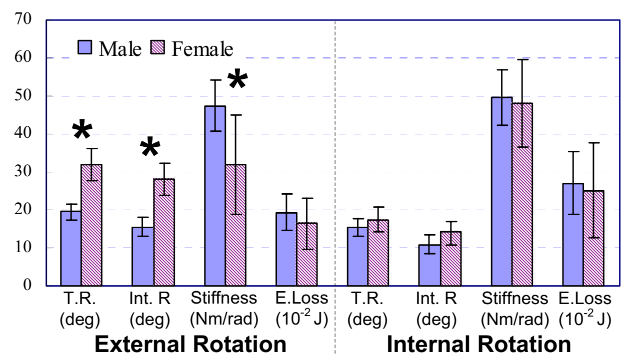

Figure 3.Passive knee joint properties in tibial rotation in men and women.

CONCLUSIONS

With the narrower notch and larger laxity in tibial external rotation, female knees are more prone to having ACL impingement and thus ACL injury. This study presents an in vivo and accurate characterization of knee biomechanical properties in tibial rotation in men and women, which may help us understand the mechanisms underlying the several fold higher ACL injury rate in women than in men. Clinically, rehabilitation protocols may be developed accordingly to strengthen muscles crossing the knee and modify joint properties in tibial external rotation, especially in women, to reduce ACL injuries.

REFERENCES

1. Shelbourne KD, et al. *Am J Sports Med* **26**, 402-408, 1998
2. Fung DT & Zhang L. *Clin Biomech,* **18**, 933-941, 2003
3. Mills OS & Hull ML. *J. Biomech*, **24**, 673-690, 1991

ACKNOWLEDGEMENT

This work was supported in part by NIH and NIDRR.

GENDER-BASED POSTURAL RESPONSES TO SEATED EXPOSURES

Nadine M. Dunk and Jack P. Callaghan
Faculty of Applied Health Sciences, Department of Kinesiology, University of Waterloo
E-mail: nmdunk@uwaterloo.ca
Webpage: www.ahs.uwaterloo.ca/kin/people/faculty/callaghan.htm

INTRODUCTION

Extensive research has attempted to determine the "optimal" seating position for the human spine to reduce the risk of low back pain. Thus, different chair designs have emerged to allow individualized optimal seated postures while maintaining comfort and functionality of the chair. However, individuals may respond differently to different chair designs and the factors that influence these sitting behaviours are not well understood. In particular, anecdotal observations of potential gender-specific sitting behaviours led to the primary purpose of this project which was to test the influence of gender on the responses to different seated postural conditions. A secondary purpose included determining if and/or how males and females respond to different seated computer-based tasks.

METHODS

Sixteen healthy university students (8 males and 8 females) were tested on 4 different chair configurations, each on a separate day. The four chairs included: 1) a fixed chair with no back rest, 2) a pivoting chair with no back rest, 3) a pivoting chair with a back rest and 4) a freely pivoting spring-post stool. Participants performed three 15-minute intervals of simulated office work (mousing, typing and a combination of the two; Figure 1). Kinematics were recorded using OPTOTRAK; spinal angles and upper body centre of mass (CoM) were calculated. The seat pressure profile was collected using a pressure mapping device (XSensor) and was used to obtain the location of the centre of pressure (CoP), peak pressure over time and the average peak pressure for each 15-minute interval. Ratings of perceived discomfort (RPD) were taken 9 times at 7.5 minute intervals.

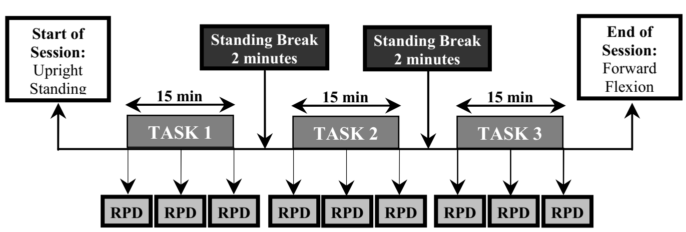

Figure 1: Study Design – For each testing session, participants completed three tasks (mousing, typing, or combination). Ratings of perceived discomfort (RPD) were taken at the beginning, middle and end of each of the three tasks.

RESULTS & DISCUSSION

Regardless of the chair used or the task performed, average lumbar and trunk angles were significantly more flexed for males than for females (Table 1). The pelvis was posteriorly rotated for males and anteriorly rotated for females (Table 1). The task performed had an effect on the average lumbar angle of all subjects ($p = 0.0029$); the lumbar spine was the least flexed during the typing task (52.5° ± 20.8°), followed by the combination task (57.9° ± 22.1°) and the mousing task (62.1° ± 20.7°). Significant gender*chair interactions of the location of the individual on the chair seat were most marked for the pivoting chair with a back rest. Females positioned their CoM and hip joints anterior to the chair pivot point while males' CoM and hip joints were located posterior to the pivot point. Females also sat with their CoM closer to the seat pan CoP than males when a back rest was present. Average ratings of perceived discomfort for each chair were analysed, revealing a significant chair effect for the upper back and overall discomfort. Both male and female participants had significantly less upper back discomfort ($p = 0.018$) and overall discomfort ($p = 0.012$) using the pivoting chair with a back rest when compared to all other chairs.

Table 1: Thoracic, lumbar, trunk and pelvis angles averaged over chair and task.

Measurement		Male	Female	P-value
	Thoracic	**8.6** *(12.0)*	**3.1** *(8.1)*	p = 0.201
% max flexion	**Lumbar**	**65.4** *(16.2)*	**49.6** *(23.1)*	p = 0.047
	Trunk	**29.8** *(28.3)*	**-3.3** *(20.4)*	p = 0.0026
Deviation from vertical (degrees)	**Pelvis**	**7.6** *(8.2)*	**-5.5** *(9.3)*	p = 0.0008

Taken as a whole, these findings suggest that men tended to slouch against the back rest while females perched closer to the front of the seat pan. It follows that males and females may be exposed to different loading patterns and may experience different injury pathways. Maintaining spine postures near neutral alignment, avoiding excessive spine flexion, and minimizing joint loading by adopting an upright posture are important factors in maintaining back health and preventing low back pain. Accordingly, males may be more susceptible to developing low back pain from prolonged sitting due to the adoption of a more flexed spine posture that increases the risk of disc herniations (1), and the increased probability of exhibiting seated flexion relaxation (2). Females may be more susceptible to back muscle pain since upright sitting postures require higher muscle activation than slumped sitting (2) and prolonged low level activation has been linked to muscle pain (3).

The identification and exploration of gender differences in seated work has implications for the differential prevention and treatment of injuries as well as the alteration of chair designs to accommodate both genders and knowledge of safe levels of exposure to prolonged sitting in occupational settings.

REFERENCES

1. Wilder DG, et al. *J Spinal Disord*, **1**, 16-32, 1988.
2. Callaghan JP, Dunk NM. *Clin Biomech,* **17,** 353-60, 2002.
3. Veiersted KB, et al. *Int Arch Occup Environ Health,* **62**, 31-41, 1990.

ACKNOWLEDGEMENTS

This study was supported by KEILHAUER.

MECHANICAL CONSTRAINTS DO NOT CHANGE THE STRENGTH OF LOCOMOTOR-RESPIRATORY COORDINATION DURING RUNNING

[1] William McDermott, [1]Richard E.A. Van Emmerik and [2]Joseph Hamill
[1]Motor Control and [2]Biomechanics Laboratories, University of Massachusetts, Amherst. Email: wm@excsci.umass.edu

INTRODUCTION

Coupling between movement and breathing rhythms is thought to be a consequence of mechanical constraints placed on these systems. During locomotion, proposed mechanical constraints have taken the form of a visceral piston resulting from the visceral mass moving relative to the trunk cavity [1], the sagittal plane orientation of the trunk [4], and/or the demands placed on the respiratory musculature in controlling the trunk against perturbations [2]. Currently, little is known about the extent to which these constraints influence locomotor-respiratory coordination (LRC) due to limitations in many methods used to evaluate LRC [3] and because these constraints have previously not been measured.

The purpose of this study was to examine the influence of mechanical constraints that are induced by different uphill and downhill slopes on LRC during running. It was expected that greater constraints in terms of trunk flexion and accelerations of the trunk would result in greater strength of LRC.

METHODS

Thirteen male runners whose mean age was 27.4 (±11) years and ran 49.9 (±15.9) km/week participated in this study. The experimental conditions consisted of running at the preferred speed at level (0%) grade, followed by –9%, -6%, +6%, +9% grades in a random order. During the last 2.5 minutes of each condition, 3D motions of the thoracic trunk and pelvis were recorded (Qualisys, Inc.) along with the timing of right heel strike (tibial accelerometer, Entran Devises) and respiratory volume (respiratory airflow integrated with respect to time, Teem 100, Medical Graphics Corp.).

Mechanical constraints were evaluated at the trunk over 20 randomly selected strides by: 1) sagittal plane orientation, 2) magnitude of peak vertical linear accelerations and 3) magnitude of peak sagittal plane angular accelerations. LRC was obtained by first calculating the relative phase between each heel strike and end-inspiration [3]. The strength of LRC frequency coupling was quantified through return maps and time lags, and was defined as the extent to which the dominant frequency coupling occurred. The strength of phase coupling was quantified by the regularity of consecutively occurring phase relations [3].

RESULTS

Increases in slope resulted in systematic increases in overall trunk flexion from 5.3° during the –9% to 15.1° during the +9% condition (p's <0.0002). Accelerations of the trunk were primarily influenced by the downhill conditions (Figure 1). The peak forward and backward directed angular accelerations (left panel) as well as the peak vertical linear accelerations (right panel) were greater during the downhill grades than during the level and uphill grades (p’s<0.05). Despite these changes there were no consistent changes in the strength of locomotor-respiratory frequency and phase coupling (Figure 2) in response to the imposed uphill and downhill running slopes (p’s>0.05). Correlation analyses showed that the timing of peak angular trunk acceleration was associated with the intra-subject variability of LRC (r=0.32, p= 0.01).

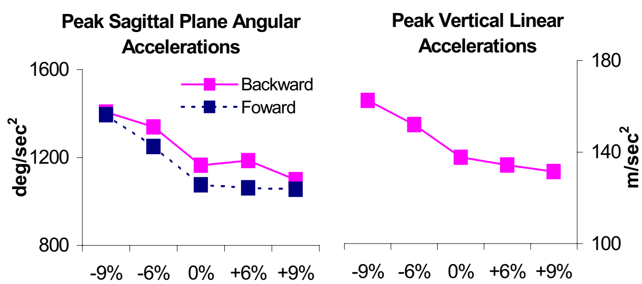

Figure 1: Peak angular and linear accelerations of the thoracic trunk.

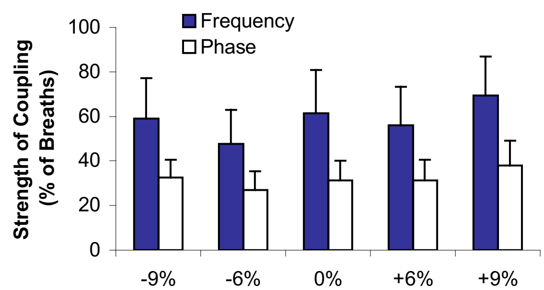

Figure 2: Strength of frequency and phase coupling between the locomotory and respiratory rhythms.

CONCLUSIONS

The results of this study indicate that proposed mechanical constraints do not act to couple locomotory and breathing rhythms in a way that increases the strength of coupling. Results from coupling analyses also suggest that increases in the *variability*, not strength, of LRC may be associated with changes in mechanical constraints. Increases in mechanical constraints imposed may therefore not result in greater coupling between locomotion and respiration, but in enhanced variability in their coordination and decoupling.

REFERENCES

1. Bramble DM and Carrier DR. *Science* **219**, 251-256, 1983.
2. Hodges PW, et al. *J Physio* **537**, 999-1008, 2001.
3. McDermott WJ, et al. *Eur J Appl Physiol* **89**, 435-444, 2003.
4. Takano N. *Jpn J Physiol* **45**, 47-58, 1995.

ACKNOWLEDGEMENTS

This work was funded in part by a grant from NSF (BCS-0341767).

HUMAN MANDIBLE RESPONSE TO IMPACT LOADING OF CHIN

[1] Matthew Craig, [1]Cynthia Bir, [1]David Viano and [2]Scott Tashman
[1]Wayne State University – Detroit, Michigan, matthew.craig@wayne.edu
[2]Henry Ford Hospital - Bone and Joint Center - Detroit, Michigan

INTRODUCTION

Load versus deflection response of the human mandible has been evaluated in the testing of cadaveric specimens in three general impact orientations. The output of the study provides a comprehensive look at the mandible, temporomandibular joint (TMJ) and basilar skull response to impact loading at the chin. Three-dimensional tracking of the mandible coupled with measured loading from an impacting drop mass was used to define response corridors of the human mandible. These corridors are to be used in the development of a surrogate mandible for use in automotive and sports equipment testing.

METHODS

A 5.2 kg drop mass is dropped from various heights onto the chin point of cadaveric specimens. The specimens are potted in an adjustable stand that allows for testing in three pre-determined orientations. The drop stand, previously used by Walilko, et al [1] and refined for use in this study, supports a PVC tube that is used as the drop mass guide. The mass is secured using an electromagnet. Drop mass acceleration is measured with a pair of accelerometers whose data is collected using TDAS PRO™ (DTS, Inc.).

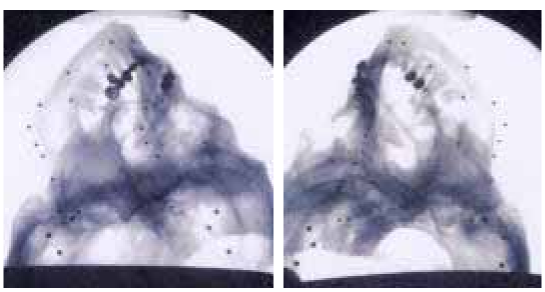

Figure 1: Images of bi-planar x-ray coverage of specimen prepared with markers

A high-speed bi-planar x-ray system was used for tracking displacements within the mandible and TMJ. The x-ray system emits an x-ray beam that is digitally recorded at a rate of 1000 frames per second by cameras at the rear of an image intensifier. The motion of lead markers (2-and 4-mm in diameter) placed on the surface of the mandible and skull are recorded and post-processed to produce x, y and z coordinates of the markers versus time (See Figure 1 for images of prepared specimen pre-test). The resulting three-dimensional motion of the markers is then used to evaluate motion between segments within the mandible and between the mandible and skull. That resulting motion is then plotted against drop mass impact force to develop force versus deflection response of the mandible.

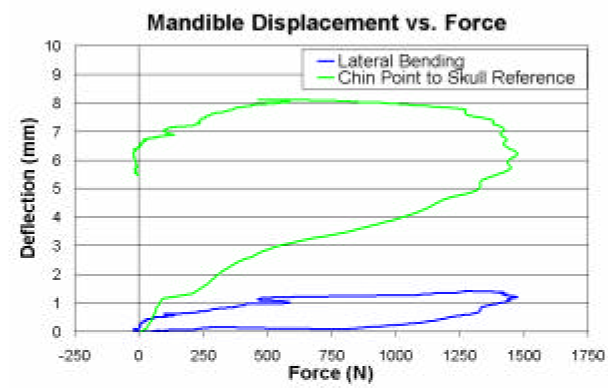

Figure 2: Load versus deflection for single test on cadaveric specimen.

RESULTS AND DISCUSSION

Load versus deflection was evaluated for a number of segments within the mandible and between the mandible and skull. Four key segments of deflection were evaluated: (1) chin point (point of drop mass impact) to a subcondylar marker just inferior to the condyle, (2) lateral deflection at 2nd molar, (3) sub-condyle to skull fixed reference, and (4) chin point to skull fixed reference. A sample output for the 1st and 2nd type of measurement listed above plotted versus the drop mass load can be seen in Figure 2. The output from the study is a set of load versus deflection corridors, one for each segment described.

CONCLUSIONS

The load versus deflection corridors produced in this study provide a complete picture of the response of the human mandible and TMJ joint to direct loading at the chin point under various loads and impact orientations. The corridors will form the basis for a work in process by the author to develop a human mandible surrogate that will be added to existing surrogate headforms for future use in sports equipment (mouthguard, helmet, chinstrap, etc.) testing and possible application in the anthropomorphic test devices used by the automotive industry.

REFERENCES

1. Walilko T, *Biomechanical response of the temporomandibular joint from impacts in boxing*, PhD Dissertation, Wayne State University, 2004.

ACKNOWLEDGEMENTS

National Football League Charities

Foot pronation in vivo – combined midfoot and hindfoot kinematics

[1] Michael Voigt, [2]Marianne Christensen and [2]Ole Simonsen
[1]Dept of Health Science and Technology, Aalborg University, mv@hst.aau.dk
[2]Department of Therapy, Aalborg Hospital, [3]Northern Orthopedic Division, Aalborg Hospital. Denmark

INTRODUCTION

Tibiocalcaneal (hindfoot) mobility has previously been described in vivo as a measure of foot pronation (e.g. [1]). However, this measure does not include the possible contribution of midfoot motion to foot pronation. The aim of the present study was to describe the combined mobility of the hindfoot and the midfoot in vivo in relation to the level of foot pronation.

METHODS

Fifteen volunteers participated in the study (4 females and 11 males). Age 43, SD 13 years, height 1.75, SD 0.1 m, weight 78, SD 13 kg, shoe size 42 SD 3 European.
The level of foot pronation was determined as the height of the medial arch of the foot during static loading ('reference navicular height') and the dynamic variation in this height ('dynamic navicular drop') during barefooted treadmill walking at 5.5 km hr^{-1} was measured using a combination digital photography and electrogoniometry [2].
Three-dimensional hindfoot and midfoot motion was determined using a motion analysis system (Qualisys, ProReflex, 4 cameras, 240 frs s^{-1}) and derived from bone mounted clusters of reflective markers during barefooted treadmill walking at 5.5 km hr^{-1} and a series of full range voluntary ankle-foot movements. Hindfoot motion was determined as the relative tibio-calcaneal rotations and midfoot motion was determined as the relative calcaneo-navicular rotations. During local anaesthesia small pins made of Kirschner wire (K-wire, 50 mm long, 2 mm thick) were inserted about 25 mm in depth into: 1. the lateral epicondyle of tibia, 2. the upper part of the lateral wall of calcaneus and 3. the dorsomedial wall of the navicular bone of the right leg. On each of these pins clusters consisting of three reflective markers (marker diameter 19 mm and distance between markers 60 mm) were mounted. The K-wire in the navicular bone was inserted guided by X-ray to ensure a proper positioning and due to the dorso-medial direction of the inserted pin (fig. 1) the marker cluster on this pin was mounted via a small mechanical joint and thereby directed towards the dorso-lateral side of the foot. The bone orientations were referenced to the orientations during upright standing with full body weight on the foot.

Figure 1. K-wires inserted guided by X-ray in calcaneus (upper dark line) and navicula (lower dark line)

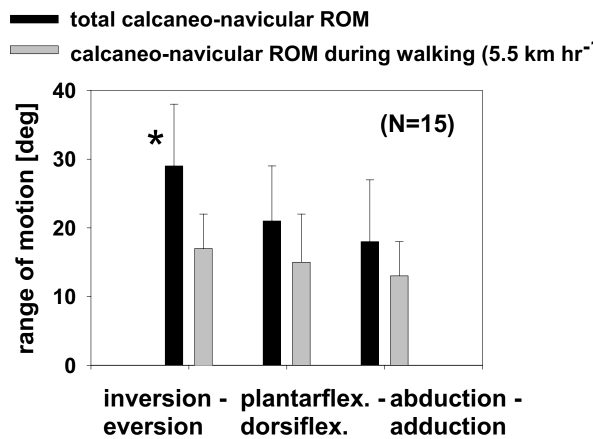

Figure 2. In vivo midfoot full range of motion (ROM) and ROM during walking (mean & SD). * = total inversion-

RESULTS AND DISCUSSION

The preliminary analyses have demonstrated that the reference navicular height ranged between 30 and 60 mm (mean 44, SD 8 mm) representing a wide range medial arch architectures. The dynamic navicular drop ranged between 14 and 61% (mean 30, SD 14%) of the reference navicular height during walking. The total calcaneo-navicular range of motion (ROM) (Fig 2, black bars) was similar to the talo-navicular ROM previously described in vitro [3]. The largest total calcaneo-navicular range of motion was observed in inversion-eversion. During walking the calcaneo-navicular ROM was between 60 and 70 % of the total ROM (Fig. 2, grey bars) with no significant differences between the movement directions. It was expected that tibio-calcaneal eversion and calcaneo-navicular eversion and dorsi-flexion would be correlated to flattening of the medial arch of the foot. However, no significant correlations were found between the level pronation (dynamic navicular drop) and the ROM in any direction of tibio-calcaneal or calcaneo-navicular movement.

CONCLUSIONS

Due to inter-individual variation in: joint geometry, ligament architecture and mechanical properties, architecture of muscle-tendon attachments, muscle strength and coordination it seems that foot pronation is achieved inter-individually through a wide range of combinations of mid- and hindfoot rotations.

REFERENCES

1. Reinschmidt et al. (1997) Gait & Posture 6: 98 – 109.
2. Voigt M et al. (2005) XXth Congress of the International Society of Biomechanics
3. Ouzounian et al. (1989) Foot & Ankle 10:140 – 146.

THE ACCURACY OF USING POSTURAL ASSESSMENT TO DETERMINE CUMULATIVE EXPOSURE

[1]Chad A. Sutherland, [1]Wayne J. Albert, [2]Jack P. Callaghan, and [1]Allan T. Wrigley
[1]Department of Kinesiology, University of New Brunswick, Fredricton, NB, Canada
[2]Department of Kinesiology, Faculty of Applied Health Sciences, University of Waterloo, Waterloo, ON, Canada
email: chads@uwindsor.ca

INTRODUCTION

Cumulative loading, a know risk factor for low back pain [1] that is separate from peak loading [2] must be investigated to aid in workplace safety. Video-based task analysis in the workplace is often limited by equipment location and production line arrangement, therefore making it difficult to capture the motion in the sagittal plane. The purpose of this paper was to investigate the amount of error in calculating cumulative loading variables (compression, joint anterior shear, joint posterior shear, reaction anterior shear and extension moment) using a posture matching approach (3DMatch; [3]) compared to a 3D coordinate modeling approach (FASTRAK™ electromagnetic tracking system).

METHODS

Six participants (3 males & 3 females) performed five repeats of two symmetrical and two asymmetrical stoop lifts while being simultaneously recorded from different camera views. The lifts were videotaped at 0^0, 45^0, 60^0 and 90^0 from the frontal plane. For modeling purposes, participants were suited with eight FASTRAK™ sensors located on the occipital protuberance, posterior surface of the second metacarpal-phalangeal joints, center of mass of the posterior surface of the trunk, upper arms and lower arms.

Four hundred and eighty lifting trials (6 subject * 20 lifts * 4 camera views) were analyzed using 3DMatch. 3DMatch uses postures of the trunk and upper extremities that are selected on a frame-by-frame basis from a set of predetermined posture categories (bins), which are used along with the subjects' anthropometric measures and hand forces to calculate the peak and cumulative variables. Relative error scores were calculated between the cumulative values derived from posture matching for each camera view (3DMatch) and those derived from the coordinate data (FASTRAK™). Both approaches used the same biomechanical model.

RESULTS AND DISCUSSION

No significant difference ($p<.05$) in the relative error for any of the cumulative loading variables across the four different camera views were found. Furthermore the relative error for compression, joint anterior shear, reaction anterior shear and

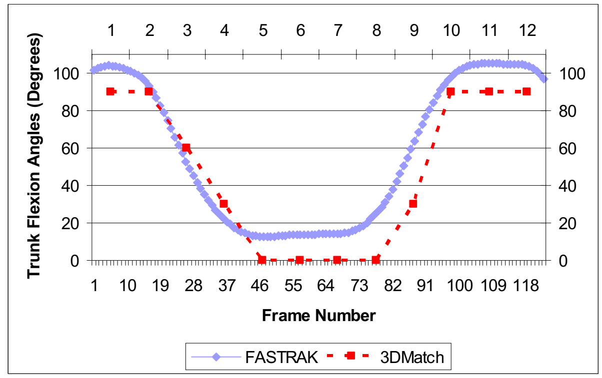

Figure 1: A trunk flexion angle graph representing a large difference between the data from the two model inputs.

extension moment were all below 11% (Table 1). The high relative error for joint posterior shear was due to the different techniques used to determine the segment angle. The posture bin for the trunk was a 30^0 range with the neutral bin postures ranging from -15^0 to $+15^0$. The midpoint bin value (0 in this example) is used as input to the 3DMatch model, whereas FASTRAK™ uses the recorded segment angle. Figure 1 illustrates this problem. During frames 5 through 8 the neutral posture category was correctly chosen as the angle was $\sim 14^0$ and therefore a segment angle of 0 was used. However, comparison with FASTRAK™ where the actual 14^0 angle was used, the simplification of choosing the midpoint of a category inflates the error.

CONCLUSIONS

These results suggest that 3DMatch is a promising tool for calculating cumulative low back loads as the relative error for all variables was below 11% when compared to a 3D biomechanical model.

REFERENCES

1. Kumar S. *Spine* **15**, 1311-1316, 1990
2. Norman R., et al. *Clinical Biomechanics*, **13**, 561-573, 1998
3. Callaghan JP., et al. *Proceedings of the 34th Association of Canadian Ergonomists, London, Ontario, Canada*, 2003.

Table 1: The relative mean (± standard deviations) percent error for each camera view across the four tasks

Variable	Camera View				
	0^0 view	45^0 view	60^0 view	90^0 view	Variable Mean
Compression	8 ± 6.0	8 ± 5.6	8 ± 5.9	7 ± 4.7	8 ± 5.6
Joint Anterior Shear	10 ± 7.8	10 ± 8.0	12 ± 10.5	11 ± 9	11± 8.9
Joint Posterior Shear	257 ± 611.8	252 ± 680.9	261 ± 686.5	260 ± 676.5	256 ± 662.4
Reaction Anterior Shear	9 ± 6.8	7 ± 5.9	8 ± 7.3	7 ± 5.4	8 ± 6.4
Extension Moment	9 ± 6.8	9 ± 6.8	10 ± 7.6	11 ± 7	10 ± 7.2
View Mean	58 ± 111.1	57 ± 108.8	60 ± 112.5	59 ± 112.0	59 ± 111.1
View Mean Excluding Joint Posterior Shear	9 ± 0.7	9 ± 1.4	9 ± 2.2	9± 2.4	9 ± 1.6

ELECTROGONIOMETRIC EVALUATION OF FOOT KINEMATICS DURING WALKING AT DIFFERENT VELOCITIES

[1]Michael Voigt, [2]Marianne Christensen [2]Ole Simonsen
[1]Dept. of Health Science and Technology, Aalborg University; email: mv@hst.aau.dk
[2]Department of Therapy, Aalborg Hospital, [3]Northern Orthopedic Division, Aalborg Hospital. Denmark

INTRODUCTION

Exaggerated pronation of the foot (hyperpronation) is a factor that induces painful conditions in the foot and eventually musculo-skeletal problems in the more proximal parts of the lower extremities e.g. shin pain, medial knee pain. However, evaluation of the relationship between the degree of foot pronation and musculo-skeletal disorders in the lower extremities is difficult because the quantification of foot pronation is either based on simple static measurements with a rather low repeatability (Weiner-Ogilvie and Rome, 1998, Vinicombe *et al.*, 2001) or rather complicated 3-dimensional movement analysis of the structure and foot kinematics which are costly and time consuming in daily clinical practice. Consequently, the purpose of this study was to develop and test a clinical applicable method which with good accuracy quantifies the degree of foot pronation both the statically and dynamically (Leardini *et al.*, 1999).

METHODS

Fifteen persons participated in the study (8 females and 7 males), age 40 yrs (S.D., 8 yrs), height 1.76 m (S.D., 0.10 m), and body weight 72 kg (S.D., 16 kg) and shoe size 41 European sizes, (S.D., 3 European sizes).

The quantification of foot pronation was based on a combination of static photographs of the foot and electrogoniometric measurements of the calcaneal angle and the height of the medial arch of the foot respectively: 1) Calibrated digital photographs were taken of the loaded foot during upright standing in the frontal plane from the dorsal side and in the sagittal plane from the medial side. 2) Two flexible wire goniometers (Biometrics®) were skin mounted one measuring the angle of calcaneus in relation to the shank in the frontal plane and one measuring the angle between the calcaneus and the first metatarsal bone in the sagittal plane. Additionally, two foot switches were placed under the heel and the forefoot respectively to measure temporal gait parameters.

The participants were asked to walk barefooted on a treadmill at three different velocities: 2.0, 4.5 and 5.5 km/hr while data were collected. All signals were sampled at 1000 Hz with a PC-based data acquisition system and processed in Matlab®. All procedures were repeated two times to evaluate the re-test reliability of the method. Two static measures were extracted from the digital photographs: the calcaneal angle in the frontal plane and the vertical height of the navicular bone and from the goniometer signals the dynamic changes in same parameters over the full step cycle were obtained.

RESULTS AND DISCUSSION

The comparison of selected parameters between the two tests did not reveal any statistical test-retest differences related to the test procedures.

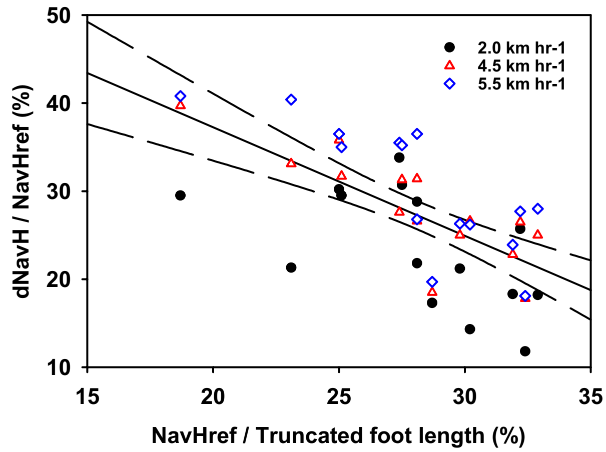

Figure 1: The relationship between the normalized static navicular height and the normalized dynamic navicular drop during walking at different velocities.

The static navicular height had a range of 36 – 62 mm between participants in the examined group (group mean 51, S.D., 7 mm), and the amplitude of the navicular movement during a full step cycle during walking at 4.5 km hr^{-1} ranged between 9 – 17 mm (group mean 14, S.D. 2 mm). The static calcaneal angle in the frontal plane ranged between -2 – 10 deg (group mean 6, S.D., 4 deg) and the corresponding amplitude of calcaneal rotation during the step cycle walking at 4.5 km hr^{-1} ranged between 8 and 33 deg (group mean 20, S.D., 5 deg). The magnitude of both calcaneal and navicular movement increased with increasing velocity. An inverse relationship between the normalized static navicular height and the normalized changes in navicular height during walking could be demonstrated (Fig.1).

CONCLUSIONS

We believe that we have developed a clinically applicable method to evaluate the degree of static and dynamic foot pronation with good accuracy. The method represents a tool for evaluation of the quality/efficiency of a wide variety of operative procedures and/or rehabilitation/training procedures that aim to correct for hyperpronation of the foot.

REFERENCES

1. Leardini et al. (1999) *Clin.Biomech.(Bristol., Avon.)* **14,** 528-536.
2. Vinicombe et al. (2001) *J.Am.Podiatr.Med.Assoc.* **91,** 262-268.
3. Weiner-Ogilvie et al. (1998) *J.Am.Podiatr.Med.Assoc.* **88,** 381-3

THE EFFECTS OF AN OVER-THE-COUNTER ORTHOTIC ON LOWER EXTREMITY KINEMATICS IN MALE AND FEMALE RECREATIONAL RUNNERS

Samuel Brethauer, Aric Warren and Robert Gregory
Biomechanics Laboratory, University of Kansas, Lawrence, KS, USA;
email: rwg@ku.edu, web: www.soe.ku.edu/hses/

INTRODUCTION

Abnormal foot mechanics during the stance phase of running may affect the kinematics of the lower extremities and predispose an individual to injuries of the foot, ankle, and knee. Custom-made foot orthotics are often prescribed to correct abnormal mechanics during running by restoring dynamic stability to the closed chain of the lower extremity. However, there has been no research done to examine the efficacy of using an over-the-counter orthotic to correct abnormal gait mechanics. In addition, females are reported to demonstrate different lower extremity mechanics during running as compared to males [1]. The goals of this study were: (1) to examine the effects of an over-the-counter orthotic on ankle and knee joint kinematics during running in individuals identified as excessive pronators, and (2) to determine if there are any gender-specific effects of orthotics on ankle and knee joint kinematics during running.

METHODS

Thirty college-age recreational runners (15 males, 15 females) identified as being excessive pronators participated in this study. Excessive pronators were defined as those individuals with a navicular drop of greater than or equal to 9 mm.

Subjects were required to perform two testing sessions in which they ran with and without orthotics. All subjects used the same model of soft, over-the-counter orthotic (Flat Foot Products, Marathon Shoe Co.) and the same model running shoe (Air Max Moto II, Nike Inc.) during testing. During both testing sessions, the subjects ran on a treadmill at a velocity of 3.35 $m \cdot s^{-1}$ for 15 min. A three-dimensional motion capture system (Visualeyez VZ3000, PhoeniX Technologies, Inc.) was used to record the position of light emitting diodes placed on the foot, shank, and thigh segments at 100 Hz for 50 complete gait cycles during the last 5 min of each testing session.

Range of motion, peak angular velocity, and peak angular acceleration of the ankle and knee joints were calculated for the frontal, sagittal, and transverse planes of motion according to the methods outlined by Eng and Pierrynowski [2]. A two-way analysis of variance was used to assess the effects of orthotic and gender on all kinematic variables.

RESULTS AND DISCUSSION

No differences between the orthotic and non-orthotic conditions across gender were found for ankle joint kinematics (range of motion, peak angular velocity, and peak angular acceleration) in the frontal, sagittal, and transverse planes of motion. One finding of note is that there was no difference in the amount of pronation between the orthotic (4.1±2.7°) and non-orthotic (3.5±2.8°) conditions. This contradicts previous findings that soft orthotics reduce pronation [2,3].

In addition, no differences between the orthotic and non-orthotic conditions were found for knee joint kinematics (range of motion, peak angular velocity, and peak angular acceleration) in the frontal and sagittal planes of motion. However, there was significantly greater ($p<0.05$) transverse plane motion in the orthotic (4.6±2.9°) versus the non-orthotic (1.7±1.2°) condition. Increased knee joint range of motion in the transverse plane when using soft orthotics has been documented previously [2].

Finally, it should be noted that there were no significant interaction effects between gender and orthotics on ankle and knee joint kinematics. While there was significantly greater ($p<0.05$) pronation in the female (7.2±1.5°) versus male (4.0±1.4°) runners across orthotic condition, the use of orthotics did not reduce pronation to a greater extent in female as compared to male runners.

CONCLUSIONS

The results demonstrate that the over-the-counter orthotic used in this study was not effective in altering lower extremity kinematics in male and female runners identified as excessive pronators. It can be concluded that over-the-counter orthotics provide mostly cushioning and little, if any, functional control. For individuals with gait pathomechanics, the use of a custom-made rigid or semi-rigid orthotic may be necessary.

Also, while there were differences in lower extremity kinematics between male and female runners, there were no gender-specific effects of orthotics on ankle and knee joint kinematics during running. Therefore, the over-the-counter orthotic used in this study was no more effective in reducing abnormal gait mechanics in female versus male recreational runners.

REFERENCES

1. Ferber R, et al. *Clin Biomech* **18**, 350-357, 2003.
2. Eng JJ, Pierrynowski MR. *Phys Ther* **74**, 836-843, 1994.
3. Smith LS, et al. *J Am PodiatrMed Assoc* **76**, 227-233, 1986.

ACKNOWLEDGMENTS

This study was funded by a grant from the Mid-America Athletic Trainers Association. The orthotics used in this study were provided by Marathon Shoe Co.

CINEMATIC MEASUREMENT OF CARTILAGE PLUGS IN UNCONFINED COMPRESSION

[1,2] Douglas R Pedersen, [1]James A Martin, [2]Nicole A Kallemeyn and [1,2]Nicole M Grosland
[1]Department of Orthopaedics and Rehabilitation, [2]Department of Biomedical Engineering, University of Iowa
email: doug-pedersen@uiowa.edu : mnypt.obrl.uiowa.edu

INTRODUCTION

Modeling natural diarthrodial contact requires material constitutive properties that accurately describe the dynamic deformation patterns of articular cartilage. To fill the knowledge gap between whole joint loading experiments and measurements of chondrocyte and cell substructure material properties, we adapted a SMITH+NEPHEW Dyonics arthroscopy system 4-mm 0° arthroscope (Figure 1A) to record real-time streaming video of cyclic cartilage loading in a purpose-designed triaxial compression vessel [1].

METHODS

Endoscope optics produce a 'fisheye' view (Figure 1B), which is deconvoluted by a transform that was generated by placing the arthroscope tip 4 mm from a geometrically homogenous pattern and unwarping the digital image to known fiducia [2].

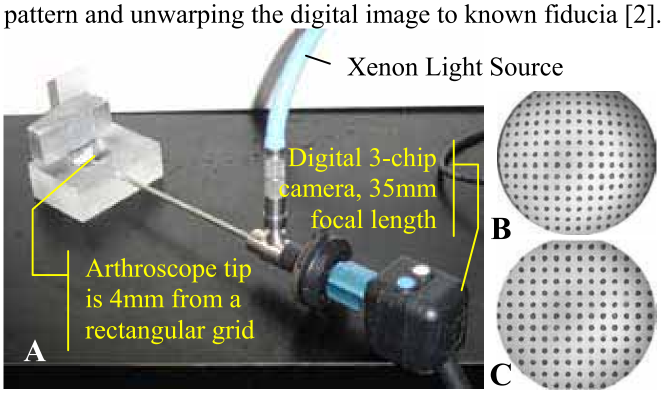

Figure 1 (A) Arthroscope configured for image calibration. The 'fisheye' view of an arthroscopic image (B) is deconvoluted (C) to the known grid geometry.

A 4-mm right-circular cylinder (plug) of human tibial plateau articular cartilage, 1.9 mm thick, was cyclically compressed with 0.1–2.0 MPa between porous platens in the nutrient-filled triaxial chamber (Figure 2). The 4 mm-wide platen (400 pixels, 10μm resolution) provided an in-image scale. Vertical movement of the upper platen was measured directly within each cine-frame (30/second) via pixel separation of fiducial grooves on the upper and lower platens. Motion of the upper platen was also recorded by a DVRT monitoring movement of the driving axial piston.

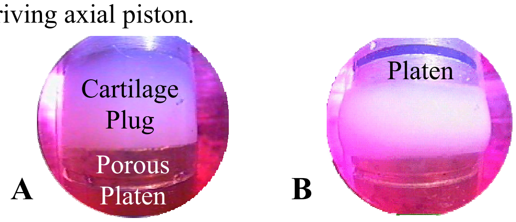

Figure 2 (A) The cartilage plug as seen before loading and (B) after 0.6 mm of axial compression.

Cartilage was stained with calcein-AM to fluorescently label live chondrocytes. An excitation filter (488 nm) was inserted between the xenon light source and the arthroscope and a yellow dichroic barrier ($\geq$515 nm transmission) was inserted at the eyepiece to allow visualization of live cell distribution in the matrix (Figure 3A). Optical resolution is sufficient to distinguish local chondrocyte columns in the deep zone (Figure 3B).

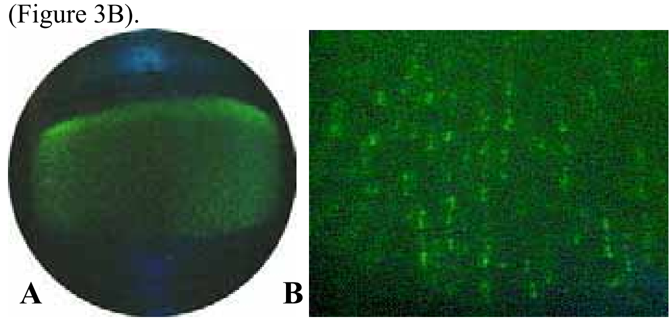

Figure 3 Chondrocyte morphometry in arthroscopic images; (A) Whole plug with highly fluoresced superficial zone. (B) Chondrocyte columns fluoresce in the deep zone.

RESULTS AND DISCUSSION

During unconfined axial compression between porous platens, an articular cartilage plug will bulge radially (Figure 2). The tissue will gradually lose height as water is forced from matrix voids under 1 Hz cyclic compression (Figure 4).

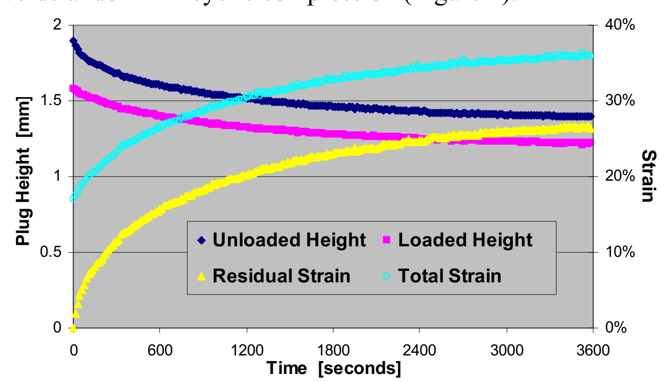

Figure 4 Plug heights and axial strains over 1 hour of loading

Articular cartilage consists of fluid and solid components. The changing shape of the cartilage plug's silhouette is indicative of the underlying biphasic material behavior. Finite element poroelastic model values of void ratio-dependent hydraulic permeability and depth-dependent modulus can be varied to match dynamic deformation patterns [3].

We present a method of real-time visualization and measurement of tissue deformation in living cartilage. Fluorescence labeling of chondrocytes provides internal fiducial markers that can be used to analyze intra-tissue strains and cell viability during dynamic loading.

REFERENCES

1. Heiner, A.D. and J.A. Martin, *J Biomech* **37**, 689-695, 2004.
2. Davis, et al., *IEEE Trans on Medical Imaging* **16**, 1997.
3. Vos, et al., *Osteoarthritis and Cartilage* **12B**, P254, 2004.

ACKNOWLEDGMENT Whitaker Foundation

FINITE ELEMENT ANALYSIS OF SHOCKWAVE PROPAGATION IN CORTICAL BONE

[1] Andrea E Tami, [2]Ulf Knothe and [1]Dwight T Davy
[1]Department of Mechanical and Aerospace Engineering, Case Western Reserve University, Cleveland, OH,
[2]Orthopaedic Research Center, The Cleveland Clinic Foundation, Cleveland OH;
email: dwight.davy@case.edu, web: mae1.cwru.edu/mae/Pages/Facilities/mmm/pages/mmm-main.html

INTRODUCTION

Osteoporosis on Earth and disuse osteopenia associated with prolonged exposure to microgravity show parallels including loss of bone mass and changes in cellular remodeling activity. Knothe and colleagues [1] have proposed the use of extracorporeal shock waves (ESW) as a means to combat bone loss. Results from in vitro pilot experiments have demonstrated the feasibility of creating microcracks in cortical bone similar to those occurring during physiological loading [1]. Based on the global hypothesis that microdamage acts as a trigger for the onset of remodeling by altering fluid flow and cell signaling, we propose that controlled application of ESW to bone tissue stimulates bone turnover. In order to better understand the therapeutic effect of ESW and to effectively develop this as a potential clinical application, the actual mechanics of the wave propagation and its interaction with local microstructure were analyzed using finite element models.

METHODS

The finite element analysis was run on the implicit solver of Abaqus 6.4 (HKS Inc., Pawtucket, RI). The basic shape for the model was a prismatic beam with isotropic, homogeneous material properties (Fig. 1A). Structural characteristics corresponding to the micro-architectural features of cortical bone tissue, i.e. lamellae, osteons with Haversian canal, and lacunar spaces, were subsequently included in distinct models (Fig. 1C-D). Comparable to the technical specifications of the lithotripter, the shockwave pulse was implemented as a haversine wave with high compressive amplitude (50-100Mpa), quick build-up time and short pulse width (1microsec). Parametric studies were carried out for different material and wave properties [2,3]. The effect on wave propagation along the beam due to changes in stiffness, density, pulse width and amplitude, as well as due to lamellar thickness and the presence of cavities was evaluated.

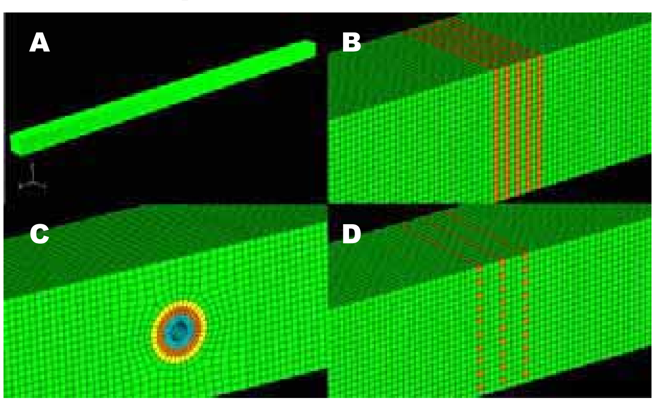

Figure 1: Basic model (A) and three modeled scenarios: lamellae (B), osteon (C) and lacunae (D).

RESULTS AND DISCUSSION

Noticeable changes in stress distribution of the propagating shockwave occurred when interfaces were modeled with very low stiffness (e.g. lacunae and Haversian canals) (Fig.2C-D). In these cases, the stress transmitted through the interface rapidly decreased with increasing interface thickness. Furthermore, in front of those inhomogeneities stress quickly changed from maximal compression to maximal tension due to reflection. When the change in stiffness was less than an order of magnitude, the interface had little effect on the traveling wave and, thus, the stress was not altered considerably.

CONCLUSIONS

In this study a model was designed that had the necessary spatial resolution for the characterization of bone properties like osteons, lamellae and lacunae, and at the same time could adequately represent the temporal resolution of a real shock wave pulse. More insight into the propagation pattern and stress distribution of a shock wave traveling in an isotropic, though inhomogeneous material was obtained. The possible effects of various interfaces were assessed. The next step will be the implementation of non-linear material behavior and algorithms incorporating the effect of damage.

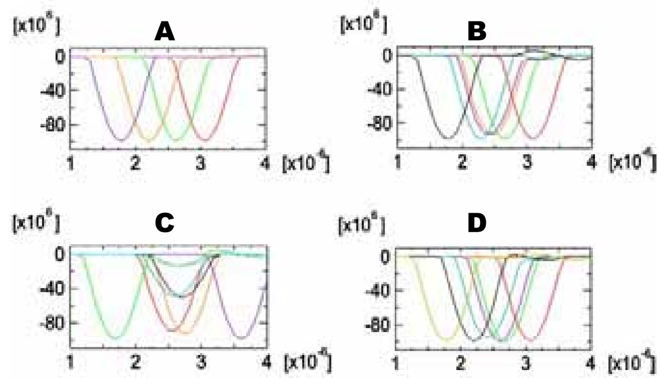

Figure 2: Stress distribution at different locations along the beam, corresponding to the modeled scenarios of Fig.1 (x-axis: time in sec, y-axis: stress in Pa).

REFERENCES

1. O'Leary JM, et al. *Trans ORS*, Washington DC, Abstract 1124, 2005.
2. Johnson W, *Impact Strength of Materials*, Edward Arnold Publishing, London, 1972.
3. Bossy E, et al. *J Acoust Soc Am* **115**(5), 2314-24, 2004.

ACKNOWLEDGEMENTS

NASA John Glenn Bioscience and Engineering Consortium (JGBEC NCC3-1000).

Velocity Sense in the Lumbar Spine is Modulated by the Vestibular and Proprioceptive Systems

[1] Joseph S. Soltys and [2] Sara E. Wilson
[1]Mechanical Engineering, University of Kansas, email: sewilson@ku.edu

INTRODUCTION

To maintain stability and normal motion of the spinal column, sensory information is necessary[1]. While studies have investigated position sense of the low back, few studies have examined velocity sense. A number of sensory systems may contribute to the perception of velocity of trunk motion. Muscle spindle organs have been shown to sense both joint position and velocity in the extremities[2]. The vestibular system could also contribute to the sense of trunk motion. In this study, the vestibular and proprioceptive contributions to the sense of low back movement were examined. It was hypothesized that altering vestibular and proprioceptive inputs would alter the sense of lateral trunk motion.

METHODS

Eight healthy subjects were recruited for the study, which was approved by the Human Subjects Committee, University of Kansas. Galvanic vestibular stimulation was applied via electrodes placed on the mastoid process behind each ear. The stimulation was set below the cutaneous threshold[3]. A vibratory stimulus device was fitted on the subject's back at L3 and adjusted to provide a 30 Hz stimulus to the underlying paraspinal muscle groups on either side of the spine independently. Subjects lay prone on a platform with their pelvis fixed, allowing only lateral trunk movement. Rotation from an optical encoder was used to provide a single audible tone for every 7^{o} of angular displacement. Subjects were blindfolded and asked to flex laterally so that the platform generated audible tones to match a digital metronome. Target paces were 10, 15, and 20 degrees/sec. The protocol consisted of alternate training (w/ audible pace and feedback) and assessment (no audible pace or feedback) trials for each of six conditions, block randomized, for each target speed. The stimulus conditions were defined as follows: NS – no stimulation, GSL/GSR – galvanic cathode at left/right ear, VL/VR – vibration left/right sides. Each trial consisted of two consecutive right to left movements across the maximum comfortable range of lateral trunk motion.

RESULTS AND DISCUSSION

The differences between consecutive right and left movement velocities for mid-range movement were assessed. Movements were found to be faster to the right with vibration of the left paraspinal muscles than with vibration of the right paraspinal muscles. Cordo et al. found that perception of velocity of movement in the elbow could be altered for frequencies between 20 and 40 Hz with slower frequencies being perceived as slower motion[2]. The muscle vibration used here was found to be interpreted as a slower lengthening, leading to a faster movement in the non-stimulus direction to compensate for the perceived slow-down. This was particularly pronounced at the higher speed where the difference between perceived and actual speed would be greater.

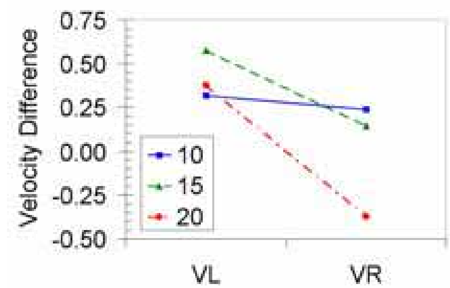

Figure 1: Right-Left velocity differences were found to be higher with vibration of the left paraspinal muscles (VL) than with vibration of the right paraspinal muscles (VR). This difference was found to increase with speed (10, 15, 20 deg/sec).

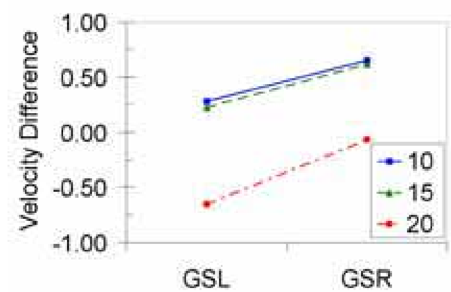

Figure 2: Right-Left velocity differences were found to be lower with galvanic vestibular stimulation with a left cathode (GSL) compared to with a right cathode (GSR). This change was found to be independent of speed (10, 15, 20 deg/sec).

With galvanic vestibular stimulation (GVS), movement towards the cathode was found to be faster for both left and right stimuli at all speeds of movement. GVS has previously been shown to induce a perceived motion towards the cathode in studies of dynamic sway[3]. This suggests that the vestibular system also plays a role in perception of velocity.

CONCLUSION

Both the proprioceptive and vestibular systems have been shown to play a role in the sense of lateral, low-back velocity. Vibration-induced changes in kinesthesia have been found to be a function of the speed of motion. Future research should examine the frequency dependence of these changes.

REFERENCES

1. Panjabi, M.M., *J Spinal Disord,* **5**(4), 383-9, 1992.
2. Cordo, P., et al., *J Neurophysiol,* **74**(4), 1675-88, 1995.
3. Latt, L.D., et al., *Gait Posture,* **18**(2), 64-72, 2003.

ACKNOWLEDGEMENTS

This publication was made possible with support from the Madison and Lila Self Graduate Fellowship and the Whitaker Foundation.

MODELING AND SIMULATION OF REACTION FORCES IN A REDUCED GRAVITY EXERCISE SYSTEM

[1]Marcus L. Just, [1]Carlos Grodsinsky, [2]Gail Perusek, [3]Brian Davis, [3]Peter Cavanagh
[1]Zin Technologies, Inc., Brookpark, OH; email: marcus.just@zin-tech.com; web: www.zin-tech.com
[2]NASA, Glenn Research Center, Cleveland, OH
[3]Cleveland Clinic Foundation, Cleveland, OH

INTRODUCTION

NASA Glenn Research Center (GRC) and the Cleveland Clinic Foundation (CCF) are collaborating to study aspects of exercise as a mitigating countermeasure to the phenomenon of bone density loss experienced by astronauts in extended space missions, despite implementing a rigorous exercise regimen. It is suspected that the reduction of reactive forces introduced by necessary vibration isolation systems make the workout less effective, thus contributing to the persistence of the phenomenon. Isolators are needed at the exercise system interface to attenuate forces that are transmitted into the space vehicle. A 1-Degree of Freedom (1-DOF) ground-based treadmill test bed known as the Enhanced Zero-g Locomotion Simulator (eZLS) has been designed which will allow researchers the ability to simulate an on-orbit reduced gravity environment in one axis. A dynamic model of the eZLS has been built to understand system dynamics and their affect on foot-treadmill reaction forces. One of the goals of the project is to experiment with isolators of different properties and determine their effect on foot reaction forces.

METHODS

The exercise system has six distinct elements that were included in the simulation (see Fig. 1).

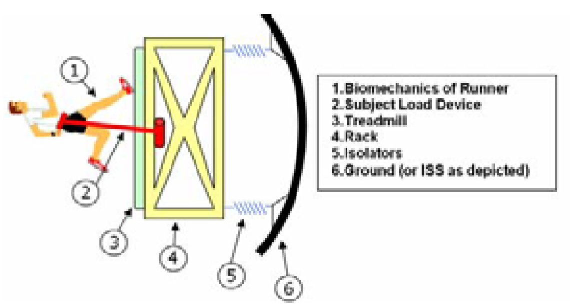

Figure 1: Zero-g Exercise Schematic

The model aimed to simulate rigid body dynamics of the treadmill and rack (items 3 and 4 in Fig. 1) as the runner foot forces (1) excited the dynamics of the isolator elements (5). The isolators were assumed to be grounded at (6). Foot forces were approximated as a sinusoidal, displacement driven body load into the runner's legs. Leg stiffness and damping values were chosen to obtain foot force input loads of 2.5 BW peak force [Ref. 1] into solid ground. The cadence was set to a frequency of 3 Hz. The input signal was half-wave rectified since the foot force could only be directed into the treadmill surface. The treadmill and rack were modeled as a rigid body, the position of which was subtracted from the displacement driven runner load. Isolator stiffness and damping properties were calculated so that certain desired resonances could be studied. Since the position of the treadmill was driven by the runner, depending on isolator stiffness and damping, the treadmill surface tended to dynamically yield against the foot. Output from the model was treadmill deflection, foot reaction forces, and ground reaction forces.

RESULTS AND DISCUSSION

The model was used to gage the potential effect that various isolator designs may have on foot reaction forces. Four simulated isolators were set to resonances of 1 Hz, 3 Hz, 10 Hz, and 25 Hz. Model output is presented in Table 1. The 1 Hz isolator set naturally produced the best attenuation of forces transmitted into the ground, however at the expense of 8.7% less total foot reaction forces compared to the baseline 25 Hz case, which is nearly hard-mounted. While the 1 Hz case peak forces only dropped by about 4.7%, the sum of the forces, which is a way of measuring total workout, increased in a non-linear fashion. Also, the model showed that a 3 Hz isolator resonance will of course couple with the cadence frequency and cause many undesirable effects such as amplified ground interface forces and treadmill oscillations, and a 43.5% reduction in summed foot reaction forces.

CONCLUSIONS

The initial rigid body model provides a good illustration of the effects that the eZLS project is setting out to study and serves as a starting point for building more sophisticated models of exercise systems for use in long duration manned spaceflight. Adding more detail regarding bio-mechanical simulation of the runner, higher-order treadmill and rack dynamics, and an active subject loading device will greatly enhance the model. The model can then be validated against tests performed on the eZLS in normal earth gravity and modified for use in 6-DOF in order to simulate performance of astronaut exercise aboard the International Space Station, or Long Duration Lunar and Mars Exploration Missions.

REFERENCES

1. Cavanagh P, et al. J Biomechanics **13**, 397-406, 1980.

Table 1. Effect of Isolator Stiffness on Foot Reaction Force

	Isolator Design Frequency			
	1 Hz	*3 Hz*	*10 Hz*	*25 Hz*
K_{total} (lbf/in)	178	1690	18e3	112e3
b_{total} (lbf/(in/s))	2	2	2	2
Max dZ of Treadmill (in)	0.699	2.629	0.026	0.003
Max Foot Force (lbs) *[% from Baseline]*	343 *[4.7% drop]*	206 *[42.7% drop]*	359 *[0.3% drop]*	360 *[baseline]*
Max Treadmill Force into Ground (lbs)	125	4232	470	382
Sum of Foot Forces *[% of Baseline]*	8.4e5 *[8.7% drop]*	5.2e5 *[43.5% drop]*	9.2e5 *[0% drop]*	9.2e5 *[baseline]*

REPDODUCING PHYSIOLOGIC MOMENT ARMS WITH AN ELBOW SIMULATOR

[1]Laurel Kuxhaus, [2]Jeffrey S. Vipperman, [3]Mark E. Barratz, [2]Joshua P. Magnusen, and [2,3]Mark C. Miller
Departments of [1]Bioengineering and [2]Mechanical Engineering, University of Pittsburgh, Pittsburgh, PA
[3]Orthopaedic Biomechanics Research Laboratory, Allegheny General Hospital, Pittsburgh, PA
email: mcmiller@wpahs.org

INTRODUCTION

The elbow is critical to activities of daily living, for gross tasks such as lifting heavy objects and finer tasks such as grooming. Some treatments of elbow injury, including replacement and/or reconstruction, do not restore stability or complete function. Tools are lacking to evaluate kinematics and stability of surgical treatments *in vitro*. An elbow simulator described in the literature has actuated its muscles with open-loop force control [1] and lacked antagonist muscle control making accurate positioning difficult at best. A wrist simulator's success using force and position control illustrates that proportional-integral-derivative control can replicate physiologic motion in an upper extremity joint [2].

The purpose of the current work was to construct an apparatus to replicate realistic, accurate motion and neuromuscular control of a cadaver elbow while maintaining moment arms similar to the broad range of those reported in the literature. Fulfillment of these design requirements will permit the study of force and motion control strategies.

METHODS

The apparatus controls the dominant movements (flexion-extension (f/e) and pronation-supination (p/s)) via the *brachialis*, *biceps brachii*, *triceps*, *pronator teres*, and *brachioradialis*. A custom frame (Figure 1) supports five servoelectric cylinders (Exonic Systems, Pittsburgh, PA) coupled with Gemini servo drives (Parker Hannifin Corp., Cleveland, OH) to actuate the muscles. Each muscle is connected to its actuator via a cable that passes through a muscle-specific custom pulley system which maintains physiologic alignment (and thus accurate moment arms) throughout the motion. The cables to extend the *biceps brachii*, *brachialis*, and *triceps* do not undergo large alignment changes during elbow motion and require only stationary pulleys. However, the *brachioradialis* and *pronator teres* undergo marked alignment changes with elbow flexion and thus a more advanced pulley system is required to allow multiple rotations (Figure 1, inset) and to prevent cable dislocation with elbow motion.

To evaluate the apparatus, a mock elbow with realistic size and mass properties that could move in both f/e and p/s was constructed. The muscle origins were adjustable to encompass the range of values previously reported [3]. The moment arms of the mock elbow's five muscles in our apparatus during 140° of elbow f/e were calculated.

RESULTS AND DISCUSSION

A realistic elbow simulator has been constructed. The versatile design can accommodate both right and left arm specimens and can test elbows in both varus and valgus

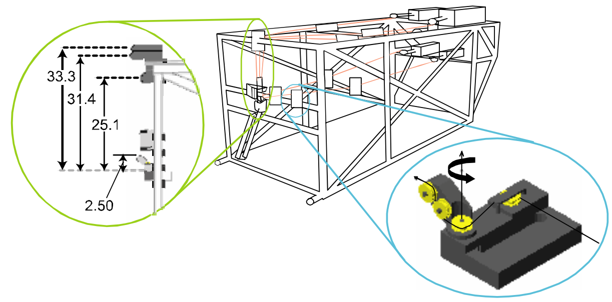

Figure 1: Schematic of frame and custom pulleys (insets), dimensions in cm.

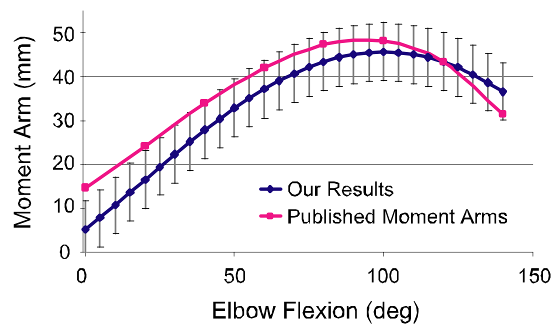

Figure 2: Moment arm results for *biceps brachii*. Error bars indicate the moment arms within the range of those reported in the literature.

orientations. Custom pulleys (Figure 1) allow the muscles to maintain their physiologic lines of action and moment arms throughout the elbow's range of motion. Calculated moment arms agree closely with previously-published results [4] (Figure 2 shows one of the five outcomes).

As a validation, the apparatus successfully moved the mock elbow through complete f/e and p/s cycles. This design can flex and extend a cadaver elbow at 300°/s (a realistic movement speed) and lift a 7 kg weight in the hand.

REFERENCES

1. Johnson J.A., et al. *J Biomech*, **33**(5), 635-9, 2000.
2. Werner F.W., et al. *J Orthop Res*, **14**(4), 639-46, 1996.
3. Magnusen, J.P. *Design and Fabrication of an Elbow Motion Simulator.* MS Thesis, University of Pittsburgh, 2004.
4. Pigeon P. et al. *J Biomech*, **29**(10), 1365-1370, 1996.

ACKNOWLEDGEMENTS

The authors thank Mr. Pete Bisnette, fabricator, for his assistance. This work was in part supported by an NSF IGERT fellowship (LK) and the American Society for Surgery of the Hand (MEB).

EVALUATE THE POTENTIAL CONTRIBUTIONS OF SWING LEG TO THE STABILITY OF BODY DURING SINGLE FOOT SUPPORT PHASE OF WALKING

[12] Ming Wu, [3]Dewen Jin, [3]Linhong Ji, [124]Brian D. Schmit
[1]Sensory Motor Performance Program, Rehabilitation Institute of Chicago, Chicago, IL, USA
[2]Northwestern University Medical School, Chicago, USA
[3]Department of Precision Instrument, Tsinghua University, PR China
[4]Department of Biomedical Engineering, Marquette University, Milwaukee, WI, USA

INTRODUCTION

Evaluation of the stability of the body during walking is critical to understanding the mechanisms of balance control. However, the current evaluation index, which is used in biped robot control [1], is not applicable to measurements of the stability of the human body. A critical limitation of this index is that it uses the stability index of the support leg to represent the stability of the whole body while neglecting the contribution of the swing leg. The purpose of this study, therefore, was to evaluate the contribution of the swing leg to the stability of whole body during the single-foot support phase of walking using an energy-work approach.

METHODS

A simplified five-segmental sagittal model of human body during single-foot support phase of walking is shown in Fig. 1.

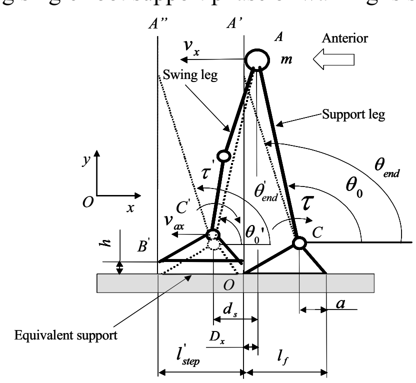

Fig. 1: A 5 links model of human body during single foot support phase of walking.

Although the swing leg does not provide support to the body during swing, the foot of the swing leg can move downward/ forward to touch the ground and form a new support, if a forward perturbation is imposed to the body. After foot touchdown, plantarflexion torque can be generated by the ankle joint to prevent forward rotation of the body. Consequently, the swing leg holds the potential to support the body and this could contribute to the stability of whole body.

We used an equivalent support to estimate the contribution of the swing leg to the stability of human body. The equivalent support consisted of a foot and a leg (without knee flexion) and could provide the same functional contributions to the stability of the body as the actual swing leg would after it touched down, as Fig. 1 shows.

After perturbations, the kinetic energy of the mass of the body transforms into two parts: one of them is the increment in potential energy of the mass when the human moves from its initial position A to the final position A"; the other one is the energy absorbed by the ankle joints, including the ankles of the supporting leg and the swing leg after it touches the ground. This corresponds to when they generate plantar-flexion torques to prevent forward rotation of the body. Thus, we define the stability reserve of the human body during a single foot support phase as

$$S^{b}_{anterior} = W - (E - (P_{end} - P_0)) \text{ (J)} \qquad (1)$$

where E is the kinetic energy of the human body at the initial position or after perturbations. P_0 and P_{end} are potential energies of the mass at initial and final positions. W is the energy absorbed by the ankle joints of the supporting and swing leg after touchdown.

RESULTS AND DISCUSSION

The stability reserve of the human body during the single support phase is shown in Fig. 2. The center of mass moved from Dx =1.8 (after the toe off the ground) to -.3 (before the heel touches with the ground). The stability reserve of the whole body was large before the foot of the swing leg touched the ground. This is consistent with the actual stability of the human body during walking.

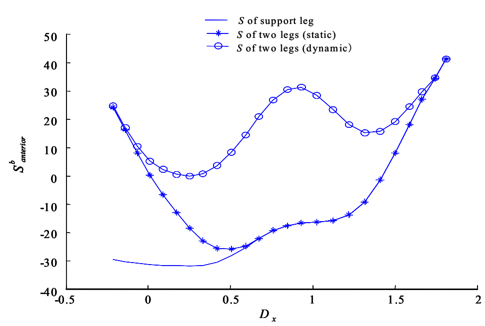

Fig. 2: The stability reserve of human body during single foot support phase. The D_x has been normalized by the length of foot.

CONCLUSIONS

The swing leg potentially contributes to the stability of the body and should be involved in the evaluation of the stability during walking.

REFERENCES

1. Furuta T. et al. *Robotics and Autonomous System,* **37**, 81-10, 2001.

ACKNOWLEDGEMENTS

This study was supported by National Science Foundation of China (30170242).

BIOMECHANICAL COMPARISON OF ADJACENT LEVEL SEGMENTAL MOTION IN THE CERVICAL SPINE WITH VARYING DEGREES OF LORDOTIC ALIGNMENT

[1] Mark Kayanja, [2] Soo-hyun Hwang, [1] Ryan Milks, [1] Edward Benzel
[1] Cleveland Clinic Spine Institute, Cleveland Clinic Foundation, 9500 Euclid Avenue Cleveland Ohio 44195
[2] Department of Neurosurgery College of Medicine Gyeongsang National University Jinju, Gyeonsangnam-do, South Korea
Presenting author = Ryan Milks; email: Milksr@ccf.org

INTRODUCTION

The anterior cervical diskectomy and fusion procedure is a well established technique with a fusion rate of approximately 95 % in non-smoking patients [1, 2]. However, approximately 25 % of these patients will suffer from degenerative disc disease at levels adjacent to the fusion within 10 years of the initial surgery [3]. It has been shown that there is a significant increase in intra-discal pressure and segmental motion at levels adjacent to a fusion during normal range of motion [4]. Graft size affects the lordotic posture of the spine which in turn affects adjacent level segmental motion. Theoretically reduction of adjacent level segmental motion should lead to a reduction of adjacent level degenerative disease. This study was designed to investigate the affect of varying configurations of cervical spine alignment on adjacent level segmental motion following a simulated cervical fusion.

METHODS

Eight human cadaveric cervical spine specimens (aged 45 to 57 years, 4 male and 4 female) were X-rayed to ensure that no major structural abnormalities were present. C2 and C7 of each specimen were potted in customized gripping fixtures and sagittal angle markers were carefully inserted into the anterior aspects of each of the vertebral bodies C3-C6. After determination of the centers of rotation of the segments, they were tested to 0.5 Nm in extension and 0.7 Nm in flexion measuring range of motion (ROM) by image analysis using Scion Image (Beta 4.0.2, Scion Image, Frederic, MD, USA). Simulated fusion was performed by a diskectomy at C4-C5 and insertion of a 6 mm interbody graft followed by a plate and screws (Orion system, Medtronic Sofamor Danek, Memphis, TN, USA) ventrally. The biomechanical tests were repeated measuring ROM as before. A second simulated fusion was then performed using a 9 mm interbody graft followed similarly by a plate and screws, achieving greater lordotic alignment. The biomechanical tests were repeated measuring ROM as before. The ROM at each level was analyzed using an ANOVA with repeated measures to determine the difference among the values for the intact state, 6 mm interbody graft fusion and the 9 mm interbody graft fusions, with the significance level at the 0.05 level.

RESULTS AND DISCUSSION

Two of the spines were inadvertently fractured during testing and were excluded from analysis. The mean values for the sagittal lordotic angle at C4-C5 were as follows: intact = 6.4 ± 1.3°, 6 mm spacer = 8.8 ± 1.4° (intact/6 mm graft, $p = 0.08$) and 9 mm spacer = 12.4 ± 0.9° (intact/9 mm graft, $p = 0.01$). Table 1 shows the measured ROM, compared to the intact there was no significant difference in adjacent segmental motion at C3-C4 with either the 6 or 9 mm interbody graft. Greater amount of adjacent segmental motion was seen at C5-C6 following the 6 mm interbody graft ($p \leq 0.02$), but not with the 9 mm graft. There was a significant increase in inferior adjacent ROM with the 6 mm interbody graft.

CONCLUSION

The attainment of cervical lordosis at the time of fusion reduces the subsequent adjacent level range of motion particularly at the inferior adjacent level.

REFERENCES

1. Brodke D, Zdeblick T. Modified Smith-Robinson procedure for anteriorcervical diskectomy and fusions. *Spine* 1992, 17: 2427-30.
2. Emery S, Bolesta M, Banks M, Jones P. Robinson anterior cervical fusion: Comparison of the standard and modified techniques. *Spine* 1994, 19: 660-3.
3. Hilibrand A, Carlson G, Palumbo M, Jones P, Bohlman H. Radiculopathy and myelopathy at segments adjacent to the site of previous cervical arthrodesis. *JBJS* 1999 (Am) 81: 519-28.
4. Eck J, Humphrey S, Lim T, Jeong S, Kim J, Hodges S, An H. Biomechanical study on the effect of cervical fusion on adjacent level intradiscal pressure and segmental motion. *Spine* 2002, 27: 2431-4.

Table 1 – Mean segmental motion following cervical fusion with 6 mm and 9 mm grafts at C4-C5

ROM Measurement	Intact (degrees)	With 6 mm graft (degrees)	With 9 mm graft (degrees)
C3-C4 segmental motion in flexion	4.5 ± 0.3	6.3 ± 0.6	4.7 ± 0.3
C5-C6 segmental motion in flexion	3.8 ± 0.4	5.8 ± 0.1	4.2 ± 0.2
C3-C4 segmental motion in extension	2.6 ± 0.2	3.7 ± 0.4	2.5 ± 0.3
C5-C6 segmental motion in extension	3.4 ± 0.4	4.8 ± 0.2	2.8 ± 0.6

Note: ROM = range of motion in degrees

COMPRESSIVE MECHANICS OF THE MATURING HUMAN SPINE

David J. Nuckley, Eno M. Yliniemi , Amy M. Cohen, Richard M. Harrington and Randal P. Ching
Applied Biomechanics Laboratory, University of Washington, Seattle, Washington,
e-mail: dnuckley@u.washington.edu, website: http://depts.washington.edu/uwabl/

INTRODUCTION

Child neck injury is a devastating trauma outcome with fatal or life-long debilitating consequences. Although spinal injuries to the pediatric populace account for less than 15% of all spine injuries, their subsequent fatality and spinal cord injury rates eclipse those of the adult population. Despite the devastating socioeconomic sequelae from pediatric neck injuries, the biomechanical characterization of neck properties and injury thresholds remains incomplete, hindering progress on advanced child neck injury prevention strategies.

Therefore, over the past five years our research team has been committed to measuring and documenting mechanical properties and injury tolerance of the cervical spine as a function of developmental age. Due to limited pediatric human tissues, this research has been performed using a baboon model (Papio anubis). A few biomechanical studies have demonstrated a correlation between baboon and human tissues with a scaling ratio of 0.70 : 1.0.[1-3] The current study was designed to understand the compressive properties of human pediatric tissues and relate them to data collected for the baboon model. Thus, we aimed to validate our baboon model and understand the compressive mechanics of the human spine throughout maturation.

METHODS

This research effort involved the biomechanical testing of eleven (11) human cadaver cervical spines across the developmental spectrum (2-to-28 years old). These specimens were dissected into 2-FSU constructs (C3-C5), wired, and embedded in PMMA for compression experimentation (Fig.1). The constructs were preconditioned and tested non-destructively up to 75% body weight in compression using a servohydraulic loading frame (MTS, Eden Praire, MN). Three loading rates were investigated: 0.1, 1.0, and 10-mm/sec and the load-displacement data were collected at 200-Hz. The stiffness was measured as the slope of the linear portion of the load-displacement curve. This protocol mimics the algorithm previously used to test our baboon specimens.[4]

Figure 1: Human Cervical Spine C3-C5 Segments Prepared for Testing. A 5-year old (left) and 18-year old (right) are shown wired on top and embedded in PMMA for testing (bottom).

RESULTS AND DISCUSSION

The human cervical spine compressive stiffness increased with spinal maturation and consistently exhibited greater values throughout development compared to baboon constructs (Fig.2). The baboon data were fit with a 2nd order polynomial growth curve which was then shifted upwards to examine its ability to model the human response. The optimal y-intercept was found using a least-squares iteration method. The human cervical spine stiffness data were found to closely match the shifted baboon growth trajectory (r^2 =0.925).

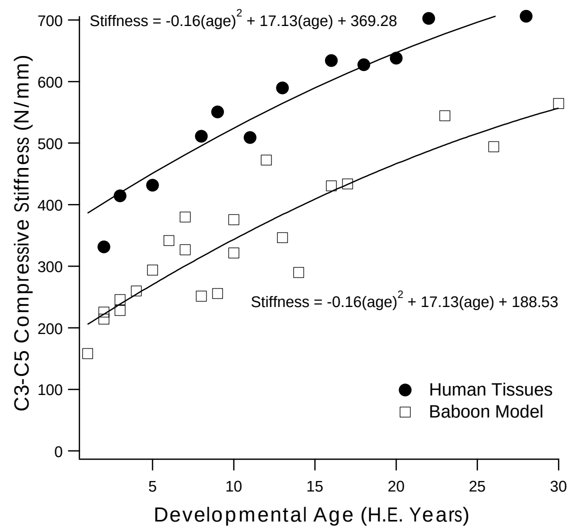

Figure 2: Compressive Stiffness of Human and Baboon C3-C5. Baboon data was fit with a 2nd order polynomial. The human data fits this shifted baboon curve (r^2=0.925).

These human cervical spine biomechanical stiffness data, the first of their kind, demonstrate an increase over baboon spinal stiffness similar to that previously reported in the literature. This relationship provides strong confidence in our baboon model and our ability to scale its spinal mechanics to humans.

CONCLUSIONS

Neck compressive stiffness significantly increased with child development and was found to follow a similar growth trajectory as baboon data. Together, these data facilitate our use of the baboon model for the establishment of child neck safety criteria and the development and analysis of advanced safety systems on playgrounds, for sports, and in automobiles.

REFERENCES

1. Dickman, CA, et al. *Spine* **19,** 2518-2523, 1994.
2. Little, R, et al. *Tech. Report* AFAMRL-TR-81-40, 1981.
3. Setton, LA, et al. *J Orthop Res*. **11**, 228-239, 1993.
4. Nuckley DJ, et al. *Stapp Car Crash J.* **46**, 431-440, 2002.

ACKNOWLEDGEMENTS

Support provided by the NCIPC (CDC) and NHTSA (DOT).

KNEE STABILITY: MECHANICAL CONTRIBUTIONS OF INDIVIDUAL MUSCLES

Aaron Derouin, Jim Potvin
Department of Kinesiology, University of Windsor, Windsor, Ont, Canada, email: derouin@uwindsor.ca

INTRODUCTION

The knee joint is an inherently complex structure that relies less on the shape of its articulating surfaces for stability than any other joint in the lower extremity [1]. The anatomical structure of the knee, and its location between the body's two longest weight-bearing bones, make it particularly susceptible to injury and subsequent instability. Non-operative treatment options, such as functional training and functional knee brace use, have qualitatively been shown to restore knee joint stability by improving muscular recruitment of key stabilizers. However, little is known about the potential contributions of individual muscles to the rotational stability of the knee. Mechanical stability is defined as the "the ability of a loaded structure to maintain static equilibrium even at small fluctuations around the equilibrium position" [2]. Recently, a new approach to calculate stability about any joint has been proposed by Potvin & Brown [3]. The objective of this paper is to use this method to determine the individual contributions, of the 13 knee muscles, to rotational stability about the valgus-varus and the flexion-extension axes of the knee.

METHODS

A seven segment biomechanical model of the lower extremity was developed based on the work of Delp *et al* [4] and was used to describe the relative joint rotational and translational characteristics of each segment. The inputs to the stability model were: 1) muscle force (assumed to be 100% of maximum), 2) three-dimensional muscle length, 3) functional moment arm and 4) local muscular coordinates with respect to the knee joint, defining either the origin and insertion or, when applicable, nodes on either side of the joint. These data were determined for rotations about the knee's flexion-extension (z) and the valgus-varus (x) axes for two different functional positions (a neutral and a squat position with the hip and knee both flexed to 90°). Fifth order polynomial equations were fit to Nisell's data [5] to determine the exact x and y translations of the femoral-tibial joint and the patella that occur simultaneously with knee flexion-extension. Additionally, seventh and third order polynomial equations were used to predict the active and passive muscle force length effects, respectively, for both postures.

RESULTS AND DISCUSSION

Overall, the average summed stability in the squat position was approximately 1.3 times higher than in the neutral posture for both the flexion-extension and the varus-valgus axes. Table 1 provides a brief summary of the dominant muscles that provide the greatest stabilizing potential when activated to 100%. Muscles with greater cross-sectional areas and high geometric stability (related to having large functional moment arms and short fibre lengths) proved to be the greatest contributors to knee stability. The semimembranosus (SM), for example, has a physiological cross-sectional area that is an average of 3 times greater than that of semitendinosus (ST), biceps femoris long head (BFL) and short head (BFS) [6]. Interestingly, the stability provided by the BFS ranked third as a flexing stabilizer in the squat position. Its geometric stability in this posture is slightly greater than that of SM and is 2.75 times greater than the ST. The maximum force potential of the BFS is about 1.2 times higher than the ST, while its stabilizing potential is about double. The BFS, it seems, almost qualifies as the ideal stabilizer, as it has a relatively short length and a long flexor moment arm [3].

Identification of the key knee stabilizers may prove to be useful during rehabilitation following ligamentous injury, and in setting surgical decision-making criteria. For example, the SM has great potential to stabilize the ACL deficient knee about the flexion-extension axis, particularly beyond 20° of knee flexion. Unfortunately, injury to medial or lateral structures leaves the knee rather vulnerable to valgus or varus instability. In the squat posture, the tensor fascia latae offers the second greatest stability potential. Results of a dissection study revealed that the tensor fasciae latae (TFL) has a greater role in stabilizing the knee than the fibular collateral ligament, as the knee is less resistant to varus angulation when the TFL is sectioned [1]. However, its potential to stabilize the knee is only 20% of that from SM. Rationale for surgery or functional knee bracing would seem to be indicated in severe LCL injuries, as the lateral knee stabilizers offer less support in either posture compared to muscles acting in the flexion-extension axis.

CONCLUSIONS

The stability model used in this study offers great insight into the stabilizing potential of the individual knee muscles. In a future project, this methodology will be used to determine the potential stabilizing benefits that functional knee braces may provide to ACL deficient patients.

REFERENCES

1. Laurence, M et al. *Proc Roy Soc Med*, **63**, 758-759,1970.
2. Bergmark, A. *Acta Orthop Scand Suppl* **60**, 1-54, 1989.
3. Potvin, J, Brown, S. *J Biomech* (in press), 2005
4. Delp, S et al. *IEEE Trans Biom Eng* **37**, 757-767, 1990.
5. Nissell, R. *Acta Orthop Scand Suppl* **216**, 5-42, 1985.
6. Friederich, JA, Brand, RA. *J Biomech* **23**, 91-95, 1990.

Table 1. Top two ranked individual muscle contributors to knee joint stability. Overall rank given in brackets.

Z-axis (Flexion-Extension)				X-axis (Valgus-Varus)			
Neutral		Squat		Neutral		Squat	
Extensors	Flexors	Extensors	Flexors	Lateral	Medial	Lateral	Medial
Rect fem. (1)	Med Gas (5)	Vas Lat (3)	SM (1)	Lat Gas (2)	Med Gas (1)	Lat Gas (2)	Med Gas (1)
Vas Lat. (2)	SM (6)	Vas Med/Int (4)	BFL (2)	Vas Lat (3)	SM (9)	TFL (3)	none

DISCOORDINATION IN STROKE MEASURED DYNAMICALLY USING THE ACT-3D ROBOT

[1,2] Theresa M Sukal, [2] Michael Ellis and [1,2,3] Julius PA Dewald
Northwestern University Depts of [1]Biomedical Engineering, [2]Physical Therapy and Human Movement Science, and [3] Physical Medicine and Rehabilitation; email: t-sukal@northwestern.edu.

INTRODUCTION

Abnormal synergy patterns, or pathological coupling of joint torques, have been shown to constrain functional reaching in patients beyond that which can be explained by simple muscle weakness [1]. These synergies have also been explored dynamically using an air bearing device. It was found that when a subject's limb was fully supported, they were able to reach targets that were well outside of their active range of motion, which was measured when they were required to lift their arm against gravity [2]. But this leaves to question how stroke subjects are able to do so well under the supported condition. The hypothesis for the current work is that they were simply working into the extension synergy and coupling elbow extension with a great deal of shoulder adduction (i.e. pushing into the table) in order to reach the target. For the first time, we measure the amount of adduction used to reach targets within the workspace under dynamic conditions.

METHODS

In the current study, we use a modified HapticMASTER robot (FCS Control Systems, The Netherlands) which has been integrated with a Biodex experimental chair (Biodex Medical Systems, Shirley, NY) to form the first generation Arm Coordination Training 3-D (ACT ^{3D}) device. The advantage of this system is that it incorporates the ability to measure 6 degrees of force and torque measurements while allowing the subject to move in 3-D workspace, features unavailable in the previous protocols. Here, the ACT ^{3D} is used to explore how shoulder adduction is coupled with reaching and retrieval motions when the arm is fully supported on a haptic table. A series of 5 targets were presented to each subject such that both single joint and multi joint movements in elbow and shoulder flexion and extension were tested, as described previously [3]. Online feedback was given via a 3 dimensional arm on a computer screen, and the subject was instructed to move as quickly as possible to the target without regard to specific endpoint accuracy. By examining only the first 100 ms after movement onset, we focused on the open loop control portion of the movement. Force and torque information in 3 dimensions (JR3 load cell, Woodland, CA) as well as angles recorded by the instrumented gimbal on the ACT ^{3D} were recorded during trials and saved for later analysis.

RESULTS AND DISCUSSION

For each trial, HM position arm angles were used to calculate the torques at the shoulder and elbow using inverse dynamics and a Jacobian matrix. Here, we compare a severely impaired stroke subject (Fugl-Meyer upper extremity score 30 out of 66; Chedoke-McMaster arm score 3 out of 7) and a healthy control subject whose speeds of movement to the target were similar. For the elbow extension target (target placement required 30° of elbow extension in order to reach it), the stroke subject coupled the elbow extension movement with a significantly greater amount of shoulder adduction ($p = .002$), compared to the healthy control subject. These results are shown in Figure 1.

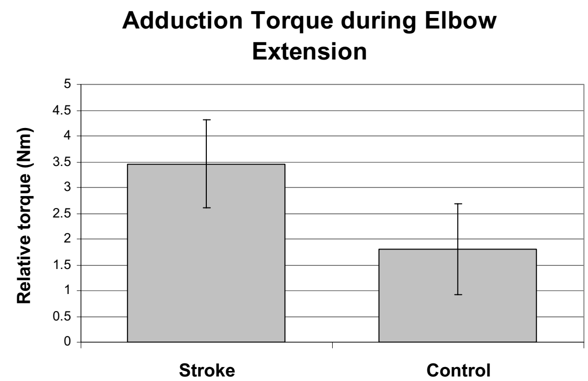

Figure 1: Relative adduction torque (that beyond limb weight) measured during elbow extension task.

CONCLUSIONS

Results indicate that subjects need to use much larger amounts of adduction torque in order to produce the same amount of elbow extension torque when compared to healthy subjects. This information supports the hypothesis that they are simply working within their extension synergies in order to accomplish the elbow extension task when supported by the haptic table. With the current setup, we can also vary the amount of limb support that is given to the subject during arm movements, so a greater resolution can be achieved between supported and unsupported conditions. This will allow us to gain a better understanding of the dynamic expression of synergies and their effect on the reduction of workspace as a function of limb support, and is the subject of ongoing investigation in the lab.

REFERENCES

1. Dewald JPA, Beer RF. *Muscle & Nerve* **24**: 273-283, 2001.
2. Beer RF, et al. *Exp Brain Res* **131**(3): 305-19, 2000.
3. Beer RF, et al. *Exp Brain Res*. **156**: 458–470, 2004.

ACKNOWLEDGEMENTS

This work was funded by NIDRR Grant H133G030143 and an individual NSF Graduate Research Fellowship to TM Sukal.

MOTOR CONTROL STRATEGY TO MANAGE CENTRAL FATIGUE

[1]Jing Z. Liu, [2]Vinod Sahgal and [1,2]Guang H. Yue
Departments of [1]Biomedical Engineering and [2]Physical Medicine & Rehabilitation,
The Cleveland Clinic Foundation, Cleveland, Ohio 44195

INTRODUCTION

Muscle fatigue is a common phenomenon that causes loss of force generation ability. Mechanisms underlying peripheral fatigue are well understood [1]. However, how the brain manipulates the fatiguing muscle is little tackled due to technical limitations and the difficult nature of the issue itself. More specifically, whether the brain suffers a central fatigue or it has other "smart" strategies to manage the situation is mostly unclear. Here we present our recent studies on this important issue of motor control using advanced functional neuroimaging methods.

METHODS

Fatigue Tasks: Intermittent handgrips of the right (dominant) hand were performed by a group of normal subjects at maximal voluntary contraction (MVC) level.

Force and EMG Recording and Analysis: Handgrip force and electromyogram (EMG) from involved muscles were recorded using a custom-built data recording system compatible with fMRI and EEG lab environments [2].

fMRI Data Recording and Analysis: Functional magnetic resonance imaging (fMRI) data were collected using EPI sequence on a 1.5 T Siemens scanner during rest and task-performance periods. Data of the two periods were statistically compared using *t*-test combined with other noise reduction procedures to determine which voxels of the brain were activated [3]. The number of activated voxels was calculated in each motor-related cortical region of interest (ROI) including both the primary sensorimotor cortices (SMI) and the higher order ones.

EEG Data Recording and Analysis: EEG data were recorded using a NeuroScan 64-channel system. Movement-related cortical potentials (MRCPs) were measured at motor-related locations. Sources that generated the signals were determined in the frame of current dipole model and effects of fatigue on their strengths and locations were analyzed.

RESULTS

1. Force and EMG decreased substantially to about 40% of initial MVC levels.
2. fMRI and MRCP-represented cortical activation levels stayed relatively unchanged while showing slight decreases (Figs. 1,2).
3. The strength of the current dipole source was little changed by fatigue, however, the source location showed substantial rotation in comparison to the result of the non-fatigue control condition (Fig. 3).

Figure 2: cortical activation level along fatigue (time). (a) fMRI results; (b) EEG (MRCP) results.

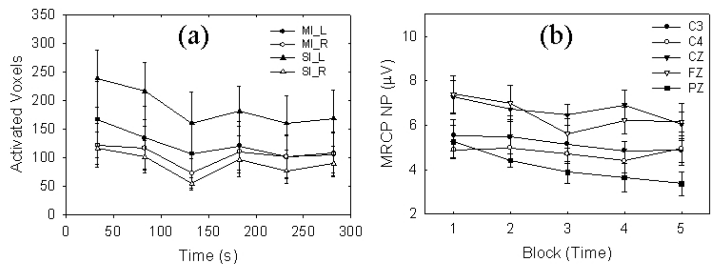

Figure 3: Distribution of source location. (a) fatigue condition; (b) non-fatigue control condition.

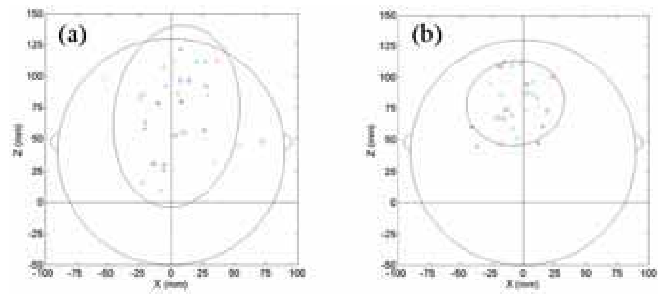

CONCLUSIONS AND DISCUSSION

The results suggest that there is a ceiling level for the cortical activation. The slight decreases indicate that central fatigue had factored in; however, the brain had successfully managed to maintain the task by recruiting additional cortical parts as indicated by the rotation of source location. These data support the concept that the neurons are activated in an alternate way so that the brain's power of motor control can be optimized/maximized, especially during severe situations such as fatigue.

REFERENCES

1. Enoka RM, Stuart DG. *J Appl Physiol* **72**, 1631-48, 1992.
2. Liu JZ, et al. *J Neurosci Methods* **101**, 49-57, 2000.
3. Liu JZ, et al. *Brain Res*, in press.

ACKNOWLEDGEMENTS

Supported by NIH and DoD grants (NS 37400-01, HD 36725, DAMD17-01-1-0665-02).

Figure 1: fMRI-determined cortical activation along the progress of fatigue (time), represented by the color points.

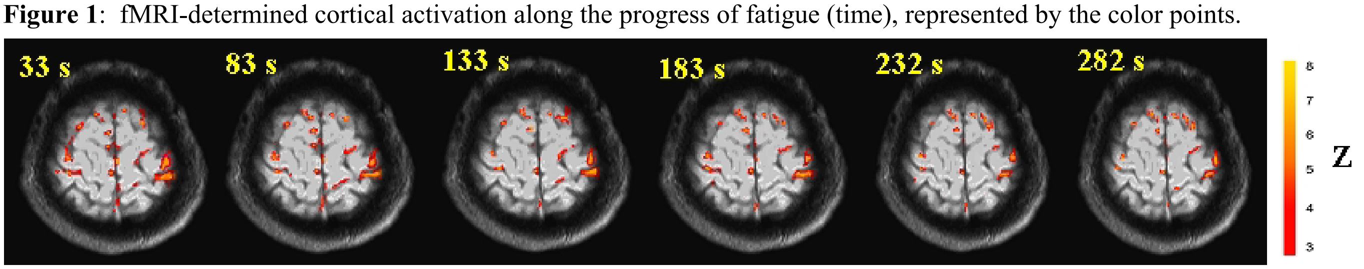

HOW DOES BONE TISSUE MICROSTRUCTURE RELATE TO *IN VIVO* BONE STRAINS IN THE GOAT RADIUS THROUGH ONTOGENY?

Russell P. Main and Andrew A. Biewener
Concord Field Station, Harvard University; email: rmain@oeb.harvard.edu

INTRODUCTION

Past hypotheses concerning a link between form and function in vertebrate limb bones have generally sought to explain how the architecture of both trabecular and cortical bone reflect habitual loading within the limb skeleton. The goal of this study is to examine how ontogenetic changes in limb bone geometry and certain microstructural features within the cortex of the limb bone diaphysis in the goat radius relate to ontogenetic changes in the measured strain environment in the radius.

METHODS

In vivo bone strain data were collected from the cranial, caudal, and medial midshaft surfaces of the goat radius in animals of three age/size groups: 'small' (<6 kg), 'intermediate' (6-11 kg), and 'adult' (>15 kg) [1]. In the weeks prior to strain data collection, fluorescent bone labels were given to the animals to be incorporated in to the growing/ remodeling bone. After the strain data were collected, cross-sectional histological thin-sections were prepared from each radius at the site of strain gauge attachment. Using a microscope equipped with a digital camera, digital images were taken of the thin-sections from each goat using plain, fluorescent, and circularly polarized light microscopy to quantify bone porosity, secondary osteon density, periosteal growth rates, and the orientation of the collagen fibers, which were classified as either being aligned primarily longitudinally (L), transversely (T), or intermediate between the two (I).

The mean and maximal normal cross-sectional strain distributions were mapped on to each bone's cross-section. Using the strain distribution and the anatomical bone axes, each cross-section was divided into eight sub-divisions (Figure 1) and the above histological variables measured in each, using custom MATLAB software.

RESULTS AND DISCUSSION

Measurements from the single 'small' goat examined thus far provide interesting preliminary results. The greatest porosity generally occurs in cranial sub-divisions 1, 2, and 3 (Table 1), which are loaded in tension during maximal strain in the radius midshaft (Figure 1). A lower percentage of longitudinally oriented collagen fibers were observed in caudal sub-divisions 6 and 7, where maximal compression occurs (Table 1). However, there was also a caudal sub-division loaded in compression (6) with a high pore density and a cranial sub-division loaded in tension (3) with a similar collagen fiber profile as sub-division 6. At least in the midshaft of this goat's radius, there are no distinguishing microstructural differences between regions of the bone loaded in tension or compression. Because measurements were made from a young goat, no secondary osteons were observed. However, preliminary observations from older, larger goats show a greater frequency of remodeling in the radius with a greater number of secondary osteons in the caudal regions of the radius. High periosteal growth rates laterally and low growth rates cranially (Table 1) do not correspond to differences in the underlying strain environments in these regions, but are consistent with the growing radius maintaining a higher second moment of area in the medio-lateral, than in the cranio-caudal direction, which has been argued to increase load and bending predictability in the goat radius [1].

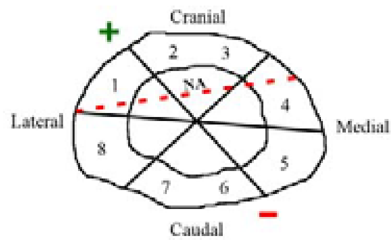

Figure 1: Goat radius divided into eight sub-sections for histological analysis. The dashed line labeled 'NA' represents the position of the neutral axis of bending when longitudinal strains are maximal; loading the cranial and caudal surfaces in tension and compression, respectively.

Further inclusion of more samples from goats over a wider range of ages/sizes would allow for stronger conclusions and possible identification of a link between bone architecture and the mechanical environments in which bone growth and remodeling occur.

REFERENCES

1. Main RP and AA Biewener. *J Exp Biol* **207**, 2577-2588, 2004.

Table 1: Measurements of periosteal growth rate, porosity, and collagen fiber orientation in the different goat radius sub-divisions.

	Numbered Sub-division of the Goat Radius Cross-section							
	1	2	3	4	5	6	7	8
Periosteal growth rate (μm/day)	8.7 ± 0.8	2.7 ± 0.7	4.0 ± 0.4	4.1 ± 0.3	5.6 ± 0.5	5.1 ± 0.5	6.7 ± 0.4	18.0 ± 0.2
Porosity (pores/mm^2)	13 ± 0	13 ± 1	11 ± 4	8 ± 0	9 ± 2	12 ± 5	9 ± 5	6 ± 0
Collagen fiber orientation (% L, % I, % T)	97 ± 2 3 ± 2 0 ± 0	97 ± 1 3 ± 1 0 ± 0	79 ± 3 17 ± 1 4 ± 3	97 ± 2 2 ± 1 1 ± 1	97 ± 1 3 ± 1 0 ± 0	83 ± 3 16 ± 2 1 ± 2	55 ± 5 26 ± 6 20 ± 1	93 ± 2 5 ± 2 1 ± 1

HIP STABILITY: MECHANICAL CONTRIBUTIONS OF INDIVIDUAL MUSCLES

Jim Potvin, Aaron Derouin
Dept of Kinesiology, University of Windsor, Windsor, Ont, Canada, email: jpotvin@uwindsor.ca

INTRODUCTION

The hip is a joint that is subjected to high forces during both dynamic and static activities. In the physiological range, translational hip stability is provided by: 1) muscle, 2) the acetabular cup, 3) ligaments. However, in this range, muscles are almost exclusively responsible for rotational stability. Little is known about the potential contributions of individual muscles to the rotational stability of the hip. Recently, a method has been developed to allow for such a calculation with knowledge of the muscle line of action and force generating potential [3]. The purpose of this study was to determine the individual hip muscle contributions to rotational stability about the flexion/extension and abduction/adduction axes in a neutral and flexed posture.

METHODS

The biomechanical model of Delp et al [2] was used to characterize the joint rotational and translational characteristics and the muscle lines of action of 19 muscles crossing the hip (with a total of 27 separate fascicles). Stability analyses were performed about the: 1) flexion/extension and 2) abduction/adduction axes in the: 1) neutral standing posture and 2) with the knee and hip both flexed to 90 degrees.

The model of Potvin and Brown [3] was used to calculate individual muscle contributions to joint stability for each of the four axis/posture combinations. The minimum potential energy (V) approach was used to calculate stability. This method assumes that a system is stable if its total V is at a minimum. In other words, the second derivative of the system V must be positive definite [1]. For a particular muscle, V was calculated as the elastic energy stored in the muscle plus the work done by the muscle for small rotations:

$$U(m) = F\,\Delta\ell + \frac{1}{2}k\,\Delta\ell^2 \qquad (1)$$

where: U(m) = potential energy stored in the muscle, F = muscle force (N), k = muscle stiffness (N/m), r = muscle moment arm (m), ℓ = muscle length (m) defined from the origin (A) to insertion (B). A and B can also be used to define nodes on either side of a joint and are expressed relative to the hip coordinates. The change in length was a function of the rotation (θ). For the hip joint, the anatomical axes were: abduction/adduction (x), internal/external rotation (y) and flexion/extension (z).

The stability contribution of a muscle about the z axis (Sz), is calculated as the second derivative of U(m) with respect to an small rotation angle ($d\theta$) using a Taylor Series expansion, differentiating twice with respect to θ, and simplifying. A further substitution of $k=qF/\ell$ [1] was made yielding equation (2). For muscles without nodes, L = ℓ. Otherwise ℓ is the distance between nodes and L is the total muscle length. All analyses were run with maximal muscle forces, after correcting for the active and passive force length effects.

$$S(m)_z = F\left[\frac{\mathrm{A_X B_X} + \mathrm{A_Y B_Y} - r_z^{\,2}}{\ell} + \frac{q r_z^{\,2}}{L}\right] \qquad (2)$$

RESULTS AND DISCUSSION

Flexion/Extension axis: In the neutral posture, the semimembranosus (SM) was found to be the dominant hip stabilizer about the flexion/extension axis, with values 68% and 132% higher than the next highest muscles; biceps femoris long head and rectus femoris (RF), respectively. These muscles have the highest force potential in this posture and each are oriented in such a way as to optimize their geometric potential to contribute to joint stiffness (termed "geometric stability" or S_G and related to having large moment arms and/or short lengths). The stability values were found to be much lower when the knee and hip were both flexed to 90º, with the largest contributors being: RF and SM (due to high force potential) and adductor magnus 3 (due to its moderate force and high S_G). It should be noted that the SM was observed to have values in the flexed posture that were only 33% of that in the neutral posture. In addition, all three hip adductor muscles were found to have greatly enhanced flexion/extension stabilizing potential in the flexed, compared to the neutral, posture. While somewhat unrealistic (because the resulting net moment is not zero), the total maximum stability potential was approximated by setting each muscle force to 100% of maximum and summating across muscles. For the flexion/extension axis, the total stability in the neutral posture was 2.6 times higher than that in the flexed posture.

Abd/Adduction axis: In the neutral posture, the dominant stabilizers were gluteus medius 1 (due to high force and S_G) adductor magnus 1 (due to very high S_G) and adductor longus (due to moderate force and high S_G). However, in the flexed posture, the gluteus medius 1 and adductor magnus 1 dropped to 8% and 22% of their neutral values and the adductor longus increased somewhat to be the dominant stabilizer (due to a very high S_G), followed by the adductor magnus 3 and the psoas. Overall, the neutral posture was found to have a maximum abd/adduction stabilizing potential 4.4 times higher than the flexed posture.

CONCLUSIONS

This study demonstrates the utility of a simple stability equation for accurately dissecting the individual muscle contributions to hip stability. It is anticipated that this work will lead to a better understanding of the factors that lead to hip instability and injury.

REFERENCES

1. Bergmark A. *Acta Orthop Scand* **230**(suppl):1-54, 1989.
2. Delp et al. *IEEE Trans Biom. Eng.* **37**, 1990
3. Potvin JR, Brown SHM. J Biomech (in press), 2005.

CONTROL OF REACH-TO-GRASP REACTIONS DURING PERTURBED LOCOMOTION IN FAMILIAR AND UNFAMILIAR ENVIRONMENTS: WHEN DOES VISUAL FIXATION OF THE HANDRAIL OCCUR?

[1,2]Charles Cejka, [1]Tracy A. Lee, [1,3]William E. McIlroy and [1,2]Brian E. Maki
[1]Centre for Studies in Aging, Sunnybrook and Women's College Health Sciences Centre, Toronto, Ontario, Canada
[2]Institute of Medical Science, University of Toronto, Ontario, Canada; email: charles.cejka@utoronto.ca
[3]Department of Rehabilitation Science, University of Toronto, Ontario, Canada

INTRODUCTION

In many situations, successful execution of a balance-recovery reaction requires visual information about the environment. In particular, reactions that involve rapid limb movement, such as stepping or reaching, must be controlled to accommodate environmental constraints, i.e. objects or architectural features that can obstruct stepping or serve as handholds to grasp for support [1]. The location of these constraints, in relation to the body, continually changes as we move about in our daily lives.

In this study, we examined the mechanisms by which the central nervous system acquires the critical visuospatial information needed to execute rapid reach-to-grasp reactions in response to sudden, unexpected loss of balance. We hypothesized that: 1) the initial arm motion toward a handrail would rely on spatial information acquired via the visual scanning that automatically occurs when ambulating in an unfamiliar environment; and 2) the later phases of the arm movement and the prehension of the handrail would be guided by visual fixation of the rail occurring after initiation of the arm reaction.

METHODS

Testing involved a moveable 6.4m walkway, which was surrounded by curtains; a door at the entrance prevented any viewing of the walkway prior to the start of each trial. Eight healthy young adults (ages 24-35) were randomly assigned to either a *handrail* group (handrail located by a stair mounted near the end of the walkway; see Figure 1) or a *control* group (no objects on the walkway). In the first trial, subjects opened the door to view the walkway for the very first time, and then walked to the opposite end at a self-selected cadence. The walkway was controlled to unexpectedly translate forward during right single-support phase when the subject was in the vicinity of the handrail and stair (*handrail* group) or in a similar location (*control* group). A deception was used to ensure that the first perturbation was truly unexpected. In the remaining 59 trials, subjects knew that the walkway might move; however, walkway translations (forward or backward) occurred in only 30% of trials. During each trial, we monitored gaze behavior and arm motion.

RESULTS AND DISCUSSION

In the very first trial, *control* subjects tended to fixate on the travel path, with few eye movements directed toward the periphery. In contrast, *handrail* subjects fixated on the rail immediately after opening the door (mean dwell time: 483ms). During the subsequent ambulation, gaze was primarily directed at the travel path but typically did return to the handrail one or more times. When the perturbation occurred, all four *handrail* subjects initiated rapid lateral arm movement toward the rail. In all cases, gaze was not directed at the rail at perturbation onset, but was redirected toward the rail after the initiation of the reaching movement. It is clear that the initial arm motion was not simply a stereotyped response, since the predominant direction of the motion in the *control* group was distinctly different (forward rather than lateral).

With repeated trials, reaching movements occurred less frequently (11% of perturbation trials) and the gaze behavior more closely resembled that of the *control* group (i.e. gaze directed primarily along the travel path). In 3 of the 8 trials where reaching occurred, there was no visual fixation of the rail at any point prior to perturbation onset.

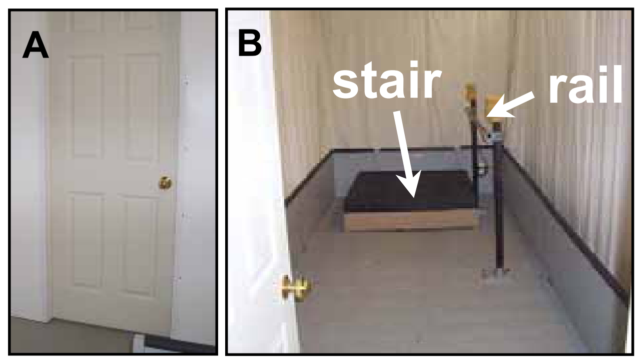

Figure 1: View of moveable walkway (*handrail* subjects) from the entrance, with door closed (A) and open (B).

CONCLUSIONS

These findings suggest that a pre-formed visuospatial map of the surroundings is used to initiate rapid reach-to-grasp reactions. This map is formed automatically (even when there is no expectation that a perturbation may occur) via visual scanning when ambulating in an unfamiliar environment. The capacity to utilize spatial information 'remembered' from previous trials may reduce the need for visual scanning, i.e. when the environment is familiar. Online visual feedback may be used later in the trajectory to guide the arm to its endpoint and/or assist in prehension of the rail. Use of a pre-formed map presumably serves to facilitate more effective balance recovery by allowing an appropriately-directed arm movement to be initiated as rapidly as possible, thereby avoiding delays that would occur if instead the visual scanning of the environment had to be performed after perturbation onset [1].

ACKNOWLEDGMENTS

Supported by the Canadian Institutes of Health Research.

REFERENCE

1. Ghafouri M, et al. *Exp Brain Res* **155**, 532-536, 2004.

WORK TIME AND REST PERCENTAGE DURING PICK-AND-PLACE TASK

Reuben Escorpizo and Anne Moore
School of Kinesiology and Health Science, York University, Toronto, ON
E-mail: reuben@yorku.ca, Web: www.yorku.ca/kahs

INTRODUCTION

In the context of machine-paced tasks, it is of interest to know how production rate affects the physical demands imposed on the worker. The time available to perform a cycle (CT) is a critical factor in determining both the resulting speed the work is performed at, and the rest time available to the worker. Pick and place tasks are a common machine paced task. They have been studied from the perspective of loads[1, 2], but the relationship between time based measures is unclear. The objective of this study was to measure the effects of shortening cycle time on work time (WT) and the overall available rest (%rest) during a cyclical pick-and-place task.

METHODS

Six right-handed participants (3m, 3f) with a mean age of 28 yrs (SD=6.9), and mean height of 176.3 cm (SD=14.2) were recruited. The participants performed a cyclical task transferring a 0.7 kg object 0.5 m from one bin to another based on an auditory metronome. Measurements of muscle activation (EMG), hand grip force, wrist posture and error rate were made. WT was defined as the time the hand was in contact with the object (force>0), and task rest was defined as (CT-WT)/CT * 100. Surface RMS EMG was collected from flexor digitorum superficialis (FDS) and extensor carpi radialis (ECR) using a commercial system (ME3000P8, MEGA, Finland). It was analyzed using a gaps analysis[3] which provides a measure of the actual rest taken by the muscles. A (4 x 2) repeated measures design was used, with two independent variables: CT (1, 2, 5, and 10s) and grip type (power, chuck).

RESULTS AND DISCUSSION

WT significantly decreases as a function of CT and grip type (Figure 1) as does %Rest (Figure 2). The chuck grip task had a significantly longer WT and associated shorter rest time at all CTs. These indicate that as the cycle time is reduced, the task is sped up; however, more time is taken out of the rest portion of a task. The relationships between the cycle time and both work time and %Rest are non-linear. Although at a one second CT, the nominal rest in the activity was at least 10% of the time, the electromyographic data found that by 2-second CT the muscle activity already occupied 100% of the time (Figure 2). To achieve even 10% muscle recovery, a CT of >3s is required. This data coupled with the EMG will allow us to model optimal CT.

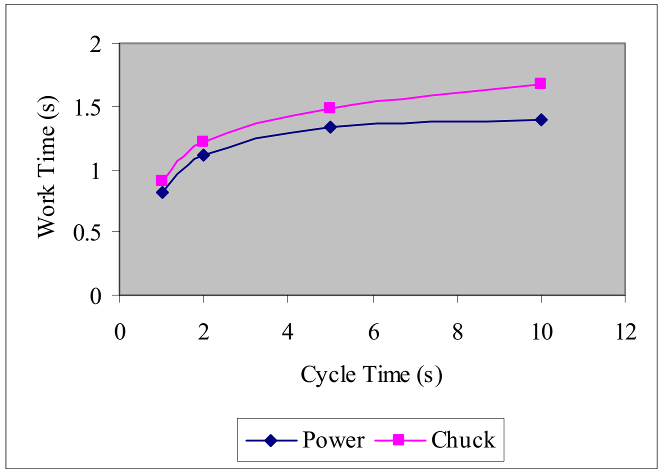

Figure 1: WT decreases as CT decreases ($CT\ p<0.01$, grip $p<0.001$)

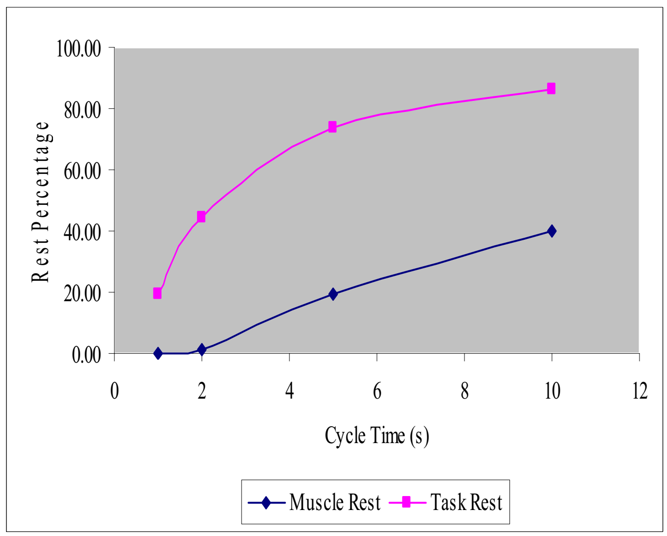

Figure 2: Calculated rest percentage based on grip force (task) and gaps (ECR muscle) during power grip

REFERENCES

1. Krawczyk S, et al. *Proceedings of the International Scientific Conference on Prevention of Work-related Musculoskeletal Disorders*, Stockholm, Sweden, 1992.
2. Chadwick EKJ, Nicol AC. *J Biomech* **33**, 591-600, 2000.
3. Veiersted et al. *Int Arch Occup Environ Health* **62**, 31-41, 1990.

ACKNOWLEDGEMENTS

This work was supported by NSERC (Canada) 238240-01.

TOE OUT GAIT AND REDUCTION OF KNEE OSTEOARTHRITIS PAIN

[1] Thomas R. Jenkyn, [1]Michael A. Hunt, [1]Trevor B. Birmingham
[1]Wolf Orthopaedic Biomechanics Laboratory, University of Western Ontario, London, Ontario, Canada
Email: tjenkyn@eng.uwo.ca

INTRODUCTION

Osteoarthritis (OA) commonly affects the knee joint. The medial compartment is affected 2.5 times more than the lateral [1,2]. During stance phase, an adduction moment acts on the knee that is thought to increase compression in the medial compartment. Individuals with knee OA often walk with a toe-out gait, which seems to reduce pain during weight-bearing. In toe-out gait, the leg is externally rotated with the toe angled laterally to line of progression.

The common explanation for this pain reduction reasons that toeing out moves centre of pressure laterally, orienting the ground reaction force (GRF) so that it passes through the knee joint. This would reduce the moment arm of GRF in the frontal plane, reducing knee adduction moment and medial compartment compression. However, this mechanism would not produce a reduction of adduction moment in early stance when the centre of pressure is under the heel.

This study suggests another mechanism Toeing-out rotates the anatomy of the knee and transforms a portion of the adduction moment into a knee flexion moment, thus reducing the compression on the medial compartment.

METHODS

Prior to corrective surgery (high tibial osteotomy), gait analysis was performed on 125 patients (98 males; mean age=46.8 yrs) with knee joint OA primarily affecting the medial compartment. Patients walked at a self-selected speed while three-dimensional kinetic and kinematic data were collected bilaterally. The inverse dynamic method calculated resultant knee moments in both laboratory-fixed and the tibia-fixed frames of reference. Patient progression coincided with the lab x-axis. The perpendicular distance from GRF line of action to knee joint centre (moment arm) was also calculated in each frame.

RESULTS

The moment arms and moments experienced in the lab-fixed and tibia-fixed frames of references are shown in Figure 1. With no toe-out angle, these frames would be coincident. Figure 1 shows that by toeing out an average of 10.6° on the affected limb, the flexion-extension moment arm and moment are increased in the tibia-fixed frame and the adduction-abduction moment arm and moments are reduced.

Table 1 shows a comparison of the peaks values of adduction and flexion moment arms and moments for the affected and unaffected limbs.

CONCLUSIONS

Toeing-out has been shown to rotate the anatomy of the knee such that a portion of the knee adduction moment is transformed into a flexion moment. Flexion moments are carried by the musculature of the knee, thereby reducing the compressive loading in the medial compartment. Such a reduction of medial compartment loading could be responsible for the reported pain relief experienced by patients with OA of the knee during walking gait.

REFERENCES

1. Schipplein OD, Andriacchi TP. *J Orthop Res* **9**, 113-9, 1991.
2. Cooke D, et al. *Osteoarthritis Cartilage* **5**, 39-47, 1997.

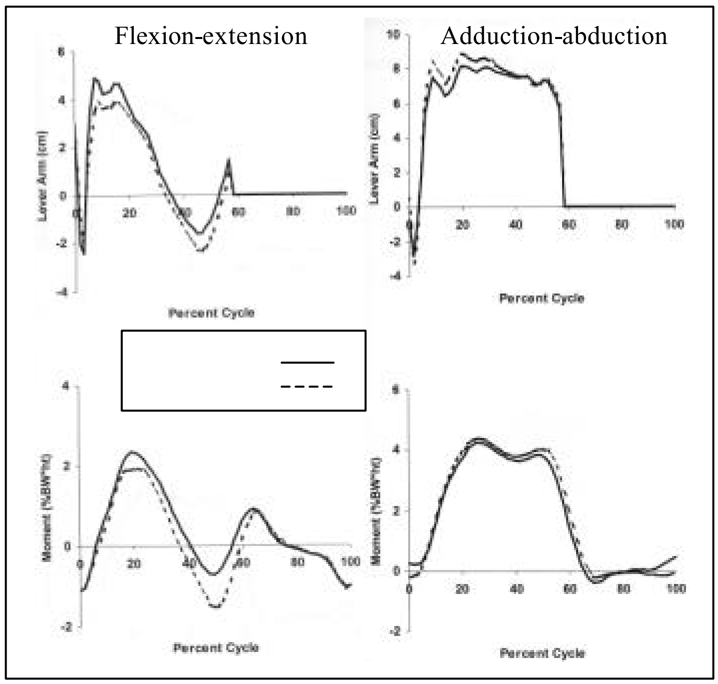

Figure 1: Flexion (left) and adduction (right) moment arms (top) and moments (bottom) in the lab-fixed (dashed line) and tibia-fixed (solid line) reference frames.

Table 1: Mean (SD) peak adduction moment (AM), peak extension moment (EM), peak flexion moment (FM), peak frontal moment arm (FPL), peak sagittal extension moment arm (SPEL), peak sagittal flexion moment (SPFL) and toe-out angle (TOE). Note that the flexion and extension moments and moment arms are increased in the tibial frame for the affected knee, while the adduction moment and moment arm are reduced.

	Laboratory Frame of Reference							Tibia Frame of Reference						
	A.M	E.M	F.M	FPL	SPEL	SPFL	Toe	A.M	E.M	F.M	FPL	SPEL	SPFL	Toe
Affected	3.07	2.18	1.72	6.17	4.55	2.01	10.6	2.94	2.24	1.96	5.80	4.68	3.58	n/a
	(1.0)	(1.3)	(0.7)	(2.1)	(3.4)	(1.8)	(6.5)	(0.9)	(1.3)	(1.0)	(2.0)	(3.5)	(1.9)	
Unaffected	2.72	2.55	1.91	5.43	4.65	1.64	12.6	2.59	2.56	2.15	5.11	4.70	2.97	n/a
	(0.9)	(1.4)	(0.8)	(1.6)	(3.4)	(1.9)	(8.3)	(0.9)	(1.4)	(0.9)	(1.5)	(3.5)	(1.9)	

PREDICTION OF FOREARM MUSCLE ACTIVITY DURING GRIPPING

Peter J. Keir, PhD and Jeremy P.M. Mogk, MSc
School of Kinesiology & Health Science, York University, Toronto, Ontario, Canada
email: pjkeir@yorku.ca

INTRODUCTION

There is a strong association between upper extremity musculoskeletal disorders and jobs involving forceful grip exertions and deviated wrist postures [1]. The inherent difficulty in measuring hand and finger forces in the workplace, without interfering with a worker's normal movement patterns, has led to the use of EMG-based mathematical relationships to predict grip force [2-4]. Prediction of grip force is valuable, however, EMG collection in the workplace is an expensive and tenuous task. In addition, predicting grip force itself does not necessarily provide information on which muscles may be at risk of injury or fatigue. Accurate prediction of muscle activity without an elaborate biomechanical model would improve our understanding of muscular loading in the workplace. The purpose of this study was to predict muscle activity of six forearm muscles from grip force and posture using an existing dataset [5].

METHODS

The dataset [5] was comprised of surface EMG of 6 forearm muscles (FCR, FCU, FDS, ECR, ECU and EDC) collected during 10s static grip force contractions on each of two days. All combinations of 3 forearm postures (pronation, neutral and supination) and 3 wrist postures (45° extension, neutral, 45° flexion) were used. Grip force and EMG were collected at 4 relative effort levels (5, 50, 70 and 100% $Grip_{max}$) and an absolute force of 50 N. EMG and grip force were normalized to maximum. AEMG was calculated from the 3 Hz linear envelope EMG over a 3 s plateau at the target force and during baseline prior to each exertion.

Forward stepwise regression analyses were performed to develop equations to predict AEMG for each of the 6 forearm muscles from grip force and posture using Day 1 data, using STATISTICA (version 6.0, StatSoft Inc., Tulsa, OK). Analyses included linear, factorial and polynomial regressions. All models included the AEMG and measured grip force data from each of the five exertion levels, in each combination of wrist and forearm posture. The predictive ability of each model was judged based on the adjusted r^2 and $RMSE_{model}$ (in % MVE). The validation process used Day 2 data as input into the equations developed from Day 1 data, and were evaluated using r^2 and $RMSE_{valid}$.

RESULTS AND DISCUSSION

Second order regression models improved the prediction of extensor muscle activity over linear regression with r^2 and $RMSE_{model}$ improving by as much as 4% and 0.7%, respectively. The generic form of each equation is:

$$AEMG_i = (a_1 \cdot G)+(b_1 \cdot G^2)+ (a_2 \cdot W)+ (b_2 \cdot W^2)+ (a_3 \cdot F)+ (b_3 \cdot F^2)+c$$

where, $AEMG_i$ is percent muscle activation (i=1-6), G is relative grip force, W is wrist posture (extension = 1, neutral = 2 and flexion = 3), F is forearm posture (pronation = 1, neutral = 2 and supination = 3), and c is a constant. Coefficients were included in each model if they were significant at $p < 0.05$; most were significant at $p < 0.001$.

Posture explained less than 2% of the variance. However, when combined with grip force, inclusion of both wrist and forearm posture reduced $RMSE_{model}$ to less than 9% MVE for all equations (Table 1). Using the measured wrist angle (in degrees) resulted in weaker models than using nominal wrist posture. Forearm posture had little effect on the prediction of average finger muscle and wrist flexor activations, but improved r^2 and $RMSE_{model}$ of the wrist extensors by as much as 4.7% and 0.9% MVE, respectively.

Day 2 AEMG was predicted very well using the equations developed from Day 1 data and was often lower than the development data ($RMSE_{valid}$ vs $RMSE_{model}$, Table 1). Each target force level was also evaluated in isolation to determine the ability of each equation to predict muscle activation across the full range of grip forces. The error in predicting muscle activation was greater with increasing grip force. The RMSE for forces = 50% $Grip_{max}$ was 0.9-2.3% lower than the overall $RMSE_{valid}$ which ranged from 6.6-9.8%. The RMSE values of predicted muscle activity for grip forces above 50% were 3.7-7.3% MVE higher than $RMSE_{valid}$. Preliminary tests using verbal estimates of grip force indicate that the equations are robust, as the predictive capacity was the same as with measured grip force.

These equations provide a simple and accurate tool to predict forearm muscle loading in the workplace, and may be used to complement existing workplace screening tools.

REFERENCES

1. Silverstein, B. et al. (1986) *Br.J.Indust.Med.* **43**, 779-784.
2.Armstrong, T.J. et al. (1979). *J Biomech*, **12**, 131-133.
3. Claudon, L. (1998). *Int J Occup Safety Ergon*, **4**, 169-184.
4. Duque, J. et al. (1995). *Appl Ergon*, **26**, 61-66.
5. Mogk, J.P., Keir, P.J. (2003) *Ergonomics* **46**, 956-75.

ACKNOWLEDGEMENTS

This work was funded by NSERC (Canada), grant #217382.

Table 1. Coefficients and error estimates for the quadratic equations to predict muscle activity in six forearm muscles.

Muscle	Equation coefficients							Goodness of fit and error			
	a_1	a_2	b_1	b_2	a_3	b_3	c	r^2	$RMSE_{model}$	r^2 (valid)	$RMSE_{valid}$
FCR	0.514	*	*	0.640	2.112	*	-5.143	0.823	7.1	0.842	6.6
FCU	0.550	*	*	0.501	-1.589	*	1.616	0.797	8.2	0.827	7.2
FDS	0.550	*	*	0.823	1.361	*	-5.071	0.826	7.5	0.823	7.3
ECR	0.811	-0.004	-6.68	2.420	*	-0.738	9.726	0.798	8.2	0.800	7.4
ECU	0.736	-0.002	*	0.654	-13.049	2.031	17.551	0.791	8.6	0.730	9.4
EDC	0.826	-0.004	*	1.358	*	0.264	-0.269	0.773	8.9	0.707	9.8

REGIONAL FOOT PRESSURE DURING RUNNING, CUTTING, JUMPING AND LANDING

Michael Orendurff[1], Eric Rohr[1], Ava Segal[1], Chris Kweon[2], Jon Medley[1], John Green III[2], Nancy Kadel[2]
[1]Motion Analysis Lab, Rehab R & D, VA Hospital, [2]Department of Orthopaedics and Sports Medicine, University of Washington, Seattle, WA, USA. email: michael.orendurff@med.va.gov web: www.seattlerehabresearch.org

INTRODUCTION

Foot pressure studies have generally focused on walking [1,2] and running [3,4] in a straight line to determine shoe-foot interactions at specific regions of the foot. However, it is likely that for several regions of the foot, straight line running and walking do not adequately quantify the complete range of plantar pressures. Ellis et al [5] has shown that during cutting movements peak pressures at the hallux increase by 40%, while the lateral forefoot undergoes a 54% decrease compared to running straight. The purpose of this study was to compare the peak pressures at seven regions of the foot during straight running, cutting, jump take-off and jump landing with two different shoe types.

METHODS

Subjects were ten healthy college athletes. All subjects signed an IRB-approved consent form. (Ht. 186.8 ± 5.3 cm; Wt. 102.3 ± 18.9 kg; Age. 20.5 ± 1.0 years). Each subject was asked to run at 75% maximum speed through a course of cones (figure 1), once wearing a wide turf shoe (Air Pro Turf Low; Nike, Beaverton, OR, USA) and once wearing a narrow cleat (Nike Speed TD) in random order. The surface was Fieldturf® (Montreal, Canada). Plantar pressures were measured using insoles (PEDAR Mobile; Novel GmbH, Munich, Germany). Only right insoles were sampled at 99 Hz. Each trial was filmed with a digital video camera (30 Hz); first and second trial times were within 5%. Each step from the foot pressure files processed from Emedlink (Novel) was matched to the corresponding step in the video to determine what maneuver was being performed. Two-way repeated measures ANOVAs were used to compare peak plantar pressure across seven regions (figure 2): great toe (T), medial forefoot (1), central forefoot (C), lateral forefoot (5), medial midfoot (MM), lateral midfoot (LM) and heel (H) during running straight, cutting right, cutting left, jump take-off and jump landing (2 shoe types by 5 maneuvers). Scheffe's tests were used for individual comparisons *post hoc*.

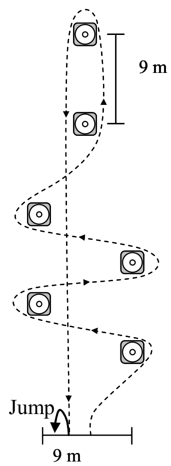

Figure 1: Running course

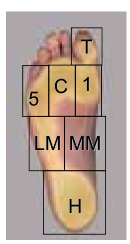

Figure 2: Mask regions

RESULTS AND DISCUSSION

The Speed TD had significantly higher peak pressures than the Pro Turf Low for all regions ($p < 0.0001$ to 0.03) except the LM ($p = 0.19$), meaning that the turf shoe had better overall cushioning. For the heel, straight running pressures were ⅓ that of cutting, jumping or landing activities ($p > 0.0001$). This suggests that hindfoot cushioning characteristics of sport shoes might be more robustly assessed by evaluating activities other than straight line running. For the great toe (T) similar high pressures were observed running straight, cutting left and jump landing, which were significantly lower than during cutting right and jump landing ($p < 0.03$). Comparing left and right cutting, the left cut produced higher pressures at the medial foot regions (T, 1 and MM; $p < 0.02$) whereas the right cut showed higher pressure at the lateral regions of the foot (5, LM) ($p < 0.0001$). The data suggest we run like we ski: by cutting our inside edges into the surface to carve the turn. All regions of the foot appears to have similar peak pressures for jump take-off and jump landing ($p > 0.12$), except T where jump take-off pressures were significantly higher than landing ($p < 0.0008$).

CONCLUSIONS

Assessing regional foot pressure over a range of movements may provide a more appropriate and sensitive evaluation of sport shoe performance.

REFERENCES

1. Segal, A, et al. *Foot Ankle Int.* 2004, 25:926-33.
2. Burnfield, JM, et al. *Clin Biomech.* 2004, 19:78-84.
3. Verdejo R & Mills NJ. *J Biomech.* 2004, 37:1379-86.
4. Nigg BM, et al. *Med Sci Sports Exerc.* 2003, 35:314-9.
5. Ellis, E, et al. *Am J. Sports Med.* 2004, 32:140-45

ACKNOWLEDGEMENTS

This work was funded by Dept. of Veterans Affairs Grant #A2661C.

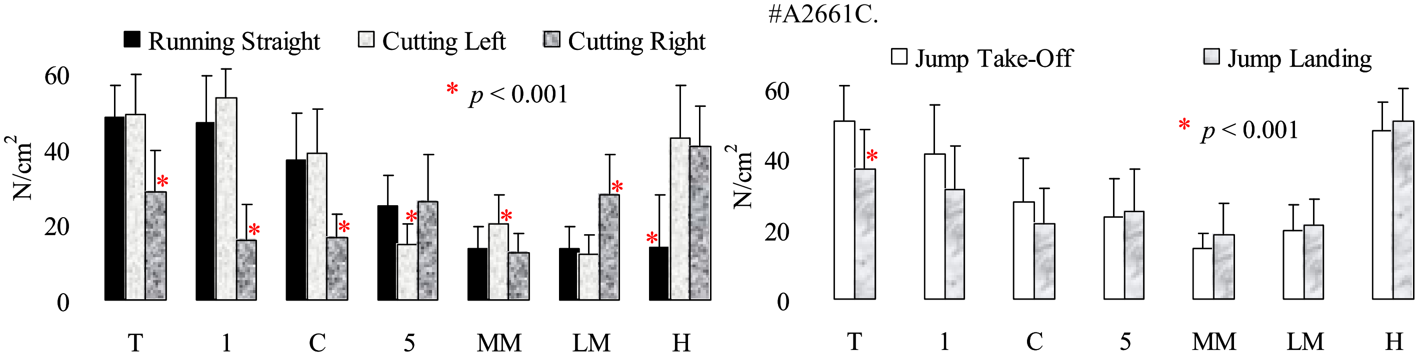

Figure 3: Peak plantar pressure over 7 regions of the right foot during running straight, cutting left, cutting right, jump take-off and jump landing. Significant differences between movements within each region are marked with *.

INVESTIGATION OF SIT-TO-STAND PERFORMANCE FOR INDIVIDUALS AFTER TOTAL KNEE ARTHROPLASTY

Catherine A. Stevermer, Shashank Raina, and Jason C. Gillette
Department of Health and Human Performance, Iowa State University, Ames, Iowa, USA; email: ktsteve@iastate.edu

INTRODUCTION

Moving from a seated position to standing is an essential transition for basic activities of daily living and is a prerequisite for ambulation. Many older adults find sit-to-stand to be challenging without additional support [1] due to lower extremity limitations associated with pathology and/or reduced dynamic stability. In contrast to healthy elderly, Cheng, et al. [2] indicated weight-bearing asymmetry and increased postural sway during sit-to-stand may increase the risk of falls in a neurologically impaired population. Before and after total knee arthroplasty, osteoarthritic adults may also have difficulty with this task due to limited range of motion and/or strength deficits [3]. Therefore, sit-to-stand technique may differentiate between standing independently, standing with assistance, or an inability to perform the task.

Janssen, et al. [4] indicated variations in lower extremity positioning, upper extremity assistance, seat height, and movement pattern may affect sit-to-stand performance. Previous research has focused on an assumption of bilaterally equivalent anthropometrics, joint timing and weight-bearing during sit-to-stand. These assumptions may be inappropriate for individuals with weakness and/or mobility limitations due to potential movement asymmetry. The goal of the present study is to determine therapeutic recommendations for foot placement during sit-to-stand in an orthopedic population.

METHODS

Two individuals with total knee arthroplasty (TKA 2 ± 0.5 yr post-surgery) participated in this experiment (2 males, age 72 ± 5 yr, mass 88 ± 12 kg). Two individuals (1 male/1 female, age 70 ± 3 yr, mass 84 ± 15 kg) without any musculoskeletal disorder participated as healthy control subjects. An eight-camera video system (Peak Performance, Englewood, CO) was used to track 10 reflective markers placed bilaterally on each subject. The subjects sat on a bench (height 45 cm) with their feet on separate force platforms (AMTI, Watertown, MA). Two triaxial force sensors (Kistler, Amherst, NY) measured hand forces applied to the bench. Individual knee range of motion and anthropometrics were measured.

The subjects placed their feet at a comfortable width. Initial foot placements included: feet placed bilaterally at 90° of knee flexion (Foot-neutral), the feet more posterior relative to the knees (Foot-back) at an angle of 100° degrees of knee flexion, and a self-selected position with the dominant foot posterior (Staggered). Lower extremity positions were combined with and without upper extremity assistance. Hand support forces were measured and joint torques were calculated for sit-to-stand movements in each condition. Each subject completed three repetitions of the six sit-to-stand conditions for a total of 18 trials.

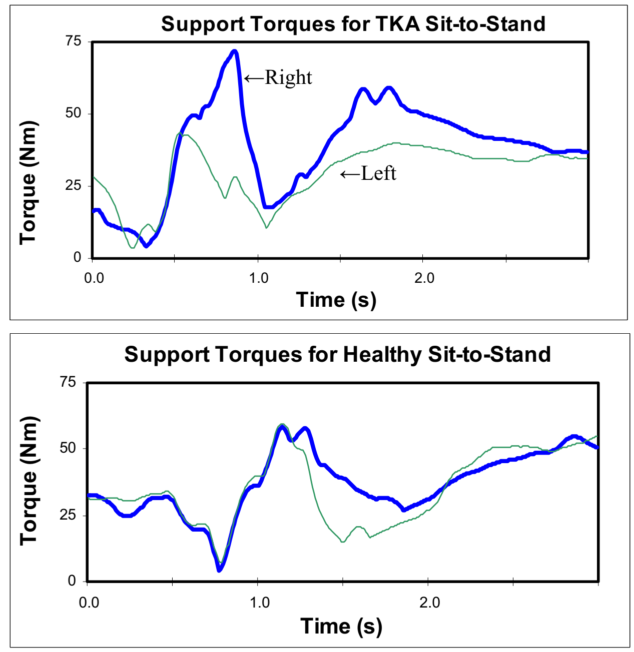

Figure 1: Left/right asymmetry is noted in maximal combined torque during the sit-to-stand ascension phase for an individual after total knee arthroplasty compared to a healthy older adult.

RESULTS AND DISCUSSION

Relative to healthy older adults, TKA subjects demonstrated greater right/left asymmetry (62%/38% in Foot-neutral) in torque production and larger variation in bilateral joint timing across sit-to-stand conditions (Figure 1). TKA subjects also exhibited increased hip flexion torques (38 Nm vs. 14 Nm), indicating they may rely on upper body momentum generation to compensate for lower extremity deficits.

TKA subjects demonstrated greater symmetry in support torques in the Staggered foot position. Healthy older adults demonstrated greater support torque symmetry and improved joint timing in the Foot-back condition relative to the Foot-neutral condition, likely due to increased ankle contributions and reduced hip strength associated with aging. These results indicate appropriate foot placement may compensate for physical limitations in older adults. In addition, alternative foot placements during the sit-to-stand movement may be used for therapeutic goals of improving dynamic stability, enhancing lower extremity strength and maximizing functional independence for individuals following total knee arthroplasty.

REFERENCES

1. Papa E & Cappozzo A. *J of Biomech* **33**, 1113-1122, 2000.
2. Cheng, et al. *Arch Phys Med Rehabil* **82**, 1650-1654, 2001.
3. Su, et al. *Clin Biomech* **13(3)**, 176-181, 1998.
4. Janssen WGM, et al. *Phys Ther* **82**, 866-870, 2002.

CAN PASSIVE DYNAMIC ANKLE FOOT ORTHOSES REPLICATE NATURAL ANKLE STIFFNESS?

Alexander R. Razzook, Kelly M. Nelson, Karen Lohmann Siegel, and Steven J. Stanhope
Physical Disabilities Branch, National Institutes of Health, Department of Health and Human Services, Bethesda, MD
email: arazzook@cc.nih.gov, web: http://pdb.cc.nih.gov

INTRODUCTION

A Passive Dynamic Ankle-foot Orthosis (PD-AFO) is a type of ankle brace that acts like a torsional spring [1]. PD-AFOs are prescribed to patients with weakened plantar flexors. PD-AFOs are designed to be effective by supporting the natural forward progression of the shank over the stance foot [2] (Figure1). Natural Ankle Stiffness (NAS) has been defined as the instantaneous slope of ankle moment plotted as a function of ankle angle [3]. The purpose of this study is to characterize NAS using an implied torsional spring PD-AFO model (PD-AFOm) as a basis.

METHODS

A video-based motion capture system (Oxford Metrics Inc., Oxford, UK) was used to capture the 3D lower extremity gait kinematics and barefoot stance phase kinetics (AMTI, Watertown, MA) of seven normal volunteers (age 26±5yr, body weight (BW) 608.2±78.5N, standing height (H) 1.77±.07m). Gait data were obtained from targeted walking velocity (Wvel) trials at 25%, 50%, 75%, 100%, 125% of normal walking velocity (.785 H/s) [4]. Net plantar/dorsiflexion ankle moments and corresponding ankle angles for three trials at each Wvel were calculated over the stance phase using Visual3D (C-Motion, Inc., Rockville, MD). The period of ankle dorsiflexion from foot flat (FF) to maximum ankle dorsiflexion (MD) was isolated and subdivided into regions R1 and R2 based on the ankle joint neutral reference position (NRP) (Figure 1). Visual inspections of existing PD-AFOs implied the resting position of the PD-AFOm should be aligned to NRP (0.0°) of the ankle obtained from a quiet standing trial. Ankle moment data were scaled by subject BW and H, and combined with angle data in R1 and R2, interpolated to 101 values and averaged for each of the five Wvels. A NAS value for each region was obtained from linear regression.

RESULTS AND DISCUSSION

Linear regression indicated that the PD-AFOm depicted NAS when evaluated in R1 and R2 (r^2>.940). R1 and R2 NAS each increased with Wvel, 12.3% and 19% respectively (Table 1). R2 averaged 58.4% stiffer than R1 over the range of Wvels. At 100% Wvel, the difference in NAS between R1 and R2 is 61%, and the difference in NAS in R2 between 100% Wvel and 25% Wvel is 47%. As R1 NAS increased, the x intercept angles decreased. The non-zero y intercepts of R2 indicated that the ankle was loaded in the NRP contradicting the assumption in the PD-AFOm. Unloading the PD-AFOm would require moving the NRP of the model by the suggested plantar flexion offsets derived from the Wvel dependent x intercept data changing the origin (NRP) of the model. Despite the origin aligned at the x intercept, patients with sufficiently impaired plantar flexors might never reach FF from heel strike (Figure 1). This data appears to isolate R2 as the dominant region for PD-AFOm fitting and potential enhancement of PD-AFOs by using suggested x intercept angles from R1 to optimize for a targeted Wvel (Table 1).

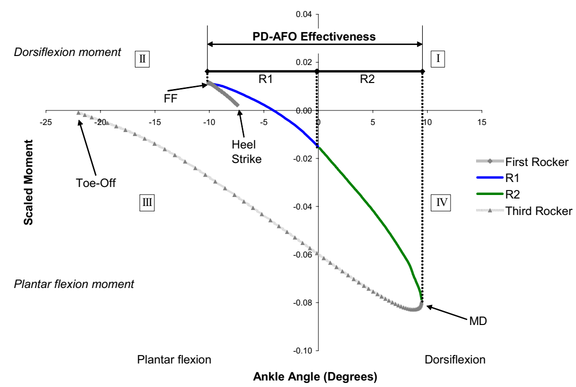

Figure 1: Mean NAS for 75% normal walking velocity

CONCLUSIONS

We have developed a novel method to characterize NAS using a PD-AFOm. Although the model indicated two regions for potential application, R1 does not seem feasible in supporting the natural forward progression of the shank over the stance foot (Figure 1). R2 NAS might be modified but supplementary study is needed to identify what adaptive movement control strategies may be necessary to overcome increased stiffness at the higher Wvels. Understanding normal and patient NAS along with robust PD-AFO modeling will be necessary to systematically enhance discrete regions of gait function where a PD-AFO could optimize human mobility.

REFERENCES

1. Nelson, KM et al. *Proceedings of ASB*, Abstract 2003.
2. Yammoto et al. Arch Phys Med Rehabil, **86**, 162-166, 2005.
3. Davis et al. *Gait and Posture*. **3**, 173, 1995.
4. Holden et al. *Clinical Biomechanics*. **12**, 375-382, 1997.

Table 1: NAS across five walking velocities with corresponding x intercepts (x=degrees) and y intercepts (y=scaled moment)

NAS (1/BW*H)	Walking Velocity (% of 0.785 H/s)				
	25%	50%	75%	100%	125%
R1	-.00201 x=-7.34	-.00247 x=-6.06	-.00270 x=-4.98	-.00318 x=-3.23	-.00340 x=-2.2
R2	-.00433 y=-.0207	-.00542 y=-.0248	-.00627 y=-.023	-.00818 y=-.0164	-.00999 y=-.0212

PREDICTING CHANGES IN KNEE ADDUCTION MOMENT DUE TO LOAD-ALTERING INTERVENTIONS FOR MEDIAL COMPARTMENT KNEE OA FROM PRESSURE DISTRIBUTION

[1]Jennifer Erhart, [1,2]Anne Mündermann, [1]Lars Mündermann, and [1,2,3]Thomas P. Andriacchi
[1]Department of Mechanical Engineering, Stanford University, Stanford, CA; email: amuender@stanford.edu
[2]Bone and Joint Center, Palo Alto VA, Palo Alto, CA
[3]Department of Orthopedic Surgery, Stanford University, Stanford, CA

INTRODUCTION

Current interventions for the treatment of medial compartment knee OA aim to reduce the knee adduction moment to decrease the load transferred through the medial compartment of the knee when walking. The most frequently used non-invasive load-altering interventions are footwear modifications [1,2] and bracing [3,4]. Thus, it seems logical that changes in the adduction moment could be predicted by changes in foot contact patterns. The purpose of this study was to test the hypothesis that changes in knee adduction moment due to load-altering interventions for medial compartment knee OA can be predicted from pressure distribution during walking.

METHODS

Fifteen physically active adults (6 male, 9 female; age: 31.9 ± 5.9 yrs; height: 1.74 ± 0.10 m; mass: 70.7 ± 15.9 kg) without pain or previous injury in their lower extremity participated in this study after giving written consent in accordance with the Institutional Review Board. Subjects performed 3 walking trials at self-selected slow, normal, and fast speeds in each of 3 shoes with identical uppers: 0° valgus (control); 4° valgus; and 8° valgus. Kinematic and kinetic data were collected using an 8-camera optoelectronic system and reflective markers [5]. Pressure distribution data were collected synchronously using a pressure mat placed on the force plate level with the walkway. First and second peak knee adduction moments were calculated for each trial. The pressure region was divided into four zones, medial and lateral heel and forefoot, respectively (Figure 1). The ratio between the medial and lateral maximum force values were calculated for the heel and the forefoot regions. Average values for each shoe, speed, and subject were calculated. Non-parametric statistics were used to determine the success rate in predicting changes in knee adduction moments compared to the control shoe from pressure distribution.

RESULTS AND DISCUSSION

In general, interventions designed to reduce the knee adduction moment during walking were successful. The 4° valgus shoe reduced the 1st and 2nd peak knee adduction moment for 35 and 42 of 45 total subject × speed cases (77.8 and 93.3%), respectively. The 8° valgus shoe reduced the 1st and 2nd peak knee adduction moment for 43 and 42 subject × speed cases (95.6 and 93.3%), respectively.

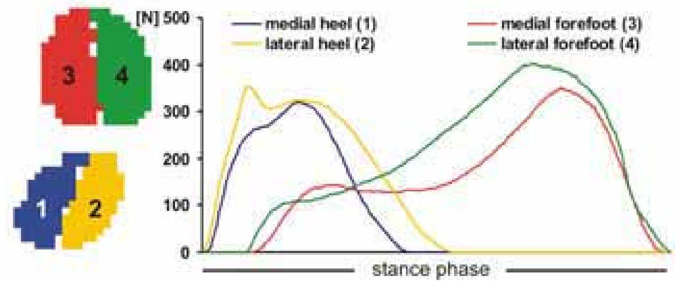

Figure 1: Force curves for one representative trial for the four zones of the foot taken from the pressure mat.

These results suggest that there are multiple ways to respond to the intervention. The ratio between the medial and lateral maximum force values successfully predicted changes in the 1st peak knee adduction moment at a greater rate for the 8° valgus shoe than for the 4° valgus shoe (Table 1). The strong prediction of changes in the knee adduction moment from the force ratio indicates that the more severe intervention (8° valgus shoe) dominated the mechanism of altering the load for most subjects, whereas with the 4° valgus shoe the mechanism of altering load was influenced by other factors such as limb alignment or upper body movement. Thus, interventions that alter load only slightly could have substantial variations in their load-modifying capacity since other factors may play an important role in the way subjects adjust their gait. A validation of these observations is required for patients with medial compartment knee OA.

REFERENCES

1. Kerrigan DC, et at. *J Rheumatology* **30**, 529-533, 2003.
2. Kerrigan DC, et al. *Arch Phys Med Rehab* **83**, 889-893, 2002.
3. Lindenfeld TN, et al. *Clin Orthop Rel Res* **344**, 290-297, 1997.
4. Pollo FE, et al. *Am J Sports Med* **30**, 414-421, 2002.
5. Andriacchi TP, et al. *J Biomech Eng* **120**, 743-749, 1998.

ACKNOWLEDGEMENTS

RSscan for providing the pressure mat; VA grant # A02-2577R.

Table 1: Rate of success of predicting changes in the 1st peak knee adduction moment compared to flat control shoe using a pressure mat. Correct positive: predicted and measured reduction; correct negative: predicted and measured increase; false positive: predicted reduction, measured increase; false negative: predicted increase, measured reduction.

Prediction	4° valgus shoe			8° valgus shoe		
	Slow speed	Normal speed	Fast speed	Slow speed	Normal speed	Fast speed
Correct positive	11 (73.3%)	9 (60.0%)	11 (73.3%)	14 (93.3%)	15 (100.0%)	14 (93.3%)
Correct negative	0 (0.0%)	0 (0.0%)	1 (6.7%)	0 (0.0%)	0 (0.0%)	0 (0.0%)
False positive	3 (20.0%)	3 (20.0%)	3 (20.0%)	1 (6.7%)	0 (0.0%)	1 (6.7%)
False negative	1 (6.7%)	3 (20.0%)	0 (0.0%)	0 (0.0%)	0 (0.0%)	0 (0.0%)
Total Correct	**11 (73.3%)**	**9 (60.0%)**	**12 (80.0%)**	**14 (93.3%)**	**15 (100.0%)**	**14 (93.3%)**

DURABILITY OF ICE HOCKEY HELMETS TO REPEATED IMPACTS

David J. Pearsall, Roghieh Hakim-Zadeh
Department of Kinesiology & Physical Education, McGill University, Montréal, Québec, CANADA
email: david.pearsall@mcgill.ca

INTRODUCTION

Various sports activities that involve protective head gear have different safety testing criteria (Hodgson, 1991). In ice hockey, helmets need to fulfill their function after multiple impacts. Current standards typically involve three repeated impacts at specified helmet sites at a specific energy (Newman, 1993). Since helmets may be used for several competitive seasons, the mechanical durability of these helmets is unknown (i.e. do helmets sustain their impact attenuation properties after numerous repeated impacts?)

METHODS

A monorail drop apparatus was used to conduct controlled impact tests according to standard CSA-Z262.1-M95. A uniaxial linear piezoelectric ± 500 g accelerometer (353B04 , Dalimar) was located at a headform's center (ISO, large size, M) to measure peak linear deceleration at impact (sampling rate 10 KHz; filtered at 1000 Hz) in g's (9.81 m/s/s). The helmet/headforms impact energy was set at 40 J. Three samples of five different models of helmet (size large) were used and four impact sites were evaluated: front, rear, side, and crown. Each site was impacted 50 times. Each helmet received a total of 200 impacts.

RESULTS AND DISCUSSION

Each helmet tested satisfied the safety test criteria at 40 J for the first three impacts (i.e.<275g). The side site showed higher g's than the other sites ($p<0.001$, Fig 1). After several impacts the degradation in impact attenuation properties would plateau and, in some model sites, peak g's would eventually exceed 275g's. The rate of attenuation properties varied with site and helmet model ($p<0.05$, Fig 2).

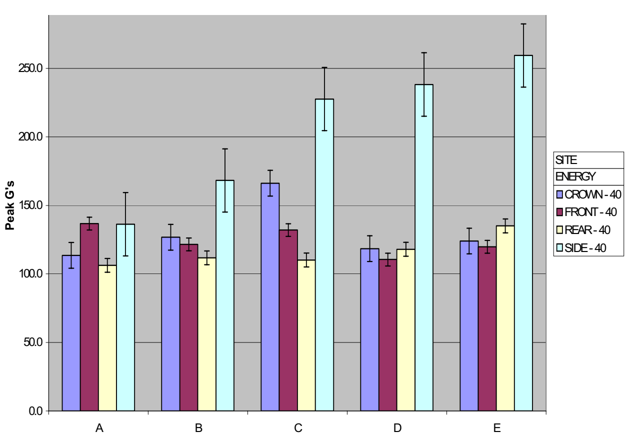

Figure 1: Comparison of peak G between the sites and helmet models at the third repeated impact.

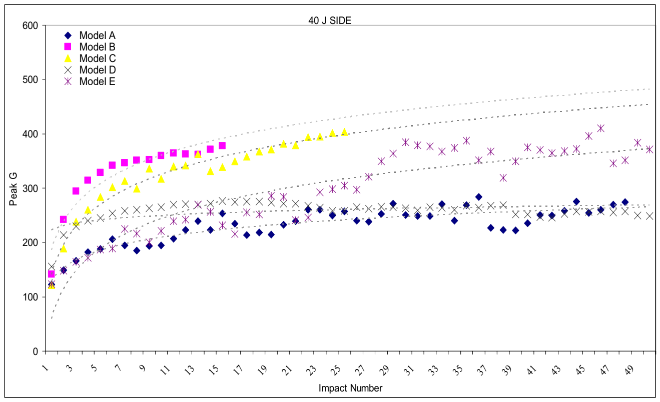

Figure 2: Comparison of side impact site peak G measures by helmet models for up to 50 repeated impacts.

The gradual decrease in impact attenuations properties (i.e. increased peak G with repeated impacts) varied with helmet model due to various liner padding materials, shapes, thickness, and outer shell geometry.

CONCLUSIONS

The above results help to predict the behaviour of helmets under an extreme number of multiple impacts. It also showed the heterogeneous impact response by helmet site; notably different for side impacts. This information may assist in establishing the expected lifetime usage for helmets. Safety standard committees, manufacturers, and national ice hockey associations need to consider this information carefully. Further study is needed to determine the typical mechanical stability of helmets over a normal season-to-season use.

REFERENCES

1. Hodgson, V.R. Impact Standards For Protective Equipment. In: Athletic Injuries to the Head, Neck, and Face. Second edition (ed Torg JS), pp. 28-43. (1991)
2. Newman, J.A. Biomechanics of Human Trauma: Head Protection. In: Accidental injury: Biomechanics and Prevention (eds Nahum A.M & Melvin J.W). pp. 292-310. Springer-Verlag, New York Inc. (1993)

ACKNOWLEDGEMENTS

Financial support was received from the National Science and Engineering Research Council (NSERC) of Canada and Bauer-Nike Hockey Inc.

A PARADIGM TO ASSESS ELECTROMYOGRAPHIC AND KINEMATIC RESPONSES DURING ANTEROPOSTERIOR SURFACE TRANSLATIONS IN SITTING FOLLOWING WHIPLASH INJURIES

[1,2] Isabelle Patenaude, [1,2] Julie Côté, [2,3] Nancy St-Onge and [2,3] Joyce Fung
[1] Department of Kinesiology and Physical Education, McGill University,
[2] Jewish Rehabilitation Hospital Research Center (CRIR),
[3] School of Physical and Occupational Therapy, McGill University;
email: isabelle.patenaude@mail.mcgill.ca

INTRODUCTION

Support surface perturbations are used in research to study the postural control system in humans. In standing healthy subjects, appropriate movement patterns and muscle actions are generated by the central nervous system to restore the projection of the body's center of mass (COM) within the base of support following multidirectional surface translations [1]. Similar studies have been done in sitting [2]. Persons with whiplash associated disorders (WAD) display clinical manifestations resulting from neck trauma. A protocol using low-intensity support surface translations could also be used to evaluate the integrity of the postural control system of WAD individuals [3]. The goal of this study was to identify a low-intensity surface translation characterized by stereotypical postural responses in healthy sitting subjects, with a long-term goal of administrating this protocol to WAD individuals.

METHODS

Healthy subjects (N = 3) sat on a chair fixed on a moveable support surface which was servo-controlled by electro-hydraulic actuators. Pilot tests were initially performed to identify the weakest translational perturbation that provoked stereotypical postural responses. Subjects were then submitted to a randomized sequence of 15 perturbation trials at the identified threshold intensity, with 5 forward translations, 5 backward translations and 5 unperturbed trials. Electromyography (EMG) of eight trunk and neck muscles was recorded bilaterally using a system of bipolar surface electrodes (Noraxon©). Reflective markers were fixed on the subject's head, trunk and arms and their position was recorded using a 6-camera high-resolution passive motion capture system (VICON©). EMG onset was identified when the signal surpassed two standard deviations above the mean of the baseline signal. EMG amplitude was determined by calculating the root mean square (RMS) values over 50 ms intervals. The position of the head, arms and trunk center of mass (HATCOM) was determined using marker coordinates and anthropometric data. The onsets of platform, head and trunk, and HATCOM displacements were identified when their velocities surpassed 5 % of maximum value.

RESULTS AND DISCUSSION

The weakest perturbation that elicited stereotypical muscle and kinematic responses was a support surface translation of 15 cm in 500 ms. For forward perturbations, neck and trunk flexors were activated first (150-250 ms after platform onset), followed by the extensors (600-650 ms). For backward perturbations, extensors were activated first (100-250 ms after platform onset), followed by flexors (450-600 ms). In both directions, flexors were activated for a shorter period as compared to extensors. Trunk and head segment onsets occurred 0-220 ms and 100-500 ms after platform onset, respectively. Trunk and head angular displacements ranged from 2 to 12 degrees, with head movement about 3 degrees smaller than trunk movement. HATCOM began moving 0-100 ms after platform onset. HATCOM stabilised within 2 seconds after overshooting its final position.

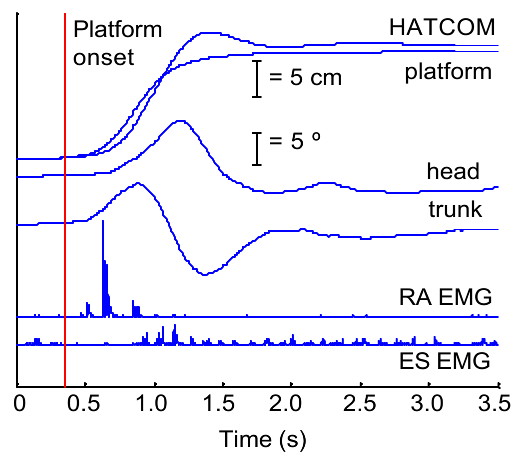

Figure 1: Kinematic and muscle responses to a forward support surface perturbation in a typical subject. RA EMG: left rectus abdominis; ES EMG: left erector spinae.

Our results show that in healthy subjects, the selected translations elicited stereotypical muscular and kinematic responses. At this threshold perturbation, the muscular response pattern is such that muscles stretched due to segmental displacement are activated first, as was shown in other studies using higher intensity perturbations [1-2]. We predict that when submitted to this protocol, WAD individuals will display a variety of inappropriate postural responses which may be caused by deficits at the musculoskeletal or proprioceptive receptor levels associated with their WAD [3].

CONCLUSIONS

Pilot studies were done to identify a low-intensity perturbation that provoked stereotypical postural responses in healthy subjects. This protocol could be used to assess the integrity of the postural control system in WAD individuals.

REFERENCES

1. Henry SM et al., *J Neurophysiol*, **80**, 1939-50, 1998.
2. Forssberg H et al.. *Exp Brain Res*, **97**, 515-527, 1994.
3. Blouin JS, et al.. *Exp Brain Res,* **150**, 458-464, 2004.

ICE HOCKEY STICK RECOIL MECHANICS

Alejandro Villaseñor, David J. Pearsall, and René Turcotte
Department of Kinesiology & Physical Education, McGill University, Montréal, Québec, CANADA
email: david.pearsall@mcgill.ca

INTRODUCTION

Several studies have been conducted with respect to the performance of shooting (1,2). From these studies, the authors suggested that movement patterns of elite players were predominant factors in determining critical outcomes such as puck velocity despite the variation of stick stiffness. However, the effect of the different mechanical factors (e.g. stick bend, puck velocity, puck contact time) on shooting performance is not completely understood. For instance, how do these parameters affect the catapult or recoil effect of the stick during a shot? Hence, the purpose of this study was to identify the recoil effect of the ice hockey stick shaft during a stationary slap shot as observe for elite and recreational players.

METHODS

Nine male Hockey players were selected as subjects for this study (four 'elite', five 'recreational'). The subjects wore ice hockey gloves and stood on a 3 m square piece of 0.004 m thick polyethylene (artificial ice) and were asked to complete eight to ten stationary slap shots for one model stick. Performance measures included: puck acceleration, stick shaft bending and kinetic energy. Data collection consisted of the simultaneous use of a high speed video recording at 1000 Hz (HSC Motion Scope RedLake Imaging, Model PCI 1000), and a piezoelectric triaxial accelerometer (Kistler Inst. Co., model 8792A500) linked to a coupler (Charge Amplifier Type 513m4, Kistler Instrumentation Corp., Amherst, NY,USA) then to a data acquisition card (AT-MIO-16X PC DAQ board, National Instruments). Blade-puck contact time was recorded (LabView 4.1® software) using the same DAQ by means of wrapping the blade of the hockey stick and the puck with a metal foil, thereby creating a ±5v contact circuit which allowed the synchronization of both systems (Figure 1).The shaft kinematics was processed using APAS Software (Ariel Dynamics Inc.).

RESULTS AND DISCUSSION

As Figure 2 shows, differences in both the magnitude and sequence of the two main phases identified (i.e. stick shaft bend and recoil) were observed between groups. For instance, a consistent bend-recoil sequence of the three stick shaft segments examined for the 'elite' group was observed in contrast to the 'rec' group, where a 'recoil' phase was relatively non existent. For the 'elite' group, the bending occurred shortly before or at the instant of first contact (t1) until 28.8 % of blade-puck contact window, followed by the recoil-phase, which lasted until 59.8 % after bend phase or 88.6 % after first touch. Conversely, the "rec" group showed a different sequence, such that the bend phase began only after half way through the contact window (i.e. 44.4 %), and then lasting for only 18.2 % of 'T_A ' before initiating the stick recoil (up to 35.4 % of contact time remaining).

On average, the 'elite' group achieved higher puck velocities than the 'rec' group within a range of 120.8 ± 18 km/h and 80.3 ± 11.6 km/h, respectively. In addition, significant differences were observed in the stick elastic (bend) energy , whereby the 'elite' and 'rec' groups showed 16.49 ± 13.29 joules versus 2.10 ± 2.10 joules, respectively. Furthermore, strong relationships were found between puck velocity and stick bending energy and between puck velocity and blade-puck contact times.

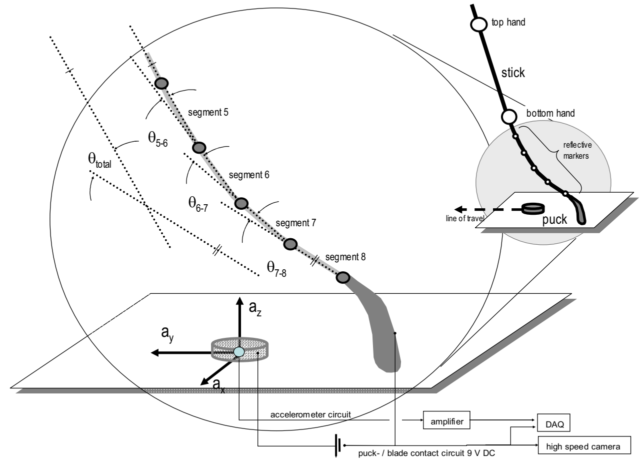

Figure 1 Set up of the experiment. Stick angle deflections (θ5-6, θ6-7, θ7-8, θtotal) and system synchronization .

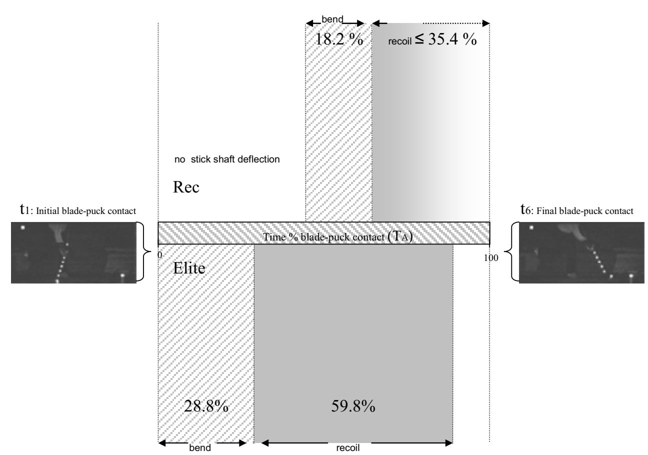

Figure 2 Percentage bend-recoil during puck-blade contact time in the slap shot.

CONCLUSIONS

Stick elastic bend energy (i.e. Ed) and blade puck contact times (i.e. T_A, T_B) were identified as the two main factors highly related to final puck velocity. From these results, a better understanding of the impact blade-puck event during a stationary slap shot was obtained

REFERENCES

1. Marino, G.W. (1998) Proc ISBS, pp. 184-187.
2. Pearsall, D.J. et al. (1999) Sports Engineering. 2, 3-11.

ACKNOWLEDGEMENTS

Financial support was received from the National Science and Engineering Research Council (NSERC) of Canada and Bauer-Nike Hockey Inc.

NON-LINEAR ELASTIC BEHAVIOR OF SMALL INTESTINAL SUBMUCOSA

[1] Brent S. Mitchell, [2]Lori Sahakian, [2]Prasanna Malaviya, and [1]Glen L. Niebur
[1]Tissue Mechanics Laboratory, University of Notre Dame, Notre Dame, IN,
[2]DePuy Orthopaedics, a Johnson & Johnson Company, Warsaw, IN

INTRODUCTION

Small intestinal submucosa (SIS) has been used as a bioactive scaffold for repair of soft tissue injuries. For load bearing and tissue engineering applications, knowledge of the material properties of the implanted scaffold is essential. The properties of SIS have been characterized by linear elastic constant[1]. However, most soft tissues exhibit non-linear elastic behavior. The goal of this study was to characterize the non-linear elastic behavior of SIS laminates.

METHODS

Five 20-layer SIS samples were cut into a dog bone shape with the gage length of 60 mm, cross sectional width of 25 mm, and 40 mm tabs. While dry, a speckle pattern was painted on the samples using an airbrush to facilitate the strain measurement using a digital speckle displacement measurement technique (Fig. 1).

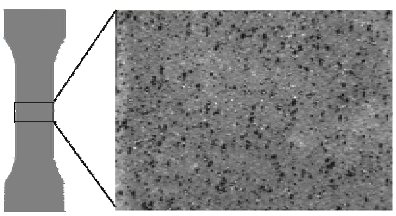

Figure 1. Dog-bone specimen shown with location of strain correlation.

The dry mass of each specimens was measured after which they were soaked in deionized water for two hours for full hydration prior to testing. The hydrated samples were weighed and the new dimensions were measured. They were then placed into cryogenic tissue grips on a material testing machine (Instron 8821, Instron, Canton, MA). A uniaxial tensile test was performed at a strain rate of 100%/s to specimen failure. During the test, video images were taken using a black and white CCD video camera (Sony XCD-X710, Sony Corporation, Tokyo, Japan) at 30 frames per second. A two-dimensional strain field was computed from the images using Vic-2D (Correlated Solutions, West Columbia, SC) optical displacement measurement software. Due to the strains uniformity in each (Fig. 2a) image the average strain values were used to generate stress-strain curves. The out-of-plane strain was calculated by assuming incompressible behavior. The force, stress, and strain at failure were also recorded.

A nonlinear constitutive model was constructed using an exponential strain energy function of the form:

$$W = C(e^{b_1(I_1-3)+b_2(I_2-3)} - 1) \qquad (1)$$

where W is the strain energy , C, b_1, and b_2 are constants, and I_1 and I_2 are the invariants of the right Cauchy Green deformation tensor.

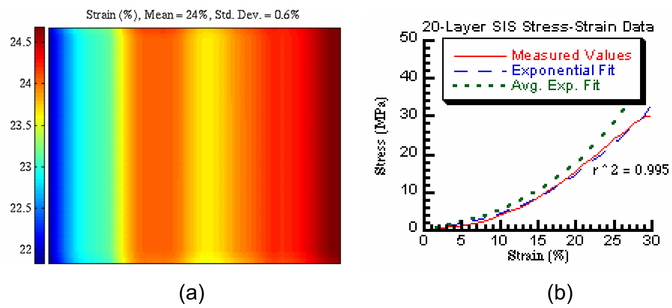

Figure 2. (a) A typical strain field demonstrating uniformity with a size of 25 mm by 10 mm. (b) Stress-strain behavior of laminated SIS. The dashed line is the fit of the data shown by the solid line. The dotted line is the model prediction using the mean coefficients from five specimens.

RESULTS AND DISCUSSION

The hydrated samples had an 80% change in cross-sectional area and an increase of mass of over 100%. Based on the hydrated cross-sectional area the average ultimate tensile strength was 30.5±2 MPa. The constants C, b_1, and b_2 in the nonlinear material model (Eqn. 1) had values of 3.268±1.4 MPa, 0.076±0.84, and 1.045±0.25 (mean ± std. dev.), respectively (Fig. 2b).

Variations of this model have been used to characterize the biaxial mechanical data of SIS [2], pressure properties in a rabbit aorta [3], and blastula wall stiffness[4]. Although this non-linear neo-Hookean exponential constitutive model agreed with the experimental data, other models can also be applied to this data to assess which model best describes the material behavior.

CONCLUSIONS

An exponential neo-Hookean constitutive model was found to correlate well with the measured stress-strain behavior of layered laminated SIS. This constitutive model can be applied to further research of SIS soft-tissue composites to predict the strength of the construct as a load bearing scaffold.

REFERENCES

1. Raghavan D, et al., *J Biomed Mater Res A* 2005.
2. Gloeckner DC, et al., *J Biomed Mater Res* **52,** 365-7, 2000.
3. Chuong CJ, et al., *J Biomech Eng* **108,** 189-92, 1986.
4. Davidson LA, et al., *Dev Biol* **209,** 221-38, 1999.

ACKNOWLEDGEMENTS

DePuy Orthopaedics, a Johnson & Johnson Comany

EVALUATION AND QUANTIFICATION OF BRUISING

[1] Don Sherman, [1]Cynthia Bir, [1]David Viano and [1]E. Mark Haacke
[1]Wayne State University - Detroit, Michigan email: dsherman@wayne.edu

INTRODUCTION

In the United States there were 903,000 estimated cases of child abuse or neglect in the year 2001 [1]. Despite this high number, many cases go unreported each year due to an inability to positively identify a case of abuse. In fact, a child will be seen several times in the acute care setting before an exact diagnosis and proper intervention can occur. This delay is partly due to subjectivity that results when dealing with cases of bruises with unknown etiology and the lack of proper documentation. The accuracy of a physician's assessment in terms of timing of a bruise based on physical examination has been previously reported to be less than 48% [2]. Therefore, there is an urgent need to objectively quantify bruises in order to document the occurrences early in the treatment process.

The purpose of this research is to develop a model for bruising to evaluate methodologies to assist in the quantification of bruises with known impact conditions.

METHODS

The gastrocnemius muscle complex of the adult Wistar rat was selected for impact based on the relative size of the complex and the ease of access. 30 adult female Wistar rats weighing between 300 to 375 grams were tested. Prior to testing, approval from the Animal Care Committee at Wayne State University was granted.

As part of this effort, a pneumatic impactor was developed to achieve a wide range of impact conditions. The pneumatic system consists of a pressure accumulator which is attached to a tube or barrel by way of an electric solenoid. A projectile is placed into the barrel and when triggered the solenoid opens and the pressure accelerates the projectile which is allowed to drive into the specimen. Three impactors ranging in mass from 50 to 100 grams were used. Each impactor surface has a diameter of 1.27 cm and a cross-sectional area of 1.27 cm^2. The impactor surfaces are a flat circle with 1 mm radius around the entire circumference to reduce the edge loading effects.

After anesthetization, the hind limbs of each specimen were shaved to expose the gastrocnemius muscle complex which includes the gastrocnemius, soleus, and plantaris muscles. Both hind limbs of the specimen were then scanned in a 4.7 T MRI to establish a baseline image. Next, one hind limb from each animal was randomly selected for impact with the other limb serving as a control. The specimen was placed in sternal recumbency with the selected hind limb extended and 90° of dorsiflexion in the ankle. The gastrocnemius complex was impacted with one of the six impact conditions list in table 1. After impact the hind limbs of the specimen were scanned again to determine the volume of the contusion that was created.

Table 1: Impact Conditions for the Six Impact Groups

Impactor Mass (g)	Impactor Velocity (m/s)	Impact Energy (J)
50	14.14	5.00
75	11.55	5.00
100	10.00	5.00
50	16.73	7.00
75	13.66	7.00
100	11.83	7.00

RESULTS AND DISCUSSION

The impact conditions were selected based on preliminary pilot studies. Multiple masses were selected to assess the effect of varying mass and velocity while maintaining impact energy. Two impact energies were selected to assess the effect of increasing velocity while maintaining the mass. Impact energies were selected based on preliminary studies and published data [3]. Figure 1 is an MRI scan of the contusion created at the 4.92 J energy level.

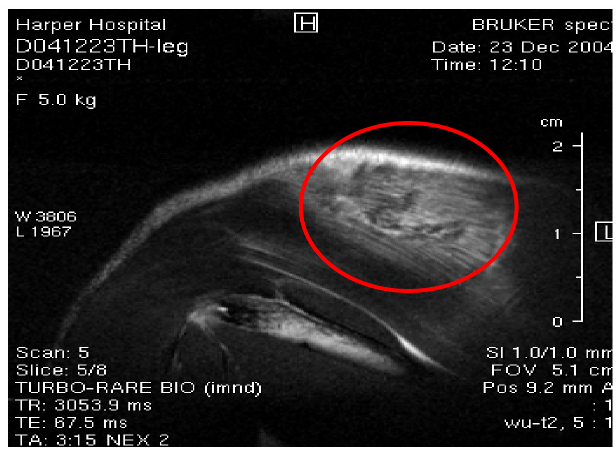

Figure 1 : A T2 weighted MRI scan of an impacted gastrocnemius (Impact energy was 4.92 J)

CONCLUSIONS

This model is capable of producing bruises on the adult Wistar rat. The 4.7 T MRI provides a viable method for visualizing and quantifying a bruise in vivo.

REFERENCES

1. Administration on Children, Youth, and Families, Child Maltreatment 2001. U.S. Department of Health and Human Services: Washington (DC), 2003.
2. Bariciak, E.D., et al., Dating of bruises in children: an assessment of physician accuracy, *Pediatrics* **112**, 804-807, 2003.
3. Crisco, J.J., et al., A muscle contusion injury model. Biomechanics, physiology, and histology, *The American Journal of Sports Medicine* **22** (5), 702-710, 1994

HIP ABDUCTOR STRENGTH MAY BE CRITICAL FOR SUCCESSFUL GAIT COMPENSATION IN PATIENTS WITH MEDIAL COMPARTMENT KNEE OSTEOARTHRITIS

[1]Anne Mündermann, [1]Chris O. Dyrby, and [1,2]Thomas P. Andriacchi
[1]Dept of Mechanical Engineering, Stanford University, Stanford, CA; Bone and Joint Center, Palo Alto VA, Palo Alto CA
[2]Dept. of Orthopaedic Surgery, Stanford University Medical Center, Stanford, CA; email: amuender@stanford.edu

INTRODUCTION

The external adduction moment at the knee during walking has been shown to be a strong predictor for medial compartmental knee osteoarthritis (OA) severity (1) and rate of progression (2). A recent study (3) showed that the knee adduction moment is only elevated compared to matched control subjects for patients with more severe knee OA. The reasons for differences in the adduction moments based on severity are not well understood. It has been suggested (4) that hip musculature could be an important factor in a patient's ability to reduce the knee adduction. However, this study did not did not segregate patients of different disease severity. The purpose of this study was to test the hypothesis that a reduction in the knee adduction moment is related to the hip adduction moment during walking and that this relationship is dependent on the severity of the disease.

METHODS

Forty-two patients (22 female, 65.1 ± 10.2 yrs, 169.1 ± 10.1 cm, 79.2 ± 13.3kg) with OA in the medial compartment of the knee participated in this study after giving written consent in accordance with the Institutional Review Board. Inclusion criteria have been defined previously (3). Patients were classified as less or more severe based on the K-L grades of both knees (less severe: K-L grade ≤ 2; more severe: K-L grade ≥ 3). For each patient, an asymptomatic control subject matched for gender, age, height and weight (62.8 ± 10.6 yrs, 169.3 ± 8.5 cm, 76.6 ± 12.9 kg) was selected after giving written consent in accordance with the Institutional Review Board. All control subjects had no clinical diagnosis of OA or rheumatoid arthritis or a history of knee trauma or pain.

All patients and control subjects performed walking trials walking at their self-selected normal speed. Kinematics and kinetics were collected using a previously described method (5). A MANOVA was used to detect an overall significant difference in gait pattern between groups. Upon a significant result of the MANOVA, separated repeated measures ANOVAs were used to detect significant differences in discrete variables describing the intersegmental angles, moments and forces between groups ($\alpha \leq 0.05$).

RESULTS

Patients with less severe knee OA had normal hip adduction moments while patients with more severe knee OA had substantially lower hip adduction moments compared to their control subjects (-29.0%; $P < 0.001$; Figure 1). In contrast, patients with more severe knee OA had greater knee adduction moments (+11.4%; $P = 0.039$). Irrespective of severity, all patients had a more rapid increase in the ground reaction force (+50.1%; $P < 0.001$), greater medial ground reaction forces (+54.0 %; $P < 0.001$) and greater hip abduction moments immediately following heel-strike (+100.7%; $P < 0.001$; Figures 1 and 2) combined with the knee in a more extended position at landing (+5.3°; $P = 0.003$) suggesting a tendency for a rapid shift of the body's load to the contralateral limb.

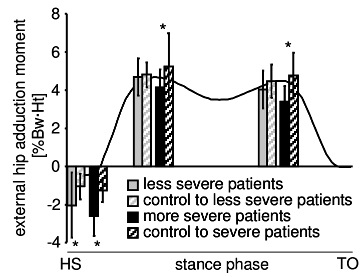

Figure 1: Hip adduction moments for patients with less and more severe knee OA and matched asymptomatic control subjects (* $P < 0.05$).

DISCUSSION

The results support the conclusion that the hip adduction moment could influence the patient's ability to reduce the knee adduction moment, suggesting that patients with less severe knee OA have sufficiently strong hip abductor muscles to maintain a position of the trunk associated with a lower adduction moment whereas more severe patients may lack sufficient hip adductor strength (Figure 2).

The more rapid shift of the body's weight from the contra-lateral limb to the support limb and a lateral shift of the trunk represent a potential mechanism of reducing the knee adduction moment later in stance if the hip abductor muscles can maintain the truck position. Thus, strengthening hip abductors especially in patients with more severe knee OA may be an effective yet non-invasive treatment for medial compartment knee OA.

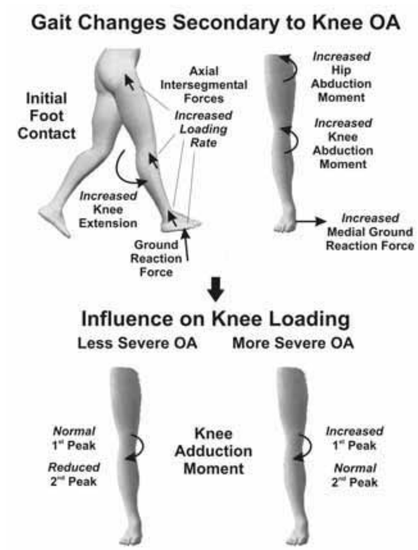

Figure 2: Similar compensation mechanisms lead to different knee adduction moments in patients with less and more severe knee OA.

REFERENCES

1. Sharma L, et al. *Arthr Rheum* **41**, 1233-1240, 1998.
2. Miyazaki T, et al. *Ann Rheum Dis* **61**, 617-622, 2002.
3. Mündermann A, et al. *Arthr Rheum* **50**, 1172-1178, 2004.
4. Mündermann A, et al. *Trans Orth Res Soc* **41**, 1406, 2005.
5. Andriacchi TP, et al. *Basic Orthopaedic Biomechanics*, 1997.

ACKNOWLEDGEMENTS

This project was funded in part by NIH grant # AR 39239 and VA grant # A02-2577R.

THE EFFECT OF SPEED ON GROUND REACTION FORCES DURING LOCOMOTION IN WEIGHTLESSNESS

[1]John DeWitt, [2]Grant Schaffner, [2]Jason Bentley and [3]R. Donald Hagan
[1] Bergaila Engineering Services, Houston, TX, USA; [2] Wyle Life Sciences, Houston, TX, USA;
[3] NASA Johnson Space Center, Houston, TX, USA; email: john.k.dewitt1@jsc.nasa.gov

INTRODUCTION

During long-term space missions, astronauts perform treadmill locomotion as an exercise countermeasure. One of the goals of the exercise is to apply force to the musculoskeletal system via the ground reaction force (GRF). Keller et al. [1] have shown that vertical GRF increases with increasing speed during locomotion at various speeds in normal gravity (1G). The purpose of this investigation was to determine how gait speed affects GRF during locomotion in weightlessness (0G). It was hypothesized that the interaction of speed and peak GRF will be affected by gravitational condition.

METHODS

Four subjects (2M/2F; 172.75 ± 11.14 cm; 73.18 ± 14.03 kg) performed locomotion at 1.34 (walk), 2.23 (jog) and 3.13 (run) m/s on the ground (1G) and during 0G onboard NASA's KC-135 airplane. Vertical GRF data were collected at 250 Hz for 25 sec during multiple trials with a GRF-measuring treadmill (Kistler Gaitway, Amherst, NY).

During 0G trials, the subjects wore a harness that attached at the hip to an external load (EL) set at 1.0 bodyweight (BW) during quiet standing. Bilateral dynamic loading forces were measured at 120 Hz with load cells (ELPS-T3E-500L, Entran Devices, Inc, Fairfield, NJ) placed inline with the EL configuration. The mean dynamic EL for each trial was calculated throughout the entire trial. During 1G trials, subjects ran without the harness.

Peak impact force (PIF) and peak propulsive force (PPF) were determined for eight consecutive footfalls (4 left and 4 right) from each trial. Trial means for all eight footfalls were computed for each GRF variable. All variables were normalized to subject body weight (BW).

A 2-way (gravitational condition × speed) ANOVA was performed on each outcome variable to identify any significant interactions. Bonferroni (all-pairwise) multiple comparison tests were used to determine differences at each speed. Results were considered significant at p<.05.

RESULTS AND DISCUSSION

Dynamic mean EL was determined to be 0.91 BW during the 0G trials. Mean PIF and PPF were between 1.0 and 2.4 BW depending on the speed and gravitational condition (see Table 1). The ANOVA analysis revealed significant effects for speed, and a significant interaction between speed and gravitational condition for both PIF and PPF. This suggests that each of these variables is affected by speed and that the speed effect is different between 0G and 1G (see Figures 1-2). The PIF were similar during 0G and 1G locomotion at each speed, but the PPF were different.

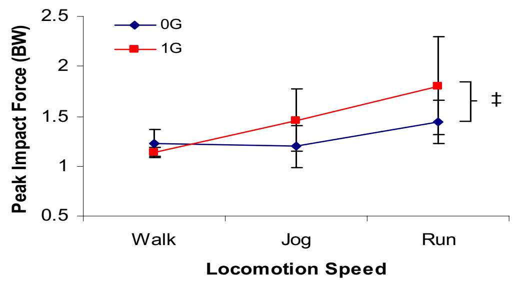

Figure 1: Mean peak impact force at varying speeds during locomotion in 0G and 1G. ‡ Significant speed × gravitational condition interaction, p<.05.

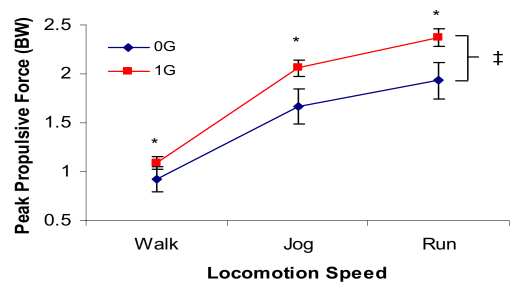

Figure 2: Mean peak propulsive force at varying speeds during locomotion in 0G and 1G. ‡ Significant speed × gravitational condition interaction, p<.05.*Significant speed effect, p<.05.

CONCLUSIONS

In both 0G and 1G, increases in locomotion speed affect the GRF. However, the affect is different between gravitational conditions. While locomotion in 0G may create similar PIF at varying speeds, PPF are less than those occurring at similar speeds in 1G. It is possible that the decreased PPF in 0G may be related to the harness-EL system that is necessary to allow locomotion during 0G exercise. The decreased PPF may result in different training effects during 0G locomotive exercise than that occurring during 1G exercise.

REFERENCES

1. Keller TS, et al. *Clinical Biomech* **11(5)**, 253-259, 1996.

Table 1: Mean ± SD of Peak Impact Force and Peak Propulsive Force during locomotion in 0G and 1G; *p<.05.

Gravitation Condition	Peak Impact Force (BW)			Peak Propulsive Force (BW)		
	Walk	Jog	Run	Walk	Jog	Run
0G	1.23 ± .13	1.20 ± .21	1.44 ± .22	0.92 ± .13*	1.67 ± .18*	1.93 ± .18*
1G	1.14 ± .05	1.46 ± .31	1.80 ± .49	1.09 ± .07	2.06 ± .08	2.37 ± .09

The Talocrural and Subtalar Helical Axes are not fixed during Plantarflexion

[1,2]Frances T. Sheehan, [1] Andrea J. Rebmann, and [1,3]Jeanine M. Graham
[1]National Institutes of Health, Physical Disabilities Branch, University of Maryland School o f Medicine,
Physical Therapy & Rehabiliation Sciences Department., [3]The Catholic University of America; email: fsheehan@cc.nih.gov

INTRODUCTION

In an attempt to understand the etiology of ankle joint injury and degeneration, numerous models of this joint have been created as a means to estimate ankle joint forces. Due to a lack of non-invasive *in vivo* measurement techniques, the kinematics required to drive these models have typically been acquired in cadavers or using external markers to infer internal bone motion. This has left some uncertainty as to the validity of the two most common model simplifications (assuming that the talocrural joint is a locked joint or that both joints are simple hinge joints). Thus, the purpose of this study was to quantify the 3D finite helical axis of the subtalar and talocrural joints non-invasively *in vivo* during plantarflexion, in order to test if the above assumptions were true.

METHODS

Four healthy male subjects participated in this IRB approved study. In total data for 6 ankles were collected (age=26.2±5.0 years, mass=79.5±11.6 kg, height=173.6±1.3cm). Subjects were placed supine in a 1.5T MR imager (LX; GE Medical Systems, Milwaukee, WI, USA) after obtaining informed consent.

A specialized ankle loading device, which allowed 3 degrees of rotational freedom at the ball of the foot, was used to apply load during plantarflexion. Time permitting, both ankles were studied. Plantarflexion (PF) was defined as the rotation of the calcaneus about the tibial medial-lateral (M-L) axis. Zero degrees PF was defined as when the long axis of the tibia was perpendicular to the plantar surface of the foot. While subjects cyclically plantarflexed and dorsiflexed their ankle at 35 cycles/min, aided by an auditory metronome, fast-PC MR images (anatomic and x, y, and z velocity images, temporal resolution=72 ms, imaging time=2:48) were collected. The imaging parameters were consistent with prior studies [1]. The sagittal-oblique imaging plane contained the soleus musculotendon junction, tibia, calcaneus, and talus. The 3D time dependent attitude of the tibia, talus and calcaneus was derived through integration of the velocity data [2]. From these data the FHA was determined. Since it is undefined as the angular velocity goes to zero, the FHA was not reported for angular velocities less than 0.25 rad/s. For clarity, on PF is being reported.

RESULTS AND DISCUSSION

The subtalar joint rotation for all subjects occurred primarily about the medial-lateral axis (Fig 1B&C) during plantar-flexion. Yet the FHA was not oriented solely in the M-L direction and rotation of subtalar FHA with minimal displacement during plantarflexion was seen across all subjects. The lateral side of the FHA began PF angled towards the anterior and inferior direction and as the ankle plantarflexed it rotated posteriorly and superiorly. One

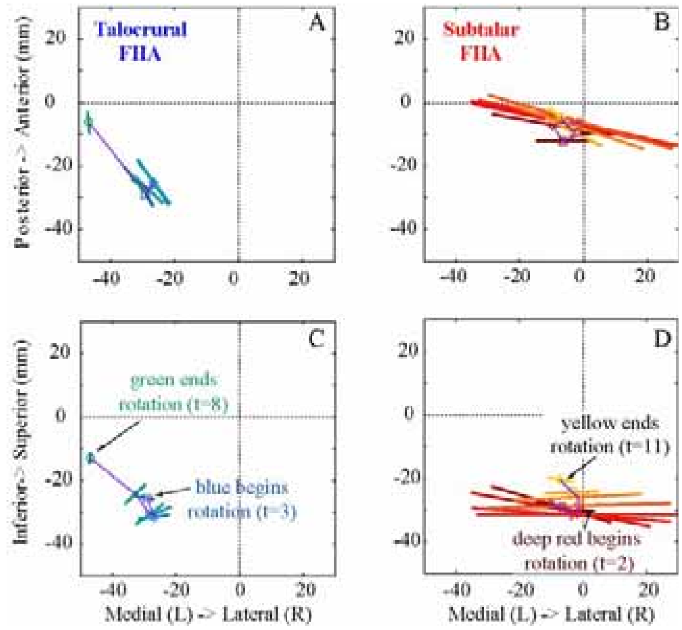

Figure 1: ***3D Talocrural (A&C) and Subtalar (B&D) FHAs During Plantarflexion for subject 9821R***. All FHA's are plotted relative to the tibial coordinate system. The talocrural joint changes from blue to green and the subtalar FHA changes from deep red to yellow as the ankle plantarflexes. **A&B.** a view from above the ankle (AP vs. ML) **C&D.** a frontal view (IS vs. ML). The length of the FHA indicates the magnitude of the angular velocity. The center of the FHA is the closest point the the talar origin (A&C) or the tibial origin (B&D). PF angle for this subject ranged from 1.9° to 39.4°.

exception was seen in one subject, where lateral side of the FHA pointed posteriorly and inferiorly at the beginning of PF and rotated further posteriorly and superiorly. The talocrural FHA was directed primarily in the anterior-posterior direction (Fig 1A&C). The amount of angulation in the M-L and superior-inferior directions did change during PF, but was variable across subjects. The angular velocity of the talocrural joint was smaller than that of the subtalar joint.

The data from this study clearly indicate that neither joint is a simple hinge joint, nor is the talocrural joint a locked joint. One interesting kinematic result of the latter is that inversion occurs about the talocrural joint, while eversion occurs about the subtalar joint during plantarflexion. Thus, the eversion that is seen externally is much smaller than that which is occurring at the subtalar joint. The tendency of the subtalar and talocrural joints to rotate and translate will impact the calculation of tendon and ligament moment arms and, thus, alter the moment producing capabilities of the force generating structures at the ankle joint. Therefore, future modeling studies should investigate the sensitivity of the model outputs to variations in the FHA direction and location.

REFERENCES

[1] Rebmann and Sheehan *JMRI* **17** 206-213, (2003)
[2] Sheehan FT et al *Clin Ortho & Rel Research* **370** 201-207 (2000)

In Vivo Patellar Tendon Moment Arm and Tibial-Femoral Helical Axis

[1,2]Frances T. Sheehan, [1] Andrea J. Rebmann, and [1,3]Jeanine M. Graham
[1]National Institutes of Health, Physical Disabilities Branch, University of Maryland School o f Medicine,
Physical Therapy & Rehabiliation Sciences Department., [3]The Catholic University of America; email: fsheehan@cc.nih.gov

INTRODUCTION

To further improve and validate knee joint models and to develop better surgical and rehabilitative protocols for knee joint injury, a complete understanding of *in vivo* knee joint kinematics and kinetics is critical. Specifically, patellar tendon (PT) moment arm length relative to the tibial-femoral finite helical axis (FHA) plays a crucial role in joint tissue loading and thus, by extension, in the etiology of knee joint pathology. Yet a clear quantitative *in vivo* measurement of this important factor is lacking, due to the fact that the majority of previous studies have been 2D, static and cadaver based. A recent study [1] did investigate 3D PT moment arm, but it was limited to a cadaver model. Thus, the purpose of this study was to experimentally quantify the PT moment arm non-invasively and *in vivo* during a volitional leg extension task in healthy volunteers. A secondary goal was to quantify the tibial-femoral FHA in these subjects in order to determine if the tibia primarily rotates or rotates with translation relative to the femur during extension. The final goal was to determine if the rotation and translation of the FHA was consistent across healthy subjects, thus indicating the applicability of a general model.

METHODS

Twenty knees [9M/11F, age=24.5±6.0years, height=172.8±7.7 cm, mass= 65.6± 12.8kg] from fifteen healthy subjects with no prior history of knee problems or pain participated in this IRB approved study. After obtaining informed consent, subjects were placed supine in a 1.5-T MR imager (LX; GE Medical Systems, Milwaukee, WI, USA).

Subjects cyclically extended and flexed their knee in a supine position at 35 cycles/min, aided by an auditory metronome. Using a sagittal imaging plane, which was perpendicular to the femoral epicondyles and bisected the patella, a full fast-PC data set was collected (anatomic and x, y, and z velocity images, temporal resolution=72 ms, imaging time=2:48). The imaging parameters were consistent with prior studies [2]. If time permitted, both legs were studied. Using rigid body mechanics, the 3D attitude of the patella, femur and tibia were quantified through integration of the 3D velocity data [3]. The insertions of the PT were defined in a single time frame and

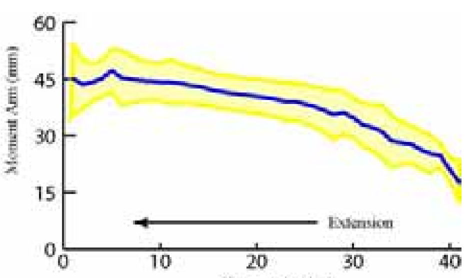

Figure 1: Average Patellar Tendon Moment Arm (blue) ± 1 SD (yellow)

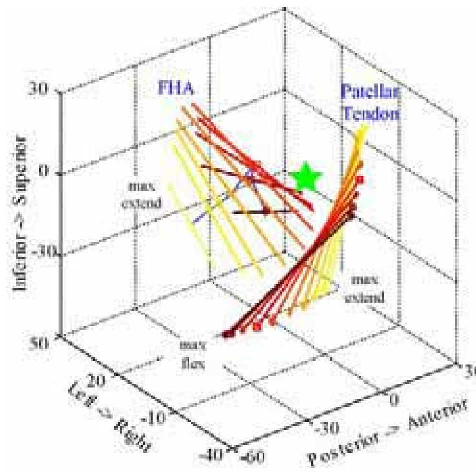

Figure 2: ***FHA and PT Moment arm for Subject 6468R***: The transition from deep red to yellow indicates extension. Deep red line w/ star = full flex ... yellow line w/diamond = full ext. Green star indicates the origin of the femoral coordinate system (0mm,0mm,0mm). The length of the FHA indicates the magnitude of the angular velocity. All axes are in mm.

tracked throughout the cycle based on the 3D patellar and tibial attitude. The FHA was defined by the direction of the angular velocity vector of the tibia relative to femur and the perpendicular vector connecting the tibial origin to the FHA.

RESULTS AND DISCUSSION

All 20 subjects had very similar profiles for the PT moment arm, FHA translation and FHA rotation.. The moment arm increased from max flexion to max extension by 28.4mm (Fig 1). On average, the FHA shifted posteriorly (19.0mm) and superiorly (12.1 mm) and rotated externally (28°) relative to the femoral coordinate system (Fig 2).

This study is the first to measure both the 3D PT moment arm and FHA attitude *in vivo* during a volitional, weighted task using a completely non-invasive measurement system. One interesting point of note is that the moment arm increased as the knee extended, contrary to that which was reported in a recent 3D cadaver study (1). This increase is consistent with the kinematic data collected in that the FHA tended to shift posteriorly while the PT rotated laterally. The discrepancy between these two studies is likely due to the differences in experimental set-up. In addition, the remarkable similarity in kinematic profiles indicates that a general kinematic model may be appropriate for the general population. The next steps in this project will be to determine if these profiles are consistent across an older population and across populations with specific impairments.

REFERENCES

[1] Krevolin et al. *J. of Biomech* 37:785-788 (2004)
[2] Rebmann and Sheehan *JMRI* **17** 206-213, (2003)
[3] Sheehan FT et al *Clin Ortho & Rel Research* **.370** 201-207 (2000)

THE INFLUENCE OF INCLINED SUPPORT SURFACE ON THE BIOMECHANICS OF ECCENTRIC OVERLOAD IN SQUATS

[1]Kjartan Halvorsen, [2]Anna Frohm and [1]Alf Thorstensson
[1]University College of Physical Education and Sports, Stockholm, Sweden, email: kjartanh@ihs.se
[2]Elite Sports Centre, Swedish Sports Confederation, Bosön, Sweden

INTRODUCTION

Eccentric overload training, i.e. resisting a moving force that exceeds what the body is able to move concentrically or hold statically, is widely used both for high performance training and for rehabilitation training. At the Elite Sports Center in Bosön, Sweden, a device has been developed to offer eccentric squat training under safe and controlled conditions (Frohm et al. 2005). It consists of a barbell suspended from two steel wires, which is raised and lowered by a hydraulic machine.

Recently, a pilot study on squat training as rehabilitation of patellar tendinopathy has suggested that performing the squat on an inclination board is more efficient (Purdam et al. 2004). The reason indicated is that the inclination board facilitates a technique that gives more load on the knee extensors. This is the hypothesis we have set out to test.

METHODS

The barbell was loaded with 320kg, and the velocity during descent was set to 0.11m/s (unresisted velocity). The subjects stood on two force platforms (60cm × 40cm, 50cm distance center-center; Kistler AG, Switzerland). The movement was measured using a seven-camera motion capture system (ProReflex, Qualisys Medical AB, Sweden) with four reflective markers on the pelvis (ASIS and PSIS), three markers on each of four clusters taped to the thighs and shanks, and markers at the lateral malleolii, the heels and the base of the second phalanxes. Force and motion was recorded on a single PC; data sampled at 2kHz and 200Hz, respectively. Bilateral measurements of the activity of the *biceps femoris, vastus lateralis* and *gastrocnemius* was performed using surface EMG electrodes and recorded on a separate PC with a sampling frequency of 1kHz (Powerlab, ADInstruments Pty Ltd, UK). A single channel of raw force data from the Kistler amplifier was split and fed to both computers to serve as synchronization signal.

Five well trained individuals (18-23years, 60-95kg, 1.70-1.80m) have so far been tested, performing squats in the machine. Starting from the upright position, the subjects were instructed to let the barbell descend about 10cm, and then resist the movement all the way to the bottom position, which corresponded to about 90° knee flexion. During the upward movement, the subjects did not assist nor resist the movement. Four different conditions were tested: Subjects standing either on a horizontal plane or on an inclination board (25° plantar flexion at the ankle), and performing either maximal resistance, or submaximal resistance. The submaximal resistance was instructed to be 80% of the maximal resistance produced isometrically in a squatting position of 90° knee flexion. The submaximal resistance was controlled by providing a visual feedback of the ground reaction force to the subject. A recording was done with the subject in a neutral standing position with extra markers laterally from the knee centers. The centers of the knee and ankle joints were determined with the knowledge of the width of the knees and ankles. The locations of the hip joint centers were estimated from motion capture data (Halvorsen, 2003), taken when the subjects moved their legs using as much of the range of motion of the hip as possible.

In the post-processing step, the data series (3D marker data, force data and EMG data), were aligned in time, saved in C3D files, and analyzed using Visual3D (C-Motion, Rockville, USA). Moments at the ankle, knee and hip joints were calculated using inverse dynamics.

RESULTS AND DISCUSSION

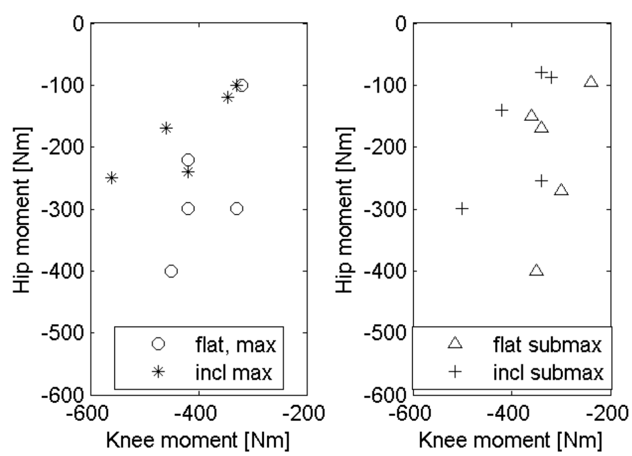

Figure 1 Peak joint moments. Negative values means that an extending muscle force is required.

The most obvious effect that the inclination board has is to remove the limitation that a poor range of motion in the ankle sets on the squatting technique. If the subject cannot dorsi-flex the ankle enough, more flexion at the hip is needed to stay in balance, thus leading to larger moment about the hip and less about the knee. This pattern is indicated in figure 1, with peaks for the inclined squats lying on a higher diagonal line than for flat squats. Two subjects did not exhibit limitation of ankle range of motion, and performed the two types of squats with only small differences in kinematics and joint moments.

REFERENCES

1. Frohm A, et al. *Eur J Appl Physi,,l* In Press, 2005.
2. Purdam et al. *Br J Sports Med* **38**: 395-397, 2004.
3. Halvorsen *J Biomech* **36**: 999-1008, 2003.

HIP CONTROL IN LOCOMOTION

Andre Seyfarth, Susanne Lipfert and Jürgen Rummel
Locomotion Laboratory, University of Jena
email: oas@uni-jena.de, web: www.lauflabor.de

INTRODUCTION

In walking and running the leg retracts during stance phase and protracts during flight phase. Proper timing of retraction and protraction seems to be crucial to obtain stable locomotion [1]. Therefore, we ask whether the difference in duty factor (ratio between stance and cycle time) between walking and running requires gait-specific timing of protraction and retraction in running and walking. Furthermore, we investigate to what extend passive joint mechanisms could help to simplify hip control.

METHODS

1) Hopping Robot. A two-segmented leg is constructed with an elastic joint between the two leg segments and a kinematically driven upper joint (servo motor with sinusoidal control function). For the given joint stiffness, stable hopping patterns exist for certain combinations of hip frequency f and offset angle φ of the servo motor control function.

2) Human Locomotion. In an experimental study on treadmill locomotion, subjects were asked to switch between walking and running every 9 seconds at a given speed. Leg kinematics (QUALISYS) and ground reaction forces (instrumented ADAL3D treadmill) are recorded for later analysis.

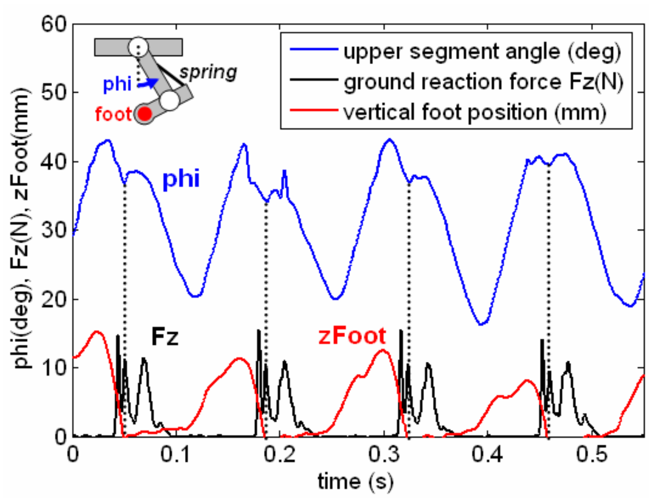

Figure 1: Kinetics and kinematics of the hopping robot.

RESULTS AND DISCUSSION

1) Robot Locomotion. Stable hopping exists in different regions in the control space (f, φ) of the servo motor (details in: Rummel et al., this conference). During the fastest configuration, stable hopping is observed with the leg joint pointing to the forward direction. Although the motor is controlled using a perfect sine function, the upper segment kinematics showed a reset (re-initiation of the sine wave) at touch-down during the retraction phase (dotted lines).

2) Human Walking and Running. The thigh kinematics during walking and running are similar to the robot kinematics. In both gaits, the thigh protracts during about 35% of the gait cycle. Leg retraction is briefly interrupted at touch-down.

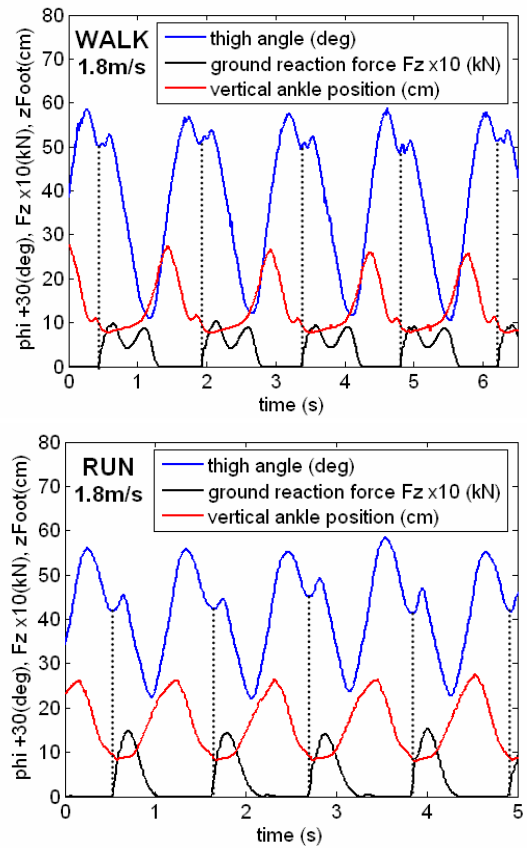

Figure 2: Kinetics and kinematics in human walking and running at 1.8m/s.

CONCLUSIONS

The results indicate that hip control during locomotion could be very similar during walking and running. The duration of the stance phase with respect to the gait cycle could be modulated by the knee function depending on the gait.

The asymmetry in protraction and retraction does not imply that the biological hip controller (e.g. CPG) needs to work asymmetrically. The simple hopping robot demonstrates that joint play and compliant actuator properties could result in the experimentally observed acceleration of the protraction phase.

REFERENCES

1. Seyfarth A, et al. *J Exp Biol* **206**, 2547-55, 2003.

ACKNOWLEDGEMENTS

This research is supported by the German Research Foundation (DFG, SE1042/1-4).

WALKING AND RUNNING ON PLACE

Andre Seyfarth and Susanne Lipfert
Locomotion Laboratory, University of Jena
email: oas@uni-jena.de, web: www.lauflabor.de

INTRODUCTION

A central question in locomotion research is to understand how leg movements are generated. In the last decade a number of experimental and analytical approaches were undertaken to reveal basic mechanisms for stable leg operation in running and hopping. As a result of this research we do believe that the leg function can be compared to a mechanical spring [1]. This means that leg forces during contact increase with the amount of leg shortening. A similar description of the leg operation in walking will be presented at this conference (Geyer et al.).
To improve our understanding of leg operation, we ask whether the well-known shape of the force patterns (Fig. 1) could be a result of the gait-specific longitudinal leg shortening and extension rather than an effect of the leg rotation (retraction during stance).
To approach this issue we investigate the leg behavior during walking and running on place. Here, the backward rotation of the stance leg (retraction) can not contribute to the leg force generation.
Our hypothesis is that the leg force patterns are primarily dependent on gait-specific leg compression dynamics and therefore similar to forward locomotion when walking and running on place.

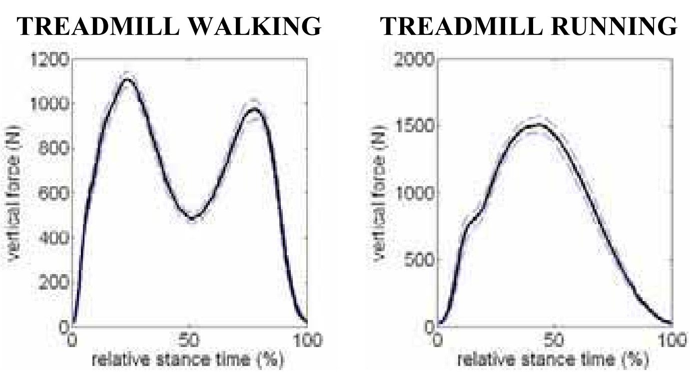

Figure 1: Vertical ground reaction forces (mean ± S.D.) in treadmill walking and running at preferred walk-run transition speed (1.9 m/s).

METHODS

Three subjects (body mass m=54, 73, 67kg; body height h=167, 182, 182 cm) were asked to walk and run on two adjacent KISTLER force plates. The kinematics of the right toe, ankle, knee, hip and shoulder were recorded using a high-speed camera system (QUALISYS).
First, subjects were asked to select their preferred gait at frequencies between 1 and 4 Hz. Then, they were required to change gait every 10 contacts at their preferred gait transition frequency. Using the marker data the inner leg joint angles (ankle and knee) were calculated.

RESULTS

The analysis of walking and running on place shows a high similarity in the ground reaction force patterns (Fig. 2) compared to forward locomotion (Fig. 1). In *running*, a single force peak (circle **3**) is observed. For *walking* on place, a double humped (circles **1** and **2**) force pattern - similar to forward walking - is present. In comparison with forward walking, however, the second hump (circle **2**) is slightly reduced in magnitude.
Walking kinematics: During stance, large extension-flexion cycle of the knee (ca. 135-175 deg) and two ankle flexion-extension cycles (ca. 105-115 deg) are observed.
Running kinematics: Leg shortening during stance is mainly achieved by the ankle joint (125-100 deg).

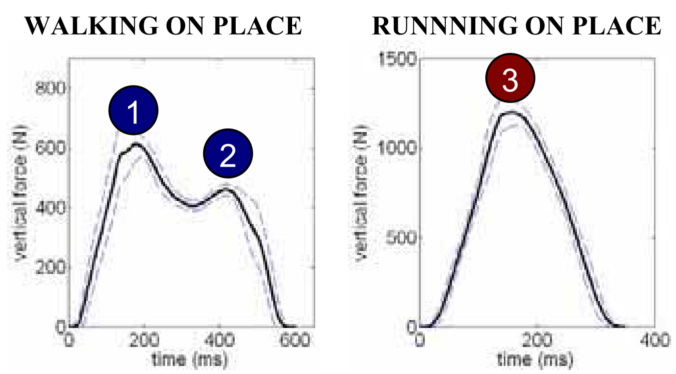

Figure 2: Vertical ground reaction forces (mean ± S.D.) during walking and running on place at preferred transition frequency (2.8 Hz).

DISCUSSION

Both, walking and running on place keep general features of forward locomotion, such as *maximum leg force* at midstance in running and *two local force maxima* and *one local minimum at midstance* in walking. On the joint level, a clear distinction of knee and ankle operation between walking and running can be found.
In conclusion, we suggest that the organization of the leg behavior during stance does primarily rely on the longitudinal dynamics of leg compression and extension. Further research needs to be done to evaluate the effects of forward movement on the leg function during locomotion.

REFERENCES

1. Blickhan, R. *J. Biomech.* **22**, 1217-1227, 1989.

ACKNOWLEDGEMENTS

This research is supported by the German Research Foundation (DFG, SE1042/1-4).

INTERSEGMENTAL DYNAMICS OF THE SWING PHASE OF WALKING IN TRANS-TIBIAL AMPUTEES

[1]Jeremy D. Smith, [1]Philip E. Martin and [2]Sarah J. Mattes
[1]Department of Kinesiology, Penn State University, University Park, PA 16802,
[2]Department of Kinesiology, Arizona State University, Tempe, AZ 85287; email: jds431@psu.edu

INTRODUCTION

Unilateral, trans-tibial amputees reflect significant inertial asymmetries between the intact and prosthetic limbs [1] and also exhibit temporal, kinematic, and kinetic gait asymmetries during walking [2]. Early modeling research [3] suggested lower extremity inertial symmetry may lead to more symmetrical gait patterns in unilateral amputees. Mattes et al. [1], however, found that matching inertial properties exacerbated existing temporal asymmetries. In an effort to better understand the influence of inertial manipulation on swing phase dynamics for unilateral, trans-tibial amputees, we examined the effect of matching the inertial properties of prosthetic and intact legs on intersegmental dynamics at the knee and hip during walking.

METHODS

Six males with unilateral, trans-tibial amputations (age: 32±12 yrs, body mass: 85±6 kg, body height: 179±6 cm, time since amputation: 3-15 yr), using energy storing prosthetic limbs, were first acclimated to treadmill walking and prosthesis load conditions. Inertial properties of the intact and prosthetic limbs were measured or estimated [4]. In a separate session, subjects completed overground walking at 1.34 m/s as sagittal plane motion and ground reaction force data were sampled (60 Hz and 480 Hz, respectively) under three prosthetic limb inertial conditions: 1) a baseline condition in which no load was added to the prosthetic limb, 2) a 100% mass condition in which prosthetic limb mass and moment of inertia about a transverse axis through the knee were matched to those of the intact limb, and 3) a 50% mass condition in which the added load was half that added to the limb for the 100% condition.

An intersegmental dynamics approach was used to partition net moments about the knee and hip into interaction, gravitational, and muscle components [5]. Absolute angular impulses for each moment component were computed and used to express each as a percentage of the total of the three components.

RESULTS AND DISCUSSION

Net moments and moment components attributed to muscle, gravitational, and interaction during the swing phase (Figure 1) of walking were consistent in amplitude and pattern with published data for able-bodied walking [5]. Intersegmental dynamics at the knee and hip of the intact limb were not affected by inertial increases of the prosthetic limb. In contrast, the magnitude of moment components at both the hip and knee of the prosthetic leg increased systematically as prosthesis inertia was increased. In addition, the relative contributions of the individual moment components were altered, particularly at the knee where the relative contribution of muscle increased and interaction contribution decreased (Figure 2). Increased muscle moments at the hip and knee as prosthesis inertia increased paralleled higher metabolic costs of walking observed by Mattes et al. [1] for the same load conditions.

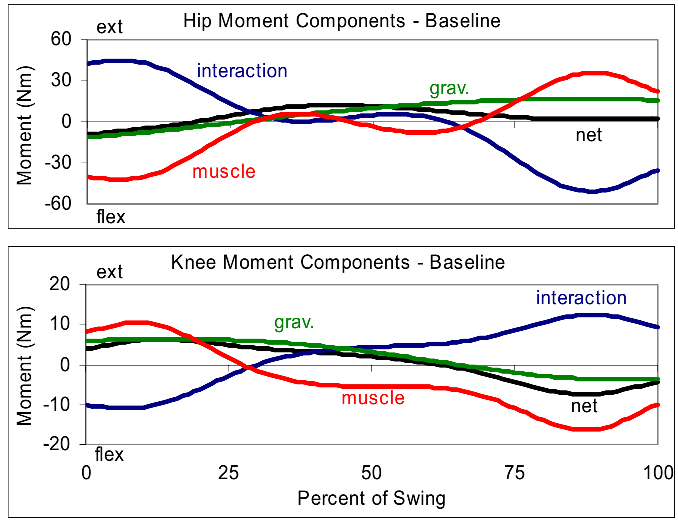

Figure 1. Net joint moment and partitioned components for the hip and knee joints of the prosthetic leg (unloaded condition; swing phase only). Note the counterbalancing effects of the muscle and interaction components at both joints. The intact leg showed similar patterns.

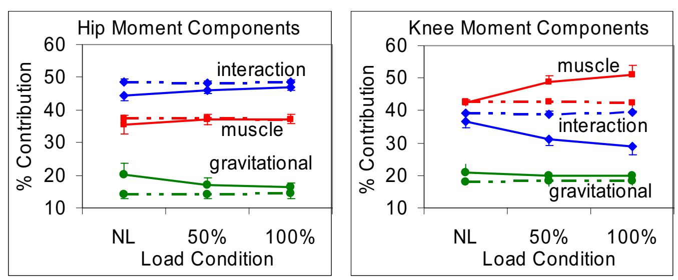

Figure 2. Relative contributions of the muscle, gravitational, and interaction components for prosthetic leg (solid lines) hip and knee were altered as prosthetic limb inertia increased. There were no changes for the intact leg (dashed lines).

CONCLUSION

The increased relative contributions of the muscle moments to the net moments at the hip and knee suggest that the prosthetic limb requires more active control by the musculature as prosthesis inertia increases.

REFERENCES

1. Mattes SJ. et al. *Arch Phys Med Rehab*, **81**, 561-68, 2000.
2. Sanderson D & Martin P. *Gait & Posture*, **6**, 126-36, 1997.
3. Tsai CS & Mansour JM. *J Biomed Eng*, **108**, 65-72, 1986.
4. de Leva P. *J Biomech*, **29**, 1223-30, 1996.
5. Zernicke R. et al. *Adaptability of Human Gait* (A. Patla, Ed.), Elsevier Science, North-Holland, 1991.

BIOMECHANICAL ANALYSIS OF SIT-TO-STAND AFTER BILATERAL TOTAL KNEE REPLACEMENT

[1] H. Wang, [2]K. Simpson, [2]M. Ferrara, [3]S. Chamnongkich, [4]T. Kinsey, and [4]O. Mahoney
[1]Queens College, [2]University of Georgia, [3]Chiangmai University, [4]Athens Orthopedic Clinic;
email: hewang@forbin.qc.edu

INTRODUCTION

As the trend of longer life span continues, more and more people receive bilateral total knee replacements (TKR) in their lifetime. It is common that many patients have two different TKR systems implanted, one on each side. The functional performance of bilateral TKR patients with two different systems during daily activities is not well understood. Although it was reported that a single-radius TKR (SR) compared to a multi-radius TKR (MR) could facilitate unilateral TKR patients' sit-to-stand (STS) movement [1], it is not known if bilateral TKR patients with an SR and an MR on each side rely on their SR limbs to perform a STS movement.

The purpose of this study is to investigate the influence of an SR and an MR TKA on functional performance during a STS performed by bilateral TKR patients.

METHODS

Eight healthy participants (age = 71 ± 9 yr.) with an SR (Scorpio™ PS, Stryker Orthopaedics Inc.) and an MR (S-7000™ PS, Stryker Orthopaedics, Inc. and P.F.C.™ PS, Johnson & Johnson, Inc.) on each side took part in this study. Three high-speed video cameras (120Hz) were used to track participants' motion. An EMG system (1080 Hz) and a force platform (1080 Hz) were used to monitor leg muscles' activation and ground reaction force (GRF), respectively. Participants performed four STS trials for each leg.

An inverse dynamic method [2] was used to calculate joint reaction forces (JRF), moments, and powers of ankle, knee, and hip joints. Horizontal and vertical impulses were calculated for the forward-thrust phase and extension phase of the STS. Normalized root-mean squared (RMS) EMG was used to quantify the contractions of quadriceps and hamstrings. Paired Student t-tests were used to determine the kinematic, kinetic, and EMG differences between the SR and the MR limbs ($\alpha = 0.05$).

RESULTS AND DISCUSSION

Compared to the MR limb, the SR limb exhibited greater: peak antero-posterior (AP) GRF; peak AP JRFs of the ankle and knee joints; and AP impulse during the forward-thrust phase (Table 1). However, the vastus lateralis (VL) RMS EMG of the SR limb (1.185 ± 0.508) was less than the MR limb (1.354 ± 0.031).

Due to the greater peak AP GRF, the SR limb had greater peak AP JRFs in the ankle and knee joints compared to the MR limb. Greater AP GRF accounted for the greater AP impulse during the forward-thrust phase. During this phase, the trunk segment rotates around the hip joint so that the upper body mass can be shifted from the seat to the feet. The increased AP impulse associated with the SR limb might help produce trunk rotation by producing extra rotational momentum.

As the moment arm length for the quadriceps force acting on the tibia via the patella tendon is longer for the SR design than the MR designs used in this study [3, 4], we anticipated that the MR limb would produce more quadriceps activation during the STS. However, we only found a weak support for this notion. The increased VL activation seen in the MR limb might be due to the TKR design differences but could also be related to knee stability.

Surprisingly, we did not detect the significant differences between the limbs for the lower extremity joint moments. Likely it was due to small sample size and high inter-individual variability.

CONCLUSIONS

Bilateral TKR patients with an SR and an MR on each side showed unique GRF differences and different VL muscle activation between the two limbs.

REFERENCES

1. Wang, et al. *Proceedings of 70th AAOS*, New Orleans, LA. 402, 2003.
2. Winter. *Biomechanics and motor control of human movement*. 75-102, 1990.
3. D'Lima, et al. *Clin. Orthop. Rel. Res*. (392), 213-220, 2001.
4. Mahoney, et al. *J. Arthroplasty*. 17(4), 416-421, 2002.

ACKNOWLEDGEMENTS

This study was funded by Stryker Orthopaedics, Inc. and CUNY Research Foundation.

	SR	MR	P value
Peak AP GRF (N)	60.5 ± 8.5	50.3 ± 10.0	0.007
Peak AP JRF of ankle (N)	60.5 ± 8.5	50.3 ± 10.0	0.007
Peak AP JRF of knee (N)	60.4 ± 9.8	50.9 ± 10.9	0.01
AP impulse of the forward-thrust phase (N*s)	13.9 ± 3.6	10.4 ± 3.5	0.006

Table 1. Peak AP ground reaction force, joint reaction forces of ankle and knee, and antero-posterior impulse between the SR and the MR limbs.

AXIAL CYCLIC AND FAILURE LOADING OF PEDICLE SCREWS

Mike Ehlert, Serkan İnceoğlu and Robert McLain
Spine Research Laboratory, Spine Institute, The Cleveland Clinic Foundation
e-mail: inceogs@ccf.org

INTRODUCTION

Screw loosening and pullout are common ways of fixation failure in clinic preventing fusion and causing pain. Standard pullout test is used to assess the mechanical behavior of the bone-screw interface. In the pullout test, the screws are placed in either synthetic or bone specimens and are withdrawn by applying an axial load at a constant rate. Although bone is known to be a viscoelastic material and thus produce a mechanical response to the loading depending on the application rate, it is still not clear if the bone-screw interface behaves similarly. Therefore, we designed this study to test the effects of loading rate on the mechanical performance of the pedicle screw in pullout.

METHODS

For this purpose, 20 conical pedicle screws (Xia, Stryker Spine, Allendale, NJ) with a size of 6.5x40mm were inserted into a foam material (Sawbones, Pacific Research Laboratories, Vashon, WA) with a density of 0.32 g/cc and axially cycled at four different rates, i.e., 0.1, 1, 5, 50 mm/min -and 1 mm/min again for diagnosis-, up to a pre-yield load (500 N) and pulled out. Then, another 40 of the same screws were inserted in foam blocks and immediately pulled out. The aforementioned loading rates were used for pullout tests, i.e., yielding 15 screws for each rate. Additionally, a lumbar bovine spine was cleaned of soft tissue and separated into vertebral levels (L1-5). Ten pedicle screws were inserted in 5 calf lumbar vertebrae according to the standard surgical technique. After instrumentation, the vertebral specimens were cut in half sagittally isolating each pedicle for testing. After embedding, one of each pair of screws in each calf specimen was pulled at a rate of either 0.1 or 50 mm/min after cycled axially at the rates of 0.1, 1, 5, 50 mm/min, sequentially, around a pre-yield load (500 N). All the testing was conducted using an MTS testing machine and custom adapters. The gripping fixtures were carefully adjusted so that there was no laxity in the system to allow cycling without losing the contact. Stiffness was calculated as the slope of the load-displacement curve in the interval of 50-450 N. The peak load was the highest load encountered during destructive testing.

RESULTS AND DISCUSSION

The results showed that the strength and stiffness were significantly affected by the loading rate. The stiffness at 1 mm/min was higher than that at 0.1 mm/min ($p<0.001$) and lower than that at 5 mm/min loading rate ($p<0.001$). The stiffness significantly dropped at the 50 mm/min ($p<0.05$) compared to the 5 mm/min in the foam group but it was still significantly higher than that at 0.1 mm/min ($p<0.001$). In bone group, the stiffness at the 5 mm/min rate was higher than those at the 0.1 mm/min ($p<0.05$) and 50 mm/min ($p<0.05$) but not 1 mm/min ($p>0.05$). The difference between the 0.1 mm/min and 50 mm/min loading rates was not significant ($p>0.05$). The peak load at the 50 mm/min rate was significantly higher than other loading rates ($p<0.01$) in the foam group except for the 1.0 mm/min ($p>0.05$). The peak load at 50 mm/min was significantly higher than that at 0.1 mm/min in the bovine group ($p<0.05$). The effects of loading rate on the hysteresis curves are shown in Figure 1.

The bone-screw interface usually exhibits completely different mechanical and viscoelastic behavior than bone alone. However, our results showed that the mechanics of the interface was significantly affected by the loading rate, as similarly to bone alone. The results also showed that the mechanical behavior of the foam-screw interface was similar to that of the bone-screw interface. However, the hysteresis behavior of the interface in the elastic region was surprisingly different from those of bone and foam and totally new to the current literature. The authors speculated that the data collected during the unloading phase of cycling could source from loading of different sites of the foam or bone threads and cause the load-displacement data to draw this unexpected curve. Further analysis needs to be conducted.

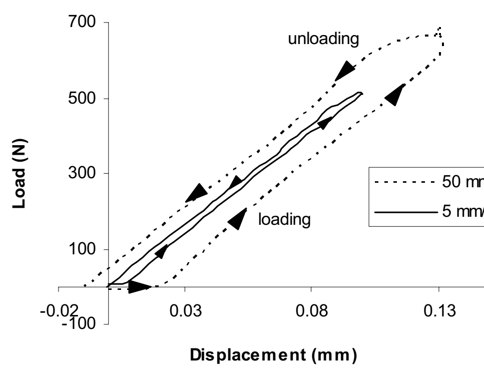

Figure 1: High loading rate caused increased hysteresis. The hysteresis behavior of the interface in pre-yield region was different than those seen in foam or bone. This unexpected trend of unloading curve might source from loading of other sites of the bone or foam threads.

CONCLUSIONS

This study investigated the axial cyclic behavior of a bone-screw interface in pre-yield load level at different rates for the first time in the literature. The results showed that the loading rate significantly affected the strength and stiffness of the interface. This suggests that for a fair comparison between screw pullout tests in the literature, the pullout rate needs to be matched. In the future, these results should be confirmed for other screw designs. The stress-strain behavior of a bone thread also needs to be investigated in a greater detail.

ACKNOWLEDGEMETNS

This study was supported in part by NASS Grant.

SHOULDER KINEMATICS DURING CLINICAL GLENOHUMERAL TESTS. DIFFERENCES BETWEEN NO-PLAYERS AND WATER POLO PLAYERS

[1] Catarina Tainha and [2]Augusto Gil Pascoal
[1]Health Superior School of Alcoitão, Estoril, PORTUGAL,
[2]Faculty of Human Kinetics, Lisbon, PORTUGAL; email: catarina.tainha@netcabo.pt

INTRODUCTION

Water polo combines the skills of swimming and throwing. On both the shoulder movement is according a pattern that combines adduction and internal arm rotation, in an elevate arm position. This pattern cause retraction on the anterior glenohumeral structures (capsule-ligamentous and/or muscular) and is assumed to be one of the most important aetiology factor involve in water polo players shoulder injuries, as glenohumeral instability and shoulder impingement [1,2]. The identification of this anterior glenohumeral retraction is made by clinical tests that putt the arm (passively or actively) on a maximal available external arm rotation or arm abduction position. The advantage of the active tests is that mostly the passive structures are stretching given that the anterior shoulder muscles are inhibit. The active test is a global arm movement that involves the glenohumeral joint and the shoulder girdle. However, diagnose is over a predisposed factor for shoulder injury on the glenohumeral joint, assuming the shoulder girdle as a stable platform. Thus, the purpose of this study was to identify the anterior glenohumeral retraction in water polo players and additionally to describe the shoulder girdle involvement during two glenohumeral active clinical tests: external rotation test and horizontal abduction test.

METHODS

The dominant shoulders of a group of five female elite water polo players (age = 20 ± 2.1) and a group of five no-players female subjects (age = 21 ± 2.3) were tested during two glenohumeral active clinical tests: external rotation test and horizontal abduction test. The subjects were asking to move slowly the arm to a maximal position (external rotation or horizontal abduction), while the arm was artificially supported in an elevated position. Each subject performs three repetitions of each test. Shoulder rotations were recorded by mean of a six-degree-of-freedom electromagnetic tracking device (Flock of Bird System) and described as Euler angles with respect to the thorax local coordinate system, according to a standardization protocol [3]. A "*scapulalocator*" device, similar to Pascoal et al. [4], was used for recording scapular 3D position.

Differences between both group in humeral (arm elevation, axial rotation and horizontal abduction) and scapular rotations (protration, latero-rotation and spinal tilt) were analyzed by mean of a *t*-test approach.

All statistical analysis was performed with SPSS (version 10) and the alpha-level set as 0.05.

RESULTS AND DISCUSSION

The non-player group showed greater values of external rotation and horizontal abduction than the water polo players group. However, scapular rotations are greater in the water polo players group on both tests. All these differences are statistically significant with exception for scapular latero-rotation's angles. These results are in contradiction with those reported by other studies that showed larges active ranges of humeral lateral rotation in overhead sports players [5]. A possible explanation is that on the water polo the arm movement must be done without leg ground fixation. Thorax and scapula are not used as fixed points but as essential elements inside a kinetics chain that connects the hand to the trunk. On these conditions, humeral rotations are reduced and scapular rotations augmented. According with Ludewig & Cook [6] the excessive contribution of scapula during arm movement is a sign of shoulder impingement pathology, caused by the decreases in serratus anterior muscle activity and increases in upper trapezius muscle activity or to an imbalance of forces between the upper and lower parts of the trapezius muscle.

CONCLUSIONS

During clinical active shoulder tests, water polo players showed reduced values of external and horizontal abduction rotations, when compared with no-players subjects. Inversely, scapular protraction and spinal tilt rotations are greater in water polo players. These results seem to be related with specific shoulder demand in water polo where the throwing arm is moving again a less fixed trunk. The increased scapular rotations during maximal active arm external and horizontal abduction rotations, observed in water polo players, could be a predispose factor for some shoulder pathologies as shoulder impingement.

REFERENCES

1. Colville, J.M. and B.S. Markman, *Competitive water polo. Upper extremity injuries.* Clin Sports Med, 1999. **18**(2): p. 305-12, vi.
2. Elliott, J., *Shoulder Pain and Flexibility in Élite Water Polo Players.* Physiotherapy, 1993. **79**(10): p. 693-697.
3. van der Helm, F.C.T., *A standardized protocol for motion recording of the shoulder*, in *Proceedings of the 1st Conference International Shoulder Group*, H.E.J. Veeger, F.C.T. Helm, and P.M. Rozing, Editors. 1996, Shaker Publishers BV: Mastricht. p. 7-12.
4. Pascoal, A.G., et al., *Effects of different arm external loads on the scapulo-humeral rhythm.* Clinical Biomechanics, 2000. **15**(Sup. nº 1): p. S21 - S27.
5. Richardson, A.B., *Overuse syndromes in baseball, tennis, gymnastics, and swimming.* Clin Sports Med, 1983. **2**(2): p. 379-90.
6. Ludewig, P.M. and T.M. Cook, *Alterations in shoulder kinematics and associated muscle activity in people with symptoms of shoulder impingement.* Physical Therapy, 2000. **80**(3): p. 276-291.

CAN THE PATELLAR TENDON MOMENT ARM LENGTH BE PREDICTED FROM ANTHROPOMETRIC CHARACTERISTICS?

Dimitrios Tsaopoulos, Constantinos N. Maganaris and Vasilios Baltzopoulos
Institute for Biophysical & Clinical Research into Human Movement, Manchester Metropolitan University, Alsager, U.K.

INTRODUCTION

It has been suggested that muscle moment arms are related to anatomical differences and could be predicted from anthropometric characteristics [e.g. 1-2]. If moment arms can be predicted from easily measured anthropometric variables then analysis of muscle and joint forces could become significantly easier without the need for complicated imaging techniques. More recently, Krevolin et al. [3] reported that when the patellar tendon moment arm was normalized to femoral condyle width, it remained roughly constant across individuals, suggesting that prediction of patellar tendon moment arm length from relevant anatomical or anthropometric measurements would be possible.

The purpose of this study was to examine the relationship between patella tendon moment arm and relevant anthropometric characteristics.

METHODS

Twenty-two males (age: 25.7±5.7 years) without any musculoskeletal injuries in the lower limbs volunteered to participate after the study was approved by the local Ethics Committee. The patella tendon moment arm was measured at rest with a 0.2 T MRI system (Esaote Medical, Italy) with the knee in full extension. The 3D MRI images (52 slices 1.7 mm apart) were analysed as follows to determine the patellar tendon moment arm. The contact points of the lateral and medial condyles were first determined as the midpoint of the shortest distance between the condyles and the tibial plateau. The specific sagittal plane slices in the medial and lateral side were chosen by examining the condyle-tibial plateau distances in the frontal plane slices. The knee contact point was calculated as the midpoint of the line connecting the medial and lateral condyle contact points. The sagittal slice corresponding to that point was used to measure the moment arm as the length of the perpendicular (shortest) line between the patella tendon and the knee contact point in the sagittal plane. In addition the following anthropometric measurements were taken: Height, mass, knee circumference, mediolateral (M-L) knee width, anteroposterior (A-P) knee width, femur (greater trochanter-tibial plateau) length, tibia (tibial plateau-malleolus) length and leg length (greater trochanter-malleolus) length. Pearson correlation coefficients and multiple regression were used to examine the relationships between the anthropometric measurements and the patellar tendon moment arm.

RESULTS AND DISCUSSION

The Pearson correlation coefficients obtained ranged from -0.04 to 0.42 (Table 1). None of the correlations examined was statistically significant ($P>0.01$), The variable with the best correlation with the moment arm was knee circumference ($r=0.49$, $P<0.05$) but the coefficient of determination R^2 was only 0.179 (Figure 1) indicating that only about 18 % of the variance in PT moment arm can be explained by knee circumference.

Table 1. Descriptive statistics of the anthropometric parameters examined and correlation coefficients with patella tendon moment arm.

	Mean±sd	**r**	**P**
Height (cm)	181.90±7.98	0.31	0.076
Mass (kg)	79.19±7.56	0.40	0.036
Knee Circumference (cm)	37.52±1.66	0.42	0.024
Knee Width (M-L) (cm)	11.04±0.47	0.25	0.133
Knee Width (A-P) (cm)	12.66±0.54	0.21	0.166
Leg length (cm)	86.91±4.30	0.18	0.201
Femur Length (cm)	43.12±3.09	-0.04	0.419
Tibia Length (cm)	42.24±2.99	0.30	0.086

Multiple regression entering all the above anthropometric variables generated a slightly higher multiple correlation coefficient ($R=0.52$) with the overall coefficient of determination $R^2=0.27$. These results indicate that the anthropometric variables examined in this study cannot be used for accurate prediction of the patellar tendon moment arm.

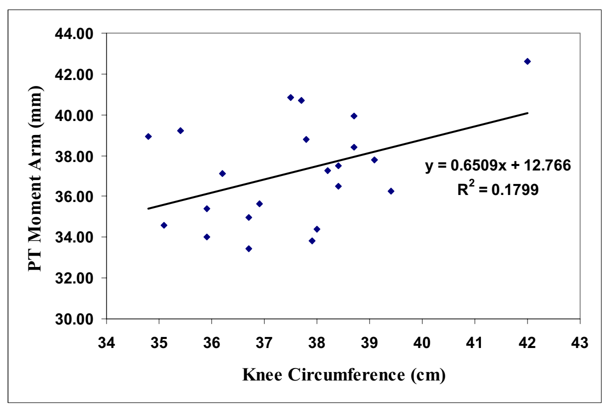

Figure 1: Scatter plot and linear regression between Patellar Tendon (PT) moment arm and knee circumference.

REFERENCES

1. Reid JG et al.. *Spine* **12,** 273-275, 1987.
2. Visser JJ et al.. *Eur. J. Appl Physiol* **61,** 453-460, 1990.
3. Krevolin JL, et al.. *J Biomech* **37,** 785-788, 2004.

EFFECTS OF ISOMETRIC AND ISOKINETIC CONTRACTIONS ON THE PATELLAR TENDON MOMENT ARM

[1]Dimitrios Tsaopoulos, [1]Vasilios Baltzopoulos, [1]Costis Maganaris and [2]Paula Richards
[1]Institute for Biophysical & Clinical Research into Human Movement, Manchester Metropolitan University, Alsager, U.K.,
[2] North Staffordshire University Hospital & Keele University, U.K.; email: d.tsaopoulos@mmu.ac.uk

INTRODUCTION

The purpose of this study was to examine the effects of contraction on knee joint mechanics and more specifically the effects of isometric and isokinetic contractions on the patellar tendon moment arm.

METHODS

Three males (age 27±6.93 years, mass 77±4.36 kg, height 1.76±0.05 m) without any musculoskeletal injuries of the lower limbs volunteered to participate after signing informed consent and radiation risk information forms. The study was approved by the local Ethics Committee. The movements were performed on a CYBEX Norm fitted with an extended input arm, to allow an adequate gap (45 cm) between the chair and the main unit to accommodate the image intensifier of a GE FlexiView 8800 C-arm X-Ray system (Figure 1). The participants were positioned on the chair and were stabilised with the standard belts and thigh straps. The most prominent point of the femoral epicondyle on the lateral surface of the knee joint and a metal disc on a strip of Perspex glass that was rigidly attached to the chair were aligned with the dynamometer axis of rotation using a special laser pointing device.

Figure 1: Photograph of the experimental set-up.

The participants performed a passive and an isokinetic knee extension at 30 deg/s and an isometric knee extension at 20 deg of knee flexion. Moment and angular displacement data from the CYBEX were captured at 200 Hz and the movements were also recorded using a pulsed mode X-ray video at 25 frames/s. The patellar tendon (PT) moment arm was measured from the X-ray video based on the methods described before [1]. Distortion correction of the images was based on a thin-plate splines method [2].

RESULTS AND DISCUSSION

There was an almost linear increase in the PT moment arm with intensity up to 75% MVC (Figure 2). The difference between moment arm values at rest and a given isometric contraction intensity was up to almost three times greater than

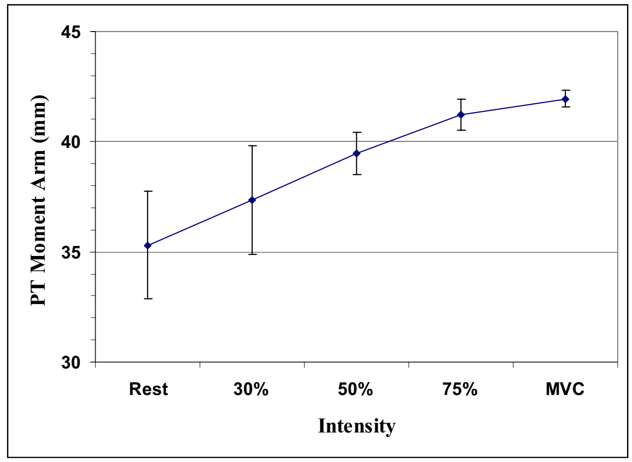

Figure 2: Patellar tendon moment arm (mean±sd) at rest and at different intensities of isometric contraction.

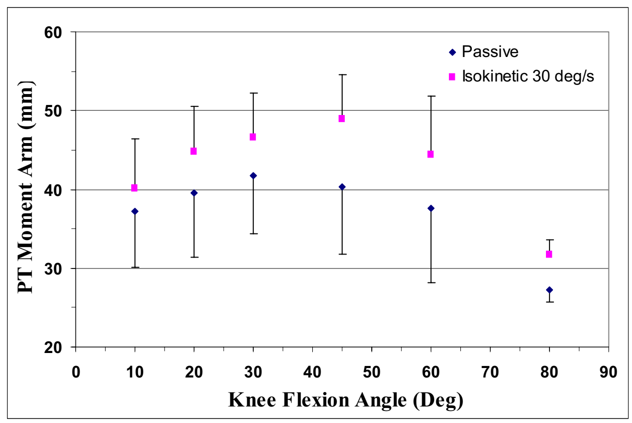

Figure 3: Patellar tendon moment arm (mean±sd) in different knee flexion angles in passive conditions (relaxed) and during isokinetic 30 deg/s knee extension.

that shown in Figure 2 when accounting for changes in tibio-femoral joint angle induced by contraction. There was also an increase in the PT moment arm between the passive movement and the isokinetic knee extension (Figure 3). The maximum average difference was recorded at 45 deg of knee flexion (8.7 mm). These results show that there are significant changes in the knee joint dynamics with contraction. Estimation of PT and knee joint reaction forces, for example, from the joint moment using PT moment arm data at passive conditions from the literature will significantly overestimate muscle and knee joint forces.

REFERENCES

1. Baltzopoulos V. *Clin Biomech.* **10**, 85-92, 1995.
2. Fantozzi S. et al. *Med. Phys.* **308**, 124-131, 2003.

QUANTIFICATION OF ENERGY ABSORBED BY THE LOWER EXTREMITY DEPENDS ON ENDPOINT OF THE IMPACT PHASE

Saori Hanaki and Steven T. McCaw
Illinois State University, Normal, IL;
email: shanaki@ilstu.edu: web www.cast.ilstu.edu/mccaw

INTRODUCTION

Landing is a complex task essential in physical activity. The lower extremity initially absorbs kinetic energy present at contact using eccentrically controlled hip and knee flexion and ankle dorsiflexion, momentarily stabilizes the body in a knee flexed position, and finally generates energy to extend the body into upright posture or a subsequent movement. The work performed by the eccentrically active muscles is estimated as the integral of the negative phase of the ankle, knee and hip joints mechanical power-time curves [1] Several researchers have investigated the relative contribution of the leg joints to energy absorption during different landing techniques[2,3], and reported differences in relative joint contributions. However, the use of different end points to define the impact phase confounds comparison of the results. The purpose of this study was to compare the absolute and relative amounts of negative work performed at each joint using different methods to define the impact absorption phase.

METHODS

Eighteen college age females, free of lower extremity trauma, volunteered as participants. In one session, 10 trials of landing from a 38 cm stool were performed; instructions were to "land comfortably." Joint kinetics (JMF) were calculated [1] using inverse dynamics from synchronized video (120 Hz) and force platform (960 Hz) data beginning before contact to beyond maximum knee joint flexion; joint mechanical power (JMP) was calculated as JMF·ω. The JMP-time curves were integrated to calculate negative mechanical work beginning with first ground contact; three end points were used: 1) when the vertical GRF leveled out or reached a minimum [3] (EP_{grf}), 2) when the lowest C of G was reached, or max knee flexion [2] (EP_{knee}), and 3) when the negative power at the knee was equal to 20% of the maximum negative knee power (EP_{pwr}), based on the observation that subsequent kinetics are more related to stabilization than energy absorption. Total work was calculated as the sum of the ankle, knee and hip works. Impact phase duration, absolute negative work and relative % work ($Work_{joint}$ / $Work_{total}$) was calculated for each of the three defined impact phases. The 10-trial mean values were entered into a repeated measure ANOVA (α=.05), with Bonferroni adjustment to the *post hocs.*

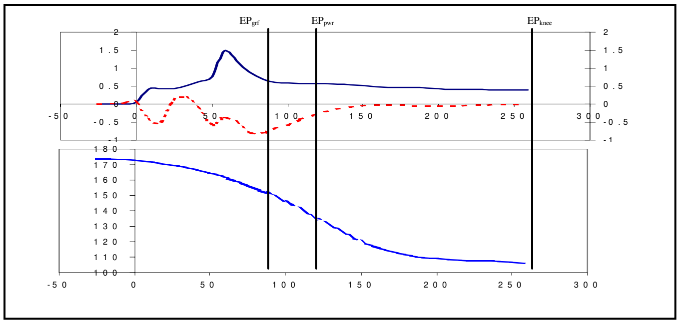

Figure 1. Typical vertical GRF (top), knee power (middle), and knee position (bottom) curves.

RESULTS AND DISCUSSION

Impact phase duration was significantly different among the techniques, shortest when defined by the GRF and longest when defined by max knee flexion (table 1). The total work and individual joint works also increased, but not significantly at the hip joint. Basically, the longer the impact phase, the greater the energy absorbed. However, for % total work, differences EP_{grf} differed from the other methods at the ankle and the knee, but not at the hip joint. EP_{pwr} and EP_{knee} did not differ for % total work at any joint. For EP_{grf}, the ankle and knee joints absorbed similar % total energy, but for both EP_{pwr} and EP_{knee} the knee absorbed significantly more energy than the ankle.

CONCLUSIONS

The method of identifying the end of the impact absorption phase affects the total and joint work calculated. The hip joint is least affected by the definition used. Most importantly, since the % contribution of joints to total energy absorption is used as a reflection of neuromuscular strategies [2,3], the comparison of the conclusions on neuromuscular adaptations must consider the different definition used in the studies.

REFERENCES

1. Winter DA. *Biomechanics and Motor Control of Human Movement.* 3rd ed., 2004.
2. Zhang, S et al. *Med Sci Sprt Ex*, **32**, 812-819, 2000.
3. DeVita P & Skelly WA. *Med Sci Sprt Ex*,**24**,108-115, 1992.

Table 1: Descriptive statistics of the power and the duration values of the different methods

		EP_{grf}		EP_{pwr}		EP_{knee}	
		Actual (J/kg)	%	Actual (J/kg)	%	Actual (J/kg)	%
Power	**Hip**	.347 ± .129	19.3 ± 7.19	.413 ± .190	17.9 ± 7.84	.510 ± .376	19.2 ± 10.81
	Knee	.744 ± .162	41.5 ± 9.41	1.087 ± .239	47.5 ± 9.97	1.177 ± .285	47.2 ± 10.89
	Ankle	.722 ± .259	39.2 ± 11.04	.801 ± .263	34.7 ± 10.91	.835 ± .266	33.6 ± 11.52
	Total	1.81 ± .253		2.30 ± .312		2.52 ± .457	
	Duration (ms)	.084 ± .012		.135 ± .028		.217 ± .078	

FE MODELING AND ANALYSIS OF COMPRESSED HUMAN BUTTOCK-THIGH TISSUE

[1,4] Qunli Sun, [1,2,4] Fang Lin, [1,3] Lissette Ruberte, [6] Ellis Nam, [5] Ronald Hendrix, [1,2,4] Mohsen Makhsous
[1] Sensory Motor Performance Program, Rehabilitation Institute of Chicago
Depts of [2] Physical Therapy & Human Movement Sciences, [3] Biomedical Engineering,
[4] Physical Medicine & Rehabilitation, and [5] Radiology, Northwestern University
[6] Dept of Orthopaedic Surgery, St. Joseph Hospital, Chicago, IL, USA
email: m-makhsous2@northwestern.edu , web: www.smpp.northwestern.edu/bossm

INTRODUCTION

Prolonged high compressive sitting stress in the buttock soft tissue of wheelchair users increases the risk of pressure ulcer (PU). However, interface pressure is currently the only available clinical tool to assess sitting load. The objective of this study was to develop a 3D finite element (FE) model to investigate how the buttock-thigh soft tissue responds to external sitting load. It was expected that this FE model would be a powerful tool for better understanding of the biomechanical response of buttock tissue to sitting load.

METHODS

A healthy subject was posed and loaded in a customer-designed apparatus at a simulated sitting posture. MRI scan was performed with two loading conditions: "No Load" and "Sitting Load". Volumetric sagittal MR images of the right buttock-thigh were acquired in the two loading conditions.

The "No Load" image sequence was segmented to reconstruct the geometry for femur, pelvis, muscles, fat and skin. Based on the geometry, the FE mesh of the buttock-thigh was created with tetrahedral elements (Fig. 1). Neo-Hookean material was employed to model each soft tissue with published data.

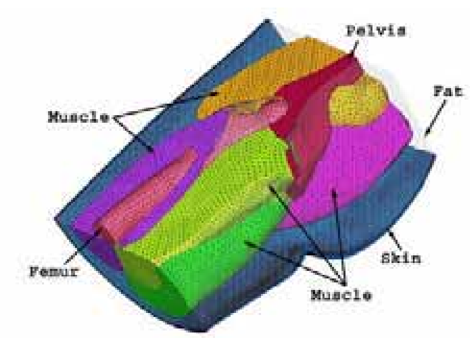

Figure 1: FE model of the buttock-thigh.

The bones were assumed as fixed boundary. Since the simulation was focused on the sitting area, the upper plane was assumed to be fixed while the longitudinal ends of muscles and skin that connect the rests of thigh or buttock structures were constrained from longitudinal motion. The medial buttock plane was assumed to be constrained from the medial-lateral motion due to the symmetry of the buttocks. The measured interface pressure (157-160mmHg) was applied on the skin in the sitting area. The static FE analysis was performed using ABAQUS. The results were examined for three regions of the tissues in the sitting area that represented the soft tissues under IT, under femur, and with no bone above, respectively.

RESULTS AND DISCUSSION

The results of the simulations showed that the internal compressive and shear stress distributions were substantially different among muscles, fat, and skin. The maximum compressive stress occurred in the muscle under IT (Table 1), which is consistent with the experimental observation from other researchers [1]. The compressive stress in fat layer was distributed relatively uniform, while in muscle and skin layers, the soft tissue under bony prominences bore substantially higher internal compressive stress (Table 1). The maximum shear stress occurred within muscle under IT and skin under femur. The shear stress within muscle and skin were significantly higher than that in fat. This supports the conclusion that the shear stress may be one of factors to form PU's in the skin by other researchers [2]. The study also showed that the soft tissues were deformed significantly and the deformation was not uniform among the soft-tissue layers of the sitting area: The maximum deformation involved the deep layer, i.e. muscular layer, which was consistent to the observation from the unloaded and loaded MRI images.

Table 1: Comparison of the compressive and shear stress levels in deep soft tissues.

Region	Layer	Compressive Stress (mmHg)		Shear Stress (mmHg)	
		Mean ± SD	Max	Mean ± SD	Max
Under IT	**Muscle**	316.9 ± 99.1	568.6	144.4 ± 28.2	205.3
	Fat	182.5 ± 7.1	200.8	20.7 ± 1.3	25.3
	Skin	280.4 ± 81.8	527.9	41.3 ± 13.5	67.3
Under Femur	**Muscle**	245.6 ± 81.8	458.7	96.7 ± 13.6	136.4
	Fat	189.1 ± 20.1	233.2	42.5 ± 7.5	56.5
	Skin	325.2 ± 91.8	486.9	159.4 ± 26.9	234.8
No Bone Above	**Muscle**	206.3 ± 22.5	262.9	96.9 ± 7.9	117.5
	Fat	183.3 ± 21.7	252.3	24.8 ± 4.3	38.6
	Skin	271.2 ± 58.9	419.4	75.8 ± 15.2	133.9

The study indicates that tissue necrosis may first occur in the deep buttock-thigh soft tissue of wheelchair users because the higher internal pressure would clog the vascular system and thus reduce or terminate the supply of blood. The high shear stress within the skin and muscle may contribute to the formation of PU's in skin and muscle. The FE model will be further improved to predict the normal biomechanical response, the outcomes from potential interventions, and the interaction between the buttock-thigh and cushion.

REFERENCES

1. Linder-Ganz E et al. J Appl Physiol, 96, 2034-2049, 2004
2. Bouten CV, et al. Arch Phys Med Rehabil 84, 616-619, 2003

ACKNOWLEDGEMENTS

Supported in part by PVA Award #2321-01, R24 Rehab Network, NIH Award #R21 HD046844-01A1, NIOSH Award #R21 OH007737, Medical Technology Systems and Falk Medical Research Trust.

EFFECTS OF REPETITIVE WORK ON DISCOMFORT AND PERFORMANCE DURING COMPOSITE TASKS

Kathleen Shyhalla
Department of Industrial Engineering, University at Buffalo, email: shyhalla@eng.buffalo.edu

INTRODUCTION

Precision work has been associated with certain musculoskeletal disorders that develop when some muscle fibers do not rest. The level of task precision might impact the development of such disorders. During short tasks people moved a probe repetitively between a Home and precision target. The activation of the descending trapezius increased and the kinematics of the forearm and wrist changed with increased task precision (1).

Additional information about the impact of precision work on the extremities required understanding how and why movement patterns change during longer duration work. During a recent experiment participants performed repetitive tapping tasks for seven minutes. These tasks were preceded and followed by Composite Tasks where work was at three levels of precision. It was hypothesized that movement patterns would change after seven minutes of repetitive work and affect performance on subsequent tasks. People's performance on the Composite Tasks and their responses to discomfort surveys are described below.

METHODS

During Main Tasks participants, who had been trained in all work administered, repetitively tapped with a probe, between a Home and a precision target for seven minutes. Main Tasks were in two layouts to elicit movements in either the scapular or sagittal planes. Targets of 48 mm, 19 mm, 10 mm, and 3.2 mm diameter created no, low, medium, and high precision conditions. Composite Tasks elicited movements in the same place as the intervening Main Task, and were performed before and after each Main Task. Composite Tasks required tapping between the Home and a ray of disks in a predefined sequence for 45 seconds. Two high precision, two medium precision, and two low precision disks were on the ray. Discomfort surveys were administered before the Main Task and after the later Composite Task. Breaks were provided after later Composite Tasks. Nine participants worked in the sagittal plane only, eleven worked in the scapular planes, and nine worked in both the scapular and sagittal planes.

RESULTS AND DISCUSSION

Discomfort increased significantly during work on the Main Tasks ($P = 0.027$). The level of precision during the Main Task significantly impacted discomfort ($P < 0.001$), with high precision work leading to greater discomfort than other work. A statistically significant interaction between precision and Task Unit Number ($P < 0.001$) occurred since discomfort ratings increased greatly with Task Unit Number after high precision work, whereas discomfort ratings after work at lower levels of precision were not sensitive to Task Unit Number. The significant interaction reveals that high precision work exacerbated residual discomfort even after breaks. Errors, or the number of deviations from the pre-defined sequence, increased after work ($P = 0.043$). Errors did not depend on precision ($P = 0.712$) or Task Unit Number ($P = .960$). The time to make Home to target movements declined significantly after repetitive work ($P < 0.001$). The change in timing impacted Phase II ($P < 0.001$), with these movements requiring 0.478 seconds after work whereas they required 0.517 seconds before work. The timing of Phase I movements were not significantly affected after work ($P = 0.131$). Declines in the times to reach each disk in the Composite ray were similar ($P = 0.973$). The Main Task's precision barely impacted the time necessary for Phase II movements ($P = 0.103$). Post-hoc analysis revealed that Phase II movements were faster after low precision work than after high precision work, with times required after medium and no precision tasks were intermediate between those two.

Results show that changes to movement patterns occurred after repetitive work. The Phase II movement iteratively corrected for differences in the position of the probe and the target, and practice on this movement might have affected its timing. Practice on the proprioceptive Phase I might also have affected Phase II. If the spatial endpoint from the Phase I movement was repeatedly optimally located to reduce the need for corrective actions, the average Phase II time would have been shortened. Since Phase II movements were shortened by approximately 0.04 seconds for all target precision levels a common learning effect, not one sensitive to the target's precision, was impacting Phase II. Additional data, already collected, will provide more information about the development of Phase I and Phase II trajectories.

REFERENCES

(1) Shyhalla, K. (2003). Wrist and forearm movements while homing in on precision Targets. Proceedings of the 47th Annual Meeting of the Human Factors and Ergonomics Society, Denver, Colorado, September 13-September 17, 2003. Human Factors and Ergonomics Society, Santa Monica, California.

ACKNOWLEDGEMENTS

I would like to acknowledge the 2004 Matching Dissertation Grant from the International Society of Biomechanics, and a grant from the National Institute of Occupational Safety and Health, Grant #1-R03-OH07532-01.

THE ANALYSIS OF PRESSURE RESPONSE IN HEAD INJURY: A VALIDATION STUDY

[1]Johnson, E. A. C. and [1,2]Young, P. G.
[1]School of Engineering and Computer Science, University of Exeter, Exeter, UK Email: e.a.c.johnson@ex.ac.uk
[2]Simpleware Ltd, Innovation Centre, Rennes Drive, Exeter, UK. Email: p.young@simpleware.com
Web: www.simpleware.com

INTRODUCTION

The study of head injuries is of obvious importance with approximately 1 million head injury cases reported in the UK each year. 60% of all such injuries are caused by motor vehicle accidents but even a simple fall or blow to the head can result in serious damage. In the present study a new approach to generating physical and numerical models of the human head is presented. We aim to investigate whether it is possible to predict the response of the head for a particular impact scenario using these modelling techniques. Firstly, by predicting the global response characteristics of the head such as the duration of impact (T_p) and secondly, by studying the pressure response of the intra-cranial tissues. An approximate analytical model based on full 3D elasticity equations was developed by one of the authors and implicit analytical expressions proposed to predict the response to blunt impact [1]. The model is based on significant geometric and material simplifications and so in order to test the validity of the assumptions on which the analytical model is based, experimental and numerical models were developed for comparison. The predictions from this model were validated using finite element (FE) and rapid prototyped (RP) models generated from MRI scans obtained *in vivo*. Both the numerical and physical models were generated from the conversion of 3D image data using an in-house software package, Scan FE/IP™.

METHODS

The analytical model, presents a blunt direct impact with a solid, elastic spherical shell of isotropic homogeneous linear elastic material properties and filled with an inviscid compressible fluid. Even for this simplified case the response is dependent on a number of material and geometric parameters including the shell thickness (h), radius of curvature (R), Young's Modulus (E) and Poisson's Ratio (ν).

MRI scan data of an adult male was obtained and an STL file was created using an in-house software package, Scan IP™ [2]. The STL file was used to manufacture a 3D, patient specific, rapid prototyped (RP) model of the human skull using Duraform™ Polyamide, a material used typically for strong, functional applications. A 3D FE mesh of the skull and intra-cranial contents was also generated from the same MRI dataset, using the in-house software package ScanFE™. The FE model consisted of over 200,000 hexahedral and tetrahedral elements and a sliding contact surface was assumed at the brain-skull interface. The material properties for the RP material and a steel impactor were incorporated into the model and LS-DYNA3D was used to perform the numerical solutions.

RESULTS AND DISCUSSION

The authors have previously reported [3] on the excellent agreement between the three modelling modalities for the measurement of global response characteristics such as impact duration, acceleration and peak force. The emphasis of this current paper is, therefore, on the pressure response of the intracranial fluid. Impacts of low duration, for example, have often been associated with increasingly large pressure transients as illustrated in Figure 1 and carry significant implications for the occurrence of brain tissue damage.

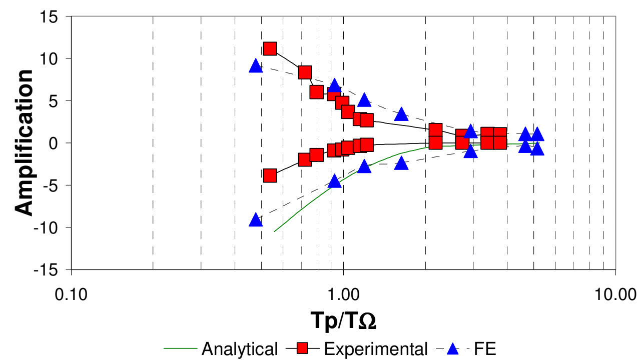

Figure 1. Peak positive and negative pressure values as obtained using the three modelling methods

The remarkable conformity between the three modelling techniques is clear and corroborates the prediction of increasing pressure amplification at the site of impact, for impacts of low duration.

CONCLUSIONS

In addition to the obvious significance in the area of head injury biomechanics, the study demonstrates how numerical and biofidelic physical models, can be generated from 3D medical imaging modalities and used effectively to simulate physical processes.

REFERENCES

1. Young, P. G., An analytical model to predict the response of fluid-filled shells to impact - A model for blunt head impacts, *J. Sound & Vibration,* **267,** 1107-1126, 2003
2. Simpleware Ltd. www.simpleware.co.uk
3. Johnson E. A. C., Young P. G., On the use of a patient specific rapid prototyped model to simulate the response of the human head to impact and comparison with analytical and finite element models, *J. Biomech.*, **38**, 39-45, 2005

OFFLOADING THE DIABETIC FOOT USING FOREFOOT OFFLOADING SHOES

[1] Sicco Bus, [2]Robert van Deursen, [2]Rajani Kanade, [1]Marieke Wissink, and [1]Erik Manning
[1]Diabetic Foot Unit, Department of Surgery, Twenteborg Hospital, Almelo, The Netherlands
[2]Research Center for Clinical Kinesiology, Department of Physiotherapy, Cardiff University, Cardiff, UK
email: s.bus@twenteborg.nl

INTRODUCTION

Most plantar foot ulcers in diabetic patients are caused by a combination of neuropathy and elevated plantar pressure and develop in the regions of forefoot and toes. Casting devices (i.e. Total Contact Cast or Mabal shoe) are commonly used for offloading these ulcers. Alternatively, in many diabetic foot centers where casting technicians are absent, prefabricated forefoot offloading shoes (FOS) are used for ulcer treatment. However, little is known about the biomechanical effectiveness of the FOS. Therefore, the purpose of this study was to assess the effectiveness of FOS in offloading the forefoot in diabetic patients with peripheral neuropathy.

METHODS

Twenty-four diabetic patients (20 men, 4 women) with peripheral neuropathy participated. Mean (SD) age, height, and weight was 60.0 (7.0) years, 1.72 (0.07) m, and 92.0 (15.2) kg, respectively. Loss of protective sensation due to neuropathy was confirmed using a 10-grams monofilament. Four FOS were tested: the Thanner Cabrio (www.thanner-gmbh.com), Rattenhuber Talus (www.rattenhuber.de), Fior&Gentz Hannover, and Fior&Gentz Luneburg (www.fior-gentz.de), together with a Pulman shoe (www.fld.fr) used as control condition. The Mabal fiberglass cast shoe was also added for comparison [1].

Patients walked at their own preferred speed across a 18-m walkway wearing the test shoe on the right foot and their own shoe on the left foot. Shoes were randomly assigned to each patient. In-shoe plantar pressure was measured using the Pedar system (Novel, Germany). A minimum of 20 steps in 3 trials were collected. Walking speed was measured using a stopwatch. Peak pressure, pressure-time integral (PTI), and force-time integral (FTI) were calculated for 6 different anatomical foot regions: heel, midfoot, MTH1, MTH2-5, hallux, and lesser toes. Comfort of walking was assessed on a scale from 0 (very uneasy) to 10 (very easy). ANOVA was used for statistical comparisons between the shoes ($P < 0.05$).

RESULTS

Walking speed varied from 1.99 m/s in the F&G Luneburg to 2.07 m/s in the control shoe and was not significantly different between shoe conditions. At the MTH regions, peak pressure and PTI were significantly reduced (by 38-58%) in all FOS and the Mabal cast shoe when compared with the control shoe (Table 1) ($P<0.001$). Loading (FTI) of the heel was similar between shoe conditions, but midfoot FTI was substantially increased in the FOS when compared with the control shoe (up to 162% in the F&G Luneburg). Walking comfort varied substantially between conditions with the control shoe being the most comfortable and the F&G Luneburg the least comfortable shoe (Table 1).

DISCUSSION

All four FOS were equally effective in offloading the forefoot of the neuropathic diabetic patients, with only minor differences between the shoes. The action of the FOS to transfer pressure from the forefoot to proximal regions was clearly illustrated by the substantially increased midfoot loads when compared with the control shoe. Compared with the Mabal cast shoe, which has been shown to be effective in healing relatively small neuropathic plantar ulcers [1], the FOS reduced MTH peak pressure to a greater extent. Although we do not know how much offloading is required to heal ulcers, these data suggest that the FOS may be effective for this purpose. We are currently studying the efficacy in healing neuropathic plantar forefoot ulcers using the FOS. Due to its low perceived comfort of walking, the Fior&Gentz Luneburg should not be used as therapeutic shoe for diabetic patients.

REFERENCES

1. Hissink et al. *Foot and Ankle* **21**, 320-323, 2000.

ACKNOWLEDGEMENTS

The authors are grateful to Michelle Evans and Sally Rees-Mathews for their contributions to this study.

Table 1: Mean (SD) results for pressure data and walking comfort

Shoe condition	Peak pressure (kPa)		Pressure-time integral (kPa.s)		Force-time integral (N.s)		Walking comfort
	MTH1	MTH2-5	MTH1	MTH2-5	Midfoot	Heel	
Control shoe	364 (102)[a]	272 (90)[a]	93.1 (35.9)[a]	75.8 (30.3)[a]	28.2 (38.5)	110.6 (22.1)	8.2 (1.5)[c]
Thanner Cabrio	153 (43)	128 (42)	50.0 (17.4)	44.2 (19.0)	58.2 (38.9)	105.6 (36.6)	5.9 (2.4)
Rattenhuber Talus	156 (40)	130 (46)	47.0 (14.8)	46.2 (21.4)	66.3 (41.7)[b]	92.6 (31.3)	4.6 (2.4)
F&G Hannover	165 (43)	127 (48)	55.7 (19.6)	46.9 (17.9)	66.3 (44.2)[b]	88.8 (29.7)	4.7 (2.5)
F&G Luneburg	153 (57)	135 (43)	50.2 (20.5)	45.3 (18.7)	73.8 (53.6)[b]	111.0 (46.7)	2.7 (2.2)[a]
Mabal cast shoe	203 (65)	166 (59)	54.2 (22.0)	46.6 (18.6)	61.6 (39.0)	86.6 (23.4)	6.8 (1.9)[d]

Significantly different to [a]any other condition, [b]control shoe, [c]all other FOS, and [d]Rattenhuber and both F&G shoes ($P<0.05$)

POWERING THE KNEED PASSIVE WALKER WITH BIARTICULAR SPRINGS

[1] Jesse C. Dean and [2]Arthur D. Kuo
[1]Dept. of Biomedical Engineering, [2]Dept. of Mechanical Engineering
University of Michigan, Ann Arbor, MI. E-mail: jcdean@umich.edu

INTRODUCTION

Passive dynamic walking can be powered by push-off impulses applied along the trailing leg. This form of powering is possible in both straight-legged models [3, 4] and following the addition of knees [1]. In the kneed model, the addition of torsional springs at the hip and knee—as an analogue for muscular torque generation—allows for a wider range of stable gaits. These springs also can reduce energetic losses associated with redirecting the body center of mass during step-to-step transitions [3]. The hip spring helps to generate human-like step frequencies, and the knee spring facilitates proper knee lock timing. Here we show that similar effects can be achieved with a single biarticular spring crossing the hip and knee joints of the swing leg. The spring produces forces similar in phase to those expected from the biarticular muscle activity seen in humans. It appears to be theoretically advantageous to produce higher torques about the hip than the knee, because a human-like gait can be achieved with the lowest spring forces.

METHODS

While torsional springs can be used to model the torques produced about the joints, the human leg also has biarticular muscles which cross both the hip and knee joints. Of particular interest in gait are the rectus femoris, which can produce hip flexion and knee extension, and the long head of the biceps femoris, which generates hip extension and knee flexion. Biarticular springs with attachments above the hip and below the knee can model the action of these two muscles. We used dynamical simulations to determine the effect of a biarticular spring on the kinematics, energetic costs, and stability of the kneed walking model.

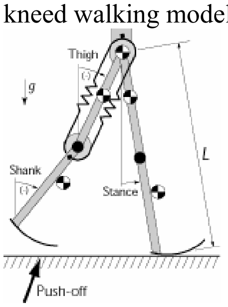

Figure 1. Side view of the walking model. The stance leg is actuated by an impulsive push applied along the leg prior to heel strike, and the joints are actuated by biarticular springs on the anterior and posterior sides of the swing leg. Stance, swing thigh, and swing shank angles are measured counter-clockwise with respect to vertical.

Our planar kneed walking model was similar to McGeer's [4], consisting of four segments with anthropometrically distributed mass, and curved feet offset forward from the legs (Fig 1). Hyperextension of each knee was prevented by a passive mechanical stop. We added a push-off impulse applied at the ground contact point of the stance leg and directed toward the hip, and a variable stiffness spring with one attachment point directly above the hip, and the other on the shank below the knee. The moment arms about the hip and the knee, as controlled by the attachment points, were variable. The model was made non-dimensional by normalizing by body mass (*M*), leg length (*L*), and gravity (*g*).

The periodic gait was powered solely by push-off. During a gait cycle, knee lock and heel strike, modeled as impulsive inelastic collisions, produced instantaneous changes in segment speeds with accompanying energy losses.

RESULTS AND DISCUSSION

As found in the model with torsional springs, step length was predominantly governed by push-off impulse. Step frequency was controlled by the biarticular spring stiffness and the moment arm about the hip. At higher speeds, a minimum spring stiffness is required for stability, and to generate high step frequencies. For a given spring stiffness and hip moment arm, there is a minimum knee moment arm required to ensure that knee lock occurs before foot touchdown.

The configuration of the biarticular spring on the swing leg causes hip flexion and knee extension torques early in the swing phase, and hip extension and knee flexion torques late. This pattern is similar to the torques expected from rectus femoris and biceps femoris muscle activity [2].

Stable gaits at the preferred human speed and step frequency (1.2 m/s, 1.8 Hz) can be generated by appropriate choice of parameters. Push-off is approximately constant across the possible range, but the peak forces or torques produced by the springs, representing muscular forces, can be minimized by producing more torque about the hip than the knee. This may be accomplished by choosing a weak spring about the knee in the torsional spring model (Fig 2a), or springs with a smaller moment arm about the knee than the hip in the biarticular model (Fig 2b).

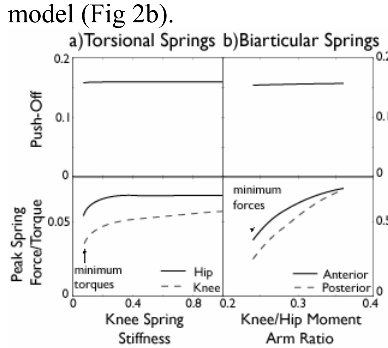

Figure 2. Human-like gaits can be generated using (a) torsional or (b) biarticular springs. In both models, spring forces or torques are minimized by generating less torque across the knee than the hip.

REFERENCES

1. Dean JC, Kuo AD. *Proceedings of the ASB*, Portland, OR, Abstract 383, 2004.
2. Hof AL et al. *Gait Posture*, **16**, 78-86, 2002.
3. Kuo AD. *JBME* **124**, 113-120, 2002.
4. McGeer T. *Int J Rob Res*, **9**, 68-82, 1990.

ACKNOWLEDGEMENTS

Supported by the UM Institute of Gerontology, and NIH grant R21DC6466.

LOCATING FATIGUE MICROCRACKS OCCURRING IN CEMENTED TOTAL HIP ARTHROPLASTY

Jihui Li[1] and Gang Qi[1,2]
[1]Dept. of Biomedical Engineering, [2]Dept. of Mechanical Engineering. The University of Memphis, Memphis, TN 38152
E-mail: jihuili@memphis.edu Web: http://www.me.memphis.edu/mar_lab/mar_lab/home.htm

INTRODUCTION

Accumulation of fatigue microcracks (MCs) has been reported as a major cause of the loosening of cemented total hip arthroplasty (THA). Although experimental models were developed to locate MCs in the cement layer [1-2], they were often limited to certain cross-sections and loading cycles. Acoustic emission (AE) is a non-destructive technique that is capable of locating a MC when its signals are received by four or more AE sensors, but the traditional AE algorithm using an iterative approach worked poorly when applied to THA specimen that had multiple layers of materials [3]. The purposes of this work were to: 1) investigate the drawbacks of the traditional algorithm and improve it accordingly; and 2) examine the error level of calculated locations of fatigue MCs.

METHODS

A cemented THA specimen was prepared for this study using Spectron stem, Palacos R cement and Sawbone femurs. 8 AE sensors were attached on the specimen's surface to monitor the MCs. Theoretically, parameters involved in MC location calculation included: receiving time and velocity of the AE signals, and the sensors spatial coordinates. There were three layers of materials in THA specimen, AE signals reflected and/or refracted a number of times at the interfaces before being received by sensors. Inhomogeneity and anisotropy of cement and bone complicated the signal propagation as well. As a result, the velocity was frequently delayed (receiving time was linear correlated to velocity and ignored in analysis). The delay induced significant errors in MC locations when using the traditional algorithm, in which velocity was an estimated constant assigned to all signals. In the improved algorithm, velocity was set as a variable that could be adjusted based on the magnitude of the residual of the signal's receiving time. The improved algorithm was first verified using artificial MCs (pencil lead break, PLB) generated on the THA surface. Then it was used to locate fatigue MCs. The area that the most MCs cumulated was sectioned and inspected using SEM. Location error was evaluated by overlaying the calculated MCs to the observed MCs.

RESULTS AND DISCUSSION

The improved algorithm reduced location errors of artificial MCs from 7.1 mm (using the traditional algorithm) to 4.2 mm. Most calculated fatigue MCs located in the proximal THA, whereas many of them were out of THA when computed by the traditional algorithm (Fig. 1). Six short discontinuities were observed along the stem-cement interface on Section A, adjacent to most calculated MCs (Fig. 2). When comparing the locations of these two sets of MCs overlaid on the same section image, the average error in X direction was 3.3 mm and 1.7 mm in Y direction. Considering the overlay could induce an average error of 3 mm (generally less than this), the total absolute error in X-Y plane was 4.77 mm. Error in Z direction was unavailable because the information was limited to only one section.

It was found that the range of adjustment on velocity was different among sensors. Generally the range was small for sensors that were close to the MC, and large for sensors far away from the MC. The range was small in artificial MCs (high strength) and large in fatigue MCs. This indicated that the delay of velocity was influenced by material distribution, signal strength and travel path (related to signal attenuation).

CONCLUSIONS

This study found that, in the traditional AE location algorithm, the major reason for inaccurate MC locations was the delay of signal velocity. The algorithm was improved by adjusting the value of velocity in computation. The new algorithm improved the accuracy of MC location significantly and achieved an average error of 4.77 mm in the X – Y plane.

REFERENCES

[1] McCormack et al., J Biomech 1999; [2] Race et al., ibid, 2003; [3] Qi et al., J Biomed Mater Res. 2004.

ACKNOWLEDGEMENTS

The project was supported in part by the Whitaker Foundation RG-01-0482.

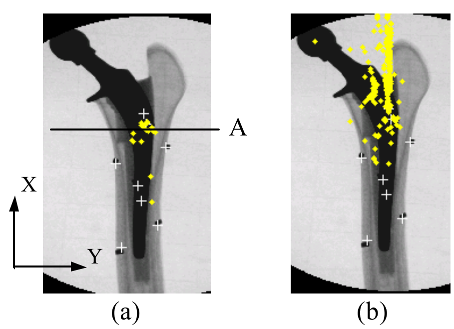

Fig. 1 (a) Calculated MCs using improved algorithm. The specimen was sectioned at A. (b) Calculated MCs using original algorithm.

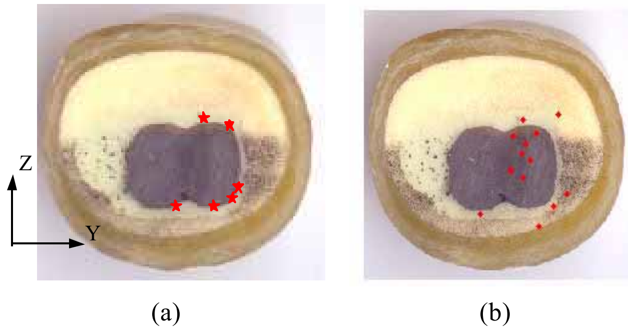

Fig. 2 (a) MCs distribution on Section A observed by SEM, (b) calculated MC locations on section A.

OPTIMAL CONTROL SIMULATIONS DEMONSTRATE HOW USING HALTERES (HAND-HELD WEIGHTS) CAN INCREASE STANDING LONG JUMP PERFORMANCE

Blake M. Ashby
Department of Mechanical Engineering, The University of Texas at Austin
email: blake.ashby@stanfordalumni.org

INTRODUCTION

Swinging the arms during the standing long jump has been shown to increase distance performance [1,2]. Studies have also suggested that using halteres (hand-held weights) as the ancient Greek Olympians did can further improve jump distance by at least 17 cm [3]. Since the combined body and halteres system must follow a parabolic trajectory during flight, throwing the halteres backwards just before landing could further enhance performance by thrusting the body forwards [3].

The present study used optimal control simulations of the standing long jump to assess if performance is improved by using halteres, and if so, how the performance increase is achieved. In addition, simulations were performed to determine how the size of the halteres influences jump distance and if further performance gains can be achieved by releasing the halteres before landing.

METHODS

The take-off and flight phases of the standing long jump were simulated using a 2-D seven segment (foot, shank, thigh, head-neck-trunk, upper arm, forearm, halteres) link model of the human body [2] (Figure 1). The ankle, knee, hip, shoulder, and elbow joints were modeled as revolute joints and were actuated by individual joint torques. The magnitude of torque generated by the joint actuators was governed by the activation, joint angle, and joint angular velocity [2].

The optimal activations that would maximize jump distance were found using a simulated annealing algorithm. Optimal solutions were determined for three types of jumps: i) jumping without halteres, ii) jumping with halteres (different total masses of 4, 6, 8, 10, and 12 kg) without releasing them during the flight, and iii) jumping with halteres with the option of releasing them during flight to improve jump distance.

RESULTS AND DISCUSSION

Using halteres during the standing long jump improved performance by much more than the 17 cm suggested by Minetti and Ardigó [3]. The jump distance for the nominal simulation (no halteres used) was 2.35 m (Table 1). Performance improved for all the different masses, but was greatest for the simulations using the 8 kg halteres. For the case in which releasing the halteres before landing was not allowed, the simulated jump distance was 2.74 m, an improvement of 39 cm.

Analysis of the simulation mechanics showed that 12 cm of this 39 cm improvement was due to the greater horizontal position of the center of gravity at take-off due to extending the halteres ahead of the body. The remaining 27 cm of improvement was due to the 22% greater velocity of the center of gravity at take-off. This greater velocity was primarily due to the increased kinetic energy (292 J) (obtained by swinging the arms back and forth before take-off [3]) and potential energy (45 J) of the halteres at the beginning of the simulation. However, some of the improvement in the take-off velocity for the jump with halteres can be explained by the additional 45 J of work performed by the joint actuators during the propulsive phase.

Table 1: Jump distances for the three types of jumps.

Type of jump	Jump distance
i) jump without halteres	2.35 m
ii) jump with 8 kg halteres without release	2.74 m
iii) jump with 8 kg halteres with release	2.89 m

Releasing the halteres during flight increased the jump performance an additional 15 cm, for a total jump distance of 2.89 m. However, optimal performance was not obtained by releasing the halteres just before landing as previously suggested [3]. The optimal time to release the halteres was about 0.18 s after take-off when the arms were extended above the head near the top of the jump (Figure 1). Releasing the halteres just before landing only resulted in an improvement of about 1 cm relative to not releasing them.

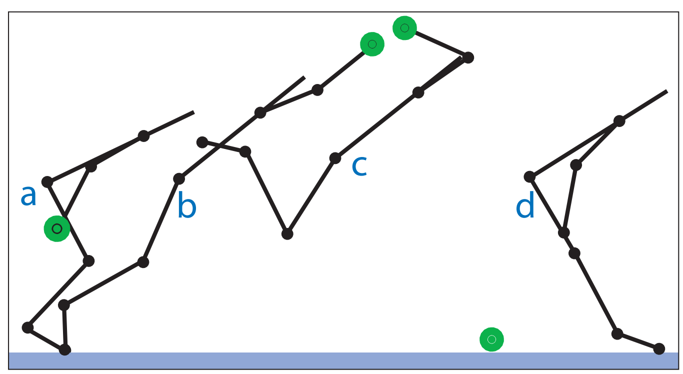

Figure 1: Body configurations at the starting point (a), take-off (b), the point where the halteres are released (c), and landing (d) for the simulated jump with 8 kg halteres.

REFERENCES

1. Ashby BM and Heegaard JH, *J Biomech* **35**, 1631-1637, 2002.
2. Ashby BM and Delp SL, *J Biomech*, submitted.
3. Minetti AE and Ardigó LP, *Nature* **420**, 141-142, 2002.

AGGRESSIVE INLINE SKATING: BIOMECHANICS OF LANDING AND BALANCING ON A GRIND RAIL

Matthew J. Major, Armand Beaudoin, Peter Kurath, and Elizabeth T. Hsiao-Wecksler
Department of Mechanical and Industrial Engineering
University of Illinois at Urbana-Champaign, Urbana, Illinois, USA
email: mmajor@uiuc.edu, web: http://www.mie.uiuc.edu/hsiao-wecksler/hdcl/hdcl.html

INTRODUCTION

Aggressive inline skating, or trick skating, is a relatively new sport. Previous studies of aggressive skating have only examined epidemiological data of skate park injuries [1]. This novel biomechanical study of aggressive skating focused on the “stall”, a basic balance training activity where the skater repeatedly jumps on an elevated surface (concrete bench edge, metal hand rail, or specially designed skate park “grind” rail). We were interested in understanding how skaters are able to successfully land and maintain balance over such a narrow base of support. Specifically, we examined sagittal-plane biomechanics of the lower extremities to see how impact force, skater experience, and joint behaviors (maximum flexion, net eccentric/concentric contraction and work) were related. We hypothesized that, to smoothly decelerate the body and minimize impact forces, this exercise emphasizes development of muscle control though eccentric contractions of the lower extremity joints. We also hypothesized that more experienced skaters would minimize impact force.

METHODS

Ten male skaters (21.8 ± 8.5 years, 179.0 ± 6.5 cm, 78.3 ± 8.0 kg) performed 10 stalls each. Each subject was instructed to jump onto a grind rail, maintain balance (1-3 s), and jump down. No constraints were placed on landing and balancing techniques, allowing the skater to maintain his unique style of performance. A simply-supported, steel grind rail (5 cm diameter pipe, 178 cm length x 26 cm height) was constructed to sustain no moments at the supporting ends. Load cell data (MTS Systems, Minneapolis, MN; 1000Hz sampling rate) from each end were used to compute vertical impact force (% body weight). Joint flexion at the ankles, knees and hips were determined from kinematic data collected with a 6-camera motion capture system (VICON 460, Oxford, UK; 100 Hz sampling rate). The landing phase was defined as the period between initial contact with the rail (S) and point of greatest flexion of the joint (F_i, where i = L or R) (e.g., Figure 1 for knee). For each joint, maximum flexion during the landing phase was defined as the magnitude difference in flexion between S and F_i; similarly, eccentric work during the landing phase was defined as the area under the negative power curve between S and F_i. Finally, the parameters, maximum joint flexion and eccentric work, were computed from the average of the right and left values. To test our hypotheses, correlation analyses assessed whether peak impact force associated with skater experience or maximum joint flexion.

RESULTS AND DISCUSSION

Peak impact force was found to significantly decrease as skater experience increased (r = -0.842, p = 0.002). Less-experienced skaters were not capable of reducing impact force while successfully landing and maintaining balance. Peak impact force was also found to significantly decrease with increasing knee flexion for six of ten subjects ($p \leq 0.041$). Three of four subjects with no correlation had the least amount of experience. The remaining experienced skater displayed a significant correlation between decreasing peak impact force and increasing ankle flexion. No significant correlation was found between hip flexion and peak impact force for any subject. During the landing phase, skaters utilized eccentric contraction of all lower extremity joints in order to decelerate the body and absorb energy. Of the three lower extremity joints, the knees performed on average the most eccentric work during the landing phase (50.6 ± 12.0% (SD)), followed by the hips (30.1 ± 13.5%) and ankles (20.5 ± 12.9%).

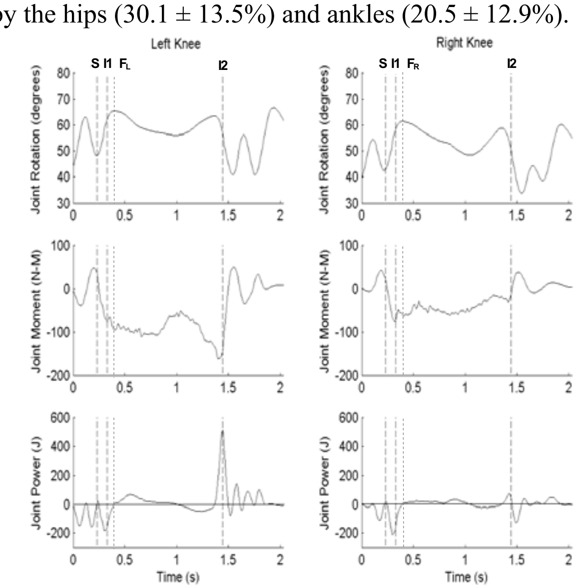

Figure 1: Typical profiles for left and right knee. Vertical lines identify instants of initial rail contact (S), first peak impact force -- used in correlation analyses (I1), greatest joint flexion (F), and second peak impact force (I2). Flexion angle, flexor moments, and concentric contraction are defined as positive.

CONCLUSIONS

Increasing knee flexion (or net eccentric contraction of the thigh muscles) immediately after contact with the rail and throughout the landing phase was extremely effective in reducing peak impact forces. Subjects who did possess a joint flexion correlation with peak impact force had significantly more experience than those who did not. Less-experienced skaters may be more concerned about maintaining balance, rather than refining their technique to (subconsciously) minimize impact force.

REFERENCES

1. Everett, W.W. J Emer Med; 23(3): 269-274, 2002.

MODELING EXTRINSIC FINGER FLEXOR TENDON KINEMATICS

Jeremy P.M. Mogk, MSc and Peter J. Keir, PhD
School of Kinesiology & Health Science, York University, Toronto, Ontario, Canada
email: pjkeir@yorku.ca

INTRODUCTION

Trauma to the tendons and nerves of the hand and wrist has been attributed to chronic tissue stress experienced during their interactions with surrounding osseous and soft tissues. Biomechanical modelling has become a common non-invasive method to estimate tissue and joint forces. While a number of models of the hand and wrist exist, recent evidence suggests improved joint kinematics are needed to increase the accuracy of predicted force transmission [1]. Tendon excursion for the same finger motion has been shown to vary depending on wrist posture using both an analytical model [2] and in canine limbs *in vivo* [3]. In addition to excursion itself, the effects of tendon motion also require investigation, as movement of the tendons relative to each other, as well as bone surfaces, likely alter tissue loading (tensile, compressive and shearing forces). The purpose of this study was to develop a model of finger flexor tendon motion that incorporates the interactions between the tendons and their surrounding tissues during finger motion.

METHODS

A three-dimensional dynamic model of the hand was developed using Maya™ v5.0 software (Alias®, Toronto, Canada). Each of the fingers was constructed as a series of four rigid body segments, sculpted to represent the metacarpal and phalangeal bone surfaces (Figure 1). A coordinate system positioned at each of the MCP, PIP and DIP joint centres defined locations and orientations of the tendons and bone segments, and defined joint posture. Scalable relationships were used to determine segment lengths, joint centre locations, and tendon centre locations of the flexor digitorum profundus and superficialis muscles proximal and distal to each finger joint space [4,5]. The annular pulley system of each finger was modelled as a series of modified rigid body cylinders attached to the palmar surface of each phalanx, to constrain palmar and mediolateral displacement of the flexor tendons. In order to utilize the mechanics of solid materials inherent in the software, each tendon was defined as a string of rigid body spheres, affixed to one another via pin joints. Tendon excursion and resultant joint motions were dependent on the interactions between the spheres, as well as with the pulleys surfaces. Initial testing focused on tendon excursion and changes in moment arm magnitude during isolated joint movements in the flexion-extension plane, allowing results to be compared to those found in the literature. For this communication, analyses were limited to the deep (FDP) and superficial (FDS) flexors of the index finger.

RESULTS AND DISCUSSION

While model development and testing are ongoing, this study represents one step in the development of a biomechanical model of the hand and wrist. Flexor tendon excursions for the index finger are in agreement with those in the literature with greater FDS than FDP excursion during MCP flexion [4]. DIP flexion of 90° resulted in 6.7 mm of FDP excursion. In addition, the physical interactions between the tendons resulted in slight FDS movement when tension was applied to the FDP tendon (1-2 mm depending on condition). And, with tension applied to both FDS and FDP, concurrent flexion of all three finger joints resulted.

While the hand and wrist model is still in its relatively early stages, the benefits are readily visible. This method enables tendon thickness and natural restraints created by the bone, tendon and pulley surfaces to predict tissue interactions and force transmission. In the future, the shape and cross-sectional area of each tendon can be incorporated from existing MRI data to improve the anatomic fidelity. By incorporating tendon excursion and changes in moment arm lengths into our existing model of the carpal tunnel [6], a more realistic and complete understanding of three-dimensional tendon movement through the carpal tunnel will result. This will enable investigation of soft tissue interactions within the carpal tunnel, including median nerve compression. A model that includes differential tendon excursion and interaction, with the potential to add frictional effects, is an important step in understanding injuries at the wrist, such as carpal tunnel syndrome and tenosynovitis.

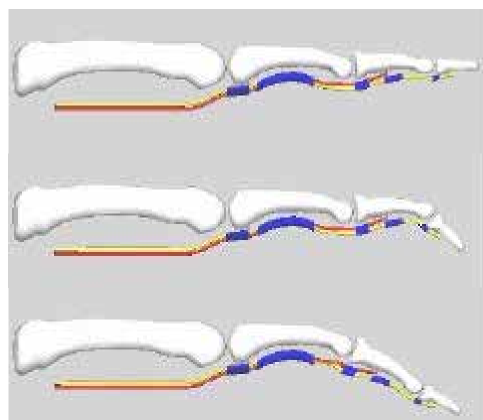

Figure 1. Excursions were measured from the straight finger (top) and included DIP (middle) and PIP (bottom) joint flexion.

REFERENCES

1. Valero-Cuevas, F.J. et al (2003). *J Biomech*, **36**, 1019-1030.
2. Nelson, J.E. et al (2000). *Clin Biomech*, **15**, 489-498.
3. Lieber, R.L. et al. (1999). *J Biomech*, **32**, 175-181.
4. Chao, E.Y. et al (1989). *Biomechanics of the Hand*, World Scientific Publishing Co., Inc., Singapore.
5. Buchholz, B. et al (1992). *Ergonomics*, **35**, 261-273.
6. Mogk & Keir (2004). *Proc. of 13th CSB Conference*.

ACKNOWLEDGEMENTS

Special thanks to Cory Mogk for his invaluable assistance and expertise with the Maya™ software. This work was funded by NSERC (Canada), grant #217382.

FATIGUE EFFECTS ON BAR KINEMATICS DURING THE BENCH PRESS

[1]Michael J Duffey and [2]John H Challis
[1]Department of Physical Education, The United States Military Academy, West Point, NY
[2]Biomechanics Laboratory, The Pennsylvania State University, USA
email: mike.duffey@usma.edu, jhc10@psu.edu

INTRODUCTION

The kinematic patterns of the bar during a single lift bench press have been reported [1], however, there is no report of how bar movement changes as a subject performs multiple repetitions to failure. Multiple repetitions of an exercise are often used to train for a single exertion for example in powerlifting, or as means of training a particular muscle group. If the kinematics of the task change with increasing number of repetitions the specificity of the training must be questioned, as can its training effect on a particular muscle group. The purpose of this investigation was to examine the effects of fatigue on the movement of the bar during a free weight bench press.

METHODS

Eighteen male and female subjects were recruited after completion of a college level introductory weight training course. They had a range of maximal bench presses from 52 to 166% of body weight. All subjects were considered experienced recreational lifters. Maximal single repetition bench press load (1-RM) was determined, and then subjects were asked to perform as many repetitions as possible at 75% of 1-RM load. A Pro-Reflex motion analysis system was used to determine bar path during each trial. Subsequent processing of these data provided bar velocity, and the timings of key kinematic events. For each repetition the start of lowering was considered 0% of movement time, and the end of raising the bar 100% of movement time. Repeated measures ANOVA was used to compare across various metrics of bar path and trajectory across repetitions. Alpha was set at $p \leq 0.05$.

RESULTS AND DISCUSSION

Subjects were able to complete between 4 and 16 repetitions with 75% of their 1-RM load. All data are presented as the group mean and standard deviation for the first and last repetitions. The time to lower the bar (1.43 ± 0.54 s) and the distance the bar traveled in each lift (0.33 ± 0.04 m) remained nearly constant throughout the trials.

As the subjects progressed from their first to last repetition, several changes were observed. The time to lift the bar increased from 1.08±0.26 s to 2.38±0.66 s ($p<0.01$), which accompanied a decrease in average vertical velocity from 0.33±0.07 $m.s^{-1}$ to 0.15±0.04 $m.s^{-1}$ ($p<0.01$) and a decrease in peak vertical velocity from 0.46 ± 0.11 $m.s^{-1}$ to 0.25 ± 0.08 $m.s^{-1}$ ($p<0.01$). Most notably, the timing of the peak vertical velocity changed from occurring late in the lift phase (65 ± 15% of upward lift phase) to very early in the lift phase (18 ± 21% lift phase, $p<0.01$). This pattern change is illustrated in Figure 1.

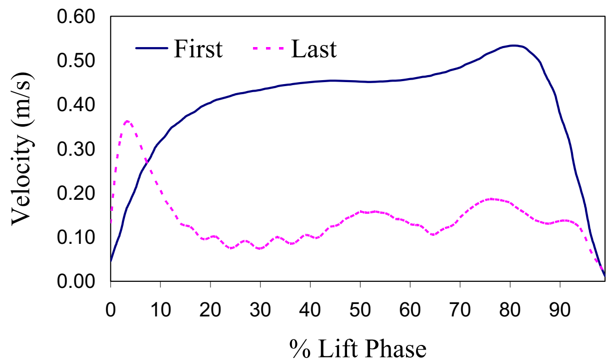

Figure 1: Bar vertical velocity for the lift phase of the first and last repetitions of a representative subject.

In the horizontal plane, subjects kept the bar more directly over the shoulder as the number of repetitions increased. The mean horizontal distance between the bar and the shoulder decreased from 0.108 ± 0.025 m to 0.073 ± 0.039 m ($p<0.01$) but change in maximal horizontal deviation of the bar from the shoulder was not found to be significant 0.142 ± 0.0027 m to 0.131 ± 0.030 m ($p=0.075$).

CONCLUSIONS

This study has demonstrated differences in bar path and trajectory over a set of free weight bench presses. These results have implications of the training effect of multiple repetitions of this exercise. The pattern of keeping the bar more directly over the shoulder during the later repetitions is believed to be a strategy to reduce the moment produced by the weight of the bar about the shoulder, as suggested by Madsen and McLaughlin [1]. Their study, however, looked at differences in single, maximal lifts between world and national caliber lifters. They found that the strongest lifters kept the bar closer to the shoulder. It is unclear why lifters would not use this strategy throughout all of the repetitions, unless the strategy used by the lifters is in some way distributing fatigue across the available muscles.

REFERENCES

1. Madsen N & Mclaughlin T. *Med Sci Sport Exer,* **16,** 376-381. 1984

THREE-DIMENSIONAL BONE KINEMATICS IN AN ANTERIOR DRAWER TEST OF THE ANKLE JOINT

[1] Leendert Blankevoort, [1]Gino M.M.J. Kerkhoffs and [2]Idsart Kingma
Institute of Fundamental and Clinical Human Movement Sciences (IFKB);
[1]Orthotrauma Research Center Amsterdam, Academic Medical Center, Amsterdam;
[2]Faculty of Human Movement Science, Free University, Amsterdam; email: orca@amc.uva.nl

INTRODUCTION

For evaluating the function of the anterolateral ligaments in the ankle joint an anterior drawer test can be performed [1]. The heel is forced forward relative to the shank. The anterior displacement of the calcaneus relative to the tibia is a measure for the anterior laxity of the ankle joint, which actually should represent the displacement between the talus and tibia. The assumption is that the calcaneus moves with the talus for the intact ligaments as well as for the ruptured ligaments [2]. The motions between the talus and calcaneus may affect the measurement in a newly designed instrumented tester. This study addressed the question to what extent the talus and calcaneus move as one in a test that is aimed at quantifying anterior ankle joint laxity.

METHODS

Five fresh-frozen cadaveric tibia-foot specimens were used. Simultaneous measurements were made with an instrumented anterior ankle laxity tester and a three-dimensional kinematic analysis system (Optotrak). Tracking LEDs were fixated to tibia, fibula, talus and calcaneus. From the continuous motion data, the three-dimensional translations and rotations of those bones were determined for anterior drawer forces up to maximally 150 N. The translations were calculated for a point at the center of the talocrural joint as marked after finalization of the drawer experiments. This point moved either with the talus or with the calcaneus. The drawer test was repeated after sequential cutting of the anterior talofibular ligament (ATFL), the calcaneofibular ligament (CFL) and the posterior talofibular ligament (PTFL).

RESULTS AND DISCUSSION

In one specimen, a luxation of the ankle joint was observed. This specimen was excluded from further analyses. For the remaining four specimens, the major motion was an anterior translation. The other translations and rotations were small and variable as illustrated by the data at 100 N anterior force (Figure 2). The anterior translation of talus and calcaneus showed a significant increase with increasing ligament damage and with increasing loads (ANOVA; $p<0.05$). On average, the motion differences between the talus and calcaneus were small, i.e. less than 1.5 mm and 2 degrees at 100 N (Figure 2). Surprisingly, the effect of cutting the ATFL was greater for the talus anterior translation than for the calcaneus anterior translation due to the altered kinematics in the subtalar joint after ligament cutting. In all 4 joints the motion coupling was mainly affected after cutting the ATFL.

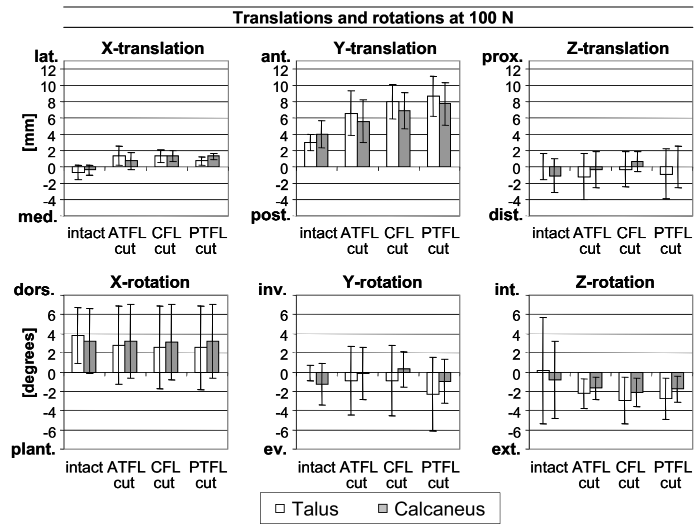

Figure 1: The translations and rotations at 100 N (average +/- s.d.) of the intact specimens (N=4) and after sequential cutting of the ATFL, CFL and PTFL. The translations are calculated for a point in the center of the talocrural joint that moves with the talus and for the same point that is virtually attached to the calcaneus and moves with the calcaneus. The motion data are calculated relative to the translation- or rotation readings at 0 N. Explanation of the abbreviations: lat. = lateral; med. = medial; ant. = anterior; post. = posterior; prox. = proximal; dist. = distal; dors. = dorsal; plant. = plantar; inv. = inversion; ev. = eversion; int. = internal; ext. = external.

CONCLUSIONS

If testing the anterior drawer of the ankle joint by evaluating the motions between the calcaneus and the tibia, then the actual translation measurement is affected by the motions between the calcaneus and the talus. This effect is small relative to the measured anterior translation. The motion coupling between the calcaneus and the talus is changed after sectioning the anterior talofibular ligament.

REFERENCES

1. Kannus P & Renstrom P. *J Bone Joint Surg (A)* **73**, 305-312, 1991.
2. Tohyama H, et al. *Am J Sports Med* **31**, 226-232, 2003.

GAIT PATTERNS OF CHILDREN WITH HYPOTONIA

[1] Victoria Chester, [2]Maureen Tingley and [3]Edmund Biden
[1]Faculty of Kinesiology,[2]Department of Mathematics and Statistics,
[3]Department of Mechanical Engineering; email: vchester@unb.ca

INTRODUCTION

Hypotonia, or decreased muscle tone, is a common diagnosis in infants and children. The presence of hypotonia is generally indicative of an underlying neuromuscular or genetic disorder, including Down syndrome. In conjunction with decreased muscle tone, children with hypotonia typically exhibit ligamentous laxity and instability of the lower limb joints, which may result in abnormal walking patterns [1]. We currently know very little about hypotonic gait patterns and treatment strategies for this disorder are controversial. The purpose of this study was to identify gait parameters that differentiated between hypotonic and normative gait patterns using statistical classifiers. A greater understanding of hypotonic walking patterns will lead to improved treatment procedures and a reduction in health care demands.

METHODS

Fifteen children, aged 3-13 years, diagnosed with hypotonia participated in the study with parental consent. Participants were recruited from the Stan Cassidy Centre for Rehabilitation in Fredericton, NB. A six-camera Vicon 512 motion capture system (Oxford Metrics Ltd.) was employed to track the three-dimensional trajectories of twenty reflective markers placed on the participants' skin at a sampling frequency of 60 Hz. Two force plates (Kistler 9281B21, AMTI BP5918) collected the three-dimensional ground reaction forces and moments during each gait cycle at a sampling frequency of 600 Hz.

A comprehensive kinematic and kinetic analysis of each child's gait was performed. The body was modeled as a series of rigid links joined by 3 degree of freedom articulations. The model consisted of the left and right foot, shank, thigh and the pelvis and trunk. Joint center locations were estimated in accordance with Davis et al. [2]. Joint angles were computed from the relative orientations of the embedded coordinate systems using Euler angles. A mathematical model (elliptical cylinder method) of the human body was used to estimate the segment inertial properties of each child [3]. Net joint moments and joint power for the hip, knee, and ankle joints were estimated using the Inverse dynamics approach.

Statistical classifiers were used to determine whether hypotonic data were significantly different from age-matched normative data. The classifier generates eight one-dimensional indices of normality for the hypotonic data [4]. The classifier examines differences in amplitude and pattern of patient gait compared to normative data. The computation of the one-dimensional indices is based on the Hotelling's T-statistic (Equation 1), which uses the normative covariance structure (Σ_B), and the difference in the means between the normative and hypotonic gait data ($B^{(i)}$).

$$D^{(i)} = \frac{82-11+1}{82\times 11}\left(B^{(i)}\right)^T \sum\nolimits_B^{-1} B^{(i)} \qquad (1)$$

The input data for statistical tests were the eight one-dimensional indices of normality (or scores) for the hypotonic and normative groups. Four of these scores were based on kinetic gait parameters, three of these scores were based on kinematic gait parameters, and the eighth score was an overall combination of all seven scores. A series of nonparametric Mann-Whitney tests were used to test for significant differences in the median score results between the two groups of data.

RESULTS AND DISCUSSION

Significant differences were found for all scores, with the hypotonic group showing higher median (and mean) values across all scores ($p<0.05$). Therefore, as a group, hypotonic gait patterns were distinguishable from normative gait patterns based on the indices of normality. To further explore the reasons for these differences, we decomposed the indices of normality into their subcomponents and examined differences in standardized means and covariance structures between the two groups.

Differences in standardized means and covariance structures between the hypotonic and normative groups showed that hypotonic abnormalities were most readily identified by specific kinematic indices of normality. These parameters were trunk obliquity and rotation, pelvic angular acceleration, sagittal knee and ankle angles, and shank angular velocity. Kinetic parameters that contributed to the identification of hypotonic gait patterns were sagittal ankle moment, ankle power, frontal hip moment, and hip power.

Numerous differences in correlations between gait parameters were also found for the hypotonic group compared to normative data. This suggests differences in coordination and control in the hypotonic group.

CONCLUSIONS

This study identified gait parameters that could distinguish between hypotonic and normative gait patterns. A greater awareness of the gait parameters that deviate from normative values will increase our understanding of the disorder and aid in treatment planning and evaluation.

REFERENCES

1. Caselli MA,et al. *Journal of the American Podiatric Medical Association*, **81**(3), 119-127, 1991.
2. Davis RB, et al. *Human Movement Sciences* **10**, 575-587, 1991.
3. Jensen RK. *Journal of Biomechanics,* **22**(6/7), 529-536, 1989.
4. Chester VL, et al. *Gait & Posture* (in review).

ACKNOWLEDGEMENTS

Support for this research was provided by NSERC and the NB Women's Doctoral Scholarship.

DO LOWER LIMB MUSCLE ACTIVITY PATTERNS CHANGE WITH PROLONGED LOAD CARRIAGE?

[1] Katrina M Simpson, [1]Julie R Steele and [1]Bridget J Munro
[1]Biomechanics Research Laboratory, University of Wollongong, Wollongong, Australia, kms99@uow.edu.au

INTRODUCTION

In occupational, military and recreational activities, loads are often carried in a backpack. Modern backpacks utilise a hip belt and shoulder straps to redistribute the load from the back to the large muscle groups surrounding the hips and legs in an attempt to protect the lower back from injury. However, by redistributing these loads the lower limbs are subjected to repetitive mechanical stress during prolonged load carriage while wearing heavy backpacks, which may, in turn, lead to lower extremity overuse injuries.

Numerous studies have identified gait and posture adaptations to carrying load, including changes to stride length, stride frequency, double and single support time, knee and trunk flexion, vertical and horizontal ground reaction forces [1,2]. However, little research has investigated changes in muscle activity during load carriage. Increased EMG activity with load has been reported for the gastrocnemius, hamstring, and quadriceps muscles [4]. Other research has found load carriage prolonged the duration of EMG activity for vastus lateralis, although hamstring EMG duration remained unchanged with load [5]. However, most of this previous research has focused only on the effects of short duration load carriage on changes in muscle activity, despite the fact that loads are often carried in a backpack for extended periods of time. Therefore, this study aimed to investigate the effects of prolonged load carriage on lower limb muscle activation patterns during gait.

METHODS

Fifteen healthy female recreational hikers (age = 22.3 ± 3.9 years) participated in the study. Each trial involved the subjects walking an 8 km circuit at a self selected speed carrying 30% of their body weight in a backpack. Data were collected at the start of the course and at 2 km intervals during the load carriage trial. During each trial muscle activity was sampled using a Noraxon Telemyo System (1000 Hz; 16 - 500Hz bandwidth) for six superficial lower limb muscles while the ground reaction forces generated at foot-ground contact were collected (1000 Hz) a Kistler force platform. The vertical GRF data were used to determine initial foot-ground contact (IC) and peak braking force (IC-peak). The EMG signals were full-wave rectified, filtered using a zero phase 4th order Butterworth low pass filter to create linear envelopes. Temporal characteristics of each muscle burst (see Table 1) were then determined using a threshold detector whereas the intensity of muscle activity was calculated by integrating the muscle bursts of interest. To determine whether there were any significant ($p < 0.05$) differences in the muscle activity patterns displayed with increasing hiking distance, a one-way repeated measures ANOVA design was used.

RESULTS AND DISCUSSION

Means and standard deviations calculated for the dependent EMG variables are presented in Table 1. No significant differences were noted for the temporal characteristics of tibialis anterior (TA), medial gastrocnemius (GM), rectus femoris (RF) or biceps femoris (BF) with increasing distance during load carriage. However, a significantly shorter semitendinosus (ST) muscle burst duration was evident when comparing the values obtained at the start of the 8 km circuit and all other distances. ST also was found to turn on significantly later between the start and the 8 km distance. The intensity of the vastus lateralis (VL) muscle burst also decreased from the start of the 8 km circuit in comparison to all other distances. Irrespective of any main effects of walking distance, all subjects displayed high variability in their EMG data, as is evident via the high standard deviations in Table 1.

The findings suggest that lower limb muscle activation patterns are relatively unchanged during prolonged carriage when subjects walk at a self selected speed over an 8 km circuit. However, the significantly shorter ST duration and later ST onset at the end of the load carriage trial may indicate that this muscle group is fatiguing and, in turn, may not be able to control deceleration of the limb in preparation for initial foot-ground contact. This lack of control of the leg by the hamstring muscles may predispose the knee to increased loading. However, further investigation of the internal forces acting on the lower limb is required to confirm or refute this notion.

REFERENCES

1. Quesada PM et al. *Gait and Posture* **4**, 201 – 202, 1996.
2. Kinoshita H. *Ergonomics.* **28,** 1347 – 1362, 1985.
3. Harman EK et al. *Medicine & Science in Sports & Exercise.* **24**, S129, 1992.
4. Ghori GM. & Luckwill RG. *European Journal of Applied Physiology* **54**: 145–150, 1985.

Table 1: Mean (±standard deviation) muscle activity variables displayed by the subjects at 2 km intervals during prolonged load carriage

Variable	Muscle	Start	2 km	4 km	6 km	8 km
Muscle burst duration (ms)	RF	341±72	355±130	355±113	322±99	334±108
	VL	324±56	295±67	301±75	304±86	299±77
	ST	271±46*	250±58*	243±55*	246±50*	252±52*
	BF	290±64	278±83	275±73	281±67	288±94
	TA	412±132	376±129	398±146	400±162	390±153
Muscle burst onset time to IC peak (ms)	RF	233±35	233±43	346±334	217±35	220±71
	VL	252±55	236±46	263±109	226±443	211±66
	ST	335±41*	313±82	351±108	326±32	311±51*
	BF	385±177	347±187	542±412	371±154	359±163
	TA	486±227	429±200	533±310	512±331	443±237

PREPARATION TO A PREDICTABLE PERTURBATION DURING MULTI-FINGER FORCE PRODUCTION

Sun Wook Kim, Jae Kun Shim, Vladimir Zatsiorsky, and Mark Latash
Department of Kinesiology, The Pennsylvania State University, University Park, PA 16802
email: mll11@psu.edu

INTRODUCTION

Two recent studies (Shim et al. 2005, Olafsdottir et al. 2005) have described changes in covariation patterns among finger forces involved in a multi-finger force production task in preparation to a change in the total force. This novel phenomenon has been termed anticipatory covariation (ACV). During steady-state total force production, individual finger forces typically show negative covariation both along a trial and across trials. This negative covariation stabilizes the total force, i.e. resists its deviations from the steady-state level. ACV has been assumed to facilitate planned changes in the total force by decreasing the negative covariation.

We investigated patterns of finger force covariation in experiments with force perturbations applied during the task of four-finger total force production at a comfortable constant level. The perturbations were triggered either unexpectedly or by the subject himself/herself. We hypothesized that ACV would be observed prior to the moment of force perturbation in trials with self-triggered perturbations but not in trials with perturbations triggered by the experimenter unexpectedly.

METHODS

Twelve healthy, right-handed volunteers, six males and six females participated in the experiment. The subjects sat comfortably in a chair and positioned the right forearm on the horizontal board directly in front of the subject. The fingertips of the right hand were placed on unidirectional force sensors spaced to fit the subject's individual anatomy. Changes in the forearm and hand position were prevented by a set of Velcro straps and using a custom-fitted wooden piece placed under the palm. A loop was placed on each finger and positioned under the distal interphalangeal joint. Each loop was connected to a 0.3 N load through a pulley system and an electromagnetic lock. The loads created forces acting on the fingers upwards. The subjects watched a 17" monitor that showed a target force level and the actual total force measured by the four sensors.

The subjects were required to press naturally on the sensors and to match the total force as accurately as possible with the target level. The target force was set at 8 N. There were four series (12 consecutive trials each) presented in a balanced order. Each trial lasted 10 s and involved unloading of one of the fingers disengaging the lock at some time over the second half of the trial. After the unloading, the subjects were required to bring the total force back to the required level as quickly as possible. Two series involved unloading of the index finger (I), either unexpectedly by the experimenter (I-Exp) or by the subject (I-Self); two other series involved unloading of the ring finger (R-Exp and R-Self).

All trials within a series were aligned by the time of unloading (t_0). Average time profiles of the total force and individual finger forces were computed for each series and each subject separately. Further, variance of the total force (V_{TOT}) and the sum of the variances of individual finger forces ($\sum V_{Fi}$) were computed and used to compute an index of finger force covariation, $\Delta V = (\sum V_{Fi} - V_{TOT})/\sum V_{Fi}$. The time of ΔV changes associated with the unloading was defined when it deviated from its average level over the steady-state force production by over 2 standard deviations.

RESULTS

No changes in the total force level were observed prior to the unloading in all series. An unloading was accompanied by an increase in the force produced by the unloaded finger on its sensor followed by corrections of all finger force. During steady-state force production, ΔV was about 0.75 in all series corresponding to negative covariation of finger forces. In I-Exp and R-Exp series, a drop in ΔV was observed on average about 25 ms after t_0. In contrast, during I-Self and R-Self series, these changes started, on average more than 100 ms prior to t_0. Following a perturbation, ΔV dropped dramatically and reached, on average -0.20 for I-Exp and R-Exp series and -0.10 for I-Self and R-Self series.

DISCUSSION AND CONCLUSIONS

Our observations support the hypothesis that humans can change patterns of finger force covariation in anticipation of a planned change in the total force. These observations extend results of the earlier studies (Shim et al. 2005, Olafsdottir et al. 2005) to ACV in preparation to a quick correction of the total force following a self-triggered perturbation. In that sense, the phenomenon of ACV is somewhat similar to the anticipatory postural adjustments. Apparently, ACV allowed subjects to avoid excessive total force destabilization over the period of correction as reflected in less negative ΔV values in I-Self and R-Self series.

REFERENCES

1. Shim JK, Olafsdottir H, Zatsiorsky VM, Latash ML (2005) The emergence and disappearance of multi-digit synergies during force production tasks. Exp Brain Res (in press)
2. Olafsdottir H., Yoshida N., Zatsiorsky V.M., Latash M.L. (2005) Anticipatory covariation of finger forces during self-paced and reaction time force production. Neurosci Lett (in press).

ACKNOWLEDGEMENTS

This research was supported in part by NIH grants AG-018751, NS-035032, and AR-048563.

MUSCLE FUNCTION LOCALLY MEDIATES BONE HOMEOSTASIS

Sarah E. Warner, Sundar Srinivasan and Ted S. Gross
University of Washington, Seattle, WA
tgross@u.washington.edu

INTRODUCTION

Muscle contractions serve as one of the two major sources of mechanical loading on bones and thereby directly effect bone homeostasis [1]. However, the means by which muscle function serves to maintain bone health is poorly understood. Recently, we observed that acute muscle paralysis induced by Botulinum neurotoxin (Botox) injection rapidly precipitates substantial muscle and bone degradation in mice [2]. As well, preliminary data from the model indicated that individual mice demonstrating the greatest loss of muscle also experienced the greatest bone degradation [3]. Here, we examine the hypothesis that local muscle function is required to maintain local bone homeostasis.

METHODS

Twenty female C57B6 mice (16 wk) were randomized into three groups: 1) saline (S; n = 5), 2) quadriceps and calf Botox injections (QC; n = 5), and 3) quadriceps Botox injection (Q; n = 10). At day zero, each IM injection consisted of either 2.0 unit/100 g body weight of Botox or equal volume of saline. This dose of Botox is within the range approved for human use. All mice were allowed free cage activity and food and water ad libitum for 3 weeks. At sacrifice, the quadriceps and calf wet mass were determined. The right femurs and tibiae were imaged via micro-CT at a 10.5 µm voxel resolution (Scanco Viva CT). Bone volume/total volume (BV/TV, %) are reported for the distal femur epiphysis and proximal tibia metaphysis. At the tibia mid-shaft, a 0.1 mm thick transverse cross section was assessed for cortical volume (Ct.V; mm^3) and endocortical volume (Ec.V; mm^3). Treatment effects were evaluated using ANOVA ($p = 0.05$) while linear regression was used to explore relations between muscle mass and site-specific bone alterations.

RESULTS AND DISCUSSION

Intramuscular injection of Botox induces temporary muscle paralysis by blocking the release of acetylcholine into the neuromuscular junction [4]. In the murine Botox model, lameness is maximal by 3 days post-Botox injection, with gradual restoration of weight bearing occurring within 2 wk. Weight bearing remains compromised compared to control mice for 4 to 6 wk. Muscle mass was significantly diminished at each Botox injection site when compared to S (range: -52% to –60%). In contrast, calf muscle mass in the Q group was diminished –29% (Table 1). Both Botox groups demonstrated similar degradation of femur and tibia BV/TV when compared to S (QC: -52 and -70%; Q: -46 and -51% respectively, $p < 0.05$; Table 1). However, while QC mice demonstrated a 15% loss of cortical volume due to endocortical expansion, the tibae of Q mice were not altered compared to S mice (Figure 1). Quadriceps wet mass was strongly predictive of femoral BV/TV for all Botox mice (QC: $r = 0.995$, $p < 0.001$ and Q: $r = 0.957$, $p = 0.011$), but calf wet mass was related to tibia Ct.V only in the presence of calf paralysis (QC: $r = 0.751$, $p < 0.001$ and Q: $r = 0.334$, $p > 0.05$).

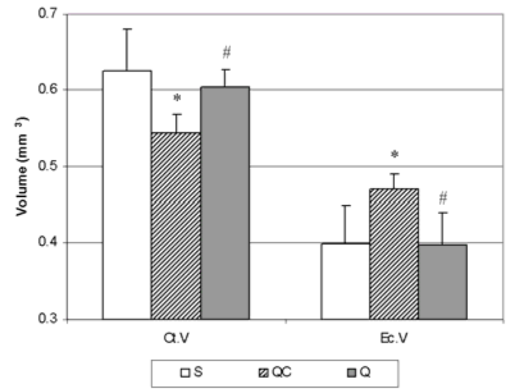

Figure 1: Tibia cortical bone volume and endocortical volume. *QC different from S, #Q different from QC.

The only observed functional difference between the Botox injected groups was that the Q mice continued to perform calf contractions during attempted ambulation, while the QC mice were unable to contract the calf muscles. As such, it is likely that the Q mice maintained a physiologic level of small magnitude muscle contractions in the face of minimal large contractions (due to limited weight bearing). Thus, the absence of tibial cortical bone loss in the Q mice supports our initial hypothesis while implicating small muscle contractions as one mechanism by which muscle function may locally mediate bone homeostasis.

REFERENCES

1. Rittweger J., *J Gravit Physiol.* 6:133-6, 1999.
2. Warner, S.E., *Bone*, in review.
3. Warner, S.E., *Trans ORS, 1552, 2005.*
4. Hambleton, P., *J Neurol*, 239:16-20, 1992.

ACKNOWLEDGEMENTS

This work was supported, in part, by NIH AR45665 and the Sigvard T. Hansen, Jr. Endowed Chair.

Table 1: Muscle wet mass and bone parameters *QC different from S, ^Q different from S, #Q different from QC, $p<0.05$.

	Muscle Wet Mass (mg)		Femur Epiphysis	Tibia Metaphysis
	R Quadriceps	**R Calf**	**BV/TV (%)**	**BV/TV (%)**
Saline	201.8 ± 7.4	142.6 ± 4.7	27.6 ± 1.5	7.7 ± 1.9
Botox QC	96.0 ± 16.0*	57.4 ± 6.1*	13.3 ± 3.3*	2.3 ± 0.8*
Botox Q	97.4 ± 3.9^	101.1 ± 2.3^#	15.0 ± 2.1^	3.8 ± 0.5^

KINETICS AND KINEMATICS OF MALES AND FEMALES DURING TWO STYLES OF DROP LANDING

[1]Rhonda L. Boros and [2]John H. Challis
[1]Biomechanics Laboratory, Texas Tech University, [2]Biomechanics Laboratory, The Pennsylvania State University
Email: rl.boros@ttu.edu, web: www.hess.ttu.edu/rboros

INTRODUCTION

Female athletes are six times more likely than males to suffer a "non-contact" anterior cruciate ligament (ACL) injury [1], and landing from a drop has been identified as a movement stressful to the ACL [2]. The kinematics and kinetics of landing from a drop have been studied extensively. The consensus is that males demonstrate greater body weight normalized vertical ground reaction forces (VGRF) compared with females, while females tend to land on more extended knees with greater trunk lean [3] and exhibit longer landing phase durations [4]. Specific gender comparisons across more than one style of landing are lacking; and many studies selected a single trial for analysis, potentially skewing performance characteristics and statistical comparison.

Previous studies typically assumed a rigid body model and thus ignored skin- mounted marker movement, compromising the accuracy of subsequent kinetic calculations [5]. Efforts to minimize this error have been made previously [6] and similar efforts were adopted in the present study. The purpose of this study was to examine kinetic and kinematic differences between males and females during two styles of landing from a drop (flat-footed and toe) utilizing an externally affixed rigid link device as representative of underlying skeletal motion.

METHODS

Simultaneous 2D kinematic (240 Hz) and kinetic (1920 Hz) data were collected as 10 subjects (5 male, 5 female) performed 5 trials each of two-footed hanging drop landings onto flat feet and toes. A rigid link device was secured to the right lower extremity of the subjects, and the intersection of the lines representing the two segments of the device served to determine the knee joint center for kinematic analysis. Torso and foot kinematics were obtained from markers placed on the acromion process, greater trochanter, lateral maleolus, calcaneal tuberosity and fifth metatarsal. Two additional markers were placed on the anterior portion of the thigh in an effort to quantify the magnitude of soft tissue motion relative to the rigid link. The instant of impact was considered time zero for all parameters, and kinetic and kinematic data were time-synched to this instant. Peak VGRF, loading rate, joint angles, angular velocities, angular accelerations, resultant joint moments (RJM), and phase durations were calculated and compared across gender. All comparisons were tested utilizing a repeated measures ANOVA ($P < 0.05$).

RESULTS AND DISCUSSION

No significant differences were observed between the genders across landing conditions in force plate derived temporal variables. Mean landing duration for both styles ranged from 1.5 to 1.7 seconds. Both groups demonstrated significantly greater VGRF during the flat-footed compared with toe landings (7.4 ± 2.1 and 4.9 ± 1.7 versus 6.5 ± 1.4 and 4.2 ± 0.9 BW for males and females, respectively). Males also demonstrated slightly greater rates of loading.

Contrary to the literature, males had significantly greater knee extension at impact and at the time of peak VGRF for both landing styles. Toe landings resulted in significantly greater ankle joint angular velocities compared with flat-footed landings, and such velocities were significantly greater for males during toe landings, perhaps indicative of an alternate ankle joint strategy compared with females. Flat-footed landings resulted in more rapid onsets of peak RJM for both genders compared with toe landings. Males exhibited significantly greater RJM at the hip during toe landings and experienced these greater moments later in the landing phase compared with females. Albeit not statistically significant, females demonstrated substantially greater resultant joint moments at the hip during flat landings compared with males. Greater RJM at the hip during impact could lead to an increased risk of knee injury if the heel were to remain firmly planted and a horizontal acceleration were introduced, as occurs during an off-balanced landing. Females also demonstrated significantly greater horizontal and vertical displacement of the soft tissue compared with males across landing styles, possibly affecting true joint kinetics. No other kinematic differences were observed.

CONCLUSIONS

Methodological differences (e.g. knee joint center kinematics, repeated versus single trial analysis) may account for the discrepancies between the present kinematic results and the literature. Considering the rigid body assumption for kinetic analysis, gender differences in soft tissue motion suggest that females may be experiencing different joint loads compared with males. Quantification of this soft tissue motion and its contribution to knee joint load may provide some insight into the predisposition of females to ACL injury.

REFERENCES

1. Arendt E & Dick R. *Am J Sports Med* **23**, 694-701, 1995.
2. Lephart SA et al., *Curr Opin Orthopedics* **14**, 168-173, 2002.
3. Cowling EJ & Steele JR. J. *Electromyogr Kinesiol* **11**, 263-268, 2001.
4. McNitt-Gray JL et al., *J Applied Biomech* **10**, 237-252, 1994.
5. Gruber K, et al., *J Biomech* **31**, 1998
6. Bobbert et al., *J Biomech* **24**, 1095-1105, 1991

ACKNOWLEDGEMENTS

This study was partially funded through the Albert and Lorraine Kligman Research Fellowship Endowment through the College of Health and Human Development at The Pennsylvania State University.

EXPLORING MECHANICAL LOADING INDUCED CA^{2+} OSCILLATIONS IN OSTEOCYTES

Brandon J. Ausk, Ted S. Gross and Sundar Srinivasan
Orthopaedics and Sports Medicine, University of Washington, Seattle; email: bjausk@u.washington.edu

INTRODUCTION

Bone is highly sensitive to alterations in its mechanical environment. In fact, extremely brief loading sessions (e.g., 100 s of exogenous loading) are sufficient to activate mechanosensory osteocytic cells within minutes and presumably drive osteoblastic bone formation days and weeks later[1]. One potential signaling pathway that would satisfy these observations is the Ca^{2+} ion second messenger system, which permits real-time cell responses to a variety of agonists, including mechanical stimuli[2,3]. However, given the inaccessibility of osteocytes, it is not possible to confirm this mechanism *in vivo*. As a potential solution, we have developed a novel agent based model of real time Ca^{2+} signaling. We examined the validity of the model by simulating Ca^{2+} oscillations induced in osteocytic cells challenged by either cyclic or rest-inserted mechanical stimuli.

METHODS

Cytosolic Ca^{2+} oscillations induced in osteocytic cells by mechanical stimuli were simulated in an agent based modeling environment (Netlogo 2.1). Ca^{2+} oscillations were governed by the following cellular functions previously identified *in vitro*[2,4]: 1) at steady state, Ca^{2+} influx occurs at a low-rate from the extracellular milieu, 2) for homeostasis, the resulting cytosolic Ca^{2+} build-up is removed via a concentration dependent efflux across the plasma membrane and uptake into the cell mitochondria, 3) mechanical stimuli causes a strain dependent influx of Ca^{2+} (via stretch activated Ca^{2+} channels), 4) when cytosolic Ca^{2+} concentrations exceed thresholds, endoplasmic reticulum (ER) Ca^{2+} stores are released into the cytosol, 5) the threshold for Ca^{2+} release from ER is inversely related to ER Ca^{2+} store concentrations, 6) the rate of Ca^{2+} release from the ER is strain and concentration dependent, and lastly, 7) when cells are quiescent, ER Ca^{2+} stores are replenished from the mitochondria in a concentration dependent manner. Using this model, Ca^{2+} oscillations induced by 500 s of cyclical (1-Hz) and rest-inserted stimuli (10-s rest between load cycles) were contrasted.

RESULTS AND DISCUSSION

Real-time Ca^{2+} oscillations induced by cyclic loading followed one of three fundamental responses (Fig 1a). A small subset of cells were non-responsive (~20%), while a majority of cells displayed either a high-magnitude transient Ca^{2+} oscillation followed by low-level steady state fluctuations (40%), or an additional secondary Ca^{2+} transient upon cessation of the stimulus (40%). The number of responsive cells was increased when the magnitude of the stimulus was increased, regardless of the waveform (Fig 1b). In contrast to the response to cyclic stimuli, multiple high-magnitude Ca^{2+} oscillations were induced when cells were subjected to rest-inserted stimuli (Fig 1c).

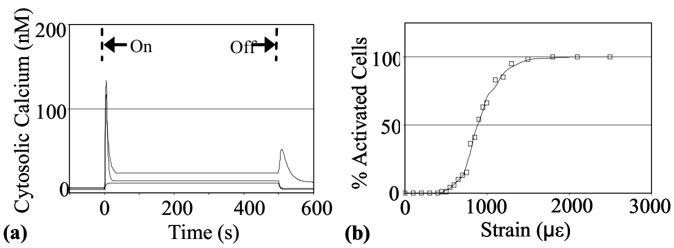

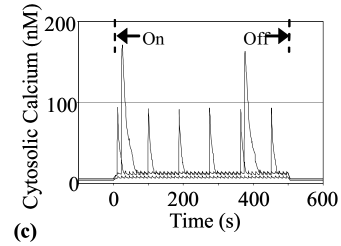

Figure 1: Cytosolic Ca^{2+} oscillations in three representative osteocytes exposed to cyclic stimuli (a). Increasing strain magnitudes increased the number of responsive cells in a sigmoidal dose-response fashion (b). Rest-inserted stimuli induced multiple high-magnitude Ca^{2+} transients in osteocytes (c).

In our agent based model of Ca^{2+} ion balance, distinct Ca^{2+} 'fingerprints' were not explicitly 'hardwired' within the model. Instead, they emerge via interactions between real cellular attributes (e.g., Ca^{2+} influx via stretch activated channels, ER Ca^{2+} stores). In our view, such an emergence based approach substantially extends model robustness and utility. Importantly, all Ca^{2+} response characteristics observed here (heterogeneous cell response, sigmoidal dose-response relations and multiple transients elicited by rest-inserted stimuli) were consistent with previous *in vitro* studies[3,5,6].

More broadly, it is possible to determine adaptation induced by mechanical waveforms at a variety of levels *in vivo* (from protein expression to cell proliferation and differentiation). Our model now provides a framework to functionally relate these adaptive events with unique Ca^{2+} fingerprints elicited *during* brief bouts of mechanical stimuli[2]. As a result, it may be possible to decipher the mechanisms underlying the distinct adaptive outcomes elicited by specific mechanical stimuli (e.g., why rest-inserted stimuli is dramatically osteogenic, but cyclic stimuli at identical loading magnitudes is not)[7]. Ultimately, the model and its expansions could serve as a powerful tool for optimization of bone tissue adaptation by enabling tailored design of loading waveforms that enhance cellular responses on the order of seconds.

REFERENCES

1) Dodds et al *JBMR* **8**:261-7; 2) Berridge *Nature* **395**:645-8; 3) Hung et al *Clin Orthop* **313**:256-69; 4) Clapham *Cell* **80**:259-68; 5) Charras et al *Biophys J* **82**:2970-81; 6) Batra et al *49th ORS* 129, 7) Srinivasan et al *JBMR* **17**:1613-20.

ACKNOWLEDGEMENTS

Funding from the Whitaker Foundation (SS) and NIH (TSG).

CELL DEFORMATION IN RESPONSE TO LOCAL MATRIX STRAIN

[1] Rachna Sah, [2,3] Markus Wimmer and [2,3] Amarjit Virdi
[1] Department of Bioengineering, University of Illinois at Chicago, Chicago, IL; [2] Department of Orthopedics, [3] Department of Anatomy and Cell Biology, Rush Medical Center, Chicago, IL; e-mail: markus_a_wimmer@rush.edu

INTRODUCTION

Chondrocyte deformation within compressed extracellular matrix (ECM) and/or agarose composites has been studied extensively during the past years [e.g. 1,2]. Since the elastic modulus of the cells is some magnitudes smaller than that of ECM, a stress concentration exists on the micro-level around the chondrocyte [3]. This needs to be taken into consideration for tissue engineering because the initial elasticity modulus of the cell-seeded artificial matrix is typically lower than that of mature ECM. In order to evaluate stresses and strains at the micron-level numerical models may be used. For the input a precise description of the matrix deformation in the immediate vicinity of the cell is necessary. In this study we employed a technique based on grayscale correlation of microscopy images. We hypothesized that considerable strain perpendicular to the primary loading axis occurs and strains are affected by cell type.

METHODS

Metacarpalphalengeal joints from 18–months old steers were dissected to obtain samples from articular cartilage. Superficial (~15% uppermost) and deep (rest) zones were separated by slicing manually. Chondrocytes were isolated by digesting the slices with pronase and collagenase. Isolated cells were labeled with calcein dye and cell/agarose constructs were prepared by mixing 5.7×10^6 cells ml^{-1} of 3% agarose. In addition, fluorescent beads (molecular Probes) were added as extracellular markers. After solidification at 4ºC, constructs were cut into ten 10mm cubes each. A loading apparatus (Fig. 1) was used to apply unconfined compression in steps of 500 microns up to 2 mm. The corresponding local agarose deformation was studied using a confocal laser microscope capturing the relative displacement of the fluorescent beads. The sets of images were analyzed using VEDDAC™- an image correlation software which uses grey scale data to give a vectorial representation of displacement. Creating a grid of measurement points with an X & Y pitch of 65µm, the grey scale information from a $4350 \mu m^2$ correlation area around each point was used to identify the displacement. The search area was limited to $33000 \ \mu m^2$. A strain calculation algorithm based on linear regression was added to determine the local principal strains. The deformation index (Fig.1) and perimeter of cells were quantified for ten cells per cube and load step.

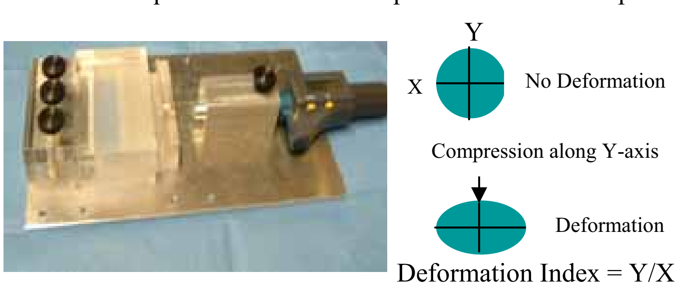

Figure 1: Compression apparatus

RESULTS AND DISCUSSION

A homogenous gradient of deformation was observed for all samples both in axial and lateral direction (Fig.2). On average, the local axial strain was similar to applied 'global' strain, however, individual values varied greatly among samples as well as between deformation steps. Thus, a nominal 5% step generated local strains from as low as 1.3% to as high as 8.8%. The local lateral strain was dependent on applied load and decreased with increasing axial strain (Fig.2) Thus, the Poisson-like values started from 0.45 and decreased with increasing strain to 0.26 and 0.32 for the superficial and deep cell-agarose composites respectively. Also deformation on the cellular level differed between the two cell populations. The slope of the deformation index was steeper for the deep cells (Fig.3). Interestingly, the cells behaved differently with regard to their perimeter (Fig.3) suggesting a growing cell volume for the deep cells and a shrinking volume for the superficial cells with increasing strain (Fig.3).

CONCLUSIONS

Locally generated strains were variable among samples and appeared to be affected by cell type and loading. Grayscale correlation is helpful in the precise computation of local strain.

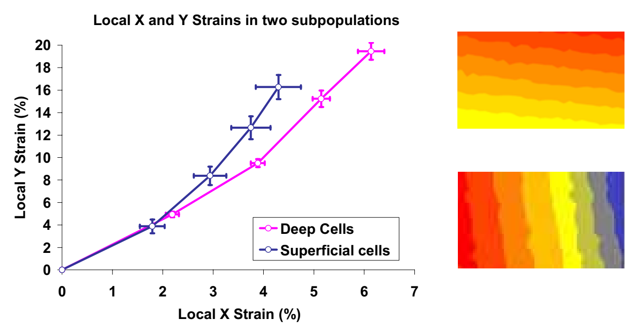

Figure 2: Local axial (Y) and lateral (X) strains for deep and superficial cell agarose constructs. Mean ± S.E., N=10. Contours depicting the local Y and X deformation gradients

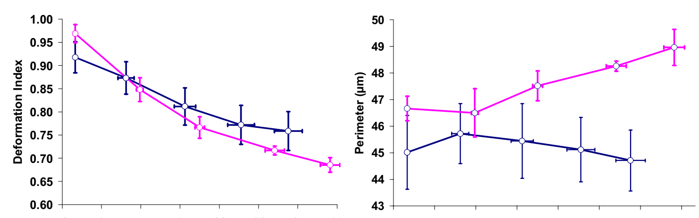

Figure 3: Deformation Index and Perimeter as a function of Local Strain for Deep and Superficial cells. Mean ± S.E., N=10. X axis = Local Strain (%)

REFERENCES

1. Freeman PM, et al. *J Orthop Res*. **12:** 311-320, 1994
2. Lee DA, et al. *J Biomech*. **33**: 81-95, 2000.
3. Guilak F, et al. *J Biomech* **33**: 1663-1773, 2000

CAN A SINGLE SCALE FACTOR BE USED TO SCALE FEMUR BONE MODELS?

[1,2] Weidong Luo, [2]Zohara Cohen and [2, 3]Frances Sheehan
[1]Physics Department, Catholic University of America; [2]Physical Disabilities Branch, National Institutes of Health;
[3]Department of Physical Therapy and Rehabilitation Science, University of Maryland School of Medicine
email: wluo@cc.nih.gov, web: http://pdb.cc.nih.gov/

INTRODUCTION

A generic bone template must be scaled to quantify the shape differences between it and a particular bone. Computational joint models rely on the scaling of a generic model to approximate the bone geometry of an individual subject. Previous modeling studies have used both single [1-3] and multiple scale factors [4] to approximate individual femurs from templates. The objective of this study was to determine whether a single scale factor is sufficient. We examined normal subjects to determine whether consistent relationships exist between designated femur lengths. We hypothesized that multiple scale factors would be necessary: three factors for the superior-inferior direction (corresponding to proximal, mid-shaft, and distal sections of the femur) and one scale factor each for the anterior-posterior and medial-lateral directions.

METHODS

Landmark coordinates for 52 skeletal femur specimens were obtained from an existing database [3]. Landmark coordinates for ten volunteers were obtained from geometric models generated using Geomagic Studio (Research Triangle Park, NC) based on data segmented from T1-weighted MRI scans. Volunteer and skeletal specimens were all skeletally mature and free from known orthopaedic abnormalities. Relevant lengths were measured as the distances between the following pairs of landmark points: the most lateral points on the greater trochanter and on the femoral epicondyle (LE) (referred to as "palpable length" due to the accessibility of the landmarks); the top of femoral head and the inferior base of lesser trochanter (LT) ("proximal length"); the superior corner of adductor tubercle (AT) and the most inferior point on the femur ("distal length"); LT and AT ("shaft length"); the most medial point on the femoral epicondyle and LE ("width"); and the origin of the VMO fibers (near the anterior-medial corner of the patellar groove) and a line connecting the most posterior points on the medial and lateral distal condyles ("depth"). Kolmogorov-Smirnov (K-S) normality tests were performed to ensure normally distributed measurements and that further statistical testing was appropriate. Correlations were sought between the palpable length, a measurement that could potentially serve as the basis for a uniform scale factor, and each of the other lengths. For each correlation, the lower and upper bounds on the 95% confidence interval were found. Measurements were normalized by their respective mean values and linear regression analysis (with y intercept=0) performed to determine the rate of change of each length with change in palpable length. The regression coefficients for these normalized data were compared.

RESULTS AND DISCUSSION

The palpable length for the 62 test subjects was 382 ±25 mm. The standard deviations for the five test measurements, when normalized by their means, ranged from 6% to 13% (Table 1, row 1). The distribution of these data was found to be normal in all cases; the Lilliefors significance level was well above 0.05 for the K-S tests (row 2). Significant (p-values <0.0001) correlation values (R) relating each of the five dependent measures to the palpable length ranged from 0.50 for (depth) to 0.96 (shaft length) (row 3). The 95% confidence intervals were narrow and the lower bounds found for R were never lower than 0.29 (row 4) and the upper bounds were as high as 0.98. The strong correlations for the three length measurements indicate that individual femoral sections change size proportionally to changes in femoral length. The width and depth correlations indicate that the changes in the two orthogonal dimensions are also proportional to the superior-inferior femoral dimension. The linear regression model proved valid as all models demonstrated significance (t-value >>2 and significance << .01). The most important finding was that the regression coefficients for the normalized data were all the same (row 5), indicating that, not only do all five parameters vary with the palpable length, they vary at the same rate. Thus, we have shown that when scaling a model femur to match an individual femur, a single scale factor is sufficient to match the three sections and three dimensions of the bone.

REFERENCES

1. Arnold AS, et al. *Comput Aided Surg* **5(2)**, 108-19, 2000.
2. Jenkins, SE, et al. *Gait Posture* **18(1)**, 13-22, 2003.
3. Kepple, TM, et al. *J Biomech* **31**, 77-80, 1998.
4. Arnold AS, et al. *Ann Biomed Eng* **29(3)**, 263-74, 2001.

ACKNOWLEDGEMENTS

We are grateful to the PDB investigators at the NIH who shared with us the skeletal specimen data.

Table 1: Statistical measurements

	proximal length	shaft length	distal length	width	depth
1 **Mean ± Standard Deviation (mm)**	98.4±9.3	328.2±23.0	49.1±5.0	87.3±9.1	77.9±10.5
2 **Lilliefors significance for K-S Test**	0.85	0.82	0.54	0.37	0.77
3 **Pearson's R Value**	0.56	0.96	0.56	0.54	0.50
4 **Lower Bound for 95% CI for R**	0.36	0.94	0.36	0.34	0.29
5 **Normalized regression coefficients**	1.00±0.01	1.00±0.01	1.00±0.01	1.00±0.01	1.00±0.01
6 **Standard error of estimation (mm)**	7.8	6.4	4.1	7.7	9.1

COMBINED VALGUS AND INTERNAL ROTATION MOMENTS STRAIN THE ACL MORE THAN EITHER ALONE: IMPLICATIONS FOR NON-CONTACT ACL INJURIES

[1]Choongsoo S. Shin, [1]Ajit M. Chaudhari, and [1,2]Thomas P. Andriacchi
[1]Dept. of Mechanical Engineering, Stanford University,
[2]Bone & Joint Center, VA Palo Alto Health Center; email: scslove@stanford.edu, web: biomotion.stanford.edu

INTRODUCTION

Video observations of non-contact injuries to the anterior cruciate ligament (ACL) suggest that the injury occurs during the deceleration phase of landing on a single limb with a combination of valgus and internal or external rotation [1]. A cadaveric study supports the conclusion that combined internal torque and valgus moment increase forces in ACL [2]. However, the dynamic effect of combined loading at physiologic levels on ACL strain during landing has not been studied. This study tested the hypothesis that the strain in the ACL is higher under combined valgus and internal rotational moments during landing than with either applied individually. The study was conducted by applying actual *in vivo* loading data to a validated simulation model of the knee to predict ACL strains.

METHODS

A combination of valgus moments, internal rotation moments, and vertical landing forces were used to drive dynamic simulations of a previously validated knee model constructed from MRI of the distal femur, proximal tibia, patella, and cartilage of a cadaveric knee (Figure 1) [3]. Peak valgus moments for valgus landers and neutral landers were obtained from the results of a previous study on sidestep cutting [4] and normalized to an average-size person (height=1.75m, weight=750N) to choose 4 physiologic levels of valgus moment for the simulations (Table 1). Four physiological levels of peak internal rotational moments were obtained from another single limb landing experiment using 30 subjects (21 female, 9 male) with no history of musculoskeletal injury (Table 1). The vertical impact force used had a peak of 1400N. Other values of valgus and internal rotation moment were also tested to illustrate the shape of the response surface. The valgus and internal rotational moments were applied at the midpoint of the trans-tibial line, while the impact force was applied at the top of femoral axis of the upper limb. The strains in both bundles of ACL were calculated, but only the anteromedial bundle strain is presented since it was the higher of the two.

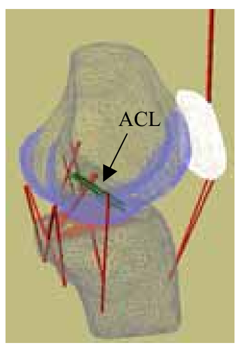

Figure 1. Knee model showing ligaments.

Table 1. Physiologic levels of valgus and internal rotational moments applied to the simulation model.

Valgus moment	**Minimum**	**Average Neutral**	**Average Valgus**	**Maximum Valgus**
	0 Nm	8 Nm	24 Nm	51 Nm
Int. Rot. moment	**Null**	**Minimum**	**Average**	**Maximum**
	0 Nm	3.6 Nm	11.5 Nm	25.9 Nm

RESULTS AND DISCUSSION

The strain in the ACL due to combined physiological maximum valgus (51 Nm) and internal rotational moment (25.9 Nm) was 10.5%, which is in the reported range for ACL rupture of 9-15% [5,6]. When applied individually, neither of the two rotational moments caused ACL strain higher than 7.7%, and the effect of each moment reached a plateau at or near the maximum level observed *in vivo.* However, when applied in combination the two rotational moments had a much larger effect, and the sensitivity of ACL strain to increases in either quantity was much higher when the other was held at a high level (Fig. 1).

Moreover, subjects whose typical valgus and internal rotation moments are high may be at greater risk because ACL strain is most sensitive to perturbations in the applied moments at those levels, as shown by the steepest slope of the surface when valgus moment is between 24 and 51 Nm, and internal rotation moment is between 11.5 and 25.9 Nm (Figure 1).

This work has shown that the combination of valgus and internal rotation moments that occur *in* vivo during simple cutting and landing maneuvers can cause ACL strains that may be high enough to cause injury, even in the absence of an anterior shear force.

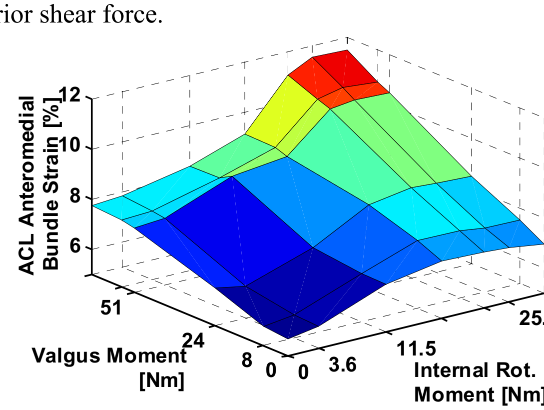

Figure 1. Response of ACL anteromedial bundle strain to applied valgus, internal rotation, and combined moments.

REFERENCES

1. Olsen OE et al. *Am.J.Sports Med.*, 32(4), 1002-1012, 2004.
2. Markolf KL et al. *J. Orthop. Res.,* 13, 930-935, 1995.
3. Chaudhari AM et al. *51st Annual meeting of ORS*, Washington DC, Abstract 1516, 2005.
4. Chaudhari AM et al. *ASME Bioengineering Conference,* Key Biscayne, FL, pp. 395-396, 2003.
5. Butler DL et al. *J.Biomech.*, 25(5), 511-518, 1992
6. Momersteeg TJA et al. *J. Biomech.,* 28(6), 745-752, 1995.

ACKNOWLEDGEMENTS

Partial funding from NIH Grant No. R01-AR39212.

KINETIC LIMITATIONS OF MAXIMAL SPRINTING SPEED REVISITED

[1,2] Stephen C. Swanson and [1]Graham E. Caldwell
[1]Biomechanics Lab, University of Massachusetts, Amherst, MA USA,
[2]The Orthopedic Specialty Hospital, Salt Lake City, UT USA; email: tosswans@ihc.com

INTRODUCTION

Many studies have examined running biomechanics, but few have addressed the factors that limit maximal sprinting speed. As running speed increases above 9 m/s, the athlete must produce large ground forces in a very short time (< 110 ms; [2]). Skillful coordination of the lower extremity during recovery may be an important aspect of realizing effective ground forces during stance. Chapman and Caldwell [1] identified energy absorption by eccentrically acting knee muscles during recovery as a key variable in limiting sprint speed. However, their analysis was limited to the planar motion of a single elite subject. The goal of the present study is to examine limitations in maximal running speed in multiple subjects with three-dimensional (3D) kinetic analysis; due to space limitations only 2D sagittal kinetics are reported here.

METHODS

Eight skilled male sprinters (19.2± 2.6 yrs., 1.83 ± .04 m, 85.7 ± 6.2 kg) ran on a high-speed treadmill at 100%, 95%, 90%, 85% and 80% of their maximal speed (9.46 ± .4 m/s). The 3D motion of 47 reflective markers on the arms, trunk, pelvis, and lower extremities was recorded with eight Motion Analysis™ digital cameras at 200 Hz. Marker trajectories were smoothed at 12 Hz. 3D kinematics and kinetics were computed with Visual3D™ software. Stance and swing were identified from the kinematics of markers on the 1st and 5th metatarsal heads, using event identification algorithms validated in a pilot study with a force treadmill. Net joint moment and power data from the hip and knee were selected from five consecutive strides in each speed condition and peak power values were calculated for distinct periods of swing. The effect of speed on peak powers at the hip and knee was tested with a within-subject repeated-measures ANOVA using post-hoc orthogonal contrasts (SPSS™). All differences reported have $p < 0.05$.

RESULTS AND DISCUSSION

Table 1 presents bi-lateral peak power data during periods of concentric hip extension (Conc HE) and eccentric knee flexion (Ecc KF). Peak Conc HE and Ecc KF power values increased in magnitude with treadmill speed from 80-95%. At maximal speed, each power reached a plateau and was similar in magnitude to the 95% condition. The within-subject stride-to-stride variability of the peak power values *increased* at maximal speed (SD values in *italics*) compared to all other speeds. Further, as illustrated for one subject in Figure 1, significant differences *between limbs* in Conc HE, Ecc KF peak power, or both measures were observed in 5 of the 8 subjects. The bilateral differences were unique to each subject. The data suggest that changes in energy generation at the hip and energy absorption at the knee may be key variables in the limitation of maximal sprint speed. Bi-lateral asymmetry and increased variability in hip and knee kinetics at maximal speed may indicate a failure in lower extremity coordination during swing that hinders effective force application during the subsequent stance phase. To definitively examine this possibility and to gain further insight into the limitations of maximal sprinting speed, additional research on stance phase kinetics of elite sprinters is needed.

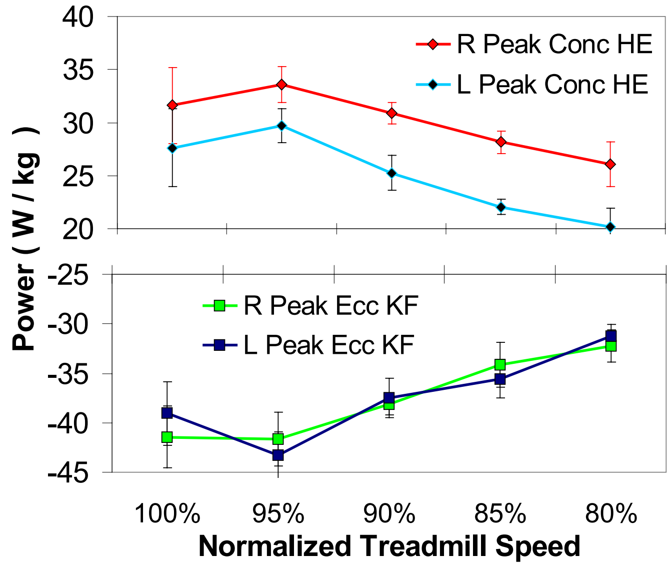

Figure 1: Bi-lateral mean peak Conc HE and Ecc KF power values across speeds for one subject. Error bars are ± 1 SD.

REFERENCES

1. Chapman, AE & GE Caldwell, *J Biomech* **16**, 73-83, 1983.
2. Kuitenen, S et. al. *Med. Sci. Sport. Exc.* **34**, 166-173, 2002.

ACKNOWLEDGEMENTS

Financial assistance of Frappier Acceleration Sports Training and The Orthopedic Specialty Hospital is appreciated.

Peak Power by Phase (w/kg)	Normalized Treadmill Speed (% maximum)									
	100%		95%		90%		85%		80%	
R Conc HE	30.0	*(3.9)*	*31.5	(2.1)	26.7	(2.3)	24.3	(1.6)	21.6	(1.6)
L Conc HE	28.7	*(5.3)*	*31.1	(2.8)	26.5	(2.4)	23.5	(2.3)	21.0	(2.0)
R Ecc KF	-38.8	*(4.2)*	*-40.0	(2.5)	-35.6	(2.4)	-32.6	(1.7)	-29.2	(1.9)
L Ecc KF	-41.2	*(4.5)*	*-41.8	(3.0)	-36.3	(2.3)	-32.7	(2.1)	-28.3	(1.6)

Table 1: Peak power values for the hip and knee in late swing [mean (SD)]. *Indicates values similar to the 100% speed condition, all others are different than 100% speed (p<.05).

Metabolic Cost of Walking Varies with Foot Roll-Over Radius

[1]Peter Gabriel Adamczyk, Kaitlin A. Schneider, Arthur D. Kuo
Department of Mechanical Engineering
University of Michigan, Ann Arbor, MI USA
[1]email: padamczy@umich.edu

INTRODUCTION

Humans perform simultaneous positive and negative work during the double support phase of walking [1]. In order to redirect the body center of mass (COM) velocity between steps, the leading leg performs negative work on the COM as the trailing leg pushes off with positive work. A simple passive dynamics-based model of walking predicts that the mechanical work required at push-off should decrease quadratically as the effective roll-over radius of the feet increases [2]. Because mechanical work requires metabolic energy, we hypothesize that a similar trend should appear in metabolic rate with variation in roll-over radius. We artificially varied the effective shape of subjects' feet by attaching cylindrical arc-soled boots to the lower leg. We measured metabolic rate while subjects walked on arcs of several sizes. We found that metabolic rate decreased substantially with higher radius of curvature, suggesting that simultaneous positive and negative work during double support is a major contributor to the total metabolic cost of walking.

METHODS

We measured metabolic energy consumption as human subjects walked on different-sized wooden arcs. The experimental setup consisted of a speed-controlled treadmill, a breath gas analyzer, and seven pair of wooden arc shapes used to give the subject a specific foot roll-over radius (arcs' radii of curvature were 2, 5, 10, 15, 22.5, 30, and 40 centimeters). These arcs were attached to the legs of the subject through a pair of Aircast PneumaticWalker boots modified to allow the interchange of foot shapes (Figure 1a). The boots immobilized the ankle, causing the subject's leg to function much like that of the passive walking model. When standing upright, the contact point of the arcs with the ground was about 7.6 cm in front of the tibia, near the metatarsal head.

Ten healthy young adults (five male, five female) were recruited to perform this study. Each subject's rate of oxygen consumption was measured during treadmill walking at 1.3 meters per second using each of the wooden arcs in random order. Step frequency was held constant across all trials in order to eliminate possible energetic variation due to swinging of the legs; frequency was set to the subject's preference when walking on the largest (40 cm) arcs. Average metabolic rate was estimated in Watts, and then non-dimensionalized using the subject's mass (m) and leg length (L) and the gravitational acceleration (g). Collision losses experienced by passive walking models decrease with increasing radius of curvature [3], because roll-over arcs greatly affect the change in COM velocity during double support. The theoretical relationship between mechanical work (W_{mech}) per step and radius of curvature R is given by [1, 3]

$$W_{mech}/\text{step} = \alpha^2 \left(1-(R/L)\right)^2, \qquad (1)$$

where α is the half-angle between the model's legs at heel strike. We hypothesized that this mechanical work would exact a proportional metabolic cost [1]. At constant step frequency, the relationship between mechanical work per step and the hypothesized metabolic rate P_{met} has an unknown constant of proportionality [2]. Allowing for different offsets above basal metabolism, data were therefore fit to the curve

$$P_{met} = C * \left(1-(R/L)\right)^2 + D. \qquad (2)$$

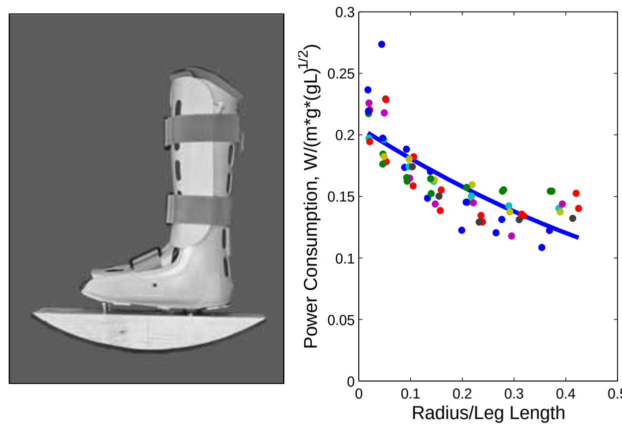

Figure 1: (a) One of the experimental boots, with 40 cm radius attachment. Metabolic rate decreased substantially with increasing radius of curvature. (b) Metabolic power vs. radius of curvature, with theoretical curve fit (Eq. 2).

RESULTS AND DISCUSSION

Average net metabolic power expenditure decreased significantly with radius of curvature (Fig. 1b). Net metabolic rate was highest at the smallest radius of curvature. Expenditures using the smallest arcs averaged 218% greater than normal walking (511 vs. 203 W above resting); expenditures using the 30 cm arcs averaged only 46% greater (296 W above resting).

The results indicate that metabolic rate roughly followed the trend predicted theoretically. Fig. 1b also shows the best fit of these data to the theoretical curve of Eq. 2: C = .134, D = 0.072, R^2 = 0.79. There are several reasons why the results do not agree entirely with the theoretical curve. Visually, it appears that the best quadratic fit to the data is not the theoretical curve, but rather one centered around R/L = 0.3. This early upturn suggests that phenomena not included in the simple model may cause humans to expend more energy when the radius of curvature causes the effective foot length to be greater than normal. An explanation noted by McGeer [3] is that in the models, bipeds with mass distributed near the feet have lower efficiency than those with mass closer to the hip (as used to derive Eq. 1). Early simulation results suggest that anthropomorphic mass distribution may explain the optimum roll-over radius observed here.

REFERENCES

1. Donelan JM et al. *J. of Biomech* **35**, 117-124, 2002.
2. Kuo AD. *ASME J. of Biomech Engrg* **123**, 264-269, 2001.
3. McGeer T. *Int. Journal of Robotics Research* **9(2)**, 62-82.

ACKNOWLEDGEMENTS

This work supported in part by NIH DC006466.

THE SPRING-MASS MODEL FOR WALKING

[1,2]Hartmut Geyer, [1]Andre Seyfarth and [2]Reinhard Blickhan
[1]Locomotion Laboratory, Jena University, Dornburger Str. 23, D-07743 Jena, Germany
[2]Dept. of Motion Science, Jena University, Seidelstrasse 20, D-07749 Jena, Germany

INTRODUCTION

In general, two different models are employed when addressing animal and human locomotion on a simple mechanical level: the *inverted pendulum model for walking*, where the body is reduced to a point mass m at the center of mass (COM) vaulting over a rigid stance leg of length ℓ_0, and the *spring-mass model for running* or hopping, where the rigid stance leg is substituted by a compressing spring of rest length ℓ_0 and stiffness k.

The spring-mass model reproduces salient features of the characteristic ground reaction force (GRF) pattern observed in running, which renders it ideal to explain experimental observations, predict functional dependencies, and formulate biological control hypotheses.

By contrast, the inverted pendulum model suffers from GRF patterns inconsistent with experimental observations. Consequently, experiments also demonstrate that instead of vaulting over rigid legs (characterized as 'compass gait'), the COM experiences much less vertical excursion necessitating significant stance limb compressions, which at high speeds are even comparable to those observed in running [e.g. 1].

Motivated by these experimental findings, we here ask in how far the characteristic GRF patterns of walking can be explained by purely elastic leg behavior.

MODEL

To address this question we extend the planar spring-mass model for running [2] by a second idealized leg spring and investigate a single walking step characterized by two subsequent apices (**Fig. 1**).

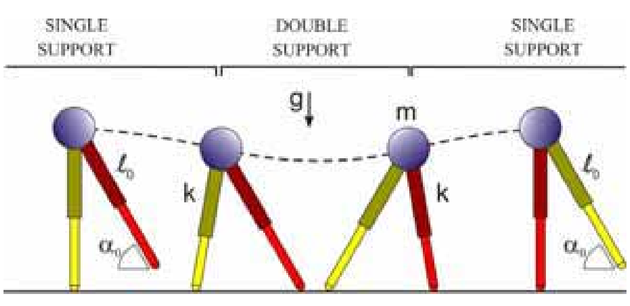

Fig. 1: Two-legged spring-mass walking model.

Starting in single support, the stance leg compresses due to the acting gravitational force (gravitational acceleration: g). The swing leg, however, remains in a fixed leg orientation (angle of attack α_0) until it touches the ground initiating the double support phase. During this phase, the COM is redirected upwardly since both spring forces together exceed the counteracting gravitational force. Maintaining forward progression, the rear leg-spring relaxes and eventually reaches its rest length initiating the subsequent single support phase.

RESULTS AND DISCUSSION

By scanning the model's behavior throughout the parameter space (angle of attack, spring stiffness, and system energy), we find that (i), similar to spring-mass running [2], the extended model describes self-stable and robust periodic locomotion if the parameters are properly chosen. (ii) Furthermore, the resulting steady state trajectories yield GRF patterns similar to those observed in animal and human locomotion (**Fig. 2**) suggesting leg compliance to be an essential feature not only in running but also during walking.

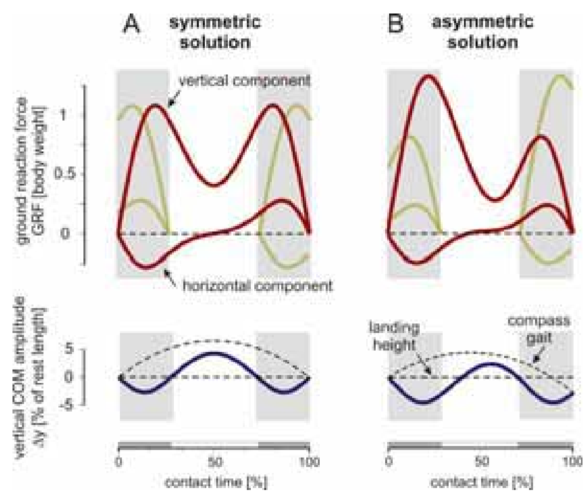

Fig. 2: Steady-state patterns of GRF and vertical COM amplitude in spring-mass walking. Dependent on the actual parameters, (**A**) symmetric and (**B**) asymmetric steady-state trajectories can be observed.

CONCLUSIONS

The bipedal model put forth in this study is probably the simplest mechanical model describing GRF patterns similar to those observed in walking. In comparison to the inverted pendulum model it establishes two new qualities. First, it emphasizes the importance of the double support. Second, it incorporates the experimentally observed motion along the leg axis as an additional degree of freedom. Moreover, as a direct derivative of the spring-mass model for running, the bipedal model allows to describe the two fundamental gait patterns within a single framework unifying the investigation of legged locomotion on the mechanical level from walking to the walk-run transition to running.

REFERENCES

1. Lee C, Farley C. *J Exp Biol* **201**, 2935-2944, 1998.
2. Seyfarth A, et al. *J Biomech* **35**, 649-655, 2002.

ACKNOWLEDGEMENTS

This research is supported by an Emmy-Noether Grant of the German Science Foundation (SE1042/1-4) to AS.

A PARAMETRIC MADYMO ANALYSIS FOR DETERMINING SEAT BELT USAGE IN A FRONTAL COLLISION

David E. Raymond, Jon B. Landerville, Jeffrey B. Wheeler, David A. Dainty
Vector Scientific, Inc., Los Angeles, California
draymond@vectorscientific.com

INTRODUCTION

Forensic biomechanics is often called upon for the purposes of determining whether a seat belt was utilized in automotive collisions. A parametric analysis utilizing MADYMO was performed to elucidate seat belt usage in a high speed frontal collision based upon the known injury outcome.

METHODS

Vehicle accident reconstruction was performed utilizing PC-Crash to determine the impact severity. Since PC-Crash does not have the ability to generate a crash pulse, two pulses were assumed: AAMA generic MVSS 208 sled pulse and a NCAP pulse from the NHTSA vehicle crash test database. The AAMA pulse was felt to represent the lower bound of the impact severity and the NCAP the upper bound of the impact severity based upon the vehicle reconstruction analysis.

Medical records were reviewed that revealed a C2 fracture, intimal rupture of the aortic arch and right tibial plateau fracture. Geometric measurements of the vehicle determined from NHTSA's vehicle database were used to generate a MADYMO model of the right front passenger compartment [1]. A generic passenger side airbag model was utilized. The Hybrid III 5th percentile female ellipsoid model was chosen as best representing the subject. Additional unknowns were included leading to an overall matrix of two collision pulses, three fore/aft passenger seat positions, and four deployment times of the passenger side airbag for both belted and unbelted conditions. For the belted condition, a generic MADYMO belt was utilized. Injury assessment values were monitored for the neck, chest and lower extremities. Injury indices (Nij, Chest G, Tibial Index) were calculated and related to MVSS 208 injury criteria.

RESULTS AND DISCUSSION

The subjects C2 fracture was consistent with biomechanical literature on compression-extension injury mechanisms to the upper cervical spine [2]. Figure 1 demonstrates representative kinematics of both belted and unbelted conditions. Nce (compression-extension) values were significantly higher for both AAMA and NCAP pulses for unbelted than belted conditions but only exceeded the injury criteria of 1.0 for the unbelted NCAP conditions as seen in Figure 2. Ncf (compression-flexion) values were also found to exceed the injury criteria in the NCAP unbelted condition with airbag deployments of 40-50 milliseconds (ms) for all three seating positions. Upper tibial indexes were also significantly higher for unbelted conditions for both AAMA and NCAP pulses and exceeded the injury criteria in all unbelted conditions but met for belted conditions. Chest acceleration (3 ms clip) was not significantly different between belted and unbelted AAMA pulse conditions. Chest accelerations did exceed the 60 G criteria in the NCAP, unbelted conditions for all three seat positions for the 40-50 ms airbag deployment times as a result of bottoming out the bag and striking the dummy's chest to the dashboard.

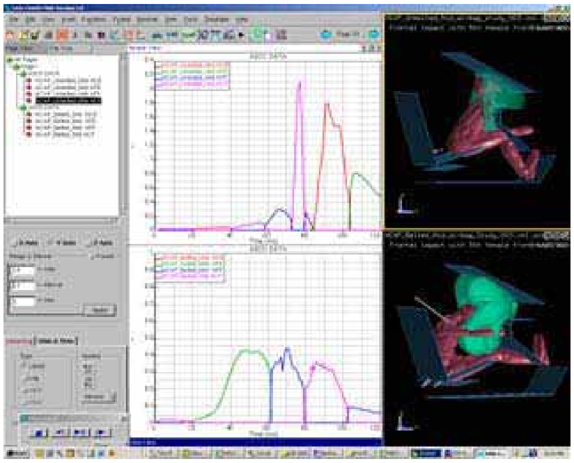

Figure 1

Tibial indexes and Nce increased as seat fore/aft position increased. Chest accelerations had an increasing trend when in closer proximity to the deploying airbag.

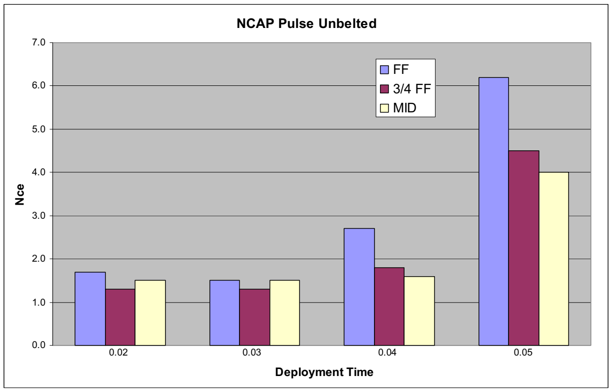

Figure 2

SUMMARY

A parametric MADYMO study was performed to determine seat belt usage in a frontal collision based upon known injury outcome. Analysis of accepted injury indices and criteria demonstrated a significantly higher probability of injury in the unbelted scenario with the occupant located at the approximate mid fore/aft position at the time of impact.

REFERENCES

1. MADYMO Users Manual
2. Myers BS, Winkelstein BA. *Critical Rev in Biomedical Engineering*, 23(5&6): 307-409, 1995.

OCCUPANT KINEMATIC ANALYSIS OF AN UNBELTED MINIVAN PASSENGER: A FREE BODY APPROACH

David E. Raymond, Edward C. Fatzinger Jr., Thomas J. Connors, Jeffrey B. Wheeler
Vector Scientific, Inc., Los Angeles, California
draymond@vectorscientific.com

INTRODUCTION

A case analysis is presented where an unbelted second row passenger of a minivan claimed to have been ejected through the second row passenger side window when his vehicle was struck on the passenger side at an intersection. A vehicle dynamics analysis, occupant kinematic analysis, and vehicle interior dimensional analysis, were utilized to develop an understanding of the occupant kinematics.

METHODS

Medical records were reviewed that revealed a minor laceration to the right cheek and minor knee contusions. Examination of an exemplar minivan was also carried out. Geometric measurements of the vehicle were recorded for use in analysis. Occupant kinematics were based on results of vehicle collision dynamics along with pre-impact body position evidence. Vehicle dynamics were determined using accident reconstruction engineering techniques and analysis. Occupant kinematics were determined using methods outline by Bready et al. and interior dimensional analysis [1].

RESULTS AND DISCUSSION

Vehicle kinematics were used to establish the pre-impact heading of the unbelted second row occupant. Since the occupant was unbelted the assumption was made that the second row occupant would act as an uncoupled body in the crash and continue along his pre-impact heading until acted on by an interior vehicle component. Once the heading was determined, the occupant position at coincidental time intervals as the vehicle dynamics data was determined and plotted. Once this was done the two are merged to give gross occupant kinematics assuming no interior contacts. Offset of the occupant initial position was made based on testimony of the occupant and interior vehicle measurements of the second row bench seat.

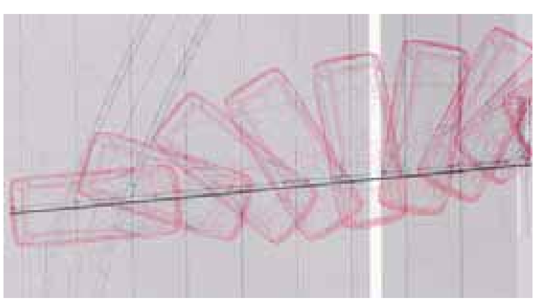

Once this was done, the coordinates were transformed into the vehicle coordinates system.

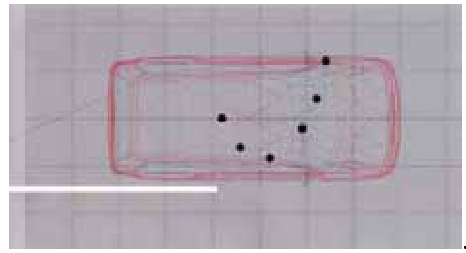

This trajectory was used to then render a 3-D drawing of occupant motion relative to vehicle interior components.

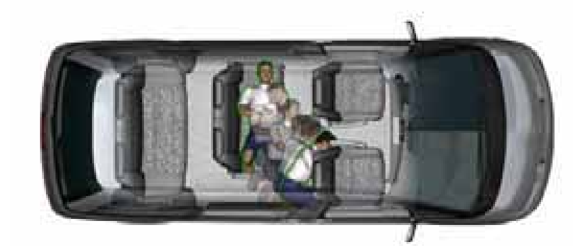

An 11-14 inch offset existed between the top of the bench seat and the bottom of the passenger side second row window. 3-D analysis revealed that the occupant would not have ejected out of the side window but rather contacted the front passenger seat as shown below. This is mostly due to the rotation of the minivan upon impact. The occupant is shown in a position close to the floor of the van which is an effect of both gravity and ramp effect of the seat back. The occupant presented with a facial laceration to the right cheek that coincided with contact of the right front seat inboard armrest as shown below.

SUMMARY

An occupant kinematics study was undertaken to investigate whether an unbelted second row occupant in the prone position, would eject through the passenger side window during a side impact. Published methods of occupant kinematic analysis, vehicle reconstruction techniques, and 3-D rendering were used to determine that the occupant would not have ejected through the passenger side window.

REFERENCES

1. Bready, J.E., et al. (2002). *SAE Technical Paper Series*, *2002-01-0536*.

WRIST ELECTROMYOGRAPHY AND KINEMATICS WHEN PROPELLING STANDARD, COMPLIANT, AND POWER-ASSISTED PUSHRIM WHEELCHAIRS: A PILOT STUDY

Philip Requejo, Ernest Bontrager, Craig Newsam, Valerie Eberly, Joanne Gronley, and Sara Mulroy
Pathokinesiology Laboratory, Rancho Los Amigos National Rehabilitation Center, Downey, CA, USA
email: prequejo@larei.org, web: www.larei.org

INTRODUCTION

Alternative modes of manual wheelchair (WC) propulsion offer a way to reduce demands on the upper extremities [1]. A compliant pushrim can reduce the impact forces on the hands during the push-phase of propulsion [2]. A pushrim-activated power-assisted WC (PAPAW) that applies power to the hub at each push requires less effort [3] than standard unassisted WC. While the demands on the upper extremities when propelling on a standard WC are well documented [4], measurement of muscle activity allows us to determine the muscular demands when propelling with alternative modes of WC propulsion. The purpose of this pilot study was to document the electromyographic activity of the wrist muscles and range of motion of the wrist joint when propelling a standard and two alternative pushrim designs. We hypothesized that these alternative pushrim designs can reduce the demands on the wrist musculature during manual WC propulsion.

METHODS

A non-disabled adult male served as a subject for this preliminary study. He read and signed an IRB approved informed consent form before participating. The subject propelled a Standard pushrim, a compliant pushrim design (FlexRim) [1], and a PAPAW (i-GLIDE^{TM}) [2] design positioned on a stationary custom wheelchair ergometer [4]. Data were recorded at a self-selected free and fast propulsion speed (level ground simulation) and at a simulated 8% grade. Switches were taped to the right palm to determine the push and recovery phase timing. Wrist muscle activity was documented with bipolar, fine-wire electrodes inserted into the flexor digitorum sublimis (FDS), flexor carpi radialis (FCR), extensor carpi radialis longus (ECRL), extensor digitorum communis (EDC), opponens pollicis (OP), flexor pollicis brevis (FPB), supinator (SUP), and pronator teres (PT) muscles. EMG signals were transmitted via a co-axial cable and digitized (2500Hz) using a data collection computer. The EMG data were full wave rectified and integrated over 0.01sec interval. The EMG values during propulsion were normalized by the highest 1 second of activity obtained in a maximal effort manual muscle test for each muscle (%MAX). The average integrated EMG was determined at each 1% of the propulsion cycle. Three-dimensional motion of the right upper extremity and trunk was recorded (50Hz) during each 10-sec propulsion trial using a Vicon (Oxford Metrix) motion analysis system. Wrist joint kinematics was calculated from the recorded data using an Euler/Cardan rotation sequence.

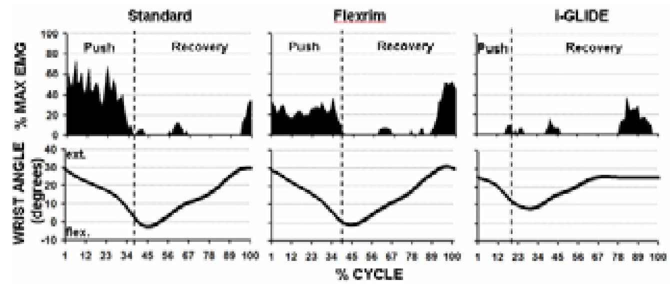

Figure 1: FDS activity during push and recovery phase of graded propulsion with a Standard, Flexrim, and i-GLIDE

RESULTS AND DISCUSSION

Five muscles had their primary activity during the push phase while three muscles were primarily active during recovery. Intensities of these muscles increased primarily in the fast and graded propulsion with Standard and FlexRim but remained low with the i-GLIDE (Table 1), particularly in the graded propulsion (Figure 1). All push-phase muscles had an onset late in recovery. Intensities of these muscles were highest primarily in the Standard. Intensities of the grip muscles (OP, FPB, and FDS) were less in the FlexRim than Standard during free and fast propulsions. During graded propulsion, the push-phase time was 52% less (42 vs. 20% cycle) for the i-GLIDE compared to Standard and FlexRim. In the graded propulsion, the push-phase flexion/extension range of motion in the i-GLIDE was 57% less (31 vs. 13degrees) than Standard and 52% less (13 vs. 28degrees) than the FlexRim (Figure 1). The lower EMG, reduced push phase timing and range of motion is indicative of reduced muscular demands. Use of alternative WC pushrim designs has the potential to benefit WC users, particularly when propelling in more demanding terrains. Assessment of wrist demands in everyday WC users remains as future work.

REFERENCES

1. van der Woude, L. H., et al. *Am J Phys Med Rehabil* **80**(10), 765-777, 2001
2. Richter, W. M., et al. *Processdings of RESNA*. 2000.
3. Levy, C. E., et al. *Arch Phys Med Rehabil,* **85**(1), 2004
4. Mulroy, S. J., et al. *Arch Phys Med Rehabil*, **77**(2), 1996

ACKNOWLEDGEMENTS

NIDRR grant H133E020732, Beneficial Designs, Independence Technology.

	Mean Push-Phase EMG (%MAX)															Mean Recovery-Phase EMG (%MAX)								
	FDS			EDC			OP			FPB			SUP			PT			ECRL			FCR		
	fr	ft	gr	fr	ft	gr	fr	ft	gr	fr	ft	gr	fr	ft	gr	fr	ft	gr	fr	ft	gr	fr	ft	gr
Standard	13	33	37	7	10	21	27	44	64	8	18	28	15	25	60	1	15	16	0	6	12	1	7	10
FlexRim	6	6	21	2	9	13	9	29	68	1	4	29	8	29	33	3	21	14	4	8	4	0	6	5
i-GLIDE^{TM}	1	13	1	11	2	1	12	11	4	0	4	0	9	7	6	3	15	1	2	7	19	0	1	0

Table 1: Mean EMG intensities of the push and recovery phase muscles during free(fr), fast(ft), and graded (gr) propulsion.

THREE DIMENSIONAL MULTISCALE RECONSTRUCTION OF EMU FEMORAL HEAD OSTEONECROSIS: FROM CELL TO ORGAN LEVEL

[1] Jessica Goetz, [1]Thomas Baer, [1]Gail Kurriger, [1]Douglas Pedersen, and [1]Thomas Brown
[1]Department of Orthopaedics and Rehabilitation University of Iowa;
email: jessica-goetz@uiowa.edu, web: poppy.obrl.uiowa.edu.

INTRODUCTION

Osteonecrosis of the femoral head is a disorder whose mechanical pathogenesis (collapse) is significantly affected by the geometric details of the necrotic lesion. The (bipedal) emu model of osteonecrosis, unlike other animal models, mimics human clinical collapse. For lesions induced by liquid nitrogen insult, systematic studies of the resulting structural compromise require delineation of zones of necrosis in three dimensions relative to the global femoral head. Unfortunately, the gold standard for determining osteonecrosis is by time-consuming histologic evaluation, thus requiring novel multiscale analysis.

Automated histologic image analysis [1], which can determine osteocyte viability, requires that global orientation of the femoral head be preserved throughout histologic processing and analysis. Post-analysis, data from multiple slides need to be reassembled into a three-dimensional global map of osteocyte survival.

METHODS

Immediately post-necropsy, the proximal portion of emu femur is fixed in formalin. After fixation, the femur is landmark leveled and potted upright in PMMA. The potted specimen is then transferred to a custom drill guide and two parallel holes, 1.6 mm in diameter and 10 mm apart, are drilled through the femoral neck (Figure 1). Two orthogonal cuts are made 3.8 mm from the holes to remove the femoral head and neck from the remainder of the proximal femur. The femoral head is then decalcified in formic acid.

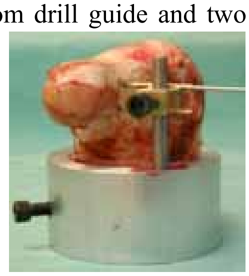

Figure 1: Potted femur in drill guide.

Since there is no practical way to preserve serial section registry after paraffin embedment and conventional microtoming, it was necessary to introduce fiducial markers that had the unique attributes of accurate shape preservation during subsequent histological processing, yet sufficient friability to not damage the delicate microtome blades. After investigating many candidates, we found that ordinary household potato had that combination of properties.

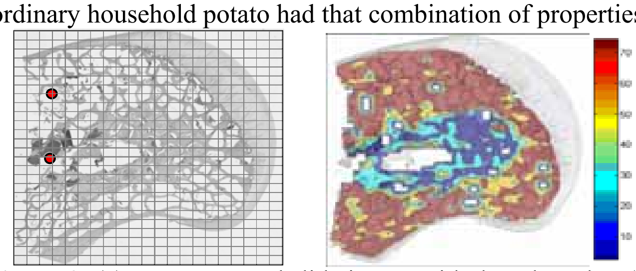

Figure 2: (a) Reconstructed slide image with dowel marker (red) and grid lines between every second subimage. (b) Two dimensional contour plot of osteocyte survival.

Upon decalcification, two 1.5 mm diameter dowels of potato, dried for 48 hours in a 42˚C oven, are inserted through the two holes in the femoral neck. The femoral head, with fiducial dowels in place, is then dehydrated in ethanol, cleared in xylene, and embedded in paraffin. Serial sections are taken every 0.5 mm through the entire thickness of the head. Each section is mounted and stained in Wiegert's hematoxylin and eosin.

Each slide is scanned on a stepper-motor-driven microscope stage, and saved in the form of approximately 2000 subimage .tif files. Every subimage is analyzed to measure fractional osteocyte survival. These individual subimages are then reconstructed in Matlab into a whole-section image, and osteocyte viability data for each slide are reassembled into a corresponding two-dimensional matrix (Figure 2). Each two-dimensional whole-head section is rotated and translated until the centroids of its two dowel fiducial markers are coincident with those from the other sections (Figure 3). After this affine transformation, these sections are assembled into a three dimensional matrix, and interpolated to output the three-dimensional distribution of osteocyte necrosis.

RESULTS AND DISCUSSION

The present three-dimensional arrays of fractional osteocyte viability represent the first instance of histology-based osteocyte status being mapped at the whole-bone level. This allows direct registration of the cryo-induced lesion relative to osseous stresses that result from external loading of the joint, toward the goal of understanding the role of lesion pathogenesis in global mechanical collapse.

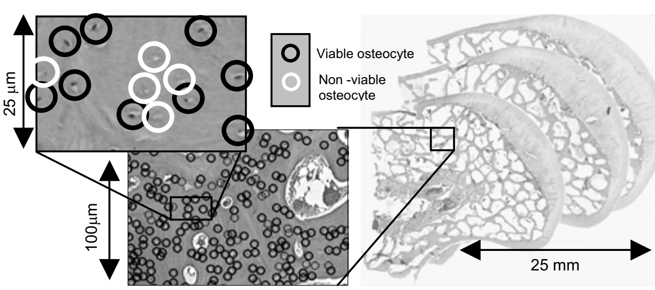

Figure 3. Stacked sections of femoral head with zoomed-in insets of an individual subimage and further zoom in of individual osteocytes.

REFERENCES

1. Reed KL, et al. *Computer Methods in Biomechanics and Biomedical Engineering* **7**(1) 25-32, 2004.

ACKNOWLEDGEMENTS

NIH AR 49919, Mr. Erich Stoermer, Dr. James Martin.

IN VITRO VALIDATION OF THERMAL FINITE ELEMENT ANALYSIS OF CRYOINSULT DELIVERY FOR EMU FEMORAL HEAD NECROSIS

[1] Jessica Goetz and [1]Thomas Brown
[1]Department of Orthopaedics and Rehabilitation University of Iowa;
email: jessica-goetz@uiowa.edu, web: poppy.obrl.uiowa.edu.

INTRODUCTION

In ongoing work with the emu as a bipedal animal model of osteonecrosis, lesions are induced by means of a custom built cryoprobe surgically inserted into the femoral head [1]. In order to study the factors governing the size of these lesions, a thermal finite element model has been developed to quantify freeze and thaw rates, as well as freeze front geometry, as a function of operator-controlled parameters during surgery.

Initial validation of the finite element model had been performed in a geometrically simplified agarose preparation [2]. Because this model needs to accurately model the freeze cycle as it occurs intraoperatively, further benchtop testing has been performed in fresh emu femur specimens.

METHODS

Six emu femurs were obtained fresh from an abattoir. PMMA molds were made of the lateral side of each femur and used as a drill guide. A 4 mm diameter drill hole and four 0.8 mm diameter drill holes were drilled through the PMMA. The drill guide was attached to the femur and holes drilled approximately 50 mm into the femoral head. Copper-constantan thermocouples embedded in 0.8 mm diameter tubing were inserted into the four small drill holes.

A custom built cryoprobe [2] was inserted into the femoral head through the main drill hole, and the femur was positioned with its head embedded in a reservoir of 1% agarose, to provide thermal inertia (Figure 1a). A seven-minute freeze from room temperature to –30°C was performed followed by a passive seven-minute thaw. Temperatures were recorded for the four thermocouples in the femoral head, and one each at the tip of the probe, in the probe shaft, and in the agarose 1 mm from the medial side of the femoral head. Post-thaw, the femoral head was cut open and the actual locations of the thermocouples measured for verification.

The finite element model reflected the geometry of probe used for the experimental testing, and was driven from the time-temperature curve recorded at the tip thermocouple during each benchtop test. Both non-homogeneous conductive effects and phase change latent head nonlinearity were included. Temperature curves for nodes corresponding to the location of the thermocouples were extracted and compared to the experimental temperature curves.

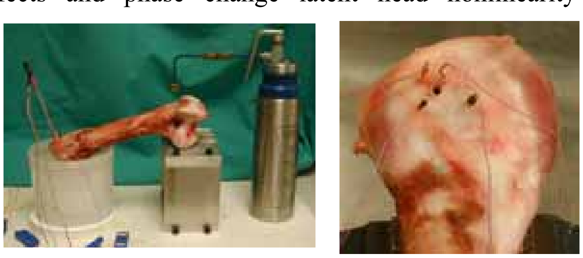

Figure 1: (a) Experimental set-up with femur in agarose and probe and thermocouples inserted into femoral head from lateral side of femur. (b) Close-up of thermocouple insertion.

RESULTS AND DISCUSSION

The current FEA parameter set results in a model that is capable of replicating experimentally measured temperatures to within 3˚C (Figure 3). Because of the accurate results obtained from the testing in this preparation, the finite element model is suitable to model the freeze cycles occurring intraoperatively, with due accommodation of tissue heating effects.

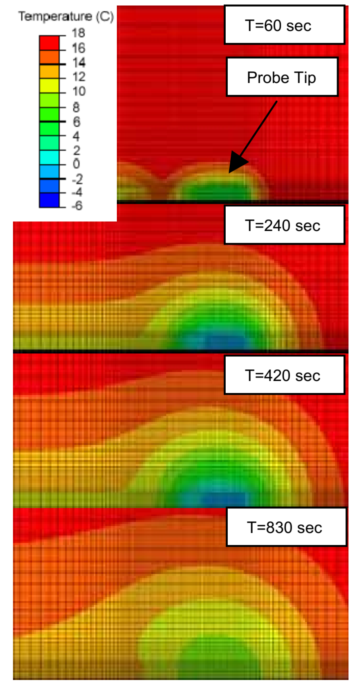

Figure 2: Finite element run of a seven-minute freeze followed by a seven minute thaw.

CONCLUSIONS

The finite element model of cryoinsults to a cadaver emu femoral head accurately models in vitro thermal behavior.

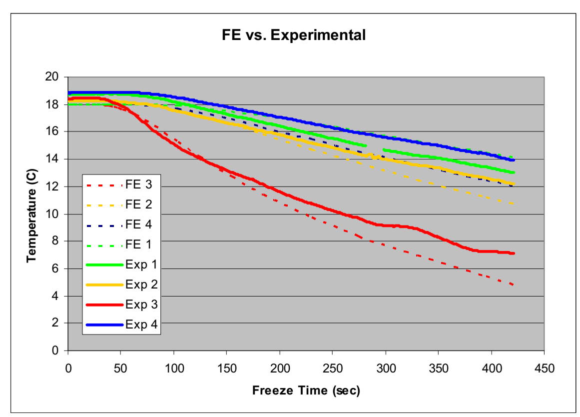

Figure 3: Temperature curves for thermocouples in the femoral head during a 7-minute freeze (thick lines) and the corresponding nodal temperature curves.

REFERENCES

1. Conzemius M, et al. *J Orthp Res* **20,** 303-309, 2002.
2. Reed KL, et al. *J Biomech* **36**, 1317-1326, 2003.

ACKNOWLEDGEMENTS

NIH AR 49919, Dr. James Martin for technical assistance.

PREDICTORS OF SUCCESS IN THE 3000M STEEPLECHASE WATER JUMP

Bryan K. Lindsay and Iain Hunter
Department of Exercise Sciences, Brigham Young University, Provo, UT, USA
email: bkl8@email.byu.edu, web: biomech.byu.edu

INTRODUCTION

While the steeplechase has been contested for over 150 years, relatively little research has been completed regarding the technique involved in this unique event. In our research, we looked at six different characteristics of the water jump barrier technique: Minimum hip angle of the lead leg at take-off, knee angle of the support leg (pushing off the barrier), take-off distance, center of mass height above the barrier, approach speed, and landing distance (see figure 1). These characteristics were chosen due to past work by coaches and researchers [1,2]. This study determined which characteristics are significant predictors of the ratio of race pace to speed through the water jump.

Figure 1: Definitions of some of the measured characteristics.

METHODS

Seventeen women and 19 men were filmed and digitized to measure two-dimensional characteristics of water-jump technique in the 3000-meter steeplechase using Peak Motus 8.2 (Centennial, CO). Subjects were filmed at three different meets during 2004: The Cardinal Invite (Palo Alto, CA), The Oxy Invite (Eagle Rock, CA), and The Olympic Trials (Sacramento, CA). These meets provided a range of athletes from Division II NCAA athletes to Olympic qualifiers, including one Olympic Finalist.

Multiple linear regression was used to determine which characteristics of technique significantly predict the ratio of race pace to speed through the jump. Speed through the jump was measured between 2.5 m prior to the barrier and 2.5 m past the water. The ratio of speeds was chosen to normalize speed between athletes.

RESULTS AND DISCUSSION

Approach speed and landing distance were significant predictors of speed divided by race pace for men and women (Tables 1 and 2). All other variables in the full model were rejected due to non-significance at the 0.05 alpha level. The ratios of race pace to speed through the water jump for women and men respectively were 0.89 and 0.92.

While approach speed and landing distance were significant predictors of the ratio of race pace to speed through the jump, they were very different in how much variance they explained for each model. Approach speed was clearly the most noticeable factor for women. However, for men, landing distance was much more critical. With the event being fairly new for women, race times are dropping rapidly. This should increase their approach speed, which may lead to landing distance explaining more of the variance for women in the future as is seen with the men.

Table 1: Prediction for speed divided by race pace for women.

Variable	β	Partial R^2	*p*-value
Approach Speed (m/s)	0.113	0.614	<0.001
Landing Distance (m)	0.067	0.078	<0.001
Intercept	0.013		0.016

Table 2: Prediction for speed divided by race pace for men.

Variable	β	Partial R^2	*p*-value
Approach Speed (m/s)	0.013	0.015	0.044
Landing Distance (m)	0.136	0.605	<0.001
Intercept	0.443		<0.001

CONCLUSIONS

Success in completing the water-jump of the 3000m steeplechase without dropping from race pace dramatically can be accomplished by accelerating during the approach to the barrier and accomplishing a relatively long landing distance. There are obviously limits to how much acceleration and how far of a jump off the barrier should be attempted. However, with the athletes analyzed in this study, the larger the approach speed and the longer the jump into the water, the better the athletes were able to keep their water-jump horizontal velocity close to their race pace.

REFERENCES

1. Fix D, et al.. *Track and Field Q Rev*, **84**, 23-25, 1984.
2. Benson T. *Mod Athlete and Coach*, **38**, 15-18, 1993.

COMPARISON OF ARTHROMETER (PASSIVE) AND FUNCTIONAL ACTIVITY (ACTIVE) ANTERIOR TIBIAL DISPLACEMENTS

[1] Robert Deusinger, [1]Dequan Zou, [1]Keith Minor, and [1]Ben Seedorf
[1]Human Biodynamics Lab, Program in Physical Therapy, Washington University School of Medicine,
4444 Forest Park Blvd., Campus Box 8502, St. Louis, MO Email: deusingerb@msnotes.wustl.edu

INTRODUCTION

KT-1000 and KT-2000 arthrometers commonly are used as diagnostic aids by clinicians to passively detect excessive amounts of anterior tibial displacement (ATD) associated with disruption of the anterior cruciate ligament (ACL) as well as during reconstructive surgery and subsequent rehabilitation as a means to determine levels of restored and maintained ACL integrity [1]. However, these devices assess only passive ATD during non-weight-bearing. Because many daily functional activities involve active movement on weight-bearing limbs, it is important to know whether the passive ATD measures imply anything about ACL integrity during actively performed non-weight-bearing (NWB) as well as weight-bearing (WB) functional activities. The purposes of this presentation are to examine whether: 1) there is concurrent validity of passive KT-1000 and active movement, functional activity ATD measurements; 2) joint surface kinematics of ATD, % rolling, and % gliding differ between a NWB and WB activity; and 3) tibiofemoral % rolling and % gliding reflect ATD during the active movement functional activities.

METHODS

Data were collected on 12 subjects (3 males and 9 females, mean age 24.8±2.1 yrs, mean weight 138.4±22.6 lbs.) and a history of no injury to the test knee within the last 5 years.

Passive anterior tibial displacement was measured at maximum manual force using a KT-1000 arthrometer. The measurements were obtained between 25°-30° knee flexion based on patient size and comfort, and according to manufacturer guidelines. Active movement ATD, % rolling, and % gliding measurements were obtained by inputting 3-D videographic motion analysis kinematic data into a computational geometric knee model [2] for a sitting knee extension (NWB) and a sit-to-stand (WB) activity. Based on the model, a slip ratio [3] was computed from which percent rolling and gliding were calculated. Using femoral arc length and tibial contact point displacement components of the slip ratio, active movement ATD measures were obtained. All knee arthrometer and active movement knee model data were averaged over three trials at respective subject-specific, knee arthrometer test angles.

Analysis: A Pearson correlation between knee arthrometer passive and knee model active movement ATD of the NWB and WB activities was used to establish concurrent validity. ANOVA was performed to determine whether meaningful differences occurred between the NWB and WB activities for ATD, % rolling, and % gliding. A multiple regression was used to identify whether tibiofemoral % rolling and/or % gliding reflect active movement ATD during NWB and WB activities.

RESULTS AND DISCUSSION

The mean passive ATD was 6 times greater than the active movement ATD of the NWB and WB activities whereas ATD for the NWB and WB activities were similar (Table 1). Pearson r-values ($r = 0.572$; $r = 0.488$) strongly support no concurrent validity between the passive and active measures of ATD suggesting they measure different aspects of ATD. High correlation values ($r = 0.978$ to 0.993) between active ATD and % rolling and % gliding demonstrate a strong association of ATD to rolling and gliding (Table 2). The lower value of active ATD for NWB likely reflects stabilizing effects of muscle activity while the lower ATD for WB likely reflects the role of both muscle activity and joint compression effects that minimize ATD, while enhancing joint stability. Conversely, the greater passive ATD may indicate tibiofemoral stability without constraints of muscle activity and joint surface compression.

Table 1. Mean Passive and Active ATD Values

Passive ATD (mm)	NWB ATD (mm)	WB ATD (mm)
8.94 ± 1.80	1.56 ± 0.05	1.37 ± 0.07

Table 2. Multiple Correlation of Functional Activity (Passive) ATD with Percent Rolling and Gliding

	NWB ATD	WB ATD
% Rolling	-0.993	-0.978
% Gliding	0.993	0.978

CONCLUSIONS

We analyzed both passive NWB and active NWB and WB measures of anterior tibial displacement in healthy knees. A similar analysis is planned for ACL deficient knees. We believe our preliminary results provide a foundation for further investigation. Substantiating a combined use of passive and active ATD measures may help differentiate whether impairments of appropriate muscle activity patterns and/or joint surface alignment contribute to abnormal joint surface kinematics with ACL disruption.

REFERENCES

1. Daniel DM, Malcolm LL, et al. JBJS-Am, 67, 720-726, 1985.
2. Hollman JM, Deusinger RH, et al. J Sport Rehabil, 12, 143-161, 2003.
3. O'Connor JJ, Zavatsky A, Biomech. Diarthoidal Joints-Vol.II, NY, NY: Springer-Verlag, 1990.

STABILITY OF PLATE FIXATION CONSTRUCTS WITH LOCKED AND NON-LOCKED SCREWS

[1]Larry W. Ehmke, [1]Michael Bruehl, [2]Daniel C. Fitzpatrick, and [1]Michael Bottlang
[1]Biomechanics Laboratory; Legacy Clinical Research & Technology Center, Portland, OR,
[2]Orthopedic Healthcare Northwest, Eugene, OR; email: mbottlang@biomechresearch.org

INTRODUCTION

The development of locked plate technology represents a changing approach to fracture fixation. Locked plates function as internal fixators and allow secondary bone healing through endochondral ossification [1]. The mechanics of locked plates are fundamentally different from conventional non-locked plates and so require a revised understanding of the plate-bone construct stability.

This study was designed to investigate the stability of unicortical and bicortical locked plate constructs relative to conventional, non-locked constructs in an osteoporotic long bone model. We hypothesized that locked unicortical and bicortical constructs were at least as stiff and strong as conventional non-locked constructs.

METHODS

To represent osteoporotic bone, 27 cylindrical surrogate specimens were machined from 30pcf foam blocks (G.P., Tacoma, WA) to 30mm outer diameter, 3mm wall (cortex) thickness, and 200mm length. A 10-hole 4.5mm narrow LCP (Synthes, Paoli, PA) was affixed to bone surrogates by either 4.5mm non-locking or 5.0mm locking screws. A 10mm fracture gap was simulated by fixing the LCP to surrogate bone on one side and to a rigid aluminum cylinder on the other (representing stiff diaphyseal bone).

Plate-specimen constructs were loaded into a material test machine (Instron 8874) to be tested in torsion, axial compression, and 4-point bending under progressive dynamic loading. Cyclic amplitude was increased with each loading cycle until construct failure or plate separation. Construct stiffness was assessed at the beginning of cyclic loading, before the onset of implant loosening or construct plastic deformation. Strength was defined as the maximum force, torque, or bending moment required for construct failure (considered as specimen breakage or plate loosening).

Three groups of screw types were tested in a 1,3,5-screw configuration: conventional non-locked (Non-Lock), locked unicortical (Lock-Uni), and locked bicortical (Lock-Bi). A one-way ANOVA was used to detect differences among groups. Subsequently, a Dunnett's test was conducted to determine significance versus Non-Lock constructs ($\alpha<0.05$).

RESULTS

Construct Stiffness: In torsion, Non-Lock constructs were 7% less stiff than Lock-Bi constructs ($p<0.05$), but were 60% stiffer than Lock-Uni constructs ($p<0.05$) (Fig. 1). In compression and 4-point bending no significant difference in stiffness was detected among groups.

Construct Strength: In torsion, Non-Lock constructs were 27% weaker than Lock-Bi constructs ($p<0.05$), but were 63% stronger than Lock-Uni constructs ($p<0.05$) (Fig. 1). In compression, Lock-Bi and Lock-Uni constructs exhibited 72% ($p<0.05$) and 16% ($p<0.05$) larger peak loads as compared to Non-Lock constructs, respectively. In 4-point bending, Lock-Bi and Lock-Uni constructs sustained 33% ($p<0.05$) and 45% ($p<0.05$) lower peak bending moments as compared to Non-Lock constructs, respectively.

In both torsion and 4-point bending, failure of all constructs was dominated by breakage of foam specimens through the screw hole furthest from the fracture gap. Plate loosening was primarily responsible for construct failure during compression.

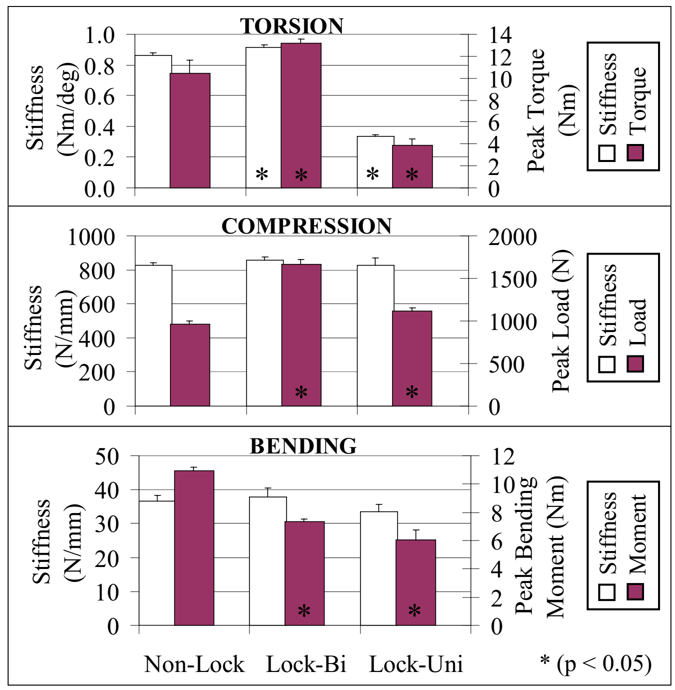

Figure 1: Stiffness and strength for locked and non-locked screw types in a) torsion, b) compression, and c) 4-point bending (*=p<0.05).

DISCUSSION

Results of this study provide a better understanding of the role of locked plating in comparison to non-locked techniques. Stiffness represents the initial fixation characteristics of the plate-bone construct. Similar to Pater et al., our results show that bicortical screw constructs provide greater stiffness and strength in torsion than unicortical locked constructs [2]. Under both torsion and compression locked bicortical constructs exhibited the highest load to failure. Interestingly, in bending, conventional non-locked constructs provided the highest resistance to failure, which may be in part due to smaller diameter screw holes.

REFERENCES

1. Egol KE, et al. *J Orthop Trauma*, 18(8), 488-93, 2004.
2. Pater TF, et al. *20th Meeting OTA*, Hollywood, Florida 2004.

ACKNOWLEDGEMENTS

Financial support provided by Synthes USA.

UPPER LIMB MOTION DURING SNOW SHOVELING WITH REGULAR AND MODIFIED SHOVEL

[1]Hitoshi Yanagi, [2]Noriyuki Yamamoto, [1]Xiaohui Gai, [1]Katsumi Miyakoshi and [3]Tadao Isaka
[1]Satellite Venture Business Laboratory, Kitami Institute of Technology,
[2]Japanese Red Cross Hokkaido college of Nursing,
[3]Ritsumeikan University; email: yanagi@mail.kitami-it.ac.jp

INTRODUCTION

Snow shoveling is a hard labor routine in a cold northern region in the winter. The task should be considered a physically intensive activity and associated with local muscle pain of the lower back. Freivalds [1] stated in his review that a second handle on a shovel might improve shoveling performance by reducing the amount of stooping. We confirmed that the amount of the thorax forward tilt, the lower limbs flexion and the center-of-gravity distance traveled were significantly smaller when using a shovel with a second handle [2, 3]. However, the effects of the second handle on the upper limbs have never been studied. Thus, this study attempted to determine how different types of shovel affect the motion of the upper limbs during the shoveling of snow.

METHODS

Five right-handed male subjects volunteered to participate in the laboratory experiments. The mean values $\pm$ *SD* of their heights, weights, and ages were 1.68$\pm$0.06 m, 66.3$\pm$10.6 kg, 28.2$\pm$8.7 yrs., respectively. They received an explanation of the experimental protocol and provided informed consent prior to testing.

Two types of shovel were compared in the study, a regular shovel and a modified shovel with a second handle. The regular shovel is a commonly used one and consists of a 1.5-m main shaft and a plastic blade. The modified shovel resembles the regular shovel in its blade and main shaft but an additional second handle is mounted perpendicularly to the main shaft.

Subjects shoveled simulated snow with the two different shovels in the laboratory. The simulated snow was stuffed bags with shredded paper in three different weights. For each bout, subjects used one of the two shovels, and were required to scoop up one bag placed diagonally left in front of their left foot and throw it onto a 0.7-m-height box 1.75 m away from them.

The measurements of kinematic data during the shoveling were established using the VICON 460 motion analysis system (Vicon Motion Systems, UK) with six cameras at 120 Hz placed on the laboratory ceiling. The flexion angles of the elbow joints were chosen in order to describe the motion of the upper limbs while shoveling. The shoveling was divided into the three phases; squatting, lifting and throwing according to the previous study [2, 3].

The kinematic data during the shoveling were expressed as mean $\pm$ *SD*. A Student's paired *t*-test was used to determine significant differences between the two types of shovel on measured variables. The *p*-value was considered significant when it was found to be less than the usual level of significance 0.05.

RESULTS AND DISCUSSION

Table 1 shows the flexion angles of the elbow joints during the shoveling with the regular and modified shovel. The minimum left elbow flexion angle was significantly smaller in the squatting phase when the subjects used the modified shovel than when they used the regular shovel. Although the maximum left elbow flexion angle was slightly larger when using the modified shovel, there was no significant difference between the two shovels. Moreover, the angular displacement of the left elbow joint was significantly larger when shoveling with the modified shovel. The right elbow flexion angles were significantly smaller both in the squatting and the lifting phases when using the modified shovel. Bending the left elbow would be needed to keep the blade horizontal with the ground so as not to let the snow slip off. Consequently, more stresses may be imposed on the left elbow flexor muscles when using the modified shovel. In order to reduce the amount of the left elbow flexion it may be necessary to increase the lift angle between the blade and the main shaft or to lower the second handle height. Further shovel modification would help users shovel snow more comfortably.

REFERENCES

1. Freivalds, A., *Ergonomics* **29**, 3-18, 1986.
2. Yanagi, H., et al., *Proceedings of the International Workshop on Modern Science and Technology 2004*, Kitami, Japan, pp. 371-374, 2004.
3. Yanagi, H. et al., *Proceedings of the 18th Japanese Society of Biomechanics Congress*, Kanoya, Japan, 2004. (in Japanese, in press)

Table 1: Flexion angles of the elbow joints during shoveling with the regular and modified shovel.

				Regular shovel		Modified shovel
Elbow Flexion Angle [deg]	Left	Squatting	Minimum	35 $\pm$ 2	*	32 $\pm$ 2
		Lifting	Maximum	45 $\pm$ 4		49 $\pm$ 7
	Right	Squatting	Minimum	38 $\pm$ 7	**	35 $\pm$ 6
		Lifting	Maximum	42 $\pm$ 6	**	39 $\pm$ 5

** and * indicate significant differences between the two shovels at $p < 0.01$ and $p < 0.05$, respectively.

SIMULATION OF BLOOD FLOW AND DEFORMATIONS OF MECHANICAL HEART VALVES USING BOUNDARY INTEGRAL TECHNIQUES

[1]Alejandro Roldán, [2]Naomi Chesler, [3]John Bustamante, [1]Tim Osswald
[1]Department of Mechanical Engineering, University of Wisconsin-Madison
[2]Department of Biomedical Engineering, University of Wisconsin-Madison
[3]Universidad Pontificia Bolivariana, Medellín-Colombia
e-mail: roldan@wisc.edu

INTRODUCTION

Approximately 170,000 individuals worldwide receive prosthetic heart valves every year; 95% of these are mitral and aortic valve replacements, and more that 60% of those are mechanical heart valves. In general, mechanical heart valves tend to last longer than biological prosthetic valves, but they also carry a greater long-term risk of cardiovascular complications. Such complications are thought to be caused by high blood shear stress, turbulence and the overall complexity of hemodynamics in the mechanical heart valves. So far, important advances have been achieved in the implementation of computational fluid dynamics to study cardiovascular physiology using numerical techniques that require domain discretization, such as finite element methods or finite difference techniques. However, these cannot fully represent the moving and deforming boundaries present in an operating valve, an issue that can be approached using the Boundary Element Method (BEM), a numerical technique that has not yet been applied in cardiovascular modeling.

The main goal of this project is to develop a mathematical and numerical model to simulate blood flow through bileaflet prosthetic valves based on the BEM. This technique will be suitable for modeling the flow in these geometrically complex systems which are dominated by moving and deforming boundaries.

METHODS

The flow of blood in the cardiovascular system can be considered incompressible and Newtonian. Therefore, the momentum equations are reduced to the Navier-Stokes equations, a system of partial differential equations that basically describe fluid flow; though fundamental and rigorous, they are nonlinear, non-unique, complex and difficult to solve. They do not have a general solution, and so far only a few particular solutions have been found. These exact solutions are important because basic phenomena described by the mathematical model can be analyzed; also they can be used as standard solutions to compare with the approximate numerical solutions. However, in almost every practical situation, it is necessary to use numerical methods in order to obtain a solution of the Navier-Stokes equations.

Through mathematical manipulation, the governing equations were transformed into boundary integrals, requiring a boundary-only discretization for their solution. This solution scheme of the complex equations, which include moving boundaries, is the BEM.

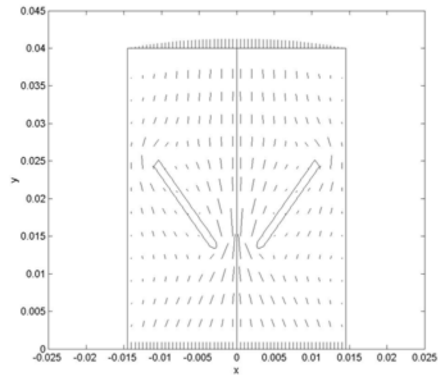

Figure 1: Snapshoot of flow through the valve.

A two-dimensional (2D) model of the mechanical bileaflet valve geometry was developed, which consisted of a cylindrical tube containing a bileaflet valve. Due to the symmetry the simulation was performed to half the domain (see Figure 1). The valve diameter and thickness were 29 mm and 1 mm, respectively; the length of the tube was 40mm. The gap between the leaflet and the tube wall in the closed position was fixed to 0.1 mm. The constant values used for density and viscosity were 1,000 kg/m^3 and 0.004 kg/m-s, respectively. The non-slip boundary condition was used on the tube wall.

RESULTS AND DISCUSSION

Simulations were performed on 10 valve positions between 0° and 70° with respect to the transverse axis of the tube. Figure 1 shows the velocity vectors through an opening valve (55° position). At small opening positions, vortices between the two leaflets were generated due to high flow acceleration in that region. As the valve opens, the flow stabilizes and shows a characteristic parabolic profile downstream.

REFERENCES

1. C. S PESKIN, “Modeling Prosthetic Heart Valves for Numerical Analysis of Blood Flow in the heart”, *Journal of Computational Physics*. **37**, 113 – 132, (1980)
2. S. ALURI and K. B. Chandran, “Numerical Simulation of Mechanical Mitral Heart Valve Closure”, *Annals of Biomedical Engineering*, **29**, 665 – 676, (2001).
3. A. QUARTERONI, “Modeling Cardiovascular System a Mathematical Adventure: Part I”, *SIAM News*. **34**, number 5. (2001)
4. M. A. NICOSIA, R. P. Cochran, D. R. Einstein, C. J. Rutland, “A Coupled Fluid – Structure Finite Element Model of the Aortic Valve and Root”. *Journal of Heart Valve Disease*, **12**, No6, 781 – 789 (2003).

QUANTITATIVE PREDICTION OF PROGRESSION OF ARTICULAR CARTILAGE DEGENERATION FOLLOWING INCONGRUOUS INTRA-ARTICULAR FRACTURE REDUCTION

Yang Dai[2], Thomas D. Brown[1, 2], J. Lawrence Marsh[1]
[1]Department of Orthopaedics and Rehabilitation, [2] Department of Biomedical Engineering
University of Iowa, Iowa City, IA; email: tom-brown@uiowa.edu

INTRODUCTION

Intra-articular fracture reduction is a very difficult orthopaedic procedure since it is widely believed that the residual incongruity can induce stress aberration in the articular cartilage and then provoke a mechano-response leading to degeneration of cartilage (secondary osteoarthritis).

The degeneration of cartilage is a chronic procedure. From a mechanical perspective, the neighboring healthy cartilage will endure elevated load since degenerative cartilage becomes more compliant. Therefore, healthy cartilage may degenerate with time, a cascading effect leading to whole joint degeneration.

Here, Discrete Element Analysis (DEA)[2] was used to quantitatively calculate the possible degeneration area in an acetabular fracture, as an example to show the effect of progressive degeneration when the cascade effect is taken into account.

METHODS

A hip joint model was created from the CT slices and the potential contact area was selected between the femoral head and acetabulum. [3] Treating the femoral head and acetabulum as rigid bodies, the region between them, *viz.* the cartilage, is represented as an array of linear elastic compressive springs. The springs' stiffnesses in the normal direction (Equation 1) depend on the cartilage modulus (E), Poisson ratio (ν) and thickness (h). Shear can also be addressed in DEA, but due to joint lubrication, the stiffness in shear here is assumed to be negligible.

$$k_n = \frac{E(1-\nu)}{(1+\nu)(1-2\nu)h} \qquad [1]$$

A trans-tectal displaced fracture model was created. A gait cycle with 16 instances was used to calculate the contact stress distribution. Cumulative pressure exposure (P_c) for the cartilage was then calculated [3]. The results were scaled to compare with literature on chronic cartilage pressure tolerance. [1]

The potential degeneration area is defined as any area with P_c large than 10 MPa-years. Here, a year was used as a time span. The cartilage modulus in any region with degeneration was reduced to only 20% that of normal. The same procedure was used to calculate the potential degeneration area in the next year and so on.

RESULTS AND DISCUSSION

For different residual step-offs (2.5, 2.0, 1.5, 1.0, 0.5 and 0mm), the cumulative pressure exposures were calculated for a 2-year time span. Also, progressive degeneration was calculated. (Figure 1)

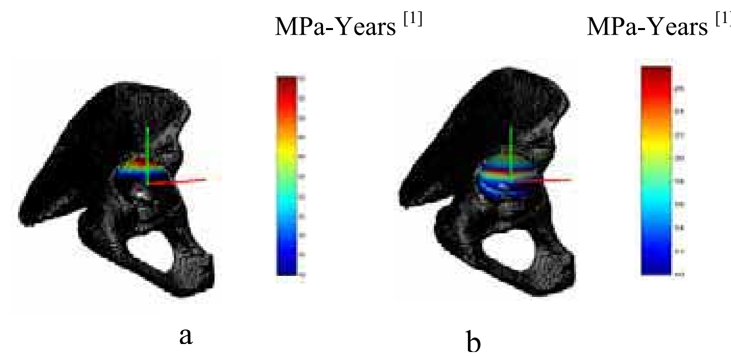

FIGURE 1 DISTRIBUTION OF CUMULATIVE PRESSURE EXPOSURE AT 2 YEARS, FOR A 2MM STEP-OFF
(a) Without progressive degeneration (b) with progressive degeneration

Step-off (mm)	2-year Overpressure Area (mm^2) without cascade effect	2-year Overpressure Area (mm^2) with cascade effect
0	0	0
0.5	6.68	845.64
1.0	486.89	1688.50
1.5	576.34	1747.80
2.0	700.60	1798.10
2.5	988.94	1954.00

Table 1: Cartilage area experiencing over 10MPa-years of cumulative over-pressure (Total potential contact area = 3402.9mm^2)

Areas of cartilage degeneration are much larger when cascading progressive degeneration is taken into account. So, mechanical degeneration may substantially accelerate the pathogenesis of whole joint OA.

The percentages of the degeneration area are 24.8%, 49.6%, 51.4%, 52.8% and 57.4% of the available contact area. From this perspective, any fracture reduction with residual step-off greater than 1mm step-off faces high OA risk at a 2-year span.

REFERENCES

[1] Hadley et al: *J. Ortho. Res. 8:* 504-513, 1990 [2] Kawai et al: *Conf. Comp. in Civ. Engn.*: 1-16, NY ,1981 [3] Dai et al: *ASB 2004* , Portland, 2004

ACKNOWLEDGEMENTS

Supported in part by NIH AR46601

RECRUITMENT ORDER HAS LITTLE EFFECT ON THE SHORT-RANGE STIFFNESS OF FELINE MEDIAL GASTROCNEMIUS MUSCLE

[1]Lei Cui, and [2]Thomas Sandercock
Department of [1]Biomedical Engineering and [2]Physiology, Northwestern University
email: t-sandercock@northwestern.edu

INTRODUCTION

The ultimate goal of our research is to determine the contributions of both individual muscles and muscle combinations to whole limb endpoint stiffness in 3 dimensional space. A computer muscle model, capable of predicting whole muscle short-range stiffness (SRS) based on anatomical properties, is believed to be necessary for accomplishing this goal. Knowledge of the effect of motor unit composition and muscle architecture on SRS is essential for developing such a muscle model.

Slow motor units have been shown to be 1.3 times stiffer than similar fast motor units [2]. In spite of this difference muscle architecture—fiber length and tendon properties—may be the principle determinants of whole muscle SRS.

The goal of this study is to test the hypothesis that the recruitment order of motor unit types has little effect on the SRS versus force characteristics of a muscle. Preliminary results are reported here.

METHODS

The hypothesis was tested in 5 cat medial gastrocnemius (MG) muscles. The cats were mounted in a rigid frame with all muscles in the left hindlimb denervated except for the MG. The MG was partially freed from surrounding tissue with its nerve and blood supply left intact. The calcaneous was cut and attached to a muscle puller allowing force to be measured during step changes in length (1.2 mm in 7 ms). The cats were decerebrated allowing activation of the MG using normal recruitment via the crossed extension reflex (CXR). A laminectory exposed the ventral roots, which were cut after the CXR measurements were complete, and stimulated with hook electrodes.

SRS was measured during three types of muscle activation: 1) CXR activation; 2) Rate modulation; and 3) Partial muscle activation. CXR modulation preserves the normal recruitment order and rate modulation of slow and fast motor units. Rate modulation was achieved by dividing the ventral roots into 4 to 6 bundles, and stimulating the bundles asynchronously to keep whole muscle force smooth, even at low frequencies [1]. Thus the whole muscle was active but at a low frequency. Partial muscle activation was achieved by stimulating part of the ventral roots at 100 Hz.

RESULTS AND DISCUSSION

The most complete results from as single cat are shown in Figure 1. Total force from CXR activation was limited and never exceeds 20% of maximum tetanic force. In contrast, steady low force is difficult to achieve with rate modulation, so these two protocols were not studied over the same force

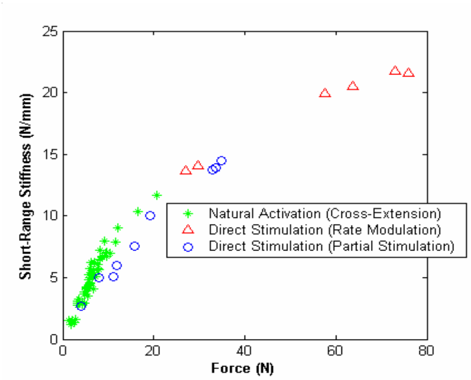

Figure 1: Results from one cat showing SRS plotted against Force (mean value 50 milliseconds before perturbation) using three different types of activation (see text).

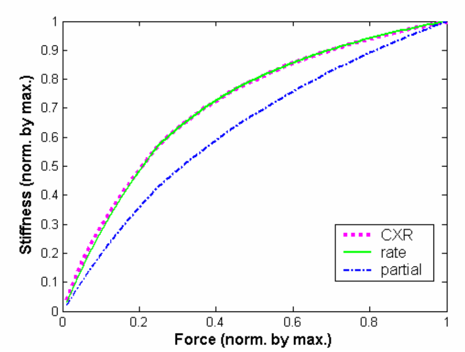

Figure 2: Normalized SRS plotted against normalized Force based on the common tendon model simulation.

range. Still, rate modulation seems to closely match the CXR data, even thought rate modulation does not employ normal recruitment. Similar results were obtained in the other cats.

Figure 2 shows predictions made using a simple common tendon model [3]. Slow units were assumed to comprise 25% of the muscle fibers and were fully recruited by 25% of muscle force. The model provides a reasonable fit to the experimental data.

CONCLUSIONS

Recruitment order of motor units has little impact on SRS of cat MG muscle. If these preliminary results are supported, it suggests recruitment order can be ignored in the hind limb models of stiffness.

REFERENCES

1. Rack MHP and Westbury DR, *J Physiol* **240**, 331-350, 1974.
2. Petit J, Filippi GM, Emonet-Denand F, Hunt CC and Laporte Y, *J Neurophysiol* **63**, 190-197, 1990.
3. Sandercock TG, *J Appl Physiol* **89**, 2206-2214, 2000.

EFFECTS OF SMOOTH VS "PRICKLY" SURFACE CONDITIONS ON TILTBOARD PERFORMANCE

[1] Peter M. Quesada, [2]Michael P. Durham, [2]Robert V. Topp, [3]Ann M. Swank and [1]Danielle Biton
[1]Department of Mechanical Engineering University of Louisville,
[2]School of Nursing, [3]Department of Health & Sport Sciences; email: pmques01@louisville.edu

INTRODUCTION

The somatosensory system, along with vestibular, visual, and proprioceptive functions, coordinates with neuromuscular systems to maintain postural stability. Investigations of somatosensory influence have often involved comparisons of diminished and normal function [1-3]. These efforts have demonstrated that compromised somatosensory function is associated with reduced postural stability. Such assessments have commonly involved measurements obtained during static standing, or with imposed perturbations. Neither approach, however, evaluates balance capacity or mechanisms associated with passively unstable surfaces.

The present study investigated the effects of a "prickly" standing surface versus a smooth surface on the performance of a tiltboard balance task. A basic tiltboard is a flat circular standing platform with a solid hemisphere attached to it. The addition of a prickly texture on the surface of a tiltboard was intended to enhance plantar surface sensation. The use of a tiltboard was intended to provide a passively unstable surface.

METHODS

Thirteen healthy subjects (8 males, 5 females), with mean height and weight of 176±8 cm and 71±10 kg, participated in this study, Each individual signed an informed consent form that approved by this institution's IRB. Each subject was provided an opportunity to "warm up" with a tiltboard prior to testing. Three reflective markers were placed at 90° intervals at the edges of the tiltboard. These markers represented right, left, and rear edges. Body markers were placed in a Helen Hayes arrangement, and surface EMG electrodes were also placed bilaterally over the gastroc/soleus, tibialis anterior, quadriceps, and hamstring groups.

For each tiltboard balancing trial, feet were positioned, such that the dorsal crease at the tibial/midfoot junction was aligned along the diameter line between the right and left tiltboard markers. For each trial the subject was instructed to maintain the tiltboard as stable as possible for an extended duration, while marker spatial coordinates were obtained at 100 Hz, with a Hawk Motion Tracking System (Motion Analysis Corp.). This duration was intended to be 35 seconds for all subjects; however, three subjects were tested with 20 second durations, and one individual performed 25 second trials. The 20 second trials were also performed without placement of body reflective markers or surface electrodes. A random draw determined whether the first trial would be performed with a "prickly" or smooth surfaced tiltboard. The second trial was then performed with the remaining surface. Another random draw then determined the order of the third and fourth trials.

Data processing has focused, to this point, on results obtained from the tiltboard reflective markers. These marker coordinate trajectories were used to determine tilt angle magnitude, and tilt direction (relative to an anterior/posterior axis) for each sampling interval. Tilt angle means and standard deviations were determined for each trial, and values from prickly and smooth surface trials were compared, using ANOVAs, to determine effects of tiltboard surface type. Plots of tilt angle magnitude vs. tilt direction were more qualitatively evaluated to assess preferred balancing orientations. EMG evaluation was intended to assess muscle activity durations.

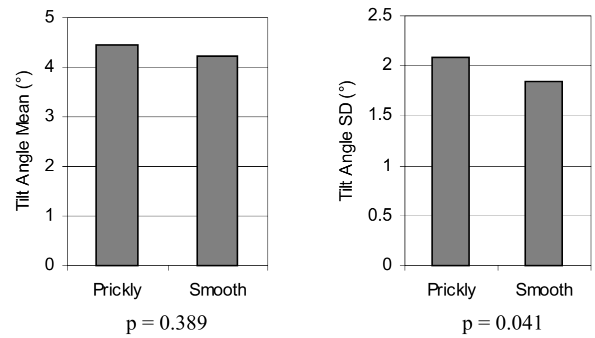

Figure 1: Mean & SD of tilt angle magnitude for prickly and smooth tiltboard surfaces

RESULTS AND DISCUSSION

Tiltboard surface type did not have a statistically significant effect on tilt angle magnitude mean values ($p = 0.389$), while standard deviations of tilt angle magnitudes were found to be significantly larger for the prickly surface ($p=0.041$). This result suggested that balance performance was poorer with the prickly surface, although this surface was intended to intensify plantar surface somatosensory input. This finding seems somewhat contrary to some previous reports that demonstrated improved balance performance with better plantar surface sensation. It was noted, however, that such improved performance was generally associated with more static balance tasks. While Horak [2] reported that healthy vs neuropathic balance differences were mitigated when sway referencing was introduced, neither the effects of an intervention directed towards intensifying somatosensory input, nor the influence of an inherently unstable surface was considered.

Analyses of tilt angle magnitudes vs tilt orientations, and of EMG recordings are more preliminary at this time. Tilt magnitude vs tilt orientation findings, however, suggest that anterior/posterior or medial/lateral tilt orientations are more prevalent during tiltboard balance tasks. EMG results indicate little, if any, periods of inactivity of lower extremity muscles.

REFERENCES

1. Corriveau H, et al. *Diabetes Care* **23**, 1187-91, 2000.
2. Horak FB, *Somatosensory & Motor Res* **19**, 316-326, 2002.
3. Meyer PF, et al. *Experimental Brain Res* **156**, 505-12, 2004.

HETEROGENEITY OF CHANGE IN MUSCLE CIRCULATION AMONG SYNERGISTS DURING DYNAMIC MUSCLE ACTION

[1] Yoshiho Muraoka, [2]Atsuko Kagaya
[1]Faculty of General Education, Meisei University,
[2]Research Institute of Physical Fitness, Japan Women's College of Physical Education
e-mail: muraoka@ge.meisei-u.ac.jp, web: http://www.meisei-u.ac.jp/

INTRODUCTION

In case of a single muscle, muscle contraction impairs blood inflow to a muscle with an increase of intramuscular pressure. Some studies have reported that muscle circulation of synergists interacted among themselves. For example, the significant decrease in muscle blood volume detected by near-infrared spectroscopy (NIRS) was found in medial gastrocnemius but not in the lateral gastrocnemius during static plantarflexion [1]. However, the result of muscle circulation in static muscle action might not be directly applicable to that in dynamic muscle action.

The purpose of present study was to clarify the heterogeneity of change in muscle circulation among synergists during dynamic muscle action. For this purpose, we investigated muscle blood volume and oxygenation in triceps surae muscle during calf-raise exercise using NIRS.

METHODS

Subjects were five healthy males. They were asked to sit quietly for more than 3 min as a control period. Then they stood up and performed 4 s calf raise consisted of 2 s heel up phase and 2 s heel down phase. They repeated the calf-raise 20 times leaded by an electric metronome.

Surface electromyogram (EMG) was recorded from medial and lateral gastrocnemius (MG and LG) and soleus (SOL) using bipolar electrode (SX-230, DKH, Japan).

To estimate the oxygenated hemoglobin and myoglobin (O_2Hb/Mb), deoxygenated hemoglobin and myoglobin (HHb/Mb), total hemoglobin and myoglobin (cHb/Mb) content and tissue oxygenation index (TOI) in target muscles, two channels optical probes NIRS were firmly placed on the skin surface of muscle belly (NIRO-200, Hamamatsu Photonics, Japan). Firstly, MG and LG muscles were measured at once, and MG and SOL muscles were measured using the same protocol. O_2Hb/Mb, HHb/Mb and cHb/Mb were expressed as changes from rest values, and TOI was expressed as a percentage (%).

The change of ankle joint angle was measured using an electric goniometer (SG110/A, DKH, Japan).
The data of EMG, NIRS and joint angle were stored on a personal computer by using an analog-to-digital converter (PowerLab/16sp, ADInstruments).

RESULTS AND DISCUSSION

The mean amplitude of EMG (mEMG) increased greater in MG than in LG, and mEMG of SOL showed almost constant value during exercise.

O_2Hb/Mb of all three muscles decreased during the exercise, and a marked decrease in the value of MG was observed. HHb/Mb of all three muscles decreased at the onset of exercise, then the great increase was observed in MG. The decline of TOI was greater in MG than LG. The TOI values at the last (20^{th}) calf-raise were 29.4 ± 3.6%, 47.9 ± 3.8% and 56.1 ± 4.0% for MG, LG and SOL, respectively.

Muscle blood volume of all three muscles decreased rapidly at the beginning of exercise. Then the blood volume in MG and LG increased gradually, but that in SOL continued to decrease until the end of exercise (**Figure 1**).

The present results suggest that muscle circulation among synergists was different from each other during dynamic exercise such as calf-raise exercise.

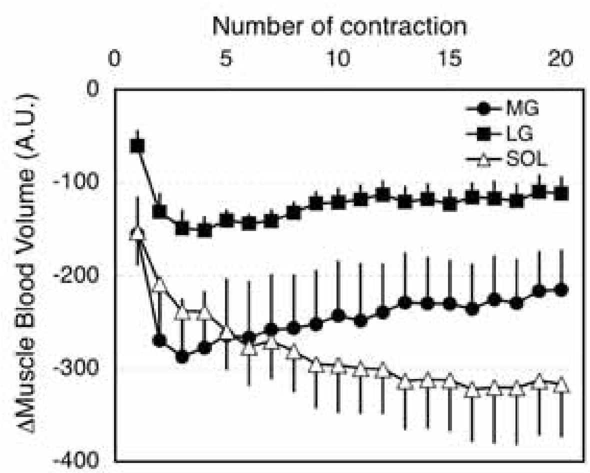

Figure 1: The changes of muscle blood volume during calf-raise exercise in MG, LG and SOL. Values are the mean ± SE

REFERENCE

1. Muraoka and Kagaya *Proceedings of ISB XIX*, Dunedin, New Zealand, 2003.

ACKNOWLEDGEMENTS

This research was partially supported by the Ministry of Education, Science, Sports and Culture, Grant-in-Aid for Young Scientists (B) 16700473, 2005.

COMPARISON OF METHODS USED TO DETERMINE INDUCED VERTICAL GROUND REACTION FORCE

[1]Zachary J. Domire, and [2]John H. Challis
[1]Division of Kinesiology and Health, The University of Wyoming, Laramie, WY, USA
[2]Biomechanics Laboratory, The Pennsylvania State University, University Park, PA, USA
email: zdomire@uwyo.edu, jhc10@psu.edu

INTRODUCTION

Every muscle action contributes to the ground reaction force via joint reaction forces passed through the system. Calculation of these effects is of interest, as it gives insight into a muscles role during a particular movement. Direct dynamic simulations have been used determine the role of individual muscle during gait [1,5], however different methodologies have been used. Neptune et al. [5] determined an individual muscle's contribution to the ground reaction force at each instant in time by taking the difference of the actual ground reaction force and the ground reaction force caused by all forces except the muscle of interest. Anderson and Pandy [1] determined an individual muscle's contribution to the ground reaction force by applying each muscle force in isolation and determining the resulting ground reaction force. The purpose of this study was to determine the induced vertical ground reaction forces during jumping using both methods and compare the summed induced vertical ground reaction forces with the actual vertical ground reaction force.

METHODS

An optimal control, direct dynamics simulation model was used to simulate vertical jumping. The model had four rigid links (foot, shank, thigh, and a combined head, arms, and trunk), connected by frictionless hinge joints. The foot was connected to the ground by a hinge joint at the metatarsal-phalangeal joint. It had a rotational spring-damper at this joint to represent the floor-heel interaction [6]. The equations of motion were formulated as mixed differential-algebraic equations [4]. The model was actuated by six muscle models representing the major muscle groups of the lower extremity. Each muscle was represented by a Hill-type model consisting of a series elastic element and a contractile element [2]. A genetic search algorithm [3] was used to select sequences of muscle model neural excitations for each of the muscles so that the total potential and kinetic energy of the center of mass was maximized at the instant the foot lost contact with the ground.

Induced vertical ground reaction forces were calculated using the methodology of Neptune et al., [5] (Method 1) and Anderson and Pandy [1] (Method 2). The induced ground reactions force for each muscle were summed and compared to the actual ground reaction force.

RESULTS AND DISCUSSION

The procedures for determining induced vertical ground reaction force produced similar results. When the individual, induced vertical ground reactions forces were summed, the total was similar to the actual vertical ground reaction force for both methods examined (Figure 1).

Method 2 produced a larger total vertical ground reaction force than method 1, with method 1 being closer to the actual values. This difference was fairly consistently spread across all of the muscles. The reasons for this difference are not completely clear, however method 1 allows for the possibility that a muscles contribution to the ground reaction force can change based upon the activity of other muscles.

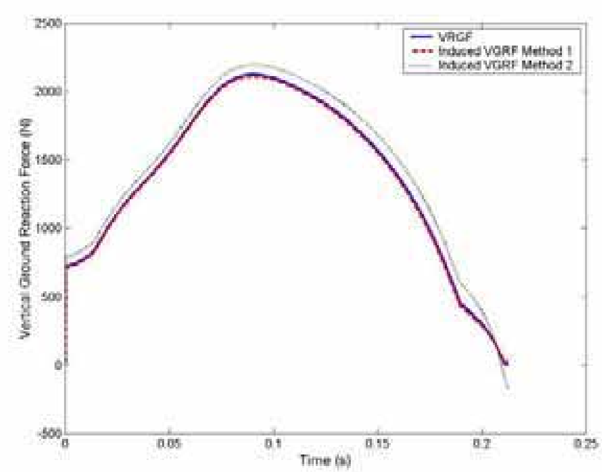

Figure 1: Total induced vertical ground reaction force for each method compared to actual vertical ground reaction force (VGRF).

CONCLUSIONS

Calculation of induced ground reaction forces can provide insight into a muscles role during a particular movement. Determining a muscles induced ground reaction force by subtracting the ground reaction force caused by all other forces from the total ground reaction force at each instant in time produces results closer to the actual ground reaction force than does applying each muscle force in isolation and determining the resulting ground reaction force.

REFERENCES

1. Anderson FC & Pandy MG. *Gait & Pos* **17,** 159-69, 2003.
2. Gallucci JG & Challis JH. *J App Biomech* **18**, 15-27, 2002.
3. Goldberg DE. *Genetic algorithms in search, optimization, and machine learning*, Addison-Wesley Pub. Co., Reading, Mass.
4. Haug EJ. *Computer Aided Kinematics and Dynamics of Mechanical Systems - Volume 1: Basic Methods.* Allyn and Bacon, Boston, Mass.
5. Neptune RR, et al.. *J Biomech* **34,** 1387-98, 2001.
6. Selbie WS & Caldwell GE. *J Biomech* **29**, 1137-46, 1996.

ACKNOWLEDGEMENTS

Supported in part by a grant from The Whitaker Foundation.

MUSCLE OPERATING RANGE INCLUDES OPTIMAL LENGTH AT EXTENDED JOINT POSTURES FOLLOWING BRACHIORADIALIS TENDON TRANSFER

[1]Wendy M. Murray, [1]M. Elise Johanson, [1]Anca Velisar, [1]Niels Smaby, and [1,2]Vincent R. Hentz
[1]Bone and Joint Center, VA Palo Alto HCS, Palo Alto, CA
[2]Department of Surgery, Stanford University, Stanford, CA;
email: murray@rrdmail.stanford.edu, web: guide.stanford.edu

INTRODUCTION

Intraoperative sarcomere length measurements have provided evidence that transferred muscles are often attached longer than optimal length during tendon transfer surgery [1]. These data suggest that outcomes of tendon transfers may be sub-optimal because muscles are too long to generate adequate active force. However, minimal data are available that describe active muscle function following tendon transfer. As a result, the influence of surgical tensioning on clinical outcomes has not been established in patients.

Brachioradialis, an elbow flexor, is commonly transferred to the paralyzed FPL, a thumb flexor, following cervical spinal cord injury. This procedure is intended to restore active lateral pinch and to improve the ability to use the hand. Because brachioradialis (Br) changes length with elbow flexion, we expect pinch force to vary with elbow position following this transfer. The aims of this study are: (i) to quantify changes in pinch force with elbow flexion following Br-FPL transfer and (ii) to estimate the operating range of the transferred muscle on the isometric force-length curve.

METHODS

Lateral pinch force produced during maximum effort was quantified in 7 subjects (8 limbs) with Br-FPL tendon transfers. Pinch force was measured with the shoulder positioned at 90° flexion and in both an extended (0°-25° flexion) and a flexed (80°-126° flexion) elbow posture. The elbow was externally stabilized; wrist position was not constrained but was recorded during testing. Passive force was also quantified as a function of elbow and wrist position. The component of lateral pinch force due to active muscle contraction was calculated by subtracting the passive force at the appropriate posture from the measured pinch force.

Using a computer model of the upper extremity [2] we estimated the length of the Br-FPL transfer as a function of elbow and wrist position. The muscle-tendon path of Br was altered in the model to simulate transfer to FPL. PCSA, optimal fiber length, and pennation angle for the transfer were defined to be the same as for Br. Tendon slack length was adjusted to simulate 30 different surgical attachment lengths. For each subject, we calculated the attachment length that best matched the observed change in active pinch force given the measured elbow and wrist positions. The simulations assume full activation and that the observed differences in active pinch force result from isometric force-length properties.

RESULTS AND DISCUSSION

Median lateral pinch force produced by the subjects was 25.2 N with the elbow extended (range = 7.9 N-45.9 N) and 17.5 N with the elbow flexed (5.0 N–36.1 N). Subjects extended their wrists while pinching; median wrist position was 51° extension with the elbow extended and 57° extension with the elbow flexed. In the wrist postures adopted during maximum effort, median passive force was 1.2 N (0.6 N-2.7 N) with the elbow extended and 1.0 N (0.5-1.5 N) with the elbow flexed.

Differences in active pinch force ranged from a 15% increase to a 39% decrease with elbow flexion. Based on these data, the computer simulations indicate that the transferred brachioradialis operates at lengths that include optimal length when the wrist is extended (Fig. 1). We estimate that median resting sarcomere length (zero activation, 10° elbow flexion, wrist in neutral) is 2.83 µm among these subjects (circles and labels in Fig. 1 indicate range). This length is approximately 20% shorter than the average resting sarcomere length measured in the transferred Br during surgery (different patients). With a resting sarcomere length of 2.83 µm and with the wrist extended between 50° and 60°, optimal length (i.e., peak force) occurs between 34° and 44° elbow flexion.

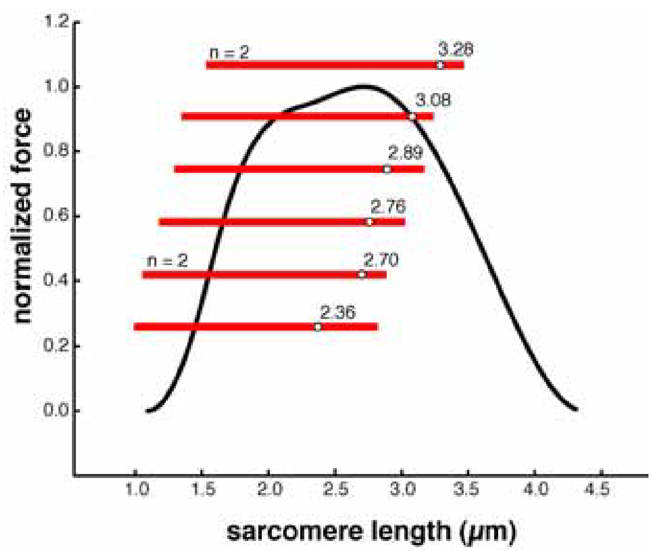

Figure 1. Br-FPL operating ranges as a function of elbow flexion (8 subjects). Wrist position is 55° extension, forearm is neutral, thumb is positioned for lateral pinch. Red bars indicate sarcomere length ranges during full muscle activation from 0° to 130° elbow flexion. Circles indicate resting length at 10° elbow flexion, neutral wrist and forearm, and the same thumb posture.

CONCLUSIONS

The data are consistent with length ranges that maximize force with both the elbow and wrist extended. This work suggests that the surgical attachment length chosen (which was not quantified in these subjects) did not result in post-operative lengths that were too long for active force generation.

REFERENCES

1. Fridén J, et al., *J Hand Surg [Am]* **23**, 105-110, 1998.
2. Holzbaur K, et al., Ann Biomed Eng**, accepted**.

ACKNOWLEDGEMENTS

This research was supported by the Rehabilitation R&D Service of the Department of Veterans Affairs (#B2785R)

SIGNIFICANCE OF SURGICAL ATTACHMENT LENGTH FOR HAND FUNCTION FOLLOWING BRACHIORADIALIS TENDON TRANSFER

[1]Wendy M. Murray, [2]Vincent R. Hentz, [3]Jan Fridén, and [4]Richard L. Lieber
[1]Bone and Joint Center, VA Palo Alto HCS, [2]Dept. of Surgery, Stanford University,[3]Dept. of Hand Surgery, Sahlgrenska University Hospital, Göteborg, Sweden,[4]Depts. of Orthopaedics and Bioengineering, UCSD and VAMC, San Diego;
email: murray@rrdmail.stanford.edu, web: guide.stanford.edu

INTRODUCTION
Intraoperative sarcomere length measurements have provided evidence that transferred muscles are often attached longer than optimal length during tendon transfer surgery [1]. It is possible that surgical outcomes could be compromised if post-operative muscle fibers are too long to generate active force. However, the relationship between surgical attachment length and functional outcome remains unclear.

Brachioradialis (Br), an elbow flexor, is the most commonly utilized donor muscle to restore hand function following tetraplegia. The aims of this study are (i) to quantify the sarcomere length of the brachioradialis chosen by surgeons at the time of tendon transfer and (ii) to evaluate theoretically muscle operating ranges given the current surgical approach.

METHODS
Sarcomere length was measured *in vivo* using laser diffraction in 13 individuals (14 limbs) with tetraplegia undergoing tendon transfer of brachioradialis to FPL (n = 12), ECRB (n = 1), or FDP (n = 1). All patients provided informed consent. Sarcomere length was measured both *in situ* and following transfer in 11 limbs, and following transfer only in 3 limbs. Measurements were taken with the elbow positioned in extension (approximately 0°-20° elbow flexion), the forearm in neutral rotation, the wrist in neutral, and the thumb in a lateral pinch posture.

A model of the Br-to-FPL tendon transfer was developed using a computer-graphics-based model of the upper extremity [2]. We assumed the line of action of the transfer was identical to the path of brachioradialis at the elbow joint and to the path of FPL at the wrist and thumb joints. Sarcomere length of the transferred brachioradialis in the model was set at the surgical attachment length measured intraoperatively, assuming the same limb posture and zero muscle activation. We then estimated the length of the transferred Br under full activation as a function of elbow, wrist, and CMC joint positions.

RESULTS AND DISCUSSION
The average sarcomere length of the brachioradialis following tendon transfer was 3.59±.27 μm. Transferred sarcomere lengths ranged from 3.10 μm to 3.90 μm across subjects. For the eleven limbs in which sarcomere length was measured both *in situ* and after tendon transfer, transferred length was significantly correlated to *in situ* length ($r = 0.76$, $p < 0.01$). The paired *in situ* and transferred lengths indicate that chosen surgical attachment lengths were slightly shorter ($p < 0.01$) than *in situ* lengths (mean = 3.78±.27 μm). *In situ* lengths ranged from 3.39 μm to 4.15 μm.

After transfer to the FPL, the Br changes length as a function of elbow, wrist, and thumb position. Based on the intra-operative data, we estimate that, with the wrist in neutral and the thumb in a lateral pinch posture, Br lengths span the plateau of the isometric force-length curve, and are comparable to lengths of the *in situ* Br (Fig. 1, compare red bars). Individuals with tetraplegia and Br-FPL transfers tend to extend their wrists when using their hands to augment the tenodesis effect; CMC extension is needed to grasp larger objects. Wrist extension and CMC extension both increase the transferred Br's length. With the elbow fully extended, the wrist at 70° extension, and the CMC joint at 45° extension, we estimate the sarcomere length of the transferred Br is approximately 13% longer than the measured surgical attachment length and 8% longer than the *in situ* length.

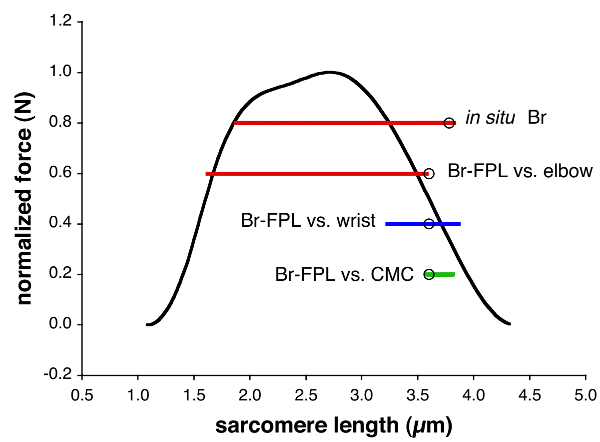

Figure 1. Br operating ranges as function of elbow position (red bars, 0°-130° elbow flexion), wrist position (blue bar, 70° extension to 70° flexion) and CMC position (green bar, 45° extension to 0° flexion). Open circles indicate sarcomere length measured *in situ* and following transfer at 10° elbow flexion, neutral forearm and wrist, and the thumb in a lateral pinch posture (0° CMC flexion).

CONCLUSIONS
This analysis suggests that the surgical attachment lengths documented intraoperatively could result in muscle lengths that are sub-optimal for force development in extended joint postures, which are functionally important. We expect that the sarcomere lengths observed here could either compromise clinical outcome in extended postures or promote structural adaptations in the transferred muscle [3].

REFERENCES
1. Fridén J, et al., *J Hand Surg [Am]* **23**, 105-110, 1998.
2. Holzbaur K, et al., Ann Biomed Eng**, accepted**.
3. Fridén J, et al.*J Hand Surg [Am]* **25**, 138-43, 2000.

ACKNOWLEDGEMENTS
This research was supported by the Rehabilitation R&D Service of the Department of Veterans Affairs (#B2785R)

STRAIN FIELD ACQUISITION ON OVINE FRACTURE CALLUS WITH ELECTRONIC SPECKLE PATTERN INTERFEROMETRY

[1]Tanja Augustin, [1]Wangdo Kim, and [2] Lutz Claes, [1]Michael Bottlang,
[1]Biomechanics Laboratory, Legacy Research & Technology Center, Portland, Oregon, USA
[2]Institute for Orthopaedic Research and Biomechanics, Ulm, Germany
email: mbottlan@lhs.org

INTRODUCTION

Fracture callus exhibits structural and constitutive heterogeneities, which provide biomechanical conditions inductive for fracture healing[1]. Quantifying strain gradients in fracture callus provides a unique opportunity to characterize biomechanical conditions which affect callus differentiation and fracture healing. This study assessed compressive strain distributions in an ovine fracture callus using an optical strain measurement approach based on the Electronic Speckle Pattern Interferometer (ESPI) [2-3].

METHODS

The fracture callus of an ovine tibia with heterotrophic non-union was harvested and frozen. A 3 mm thick sagittal cross-sectional slice of the callus was extracted with a diamond saw and thawed. First, its gross histology was documented photographically. Subsequently, a contrast powder was applied, ensuring adequate reflective properties of the specimen surface for optical strain measurement. The specimen was mounted in a custom-built compression stage. Specimen ends were rigidly clamped to induce unconfined axial compression over a 50 mm long section under displacement control. Displacement was applied manually with a micrometer screw in combination with a precision linear translation stage. The entire setup was assembled on a rigid base plate, ensuring stable conditions for laser-based strain acquisition with an Electronic Speckle Pattern Interferometer (ESPI, Q100, Ettemeyer AG, Nersingen, Germany). This laser-based non-contact measurement system generated speckle images of the specimen surfaces before and after callus compression. Subsequent speckle image subtraction and fringe analysis algorithms enabled quantification of surface strain fields in absence of specific surface markers. The particular ESPI system used in this setup sequentially captured speckle images from three linear independent illumination directions for computation of three-directional surface displacement vectors. It acquired three-directional displacement reports at 512 x 512 individual locations over a 25 x 50 mm region of interest (ROI). Not to exceed the measurement range of the ESPI system, displacement was applied in 50 increments of 1 µm, and the sum of all 50 displacement reports was calculated. Based on this summary displacement report in response to 0.1% specimen compression, the minimal principal strain distribution (i.e., compression) was computed over the callus ROI. Throughout the measurements, the callus specimen remained in a humidified atmosphere.

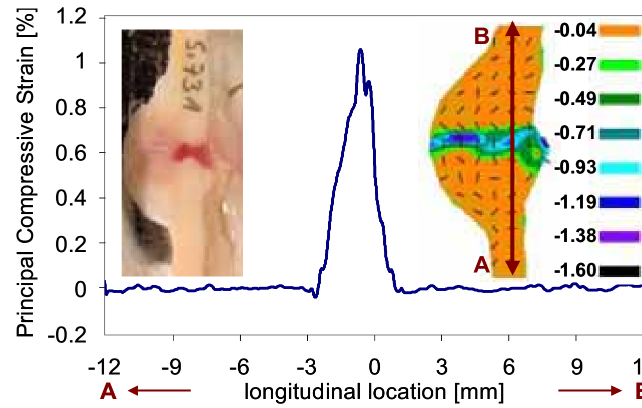

Figure 1. Principal compressive strain distribution on fracture callus.

RESULTS AND DISCUSSION

ESPI measurements on the cortex and callus delivered continuous strain reports. In callus, a clearly demarcated layer of elevated strain was observed which bisected the fracture callus transversely. This high-strain region correlated closely to the fibrous non-union layer visible on the specimen cross-section. Compressive strain in this fibrous zone exceeded 1% in response to 0.1% overall specimen compression. Corresponding strain vectors were perpendicular to the orientation of the fibrous layer. In the reminder of the callus tissue and on cortical bone, compressive strain remained below 0.1%, and was one order of magnitude smaller than that in the fibrous non-union layer. This small strain magnitude did not allow for consistent calculation of compressive strain vectors. Soft tissue in the intramedullary cavity of the ovine specimen was structurally unstable and had geometric incontinuities, for which reason it was excluded from continuous strain field acquisition with ESPI.

CONCLUSIONS

ESPI provided the unique ability to measure minute surface deformation and strain over a considerably large ROI, which allowed capturing of continuous strain maps over an entire fracture callus cross-section. Results reflect constitutive heterogeneities of a fracture callus in a quantitative manner. As such this approach provides a unique tool for analysis of mechano-biological factors in fracture healing and for validation of computational models thereof.

REFERENCES

1. Claes LE, et al. *J Clinil Orthop & Rel Res*, **355S**, 132-147, 1998.
2. Erne OK, et al. *J Biomech* ,in press, 2004.
3. Jones R, et al. *Holographic and Speckle Interferometry*, Cambridge University Press, Cambridge.

FIBER SELECTIVE MUSCLE ATROPHY IN ANKLE ARTHRITIS

[1,2,4] Victor Valderrabano, [1] Vinzenz von Tscharner, [1] Benno M. Nigg, [2] Beat Hintermann, [1,4] Cyril Frank, [3] Beat Göpfert
[1] *Human Performance Laboratory, University of Calgary, Canada*
[2] *Orthopaedic Department, University Hospital of Basel, Switzerland*
[3] *Laboratory of Orthopaedic Biomechanics, University of Basel, Switzerland*
[4] *Orthopaedic Department, University of Calgary, Canada*
email: v.valderrabano@kin.ucalgary.ca, *web:* www.kin.ucalgary.ca/hpl

INTRODUCTION

Recently, the occurrence of ankle arthritis has increased due to an increase of injuries and people's life span [1]. Biomechanical studies of the normal ankle joint complex provided knowledge on range of motion, movement coupling between calcaneus and tibia, gait kinematics and kinetics and functional zones of foot and lower leg [2, 3]. Only a few studies addressed the kinematic characteristics of the disabled ankle in vivo [4]. However, no studies addressed the clinically seen muscle atrophy of the lower leg muscles for subjects with ankle arthritis.

Therefore, the aim of the present study was to analyze the electromyogram and the strength of the lower leg muscles during isometric maximal voluntary dorsi- and plantar-flexion contraction of the arthritic ankle. The results were compared to the contralateral healthy side and a normal population, as well as to clinical orthopaedic and radiological variables.

METHODS

Seven patients and 7 healthy control subjects participated in the study. The patients (3 males and 4 females with an average age of 49 years (range between 43-57 years)) suffered from unilateral posttraumatic end-stage ankle arthritis. The control subjects were age matched with no muscular-skeletal pathologies of the lower extremity.

The clinical variables assessed through an orthopaedic examination included subjective pain score (visual analogue scale 0-10), functional American Orthopaedic Foot and Ankle Society (AOFAS) hindfoot score (0-100 points), hindfoot alignment (valgus, varus degree), muscle mass (shank circumference), ankle range of motion, latency time between injury and symptomatic ankle arthritis, and ankle arthritis degree (X-rays). The biomechanical variables included electromyography (EMG; frequency, intensity) and muscle force (ankle joint torque). Muscle activity was quantified using surface EMG during maximal voluntary dorsi- and plantar flexion for the tibialis anterior, gastrocnemius medialis, soleus, and peroneus longus. Electromyograms were analyzed using a wavelet analysis by decomposition the EMG for specified wavelets into an intensity pattern resolving the power of the signal in time and frequency) [5].

RESULTS AND DISCUSSION

The results showed a significant pathology of all clinical variables of patients suffering from ankle arthritis compared to the healthy population. There was a significant decrease of the torque produced by the arthritic joint compared to the torque produced at the contralateral side and the normal population for maximal voluntary dorsi- and plantar flexion. Compared to

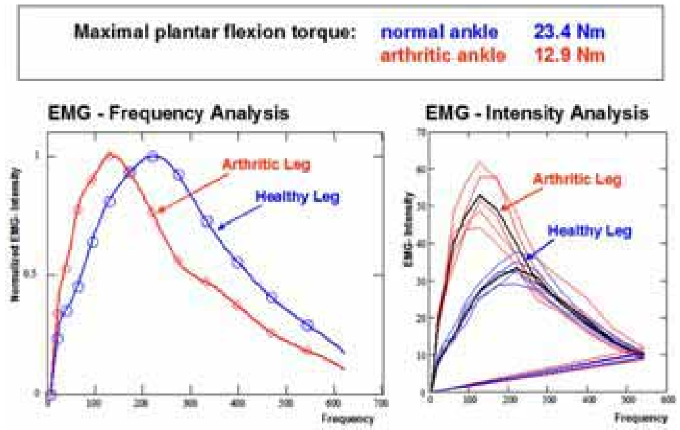

Figure 1: **Gastrocnemius Medialis – Force and EMG of Arthritic and Healthy Leg**. Force, EMG-frequency, and EMG-intensity of the Gastrocnemius medialis during maximal voluntary plantar flexion on the arthritic (red) and the healthy lower leg (blue).

the contralateral healthy side and the normal population, posttraumatic ankle arthritis also changed the EMG signal of the surrounding muscles (gastrocnemius, tibialis anterior; Figure 1), resulting in a frequency shift towards lower frequency pattern. This phenomenon may be caused by fiber specific changes in the muscle, a hypo-/atrophy of the fast twitched fibers (200-600 Hz). It is speculated that, during maximal contraction, the atrophic muscles attempted to compensate for this shortcoming by increasing the intensity of the remaining pool of slow twitch fibers (Figure 1).

CONCLUSIONS

To the author's knowledge, this is the first study quantifying the effect of posttraumatic ankle arthritis on lower extremity muscle activation, associated with fiber selective muscle degeneration: a fast-twitch fiber hypo-/atrophy. It is proposed that this knowledge may be applied for surgical treatment and rehabilitation programs.

REFERENCES

1. Baumhauer JF, et al.. *Am.J.Sports Med.* 23:564-570, 1995.
2. Hintermann B, Nigg BM. *Foot Ankle Int.* 16:514-518, 1995
3. Valderrabano V, et al. *Foot Ankle Int* 24:888-896, 2003
4. Shih LY, et al. *Foot Ankle Int* 14:97-103, 1993.
5. von Tscharner V. *J.Electromyogr. Kin.* 10:433-445, 2000

ACKNOWLEDGEMENTS

This study was supported by a grant of the Swiss National Science Foundation (SNF).

DYNAMIC SYMMETRY IN FEMALE RUNNERS WITH A HISTORY OF TIBIAL STRESS FRACTURES

[1]Joseph Seay, [1]Jeffry M. Haddad, [2]Clare E Milner, [2,3]Irene S Davis, [1]Joseph Hamill
[1]University of Massachusetts, Amherst, MA, [2]University of Delaware, Newark, DE, [3]Drayer Physical Therapy Institute, Hummelstown, PA
email: joeseay@excsci.umass.edu

INTRODUCTION

Change in gait symmetry, assessed using a variety of kinetic or kinematic measures, is observed across many pathologies affecting gait [1]. The observed asymmetries are typically viewed clinically as a pathological by-product of the affliction and efforts are expended to correct the asymmetry [2]. Newer research has however suggested that some degree of asymmetry is present in healthy non-afflicted individuals and may actually be functional [1]. Further, spatio-temporal symmetry measures derived from dynamical systems techniques, such as continuous relative phase (CRP), have been shown to change in locomotion based on the constraints of the task [3]. This past research suggests that changes in limb symmetry may not be a symptom of pathology, but rather a functional mechanism utilized by the body to cope with altered mechanical constraints caused by injury.

The purpose of this study was to examine changes in spatio-temporal gait symmetry in asymptomatic female runners who had previously experienced a unilateral tibial stress fracture (TSF) compared to a control group (CTRL) of mileage matched female runners. It was hypothesized that the TSF group would show increases in limb asymmetry compared to the CTRL group.

METHODS

Fifteen female runners with a unilateral retrospective tibial stress fracture (TSF) and 15 mileage matched control (CTRL) subjects were recruited for this study. All volunteers were female, rearfoot strikers who ran at least 20 miles per week and were free of any lower extremity injuries at the time of data collection.

Subjects ran along a 25 m runway at a speed of 3.65 m/s (± 5%). Three-dimensional kinematic data (120 Hz) were collected using a six-camera high-speed motion capture system. Five trials were collected for both the left and right limbs. For each subject, the profiles of the ankle, knee and hip sagittal view angles were interpolated to 100% of stance.

CRP was calculated bilaterally in the hip-knee and knee-ankle coupling of both groups. Spatio-temporal asymmetry was calculated as the difference in CRP patterns between involved and contralateral limb of the TSF subjects and the right and left limbs of the CRTL subjects in the hip-knee and knee-ankle couplings. Through these calculations, a time series about 0° indicates perfect spatio-temporal symmetry across the stance phase whereas deviations from zero represent a magnitude of asymmetry.

Effect size (ES) was calculated to express differences between groups relative to the pooled standard deviation. Cohen (1988) proposed that ES values of 0.2 represented small differences; 0.5, moderate differences; and 0.8+, large differences [4]. Effect sizes greater that 0.5 were considered clinically important.

RESULTS AND DISCUSSION

In both hip-knee (ES=0.52) and knee-ankle (ES=0.50) couplings moderate effects were seen between the TSF and CTRL group, where increases in asymmetry were seen in the TSF group (Figure 1).

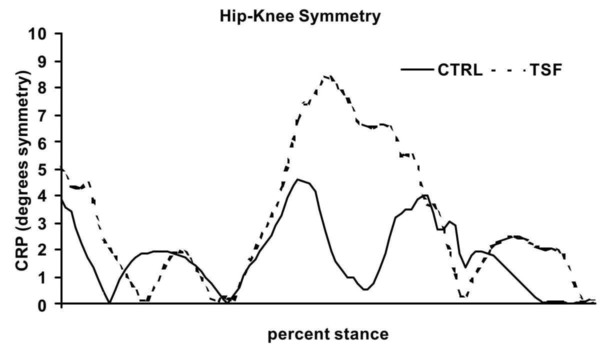

Figure 1: Between subject average of hip-knee CRP symmetry in both the stress fractured and control group.

Although effect sizes between groups were only moderate, it is interesting to note that all subjects were asymptomatic at the time of collection, showing that spatio-temporal asymmetry is present in female runners with a history of tibial stress fractures.

CONCLUSIONS

Female runners with a history of stress fractures show differences in spatio-temporal gait asymmetry compared to a healthy group. Although prospective studies are needed to determine whether this asymmetry is a cause or a result of the injury, this study adds to a growing body of literature that suggests gait asymmetry may be a functional adaptation utilized to cope with the injury.

REFERENCES

1. Sadeghi H, et al., *Gait & Posture* **12,** 34-45, 2000.
2. Seeger BR, et al., *Arc Phys Med Rehab* **62,** 364-368, 1981.
3. Haddad JM, et al., *Gait & Posture,* under review, 2005.
4. Cohen, J., Erlbaum, New Jersey, 1988.

ACKNOWLEDGEMENTS

This study was supported by Department of Defense grant DAMD17-00-1-0

INTRALIMB COORDINATION IN FEMALE RUNNERS WITH TIBIAL STRESS FRACTURES

[1]Joseph Hamill, [1]Jeffry M. Haddad, [2]Clare E Milner, [2,3]Irene S Davis
[1]University of Massachusetts, Amherst, MA, [2]University of Delaware, Newark, DE, [3]Drayer Physical Therapy Institute, Hummelstown, PA
email: jhamill@excsci.umass.edu

INTRODUCTION

Tibial stress fractures are a common injury suffered by female runners. Studies looking at traditional kinematic or kinetic (such as ground reaction forces) differences between injured and uninjured populations during running have been unsuccessful at determining a causal factor associated with the injury [1]. The nature of differences that exist between groups may better be captured using dynamical systems techniques that capture the spatio-temporal dynamics of gait [2]. Dynamical systems analysis techniques have been shown to be more sensitive to subtle differences in human movement analyses. For example, gait variability as measured through continuous relative phase (CRP) has been shown to decrease in subjects with patellofemoral pain relative to an asymptomatic group [3].

The purpose of this study was to examine changes in gait variability in asymptomatic female runners who had previously suffered from a tibial stress fracture (TSF) compared to a control group (CTRL) of mileage matched female runners. It was hypothesized that the TSF group would have a significant difference in CRP variability between the stress fractured limb and the contralateral limb while the CTRL group would have no difference in CRP variability between limbs.

METHODS

Fifteen female runners with a unilateral retrospective tibial stress fracture and 15 mileage matched control subjects were recruited for this study. All volunteers were female, rearfoot strikers who ran at least 20 miles per week and were free of any lower extremity injuries at the time of data collection.

Subjects ran along a 25 m runway at a speed of 3.65 m/s (± 5%). Three-dimensional kinematic data (120 Hz) were collected using a six-camera high-speed motion capture system. Five trials were collected for both the left and right limbs. For each subject, the profiles of the ankle, knee and hip sagittal view angles were interpolated to 100% of stance.

Bilateral hip, knee and ankle 3-D angles were calculated over each stride. Variability in intralimb coordination was assessed through measures of CRP for the hip-knee and knee-ankle coupling of both the involved and contralateral limb of the TSF subjects and the right and left limbs of the CRTL subjects. CRP variability was defined as the average standard deviation of CRP across each stride.

Effect size (ES) was calculated to express differences relative to the pooled standard deviation. Cohen (1988) proposed that ES values of 0.2 represent small differences; 0.5, moderate differences; and 0.8+, large differences.

RESULTS AND DISCUSSION

In the control group no effect was observed between the right and left limb in either the hip-knee or knee-ankle coupling (ES<0.1). In the TSF group, CRP variability decreased in the involved limb relative to the contralateral limb in the hip-knee (ES=.26) and the knee-ankle coupling (ES=.87) (Figure 1).

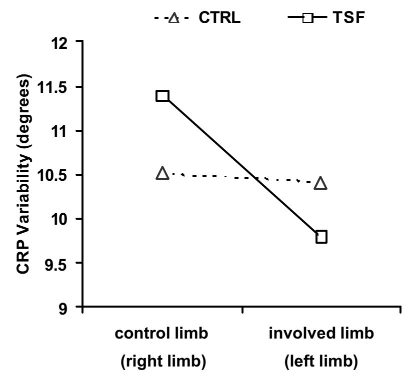

Figure 1: Mean CRP variability in the knee-ankle coupling for involved and contralateral limbs of TSF group and right and left limbs of the CTRL group.

Although the largest effect in the TSF group was observed in the knee-ankle coupling, a small effect was also observed in the hip-knee coupling, showing that a distal injury may also affect more proximal coordinative patterns. The results from both the TSF and CTRL groups support the hypothesis. It has been proposed that reduced CRP variability indicates a less flexible or less adaptable movement pattern [2, 3]. A less flexible pattern may exacerbate the injury or cause further injury to a TSF runner.

CONCLUSIONS

While the results of this study support the hypothesis that reduced CRP variability and thus less flexible/adaptable patterns are indicative of an injured condition, it is still not evident whether this less flexible pattern is a cause or a result of the injury. Although prospective studies are needed to determine cause-effect of this phenomenon, this study adds to a growing body of literature that suggests CRP variability may be a functional adaptation utilized to cope with the injury.

REFERENCES

1. Bennell K, et al., *Med Sci Sports Exerc* **36,** 397-404, 2004.
2. van Emmerik REA, et al., *J Appl Biomech* **20**, 396-420, 2004.
3. Hamill J, et al., *Clinical Biomech* **14**, 297-308, 1999.
4. Cohen, J., Erlbaum, New Jersey, 1988.

ACKNOWLEDGEMENTS

This study was supported by Department of Defense grant DAMD17-00-1-05

DIFFERENCES IN MIDFOOT ROTATIONS BETWEEN FOOT TYPES

[1]Matthew Cowley, [2]Lisa Berti, [2]Maria Grazia Benedetti, [1]Eric Rohr, [1]William Ledoux, [1]Michael Orendurff
[1] VA RR&D Center, Seattle, WA; email: Matthew.Cowley@med.va.gov, web: www.seattlerehabresearch.org
[2] Movement Analysis Laboratory, Istituti Ortopedici Rizzoli, Bologna, ITALY

INTRODUCTION

Typical full-body models used in gait analysis view the foot as a single rigid segment and essentially ignore the complex motions of the foot. Using newer motion capture technology and smaller markers, detailed foot models can now be incorporated into the full-body model. Several groups have reported more detailed models to determine the kinematics of various foot segments[1-3]. One of the main purposes of a foot model is to distinguish deviations from a "normal" foot. This project looks at the midfoot rotations for four different foot types to see if a novel foot model can be used to distinguish between foot types.

STATEMENT OF CLINICAL SIGNIFICANCE

Detailed foot models can provide an important tool for studying outcomes of foot surgeries and for pre-operative planning. An improved kinematic model will enhance our understanding of foot biomechanics and subsequently help to improve surgical outcomes.

METHODOLOGY

The left feet of 23 adult subjects walking at self-selected speeds were analyzed with an eight-camera Vicon 612 system recording at 120 Hz. The subjects were examined by an orthopedic surgeon and classified into 4 categories; 13 neutrally aligned feet (N), 6 flat feet (F), 2 high arched feet (H), and 3 slight equinus feet (E). All of the non-normal feet were asymptomatic and of mild pathology. Twenty reflective markers (9.4 mm in diameter) were placed on bony landmarks of the foot and lower leg. The following segments were studied: shank (tibia and fibula), hindfoot (calcaneus), midfoot (navicular, cuboid and cuneiforms), forefoot (metatarsals) and hallux (proximal and distal). Axial rotations were determined through a custom Vicon BodyBuilder model. Local coordinate systems were created to approximate the actual joint centers using distances and directions taken from a static trial of the subject.

RESULTS

The Figure 1A shows that all four foot types have the same general shape, although all four curves differ in range and magnitude. The Figure 1B illustrates the normal and flat foot groups are very similar in magnitude and pattern, while the other two are similar in pattern. The Figure 1C shows all four foot types to be somewhat similar in range and shape. The Figure 1D again shows all of the foot types to have similar shapes, but not ranges of values. In the Figure 1A the flat foot group is shown to be more dorsiflexed than the high arch group. The Figure 1B rotations show that the flat foot and the normal foot are nearly identical while the high arch is more inverted and the slight equinus is more everted. Only the means are reported because the n in each group were too small to get statistically significant results.

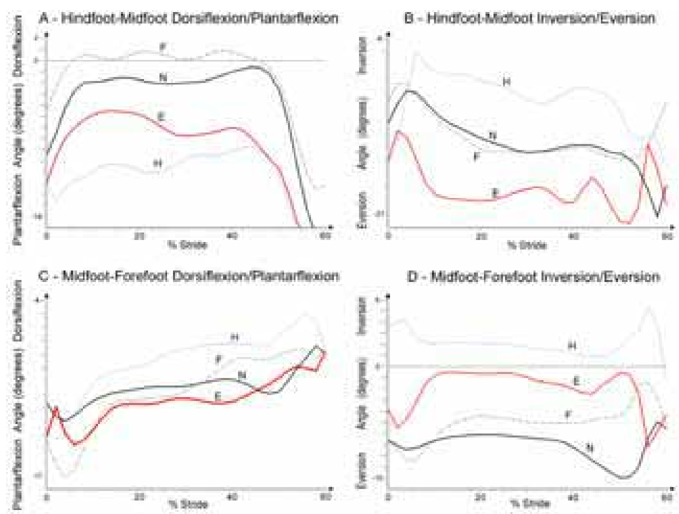

Figure 1A-1D. Mean joint rotations for the hindfoot-midfoot and the midfoot-forefoot. The four foot types shown are neutral aligned (N), flat foot (F), high arch (H), and slight equinus (E)

DISCUSSION

The fact that the rotations in the midfoot-forefoot plantarflexion/dorsiflexion graph are all similar in curvature and range, while the hindfoot-midfoot plantarflexion/ dorsiflexion and the midfoot-forefoot inversion/eversion are similar in curvature but not in ranges implies that the model seems to be sensitive enough to see differences and similarities between foot types. If the model was not able to distinguish between the foot types, one would expect to see the same general relationships in the rotations of all four of the graphs. These outcomes indicate that a large population study is feasible and needed in order to statistically analyze the findings and make any clinical predictions of foot type and function. These results look similar to the results in the aforementioned papers. The shortcomings of this study were the lack of clearly defined pathologies and the relatively small numbers of pathologic feet.

REFERENCES

1. Kidder, S.M., et al. *IEEE Trans Rehabil Eng* **4**, 25-32, 1996.
2. Leardini, A., et al. *Clin Biomech (Bristol, Avon)* **14**, 528-536, 1999.
3. MacWilliams, B.A., et al. *Gait Posture* **17**, 214-224, 2003.

ACKNOWLEDGEMENT

Supported in part by the Department of Veterans Affairs, RR&D service grant number A3030R.

EFFECT OF MARKER PLACEMENT METHODS ON CALCANEAL ROTATIONS

[1]Matthew Cowley, [2]Lisa Berti, [2]Alberto Leardini, [1]Eric Rohr, [1]William Ledoux, [1]Michael Orendurff
[1] VA RR&D Center, Seattle, WA; email: Matthew.Cowley@med.va.gov, web: www.seattlerehabresearch.org
[2] Movement Analysis Laboratory, Istituti Ortopedici Rizzoli, Bologna, ITALY

INTRODUCTION

Most full-body models used in gait analysis view the foot as a single rigid segment and ignore the complex sub-segment motions in the foot. Newer motion capture technology and smaller markers have allowed more comprehensive foot models to be created. Several groups have reported detailed models to determine the kinematics of various foot segments (e.g., [1, 2]). Some deformities may hinder the placement or obstruct the view of markers placed on the sides of the calcaneus. This paper will compare a common method to a more robust marker placement method, which removes the side calcaneal markers and uses only the calcaneal tuberosity for the segment's primary definition.

STATEMENT OF CLINICAL SIGNIFICANCE

Detailed foot models can provide an important tool for studying outcomes of foot surgeries and for pre-operative planning, much like the full body gait models commonly used today for lower limb procedures. An improved kinematic model will enhance our understanding of foot biomechanics and subsequently help to improve surgical outcomes.

METHODOLOGY

The left feet of 23 adult subjects walking at self-selected speeds were analyzed with an eight-camera Vicon 612 system recording at 120 Hz. The cameras were located around the perimeter of a 30 ft. by 40 ft. room. Kinematics were determined with a custom Vicon BodyBuilder model. Joint rotation means and standard deviations for both methods were calculated and paired t-tests were performed on the min/max peak joint rotations. Both marker sets were placed on the feet at the same time to reduce marker placement error. This first method is a common calcaneal marker method (CC) where markers were placed on the most medial projection of the sustentaculum tali, the lateral apex of the peroneal tuberacle, and the upper ridge of the calcaneal tuberosity. The second method used is referred to here as the paired calcaneal marker method (PC). Markers were placed superiorly and inferiorly on the calcaneal tuberosity.

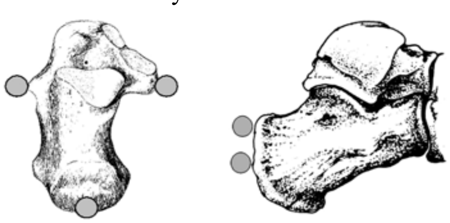

Figure 1. Marker placement for the CC method (left – superior view) and the PC method (right – sagittal view)

RESULTS

There were no significant differences in maximum or minimum values between the two marker methods along any axis of rotation (see Fig. 2). The paired t-test of the peak values was performed and showed no significant difference. In Inversion/Eversion the PC method has approximately 10 degrees of static offset from the CC method. Both methods have a similar pattern, but the PC method has a 140% greater range of motion. Dorsiflexion/Plantarflexion rotations of the two methods are closely aligned with no significant difference in the min/max peak values. The Internal/External rotation of both methods followed the same pattern. There is a slight static offset between the two methods of about 3 degrees, but there is no statistical difference between the two methods.

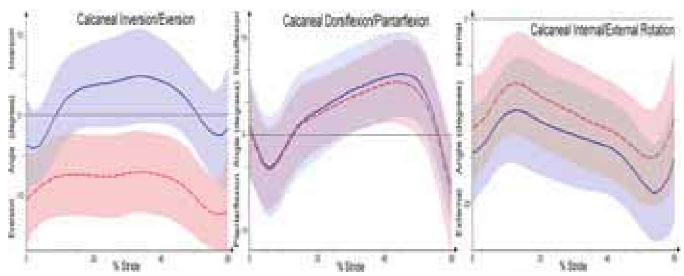

Figure 2. Rotations for the calcaneus with respect to the tibia during the stance phase of gait. The PC method is the solid blue line, the CC method is the dashed red

DISCUSSION

The lack of statistical significance between the two methods and the good shape agreement in all three planes of rotation indicates that the two methods can be used interchangeably when looking at these particular planes of motion. The offset between the PC and CC methods in the Inversion/Eversion and Internal/External rotation is due to the difference in location of the calcaneal center and talonavicular joint, which are used to define the segmental orientations. The larger range of motion of the PC method in Inversion/Eversion is comparable to the ranges reported by a calcaneal tuberosity defined calcaneus[3]. The differences in the range are most likely the result of soft tissue movement influencing one method more than the other. Further testing can determine the accuracy of each of the methods.

REFERENCES

1. MacWilliams, B.A., et al. *Gait Posture* **17**, 214-224, 2003.
2. Leardini, A., et al. *Clin Biomech (Bristol, Avon)* **14**, 528-536, 1999.
3. Cornwall, M.W., et al. *J Am Podiatr Med Assoc* **92**, 67-76, 2002.

ACKNOWLEDGEMENT

Supported in part by the Department of Veterans Affairs, RR&D Service grant number A3030R.

A PROSPECTIVE LOOK AT FOOT SHAPE AND FOOT ULCER DEVELOPMENT

[1]Matthew S. Cowley, [1]William R. Ledoux, [1]Jane B. Shofer, [2]Jessie H. Ahroni, [2]Edward J. Boyko
[1]VA RR&D Center, Seattle, WA; [2]VA Puget Sound, Seattle, WA
email: Matthew.Cowley@med.va.gov, web: www.seattlerehabresearch.org

INTRODUCTION

Diabetic foot ulceration and lower limb amputations cause significant mobility, morbidity and mortality issues as well as substantial health care costs. To date, little prospective data exists on this subject. Prospective analyses will help predict which patients may be at high risk for ulceration. We examined the foot structure of 2939 feet (1484 subjects) and the prospective ulcer occurrence of veterans with diabetes as an extension of the Seattle Diabetic Foot Study [1].

METHODS

All patients of a general internal medicine clinic who were diabetic, ambulatory and did not have foot ulcers were eligible for the study. Exclusion criteria included current foot ulcer, non-ambulatory, or inability to cognitively participate in the study. Subjects were followed prospectively for 3.2 years ± 2.5 years (mean ± SD), to determine which risk factors could be linked to ulceration. Subjects were removed from the study upon ulceration, amputation or death. Subjects were reexamined yearly and were contacted quarterly to ascertain any incidence of foot ulceration. A physical exam conducted by an LPN determined the foot type, presence of foot deformity and neuropathy. Either a t-test (continuous variables) or a chi-squared analysis (categorical variables) was performed to examine demographic differences between the ulcer and non-ulcer groups. A Cox regression analysis was performed to determine the Hazard Ratios (HR) and confidence intervals(CI). An α-level of 0.05 was chosen.

RESULTS

Demographic parameters that were statistically significant between the non-ulcer and ulcer group were: BMI, type 1 diabetes, diabetes duration, insulin use, sensory neuropathy, amputation history, ulcer history (Table 1). Several foot shape or foot deformity variables also significantly differed between groups (Table 2).

Table 1: Demographics of non-ulcer and ulcer feet (mean ± SD or %).

Measurement	Non-ulcer (n=2709)	Ulcer (n=230)	p-value
Age (yr)	62.5 ± 10.7	62.3 ± 9.3	.7
BMI (kg/m^2)	31.0 ± 6.9	30.3 ± 5.9	.083
Female	1.9	1.7	1.0
Type 1 Diabetes	4.3	8.7	.0042
Duration Diab. (yr)	10.0 ± 9.2	12.4 ± 10.1	.0003
Insulin Use	39.1	59.1	<.0001
Sensory Neuropathy	37.3	66.1	<.0001
Amputation History	3.0	13.9	<.0001
Ulcer History	20.0	45.7	<.0001

CONCLUSION

Foot shape and foot deformity parameters such as hammer/claw toes, bony prominences, pes cavus and 'other' foot types were significantly associated with ulceration. (The foot type 'other' consisted of Charcot deformity and drop foot classifications.) Although we did not measure plantar pressure, these biomechanical deformities all tend to increase pressure on the tissues in certain areas of the foot during normal walking. Since these deformities are easily identifiable, measures to protect the feet could be implemented without difficulty. Further analyses will include the consideration of ulcer location to determine if certain foot deformities are more likely to cause ulcers at a certain location on the foot.

REFERENCES

1. Boyko, E.J., et al. *Diabetes Care* **22**, 1036-1042, 1999.

ACKNOWLEDGEMENT

Supported in part by the Department of Veterans Affairs, RR&D service grant numbers A2661C and A99-1499RA.

Table 2: Foot shape and foot deformity parameters for non-ulcer and ulcer feet. (Adjusted for age, gender, BMI, diabetes treatment and amputation history; stratified by presence of neuropathy and ulcer history.) HR=hazard ratios, CI=confidence interval (CI)

Measure	Non-ulcer (n=2709)	Ulcer (n=230)	Adjusted HR (95% CI)	P
Hallux Valgus (%)	45.6	31.3	0.84 (0.63, 1.11)	.2
Hallux Limitus (%)	35.9	30.9	1.03 (0.77, 1.37)	.9
Hammer/Claw Toes (%)	57.4	72.3	1.44 (1.06, 1.95)	.021
Prominent Metatarsal Heads (%)	60.0	69.1	1.25 (0.94, 1.66)	.12
Plantar Callus (%)	51.6	55.2	1.01 (0.77,1.32)	.9
Muscle Atrophy (%)	59.0	63.1	1.26 (0.93, 1.72)	.14
Bony Prominences (%)	59.6	68.3	1.44 (1.05, 1.98)	.022
Foot Type				
Normal (%)	60.1	49.6	1.48 (0.83, 2.62)	.18
Pes Cavus (%)	21.4	28.7	1.91 (1.06, 3.45)	.031
Pes Planus Rigid (%)	7.6	6.1	1.0	
Pes Planus Flexible (%)	8.5	8.3	1.60 (0.78, 3.29)	.2
Other (%)	2.3	7.4	3.11 (1.42, 6.81)	.0044

THE METHOD OF USING PHASE PLANE PORTRAITS AND FIRST RETURN MAPS TO EXAMINE TURNING

Ava Segal[1,2], Michael Orendurff[1], and Glenn Klute[1-3]
[1]Dept. of Veterans Affairs, Seattle, Washington USA
Depts. of [2]Mechanical Engineering and [3]Electrical Engineering, University of Washington, Seattle, Washington USA.
email: avasegal@hotmail.com, web: www.seattlerehabresearch.org

INTRODUCTION

The risk of falling and injury maybe exacerbated during complex tasks such as avoiding obstacles and turning corners, which occur during daily community and household ambulation. Previous research has shown falls that occur during a turn are more likely to result in serious injury [1]. Recent publications of able-bodied subjects have highlighted the kinematic and kinetic differences associated with turning [2,3]. This study examined the effect of turning on dynamic equilibrium using phase plane portraits and first return maps [4].

METHODS

One able-bodied subject gave informed consent to participate in this IRB approved protocol. Average self-selected walking speed (SSWS) over five straight walking trials was determined using a timing light system. Steady-state straight-line walking data was collected over 100 continuous steps on a treadmill at SSWS. Full body gait kinematics were collected using a 10-camera Vicon 612 system and Plug in Gait (Lake Forest, CA.). Next, the subject walked along a 1m-radius circular path at the previously measured straight-line SSWS speed and data was collected over 100 steps. A constant speed 1m-radius path was selected to elucidate the mechanisms of turning while under steady-state conditions [2]. Angular velocity was calculated by numerically differentiating the angular position data. Hip, knee and ankle sagittal plane angle were then plotted versus angular velocity. Toe off was identified at the moment of peak ankle joint center vertical velocity. The toe off event was then used to create first return maps of sagittal plane angle (θ_i) at toe off versus the angle at the next consecutive toe off (θ_{i+1}).

RESULTS AND DISCUSSION

The phase plane portraits for straight-line walking were reasonably consistent with previously reported data [4]. Average center of mass velocity was determined post data collection to be 1.6 m/s, which is within 10% of the straight-line SSWS (1.5 m/s). Therefore, differences between turning and straight kinematics were not likely related to changes in walking speed [2]. Turning demonstrated increased stride to stride variability (figure 1). Toe off during turning occurred at higher angular velocities compared to straight-line walking (figures 1A & 1B). Stride to subsequent stride ankle angle differences were larger for turning than straight (3.5 $\pm$ 2.7 vs. 2.0 $\pm$ 1.6 degrees, respectively). The first return maps portray the wider distribution of stride to stride ankle angle of turning compared to straight (figures 1C & 1D). The circles in these figures, whose radii are two standard deviations from the mean and centered on the diagonal line, signify dynamic steady-state. The standard deviation from the mean for turning was larger than straight (3.9 vs. 2.8 deg, respectively).

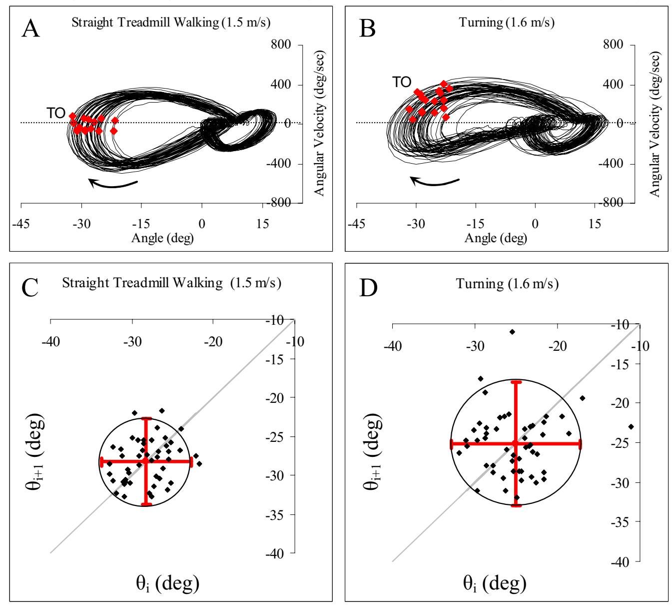

Figure 1: Ankle phase plane portraits of straight treadmill walking (A) and walking along a 1m-radius circular path (B). The red data points signify toe off (TO) over multiple strides. The arrow indicates direction of progression. Example first return maps for the ankle at toe off comparing treadmill straight-line walking (C) to turning (D). The radii of the circles signify two standard deviations from the mean.

More subjects must be examined to determine whether these differences are statistically significant. The preliminary data suggests that these graphical tools demonstrate the ability to identify increased variability associated with more complex tasks, which may relate to falls and injury. Pathologic individuals have an increased risk of falling, which may be associated with an increase in stride to stride variability. Therefore, these tools may be capable of determining the efficacy of rehabilitation treatments, surgical procedures and prosthetic componentry.

REFERENCES

1. Cumming, RG, et al. *J Am Geriatr Soc* **42**(7), 774-8, 1994.
2. Orendurff, MS, et al. *Gait & Posture* In press, 2005.
3. Courtine, G, et al. *Eur J Neurosci* **18**(1), 177-90, 2003.
4. Hurmuzlu, Y, et al. *J Biomech* **27**(12), 1495-9, 1994.

ACKNOWLEDGEMENTS

This work was funded by Dept. of Veterans Affairs Grants #A2661C and A3611I.

COMPARISON OF THE KNEE JOINT BETWEEN THE SKILLED AND UNSKILLED SUBJECTS DURING THE KIP MANEUVER ON THE HORIZONTAL BAR

[1] Tetsu YAMADA, [2] Michiyoshi AE and [2] Norihisa FUJII
[1] Doctoral program in Health and Sport Sciences, University of Tsukuba, Tsukuba, Japan.
tetsu@lasbim.taiiku.tsukuba.ac.jp,
[2] Institute of Health and Sport Sciences, University of Tsukuba, Tsukuba, Japan.

INTRODUCTION

In general, the knee joint flexion will not be used in executing the kip maneuver on the horizontal bar. However, most of the unskilled subjects bend their knees during the kip maneuver. The knee flexion will be attributed to not only body position, but also poor technique. There is little information of the effect of the knee joint on the execution of the kip maneuver. The purpose of this study was to investigate the effect of the knee joint flexion on the mechanical work, comparing the skilled with unskilled subjects of the kip maneuver on the horizontal bar.

METHODS

Ten varsity gymnasts as skilled subjects performed the kip maneuver on the horizontal bar, and five non-gymnast subjects were selected as unskilled subjects. Their maneuver was videotaped in the sagittal plane with a VTR camera (60Hz) to obtain kinematics and kinetics data by a motion analysis technique. The data were normalized by the time from the instant that the center of mass (CoM) passed under the bar in the forward swing to the same instant in the backward swing, and then averaged. The difference between the skilled and unskilled subjects was tested by Mann-Whitney test ($p < 0.05$).

RESULTS AND DISCUSSION

Figure 1 shows the maximum and minimum knee joint angles during the kip maneuver for the skilled and unskilled subjects. Although there was no difference in the maximum knee joint angle between the skilled and unskilled subjects, the minimum knee joint angle of the unskilled subjects was smaller than that of the skilled subjects ($p < 0.01$). This indicated that the unskilled subjects flexed their knee joint deeper than the skilled subjects. This would help the unskilled subjects raise their leg easier because of smaller moment of inertia about the hip joint.

Figure 2 shows the mechanical works done by the shoulder, hip and knee joint torques for the skilled and unskilled subjects in the kip maneuver. The mechanical work of the shoulder joint for the skilled subjects was larger than that of the unskilled subjects ($p < 0.05$), but there was no difference in the mechanical work of the hip joint. The mechanical work of the knee joint for the skilled subjects was close to zero and smaller than that of the unskilled subjects ($p < 0.05$). Most of the mechanical work for the skilled subjects was developed by the shoulder joint torque. Although the mechanical work of the knee joint for the unskilled subjects was much smaller than those of the shoulder and hip joints, this would compensate for smaller work of the shoulder joint to increase the mechanical energy of the whole body.

Since the knee joint flexion during the execution of the kip maneuver is considered to be undesirable body position and technique, the mechanical work done by the knee joint torque will not be recommended to gymnasts. However, in physical education class, increasing the mechanical work done by the shoulder and hip joint torques should be more focused, correction of the knee joint flexion was less important in succeeding the kip maneuver.

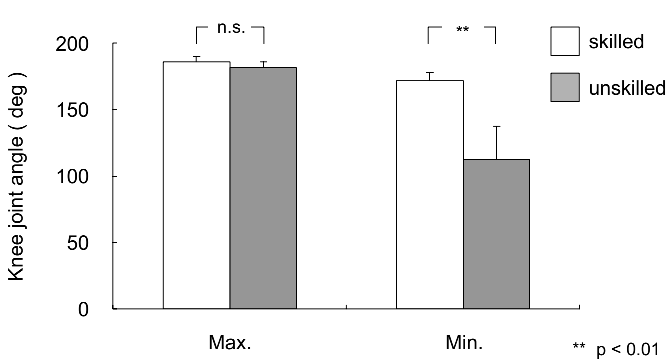

Figure 1: The maximum and minimum knee joint angles during the kip maneuver for the skilled and unskilled subjects.

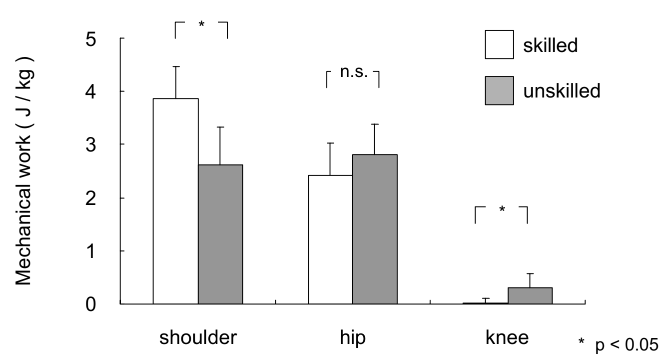

Figure 2: The mechanical works done by the shoulder, hip and knee joint torques in the kip maneuver.

A DEVICE TO MEASURE IN VIVO TRANSLATIONAL AND ROTATIONAL LAXITY OF RABBIT KNEES

Anneliese Heiner, Jim Rudert, and Todd McKinley
Department of Orthopaedics and Rehabilitation, University of Iowa, Iowa City, IA, 52242
Email: anneliese-heiner@uiowa.edu Web: www.uihealthcare.com/depts/med/orthopaedicsurgery/

INTRODUCTION

Successful orthopaedic management of intra-articular fractures, to forestall post-traumatic osteoarthritis (OA), depends on avoidance of a mechanical environment that is deleterious to articular cartilage. Instability associated with excessive joint laxity is a factor that has been implicated in progression of post-traumatic OA. Work is ongoing to explore the pathomechanics, using New Zealand white rabbits, a well-established OA model in which transections of the anterior cruciate ligament (ACL) induce knee laxity. To measure joint laxity as a function of the degree of ACL transection, we have designed a specialized testing device to determine both translational and rotational stiffness of rabbit knees.

METHODS

The device consists of a main cradle (Figure 1a) with an integral femur clamp, a free-floating tibia clamp, and interchangeable linear stepper motor/load cell modules – one for translational (Figure 1b) and one for rotational (Figure 1c) testing. The rotational test module incorporates a rack-and-pinion linkage to convert linear to rotary motion. Both modules include a method to adjust knee flexion angle to 90 or 135 degrees. Test control and data acquisition are by user-written LabView programs running on a laptop computer.

To prepare a rabbit for testing, coronal plane transverse pins are inserted through the leg, two in the tibia (Figure 1c) and one in the distal femur. The pins are accurately placed using a drill guide, and serve to reproducibly position the leg in the test device for repeated testing at successive time points after ligament transection. During testing, the cradle supports the rabbit on its back, with the femur held fixed vertically. The translational module draws the tibia upward for a specified distance and speed, then returns to the home position. Stepper motor displacement and load data are displayed in real time and recorded (Figure 2). The rotational module rotates the tibia in one direction and then the other, then returns to the home position; test angles, speed, and starting direction are user-defined, and angle and torque data are recorded. As a safeguard, if a preset maximum load is exceeded on either module the test will terminate and return to the home position.

RESULTS AND DISCUSSION

A series of translational tests demonstrated that the testing device can measure the difference in stiffness of a rabbit knee when the ACL is intact, partially transected, and fully transected (Figure 3). It also demonstrated that knee flexion angle affects knee stiffness. Note that the intact knee at 90 degrees reached the preset load limit of 75 N before the full 3 mm test displacement was obtained. Multiple test sessions with this device have shown it to be an accurate and efficient method of determining rabbit knee stiffness in vivo.

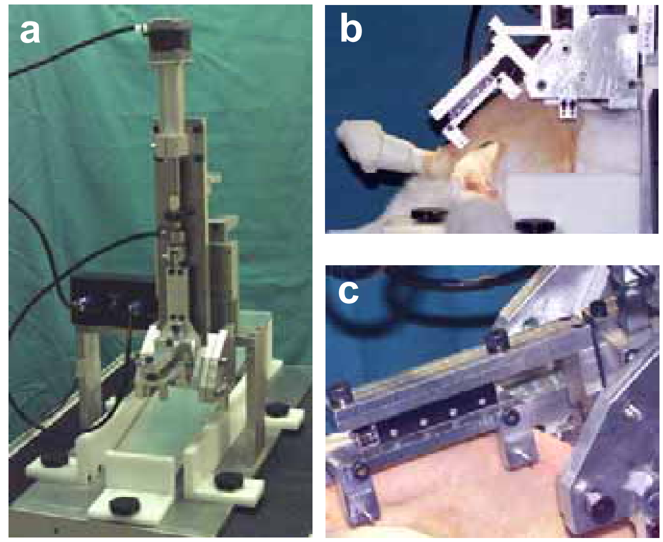

Figure 1: Rabbit knee testing system (a), with translational (b) and rotational (c) modules.

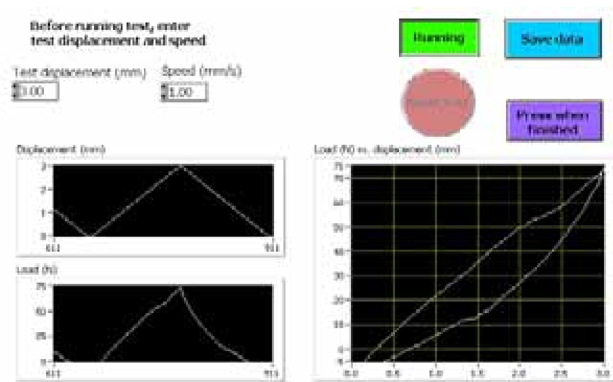

Figure 2: Control menu and screen graphics for translational testing of a rabbit knee.

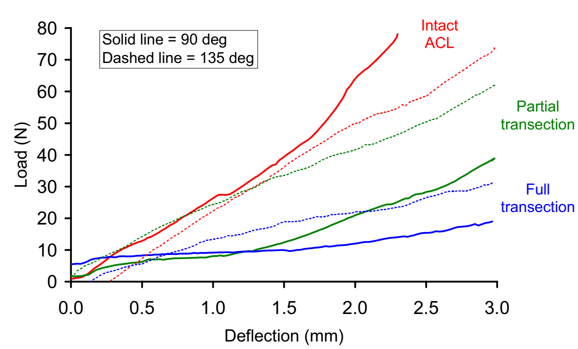

Figure 3: Effect of partial ACL transection and knee flexion angle on translational stiffness.

ACKNOWLEDGEMENT

Supported by award 5 P50 AR048939, NIH Specialized Center of Research for Osteoarthritis.

AN EXPERIMENTAL METHOD FOR MECHANICAL ANALYSIS OF THE INTERSPINOUS AND SUPRASPINOUS LIGAMENTS

Brian Beaubien[1], Joan Bechtold[1], William Lew[1], Pascal Swider[2]
[1]Midwest Orthopaedic Research Foundation, Minneapolis, MN
[2]Laboratory of Biomechanics, Toulouse, France
e-mail:bbeaubien@morfn.org; web: www.morfn.org

INTRODUCTION

Differences in the interspinous ligaments (ISLs) and supraspinous ligaments (SSLs) have been observed in patients with kyphotic and scoliotic spines. These differences are to be evaluated mechanically, but the appropriate test method is unclear. Specifically, a protocol to compare the combined and individual viscoelastic contributions of the ISL and SSL needs to be developed. The objective of this study was to select a rigorous but interpretable model and experimental method to use in comparing clinically obtained tissues. Sample data from porcine ligaments were evaluated using this method.

METHODS

The quasi-linear viscoelasticity (QLV) model was chosen to model the stress-relaxation behavior of the ligaments. This method assumes separable time-dependent relaxation and strain-dependent elastic functions. The relaxation function was the focus of this study, and was represented by a three-element Maxwell model (Eq.1):

Eq. 1 $$G(t) = [G_1 e^{\beta_1 t} + G_2 e^{\beta_2 t} + G_2 e^{\beta_3 t} + G_\infty]$$

Relaxation time constants (β_i) were fixed at 10ms, 100ms, and 1s, respectively, in order to provide an accurate but more constrained curve fit, and to facilitate physical interpretation. Furthermore, because G(t) is normalized to the instantaneous strain, G(0) was constrained to be 1.

Models were fit to sample relaxation data acquired from porcine bone-ligament-bone ISL-SSL constructs (N=4). These constructs were preconditioned and subjected to a “step input” of 25% strain and allowed to relax for 1000s. Ligaments were returned to zero strain and tested again after separation of the ISL and SSL with a scalpel blade (without disruption of the ligament-bone interface), and after removal of the SSL (n=2) or ISL (n=2). The remaining ligament was tested to failure at 0.1 mm/s, and the failure stresses and strains were calculated. Two additional bone-ligament-bone constructs were evaluated histologically to observe the ISL and SSL fiber orientation. The mean and standard deviation were calculated for each relaxation variable.

.

RESULTS AND DISCUSSION

The relaxation function fit the data well (Table 1). Separating the ligaments reduced the maximum and equilibrium stress of the bone-ligament-bone complex by 31% and 19%, respectively. Removing the SSL further reduced the instantaneous and equilibrium stress of the ISL to approximately 90% and 89% of the respective sectioned states. With the ISL removed, the mean instantaneous and equilibrium stresses of the SSL alone were 25% and 15% of the sectioned sate stresses, respectively. The ISL’s failed at a mean 1122kPa and 72% strain, and SSL’s failed at a mean 1720kPa and 42% strain. Histology revealed ISL fibers parallel to the spinous processes, SSL fibers perpendicular to the processes, and many fibers spanning the two ligaments.

	G_∞	G_1	G_2	G_3	R^2
Specimen 1	0.643	0.152	0.112	0.107	0.997
Specimen 2	0.651	0.123	0.086	0.129	0.997
Specimen 3	0.698	0.111	0.095	0.094	0.996
Specimen 4	0.666	0.105	0.095	0.118	0.998
Mean	0.664	0.123	0.097	0.112	
St. Dev.	0.024	0.021	0.011	0.015	

Table 1- Reduced relaxation function coefficients and residual values

CONCLUSIONS

The three-element relaxation function provided a close and relatively repeatable fit to stress-relaxation data to ISL-SSL construct. The stress in the intact ligaments decreased greatly when the ISL and SSL were separated. This decrease may be attributed to cutting the fibers that were seen to span the two ligaments. The stresses in the SSL alone during the relaxation experiment appeared to be lower than those for the ISL, but the failure load for the SSL appeared to be higher. This discrepancy may exist because the SSL spans several spinal levels *in vivo*, and its unloaded length may therefore differ from that of the ISL in single-level constructs.

The QLV model employed as described here will be used to test clinically obtained tissue. The ISL and SSL can be sectioned to determine the properties of the two ligaments individually, but care should be taken in considering the interaction of these non-discrete ligaments. A larger study is needed to statistically describe the findings in this study.

ACKNOWLEDGEMENTS

The author thanks the Minneapolis Medical Research Foundation for financial support.

QUASI-LINEAR VISCOELASTIC PROPERTIES OF THE PLANTAR SOFT TISSUE IN COMPRESSION

[1]William R. Ledoux, [1]Joanna J. Blevins, and [1]Bruce J. Sangeozan
[1]VA RR&D Center, Seattle, WA; email: wrledoux@u.washington.edu, web: www.seattlerehabresearch.org

INTRODUCTION

Mechanical testing of the plantar soft tissue has consisted of primarily structural heel pad testing.[1-4] One group studied material properties and demonstrated that the subcalcaneal tissue is homogeneous.[5] However, there has been little research on other areas, and temperature, age, and vascular status are often not accounted for. The purpose of this study was to model the relaxation behavior of the plantar soft tissue the using quasi-linear viscoelastic (QLV) theory[6] at six locations: the subcalcaneal, subhallucal, lateral submidfoot and the first, third and fifth submetatarsal.

METHODS

Specimens were obtained from ten fresh frozen feet (36 ± 8.7 years, 798 ± 131 N) from seven non-diabetic donors. The plantar soft tissue was removed as 2 cm x 2 cm blocks without skin. The specimen was placed between two aluminum platens in a materials testing machine with an environmental chamber. The top platen was lowered until a force of 0.5 N was detected. The distance between the platens was the initial specimen thickness. Hot moist air was circulated to keep the specimen at 35˚ C and near 100% humidity. The target loading level for the tissue was based on ground reaction force data.[7] In load control, the specimen underwent ten 1Hz sine waves from 10 N to the target load. The displacement at the target load was noted. Using displacement control, a stress relaxation test was performed. In this test, the tissue was compressed to the noted displacement in 0.1 s and held at a constant strain for 300 s. The relaxation curves were normalized by the peak force value. The normalized curves were fit to the QLV with a non-linear least squares regression. An analysis of variance determined if the fit parameters differed across areas.

RESULTS

The long term relaxation constant, τ_2, was significantly larger for the subcalcaneal than the other areas except for the fifth submetatarsal (Table 1). No significant differences were found for the other parameters, including the short term time constant, τ_1, the amplitude of the viscous damping, c, and the elastic constants A and B. However, the two areas, the lateral submidfoot and the third submetatarsal, with the largest c also experienced the most relaxation (Figure 1).

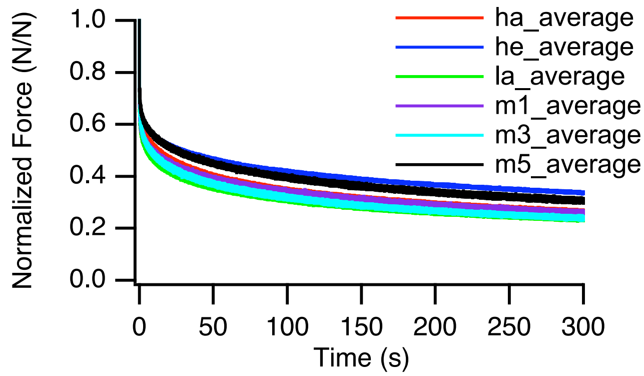

Figure 1: The average relaxation curves for the six areas.

DISCUSSION

These data indicate that some differences in the relaxation properties exist between certain areas of the foot. In particular, the large values of τ_2 seen for the calcaneus and fifth metatarsal indicate that these areas require more time to achieve steady state. The curve fits were sensitive to the initial guesses. However, we did use the same initial guesses for all specimens in each area. Also, the τ_2 obtained were greater than the length of the experiment, indicating that the experiment was terminated before steady state was achieved. Therefore in future testing, the specimen should be held at the maximum strain longer than 300 s. It should be noted that other than τ_2, there were no differences in the relaxation properties of the different areas. This has implications for computational foot models that incorporate the plantar soft tissue.

REFERENCES

1. Ker, RF, *et al.*, Proc Inst Mech Eng <H>, **203** 191-6, 1989.
2. Bennett, MB and RF Ker, J Anatomy, **171**, 131-8, 1990.
3. Kinoshita, H, *et al.*, E J App Phy & Oc Phy **73**, 404-9, 1996.
4. Aerts, P, *et al.*, J Biomech, **28**, 1299-1308, 1995.
5. Miller-Young, JE, *et al.*, J Biomech **35**, 1523-31, 2002.
6. Fung, YC, *Biomechanics* 1993, Springer-Verlag: NY.
7. Ledoux, WR and HJ Hillstrom, Gait Posture **15**, 1-9, 2002.

ACKNOWLEDGEMENTS

The Department of Veterans Affairs projects no. A2362R and A2661C.

Table 1: The QLV parameters for each of the six soft tissue locations.

area	A (N)	B (mm/mm)	c (s)	τ_1 (s)	τ_2 (s)
Subhallucal (ha)	19.88 (17.74)	9.24 (7.34)	0.848 (0.253)	0.004 (0.012)	8930 (9390)
Subcalcaneal (he)	14.84 (12.83)	87.74 (213.9)	0.523 (0.189)	0.019 (0.054)	20170 (15060)
lateral submidfoot (la)	3.75 (7.10)	53.93 (58.49)	1.028 (0.950)	0.00012 (0.0002)	6810 (7280)
first submetatarsal (m1)	16.98 (15.76)	87.26 (131.9)	0.685 (0.309)	0.005 (0.011)	5360 (2540)
third submetatarsal (m3)	14.66 (17.94)	107.3 (262.9)	0.926 (0.397)	0.005 (0.008)	7840 (8480)
fifth submetatarsal (m5)	11.47 (10.93)	13.42 (10.18)	0.814 (0.286)	0.019 (0.031)	15360 (12090)
p-value	0.21	0.74	0.43	0.53	0.035 [a]

[a] The subcalcaneal tissue was greater than all areas except the fifth submetatarsal.

NEUROMUSCULAR ADJUSTMENTS TO HOPPING WITH AN ELASTIC ANKLE-FOOT ORTHOSIS

Zaineb Bohra, Jamie Lukos, Catherine Kinnaird, Daniel P. Ferris
Division of Kinesiology, University of Michigan, Ann Arbor, MI; email: zbohra@umich.edu

INTRODUCTION

When humans hop or run on elastic surfaces, they adjust the effective stiffness of their legs to perfectly offset changes in surface stiffness [1, 2]. As a result, the addition of a surface spring in series with the leg spring does not alter global movement parameters such as ground contact time or displacement of the center of mass. The purpose of this study was to determine if humans would show similar neuromuscular adjustments when hopping with a spring in parallel to their leg spring. Farley and colleagues have demonstrated that ankle stiffness primarily determines leg stiffness during hopping [3, 4] so we focused on adding a spring in parallel with the ankle joint. We hypothesized that humans would decrease their ankle joint stiffness when hopping with a plantar flexor spring added to an ankle-foot orthosis compared to hopping without a spring added to the orthosis. This adjustment would allow them to compensate for joint stiffness added by the orthosis spring.

METHODS

Four healthy subjects (ages 24-27 years) participated in this study. The University of Michigan Institutional Review Board approved the study protocol and each participant gave informed consent. Each subject hopped on their left leg at four frequencies (2.2, 2.6, 3.0 Hz, and their preferred frequency) under two orthosis conditions. In one condition (SPRING), the subjects hopped while wearing an ankle-foot orthosis with a linear extension spring providing plantar flexor torque (k=6.7 kN/m, resulting in ~1.1 Nm/deg). In the second condition (NO SPRING), subjects hopped wearing the ankle-foot orthosis without the spring attached. After subjects practiced for ~15 seconds under the two conditions, they completed trials in a randomized order.

We collected joint kinematics, ground reaction forces, and electromyography (EMG) for two trials at each condition. We recorded spring force with a load cell. Using Visual3D software, we determined internal joint moments about the ankle, knee, and hip. We calculated leg and joint stiffnesses from vertical ground reaction force, center of mass displacement, joint displacements, and joint torques [4]. We used a three-way ANOVA to test for significant differences.

RESULTS AND DISCUSSION

At each hopping frequency, subjects demonstrated the same effective leg stiffness for both orthosis conditions ($p=0.07$). At preferred frequency leg stiffness was 6.2±2.0 kN/m for NO SPRING and 7.3±2.2 kN/m for SPRING conditions (mean±s.d.). The invariant leg stiffness was possible because subjects decreased their ankle joint stiffness ($p<0.001$) to offset orthosis stiffness added by the spring (Figure 1). The spring contributed ~24% of the total stiffness about the ankle joint (ankle stiffness + orthosis stiffness) during the preferred frequency SPRING condition and less at faster frequencies.

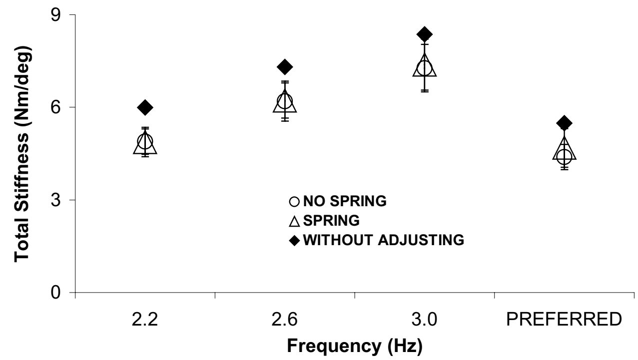

Figure 1: Total stiffness about the ankle joint. The WITHOUT ADJUSTING values reflect what the total stiffness would have been in the SPRING condition if the subjects maintained the same ankle stiffness as during the NO SPRING condition. The total stiffness was independent of orthosis condition ($p=0.46$).

As a result of the adjustments in ankle stiffness, there were no differences in peak vertical ground reaction force, center of mass displacement, or ground contact time between conditions ($p>0.20$). EMG data revealed that subjects decreased soleus, medial gastrocnemius, and lateral gastrocnemius activation amplitudes during ground contact for the SPRING condition compared to the NO SPRING condition (22%, 21%, & 22% decreases, respectively; $p<0.05$).

CONCLUSIONS

When hopping unilaterally with an energy storing ankle-foot orthosis, our subjects decreased their ankle stiffness to offset the added stiffness of the orthosis. As a result, global movement dynamics were not affected by the added orthosis stiffness. Subjects appeared to achieve the decreased ankle stiffness by reducing triceps surae activation. These findings provide important insight into the neuromuscular control of bouncing gaits (i.e. hopping and running). The results also have important implications for the design of braces and orthoses for improving human performance and/or preventing injury.

REFERENCES

1. Ferris DP, et al. *J Appl Physiol* **82**, 15-22, 1997.
2. Ferris DP, et al. *Proc Roy Soc Lond B* **265**, 989-994, 1998.
3. Farley CT, et al. *J Appl Physiol* **85**, 1044-1055, 1998.
4. Farley CT, et al. *J Biomech* **32**, 267-273, 1999.

ACKNOWLEDGMENTS

The authors would like to thank Keith Gordon and Greg Sawicki for their help with data analysis and interpretations. Supported by NIH R01NS045486 and NSF BES-0347479.

BRACING ALTERS PATELLOFEMORAL CONTACT MECHANICS DURING THE GAIT CYCLE: A DYNAMIC BIOMECHANICAL STUDY

[1] Nicole A. Wilson, [2]Tom Mazahery, MD, [2]Jason Koh, MD, and [1,2]Li-Qun Zhang, PhD
[1]Rehabilitation Institute of Chicago, [2]Northwestern University; email: l-zhang@northwestern.edu

INTRODUCTION

Patellofemoral (PF) pain is one of the most common knee disorders seen in orthopaedic practice [1]. However, the etiology of PF pain remains unclear and functional outcomes after treatment are unpredictable and often unsatisfactory [2]. Clinical decreases in PF pain symptoms with the application of bracing have been demonstrated [1]; yet, the mechanism by which an individual brace reduces pain is not well understood. The purpose of this study was to evaluate the effects of three PF braces in altering contact mechanics during gait.

METHODS

Three fresh-frozen human cadaveric knees were tested during simulated free-speed walking under the following five test conditions: (1) no brace; (2) three DonJoy™ PF braces including, the Tru-Pull™, Lateral "J", and an elastic sleeve; and (3) after a lateral release had been performed. The major individual muscles crossing the knee joint were moderately loaded according to their physiological cross-sectional areas [3]. A Tekscan™ sensor was inserted into the PF joint, through a medial parapatellar arthrotomy.

Fifteen strides were collected with each knee under each test condition. Differences in contact area, total contact pressure, peak pressure and center of pressure due to application of the three braces and the lateral release were analyzed using ANOVA with multiple comparisons (i.e. Tukey's HSD) with the non-braced condition set as the control group.

RESULTS AND DISCUSSION

Biomechanical variables, including peak pressure, contact area, and center of pressure, varied systematically with the gait stride (Figure 1a, 1b). Peak PF pressures during mid-stance were significantly reduced when compared with the unbraced condition by the Lateral "J", the Tru-Pull, the elastic sleeve, and the lateral release (Figure 1a, $p<0.03$). The Lateral "J" reduced peak pressure during mid-stance by 21%; Tru-Pull by 19%; elastic sleeve by 19%; the lateral release by 22%. The Tru-Pull, elastic sleeve, and the lateral release also reduced peak pressure throughout swing phase (Figure 1a, $p<0.04$). The Lateral "J" did not significantly reduce peak pressure during the swing phase of the gait cycle. The elastic sleeve increased PF contact area by 79% during the double-support phase of the gait cycle ($p<0.05$). However, the Tru-Pull decreased contact area by 32% during mid-stance ($p<0.03$). Contact area did not significantly change with the Lateral "J". Application of the Lateral "J" shifted the center of pressure medially during single-leg support (Figure 1b, $p<0.02$).

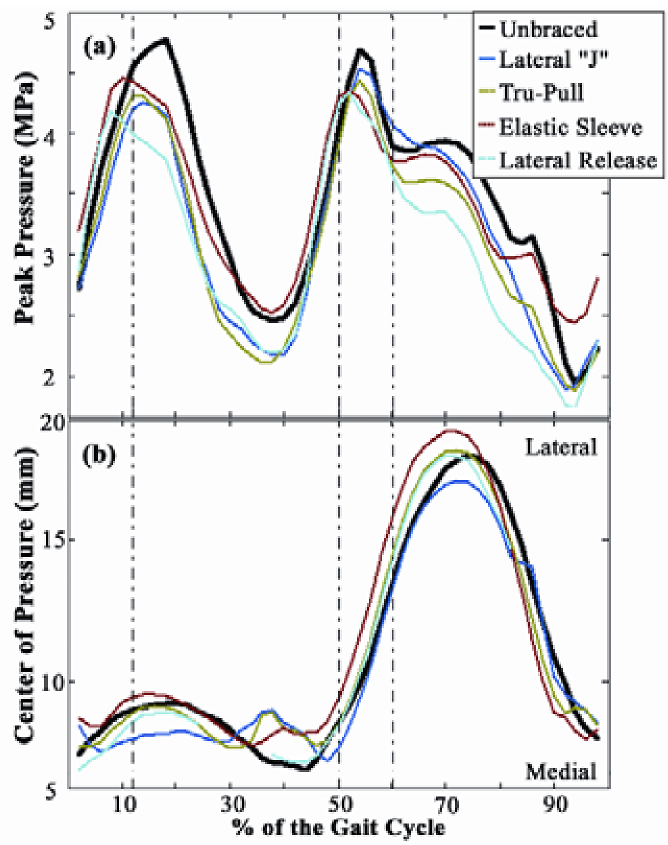

Figure 1. (a) Peak pressure and (b) Center of pressure, (x-coordinate) vs. % of the gait cycle. The three vertical lines (located at 11.8, 50.7, and 60.5% respectively) correspond to the onset of single-leg support, the onset of the second double-leg support, and the end of the stance phase, respectively. In (b) lateral and medial directions are as indicated.

CONCLUSIONS

This study presents a quantitative approach to the evaluation of PF contact mechanics with a range of clinical interventions during simulated locomotion and can aid understanding of the factors that contribute to PF pain and the mechanisms underlying symptom reduction associated with bracing.

The demonstrated reduction in peak PF pressure, for example, is a potential mechanism for pain relief associated with bracing. Limitations of this study include the small sample size, specimens not necessarily having a PF disorder, open-chain movement, and moderate muscle loads. A follow-up study is planned.

REFERENCES

1. Fulkerson JP. *Am J Sports Med* **30**:447-456, 2002.
2. Lin F, et al. *Clin Biomech* **18**:401-409, 2003.
3. Wickiewicz TL, et al. *Clin Orthop*. **179**:275-83, 1983.

ACKNOWLEDGEMENTS

The authors would like to acknowledge the partial support of NIH and DJ Ortho, Inc.

ENSLAVING EFFECTS OF FINGER MOVEMENT ON PRESSING FORCES OF OTHER FINGERS

[1]Byung Hoon Woo, [1]Sun Wook Kim [1]Vladimir M. Zatsiorsky, [1]Mark L. Latash, and [1,2] Jae Kun Shim
[1]The Pennsylvania State University and [2]University of Maryland
email: shimjaekun@hotmail.com

INTRODUCTION

Studies of finger kinetic and kinematic interactions have shown that fingers are interdependent each other (for a review see Schieber and Santello 2004). Kinetic and kinematic enslaving effects are larger in neighboring fingers (e.g. in the index finger-middle finger or middle finger-ring finger pairs) then in the fingers positioned farther from each other (e.g. in the index finger-ring finger pair). These effects were studied both in static force production tasks (Zatsiorsky et al. 1998) and during finger movements (Hager-Ross et al. 2000; Li et al. 2004). However, interdependence between the static force production and finger movement has not been addressed. The purpose of the current study was to investigate the effects of finger movement on the finger-tip forces of other fingers. We hypothesized that the effects depend on the fingers proximity and are the larger the closer the fingers to each other (proximity hypothesis).

METHODS

Equipment: One goniometer (Sensor SG65 Biometrics Ltd.) and six piezoelectric sensors (Model 208C02, Piezotronic, Inc.) were used (Figure 1) to record metacarpophalangeal (MCP) joint angles of a finger in motion (task finger) and finger-tip forces of the rest of fingers (non-task fingers). The sensors were horizontally movable on an aluminum panel, and they were fixed according to hand anatomy of individual subjects. The hand position was maintained constant, but the aluminum panel was vertically moved so that a task finger could move through the slot.

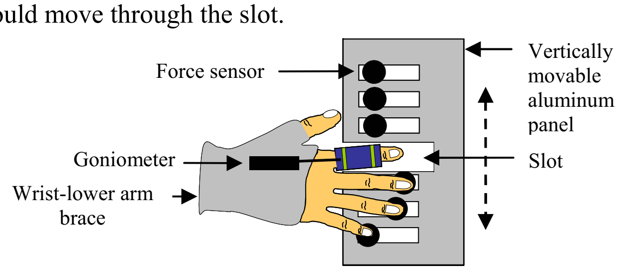

Figure 1. Experimental setup.

Experimental Procedure: Ten healthy, right-handed volunteers, five males and five females participated in the experiment. Subjects sat on a chair with their right lower arms positioned on a table and strapped with a set of Velcros. A wrist-forearm brace (EBONITE Inc.) was used to immobilize the wrist. A small aluminum bar was used to restrict the movement of proximal and distal interphalangeal joints of a task finger. Before each trial, subjects extended all phalangeal joint angles into approximately 180° with the thumb pointing upward. Subjects flexed the MCP joint of one finger each time to its maximum range of motion through a hole at a comfortable speed, and isometric pressing forces on finger-tips of non-task fingers were recorded. Non-task finger forces at the time of the maximum range of motion of a task finger were extracted to quantify enslaving forces of non-task fingers.

RESULTS

Neighboring fingers of a task finger produced approximately 67% of the total force, and non-neighboring fingers generated about 33%. In the tasks with two neighboring fingers (e.g. middle and ring finger tasks), index and middle fingers showed larger enslaving forces than the other neighboring fingers. During index and little finger tasks, the enslaving force magnitudes decreased with distance to the task fingers (i.e. index finger enslaving force was the smallest during the little finger task).

CONCLUSIONS

Our observations support the proximity hypothesis; fingers positioned closer to a task finger produce larger enslaving forces. These observations extend results of the earlier studies of kinetic and kinematic enslaving (Zatsiorksy et al. 1998; Hager-Ross et al. 2000; Li et al. 2004) to enslaving of non-task finger forces in response to a kinematic movement of a task finger.

REFERENCES

1. Schieber and Santello. J Appl Physiol **96**(6):2293-2300, 2004
2. Zatsiorsky VM et al. *Exp Brain Res* **131**:187–195, 1998.
3. Hager-Ross CK et al. *J Neurosci* **20**:8542-8550, 2000.
4. Li et al. *Motor Control* **8**:1-15, 2004.

ACKNOWLEDGEMENTS

AG-018751, NS-035032, and AR-048563.

Table 1: Finger-tip pressing force responses in non-task fingers to a maximum MCP joint flexion of a task finger (Mean ± S.D.)

Task fingers	Non-task finger force responses (% sum of all finger forces)			
	Index	Middle	Ring	Little
Index	-	59.51 ± 5.24	25.22 ± 3.92	15.27 ± 3.18
Middle	52.92 ± 7.22	-	35.03 ± 4.56	12.05 ± 2.12
Ring	16.32 ± 3.49	59.99 ± 5.00	-	23.69 ± 4.01
Little	18.38 ± 4.00	24.84 ± 4.93	56.78 ± 6.46	-

RELATING FRACTURE ENERGY TO CLINICAL OUTCOME IN TIBIAL PILON FRACTURE CASES

Thaddeus Thomas, Donald Anderson, Evan Hermanson, Valerie Muehling, J Lawrence Marsh and Thomas Brown
Department of Orthopaedics and Rehabilitation, The University of Iowa,
email: don-anderson@uiowa.edu, web: poppy.obrl.uiowa.edu

INTRODUCTION

Post-traumatic osteoarthritis (OA), evidenced in part by early radiographic changes, is a frequent outcome following intra-articular fracture. Residual altered articular surface anatomy is believed a primary culprit, subjecting cartilage to chronically aberrant contact stress distributions predisposing to OA. But this dogma has evolved from clinical studies unable to control for the initial mechanical insult to peri-articular tissues, another reasonable factor predisposing to early OA.

We have implemented a CT-based technique to objectively quantify injury severity in complex fractures.[1] The technique exploits the principle that mechanical energy is required to create new free surface area in a brittle solid, and that the amount of energy required is directly related to the amount of *de novo* surface area. In tibial pilon fractures, the fracturing energy is delivered directly through ankle joint cartilage.

In the present study, fracture energy measures were used to quantify injury severity in a series of fracture cases, and these results were compared to the clinical judgment of two experienced orthopaedic surgeons. Cartilage appearance on double contrast CT scans of the healed fractures were graded and correlated with fracture energy measures.

METHODS

Injury severity was quantified in a series of ten tibial pilon fracture cases, utilizing CT studies obtained during standard clinical care. Contralateral limb scans provided intact bone surface areas over a comparable distal segment of the patient's tibia, for taring. Bone free surface area measurements were extracted from CT datasets using validated digital image analyses.[2] The *de novo* surface area liberated during fracture was inferred from the difference between free surface areas measured on fractured and intact tibias of each patient.

In independent grading sessions, the fracture cases were rank ordered by two experienced orthopaedic traumatologists from lowest to highest severity, based on the appearance of A-P and lateral radiographs.[3] One rater participated in two independent sessions. Raters were blinded to the surface energy data. Concordance values were calculated to measure agreement between the two raters and between each rater and the CT-based measure of fracture energy.

At the time the fracture had healed (4-8 months post-op), double-contrast (contrast agent followed by air) CT scans were obtained. Articular cartilage integrity was graded from by one of the orthopaedic traumatologists and by two musculoskeletal radiologists using a scale ranging from 0 (all cartilage apparent) to 4 (no visible cartilage). Mean values of the cartilage gradings were compared to fracture energy data.

RESULTS AND DISCUSSION

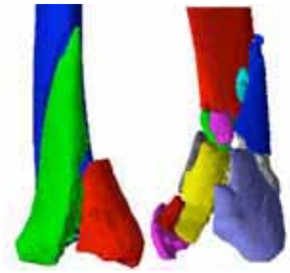

Figure 1. These two cases span the comminution spectrum studied.

Fracture-liberated surface areas ranged from 1765 to 9406 mm^2, reflecting a wide range in fracture severity (Figure 1). There was excellent agreement between all injury severity measures (Figure 2). Concordance between the raters was .912 ($p<0.0001$). The concordance between the first rater's assessment of injury severity and that of the CT-based measure was .844 ($p<0.0001$), and for the second rater it was .800 ($p<0.0006$). The range of graded cartilage integrity did not correlate as well with fracture energy measures, though results are too preliminary to warrant statistical comparisons.

Figure 2: Graphical representation of agreement between different injury severity rank-orderings.

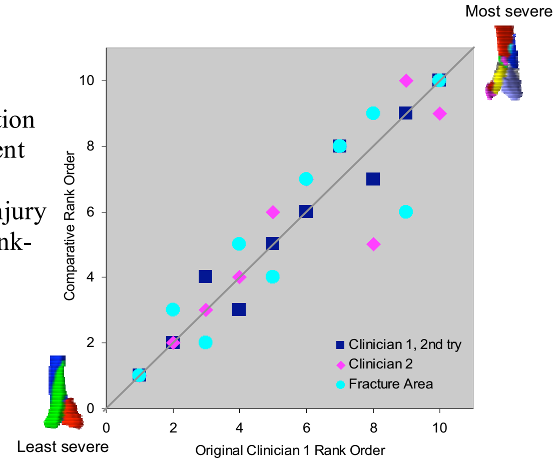

CONCLUSIONS

We have developed estimates of the fracture-liberated bone surface area associated with a series of clinical pilon fractures. Our previous work has shown that this parameter correlates closely with fragmentation energy. The energy measures here calculated agree favorably with the clinical impression of experienced orthopaedic surgeons, in terms of a rank ordering of injury severity. This opens new possibilities in studying the link between initial injury severity and the onset of post-traumatic OA in an actual clinical population.

REFERENCES

1. Anderson D, et al. *Trans 50th ORS Meeting*, **29**, 488, 2004.
2. Beardsley C, et al. *J Biomech*, **35**, 331-8, 2002.
3. DeCoster T, et al. *Foot & Ankle Int'l*, **20**(1):44-9, 1999.

ACKNOWLEDGEMENTS

Supported by grants from the Arthritis Foundation and the NIH (AR46601 and AR048939).

SUPERPOSITION OF OPTIMAL SUBMOVEMENTS IN FEEDBACK-CONTROLLED REACHING

Kevin A. Rider, Bernard J. Martin
University of Michigan; email: riderk@umich.edu, web: www.humosim.org

INTRODUCTION

The inverse relationship between speed and accuracy of rapid target-directed movements is a result of the combined use of visual and somatosensory feedback systems by the central nervous system (CNS). Feedback loops allow for comparisons between the desired movement plan and actual execution in discrete intervals [1]. Optimal rapid movements have been shown to exhibit bell-shaped speed profiles [2], although speed profiles exhibit multiple peaks due to compensatory adjustments made when the movement is perceived to no longer satisfy the desired goals. Composites of superimposed optimal speed profiles of submovements were generated and compared with actual speed profiles of rapid, three-dimensional reaching tasks under stationary and random whole-body vibration.

METHODS

Participants (N=20) performed rapid pointing tasks under stationary and motion conditions to targets presented on three touchpanel displays. A ten-camera VICON motion capture system recorded trajectories of reflective marker placed on the participants' torso, head, and arms. Fingertip trajectories were extracted and averaged to determine participant's optimal path for each motion condition [3]. Speed profiles were generated from the tangential velocity of the fingertip marker.

Random six degree-of-freedom (6DOF) ride motion was recorded from a High Mobility Multi-Wheeled Vehicle (HMMWV). Motion conditions (Roll, Pitch) were extracted, each with dominant vehicle acceleration about the longitudinal and lateral axes respectively. These motion files were simulated on a 6-DOF Ride Motion Simulator (RMS) (Figure 1a). Three touchpanel displays were mounted to the RMS to display targets and record endpoint locations (Figure 1b).

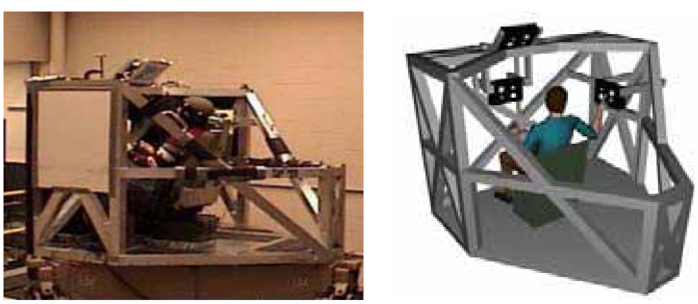

a) b)

Figure 1. The RMS (left) configured with three touchpanel displays and depicted in simulation (right).

Modeling began with an optimal bell-shaped speed profile of the fingertip, initially generated based on the time and magnitude of the peak tangential velocity (Figure 2a). As the fingertip deviates from the optimal path, a compensatory submovement is made with a sensorimotor delay of 100 ms. Submovements were assumed to have optimal bell-shaped profiles. The optimal path was then adjusted using a decreasing gradient in the vector of radial deviation to create a new optimal path, from which the continuing trajectory of the fingertip was evaluated. This recursive process continued until task completion. Submovements were superimposed to form composite speed profiles (Figure 2b).

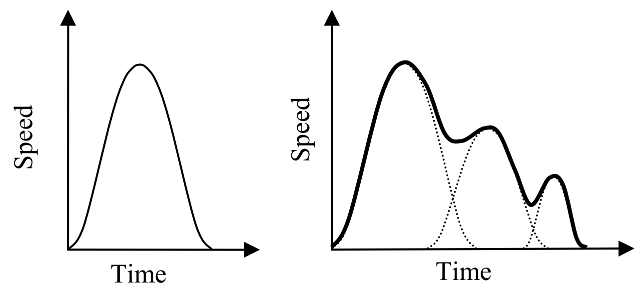

a) b)

Figure 2. a) Optimal open-loop bell-shaped speed profile and b) Closed-loop profile with superimposed submovements.

RESULTS AND DISCUSSION

Composite speed profiles compared favorably with actual fingertip speed profiles in the latter portion of the movement, when the fingertip entered the field-of-view. Our results suggest that the initial phase of movement is to accelerate away from the origin without specific accuracy requirements. It is possible that somatosensory feedback is used only for movement planning and not for feedback control. It is unclear whether the CNS does not discern initial deviations from the optimal path, or if comparisons are weighted more heavily toward the destination. Reaches performed without ride motion did not have observable movement corrections, rather near-optimal speed profiles. This may be due to corrections that were either imperceptible or not present. These and other discrepancies between composite and actual speed profiles may be due to additional movement strategies such as non-linear trajectories, time-varying goals (lift-off vs. landing phases), and biodynamic responses to the vibration stimulus.

REFERENCES

1. Desmurget M, et al. *Neurosci Behavioral Review* ***22***: 761-788, 1998.
2. Morasso P. *Exp. Brain Res.* ***42***: 223-227, 1981.
3. Faraway J. Proceedings of SAE Digital Human Modeling Conference, Report, 2000.

ACKNOWLEDGEMENTS

Thanks to the Automotive Research Center (ARC); a collaboration between the University of Michigan and the US Army. Special thanks to Charles Woolley and additional support of the HUMOSIM Laboratory for their time in setting up the displays and data acquisition systems used.

USE OF THE LONG FLEXOR AND INTRINSIC THUMB MUSCLES TO RESTORE LATERAL PINCH IN THE TETRAPLEGIC THUMB: A CADAVER STUDY

[1]Joseph D. Towles, [2]Vincent R. Hentz, and [3]Wendy M. Murray
[1]Sensory Motor Performance Program, Rehabilitation Institute of Chicago; [2]Dept. of Surgery, Stanford University;
[3]Bone and Joint Center, VA Palo Health Care System; email: towles@northwestern.edu

INTRODUCTION

In tendon transfer surgeries designed to restore lateral pinch following tetraplegia, the donor muscle is commonly attached to the insertion of the paralyzed flexor pollicis brevis muscle (FPL), a thumb flexor [1]. However, the nominal direction of the thumb-tip force that FPL produces may cause the thumb to slip during lateral pinch [2]. The aim of this study was to evaluate if actuating additional thumb muscles via tendon transfer could orient the thumb-tip force more appropriately for lateral pinch.

METHODS

Thumb-tip forces produced by the extrinsic and intrinsic muscles of the thumb were measured in 11 upper extremity cadaveric specimens by adapting an experimental approach previously developed for the index finger [3]. Briefly, a force of 10 N was applied to the tendons of nine muscles and the resulting three-dimensional (3D) thumb-tip force was quantified using a force sensor. The wrist was positioned in neutral and the thumb was fixed so that the trapezio-metacarpal joint was extended 29^o, the metacarpo-phalangeal joint was flexed 27^o, and the interphalangeal (IP) joint was flexed 50^o to simulate lateral pinch.

For each muscle, median components of the measured thumb-tip force vectors were computed. Using this data, we calculated the resultant thumb-tip force vector from linear combinations of (1) the forces produced by FPL and one other muscle, and (2) the forces produced by FPL and two other muscles. Direct comparisons of the directions of the force vectors resulting from the linear combinations of multiple muscles were compared to the nominal FPL direction to evaluate if actuating more than one muscle could better orient thumb-tip force. We used the Mardia-Watson-Wheeler Test for circular statistics (Kovach Computing Services, Anglesey, Whales, UK) to test for significance ($\alpha = 0.05$).

RESULTS AND DISCUSSION

When the tendon of FPL was loaded with 10 N of force, the median (interquartile range) magnitude of the force was 1.7 N (1.5 N to 3.9 N) and the force was oriented obliquely at 49^o (19^o to 54^o) with respect to the palmar direction in the flexion-extension plane (Fig. 1). We estimate that if equal force is applied to the tendons of the ulnar head of the flexor pollicis brevis muscle (FPBu) and FPL, i.e., if these muscles were simultaneously actuated by a single donor muscle, the resultant thumb-tip force direction is 15^o (-20^o to 27^o). A single donor muscle actuating three muscles, FPL, FPBu and the radial head of the flexor pollicis brevis, also re-orients the force; the new orientation being -9^o (-49^o to 2^o) with respect to the palmar direction.

Surgical restoration of lateral pinch following cervical spinal cord injury often leaves a donor-muscle-actuated FPL as the only muscle producing force at the thumb. Based on the

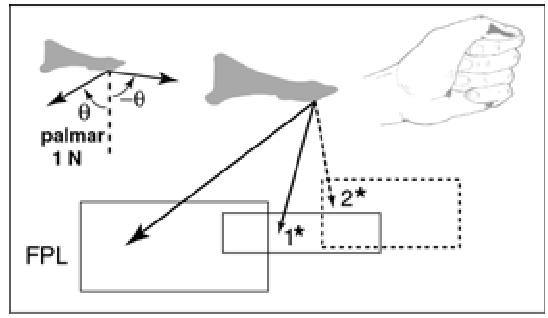

Figure 1: Median thumb-tip force directions. FPL and FPBu combined (1) and FPL, FPBu, and FPBr combined (2) yield force directions that are less oblique (more palmarly directed) than FPL alone. Boxes indicate the interquartile ranges of the thumb-tip force components. (*$p < 0.05$)

coefficients of friction between skin and objects of different materials [4], we estimate that the force applied to an object by the thumb should be oriented to within 15^o to 33^o of the palmar direction to stably grasp objects. The direction of FPL's nominal force lies outside this range. This mis-direction likely explains the need for procedures that stabilize the IP joint, frequently performed concomitantly with tendon transfers that restore lateral pinch [5]. This study suggests that simultaneously actuating additional muscles with the same donor muscle has the potential to improve thumb-tip force direction. This approach could reduce the need for joint stabilization procedures that restrict joint movement, such as percutaneous pin fixation.

Limitations of this work should be considered when interpreting the results. First, thumb-tip force directions should also be evaluated in three-dimensions to evaluate how actuating multiple muscles would influence function in other planes. Second, we assume forces produced by multiple muscles can be combined linearly. The sensitivity of our results to this assumption should be further evaluated [6].

CONCLUSIONS

Actuating the paralyzed intrinsic musculature of the thumb via tendon transfer has the potential to improve lateral pinch function following tetraplegia.

REFERENCES

1. House, J, et al. *J Hand Surg [Am]* **1**, 152-9, 1976.
2. Towles, JD, et al. *J Hand Surg [Am]* **29**, 1056-1062, 2004.
3. Valero-Cuevas, FJ, et al. *J Biomech* **33**, 1601-1609, 2000.
4. Buchholz, B, et al. *Ergonomics* **31**, 317-325, 1988.
5. Moberg, E. *J Bone and Joint Surg* **57A**(2), 196-206.
6. Pearlman, JL, et al. *J Orthop Res* **22**, 306-312, 2004.

ACKNOWLEDGEMENTS

Supported by the Rehabilitation R&D Service of the Department of Veterans Affairs (#B1967R and #B2785R).

EXTRACTION OF THE IMPACT FROM VERTICAL GROUND REACTION FORCES

T.R. Derrick, J.C. Gillette and J.M. Thomas
Department of Health and Human Performance, Iowa State University, Ames, IA, USA
email: tderrick@iastate.edu

INTRODUCTION

Vertical ground reaction forces (VGRF) are composed of a high frequency (impact) and a low frequency (active) component. The impact component is associated with the acceleration the stance leg during running [1]. This impact component has been associated with both positive (bone strengthening) and negative (injury) effects. The impact and active components are superimposed in the time domain and contain significant overlap in the frequency domain. Therefore, spectral methods are inadequate as a means of separating the components. The purpose of this research was to determine if spline techniques could be used to separate the impact from the active portion of a VGRF.

METHODS

A cubic smoothing spline with a weighting variable was used to remove the impact peak from a VGRF curve. The curve was split into 4 regions (Figure 1). Region A consisted of the first 8 ms of the curve. The values were set to the reverse of the last 8 ms of the curve and the weights were set to 0.1. Region B was from 8 ms to approximately twice the time to the impact peak. This assumes a symmetric impact curve. The weights were set to 0.0 in this region. Region C was from the end of Region B to one data point prior to the end of the VGRF. The weights in this region were set to 0.1. The final data point was set to 1.0 to force the curve through this value. Application of the spline resulted in the active force. The impact force was obtained from subtraction of the active force from the VGRF.

A mass-spring model was used to simulate impact curves. Stiffness was originally set to 100 kN/m, mass was 8.5 kg and initial velocity was -1.0 m/s. The active curve was simulated

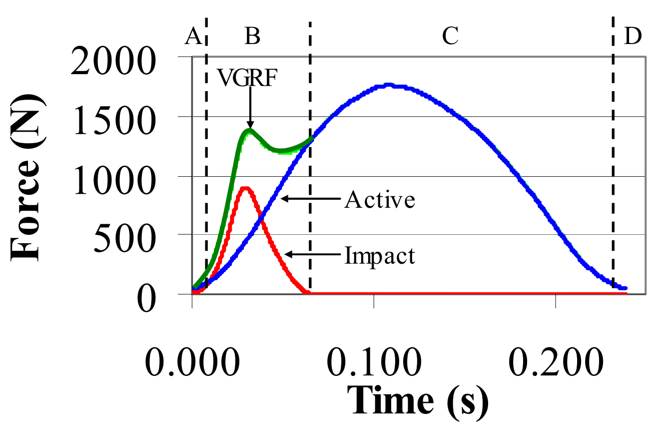

Figure 1. Spline extraction of the impact portion of an actual running vertical ground reaction force curve. Regions A, B, C and D indicate different weights of the spline.

using a Kaiser window (β=5) scaled in magnitude to 1200 N and scaled in time to 0.25 s. Simulated VGRF curves were constructed by adding the impact and active curves. The ability of the spline to accurately extract the impact portion of the curve was assessed by comparing the actual mass-spring impact peaks to the extracted impact peaks while changing the parameters of spring stiffness, impact velocity and stance time.

The spline method of impact extraction was also applied to actual VGRF curves obtained while running across a force platform in 4 conditions. Seven subjects (mass: 66±7.5 kg) were first asked to run at a normal pace. They were then asked to run at the same pace off of a raised platform while flexing the knee normally, with excessive flexion and with minimal flexion. Ten trials of force platform data were recorded at 1000 Hz for each of the four conditions. Actual running VGRF impact peaks were compared to impact peaks extracted using the spline technique.

RESULTS AND DISCUSSION

Although simulated VGRF impact peaks ranged from 649 to 1543 N, the extracted impact peaks were never more than one N different than the mass-spring simulated impact force peaks.

Table 1 indicates the average VGRF and extracted impact peaks for each running condition. Note the magnitudes are substantially different, yet there is a correlation of 0.98 between actual and extracted peak values.

Extraction of impact peaks allows the determination of impact parameters independent of the active portion of the curve. This has applications for assessing both the injury and osteogenic potential of impacts. The extracted impact forces could be used to estimate the effective mass of an impact.

Table 1. Peak impact values for actual VGRF curves.

Running Condition	Peak VGRF Impact Force (N)	Peak Extracted Impact Force (N)
Normal	1182±227	705±227
Platform Normal	1925±404	1484±379
Platform Flexed	1855±479	1569±457
Platform Extended	2290±539	1888±538

REFERENCES

1. Bobbert, et al., *J. Biomech.*, **24**:1095-1105, 1991.

IMPLEMENTING DATA-DRIVEN MODELS OF THE HUMAN THUMB INTO A ROBOTIC GRASP SIMULATOR TO PREDICT GRASP STABILITY

[1] Veronica J. Santos, [2] Andrew Miller, [2] Peter Allen, and [1,3] Francisco J. Valero-Cuevas
[1] Neuromuscular Biomechanics Laboratory, Cornell University, NY, USA,
[2] Department of Computer Science, Columbia University, NY, USA, [3] The Hospital for Special Surgery, NY, USA
email: fv24@cornell.edu; web: www.mae.cornell.edu/nmbl, www.cs.columbia.edu/~amiller/graspit

INTRODUCTION

What are the features of the human hand that enable dexterous manipulation functionality that transcends that of state-of-the-art robotic hands? Understanding and emulating the biologically evolved solutions to the manipulation problem in humans would empower both biomechanists and roboticists alike. In this interdisciplinary work, we present the computational foundations to simulate and predict the functional advantages of multi-finger grasps with a biomechanically realistic model of the human hand.

METHODS

We translated the anatomical description of the "virtual five-link" thumb kinematics into a standard robotics notation (Denavit-Hartenberg (D-H)) using 3D geometry and D-H conventions [1]. We added musculoskeletal parameters (e.g., moment arms) to the kinematics, resulting in a 50-parameter robotics-based model capable of producing thumbtip forces and torques. We then used Markov Chain Monte Carlo simulations to find parameters that achieved a least squares best fit to experimental thumbtip forces [2].

As a first approximation, we implemented these best fit D-H parameters for the thumb in *GraspIt*! [3], our visualization and simulation engine designed for the study of grasp planning in robotic hands. The other fingers were simulated using universal joints at the metacarpophalangeal joints, and simple hinges at the interphalangeal joints [4]. With this program, grasps of arbitrary objects can be dynamically simulated, optimized for grasp stability, and objectively quantified for feasibility and grasp quality.

To quantify grasp quality, we use a robotics-based mathematical representation of grasp that employs a "grasp matrix" to relate fingertip contact forces (and torques if using soft fingertips) to the effective force and torque on the grasped object (the grasp "wrench"). The rank of the grasp matrix, for given object geometry and friction characteristics, is affected by fingertip placement and the margin of error permitted by the friction cones associated with each fingertip contact force, and is a measure of how many degrees of freedom of the object can be controlled [5]. We evaluate the ability of a quasi-static grasp to reject disturbances by building the 6D space of forces and torques that can be applied by the grasp using convex hull theory. We propose the hyper-volume of this space as one possible measure of grasp quality, since a larger volume of this space means that the grasp is more efficient at rejecting force and torque perturbations [3].

RESULTS AND DISCUSSION

The D-H representation of the anatomy-based, non-intersecting, non-orthogonal axes of rotation for the thumb provides a new biomimetic direction for comparative kinematic studies of robotic and human hands, and may help elucidate whether and how these kinematic features enable dexterous manipulation in humans (Fig. 1). Traditionally, simple orthogonal axes of rotation are used to model thumb kinematics in robotic hands, but our work suggests these articulations cannot realistically predict 3D static thumbtip forces [6].

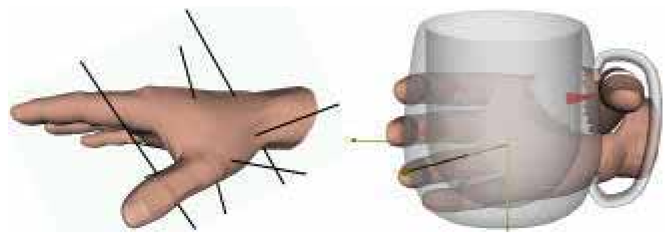

Figure 1: Left: The anatomy-based model represents more faithfully the thumb's five non-orthogonal, non-intersecting joint axes. Right: The hand model grasps a mug.

We have adapted a computational environment to quantify grasp quality of biomimetic human hands. Our critical challenge now is to determine the level of model complexity that is necessary and sufficient for predicting realistic multi-finger manipulation function. We are currently investigating adaptive refinement finite element methods to account for finger pad compliance and skin deformation, tendon interconnections within and across fingers, and will use accurate skeletal geometry to constrain the innermost elements. This computational platform will allow us to investigate the relative contributions of passive anatomical elements and active neuromuscular elements to dexterous manipulation.

REFERENCES

1. Santos VJ, Valero-Cuevas FJ. *Trans Biomed Eng*, in review.
2. Santos VJ, Valero-Cuevas FJ. *Proceedings of IEEE EMBS*, San Francisco, CA, Session 11.8.1, 2004.
3. Miller A, et al. *Ind Robot* **32**, in press.
4. Valero-Cuevas FJ, et al. *J Biomech* **31**, 693-703, 1998.
5. Murray RM, et al. *A Mathematical Introduction to Robotic Manipulation*, CRC Press, Boca Raton, FL.
6. Valero-Cuevas FJ, et al. *J Biomech* **36**, 1019-1030, 2003.

ACKNOWLEDGEMENTS

This material is based upon work supported under grants from the National Science Foundation (NSF) ITR-0312271 (to FVC and PA), GRF (to VJS), and CAREER BES-0237258 (to FVC), and Grants RG-00-0397 from the Whitaker Foundation and R01-050520 from NIH (to FVC).

IN VIVO ASSESSMENT OF CONGRUENCE IN THE PATELLOFEMORAL JOINT OF HEALTHY SUBJECTS

[1]Kim McLaughlin, [1]Janet Ronsky, [2]Richard Frayne
[1]Department of Mechanical and Manufacturing Engineering, University of Calgary, kim@kin.ucalgary.ca
[2]Departments of Radiology and Clinical Neurosciences, University of Calgary

Introduction

Joint congruence indicates how well mating surfaces fit together. A mismatch between contacting surfaces may cause abnormal joint forces and stresses. Joint congruency has been suggested as a potential risk factor in patellofemoral (PF) pain syndrome [1] as well as in the initiation and progression of osteoarthritis [2]. Radiography is the most widely used imaging modality for the clinical assessment of joints. However, this technique is limited for measures of joint congruency. It provides only subchondral bone shape which does not necessarily match the contour of the articulating cartilage [3]. In addition, the joint is typically examined in only one position. The complex 3D geometry of the joint throughout a range of motion may not be adequately characterized by this 2D measurement. Magnetic resonance (MR) imaging overcomes the limitations of current x-ray approaches for assessing joint congruence and has been used to study the knee joint [2]. However, the effect of joint angle and physiological joint loading on knee joint congruency has not been examined. The purpose of this research was to quantify in-vivo PF joint congruence and to examine effects of flexion in a loaded condition.

Methods

MR imaging (3.0T GE unit, 3D FIESTA, 3 mm slice thickness, 2.5 min. data acquisition) was used to quantify the PF joint geometry of 4 healthy female adults (mean age = 25.5 years, height = 160.6 cm, weight = 61.5 kg). Ethics approval for all procedures was provided. The knee was imaged during physiological loading at three alignments (15°, 30° and 45° flexion) using a custom designed loading apparatus. A mathematical joint model was developed through image segmentation, 3D reconstruction of each surface using a thin plate spline and contact determined with a proximity algorithm (Figure 1) [4]. The principal curvatures at each surface point were calculated and averaged over the contact area for the patella and femoral surfaces [5]. Based on the average curvature for each surface, an equivalent surface was created and compared to a flat plane.

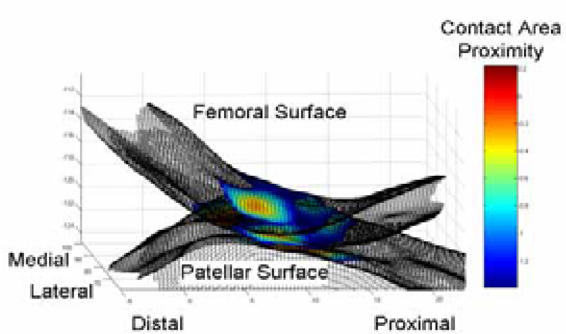

Figure 1: PF joint contact area plotted on the 3D reconstruction of the patellar and femoral surfaces.

The relative curvatures (K^e_{max}, K^e_{min}) were determined for the equivalent surface. A congruence index (CI), zero for perfect congruence, was found using: $CI = K^e_{RMS} = [(K^e_{min})^2 + (K^e_{max})^2 /2]^{1/2}$ [2]. Changes during flexion in the loaded knee joint were examined. Differences were compared using a paired t-test with a p-value < 0.05 indicating significance.

Results and Discussion

The patellofemoral joint (n=4) became more congruent as the knee joint angle increased (Figure 2). The CI at 30 degrees was found to be significantly different from both 15 degrees (p-value = 0.008) and 45 degrees (p-value = 0.002).

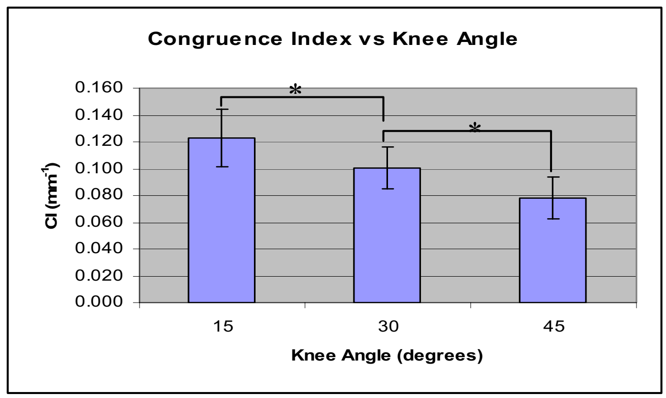

Figure 2: Average CI (mean ± 1 SD) of the loaded PF joint at 15°, 30° and 45°of flexion. (* = p-value<0.05)

The CI enables detailed characterization of subject specific joint congruence over a range of motion. Increased joint congruence can be accomplished by deforming the cartilage, changing the location of the surfaces relative to one another or a combination of both. More congruent joints may allow forces to be better distributed and therefore, minimize potentially deleterious local stress concentrations with increasing flexion angle.

Conclusions

Initial results indicated that the PF joint became more congruent as the angle increased in healthy females. Congruence could potentially be a factor in certain knee joint pathology. On-going work involves investigating the relationship of CI and knee angle in individuals with PFPS.

References: 1: Doucette, S. et al.. *Am. J. of Sport Med*, **20**(4), 434-440, 1992. **2**: Hohe, J. et al.. *Magn. Reson. Imaging*, **47**, 554-561, 2002. **3**: Adam, C. et al.. *J Anat*., **193**, 203-14, 1998. **4**: Baker: *MSc Thesis – U of Calgary*, 2001. **5**: McLaughlin et al. *Proceedings of CSB XIII*, Halifax, Nova Scotia, poster, 2004

Acknowledgements
NSERC, CRC, Calgary Health Region, GEOIDE

THE CHARACTERISTICS OF GAIT PATTERN ON THE SLIPPERY SURFACE

[1] Noriyuki Yamamoto, [1] Emi Miyai, [1] Erina Narita, [2] Hitoshi Yanagi, [2] Xiaohui Gai,
[3] Tadashi Wada, [3] Kouji Sakurama, [4] Tadao Isaka
[1] Japanese Red Cross Hokkaido college of Nursing,
[2] Satellite Venture Business Laboratory, Kitami Institute of Technology, [3] Tokushima Bunri University,
[4] Ritsumeikan University, email: yama@rchokkaido-cn.ac.jp

INTRODUCTION

Icy and snowy surface roads near melting temperature are more slippery than normal one. There have been many fall accidents caused with slip on icy and snowy surfaces in cold regions and in the winter season in many parts of the world. The biomechanics researches on slip are an important component in the prevention of fall-related injuries. The purpose of present study was to compare the biomechanics of human gait from slippery floor surface to that from non-slippery floor surface in healthy subjects.

METHODS

Five male subjects volunteered to participate in the laboratory experiments. The mean values ± *SD* of their heights, weights, and ages were 1.72 ± 0.05 m, 65.2 ± 8.9 kg, 23.2 ± 7.8 yrs., respectively. They received an explanation of the experimental protocol and provided informed consent prior to testing. A slippery (coefficient of friction: 0.125-0.225μ) and non-slippery floor surface was placed on the walking track over the force plate (KYOWA, Japan). The subject was performed to walk with three different strides; preferred, long and short strides. The cadence of walking was fixed with 90 steps per a minute. The measurements of kinematic data during the walking were collected by using the VICON 460 motion analysis system (Oxford's Metrics, Oxford, UK) with six cameras at 120 Hz placed on the laboratory ceiling. The motion of the subjects' walking was recorded with this system and reflective markers. VICON Workstation software was used to calculate position of the subject's center of gravity (CG) and the relative angles between coordinate systems of each segment in the lower limb and the laboratory coordinate system. The electromyography (EMG) system (WEB-5000, Nihon Kohden, Japan) was used to collect muscle activity from the rectus abdominis, erector spinae, vastus lateralis, hamstrings, tibialis anterior and gastrocnemius. The EMG signals were amplified and recorded by a computer via an A/D converter. A Student's paired t-test was used to determination differences between the kinematic variables when walking either the slippery and non-slippery floor surface. Probability values of $p < 0.05$ were accepted as being statistically significant.

RESULTS AND DISCUSSION

Figure 1 shows the kinematic data of the CG when the subjects walked on slippery and non-slippery floor surface. The highest CG position during one cycle was significantly lower when walking on the slippery floor surface than on the non-slippery. Differences between the maximum and minimum value in the vertical CG position during one cycle of walking were 5.1 and 3.5 cm for non-slippery and slippery

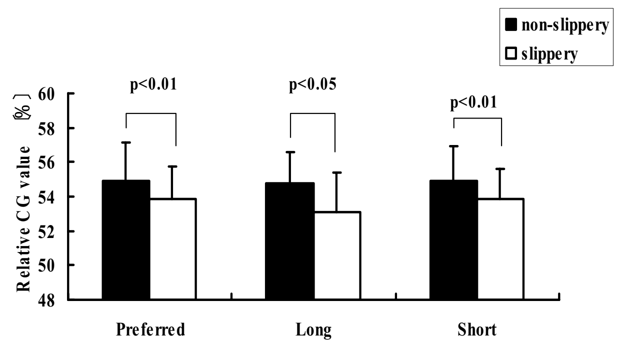

Figure 1: Comparisons of the highest value of the vertical CG position to relative body height during one cycle between slippery and non- slippery floor surface.

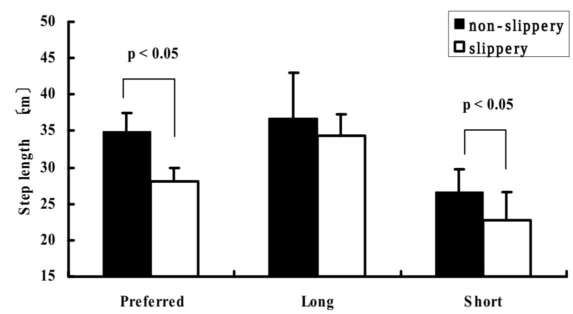

Figure 2: Comparisons of step length between slippery and non-slippery floor surface.

floor surface, respectively. This seemed to lower CG in order to stabilize the body in slippery floor surface. Figure 2 shows change of the step length when the subjects walked on slippery and non-slippery floor surface. The step length was significantly shorter slippery floor surface than non-slippery floor surface. Additionally, there was significant difference in walking speed between slippery and non-slippery floor surface. Pronounced EMG activity was found in rectus abdominis and tibialis anterior muscle during the walking on the slippery floor surface. These results indicated that the lower vertical position and smaller vertical variation of the CG during the walking on the slippery floor surface would be due to the shorter step length and larger ankle dorsiflexion and knee flexion compared to the non-slippery floor surface.

CONCLUSIONS

These findings suggest that the gait patterns were changed with depending on slippery or non-slippery floor surface. Especially, the transition of the CG on slippery was lower because of shorter step length and larger knee flexion. This changed gait pattern on slippery seems to avoid naturally for slip and fall.

THE EFFECTS OF MECHANOSENSITIVITY ON THE PREDICTION OF BONE FORMATION RATE

S.A. Meardon, T.R. Derrick, & T.J. Tauber
Department of Health and Human Performance, Iowa State University, Ames, IA, USA
E mail: smeardon@iastate.edu

INTRODUCTION

Impacts have the potential to be an influential factor in both the etiology of overuse injury and the promotion of bone strength. Models of canalicular fluid flow [1] and recent animal studies suggest impact patterns influence variables related to osteogenesis independent of magnitude and number of impacts. Repeated impacts can saturate the sensitivity of bone to mechanical stimuli. Rest between impacts or between impact bouts allows bone to recover mechanosensitivity. Knowledge of optimal patterns of loading will allow exercise routines to be developed that maximize osteogenic potential. The purpose of this study was to determine if a model of impact activity that accounts for the effects of saturation and recovery on mechanosensitivity will better predict changes in bone formation than a stimulation model based solely on magnitude and number of impacts.

METHODS

Animal studies which investigated the magnitude, number of impacts or time between impacts were used to evaluate the two models. Studies were included if loading was measured in units of microstrains (μs) and the dependent variable was bone formation rate (BFR). At present, six studies were found to meet these qualifications. *Osteogenic stimulation* was defined as the product of impact magnitude and the total number of impacts. *Osteogenic activation* was determined by the magnitude and the pattern of impacts, as influenced by the current state of mechanosensitivity. Saturation was modeled as 1/N, where N was the number of impacts [2]. Recovery was modeled as $1\text{-}e^{-t/\tau}$, where t was the time from the last impact [2]. In this study τ was optimized by finding the value that maximized the Spearman correlation between the model derived activation and the BFR from all studies combined (Figure 1).

Once the optimal τ was determined, the stimulation and activation models were correlated with BFR using a Pearson correlation for each individual study that contained more than 2 treatment conditions.

RESULTS AND DISCUSSION

The value for τ that was optimized across studies was 1.1 hours. This corresponds to 99% recovery in approximately six hours of rest. Data from each of the six studies is summarized in Table 1. In all studies, Pearson correlation coefficients indicated ostoegenic activation model was a better predictor of BFR than the stimulation model.

Both stimulation and activation models assume that strain magnitude is directly related to the osteogenic stimulus. In addition the activation model incorporates bone saturation and recovery effects. Previous research has shown that strain rates, which we did not include, play an important role [8]. In addition, neither model takes into consideration the effects of accommodation [9]. Future models will need to incorporate these variables for better prediction of bone formation rates.

Models used to predict optimal exercise patterns must take into account the effects of saturation and recovery. Use of such models would bring us one step closer to developing exercise routines that maximize human osteogenic potential.

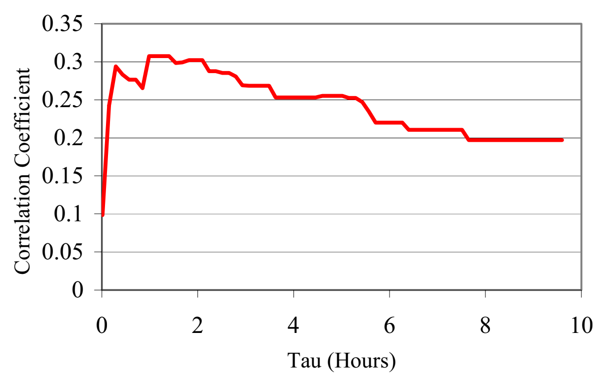

Figure 1: Optimization of tau (τ) across studies.

REFERENCES

1. Srinivasan S, et al. *Med Eng Phys*, **22**, 127-133, 2000.
2. Turner CH, et al. *Exerc Sports Sci Rev*, **31**, 45-50, 2003
3. Srinivasan S, et al. *Bone*, **33**, 946-955, 2003.
4. LaMothe JM et al. *J Appl Physiol*, **96**, 1788-1793, 2004.
5. Robling AG, et al. *J Bone Miner Res*, **15**, 1596-1602, 2000.
6. Robling, AG, et al. *J Exp Biol*, **204**, 3389-3399, 2001.
7. Srinivasan, S, et al. *J Bone Min Res*, **17**, 1613-1620, 2002.
8. Turner CH, et al. *Am J Physiol*, **269**, E438-442, 1995.
9. Schriefer JL, et al. *J Biomech*, In Press.

Table 1: Summary data for 6 studies of mechanical loading. Correlation coefficients were significant at $p<0.01$ (†) except study 6 stimulation model which was significant at $p> 0.05$ (††).

Reference	Independent Variable(s)	Specimens	Stimulation Model Correlation	Activation Model Correlation
1 [3]	Magnitude, time between impacts, # of impacts	49 mice/6 conditions	0.51†	0.64†
2 [4]	# of bouts	18 mice/2 conditions	Only 2 conditions	Only 2 conditions
3 [5]	# of bouts	36 rats/4 conditions	No variability	0.88†
4 [6]	Time between bouts	54 rats/6 conditions	0.65†	0.8†
5 [6]	Time between bouts	36 rats/4 conditions	No variability	0.76†
6 [7]	Magnitude and # of impacts	18 rats/3 conditions	0.59††	0.72†

VALIDATION OF A THEORETICAL ROWING MODEL USING EXPERIMENTAL DATA

[1,3] Alan Lai, [2,3]Daniel A. James, [1,3]Jason P. Hayes, [4]Anthony Rice and [1,3]Erol C. Harvey
[1]Industrial Research Institute Swinburne, Swinburne University of Technology, Australia,
[2]School of Microelectronic Engineering, Griffith University, Australia,
[3]Cooperative Research Centre for microTechnology, Australia,
[4]Australian Institute of Sport; email: alai@swin.edu.au

INTRODUCTION

The identification of key parameters in acceleration profiles as a means to evaluate rowing performance has traditionally been difficult to achieve. A review of the literature shows that no publication to date has attempted this, possibly due to the mechanical complexity of rowing. In this paper a single-scull rowing model, created using MathWorks' Matlab® and Simulink®, is presented. The model has been created to investigate the feasibility of monitoring shell acceleration as a means to assess single rower technique.

METHODS

The developed model describes the rower as linkages (Figure 1) rather than a series of lumped masses; a distinction from many of the existing rowing models [1-3]. The motivation for modelling the rower in such great detail is to generate a more realistic shell acceleration trace. Each body segment of the rower model was based on cadaver limb dimension data [4]. Input parameters and boundary conditions for the rower motion were based on 3D acceleration and video data collected from a single heavyweight male sculler in one session.

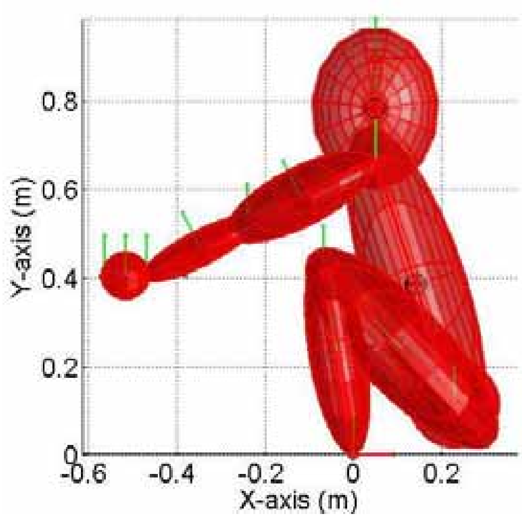

Figure 1: Rower model. The ellipsoids represent the inertial properties of the body segments.

RESULTS AND DISCUSSION

The resultant shell acceleration trace (Figure 2) from the initial attempt in simulating the rower motion does show similar characteristics to the measured shell acceleration trace (Figure 3). Further fine-tuning of the rower motion description is now in progress.

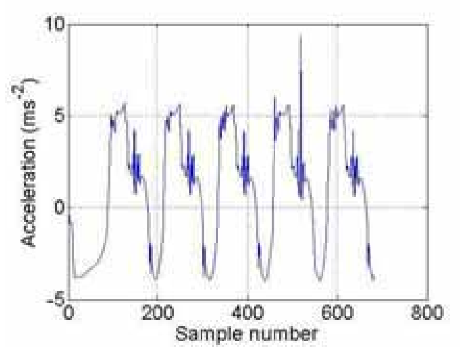

Figure 2: Simulated shell acceleration trace.

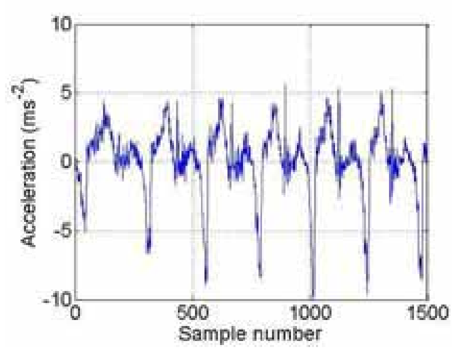

Figure 3: Measured shell acceleration trace.

CONCLUSION

The variability of the shell acceleration profile of each stroke reflects the rower's consistency. The model is an important step towards understanding the measured acceleration profile and relating the variability in the shell acceleration profiles to the timing of the rower's motion.

REFERENCES

1. Millward A. *Journal of Sports Sciences* **5**, 93-103, 1987.
2. Brearley M, et al. *3rd Conference on Mathematics and Computers in Sport*, Queensland, Australia, 35-46, 1996.
3. Atkinson WC. www.atkinsopht.com/row/rowrpage.htm, last accessed on 25th January 2005.
4. de Leva Paolo. *J Biomech* **29**, 1223-1230, 1996.

ACKNOWLEDGEMENTS

I would like to sincerely thank Emeritus Professor Marinus van Holst of Delft University of Technology for his help in constructing the rowing model.

CLINICAL USEFULNESS OF FOUR FUNCTIONAL KNEE AXIS ALGORITHMS

[1]Adam M. Fullenkamp, [1]Alicia M. Adams, [1]David J. Hudson, and [1]James G. Richards
[1]The Human Performance Laboratory, University of Delaware, Newark, DE ,
email: jimr@udel.edu

INTRODUCTION

Four functional algorithms have been proposed to resolve the challenge of identifying the true flexion/extension (F/E) axis of the knee during gait. The functional axis algorithms of Woltring [1], Halvorsen et al. [2], Schwartz and Rozumalski [3] and Baker et al. [4] were selected for comparison. A majority of these algorithms attempt to minimize ab/adduction (A/A) motion on the premise that the knee operates as a 1 (F/E) or 2-degree of freedom joint (F/E, I/E). Woltring's method involves the calculation of instantaneous helical axis vectors between thigh and shank anatomical coordinate systems. Halvorsen's method tracks the movement of a single point on the shank within the thigh's anatomical coordinate system, and then identifies the eigenvector associated with smallest eigenvalue as the knee axis. Schwartz and Rozumalski find the knee axis by determining the null space between the thigh and shank anatomical coordinate systems. Baker manipulates the orientation of the thigh coordinate system to minimize knee A/A motion. While mathematical details of each approach are available in the literature, little information is presented as to their clinical usefulness. The purpose of this investigation was to examine the performance of each of the four algorithms with respect to their agreement with static anatomical measures of tibial torsion and their ability to minimize A/A.

METHODS

Four subjects were used in this study. Tibial torsion was measured using ultrasound by subtracting readings from proximal and distal landmarks on the bone. The amount of torsion in the tibia approximates the axis formed by the medial and lateral malleoli WRT the knee axis in the transverse plane., The standard Helen Hayes marker set was used to test each method during walking trials. For subject A, data was collected with medial and lateral knee markers in the position identified by the clinician. For subsequent trials, each knee marker was shifted in the opposite direction along the AP axis in increments of 0.5cm until each marker was moved a distance of $\pm$2cm. For each trial, the functional knee axis was calculated using each of the methods described above. In addition, functional knee axes were calculated for three additional subjects while wearing markers in standard clinical locations. Tibial torsion was calculated from marker data using the tibia coordinate system and the femur coordinate system with orientation determined by the functional axis. A/A motion was also examined for each subject.

In addition to testing the algorithms as presented in the literature, modifications were made to three of the methods in the hopes of improving accuracy and/or computational efficiency. Woltring's velocity threshold was changed to a 5° displacement threshold, Halvorsen's arbitrary selection of points separated by (n/2) frames was changed to compare pairs of frames associated with ~5° of tibial motion, and Schwartz and Rozumalski's method of comparing each frame of data in a trial to all other frames within the trial was changed to compare pairs of frames associated with ~5° of tibial motion.

RESULTS AND DISCUSSION

Data from subject A indicated that Baker's method of minimizing A/A motion produced results most consistent with the ultrasound measure of tibial torsion regardless of knee marker offset (Figure 1). Schwartz's original and modified methods produced similar deviations (7.6° and 4.2° respectively), although the modified method ran in a fraction of the time.

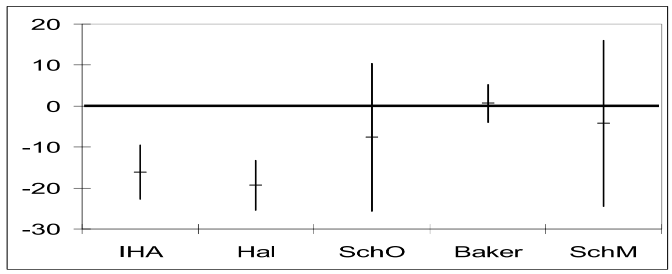

Figure 1: Rotational deviation in degrees from ultrasound measure for Subject A. Both the average and range are indicated. IHA: helical, Hal: Halvorsen modified, SchO: Schwartz original, SchM: Schwartz modified.

Data from the three additional subjects showed Baker's method to be the most consistent in the estimation of tibial torsion, while Schwartz's method performed poorly when the clinical marker placement was accurate. The remaining methods, though more consistent than those of Schwartz, showed less agreement with the ultrasound measures on average. Halvorsen's original method produced clinically irrelevant results.

CONCLUSIONS

While many of the methods represent sophisticated attempts to identify the knee axis by minimizing A/A motion, the most direct method (Baker) produced the most anatomically consistent results relative to ultrasound measures of tibial torsion. Conversely, while Schwartz's method performed well when clinical marker placement was slightly errant, it worsened the knee axis estimate considerably when the initial placement of markers provided a close approximation of the functional knee axis.

REFERENCES

1. Woltring HJ. *Biomechanics of Human Movement*. Bertec Coporation, Worthington, pp. 203-237, 1990.
2. Halvorsen K, et al. *J Biomech* **32**, 1221-1227, 1999.
3. Schwartz MH, et al. *J Biomech* **38**, 107-116, 2005.
4. Baker R, et al. *Hum Mov Sci* **18**, 655-667, 1999.

MECHANICAL PROPERTIES OF THE HUMAN HEEL PAD: A COMPARISON BETWEEN POPULATIONS

John H. Challis and Chloe Murdock
Biomechanics Laboratory, The Pennsylvania State University, USA
email: jhc10@psu.edu

INTRODUCTION

The initial point of impact during many footfalls is the heel pad, its role is to help absorb and dissipate the impact forces [1]. It is composed primarily of collagen reinforced chambers filled with densely packed fat cells [2]. The mechanical properties measured in vivo suggest the heel pad has low stiffness at loading of one body weight, and exhibits large energy losses [3].

There is evidence that human heel pad mechanical properties change with age [3], and certain disease or clinical abnormality (e.g. diabetes [4]). The reasons for these changes in mechanical properties are not clear, and one potential reason is due to changes in weight bearing activity levels. The purpose of this study was to compare the mechanical properties of the heel pad between runners, who repetitively load the heel pad during training, and cyclists, who during training do not load their heel pad.

METHODS

Ten competitive long distance runners (height: 1.66 m ± 0.06, mass 56.3 kg ± 5.7), and 10 competitive cyclists (height: 1.77 m ± 0.08, mass 71.1 kg ± 12.1) volunteered for this study. All subjects had no previous or current plantar foot injury, and the cyclists had no running history (determined to be more than 2 days a week of running). The subjects provided informed consent, with all procedures approved by the Institutional Review Board.

Thickness of the unloaded heel pad was measured using real-time B-mode ultrasonography (Aloka SSD-625, Conneticut, USA) with a 7.5 MHz linear array scanhead. Measurements were taken after the subject had not placed weight on their heel pad for 10 minutes. The ultrasound images were digitized (Scion Image for Windows) and the mean of five measurements used to compute heel pad thickness.

A heel pad indentation device, adapted from the one described in Rome and Webb [5], was used to measure the mechanical properties of the heel pads. Heel pad deformation and applied force were measured via the indentation device, for 5 trials per subject. The displacement and force data were low pass filtered with a second order Butterworth digital filter (cutoff = 4 Hz). Numerical integration was used to compute the ratio of the area within the hysteresis loop and the area under the loading curve; this indicated the energy loss between loading and unloading. A model was fitted to the force-deformation data [6], and then used to estimate heel pad stiffness at the same relative loading for each subject (5 % of body weight).

To evaluate the differences between the runners and cyclists heel pad properties a repeat measures analysis of variance (ANOVA) was used ($p < 0.05$).

RESULTS AND DISCUSSION

Heel pad thickness was statistically significantly greater for the cyclists (14.9 mm ± 1.5) compared with the runners (13.6 mm ± 1.2), but if this thickness was expressed relative to subject height then there was no significant difference (cyclists: 0.75 % ± 0.07; runners: 0.82 % ± 0.08).

There was no significant difference between the groups in percentage energy loss during loading and unloading (runners: 61.4 % ± 8.6; cyclists: 62.5 % ± 4.6). Model fits to the data produced R^2 values in excess of 0.96. Heel pad stiffness for the runners was significantly less than that of the cyclists (runners: 17.1 $N.mm^{-1}$ ± 3.0; cyclists: 20.4 $N.mm^{-1}$ ± 4.0).

CONCLUSIONS

The two populations showed no differences in heel pad thickness or energy loss due to hysteresis, but did have different pad stiffnesses. This difference in heel pad stiffness would influence the forces experienced by the body during gait containing a heel strike [7]. The indentation device used for measuring the mechanical properties only applied low loads to the heel pad, but has the advantage that measurements can be made *in vivo*, and that compared with other methods for making these measurements *in vivo* soft tissue motion does not contaminate the results [8]. These results indicate that the nature of the activity undertaken by subjects influences their heel pad properties. This finding may be important, for example, when considering differences in heel pad properties between the young and elderly [e.g., 3].

REFERENCES

1. Ker, R.F., et al. *Proc Inst Mech Eng [H]* **203**, 191-196, 1989.
2. Jahss, M.H., et al. *Foot Ankle* **13**, 233-242, 1992.
3. Kinoshita, H., et al. *Eur J Appl Physiol Occup Physiol* **73**, 404-409, 1996.
4. Hsu, T.C., et al. *Clin. Biomech* **17**, 291-296, 2002.
5. Rome, K., & Webb, P. *Clin. Biomech* **15**, 298-300, 2000.
6. Fung, Y.C. *Am. J. Physiol* **213**, 1532-1544, 1967.
7. De Clercq, D., et al. *J Biomech* **27**, 1213-1222, 1994.
8. Pain, M.T.G., & Challis, J.H. *J Biomech* **34**, 327-333, 2001.

THE RULE OF CREEP IN THE SEX DIFFERENCES OF LONG BONE RESISTANCE TO FATIGUE FAILURE

[1,2] Luisa Moreno, [2]Angela Cheung and [1]Marc Grynpas
[1]Samuel Lunenfeld Research Institute, Mount Sinai Hospital, [2] Osteoporosis Program, University Health Network and Mount Sinai Hospital, University of Toronto; e-mail: moreno@mshri.on.ca

INTRODUCTION

Stress fractures can be caused by prolonged exercise and are associated to cyclic loading. Fatigue is the accumulated damage that results from cyclic loading. This is of special concern for athletes and army recruits. Existing literature shows that the rates of stress fracture for female athletes and army recruits are higher than for their male counterparts [1].

In this study we used an ex-vivo rat model to investigate the fatigue response of female and male rat bones.

METHODS

In this model, 16 weeks old Sprague-Dawley rats were used. Fresh excised tibias were loaded at different strains from 0.5% to 1% ε to determine the strain versus cycles to failure curve (S/N curve) and endurance limit at the physiological frequency of 2Hz.

The tibias were loaded in three-point bending under load control on the medial side, using a servo-hydraulic material testing machine (Instron 8511) equipped with a 220N load cell. Displacement was measured by means of an external high precision LVDT with 10mm travel. The gauge length was 32 mm, and it was kept constant for male and female bones. Strain was calculated from the individual cross sectional dimensions directly measured with calipers at the point of striker contact. Bones were wrapped in gauze continuously soaked with saline and kept moist for the duration of the test. Using MATLAB® the individual cycle data was fitted using the least-squares method. The tangent stiffness was determined by the slope of the line that passes through the minimum and maximum points of the hysterisis curve.

To study the creep behavior, the accumulated strains from each cycle was plotted versus time. The data fitted a characteristic creep curve, with an initial fast creep followed by a steady-state deformation and a subsequent tertiary creep, followed by sudden failure. The strain damage rate was determined by the slope of the line that best fit the steady-state region of the creep data. Strain-to-failure was defined as the maximum strain the bone undergoes before fracture. The statistical analysis was done using SPSS software.

RESULTS AND DISCUSSION

The fatigue data revealed that for the same strain level the endurance limit of the female bones is 20% lower than the males. It has been suggested that the high levels of stress fracture among athletic women occur because their bones are subjected to higher strains [1]. This study shows that even if female bones are subjected to the same strains as males the female bones are still at higher risk of stress fracture.

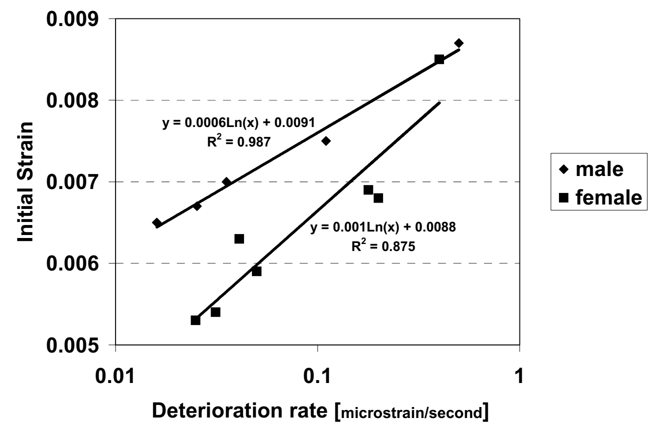

Figure 1:Plot of strain versus deterioration rate for male and female rat tibia

The creep data revealed that the strain-to-failure is similar for both genders; it seems that there is a maximum strain limit before bone fractures. However the higher deterioration rate of the female bones versus strain data (Figure 1), indicate that female bones reach this critical strain at a faster rate than male bones.

CONCLUSIONS

From this study we learned that independently from muscular of biological body response, female bones stressed to the same strain levels as male bones over a period of time, are more likely to experience stress fracture.

In the context of our study, we concluded that the female whole 'bone material' is relatively weaker, i.e. has a lower fatigue resistance than male bone material. For a given initial strain, the deterioration rate was higher for female than male bones. Hence we concluded that the fatigue life of the tibia might be determined by how fast the bone deteriorates.

This study suggests that less intensive exercises may not be enough to address the fast deterioration rate of female bones. Hence, shorter training sessions or frequent training interruptions may allow bone creep relaxation, which may prolong bone fatigue life. This may reduce the rates of stress fractures within female athletes and army recruits.

REFERENCES

1. Burr DB and C. Milgrom. CRC Series in Exercise Physiology. *Musculoskeletal Fatigue and Stress Fractures. 2001.*

Electromyography and leg stiffness comparison between old and young adults in descent stair walking

[1] Chia-Huei Shen, [2]Ming-Feng Kao and [1]Chien-Lu Tsai
[1] Department of Physical Education, National Taiwan Normal University,
[2] Department of Physical Education, National Taiwan College of Physical Education; email: true_shen@yahoo.com.tw,

INTRODUCTION

Old people experience an increased susceptibility to falls. Four out of five falls on stairs occur in descent stair walking. Descent stair walking challenges elder person's sensoriomotor reaction because it requires the elder person to overcome the perturbation from rapid change in ground reaction force. Initial mechanism of overcoming this perturbation is to adjust leg stiffness rapidly. Intrinsically, muscle activity of the lower extremity must also be alternated. Understanding leg stiffness and muscle activity during descent stair walking for elder person may provide strategy in prevention of fall occurrence. Therefore, the purpose of this study was to investigate the differences in EMG of knee extensors and flexors and leg stiffness between old and young men during descent stair walking.

METHODS

Subjects for the study were 16 old men (72 ± 4.5 years old) and 16 young men (21.2 ± 0.5 years old). Subjects performed one test session of descent stair walking from designed stairs to an elevated force plate. In order to perform quantifiable analysis, the movement was divided into three phases: pre-landing (T_1), impact (T_2), and push-off. (T_3). Electromyograpphy (EMG) signals were recorded from the rectus femoris and biceps femoris of each subject's right leg, while an electrogoniometer measured knee joint angle changes. Leg stiffness was calculated by dividing the first relative maximum of force applied on hip by its corresponding leg displacement. The Student's t-test was used to examine the differences between the two test groups. The significant difference was set at $\alpha < 0.05$.

RESULTS AND DISCUSSION

Table 1 lists the data of all the parameters. During the pre-landing phase, the old subjects were found greater EMG readings for knee extensor muscle control and greater muscle co-contraction. This suggests that the old subjects used greater anticipatory control of the lower limb's muscles to have a safer descent stairs movement. The old subjects had greater leg stiffness at impact phase may indicate that they used a conscious effort to set the limb position prior to impact. This may have helped them anticipate a safer landing, but this posture would result in greater reliance on the skeletal system for impact absorption during landing, and less reliance on the muscles [1]. At push-off phase, in order to decrease sudden ground reaction force applied on the lower extremity, the strategy in old subjects was to increase time in push-off leg. This compensatory mechanism could increase the stability but could also be associated with degradation of muscle strength and slower rate of muscle force production [2].

CONCLUSIONS

Old individuals developed a different strategy for descent stair walking. They relied much more on skeletal system instead of muscle system of the lower extremity to anticipate a safer descent stair walking. The characteristics of their descent stair walking strategy included increased pre-activity and coactivity in thigh muscles at the pre-landing phase; increased leg stiffness at the impact phase; and increased support time at the push-off phase. These changes in mediating leg stiffness and muscle activity might help them anticipate safer descent stair walking.

REFERENCES

1. Skinner HB, Barrack RL, Cook SD. *Clin Orthop* **184**, 208-211,1984.
2. Häkkinen K, Alen M, Allinen M, Izquierod M, Jokelainen K, Lassila H, Mälkiä E, Kraemer W, Newton R.. *J Aging Phys Activ* **62**,32-47,1998.

Table 1: Maximal Ground Reaction Forces Applied to the Foot, Leg Stiffness, EMG, and Coactivity Data During Descent Stair Stepping Testing for Older and Younger Subjects

	Phase	Old (n=16)	Young (n=16)	% diff	P
Maximal force, N	-	1291.0	1281.8±0.33	0.72	0.31
Knee flexion angle; deg	T_2	10.6±14.0	19.5±8.2	-45.6	0.01*
Max leg displacement; m	T_2	0.035±0.01	0.065±0.02	-46.2	0.00*
Maximal leg stiffness; kN/m	-	36.8±9.96	21.4±14.8	26.5	0.02*
Knee extensor; %MVC	T_1	24.57±12.02	13.76±5.34	78.6	0.02*
	T_2	38.70±11.49	34.29±11.73	12.3	0.32
	T_3	29.56±7.67	28.02±6.59	5.5	0.57
Knee flexor; %MVC	T_1	23.28±11.86	6.14±2.15	279.1	0.05
	T_2	30.10±8.80	15.49±6.18	94.3	0.83
	T_3	24.31±9.09	14.19±4.82	71.3	0.26
Muscle coactivity;	T_1	1.21±0.71	0.53±0.26	128	0.03*
	T_2	0.87±0.42	0.47±0.21	85.1	0.05
	T_3	0.90±0.47	0.52±0.18	73.0	0.12
Contact time; sec	T_2	0.32±0.03	0.35±0.03	-8.6	0.03*
	T_3	0.72±0.25	0.37±0.06	94.6	0.00*

BRIDGING ORGAN- AND TISSUE LEVEL COMPUTATIONAL MODELS OF BONE TO IMPROVE LOAD-INDUCED FLUID FLOW PREDICTIONS

[1] Roland Steck, [2]Hansjörg Sidler, and [1,3]Melissa L. Knothe Tate
[1]Orthopaedic Research Center, Cleveland Clinic Foundation, Cleveland OH, USA,
[2]Institute of Biomedical Engineering, Swiss Federal Institute of Technology, Zurich, Switzerland,
[3]Depts. of Biomed. Eng. and Mech. & Aeorspace Eng., Case Western Reserve University, Cleveland OH, USA;
email: knothetate@case.edu, web: bme.case.edu/mechbio

INTRODUCTION

Mechanical loading of bone has been shown to enhance extravascular molecular transport [1]. This convective transport of nutrients and bioactive molecules from the blood supply to the osteocytes embedded in the mineralized bone matrix, and between osteocytes, osteoblasts and osteoclasts, acts in addition to baseline diffusive and intracellular transport mechanisms. Due to the inaccessibility of the fluid spaces in bone for direct experimental observation, theoretical and computational models aid substantially in understanding the generation and effects of load-induced fluid movement.

Bone, like most biological tissues, is a highly hierarchical structure and possesses fluid spaces at several different length scales. It is therefore important to apply methods that are appropriate to simulate interstitial fluid flow effects at a given level of porosity. In our laboratory we have developed poroelastic finite element models to predict interstitial fluid movement in mechanically loaded bone on an organ level [2], and stochastically generated network models [3] to study the influence of cell density and connectivity on the bone tissue permeability on a tissue level. In this study we report on a method to integrate insights gained from tissue level simulations into calculations on an organ level in order to improve the accuracy of the computational predictions.

It has been reported that porosity of bone is site specific with respect to the distance from the bone surfaces (near endosteum, mid-cortex, or near periosteum), as well as with respect to the loading mode, to which a given area of the cross section is predominantly subjected to (*i.e.* tensile- or compressive load). In addition, porosity and permeability (one of the most important parameters for the prediction of interstitial fluid movement of a tissue) are intimately related. The goal of this study was to determine to what degree varying porosities in different aspects of the bone cross section affect the predicted macroscopic fluid movements. For this purpose we measured the site-specific porosities in a rat ulna, used these values to determine the local tissue permeability, which was then applied to predict the pore pressure distribution in a mechanically loaded bone model.

METHODS

The porosity attributed to the vascularity of a rat ulna was measured from high resolution μCT scans (6 μm, μCT 40, Scanco Medical AG, Switzerland). Photomicrographs from histological sections were used to measure the lacunocanalicular pore spaces and the osteocyte connectivity. The measured parameters served as input for stochastically generated network models [3] that allowed for the calculation of site specific, anisotropic permeability. These values, in turn, were used in an idealized, cylindrical bone model, representing a rat ulna, to calculate the fluid pore pressure in a bone subjected to a cyclic, combined compression-bending load acting at a frequency of 1 Hz.

RESULTS AND DISCUSSION

Most blood vessels within the bone cortex, and therefore the highest vascular porosity, were found in the region adjacent to the endosteal surface, as the analysis of the μCT scans showed. With respect to the lacunocanalicular porosity, the photomicrographs unveiled that for the specific case of the rat ulna the bone cortex can be divided into 3 concentric shells. Two of the shell layers are located near the endosteal and near the periosteal surfaces, respectively, where a relatively low number of osteocytes, and therefore low lacunocanalicular porosity, are arranged with a high degree of organization. A mid-cortex shell can be identified with a much lower degree of organization but higher number of osteocytes and therefore bigger porosity. A shell model incorporating these findings was therefore used for the parametric finite element study, whereas the site-specific material properties for each shell layer were calculated using the stochastically generated network models. While the overall pore fluid pressure distribution calculated with this poroelastic shell layer model was comparable to the pressure distribution determined with a model with uniform material parameters, local fluid pressures and fluid velocities changed significantly. Higher porosity and therefore permeability generally lead to lower fluid pressures, but higher fluid velocities. However, all calculated fluid velocities remained within the same order of magnitude.

CONCLUSIONS

This study confirmed the importance of site specific material parameters in the prediction of interstitial fluid flow in mechanically loaded bone. These insights will lead to the development of a next generation of computational models that will allow for a direct comparison with the results of experimental tracer studies.

REFERENCES

1. Knothe Tate ML, et al. *J Exp Biol* **203**, 2737-2745, 2000.
2. Steck R, et al. *J Theor Biol* **220**, 249-259, 2003.
3. Steck R, et al. *Ann Biomed Eng* **33** (1): 87-94, 2005.

ACKNOWLEDGEMENTS

This study was funded in part by a grant from the AO Research Foundation (04-S4)

THE MOUSE AS A MODELORGANISM FOR HUMAN SKELETAL DISEASES – A BIOMECHANICAL STUDY

[1]Nils Goetzen, [2]Tobias Kummer, [2]Arndt Schilling, [2]Michael Amling and [1]Michael M. Morlock
[1]Hamburg University of Technology, Biomechanics Section, Germany; email: goetzen@tuhh.de,
[2]Hamburg University School of Medicine, Department of Trauma, Hand and Reconstructive Surgery, Germany

INTRODUCTION

Our understanding of the biology of the skeleton has been transformed dramatically since the first successful introduction expression of selected genes into the germline of mice [1]. Transgenic, knock-out or knock-in strategies – particular through the use of homologous recombination in embryonic stem cells – allow the generation of specific animal models for human diseases to study the regulation and function of genes within mammalian organisms. The power of genetics has also initiated the molecular understanding of the skeleton system and identification of genes responsible for murine and human skeletal abnormalities. Since decades many inbred strains of mice are available, which helped to detect the loci of specific genes responsible, for instance, for the bone mineral density. The biomechanical description of these phenotypes is, although straight, quite challenging due to the size of the analyzed bones. The objective of this study is the integrated biomechanical analysis of various mouse models – inbred and transgenic – representing a broad spectrum of skeletal defects or abnormalities.

METHODS

Five mice-models were selected from the variety of available types: C57BL/6 and FVB/N (age: 12 weeks) as a typical starting model for transgenesis [2,3]; SAM/P6 (age: 12 & 52 weeks) as a model for senile osteoporosis [4]; Calc-$A^{-/-}$ (12 weeks) as a calcitonin knock-out [5]; and $src^{-/-}$ (12 weeks) as an osteopetrosis model [6]. The biomechanical analyses were conducted at the lumbar vertebrae (L4-L6) because they contain a higher amount of trabecular bone than femora. The following methodologies were used: Morphometry: all vertebrae were µCT-scanned (Scanco µ40; resolution: 10µm) and typical parameter like BV/TV, MIL, and trabecular thickness/separation etc. were quantified; Densitometry: bone mineral content (bmc) and density (bmd) were determined experimentally and with the help of a specially designed integrated µCT phantom.; Biomechanics: the failure load and overall stiffness of the vertebrae was determined experimentally with micro-compression test (Figure 1 left) and specimen specific finite element analysis were generated to allow an estimation of yield and ultimate stress at a local tissue-level. These methodologies were combines a the specimen-level to improve the quality of the analysis and inferences

RESULTS AND DISCUSSION

SAM/P6 shows no age-dependent variation in BMD but a distinct loss of BV/TV (from 25 to 17%). Trabecular thickness did not change either but separation increased from 360 to 530µm. Fracture load increased with age although corrected for the size effect of the vertebrae.

FVB has a slightly lower bmd-level than BL6 and failure load is not significantly different when only corrected for the size effect but lower when also corrected for the BV/TV influence – indicating a less strong tissue.

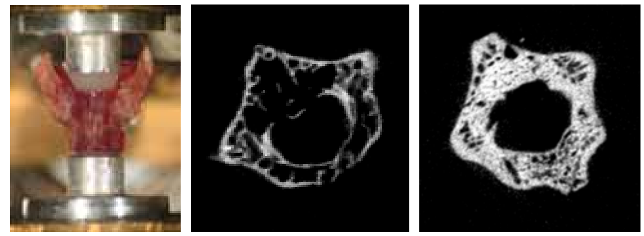

Figure 1: left: micro-mechanical compression test of a vertebra, middle: transverse cross-section of BL6-L4 and right: SRC-L4.

Calc-A has a surprisingly high BV/TV-level compared with the BL6 strain (22% versus 25%) but a reduced trabecular thickness (66µm versus 72µm). The size corrected failure load did not show any significant difference.

The failure load of the $src^{-/-}$ mice is extremely higher than in all other models: 113.7N compared with 32.7 (BL6) but the same is true for the BV/TV-ratio (Figure 1 middle/right): 90% versus 25% (BL6). BMD is also highest of all analyzed mice-models but the difference in the failure load can be largely explained by the size effect and the BV/TV ratio yielding a slightly lower fracture strength in the src-model than in the BL6-strain.

CONCLUSIONS

The analyzed mice-models represent a broad spectrum of skeletal phenotypes and large variations in morphometrical, densitometrical, and biomechanical parameter were measured. The src-model shows the most dramatic variations and indicates the effect of missing osteoclastic activities – yielding a highly mineralized and compact but less strong bony tissue. SAM/P6 shows typical (human) osteoporotic indications like lower BV/TV and higher trabecular separation but lacks reduced compressive strength. Final results of the numerical analyses will additionally give more insight into the tissue strength than current analyses. All vertebrae show a high degree of inhomogeneity and derived morphometric parameters should be treated carefully.

REFERENCES

1. Palmiter et al.. *Nature* **300**, 611, 1982.
2. Akhter et al.. *Calcif Tissue Int* **67**, 337-44, 2000.
3. Arita et al.. *Osteoarthritis Cartilage* **10**, 808-15, 2002.
4. Silva et al.. *Bone* **35**, 425-31, 2004.
5. Hoff AO, et al.. *J Clin Invest* **110**, 1849-57, 2002.
6. Amling M, et al.. *Bone* **27**, 603-10, 2000.

PREDICTING ANKLE JOINT MOMENTS IN SUBJECTS WITH NORMAL AND ABNORMAL GAIT

Daniel N. Bassett, Kurt Manal, Qi Shao, and Thomas S. Buchanan
Center for Biomedical Engineering Research, University of Delaware, Newark DE 19716

INTRODUCTION

Biomechanical models have been developed to analyze the motion of healthy individuals that walk with normal gait patterns. Such models are important for the study of muscle stimulation, prototype design, and limb control. We have created a biomechanical model of the ankle designed to predict joint moments in both unimpaired subjects and those who have had neuromuscular disorders. In this paper we will use this approach to study ankle moments in patients who have had strokes. Future research could apply the model to help subjects having abnormal gait patterns learn how to correct their muscle activation patterns through increased limb control and functional electrical stimulation.

METHODS

Three types of data were collected on normal and stroke affected subjects during isokinetic and gait trials: EMG from the tibialis anterior, medial gastrocnemius, lateral gastrocnemius, and soleus, joint position, and reaction forces (from the ground or dynamometer). Forward dynamics, using EMG and joint position data, were used to estimate the joint moments. This was verified by comparison with the inverse dynamics calculation.

The forward dynamics calculation was comprised of three elements: (1) muscle activation dynamics, (2) muscle contraction dynamics, and (3) musculoskeletal geometry. Muscle activation dynamics started from raw EMG which was rectified, filtered, and normalized. The EMG activation was then passed through a discretized recursive filter that gave neural activation. Muscle activation was calculated by non-linearizing neural activation. Muscle contraction dynamics was based on a Hill-type model approach deriving muscle force from a combination of active, passive, and fiber-velocity-dependent forces which were calculated from muscle activation and the muscle tendon lengths [1]. Calculation of both activation and contraction dynamics involves the use of unknown physical parameters. Relevant musculoskeletal geometry was the muscle moment arms which, along with muscle force, gave total joint moment [2].

The model was calibrated by optimizing the forward dynamics joint moment to fit the inverse dynamics calculation. The calibration process was done by varying unknown parameters using simulated annealing [3]. Once the fit was achieved, the parameters were used in the forward dynamic prediction of joint moment for trials for which the model had not been calibrated.

RESULTS AND DISCUSSION

The results of the calibrations and predictions of joint moments for unimpaired and post-stroke subjects were very similar, (Figure 1). The joint moment patterns (from both the model and inverse dynamics), r-squared values, and RMS error were all comparable. Muscle forces and fiber lengths were consistent with literature, indicating the model is potentially a valuable tool to deliver realistic joint moment predictions.

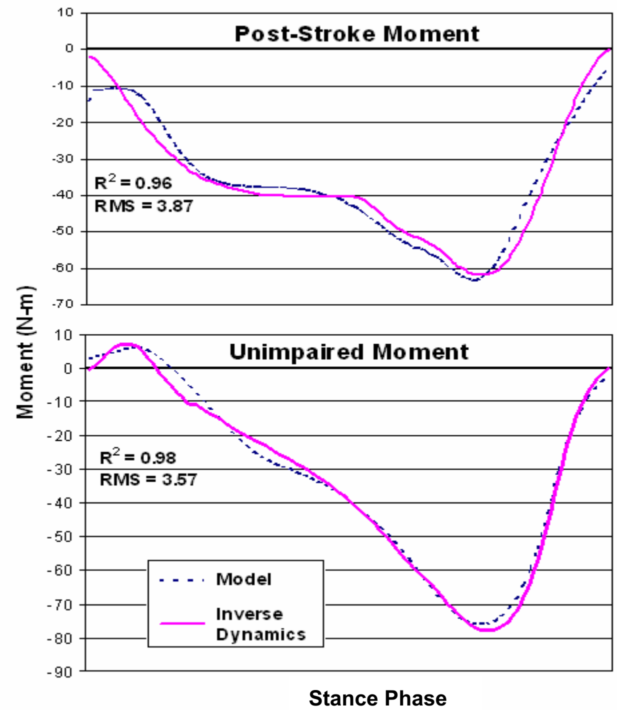

Figure 1: Comparison of calibration between a stroke patient and healthy subject.

The differences noted between subject groups were in the muscle activations and force. According to the model, an unimpaired person produces the predominance of the joint moment with their medial gastrocnemius and soleus while walking, the rest created by the lateral gastrocnemius, implying insignificant torque contribution by the tibialis anterior. Whereas a post-stroke patient produces an antagonist moment with the tibialis anterior to compensate for the enlarged moment generated by the gastrocnemii and soleus. The discrepancy is not deemed to be an error of the model; it can be explained by the fact that an individual who has spasticity due to a stroke has increased triceps surae forces.

CONCLUSIONS

In our testing, the model was able to accurately predict joint moments in novel trials for subjects with normal and abnormal gait patterns.

REFERENCES

1. Delp SL, et al. *Comput Biol Med* **25(1)**, 21-34
2. Buchanan TS, et al. *J App. Biomech*, 2004, **20**, 367-395.
3. Goffe WL, et al. *J Econometrics*, 1994, **60**, 65-99

ACKNOWLEDGEMENTS

Supported by NIH R01-HD38582

VERTICAL GROUND REACTION FORCE DIFFERENCES IN RUNNERS WITH LEG LENGTH DISCREPANCY

[1]Carla Sonsino Pereira, [1]Mariane Silva de Andrade, [1]Isabel de Camargo Neves Sacco and [1,2]Eneida Yuri Suda.
[1] Physical Therapy, Speech and Occupational Therapy department, School of Medicine, USP, Brazil; email: carlaspd@usp.br
[2] Centro Universitário Capital - Physical Therapy Course

INTRODUCTION

Leg Length Discrepancy (LLD) is so common that is considered normal by many authors and frequently it has occurred concomitant to low back pain (LBP), stress fractures (SF) and osteoarthritis (OA). The investigators have not found yet how many difference of LLD is necessary to provide these problems [3]. Large differences are generally diagnosed in youth, but smaller amounts of LLD may be unrecognized until some symptom come up. An anatomic disparity could be partial or totally compensate by functional adaptations. Biomechanical gait analysis could help discriminating between functional and structural LLD [2]. Therefore, we compared vertical ground reaction force (GRF) during running in two LLD groups of runners and one control group without inequality in order to identify if this structural inequality may cause changes and dynamic adaptations of gait.

METHODS

175 physically active subjects were submitted to a personal interview and anthropometric measurements of the lower limbs to investigate run training, symptoms and to identify possible leg differences. Subjects with LLD detected by clinical measurements done in the first stage of the study were oriented to perform a Scanogram to certify the difference. From these subjects, we formed our experimental groups: Discrepancy and Symptom Group (DSG)-40 LLD runners higher than 0.3cm with LBP and/or SF, mean age 31±5 yrs; Discrepancy Group (DG)-15 LLD runners higher than 0.3cm without symptoms, mean age 27±4 yrs; and Control Group (CG)-15 physically active subjects with zero to 0.3cm leg discrepancy, mean age 32±5 yrs. Vertical GRF were analyzed during running at a self-selected speed using a Force Plate AMTI [2]. The subjects wore their habitual running shoes during analysis. Five trials of each lower limb of each subject were acquired at a sampling rate of 200 Hz. The vertical GRF variables analyzed were: first peak of force (Fy_{1}); second peak of force (Fy_2); time to reach Fy_2 (Δt_2) and rate of loading ($RL=Fy_1/\Delta t_1$). The groups were compared using ANOVA post hoc Scheffé and between legs for each group dependent t-test. We adopted $p<0.05$ for significant differences.

RESULTS AND DISCUSSION

GRF data and p values are showed in the table 1. According to literature [1], DG presented greater Fy_2 at the longer limb, and greater values in comparison to CG and DSG. These findings could be related to the smaller values of Δt2, it could represent high mechanical loads at toe-off phase in subjects with LLD. The cumulative effect of overload during long periods on the longer limb could generate symptoms, as OA of the hip. The inclination of the pelvis to the shorter side could create a decreased area of loading at the acetabulum and the association of higher loads at the longer limb could lead to the OA [1]. Contradicting literature, that assume higher values of Fy_1 at longer limb, DSG and DG presented higher Fy_1 at shorter limb [2, 3, 4]. In agreement to some authors [1, 2, 3], this could represent a light compensatory mechanism adopted in mild discrepancies capable to minimize overloads. DSG showed significant lower values of Fy_1 related to CG. This fact might be related to symptoms observed in DSG subjects and could be explained as a dynamic strategy adopted in both sides to minimize mechanical overloads. DSG subjects also showed smaller values of RL in comparison to the other groups and this finding could be possibly explained as an anticipatory reaction in order to reduce overload at heel strike [1, 4]. DSG presented higher values of Δt_2 at shorter limb in comparison to CG, and at longer limb in comparison to CG and DG, representing greater time to reach a small Fy_2.

CONCLUSIONS

DSG presented smaller vertical force peaks and greater time to reach them in comparison to the other experimental groups. These results could be related to a dynamic strategy adopted in both sides of subjects with LLD in order to reduce overloads that might be leading to the symptoms observed in LLD subjects. DG showed higher Fy_2 at longer side and it could generate symptoms as LBP, stress fractures and precocious joint degeneration.

REFERENCES

1. Bhave et al. Improvement in gait parameters after lengthening for the treatment of limb length discrepancy. *J. Bone Joint Surg*., **.81A (4),** 529-34, 1999.
2. Kaufman, K.R. et al. Gait asymmetry in patients with limb length inequality. *J. Pediatr Orthop* **, 16**, 144-50, 1996.
3. McCaw, S.T. et al. Biomechanical implications of mild leg length inequality. ***Br. J. Sport. Med***., **25 (1)**, 10-13, 1991
4. Perttunen, J.R. et al. Gait asymmetry in patients with limb length discrepancy. Scan *J. Med. Sci.Sports*, **14,** 49–56, 2004.

ACKNOWLEDGEMENTS

We thank FAPESP for financial support (03/08165-7).

Table 1: GRF data and p-values of the experimental groups.

	CG		DSG		DG		p-value	
	greater	**shorter**	**greater**	**shorter**	**greater**	**shorter**	**greater**	**shorter**
Fy_1	1.48±0.31 [a]	1.50±0.29	1.28±0.27 [a]	1.37±0.28	1.40± 0.24	1.50±0.20	0.1724	0.1036
Fy_2	2.10±0.26 [a]	2.09±0.35 [c]	2.13 ±0.24 [b]	2.13±0.18 [d]	2.42± 0.15 [a, b]	2.35± 0.18 [c, d]	0.0482	0.1837
Δt_2	0.12± 0.01 [a]	0.12±0.00 [c]	0.13 ±0.02 [a, b]	0.13±0.01 [c]	0.11± 0.01[b]	0.12± 0.01	0.0002	0.0242
$Fy1/\Delta t1$ y	32.93±7.63 [a]	29.89±9.42 [c]	25.19 ±6.63 [a, b]	26.55±6.09 [c, d]	35.55± 17.63[b]	31.82±9.55 [d]	0.0710	0.1172

INFLUENCE OF THE PERICELLULAR MICROENVIRONMENT ON CHONDROCYTE MODELLING

[1]Sang-Kuy Han, [1]Salvatore Federico, [2]Alfio Grillo, and [1]Walter Herzog
[1]University of Calgary, Calgary, Alberta, Canada, [2]University of Catania, Catania, Italy
Email: shan@ucalgary.ca

INTRODUCTION

Chondrocytes, the living cells in articular cartilage, synthesize and maintain the extracellular matrix. The mechanical environment of chondrocytes is known to influence the health of joints. Previous experimental studies have shown that the magnitude of cell deformation is less than what would be expected based on the large differences in material properties between cell and extracellular matrix [1]. This means that cells may have a mechanism to protect themselves from high deformation in the surrounding extracellular matrix. A possible protective mechanism may be the presence of the pericellular matrix and the capsule, which, together with the chondrocyte itself, constitute the chondron. The function of the chondron is not fully understood. It has been speculated that it functions to protect chondrocytes during cartilage loading [2]. This hypothesis is supported by theoretical models of cell-matrix interactions in cartilage [3]. However, previous theoretical cell-matrix models did not entirely explain the cell deformations observed in experiments. Therefore, we hypothesised that the pericellular microenvironment, represented by the material gradient in pericellular matrix and capsule, may be responsible for the observed cell deformations.

METHODS

In order to model cell deformation, we used a multi-scale step method [3] [4]. Cartilage was assumed to be biphasic, and the elastic solid phase was modelled as a transversely isotropic, transversely homogeneous composite material [5] comprised of a proteoglycan matrix, cell inclusions, and a depth-dependent, statistically oriented collagen fibre inclusion phase. The fluid phase was assumed to be inviscid, incompressible, and associated with a deformation-dependent permeability. The cartilage specimen was assumed to be cylindrical, 1.0*mm* thick, and with a diameter of 6.0 *mm*. A spherical cell (5 μm radius) from the middle zone was modelled as a biphasic inclusion embedded in the extracellular matrix (ECM). In order to model the pericellular microenvironment, we assumed that the pericellular matrix (PCM) is 2.5 μm thick, and the pericellular capsule (PC) is 0.5 μm thick with a high volume fraction of collagen fibres, which has been observed by scanning electron microscopy [2]. All material properties for the cartilage, cell model were taken from the literature [6] [7]. Numerical simulations were performed by means of the commercially available software ABAQUS v6.3. The cartilage specimen was subjected to a 15% unconfined compression test, at a constant rate during a ramp period of 300 *s*, and the deformation was then kept constant until 1200 *s*.

RESULTS

The study of the axial displacement fields shows that the presence of the pericellular capsule influenced the discontinuity of the normal strain in the axial direction at the interface between the chondron and the surrounding matrix (Fig 1). The prediction of the ratio between cell height decrease (H_c) and local tissue strain (E_t) is more accurate when considering the capsule (Figure 2) compared to the case when the capsule is neglected, which causes an overestimation of, the predicted cell height decrease and the ratio H_c/E_t observed in experiments (Fig 2).

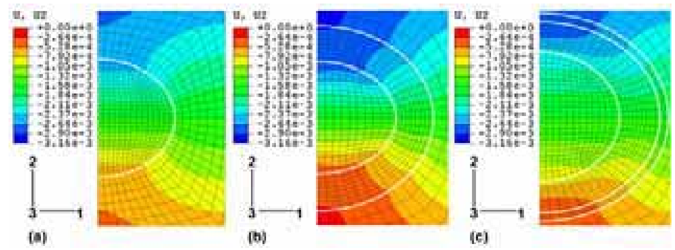

Figure 1. Comparison of the axial displacement around cell inclusions; (a) cell and ECM model (b) cell, PCM and ECM model (c) cell, PCM, PC, and ECM model.

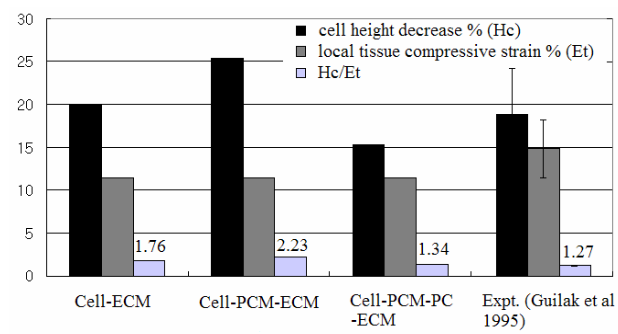

Figure 2. Comparison of cell height decrease, local tissue compressive strain, and the ratio between the two for different cell inclusion configurations.

DISCUSSION

The present analysis demonstrated that the pericellular microenvironment might explain why cells deform much less than expected during articular cartilage loading. In further studies, cell modelling should be extended to the superficial and the deep zones, where cells are no longer spherical (i.e., they are flattened and elongated, respectively). Another improvement of the current model might be achieved by incorporating the osmotic and biochemical environments.

REFERENCES

[1] Guilak, F. et al., 1995. *J. Orthop. Res. 13, 410-421*. [2] Poole, C.A. et al 1987 *J. Orthop. Res* 5, 509-522. [3] Guilak, F., Mow, V.C. 2000 *J. Biomech.* 33, 1663-1673. [4] Wu, J.Z., Herzog, W. 2000 *Ann. Biomed. Eng.* 28, 318-330. [5] Federico, S. et al. 2005 *J. Biomech.,* in press. [6] Shin, D., Athanasiou. K. A. 1997 *Trans. Orthop. Res. Soc*. 22:1: 352. [7] Alexopoulos et al. 2003 *J. Biomech. Eng*, 125, 323-333.

ACKNOWLEDGEMENTS

Dr. Les Sudak, NSERC, CHIR, Arthritis Society of Canada, Canada Research Chair Programme, Alberta Ingenuity Fund.

VARIABILITY IN THE DIRECTION OF SUBSTRATE REACTION FORCES IN THE LOCOMOTOR REPERTOIRE OF THE PRIMATE *LEMUR CATTA*

[1] Anne Su, [2]Kristian J. Carlson, [2]William L. Jungers and [2]Brigitte Demes
[1]Interdepartmental Doctoral Program in Anthropological Sciences, Stony Brook University, Stony Brook NY 11794-4364
[2]Department of Anatomical Sciences, Stony Brook University, Stony Brook NY 11794-8081
Email: ansu@ic.sunysb.edu

INTRODUCTION

Long bone cross-sectional geometry has been used in anthropological studies to infer activity patterns of fossil primates (e.g. Trinkaus and Ruff, 1999). However, our knowledge about how activity patterns of living non-human primates translate into loading patterns, and the variability of those patterns, is limited.

The goal of this study was to examine the variability in direction of substrate reaction forces (SRFs) in the locomotor repertoire of the primate species *Lemur catta*. These Malagasy primates travel predominantly on the ground with quadrupedal gaits, while in trees they travel by performing a series of runs and leaps. An attempt was made to experimentally simulate this combined terrestrial and arboreal locomotor repertoire, additionally incorporating quick changes in direction to simulate obstacle or predator avoidance and rapid movement across 3-dimensional arboreal substrates.

METHODS

Three adult individuals of *L. catta*, two females and one male (3.1 ± 0.2 kg) were included in this study. The substrate reaction forces (SRF) of the animals were recorded as they traversed a 10.5m Lexan-enclosed runway with a standard forceplate (Kistler 9281B) embedded in the center. For simulated arboreal locomotion, a 5 cm long piece of 3.2 cm diameter PVC tubing was attached to the force plate and aligned with 2 m long PVC poles of the same diameter on either side. The simulated branch was mounted 15 cm above the runway. Quick changes in movement direction were imposed by installing obstacles along the runway around which the animals were required to move, resulting in a weaving, zig-zag movement. The four test conditions were therefore: 1. linear movement on ground (LinGr, n=39); 2. linear movement on the simulated branch (LinBr, n=45); 3. turning movement on ground (TurnGr, n=26); and 4. turning movement on branch (TurnBr, n=18).

Vertical, fore-aft, and mediolateral force components were recorded digitally at 2700 Hz. Forces were low-pass filtered at 65 Hz and normalized by body weight. The direction of the peak resultant force vector was computed and normalized according to direction of travel and limb side such that a braking force was negative, propulsive force was positive, medially-directed force was negative, and laterally-directed force was positive. The forelimbs and hindlimbs were assessed separately.

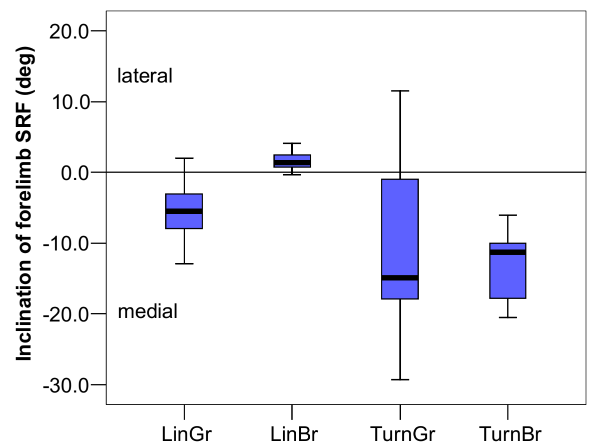

Figure 1: Mean inclination of SRF vector in the frontal plane for the forelimb in the four locomotor conditions.

RESULTS AND DISCUSSION

There is variability in the inclination of the peak SRF vector in both frontal and sagittal planes across substrates and movement tasks. The mean angle of inclination in the frontal plane ranges from -10.6 to 1.7 degrees in the forelimb (Figure 1) and -14.5 to -1.0 degrees in the hindlimb. In particular, angles associated with turning behaviors differ from those associated with linear locomotion. The mean angles in the sagittal plane range from -9.2 to -8.6 degrees in the forelimb and -0.5 to 8.4 degrees in the hindlimb. This suggests that limbs experience a range of substrate reaction force directions indicative of variation in loading regimes.

CONCLUSIONS

These data suggest that treadmill or purely linear locomotion studies of limb loading (e.g., Lieberman, 2004) may not adequately capture the range of limb loadings experienced by animals in their natural habitat. Animals such as arboreal primates with a versatile locomotor repertoire experience a range of substrate reaction force directions and their limb bones are likely exposed to multidirectional bending.

REFERENCES

1. Trinkaus E, Ruff CB. *J Archaeo Sci* **26**:409-424, 1999.
2. Lieberman, et al. *Am J Phys Anthropol* **123**, 156-171, 2004.

ACKNOWLEDGEMENTS

Supported by NSF BCS 0109331.

DESIGN OF A GAIT LABORATORY TO ENABLE BIOMECHANICAL ANALYSIS OF INDIVIDUALS WITH POST-STROKE WALKING DEFICITS: FORCE PLATFORM POSITIONING

[1] Lise C. Worthen, [1]C. Maria Kim and [2]Steven A. Kautz
[1]Rehabilitation, Research and Development Center, VA Palo Alto Health Care System, Palo Alto,CA
[2]Brain Rehabilitation Research Center, Malcom Randall VA Medical Center, Gainesville FL; [2]Department of Physical Therapy, University of Florida, Gainesville FL; [2]UF Brooks Center for Rehabilitation Studies, Gainesville FL
worthen@rrd.stanford.edu, http://guide.stanford.edu/people

INTRODUCTION

Measuring bilateral ground reactions forces in persons with post-stroke hemiparesis can be quite difficult because of the wide range of asymmetry in step lengths with which they present. The purpose of this work is to outline considerations and propose solutions for laboratory design related to recording ground reaction force data (Fx,y,z; Mx,y,z) from these individuals. Design considerations include: 1) force platform (FP) placement 2) resonant frequency signals from mounting materials, 3) order of FP strikes (paretic/non-paretic) and 4) mobility aid use (i.e. cane, AFO).

This presentation primarily addresses optimal FP placement, which we define as allowing for the collection of two consecutive footfalls in order to enable analysis of forces associated with one compete walking cycle: paretic stance, non-paretic stance and the transition between stance phases. Force platform positioning is primarily dependent on step length because it determines whether ipsilateral and contralateral steps will strike two separate platforms cleanly in one stride. Specifications for spacing multiple FPs based on 76 measured step lengths are described.

METHODS

Step length data from 38 independent ambulators with post-stroke walking deficits, collected as part of a separate study, were analyzed. All volunteers demonstrated Functional Independent Motor scores of 5 to 7 (max = 7). Step length data were acquired and calculated using a 4.6 meter long GAITRite portable walkway system (CIR Systems, Inc., Clifton, NJ 07012). Paretic and non-paretic data were grouped because collecting two footfalls requires knowing only one step length.

RESULTS AND DISCUSSION

Step lengths ranged from 19.57 to 79.60 cm. While the range of step lengths demonstrated a continuum of values, step lengths were grouped into four step clearance patterns in order to make decisions about FP positioning: minimal (T) or step-to gait, short (S), medium (M) and long (L). In addition, within the S, M and L patterns (not T), volunteers demonstrated midline cross (x), i.e. a narrow base of support in which the contralateral heel crossed in front of the ipsilateral heel (Figure 1), or no midline cross.

Six of the seven step length patterns (not Sx) were accommodated with three FPs and two orthogonal walkway usage orientations (Figure 1). We related step lengths to commercially available FP dimensions: 40 x 60 cm and 46.4 x 50.6 cm. In step pattern analyses, to account for recommended space between FPs, 2 mm were added to each side length. Group T step lengths did not clear the shortest length of 40.2 cm. Group S cleared 40.2 but not 46.6 cm. Group M cleared 46.6 but not 60.2 cm. Group L cleared 60.2 cm (Table 1).

Based on these findings, Figure 1 below illustrates the design implemented to accommodate the six patterns. One 10-meter walkway (direction AB) plus a second, orthogonal, 6-meter walkway (direction CD) were created. The overlapping, central walkway area was equipped with embedded FPs: FP1 and 2 dimensions are 46.4 x 50.6cm (Advanced Medical Technology, Inc., Watertown, MA), and FP3 dimensions are 40 x 60 cm (Bertec Corporation, Columbus, OH). Note that different step patterns may be required depending on whether the paretic or non-paretic footfall is desired to be first for subjects with a substantial step length asymmetry.

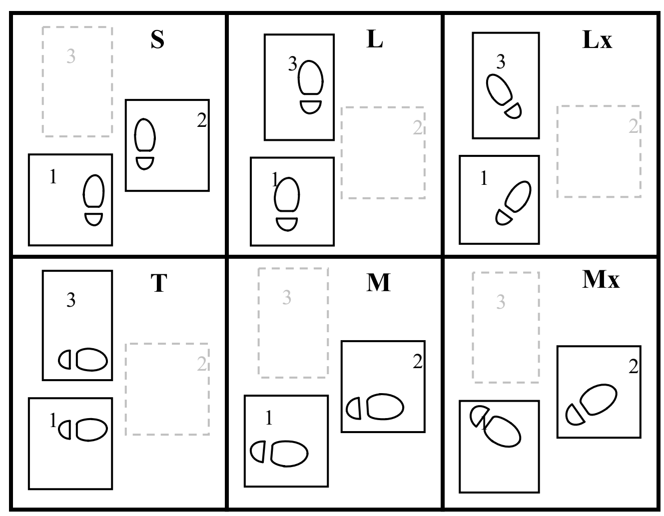

Figure 1. Step patterns are illustrated. Drawing not to scale. Top row = AB & bottom row = CD walkway orientation.

ACKNOWLEDGEMENTS This work was supported by VA Rehabilitation R&D Service Merit Review grant B2748R (Gary S. Beaupre; Steven A. Kautz).

Table 1. Step pattern data presented by group.

Step Pattern	Walkway Orientation	Platforms	n (76 total)	Step Length Mean	Step Length Range
T	CD	1 & 3	17	29.21	19.57-38.49
S	AB	1 & 2	11	43.30	41.71-45.99
M/Mx	CD	1 & 2	26	53.77	46.72-60.20
L/Lx	AB	1 & 3	22	68.56	60.28-79.60

THE DODGE MOVEMENT DURING THE LAT PULL-DOWN EXERCISE INCREASED SCAPULA ROM

Yasushi Koyama, Hirofumi Kobayashi and Shuji Suzuki
Graduate School of Human Sciences, Waseda University, Tokorozawa, Japan
email: koyama@asagi.waseda.jp, web: www.f.waseda.jp/shujiwhs/index-j.htm

INTRODUCTION

There is a skilled technique, known as the “dodge movement”, in the Beginning Movement Load Training (BMLT) method developed by Y. Koyama (1994). Numerous Japanese athletes, including Ichiro Suzuki (Mariners) and Isao Aoki (golfer), have trained with the BMLT technique.The dodge movement at lat pull-down exercise involves rapid supination and then pronation of the forearm at the transition from the eccentric to concentric contractions under rather relaxed conditions.The BMLT movement is expected to suppress the coactivation of agonist and antagonist muscles, and thereby enhance optimal power output during multi-joint movements (ISEK 2004, ACSM 2005). The purpose of this study was to determine the effect of the dodge movement during the lat pull-down exercise on the ROM of the scapula.

Figure 1: Lat pull down exercise with BMLT machine.

METHODS

Five healthy male subjects (28.6±5.1 yrs; 1.72±0.37 m; 71.2±3.8 kg), who were familiar with the BMLT, performed the lat pull-down exercise under the condition of having or not having the dodge movement at a moderate speed (ca 1.6 s per cycle) with a load of 30% 1RM (Fig. 1).Two digital video cameras operating at 60 Hz captured the entire motion for subsequent measurement of the superior and inferior angles of the scapula, L1 lumbar SP, elbow and wrist joints of the right side.The locations of the superior and inferior scapula angles were identified and marked by palpation before the experiment, and the medial-lateral and elevation-depression displacements were determined.

RESULTS AND DISCUSSION

The vertical displacement of the wrist join in the up-down direction was not significantly different for the two conditions. In contrast, the ROM in the medial-lateral and the elevation-depression directions for scapula angles were greater when the dodge movement was performed during the lat pull-down exercise compared with when it was not performed (Table 1).The maximal ROM of the superior and inferior scapula angles during the lat pull-down exercise with the dodge movement were 4.3 and 11.4 cm, respectively, in the medial-lateral direction and 4.3 and 7.5 cm, respectively, in the elevation-depression direction.

CONCLUSION

Inclusion of the dodge movement during the lat pull-down exercise increased the range of motion of scapula.

REFERENCES

1.Yoshida M, et al. Synergistic muscle activation and optimal power output in lat pulldown exercise, *Proceedings of the XVth Congress of the ISEK,* Boston, MA USA, 136, 2004.

2. Koyama Y, et al. Scapular kinematics and EMG activity of the lat pull-down with a dodge movement. *Medicine and Science in Sports and Exercise,* 37:5 Supplement (in press).

ACKNOWLEDGMENT

Supported by Grant-in-Aid for Scientific Research, Japan (No: 15650137)

Table 1: Average displacements of the superior and inferior angles of the scapula (Values are mean ±SD)

Dodge Movement	Superior Angle (cm)		Inferior Angle (cm)	
	Lateral Displacement	Vertical Displacement	Lateral Displacement	Vertical Displacement
Absent	1.50 ± 0.43	1.28 ± 0.26	6.98 ± 0.90	4.24 ± 0.86
Present	3.12 ± 1.24*	2.76 ± 1.00*	9.98 ± 1.25**	6.46 ± 1.37*

* P < 0.05; ** P < 0.01

3D LASER SCAN BASED ACCURACY TEST OF IN-VIVO CARTILAGE THICKNESS MEASUREMENT FROM MRI

[1]Seungbum Koo, [1,2,3]Nicholas J. Giori, [1,2,3]Chris O. Dyrby, [4]Garry E. Gold and [1,2,3]Thomas P. Andriacchi
[1]Department of Mechanical Engineering, Stanford University, [2]Department of Orthopaedic Surgery, Stanford University
[3]VA RR&D Center, Palo Alto, CA, [4]Department of Radiology, Stanford University
email: skoo@stanford.edu, web: http://biomotion.stanford.edu

INTRODUCTION

Osteoarthritis (OA) is a highly prevalent joint disease and a leading cause of disability. Diagnosis and monitoring of OA progression is usually determined using radiographs, computer tomography and magnetic resonance (MR) imaging. Among these modalities, MRI has shown excellent capability in imaging soft tissues and has been used to quantify cartilage morphology [1]. Three-dimensional (3D) cartilage models reconstructed from plain MR images can provide important quantitative information on articular cartilage surface area, thickness and volume. However, there remains a need to evaluate the factors influencing the *in vivo* accuracy of MRI derived geometry. The purpose of this study was to test the accuracy of articular cartilage thickness measurement from MR images by using a 3D laser scanner.

METHODS

Data was obtained from two total knee replacement (TKR) patients (age 79 and 82, both male) after IRB approval and informed consent were obtained. Prior to TKR surgery, MR images of the knee were acquired using a 1.5T GE Signa Scanner (GE Healthcare, Milwaukee, WI). We used a 3D spoiled gradient echo sequence in the sagittal plane with fat-saturation, TR=60ms, TE=5ms, flip angle=40°, matrix 256x256, rectangular field of view 140x140mm, slice thickness 1.5mm, 60 slices. Tibial articular cartilage in the MR images was segmented and reconstructed into 3D surface models using custom software [2].

After TKR surgery, the entire resected tibial plateau was immediately taken into the laboratory to measure the actual shape of the cartilage using a 3D laser scanner (Model-15, Cyberware, Monterey, CA). This scanner has an average accuracy of 50-200 µm [3]. The cartilage surface was properly coated using a powder spray of negligible thickness to prevent laser scan error due to optical properties of the cartilage before acquiring the 3D surface shape of the cartilage [4]. After laser scanning, the articular cartilage on the tibial plateau was removed using a 6.0% sodium hypochlorite solution. A second laser scan was then performed to obtain the 3D surface of the subchondral bone. Data from the laser scans obtained before and after articular cartilage removal were then aligned and combined to estimate the true articular cartilage thickness.

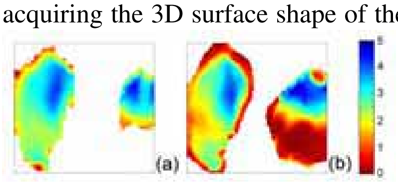

Figure 1: Tibial cartilage thickness maps of the first subject calculated using (a) MRI and (b) 3D laser scan.

Thickness maps were calculated for both 3D cartilage models, one from MR images and the other from 3D laser scans, by calculating the Euclidean distance between cartilage surface and bone-cartilage interface surface, and encoded on the surfaces of the models. The two models were aligned and projected onto a plane as shown in Fig. 1 to compare thickness measurements across the entire surface.

RESULTS AND DISCUSSION

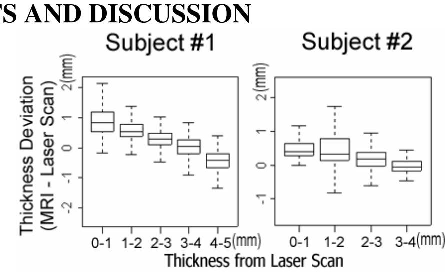

Figure 2: Comparison of thickness measurements for the tibial cartilage between 3D models from MR images and laser scan data. The graphs in the lower rows show the deviation of the MR-based cartilage thickness measurement from the laser scan-based measurement.

The correlation coefficients (R^2) between the thickness measurements from the MR images and the 3D laser scan were 0.7463 ($p<0.001$) and 0.7068 ($p<0.001$) for the first subject and the second subject, respectively. The deviation graphs show that MR will overestimate the true thickness of articular cartilage for thin cartilage (<3mm).

This result is consistent with other studies [4]. The high voxel anisotropy caused by a through plane resolution of 1.5mm vs. in-plane resolution of 0.6 mm has the effect of over-estimating cartilage thickness in regions of thin cartilage.

CONCLUSIONS

Cartilage thickness measurements from MR images have a good correlation with the measurements from laser scan data that best estimate the actual thickness. Thin cartilage less than 3mm has an inclination to be overestimated in MR images with high voxel anisotropy. This result has important implications for protocol design in longitudinal studies that follow cartilage volume and thickness with MRI.

REFERENCES

1. Eckstein F, et al. *Osteoarthr Cartilage* **9**, 101-111, 2001
2. Koo S, et al. *2003 ASME Summer Bioengineering Conference*, Key Biscayne, FL, 2003.
3. Cyberware, Model-15 manual, http://www.cyberware.com
4. Koo S, et al. *Proceedings of 28th ASB*, Portland, OR, Abstract 166-167, 2004.
5. Sato Y, et al. *IEEE T Med Imaging* **22**, 1076-1088, 2003.

ACKNOWLEDGEMENTS

We thank Barbara Elspas for her coordination of this study. This study is funded by NIH EB0002524 and NIH AR049792-01. The laser scan data were processed using the RapidForm (INUS tech, Korea).

AN INNOVATIVE TOOL FOR GENERATING NUMERICAL MODELS OF THE HUMAN FOOT – A NEW AGE OF TAILOR MADE RUNNING SHOES?

[2]E. Dejuniat, [1]E. A. C. Johnson, [1,2]P. G. Young
[1]School of Engineering and Computer Science, University of Exeter, Exeter, UK Email: e.a.c.johnson@ex.ac.uk
[2]Simpleware Ltd, Innovation Centre, Rennes Drive, Exeter, UK. Email: p.young@simpleware.com
Web: www.simpleware.com

INTRODUCTION

The human foot is a complex, multifunctional system that serves as the primary physical interaction between the body and the environment during gait and understanding the impact mechanics during human motion is important for research in motion analysis and footwear design. Many fundamental and applied human motions are influenced by complex deformations, internal stresses and shock waves of the foot skeletal system but it is difficult to directly examine the relationship between foot structure and function *in vivo*.

A new technique is emerging in the advancement of motion analysis and image processing. The ability to automatically convert any 3D image dataset into high quality meshes, is becoming the new *modus operandi* for studying the mechanical loading of complex structures. Novel proprietary techniques have been developed for the automatic generation of volumetric meshes from 3D image data including image datasets of complex structures composed of two or more distinct materials at resolutions down to the sub-micron level. The techniques guarantee the generation of robust, low distortion meshes from 3D data sets for use in finite element analysis (FEA). Such a model could generate simulations of normal and pathological foot behaviour.

The purpose of this study was to develop a complex skeletal model for finite element analysis of physical exercise, sports injury and footwear design.

METHODS

Magnetic Resonance Image (MRI) scan data was obtained from the Medical Physics department of the University of Exeter. The original scan had a plane resolution of 0.75mm and a slice-to-slice separation of 0.75mm. A first generation finite element (FE) model of the foot, that had been preliminarily validated against cadaveric data, was developed (Figure 1) using an in-house software package, Scan IP™ [1]. The model consisted of 26 foot bones (including the distal tibia and fibula), 51 ligaments (including the plantar aponeurosis) and the plantar soft tissue (flesh).

Material properties of each tissue structure were assigned to the model and appropriate loading conditions according to the mass of a 70kg human, were introduced thus imitating the impact of the weight on the articulations.

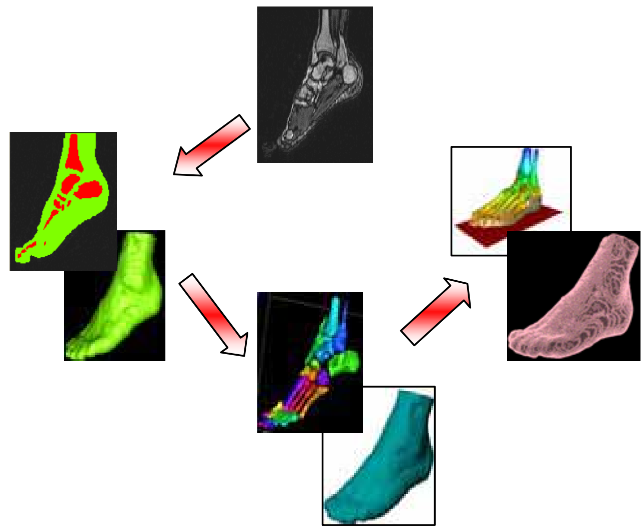

Figure 1: Development of the model from MRI scan to numerical (FE) model

RESULTS AND DISCUSSION

The aim of the study was successfully achieved in the development a high quality, complex mesh of unprecedented sophistication for use in FE analysis. The model is true to form and patient specific which opens the door to a vast array of applications in biomechanics. Parametric analyses can be performed to explore the function of different regions of the foot. Various treatment strategies could be simulated to quantify their efficacy in treating foot pathology. In addition to the obvious potential for sports injury and physical exercise analysis, it leads the way to mass customization of subject specific products such as running shoes or football boots.

REFERENCES

1. Simpleware Ltd. www.simpleware.co.uk

THE ACCURACY OF SURFACE MEASUREMENT FOR OSTEOPOROTIC SPINE MOTION ANALYSIS

ZY Yang, LW Sun, JF Griffith, PC Leung, [1]Raymond YW Lee
Department of Rehabilitation Sciences,
The Hong Kong Polytechnic University, HKSAR, China
[1]Corresponding author, email: rsrlee@polyu.edu.hk, web: http://www.rs.polyu.edu.hk/rlee

INTRODUCTION

The surface method of measuring lower thoracic and lumbar spine motion with Fastrak® was examined for validity. There is an increasing awareness of the health risks of exposure to radiation associated with repeated radiographic assessment of spinal curvature and spinal movements. As a skin-surface measurement device, Fastrak® was employed to study the effect of low bone mineral density on spine motion. However, the reliability and validity of data recorded has not been established. The purpose of this study was to develop a methodology to determine the accuracy of the surface measurement device when it is applied on osteoporotic spine motion analysis.

METHODS

The Fastrak® system consists of a source of pulsed electromagnetic waves and four sensors of signals. The source was placed in fixed positions close to the subject. The sensors of signals were attached to the skin overlying spinous processes. The angle and distance between each sensor and the source were then sampled at 30 Hz and input to computers for calculation.

Nine volunteers (3 men, 6 women, 73±4 yrs old) with different level of bone mineral density (2 normal, 5 osteopenia, 2 osteoporosis) agreed to participate. In this study, the region of interest is lower thoracic spine and lumbar spine. The tips of the spinous processes of the seventh thoracic (T7), the first lumbar (L1), and first sacral (S1) vertebrae were identified by palpation and three sensors were placed over them. Three more sensors were evenly distributed on the spine between T7 and L1 and two more between L1 and S1 to reconstruct the spine curvature. Two sets of Fastrak® systems were used in this study.

With sensors attached, the subjects were requested to take lateral radiographs in three postures: neutral upright, full flexion, and full extension. In order to facilitate the image processing, two radiopaque lead markers were fixed on each sensor as shown in Figure 1.

The sagittal rotation and translation of vertebrae and sensors were then calculated from the radiographs. The vertebral body corners of T7, L1, and S1 were marked out on the three radiographs using the method presented by Frobin [1]. The translation and rotation of the overall lower thoracic spine and lumbar spine were calculated from the corners points of T7, L1 and that of L1, S1, respectively. As for the sensors, the lead markers were easily identified on the radiographs and two lead markers on one sensor could determine the orientation and location of that sensor. Therefore, the movement of sensors on T7, L1, and S1 could be calculated.

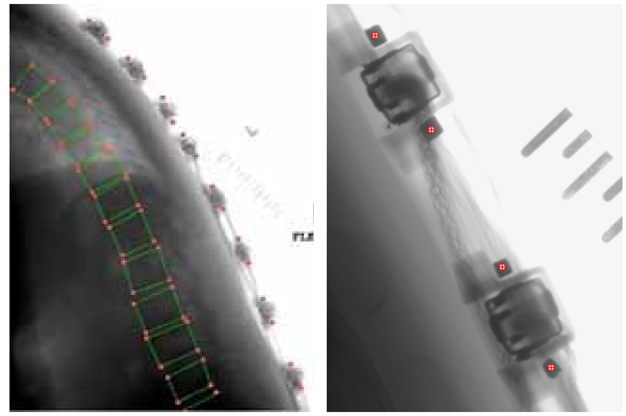

Figure 1: Manual 4 points quadrangles and sensors with radiopaque markers mounted on skin.

RESULTS AND DISCUSSION

Table 1 shows the differences of rotation angle and translation distances in two orthogonal directions calculated from vertebrae corners and lead markers on the sensors. The differences are relative differences in percentage, i.e., the calculated differences are divided by the motion range calculated from vertebrae corners. These differences were regarded as the error of the surface measures with respect to radiographic measures. It can be observed the accuracy is poor. It might be caused by the fatty bagged back of the aged subjects and the inaccurate palpation of osteoporotic spines.

	T7-L1		L1-S1	
	F / N	**E / N**	**F / N**	**E / N**
Rotation Angle	5.62%	12.3%	8.31%	10.85%
Translation X	16.30%	8.56.3%	9.47%	4.59%
Translation Y	9.34%	11.40%	2.41%	7.83%

Table 1: The accuracy of surface measures and radiographic measures. (F/N: Flexion-Neutral, E/N: Extension-Neutral)

CONCLUSIONS

Radiographs taken with 3D sensors are demonstrated as a method of accuracy estimation of surface measurement. It is expected that the relationship between the measured data obtained with the two methods can be established when sufficient subjects are examined and the surface measured data can be compensated. Therefore, more accurate data could be collected and radiographic risk eliminated. Although the accuracy calculation method is applied on elderly people with osteoporotic spine in this study, it is obvious that the method is applicable to normal healthy person as well.

REFERENCES

1. Frobin W, Brinckmann P, Leivseth G, Biggemann M, Reikeras O. Precision measurement of segmental motion from flexion-extension radiographs of the lumbar spine. *Clin Biomech* **11**(**8**), 457-465, 1996.

AN ORGANOTYPIC MODEL OF TRAUMATIC BRAIN INJURY CAUSED BY ACCELERATION-INDUCED SHEAR STRAIN

[1]Mark B. Sommers, [1]Katrin Weidner, [2]Theresa A. Lusardi and [1]Michael Bottlang
[1]Biomechanics Laboratory, Legacy Research & Technology Center, Portland, OR
[2]Robert S. Dow Neurobiology Laboratories, Legacy Research & Technology Center, Portland, OR;
email: mbottlang@biomechresearch.org

INTRODUCTION

Traumatic Brain Injury (TBI) in form of diffuse axonal injury is commonly inflicted by head acceleration, which subjects brain tissue to shear strain. This tissue level injury cascade can be simulated by *in vitro* TBI models based on organotypic brain cultures, which closely replicate the *in vivo* apparent cell heterogeneity and spatial cell architecture. However, these models typically subject cultures to stretch and fall short to employ defined shear strain as the primary mechanical insult.[1,2] This abstract presents an organotypic TBI model, which inflicts controlled, graded neuronal injury to organotypic hippocampal cultures by means of acceleration-induced shear strain.

METHODS

Hippocampi from 8-day old rat pups were harvested and sliced into 400µm thick coronal cross-sections using a tissue slicer. Hippocampal slices were plated onto Millicell culture inserts (Millipore, Bedford, MA) in a 6-well dish containing 1.1 ml of culture medium (50% MEM, 25% horse serum, 25% HBSS, 5 mg/ml glucose, and 1mM glutamine). Slices were maintained in a 37°C humidified incubator with a 5% CO enriched atmosphere for 12 days before the TBI experiment. A custom-designed linear acceleration device was utilized to produce controlled, inertia-induced shear strain in organotypic cultures (Figure 1). An electromechanical actuator impacted the acceleration module, which contained up to six Millicell culture inserts. The acceleration magnitude could be adjusted up to 12,000g. The acceleration history was measured with a piezo-resistive accelerometer (350B03, PCB Piezotronics, Depew, NY) attached to the acceleration module, and was stored with a digital oscilloscope (54603B, HP, Palo Alto, CA) at a sampling rate of 60 MHz. Following rapid linear acceleration, the acceleration module was decelerated with a constant breaking force along a 400 mm long chute with a viscoelastic foam end stop.

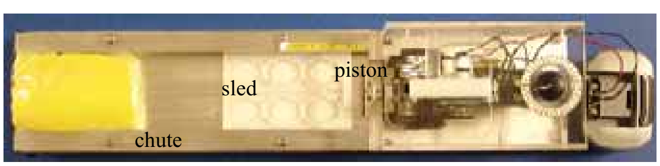

Fig. 1: TBI device with 6-well culture module.

Nine cultures each were subjected to an acceleration magnitude of 450g, 9,000g and 11,500g. Nine additional slices served as sham cultures, which were removed from the incubator, placed onto the TBI device, but were not accelerated. 21 cultures were used as control and remained in the incubator. Cellular response was measured in terms of cell death determined by propidium iodide (PI) which labels the nucleus of dead cells. Subsequently, cultures were treated with 1 mM NDMA, which caused 100% death of the neuronal cell population. This allowed expression of the initial PI labeling results as a percentage of maximum neuronal cell death. Statistical analysis was conducted using ANOVA with a Fisher's posthoc test using a confidence level of α=0.05.

RESULTS AND DISCUSSION

Viability of hippocampal cultures was not affected by placing slices onto the TBI device as shown by comparison between cell death rates in the control group (7.1±2.3%) and sham group (7.3±1.4%) (Fig. 2). Acceleration of 450g did not produce significantly elevated death of neuronal cells. Acceleration of 9,000g produced 33.6±21.9% cell death, which was significantly higher compared to sham cultures ($p<0.01$). Cell death was observed mainly in the CA1-CA3 regions and in the dentate gyrus, which are densely populated with neuronal cells (Fig. 3). 11,500g acceleration resulted in over 100% cell death, which suggests that cell death had been inflicted not only in the neuronal cell population, but extended to other cell phenotypes in the hippocampus.

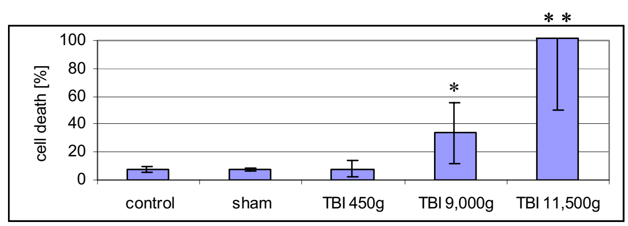

Fig. 2: Cell death response (mean +/- SD)

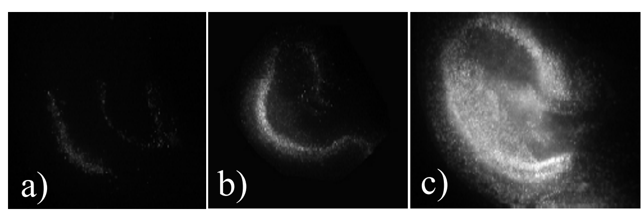

Fig. 3: PI results: a) sham; b) after 9,000 g; and c) 11,500 g.

Conclusion

The presented TBI model was able to induce acceleration-induced shear strain injury in organotypic brain slices in a graded, reproducible manner. Further characterization of this model will include measurement of the tissue–level shear strain during acceleration, a more accurate predictor of TBI.

REFERENCES

1. Morrison, B., et al., Annals Biomed Eng, 26, 1998
2. Cater, H.L., et al.. *Proceedings of Neuroscience*, San Diego,CA, 2004.

ACKNOWLEDGEMENTS

Supported by a grant of NIH/NINDS, R01NS 42946

AN ANALYTICALLY TRACTABLE MODEL FOR A COMPLETE GAIT CYCLE

Sujatha Srinivasan and Eric R. Westervelt
Department of Mechanical Engineering, The Ohio State University
email: {srinivasan.54, westervelt.4}@osu.edu

INTRODUCTION

Human walking is complex due to a human's many degrees of freedom (DOF) and the periodic impacts that occur at leg exchange. This has resulted in models of walking that either deal with only limited aspects of the gait, for example, models of only the swing phase, or models that attempt to be all-inclusive that include, for example, all of a human's DOF and musculature [1]. As a result, these models have limited use for clinical judgments, which are usually based upon gait analysis heuristics or statistical comparisons. The work described here deals with the development of an analytically tractable hybrid model to model an entire gait cycle of human walking (a forward-dynamic model). The model is validated using experimental data for normal gait reported by Winter [2].

This analytical model, in turn, will lead to a low-dimensional model that captures the essential dynamics of human walking. Such a *template* dynamical model is considered possible because of the observed parsimony of human gait (Figure 1). Having such a model has important implications for clinical applications and could lead to the development of analytical tools that, for example, predict the effect of anthropometric changes, or enable analysis of systematic changes to prosthetic alignment instead of relying on heuristics.

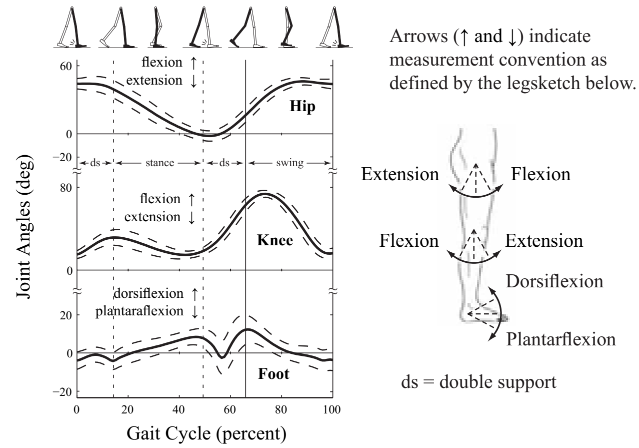

Figure 1: Average joint angles for five subjects using five trials each. Note strikingly small variation in the joint trajectories, which indicates that humans use their DOF parsimoniously, and with uniformity, while walking. Data courtesy of J. Linskell, Limb Fitting Centre, Dundee, Scotland.

METHODS

Since the gross motions during human walking take place in the sagittal plane, a 2D model is developed. (Extension of the model to three dimensions is planned.) The hybrid dynamic model consists of three parts, the single support phase, a leg-ground contact event, and a double support phase. The analysis of the continuous phases (single and double support) is developed using standard robotics analysis: Kinematics are obtained via the Denavit-Hartenberg convention and then Lagrange's method is used to derive the equations of motion [3]. The discrete phase, (leg-ground contact event) is modeled as a rigid impact. We term this approach "robomimetic" in that the inspiration for this approach is from a framework developed for the systematic design and analysis of controllers to induce stable walking in planar biped robots [4].

The single support phase model is of five rigid links: two shanks, two thighs and a HAT segment. The weight-bearing leg has a rocker foot, the shape of which is determined using the roll-over shape model of Hansen [5]. The single support model is valid from heel contact to opposite heel contact.

A rigid impact model, which acts instantaneously, is used to model the transition from single support to double support. The model captures the energy loss associated with this event.

The model for double support (DS) is of six rigid links, with the trailing limb's ankle joint being actuated. This additional DOF is to enable the model to capture the impulse at toe-off.

To validate the model, the energies of the segments are computed using the hybrid model and compared with the data for a single normal gait cycle reported by Winter [2].

RESULTS AND DISCUSSION

The analytical model described is a first step in the development of a low-dimension model of human gait. Preliminary comparisons of the data generated from this analytical model show that the model is able to capture well the energetics in the single support phase. Note that, in a first analysis, the DS model's trailing limb ankle was not actuated. This model was not able to accurately capture the energetics of the DS phase. With the addition of an actuated ankle, the energy burst that appears at toe-off is captured.

The parsimony of human gait and the successful use of an analytically tractable low-dimension model to implement stable walking in a biped robot [4] suggest that a template dynamical system for human walking is possible. The model developed here provides the foundation for this approach.

REFERENCES

1. Zajac FE, et al. *Gait and Posture* **17**, 1-17, 2003.
2. Winter DA. *Biomechanics and Motor Control of Human Movement,* John Wiley & Sons, 2004.
3. Spong MW, et al. *Robot Modeling and Control*, John Wiley & Sons, 2004.
4. Westervelt ER, et al. *IEEE Transactions on Automatic Control*. **48**, 42-56, 2003.
5. Hansen AH et al. *Clin. Biomech.* **19**, 407-414, 2004.

INFLUENCE OF SEAT HEIGHT ON PITCH ANGLE AND PUSHRIM KINETICS DURING A WHEELIE ACTIVITY

[1,2]Po-Chou Lin, [1]Fong-Chin Su, Kenton R Kaufman[2] and Kai-Nan An[2]
[1]Institute of Biomedical Engineering, National Cheng Kung University, Tainan, TAIWAN; email: fcsu@mail.ncku.edu.tw
[2]Biomechanics and Motion Lab, Div. of Orthopedic Research, Mayo Clinic, Rochester, MN, USA

INTRODUCTION

A wheelie is a high level skill performed when the user pops the front casters off the ground and keeps balance on the rear wheel. The pitch angle is the tilt angle of the rear wheel axle when maintaining the wheelie . Bonaparte et al. suggested wheelie performers appear to use a proactive balance strategy in maintaining a stationary wheelie[1]. The seat height affects manual wheelchair propulsion[2, 3]. Pushrim kinetics plays a very important role in wheelie activity, but the influence of seat height has not been studied. Therefore, the purpose of this study was to compare the pushrim kinetics of individuals in different seat height when performing a wheelie.

METHODS

Five experience spinal cord injury males (age 26.6±1.5 years old, weight 64.7±6.3kg, and height 171.3±5.2cm) participated in this study. A six-camera Expert Vision™ motion analysis system (Motion Analysis Corp, CA, USA) was used to collect the three-dimensional trajectory data of 8 markers placed on the wheelchair. A standard type manual wheelchair instrumented with a six-component load cell was used to collect the forces and moments applied on the hand-rim by users. Subjects were requested to keep their balance as stable as possible during tests which lasted 10 seconds at each of three different seat heights. The standardized seat height adjusted by a suitable seat cushion, were defined as 80, 60 and 40 degrees of elbow flexion for low, neutral and high seat positions, respectively, when the hands were placed on top-dead-center of the rim. We defined the time after 3 minutes as the balance phase when maintaining wheelie balance. Statistical analysis using ANOVA with repeated measurement was used to compare the pitch angles and pushrim kinetics among the different seat heights.

RESULTS AND DISCUSSION

Increased seat height decreased the peak pitch angle which occurred durring popping the wheelchair up and the mean pitch angle during the balance phase (Figure 1). Because the center of mass (COM) of the whole user-wheelchair system was moved from the front of the axle to the top, the angle between the vertical through the rear axle and a line connecting the rear axle and the system COM is less in the high seat which will cause a lower pitch angle. The maximum peak tangential and axial components of applied handrim

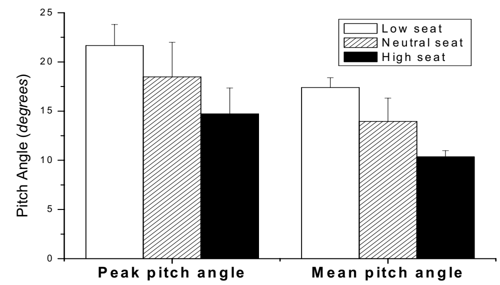

Figure 1: Mean pitch angle when keeping wheelie balance and peak pitch angle.

contact forces occurred at the neutral seat position (Table 1). At this position, bodyweight compensation helped to keep the wheelie balanced and may increase more than other seat positions. The peak radial force on the pushrim was largest at the high seat position, because less elbow flexion resulted in a larger radial force to push on the hand rim. In contrast, the mean tangential and axial forces were significantly smaller at the high seat position. The high seat position results in not only a lower effective biomechanical mechanism in wheelchair propulsion but also lower effective (tangential) force in peak force and mean force during the balance phase of a wheelie activity. We suggest that the effective force is used to against the stability of the wheelchair.

CONCLUSIONS

The results indicate that the seat height significantly affects the pushrim kinetics in during a wheelie activity. Our findings show that the effective force may be compensated by the body weight.to maintain the wheelie balance force.

REFERENCES

1. Bonaparte JP et al. *Arch Phys Med Rehabil* **82**, 475-479, 2001.
2. Kotajarvi, BR, et al. *J Rehabil Res Dev* **41**, 403-414, 2004.
3. van der Woude et al. *J Rehabil Res Dev* **26**, 31-50, 1989.

ACKNOWLEDGEMENTS

This study is supported by National Health Research Institutes grant NHRI-EX93-9318EI, TAIWAN.

Table 1: Peak applied handrim contact force in wheelie activity.

	Peak force in whole wheelie activity			Mean force when keep in balance phase		
	Radial	Tangential	Axial	Radial	Tangential	Axial
High seat	56.83 ± 1.17	23.41 ± 13.83	12.76 ± 3.37	41.43 ± 1.99	5.69 ± 1.12	3.19 ± 1.57
Neutral seat	36.08 ± 6.46	59.85 ± 9.06	23.95 ± 4.38	18.25 ± 5.57	27.82 ± 3.87	5.24 ± 1.73
Low seat	38.18 ± 5.78	53.78 ± 7.21	18.83 ± 5.16	28.45 ± 4.74	27.43 ± 2.98	5.54 ± 1.97

MEASUREMENTS AND MODELING OF THE DESCENDING COLON

[1]M. Higa, [1]Y. Luo, [2]T. Okuyama, [3]Y. Shiraishi, [2]T. Takagi, [3]T. Yambe
[1]Biomedical Engineering Research Organization, Tohoku University
[2]Institute of Fluid Science, Tohoku University
[3]Institute of Developing, Aging and Cancer, Tohoku University
email: masaru@tubero.tohoku.ac.jp

INTRODUCTION

Stress-strain data obtained from animal and human tissue have several applications including medical diagnosis, assisting in surgical instrument design and the production of realistic computer-based simulators for training in minimal access surgery. Up to the present time, about gastrointestinal organs, some researchers have reported the extensive investigations. The common problem of the methods employed in these works, however, has been the extirpation of the organs from the experimental animals or human, so-called in vitro experiment. The object of this study is to determine the passive mechanical properties of large intestine under the condition in vivo. Experiments to determine the mechanical properties are to be performed on intact living organs.

METHODS

1. In vivo indentation experiments

Experiments were performed in the descending colons of a female goat under general anesthesia. Through an incision in the skin the large intestine were laterally exposed. A supporting plate of the indentation test was inserted into it through the incision on the intestinal wall, preserving the neurovascular supply. The indenter was cylindrical and flat-ended in ϕ1 mm, and applied to the tissue perpendicularly. Three indentation rate were chosen; 0.02, 0.5, and 5 mm/s. Load values and indent depth were measured at each experiment. The thicknesses of layers were also measured.

2. Finite element analysis

The biomechanics of compression behavior of descending colon was analyzed using a 3-dimensional finite element (FE) model. FE model consists of 3861 hexahedral and wedge shaped iso-parametric elements (Figure 1). The indenter was assumed to be a rigid body. The dimensions of the model and boundary conditions were assumed to be one of the representative model of the in vivo experiment. Descending colon was assumed to be incompressibility and homogeneous. Mechanical properties of descending colon were calculated as a inverse problem. The commercial FE software package ANSYS (Cybernet Systems, Co., LTD) was applied for analysis.

RESULTS AND DISCUSSION

The relation between indentation depths and load values is shown in Figure 2. These curves are results of in vivo experiment. The influence of the heartbeat and the respiration is apparent. Values of elastic modulus were derived from these curves using Heyes' formula [1]. Average value of elastic modulus was 99.93 kPa. This value was same as the elastic modulus of the spleen [2] approximately. Elastic modulus derived from FE analysis was nearly consistent with the result of in vivo experiment. As a conclusion, the elastic modulus of descending colon was measured by in vivo indentation tests and the results of experiments were validated by FE analysis.

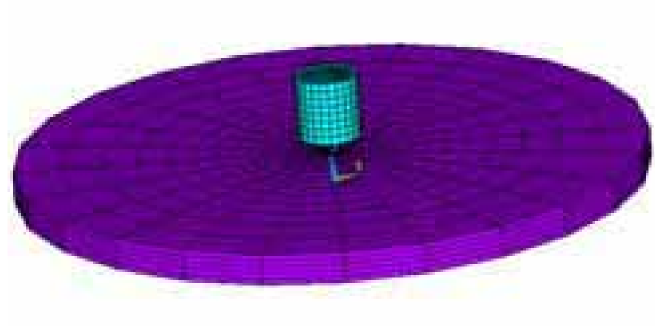

Figure 1: FE model of intestinal wall and rigid indenter

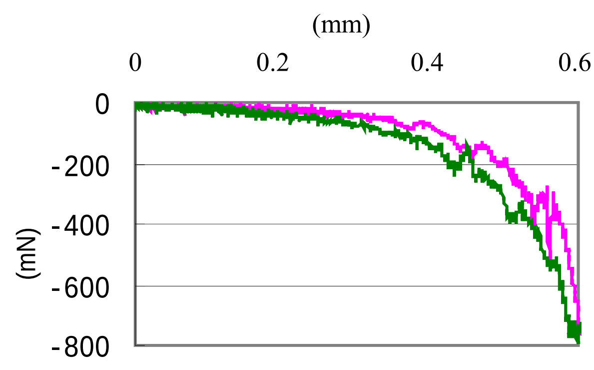

Figure 2: Results of in vivo experiments

REFERENCES

1. Heyes W., et al., A mathematical analysis for indentation tests of articular cartilage, *J. Biomechanics*, 1972, **5**, pp541-551.
2. Carter F. J., et al., Measurement and modeling of the compliance of human and porcine organs, *Medical Image Analysis*, 2001, **5**, pp231-236.

Computer Modelling

FROM REALITY TO MODEL IN MINUTES OR ON THE AERODYNAMICS OF A THANKSGIVING TURKEY

[1]V. Bui Xuan, [1]A. Benattayallah, [1]G.R. Tabor, and [1,2]P.G.Young, [2]T.B. West
[1]School of Engineering and Computer Science, University of Exeter, Exeter, UK
[2]Simpleware Ltd, Innovation Centre, Rennes Drive, Exeter, UK

INTRODUCTION

Novel techniques have been developed to convert 3D image data as obtained from a range of imaging modalities (MRI, CT, Ultrasound) into numerical meshes suitable for finite element or computational fluid dynamics analyses. These new meshing techniques provide a significant qualitative and quantitative improvement compared to currently available methods.

A number of example cases will be shown to illustrate the use of these techniques in a wide range of fields including Finite Element models of a hip implant and CFD models of cooling of a thanksgiving turkey in a light breeze.

METHODS

The steps involved in the generation and processing of finite element models based on medical imaging data are listed below.

(1) Scan and Image Processing
ScanIP is Simpleware's Image processing software tool. It offers a user friendly environment and a wide range of image processing tools to assist the user in visualizing and segmenting regions of interest from 3D data.

(2) Finite Element Model Generation
ScanFE, Simpleware's meshing software tool automatically generates the mesh from the parts (masks) generated by ScanIP. The proposed automated mesh generation from scan data simplifies has several important advantages:

1) finite element mesh sub-voxel geometry accuracy;
2) automatic multiple part structures meshing;
3) variations in material properties throughout the medium can be reflected in the finite element model
4) interfacial contacts can be modelled;
5) both scan and experiments can be performed simultaneously within the imaging modality.

(3) Export to FE mesher
Nodes, elements, material properties, contact surfaces for any or all meshed parts may be exported to input-format files for a variety of FE and CFD packages.

(4) Export to RP facility
Mesh surfaces for any or all parts may also be exported in STL file format. It allows the generation of an exact physical replica of any part for which a volumetric mesh has been generated and can, for example, be used to provide experimental corroboration of FE simulations.

RESULTS AND DISCUSSION

(1) Hip Implant
A male patient with a Total Hip Replacement (THR) was CT scanned (cf. Figure 1-a). The data was then segmented in 6 different parts and meshed. RP models were generated and an FE analysis was conducted with different mesh density models, taking into account material properties derived from the original grayscales, boundary conditions and loads were applied. Excellent qualitative and quantitative agreement was obtained for predicted stresses using both low and high element density models.

(2) Thanksgiving Turkey
A frozen turkey was scanned in an MRI scanner (cf. Figure 1-b). The segmentation was carried out based on grayscale intensities and the mesh was created in minutes. Airflow past the turkey was modelled to obtain effective lift and drag coefficients. The lift /drag ratio = 0.09 - frankly, it won't fly!

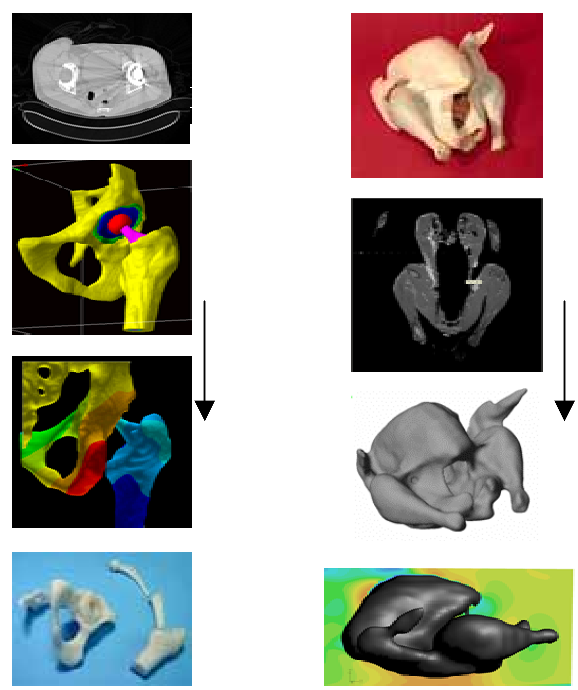

Figure 1: a) Total Hip replacement: from CT scan to FE analysis and RP model. b) Turkey: from actual turkey to CFD analysis.

CONCLUSIONS

These studies have clear implications for the future of Biomechanical modelling. Models of unmatched sophistication can now be generated with ease which opens up a wide range of previously difficult or intractable problems to numerical analysis.

A NOVEL ROBOTIC DEVICE WITH HAPTIC FEEDBACK FOR LOWER LIMB REHABILITATION

[1]Ann M. Barkowitz, [1,2]Daniel P. Ferris
[1]Dept. of Biomedical Engineering & [2]Dept. of Movement Science, University of Michigan, Ann Arbor
email: abarko@umich.edu

INTRODUCTION

After a stroke, many individuals have difficulty producing symmetric forces with their limbs. Several rehabilitation devices currently use visual biofeedback in attempts to increase this symmetry, but studies have shown only small changes in function when compared to no feedback controls [1]. A novel alternative is to use force-sensing feedback, or haptics, for rehabilitation. This technique uses computer controlled force feedback and has been suggested as a means to improve coordinated bilateral movements in the upper limbs of stroke subjects [2]. We developed a lower limb robotic device that uses haptics to investigate motor learning after stroke. In haptic feedback mode, subjects perform lower limb extensions while computer control increases resistance proportional to lower limb force asymmetry. We propose that practice with this form of direct haptic feedback will promote improved lower limb symmetry during leg extensions.

METHODS

We modified a commercially available exercise machine (Plyo-Sled, Lifestyle Sports) by adding a computer controlled electrical motor for providing resistance (Kollmorgen MT706C1-R1C1 Goldline XT Servomotor) (Figure 1). Subjects lie supine on a sled with rollers and place their feet on a vertical footplate to perform lower limb extensions. The motor affects sled movement through a rack and pinion attachment. Computer software (RT-Lab Solo, Opal-RT Technologies) controls the real-time processor to determine motor resistance. We attached a force platform (Model OR6-7MA, AMTI) to the footplate to capture center of pressure during lower limb extensions. From center of pressure data we can discern the relative symmetry between the right and left foot forces. Safety measures include an emergency stop button and electrical and mechanical stops.

In haptic feedback mode the computer controls resistance based on center of pressure from the force platform. If foot forces are equal (i.e., the subject's center of pressure remains directly in between his/her feet), the motor resistance will stay at baseline levels. If foot forces are unequal (i.e., the subject's center of pressure moves away from the center line and towards one of the feet), the computer will increase the motor resistance above baseline levels. This controller provides immediate force feedback of the amount of relative symmetry in the lower limbs. The resistance is proportional to the amount of asymmetry of the subject's foot forces. Feedback in this mode includes person-in-the-loop, where the subject can perceive increases and decreases in resistance and adjust their foot forces accordingly. If stroke subjects rely more on their non-paretic limb, they will perceive the increase in resistance and presumably increase force in their paretic limb (or decrease force in their non-paretic limb).

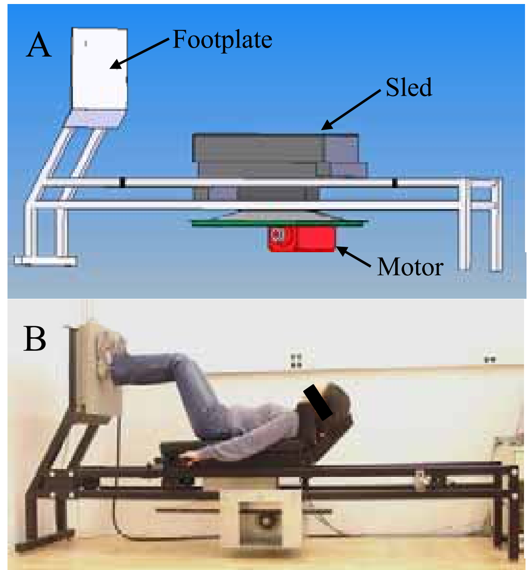

Figure 1. (a) Computer renderings of the robotic device. (b) Robotic device in use on a healthy subject.

Three healthy subjects performed leg extensions on the robotic device. Each subject performed 20 repetitions at a frequency of 0.5 Hz under two conditions; a) against baseline resistance of ~50% body weight, and b) in haptic feedback mode where the resistance was increased above baseline in proportion to the asymmetry in lower limb forces. We measured root mean square (RMS) of center of pressure excursion over the last 10 repetitions. We hypothesized that the center of pressure excursion (measure of symmetry between lower limbs) would decrease in haptic feedback mode compared to the condition with constant resistance.

RESULTS AND DISCUSSION

While providing haptic feedback to subjects, we are able to produce variable resistances up to 1200 N. Our results showed that while performing leg extensions against a constant resistance, the center of pressure excursion RMS was 3.1 ± 0.4 cm. While subjects performed leg extensions in haptic feedback mode, their center of pressure excursion RMS was 2.2 ± 0.4 cm. These results support our hypothesis and provide a basis for further testing on the robotic device in stroke subjects.

REFERENCES

1. Geiger RA, et al.. *Phys Ther* **81**, 995-1005, 2001.
2. Johnson MJ, et al.. *Robotica* **21**, 13-23, 2003.

ACKNOWLEDGEMENTS

Supported by NIH R01NS045486 and NSF GRFP.

CHILDREN'S POSTURAL CHANGES AT ADULT COMPUTER WORKSTATIONS

Carol Murphy and Joan Stevenson.
Biomechanics/Ergonomics Laboratory, 148PEC, Queen's University, Kingston, Canada, dcmurph@cogeco.ca

INTRODUCTION

The increasing incidence and disability associated with RSI and MSD and their frequency among computer users has led to concern. (Gerr, 2002) This concern has been extended to young children who are potentially also at risk for these injuries. Jacobs (2002) has shown that children are reporting moderate amounts of musculoskeletal discomfort and this discomfort can be related to computer use. This risk is increased by the fact that children are often required to play and work on computer workstations which are designed for adult anthropometrics. The purpose of this research study was to examine the quality and quantity of postural movements exhibited by five and six year olds when using an adult workstation to play a computer game. The quantitative measures children's postures and joint and segmental angles and the qualitative analysis was examined by time-motion analysis.

METHODS

Six physically active 5 and 6 year old boys and girls were asked to participate in the study. After ethics approval by parents, children were asked to give verbal assent. Each child was asked to wear a dark shirt. Joint markers were placed on the shoulder, elbow, wrist, and third knuckle for upper limb joint angles. For head orientation, the earlobe and two sweat-band markers were used. For back orientation, bilateral extended markers were placed at the level of T1, T7, and L5. Although not always visible at all times, the hip, knee and ankle were marked for lower limb kinematics.

Once outfitted, each child was asked to play a pre-selected computer game for 20 minutes. The game set-up involved use of the keyboard initially, but thereafter it was primarily mousing. Digital images were taken perpendicular and posterior to the subject for the total time. After 20 minutes, each child was asked to complete a series of shoulder shrugs and head flexion, extension, lateral bending and rotation to determine their full range of motion. Neutral resting posture was also recorded.

Using Pinnacle Studio DV software, the time that subjects spent in static postures and the frequency and nature of their postural changes were recorded from the time counter. Then, individual images were extracted from each segment in order to evaluate the posture that the child was assuming. The specific postures of interest from the side camera were: 1) joint angles of the a) upper trunk, b) elbow c) lower trunk, and segment angles of a) upper trunk, b) lower trunk, c) elbow, d) forearm and e) wrist. From the rear camera, the points of interest were angles from the horizontal of a) T1, b) T7, c) L5, d) shoulder abduction, e) elbow and f) wrist. Data were analyzed using descriptive statistics and comparing their postures to recommended postures for office ergonomics.

RESULTS AND DISCUSSION

In analyzing children's postures it was observed that all children show the same postural movement patterns with a greater number of postural shifts occurring in the feet and legs. Children show little change in their upwardly tilted head position throughout the 20 minutes. Joint and segment angles were surprisingly similar between subjects. The children chose one of three arm and hand positions when using the mouse. All involved abduction of the shoulder averaging 67º and elbow displacement of 9.2 cm which exceeded the limit recommended as 0º abduction and minimal displacement. The forearm segment angle was 20º, above the recommended horizontal position. The spinal posture was also rounded from their natural upright sitting posture.

Analysis of children's postures at adult workstations show four main areas of concern: 1) spinal curves were compromised from their neutral positions; 2) their heads were upwardly inclined; 3) their arm postures were compromised in that: a) the forearm of their mouse hand rested on the desk; b) their arms were held in 90º of abduction; and, c) their wrist of the mouse hand rested on the edge of the desk; and, 4) children's frequent postural shifts indicate discomfort.

CONCLUSION

Based on these results it would be advisable to devise recommendations and guidelines for children's workstation design. This need is deemed to be imperative based on the increasing use of computers both in school and at play and the increasing amount of time spent at the computer on a daily basis. (Jacobs, 2002)

REFERENCES

Gerr, F. et al *American Journal Industrial Medicine.* 2002 Apr;41(4):221-35.
Jacobs, K. Baker, NA. *Work.* 2002;18(3):221-6

ACKNOWLEDGEMENTS

The authors would like to acknowledge the contribution of the Ontario Chiropractic Association.

MEDIAL LONGITUDINAL ARCH MOTION AND THE WINDLASS EFFECT DURING GAIT USING A MULTI-SEGMENT FOOT MODEL

[1]K Anas and [1,2] TR Jenkyn
[1]Department of Biomedical Engineering, [2]Wolf Orthopaedic Biomechanics Laboratory, University of Western Ontario
London Ontario, Canada
email: tjenkyn@eng.uwo.ca

INTRODUCTION

Current gait analysis practice treats the foot as a single rigid segment and is therefore unable to measure clinically important motion of the joints of the foot. Several multi-segment foot models have been developed to address this deficiency [1,2]. This study uses a multi-segment foot model to examine the behaviour of the medial longitudinal arch and the hallux during normal level walking. The movement of these structures has had limited study [3] due to the difficulties in tracking six degree of freedom motion of the required segments in vivo. However, there has been much speculation on the role of the medial longitudinal arch and the windlass effect of the dorsiflexing hallux, and how these structures allow the foot to transition from a flexible and compliant structure in early stance to a rigid lever in late stance. However, this has yet to be clearly demonstrated in a large population in vivo.

Since much of the clinical practice in podiatrics and pedorthics presumes this behaviour, it seems important that this assumption be validated. Proper characterization of normal arch function and its disruption due to pathology would improve clinical understanding and treatment.

METHODS

One subject (age 26, weight 85.5 kg, height 82.5 cm) with no prior history of foot or ankle problems performed level barefoot walking at self-selected pace. 3D kinetic and kinematic data were collected with a Helen Hayes full body marker set and a multi-segment right foot marker set (Motion Analysis Corp). The foot was functionally divided into six rigid segments: talus, hindfoot, midfoot, medial and lateral forefoot and the hallux. Each segment (except for the talus) was tracked in six degrees of freedom with a three marker cluster (marker diameter 8mm, separation 24mm, carbon-fiber stalks, 16mm delrin base).

11 bony landmarks were digitized during an initial static trial and tracked during walking. Three are used in this study: lateral distal calcaneus (CL), navicular tuberosity (NT) and lateral eminence of the 1st metatarsal head (M1). The length (L) of the medial longitudinal arch is defined as the distance from CL to M1. The height (h) of the arch is the perpendicular distance from NT to the arch length vector. The ratio h/L was found and normalized to 1.0 in quiet standing. Dorsiflexion/plantarflexion of the hallux was defined as the angle of the long axis of the hallux segment with respect to the shaft of the 1st metatarsal. This approximately to 180° in quiet standing. Decreasing angle represents dorsiflexing motion.

RESULTS

The medial longitudinal arch was shown to be flatter and longer in early stance and higher and shorter in late stance (Figure 1). An unexpected small rise in the arch was seen between 10% and 40% stance. The hallux was found to be equally dorsiflexed early and late in stance and more neutral from 20% to 70% stance (Figure 2).

DISCUSSION

Early in stance, the arch was low and long but the hallux was dorsiflexed as much as in late stance. This likely represents the activity of the extensor hallucis longus acting to dorsiflex the ankle between heel strike and foot flat. In terminal stance during toe-off, the arch was found to be high and short with the hallux dorsiflexed. The hallux is likely acting as a windlass to tighten the plantar fascia and stabilize the arch as has been previously speculated. The lower peak in the h/L ratio of the arch between 10% and 40% stance was unexpected and deserves further study to determine its clinical significance.

REFERENCES

[1] Carson, MC et al. *J Biomech* **34**, 1299-1307, 2001.
[2] Leardini, A et al. *Clin Biomech* **14**, 528-536,1999.
[3] Kappel-Bargas A, et al. *Clin Biomech* **3,** 190-194, 1998

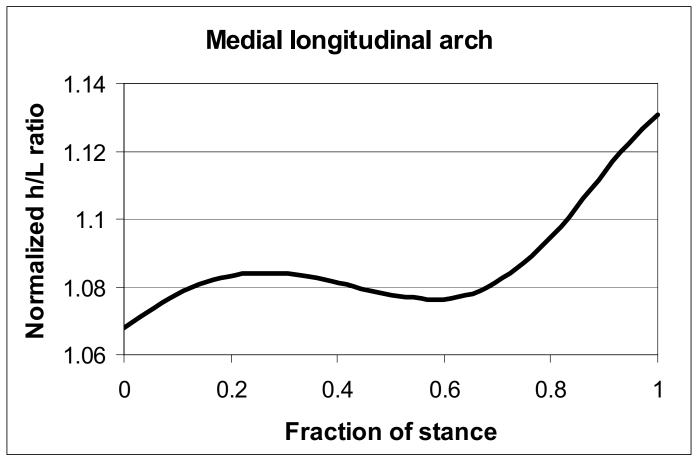

Figure 1: Normalized h/L ratio of the medial longitudinal arch shows the arch is raised higher and shorter than quiet standing. The arch showed an unexpected low peak in height early in stance and then the expected high peak in height in late stance.

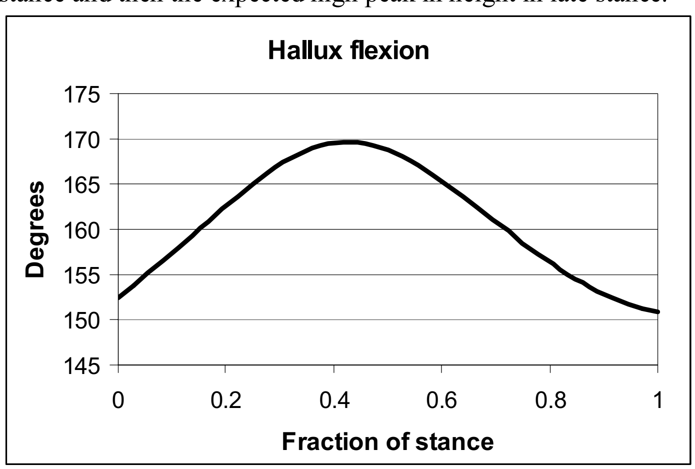

Figure 2: Hallux flexion angle in the sagittal plane where 180° defines the hallux in line with the 1st metatarsal and smaller angles represent dorsiflexion. Note the equal amounts of dorsiflexion early and late in stance, with more neutral positioning in midstance.

THE INFLUENCE OF AGING ON THE MATERIAL PROPERTIES OF TENDON

[1] Sarah Calve, [2] Keith Baar, [1]Kevin Mundy and [1] Ellen M. Arruda
[1]University of Michigan,
[2]University of Dundee; email: scalve@umich.edu

INTRODUCTION

Our lab studies the effect cyclic and static mechanical loads have on soft tissue. Specifically, we are interested in quantifying how material properties of tendon change during development and aging. We have shown that the tibialis anterior (TA) tendons of rats have varying material properties along their length, and when loading was removed by functional denervation, the entire tendon stiffened up and displayed homogeneous material properties [1]. It has previously been shown that there are age related changes in the musculoskeletal system, but very little data exist specifically on tendon. In order to examine the effects of aging on both the average end-to-end response and the heterogeneity of the response of old tendon, we compared local and average σ-ε responses of young and old rat TA tendon.

METHODS

The TA tendon unit (TA muscle, TA tendon, and the 5th metatarsal) was removed from young (8 months) and old (38 months) Fisher x Brown Norway F-1 Hybrid rats and stored in sterile PBS prior to determination of the stress vs. strain response curve. The cross-sectional area (CSA) of the tendon was determined by placing the specimen in DPBS and measuring the diameter at three 60° orientations and calculating the area of the ellipse described by these data. The optical stress-strain device consisted of an optical force transducer of our own design with a force resolution of 0.2 to 200 mN, two uniaxial servomotors controlled using LabVIEW, and a Basler digital video camera connected to a Nikon (SMZ800) dissecting microscope. Spots of tissue marking dye were placed at equal intervals along the length of the tendon to allow optical measurement of tissue displacement. The samples were loaded at a constant strain rate until failure and the synchronized force and image recordings were compiled using LabVIEW. The raw load vs. optical displacement data were converted to nominal stress (load/CSA) vs. nominal strain (change in separation of ink marks/initial separation). The (maximum) tangent stiffness was determined by calculating the secondary slope of the nominal stress vs. nominal strain data.

Hydroxyproline concentration was determined following the method of Woessner [2]. Constructs were dried at 110°C, weighed immediately then placed in 6 N HCl and hydrolyzed for 3 hours 130°C. After neutralizing to pH = 7 with NaOH, Chloramine T was then added, and the tubes were incubated for 20 minutes at room temperature. The chloramine T was inactivated by the addition of perchloric acid before adding an equal volume of Ehrlich's reagent. The tubes were incubated at 60°C for 20 minutes, cooled, and absorbance measured at 560 nm. Results were converted to collagen concentration by assuming hydroxyproline accounts for 13.8% of the dry weight of collagen.

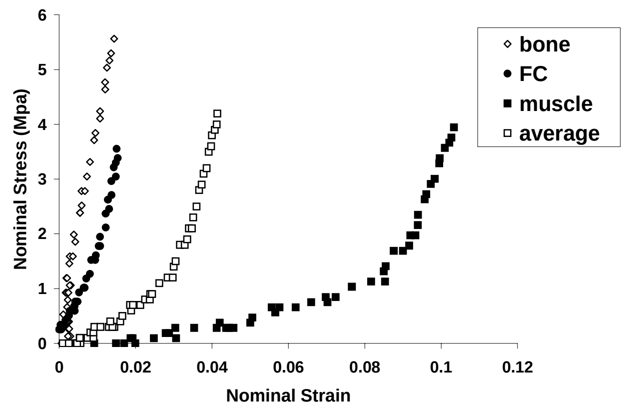

Figure 1: The young TA tendon displays heterogeneous material properties across the different regions of tendon. Bone = region closest to osteotendinous junction, FC= fibrocartilage region, Muscle = region closest to myotendinous junction.

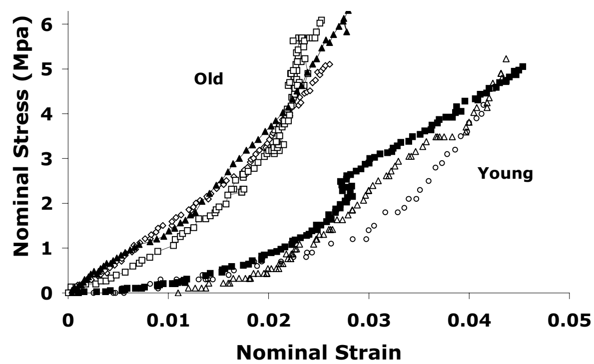

Figure 2: The stress-optical strain response reveals that the TA tendon becomes stiffer and less compliant in old rats.

RESULTS AND DISCUSSION

The old tendons maintained the graded mechanical response previously recorded for young adult TA tendon (Figure 1), but there was a significant reduction in the length of the toe region and an increase in tendon stiffness (Figure 2). The maximum tangent modulus increased from 195 +/- 36 MPa at 8 months to 461 +/- 193 MPa at 38 months. Interestingly, the collagen concentration did not change as the animal aged (data not shown). This pronounced extensibility of the tendon region nearest the muscle is presumed to protect the muscle fibers from injury. The loss in tendon extensibility with aging may partially explain the increased incidence of both muscle and tendon injury with aging [3].

REFERENCES

1. Arruda EM, et al. Submitted to *J. Physiology* 2005.2
2. Woessner JF. *Arch. Biochem Biophys*. **93**, 440-447, 1961.
3. Maffulli N, et al. *Clin J Sport Med*. **9**, 157-60, 1999.

DIFFERENCES IN JOINT KINETICS IN GIRLS DUE TO CHOICE OF BODY SEGMENT PARAMETERS

[1,2]Michelle Sabick, [1,3]Kristof Kipp and [1,3]Ron Pfeiffer
[1]Center for Orthopaedic & Biomechanics Research, [2]Department of Mechanical Engineering,
[3]Department of Kinesiology, Boise State University, Boise, ID USA; email: MSabick@boisestate.edu
web: coen.boisestate.edu/cobr

INTRODUCTION

The effects of gender on lower extremity mechanics during landing have been studied extensively in adults, but little is known about landing mechanics in preadolescent populations. By studying landing strategies in preadolescent children, body morphology differences between the genders are essentially eliminated. However, joint kinetics calculated during landing using inverse dynamics are affected by the method used to estimate body segment parameters (BSPs) [1]. Some BSP data sets contain primarily elderly specimens, and many contain primarily males [1].

For preadolescents and young adults, not many studies have provided equations to estimate BSPs. According to Zatsiorsky et al [2], BSPs for girls from 9 to 10 years old (28 to 30 kg) can be calculated with little error using the equations for boys the same age. BSPs for boys, in turn, are calculated using equations for men as long as the boys have normal tissue composition (body fat between 15% and 20%). Our subject group, girls between the ages of 9 and 12, spans the suggested age dividing line for using male or female data. Therefore, it was not clear whether their BSPs should be calculated using the equations for men or women. The purpose of this study was to compare the joint kinetics from the same landing trials when calculated with male and female BSP data. To our knowledge, this is the first study to examine the effect of body segment parameters on joint kinetics during landing.

METHODS

From a larger study of gender effects on landing mechanics, a subset of five female subjects (10 to 12 years of age) were randomly selected for this study. In the larger study, subjects dropped from a horizontal bar (net drop 30.5cm) landing barefoot on one leg. The test leg was randomized. The landing surface was a force platform sampling at 1250 Hz. Each subject performed 5 to 10 trials and the first five successful trials were analyzed.

Pelvis and lower extremity kinematic data were collected at 250 Hz. The 3-D marker coordinate data were smoothed using a 4^{th} order Butterworth filter with a cutoff frequency of 17 Hz. Kinematics of the pelvis, hip, knee, and ankle were calculated using Euler angles.

Internal joint resultant forces and moments for the instrumented lower extremity were calculated using inverse dynamics. Body segment parameters for all subjects were computed using data from de Leva [1] referencing Zatsiorsky [2], first using data from female subjects and then using data from male subjects [1]. Comparisons of joint kinetic variables between the data processed using male and female BSPs were made using two tailed Student's t-tests with an α level of 0.05.

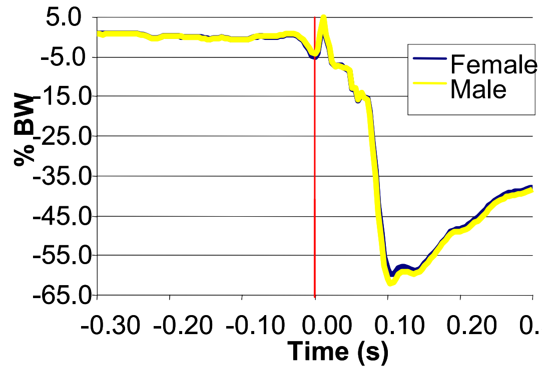

Figure 1: Hip anterior-posterior shear force computed using male and female BSP values.

RESULTS AND DISCUSSION

In most cases the joint force and moment components were not significantly different when computed with different BSP data. Differences between variables calculated with male and female BSPs ranged from –8.8 to 7.3%, and were usually more pronounced for components in which the ground reaction force had little effect (Fig 1). Peak knee distraction force was significantly greater for trials in which female BSPs were used (5.51±0.20 %BW vs. 5.15±0.19 %BW, p=0.018), although peak knee compression was the dominant force in the superior-inferior direction and its at values were not significantly different between groups (235±43 %BW vs 237±44 %BW, p=0.939).

Although not necessarily statistically significant, differences in joint kinetic values of 5-8% might be clinically significant. Many studies comparing landing mechanics data between genders do not specify how BSPs were calculated. Differences in joint kinetics between groups could be either positive or negative, so group differences may be either minimized or inflated by the use of BSPs from a data set that does not adjust for gender.

CONCLUSIONS

For most variables of interest, use of male or female BSPs did not significantly affect our results. However, differences of as much as 8.8% in certain joint force components were due solely to differences in BSPs, even with the same ground reaction forces and joint kinematics. The use of inappropriate BSPs may influence the results of a gender comparison either positively or negatively.

REFERENCES

1. de Leva P. *J Biomech* **29**, 1223-1230, 1996
2. Zatsiorsky VM, et al. *Contemporary Problems of Biomechanics*, CRC Press, Boca Raton, FL.

CONTROLLED ENERGY STORAGE AND RETURN PROSTHESIS REDUCES METABOLIC COST OF WALKING

Steven H. Collins and Arthur D. Kuo
Dept. Mechanical Engineering, University of Michigan, Ann Arbor, MI USA
email: shc@umich.edu, web: www.umich.edu/~shc

INTRODUCTION

Humans actively push off with the trailing leg just before and during the double support phase of walking. Push-off compensates for the energy lost as the leading leg performs negative work during the transition between steps [1]. Simple models predict that the energy used in walking is strongly linked to the mechanics of this step-to-step transition; pushing off just before double support can theoretically reduce the step-to-step transition work by a factor of four [2].

Lower-limb amputees have a reduced capacity for ankle push-off during walking [3] contributing to a 20-30% greater energy demand than intact individuals [4]. A variety of prosthetic feet have been designed with elastic properties to compensate for lost ankle function, but none have significantly reduced the metabolic cost of walking compared to the conventional Solid Ankle Cushion Heel (SACH) foot [4]. We hypothesized that mechanical energy should optimally be stored during load acceptance and released during push-off, as opposed to being spontaneously returned as in existing elastic prostheses. We tested this hypothesis by constructing a prototype prosthetic foot with *Controlled Energy Storage and Return* (CESR), and by measuring the resulting metabolic cost of walking.

METHODS

We tested intact individuals using a foot prosthesis simulator, a boot that securely constrains the ankle and has a foot prosthesis attachment at its base. Each subject wore the prosthesis unilaterally (ipsilateral foot) with a rocker-bottomed lift on the contralateral foot to compensate for the 10 cm height of the prosthesis attachment. We tested 5 male subjects (ages 20-25 yrs, mass 73-90 kg), walking on a treadmill at 1.3 m/s. Metabolic rate (VO2, Physio-Dyne Max-II) was averaged over the last 3 minutes of each 7 minute walking trial to allow subjects to approach steady state. We also recorded ground reaction forces in 6 identical over-ground trials, and computed work performed on the body center of mass by each leg [1]. We defined push-off as positive work by the trailing leg during double support, and collision as simultaneous negative work by the leading leg. Experimental conditions included normal walking, CESR prosthesis, and SACH prosthesis.

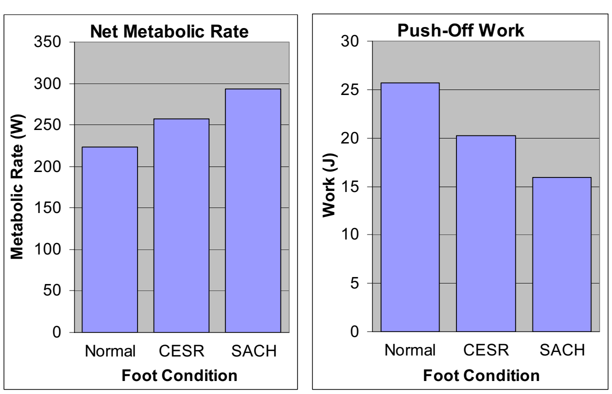

Figure 1: Left: Net metabolic power consumed while walking with different foot prostheses: Controlled Energy Storage and Return (CESR) prototype and conventional Solid Ankle Cushion Heel (SACH) foot. **Right:** Push-off work performed on body center of mass. The CESR significantly reduced metabolic rate and increased push-off work compared to The SACH foot.

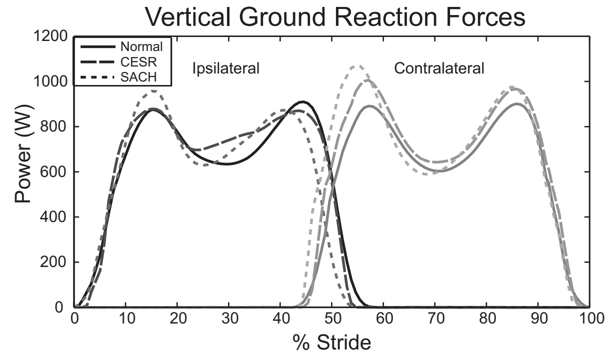

Figure 2: Average vertical ground reaction forces over one stride. Prototype CESR prosthesis yielded more normal forces (greater push-off and lower collision) than the SACH foot, for the ipsi- to contralateral transition (about 50-60% stride).

RESULTS AND DISCUSSION

Walking with the SACH foot resulted in a 69 W increase in metabolic rate over normal walking, or about 31% ($p < 0.005$, Fig. 1). This increase is consistent with results for amputees, though simulator mass and height may also have contributed to metabolic cost. With the CESR foot, subjects used 36 W less metabolic power than with the SACH foot ($p < 0.005$).

The CESR foot appears to partially compensate for the loss of push-off (Fig. 1). Work produced by the trailing leg with the CESR during push-off was 27% greater than that with the SACH foot ($p < 0.02$). Both prostheses produced lower push-off and greater collision or load acceptance forces than in normal walking (Fig. 2). The mechanical power capacity of the CESR foot was about 14 W, not all of which was successfully returned at push-off. Newer prototypes have been constructed that may improve on energy return.

CONCLUSIONS

We have developed a prototype prosthetic foot that stores and returns mechanical energy during successive step-to-step transitions, significantly reducing metabolic energy consumption compared to a conventional prosthesis. Simultaneous positive and negative work during the step-to-step transition seems to be a significant determinant of the metabolic cost of walking, a determinant with clinical applications.

REFERENCES

1. Donelan, JM, et al. *J Exp. Biol.* **205**: 3717-3727, 2002.
2. Kuo, AD. *J. Biomech. Eng.* **124**: 113-120, 2002.
3. Whittle, MW. *Gait Analysis: An Introduction*, 1996.
4. Waters, RL, et al. *Gait & Posture*. **9**(3): 207-231, 1999.
This work funded by an NSF Biotechnology STTR grant.

DENERVATION IMPAIRS ACHILLES TENDON HEALING IN RAT MODEL

[1] Chi Keung Yeung BSc, [1]Xia Guo MD and [1]Gabriel Yin Fat Ng PhD
[1]Department of Rehabilitation Sciences, The Hong Kong Polytechnic University

INTRODUCTION

With the advance of immunohistochemical techniques, the role of nervous system in successful repair of injured tissue has been recognized. Evidences have shown the importance of innervation in promoting wound, bone and ligament healing. [1,2] How peripheral nervous system contributes to repair of tendon remains unknown. In this study, we investigated the effect of denervation on healing of rats using biomechanical and histological methods.

METHODS

Hemi-transection of the right Achilles tendon was performed on 28 adult male Sparague-Dawley rats. An additional sciatic neurectomy (SN) (n=14) or patella tenotomy (PT) (n=14) was also performed on the limb with AT injury. At 4 weeks after surgery, all rats were sacrificed and their bilateral Achilles tendons were subject to biomechanical test/histological analysis.

The medial portion of Achilles tendon, with the intramuscular tendinous fibers and the calcaneal bone were dissected out, and was attached to the MTS Synergie 200 machine (MTS Systems Corporation, Minnesota). The tendon was subjected to ultimate tensile testing at an elongation rate of 500mm per minute until failure. [2] The load-displacement curve was plotted with the peak of the curve representing the ultimate tensile strength (UTS) and the gradient in the linear portion representing the stiffness. (Figure one) Finally, all the above values of right leg were normalized against the left leg of the same animal for further analysis.

Statistical tests were used for the result of biomechanical test. Student t-test was used to compare the difference between the means of biomechanical test parameters (UTS, Stiffness and load relaxation) of injured legs between PT and SN groups, as well as the normalized UTS, stiffness and load relaxation. α was set at 0.05 for all tests.

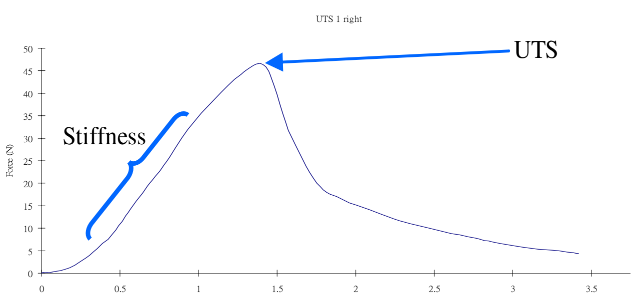

Figure one: **Load-displacement curve of tendon**

RESULTS AND DISCUSSION

The mean ultimate tensile strength (UTS) of the injured tendon in SN group was significantly lower than of the PT group. (*:$p<0.05$, Figure two) However, no significant difference in stiffness and load relaxation was found between these two groups. After normalizing the right leg values (UTS, stiffness and load relaxation) with that of the left leg, no significant difference in all normalized values was found among three groups. (Figure three) Denervation result in scar tissue with irregular collagen alignment and higher cell to matrix ratio. Whereas immobilization with patella tenotomy revealed a relatively mature scar tissue with more mature fibroblasts and better alignment of collagen matrix. (Figure four)

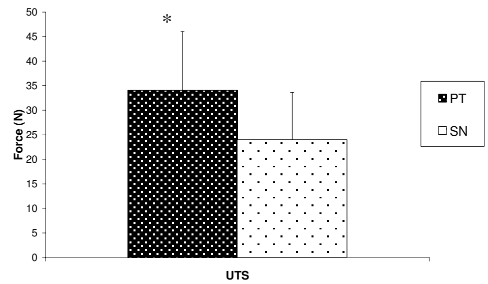

Figure two: Mechanical test result: Right leg UTS

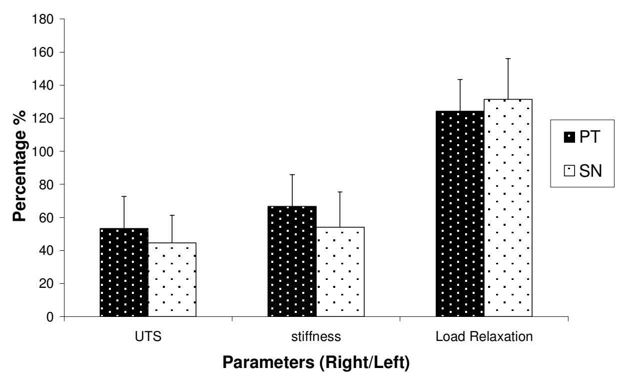

Figure three: Mechanical test result: Right/leg %UTS, stiffness and load relaxation

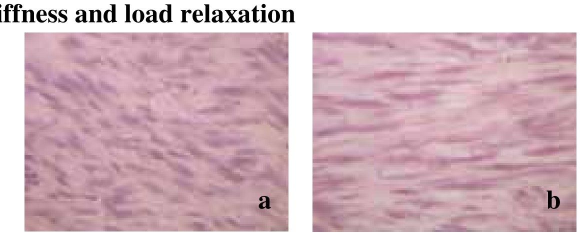

Figure four: Histology of scar tissue in SN (a) and PT (b) group

CONCLUSIONS

Denervation affects tendon healing, during which the scar tissue is biomechanically and morphologically inferior to that of innervated tendon. An intact nervous system is vital for normal healing of tendon.

REFERENCES

1. Ivie TJ, et al. *J Ortho Res* 25, 990-995, 2002
2. Madsen JE, et al. Clin Ortho, 351, 230-40, 1998
3. Ng COY, et al. Ultrasound Med Biol 29,1501-6, 2003

QUANTITATIVE TRAIT LOCI INFLUENCING BONE QUALITY IN YOUNG AND OLD MICE

[1,2] Dean H. Lang, [1]Neil A. Sharkey [1]George P. Vogler, [1]David J. Vandenbergh, [1]David A. Blizard, [1]Joseph T. Stout, and [1]Gerald E. McClearn
[1]The Pennsylvania State University, University Park, PA, USA
[2] email: tcl133@psu.edu

INTRODUCTION

C57BL/6J and DBA/2 inbred mouse strains have been shown to differ in their skeletal response to aging. This study was designed to increase our understanding of the genetic architecture responsible for the maintenance of bone quality across the lifespan. Our primary aim was to identify quantitative trait loci (QTL) linked to bone quality in young (200 day) and old (800 day) C57BL/6J X DBA/2 (BXD) recombinant inbred (RI) mice. Identifying QTLs in both cohorts adds confirmation of the locus while the identification of QTLs in either the 200 or 800 day old cohort suggests that these loci are operating on bone quality at specific ages.

METHODS

Skeletal measures of strength and architecture were assessed in C57BL/6J X DBA/2 recombinant inbred (RI) mouse strains at both 200 and 800 days of age. The young adult (200 day) population included 23 RI strains with 10 male and 10 female mice per strain. A second population was bred to achieve similar numbers of mice at old age (800 days of age). The original study was designed to target 10 male and 10 female mice per 23 strains at 800 days of age taking into account known attrition rates. Despite these precautions, adequate numbers of mice per strain were unable to be maintained to 800 days of age. Those strains that did not have at least 3 mice for each male and female strain were not included in the QTL analyses. This resulted in 15 strains in the female analysis and 18 strains in the male analysis. The average number of 800 day old mice included in the QTL analyses was 6 per strain. Strain means were used in quantitative trait loci analysis to search for chromosomal regions influencing skeletal phenotypes at 200 and 800 days of age.

A three-point bending test was used to assess the mechanical integrity of the mid-shaft of femora and tibiae and a shear test was performed on the femoral neck to assess the mechanical integrity of this functionally significant skeletal site. Gross morphological measurements were made on both bones. Percent water, organic, ash, and mineralization were also measured. Separate sex-specific QTL analyses were performed using QTL Cartographer. Genotypes for the RI lines consisted of 672 microsatellite markers in each BXD strain. LOD scores of 3.3 or greater were considered significant while scores between 1.9 and 3.3 were considered suggestive.

RESULTS AND DISCUSSION

The QTL results from the sex-specific interval mapping analyses are presented in Table 1 (cM corresponds to peak centimorgan position of the maximum LOD score or logarithm of the odds that linkage between a marker and a trait did not occur by chance). Significant LOD scores are highlighted with grey shading. Numerous QTLs for skeletal phenotypes mapped throughout the mouse genome. Table 1 summarizes the QTL results for those traits that had a LOD score of 3.3 or greater in either the 200 or 800 day old analyses.

Table 1: Interval mapping results from QTL analyses of 200 and 800 day BXD RI mice. R indicates QTLs detected using data adjusted for animal size.

Chr.	Trait	Sex	200 Day		800 Day	
			cM	LOD	cM	LOD
1	Femur Length	F	89	2.9	90	1.9
1	Femur Length	M	90	3.3		
1	Femur Length - R	M	90	4.7		
1	Femur Stiffness - R	F	85	4.3		
1	Tibia Length - R	M	78	1.6	62	3.3
1	Tibia Length - R	M	89	4.0	90	2.0
4	Femur Coronal Width	F			7	3.3
4	Femur Coronal Width - R	F			7	3.8
5	Femur Epiphyseal Width	F	44	3.5	43	1.6
5	Tibia Length - R	M	20	2.1	3	3.5
9	Femur Stiffness	F	21	3.5		
9	Femur Stiffness - R	F	21	4.5		
9	Tibia Length - R	F	21	3.3		
10	Femur Neck Ult. Work	F	4	2.7	2	4.0
13	Femur Yield Load	M	70	3.3		
13	Femur Yield Work	M	68	3.8		
13	Femur Yield Work - R	M	68	3.7		
15	Tibia Length	M	54	3.4		
15	Tibia Length	F	48	3.5	48	2.5
15	Tibia Length - R	F	48	3.8	48	2.5
15	Tibia Yield Work	M	41	3.3		
15	Tibia Yield Work - R	M	41	3.3		
16	Femur Stiffness	F			16	3.8
16	Femur Stiffness - R	F			16	3.5
16	Femur Ult. Load - R	F	12	1.5	18	3.3
16	Femur Ult. Work	F			21	4.1
16	Femur Ult. Work - R	F			21	3.6
17	Tibia Length	F	23	2.8	24	3.8
17	Tibia Length - R	F	23	2.3	24	4.0
18	Femur Stiffness - R	F	8	4.0		
18	Tibia Stiffness	M			49	3.3
20	Femur Ult. Displacement	F			30	3.5

Of primary interest are the QTLs that were identified in either the 200 or 800 day analyses suggesting these loci are operating at specific time points throughout the lifespan on chromosomes 1, 4, 9, 13, 15, 16, 18, and 20. These data illustrate the complex nature of genetic influence on bone quality and suggest that some genes exert their effects in an age dependent manner.

ACKNOWLEDGEMENTS

This work is funded by the National Institute on Aging (grants P01 AG14731, R01 AG21559, and T32 AG00276).

CAT HINDLIMB MUSCLE RESPONSE TO SLOW MOVEMENT SHOWS POOR RELATIONSHIP TO LENGTH-TENSION PROPERTIES

[1] Thomas G Sandercock, [1]Aaron Daub, and [2]Eric J. Perreault
[1]Dept. Physiology and [2]Biomedical Engineering; Northwestern University; email: t-sandercock@northwestern.edu

INTRODUCTION

The ultimate goal of our research is to determine the contributions of individual muscles and muscle combinations to whole limb endpoint stiffness in 3 dimensional space. Initially we are examining the intrinsic muscle properties without reflex contributions. For this particular task, i.e. characterizing endpoint stiffness, a central consideration is how a muscle's force changes when a small change in joint angle is imposed on it. This particular study examines tetanic activation with relatively slow movement (short range stiffness properties are ignored). Several well known contractile properties play a role in the total response. They include: length-tension-frequency, force-velocity, and persistent tension excess or deficit properties. Muscle models often use the tetanic length-tension and force-velocity curves but the results here show this leads to substantial errors, and false estimates of endpoint stability.

The purpose of this study is to test the hypothesis that within the physiological range of a muscle, slow stretch of a tetanically active muscle will always result in more force, and slow shortening of a muscle will always result in less force, irregardless of the position on the length tension curve.

METHODS

Data were collected from 3 cats (2-3kg) under deep anesthesia (pentobarbital). Three muscle groups, accessible with minimal disruption of the surrounding connective tissue, were examined: the medial gastrocnemius (MG), the lateral gastrocnemius and soleus (LG/S), and the Tibialis Anterior and Extensor Digitorum Longus muscles (TA/EDL). Muscles were stimulated in pairs when nerve separation would have caused an undesired level of connective tissue disruption. During all measurements, muscles were maximally stimulated (100Hz) using peripheral nerve cuff electrodes. Reflex activation was eliminated by cutting the ipsilateral dorsal roots.

The cat foot was rigidly attached to a 6 degree-of-freedom load cell (JR3) coupled to a 6 degree-of-freedom robotic manipulator (Staubli RX60). Each trial (Fig. 1) consisted of an initial isometric stimulation period (0.25 sec), followed by a robot-controlled joint rotation (5 degrees in 0.37 or 0.75 s) around the ankle. Isometric muscle force was measured immediately prior to the imposed movement and fit with a polynomial to determine the static length-tension properties.

RESULTS AND DISCUSSION

Figure 1 shows typical results from the combined LG/S muscles. The cat's knee was extended allowing the LG to be studied on the descending limb of the length-tension curve. The dark line shows the static moment-angle properties. The superimposed traces show moments measured during

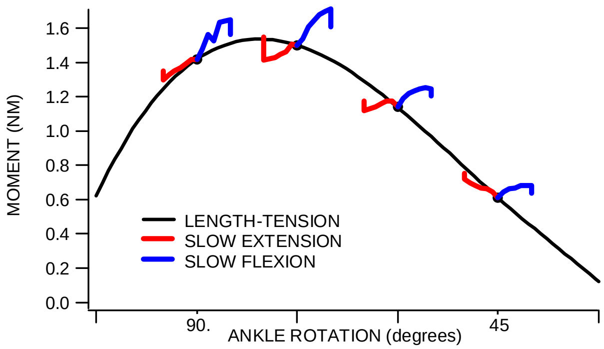

Figure 1: Torque-Rotation (flexion-extension) curve for combined LG and SOL muscles.

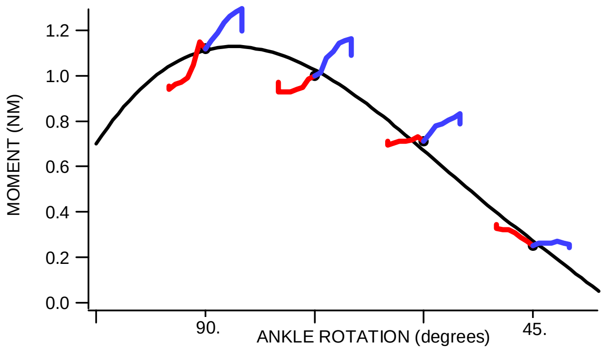

Figure 2: Torque-Rotation (flexion-extension) curve for MG.

extension (blue) and flexion (red) movements (5 degree rotations over .75s) followed by a .25 isometric hold. The movement is slow so force-velocity properties play a trivial role. Note that the hypothesis is supported at all but the longest muscle length.

Figure 2 shows typical results from the MG. Similar results were obtained for the TA/EDL which was primarily on the ascending limb of the length-tension curve for the same leg position. The results shown here were supported by data from the other 2 cats.

CONCLUSIONS

The hypothesis was disproved at the longest muscle lengths. However, over a wide range of muscle lengths, muscle force increased during slow stretch and decreased during slow shortening, irregardless of the position on the static length-tension curve. This suggests muscle is intrinsically stable, even in the absence of reflex mechanisms.

ACKNOWLEDGEMENTS

Supported by NIH R01 AR041531.

DOES WARMING UP WITH A WEIGHTED BAT HELP OR HURT BAT SPEED IN BASEBALL?

Young-Kwan Kim and Richard N. Hinrichs
Department of Kinesiology, Arizona State University, Tempe, AZ, USA
email: Young-Kwan.Kim@asu.edu

INTRODUCTION

Although baseball players may believe that by warming up with a heavy bat they will increase their swing speed, past research indicates that following warm-up with heavy bats, swing patterns are significantly altered resulting in lower velocities than warm-ups with a standard bat [1]. Further, it was demonstrated that prior to impact with a ball on the first swing following a weighted warm-up there is a 3.3% reduction in linear bat velocity at the trial right after weighted bat swing [2]. The purpose of the current study was to identify if warm-ups with different weighted bats prior to bat swing alter the bat speed and determine whether bat speed agrees with kinesthetic feeling from subjects.

METHODS

Thirteen subjects ranged from 22 to 28 years (eight males and five females) participated in this study. They came in three different days for three different bat warm-ups. Three different weighted bats, such as a lighter bat (wiffle bat, 113g), a standard bat (909g), and a heavier bat (standard bat + 568g donut weight), were used for each warm-up condition. Subjects were asked to perform total 15 trials of swing as fast as they could per day. The first five trials were PRE-warm-up swings with a standard bat. Following two minutes break, the next five trials were warm-up swings with a randomly selected bat. The last five trials following two minutes break were POST-warm-up swings with a standard bat again. Subjects were asked to rate the kinesthetic feeling of each swing on a scale from –5 (very slow) to +5 (very fast) after each trial during POST-warm-up swings.

A seven-camera VICON system (sampling rate: 120 Hz) was used to collect kinematic data of the bat. Seven reflective markers on a bat and upper arms were attached to measure the trajectories and to determine pattern changes. Peak tangential velocity and time-to-peak velocity at each landmark were dependent measures for the analysis.

RESULTS AND DISCUSSION

Repeated measures ANOVA on bat speed indicated that there were significant differences between PRE-warm-up and warm-up conditions and between warm-up and POST-warm-up ones, while there was no significant difference between PRE- and POST-warm-up conditions. Bat speed of the lighter bat at warm-up (22.0 m/s) was significantly faster than the heavier bat (14.4 m/s) and the standard bat (16.0 m/s) (see Figure 1). One-way ANOVA on kinesthetic feeling at POST-warm-up swing indicated significant main effect of different weighted bat warm-up (see Figure 2). Subjects felt significantly faster bat speed following a heavier bat warm-up (2.55 ± 1.29) than any other bat warm-ups (–.38 ± 1.75 and .35 ± .82) regardless of non-difference on bat speed. No pattern change was found following warm-ups. However, there were changes of the differences on time-to-peak velocities between bat and wrists and between wrists and elbows in leading and trailing arm, respectively.

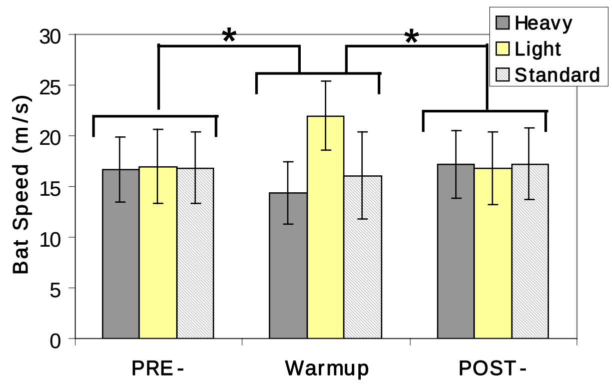

Figure 1: Changes in bat speed among PRE-Warm-up, Warm-up, and POST-Warm-up with different weighted bats. Significant differences are shown with an asterisk.

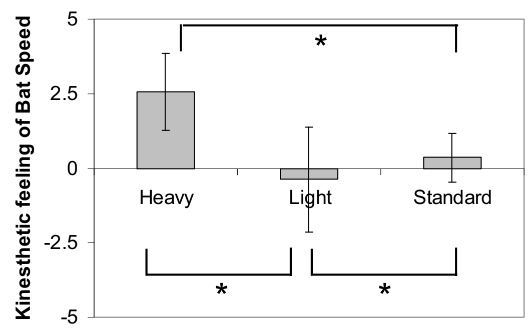

Figure 2: Kinesthetic feeling of bat speed at POST-Warm-up swings following different weighted bat warm-ups. Scale ranged from –5 (very slow) to +5 (very fast) with indication of 0 (no difference). Significant differences are shown at each different POST-Warm-up swing.

CONCLUSIONS

Warm-up with different weighted bats provides no significant differences on bat speed following warm-ups, while it provides significant different kinesthetic feelings of bat speed. The kinesthetic feeling during POST-warm-up swing may result from the shortened differences on time-to-peak velocity between wrists and elbows. Finally, there is no benefit on bat speed with a heavier bat warm-up.

REFERENCES

1. Southard, D & Groomer, L *Research Quarterly for Exercise and Sport,* **74,** 270-276, 2003.
2. Otsuji, T. *et al.*, *Perceptual and Motor Skills*, **94,** 119-26, 2002.

IN VIVO FASCICLE VELOCITY OF CAT GASTROCNEMIUS AND SOLEUS MUSCLES DURING THE PAW-SHAKE

Boris I. Prilutsky, Huub Maas and Robert J. Gregor
Center for Human Movement Studies, School of Applied Physiology, Georgia Institute of Technology, Atlanta, GA, USA
Email: boris.prilutsky@ap.gatech.edu

INTRODUCTION

During the paw-shake (PS) in the cat a differential activation of ankle extensor synergists, the two-joint gastrocnemius (GA) and the one-joint soleus (SO), occurs: the GA demonstrates very high activation, whereas SO is either inactive or its activation is substantially reduced [1,5]. The two muscles are activated during the lengthening phase of the muscle-tendon complex (MTC) [1,4], in which substantial activation of SO and GA Ia- and Ib-afferents has been reported [4]. Thus, both velocity-dependent (Ia) and force-dependent (Ib) feedback might be used to regulate the differential activation of the two muscles.

The velocity-dependent feedback is related among other factors to muscle fascicle velocity rather than to MTC velocity. Therefore, the role of MTC and fascicle velocity in the regulation of muscle activity in the PS remains unclear. High shortening velocity in muscle fascicles during PS can also be a limiting factor in muscle force production. The aim of this study was to determine fascicle and MTC velocities of the cat medial gastrocnemius (MG) and SO during the PS.

METHODS

Four cats were surgically instrumented with EMG electrodes in SO and MG [2]. Selected cats were also instrumented with sonomicrometry crystals to measure fascicle length [3]. After recovery, the PS was elicited by attaching a sticking tape to the paw and allowing the animal to walk on a walkway. Reflective markers on the animals were video-filmed using high-speed (120 Hz) motion capture system (Vicon, UK) with simultaneous recordings of EMG or sonomicrometry signals. The recorded kinematics and a geometric model of the hindlimb were used to calculate the origin-to-insertion (MTC) lengths of MG and SO. Joint velocities, moments and powers were also calculated for the major hindlimb joints.

RESULTS AND DISCUSSION

During the PS, MTC shortening velocity peaks of MG and SO were up to 0.2 m/s (Fig.1) or 80 and 120% of their in-situ MTC V_{max} [6], respectively. Fascicle shortening velocity peaks reached much smaller values of 0.1 and 0.05 m/s for MG and SO, respectively, (Fig. 1) which corresponded to 40 and 27% of V_{max} expressed in fiber lengths of each muscle [6]. The above results may be explained, in part, by in-series compliance of the tendons and aponeuroses of MG and SO.

MG fascicle and MTC velocities changed in phase during steady state PS cycles (Fig.1), whereas SO fascicle velocity changes were delayed with respect to the MTC velocity (Fig. 1). These results suggest that velocity-dependent feedback from the two muscles during the PS might be different and thus could contribute to their differential activation.

Stretch velocity peaks of MG fascicles typically coincided with the switch of joint moment directions: from ankle flexion/knee extension/hip flexion to ankle extension/knee flexion/hip extension (Fig. 1). Thus, signals from MG velocity-sensitive afferents might be involved in phase regulation between the flexors and extensors during the PS.

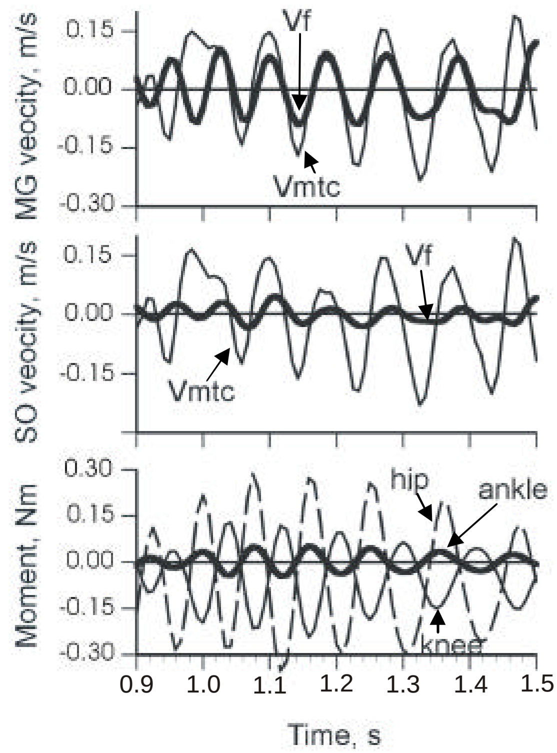

Figure 1: Velocity of muscle fascicle and MTC of MG (top panel) and SO (middle panel) and moments at the hindlimb joints (bottom panel) during a paw-shake. Positive velocities correspond to muscle shortening, positive joint moments correspond to extension.

REFERENCES

1. Fowler EG, et al. *Exp Neurol*, **99**, 219-224, 1988.
2. Gregor RJ, et al. *Proceedings of the 34th IUPS Congress*, San Diego (CA), 2005.
3. Hoffer JA, et al. *Prog Brain Res*, **80**, 75-85, 1989
4. Prochazka et al. *J Neurophysiol*, 61:550-562, 1989.
5. Smith J, et al. *J Neurophysiol*, **40**, 503-513, 1977.
6. Spector SA et al. *J Neurophysiol*, **44**, 951-960, 1980.

ACKNOWLEDGEMENTS

Supported by NIH HD032571 and the CHMS at Georgia Tech.

VALIDATION OF THE VICON 460 MOTION CAPTURE SYSTEM™ FOR WHOLE-BODY VIBRATION ACCELERATION DETERMINATION

[1] Robert J. Jack, [1,2] Michele Oliver, [2] Gordon L. Hayward
[1] Department of Biophysics, University of Guelph, Guelph ON; email: rjack@uoguelph.ca
[2] School of Engineering, University of Guelph, Guelph ON

INTRODUCTION

With mobile equipment operators experiencing root mean square (RMS) average accelerations (A_{rms}) ranging from 0.1g to 0.3g [3], the ultimate goal of this research program is to recreate and monitor in a laboratory environment the whole-body vibration (WBV) exposure levels experienced by forestry equipment operators in a field setting. Since the research questions being asked are concerned with investigating the transmission of WBV for frequencies up to 20Hz, coupled with the fact that the body can have transfer functions approaching 2 [2], the ability to measure an A_{rms} of 0.6g up to a frequency of 20Hz is required.

To better understand the body's response to WBV more detailed studies need to be conducted, where vibration levels are monitored at many levels of the spine in concert with muscle activation and posture measurements. This requires many markers, accelerometers, and electrodes to be placed on the subject. If multiple measurement systems are used, subject preparation is time intensive, large amounts of memory for data storage and processing are required, and results can be affected by skin artifacts and the encumbrance of the subject. Using a high sample rate/high resolution camera system to determine accelerations can reduce some of these problems. Thus, the purpose of this study was to determine if a VICON camera system could measure WBV acceleration levels within the range established above, eliminating the need for accelerometers.

METHODS

A Bruel and Kjaer™ 4810 electromechanical shaker was used to produce RMS accelerations of 1.09±0.11g, 0.74±0.06g, 0.33±0.06g, and 0.13±0.01g at each of 30Hz, 25Hz, 20Hz, 15Hz, 10Hz, 5Hz, and 3Hz frequency levels. A VICON™ 460 motion capture system (with six M^2mcam cameras) recorded a reflective marker vibrated at each amplitude and frequency combination while a Crossbow™ CXL04LP3 accelerometer recorded the acceleration. Each amplitude and frequency combination was recorded for a 5 second duration at a sampling rate of 250Hz.

The raw digitized VICON and accelerometer data were fourth order zero lag Butterworth filtered (cutoff frequency of 45Hz [1]). The VICON data were then double differentiated using a three point method to provide acceleration values. A 1/3-octave band-pass filter was then applied to the VICON and accelerometer data and the overall A_{rms} acceleration levels were calculated for each combination of the input acceleration and frequency levels using the 3.15Hz to 31.5Hz 1/3 octave bands. The percent difference between the VICON and accelerometer overall A_{rms} acceleration values were compared for all acceleration and frequency combinations.

RESULTS AND DISCUSSION

When comparing the overall A_{rms} acceleration values it was found that the percent difference between the VICON 460 motion capture system and the accelerometer was 4.43±8.23% for frequency and acceleration combinations ranging from 5Hz to 25Hz, and 0.33g to 1.09g (Table 1). Larger errors were observed at the 3Hz and 30Hz frequencies, as well as the 0.74g accelerations (Table 1). While errors were greater than 10% for some acceleration frequency combinations, for the most part, these errors resulted from the shaker having small displacements (<1mm) which are probably within the error of the VICON system. Field measurements indicate that displacements at all frequencies of interest are in excess of 1 mm suggesting that the VICON system can be used to predict acceleration in laboratory studies which simulate field vibration profiles.

Results are promising and further validation studies will be conducted using acceleration profiles from actual field data.

REFERENCES

1. International Organization for Standardization. IS0 2631-1, 1997.
2. Jack RJ, et al.. *Int J Ind Ergon,* (In Revision).
3. Neitzel R, et al.. *Department of Environmental Health*, Seattle, Washington, Unpublished Manuscript, 2001.

Table 1: Percent difference between overall RMS accelerations measured with a VICON™ 460 Motion Capture System and a Crossbow™ CXL04LP3 accelerometer

Frequency (Hz)	Overall RMS Acceleration (g)		
	VICON System	Accelerometer	Percent Error (%)
5	0.38	0.32	19.58
	0.77	0.75	3.95
	0.97	0.94	2.83
10	0.46	0.39	16.38
	0.82	0.78	4.79
	1.22	1.19	2.67
15	0.40	0.36	9.84
	0.85	0.82	3.69
	1.18	1.15	2.55
20	0.33	0.33	-1.99
	0.68	0.74	-7.58
	1.23	1.14	7.72
25	0.21	0.24	-10.05
	0.63	0.64	-1.85
	1.15	1.01	13.98

THE CONTINUUM OF MIXTURES OF FEEDBACK AND FEEDFORWARD CONTROL STRATEGIES USED IN DYNAMICAL DEXTEROUS MANIPULATION CAN BE EXPLORED AT THE BOUNDARY OF INSTABILITY

[1]Madhusudhan Venkadesan*, [1]Stephanie Roach, [2]John M. Guckenheimer and [1]Francisco J. Valero-Cuevas
[1]Department of Mechanical & Aerospace Engineering, [2]Department of Mathematics, Cornell University, Ithaca, NY, U.S.A.
*email: mv72@cornell.edu, web: www.mae.cornell.edu/nmbl

INTRODUCTION

Characterizing the roles of feedback and feedforward control, during any motor behavior is essential, albeit challenging, to further our understanding of the human sensorimotor system. The repertoire of control methodologies used by the sensorimotor system to accomplish any task can be classified as (i) passive mechanics (e.g., soft contact of finger pulp, etc) (ii) feedforward control (e.g., high stiffness, internal model, etc.), or (iii) feedback control (e.g., visual, tactile, etc.). The sensorimotor system may use any control strategy chosen from a continuum of mixtures of the above methodologies. Additionally, activities of daily living often necessitate active and dynamic regulation of fingertip position and forces to stabilize objects (e.g., rolling a pen)[1]. Our past studies [2] have suggested that nonlinear dynamical analysis of a neuromuscular system at the boundary of instability is a powerful paradigm for understanding complex dynamical sensorimotor behavior. In this study, we extend our past work to explore the continuum of control strategies used by the sensorimotor system during dynamical dexterous manipulation by exploiting the dependence of its behavior at the boundary of instability on the specific composition of the control strategy.

METHODS

As in our previous work [2], 13 consenting unimpaired subjects (25±2 yrs, 8 males) used their thumbpad to compress and hold at maximum possible compression, a slender spring (D=8.7mm,d=0.787mm,N=24,L_0=76mm) prone to buckling while we recorded 3D position/orientation of the spring's endcap and vertical compressive spring force (Fig 1). Audio feedback was provided as a tone of diminishing volume for increasing vertical load. The goal was to maximize vertical compressive load, i.e., minimize the volume of the audio feedback. The protocol consisted of 2 days: Day1 – "testing" before and after 110 trials of practice; Day2 – "testing" before and after a digital nerve block of the thumb (1% Lidocaine at the base of proximal phalanx, blocking the digital nerve branches of the median and radial nerves). A "test" is defined as at least 3 satisfactory compressions (a steady hold within 90% of the maximal load ever reached by the subject). The response variable used for all analyses presented here is $\boldsymbol{\mu_S}$ (Fig 1). Mixed-model ANOVA using contrasts for post-hoc tests were used to test for differences in μ_S with changes in tactile feedback and learning. Maximal static key and opposition pinch strength were also recorded in all subjects.

RESULTS AND DISCUSSION

The value of μ_S after practice on Day 1 was 305gm ± 4.8%. The mixed-model ANOVA results show a significant drop due to loss of tactile feedback (23gm, $p<0.0001$) and a significant, but smaller rise due to learning (11gm, $p=0.0086$) in μ_S that carried over to the next day. The deficit in μ_S after the nerve

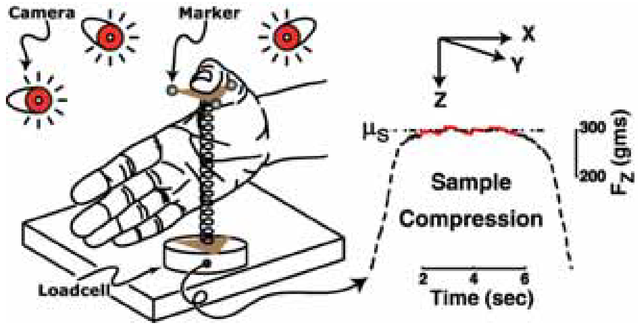

Figure 1: Schematic of the experiment. The unused digits were restrained against a vertical post and the arm using a vacuum pillow (not shown). μ_S is the mean sustained vertical load (F_Z).

block quantifies and characterizes the role of tactile feedback. The performance after the nerve block by itself, characterizes the combined contribution of other sensory feedback (e.g. visual), feedforward control and passive mechanics.

With tactile feedback, μ_S was strength independent (R^2=0.01,p=0.81;[2]), but without tactile feedback, μ_S was not strength independent (R^2=0.64,p=0.02). Together with the previous result, this strongly indicates that without tactile feedback, a high stiffness strategy (feedforward) dominates, with little contribution from vision or passive mechanics. Interestingly, we observe that stiffening is not the best strategy when tactile (short latency) feedback is available.

CONCLUSIONS

The sensorimotor system has a different behavior at the boundary of instability for every distinct condition of sensory feedback or quality of feedforward control used (i.e., learning), as seen above. Hence, we can quantify and characterize the contributions of the feedback, feedforward and passive components at the boundary of instability. The set of control strategies available to the sensorimotor system is a continuum of mixtures of feedback and feedforward strategies. Each member of this continuum of control strategies causes a different type of instability. This feature of our paradigm that maps different controller compositions to different behavior at the boundary of instability facilitates the exploration of the continuum of control strategies used during dynamical dexterous manipulation. This can be extended to sensorimotor behavior in general using an appropriate dynamical task.

REFERENCES

1. Valero-Cuevas FJ, et al. *J Biomech* **36**, 265-270, 2003.
2. Venkadesan M, et al. *Adv in Comp Motor Control II. Symposium at the 33th Annual Meeting of the Soc for Neurosci*, New Orleans, LA, 2003.

ACKNOWLEDGEMENTS

This material is based upon work supported by the National Science Foundation under Grant No. 0237258 (CAREER award) to F.J.Valero-Cuevas

CHARACTERISTICS OF MUSCLE ACTIVITY IN DISTAL AND PROXIMAL UPPER EXTREMITIES IN DIFFERENT PHASES FOR TAIWAN OLYMPIC FEMALE ARCHERY PLAYERS

Chien-Nan Liao[1] , Wen-tzu Tang[1,2] , and Tzyy-Yuang Shiang[3]
[1]Institute of Coaching Science , National College of Physical Education and Sports
[3]Institute of Sports Equipment Technology Taipei Physical Education College
[2]email: wttang@mail.ncpes.edu.tw

INTRODUCTION

The performance ofan elite archer can be affected by effective control of muscle in the upper extremities. Moreover, archery can be described as a comparatively static sport requiring strength and endurance of the upper body, in particular of the forearm and shoulder girdle [1]. Thus, EMG provides useful information to investigate the static skill sof archery. So far, a contraction and relaxation strategy with regard to forearm muscles during the release of the bowstring has been observed and studied through EMG for different skill levels of players [2,3]. These studies showed that archers released the bowstring by active contraction of the forearm extensors, whereas a clear relaxation characterized the forearm after release. Improper contraction may lead the incorrect movement and hasten fatigue of the muscle, as seen in beginner archers. However, most studies of the relaxation of release only focus on either the forearm or certain shoulder muscles (e.g., the right trapezius). There is no study that investigates how different contraction and release strategies might apply from the distal to proximal segments of the upper extremities, especially in world rank elite archers. Thus, the purpose of this study was to (1) investigate this strategy in the limb extremities from distal to proximal segments using Olympic Female Archery Players, (2) quantify relaxation strategy which was indicated by reduction in muscle activation before and after the release, and (3) determine the characteristic of reduction level of muscle activities in supplemental studies of anchoring and aiming. These studies can provide archers and coaches with the possible assessments of optimal skill patterns.

METHODS

The Chinese Taipei 2004 Athens Olympic archery team was used in this study. The national rankings of team members were Archer A: fourth position, Archer B: sixth position, and Archer C: fiftieth position. Measurements were made under simulated Olympics conditions on the outdoor court of the Taiwan National Training Center. Biovison surface electrodes were placed on the central portion of each muscle. Electromyography activity of the M. extensor digitorum, trapezius muscle, and deltoid muscle were recorded at a sampling frequency of1000Hz using synchronized electronic signals for 24 shots by each participant. The mean amplitude of EMG activity during (1) one second of pre- and post-anchoring start point, (2) pre- and post- release timing, and, (3) the first second and last second of the aiming phase were obtained using standard processing. Reduction in the level of muscle activity at anchoring and release were calculated to evaluate release skill in the 0.1 s duration prior to (X) and after specific timing (Y) using the following equation:

$$\text{Reduction in muscle activity} = 1 - Y/X \qquad (1)$$

A higher positive reduction ratio represented a higher reduction in muscle activation, whereas a negative value represented an increase in muscle activation.

RESULTS AND DISCUSSION

The reduction ratio is shown in Figure 1 from proximal to distal segments for three phases. A greater reduction of muscle activation was seen in the more distal of muscle groups at release. However, anchor and aiming phases did not exhibit such a tendency. During the aiming phase, the extensor carpi of the draw arm increased , unlike other muscle groups. During the anchor phase, proximal muscle groups increase activation whereas distal muscle groups tend to reduce activation.
onthe other hand Reduction levels and variation in activation were compared among players using One-way ANOVA and post-comparisons (LSD). There were no significant differences between the three archers in reduction of muscle activation during anchoring and release phases. However, during the anchor phase, player A exhited a significantly greater reduction level relative to other players for the distal muscle groups (right extensor carpi, left detoideus, and right detoideus). This may imply that player A with a better performance may be due to a better relaxation strategy that yields more consistent performance.

Figure1: Reduction level in muscle activation for three archers

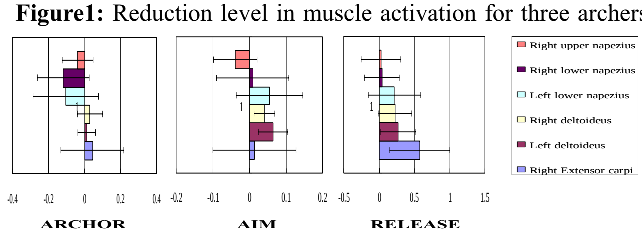

in three phases. (n=72)

CONCLUSIONS

This study indicates that the proximal muscles exhibit a lower redu ction level of muscle activation than do distal muscles for three archers after release. Archer A with a better Olympicsranking had the more coherent reducing muscle activation for all muscle groups at release phase, and reduced with distal muscle group during aiming phase. This may imply such relaxation strategy leads to better performance.

REFERENCES

1. Mann DL & Littke, N. Shoulder injuries in archery. Canadian Journal of Sport Sciences, **14(2)**,85–92. (1989)..
2. Tsung-Yi Wu. *For Archers*. Chinese Culture University,Taipei (1998).
3. H Ertan H, et. al., *Hum Mov Sci*, **22**, 37-45 (2003).TITLE?

ACKNOWLEDGMENT

Thanks for the grant of National Council on Physical Fitness and Sports and Chinese Taipei Amateur Archery Association for cooperatio

A NEW FRONTAL PLANE FOOT MODEL SHOWS THE EFFECT OF NARROWED BASE OF SUPPORT ON UNIPDEDAL BALANCE

[1] Jaebum Son and [1] James A. Ashton-Miller
[1] The University of Michigan, Ann Arbor
email: jaebum@engin.umich.edu

INTRODUCTION

Despite balancing on one leg being widely used as a clinical test of frontal plane balance, comparatively little is known about the biomechanics of this task. The foot is generally described as a ground-attached pivot that transfers the ankle torque to the ground 'transparently' and this assumption forms the basis for using an inverted pendulum to model balancing on one foot. Two common ways to increase the difficulty of balancing tasks are to ask the subject to stand on a compliant surface or on a narrowed base of support. In the latter case, balancing on a narrow beam limits the transmission of ankle torque to the support surface. In this paper we will show that a narrowed base of support also changes the effective compliance of the foot-ground interface, an effect that is often neglected in the simple inverted pendulum model.

METHODS

Let us first posit that the compliance of the foot-ground interface changes the passive dynamics of balancing on one foot. To prove this, we developed an analysis method called *ground pressure decomposition (GPD)* whereby the ground pressure profile is decomposed into pure force (P_f) and pure moment (P_m) components.

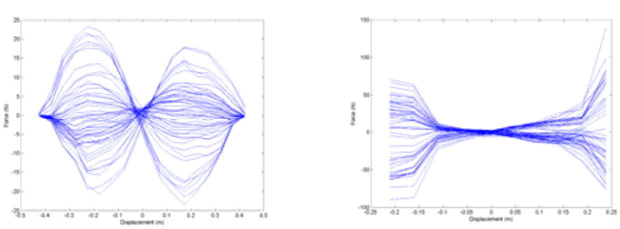

(b) P_m for a compliant surface (c) P_m for a narrow beam

Figure 1: Profile of pure moment component (P_m)

We assume that the frontal plane motion of the foot can be modeled as the sum of a deflection and a rolling component ($\Delta X_{ankle} = K_1\Delta COP + K_2\Delta\varphi_{limb}$) [where COP denotes center-of-pressure]. In this we hypothesize that the deflection coefficient (or effective stiffness) K_1 is inversely proportional to the square of beam width (**H1**). The existence of the deflection suggests that there exists a critical beam width (CBW) at which it is no longer possible to balance upon: a base of support narrower than CBW (**H2**).

To test above hypotheses (**H1** & **2**), 11 healthy young adults (ages 23-32 yrs., 5 females) were recruited. They were asked to balance for 30s on one foot placed on one of six beams of increasing widths (1.75 cm to 7 cm) presented in a randomized order (total 15 trials for each subject). The kinematics and the ground reaction force were measured at 100 Hz using three Optotrak® markers and two AMTI® force plates and filtered with a 4^{th}-order bidirectional low-pass (7-Hz cut-off) Butterworth filter.

RESULTS AND DISCUSSION

Of a total of 165 trials from the 11 subjects, 141 trials exceeded 20 s and analyzed. In Figure 1a & b we see that the deflection component gain, K_1, increased while the rolling component gain, K_2, remained constant. Figure 1c shows that the change of K1 has an optimal regression exponent, n=1.9, close to our expected value of n=2.0, thereby supporting **H1**. Figure 1(d) shows the change of K1 against beam width normalized about CBW. No subject could stand on beams narrower than CBW, supporting **H2**.

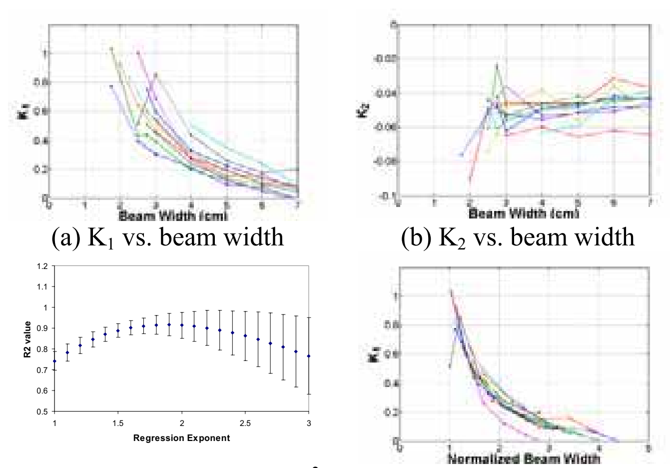

(a) K_1 vs. beam width (b) K_2 vs. beam width

(c) Regression Exponent vs. R^2 (d) K_1 vs. normalized BW

Figure 1: Least square regression result result using $\Delta X_{ankle} = K_1\Delta COP + K_2\Delta\varphi_{limb}$.

So, balancing on a narrow beam has two characteristics: COP saturation and a compliant interface. As the compliance increases, the axis of the torque source (i.e., ankle jt.) is translated laterally causing relative system instability.

CONCLUSIONS

1) The foot has both compliance and rolling characteristics in the frontal plane.
2) This compliance reduces the transmission of the ankle torque to the ground, and defines a critical beam width (CBW) that limits balancing in a pure ankle mode.

FACTORS AFFECTING THE JAVELIN'S ATTITUDE ANGLE IN AMERICAN JAVELIN THROWERS

Michele LeBlanc and Rachael G. Mooney
California Lutheran University
email: mleblanc@clunet.edu

INTRODUCTION

The distance a javelin travels is affected not only by its release velocity and angle, but the javelin's orientation with the horizontal plane (its attitude angle). Several authors have reported optimal values for these release angles [1,2]. Recent work has found that during the final release phase, American female javelin throwers exhibit much larger attitude angles while having similar release angles to their male counterparts [3]. These large attitude angles are detrimental for the javelin's flight and can lead to shorter throw distances [1,2]. The American females' trunk forward/backward lean angles also differed from the males' during the early part of the release phase. However, a significant relationship between the trunk's lean angle and the javelin's attitude angle did not exist and so other differences should be investigated.

The purpose of this study was to further examine the differences in the javelin's attitude angle between American female and male elite-level javelin throwers. In particular, to determine how the throwing arm's wrist position relative to the shoulder position may contribute to the attitude angle differences observed.

METHODS

The nine finalists for the men's and for the women's javelin throw competition at the 2003 US National Championships were filmed at 60 Hz with two cameras. Standard DLT methods were used to obtain 3D coordinates for 21 body landmarks and 3 javelin landmarks. The 3D coordinates were expressed in an orthogonal reference frame in which the X axis pointed toward the right, the Y axis pointed forward, and the Z axis pointed upward (see Fig. 1).

For each athlete, the two best analyzable throws were used. At the end of the run-up, the right-handed javelin thrower performed a crossover step onto their right foot (RTD), planted their left foot (LTD), and released the javelin (REL). Each throw was digitized from before RTD past REL. The relatively low frame rate was adequate for this study as the parameters investigated exhibited small changes during the time frame studied.

The javelin's attitude angle (ATT) was defined as the angle between the projection of the javelin's long axis on the YZ plane and the +Y axis. The arm angle (ARM) was defined as the angle between the projection of the vector pointing from the right wrist to the right shoulder onto the YZ plane and the +Y axis. These angles were computed at RTD and at LTD. The difference between these two angles created with the horizontal (DIFF) was also computed.

Figure 1: Sequence of the release phase of the javelin throw.

Mean and standard deviation values were computed for the male and female groups. Student's t-tests were used to determine if differences existed between the male and female values. An experiment-wise $\alpha = 0.05$ was used with a correction made for multiple comparisons. Correlation coefficients were computed between ATT and ARM values at RTD and LTD for each gender and for the pooled data.

RESULTS AND DISCUSSION

Table 1 gives the mean and standard deviation values for the male and female groups. There was a statistically significant positive correlation between ATT and ARM at RTD for the pooled data as well as each gender separately. At LTD, none of these correlation coefficients were statistically significant. DIFF values were significantly different at both RTD and LTD indicating that there are differences in the angle between the thrower's arm and the javelin's long axis which are presumably due to differences in wrist angles.

Results suggest that by raising their throwing wrist, females may be able to decrease their attitude angle at RTD. There is a strong relationship between the javelin's attitude angle at RTD with its value at LTD and REL. Thus, having a smaller value at RTD may be enough to create a more favorable attitude angle at REL. Wrist flexion/extension angles should also be considered.

REFERENCES

1. Hubbard & Alaways, *Int J Sp Biomech, 3*,207-22*1*,1987.
2. Best, R. J. et al.. *J Applied Biomech*, **11**, 371-394, 1995.
3. LeBlanc, M. & Mooney, R. *Eng in Sport 5*, 182-188, 2004.

ACKNOWLEDGEMENTS

This work was funded by a grant from USA Track & Field.

Table 1: Mean (standard deviation) values (given in degrees) for the javelin's attitude angle, arm angle and their difference at RTD and LTD for males and females. * denotes statistical significance.

	ATT-RTD*	ARM-RTD*	DIFF-RTD*	ATT-LTD*	ARM-LTD	DIFF-LTD*
Males	26.3 ± 5.3	8.8 ± 6.6	17.1 ± 6.0	31.3 ± 5.2	8.4 ± 4.4	22.8 ± 8.0
Females	35.7 ± 9.0	13.4 ± 5.2	22.3 ± 6.5	40.3 ± 5.3	6.7 ± 3.4	33.6 ± 6.6

OPTIMIZATION OF FEEDFORWARD AND FEEDBACK CONTROL DURING WALKING

Shawn M. O'Connor, Arthur D. Kuo
Department of Mechanical Engineering and Biomedical Engineering
University of Michigan Ann Arbor, MI USA
Email: smoconno@umich.edu

INTRODUCTION

We used a simple walking model to study how feedforward (FF) and feedback (FB) control can be optimally combined to produce steady walking motions. We interpret combined FF and FB control in terms of an internal model that is updated by sensory information. The theory of state estimation suggests there is an optimal balance of FF and FB control for improved performance in the presence of noise.

Biological systems function despite imperfect sensors and the presence of disturbances. Neural oscillators are thought to act as Central Pattern Generators (CPGs) of rhythmic motor commands, producing FF commands even in the absence of sensory FB. But this FB is also thought to play an important role in normal behavior, and FF compensates poorly for disturbances. How can the apparent feedforward behavior of CPGs be reconciled with FB? We previously proposed [1] that the neural oscillators could be interpreted as an internal model of limb dynamics. In control theory, internal models can estimate the system state and associated sensory output. Errors in sensory prediction are used to refine the state estimate, which is then used for FB control. In this interpretation, the internal model produces FF commands even when error FB is removed. The optimal motor combination of FF and FB is determined by the presence of two types of noise: *process noise* refers to unpredictable disturbances that are detrimental to pure FF control, and *sensor noise* refers to sensor imperfections that are detrimental to high gain FB. To demonstrate this interpretation, we applied a controller with state estimation to a simple walking model under the presence of both types of noise. We tested whether step variability would be minimized with a predicted optimum combination of FF and FB, as opposed to using either control strategy alone.

METHODS

We employed a simple passive dynamic model of two-dimensional, straight legged biped walking [2], but with added actuation of the hips. The hip torque had two components: a torque applied in proportion to the angle between the legs, as estimated by the internal model, and a constant torque to add energy lost in collisions during double support.

The control system (Figure 1) uses a CPG to model the dynamics of limbs, producing an estimate of the system state used to drive hip torque. The error signal, from model stretch sensors, was used to refine the state estimate via an estimator feedback gain, L, which scales the relative influences of FF and FB on the controller (i.e. small L produces pure FF and large L produces pure FB control). State estimation theory predicts an optimal value of L given characteristics of process and sensor noise.

Walking simulations were conducted over many steps for a range of L between pure FF and pure FB. Process and sensor noise were applied to the system with equal weight such that both had the equivalent strength of 10% of the maximum hip torque produced by the walker. Step-to-step variability was calculated from the standard deviation of leg angles and velocities at the end of each double support period.

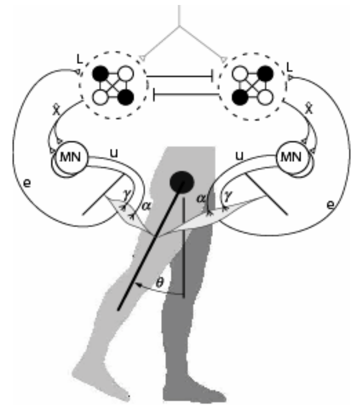

Figure 1: Model of CPG control of hip torque

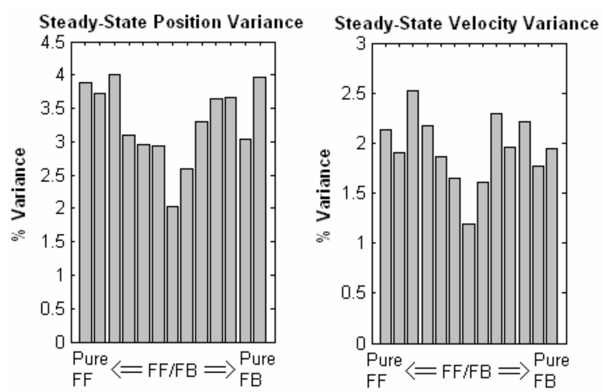

Figure 2: Percent variation of leg angle and velocity over a range of values of the estimator feedback gain.

RESULTS AND DISCUSSION

The model demonstrates (Figure 2) that step-to-step variability is minimized when the relative roles of FF and FB are appropriately balanced. In the presence of noise, there is an optimal combination that produces better performance over either FF or FB alone. CPGs may be interpreted to act as local internal models of limb dynamics. In this sense, CPGs are not seen to simply produce motor commands for muscle activation, but also to process sensory information. Further application of state estimation theory may provide insight into the role of CPGs in biological movement.

REFERENCES

1. Kuo A. *Motor Control* **6**, 129-145, 2002.
2. McGeer, T. *Int'l J Robot Res.* **9**(2):62–82, 1990.

ACKNOWLEDGEMENTS

Rollin M. Gerstacker Foundation

BIOMECHANICS OF THE FLEXRIM LOW IMPACT WHEELCHAIR HANDRIM

W Mark Richter, Russell Rodriguez, Kevin Woods, and Peter Axelson
Beneficial Designs BioMobility Lab, Nashville TN
mark@beneficialdesigns.com www.beneficialdesigns.com

INTRODUCTION

Handrims are the primary interface by which a wheelchair user controls the wheelchair. The standard handrim is anodized aluminum and relatively slippery. As a result, the user must grip it tight to keep their hand from slipping. A vinyl-coated handrim provides increased friction so the user does not have to grip as much. Because the vinyl coating is a heat insulator, it can burn the hand when braking downhill. However, its benefits to propulsion are important to take advantage of, since decreasing physical demand on the wheelchair user may serve to delay or prevent the development of upper extremity repetitive stress injuries.

In a study of 9 wheelchair users pushing on a treadmill set to a range of grade conditions, we found the use of a vinyl-coated handrim resulted in a 9% average decrease in metabolic demand during propulsion [1]. In a similar study of 25 wheelchair users, we found subjects tended to push with an average of 10% more power during the push [2]. As a result users spent less time pushing and more time coasting. However, this increased push intensity also resulted in a higher rate of loading in the radial direction, which has been associated with incidence of repetitive stress injuries. Use of a compliant handrim has been shown to reduce the rate of loading during propulsion [3]. The FlexRim is a new handrim that incorporates a high friction grip surface with a compliant interface to reduce impact loading (Figure 1). The outer rim is uncoated, so the FlexRim preserves the ability to brake downhill. The purpose of this study was to assess the biomechanics of the FlexRim during propulsion.

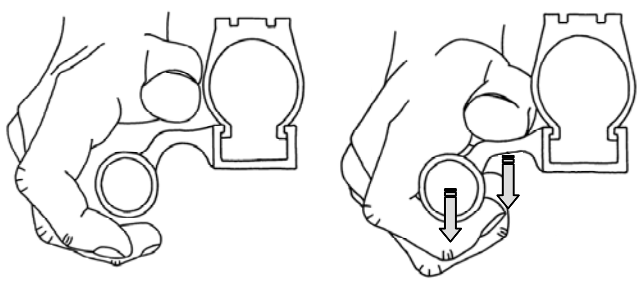

Figure 1: The FlexRim has a high friction compliant interface for the hand that is designed to improve grip and reduce impact loading during propulsion.

METHODS

Full-time manual wheelchair users were recruited to participate in this study. Subjects were asked to propel their wheelchair (with instrumented wheels) on a treadmill using one of either the FlexRim handrim or the standard handrim. Handrim order was randomized. Subjects propelled at predetermined self-selected (comfortable) speeds for 35 pushes on level, 30 pushes at 3 degrees, and finally 25 pushes at 6 degrees. Kinetic and kinematic measures were made continuously over each handrim trial. The last 20 pushes from each grade condition were used in the analysis. For each push analyzed, target temporal and kinetic characteristics were determined and averaged over the entire 60-push set. Biomechanical metrics were then compared between the handrim conditions using a paired samples t-test and determined to be statistically significant for $p<0.05$.

RESULTS AND DISCUSSION

Twenty-five (25) subjects, with an average of 17 years of wheelchair experience (sd=11) participated in the study. The resulting temporal and kinetic biomechanical measures are given in Table 1. The magnitude and rate of loading radially into the handrim (Fr, dFr/dt) were maintained due to the compliance of the FlexRim. The axial moment (Ma) and moment generated by the hand (Mh) were both found to be significantly higher, by 15.5% and 27.8% respectively for the FlexRim. The FlexRim did not affect push frequency. Similar to the vinyl-coated handrim, use of the FlexRim resulted in improvements in the ratio of time spent pushing to coasting, as well as in the amount of power generated during the push. The FlexRim resulted in a 13.2% increase in the average power generated, even greater than that found for the vinyl-coated handrim in an earlier study [2].

CONCLUSIONS

Improving the ergonomics of wheelchair propulsion is important as it may serve to delay or prevent the development of repetitive stress injuries. The FlexRim low impact handrim was found to result in dramatically improved power generation during the push without the adverse effects found for the vinyl-coated handrim. Longitudinal studies of injury development will be necessary to evaluate the long-term injury prevention potential of the FlexRim.

REFERENCES

1. Richter WM, et al. *Proc of ASB*, Cincinnati OH 2003.
2. Richter WM, et al. *Proc of RESNA*, Orlando FL 2005.
3. Richter WM, et al. *J Rehabil Res Devl*, (in press) 2005.

ACKNOWLEDGEMENTS

This research was funded by NCMRR in the NICHD at the NIH through SBIR Phase II Grant #2 R44 HD36533-02A2.

Table 1: Biomechanical results for the standard and FlexRim handrims. Bold values represent statistically significant differences.

Handrim	Max Fr (N)	Max dFr/dt (N/s)	Avg Ma (Nm)	Avg Mh (Nm)	Push Freq (Hz)	Push/Coast Time Ratio	Power/Push (W)
Standard	69.4 ± 21.2	1357 ± 370	10.2 ± 2.8	2.7 ± 1.4	1.02 ±0.19	0.29 ± 0.06	15.7 ± 5.5
FlexRim	68.4 ± 19.1	1353 ± 269	**11.8 ± 2.3**	**3.5 ± 1.3**	1.03 ±0.20	**0.31 ± 0.06**	**17.8 ± 5.3**

HIP- SPINE INTERACTION DURING SIT-TO-STAND IN HEALTHY YOUNG SUBJECTS

Fotoohabadi MR, Tully EA**,** and Galea MP.
School of Physiotherapy, The University of Melbourne, Parkville,Victoria 3010.
email: m.fotoohabadi@pgrad.unimelb.edu.au, web: www.physioth.unimelb.edu.au/

INTRODUCTION

Standing up from sitting (STS) is essential for walking and therefore independent function**.** However, little is known about the contribution of the thoracolumbar spine during STS. It has been suggested that minimal movement occurs in the spine during STS, with trunk forward lean prior to buttock's lift off (LO) being produced solely by flexion of the hips[1,2]. The aim of this study was to use computer-aided video analysis to determine the sagittal contribution of lumbar and thoracic spine, hip and knee joints during STS in a group of healthy young adults.

METHODS

Forty-seven healthy young adults with reflective markers attached over the mid-line thoracolumbar spine, right lateral pelvis and lower limb were videotaped (i) performing STS at their preferred speed from a chair set at 100% knee height, and (ii) undertaking tests for maximal available thoracic, lumbar and hip joint flexion. The automatic digitization mode of the 2D Peak Motus was used to track the marker movement on the videotape at 50Hz. Following (Butterworth) filtering of the data sagittal thoracic, lumbar, hip, and knee angles were calculated. All angular data were normalized to 100% movement duration to accommodate speed variations between subjects.

RESULTS AND DISCUSSION

Forward trunk lean prior to LO was accomplished by concurrent lumbar and hip flexion; 1° lumbar flexion for every 2.7° hip flexion. As the lumbar spine flexed the thoracic spine extended resulting in a LO trunk angle of 45.7°(±5.8°). Following LO, the hip(s) and lumbar spine extended and the thoracic spine flexed, with the standing thoracic angle approximating the initial thoracic flexion posture in sitting. During STS subjects used 95.5%, 65.9%, and 57.7% of their maximal available hip, lumbar and thoracic spine flexion respectively.

CONCLUSION

Improved knowledge of sagittal thoracolumbar and hip-spine movement patterns in healthy subjects will facilitate rehabilitation of dysfunctional STS.

REFERENCES

1.Carr JH, Shepherd RB. *Stroke Rehabilitation*. Edinburgh: Butterworth-Heinmann, 2003.

2.Cahill BM, Carr JH. Inter-segmental co-ordination in sit-to-stand: an age cross-sectional study. *Physiotherapy Research International* 1999; **4**:12-27.

KINETIC CHARACTERISTICS OF MIDDLE-AGED AND OLDER ADULTS DURING WALKING

[1] Hidetaka Okada, [2]Shinya Kuno, [2]Mitsuo Matsuda and [2]Michiyoshi Ae
[1]The University of Electro-Communications, Japan; e-mail: hidetaka@e-one.uec.ac.jp
[2]University of Tsukuba, Japan

INTRODUCTION

The ability to walk is one of the most important factors for us to live actively. It may be a strong determinant for independent daily living, especially for elderly people. Unfortunately, the ability of the elderly to walk seems to deteriorate with aging. However, we can find the biomechanical causes of that deterioration and show how the elderly can maintain the ability to walk from the results of kinetic analyses of their motion.

The purpose of this study is to clarify the kinetic characteristics for middle-aged and older adults during walking and to present findings useful for maintaining or enhancing their ability to walk.

METHODS

The subjects were 326 healthy Japanese adults, including 49 middle-aged, 265 elderly and 12 young adults (Table 1). They were instructed to walk about 10m as they usually did in their daily lives. In order to analyze the motion in the sagittal plane, we videotaped them during walking with a digital VTR camera at 60fps. The ground reaction forces on the right foot were measured by a force platform installed below the walkway. Two-dimensional coordinates of the eight body landmarks were obtained by using a video digitizing system (Frame-DIAS, DKH Co., Ltd.). The coordinates were smoothed by a fourth-order, zero-phase-shift Butterworth digital filter at the optimal cut-off frequencies that were derived from residual analysis (Winter, 1990). After synchronizing the smoothed coordinate data and ground reaction forces, we calculated joint torques at the ankle, knee and hip using a link-segment model based on the inverse dynamics method. Joint torque powers were next calculated by multiplying the joint torque by the joint angular velocity. Finally, joint mechanical work was calculated by integrating the joint torque power over time.

RESULTS AND DISCUSSION

Figure 1 depicts the joint mechanical work of the ankle, knee and hip during normal walking for each age group. From these results, it appeared that positive work of ankle and knee and negative work of each joint for M, E1, E2 and E3 were smaller than those for Y. The positive ankle work was remarkably smaller in older groups. In contrast, the positive hip work was larger in older groups than the younger group.

Table 1 Subjects and age groups

Group	Abbr.	n	Age (yr.)	
			Mean±SD	Range
Young	Y	12	24.5±1.8	22.02–27.54
Middle-aged	M	49	59.7±4.8	45.30–64.97
Elderly 1	E1	97	67.6±1.3	65.14–69.99
Elderly 2	E2	109	72.5±1.4	70.05–74.98
Elderly 3	E3	59	77.7±2.2	75.31–86.32

Positive ankle power is exerted only in the second half of the stance phase (push-off phase) in walking. In this phase, positive power is generated by concentric contraction of the ankle plantar flexors, in which plantar flexion torque is exerted as the joint moves in the direction of plantar flexion. We therefore believe that the function of plantar flexors during walking deteriorates with aging and the hip joint must then exert more power to compensate for the decline in ankle function.

CONCLUSIONS

The most remarkable characteristic of walking kinetics for middle-aged and older people is the decrease in positive ankle work. Therefore, preventing the decline in ankle plantar flexor function during walking may be the key for maintaining or enhancing the ability of the elderly to walk.

REFERENCES

1. Judge, JO, et al.. *J Geront* **51A**, M303-M312, 1996.
2. Okada H, et al.. *Proceedings of ISB XIX*, Dunedin, New Zealand, Abstract 303, 2003.
3. Winter, DA, et al.. *Phys Ther* **70**, 340-347, 1990.

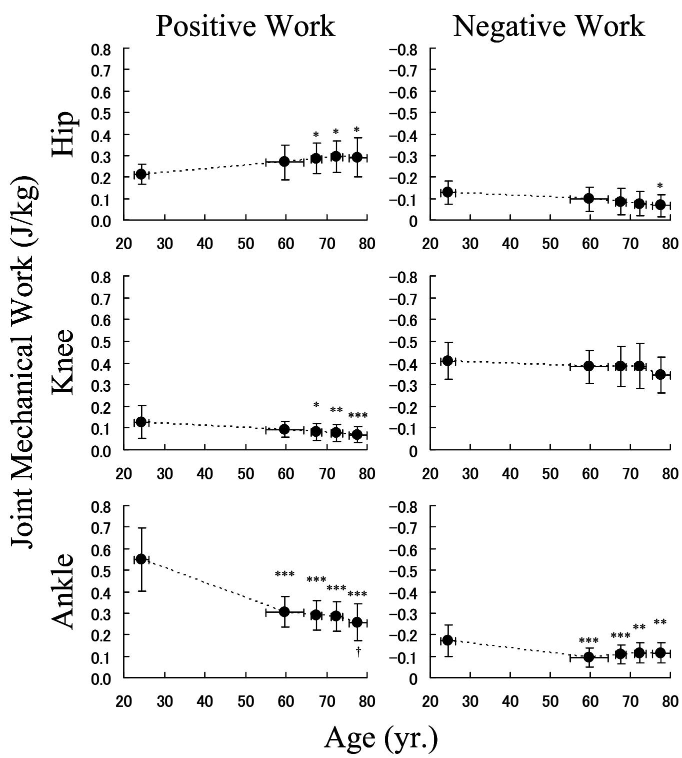

Figure 1 Joint mechanical work of lower limb during normal walking

Asterisks mean significant differences from the YOUNG in the multiple comparison (Scheffe's method) after ANOVA (* p<.05, **p<.01, ***p<.001). Crosses mean significant difference from the MIDDLE-AGED in the multiple comparison (Scheffe's method) after ANOVA († p<.05).

DYNAMIC STABILITY IN A ROUGH ENVIRONMENT: THE INFLUENCE OF INITIAL LIMB POSTURE ON BODY DYNAMICS DURING AN UNEXPECTED PERTURBATION.

Monica A. Daley and Andrew A. Biewener
Concord Field Station, Harvard University; mdaley@oeb.harvard.edu

INTRODUCTION

Little is currently known about the capability, mechanics and time-course of recovery from the types of perturbations that animals face while running in the natural world. Work on humans reveals that changes in k_{leg} help maintain similar CoM motions over surfaces of varying compliance [e.g., 1, 2], and these changes in k_{leg} can occur through intrinsic changes in limb mechanics [3]. Furthermore, stability of running can be improved by adjusting leg contact angle, which can be accomplished automatically if the leg retracts during late swing phase [4]. Thus, proper tuning of limb parameters in the face of a changing external environment is required to maintain locomotor stability. However, the relative importance of different control mechanisms during real-world perturbations is not yet clear. In this study, we perturb the running of guinea fowl by subjecting them to an unexpected drop in substrate height (ΔH). The goal of this study is to investigate how body centre of mass (CoM) mechanics deviate from steady running dynamics in response to an unexpected ΔH, and how limb dynamics mediate the response.

METHODS

The drop in substrate height is camouflaged to remove any visual cue about the upcoming change in terrain (Figure 1). Ground reaction forces (GRF), measured in the vertical and fore-aft directions, were recorded at 5000Hz and used to calculate instantaneous kinetic and potential energies of the CoM. Limb kinematics during the response were obtained from synchronized high-speed digital video recorded in lateral view at 250 frames s^{-1}.

RESULTS AND DISCUSSION

The birds stumbled or fell in fewer than 6% of the unexpected perturbations. In contrast, during visible substrate drops, they stumbled or fell in 20% of the cases, and came to a complete stop in an additional 25%. Due to altered timing between limb retraction and limb loading, an exchange between potential

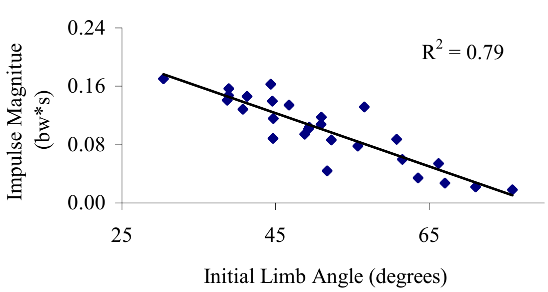

Figure 2: The relationship between limb contact angle and GRF impulse magnitude.

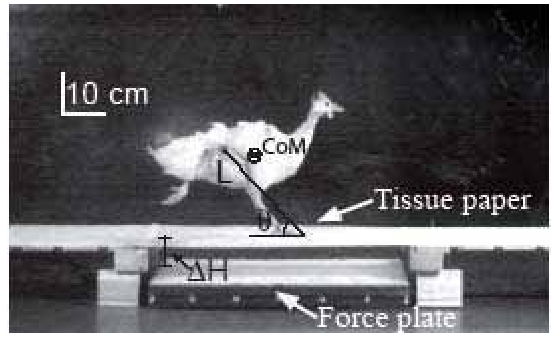

Figure 1: Still frame of a guinea fowl as it encounters a hidden drop in terrain, illustrating the experimental setup.

and kinetic energy occurs during the perturbed step, unlike during steady running. The birds exhibited three CoM energy exchange patterns in response to the unexpected ΔH, each characterized by a distinct combination of altered magnitude and direction of the ground reaction force (GRF) impulse.

Overall, the results suggest that decoupling of limb retraction from limb loading plays a primary role in determining the dynamics of the response. Limb angle at the time of ground contact explains much of the variation in CoM dynamics during the response (Figure 2). In contrast, k_{leg} during the unexpected ΔH varies dramatically but does not predict the CoM dynamics. Therefore, it appears that limb posture at ground contact plays a larger role in the response to the perturbation than does k_{leg} alone. The variation in stance phase CoM dynamics during the perturbation likely relates to altered intrinsic mechanics when the leg contacts the ground with a different posture.

CONCLUSIONS

Despite large changes in CoM dynamics and a great deal of variability in the response to an unexpected ΔH, guinea fowl are quite successful in maintaining dynamic stability, as they rarely stumble or fall. Further investigation of the joint and muscle dynamics underlying this variation could yield further insight into the control mechanisms that allow such robust dynamic stability during running in the face of large, unexpected perturbations.

REFERENCES

1. Ferris, D. P., Liang, K. & Farley, C. T. (1999) *J Biomech* **32,** 787-794.
2. Kerdok, A. E., Biewener, A. A., McMahon, T. A., Weyand, P. G. & Herr, H. M. (2002) *J Appl Physiol* **92,** 469-478.
3. Moritz, C. T. & Farley, C. T. (2004) *J Appl Physiol* **97,** 1313-1322.
4. Seyfarth, A., Geyer, H. & Herr, H. (2003) *J Exp Bio* **206,** 2547-2555.

SHORT AND LONG-TERM INFLUENCE OF A CUSTOM FOOT ORTHOTIC INTERVENTION ON LOWER EXTREMITY DYNAMICS IN INJURED RUNNERS

Christopher L. MacLean and Joseph Hamill
Biomechanics Laboratory, University of Massachusetts-Amherst, Amherst, Massachusetts, USA
E-mail: cmaclean@excsci.umass.edu

INTRODUCTION

Prior research on the influence of custom foot orthotic (CFO) intervention has primarily focused on the short-term dynamical influences at the ankle and knee in healthy runners. That is, subjects in the study were dispensed custom foot orthoses and tested immediately with no controlled period of wear. In addition, for the most part, subjects included in these studies have been healthy subjects who are not typically candidates for this intervention (Mundermann et al., 2003). Therefore, the purpose of this study was to analyze the short and long-term influence of a CFO intervention on the lower extremity dynamics in a sample of runners who had a history of running related knee injury.

METHODS

Eight female runners (at least 10+ miles per week) with a history of a knee-related running injury were selected for participation in the study. Each subject performed 5 acceptable over-ground running trials with a CFO and without a CFO (SHOD) (Paris Orthotics Lab, Vancouver, BC, Canada). Subjects were tested at the time of orthotic dispense and following 6 weeks of orthotic wear during all running activity.

Kinematic data were collected using Qualisys® software (Gothenburg, Sweden) at 240Hz and kinetic data were collected using an AMTI® force platform (Watertown, MA, USA) at 1920Hz. Data were processed using Visual 3D® (C-Motion, Inc. Rockville, MD, USA) for the calculation of ankle and knee angles and internal joint moments. Data were statistically analyzed using a Condition X Time X Subjects repeated measures ANOVA. Significant main effects and interactions were indicated with a criterion alpha level of 0.05.

RESULTS AND DISCUSSION

CFO intervention resulted in significant main effects for Condition (CFO vrs Shod) but not for Time (0 vrs 6 weeks). Short and long-term intervention led to significant decreases in maximum values for rearfoot eversion angle (Figure 1), rearfoot eversion velocity (Figure 2) and internal ankle inversion moment (Figure 3).

The results of this study reveal that 3-D frontal plane dynamics of the ankle were affected by CFO intervention in subjects with a history of running-related knee injury. Results from this sample of runners indicate that the influence of CFO intervention might be realized immediately and that changes in dynamical variables were not significantly influenced by prolonged wear following dispense.

Figure 1: Mean peak rearfoot eversion angles (CFO condition: gray; Shod condition: white).

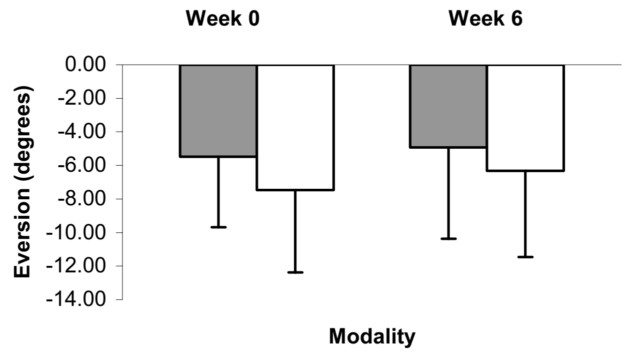

Figure 2: Mean peak rearfoot eversion velocity. (CFO condition: gray; Shod condition: white).

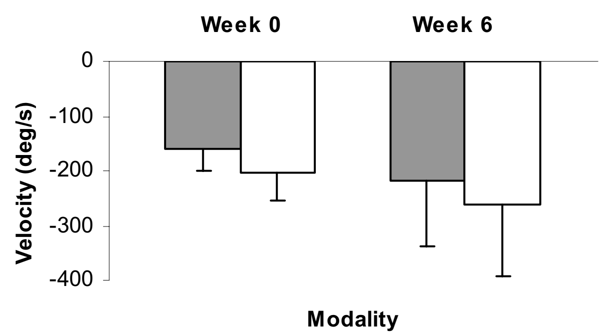

Figure 3: Mean peak ankle inversion moment. (CFO condition: gray; Shod condition: white).

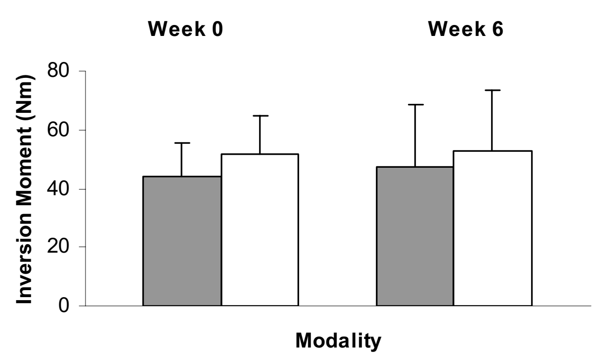

REFERENCES

Mundermann et al., (2003). *Clinical Biomechanics*, **18**, 254-262.

ACKNOWLEDGEMENTS

This study was supported by a grant from PFOLA.

PATELLAR LIGAMENT INSERTION ANGLE INFLUENCES QUADRICEPS USE DURING STAIR CLIMBING: EFFECT OF AN ANTERIOR CRUCIATE LIGAMENT DEFICIT

[1]Ajit Chaudhari, [1]Choongsoo Shin, [1,2]Chris Dyrby and [1,2]Thomas Andriacchi
[1]Dept. of Mechanical Engineering, Stanford University,
[2]Bone & Joint Center, VA Palo Alto Health Center; email: ajit.chaudhari@stanford.edu, web: biomotion.stanford.edu

INTRODUCTION

The patellar ligament transfers the force of quadriceps muscle contraction to the tibia, The orientation of the force transferred to the tibia is influenced by the patellar ligament insertion angle (PLIA), defined as the angle between the patellar ligament and the tibial shaft, since the PLIA determines how quadriceps force is decomposed into the anterior and superior directions. In individuals with an anterior cruciate ligament deficit (ACL-D), this anterior component of the force may cause anterior tibial translation. One of the explanations for why ACL-D individuals often reduce quadriceps force gait during walking is to prevent excessive anterior tibial translation [1]. Based on this explanation one would expect that anatomical variation in the PLIA would influence the tendency of patients to reduce quadriceps contraction. While it has been observed that ACL-D knees have a reduced PLIA relative to the contralateral knee or control knees [2], the relationship between this reduced PLIA and the reduction or avoidance of quadriceps usage has not been explored.

This study tested the hypothesis that in ACL-D knees, the peak external knee flexion moment during stair climbing would be negatively correlated to the PLIA, while in the contralateral or control limbs no such correlation would occur.

METHODS

Seventeen subjects were studied after giving IRB-approved informed consent – nine unilateral ACL deficients (age=40.1±12.7 years, 7 male, 2 female, average 178 months past injury) and eight controls with no history of musculoskeletal injury (age=34.3±9.9 years, 6 male, 2 female). Sagittal-plane magnetic resonance images (3DSPGR) were taken of each subject's knees in a fully extended, non-weight-bearing position. PLIA was defined as the angle in the sagittal plane between the patellar ligament and the tibial shaft, as described previously [2].

All subjects climbed a set of 21-cm steps while being recorded using an opto-electronic motion capture system with six markers on each lower limb. A force plate under the first step recorded the ground reaction force. A previously-described link model was used to estimate the net external forces and moments acting at the joints [3]. Three trials were captured for each leg, and the peak external knee flexion moments for the three trials were averaged together for subsequent analysis.

Linear regressions were performed to examine the strength of the correlations between the PLIA and the peak knee flexion moment, with a significance level of α=0.05.

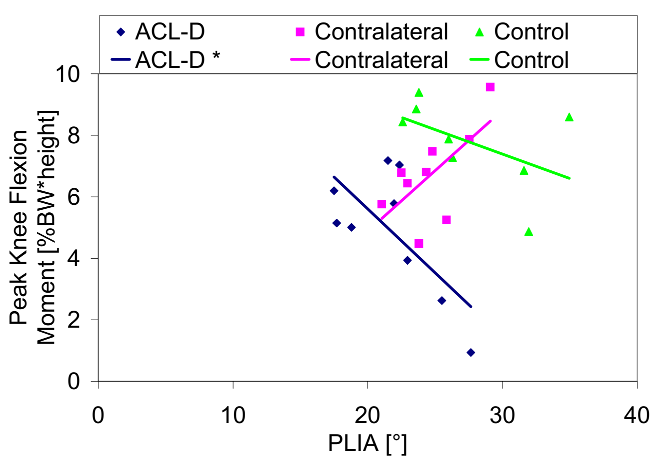

Figure 1: Peak external knee flexion moment vs. PLIA for ACL-deficient, contralateral, and control knees. * denotes slope significantly different from zero.

RESULTS AND DISCUSSION

The significant negative (slope=-0.41, p=0.04, R^2=0.48) relationship between PLIA and knee flexion moment (Figure 1) for the ACL-D knees suggests that individuals with a smaller PLIA experience less of an anterior pull on the tibia when the knee extensors are active, and therefore they show less of a tendency to avoid using these muscles.

Although it fell short of statistical significance, the positive slope observed in the contralateral knees (slope=0.39, p=0.05, R^2=0.43) appears to be different from the control knees and deserves further study. For the control knees, no relationship was observed (p=0.19, R^2=0.26).

CONCLUSIONS

The results of this study indicate that differences in the orientation of the patellar ligament can influence the tendency of ACL-D patients to reduce quadriceps contraction. Moreover, this study may help to explain why some researchers have reported observing quadriceps avoidance [1] while others have not [4], since the PLIA variability between ACL-D subjects can be considered as a confounding factor in those earlier studies.

REFERENCES

1. Berchuck M, et al. *J Bone Joint Surg* **72-A**, 871-877, 1990.
2. Shin CS et al. *28th Meeting of ASB,* Portland, 167, 2004.
3. Andriacchi TP, et al. in *Basic Orthopaedic Biomechanics,* Lippincott-Raven, Philadelphia, 37-68, 1997.
4. Torry MR, et al. *Med Sci Sports Exerc* **36**, 1403-1412, 2004.

ACKNOWLEDGEMENTS

Support for this study was received from NIH R01-AR392.

SENSORY REGULATION OF MUSCLE ACTIVITY DURING WALKING IN CONSCIOUS CATS

[1]J. Maxwell Donelan, [2]Atsumichi Tachibana, [2]David A. McVea, and [2]Keir G. Pearson
[1]Simon Fraser University, Canada; [2]University of Alberta, Canada;
email: mdonelan@sfu.ca

INTRODUCTION

Our previous work on decerebrate cats suggested that force feedback, originating from Golgi tendon organs (GTOs), makes a substantial contribution to ankle extensor activity accounting for approximately 50% of suprathreshold activity at longer muscle lengths [1]. To test the functional significance, we determined the contribution of force feedback to muscle activity during walking in conscious cats with intact central nervous systems.

METHODS

We trained 2 cats to walk on a pegway that could be adjusted to different slopes (Figure 1; +25, +10, 0, -10, -25 degrees). One peg measured ground reaction force. Video analysis yielded joint kinematics. To isolate the MG muscle, other major ankle extensors (LG, Sol, and Pl) were denervated 4 days prior to data collection. Implanted EMG electrodes measured muscle activity. Using inverse dynamics and moment-arm measurements, we estimated MG force, length, and velocity. The estimates allowed the use of mathematical models [2] to predict muscle spindle (Ia and II afferents) and GTO activity (Ib afferents).

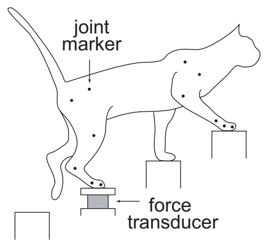

Figure 1:

RESULTS AND DISCUSSION

As expected, greater slopes resulted in increased muscle activity and force at longer muscle lengths during stance (Figure 2). Due to this increase in force, predicted Ib activity increased strongly with length. Predicted Ia and II activity, however, was nearly independent of length because muscle velocity decreased at longer muscle lengths. This suggested that changes in muscle activity were due primarily to force feedback allowing the use of a simple model of the neuromuscular system to estimate the pathway loop gain ($K{\cdot}M$; Figure 3). This gain ranged from ~0.2 at short muscle lengths to ~0.6 at longer muscle lengths demonstrating that force feedback was of modest importance downhill, accounting for 20% of total activity and force, and of substantial importance uphill, accounting for 60%. This length dependence was due to the intrinsic force-length property of muscle, M. The gain of the pathway that converts muscle force to motoneuron depolarization, K, was independent of length. These findings emphasize the general importance of feedback in generating ankle extensor activity during walking in the cat and suggest the intriguing possibility that feedback automatically compensates for changes in slope without requiring different descending commands.

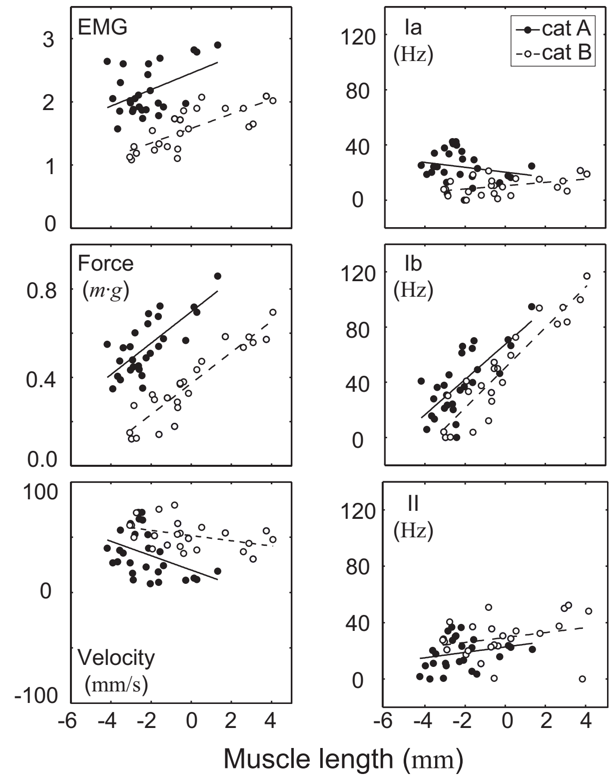

Figure 2: Relationship between muscle length and muscle activity, force, velocity, and predicted proprioceptor activity during stance. A positive velocity denotes a lengthening muscle. Symbols represent the average value over 50 ms beginning 50 ms after ground contract. Lines are best-fit linear regression lines.

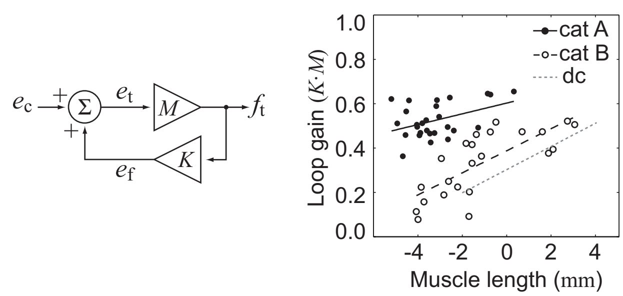

Figure 3: Left: Force feedback model. Total muscle activity, e_t, and force, f_t, are measured variables. e_c, the central contribution to e_t, was estimated as the y-intercept of the regression line for the relationship between e_t and f_t. We solved for the remaining variables. Right: Relationship between loop gain and muscle length. Symbols represent the average values and lines represent linear regressions. The dotted line shows that previous decerebrate experiments yielded similar results to current findings.

REFERENCES

1. Donelan JM, et al.. *J Neuro Physiol* **92**, 2093-2104, 2004.
2. Prochazka A. *Prog Brain Res* **123**, 133-142, 1999.

APPROACH VELOCITY PROFILES OF ELITE MALE AND FEMALE LOWER-LIMB AMPUTEE LONG JUMPERS

[1]Benjamin L. Patritti, [2]Kathy J. Simpson and [3]Lee Nolan
[1]Department of Physical Medicine and Rehabilitation, Spaulding Rehabilitation Hospital, Boston, MA, USA
[2]Department of Kinesiology, University of Georgia, Athens, GA, USA
[3]Laboratory for Biomechanics and Motor Control, Karolinska Institute, Stockholm, Sweden email: leen@ihs.se

INTRODUCTION

The approach velocity is accepted as a key determinant of successful long jump performance for elite able-bodied athletes [1,2]. Whether a similar relationship underlies the performance of disabled athletes, such as lower-limb amputees, is not well known. There is evidence that greater approach speed at take-off (TO) contributes positively to distance jumped for male below-knee amputees (BKA) and also for male above-knee amputees (AKA) with some slight adjustments in technique [3]. However, compensatory kinematics due to a prosthetic knee joint likely influences the regulation of velocity on the long jump approach [4]. The aim of this study was to compare approach velocity profiles of elite AKA and BKA, and the relationship between approach velocity and distance jumped.

METHODS

The velocity profiles of the approach runs of 14 AKA (male = 6, female = 8) and 20 BKA (male = 11, female = 9) were investigated during the long jump finals at the 2004 Paralympic Games. Approach velocities were sampled (100 Hz) using a laser Doppler device (Laveg, Jenoptik, Germany) positioned behind the long jump pit and targeted on the torso of each athlete during the run up. Velocity for the entire run up was recorded for each successful jump, corrected for perspective error and smoothed using Laveg Sport® software. Mean (± SD) data of selected velocity variables for positions 0m (take-off (TO) board), 1m, 6m, and 11m before the take-off board were calculated for each group using the greatest official distance jump of each athlete (Table 1). Differences between classification (AKA vs BKA) for each gender were determined using Students t-test. Relationships between variables were analysed using Pearson correlation and linear regression. Significance was set at $p < 0.05$.

RESULTS AND DISCUSSION

Female AKA approach velocity and distance jumped were lower than female BKA (Table 1), and lower than those reported for skilled able-bodied jumpers [1]. Likewise, the male athletes ran slower and jumped less far with increasing level of amputation, supporting previous research [3]. The positive relationship between approach velocity and distance jumped was strongest for male BKA athletes (Figure 1). Male AKA and female BKA athletes showed a slightly weaker relationship, partly conforming to the accepted long jump model [2,3]. Female AKA, however, exhibited a weak relationship indicating that for a given increase in approach velocity, the gain in distance jumped is minimal. Female AKA had a greater increase in approach velocity between 11-6m compared to the other athletes (Table 1). They also were the only group to have a relationship (r = –0.77) between this variable and distance jumped, and the only group to exhibit a weak relationship (r = 0.25) between average velocity at 11-6m and distance jumped. Thus, female AKA may be compensating for their slow approach velocity by continuing to accelerate between 11-6m from the TO board. This has a negative effect on their jump performance. The mechanisms which prevent female AKA from performing long jump technique in the same manner as female BKA or male AKA are not known and warrant detailed kinematic analysis.

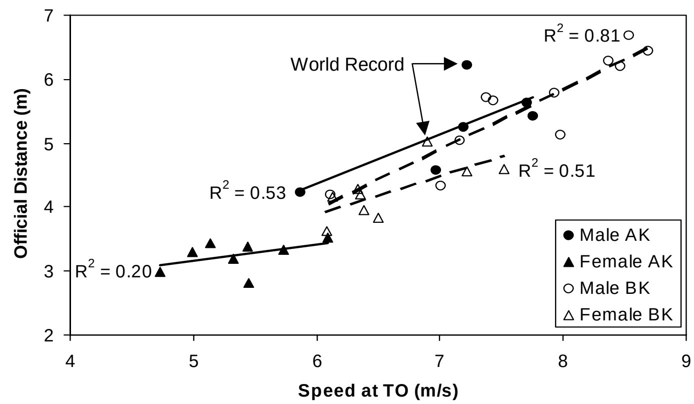

Figure 1: Relationships between approach velocity and distance jumped for male and female AKA and BKA athletes.

REFERENCES

1. Lees A, et al. *J Sport Sci* **11**, 303-314, 1993.
2. Lees A, et al. *J Sport Sci* **12**, 61-78, 1994.
3. Nolan L and Lees A. *Ergonomics* **43**, 1637-1650, 2000.
4. Simpson KJ, et al. *Proc NACOB*, Waterloo, 465-466, 1998.

Table 1: Means (± SD) for distance jumped and approach velocity variables for the male and female AKA and BKA groups.

	MALE		FEMALE	
	AKA	BKA	AKA	BKA
Official distance (m)	5.23 ± 0.72	5.59 ± 0.83	**3.25 ± 0.24**	4.25 ± 0.43
Velocity at TO (m s^{-1})	7.12 ± 0.69	7.73 ± 0.79	**5.36 ± 0.43**	6.60 ± 0.50
Av. velocity 11-6m from TO board (m s^{-1})	**7.31 ± 0.71**	8.08 ± 0.68	**5.32 ± 0.23**°	6.76 ± 0.49
Av. velocity 6-1m from TO board (m s^{-1})	**7.67 ± 0.59**	8.30 ± 0.66	**5.67 ± 0.24**	7.05 ± 0.45
Δ velocity 11-6m from TO board (m s^{-1})	0.51 ± 0.42*	0.54 ± 0.58*	**0.70 ± 0.32***	0.25 ± 0.48
Δ velocity 6-1m from TO board (m s^{-1})	–0.22 ± 0.44 [A]	–0.41 ± 0.64 [A]	0.36 ± 0.42	0.34 ± 0.43

[A]: negative (–) sign denotes decrease in velocity; **bold**: significant difference between classifications (AKA and BKA) for each gender;
°: significant difference between Av. velocity 11-6m vs. 6-1m for a given group; *: significant difference between Δ velocity 11-6m vs 6-1m for a given group.

WHAT FACTORS EFFECT THE ACCURACY OF SOLID MODELS MADE FROM CT DATA?

Heidi-Lynn Ploeg[1], Nick Byrne[1], Sylvana Garcia[1], Mariana Kersh[1], Andrew Van de Weghe[1]
[1]Departments of Mechanical and Biomedical Engineering, University of Wisconsin, Madison, WI, USA
email: ploeg@engr.wisc.edu, web: http://www.engr.wisc.edu/me/faculty/ploeg_heidi-lynn.html

INTRODUCTION

Computer models of bones are essential tools for research in orthopaedics, preclinical analysis of orthopaedic implant designs, and in computer-aided surgery. In these applications, solid models of bones are routinely created from computed tomography (CT) scan data; however, there are few studies [1-3] that have quantified the effects of the process parameters, on the error of the resulting geometry. The purpose of this study was to determine the magnitude of the error in solid models generated from CT-scan data and to which factors the error was most sensitive.

METHODS

This study compared the volumes of simple shapes derived from their measured dimensions and their segmented CT data. Cubes and cylinders were constructed from aluminum 6063 and polyurethane (PU) foam and their geometric dimensions were measured. Solid models based on the measured dimensions of the pieces were constructed with Unigraphics NX 2.02 from EDS, Plano, TX. In addition, the pieces were CT scanned (120 kV, 30 mA ,GE Litespeed[16] CT scanner from GE Medical Systems, Waukesha, WI at the University of Wisconsin Hospital), and their geometry was reconstructed by segmenting (Mimics 8.11 from Materialise, Ann Arbor, MI) the grey values of CT data that represented the density of the shapes.

The volumes of the shapes reconstructed from the CT data were normalized to the volumes of the solid models constructed from the measured dimensions. The effect of 7 factors at 2 levels each on the normalized volume of the segmented models was investigated using a one quarter fractional factorial design. 32 (2^{7-2}) treatments were run without replication in random order. The 7 factors and each of their high and low levels were:

1. CT-scan axis orientation: parallel and perpendicular to sample axis;
2. CT-scan slice thickness: high (1.25 mm) and low (0.625 mm);
3. CT-scan slice spacing: high (1.25 mm) and low (1.625 mm);
4. Density: high (aluminum 6063, 2700 kg/m^3) and low (solid rigid PU foam, 320 kg/m^3);
5. Fill: full and hollow (wall thickness 3.18 mm);
6. Feature: with and without a 3.3 mm wide by 6.6 mm deep, centered slot; and,
7. Shape: cube (25.4 mm^3) and cylinder (25.4 mm diameter x 25.4 mm height).

RESULTS

The mean of the normalized volumes of all the segmented shapes was 96% (79%-115%). A normal probability plot of the effect estimates from the fractional factorial analysis found that density was the only main effect that was likely to be important. The normalized volume of the aluminum and PU samples were 105% (93-115%) and 88% (79-96%) respectively. In contrast, all the highs and lows of the other main effects differed by less 2% (95-97%). In Table 1, the qualitative effects of the scanning parameters on the segmented models are demonstrated.

Table 1. The Effects of Scanning Parameters

a) Scan Axis Perpendicular to the Sample Axis.

	Fine Spacing	Coarse Spacing
Fine Thickness		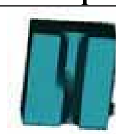
Coarse Thickness	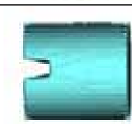	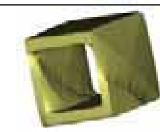

b) Scan Axis Parallel to the Sample Axis.

	Fine Spacing	Coarse Spacing
Fine Thickness	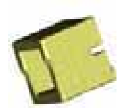	
Coarse Thickness	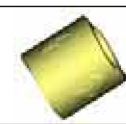	

DISCUSSION

Even though, normalized volume is a relatively insensitive result, density was found to be an important main effect. Volumes were under and over-estimated for low and high density pieces respectively. The scanning parameters had a qualitative effect on the models; however, it remains to be investigated, if a more sensitive result would find quantitative effects.

REFERENCES

1. Viceconti, M. et al. *J. Medical Engineering and Technology*, **23**(2):77-81, 1999.
2. Zannoni, C. et al. *Medical Engineering & Physics*, **20**(9): 653-659, 1998.
3. Testi D, et al. *Comput Methods Programs Biomed* **65**, 175-82, 2001.

EFFECTS OF SHORT-TERM WALKING EXERCISE IN ELDERLY

Sukhoon Yoon, Jeff Casebolt, Sunghoon Shin, Jaewoong Kim, and Young-Hoo Kwon
Biomechanics Laboratory, Texas Woman's University, Denton, TX 76205-5647
email: g_2yoon@mail.twu.edu, web: http://www.twu.edu/biom

INTRODUCTION

Falls among the elderly are quickly becoming an enormous concern for the United States in the 65-plus age group population. Tripping is one of the main causes for concern and is usually attributed to decreased lower extremity strength, stability, and range of motion. Minimizing the potential for tripping when maneuvering around or over an obstacle requires body control and working within a safe distance of the obstacle in question. Furthermore, if an obstacle is of a different height, then additional strength and coordination are needed from the lower extremity to perform the appropriate action.

The purpose of this study was to determine the effectiveness of: 1) a three month regular walking program, and 2) three different walking groups to improve an elderly individual's ability to interact with a series of obstacles in a safe and effective manner.

METHODS

Subjects were medically screened and cleared by a doctor to participate in the study. Thirty-three subjects volunteered and met all the criteria for participation (mean age: 73.2 ± 5.5 yrs). Thirteen males and twenty females were randomly assigned to one of three walking groups: 1) walking without equipment (C), 2) walking with ski-poles (T1), and 3) walking with equipment where the poles attached to a vest and were allowed to swing freely by the participants side (T2). The walking program lasted for twelve weeks and included three sessions per week at forty-five minutes per session.

Each participant was asked to perform three distinct tasks at a self selected pace using both their Preferred (P) and Non-Preferred (N) leg: 1) Step-Over (SO), 2) Step-Up (SU), and 3) Step-Down (SD). The SO consisted of an obstacle placed in the path of the participant at a height of 30% of leg length. During SU and SD the subjects were asked to step on to or down from a platform at a self-selected pace. The height of the platform was set at 30% of leg length.

Participants' motions were recorded in both right and left sagittal planes at 60-Hz video cameras (Panasonic AG450) and digitized with Kwon3D motion analysis software (Visol, Inc., Seoul, Korea). Ground reaction forces were collected using two force plate (AMTI OR6-5).

The 3 x 2 (groups x periods) factorial ANOVAs were performed to see significance in dependent variables ($\alpha < .05$).

RESULTS AND DISCUSSION

During SO, Maximum Vertical Heel Clearance (MVHC) was calculated as the vertical distance between top of the obstacle and heel of the lead leg at the instant of the leg crossing the obstacle. Toe Clearance (TC) was defined as the horizontal distance between the toe of the lead leg and the obstacle prior to crossing the obstacle. Heel Clearance (HC) is the horizontal distance between the heel and the obstacle at post crossing obstacle. The significant crossing clearance differences in step over among groups were shown (Table 1). SU elicited different GRF loading times among groups ($p < 0.05$). Longer propulsive force loading time were demonstrated in T2 versus T1 in both SU_N and SU_P, while T2 showed longer pulling force loading time compare with T1 in SU_P.

Pulling force loading time may indicate the index of confidence for falling. If an elderly walker has confidence to step up onto an obstacle in a safe manner, the trail foot will remain in contact with ground until leading foot is fully secure on the top of the platform.

While we expected a training effect, none was noted. This is probably due to the relatively short training period (12 weeks) coupled with the relatively low intensity training (walking). One possible reason for lack of significant data may be the duration of the training period. O' Neill et al. reported positive resistance training effects within 3 months [1], but the current study may have been hindered due to the low-intensity activity of walking given the time frame [2].

CONCLUSIONS

The current study revealed obstacle clearance and loading time differences among groups. At the present time, we cannot attribute these differences to the relatively short training period and low-intensity activity. A longer training period seems warranted, and further studies with longer training periods are in progress.

REFERENCES

1. O'Neill DET, et al.. *Journal of Aging and Physical Activity* **8**, 312-324, 2000.
2. Hamdorf, PA, et al.. *Archives of physical medicine and rehabilitation* **73**, 603-608, 1992.

Table 1: Summary of obstacle clearance parameters among groups in period (Mean ± SD).

	Pre-Test									Post-Test								
	C			T1			T2			C			T1			T2		
	MVHC	HC	TC	MVHC	HC	TC	MVHC	HC	TC	MVHC	HC	TC	MVHC	HC	TC	MVHC	HC	TC
SOR_P	8.1±4.7	16.6±6.3	65.0±11.6	7.4±5.7	18.0±3.5	75.4±13.7[2]	5.5±2.9	16.6±6.9	60.6±11.7	15.6±7.0	17.1±5.6	58.5±12	14.2±6.1	19.9±8.1	66.9±11.3[2]	12.3±5.1	18.0±6.7	67.8±7.9
SOR_N	11.8±6.5[1]	17.2±5.0	57.9±15.4	11.8±9.1	16.9±4.5[3]	70.8±14.4	8.1±4.1	14.4±5.2	57.5±10.5	15.7±7.8[1]	18.1±4.3	65.6±12.2	13.6±7.9	19.5±8.0[3]	65.5±8.4	8.1±4.3	14.1±5.6	67.9±9.1

[1]- significantly different from T2; [2]- significantly different from C; [3] significantly different from T2 ; All measurement in cm

VIBRATIONAL ANALYSIS OF NORMAL AND OSTEOPENIC TRABECULAR BONE USING RAPID PROTOTYPED DUPLICATES

[1]Wafa Tawackoli, [1]Jeremy Lemoine, [1]Matthew Wettergreen, [3]Chamith Rajapakse, [3]Gemunu Gunaratne, [2]Pol D. Spanos, and [1]Michael AK. Liebschner
[1]Department of Bioengineering and [2]Department of Mechanical Engineering and Materials Science, Rice University, Houston, TX, USA
[3]Department of Physics, University of Houston, TX, USA
email: wtawacko@rice.edu, web: www.rice.edu/cebl

INTRODUCTION

Osteoporosis is a systemic skeletal disease which increases bone fragility and susceptibility to fracture. Osteoporosis afflicts about 200 million people around the world [1] and osteoporotic fractures are estimated to be several millions annually in the US alone and cost tens of billions of dollars [1]. Characterization of bone quality in osteoporotic patients is very important with respect to monitoring treatment efficacy, however, currently quite limited. While some technical hurdles in developing a diagnostic tool using low frequency vibration have been overcome, many questions still remain including data interpretation and analysis. In particular, changes in the frequency response signal of bone have not been investigated at the various bone organizational levels. Our principal hypothesis is that the vibrational modes of bone tissue changes significantly with the deterioration of bone micro-architecture and that these modes can be captured by sensors to infer a structural compromise.

METHODS

Bone Models: Rapid prototyped duplicates of trabecular bone samples were fabricated based on digital scans of a lumber vertebra excised from a female cadaver and obtained on a μCT80 (Scanco Medical) with an isotropic resolution of 30 μm. Through image manipulation, triangulated surfaces of a randomly selected bone cube taken from the lateral aspect of the vertebra were generated using the thresholded μCT scans. This bone cube measured a bone mineral density (BMD) of 127 mg/cm^3, with is within the normal range [2]. An available custom algorithm was used to reduce the overall bone mass of the normal bone cube to an osteopenic stage (BMD of 86 mg/cm^3). After scaling both models, digital files were exported to a rapid prototyping system, which fabricated a scaled up duplicate of both bone cubes with 20 cm edge length (Figure 1).

Vibrational Analysis [3, 4]: Dynamical responses were carried out by attaching the bone cubes to an active electro-dynamic shaker while simultaneously recording acceleration and dynamic force. Frequency Response Function (FRF) measurements were made using random broad band excitation signal. A sample rate of 2000 S/s with a Hanning time domain window allowed for a frequency resolution of 0.1 [Hz]. The experiments on the cubes were repeated three times in alternative order to ensure accuracy of the results. The power spectrums of the force and acceleration signals were computed. Acceleration signals were processed to derive velocity and displacement signals. Dynamic stiffness, half-peak bandwidth, and damping ratio (ζ) for both bone cubes were calculated using FRF measurements, and other techniques.

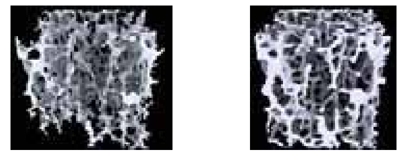

Figure 1: Scaled version of a normal (right) and osteopenic (left) bone cubes were made using rapid prototyping system.

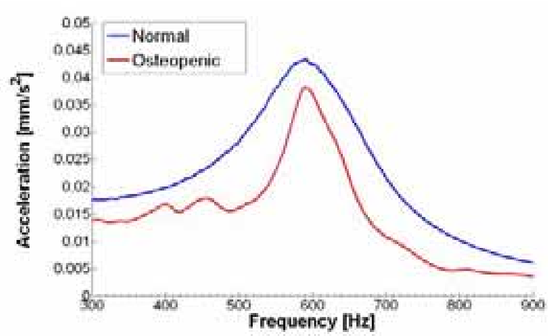

Figure 2: Power spectrums of acceleration signals from normal and osteopenic bone models (peak at 595 [Hz]).

RESULTS AND DISCUSSION

The normal bone model showed a light modal coupling in power spectrum, whereas the osteopenic bone model showed a heavy modal coupling with both models exhibiting a strong peak at 595 [Hz] (Figure 2). The half-peak bandwidths for the normal and the osteopenic bone were determined to be 265 (ζ = 0.10) and 130 (ζ = 0.08) [Hz], respectively. The dynamic stiffness of the osteopenic bone model was about one third of the normal bone model.

CONCLUSIONS

The results of the experimental modal analysis of the bone cube models representing the normal and osteopenic stages of trabecular bone have been discussed here. Although at a preliminary stage, the results have showed a clear difference between these two architectures. Current and further studies are underway to ensure the feasibility and reliability of a structural dynamics approach to detect early stages of bone loss.

REFERENCES

1. *International Osteoporosis Foundation World Congress on Osteoporosis*, Lisbon, Portugal, 2002.
2. Kiberstis, P., O. Smith, and C. Normal. Bone Health in the Balance. *Science* **289,** 1497, 2000.
3. B.J. Schwarz and M.H. Richardson, "Experimental Modal Analysis", *CSI Reliability Week*, Orlando, FL, 1999.
4. Ewins,D.,J, "Modal Testing: Theory and Practice", *Research Studies Press LTD*, Baldock, England,2000.

CENTER OF PRESSURE MEASURES PREDICT HEMIPARETIC GAIT VELOCITY

Chris Mizelle[1], Larry Forrester[1, 2], Mary Rodgers[1]
[1]Department of Physical Therapy and Rehabilitation Science, University of Maryland School of Medicine,
[2]Veterans Affairs Maryland Health Care System, Baltimore, Maryland
email: cmizelle@som.umaryland.edu web: http://pt.umaryland.edu

INTRODUCTION

Stroke is the leading cause of disability in the US, leaving two-thirds of survivors with abnormal motor function, including hemiparetic gait. Gait velocity is commonly used to assess locomotor function in this population, though velocity alone provides only a general index of function (1). A more detailed description of hemiparetic gait can be derived from center of pressure (CoP) time series measurements taken at each foot during the gait cycle. These measures may reflect aspects of the underlying motor control for walking and have been used to characterize asymmetries in hemiparetic gait (2). The goal of this study was to identify paretic and nonparetic foot CoP characteristics that may have a predictive relationship with the global functional measure of gait velocity.

METHODS

Thirty-three chronic stroke survivors > than 6 months post-stroke (10 female; 22 with left hemiparesis; mean age 67±10 yrs) were evaluated during walking at a self-selected speed on an instrumented gait mat (GaitRite®, CIR Systems, Clifton, NJ, USA). Patients wore pressure sensitive shoe insoles (Pedar®, Novel, Munich, Germany) and completed 15 steady-state gait cycles (five from each of three trials). Walking velocity and center of pressure parameters were measured during each cycle. Multiple regression analyses were used to model 58 CoP and symmetry parameters as predictor variables of gait velocity in all possible combinations. For the final model, parameters were evaluated using an adjusted regression model with $\alpha \leq 0.05$ and independence defined as a Variance Inflation Factor <10.

RESULTS

Table 1 shows the intercept and 11 parameters used to construct the final model, including bilateral variability of CoP mean location and displacement in anteroposterior (A-P) and mediolateral (M-L) directions, bilateral peak force, variability in stance time symmetry, and variability in CoP path length symmetry index. All parameters in the resulting final model contributed significantly and independently to the prediction of gait velocity. CoP and symmetry parameters in this model accounted for a large portion of the variance in hemiparetic gait velocity ($R^2_{adj} = .90$), showing strong predictive ability in this group of patients with chronic stroke.

DISCUSSION AND CONCLUSIONS

In the present study, 8 of the 11 variables used to predict hemiparetic gait velocity were derived from CoP time series. In addition, the relationships between the variability of the CoP parameters to gait velocity suggest a connection to motor control deficits at the foot and ankle during hemiparetic stance in both limbs. For example, velocity is positively related to variability of the nonparetic mean M-L CoP location, but is negatively related to the variability of A-P CoP location. Thus increased walking velocity may improve consistency of loading related to nonparetic dorsi-plantar flexor control, but it simultaneously introduces less predictable loading through the range of inversion-eversion. This latter effect is underscored by increasing ranges and variability on M-L loading of the paretic foot. The notion of improved motor control with higher velocities is also supported by the decreased variability in the symmetry ratio of paretic-to-nonparetic stance times, an indication of more consistent interlimb patterning. The significance of these results is that foot CoP measures not only successfully index functional locomotor status, but they may also be useful in determining adaptive mechanisms of recovery associated with specific therapeutic interventions.

REFERENCES

1. Richards & Olney. *Gait & Posture* (**4**), 149-162, 1996.
2. Rodgers et al., *Proceedings of ASB XXVIII*, Portland, Oregon, 2004.

ACKNOWLEDGEMENTS

This work was supported by Claude D. Pepper OAIC (NIH P50 AG12583) and Department of Veterans Affairs: Rehabilitation Research and Development Service Advanced Career Development Award (B3390K).

Table 1: Multiple regression results from combined paretic and nonparetic parameters to predict velocity.

Final Model	Parameter Estimate	Standard Error	t value	Pr > | t |	Variance Inflation
Intercept	88.34	10.15	8.70	< 0.01	0
Max M-L Paretic CoP displacement	0.86	0.17	5.14	< 0.01	1.73
SD Max M-L Paretic CoP displacement	2.09	0.96	2.18	0.04	1.65
SD Max A-P Paretic CoP displacement	-0.53	0.21	-2.55	0.02	1.90
Mean Peak Force: Paretic Foot	-0.06	0.01	-5.39	< 0.01	5.29
Mean A-P Location: Paretic CoP	-0.19	0.06	-3.25	< 0.01	1.63
Mean Peak Force: Nonparetic Foot	0.07	0.02	4.14	< 0.01	5.58
Mean Nonparetic Stance Time	-44.97	3.88	-11.58	< 0.01	1.45
SD Mean M-L Location: Nonparetic CoP	7.45	1.26	5.92	< 0.01	1.19
SD Mean A-P Location: Nonparetic CoP	-0.92	0.32	-2.85	< 0.01	1.26
SD Symmetry Ratio of Stance Time	-9.60	3.19	-3.01	< 0.01	1.35
SD Symmetry Index of Total CoP Path Length	0.40	0.08	5.01	< 0.01	1.49

IMAPACT OF RESTRICTED PIP JOINTS ON MCP JOINT MOTION IN THE HUMAN HAND

Jessica Woodworth*, Matthew McCullough*, Nicole Grosland[+]* and Brian Adams[+]*
Departments of Orthopaedic Surgery[+] and Biomedical Engineering*, University of Iowa, Iowa City, IA
Email: jessica-woodworth@uiowa.edu

INTRODUCTION

Loss of motion of the metacarpophalangeal (MCP) and proximal interphalangeal (PIP) joints caused by trauma or degenerative processes impairs hand function. Patients with arthritis often have involvement of multiple finger joints, which further decreases function. Surgical alternatives for severe PIP arthritis are arthrodesis and implant arthroplasty. Arthrodesis provides a pain-free and stable joint, but sacrifices motion, resulting in a need for compensatory increased motions at neighboring joints. Arthroplasty is an attractive option, but its risks should be weighed against the impairment caused by fusion. The impact of stiff finger joints on the performance of activities of daily living is unclear. In this study we aim to determine the affect of restricting PIP motion on the range of MCP motion while performing several manual tasks.

METHODS

After obtaining IRB approval, 15 subjects (5 male/9 female) without upper extremity compromise were recruited from the local community. Subsequently, informed consent was obtained from each subject. The goal was to evaluate the motions used by the MCP joints of the dominant hand for a series of thirteen activities of daily living (ADL) with the PIP joints free and splinted. Tasks included: tying a shoe, buttoning a shirt, turning a doorknob, drinking, opening a jar, answering a phone, pouring milk, stirring rice, picking up small objects, eating soup, typing, wringing out a washcloth and signing ones name.

Motion of each finger was monitored using an Optotrak (Northern Digital, Inc., Waterloo, Ontario) motion analysis system with two position sensors. Each task was evaluated under two conditions: 1) unrestricted PIP and MCP motion (i.e. without the use of splints), and 2) fully restricted PIP motion of each finger (excluding the thumb) with unrestricted MCP motion.

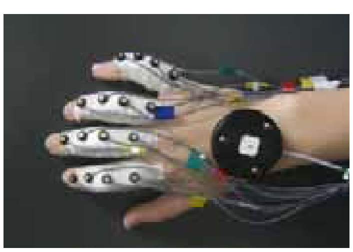

Figure 1. Splinted Finger Setup

For the first condition, four LEDs were affixed to each finger and the respective MCP joint was digitized with respect to a sensor placed on the back of the hand. Subjects were instructed to begin and end each task in the neutral position (i.e. with their fingers in line with the long axis of the third metacarpal). For the second condition, all four of the PIP joints were splinted at 40 degrees of flexion using small aluminum splints covered with self-adherent Coban (3M) and secured to the fingers with tape. The position sensor remained on the back of the hand and markers were applied directly to each splint (Figure 1). Each task was performed at a self-selected pace, while finger motions were recorded.

Data was processed using a Motion Monitor System (Innovative Sports Training, Chicago, IL) and then exported to a custom written Matlab program that used Euler angle transformation to compute the three-dimensional positions of the markers with respect to a local hand coordinate system. Differences in the maximum range of motion measurements were measured between the splinted and non-splinted trials for each task.

RESULTS AND DISCUSSION

A significant increase occurred in the amount of MCP flexion used to perform some of the tasks during the splinted trials. Tasks normally involving substantial PIP motion typically produced an increase in MCP flexion when the PIP joints were restricted. For example, buttoning a shirt showed a significant increase in MCP flexion ROM at all four fingers ($p<0.05$) when splinted (Figure 2). Although recorded, increases in the amount of MCP flexion for most tasks were small and did not display great changes statistically due to high standard deviations.

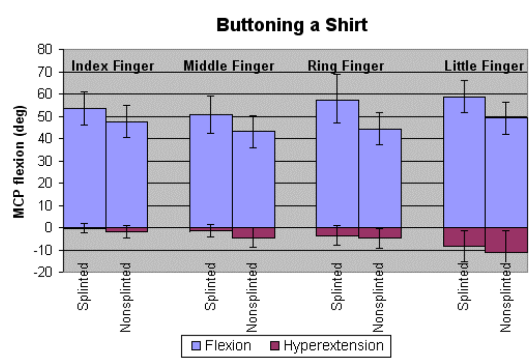

Figure 2. MCP flexion/hyperextension while buttoning

This investigation lends insight into the amount of compensatory motion used by the MCP joints when PIP joint motion is restricted at 40° of flexion. A wide range of required flexion was used by each subject indicating individuals accommodate well when PIP joints are splinted in this position. Since the finger DIP joints and thumb were neither monitored nor restricted, the affects of PIP restriction may have been underestimated in arthritic patients who often have multiple joint involvement. In fact, we observed that subjects altered thumb use to compensate for the restricted PIP joints in tasks such as tying a shoe and stirring rice.

ENERGETICS OF LEGGED LOCOMOTION: WHY IS TOTAL METABOLIC COST PROPORTIONAL TO THE COST OF STANCE WORK?

Manoj Srinivasan
Cornell Bio-robotics and Locomotion Lab, Theoretical and Applied Mechanics
Cornell University, email: ms285@cornell.edu, web: http://www.tam.cornell.edu/~ms285

INTRODUCTION

What are the major contributors to the metabolic cost of legged locomotion? During the stance phase of a gait, energy is required to periodically redirect the velocity of the center of mass from down to up. This **"cost of stance"**, typically approximated by external work calculations, is a substantial fraction of the total metabolic cost. Another large fraction is the **"cost of swinging"**, relating to the energy required to swing the legs and other body parts faster than they would move passively.

In treadmill experiments [1], where an animal or a human runs at a number of speeds, researchers have found that the stance work (estimated by external work on the body) is approximately proportional to the total metabolic cost. And in a recent study, Marsh *et al* [2] showed that in running turkeys, over a range of speeds, the metabolic cost of swinging the leg is proportional to the metabolic cost of stance. While these two experimental results are consistent with each other, how can the proportionality be simply explained? We show that it can be explained by metabolic cost optimization.

METHODS

The total cost of locomotion, minus the resting metabolic cost, is modeled as the sum of the two terms – the cost of swing and the cost of stance. The magnitude of these terms will depend both on the speed v of locomotion and on the stride rate f, or equivalently, the step-length d. For example, keeping the speed constant and varying the stride rate, or vice versa, changes the magnitudes of the terms. In particular, while swing cost and stance cost do depend on the details of the muscular coordination, for simplicity, they can be assumed to be functions of only the speed and the stride rate. This assumption might be also interpreted as using the costs for the optimal muscular coordination for a given speed and stride rate.

For simple models of the animal's mechanics, and in experiments, the individual cost terms are relatively well-approximated by power laws (e.g., [2]). Typically, the stance cost per unit distance is of the form: $E_{stance} = c_1 v^m f^n$.

Assuming a metabolic cost proportional to work, maximum force, integral of force, or any other reasonable quantity, results in such a power law, in walking [3] and in running [5]. For much of the following discussion, however, how exactly the power law is derived is not important, but only that it be a power law.

The swing cost per unit distance is assumed to have the same functional form, $E_{swing} = c_2 v^p f^q$. This has also been verified by systematic experiments (e.g., [3]). In experiments and in models, for a given speed, E_{stance} decreases with increasing f, so $n<0$. E_{swing} increases with increasing f, so $q>0$. Other than these two conditions, the actual values of the various coefficients and exponents in these formulas are not important for obtaining the main result of the paper.

The total cost of locomotion is given by:

$$E_{total} = E_{stance} + E_{swing} = c_1 v^m f^n + c_2 v^p f^q. \quad (1)$$

RESULTS AND DISCUSSION

It is well-established that, for a given velocity v, humans and animals pick the stride rate f_{opt} that minimizes their cost of locomotion (e.g., [6]). The optimal stride rate f_{opt} might be obtained by differentiating Eq.1 with respect to f, and setting it equal to zero. Substituting this expression for f_{opt} in the respective formulas for the costs, we get:

$$E_{stance} / E_{swing} = -q / n \quad (2)$$

Thus, as experimentally determined by Marsh *et al* [2], our simple theory predicts that the ratio of the cost components is independent of the speed. Eq.2 also suggests that E_{stance} is proportional to the total metabolic cost, independent of speed. Assuming that the cost of stance E_{stance} is proportional to muscle work and that the elastic recovery is a constant fraction of the stance work, we predict that the metabolic cost is proportional to stance work alone, as observed by early investigators [1].

CONCLUSIONS

We have presented a simple way of understanding the apparently constant partitioning of the metabolic cost of legged locomotion observed in experiments, both old and new. More generally, the result provides a justification for the use of force plates as approximate ergometers [7], to estimate the total metabolic cost. The result is general in that it is independent of many details of the actual cost laws assumed. And it is likely to be applicable whenever the total metabolic cost of locomotion is modeled by sum of two terms, both of which are well-approximated by power laws.

REFERENCES

1. Cavagna GA *et al, J Appl. Physiol.*, **19**, 249-256, 1964.
2. Kuo AD. *ASME J Biomech Engg.*, **124**, 113-120, 2002.
3. Doke J, *et al. Proc. 27th annual meeting ASB.* 2003.
4. Marsh *et al. Science*, **303**, 80-83, 2004.
5. Ruina A *et al. J theor. Biol.*, in press, 2005.
6. Bertram J and Ruina, *J theor. Biol.*, **209**, 445-453. 2001.
7. Cavagna GA, *J Appl. Physiol.*, 39, 174-179. 1975.

ACKNOWLEDGEMENTS

The author thanks Andy Ruina's encouragement

Aerodynamic Characteristics of Baseballs Delivered from a Pitching Machines

Tsutomu Jinji and Shinji Sakurai
School of Health and Sport Sciences, Chukyo University

INTRODUCTION

The purpose of this study was to compare aerodynamic characteristics of baseballs delivered by actual pitchers and by pitching machines. The results of this study would suggest useful ideas for the usage of a pitching machine in batting practice.

Although many studies using the wind-tunnel experiment have clarified aerodynamic forces on a pitched baseball, the spin characteristics, such as spin rate and spin axis directions, during the actual ball flight have been hardly quantified. To elucidate the aerodynamics of a baseball more closely, we obtained three-dimensional trajectory, angle of spin axis and the spin rate of the actual pitched baseball.

METHODS

All experiments were conducted indoors in order to minimize wind influence. Nine collegiate pitchers pitched 10 fastballs of 4-seam (FB) and 10 curve balls (CB), respectively. A pitching machine with a propulsion system of spinning wheels was used to fire 10 FBs of 4-seam and 10 CBs.

Trajectories of these balls were filmed with four synchronized video cameras (60Hz) and were analyzed using DLT procedures. The global coordinate system was set as follows; the Z-axis was defined as vertical, the Y-axis was defined as horizontal and pointing toward home plate and X-axis was then defined as the cross product of the Y- and Z-axes, with the origin at the center of the front edge of the pitching rubber. Polynomial function using the least square method was used to derive time-displacement relationships of ball coordinates during flight for each pitch.

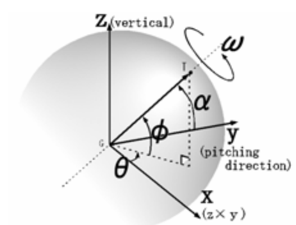

Figure1: Definition of spin axis. The orientation of the angular velocity vector ω is specified by two angles θ and ϕ. α is angle between spin axis and y−axis.

To obtain the ball rotation axis and spin rate, the baseball was filmed just after the delivery with a high-speed video camera (250Hz) set with the lens axis along the Y-axis of the global coordinate system. The direction of spin axis and the spin rate were calculated using positional changes of drawn marks on the ball surface. The direction of the spin axis was defined by two angles, θ (azimuth) and φ (elevation), an angle between spin axis and y axis (α) was also obtained. The spin parameter (r**ω**/**V**; **V** is the free-stream velocity, r is radius of the ball and **ω** is the ball angular velocity) was obtained, following previous studies.

RESULTS AND DISCUSSION

Initial velocity and spin rate of the balls from pitching machine were within the ranges of those for the actual pitchers. However, there was a significant difference in the mean values of total break (composition ⊿X and ⊿Z) between the balls from a pitching machine and the balls pitched by actual pitchers for both FB and CB pitches ($p<0.001$). FB pitches tended to break in the opposite direction to the CBs. The mean value for the break of CBs by pitching machine was approximately 1.9 times larger compared to those for actual pitchers.

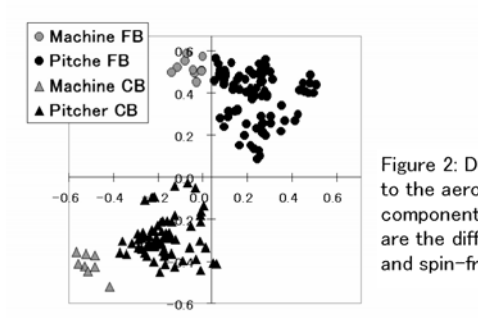

Figure 2: Deflections of trajectory due to the aerodynamic force. The two components of break, X and Z direction, are the differences between the fitted and spin−free trajectories at 18.44m.

Watts and Ferrer (1987) suggested that lift coefficient was proportional to r**ω**/**V** in the wind tunnel. However, in this study, the lift coefficient did not depend on r**ω**/**V** ($r=0.429$), but had a close relationship with **ω**sinα ($r=0.860$). This parameter, **ω**sinα, represents the actual effect of spin on lift force.

Magnus effect occurs from rotation of the ball, and act perpendicular to the axis of spin. Magnus effect is largest when the angular and translational velocity vectors are perpendicular to each other, and it indicates that the break of the pitched baseball is decreased when the angle between the two vectors comes closer to 0°. To adapt the features of the balls by a pitching machine to the actual pitchers' balls, it would be necessary to set the propulsion condition of a "screwball" for a fastball, and reduce the spin rate for curve ball.

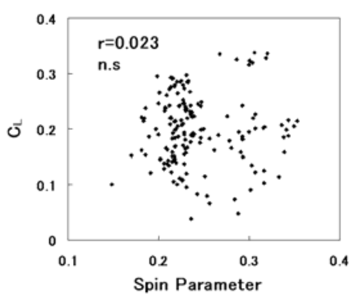

Figure 3: The relation between lift coefficient and Spin Parameter ($r\omega/V$)

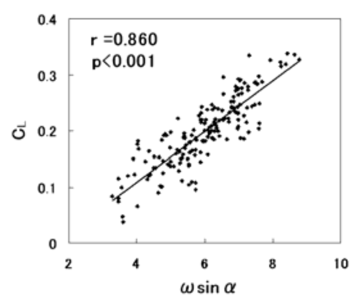

Figure 4: The relation between lift coefficient and $\omega \sin\alpha$

CONCLUSIONS

Balls delivered from a pitching machine whose axis was close to vertical to the pitching direction broke more largely than actual pitcher's balls.

REFERENCES

1. Bearman, P.W., & Harvey, J.K. *Aeronautical Quarterly*, **27**, 112-122, 1976.
2. Watts, R.G.., and Ferrer, R.. *American Journal of Physics*, **55**, 40-44, 1987.

A 3-DIMENSIONAL CAMERA CALIBRATION ALGORITHM FOR UNDERWATER MOTION ANALYSIS WITH REFRACTION CORRECTION CAPABILITY

Young-Hoo Kwon
Biomechanics Laboratory, Texas Woman's University, Denton, TX, USA
email: ykwon@mail.twu.edu

INTRODUCTION

The DLT (Direct Linear Transformation) algorithm, the most frequently used calibration algorithm, is based on the so-called collinearity condition; i.e. the object, image, and projection center form a straight line. This condition, however, does not hold in an underwater analysis setting due to the nonlinear image deformation caused by refraction at the water-air interface (Figure 1) [1]. The immediate outcome of the image deformation is an increased calibration/reconstruction error when compared to its above-water counterpart.

Reconstruction accuracy can be improved to a certain extent by maintaining large interface-object distance and/or camera-interface distance [1], by using localized sub-volumes (localized DLT) [2], or by manipulating the characteristics of the calibration frame [1]. Although these methods are useful, the ultimate solution is to use a calibration algorithm that has the refraction correction capability. The purposes of this study are (a) to develop a calibration algorithm that allows refraction correction, and (b) to test its applicability through a simulation.

METHODS

A comprehensive refraction model was developed with 12 experimental factors incorporated (Figure 1): position and orientation of the calibration frame with respect to the interface plane (6), camera position and orientation with respect to the interface plane (3), and the internal factors of the camera (3). Due to the complexity imposed by the nonlinear refraction equation, no simple direct solution is available and a special optimization strategy must be developed.

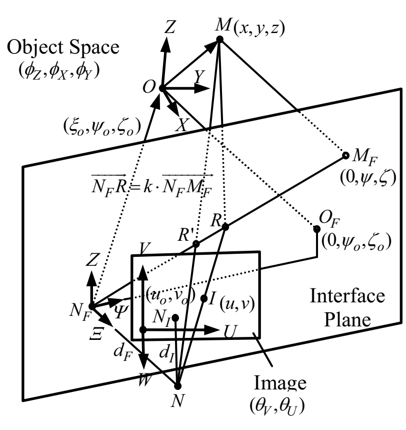

Figure 1. Refraction Model with 12 Experimental Factors

The new method proposed in this study is mainly based on the collinearity among the refraction point (R in Figure 1; not the object), image point (I), and the projection center (N). The coordinates of the refraction point were described as a fraction of the coordinates of point M_F by a ratio k (Figure 1). Although k is a high-order function of the position and angle factors, it was considered as a constant in the cost function for simplicity. As a result, the interface-to-calibration-frame distance was optimized separately from the others since this factor is involved only in the computation of ratio k. All other factors are present in the cost function and can be computed through an iterative approach using the Newton method. The interface-frame distance was optimized based on the calibration error. A converged set of experimental factors were obtained for every level of interface-to-frame distance. The distance that shows the smallest calibration error was selected as the optimal interface-frame distance.

A simulation was performed to assess the performance of the new algorithm. A 3 m x 1 m x 1m calibration frame with 56 control points was used. An arbitrary set of experimental condition was used (interface-frame distance = 4.0 m, camera-interface distance = 0.8 m, etc.) to generate the image coordinates of the control points. A series of calibrations were performed based on the real-life coordinates and the simulated image coordinates.

RESULTS AND DISCUSSION

Only 7 distance and internal camera factors were subject to optimization in this paper. Calibrations were repeated with various initial values. In all cases the distance and camera factors fell within 2 cm of the actual values used in the simulation. In terms of calibration error, the new algorithm outperformed the DLT algorithm considerably. Moreover, the calibration error showed a quadratic pattern with the minimum value coming from the optimized interface-frame distance. The calibration error increased when random errors were introduced to both the real-life coordinates and the image coordinates. However, the algorithm consistently generated stable (converged) solutions.

CONCLUSIONS

The new algorithm was deemed applicable in the underwater analysis. Due to its refraction correction capability, the algorithm will be useful especially in situations with poor experimental conditions, such as short camera-interface distance and interface-frame distance. Distortion correction also means considerably less extrapolation error outside the control volume.

REFERENCES

1. Kwon, Y.-H. Journal of Applied Biomechanics, **15**, 396-403, 1999.
2. Kwon, Y.-H. et al. *XVIII International Symposium on Biomechanics in Sports. Applied program: Application of Biomechanical Study in Swimming*. Hong Kong, 2000.

QUADRICEPS-HAMSTRING MUSCLE SYNCHRONY DURING LANDING MOVEMENTS: IS IT AFFECTED BY MOVEMENT DIRECTION?

Bridget Munro and Julie Steele
Biomechanics Research Laboratory, Department of Biomedical Science, University of Wollongong, NSW, Australia, 2522
email: bmunro@uow.edu.au, web: www.uow.edu.au

INTRODUCTION

One of the most frequent non-contact mechanisms of isolated injury to the anterior cruciate ligament (ACL) occurs when landing from a jump, particularly when players land and rapidly decelerate their forward progression [1]. Past research has suggested that to protect the ACL from injury, athletes should land with more vertical rather than horizontal momentum and use run-on steps where possible [1]. Although appropriate muscle activation patterns that control the lower limb at initial contact (IC) have been suggested to protect the ACL, little is know as to how or whether these patterns change with different movement types and with different post-landing strategies. Therefore, the purpose of this study was to assess whether quadriceps-hamstring muscle synchrony are affected by different landing movements and/or the need to decelerate abruptly or not.

METHODS

Thirty-six athletes (mean 23.6 years, range 19-30) involved in landing sports and with no history of knee joint injury volunteered to participate in the present study. All subjects underwent laboratory-based assessment of their landing technique when performing two landing movements (vertical mark, horizontal stride) and two post-landing strategies (rapid deceleration at IC, run-on after IC).

During the five trials per condition, electromyographic (EMG) data were sampled (1000 Hz; bandwidth, 0-340 Hz) for the rectus femoris (RF), vastus lateralis (VL), biceps femoris (BF) and semitendinosus (S) muscles of each subject's dominant lower limb using a Noraxon Telemyo system. Following zero offset removal, raw EMG signals were filtered using a fourth order zero-phase-shift Butterworth high pass filter (f_c = 15 Hz). The filtered muscle activity data were then full-wave rectified and low pass filtered (f_c = 20 Hz) and the resultant linear envelopes were screened with a threshold detector (7% of maximum amplitude) to determine the temporal aspects of each muscle burst with respect to IC. IC was confirmed against ground reaction force data collected (1000 Hz) using a Kistler force platform.

RESULTS AND DISCUSSION

Two-way repeated measures ANOVA results indicated that, although there was no main effect of post-landing strategy on muscle activity, there was a significant main effect of movement type on quadriceps-hamstring muscle synchrony (Figure 1). That is, RF and VL were activated significantly earlier and S and BF were activated significantly later when subjects performed the vertical mark compared to the horizontal stride (Figure 1). When striding, a horizontally directed movement, subjects appeared to follow the typical sequential recruitment pattern of hamstrings followed by quadriceps activation. This pattern is suggested to protect the ACL by maximizing the efficacy of the hamstring muscles to produce posterior tibial drawer [2]. In comparison, when subjects performed the vertical mark, the thigh muscles showed a more simultaneous activation pattern, indicating greater co-contraction and preparation of the lower limb to absorb a more vertically directed ground reaction force and prevent collapse of the lower limb during landing. Interestingly, these two muscle activation strategies used during the two different movement types were unchanged regardless of the post-landing strategy to be performed.

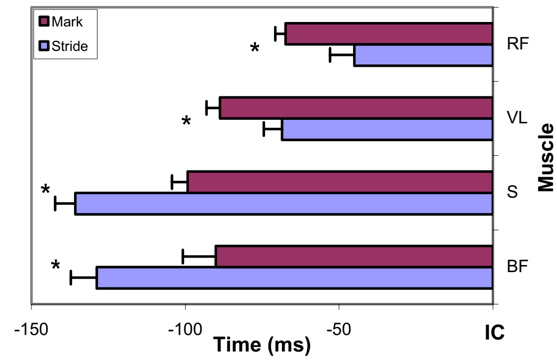

Figure 1: Quadriceps and hamstring muscle synchrony when subjects performed the mark and stride movements (IC = initial contact; * indicates $p < 0.05$).

CONCLUSIONS

It was concluded that, although the direction of landing movement may alter quadriceps-hamstring muscle synchrony at IC, the movement to be performed after landing did not influence this muscle synchrony. However, research is warranted to determine whether the quadriceps-hamstring muscle synchrony noted for the vertical mark was more advantageous in terms of preventing ACL injury relative to the strategy used during the horizontal landing. Furthermore, whether unanticipated post-landing strategies, relative to anticipated strategies, could alter the quadriceps-hamstring muscle synchrony in a way that could predispose the athlete to ACL injury requires investigation.

REFERENCES

1. Steele J. *Sports Med* **10,** 88-102, 1988.
2. Kain, et al. *Am J Sports Med* **16,** 147-152, 1988.

ACKNOWLEDGEMENTS

This project was funded by the Australian Football League Research Board and New South Wales Sporting Injuries Committee.

Gait Affects Tibial Component Migration in Unicondylar Knee Arthroplasty

[1&2] Brendan Joss, [2]Ming Guo Li,[2]David Wood and [1]David Lloyd
[1]School of Human Movement and Exercise Science, University of Western Australia
[2]Perth Orthopaedic Institute, Perth Western Australia
bjoss@cyllene.uwa.edu.au

INTRODUCTION

The processes behind tibial component migration in Unicondylar knee arthroplasty (UKA) have been relatively unstudied. The force applied to the prostheses during walking increases the shear stress at the bone cement interface, which may lead to aseptic loosening[1]. Knee compressive forces in gait may also cause prosthesis migration[1]. By participating in a large amount of walking, the UKA prosthesis may be highly exposed to these knee loads, exacerbating the migration thus loosening. Roentgen stereophotogrammetric analysis (RSA) can accurately measure component migration[2]. In addition, by using three-dimensional (3D) gait analysis and wearing daily activity monitors, respectively we examined if knee joint loading during gait and exposure to this loading is related to UKA tibial component migration.

METHODS

11 patients who received a Millar Glante (Zimmer) UKA for medial compartment Osteoarthritis with suitable RSA films for analysis at 2 years post surgery were studied with 3D gait analysis. The sample is part of a larger sample still to be collected and analyzed. The Vicon 370 (Oxford Metrics, Oxford UK) motion analysis system with 7 infra red camera at 50 hertz and two ATMI force plates were utilised to measure the lower limb joint kinematics and kinetic with the cluster marker model and optimized joint axes and centres[3]. Kinematic variables were normalized to bodyweight x height and expressed as external joint moments. Patients were instructed to walk at their self-selected, normal walking speed for analysis. Prior to the gait analysis session, each subject also wore an activity monitor. Nine age matched control subjects were also tested using the same procedures for comparison.

RESULTS AND DISCUSSION

The UKA group walking with higher peak knee adduction and flexion moments during the stance phase compared to the control group. There was no correlation between peak knee adduction moment and tibial component migration. However peak knee flexion moments showed moderate correlations with distal subsidence (r=0.48) and posterior tilt (r=0.43) of the tibial component. Higher correlations were found between average number of steps per day and lateral (r=0.57) and posterior subsidence (r=0.52) and varus tilt (r=0.62).

High peak knee flexion moments in total knee arthroplasty patients have also been associated with increased tibial component migration, leading to the potential early onset of aseptic loosening[1]. High peak flexion moments also predict the presence and severity of anterior knee pain following total knee arthroplasty[4].

The preliminary results are also the first to show an association with physical activity and component migration in knee replacement, supporting a long held belief by orthopaedic surgeons. When the peak knee flexion moments were multiplied by the average number of steps taken per day the correlations with components migration were strengthened (r=0.68 for distal subsidence and r=0.61 for varus tilt of the tibial component). These stronger correlations suggest the amount and frequency of knee joint loading has the greatest affect on potential tibial component loosening.

CONCLUSIONS

The results from this small sample of a larger study group to be tested suggests that high flexion moments have a negative effect on the tibial component in UKA, similar to that seen in total knee replacement[1]. This sample is the first reported evidence of the frequency of joint loading having larger affect on migration, which is further strengthening when combined with high joint moments.

REFERENCES

1. Hilding, M. B., Ryd, L., Toksvig-Larsen, S., Mann, A., & Stenstrom, A.. Gait affects tibial component fixation. *Journal of Arthroplasty, **14**(**5**),* 589-593, 1999.
2. Ryd, L., Albrektsson, B. E., Carlsson, L., Dansgard, F., Herberts, P., Lindstrand, A., et al.. Roentgen stereophotogrammetric analysis as a predictor of mechanical loosening of knee prostheses. *J Bone Joint Surg Br, **77***(**3**), 377-383, 1995.
3. Besier T.F., Sturnieks, D.L., Alderson, J.A, And Lloyd D.G., Repeatability of gait data using a functional hip joint centre and knee helical axis. *Journal of Biomechanics*, **36**(**8**), 1159-1168, 2003.
4. Smith A.J., Lloyd D.G. and Wood D.J. Presurgery knee joint loading patterns during walking predict the presence and severity of anterior knee pain after total knee arthroplasty. *Journal of Orthopaedic Research*, **22**(**2**), 260-266, 2004.

PARAMETRIC FINITE ELEMENT MODEL OF FEMUR FROM CT DATA

[1] Mehran Armand and [1]Liming Voo
[1]Johns Hopkins University Applied Physics Laboratory, Laurel, MD. 21044

INTRODUCTION

The investigation of the individual effects of structural and geometrical parameters on the bone strength can lead to a better understanding of the mechanisms and risk factors associated with a range of bone problems including fracture, aging, osteoporosis, and bone loss in microgravity. A semi-automatic technique is used to develop a finite element model of the femur bone from the CT data. The major difference between this technique and other FE models of the femur is that it is based on the parameterization of the bone; therefore, it directly lends itself to a sensitivity analysis of the femur's structural and geometrical factors. This work is the extension to the elliptical model reported previously [1], and generates a more accurate geometry.

METHODS

A proximal femur of an average male cadaver was scanned using a CT scanner. The steps towards developing FE mesh were as follows: 1) Semi-automatic custom algorithms were applied to extract the bone's outer contours and density information from the CT data; 2) A piecewise continuous cubic spline fit was applied to parametrize the outer contours; 3) The inner contours were calculated such that the constraint equations for cross-sectional mass and moment of inertia along femoral shaft and neck axes were satisfied; 4) Scaling was performed on the regions of interest; 5) An automated algorithm generated the volumetric model including outline of the bone and the inner cortex boundaries. 5) The bone volume was meshed automatically with 20-node brick elements, as needed for finite element simulations.

Semi-automatic custom algorithms were applied to extract the bone's outer contours and density information from the CT data. The algorithm re-sliced images along the axis of the shaft and neck of the femur (the transition from shaft axis to neck axis was defined by a hyperbolic fit). Edge extractions were performed for the outer boundaries of the femur using the re-sliced sections along the femur's neck and shaft axes [2].

The algorithm performed a piecewise continuous cubic spline fit on the new reformatted slices along shaft and neck axis. A minimum number of control points that would adequately approximate the true geometry were found for each cross-section. The cross-sections were also visually inspected for the any potential imperfection.

The main challenge in creating accurate parametric bone geometry is the extraction of the contours of the inner cortex. We derived a theoretical and algorithmic technique for analytical calculation of the inner contour from the outer cortical boundary geometry. These calculations satisfy the mechanical properties of each cross section of the bone while producing a comparable geometry to the original bone. We

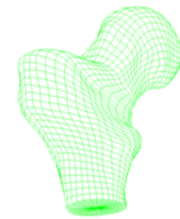

Figure 2: A finite element mesh of a proximal femur with neck-shaft angle reduced by 15^o

calculated the cortical/cancellous and cortical/marrow boundary such that the cross-sectional moment of inertia (CSMI) and cross-sectional area (CSA) of the model and the original bone remained equal (note that both are calculated from the mass of the cross-section based on one voxel thickness). We used the density map data for each cross-section plus the CSMI and CSA equations to calculate the appropriate spline fit to the cortical/cancellous or cortical/marrow boundaries. This enabled us to define the bone geometry and its material distribution with a finite number of control points for each cross-section. Thus, a full parametric model of the femur was created.

The regions of interest (e.g. neck angle, neck length) and cortical thickness was scaled using the cross-sectional geometries. An automated algorithm was developed to create surfaces on these cross-sections and mesh the generated volumes with 20-node hexahedral elements.

A TYPICAL EXAMPLE

The simulations were performed using SDRC-IDEAS finite element software. A typical example of the scaled bone is shown in Figure 1. The neck-shaft angle in this model was reduced by 15^o from the original CT data. The model had approximately 12000 hexahedral elements. Both cortical and cancellous layers had quality elements with maximum distortion less than 30%. In summary, the model from CT data included more accurate geometry than the previously reported elliptical model [1]. Additional user interaction, however, was required to verify the quality of the spline fits.

REFERENCES

1. Armand et al. *Proceedings of ASME Summer Bioengineering Conference,* Key Biscayne, Florida 2003.
2. Oden Z.M., Selvitelli D.M., and Bouxsein M.L., 1999, "Effect of local density changes on the failure load of the proximal femur," *J Orthop Res* 17(5):661-667.

ACKNOWLEDGEMENTS

This work was supported by USA MRMC grant number DAMD17-03-0711.

THERAPIST CONTROLLED POWERED LOWER LIMB ORTHOSES TO ASSIST LOCOMOTOR TRAINING

[1,2]Gregory S. Sawicki, [1]Antoinette Domingo and [1,3]Daniel P. Ferris
Departments of [1]Movement Science, [2]Mechanical Engineering, & [3]Biomedical Engineering,
University of Michigan, Ann Arbor, MI; email: gsawicki@umich.edu

INTRODUCTION

Locomotor training with manual assistance can greatly improve walking ability after neurological injury. However, manual assistance is labor intensive and variable from trainer to trainer. Robotic assistive devices are currently being developed to assist locomotor training, but no current device can assist ankle plantar flexion, the major source of work during normal walking. Therapist-controlled, powered lower limb orthoses for locomotor training could decrease therapist labor requirements, increase walking speed during training and lead to increased muscle activation and improved gait kinematics. However, because sensorimotor feedback contributes to muscle activation, plantar flexor assistance could decrease muscle activation of the triceps surae. The purpose of this study was to test therapist-controlled, powered ankle-foot orthoses (AFOs) to facilitate gait rehabilitation after spinal cord injury. We assessed the impact of localized powered assistance at the ankle on muscle activation patterns and joint kinematics during walking with partial bodyweight support in individuals with incomplete spinal cord injury.

METHODS

Four subjects (ASIA C or D) with chronic incomplete spinal cord injuries walked at 0.54 m/s under three different conditions: (1) without the AFOs, **WO;** (2) with passive bilateral AFOs, **PA;** and (3) with active bilateral AFOs under push-button control by a therapist, **TC**. Body weight support was provided at either 30% or 50% depending on the weight-bearing ability of the subject. When necessary, elastic cords provided lateral stability.

Figure 1: (a) Powered Ankle-Foot Orthosis (AFO). A lightweight carbon fiber orthosis (~1.5 kg) fit with an artificial pneumatic plantarflexor muscle. (b) **Therapist Control.** A therapist uses push-buttons to control the timing of active AFO assistance at the ankle as an ASIA D 24 yr. old male trains with partial body weight support.

RESULTS AND DISCUSSION

The passive condition and therapist control condition produced higher stance phase RMS EMG muscle activation in all three triceps surae muscles (SOL, MG, LG) than the without condition (Figure 2). The tibialis anterior demonstrated decreased stance phase activity in the passive condition and therapist control condition compared to the without condition.

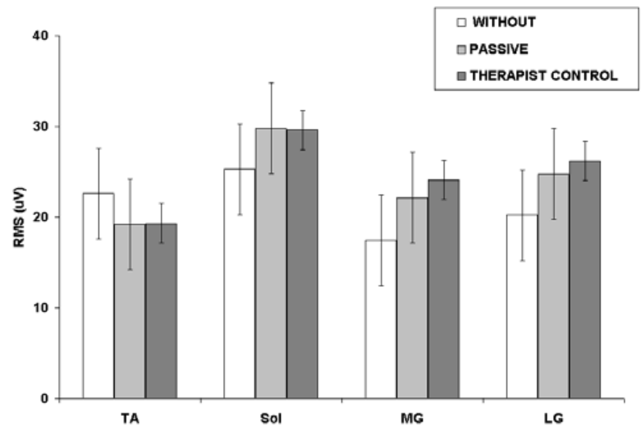

Figure 2: Stance phase averaged rectified RMS EMG for tibialis anterior (TA), soleus (Sol), medial gastrocnemius (MG) and lateral gastrocnemius (LG). Bars are mean and standard error of the mean.

CONCLUSIONS

These findings suggest that powered plantar flexion assistance does not decrease plantar flexor muscle recruitment during gait in incomplete spinal cord injury subjects. Thus powered lower limb orthoses may be a viable aid to assist therapist during locomotor training.

Our powered AFO comfortably delivered ~50% of normal ankle plantar flexor torque. Therapist labor intensity was reduced considerably, allowing the therapist to focus more on gait quality. Another possibility is that the push button control could come directly from the patient during gait rehabilitation.

ACKNOWLEDGEMENTS

Supported by Christopher Reeve Paralysis Foundation Grant FAC2-0101 and NSF BES-0347479.

MOTOR ADAPTATION TO A POWERED ANKLE-FOOT ORTHOSIS UNDER FOOT SWITCH CONTROL

[1]Stephen M. Cain, [2]Keith E. Gordon, and [2,3]Daniel P. Ferris
Departments of [1]Mechanical Engineering, [2]Movement Science, & [3]Biomedical Engineering
University of Michigan, Ann Arbor, MI; email: smcain@umich.edu

INTRODUCTION

Powered orthoses are an innovative way to study how humans adapt and change control strategies during walking. A previous study [1] using a powered ankle-foot orthosis (AFO) under proportional myoelectrical control (soleus EMG) to provide plantar flexion assistance found a decrease in soleus EMG amplitude without concomitant decreases in gastrocnemius EMG amplitude. We hypothesized that using foot switch control, in which the nervous system has no direct control over plantar flexion assistance, would result in simultaneous decreases in soleus, medial gastrocnemius, and lateral gastrocnemius EMG.

METHODS

Two healthy subjects (ages 23 and 24) participated in this study. The University of Michigan Institutional Review Board approved the study protocol and each subject gave informed consent. Each subject walked without an orthosis at a speed of 1.25 m/s on a treadmill and also while wearing a powered AFO as described by Gordon et al. [2] on the left leg. The powered AFOs used artificial plantar flexors (pneumatic muscles) that were controlled using an on/off (i.e., bang-bang) controller. The forefoot portion of a footswitch provided the signal to the controller to activate the artificial muscle. Each subject had two training sessions three days apart. A session consisted of walking without an AFO (no AFO) for 5 minutes, with a passive AFO (pre-passive AFO) for 10 minutes, with an active AFO (active AFO) for 30 minutes, and with a passive AFO (post-passive AFO) for 15 minutes. We collected and analyzed lower limb kinematics and electromyography (EMG) for 9 muscles (Motion Analysis system & Visual3D). We calculated average EMG RMS values normalized to the final minute of the pre-passive condition.

RESULTS AND DISCUSSION

The powered orthosis produced a peak plantar flexion torque of ~55 Nm, which resulted in increased plantar flexion from mid-stance through swing phase when wearing the powered AFO (Figure 1A). The subjects decreased soleus (SOL), medial gastrocnemius (MG), and lateral gastrocnemius (LG) muscle activation when the AFO was active (Figure 1B). During the last 10 minutes of the active AFO condition, EMG was reduced to ~77, 68, and 72% of pre-passive values for SOL, MG, and LG, respectively. When the powered AFO was turned off, SOL, MG, and LG EMG returned to ~100, 87, and 100% of pre-passive values. Both subjects were able to adapt to the powered AFO more quickly on the second day of training. As hypothesized, both subjects decreased muscle activity in all three triceps surae muscles (SOL, MG, LG) when walking with the powered AFO. However, even after two days of training, ankle kinematics were substantially different from passive AFO walking.

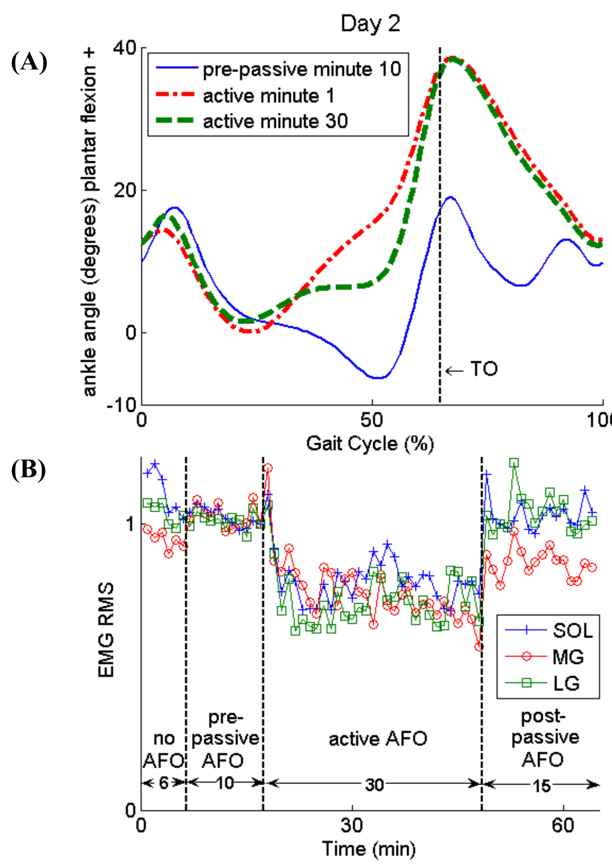

Figure 1: A) Ankle flexion versus gait cycle (left heel strike to left heel strike). Subjects walked with increased plantar flexion with the artificial plantar flexor powered ankle-foot orthosis (AFO). **B)** EMG RMS normalized to the last pre-passive minute versus time for soleus (SOL), medial gastrocnemius (MG), and lateral gastrocnemius (LG). With the powered AFO, subjects decreased muscle activity in SOL, MG, and LG simultaneously.

CONCLUSIONS

When a foot switch was used to control a plantar flexor-assist AFO instead of soleus EMG, muscle activity in all three triceps surae muscles (SOL, MG, LG) decreased synergistically. This study emphasizes that neural adaptations to a powered orthosis during gait depend on the type of controller used. Proportional myoelectric control [1] resulted in faster kinematic adaptation than foot switch control.

REFERENCES

1. Ferris, et al. *Proc 25th ASB*, San Diego, CA, 2001.
2. Gordon, et al. *Proc XXth ISB / 29th ASB*, in review, 2005.

ACKNOWLEDGEMENTS

Supported by NIH R01NS045486, NSF BES-0347479, and NSF GRFP.

POSTURAL SWAY ADAPTATION DURING INITIAL EXPOSURE TO PERIODIC AND NON-PERIODIC OPTIC FLOW

Mark Musolino[1,2,4], Patrick Loughlin[1,2,3] , Patrick Sparto[1,2,4] and Mark Redfern[1,2,4]

[1]Human Movement and Balance Laboratory
[2]Dept. of Bioengineering, [3]Dept. of Electrical Engineering, and [4]Dept. of Otolaryngology
University of Pittsburgh, Pittsburgh, PA, USA
Email: markmuso@pitt.edu Web: www.mvrc.pitt.edu

INTRODUCTION

Previous work in our laboratory showed that postural sway power in a group of six healthy adults was significantly larger in response to a periodic sum-of-sinusoids (SOS), compared to a spectrally similar non-periodic SOS [1], but only at the highest component frequency of the stimulus (0.5Hz). The objective of the current study was to determine whether this behavior could be reproduced in a larger group of subjects, and for a wider variety of SOS optic flow stimuli.

METHODS

Postural sway was examined in twenty healthy young adults during exposure to 90-second trials of various periodic and non-periodic optic flows, in a virtual reality setting [2] (Fig. 1b). Visual scene motion for each trial was driven by one of ten signals (Fig. 1a). Scene movements were presented only once, and in random order. Postural responses were examined through center-of-pressure (COP) excursions in the sagittal plane, measured via a force platform beneath the feet. Sway power at each stimulus component frequency was used as the means of comparison among PSUM and NPSUM groups. Differences were tested for statistical significance using a full-factorial repeated measures ANOVA (α=0.05).

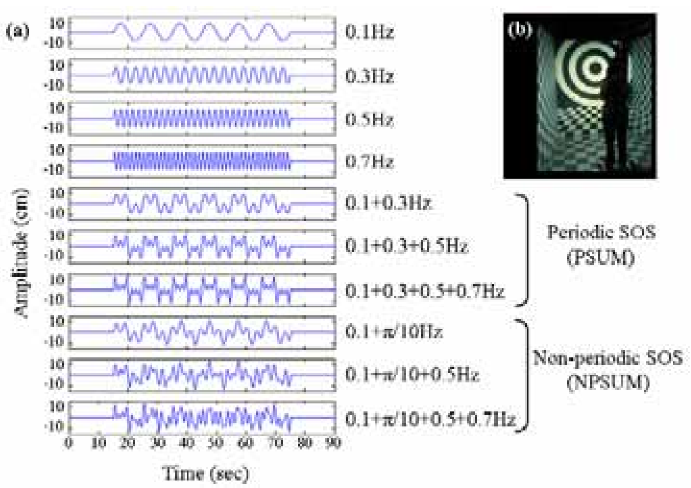

Figure 1: (a) Time-series of signals used to generate optic flow (60-seconds of motion, bounded at beginning and end by 15 seconds of stationary scene); **(b)** Subject standing on force platform, viewing the optic-flow pattern.

RESULTS AND DISCUSSION

Postural responses to PSUM and NPSUM optic flow were not significantly different at any of the stimulus frequencies, contrary to previous observations. However, sway power was again largest at the highest stimulus frequency (0.7Hz), suggesting that subjects were influenced by stimulus velocity, as others have reported [3]. In addition, an unusually strong trial effect was observed in 16 subjects, in which sway power for trial 1 was significantly larger than that for trials 2 through 10. Time-frequency analysis revealed *adaptation* (i.e. a within-trial decline in sway amplitude at the stimulus frequency [4]) in trial 1 (Fig. 2). That is, subjects responded strongly during initial exposure to optic flow, but the amplitude of this response decreased substantially during trial 1, and remained at an attenuated level for subsequent trials.

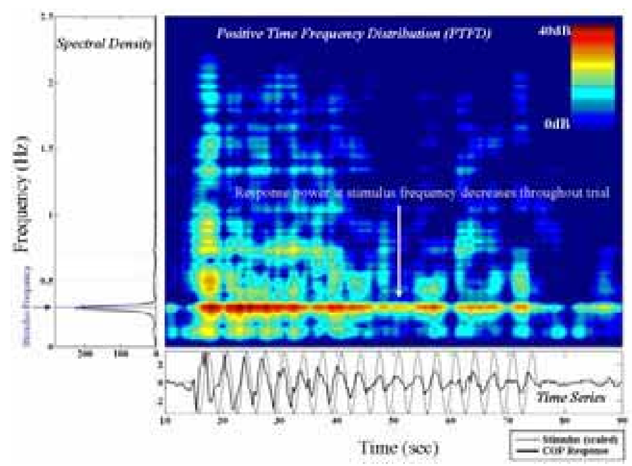

Figure 2: PTFD (see [4] for details) showing adaptation of sway response to 0.3Hz sinusoidal stimulus (subject 216).

This trial effect could not be completely addressed in the statistical analysis (due to insufficient power), so it is unclear whether or not this effect contributed to the current finding that responses to PSUM and NPSUM optic flow were not significantly different, which is contrary to prior observations.

CONCLUSION

Previous results were not entirely reproduced, perhaps due to the confounding influence of a strong trial effect. Further study is required to better understand these findings.

REFERENCES

1. Musolino MC, et al. *Proceedings of the 28th ASB*, Portland, Oregon, Abstract 289, 2004.
2. Jacobson J, et al. *Proceedings of the Virtual Reality Software & Technology Mtg*, 2001.
3. Dijkstra TM, et al. *Biol Cyb* **71(6)**, 489-501, 1994.
4. Loughlin PJ, et al. *IEEE EMB Mag*, March, 69-75, 2003.

GENERATION OF FORWARD ANGULAR IMPULSE IN TASKS WITH BACKWARD TRANSLATION IS ACHIEVED BY REDIRCTING THE REACTION FORCE RELATIVE TO CENTER OF MASS

[1] Witaya Mathiyakom and [2] Jill L McNitt-Gray
[1]Andrus Gerontology Center and [2]Department of Kinesiology, Biomedical Engineering, Biological Sciences, and University of Southern California; e-mail: mathiyak@usc.edu

INTRODUCTION

Successful performance of whole body movements is dependent on the ability of the performer to satisfy both linear and angular impulse requirements of the task during contact with the environment [1]. Previous research indicates that mechanisms of generating linear and angular impulse vary with tasks [2]. While linear impulse in both forward and backward translating tasks is affected by the orientation of the hips relative to the feet (leg angle) and lower extremity muscle activation patterns, angular impulse is affected by the moment arm between the reaction force and the center of mass (CoM) and the magnitude of the reaction force. During forward translating somersaults (e.g. reverse somersault), modification in CoM position relative to the center of pressure (CoP) is limited by anatomical constraints (e.g. dorsiflexion). As a result, the magnitude of the moment arm is regulated by redirecting the reaction force. In contrast, during backward translating somersaults (e.g. back somersault), the moment arm is regulated by reorienting the CoM relative to the CoP prior to rapid joint extension during the push phase. During the take-off phase of the inward somersault (backward translation, forward rotation), the foot contact duration is approximately half of the back and reverse somersaults and the reaction force passes posterior relative to the CoM. This time limitation for generation of linear and angular impulse led us to hypothesize that magnitude of the moment arm during the take-off phase of the inward somersault would be regulated by redirecting the reaction force rather than altering the CoM position relative to the CoP. Redirecting the reaction force was expected to be achieved by redistributing the lower extremity NJMs.

METHODS

Six (2 females and 4 males) highly skilled divers performed a series of the inward somersault (IS) and inward timer (IT) take-offs from a force platform onto a landing pit using their competitive style. Sagittal plane kinematics and reaction force data were simultaneously collected and synchronized at the time of plate departure. Newtonian mechanics were used to compute the lower extremity NJMs.

RESULTS AND DISCUSSION

Between-task differences in reaction force direction and trunk-leg coordination indicated that angular impulse is generated by redirecting the reaction force relative to the CoM (Figure 1). Redirection of the reaction force was achieved by a redistribution of the knee and hip NJMs during the take-off phase. These results support the hypothesis that angular impulse is regulated by redirecting the reaction force. As expected, more posterior directed reaction forces were associated with trials with large knee NJMs in relation to hip NJMs (Figure 2).

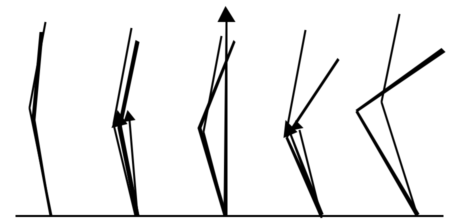

Figure 1. Orientation of the trunk, leg, and reaction force (arrow) from initiation (left) to plate departure (right) during the take-off phase of the inward timer (thin line) and inward somersault (think line).

Redistribution of the lower extremity NJMs and a more posterior oriented hip relative to the CoP (leg angle greater than 90 degrees) affected the orientation of the reaction force. At the time of peak horizontal reaction force, leg orientation and magnitude of the horizontal reaction force were significantly larger during the take-off phase of the IS as compared to the IT. The leg orientation explained only 55% of the variance in the reaction force direction, whereas the difference in the knee and hip NJMs explained 88% of the variance in the reaction force direction (Figure 2). These results further substantiate the role of redistribution of NJMs on reaction force redirection relative to the CoM in whole body movements [3].

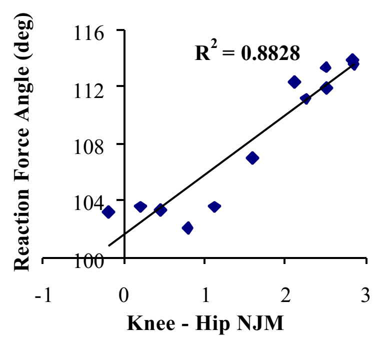

Figure 2. Correlation between the differences in knee and hip NJMs and reaction force direction at the time of peak horizontal reaction force.

CONCLUSIONS

Generation of the forward angular impulse and backward linear impulse during take-off phases with limited foot contact duration is primarily achieved by redirecting the reaction force relative to the CoM. Backward leg orientation facilitates generation of backward directed reaction force in global space. In addition, redistribution of the lower extremity NJMs redirects the reaction force relative to the leg and CoM.

REFERENCES

1. Miller DI, *Biomechanics in Sports*, 326-348. 2000.
2. Mathiyakom et al., *J Applied Biomech* (submitted).
3. van Ingen Schenau et al., *Neuroscience*, 197-20. 1992.

REGULATION OF REACTION FORCE DIRECTION AND ANGULAR IMPULSE DURING JUMPING TASKS VIA REDISTRIBUTION OF KNEE AND HIP NET JOINT MOMENTS

[1] J. L McNitt-Gray, [2] W. Mathiyakom, [3]P.S. Requejo, and [4]H. Flashner
[1]Departments of Kinesiology, Biomedical Engineering, Biological Sciences, [2]Andrus Gerontology Center, [4]Aerospace and Mechanical Engineering, University of Southern California; [3]Rancho Los Amigos National Rehabilitation Center
e-mail: mcnitt@usc.edu

INTRODUCTION

Previous study of goal-directed whole body movements requiring the generation of reaction forces during interaction with the environment indicates that the nervous system organizes the human body using a structure that enables the performer to satisfy a variety of task objectives with minimal modification in control [1, 2]. In this study, we hypothesized that the redistribution of the knee and hip net joint moments (NJM) serves as a mechanism for altering the direction of the reaction force and magnitude of the angular impulse generated during the take-off phase of jumping-related tasks. We expected that relative magnitude of knee and hip NJMs would be regulated via reciprocal activation of bi-articular muscles crossing the knee and hip as previously observed during seated tasks [1]. We tested this hypothesis by comparing reaction forces, center of mass trajectories, lower extremity joint kinetics, muscle activation patterns of seven lower extremity muscles during the performance of forward (reverse, R) and backward (back, B) translating jumps performed with (BS, RS) and without rotation (BT,RT) about the somersaulting axis of the body and by determining the sensitivity of trunk and leg motion to redistributions of knee and hip NJMs using an experimentally validated dynamic model[3, 4].

METHODS

Seven national level divers performed each task from a force plate onto a foam landing pit in accordance with the Institutional Review Board. Reaction forces (2000 Hz, Kistler, Amhurst, MA), sagittal plane kinematics (200Hz, NAC C^2S), and muscle activation patterns (2000 Hz, Konigsberg, Pasadena, CA) were collected simultaneously[2]. Body landmarks (deLeva, 1996) were digitized (Motus, Peak Performance, Inc.) and filtered using a fifth-order spline (Woltring, 1986).

A dynamic model was used to determine the sensitivity of leg and trunk motion to alternations in the relative magnitude of the knee and hip NJMs [3, 4].

RESULTS and DISCUSSION

The leg angle during the push phase and the redistribution of NJMs via reciprocal bi-articular muscle activation affected reaction force direction and angular impulse generation. The direction of the reaction force was affected by the orientation of the hip relative to the center of pressure (leg angle) during the tip phase and muscle activation patterns during the push phase. The relative magnitudes of knee and hip NJMs were affected by the orientation of the reaction force relative to the lower extremity segments resulting from reciprocal activation of the biarticular muscles (hamstrings and rectus femoris). No significant differences in NJMs or biarticular muscle activation patterns were observed between the BS and RS tasks and the BT and RT tasks (Figure 1A). The redistribution of knee and hip NJMs were shown to affect both leg and trunk angles during the push phase (Figure 1B) and affected the magnitude of the moment arm between the reaction force and center of mass. These results suggest multiple and diverse task objectives can be satisfied with minimal modifications in control.

REFERENCES

1. van Ingen Schenau et al., *Neuroscience*, 197-20, 1992.
2. Mathiyakom et al., *J Applied Biomech* (submitted).
3. Requejo et al., *Biological Cybernetics*, 2004
4. McNitt-Gray et al., *Biological Cybernetics*, (submitted)

ACKNOWLEDEMENTS US Diving, WiSE, Intel

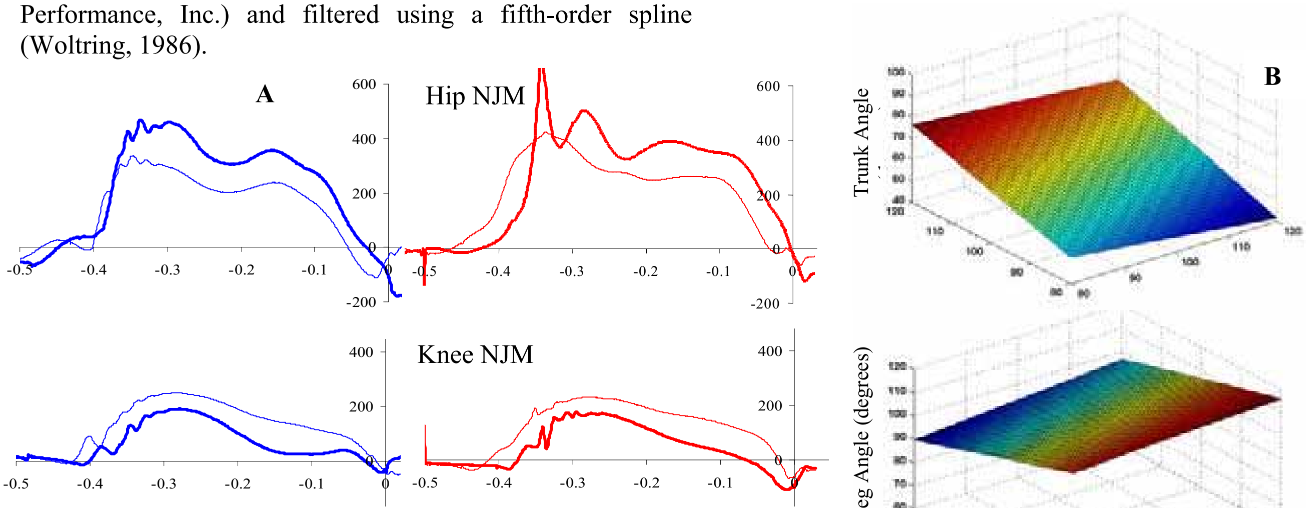

Figure 1.A. Comparison of the knee and hip net joint moments (NJM) during the take-off phase of BS (thick blue), BT(thin blue), RS(thick red), and RT(thin red) tasks. B Sensitivity of leg and trunk angle during push to redistribution of knee and hip NJMs during take-off phase of BS.

THEORETICAL BASIS FOR A LOAD CARRIAGE LIMIT EQUATION

[1]Joan Stevenson, [2]Timothy Bryant, [3]Evelyn L. Morin, [1]Susan A. Reid
[1]Physical & Health Education, [2]Mechanical Engineering, [3]Electrical & Computing Engineering and
[4]Ergonomics Research Group, Room #148 PEC, Queen's University, Kingston, Canada, stevensj@post.queensu.ca

INTRODUCTION

Carrying heavy loads has always been the bane of existence for military soldiers, explorers and weekend trekkers. As a result, under certain conditions, people become 'beasts of burden'. In a recent military report entitled *Modern Warrior's Combat Load* about Afghanistan dismounted operations, U.S. rifle squads carried average approach loads of 43 kg (95 lbs) which was 35% BW and emergency approach marches of 63 kg (138.4 lbs) an amount that was 73.6% BW. The authors argued that this plight would not be solved until sufficient resources were put in place to lighten and reduce the size of combat items, increase the versatility of load carriage items and rethink the logistics and doctrine of operations and supply.

One difficulty for operations personnel is to appreciate the impact that various loads will have on foot soldiers. Even though payload items and their weights are known, there are only a few strategies to calculate the impact of these weights on the soldiers. For example, physiological regression equations were developed by (Pandolf et al., 1977; Holewijn and Meeuwsen, 2001) help determine the metabolic cost of various loads and load carrying conditions. However, the equations output information in percent maximal energy cost, units that most operations personnel would not understand. It is important to develop a predictive equation that encompasses more of the major variables that limit performance in the field.

OBJECTIVE

The objective of the study was to use empirical data to develop a Load Carriage Limit equation that would provide backpackers and military with a simple guideline to assess the loads they could reasonably carry on a backpack.

THEORETICAL MODEL

The concept to be investigated is whether a multi-dimensional load carriage limit (LCL) could be developed similar to the National Institute of Occupational Safety and Health's (NIOSH) guideline for lifting in industry. This NIOSH lifting guideline is structure around a load constant of 23 kg. (50 lbs). Then multipliers less than 1 are used to discount for non-ideal factors such as load horizontal distance or frequency of lifts. For the LCL, a similar concept would be used. The proposed equation is:

$$LCL = (\text{Load Constant} * PF * BF * DF * RF) * \text{Time}$$

Where:

- PF is derived from physiological demands
- BF includes shoulder and hip reaction forces, pack motions, contact pressures
- DF includes body size, gender, and age
- RF includes soldier readiness, fitness and injury factors
- Time represents the mission expectations in terms of time/distance to be traveled.

METHODOLOGY

The methodology for this model is based on a series of separate data collections over a period of eight years. Physiological data have been extracted from a data set by Morin et al. (2004) combined with findings of Pandolf et al. (1997) and Holewijn and Meeuwsen,(2001). Maximum aerobic capacities were taken from 10 fit male subjects. On separate days subjects completed one of four test batteries, (either 0 kg and 38.7 kg at different speeds or inclines or 16.6kg and 25.9 kg at different speeds or inclines) while wearing a common backpack. A TEEM 100 metabolic cart was used to collect oxygen consumption in 20 sec intervals.

Biomechanical data were collected an objective load carriage simulator (Stevenson et al., 2004a,b) which has been validated by soldiers' opinions. Additional biomechanical data have been collected during a human trial fatigue tests where subjects were asked to provide feedback on discomfort as they completed a 45 minute treadmill march with loads of 0, 15, 25, 35 and 50 kg. These results have been distilled into important factors, such as: lumbar shear force, shoulder reaction forces, pack-person motion and other variables.

The demographic factor (DF) and readiness factor (RF) have been determined from the scientific literature. The load constant (LC) will be a high number that is discounted based on the conditions. Based on previous combat situations, loads of 63 kg and 68 kg were carried by soldiers in Afghanistan and the Falkland Islands respectively (McGaig and Gooderson, 1986). Based on injury data, these weights are too high thus a 50 kg (110 lbs) load was recommended as the starting point. At these extreme loads, the duration of load carriage will be minimal (under 1 hour) but humanly possible.

DISCUSSION AND CONCLUSION

A discussion of results will be presented based on the empirical data for various examples of load conditions. This theoretical model remains to be validated by military field trials across a number of operational conditions.

REFERENCES

Holewijn et al. NATO Specialist Meeting 9, 1-7, 2001.
McGaig RH & Gooderson. *Ergonomics* **29**(7) 849-857, 1986.
Morin EL et al. PWGSC W7711-03-7863-01. 76 pgs.
Pandolf KB et al. *Ergonomics* **19**:683-690, 1976.
Stevenson JM et al. *Ergonomics*, **47**(11):1160-1179, 2004
Stevenson JM et al. *Ergonomics,* **47**(12): 1272-128, 2004.

ACKNOWLEDGEMENTS

This work was supported and funded by Defence Research and Development Canada - Toronto; Scientific Authority: Walter Dyck.

MUSCLE ACTIVATION DURING MANUALLY ASSISTED TREADMILL TRAINING AFTER INCOMPLETE SPINAL CORD INJURY

[1]Antoinette Domingo, [1,2]Gregory Sawicki and [1,3]Daniel P. Ferris
Departments of [1]Movement Science, [2]Mechanical Engineering, & [3]Biomedical Engineering
University of Michigan, Ann Arbor, MI; email: adomingo@umich.edu

INTRODUCTION

Figure 1: Manually assisted locomotor training

Partial body weight supported training (BWST) is effective in improving the gait of those with incomplete spinal cord injury [1,2]. In this treatment, the patient is suspended above a treadmill with a harness so that the patient bears only a portion of her weight on her legs (Figure 1). A therapist on each side of the patient manually assists the patient's legs through the motions of walking. Although this treatment is effective in improving walking ability, the neural mechanisms of locomotor recovery are not clear.

There are two competing hypotheses on how electromyographic (EMG) activity might be affected by BWST. One possibility is that manual assistance decreases the patient's effort, reducing EMG amplitudes. An alternative possibility is that manual assistance provides more normal kinematic patterns, thus resulting in more appropriate sensory feedback and increasing EMG amplitudes. The purpose of this study was to determine how manual assistance at the lower limbs specifically modifies EMG activity.

METHODS

Four subjects with incomplete spinal cord injury (ASIA Impairment Scale Classification of C or D) at the cervical or thoracic level participated in the study. Subjects were at least 12 months post-injury and free of any conditions that would limit their ability to safely complete testing. Subjects were community ambulators with preferred overground walking speeds of 0.41-0.95 m/s. Three of the four subjects used canes. All subjects gave informed consent prior to participating.

Subjects stepped with and without manual assistance at 0.36 m/s with body weight support (30% or 50%, depending on the subject's tolerance). The same trainers manually assisted all subjects following the procedures described by Behrman and Harkema for locomotor training with partial bodyweight support [1]. While walking under the two experimental conditions, we collected kinematic and EMG data (tibialis anterior, TA; soleus, SO; medial gastrocnemius, MG; lateral gastrocnemius, LG; vastus lateralis, VL; vastus medialis, VM; rectus femoris, RF; and medial hamstring, MH). After averaging EMG RMS for each muscle, we normalized to the highest RMS that occurred without manual assistance. We also found separate RMS values for the stance and swing phases of gait. We used a two-way ANOVA to test for significant differences.

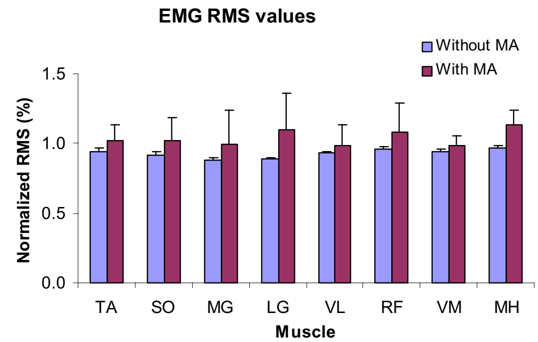

Figure 2: Averaged and normalized EMG RMS values with standard error bars. EMG amplitudes were greater in all muscles with manual assistance, but not significantly ($p > 0.3$).

RESULTS AND DISCUSSION

EMG RMS values for the complete gait cycle were greater with manual assistance, but the differences were not significant (Figure 2). Stance phase and swing phase EMG RMS were similar to the overall gait cycle EMG RMS. Power analyses revealed that effect sizes for EMG amplitudes were all less than 0.11, indicating any real difference between conditions would be very small. To have at least a 50% chance of detecting a significant difference would require ~245 subjects [3].

CONCLUSIONS

The two competing hypotheses are based on valid neural control principles. It is likely that both ideas are at least partially correct in explaining how manual assistance affects muscle activation during BWST. The overall result, however, is that EMG amplitudes change little with manual assistance for subjects with this level of incomplete spinal cord injury. Thus, therapists' fears that manual assistance will promote passivity by subjects are unfounded.

REFERENCES

1. Behrman & Harkema. *Phys Ther* **80**, 388-700, 2000.
2. Wernig, et al. *Spinal Cord* **36**, 744-749, 1998.
3. Sall, et al. *JMP Start Statistics*, Thomson Learning, 2001.

ACKNOWLEDGEMENTS

Supported by a grant from the Christopher Reeve Paralysis Foundation and a Student Award Program grant from the Blue Cross Blue Shield of Michigan Foundation.

FORWARD SOLUTION SIMULATION OF THE MIXED ACTION IN CRICKET FAST BOWLING

[1]René Ferdinands and [2]Uwe Kersting
[1]Department of Physics & Electronic Engineering, University of Waikato; email: rene@waikato.ac.nz
[2]Department of Sport & Exercise Science, University of Auckland; email: u.kersting@auckland.ac.nz

INTRODUCTION

The objective of fast bowling in cricket is to deliver the ball with a straight arm so that it reaches the batter at high speed after having first bounced once off the ground. The faster the ball, the less time the batter has to respond. However, fast bowlers require high run-up speeds, generate large ground reaction forces, and produce high joint torques [3]. With the loading placed on the body, it is not surprising that fast bowling is associated with a high incidence of lower lumbar injury. The susceptibility to such injury is correlated with shoulder counter-rotation during delivery stride [2]. The purpose of this study was to develop a forward solution model to predict the causal factors associated with the counter-rotation of fast bowlers. This approach potentially gives the cricket coach a scientific means of modifying the technique of mixed action bowlers to reduce their susceptibility to lower lumbar injury.

METHODS

A three-dimensional (3D) forward solution dynamics model of the human body was used to simulate the motion of fast bowling in cricket. This model provides a mechanical basis for the remediation of fast bowling techniques that are correlated with an increased injury risk. Thirty-four fast bowlers were selected for study and divided into four groups according to ball release speed. An 8-camera 240 Hz motion analysis system (Motion Analysis Corp.) tracked markers placed on the bowler delivering a series of balls at a target approximately on a 'good length' in line with the wickets, and a Bertec force plate was used to measure ground reaction forces. The marker arrangement allowed for the 3D motion tracking of all major body segments. Kinematic alignment factors were calculated to classify bowlers according to bowling type: side-on, front-on, and mixed.

A forward solution model of the bowler was developed using *Mathematica's Mechanical Systems Pack*. This is a set of packages designed for the analysis of spatial rigid body mechanisms by implementing a dynamics formulation with Lagrangian multipliers. The computer model gives a 3D representation of the human body as a system of fifteen rigid body segments with mass and inertia properties. The forward solution model was used to test the effectiveness of technical hypotheses to correct a mixed action.

RESULTS AND DISCUSSION

According to a modified classification for action type [3] only 11.8% were side-on, 27.5% front-on, and 61.7% mixed. The mixed action bowlers had higher shoulder-hip separation angles than the side-on and front-on bowlers (Table 1). Mixed action bowlers also have more lateral flexion and hyperextension of the lumbar spine during delivery stride [1].

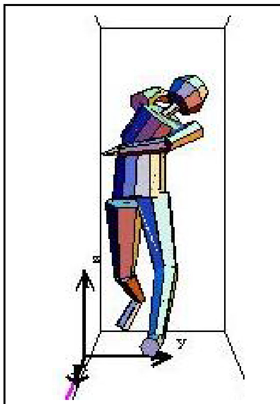

Figure 1: Simulated mixed action

The forward solution was run to test the effects of increasing the shoulder-hip separation angle of a front-on bowler. This was performed by increasing the anticlockwise upper trunk torque about the longitudinal axis and decreasing the corresponding torque of the lower trunk. This was represented by the shoulder to hip torque differential factor (γ) in the forward solution.

The simulation of the bowler under these modified torque inputs (γ = 1.3) increased the amount of lateral lean (15.3º), hyperextension (10.2º), and shoulder counter-rotation (8.0º) at front foot contact. Increasing γ from 1 to 1.3 increases the severity of those factors that constitute a mixed action. As γ was increased more than 1.3 the solution become unstable. The kinematic data and the forward solution simulation suggest that a strong torquing between the shoulders and hips can promote shoulder-counter-rotation in bowling.

CONCLUSIONS

This study showed that the mixed technique can be produced by changing the trunk torques in a forward solution. Despite their inherent stability problems, the further development of forward solutions should be pursued to give biomechanists a tool that not only achieves the objective of reducing shoulder counter-rotation, but that can also be used to improve other areas of performance.

REFERENCES

1. Burnett AF et al. *Clin Biomech* **13**, 574-583, 1998.
2. Elliott BC. *J. Sports Sci* **38**, 983-991 ,2000.
3. Ferdinands RED. PhD thesis (University of Waikato), 2004.

ACKNOWLEDGEMENTS

I wish to thank New Zealand Cricket for funding the post-doctoral component of this study.

Table 1: Shoulder and hip alignment characteristics show that mixed bowlers tend to have higher separation angles.

ACTION TYPE	Shoulder Angle BFC(°)	Shoulder/Hip Separation BFC (°)	Shoulder Counter Rotation (°)
Side-on	21.7 ± 1.8	10.2 ± 3.3	11.0 ± 5.4
Front-on	41.6 ± 3.4	9.07± 3.1	21.5 ± 2.4
Mixed	61.1 ± 2.7	28.4 ± 2.8	36.6 ± 2.3

A NUMERICAL METHOD FOR DETERMINING IDEAL CAMERA PLACEMENT

[1] Joseph D Gardinier, [1]Kurt Manal
[1]Center for Biomedical Engineering Research, University of Delaware

INTRODUCTION

Data piloting is important to ensure accurate coordinate data and to minimize camera drop-out. Camera drop-out occurs when a marker fails to be imaged by a camera; often due to marker merging and occlusion. In this paper, we present the conceptual framework of a numerical method for determining where video cameras, if placed, would have an occluded or a merged view of the markers. Experimental data are used to demonstrate the efficacy of the method as an effective tool to complement existing data piloting procedures.

METHODS

The method is best described by considering two markers within a motion capture volume. The motion capture volume is a subspace of a larger laboratory volume, both of which are defined by 4 walls, a floor and a ceiling (Figure 1). The apex of a cone is set at the midpoint between the markers, opening in the direction of one of the markers, and encircling its perimeter exactly. The cone continues outward, intersecting the walls, floor or ceiling of both volumes. A camera placed within this cone will have an occluded or merged view of the markers. This process is expanded to every possible marker pairing and at every point in time. Regions of intersection are displayed graphically to portray problematic camera locations. An exemplar graphical display is shown in Figure 1. The darker the shade of gray, the more frequently a camera in that location will drop-out. The method was tested using 3 video cameras positioned symmetrically as depicted by the circles in Figure 1 (Experiment 1). Markers were placed on the right leg and shoe of a subject using a modified Helen Hayes marker set. The distance between select markers was determined from data collected during a standing reference trial, and subtracted from distances measured during walking as an estimate of error due to camera drop-out. Note that camera 3 was initially positioned in a problematic location. In a second experiment, camera 3 was moved to a more favorable location (square in Figure 1) and the distance between the markers was computed once again.

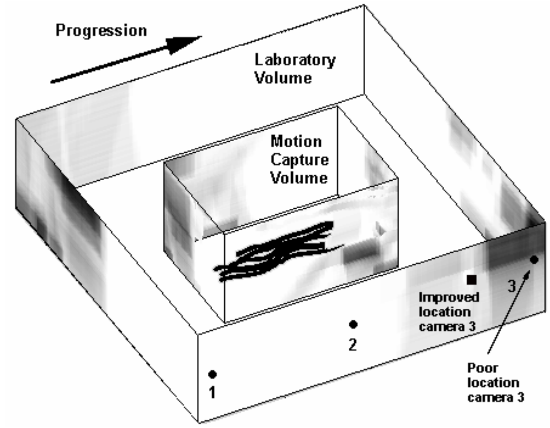

Figure 1: Gray regions depict problematic camera locations. The numbers identify the cameras. The black lines within the motion volume are marker trajectories.

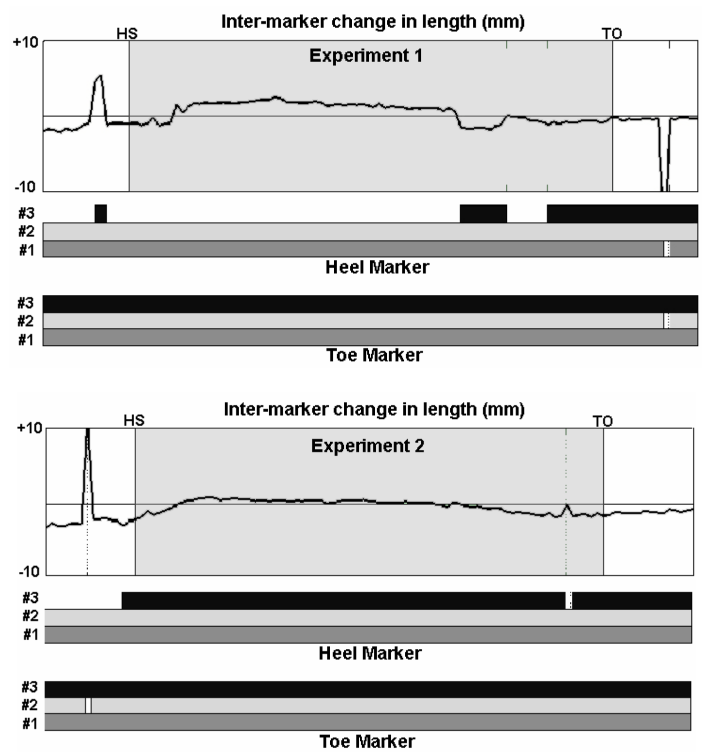

Figure 2: Errors due to camera drop-out when camera #3 was located in a bad region (Experiment 1). The bar graphs indicate which cameras contributed to the spatial location of the markers. Cameras are identified as #1 - #3. HS = heel strike, TO = toe off. In contrast, the errors are smaller in experiment 2 when camera 3 was moved to a better location. Notice how camera 3 contributed to the location of the heel marker in all but 1 video frame.

RESULTS AND DISCUSSION

Only results for markers over the heel and toe are reported. The change in the distance represents errors due to camera drop-out since markers on the shoe are not subject to soft tissue error. Notice the large interval during stance in Experiment 1 when only cameras #1 & #2 contributed to the spatial determination of the heel marker. In contrast, camera 3 exhibited minimal drop-out and only small errors were noted during experiment 2.

CONCLUSIONS

The method can be used to assist data piloting. It affords an objective and practical solution to minimizing errors associated with camera placement.

ACKNOWLEDGEMENTS

Supported by NIH RR16458

VALIDATION OF A MARKERLESS MOTION CAPTURE SYSTEM FOR THE CALCULATION OF LOWER EXTREMITY KINEMATICS

[1]Lars Mündermann, [2]Dragomir Anguelov, [1]Stefano Corazza, [1]Ajit M. Chaudhari and [1,3,4]Thomas P. Andriacchi
[1]Department of Mechanical Engineering, Stanford University, Stanford, CA; Email: lmuender@stanford.edu
[2]Department of Computer Science, Stanford University, Stanford, CA
[3]Bone and Joint Center, Palo Alto VA, Palo Alto, CA
[4]Department of Orthopedic Surgery, Stanford University, Stanford, CA

INTRODUCTION

New methods for the capture of human movement motivated by technological advances aiming to use non-intrusive or markerless motion capture [1] offer the potential to address some of the limitations of current methods for human gait analysis and open the door for new opportunities for the study of normal and pathological motion. While theoretical studies [2,3] showed that human kinematics can be accurately estimated in a virtual environment, these methods have not been tested with laboratory data. The purpose of this study was to evaluate the accuracy of human body kinematics extracted from experimental data using a visual hull markerless motion capture system.

METHODS

Full body movement was captured using a marker-based and a markerless motion capture system simultaneously. The marker-based system consisted of an 8 Qualisys camera optoelectronic system monitoring 3D marker positions for the hip, knees and ankles at 120 Hz. The markerless motion capture system consisted of 7 Basler CCD color cameras capturing synchronously images at 76.9 fps. Movement was determined by first constructing visual hulls [2] and subsequently tracking an articulated body using an iterative closest point (ICP) tracking algorithm for articulated bodies [3]. The subject was separated from the background in the image sequence of all cameras using intensity and color thresholding compared to background images (Figure 1). The separated image information was projected into 3D and a visual hull (bounding surface) was constructed for each frame (Figure 2). The articulated body was created from a detailed full body laser scan with markers affixed to the subject's joints (Figure 1). The articulated body consisted of 15 body segments (hip, upper trunk, head, and left and right shoulder, forearm, hand, thigh, shin and foot) and 14 joints connecting these segments. Virtual markers were used to define segment coordinate axes. The joint angles (sagittal and frontal plane) for the knee calculated as angles between corresponding axes of neighboring segments, were used as preliminary basis of comparison between the two systems.

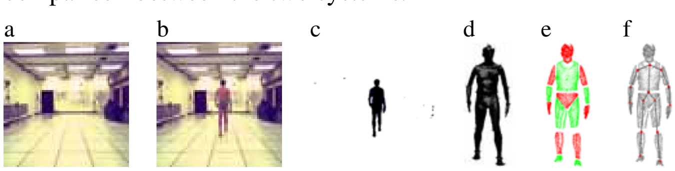

Figure 1: a) Background image. b) Image. c) Separated subject data. c) Laser scan. d) Body segments. e) Joint centers.

RESULTS

The 15 articulated body segments defined from the laser scan were tracked through a gait cycle for both the markerless and marker system (Figure 2). The kinematics from the markerless and marked system produced comparable results (Figure 3) for knee joint angles in the sagittal and frontal plane.

Figure 2: Visual hulls constructed using 7 cameras (top). Articulated body matched to visual hulls (bottom).

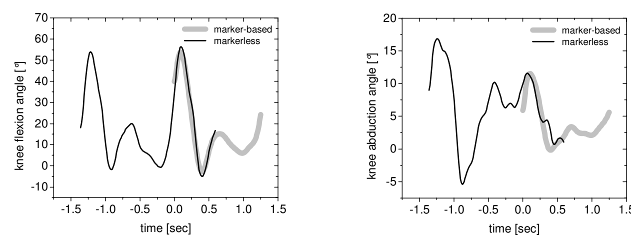

Figure 3: Motion graphs for knee flexion and knee abduction angles (gray = marker-based; black = markerless).

DISCUSSION

The image processing modules used in this study including background separation, visual hull and iterative closest point methods yielded results that were comparable to a marker based system for motion at the knee. While additional evaluation of the system is needed, the results demonstrate the feasibility of calculating meaningful joint kinematics from subjects walking without any markers attached to the limb.
The markerless framework established in this study can serve as a basis for developing the broader application of markerless motion capture. Each of the modules can be independently evaluated and modified as newer methods, cameras and processors become available, thus making markerless tracking a feasible and practical alternative to marker based systems.

REFERENCES

1. Moeslund T, et al., *Computer Vision and Image Understanding* **81**, 231-268, 2001.
2. Mündermann L, et al., *Videometrics VIII IS&T/SPIE* **5665**, 268-287, San Jose, CA, 2005
3. Mündermann L, et al., submitted to *ASME/SBC 2005*.

ACKNOWLEDGEMENTS

Funding provided by NSF #03225715 and VA #ADR0001129.

FOREFOOT PLANTAR PRESSURE IS RELATED TO 3-D CT DERIVED MEASURES

[1] William R. Ledoux, [1] Eric S. Rohr, [1] Jane B. Shofer, [1] Randal P. Ching and [1] Bruce J. Sangeorzan
[1] VA RR&D Center, Seattle, WA; email: wrledoux@u.washington.edu web: www.seattlerehabresearch.org

INTRODUCTION

The relationship between foot structure and foot function is complex and not completely understood. Previous research has employed static X-ray parameters[1] or static X-ray parameters in conjunction with additional measures of foot structure and function,[2] including, among others, joint range of motion, tissue parameters, EMG, etc., to explain 35% and 50% of the variability of the plantar pressure, respectively. Our group has recently completed a study of the 3-D structure of feet ranging from flat to high arched feet.[3] Additionally, we compared plantar pressure data between these subjects.[4] In both studies, we found significant differences between foot types. The purpose of this study was to combine the work of the previous two studies to determine if 3-D measures of foot shape were related to forefoot plantar pressure.

METHODS

A total of 40 subjects were enrolled with ten in each of four foot type groups: pes cavus (high arch), neutrally aligned, asymptomatic pes planus (low arch) and symptomatic pes planus. If the foot type was bilateral both feet were included (n=64 feet). Foot type was determined via clinical examination by an orthopaedic surgeon. Each foot was X-rayed (AP and lateral) and a weight-bearing CT scan was performed. Age, weight, height and gender were recorded. Ten trials of barefoot plantar pressure data were collected with an EMED-SF system and velocity was recorded. Peak pressure was determined over the entire foot as well as 6 subdivisions: the hallux and the 1st through 5th metatarsal heads. These subdivisions were obtained by overlaying the AP X-ray on top of an actual-size composite peak plantar pressure print out. Simulated weight bearing CT scans of the subject's foot were generated. Using techniques defined elsewhere, local coordinate systems (inertial matrices) were determined based on the bone morphometry.[5] These axes were then used to describe bone to bone orientation using the Z, Y', X" Euler angles. Euler angles were calculated between the 1st Metatarsal-Talus (M1Tal), 5th Metatarsal-Talus (M5Tal), Calcaneus-Talus (CalTal), 2nd Metatarsal-1st Metatarsal (M2M1), Calcaneus-Fibula (CalFib), Cuneiforms-Talus (CunTal), Cuneiforms-Navicular (CunNav), and Navicular-Talus (NavTal), resulting in 24 total angles. Linear regression models of mean pressures (per subject) on Euler angles were calculated; age, BMI and mean velocity were adjusted for.

RESULTS

To visualize trends for each location, a plot of the data with a loess-smoothed curve was generated (Figure 1). The regression for each location required only 3 or 4 of the 24 possible angles; additional angles made no improvement. For the hallux, the CunTalZ, M1TtalZ, and the M2M1Y' angles explained 46.4% of the variability in peak plantar pressure. The 1st metatarsal data indicated that the CalFibX", M2M1Z, M1TalY', and CalTalX" angles were significant and could

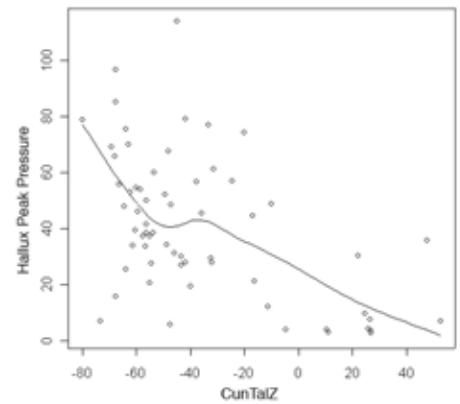

Figure 1: The hallux peak pressure vs. the CunTalZ angle.

account for 47.7% of the variability in peak plantar pressure. The 2nd and 3rd metatarsals only showed significance with one angle, the NavTalX" and M2M1Z, respectively, and only 21.5% and 3% of the variability could be explained. The 4th metatarsal showed that the CunTalZ, M2M1Z, CalFibX", CalTalZ angles were significant and able to describe 51.2% of the variability in peak plantar pressure. And finally for the 5th metatarsal we found that 44.7% of the pressure variability over this region could be accounted for when the M5TalX", M1TalX", CalFibX", and CunNavX" angles were analyzed.

DISCUSSION

This study indicates that for several locations on the forefoot (hallux, and the 1st, 4th and 5th metatarsals) the 3-D static angles describe more of the variability of the plantar pressure then just X-ray parameters.[1] In fact, for these areas the 3-D static angles were as predictive as the range of foot structure and functional parameters used elsewhere.[2] However, for other locations, our analysis was a very poor predictor (2nd and 3rd metatarsal). It is not clear why these locations did not perform well; they were not emphasized in the selection of bony relationships to study, but neither was the 4th metatarsal and it had the highest percentage. Nevertheless, areas such as the hallux and the 1st and 5th metatarsals are important areas for ulcer occurrence. The data present here demonstrate that 3-D CT angles useful for predicting peak plantar pressure.

REFERENCES

1. Cavanagh, PR, et al. *J Biomech* **30**, 243-250, 1997.
2. Morag, E and PR Cavanagh, *J Biomech* **32**, 359-70, 1999.
3. Rohr, ES, et al. *Proceedings of the 49th ORS*, 2003.
4. Ledoux, WR, et al. *Proceeding of the 28th ASB*, 2004.
5. Camacho, DLA, et al. *JRR&D* **39**, 401-10, 2002.

ACKNOWLEDGEMENTS

Supported in part by the Department of Veterans Affairs, RR&D service grant number A2180R.

STEPPING-OVER GAIT CHARACTERISTICS IN CHILDREN WITH DOWN SYNDROME

[1]Bee-Oh Lim, [1]Joong-Hyun Ryu , [2]Dong-Ki Han, [1]Gary Christopher and [1]Young-Hoo Kwon
[1]Biomechanics Laboratory, Texas Woman's University, Denton, TX, USA
[2]Dept. of Physical Education, Seoul National University, Seoul, Korea
email: imabo@korea.com, web: www.twu.edu/biom

INTRODUCTION

Approximately 80% of children with DS exhibit difficulty in walking [1]. Most studies on gait characteristics in children with DS have concentrated on level walking. We are not aware of any study dealing with stepping over obstacles, despite the frequency with which this must be done in everyday life and the potential consequences of falls [2]. The purpose of this study was to investigate the step-over gait characteristics of children with Down syndrome (DS) as they approached and stepped over obstacles of different heights. We tested the null hypothesis that no differences exist in dependant variables when stepping over obstacles of different heights.

METHODS

Thirteen boys with DS initially participated in this study but analysis has been completed for only five (age: 12.0 ± 0.9 yrs; height: 134.9 ± 9.7 cm; mass: 34.4 ± 8.4 kg) of them due to difficulties in obstacle clearance. A 10.0 m x 1.3 m walkway with a firm dark surface was used for data collection. An AMTI force plate was embedded in the walkway such that the first footfall after obstacle clearance occurred on the force plate. Three-dimensional motion analyses and ground reaction force analyses were performed to obtain dependant variables. One-way repeated-measure ANOVA was performed to determine whether obstacle height had a significant effect on the dependent variables. Four levels of obstacle height were used: 0, 2.5, 5.2, and 15.2 cm [1].

RESULTS AND DISCUSSION

As obstacle height increased, the subjects exhibited greater vertical foot clearance, obstacle to heel horizontal distance, hip sway angle, joint ROM (knee & hip), impulse, 1st peak force (Figure 1), and support time compared to obstacle free gait. Hip ROM at swing phase, impulse and support time increased and knee angle at step over decreased as obstacle height increased (Table 1). The results of this study show that obstacle height gait differ in some ways from obstacle free gait. The fact that subjects had similar toe to obstacle horizontal distance, obstacle to heel horizontal distance and vertical foot clearance for each obstacle suggests a commonality in the strategy used for negotiating obstacles. The results suggest that this strategy places great emphasis on avoiding toe contact with the obstacles.

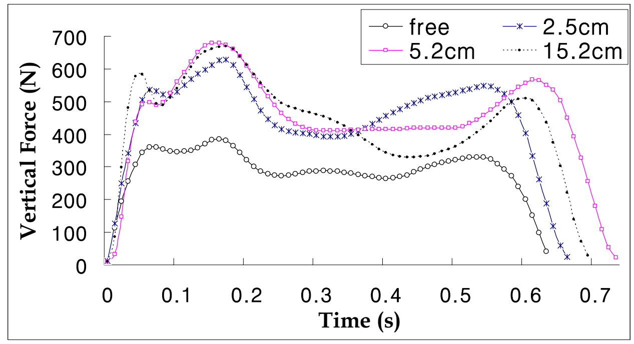

Figure 1: Vertical ground reaction force (subject 5). The ground reaction force pattern was characterized by a wide spectrum of individual differences. In some participants (subject 5), however, vertical force patterns similar to the normal pattern were observed.

REFERENCES

1. Matteo C. *Physical Medicine and Rehabilitation* **16**, 303-321, 2002.
2. Chen HC, et al. *J Gerontology* **46**, M196-203, 1991.

Table 1: Summary of the changes in the kinematic and ground reaction force data (Mean ± SD)

Parameter	Obstacle Height (cm)			
	0	**2.5**	**5.2**	**15.2**
Vertical foot clearance (cm)	4.8 ± 0.8	13.5 ± 3.6	11.2 ± 2.4	13.6 ± 1.0 *
Toe - obstacle distance (cm)	31.0 ± 17.5	21.2 ± 2.3	24.7 ± 8.2	21.0 ± 5.9
Obstacle - heel distance (cm)	13.2 ± 1.1	21.5 ± 3.0	22.2 ± 2.1 *	21.3 ± 1.6
Knee angle at step over (°)	161.6 ± 3.5	123.1 ± 28.6	108.1 ± 4.1 *	90.8 ± 0.2 *
Hip sway angle at step over (°)	-9.2 ±1.1	-0.8 ± 6.5	7.0 ± 1.6 *	4.2 ± 2.4
Knee ROM at swing phase (°)	37.8 ± 3.7	60.5 ± 15.1	53.1 ± 3.0 *	77.9 ± 2.9 *‡
Hip ROM at swing phase (°)	27.4 ± 2.9	34.4 ± 1.2	51.9 ± 0.2 †	65.3 ± 0.1 *†‡
Impulse(%BW-s)	0.4 ± 0.1	0.6 ± 0.0 *	0.6 ± 0.0 *	0.7 ± 0.1 *†
1st peak force(%BW)	1.1 ± 0.1	1.3 ± 0.1	1.3 ± 0.1 *	1.1 ± 0.1
Post obstacle clearance support time (s)	0.59 ± 0.04	0.68 ± 0.03 *	0.70 ± 0.48 *	0.90 ± 0.67 †

* Significantly different from the 0-cm condition ($p < .05$). † Significantly different from the 2.5-cm condition. ‡ Significantly different from the 5.2-cm condition.

ELBOW ANGLE EXCURSION SLOPE AS A DETERMINANT OF BOWLING LEGALITY

[1] René Ferdinands and [2]Uwe Kersting
[1]Department of Physics & Electronic Engineering, University of Waikato, Hamilton, New Zealand,
[2]Department of Sport & Exercise Science, University of Auckland, Auckland New Zealand

INTRODUCTION

The legality of a bowler's action in cricket has been established in accordance with Law 24.3 of the International Cricket Council (ICC) rules, which state that "once the bowler's arm has reached the level of the shoulder in the delivery swing, the elbow joint is not straightened partially or completely from that point until the ball has left the hand" (MCC, 2002). However, fast bowlers seldom use a rigid straight arm, and the elbow angle generally increases after reaching shoulder height [1,3].

The ICC in keeping with these facts set a range of allowable elbow extension angles: 10° for fast bowlers, 7.5° for medium-pace bowlers, and 5° for spin bowlers. However, in a laboratory study of 42 subjects Ferdinands and Kersting [1] showed that there was no correlation between elbow extension angle and bowling type, and recommended a 15° flat tolerance level. The aim of this study was to further examine bowling action legality by measuring the elbow extension angle, and the elbow excursion angle slope through ball release of a sample of 67 bowlers using an 8-camera three-dimensional (3D) motion analysis system (240 Hz). The results suggest that elbow excursion angle is an important determinant of bowling action legality.

METHODS

Sixty-seven bowlers were selected for the study, and grouped into fast, med-fast, medium, slow, and finger-spin categories. Also, 8 bowlers in this sample were observed as possibly having a throwing-type action. Each subject was filmed by an 8-camera marker-based 240 Hz motion analysis system. A 10-marker static calibration marker system was used. This was reduced to a 7-marker bowling set, which is the minimum required to carry out a 3D analysis of the arm based on an anatomically based joint coordinate system (JCS). The 3D elbow angles were calculated from the relative orientation of the forearm to the upper arm based on a joint coordinate system [2]. Six trials per subject were recorded. Elbow excursion angle slope was calculated as the rate of elbow angle change from two frames before to two frames after ball release.

RESULTS AND DISCUSSION

The mean elbow extension angles for the groups were fast: 6.23±0.65º, med-fast: 4.79±0.63º, medium: 7.27±0.93º, and slow: 6.74±1.59º. There was no correlation found between elbow extension angle and ball release speed. Also, there was some variability in the mean elbow extension angles per subject. Eight bowlers had elbow extension angles in excess of 10º, and rare individual trials could have up to 15º extension. However, only one of these bowlers was suspected of throwing.

The elbow excursion angle slope was negative for 70.1% of the bowlers, which means that after an initial elbow extension, the elbow flexed through release (Figure 1). For the remaining bowlers, the elbow excursion angle slope was positive, indicating that the elbow extended through release. This is partially consistent with the 4th edition of the MCC 1947 code (1970) which defined a legal bowl when the "process of straightening the bowling arm, whether it be partial or complete, takes place during that part of the delivery swing which directly precedes the ball leading the hand." However, according to this law there would still be too many illegal bowlers. However, above an elbow excursion angle slope of a 100 º/sec, only 11.9% of the bowlers would be considered illegal, including all eight bowlers who had been previously observed as having suspect actions.

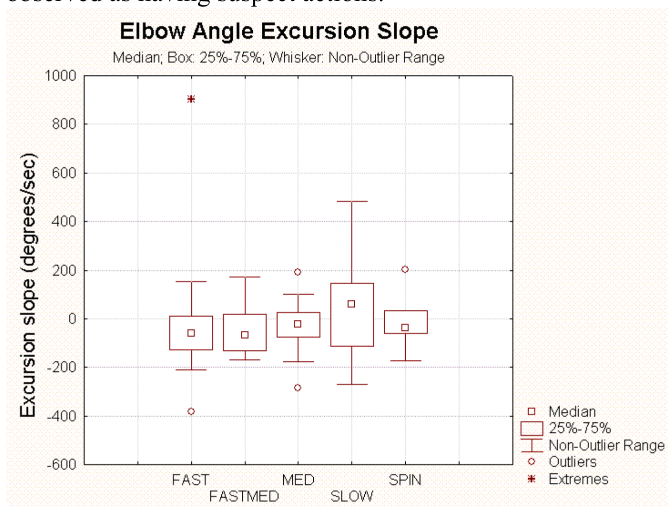

Figure 1: Elbow excursion angle slope for all bowling groups. Positive means extension through release.

CONCLUSIONS

The findings suggest that a new bowling law should not only specify a flat tolerance level for elbow extension angle, but examine the new concept of elbow excursion angle slope through ball release. It is also possible that elbow excursion angle slope has a better correlation with a visual determination of bowling legality. From a biomechanical perspective, an extending arm through release is able to use both humerus internal rotation and elbow extension as a contribution to ball speed, as in a throw. More research is needed to determine the legal level of excursion angle slope. Also, the mean elbow extension data indicates that a 15º tolerance level may be excessive, particularly if there is no consideration of elbow excursion angle slope.

REFERENCES

1. Ferdinands, R. & Kersting. (2003) Elbow angle extension and the legality of the bowling action in cricket. 5th ABC, Sydney.
2. Grood, E.S. & Suntay, W.J. (1983). J. of Biomech. Engineering, 11, 443-459.
3. Portus, M., at al., (2003). Sci. and Med. in Cricket, South Africa, 41-54

ESTIMATION FOR DYNAMIC MEASUREMENT OF SCAPULA KINEMATICS USING ELECTROMAGNETIC TRAKING DEVICE

Koh Inoue and Shuji Suzuki
Graduate School of Human Sciences, Waseda University, Tokorozawa, Japan,
e-mail: k.inoue@ruri.waseda.jp

INTRODUCTION

Scapula motion is an important element of upper limb movement, and therefore several investigators have developed methods for measuring three-dimensional and dynamic scapula kinematics. Recently, *acromial method* [1] using electromagnetic sensor was investigated. Although this method is three-dimensional, dynamic, noninvasive and practical, sliding of scapula under skin prevents accurate measurement [2]. The purpose of this study was to examine the error pattern in *acromial method* during humerus elevation.

METHODS

Six adult subjects with functionally normal shoulder girdles participated. Kinematic data were collected with electromagnetic tracking device (Plhemus, LIVERTY). Sensors were attached to the skin on acromion, sternum and a three-pin device according to Johnson [3], which was scapula locator by palpating landmark. Scapula orientations from thorax coordinate system were recorded during humerus elevation, and expressed in Euler angle, which are comprised of three angles. These angles represented external rotation (ER), upward rotation (UR) and tilting (TI). Humerus elevations were performed in 76 positions: 19 humerus elevations per 10˚ and 4 elevation planes per 30˚. The error of bone and skin based measurement was computed for each angle. Each rotation error was separately compared with a 19 (humerus elevation: HE) × 4 (elevation plane: EP) repeated measures ANOVA.

After examinating the error pattern, estimation was tested. Estimation models were developed for each subject. The models were made by multiple linear regression: predictor was skin orientation and estimator was Scapula orientation. For practical application, samples were required to be small and easy to obtain. Therefore, 25 positions, 6 humerus elevations × 4 elevation planes in steps of 30˚ + 1 rest position, were selected. As the number of samples decreased from 25 to 2 samples, root mean squared error on average in all subjects (ARMSE) was observed and evaluated.

Table 1: The error of scapula and skin orientation.

Rotation	Factor	DOF	f-value	p-value
ER	HE	18	19.827	.000 **
	EP	3	0.417	.743
	HE×EP	54	2.280	.000 **
UR	HE	18	14.828	.000 **
	EP	3	12.315	.000 **
	HE×EP	54	2.370	.000 **
TI	HE	18	9.996	.000 **
	EP	3	5.990	.007 **
	HE×EP	54	1.952	.000 **

** p<.01

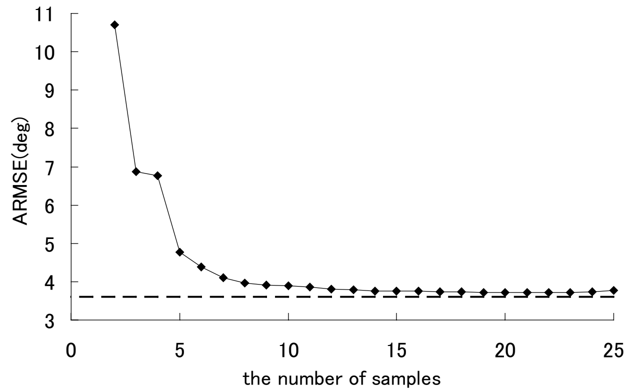

Figure 1: The change of ARMSE for the number of samples. Broken line expressed ARMSE by regression using all samples.

RESULTS AND DISCUSSION

All errors had HE × EP interaction (Table 1), therefore HE differently affected to error patterns in each EP. These complex errors were caused by slack of skin. During humerus elevation, the distance between scapula and humerus was partly contracted then the skin on acromion was slacked. Though the amount of the errors was individually different, the error patterns across all subjects were identified.

Systematic error pattern allowed estimation of regression. ARMSE was decreased from 20.3˚ (no regression) to 3.6˚ (using all samples). Focusing the number of samples (Figure 1), ARMSE obviously increased under 10 samples, while it did not clearly changed over 15 samples. To consider estimation accuracy and time cost for sampling, using about 10 to 15 samples was practical. Then, the number of samples decreasing, remained samples were based between low elevation in frontal plane and high elevation in sagittal plane. It was suggested that employing sampling position was based on this positions.

CONCLUSIONS

The error patterns were examined for humerus elevation and elevation plane. Employing linear regression, dynamic measurement of scapula kinematics from skin is possible. For practical way, the number of samples and sampling humerus positions were suggested.

REFERENCES

1. McQuade KJ, et al. *JOSPT*, 27 (2), 125-133, 1998.
2. Karduna AR, et al. *J Biomech Eng,* 123**,** 184-190, 2001.
3. Johnson GR, et al. *Clinic Biomech*, 8 (5), 269-273, 1993

CENTRAL AND PERIPHERAL CONTROL OF MUSCLE STIFFNESS IN HOPPING

Hiroaki Hobara, Masashi Yoshida and Shuji Suzuki
Graduate school of Human Sciences, Waseda University, Tokorozawa, Japan
Email: h_hobara@moegi.waseda.jp

INTRODUCTION

In stretch-shortening cycle (SSC), a transition period from the eccentric to the concentric phases is called coupling time (Ct). If duration of Ct increases, the release of the elastic energy in the concentric phase would decrease. Thus, minimizing Ct is important for the elastic energy utilization in SSC.

Although Ct depends on the total movement time [2], the mechanisms responsible for this phenomenon were not well-known. Lansel-Corbeil and Goubel (1990) reported that an increase in muscle stiffness during the eccentric phase would reduce Ct. Therefore, it is hypothesized that stiffness regulation during the eccentric phase could be key to solve above-mentioned problem.

The purpose of this study was to investigate the neural control mechanism of the triceps surae to reduce Ct during hopping.

METHODS

Seven male subjects performed two-legged hopping at the preferred and the lowest frequency (PF, LF, respectively). The subjects determined these frequencies voluntarily. To differentiate Ct, two different ground contact time were manipulated during stance phase at each frequency: preferred and the shortest possible time (PCT and SCT, respectively).

An ankle angle was measured by a goniometer to calculate Ct, which was computed as the time period of 5 % threshold levels above the minimum ankle angle [1]. The surface electromyography (EMG) activities of the medial gastrocnemius (MG) and soleus (SOL) muscles were recorded with telemetric system. Obtained EMG signals were amplified, full wave rectified, and then integrated over the fixed interval of 20 ms. All data were compared PCT with SCT conditions.

RESULTS AND DISCUSSION

As shown in Table 1, we could differentiate Ct by manipulating ground contact time in same hopping frequency.

The most important finding of this study was that increased pre- and post-landing EMG activity was observed in SCT conditions at each frequency (Figure 1).

Table 1: Mechanical data for PCT and SCT.

	Preferred frequency		Lowest frequency	
	PCT	SCT	PCT	SCT
Hopping frequency (Hz)	2.12 ± 0.1	2.11 ± 0.08	1.87 ± 0.2	1.87 ± 0.2
Ground contact time (ms)	238 ± 32	203 ± 32**	210 ± 33	198 ± 28**
Coupling time (ms)	39 ± 15	32 ± 9 **	33 ± 11	29 ± 10**

** $p < 0.01$

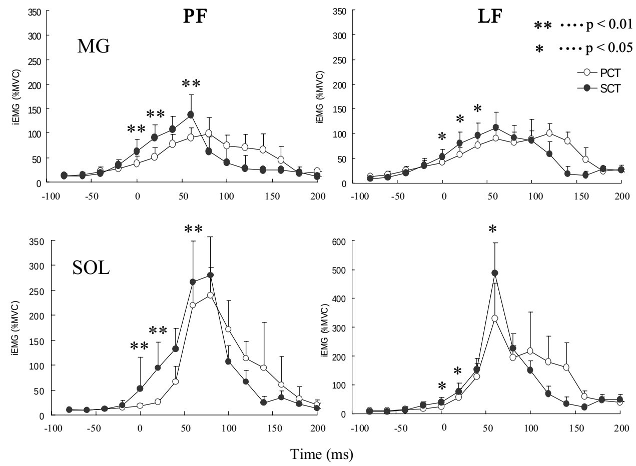

Figure 1: Representative EMG activities during hopping. The records were lined up with ground contact as reference (Zero time).

EMG activity observed at pre-landing was thought to be feed-forward motor program that made in central nervous system [3]. In addition, post-landing EMG is mentioned as short-latency stretch reflexes triggered by dorsiflexion [5]. Both EMG activities have an effect to regulate muscle stiffness during the eccentric phase [3, 5].

Considering that an increase in muscle stiffness during the eccentric phase would reduce Ct [4], increased EMG activity in SCT conditions can be interpreted as adaptations to regulate muscle stiffness for reduction of Ct by central and peripheral nervous system.

CONCLUSIONS

Neuromuscular control of the triceps surae to reduce Ct was investigated. These results clearly show that stiffness regulation by central and peripheral nervous system contributes to reduce Ct.

REFERENCES

1. Aura O., Komi PV. BIOMECHANICS X-A, 507-501, 1987.
2. Bosco C., Rusko H. Acta Physiol Scand **119**, 219-224, 1983.
3. Golhofer A., Kyrolainen H. Int J Sports Med **12**, 34-40, 1991.
4. Lansel-Corbeil G., Goubel F. J Biomech **23**, 121-126, 1990.
5. Voigt M., et al. Acta Physiol Scand **163**, 181-194, 1998.

A VALIDATION STUDY: USING CT SCANS TO CALCULATE VOLUME, WEIGHT AND DENSITY

[1]Sylvana García, [1]Jill Schmidt, [1]Heidi Ploeg
[1]Department of Mechanical Engineering, University of Wisconsin-Madison
email: garcia1@wisc.edu, web: www.engr.wisc.edu/groups/BM/

INTRODUCTION

Virtual modeling is a rapidly growing pre-clinical evaluation tool in the biomedical field. Not only is it a non-invasive method to predict biomechanical behavior, but it can also be performed to gain insights before clinical applications [1-4], thus increasing the efficiency of the design process. Computerized Tomography (CT) scans can provide data on the shape and density distribution [5] of a tissue required for a virtual a model.

The purpose of this study was to determine an empirical relationship between the CT gray values (Hounsfield Units, HU) and the density of polymeric materials, and to apply this relationship to volumes constructed from the segmented CT data. These results were compared to physically measured volumes and weights.

METHODS

In this study, cylinders made from 8 materials were scanned with a clinical CT scanner: low density polyethylene, high density polyethylene, polymethylmethacrylate, polypropylene, Nylon 66, and low density polyurethane (LDPU) were 10 mm diameter by 7 mm height; and, high density PU (HDPU), and aluminum, were 10 mm diameter by 5 mm height. Each cylinder was measured and weighed prior to CT scanning (UW Hospital, 120 kV, 30 mA, 0.43 mm pixel size, GE LiteSpeed[16], GE Medical Systems). The cylinders were CT scanned with their axes oriented in a vertical direction.

The CT data were imported into Mimics 8.11 (Materialise, Ann Arbor, MI) software. Using the thresholding procedure "masks" were created which consisted of a group of pixels within the relevant range of HU's. The masks were not manually edited in this protocol. A mean value of HU was recorded for each material. Based on the masks, a 3D model of each material was constructed and its volume was determined. The 3D models were surface-meshed with triangles using Mimics and imported into MSC/Patran 2003 (MSC.Software, Santa Ana, CA) to create a volume mesh with tetrahedral-shaped elements, which was imported back into Mimics, to assign density to each element, based on the HU's. The volume mesh with assigned density was then re-imported into MSC/Patran 2003 to find its volume and weight.

RESULTS

An empirical relationship between HU and the polymeric densities (measured mass/volume) was derived (Figure 1). A mean of the absolute errors of 12% (-7%-19%) between the Mimics derived volumes and the measured volumes was found. The error between the Mimics and MSC/Patran volumes was insignificant. A comparison of the measured weights and densities to the MSC/Patran derived values found a mean of the absolute errors of 7% (-15% to -1%) and 12% (-17% to 20%), respectively, excluding the results from PU foams, which produced the largest errors (76% and 183%) on the weights of the HDPU and LDPU, respectively.

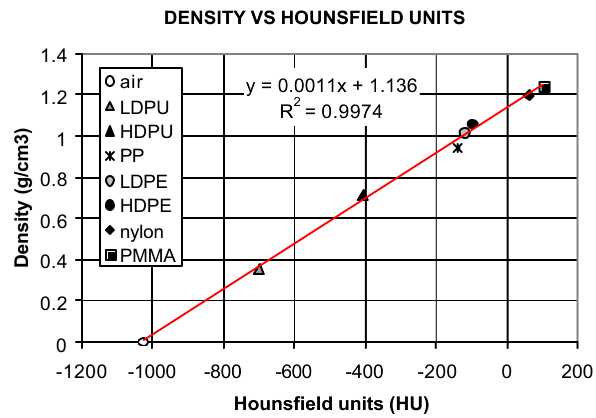

Figure 1: Density versus Hounsfield units for 7 polymers and air (ρ = 0 g/cm^3, at HU = -1024).

DISCUSSION AND CONCLUSIONS

The volume error of segmented models was due to CT scanning resolution which caused the cylinders to be slightly sectioned perpendicular to the scanning direction. Also, the thresholding procedure was imprecise at the base of the cylinders due to the material interfaces. The large errors in the weights and densities of LDPU and HDPU foams were caused by modeling them as a continuum. This result is particularly relevant to similarly derived models of trabecular bone and the study of its micro- and macro-mechanical properties.

CT scans of cylinders of various materials were used to construct 3D virtual models. A linear relationship (R^2 = 0.997) between HU and density for 7 polymers and air was used to assign density to a volumetric mesh. The measured and constructed properties (volume, weight and density) for the cylinders were compared, finding errors in weight and density of 7% and 12%, respectively, excluding the results from the LDPU and HDPU. The sources of error were: CT scanning resolution, thresholding at material interfaces, and modeling of foam on a macro-scale. The relationship between micro- and macro-mechanical properties needs to be further investigated.

REFERENCES

1. Taylor, W.R., et al. *J Biomech* **35,** 767-773, 2002.
2. Donahue TL, et al. J Biomech Eng 124, 273-280, 2002.
3. Keyak JH et al. J Biomed Eng 12, 389-397, 1990.
4. Merz B, et al. J Biomech Eng 118, 387-390, 1996.
5. Prendergast PJ. Clin Biomech 12, 343-366, 1997.

INFLUENCE OF VOLUNTARY POSTURE SELECTION ON ENDPOINT STIFFNESS

Eric J. Perreault
Departments of Biomedical Engineering and Physical Medicine and Rehabilitation
Northwestern University, Evanston, IL,

INTRODUCTION

The endpoint stiffness of the human arm describes the relationship between postural perturbations applied at the hand and the steady-state forces generated in response to those displacements. As such, it characterizes the mechanical properties of the arm as seen at the point of contact with the environment and can be used to quantify limb stability. The stiffness properties of a limb are not fixed, but rather depend strongly on limb posture [1] and muscle activation [2]. It has been proposed that humans modulate limb stiffness to optimize the mechanical properties of a limb in a task-dependent manner [3]. However, most studies examining endpoint stiffness only have characterized 2D stiffness with the arm in the horizontal plane. Under these conditions, the direction of maximum stiffness is oriented approximately along the line connecting the shoulder and hand, and it appears that this orientation cannot easily be modified for a fixed arm posture. In contrast to these studies, functional tasks rarely are restricted to the horizontal plane. Hence, a more complete understanding of how endpoint stiffness is regulated during functional tasks requires an assessment 3D endpoint stiffness at self-selected arm postures. The purpose of this study is to quantify the 3D stiffness properties of the human arm and to examine if individuals voluntarily choose postures that optimize endpoint stiffness in a task-dependent manner.

METHODS

Endpoint stiffness was measured using a 3D robotic manipulator [HapticMaster; FCS Control Systems, The Netherlands], configured as a stiff position servo. The robot was used to apply random 3D displacements to the arm and to measure the 3D forces generated in response. Subjects were strapped into an adjustable height chair so that the trunk was fixed and positioned to that the hand was at shoulder height, approximately in front of the sternum. Although the shoulder and hand were fixed, the position of the elbow was free. In each trial subjects were instructed to exert a constant level of force against the robot and were assisted in this task by a 3D visual display of the force measured by the robot. Data were collected either with the arm positioned in the horizontal plane or positioned at a posture selected by the subject. The presented data focus on forces generated along the ±X-axis (Fig. 1), which corresponds pushing or pulling along the intersection of the sagittal and horizontal planes.

Endpoint stiffness was estimated from the measured endpoint displacements and forces using system identification techniques presented previously [2, 4].

RESULTS AND DISCUSSION

When the arm was kept in the horizontal plane, our 3D stiffness estimates were consistent with the 2D results that we and others have reported previously [1,2]. When allowed to self-select an arm posture, subjects always chose one in which the elbow was dropped below the horizontal plane connecting the shoulder and hand. Fig. 1 compares the stiffness estimated at two self-selected postures (purple) to those measured with the arm in the horizontal plane (green). Each ellipsoid represents the results of a separate endpoint force condition, indicated by the labels; the overlaid ellipsoids were collected at matched forces. The self-selected postures resulted in increased stiffness for forces along the –X axis, which tend to decrease limb stability [5], and increased stiffness for forces in the opposite direction, which tend to increase stability. Hence these postures may have been chosen to compensate for the effects of the constant forces applied at the hand.

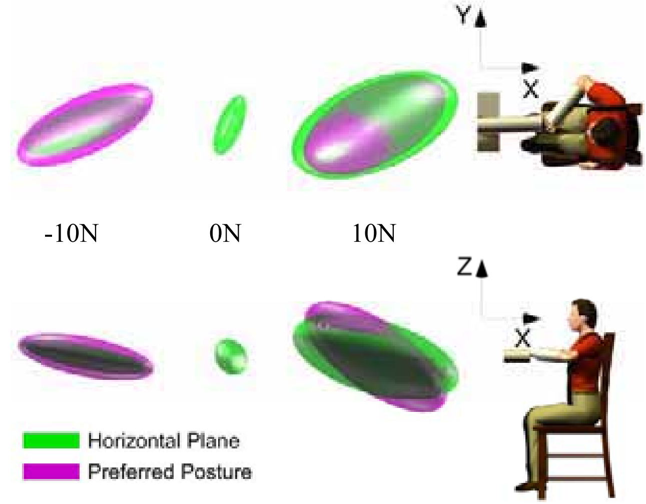

Figure 1: Endpoint stiffness measured at three different voluntary force levels along the X-axis.

CONCLUSIONS

These initial results demonstrate our ability to measure endpoint stiffness in the three degrees of freedom relevant to most functional tasks. In addition, they demonstrate that subjects often work outside of the horizontal plane characterized in most previous studies and that these alternate postures influence endpoint stiffness. We currently are examining how self-selected postures influence limb stiffness and stability in a variety of tasks.

REFERENCES

1. FA Mussa-Ivaldi, et al. *J Neurosci*, v. 5, pp. 2732-43, 1985.
2. EJ Perreault, et al. *Exp Brain Res*, v. 141, pp. 312-23, 2001.
3. N Hogan, *Biol Cybern*, v. 52, pp. 315-331, 1985.
4. EJ Perreault, et al. *Biol Cybern*, v. 80, pp. 327-337, 1999.
5. J McIntyre, et al. *Exp Brain Res*, v. 110, pp. 248-264, 1996.

ACKNOWLEDGEMENTS

This work was supported by NIH grant K25-HD044720 and by The Whitaker Foundation.

A BIOMECHANICAL COMPARISON OF KENYAN AND JAPANESE ELITE LONG DISTANCE RUNNER'S TECHNIQUES

[1] Yasushi Enomoto and [2]Michiyoshi Ae
[1]Faculty of Education, Kyoto University of Education; enomoto@kyokyo-u.ac.jp
[2]Institute of Health and Sport Sciences, University of Tsukuba

INTRODUCTION

It is recognized that Kenyan runners have an excellent record in running events of various distances: they have mastered running techniques for the acquisition and maintenance of high speed over long distances. Although there are many world class Japanese long distance runners, comparing their running techniques with those of Kenyan elite runners seems to reveal differences in efficiency. This study will attempt to show reasons for the high performance of Kenyans through biomechanical analysis of their running techniques. The purpose of this study is to compare the running techniques of Kenyan and Japanese elite male long distance runners in 5000 m races.

METHODS

Official 5000 m races were videotaped with a digital video camera at 60 Hz in the 2003 IAAF Grand Prix in Osaka; the 2004 Super Athletic Meets in Yokohama; and the 2004 Inter-high School Athletic Competition. Videotapes of nine Kenyan and nine Japanese runners were digitized through out the running cycle at the 2000 m and 4000 m marks. Their height, body mass, and race record were 1.69 m, 55.1 kg, 13 min 24.08 sec for Kenyans and 1.73 m, 55.8 kg, 13 min 34.92 sec for Japanese, respectively. Kinematic and kinetic variables were calculated using two-dimensional motion analysis. Joint and segment angles, center of mass, joint torque, and power of the lower limb were calculated for the evaluation.

RESULTS AND DISCUSSION

Running velocity at the 2000 m and 4000 m marks was 6.16 and 6.28 m/s for the Kenyan and 6.08 and 6.11 m/s for the Japanese. There was no significant difference in running velocity, step length and step frequency. However, relative step length to the body height was greater in the Kenyans than the Japanese.

There were few significant differences in lower limb angles and angular velocities between the Kenyan and the Japanese runners. One of the greatest differences was shown in the mean torso angle of the cycle, which indicates that Kenyan runners ran with greater forward lean of the torso than the Japanese. Ankle joint angle at toe-off and angular displacement in the second half of the support phase were greater in the Japanese than the Kenyans. Thigh and shank angular velocity in the recovery phase tended to be greater in the Kenyans than the Japanese but there was not a statistically significant difference. The peak values of the joint torque and power at knee joint in the late recovery phase were greater in the Kenyans than the Japanese. These results suggest that hip and knee joint movement relative to the ankle joint was greater in the Kenyans than the Japanese.

The figure below shows stick pictures at each point in the cycle and the locus of the center of mass of the lower limb (CMleg) for typical subjects at the 4000 m mark, subject A is a Kenyan and subject B is a Japanese runner. It is shown that the locus of CMleg for subject A shows a wider and higher ellipse than subject B. There were significant differences in the horizontal displacement (range of horizontal movement) of CMleg relative to the body height and the maximum horizontal (forward) velocity of CMleg relative to the center of mass of the body between the Kenyan and Japanese runners. It is important for a distance runner to swing both legs forward and backward coordinately in order to reduce energy waste [1]. These results suggest that the Kenyan runner swung the leg forward faster and more broadly so as to efficiently acquire the higher running velocity.

CONCLUSIONS

One of the most significant characteristics of the Kenyan runner was the forward lean of the torso. Movement of the center of mass of the lower limb was greater and faster for the Kenyans than the Japanese, which indicates that the Kenyan runner could swing the leg forward faster and more broadly.

REFERENCES

1. Williams KR, Cavanagh PR. *Journal of Applied Physiology* **63**, 1236-1245, 1987.

ACKNOWLEDGEMENTS

This study was supported by the Japan Amateur Athletic Federation (JAAF) Scientific Committee.

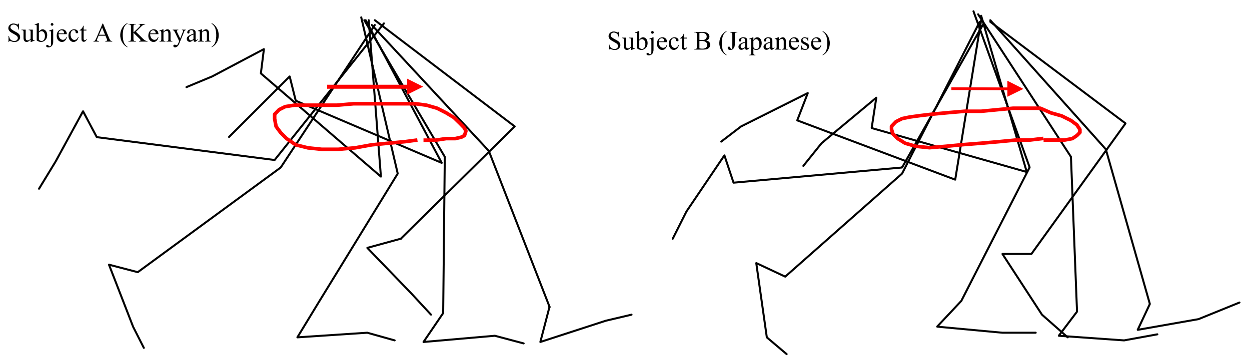

Figure Stick pictures at each point in a cycle and a locus of the center of mass of lower limb for typical subjects at 4000 m mark.

THE KINEMATIC CHANGES OF PITCHING DURING A SIMULATED BASEBALL GAME

[1] Daisaku HIRAYAMA, [2] Norihisa FUJII
[1]Graduate School of Comprehensive Human Science, University of Tsukuba, Japan
[2]Institute of Health and Sport Sciences, University of Tsukuba, Japan
e-mail: daisaku-h@lasbim.taiiku.tsukuba.ac.jp

INTRODUCTION

Maintaining consistent maximum ball velocity is an important factor for baseball pitchers. At the latter half of the game, ball velocity and control decrease due to fatigue by excess of pitching. Therefore, it is difficult for a baseball pitcher to pitch the whole game in many cases. The purpose of this study was to investigate the effect of fatigue on changes of pitching kinematics during a simulated baseball game.

METHODS

Six male college baseball pitchers threw 15 pitches in an inning for 9 innings (135 pitched) in an indoor pitcher's mound. Rest time between innings was 6 minutes.

Three-dimensional positions of 47 reflective markers attached to subjects were tracked by an optical motion capture system (Vicon Motion System 612, Oxford Metrics) with eight cameras (250Hz). For each subject two fastball pitches (one in the 1st inning and one in the 7th inning) were chosen for analysis.

The pitching motion was divided into three phases by four instants of motion events: the first phase was defined as a phase from the instant for maximal knee height of the stride leg (MAXknee) to the instant for minimal ball height (MINball), the second phase from MINball to stride foot contact (SFC), and the third phase was from SFC to ball release (REL).

Differences among kinematic parameters were analyzed by paired t-test with significant level of 5%.

Kinematic parameters were analyzed as follows: ball velocity, knee angle of lead leg, shoulder rotation angle (Figure1), pelvis rotation angle, abduction angle and horizontal abduction angle of throwing arm, forward tilt angle (Figure2) and lateral tilt angle of trunk, backward tilt angle (Figure2) and lateral tilt angle of shank.

RESULTS AND DISCUSSION

Four of ten kinematic parameters changed significantly between 1st inning and 7th inning (Table1).

1) The ball velocity of 7th inning was significantly smaller than that of 1st inning. It is generally accepted that the ball velocity often decreases when a pitcher throws about 100 pitches. Therefore, this research had the same tendency as the generally considered one.

2) The shoulder rotation of 7th inning at SFC was significantly larger than that of 1st inning. It shows that the shoulder is open up at SFC. Stodden et al.[3)] indicated that pitchers could generate larger momentum and transfer it from the trunk to the throwing arm when they were in a proper position to optimally rotate the pelvis and upper torso (shoulder). Therefore, it is important to twist the trunk appropriately.

3) The forward trunk tilt of 7th inning at REL was smaller than that of 1st inning. Matsuo et al[1)] found that ball velocity increased as forward trunk tilt increased. It is inferred that forward trunk tilting at REL might be appearance that the pitcher tried to enlarge the ball velocity.

4) The backward shank tilt of 7th inning at REL was larger than that of 1st inning. Murray et al.[2)] showed that the knee flexion angle at REL might indicate muscle fatigue. In turn, less energy was transferred from the support leg to the trunk, subsequently decreasing the amount of energy in the throwing arm at 7th inning.

REFERENCES

1. Matsuo T, Escamilla R F, Fleising G S, et al (2001): Comparison of Kinematic and Temporal Parameters Between Different Pitch Velocity Groups. Journal of Applied Biomechanics 17: 1-13
2. Murray T A, Cook T D, Werner S L, Schlegel T F et al (2001): The Effects of Extended Play on Professional Baseball Pitchers. The American Journal of Sports Medicine 39(2): 137-142.
3. Stodden D F, Fleisig G S, McLean S P, et al (2001): Relationship of Pelvis and Upper Torso Kinematics to Pitched Baseball Velocity. Journal of Applied Biomechanics, 17: 164-172

Table 1: Kinematic differences between 1st inning and 7th inning

Parameters	1st inning	7th inning	P value
Ball velocity (m/s)	34.5	33.1	0.020
Stride foot contact			
Shoulder rotation (deg)	67.7	69.7	0.014
Ball release			
Forward trunk tilt (deg)	57.1	54.6	0.025
Backward shank tilt (deg)	99.1	102.7	0.032

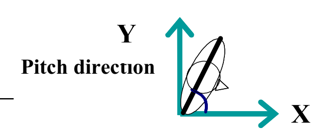

Figure 1: Shoulder rotation

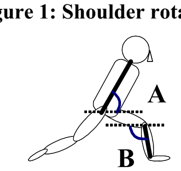

Figure 2:
A) Forward trunk tilt
B) Backward shank tilt

THE ROLE OF MUSCLE IN GLENOHUMERAL JOINT STABILITY DURING BASEBALL PITCHING

[1]Hwai-Ting Lin, [2]Fong-Chin Su and [2]Edmund Y.S. Chao
[1]Institute of Biomedical Engineering, National Cheng Kung University, Tainan, Taiwan
[2]Department of Orthopaedic Surgery, Johns Hopkins University, MD, U.S.A.
email: fcsu@mail.ncku.edu.tw

INTRODUCTION

Joint instability is one of the most common human afflictions. Capsulolabrum, articular surfaces, intracapsular pressure and muscle contractions are the factors in maintaining joint stability. The glenohumeral joint is a common dislocated large joint of the body [1]. Shoulder motion with improper muscular coordination or need of explosive muscle contraction is easy lead to joint dislocation such as baseball pitching. The purpose of this study was to examine how the muscle functions response for joint stability during baseball pitching. We hypothesize that muscle contraction force contributed the most to balance external loading to keep joint stability.

METHODS

A graphic-based musculoskeletal model of the shoulder was utilized for the dynamic analysis [2] (Fig. 1). Ten muscles with fifteen action lines were included in the shoulder model. The pitching motion of a college baseball pitcher was captured using a Qualisys^{TM} motion analysis system (Qualisys AB, Sweden) at a 500Hz sampling rate. Using the inverse dynamic problem solution and Newtonian analysis, the joint resultant forces and moments at shoulder were quantified. The indeterminate problem was solved using an optimization technique by minimizing the sum of the squares of muscle stresses. Additional inequality constraints on muscle stress were considered, thus making the present formulation a "mini-max" problem. Sequential quadratic programming and a steepest decent algorithm were used to search for the muscle contraction force. The magnitude and action line of resultant joint force, joint constraint force (joint contact force and passive element forces) and muscle contraction force was used to identify the contribution to joint stability. For the results presentation, the action line of the muscle, resultant joint force, and joint constraint force were projected to scapular coordinate and expressed as anterior/posterior (z-axis), superior/inferior (y-axis), centripetal/centrifugal (x-axis).

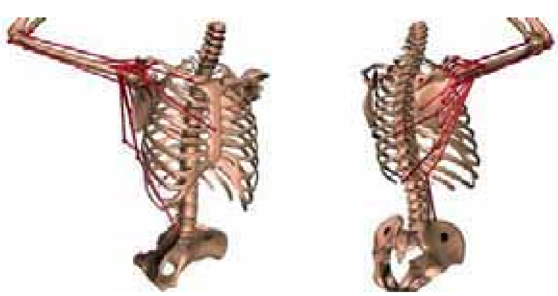

Fig. 1 The graphic_based musculoskeletal model of the shoulder.

RESULTS AND DISCUSSION

Results showed that the resultant joint force has significant loading force until the end of late cocking phase. The maximum resultant joint force in centripetal direction (851N) was occurred in ball releasing, and inferior direction (479N) at the end of late cocking phase. The force in anterior/posterior direction was relative small and found the maximum loading force in follow through phase about 390N. From the muscle forces analysis, the joint constraint forces contributed very little to keep joint stability from the end of late cocking phase to the acceleration phase. During this period, eight of fifteen muscle action lines are mainly in the inferior direction (Table 1). Among these muscles, sternal and clavicle branch of the pectoralis major, infraspinatus, and supraspinatus had significant contraction forces. At this moment, glenohumeral joint could not rely on its geometry to keep joint stability. These muscles forces contribute to both joint motion and stabilization. On the contrary, at the ball release, only four muscle action lines are in the centripetal direction and only latissimus dorsi had significant contraction force. That means that joint contact force could provide enough joint stability.

Table 1. The magnitude and orientation of action line of joint resultant force and muscles at the end of late cocking phase.

	Orientation	Force (N)
Joint resultant force	(0.45, -0.89, 0.09)	479
Pectoralis major (sternal)	(-0.52, -0.84, -0.19)	95
Pectoralis major (clavicle)	(-0.18, -0.98, 0.11)	135
Infraspinatus	(0.46, -0.79, -0.41)	276
Supraspinatus	(0.35 -0.93, 0.06)	82

CONCLUSIONS

This quantitative model improves our understanding of the role of shoulder muscles in glenohumeral joint during the baseball pitching. Muscles not only play the movers but also stabilizers especially when joint had anterior/posterior and superior/posterior external loading. Future study may optimize muscles strengthening to maximize compressive forces to keep joint stability

REFERENCES

1. McMahon et al. *Clin Orthop*. 403S, S18-25, 2002.
2. Lin HT, et al. *J Biomech Eng*, 2005 (in press).
3. Labriola et al. *Clin Biomech.* 19, 801-809, 2004.

ACKNOWLEDGEMENTS

Support from National Science Council, NSC91-2320-B-006-047, Taiwan.

The Effects of Locomotor Training on Neural and Muscle Activation.

Gail F Forrest[1], Sue Ann Sisto[1], Dr Steven Kirshblum[2], Janina Wilen[1], Quin Bond[3], Scott Bentson [1], Susan Harkema[4]
[1]Kessler Medical Rehabilitation Research and Education Corporation
[2]Kessler Institute of Rehabilitation
[3]BioMotion of NJ
[4]School of Medicine, Department of Neurology, University of California, Los Angeles
email:gforrest@kmrrec.org

INTRODUCTION

There is generally limited quantitative kinematic and electromyography (EMG) regarding the effect of Locomotor Training using body weight support Treadmill Training (BWST) for an extended period of time on a person with ASIA B classification. The objective of this case study is to determine the effects of Locomotor Training using BWST on kinematics, neural, and muscle activation changes for an individual with an incomplete SCI, one year post injury.

METHODS

The participant (male, 26 years, ASIA B, no motor function below level of injury, injury level C6) trained for 35 sessions of Locomotor Training (T1), stopped training for 8.6 weeks, and recommenced training for another 62 sessions (21 weeks) (T2). Before T1 (PRE-T1), and before T2 (MID) kinematic and EMG data were collected [at 60% and 40% body weight support (BWS), treadmill speed at 1.6 mph]. After T2 (POST-T2) was completed, kinematic and EMG were collected bilaterally for 60%, 40% and 20% BWS.
A 6-camera Vicon system (sampled at 60Hz) was used to collect kinematic data. Spherical reflective markers were placed on right and left second and fifth metatarsal, calcaneous, tibial tuberosity, femoral epicondyle, greater trochanter, anterior inferior iliac spine, posterior inferior iliac spine. EMG was recorded using surface EMG for left and right medial gastrocnemius (L/R G), tibialis anterior (L/R TA), rectus femoris(L/R RF) and bicep femoris(L/R BF). EMG was collected at a bandwidth of 10-600 Hz, and sampled at 1500 or 1560 Hz. Raw EMG signals were filtered at a bandwidth of 30-150 Hz, full-wave rectified, then root mean squares (RMSs) were calculated over a 120ms window (2). EMG data was processed using MATLAB (MathWorks Inc., Version 6.1). Calculation of sagittal plane segment motion for the thigh, shank and foot was determined using MATLAB.
Limb kinematics were calculated in the local moving plane with calculation of orientation angles for each segment relative to the right horizontal (3). 6-8 gait cycles were analyzed per condition.

RESULTS AND DISCUSSION

After training, EMG firing patterns were consistent to kinematic profiles at the hip and knee. Before training the EMG firing profiles were not. Higher EMG amplitudes were observed after training [Pre vs. post (60%BWS): LBF: 19.64±.23 vs. 43.76 ±5.10uV; LR: 19.64 ± 1.36 vs. 43.76 ± 1.13uV; LG:3.96 ± 1.29 vs. 23.73 ± 1.01uV].
For the LRF, LBF, and LTA the EMG activity were more rhythmical and less tonic after the first series of Locomotor Training sessions (Figure 1). Significantly, at PRE-T1, the LBF was firing for most of the gait cycle (GC) [i.e., mean burst duration (BD) was 88.1 ± 6.1% of the GC] whereas at MID, the mean BD decreased to 55 ±15% of the GC and at POST-T2 its BD decreased further to 41±15%. In general, the BD for the LTA and LG at MID and POST-T2 decreased with increasing load.
Further, there was a positive linear response in mean EMG amplitude to bodyweight (BW) load. At mid, mean EMG amplitudes for all muscles (LR, LBF, LTA, and LG) increased with loading from 40% to 60% BW and at POST-T2 the mean EMG amplitude for LG (at 40%, 60%, and 80% BW load) also increased. The results for LBF and LTA were more variable. Both of these muscles showed a decrement in mean EMG RMS amplitude (from 40% to 60% BW load) followed by an increase (from 60% and 80% BW load).
All of these results demonstrate the positive neural and muscle activation changes that occur after Locomotor Training for an individual with an incomplete SCI (ASIA B, 1-year post).

REFERENCES

1. Dietz V, et al., *Physical Therapy*. **77**(5): 508-516, 1997
2. Wilen J, et al., *A of Biomed Eng.* **39**:97-106, 2002

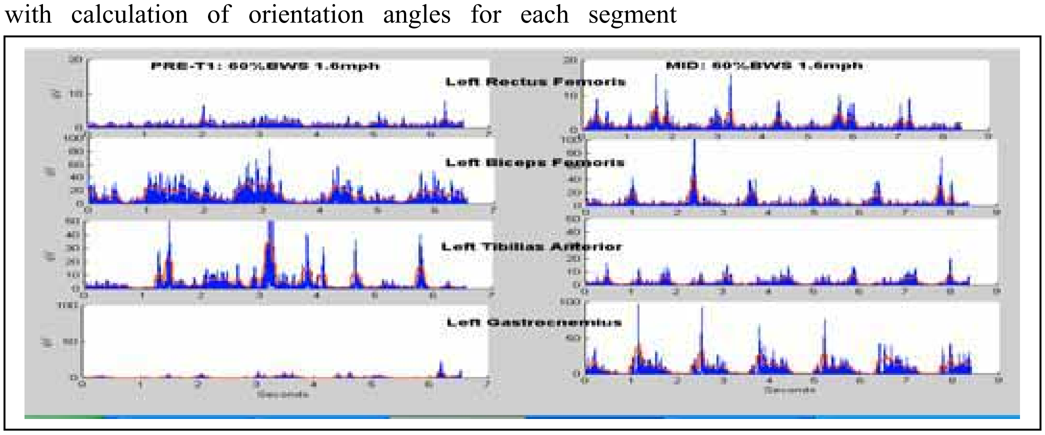

Figure 1. At PRE –T1 & MID. Rectified EMG and EMG RMS amplitude (uV) versus time (sec) for 5 gait cycles LRF, LBF, LTA, LG.

ACKNOWLEDGEMENT:
New Jersey Commission on Spinal Cord Research

PARAMETERIZATION OF JOINT KINEMATICS USING QUATERNIONS

[1] Laura Held, [1,2,3]J. L. McNitt-Gray, and [4]Henryk Flashner
Biomechanics Research Lab; [1]Departments of Biomedical Engineering, [2]Kinesiology,
[3]Biological Sciences, and [4]Aerospace and Mechanical Engineering;
University of Southern California, Los Angeles, CA
email: held@usc.edu

INTRODUCTION

Several methods exist to parameterize 3D segment orientation of a multijoint system. Any method of attitude characterization requires coordinate data of a minimum of three non-collinear points located on each body segment during the movement (tracking markers). The method used to acquire the kinematic data and characterize the motion must be consistent with the research question and insensitive to the error introduced during the motion detection process. Choosing an appropriate method for a given research question depends on its performance in the following areas: immediate physical meaning, ease of calculations, singularities, smooth transition around 180°, and ability to describe sequential rotations [1].

In this study, we investigated the ability of the quaternion parameterization of rigid body orientation to characterize lower extremity joint kinematics during 3D human movements using experimental data.

A quaternion is an extension of complex numbers of the form:

$$\mathbf{q} = [\cos\theta, \cdot (\sin\theta \cdot n_1, \sin\theta \cdot n_2, \sin\theta \cdot n_3]^T$$

The four parameters represent the rotation of a rigid body about a unit vector **n** by an angle 2θ [2]. Quaternions are advantageous because the addition of a fourth parameter avoids the singularities inherent in the Euler parameterization, the implementation is algebraic, and successive rotations are handled as an addition operation. Further, the axis/angle information embedded in the quaternion can be used to quantify out of plane motion and changes in the axis of rotation within a joint during movements.

METHODS

Footwork skills were performed by a skilled athlete in accordance with the Institutional Review Board. Three non-collinear markers were mounted onto orthoplast and attached to the lateral aspect of the thigh and shank over a neoprene sleeve to minimize marker movement. Sagittal and frontal plane kinematics were recorded during the task using digital video (200 Hz, NAC C2S, Burbank, CA). Tracking markers and joint centers were manually digitized for the entire task (Peak Performance Inc, Englewood, CO). Bony landmarks were digitized for one frame to calibrate segment reference systems. 3D coordinate data for all points was acquired using direct linear transformation. Raw coordinate data was filtered using quintic splines and exported into Matlab.

Quaternions were calculated for both segments at each time step [3]. The shank and thigh quaternions were then used to calculate the knee angle. To validate the quaternion algorithm, these knee angles were compared to knee angles calculated using the digitized joint center coordinates (Figure 1).

RESULTS AND DISCUSSION

Comparison of the joint angles calculated using digitized joint centers versus quaternions demonstrated the ability of the quaternion to accurately parameterize segment configuration. The RMS error for the knee angle calculated with the knee and hip quaternions was 2.53˚ By increasing the number of tracking markers on each segment to four or five, this RMS error is likely to be reduced.

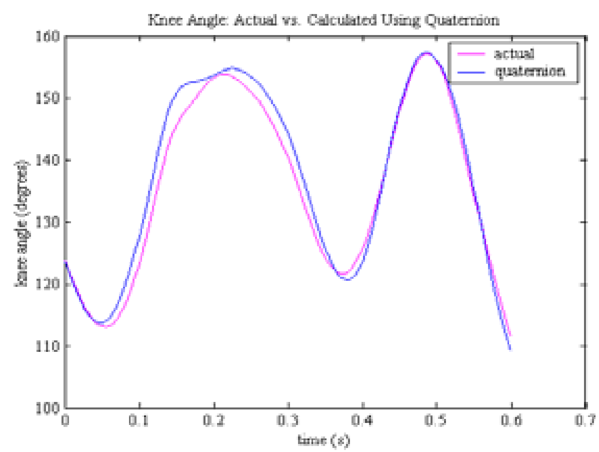

Figure 1. Comparison of knee angle computed using 3D coordinate data and knee angle determined using quaternion parameterization.

These results demonstrate that the quaternion parameterization of segment configuration can be used to characterize knee motion during foot work skills as performed in this study.

CONCLUSIONS

The quaternion parameterization of rigid body orientation was found to be a reasonable method for characterizing lower extremity joint kinematics during 3D human movements. This parameterization provides advantages over alternative methods (Euler angles, screw method) because it provides biomechanically relevant information, is easy to implement, and avoids singularities. The axis/angle information embedded in the quaternions for each segment can be used to validate assumptions about joint characteristics and to quantify out of plane motion between adjacent segments.

REFERENCES

[1] Zatsiorsky. *Kinematics of Human Motion*.1998.25-60
[2] Kim, Injung et al. *Kalman filtering using the quaternion extracted from vector measurements*. AAS 01-142. 571-586
[3] Kuipers. *Quaternions and Rotation Sequences*.1999.

ACKNOWLEDGEMENTS

Intel, Women in Science and Engineering Fellowship, Oakley Fellowship, Witaya Mathiyakom, Lauren Deutsch

REPEATABILITY OF DRT4 LASER DOPPLER MICROVASCULAR MEASUREMENTS

[1, 2] James A. Furmato, [2]Jinsup Song and [2, 3] Howard J. Hillstrom
[1]PhD Student, [3]School of Biomedical Engineering, Drexel University, Philadelphia, PA,
[2] Gait Study Center, Temple University School of Podiatric Medicine, Philadelphia, PA

INTRODUCTION

The Moor DRT4 Laser Doppler Monitor (Moor Instruments, Devon, UK) uses fiber optic cables to deliver two channels of 780 nm, 1.0 mW laser light to the interrogated tissue. The system is designed to evaluate microcirculation in 1 mm^3 of tissue at a depth of 1.0 mm. Like other systems, the DRT4 is not able to provide flow output in physical units since the geometry of the capillary bed is unknown. This limitation is overlooked clinically since the monitor allows functional testing of microcirculation, provides sufficient screening of those vessels and is not used for absolute measurements[1].

Use of laser Doppler (LD) monitors to provide follow up studies at the same site depends on finding the same capillary structure. Measurements may also be affected by temperature of tissue, tissue thickness, location of the probe and its orientation. Where repeated measures are needed for a research study, the reliability of measurements comes into question. If repeated measures can be taken at the same location and with controlled amounts of displacement from the original site, similar signals should be captured.

METHODS

Ten subjects from the general population were asked to refrain from eating, consuming alcohol or using nicotine products at least one hour before being studied. Each was studied in a reclined position that was relaxed and quiet. One LD probe was placed on the plantar hallux and the other under the first metatarsal head of the right foot as a control. Note that the control probe was never moved during the course of the experiment. The hallux location was marked with ink. The cable from the probe was directed proximally to register the orientation. Each probe collected data related to red blood cell motion (flux) and intensity of reflection (concentration).

Table 1: Interclass Correlations Coefficients (k=3. N=10). F=flux and C=concentration, both in arbitrary units; (1) sub-hallucial, (2) sub 1st metatarsal head [2].

Condition	F1	F2	C1	C2
Fixed position	0.94	0.97	0.94	0.97
Remove probe and replace	0.94	0.93	0.95	0.98
Remove probe and rotate 90	0.97	0.96	0.97	0.97
Remove probe and relocate 2 mm laterally	0.96	0.96	0.90	0.97
Remove probe and relocate 2 mm medially	0.92	0.92	0.90	0.98
Pooled Conditions	0.92	0.95	0.97	0.99

Data was collected in two-minute segments with approximately a one minute pause between measurements under five conditions for three trials each (see Table 1). Mean Flux and Concentration were evaluated using a Repeated Measures Analysis of Variance (ANOVA) in Staview™ 5.0. Intra-class correlation coefficients (ICC(2,1)) of Fluxes and Concentrations were determined as described by Denegar and Ball[2].

RESULTS AND DISCUSSION

ICCs were greater than 0.9 indicating that minor differences in DRT4 probe location were well tolerated in this test setting. The plantar big toe (hallux) has a high density of arterio-venous anastamoses presenting the best opportunity for interrogating microvascular flow with an LD on a repeatable basis[3]. Popel suggests the geometry of capillaries is not important since tissue is supplied from a network of vessels[4].

CONCLUSIONS

The Moor DRT4 LD Monitor has excellent reliability and hence may be appropriate for evaluation of hallucial microcirculation. Future efforts should apply similar technique to assess repeatability at other locations.

REFERENCES

1. Fagrell, B., *Advances in microcirculation network evaluation: an update.* Int J Microcirc Clin Exp, 1995. **15 Suppl 1**: p. 34-40.
2. Denegar CR, B.D., *Assessing Reliability and Precision of Meaurement: An Introduction to Intraclass Correlation and Standard Error of Measurement.* J Sport Rehab, 1993. **2**: p. 35-42.
3. Castronuovo, J.J., Jr., et al., *Noninvasive determination of skin perfusion pressure using a laser Doppler.* J Cardiovasc Surg (Torino), 1987. **28**(3): p. 253-7.
4. Popel, A.S. and J.F. Gross, *Analysis of oxygen diffusion from arteriolar networks.* Am J Physiol, 1979. **237**(6): p. H681-9.

ACKNOWLEDGEMENTS

JAF acknowledges the help of his father, Matthew Furmato, in establishing the protocols for this study.

EFFECTS OF ARCH HEIGHT AND ACCOMODATION ON POSTURAL STABILITY

Esther H. Kim, Howard J. Hillstrom, Jinsup Song, and Benjamin P. Heilman
Gait Study Center, Temple University School of Podiatric Medicine
email: ekim@tuspm.temple.edu

INTRODUCTION

The primary purpose of this study was to examine the effects of sandal arch height on postural stability. Secondarily the effects of a two-month wear period on posture were determined as well. Five models of sandals were tested: Santa Cruz (SC), Iceland (IC), Arizona (AS, soft footbed), Arizona (AP, pronounced footbed), and Fulda (FU). Note that each of the aforementioned models shared similar footbed technology yet had progressively larger arch heights.

METHODS

Data was collected on 20 healthy subjects with moderate pes planus feet. Each subject was tested in 5 different sandal conditions (Table 1). Center of pressure (COP) data was collected on each subject, in each shoe condition at 120 Hz using a Kistler™ (9261A) force plate. The subject was asked to stand upon the force plate in their comfortable angle and base of support. The subject's feet were then traced onto a white paper that was adhered to the force plate to ensure repeatability in each subject's foot position across all trials. Each subject stood for a total of 1 minute while only the last 40 seconds of data was analyzed to eliminate transient effects [1]. A total of 3 trials were collected for each shoe condition at the baseline visit. Data was also collected after 2 months in the Birkenstock® Arizona Sandal to examine the effects of accommodation. Best-fit elliptical and circular areas of COP excursion were calculated (Figure 1). Deviation from a postulated ideal COP position (i.e. the midpoint between the left and right feet at the posterior third of the foot length) was determined as well. A 2-way mixed effect ANOVA was performed for statistical analysis and all post-hoc analysis used the Bonferroni-Dunn test with significance at $P < 0.005$.

RESULTS AND DISCUSSION

Mean elliptical sway area increased as a function of sandal arch height. Mean elliptical area for SC (lowest arch height) was 166.22 mm^2, while mean elliptical sway area for FU (highest arch height) was 227.75 mm^2 (Table 1). Post-hoc's revealed that the SC and IC sandals were both statistically significantly smaller in sway area compared with FU. Following a 2-month accommodation period the mean elliptical sway area was reduced from 196.39 mm^2 to 172.28 mm^2 (Table 2) however this change was not significantly different.

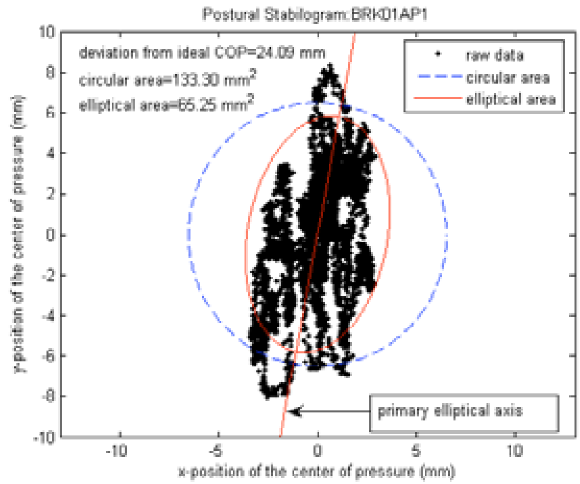

Figure 1: Sample postural stability analysis

CONCLUSIONS

Comparison of postural sway areas across the 5 different sandal models suggests that the mean circular and elliptical sway areas are the smallest in the IC and SC sandals while largest for FU. This result suggests that there may be an optimal arch height in sandals for minimum postural sway. With a 2-month accommodation of the AP sandal, there was a trend toward decreasing sway at follow-up. If postural sway can be minimized by appropriate selection of arch support then these findings may have important implications for those at risk of falling.

REFERENCES

1. Carroll, J.P., et al., *J Biomech*. **26**: 409-16, 1993.

ACKNOWLEDGEMENTS

This study was funded by Birkenstock USA

Table 1: Sandal Arch Height: Elliptical Sway Area

ID	Arch Height	Elliptical Sway Area			
		Mean (mm^2)	SD	p-value	Post-Hoc
SC (a)	4.0 cm	166.22	77.46	0.0477	e
IC (b)	4.2 cm	162.95	78.43		e
AS (c)	4.3 cm	180.50	77.46		
AP (d)	4.4 cm	196.39	79.38		
FU (e)	4.6 cm	227.75	79.38		a, b

Table2: 2-month Accomodation: Elliptical Sway Area

ID	Time	Elliptical Sway Area		
		Mean (mm^2)	SD	p-value
AP (a)	Baseline	196.39	65.74	0.1546
AP2 (b)	2-month Post	172.28	64.16	

HOW DOES SHOE UPPER DESIGN INFLUENCE PLANTAR PRESSURE DISTRIBUTION?

Howard Hillstrom, Jinsup Song, Esther Kim, and Benjamin Heilman
Gait Study Center, Temple University School of Podiatric Medicine; email: hhillstrom@tuspm.temple.edu

INTRODUCTION

The purpose of this study was to examine the immediate effects of footwear design on in-shoe plantar pressures during gait. This study is part of a larger investigation of the structural properties of Birkenstock® footwear technologies and their effect upon lower extremity function. Each of the shoe designs studied employed the identical Birkenstock footbed (ie. a deep heel cup with a 'pronounced' medial longitudinal arch support). The design differences were confined to the 'uppers' whereby the Boston (BO) was a clog, the London (LO) was a shoe, and the Arizona (AZ) was a sandal. The following research question was addressed: *Does the upper design affect shoe structure and foot function?*

METHODS

Data was collected on 20 subjects (mean age=27) with moderate pes planus, each wearing the three shoe models described. The Novel Pedar-X system was used to measure in-shoe plantar pressures at a sampling frequency of 50 Hz. Following a 5-minute accommodation period, four trials of in-shoe plantar pressures were collected for each shoe condition while each subject walked at his or her self-selected comfortable speed. Each trial of plantar pressure data was analyzed using three separate masks (anatomical, medial-lateral, and anterior-posterior). The anatomical mask determined plantar loading as shown in Table 1. The medial-lateral mask determined plantar loading from the medial half versus lateral half of the shoe (*about its long axis*). The anterior-posterior mask determined plantar loading from the anterior half versus the posterior half of the shoe. Two parameters were calculated for each region in the aforementioned masks: peak pressure (N/cm^2) and Pressure-time integral (Ns/cm^2). Gait speed was captured with a light-based timing system. Two-way mixed effect Analysis of Co-Variance was performed, utilizing gait speed as a covariate. Post-hoc analysis consisted of the Bonferroni-Dunn test.

RESULTS AND DISCUSSION

When examining pressures from the anatomical mask the LO had the lowest peak values and AP had the highest beneath the metatarsalphalangeal joints (MTPJ). In the medial/lateral mask the LO design had the lowest medial and lateral Pressure-time integral (PTI) and Peak pressure (PP) values. LO had the lowest anterior PTI, anterior PP, and Ant/Post ratios while AP had the highest. One plausible explanation for these differences in shoe gear with identical footbeds is that load sharing was afforded by the more extensive uppers in the LO design which could effectively reduce forefoot loading.

Figure 1: Peak In-Shoe Plantar Pressure

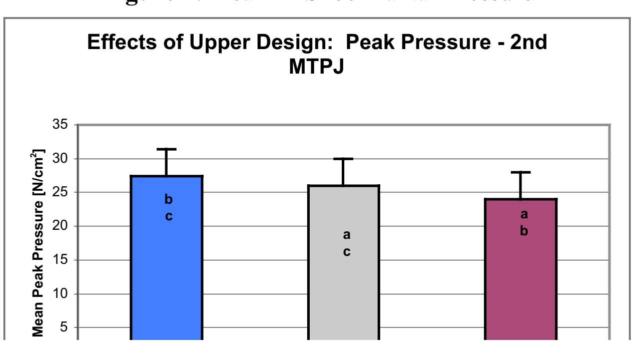

Location	Shoe	Mean	SD	p-value	Post-Hoc
Medial Heel (N/cm^2)	AP	24.539	4.117	0.0259	b,c
	BO	26.151	4.149		a,c
	LO	23.533	4.117		a,b
Lateral Heel (N/cm^2)	AP	22.520	4.149	0.3330	
	BO	23.678	4.180		
	LO	23.713	4.149		
Medial Arch (N/cm^2)	AP	12.398	2.346	0.6718	
	BO	12.255	2.365		
	LO	12.049	2.340		
Lateral Arch (N/cm^2)	AP	15.732	2.517	0.1533	
	BO	15.373	2.536		
	LO	14.669	2.517		
1st MTPJ (N/cm^2)	AP	14.383	3.478	0.0005	c
	BO	14.398	3.510		c
	LO	17.273	3.478		a,b
2nd MTPJ (N/cm^2)	AP	27.407	3.946	0.0014	b,c
	BO	25.981	3.978		a,c
	LO	24.039	3.946		a,b
3rd MTPJ (N/cm^2)	AP	28.181	3.845	$<$ 0.0001	b,c
	BO	26.596	3.877		a,c
	LO	24108	3.845		a,b
4th MTPJ (N/cm^2)	AP	23.249	3.156	$<$ 0.0001	b,c
	BO	20.977	3.181		a,c
	LO	19.839	3.156		a,b
5th MTPJ (N/cm^2)	AP	14.433	2.087	0.2683	
	BO	14.554	2.106		
	LO	13.855	2.087		
Hallux (N/cm^2)	AP	30.450	7.519	0.1574	
	BO	27.142	7.582		
	LO	28.818	7.519		

Table 1: Peak Pressure for Each Anatomical Region

CONCLUSIONS

The shoe upper design can influence biomechanical foot function.

ACKNOWLEDGEMENTS

This study was funded by Birkenstock USA

CAN A SANDAL ARCH SUPPORT REDUCE PLANTAR HALLUCIAL MICROCIRCULATION?

Jinsup Song, Howard Hillstrom, Nina Babu, and Yoko Miyazaki
Gait Study Center, Temple University School of Podiatric Medicine, email: jsong@temple.edu

INTRODUCTION

It was postulated that the three-dimensional footbed of the Birkenstock sandal could improve weight distribution and promote improved microcirculation to the feet. To test this concept, plantar hallucial cutaneous microcirculation was captured at baseline and following a 2-month wear period of the Birkenstock Arizona sandal while non-weightbearing. In addition, weight-bearing plantar hallucial microcirculation was measured in the barefoot and sandal conditions.

METHODS

Twenty healthy subjects with mild to moderate pes planus feet were evaluated at baseline and following a 2-month use of Arizona sandals. Using a technique described previously [1], cutaneous microcirculation was assessed at the plantar hallux for a 2-minute resting condition, a 2-minute challenge of skin heating to 42ºC, and following 5-minutes of occlusion. Mean flux (in arbitrary units) and skin temperature (°C) were measured using the DRT4 laser Doppler flowmeter (Moor Instruments, Willington, DE). Cutaneous microcirculation was also measured at the thumb (i.e. pollex) as a control. All subjects refrained from eating and drinking caffeinated beverages for greater than 1.5 hours prior to the assessment.

In addition, plantar hallucial microcirculation was measured while each subject stood in barefoot (BF), Arizonal sandal with a pronounced arch support (AP), and the Arizonal sandal with a soft foot bed (AS). For the barefoot condition, each subject stood on a 3/8” wooden platform, which had a 5mm diameter channel drilled for the DRT4 laser probe. Similarly, a 5mm diameter was also drilled through each sandal to allow for weight bearing plantar hallucial measurements. The DRT4 was placed leveled to the supporting surfaces. In each shoe condition, the laser Doppler flow meter was obtained during 2 minutes of sitting, 2 minutes of standing, and 2 additional minutes of sitting.

A repeated measures analysis of variance (ANOVA) model was utilized to ascertain group differences. Bonneferoni-Dunn post hoc analysis was conducted for significant ANOVA results for the weight-bearing assessment.

RESULTS AND DISCUSSION

As shown in Table 1, the ratio of reactive hyperemia (RH) during the first minute post occlusion and the 2 minute resting

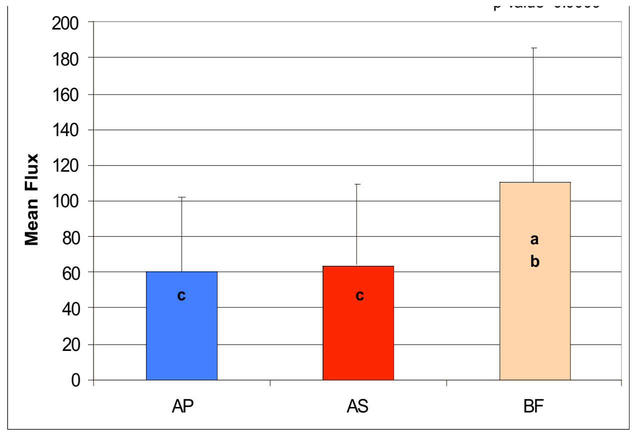

Figure 1: Mean flux (in a.u.f.) at the plantar hallux following 2-minutes of standing (reactive hyperemia) in 3 shoe conditions.

mean flux (RH1/Resting) was higher at 2 month follow up than at baseline (p value=0.0159). Mean flux during heating and peak flux during reactive hyperemia at the pollex also increased at 2-months. These changes were not accounted for by the room temperature.

During quiet comfortable stance, mean flux during reactive hyperemia reduced significantly in the Birkenstock sandal conditions as compared to barefoot (see Figure 1). This implies that there was less oxygen deprivation in the sandal conditions thereby requiring a reduced hyperemic response.

CONCLUSIONS

These results suggest that the improved alignment as well as the increased contact area afforded by Birkenstock footbed technologies may help to minimize transient hypoxia in the plantar tissues while standing. It is also possible that wearing the Arizonal sandals for 2 months may influence endothealial-mediated valsodilation. Further studies are needed to confirm these findings.

REFERENCES

1. Song J, et al. *Submitted for publication, JAPMA*.

ACKNOWLEDGEMENTS

This study was funded by Birkenstock USA.

Table 1: Mean Hallucial and Pollex Flux (Pre/Post)

Mean flux in a.u.f. (Arbitrary Unit of Flux)	Plantar Hallux			Palmar Pollex		
	Pre	Post	P value	Pre	Post	P value
At 2-minute Resting	70.6 ± 75.0	90.6 ± 123.7	0.5523	195.8 ± 97.1	275.2 ± 187.7	0.0625
Localized skin heating to 42ºC	236.9 ± 157.4	277.8 ± 182.3	0.4405	274.4 ± 92.1	392.5 ± 174.9	0.0120
Reactive hyperemia (RH1)	114.1 ± 102.1	189.9 ± 168.7	0.1190	217.0 ± 81.4	309.8 ± 179.8	0.0396
RH1/Resting	2.3 ± 1.8	3.5± 2.0	0.0159	1.6 ± 1.7	1.5 ±1.3	0.4288
Room temperature (ºC)	23.8 ± 2.1	23.3 ± 1.0	0.5143	23.8 ± 2.1	23.3 ± 1.0	0.5143

DEVELOPMENT OF A NOVEL BAREFOOT TORSIONAL FLEXIBILITY DEVICE: A PILOT STUDY

Laura E. Bray, M.S.; Esther H. Kim, B.S.; Howard J. Hillstrom, Ph.D.; Jinsup Song, Ph.D, DPM; and Benjamin P. Heilman, M.S.
Gait Study Center, Temple University School of Podiatric Medicine

INTRODUCTION

A novel instrument was developed to assess the torsional flexibility of the human barefoot to establish a common basis for comparison of the flexibility properties of foot wear and bare feet. Data was collected on the left foot of five subjects, with each subject being tested in weight bearing and non-weight bearing conditions. Torsional flexibility data was also collected for the Arizona Soft Birkenstock® sandal model. The comparison between the barefoot and sandal torsional flexibilities was made to ascertain differences between man-made shoe gear and man.

METHODS

The Barefoot Torsional Flexibility Device mechanically grounded the heel while the forefoot was positioned on a plate that was rotated about the longitudinal axis of the foot (Figure 1). The goal was to measure the maximum moment and anglular excursion of the foot when it was loaded in inversion and eversion. A torque was applied to each foot in inversion and eversion, cycling three times for each of the three trials collected. Only the inversion segment of each cycle was analyzed for this study, to simulate in vivo loading during propulsion. The sandal flexibilities were quantified with an Instron 4201 structural testing machine (*sampling rate = 20Hz*). Each sandal (size matched for a given subject) was loaded in inversion with the heel mechanically grounded.

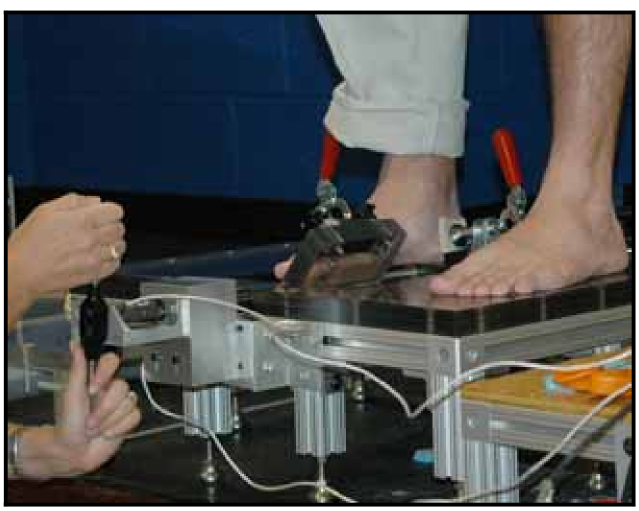

Figure 1: A subject's foot was loaded in inversion using the proposed Barefoot Torsional Flexibility Device.

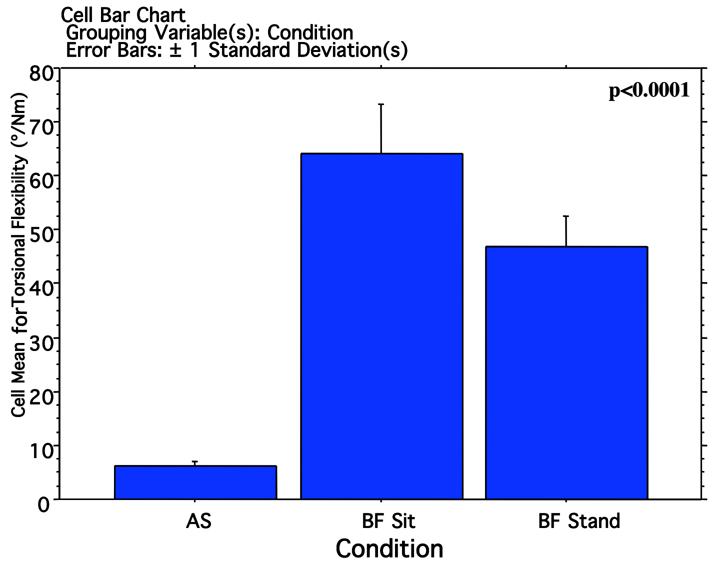

Figure 2: Mean Torsional Flexibilities for all subjects, across all conditions.

RESULTS AND DISCUSSION

The Arizona Soft sandal had the lowest torsional flexibility (i.e. was the most stiff). Barefoot Torsional Flexibility was much higher, with non-weight bearing being the least stiff. A mixed effects analysis of variance (ANOVA) was used to test statistical significance in the three conditions. All of the torsional flexibility conditions were statistically different, the interaction between condition and subject was significant, and the relationship between subjects was not significant. A Bonferroni-Dunn post-hoc analysis was performed and all three conditions were significantly different ($p<0.0001$) from each other. Intra-class Correlation Coefficients (ICC(2,1)) demostrated that the Seated Barefoot Torsional Flexibility (ICC=0.75) and Sandal Torsional Flexibility (ICC=0.99) tests were reliable. Standing Barefoot Torsional Flexibility had a lower reliability (ICC=0.45), which could be a result of non-stationary active contractile processes (i.e. muscles firing during standing).

CONCLUSIONS

The lower flexibility of sandals compared to human bare feet indicate that sandals are likely to modify the function of feet. Because sandals are stiffer than feet, pedal movements may be restricted compared to that of barefoot. Further studies are needed to determine if, the structure of the sandal imposes a change in the function of feet during gait and posture.

REFERENCES

1. Stacoff, A., et al., Med Sci Sports Exerc, 23(4), 1991.

BIOMECHANICS REALATED TO RACKETS DESIGN AND CUSTOMIZATION

Federico Casolo, Michele Camposaragna, Barbara Cattaneo
Politecnico di Milano : federico.casolo@polimi.it camposaragna@mech.polimi.it, cattaneo@mech.polimi.it

INTRODUCTION

The new composite materials applied to tennis, supply the racket designers of many degrees of freedom. It is now possible, for instance, to build very light rackets, to differentiate the stiffness along the frame, to chose the mass distribution; to vary the position of the vibration nodes, the position of the center of percussion and the one of the point of maximum rebound. The impact sound can also be changed. To take advantage of the design freedom for this technological piece of equipment a computer simulation approach is essential. The same approach is profitable to identify the best suited racket for a specific player and to evaluate the consequences of the racket customization. Customization is usual for the elite athletes equipment – because they often are forced to use rackets chosen by their sponsors – but it is also very common among non professional players. A racket is often customized by adding extra masses, by stringing the oval by means original procedures or by adding some kinds of shock absorbers. Many customization procedures can produce some not desired, collateral effects which affect both the stoke and the action transmitted to the body of the athlete . This work mainly deals with the theoretical and experimental analysis of the customization concerning racket comfort.

METHODS

A quantitative approach to the problem require to build complex models capable to simulate the impact dynamics.

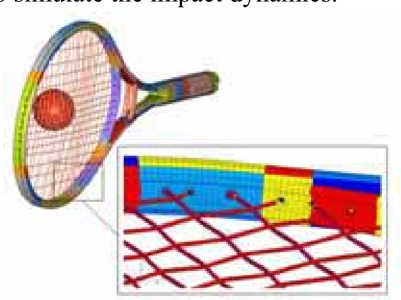

Figure 1: F.E. model that take into account the orientation of the reinforce fibers of the layers of the frame and of the interaction among the strings

The main parameters to be monitored are: center of percussion location, the frequency and the nodes of the vibration modes, the strings tension and moment of inertia with respect to the handle.
Experimental tests are required to validate the models and also to identify level of the parameters related the subjective feeling of comfort with a racket.

RESULTS AND DISCUSSION

As an example the influence of an extra mass, added in two locations on a popular racket frame, is analyzed. (10 grams are added at the top or at the bottom of the stringed oval). Influences on maneuverability (J) can be easily evaluated, such as the influences on the position of the racket centre of percussion. About vibration (fundamental mode) fig.3 shows that when the racket is handled (the hand is represented by the black dot) one of the vibration nodes (white triangle) is forced to move at the handle (a) and is not influenced (c)(d) by the extra mass. This mass affects, on the contrary, the position of the other node that is the point to which the impact don't excite that vibration mode. The little added mass, placed at the racket top, has a significant effect in lowering the fundamental mode of vibration frequency (fig.2)

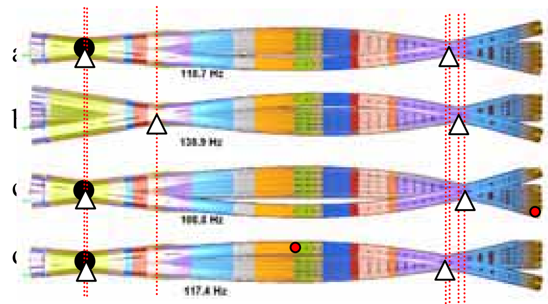

Figure 2: extra mass influence on the fundamental mode

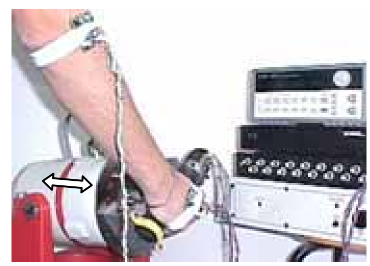

Figure 3: shaker and arm instrumented by accelerometers

Experimental tests (fig.3) prove that lower frequencies propagate more on the arm and are less comfortable. Strings tension also affects rebound and comfort but the simulation of the stringing procedure show (fig.4) that at the end of the process string tension are different by the theoretical tension set on the stringing machine because of the frame deformation

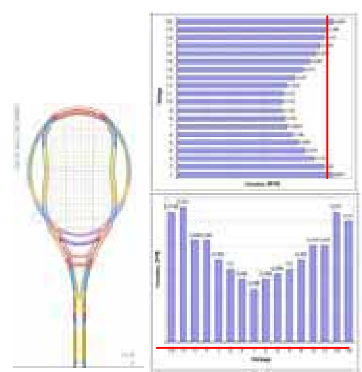

Figure 4: a) Deformation of the frame (amplified) under the strings forces b)Graph of the string tension at the end of the stringing process.
The red line is the theoretical string tension

CONCLUSIONS

Racket customization must be accurately planned and simulated to avoid collateral negative effects on the player. Special stringing techniques must also be tested to check the effective string tension on the frame at the end of the process.

REFERENCES

1. Casolo F., Ruggieri G. *Dynamic analysis of the ball-racket impact in the game of tennis,* Meccanica, 1991

Effects of Knee Joint Angle on the Force-length and Velocity Characteristics of Gastrocnemius Muscle

[1] Taku Wakahara, [2]Hiroaki Kanehisa, [3]Yasuo Kawakami and [3]Tetsuo Fukunaga
[1]Graduate School of Human Sciences, Waseda University ; e-mail waka1002@fuji.waseda.jp
[2]Department of Life Sciences (Sports Sciences), University of Tokyo
[3]Faculty of Sport Sciences, Waseda University

INTRODUCTION

Static plantar flexion torque developed in a knee extended position is greater than that in knee flexed position[1], in which the muscle fibers of gastrocnemius shorten. In concentric actions, however, the difference in torque between the knee extended and flexed positions decreases with increasing angular velocity of the ankle[2]. The reasons for this torque discrepancy between the static and concentric actions have not been clarified. This study aimed to examine the effect of knee joint angle on the plantar flexion torque from the viewpoint of the length-force and force-velocity relationships in the muscle fiber (fascicle) of the medial gastrocnemius (MG).

METHODS

Six male subjects performed static and concentric plantar flexions at two different knee joint angles [fully extended (K0) and flexed at 45º (K45)] with the maximal effort. The ankle joint was fixed at 0º (neutral position) in the static action. The range of motion of the ankle joint in the concentric actions was –10º (dorsiflexed) to 30º (plantar flexed) and the angular velocities were set at 30 and 350º/s by a dynamometer.

The Achilles tendon force was calculated from the measured plantar flexion torque divided by the moment arm of the Achilles tendon. The fascicle length, pennation angle at the mid belly of MG, and the length change of the external tendon of MG were measured by two ultrasound apparatuses. Surface electromyograms (EMGs) were recorded from the MG, lateral gastrocnemius (LG), soleus and tibialis anterior muscles.

RESULTS AND DISCUSSION

The difference in peak torque and tendon force between K0 and K45 decreased with increasing angular velocity of the ankle, i.e. no significant differences at higher angular velocity (Table 1). The average EMG activity of MG at 350º/s was significantly lower in K45 than in K0 (Table 1), while no significant differences were observed between K0 and K45 in the other angular velocities for MG and at all velocities for the EMGs of LG and soleus muscle.

We estimated the sarcomere lengths which were calculated from the fascicle lengths obtained from ultrasonography. It is considered that the MG muscle at the peak force had a greater force potential in K0 at static and 30º/s (Figure 1). However in the case of 350º/s, the MG fascicle may perform with higher force potential in K45 than in K0 (Figure 1).

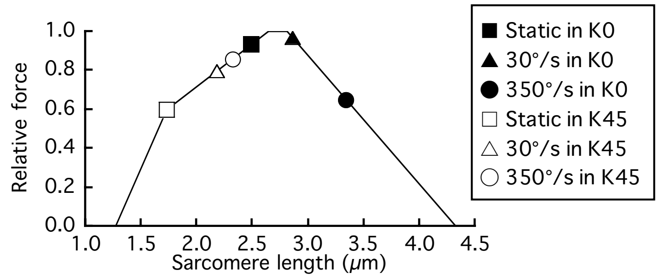

Figure 1: Estimated sarcomere lengths at peak tendon force and the length-force relationship of human sarcomeres[3].

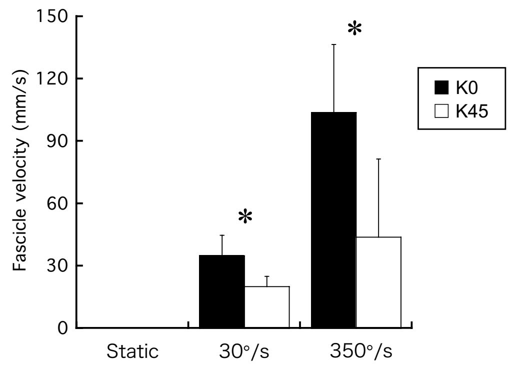

Figure 2: Shortening velocity of fascicle at the peak tendon force. * denotes a significant difference between K0 and K45.

The fascicle velocities were significantly lower in K45 than in K0 (Figure 2), even though nearly identical angular velocities. Thus, MG fascicles in K45 were more advantageous for producing force in the concentric actions, according to the force-velocity characteristics of a muscle.

CONCLUSIONS

The present study showed the plantar flexion torque developed during concentric actions did not always decrease with knee flexion. This would be attributed to the length-force and force-velocity relationships and activation levels of the MG.

REFERENCES

1. Sale et al. *J Appl Physiol*. **52**, 1636-42, 1982
2. Fugl-Meyer et al. *Acta Physiol Scand.* **107**, 47-56, 1979
3. Walker & Schrodt. *Anat Rec*. **178**, 63-81, 1974

Table 1: Peak values of plantar flexion torque and tendon force, and mEMG of MG.

	Static		30°/s		350°/s	
	K0	K45	K0	K45	K0	K45
Peak torque (Nm)	122 ± 18**	92 ± 10	84 ± 13	70 ± 12	58 ± 10	57 ± 13
Peak force (N)	2653 ± 437*	2006 ± 257	1814 ± 289	1566 ± 276	1322 ± 229	1320 ± 295
mEMG of MG(μV)	198 ± 84	145 ± 61	221 ± 91	129 ± 36	325 ± 138*	157 ± 37

* denotes a significant difference between K0 and K45.

MEASUREMENT SYSTEM WITH NANO-RESOLUTION FOR MICROSCOPIC BONE PROPERTY

J. H. Hong and Y. H. Park
Department of Control and Instrumentation Engineering, Korea University, Republic of Korea

INTRODUCTION

To understand physiological and pathological behavior of human skeletal system, the accurate measurement of biomechanical properties for bone is the one of important works. Particularly, the microscopic measurement of human bone is important since the biomechanical behavior at the small scale of bone could be closely related to the remodeling of bone. The remodeling processes of bone have been investigated by using various mechanobiological models [1]. Thus, significant attempts have performed to directly measure the microscopic biomechanical properties of human bone using small scale specimens. They used the three-point or four-point bending, and tensile tests [2-4]. However, the use of coarse microtesting machines and irregular shape of micro-specimens could cause significant measurement errors. For example, the microscopic elastic modulus could vary from 4.59 GPa to 10.4 GPa for the human trabeculae at the same anatomical site depending on the selection of the test method [2-4]. In this study, a small scale compressive testing machine was developed to measure accurate microscopic elastic moduli of bone.

METHODS

Fig. 1 (a) shows a schematic diagram of the small scale compressive testing machine. The testing machine had a PZT actuator (PI Gmbh, Germany) for axial loading. The axial loading PZT actuator could load up to 3000 N with a full displacement range of 120 ㎛. When a loading displacement was measured with l2-bit A/D converter, the resolution of the testing machine was 30 ㎚. To check the accuracy of the testing machine, A6061S-T6 aluminum alloy rectangular parallelepiped having the compressive strength of 265 MPa (2 x 2 x 4 ㎜^{3}) was manufactured and subjected to the compression test to examine the accuracy of measuring the compressive strength. When aluminum specimens were loaded up to a strain of 0.5 %, the measurement error was about 0.2 %. Thus the measurement system was accurate.

Five bovine cortical bone specimens were used in this study. A micro-milling machine (EGX-300, Roland, Japan) was used to obtain rectangular parallelepiped cortical specimens (300 x 300 x 600 ㎛^{3}) from near the spinous process of lumbar vertebra. Fig. 1 (b) shows this specimen. Compressive strain of up to 1% was applied using the PZT actuator at a strain rate of 0.001/sec. The linear regression analysis was performed to represent the stress-strain relationship. The Young's modulus was determined as the slope of the tangential line to the regression curve.

RESULTS

Figure 2 shows the mean stress-strain behavior. The mean Young's modulus of the bovine lumbar vertebral cortical bone measured in this study was 10.3 GPa (SD ± 0.7). Based on the previous studies, the elastic moduli of cortical bone obtained from bovine femur were about 14 GPa in the macroscopic level [5], and 21 GPa at the osteon [6]. Since the microscopic elastic modulus in this study was obtained using bovine lumbar vertebrae, which are weaker than femur, the results would be reasonable.

(a) (b)

Figure 1: Developed measurement system and fabricated microscopic cortical specimen

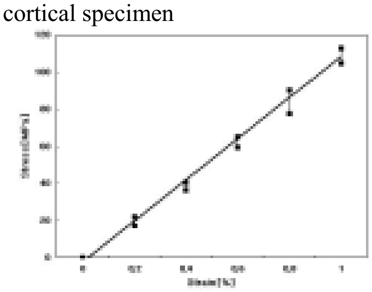

Figure 2: Obtained stress-strain curve with the standard deviation error bar

CONCLUSIONS

In this study, a small scale compressive testing machine was developed to measure accurate microscopic elastic moduli of bone. Experiments were also conducted to validate the accuracy and suitability of the measurement system. The developed system will be useful to understand the biomechanics of the bones at a micro-scale.

ACKNOWLEDGEMENTS

This work was sponsored by the Interdisciplinary Research Grants (R01-2004-000-10798-0) of Korean Science and Engineering Foundation.

REFERENCES

[1] Bone Mechanics Handbook, Cowin SC Edited, CRC, NY, 2001; [2] Choi K et al., J Biomech 23, 1103, 1990; [3] Choi K and Goldstein SA, J Biomech 25, 1371, 1992; [4] Rho JY et al., J Biomech 26, 111, 1993; [5] Iyo T et al., J Biomech 37 1433, 2004; [6] Rho JY and Pharr GM, J Mat. Sci.: Mat. In Medicine 10, 485, 1999.

IMPACT FORCES, REARFOOT MOTION AND THE REST OF THE BODY IN HEEL-TOE RUNNING

[1] Uwe G. Kersting, [2]René E.D. Ferdinands
[1]Department of Sport and Exercise Science, The University of Auckland, New Zealand,
[2]Department of Physics and Electronic Engineering, The University of Waikato, New Zealand
e-mail: u.kersting@auckland.ac.nz , web: http://www2.auckland.ac.nz/tmk/ses/

INTRODUCTION

The high incidence of overuse injuries in heel-toe running has inspired numerous researchers to identify their mechanical causes. High internal stresses experienced during the impact phase and excessive ranges of rearfoot motion have been the focus of interest in the past [1]. Recently a new paradigm has been proposed [2] which states that muscular activities being modulated by foot-shoe-ground interactions may play an important role in the development of overuse syndromes. If this is the case it can be expected that a variation in muscular activities would affect joint powers, energy transfer between body segments and therefore movement efficiency. Only a limited number of studies have taken into account full body mechanics in comparing effects shoe modifications.

The purpose of this study was to apply a three-dimensional model of the human body to heel-toe running. Systematic variations of rearfoot movement were compared with regard to their effect on torques and powers at various joints of the body.

METHODS

Twelve trained distance runners served as subjects for this study. They were equipped with reflective markers to represent body segments and determine joint centers using static markers on anatomical landmarks. Runners had to run for 1.5 km in a standard running shoe (Nike Pegasus) prior to the collection of ground reaction forces (GRF) and kinematic data while running through the laboratory. Three versions of a heel insert were applied in randomized order (8 deg varus, neutral, 8 deg valgus). For each shoe insert runners had to hit the force platform five times with each foot.
Using an 8-camera 240 Hz motion analysis system (Motion Analysis Corp.) markers placed on the runner were recorded and tracked. A force plate (Bertec, 1200 Hz) was used to collect ground reaction forces. Ratings of perceived comfort and efficiency were recorded using visual analogue scales.

An inverse dynamics model of the runner was created using *Mathematica's Mechanical Systems Pack*. This is a set of packages designed for the analysis of spatial rigid body mechanisms by implementing a dynamics formulation with Lagrangian multipliers. The computer model gives a 3D representation of the human body as a system of fifteen rigid body segments with mass and inertia properties (Fig. 1). Joint kinematics, torques and joint powers were derived.

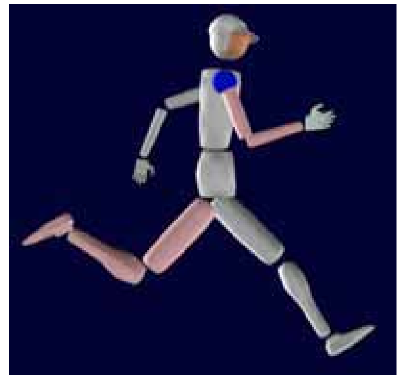

Figure 1: Graphical representation of the 15 segment model.

RESULTS AND DISCUSSION

Results show that rearfoot movement varied systematically and consistently with the insert being used. However, GRF did not vary according to a frontal plane model proposed by Denoth [3]. In 58% of the subjects ankle flexion kinematics showed significant differences between shoe conditions. Thirty-three per cent of the runners demonstrated modified knee joint kinematics in this comparison. These differences were accompanied by significant variations in joint kinetics and power flows up the hip and trunk joints.

CONCLUSIONS

The results of this study suggest that relatively subtle kinematic changes in foot placement and GRFs may be accompanied by considerable variations in segmental kinetics and energy transfer at the joints of the human body. It is likely that these variations will affect running efficiency and may therefore influence fatigue and overloading in distance running.

REFERENCES

1. Taunton, J.E. et al. (2002) Br J Sports Med. 36(2): 95-101.
2. Nigg, B.M. (2001) Clin J Sport Med. 11(1): 2-9.
3. Denoth (1986) in Nigg, B.M. (ed.) Biomechanics of Running Shoes. Human Kinetics Publishers.

ACKNOWLEDGEMENTS

We thank NIKE Inc. for the generous provision of the footwear used in this study.

BIODYNAMIC CHANGES ACCOMPAYING AGE AND INACTIVITY IN FEMALES

Lee Cabell[1], David Pienkowski[2, 3] Robert Shapiro[4]
[1] School of Graduate Medical Education, Seton Hall University, South Orange, NJ 07079
[2] Center for Biomedical Engineering, University of Kentucky, Lexington, KY 40507
[3] Department of Orthopaedic Surgery, School of Medicine, University of Kentucky, Lexington, KY 40536
[4] Department of Kinesiology and Health Promotion, University of Kentucky, Lexington, KY 40506

INTRODUCTION

Bone fractures secondary to falls in the elderly continue to be a major healthcare and economic problem [1]. A greater understanding of the processes that contribute to the propensity of elderly females to fall may be obtained by kinematic and kinetic gait studies [2]. The purpose of this study was to examine the 3-D gait parameters in female subjects to determine the effects of aging and activity on selected biomechanical parameters and to determine if any measures might predict a predisposition to musculoskeletal dysfunctions and subsequent remedial intervention.

METHODS

Younger (24 ± 1.6 yrs) and older (67 ± 7.1 yrs) healthy female volunteers (n=17 total) were divided into active and sedentary subgroups in this IRB approved study. Data from three-dimensional video images were collected by 5 high-speed (60 Hz) video cameras (FALCON HR 240, Motion Analysis Corporation, Santa Rose, CA). The basic simplified ("Helen Hays") marker set of 15 retro-reflective external markers were attached to significant anatomical locations of the right lower extremity. Resulting video images were digitized by using the Motion Analysis HiRES analysis package. Ground reaction forces were measured by a Kistler force platform at 1000 Hz. Each subject was asked to walk at a self-selected pace across the force platform in a 20m walkway during which kinematic and kinetic data were collected for three seconds and analyzed during the stance phase of the gait cycle. The data were analyzed by repeated measures ANOVA and each model included the two factors of age and activity level. The Scheffe criteria was used for multiple group corrections. P-values less than 0.05 were considered indicative of significant difference.

RESULTS AND DISCUSSION

As expected, the elderly group had greater functional and mobility limitation in their lower extremity joints compared to the younger group [3], and of these, he largest differences were observed in the ankle (Fig. 1). Knee joint biodynamics were related to both activity and age. The hip was the most effected joint in sedentary population (Fig. 2). These findings led us to postulate that lower limb gait alterations may begin at the ankle, progress up the lower extremity, and eventually act in concert to predispose elderly and sedentary women to gait imbalances and subsequent slip-induced fall or low energy bone fracture. This is important because it means that there may exist specific physical activities involving targeted controlled 3-D muscle movements which help maintain lower limb joint kinematics, kinetics and their accompanying intrinsic postural control strategies that together help prevent gait imbalances and subsequent falls.

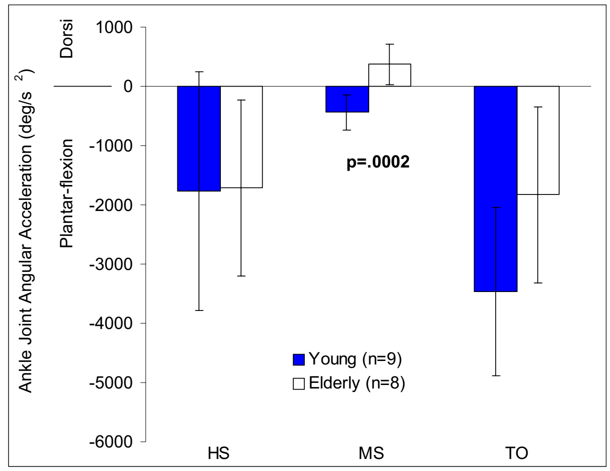

Figure 1: Comparison of ankle joint dorsiflexion / plantar flexion angular acceleration.

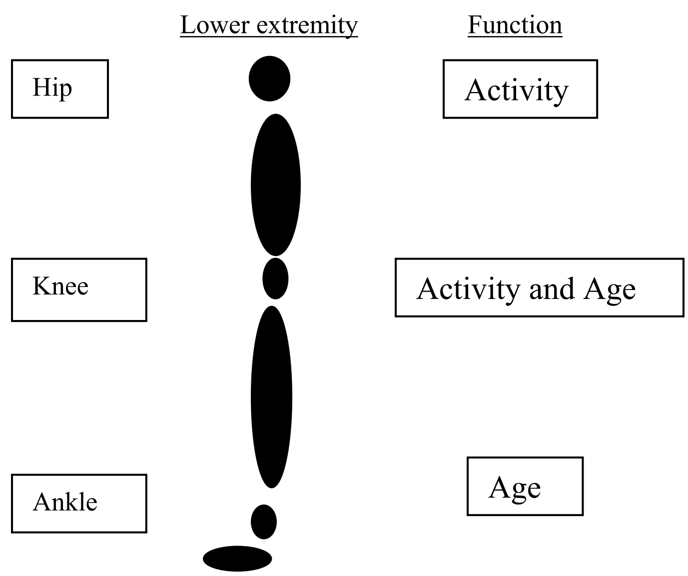

Figure 2: Model of the lower extremity noting the key biodynamic factors most effecting the indicated joints.

Address questions or comments to cabellle@shu.edu

REFERENCES

1. Daubney ME, Culham EG. Lower-extremity muscle force and balance performance in adults aged 65 years and older. Phys Ther **79**, 1177-85 1999.
2. Owings TM, Grabiner MD. Variability of step kinematics in young and older adults. Gait Posture **20**, 26-29, 2004.
3. Finley FR, Cody KA. Locomotive characteristics of urban pedestrians. Arch Phys Med Rehabil **51**, 423-6, 1970.

ACKNOWLEDGEMENTS

Thank you to Dr. Doreen Stiskal for her clinical comments.

AN APPROACH TO CALCULATING LINEAR HEAD ACCELERATIONS IS NOT AFFECTED BY ROTATIONAL HEAD ACCELERATIONS

[1] Joseph J. Crisco, [2]Jeffrey J. Chu and [2]Richard M. Greenwald
[1]BrownMedical School/Rhode Island Hospital, [2]Simbex
email: joseph_crisco@brown.edu, web: brownbiomechanics.org

INTRODUCTION

Mild traumatic brain injury (MTBI), or concussion, is a growing health concern especially for young athletes. A critical piece in the puzzle for understanding MTBI is the link between the mechanical input (trauma) that causes injury and the clinical outcome. We hypothesize that head acceleration due to impact is predictive of the type and severity of concussion, and correlates to specific clinical measures of concussion. One major limiting factor in testing this hypothesis and the development of strategies to reduce MTBI is the lack of sufficient *in vivo* biomechanical head impact data. Previously, we developed and validated the Head Impact Telemetry (HIT) System as an approach to measure linear head acceleration of a helmeted athlete [1]. The purpose of this work was to determine if the theoretical accuracy of calculating linear head acceleration using this approach was affected in the presence of rotational accelerations.

METHODS

Theory. The HIT System consists of six linear accelerometers placed within the liner of a football helmet in close proximity and orthogonal to the skull. The system estimates the linear acceleration of the center of gravity of the head ($\vec{H}$) due to an impact, with its direction specified in spherical coordinates (azimuth θ and elevation α). The value of each accelerometer ($\vec{a}_i$), located at (θ_i, α_i), is used to minimize the least-square error,

$$\sum_{i=1}^{6}\left(\left\|\vec{H}\right\|\left(\cos\alpha_i \cos\alpha_H \cos\left(\theta_i-\theta_H\right)+\sin\alpha_i \sin\alpha_H\right)-\left\|\vec{a}_i\right\|\right)^2,$$

and to obtain an estimate of the magnitude of the linear head acceleration $\left\|\vec{H}\right\|$ and its impact location (θ_H, α_H). Rotational accelerations were estimated assuming a fixed rotation point 10 cm inferior to the center of gravity of the head.

Experiment. Laboratory experiments were performed using a Hybrid III headform, neck and torso fit with a commercially available football helmet that was impacted (n=48) with a weighted pendulum (8.2 kg) at various locations about the helmet and at 3 impact speeds (3, 5, and 7 m/s). The linear and rotational accelerations of the Hybrid III headform were computed using a standard 3-2-2-2 accelerometer package and established algorithms (Biokinetics, Ottawa, CA). These experimentally measured accelerations were used to predict the accelerations of each HIT system accelerometer, which were then feed back into the theoretical algorithm. The differences between the experimentally measured headform accelerations (linear and rotational, GSI, and HIC15) and those predicted from the theoretical algorithm were compared using root mean square error (RMSE)

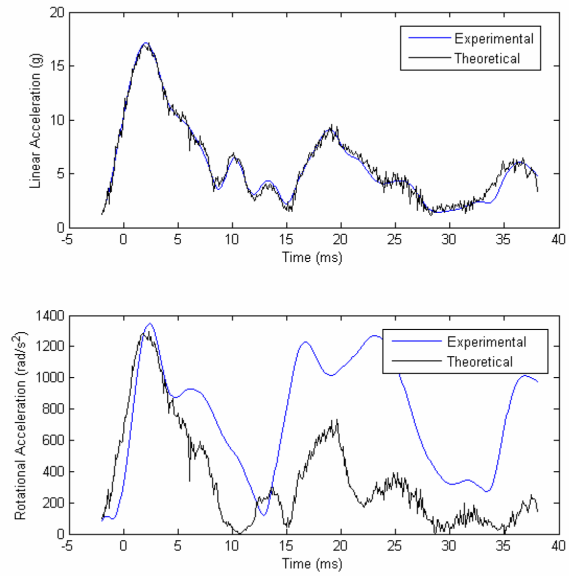

Figure 1: Typical acceleration-time curve.

RESULTS AND DISCUSSION

A typical theoretical linear acceleration-time curve was in excellent agreement with the experimental curve, but there was only limited agreement with the rotational acceleration-time curve (Fig. 1.). The RSME errors for the peak linear acceleration, peak rotational acceleration, GSI, and HIC15 were 2.9g [experimental range of values: 15–82 g], 31 GSI [6.6–294 GSI], 16 HIC15 [4–232 HIC 15], 757 rad/s^2 [1201–4555 rad/s^2], and the mean (1 s.d.) percent error was -4% (5), -17% (16), -10% (14), and -20% (32), respectively.

CONCLUSIONS

Using helmeted impacts within a laboratory setting we were able to demonstrate that our previously reported algorithm is quite robust and can accurately (RSME 3 g's) predict linear head acceleration even when these impacts are associated with a wide range of rotational accelerations. An algorithm for more accurately measuring rotational acceleration with this approach remains to be further developed.

REFERENCES

1. Crisco JJ, Chu JJ, Greenwald RM. An Algorithm for Estimating Acceleration Magnitude and Impact Using Multiple Non-Orthogonal Single-Axis Accelerometers, Journal Biomechanical Engineering, **In Press.**

ACKNOWLEDGEMENTS

Funded by Simbex, Lebanon, NH and NIH R43HD40473.

BILATERAL COMPARISONS OF ISOKINETIC KNEE STRENGTH IN UNILATERAL TOTAL KNEE REPLACEMENT INDIVIDUALS

[1]John W. Chow, [1]Dana M. Otzel, [1]Mark D. Tillman, and [2]Richard Vlasak
[1]Department of Applied Physiology and Kinesiology, [2]Department of Orthopaedics and Rehabilitation
University of Florida, Gainesville, FL, USA; e-mail: jchow@hhp.ufl.edu

INTRODUCTION

Knee function after total knee replacement (TKR) has been studied extensively. Several studies compared isokinetic knee flexion and extension strength of TKR knees with the uninvolved knees in unilateral TKR subjects and healthy knees in control subjects [1,2,3] and the results were equivocal. For example, Berman et al. [1] found significantly lower peak knee extension torques for 60 °/s in TKR knees at 2-yr post-op. However, Walsh et al. [3] did not find any significant bilateral differences in peak knee extension torques in unilateral TKR subjects. They only reported significantly lower peak knee flexion torques for speeds of 90 and 120º/s in TKR knees at 1-yr post-op in their male subjects (no differences in their female subjects). Interestingly, the knee angles at which peak torques occurred were not reported in previous studies. The purpose of this study was to examine the knee strength at different isokinetic speeds and the peak torque angles in unilateral TKR individuals.

METHODS

Seven females and four males (age 67.6±10.9 years, height 168.7±8.0 cm, weight 876.3±218.5 N) with unilateral TKR knee (3.8±3.4 years post-op; 9 right involved knee, 2 left involved knee) participated in this study. Knee flexion and extension torques were assessed using a KinCom AP125 isokinetic dynamometer at speeds of 60, 180, and 240 °/s. Two maximum effort trials of three reciprocal repetitions were completed for each joint motion-speed-side condition. For each condition, the largest torque value among the six repetitions was identified as the *peak torque*. The *peak torque angle* was the knee flexion angle associated with a peak torque. T-tests with repeated measures were used to determine if bilateral differences exist (alpha = .05). No adjustment was made for multiple tests due to the exploratory nature of this study.

RESULTS AND DISCUSSION

Significantly lower peak knee extension torques were found in the involved knees for the speeds of 60 and 180 º/s, but not in the 240 º/s (Table 1). On average, peak torques of the involved knees were 73% and 80% of the uninvolved knees for the 60 and 180 º/s, respectively. These results support the quadriceps deficit reported by Berman et al. [1].

No bilateral difference in peak knee flexion torque was found for any of the isokinetic speeds (Table 1). This is in contrary to the findings of Walsh et al. [3]. It should be emphasized that the different durations of post-operation may explain some of the differences in findings reported in different studies.

Trends were detected in peak torque angles associated with the peak knee flexion torques for 180 and 240 º/s (Table 1). However, the average differences are relatively small and probably do not carry any functional significance.

The average flexion/extension ratios for the involved knee were 0.55, 0.88, and 1.06 for speeds of 60, 180, and 240 °/s, respectively. The corresponding values for the uninvolved knees were 0.44, 0.70, and 1.08, respectively. These values are comparable to those reported in the literature.

CONCLUSIONS

Reduced knee extension strength seems to be common in TKR knees. Future studies should examine the possible causes of such a deficit.

REFERENCES

1. Berman AT, et al. *Clin Orthop* **271**, 106-113, 1991.
2. Huang CH, et al. *Clin Orthop* **328**, 147-154, 1996.
3. Walsh M, et al. *Phys Ther* **78**, 248-258, 1998.

ACKNOWLEDGEMENTS

Supported in part by the University of Florida Opportunity Fund.

Table 1: Means (standard deviations) of isokinetic peak torques (Nm) and peak torque angles (º).

	Flexion						Extension					
	60 °/s		180 °/s		240 °/s		60 °/s		180 °/s		240 °/s	
	Torque	Angle	Torque	Angle	Torque	Angle	Torque	Angle	Torque	Angle	Torque	Angle
Involved Knee	29.8 (16.4)	79.2 (16.3)	47.2 (17.1)	78.4 (5.0)	58.9 (16.2)	75.5 (10.1)	63.6 (22.5)	62.8 (12.3)	59.0 (24.6)	55.8 (14.4)	59.9 (21.7)	61.7 (7.7)
Uninvolved Knee	34.9 (13.8)	68.6 (32.9)	52.2 (24.8)	81.7 (4.5)	66.5 (25.0)	80.6 (6.4)	86.9 (40.1)	62.8 (13.3)	73.9 (24.9)	63.5 (13.0)	63.9 (25.9)	52.5 (24.1)
P-value	.344	.294	.318	.067#	.161	.062#	.043*	.999	.047*	.163	.554	.163

* Significant different at $p < 0.05$.
# Statistical trend.

EMOTIONALLY-RESPONSIVE CLOTHING FOR LEISURE AND EXERCISE ACTIVITIES

[1]Peter Dabnichki, [2]Sharon Baurley and [2]Lisa Stead
[1]Department of Engineering, Queen Mary, University of London, e-mail: p.dabnichki@qmul.ac.uk
[2] Central Saint Martins College of Art and Design, University of Arts London, email: s.baurley@csm.arts.ac.uk

INTRODUCTION

The possibility of augmenting high-specification sportswear, for a broad range of users from enthusiasts to non-sporting people, through the integration of textile sensors and actuators that can monitor and respond to the emotional status of wearers, is being explored. The long-term aim is to develop clothing that could help wearers manage their emotional intelligence. Physiological sensors, such as heart rate monitor, sweat pads, etc., are widely used in sports and medical areas. However such sensors can also be used to gain an insight into the condition of affect in people. Body actions and gestures are well known to be reliable indicators of temporary emotional status in humans. It is, however important to classify and quantify in a systematic and to establish reliable set of controlled variables that allow to assess and control psychological status.

METHODS

The current study focused on the on the initial design of close loop system for assessment and control of emotional responses by the sole use of kinematic and postural parameters, such as joint angels and joint angular velocity as an initial stage of the development.
Initial consideration was given to most common postures and gestures that allow reliable measurement through integrated textile sensors.

RESULTS AND DISCUSSION

A key focus is to identify the possible emotional meanings of physiological and behavioural information within a range of sports/training contexts, and to determine whether these signals can be translated into a *language of emotions*, which wearers and trainers can use to manage emotions to positive effect in exercise and leisure activities. It is essential (Fig.1) to provide the clothing system with appropriate self-calibrating facilities to allow it to learn from its wearer, so that emotional identification and response become uniquely attached to that person. By being able to monitor an individual's emotional status, the amount of training or sports activity engaged in could be modulated and enhanced, thereby reducing the risk of over-training. Such a clothing system might also help with motivation, as hormones produced as a result of physical exercise are known to promote feelings of happiness, with the possible advantage of combating life/work stress. In general the idea is to shift the focus of the exercise from performance targets to level of satisfaction and sense of achievement that will allow to offset the boredom factor that stops many people from undertaking exercise. By monitoring and enhancing technique through force feedback actuators, a sense of achievement might be attained quickly, thereby enhancing wellbeing, and consequently motivation. Clothing that changes [e.g., colour, emits aroma] or produces sound/music according to mood, emotions, and environmental context should help influence/modulate mood, promoting positive self-esteem. Integrated mobile communications, would enable the remote exchange of emotional impulses between wearers.

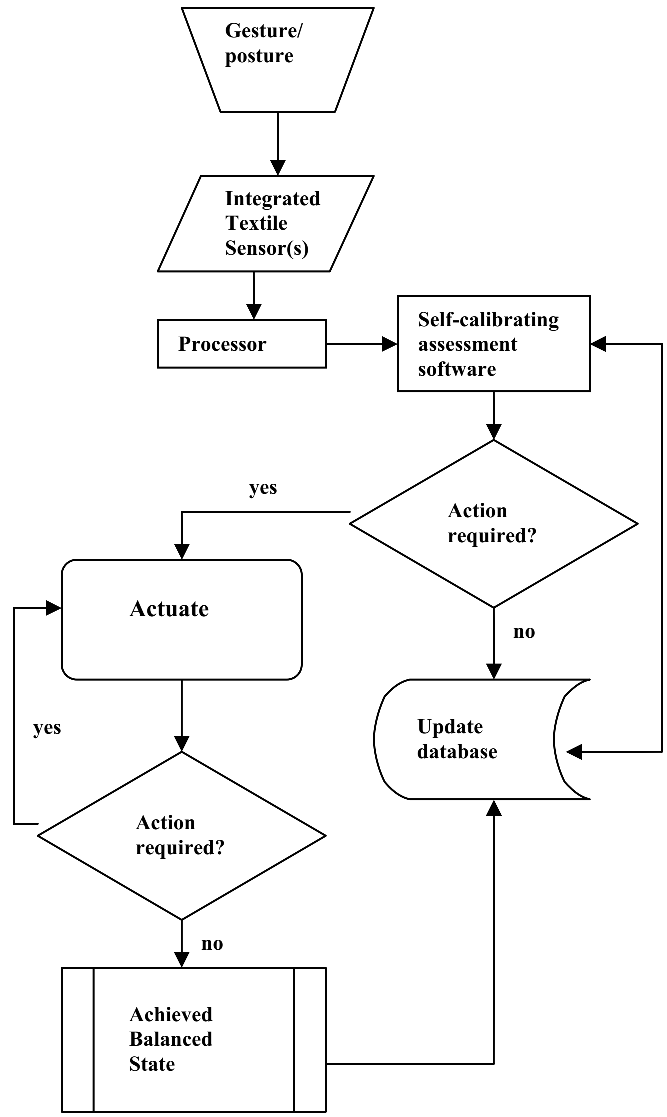

Fig.1 Proposed design for emotionally responsive clothing.
The project is in its infancy (although clothing with built-in electronic devices has been developed and used) and is to be expanded in the next few years as some large hardware and software manufacturers are to be involved in it.

ACKNOWLEDGEMENTS

The results are partially based on work by Dr. Sharon Baurley, supported by the Arts and Humanities Research Board through the AHRB's Fellowships in the Creative and Performing Arts scheme, UK. Some results are also from a PhD study by Lisa Stead, within the Fashion and Modernity project, supported by the Arts and Humanities Research Board, UK

IS CHILD WEIGHT TO BAG WEIGHT THE BEST WAY TO ASSESS RISK OF LOW BACK PAIN IN CHILDREN DUE TO BACKPACK USE?

[1] Rebecca Whissell, [2]Eric Labrosse and [1,3]Sylvain Grenier
[1]Laurentian University,
[3]Sudbury and District Public health Unit, Health Promotion Division
[3]Occupational Health Clinics for Ontario Workers; email: Ssgrenier@laurentian.ca, web: www.humankinetics.laurentian.ca, http://www.ohcow.on.ca/

INTRODUCTION

Studies of lower back-pain caused by the carrying of school bags have typically been investigated by using the weight of the bag, the weight of the person, or the height of the person as predictors of low pack pain. It is possible that an interaction of these variables such as a body mass index (BMI) to weight of the bag ratio could be more effective in understanding what causes back pain.

METHODS

In this study, 119 children were measured for height, weight, mass of school bag, type of bag, method of carrying, method of getting home, distance from home and self-perceived lower back pain (due to running carrying and lifting), were recorded.

The validated questionnaire [1] was administered to volunteer students (as well as parents/guardians). The study addressed a representative sample of francophone students within grades 4-6 from the Conseil Scholaire du Grand Nord de l'Ontario. Students and their backpacks were weighed at the school on the testing day with a calibrated spring scale. At this time, students also completed the questionnaire. The questions asked were as follows:

How do you get to school?
How long does take to travel from home to school?
How long do you carry your bag for?
How do you carry your bag?
Are there days when you bring your bag home and don't use the contents?
Does carrying your bag make you tired?
Do you think your bag is too heavy?
If you have back pain is it made worse by carrying, lifting or running with your bag?

Each question had a limited selection of answers. Prior to the testing day the parents had consented to participation.

RESULTS AND DISCUSSION

A linear regression showed that, in the children tested, lower back pain could be predicted (R^2=0.41) from variables such as weight, height, bag weight, BMI, BMI/bag weight. Among the physiological measures, the BMI to bag weight ratio had the greatest effect on the linear regression equation (Standardized beta weight=1.11).

Lower back pain due to carrying could also be predicted (R^2=0.48). In this case, among the physiological measures, the BMI to bag weight ratio again had the greatest effect on the linear regression equation (Standardized beta weight=1.19).

Lower back pain due to lifting could also be predicted (R^2=0.36), however in this case, of the physiological measures the weight of the person had the greatest effect on the linear regression equation (Standardized beta weight=1.815), but only slightly better than the BMI to bag weight ratio (Beta=1.41).

Lower back pain due to running was not found to be significantly predictable. When a discriminant analysis was performed to distinguish between those that had back pain and those that did not, the generated function correctly predicted 80.4% of the cases and the BMI to bag weight ratio was found to be the variable that contributed the most to the equation (s.c.c.c. 2.207).

CONCLUSIONS

The results suggest that considering the ratio of backpack weight to body weight may not be sufficient. A more complex interaction of variables which account, at least partially, for activity level seems to provide a better indicator of LBP risk in children.

REFERENCES

1. Negrini S, et al. *Spine* **27(2)**, 187-95, 2002.

ACKNOWLEDGEMENTS

Conseil Scholaire du Grand Nord de l'Ontario for allowing us into their schools.
Sudbury and District Health Unit, Public Health Research, Education and Development (PHRED) for funding this project.
Special thanks to Dar Malaviarachchi for statistical advice.

THE EFFECT OF FOREARM SUPPORT ON EMG ACTIVITY OF THE UPPER EXTREMITIES DURING COMPUTER WORK: A CHAIR INTERVENTION STUDY

[1] Jaworski, K, [1]Moore, A, [2]Amick, B, [3]Robertson, M, [4]Bazzini, L, [4]Rooney, T, [5]DeRango, K, [6]Harrist, R and [3]Jackson, J
[1] School of Kinesiology and Health Science, York University, Canada email: karl@yorku.ca,
[2]University of Texas School of Public Health, USA; [3]Liberty Mutual Research Institute for Safety, USA; [4]Health and Work Outcomes, USA; [5]Upjohn Research Institute, USA [6]Texas Program for Society and Health, Rice University, USA;

INTRODUCTION

The use of computer keyboards has been linked to a number of musculoskeletal symptoms of the upper extremities. While proper workstation setup is a key element to reducing the risk of developing musculoskeletal disorders, the use of forearm support has been shown to increase comfort as well as to reduce the muscular load of the neck and shoulders [1]. Most of these results, however, are based on laboratory experiments or on studies where the arm support condition is compared with a "floating" or no-support condition. There is a need for further exploration of this topic, specifically whether workers use arm supports when provided and whether there is a greater benefit of a highly adjustable chair in comparison with an office chair with fixed arms height.

METHODS

Thirty five participants were recruited from a medical insurance call centre and randomly assigned into either a control or intervention group (16 control, 19 intervention). The intervention consisted of supplying the workers with a chair with adjustable (both vertically and horizontally) forearm supports and office ergonomics training, while the control group remained with their existing office chair which had fixed forearm supports. Each participant took part in two, one-hour observation sessions before and after the intervention. During each of the four observations, the subjects were videotaped from the frontal and sagittal views while doing their usual office duties. The video was analyzed using commercial software (Observer Pro 5.0, Noldus Technology, Netherlands) to determine when participants were keyboarding, using a mouse or performing other office duties as well as whether the participants were using chair forearm supports. RMS EMG was collected at 10 Hz using a commercially available portable system (ME3000P8, MEGA Electronics, Finland) from the trapezius and extensor carpi radialis brevis (ECRB) muscles bilaterally. Changes in the static level of APDF[2] were analyzed. A 2 (pre, post) x 2 (control, intervention) repeated measures ANOVA was performed.

RESULTS AND DISCUSSION

There was an increase in left armrest use for both groups post intervention (Figure 1), However there was a significant (p=.02134) interaction term indicating that there was a much greater increase in armrest use with the highly adjustable arm rests. While the associated levels of the static EMG reflect these changes, the results were not significant.

The results for the right side reflect the more complex activity that occurs in the dominant arm. There was a small but not significant increase in armrest use on the right side. However at the same time there was an increase in mouse use post intervention (Figure 2). These conflicting results may be responsible for the lack of significant changes in the static EMG in the right trapezius.

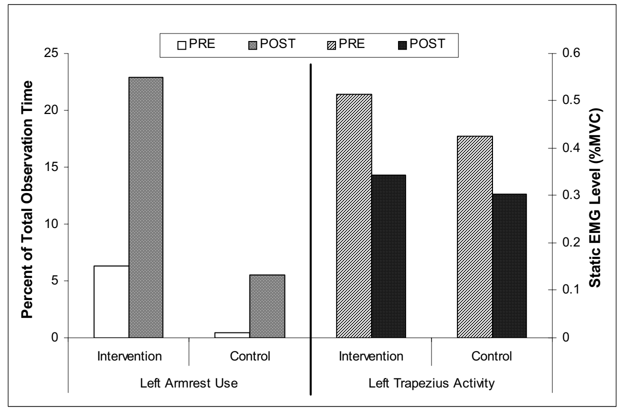

Figure 1. Left armrest use and associated static level EMG (left trapezius)

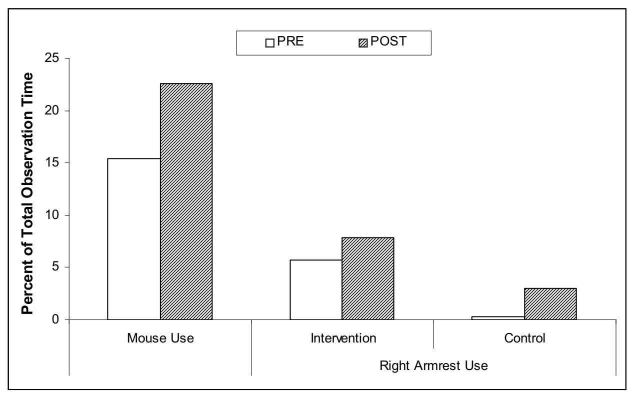

Figure 2 Mouse use (right hand) and Right Armrest use

CONCLUSIONS

Arm rest use on the left side in the workplace is significantly affected by chair design and training. However intervention use on the right is complicated by task changes. Further studies will isolate the EMG associated with arm rest use.

REFERENCES

1. Cook C, et al. *Applied Ergonomics* **35**, 285-292, 2004.
2. Jonsson B. *J. Human Ergl*. **11**, 73-88, 1982.

IMPACT OF LIFT ASSISTIVE DEVICE ON LUMBAR COMPRESSIVE FORCE

Mohammad Abdoli E*. Michael Agnew, Joan Stevenson, Christy Lotz
Ergonomics Research Group, Rm 148, PEC, Queen's University,
Kingston, Ontario, Canada, *0ema@qlink.queensu.ca

INTRODUCTION

The goal of this research is to develop a strategy to reduce the lifting force requirements of back muscles and thus allow provide some support to returning injured workers to their jobs more quickly. To accomplish this goal, a personal lift assistive device (PLAD) was developed using elastic elements and attachment points at the shoulders, waist and knees. The PLAD acts parallel to the back muscles and can be thought of as an external force generator that provides additional elastic energy for lifting tasks, thus allowing the user to accomplish a lift using less of his/her own muscle force. During a lift, these internal forces are transferred by the PLAD to the shoulders, pelvis and lower legs during the down phase of lift and energy returned to the worker during the up phase of the lift. The purpose of this study is to demonstrate the effectiveness of the PLAD on the compressive force on the L4/L5 disc during a variety of lifting tasks.

METHODS

To validate these findings, nine male subjects with no history of back pain executed a variety of lifting tasks (symmetric /asymmetric, light/medium/heavy, free/stoop/squat) under the PLAD and No-PLAD conditions. Three Fastraks® were synchronized into one computer in order to provide 12 electromagnetic sensors with 6 dof. Simultaneous data were acquired at 30 Hz. On a slave computer, sampling at 1000 Hz, six custom strain gauges and eight EMG channels were recorded with all data synchronized using a hand switch. Fastrak® sensors were positioned at the centre of gravity of the hands, forearms, arms, thighs, as well as on the head, C7, T9 and L5. The fully dynamic 3D moments at L4/L5 were calculated using the Hof [1] validated model. A polynomial model [2] was used to predict the lumbar compressive force by the 3D estimated moments. Two approaches were used to determine the impact of the PLAD on back moments. When there is no PLAD, conventional LSM 3D dynamic calculations were used. When PLAD was worn two strategies were employed: first, the force contributions of the elastic elements were subtracted from the total L4/L5 moments so that the contribution due to the PLAD could be calculated. Second, the PLAD force contributions were ignored to see if postural effects alone influenced the results. Results of peak lumber compressions were compared in symmetrical lifting for 3 different loads (5kg, 15kg , 25 kg) with 3 different styles (stooped, squat, free) under 2 conditions of PLAD/No-PLAD. Two 3-way repeated measure ANOVAs were used to examine the impact of peak compression under various conditions.

RESULTS AND DISCUSSION

Figure 1 shows that regardless of load or style, the PLAD conditions were less than the no PLAD conditions by 5% to 20% ($p<0.001$). This difference was greatest for stoop conditions and least for freestyle lifts. Future designs could correct this problem. It also shows the ability of PLAD across different lifting styles ($p<0.05$) as well as for various loads

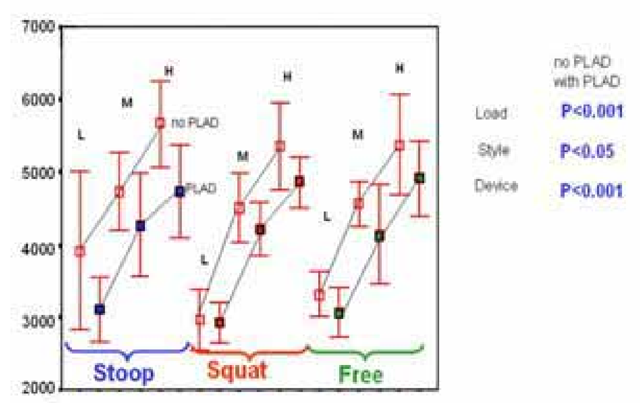

Figure 1: PLAD/no-PLAD comparison of 3 styles of lifting at 3 different types of loads.

($p<0.001$). Hence, regardless of the comparison, the PLAD proved to be effective at reducing the L4/L5 moments and compressive forces.

In Figure 2, when the impact of PLAD was removed mathematically, results revealed that there was no significant

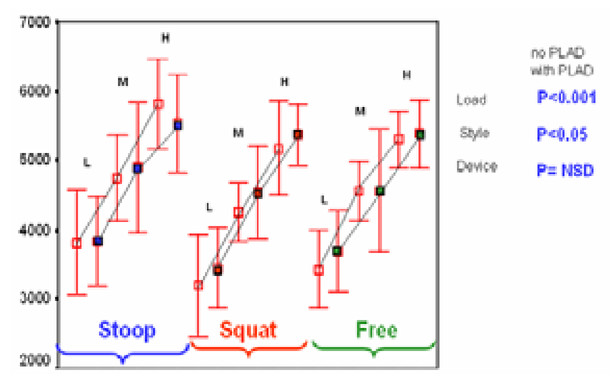

Figure 2: Influence of posture on PLAD/no-PLAD comparison of 3 styles of lifting at 3 different types of loads.effect.

different in peak compressive force across all conditions.

CONCLUSIONS

These results prove that the PLAD does reduce the compressive force on the L4/L5 disc across a number of lifting conditions. Hence, it could be considered as a good device to increase the margin of safety for tissue tolerances in the spine during lifting tasks. Further research is needed to confirm its effectiveness in terms of electromyography and spinal stability as well as examining the impact of the PLAD over extended user trials.

REFERENCES

1. Hof AT. An explicit expression for the moment in multibody systems. J Biomech 1992;25:1209-11.
2. McGill, S. M., Norman, R. W., Cholewicki, J., (). A simple polynomial that predicts low-back compression during complex 3-D tasks. Ergonomics 1996:39, 1107-1118.

THE EFFECTS OF QUANTITATIVE FEEDBACK ON THE REDUCTION OF LANDING FORCE

[1]Sara C. Novotny and [1]Richard N. Hinrichs
[1]Department of Kinesiology, Arizona State University; email: novotns@ccf.org

INTRODUCTION

Many sports involve regularly landing from a jump. Repetitive, high force landings have been associated with an increase in lower extremity injuries in active individuals [1]. Recently, the use of feedback has been implemented to aid athletes in reducing their landing forces. However, the feedback has generally been qualitative in nature [2]. This study aimed to evaluate the usefulness of providing quantitative feedback regarding landing force and landing sound.

METHODS

Forty recreationally active males and females were assigned to one of four feedback groups. Each group was comprised of five males and five females. The groups were given feedback about peak force only (Force), feedback about peak sound only (Sound), feedback about both peak force and peak sound (Both), or feedback about neither peak force nor peak sound (Control).

All subjects performed a series of drop landings from a set height onto a force platform, and vertical ground reaction force (GRF) and sound level were recorded for each landing. Subjects performed three trials without feedback, establishing baseline force and sound values. The appropriate feedback was given after each of the next five landings. The feedback was presented on a 1 to 10 scale, with 10 representing 100% of the baseline value. All subjects returned one week later to perform three landings without feedback. The effects of feedback on peak vertical GRF were computed using a 2 (peak sound level) × 2 (peak force) repeated measures ANOVA.

RESULTS AND DISCUSSION

The main effect for time on peak force was significant, $p<.01$. Pairwise comparisons for peak force indicated that subjects significantly changed their landing forces from the baseline measures to the feedback measures, $p<.01$, and the baseline measures were significantly different from the retention measures, $p<.01$ (Figure 1).

Overall, the feedback groups reduced their peak force by 0.80-1.39 times body weight (BW). However, the main effect for feedback group and the interaction effect between feedback group and time were not significant, $p>.01$. Since the main effect for group was non-significant, the differences between the feedback groups over time were examined by looking at the effect sizes between the four feedback groups. The effect size for the difference between the baseline and feedback measures was moderate to large when the each group was compared to the Control group, -1.16, -0.82, and -0.69 for Force, Sound, and Both groups respectively. (An effect size ≤ 0.2 was considered small. An effect size of approximately 0.5

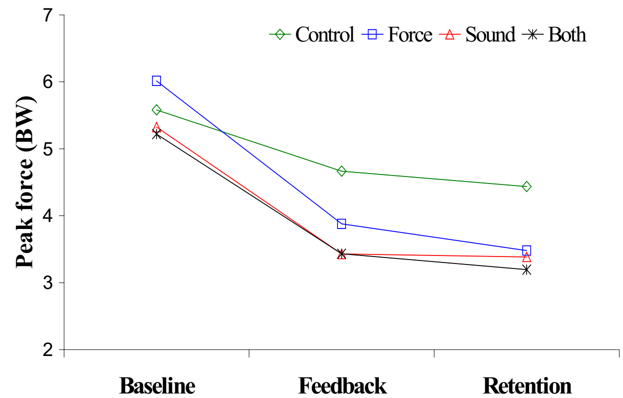

Figure 1: Changes in peak force over time for different feedback groups.

was moderate and ≥ 0.8 was large. [3]). Similar effect sizes occurred for the difference between baseline and retention measures when the Control group was compared to the Force, Sound and Both groups, -1.17, -0.65, and -0.66 respectively. The effect sizes between the Force and Sound group were 0.21 from baseline to feedback and 0.52 from baseline to retention, while the effect sizes between the Force and Both groups were 0.29 and 0.41 for the same difference scores.

CONCLUSIONS

All subjects decreased their landing force over the course of the study due to learning. The reduction in force was greater for the feedback groups, though not significantly greater. However, effect sizes indicated a trend towards any type of feedback being better than no feedback at all. An increased number of subjects per group might have solidified this trend. Feedback on peak force was the most effective feedback, as the feedback group had the largest effect sizes between both baseline and feedback and baseline and retention when compared to the other groups. Feedback on sound level was also effective, raising interesting questions about the potential for a more accessible method of providing feedback on landings. Sound has previously been shown to be a significant predictor of force, allowing for inferences of relative force to be made from relative sound [4].

REFERENCES

1. Hreljac, A, et al.. *Med Sci Sports Exerc*, **32**, 1635-1341, 2000.
2. McNair, PJ, et al.. *Br J Sports Med*, **34**, 293-296, 2000.
3. Cohen, J. *Statistical Power Analysis for the Behavioral Science*, Academic Press, New York, NY
4. Novotny, SC & Hinrichs, RN. *Proceedings of ASB XXIIX*, Portland, OR, Abstract 166, 2004.

THERAPEUTIC FOOTWEAR DESIGN: A FINITE ELEMENT MODELING APPROACH

[1]Ahmet Erdemir, [1,2]Marc Petre, [1,3]Sachin Budhabhatti, [1]Todd Doehring, [4]Steven Goske, [1,2]Pavan Thangudu, [1,2]Josh Considine, [5]Donald Bly, [6]James Wyllie, and [1,7]Peter R. Cavanagh
[1]Dept. of Biomedical Engineering, Cleveland Clinic Foundation, [2]Dept. of Biomedical Engineering, Case Western Reserve University, [3]Dept. of Chemical & Biomedical Engineering, Cleveland State University, [4]Dept. of Biomedical Engineering, Saint Louis University, [5]Dept. of Engineering Sciences, Dartmouth College, [6]School of Electrical Engineering & Computer Science, Ohio University, [7]Dept. of Orthopaedic Surgery and Orthopaedic Research Center, Cleveland Clinic Foundation
e-mail: cavanap@ccf.org, web: www.lerner.ccf.org/bme/cavanagh

INTRODUCTION
Foot ulceration is a common complication among diabetic patients with peripheral neuropathy [1]. Elevated foot pressures can cause skin breakdown that might lead to ulceration (Fig. 1). Therapeutic footwear is a typical intervention for relieving plantar pressures which can lead to ulceration [2], but scientific guidelines for selection of footwear are not well defined [3]. Although some experimental studies have attempted to establish such guidelines, e.g. [4], the systematic testing of multiple design variables is difficult. In practice, footwear selection still relies on the experience of the healthcare provider and on trial-and-error.

Finite element (FE) analysis allows the investigation of complex biological structures under load by discretization of the geometry into small uniformly shaped elements [5]. When boundary conditions, loading and friction at the foot-shoe interface are defined, the models can predict stresses under the foot. This approach permits the examination of a large number of footwear designs without the burden of high-volume experimentation. Once validated, the models can simulate variations in anatomy and footwear: for example, the insole geometry and material can be systematically varied to guide strategies for the prescription of therapeutic footwear. Our objective is to establish an integrated approach and use FE modeling for design of therapeutic footwear.

METHODS
The modeling strategy employed includes representations of foot anatomy, footwear geometry, soft tissue properties, footwear materials, foot kinematics and loading and foot-footwear-ground interactions. Barefoot and in-shoe pressure measurements provide foot loading as well as validation data. Subject specificity is established by optimization protocols to map model predicted pressure measurements to those measured experimentally. Foundations of FE simulations rely on computational and experimental research in the areas listed above; the integrated approach provides the necessary input to develop two- and three-dimensional FE models (Fig. 2).

A variety of design criteria for therapeutic footwear are tested by systematically changing footwear properties (e.g. geometry, material) in FE models. It is possible to identify designs that result in effective pressure reduction overall. Footwear interventions to relieve local pressures under focal areas of the foot (e.g. heel pad, metatarsal head) are also investigated by FE simulations.

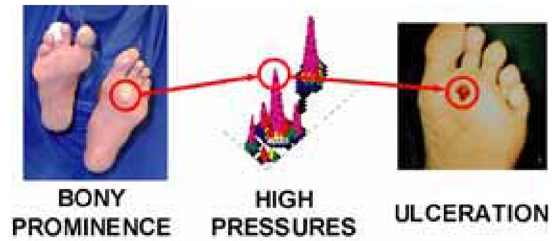

Figure 1: Potential pathway to foot ulceration in diabetic patients with peripheral neuropathy.

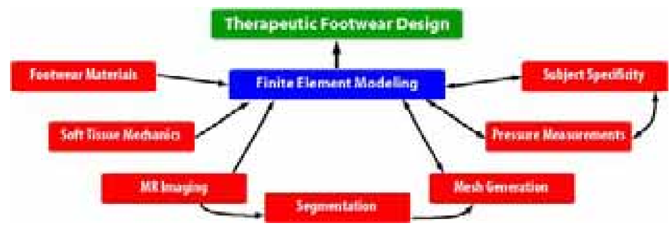

Figure 2: An integrated approach for therapeutic footwear design based on finite element modeling.

EXAMPLES
Simulations using a plane strain model of the second metatarsal region have identified favorable plug designs to relive local pressures underneath the metatarsal head. A plane strain model of the heel pad has provided guidelines on the selection of insole thickness, material and conformity to reduce heel pressures. A three-dimensional model of the first metatarsal and hallux has quantified the influence of material selection on plantar pressure reduction under the first ray.

Among the models under development are a planar heel-pad model to explore shear prediction under the foot; a three-dimensional forefoot model for evaluating load redistribution among the metatarsal heads; and a whole foot model to investigate transfer of forefoot loads to the arch using footwear.

REFERENCES
1. Veves A, et al. *Diabetologia* **35**, 660-663, 1992.
2. Brill LR, et al. **No. 5**, 1994, Treatment of Chronic Wounds, East Setauket, NY.
3. Ulbrecht JS, et al. *in Kominsky SJ,* 29-45, 1994, Mosby Year Book, St. Louis, MO.
4. Ashry HR, et al. *J Foot & Ankle Surg* **36**, 268-271, 1997.
5. Huiskes R, et al. *J Biomech* **16**, 385-409, 1983.

ACKNOWLEDGEMENTS
This study was funded by the NIH Grant # 5R01 HD037433.

REDUCTION OF PLANTAR HEEL PRESSURES: INSOLE DESIGN USING FINITE ELEMENT ANALYSIS

[1] Steven Goske, [2]Ahmet Erdemir, [2,3]Marc Petre, [2,4]Sachin Budhabhatti and [2,5]Peter R. Cavanagh
[1]Dept. of Biomedical Engineering, Saint Louis University, [2]Dept. of Biomedical Engineering, Cleveland Clinic Foundation,
[3]Dept. of Biomedical Engineering, Case Western Reserve University, [4]Dept. of Chemical & Biomedical Engineering,
Cleveland State University, [5]Dept. of Orthopaedic Surgery and Orthopaedic Research Center, Cleveland Clinic Foundation
e-mail: cavanap@ccf.org, web: www.lerner.ccf.org/bme/cavanagh

INTRODUCTION

Plantar loading of the heel during daily locomotion can result in high local pressures that need to be relieved in the case of heel pain [1]. In-shoe interventions are commonly used to reduce plantar heel pressures by using custom or off-the-shelf insole products, e.g. [2]. The design process for these products is often intuitive in nature and does not always rely on scientifically derived guidelines [3].

Finite element analysis provides an efficient computational framework to investigate the performance of a large number of designs for optimal plantar pressure reduction. The objectives of this study were to develop a finite element model of the heel pad and footwear and to explore the insole design space in order to quantify the effects of i) insole conformity, ii) insole thickness, and iii) insole material on pressure relief.

METHODS

A 55 mm thick plane strain model of the heel pad was developed. Heel geometry was obtained from MRI of the right heel of a healthy adult male (23 years, 89 kg, 1.88 m). Bone was assumed to be rigid; soft tissue was modeled as incompressible hyperelastic. A barefoot simulation was conducted during which the heel was loaded vertically to simulate maximal loading of the heel at first step of walking. This simulation provided the baseline peak pressure that needed to be relieved by insole intervention. Barefoot pressure measurements validated model predicted peak heel pressure. For simulations regarding insole design, footwear was included into the model (Fig. 1). A 20 mm thick midsole was modeled as Firm Crepe (compressible, hyperfoam) and the shoe sidewalls were modeled as stiff leather (linearly elastic).

Three insole design variables were investigated: conformity (flat, half, full); thickness (6.3 mm, 9.5 mm, 12.7 mm); and compressible hyperfoam material (Microcel Puff [hard], Microcel Puff Lite [medium], Poron Cushioning [soft]). All simulations were conducted using ABAQUS (Abaqus, Inc.) and percent reduction in peak heel pressures was calculated compared to model prediction of peak barefoot pressure.

RESULTS AND DISCUSSION

Conformity had the most profound effect in pressure reduction (Table 1), possibly due to larger contact surfaces. Thickness was also influential in reducing plantar heel pressures (Table 1). Material had a limited effect; pressure reduction slightly improved while using a softer material. It was possible to reduce peak heel pressure by 15-24% (compared to barefoot condition) by simply using a flat insole. Through careful selection of insole properties, it was possible to increase this reduction up to 44% when compared to barefoot values.

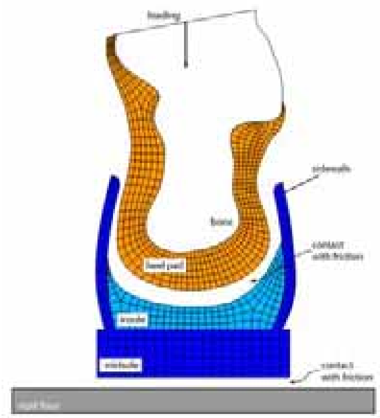

Figure 1: Plane strain model of the heel pad, insole and the remaining components of the shoe.

Table 1: Percent reduction in peak heel pressures (for each insole) compared to barefoot peak pressure (435 kPa).

			Thickness (mm)		
Conformity			6.3	9.5	12.7
Flat	Material	Microcel Puff	15.2	20.5	23.0
		Microcel Puff Lite	16.3	20.7	23.9
		Poron Cushioning	16.8	20.7	24.1
Half		Microcel Puff	26.7	28.7	31.3
		Microcel Puff Lite	26.2	29.7	34.7
		Poron Cushioning	25.1	28.5	33.8
Full		Microcel Puff	37.5	38.9	40.7
		Microcel Puff Lite	37.9	40.7	43.7
		Poron Cushioning	35.6	38.9	43.4

The finite element analysis allowed a cost-effective investigation of multiple insole design criteria to reduce plantar heel pressures. The approach also advanced previous modeling studies of the heel/footwear, e.g. [4], by adapting a plane strain approach in order to capture heel anatomy and representation of the various components of the shoe.

REFERENCES

1. Alridge T *Am Fam Phys* **70**, 332-338, 2004.
2. Ashry HR, et al. *J Foot & Ankle Surg* **36**, 268-271, 1997.
3. Ulbrecht JS, et al. *in Kominsky SJ,* 29-45, 1994, Mosby Year Book, St. Louis, MO.
4. Verdejo R and Mills NJ *J Biomech* **37**, 1379-1386, 2004.

ACKNOWLEDGEMENTS

This study was funded by the NIH Grant # 5R01 HD037433.

THE INFLUENCE OF GASTROCNEMIUS GEOMETRY ON ITS ACTION AT THE KNEE DURING STANCE

Saryn R. Goldberg[1], Frank C. Anderson[2], and Scott L. Delp[2,3]
[1] Physical Disabilities Branch, National Institutes of Health, Department of Health and Human Services, Bethesda, MD, USA
[2] Biomechanical Engineering Division, Mechanical Engineering Department, Stanford University, Stanford, CA, USA
[3] Bioengineering Department, Stanford University, Stanford, CA, USA
email: goldbergs@cc.nih.gov, web: http://pdb.cc.nih.gov

INTRODUCTION

The gastrocnemius plays an important role in support of the body during stance [1] and in preparation of the limb for swing [2,3]. However, the action of this muscle at the knee is unclear; some dynamic analyses show that gastrocnemius acts mainly to flex the knee during double support [2], while others demonstrate that the muscle accelerates the knee into extension [3]. To clarify the action of gastrocnemius at the knee, we systematically altered the ratio of the moment arms of gastrocnemius to determine how changes in the geometry of this muscle affect its capacity to accelerate the knee during stance. Our objective was to determine the knee-to-ankle moment arm ratio that would result in zero knee acceleration, as this ratio represents the ratio at which muscle function changes from knee flexion to knee extension.

METHODS

To calculate the acceleration of the knee joint generated by various gastrocnemius geometries, we fixed a 3-dimensional model of the lower extremity with a 2-degree-of-freedom ankle and 2-segment foot [4] in positions corresponding to every 2% of normal stance phase kinematics [4], assumed rigid contact of the foot with the ground [1], and applied moments about the knee, ankle, and subtalar joints corresponding to a range of knee-to-ankle moment arm ratios for gastrocnemius. Specifically, for each stance phase position, the ankle moment was set to 1 Nm, the subtalar moment was set to its normal size relative to this ankle moment, and the knee moment was varied until the knee was not accelerated. The relative values of the ankle and subtalar moments were chosen to correspond to those generated by gastrocnemius during normal gait [4]. Values for the knee-to-ankle moment arm ratio that gave rise to zero knee acceleration were insensitive to the absolute sizes of the knee and ankle moments; only their ratio mattered.

RESULTS AND DISCUSSION

The knee-to-ankle moment arm ratio for gastrocnemius that resulted in zero knee acceleration was near or below a value of 0.4 until about 55% of the gait cycle (Figure 1). After the metatarsal joint left the ground, leaving only the toe in contact, the ratio rose dramatically to values ranging from 1.2 to 1.8 (Figure 1). Experimental data from cadavers places the knee-to-ankle moment arm ratio for gastrocnemius above 0.4 and below 0.7 for nearly all of stance [5,6,7] (Figure 1). This suggests that gastrocnemius, when generating force, would accelerate the knee into flexion for most of stance. After metatarsal-off, however, any normal moment arm ratio would result in gastrocnemius acting to extend the knee (Figure 1). Given that gastrocnemius flexes the knee during most of stance but extends it in late stance, it is difficult to determine

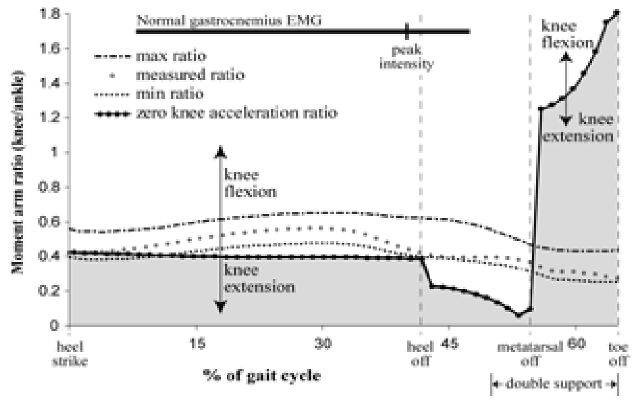

Figure 1. The gastrocnemius knee-to-ankle moment arm ratio that resulted in zero acceleration of the knee during stance compared to ratios estimated from experiments [5,6,7] and normal gastrocnemius EMG activity [8]. Ratios above (below) the zero-knee-acceleration ratio would accelerate the knee into flexion (extension). The measured ratio was based on data collected from a single specimen [5]. The max and min ratios were based on data from separate knee and ankle joint studies and represent the theoretical extremes of this ratio during stance [5,6,7].

the net action of this muscle. Since gastrocnemius typically generates the largest forces near heel-off [4,8], and since forces generated at the beginning of a movement are the most influential in determining the resulting net action over a period of time [2], it is likely that gastrocnemius acts in net to flex the knee. This is likely true even over double support, when gastrocnemius is generating force due to muscle deactivation. Indeed, perturbation analyses support this conclusion [2]. However, further investigation is needed before such conclusions can be drawn definitively. Specifically, future work will determine how other modeling variables, such as the way in which the foot and its contact with the ground are represented, affect the action of gastrocnemius at the knee.

REFERENCES

1. Anderson FC, et al. *Gait & Posture* **17**, 159-169, 2003.
2. Goldberg SR, et al. *J Biomech* **37**, 1189-1196, 2004.
3. Neptune RR, et al. *J Biomech* **34**, 1387-1398, 2001.
4. Anderson FC and Pandy MG. *J Biomech Eng-T ASME*, **123**, 381-390, 2001.
5. Spoor CW, et al. *J Biomech* **23**, 1247-1259, 1990.
6. Magnaris CN, et al. *Eur J Appl Physiol* **83**, 363-369, 2000.
7. Magnaris CN. *Clin Anat* **16**, 215-223, 2003.
8. Perry J. *Gait Analysis*, SLACK Inc., Thorofare, NJ, 1992.

ACKNOWLEDGEMENTS

This work was supported in part by NIH R01 HD38962.

NEW OPEN-SOURCE TOOLS FOR 3D RECONSTRUCTION FROM MEDICAL IMAGES

[1]Todd Doehring, [2]Pavan Thangudu, [2]Josh Considine, [1]Peter R. Cavanagh
[1]Department of Biomedical Engineering, Cleveland Clinic Lerner College of Medicine of CWRU
[2]Department of Biomedical Engineering, CWRU

INTRODUCTION

With the advent of new medical imaging technologies and options for non-invasive means of patient diagnosis, the need for better 3D segmentation and reconstruction tools for research and clinical practice is increasing. Unfortunately, segmenting and generating 3D anatomical models from 2D medical images is currently a time consuming process, usually requiring large amounts of manual labor and expensive, proprietary software. The available commercial software [1] is "closed-source", restricting research and experimentation with the underlying algorithms. Also, commercial software is often not well suited to reconstruction of complex tissues from noisy magnetic resonance images (MRIs).

Because of these limitations of commercial software, the purpose of this research was to develop new software tools ("Super//Slicer") for 3D segmentation and reconstruction from medical images, with an emphasis on reconstructing connective tissues. In this report we describe the basic components of the software. Super//Slicer is written in Matlab (Mathworks, Inc.) and is freely available [2].

METHODS

A graphical user interface (GUI) was developed to maximize interactivity and user control. Image sequences can be loaded and saved, as well as entire segmentation sessions. The software has for main components: (1) a set of filters, including cropping, thresholding, noise reduction, and other filters, (2) a threshold-based contouring algorithm, (3) manual contour tracing and editing, and (4) a surface generation algorithm for generating spline-smoothed contour data and 3D "water-tight" triangular polygon surfaces. The contours and surfaces are output in "obj" format (Wavefront format, Alias, Inc.) compatible with most 3D solid modeling software. Once a contour is selected, the software uses an automatic selection algorithm to identify and select contours in adjacent images that are associated with the object that is being segmented. The user can specify multiple threshold values to vary the shape of the contour ("keyframing"). Manual tracing and editing functions were also included to enable the user to trace regions that could not be segmented with the contour function.

A typical process of segmentation and reconstruction is: (1) open the image files, (2) crop to the region of interest, (3) adjust the contour threshold and set keyframes to best fit the object to be segmented (i.e. ligament, muscle, bone, etc.), (4) automatically detect and select similar object contours (i.e. "super slice"), (5) add or delete contours as needed, using manual editing if necessary, and (6) automatically generate and output the contour data and resulting surface mesh.

Super//Slicer was designed to be easy to understand and program. The user can reprogram filters, add new filters, and otherwise modify the segmentation and surface generation codes. The current contouring and segmentation algorithms are simple, however, more advanced methods, such as active contours and neural network training are under development.

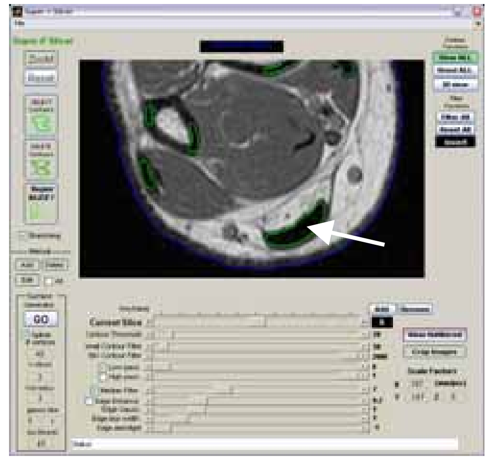

Figure 1: GUI and contoured image of the Achilles tendon.

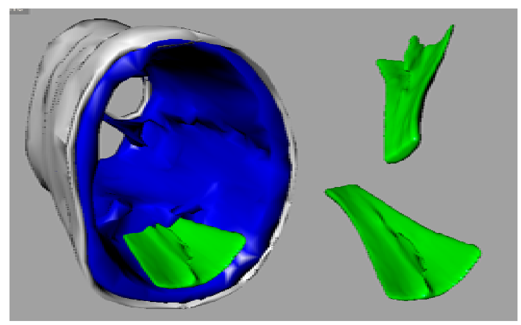

Figure 2: Reconstructions of lower leg skin, fatty tissues, and Achilles tendon (shown in two views for clarity).

RESULTS AND DISCUSSION

Development of Super//Slicer is ongoing, but already several complex 3D reconstructions of foot-related tissues have been performed (Fig. 2).

CONCLUSIONS

The goal of this project was to construct a simple and efficient framework for development of new methods for 3D segmentation and model generation from medical images. Super//Slicer has exhibited potential in its ease of use, and ability to generate accurate models in a short amount of time. It is hoped that open-source availability will spark new research and development of improved methods for analysis of MRI and CT medical images.

REFERENCES

1. http://biocomp.stanford.edu/3dreconstruction/software/
2. Email doehrint@ccf.org for code and information.

ACKNOWLEDGEMENTS

Funded by NIH (F32 HL72598) and 5R01 HD037433

MECHANICAL EFFICACY OF TENDON TRANSFER OPERATIONS FOR FOOT DROP

[1]Tsuyoshi Jotoku; [1]Kristin Zhao; [2]Harold Kitaoka; [1]Lawrence Berglund;[1]Kota Watanabe; [1]Kenton Kaufman
[1]Biomechanics Laboratory, Division of Orthopedic Research, Mayo Clinic Rochester, MN;
[2]Department of Orthopedic Surgery, Mayo Clinic Rochester, MN;
Email: zhao.kristin@mayo.edu

INTRODUCTION

There are multiple operations described for foot drop. Conventional posterior tibial tendon transfer through the interosseus membrane (IOM) is popular, but there are concerns that it may not be adequate to obviate continued bracing. The Bridle procedure (BRI) is promising [1] but involves 5-7 incisions and a higher potential for complications. The purpose of this study was to compare results of these two operations in cadaveric lower extremities using a dynamic ankle-foot simulator.

METHODS

Seven fresh-frozen lower extremities without foot-ankle pathology were evaluated. The tibia and fibula were embedded in PMMA and specimen mounted in a previously-validated dynamic ankle-foot simulator [2], designed to recreate late swing phase and entire stance phase of gait in cadaveric specimens (Fig 1). Input data derived from anatomic, electromyographic, and gait analysis studies were used for ground reaction force profiles, tibial advancement, and application of forces to 6 distinct muscle groups. Axial and fore-aft shear forces were applied with servomotors, with profiles from gait analysis data [3]. Each specimen was pre-tested three times to reduce viscoelastic effect of soft tissue structures.

Three-dimensional kinematics were measured using a magnetic tracking device (3Space Fastrak system, Polhemus, Colchester, VT), focusing upon metatarsal motion relative to talus. Motor control and data acquisition were accomplished using Labview (National Instruments, Austin, TX). Specimens were tested in 4 conditions: 1) intact, 2) foot drop (tibialis anterior, extensor hallucis longus, extensor digitorum longus, and peroneals forces removed), 3) after IOM, and 4) after BRI. Statistical analysis included repeated measures ANOVA to evaluate the effect of each test condition on foot kinematics, with statistical significance set at $p<0.05$ level.

RESULTS AND DISCUSSION

Typical metatarsal-tibial sagittal motions for normal, foot drop, BRI and IOM are shown in Figure 2. The position of the foot at initial contact in all three planes differed significantly between the intact and foot drop conditions, with the intact foot in a position of dorsiflexion (4.6±5.5 deg), eversion (4.4±4.9 deg), and external rotation (3.3±6.3 deg) and the foot drop in a position of plantarflexion (-18.5±5.4 deg), inversion (-13.1±3.8 deg), and internal rotation (-9.8±6.1 deg). Both operations improved foot position, as compared to foot drop, in all three planes. Neither the IOM nor the BRI conditions differed significantly from the intact condition, except for the sagittal position of the foot after the BRI procedure.

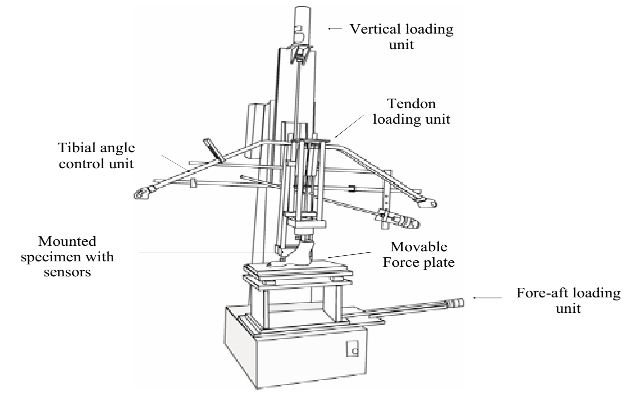

Figure 1: Dynamic ankle-foot simulator.

CONCLUSIONS

These data suggest that the IOM and BRI procedures were successful in restoring the kinematics of the foot at heel strike in this cadaveric model of gait. The mechanical effects of these two procedures are similar, suggesting that either may be employed for the improvement of gait in patients with foot drop.

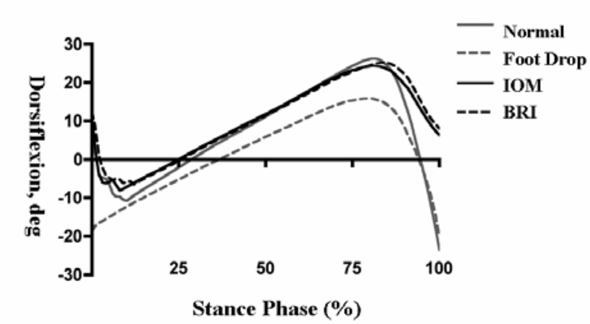

Figure 2: Metatarsal-tibial sagittal motion in intact, foot drop, IOM, and BRI conditions.

REFERENCES

1. Rodriguez R. *Foot Ankle* **13**, 63-9, 1992
2. Kim, KJ, et al. J Musculoskeletal Res, **5**, 113-121, 2001
3. Perry J. *Gait Analysis -Normal and Pathological Function,* Slack, Thorofare, NJ, 1992

ACKNOWLEDGEMENTS

The authors gratefully acknowledge the assistance and support of: S. Ringleb, K. An, T. Tsubone, X. Crevoisier, and the Mayo Foundation.

SARCOMERE LENGTH MEASUREMENT PERMITS HIGH RESOLUTION NORMALIZATION OF MUSCLE FIBER LENGTH IN ARCHITECTURAL STUDIES

Amanda Felder, Samuel R. Ward and Richard L. Lieber
Departments of Orthopaedic Surgery and Bioengineering, University of California
and Department of Veterans Affairs Medical Centers, San Diego, CA; email: rlieber@ucsd.edu

INTRODUCTION

The reliability of architectural information depends heavily on accurate fiber length (L_f) values. One difficulty in obtaining accurate L_f values is compensating for the fiber length variation that occurs because muscles are fixed at various joint angles. The procedure typically used to compensate for such variation is to use sarcomere length measurements to normalize fiber length to a standard sarcomere length, using the equation:

$$L_f(cm) = \frac{L_f'(cm) \bullet L_s(\mu m)}{L_s'(\mu m)} \qquad \text{(Equation 1)}$$

where L_f is the normalized fiber length, L_f' is the experimentally measured (raw) fiber length, L_s is the standard sarcomere length and L_s' is the experimental sarcomere length measured at the experimentally measured fiber length. The purpose of this study was to test the accuracy and resolution of this method of fiber length normalization.

METHODS

The mouse hindlimb was used as a model system. Limbs were disarticulated at the hip, the knee joints were set to 90°, ankle joints were set to angles ranging from 30° to 150° (n=2-4/group), and the limbs were fixed in formalin. To determine the precise tibiotarsal and tibiofemoral angles of fixation, lateral radiographs were obtained of the limbs, and joint angles were digitized.

Tibialis anterior (TA), extensor digitorum longus (EDL), and soleus muscles were removed from limbs and digested in 15% H_2SO_4 to facilitate fiber bundle dissection. Small fiber bundles were dissected from the whole muscles under 8X-20X magnification, with care to remove the entire bundle from tendon to tendon. Three to four bundles were removed from each muscle. Fiber bundle length was measured to the nearest 0.01 mm. After mounting the fibers, sarcomere length was measured at three different points along each bundle using laser diffraction as previously described [1].

Raw fiber lengths were normalized to a standard sarcomere length of 2.5 μm using equation 1 shown above. Linear regression of raw and normalized fiber lengths over ankle angle was performed for each muscle. Additionally, raw and normalized fiber lengths were compared across angle groups by one-way analysis of variance (ANOVA). Finally, resolution of the normalization procedure was defined using the standard statistical power equations.

RESULTS AND DISCUSSION

As anticipated, raw fiber bundle length was strongly dependent on tibiotarsal angle (Fig. 1A; $p<0.002$ for all muscles, r^2 range from 0.20-0.68), although the magnitude of the change was muscle-dependent, based on the different fiber

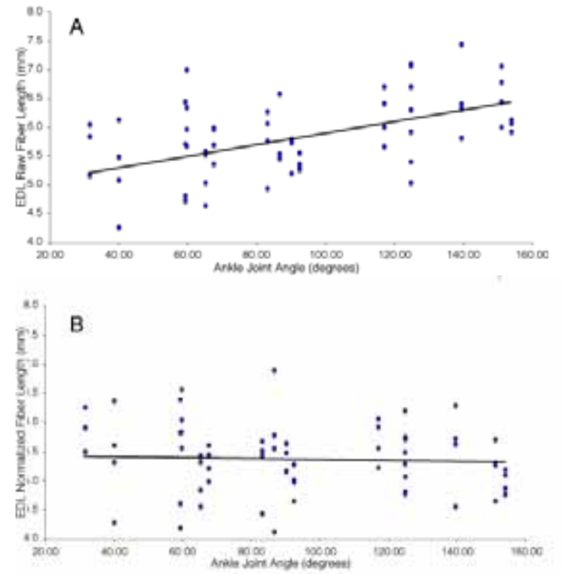

FIGURE 1: (A) EDL raw fiber length *vs*. ankle angle. (B) EDl normalized fiber length *vs*. ankle angle. Results from EDL are representative of TA and soleus as well.

length-moment arm relationships of each muscle [2]. Sarcomere length normalization eliminated the joint-angle dependent variation in fiber length in all muscles, as evidenced by both linear regression (Fig 1B; $p>0.3$, r^2 range from 0.009-0.022) and one-way ANOVA ($p>0.1$). There was no significant variation of animal mass or tibial length across groups ($p>0.9$, $p>0.8$, respectively). A large degree of natural fiber length variation occurs which is not eliminated after sarcomere length normalization. Statistical power analysis revealed a ~90% chance of detecting a 15% fiber length difference and a ~60% chance of detecting a 10% variation.

CONCLUSIONS

We demonstrated that sarcomere length normalization eliminates the fiber length variability due to variation in joint angle. The use of sarcomere length normalization easily permits resolution of fiber length variations of 15%.

REFERENCES

1. Lieber, R. L., B. M. Fazeli and M. J. Botte, 1990. Architecture of selected wrist flexor and extensor muscles. *Journal of Hand Surgery* (American Vol.) **15A**, 244-250.
2. Lieber, R. L., 1997. Muscle fiber length and moment arm coordination during dorsi- and plantarflexion in the mouse hindlimb. *Acta Anatomica* (Basel) **159**, 84-89.

ACKNOWLEDGEMENTS

Department of Veterans Affairs and NIH grant AR40050.

EXERCISE COUNTERMEASURES LABORATORY AT NASA GLENN RESEARCH CENTER – A NEW GROUND-BASED CAPABILITY FOR ADVANCING HUMAN HEALTH AND PERFORMANCE IN SPACE

[1]Gail Perusek, [1]Miguel Polanco, [2]Carlos Grodsinsky, [2]David Root, [3,4]Andrea Rice, [3,4]Kerim Genc, [3,4,5,6]Brian Davis, [3,4,5,6]Peter Cavanagh
[1]NASA Glenn Research Center, [2]ZIN Technologies, [3]The Cleveland Clinic Foundation Center for Space Medicine, [4]Departments of Biomedical Engineering and [5]Orthopaedic Surgery and the [6]Orthopaedic Research Center
email: Gail.P.Perusek@nasa.gov

INTRODUCTION

To mitigate the detrimental effects of microgravity on the human musculoskeletal system, astronauts on the International Space Station (ISS) currently exercise on three exercise countermeasures devices (TVIS, CEVIS, and iRED). However, it is known that astronauts on the first 6 Expeditions to the ISS lost lower-extremity bone mass despite exercising on these devices. Peak magnitude and rate-of-change of force elicited under the feet (F and dF/dt, respectively) are widely believed to be important criteria for efficacy of countermeasures against loss of bone mass, but there is no information in the literature to demonstrate F and dF/dt imposed on the lower extremities during exercise throughout the range of available gravity-replacement loads imposed on the subject during exercise on ISS. To address these issues, NASA Glenn Research Center and The Cleveland Clinic Foundation Center for Space Medicine have developed the Exercise Countermeasures Laboratory (ECL), a new ground-based test capability, for providing a more flight-like simulation of exercise and reduced-gravity locomotion. Finite element analysis (FEA) of crucial system components was used to verify structural modes of vibration do not couple with ground reaction force measurements in the simulator.

METHODS

The ECL incorporates an enhanced Zero-g Locomotion Simulator (eZLS) which includes interface dynamics of those seen on the ISS, and the ability to provide variable structural dynamic interdependence to mimic variable interface configurations as seen on the ISS and other possible vehicle carriers. To allow interface forces to be accurately measured, non rigid-body structural modes of the ground-based testbed were analyzed using FEA, to ensure that the forcing function induced by the subject and subject load device are decoupled from non-rigid body modes of the simulator (Figure 1). Components of the simulator that were modeled included (i) the inertial ground frame reference, or ground reaction frame, (ii) the exercise device, and (iii) the 1 DOF off-loading and translation system for the exercise device. Target modes were set at 1.7 times the highest bandwidth of interest in the ground reaction force Z-axis component. The Z-axis is oriented normal to the running surface. Frequency content of human ground reaction force has been shown to be below 25Hz [1]. Acceptable non-rigid body structural modes were established to be 43 Hz or higher, to minimize structural interactions with the foot force measurements.

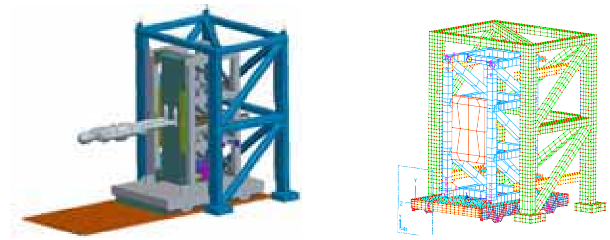

a.) **b.)**

Figure 1: (a) Solid model of test subject in enhanced Zero-g Locomotion Simulator (eZLS). Subject suspension system not shown. (b) Finite element model of simulator components.

RESULTS AND DISCUSSION

The inertial ground frame reference, or ground reaction frame, is a carbon steel box-tubing welded framework with grouted base pads which accept concrete anchors. Modes of vibration of this structure were found to meet the established criterion, with the first mode in the Z-axis direction at 70 Hz. The treadmill frame, which accommodates treadmill mechanical and electrical components, forceplate, and subject load device system, is an aluminum box-tubing welded framework. The treadmill base mounts to the 1 DOF linear translation system, or “Z-slide”, which offloads the weight of the treadmill system and allows frictionless movement in the Z-axis via air bearings. The treadmill frame and Z- slide assembly modes were also found to be acceptable, with the first Z-axis mode at 45 Hz.

CONCLUSIONS

Interface forces to the subject, as well as to the exercise equipment and ground reaction frame, will be measured in the eZLS for various exercise modalities to develop a more detailed understanding of the human, subject load device, and exercise countermeasure equipment interactions, without interference from unwanted non-rigid body modes of the structural components in the system. FEA informed the design decisions for the system components and their interfaces, including the attachment method to ground for the ground reaction frame. The outcome will be that an integrated load (duration, intensity, frequency, time rate of change) may be identified for maximum benefit of counteracting the degenerative effects of space flight.

REFERENCES

1. Kram R, et al.. *J Appl Physiol* **85**(2), 764-769, 1998.

ACKNOWLEDGEMENTS

This work funded in part by the National Space Biomedical Research Institute grant BL00402 through NASA NCC 9-58.

SUB-CALCANEAL FAT-PAD INFILTRATION AND ITS EFFECT ON PLANTAR HEEL PRESSURES IN THE DIABETIC NEUROPATHIC FOOT

[1,3] Sicco Bus, [2]Mario Maas and [2]Erik Akkerman
Department of [1]Internal Medicine and [2]Radiology, Academic Medical Center, University of Amsterdam, The Netherlands
[3]Diabetic Foot Unit, Department of Surgery, Twenteborg Ziekenhuis, Almelo, The Netherlands
email: s.a.bus@amc.uva.nl

INTRODUCTION

Diabetes mellitus and its complications are associated with several structural and physiological abnormalities in the foot, which can increase the risk for plantar ulceration [1]. These abnormalities also include changes in the sub-calcaneal and sub-metatarsal fat-pads used for cushioning. Micro-hemorrhage of sub-cutaneous tissue has been reported [1,2] and non-enzymatic glycosylation of proteins may lead to systemic fat pad tissue changes [3]. The purpose of this study was to use magnetic resonance imaging (MRI) to quantify pathologic changes in the sub-calcaneal fat pads and to determine the association with plantar pressures measured in the heel region in diabetic patients with peripheral neuropathy.

METHODS

Fourteen diabetic patients with peripheral neuropathy (mean age 57.9 years (SD 6.9), body mass 81.7 kg (SD 11.4)) and five healthy age-matched control subjects (mean age 58.0 years (SD 1.7), body mass 73.4 kg (SD 6.1)) underwent MRI examination and plantar foot pressure measurement. Two-point Dixon chemical shift imaging was performed at 1.5-T using a Siemens Magnetom 63SP/4000 imager. Fat-only and water-only (fat-suppressed) images were created from which the fraction of fat signal in each pixel could be determined [4]. All images were high-resolution (512x512 pixels) T_1-weighted sagittal plane spin-echo images of the foot and were obtained non-weight bearing. One centrally located slice was selected for quantitative analysis. Using Scilimage a region of interest (ROI) was defined in the heel and the fat signal fraction in this ROI was calculated (Figure 1).

Figure 1: Water-only image in which ROI was defined between 1/12 and 3/12 of the foot length from the heel

Barefoot plantar pressures during gait were measured using an EMED pressure platform (Novel, Germany) while obtaining a second-step approach to the platform. Five repeated trials were collected from each subject. Peak pressures were calculated for the heel region. Mann-Whitney non-parametric tests were used to determine statistical significance between the groups ($P<0.05$).

RESULTS

The mean fat signal fraction was 0.72 (SD 0.03, range 0.70-0.76) for the healthy control subjects and 0.55 (SD 0.11, range 0.34-0.67)) for the diabetic patients; the mean difference was statistically significant ($P<0.005$). Peak pressure in the heel was 325 kPa (SD 53) and 391 kPa (SD 119) for the healthy controls and diabetic patients, respectively, which was not significantly different. Figure 2 shows examples of healthy and infiltrated sub-calcaneal fat-pad tissue. A significant inverse correlation of -0.59 was present between fat signal fraction and heel peak pressure ($P<0.01$).

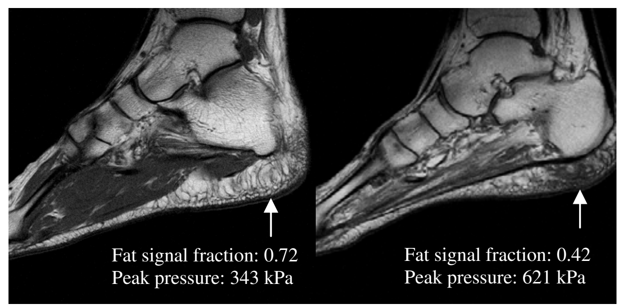

Figure 2: Healthy subject with normal sub-calcaneal fat pads (left) and diabetic patient showing fat-pad infiltration (right)

DISCUSSION

A substantial reduction in the ratio of fat to water signal in the sub-calcaneal fat pads was shown in a large percentage of neuropathic patients when compared with healthy control subjects. These results are consistent with data from Kao et al. [3] showing increased T_1-relaxation times in cadaver diabetic heel fat pads. Increased amounts of collagen as a result of non-enzymatic glycosylation or micro-hemorrhage caused by repetitive minor trauma may explain these pathologic changes [1,2,3]. The data suggests reduced functionality of the sub-calcaneal fat pad as shown by the significant association between reduced fat signal fraction and increased pressure levels in the heel. Whether fat-pad infiltration or elevated mechanical pressure is the primary event in this association requires further prospective analysis. The findings from this study contribute to our understanding of the relationship between structural and functional parameters in the diabetic foot. Although heel ulcers are not common in the diabetic foot, fat-pad infiltration may play a role in their pathogenesis.

REFERENCES

1. Delbridge L, et al. Br J Surg 72, 1-6, 1985
2. Brash PD, et al. Diabetic Med 13, 973-978, 1996
3. Kao, PF, et al. Magn Res Imag 17, 851-857, 1999
4. Maas M, et al. Radiology 210, 189-193, 1999

DYNAMIC STABILITY STRATEGY FOR ELITE JUDOISTS IN BALANCE CONTROL FOR ANTERIOR AND POSTERIOR PERTURBATIONS

Chih-Hang Lien[1] and Wen-Tzu Tang[1,2]
[1]Graduate Institute of Coaching Science, National College of Physical Education and Sports, Taiwan.
[2]Email: wttang@mail.ncpes.edu.tw

INTRODUCTION

Balance control abilities are essential for top athletes to reach optimal performance in competitions, especially for judoists [1]. Judo can be divided into attack and defence abilities, both of which influence winning. For response to attack, control of proper distance and force application to destabilize the rival through movement derives from control in balance. Stability of the centre of body weight must be maintained through intersegmental controlling. In order to avoid being attacked and falling, training for balance control of the body is important to the judo player[2]. Several studies have shown that judoists represent high balance performance, as measured from the through size of the COP area or scores on a balance system [2] with unstable platform perturbation. However, quantitative principles of balance strategy for judoists are still unknown, especially with waist perturbation similar to that in judo throwing. Therefore, this study investigated responses in terms of balance performance (using COP) and balance responses as measured using reaction forces to direction-dependent perturbation without anticipation. Postural control in two directions (forward, backward) for different skill levels of judoists was measured using force plates. These results may provide valuable information for selecting and training judoists scientifically.

METHODS

Experimental data were collected from fourteen elite-level judoists (Top twelve national level, Age: 21.2±1.9 years), fourteen subelite-level judoists (regional level from university teams, Age: 21.0±1. years), and fourteen non-judoist college students (Age: 21±2 years) performing perturbation balance control tests. All judoist subjects had a minimum number of five years of practice and no mechanical or functional instability from ligamentous, articular or muscle trauma or injury in the past three months. The perturbation test was performed by imposing a 10% body weight in 20 cm free-fall= without anticipation (Figure 1). An AMTI force plate (1000 Hz) was used to measure the reaction of participants with ground reaction force and COP trajectory. The balance response variables included maximum reaction force and balance performance variables including Maximum of Center of pressure (COP), total COP displacement, and averaged COP velocity. Three trials were collected for each test. Variables with length or weight units were normalized by height and weight of subjects, respectively. *T*-tests were performed between judoists and non-judoist groups.

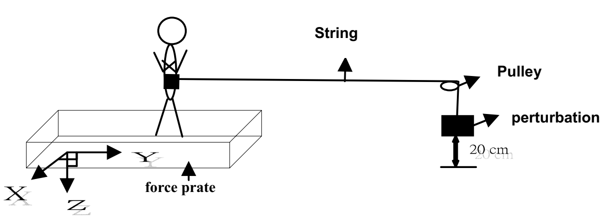

Figure1. Unanticipated direction-dependent perturbations

RESULTS AND DISCUSSION

In forward perturbation tests, both levels of judoists demonstrated significantly lower values than the non-judoist group for the COP averaged moving speed and total displacement (Table 1; p<.01). In addition, only the elite group showed significantly lower values for COP reaction force than the non-judoist group. Postural adaptations of judoist group are more efficient, especially for elite groups, than the control group. Judoists can change their intersegmentary coordination in order to accommodate specific unpredictable perturbation of tasks, as in the judo throwing attack (Seoinage-drop-knee). The main reason that judoists perform better in balance control is not due to leg muscle strength, which should yield greater reaction force, but because of balance control as demonstrated by lower reaction force with less COP displacement and lower COP moving speed.

Table 1 One-way ANOVA in National judoists (elite group), Regional judoists (subelite group) and Control group during unanticipated forward and backward perturbations

Forward	Group	m (SD)		One-way	ANOVA	
N=14	National Judoists (N)	Regional Judoists (R)	Controls (C)	Fishers N/R	PLSD R/C	N/C
Cop-X	0.07±0.07	0.09±0.06	0.56±1.68	NS	NS	NS
Cop-Y	0.08±0.02	0.1±0.03	0.61±1.73	NS	NS	NS
Fz	1.23±0.22	1.31±0.23	1.52±0.29	NS	NS	0.01
Avg velocity	66.5±22.4	77.6±11.8	99.9±22.5	NS	0.01	0.00
Length	261±88	305.5±46.6	415±73	NS	0.01	0.00
Backward						
Cop-X	0.17±0.03	0.15±0.01	0.15±0.01	NS	NS	0.02
Cop-Y	0.13±0.02	0.15±0.01	0.17±0.02	NS	NS	0.00
Fz	1.46±0.24	1.5±0.29	1.62±0.42	NS	NS	NS
Avg velocity	80±24.8	88.5±13.2	115±19.3	NS	0.00	0.00
Length	317±97	348±52	455±76	NS	0.00	0.00

In backward perturbation, both levels of judoists demonstrated significantly lower values than non-judoists for the COP-averaged moving speed and total displacement (p<.01). In addition, only the elite group showed significantly lower values for COP y direction displacement and greater values for COP x direction displacement (p<.01) than the control group. Elite judoists also tend to use more lateral movement skills to maintain balance and to control COP displacement. Postural adaptations of judo group are more efficient, especially for the elite group, relative control group.

CONCLUSIONS

In this study, elite and subelite judoists showed a postural adaptation strategy of significantly lower values for COP-averaged moving speed and total displacement, and also lower reaction force following unpredictable perturbation relative to the control group. Elite and subelite judoists did not differ significantly in these variables. Postural adaptations of judoists are more efficient, especially in the elite group. Kinetic parameters can be utilized to evaluate the efficient strategy in judo balance control for different attack directions.

REFERENCES

1. Perrin P, et. al *Gait and Posture* **15**,187-194,2002.
2. Perrot C, et. al. *Scandinavian J of Med & Sci in Sports*,**10**, 292-297,2000.

ELELECTROMYOGRAPHIC LINEAR ENVELOPE ANALYSIS OF GOLF SWING FOR TRUNK MOTION IN ASIAN PLAYERS: A CASE STUDY

Chia-Nen Chan[1] and Wen-Tzu Tang[2]
[11]Chang-Gang University, Taoyuan, Taiwan, and[2]National College of Physical Education and Sports, Taoyuan, Taiwan
email: wttang@mail.ncpes.edu.tw

INTRODUCTION

Despite the significant prevalence of back pain among golfers at all levels of ability, the current literature does not fully address specific mechanisms responsible for this injury. The approach of studying trunk motion includes motion analysis and EMG measurements. Some studies show differences in trunk motion with kinematic variables for two groups with non-back pain and back pain, respectively [1]. Most EMG studies have measured EMG amplitude in each phase to understand general on/off activation of trunk muscles in different phases. However, little work evaluates back muscle activation patterns with the EMG envelope, which provides information on the the timing and duration of the burst, and also detail smuscle activation characteristics integrated with kinematics variables. Moreover, most studies have recruited western players as participants who usually have higher anthropometric scores. Recently, Asian professional golf players have successful performances in American and Europe, albeit with lower anthropometric scores. . Investigation of trunk muscle activation pattern in an elite Asian player without pain history may provide useful information to explore the optimal swing for back loading. Therefore, this study identifies reproducible patterns of trunk muscle activity through use of the EMG envelope integrated the kinematic variables. We analyze the swing of a golfer who won a Gold Medal in 2002 Busan Asian Games. The participant had a low anthropometric anthropometry score relative to western players.

METHODS

One male Gold Medal winner in 2002 Busan Asian game aged 25 yearswith height 160 cm and weight 65 kg, with 15 years of training, participated in this study. The subject is a typical right-handed player. Surface EMG data at sampling rate of 1200 Hz were collected by Biovision EMG System (Wehrheim, Germany). The muscles of abdominal oblique, erectus spinae, latissimus dorsi, and upper rectus abdominis in both right and left sides were studied. The distance of the interelectrode was 20 mm, and the placement of electrode was as described by Zipp (1982). A JVC 9800 digital camera at a sampling rate of 120 Hz captured the subject's swing with a #7 iron via markers on club, shoulder, elbow, wrist, ilium, and knee. EMG and video data were synchronized with a simple circuit that simultaneously lit an LED and sent a voltage signal to the Biovision input box. Kinematic data were analyzed by the Kwon3D Software. The swing was divided into five phases: Phase I, upswing; Phase II, forward swing; Phase III, acceleration; Phase IV, early follow through; Phase V, late follow through [2]. The subject was asked to perform 10 swings after a proper warm-up. The four best and most consistent strokes were chosen by the subject for later data analysis. The EMG signal was band-pass filtered at 4 to 500 Hz (Butterworth digital fliter), full-wave rectified, and low-

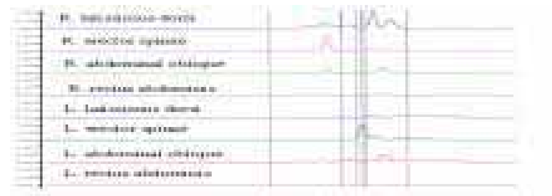

Figure 1: EMG activity patterns of shoulder and trunk muscles on left and right sides during five swing phases

pass filtered at 8 Hz by DasyLab 6.0 System to derive the EMG linear envelope.

RESULTS AND DISCUSSION

To analyze the timing and duration of the firing pattern of back and shoulder muscles of the participant, the EMG linear envelope as shown in Figure 1 was studied for each muscle. In the early phase of the takeaway, all muscles presented extremely low activation. However, the latissimus dorsi on both sides started to activate during the tak-away. In particular, the latissimus dorsi on the right side continued activation until the top point of the takeaway phase. This muscle presented a similar pattern in the forward swing phase. Comparing the two sides, the left latissimus dorsi presented less activation, and the latissimus of both sides were silent until the end portion of the late follow through. The left and right erect spinae and right obdominal oblique presented significant activation until the top point of the take away, then decline. Overall, the forward and acceleration phases muscles on the upper torso did not showed burst activbity except for the left erect spinae in acceleration phases. Other studies have demonstrated greater activation levels on the forward swing and acceleration relative to the upswing and follow through, as characterized by MVC percentage. The burst peak may be reduced in MVC percentage because of the long duration of the upswing and follow through phase. Furthermore, not many trunk muscle groups in our study exhibited a burst in the forward and acceleration phases, and it is possible that other deep trunk muscles not involved in this study may play an important role for these two phases, which should be further investigated for back pain research.

CONCLUSIONS

From previous studies using EMG amplitude analysis for different swing phases, information is available on the general roles of each muscle in different phases. However, this work demonstrates dilution of the burst which may associate with back pain because of repetitive and cumulative acute motion. Also, reduced burst activation in the forward swing and acceleration which may imply the relevance of exploring deep muscles during the forward swing and acceleration.

REFERENCES

1. Lindsay D et. al., *J Sports Sci*, **20**, 599-605,2002.
2. Pink M et. al., *Am J Sports Med*, **18**, 137-140,1990.

THE COMPARSION OF EFFECTIVENESS BETWEEN GRAB START AND TRACK START IN COMPETITIVE SWIMMING

Shu-ting Chen, Weng-tzu Tang
Institute of Coaching Science in National College of Physical Education and Sports, Taipei, Taiwan
Email:wttang@ncpes.edu.tw

INTRODUCTION

Performance in competitive swimming is influenced by swimmer's physique, strength and endurance of muscle factors, etc., but the most important and key factors are swimming techniques, including stroke, kick, turn, touch wall and start. The time a swimmer spends in the start ranges from 0.8% to 26.1% of the overall race time, depending on the event [1]. So the shorter the race distance, the more important the effect of the start. Many starting techniques are used in competitive swimming, such as the grab start, track start and swing start. The grab start and track start are the most popular techniques presently employed for individual events. Studies regarding the comparison of both starts have been investigated through kinematic and kinetics variables [1,2]. Kinematics variables are the outcome of kinetics variables, which provide information for coaches. However, the efficiency of integrated variables with kinematic and kinetics parameters, can provide further information for technique, but has not been studied. Therefore, the purpose of this study was to compare the grab start with the track start in kinematics (horizontal distance of entry) and kinetics variables (peak ground reaction force, peak vertical and horizontal force, speed strength index, i.e., SSI, impulse), and to integrate variables to estimate the starting efficiency (SSI-efficiency index, impulse-efficiency index) for both starts. The results of this study can provide coach and swimmer with different perspectives on comparative advantages of start techniques.

METHODS

Eight competitive swimmers were used in this study: four males (19.75±0.96 years of age, 170.25±5.80 cm in height, 66.35±5.32kg in body mass) and four females (20.75±2.36 years, 161.75±5.87 cm, 56.83±7.98 kg).Participants had trained at least six years with no injury. Four participants had a grab start preference, and four participants used track starts; both groups had practiced both starts for at least three months after recruitment. All subjects were required to perform two start tests in random order (three trials by each subject for each of the grab start and and the track start).

A digital video camera (JVC/9800, 60 Hz)and a Kistler force plate (1000 Hz) were used to collect motion data and kinetic variables (peak resultant ground reaction force, vertical and horizontal force, SSI, and impulse). The SSI efficiency is derived as the horizontal distance of entry divided by SSI. Impulse efficiency is derived as the horizontal distance of entry divided by the impulse. All kinetics variables were normalized by body weight, and kinematics variables were normalized by body height. The force plate was fixed above the starting platform, and the camera was setting in the sagittal plane (Figure 1). An electronic trigger with light bulb synchronized the force plate to the video camera.

Data were analyzed by t-tests with repeated measures. Measured kinetic parameters included peak ground reaction force (Fx,y), vertical and horizontal force (Fx,Fy), speed strength index (SSI), impulse, horizontal distance of entry, the SSI-effectiveness index, and the impulse-effectiveness index.

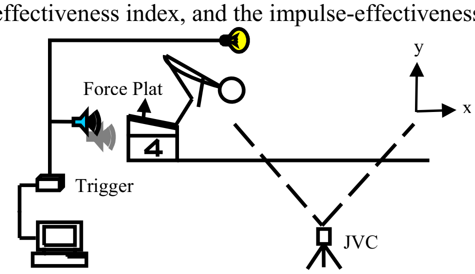

Figure 1: The diagram to show testing location.

RESULTS AND DISCUSSION

Significant differences were found between the two start types in peak ground reaction force, SSI, impulse, horizontal distance of entry and impulse- efficiency index. However, there were no significant differences between the two starts either in peak vertical and horizontal force or SSI-efficiency index (Table 1). This may derive from difference in lower limb joint flexion and in the absence of coincidence of peak force (Fx,y_{max}) of both limbs.

The impulse was a significant factor influencing flight velocity after takeoff. Impulse and horizontal distance of entry for the grab start were greater than for the track start in this study. However, the effectiveness of the track start was higher than that of the grab start (as measured by the impulse-efficiency index). The reason may due to the increased takeoff angle of track start, and then a higher flight trajectory. Such integration of kinetic and kinematics data together with derived efficiencies can provide coaches and competitive swimmers with specific technique information for swim starts.

CONCLUSIONS

The general principles of a good start are high velocity, longer horizontal distance of entry, optimal entry angle, and similar parameters. However, quantitative assessment of starts may indicate not just one aspect of greater distance performance (e.g., grab start) or of reaction force, but also a greater efficiency (as in the track start) that will provide more insight into better starting skills.

REFERENCES

1. Cosser & Mason, *Proceedings of XIX Symposium on Biomechanics in Sports,*2001.
2. Breed RVP, Mcelroy GK, *Journal of Human Movement Studies*, **39**,277-293,2000.

Table 1: Comparison of grab start and track start in kinematic and kinetic variables. (BW:body weight, BH:body height,* : p<.05)

	SSI (s^{-1}•B.W.)	Impulse (s•B.W.)	Entry Distance (B.H.)	SSI-Effectiveness Index (kg^{-1}•s2)	Impulse-Effectiveness Index (kg^{-1})
Grab start	2.16 ± 0.366	0.50 ± 0.045	1.77 ± 0.096	0.84 ± 0.121	3.57 ± 0.262
Track start	1.55 ± 0.372	0.38 ± 0.074	1.66 ± 0.115	1.24 ± 0.537	4.59 ± 0.808
P	0.002*	0.003*	0.006*	0.053	0.010*

ROTATION CHARACTERISTICS OF THE SHOULDER, TORSO, AND PELVIS DURING PITCHING FOR TAIWAN ELITE AND SUBELITE COLLEGIATE BASEBALL PITCHERS

Yi-Ling Chiang[1] and Wen-Tzu Tang[1,2]
[1]Graduate Institute of Coaching Science, National College of Physical Education and Sports, Taiwan
[2]email: wttang@mail.ncpes.edu.tw

INTRODUCTION

Many kinematic variables from each phase of the baseball throw have been identified as being important to maximal throwing velocity[1] as well as to the potential for injury, especially in the elbow, shoulder, and hip joints. Although torso motion can produce high force relative to distal extremeties, very few of the trunk kinematic variables were described, only trunk tilt and later trunk tilt angle, trunk flexion [2,3].

However, trunk rotation and twist rotation in terms of the stretch X-factor, which in golf is the difference between shoulder and pelvis rotation during the swing, have not been studied for the baseball throw. It is believed that extra stretch during the early down swing allows the upper-body muscles to contract more forcefully and hence to provide more power**.** Therefore, this study investigates kinematics of the upper torso and pelvis, including the horizontal rotation of upper torso and pelvis, twist of the trunk (i.e., the X-factor, the difference of the included angle between shoulder and pelvis), and flexion of the trunk during windup, stride, arm cocking, arm acceleration, arm deceleration and follow-through [4]. Integrated study of the torso, shoulder, and pelvis motions may not only contribute to pitching strategy, but also could be helpful to reduce the harm to the shoulder. Through studying Taiwan Elite pitchers and subelite pitchers who usually has less muscle mass and weight, and different pitching pattern compared to west pitchers.

METHODS

3D motion data of the entire body during fastballs thrown by ten collegiate pitchers were collected at 250 Hz by seven high speed cameras attached to a VICON 3D motion analysis system (Oxford Metrics, UK) . Pitchers were chosen from the top four collegiate teams in Taiwan, and represented both elite and sub-elite groups.. Reflective markers were attached at multiple points on the entire body of subjects.. Using calculated 3D positional data of the entire body, kinematic characteristics of the pitch, including horizontal rotation of upper torso and pelvis, twist of trunk (X-factor), and trunk flexion of trunk were obtained. X-factor, the difference of the included angle between shoulder and pelvis from maximum backward twist to ball release, was illustrated in Figure 1.

(a) at max. backward twist (b) at release

Figure 1: Definition of X-factor: (a) and (b) are top-view of the subject, X-factor is equal to $\theta_r - \theta_b$, where θ_r is negative.

RESULTS AND DISCUSSION

Representative data from the two groups are presented in Table 1. Elite pitchers exhibited proper sequential movement of the entire body, with a greater angular velocity of twist and flexion motions, and larger X-factors. They also pitched faster, and the net torques at the shoulder before ball release, as calculated by inverse dynamics, were higher.

Such proper mechanics also delay the onset of fatigue, leading to more consistent performance [5]. In the long term, overuse injuries, which may result from cumulative microtrauma, may be reduced through utilizing aforementioned techniques.

CONCLUSIONS

The experimental data may give more detail look to the integrated shoulder, torso, and pelvis motion. Greater range and speed of trunk flexion and twist rotation demonstrate better ball speed performance. The results confirmed the point of view that the motion of trunk, in proper order, is also an important factor to the speed of pitched ball [6] and help to achieve the optimal pitching and contribute to injury prevention of shoulder in baseball players.

REFERENCES

1. Matsuo T, et.al., *J of App Biomech*, **17**, 1-13,2001.
2. Escamilla E, et. al.,*Sports Biomech*, **1**, 213-228,2002.
3. Escamilla, et. al, *J Sports Sci*, **19**, 665-676,2001.
4. Dillman CJ,et. al., *J Orthop Sports Phys Ther*, **18**, 402-408,1993.
5. DeVon HA, et. al.*West J Nurs Res*, **26**, 547-560,2004.
6. Fleisig, et. al., *23rd annual meeting of ASB*, 21-23, 1999.

Table 1 The rotation variables of shoulder, torso, and pelvis in pitching motion from elite and subelite picthcers

	Speed of ball	Trunk flexion angle	Max. flexion angular speed	X-factor stretch (twist angle)	Max. twist angular speed	Max. net torque at shoulder
Sub-elite	35.25 m/s	32.73 °	309.63 °/s	66.12 °	733.14 °/s	52.6 N-m
Elite	36.93 m/s	42.89 °	454.03 °/s	88.31 °	943.70 °/s	57.6 N-m

NOVEL *IN SILICO* VIRTUAL & SCALED UP PHYSICAL MODEL PLATFORM TO BRIDGE GAPS IN UNDERSTANDING *IN SITU* FLOW REGIMES AT MULTIPLE LENGTH SCALES IN BONE

[1]Eric J. Anderson, [1]Steven Kreuzer, [1,2]Melissa L. Knothe Tate
[1]Dept. of Mechanical & Aerospace and Biomedical Engineering, Case Western Reserve University, Cleveland, OH
[2]Orthopaedic Research Center, Cleveland Clinic Foundation, Cleveland, OH
knothetate@case.edu

INTRODUCTION

Fluid flow through the pericellular network plays a key role in molecular transport through the dense tissue of bone. Fluid flow also serves as the dominant mechanism by which exogeneous mechanical stimuli are translated to cells and trigger cellular remodeling activity as well as tissue level adaptation. Osteocytes, the putative mechanosensors in bone, are organized in a functional syncytium that provides a biological network for transport and communication within and across bone tissue. Although osteocyte mechanobiology has thrived as a research arena in recent years, we still do not understand the prevailing mechanobiological environment of osteocytes *in situ* or how extrinsic stimuli are transduced at a cellular level. Here we implement a novel approach to bridge gaps in understanding between cell and tissue mechanobiology in bone using *in silico* virtual as well as scaled up physical models; these experimentally validated models give us a novel platform to extrapolate prevailing *in situ* flow regimes around single cells and networks of cells (which, together with their extracellular matrix comprise bone tissue) that are currently impossible to measure or observe directly.

METHODS

In Silico Models:

To explore fluid flow at the level of the cell and within the pericellular space of the lacunocanalicular network, an idealized osteocyte was modeled with multiple connecting canaliculi using a computational fluid dynamics package (CFD-ACE). Fluid flow was induced by a pressure gradient of 300 Pa over the length of the osteocyte with a perfusate medium similar to water (ρ=997 kg/m^3, μ=0.000855 kg/ms). Simulations of steady flow (governed by Navier-Stokes equations) provided velocity and pressure profiles within the fluid space, where shear stress at the surface of the cell and processes was calculated from wall strain rate and laminar viscosity [*after* 1]. In order to address lower length scales, we studied parametrically the effect of subcellular structures on prevailing flow regimes and network permeability. This was accomplished by calculating velocity and pressure profiles as a function of i) the presence and state of the macromolecular network in the pericellular space as well as ii) differences in relative gap size for flow between the osteocyte body–lacuna and the osteocyte process–canaliculus.

Scaled-Up Physical Models:

To study fluid flow at the tissue level (flow around networks of cells), experimental tissue permeability measurements were carried out on scaled-up (1000x), anatomically accurate (hollow) physical models of the lacunocanalicular network. Specimens were obtained from the cortical sheath of the femoral neck from human patients undergoing orthopaedic surgery (IRB approved). Hard-tissue histological sectioning and the creation of a three-dimensional image stack using confocal microscopy (SP2 AOBS, Leica) was used as the template for the rapid prototyping of a physical scaled-up (1000x) model. Permeability was tested in the transverse plane of the specimen for both water and viscous silicone oil (1000x viscosity of water, to counter effect of scaling) as the perfusate medium. By incorporating this scaling coefficient, appropriate permeability estimates can be made of the osteocyte syncytium by scaling back down to cellular length scales. Darcy’s Law was used to calculate permeability for a specific mass flow rate and pressure gradient [*after* 2].

RESULTS AND DISCUSSION

Cell level *in silico* models show that fluid flow resulting from mechanical loads subjects the virtual osteocyte surface to hydrodynamic pressure of nearly constant magnitude within the lacuna, and high gradients of shear stress along the processes within the canaliculi. Incorporation of subcellular structures into this virtual model reveals a dominant effect of gap size ratio (between fluid gap size within the lacuna and within canaliculi) as compared to the presence of a fluid saturated macromolecular mesh within the pericellular space. Tissue level physical models allow for actual measurements of permeability based on scaled-up, anatomic cell network dimensions. In the scaled-up physical model, permeability is calculated to be 2.78x10^{-10} m^2 with 1.8% uncertainty in the transverse direction using silicone oil. Using the scale-factor relationship, specimen permeability at the cellular length scale is 2.78x10^{-16} m^2 for hollow geometry. Hence, actual permeability can be calculated from model-based experimentally determined permeability using,

$$k_{1x} = \frac{k_{1000x}}{scalefacto\ r^2}$$

The differently scaled models are then bridged by applying the relationship acquired in the sub-/cellular *in silico* models to the experimentally measured data of the hollow physical network model to calculate permeability for a partially (cell and process) filled virtual network model (Figure).

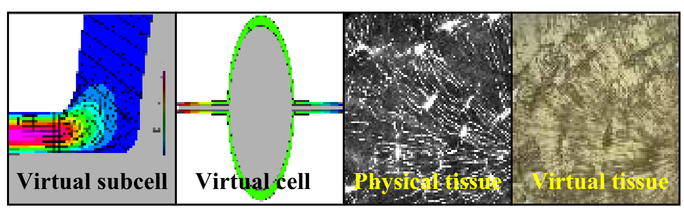

CONCLUSIONS

These studies provide, for first time to our knowledge, a novel platform to elucidate fluid flow within the lacunocanalicular network of bone across length scales, from the subcellular to the tissue level. An accurate description of flow across length scales paves the way for understanding the prevailing mechanical environment of bone cells, which will yield unique insight regarding translation of extrinsic signals to the cellular, tissue and organ level and its role in bone (patho)physiology.

REFERENCES [1] Anderson EJ, *et al*. *Ann Biomed Eng* 33, 52-62, 2005. [2] Anderson EJ, *et al*. Trans *BMES* 2004, 1215.

INTERMUSCULAR COORDINATION ANALYSIS OF SKILLED DOUBLE-HANDED BACKHAND AND SINGLE-FOREHAND PLAYERS

Yi-Ming Huang[1], Wen-Tzu Tang[1,2], and Shi-Ting Wang[1]
[1]*Graduate Institute of Coaching Science, National College of Physical Education and Sports, Taiwan*
email: wttang@mail.ncpes.edu.tw

INTRODUCTION

Experienced coaches and players may easily identify performance by visual observation, whereas testing tools have been used to evaluate players' motor performance to understand coordination mechanisms [1]. Electromyography (EMG) has been widely applied in studies of intermuscular coordination, and is helpful to categorize and understand the agonist and antagonist muscular activity at different skill levels in many sports, including tennis. In tennis, each player usually has a better skill level for one single stroke (e.g., forehand or backhand), and also has his or her own advantage in side movements. Although this phenomenon can be easily judged by professional coaches, the underlying EMG patterns are unknown. Agonist-antagonist co-contraction patterns for stability and the strong agonist pattern for acceleration has been studied in simple fast goal-directed movement [2,3], but not for tennis. Therefore, agonist-antagonist pattern in terms of onset-offset and normalized amplitude with MVC (Maximum Voluntary Contraction), and their ratio were analyzed to understand EMG patterns and to examine whether the agonist-antagonist ratio can be an effective parameter to assess intermuscular coordination in single- forehand and double-handed backhand strokes.

METHODS

Female tennis players participating in this study were characterized into two groups: skilled single-forehand and double-backhand. Subjects were typically right-handed players. A reliability assessment for identifying skilled single-forehand or double-backhand abilities was obtained from three expert tennis coaches prior to the study, and was highly consistent. Surface EMG data at a sampling rate of 1200 Hz, were collected with a Biovision EMG System synchronized with a JVC digital camera at sampling rate 120 Hz by a simple circuit with LED. Muscles measured were the biceps brachii, triceps brachii, flexor carpi and extensor carpi muscles on both right and left arms. The backhand and forehand stroke was divided into three phases: Phase I, the preparation, began with the backswing and ended with the first forward motion of the racket; Phase II, acceleration, ended at impact; Phase III, the follow-through, ended with completion of the swing (Figure 1).

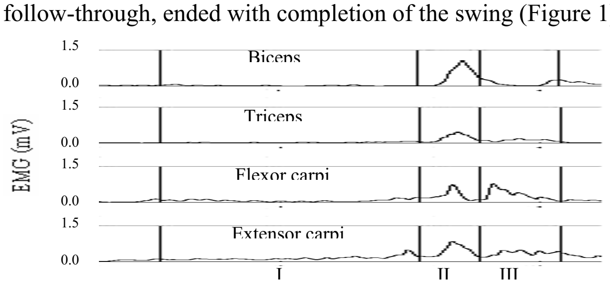

Figure 1 The EMG patterns of dominant (right) arm during double-handed backhand.

We analyzed individually the four best strokes (as evaluated by both subject and experts' observation) from a total of 15 backhand and 15 forehand strokes after a proper warm-up. Maximum voluntary isometric contraction (MVC) for each muscle was used to normalize values. The EMG signal was band-pass filtered at 10 to 500 Hz, full-wave rectified, and the integrated.

RESULTS AND DISCUSSION

Elbow flexor/extensor EMG ratio in the acceleration phase differed significantly between the two groups, as demonstrated for both forehand and backhand strokes with the example data (Table 1). A higher elbow flexor/extensor EMG ratio characterized the left arm of skilled double-handed backhand players and the right arm of skilled single-handed forehand players, although both groups are right-arm dominant. For skilled left double-handed backhand players, a stronger agonist activation pattern was evident in double-handed movements but also demonstrated was stronger co-contraction pattern for forehand movements. However, the opposite trend was seen for skilled right forehand players, who demonstrated stronger agonist activation in forehand movements, but also stronger co-contraction patterns for double backhand movements. The characteristics of elbow acceleration were clear in terms of a stronger agonist in the preferred skilled movement (either double back hand or forehand), and showed a stabilization function in terms of higher co-contraction for the less skilled movement. The elbow uncocking movement skill was different from the traditional method in that only shoulder joint was unlocked. However, the wrist flexor/extensor normalized EMG ratio demonstrated a stabilization function even for the skill movement, which differed from what was seen in the elbow. This may derive from the necessity of stabilization in the distal segment for withstanding impact.

Table 1: Ratio of elbow flexor/extensor normalized EMG for skilled double- backhand and single- forehand players

Elbow(n=4)	**Group I** Skilled double-backhand		**Group II** Skilled single-forehand	
Movement Arm	forehand right hand	backhand lefthand	Forehand right hand	Backhand left hand
Phase I	1.55±0.30	3.26±0.81	3.76±0.59	0.78±0.17
Phase II	1.84±0.28	8.71±1.61	6.87±0.49	1.38±0.22
Phase III	0.99±0.17	1.60±0.30	1.80±0.60	0.69±0.10

CONCLUSIONS

Tennis players showed a higher elbow flexor/extensor ratio for their preference arm during the acceleration phase of their stroke when performing their skilled movement. This may increase the elbow joint acceleration more efficiently. In addition, the parameter of the ratio of agonist to antagonist EMG can usefully assess coordination performance in skilled tennis strokes.

REFERENCES

1. Wang ST et al, *Physical Edu J*, **36**, 85-94,2004
2. Milner TE, , *Exp Brain Res*,**143**, 406-416,2002
3. Jaric S et al., *Eur J Appl Physiol Occup Physiol*, **71**, 464-468,1995.

MUSCLE ACTIVATION BY OLYMPIC FEMALE ARCHERS AT DIFFERENT RELEASING RHYTHMS

[1]Cheng-Ming Hu and [2]Wen-Tzu Tang
[1,2]National College of Physical Education and Sports, Graduate Institute of Coaching Science,
[2]email: wttang@mail.ncpes.edu.tw

INTRODUCTION

Archery is a comparatively static sport requiring strength and endurance of the upper body, in particular of the forearm and shoulder girdle [1]. Through analysis of muscle activation of the shoulder girdle and forearm, stability and accuracy for archers can be evaluated [2,3]. However, archery conducted outside with disturbance from the environment disturb archers during the process of arrow release, and archers must utilize different releasing rhythms within a time limitation. Little is known about optimal release rhythms and variation in muscle activation with faster rhythms. Thus, the purpose of this study was to analyze muscle activation patterns of archers' forearm and shoulder for both normal and fast releasing rhythms and to find an effective index to assess release performance.

METHODS

Two female archers from the 2004 Olympic Chinese archery team were involved in this study. They were characterized as elite (awarded Fourth in Olympic Games 2004) and subelite archers (Fifty-fifth in Olympic Game 2004). Measurements were made under simulated Olympics game conditions on outdoor courts. Each participant completed two trials of 24 successful shots to get acquainted with measurement conditions. Timing of the anchor and release moments were determined with an electronic trigger controlled by the coach. Surface electrodes were placed on the central portion of principal muscles with Biovision EMG System (Wehrheim, Germany). Electromyographic activity of the shoulder and trunk muscles (i.e., M. extensor digitorum, trapezius muscle, and deltoid muscles) were recorded at a sampling frequency of 1000 Hz using synchronized electronic signals for a total of 24 shots by each participant. EMG activity amplitudes were determined during the anchoring phase to the time of release, and the reduction in level of muscle activity at release, were derived to evaluate release skill from the 0.1 s duration prior to (X) and after release (Y) from the following equation:

$$\text{Reduction in muscle activity} = 1-Y/X \qquad (1)$$

Mean scores and SD's (standard deviation) in amplitude and reduction level for back and shoulder muscles were calculated for each subject's shots under both fast and normal releasing rhythms. T-*tests* assuming independent samples were used for each participant to assess differences between the two release rhythms. A probability of α=0.05 was selected to indicate statistical significance.

RESULTS AND DISCUSSION

For the elite archer, the electromyographic amplitude of right upper trapezius and left deltoid activity from anchoring to release was significantly different between fast and normal releasing rhythms (Table 1). The elite archer used more of the right upper trapezius in drawing the bow, and less of the left deltoid controlling the bow in fast releasing. For the subelite archer, the left lower trapezius, left deltoid, and right upper trapezius were significantly between the two releasing rhythms. The subelite archer used more muscle activity from the holding hand to supply sufficient power for fast release. Only the right deltoid of the elite archer was significantly between the two releasing rhythms. Overall, there was no strong difference in the reduction level of muscle activity between the two releasing rhythms (Table 2).

Table 1 The amplitude of muscle activity during anchoring for archers using two different releasing rhythms.

Fast VS Normal	Left lower Trapezius	Right Lower Trapezius	Left Deltoid	Right Deltoid	Right Upper Trapezius	Right Wrist Extensor
Elite Archer	none	none	*(N>F)	none	*(F>N)	none
Sub Elite Archer	*(F>N)	none	*(F>N)	none	*(F>N)	none

α<.05 (F=Fast; N=normal)

Table 2 Reduction level of muscle activation at release for archers using two different releasing rhythms

Reduction level (F Vs N)	Left lower Trapezius	Right Lower Trapezius	Left Deltoid	Right Deltoid	Right Upper Trapezius	Right Wrist Extensor
Elite Archer	none	none	none	*(F>Nl)	none	none
Sub Elite Archer	none	none	none	none	none	none

α<.05 (F=Fast; N=Normal)

CONCLUSIONS

Compared to the subelite archer, the elite archer presented a greater reduction in muscle activation at release and a more consistent pattern adaptation when using the fast releasing rhythm. The amplitude and reduction level can be useful indices to quantify release skill. These experiments have monitored differences of muscle activation for elite female archers for different releasing rhythm, and also supplied a guide for fast releasing training.

REFERENCES

1. Mann, D. L., & Littke, N. *Shoulder injuries in archery.* Canadian Journal of Sport, **14(2)**, 85-92, 1989.
2. Tsung-Yi Wu. *EMG and Stability Analyses at Pre and Post Releasing Moment For Archers*. Chinese Culture University, Taipei. 1998
3. Martin, P. E., Siler, W. L., & Hoffman, D. *Electromyographic analysis of bowstring release in highly skilled archers*. Journal of Sports Science, **8**, 215-221, 1990

ACKNOWLEDGEMENT

Thanks for the grant of National Council on Physical Fitness and Sports and Chinese Taipei Amateur Archery Association for cooperation.

LOWER LIMB KINEMATICS THROUGH MODEL-FREE MARKERLESS MOTION CAPTURE

[1]Stefano Corazza, [1]Lars Mündermann and [1,2,3] Thomas P. Andriacchi
[1]Department of Mechanical Engineering Stanford University Stanford, CA
[2]Bone and Joint Center, Palo Alto VA, Palo Alto CA
[3] Department of Orthopedic Surgery, Stanford University Medical Center, Stanford, CA
email: stefano.corazza@stanford.edu, web: biomotion.stanford.edu

INTRODUCTION

In recent years, the development of new techniques for motion capture not involving the use of skin markers is receiving great interest. This is mainly due to several potential advantages that a non-invasive (markerless) technique has over stereophotogrammetry. These are mainly: i) no subject preparation, ii) intrinsically more robust with respect to soft tissue artifacts, and iii) potentially applicable in outdoor environments. A common way of capturing human motion is the construction of visual hulls. Human body segments are typically extracted by employing an articulated model. In this study a model-free approach for extracting human body kinematics from visual hull sequences through Laplacian Eigenmaps is presented.

METHODS

A virtual gait sequence of 120 frames of a human form was created using Poser (Curious Labs, CA). Visual hulls of different quality using 8, 16 and 64 cameras were created using most favorable camera configurations [1]. Each visual hull was constructed as volume data set with a resolution of 2 cm. Human body segments were identified by mapping visual hulls to a multi-dimensional space through Laplacian Eigenmaps [2,3] (implementation code by Belkin, Surendran, and Bundschoten, University of Chicago). The resulting mapping (location) in the multi-dimensional space was invariant with respect to pose and position in the original Euclidean space, that is the same body segment mapped to the same location. Locations for the head, neck, torso, arms, forearms, hands, thighs, shanks and feet were determined allowing the identification of these segments in all frames in the Euclidean space (Figure 1a). The main geometric axes were calculated, approximating a segment's anatomical axes. Joint angles for the sagittal and frontal plane were calculated as angles between corresponding axes of neighboring segments. Accuracy of human body kinematics was calculated as the average deviation of joints angles derived from visual hulls compared to joints angles derived from the Poser sequence over the gait cycle.

RESULTS

The accuracy of visual hulls is greatly affected by the number of cameras used [1], which potentially affects body segment identification. Body segments were identified accurately for visual hull sequences constructed using 16 or more cameras. The patterns of sagittal and frontal plane kinematics derived from all visual hulls were very similar to those derived from Poser (Figure 1). The accuracy of hip, knee and ankle flexion-extension and ab-adduction angles for visual hulls constructed using 16 cameras was 1°, 3° and 8°, and 3°, 3° and 5°, respectively.

DISCUSSION

This study demonstrates the feasibility of accurately measuring 3D human body kinematics using a model-free markerless motion capture system on the basis of visual hulls and Laplacian Eigenmaps. The ankle joint angles are the most critical to measure due to the small size of the foot. The approach can be easily extended to upper limb measurements.
The model free approach described here represents an important step towards making markerless motion capture practical, since the total time and manual intervention for a complete analysis are substantially reduced. The presented gait cycle of 120 frames takes approximately 3 hours to be processed in the Matlab code on a 3GHz pc.
Limitations of this study are the use of a rigid human form for constructing visual hulls. However, inaccuracies in visual hull construction, might outweigh segment deformations in the living human. Thus, it is expected that similar results will be obtained in experimental set-ups with limitations due to camera calibration and fore-background separation.

REFERENCES

1. Mündermann L, et al., *IS&T/SPIE* **5665**, 268-287, 2005.
2. Belkin M., Niyogi P., *Neural Comp.* 15 **6**, 1373-1396, 2003.
3. Von Luxburg U., Bousquet O., Belkin M., *NIPS*, 2004.

ACKNOWLEDGEMENTS

Thanks to Dinoj Surendran, University of Chicago for providing the help on Laplacian Eigenmaps code. Funding provided by NSF#03225715 and VA#ADR0001129.

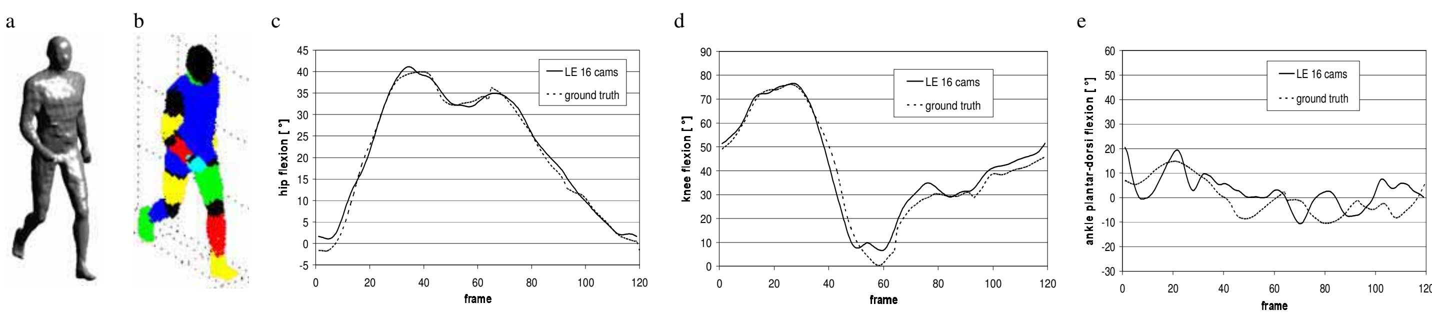

Figure 1: a) Visual hull and b) identified body segments. c) Hip, d) knee flexion, and e) ankle plantar-dorsiflexion.

PROXIMO-DISTAL DISTRIBUTION OF MECHANICAL WORK AND CAPACITY FOR ELASTIC ENERGY STORAGE IN THE LIMB JOINTS OF RUNNING GOATS

David V. Lee, M. Polly McGuigan, and Andrew A. Biewener
Concord Field Station, Harvard University
email: dvlee@fas.harvard.edu, web: http://www.oeb.harvard.edu/cfs/

INTRODUCTION

The legs of running animals generally shorten during the first half of stance and lengthen during the second half. In a multi-segment limb, this basic pattern requires flexion (or closing) followed by extension (or opening) of at least some the joints, thus presenting opportunities for storage and return of elastic strain energy via springs.[1] The Equine metacarpo-phalangeal (MCP) joint provides an elegant example of such a springy joint, the flexion of which is linearly related to the ground reaction force at the foot.[2] In fact, the long digital flexor tendons acting about this joint have almost no capacity to actuate the joint, due their extremely short muscle fibers. Nevertheless, joints proximal to the MCP (or MTP in the hindlimb) lack these anatomical constraints and are often actuated by muscles with longer fibers and shorter tendons. Here we investigate the joint mechanical work that is done by actuators and that which may stored and returned. Forelimb (elbow, wrist, and MCP) and hindlimb (knee, ankle, and MTP) joints were measured in running goats and a simple model was used to identify spring and actuator components of joint work. Distal joints were predicted to have greater capacities for elastic energy storage and return than more proximal joints.

METHODS

Three goats were run at various speeds across a pair of force platforms in series and ground reaction forces were recorded at 2,400 Hz. Concomitantly, an infrared motion capture system tracked joint and trunk positions at 240 Hz. Joint angles were determined from motion capture data and joint moments were given by the cross product of joint position and ground reaction force vectors. Joint work was determined by integrating the product of joint angular velocity and moment over the stance time of a given footfall. Using measured joint angles and moments, a simple model comprising an in-series rotational actuator and rotational spring was implemented to examine the potential for elastic energy storage and return. This was done by manipulating the spring constant and constraining the actuator to match the experimental joint angles while the experimental joint moments were applied. Searching the parameter space produced a spring constant that minimized positive + negative actuator work. Expressing this rectified actuator work as a fraction of rectified joint work provides a useful index of the actuator work contribution.

RESULTS AND DISCUSSION

As expected, the proximal most joints investigated (i.e., the elbow and knee) showed the greatest actuator contributions (values > 0.80) (Figure 1). The MCP and ankle showed the smallest actuator contributions (approximately 0.40), indicating substantial elastic energy storage and return (Figure 1). Surprisingly, similarly low values were not observed in

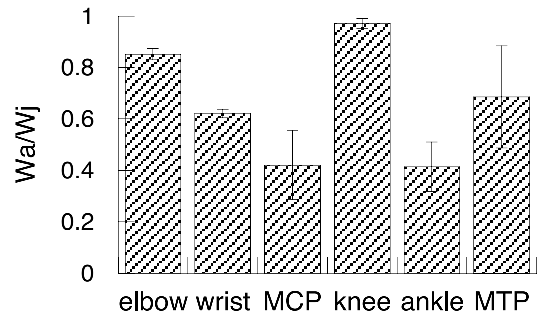

Figure 1: Ratio of rectified actuator work to rectified joint work in three forelimb and three hindlimb joints. Smaller values indicate greater spring contributions. Error bars show 95% confidence intervals.

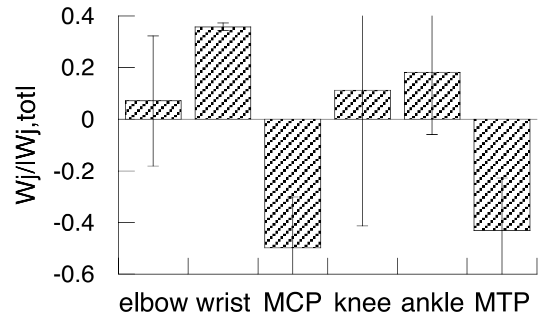

Figure 2: Ratio of joint work to the sum of joint work magnitudes across the three joints of the forelimb or hindlimb. Error bars show 95% confidence intervals.

the MTP, the distal most hindlimb joint. The wrist and MTP showed intermediate actuator contributions between 0.60 and 0.70 (Figure 1). This may be due in part to the function of the MTP as a damper, although the MCP also shows substantial negative net work (Figure 2). In contrast, the wrist shows substantial positive net work, while the elbow, knee, and ankle do little net work (Figure 2).

CONCLUSIONS

Greater actuator contributions were found at the more proximal joints. Although the joints with the greatest capacity for elastic energy storage were a distal (MCP) and a mid (ankle) joint, the predicted proximo-distal pattern generally held.

REFERENCES

1. Alexander, R. McN. (1984) *Elastic Mechanisms in Animal Movement*. Cambridge: Cambridge University Press.
2. McGuigan, M. P. & Wilson, A. M. (2003) *J. Exp. Biol.* **206**,1325-1336.

TRANSFER OF ANGULAR MOMENTUM IN THE BASEBALL BATTING

Tomohisa Miyanishi
Faculty of Physical Education, Sendai College, Miyagi, Japan
email: tm-miyanishi@scn.ac.jp, web: www.sendaidaigaku.jp

INTRODUCTION

In a full swing batting motion, one of the most important factors should be to obtain a large amount of angular momentum from the ground, and then transfer as much of it as possible to the batting arms and also bat. Angular momentum for the combined batter-plus-bat system can be separated into two parts, associated respectively with the motions of the body-minus-batting arms ("body-minus-arms") and of the batting arms-plus-bat ("arms-plus-bat"). The purpose of this study was to clarify the changes in the angular momentum for the system during the baseball batting, and the transmission of angular momentum to the arms-plus-bat system.

METHODS

After the take-off of the lead leg (LOF), a right-handed batter elevates the lead leg and turns the trunk toward the right, steps forward, plants the lead leg (LON), and impacts the ball (IMP) in general. The batter is in single-support (SS) phase between LOF and LON, and in double-support (DS) phase between LON and IMP. Batting motions with maximum effort by eight right-handed male varsity batters were videotaped using three-dimensional (3D) DLT procedures. The 3D coordinate data of the 21 body landmarks, the 2 bat's portions (tip and tail) and the ball center were obtained for the best battings (hit a ball squarely toward a center field) of each subject, and smoothed using quintic spline as selected by the optimal cutoff frequencies for each coordinate [3]. The coordinates were expressed in an orthogonal reference frame: The X axis pointed toward the right (normal to the direction of pitcher's mound), the Y axis the pitcher's mound, and the Z axis upward. The angular momentum values of 16 body segments and of the bat were calculated using a method based on previous study [1]. The location of the center of mass and the moment of inertia about the transversal axis of bat were measured using the balance and pendulum methods, respectively. The SS and DS phases were each divided into two equal time periods. The 3D angular momentum of the body-minus-arms, arms-plus-bat and combined system were calculated for five instants: (1) LOF, (2) the mid-point of SS, (3) LON, (4) the mid-point of DS, and (5) IMP.

RESULTS AND DISCUSSION

Average angular momentum values for the eight swings are shown in Table 1. To facilitate the following discussion, the terms "clockwise" (CW) and "counterclockwise" (CCW) will replace the signs of the X, Y and Z angular momentum components; the directions will correspond to views from the right, from behind and from overhead for the H_X, H_Y and H_Z angular momentum components, respectively.

Table 1. Angular momentum ($kg{\cdot}m^2/s$). (M±SD)

Times:	1	2	3	4	5
	LOF		LON		IMP
H_X					
body-minus-arms	1±2	1±2	1±3	3±4	3±4
arms-plus-bat	0±0	0±0	2±1	1±1	3±1
system	1±2	1±2	3±3	3±3	6±4
H_Y					
body-minus-arms	-1±3	0±3	2±4	1±3	3±3
arms-plus-bat	-1±1	-1±1	0±1	4±1	-3±2
system	-2±3	-1±2	2±4	5±3	0±4
H_Z					
body-minus-arms	-2±1	0±2	4±2	9±2	3±2
arms-plus-bat	0±1	-1±0	0±1	8±2	21±4
system	-2±2	0±2	4±2	17±2	23±4

Note: Some of the values in this table may not fit perfectly with each other, because of rounding off.

The changes of the system angular momentums depend on the angular impulses of the ground reaction forces (GRFs) received by the batter's feet. The changes in the system H_X and H_Y values were much smaller than those of the system H_Z value because little angular momentum was needed in these directions. Therefore, in this discussion, we will concentrate on the changes in the H_Z value.

At LOF the system had a CW H_Z of 2 $kg{\cdot}m^2/s$. This value changed to a CCW H_Z of 4 $kg{\cdot}m^2/s$ at LON. Since the GRF in the XY plane pointed rightward (toward a catcher) of both feet before LOF and leftward (toward a pitcher) of pivot foot after LOF [2], the change of the H_Z was produced by the horizontal GRF. The change from a CCW H_Z of 4 $kg{\cdot}m^2/s$ at LON to a CCW H_Z of 23 $kg{\cdot}m^2/s$ at IMP was produced by the backward and rightward GRFs of lead foot and also the forward and leftward GRFs of pivot foot during the DS [2].

At LOF, all the H_Z of the system was in the body-minus-arms, and most of the changes produced in the CCW H_Z during the SS by the GRF also went into the body-minus-arms. During the 1st half of DS there was a gain of H_Z, half of which was transmitted from the ground through the legs and trunk to the batting arms and also was generated by the legs and trunk, the remains was generated by the batting arms. During the 2nd half of DS there was a gain of H_Z, most of which was generated by the arms and bat.

REFERENCES

1. Dapena J. *J Applied Biomech* **13**, 239-253, 1997.
2. Hirano Y, et al. *Sci hum mov V*, Kyorin-shoin Inc, Tokyo, 260-267, 1983.
3. Miyanishi T, et al. *Proceedings of ISB XIX*, Dunedin, New Zealand, Abstract 269, 2003.

Optimal or Antagonistic? Muscle force solutions in the lower limb.

[1] Stansfield BW, [1]Nicol AC, [1]Paul JP, [2]Graichen F and [2]Bergmann G
[1]Bioengineering Unit, University of Strathclyde; email: benedict.stansfield@strath.ac.uk
[2]Biomechanics Lab., Charité - University Medicine Berlin; web: www.biomechanik.de

INTRODUCTION

The musculature of the lower limb is redundant in nature. When calculating the muscle forces using a mathematical musculo-skeletal model it is necessary to select a criterion for muscle force distribution. For example, optimization may be used to minimize the sum of muscle forces, or minimize the maximum muscle stress. One method of validating these internal force distribution calculations is to use internal force measurements made with instrumented implants [2,4].

The current paper provides evidence of the appropriateness of various muscle force distribution protocols in a musculoskeletal model of the lower limb [1]. Calculated hip joint contact forces (HJCF) are directly compared with simultaneously acquired in vivo loads.

METHODS

HJCF were measured in-vivo using instrumented femoral prostheses [3,4]. These measures provided the 'gold standard' for comparison with calculated forces. HJCF were calculated using a lower limb musculoskeletal model [1]. This model described the 3D anatomy of the lower limb including hip, knee and ankle. Inverse dynamic methods were applied to motion and force plate data. Two subjects took part in various tasks and results are presented for one male (170.4cm, 92.3kg, 58 years, 36 months post-op., right side THR). The calculations of HJCF during one typical walking trial are examined here.

The muscle force distribution problem was solved using four different optimization criteria (C):
C1. Minimization of the sum of muscle forces
C2. Minimization of the sum of the square of muscle forces
C3. Minimization of the sum of the cube of muscle forces
C4. Minimization of the maximum muscle stress

RESULTS AND DISCUSSION

Figure 1 provides a comparison of HJCF calculated using the musculoskeletal model with forces simultaneously measured, using the instrumented implants. The forces are illustrated in an axis set attached to the femur with neutral orientation based on radiographs incorporating femoral neck anteversion.

Direct comparison of the calculated and measured forces illustrates a number of points:
- It was possible to provide a muscle force solution that satisfied equilibrium, but that consistently underestimated HJCF (C1) suggesting that the physiological solution does not use minimization of joint force as a criterion.
- Although solutions exist that 'optimize' criteria associated with muscle force, none of those used provided consistent agreement with the measured forces, e.g. C4 overestimated at some points in the gait cycle and underestimated at others.
- All criteria underestimated the HJCF during late stance suggesting that the body uses antagonism to provide extra stabilization at the joints during this phase of walking, or that the hip joint was hyper extended producing force in the ilio-femoral ligament that was not accounted for in the model.

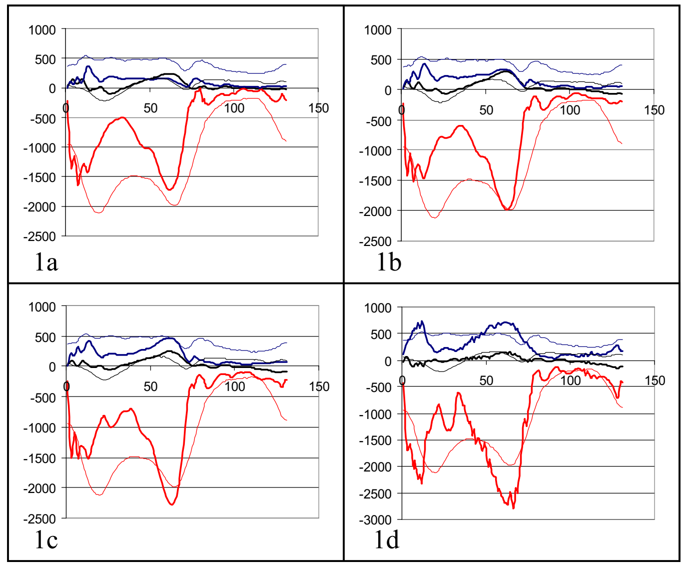

Figure 1 Calculated (thick lines) and measured (thin lines) HJCF (Newtons force vs. samples at 120Hz). Black – X (anterior-posterior); Red – Y (femoral long axis), Blue – Z (medio-lateral). 1a) C1; 1b) C2; 1c) C3; 1d) C4.

CONCLUSIONS

Although the authors recognize the significant contribution of the musculoskeletal model in determining HJCF, the results suggest that the physiological solution to the redundancy problem is not to operate an optimal criterion aligned with any of those investigated.

The results also suggested that the body uses a degree of antagonism above that required to provide stability at certain instances during the walking cycle or, as at the knee, moments may be transmitted by forces in ligaments.

REFERENCES

1. Stansfield BW & Nicol AC. *Clinical Biomechanics* **17**, 130-139, 2002.
2. Stansfield BW, et al.. *J Biomech* **36**, 929-936, 2003.
3. Bergmann, G., 2001. Hip98. Free University, Berlin. ISBN 3980784800 (compact disc).
4. Graichen F, et al.. *J Biomech* **32**, 1113-1117, 1999.

ACKNOWLEDGEMENTS

This work was funded by the United Kingdom EPSRC

JOINT VELOCITY SEQUENCE OF THE UPPER EXTREMITY DURING FLY-CASTING

[1] Katie B. O'Keefe, [1]Joshua R. Allen, [2]Timothy J. McCue and [1]Michael E. Hahn
[1]Movement Science Laboratory, Montana State University, Bozeman, MT, USA
[2]Fly Casting Institute, Missoula, MT, USA
email: mhahn@montana.edu

INTRODUCTION

Segmental chain analysis of the upper extremity can contribute to a deeper understanding of the coordination and control strategies used during overhand throwing tasks. The fly-casting stroke parallels throwing tasks in that the ultimate goal is accurate placement of a projectile at some distance from the body. Previous studies have shown differences in the sequence of peak joint velocities, based on the skill vs. power required for the task [1,2]. The focus of this study is to determine whether upper extremity sequencing during fly-casting is proximal-distal or distal-proximal. Establishing the order of sequence should add to the basic understanding of coordination involved in fly-casting.

METHODS

The sample consisted of six subjects (five males, one female) ranging in age from 22 to 38. Each subject signed an informed consent and was medically evaluated for upper extremity health. Within the medical evaluation, subjects were asked to state the number of days spent fly-fishing per year. Responses varied from 3 days/year to over 100 days/year indicating a variety of experience. Segments of the upper body were defined by 25 spherical, reflective markers placed on bony landmarks (adapted from Rab et al. [3]). Marker position data were collected at 200 Hz using a 6-camera Vicon 460 system (Vicon Motion Systems, Lake Forest, CA).

Subjects were required to perform a series of casting trials, including 2-3 "false casts" followed by the "shooting" cast. The shooting cast from each of three trials was evaluated for each subject.

The upper extremity was modeled as a system of rigid bodies connected by pin joints. The wrist was modeled with a two-axis pin joint, the elbow as a one-axis pin joint, and the shoulder as a three-axis ball and socket joint. Time and magnitude of peak angular velocities were examined during the forward cast. Angular velocities were calculated using the central difference method and smoothed with a 4^{th} order Butterworth low pass filter (cutoff = 2Hz). The peak velocities examined included shoulder internal rotation, elbow extension, and wrist ulnar deviation.

RESULTS AND DISCUSSION

The motion of fly-casting includes a back cast in which the line is lifted and brought behind the caster followed by a pause. During the pause, the line is drawn behind the caster due to the inertial force. This causes the line to load the rod at which point the caster will enter the forward cast. It is during this last phase that the line is directed to the target.

Segmental chain analysis revealed a pattern of proximal-to-distal motion of the upper extremity during the final forward casting phase. Figure 1 shows an example trial of the peak wrist, elbow and shoulder velocities as they occurred during the forward cast. Overall, the shoulder velocity peaked at an average of 80.5% (± 8.5%) of the total casting time, elbow velocity at 86.3% (± 8.3%), and wrist velocity at 89.1% (± 8.8%). Each subject's time to peak velocity is presented in Table 1.

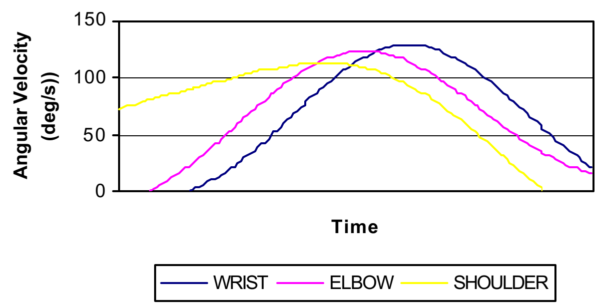

Figure 1: Peak angular velocities during the forward cast.

Peak velocities generally corresponded to the expertise of the fly-caster. Those who fished 10 days/year or less were more likely to have a wrist velocity much higher than shoulder or elbow velocities and those who were more experienced (i.e. fishing guides) had a much higher shoulder velocity.

CONCLUSIONS

Initial findings of this study indicate a proximal-to-distal sequence for angular velocities of the upper extremity joints during fly-casting. Though generally considered a skill-driven motion, a secondary goal is to produce high line velocities during the forward cast. This goal may require a more forceful coordination sequence similar to overhand throwing.

REFERENCES

1. McDonald PV, et al. *J Mot Behav* **21**, 245-264, 1989.
2. van den Tillaar R, et al. *Percept Mot Skills* **97**, 731-742, 2003.
3. Rab G, et al. *J Biomech* **15**, 113-119, 2002.

Table 1: Percent time to peak velocity.

% Total Time to Peak Velocity	Subject 1	2	3	4	5	6
Wrist	87.68%	83.74%	91.46%	93.07%	89.77%	89.20%
Elbow	85.91%	80.51%	90.28%	90.81%	80.41%	85.44%
Shoulder	76.31%	80.89%	85.15%	78.98%	79.24%	82.26%

Biomechanical and physiological determinants of skiing locomotion development

Formenti F., Ardigo' L.P., Minetti A.E.
Manchester Metropolitan University, Institute for Biophysical and Clinical Research into Human Movement
e-mail: f.formenti@mmu.ac.uk, web: www.cheshire.mmu.ac.uk/exspsci/research/biomex/Biomech.html

INTRODUCTION

How far could man travel on snow five thousand years ago? What did man empirically understand to be the limiting factors for his skiing performance, from its very beginning to date? Very little research focused on the biomechanics and physiology of the development of cross-country skiing [1]. In the present study the evolution of skiing locomotion from 3000 BC to date is explored by investigating how humans adapted to move effectively in lands where a cover of snow, for several months every year, prevented from travelling as effectively as on dry ground. Following historical research, a few sets of skis were identified as the 'milestones' of skiing evolution in terms of ingenuity and technology. Their replicas were built and the metabolic energy associated to their use was measured in a climatic-controlled tunnel.

METHODS

Seven sets of skis were tested, covering a span of about five thousand years. Original archaeological specimens could not be used for the present study, so accurate reproductions of the originals were made (Department of Design and Technology – MMU, Cheshire). Experiments took place at the Vuokatti ski tunnel, Finland, where temperature (mean±s.d., air –5.2±1.1 °C, snow -4.5±0.5 °C, n=115) and humidity (83.6±1.4 %, n=115) are monitored and controlled 24 hours a day by a computer controlled air conditioning system. Five healthy adult non-professional skiers took part in the experiments (age 33.8±11.8 years, stature 176±2.8 cm and body mass 73.0±4.8 kg). Participants were requested to adopt two subjectively chosen speeds, the former defined as sustainable for 7 to 8 hours ('migration'), the latter for just 3 to 4 hours ('hunting'). When skiing with the 2004 AD models (classical and skating techniques) participants travelled at two additional faster speeds, the fastest being 70% of their maximum speed. Participants were equipped with a portable metabograph (Cosmed K4b2) that measured their heart rate (HR) (b min^{-1}), carbon dioxide output (VCO2) (l min^{-1}) and oxygen uptake (VO2) (l min^{-1}) on a breath-by-breath basis. Oxygen uptake at rest was measured and was used to calculate the net oxygen consumption for skiing with each set of skis. VO2 measurements (mlO_2) were converted into equivalent units (J) according to the obtained respiratory quotient coefficient [2]. The metabolic cost of skiing (J/(kg m)) was calculated by integrating the net oxygen consumption over each trial duration and dividing it by the length of the track (2.5 km) and by the (body) mass. Kinematic variables relative to the skiers' movement were recorded by means of inertial sensors (MT9, Xsens) placed on the skiers' right thigh and shank. A stride has been defined as the distance/time between the ends of two successive kicks performed by the same leg. Euler angles from the data recorded on the legs were used to calculate the stride frequency (Hz) and estimate the internal work [3]. Ski friction was measured for all the pairs of skis by means of two inertial sensors during passive deceleration manoeuvres.

RESULTS AND DISCUSSION

The decision to perform the experiments in the ski tunnel allowed recording data in standard conditions, hence reducing to a minimum the variability due to temperature changes.

Results from the present study show that: a) for the same amount of metabolic power today it is possible to travel at twice the speed of ancient times (Figure 1) and b) the cost of transport is speed-independent for each ski model. By combining this finding with the physiological relationship between time of exhaustion and the fraction of sustainable metabolic power [4], a prediction of the maximum skiing speed according to the distance travelled is provided for all past epochs and can predict with a good precision modern competitions.

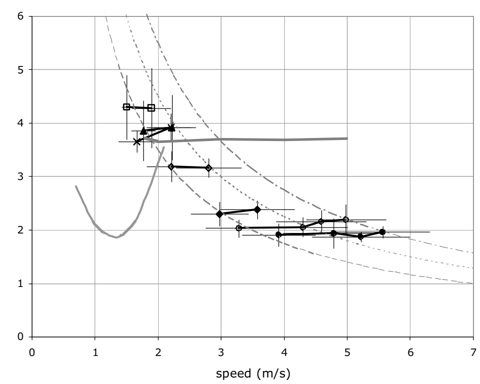

Figure 1: the metabolic cost (J/kg m) of skiing is here plotted against the speed for all the investigated skis. For sake of comparison, lines reporting walking and running costs are shown (walking in the tunnel is represented by the grey circle). Iso-power curves show the power chosen by participants.

Total stride length increased from 14.0% to 60.5% in the chronological ski sequence. We did not directly measure the 'body centre of mass' part of the external mechanical work, but it is expected to decrease along skiing history since the increase in the sliding length will allow distributing the raise of the body centre of mass across a longer distance. This was confirmed (-86.8%) when we calculated an 'estimated version' of it by subtracting from the measured cost the metabolic equivalent of both the work against friction and the internal work.

CONCLUSIONS

Results from the present study will help historians to understand the times needed and distances covered during migrations in cold regions in the past. Our research shows that the performances of two legendary historical journeys (1206 and 1520 AD) on snow, the performances of races originating from them (Birkebeiner and Vasaloppet) and those of other modern competitions (skating vs. classical techniques) are well predicted by the evolution of skiing economy.

REFERENCES

1. Street, G.M. *Med. Sci. Sports Exerc.* **24**, 1048-1054, 1992.
2. di Prampero, P.E. *Int J Sports Med.*, **7**, 55-72, 1986.
3. Minetti, A.E. *J. Biomech.,* **31**, 463-468, 1998.
4. Minetti, A.E. *J. Exp. Biol.,* **207**, 1265-1272, 2004.

ISB XXth Congress - ASB 29th Annual Meeting
July 31 - August 5, Cleveland, Ohio

SIMULATION OF LONGITUDINAL ARTERIAL STRETCH IN THE LOWER LIMBS DURING GAIT

Richard J. Beck, Antonie J. van den Bogert, Azita Tajaddini, and Brian L. Davis
Biomedical Engineering Department, Cleveland Clinic Foundation, Cleveland, OH
email: beckr2@ccf.org

INTRODUCTION

Peripheral arterial disease is common in patients with diabetes and is a major risk factor in the etiology of gangrenous lesions that can, in turn, lead to lower extremity amputations. Correction of stenosis using stents can maintain patency in affected vessels; however, these devices are susceptible to mechanical problems. A fractured strut within a stent can initialize new obstructions in the lumen. The incidence of fractures corresponds to the length of the stented segment and the number of implants [1].

The present study was based on the hypothesis that activities of daily living impose longitudinal stretch on arteries traversing the hip and knee regions, and that this elongation may play a role in stent failure. Thus the purpose of the current study was to estimate arterial stretch during gait and to relate this to joint excursions.

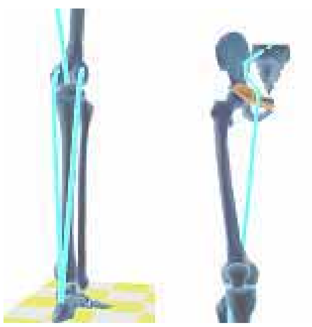

Figure 1: Views of the adapted SIMM graphical model.

METHODS

Using SIMM (Software for Interactive Musculoskeletal Modeling, V.4.0.1, MusculoGraphics, Inc., Motion Analysis Corp., Santa Rosa, CA), a model of the lower extremity was modified to include representatives of the iliac, femoral, and popliteal arteries. This software sets realistic geometrical constraints on muscle objects by conforming the muscle length and orientation to the motion of the bones [2]. An object created as a muscle and placed in the location of an artery will follow the same geometric rules. Using a SIMM leg model of an adult subject with height of about 1.8 meters and weight of about 75 kg, attention was given to the general anatomical route of the vessels. The mechanical anchor that perivascular connective tissue provides was modeled as origin and insertion. The arteries are subjected to the influence of residual strain and constant tension, therefore the resting lengths of the model arteries are assumed to be identical to the resting lengths of the surrounding muscles.

To demonstrate iliofemoral stretch, a new digital muscle was created, with origin in the sacral region and insertion on the proximal tibia (Figure 1). The SIMM default placements of the medial and lateral heads of the gastrocnemius were used to model the popliteal artery (Figure 1). For both iliofemoral and popliteal regions, the relationship of arterial length as a function of the gait cycle was predicted using SIMM.

RESULTS AND DISCUSSION

Plots generated from SIMM indicate the estimated length change for the iliac and femoral arteries together to be about 2.5 cm (Figure 2A). Likewise, the popliteal artery stretches an estimated 4 cm (Figure 2B). These geometrical demands associated with normal gait illustrate the necessity for compliance in vascular tissue. Modern stents and vascular tissue have dissimilar properties, providing undesirable stresses at their interface. Arterial stretch may therefore play an important role in stent failure.

Limitations of the current approach include (i) selecting origin and insertion points that may not replicate normal anatomy, (ii) restricting the analysis to gait, (iii) modeling a single subject, (iv) estimating global rather than local stretch, and (v) including wrapping surfaces that may not replicate the exact course of an artery. Nevertheless, predictions from the model suggest that lower extremity arteries undergo substantial longitudinal stretch, and that stent and vascular graft designers should be cognizant of these biomechanical demands.

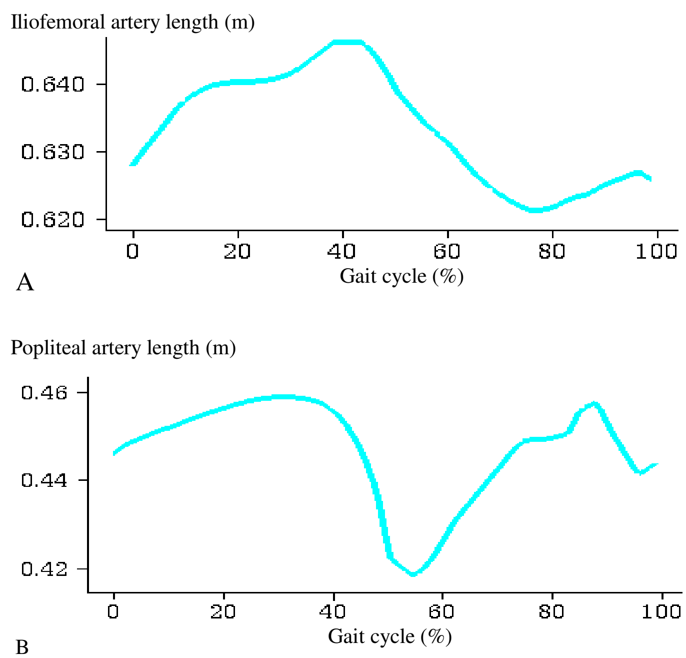

Figure 2: Iliofemoral length (A) and Popliteal length (B) plots from the SIMM model.

REFERENCES

1. Scheinert D, et al. *J. Am Coll Cardiol* **45(2)**, 312-315, 2005.
2. Delp, S. L. and Loan, J. P. *Computing in Science &Engineering,* **2**, 46-55, 2000.

CALIBRATION AND MONITORING OF PIEZORESISTIVE CONTACT STRESS SENSOR ARRAYS USING A TRAVELLING PRESSURE WAVE PROTOCOL

[1]Thomas E Baer, [1]Douglas R Pedersen, [1]M James Rudert, [1]Nicole A Kallemeyn, [1]Nicole M Grosland, [1]Thomas D Brown
[1]University of Iowa, Iowa City, IA, email: thomas-baer@uiowa.edu web: http://mnypt.obrl.uiowa.edu

INTRODUCTION

To improve the accuracy and efficiency of measuring the distributions of intra-articular contact stresses during dynamic loading of cadaveric joint specimens, a novel hardware and software regime has been developed for calibrating Tekscan sensors.

In many experiments measuring contact stress, especially those involving cadaveric joints with malreduced fractures or total joint replacement prostheses, high localized stresses lead to significant local changes in sensor responses during a given testing session. The ability to easily and frequently recalibrate sensors is therefore desirable.

Figure 1. The calibration device with a sensor between the rollers.

METHODS

To meet this challenge, a novel "wringer" device was built (Figure 1). Regulated air pressure applies a known force across a pair of elastomeric rollers. As the sensor is drawn between them, a traveling pressure wave is recorded (Figure 2A). Passage of the wave over each sensel is recorded as a time series signal. A finite element solution of the contact between parallel elastic cylinders provides a normalized distribution of pressure as a function of contact patch width. The spatial position of every sensel within the contact patch is known, allowing local pressures at every point in time to be based on the FE solution. A provisional calibration is derived using iterative power law curve fitting to the sensel-specific signal-pressure data arrays.

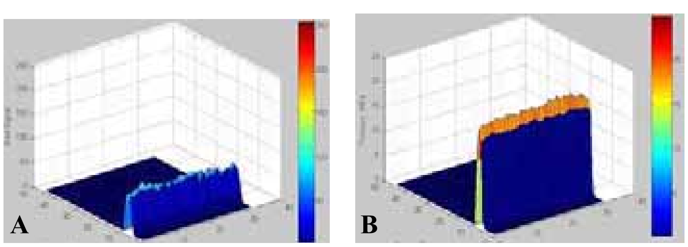

Figure 2. Traveling wave of raw (**A**) and pressure calibrated (**B**)

In these sensors, the area of the active pressure sensing elements constitute only about 10 percent of the total area over which the pressure is calculated. Calibration therefore depends on the distribution of load between sensing and non-sensing areas of the sensel and is strongly affected by the compliance of the surfaces between which the sensors are used.

After the provisional calibration, a sensor was inserted into a joint specially prepared so that all the load across it is carried by the sensor, and the calibration was "fine-tuned" at a series of known loads to the specific surface compliance properties of the joint's intra-articular environment. A *cartilage tuning factor* of 1.36 (the ratio of load applied to load recovered using the provisional calibration) was then used to adjust the provisional curves for each sensel. (Figure 3A). These final calibration curves were applied to eight other ankle loading experiments (Figure 3B).

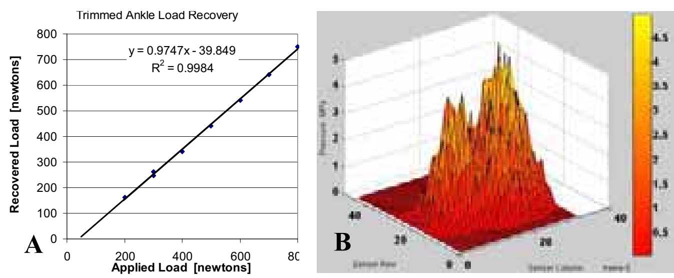

Figure 3. (**A**) Recovered load versus applied load is linear. (**B**) Pressure distribution in a cadaveric ankle loaded to 800N.

RESULTS AND DISCUSSION

The traveling wave technique serially calibrates the entire array of piezoresistive sensing elements over its full functional range while obviating the prohibitively high forces required for calibration using conventional whole-sensor-loading techniques.

At intervals during a typical experimental session, the sensor is removed from the joint and run through the device. Using the tuning factor already calculated, an updated calibration is calculated for each sensel. The sensor is then placed back in the joint and the experiment continues. If too much change (implicitly degradation) is seen to have occurred, the sensor is replaced. With minimal disruption of the protocol, the sensor's performance can be evaluated as often as desired during the course of an experiment. Data that might otherwise be lost to sensor artifacts can be saved by these on-the-fly recalibrations.

CONCLUSIONS

The manufacturer's calibration procedure, which restricts sensel loadings to the low end of the functional range and cannot provide sensel-by-sensel calibrations, may be problematic in many research environments. The new device and method effectively overcome these limitations.

ACKNOWLEDGEMENTS

NIH grant 5 P50 AR048939 and CDC grant R49 CCR721745.

The Effects of Plyometric Versus Dynamic Stabilization and Balance Training on Lower Extremity Biomechanics

[1]Gregory D. Myer, [1]Kevin R. Ford, [2]Scott G. Mclean and [1,3]Timothy E. Hewett
[1]Cincinnati Children's Hospital Medical Center, Sports Medicine Biodynamics Center,
[2]Department of Biomedical Engineering and Orthopaedic Research Center, Cleveland Clinic Foundation
[3]University of Cincinnati, College of Medicine; email: greg.myer@cchmc.org, web: www.cincinnatichildrens.org/sportsmed

INTRODUCTION

Females who participate in pivoting and jumping sports suffer anterior cruciate ligament (ACL) injuries at a 4 to 6-fold greater rate than males participating in the same sports. Neuromuscular training protocols that combine plyometric and dynamic stabilization and balance exercise components have been shown to significantly alter potentially hazardous lower limb biomechanics and reduce ACL injury risk in female athletes [1-4]. Currently, no studies have compared the effects of plyometric and dynamic stabilization training as a means to delineate the mechanism behind the successful modification of female biomechanics linked to ACL injury risk. The purpose of the current study was to compare the effects of maximum effort plyometric training (PLYO) versus dynamic stabilization and balance training (BAL) on female lower extremity kinematics during a drop vertical jump (DVJ) and a single leg medial drop landing (MDL). Specifically, we examined the effects of each training mode on resultant frontal and sagittal plane motions during each of these tasks, which incorporate potential high-risk neuromuscular control effects[1, 3].

METHODS

Eighteen high school female athletes were randomized into one of two (BAL or PLYO) training (3 X/week) regimens for 7 weeks. The BAL (n=10) group performed dynamic stabilization and balance exercises and the PLYO (n=8) group performed maximum effort jumping and cutting tasks during training. Subjects had lower extremity (bi-lateral) three-dimensional (3D) kinematics data recorded during the execution of three DVJ and three MDL tasks, pre and post training. The 3D coordinates of external skin markers were recorded at 240 HZ during each trial using a high-speed motion analysis system (Motion Analysis, Santa Rosa CA). These data were submitted to Mocap Solver 6.17 to solve for each lower limb rotational degree of freedom. Ground reaction force data for each leg were collected at 1200Hz via AMTI force plates and used to normalize joint kinematic data to stance. Coronal and sagittal plane kinematics were calculated for the hip, knee and ankle. A mixed design ANOVA was utilized to test for the main effects of gender, task and side with alpha level of 0.05.

RESULTS AND DISCUSSION

During the DVJ, both PLYO and BAL training reduced initial contact (IC) (p=0.002), and maximum hip adduction angle (p=0.015) and maximum ankle abduction angle (p=0.02). When performing the MDL, both groups decreased IC (p=0.002) and maximum knee abduction angle during stance (p=0.038). While each training approach had a similar impact on coronal plane measures, distinct training effect differences were observed for the sagittal plane. . Specifically for PLYO training significantly increased maximum hip (p=0.041) and knee (p=0.031) flexion during DVJ tasks but not during the MDL (Figure 1A). Conversely, BAL training increased knee

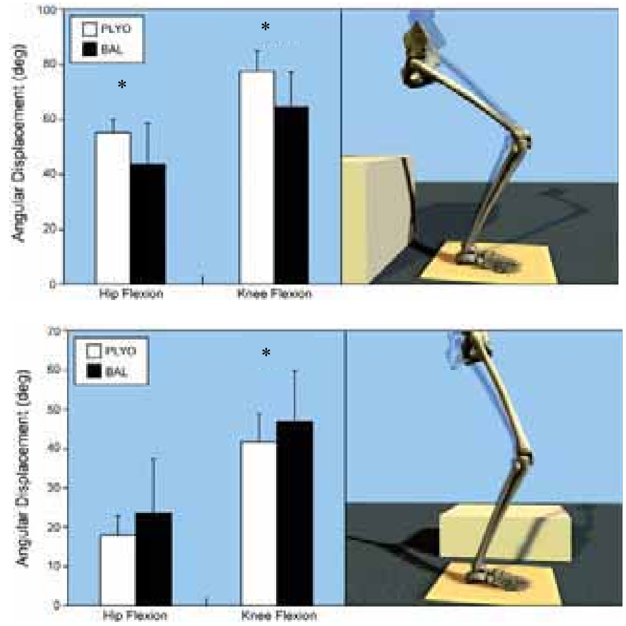

Figure 1. Effect of BAL (solid) and PLYO (transparent) training on hip and knee flexion during (A) DVJ and (B) MDL tasks.

(p=0.005) flexion during the MDL but not during the DVJ (Figure 1B). The results of the current study demonstrate that a reduction in lower limb dynamic valgus can be achieved via both PLYO and BAL training. The impact of each type of training exercise on potential sagittal plane risk factors however, appear to be most pronounced during movement tasks that incorporate similar underlying neuromuscular requirements (plyometric versus stabilization). If the ACL injury mechanisms is indeed governed by both coronal and sagittal neuromuscular factors therefore, then the inclusion of both BAL and PLYO training components appear warranted

CONCLUSIONS

The results of the current study do not support excluding either plyometrics or dynamic stabilization exercises from an ACL injury prevention protocol. Future research should evaluate whether the combinatorial effects of these training methods in more detail to maximize both risk prevention and athlete compliance. Additionally, further investigation into the role of athlete awareness of potentially dangerous positions and feedback during dynamic tasks is warranted.

REFERENCES

1. Hewett, T.E., et al., *Am J Sports Med*, **33**(4) 2005..
2. Myer, G.D., et al., *J Strength Cond Res*, **19**(1) 2005..
3. Olsen, O.E., et al., *Am J Sports Med*, **32**(4): p. 1002-12. 2004.
4. Hewett, T.E., et al., *Am J Sports Med*, **27**(6): p. 699-706. 1999.

ACKNOWLEDGEMENTS

This work was supported by NIH Grant R01-AR049735-01A1 (TEH)

MECHANOBIOLOGICAL INFLUENCES ON ENDOGENEOUS BONE TISSUE ENGINEERING STRATEGIES

[1,3]Kreuzer, S, [1]Ritzman, TF, [1]Knothe, UR, [2]Schneider E, [1,3]Knothe Tate, ML
[1]Orthopaedic Research Center, The Cleveland Clinic Foundation, Cleveland, OH; [2]AO ASIF Research Institute, Davos, CH;
[3]Depts. of Mechanical & Aerospace and Biomedical Engineering, Case Western Reserve University, Cleveland, OH

INTRODUCTION

In this study we implemented a previously developed surgical model [1, Figure] to quantify specific mechanobiological influences on endogeneous bone tissue engineering strategies.

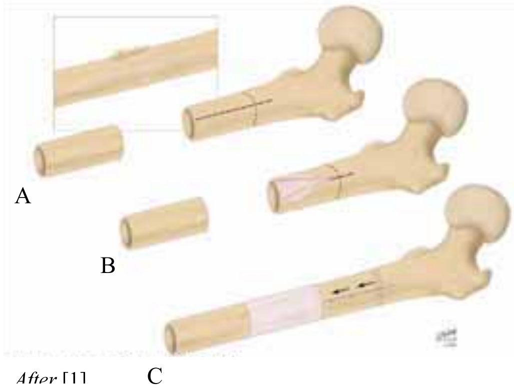

This surgical model allows for osteogenesis, osteoconduction and osteoinduction to take place *in situ*. The **periosteum** serves as a source of osteoprogenitor cells and osteoblastic precursors as well as a well-vascularized tissue bed. The periosteal sleeve also acts as a barrier to ingrowth of fibrous granulation tissue and allows for establishment of chemical gradients, *e.g.* of osteogenic substances, that otherwise could diffuse out to the surrounding soft tissue. In addition, use of vascularized and/or morcellized **bone grafts** may provide osteoblasts for *de novo* bone generation, a scaffold for osteoconduction and/or release of osteoinductive substances from the bony matrix of the host graft. Finally, an intramedullary nail provide mechanical stability for the entire construct. In implementing this model, we aimed to elucidate the influence of mechanics, availability of osteoprogenitor cells (from the periosteum), and autologous bone graft on density and spatial distribution of bone tissue regenerate.

METHODS

An ovine femur model was implemented with a critical size (2.6 cm) diaphyseal defect in skeletally mature, females (n = 35)‡. The periosteum was elevated circumferentially off the proximal femoral diaphysis adjacent to the defect. The healthy "donor" bone was then osteotomized (Fig A) and transported distally over a retrograde IM nail to fill the defect (Fig B), thereby creating a new defect around which the healthy periosteum was sutured to form a sleeve (Fig C). The entire construct was stabilized with a custom made, interlocking, retrograde IM nail. Five groups of 7 sheep were investigated. In the control group, no periosteal sleeve enveloped the defect. The sleeve alone enveloped the defect in a 2nd group. Autogenous cancellous bone graft was placed within the sleeve of the 3rd group. Vascularized bone chips were left adhering to the periosteum in the 4th group. Bone graft and adherent bone chips were included in the 5th group.

‡All animal protocols were approved by the IACUC.

Mean density and spatial distribution of bone regenerate were calculated from high-resolution (20 µm) µ-CT data sets (Scanco Medical, Bassersdorf, Switzerland). Inter-group differences were assessed using ANOVA and Fisher's protected least significant difference (PLSD) post-hoc tests (StatView, SAS Institute, Inc., Cary, NC). A p-value < 0.05 was considered to be statistically significant.

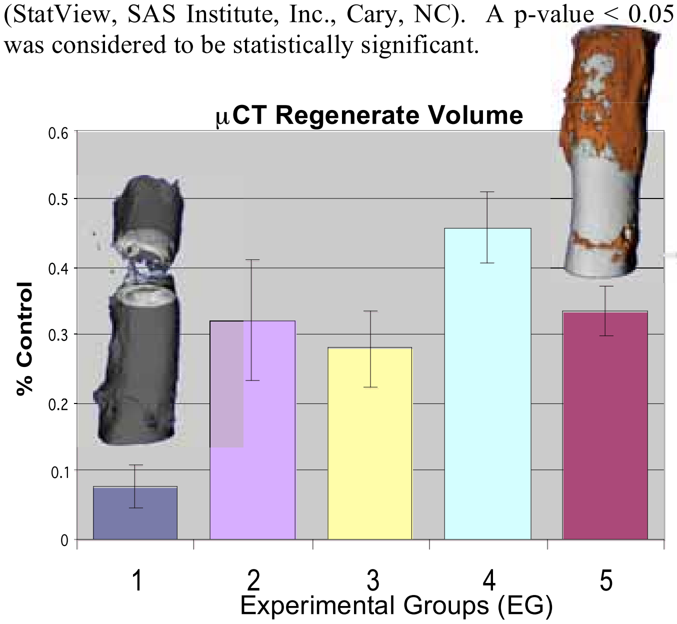

RESULTS AND DISCUSSION

All groups in which the periosteal sleeve was retained (EG 2-5, Fig.) exhibited significantly greater *volume of regenerate bone* within the defect zone than the group without periosteal sleeve (EG 1, Fig., $p<0.0001$). The addition of bone graft (EG 3) in the defect zone did not increase regenerate volume compared to the periosteal sleeve alone (EG 2). The addition of graft (EG 5) in the defect zone resulted in a significantly decrease in regenerate volume compared to the periosteal sleeve with adherent, vascularized bone chips (EG 4). However, the observed increase in regenerate with addition of adherent, vascularized bone chips (EG 4) was not statistically significant, as compared to the periosteal sleeve alone (EG 2). Currently we are measuring the spatial distribution of the regenerate as a function of distance from the blood supply as well as the neutral axis. These data will allow us to colocalize distance to blood supply as well as predominate modes of mechanical loading (via matrix deformation and/or fluid flow) to spatially-resolved regenerate density data.

CONCLUSIONS

For the first time to our knowledge, this experimental model provides a novel means to elucidate the relative influence of intrinsic and extrinsic factors on successful functional engineering of bone tissue replacements.

REFERENCES [1] Knothe U, Springfield DSS, *World J Surg Onc*, 2005. [2] Ritzman *et al. Trans ORS*, 2005.

FOOT PROGRESSION ANGLE AND THE KNEE ADDUCTION MOMENT IN INDIVIDUALS WITH MEDIAL KNEE OSTEOARTHRITIS

[1] Kurt Manal and [1]Mengtao Guo
[1]Center for Biomedical Engineering Research, University of Delaware

INTRODUCTION

Progression of medial knee OA is associated with the external knee adduction moment [1]. Treatments to reduce the magnitude of the moment are therefore indicated for patients with knee OA. Regression analysis has revealed an inverse relationship between the adduction moment and an individual's self-selected foot progression angle (FPA) [2]. No study has examined if walking with a greater than self-selected FPA will further reduce the peak moment in this population. This simple strategy may be an effective method of reducing knee joint loading during activities of daily living for subjects with medial knee OA. The purpose of this study was to examine the effect of increasing FPA on the knee adduction moment during walking, stair ascent and descent in subjects with knee OA.

METHODS

10 subjects with mild to moderate medial compartment knee OA participated in this study (mean age = 63 ± 5 years, weight = 81.8 ± 12.7 kg, height = 1.68 ± 0.08 m). Subjects performed 5 walking, 5 stair ascent and 5 stair descent trials for each of two conditions: (1) self-selected FPA, and (2) increased FPA (self-selected FPA + 15 degrees). Video and force data were collected, and Visual3D (C-motion Inc.) was used to compute the normalized (% BW*Ht) external knee adduction moment. The knee adduction moment has a characteristic 2 hump pattern (see Figure 1). Dependent t-tests were used to assess the effect of increasing FPA on the 1st and 2nd peak moments during walking, stair ascent and descent. The 1st and 2nd peak moments within each task were analyzed separately.

RESULTS AND DISCUSSION

During walking, the 1st peak adduction moment did not change with increasing FPA, but the magnitude of the 2nd peak decreased significantly (Table 1). During stair ascent, a strong trend (p=0.051) towards a reduced 2nd peak adduction moment was noted for the increased FPA condition. The potential benefit of a smaller 2nd peak moment however was likely overshadowed by a significantly greater 1st peak adduction moment with increased FPA. No differences in the peak moment were noted during stair descent. The results of this study suggest that walking with an increased FPA can reduce the magnitude of the 2nd peak knee adduction moment in subjects with knee OA. The adduction moment is an indirect estimate of joint loading [3], and thus, this finding suggests that walking with an increased FPA can reduce joint contact forces.

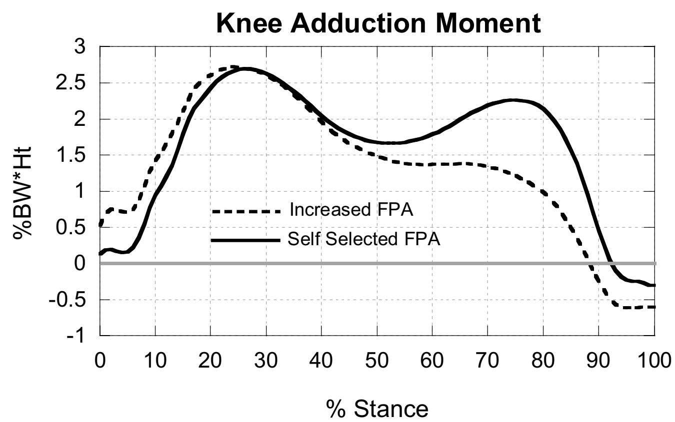

Figure 1. External knee adduction moment during the stance phase of walking. The magnitude of the 2nd peak moment was significantly smaller when walking with an increased FPA.

CONCLUSIONS

Increasing the degree of toe-out during walking decreased the peak adduction moment and presumably joint contact forces for subjects with medial compartment OA. This strategy may have beneficial effects, however it is premature to assert so at this time because the effect of increasing FPA at other joints, specifically the hip has not addressed. This will be the focus of future work.

REFERENCES

1. Sharma L, et al. *Arthritis Rheum* **41**,1233-40, 1998.
2. Hurwitz DE, et al. *J Orthopaed Res* **20**, 101-107, 2002.
3. Andriacchi, TP. *Orthop Clin N Am* **25**, 395-403, 1994.

ACKNOWLEDGEMENTS

Supported in part by NIH RR16458

Table 1: Peak knee adduction moments. The mean and (SD) are reported as (%BW*Ht). The cells shaded gray indicate a statistically significant difference ($p < 0.05$). A strong trend ($p = 0.051$) was noted for a reduced 2nd peak during stair ascent with increased FPA.

FPA	Walking		Stair Ascent		Stair Descent	
	Peak 1	Peak 2	Peak 1	Peak 2	Peak 1	Peak 2
Self-selected	2.81 (0.49)	2.27 (0.63)	3.18 (1.02)	2.60 (0.94)	4.37 (0.77)	2.78 (0.73)
Increased	2.85 (0.44)	1.37 (0.53)	3.53 (1.00)	2.31 (0.83)	4.28 (0.77)	2.61 (0.80)

LIGAMENT ESTIMATION FROM *IN VIVO* KNEE MOTION: AN INVERSE-KINEMATICS MODEL

[1]Elvis C.S. Chen and [1,2]Randy E. Ellis
[1]School of Computing, Queen's University, Canada, [2]Harvard Medical School, U.S.A.
email: chene@cs.queensu.ca, ellis@bwh.harvard.edu

INTRODUCTION

A forward-kinematics knee (FKK) model was previously introduced [1]: given a joint angle, the precise knowledge of the articular geometry plus mechanical properties of knee ligaments, the FKK model predicted where the femoro-tibial contacts were based on the principle of ligament energy-minimization. Knee motion was simulated by finding successive contacts from full extension to full flexion. We now introduce an inverse-kinematics knee (IKK) model that performs the opposite: given an observed knee motion, determine the joint angle and the *in vivo* femoro-tibial contact. The *in vivo* contacts were validated using Fuji-films. Together, the FKK/IKK pair form a *predictor-corrector* loop that can then be used in a parameter-estimation algorithm to find the ligament insertion locations and neutral length of the individual patient.

METHODS

Articular surfaces of aTotal Knee Replacement (TKR) prosthesis were laser-scanned at 0.25mm resolution and computer models of the surfaces, in the form of point clouds with surface normals, were reconstructed. TKR components were mounted to a knee-jig in which they were held in contact by tensile forces of 6 springs: 3 mimicking MCL, 3 mimicking LCL. The mechanical properties of each of the 6 springs, including length, spring constant, and insertion location relative to TKR components, were previously measured.

TKR components were attached with Dynamic Reference Bodies and their motion, while in contact with each other, were tracked by a 3D optical tracker. An image-free contact-determination algorithm was developed to find the *in vivo* femoro-tibial contacts. Based on proximity search and facilitated by a KD-tree, this algorithm was able to find the femoro-tibial contact under 1sec for each joint pose. For experiments involving Fuji-films, the entire knee jig was mounted to a FORCE5 manipulator that applied 100lb of downward force to produce imprints on Fuji-films

Two sets of contact locations were determined for each joint angle: one *predicted* from the FKK model and the other *observed* from the contact-determination algorithm. Together, they form a *predictor-corrector* pair that can then be fed into a parameter-estimation algorithm, in which the parameters to be estimated were the ligament mechanical properties (neutral length, insertion locations, and spring constant) that would produce the observed knee motion.

RESULTS AND DISCUSSION

A size-3 Sigma Knee (Johnson & Johnson), represented by approximately 31,000 and 19,000 points for the femoral and tibial components respectively, was used for this study. The contact-determination algorithm was first validated using Fuji-films: the perimeter of the Fuji-film contacts were digitized and superimposed to those found by our algorithm. They showed high degree of conformity.

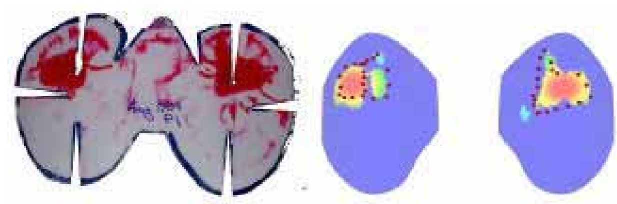

For each recorded joint pose, the joint angle (without translation), along with known ligament information, were fed to the FKK model. The FKK model produced an *energy map* and regions with the lowest energy were selected as the *in vitro* contact. The same pose was also fed into the contact-determination algorithm and the *in vivo* contact was produced. Numerically, the difference in the translations found between the *in vitro* and the *in vivo* contacts were less than 1mm.

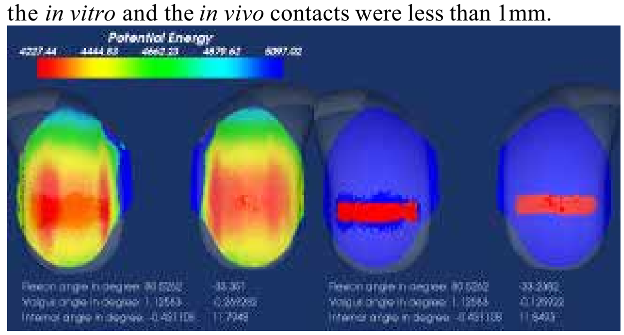

These sets of predicted *in vitro* and observed *in vivo* contacts were then used in a parameter-estimation algorithm in which the ligament information was treated as the unknown. Our implementation was able to correctly estimate the ligament insertions that were intentionally and erroneously guessed at 10mm away from the correct location. The *predictor-corrector* paradigm can also be used to test different hypotheses of ligament model: simulations suggested that a single-fibre ligament model could produce kinematics that was similar to a multi-fibres (3) ligament model in Sigma Knee.

CONCLUSIONS

We proposed an inverse-kinematics knee model. Combined with a forward-kinematics model, this *predictor-corrector* pair can be used to estimate ligament parameters such as ligament insertions. Furthermore, it can be used to test different hypotheses of the ligament model, based solely from a sequence of *in vivo* knee motion. We also introduced an image-free, nearly real-time contact-determination algorithm. Application includes, but not limited to, post-TKR assessment.

REFERENCES

1. Chen *et al* (2001). *Medical Image Analysis* **5**(3), 317-330

ACKNOWLEDGEMENTS

Joel Lanovaz assisted in the development of the knee jig.
Support in part was provided by NSERC, CITO, and ORDCF.

LASER INDUCED AUTO-FLUORESCENCE (LIAF) AS A METHOD FOR ASSESSING SKIN STIFFNESS PRECEDING A DIABETIC ULCER FORMATION

[1] Azita Tajaddini, [1] Heather M. Scoffone, [2] Georgeanne Botek, and [1] Brian L. Davis
Departments of [1]Biomedical Engineering /ND20, and [2] Orthopaedic Surgery
The Cleveland Clinic Foundation
Cleveland, OH 44195; email: tajadda@ccf.org

INTRODUCTION

Diabetic foot ulceration is a leading cause of non-traumatic amputations. Discrepancy between the stiffness of the skin and the plantar soft tissues may influence the likelihood of ulceration. Changes in tissue properties with diabetes are mainly due to accumulation of glucose in tissues which promotes non-enzymatic glycation of structural proteins [1] such as collagen and keratin. Such intermolecular cross linking will alter the structure of the fibers and lead to their stiffening [2]. Our objective was to develop a non-invasive method for assessing skin properties in the context of ulcer formation on plantar surface of the foot in diabetic patients.

METHODS

A nitrogen laser (Laser Science VSL-337 ND) with excitation wavelength at 337 nm was used to induce fluorescence of the plantar skin of hallux and fifth metatarsal head from 9 male subjects (age 70-82, Table 1). The auto-fluorescence spectra were collected from each site with a fiber optic probe using over 500 diodes in the detector, corresponding to wavelengths of 300 to 650 nm. The spectral area under the curve (AUC) was calculated in arbitrary units after background subtraction and normalization. The diabetic subjects were monitored more frequently than the control subjects. Data was not collected from callused or open wound areas. Two-way ANOVA and student's t-test were used for statistical testing as appropriate.

RESULTS AND DISCUSSION

The two-way ANOVA of AUC indicated a significant difference among the three groups, but not due to skin sites. The AUC is significantly ($p<0.05$) higher for diabetic than in the non-diabetic individuals (Table 1). No significant difference was observed between the AUC of diabetic individuals based on ulcer formation. However most of those who developed an ulcer appear to have a sharp decrease in AUC about when the ulcer was detected (Figure 1). Only in one subject, the lowest point of AUC may have been missed since he started in the study while healing from an ulcer.

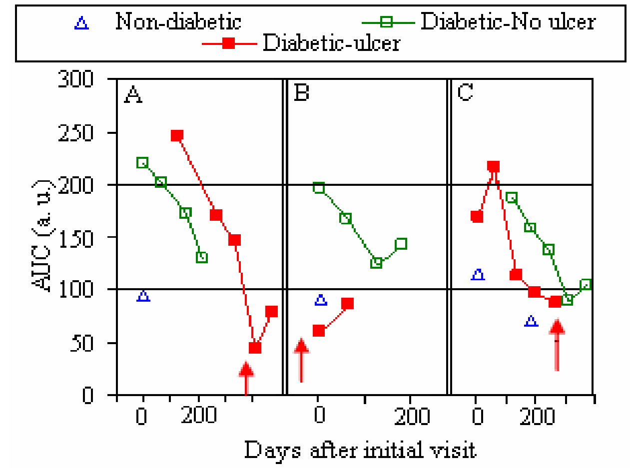

Figure 1: Spectral characteristics of the plantar skin area of interest in age-matched subject groups based on time from their initial visit. AUC=area under the curve, au=Arbitrary Units. Arrows indicate ulcer.

CONCLUSIONS

The LIAF data indicates a higher signal for the diabetic individuals due to their altered state of intermolecular bonds. However, the AUC decreased prior to an ulcer formation suggesting its potential as a marker of tissue stiffness and thickness changes which precede ulceration in the diabetic foot. Additional data are needed to evaluate the differences within the diabetic population which predispose some to ulceration.

REFERENCES

1. Brownlee, M. *Nature* **414**(6865), 813-820, 2001.
2. Monnier, VM, *et.al. The New England Journal of Medicine* **314**(7):403-408, 1986

ACKNOWLEDGEMENTS

Support was provided by the Juvenile Diabetes Research Foundation, the National Science Foundation Research Education for Undergraduates program, and the NIH, NCRR, General Clinical Research Center Grant.

Table 1: The AUC of LIAF spectra and age of the subjects (n=9). Groups A, B, and C correspond to Figure 1based on ulcer site.

Max.AUC (arbitrary unit)	Group (Fig 1)	Non-Diabetic	Diabetic-No Ulcer	Diabetic-Ulcer
Hallux		130.7	196.9	126.7
	A	95.4	220.0	245.3
		98.3	178.0	92.4
5^{th}Metatarsal		96.8	205.4	202.0
	B	91.3	198.5	85.8
	C	115.0	187.4	217.6
Age (Years)		76.7 ± 4.6	76.3 ± 3.2	73.7 ± 5.5

DENSITY CHANGES IN BOVINE TENDON RESULTING FROM BUFFERED AND UNBUFFERED SOLUTIONS

[1]Robin Adams, [2]Michele Oliver and [2]Taylor Murphy
[1]School of Biomedical Engineering, Dalhousie University, Halifax, Nova Scotia
[2]School of Engineering, University of Guelph, Guelph, Ontario; email: Robin.Adams@dal.com

INTRODUCTION

Standard engineering materials can be characterized with a variety of parameters including elastic modulus, yield stress, and ultimate tensile strength. Many engineering materials behave in a well-characterized fashion, however, when applying the same methods to biological materials their performance is varied, and highly dependent upon the methods of *in-vitro* preparation. This has led to a variety of complications in biological materials research. The objective of this work was to address the issue of cross-sectional area prediction of biological tissues. One method, in particular, uses mass and length measurements and assumed values for tissue density to determine an average cross-sectional area as per the formula [1].

$$\frac{m}{dL} = \overline{A} \quad (1)$$

Where
d is the density of the specimen
m is the mass of the specimen
L is the length of the specimen and
$\overline{A}$ is the average cross-sectional area.

Using the definition of engineering stress, there is an inverse relationship between stress and average cross-sectional area.

$$\sigma = \frac{F}{\overline{A}} = F \times \frac{dL}{m} \quad (2)$$

Where
F is the force applied and
σ is stress.

Tissue volume can be determined through fluid displacement. In itself this is not a problem; however, the submersion does bring into question how the tissue dimensions and density change in *in-vitro* solutions. Unbuffered hyper- or hypo-tonic solutions may cause bulk fluid transfer, changing the density of the sample as well as the overall sample dimensions [1]. Because submersion affects fluid retention, it is difficult to determine pre- and post-volume measurements. However, length and mass measurements may be performed independent of submersion with changes in this dimension being used to determine the sensitivity of a tissue to submersion. In this manner, the effect on the change in predicted stress ($\Delta\sigma$) may be approximated.

$$\therefore \Delta\sigma \cong \left(\frac{FdL_0}{m_o}\right) - \left(\frac{Fd\left(L_0 + \delta_{Length}\right)}{(m_o + \delta_{mass})}\right) \quad (3)$$

Where
δ_{Length} is the change in sample length
δ_{mass} is the change in sample mass

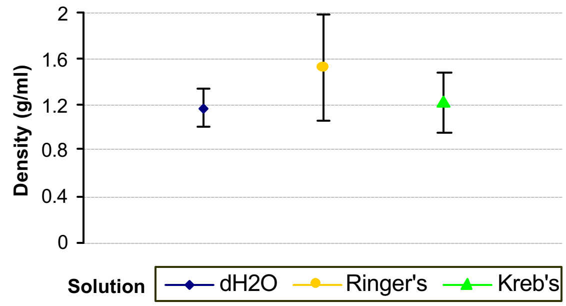

Figure 1: Predicted tissue densities for a 60 second submersion (mean±standard deviation).

METHODS

Three solutions were prepared (Ringer's Solution, Kreb's Solution and deionized water (dH_2O)). Bovine hoof tendon samples (n=14) were obtained from the Ontario Veterinary College within one hour of slaughter and dissected longitudinally into 80mm lengths. Sample lengths and masses were evaluated pre- and post- submersion. All length measurements were made in triplicate using a MicroScribe™ 3D Digitizer (Immersion Corporation, San Jose, CA, USA). Tendon samples from each cow were submerged in one of the three solutions for approximately 60 seconds and their volumes were determined by their fluid displacement. A system of syringes was created for this purpose. Density was determined from the volume and the post-mass measurements.

RESULTS AND DISCUSSION

No significant post- minus pre-immersion changes in mass ($p=0.73$) or sample length ($p=0.15$) were observed as a result of solution type. However, a significant solution effect was found in the density values ($p=0.01$) where the Ringer's solution tissue had higher values for density than the dH_2O or the Kreb's solutions. Interestingly there was no difference observed for stress variability ($\Delta\sigma$) by solution ($p=0.89$) indicating that solution type did not alter the predicted stress.

CONCLUSIONS

Results suggest that while solution type affects density, any effects on predicted stress cancel out probably as a result of subtle mass and length changes in the tissue sample.

REFERENCES

1. Ker RF, et al., *J. Zool., Lond.* **216**, 309-324, 1988.
2. Zanaboni G, et al.. *Matrix Biology* **19**, 511-520, 2000.

ACKNOWLEDGEMENTS

This work was supported by an NSERC Discovery grant to M. Oliver and an NSERC Summer Student grant to R. Adams.

CYTOSKELETON DYNAMICAL BEHAVIOR APPROACHED BY A GRANULAR TENSEGRITY MODEL

[1]Jean-Louis Milan, [1]Sylvie Wendling-Mansuy, [2]Michel Jean and [1]Patrick Chabrand
[1]Laboratoire d'Aérodynamique et de Biomécanique du Mouvement, CNRS-USR2164
[2]Laboratoire de Mécanique et d'Acoustique, CNRS-UPR 7051
Université de la Méditerranée, Marseille, France. email: milan@morille.univ-mrs.fr

INTRODUCTION

The mechanical behavior of cells plays a fundamental role in the tissue development and adaptation. Adherent cells are supported by their cytoskeleton (CSK), an internal pre-stressed framework composed of numerous interconnected filaments. For instance, contractile actin filaments (AF) generate tension forces toward the whole cell, especially in the basal side to strengthen the cell attachment to the extracellular matrix. This internal tension is balanced by microtubules (MT) associated to intermediate filaments (IF) that appear to resist to compression. By polymerization or depolymerization of AF and MT, the CSK continuously reorganizes itself according to the external mechanical microenvironment. Classical models based on tensegrity concept are consistent with biological observations of mechanical behavior of adherent cells such as strain-hardening, prestress-induced stiffening, viscoelastic properties [2,3] nonetheless the fixed connectivity between their constitutive elements (cables and struts) limits the description of the CSK reorganization. The aim of the present study is to develop a mechanical model based on divided medium theory to estimate the dynamical behavior of the CSK pre-stressed structure.

METHODS

To describe the CSK of an adherent cell, our 2D model is composed of numerous rigid disks arranged in a compact configuration whose shape is a 80 µm-diameter half disk and whose basal side is stuck on a flat substrate. Among these disks a larger one represents the nucleus (Figure 1). Within this assembly of elements in cohesive contact are distinguished several collections of elements on which particular interaction laws are applied. To represent the cell adhesion some disks of basal side interact with the substrate according to a highly cohesive contact law. To characterize the stress fibers that generate internal tension toward the whole cell a network of at-a-distance interactions of elastic tension are defined between some disks of the model boundary and especially between disks of the basal side that adhere to the substrate. The large disk that represents the nucleus interacts in the same way with those singular bodies. At-a-distance elastic tensions are also defined between disks of the apical side of the model to represent the cortical actin network located under the cell membrane. The model is then submitted to uniaxial compression at 3.10^{-3} m/s for a final deformation of 30%. The mechanical equations are resolved using a numerical method of non-smooth contact dynamics [3].

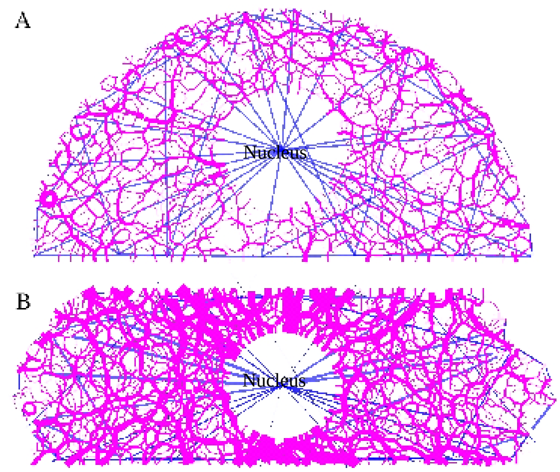

Figure 1: Distribution of forces within the granular tensegrity model. (A) at reference state (before loading) and (B) at 30%-compressed state. The blue straight lines represent at-a-distance forces of tension and the purple diffused lattice shows the network of compression forces.

RESULTS AND DISCUSSION

The first results obtained by the 2D granular tensegrity model show the internal force distribution (Figure 1). To balance the at-a-distance or cohesion tension forces, some elements in contact form chains of compression and thus a compression network inside the whole structure. Under compressive loading, elements rearrange themselves modifying their connectivity and the magnitude of interactions to balance the external applied force. Some at-a-distance elastic tensions vanish, new ones appear. Considering the prestretched actin network in analogy with the tension distribution and the MT associated to the IF network in analogy with the compression distribution, the 2D granular tensegrity model shows the organization of the CSK filaments and its variation under external applied stress and thus should provide a useful approach for investigating how each of the CSK substructures may be involved in the mechanical response of living cells.

REFERENCES

1. Cañadas P., Laurent V.M. et al.; *J. Theor. Bio.* **218**, 155-173, 2002.
2. Wendling-Mansuy S., Cañadas P., Chabrand P.; *Comp. Methods in Biomech. and Biomed. Eng.* **6**(1), 45-52, 2003.

Jean M.; *Comp. Methods in Applied Mech. and Eng.* **177**, 235-257, 1999.

REPETITIVE HEAD LOADING: ACCELERATIONS DURING CYCLIC, EVERYDAY ACTIVITIES

[1]Darrin Richards, [1,2]Irving Scher, [1]Vinod Vijayakumar,[1]Michael Carhart,[1]Robert Larson,[3]Sara Taylor, and [1]Catherine Ford Corrigan
[1]Exponent, Failure Analysis Associates, Inc.
[2]University of Southern California, Los Angeles, California
[3]University of Alabama at Birmingham, Birmingham, Alabama

INTRODUCTION

Closed head injury research has primarily focused on acceleration and force thresholds for isolated impulses, such as those experienced in motor vehicle accidents or falls. The effects of activities that result in long duration cyclic exposure have been studied for the thoracic and lumbar spine and standards for vibration dosage have been generated. The international standard ISO 2631-1 [1] provides guidance on measuring and frequency weighting vibration input. This is done for a seated occupant from the seat bottom and seatback, and for person who is standing or recumbent. Health guidance limits are defined for the vibration exposure for a seated occupant, but are mainly related to the lumbar spine and connected nervous system. Little has been done with the head.

When involved in a cyclic activity, such as running or hopping, motion of the torso and neck result in head motion. The frequency content of the accelerations experienced by the head differs from the input. Goldsmith [2] stated that the head resonance is most pronounced at 8Hz for forced harmonic resonances at whole-body frequencies. This could result in signal amplification at response frequencies near 8Hz. The purpose of this study was to investigate the frequency content of linear head accelerations during various repetitive, common activities and determine if there is significant loading at 8Hz.

METHODS

A head accelerometer apparatus was designed and constructed with linear accelerometers mounted to an adjustable lightweight headband. The sensor group had a range of ±10Gs (resolution: 0.0003Gs) along each axis. Each channel was low-pass filtered using a 100Hz anti-aliasing filter then digitally sampled at 500Hz. For testing, the headband was positioned so that the sensors were at the top of the head and its axes were coincident with the mid-sagittal plane and the coronal plane through both external auditory meati. The complete head apparatus weighed 85g.

Fifteen male and fifteen female participants voluntarily performed the activities chosen for the study: hopping (with two feet), running with an abrupt stop, jump rope, and running up and down stairs. Participants exhibited a wide range of age (from 18 to 44 years old), height (1.56 to 1.89m, mean 1.72m), and weight (51 to 106kg, mean 73kg). The subjects were asked to perform the tasks in a quick and precise manner.

The data from the sensors were filtered digitally using a 50Hz low-pass filter. The linear acceleration data were used to determine the accelerations at the approximate center of gravity (CG) of the head. The distance from the sensor to the head CG was estimated using anthropometric measurements and regression formulae given by Zatsiorsky [3].

RESULTS

All thirty participants were able to complete the tasks with no reports of injury or pain. A power spectrum density (PSD) analysis for each task across all subjects revealed that the magnitude decreased consistently by more than 30dB beyond 9Hz (see Figure 1). The largest loading was usually between 1 and 5Hz (see Figure 2). Not surprisingly, the torso and neck essentially acted as a low pass filter, not allowing the higher frequency loading to reach the head. The average number of impulses above 3Gs (a measure of dosage) was computed for each subject and each trial. On average, subjects experienced 58, 84, 24, and 4 impulses above 3Gs per minute for hopping, skipping rope, running, and stair running, respectively.

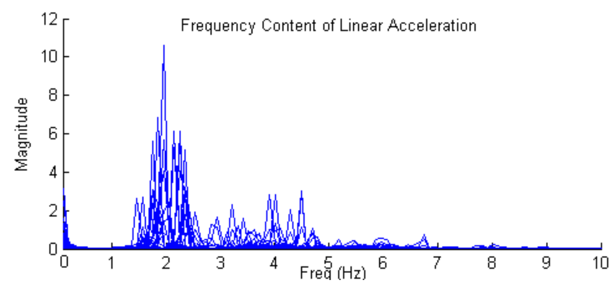

Figure 1: Compiled PSD of head acceleration while skipping rope, for all 30 subjects. The other tasks had similar plots.

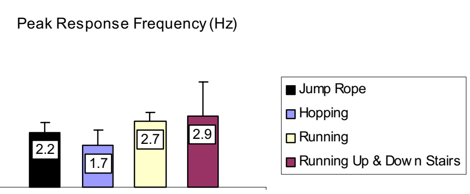

Figure 2: Peak frequency response (mean ± standard error).

DISCUSSION AND CONCLUSIONS

Previous studies have documented forced resonance values of the head, but there is limited information available describing the frequency content of head accelerations during repetitive activities. In this study, we quantified the frequency content associated with a several non-injurious repetitive activities by measuring head accelerations. The response frequency of the head was generally between 0.1 and 9Hz, with the most significant frequency falling between 1 and 5Hz.

REFERENCES

1. ISO 2631-1, Mechanical Vibration and Shock—Evaluation of Human Exposure to Whole Body Vibration, 1997.
2. Goldsmith, W. *Critical Reviews in Biomedical Engineering*, **29(5&6)**, 441-600, 2001.
3. Zatsiorsky, V, et al. *Proceedings of the Ninth International Congress of Biomechanics*, Waterloo, Ontario, 1983.

A NEW APPROACH FOR MODELING AND ANALYZING THE VISCOELASTIC BEHAVIOR OF BLADDER WALL TISSUE

[1] Jiro Nagatomi, [2,3]Michael B. Chancellor, and [1,3]Michael S. Sacks
[1]Department of Bioengineering, [2]Department of Urology, [3]McGowan Institute for Regenerative Medicine
University of Pittsburgh, Pittsburgh PA 15261; email: msacks@pitt.edu

INTRODUCTION

Previously our laboratory demonstrated using biaxial stress relaxation tests that the viscoelastic behavior of rat bladder wall is dependent on the health state (normal vs. neurogenic) as well as on the initial stress level [1]. Although these mechanical testing results were fitted relatively well to a reduced relaxation function (RRF: part of the Fung QLV theory [2]) we observed time-dependent residuals between the model prediction and the experimental data [1] Since the bladder is composed largely of smooth muscle with varying amounts of collagen and elastin in the extracellular matrix, we hypothesized that modeling of the bladder wall would require multiple RRFs specific for each component.

The present study, thus, proposes a new modeling approach to predict the stress relaxation response of the bladder wall. Furthermore, an experimental method has been established to test the stress relaxation behavior of the decellularized bladder extracellular matrix in order to determine the contribution of the matrix on viscoelasticity of the bladder wall tissue.

METHODS

New Approach for Viscoelastic Modeling of Bladder Tissue

In an attempt to dissociate the contributions of the extracellular matrix and the smooth muscle components of the bladder wall tissue, the following form of the reduced relaxation function, RRF, was suggested.

$$G_{total}(t) = (1 - e^{-\beta\sigma}) \cdot G_{ECM}(\mathrm{t}) + e^{-\beta\sigma} \cdot G_{sm}(t) \qquad (1)$$

In this formulation, the total RRF consists of two independent RRF's for the ECM and for smooth muscle, bound by an exponential recruitment function that is dependent on the initial stress level, σ, under the assumption that the higher the stress, the more ECM is loaded and contributes toward the overall stress relaxation response of the tissue.

According to the Fung QLV model, the RRF is formulated with a continuous relaxation spectrum. In the present study, based on the literature reports on the stress relaxation behavior of smooth muscle [3], we assumed that the smooth muscle component of the bladder tissue would follow this spectrum. For the extracellular matrix of the bladder, however, based on our previous results we assumed that the relaxation spectrum could not be described with a constant. Therefore, as a first attempt, we suggested that the following dual Gaussian form of the relaxation spectrum for the bladder ECM.

Decellularization of Bladder Tissue Specimen and Biaxial Stress Relaxation Tests

Whole bladders were harvested from female Sprague-Dawley rats and were placed immediately in tris-buffered saline (TBS) at 4 °C for up to 48 hours. The bladders were then treated in a series of detergent solutions to decellularize using a method adapted from the literature [4].

Equi-biaxial stress relaxation tests were performed using a custom-made biaxial testing device [5] in modified Kreb's solution at 37 °C for up to 3 hours according to the established protocol [1]. Briefly, an equi-biaxial quasi-static testing run with 12 loading-unloading cycles was performed to precondition the tissue (at either 25 or 100 kPa) and to determine the strain levels necessary for the subsequent equi-biaxial stress relaxation run. Next, the specimen was loaded to the strain-levels representative of 25 or 100 kPa stress in both axes in 50-millisecond ramping time and was held at these strain levels to relax for the following 10,000 seconds (2 hours 47 minutes).

RESULTS AND DISCUSSION

Decellularized bladder specimens were used in biaxial stress relaxation tests to determine the contribution of the extracellular matrix to the viscoelastic behavior of the bladder wall tissue. The results of stress relaxation tests provided evidence that compared to intact bladder tissue, the decellularized bladder tissue relax less over the testing period of 10,000 seconds. Based on these findings, the RRF for the extracellular matrix, G_{ECM}, was determined.

Finally, the stress relaxation data for normal rat bladder tissue were fitted successfully ($r^2 > 0.99$) with our new viscoelastic model, which produced smaller residuals compared to the conventional QLV (data not shown).

CONCLUSIONS

The present study demonstrated for the first time that stress relaxation response of the bladder tissue can be divided into the contributions of the extracellular matrix and smooth muscle components. Further experimental validation and detailed analyses of the structure of the ECM will allow development of this model into a structure-based viscoelastic model of the bladder.

REFERENCE

1. Nagatomi, J., et al., Ann Biomed Eng. **32**: 1409-1419,2004.
2. Fung, Y.C., *Biomechanics: Mechanical Properties of Living Tissues*. 1993.
3. Price, J.M., et al. Am J Physiol. **236**: C211-20,1979.
4. Brown, A.L., et al., Biomaterials. **23**: 2179-90,2002.
5. Sacks, M.S. J Elast. **61**: 199-246,2000.

ACKNOWLEDGEMENTS

Source of funding: Spinal Cord Research Foundation (#2289-02); NIH (NICDH: P01-HD39768)

THREE VERSUS FOUR PEGGED GLENOID COMPONENTS: A BIOMECHANICAL EVALUATION OF FIXATION STABILITY WITH CYCLICAL LOADING

[1] David Wellman, [1]Paul Weinhold, [2]Carly Kreps, [1]Matthew Raynor, and [3]Spero Karas
[1]University of North Carolina-Chapel Hill, Department of Orthopaedics, [2]University of Virginia School of Medicine, [3]Emory University Department of Orthopaedics; email: weinhold@med.unc.edu

INTRODUCTION

The most common complication in total shoulder arthroplasty is glenoid loosening [6, 2, 4]. Past studies analyzing loosening have concluded that some glenoid designs are superior to others. Rough-backed is better than smooth-backed [1, 2], curve-backed superior to flat-backed [1,2], all polyethylene better than metal-mesh backed [5, 1, 3], and pegs preferred over a keeled design [1]. To date, no studies have investigated the difference between a 4 peg and 3 peg glenoid design. The objective of this study was to characterize the loosening performance of a commonly used 3-peg design (Encore Foundation Total Shoulder Glenoid) versus a 4-peg design (Zimmer Anatomical Total Shoulder Glenoid).

METHODS

Fourteen glenoid components were cemented into bone stock (Model 1522-12, Pacific Research Labs) using standard surgical methods. Loosening of the components was evaluated by a previously established dynamic testing method (ASTM F2028-02) with slight modification. Four of the samples were used to determine the 90% subluxation distance to be utilized in the dynamic testing method. This distance was found to be 4mm. The remaining ten samples were subjected to dynamic testing (n=5 per design).

A linear pneumatic cylinder aligned normal to the glenoid plane was used to compress the humeral head horizontally into the glenoid component at 112 lbs (+/- 11 lbs). The actuator of a servohydraulic materials testing system was used to displace the humeral head sinusoidally to 90% of the subluxation distance in the superior and inferior directions. Samples were subjected to 100,000 cycles at 2 Hz.

Loosening was measured by two eddy current sensors (Model 4U, Kaman Inc.) aligned normal to the glenoid plane that detected the rocking motion of aluminum targets attached to the superior and inferior edges of the glenoid component . A 21 point calibration of the sensors was completed using a non-rotating micrometer with 0.001'' resolution. Dynamic tests were paused at the following load cycles so that static edge displacements could be recorded after the humeral head was displaced to 90% of the subluxation distance: 1K-10K(in 1K increments), 20K, 30K, 40K, 60K, 80K, 100K.

Superior and inferior edge displacements were compared between the glenoid designs at equivalent cycle numbers by a student's T-test. In addition, a two-way ANOVA was used to compare displacements as a function of glenoid design and cycle number. Edge displacements were also plotted as a function of cycle number. Logarithmic regressions of these plots were compared for each design using a dummy variables statistical approach.

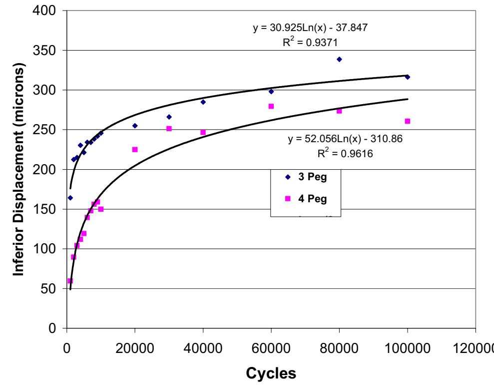

Figure 1: Mean inferior edge displacement of glenoid as a function of cycle number for the 3 and 4 peg designs.

RESULTS AND DISCUSSION

Both inferior and superior edge displacements were found to increase significantly with cycle number (Figure 1). While statistical analyses revealed the regressions of displacement versus cycle number differed with design, comparisons of displacements at specific cycle numbers revealed no difference with design except in the inferior displacement at 1000 cycles. Thus, while the 4 peg design displayed a slightly more stable fixation early, this did not prove to be significant over extended cycles. It is important to recognize that while the two designs did differ in peg number, they also differed in threading pattern of peg and in the width of the articular surface at the inferior pole. A limitation of this study is that inclination and cement mantle thickness were not controlled for.

CONCLUSIONS

Both the 3 and 4 peg design displayed similar loosening over extended cycles. Clinically, the difference over time between the two is unlikely to be detected by the patient. However, further clinical studies involving patient surveys and radiographic analyses are needed to confirm these *in vitro* results.

REFERENCES

1. Anglin, et al. *Clin Biomech* **16**(2): 144-50, 2001.
2. Anglin, et al. *J Shoulder Elbow Surg* **9**(4): 323-31, 2000.
3. Boileau, P., et al. *J Shoulder Elbow Surg* **11**(4): 351-9, 2002.
4. Lacroix, D., et al. *J Biomech Eng* **122**(4): 430-6, 2000.
5. Stone, K. D., et al. *J Shoulder Elbow Surg* **8**(2): 151-8, 1999.
6. Wirth, M. A. and C. A. Rockwood, Jr. *J Bone Joint Surg Am* **78**(4): 603-16, 1996.

MMP-I UP-REGULATION AS A POTENTIAL MECHANISM FOR INCREASED COMPLIANCE IN MUSCLE-DERIVED STEM CELL-SEEDED SIS FOR UROLOGIC TISSUE ENGINEERING

Long, RA [1], Nagatomi. J [1,2], Chancellor, MB [2,3], and Sacks, MS [1,2]
[1] Department of Bioengineering, University of Pittsburgh, Pittsburgh, PA, USA
[2] McGowan Institute for Regenerative Medicine, University of Pittsburgh, Pittsburgh, PA, USA
[3] Department of Urology, University of Pittsburgh, Pittsburgh, PA, USA; email: ral11@pitt.edu

INTRODUCTION

Porcine small intestinal submucosa (SIS, Cook Biotech) can be used as a sub-urethral sling device for treatment of Stress Urinary Incontinence (SUI). However, SIS, along with other biologically derived sling materials, has the tendency to degrade and lose mechanical integrity in vivo over time. In order to improve integrity and function, SIS may be seed with cells. Previously, we demonstrated that SIS seeded with MDSC formed a calcium-dependent contractile muscle-like tissue after 4 weeks of culture(1). We have also shown that MDSC seeded onto SIS increase the mechanical compliance of SIS (2). To date, however, the mechanisms by which the MDSC/SIS construct becomes more compliant are yet to be elucidated.

One possible mechanism responsible for an increase in compliance is the release of matrix metalloproteinase-I (MMP-I), which degrades collagen type-I, the main component of SIS. We hypothesize that the release of MMPs and break down in collagen fibers by MDSCs seeded onto SIS is a potential mechanism responsible for a change in the mechanical properties of MDSC/SIS compared to unseeded SIS. In the present study, we examined the impact of MMP-I on the mechanical properties and surface characteristics of SIS as well as the MMP-I activity of MDSC seeded onto SIS .

METHODS

Samples of SIS (Cook Biotech) were cut into circles and attached with an o-ring to a modified costar transwell cell culture insert (Fisher Scientific) such that the growth area of the SIS was 4.7 cm^2. SIS samples in the constructs were placed in 6 well tissue culture dishes. Mc13 cells (murine, transfected with a plasmid encoding for the b-galactosidase for the tracking purpose) passages 8-10, were seeded at $1x10^6$ cells/ insert in 5.5 mL of in DMEM supplemented with 20% FBS, 1% penicillin streptomycin, and 500 μg/mL G418. Media were changed every 48 hours and supernatant and cell lysates were collected at time points of 1, 3, 5, 7, and 10 days for assays.In order to examine cell proliferation, a PicoGreen dsDNA quantitation kit (Molecular Probes, Eugene, OR) was used on cell lysates. MMP-I activity of MDSC on SIS in culture media at 1, 3, 5, 7, and 10 days was determined using a collagenase assay kit (Chondrex Inc.). The data were normalized by total protein concentration, which was determined using Coomassie Blue total protein kit (Fisher Scientific) as per the manufacturer's instructions.

Twenty samples of SIS were cut in 1 cm^2 squares, sterilized in 70% EtOH, and rehydrated in HBSS for 2 hours. Sixteen of the twenty samples were treated with culture media containing 0.16 U/mL collagenase type I (an equivalent amount of collagenase activity as found at day 1 in the MDSC/SIS seeded samples) in DMEM for 3, 4.5, 5, and 24 hours. The enzyme reaction was stopped in 0.5 mM EDTA for 10 minutes. Four samples of SIS were treated in culture media not containing collagenase-I for 24 hours were used as a control. Biaxial testing was performed on all samples as described previously(2).

Six samples of MDSC/SIS and SIS digested in collagenase-I at varying time points were fixed in 2.5% gluteraldehyde, rinsed in PBS, soaked in 1% OsO4, and dehydrated in EtOH. Samples underwent critical point drying and sputter coating. Then, samples were viewed with a JSM6330F Scanning Electron Microscope in order examine initial cell attachment and surface degradation.

RESULTS AND DISCUSSION

The results of biaxial mechanical testing provide evidence that digestion of SIS with collagenase-I for 5 hours increased up to 7%. This increase in compliance was statistically similar ($p=0.356$) to the compliance of MDSC seeded SIS at 10 days.

Furthermore, DNA quantification showed that the DNA content of MDSC/SIS increased over time indicating that SIS supports cell growth and proliferation. The MMP assay revealed that there was a significant amount ($p<0.05$) of MMP-I present in supernatant from soaked, unseeded SIS compared to media alone. Additionally, MMP-I activity of the MDSC seeded SIS was significantly higher ($p<0.0025$) after one day in culture compared to samples collected from subsequent time points and the unseeded control. These results suggest that the MDSC synthesize and release MMP-1 into the ECM to digest the SIS substrate, which may allow the cells to penetrate and to integrate into the substrate.

CONCLUSIONS

The increase in mechanical compliance seen in MDSC seeded SIS may be mimicked with collagenase-I digestion. MDSC initially respond to SIS by releasing MMP-I, as exhibited through biological assays. The released MMP-I subsequently breaks down the collagen fibers in the SIS. The break down of collagen fibers, in turn may lead to the increase in compliance seen in the MDSC seeded SIS.

REFERENCES

1. Lu, S.H., et al. *Urology*. 61:1285-91, 2003.
2. Lu, S.H. et al. *Biomaterials* 26: 443-449, 2005.

ACKNOWLEDGEMENTS

Source of funding: NIH AR-49398
The authors would like to thank Cook Biotech and Cook MyoSite for materials and technical assistance.

AUTOMATIC MEASUREMENT OF LUMBAR SPINAL KINEMATICS FROM LATERAL RADIOGRAPHS

LW Sun, Steven Yang and Raymond YW Lee

Department of Rehabilitation Sciences,
The Hong Kong Polytechnic University, HKSAR, China
Email: lwsun.mike@polyu.edu.hk

INTRODUCTION

A quantitative method for lumbar spinal kinematics has been developed by composing of the rapid and accurate measurement of vertebral shape and the reproducible and reliable determination of the intervertebral movements of the lumbosacral spine when performing Flexion-Extension motions. Current quantitative methods have suffered from the limitations of the variability of detecting vertebral body landmarks, labour and time-consuming of manual point placement and incompletely describe of the vertebral body shape. Techniques described herein intend to eliminate the limitations. This paper describes the accuracy and feasibility of an active shape model (ASM) and Genetic Algorithm (GA) to measure spine kinematics.

METHODS

Twelve normal male subjects of mean age 21 years (Range, 20-22 years) were examined in this study. Lateral radiographs of the lumbar spine of each subject were taken in a neutral upright position, in full flexion and extension. The capital rotation and translations of the vertebrae on inter-segmental level from L1 to Sacrum were determined and compared between manual 4 corners quadrangles and ASM search finally. Intra class correlation was employed to determine the reliability of these data.

An active shape model (ASM) [1], a general contour method from the field of computer vision, to locate and measures the shapes of vertebrae in images. An ASM contains two separate components. Vertebral shape is described by means of a point distribution model (PDM) with 73 landmarks points along the vertebral contour, which is generated by performing statistical analysis of the object shapes observed over the set of training images. Then, principal component analysis is performed of the set of training profiles for that landmark point as a mean profile plus a set of modes of profile variation. Fourier descriptors were used to represent the vertebral shape. According to Fourier theory, a curve $c(t)$ defines the positions of its points on the vertebral contour

$$c(t)=\begin{bmatrix} C_x(t) \\ C_y(t) \end{bmatrix} = a_0 + \sum_{k=1}^{8} \begin{bmatrix} a_{xk} & b_{xk} \\ a_{yk} & b_{yk} \end{bmatrix} \begin{bmatrix} \cos(k\omega) \\ \sin(k\omega) \end{bmatrix} \qquad (1)$$

Genetic algorithms, is a class of stochastic search methods, operate on a population of solutions. The relative motions between two vertebrae on images are determined by using searching of the ‘best’ value of coefficient of multiple correlations on GA. In this study, the angle of rotation θ and translations of the vertebrae $(x \quad y)$ are the solutions. It encodes in a structure (genome or chromosome). The GA

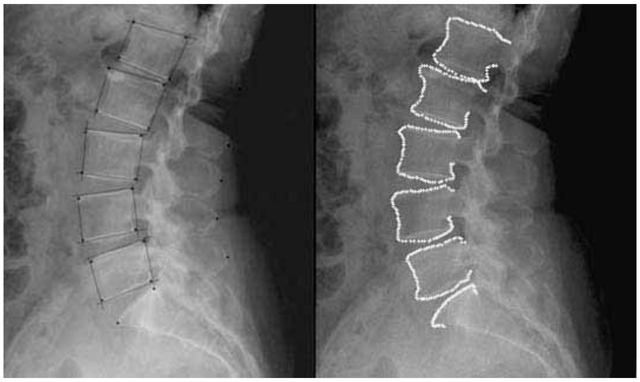

Figure 1: Manual 4 corners quadrangles and ASM search on lumbosacral images.

creates a population of genomes then applies crossover and mutation to the individuals in the population to generate new generation. The objective function (fitness) determines how 'good' each individual is and the best individuals for mating to keep the population evolve.

RESULTS AND DISCUSSION

Figures 1 show the Manual 4 corners quadrangles and ASM search on lumbosacral images. Table 1 summarized the mean of the kinematics on 4 corners quadrangles and ASM method for each vertebral level. High R value (0.998) of ICC(3,1) among subjects was reported.

Ang/°	L1/2	L2/3	L3/4	L4/5	L5/S
4 point	9.0	14.8	11.9	15.4	16.8
ASM	9.2*	14.2*	12.1*	15.3*	17.0*

Table 1: Mean value of angle of rotation (* R>0.995)

CONCLUSIONS

This study demonstrated the accuracy and feasibility of using ASM and GA to determine the intervertebral movements. Less variance and high R value showed that the method was studied to be valid.

REFERENCES

1. Smyth P et al., Automatic measurement of vertebral shape using active shape models, 1997 RSNA scientific assembly, Radiology 1999; 211; pp. 571-578.
2. Genetic Algorithm & Direct Search Toolbox http://www.mathworks.com/access/helpdesk/help/toolbox/gads/

ACKNOWLEDGEMENTS

The author would like to thanks to the Duchess of Kent Children’s Hospital for providing the radiographs.

THE EFFECT OF ACUTE FATIGUE ON NEUROMUSCULAR ACTIVATION PATTERN DURING SIDE-CUTTING IN FEMALE TEAM HANDBALL PLAYERS

[1] Mette K. Zebis, [3]Jesper Bencke, [1]Michael Kjær and [1,2]Per Aagaard
[1]Institute of Sports Medicine Copenhagen, Bispebjerg Hospital, Denmark
[2] University of Southern Denmark, [3] Gait Laboratory, Hvidovre University Hospital, Denmark
email: mkz01@bbh.hosp.dk

INTRODUCTION

Female handball players have a 2-8 fold higher incidence of non-contact injury to the anterior cruciate ligament (ACL) compared to their male counterparts (Myklebust G et al., 1998). Alternated motor control strategies have been identified as a potential risk factor (Malinzak RM et al., 2001). Furthermore it has been shown that fatigue may alter the movement strategy (Wojtys EM et al., 1996), and that the majority injuries occur in the late stage of a match (Gabett TJ, 2000; Pinto M et al., 1999).

The purpose of this study therefore was to investigate if muscle fatigue induced by a simulated handball match would result in altered leg muscle motor patterns during side-cutting movements in female elite team handball players. It was hypothesized that motor patterns would change following the simulated match in a way that could contribute to the increased risk of ACL injury.

METHODS

Neuromuscular activity (EMG; vastus lateralis and medialis, rectus femoris, biceps femoris, semitendinosus) was recorded (1 kHz) during a standardized side-cutting maneuver in fourteen female elite team handball players, pre and post a simulated handball match. Furthermore EMG was obtained during maximal isometric quadriceps and hamstring contraction (MVC) at a knee joint angle of 70° (0°=full extension). All EMG signals were highpass filtered (5 Hz cutoff) and smoothed by a moving RMS filter (30 ms time constant). EMG activity (mean average amplitude) during side-cutting was normalized to the peak EMG amplitude recorded during MVC. Median power frequency was determined by FFT analysis of the raw EMG signals subsequent to a Hanning window procedure.

The simulated handball match consisted of a series of intermittent exercises (side steps, cross over steps, jumps, high and low intensity running and sprinting) mimicking handball match activity (50 min).

RESULTS AND DISCUSSION

The simulated handball match protocol caused a marked decrease in quadriceps (-21%) and hamstring (-16%) MVC ($p<0.05$). During the ground contact phase (in time intervals 10, 50, 100 and 200 ms after toe-down) the neuromuscular activity of semitendinosus decreased by 47-55% (Fig.1). A tendency towards an increase in activity of biceps femoris was observed (50, 100 and 200ms after toe down, $p<0.10$) (Fig.1). Median power frequency (MPF) in biceps femoris increased after the simulated handball match from 109 ± 19 to 122 ± 32 Hz ($p<0.05$). In contrast, MPF remained unchanged in semitendinosus, 97 ± 25 vs 90 ± 14 Hz. EMG activity (RMS amplitude) and MPF remained unchanged in all other muscles examined.

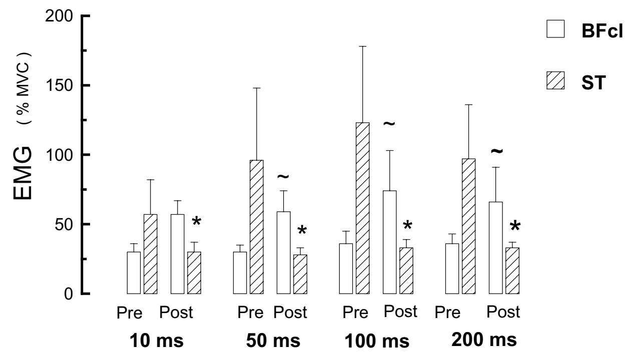

Figure 1: EMG activity of biceps femoris (BFcl) and semitendinosus (ST) during braking phase in a side-cutting maneuver. *denotes significant difference ($p<0.05$).~denotes a tendency towards a difference ($p<0.1$).

CONCLUSIONS

This study indicates that acute fatigue induced by handball match play, involving substantial eccentric and rotational forces, cause changes in the neuromuscular motor pattern during a standardized side-cutting maneuver.

The simulated handball match resulted in substantial decreases in maximal quadriceps and hamstring contraction strength. Likewise, alterations were observed in the neuromuscular activation pattern: Median power frequency increased in biceps femoris which could indicate recruitment of more type II motor units and/or a decrease in the amount of motor unit synchronization at the end of the simulated match. Furthermore, reduced EMG activity was found in the semi-tendinosus muscle in response to match-induced fatigue, which may potentially represent an elevated risk factor for ACL-injury. The typically female non-contact rupture of the anterior cruciate ligament (ACL) involves the knee in valgus, the foot fixed on the ground, and external rotation of the tibia. Since m. semitendinosus acts as an internal rotator of the tibia, the observed decrease in m. semitendinosus EMG activity may predispose for excessive external tibia rotation during side-cutting, thereby increasing the risk of ACL overloading.

REFERENCES

1. Gabbett TJ. *Br J Sports Med* 34: 98-103, 2000.
2. Pinto M, et al. *Clin J Sport Med* 9: 70-74, 1999.
3. Myklebust G. et al. *Scand J Med Sci Sports* 8:149-153, 1998
4. Wojtys EM, et al. *Am.J Sports Med* 24:615-21, 1996
5. Malinzak RA, et al. *Clin.Biomech* 16:438.-45, 2001

EFFECTS OF CORRECTIVE SHOEINGS ON THE EQUINE SUPERFICIAL DIGITAL FLEXOR TENDON LOAD, EVALUATED BY A NON-INVASIVE ULTRASONIC TECHNIQUE

Nathalie Crevier-Denoix, Bérangère Ravary, Jean-Marie Denoix and Philippe Pourcelot
UMR INRA/ENVA Biomécanique et Pathologie Locomotrice du Cheval, Ecole Vétérinaire d'Alfort, France

INTRODUCTION

Corrective shoeings are often recommended for tendinitis management, although their effects on tendon tension lack scientific evidence. Previous studies dealing with the quantification of the effects of corrective shoeings on equine tendon loads are indeed few [1,2], mainly because of the difficulty to obtain reliable in vivo data about tendon loads or strains, and because of the invasive nature of the techniques used so far (implanted transducers). A non invasive method to measure tendon loads has been developed [3]. This method is based on the measurement of the propagation velocity of ultrasound (US) in the tendon. It has been demonstrated that the speed of sound (SOS) changes in a logarithmic manner with the load applied to the tendon.
The objective of this paper is to report results of evaluation of the effects of 4 corrective shoes on the equine superficial digital flexor tendon (SDFT) load using this novel non-invasive technique.

METHODS

Ultrasonic (US) measurements were performed on a group of 4 sound horses (8.5±4.0 years; 501±28 kg) using a dedicated device composed of an electronic battery-powered module (placed on the horse back by means of a saddle) and an ultrasonic probe. The probe is made of 6 transducer elements, one acting as an emitter and the others as receivers. The SOS was measured using the axial transmission method along the long axis of the tendon. Skin facing the right SDFT in the palmar metacarpal area was clipped. The probe was placed in contact with the skin by means of a gaiter.
After preliminary trimming, both front hooves of each horse were equipped with a support shoe (nailed). The standard and corrective shoes to be tested (6° toe and 6° heel elevation on hard ground, reverse shoe and wide toe-narrow branches shoe on soft ground) were successively screwed on the support shoes of both limbs. For each shoe test, a 10 minute habituation was performed then horses were led at the walk along a 30 m long track. Ultrasonic and accelerometric recordings (100 Hz) were repeated 3 times.
For each recording, a mean pattern of SOS was calculated after time normalization by averaging the SOS data over 10 successive strides. Finally, data from the 3 recordings of a shoe test were averaged.
The SOS values at the beginning, the 2 peaks and the end of the stance phase, as well as the corresponding temporal parameters (in % of stride duration) were considered for statistical analysis. An ANOVA was performed to test the effects ($P<0.05$) of the different shoes, each corrective shoe being compared both with the standard shoe and the opposite shoe, on a given ground (toe vs. heel elevation on hard ground, reverse shoe vs. wide toe-narrow branches shoe on soft ground).

RESULTS AND DISCUSSION

Comparison of the SOS patterns demonstrated that heel elevation and reverse shoe induce a significant increase of both the intensity (about 0.2 to 0.3 N/kg of bodyweight, at the second peak), and the relative duration, of tendon loading during the stance phase (especially propulsion, i.e. second part of the stance), compared with standard shoe. The inverse effects were observed with toe elevation (about 0.2 N/kg of bodyweight load decrease) and, to a lesser extent, with wide toe shoe. In terms of loading intensity, the effects of toe vs. heel elevation on hard ground were more marked than those of wide toe vs. reverse shoes.

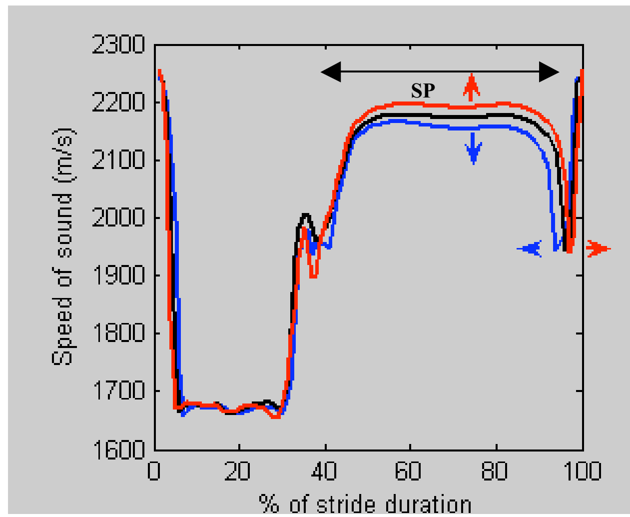

Figure 1: Effects of toe (blue) and heel (red) elevation, compared with a standard shoe (black), on the ultrasonic velocity pattern, at the walk on hard ground (SP = stance phase).

CONCLUSIONS

This study confirms the results reported by the two previous studies [1,2] dealing with the effects of heel/toe elevation on the SDFT loading (increased / decreased tendon tension). It brings new information about reverse shoes and wide toe shoes, more recommended in practice, and tested on soft grounds as those used for training and competition. This study also revealed significant changes in tendon loading duration, induced by the corrective shoeings tested, on both ground surfaces.

REFERENCES

1. Riemersma DJ, et al. *Equine vet J* **28**, 126-132, 1996.
2. Stephens PR, et al.. *Am J Vet Res* **50**, 1089-1095, 1989.
3. Pourcelot P, et al.. *J Biomech* in press.

Quantitative Match Analysis of Soccer Games with Two Dimensional DLT Procedures

Sumiyo Toki and Shinji Sakurai
School of Health and Sport Sciences, Chukyo University, Japan

INTRODUCTION

Match analysis has been widely executed for soccer games. For many years these analyses were mainly based on “observation sheets” methods, in which a tester took charge of a player to draw his trajectory on a sheet. Ohashi et al (2000) developed a quantitative method for the match analysis using trigonometric surveying with two potentiometers. However, it is not realistic to analyze the movement of all the players in a match, because these methods basically need at least one or two testers for one player. The purpose of this study was to develop a new simple quantitative method for match analysis of soccer games with a single video camera filming.

METHODS

Two-dimensional DLT procedures were used for the calculation of the players’ positions, with an assumption that all the players’ movement was on the same level (Z=0). A game of Japanese Professional Soccer League (J-League, Nagoya vs. Kashima) was filmed with a video camcorder set at the highest point of the audience stand of a stadium. The actual image of the video was shown in Figure 1. Two-dimensional coordinate system was set as shown in the Figure 1 with X and Y axes along the goal line and the touchline, respectively. Twenty-nine points with an already known coordinates on the field, such as the intersection point of a touchline and the center line, were used for the reference points for 2D-DLT calculation. Standard errors for the estimation were X=0.40m and Y=0.55m. All the players were digitized every 0.5 second (2Hz) throughout the game. Trajectory, distance covered, and running speed were obtained for each player.

Figure 1: Video image and the coordinate system for the analysis

RESULTS AND DISCUSSION

Figure 2 shows moving trajectories of three players (defense=BK, midfielder=MF, and forward=FW) of Nagoya team during 2nd half of the match. The trajectories show the distinctive features of the players and the positions.

Distance covered by each player was obtained every 5minutes in the 2nd half of the match and the changes are shown in Figure 3 for all the field players of Nagoya team. The average distance covered was 5886m. There was about 4 minutes interruption (29-33 min) over a judgment of a foul. The graph

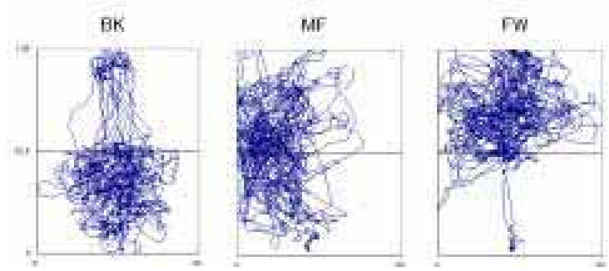

Figure 2: Trajectories of three players with different positions

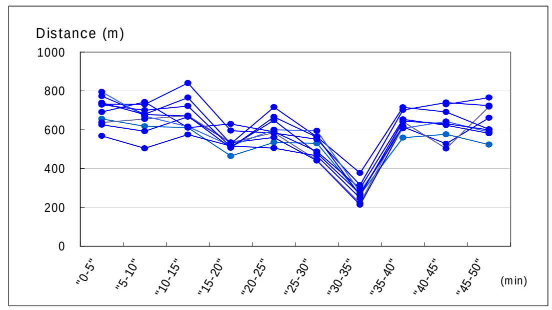

Figure 3: Changes of distance covered of all the players

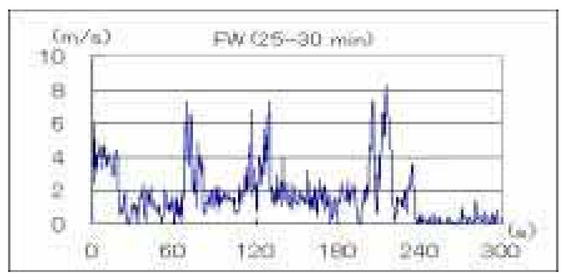

Figure 4: Speed changes of a forward player

well indicates an overall decreasing trend of the running distance with the progress of the match. It also clearly shows a short distance covered for all of the players during the interruption.

Speed changes were calculated from displacement changes for all of the players. Figure 4 shows an example of the speed changes of a forward player for 25-30 minute of the 2nd half. Forwards tended to move faster while their team played offense. Players far from the ball tended to move slower..

CONCLUSIONS

These results suggested useful information could be obtained from individual players’ movement with this method. Moreover, team tactics or strategy can be examined because all the players’ movement are clarified.

REFERENCES

1. Ohashi, J. et al.: Application of an analysis system evaluating intermittent activity during a soccer match. Science and Football IV, 133-136

METATARSAL AND TOE LOADING PATTERNS IN DIABETIC PATIENTS: POSSIBLE ROLE IN THE ETIOLOGY OF CHARCOT FOOT COMPLICATIONS.

Brian L. Davis, Ph.D., Kristian Walker, Heather Scoffone
Department of Biomedical Engineering (ND20), Cleveland Clinic Foundation, 9500 Euclid Ave, Cleveland, OH 44195
Email: davisb3@ccf.org

INTRODUCTION

Charcot foot deformities are a complication for diabetic patients with neuropathy. The etiology is poorly understood, though many patients report minor trauma preceding the collapse of their foot. Under normal foot conditions there is a balance[1] in bending stresses applied to the first metatarsal (Figure 1). For this study, it was hypothesized that patients at risk for Charcot complications would exhibit higher imbalances in these loading profiles.

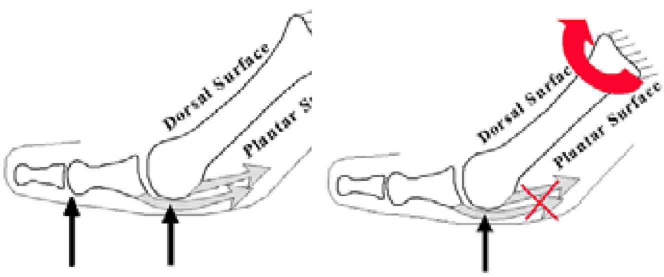

Figure 1. With normal foot conditions, the dorsiflexing forces under the metatarsal heads (vertical black arrow) are balanced by intrinsic muscle contractions (grey arrows). If intrinsic plantar flexor muscle forces are reduced (either through a surgical release or because of pathological changes) the metatarsals will experience greater bending moments.

METHODS

Twelve subjects (five control patients, mean age 58.8 ± 7.89, and seven diabetic patients, mean age 57.33 ± 7.42) were assessed. All diabetic subjects had plantar structural deformities related to Charcot foot disease. The subjects were not age matched, however age has not been found to be a significant factor in plantar pressure distribution. Written informed consent was obtained from all volunteers before data collection, in accordance with Institutional Review Board policies.

For all subjects, recordings of toe and metatarsal head forces were obtained during gait using an EMED pressure measurement system. Three trials were completed for each foot. Pressure masks were designed using Novel Multimask Evaluation software to divide the plantar footprint into anatomical regions, specifically, hallux, second toe, 1st metatarsal head (MTH) and 2nd MTH. Measurements of the arch index[2] for were obtained, with an increased arch index representing a flattened arch.

In terms of statistical analyses, a regression approach was used to relate the ratio of toe and MTH loading to arch index. Finally, ANOVA techniques were used to compare diabetic and control groups (level of significance was 0.05).

RESULTS AND DISCUSSION

Control subjects exhibited a balance between toe and metatarsal loading, whereas diabetic patients had significantly reduced toe loads (Figure 2). The ratio of toe to metatarsal loading was significantly related to arch index (Figure 3).

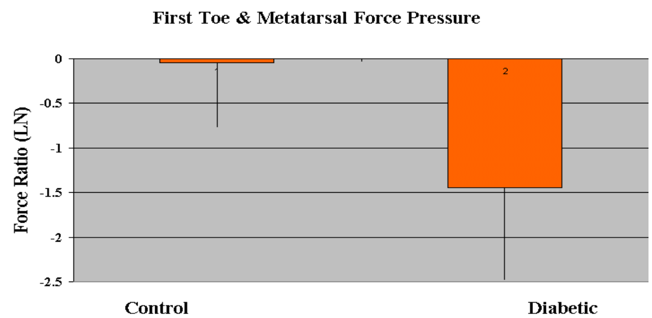

Figure 2: The relationship between forces of the first toe and metatarsal for each experimental group. In control subjects, there is a balance between toe and metatarsal loading, as evidenced by the logarithm being close to zero.

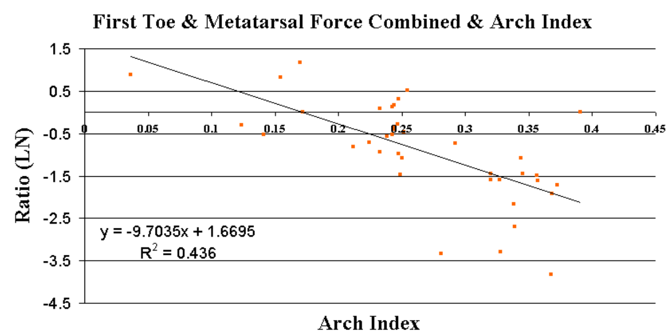

Figure 3. The ratio of toe loading to metatarsal loading was related to arch index ($p<0.05$), with the relationship given by: Log(loading ratio) = 1.67 - 9.7(arch Index)

CONCLUSIONS

The fact that diabetic patients with signs of Charcot foot had (i) smaller forces in the first toe compared with non-diabetic patients, and (ii) increased values for their arch index, supports the hypothesis that diminished plantar muscle forces may increase the likelihood of Charcot foot problems.

REFERENCES

1. Stokes IA, Hutton WC, Stott JR (1979) Forces acting on the metatarsals during normal walking. J.Anat. 129: 579-590
2. Cavanagh PR and Rodgers MM (1987). The arch index: a useful measure from footprints. J.Biomech. 20: 547-551

ACKNOWLEDGEMENTS

The authors acknowledge funding from the National Science Foundation (for HS) and Philips Medical Systems (for KW).

SHORT STATURE OR TALL STORY? HYPOTHESIS AND IMAGINATION IN BODY SIZE RECONSTRUCTION OF LB1 FROM FLORES, INDONESIA

[1]Robert B. Eckhardt, [1]Adam Kuperavage, [2]H. Joseph Sommer, III, and [3]Karol Galik
[1]Laboratory for the Comparative Study of Morphology, Mechanics and Molecules, Department of Kinesiology, The Pennsylvania State University; email: eyl@psu.edu; [2]Department of Mechanical Engineering, The Pennsylvania State University; [3]Laboratory of Orthopedic Biomechanics, Allegheny General Hospital

INTRODUCTION

The LB1 partial skeleton was recovered in September 2003 at a depth of 5.9 m during archeological excavations at the Liang Bua site on the island of Flores, Indonesia [1]. The individual has been diagnosed as female and dated to about 18 kyr, an estimate bracketed by thermoluminescence dates of 35$\pm$4 kyr and 14$\pm$2 kyr, although these figures are disputed [2]. This specimen has been described as the holotype (to which an associated left mandibular P_3 was referred) of a new hominin species, *Homo floresiensis*. Among the features used to support the creation of this new taxon are some estimated dimensions that are extreme in relation to other human populations from this time period, including an endocranial volume of 380 cm^3 and a stature of 106 cm. Here we focus on alternative stature reconstructions and their implications.

METHODS

In the original report, the extremely short stature of 106 cm for LB1 had been reconstructed [1] using an average of results from three regression formulae derived from human pygmies [3]: least squares (LS), 109 cm; major axis (MA), 104 cm and reduced major axis (RMA), 106 cm. Because this result differed so widely from other human population means and no justification was given for the choice of formulae, we surveyed the substantial existing literature for alternative methods that had been used on populations broadly comparable to LB1.

All results reported in the following section are based on the data originally reported in [1]:
LB1 femur length (FL) = 28.0 cm, tibia length (TL) = 23.5 cm

RESULTS AND DISCUSSION

Details of alternative samples and methods for stature estimation are provided in specific references cited below.

[4] African Pygmies, regression lines:
Stature = 1.74 (FL) + 84.5 = 133.2 cm
Stature = 1.85 (TL) + 88.8 = 132.3 cm
Stature = 1.31 (FL + TL) + 55.3 = 122.7 cm
[4] African Pygmies, correlation axis:
Stature = 3.42 (FL) + 17.1 = 112.9 cm
Stature = 3.29 (TL) + 37.8 = 115.1 cm
Stature = 1.61 (FL + TL) + 32.6 = 115.5 cm
[5] Mongoloid, regression:
Stature = 2.15 (FL) + 72.57 = 132.8 cm
Stature = 2.39 (TL) + 81.45 = 137.6 cm
Stature = 1.22 (FL + TL) + 70.37 = 133.2 cm
[6] Javanese females, regression:
Stature = 36.5 + 2.98 (FL) = 119.9 cm
Stature = 52.0 + 3.08 (TL) = 124.4 cm

The unweighted average of the preceding 11 estimates is 125.4 cm, far closer to the estimate of 120 cm [2], which in turn approximates the regression based on femur length for Javanese females, than it is to the original estimate of 106 cm [1]. A stature of 120 to 125 cm is low for extant humans, but is only moderately below those recorded for insular Asian populations exhibiting normally short stature, such as a sample of 15 Andman Island females averaging 137 cm [7].

CONCLUSIONS

Representation of LB1 as the holotype of a new hominin species [1] was challenged initially, with the alternative hypothesis that the specimen instead was a microcephalic individual [8] accounting for the extremely low endocranial volume, which is about one third the average of extant *Homo sapiens* and comparable to chimpanzees and Plio-Pleistocene fossil hominids. The microcephalic hypothesis has been buttressed by subsequent studies of LB1 [2] and our own research on previously known Flores human specimens, which are short (152 cm) but not dwarfed. The idea of individual abnormality rather than phylogenetic novelty gains additional support from other features of the LB1 skeletal remains, comprising a skull vault that exhibits early fusion of cranial sutures, as well as the presence of several dental abnormalities, including tooth crowding, with both maxillary P^4s being rotated parallel to the tooth row, plus a congenitally absent left M^3. These and other postcranial details support the hypothesis that the endocranial volume and stature of the LB1 individual are consistent with known microcephalic members in extant *Homo sapiens* populations [9] of small stature.

REFERENCES

1. Brown P, et al. *Nature* **431**, 1055-1061, 2004.
2. Jacob, T. Personal communication, 17 December 2004.
3. Jungers WL. *Am. J. Phys. Anthrop.* **76**, 227-231, 1988.
4. Olivier G. *J. Hum. Evol.* **5**, 529-534, 1976
5. Trotter M, Gleser GC. *Am. J. Phys. Anthrop.* **16**,79-123, 1958.
6. Bergman RAM, The TH. *Documenta de Medicina Geographica et Tropica* **7**, 197-214, 1955.
7. Quatrefages, A de. *The Pygmies*, Macmillan, New York, 1894.
8. Henneberg M, Thorne A. *Before Farming,* in press.
9. Hall JG et al. *Am J. Med. Genet.* **130A**, 55-72, 2004.

ACKNOWLEDGEMENTS

We thank Dr. Teuku Jacob of Gadjah Mada University in Jogjakarta, Indonesia, for helpful discussions concerning the LB1 specimen as well as access to his unpublished findings.

WAS THE EARLY HOMINID BRAIN MUSCLEBOUND?

Robert B. Eckhardt and Adam Kuperavage
Laboratory for the Comparative Study of Morphology, Mechanics and Molecules, Department of Kinesiology, The Pennsylvania State University, email: eyl@psu.edu

INTRODUCTION

Stedman et al. [1] explored the possible influence that a gene encoding the myosin heavy chain (MYH) might have on the development of hominid masticatory muscles, mandibles and brains, with explicit attention to causal relationships between genetics and morphology in development and evolution. In this context, we read their concluding statement that "findings on the age of the inactivating mutation in the MYH16 gene raise the intriguing possibility that the decrement in masticatory muscle size removed an evolutionary constraint on encephalization..." as embodying a testable hypothesis.

METHODS

It was noted [1] that "experimental animal models of the masticatory muscle resection or transposition have demonstrated the correlation between craniofacial morphology and the force of masticatory muscle contraction" [2]. However, in the rabbits subjected to manipulation of the temporal muscle attachment, no statistically significant changes in brain size were documented; while skull width decreased, length increased, suggesting conservation of endocranial volume. Classic experiments in this area include those in which Washburn [3] removed various muscles from one side of the skull in newborn rats, producing temporal lines either absent altogether or displaced far down in the temporal fossa; but brain endocasts were unchanged on the operated side.

Observationally, many domestic animals have jaws, teeth and brains that all are evolutionarily reduced relative to their wild ancestors. In comparison with skull morphology of *Canis lupus arctos*, cranial capacities of husky dogs are diminished along with measures of jaw size [4]. Among free-living hominoid primates, the largest nonhuman cranial capacity was recorded for a West African gorilla [5]. Its endocranial volume of 752 cc not only exceeds by 40% the average for 400 conspecifics, but also is higher than many of the fossil hominid crania for several hundred thousand years following the 2.4 ± 0.3 my time estimated for the MYH16 mutation. The large gorilla skull also had a markedly high sagittal crest, indicative of massive jaw muscles.

Among extant humans, jaw musculature also can vary quite independently of endocranial volumes. For example, Smith Sound Eskimo were characterized by skulls high in internal volume that nonetheless externally showed markings for the large temporal muscles developed from a traditional diet that required heavy chewing. One male exhibited an intertemporal distance of only 7 mm, less than in some gorillas with endocranial volumes less than half as great [6]. His cephalic index ([head breadth/head length]x100) was 73.1, reflecting a low ratio of cranial width to anterior-posterior length. However, this pattern was not interpreted to mean that a more elongated form of the hominoid skull is produced by greater lateral pressure of the temporal muscles, but rather that higher temporal lines are due to the more reduced insertion area for temporal muscles on skulls elongated for other reasons. Although the most dolichocephalic skull in the sample [7], its cranial capacity was 1545 cc, nearly at the 1563 cc mean for 9 skulls, some of which differed in proportions. An older study [8] of microcephalic human skulls discussed by the same author [6] showed that in these, the intertemporal distance varied tenfold (from 5 to 50 mm), while cephalic index ranged from 75 to 85 (dolichococephalic to brachycephalic), with the lowest intertemporal distance occurring in the most brachycephalic skull. Furthermore, the form of these small-brained skulls was not attributable to premature suture fusion, since the sutures remained open in most of the specimens. Last, the skull of LB1, a very small human discovered recently on the island of Flores, Indonesia, combines a low endocranial volume, in the range of 380 mm^3 [10] to 430 mm^3 [11], with a mandibular corpus that is proportional to its size.

RESULTS AND DISCUSSION

The experiments and observations outlined above establish that in mammals, including hominoid primates, there is no effective constraint by masticatory muscles on encephalization.

CONCLUSION

Our findings demonstrate that the size and attachment of jaw muscles make their marks principally on the external surfaces of the skulls rather than determining internal forms and volumes. Consequently, the idea that the early hominid brain was fettered by muscles whose confines were struck off by a single mutation stands as intriguing but as yet unproved. Nonetheless, it is important to note that although "Recently, evolutionary studies have been revitalized and revolutionized by an infusion of genetics into paleontology and systematics"[9], much of the promise remains to be realized.

REFERENCES

1. Stedman H, et al. *Nature* **428**, 415-418, 2004.
2. Brennan M & Antonyshyn O. *Plast. Reconstr. Surg.* **97**, 13-24, 1996.
3. Washburn SL. *Anat. Rec*. **99**, 239-248 1947.
4. Clutton-Brock J, et al. *J. Zool. Soc. Lond.* **233**, 19-36, 1994.
5. Schultz AH. *Anthrop. Anz.* **25**, 197-203, 1962.
6. Riesenfeld A. *Am. J. Phys. Anthropol*. **13**, 599-620, 1995.
7. Hrdlicka A. *Anthropol. Papers Am. Mus. Nat. Hist*. **5**, 177-280, 1910.
8. Vogt CH. *Arch. f. Anthrop*. **2**, 129-284, 1867.
9. Washburn SL. *Trans. N. Y. Acad. Sci*. **13**, 298-304, 1954.
10. Brown P, et al. *Nature* **431**, 1055-1061, 2004.
11. Jacob T. Personal communication, 17 December 2004.

USING DATA FROM MULTIPLE TESTS TO DETERMINE FOAM PARAMETERS: MODELING IMPLICATIONS

[1,2] **Marc Petre,** [1]**Ahmet Erdemir and** [1-3]**Peter R. Cavanagh**
[1]Dept. of Biomedical Engineering, The Cleveland Clinic Foundation, Cleveland OH
[2]Dept. of Biomedical Engineering, Case Western Reserve University, Cleveland OH
[3]Orthopaedic Research Center & Dept. of Orthopaedic Surgery, The Cleveland Clinic Foundation, Cleveland, OH
e-mail: cavanap@ccf.org, web: www.lerner.ccf.org/bme/cavanagh/lab

INTRODUCTION

Elastomeric foams are represented in finite element (FE) models using constitutive equations containing one or more material specific parameters. Previous work has suggested that the test data used in material parameter determination may have a large effect on simulation results [1]. Specifically, parameters for simulations involving multi-mode deformations should be determined from test data describing all simulated deformation modes. The practical implications of multi-test parameter determination have not been shown in a FE simulation for footwear applications.

This investigation illustrates the effects of using data from multiple tests for foam parameter determination on predictions of clinical interest by simulating the indention of a foam mat by the human heel pad.

METHODS

Two sets of Poron® foam parameters for a common compressible hyperelastic model [2] were determined using custom Matlab® optimization scripts. One parameter set was determined from uni-axial compression data alone and the other from a combination of uni-axial compression, simple shear, and volumetric compression data. The material parameters were incorporated into a pre-existing hyperfoam material model inherent in ABAQUS® FE software.

A plane-strain heel pad model described elsewhere in detail [3] was used to indent a 10mm thick foam mat (Figure 1). The simulation was run twice, once with each set of material parameters. Peak normal stress (plantar pressure) and shear stress were extracted.

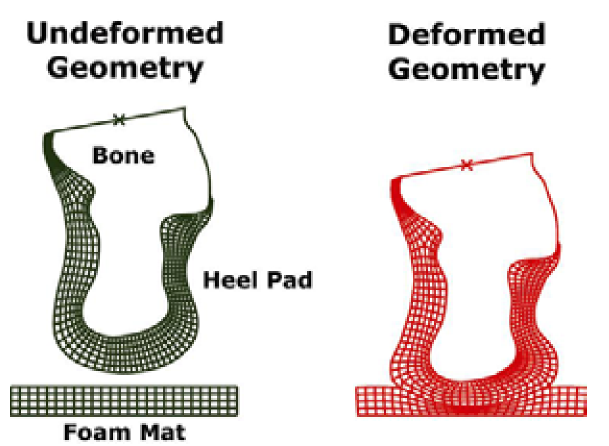

Figure 1. The undeformed and deformed heel pad indentation model. Final geometry was similar for both parameter sets.

RESULTS AND DISCUSSION

Fitting parameters to compression data alone led to high errors in material model prediction of the shear and volumetric test data. Simultaneous fitting of all three deformation modes provided reasonable predictions (RMS error < 5% of maximum) of all test data (Table 2).

Test Data Used in	Order	Errors (RMS as a % of maximum)		
		Uni-axial Compression	Simple Shear	Volumetric Compression
Uni-axial Compression	1	0.67	1.34×10^6	58.5
Compression, Shear, Volumetric	3	4.24	1.30	2.04

Table 1. Material model errors for the two sets of Poron® parameters.

Although the heel pad simulation involves a strictly compressive load, non-linear geometry and friction lead to the generation of multi-axial deformation. When different test data sets were used in parameter determination, large differences between predicted peak stresses were present (Table 2).

Test Data Used in Parameter Determination	Order	Peak Pressure (kPa)	Peak Shear Stress (kPa)
Uni-axial Compression	1	288	62
Compression, Shear, Volumetric	3	258	36

Table 2. Simulation predictions of peak stresses vary with the amount of data used in parameter determination.

Parameters determined from compression alone can not accurately predict shear behavior, leading to an over estimation of about 72%. There is also a discrepancy in the peak pressure prediction that could be due to extrapolation error because the simulation strain has exceeded the maximum strain supplied in the test data.

REFERENCES

1. Petre, *et al. Summer Bioengineering Conference*, Vail, Colorado, Abstract Submitted, 2005.
2. Hill, R. *Advances in Applied Mechanics*, 1-72, 1978.
3. Goske, et al. *J.Biomech*, in review.

ACKNOWLEDGEMENTS

This work was supported by NIH Grant # 5R01 HD037433 and Marc Petre was supported by NIH Grant # T32 EB04314.

INFLUENCE OF FOOT ORIENTATION AND BONE STRUCTURE ON PLANTAR PRESSURE DISTRIBUTION

[1,2] Sachin P. Budhabhatti, [2]Ahmet Erdemir, and [2,3]Peter R. Cavanagh
[1]Dept. of Biomedical Engineering, Cleveland Clinic Foundation
[2]Dept. of Chemical & Biomedical Engineering, Cleveland State University
[3]Dept. of Orthopaedic Surgery and Orthopaedic Research Center, Cleveland Clinic Foundation
e-mail: cavanap@ccf.org, web: www.lerner.ccf.org/bme/cavanagh

INTRODUCTION

Foot orientation is an important component of variability in barefoot plantar pressures [1], a standard approach for assessing risk of ulceration in patients with diabetic neuropathy. Modeling of plantar pressure distribution can be used for the design of therapeutic footwear. In recent three-dimensional finite element (FE) models [2, 3], the orientation of the foot and the relative alignment of the bones was either based on unloaded positioning at the time of imaging or was roughly approximated by using kinematics information. The goal of the present study is to perform sensitivity analyses of i) foot orientation in the frontal plane and ii) relative metatarsal (MT) alignment on plantar pressure distribution.

METHODS

Magnetic resonance images were obtained from the right foot of a male subject (24 yrs, 95 kg, 1.88 m). Bones (MT, phalanges, and sesmoids) and soft-tissue (ST) contours were digitized using custom Matlab (Mathworks Inc., Natick, MA) code and a FE mesh (57,544 eight-noded hexahedral elements) was generated using TrueGrid (XYZ Scientific Inc.) (Figure 1).

The bones were modeled as rigid and ST as incompressible hyperelastic material. Frictional contact between the plantar surface of the foot and the rigid floor was modeled.

The foot was first positioned such that the inferior aspects metatarsal heads (MTH) were approximately parallel to the floor (neutral position). The floor was then displaced towards the foot to obtain contact and horizontal and vertical forces of 500 N and 90 N respectively were applied. The frontal plane orientation of the foot was changed by ±1° from neutral position to test the sensitivity of plantar pressure distribution to this variable. In an additional simulation, of one of the rotated models (neutral + 1°), the second MT was plantarflexed by 1.5 degrees and the first MT was dorsiflexed by 1.5 degrees. The bones were constrained to stay fixed with respect to each other once loading commenced.

Figure 1: Three-dimensional FE model of the forefoot. Arrows show the application of loads to the floor.

RESULTS AND DISCUSSION

In the neutral model, there were no focal areas of high pressure (Figure 2a). Eversion by only one degree loaded MTH4 more prominently (MTH4: 40% increase); inversion by the same amount elevated MTH1 pressures by 35%. Dorsiflexion of MTH2 with respect to MTH1 allowed transfer of loads from MTH1 to MTH2 areas (MTH1: 30% decrease, MTH2: 15% increase with respect to the base model) (Figure 2b).

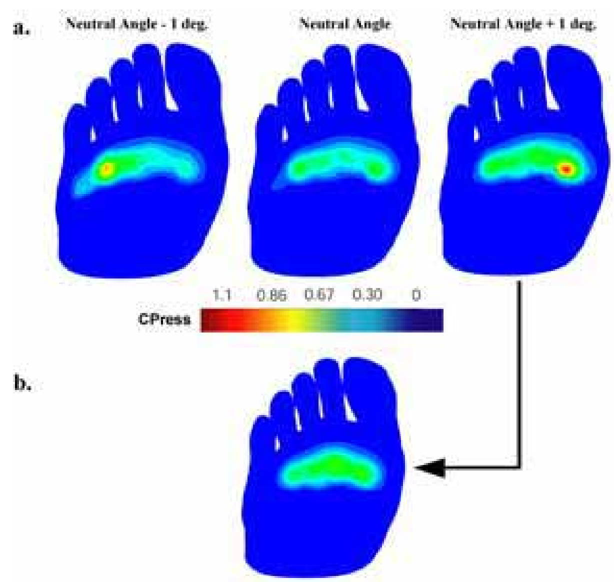

Figure 2: **a.** Plantar Pressure for orientation of the foot. **b.** Increase in MTH2 pressure.

These results show that the prediction of plantar pressures using the current FE model is acutely sensitive to foot orientation and bone alignment, probably much more sensitive than an actual foot in vivo. Before conducting simulations for footwear design, an optimization protocol could be used to provide the bone configuration and foot orientation that best represents experimental barefoot pressures. This study also demonstrates the possibility of changing the alignment of a generic model in order to represent different plantar pressures distributions (e.g. MTH1 predominant).

REFERENCES

1. Morag E, et al., *J Biomech,* **32(4)**, 359-370, 1999.
2. Gefen A. et al., *J Biomech,* **122**, 630-638, 2000.
3. Chen WP et al., *Clinical Biomech.*, **18,** S17-S24, 2003.

ACKNOWLEDGEMENTS

This study was supported by NIH Grant #5R01 HD0374.

LOWER LIMB STRUCTURE AND FUNCTION PREDICT BONE DENSITY OF THE PROXIMAL TIBIA

David Hudson, James Richards, and Todd Royer
University of Delaware, Newark, DE; email: dhudson@udel.edu

INTRODUCTION

Hardening of subchondral bone is a hallmark of advanced osteoarthritis (OA) and is suspected to play a role in the pathogenesis of the disease[1]. Frontal plane knee alignment and moments have been linked to both subchondral bone mineral density (BMD) of the proximal tibia and knee OA[2, 3, 5]. The severity of knee OA has also been linked with medial tibial torsion and limited hip mobility; however, their association with tibial BMD has not been studied[6, 7]. This experiment determined if measures of lower limb structure and function could be used to predict BMD of the proximal tibia.

METHODS

Fifty healthy limbs from 17 females and 8 males; average age: 34 (21-56); average BMI: 24.7 (21.2-28.0) were studied. Eight cameras operating at 120 Hz (Eagle; Motion Analysis Corporation, CA) and 2 force plates operating at 480 Hz (AMTI; MA) were used to collect gait data using a standard Helen Hayes marker set. Orthotrac software calculated the varus/valgus knee angles and moments.

Ultrasound (Sonosite 180plus; MA) was used to image the planes of the posterior tibial plateau and the distal anterior capsular margin. A digital inclinometer (AeroAngle PRO 160, Macklanburg-Duncan, OK) was mounted on the transducer to measure the angular difference between the proximal and distal landmarks. Subjects sat with the foot secured in a custom frame mounted on the wall with the knee flexed and the tibia parallel to the floor (Figure 1).

Hip internal and external rotations were measured using the inclinometer with subjects prone and the knees flexed. A hip rotation index was calculated as the difference between internal and external rotation.

Figure 1. Distal tibial measurement. The arrow points to ultrasound image of the anterior capsular margin; the inclinometer measures the tilt of the transducer when the image is horizontal on the screen.

BMD within the medial and lateral compartments of the proximal tibia was measured using dual energy x-ray absorptiometry (Hologic Delphi W; MA). Compartment widths were ½ the proximal tibia width, and the height was from the cortical line to the superior margin of the fibular head.

Simple and forward stepwise regression was used to determine if maximal knee varus, maximal abduction moments, the hip rotation index and tibial torsion could predict the ratio of the medial to lateral compartment BMD in the proximal tibia.

RESULTS AND DISCUSSION

The hip rotation index, tibial torsion, knee alignment and abduction moments were able to predict a significant portion of the variance associated with BMD distribution ($r^2 = 0.68$; $p = 0.004$). Individual relationships determined from simple regression are listed below (Table 1).

Table 1. Results of simple regression analyses.

Variable	r	sig.
hip rotation index	-0.58	0.001
tibial torsion	-0.40	0.004
abduction moment	0.40	0.005
knee alignment	-0.16	0.318

These results indicate that limb structure and function contribute significantly to BMD of the proximal tibia. Hip rotation and tibial torsion had not previously been investigated and appear to play an important role in this relationship. Knee alignment was less important in this experiment than previously reported[4]

CONCLUSIONS

Limited internal rotation of the hip and medial tibial torsion were related to increased subchondral BMD in the medial compartment of the proximal tibia, and may play a role in the pathogenesis of knee OA.

REFERENCES

1. Burr, D.B., *Osteoarthritis Cartilage*, 2004. **12 Suppl A**: p. S20-30.
2. Christensen, P., et al., *Acta Orthop Scand*, 1982. **53**(6): p. 889-95.
3. Hurwitz, D.E., et al., *J Biomech*, 1998. **31**(5): p. 423-30.
4. Hurwitz, D.E., et al., *J Orthop Res*, 2002. **20**(1): p. 101-7.
5. Sharma, L., et al., *JAMA*, 2001. **286**(2): p. 188-95.
6. Steultjens, M.P., et al., *Rheumatology* (Oxford), 2000. **39**(9): p. 955-61.
7. Yagi, T., *Clin Orthop*, 1994(302): p. 52-6.

PROPRIOCEPTIVE DISTURBANCES IN RSI: A COMPARISON WITH CRPS

[1,2] DirkJan Veeger, [2]Mark Arts and [2]Alfred Schouten
[1]Vrije Universiteit Amsterdam,
[2]Delft University of Technology; email: h_e_j_veeger@fbw.vu.nl

INTRODUCTION

Repetitive Strain Injury (RSI) is a syndrome causing sickness absenteeism all over the world. An often reported symptom of RSI is dystonia, in which there are strong indications for the presence of proprioceptive disturbances. Since RSI is sharing a clinical spectrum along with Complex Regional Pain Syndrome (CRPS), it has been suggested that chronic RSI and CRPS might be related. Chronic RSI might be maintained as the consequence of sensory and proprioceptive disturbances, resulting in co-contraction, tremor, or disturbed proprioceptive response. RSI patients suffering from dystonia may show comparable deficits in performance as CRPS patients. To evaluate the existence of tremors, or deviating force control in patients with chronic RSI, RSI and CRPS patients and controls performed a bradykinesia experiment and a force-control task. We hypothesized that RSI patients would perform worse than controls, but still better than patients with CRPS.

METHODS

Nine RSI patients, 5 CRPS patients and 10 healthy subjects participated. Six RSI patients and all CRPS patients were diagnosed as having dystonia. All subjects filled in the Disabilities of Arm, Shoulder and Neck (DASH) questionnaire and the Shoulder Pain questionnaire.
In the bradykinesia test subjects were asked to open and close their thumb and index finger, as wide and as fast as possible for a period of 30 seconds. From recordings we derived the Total reached distance (TRD), root mean square (RMS) and median frequency (MF), for both the full 30 seconds and three consecutive 10-s intervals.
The force-control task was administered with a handle, positioned in front of the subject. Subjects were sitting with their arm in zero degrees elevation, the elbow in 90° flexion and pronation. Subjects were asked to follow a tracing signal on a computer screen that indicated the required force level. Applied force was plotted on-line (Figure 2). During the task EMG of two shoulder flexors and extensors was recorded. Mean Absolute Amplitude (MAA), transition time (TT) and muscle co-activity were analyzed.

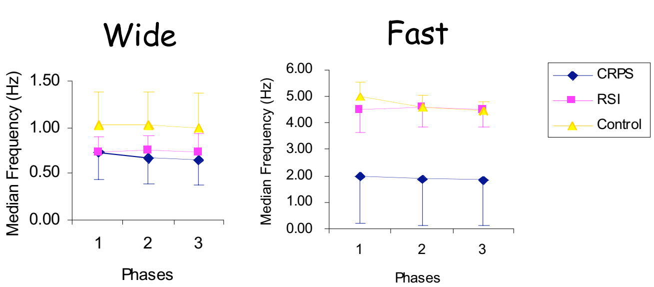

Figure 1
Median frequencies as measured in the bradykinesia test. Phases indicate following 10-second windows during the 30-s test.

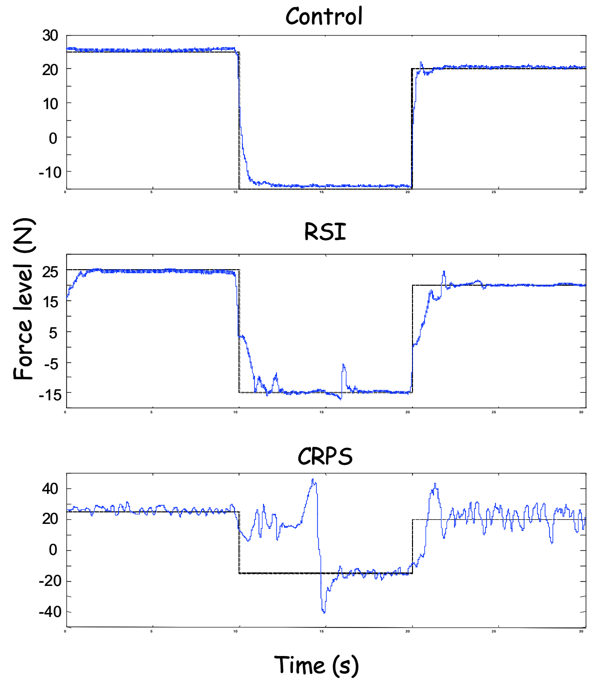

Figure 2
Typical examples of results for the force-control task. Top:

Differences between groups were determined using ANOVA and a Bonferroni post-hoc evaluation.

RESULTS AND DISCUSSION

CRPS patients performed the bradykinesia experiment with a lower MF and a shorter TRD than RSI patients and controls (Figure 1). No significant differences were found between RSI and controls. The median frequency dropped marginally over the three 10-s periods, but not different for the three groups.
Force-control parameters were not different between subjects with RSI and controls, but CRPS patients did show significantly shorter TT and a higher MAA (Figure 2).
RSI patients and CRPS patients show not show a higher co-activation in the shoulder muscles than controls.

CONCLUSIONS

On the basis of the bradykinesia- and force-control test, it could not be concluded that RSI patients had proprioceptive disturbances. As such, these results could not support the theory by Johansson et al. (1) related to the development of RSI could not yet be supported. Evaluation of co-a

REFERENCES

1. Johansson, H & Sojka, P, 1991. Medical Hypothesis, 35: 196-203.

3-D FINITE ELEMENT MODELS OF ARTERIAL CLAMPING WITH FLUID-STRUCTURE INTERACTIONS - A STEP TOWARD SIMULATING CARDIOVASCULAR SURGERY

Henry Yu Chen[1,2], Daniel R. Einstein[3], Kinon Chen[1,2], Ivan Vesely[1]
[1]The Saban Research Institute of Childrens Hospital Los Angeles, CA, United States;
[2]Dept. of Biomedical Engineering, University of Southern California, CA
[3]Pacific Northwest National Laboratory, Richland, WA, United States
Email: HenryChen@chla.usc.edu; Web: http://www.childrenshospitalla.org/body.cfm?id=180

INTRODUCTION

Patient-specific computational modeling can be a useful component of pre-operative planning of cardiovascular surgeries such as those of valves and arteries. The deformation and stress analysis could also provide valuable insights into the tissue injury mechanisms.[1] The objective of this study was to simulate clamping of the aorta, a particularly challenging step, as it is computationally demanding and involves contact between rigid clamps and flexible aorta, contact within the artery walls, large deformations in tissues, and fluid-structure interactions (FSI).

METHODS

The models were created using Finite Element Analysis as well as Computer Aided Design packages. The aorta was modeled as a soft, non-linear material and the clamp was modeled as rigid. The soft tissue material was modeled using a custom in-house subroutine.[2,3] The fluid was modeled as Newtonian, incompressible and transient flow. For validation purpose, ascending porcine aortas were dissected from fresh unfixed hearts and clamped with actual surgical clamps. The external deformation profiles of the pinched aorta were imaged and compared with those of the simulations.

RESULTS AND DISCUSSION

Clamping of the aorta was simulated, producing occlusion of blood flow. The deformation profile of the simulated aorta matched well with that of the real tissue (see Figure 1), indicating that our material model and the simulation were reasonable. The computed deformation profile and stress distributions within the aorta, with and without the internal fluid, indicated significant difference between the two simulations, suggesting the importance of FSI in surgical modeling. The flow fields within the aorta were also computed (see Figure 2).

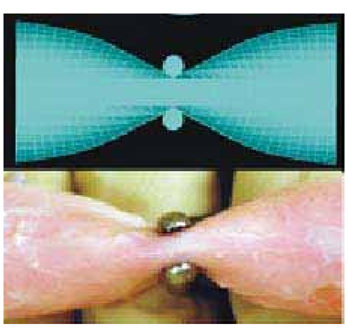

Figure 1. The simulated clamp test showing the deformed profile of the aorta that can be matched to real experiment data of the same deformation.

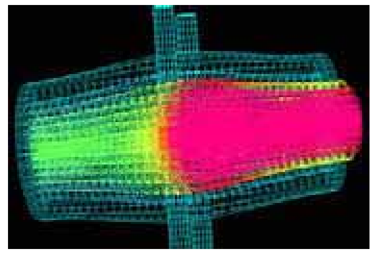

Figure 2. Top view of the fluid flow fields within the aorta during the clamping process; the colors correspond to magnitudes of flow velocities.

CONCLUSIONS

Clamping of a fluid-filled aorta, an important first step towards simulating of surgical procedures, was successfully modeled. The simulation was compared with actual aortic clamping, and deformation profiles of the simulations matched the experiment. The techniques developed in this project are applicable to valve FSI models and further surgery simulations. This model could also be linked with systemic Matlab simulations to have even more realistic modeling.

REFERENCES

1. Gasser TC, Schulze-Bauer CA, Holzapfel GA, A three-dimensional finite element model for arterial clamping. *J Biomech Eng.* 2002 Aug;124(4):355-63.
2. Freed AD, Einstein DR, Vesely I: Invariant Theory for Dispersed Transverse Isotropy: an Efficient Means for Modeling Fiber Splay, *Biomechanics and Modeling in Mechanobiology,* Accepted June 2004.
3. Einstein-D, Reinhall-P, Kunzelman-K, Nicosia-M, Cochran-RP: Dynamic Finite Element Implementation of Nonlinear, Anisotropic Hyperelastic Biological Membrane: *Computer Methods in Biomechanics and Biomedical Engineering*, 2003; 6(1): 33-44.

THE EFFECT OF GLYCOSAMINOGLYCANS AND HYDRATION ON VISCOELASTIC PROPERTIES OF AORTIC VALVE

[1] Abhijit Bhatia, [1] Ivan Vesely
[1]Childrens Hospital Los Angeles
email: abhatia@chla.usc.edu

INTRODUCTION

Glycosaminoglycans (GAG's), long chain sugar molecules that bind water due to their negative charge density, have been thought to be important in defining the viscoelastic properties of soft tissues such as skin [1]. Their importance in aortic valve mechanics however, has not been studied in detail. It has also been showed that cross-linked, commercially available bioprosthetic heart valves have less water content and less viscoelasticity. Therefore, the objective of this study was to determine the relative roles of hydration and GAG content on aortic valve cusp viscoelasticity.

METHODS

To extract the GAGs from porcine aortic valve leaflets, specimens were immersed in three consecutive baths of 0.1M NaOH at room temperature, followed by three consecutive solutions of distilled water. GAG extraction was verified by the protianase-K method (β elimination) [2]. Stress relaxation and failure tests were performed on circumferential specimens before and after GAG extraction. To vary the degree of hydration of GAG-depleted specimens, samples were subjected to deswelling media such as mineral and baby oil, and swelling media such as water, sodium dodecyl sulfate and phosphate-buffered saline solution. After equilibrium was attained, the samples were subjected to a mechanical stretch and hold protocol and their Quasi-Linear Viscoelastic (QLV) parameters ($\tau 1$, $\tau 2$, C) were obtained. Similar stress relaxation tests were performed on non-GAG depleted tissues, hydrated in swelling and deswelling media, and native tissue (control), tested immediately after harvesting.

RESULTS AND DISCUSSION

The native tissues equilibrated in deswelling media showed a significant decrease in the QLV parameter C relative to unswelled native control tissue (0.12 + 0.01 vs. 0.15 + 0.02). In contrast, samples equilibrated in swelling media showed an increase in C (0.21 + 0.03 vs. 0.15 + 0.02). Swelling and water content therefore, affect the QLV parameter C. GAGs extracted tissues had a lower C value whether equilibrated in swelling (0.11 + 0.04) or deswelling media (0.09 + 0.02) as compared to the native control tissue (0.15 + 0.02). GAG content therefore, also affects C in ways similar to water content. Regression analysis of the various samples in different media, with and without GAGs, showed an overall increase in the QLV parameter C with the swell ratio (Figure 1) and hence with water content. However, there was no significant difference in the slopes of the regression lines for tissues swelled with and without GAGs.

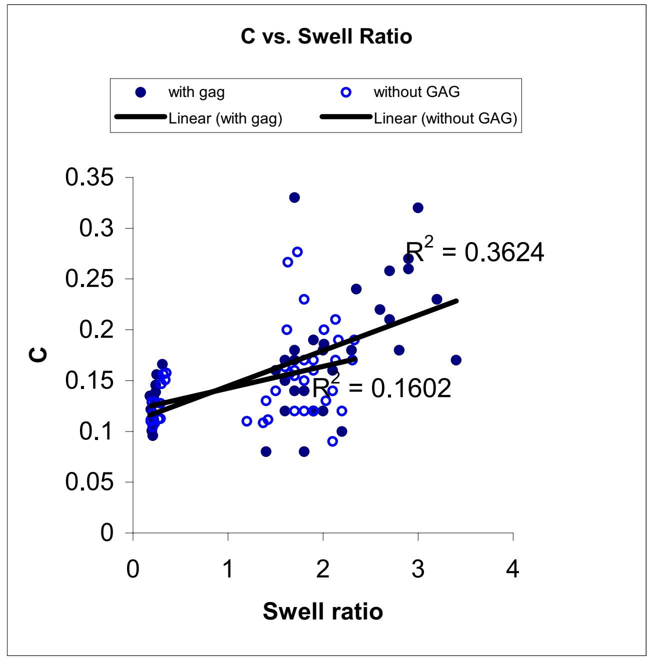

Figure 1: Comparison of QLV parameter C for tissue samples (swelled and deswelled in various media) with and without GAGs.

CONCLUSIONS

GAG depletion appears to affect the viscoelastic response of aortic valve tissue, although the major portion of this effect correlates with water content. Thus, it may be concluded that both GAGs and water content contribute to tissue viscoelasticity, with water being the major contributor.

REFERENCES

1. Fung, et al. *J of Biomechanics* ***9(10)**, 649-657*, 1976.
2. Grande AJ, et al. *J Biomed Mater Res* ***65A***, 251-259, 2003.

LOWER EXTREMITY LOADING DURING ENTIRE DAYS OF SPACE FLIGHT

[1,2,3,4]Peter R. Cavanagh, [1,2]Kerim O. Genc, [5]Christian C. Maender, [6]Ruth S. Ochia, [7]Jess G. Snedeker, and [1,2]Andrea J. Rice
[1]The Cleveland Clinic Foundation Center for Space Medicine, [2]Departments of Biomedical Engineering and [3]Orthopaedic Surgery and the [4]Orthopaedic Research Center, Cleveland, OH, USA
[5]NASA Johnson Space Center, Houston, TX, USA
[6]Rush Presbyterian-St. Luke's Medical Center, Chicago, IL, USA
[7]ETH, Zurich, Switzerland
email: cavanap@ccf.org

INTRODUCTION

Bone loss in the lower extremities is an established consequence of long-duration human space flight, whereas bone mass in the upper extremities appears to be maintained [1]. This difference may be the result of disuse of the lower extremities in space. Reduction in load bearing on the feet may play a key role in these changes, but no quantitative data showing loads in-orbit currently exist.

The purpose of the present experiment was to measure loads on the feet over an entire day in the same subject during daily life on the ground and on the International Space Station (ISS).

METHODS

In-shoe forces were monitored with modified Pedar insoles (Novel Gmbh, Munich, Germany) placed inside the shoes of a single astronaut on a 161-day ISS mission. DXA scans were also performed pre- and post-flight. All instrumentation was built into a Lower Extremity Monitoring Suit custom made for the subject, who gave informed consent to participate in the IRB-approved experiment. The force data were analyzed by a custom routine written in MATLAB (Mathworks Inc.).

Daily load stimulus (DLS), a mathematical model used to relate changes in bone mineral density to daily loading histories, was calculated using in-shoe force profile data [2].

RESULTS AND DISCUSSION

Average monthly BMD losses in the proximal femur, total hip, and lumbar spine regions were 0.64%, 0.72% and 2.31%, respectively. There was a net BMD gain of 0.32% per month in the arms.

Peak force histograms from sample days in 0g and 1g (Figure 1) show a marked shift in the two main modes of loading (walking and running from 260% and 120% BW in 1g to 160% and 90% BW in 0g). The total number of peaks above 5% BW is greatly reduced (10,112 peaks in 1g vs. 2,569 peaks in 0g) and force peaks greater than 200% BW are absent in 0g.

The ratio of mean DLS in 0g to that in 1g varied from 0.44 to 0.55 (using values of m between 3 and 8). Thus, exercise in space over an entire work day provided only approximately half the stimulus to bone experienced during a typical work day on Earth.

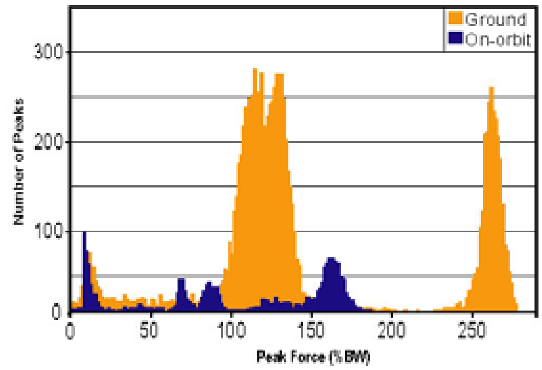

Figure 1: Peak force histograms in percent body weight (%BW) units for typical days on Earth (light – yellow) and on the ISS (dark – blue).

CONCLUSIONS

A number of countermeasures have been attempted, so far unsuccessfully, to prevent loss of bone mass during long-duration space flight. The fact that cosmonauts and astronauts have lost bone mass despite exercising on-orbit has led some authorities to suggest that exercise is not a suitable countermeasure. When the reduced loading during locomotion on-orbit found in the present experiment is considered together with what appears to be a markedly lower total daily load to the feet, these results, if confirmed by ongoing measurements on other ISS astronauts, will present strong evidence that the "mechanical dose" derived from exercise needs to be increased. Such an increased dose could be obtained by increasing the load in the SLD, increasing the speeds available on the ISS treadmill, or by novel exercise. Since ground experiments in simulated zero gravity have shown that subjects can tolerate SLD loads of 1 BW [3], we believe that SLD loads should be increased for exercise on future ISS increments.

REFERENCES

1. LeBlanc et al., *J Bone Miner Res*, **11**, S323, 1996.
2. Fischer KJ et al., *Bone* **19**, 127-135, 1996.
3. McCrory et al., *Aviat Space Environ. Med,* **73**, 625-631, 2002.

ACKNOWLEDGMENTS

This work was supported by NASA cooperative agreement NCC 9 153. The remarkable cooperation of the subject is gratefully acknowledged.

EFFECTS OF LONG-TERM SPACE FLIGHT ON MUSCLE VOLUME

[1,2]Raghavan Gopalakrishnan, [1,2]Kerim O. Genc, [1,2]Andrea J. Rice, [5]Christian Maender, [6]Harlan Evans, [1,2,3,4]Peter R. Cavanagh
[1]The Cleveland Clinic Foundation Center for Space Medicine, [2]Departments of Biomedical Engineering and [3]Orthopaedic Surgery and the [4]Orthopaedic Research Center, Cleveland, OH, USA
[5]NASA Johnson Space Center, Houston, TX, USA, [6]Wyle Laboratories, Houston, TX, USA
email: cavanap@ccf.org

INTRODUCTION

In a microgravity environment, the disuse of the lower extremities is known to cause physiological deconditioning of muscle. Previous studies have reported that considerable lower extremity muscle volume loss occurs during both short (Shuttle) and long-duration space flights (MIR), 3-10% and 5-17% loss respectively, even with exercise countermeasures [1]. It has been speculated that disuse of the lower extremity may be the principal mechanism of atrophy. The purpose of this study is to quantify the atrophy that occurs in the individual muscle groups of the lower and upper extremities of crewmembers on the International Space Station (ISS). This information will later be coupled with activity and strength data obtained from the same subjects.

METHODS

Muscle volume changes were calculated using Magnetic Resonance (MR) images taken from two male ISS crewmembers before and after space flights of 161 and 194 days. Images of the thigh, calf, and arm were acquired pre- and post-flight (within 5 days of re-entry). Images of standard cylindrical calibration phantoms were also obtained to allow quantification of distortion in the images. The muscle groups of interest were the quadriceps, hamstrings, medial gastrocnemius, soleus, anterior calf, and anterior and posterior arm. The non-anatomical groupings (e.g. anterior calf) were used because of the difficulty in identifying individual muscles on MRI.

Each muscle group was traced manually from individual slices using custom MATLAB (MathWorks Inc.) software and then corrected for MRI distortion. The offset between pre- and post-flight images was accounted for by aligning each scan according to the endosteal area of the femur, tibia, or humerus. This alignment ensured that comparable regions were evaluated pre- and post-flight. The traced muscle contours were reconstructed using Rhinoceros 3D Modeling software (Robert McNeel & Associates) to visualize the muscle mass and volume measured.

In order to estimate the user-reliability of the manual tracings, statistical analyses were performed in terms of intra-class correlation coefficient (ICC) based on two-way ANOVA. Three users traced three groups of muscles three times each in order to calculate the ICCs.

RESULTS AND DISCUSSION

The mean intra-observer ICCs of all the muscle groups, calculated based on muscle cross-sectional area (CSA), for all observers were $\geq$ 0.99, the mean inter-observer ICC for all muscle groups based on muscle CSA were $\geq$ 0.98. These high values indicate good agreement between and within observers.

The mean percentage volume changes, over the duration of the missions, of the quadriceps, hamstrings, medial gastrocnemius soleus, and the anterior calf, were found to be -6.4%, -4.4%, -7.7%, -16.4% and -11.9% respectively. In the anterior and posterior arm groups of muscles, the volume changes were 1.7% and no change respectively.

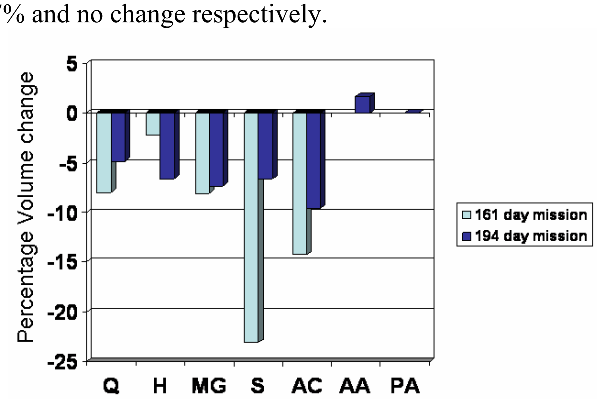

Figure 1: Percentage muscle volume changes for two subjects during 161- and 194-day missions on the ISS. Quadriceps (Q), hamstrings (H), medial gastrocnemius (MG), soleus (S), anterior calf (AC), anterior arm (AA), and posterior arm (PA)

CONCLUSIONS

Although exercise countermeasures were performed on-orbit, significant muscle loss was observed in the lower extremities while no loss occurred in the arms (Figure 1). This atrophy is likely due to disuse of the lower extremity which was not adequately protected by the exercise regimens performed on-orbit [2]. The absence of substantial change in muscle volume in the arms is possibly due to the continued daily use of the upper extremities on-board the ISS. More research is needed to design and implement effective countermeasures to the changes observed and data from additional subjects will be available on future ISS missions. Current experiments using bedrest to evaluate proposed countermeasures and exercise prescriptions will provide valuable insights into muscle loss and its prevention during long-duration space flight.

REFERENCES

1. LeBlanc, A et al., *J Appl Physiol*, **89**: 2158-2164, 2000.
2. Rice, AJ et al., *J Bone Miner Res*, **19**:S95, 2004.

ACKNOWLEDGMENTS

This work was supported by NASA cooperative agreement number NCC 9 153. The remarkable cooperation of the subjects is gratefully acknowledged.

TREADMILL EXERCISE ON THE INTERNATIONAL SPACE STATION: THE EFFECTS OF EXTERNAL LOADING

[1,2,3,4]Peter R. Cavanagh, [5]Kenneth D. Bowersox, [1,2]Andrea J. Rice, [5]Christian C. Maender, and [1,2]Kerim O. Genc
[1]The Cleveland Clinic Foundation Center for Space Medicine, [2]Departments of Biomedical Engineering and [3]Orthopaedic Surgery and the [4]Orthopaedic Research Center, Cleveland, OH, USA
[5]NASA Johnson Space Center, Houston, TX, USA
email: cavanap@ccf.org

INTRODUCTION

Bone loss in the lower extremities during space flight has been a feature of post-flight reports since the Gemini missions. Although these early findings from short-duration flights were later found to be incorrect and linked to inappropriate biomedical instrumentation, the first definitive study on Skylab IV indicated the severity of the problem. Later studies of MIR Station flyers and now data from the first 6 crews on the International Space Station (ISS) have confirmed that bone continues to be lost in long-duration space flight today despite exercise countermeasures [1,2].

Providing Earth-like gravity replacement loads (GRL) during exercise on long-duration space missions may be critical to the maintenance of bone mass. Two devices are currently used on the International Space Station (ISS) to provide a restoring force to return the astronaut to the treadmill surface during treadmill exercise: a subject load device (SLD) and various bungee cord (BC) configurations.

METHODS

In this experiment, the loads on the feet during treadmill exercise on the ISS were measured while different combinations of GRLs were used. The results were compared to similar exercise protocols from the same subject on Earth. In-shoe forces were monitored using modified Pedar insoles (Novel Gmbh, Munich, Germany) placed inside the shoes of a single astronaut, who gave his informed consent to participate in the IRB-approved experiment. Data were recorded at 128 Hz on a wearable computer and saved to a PCMCIA flash memory card. Thirty seconds of exercise data during 10 different loading conditions on orbit were collected and low-pass filtered using a 50 Hz cutoff frequency.

RESULTS AND DISCUSSION

All on-orbit loading profiles showed a marked decrease in peak ground reaction force when compared to 1g loading. The mean active peak force was significantly larger in 1g compared to 0g for all ISS loading conditions (Figure 1).

Daily load stimulus (DLS), a mathematical model used to relate changes in bone mineral density to daily loading histories, was also calculated from the force data for each loading condition using an exponent, m, of 5. During treadmill running the ratio of DLS for a 30 second period of activity in 0g to that in 1g varied from 0.50 to 0.78 over the range of loading configurations. Thus, treadmill exercise in space provided a maximum of only approximately 75% of the stimulus to bone experienced during typical exercise on Earth.

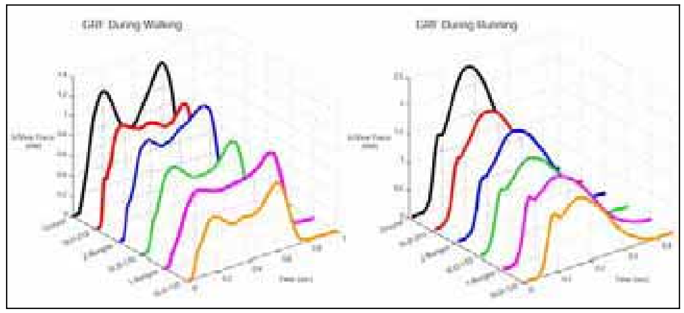

Figure 1: Typical in-shoe force curves for running and walking over-ground (black – far left in each graph) and on-orbit using five different gravity replacement modalities.

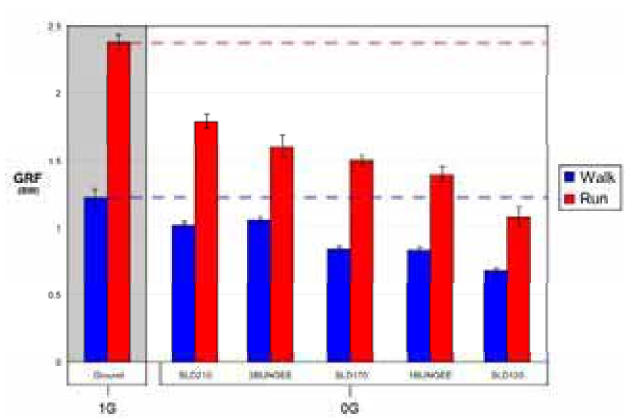

Figure 2: Mean active peak force values for 30 seconds of 0g walking (blue) and running (red) using different loading modalities compared with the values for 1g (shaded area, also indicated by the dashed lines.)

CONCLUSIONS

In order to evaluate treadmill exercise as an effective countermeasure, crewmembers must be able to comfortably apply a GRL of full body weight. However, these data suggest that the common loading conditions studied here that are currently used on the ISS do not produce loading of this magnitude. Further research is needed to improve SLD and harness design so that both load and comfort are improved in order to maximize the osteogenic effects of exercise in space.

REFERENCES

1. LeBlanc et al., *J Bone Miner Res*, **11**, S323, 1996.
2. Lang et al., *J Bone Miner Res*, **19**, 1006-1012, 2004.

ACKNOWLEDGMENTS

This work was supported by NASA cooperative agreement NCC 9 153

MICROMECHANICAL MODELING OF NONLINEAR VISCOELASTIC BEHAVIOR OF MITRAL VALVE CHORDAE

[1]Murat Surucu, [2]Daniel Einstein [1]Ivan Vesely
[1]Childrens Hospital Los Angeles, USC, Los Angeles, CA
[2]Pacific Northwest National Laboratory, Richland, WA
email: msurucu@chla.usc.edu, web: http://www.childrenshospitalla.org/body.cfm?id=658

INTRODUCTION

Biological tissues, such as heart valves, consist of stiff fibers embedded in a soft matrix. Most computational analyses of the highly non-linear mechanical response that results are based on the concept of a continuum in which a constitutive model is postulated for an averaged volume. In order to more accurately model the specific interaction of tissue constituents, we have applied a micromechanical modeling approach, in which the macroscopic behavior emerges from the mechanical interaction of the internal microstructure. Our vision is to associate subgrid mechanics based on measured tissue microstructure with macroscopic computational models in order to resolve stress at the physiologically relevant scale.

METHODS

Micromechanics Model and Geometry

We have implemented a high-fidelity modeling system that uses the generalized method of cells to represent the viscoelastic response of periodic materials with continuous reinforcement along the X1 direction. The model is characterized by a repeating unit cell with an arbitrary microstructure in X2-X3 plane [1]. The micromechanics analysis of the periodic multiphase material is based on approximating repeating unit cell by a rectangular grid (Fig.1).

Microscopic Constituents

The microstructure of mitral valve chordae was assumed to be composed of nonlinearly viscoelastic, crimped collagen fibrils, embedded in a nonlinearly elastic matrix. The nonlinear elastic response of both phases was modeled as a Mooney-Rivlin material, whose strain energy function (W) is:

$$W = c_{10}(I_1-3) + c_{01}(I_2-3) \quad , \tag{1}$$

where c_{10} and c_{01} are material parameters. The viscoelastic response of the collagen fibers was assumed to be quasi-linear (QLV). Generally, the elastic response of each constituent is determined from the relationship between the second Piola-Kirchhoff stress $\mathbf{S}^e$ and the right Cauchy-Green deformation tensor [1]

$$\mathbf{S}^e = 2\frac{\partial W}{\partial \mathbf{C}} \cdot \tag{2}$$

Following the discrete spectrum approximation of Puso and Weiss [2], the time-dependent response is represented as:

$$\mathbf{S}_{(t+\Delta t)} = G_e \mathbf{S}^e{}_{(t+\Delta t)} + K\sum_{I=0}^{N}\left[\begin{array}{l} \exp\left(\Delta t/_{v_I}\right)\mathbf{H}_{I(t)} + \\ \left(\mathbf{S}^e{}_{(t+\Delta t)} - \mathbf{S}^e{}_{(t)}\right)\left[\dfrac{1-\exp\left(\Delta t/_{v_I}\right)}{\Delta t\, v_I}\right] \end{array}\right]$$

$$K = \frac{G_0 - G_e}{Nd+1}; \quad v_I = 10^{I+I_0}; \quad \mathbf{H}_I = \int_0^t \exp\left(-(t-s)/_{v_I}\right)\frac{d\mathbf{S}^e}{ds}ds$$

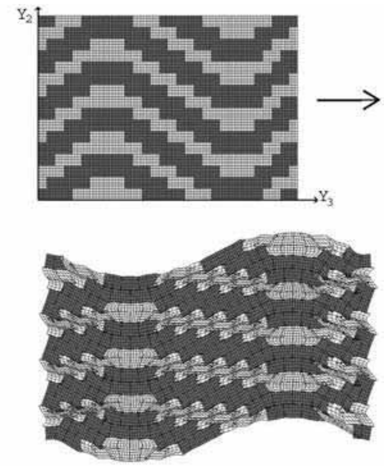

Figure 1: A wavy mesh representing crimped structure of collagen embedded in a nonlinearly elastic matrix: undeformed mesh (top), deformed mesh (bottom). Collagen fibers are in black.

Ge is the equilibrium modulus, G0 is the initial modulus, Nd is the number of decades in the transition and 10Io is the lowest discernable relaxation time. As indicated by Puso and Weiss [2], these four parameters can be determined graphically from a logarithmic plot of G(t). A non-zero deformation was applied in 33-direction ($F_{33}\neq 0$). All tractions other than T_{33} were zero. Deformation was applied for 1.25 s at a strain rate of 40%/sec. From t = 1.25 sec. to t = 3.25 sec., extension was held constant to examine stress relaxation.

RESULTS AND DISCUSSION

The deformation and stress distribution of the unit cell was as expected. Figure 1 shows both undeformed and deformed configurations. Extension of collagen crimp produced a toe region of the stress strain curve. As the collagen begins to bear the load, the stress-strain behavior becomes progressively linear. During the hold phase, stress in the fibers is relaxed.

CONCLUSIONS

The nonlinear, viscoelastic response of chordae results from the interplay of its microstructure. This behavior was simulated in a subgrid micromechanics method. We continue to develop this micromechanical approach, toward the goal of resolving stress and damage on a scale that better inform devise design and clinical understanding.

REFERENCES

1- Aboudi, J. "High-Fidelity Micromechanical Modeling of Viscoelastic Multiphase Materials Undergoing Finite Deformations" EMC Report No. 2003-01, 2004-01, Eng. Mat. Concepts, LLC, Charlottesville, VI
2- Puso, M.A, Weiss, JA. Finite element implementation of anisotropic quasi-linear viscoelasticity using a discrete spectrum approximation. J. Biomech. Eng. Vol: 120, pp:62-67

ACKNOWLEGDEMENTS

This study is funded by DHRP Grant No. DAMD17-01-1-0673.

POSTURAL CONTROL AND POSTURAL MECHANISMS IN OBESE AND CONTROL CHILDREN.

[1,2]Julie Nantel, [1,2]Hugo Centomo and [1,2,3]François Prince

[1] Department of Kinesiology, University of Montreal, Canada
[2] Gait and Posture Laboratory, Marie Enfant Rehabilitation Center, Montreal, Canada
[3] Department of Surgery, Faculty of Medicine, University of Montreal, Canada
email: francois.prince@umontreal.ca

INTRODUCTION

The obesity is in constant increase since the last two decades and the problem is taking epidemic proportion in children [1]. Only few investigators looked at the possible effects of the obesity on the postural control in children. The two principal variables generally assessed in postural balance control are the center of pressure (COP) and the center of mass (COM). To control the equilibrium of the body during quiet standing, the COP must oscillate either side of the COM [2]. Furthermore, Winter et al. [2] demonstrate that postural equilibrium, for healthy adults, was regulated by two different mechanisms according to the observed direction of oscillation. In the anterior-posterior (A/P) direction, the COP_{net} is mostly controlled by an ankle strategy called COP_c. In the medio-lateral (M/L) direction, COP_{net} is controlled by the hip abductor and adductor muscles and it is called hip strategy (COP_v) and more specifically a load/unload strategy. The purpose of the present study is to compare the postural control between obese and non obese children during quiet standing and to assess degree of maturation compare to adult population.

METHODS

Nine non obese children (mass: 32.5; SD: 8.9kg) and nine obese children (mass: 54.1; SDd: 16.6kg) aged between 8 and 13 years participated in the study. The criterion for obesity was a BMI above 95e percentile for the age. Subjects were instructed to stay as still as possible in upright position with a comfortable width between the feet. Two trials of 120 seconds were collected at 60 Hz on two dynamometric force platforms (AMTI). The root-mean-square (RMS) of the centre of pressure velocity (V_{COP}) and RMS amplitude of load/unload mechanism (COP_v), the COP mechanism (COP_c) and the COP_{net} in the A/P and M/L directions were calculated. Finally, the contribution (in %) of the COP_v and COP_c to the COP_{net} was also estimated. Data were also compared to adults[2]. Statistical analysis was realized with a one-way ANOVA. The statistical significant level was set at $p < 0.05$.

RESULTS AND DISCUSSION

Figure 1 shows that the RMS amplitude of the COP_v in the M/L direction was significantly superior in the obese group (X: 4.7; SD: 1.8mm) compared to control (X: 2.4; SD: 1.1mm). The RMS amplitude of the COP_{net} in the M/L direction was also larger in obese children (X: 4.8; SD:

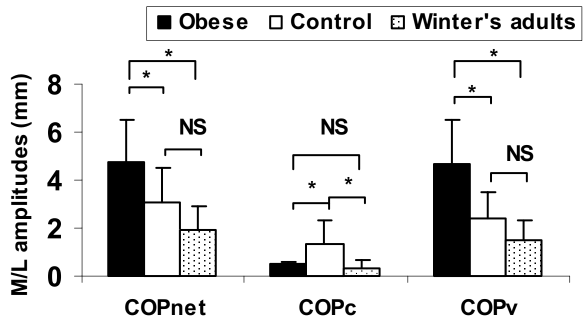

Figure 1: RMS amplitudes of COP_{net}, COP_c and COP_v in M/L direction for the obese and control children. * p< 0.05, NS = not significant.

1.7mm) than in control (X: 3.1; SD: 1.4mm) indicating that obese children could have problem with there postural balance. The contribution of the COP_v on the COP_{net} in the M/L direction was significantly different (X: 96.8; SD: 4.5%) for obese children compare to (X: 78.7; SD: 24.5%) the non obese children. Finally, the V_{COP} in the M/L direction was statistically smaller in the obese group (X: 5.8; SD: 0.9mm/s) when compared to the control group (X: 9.85; SD: 4.7mm/s). No difference was found in any of the parameters in the A/P direction. In regards to the COP_v contribution to the COP_{net} (96.8%) and to the V_{COP} in the M/L direction (5.8 mm/s), obese children demonstrated a more mature postural control, much like the adults population [2], than the non obese children. However, because of there larger COP_{net} amplitude in M/L direction (Figure 1), obese children could be more at risk of falls than normal-weight children.

CONCLUSIONS

Results showed a difference in the postural control of the obese children compare to non obese in the M/L direction. Indeed, the contribution of the COP_v to the COP_{net} was more pronounced in the obese group, indicating an increased involvement of the abductor/adductor muscles to achieve postural stability. Notwithstanding, because of their higher body inertia obese children have difficulty to control there equilibrium.

REFERENCES

1. Weiss R et al. Obesity and the metabolic syndrome in children and adolescents. N Engl J Med 35, 2362-74, 2004.
2. Winter DA et al. Medial-lateral and anterior-posterior motor responses associated with centre of pressure changes in quiet standing. Neurosci Res Commun 12, 141-8, 1993.

LOCAL DYNAMIC STABILITY OF PASSIVE DYNAMIC WALKING ON AN IRREGULAR SURFACE

Jimmy Li-Shin Su [1] and Jonathan B. Dingwell [2]
[1] Department of Biomedical Engineering, University of Texas, Austin, TX, USA
[2] Nonlinear Biodynamics Lab, Dept. of Kinesiology, University of Texas, Austin, TX, USA
E-mail: jdingwell@mail.utexas.edu Web: http://www.edb.utexas.edu/faculty/dingwell/

INTRODUCTION

Previous experiments have shown that stride-to-stride fluctuations in human walking kinematics are statistically distinguishable from linearly filtered white noise [1]. However, the human musculoskeletal system is very nonlinear. Therefore, these nonlinear fluctuations may still be due to a white noise source (of either biological and/or environmental origin) that is being nonlinearly filtered by the mechanics of the system. If this were the case, the perturbations induced by this process should dissipate very quickly. The purpose of this study was to determine how quickly local perturbations from a purely white noise source dissipate in a mechanical model of walking.

METHODS

We modified an existing "simplest" model of passive dynamic walking [2] to allow us to examine the local dynamic stability characteristics [1,3] of walking in the presence of amplitude increasing white noise. Random perturbations were applied to the step transition constraint, making the task equivalent to walking down a "bumpy" slope (i.e., transitions occurred slightly earlier or later) The modified transition equation was:

$$\phi(t) - 2\theta(t) = \varepsilon \cdot U[-0.5, +0.5] \qquad (1)$$

where ϕ = the angle between the stance leg and the swing leg, θ = the angle of the stance leg with respect to the slope normal, and ε was the amplitude (in rad) of the uniform white noise, U, applied to the system. Five trials of 300 strides (600 steps) of perturbed walking were simulated for each of 6 perturbation amplitudes (0 = ε = 0.1 rad). All trials simulated walking down a slope of angle γ= 0.009 rad, corresponding to stable period-1 limit cycle motion. Per-turbations were applied randomly to each step in each trial.

We used a previously established method [1,3], to calculate exponential divergence for each trial for each perturbation amplitude. Mean log divergence was calculated out past 2.5 strides (5 steps) (Fig. 1A). Local dynamic stability, defined as the exponential *rate* of divergence, was quantified from the instantaneous slopes of these curves, using a standard 3-point difference formula.

RESULTS AND DISCUSSION

The amplitudes of the mean log divergence curves increased with increasing noise amplitude (Fig 1A). The slopes of the divergence curves, however, remained nearly identical (Fig 1B). Thus, the *rates* of divergence were controlled primarily by the inherent stability of the limit cycle motion, rather than by the amount of noise present. In fact, the rates of divergence dropped to near zero after only 2 steps, and were virtually zero after 3 steps.

This shows that this simple mechanical model of walking can dampen out the effects of these local perturbations very quickly. This capacity does not depend very strongly on the amplitude of the perturbations (i.e. noise amplitude).

In humans, local perturbations exhibit continued divergence for well beyond 10 strides [1]. The present results suggest that this extended divergence seen in humans may not be due exclusively to the nonlinear filtering properties of this highly nonlinear mechanical walking mechanism. Rather, these results provide additional evidence that suggests the source of the nonlinear fluctuations in experimental walking data is at least partly biological (e.g., possibly due to reflex mechanisms) in origin and is not purely mechanical.

Future work will refine the walking model by making it more anthropometric, adding knees, and adding more biologically inspired control mechanisms. These efforts will allow us to determine the relative influences of different types of both biological and environmental noise on the local dynamic stability of walking.

REFERENCES

1. Dingwell JB & Cusumano JP *Chaos*. **10**: 848-863, 2000.
2. Garcia M et al. *J. Biomech Eng*. **120**: 281-8, 1998.
3. Rosenstein MT et al. *Physica D*. **65**: 117-134, 1993.

ACKNOWLEDGEMENTS

This work was supported by a Biomedical Engineering Research Grant from the Whitaker Foundation.

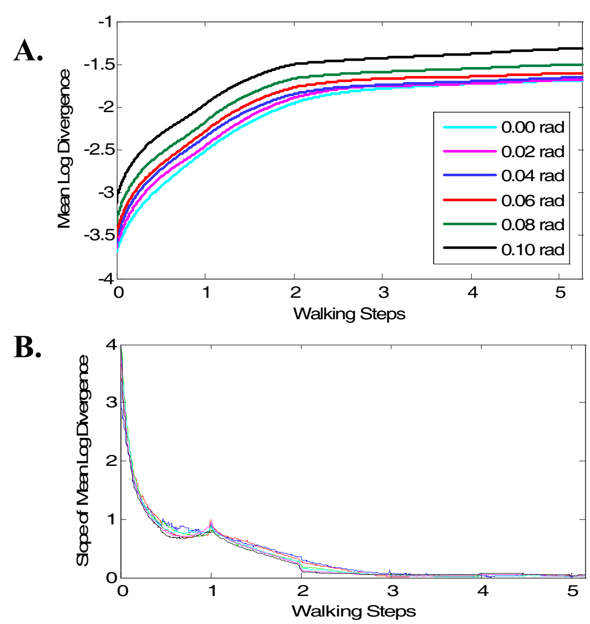

Figure 1: A. Mean log divergence curves averaged over 5 trials at each noise level. Divergence amplitudes increased for increasing ε (Eq. 1). **B.** Slopes of the divergence curves in **A**. Excluding the initial value, these curves were very similar. Note the slight jumps at steps 1 and 2. By the 3rd step, the divergence was negligible.

DIRECTION SENSITIVE SENSOR PROBE FOR THE EVALUATION OF VOLUNTARY AND REFLEX PELVIC FLOOR CONTRACTIONS

[1]Qiuy.Y. Peng and Chris. E. Constantinou
Urology, Stanford University Medical School, Stanford, CA. USA
Email: ceconst@stanford.edu

INTRODUCTION

Reliable measurement of the ability of pelvic floor muscles (PFM) to contract voluntarily can be of clinical value in the assessment of women with urinary incontinence. Currently available devices, expected to measure PFM strength such as surface EMG or periniometry, are of limited anatomic specificity. Digital palpation, although more specific and reliable remains a subjective measurement. In this presentation we demonstrate the development of a novel sensor system to be used for the reliable measurement and recording of PFM strength emulating palpation.

METHODS

Prototype probe is equipped with 4 pairs of contact-force sensors and displacement transducers, each designed to move independently. For patient protection, probe is inserted in the vagina using a female condom placed over the sensor. By inserting the device into vagina, the movement and the force of PFM in the different four directions (anterior, posterior, right and left) were measured at a sample rate of 25Hz and presented on the computer screen as feedback to the patient. This system was used in the evaluation of 12 incontinent patients (mean age 63.2) recruited for this study. The PFM strength was first assessed in the lithotomy position using manual muscle testing and subsequently employing the probe of the sensor system. During the measurement, the patients were asked to perform 3 times voluntary pelvic floor muscle contractions (VPFMC) and 3 times coughing (CPFMC).

RESULTS

Figure 1 shows the typical force (a) and movement (b) measured in the middle of the vaginal wall of a patient with urinary incontinence (UI). The measurements in the anterior direction and in the posterior direction are shown by the solid line and the dotted line respectively.

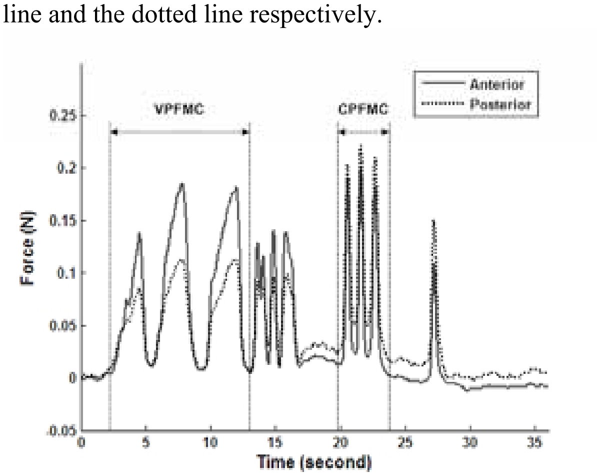

Figure 1a: Typical recording of force of contraction.

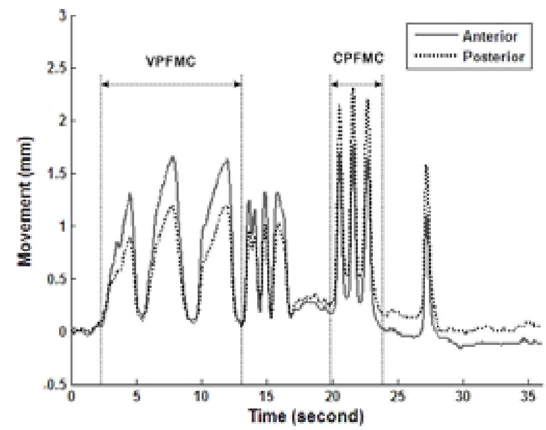

Figure 1b: Typical recording of displacement produced.

Force signals, Fig 2 during CPFMC have high-frequency components (0.5Hz to 4.4Hz). In contrast, VPFMC have much more the low-frequency components (0.25Hz to 0.5Hz).

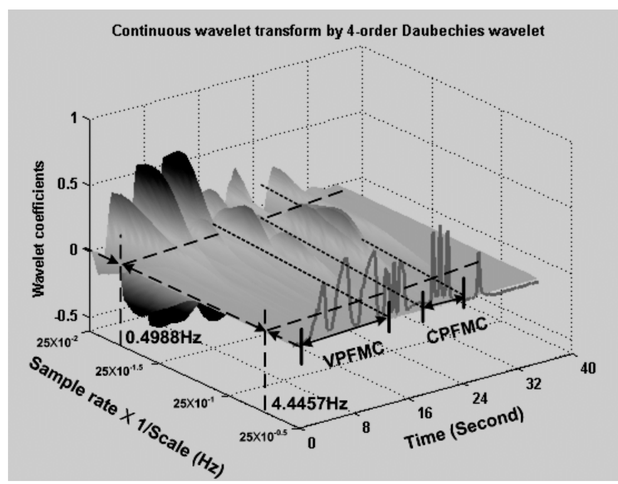

Figure 2: Time-frequency distribution of the force signals in the anterior direction of the middle vaginal wall. Y-axis is the product of sample rate and the reciprocal of the scale of Continuous Wavelet Transform CWT.

CONCLUSIONS

Sensor system provides direct measurements PFM strength and displacement. Analysis suggests that the modes of PFM contraction are different between voluntary PFM contraction and cough induced reflex PFM contraction.

ACKNOWLEDGEMENTS

Funded in part by NIH-NIBIB 1-R21-EB001654

THE DIFFERENCE OF FITNESS LEVEL EVALUATED FROM THE MECHANICAL AND EXTERNAL WORK DURING BICYCLE EXERCISE

[1] Takayuki Sato and [1] Tetsunari Nishiyama
[1] Human Performance Laboratory, Nippon Sport Science University
email: takayuki@nittai.ac.jp, web: http://www.nittai.ac.jp/

INTRODUCTION

The conventional bicycle exercise test has traditionally been used to evaluate physical fitness. The load pedaled by the subjects in the traditional fitness test is actually the resultant force of the tangential and radial forces relative to the crank arm. Whereas the tangential work or power used in the fitness test has been based on the tangential load. Thus variation in the pedaling skill of the subjects will result in under- or over-estimation of the evaluated fitness level. The purpose of this study is to examine the difference in the evaluated levels determined for tangential and resultant pedal loads in bicycling exercise.

METHODS

Seven male subjects (28±4.1 yr, 174±6.2 cm, 67±4.7 kg) participated in this study on two different days. To estimate the $\dot{V}o_2$ max, on the first day of testing the subjects performed an incremental test on a bicycle ergometer. The resistance load was increased at each 0.5 kp every 2 min a target rate 70 rpm continuing until the subject was exhausted. Vo_2 was measured breath by breath using a Metamax system (Cortex Inc.). On the second day of $\dot{V}o_2$ max testing, the subjects pedaled while maintaining an intensity of 30, 50 and 70% of $\dot{V}o_2$ max. Each resistance load test consisted of exercise periods of 5 min with a resting interval of 5 min between each resistance load. Vo_2 were also measured. The original measurement system was constructed to obtain information on the load which was applied to the pedal. The pedal load was measured at the pedal shaft using a strain gauge. The feet were fixed to the pedals with toe clips and straps. The height of the seat position was set to 107% of the symphysis pubis height from the floor. Tangential, radial pedal load and crank angular velocity data were collected and averaged over thirty pedaling cycles at the end of each resistance load. The work rate of the tangential (Tan-w) and resultant (Res-w) components were calculated. An index of effectiveness was calculated using the equation (Tan-w) / (Res-w).

RESULTS & DISCUSSION

Tan-w has been used for conventional physical fitness evaluation, such as the physical work capacity test (Fig.1, Tan-w). But this Tan-w is calculated from tangential pedal load, which is only a part of the subject-induced pedal load. Therefore, we also evaluated the resultant pedal load to eliminate the dependence on the subject's pedaling skill (Fig. 1, Res-w). Table 1 shows Tan-w and Res-w for each %$\dot{V}o_2$ max. The order of fitness level based on Tan-w was clearly different to that based on Res-w. If, based on Res-w, a subject has a higher fitness than another when their level is similar based on Tan-w, it is thought that the subject has an excellent fitness level but poor pedaling skill. The conventional bicycle exercise test is an excellent method to evaluate the bicycle exercise ability. In the case of evaluating physical fitness on a bicycle, both physical fitness and pedaling skill need to be considered.

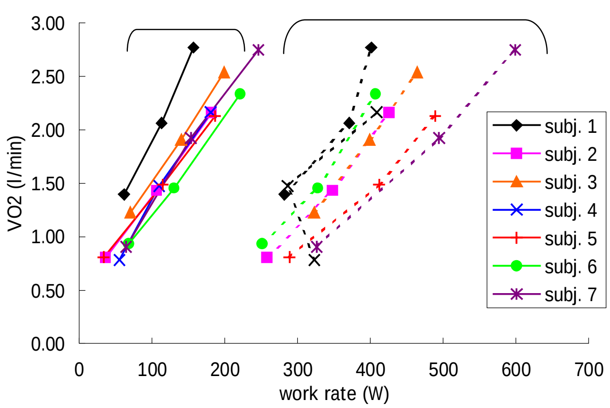

Fig. 1; The relationship between each work rate and $\dot{V}O_2$.

Table 1; Tan-w and Res-w in each %$\dot{V}o_2$ max.

	$PWC_{30\%Vo2max}$		$PWC_{50\%Vo2max}$		$PWC_{70\%Vo2max}$	
	Tan-w	Res-w	Tan-w	Res-w	Tan-w	Res-w
subj. 1	61	282	113	371	157	401
subj. 2	36	258	106	348	182	426
subj. 3	70	323	140	399	199	464
subj. 4	55	323	110	286	180	409
subj. 5	33	289	115	412	186	489
subj. 6	68	251	130	328	221	407
subj. 7	64	326	153	495	246	599
AV.	55	293	124	377	196	456
S.D.	15	32	18	67	29	71

* The values are w.

TIME-COURSE CHANGES IN THE MECHANICAL PROPERTIES OF THE RAT URINARY BLADDER FOLLOWING SPINAL CORD INJURY

[1, 3]Kevin K. Toosi, [1, 2]Jiro Nagatomi, [2, 3]Michael B. Chancellor, [1, 2]Michael S. Sacks
[1]Department of Bioengineering, University of Pittsburgh, Pittsburgh, PA
[2]McGowan Institute for Regenerative Medicine, University of Pittsburgh, Pittsburgh, PA
[3]Department of Urology, University of Pittsburgh, Pittsburgh, PA
email: msacks@pitt.edu , web: www.pitt.edu/~msacks/etml.html

INTRODUCTION

The urinary bladder is a smooth muscle organ whose main functions are to store urine and to void when necessary. Since the most important aspect of the storage function of the bladder is to maintain low intravesical pressure in order to protect the upper urinary tract from backflow of urine, the compliance of the bladder wall is one of the key functional parameters to assess the health of this organ. Previously, using planar biaxial testing, we demonstrated that the mechanical compliance of bladder wall tissue in spinal cord injury (SCI) rats at 10 days post-injury was significantly greater compared to that of normal bladders under biaxial stretch [1]. These results contrasted typical, non-compliant bladder conditions found in chronic SCI patients [2]. In order to determine long-term alterations in the urinary bladder mechanical behavior due to SCI, the present study examined the biaxial mechanical properties of bladder wall tissues at various time points post-SCI. In addition, biochemical assays were used to quantify collagen and elastin contents of SCI bladders to correlate with tissue-level findings of biomechanical properties.

METHODS

Female SD rats in the test group were subjected to complete transection of the spinal cord at the T9-T10 level, and the bladders were harvested at 3-week, 6-week and 10-week post-SCI. Normal rats were used as controls. Using our custom planar biaxial testing device, bladder specimens were subjected to equibiaxial stress (100kPa), and areal strain of the rat bladder wall, as an index of the mechanical compliance, was calculated for each group.

Following biaxial mechanical testing the bladder specimens were weighed, cut into smaller strips, and digested in 0.5N acetic acid supplemented with 1 mg/mL pepsin at 4 °C overnight. Acid-soluble collagen in the supernatant solution was quantified using a commercially available assay kit. The insoluble tissue materials (following acetic acid digestion) were further treated with 0.25M oxalic acid at 95 °C for 180 minutes. Elastin concentrations in these supernatants were also quantified using a commercially available assay kit. The data were normalized by wet tissue weight and expressed as average ± SEM, analyzed using a t-test when compared to that of normal and 3-week SCI bladders from our previous study and the difference was considered significant if $p<0.05$ [3].

RESULTS AND DISCUSSION

Bladder wall compliance was significantly greater at three and six weeks after spinal cord injury, when compared to normal. The increase in compliance, however, diminished by ten weeks post-injury, and was similar to that of normal bladder. Furthermore, when maximum axial stretches in two anatomical directions were compared, it was significantly ($p<0.05$) greater in the circumferential direction than in the longitudinal direction in 3-, 6- and 10-week SCI bladders. The different mechanical responses in two directions found in 3-, 6- and 10-week SCI bladder tissues indicate material anisotropy in these samples. This finding contrasted the isotropic behavior found in 10-day SCI bladders, suggesting that material class of bladder tissue continues to change from 10-day to 10-week after SCI.

Collagen concentrations (*i.e.* collagen mass normalized by wet tissue weight of bladder sample) of the 3-week and 10-week SCI rat bladders were similar to each other but significantly lower compared to the normal bladders, due to increased mass of hypertrophied bladder. However, the collagen content (*i.e.* total collagen mass per bladder sample) of 10-week SCI bladders was significantly greater than both normal and 3-week SCI samples, indicating increased collagen production by smooth muscle cells between three and ten weeks after injury. Elastin concentrations (and contents) of the 3-week and 10-week SCI bladders were similar to each other and significantly higher than that of normal bladders. These results suggest that elastin content primarily increases over the first three weeks following injury and remains constant after that.

CONCLUSIONS

The changes in the tissue mechanical compliance, composition and material class of bladder wall over a 10-week period of time post-SCI indicate that the bladder tissue continuously remodels after spinal cord injury. The results of the present study provide first evidence that early and late responses of bladder tissue following spinal cord injury were distinct from each other. Understanding that the bladder wall functional behavior continuously alters over the time, urologists may need to choose different clinical approaches regarding treatment of non-compliant bladder in SCI patients, based on injury's time-course.

REFERENCES

1. Gloeckner, D.C., et al., *Passive biaxial mechanical properties of the rat bladder wall after spinal cord injury.* J Urol, 2002. **167**(5): p. 2247-52.
2. Hackler, R.H., M.K. Hall, and T.A. Zampieri, *Bladder hypocompliance in the spinal cord injury population.* J Urol, 1989. **141**(6): p. 1390-3.
3. Nagatomi, J., et al., *Changes in the biaxial viscoelastic response of the urinary bladder following spinal cord injury.* Ann Biomed Eng, 2004. **32**(10): p. 1409-19.

DYNAMOMETRY TO MEASURE PELVIC FLOOR FUNCTION

[1]Chantale Dumoulin, [1]Daniel Bourbonnais, [1]Denis Gravel, [2]Marie-Claude Lemieux, [1]Mélanie Morin,
[1]School of rehabilitation, University of Montreal,
[2] Faculty of Medicine, University of Montreal; dumoulin@sympatico.ca

INTRODUCTION

Evaluation of the pelvic floor muscle (PFM) function is an important parameter in clinical and scientific issues regarding PFM training, the first-line treatment of Stress Urinary Incontinence (SUI) [1]. Until recently, clinicians have been relying on digital assessment, a subjective measure that lack sensitivity, or on indirect sources of measurements of the PFM function such as surface EMG and pressure measurements, which do not offer adequate specificity [2]. This research report addresses the development and psychometric evaluation of a new dynamometer for measuring PFM function in women.

METHODS

The new dynamometer comprises a computerized central unit and a peripheral, a dynamometric speculum.

Through *in vitro* calibration studies, the dynamometer was assessed for linearity, repeatability and its capacity to measure a force independently of its point of application on the dynamometer branch. Subsequently, 29 female subjects aged between 27 and 42 and presenting different severity levels of SUI participated in an *in vivo* test-retest reliability study where the PFM evaluation was repeated in three successive sessions. During each session, maximum strength at 19mm and 24mm vaginal aperture, endurance, speed and rapidity of PFM contraction were recorded.

RESULTS AND DISCUSSION

The calibration results suggest that the voltage outputs of the apparatus are linearly related to applied forces. Repeated calibration with dead weights has shown that the force measurements are also repeatable. Furthermore, calibration performed by applying forces at different locations on the moving branch of the dynamometer confirms that the measurement is independent of the site of application of the resultant force.

The reliability coefficients found in the test-retest reliability study (coefficient of dependability and standard error of measurement) indicated good to very good reliability of all PFM measurements (Table 1). Furthermore, the subjects' unanimous appreciation implied that the instrument is acceptable and the measuring procedure comfortable.

CONCLUSIONS

This study demonstrates that the new dynamometer accurately measures forces applied to its instrumented branch, takes reliable measurements of the PFM function and is deemed acceptable by women.

REFERENCES

1. Wilson P., Bo K., Hay-Smith J., Staskin D., Wyman J., Nygaard I. Conservative treatment in women. In Abrams P., Cardozo L., Khoury S., Wein A. Editors. Incontinence. *Second international consultation on incontinence*. 2nd Edition. UK: Health Publication Limited, 2002: **571-623.**

2. Peschers U., Gingelmaier A., Jundt K., Leib B., Dimpfl T. Evaluation of pelvic floor muscle strength using four different techniques. *International Urogynecology Journal and Pelvic Floor Dysfunction* 2001; **12:27-30**.

ACKNOWLEDGEMENTS

This study was financially supported by: The Canadian Institute of Health Research and Laborie Medical Technologies Inc. through a CIHR-Industry grant and by l'Ordre Professionel de la Physiothérapie du Québec through a clinical research grant.

Table 1: **Dependability coefficients and standard error of measurements for the PFM function measurements**

Parameters	**Maximal strength at 19mm vaginal aperture**	**Maximal strength at 24mm vaginal aperture**	**Endurance**	**Speed of contraction**	**Number of rapid contraction**
Dependability coefficient	0.71	0.88	0.81	0.92	0.79
Standard error of measurement	1.22 N	1.49 N	2.98%	1.39N/s	1.4 contraction

AN INSTRUMENTED SCAFFOLD TO MONITOR LOADING OF CARTILAGE IN THE KNEE JOINT

Szivek JA[1], Bliss CL[1], Ruth JT[1], Schnepp AB[1], DeYoung DW[2], Vaidyanathan RK[3]
[1] Orthopaedic Research Lab, Dept. of Orthopaedic Surgery, University of Arizona, Tucson, AZ USA
[2] University Animal Care, University of Arizona, Tucson, AZ USA
[3] Advanced Ceramics Research, Tucson, AZ USA
szivek@u.arizona.edu

Introduction

Tissue engineered cartilage covered scaffolds offer one solution to resurfacing damaged cartilage in young and active arthritis patients. Cyclically loading cells is expected to provide more rugged aligned tissues than those grown in static culture. No direct in vivo measurements of loads during gait, acting on cartilage tissues are available, making it difficult to select appropriate loads to apply during tissue growth. In addition no monitoring technique currently exists to monitor loading of implanted tissue engineered constructs. It was the goal of this study to develop a monitoring system and use it in an animal model to collect in vivo cartilage load measurements.

Methods

Polybutylene terephthalate(PBT) scaffolds were manufactured using an extrusion freeform fabrication rapid prototyping process. A grid pattern, which developed bone ingrowth in a previous study, was modified so that strands were rotated 45° between layers.

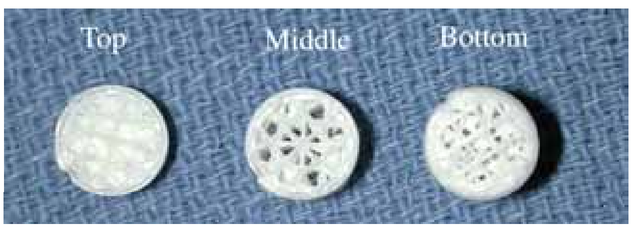

Figure 1: Scaffold showing cross layered polymer pattern. Layer labeled top is solid and has a dome shaped section above it to support tissue engineered cartilage.

Three 1000 ohm single element strain gauges were aligned and attached along the long axis of the scaffold surface with a 120 degree separation. Gauges were wired to a cable and waterproofed using a published procedure. Scaffolds were loaded in confined compression on an MTS at a load rate simulating gait speeds and load vs. strain calibration curves were prepared. Wired scaffolds were cleaned, sterilized using ethylene oxide and aerated.

Six tall male hounds weighing between 29 and 35 Kg were selected for implantation surgery. The NIH Guide-lines for animal care and use were observed during animal experiments. Following preparation of one hind limb of each of six hounds, an incision was made exposing the medial femoral condyle and a scaffold was implanted by drilling two concentric holes (one for the cable and the second for the scaffold). The cable exited the lateral aspect of the femur and was coiled subcutaneously for later retrieval. Following a 3 month holding period retrieved wires were connected to a hard wired and/or a radio transmitter system. Strains were collected while dogs walked on a treadmill and calibration curves were used to assess loading. Following *in vivo* monitoring bones were explanted and loaded using a bench top loading system. Finally bones were dehydrated and embedded using a published undecalcified tissue embedding technique. They were sectioned and stained and histomorphometry was used to assess bone growth.

Results

Strain vs. load curves for gauged scaffolds were noted to be linear up to the peak test load of 147 N (15 Kg). *In vivo* strain patterns were similar to patterns collected directly from the mid-diaphysis of the femora of dogs during earlier *in vivo* studies. Each gait cycle contained a low load swing phase which was assigned the zero strain value. Load vs. time graphs converted by using calibration curves indicated that peak loads ranged from approximately 80 to 120 N during gait (Figure 2) for this test animal (weighing 34 Kg). Standing relaxed prior to and following gait, a load of 65 ± 6.5 N was recorded from this animal.

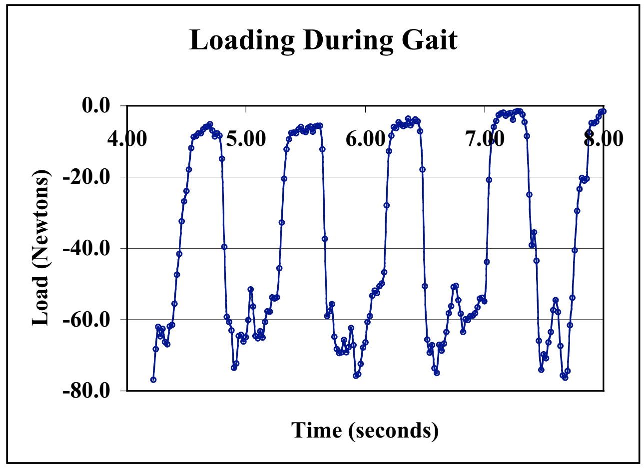

Figure 2: Representative load patterns determined from strains collected during gait. Measurements were zero adjusted assuming the lowest combination of bodyweight and muscle loads during swing phase. At this gait speed swing phase lasts approximately 0.3 seconds.

Gross examination of knee surfaces in the explanted hind limbs, showed that scaffolds were adequately recessed but mild scoring of the tibial cartilage was noted in some animals. Scaffolds were securely fixed by extensive bone in-growth with no visible adverse reaction to the scaffold material. Cables were surrounded by a thin fibrous tissue layer which prevented them from migrating. Fluid infiltration into cables lead to some visible corrosion and precluded monitoring of some strain gauges.

Discussion

Load measurements collected from strain gauged scaffolds were in general agreement with observations that dogs loaded at most 2 legs (one front and one back) simultaneously during gait at this speed. Results were also in agreement with evidence showing that, during stance, 40% of the dogs body weight is carried on the hind limbs (in this case 6.8 Kg/leg (67 N/per leg)). Telemetry was noted to function well when the exciting coil was accurately aligned with the subcutaneous transmitter but stopped transmitting when the power coil was slightly misaligned . Monitoring of telemetry output over a period of several days provided a consistent output suggesting that this system could be used over an extended period even though fluid infiltration was likely to incapacitate the system eventually.

Ongoing studies using cartilage covered "sensate" scaffolds are evaluating the effect of a tissue engineered cartilage layer. Development of better waterproofing coatings for connections between gauges and lead wires, and between lead wires and transmitters is expected to increase the length of time that these systems are able to provide measurements.

Acknowledgements

The authors thank the NIH and NIBIB for support through grant RO1-EB000660.

CHANGES OF SPRING–LIKE LEG BEHAVIOR ACCORDING TO DIFFERENT TOUCH DOWN VELOCITIES IN DROP LONG JUMPS

[1] Koji Zushi, [1] Yasumitsu Ishii and [2] Bruce Elliott
[1] National Institute of Fitness and Sports in Kanoya, Japan ; email : zushi@nifs-k.ac.jp
[2] The School of Human Movement and Exercise Science, The University of Western Australia

INTRODUCTION

Shortening and lengthening of the leg is a characteristic of hopping on the spot. On the other hand, jumping with the aim of moving forward consists of shortening-lengthening and rotation of the leg. The contribution of these two components may change according to the vertical and horizontal velocity of the center of mass (COM) and attack angle at the instance of touchdown. Moreover leg stiffness during the contact phase is affected by both the velocity and angle. A spring mass model was developed that represents the mechanical behavior of the integrated muscle-tendon system. The purpose of this study was to investigate the differences in spring-like leg behaviors of hopping on the spot and hopping following drop long jumps (Fig.1) with different touchdown velocities.

METHODS

Nine college jumpers participated in this study. Subjects performed hopping on the spot (HJ) and hopping following a drop long jump (DLJ). Subjects were required to vary their running speed on the box (2m long, 0.3m high) to achieve landing distances of 1m, 2m and 3m onto a force platform (Fig.1). Vertical and horizontal GRF signals from the force platform were sampled at 1080Hz. 3D motions of the body were recorded at 120 Hz using a VICON motion analysis system (VICON612 Oxford United Kingdom). Selected 2D parameters were then placed into the model. Spring-like leg behaviors during the contact phase of HJ and DLJ were evaluated using the spring mass model (McMahon et al., 1990; Arampatzis et al., 1999 ; Farley et al., 1998) (Fig. 1). As the velocity of the COM is derived from leg rotation and shortening-lengthening, these were calculated by geometrics related to changes of rotating angle and the length L (Jacobs et al., 1992).

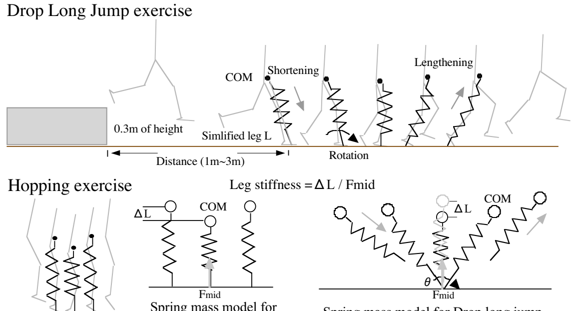

Fig. 1 Spring mass models for hopping in place and drop long jumping

RESULTS AND DISCUSSION

Velocity of the COM and the attack angle at the instance of touch down and during early stance, as the jump distance increased, is related to greater compression of the leg L (ΔL) and larger vertical and horizontal GRF. However, leg stiffness decreased and contact time shortened over this period (Fig.2). The model showed an approximate linear relationship between vertical GRF and ΔL in the HJ but was non linear in each DLJ (Fig.3). Correlation coefficients between leg stiffness of HJ and each DLJ were not significant. These results suggest different spring-like leg behaviors in both HJ and DLJ. Horizontal and vertical velocity of the leg rotation markedly increased during contact phase as the jump distance increased. On the other hand, the influence of the leg shortening-lengthening on horizontal and vertical velocity increased with compression during the early stance but did not change during the recoiling motion latter in the stance phase (Fig.4). We concluded that the leg spring becomes compliant and does not recoil because of limitations of the muscle-tendon elasticity with a high impact GRF, while the rotary motion of the leg spring acts strongly as horizontal velocity increases in forward jumping following a faster approach.

REFERENCES

1. McMahon T. A. et al. J Biomech, 23, Suppl. 1.65-78, 1990.
2. Arampatzis, A. et al. J Biomech, 32, 1349-1353, 1999.
3. Farley C. T. et al. J. Appl. Physiol. 85, 1044-1055, 1998.
4. Jacobs R. et al. J Biomech, 25, 953-965, 1993.

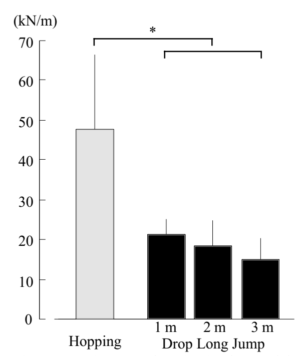

Fig. 2 Leg stiffness of hopping in place and drop long jumpings according to different distance.

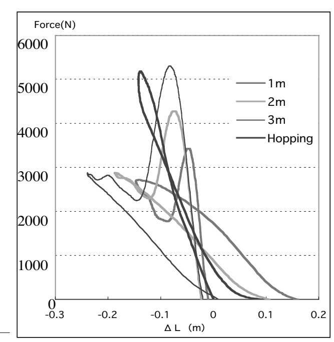

Fig. 3 Vertical ground reaction force versus lenght of shortening-lengthening in place and drop long jumpings according to different distance.

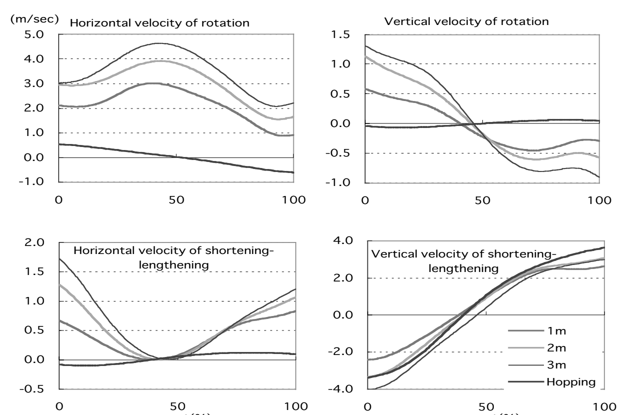

Fig. 4 Vertical and horizontal velocity of the leg rotation and shortening-lengthening components according to defferent distances.

EVALUATION OF THE FATIGUE PROPERTIES OF RUBBERY BIOMATERIALS USING THE HYSTERESIS METHOD

[1] Judit E. Puskas, [2]Miroslawa El Fray, [3]Volker Altstädt

[1]The University of Akron, OH, USA
[2] Technical University of Szczecin, Poland; [3] University of Bayreuth, Germany
email: jpuskas@uakron.edu

INTRODUCTION

Thermoplastic elastomers (TPE) constitute a relatively new group of polymeric materials classified as a separate category of rubbers. TPEs do not need to be vulcanized and therefore offer many advantages over chemically crosslinked elastomers, while being processible as classical thermoplastics. High performance TPEs with good solvent resistance, elasticity, tear strength and flex fatigue properties have found a wide range of applications in medicine such as medical tubing or equipment parts. Selected TPEs are also used for implant applications [1].

This paper will discuss the dynamic fatigue properties of medical grade silicone (SIL), a chemically crosslinked elastomer, and polyurethane (PU), a TPE, and two new TPE biomaterials: polystyrene-*b*- polyisobutylene-*b*-polystyrene (SIBS), recently FDA-approved as medicated coronary stent coating, and a segmented polyester TPE containing dimerized fatty acid (PED).

METHODS

Fatigue testing was carried out using a servo-hydraulic test machine with a digital controller (Instron 8400/8800), equipped with a 200-N load cell, a 10 kN cylinder and an environmental chamber. For all tests, the load ratio R = $\sigma_{min}/\sigma_{max}$ was held constant at 0.1. The strain was measured as the real-time clamp displacement. The possible phase shift between the stress and strain signals were minimized below 20 µs by the experimental set-up. Testing in simulated body fluid (SBF) was carried out at 24 and 37°C. Testing was carried out using the SILT (Stepwise Increasing Load Test) and SLT (Single Load Test) methods. The DynMat Hysteresis Measurement Software V.1.1.0.1 was used for the evaluation of the hysteresis loops [2].

RESULTS AND DISCUSSION

With SILT, SIL showed extremely low dynamic modulus, and large instantaneous elastic deformation. SIBS performed much better, with nearly ten times higher modulus than SIL, bridging the gap between SIL and PU. PED showed an intermediate behavior between SIBS and PU. SIBS and PED both displayed high damping. Figure 1 shows the hysteresis loop patterns. SIBS30 shows the largest area under the hysteresis loop, indicative of its high damping. The hysteresis loop of SIL exhibits large displacement at low forces. The much broader hysteresis loops of PU and SIBS compared to PED indicate structural changes, accompanied with high energy dissipation and larger creep.

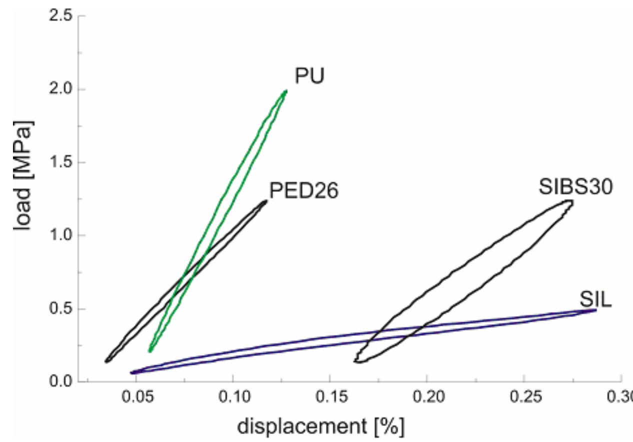

Figure 1: Hysteresis loop patterns.

SIBS demonstrated superior creep resistance compared to SIL *in vitro* (SBF, 37 °C), approaching the performance of PU and PED.

CONCLUSIONS

The hysteresis method seems to be a useful new method to evaluate the dynamic behavior of biomaterials. The recently developed dendritic SIBS materials are expected to have improved dynamic fatigue and creep properties, on account of their branched structure [3]. This, coupled with the biocompatibility of SIBS, predicts a bright future for this novel biomaterial.

REFERENCES

1. Puskas JE, et al. *J.Polym. Sci., Chem*., **42**, 3091-3109 (2004)
2. M. El Fray et al. *Rubber Chem.Tech.,* submitted, 2004
3. Puskas JE, et al. US Patent 6,747,098, 2004.

ACKNOWLEDGEMENTS

Financial support by Lanxess Inc. (Bayer) and DFG is acknowledged.

IMPACT RESPONSE ANALYSIS OF THORAX BY THE THIN-LAYER METHOD

Abir Chakraborty
India Science Lab, General Motors Tech. Centre - India, ITPL, Bangalore-560066

INTRODUCTION

Development of lung injury criteria is essential to understand the damage incurred by automobile accidents or high velocity projectile impacts. While the car accidents are characterized by low velocity, high mass transferring energy to the thoracic tissues over a relatively long time period (~60 ms), the bullet impacts generate two waves arriving at around 100 µs and 1 ms. Thus, the thorax is subjected to a broad-band frequency loading throughout its life and it is essential to have a tool to characterize its behavior for both long and short duration loading.

A realistic Finite Element (FE) model of thorax with all its complexities is computationally very expensive especially for high frequency loading [1]. Following [1], it is assumed in this work that the thorax can be modeled as an assemblage of two-dimensional layered media. Among the existing methods, the Thin-Layer Method (TLM) is tailor-made for analyzing this kind of structure. The formulation is based on Fourier series representation of the unknown displacement components, which reduces the dimension of the problem and thus the cost of computation.

The method is employed to analyze thorax for several different stress pulses, which bring out the wave nature of the response (short duration load) and quasi-static behavior (large time load).

METHODS

The layered model is assumed finite in the Z direction only. The TLM starts by Fourier series representation of the displacement field in the X direction, which upon substitution in the elastodynamic equation generates a set of partial differential equations, where z and t are the only independent variables. This equation is supplemented by the displacement and stress boundary conditions. Discretizing this reduced set of equations by following the regular FE procedure, a set of ordinary differential equation (ODE) is obtained. Both implicit Newmark method and explicit central difference methods are adopted to solve the ODE. Thus, along with regular constrained structures, unconstrained media can also be analyzed using this method, which is instrumental in modeling the thorax. Further, sliding contact condition without friction is also incorporated in the formulation, which is useful in modeling the interface between the bone and the lung.

RESULTS AND DISCUSSION

The thorax is modeled by three layers of muscle, bone and lung, where the material properties and thickness of each layer are same as that given in Ref. [1]. Each layer is modeled with only 10 elements (system size 61×3). Three different unit stress pulses are applied on top of the layer, whose time dependency is given by Blackman window function; with duration of 50, 100 and 200 µs. The stresses are considered as point loading in space for simplification although any kind of variation can be taken. Figure 1 shows the displacement of the thorax at the loading surface and interfaces for the three different stress pulses. For 50 µs, considerable difference in displacement can be observed between the top layer and the interfaces, which suggests the predominant nature of the wave. However, for the longer duration loadings, all the three layers behave in the similar fashion, which signifies the quasi-static nature of the layers.

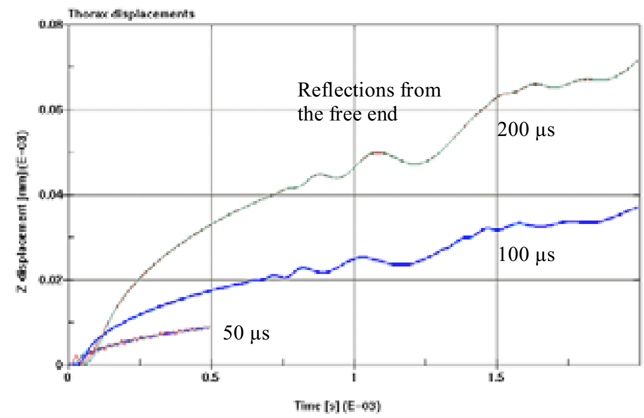

Figure 1: Displacement histories at the surface and interfaces

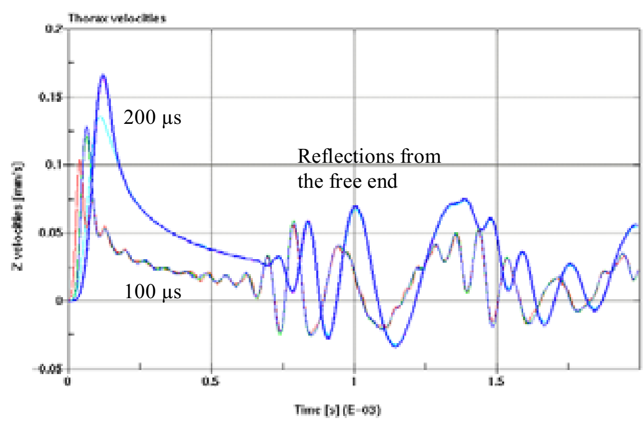

Figure 2: Velocity histories at the surface and interfaces

Figure 2 shows the velocity histories, where appreciable differences can be observed between surface and interface responses for 100 µs, which is missing for 200 µs loading. Further, the response is similar to that of a cantilever beam, whereas, for 50 µs loading the response is that of a rod (not shown here). These observations can be used to make one-dimensional model of the thorax, which will be helpful in establishing the injury criteria. Overall, the example shows the efficiency of the TLM as a tool for analyzing thorax.

REFERENCES

1. Grimal Q., et al. *Int. J. Impact Engineering,* **30**, 665-683, 2004.

Towards an advanced clinical expert system for patient-specific modeling and musculo-skeletal (MS) analysis?

[1]Serge VAN SINT JAN
[1]Department of Anatomy, Faculty of Medicine, Université Libre de Bruxelles (Belgium)
email : sintjans@ulb.ac.be, web: www.ulb.ac.be/~anatemb

INTRODUCTION

Current data collection procedures include numerous tools to collect data related to any part of the musculoskeletal system (MS) and its functions. Unfortunately, the MS complexity makes the simultaneous use of the above procedures difficult. The amount of procedures to possess is so large that no research center possesses them all. Therefore, inhomogeneous datasets must be first obtained from various sources (e.g., literature, colleagues), and registered if one wished to build complex MS models. Data format conventions and validation is therefore an important issue to insure the quality of the final models. Clinical data collection is even more problematic because of ethical constraints (no use of invasive tools), and time constraints (some category of patients are rapidly tired).
Clinical MS analysis of patients is highly complex [1]. However, clinicians mostly rely on their experience and expertise to draw therapeutic conclusions because of the lack of other efficient tools. This lack is due to the current shortages (see above) of the state-of-the-art to generate a fully anatomically accurate and patient-customizable MS model.
Technologies found in modern simulations systems include advanced registration algorithms [2,3], state-of-the-art display [4], dynamic simulation [5], decision-making analysis [6,7] and knowledge-based management [8]. Most of them answer some local practical questions, either at fundamental research level or at clinical level. Unfortunately, most of these efforts appear to become not usable once it is exported to other locations where local needs or local resources are different.
This poor transportability of resources (data, hardware, protocols, software code, people, etc) can be explained at various levels: - complexity of the problems; - non-inhomogeneous data; - multidisciplinarity; - lack of standardization; - lack of consensus about the goals to reach; - etc.
In summary, numerous efforts are currently spent in the world to answer local clinical needs. Unfortunately, none of them has been large enough to deliver a truly patient-specific clinical analysis tools.

METHODS

A potential ideal system (Figure 1) would combine most above available technologies. It should be based on an anatomically accurate database including all components necessary to generate generic MS models using advanced registration tools (full arrow). Some parameters of the MS models will be registered to patient-specific data obtained through clinical analysis (dotted arrows). Knowledge-based algorithms that will offer a decision-making support to clinicians will then statistically analyze the "patient-customized" models.

RESULTS

The final report produced by the system would help clinicians to orientate their diagnosis and final conclusions based on objective data analysis.

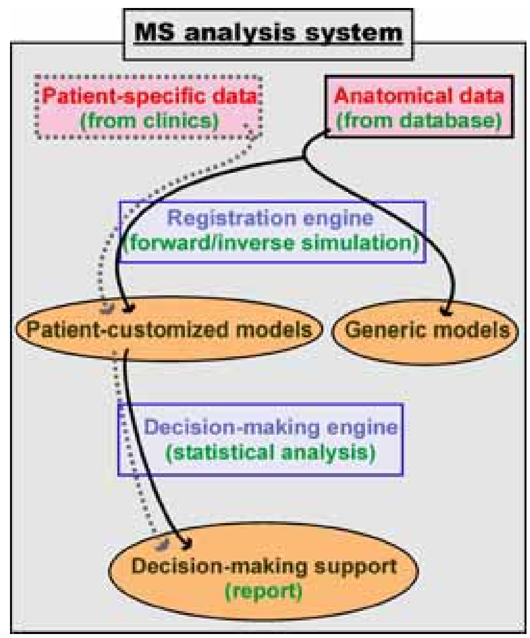

Figure 1. Sketch for MS analysis system.

DISCUSSION

Such system is technologically possible, but will need an important, and well-organized multidisciplinary effort to gather all necessary expertises. This paper would like to emulate a discussion to determine is such effort is practically achievable. This will require a long-term effort coming from all fields available in Biomechanics.

REFERENCES

1. Fabry G, et al. *J Pediatric Ortho* **9**, 170-179, 2000.
2. Neu CP, et al. *J Biomech* **34**, 1429-1438, 2001.
3. Van Sint Jan S et al. *J Biomech* **35**, 1475-1484, 2002.
4. Viceconti M et al. *Proceedings of ESB XIV*, 's-Hertogenbosch, Netherlands, 2004.
5. Daryl G et al. *J Biomech* **36**, 321-328, 2003.
6. Õunpuul S et al. *Gait & Posture* **4**, 62-78, 1996.
7. Ahmed AA et al. *Gait & Posture* **19**, 252-262, 2004.
8. Loslever P et al. *Gait Posture* **7**, 39-44, 1998.

ACKNOWLEDGEMENTS

Special thanks to Dr. G. Molenaers and Dr. K. Desloovere (Pellenberg Hospital, University of Leuven, Belgium) for their very valuable input in the above system sketch (Figure 1).

THE EFFECT OF AGING ON STROKE PARAMETERS IN SWIMMING

[1,2] Bryan Morrison, [2]Richard Hinrichs and [2]Bethany Larsen
[1]Valparaiso University, Department of Physical Education
[2]Arizona State University, Department of Kinesiology; email: Bryan.Morrison@valpo.edu

INTRODUCTION

Recent studies have shown that swimming performance can be maintained through 35 years of age, but then linearly slows 9% for men and 5% for women per decade to age ~70 when women begin to slow at a greater rate than men [1]. They attribute this decline to a reduction in physiological functional capacity, which is the ability to perform the physical tasks of daily life and ease with which these tasks can be performed. Wilmore and Costill describe these changes more specifically as cardiorespiratory endurance, muscular strength, muscular endurance, flexibility, and body composition. These changes are likely to affect both the stroke rate (SR) and stroke length (SL). Hay [2] demonstrated that the changes in SR and SL with increased velocity for many activities including walking, running, and swimming are similar. Recently the relationship between running performance and age was investigated by Korhonen and colleagues [3] who reported similar declines of 5 % per decade in sprinters. They discovered that this was caused by a reduction in step length and no reduction in step rate. In longer races step rate was greater and step length was lower at the self-selected running velocity and was due to a significantly lower propulsive force. Swimmers appear to behave differently than runners. This can be seen at swim meets when the older swimmers tend to have a reduced SR during their races.

This leads to questions of why the SL-SR relationship with velocity is different for individuals and why it changes with age. If we are to train older swimmers to their potential, we have to determine what are the most important stroke techniques. Typically, journal and magazine articles are based on data from elite twenty-year-olds. This may or may not apply to older swimmers as they age and their bodies change. This research hopes to demonstrate the need for age-specific research in the SR-SL relationship and aging in swimming.

METHODS

Two masters national swim meets were videotaped and analyzed. This gave 695 men and 276 women ranging in age from 19 to 88. The videotaping procedure involved setting up a 60 Hz camera in such a way as to be unobstructed throughout the races of interest. The second length of a short course 100-yard freestyle was used for analyses. This videotape was time coded to allow accurate frame specific times. Velocity was determined by measuring the time for the 15 yards between the flags from the time code on the videotape. The SR was determined from the elapsed time for three stroke cycles (first water contact of the right hand to the next water contact of the right hand). SL was then be computed by dividing the velocity by the SR.

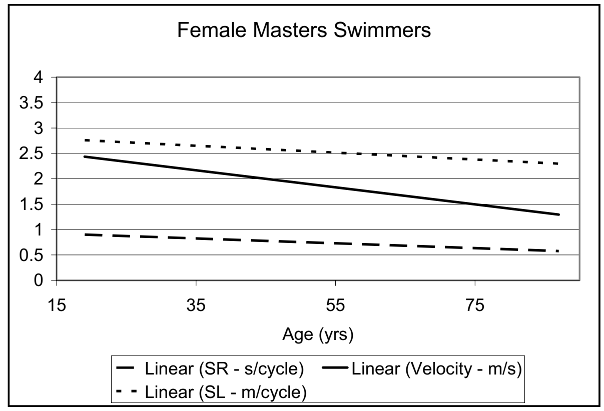

Figure 1: The best fit lines for velocity, SR, and DPS of female masters swimmers.

RESULTS AND DISCUSSION

Velocity decreased as expected at a rate of 5.2 %/decade and 6.1 %/decade for men and women (Figure 1), respectively. This was due to a decrease in men of 9.6 %/decade and in women of 12.1 %/decade in SR. The SL declined slightly in both men and women to help increase the velocity reduction per decade. The SL for women declined 2.4 %/decade and the men declined 1.5 %/ decade.

CONCLUSIONS

The reduction in velocity seen by men and women masters swimmers can mainly be associated with a reduction in SR. The SL reduced slightly in both. However, the women were more affected by a reduction in SL. This demonstrates the need to promote tempo training with aging to help slow this velocity loss.

REFERENCES

1. Donato, AJ, et al. *Journal of Applied Physiology,* **94**, 764-769, 2003.
2. Hay, JG. *Journal of Applied Biomech,* **18**, 257-270, 2002.
3. Korhonen, MT, et al. *Med Sci Sports Exerc, 35*(8), 1419-1428, 2003.

ACKNOWLEDGEMENTS

This research project was sponsored by an USMS Endowment Grant and an ISB Matching Dissertation Grant.

CENTER OF PRESSURE TRAJECTORY DURING WHOLE BODY REACHING IN HEMIPLEGIC PATIENTS

[1,2]Jen-Suh Chern, [2]Saiwei Yang and [2]Wen-hun Yao
[1]Chang Gung University,
[2]Corrosponding author, Yang Ming University; email: swyang@bme.ym.edu.tw

INTRODUCTION

Center of pressure (COP) trajectory is one of the most common methods used to characterize the balance control of both normal subjects and patients with neurological disorders, such as stroke. Voluntary movements, such as targeted reaching, are practical essence for daily function and have been proved to be more effective in challenging and training the balance ability than simulated balance perturbations such as moving platforms [1,2]. Seated reaching for targets in different directions at the level of shoulder height has been shown to affect COP trajectory significantly. Whole body reaching (WBR) requires the subjects to pick up a target on the floor and the target distances were found to affect the movement of COP and activation patterns of postural muscles [3]. The purposes of this study were to compare the performance of WBR with different balance ability and the effects of target distances (10% body height vs 30% body height measured from the midpoint of both big toes) and directions (middle, M; left, L) on COP trajectory as measure by COP path excursion (WTP), COP maximum displacement in frontal (MML and sagittal (MAP) direction.

METHODS

Fifteen normal adults and 23 stroke subjects who fulfilled the inclusion criteria participated in this study. They were instructed to pick up a light weighted bean bag on the floor in two directions (in the middle and to the left or paretic side) at two distances (away from the big toe for 10% and 30% of body height) while standing erectly on RSSCAN pressure mat. A total of 12 trials (3 x 2x 2) were required. The functional reach distance (FR) was also measured as an indicator of balance ability.

The COP trajectory data were normalized (WTP to body height and foot length, MML to foot width, and MAP to body height and foot length) and averaged for statistical analysis. The FR was normalized by body height.

One way analysis of variance was used to compare the difference between normal and hemiplegic subjects. Repeated-measure analysis of variance was used to examine the target location effects. Pearson correlation coefficients were used to examine the performance of WBR for targets at various locations. The statistical significant level was set at α =.05 and all statistical analysis was performed using SPSS 8.0 software package for Windows.

RESULTS AND DISCUSSION

As shown in table 1, FR was different between normal and hemiplegic subjects indicating that baseline balance ability of hemiplegic patients was inferior to the balance control of normal subjects. The significant difference in COP trajectory between groups(Table 1) suggested that control of COP during whole body reaching could be an indicator of level of balance. Descriptive analysis showed that the amount of WTP, MML and MAP was larger in hemiplegic patients than in normal subjects, indicating that hemiplegic patients was not able to shift their COP according to the target location as much as normal subjects did. Targets locations were found to imposed graded dynamic balance challenge for both group [3].

Table 1. Comparison of group differences.

	S of MS	DF	F	P
10MWTP	0.001	1	30.602	**0.000**
MAP	0.003	1	42.147	**0.000**
MML	0.220	1	7.889	**0.008**
30MWTP	0.000	1	16.033	**0.000**
MAP	0.001	1	89.607	**0.000**
MML	0.258	1	6.101	**0.018**
10L WTP	0.002	1	8.075	**0.008**
MAP	0.004	1	41.976	**0.000**
MML	0.227	1	5.736	**0.023**
30LWTP	0.000	1	25.940	**0.000**
MAP	0.001	1	75.414	**0.000**
MML	0.278	1	5.468	**0.025**
FR	0.059	1	30.811	**0.000**

The correlation coefficients between FR and COP trajectory were negative, significant and moderate, indicating that the subjects with shorter FR shifted COP less in both frontal and sagittal directions than subjects with longer FR distance [4]. The correlations between FR and COP trajectory in frontal direction were the lowest indicating that FR might not be able to measure the balance control in frontal direction.

CONCLUSIONS

The results of this study suggested that analysis of COP trajectory during WBR can distinguish subjects with different level of balance ability as measured by FR, indicating that WBR could be a dynamic balance training and evaluation tool for hemiplegic patients. Questioning of FR in measuring balance control in frontal direction [4] was supported by the correlation analysis in this study. Analysis of muscle activation patterns might be valuable for interpretation of balance mechanism.

REFERENCES

1. Streepey JW, Angulo K. Hum Move Sci, 21:423-438, 2002.
2. Goldie PA, et al. Clin Biomech,11:333-342, 1996.
3. Kim CM, Eng JJ. Gait Posture, 18:23-28, 2003..
4. Wernick-Robinson M, et al. Arch Phys Med Rehabil, 80:262-9, 1999

Table 2: Pearson correlation coefficients between FR and parameters during whole body reaching.

	10MWTP	10MAP	10MML	30MWTP	30MAP	30MML	10LWTP	10LMAP	10LMML	30LAWTP	30LMAP	30LMML
FR	**-0.492**	**-0.569**	-0.285	**-0.381**	**-0.579**	-0.231	-0.314	**-0.526**	-0.266	**-0.472**	**-0.554**	-0.118

A NOVEL APPROACH FOR A SOLID OBJECT IMPACT ON HUMAN HEAD

S. W. Gong, H. P. Lee, C. Lu
Institute of High Performance Computing, 1 Science Park Road,#01-01 The Capricorn
Singapore Science Park II, Singapore 117528 Email: gongsw@ihpc.a-star.edu.sg

INTRODUCTION

This paper proposes a feasible methodology to estimate contact force between a solid striker and human head and to predict the human head response to the contact impact via an integration of a simple striker-head contact force model with finite element methods. The computational results from present methods were compared with Nahum's experimental data [1]. The results closely matched the experimental data, showing that present approach facilitates the study on the problem of a solid object impacting on human head.

METHODS

Consider a solid object impacting on a static human head. The three-dimensional finite element model consists of both the head and striker as shown in Fig.1(a). The head model includes the skull, the brain, cerebrospinal fluid (CSF) and the neck. The striker is a solid cylinder attached with soft robber padding. It has a total weight of 5.6kg and impacted on the frontal bone of the head at 9.94m/s along the mid-sagittal plane, which is the similar with the condition used in Nahum's test.

To estimate contact force between the solid object and human head during impact, a simple striker-head contact force model is proposed, as shown in Fig. 1(b). The striker-head contact force model contains five parameters; they are the head mass m_1, the striker mass m_2, the equivalent stiffness K_1 of the human head and neck, the effective contact stiffness K_2^* and the initial striker velocity V.

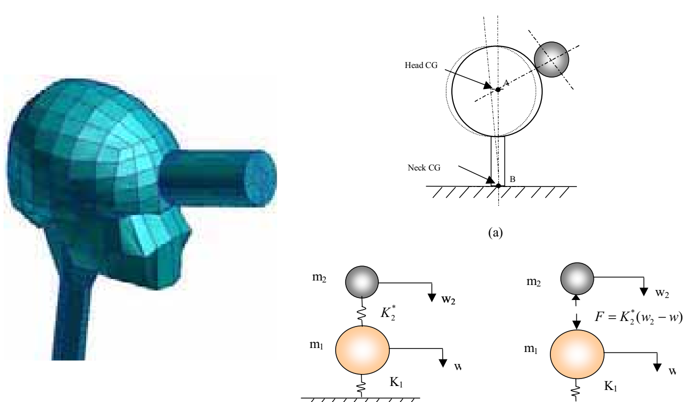

(a) (b)

Figure 1: (a) 3D FE head and striker model; (b) Striker-Head Contact force model.

Based on the striker-head contact force model, the contact force function is formulated in terms of the five parameters as follows:

$$\mathbf{F(t)} = \begin{cases} \mathbf{K_2^*[a_1(c_1-1)\sin(\omega_1 t) + a_2(c_2-1)\sin(\omega_2 t)]} & \mathbf{0 < t < T} \\ \mathbf{0} & \mathbf{t > T} \end{cases} \tag{1}$$

In the force function, T is the contact duration and

$$\omega_{1,2}^2 = \frac{1}{2}\left(\frac{K_1 + K_2^*}{m_1} + \frac{K_2^*}{m_2}\right) \mp \sqrt{\frac{1}{4}\left(\frac{K_1 + K_2^*}{m_1} - \frac{K_2^*}{m_2}\right)^2 + \frac{K_2^{*2}}{m_1 m_2}}$$

$$c_1 = \frac{K_2^*}{K_2^* - \omega_1^2 m_2} \qquad c_2 = \frac{K_2^*}{K_2^* - \omega_2^2 m_2} \qquad a_1 = \frac{V}{\omega_1(c_2 - c_1)} \qquad a_2 = \frac{V}{\omega_2(c_1 - c_2)}$$

The contact force predicted by Eq (1) can be directly applied to the FE head model to substitute the FE striker model.

RESULTS AND DISCUSSION

Figure 2(a) shows the contact force histories estimated by contact force function (1), computed by contact-impact algorithm implemented in the commercial code DYNA3D, and recorded from Nahum's experiment, respectively. The comparison shows that the present contact force function (1) produces a reasonable result. Figure 2(b) shows a comparison between Nahum's test results, Ruan's numerical data [2] and present simulation outcomes. The present result has good agreement with the experimental results.

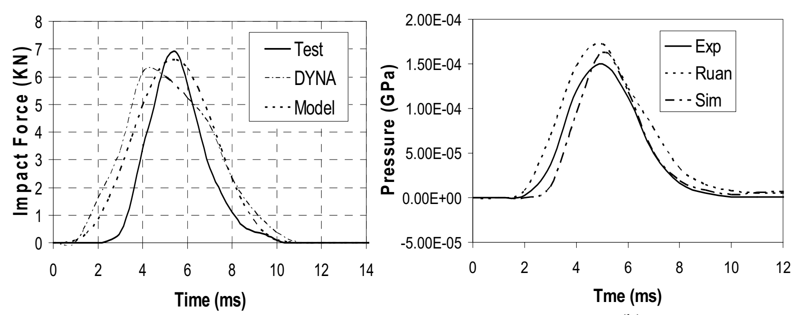

(a) (b)

Figure 2: (a) Comparison of contact forces; (b) Comparison of Coup Pressures

CONCLUSIONS

The proposed approach facilitates the estimation of striker-head contact force and the prediction of human head response to solid contact impact. It can also be used to evaluate the influences of a solid striker's material properties, mass and velocity on head injury.

REFERENCES

1. Nahum, A. M., Smith, R., and War, C. C., 1977. Intracranial Pressure Dynamic During Head Injury. 21st Stapp Car Crash Conference Proceedings, SAE 770922.
2. Ruan, J. S., Khalil, T. B., King, A. I., 1994. Dynamic response of the human head to impact by three-dimensional finite element analysis. *Journal* of Biomechanical Engineering 116, 44-50.

ISB XXth Congress - ASB 29th Annual Meeting
July 31 - August 5, Cleveland, Ohio

Postural Control Against Perturbation During Walking

[1] Misono SAKAI, [2]Shuichi OBUCHI,[3]Yoshitaka SHIBA, [3]Haruhiko SATO and [1]Toshiro FUTAMI
[1]Graduate School of Medical Science, Kitasato University
[2]Tokyo Metropolitan Institute of Gerontology
[3]School of Allied Health Science, Kitasato University; email: dm04023w@st.kitasato-u.ac.jp

INTRODUCTION

To maintain stability of the body when the perturbation was given while moving, the postural control is required otherwise it will cause falling. Although many studies reported on postural control to perturbation in standing[1,2], few study reported on postural control against to perturbation during walking[3]. The purpose of this study was to examine postural control against perturbation during treadmill walking. In addition, we hypothesized a strategy of postural control in such a situation and suggested the effect of aging on postural control.

METHODS

Ten young and twenty-nine elderly subjects participated in this study. We used a separated-belt treadmill (Figure 1), and perturbations were produced by rapidly decelerating one side of the walking-belt for 500 ms while walking. To young subjects, two types of the perturbation were given five times each in three minutes walking: 50% deceleration of the initial speed (moderate perturbation) and 100% deceleration of the initial speed (strong perturbation). To elderly subjects moderate perturbations were given five times in three minutes of walking. The electromyogram responses of leg, thigh, and trunk muscles on the both sides and the acceleration at the pelvis were measured .We classified subjects from reaction patterns of muscles, and compared them.

Figure 1: Separated-belt treadmill (PW21; Hitachi, Japan)

RESULTS AND DISCUSSION

Four reaction patterns of muscles were observed: "ankle strategy", "mixed ankle and hip strategy", and others (Figure 2). Comparing the ankle strategy seen in young and elderly subjects, the response of tibialis anterior on the perturbed side after the perturbation was significantly delayed in elderly subjects (p<. 05)(Figure 3).

The "mixed ankle and hip strategy" observed in this study did not change with advancing trials, although the mixed strategy in standing is defined as the transitory pattern to pure ankle strategy or hip strategy when the stimulus exceeds the control limit. We therefore concluded that the mixed strategy observed in this study was different from the mixed strategy seen in standing. The pattern of muscle recruitment was immediate antero-distal muscle activities followed by postero-proximal muscle activities after perturbation. This pattern resembled whiplash. We suggest this mixed strategy be established as a new strategy. It is thought that the posture of a subject moves like striking a whip since this new strategy showed the ankle strategy followed by the hip strategy, and we considered this new strategy to be a "whiplash strategy". Also, this new strategy was seen when the body shake was large, so it is suggested that it is an important strategy for subjects who have low ability of postural control.

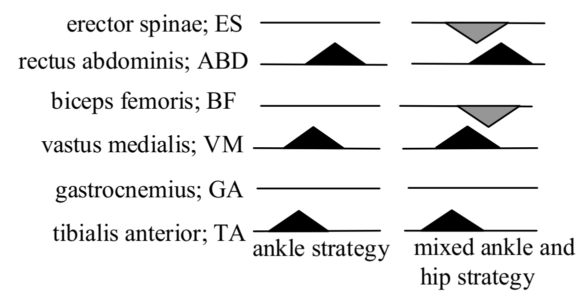

Figure 2: Reaction patterns of muscles

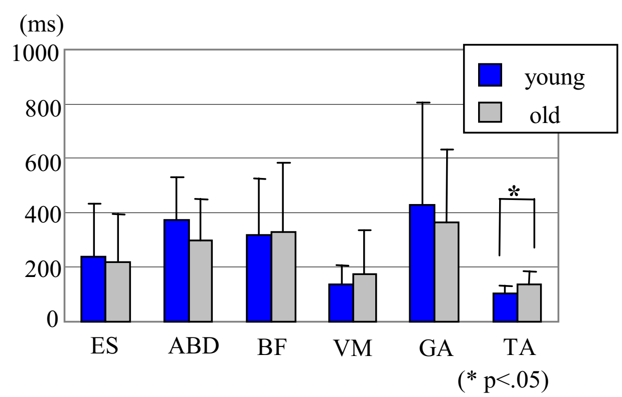

Figure 3: Comparing the ankle strategy (perturbed side)

CONCLUSIONS

From these results, we concluded that there is a specific postural control strategy in walking, and there are differences in postural control ability between elderly and young subjects.

REFERENCES

1. Horak FB, et al. *J Neurophysiol.* **55(6)**, 1369-1381, 1986.
2. Nashner LM. *Exp Brain Res.***30**, 13-24, 1977.
3. Tang PF, et al. *J Gerontol.* **54**, M89-M102, 1999.

MODELING OF PELVIS AND THORAX ROTATIONS IN HEALTHY AND PATHOLOGICAL GAIT

[1]Jaap H. van Dieën, [1,2]Onno G. Meijer, [1]Claudine J.C. Lamoth and [2]Wenhua Wu
[1] Institute for Fundamental and Clinical Human Movement Sciences, "Vrije Universiteit Amsterdam", the Netherlands;
[2]Second Affiliated Hospital of Fujian Medical University, QuanZhou, China; email: J_H_van_Dieen@FBW.VU.NL

INTRODUCTION

During gait the pelvis and thorax rotate in the transverse plane in a near sinusoidal pattern [1]. With changes in gait velocity, the relation between these rotations changes, especially in terms of the relative timing. Whereas at low velocities the rotations are almost in phase, phase lead of the pelvis increases at increasing velocities up to around 2.5 radians (140 degrees; Figure 1). In several pathological conditions, among which low back pain [1] and pregnancy-related pelvic girdle pain (PPP) [2] this increase in phase difference has been shown to be less pronounced (Figure 1).

The out-of-phase relationship between pelvis and thorax rotation in healthy gait has been interpreted as a coordinative strategy to reduce body angular momentum around the vertical axis [3]. However, since stride frequency increases with gait velocity, it may be the case that this phase relationship emerges from second order dynamics of the system without any active coordination. The reduced phase difference in patients with disorders such as low back pain could then be accounted for by an increased stiffness, consequent to increased cocontraction [4]. Thus, we set out to model the relative rotations of pelvis and thorax in healthy and pathological gait as second order linear dynamics.

METHODS

Data were derived from an earlier study on healthy nulliparous women, healthy pregnant women, and pregnant women with PPP [2]. Relations between pelvis and thorax rotations in the transverse plane were characterized as group averaged frequency responses (gain and phase as function of stride frequency).

Analytical solution of a linear second order system with harmonic position forcing was used to express gain and phase as function of frequency, inertia (of the thorax), stiffness and damping. Thorax inertia was estimated based on literature data [5]. First, this model was fitted to the experimental frequency response by optimizing a constant stiffness and gain. Then, a second model was developed in which stiffness and damping were modeled as sigmoidal functions of stride frequency.

RESULTS AND DISCUSSION

The model with constant stiffness and damping did not permit an acceptable description of the experimental data.

The second model adequately described the data of all three groups (Figure 1). The model predicted stiffness and damping to decline above stride frequencies of 0.65 Hz. The declining stiffness and damping might be due to reduced activity of muscles, for example of left rotating muscles active when the trunk is right rotated (stiffness) or rotating to the right

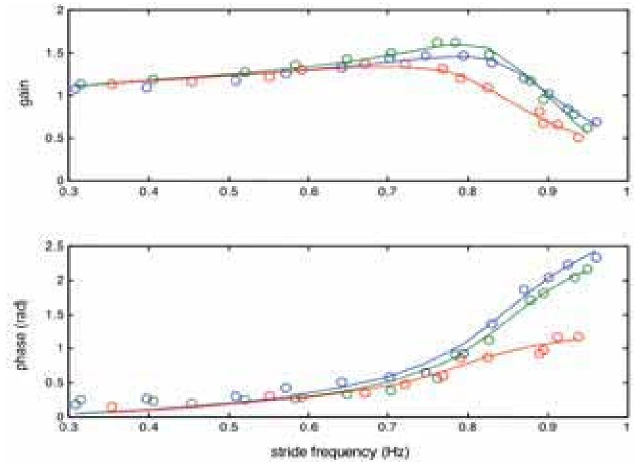

Figure 1: Actual relations between transverse pelvis and thorax rotation (circles) during gait in healthy nulliparous (blue) pregnant (green) and pregnant women with PPP (red) modeled as the frequency responses of second order systems (lines) with stiffness and damping declining with frequency.

(damping). The stiffness, however, declines below values expected on the basis of passive trunk stiffness [6], which implies that at higher velocities active counter rotation is required to obtain the kinematics observed. This can be explained by increased activity of muscles producing for example left rotation when the trunk is already left rotated. For damping no reference data are available, but similarly the decreased damping could be a consequence of increased activity of left rotators when the trunk is rotating to the left and vice versa. The PPP patients differ from the healthy controls mostly in that the damping at higher stride frequencies is reduced less than in the controls.

CONCLUSIONS

Relative transverse rotation between pelvis and thorax during gait can not be modeled as a passive second order system. With increasing stride frequency stiffness and damping are reduced, which suggests that counter rotation of the thorax is actively coordinated. This counter rotation is less pronounced in subjects with PPP than in healthy controls.

REFERENCES

1. Lamoth CJC, et al. *Spine* **27**, E92-E99, 2002.
2. Wu, WH, *Pregnancy-related pelvic girdle pain*. *PhD Thesis*, Vrije Universiteit Amsterdam, 2004.
3. Nottordt JW, et al., *J Hum Mov Stud* **8**, 27-40, 1982.
4. van Dieën JH et al. *Spine* **28**, 834-841, 2003.
5. McConville JT, Churchill TD *Anthropometric relationships of body and body segment moments of inertia.* Air force aerospace medical research laboratory, Ohio, 1982.
6. McGill SM, et al. *Spine* **19**, 696-704.

CAN REPETITIVE SHEAR LOADING OF SPINAL MOTION SEGMENTS CAUSE DISC INJURY?

[1,2]Jaap H. van Dieën, [1,3]Albert van der Veen, [1,3]Barend J. van Royen and [1,2]Idsart Kingma
[1]Institute for Fundamental and Clinical Human Movement Sciences, [2]Faculty of Human Movement Sciences, Vrije Universiteit, Amsterdam, [3]VU Medical Center; email: J_H_van_Dieen@fbw.vu.nl

INTRODUCTION

The lumbar spine, especially at the L5S1 level, is subjected to substantial anterior directed shear forces during many activities [1]. In vitro experiments have shown that shear loading of spinal segments can cause bony failure, most often of the pars interarticularis [2,3]. However, the intervertebral disc (IVD) has been reported to contribute significantly to shear stiffness [3] and may thus also be at risk of failure. Two in vitro experiments using porcine lumbar spine segments were performed to establish whether soft tissue damage could occur in repetitive shear loading.

METHODS

In experiment 1, 14 lumbar spines of immature pigs (80 kg) obtained from the slaughterhouse were fresh frozen. Maximum shear strength of the T13L1 segment was tested at a strain rate of 0.1 mm/s, while the segment was loaded with a compression force of 1600 N (800 N for 5 younger specimens tested in experiment 2). L2L3 and L4L5 segments were loaded with a sinusoidal varying shear force (0.5 Hz) between 20 and 80% of the strength of the corresponding T13L1 segment, while again the segment was statically loaded in compression. Shear displacement and force were continuously recorded at 10 Hz. The posterior elements (PE) were removed in half of the segments, leaving the IVD as the only structure providing shear resistance. The groups with and without PE consisted of equal numbers of L2L3 and L4L5 segments.

In experiment 2, 12 lumbar spines of immature pigs (40-80 kg) were used. The protocol was similar to experiment 1, except that all segments were left intact and that half of the segments were tested in the neutral position and half were tested in a 10 degrees flexed position.

The deformation within the initial cycles was determined as an indicator of shear stiffness. The time to failure (obvious discontinuity in overall deformation as well as range of deformation within the cycles; see Figure 1) was determined. Furthermore the deformation within the cycles just preceding failure and just after failure were compared to indicate changes in stiffness.

L4L5 and L2L3 segments from the same specimen were treated as dependent observations and all tests were done using a Wilcoxon matched pairs test.

RESULTS AND DISCUSSION

Shear strength of the T13L1 segments ranged from 1062 to 1985 N in experiment 1 and 428 to 2282 N in experiment 2, where spines of 40 kg animals were included.

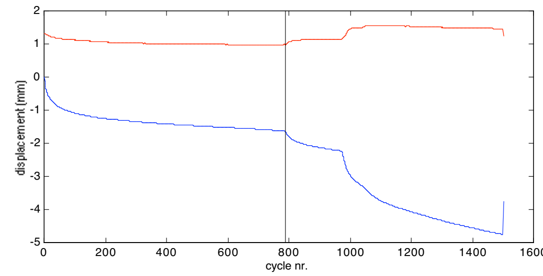

Figure 1: Mean (blue) and amplitude (red) of deformation in each of 1500 subsequent loading cycles in anterior shear of an intact segment in a neutral position. The vertical line at cycle 789 indicates the instant of failure.

In experiment 1, shear loading caused a larger deformation (1.5 vs. 1.0 mm, $p = 0.013$) during the initial cycles, when PE had been removed. In the group with PE, 6 segments did not fail within 1500 cycles. In the group without PE, 3 segments did not fail. Time to failure of the specimens that did fail was 3.3 times longer ($p = 0.017$) in the group with PE. In this group, deformation within cycles after failure was larger than that preceding failure, indicating a loss of stiffness. Whereas in the group without PE, deformation within cycles decreased after failure, indicating increased stiffness. The results suggest bony failure in the segments with PE, which was confirmed by inspection of the specimen after testing. However, when PE were removed, soft tissue injury occurred already after relatively few cycles.

Since the IVD may be less protected by the PE when the specimen is flexed, experiment 2 compared specimens tested in flexed and neutral positions. However, for none of the variables studied were significant differences found between the flexed and neutrally positioned segments.

CONCLUSIONS

Although repetitive anterior shear forces are capable of inducing IVD damage in porcine spine segments, this appears not to occur when PE are present, not even when the segment is flexed close to maximal flexion.

REFERENCES

1. Dieën J.H. van and Kingma I. *Ergonomics* in press.
2. Cyron W. *JBJS* **58B**, 462-466, 1976
3. Yingling VR, and McGill SM. *Spine* **24**, 1882-1889, 1999.

ACKNOWLEDGEMENTS

The help of our students Jaap Jansen, Stijn van Huijstee and Maddy van Straalen in data collection is gratefully acknowledged.

NONLINEAR ANALYSIS OF THE BEHAVIOUR OF THE HUMAN CORNEA

Long-yuan Li and Brian Tighe
School of Engineering and Applied Science, Aston University, Birmingham B4 7ET, UK
Email: l.y.li@aston.ac.uk and b.j.tighe@aston.ac.uk

INTRODUCTION

The biomechanical properties of the human cornea are fundamental to our understanding of corneal behaviour in response to keratorefractive surgery and aspects of corneal physiology where mechanics plays an important role. Recent research on the whole corneal structure has showed that the mechanical behaviour of the cornea is rather complicated [1-3]. The unexpected non-uniform distribution of strain in the meridian direction of the cornea measured in experiments indicates that the corneal has regionally different mechanical properties. The principal causes for the regional variability in mechanical properties of the human cornea may include the variability of the elastic modulus of fibrils, the reinforcing ratios of collagen fibrils, the orientation of fibrils, and/or the sequential recruitment of fibrils [3,4]. Previous studies showed that the diameter of fibrils is constant in the centre and para-centre, while there is increased variability in the diameter of fibrils in the corneal periphery. In the limbus, the diameter of fibrils increases. Unfortunately, no accurate quantitative determinations on the regional variation in the volume fraction of collagen fibrils are available, although variations possibly are small.

METHODS

The cornea is approximated as a spherical cap with a variable thickness. The radius of curvature of the mid-surface of the shell is assumed to be R = 7.86 mm. The horizontal diameter of the mid-surface of the shell at the edge is assumed to be D_b=15 mm (see Fig.1). The corneal thickness is assumed to increase linearly from h_{min} = 0.5 mm at the centre to h_1 = 0.66 mm at the limbus and to h_2 = 1.0 mm at the edge. The cornea is subjected to the intra-ocular pressure of p = 2.135 kPa. The boundary of the shell is assumed to be hinged at the edge. In the present nonlinear analysis the cornea is assumed to be perfectly axial-symmetric and the analysis is performed within the cross-section by using axial-symmetric plane elements.

The cornea material is modeled as an orthotropic, nonlinear elastic material with principal axes defined as in the directions of meridian and circumference. Since the reinforcing ratios of the collagen fibrils vary from the central region to the limbus the overall orthotropic moduli in meridian and circumference are not constants. The stress-strain equation in the uni-axial stress state, in the principal axes is assumed as [5]:

$$\sigma = \alpha\varepsilon^2 + \beta\varepsilon \qquad (1)$$

where σ and ε are the stress and strain, α and β are constants. The nonlinear stress-strain equations for a three-dimensional orthotropic material can be derived based on the uni-axial stress-strain equation (1).

The problem is solved using the nonlinear finite element analysis program (Femlab). Because of axial-symmetry, only half of the cornea within the axial-symmetric plane is analyzed.

RESULTS AND DISCUSSION

Fig.1 shows the deformation of the cornea and corresponding von Mises stress distribution in the cross-section. The high stresses are found mainly in the areas close to the limbus and the edge where the boundary is fixed. More results and the comparisons between the model predictions and experimental results will be shown in the conference presentation. Results on the parametric studies will also be provided in the presentation.

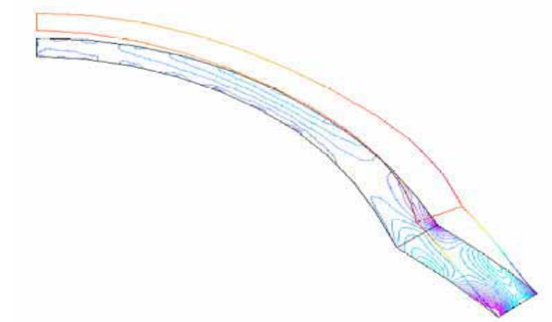

Fig.1 von-Mises stress distribution and deformed shape of the cornea subjected to intra-ocular pressure.

CONCLUSIONS

This paper presents a numerical investigation on the mechanical behaviour of human corneas by using a nonlinear finite element analysis method. After verification, the FE model is used to examine both normal and keratoconic corneas. Future extensions of this research will include the interaction between the stress analysis model and the flow model of corneal hydration [6]. The research presents here is part of a long term project to develop accurate predictive tool that can assist the clinical management.

REFERENCES

1. Hjortdal JO. Regional elastic performance of the human cornea. *J. Biomechanics* **29**, (7)931-942, 1996.
2. Jue B and Maurice DM. The mechanical properties of the rabbit and human cornea. *J. Biomechanics* **19**, 857-853, 1986.
3. Lindsay R and Atchison D. Descriptors of corneal shapes. Optom. Vis. Sci**. 75**, 156-158, 1998.
4. Shin TJ et al. The distribution of strain in the human cornea. *J. Biomechanics* **30**, (5)497-503, 1997.
5. Fung YC *Biomechanics: Mechanical Properties of Living Tissues* (2nd Edition). Springer, New York, 1981.
6. Li LY, Tighe BJ and Ruberti JW. Mathematical modeling of corneal swelling. *Biomechanics and Modeling in Mechanobiology* **3**, (2)114-123. 2004.

SYMMETRY AND ASYMMETRY IN THE LOWER LIMBS OF ATHLETES DURING GAIT

[1]Shigehito Matsubara , [1]Tetsu Yamada, [2]Sekiya Koike and [2]Michiyoshi Ae

[1] Doctoral program in Health and Sport Sciences, University of Tsukuba; email:shige-m.taiiku.tsukuba.ac.jp

[2] Institute of Health and Sport Sciences, University of Tsukuba

INTRODUCTION

Gait analysis is an effective tool for evaluating and quantifying effects of a surgical intervention or rehabilitation on a patient's gait (Schutte et all., 2000). Although gait symmetry has often been assumed to simplify data collection and analysis (Heydar et all., 2000), asymmetry of the lower limbs will be an indication for a risk of abnormality in the physical function. The similar idea may be applied to gait analysis for athletes who suffered from various injuries of the lower limbs. The symmetry-asymmetry analysis in athlete's gait will provide us with useful information to precaution and prevent from serious injuries which may be induced by the asymmetry in the lower limbs. Therefore, investigating symmetry and asymmetry in the lower limbs of athletes has a special significance. The purpose of this study was to investigate gait pattern of uninjured and injured athletes to determine symmetry and asymmetry in the lower limbs.

METHODS

The gait of 8 injured athletes (age 20.3±2.3 yrs) and 10 uninjured athletes (age 19.2±0.8 yrs) from a university track club was analyzed. After the explanation of the procedure and safety of the experiment, informed consent was obtained from the subjects. Three-dimensional coordinates of 47 reflective markers attached to the subjects were obtained with an optical motion measurement system (VICON 612) with eight cameras operating at 120Hz, which was synchronized with two KISTLER force platforms. Subjects were asked to walk in barefoot at a self-selected speed on the laboratory floor under which the force platforms were mounted.

Kinematics and force platform data were used to estimate the joint torque and joint torque power at the hip, knee and ankle of the lower extremities during the stance phase by an inverse dynamic approach. Asymmetry index of the lower limbs was calculated for gait descriptors such as step length by the following equation.

$AI = | \text{Right} - \text{Left} | * 100 / (\text{Right} + \text{Left}) / 2$

ANOVA was used to test differences in gait descriptors and asymmetry index (AI) between two groups with significant level of 0.05.

RESULTS AND DISCUSSION

Table 1 shows mean and standard deviation of AI. Although there was no significant differences in AIs of gait descriptors such step length (SL), step frequency (SF) and so forth, AI of SL and walking ratio(SL/SF) tended to be larger in the uninjured athletes than those of the injured athletes. The AI of double support time for the injured athletes was significantly larger than the uninjured athletes. Smaller AI of gait descriptors for the uninjured athletes was expected, but the results indicated that this hypothesis was not accepted, except for double support time which was a symptom of the asymmetry for the injured athletes.

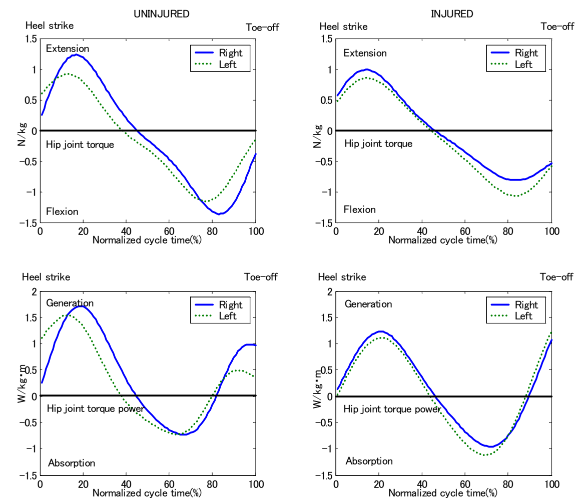

Figure 1: The hip joint torque and torque power for an uninjured and an injured athlete

Figure 1 shows hip joint torque and torque power patterns for the uninjured and injured athletes. The peak torque and torque power of the right hip for the uninjured athlete were greater than that of the injured athlete. However, no big difference was observed in the joint torque of the left leg between two athletes. This may be interpreted as an over-exertion of the torque and power at the right hip joint of the uninjured athlete because he could cancel out the asymmetry in joint kinetics through his adaptability. It is speculated from these results that injured athletes might change the gait pattern involuntarily not so as to be beyond the range of control, while uninjured athletes could control their gait pattern over their asymmetry in the lower limbs by the uninjured physical function. The other possible reason for the asymmetry of uninjured athletes may be laterality in their leg which is used as take-off leg and so forth.

Table 1: Asymmetry indexes for the athletes
*: P<0.05

	step length(%)	step frequency(%)	walking ratio(%)	STT(%)	SWT(%)	SST(%)	DST(%)
uninjured	17.9±9.4	4.8±3.0	24.2±14.4	1.9±1.9	8.9±6.3	6.1±4.5	0.08±0.01*
injured	9.2±8.0	4.7±5.4	19.2±18.3	3.6±4.8	4.4±6.8	4.4±6.8	0.1±0.02*

REFERENCES

1. Schutte L.M, et al. *Gait and Posture* 11, 25-31, 20

GENDER DIMORPHISM IN KNEE JOINT MECHANICS AFFECTS ACL LOADING

[1]Kiyonori Mizuno, [2]Jack Andrish and [2]Ton van den Bogert and [1]Scott McLean,
[1]Department of Biomedical Engineering, The Cleveland Clinic Foundation, Cleveland OH
[2] The Orthopaedic Research Center, The Cleveland Clinic Foundation, Cleveland OH; email: mcleans@ccf.org

INTRODUCTION

Anterior cruciate ligament (ACL) injury is a common and potentially traumatic knee joint injury. Women suffer ACL injuries more frequently than men (Arendt and Dick, 1995), with this disparity commonly attributed to a combination of neuromuscular, anatomical and hormonal factors. The potential for gender differences in ACL loading, and hence injury risk, stemming from a gender dimorphism in knee joint mechanics however, has not been addressed. The current study examined whether the ACL in the female knee experiences larger strain than its male counterpart, under application of the same three-dimensional (3D) knee joint loading state.

METHODS

Methods for data collection have been described previously (Mizuno et al., 2004). Joint loads (forces and torques) were applied to 5 male (57 ± 13.4 yrs) and 5 female (58.3 ± 11.5 yrs) cadaveric specimens via a custom-designed loading device and were recorded with a 6 DOF load cell fixed to the tibia. Synchronous knee flexion data were recorded via an electro-goniometer secured across the joint. ACL strain was recorded via a microminiature differential variance reluctance transducer (DVRT, Microstrain, Burlington, VT) attached to the anterior-medial bundle (AMB). Data were collected at 10 Hz while flexion angle and loads were varied continuously for about 25 minutes. Regression analysis was applied to determine how ACL strain depended on seven independent variables: anterior-posterior, medial-lateral and compression force, flexion-extension, varus-valgus and internal-external rotation torques and knee flexion angle. Specifically, single specimen data were fit to the following model:

$$\varepsilon = a_0 + \sum_{i=1}^{7} b_i x_i + \sum_{i=1}^{7} \sum_{j=1}^{i} c_{ij} x_i x_j \qquad (1)$$

where, ε corresponds to AMB strain and x_i is the ith independent loading variable. Specimen-specific regression coefficients were obtained via least-squares fitting, following which model strain predictions were validated. A clinically relevant 3D knee joint loading state, comprising combined valgus (10 Nm) and internal rotation torque (10 Nm) was then input to each specimen-specific regression model, at flexion angles of 0, 15, 30, 60, and 90 degrees (Kanamori et al., 2000). Resulting ACL strains were submitted to a 2-way ANOVA to test for gender and flexion angle effects ($P<0.05$).

RESULTS AND DISCUSSION

Male and female specimen specific regression models could predict ACL strain within 0.51% ± 0.10% and 0.52% ± 0.07% of the measured data respectively, and in each case explained more than 75% of the associated variance (Figure 1). Predicted strains in each model were also consistent with that obtained experimentally for the same loading and knee flexion conditions. Significant increases ($p<0.05$) in mean peak ACL strains were observed in female compared to male models under the same load application (Figure 2). It is not clear which aspect of gender-dimorphic joint mechanics is responsible for this ACL strain increase. It is possible that the female ACL experiences the same force as the male ACL, but is more compliant and undergoes larger strains. It is equally plausible that female knee geometry is such that the ACL experiences a larger force than in the male knee when subjected to combined valgus and internal rotation loads. Further study is needed to quantify the contributions of these two potential mechanisms.

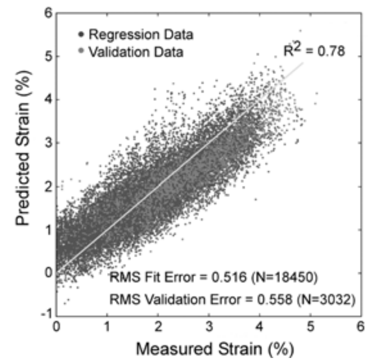

Figure 1: Model predicted versus measured ACL strain.

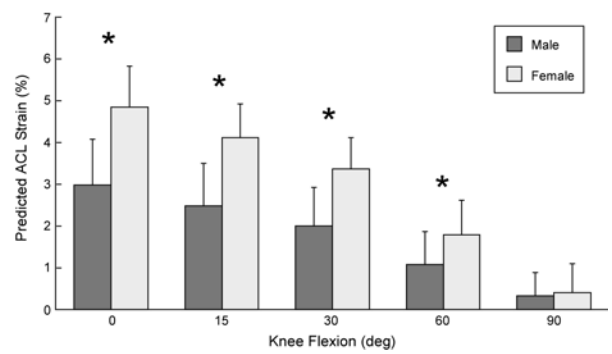

Figure 2: Gender comparisons of predicted strains.

CONCLUSIONS

A gender dimorphism in knee joint mechanics exists, which may play an important role in ACL injury risk during dynamic sports postures. The ultimate success of current injury prevention strategies, typically teaching females to adopt "male" neuromuscular patterns, may thus be severely compromised. Elucidation of the underlying causes of this gender dimorphic behavior would facilitate more effective screening and prevention of ACL injury in the future.

REFERENCES

1. Arendt et al., (1995) *Am J Sports Med* **23**: 694-701.
2. Kanamori et al., (2000) *Arthroscopy* **16**: 633-639.
3. Mizuno et al., (2004) ORS 50th Annual Meeting, #240.

ACKNOWLEDGEMENTS

Funded by NIH (AR47039) and CCF RPC (RPC 07206).

SAGITTAL PLANE BIOMECHANICS DURING SPORT MOVEMENTS DOES NOT EXPLAIN HIGHER INCIDENCE OF ACL INJURY IN FEMALES

[1,2] Scott McLean, [1]Xuemei Huang and [1,2]Ton van den Bogert
[1]Department of Biomedical Engineering, The Cleveland Clinic Foundation, Cleveland OH
[2] The Orthopaedic Research Center, The Cleveland Clinic Foundation, Cleveland OH; email: mcleans@ccf.org

INTRODUCTION

Anterior cruciate ligament (ACL) injury is a common and traumatic sports injury, particularly for females. Female neuromuscular control patterns can contribute to their increased risk of ACL injury. For example, women tend to land in a more extended (hip and knee) position than men (e.g. Malinzak et al., 2001). This places the patellar tendon in a more anterior orientation (Herzog and Read, 1993), which is theorized to increase the amount of quadriceps-induced ACL force, and thus contribute to ACL injury (DeMorat et al., 2004). During athletic movements, however, the quadriceps and ground reaction forces are not independent of flexion angle, or of each other, which is ignored in this theory. The current study quantified the contributions of gender specific sagittal plane knee biomechanics to the force in the ACL during an athletic movement linked to ACL injury.

METHODS

Ten male and ten female NCAA basketball players had lower limb 3D kinematics and kinetics quantified during the stance phase of ten sidestep cutting maneuvers. A dynamic model of the pelvis and lower extremity was generated for each subject as described previously (McLean et al. 2003). Joint angles were obtained from Mocap Solver (Motion Analysis Corporation, Santa Rosa, CA) and intersegmental 3-D forces and moments at the knee were solved using standard inverse dynamics. Intersegmental loads were defined as components of external load on the joint, expressed in a joint coordinate system. Anterior tibial shear force (F_{ant}), external flexion (M_{flex}), valgus (M_{val}), and internal rotation moments (M_{int}) were used for further analysis. ACL force (F_{ACLsag}) due to the sagittal plane joint loading mechanism was estimated as:

$$F_{\mathrm{ACLsag}} = F_{\mathrm{ant}} + \left(\frac{M_{\mathrm{flex}}}{d(\theta)} \right) \times \sin \alpha(\theta) \, ,$$

where d is the moment arm of the patellar tendon as a function of knee flexion angle θ, and α represents the angle between the patellar tendon and the long axis of the tibia in degrees, also a function of knee flexion (Herzog and Read, 1993). This equation does not incorporate hamstring force contributions, and thus represents a worst-case scenario in terms of ACL injury risk during sidestepping. Peak joint loads, F_{ACLsag} and initial contact knee flexion data were obtained from each trial, averaged for each subject, and compared between genders using a Student t-test (p<0.01 after Bonferroni correction).

RESULTS AND DISCUSSION

Women landed with less initial knee flexion (Table 1), similar to previous observations (Malinzak et al., 2001). Significant gender differences were found in peak valgus moment only (Figure 2), which is consistent with data obtained via gender specific forward dynamic simulations of sidestepping movements (McLean et al., 2004). The sagittal plane loading mechanism failed to significantly load the ACL for either gender (Figure 1). In fact, the joint forces were mainly posterior, loading the PCL rather than the ACL. Females loaded the ACL during early stance, but the magnitude was much smaller than known failure loads. The closed-chain relationship between flexion angle, external ground reaction force, and quadriceps force appears to protect the ACL from excessive sagittal plane loading. Specifically, during early stance, the ground reaction force acts posteriorly on the tibia, protecting the ACL. Quadriceps force does not become large until later in stance, when the flexion angle is such that the patellar tendon orientation is no longer harmful.

Table 1: Peak load comparisons across gender (*p<0.01).

Variable	Male	Female
θ_{init} (deg)*	30.4 ± 3.6	24.0 ± 1.3
F_{ant} (N)	294.2 ± 126.3	194 ± 85
M_{flex} (Nm)	311.4 ± 84.4	282 ± 60
M_{val} (Nm)*	36.6 ± 12.2	70.0 ± 19.8
M_{int} (Nm)	31.7 ± 14.3	20.0 ± 16.2
F_{ACLsag} (N)	378 ± 173	287 ± 110

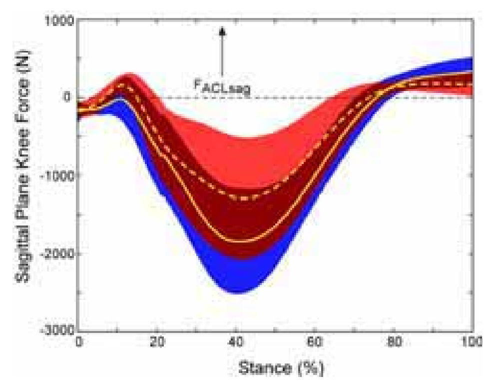

Figure 1: Male and female sagittal plane ACL force.

CONCLUSIONS

Gender differences in sagittal knee biomechanics do not alone explain the higher incidence of ACL injury in women. Gender differences observed in peak valgus moment add further support the evolving hypothesis that knee valgus is the primary extrinsic contributor to the female injury mechanism.

REFERENCES

1. DeMorat et al., *Am J Sports Med* **32**, 477-483, 2004.
2. Herzog and Read, *J Anat* **182**, 213-230, 1993.
3. Malinzak et al., *Clin Biomech* **16**, 438-445, 2001.
4. McLean et al., *J Biomech En,* **125**, 864-874, 2003.

ACKNOWLEDGEMENTS

Funded by NIH (AR47039).

CURRENT CHALLENGES IN CLINICAL GAIT ANALYSIS

Bruce A. MacWilliams and Jacques L. D'Astous
Shriners Hospitals for Children, Intermountain Unit and the University of Utah, Dept. of Orthopaedics
bmacwilliams@shrinenet.org

Video based systems for analyzing human movement began evolving in the early 1970s. By the mid 1980s, commercial systems had grown out of these early efforts. Basic, standard arrangements of reflective markers placed on the lower limbs and associated methods to compute joint angles from these markers were also developed. These marker sets were created to work with a small number of cameras (3 or 4) which by today's standards had exceedingly poor resolution. Capturing and reconstruction software was rudimentary, meaning that sometimes hours were needed to process a single trial. Thus, simplicity and a minimum number of markers were the imperative of the day. Today's gait laboratories typically have at least twice the number of cameras (8-12) that were the standard in the 1980s and 1990s. More importantly, each of these cameras has many times the resolution of their predecessors. The capturing and reconstruction software have advanced to the point where it is now possible to process data in real time. Modern systems are therefore easily capable of tracking many times the number of markers which limited the early model development. Yet with all these advances, most labs use the same commercial gait models that were developed for the earliest technology. Some of the specific clinical deficiencies of these gait models are:

Joint axis identification. There are various options for the user to attempt to align markers that reflect the axis about which knee and ankle motions occur. Attempting to specify these axes using surface markers is notoriously unreliable. This leads to a reduction in reported flexion and erroneous increases in other angles. Misalignment of the knee axis also directly affects hip rotation angles. Accurate representation of this parameter would be greatly beneficial in eliciting the effects of femoral anteversion. Errors of 10 to 15° are not uncommon, and these are of the same magnitude as pathologic values of anteversion, so this measure is not normally helpful.

Hip joint center location. In order to accurately compute hip kinematics and kinetics, the location of the femoral head must be known. Unlike the knee and ankle, the hip joint is not easily accessed. To locate hip joint centers, markers are placed on the pelvis, and the hip joint is determined using a calculation with parameters determined from normal individuals. Some or many of the patients seen for gait analysis may not fit this normal profile, particularly those with hip dysplasia. For these individuals, there are likely gross inaccuracies in hip joint kinematics and kinetics.

Skin motion. An inherent problem with any surface marker model is motion of the skin relative to the bone. The biomechanics of interest are those of the bony segments. As joints move and muscles change shape, the skin surface will translate relative to the underlying bone. Marker landmarks are chosen to avoid particularly muscular regions, but there will always be some error. In current models there is no way to assess or compensate for these inaccuracies.

Foot model. One of the greatest frustrations with current models is the lack of useful information about the foot. Many multisegmental foot models have been developed and validated, yet commercial gait models treat the foot as a single rigid segment, essentially a "foot bone" and motions within the foot are attributed to the ankle joint. This approach to foot modeling is a direct result of limitations of older systems.

Interlaboratory consistency. A recent study[1] showed that while systems in different labs produced reliable and accurate data, there were large differences between labs due to marker placement (*e.g.* hip rotations varied by as much as 28°). This study highlights some of the sensitivities and difficulties of marker placement in current models.

Additional segments. During gait the trunk is often used to compensate for distal motor deficiencies. While trunk and upper extremity models are now commercially available, standardization on their implementation is lacking. Because these were only recently developed commercially, many users had already created their own models. Thus there is little agreement on marker placement and computational methods for the trunk, head and upper extremities.

Additional quantitative parameters. Current commercial software computes joint angles, temporal parameters and, if force plate data are present, joint moments and powers. There are other parameters however which may be useful in assessing a patient's current status or outcome. These include the "gait index" and functional muscle lengths. While these data may be processed with the information from current models, additional software and processing steps are required.

Muscle Forces. While EMG provides valuable information about muscle timing, there is no way to predict muscle forces with standard software. Information about individual muscle forces could be invaluable to treatment planning. This analysis requires muscle modeling and optimization techniques and may represent the next generation of gait software.

In summary, while current commercial gait models have been providing useful clinical data for many years, there are several recognized inherent deficiencies. New cameras allow for many more markers to be visualized and real time tracking technologies could be employed to develop more sophisticated data collection methods which may address these limitations. Recent commercial programs have made strides toward some of these issues, but most laboratories have yet to adopt these.

1. Gorton et al. *Gait and Posture* 16(S1):S65-6, 2002

THE EFFECT OF ANATOMICAL AND ROBUSTNESS CONSTRAINTS ON OPTIMUM JUMPING PERFORMANCE

Maurice R. Yeadon, Cassie Wilson and Mark A. King
Loughborough University; email: M.R.Yeadon@lboro.ac.uk, web: www.lboro.ac.uk

INTRODUCTION

Using a simple criterion, such as maximum jump height, in a simulation model optimisation study may lead to a theoretical performance which is not achievable due to the violation of anatomical constraints or due to the effects of timing perturbations on performance. The aim of this study was to determine the effects of imposing anatomical and robustness constraints on the optimisation of the height reached in a running jump.

METHODS

A planar eight-segment torque-driven subject-specific computer simulation model of the contact phase in running jumps for height was developed. The model included eight torque generators, comprising contractile and elastic elements in series, situated on both sides of the ankle, knee, hip and shoulder joints to allow for co-contraction. Wobbling masses were included in the shank, thigh and trunk segments using non–linear spring-damper representations. The foot-ground interface was modelled using non-linear, spring-damper systems situated at the toe and the heel (Figure 1).

Figure 1: Eight-segment simulation model of the foot contact phase in running jumps from one leg.

The model was customised to an elite high jumper by determining subject-specific inertia and torque parameters. Anthropometric measurements of the jumper were taken and segmental inertia parameters were calculated using a mathematical model [1]. Torque measurements were taken during eccentric-concentric movements at the ankle, knee, hip and shoulder joints using an isovelocity dynamometer (Cybex NORM), with crank angular velocities ranging from 50°/s to 450°/s, in order to express maximum voluntary torque as a function of joint angle and angular velocity [2].

The simulation of a running jump for height was matched to an actual performance by varying the torque generator activation time histories and allowing small adjustments to the initial conditions in order to minimise the difference between the kinematics of simulation and performance. Using the matching simulation as a starting point, an unconstrained optimisation of the contact phase was carried out to maximise the height reached by the centre of mass during the flight phase. This was achieved by varying the torque generator activation time histories, the initial configuration conditions and the approach velocity in order to obtain a simulation with maximum height. A second optimisation was carried out using constraints to ensure that the knee and ankle joint angles remained within anatomical limits during takeoff and flight. In a third optimisation perturbations of 5 ms in activation timings of the knee extensor torque were also introduced and the score to be maximised was taken to be the minimum height reached in a group of perturbed simulations.

RESULTS AND DISCUSSION

Table 1. Optimised jump heights for the three conditions

	approach velocity [ms^{-1}]	jump height [m]
performance (track)	7.4	2.01
matching simulation	7.4	1.95
optimisation 1	7.4	2.74
optimisation 2	7.4	2.63
optimisation 3	7.4	2.32

Without any constraints the theoretical maximum jump height in optimisation 1 was an unrealistic 2.74 m while imposing anatomical constraints in optimisation 2 reduced this to 2.63 m. Perturbing the activation timings by 5 ms in optimisations 1 and 2 did not change jump heights but violated the anatomical constraints and the knee and ankle.

Requiring robustness to timing perturbations in optimisation 3 further reduced the jump height to 2.32 m. Perturbing the activation timings of optimisation 3 by 5 ms did not result in reduced jump height.

CONCLUSIONS

When maximising performance using simulations it is important that considerations of anatomical constraints and robustness to timing perturbations are taken into consideration. Failure to do this can result in maximal solutions that are unrealistic and unachievable. Since the jumper in this study had a personal best high jumping performance of 2.31 m and since perturbations at hip and ankle must be accommodated it appears that activation timing must be better than 5 ms.

REFERENCES

1. Yeadon MR. *J Biomech* **23**, 67-74, 1990.
2. Yeadon MR, et al. *J Biomech* **38**, 2005.

CHALLLENGES IN MUSCULOSKELETAL MODELING FOR CLINICAL USE

[1] John Rasmussen, [2]Michael Damsgaard, [2]Søren Tørholm Christensen and [3]Mark de Zee
[1]Institute of Mechanical Engineering, Aalborg University, Denmark, jr@ime.aau.dk
[2]AnyBody Technology, Aalborg, Denmark
[3]Department of Orthodontics, School of Dentistry, Faculty of Health Sciences, University of Aarhus, Denmark

INTRODUCTION

Musculoskeletal modeling has evolved in the past five years from a field of scientific experiments to a tool applicable to solution of practical ergonomic problems. This paper very briefly points out a number of challenges the scientists and developers within this field must face in the forthcoming years in order to make the technology applicable also to clinical use.

Much of the scientific discussion concerning musculoskeletal modeling has been focused on the basic approaches and their divisions into forward and inverse dynamics with the former capturing the complexity of activation dynamics and the latter enabling models of realistic complexity. Recently, experiments with hybrid models have been reported (see, for instance, [1]), and with the development of computational technology, it must be foreseen that reliable analysis methods will be available in the future. This leaves the scientific community with the challenge of providing models with the necessary reliability, versatility and documentation for clinical applications.

CLINICAL REQUIREMENTS OF MUSCULOSKELETAL MODELING

It is useful to attempt a categorization of the requirements for clinical use of musculoskeletal models.

Morphological complexity: Since clinical applications are diverse, models with an adequate complexity to cover a wide range of cases must be available. One of the challenges here is that it is necessary to divide many anatomical muscles into several separate mechanical units [2]. We estimate that a full body model will comprise some 1000 independent muscle units.

Physical complexity: Muscles have nonlinear elastic properties, they wrap over and slide on bones and other muscles, and their contraction is due to a complex electro-chemical process. Joints are rarely ideal hinges, and many of the reaction forces in the body are unilateral and hence form contact mechanics problems. These are some of the physical complexities that must be addressed.

Individualization: Many clinical applications require models to be individualized. This is in particular the case for modeling of physical disabilities or prospective surgical procedures. A musculoskeletal model comprises thousands of parameters, so a full individualization made operational in a clinical setting is a challenging requirement.

Reliability and validation: Clinical models are used to make decisions on diagnostics, treatment, and rehabilitation of patients, and hence they must be reliable and validated. Errors can come from many sources including input, the musculoskeletal model, and the software used to process it. Further-

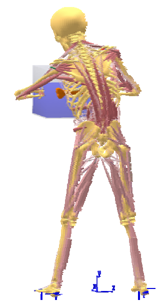

Figure 1: Musculoskeletal model of a box lift comprising roughly 500 muscles [4].

more forward dynamics models assume that the body moves optimal according to some criteria. Are these criteria still valid for patients? Proper validation must treat all these elements and do so as separately as possible from each other.

RESULTS AND STATE-OF-THE-ART

Due to space limitation, we shall focus on the issues of morphological and physical complexity. Anderson et al [3] demonstrated that a gait pattern can be reproduced in a model with reasonable morphological complexity in a forward dynamics model capturing the physical complexity of activation dynamics. Unfortunately, the computation times are prohibitive for clinical applications so far.

The AnyBody Research Group has announced an initiative [4] for assembling a public domain repository of musculoskeletal models written in the AnyScript body modeling language (Figure 1). The idea behind this initiative is that a public domain library will allow many scientists to contribute and scrutinize models, while the relation between the data and the computer model guarantees the completeness of the date. Recently, this library was reported to have been equipped with anthropometrical scaling [5] capable of partial individualization.

CONCLUSIONS

Much work remains before musculoskeletal models are generally clinically applicable. The amount of work indicates that this must be a worldwide concerted effort, and models for managing this effort must be devised.

REFERENCES

1. Thelen, DG, Anderson, FC and Delp, SL., *J. Biomech* **36**, 321-328, 2003.
2. van der Helm, F. *J Biomech* **24**, 1151-1163, 1991.
3. Anderson, FC, Pandy, M, *J. Biomech. Eng.* **123**, 381-390.
4. The AnyScript Model Repository, www.anybody.aau.dk/repository.
5. Rasmussen, J, de Zee, M, Damsgaard, M, Christensen, ST, Marek, C, and Siebertz, K. ISCSB 2005, Cleveland, Ohio.

SIMULATION-BASED TREATMENT PLANNING FOR GAIT ABNORMALITIES: VISION AND CHALLENGES

[1]Allison S. Arnold, [1]Frank C. Anderson, [1]May Q. Liu, [2]Ilse Jonkers, [1]Ayman Habib, [3]Darryl G. Thelen, and [1]Scott L. Delp
[1]Departments of Mechanical Engineering and Bioengineering, Stanford University
[2]Faculty of Kinesiology and Rehabilitation Sciences, KULeuven, Belgium
[3]Department of Mechanical Engineering, University of Wisconsin-Madison
email: asarnold@stanford.edu, web: www.stanford.edu/group/nmbl

INTRODUCTION

The management of gait abnormalities in persons with neuromuscular disorders is challenging. Theoretically, gait abnormalities can be alleviated by first identifying the biomechanical factors that contribute to abnormal movement and then *(i)* decreasing the muscle forces that disrupt normal movement (e.g., via tendon transfers or botulinum toxin injections) and/or *(ii)* increasing the muscle and ground reaction forces that have the potential to improve movement (e.g., via strengthening exercises, orthoses, or osteotomies). However, physical examination and gait analysis alone are often not sufficient to identify the cause of a patient's abnormal gait or to predict the consequences of treatments. The transformation from EMG patterns to multijoint movement is complex, and experimental approaches to infer a muscle's actions, based on the muscle's attachments, EMG activity, and measured motions of the body, cannot explain how forces produced by the muscle contribute to motions of the joints. At present, the treatment outcomes are inconsistent; some patients show dramatic improvements after treatment, while others show little improvement or get worse.

The following case study illustrates how dynamic simulation can be used, with gait analysis, to enhance our understanding of gait abnormalities and to provide a scientific basis for planning treatments. We generated a 3D muscle-actuated simulation of a subject with stiff-knee gait to determine the source of his diminished swing-phase knee flexion and to evaluate the potential efficacy of different treatments.

CASE STUDY

The subject was a 12-year-old male with cerebral palsy. Preoperatively, his peak knee flexion during swing was 33º, and he exhibited abnormal activity of the rectus femoris throughout the gait cycle. We represented the subject's musculoskeletal system by a 21-degree-of-freedom linkage that was scaled to his size and actuated by 92 muscles. We used "computed muscle control" [1] to find a set of muscle excitations that, when used to drive a simulation of the preswing and swing phases, generated gait kinematics and kinetics that closely matched the experimental data (Fig. 1). The predicted muscle excitations were consistent with the subject's measured EMG activity.

Analysis of the simulation revealed that the subject's stiff-knee gait was caused by excessive rectus femoris forces during preswing. His average knee extension and hip flexion moments in early swing were within normal limits, as were his average hip and ankle flexion moments in preswing. However, his average knee extension moment in preswing was excessive, resulting in an abnormally low knee flexion velocity at toe-off.

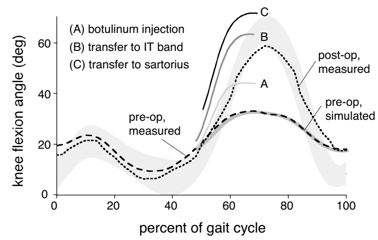

Figure 1. Knee flexion trajectories following simulated treatments. The subject's measured knee angles before and after surgery are shown for comparison. Shaded area is the normal mean ± 1SD.

Decreasing the excessive excitation of rectus femoris, simulating the effects of botulinum toxin injection, increased knee flexion by about 10º (Fig. 1, A). Eliminating the excessive knee extension moment of rectus femoris while leaving the hip moment intact, simulating a surgical transfer of the rectus femoris insertion to a site lateral (Fig. 1, B) or posterior (Fig. 1, C) to the knee, increased the peak knee flexion by about 30º. A substantial improvement was achieved regardless of whether the muscle was converted to a knee flexor. The simulated improvements were similar to the subject's actual improvements after tendon transfer surgery.

CHALLENGES

Simulation-based analyses of muscle function during walking provide insights not available from experimental methods alone [e.g., 2]. Before simulations can be widely used to guide treatment decisions for individual patients, however, advancements in the following areas are needed:

- Experimental data that more accurately describe patients' joint axes, trunk motions, and foot-floor interactions during consecutive strides.
- Models that more accurately and efficiently characterize patients' musculoskeletal geometry and joint kinematics.
- Muscle-tendon models that characterize the effects of pathology, surgery, and other treatments on the time course of muscle force generation.
- Methods for analyzing and validating simulations that better elucidate the actions of muscles and the consequences of neuromusculoskeletal impairments.
- Techniques for incorporating representations of sensory-motor control into simulations of normal and abnormal gait.
- Clinical studies that test whether subject-specific dynamic simulations can improve treatment outcomes.

REFERENCES

1. Thelen DG and Anderson FC. *J Biomech*, in press.
2. Zajac et al. *Gait Posture* 17, 1-17, 2003.

ACKNOWLEDGEMENTS

Thanks to Saryn Goldberg, Michael Schwartz, Sylvia Õunpuu, and the staff of the Center for Motion Analysis at the Connecticut Children's Medical Center. This work is funded by the NIH and the Department of Veterans Affairs.

APPROXIMATION OF BALANCED LANDINGS IN GYMNASTIC DISMOUNTS

Alison L. Sheets and Mont Hubbard

University of California, Davis, USA
email: alsheets@ucdavis.edu , web: mae.ucdavis.edu/~biosport

INTRODUCTION

Gymnastic dismount landing phases have two parts: a short duration impact phase when foot-mat contact forces are high, and a subsequent balancing phase during which the gymnast exerts active control over the resulting post-impact velocities to achieve a desired motionless terminal configuration. Simple impulse-momentum approximate models for the two phases can help in understanding what pre-impact motion states are controllable and thus are feasible targets for the end of flight.

METHODS

Approximate quasi-rigid-body gymnast models are used for both impact and balance phases. Impact is characterized by larger forces over a shorter duration (Δt = 0.04 sec) than the balancing phase [1]. Although large impulses at the feet create similar joint impulses and cause the body to deviate slightly from its presumed rigid pre-impact configuration, the short impact period motivates the approximation that the body remains rigid. Nevertheless, impact is long enough to make total rigid-body rotation (~0.3 rad) non-negligible. Whole-body rotation is included by assuming that angular velocity decreases linearly during impact and that the rigid body rotates about the ankle. Non-instantaneous linear and angular impulse and momentum relations approximate the impact phase. Horizontal and vertical impulses, ϑ_x and ϑ_y, applied to the gymnast's feet cause them to stop [1] and decrease body angular velocity according to

$$\vartheta_y = m(v_{yf} - v_{yo}) + mg\Delta t_i \quad (1)$$

$$\vartheta_x = m(v_{xf} - v_{xo}) \quad (2)$$

$$I_{cm}(\omega_f - \omega_o) = r(\vartheta_x \cos\theta_{avg} + \vartheta_y \sin\theta_{avg}) \quad (3)$$

where m is gymnast mass, r the distance from feet to center of mass (cm), g gravity, $\theta_{avg} = (\omega_o + \omega_f)\Delta t / 4 + \theta_o$ the average angle between the line from ankle to cm and vertical during impact, I_{cm} the whole body inertia about the cm, ω the angular velocity, v_x and v_y the horizontal and vertical velocities, and subscripts o and f denote prior to and after impact.

In a balanced landing, impulses reduce the angular velocity to an amount that can be controlled by multiple muscle torques during the balance phase. While the impulses may cause post-impact angular velocity to be exactly zero, balancing is possible over a range of landing configurations and velocities. Moreover, post-impact balance control is generally exerted at all joints and is a multi-input multi-output control problem. A conservative approximate model of balance allows the gymnast to attenuate the post impact angular velocity while remaining rigid and using only the ankle moment created by pressing the toe or heel into the ground. The ankle moment is limited since the ground reaction force (~mg) must pass though the foot. Minimum and maximum possible post-impact angular velocities ω_{min} and ω_{max} are calculated by solving differential equations for this motion,

$$I_{cm}\ddot{\theta}_{min} = mgr\sin\theta_{min} + mgd_t \quad (4)$$

$$I_{cm}\ddot{\theta}_{max} = mgr\sin\theta_{max} - mgd_h \quad (5)$$

where d_t and d_h are horizontal distances from ankle to toe and heel, respectively.

RESULTS AND DISCUSSION

Short and tall gymnasts with properties and bar release conditions shown in Table 1 can complete 3 and 2 dismount somersaults, respectively, and are configured differently at impact to reduce angular velocity enough to balance [2].

Table 1: Gymnast properties and bar release conditions

Ht (m)	Mass (kg)	I_{cm} (kg·m^2)	ω (rad/s)	H_{cm} (kg·m^2/s)
1.57	62.38	9.20	9.84	90.57
1.71	69.30	12.57	8.96	112.71

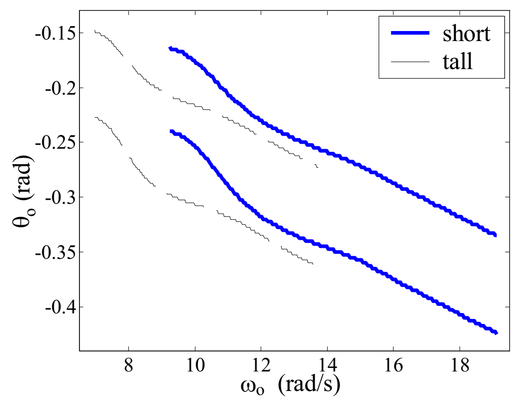

Figure 1: Ranges for pre-impact contact angles for balanced landings differ for short and tall gymnasts

The ranges of all possible landings for the short and tall gymnast's given their angular momentum H at bar release are shown in Figure 1. If the athlete has a larger impact angular velocity ω_o and small inertia, she must contact the ground with a larger body angle relative to vertical θ_o than an athlete with larger inertia and smaller angular momentum because she will rotate further during impact. The short gymnast is able to balance over a larger range of ω_o than the tall one. With a given ω_o, the tall gymnast is able to balance with a slightly larger range of θ_o due to a relatively larger foot size which increases ankle moment (Figure 1). Although the range of possible θ_o decreases for small values of ω_o, the athlete is in controllable landing configurations longer since she rotates more slowly, making a balanced landing more likely.

REFERENCES

1. McNitt-Gray, JL, et al. *J Biomech*, **34**, 1471-1482, 2001.
2. Sheets, AL & Hubbard, M. 10th ISCSB, submitted 2005.

A NEUROMUSCULAR TRACKING METHOD FOR COMPUTING INDIVIDUAL MUSCLE FORCES DURING HUMAN MOVEMENT

Ajay Seth[1] and Marcus G. Pandy[1,2]
[1]Department of Biomedical Engineering, University of Texas at Austin, U.S.A.
[2]Department of Mechanical Engineering, University of Melbourne, Australia

INTRODUCTION

Quantifying muscle forces in human performance is necessary to understand muscle coordination and to properly characterize skeletal loading. Inverse dynamics and static torque decomposition are often used to calculate individual muscle forces from joint kinematics and force measurements. In this case, the quality of the muscle forces depends significantly on the accuracy of the inverse dynamics solution. Legitimate questions about the accuracy of inverse dynamics arise when resultant torques/forces fail to drive a forward model through the observed motion. Furthermore, static decomposition can neglect the effects of muscle dynamics. While optimization of muscle controls that make forward dynamics match experimental observations is considered more accurate, the simplicity and low computational cost of inverse dynamics is often favored over the computationally intensive approach of dynamic optimization. There is a need to solve the motion-tracking problem with the accuracy of dynamic optimization, but with the solution speed of inverse dynamics.

METHODS

The optimal control problem for maximum height jumping was solved via a large-scale parameter optimization approach [1]. This solution represented the "gold-standard" for muscle force estimates during jumping in a jumping model (Fig 1.). Noise was added to the optimal solution for joint kinematics and ground-reaction forces (GRFs) to simulate experimental observations. A two-stage tracking methodology was then used to compute individual muscle forces.

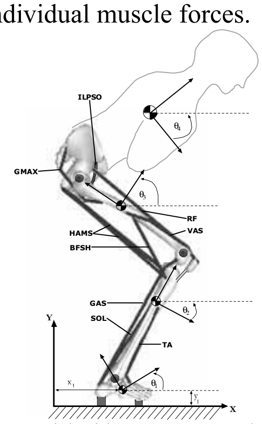

Figure 1: Planar jumping model with 4 segments, 6 dofs and 9 muscles

The method of computed torques [2] was extended to include GRFs as part of the tracking set. Because measurements of GRFs are more accurate than measured kinematics, the accuracy of the computed torques method can be improved. The complete representation of muscle dynamics, from nervous excitation to torque production at each joint, was encapsulated as a nonlinear neuromuscular system. This system was treated as its own plant, whose output torques were used to track the previously computed joint torques. Feedback linearization [3] was applied to cast the nonlinear neuromuscular dynamics into a linear system. The new system was used to formulate a linear tracker and an optimal linear-quadratic tracker (LQT), with the cost function formulated by the sum of the squared tracking errors and muscle efforts.

RESULTS AND DISCUSSION

The motion tracker produced stable joint torques that had less than 1° in segment angle and 1% of body weight tracking error. These torques were fed to the neuromuscular tracker to determine individual muscle forces (Fig. 2). The tracking solutions were computed in less than 100s on a desktop PC. In contrast, the parameter optimization required nearly 24hrs of computing. Nonetheless, the forces determined by the neuromuscular LQT were very similar to those predicted by the parameter optimization (Fig 2).

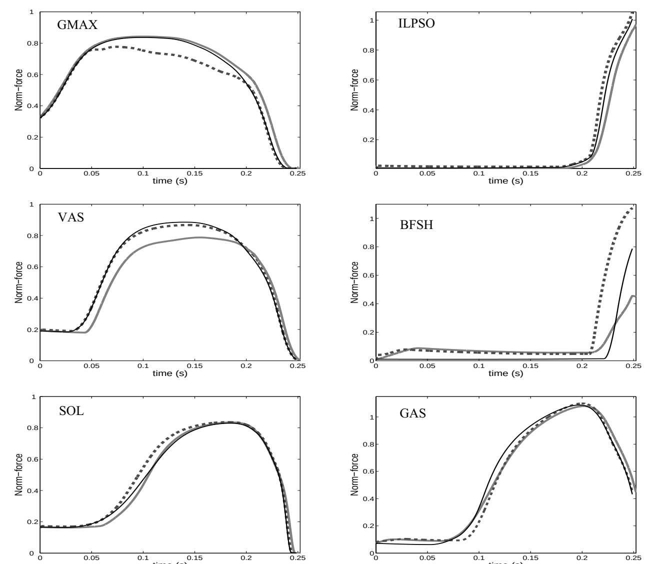

Figure 2: Normalized muscle forces obtained from a neuromuscular tracker (dashed lines) and an LQT (thick solid lines) compared to the paramater optimization solution (thin solid lines).

CONCLUSIONS

A neuromuscular tracking method was developed that can provide accurate individual muscle forces with a time-savings of nearly 3 orders of magnitude over parameter optimization.

REFERENCES

1. Pandy MG, et al.. *J Biomech Eng.* **114**, 343-63, 1992.
2. Spong MW and Vidyasagar M. *Robot Dynamics and Control*. John Wiley Sons, Toronto.
3. Slotine JJ and Li W. *Applied Nonlinear Control*. Prentice-Hall, NJ.

ACKNOWLEDGEMENTS

Supported by the NSF Engineering Research Centers Grant EEC-9876363. Additional support provided by a University of Texas Fellowship and an ISB Dissertation Grant to AS.

CREATING A SKIN STRAIN FIELD MAP WITH APPLICATION TO ADVANCED LOCOMOTION SPACESUIT DESIGN

[1]Kristen Bethke, [2]Dava J. Newman, and [3]Raul Radovitzky
[1]Man-Vehicle Laboratory, Massachusetts Institute of Technology, email: kbethke@mit.edu
[2]Professor of Aeronautics and Astronautics and Engineering Systems, Director of Technology and Policy Program, Massachusetts Institute of Technology
[3]Professor of Aeronautics and Astronautics, Massachusetts Institute of Technology

INTRODUCTION

An improved understanding of the deformation of the body's soft tissue during locomotion would enable quantitative design requirements for advanced spacesuits. A repeatable, quantitative technique for mapping the skin strain field on the human body in motion provides this understanding. The skin strain field map informs the design of a skintight spacesuit, called a mechanical counter pressure suit [1], whose fabric must stretch and rotate with the astronaut's skin to allow for maximum mobility.

METHODS

To measure the strain of the human skin *in vivo* during locomotion, the non-invasive strain measurement technique of Digital Image Correlation is applied to data sets gathered by a 3D laser scanner rather than by optical cameras [2]. In this pilot study, knee flexion from 0 to 90 degrees, for one subject, is used as the representative movement for human locomotion. The leg surface is marked with 156 position trackers that can be identified in the laser scanner's 3D virtual reconstructions of the leg surface. Each tracked point is separated by approximately 3 cm from adjacent points, and each triad of points defines a local surface reference frame with a longitudinal and a circumferential direction. Normal strains emanating out from each tracked point are estimated by comparing the initial separation of each pair of adjacent points to the deformed separation of each pair. Strain gage rosette equations transform these strains from extension/contraction along arbitrary axes to the normal and shear components of the orthogonal strain tensor, with respect to the longitudinal and circumferential axes. Eigenvalue analysis of this strain tensor provides information about the directions and magnitudes of principal strain and of minimum normal strain.

The goal of the analysis is to provide three types of strain information for all tracked body surface points: 1) the strain in the local longitudinal and circumferential directions, 2) the directions and magnitudes of purely normal strain, and 3) if they exist, the directions and magnitudes of purely shear strain. This information specifies in which directions and with what magnitudes an astronaut "second skin" pressure suit must stretch or contract at each location on the body surface.

RESULTS AND DISCUSSION

For the one subject in this pilot study, the largest stretch of the leg skin in the longitudinal direction occurs 3 cm to 9 cm below the patella; longitudinal normal strain magnitudes in this region range from 0.3 to 0.7 (Figure 1). The largest stretching in the circumferential direction occurs on the anterior surface 3 cm below the patella and on the medial surface of the mid-calf, with normal strain values of 0.6 and 0.5, respectively. Shear strain, or angular distortion of the skin, is near zero for most of the anterior and posterior surfaces of the leg.

Eigenvalue analysis transforms the orthogonal strain components into principal and minimum strain directions. The set of minimum normal strain directions suggests the "weave" direction of the tensile fibers of the spacesuit. Proper weave alignment will allow for maximum mobility and ease of locomotion, which are essential requirements for advanced spacesuit designs for future missions to the moon or Mars.

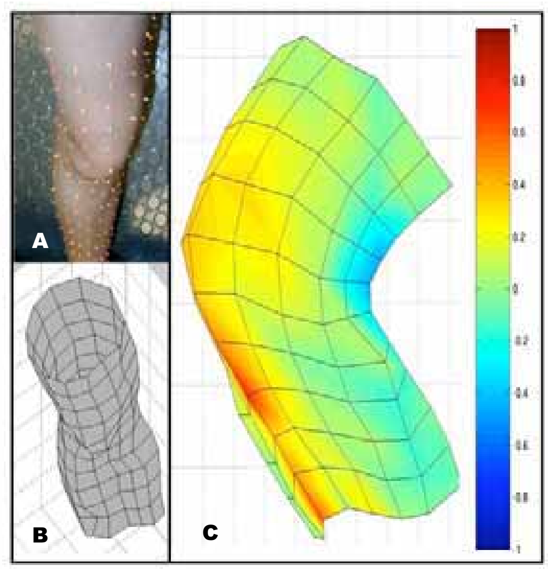

Figure 1: **A.** Raised position trackers covering the leg surface are identified in laser scans and serve as input for a virtual 3D model of the leg. **B.** Leg reconstruction in initial state, from upper thigh to mid calf, using only the positions of the tracked points. **C.** Leg reconstruction with 90-degree knee flexion angle, with the magnitude of skin's longitudinal strain overlaid in color.

REFERENCES

1. Webb P. *Aerospace Medicine*, April 1968, 376-383.
2. Helm JD, et al. *Optical Engineering* **35**, 1911-1920, 1996.
3. Marcellier, H, et al. *Skin Research and Technology* **7**, 246-253, 2001.

ACKNOWLEDGEMENTS

The authors wish to thank Natick Soldier Systems Center for the use of their whole-body laser scanner. Financial support provided by NASA Institute for Advanced Concepts and the National Science Foundation Graduate Research Fellowship.

NO SINGLE LIFTING TECHNIQUE MINIMIZES LOW BACK LOAD

[1]Jaap H. van Dieën, [1]Anja Bakker, [1]Gert Faber and [1]Idsart Kingma
[1] Institute for Fundamental and Clinical Human Movement Sciences, Faculty of Human Movement Sciences, “Vrije Universiteit Amsterdam”, the Netherlands; email: J_H_van_Dieen@FBW.VU.NL

INTRODUCTION

From the epidemiological literature, lifting emerges as an important cause of low back injury and low back pain [1], likely due to the high mechanical loads on the low back that lifting causes. To prevent low back injuries, several lifting techniques have been advised in practice. However, some of the techniques advised do not appear to consistently reduce back load [2,3] and other techniques have not been studied. The aim of the present study was to compare low back load during lifting with four different techniques under varying task constraints.

METHODS

In a repeated measures design, twelve healthy young males lifted 20 kg loads. Subjects used four techniques (stoop, squat, straddle, and archer’s technique; Figure 1). Load widths of 0.30 and 0.60 m were used. In addition, loads were lifted from an initial hand position 0.05 and 0.29 m above floor level.

3D kinematics, ground reaction forces and EMG of selected trunk muscles were measured. These data in combination with anthropometrical measurements were used to estimate net moments around L5S1 and to estimate compression and shear forces acting at L5S1 using previously described methods [4].

RESULTS AND DISCUSSION

Description of the results will in this abstract be limited to peak total (3D) net moments, since these not only reflect the overall outcomes in the present experiment fairly well, but in general appear to be predictive of peak spinal compression and anterior shear forces [5].

Peak net moments were significantly affected by main effects of technique, hand position, and load width and by both two-way interactions with technique. Post-hoc comparisons between techniques for each hand position / load width condition separately indicated the following. For low-lying narrow loads, no differences in back load occurred between techniques. For low-lying wide loads, squat and straddle techniques caused higher back loading than stoop and archer’s techniques. For high and narrow loads the stoop technique caused the highest back load, while the other techniques did not differ from each other. For high and wide loads all differences between techniques were significant. The squat technique caused the highest and the archer’s technique the lowest back load. Differences in trunk inclination as well as the distance between load and the low back appear to explain the effects found.

Differences between lifting techniques within hand position and load width conditions ranged from 10 to 50 Nm or approximately 20%. Differences between low and high hand positions within techniques and load widths ranged from 6 to 35 Nm. Differences between load widths within techniques and hand positions ranged from 16 to 70 Nm.

The interactions found are in line with findings from an earlier study on self-selected, squat, and stoop techniques [3]. This result implies that, although differences between techniques were substantial in some cases, no single lifting technique can be advised and that other aspects than lifting technique merit attention in prevention. Furthermore, the results strongly supports an approach towards lifting technique in which subjects are taught a problem solving approach, which allows them to deal with the highly varying task constraints encountered in practice, rather than a single strategy [6].

CONCLUSIONS

Back load in lifting is affected by interactions of lifting technique and other task constraints, implying that no single technique can be advised.

REFERENCES

1. Hoogendoorn WE et al., Scan J Work Environ Health 25, 387-403,1999.
2. van Dieën JH et al., *Clin Biomech* **14**, 685-696, 1999.
3. Kingma I et al., *Ergonomics* **47**, 1365-1385, 2004.
4. van Dieën JH et al., *J Biomech* **36**, 1829-1836, 2003.
5. van Dieën JH and Kingma I, *Ergonomics*, in press.
6. Gagnon M. *Clin Biomech* **18**, 601-611, 2003.

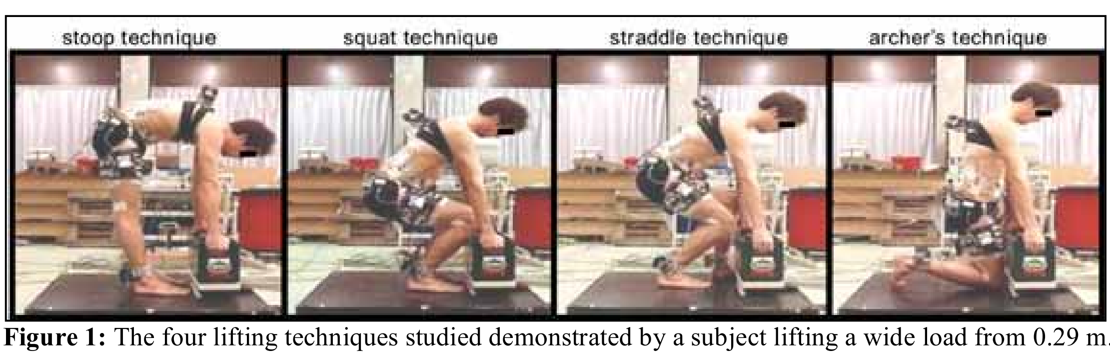

Figure 1: The four lifting techniques studied demonstrated by a subject lifting a wide load from 0.29 m.

PRESCRIBING SKELETAL MOTION CAN SUBSTANTIALLY ENHANCE MECHANICAL POWER OUTPUT; A SIMULATION STUDY

A.J. "Knoek" van Soest and Richard Casius
Faculty of Human Movement Sciences and IFKB, Free University, Amsterdam, The Netherlands
email: k.vansoest@fbw.vu.nl

INTRODUCTION

Average mechanical power output (referred to as "power output" in what follows) is a key factor in determining performance in high-intensity periodic movements like cycling and rowing. We have recently investigated how power output is affected by adding/removing kinematic constraints on skeletal motion using a modelling/simulation approach. We have predicted that the power output of rowers may be limited by the fact that they must prevent "shooting the slide", and that strapping the rower to the sliding seat (i.e. adding a kinematic constraint) may thus improve power output [1]. In the context of FES cycling we have predicted that releasing the customarily fixed ankle joint and stimulating triceps surae and tibialis anterior, does not necessarily improve power output; removing the kinematic constraint at the ankle introduces a degree of freedom that has to be controlled through muscle actions, which counteracts the power gained by the extra muscle mass [2]. Regarding isokinetic sprint cycling we have predicted that prescribing the optimal leg kinematics for unconstrained conditions (i.e. adding a kinematic constraint), and thus removing the need to coordinate leg motion, does improve power output, albeit only marginally [3]. While the latter study confirmed that upon prescription of the optimal unconstrained kinematics power output can only improve, it did not answer the question to what extent power output of the leg muscles can theoretically be improved relative to the natural sprint cycling setup when the fully prescribed leg motion is optimized. The goal of this modelling/simulation study is to find the maximal power output that can be achieved when prescribing a periodic motion of hip, knee and ankle joint in a sagittal plane model.

METHODS

For comparability we adopt a model that was used previously in a study of isokinetic sprint cycling [4], where the highest power output occurred at a pedalling rate of 120 RPM. In this study we investigate 120 "RPM" prescribed sinusoidal movements of hip, knee and ankle, parameterized by average joint angle and joint angle amplitude for each of the three joints, and phase shifts between hip, knee and ankle joints. These parameters are optimized collectively with the stimulation pattern of 8 Hill-type muscles with realistic activation and contraction dynamics. The muscles are assumed to be maximally stimulated for one part of the period time and to receive no stimulation for the remaining part. The optimization is carried out using a genetic algorithm [5], with power output as the optimization criterion.

RESULTS AND DISCUSSION

The optimal leg motion found is characterized by almost simultaneous extension (and flexion) of hip, knee and ankle joints. The hip joint range of motion is much larger than during cycling, resulting in a leg motion (Fig. 1) that is quite different from that allowed by the circular path of the MTP joint as imposed during cycling. As expected for any setup where muscles are effectively decoupled, stimulation of each muscle is tightly tuned to maximization of its power output, i.e. full stimulation during shortening and none during lengthening. Most importantly, power output was found to be 1441 W., which is 135% of the optimal power output for the natural sprint cycling setup.

It must be expected that the theoretical maximal power output of the leg muscles is even higher than that calculated here, as neither the period time nor the form of the motion has been varied. It remains to be investigated if a mechanism that enforces the optimal lower extremity motion can be built, and if subjects are able to exploit the advantages of such a mechanism. It also remains to be established if such a mechanism has advantages during prolonged exercise, where central physiological processes may be performance-limiting. Irrespective of issues of practical implementability, this study illustrates the potential of a modelling/simulation approach for preliminary evaluation of hypotheses on the mechanics and energetics of human motion.

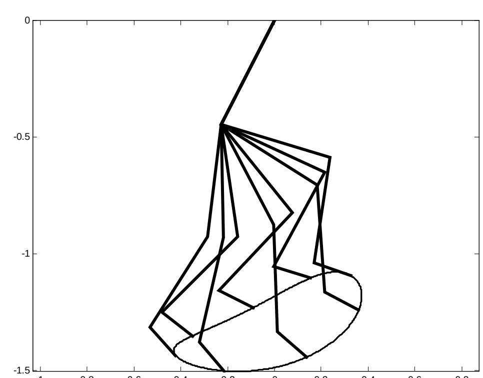

Figure 1: Optimal motion of foot, shank and thigh, plotted at regular time intervals, with fixed upper body. To facilitate comparison to the kinematics of cycling the complete path of the MTP joint is also plotted.

REFERENCES

1. Soest AJ van et al. *Proc. VIIIth TGCS Symp.*, Milan, 2001
2. Soest AJ van et al. *MSSE.*, in press, 2005.
3. Soest AJ van et al. *Proc.IVth WCB*, Calgary, 2002.
4. Soest AJ van et al. *MSSE* **32**, 1927-1934, 2000
5. Soest AJ van et al. *J. Biomech. Eng.* **125**, 141-146, 2003.

ACKNOWLEDGEMENT

We acknowledge the contribution of Andy Ruina (Cornell University) to this work.

EFFECTS OF TIMING OF MUSCLE ACTIVATION ON PERFORMANCE IN HUMAN VERTICAL JUMP

[12]Przemyslaw Prokopow, Stefan Szyniszewski[3] and [12]Ryutaro Himeno
[1]Computational Biomechanics Unit, RIKEN, Japan
[2]Department of Computer Science and Mathematics, University of Saitama, Japan
[3]Graduate School of Natural Science and Technology, Kanazawa University, Japan

INTRODUCTION

The sensitivity of human movement on precise neural control is noteworthy problem in terms of movement control and sports biomechanics. Previous studies demonstrated that human vertical squat jump is very sensitive to precise timing of muscle action [1,2]. Present study investigates quantitatively the effects of time shift of individual muscles and group of muscles on jump performance. Three research questions were addressed: (i) what is the effect of altered muscle activation timing on jump height and kinematics (ii) how disorder of muscle coordination cause decline in jump performance (iii) what is the minimal shift of muscle activation timing that significantly alter jump height.

METHODS

Forward dynamics computer simulation of vertical squat jump was used in present study [3]. A human musculoskeletal model of lower extremities was three dimensional and consisted of nine rigid body segments (i.e. head-arms-trunk, right and left upper legs, right and left lower legs, right and left feet, and right and left toes). The body was modeled as 20 degree-of-freedom linkage which was free to make and break contact with ground. A total number of 26 Hill-type musculotendon actuators drove the model. An optimal control of muscles activation pattern was found through numerical optimization where Bremermann's method was applied. As an objective function we used a maximum height reached by the mass centroid of the body. In order to evaluate the effects of timing of muscles activation on the performance of vertical jump, the optimal activation time of each muscle was systematically altered by the interval of 0.1 ms in the range ±50 ms. Altered were either muscle onset time, muscle offset time, or muscle switching time (total activation duration remained constant but onset and offset times were shifted equally). Time shift was applied separately to each of eight individual muscles (m. gluteus maximus, m. adductor magnus, hamstrings, m. rectus femoris, mm. vasti, m. gastrocnemius, m. soleus, and other plantaflexors) and to each muscle functional group.

RESULTS AND DISCUSSION

The numerical optimization procedure generated a natural-looking and smooth squat jumping motion where jump height was 34.6 cm. Muscle control (i.e. muscle activation timing) in jump was very sensitive to a shift applied to onset activation time. It was found the changing activation timing of certain muscles (i.e. mm. vasti, m. soleus and hamstrings) by as little as 2-3 milliseconds resulted in a marked (over 10%) difference in jump height (Fig. 1). Muscle control was the most sensitive to precise tuning of muscles spanning the knee joint and ankle joint, where muscle control at the knee joint depended to a large extent on co-action of the monoarticular knee extensor

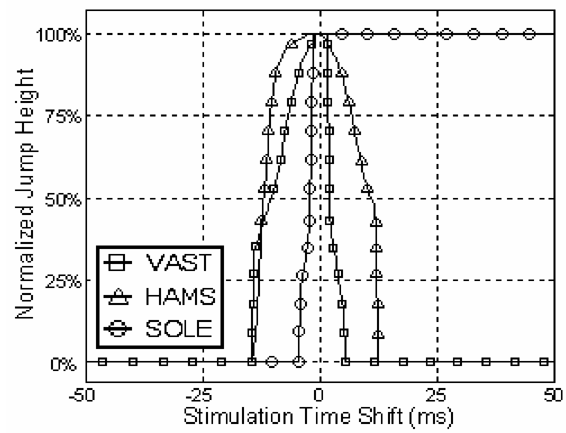

Figure 1: The effect of time shift applied to mm. vasti, hamstrings and m. soleus. Jump height is expressed as percentage of optimal jump height.

(mm. vasti) with biarticular muscles. Among individual muscles the control of mm. vasti, m. soleus, hamstrings and other plantaflexors were found to be especially important for coordination in jumping. Muscle control was found to be very sensitive to intermuscular coordination. The disintegration in coordination caused by earlier activation of mm. vasti was minimized when the hamstrings activation onset time was decreased by a similar amount. Earlier activation of other plantarflexors was found to reduce jump performance by a significantly smaller amount when hamstrings were activated jointly. Furthermore, the negative effects of other plantarflexors were mitigated by concurrent time shift in mm. vasti activation. Also the effect of later activation of mm. vasti was considerably smaller when m soleus activation was also delayed by the same amount. Mechanical effect of time shift applied to different muscles were found to be virtually the same for: earlier stimulation of mm. vasti and later stimulation of hamstrings; earlier stimulation of m. gluteus maximus and m. rectus femoris; later stimulation of m. adductor magnus and hamstrings; earlier stimulation of m. rectus femoris and m. gastrocnemius; earlier stimulation of m. gluteus maximus and m. adductor magnus; earlier stimulation of m. adductor magnus and m. rectus femoris, earlier stimulation of m. adductor magnus and m. gastrocnemius. A time shift applied to one of these two muscles had virtualy the same effect on jump kinetics and kinematics as a time shift applied to the other muscle. Therefore it can be postulated that their action in vertical jump is to some extend mechanically linked.

REFERENCES

1. Bobbert M, Zandwijk JP. *Biol Cybern* **81**, 101-108, 1999.
2. Pandy MG, et al.. *J Biomech* **23**, 1185-1198, 1990.
3. Nagano A. Dissertation, Arizona State University, 2001.

MODELING CEREBRAL ANEURYSM FORMATION AND ASSOCIATED STRUCTURAL CHANGES

Rachmadian Wulandana and Anne M. Robertson
Department of Mechanical Engineering, University of Pittsburgh
E-mail: rxwst2@pitt.edu

INTRODUCTION

Intracranial aneurysms (ICA) are saccular dilations of cerebral arteries, most commonly found at the apices of arterial bifurcations on or near the Circle of Willis. Clinical and histological evidence support the hypothesis that an ICA develops from a local weakening of the wall, possibly due to mechanical or biochemical processes. It is hypothesized, that as a result, the bifurcation apex (A) bulges into an early stage aneurysm 'bleb' with no identifiable neck (B), and then into an aneurysm with a clear neck region (C). It is further hypothesized that the process from (B) to (C) is accompanied by collagen degradation and deposition. When the two processes are well balanced, the ICA is secured from rupture and develops into a complex aneurysm, exhibiting biological responses such as calcification and thrombosis (D) [4].

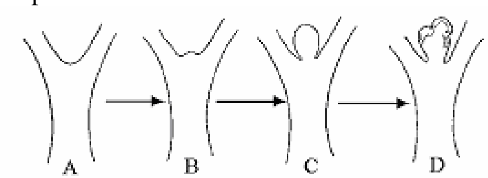

Figure 1 Stages of Aneurysm Development

We recently developed a dual-mechanism constitutive equation capable of modeling collagen recruitment and disruption of the IEL [2,3] based on the nonlinear inelastic behavior of cerebral arteries reported in [5]. This is the first ICA wall model that takes into account the IEL disruption, commonly observed in histological studies of ICA walls. This model was able to predict the "sac like" shape of the ICA and other important features of early aneurysm formation [1,2]. In this work, we extend the model to include the collagen degradation and synthesis.

CONSTITUTIVE MODEL

Three mechanisms are employed in this model representing the passive mechanical elements of artery and aneurysm walls: elastin, recruited collagen and newly synthesized collagen. Each mechanism is activated at a different deformation level and thus has a unique reference configuration. A scalar function s that depends on the deformation gradient $\mathbf{F_1}$ relative to the stress free initial reference configuration κ_1 is introduced to quantify the level of deformation. The activation and deactivation of the mechanisms commence when s reaches critical values s_a, s_b, s_c and s_d corresponding to arterial collagen activation, elastin breakage, collagen degradation and the synthesis of new collagen, respectively. Following [2-3], we suppose that $s_a < s_b$.

At sufficiently low loads, $s \leq s_a$, only the elastin mechanism, which is presumed to depend on $\mathbf{F_1}$, is load bearing. When $s = s_a$, the collagen mechanism is activated in the mechanical response and the response is a function of the deformation gradient $\mathbf{F_2}$ relative to configuration κ_2 occupied by the body at s=sa. The elastin disrupture is modeled by irreversible termination of the elastin response at $s=s_b$. Collagen degradation will be specified to commence when $s=s_c$. The gradual degradation is carried out by assigning a monotonically decreasing function b(s), which is chosen such that $b(s_c)=1$, that represents the volume fraction of the remaining material (e.g. [6]). Furthermore, collagen synthesis is modeled as continuous integration of a new mechanism that begins when $s=s_d$. Assuming the existence of an incompressible isotropic exponential type strain energy function W_3, the extra stress tensor due to collagen synthesis is

$$\tau_3 = 2\int_{s_d}^{s} a(\hat{s})\frac{dW_3}{d(I\,|_{\hat{s}})}\underline{B}\,|_{\hat{s}}\; d\hat{s} \qquad (1)$$

(see, e.g.[6] for more details) where a(s) is related to the rate of synthesis. Following [1-3], the other two mechanisms are assumed to be described by strain energy density functions W_1 and W_2, similar to W_3. For purely monotonically increasing s, the Cauchy extra stress tensor is given by,

$$\begin{aligned}
\boldsymbol{\tau} &= \boldsymbol{\tau_1} && \text{for s in } [0,s_a) \\
\boldsymbol{\tau} &= \boldsymbol{\tau_1} + \boldsymbol{\tau_2} && \text{for s in } [s_a,s_b] \\
\boldsymbol{\tau} &= \boldsymbol{\tau_2} && \text{for s in } [s_b,s_c] \qquad (2)\\
\boldsymbol{\tau} &= b(s)\,\boldsymbol{\tau_2} && \text{for s in } [s_c,s_d] \\
\boldsymbol{\tau} &= b(s)\,\boldsymbol{\tau_2} + \boldsymbol{\tau_3} && \text{for } s > s_d
\end{aligned}$$

where $s = I_1-3$, $\boldsymbol{\tau_1} = 2\, dW_1/dI_1\, \mathbf{B_1}$, $\boldsymbol{\tau_2} = 2\, dW_2/dI_2$ and $\boldsymbol{\tau_3}$ is given by (1). As is shown in [1-3], the strain energy functions W_1 and W_2 are given by $W_1 = C_1(e^{\gamma_1(I_1-3)}-1)$ and $W_2 = C_2(e^{\gamma_2(I_2-3)}-1)$ where I_1, I_2 are the first invariants of the left Cauchy Green tensors, $\mathbf{B_1}=\mathbf{F_1}\mathbf{F_1}^T$ and $\mathbf{B_2}=\mathbf{F_2}\mathbf{F_2}^T$, respectively. The material constants C_1, C_2, γ_1, and γ_2 were obtained using the experimental data of Scott *et al* [5].

REFERENCES

1. R. Wulandana and A. M. Robertson, 2001, "A Model of Early Stage Aneurysm Development Based on an Inelastic Multi-Mechanism Constitutive Model," Proceedings of the ASME Summer Bioengineering Conference, Utah.
2. Wulandana R., 2003, "A Nonlinear and Inelastic Constitutive Equation for Human Cerebral Arterial and Aneurysm Walls," Ph.D. thesis, University of Pittsburgh, Pittsburgh, PA.
3. Wulandana, R., Robertson, A. M., 2005, "A Multi-Mechanism Constitutive Model for the Development of Cerebral Aneurysms," (in review).
4. Humphrey, J.D., 2001, Cardiovascular Solid Mechanics Cells, Tissues, and Organs, ch. Vascular Disorders, pp 365-498, Springer
5. Scott, S.,Ferguson, G.G.,Roach, M. R., 1972, "Comparison of Elastic Properties of Human Intracranial Arteries and Aneurysms," Can. J. of Phys. and Pharn., Vol. 50, pp 328-332.
6. Wineman, A.S. and Huntley, H.E., 1994, "Numerical Simulation of the Effect of Damaged Induced Softening on the Inflation of a Circular Membrane," Int.J.Solids Structures, Vol.31, pp.3295-3313

ACKNOWLEDGEMENTS

The author RW acknowledges the support from the American Heart Association (AHA 0325737U)

MODIFIED METHODOLOGY TO DETERMINE HEAD ACCELERATION IN HEAD-TO-BALL COLLISIONS IN SOCCER

Mariusz Ziejewski, Radu Danescu, Michael Stewart
Department of Mechanical Engineering, Impact Biomechanics Laboratory
North Dakota State University
E-mail: Radu.Danescu@ndsu.edu, Phone: (701) 231-8841

INTRODUCTION

The cumulative effect of repetitive subconcussive head impacts with the soccer ball may lead to neurological dysfunction and permanent brain damage. Accurate information on head acceleration is therefore essential in reaching the ultimate goal of designing appropriate head protection devices. This paper proposes a set of features to be added to the test models in order to better predict the dynamics of the head/neck ensemble for the real conditions seen in a soccer game. The new features include the capability to adjust the elastic constant of the neck under bending loads in the sagittal plane and the inclusion of added linear resistance simulating the torso participation in the impact.

METHODS

The experimental evaluation was performed on a Hybrid III male head/neck model instrumented with a linear, single-axis accelerometer placed in the center of gravity of the head. The direction of impact was restricted to the front of the model's head only. By tilting the model, the elevation angle varied between 0 and 30 degrees. In some tests, the head model was removed from the neck and mounted on a rotating plate fitted with a spring opposing its rotation. In others, it was mounted on a sliding carriage that simulated the added resistance of the torso in the process of heading the ball. To account for the skill level, muscle strength, and heading technique, the resistance opposed to head movement was simulated by a spring attached to the carriage.

Acceleration data was recorded using a data acquisition system. Baseline data was initially gathered using the head/neck model without headgear. Some of the impact tests were also replicated using a commercially available headgear.

Data analysis was performed on the experimentally generated acceleration curves. A computer code was developed to estimate the following parameters: (*i*) peak acceleration; (*ii*) characteristic time length of the impact; (*iii*) average slope for the rising portion of the curve, and (*iv*) the similarly defined average slope for the descending portion of the curve.

RESULTS

Table 1 shows the acceleration peaks recorded on the head model that first rotated freely in the sagittal plane, and then was fitted with a spring opposing its rotation. Addition of the spring reduced the acceleration peak between 5.0% and 9.6%. The acceleration rate did not change significantly.

A different set of results was generated for tests where the ball approached the head model at a 30-degree elevation angle (table not included in this abstract). The relative decrease in peak acceleration was between 8.6% and 19.5%, always lower when the spring was used. Acceleration rates were also decreased between 0 and 12.5%.

With the model mounted on the sliding carriage, acceleration was compared between spring and no-spring cases (Table 2). Adding the spring reduced peak acceleration between 2.0 and 14.2% and acceleration application rate between 13.8 and 24.0%. Relative differences were higher at higher ball speeds.

The tests were repeated with a protective soccer headgear mounted on the head model. Compared to no-gear cases, acceleration peak decreased between 8.4% and 32.1% while acceleration onset rate decreased between 6.0% and 34.7%.

CONCLUSIONS

1. Addition of a spring limiting head rotation in the sagittal plane (strength, prepared player) reduces head acceleration.

2. Addition of a spring opposing translation (upper body added mass, prepared player) reduces head acceleration.

3. The maximum head acceleration occurred for the setup with no resistance to head rotational motion and no resistance to upper torso translation.

4. It is proposed to modify the existing models to account for different player's strength and skill level. New features include ability to control resistive torque at the head pivot as well as upper body dynamics.

TABLE 1 Head rotation, spring, 0 degrees

Speed (m/s)	Acceleration Peak (g)		
	No spring	Spring	% Decrease
3	8.0	7.6	5.0
9	15.6	14.1	9.6
15	24.8	23.4	5.6

TABLE 2 Base of neck translation spring, 0 degrees

Speed (m/s)	Acceleration Peak (g)		
	No spring	Spring	% Decrease
3	10.2	10.0	2.0
9	26.6	23.0	13.5
15	43.6	37.4	14.2

RELATIONSHIP BETWEEN PRESSURE AND SHEAR UNDER THE FOOT

Z. M. Hasasneh, MS[1,2], S. C. Sibole[1,3], B. L. Davis, PhD[1]
1. Department of Biomedical Engineering, The Cleveland Clinic Foundation, Cleveland, OH 44195.
2. Department of Chemical and Biomedical Engineering, Cleveland State University, Cleveland, OH
3. Department of Biomedical Engineering, University of Akron, Akron, OH

INTRODUCTION

Skin ulceration of diabetic feet is a problem that has major repercussions to both the patient and the health care system. It is generally agreed that non-mechanical factors such as peripheral neuropathy, dry skin and/or vascular problems are often major contributing causes. However, current opinion is divided as to the principal *mechanical* factors leading to ulcer formation. Possible contributors to the formation of an ulcer are localized pressures and shear stresses. The purpose of this study was to examine the relationship between pressure and shear stresses under the forefoot of non-diabetic subjects.

METHODS

The method for examination of this relationship consisted of two parts. Part one required collection of pressure and shear data for 10 non-diabetic subjects. A shear and pressure measurement device (Figure 1) employing an array of 80 force transducers (cross-sectional area of 1.61 cm^2) was used to collect data for 5 males and 5 females with a mean age of 24 years old.

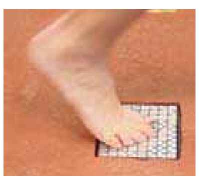

Figure 1: Subject walking on a shear and pressure device.

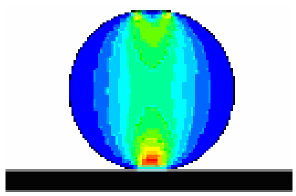

Figure 2: Finite element model of two surfaces in contact.

Data collection consisted of one trial for each subject, in which the subject walked in a straight line and had the right forefoot land on the shear and pressure device. Data were collected at 50Hz for 2 seconds. The data were processed using Matlab programs to convert the voltages into forces [1] followed by low pass filtering (Butterworth filter). Part two consisted of creating a plane-strain finite element model of a hyperelastic ball in contact with a rigid plate (Figure 2) to study the relationship between pressure and shear.

RESULTS AND DISCUSSION

By obtaining the first time derivative of the pressure data, one can not only find the peak pressure in time, but can also gain some insight into the shear behavior (Figure 3). Based on this study's results, the instant of maximum pressure was very close to the instant of maximum shear (Figures 4, 5). Plotting the shear vs. derivative of pressure for all 10 subjects showed the best-fit lines to have similar slopes between -.014 and -0.022 which indicates a good correlation between shear and derivative of pressure (Figure 6). The shear and pressure curves gathered from the finite element model had similar behavior when taking the pressure derivative with respect to position (Figure 7).

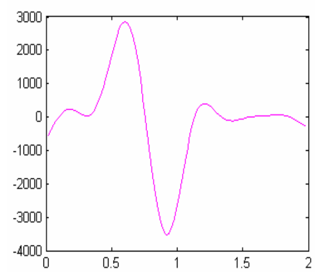

Figure 3: Pressure derivative.

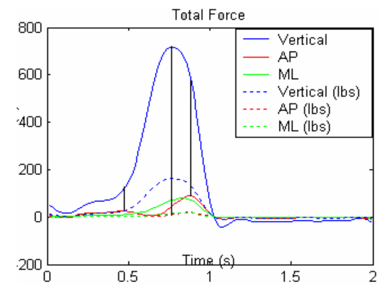

Figure 4: Pressure & shear.

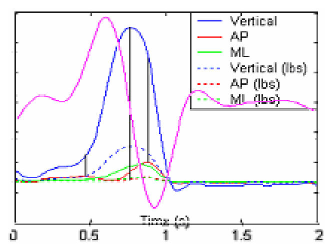

Figure 5: Derivative of pressure overlapping figure 4

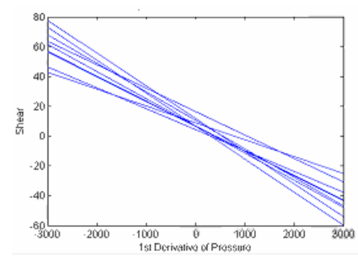

Figure 6: Best fit line of shear vs. derivative of pressure for 10 subjects.

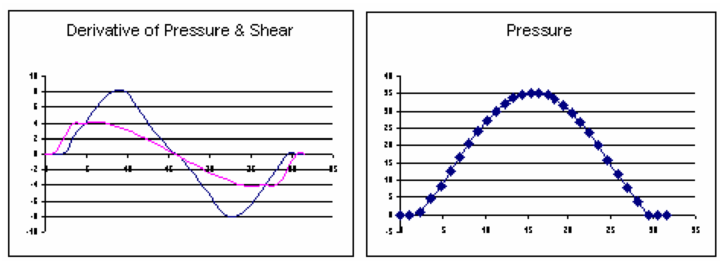

Figure 7: Pressure, derivative of pressure and shear plots of the FEM data.

CONCLUSION

One can hypothesize that maximum shear forces occur at the time and location of peak pressures, however, difficulties in shear measurement impede validation. Based on the results of these trials for control subjects, peak shear position and timing corresponded well with the derivative of pressure. Therefore, through measurement of the pressures, approximate assumptions about the shear behavior can be made.

ACKNOWLEDGMENT

A Juvenile Diabetes Research Foundation (JDRF) funded study.

REFERENCES

1. Weinans, H., Blankevoort, L. (1995) Reconstruction of bone loading conditions from in vivo strain measurements. *J. Biomechanics* Vol. **28**, No. 6, pp. 739-744.

THE VALIDITY OF ACTIVE SQUAT KEEN JOINT PROPRICEPTION TEST

Ming-Feng Kao
National Taiwan College of Physical Education
email: eric3456733@yahoo.com.tw

INTRODUCTION

Proprioception is a sense of position and movement of one's own limbs and body in the absence of vision, termed "limb-position sense" and "kinesthesia," respectively. Proprioception has been shown to diminish with injury, age, and so on. Position sensibility can be measure by many methods. Several different testing techniques have been developed to measure the conscious submodalities of propriception. There are 3 submodalities (joint position sense, JPS; Kinaesthesia and sense of tension). The JPS test measures the accuracy of position replication and can be conducted actively or passively in both open and closed kinetic chain position. Variety of equipment and instrument were developed to measure conscious appreciation of propriception, such as commercial isokinetic dynamometers, electromagnetic tracking devices, custom-made jigs, and some new device. Recently a functional squat system (FSS) was introduced by MONITORED REHAB SYSTEMS that mimics the movement co-ordination pattern of squat jump, under the control of an external load. This device can be measure propriception in actively closed kinetic chain. Compared to some open chain device, it shows more similar to daily activity. Therefore, some test need to investigate the reliability for FSS. The intraclass correlation coefficient (ICC) is used to measure inter-rater reliability. Although Pearson's r may be used to assess test-retest reliability, ICC is preferred when sample size is small (<15) or when there are more than two tests (one test, one retest) to be correlated. Therefore, The purpose of the present study was to compare repeat-measures proprioceptive test in Functional Squat System.

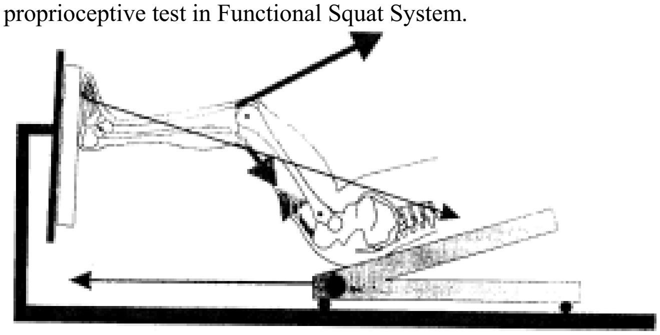

Figure 1: Functional Squat System when performed repetitive squat exercises with one leg in standardized pace.

METHODS

Eighteen college students participated in this study (male=9, female=9; mean age, 22.1±3.5 years). Subject were used FSS in propriception test program to measured low extremity in 25, 50 and 75 three different knee joint angel. For intrasession intratester reliability of the figure-of-two measurement, ICC (2,1) and the SEM were used. The ICC (2,1) was based on a subjects ×2-way analysis of variance (Shrout & Fleiss, 1979).

RESULTS AND DISCUSSION

The ICC (2,1) for repeat-measures knee propriceptive test was 0.94 (P< .05). The means, SDs, and SEMs for these measurements and the repeat-measures propriceptive test are summarized in table 1. the results of the correlations between two test are summarized in Table 2. In order to get an accurate measurements, the reliability coefficients should exceed 0.90 to ensure valid interpretations (Portney and Watkins, 1993). In this study, results demonstrated excellent intrasession intratester reliability and small measurement error for the repeat-measures propriceptive test.

Table 1: Means, SDs, and SEMs, for 3 different knee angles repeat measurement test in FSS.

Measurement	Distance (cm)		
	Mean	**SD**	**SEM**
25°	70.70	18.58	1.89
50°	123.80	21.33	2.90
75°	171.51	23.76	1.43

*Means based on 3 measurements obtained from 25 subjects.

Table 2: Pearson Product Moment correctlation coefficients (γ) of the relationship between repeat-measures propriceptive test in FSS.

Measurement	r*
25°	0.89
50°	0.84
75°	0.96

*$p < .001$

CONCLUSIONS

This study was conducted to determine the intrasession-intratester reliability and criterion-related validity of the repeat-measures knee propriceptive test. The result shows that the FSS propriception test was realiable and valid indirect method of measuring knee propriception in individuals with this test.

REFERENCES

1. Lephart SM, el al. Proprioception and Neuromuscular Control in Joint Stability, Human Kinetics Publishers, 2000.
2. Shrout, P. E., & Fleiss, T. L. (1979). Intraclass correlations: uses in assessing rater reliability. *Psychology Bull, 86*, 420-428.

CHRONIC STRESS EXPOSURE FOLLOWING INTRA-ARTICULAR ANKLE FRACTURES

[1,2]Jane K. Goldsworthy, [1,2]Donald D. Anderson, [2]Kiran H. Shivanna, [2,1]Nicole M. Grosland, [1,2]Douglas R. Pedersen, and [1,2]Thomas D. Brown
Departments of [1]Orthopaedics and Rehabilitation and [2]Biomedical Engineering, The University of Iowa,
email: don-anderson@uiowa.edu, web: poppy.obrl.uiowa.edu

INTRODUCTION

Post-traumatic osteoarthritis (OA) is a frequent outcome following intra-articular fracture. Residual incongruities have long been associated with aberrant articular contact stress distributions [1]. While these atypical stresses likely play a role in predisposing an articular joint to post-traumatic OA, little is known concerning the relationships between altered surface anatomy and associated contact stress. With the advent of patient-specific finite element (FE) modeling techniques comes the ability to address this issue objectively. Here we present work characterizing aberrant contact stress exposure following intra-articular ankle fractures in a clinical series.

METHODS

CT studies from a series of 6 patients with intra-articular ankle fractures were obtained following a standard orthopaedic protocol. Models were generated from both the fractured and intact contralateral ankles. Tibial and talar subchondral bone surfaces were segmented to yield geometric surface descriptions. An experienced ankle surgeon then used a medical data visualization program (Data Manager (beta2)) to bring these surfaces into apposition to match their weight-bearing radiographic appearance (Figure 1).

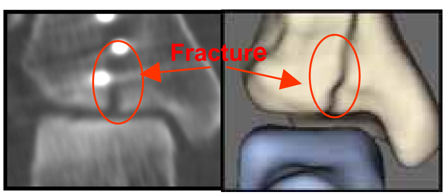

Figure 1: Post-operative CT image of fractured ankle (left) and resulting apposed surfaces (right).

Rigid bone surfaces were defined, and 1.5 mm layers of articular cartilage (E=12MPa, ν=0.42) were meshed onto them using a ray projection-based in-house computer code. Apposing cartilage surfaces were defined as deformable contact pairs with a frictionless interface. FE simulations (ABAQUS (v6.4)) entailed solving a sequence of 13 loading cases to simulate the entire stance phase of gait [2]. The tibia is rotated about a flex/extension axis, while the talus is free to rotate as required by the tibio-talar articulation. Articular cartilage contact stress exposures were characterized by multiplying computed nodal contact stress values by their resident time in the gait cycle, then summing the result over the 13 loading increments and scaling to steps per year.

RESULTS AND DISCUSSION

Computed contact stress distributions for the intact joint were continuous and relatively uniform, while distributions for fracture cases were discontinuous, and more heterogeneous (Figure 2). All 6 fracture cases showed similarly

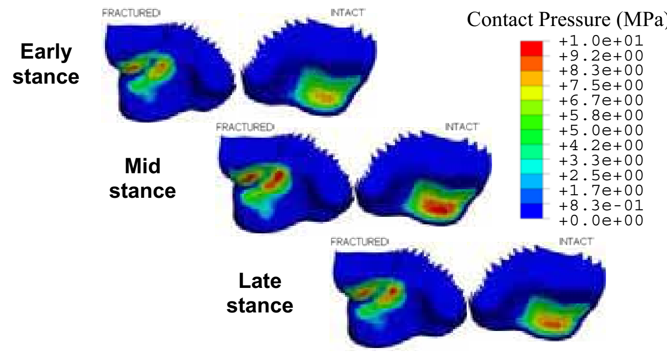

Figure 2: Anterior views of contact stress for a fractured versus intact ankle.

discontinuous and heterogeneous pressure distributions (Figure 3). From these patient-specific contact stress predictions, site-specific chronic stress exposures are

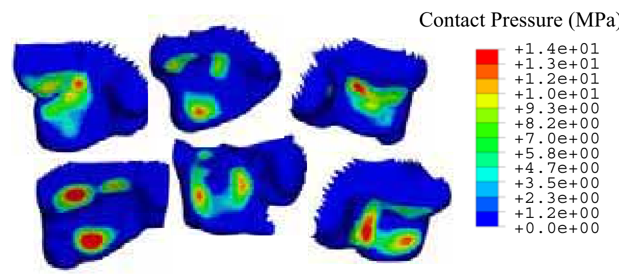

Figure 3: Anterior views of contact stress distributions for individual fractured tibias.

computed for each patient with appropriate time scaling. Comparing the chronic exposure to known chronic stress tolerance levels affords prediction of the likelihood of onset of post-traumatic OA in a given injury.

CONCLUSIONS

These patient-specific FE models of ankle loading during the stance phase of gait provide insight into the contact stress histories which articular cartilage experiences over many cycles each day. This opens new possibilities in studying the link between chronic stress exposure and the onset of post-traumatic OA in an actual clinical population.

REFERENCES

1. Fitzpatrick D, et al. (2004). *J Orthop Trauma,* 18(5):271-8.
2. Anderson D, et al. (2004). *ASB Annual Meeting,* Podium 7.
3. Stauffer R, et al. (1977). C*lin Orthop*, 127:189-96.

ACKNOWLEDGEMENTS

Supported by grants from the NIH (AR46601 and AR048939), with technical help from J.L. Marsh, and Y. Tochigi. F. Taddei and M. Viceconti (Istituti Ortopedici Rizzoli) provided assistance with Data Manager software.

PROPORTIONAL DERIVATIVE CONTROL FOR PLANAR ARM MOVEMENT

[1] Kathleen M. Jagodnik and [1,2]Antonie J. van den Bogert
[1]Department of Biomedical Engineering, Case Western Reserve University, Cleveland , OH
[2] Department of Biomedical Engineering and Orthopaedic Research Center, Cleveland Clinic Foundation, Cleveland, OH

INTRODUCTION

Functional Electrical Stimulation (FES) is a technology that entails the stimulation of nerves and muscles with electrical current to restore movement in those with neurological movement disorders. The application of FES to upper extremities (UE) requires the control of gross motor tasks with a dynamic component. To date, the timing and amplitude of these artificial stimuli have been controlled by open loop pattern generators. It is thought that performance of FES systems can be improved by feedback control. This project involves the design of a controller for an UE model that implements the Proportional Derivative (PD) algorithm, and testing such a controller on a computational UE model that includes realistic dynamic properties of muscle.

METHODS

Controller performance was evaluated using a biomechanical model for arm movement in the horizontal plane. The model had two segments and was driven by six muscles, two of which were biarticular. Each muscle was modeled using a Hill-based approach. The contractile elements (CE) had realistic force-length and force-velocity properties, as well as activation dynamics. Muscle force was transmitted to the skeleton via a nonlinear series elastic element (SEE). Equations of motion were generated using SD/FAST (PTC, Needham, MA).

The Proportional Derivative (PD) controller generates a stimulation value u for each muscle whose magnitude is proportional to the errors in shoulder and elbow angles and their time-derivatives:

$$u = K_{p,1}(\theta_1 - \theta_{1,\text{target}}) + K_{d,1}\dot{\theta}_1 + K_{p,2}(\theta_2 - \theta_{2,\text{target}}) + K_{d,2}\dot{\theta}\ ,$$

where K_p and K_d are the proportional and derivative gains, respectively. Single joint muscles were only given feedback from one joint.

Forward dynamic simulations were performed for a single-target, planar reaching task. Initial joint angles were zero, and target joint angles were 45 and 90 degrees for shoulder and elbow, respectively. The feedback gains were set to identical values for all muscles and all joints, and varied to assess their effect on the performance of the reaching movement and on muscle forces.

RESULTS AND DISCUSSION

As expected, PD controller performance depended on feedback gains (Figure 1). When gains were selected to produce movements of sufficient speed and accuracy, undamped oscillation resulted. Model perfomance improved under two conditions: (i) when inertia of the limb segments was significantly increased, and (ii) when muscle response time was reduced, either by stiffening of the SEE or reduction of time constants in the activation dynamics model.

CONCLUSIONS

This computational model strongly suggests that oscillatory behavior may be an inevitable feature of proportional-derivative control for upper extremity FES. Further work will investigate the feasibility of an 'intelligent' controller based upon the Reinforcement Learning paradigm.

REFERENCES

1. Crago PE, Lan N, Veltink PH, Abbas JJ, Kantor C. (1996) *New control strategies for neuroprosthetic systems. J Rehabilitation Res Dev* 33: 158-172.

ACKNOWLEDGEMENTS

This project was funded by NIH Training Grant T32-HD-07500.

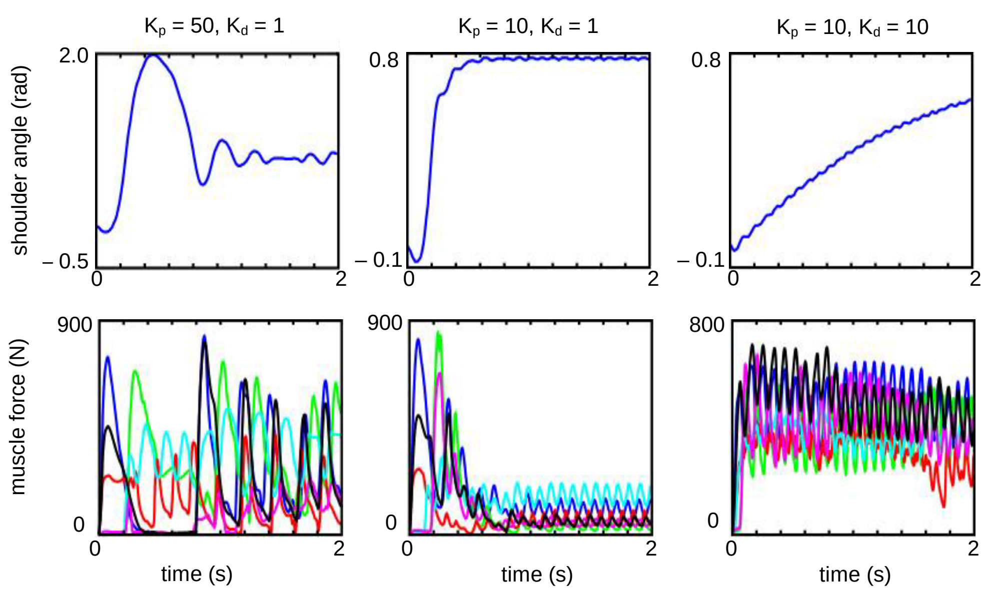

Figure 1: Simulation results: Time histories of joint angles and muscle forces for three feedback controllers

ACHILLES AND PATELLAR TENDON LOADING DURING GAIT MEASURED USING A NON-INVASIVE ULTRASONIC TECHNIQUE

[1]Philippe Pourcelot, [2]Antonie J. van den Bogert, [2]Xuemei Huang and [1]Nathalie Crevier-Denoix
[1]UMR INRA/ENVA Biomécanique et Pathologie Locomotrice du Cheval, Ecole Vétérinaire d'Alfort, France,
[2]Department of Biomedical Engineering, Cleveland Clinic Foundation, USA

INTRODUCTION

In vivo measurement of tendon and ligament loads remains a challenge. Forces acting on these structures during exercise have either estimated indirectly using EMG and inverse dynamics or measured by means of invasive techniques [2]. Recently, a non-invasive technique has been proposed, based on the measurement of the velocity of ultrasound (US) propagation in the tendon [1]. It has been demonstrated that this velocity is dependent on the force applied to the tendon (Fig. 1A). In this paper we report preliminary results of measurements performed on the Achilles tendon and patellar tendon in humans during walking.

METHODS

Ultrasonic (US) measurements were performed using a dedicated device composed of an electronic battery-powered module connected to an ultrasonic probe. The probe consists of 4 transducer elements, one acting as an emitter and the others as receivers. Knowing the distance separating these receivers, the speed of sound (SOS) is easily obtained by dividing this distance by the time required by the US waves to travel from one receiver to another.

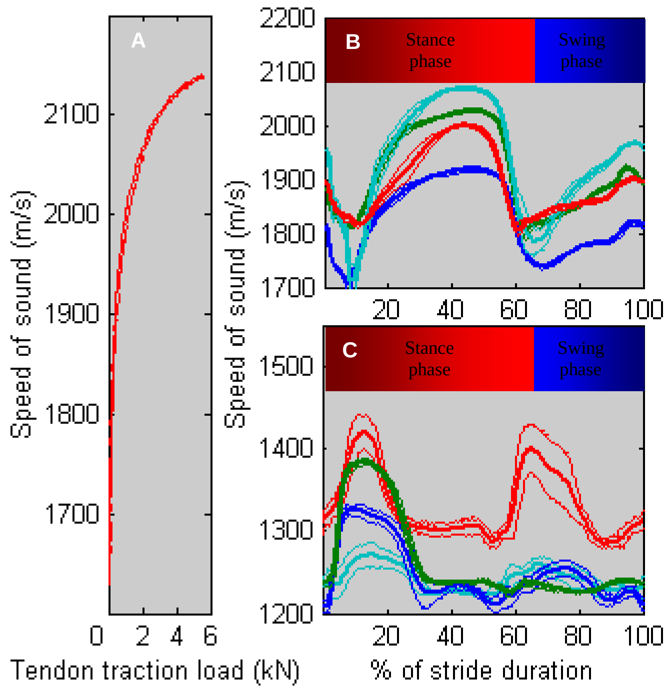

Figure 1: A - Relationship between ultrasound velocity and load in an equine superficial digital flexor tendon.
B and C - Ultrasound velocity (mean ± SD) recorded at the walk in the Achilles tendon and in the patellar tendon, respectively.

Data were collected in four subjects (1 female, 52 kg, and 3 males, 68, 80 and 88 kg). Each subject performed 10 barefoot walking trials with the US probe on the right Achilles tendon and 10 other trials with the probe on the right patellar tendon.

An extra analog input on the US device was used to record the vertical ground reaction force (Fz) from an AMTI force plate. After time normalization to percentage of stride duration, SOS and Fz data were averaged over the 10 gait cycles.

RESULTS AND DISCUSSION

Results obtained in the Achilles tendon (Fig. 1B) are consistent with those from implanted sensors. As described by Finni *et al*. [2], the tendon force decreases suddenly at heel contact on the ground followed by a steep rise in tendon load during the first part of the stance phase. The patellar tendon (Fig. 1C) shows a peak in the first half of stance, as seen in knee extensor moments during gait (Winter, 1983).

In all subjects, SOS was higher in the Achilles tendon, which may be due to higher tensile stress during gait. Between-subject differences in SOS were not related to body weight. These variations could be due to differences in muscle activation, or differences in elastic properties of the tendons. Further studies, using simultaneous EMG and inverse dynamic analyses, are needed to resolve this issue.

When compared to inverse dynamic analysis, the ultrasound method has several advantages. First, no assumptions on antagonistic co-contraction are needed. This enables direct inferences about individual muscle forces. Second, no low-pass filtering is needed and this results in better temporal resolution.

When compared to EMG, the ultrasound method has the advantage that calibration to force appears possible (Fig. 1A). Until we can non-invasively obtain a force-SOS relationship for a specific tendon in a specific subject, applications are limited to those that only require within-subject comparisons.

CONCLUSIONS

This new non-invasive technique opens up a range of investigative opportunities in various fields of research. It should also be a useful clinical tool for diagnosis, evaluation and follow-up of muscle, tendon and ligament injuries or dysfunctions.

REFERENCES

1. Pourcelot P, et al.. *J Biomech*, in press.
2. Finni T, et al.. *Eur J of Applied Physiol* **83**, 289-291, 1998.
3. Winter, DA, *Clin Orthop Rel Res* **175**, 147-154, 1983.

SHIFTING TO POPULATION-BASED MODELS AND INFERRING MODEL STRUCTURE FROM DATA ARE TWO DIRECTIONS THAT WILL ENHANCE THE CLINICAL USEFULNESS OF MODELING

Francisco J Valero-Cuevas, Hod Lipson, Veronica J Santos and Vic Anand
Sibley School of Mechanical and Aerospace Engineering
Cornell University, Ithaca, NY; email: fv24@cornell.edu, web: www.mae.cornell.edu/valero

INTRODUCTION

The clinical promise of biomechanical models lies in their ability to explain, illustrate and predict the functional consequences of injury, disease and treatment on the basis of first principles. Many advances in computational methods, computer hardware and computer graphics have greatly facilitated the creation and use of ever more complex models. We propose, however, that continuing on this path does not guarantee that modeling will revolutionize clinical care. We argue that the conceptual framework for modeling is, in general, limited because it is largely an exercise in parameter estimation that does not consider population variability. We underscore the need to adopt a population-based strategy where the structure of the model is inferred from data.

POPULATION-BASED MODELS

A model is generally taken to be a single instantiation of a biological process that results in specific predictions. This frequentist approach applies well when simulating the behavior of either a single individual or the representative (i.e., mean) behavior of a group. It is less informative of the general trend of behavior in the general population, or of how the unavoidable variability in a population produces variable performance across the population. Bayesian inference techniques like Monte Carlo simulations [1-3] are well suited to approach these questions. In this Bayesian approach, model parameters are variables that, like people, are best described as randomly drawn values from statistical distributions (called "prior distributions") instead of specific constant values. This approach produces "posterior distributions" describing the likely performance across the population. For example, the multimodal distributions of thumb kinematics arising from bone variability (Fig 1) enables the exploration of biomechanical explanations for the clinical reality that a same diagnosis leads to distinct groupings in the rate and amount of impairment and recovery after treatment. If there are truly several "types" of people, modeling can then explain why some are more/less susceptible to disease and more/less responsive to treatment.

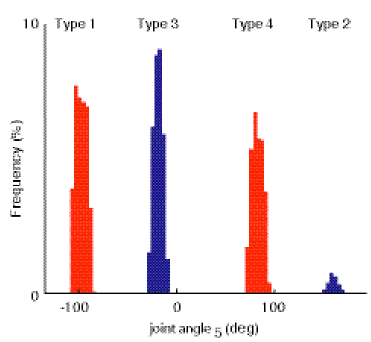

Figure 1: Monte Carlo simulations suggest there are 4 "Types" of thumb kinematics, distinguished by the angle at joint #5 needed to reach a reference configuration [1].

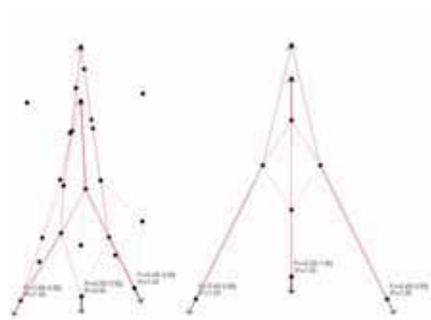

Figure 2: The tendon network at left arose from the unsupervised inference of the hidden network at right via random loading of a uniform mesh at three nodes.

INFERRING MODEL STRUCTURE FROM DATA

For complex anatomical structures such as the hand, it is necessary to explicitly distinguish between model structure (i.e., the preconceived morphology) and parameter values (i.e., the particulars of that structure). The inevitable discrepancies between predicted and measured data can be attributed to unsatisfactory parameter values, inadequate model structure or both. In contrast, today's biomechanical models consist of manually assembled structures where only the parameter values are systematically adjusted to explain and/or reproduce experimental data. Thus, improving current models necessitates that we explicitly investigate how the assumed model structure fundamentally determines and limits model behavior. Extending prior work [4], we now have unsupervised algorithms that simultaneously infer both the model structure and parameter values to best explain data (Fig 2). In this way, models can begin to clarify how disease and treatment affect the type, connectivity, properties, parameters and interactions of available "building blocks" such as bones, tissues, tendons, muscles, neural circuits, etc.

CONCLUSIONS

Population-based models with data-driven structures will enable new and powerful clinical applications of modeling.

REFERENCES

1. Santos, V.J. & F.J. Valero-Cuevas. *IEEE Trans Biomed Eng*, In review.
2. Valero-Cuevas, F.J. et al. *J Biomech*, 36, 1019-30, 2003
3. Hughes, R.E. and K.N. An. *Med Biol Eng Comput*, 35, 544-8, 1997.
4. Lipson, H. & J.B. Pollack. *Nature*, 406, 974-8, 2000.

ACKNOWLEDGEMENTS

This material is based upon work supported under a NSF GRF (VJS), The Whitaker Foundation, NSF Grants 0312271 & 0237258, and NIH Grants AR050520 and AR052345 (FVC).

MODELING AND CONTROL OF HUMAN POSTURAL SWAY

[1]Radhika Kotina, [1]Zhiqiang Gao, [2]Antonie J. van den Bogert
[1]Department of Electrical Engineering, Cleveland State University
[2]Department of Biomedical Engineering, Cleveland Clinic Foundation; email: r.kotina@csuohio.edu

INTRODUCTION

For quiet standing, the ankle strategy is used for the control of human posture in which the body moves as a rigid mass around the ankle joints. In its simplest form, the body is regarded as a single-link inverted pendulum with movement at the ankle joint controlled by the human postural control system. In patients with neurological impairment, this function might be restored by functional electrical stimulation. A critical part of such a neural prosthesis is the control algorithm. The control techniques used for such dynamic and nonlinear models need to be robust, such that they can perform well in spite of variations in the dynamics and parameters when applied on a real human. Hence, it is the purpose of our study to develop such robust control algorithms for postural control and to evaluate their performance using a computational model of musculoskeletal dynamics.

MODELING AND CONTROL DESIGN

The musculoskeletal dynamics model (Figure 1) consisted of one rigid segment, and three muscles at the ankle joint. Muscles were modeled using nonlinear differential equations from McLean *et al.* [1]. The plant model is complex and nonlinear. Furthermore, there are significant uncertainties in the model, caused by biological variation in human muscle properties. All of these make model-based control designs such as pole-placement, feedback linearization, sliding model control and H_2/H_{inf} difficult to attain. This leaves proportional-integral-derivative controller (PID) as the only common alternative. However, the limitations of PID make its performance unsatisfactory for this application, as shown later.

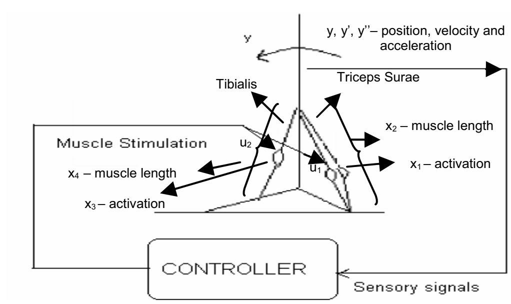

Figure 1: Closed-loop control strategy of the human ankle model

As pointed out by Gao *et al.* [2], problems like this call for a control design framework that is not overly dependent on the mathematical model of the process. In particular, we suggest that the active disturbance rejection control (ADRC) concept fits the nature of this problem well. This is because that the motion problem can be treated as

$$\ddot{y} = f + b \cdot U \tag{1}$$

where y is the output position and f represents combined effects of internal nonlinear dynamics and external disturbances of the plant, b is a parameter and U is the control signal. In the ADRC framework, a unique state observer is used to estimate the value of 'f' in real time without knowing its mathematical expression. Using this, the control law

$$U = (U_0 - f)/b \tag{2}$$

reduces the plant to a simple double integral plant, which can be easily controlled. A complete simulation model of the musculoskeletal system and both types of controller was built in Simulink. Desired posture in Figure 2 is 4° from vertical.

RESULTS AND DISCUSSION

The simulation results in Figure 2(a) were obtained at a nominal condition, for which PID and ADRC were tuned. In addition, inertia change and disturbance are added to test the robustness of the controllers as shown in Figures 2(b), 2(c).

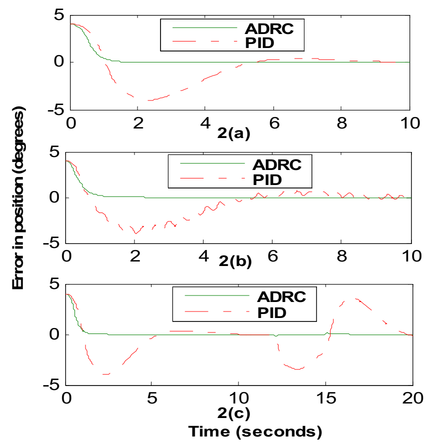

Figure 2: (a) nominal model, (b) with decreased inertia, (c) with a push of 60N-m at t = 12 secs for 3 secs

Based on the simulation results, the response of ADRC appears to be very tolerant to the uncertain and disturbed models. For the nominal condition, results of ADRC show no overshoot, reaching to steady state in less than 2 secs, whereas the control of PID takes 8 secs with a large overshoot. PID results in oscillatory response with decrease inertia by 4 times the nominal value, proving that its performance is sensitive to parameter variations whereas ADRC performance remains consistent. The maximum push that ADRC could withstand is 120N-m but with PID no more than 60N-m could be achieved. Muscle strength was sufficient to recover from a forward lean of 18°. This was attained by ADRC whereas PID could not tolerate more than 7° lean. These initial results show promise that ADRC can be extended to multiple joints for a more complete study of human postural control.

REFERENCES

1. S. G. McLean, *et al.*, "Development and Validation of a 3-D Model to Predict Knee Joint Loading During Dynamic movement", *J Biomech, Nov 2003*
2. Zhiqiang Gao *et al.*, "An Alternative Paradigm for Control System Design", *IEEE Conference on Decision and Control, 2001.*

THE EFFECT OF SHOULDER GIRDLE COORDINATION ON UPPER EXTREMITY WORKSPACE IN STROKE

[1] Ana Maria Acosta and [1,2]Jules Dewald
[1]Northwestern University, Department of Physical Therapy and Human Movement Sciences, [2]Department of Physical Medicine and Rehabilitation, Department of Biomedical Engineering ; email: a-acosta@northwestern.edu

INTRODUCTION

The extensive range of motion of the healthy shoulder is a result of the integrated movements of the sternoclavicular, acromioclavicular, glenohumeral, and scapulothoracic joints. These movements are achieved by the coordinated action of the shoulder muscles that also act to maintain joint stability. It is generally accepted that the interaction between rotator cuff muscles and the deltoid muscles is crucial for effective arm elevation while the coordinated action of trapezius, rhomboids and serratus anterior allows scapular rotation necessary for full arm elevation [1]. However, it is not known how these patterns of muscle activation change following stroke, and how this impacts the shoulder range of motion in this population. The goal of this work is to understand the effect of brain injury due to stroke on shoulder muscle coordination and its impact on arm workspace.

METHODS

The shoulder kinematics were measured in one subject with unilateral brain injury resulting in left hemiparesis. The AROM in the affected limb was limited to 90° abduction. The kinematics, including scapular rotations, were measured statically using the standardized protocol developed by van der Helm [2]. The 3D position of the trunk, arm, forearm, and scapula was measured using a motion analysis system that tracked the location of infrared LEDs (IREDS) mounted on rigid bodies. Segment kinematics were calculated based on bony landmarks [3] that define their location and orientation. The locations of the scapular bony landmarks were recorded by placing a tripod instrumented with IREDs on the bone. In addition, surface EMG of a set of shoulder and elbow muscles was recorded simultaneously with the kinematics. The subject was asked to abduct (coronal plane) and flex (sagittal plane) the arm to specific angles in increments of 15° up to the maximum voluntary elevation in the affected side and maintain each posture for 5 s while the 3D location of the IREDs was recorded. The measurements were repeated twice with resting periods between trials to avoid muscle fatigue.

RESULTS AND DISCUSSION

Figure 1 shows the scapular kinematics calculated for the

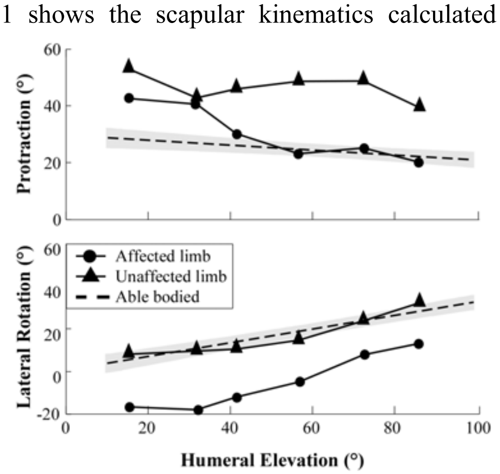

Figure 1. Scapular kinematics in a subject with stroke compared to able-bodied.

Table 1. Average EMG (%MVC) activity in upper and middle heads of the trapezius muscle in the stroke subject.

	Utrap	MTrap
Unaffected arm	84.4 ± 10.9	7.6 ± 1.6
Affected arm	42.2 ± 9.8	16.8 ± 3.7

affected (solid circles) and unaffected (solid triangles) limbs compared to able bodied (dashed line – gray area indicates 95% confidence interval). The able bodied kinematics are represented as the linear regression of the experimental data calculated from both limbs five subjects [3] with the associated 95% confidence interval. Note that the lateral rotation of the scapula, typically associated with the scapulo-humeral rhythm, in the unaffected side is similar to able bodied. However, in the affected side, the scapula is more medially rotated across arm elevations, indicating a more medial resting position. The scapulo-humeral rhythm or the relationship between the lateral rotation and the humeral elevation is similar between the affected and unaffected limbs. The mean or resting protraction angle of the scapula also differed across limbs, especially at higher elevation angles. In contrast, the tipping angle (not shown) was similar between limbs and to able bodied. Both of these angles represent the scapular winging. These results from a single subject are preliminary evidence to the alteration in muscle activation patterns. The scapular kinematics could be the explained by increased activity in the Middle Trapezius (MTrap) and Rhomboid muscles and reduced activity of Upper Trapezius (UTrap) muscle as was actually observed in the EMG measurements. The average normalized MTrap EMG while supporting the arm at 90° abduction was twice as large for the affected arm than for the unaffected arm (see Table 1), while the activity of UTrap in the affected limb was approximately half of the activity measured in the unaffected limb. These results support the notion of altered coactivation patterns responsible for changes in the scapular kinematics. The increased activity in the affected side MTrap muscle pulls the scapula to a more medial rotation compared to the unaffected side. Note that although the activity in UTrap increased with arm elevation, it is still lower in the affected side, which may provide an explanation for the reduced range of motion in the affected arm. Under normal conditions, the scapula rotates laterally to allow the head of the humerus to clear the acromion. However, if the scapular rotation is not sufficient, the head of the humerus will encounter a physical stop that prevents the arm from being elevated above this point. Future work will provide further evidence for abnormal muscle coactivation patterns by measuring the activity of additional key muscles including rhomboids and rotator cuff muscles in a representative sample of stroke subjects.

REFERENCES

[1] B. F. Morrey and K.-N. An. *The Shoulder*, vol. **1**. Philadelphia: W.B. Saunders Company, 208-45, 1990.
[2] F. C. T. van der Helm. *J Biomech*, **27**, 551-569, 1994.
[3] A. M. Acosta, et al. *Proc Inst Mech Eng [H]*, **215**, 299-307, 2001.

THE EFFECT OF TIBIOFEMORAL LOADING ON PROXIMAL TIBIOFIBULAR JOINT MOTION

Jacob Scott[1], Antonie J. van den Bogert[1,2], Ed Barber[1], Wael Barsoum[2]
[1]Department of Biomedical Engineering, Cleveland Clinic Foundation, Cleveland, OH, USA
[2]Department of Orthopaedic Surgery, Cleveland Clinic Foundation, Cleveland, OH, USA

INTRODUCTION

The posterolateral part of the knee joint has been largely ignored in past biomechanical studies. Specifically, little is known about the proximal tibiofibular joint (PTFJ) and its relationship to overall knee joint mechanics.

The proximal fibula serves as the insertion for several anatomic structures integral to knee stability – the lateral collateral ligament (LCL), arcuate ligament, posterolateral capsular complex, and biceps tendon all insert onto the proximal fibula. A recent study has shown that the force in the lateral-collateral ligament is greatest during external tibial rotation loading conditions [1].

We hypothesize that these same loading conditions could cause motion in the PTFJ. Excessive motion in this joint may contribute to the development of posterior-lateral knee pain..

METHODS

Fresh-frozen cadaveric knee specimens were tested with the knee joint fully intact. The tibia was mounted vertically on a six degree of freedom force/torque sensor (SI-2500-400, ATI Industrial Automation, Apex NC) mounted to the floor. The distal fibular connections to the tibia and talus were undisturbed during dissection and subsequent testing. Two reflective markers were mounted on pins driven into the tibial plateau and the head of the fibula at the proximal tibiofibular joint, respectively. Motion was recorded by a video camera (DALSA model #CL-C3 running Epix FrameGrabber software) at 10 frames per second. Load cell data was synchronized to the video data and recorded at 10 Hz.

The knee joint is then subjected to manual loading conditions in each of four flexion angles (0, 30, 60, 90 degrees as established by a manual goniometer). Varying loads were applied manually to a "handlebar" on the femur, in combination with a static compressive load of 40 lbs of compressive load to simulate weight bearing [2]. At each flexion angle, four discrete loading conditions were generated by the operator: varus, valgus, internal tibial rotation, and external tibial rotation. Peak moments were 20 Nm for internal-external rotation and 50 Nm for varus-valgus. To ensure standardized loading conditions, there is real time visual feedback of force/torque data.

Video images were digitized using custom Matlab software. The tibia marker was used as a reference and the displacement of the fibula marker, relative to its initial position, was computed to quantify PTFJ motion. Results from one typical specimen are presented.

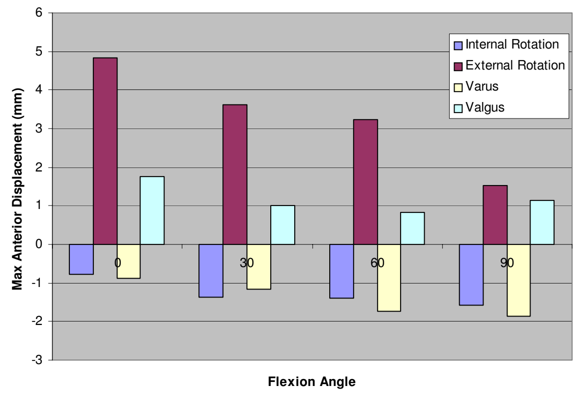

Figure 1: Maximal anterior-posterior joint motion for the sixteen knee joint loading conditions. Positive values represent an anterior translation of the fibular head relative to the tibia.

RESULTS AND DISCUSSION

Initial results indicate that there is significant tibiofibular joint motion. The greatest motion was seen in external rotation near full extension when we see the fibular head displacing more than 4 mm anteriorly relative to the tibia, at an external rotation moment of about 20 Nm. Results for all loading conditions are summarized in Figure 1.

The tibiofibular joint is a robustly encapsulated synovial joint that has very flat and smooth articular surfaces which do not mechanically resist translation. Considering the size of the joint itself (~7mm across), a translation of 4mm is substantial, and in the paradigm of any other joint would have to be considered traumatic.

While the applied rotation torques were much larger than typically seen during gait, the load-displacement relationship was nonlinear such that 2 mm displacement was already seen at 10 Nm external rotation torque which is more representative of in vivo loading. Frontal and transverse plane torques were only applied in isolation, and not combined. Because of the LCL, we would expect the PTFJ to be especially sensitive to external rotation in combination with varus loading. Further studies will investigate these interactions.

REFERENCES

1. LaPrade, *Am J Sports Med*, Vol 32, No. 7, 2004.
2. Mizuno et al., (2004) Orthopaedic Research Society 50th Annual Meeting, Paper #240.

ACKNOWLEDGEMENTS

We acknowledge Stryker Corporation and NIH (1P30AR050953) for financial support.

A DUAL TRACK ACTUATED TREADMILL IN A VIRTUAL REALITY ENVIRONMENT AS A COUNTERMEASURE FOR NEUROVESTIBULAR ADAPTATIONS IN MICROGRAVITY

[1]Samantha M. Lane, [2]Michael W. Kahelin, [3]Philip O'Connor, [3]Jay G. Horowitz and [2]Susan E. D'Andrea
[1]The University of Iowa, [2]The Cleveland Clinic Foundation, [3]NASA Glenn Research Center;
Email: susan.dandrea@gmail.com

INTRODUCTION

The neurovestibular system is primarily responsible for balance and stabilization and relies on vestibular, visual and proprioceptive cues. The microgravity environment alters these cues, resulting in sensory conflicts that cause crew members to experience gait and postural instabilities when returning to gravity environment. Longer durations in microgravity cause the adaptation process to be longer and more difficult [1]. During re-entry and post-flight, crew members suffer from disabling vertigo, oscillopsia, sudden loss of orientation, impaired coordination, sudden loss of postural ability, and overall decreased ability in standing and gait performance [2,3].

Travel to distant planets and extended durations of time aboard the International Space Station have made it necessary to develop effective countermeasure to aid in the adaptation process. The aim of this study was to determine if the dual-track actuated treadmill in a virtual reality environment significantly stimulates the neurovestibular system such that it would alleviate adverse adaptations.

METHODS

Subjects walked on the treadmill at a speed of 3.5 mph in one of three conditions:

1. Visual Only: There was a visual display and the left and right treadmill tracks were the same as the Control condition.
2. Treadmill Only: There was no visual display and the treadmill tracks raised and lowered vertically, inclined and declined, and changed speeds.
3. Treadmill and Visual: There was a visual display that coincided with the treadmill tracks as they performed like the Treadmill Only condition.

Data were collected for ten seconds both in the first and last five minutes of the 30-minute trial during the simulated activities of walking straight, around curves, uphill and downhill. Measurements were also made in control conditions before and after testing in which there was no visual display and both treadmill tracks remained the same speed and height.

Electromyography of the neck as well as and head/trunk kinematics were measured. Head acceleration was measured by a head mounted tri-axial accelerometer. Footswitches fixed to the bottom of the shoe were used to determine gait events.

RESULTS AND DISCUSSION

Results for head acceleration were analyzed to determine if the virtual reality treadmill alters the response to shock transients through the body. The resultant acceleration of the head was calculated and peak values were determined for each stride at heel strike. Accelerations were normalized by subtracting the peak values found in the initial control condition (Figure 1).

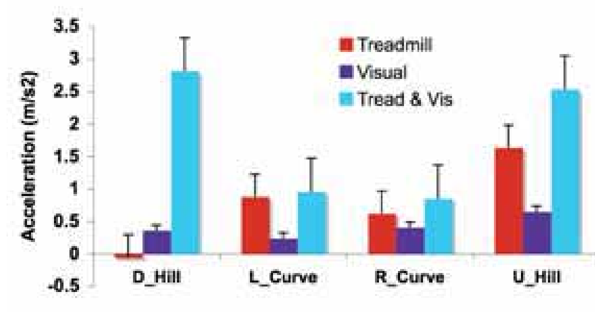

Figure 1: Normalized Head Acceleration During Five Activities By Experimental Condition

Acceleration for each activity was highly correlated to the control condition. Normalized accelerations of the head increased while walking on the dual-track treadmill compared to normal treadmill walking. Similarly, no significance was found when using paired t tests to compare the data across conditions. This can be attributed to the large variability between subjects. Treadmill and Visual trials showed significantly larger acceleration than the Visual Only trials indicating the importance of actuated belts with regard to neurovestibular stimulation. Of particular interest is the fact that the accelerations remained elevated in the final Control Condition as seen in Figure 1.

CONCLUSIONS

By increasing the input stimulus to the body, specifically the shock to the head, the treadmill forces the user to consistently activate their balance reflexes to maintain a consistent gait. This illustrates the potential for the dual track, actuated treadmill device with virtual reality to be an effective counter measure to alleviate the postural and balance distirbances after exposure to microgravity. Analysis of the muscle activation patterns and the head/neck coordination will further clarify the extent to which the treadmill stimulates the neurovestibular system.

REFERENCES

1. Layne, et al. *J. Applied Physiology*, **90**, 997-1006, 2001..
2. Bloomberg, et al. *J. Vestibular Research,* **7**:161-177,1997.
3. Reschke, et al. *Brain Research Reviews*, **28**:102-117, 1998.

ACKNOWLEDGEMENTS

The authors would like to acknowledge the John Glenn Biomedical Engineering Consortium and the contributions of Edward Eucker, Marquette University.

IN VIVO KINEMATICS OF HUMAN WRIST JOINTS: COMBINATION OF MEDICAL IMAGING AND THREE-DIMENSIONAL ELECTROGONIOMETRY.

[1] Patrick Salvia, [2] Victor Sholukha, [1]Pierre-Michel Dugailly, [1]Stéphane Sobczak, [1]Véronique Feipel , [1]Marcel Rooze and [1]Serge Van Sint Jan
[1]Laboratories of Anatomy, Université Libre de Bruxelles, Belgium
[2] Department of Applied Mathematics, Polytechnical University of St.Petersburg, Russia
email: salviap@ulb.ac.be, web: www.homepages.ulb.ac.be/~anatemb

INTRODUCTION

This paper described improvement of previous work [1] that allowed registration of both joint kinematics and medical imaging during in-vitro experiments. In that study, joint kinematics data were collected from three-dimensional (3D) electrogoniometry [2,3] and 3D bone morphological data from CT using inserted fiducial bony landmarks for registration. In parallel, Snel et al. [4] described an in-vivo method to study discrete wrist kinematics using dynamic 3D tomography.
The aim of this study was to develop a protocol of registration of in-vivo wrist kinematics using selected anatomical landmarks virtually and manually identified on both CT reconstruction and in situ.

METHODS

Subject. One subject (male, 50 years old) volunteered for the entire protocol.
Principle. The aim of the overall protocol was to register two datasets: bone morphology from medical imaging (Siemens SOMATON Volume Zoom, Siemens Corp, Iselin, N.J.) and joint kinematics data from custom made electrogoniometry. Anatomical landmark (AL) location allowed this registration. Prior to 3D electrogoniometry (3DE), the 15 ALs selected in the method were virtually identified (palpated) on the 3D reconstructed bone surface of the subject. From this virtual palpation, a booklet was produced with various views of the virtual ALs to facilitate AL representation during manual palpation. The spatial location of the same bony ALs was determined using a 3D digitizer (Faro® arm, Bronze series, USA) just before collecting joint kinematics data by 3DE on the subject.
The origins of 3D digitizer and 3DE coordinate systems were made coincident. Joint kinematics collected using the 3DE could then be registered to the 3D bone models using the AL coordinated obtained during both virtual and manual palpation. The protocol has been fully implemented in Matlab and allows quasi real-time visualization of joint motion of the subject while the latter is performing the motion. Anatomical angle and helical axis parameters were computed to describe the joint kinematics.
Precision. The precision of the manual palpation was evaluated by four experimenters repeating five times the procedure and estimated by the error norm. The palpation effect was also estimated on the anatomical angular and translational values calculated during dorsopalmar flexion, radioulnar deviation and circumduction. The intraobserver precision was 2.6 (0.3) mm and 4.8 (1.2) mm for interobserver precision. The ICC for intra- and interobservation was greater than 0.95.

RESULTS AND DISCUSSION

A view of animation is presented on Figure 1 with a set of Mean Helical Axis computed during the movement.

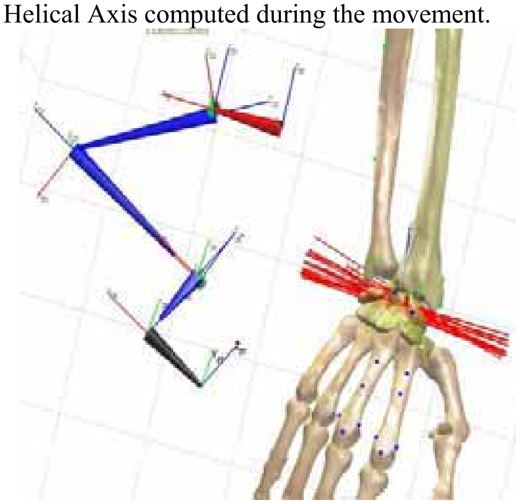

Figure 1: View of the animation. In red, the set of Mean Helical Axis during dorsopalmar flexion. The virtual representation of 3DE is also shown.

The propagation of the palpation error on anatomical angles and translation was less than 2° and 5 mm for the primary component of movement. For associated components, error curves showed some patterns underlying a “cross-talk” effect induced by the different definitions of the fixed anatomical coordinate system

DISCUSSION

A new protocol of in-vivo registration was developed. This animation of wrist kinematics helps us to better understand several kinematical parameters as orientation and position of helical axis. Precisions of our measurements are better than those shown by Della Croce [5]. This was probably due to the availability of the booklet describing manual palpation precisely, and allowing the observer to reach a higher precision.
Before proposing this technique in clinics, a study of the influence of imaging parameters on the 3D bone reconstruction quality must be done to reduce the effective dose absorbed by the subject.

REFERENCES

1. Van Sint Jan S et al., *J Biomech*. **35**, 1475-1484, 2002.
2. Sholukha et al., *Med. Eng. and Phys.* **26**, 251-260, 2004.
3. Salvia et al., *Clin.Biomech.* **15,** 103-111, 2000
4. Snel et al., *Med. Phys*. **27**, 2037-2047, 2000
5. Della Croce et al., *Med.Biol.Eng Comput.* **37** 155-161, 1999

LOWER EXTREMITY KINEMATICS DURING JOGGING: INFLUENCE OF TREADMILL SETTINGS

[1] Lan-Yuen Guo, [2]Chich-Haung Yang, [1]Wen-Lan Wu and [3]Fong-Chin Su
[1]Faculty of Sports Medicine, Kaohsiung Medical University, Kaohsiung, Taiwan
[2]Department of Physical Therapy, Tzu Chi College of Technology, Hualian, Taiwan
[3] Institute of Biomedical Engineering, National Cheng Kung University, Tainan, Taiwan

INTRODUCTION

In recent years, more and more people have chosen to exercise using a treadmill in a gym or home setting. The main options available for jogging on a treadmill are (i) speed and (ii) inclination of the belt. Increased speeds and inclination not only increase the cardiopulmonary loading but also alter the lower extremity (LE) joint movement patterns[1, 2].

The current study to investigated LE joint movements during jogging at different speed and inclination settings.

METHODS

Eighteen young males without neuromuscular or orthopedic problems were recruited in the experiment. The video-based motion capture system, HIRES Expert Vision System (Motion Analysis Corporation, CA, USA), with six CCD cameras, was used to collect kinematic data at a sampling frequency of 120Hz. Nineteen passive reflective markers were attached to bilateral lower extremities of the subject (Figure 1).

All subjects had a 5-minute warm-up period. One series of tests utilized four speeds (3.5 m/s, 3 m/s, 2.5 m/s, 2 m/s) with zero inclination. A second series of tests involved three slopes (15%, 10%, 5%) with the speed set at 3 m/s.

Figure 1: Marker setting

RESULTS AND DISCUSSION

Increased the slope resulted in the lower extremity taking off the ground earlier during the jogging cycle. The main three joints of the LE had increased maximum flexion angles during the swing phase, but the maximum extension angles at stance phase were unchanged. For increased speeds, the hip and ankle joints had increased maximum joint extension angles during the stance phase, whereas the hip and knee joint had increased maximum flexion angles during the swing phase (Figure 2-4).

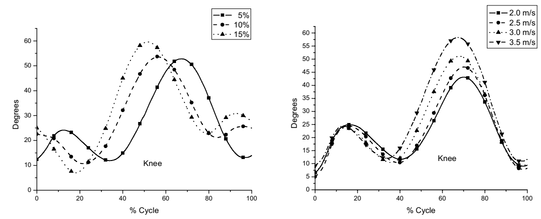

(A) (B)

Figure 2: Knee joint motion during a jogging cycle with different incline (A) and speed (B) conditions.

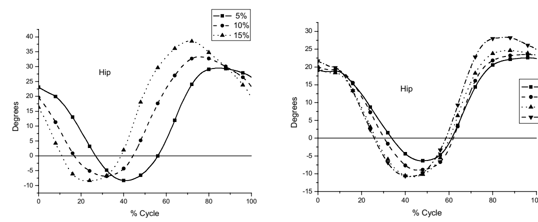

(A) (B)

Figure 3: Hip joint motion during a jogging cycle with different incline (A) and speed (B) conditions.

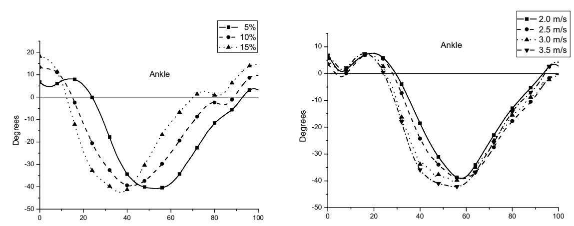

(A) (B)

F**igure 4**: Ankle joint motion during a jogging cycle with different incline (A) and speed (B) conditions.

CONCLUSIONS

Systematic kinematic investigations of the speed and incline settings on recreational treadmills show that LE joint motions are affected differently for each setting. This information can provide rehabilitation clinicians or athletic coaches with guidelines for selecting appropriate modes for jogging.

REFERENCES

1. Mann, R.A, et al.. Am J Sports Med **8**, 345-50, 1980.
2. Novacheck, T.F. Gait Posture **7**, 77-95, 1998.

ACKNOWLEDGEMENTS

Supported by grant NSC92-2320-B-277-003, Taiwan

THE EFFECTS OF HIKING DOWNHILL USING TWO TREKKING POLES WHILE CARRYING DIFFERENT EXTERNAL LOADS IN A BACKPACK

[1]Michael Bohne, [2]Julianne Abendroth-Smith and [1]Gary Heise
[1]University of Northern Colorado, Greeley, CO; email: M-Bohne@wiu.edu; gary.heise@unco.edu
[2]Willamette University, Salem, OR; email: jabendro@willamette.edu

INTRODUCTION

Hiking is commonly known as a recreational activity shown to offer significant positive effects on the human body. However, often times this requires transportation of an external load for supplies, with the most common and advantageous method by use of a backpack. Also, many people are required to walk downhill with an external load as part of their occupation. Walking downhill and the addition of an external load has been shown to increase the risk of musculoskeletal pain and injury. (1).

To alleviate some of the loading placed on the lower extremities, walking poles have become popular. The effectiveness of poles in downhill walking without packs has been demonstrated in that the poles successfully reduced forces placed on the lower extremities (2,3). Furthermore, poles used in uphill backpacking were successful in reducing muscle activity (4). It was hypothesized that the use of hiking poles would help reduce the net joint moments and net joint power for the ankle, knee and hip during the stance phase across all load conditions.

METHODS

Fifteen male subjects (ages 20-49; height 1.36 m–1.68 m and weight: 600 N-1063N) were selected from hiking clubs in the Salem, Oregon area. All subjects were experienced hikers self-proclaimed to be comfortable with the use of hiking poles.

All participants were required to complete all conditions. Conditions included with and without the use of hiking poles for each of the three backpack conditions (no pack, day pack and large expedition pack). The day pack was loaded with 15% of body weight while the expedition pack was loaded with 30% of body weight. Ten trials were completed for each condition, for a total of 60 trials for each participant. All conditions were in random order for each participant.

An average of each of the six conditions was used for analysis. The net joint moments and power at the ankle, knee and hip, as well as the net joint forces at the knee were examined statistically using a 2 X 3 (poles X packs) repeated measures ANOVA, with a family-wise alpha level of 0.05, using a Bonferonni adjustment, to protect against the running of multiple tests.

RESULTS AND DISCUSSION

A significant reduction was observed for the dominant moment at each of the joints in the lower extremity (plantar flexion at the ankle, extension at the knee and hip) (See Figures 1). These results may be due to a reduction in the muscle activity which may help the muscle maintain the ability to help stabilize the joint, and, thus, reduce risk of injury.

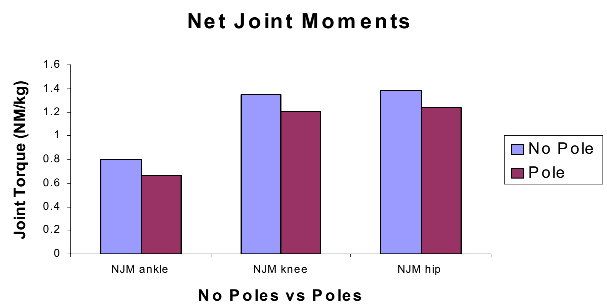

Figure 1: Changes in net joint moment for the ankle knee and hip with pole use

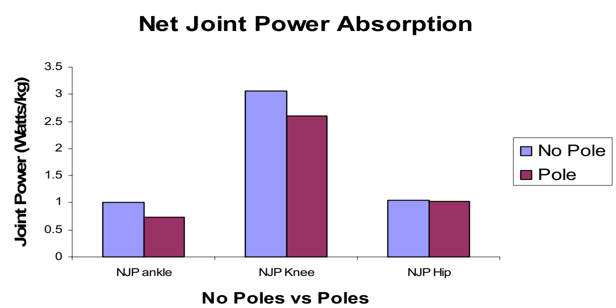

Figure 2: Changes in net joint power for the ankle knee and hip with pole use

Reductions were also observed in the peak power absorption (See Figure 2) for the ankle and knee. These reductions are believed to result in a lessening of eccentric muscle actions, which may reduce the post exercise pain felt by participants. These results held true across pack conditions, as packs seemed to only result in a larger power generation at the hip.

CONCLUSIONS

A reduction in the moments and power around the joint, with the use of poles, will help reduce the dangerous loading on the joints of the lower extremity. These reductions may lead to a larger portion of the population being able to enjoy a more active lifestyle.

REFERENCES

1. Laursen, B., Ekner, D., Simonsen, E. B., Voigt, M., & Sjogaard, G. (2000). Applied Ergonomics, 31(2), 159-166.
2. Abendroth-Smith, J., Benson, A., & Bohne, M. (2003) Med Sci Sport and Exercise, 34(5), pp. s98.
3. Schwameder, H., Roithner, R., Müller, W., & Raschner, C. (1999). Journal of Sports Sciences, 17. 969-978.
4. Knight, C., & Caldwell, G. (2000). Med Sci Sport Exercise. 32. 2093-2101.

ACKNOWLEDGEMENTS

Special thanks to the International Society of Biomechanics for helping fund the current project through their Student Dissertation Grant program.

FORCE STEADINESS, NEUROMUSCULAR ACTIVATION AND MAXIMAL MUSCLE STRENGTH IN SUBJECTS SUFFERING FROM SUBACROMIAL IMPINGEMENT SYNDROME

[1,2] Thomas Bandholm, [1,2]Lars Raundahl Rasmussen, [2]Per Aagaard, [1]Bente Rona Jensen, and [2]Louise Diederichsen
[1]Institute of Exercise & Sport Sciences, Dep. of Human Physiology, University of Copenhagen, Denmark
[2]Institute of Sports Medicine - Copenhagen, Bispebjerg Hospital, Copenhagen, Denmark,
email: thomas.bandholm@hh.hosp.dk

INTRODUCTION

The therapeutic rehabilitation regime of subjects suffering from subacromial impingement syndrome (SIS) typically includes sensory-motor training of the shoulder. The rationale for this treatment is the assumption that the SIS causes an impairment of shoulder sensory-motor control. This view is in part supported by the findings of reduced maximal shoulder muscle strength [1], deltoid muscle fiber atrophy [2], and impaired kinesthetic sense of the shoulder [3] in patients with SIS. In the present study, therefore, it was hypothesized that shoulder sensory-motor control expressed as force steadiness would be impaired in subjects suffering from SIS.

METHODS

Nine male subjects with unilateral SIS, who remained physically active in spite of shoulder pain ((mean) 28.2±1.8yrs (SEM)) and 9 healthy matched controls (27.7±1.4yrs) were included. No significant between-group differences were noted at baseline for any of the variables used to match the two groups (height, weight, involvement in upper body sports or not, and participation in strength training or not). Shoulder sensory-motor control and maximal shoulder muscle strength (MVC) were assessed using an isokinetic dynamometer (KinCom). Isometric and dynamic submaximal shoulder abduction force steadiness was determined at target forces corresponding to 20, 27.5 and 35% of the maximal shoulder abductor torque and expressed as the standard deviation (SD) and coefficient of variation (CV) for the exerted abductor force. Isometric steadiness contractions (10 seconds duration) were performed at 90 degrees of shoulder abduction in the scapular plane and dynamic contractions (15 deg/sec) were performed from 30-120 degrees of abduction in the scapular plane. Shoulder MVC´s were performed at 45 and 90 degrees of shoulder abduction. Neuromuscular activity (EMG) was assessed by surface and intra-muscular recordings in eight shoulder muscles: supraspinatus, infraspinatus, upper trapezius, lower trapezius, latissimus dorsi, serratus anterior, anterior and middle deltoid muscles.

RESULTS AND DISCUSSION

While no differences were observed for isometric force steadiness, concentric submaximal force steadiness at the 35% target force level was reduced in SIS subjects (Figure 1). Thus, shoulder sensory-motor control expressed, as isometric submaximal force steadiness was not impaired in SIS subjects. Expressed as dynamic submaximal force steadiness, shoulder sensory-motor control was only impaired during concentric contractions at the highest target force level. It is possible that the pain-induced changes in shoulder afferent feed-back with SIS can be compensated for during isometric contractions.

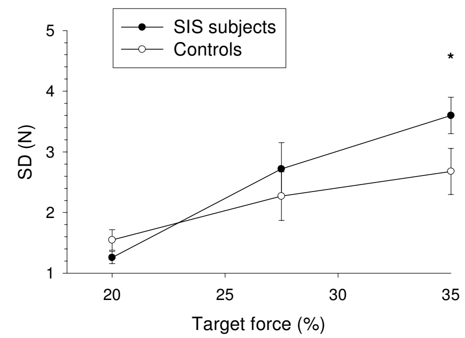

Figure 1: Dynamic (concentric) shoulder force steadiness. * denotes a statistical between-group difference.

This might not be the case during more complex movements. It seems that the control of contraction types requiring graduation of muscle force during articular movement with changes in muscle length/tension relationships, such as concentric contractions, are more prone to impairment in SIS subjects. All SIS and control subjects demonstrated activity in all of the investigated muscles for every target force level during both isometric and dynamic contractions. Muscle activity was similar between SIS and control subjects in almost all steadiness conditions examined. Only latissimus dorsi muscle activity during concentric submaximal force steadiness at the 20% target force level was elevated in the SIS subjects (SIS subjects: 16.2±3.8%EMGmax vs. controls: 9.0±1.9%EMGmax, p=0.046). No differences in maximal shoulder muscle strength were found between groups (ABD45-SIS subjects: 32.3±2.4Nm vs. controls: 32.5±2.4Nm, p=1.00, and ABD90-SIS subjects: 57.9±5.1Nm vs. controls: 54.8±2.6Nm, p=0.537). Thus, maximal shoulder abduction muscle strength was not found to be reduced in SIS subjects.

CONCLUSIONS

In conclusion, the present results suggest that shoulder sensory-motor control expressed as force steadiness is only mildly impaired, with neuromuscular activation remaining largely unaffected, and maximal shoulder abductor muscle strength unaffected in SIS subjects who are able to continue with upper body physical activity in spite of shoulder pain.

REFERENCES

1. Brox, J, et al. *Arch Phys Med Rehabil* **78**, 1260-1267, 1997.
2. Leivseth, G. & Reikeräs, O. *J Orthop Sports Phys Ther* **19**, 146-149, 1994.
3. Machner A, et al. *Acta Orthop Scand* ***74***, 85-88, 2003.

ARM MOBILITY VERSUS GLENOHUMERAL STABILITY

[1] Jurriaan H. de Groot, [1] Carel G.M. Meskers, [2]Frans Steenbrink, [2]Michiel A.J. van de Sande and [2]Piet M. Rozing
[1]Dept. Rehabilitation Medicine, Leiden University Medical Centre, The Netherlands.
[2] Dept. Orthopaedics, Leiden University Medical Centre, The Netherlands.
email: J.H.de_Groot@lumc.nl, web: www.lumc.nl

INTRODUCTION

Subacromial pathologies ranging from impingement to major cuff tearing are characterized clinically by shoulder pain and reduced arm mobility. The pathology is associated with a reduction of the subacromial space due to glenohumeral (GH) instability [1,2]. Arm mobility and GH-stability are both determined by shoulder muscle forces. Arm mobility requires a GH torque; stability requires GH force equilibrium [3,4].

We determined arm mobility, pain, external force and isometric muscle coordination before and after subacromial injection of lidocain in 6 patients with major rotator cuff tears. We will discuss our results in the scope of a torque versus force muscle function hypothesis.

METHODS

Six patients (4♂, 2♀, 61y SD=8) with irreparable rotator cuff tears, pain and reduced arm mobility were included prior to Teres Major tendon transfer surgery[1]. Before and 10 min. after sub-acromial lidocain injection (5ml, 1%) we quantified the Principal Action (PA) of 6 muscle(part)s, i.e. the direction of maximum muscle activation provoked by a force of constant magnitude rotated in a plane perpendicular to the humerus [5,6]. For this purpose, the injured arm was fixed into a splint and connected at the elbow onto a force transducer constraining only two translation degrees of freedom (dof's) perpendicular to the humerus. The arm was to be held still for the four remaining (dofs) in about 60^o elevation in the 45^o plane of abduction; the elbow was 90^o flexed, the forearm positioned at 45^o above the horizontal plane. The magnitude of the external force equaled the minimum of 12 maximum voluntary forces (MVF) generated in equidistant directions of 30^o onto the force transducer. Shoulder pain was quantified using a Visual Analog Scale (VAS) and range of arm abduction (RoM) was determined by means of electromagnetic motion tracking [7].

RESULTS AND DISCUSSION

The VAS decreased significantly after lidocain injection both in rest and during the experiment resulting in an increase of the minimum MVF with a factor 2.0 (SD 0.6). This was consistent with earlier reports [8]. The observed increase of ROM was not expected from model simulation, were transposition of the Teres Major muscle was found to be required for restoration of the insufficient GH abduction moment [4].

This study shows that the potential external muscle torque was not the limiting factor for ROM reduction. The possible explanation was found in the altered coordination of the shoulder muscles, illustrated here by the Principal Action (Figure 1). The ●-marks indicate the average normal function of the Deltoid muscle parts (Dlt), generating an abduction moment and activated around PA=0^o, and the Latisimus Dorsi (LD), Pectoralis Major (PM) and Teres Major muscles (PM), generating abduction and endoflexion moments and activated around PA=150^o – 270^o (i.e. equal to -90^o)

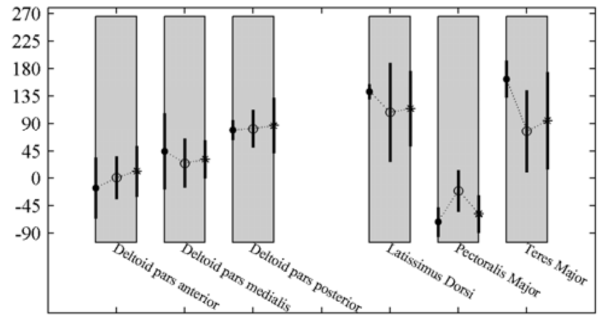

Figure 1: Principal action (degrees) of six shoulder muscles recorded by means of surface EMG for normal subjects (●) ± 95% C.I. [6] and patients with cuff tear prior to (o) and after subacromial lidocain injection (*). PA=0^o: vertical abduction; PA=90^o: horizontal adduction; PA=180^o: vertical adduction; PA=270^o: horizontal abduction.

Patients exhibit a relatively normal Deltoid PA. On average and prior to lidocain injection, the LD, PM and TM were co-activated during external abduction forces (change towards PA=0^o). Lidocain injection reduced this effect and the external abduction moment and ROM were partly restored.

The underlying hypothesis is that the patients exhibit a GH instability. Superior translation of the humerus during abduction results in a reduction of the sub-acromial space and a pain sensation. Downward and inward directed muscle forces on the humerus stabilize the humeral position into the glenoid cavity. The LD, PM and TM muscles generate these downward and inward forces, which consequently results in the reduction of the abduction moment generated by the deltoid muscle and a reduction of RoM. Lidocain reduces the GH 'pain-feedback' activation of the adducting LD and TM, thus increasing the external moment and ROM.

REFERENCES

1. Graichen H et al., *Am J Roentgenol.* **172**, 1081-6, 1999.
2. Ludewig PM & Cook TM, *Clin. Biomech* **19**, 350-7, 2004.
3. van der Helm, J.Biomech. **27**, 527-50, 1994.
4. Magermans et al., *Clin. Biomech* **19**, 116-22, 2004.
5. de Groot JH et al., *Clin. Biomech* **19**, 790-800, 2004.
6. Meskers CGM et al., *Clin. Biomech* **19**, 913-20, 2004.
7. Meskers CGM et al., *Clin. Biomech* **13**, 280-92, 1998.
8. Ben Yishay A. et al., *Orthopedics* **17**,685-8, 1994.

ACKNOWLEDGEMENTS

Hans Fraterman (technical support)

THE EFFECT OF GENERATING ANTI-GRAVITY SHOULDER TORQUES ON UPPER LIMB DISCOORDINATION FOLLOWING HEMIPARETIC STROKE

[1,2,3]Jules Dewald and [1] Jun Yao
[1]Northwestern University, Department of Physical Therapy and Human Movement Sciences, [2]Department of Physical Medicine and Rehabilitation, [3]Department of Biomedical Engineering ; email: j-dewald@northwestern.edu

INTRODUCTION

Despite the variability of lesion location and spontaneous recovery experienced by individuals following hemiparetic stroke, the commonality among subjects is the presence of abnormal muscle synergy patterns and resulting stereotypical movement behaviors. These synergies and associated pathological coupling of joint torques were first observed in the clinic [1,2] and later verified quantitatively by Dewald et al [3,4] under static conditions. The synergies are expressed in strong coupling of shoulder abduction with elbow flexion (the flexion synergy) and shoulder adduction with elbow extension (the extension synergy). In this study we will compare the expression of the flexion synergy induced by generating isometric shoulder abduction (SABD) as opposed to elbow flexion (EF) torques at a maximal and a sub-maximal effort level. The goal of this study is to understand whether generation of anti-gravity torques at the shoulder has a more profound effect on the expression of the flexion synergy as opposed to torques generated at the elbow.

METHODS

Hemiparetic stroke (n=7) and control (n=6) subjects were casted at the wrist and secured to a six degree of freedom (DOF) load cell with shoulder at 70° abduction and 40° flexion and the elbow at a 90° angle. In order to minimize the effect of trunk muscle activation, subjects were seated in a Biodex chair with the trunk secured and the shoulders strapped to the back of the chair. A computer monitor was placed in front of the subject to provide visual feedback in the form of a horizontal and vertical movement of a circular cursor on the screen representing elbow flexion-extension and shoulder abduction-adduction, respectively. Subjects were generating maximum voluntary torques (MVTs) and 25% of MVTs in the shoulder abduction and elbow flexion directions. Forces and moments measured with the load cell were converted online to torques at the elbow (flexion/extension) and shoulder (flexion/extension, abduction/adduction, and external/internal rotation) using a Jacobian transformation. Subjects generated 3-5 trials in either direction. An analysis of variance (ANOVA) was performed at the 0.05 level of significance to test for the presence differences in secondary torques between stroke and control subjects.

RESULTS AND DISCUSSION

Figure 1 shows a significant increase in elbow flexion torques in stroke compared to control subjects during the generation of maximum SABD torques. Conversely, during the generation of maximum EF no significant increases in SABD were observed. The dominance of shoulder antigravity torques on the expression of the flexion synergy persists even at the 25% of MVT level as shown in figure 2 although the significance level was reduced from $p<0.01$ to $p<0.05$.

These results indicate that the generation of shoulder abduction torques following stroke results in a strong expression of the flexion synergy whereas generating EF does not have the same effect. Apparently, the activation of postural anti-gravity muscles at the shoulder uniquely impacts arm discoordination following stroke both in static as well as during dynamic arm reaching tasks as demonstrated in our laboratory in an earlier study [5].

REFERENCES

[1] S. Brunnstrom *Movement therapy in hemiplegia*. New York: Harper & Row, 1970.
[2] T. E. Twitchell. *Brain* 1951;74:443-480.
[3] J.P. Dewald et al., *Brain* 1995;74:443-480.
[4] J. P. Dewald and R. F. Beer *Muscle Nerve* 24:273-283, 2001.
[5] R. F. Beer, J. P. Dewald, et al. *Exp Brain Res* 156(4): 458-70, 2004.

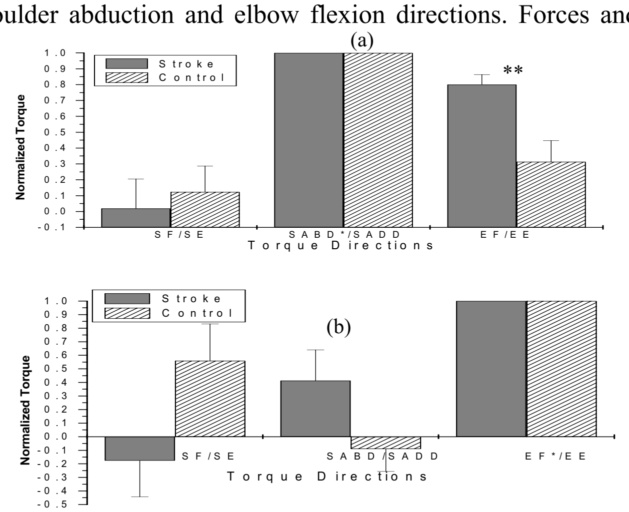

Figure 1. The group mean and standard errors of torque in each direction during the generation of (a) SABD and (b) EF torques at the **maximum** level. * P<0.05, **P<0.01.

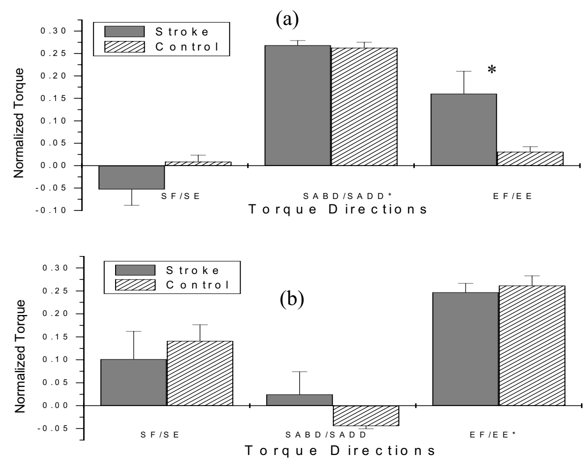

Figure 2. The group mean and standard errors of torque in each direction during the generation of (a) SABD and (b) EF torques at **25%** of MVT level. * P<0.05, **P<0.01.

SUPRASCAPULAR NERVE BLOCK DISRUPTS THE NORMAL PATTERN OF SCAPULAR KINEMATICS

Sean P McCully[1], David N Suprak [1], Peter Kosek [2], Andrew R Karduna[1]

[1]Department of Human Physiology, University of Oregon, Eugene, Oregon, USA,
[2]Pain Consultants of Oregon, Eugene, Oregon, USA
email: karduna@uoregon.edu

INTRODUCTION

Elevation of the arm is not accomplished by the motion of a single articulation, but rather is a combination of both glenohumeral and scapulothoracic motion. Previous research has demonstrated an increase in scapular upward rotation with alterations in rotator cuff activity, either due to tears [1] or fatigue. [2] We propose the use a suprascapular nerve block as an appropriate model of dysfunction of the supraspinatus and infraspinatus. It is our hypothesis that this block will result in a compensatory increase in scapular rotations, similar to what is observed due to fatigue and rotator cuff tears.

METHODS

Ten subjects with no reported shoulder pathology successfully completed a nerve block protocol (age range 23-33). Kinematic and force data were collected prior to and immediately after a suprascapular nerve block. The 3Space Fastrak (Polhemus, Colchester, VT) was used to collect kinematic data. A thoracic receiver was placed over T3 with double sided tape, a humeral receiver was mounted on a molded cuff strapped to the distal humerus, and a scapular receiver was fixed to a scapular tracking device attached to the scapular spine and acromion. [3] Data were collected for scapular plane elevation and three scapular rotations were analyzed: posterior tilting, upward rotation, and external rotation. [3] Force production during shoulder external rotation with the arm at the side was measured with a 50 kg capacity load cell (Lebow, Troy, MI). The nerve block was performed by an Anesthesiologist (PK). After sterile prep of the skin, local anesthetic was infiltrated at a point 2 cm above the scapular spine and at the junction of the outer and middle one third of the spine. A 22 gage 5 cm insulated nerve stimulator needle was advanced to the scapular notch with 0.6 mA of current at 2 Hz. When motor stimulation was seen at current of less than 0.3 mA, 1.5 ml of 1.5% lidocaine was injected. Once repeat stimulation at 0.8 mV did not result in any muscle activity, the remaining 5.7 ml of 1.5 % lidocaine (total 100 mg) were injected and the needle was removed.

Figure 1 Photograph demonstrating the location of the scapular sensor and injection of lidocaine.

RESULTS AND DISCUSSION

There was no significant effect of the nerve block on posterior tilting and external rotation. However, for upward rotation, there was a significant effect of the block ($p = 0.009$). The amount of scapular upward rotation was found to be significantly increased due to the block at humeral elevations from 20 to 90 degrees ($p < 0.01$) (figure 2). The results of the present study are similar to changes due to cuff tears and fatigue, which also result in increases in upward rotation that peak in the mid ranges of motion. [1,2] Despite the fact that the muscles innervated by a suprascapular nerve (supraspinatus and infraspinatus) do not directly control the movement of the scapula, they appear to indirectly affect the scapulothoracic rhythm. The changes in scapulothoracic and humeral kinematics noted in the present study may lead to detrimental conditions such as a reduction in the subacromial space, mal-alignment of the humeral head and glenoid fossa, and a reduction in muscle mechanics (ideal muscle length and moment arms). Alternatively, the scapulothoracic kinematic changes might be considered beneficial as they may be compensatory motions helping to maintain joint stability.

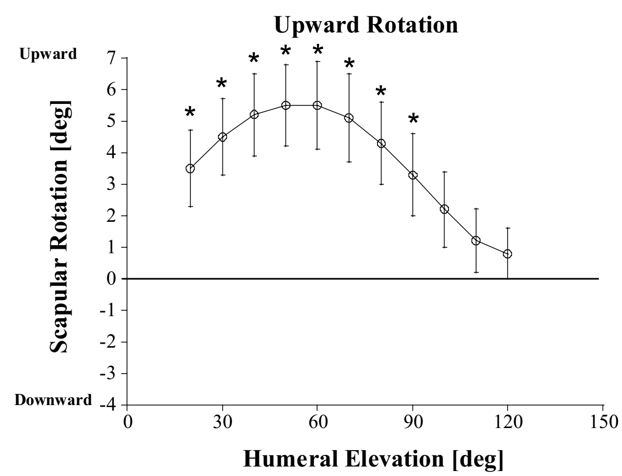

Figure 2 Changes in scapular rotations after the nerve block (Means ± SEM).

CONCLUSIONS

The results of this study indicate that abnormal kinematics patterns found in patients with rotator cuff tears may be compensatory in nature, rather than one of the underlying causes of the pathology.

REFERENCES

1. Mell AG, et al. *ASB Conferences*, Toledo, OH, 2003
2. Ebaugh DD, et al. *ASB Conferences*, Toledo, OH, 2003
3. Karduna AR, et al. *J Biomech Eng* **123**, 184-90, 2001

ALTERATIONS IN SCAPULAR KINEMATICS IN PATIENTS WITH SHOULDER IMPINGEMENT

Paula M. Ludewig
Program in Physical Therapy, School of Medicine
University of Minnesota, Minneapolis, MN
email: ludew001@umn.edu

INTRODUCTION

Subacromial shoulder impingement is defined as compression and mechanical irritation of the rotator cuff and long head of the biceps tendons beneath the coracoacromial arch during elevation of the arm. In healthy subjects, the scapula must achieve a balance of adequate mobility to allow full arm motion, while maintaining stability on the thorax. Abnormal scapular motion on the thorax has been implicated as potentially contributing to shoulder impingement.[1-6] The purpose of this paper is to present an overview of findings regarding normal and abnormal scapular motion in subjects with shoulder impingement during elevation of the arm.

METHODS

Several investigators have compared scapular kinematics in subjects with shoulder impingement to healthy controls.[1-4, 6] Subjects are identified based on a history of localized shoulder pain and clinical examination demonstrating positive impingement tests.[3,4] Methods of data collection have included two-dimensional topographic and radiographic analysis, and three-dimensional static digitizing of surface landmarks, and dynamic motion analysis with surface or bone fixed sensors on the thorax, scapular acromion process, and humerus.[1-6]

Three-dimensional (3-D) scapular data relative to the thorax are described using anatomically embedded reference frames. Ordered Cardan angles for scapular internal / external rotation (protraction / retraction); upward / downward rotation (lateral / medial rotation); and anterior / posterior tilting are described relative to thorax cardinal plane axes. Scapular angles are typically described across humeral elevation angles where shoulder impingement is believed to occur in the "painful arc" of motion (60° to 120° of humeral elevation relative to the thorax).[3] Data have been described in healthy and symptomatic populations during shoulder flexion, abduction, and scapular plane abduction.[1-6]

RESULTS AND DISCUSSION

During elevation of the arm in the scapular plane in healthy subjects, the scapula typically undergoes upward rotation, external rotation, and posterior tilting,[5] while maintaining contact of the medial border and inferior angle of the scapula against the thorax. Subjects with impingement have demonstrated reductions in each of these component motions across different investigations. The most consistent abnormality across studies is a lack of normal posterior tilting.[1-4] Lack of normal posterior tilting and external rotation result in a loss of contact of the inferior angle (Figure 1) or medial border of the scapula with the thorax.[6] Some subjects demonstrate a pattern of progressive scapular anterior tilting throughout humeral elevation (Figure 2). Reductions in upward rotation early in the range of motion and reductions in

Figure 1: Subject demonstrating anterior tilting of the scapula during shoulder flexion.

external rotation under hand held loads have also been reported in impingement subjects.[3] The average magnitude of deviations is in the range of 4° to 6°. These deviations may be causative in the development of impingement syndrome or compensatory in response to pain and muscle inhibition. Although these deviations are believed to bring the acromion process in closer proximity to the humerus, the literature is inconsistent with regard to how these deviations may impact the subacromial space.

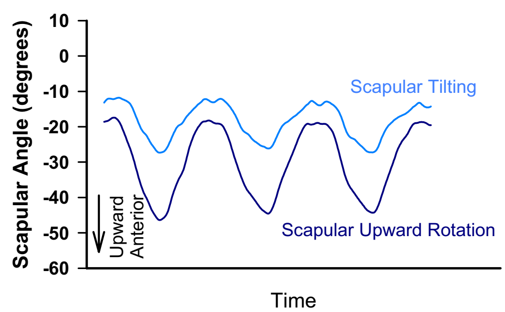

Figure 2. Graphical representation of anterior tilting pattern during three repetitions of humeral elevation.

CONCLUSIONS

Significant alterations in (3-D) scapular motions on the thorax are seen in subjects with clinical signs of shoulder impingement as compared to healthy controls. Greater understanding is needed with regard to how these deviations impact the subacromial space and pathology of the rotator cuff and long head of the biceps tendons.

REFERENCES

1. Endo K, et al. *J Orthop Sci* **6**, 3-10, 2001.
2. Hebert LJ et al. *Arch Phys Med Rehabil* **83**, 60-69, 2002.
3. Ludewig PM and Cook TM. *Phys Ther* **80**, 276-291, 2000.
4. Lukasiewicz AC et al. *J Orthop Sports Phys Ther* **29**, 574-583, 1999.
5. McClure P et al. *J Shoulder Elbow Surg* **10**, 269-277, 2001.
6. Warner JJ et al. *Clin Orthop* **285**, 191-199, 1992.

POSITION OF THE HUMERAL HEAD SHIFTS IN THE GLENOID DUE TO THE PRESENCE OF OSTEOARTICULAR LESIONS

[1] Alexis C. Wickwire, [1] Jens H. Stehle M.D., [2] Jon Sekiya M.D., [3] Patrick J. McMahon M.D., [1] Richard E. Debski Ph.D.
[1] Musculoskeletal Research Center, Dept. of Bioengineering, University of Pittsburgh, Pittsburgh, PA
[2] Bone and Joint/Sports Medicine Institute, Dept. of Orthopaedic Surgery, Naval Medical Center, Portsmouth, VA
[3] Dept. of Orthopedic Surgery, University of Pittsburgh, Pittsburgh, PA; email: genesis1@pitt.edu

INTRODUCTION

Osteoarticular lesions of the humeral head are often observed after shoulder dislocations [1]. The presence of such lesions could contribute to changes in position of the humeral head with respect to the glenoid. These alterations in the position of the humerus may lead to joint subluxation and the development of osteoarthritis [2]. The objective of this study was to determine the effects of osteoarticular lesions on the position of the humeral head during the application of a compressive force to the humerus.

METHODS

Nine fresh-frozen cadaveric shoulders (age 44.9±8.2 years, humeral head diameter 45.9±3.8mm) were dissected free of all skin and musculature except for the coracoacromial ligament and labrum. (Intact joint) The humerus and scapula were then potted in epoxy putty and fixed within a robotic/universal force-moment sensor (UFS) testing system [3]. The joint was initially oriented in the testing system at 60° of glenohumeral abduction and 0° of external rotation. A 22 N joint compressive force was applied by the testing system to the humerus while minimizing the forces in the orthogonal directions to center the humeral head within the glenoid cavity. The joint orientation was held constant during application of the compressive force. This protocol was then repeated after the joint was moved to 60° of glenohumeral abduction and 60° of external rotation. Three osteoarticular lesions on the posterolateral side of the humeral head were subsequently created to simulate an injury that would occur during joint dislocation at 60° of glenohumeral abduction and 60° of external rotation. The size of each lesion was approximately 12.5% (Lesion 1), 25% (Lesion 2), and 27.5% (Lesion 3) of the humeral head diameter and was created using an oscillating bone saw. (Figure 1) The compressive force was applied again to the shoulders at 60° glenohumeral abduction and both external rotation angles in each lesion state. The position of the humerus was recorded for each joint orientation following application of the compressive force. The change in the position of the humerus for each lesion state was then calculated and paired *t*-tests were used to determine significant differences between the position of the humerus for the intact joint and each lesion state ($p<0.05$).

RESULTS

No significant changes in joint position were found for all lesion states at 0° external rotation. (less than 1mm for each direction; $p>0.05$) The largest changes in position compared to the intact joint were found for Lesion 2 and 3 at 60° external rotation (Figure 2). The position of the humerus for Lesion 2 shifted 1.3±1.4mm and 2.5±1.6mm in the medial and posterior directions, respectively. The position of the humerus for Lesion 3 shifted 1.8±1.1mm and 1.9±1.5mm in the medial and posterior directions, respectively. These changes in position were statistically significant ($p<0.05$). No significant changes in joint position were found for Lesion 1 with the humerus shifting by less than 1mm in all directions.

DISCUSSION

This study evaluated the effect of osteoarticular lesions on the position of the humeral head with respect to the glenoid. A significant effect was found when the size of the lesion was 25% or more of the humeral head diameter (Lesions 2 & 3). However, smaller lesions did not affect bony contact between the humeral head and glenoid, and consequently the position of the humerus. In addition, the change in position was dependent on the location of the lesion and orientation of the joint. These altered joint positions could contribute to abnormal joint contact and the development of osteoarthritis [2]. In the future, the effect of the lesions on the contact forces and forces in the glenohumeral capsule will be examined.

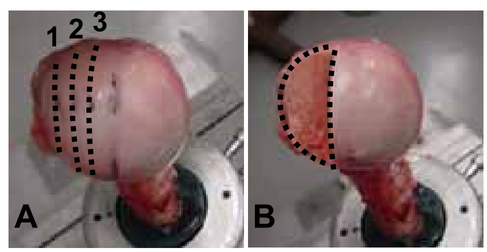

Figure 1: A) Lines on humeral head indicating borders used for creation of Lesions 1, 2, and 3; B) humerus with Lesion 3.

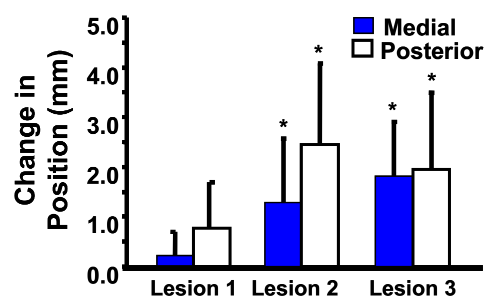

Figure 2: Change in position of humerus with respect to intact joint at 60° of abduction and 60° of external rotation (mean±SD; * $p<0.05$).

REFERENCES

1. Matsen, et al: *The Shoulder*, 1994.
2. Hawkins RJ, et al: *JBJS* **72**: 1193-7, 1990.
3. Debski, RE et al: *J Orthop Res* **17**: 769-776, 1999.

ACKNOWLEDGEMENTS

The Musculoskeletal Research Center, American Shoulder and Elbow Surgeons, Arthroscopy Association of North America.

Gait Data Collection Technology: Where are we, where are we going?

Lasse Roren
Vicon Peak, Oxford, United Kingdom
Email: lasse.roren@vicon.com

INTRODUCTION

Clinical gait analysis depends upon technology enabling the measurement of human movement. The availability of custom-designed hardware/software solutions has been key to the spread and popularity of clinical gait analysis.

MATERIALS

The current state-of-the-art in gait analysis collection technology allows labs to collect data using high resolution cameras (up to 4 mega-pixels, see figure 1 below), high collection speeds (up to 2,000 Hz), small markers (down to 4mm diameter) and user friendly software that allows collection, processing and generation of clinical reports to be done in seconds ([1], [2]). A modern lab is able to capture full-body and foot data simultaneously using a large number of small markers, process both the full-body and foot models concurrently and generate a full clinical report long before the patient leaves the lab.

Labs have thus switched their focus from obtaining and processing data to the interpretation. The fact that reports can be generated quickly means that the lab has full confidence in the data quality before the patient leaves. Having to recall the patient because the data turned out to be poor is a thing of the past. In short, the recent increases in camera and software technology has resulted in significant accuracy and time saving gains.

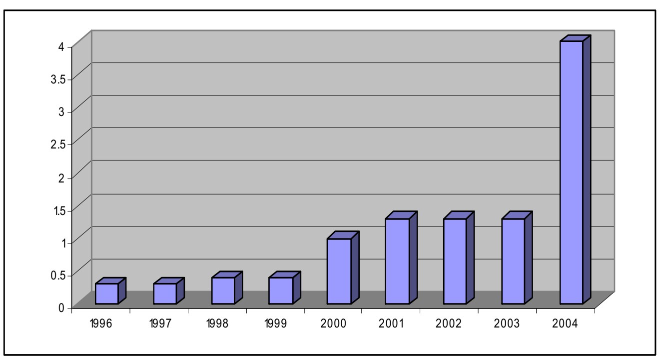

Figure 1: Maximum camera resolutions, in mega-pixels

DISCUSSION

As the attention has switched from the data collection process to the analysis, it is becoming increasingly clear that the improved collection technology exposes shortcomings in the biomechanical modeling phase. Various papers have criticized the current standard, the Conventional Gait Model ([3]). Whereas data collection systems can determine marker centroids to typical accuracies in tenths of millimeters ([4]), the process of transforming these measurements to joint centers, kinematics and kinetics is subject to various sources of errors: soft tissue artifacts, anthropometric measurements that are not subject specific, and inaccurate marker placement with respect to anatomical landmarks.

Solving these problems is currently a hot topic of research ([5]). It can be argued that the manufacturers themselves have done relatively little, although some research and development has taken place ([6]). The future will very likely see more emphasis being placed on the "next generation gait model", both from researchers and manufacturers, and we will see competitive pressures forcing the manufacturers to act.

The main attention must focus on obtaining clinically validated and repeatable results. Manufacturers have to ensure that, whichever biomechanical model and protocol is adopted, the data can be processed through the model with a high degree of automation, confidence and accuracy. To this end, a cooperation between researchers in the gait community and the commercial development departments of manufacturers must be formalized. Also, the manufacturers must recognize that it is in everybody's interest that the implementation of the model is open, published and streamlined – this will give researchers the double benefit of being able to conduct validation easily *and* having full confidence in the results.

Another topic which must be addressed is the financial viability of clinical labs. The manufacturers can address this in two ways: by developing systems that increase the intrinsic value of clinical gait through increased accuracy and standardization, and by developing systems that reduce the time and cost of conducting an analysis session.

As for the technology, initial development will focus on gradually increasing the system's specifications in terms of accuracy and usability. However, the major technology breakthrough in the next 2-3 years is likely to be the development of markerless capture. Although it is too early to predict whether the clinical accuracy requirements will be satisfied, it is obvious that removing the need for markers would bring huge benefits to both patients and operators.

REFERENCES

1. Vicon Peak, www.viconpeak.com
2. Motion Analysis Corporation, www.motionanalysis.com
3. Jenkins, S. E. M., *et al., Errors in the calculation of the hip joint centre location in children.* XVIII Congress of the International Society of Biomechanics, book of abstracts, p. 365.
4. www.ne.jp/asahi/gait/analysis/comparison2002
5. Cappozzo, A, *Are we ready for a second generation* clinical gait model? GCMAS 2005 keynote
6. Roren, L., *et Al., A New Lower Body Model using Global Optimisation to Establish Joint Centres,* GCMAS 7th Annual meeting, Chattanooga, 2002.

CALCULATING ANATOMICAL LEG STRUCTURES FROM SURFACE CONTOURS

[1] Walter Rapp, [2]Marcin Witkowski, [1]Thomas Horstmann, [3]Burkhard Lembeck, [4]Jos Vander Sloten, and [5]Kjell Heitmann
[1]Dep. of Sport Medicine, University Tübingen, [2]Dep. of Micromechanics, Warsaw University , [3]Dep. of Orthopedics, University Tübingen, [4]Dep. of Biomechanics, KU Leuven, [5]Diers International. E-mail: walter.rapp@med.uni-tuebingen.de

INTRODUCTION

The analysis of objective movement parameters plays an important role in clinical diagnoses. State of the art motion analyzing tracks reflecting markers fixed on the skin over anatomical landmarks. When using such systems however, no information about the surrounding surface structures is available. Therefore, the purpose of this project is the development of a system able to reconstruct anatomical structures from the scanned surface volume of the lower leg under dynamic conditions. It was shown that a surface analysis of the back shape could be performed using white light raster line projection (Frobin&Hierholzer 1981, Drerup&Hierholzer 1987).

To achieve a system with the capacity to analyze the full volume of the lower extremities two main changes have to be developed. First, is the synchronization of four camera projection units and second, is to change from white light to laser light line projection.

The goal of the following pre-study is to evaluate the shape of the lower extremities using white light rasterstereographic technique to find surface areas which represent bony structures for the reconstruction of a musculo-skeletal model.

METHODS

The surface contour of the lower leg was analyzed using the formetric® system (DIERS International, Germany). This system consists of a commercial slide projector and a fire wire camera which were mounted in a constant geometrical order. The maximum analyzing frequency is 15 Hz.

The method of rasterstereography is based on the curvature analysis of horizontal light lines which are projected onto the legs and stored as a video image. Transforming the light lines into a 3D-point cloud, the shape of the leg can be comprised of concave, convex and saddle shaped areas (Fig.1).

Five subjects participated in this pre-study. They were positioned in front of the recording system and performed slow knee bending during normal stance. The surface structures were scanned from an anterior, posterior and sagittal view separately. Black markers were fixed on significant anatomical landmarks, like the patella, tibial tubercle, the malleolus and the head of the fibula, for comparison with the previously palpated positions. Due to limitations of the measuring volume, the pelvis could not be analyzed. As an orientation, markers were placed 15cm beneath the spinea iliaca anterior and the trochanter major.

RESULTS AND DISCUSSION

From the sagittal view the lateral malleolus are a rather prominent landmark detectable in every subject. Looking at the knee, the patella can be detected as a prominent convex area from the frontal view and is also detectable from the lateral view (Fig. 1). At the shank, the maximum curvature of each horizontal line can be marked and linked vertically. This however, does not represent the line of the tibia due to the fact that the m. tibialis ant. obscures the tibia. As a further landmark, visible from the frontal view, the tibial tubercle is represented by a change from a convex to a saddle shaped area. As already mentioned, no significant landmarks can be detected from the thigh, neither from the frontal nor from the sagittal view. In this case alternative points must be marked manually to get the line passing the iliac spine or the trochanter. Thus a calculation of the angle in the anterior posterior and the medial lateral plane is possible.

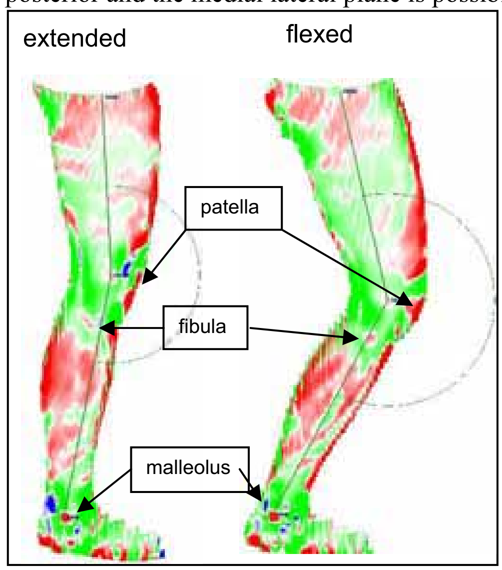

Figure 1: Image example from a sagittal view. The arrowed parts represent the detected landmarks.

CONCLUSIONS

It could be shown, that lower leg anatomical landmarks are detectable using this technique. The detection of these landmarks allows the computation of segments representing the anatomy of the lower extremities in 3D. Limitations must be seen that a movement sequence could only be analyzed from one view. The development of a four camera laser light based system, however, should solve this problem.

REFERENCES

1. Frobin W, Hierholzer E. Photogrammetric Engineering &Remote sensing, 47, 1717-1724.
2. Drerup B, Hierholzer E. J. Biomechanics, 20, 961-970.

ACKNOWLEDGEMENTS

This study was supported by the European Commission in the FP6 research program.

HAMSTRING CO-CONTRACTION DOES NOT NECESSARILY REDUCE ACL LOADING

[1] Bing Yu, [2] William E. Garrett
[1] Center for Human Movement Science, Division of Physical Therapy, The University of North Carolina at Chapel Hill, Chapel Hill, NC, USA; [2] Sports Medicine Center, Duke University; email: byu@med.unc.edu

INTRODUCTION
One of the risk factors of sustaining non-contact anterior cruciate ligament (ACL) injury proposed in literature is the strong quadriceps muscle contraction at a small knee flexion angle. Previous studies with cadaver testing show hamstring co-contraction significantly reduces ACL loading, and suggest that training for hamstring co-contraction assist in reducing the risk of sustaining non-contact ACL injuries. The results of reduced ACL loading with hamstring co-contraction, however, were obtained with reduced knee joint resultant extension moment. The purpose of this study was to investigate the effects of hamstring co-contraction on ACL loading in a stop-jump task using a computer simulation method with in-vivo lower extremity kinematic and kinetic data.

METHODS
Twenty healthy recreational athletes (10 males and 10 females) with no known history of knee injuries or disorders were recruited to collect radiographic data of the knee. Side-view roentgenographic films of the knee were obtained for each subject at 0°, 15°, 30°, 45°, 60°, 75° and 90° knee flexion bearing 50% of the total body weight. Patella tendon-tibia shaft angles (PTTS) and actual knee flexion angles were measured from the roentgenographic films. Multiple regression analyses with dummy variables were performed to express the PTTS as a function of knee flexion angle and gender. Quadriceps and hamstring muscle moment arms and ACL elevation angles from the literature were also expressed as functions of knee flexion angle using regression analyses.

Sixty healthy recreational athletes (30 males and 30 females) without known history of knee injuries or disorders were recruited for kinematic and kinetic data collection. Three-dimensional (3D) kinematics and kinetics of the lower extremities were collected for each subject in a stop-jump task. Knee joint angles and joint resultants were estimated. Multiple regression analyses with dummy variables were performed to express each of the peak knee joint resultant extension moment and peak proximal tibia anterior shear force during landing of the stop-jump task as a function of the peak posterior and vertical ground reaction forces.

A biomechanical model of the knee was developed with the PTTS, quadriceps and hamstring moment arms, and ACL elevation angle as functions of knee flexion angle, and peak knee extension moment and proximal tibia anterior shear force as functions of peak posterior and vertical ground reaction forces. The hamstring tendon was considered as parallel to the femur. Peak posterior and vertical ground reaction forces and knee flexion angle at peak posterior ground reaction force were varied based on the variations of corresponding in-vivo data. Quadriceps and hamstring muscle forces were varied to satisfy the peak knee extension moment estimated from the peak ground reaction forces. ACL loading were estimated from the peak proximal tibia anterior shear force, quadriceps and hamstring muscle forces, and ACL elevation angle.

RESULTS AND DISCUSSION
ACL loading increased as the hamstring co-contraction increased when the knee flexion angle is smaller than 15 degrees for males and 20 degrees for females (Figures 1 and 2). Hamstring co-contraction effectively reduced ACL loading when the knee flexion angle is greater than 15 degrees for males and 20 degrees for females (Figures 1 and 2).

Knee flexion angle significantly affects the relationship between ACL loading and hamstring co-contraction. Quadriceps force has to be increased to satisfy the given knee extension moment due to external loading when hamstring co-contraction increases. The anterior shear force applied on the tibia by the quadriceps increases while the posterior shear force applied on the tibia by the hamstring decreases as the knee flexion angle decreases. The gender difference in the relationship between ACL loading and hamstring co-contraction is mainly due to the gender difference in PTTS.

REFERENCES
Li G et al. J.Ortho Res, 23: 340-344, 2005.
Smidt G. J Biomech, 6: 79-92, 1973.
Nunley RA et al. Res Sports Med, 11: 173-185, 2003.

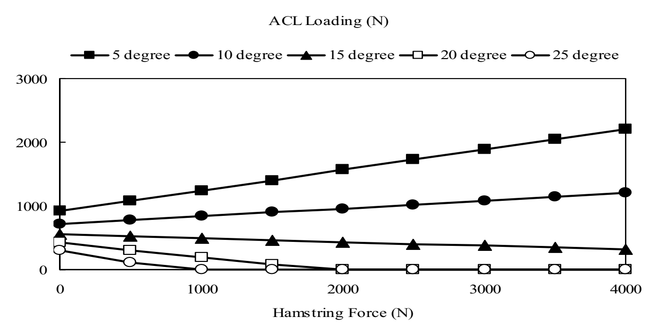

Figure 1. ACL loading as a function of hamstring force and knee flexion angle for male subjects.

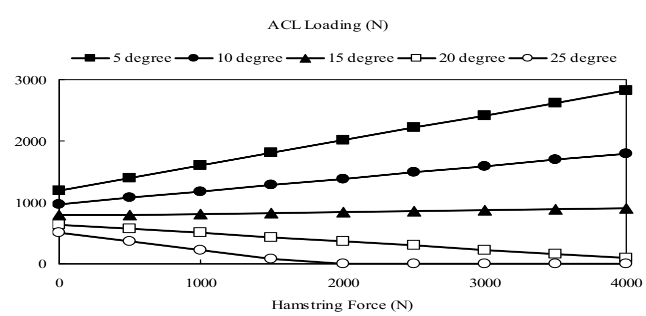

Figure 2. ACL loading as a function of hamstring force and knee flexion angle for female subjects.

A COMPARISON OF VARIOUS DIGITAL FILTERING TECHNIQUES APPLIED ON PLANTAR SURFACE PRESSURE AND SHEAR DATA

Metin Yavuz, M.S., Brian L. Davis, Ph.D.
Department of Biomedical Engineering (ND20), Cleveland Clinic Foundation, 9500 Euclid Ave, Cleveland, OH 44195
E-mail: davisb3@ccf.org

Introduction

Occurrence of ulcers on the plantar surfaces of the diabetic patients' foot can lead to serious medical complications, including limb amputation. We have employed a transducer array to measure the plantar surface pressures and shear forces whose combination may give rise to diabetic foot ulceration. However data produced by the equipment includes noise that needs to be filtered in order to perform subsequent data analyses. The aim of this study is to investigate and compare the common spatial, temporal and wavelet signal denoising procedures on the plantar surface pressure and shear force data.

Methods

The device (Figure 1) has 80 transducers that are based on strain gauge technology and capable of collecting all three force components (vertical, mediolateral and anteroposterior) simultaneously. It was designed in an 8 x 10 array architecture with 10 mm x 10 mm measuring transducers. Data were obtained at 50Hz for 2 seconds during steady state gait without adjusting step lengths prior to contact with the platform. To achieve spatial domain filtering the shear data were converted into an 8 x 10 pixel resolution 8-bit grayscale image. The median filter in Matlab's (MathWorks, Nattick, MA) image processing toolbox and a 2D Wiener filter were then employed on the spatial data. Two time domain filters, moving average and second order Butterworth, were also operated on the time series data. Cut-off frequency for Butterworth filter was calculated according to Wells *et al* (1). We utilized the Rice Wavelet Toolbox, an open source wavelet toolbox developed by the Digital Signal Processing Group at Rice University, to carry out wavelet filtering of the shear data (2).

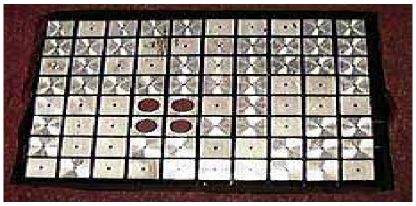

Figure 1. The transducer platform used to obtain pressure and shear data. The overall size is 14.2 cm by 11.4 cm

Results and Discussion

In order to compare the performance of the methods employed, average signal-to-noise ratio (SNR) was calculated for each filtering process. The results of SNR calculations are given in Table 1. The SNR values indicate that the wavelet filtering yielded the best noise removal. Spatial filtering was found to be inappropriate with the shear data. Figure 2 shows a representative set of results for the five filtering techniques. Temporal filtering of the shear data produced intermediate noise elimination.

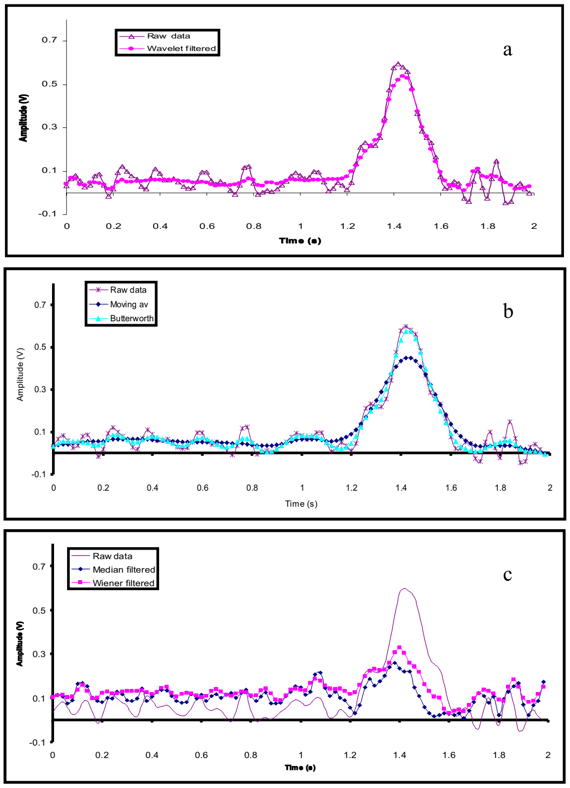

Figure 2. Results of a. wavelet filtering, b. time domain filtering, c. spatial filtering of shear data

Table 1. SNR values for each filtering process

Filter	SNR (dB)
Wavelet	8.97
Butterworth	7.13
Moving Average	4.96
Wiener	0.12
Median	-0.19

Conclusions

Wavelets were observed to perform high quality shear data filtering due to their ability to analyze both spectral and temporal information in the data compared with other noise removal procedures. Spatial filtering did not perform well, most probably due to spatial resolution of the transducer array.

References

1. Wells RP, Winter DA. Proceedings of the first Congress of the Canadian Society of Biomechanics. Human Locomotion I, Waterloo, 1980:92-93.
2. http://www.dsp.rice.edu/software/rwt.shtml

Acknowledgment

This work was possible due to support from the Juvenile Diabetes Research Foundation.

THE ENERGETICS AND BIOMECHANICS OF TURTLE LOCOMOTION

[1] Peter A. Zani, [1] Rodger Kram, [2]Audrone R. Biknevicius, and [2]Stephen M. Reilly
[1]University of Colorado, [2]Ohio University;
email: zani@colorado.edu, web: www.colorado.edu/kines/research/locomotion.html

INTRODUCTION

Tortoise muscle has been shown to be very efficient *in vitro*[1]. Likewise, a semi-aquatic turtle has been shown to walk with remarkable metabolic economy[2]. Yet, Galápagos tortoises do not conserve substantial mechanical energy during walking[3] calling into question the link between locomotor energetics and mechanics. We gave begun to investigate if turtles in general are economical walkers and if so why.

METHODS

We measured the metabolic cost of locomotion in 18 terrestrial box turtles, *Terrapene ornata*. We trained turtles to walk steadily on a treadmill for 10-20 minutes while wearing a mask (Figure 1). We then measured steady-state oxygen consumption for 5-10 trials of level walking as well as walking up a 24° incline. In addition, we collected ground-reaction forces for individuals walking across a force platform to determine whether economical walking in box turtles is due to the inverted-pendulum mechanism of energy conservation[4].

RESULTS AND DISCUSSION

Minimum cost of transport for level walking (8.0 ± 2.97 J/kg/m) was roughly one-half the expected value (15.9 ± 1.50 J/kg/m) for animals of similar size (Figure 2). When walking up an incline turtles walked much slower (0.04 ± 0.016 m/s) and with a much higher cost of transport (15.0 ± 7.10 J/kg/m). By matching level and incline trials of similar speed we were able to calculate uphill efficiency (20.2 ± 9.16 %). This value is comparable to terrestrial mammals and birds of similar size. Thus, the low cost of transport during level walking does not appear to be due to high efficiency of turtle muscle.

Examination of turtle mechanics indicates that the magnitude of kinetic-energy fluctuations (0.01 ± 0.004 J/stride) were only one-quarter of fluctuations in gravitational potential energy (0.04 ± 0.017 J/stride). These energies were only sporadically out of phase and thus, turtles recovered only 25.2 ± 3.83 % of their mechanical energy per stride. Hence, it appears that economical level walking in turtles is not due to mechanical-energy conservation. We suggest that the low metabolic cost of turtle walking is related to their extremely slow muscles, consistent with the cost-of-generating-force hypothesis[5].

CONCLUSIONS

We studied the energetics and mechanics of turtle locomotion. Despite having poor mechanical-energy conservation (~25% energy recovery), turtles are very economical at level walking (half the expected metabolic cost). Yet, this does not appear to be due to extraordinary muscular efficiency (~21%). Thus, we suggest that economical walking in turtles in general is not dependent upon effective mechanical-energy recovery. Rather, the extremely slow muscles of turtles may account for their low metabolic expenditure during walking.

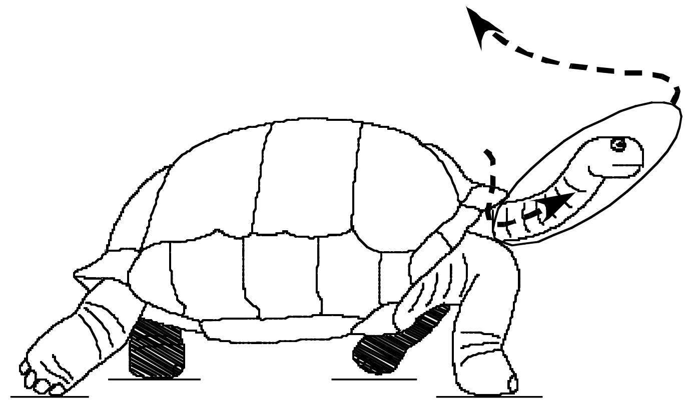

Figure 1: A walking turtle wearing an open-flow mask to collect respired air (flow direction indicated by arrows).

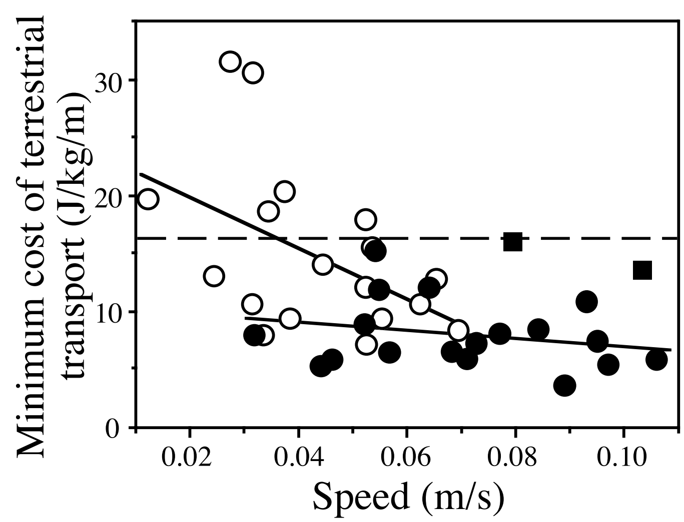

Figure 2: Minimum cost of transport vs. speed for level (filled symbols) and 24° incline (open symbols) walking in turtles. Dashed line is average expected level cost based on size.

REFERENCES

1. Woledge RC. *J. Physiol*. **197**, 685-707, 1968.
2. Baudinette RV, et al. *Physiol. Biochem. Zool.* **73**, 672-682, 2000.
3. Zani PA, et al. *Int. Comp. Biol*. **43**, 985, 2003.
4. Cavagna GA, et al. *Am. J. Physiol*. **233**, R243-R261, 1977
5. Kram R and CR Taylor. *Nature* **346**, 265-267, 1990.

ACKNOWLEDGMENTS

We thank T. Gleeson, A. LaFave, E. McElroy, K. Sidenblad, and A. Van Dijck for assistance during this project. Supported by NIH F32 AR08615 and an ASB travel grant to PAZ.

KNEE LOADING PATTERNS THAT ENDANGER THE ACL: INSIGHTS FROM EXPERIMENTAL AND SIMULATION STUDIES

[1]Ajit M. Chaudhari, [1]Choongsoo S. Shin, [1,2]Chris O. Dyrby and [1,2]Thomas P. Andriacchi
[1]Stanford Biomotion Laboratory, Dept. of Mechanical Engineering, Stanford University,
[2]Bone & Joint Center, VA Palo Alto Health Center; email: ajit.chaudhari@stanford.edu, web: biomotion.stanford.edu

INTRODUCTION

Over the past several decades, *in vivo* research addressing non-contact ACL injury mechanisms has been unable to directly examine motion of the tibiofemoral joint and the strain on the ACL during high-risk activities. Cadaver studies have attempted to identify the loading patterns that strain the ACL during such activity, but these studies are limited by practical considerations such as cadaveric tissue breakdown and experimental setup limitations.

Recent advances in measuring *in vivo* kinematics using the Point Cluster Technique (PCT) [1] now allow much more detailed examinations of the knee loading patterns and tibiofemoral motions that occur *in vivo* during high risk activities [2], and simulations of the tibiofemoral joint can be used to examine consequences of such loading patterns for ACL injury [3]. This talk will discuss the results of these techniques in improving our understanding of the ACL injury mechanism.

METHODS

Using the previously-described PCT we use an opto-electronic motion capture system to measure the 6 degree of freedom motion of the femur with respect to the tibia during activities of daily living. We have observed the anterior-posterior translation, internal-external rotation, and abduction/adduction of the knee joint during 90-degree sidestep cut and single-leg stopping maneuvers [2], as well as the net reaction forces and moments at the knee [4].

In addition, we have developed a specimen-specific simulation model of the knee built from MRI data and validated against experimental loading tests of cadaver specimens [3]. Using this model together with the physiologic loading observed during *in vivo* testing, we can estimate the strain in the bundles of the ACL to examine the relative importance of the different loading modes for the ACL injury [3,5,6].

RESULTS AND DISCUSSION

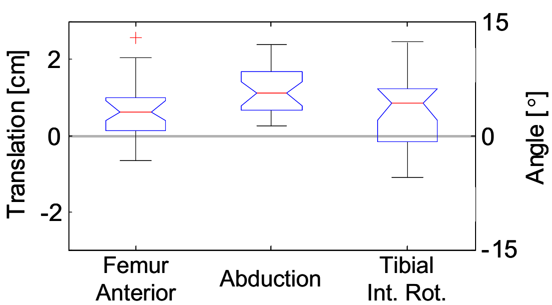

Figure 1. *In vivo* knee tibiofemoral displacement during first 100ms after foot strike during a run-to-stop maneuver.

In vivo testing using the PCT shows that anterior translation of the tibia does not occur in most subjects during single-limb landing. However, abduction and tibial internal rotation do occur in most subjects, suggesting that a mechanism involving abduction and tibial internal rotation may be the most relevant in understanding the ACL injury mechanism during these deceleration and change-of-direction activities. Joint reaction loads at the knee further support these conclusions because the external reaction force at the knee acts to push the proximal tibia in a posterior direction, while the reaction moment acts to push the tibia into abduction and internal rotation.

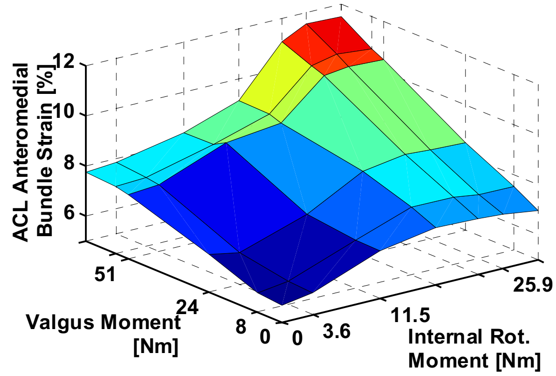

Figure 2. Response of ACL anteromedial bundle strain to applied valgus, internal rotation, and combined moments.

Applying the loading patterns observed *in vivo* to our simulation model shows the direct effects of these loads on ACL strain. Increasing the posterior force from zero to the maximum physiologically observed values reduces ACL strain. **This reduction in strain occurs even while the force in the quadriceps increases, because the force in the quadriceps is merely a reaction to the externally applied force.** In contrast, externally applied abduction and internal rotation moments result in increased ACL strains. The individual moments themselves do not appear large enough to cause rupture of the ACL, but when acting together combined abduction and internal rotation loading cause increased ACL strains that may be large enough to damage the ACL.

REFERENCES

1. Andriacchi TP, et al. *J. Biomech. Eng* **120**, 743-749, 1998.
2. Chaudhari AM, et al. *Transactions of ORS,* San Francisco, CA, Abstract 1293, 2004.
3. Chaudhari AM, et al. *Transactions of ORS,* Washington, DC, Abstract 1516, 2005.
4. Chaudhari AM, et al. *Int. Symposium on Ligaments & Tendons IV,* San Francisco, CA, Abstract 13, 2004.
5. Shin CS, et al. *Proceedings of ASME Summer Bioengineering Conference,* Vail, CO, 2005.
6. Shin CS, et al. *Proceedings of ISB XX,* Cleveland, OH, Abstract 969, 2005.

COUPLED BIOMECHANICAL-EPIDEMIOLOGICAL STUDIES FOR THE ASSESSMENT OF ACL INJURY RISK

[1, 2] Timothy E. Hewett, [1]Gregory D. Myer and [1]Kevin R. Ford
[1]Cincinnati Children's Hospital Sports Medicine Biodynamics Center
[2] University of Cincinnati College of Medicine; email: tim.hewett@cchmc.org, web: www.cincinnatichildrens.org/sportsmed

INTRODUCTION

The goal of applied biomechanical and epidemiological research aimed at decreasing injuries in general and specifically anterior cruciate ligament (ACL) injuries in athletes must be to first determine the factors that make athletes susceptible to ACL injuries, second to develop screening tools to identify these factors in individual athletes and third to develop treatment modalities targeted to these factors in an attempt to prevent of these injuries. If preventive modalities such as dynamic neuromuscular training can reduce the incidence of knee injury by even a few percentage points, thousands of knee injuries can be prevented in high school and collegiate sports annually. In addition, with the ever increasing popularity of high-risk jumping and pivoting sports like soccer, volleyball, and basketball and the rapidly growing number of participants each year, even higher numbers of ACL and other injuries might be avoided in the future.

Neuromuscular control deficits that can be identified using kinematic and kinetic techniques may be responsible for decreased knee joint control and increased injury risk in female athletes.[1] Neuromuscular training may alter active knee joint control, decreasing ACL injury rates by correcting identified neuromuscular deficits.[2] Coupled biomechanical and epidemiologic techniques have shown the effects of growth and development on neuromuscular control deficits and on ACL injury risk and the effects of neuromuscular training on both dynamic knee control and ACL injury risk in young female athletes.[2,3,4] Coupled biomechanical and epidemiologic studies clearly demonstrate the ability not only to detect but to correct neuromuscular imbalances using biomechanical techniques. These biomechanical and epidemiologic studies provide strong evidence that biomechanical screening, computer modeling and neuromuscular training used in combination may provide an effective solution to the problem of gender inequity in knee and ACL injury.

The goal of these studies is to determine whether measured neuromuscular control deficits can predict ACL injury risk. A large-scale prospective coupled 3D biomechanical and epidemiological cohort study design was employed to determine whether prescreened athletes with decreased neuromuscular control and increased valgus joint loading had increased risk of ACL injury. [3] Prior to their competitive season, 205 female athletes in the high-risk sports of soccer, basketball, and volleyball were prospectively measured for neuromuscular control during landing using 3D kinematics and kinetics.

Nine athletes who subsequently during the following sports seasons suffered confirmed ACL ruptures had significantly different knee kinematics and kinetics than the 196 female athletes who did not go on to ACL rupture. The knee abduction valgus angle at landing was 8º greater in ACL-injured than uninjured athletes. ACL-injured athletes had a

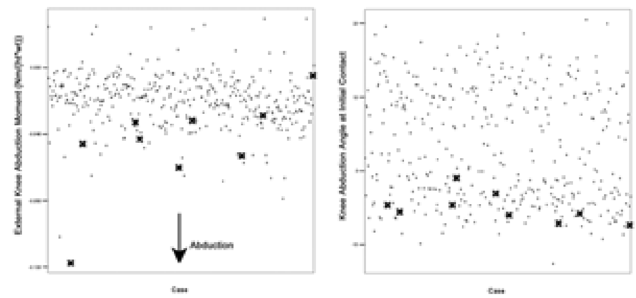

Figure 1: Knee abduction moment and knee abduction angle prospectively measured in subsequently ACL Injured (**X**) and Non-Injured Subjects.

2.5-times greater knee abduction moment and 20% higher ground reaction force. The knee abduction moment predicted ACL injury status with 73% specificity and 78% sensitivity.

CONCLUSIONS

Biomechanical and epidemiological findings demonstrate that decreased neuromuscular control, as evidenced by measures of knee abduction torque and knee abduction angle, can predict increased ACL injury risk in a high percentage of individuals.[3] Computer models show that valgus increases ACL loads.[5] A combination of computer modeling coupled with the above approach may provide the necessary answers to this problem. However, the question is whether it is possible to accurately and identify those individuals who display these potential causal factors. Effective screening programs need to be developed and put into practice that will enable identification of athletes at risk for ACL injury in order to channel them into custom-designed neuromuscular interventions.

REFERENCES

1. Hewett TE, Myer GD, Ford KR. Decrease in neuromuscular control about the knee with maturation in female athletes. *J Bone Joint Surg Am.* 2004;86-A(8):1601-1608.
2. Hewett TE, Myer GD, Ford KR, et al. Biomechanical Measures of Neuromuscular Control and Valgus Loading of the Knee Predict Anterior Cruciate Ligament Injury Risk in Female Athletes. *Am J Sports Med.* Feb 8 2005;33(4):492-501.
3. Hewett TE, Lindenfeld TN, Riccobene JV et al. The effect of neuromuscular training on the incidence of knee injury in female athletes. A prospective study. *Am J Sports Med.* Nov-Dec 1999;27(6):699-706.
4. McLean, S. G., Huang, X., Su, A., et al.: Sagittal plane biomechanics cannot injure the ACL during sidestep cutting. *Clin Biomech 19:* 828-838. 2004

ACKNOWLEDGEMENTS

The authors would like to acknowledge funding support from National Institutes of Health Grant R01-AR049735-01A1 (TEH). The authors would like to acknowledge the invaluable assistance of Scott McLean and Ton van den Bogert

BIOMECHANICAL ANALYSIS OF OCCUPATIONAL HIGH EXERTION TASKS

Don B. Chaffin, PhD, CPE, PE
Center for Ergonomics, The University of Michigan
dchaffin@umich.edu, http://www.personal.engin.umich.edu/~dchaffin/

Often extremely high levels of exertion are required in manual tasks in industry, and the preponder-ance of epidemiological evidence indicates that these tasks cause and precipitate excessive numbers of low back and other musculoskeletal pain and suffering for thousands of workers, along with high medical and compensation costs. This paper will explore the historic role that biomechanics has played in under-standing these outcomes, as well as reviewing the basis for ergonomic prevention strategies used today.

The focus of the presentation will be on occupational low back pain. The discussion begins with the fundamental biomechanical reality; that the lumbar spine is often subjected to extremely large compres-sion forces when one stoops to pick up an object, even if the object is of moderate weight. Biomechanics research has disclosed that such compression forces will cause premature vertebral disc fractures in many people. This information has provided a primary basis for the “Lifting Guideline” first proposed by NIOSH in 1981, which recommends the amount of load that can be lifted in various postures by most people. The paper will discuss this outcome of the research, as well as biomechanics research in the late 80s that lead to inclusion in 1994 of a torso twisting risk factor in the “Lifting Guideline.” Much of the biomechanics research to be reviewed in this later regard focused on the role of torso muscle antagonism during lateral bending and twisting exertions.

During the 90s measurement methods and biomechanical models became available to begin to under-stand the affects on the lumbar spine of complex motions. The need for this knowledge was predicated on a growing awareness that the recommendations to keep heavy loads off the floor and close to the body when being lifted was not sufficient to prevent all occupational low back pain incidents. The growing use of mechanical aids (hoists, articulated arms and conveyors) has done a great deal to alleviate high levels of low back stress while lifting, but too often these same devices require people to twist and push and pull objects. High torso muscle antagonistic actions and vertebral shear forces were being predicted in such activities, especially when fast motions were involved. Concern also over shoulder injuries was growing related to the use of these devices, leading to the need to develop and use models of whole body exertions in industry to understand the full complexity of the problems for various groups of people.

Recently some biomechanics research began to focus on another aspect of vertebral column function that makes it vulnerable to injury, particularly during fast motions with light loads. This vulnerability is due to the column’s reliance on well coordinated torso muscle contractions to control its inherent dynamic instability. Such instability could explain why low back pain is often associated with performance of tasks when: 1) an occasional and possibly poorly planned motion takes place, 2) a sudden or unexpected motion (such as a foot slipping) takes place, or 3) when torso muscle fatigue is present.

This presentation reviews these matters and proposes that future prevention strategies will have to be much more sophisticated than is presently the case. It will propose the need for better biomechanical risk models, and will propose work cell design strategies that take advantage of newer digital human modeling CAD technologies.

HISTORY AND FUTURE OF ANTERIOR CRUCIATE LIGAMENT RECONSTRUCTION

Masahiro Kurosaka, MD
Department of Orthopaedic Surgery
Kobe University Graduate School of Medicine, Kobe, Japan

Primary repair of the anterior cruciate ligament used to be the standard treatment for the torn anterior cruciate ligament. However subsequent follow up of these patients have shown poor healing potential of the anterior cruciate ligament. Biomechanical studies have shown that the anterior cruciate ligament is the primary anterior stabilizer of the knee. Also different bundles of the anterior cruciate ligament have been shown to play different roles in different knee flexion angle against anterior and rotational load. From 1980's anterior cruciate ligament reconstruction with some type of the graft became standard treatment technique. Among the factors that influence the results of ACL reconstruction, selection of graft materials, tibial and femoral graft position placement, orientation of the drill holes, fixation and tensioning of a graft are known to be important intra-operative factors when performing ACL reconstruction surgery. Reconstructed anterior cruciate ligament grafts with an autogenous bone-patellar tendon-bone graft and a hamstrings graft have been shown to be revascularized and remodeled after the implantation and are therefore thought to be biologically suitable materials. Thus, the use of one of these graft materials has become a common procedure. The graft material, fixation technique, preconditioning, and tensioning will influence the early postoperative graft load. We have shown that interference fit type fixation provides better stability and advantageous mechanical proterties of the reconstructed graft [1].

Regarding graft positioning, the recommended placement of the tibial graft placement has changed from an eccentric anterior medial position to a more posterior anatomic position. Theoretically more anatomically placed femoral graft positioning will also provide better biomechanical function and clinical result. Currently we are trying to do two bundle ACL reconstruction through two femoral and tibial tunnels [2]. Femoral tunnels can be prepared through two tibial tunnels or far anterior medial arthroscopic portals. Femoral positioning of the posterolateral bundle should be more posterior and distal than conventional femoral drill hole placement. Damage of the posterior neurovascular bundle and breakage of the posterior wall of the drill hole can be a possible intraoperative complication. This problem can be avoided by making deeper knee flexion angle when creating a femoral drill hole. Once two bundle grafts are passed through drill holes created they can be tensioned and fixed separately. We fix a posterolateral bundle graft first in15 degree knee flexion angle and then an anteromedial bundle graft is fixed in 70 degree knee flexion angle. Advantages and disadvantages and technical pitfalls of this procedure will be discussed both in basic and clinical aspects.

1. Kurosaka M, Yoshiya S, Andrish JT: A biomechanical comparison of different surgical techniques of graft fixation in anterior cruciate reconstruction. Am J Sports Med 15:225-229, 1987.
2. Yagi M, Kuroda R, Yoshiya S, Kurosaka M: Anatomic anterior cruciate ligament reconstruction. The Japanese experience. Operative techniques in orthopaedics. 15: 116-122, 2005.

.

BONE: THE ENGINEER'S ULTIMATE DREAM MATERIAL

Rik Huiskes
Department of Biomedical Engineering, Eindhoven University of Technology, The Netherlands

After cartilaginous bone tissue mineralizes in the embryo, the tissue is modeled to bone by bone-forming osteoblasts and bone-resorbing osteoclasts. This modeling process continues during growth, producing cortical shells and trabecular patterns that seem mechanically optimized in form, density and directionality, relative to the external forces. In maturity, bone is continuously remodeled through resorption and apposition of bone tissue at free trabecular surfaces and within the cortical shells, while maintaining structural optimality relative to external loads. Later in life trabeculae reduce in number and thickness, while cortices become thinner, when musculo-skeletal activities reduce.

The evident – though implicit – question for the scientific biomechanics community is whether effects of external forces on bones can be linked to local metabolism, so that they could be made predictable in a quantitative sense. From the mid-Eighties, several empiric theories to this end were proposed and used in computational models [1,2]. It was found, in serendipity, that the recursive formulas used in these models inherently cause trabeculation [3]. We put this to use in a new theory, by separation of ‘actor’ and ‘sensor’ functions [4]. Osteocytes within the trabeculae were considered as strain-energy-density (SED) sensors, signaling Basic Multicellular Units (BMU’s) of osteoclasts and osteoblasts at trabecular surfaces to add or remove net bone mass [4].

We refined and unified the theory to include the separate activities of osteoclasts and osteoblasts in modeling & adaptation and in remodeling of trabecular structure [5,6]. We use dynamic loading variables (SED-rate) that activate osteocytes in the bone matrix to transfer osteoblast bone-formation stimuli to trabecular surfaces, through the canalicular network. The stimulus received at the surface depends on osteocyte density, mechano-sensitivity and signal decay by distance. Bone is formed at the surface where and while the stimulus exceeds a threshold value. Concurrently, osteoclasts are assumed to resorb bone which is (micro)damaged, the sites of which are determined at random per iteration. Coupling between osteoclast and osteoblast activities in remodeling is governed implicitly by the mechanics, through SED concentrations around resorption cavities, due to a notching effect. Applied in an FEA computer simulation of a bone cube, the theory produces a mature trabecular structure, aligned to the external loads [6,7], with morphological parameters similar to reality [8].

Hence, the strain-related signaling processes producing trabecular morphology in accordance with optimal mechanical resistance can now be understood. We have discovered recently that this trabecular computational theory can be unified to also describe remodeling processes in the cortical shells. These theories can now be applied for the investigation of osteoporotic processes, in search for preventive and curative agents. A complication is still that only small bone cubes can be investigated, due to limitations in computational capacities, but we expect that these limitations can be reduced with time.

REFERENCES

1. Carter, 1987, J Biomech
2. Huiskes et al., 1987, J Biomech
3. Weinans et al., 1992, J Biomech
4. Mullender & Huiskes, 1995, J Orthop Res
5. Huiskes et al., 2000, Nature 405
6. Ruimerman et al., 2001, Comp Meth in Biomech & Biomed Engr
7. Ruimerman et al., 2005, J Biomech
8. Tanck et al., 2001, Bone.

ISB XXth Congress - ASB 29th Annual Meeting
July 31 - August 5, Cleveland, Ohio

EMERGENCE OF GAIT IN LEGGED SYSTEMS

Andre Seyfarth
Locomotion Laboratory, University of Jena
email: oas@uni-jena.de, web: www.lauflabor.de

What is special about our legs such that we do use them daily without any effort? And what makes legged locomotion special compared to other types of locomotion?

One of the basic observations in human and animal locomotion is the existence of gaits, e.g. distinct movement patterns with characteristic curves of the joint kinematics and the corresponding ground reaction forces. In humans we observe just two gait patterns, walking and running, whereas in many animals a repertoire of different gaits can be found.

What are the common design and control principles of legged locomotion from which one could derive the individual gait patterns? To approach this issue, (1) we performed experiments on human locomotion, (2) we modeled the dynamics of legs in computer simulations and (3) we built a series of legged robots to explore the behavior of a physical model in a real-world environment.

In **experiments on human locomotion**, we found that during the push-off phase there was an *in-phase* relationship of knee and ankle extension in running but an *out-of-phase* relationship of knee flexion vs. ankle extension in walking. Hence, the knee joint is extending during running but bending during walking. The ankle joint, at the same time, is extending in both gaits.

In a **computer simulation model**, we found that walking could be understood as a sequence of single and double supports of a *pair of compliant legs* similar to the well-known spring-mass model (such as the pogo stick leg, figure **A**).

Gait changes from walking to running could then be considered as an energetically driven transition from a region where double support phases do occur to a second region where only single-support phases and flight phases are present (Geyer et al., this conference). However, such a simple representation of a leg seems not sufficient to explain the experimentally observed change in the coordination of the leg joints between walking and running.

This leads us to the **role of leg segmentation**. In a series of robots with segmented legs (figures **B, C, D**) we investigated the influence of leg segmentation and joint stiffness on the dynamics of locomotion. Here, the leg was actuated only at the hip joint by an electric motor introducing a sinusoidal joint kinematics.

For elastic two-segmented legs (figures **B, C**) we found forward or backward hopping depending on the hip control (frequency, leg orientation). In contrast, stable walking patterns could be observed in a bipedal robot with elastic three-segmented legs (figure **D, E**). Here, the **experimentally observed out-of-phase coordination** of knee and ankle joint was reproduced by attaching several springs to the purely passive leg. The control of the hip joint was kept identical to that of the hopping robot. Hence, elastic properties in a segmented leg could be responsible for the observed gait-specific leg kinematics.

ACKNOWLEDGEMENTS
This research is supported by the German Research Foundation (DFG) within the Emmy-Noether Program.

A
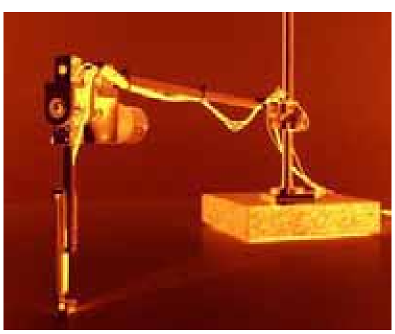
B

C

D

E
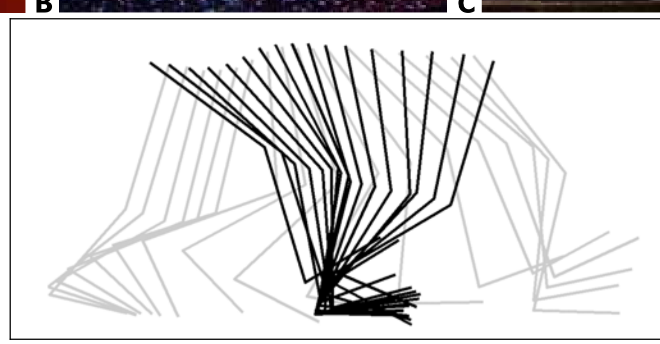

DEVELOPING TEXTILE BIOFEEDBACK TECHNOLOGY: FROM BRASSIERES TO NOISY KNEES

Julie R Steele
Biomechanics Research Laboratory, Department of Biomedical Science, University of Wollongong, NSW, Australia, 2522
email: julie_steele@uow.edu.au, web: www.uow.edu.au/health/brl

INTRODUCTION

A perpetual challenge confronting practitioners when they are evaluating and modifying human motion is to monitor the kinematics and/or kinetics characterizing human performance in the field and then to "feed" this information back to the performer in real-time so the performer can modify their motion to achieve the desired outcome. Although advances in technology have provided highly sophisticated equipment for biomechanical analyses of human performance, many of these items are unsuitable as biofeedback devices because they require extensive data processing before meaningful information can be relayed back to the performer. Other devices, particularly those attached to an individual's body, are often inappropriate as they have rigid components that do not conform to the individual's body shape, thereby interfering with their natural motion during performance of a movement and possibly posing a safety hazard.

Recent advances in polymer science, however, now enable inherently conducting polymers to be integrated into appropriate host fabrics, creating the opportunity to develop wearable sensors which offer novel biomonitoring options. These fabric sensors, with strain gauge-like properties that have a wide dynamic range, are ideal for biomonitoring applications as they can be integrated directly into existing clothing and equipment without changing the material properties or functions of these items and without interfering with normal human motion. When connected to appropriate electronic circuitry, these fabric sensors can also act as unique wearable systems capable of providing biofeedback to the wearer with respect to their joint motion. The purpose of this talk is to overview the development of these unique fabric sensors, from their initial application in monitoring breast motion to the development of an innovative fabric biofeedback system designed for use in landing training programs to reduce the rate of non-contact anterior cruciate ligament (ACL) ruptures.

WHY MONITOR BREAST MOTION?

As female breasts have limited internal anatomical support, external support, such as a sports brassiere, is usually recommended to reduce breast motion and, in turn, exercise-induced breast pain, during vigorous activity. Breast motion is restricted by compressing the breasts tightly against the chest wall and by using relatively non-elastic materials in the vertical plane. Although effective in limiting breast motion and related breast pain, the straps of most current sports bras bear much of the load generated by breast motion during physical activity. Excessive brassiere strap loading can lead to a distinct set of symptoms including deep brassiere strap furrows, malpostures and paresthesias of the fifth digit [1]. Despite potential negative consequences associated with excessive strap pressure, no research was located quantifying the loads borne by brassiere straps during physical activity. A novel method using inherently conducting polymers to directly measure dynamic brassiere strap loading during treadmill running was therefore developed and will be described.

NOISY KNEES?

Non-contact rupture of the ACL is one of the most common disabling injuries an athlete can sustain. As ACL rupture frequently results from poor landing technique, it is postulated that learning to land correctly, particularly bending the knee sufficiently, can help to protect athletes against non-contact ACL injury. The "Intelligent Knee Sleeve" (IKS) was developed, also using polymer technology, as an immediate biofeedback system to teach athletes how to land correctly. The IKS consists of a simple, inexpensive sleeve of Lycra-like material incorporating a disposable polymer coated fabric sensor that is placed over the patella. The fabric sensor, integrated into an electronic circuit, acts as a fabric strain gauge whereby as the sensor is stretched when the wearer bends their knee, resistance within the sensor decreases. At a predetermined threshold resistance, which can be varied, an audible tone is emitted to alert the wearer that the desired knee flexion angle has been achieved. The knee sleeve has the advantage over other currently available feedback devices of providing immediate individualized feedback to the wearer, thereby increasing the objectivity, frequency, and speed of feedback. How the IKS was developed and how it is used as a biofeedback system to teach safe landing technique will be described. Future applications of fabric biofeedback systems in enhancing patient rehabilitation following total knee replacement surgery will also be presented.

Figure 1: An early prototype of the Intelligent Knee Sleeve.

REFERENCES

1. Letterman G, Schurter M. *Ann Plastic Surg* 1980; 5(6): 425-431.

ACKNOWLEDGEMENTS

Thanks to the CSIRO Textile & Fibre Technology division, the NSW Sporting Injuries Committee, the Australian Football League Research Board, and the National Health & Medical Research Council Development Grant scheme for their support of this research.

NOISE-ENHANCED SENSORIMOTOR FUNCTION

J.J. Collins
Department of Biomedical Engineering and Center for BioDynamics, Boston University;
email: jcollins@bu.edu, web: www.bu.edu/abl

INTRODUCTION

Traditionally, noise has been viewed as a detriment to signal detection and information transmission. Recently, however, it has been shown that noise can enhance the detection and transmission of weak signals in certain nonlinear systems, via a mechanism known as stochastic resonance (SR). In this talk, we describe studies wherein we demonstrate SR-type behavior in model neurons, rat cutaneous afferents, and human sensory and motor function. We show that input noise (mechanical and electrical) can enhance somatosensation in young subjects, older adults, and patients with sensory deficits. We also demonstrate that the application of sub-sensory mechanical noise to the soles of the feet via vibrating insoles improves balance control in healthy young subjects, older adults, patients with diabetic neuropathy, and patients with stroke. We discuss how noise-based techniques and devices might prove useful in overcoming age- and disease-related losses in sensorimotor function.

REFERENCES

1. Collins JJ, et al. *Nature* **376**, 236-238, 1995.
2. Collins JJ, et al. *Physical Review E* **52**, R3321-R3324, 1995.
3. Collins JJ, et al. *Journal of Neurophysiology* **76**, 642-645, 1996.
4. Cordo P, et al. *Nature* **383**, 769-770, 1996.
5. Collins JJ, et al. *Nature* **383**, 770, 1996.
6. Richardson KA, et al. *CHAOS* **8**, 599-603, 1998.
7. Liu W, et al. *Archives of Physical Medicine and Rehabilitation* **83**, 171-176, 2002.
8. Dhruv NT, et al. *Neuroreport* **13**, 597-600, 2002.
9. Gravelle DC, et al. *Neuroreport*, **13**, 1853-1856, 2002.
10. Priplata A, et al. *Physical Review Letters* **89**, 238101, 2002.
11. Priplata AA, et al. *The Lancet* **362**, 1123-1124, 2003.
12. Collins JJ, et al. *IEEE Engineering in Medicine and Biology Magazine* **22(2)**, 76-83, 2003.
13. Harry JD, et al. *IEEE Spectrum*, **April**, 36-41, 2005.

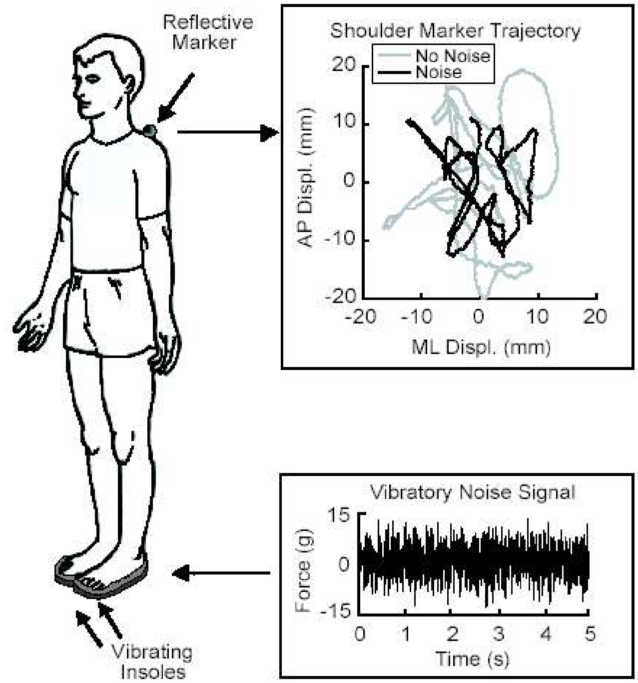

FIGURE**:** Enhancing balance control with mechanical input noise. Shown is the experimental setup with sample input noise and sample shoulder-marker stabilograms comparing the control and noise conditions.

ACKNOWLEDGEMENTS

This work was supported by the NIH and NSF.

SPINNING SPORTS BALLS

Mont Hubbard
Department of Mechanical and Aeronautical Engineering
University of California, Davis, USA
email: mhubbard@ucdavis.edu , web: mae.ucdavis.edu/~biosport

INTRODUCTION

Ball spin significantly affects how sports balls move. The production of spin, its evolution during impact and flight and its effects on the ball paths are discussed for two popular American ball sports; baseball and basketball. In baseball, the spin in flight is important because it generates substantial lift forces. These can add substantial range to that achievable with no spin and cause large lateral deviations of the path from the vertical plane. As a result a curve ball can be hit farther than a fastball, even though its pitched and batted speeds are less than those of the fastball. Furthermore, the effect of spin has implications on how different pitches should be batted optimally. In basketball free throws, aerodynamic forces are small compared to spin-generated friction contact forces that dominate. This talk examines the mechanics of spin generation and its effects on the two games.

METHODS

Improved models for the pitch, batting impact, and post-impact flight phases of a baseball can be used in an optimal control context to find bat swing conditions that produce maximum range [1]. An improved batted flight model incorporates experimental aerodynamic lift and drag force profiles (including the drag crisis) and their dependence on spin and velocity. The rigid-body model for bat-ball impact includes the dependence of the coefficient of restitution on the approach relative velocity and the dependence of the incoming pitched ball angle on speed. Undercut distance and bat swing angle are chosen to maximize range of the batted ball. Post-impact conditions are found to be independent of the ball-bat coefficient of friction. The lift force is enhanced by spin produced by undercutting the ball during batting. Contrary to popular opinion, an optimally hit curve ball will travel farther than an optimally hit fastball or knuckleball as a result of increased lift during flight. Because the curve ball has pitched topspin, less undercut is required to produce optimal batted backspin, and smaller batted ball speed and launch angle penalties must be incurred to generate backspin than when hitting a fastball optimally. Changing spin during flight is likely not important since the characteristic spin decay time is of the order of 30 s [1]. The sensitivity of maximum range can be calculated for all model parameters including bat and ball speed, bat and ball spin, and wind speed.

In contrast, the flight of a basketball is much less affected by aerodynamics but spin is important during rim and backboard contact. Friction forces caused by spin-induced relative motion of the ball contact point are important and largely determine the ball path. A dynamic model [2] is discussed for basketball motion that may contact the rim, the backboard, the bridge between the rim and board, and possibly the board and the bridge simultaneously. The model is used to investigate free throw success near the sagittal plane. Non-linear ordinary differential equations describe the ball angular velocity and ball center position. The model includes radial ball compliance and damping and contains sub-models describing slipping and non-slipping contact and purely gravitational flight. Switching between the sub-models depends on contact point velocity and friction forces. Interesting limiting dissipation-free families of trajectories allow the ball to enter and pass below the rim plane before being ejected rather than being captured. These rely importantly on continuously changing spin and precession of the consequent angular momentum by the contact forces. The dynamic models of basketball-rim and basketball-backboard interaction allow simulations for a single point ball-rim or ball-board contact, as well as the possibility of two-point contact on both board and bridge. The model can be used to study release angles, velocity, and angular velocity that maximize the probability of success. In basketball free throws in which contact forces dominate, backspin can scrub more energy from the ball in shots that hit the rim and can aid in capture, increasing the number of successful shots by about 10%, all other conditions held constant.

Generation of appropriate spin by the athlete during impact (baseball) or launch (basketball) relies on contact forces normal [3] and tangent [4] to the ball surface. Simple rigid-body models of the ball may not accurately predict post-impact spin. Although large normal compliance is obvious in high-speed images of batted balls, models including tangential compliance of the ball surface lead to two-degree-of freedom oscillations and predict significantly different post-impact spin and translational velocity than do models assuming rigid-body ball motion. Experimental measurements of baseball and basketball contact forces [5] show the possible influence of tangential compliance. Present research efforts search for the least complex model of the 1 ms baseball-bat and 11 ms basketball-rim impacts that can adequately describe these processes.

CONCLUSIONS

Accurate description of the paths of sports balls must rely on a complete understanding of the aerodynamic and contact forces caused by the interaction of the spinning ball with its environment.

REFERENCES

1. Sawicki GS, et al., *Am. J. Physics*, **71**(10), 1152-1162, 2003.
2. Okubo H & M Hubbard, *Sports Engrg.* **7**(1), 15-30, 2004.
3. Hubbard M & WJ Stronge, *Sports Engrg.* **4**(1), 49-61, 2001.
4. Stronge WJ, *Impact Mechanics*, C U Press, UK, 2000.
5. Cross R, *Am. J. Physics*, **70**, 1093-1102, 2002.

The Evolving Journey of Tendon and Joint Mechanics - Clinical Impacts from Humble Concepts

K. N. An, Ph.D.
Biomechanics Laboratory, Division of Orthopedic Research
Mayo Clinic College of Medicine, Rochester, MN 55905 – E-mail: an@mayo.edu

As integral components of the musculoskeletal system, the primary function of tendons is transmission of muscle forces to the skeletal system. Proper excursion and gliding of the tendon will determine the efficiency of this function. Studies of the tendon and joint mechanics based on two simple mechanical concepts have resulted in several significant clinical implications.

EXCURSION

A pulley-type constraint keeps the tendon path close to the bone when the tendon crosses a joint. In normal anatomy, there is an intimate relationship between tendon excursion and joint rotation that maintains the mechanical advantage of the tendon while preserving the passive and active muscle tension during joint motion. The instantaneous moment arm (r) of a tendon can be related to the tendon excursion (E) and the joint rotation (φ) as:

$$r = d E / d \varphi.$$

This simple concept has been confirmed analytically for various scenarios of tendons crossing the joint [1]. Experimentally, the tendon excursion has been measured using linear or rotary potentiometers *in vitro* or ultrasound imaging *in vivo*. Joint rotations have been monitored using goniometers, magnetic tracking devices, and imaging systems. The moment arm-tendon excursion principle has been used to examine the importance of the pulley constraint and also to compare various surgical reconstructive procedures and the options for tendon transfer and tendon reattachment [2]. For joints with additional degrees of freedom or when the tendon crosses multiple joints, muscle recruitment depends on the resultant moment at the joint [3] or all of the joints that the muscle spans. For the postoperative treatment of flexor tendon injury, it has been demonstrated that synergistic wrist motion could eliminate tendon slackness in the palm and improve tendon excursion during passive finger joint motion [4]. This concept explained why the mechanism of co-contraction of quadriceps and hamstrings at the knee joint during closed-kinetic-chain exercises resulted in favorable tension in the anterior cruciate ligament after reconstruction [5]. Finally, tendon excursion influences the functional length of the muscle-tendon unit. Due to the length-tension interaction during muscle contraction, the potential tension generated by the muscle will be influenced by the joint position and tendon excursion.

GLIDING

A tendon sliding through the pulley is analogous to a belt wrapped around a fixed mechanical pulley [6]. As the tendon moves proximally, the tensions in the tendon proximal and distal to the pulley (F_p and F_d) are related to the angle (θ) of the tendon segments across the pulley and the friction coefficient (μ):

$$F_p = F_d \, e^{\theta \mu}.$$

Based on this simple model, a system was developed that allows direct measurement of friction at the tendon-pulley interface as the difference between F_p and F_d. This relationship clearly demonstrated the importance of avoiding awkward joint postures in ergonomic consideration to reduce the repetitive injury of soft tissue. In-depth investigations of the mechanism of lubrication [7] associated with the tendon gliding provided insight related to the potential etiology of soft tissue disorders including carpal tunnel syndrome and tendonitis. Clinically, significant improvements have been made in the surgical and rehabilitation modalities for treating tendon injuries [8, 9].

REFERENCES

1. An, K.N., et al. *J Biomech*, 16:419-425, 1983.
2. Liu, J., et al. *J Bone Joint Surg*, 80A:853-860, 1998.
3. Horii, E., et al. *J Hand Surg*, 17A:559-566, 1992.
4. Su, F-C., et al. *Clin Biomech*, 20:491-497, 2005.
5. Lutz, G.E., et al. *J Bone Joint Surg*, 75A:732-739, 1993.
6. An, K.N., et al. *Biomed Sci Instr*, 29:1-7, 1993.
7. Uchiyama, S., et al. *J Orthop Res*, 13:83-89, 1995.
8. Sun, Y.L., et al. *J Orthop Res*, 22:984-989, 2004.
9. Zhao, C., et al. *J Biomech*, 36:295-299, 2003.

ACKNOWLEDGEMENTS

The contributions from colleagues, fellows and students, as well as the financial support from the NIH for various aspects of the investigations are greatly appreciated.

REHABILITATION AND BIOMECHANICS (DO THE LOCOMOTION)

Mary M. Rodgers
Department of Physical Therapy and Rehabilitation Science, University of Maryland School of Medicine
Baltimore, MD; email: MRodgers@UMaryland.edu. web: www.ptmaryland.edu

Rehabilitation is defined by the Institute of Medicine as the restoration of "some or all of the patient's physical, sensory, and mental capabilities that were lost due to injury, illness, or disease." Rehabilitation includes assisting the patient to compensate for deficits that cannot be reversed medically. It is prescribed after many types of injury, illness, or disease, including amputations, arthritis, cancer, cardiac disease, neurological problems, orthopedic injuries, spinal cord injuries, stroke, and traumatic brain injuries. It has been estimated that as many as 14% of all Americans may be disabled in some way at any given time, and that nearly 1.5 million Americans have a disability that requires use of a manual wheelchair [1].

The achievement of functional independence for individuals with disability is a primary goal in rehabilitation. Because independent locomotion is essential to independent function, rehabilitation interventions are usually directed toward this goal for those individuals who desire independent function and for whom that goal is feasible.

Studies in rehabilitation science research have incorporated combinations of variables that are not likely to be studied in separate existing basic science, health professional or engineering disciplines. Models of disability have provided a framework for examining how rehabilitation research studies address the enabling-disabling continuum [2]. Within this framework, biomechanical measures and analyses play an important role in quantifying disability related performance and factors affecting the enabling-disabling process.

This is illustrated, for example, by selected studies of walking gait and wheelchair propulsion. I will discuss how biomechanical performance measures have contributed to an understanding of disability and how rehabilitation interventions can be more individualized and effective.

CONCLUSIONS

Future work that incorporates biomechanical performance measures in the framework of "enablement" would ensure that all of those who desire to do so would be able to independently "do the locomotion" [3].

REFERENCES

1. Kaye, H.S. et al, NIDRR Mobility Device Use in the US, 2000
2. Enabling America: Assessing the Role of Rehabilitation Science and Engineering (Brandt & Pope, Eds., National Academy Press, 1997)
3. Little Eva circa 1962

ACKNOWLEDGEMENT

NIH P50 AG12583 and Veterans Affairs Rehabilitation Research & Development Service Merit Review Board Project #B2168RA.

IMPLEMENTING DATA-DRIVEN MODELS OF THE HUMAN THUMB INTO A ROBOTIC GRASP SIMULATOR TO PREDICT GRASP STABILITY

[1] Veronica J. Santos, [2] Andrew Miller, [2] Peter Allen, and [1,3] Francisco J. Valero-Cuevas
[1] Neuromuscular Biomechanics Laboratory, Cornell University, NY, USA,
[2] Department of Computer Science, Columbia University, NY, USA, [3] The Hospital for Special Surgery, NY, USA
email: fv24@cornell.edu; web: www.mae.cornell.edu/nmbl, www.cs.columbia.edu/~amiller/graspit

INTRODUCTION

What are the features of the human hand that enable dexterous manipulation functionality that transcends that of state-of-the-art robotic hands? Understanding and emulating the biologically evolved solutions to the manipulation problem in humans would empower both biomechanists and roboticists alike. In this interdisciplinary work, we present the computational foundations to simulate and predict the functional advantages of multi-finger grasps with a biomechanically realistic model of the human hand.

METHODS

We translated the anatomical description of the "virtual five-link" thumb kinematics into a standard robotics notation (Denavit-Hartenberg (D-H)) using 3D geometry and D-H conventions [1]. We added musculoskeletal parameters (e.g., moment arms) to the kinematics, resulting in a 50-parameter robotics-based model capable of producing thumbtip forces and torques. We then used Markov Chain Monte Carlo simulations to find parameters that achieved a least squares best fit to experimental thumbtip forces [2].

As a first approximation, we implemented these best fit D-H parameters for the thumb in *GraspIt*! [3], our visualization and simulation engine designed for the study of grasp planning in robotic hands. The other fingers were simulated using universal joints at the metacarpophalangeal joints, and simple hinges at the interphalangeal joints [4]. With this program, grasps of arbitrary objects can be dynamically simulated, optimized for grasp stability, and objectively quantified for feasibility and grasp quality.

To quantify grasp quality, we use a robotics-based mathematical representation of grasp that employs a "grasp matrix" to relate fingertip contact forces (and torques if using soft fingertips) to the effective force and torque on the grasped object (the grasp "wrench"). The rank of the grasp matrix, for given object geometry and friction characteristics, is affected by fingertip placement and the margin of error permitted by the friction cones associated with each fingertip contact force, and is a measure of how many degrees of freedom of the object can be controlled [5]. We evaluate the ability of a quasi-static grasp to reject disturbances by building the 6D space of forces and torques that can be applied by the grasp using convex hull theory. We propose the hyper-volume of this space as one possible measure of grasp quality, since a larger volume of this space means that the grasp is more efficient at rejecting force and torque perturbations [3].

RESULTS AND DISCUSSION

The D-H representation of the anatomy-based, non-intersecting, non-orthogonal axes of rotation for the thumb provides a new biomimetic direction for comparative kinematic studies of robotic and human hands, and may help elucidate whether and how these kinematic features enable dexterous manipulation in humans (Fig. 1). Traditionally, simple orthogonal axes of rotation are used to model thumb kinematics in robotic hands, but our work suggests these articulations cannot realistically predict 3D static thumbtip forces [6].

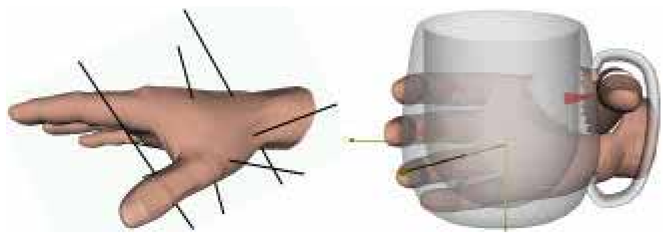

Figure 1: Left: The anatomy-based model represents more faithfully the thumb's five non-orthogonal, non-intersecting joint axes. Right: The hand model grasps a mug.

We have adapted a computational environment to quantify grasp quality of biomimetic human hands. Our critical challenge now is to determine the level of model complexity that is necessary and sufficient for predicting realistic multi-finger manipulation function. We are currently investigating adaptive refinement finite element methods to account for finger pad compliance and skin deformation, tendon interconnections within and across fingers, and will use accurate skeletal geometry to constrain the innermost elements. This computational platform will allow us to investigate the relative contributions of passive anatomical elements and active neuromuscular elements to dexterous manipulation.

REFERENCES

1. Santos VJ, Valero-Cuevas FJ. *Trans Biomed Eng*, in review.
2. Santos VJ, Valero-Cuevas FJ. *Proceedings of IEEE EMBS*, San Francisco, CA, Session 11.8.1, 2004.
3. Miller A, et al. *Ind Robot* **32**, in press.
4. Valero-Cuevas FJ, et al. *J Biomech* **31**, 693-703, 1998.
5. Murray RM, et al. *A Mathematical Introduction to Robotic Manipulation*, CRC Press, Boca Raton, FL.
6. Valero-Cuevas FJ, et al. *J Biomech* **36**, 1019-1030, 2003.

ACKNOWLEDGEMENTS

This material is based upon work supported under grants from the National Science Foundation (NSF) ITR-0312271 (to FVC and PA), GRF (to VJS), and CAREER BES-0237258 (to FVC), and Grants RG-00-0397 from the Whitaker Foundation and R01-050520 from NIH (to FVC).

ALTERED FOOT LOADING IN DIABETICS. THE ROLE OF ACHILLES TENDON AND PLANTAR FASCIA.

[1] Claudia Giacomozzi, [2]Emanuela D'Ambrogi [2]Luigi Uccioli, [1] Velio Macellari
[1]Dept. Technology and Health, Istituto Superiore di Sanità, Rome, Italy,
[2]Dept. Internal Med., Tor Vergata University, Rome, Italy; email: c_giacomozzi@yahoo.com

INTRODUCTION

The diabetic foot often undergoes abnormal plantar pressures, changing in walking strategy, ulcerative processes. Neuropathy was frequently added as the main responsible for the alteration of foot loading pattern [1]. A different approach comes from the observation that the common sign of the distinct diabetic syndromes, hyperglycaemia, promotes glycosilation of proteins and the consequent accumulation of advanced end-products in most human tissues [2]. This means that muscles, cartilages, tendons, ligaments, all might experience structural changes even before the onset of diabetic neuropathy, and might then concur to alter the gait pattern.

The present study focuses on the effects that diabetes-induced alterations of Achilles tendon, plantar fascia and 1st metatarso-phalangeal joint – both anatomical and functional - may have on foot loading.

METHODS

Sixty-one diabetic patients (27 without neuropathy, 19 with neuropathy, 15 with previous neuropathic ulcers), and 21 healthy volunteers were recruited. Thickness of Achilles tendon and plantar fascia was measured by ultrasound [3]. Flexion-extension of the 1st metatarso-phalangeal joint was measured passively by a long-arm mechanical goniometer [3]. Main biomechanic parameters of foot-floor interaction during gait were acquired by means of an integrated force/pressure device [3]. Among them, only vertical ground reaction (expressed as a percentage of body weight (b.w.)), force/time integral and relative loading time (expressed as a percentage of the whole stance phase) under the metatarsals were included in the present study. Piecewise linear regressions were applied to relate all the above measurements.

RESULTS AND DISCUSSION

Plantar fascia and Achilles tendon were significantly thicker in diabetics with neuropathy than in controls, while flexion-extension of the 1st metatarso-phalangeal joint was significantly smaller. Load under the metatarsal heads significantly increased in diabetics with neuropathy in terms of both amplitude and duration, as proved by vertical forces and integrals data. Mean values and standard deviations of all the above parameters are reported in Table 1. The increase in the vertical force under the metatarsals strongly related ($R=0.83$, explained variance = 70.1%) with the changes in the three examined structural and functional parameters.

Thickening of plantar fascia and Achilles tendon in diabetics, more evident in the presence of neuropathy, concurs to develop a rigid foot, which poorly performs the physiological impact force absorption during landing. More generally, an overall alteration of the foot-ankle complex motion likely occurs throughout the whole gait cycle, which partly explains the abnormal loading under the forefoot.

CONCLUSIONS

Even though neuropathy is still considered as the major responsible for the ulceration of the diabetic foot, we believe that several other factors should be investigated and monitored, in the attempt of preventing the formation of such severe wounds.

In the present study we observed structural alterations of the main tendinous and ligamentous structures of the foot-ankle complex in presence of mild-to-severe diabetic neuropathy. Range of motion of the 1st metatarso-phalangeal joint in the sagittal plane was also measured under passive conditions. Most important finding was that the thicker the Achilles tendon and plantar fascia become, and the more the 1st metatarso-phalangeal joint mobility is reduced, the more severe is the overall alteration of the foot loading during gait. More specifically, concurrent changes of the above factors accounted for 70.1% of the changes in metatarsals loading for all diabetics groups, with and without neuropathy. In presence of severe neuropathy only, the explained variance attained a value of 74.4%.

We do not claim the hereby measured alterations as the only factors which are responsible for the triggering of the neuropathic ulceration process. Further studies are needed to merge the contributions of the numerous structural and functional alterations of the diabetic foot, which concurrently take the forefoot plantar soft tissue under conditions of "potential damage" [4].

REFERENCES

1. Kwon OY, Mueller MJ, 2001. *Phys. Ther.* **81**, 828-35, 2001.
2. Barbagallo M, et al.. *Int. Angiol.* **12**, 365-70, 1993.
3. D'Ambrogi E, et al.. *Diabetes Care*, **26**(5):1525-9, 2003.
4. Mueller MJ, Maluf KS. *Phys. Ther.* **82**, 383-403, 2002.

Table 1: Mean values and standard deviations of the measured parameters for Healthy Volunteers (HV), Diabetics without neuropathy (D), Diabetics with Neuropathy (DN), Diabetics with Previous Neuropathic Ulcers (DPNU). Statistically significant differences (*P<0.05) were assessed by means of one-way ANOVA and Bonferroni *post hoc* test.

	Achilles tendon thickness (mm)	Plantar fascia thickness (mm)	1st met-phal joint flexion-extension (°)	Metatarsals vertical forces (% b.w.)	Metatarsals integrals (%b.w.*ms)	Metatarsals loading time (%stance)
HV	4.0 ± 0.5	2.0 ± 0.5	100.0 ± 10.0	89.9 ± 6.3	2956.8 ± 430.5	88.2 ± 4.0
D	4.6 ± 1.0	2.9 ± 1.2	54.0 ± 29.4	93.9 ± 6.7	3209.7 ± 493.3	90.1 ± 4.7
DN	4.9 ± 1.7*	3.0 ± 0.8*	54.9 ± 17.2*	96.0 ± 7.0*	3625.2 ± 695.3*	91.7 ± 6.6
DPNU	5.2 ± 1.7*	3.1 ± 1.0*	46.8 ± 20.7*	97.5 ± 7.0*	3722.1 ± 743.2*	93.0 ± 6.3*

EFFECTS OF LOW BAR AVOIDANCE AND GYMNAST SIZE ON HIGH BAR DISMOUNT PERFORMANCE

Alison Sheets, Mont Hubbard
University of California, Davis, USA
email: alsheets@ucdavis.edu , web: www.ucdavis.edu/biosport

INTRODUCTION

Required maneuver difficulty on the uneven parallel bars has increased with the maximum allowed bar spacing. Computer modeling, simulation and optimization are used to quantify the low bar's detrimental effect on the maximal number of dismount revolutions a short and a tall gymnast can complete. Two optimal low bar avoidance strategies were calculated; 1) using only planar shoulder and hip movement (2D), and 2) using planar shoulder but three dimensional hip motion (3D).

METHODS

A four-segment dynamic model of a female gymnast in a preparatory swing is optimized to maximize dismount revolutions at a specified landing height. The purpose is to quantify the low bar's effect on dismount performance and to calculate optimal joint motions for low bar avoidance resulting in minimum dismount performance decreases. Optimization constraints include maximal bar force, joint ranges of motion, and minimum landing distance. Joint torque models include angle, angular velocity, and isometric strength dependent factors. Torque activation time histories are approximated by cubic splines fit to ten nodes equally spaced throughout bar contact. Using the downhill simplex method, optimal joint torque activations and bar release time are calculated [1].

The optimal solution begins (t = 0) with the gymnast in a handstand rotating about the deflected bar with an initial angular velocity of 1.8 rad/s [2]. It ends at bar release (T), and results in maximal straight body revolutions during dismount:

$$J_o = (\omega(T)\Delta t + \gamma(T))/(2\pi) \qquad (1)$$

where $\omega(T)$ is the gymnast release angular velocity, Δt is the flight time and $\gamma(T)$ is the angle between the line from the deflected bar center to the gymnast mass center and vertical. Using the optimization criterion in eqn. (1) and constraints, three performances are calculated for two collegiate gymnasts: short=1.887m, 62.38 kg; tall=2.048 m, 69.30 kg.

RESULTS AND DISCUSSION

Both athletes completed the most revolutions when no low bar was present (Table 1). Avoiding the low bar and restricting motion to 2D decreased dismount performance 1.22% and 3.59% for the short and tall gymnasts, respectively (Fig.1). By straddling her legs, the performance decrease is reduced to 0.45% and 2.00%, respectively. The taller athlete with 2D motion was most affected by the low bar because her optimal swing was most altered to avoid low bar contact.

Table 1: Number of dismount flight revolutions

	No Low Bar	Low Bar	
		2D motion	3D motion
Short	1.556	1.537	1.549
Tall	1.503	1.449	1.473

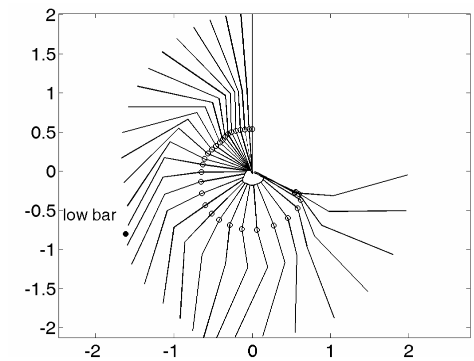

Figure 1: Stick figure sequence- tall 2D case

Absence of the low bar allowed more revolutions because joint torques applied during the swing added more energy to the system (Fig. 2). Avoiding the low bar required substantial negative work to resist hip joint extension after low bar clearance (Fig. 1), and decreased terminal system energy.

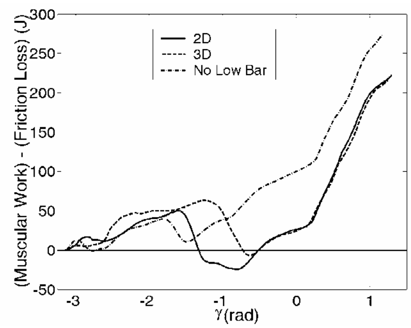

Figure 2: Net energy change during swing- tall gymnast

All performances were limited by the ability to maintain bar contact. Because the gymnast mass center cannot move instantaneously, fast joint angle flexion compresses the bar and exerts larger hand forces. Thus bar force constraints limit both joint angles and rates and, indirectly, ability to do muscular work.

In all cases, short athletes release with lower mass centers than tall ones. Short athletes minimize bar contact time because a larger percentage of initial energy is dissipated by bar friction (short-17%, tall-15%) reducing dismount performance capabilities. Frictional energy dissipation was relatively constant regardless of low bar presence. The short and tall athletes have largest release angles in the 2D case. Because of the time needed for joint extension after low bar avoidance, release is delayed to allow muscular work to be performed during bar contact.

REFERENCES

1. Nelder, JA & Mead, R. *Comp J*, 7, 308-313, 1965.
2. Hiley, MJ & Yeadon, MR. *J Appl Biomech*, 19(2), 119-130.

HIGH-SPEED COUPLING CHARACTERISTICS OF THE FOOT AND SHANK DURING THE STANCE PHASE OF RUNNING

[1] Caroline J Digby, [2]Mark J Lake and [2]Adrian Lees
[1]Dept. of Sport Science, Tourism and Leisure, Canterbury Christ Church University College, Canterbury, UK, c.digby@canterbury.ac.uk,
[2]Research Institute for Sport and Exercise Sciences, Liverpool John Moores University, Liverpool, UK;

INTRODUCTION

Motions of the foot and tibia during locomotion, or their kinematic coupling, have been highlighted as a factor that may be important in the aetiology of lower limb injury [1]. Particularly, transference of excessive eversion motion of the rearfoot to internal rotation of the tibia through the subtalar joint has been linked to overuse injuries of the knee [2,3,4]. The relative timing of motions of the foot and shank during locomotion may also be an additional factor in injury predisposition [3]. Coupling of the foot and shank has been examined by the ratio of the range of angular motion of these adjacent segments [3], although [2] indicated that differences in the rates of rotation between the two adjoining segments might be a better indication. Continuous relative phase angles have also been used [5], although many of these studies have involved low subject numbers [6]. Rotations about the longitudinal axis of the shank have been difficult to quantify accurately, primarily due to motion of skin-mounted markers relative to the underlying bone [7]. Recently, a lightweight, custom-moulded plate contoured to the shape of each subject's tibia has been used to minimise this error and allow higher frequency aspects of the motion to be captured during locomotion [8]. The aim of this study was to assess movement coupling between the rearfoot and shank during the stance phase of barefoot running, utilising high-speed kinematic analysis and an evaluation of the relative movement rates, ranges of motion and timing of peak velocities. It was hypothesised that timing and magnitudes of angular velocities of rearfoot eversion and tibial internal rotation would be influenced by the inclusion of high frequency components in the displacement data, with velocities being greater than previously recorded [8,9].

METHODS

Twenty-five healthy male subjects (mean age 26 ± 5.2 years, height 1.78 ±0.05 m and mass of 80.5 ±9.6 kg) ran barefoot (3.35 m.s^{-1}) along a runway whilst the landing kinematics of the right foot and shank on a large Kistler force platform were recorded by 8 ProReflex (Qualisys, Sweden) cameras at 1000 Hz. At least 15 dynamic running trials were collected per subject. An individually moulded plate was used to track rapid movements of the tibia [8] and foot movements were monitored using a multi-segment foot model so that eversion/inversion movements of the calcaneus segment with respect to the tibia could be calculated. Data was filtered using a standard low-pass Butterworth digital filter (cut-off freq. 40 Hz). Movement coupling was assessed by means of a coupling ratio of calcaneal eversion (EV) to tibial internal rotation (TIR) range of motion (ROM), and by determining the ratio and timing of peak angular velocity of the calcaneus and tibia.

RESULTS AND DISCUSSION

The range and velocity of EV motion of the rearfoot tended to be larger compared to the tibia, producing coupling ratios greater than 1.0 (Table 1). The ROMs and ROM coupling ratio values were similar to that found in the literature [3,4,10]. Peak ang. velocity of the tibia was more than double that previously reported [2,10], which can be explained by the maintenance of high frequency movement transients in the displacement data due to the high sample rate and marker attachment procedure used in this investigation [8]. TIR peak ang. velocities displayed greater differences to the literature than EV peak ang. velocities (4.6 times v 3.77 times greater) [10], suggesting that if a velocity ratio had been performed in that study they would have been different to that presented here. For 14 subjects (56%), peak internal rotation velocity of the tibia occurred before peak eversion velocity of the calcaneus, suggesting proximal motion control [2]. ROM ratio was significantly correlated to TIR ROM (-0.689 p=0.000), but not EV ROM (-0.026, p=0.901) suggesting TIR excursions have more influence on this ratio despite being smaller in magnitude than EV excursions [6]. This highlights the importance of reducing marker displacement error during capture of tibial rotation data.

During the impact phase, when motions of the lower limb segments combine to transmit force and attenuate shock, the relative velocity of adjacent segments and the timing of velocity changes may be more important than excursion differences for the identification of factors associated with overuse injury. At lower sample frequencies, peak ang. velocity is underestimated to varying degrees for each segment, increasing the likelihood of a misinterpretation of the velocity coupling. The present investigation will be expanded to evaluate the influence of different foot types (static and dynamic) on the high frequency coupling parameters reported here.

REFERENCES

1. Stacoff A, et al. *Clin Biomech* **15**, 54-64, 2000a.
2. Bellchamber TL, et al. *J Biomech* **33**, 1397-1403, 2000.
3. McClay I, & Manal K. *J App Biom* **13**, 109-124, 1997.
4. Nigg BM, et al. *J Biomech* **26**, 909-916, 1993.
5. Hamill J, et al. *Clin Biomech* **14**, 297-308, 1999.
6. DeLeo A, et al. *Clin Biom*, **19**, 983-991, 2004.
7. Manal K, & McClay I. *Gait & Posture* **11**, 38-45, 2000.
8. Digby CJ, et al., *Ergonomics*, in press.
9. Digby CJ, et al., *Int J Pod Biom* **1**(2), 37-38, 2003.
10. Stacoff A, et al. *J Biomech* **33**, 1387-1395, 2000b.

Table 1: Coupling parameters (group means ± SD) for barefoot running.

	Calcaneal Eversion EV	Tibial Internal Rot. TIR	Coupling Parameters	
Range of Motion (deg)	10.24 ± 2.37	7.19 ± 3.1	Ratio (EV/TIR)	1.66 ± 0.62
Peak Ang. Vel. (rad.s^{-1})	-7.70 ± 2.61	-6.95 ± 2.24	Ratio (EVpeak/TIRpeak)	1.25 ± 0.55
Time to Peak Ang. Vel. (ms)	17.16 ± 11.71	14.06 ± 7.41	TIR-EV peak time	-3.09 ± 13.76

A PRELIMINARY ASSESSMENT OF THE EFFECTS OF FOOT TYPE ON THE MOVEMENT COUPLING OF THE FOOT AND SHANK DURING THE STANCE PHASE OF BAREFOOT RUNNING

[1]Caroline J Digby*, [2]Mark J Lake, and [2]Adrian Lees
[1]Dept. of Sport Science, Tourism and Leisure, Canterbury Christ Church University College, Canterbury, UK, c.digby@canterbury.ac.uk
[2]Research Institute for Sport and Exercise Sciences, Liverpool John Moores University, Liverpool, UK;

INTRODUCTION

Kinematic coupling of the foot and shank has been highlighted as a potential factor in lower limb overuse injury aetiology, particularly if excessive eversion motion of the rearfoot is transferred to rotation of the tibia [1,2]. It has been speculated that the height of the medial longitudinal arch of the foot may play a role in the amount of movement transfer present [2,3,4] and so researchers have attempted to classify foot type [5,6,7] in an attempt to understand the effects of foot structure on dynamic foot function. Recently, a foot posture index (FPI) was devised based on a number of observational tests during normal static stance to classify feet [8]. However, it has been suggested that traditional static measurements appear not to predict dynamic function accurately [7,9,10]. The aim of this study was to examine a number of simple static parameters of foot arch structure at three different loading conditions, and several dynamic measures of foot type obtained during barefoot running to characterise foot type, and examine the relationship to movement coupling of the foot and shank during running.

METHODS

Using callipers and a ruler, repeated anthropometic measurements were recorded on the right foot of 27 healthy male subjects in static non weight bearing (NWB), normal partial weight bearing (PWB) and full weight bearing (FWB). They included truncated foot length (TFL), dorsum height (DH), and soft tissue arch height (AH). Retro-reflective markers were glued to anatomical landmarks on the foot (medial calcaneus (MED_CALC), medial aspect of the navicular tubercle (NAV_TUB), and medial aspect of the first metatarsal head (MTH1)) and tibia. At each weight-bearing condition, the Arch Ratio (AR) was calculated by DH/TFL [6]. Static relative arch deformation (SRAD) was calculated based on NWB and FWB measurements of soft tissue arch height [11]. Dynamically, min. vertical height of the NAV_TUB marker during stance and average height at NWB stance were used. A further method of classification, Arch Deformation Ratio (ADR), was developed by combining SRAD and AR [12]. From marker position data average vertical height of the NAV_TUB marker (NTMH), average Infra-Navicular Angle (INA) and navicular height (NH) [13] were calculated.

The subjects ran barefoot ($3.35 ms^{-1}$) whilst the landing kinematics of the right foot and shank were recorded by 8 ProReflex cameras (Qualisys, Sweden) at 1000Hz. An individually moulded plate was used to track rapid movements of the tibia [14], and foot pressure data was collected at 500Hz (RSscan Ltd., Belgium). For running trials, min. NTMH and NH, and max. INA during the stance phase were calculated (indicating the arch is at its flattest), along with the total deformation of the arch, and velocity of the deformation. Dynamic RAD (DRAD), Dynamic Arch Ratio (DAR) and Dynamic Arch Deformation Ratio (DADR) were calculated. A Dynamic Arch Index (DAI) (% midfoot contact) was obtained from the pressure data. Ratios of the range of motion (ROM Ratio), peak angular velocity (VEL Ratio) and time to peak velocity (TIME Ratio) for rearfoot eversion and tibial internal rotation were used to characterise movement coupling. Pearson's correlations were used to identify any significant relationships.

RESULTS AND DISCUSSION

There was no significant correlation between ROM Ratio and VEL ratio with any of the static or dynamic parameters. The DAI obtained from the pressure mat was negatively correlated with AH at all loading conditions (NWB = -0.576, p=0.002; PWB = -0.546, p=0.004; FWB = -0.563, p=0.003). SRAD was not correlated at any loading condition to any AH or AR measure or to DRAD. Equally, DRAD was not correlated to DAR. In general, the static measures were not strongly correlated to any of the dynamic parameters, with the exceptions of INA at PWB was strongly correlated to max INA (0.952, p=0.012) and min NH (-0.948, p=0.014), NH at PWB was strongly correlated to DAR (0.889, p=0.044), and NTMH at PWB was strongly correlated to DAR (0.895, p=0.040), and min NTMH (0.944, p=0.016).

Traditional static measurements do not predict dynamic function accurately [7,9,10], as observed in this study by the lack of correlation between static and dynamic parameters. It appears that static measures taken during PWB are the most accurate predictor of dynamic function, however some information about deformation of foot during locomotion is needed to improve classification of foot arch type [5,6].

Although both include valuable information about the foot, SRAD and Arch Ratio were not correlated. We must consider the amount of static deformation as well as the height of the MLA, as these may not be well correlated [15]. A more comprehensive categorisation of foot type may be achieved when static and dynamic measures are combined. This will be attempted in an extension of this study by combining the parameters measured into a single foot index.

REFERENCES

1. McClay I & Manal K. *J App Biom* **13**, 109-124, 1997.
2. Nigg BM, et al. *J Biomech* **26**, 909-916, 1993.
3. Nawoczenski DA, et al. *Phys Ther*, **78**, 404-416, 1998.
4. Hawes MR, et al. *Foot & Ankle*, **13**(1), 22-26, 1992.
5. Razeghi M & Batt ME. *Gait & Pos*, **15**, 282-291, 2002
6. Williams DS & McClay IS. *Phys Ther*, **80**, 864-871, 2000
7. McPoil TG & Cornwall MW. *JOSPT*, **24**, 309-314, 1996
8. Scharfbillig R, et al. *JAPMA*, **94**(1), 31-38, 2004.
9. Miller JE, et al. *Proc. of ISB XVII^th^*, Calgary, 513, 1999
10. Knutzen KM & Price A. *JAPMA*, **84**(4), 171-180, 1994.
11. Nigg BM, et al. *Med. Sci. SpEx.*, **30**, 550-555, 1998.
12. Digby CJ & Lake MJ. *2nd Staff Conf on Clin Biom*, 2004.
13. Razeghi M. *Unpub. doctoral thesis*, Nottingham Uni, 2001.
14. Digby CJ, et al. *Ergonomics*, in press.
15. Nachbauer W & Nigg. *Med. Sci. SpEx.*, **24**, 1264-1269, 1992.

SOFT TISSUE COMPARTMENT RESPONSE TO AN UNEXPECTED SURFACE CHANGE.

[1] Katherine A. Boyer, [2] Benno M. Nigg
Human Performance Laboratory, Departments of Mechanical Engineering[1] and Kinesiology[2] University of Calgary

INTRODUCTION

During locomotion, the body adapts to changes in surface or shoe sole properties by changing the GRF, kinematics, joint stiffness and/or muscle activity [1,2,3]. It has been speculated that one reason for these changes may be to limit vibrations of the soft tissue [4]. The amplification of the skeletal acceleration (input) for soft tissue vibrations depends on the magnitude, length and shape of the input signal. Resonance will occur when the input frequency equals the natural frequency of a given soft tissue compartment (Fig 1.). It has been shown that accelerations of soft tissue compartments remain constant and that EMG pre-activation changes with changing loading rate, G_z [5] when the input frequency is close to the natural frequency of a soft tissue compartment. Maintaining a constant acceleration level is possible if (a) damping in the soft tissue compartment is increased to reduce the accelerations [4] or (b) lower extremity kinematics are altered to change the skeletal acceleration transient rate. However, for an unexpected change of the input signal the muscle pre-activation should remain constant while the acceleration level should change. Thus, the purpose of this study was to compare the soft tissue vibrations for an expected and an unexpected excitation signal near its resonance vibration frequency. It is expected that this study will increase the understanding of the function of muscle pre-activation and the potential adaptations to changes in surface stiffness during running. The hypotheses tested were:

H(1): Frequencies: f_{nat}(expected) ≈ f_{nat}(unexpected),
H(2): accelerations: a(expected) < a(unexpected/hard),
H(3): EMG(preHS): EMG(expected) ≈ EMG(unexpected)

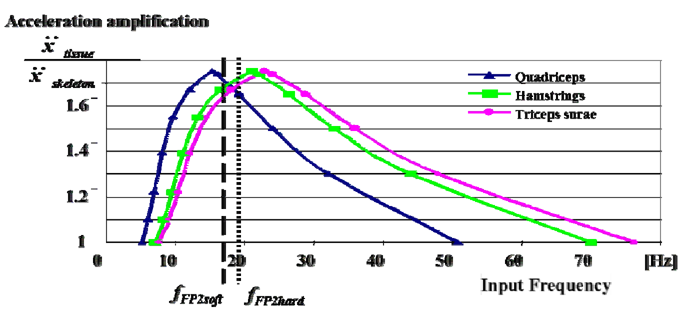

Figure 1: Theoretical response spectrum for the quadriceps, hamstrings and triceps surae soft tissue compartments, assuming a system with a simple mass and linear spring. Input is a versed sine pulse with magnitude and duration τ; thus $f_{in}=1/(2*\tau)$.

METHODS:

Fourteen male subjects ran at 4.8 +/- 0.2 m/s on a 24 m long runway instrumented with 3 consecutive force platforms (Kistler, Type Z4852/C) while soft tissue accelerations and muscle activity [5] were measured. Overlying the runway were two different flooring surfaces to change the input signal. To hide the location of the surface change a thin carpet was placed on top of the flooring. The surfaces were arranged in two different ways (Fig. 2). The experimental conditions were presented in a randomized block sequence, ABBAAB. Data was collected for the following steps of running: (Control condition) $FP1_{soft}$, $FP2_{soft}$, $FP3_{hard}$; (Test condition) $FP1_{soft}$, $FP2_{hard}$ (unexpected), $FP3_{hard}$ (expected).

Peak acceleration and the frequency power spectra were determined for each accelerometer signal. The EMG intensity was summed for a 50 ms window prior to heel-strike to determine the pre-activation EMG intensity. F_z, and G_z, were determined from the GRF data. The time of peak leg acceleration was estimated from the F_z and G_z maximums. Each subject was examined independently to determine the relationship between EMG, input signal and soft tissue accelerations. Paired t-tests and repeated measures ANOVA ($p<0.05$) were used to determine group differences between the expected and unexpected conditions.

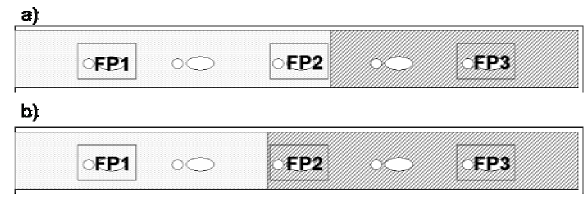

Figure 2: Experimental set-up. a) Control condition b) Test condition.
Surface 1: soft Surface 2: hard

RESULTS AND DISCUSSION:

(1) The natural frequencies of the soft tissue compartments were the same for the expected and the unexpected situation, indicating that the vibration characteristics have not been changed because the change was not expected.
(2) The soft tissue accelerations were typically higher for the unexpected than for the expected condition. They were highest when the input frequency was close to the natural frequency of a soft tissue compartment.
(3) The EMG intensities were the same for the expected and the unexpected situation since the subjects could not prepare.
(4) EMG and GRF showed no systematic changes for the third step, which suggests that the expectations and/or the applied strategies were different for the different subjects.
Specifically illustrated for subject P: The natural frequencies were estimated at 15.23 Hz, 20.95 Hz, and 22.85 Hz for the quadriceps, hamstrings and triceps surae, respectively. There was no change in the EMG pre-activation intensity between the unexpected (step $FP2_{hard}$) and the expected surface condition (step $FP2_{soft}$). There was an increase in the magnitude of the peak acceleration of 3%, 10% and 7% for the quadriceps, hamstrings and triceps surae. The input frequencies were estimate as 17.7 Hz for the soft expected and 19.0 Hz for the hard unexpected surface. As expected based on the theoretical response spectrum (Fig 1.) for a shift in the input frequency from 17.7 to 19 Hz the greatest increase in acceleration occurred in the hamstrings.

CONCLUSIONS

Increased soft tissue vibrations did occur when a runner experienced an unexpected impact with a frequency close to the natural frequency of a soft tissue compartment.

REFERENCES:

1. Dixon S. J.et al., *Med.Sci.Sports Exerc.* **32** 1919-1926 2000
2. Wakeling J. M.et al., *J.Appl.Physiol* **91** 1307-1317 2001
3. Hardin E. C.et al., *Med.Sci.Sports Exerc.* **36** 838-844 2004
4. Nigg B. M. *Curr Opin Orthopaed.* **8** 43-47 1997
5. Boyer K. A. and Nigg, B. M. *J.Biomech* **37** 1583-1588 2004

A MATHEMATICAL DEFINITION OF FEASIBLE FINGER POSTURES AND MOVEMENTS

[1] Saurabh Mahapatra, [2]John Guckenheimer and [1]Francisco J. Valero-Cuevas
[1] Neuromuscular Biomechanics Laboratory, [2] Department of Mathematics, Cornell University, NY, USA,
email: {SM387, JMG16, FV24}@cornell.edu

INTRODUCTION

It is not well understood why or how neurological diseases or injuries so easily disrupt the delicate interactions among finger muscles that produce finger postures and slow movements. Thus, we lack clear therapeutic approaches to, say, shape the hand for grasp following stroke. A first-order dynamical systems approach is applicable to this neuromuscular control problem because finger postures are combinations of joint angles, and slow finger movements are damped during transitions between postures. Our long-term goal is to explicitly define the manifold of feasible finger postures in state-space as a function of the continuous muscle inputs that drive the fingers to various configurations during slow movements. As a first step, we develop here, the mathematical tools to find such manifolds and their stable points. While our approach is reminiscent of the *deformable membrane* analogy of the equilibrium-point hypothesis, our purpose is quite different: to determine whether first-order dynamical equations derived from basic biomechanical and muscle mechanics concepts can begin to explain experimental measurements of finger postures and slow movements.

METHODS

To facilitate visualization of our methods, we present the example of a tendon-driven, 2-joint, planar finger with anatomically inspired tendon routing [1]. For quasi-static motions, muscles are modeled as simple force-length actuators with the resting lengths as parametric inputs and the tendons are modeled as elastic bands. Using geometrical constraints obtained from tendon routing, we obtain relationships between tendon stretch/excursions and joint angles (generalized coordinates). This relationship we obtain is called the transmission matrix $\boldsymbol{G}$. For a given set of muscle resting length inputs, the potential energy of the system can be written as a non-linear function of tendon stretch/excursions and joint angles. This potential energy function is a high dimensional manifold in the generalized coordinate space whose maxima/minima give the equilibrium postures for the finger. These maxima/minima when plotted as a function of the muscle input parameters also give a manifold, the local and global properties of which determine if the system is controllable locally and/or globally. We use results from manifold theory to study such properties. For example, the Implicit Function Theorem lays down the sufficient conditions for a functional relationship to exist between the muscle inputs and the output generalized coordinates [2].

RESULTS AND DISCUSSION

For the above example, we found that the transmission matrix $\boldsymbol{G}$ determines the controllability of the system. A necessary and sufficient condition for such a system to be controllable is that the rank of the matrix $\boldsymbol{G}$ should be equal to the number of joints (generalized coordinates). For two test cases, the results are shown in Figure 2. We found that the cross-over tendon m3 shown in Figure 1 (analogous to the extensor mechanism of the fingers) plays a major role in determining this rank for $\boldsymbol{G}$, hence showing the importance of anatomically faithful models.

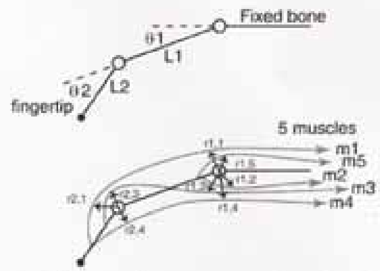

Figure 1: The tendon geometry for the 2-link 5-muscle finger.

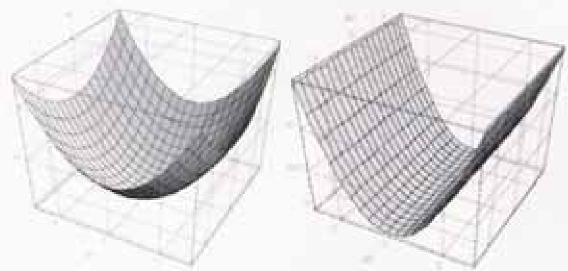

Figure 2: Left: The potential energy function manifold is a paraboloid in the joint angle space when rank ($\boldsymbol{G}$) =2. The system is fully controllable along the two degrees of freedom. Right: The potential energy function manifold reduces to a parabolic cylinder when rank ($\boldsymbol{G}$) =1. There is loss of controllability along the axis of this cylinder.

Having developed the ability to calculate the manifolds that predict stable finger postures and gradients for finger movement, our next step is to create anatomically faithful 3D models of the human finger with complex tendon geometry.

REFERENCES

1. Valero-Cuevas FJ, An integrative approach to the biomechanical function and neuromuscular control of the fingers, *J Biomech*, in press.
2. Boothby W, *Differentiable Manifolds*, Academic Press.

ACKNOWLEDGEMENTS

This material is based upon work supported by the National Science Foundation under CAREER Grant #0237258 and the National Institutes of Health Grant R01-050520 to Francisco Valero Cuevas.